



Cone Penetration Testing 2022



CRC Press
Taylor & Francis Group

Editors
Guido Gottardi & Laura Tonni

CONE PENETRATION TESTING 2022

This volume contains the proceedings of the 5th International Symposium on Cone Penetration Testing (CPT'22), held in Bologna, Italy, 8-10 June 2022. More than 450 authors - academics, researchers, practitioners and manufacturers – contributed to the peer-reviewed papers included in this book, which includes three keynote lectures, four invited lectures and 170 technical papers. The contributions provide a full picture of the current knowledge and major trends in CPT research and development, with respect to innovations in instrumentation, latest advances in data interpretation, and emerging fields of CPT application.

The paper topics encompass three well-established topic categories typically addressed in CPT events:

- Equipment and Procedures
- Interpretation
- Applications.

Emphasis is placed on the use of statistical approaches and innovative numerical strategies for CPT data interpretation, liquefaction studies, application of CPT to offshore engineering, comparative studies between CPT and other in-situ tests. **Cone Penetration Testing 2022** contains a wealth of information that could be useful for researchers, practitioners and all those working in the broad and dynamic field of cone penetration testing.



Taylor & Francis

Taylor & Francis Group

<http://taylorandfrancis.com>

PROCEEDINGS OF THE 5TH INTERNATIONAL SYMPOSIUM ON CONE PENETRATION TESTING (CPT'22), 8-10 JUNE 2022, BOLOGNA, ITALY

Cone Penetration Testing 2022

Editors

Guido Gottardi

Department of Civil, Chemical, Environmental and Materials Engineering, University of Bologna, Bologna, Italy

Laura Tonni

Department of Civil, Chemical, Environmental and Materials Engineering, University of Bologna, Bologna, Italy



CRC Press

Taylor & Francis Group

Boca Raton London New York Leiden

CRC Press is an imprint of the
Taylor & Francis Group, an **informa** business

A BALKEMA BOOK

Cover image: photo by Claudio Turci

First published 2022
by CRC Press/Balkema
Schipholweg 107C, 2316 XC Leiden, The Netherlands
e-mail: enquiries@taylorandfrancis.com
www.routledge.com – www.taylorandfrancis.com

CRC Press/Balkema is an imprint of the Taylor & Francis Group, an informa business

© 2022 selection and editorial matter, Guido Gottardi & Laura Tonni; individual chapters, the contributors

The right of Guido Gottardi & Laura Tonni to be identified as the authors of the editorial material, and of the authors for their individual chapters, has been asserted in accordance with sections 77 and 78 of the Copyright, Designs and Patents Act 1988.

The Open Access version of this book, available at www.taylorfrancis.com, has been made available under a Creative Commons Attribution-Non Commercial-No Derivatives 4.0 license.

Although all care is taken to ensure integrity and the quality of this publication and the information herein, no responsibility is assumed by the publishers nor the author for any damage to the property or persons as a result of operation or use of this publication and/or the information contained herein.

Library of Congress Cataloging-in-Publication Data

A catalog record has been requested for this book

ISBN: 978-1-032-31259-0 (hbk)
ISBN: 978-1-032-36228-1 (pbk)
ISBN: 978-1-003-30882-9 (ebk)
DOI: 10.1201/9781003308829

Table of contents

Preface	xvii
Symposium organizers	xix
Committees	xxi
International advisory board	xxiii
Reviewers	xxv
Sponsors	xxix
Keynote lectures	
New CPT methods for evaluation of the axial capacity of driven piles <i>B.M. Lehane, E. Bittar, S. Lacasse, Z. Liu & F. Nadim</i>	3
Material Point Method simulations of cone penetration and CPT interpretation <i>R. Salgado, V. Bisht & M. Prezzi</i>	16
Practical use of shear wave velocity measurements from SCPTU in clays <i>M. Long</i>	28
Invited papers	
Uncertainties associated with CPT data acquisition <i>R. Soage Santos</i>	55
CPT equipment: Recent advances and future perspectives <i>D.J. White</i>	66
Non-deterministic interpretation and applications of CPT testing data <i>M. Uzielli</i>	81
Combined use of CPT & DMT: Background, current trends and ongoing developments <i>P. Monaco</i>	94
Technical papers	
<i>Session 1: Equipment and procedures</i>	
Incorporation of SH source wave parameter “SH Polarization” within DST seismic trace characterization <i>E. Baziw & G. Verbeek</i>	109

Methodology for obtaining true cone bearing estimates from blurred and noisy measurements	115
<i>E. Baziw & G. Verbeek</i>	
Evaluation of parameters inducing desaturation of a piezocone: Saturation liquid viscosity and exposure to dry sand	121
<i>G. De Backer, R.D. Verastegui-Flores, W. Vervaele, L. Vincke & K. Haelterman</i>	
Large diameter cone penetrometers: What is an appropriate location for the transition to the rod diameter?	126
<i>D.A. de Lange, T.A. van Duinen & D.J. Peters</i>	
Issues related to piezocone sleeve friction measurement accuracy in soft sensitive clays	132
<i>B. Di Buò, M. D'Ignazio, T. Lämsivaara & M. Haikola</i>	
Flow cone – new CPTU add-on module trialled in Halden silt	138
<i>A.S. Gundersen, T. Lunne, R. Stelzer, Ø. Blaker, G.W. Tucker & L. Krogh</i>	
Estimating in-situ frozen loamy soil viscosity from CPT	144
<i>O.N. Isaev</i>	
Determination of natural stress state parameters for clay soils by using 3LSU-CPTU penetrometer	151
<i>O.N. Isaev, R.F. Sharafutdinov & D.S. Zakatov</i>	
Towards correlating seabed penetrometer and chirp sonar measurements	158
<i>R. Jaber & N. Stark</i>	
Development of free fall cone penetration testing system	164
<i>H. Kang, O. Kwon, C. Shin, J. Seo, I. Jang & M. Dong-Woo</i>	
Evaluation of statistical fluctuation of measured data from nuclear density cone penetrometer	170
<i>M. Karthikeyan</i>	
On the accuracy and precision of the seismic cone penetration test – a field test study on the seismic source	176
<i>O. Koreta, A.H. Augustesen, L. Krogh, K. Lundvig & S. Bøtker-Rasmussen</i>	
The revival of multiple pore pressure measurements in the cone penetration test	183
<i>T. Lunne, R.K. Ghanekar, G.W. Tucker, R. Santos & L. Krogh</i>	
Comparisons CPT-DMT in soft clay at Fucino-Telespazio GeoTest site	190
<i>D. Marchetti, P. Monaco, G. Totani, F. Totani & S. Amoroso</i>	
An innovative new 3MPa CPT – to detect and measure very small fs values	197
<i>A.J. McConnell & E.J.C. Wassenaar</i>	
Assessment of seismic cone penetration testing for small strain shear modulus	203
<i>N. Parasie, T. Franken & J. Peuchen</i>	
Experimental procedure for checking the saturation degree of piezocone tips	209
<i>I. Rocchi, L. Tonni, G. Gottardi & M. Marcolongo</i>	
Using penetrometer in situ and in box-core testing to obtain design information for lazy wave riser-soil interaction	214
<i>O. Safaqah, H.E. Low, S. Pant, S. Ingarfield, M.F. Bransby, M.F. Randolph & Z.J. Westgate</i>	

Calibration of cone penetrometers according to International Organization for Standardization requirements	220
<i>R. Soage Santos, E. Gómez Meyer, J. Peuchen, G. Yetginer, T. Lunne & T. Carrington</i>	
Long-term strength determination of frozen soils by CPT	225
<i>I. Sokolov & N. Volkov</i>	
Efficiency examined of hands-free Cone Penetration Testing using the SingleTwist™ with COSON	229
<i>O. Storteboom, M. Woollard & J. Verhagen</i>	
Sustainability in CPT practice: Hybrid CPT Track-Truck	235
<i>O. Storteboom, M. Woollard & B. Ooms</i>	
Elastic soil properties investigated using seismic tests to complement the CPT	241
<i>O. Storteboom, M. Woollard & J.L. Rangel-Núñez</i>	
Tensiocone: A cone penetrometer with the facility to measure negative pore-water pressure	247
<i>A. Tarantino, A. Capotosto, F. Bottaro, M. Bellio & D. Gallipoli</i>	
New portable pressiocone system for carrying out CPT+FDP tests	253
<i>G. Vinco & M. Sacchetto</i>	
Characterisation of near-surface sediments using a blend of vertical and shallow rotational penetrometers	258
<i>D.J. White, S.A. Stanier & H. Mohr</i>	
Development of an enhanced CPT system for Dogger Bank	266
<i>T.I. Yetginer-Tjelta, S. Botker-Rasmussen, M. Rose, T. Lunne, V. Meyer & C. Duffy</i>	
 <i>Session 2: Interpretation</i>	
CSi – a joint industry project into CPTUs in silty soils	275
<i>A.H. Augustesen, P. Carotenuto, C. Bilici, T. Lunne, R.C.J. Lindeboom, L. Krogh, J. van den Bosch, R. Barth, C. Erbrich, S. Ingarfield, D. Giretti, V. Fioravante, H. Dias, M.-C. Sougle, A. Barwise, S. de Wit, D. Burbury & N. Adams</i>	
Numerical investigation of piezocone dissipation tests in clay: Sensitivity of interpreted coefficient of consolidation to rigidity index selection	282
<i>A. Barati Nia, D.M. Moug, A.P. Huffman & J.T. DeJong</i>	
Correlation of CPT measurements and VibroCore penetration speed for medium, calcareous sands: A case study of the cable route survey at the North sea	288
<i>K. Bartczak & G. De Vries</i>	
CPT data interpretation for an improved characterization of the paleosol stratigraphy in the Po River Valley, Italy	294
<i>I. Bertolini, M. Marchi, L. Tonni, G. Gottardi, L. Bruno & A. Amorosi</i>	
Application of CPT to the evaluation of permeability in a Po river embankment prone to backward erosion piping	300
<i>I. Bertolini, G. Gottardi, M. Marchi, L. Tonni, A. Bassi & A. Rosso</i>	
Dissipation tests to evaluate the equilibrium pore pressure	306
<i>F.A.B. Danziger, G.M.F. Jannuzzi & A.V.S. Pinheiro</i>	

Dynamic characteristics of the soils by Cone Penetration Tests (CPT) <i>A. Cavallaro</i>	311
Validating cone penetration test in partially drained conditions using a simplified numerical modelling method <i>R.W.L. Chia, Z.Z. Wang & S.H. Goh</i>	317
Cone penetration testing to constrain the calibration process of a sand plasticity model for nonlinear deformation analysis <i>A. Chiaradonna, T.J. Carey, K. Ziotopoulou & J.T. DeJong</i>	325
Probabilistic delineation of soil layers using Soil Behaviour Type Index <i>S. Collico, M. Arroyo, M. DeVincenzi, A. Rodriguez & A. Deu</i>	332
Clustering analysis to improve total unit weight prediction from CPTu <i>S. Collico, M. Arroyo, M. DeVincenzi, A. Rodriguez & A. Deu</i>	339
Combining CPTU and UMASW to characterise Irish offshore deposits <i>M. Coughlan, A. Trafford, M. Long, S. Donohue & S. Corrales</i>	345
Cone factor from CPTU tests in very soft clays at the east of Mexico's valley <i>J.M. De La Rosa R. & F.A. Flores López</i>	351
Piezocoone testing in Nordic soft clays: Comparison of high-quality databases <i>M. D'Ignazio, B. Di Buò, T. Länsivaara, J.S. L'Heureux, P. Paniagua & J. Selänpää</i>	356
Prediction of resilient modulus of cohesive subgrade soils from CPTU data using polynomial neural networks <i>W. Duan, Z. Zhao, G. Cai, A. Wang, R. Chen, A.J. Puppala, S. Liu & S.S.C. Congress</i>	363
Effect of sand bio-cementation on cone tip resistance: A numerical study <i>M.El Kortbawi, K. Ziotopoulou, J.T. DeJong & D.M. Moug</i>	368
A data-driven approach to predict shear wave velocity from CPTu measurements <i>I. Entezari, J. Sharp & P.W. Mayne</i>	374
Interpretation and comparison of CPT derived soil properties to static and cyclic laboratory tests on unique fine-grained soils in Western Washington and Oregon <i>B. Exley, A. Pynch, J. Jacoby & B. Thunder</i>	381
Evaluation of cyclic softening potential using CPTu and assessment with cyclic triaxial test results: A case study <i>K. Fakharian, M. Bahrami, M. Kashkooli, H. Vaezian & T. Bahrami</i>	387
Application of integrated Game Theory-optimization subground stratification (-IGTOSS) model to Venetian Lagoon deposits <i>M.S. Farhadi, T. Länsivaara & L. Tonni</i>	394
Application of two novel CPTu-based stratification models <i>M.S. Farhadi, T. Länsivaara, J.S. L'Heureux & T. Lunne</i>	400
Numerical simulation of CPT in sands using DeltaSand and Hardening Soil models <i>M. Fetrati, V. Galavi, M. Goodarzi, S. Kreiter & T. Mörz</i>	407
CPT calibration in centrifuge: Effect of partial saturation on cone resistance <i>V. Fioravante, D. Giretti, E. Dodaro, C.G. Gragnano & G. Gottardi</i>	414

Calibration cone penetration testing in silty soils	420
<i>V. Fioravante, D. Giretti, T. Lunne, P. Carotenuto, A.H. Augustesen, R.C.J. Lindeboom, L. Krogh, H. Dias, M.-C. Sougla, A. Barwise, S. de Wit & D. Burbury</i>	
Comparison between coefficients of consolidation from CPTu and laboratory tests for Guaratiba's soft soil, Rio de Janeiro, Brazil	427
<i>M.M. Freire, M.E.S. Marques, M.C. Tassi & L.A. Berbert</i>	
Quantitative modelling of spatial variability of piezocone data from Venice lagoon silty soils	432
<i>G. Gottardi, M. Ranalli, L. Tonni & M. Uzielli</i>	
Thin-layer detection from the cone resistance rate of change	438
<i>H.B. Hammer, S. Nordal, J.-S. L'Heureux & H. Skrede</i>	
Recalculation of in-situ CPTu in intermediate soils using G-PFEM	445
<i>L. Hauser, S. Oberhollenzer, A. Gharehaghajlou, H.F. Schweiger, R. Marte & C. Fabris</i>	
Full-flow CPT tests in a nearshore organic clay	452
<i>S. Hov, K. Borgström & P. Paniagua</i>	
Bayesian supervised learning of 2D subsurface soil stratigraphy using limited cone penetration tests with consideration of uncertainty	459
<i>Y. Hu & Y. Wang</i>	
Estimation of constrained modulus from CPT measurements in case of Holocene sands	466
<i>Z. Illés, I. Kádár, G. Nagy, A. Mahler & L. Nagy</i>	
Evaluation of complex CPTu dissipation tests of B.E.S.T.	473
<i>E. Imre, M. Hegedűs, L. Bates & S. Fityus</i>	
Simulation of CPT penetration in sensitive clay	480
<i>J. Isaksson, J. Yannie, M. Karlsson & J. Dijkstra</i>	
A CPT-based method for estimation of undrained shear strength of sands and transitional soils	486
<i>K. Kaltekis & J. Peuchen</i>	
Comparison of frozen soil strength characteristics by cone penetration and triaxial compression testing	491
<i>D. Lagosha, I. Sokolov & N. Volkov</i>	
Fincone: A study on the use of CPT in soft sensitive clays	497
<i>T. Lämsivaara, B. Di Buò, J. Selänpää, M. Knutti & M. Haikola</i>	
CPT-based unit weight estimation extended to soft organic clays and peat: An update	503
<i>H.J. Lengkeek & R.B.J. Brinkgreve</i>	
CPT-based classification of soft organic clays and peat	509
<i>H.J. Lengkeek & R.B.J. Brinkgreve</i>	
Shear wave velocity – SCPTU correlations for sensitive marine clays	515
<i>M. Long & J.S. L'Heureux</i>	
A simplified method to incorporate the benefits of microstructure for cyclic liquefaction analyses using the SCPT	521
<i>K. Lontzetidis, P.K. Robertson & D.J. Morton</i>	

Classification of Miocene deposits using CPT data <i>A. Makra & H. Kim</i>	528
On the interpretation of piezocone dissipation testing data in clay <i>F.M. Mántaras, F.S. Pereira, E. Odebrecht & F. Schnaid</i>	534
Determination of fine-grained soil parameters using an automated system <i>I. Marzouk, F. Tschuchnigg, F. Paduli, H.J. Lengkeek & R.B.J. Brinkgreve</i>	540
Undrained shear strength of clays from piezocone tests: A database approach <i>P.W. Mayne & J. Peuchen</i>	546
Evaluating geoparameters of Maine sensitive clay by CPTU <i>P.W. Mayne, P. Paniagua, B. Di Buò & S.S. Agaiby</i>	552
CPTU evaluations in Appalachian Piedmont residual sandy silts <i>P.W. Mayne & E. Cargill</i>	559
Soil unit weight prediction from CPTs for soils and mining tailings <i>T. Menegaz, E. Odebrecht, H.P. Nierwinski & F. Schnaid</i>	566
Use of DMT and CPTU to assess the G_0 profile in the subsoil <i>Z. Mlynarek, J. Wierzbicki & P. Monaco</i>	570
Physical and numerical modelling of T-CPT for mechanisms of penetration and heat transfer <i>P.Q. Mo, L. Gao, H.S. Yu, X.L. Tao & Q.Z. Ma</i>	577
Soil stratigraphy from seismic piezocone data and multivariate clustering in alluvial soil deposits: Experience in the Lower Tagus Valley region <i>F. Molina-Gómez, D. Cordeiro, C. Ferreira & A. Viana da Fonseca</i>	584
Undrained strength from CPTu in brittle soils: A numerical perspective <i>L. Monforte, M. Arroyo & A. Gens</i>	591
Assessment of deltaic soil behavior classification using AUT: GMD database regarding CPTu records <i>M.H. Naghibi, A. Eslami & S. Heidarie Golafzani</i>	598
A review of methods for estimating undrained brittleness index from the CPT <i>Y. Narainsamy & S.W. Jacobsz</i>	604
A comparative study on CPTu-based soil classification methods: Case studies <i>T.D. Nguyen, P.S. Khin, Q.N. Pham & A.T. Vu</i>	610
Characterization of young sediments using CPTu and Medusa SDMT <i>S. Oberhollenzer, L. Hauser, F. Brand, R. Marte, H.F. Schweiger, D. Marchetti & S. Pfeifer</i>	617
PFEM modeling of CPTu tests in saturated structured soils <i>K. Oliynyk, M.O. Ciantia & C. Tamagnini</i>	623
Effect of the scatter between CPTU measured parameters in soil classification <i>P. Paniagua & J.-S. L'Heureux</i>	630
Evaluation of shear wave velocity profiles in alluvial and deltaic soils using a CPT database <i>J. Paredes & F. Illingworth</i>	636
Upscaling 1 500 000 synthetic CPTs to voxel CPT models of offshore sites <i>J. Peuchen, W. van Kesteren, V. Vandeweyer, S. Carpentier & F. van Erp</i>	641

Automated CPT interpretation with a Convolutional Neural Network <i>M. Pippi, R. Vink, J. Haasnoot & S. Bersan</i>	646
Watch out for the use of global correlations and “black box” interpretation of CPTU data <i>J.J.M. Powell & L. Dhimitri</i>	651
New methods for assessing Plasticity Index and Low-strain Shear Modulus in fine-grained offshore soils <i>N. Ramsey & K.K. Tho</i>	657
Cone penetration testing and interpretation in the holds of two ore-carrying vessels <i>N. Ramsey</i>	664
Suction influence on CPT and DMT for some Brazilian tropical soils <i>B.P. Rocha, R.A. Rodrigues & H.L. Giacheti</i>	670
Study of SPT-CPT and DP-CPT correlations for sandy soils <i>M.D. Santos & K.V. Bicalho</i>	677
Correlation between SPT and CPT tests in liquefiable deposits <i>R. Shahgholian, C. Ferreira & A. Viana da Fonseca</i>	683
CPTU-detection of thin clay layers in sand: Results from calibration chamber tests <i>H. Skrede, H.B. Hammer, S. Nordal & J.S. L’Heureux</i>	690
Determination of hydraulic conductivity using HPT & CPTu <i>M. Slowiok, S. Oberhollenzer, R. Marte & T. Freudenthaler</i>	697
DEM-FDM coupling simulation of cone penetration tests in a virtual calibration chamber <i>Y. Song, X.Q. Gu & J. Hu</i>	703
Data-driven soil profile characterization using statistical methods and artificial intelligence algorithms <i>R.L. Spacagna, A. Baris, L. Paoella & G. Modoni</i>	708
Capability of seismic CPTu and DMT in assessing propagation velocity of body waves: A comparative study <i>S. Stacul, D. Lo Presti, N. Nenci, F. Fiera, M. Perini, D. Marchetti, E. Pagani & M. Siviero</i>	715
Bayesian estimation of small-strain shear modulus from offshore CPT tests in the North Sea <i>B. Stuyts, C. Sastre Jurado, D. Gomez Bautista & A. Kheffache</i>	722
Factors influencing $CPT_U N_{kt}$ for marine clay in Singapore reclaimed land <i>C. Tanaka, M. Angeles & J.Y. Wong</i>	728
Parameters affecting the CPT resistance of reconstituted sands <i>Y. Tian & B.M. Lehané</i>	734
Practical experience with cone penetration in frozen soils <i>N.G. Volkov, I.S. Sokolov & R.A. Jewell</i>	741
A site-specific relationship between CPT data and fines content for fine grained soil in the context of liquefaction analyses <i>C. Vrettos</i>	747
Numerical modelling of cone penetration tests in spatially variable clays <i>Z.Z. Wang, S.H. Goh & X. Zheng</i>	753

Some aspects of in situ testing of clay-glacial till mixture redeposited as man-made fills <i>J. Wierzbicki, K. Stefaniak, S. Wilczyński & B. Brzeziński</i>	760
Cone penetration in a thin medium dense sand layer sandwiched by different clay layers – LDFE analysis <i>Q. Xie, Y.X. Hu, M.J. Cassidy & M. Zhou</i>	766
Study on SPT N-values and relative density through various soundings in full-scale chamber test ground <i>H. Yabe, K. Harada, T. Ito & E. Watanabe</i>	772
Correcting measured CPT tip resistance for multiple thin-layer effects <i>K.M. Yost, J. Cooper, R.A. Green, E.R. Martin & A. Yerro</i>	778
Spatial interpolation of consolidation property of clays from limited CPTU dissipation data <i>Z. Zhao, W. Duan, G. Cai, M. Wu, Anand J. Puppala, S. Liu & S.S.C. Congress</i>	784
 <i>Session 3: Applications</i>	
Evaluation of the geotechnical behavior of mining tailings through CPTU tests in the soil improvement process for the decharacterization of upstream heightened dams <i>J.L. Albino, T.A.T. Souza J. & L.S. Machado</i>	793
VCPT: An in-situ soil investigation method to validate vibratory pile-soil interaction models <i>D. Al-Sammarraie, S. Kreiter, T. Mörz, M.O. Kluger & M. Goodarzi</i>	799
Monitoring ground improvement by Rammed Aggregate Piers using a combined CPTU and SDMT approach at a silty sand liquefaction-prone site in Emilia-Romagna <i>S. Amoroso, M.F. Garcia Martínez, L. Tommi, G. Gottardi, P. Monaco, K.M. Rollins, L. Minarelli, D. Marchetti & K.J. Wissmann</i>	806
A CPT-based method for monotonic loading of large diameter monopiles in sand <i>S. Bascunan, K. Kaltekis, B. van Dijk & K. Gavin</i>	812
Automatic interpretation and statistical evaluation of soil conditions for preliminary design of offshore foundations using the cone penetration test <i>L. Berenguer Todo Bom & M. Kanitz</i>	819
Effect of dynamic pile driving parameters on vibratory penetration <i>A. Bhaskar, S. Kreiter, D. Al-Sammarraie & T. Mörz</i>	825
Application of a new q_c averaging approach for end bearing of driven piles in sand <i>E.J. Bittar, Y. Tian & B.M. Lehane</i>	832
A review of a CPT based axial capacity prediction of screw piles in sand <i>E.J. Bittar, B.M. Lehane, S. Mahdavi, A.P. Blake, D.J. Richards & D.J. White</i>	838
CPT-based liquefaction ejecta evaluation procedure <i>J.D. Bray & D. Hutabarat</i>	844
Settlement estimations for buildings founded on saturated silty sands from CPT and DMT results <i>M. Cáceres, J. Fumeron, F.A. Villalobos & R. Moffat</i>	850
Numerical modeling of static load test in drilled shaft using CPTu results <i>M.A. Camacho, C.B. Camacho & V.H. Miranda</i>	857

Characterization of geotechnical spatial variability in river embankments from spatially adjacent SCPT	863
<i>F. Ceccato, M. Uzielli & P. Simonini</i>	
Coupling site wide CPT profiles and genetic algorithms for whole-site offshore windfarm layout optimization	870
<i>J.A. Charles, S.M. Gourvenec & M.E. Vardy</i>	
CPT-based model calibration for effective stress analysis of layered soil deposits	876
<i>A. Chiaradonna, N. Ntritsos & M. Cubrinovski</i>	
Stress increase induced by impact precast pile driving	883
<i>V. Colella, G. Cortellazzo, A. Dei Svaldi, S. Amoroso, L. Minarelli & K.M. Rollins</i>	
CPT based liquefaction potential of flood defences in The Netherlands	889
<i>T. de Gast, K.G. Gavin, P.D. Notenboom, R. Abraimi & C. Reale</i>	
Application of the CPT for liquefaction assessment of gravelly reclamations at the port of Wellington	894
<i>R. Dhakal, M. Cubrinovski & J.D. Bray</i>	
Concept design of a new CPT module for direct in situ measurement of P-Y soil responses	900
<i>A. Diambra, J. Creasey, J. Leonet, A. Conn, E. Ibraim, G. Mylonakis, D. White, B. Cerfontaine, S. Gourvenec & D. Igoe</i>	
The use of dynamic probing tests and cone penetration tests to verify the effectiveness of expanding polyurethane resin injections for ground improvement	907
<i>A. Dominijanni, M. Gabassi, A. Minardi & S. Pavan</i>	
Evaluation of flow liquefaction susceptibility of a sandy-silt tailings using the CPTu	913
<i>M.P. dos Santos Junior, R. César Gomes, S.G. Silva Ribeiro & B.G. Delgado</i>	
Prospects on data mining approach for pile geotechnical design utilizing CPT and CPTu records: Case study: AUT database	920
<i>A. Eslami, S. Heidarie Golafzani & S. Moshfeghi</i>	
Evaluating mitigation of kinematic moments of precast driven piles in liquefiable layers using pre- and post-CPTu tests	926
<i>K. Fakharian, D. Mohtashamamiri, K. Behroozian, M. Bahrami, T. Bahrami & I.H. Attar</i>	
Verification of 3D FEM analysis of ground improvement works using CPT test results	932
<i>G.A. Faour & K.N. Khouri</i>	
A comprehensive design procedure for pile groups in liquefiable soils	938
<i>M. Franceschini, F. Fiorelli & E. Bandiera</i>	
Deep foundations of the new Pavilion 37 – fair quarter Bologna	944
<i>M. Franceschini, F. Fiorelli, E. Bandiera, V. Colella, G. Cortellazzo & A. Dei Svaldi</i>	
Consolidation settlement of coastal areas of the Emilia-Romagna region from cone penetration tests	949
<i>D. Giretti, V. Fioravante, L. Perini & L. Calabrese</i>	
A comparative study on liquefaction assessment of Rajarhat area of Kolkata by using different approaches	955
<i>A. Halder, K. Das, S. Nandi & K. Bandyopadhyay</i>	

Kriging analysis on CPTU data from offshore wind farm <i>R. He, J. Li, S. Yang & B. He</i>	961
Evaluation of CPT-based design method for offshore pile <i>B. Huang, E. Bittar, Y. Zhang & X. Fu</i>	967
Application of CPT based 3DFE approach for estimating monopile damping in sand <i>D. Igoe & M.B. Mohammed</i>	973
The use of CPTU for driven piles designed in a backfilled opencast ‘marl hole’ in an important post-industrial revolution area within the UK <i>D. Illingworth, C. Burton, L. Dhimitri, D. Ward & P. Shelton</i>	979
Consolidation settlement prediction using cone penetration testing <i>M. Kermani & F. Esford</i>	985
3D FE derivation of CPT based soil reaction curves for monopile lateral static design in sand <i>L.-M. Lapastoure & D. Igoe</i>	991
CPT-based assessment of densification induced by stone column installation <i>F. Marchi, E. Zambianchi, A. Boschi, A. Mastrangelo, G. Marchi, G. Gottardi & L. Tonni</i>	998
Geopier Impact technology for liquefaction risk mitigation based on CPTu investigations <i>G. Martinez, K. Wissmann, M. Franceschini, E. Bandiera & F. Fiorelli</i>	1004
Estimating bearing capacity of polar snow using the Cone Penetration Test (CPT) <i>A.B. McCallum & G. White</i>	1010
The use of CPT based metamodels to predict the performance of offshore anchor piles <i>A Mentani, L. Govoni & F. Bourrier</i>	1016
Spatial interpolation of sparse PCPT data to optimise infrastructure design <i>M.P. O’Neill, M.F. Bransby, J. Doherty & P. Watson</i>	1023
Use of CPT as a soil mixing verification tool: Some practical observations <i>A. O’Brien & I. Murray</i>	1029
Liquefaction damage assessment using Bayesian belief networks <i>L. Paolella, A. Baris, G. Modoni, R.L. Spacagna & S. Fabozzi</i>	1035
Geotechnical zoning of deltaic and alluvial soils of Guayaquil (Ecuador) using CPT and N_{kt} calibration based on FVT <i>J. Paredes, F. Illingworth & R. Luque</i>	1042
Use of piezocone with dissipation tests CPTu_Δu, in tailings dams in Mexico: Case history <i>J.L. Rangel-Núñez, E. Ibarra-Razo & R. Flores-Eslava</i>	1048
Assessment of the spatial variability of a Croatian flood embankment using the cone penetration test <i>C. Reale, M.S. Kovačević, M. Bacic & K.G. Gavin</i>	1053
Prediction of bearing capacity and settlement using penetrometer design method for shallow foundation and load transfer curves <i>P. Reiffsteck, F. Szymkiewicz, M.A. Benz Navarrete & T.A. Luong</i>	1058
Probabilistic analysis of gytja undrained strength from CPTU data for slope stability analysis <i>S. Rios, L. Sousa, A. Viana da Fonseca, P. Milheiro-Oliveira & O. Hededal</i>	1065

Monitoring ground improvement using in situ tests in Guayaquil, Ecuador <i>F. Ripalda, D. Falquez, D. Besenon, R. Luque, F. Illingworth & S. Amoroso</i>	1071
Plate anchor capacity estimation through CPT tip resistance in sand <i>A. Roy & S.H. Chow</i>	1077
CPT results and installation parameters for CFA piles in pyroclastic soils <i>G. Russo, M. Ramondini, A. Vecchiotti & G. Russo</i>	1083
Validation of CPT-based methods for estimation of footing settlement in sand <i>V.A. Sakleshpur, M. Prezzi & R. Salgado</i>	1089
Derivation of SRD for driven piles from CPT data <i>J.A. Schneider, M.F. Randolph & J.P. Doherty</i>	1095
New method for assessing soil liquefaction resistance using a cyclic cone penetrometer <i>A. Sharma, P. Rapanakis, E. Incardona, C. Dano, L. Sibille, B. Chareyre & H.H. Sadrabadi</i>	1102
Evaluation of deformation modulus during Cone Loading Tests (CLT) and settlement of shallow foundations <i>A. Teyssier, M. Rispal, C. Jacquard & P. Reiffsteck</i>	1107
Assessment of the potential for liquefaction using CPTu in the tailings dam I – Feijão <i>M. Tincopa & G. Carnero-Guzman</i>	1113
Is CPT a suitable in situ test for characterizing gravely sands? <i>G. Togliani</i>	1119
A CPT-based diameter-dependent m - θ spring model for lateral pile analysis <i>J. Tott-Buswell & L.J. Prendergast</i>	1126
An investigation into the use of the Vibdrive and β -methods for calculating the SRV of offshore piled foundations <i>M.P. Trubshaw, T. Joseph & G. Giuliani</i>	1131
Potential of the Cone Pressuremeter Test for obtaining stiffness degradation for offshore wind turbine monopile foundations <i>G.W. Tucker, C.T. Leth, L. Krogh, P. Ladefoged, T. Lunne & M. Taylor</i>	1137
Centrifuge study on the CPT based p - y models for the monopiles <i>H. Wang, D.V. van Zanten, D. de Lange, F. Pisanò, K. Gavin & A. Askarinejad</i>	1143
Using near-surface CPT data to predict foundation skirt embedment in partially drained carbonate sands <i>H.M. Wroth, M.F. Bransby, C.D. O'Loughlin, M.F. Silva, M. Cocjin, N. Levy & H.E. Low</i>	1149
The role of cone penetration testing in the Dogger Bank offshore wind farm <i>T.I. Yetginer-Tjelta, J. De Sordi, L. Cafferri, M. Rose, C. Duffy, T. Lunne, Ø. Blaker, S. Strandvik & V. Meyer</i>	1156
Procedures to evaluate seismic settlement in dry sand based on CPT Data – an update <i>F. Yi</i>	1164
Author index	1171



Taylor & Francis

Taylor & Francis Group

<http://taylorandfrancis.com>

Preface

This volume contains the contributions to the 5th International Symposium on Cone Penetration Testing, CPT'22, that took place in Bologna (Italy) from June 8th to 10th, 2022. The Symposium, built on the successful series of CPT events held in Delft (2018), Las Vegas (2014), Huntington Beach (2010) and Linköping (1995), was organized by the Italian Geotechnical Association (AGI) and the University of Bologna, under the auspices of the ISSMGE Technical Committee TC102.

Over the last decades, the use of the cone penetration testing for site investigation has steadily grown around the world, causing the CPT to be currently recognized as the major in situ testing technique in geotechnical engineering practice. Its widespread use has in turn stimulated the development of enhanced or new types of CPT equipment, aimed at both improving the accuracy of measurements and extending the field of application, along with the increasing demand for a sound understanding of penetration mechanisms and consistent interpretation methods, suitable for the characterization of a variety of soil deposits.

The CPT symposia have always provided a unique and fruitful forum for the exchange of new ideas and discussion on key issues within the largest gathering of world's experts, academics and non-academics, working in the broad and dynamic area of cone penetration testing. The objective of CPT'22 was therefore to foster a lively debate on current trends in cone penetration testing, among Researchers, Practitioners and Manufacturers, in a friendly and creative atmosphere for discussion and collaboration, as tradition of CPT events.

More than 450 Authors, coming from academic institutions, private companies and public bodies worldwide, contributed to the peer-reviewed papers included in this volume. The Symposium Organizing Committee was especially pleased with the unprecedented large number of contributions submitted, exceeding all expectations, and with the general high quality of the papers.

A total of 186 manuscripts were received and 170 of them were finally accepted for publication in the Symposium Proceedings. The papers were sorted into three well-established theme categories, according to the subject areas typically addressed in CPT events: Equipment and procedures, Interpretation, Applications. The volume also includes three outstanding keynote papers and four invited papers presented by renowned experts in specific thematic discussion sessions on selected key topics.

A significant effort was made to provide the Authors with a rigorous and fair review of the papers. The Editors are therefore very grateful to the almost one hundred Reviewers, for their generous and valuable work.

We gratefully acknowledge the support of the Italian Geotechnical Association, which organized the Symposium in cooperation with the University of Bologna. Special thanks are extended to the AGI Secretary, Mrs Susanna Antonielli, for her tireless work and patient assistance. We would also like to express our appreciation to all the Sponsors that helped us in making this conference a success.

Finally, many thanks to all Keynote Lecturers, Invited Speakers and Authors for their enthusiastic and proactive response to CPT'22, and for their contribution to this Proceedings volume.

We do hope you will find its content of valuable and long lasting use.

Guido Gottardi
Laura Tonni



Taylor & Francis

Taylor & Francis Group

<http://taylorandfrancis.com>

Symposium organizers

Italian Geotechnical Association, AGI



Alma Mater Studiorum – Università di Bologna



Under the auspices of



ISSMGE TC 102 “In-Situ Testing”



Taylor & Francis

Taylor & Francis Group

<http://taylorandfrancis.com>

Committees

ORGANIZING COMMITTEE

- Laura **Tonni** – *Chair, Università di Bologna, Italy*
Sebastiano **Rampello** – *Co-Chair, AGI Delegate, Sapienza Università di Roma, Italy*
Claudio **Soccodato** – *AGI General Secretary*
Susanna **Antonielli** – *AGI Secretary*
Sara **Amoroso** – *Università di Chieti-Pescara, Italy*
Giovanni **Biondi** – *Università di Messina, Italy*
Giovanni **Bosco** – *Università dell'Aquila, Italy*
Simonetta **Cola** – *Università di Padova, Italy*
Andrea **Dominijanni** – *Politecnico di Torino, Italy*
Laura **Govoni** – *Università di Bologna, Italy*
Carmine Gerardo **Gragnano** – *Università di Bologna, Italy*
Chiara **Iodice** – *Università della Campania Luigi Vanvitelli, Italy*
Maria Clorinda **Mandaglio** – *Università di Salerno, Italy*
Michela **Marchi** – *Università di Bologna, Italy*
Luca **Masini** – *Sapienza Università di Roma, Italy*
Claudia **Meisina** – *Università di Pavia, Italy*
Lorella **Montrasio** – *Università di Parma, Italy*
Irene **Rocchi** – *Technical University of Denmark, Denmark*
Gianpiero **Russo** – *Università di Napoli Federico II, Italy*
Ermanno **Pagani** – *Pagani Geotechnical Equipment, Italy*
Daniele **Spizzichino** – *ISPRA Istituto Superiore per la Protezione e la Ricerca Ambientale, Italy*
Stefano **Stacul** – *Università di Pisa, Italy*
Marco **Uzielli** – *Università di Firenze, Italy*
Maurizio **Ziccarelli** – *Università di Palermo, Italy*



Taylor & Francis

Taylor & Francis Group

<http://taylorandfrancis.com>

International advisory board

- Guido **Gottardi** – *Chair, Università di Bologna, Italy*
Nicola **Moraci** – *AGI President, Università “Mediterranea” di Reggio Calabria, Italy*
Marcos **Arroyo** – *Universitat Politècnica de Catalunya, Spain*
Guojun **Cai** – *School of Transportation Southeast University, China*
Misko **Cubrinovski** – *University of Canterbury, New Zealand*
Jason **DeJong** – *University of California Davis, United States*
Heraldo Luiz **Giacheti** – *São Paulo State University, Brazil*
Michael **Hicks** – *Delft University of Technology, The Netherlands*
An Bin **Huang** – *National Chiao Tung University, Taiwan*
Michele **Jamiolkowski** – *Politecnico di Torino, Italy*
Junichi **Koseki** – *University of Tokyo, Japan*
Tim **Länsivaara** – *Tampere University, Finland*
Jong-Sub **Lee** – *Korea University, Korea*
Barry **Lehane** – *The University of Western Australia, Australia*
Michael **Long** – *University College Dublin, Ireland*
Diego **Lo Presti** – *Università di Pisa, Italy*
Tom **Lunne** – *Norwegian Geotechnical Institute, Norway*
Mario **Manassero** – *Politecnico di Torino, Italy*
Alessandro **Mandolini** – *Università della Campania Luigi Vanvitelli, Italy*
Diego **Marchetti** – *Studio Prof. Marchetti, Italy*
Paul W. **Mayne** – *Georgia Institute of Technology, United States*
Paola **Monaco** – *Università dell’Aquila, Italy*
Joek **Peuchen** – *Fugro, The Netherlands*
John **Powell** – *GEOLABS Limited, United Kingdom*
Mark **Randolph** – *The University of Western Australia, Australia*
Peter K. **Robertson** – *PK Robertson Inc & Gregg Drilling Inc, United States*
Rodrigo **Salgado** – *Purdue University, United States*
Fernando **Schnaid** – *Universidade Federal do Rio Grande do Sul, Brazil*
Helmut **Schweiger** – *Graz University of Technology, Austria*
Paolo **Simonini** – *Università di Padova, Italy*
Laura **Tonni** – *Università di Bologna, Italy*
Antonio **Viana da Fonseca** – *Universidade do Porto, Portugal*
Phil **Watson** – *University of Western Australia, Australia*
David **White** – *University of Southampton, United Kingdom*



Taylor & Francis

Taylor & Francis Group

<http://taylorandfrancis.com>

Reviewers

- Glenda **Abate** – *Università di Catania, Italy*
Sara **Amoroso** – *Università di Chieti-Pescara, Italy*
Marcos **Arroyo** – *Universitat Politècnica de Catalunya, Spain*
Dusan **Berisavljevic** – *University of Belgrade, Serbia*
Silvia **Bersan** – *Crux Engineering BV, The Netherlands*
Ilaria **Bertolini** – *Università di Bologna, Italy*
Davide **Besenzon** – *Escuela Superior Politécnica del Litoral, Ecuador*
Katia V. **Bicalho** – *Federal University of Espirito Santo, Brazil*
Giovanni **Biondi** – *Università di Messina, Italy*
Giovanni **Bosco** – *Università di Messina, Italy*
Lorenzo **Brezzi** – *Università di Padova, Italy*
Vincenzo **Butticé** – *Università di Palermo, Italy*
Francesco **Calvetti** – *Politecnico di Milano, Italy*
Orazio **Casablanca** – *Università di Messina, Italy*
Zijun **Cao** – *Wuhan University, China*
Francesca **Casini** – *Università degli Studi di Roma Tor Vergata, Italy*
Francesca **Ceccato** – *Università di Padova, Italy*
Manuela **Cecconi** – *Università di Perugia, Italy*
Jared A. **Charles** – *University of Southampton, United Kingdom*
Anna **Chiaradonna** – *Università dell'Aquila, Italy*
Andrea **Ciancimino** – *Politecnico di Torino, Italy*
Matteo O. **Ciantia** – *University of Dundee, United Kingdom*
Simonetta **Cola** – *Università di Padova, Italy*
Giorgia **Dalla Santa** – *Università di Padova, Italy*
Andrea **Diambra** – *University of Bristol, United Kingdom*
Francesco **Di Buccio** – *Università di Chieti-Pescara, Italy*
Bruno **Di Buò** – *Tampere University, Finland*
Giuseppe **Di Filippo** – *Università di Messina, Italy*
Marco **D'Ignazio** – *University of Tampere, Finland*
Elena **Dodaro** – *Università di Bologna, Italy*
James **Doherty** – *University of Western Australia, Australia*
Settimio **Ferlisi** – *Università di Salerno, Italy*
Alessio **Ferrari** – *Università di Palermo, Italy*
Cristiana **Ferreira** – *Faculdade de Engenharia da Universidade do Porto, Portugal*
Aligi **Foglia** – *Fraunhofer IWES, Germany*
Fabio **Gabrieli** – *Università di Padova, Italy*
Andrea **Galli** – *Politecnico di Milano, Italy*
Domenico **Gaudio** – *Sapienza, Università di Roma, Italy*
Heraldo L. **Giacheti** – *São Paulo State University (Unesp), Brazil*

Domenico **Gioffré** – *Università di Pavia, Italy*
 Daniela **Giretti** – *Università di Bergamo, Italy*
 Guido **Gottardi** – *Università di Bologna, Italy*
 Laura **Govoni** – *Università di Bologna, Italy*
 Jürgen **Grabe** – *Hamburg University of Technology, Germany*
 Carmine Gerardo **Gragnano** – *Università di Bologna, Italy*
 Paolo Maria **Guarino** – *ISPRA Istituto Superiore per la Protezione e la Ricerca Ambientale, Italy*
 Michael **Hicks** – *Delft University of Technology, The Netherlands*
 Chiara **Iodice** – *Università degli Studi della Campania Luigi Vanvitelli, Italy*
 Maria **Iovino** – *Università degli studi di Napoli “Parthenope”, Italy*
 Stefan **Kreiter** – *University of Bremen, Germany*
 Tim **Länsivaara** – *Tampere University, Finland*
 Valentina **Lentini** – *Università degli studi di Enna “Kore”, Italy*
 Jean-Sébastien **L’Heureux** – *Norwegian Geotechnical Institute, Norway*
 Stefania **Lirer** – *Università degli Studi Guglielmo Marconi, Italy*
 Diego **Lo Presti** – *Università di Pisa, Italy*
 Tom **Lunne** – *Norwegian Geotechnical Institute, Norway*
 Claudia **Madiai** – *Università di Firenze, Italy*
 Rosa Maria Stefania **Maiorano** – *Università degli studi di Napoli “Parthenope”, Italy*
 Maria Clorinda **Mandaglio** – *Università di Salerno, Italy*
 Alessandro **Mandolini** – *Università degli Studi della Campania Luigi Vanvitelli, Italy*
 Diego **Marchetti** – *Studio Prof. Marchetti, Italy*
 Michela **Marchi** – *Università di Bologna, Italy*
 Luca **Masini** – *Sapienza Università di Roma, Italy*
 Rossella **Massimino** – *Università di Catania, Italy*
 Paul W. **Mayne** – *Georgia Institute of Technology, United States*
 Claudia **Meisina** – *Università di Pavia, Italy*
 Lucia **Mele** – *Università di Napoli Federico II, Italy*
 Fausto Andrés **Molina-Gómez** – *University of Porto, Portugal*
 Paola **Monaco** – *Università dell’Aquila, Italy*
 Lorella **Montrasio** – *Università di Parma, Italy*
 Diane **Moug** – *Portland State University, United States*
 Zhongkun **Ouyang** – *University of New Haven, United States*
 Priscilla **Paniagua** – *Norwegian Geotechnical Institute, Norway*
 Paul José **Pinedo Vilcahuamán** – *Universitat Politècnica de Catalunya, Spain*
 Nick **Ramsey** – *Fugro Australia, Australia*
 Sara **Rios** – *University of Porto, Portugal*
 Peter K. **Robertson** – *PK Robertson Inc & Gregg Drilling Inc, United States*
 Irene **Rocchi** – *Technical University of Denmark, Denmark*
 Fabio **Rollo** – *Sapienza Università di Roma, Italy*
 Alessandra **Rosati** – *Sapienza Università di Roma, Italy*
 Marco **Rosone** – *Università di Palermo, Italy*
 Giacomo **Russo** – *Università di Napoli Federico II, Italy*
 Gianpiero **Russo** – *Università di Napoli Federico II, Italy*
 Fernando **Schnaid** – *Universidade Federal do Rio Grande do Sul, Brazil*

James **Schneider** – *US Army Corps of Engineers, United States*
Britta **Søndergaard** – *COWI, Denmark*
Daniele **Spizzichino** – *ISPRA Istituto Superiore per la Protezione e la Ricerca Ambientale, Italy*
Nunziante **Squeglia** – *Università di Pisa, Italy*
Stefano **Stacul** – *Università di Pisa, Italy*
Francine Chantal **Tchamaleu Pangop** – *Università di Padova, Italy*
Laura **Tonni** – *Università di Bologna, Italy*
Giuseppe **Tropeano** – *Università di Cagliari, Italy*
Marco **Uzielli** – *Università di Firenze, Italy*
Phil **Watson** – *UWA, University of Western Australia, Australia*
Varvara **Zania** – *Technical University of Denmark, Denmark*
Ningning **Zhang** – *RWTH Aachen University, Germany*
Maurizio **Zicarelli** – *Università di Palermo, Italy*
Paolo **Zimmaro** – *Università della Calabria, Italy*



Taylor & Francis

Taylor & Francis Group

<http://taylorandfrancis.com>

Sponsors

Platinum Sponsors



Gold sponsors



Exhibitors in Outdoor Spaces



Silver Sponsors



Bronze Sponsors





Taylor & Francis

Taylor & Francis Group

<http://taylorandfrancis.com>

Keynote lectures



Taylor & Francis

Taylor & Francis Group

<http://taylorandfrancis.com>

New CPT methods for evaluation of the axial capacity of driven piles

B.M. Lehane & E. Bittar

University of Western Australia, Australia

S. Lacasse, Z. Liu & F. Nadim

Norwegian Geotechnical Institute, Norway

ABSTRACT: High costs associated with offshore foundation installations have provided strong impetus to the offshore energy sector in the search for more reliable design methods. This paper provides a summary of an Industry sponsored project that led to the development of new CPT-based design methods for the evaluation of the axial capacity of driven piles. Particular attention was given to the need for the new methods to be applicable to large diameter offshore piles given that many existing methods are derived by calibration with capacities measured in static pile load tests on smaller diameter onshore piles. The basic mechanisms supporting the general format of the expressions proposed for shaft friction and end bearing in sands and clays are described. It is shown how the new expressions, which are calibrated against a database of the most reliable load tests reported in the literature, lead to better predictions of capacity compared to other methods and can also satisfactorily predict the capacity of piles driven into deposits comprising interbedded layers of sand, silt and clay. Recommendations for the prediction of pile displacements at working loads using CPT data are also presented.

1 INTRODUCTION

The popularity of the CPT and the similarity between the mode of penetration of a cone and a driven pile have provided strong motivation in the search for direct correlations between the CPT q_t value and axial pile capacity. The best known of initial correlations proposed for pile shaft and base resistance in a range of soil types were developed about 40 years ago and include methods recommended by de Beer (1972), Schmertmann (1978), de Ruiter & Beringen (1979), Zhou et al. (1982), Bustamante & Gianselli (1982) and Van Impe (1986).

These and other methods have since been assessed using specific databases of static load tests by workers such as Briaud & Tucker (1988), Niazi & Mayne (2013), Eslami et al. (2014), Hu et al. (2012) and Amirmojahedi & Abu-Farsakh (2019). These studies show that there is no consensus of opinion regarding the relative reliability of the methods with some methods providing good predictions for a given database but poor predictions for other databases. This lack of consensus is partly due to significant inconsistencies between the respective databases which arise due to (i) different definitions of ultimate axial capacity, (ii) contradictory interpretations of load test data, (iii) uncertainty in CPT q_t values at test pile locations, (iv) inclusion or exclusion of layered/mixed soil deposits and different pile types and (v) separate assumptions relating to the effects of time,

loading direction, re-testing and loading rate. In addition, the formulations of most methods do not explicitly incorporate many characteristics of driven pile behaviour that have been well proven in experimental research programmes (discussed below).

The Offshore Energy sector recognized the advantages of a CPT-based method for axial capacity assessment but also understood the need to quantify the reliability of such a method using a database that had the backing of much of the profession. A Joint Industry Project (JIP) was set up in 2014 to achieve this objective. The JIP was managed by the Norwegian Geotechnical Institute (NGI) with support from the University of Western Australia (UWA) and was sponsored by Equinor, Ørsted, Lundin, ONGC, Petrobras and DNV GL. A ‘Team of Experts’ worked over a period of 3 years with guidance from the JIP steering committee to assess the suitability of about 600 pile load tests for inclusion in the database. A good CPT coverage close to pile tests was required and only first-time load tests on driven piles that were statically loaded to a displacement of 10% of the pile diameter were included. The final tests selected make up, what is referred to as, the ‘Unified database’ and comprises 71 test piles in silica sand and 49 pile tests in clay. Full details of the ‘Unified database’ and the steps followed in its compilation are provided in Lehane et al. (2017).

A subsequent phase of the JIP began in 2017 (sponsored by Equinor, Lundin Norway, Ørsted, ONGC, BP, Total, ExxonMobil, EnBW, EDF,

Aramco, SSER and HDEC) with the aim of developing new ‘Unified’ methods for the prediction of the axial capacity of driven piles in sand and clay. This initiative was motivated by the desire of Industry to replace the 4 CPT-based methods for driven piles in sand included in the API (2011) recommendations with a single method. The term ‘unified’ is employed as the method was developed with input from the proponents of the 4 most current CPT-based sand methods used offshore. Although no CPT method for driven piles in clay and silt are currently provided in API/ISO documentation, the inclusion of such a method was seen to be an important step forward to reduce dependence on laboratory measurements of undrained strength required by the existing ‘alpha’ method.

The JIP was concluded successfully in 2021 and the methods developed will be incorporated in the next versions of the ISO-19901-4 and API recommendations.

This paper provides an overview of the new CPT methods with a focus on justification of the basis of the formulations employed. A full description of the methods is provided in Lehane et al. (2020, 2022) and in Nadim et al. (2021). The ‘sand’ and ‘clay’ formulations were calibrated using the Unified database and their application to interbedded deposits comprising sand, silt and clay layers is examined in this paper. Recommendations are also provided to assist prediction of the displacement of driven piles at working loads using CPT data.

2 CPT METHODS FOR CAPACITY OF DRIVEN PILES IN SAND

2.1 Approaches for evaluation of shaft friction

Traditional CPT methods relate the local ultimate friction (τ_f) directly to the cone resistance (q_t) via a single factor, β :

$$\tau_f = q_t / \beta \quad (1)$$

Bustamante & Gianceselli (1982), for example, recommend β values for driven steel tubular piles of 120 and 200 in loose and dense sands respectively and propose limiting τ_f values in each of these deposits to respective maximum values of 35 kPa and 120 kPa. These and other similar recommendations reported in the literature ignore the following well-known characteristics of driven piles in sand observed from instrumented pile tests (Lehane et al. 2020):

- i. Ultimate shaft friction (τ_f) varies in direct proportion to the tangent of the interface friction angle between the sand and pile shaft ($\tan \delta$) i.e. shaft friction is governed by Coulomb’s law.

- ii. τ_f developed in any soil horizon reduces with the distance of that soil horizon from the pile tip (h); this arises largely due to the progressive cycling of sand at any particular level as installation progresses.
- iii. Smaller diameter piles generate larger frictions due to constrained dilation under shear at the interface.
- iv. Open-ended pipe piles generate lower shaft frictions than closed-ended piles due to lower levels of displacement imparted to the sand mass.
- v. Ageing effects lead to increases in shaft friction with time after pile installation.

These characteristics are not incorporated in Eqn. 1 and prompted the development of a new generation of CPT methods included in API (2011), namely those referred to as Fugro-05 (Kolk et al. 2005), ICP-05 (Jardine et al. 2005), NGI-05 (Clausen et al. 2005) and UWA-05 (Lehane et al. 2005). While all of these newer methods do not include all of the characteristics listed above, each incorporates a direct proportional relationship between τ_f and q_c and a reduction of τ_f with distance from the pile tip (h). These dependencies were first clearly revealed in experiments conducted in 1989 with the Imperial College instrumented pile in medium dense sand at Labenne, France (Lehane 1992). Figure 1 plots bounds to a large number of equalised radial stress measurements (σ'_{rc}) obtained in these experiments and displays an obvious trend for the σ'_{rc}/q_c ratio to be constant in a given soil horizon and to reduce with increasing distance of that horizon above the pile tip (noting that there is a direct relationship between τ_f and σ'_{rc} via Coulomb’s law).

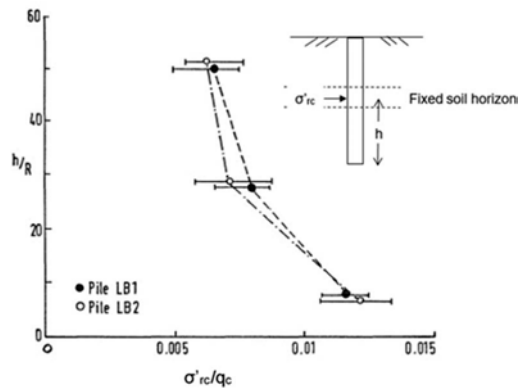


Figure 1. Dependence of equalised radial effective stress on q_c and normalised distance from the pile tip (h/R) at Labenne, France (Lehane 1992) [$R=D/2$ and τ_f varies directly with σ'_{rc}].

The trend shown on Figure 1, which has since been confirmed by Chow (1997) and others, is the key element of the shaft friction formulations of the

UWA-05, NGI-05, ICP-05 and Fugro-05 methods. These shaft frictions correspond to frictions that can be developed in the 2 to 4 week period following driving as the methods' calibrations employed static load test data recorded in the same period.

2.2 Approaches for evaluation of base resistance

Given the comparable modes of penetration, all historical CPT methods for closed-ended driven piles in sand relate the ultimate end bearing directly to the q_c value in the vicinity of the pile tip. However, the ultimate end bearing stress, defined at a displacement of 0.1D ($q_{b0.1}$), is typically only about 50% of q_c for a closed-ended pile driven in homogeneous sand deposits because a displacement of the pile tip of order of 1D is required to reach steady state penetration conditions (as exist during cone penetration). In addition to partial mobilisation at a displacement of 0.1D, Van Mierlo & Koppejan (1952) recognised the importance of the scale difference between a pile and a penetrometer. Recognition of this effect subsequently led to a variety of proposals for q_c averaging techniques, the most popular of which relates $q_{b0.1}$ to a simple average value of q_c values in a zone extending 1.5D above and 1.5D below a pile tip.

Compared with closed-ended piles, pipe piles induce lower levels of displacement (or disturbance) to the sand near their bases during installation. The degree of partial plugging (and hence disturbance) reduces as the pile diameter increases. Consequently, as shown by Gavin & Lehane (2003), the end bearing of large diameter piles under static loading (when the plug remains stationary) reduces to that of a bored pile for which $q_{b0.1}$ is typically about 15% of the q_c value (Lehane & Randolph 2002). This diameter dependence is incorporated in a number of different ways in the Fugro-05, ICP-05, NGI-05 and UWA-05 correlations for $q_{b0.1}$. No set-up of end bearing resistance has been observed for driven piles in sand.

2.3 Performance of CPT methods in API (2011)

The Fugro-05, ICP-05, NGI-05 and UWA-05 CPT methods included in API (2011) were calibrated using databases compiled specifically for the development of these methods. It is therefore of interest to examine their performance against the 'Unified database', which is fully supported by all researchers involved in the four methods. The findings from this exercise are summarised in Table 1, which presents statistics for ratios of measured to calculated capacities (Q_m/Q_c) for the four methods as well as for the earth pressure theory method in API RP2A (2011) and the new 'Unified method' (discussed below).

The results in Table 1 show that, while the earth pressure approach in API over-predicts pile capacities by an average of 66%, the mean Q_m/Q_c ratio of measured to calculated capacity for the four API

CPT methods is close to unity. The spread in predictions for the earth pressure approach, as measured by the CoV for Q_m/Q_c , is also higher than for the CPT methods and is indicative of a significantly lower level of reliability. The UWA-05 and ICP-05 methods are the best performing methods with the lowest CoVs.

Table 1. Mean (μ) and coefficient of variation (CoV) of Q_m/Q_c for the Unified database of driven piles in silica sand.

Method	All open & closed-ended piles (total capacity) 71 Piles	
	μ	CoV
API (2011), K tan δ (β) approach	1.66	0.56
Fugro-05	0.99	0.40
ICP-05	1.04	0.27
NGI-05	0.99	0.34
UWA-05	1.06	0.26
Unified Method	1.05	0.24

3 UNIFIED CPT METHOD FOR DRIVEN PILES IN SAND

While the UWA-05 and ICP-05 methods performed relatively well against the 'Unified database', a primary aim of the JIP was to develop a unified and un-affiliated method that had the support of those involved in the derivation of the API β method and the four API CPT methods. The first point of agreement was that, in line with the findings of Lehane et al. (1993), and others, the following expression should form the basis of the correlation for peak shaft (τ_f):

$$\tau_f = (\sigma'_{rc} + \Delta\sigma'_{rd}) \tan \delta_f \quad (2)$$

where σ'_{rc} is the stationary (equalised) radial effective stress, $\Delta\sigma'_{rd}$ is the increase in radial effective stress during pile loading (attributed to dilation) and δ_f is the constant volume sand-pile interface friction angle. On review of the state-of-the-art, it was agreed that the Unified method should incorporate considerations described in the following.

3.1 Interface friction angle (δ_f)

In the absence of site-specific tests to measure ultimate interface friction angles (δ_f), the ICP-05 and UWA-05 methods propose the variation with the mean effective particle size (d_{50}) indicated by the curve shown in Figure 2. This variation was deduced from direct shear box tests on steel interfaces with a roughness typical of industrial piles but that did not include pre-shearing to large relative displacements. Yang et al.

(2010), and others, have since shown that crushing of sand at the pile tip and subsequent shearing during installation reduces the grading to that of a fine sand. Interface shear angles measured in the Bishop ring shear apparatus in tests that induced a large level of pre-shearing are plotted on Figure 2 confirmed the relatively low sensitivity of δ_f to the initial d_{50} value. Similar tests reported by Liu et al. (2019) also show that δ_f has virtually no dependence on the (non-plastic) fines content of typical siliceous sands and on the normal stress level. It was therefore concluded that, in the absence of site specific ring shear interface tests, adoption of a constant δ_f value of 29° is a reasonable assumption for all piles in the load test database.

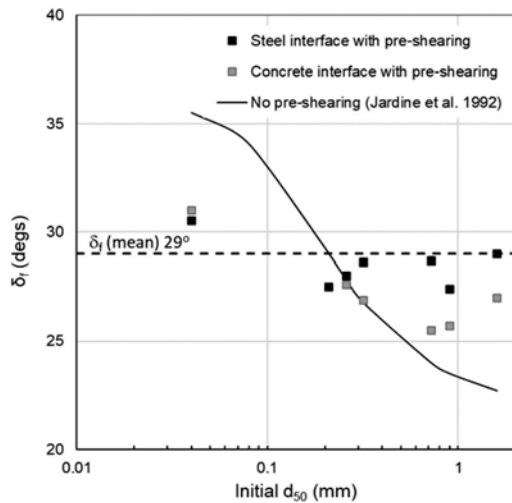


Figure 2. Interface friction angle and d_{50} for roughness typical of industrial piles (centreline average roughness of 5 to 20 μ m) (Barmopoulos & Ho, 2009); Ho et al., 2011).

3.2 Increase in radial stress ($\Delta\sigma'_{rd}$) during pile loading

The restraint to dilation at the pile shaft during pile loading provided by the surrounding sand leads to an increase in radial stress on the pile shaft ($\Delta\sigma'_{rd}$) and hence to the peak shaft friction. This increase can be assessed from cavity expansion (CE) theory, where G is the operational shear modulus of the sand mass, y is the dilation of the sand at the shaft interface and $y/2D$ is the cavity strain:

$$\Delta\sigma'_{rd} = 4Gy/D \quad (3)$$

The UWA-05 and ICP-05 methods assume that the cavity strain is small enough for conditions to be fully elastic and hence the methods equate G with the small-strain elastic value (G_0). However, data from constant normal stiffness direct shear interface

tests and tests on centrifuge piles with a range of diameters presented in Lehane et al. (2005) show that the cavity strains can be relatively large and that the operational G value is less than G_0 for typical pile diameters in the 'Unified database'. The following revised approximate expression was deduced using $\Delta\sigma'_{rd}$ measurements on jacked piles and parallel numerical analyses (Lehane et al. 2020):

$$\Delta\sigma'_{rd} = \left(\frac{q_c}{10}\right) \left(\frac{q_c}{\sigma'_v}\right)^{-0.33} \left(\frac{d_{CPT}}{D}\right) \quad (4)$$

with $d_{CPT} = 35.7$ mm, which is the usual CPT diameter.

Most piles in the Unified database have a diameter (D) between 350mm and 800mm. Equation (4) predicts that the increase in peak friction due to dilation ($=\Delta\sigma'_{rd} \tan\delta_f$) for a 20m long pile in medium dense sand is about 35% for $D=350$ mm but only 10% for $D=800$ mm. The relative influence of dilation is clearly an important consideration when extrapolating from the smaller diameter piles in the database to larger diameter offshore piles. The relative influence of dilation is also greatest in looser sands and for longer piles.

3.3 Allowance for partial plugging

Many of the pipe piles in the Unified database (with $D = 550 \pm 250$ mm) experienced partial plugging during pile driving. The additional shaft and base capacity that such plugging induces (e.g. see Gavin & Lehane 2003) needs to be accounted for correctly in the database analysis to ensure safe extrapolation to the capacity of full scale offshore piles.

White et al. (2005) used a cavity expansion analogy to deduce that the equalised lateral effective stress acting on the pile shaft (σ'_{re}) varies with the effective area ratio (A_{re}) raised to a power of between about 0.3 and 0.45 while Xu et al. (2008) present experimental data showing how $q_{b0.1}$ varies in proportion to A_{re} .

A_{re} provides a measure of the level of soil displacement in any given soil horizon, and is defined as:

$$A_{re} = 1 - IFR(D_i/D)^2 \quad (5)$$

where IFR is ratio of the change in plug length to change in pile embedment and D_i is the internal pile diameter. A_{re} varies from unity for a closed-ended or fully plugged pile to a value of $4t/D$ for a large diameter coring pile (where t is the pile wall thickness). As the IFR is not measured routinely, the analysis of the unified database substituted the plug length ratio (PLR) for IFR, noting that the PLR is the average IFR during pile driving and equal to the ratio of the final plug length to the embedded pile length.

The PLR is primarily a function of the internal pile diameter (D_i) (e.g. see Gudavalli et al. 2013) and the following approximate expression was derived based on available records ($d_{CPT} = 35.7\text{mm}$):

$$PLR \approx IFR = \tanh \left[0.3 \left(\frac{D_i}{d_{CPT}} \right)^{0.5} \right] \quad (6)$$

The database analysis examined the influence of various exponents of A_{re} in the search for a best-fit expression for τ_f .

3.4 Time effects

The shaft capacity of driven piles in silica sand increases with time over a period of least one year (e.g. Chow et al. 1998, Jardine et al. 2006, Karlsrud et al. 2014, Gavin et al. 2015). Such increases are not exhibited by bored piles and may be viewed as a recovery process following the ‘trauma’ of driven pile installation (Lim and Lehane 2014, Anusic et al. 2019). The new CPT method is calibrated using the Unified database comprising static load tests with a median equalisation period (or set-up time) of about two weeks. It is therefore likely to underestimate long term capacities and over-estimate short term capacities (including driving resistance).

3.5 Formulation for σ'_{rc}

The observed reduction in the equalised radial effective stress (σ'_{rc}) with the distance from the pile tip (h) or normalised distance from the pile tip (h/D) can be described as a power law relationship (as in the ICP-05 and UWA-05 methods) or as an exponential relationship (proposed by Randolph et al. 1994 and Salgado et al. 2011). Lehane et al. (2020) show that the bias in the database, with respect to diameter, of the ratio of measured to calculated capacities (Q_m/Q_c) can be removed when a h/D term is used instead of ‘ h ’ (as proposed by Alm & Hamre 2001). Lehane et al. (2020) also show that while the power law and exponential variations with h/D lead to very similar statistics for the Q_m/Q_c ratios, the exponential relationship tended to predict marginally larger capacities for piles with $L/D < 20$ compared with the power law form. The power law form was retained as many piles used in the offshore wind Industry have lower L/D values.

3.6 Tension compression ratio

The database piles clearly showed that shaft friction measured in tension are, on average, about 75% of the shaft friction of compression piles. Limited data exist in relation to differences in the distribution of τ_f along test piles and, in the absence of other

information, the global (best-fit) tension to compression ratio (f_L) of 0.75 was employed in the new method.

3.7 Formulation for end bearing

The Unified method relates the ultimate end bearing ($q_{b0.1}$) with the effective area ratio (A_{re}) for pipe piles in line with observations of Gavin & Lehane (2003) and as adopted in the UWA-05 method. The end bearing formulation of ICP-05 incorporates this dependency indirectly by allowing $q_{b0.1}$ for pipe piles to reduce with pile diameter.

The Unified method relates $q_{b0.1}$ with q_p , where q_p is the end bearing resistance expected for an ‘imaginary cone’ that has the same diameter as the pile being considered (or equivalent diameter for a pipe pile = $(A_{re}/\pi)^{0.5}$). The value of q_p is determined using a component of a ‘thin-layer’ procedure described by Boulanger and DeJong (2018) and its application in piling calculations is explained by Bittar et al. (2020). Although q_p is a rational and objective way of obtaining an averaged cone resistance near a pile base of given diameter, its determination requires use of software (freely downloadable from <https://faculty.engineering.ucdavis.edu/boulanger/research-interests/>) which is not appealing to many practitioners. The new ISO-19901-4 recommendations therefore suggest taking q_p as the average q_c value in the zone extending 1.5D above and below the pile tip, unless conditions at the pile tip are highly variable. Separate studies show that q_p for the Unified database piles is, on average, 20% higher than q_{Dutch} , where q_{Dutch} is the CPT resistance determined using the ‘Dutch’ averaging technique (Van Mierlo & Koppejan 1952)

3.8 Formulation of Unified CPT method in sand and predictive performance

The final formulations decided upon for the Unified CPT method for piles in sand (Zone 6 of the soil behaviour type chart) are provided in Table 2. When these are applied to the Unified database, the average ratio of measured to calculated capacities (Q_m/Q_c) is 1.05 while the CoV for Q_m/Q_c is 0.24. These statistics are a marginal improvement on those for the UWA-05 and ICP-05 methods (see Table 1). The method is, however, considered to be a significant step forward as it replaces the four API CPT methods with full support of the authors for these methods and it incorporates state-of-the-art understanding of the mechanisms controlling the axial capacity of driven piles in sand. It should be noted that the method potentially under-estimates axial capacity in gravelly sands (Zone 7 of the SBT chart), where the presence of gravels leads to higher average q_c values. The method is only applicable to piles driven in a conventional manner and should not be used for jacked piles or piles installed by vibration.

Table 2. General formulations for Unified method in sands, silts and clays (see <https://pile-capacity-uwa.com/>).

$$Q_{\text{shaft}} = \pi D \int_0^L \tau_f dz$$

$$Q_{\text{base}} = q_{b0.1} (\pi D^2/4)$$

Capacity estimate for piles for flexible piles in strain-softening clays requires load-transfer analysis using load transfer curves given in API (2011)

Sands: Zone 6 of SBT chart ($I_c < 2.1$)

$$\tau_f = f_L (\sigma'_{rc} + \Delta\sigma'_{rd}) \tan 29^\circ$$

$$q_{b0.1} = [0.12 + 0.38A_{re}]q_p; \text{ for plugged base (expected when } L/D > 5)$$

$$q_{b0.1} = A_{re} q_p; \text{ for unplugged base}$$

$$\sigma'_{rc} = (q_c/44) A_{re}^{0.3} [\text{Max}[1, h/D]]^{-0.4}$$

$$\Delta\sigma'_{rd} = (q_c/10) (q_c/\sigma'_{v0})^{-0.33} (d_{CPT}/D)$$

$$A_{re} = 1 - PLR (D_i/D)^2$$

$$PLR = \tanh [0.3 (D_i/d_{CPT})^{0.5}]$$

$$f_L = 0.75 \text{ in tension, } 1.0 \text{ in compression}$$

q_p can be taken as the average q_c within a zone 1.5D above and below the pile tip or determined using the procedure described Boulanger & De Jong (12018) and Bittar et al. (2020)

Clays: Zones 1,2,3 & 4 of SBT chart

$$\tau_f = 0.07 F_{st} q_t [\text{Max}[1, h/D^*]]^{-0.25}$$

$$q_{b0.1} = [0.2 + 0.6A_{re}]q_p$$

$F_{st} = 1$ for clays with $I_{z1} > 0$, in Zones 2, 3 and 4 on the SBT Chart ($I_c \geq 2.6$)

$F_{st} = 0.5 \pm 0.2$ clays with $I_{z1} < 0$, in Zone 1 on the SBT Chart

$D^* = (D^2 - D_i^2)^{0.5}$ for an open-ended pile and $D^* = D$ for a closed-ended pile

$$I_{z1} = Q_m - 12 \exp(-1.4F_r)$$

q_p = average q_t value in zone between the pile tip and 1D below the pile tip (closed-ended/ plugged pile) or average q_t to a depth of 20t below the pile tip (large diameter, unplugged pile)

Silts: Zone 5 of the SBT chart ($2.1 < I_c < 2.6$)

Apply equations as for Zone 6 using corrected q_c value determined as:

$$q_c = [3.93 I_c^2 - 14.78 I_c + 14.78] q_t$$

Notation

h	$L - z$, where L is pile embedment length and z is the depth)
D	Pile outer diameter
D_i	Internal diameter of a pipe pile
f_s	Cone sleeve friction
F_r	Friction ratio (expressed as a percentage) = $f_s/(q_t - \sigma_{v0})$
q_t	Total (corrected) CPT end resistance (= q_c in sands)
Q_m	Normalised cone resistance $[(q_t - \sigma_{v0})/p_a]/[(p_a/\sigma'_{v0})^n]$; p_a = ref. stress = 100 kPa
I_c	Consistency index, function of Q_m and F_r ; see Robertson (2009)
n	Stress exponent for Q_m , function of I_c and σ'_{v0} ; see Robertson (2009)
t	Pile wall thickness
SBT	Soil Behaviour type; see Robertson (2009)
σ_{v0}	Total vertical stress
σ'_{v0}	Effective vertical stress

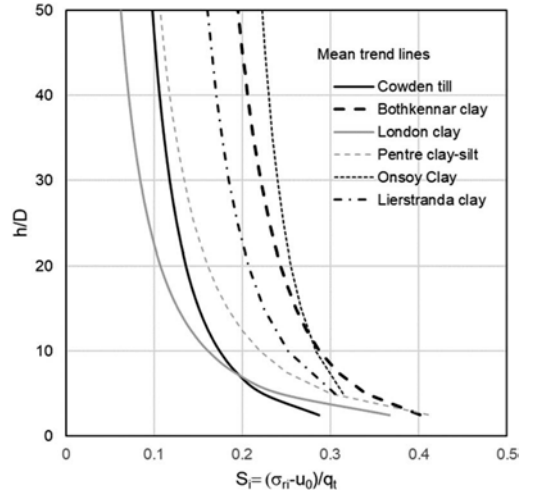


Figure 3. Mean recorded variations of normalised radial total stresses (S_i) with h/D measured during installation of closed-ended instrumented piles.

4 CPT METHODS FOR CAPACITY OF DRIVEN PILES IN CLAY

4.1 Shaft friction

Relationships between shaft friction and the measured and corrected cone resistances (q_c and q_t) for driven piles in clay have been proposed for many years e.g. Bustamante & Gianselli (1982), Almeida et al. (1996), Lehane et al. (2000, 2013), Eslami & Fellenius (1997) and Niazi & Mayne (2016). The newly proposed Unified CPT method for clays builds on these methods but is based primarily on observations made in high quality instrumented pile experiments conducted by a number of institutions, most notably at the Norwegian Geotechnical Institute and Imperial College London.

The basis of the correlation between shaft friction and the (corrected) CPT end resistance (q_t) for the new Unified method is the observation that, in any particular clay, the radial total stress developed during installation (σ_{ri}) on the shaft of a closed-ended displacement pile varies directly with q_t and reduces with the normalised distance from the pile tip (h/D). Examples of observed trends are shown on Figure 3, which plots the mean measured variation of the normalised radial total stress in six different clays against h/D , where the normalised radial total stress (S_i) is defined as follows and u_0 is the hydrostatic or ambient pore pressure:

$$S_i = (\sigma_{ri} - u_0) / q_t \quad (7)$$

The mean trend lines indicated on Figure 3 have a typical standard deviation of 25% and are evidently dependent on the clay type. Following installation,

instrumentation on driven piles shows that radial total stresses fall as excess pore pressure dissipate while radial effective stresses (σ'_r) increase. σ'_r reaches a fully equalised value (σ'_{rc}) after equalisation of radial total stresses and full pore pressure dissipation. When a pile is loaded to failure after equalisation, radial effective stresses reduce attaining a value of σ'_{rf} at peak local shear stress (τ_f).

These stages in the life of a driven pile are incorporated in the following expression for τ_f , which is based on Coulomb's friction law:

$$\tau_f = \sigma'_{rf} \tan \delta = q_t S_i (S_c / S_i) f_1 \tan \delta_f \quad (8a)$$

where

$$S_c = (\sigma_{rc} - u_0) / q_t = \sigma'_{rc} / q_t \quad (8b)$$

$$f_1 = \sigma'_{rf} / \sigma'_{rc} \quad (8c)$$

Equation (8) illustrates that the relationship between τ_f and q_t depends on the degree of relaxation of radial total stresses during equalisation (expressed by S_c/S_i), the relative change in σ'_r during load testing (f_1) and the interface friction angle between the pile and clay (δ_f). Numerical simulations such as those of Whittle & Baligh (1988), as well as experiments, indicate that S_c/S_i ratios are lower in sensitive and low OCR clays where installation causes a significant degree of remoulding and reduction in effective stress. The S_c/S_i values measured experimentally range from 0.15 in (highly sensitive) Lierstranda clay to 1.0 in the heavily overconsolidated London clay. Measured values of f_1 are in the range of 0.8 to 1.0 in all clays but average at about 0.6 in Lierstranda clay. The operational coefficient of friction ($\tan \delta_f$) is strongly affected by the clay mineralogy, amongst other factors, and for the six clays considered in Figure 3 varies by more than a factor of 2 (from a $\tan \delta_f$ value of 0.23 in London Clay to 0.55 in Bothkennar clay).

The compounding effects of differences in respective clays of the S_c/S_i , f_1 and $\tan \delta_f$ values as well as the S_i relationship with h/D (shown on Figure 3) reveal a complex relationship between τ_f and q_t . Nevertheless, when ratios of τ_f/q_t with h/D measured in instrumented pile tests are plotted, as shown in Figure 4a, it is evident that a number of compensatory factors lead to a relatively consistent relationship between τ_f/q_t and h/D in all of clays apart from Lierstranda, where the product of S_c/S_i and f_1 is, on average, about four times less than the other clays. Best-fit mean trend lines for the instrumented data included in Figure 4a are presented on Figure 4b and, as shown later, are consistent with best-fit expressions for the capacities of the piles in the Unified database.

4.2 End bearing

The contribution of end bearing to the capacity of driven piles in clay is relatively small and therefore

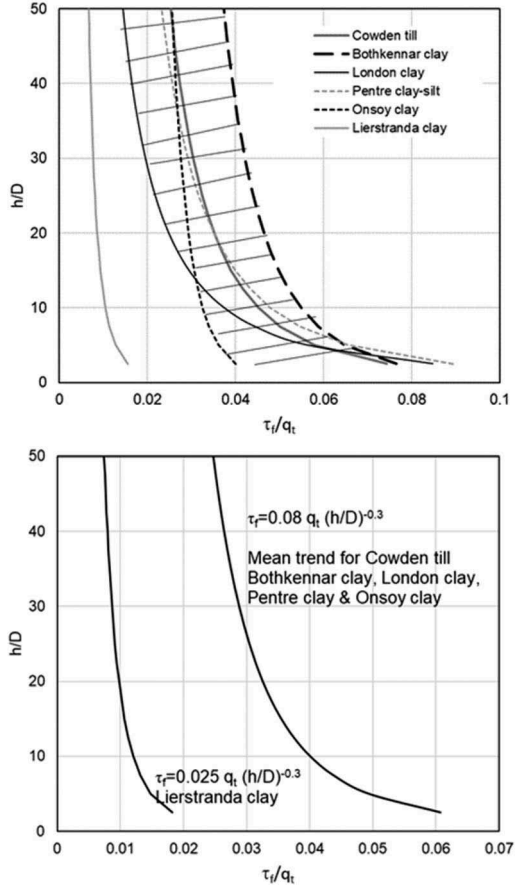


Figure 4. (a) Average measured variations of τ_f/q_t with h/D (showing envelope for all clays except Lierstranda clay), (b) best-fit mean trend lines.

has not been the subject of extensive research. The assumption of a simple direct relationship between $q_{b0.1}$ and the average q_t value near the pile tip is considered adequate for practical purposes. On the basis of a review of existing correlations, Lehane et al. (2022a) propose the following relationships for typical onshore driven piles ($D < 0.75m$)

$$q_{b0.1} = 0.8q_t \text{ (closed-ended pile)} \quad (9a)$$

$$q_{b0.1} = 0.4q_t \text{ (open-ended pile)} \quad (9b)$$

5 UNIFIED CPT METHOD DRIVEN PILES IN CLAY

The development of the new Unified CPT method for clays recognised the compensatory effects of factors evident on Figure 5a but investigated potential systematic dependence on (i) clay plasticity index, (ii) soil behaviour type (SBT), (iii) CPT sleeve friction (f_s) and

(iv) vertical effective stress level (σ'_v). The calibration of the method with the Unified database also included consideration of the aspects detailed below.

5.1 Dependence of τ_f on loading direction

Compression and tension tests on piles with identical configurations in seven different clays in the Unified database indicate that, in general, there is not a clear dependence of ultimate shaft friction on the load direction. A load direction factor (f_L) of unity was found to provide a best fit to the full Unified database.

5.2 Friction on open-ended piles

Instrumented pile test data reported by Doherty & Gavin (2011) show that lower levels of soil displacement during installation of open-ended piles lead to lower installation radial total stresses (σ_{ri}) and lower ultimate shaft frictions after equalisation. There is, however, a considerable shortage of such data in different clays and, in the absence of such data, the regression analyses conducted for the Unified method assumed the following potential dependencies (where Equation 10a is comparable to the Unified CPT sand method and Equation 10b is a similar format to the ICP-05 method for sands):

$$\tau_f = f(A_{re}, h/D) \quad (10a)$$

$$\tau_f = f(h/D^*); D^* = (D^2 - D_i^2)^{0.5} \quad (10b)$$

Lehane et al. (2017) show that Equations 5 & 6, which were derived from data for piles in sand, may also be used to approximate A_{re} values for pipe piles in clays.

5.3 Progressive failure

A number of piles in the clay database exhibit post-peak softening of shaft shear stress. The calibration of the Unified method assumed that peak shear stresses corresponded to the measured peak axial capacity or, if such a peak was not observed, to the axial resistance at a displacement of 0.1D. This approach is considered reasonable for the majority of the database (which comprised relatively rigid piles) but is moderately conservative for a few very long piles in clays where strain softening can be significant.

5.4 Silt layers

Occasional silt layers with a soil behaviour type (SBT) index, I_c , in the range 2.05 to 2.6 occur within the clay strata of the database. For these deposits, the calibration process employed the Unified sand method adopting the equivalent clean sand q_t value ($q_{t,sand}$) for the silt. This was derived using the following relationship which is equivalent to the proposal of Robertson & Wride (1998) but adapted to a simplified format and modified to give a correction factor of unity at $I_c = 2.05$:

$$q_{t,sand} = q_c = [3.93I_c^2 - 14.78I_c + 14.78]q_t \text{ for } 2.05 < I_c < 2.6 \quad (11)$$

5.5 End bearing of large diameter pipe piles

Eqn. 9 was employed in the calibration of the relatively small diameter piles in the Unified database. For large diameter offshore piles, the following expression is considered more appropriate; this was based on findings of Doherty and Gavin (2011) from measurements of twin-walled instrumented piles during installation.

$$q_{b0.1} = [0.2 + 0.6A_{re}] q_t \quad (12)$$

where q_t is the average corrected cone resistance value in the zone extending from the pile tip to a depth of $20t$ below the pile tip (t = pile wall thickness)

5.6 Formulation of Unified CPT method in clay and predictive performance

The formulations for the Unified clay method are provided in Table 2. These were established following various optimisation analyses which revealed that, as inferred from instrumentation pile test data, τ_f is primarily correlated to the CPT q_t value and the normalised distance from the pile tip (h/D^*). The analyses also showed that the shaft friction generated in high sensitivity clays (within Zone 1 of the SBT chart) is typically 50% of the shaft friction in other clays (although there is significant variability). The formulations developed are remarkably similar to those deduced independently from instrumented pile test data (compare formulae in Figure 5 with those in Table 2). Surprisingly, the fit to the capacities of the database piles was not improved by consideration of additional factors such as cone sleeve friction, plasticity index and overconsolidation ratio (inferred by examination of a q_{net}/σ'_{v0} term).

The predictive performance for the Unified clay database of the new clay method was compared by Lehane et al. (2022a) with a number of other current methods. This comparison is summarised in Table 3, which also lists the main input parameters in the τ_f correlation for each method (noting that differences in the end bearing formulations had little impact on calculated capacities). Evidently the CoV of Q_m/Q_c for the new method is a good improvement on existing methods and is significantly lower than the corresponding CoV for the existing ' $\alpha - s_u$ ' method recommended by API/ISO. It should be noted, however, that part of the reason for the substantial reduction in the CoV with respect to other methods arises due to application of a separate equation for Zone 1 (sensitive) clays.

Table 3. Comparison of predictive performance for driven piles in clay of the Unified method with other methods (in terms of mean and CoV of measured to calculated capacity ratios).

Method	Parameters controlling τ_f	Mean Q_m/Q_c	CoV for Q_m/Q_c
API (2011)	s_u & s_u/σ'_v	1.05	0.43
Fugro-96 (Kolk & van der Velde 1996)	s_u , h/D & s_u/σ'_v	1.04	0.35
ICP-05 (Jardine et al. 2005)	OCR, σ'_v , h/D^* , δ & S_t	1.12	0.55
NGI-05 (Karlsrud et al. 2005)	s_u , s_u/σ'_v , I_p & σ'_v	1.1	0.36
UWA-13 (Lehane et al. 2013)	q_t & h/D^*	1.12	0.33
Fugro-10 (Van Dijk & Kolk 2010)	q_{net} , h & q_{net}/σ'_v	0.98	0.37
Unified method (Lehane et al. 2022a)	q_t , h/D^* & S_t	0.99	0.23

The Unified method in clay is calibrated on a relatively small number of pile tests (49) and, as may be inferred from the instrumented pile test data, its relatively good predictive performance arises partly because of compensating factors. For example, interface friction angles (δ) for clays in the Unified database range from 12° to 30° , implying a range in capacities of about 2.5 if τ_f varied only with $\tan \delta$. However, encouragingly, Lehane et al. (2022a) examined the performance of the new method against a different ‘Test database’ comprising 24 pile tests in clay and found a mean Q_m/Q_c ratio of 1.09 (i.e. a 9% over-prediction, on average) and a CoV for Q_m/Q_c of 0.22; this CoV is a substantial improvement on the CoV of 0.43 determined for the API $a - s_u$ method (Table 3).

6 APPLICATION TO LAYERED DEPOSITS

The Unified CPT methods for sand and clay were calibrated against test data for piles that were driven into predominately sand or clay deposits. However, many deposits encountered in practice contain sand, silt and clay layers and it is therefore important to assess the reliability of the methods at such sites. Bittar et al. (2022) conducted such a study involving 23 load tests on piles driven into mixed stratigraphies. Ten of these load tests were on piles with diameters between 0.9m and 2m in diameter which is considerably larger than the mean D value of about 0.4m for the piles in the Unified database. An average of 55% of the layers in these case histories were coarse grained and two cases involved sensitive zone 1 soils.

Sample predictions for two driven steel pipe pile case histories examined are presented in Figure 6a for a tension test in Oakland California on a 13.3m long, 610mm pile and in Figure 6b for a compression test in Minneveka, Norway on a 40m long, 405mm diameter pile. As seen with reference to the plotted I_c profiles in these figures, a 5.5m thick layer of Zone 3 clay is present along the central portion of the pile shaft whereas the stratigraphy at Minneveka comprises alternating 1.5m to 2m thick layers of sand and clay. The calculated τ_f distributions were determined in a simple spreadsheet using the I_c dependent expressions, as summarized in Table 2; calculations can also be performed using UWA freeware at <https://pile-capacity-uwa.com/>. These τ_f distributions lead to ratios of measured to calculated capacities (Q_m/Q_c) of 1.15 at Oakland and 1.16 at Minneveka (ignoring potential strain softening).

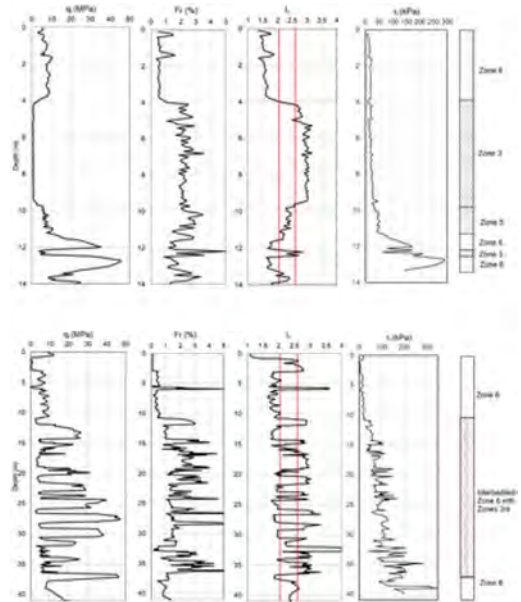


Figure 5. Stratigraphy and predicted τ_f distribution for (a) tension test on 610-mm diameter, 13.3m long pipe pile in Oakland and (b) compression tests on 405-mm diameter, 40m long pipe pile at Minneveka.

Bittar et al. (2022) show that the mean and coefficient of variation of the Q_m/Q_c values for the 23 load test database were 1.02 and 0.17 respectively i.e. the spread in predictions is less than that of the Unified databases for sand and clay sites. It can therefore be concluded that the Unified methods can be applied with the same level of confidence to layered stratigraphies as to ‘single soil type’ deposits. However well instrumented test piles that accurately measure the distribution of shaft friction in layered stratigraphies are needed for verification of the method. There is also a great shortage of skin friction data for

piles installed in in Zone 5 (silt) of the SBT chart. Such data would help to resolve the discontinuity in the expressions for τ_f at the boundary between Zone 4 and 5 (at $I_c=2.6$), where τ_f calculated using the clay expression is typically double that calculated using the clean sand correction approach for silt.

7 LOAD DISPLACEMENT RESPONSE USING THE UNIFIED CPT METHOD

The load-displacement response of piles is normally predicted in a load transfer analysis where the shear stress-displacement (τ - w) springs (also called t-z springs) at various levels along the pile shaft are scaled in proportion to the ultimate shaft friction (τ_f) and the base spring (q_b - w_b) is scaled with the ultimate end bearing ($q_{b0.1}$). The application of the new Unified CPT method to this approach is examined in the following.

7.1 Piles in sand

Lehane et al. (2020b) examined the accuracy of pile displacement predictions for driven piles in the Unified sand pile database sand using the τ - w and q_b - w_b load transfer relationships recommended in API (2011). These relationships are provided in tabular form in API (2011) but may be expressed as follows, where w_f is the displacement to peak shear stress (τ_f) and is assigned a mean value of 0.01D in API (2011):

$$\frac{\tau}{\tau_f} = 2 \frac{w}{w_f} \left[1 - \frac{w}{2w_f} \right] \quad (13)$$

$$\frac{w_b}{D} = 0.01 \left[\frac{q_b/q_{b0.1}}{1 - 0.9 (q_b/q_{b0.1})} \right] \quad (14)$$

Although Equation (14) is not a perfect match to the API tabulated values when $q_b/q_{b0.1} > 0.5$, this is not a concern as settlement predictions are required for the serviceability limit state when applied loads are rarely greater than 70% of the pile capacity.

API (2011) recommends adoption of a mean w_f/D value of 0.01. However the analyses showed that use of a constant value did not capture the tendency for softer pile responses in tension compared with compression and for stiffer responses in denser sands and longer piles. On examination of the trends shown by the piles in the Unified database, Lehane et al. (2020b) proposed the following expression for w_f/D :

$$\frac{w_f}{D} = \frac{q_c^{0.5} \sigma'_v^{0.25}}{Ap_a^{0.75}} \quad (15)$$

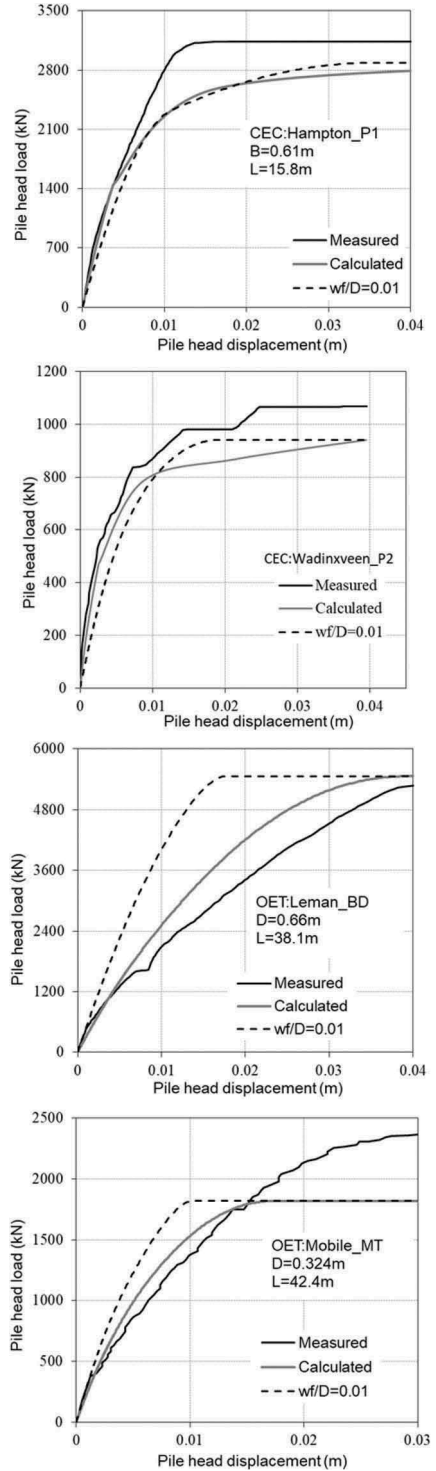


Figure 6. Comparison of measured pile load-displacement response with the calculated response using the Unified method with (i) w_f/D given by Equation 15 and (ii) $w_f/D=0.01$. The symbols CEC and OET denote closed ended piles tested in compression and open-ended piles tested in tension respectively.

where the constant A is 1250 in compression and 625 in tension.

Comparisons of measured and calculated load-displacement responses are plotted for typical cases from the Unified database on Figure 7, where calculations were performed using Equations 13 and 14 combined with the Unified method to determine τ_f and $q_{b0.1}$. Figure 7 presents calculated responses for a constant w_f/D value of 0.01 and for w_f/D values at various levels along the pile shaft determined using Equation 15. The improved fit obtained using Equation 15 for tension piles and for longer piles is evident on Figure 7. Lehane et al. (2020b) show that the error in calculated displacements at 50% of the ultimate capacity is typically about 0.002D and is less than 0.005D. Equation 15 will be included in the next version of the API/ISO recommendations.

7.2 Piles in clay

Lehane & Bittar (2022) repeated the exercise described above for the Unified database of piles in clay, for which API (2011) recommends the same format of load transfer curves apart from the allowance for post-peak softening to a shear stress of $(0.8 \pm 0.1) \tau_f$ at a displacement of $0.02D$. It was found that a combination of the Unified CPT method in clay (Table 2) with these load transfer curves provides good predictions of the displacements of both the tension and compression piles in the database. The standard deviation of the difference between measured and calculated displacements was $0.002D$.

8 CONCLUSIONS

There are clear advantages to CPT-based design approaches for the assessment of the axial capacity of driven piles. The CPT-based methods have the full support of the geotechnical community as they remove subjectivity associated with parameter assessment, provide essentially continuous profiles of soil behaviour and allow direct rapid and automated calculation of capacity at any CPT location.

There has been a concerted effort over the past decade to first quantify and then increase the reliability of design methods for piles. This was made possible by the thorough, detailed and careful compilation of a database of static pile load tests (the Unified database) that had the support of the proponents of recent existing CPT methods and the support of a large and active group of energy companies from around the world.

The creation of the Unified database highlighted the level of uncertainty associated with design methods in common use and prompted the development of the new non-affiliated 'Unified CPT method' described in this paper. The new method captures key characteristics of driven piles, as observed in high quality instrumented pile test programmes completed

over the past 30 years. The method is shown to have higher reliability than existing approaches.

As for most empirical methods, further developments and improvements are still to come. Such improvements include the need to better quantify the effects of time in various soil types and how the resistance to pile driving as well as the long term capacity can be assessed with more confidence. More static load tests on large diameter instrumented piles are clearly required while greater understanding of factors controlling the influence of the installation mode and friction in silt is needed.

It is hoped that the 'Unified database' can be expanded on an ongoing basis with each additional pile test included satisfying the strict selection criteria applied in the database development to date.

ACKNOWLEDGEMENTS

The authors gratefully acknowledge the funding and support provided under a Joint Industry Project (JIP) funded by Aramco, Equinor, Lundin, Ørsted, ONGC, BP, Total, ExxonMobil, EnBW, EDF and SSER. The significant contribution of the team of experts to the JIP, namely Prof. Richard Jardine, Dr. Philippe Jeanjean, Mr. Bas van Dijk, Dr. Mike Rattley and Mr. Pasquale Carotenuto is much appreciated.

REFERENCES

- Alm T. and Hamre L. (2001). Soil model for pile driveability predictions based on CPT interpretations. Proc. 15th Int. Conf. on Soil Mechanics and Geotechnical Eng., 1297–1302.
- Almeida M.S., Danziger F.A., and Lunne, T. (1996). Use of the piezocone test to predict the axial capacity of driven and jacked piles in clay. *Canadian Geotechnical J.*, 33 (1), 23–41.
- Amirmojahedi M. and Abu-Farsakh M. (2019). Evaluation of 18 direct CPT methods for estimating the ultimate pile capacity of driven piles. *Transport Research Record*, 2673(9), 127–141.
- Anusic I., Lehane B.M., Eiksund G., and Liingaard M. (2019). Evaluation of installation effects on the set-up of field displacement piles in sand. *Canadian Geotechnical Journal*, 56(4), 461–472.
- API (2011). ANSI/API RP 2GEO: Geotechnical and Foundation Design Considerations. ISO 19901-4:2003 (Modified), Petroleum and natural gas industries-Specific requirements for offshore structures, Part 4-Geotechnical and foundation design considerations. 1st edition. Washington, DC: API Publishing Services.
- Barmpopoulos I. and Ho T. (2009). The large displacement shear characteristics of granular media against concrete and steel interfaces. Proc Research Symp. Characterization & Behaviour of Interfaces, Atlanta, Georgia, USA Behaviour of Interfaces, 16–23.
- Bittar E., Lehane B.M., Boulanger R.W., and DeJong J. (2020). CPT filter to estimate end bearing of closed-ended driven piles in layered sands. Proc. Int.

- Symp. *Frontiers in Offshore Geotechnics*, Austin, Texas, 520–528.
- Bittar E., Lehane B.M., Nadim F., Liu Z. and Lacasse S. (2022). Assessment of the unified CPT Design Method for Axial Capacity of Driven Piles in Interlayered Deposits. *Canadian Geotechnical Journal* (submitted).
- Boulanger, R.W.W., and DeJong, J.T.T. (2018). Inverse filtering procedure to correct cone penetration data for thin-layer and transition effects. *Proc 4th Int Symp. on Cone Penetration Testing (CPT'18)*, 21-22 June, 2018, Delft, The Netherlands, 25–44.
- Briaud J.-L. and Tucker. L.M. (1988). Measured and Predicted Axial Response of 98 Piles. *Journal of Geotechnical Engineering*, 114(9), 984–1001.
- Bustamante, M. and Gianeselli, L. (1982). Pile Bearing Capacity Prediction by Means of Static Penetrometer CPT. *Proc. 2nd European Symposium on Penetration Testing*, Amsterdam, 493–500.
- Chow F. (1997). Investigations into the behaviour of displacement piles for offshore foundations. PhD thesis, Imperial College London (University of London).
- Chow, F.C., Jardine, R.J., Nauroy, J.F., and Brucy, F. (1998). Effects of Time on Capacity of Pipe Piles in Dense Marine Sand. *J. Geotech. & Geoenv. Engineering*, 124, 254–264.
- Clausen C. J. F., Aas P. M. & Karlsrud, K. (2005). Bearing capacity of driven piles in sand, the NGI approach. *Proc. 1st Int. Symp. on Frontiers in Offshore Geotechnics (ISFOG)*. Balkema, 574–580.
- De Ruitter J. and Beringen F.L. (1979). Pile foundations for large North Sea structures. *Marine Geotechnology*, 5(3), 267–314.
- Doherty, P. and Gavin, K. (2011). Shaft Capacity of Open-Ended Piles in Clay. *J. Geotech. & Geoenv. Engrg.* 137(11): 1090–1102.
- Eslami, A. and Fellenius, B.H. (1997). Pile capacity by direct CPT and CPTu methods applied to 102 case histories. *Canadian Geotechnical J.*, 34(6), 886–904.
- Eslami A., Tajvidi I. and Karimpour-Fard M. (2014). Efficiency of Methods for Determining Pile Axial Capacity – Applied to 70 Case Histories in Persian Gulf Northern Shore. *International Journal of Civil Engineering*, 12(1), 45–54.
- Hu Z., McVay M., Bloomquist D., Horhota D. and P. Lai. P. (2012) New Ultimate Pile Capacity Prediction Method Based on Cone Penetration Test (CPT). *Canadian Geotechnical Journal*, 49(8), 961–967.
- Gavin K., Jardine R., Karlsrud K., and Lehane B.M. (2015). The effects of pile ageing on the shaft capacity of offshore piles in sand. *Proc. 3rd Int. Symp. Frontiers in Offshore Geotechnics*, 1, 129–151.
- Gavin K.G. and Lehane B.M. (2003). The shaft capacity of pipe piles in sand. *Canadian Geotechnical Journal*, 40 (1), 36–45.
- Gudavalli S.R., Safaqaq O. and Seo H. (2013). Effect of soil plugging on axial capacity of open-ended pipe piles in sand. *Proc. 18th Int. Conf. Soil Mech. and Geotech. Eng.*, Paris, 1487–1490.
- Ho T.Y.K., Jardine R.J. and Anh-Minh N. (2011). Large-displacement interface shear between steel and granular media. *Geotechnique*, 61(3): 221–234.
- Jardine R.J., Lehane B.M. and Everton S.J. (1993). Friction coefficients for piles in sands and silts. In *Offshore site investigation and foundation behaviour*. Springer. 661–677.
- Jardine, R. J., Chow, F. C., Overy, R. & Standing, J. R. (2005). *ICP design methods for driven piles in sands and clays*. Thomas Telford.
- Jardine, R. Standing, J. and Chow, F. (2006). Some observations of the effects of time on the capacity of piles driven in sand. *Geotechnique*, 56 (4), 227–244.
- Karlsrud, K., Clausen, C.J.F. and Aas, P.M. (2005). Bearing capacity of driven piles in clay, the NGI approach. *Proc. Int. Symp. on Frontiers Offshore Geotechnics*, Perth. pp. 775–782.
- Karlsrud, K., Jensen, T. G., Wensaas Lied, E. K., Nowacki, F., and Simonsen, A. S. (2014) Significant ageing effects for axially loaded piles in sand and clay verified by new field load tests. *Proc. Offshore Technology Conference*, Houston, USA, OTC-25197-MS. doi:10.4043/25197-MS.
- Kolk H. and van der Velde E. (1996). A Reliable Method to Determine Friction Capacity of Piles Driven into Clays. In *Proc. Offshore Technology Conference (OTC)*, Houston, Texas, Pub No. 413532.
- Kolk H.J., Baaijens A.E., and Vergobbi, P. (2005). Results of axial load tests on pipe piles in very dense sands: The EURIPIDES JIP. *Proc. of the Int, Symp. Frontiers in Offshore Geomechanics*, ISFOG. Taylor & Francis, London. pp. 661–667.
- Lehane B.M. (1992). Experimental investigations of pile behaviour using instrumented field piles. Imperial College London (University of London).
- Lehane B.M., Chow F.C., McCabe B.M. and Jardine R.J. (2000). Relationships between shaft capacity of driven piles and CPT end resistance. *Geotech. Engrg.*, ICE, 143, 93–101.
- Lehane B.M., Gaudin C., and Schneider J.A. (2005). Scale effects on tension capacity for rough piles buried in dense sand. *Geotechnique*, 55(10), 709–720.
- Lehane B.M., Jardine R.J., Bond A.J. and Frank, R. (1993). Mechanisms of shaft friction in sand from instrumented pile tests. *Journal of Geotechnical Engineering*, ASCE, 119(1), 19–35.
- Lehane B., Li L. and Bittar E. (2020b). CPT-based load-transfer formulations for driven piles in sand. *Geotechnique Letters*, 10, 568–574.
- Lehane B., Li L. and Bittar E. (2022). CPT-based load-transfer formulations for driven piles in clay (in preparation).
- Lehane, B.M., Li, Y. and Williams, R. (2013). Shaft Capacity of Displacement Piles in Clay Using the Cone Penetration Test. *J. Geotech. & Geoenv. Engrg.*, ASCE, 139(2):253–266.
- Lehane B.M. and Randolph M.F. (2002). Evaluation of a Minimum Base Resistance for Driven Pipe Piles in Siliceous Sand. *J. Geotech. and Geoenviron. Engineering*, ASCE, 128(3), 198–205.
- Lehane, B.M., Liu, Z., Bittar, E., Nadim, F., Lacasse, S., Jardine, R., Carotenuto, P., Rattley, M., Jeanjean, P., Gavin, K., Gilbert, R., Bergan-haavik, J. and Morgan, N. (2020a). A new CPT-based axial pile capacity design method for driven piles in sand. *Proc. 5th Int. Symp. Frontiers Offshore Geotechnics*, ISFOG-21, 462–477. DFI publications, New Jersey.
- Lehane B.M., Liu Z., Bittar E., Nadim F., Lacasse S., Bozorgzadeh N., Jardine E., Ballard J-C, Carotenuto P., Gavin K., Gilbert R., Bergan-Haavik J., Jeanjean P. and Morgan N. (2022). CPT-based axial capacity design

- method for driven piles in clay. *J. Geotech. & Geoenviron. Engineering*, ASCE (under review)
- Lehane, B.M., Lim, J.K., Carotenuto, P., Nadim, F., Lacasse, S., Jardine, R.J. and van Dijk, B.F.J. (2017). Characteristics of Unified Databases for Driven piles. Proc. 8th International Conf. Offshore investigation and Geotechnics: Smarter solutions for offshore developments, Society for Underwater Technology, 1, 162–194.
- Lim J.K. and Lehane B.M. (2014). Characterisation of the effects of time on the shaft friction of displacement piles in sand. *Géotechnique*, 64(6), 476–485.
- Liu T.F., Quinteros V.S., Jardine R.J, Carraro J. A. H., and Robinson J. (2019). A Unified database of ring shear steel-interface tests on sandy-silty soils. Proc. XVII European Conf. Soil Mech. and Geotechnical Engg. Reykjavik, Iceland. doi: 10.32075/17ECSMGE-2019-268.
- Nadim F., Lehane B.M., Liu Z., Bittar E., Bozorgzadeh (2021). New CPT-based method for calculation of axial pile capacity in sand and in clay- Summary and Guidelines. Doc No. 20180089-03-R, Norwegian Geotechnical Institute, Oslo, Norway.
- Niazi F. S. and Mayne P.W. (2013). Cone Penetration Test Based Direct Methods for Evaluating Static Axial Capacity of Single Piles. *Geotechnical and Geological Engineering*, 31(4), 979–1009.
- Niazi, F.S. and Mayne P.W. (2016). CPTu-based enhanced UniCone method for pile capacity. *Engineering Geology*, 212: 21–34. Elsevier B.V.
- Randolph M.F., Dolwin J., and Beck R. (1994). Design of driven piles in sand. *Geotechnique*, 44(3), 427–448.
- Robertson, P.K. (2009). Interpretation of cone penetration tests - A unified approach. *Canadian Geotechnical J.*, 46(11):1337–1355.
- Robertson P.K., and Wride C.E. (1998). Evaluating cyclic liquefaction potential using the cone penetration test. *Canadian Geotechnical Journal*, 35(3), 442–459.
- Salgado R., Woo S. I., and Kim D. (2011). Development of load and resistance factor design for ultimate and serviceability limit states of transportation structure foundations. Rep. No. FHWA/IN/JTRP- 2011/03, Indiana Dept. of Transportation and Purdue Univ., West Lafayette, US.
- Schmertmann J.H. (1978). Guidelines for cone penetration test, performance and design. Report FHWA-TS-78-209, Washington, 145pp.
- Van Dijk B.F.J. and Kolk H.J. (2011). CPT-based design method for axial capacity of offshore piles in clays. In Proc. of the Int. Symposium on Frontiers in Offshore Geotechnics II. Taylor & Francis Group, London. 555–560.
- Van Impe W.F. (1986). Evaluation of deformation and bearing capacity parameters of foundations from static CPT-results. Proc. 4th Int. Geotechnical on Field Instrumentation and in-situ measurements, Singapore, 51–70.
- Van Mierlo, W.C. and Koppejan, A.W. 1952, ‘Lengte en draagvermogen van heipalen’, Bouw, January.
- White D., Schneider J., and Lehane B.M. (2005). The influence of effective area ratio on shaft friction of displacement piles in sand. Proc. 1st Int. Symp. Frontiers in Offshore Geotechnics, Perth, Australia. pp. 741–747.
- Whittle A.J. and Baligh M.M. (1988). A Model for Predicting the Performance of TLP Piles in Clays. Final Report Phase III to sponsors, Dept. of Civil Engineering, Massachusetts Institute of Technology.
- Xu X., Schneider J.A., and Lehane B.M. (2008). Cone penetration test (CPT) methods for end-bearing assessment of open- and closed-ended driven piles in siliceous sand. *Canadian Geotechnical Journal*, 45(8), 1130–1141.
- Yang Z.X., Jardine R.J., Zhu B.T., Foray P. and Tsuha C.H. C. (2010). Sand grain crushing and interface shearing during displacement pile installation in sand. *Geotechnique*, 60(6), 469–482.
- Zhou J., Xie Y., Zuo Z.S., Luo M.Y. and Tang X.J. (1982), Prediction of limit load of driven pile by CPT, 2nd Eur. Symp. On Penetration testing, Amsterdam, 957–963.

Material Point Method simulations of cone penetration and CPT interpretation

R. Salgado

Purdue University, West Lafayette, USA

V. Bisht

Itasca Consulting Group, Minneapolis, USA

M. Prezzi

Purdue University, West Lafayette, USA

ABSTRACT: It is now possible to realistically simulate cone penetration in either sand or clay using the Material Point Method (MPM). To do that, the following requirements must be met: (1) a realistic constitutive model must be used; (2) stress integration of the constitutive model must be accurate; (3) the explicit scheme for the solution of the governing equation must be accurate, robust and efficient; and (4) shear strain localization must be correctly captured. The paper provides an overview of how to correctly perform such simulations and then discusses the implications for the future of CPT interpretation of the availability of accurate, reliable cone penetration simulation methods.

1 INTRODUCTION

1.1 *The cone penetration test*

One of the attractions of the cone penetration test (“CPT”) as originally conceived is its simplicity. A penetrometer with a simple, axisymmetric shape is pushed into the ground, and the resistance to penetration at its tip is measured. Given the simplicity of the test, one would expect that a theoretical basis for its interpretation would have been in place for some time. Unfortunately, what is simple in concept is not necessarily so once implemented (Salgado 2012). The complexity appears when we try to develop methods of analysis for realistic interpretation of CPT results. For example, when we attempt to estimate fundamental state variables or direct functions of state variables – such as relative density (“*DR*”) for sand or undrained shear strength (“*su*”) for clay – we find out that there have not been rigorous theories to guide us.

The two main sources of difficulties in cone penetration simulation are: (1) the modeling of the soil response itself and (2) the method of solving the global equation of motion. To address (1), researchers have developed constitutive models that are now accurate and reliable, at least in the absence of cycling. To address (2), researchers have explored a variety of approaches, which are detailed next.

1.2 *Methods of cone penetration simulation*

To remedy the gap in the theoretical basis for CPT interpretation, efforts started early. Initial attempts relied on modeling the soil as a rigid-plastic material with either a Tresca or Mohr-Coulomb yield surface and applying the notion of a limiting equilibrium to an axially loaded penetrometer and a surrounding soil mass. The Durgunoglu & Mitchell (1976a) model was the most successful of these early models, but fell short when people tried to use it. A major shortcoming of the model was its reliance on perfect plasticity and an interpretation based on estimating the friction angle of the soil. As discussed elsewhere (e.g., Salgado 2012), the mobilized friction angle varies across the soil domain in any boundary-value problem involving real soil, so any method based on such an over-simplification of soil response is fatally flawed.

The next main thrust in developing a framework for CPT simulations was cavity expansion theory (e.g., Salgado et al. 1997; Salgado and Prezzi 2007; Salgado and Randolph 2001). Cavity expansion theory was an approximation to the problem based on the requirement that the cone must expand a cylindrical cavity in the soil in order to advance. With the exception of Salgado and Randolph (2001), these efforts concentrated on the use of simple elastoplastic soil models with Tresca or Mohr-Coulomb yield criteria, although with some modifications attempting to capture the effects of soil nonlinearities. It produced useful relationships

(e.g., Salgado and Prezzi 2007) that can be used in CPT interpretation, but it could not truly simulate a process that is much more involved than a simple cavity expansion process.

The strain path method (Teh and Houlsby 2009) was proposed for analysis of cone penetration in clay, and it was a reasonable approximation to the penetration process, but its impact was again limited by a simple elasto-plastic model with a Tresca yield criterion.

Early application of the Finite Element Method (“FEM”) also met with difficulties. In geomechanics applications, FEM has traditionally followed a Lagrangian approach. This means that the nodes of a mesh are tracked throughout the analysis, and it is through node displacements that solutions are obtained. Deformation follows from relative node displacements, and stress follows from deformation. After considerable deformation has occurred, mesh elements may be so distorted that accurate solutions are no longer possible. In fact, a solution may not even be possible, with the analysis crashing instead.

The Arbitrary Lagrangian-Eulerian (“ALE”) FEM approach (Belytschko and Kennedy 1978) and the material point method (“MPM”) (Schreyer et al. 1994) were proposed to avoid this limitation. In ALE FEM, mesh distortion is limited by remeshing or node repositioning after some threshold level of deformation has happened. When nodes are repositioned or a new mesh formed, we need to map the state variables from quadrature points on the old mesh to quadrature points on the new mesh. The remapping can lead to stress states that lie outside the yield surface for plasticity models with single yield surface or outside the bounding surface for bounding surface models. Remapping can be challenging with bounding surface models or complex models with several variables to map. In contrast to ALE FEM, MPM does not require remapping of variables because the state variables are carried by the same material points throughout the computations. The material point method is discussed next.

2 THE MATERIAL POINT METHOD

2.1 *Fundamentals of the method*

The material point method can be best understood as a variant of the finite element method in which Gauss points are replaced by so called material points. A material point (“MP”) may be a point (as in classical MPM), but it may also be a small area (for two-dimensional analysis) or small volume (for three-dimensional analysis). In contrast with Gauss points, material points may move within and even across elements. This key difference between FEM and MPM has a number of computational consequences.

The most important and most useful implication of the use of material points instead of Gauss points as used in ALE FEM is that the approach is a pure Lagrangian approach, with material point displacements being the basis for the solution. Whereas grid nodes do

move during a computation step, they can be repositioned to their original locations before the next computation time step. It may also be advantageous to consider parts of the grid to either translate in some direction or to compress one-dimensionally. This means that, whether the grid remains static, moves in some direction or is unidirectionally compressed in MPM, it does not get distorted as in FEM, escaping therefore the difficulties created by mesh distortion.

The second most important implication of the use of material points instead of Gauss points in an analysis is that the absolute rigor of FEM with respect to integration of the constitutive model is, to some extent, lost. This happens mainly because Gauss integration is no longer possible. This is not fatal, but a number of remedial measures must be taken to limit any error from this partial loss of rigor.

The next sub-section reviews the MPM formulation used for the analyses whose results are presented in this paper and the key steps in an MPM computation time step.

2.2 *The MPM formulation*

The MPM formulation used in the simulations discussed later is based on the uniform generalized interpolation material point method (“uGIMP” or, in this paper, also “GIMP”) variant of MPM discussed in detail by Bisht and Salgado (2018), Bisht et al. (2021b) and Salgado and Bisht (2021).

Figure 1 shows how space and matter can be discretized for a cone penetration problem. Space can be discretized in the form of a computational grid, and the soil and cone can be discretized using material points. The grid can be a rectangular grid with elements sufficiently small around the cone penetrometer. Material point discretization is achieved derivatively: the initial number of material points per element is fixed across the grid (e.g., four material points per element), and finer discretization is therefore achieved where the grid is itself made finer.

How fine the grid must be depends on whether shear strain localization is expected. The smallest element size in any zone in which shear bands are expected to form should have a width equal to the width of the shear band. We discuss this in greater detail later.

There are two other aspects of discretization that should be briefly discussed. First, the grid can be set up so that part of it moves with the cone penetrometer during penetration and another part, at the bottom of the grid, compresses vertically. Second, when material points flow into a grid element for which they are too large, they are split in a way that conserves energy, momentum and mass. What these two measures accomplish is that, when the cone moves down, together with the fine grid around it, material points located in the coarser grid elements below it will subdivide as they enter the fine grid around the cone, maintaining the required level of material discretization and a sufficient number of material points per element for adequate quadrature.

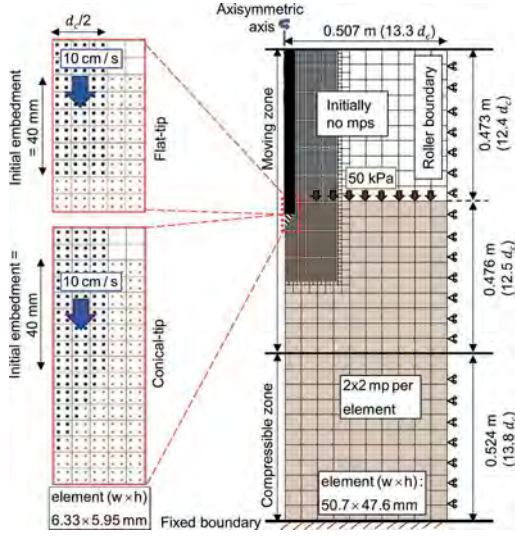


Figure 1. Spatial and material discretization for simulation of penetration of a flat-tip and a conical-tip penetrometer in sand (after Bisht 2021).

Displacement or velocity boundary conditions are straightforward in MPM: the correct displacement or velocity is directly applied on the outermost grid nodes corresponding to that boundary. Application of traction boundary conditions is more involved, requiring distribution of tractions to the material point boundaries aligned with the boundary of the body for every material point so positioned, and then redistribution of these tractions to the nodes of any element containing any part of the material point (Bisht and Salgado 2018). See Figure 2.

To model a semi-infinite soil medium using a finite grid, silent boundaries are required. Silent boundaries let energy dissipate just as it would by radiation in a semi-infinite medium. Kellezi (2000) proposed a “cone boundary” that assumes that a load applied on a free surface of a half-space would propagate within a volume expanding with increasing depth, which can be approximated as a cone. At the boundary, there is both a viscosity term to simulate the energy dissipation through radiation and a stiffness term. Bisht and Salgado (2018) adapted it for MPM, and it is their formulation that is used here.

MPM formulations for solving the global equation of motion have typically been explicit. The governing equation for a general analysis applicable to simple models and any drained simulation is:

$$\dot{p}_i^{(I)} = f_i^{(I)EXT} - f_i^{(I)INT} \quad (1)$$

The rate of the momentum $p_i^{(I)}$, external force $f_i^{(I)EXT}$ and internal force $f_i^{(I)INT}$ at node I , all appearing in (1), are given by (Bisht et al. 2021a):

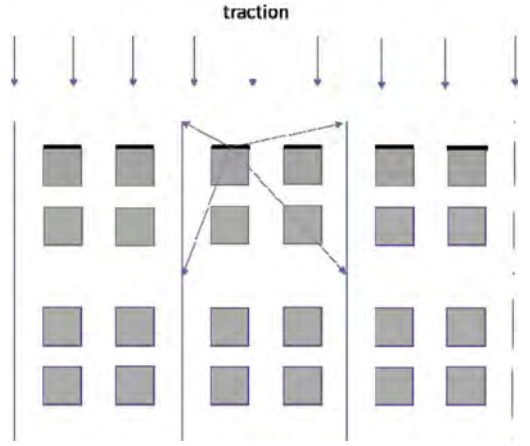


Figure 2. Application of tractions to a body in uGIMP MPM: the tractions are first applied on the edges of the material points (rep-rented by thick lines) and then, using finite element-element shape functions, mapped to the nodes of the element containing the material point.

$$\dot{p}_i^{(I)} = \sum_P S^{(IP)} \dot{p}_i^{(P)} \quad (2)$$

$$f_i^{(I)EXT} = \int_{\Gamma} N^{(I)} t_i d\Gamma + \sum_P S^{(IP)} m^{(P)} b_i \quad (3)$$

and

$$f_i^{(I)INT} = \sum_P S_j^{(IP)} \sigma_{ij}^{(P)} V^{(P)} \quad (4)$$

In Equations (2) through (4), σ_{ij} is the Cauchy stress, b_i is the body force per unit mass, $m^{(P)}$ is the mass of the material point, Γ is the boundary of the domain Ω of the problem and $t_i = \sigma_{ij} n_j$ is the traction on an arbitrary point on Γ , with n_j being the unit vector normal to Γ at that point. Also appearing in Equations (2) through (4) are the finite element shape function $N^{(I)}$ at node I , the material point shape function $S^{(IP)}$, which maps the value of a variable at the centroid of a material point P to node I , and its gradient. These last two are defined as:

$$S^{(IP)} = \frac{1}{V^{(P)}} \int_{\Omega^{(P)}} N^{(I)} \chi^{(P)} d\Omega \quad (5)$$

and

$$S_j^{(IP)} = \frac{1}{V^{(P)}} \int_{\Omega^{(P)}} N_j^{(I)} \chi^{(P)} d\Omega \quad (6)$$

where $\chi^{(P)}$ is the particle characteristic function, usually taken to be uniformly equal to 1 across the MP and zero outside it:

$$\chi^{(P)} = \begin{cases} 1 & \mathbf{r} \in \Omega^{(P)} \\ 0 & \mathbf{r} \notin \Omega^{(P)} \end{cases} \quad (7)$$

One reason for using an explicit solution scheme in MPM are the difficulties in inverting ill-conditioned stiffness matrices that result when there are only a few material points in some element or elements (Wang et al. 2016).

The Update Stress Last (USL) explicit time integration scheme, in which the stresses in the material point are computed after momentum in the grid is updated (Wallstedt and Guilkey 2008), is used here.

Explicit time integration is conditionally stable, which means that time increments must be less than some limit for the computations to converge. For nonlinear problems, the time step Δt is usually taken as:

$$\Delta t = \kappa \min \left(\text{ele} / \sqrt{E_c / \rho} \right) \quad (8)$$

where κ is the Courant number (Courant et al. 1967), elem_{in} is the minimum element size, E_c is a measure of material stiffness (the Young's modulus or the constrained modulus are common choices, depending on the problem), and ρ is the material density. For dynamic problems, $\kappa \approx 0.4$ yields suitable results for the USL approach, but higher values of κ may be used for quasi-static problems (Wallstedt and Guilkey 2008). For quasi-static problems, such as cone penetration, the time step Δt can be increased by mass scaling to reduce the overall computation time. In mass scaling, the material density ρ is artificially increased by a mass scaling parameter η :

$$\rho_{\text{scaled}} = \eta \rho \quad (9)$$

This allows the use of a larger time step Δt_{ms} :

$$\Delta t_{\text{ms}} = \sqrt{\eta} \Delta t \quad (10)$$

2.3 Volumetric locking

In numerical solutions to problems in mechanics involving incompressible or nearly incompressible materials, a phenomenon known as volumetric locking may occur. Volumetric locking is the insufficiency of variables provided by a grid discretization to allow solution of all equations. This results from the additional equation involving strain tensor components resulting from the imposition of the incompressibility

constraint on an integration point. Incompressibility or near incompressibility appears in Tresca solids in the plastic range and at critical state for any soil model. It often appears as strong spatial oscillations in the values of fundamental variables, such as stress, which appears as a checkerboard pattern when results are plotted as contour plots.

In the finite element method, volumetric locking can be avoided by using higher-order elements, which lead to a sufficient number of variables to overcome any excess equations from the incompressibility constraint. This is not an option in MPM because shape functions for higher-order elements can take negative values for some regions in an element, which in turn can lead to negative mass at the corresponding nodes from a material point located in such regions. The attending complications are discussed in detail in Bisht et al. (2021a).

An effective way to deal with volumetric locking in MPM is the use of the so-called non-linear $\bar{\mathbf{B}}$ method (Hughes 1980). The method is based on the fact that volumetric locking can be prevented by reducing the number of constraints imposed by incompressibility in each element. For example, for Q4 elements, volumetric locking can be prevented if a reduced, single-point quadrature rule is used (see Sloan and Randolph (1982)). The use of single Gauss point in reduced integration for Q4 elements is sufficient to prevent volumetric locking, but this strategy is not applicable in MPM.

For MPM, Bisht et al. (2021a) used a large-deformation formulation of the $\bar{\mathbf{B}}$ method with the deformation gradient \mathbf{F} split into a volumetric and a deviatoric component, with the volumetric component calculated only at the element center. The computational algorithm that results requires that the gradient $S_{,j}^{(IP)}$ of the material point shape functions (material point mapping functions) must be calculated also at the element center. A modified deformation gradient $\bar{\mathbf{F}}^{(P)}$ at the material point P , obtained from combining the deviatoric component of the deformation gradient with the volumetric component of it at the element center, is then used in stress integrations.

2.4 A computation time step in an MPM simulation

During a time step in an MPM simulation, we follow the steps outlined below.

1. Start with initialization of all variables at material points and grid nodes and set the time t to 0.
2. Determine an appropriate time increment Δt using Eq. (10).
3. For each material point P :
 - (a) Find every node I around the material point P to which nonzero values of material point variables must be transferred, i.e., nodes for which $\int_{\Omega^{(P)}} N^{(I)} \chi^{(P)} d\Omega \neq 0$
 - (b) Compute mapping functions $S^{(IP)}$ using Eq (5) and their gradients $S_{,j}^{(IP)}$ using Eq. (6). If the node is a hanging node, transfer mapping

functions and their gradients to surrounding nodes as explained by Bisht et al. (2021a).

- (c) For simulations in incompressible soil, compute mapping function gradients $S_j^{(IP)}(C)$ at element center C .
- (4) For each node I :
 - (a) Compute nodal mass $m^{(I)} = \sum_P m^{(P)} S^{(IP)}$ and momentum $p_i^{(I)} = \sum_P m^{(P)} v_i^{(P)} S^{(IP)}$
 - (b) Compute nodal external $\bar{f}_i^{(I)EXT}$ (Eq. (3)) and internal forces $\bar{f}_i^{(I)INT}$ (Eq. (4)).
 - (c) Compute the rate of change of momentum $\underline{p}_i^{(I)}$ using Eq. (1) and update nodal momentum using $p_i^{(I)} \leftarrow p_i^{(I)} + \underline{p}_i^{(I)} \Delta t$
 - (d) If the node is on a velocity boundary, set $p_i^{(I)} = mv_i^*$, where v_i^* is the prescribed velocity.
 - (e) Compute contact forces $f_i^{(I)CT}$ using the contact algorithm proposed by Bardenhagen et al. (2000, 2001) and update the nodal momentum using $p_i^{(I)} \leftarrow p_i^{(I)} + f_i^{(I)CT} \Delta t$
- (5) For each material point P :
 - (a) Update material point velocity $v_i^{(P)} \leftarrow v_i^{(P)} + \Delta t \sum_I S^{(IP)} \underline{p}_i^{(I)} / m^{(I)}$ and position $x_i^{(P)} \leftarrow x_i^{(P)} + \Delta t \sum_I S^{(IP)} p_i^{(I)} / m^{(I)}$
 - (b) Compute the velocity gradient $v_{i,j}^{(P)}$ and deformation gradient $F_{ij}^{(P)}$
 - (c) For simulations in incompressible soil, compute the velocity gradient $v_{i,j}^{(P)}(C)$ at the element center and compute the modified deformation gradient $\bar{F}_{ij}^{(P)}$
 - (d) Using a suitable objective rate formulation, update the stresses and internal variables using the algorithms proposed in Nazem et al. (2009).
 - (e) Update the material point volume $V^{(P)} \leftarrow (\det F_{ij}^{(P)}) V^{(P)}$
- (6) Adjust (translate/compress/reset) the background grid.
- (7) Update time $t \leftarrow t + \Delta t$. If $t > t_{end}$, go to step 2; otherwise exit.

An objective time rate is required in large-deformation, large-rotation analyses (Lubliner 2008). There is also a specific objective rate formulation that must be used to obtain the correct solution of a bound-ary-value problem (Lim, J., Salgado, R. and Prezzi, M., paper in preparation).

3 VALIDATION OF MPM SIMULATIONS OF RELATED GEOMECHANICS BOUNDARY VALUE PROBLEMS

3.1 Limit bearing capacity

If an MPM formulation is capable of modeling cone penetration, then it must be able to also model a bearing capacity problem. The Prandtl punch

problem, in which a flat plane-strain punch (a strip footing) is forced into a Tresca half-space from the surface, is a good test of the quality of the formulation because the solution to it is known exactly. But limit analysis solutions also exist bracketing the bearing capacity of footings, strip or square, embedded to various depths D in Tresca soil (Salgado et al. 2004). The values of limit unit bearing capacity qbL are given in Table 1 for strip and Table 2 for square footings. We can see very good agreement between MPM and the benchmark results, including the value for a strip footing on the surface of the half-space, which is known to be $2 + \pi$ times the yield stress c of the Tresca material and is well approximated by the MPM solution.

The MPM analyses were performed for very stiff Tresca soils. This allowed development of the limit bearing capacity for small footing deflection, before any significant change to the geometry of the problem could occur. This is important because this is a feature of the limit analysis solutions used to benchmark the MPM values of qbL .

In only three of the ten cases considered in the two tables was the MPM value outside, and only margin-ally outside, the range defined by the lower and upper bounds from limit analysis.

Table 1. Value of limit unit bearing capacity qbL of a strip footing in Tresca soil from MPM compared to values obtained using formation gradient.

D/B	L	U	MPM
0.0	5.132	5.203	5.213
0.1	5.448	5.548	5.471
0.2	5.696	5.806	5.761
0.4	6.029	6.133	5.977
1.0	6.562	6.657	6.535

B = footing width.

Table 2. Value of limit unit bearing capacity qbL of a square footing in Tresca soil from MPM compared to values obtained using limit analysis.

D/B	L	U	MPM
0.0	5.856	6.227	6.149
0.1	6.491	7.140	7.063
0.2	6.897	7.523	7.426
0.4	7.303	8.104	8.002
1.0	8.771	9.429	9.296

B = footing width.

3.2 Footing loaded to large settlements

Rather than simply producing the correct values of limit bearing capacity, the MPM formulation must also reproduce the load response of a footing to large settlements. This problem has been studied using several methods, including sequential limit analysis (da Silva et al. 2011), ALE FEM (Kardani et al.

2015; Nazem et al. 2006, 2009), a form of ALE FEM known as “remeshing and interpolation technique with small strain” (RITSS) (Wang et al. 2013) and MPM (Iaconeta et al. 2019; Sołowski and Sloan 2015; Woo and Salgado 2018).

In the validation simulations, a 1-m wide footing was modeled as a rigid material, and the soil was modeled as a weightless Tresca material with $E = 100$ kPa, $\nu = 0.49$, $\rho = 1.0\text{g/cm}^3$ and $su = 1$ kPa (the same parameter values used by Wang et al. 2013). The problem domain was discretized using an irregular background grid with a minimum element size equal to $B/20$ near the base of the footing and a maximum element size equal to $B/80$ away from the footing. Initially, each element contained 4 material points in a 2×2 configuration. The size of the domain was $10B$ in both the horizontal and vertical directions when measured from the center of the base of the footing. The Courant number κ was taken as 0.3. To simulate quasi-static conditions, the vertical penetration velocity increased linearly from 0 to 0.02 m/s over 1 s and then remained constant at 0.02 m/s after 1 s.

Comparison of the MPM formulation of Bisht et al. (2021a), noted in the legend as “B-bar GIMP,” with a variety of other methods is shown in Figure 3. The favorable comparison with the high-quality ALE FEM simulation (labeled “RITSS” in the figure) is an important validation result.

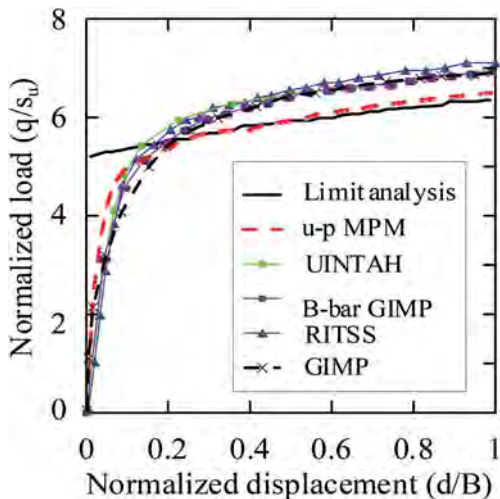


Figure 3. MPM GIMP simulations of a footing pushed to large penetration in an elasto-plastic Tresca soil compared with the solution of various other methods of analysis (after Bisht et al. 2021a).

4 CONE PENETRATION IN SAND

4.1 Constitutive model

Simulation of cone penetration in sand using MPM is less complex than in clay largely because drained penetration can be assumed a priori, there being

therefore no need to perform coupled flow-deformation analyses. Coupled analyses are required for clay, as we will discuss later.

To properly simulate penetration in sand, a realistic sand constitutive model is required. The model must be able to accurately reproduce soil element response in triaxial compression, triaxial extension and simple shear loading. A model satisfying this requirement is that of Loukidis and Salgado (2009). The analyses reported here were performed using this model.

Model parameters and the test data required for their determination are listed in Table 3. Also given in the table are the values of model parameters for Ottawa sand. It is for Ottawa sand that MPM simulations were performed. Although the number of parameters (22) may seem daunting, only 5 parameters (h_1 , h_2 , e_{lim} , μ and k_h) are determined using a trial and error approach. The remaining 17 can be directly determined by fitting the model equations to the data. Most parameters can be determined using routine tests such as drained and undrained TXC, while others can be reasonably assumed based on the corresponding values for similar sands.

Table 3. Constitutive model input parameters for Ottawa sand (after Loukidis and Salgado 2009).

	Symbol	Value	Test(s)
Small-strain(“elastic”) parameters	ν	0.15	compression w/unloading
	C_g	611	BE or RC
	n_g	0.437	BE or RC
	γ_1	0.00065	RC or TX
	a_1	0.47	TXCU
Critical state	Γ_c	0.780	TXC
	λ	0.081	TXC
	ξ	0.196	TXC
Bounding surface	M_{cc}	1.21	TXC
Dilatancy	k_b	1.9	TXC
	D_0	1.31	TXC
	k_d	2.2	TXC
Plastic modulus	h_1	2.2	TXC
	h_2	0.240	TXC
	e_{lim}	0.81	TXC
	μ	1.2	TXCU
Stress-induced anisotropy	$c1$	0.71	TXE
	$c2$	0.78	SS
	n_s	0.35	SS
Inherent anisotropy	a	0.31	TXE
	k_h	0.39	TXE
Yield surface radius	m	0.05	-

TXC: triaxial compression; TXE: triaxial extension; TXCU: un-drained triaxial compression; SS: simple shear; RC: resonant column; and IC: isotropic compression.

4.2 Cone penetration simulation scheme

A fixed time step size – determined using Eq. (10) – was used for all cone penetration simulations. For us

to use Eq. (10), certain variables and parameters must be evaluated. As will be discussed in detail in the next sub-section, the minimum element size e_{min} used for the simulations in this study was 5.95 mm, and the relative density DR for all tests was $\sim 90\%$ (implying a dry density ρ_{of} of 1.72 ton/m³). Using a reasonably high mean stress p' of 10 MPa and a void ratio e of 0.524, corresponding to a relative density DR of 90%, the small-strain shear modulus G_{max} is equal to 800 MPa using the Hardin and Richart (1963) correlation. Assuming $\kappa = 0.7$ and $\eta = 25$, a scaled time step $\Delta t_{\text{ms}} = 2.0 \times 10^{-5}$ s was computed. Simulations performed using smaller κ and smaller η values produced nearly identical results. A fixed time step $\Delta t_{\text{ms}} = 2.0 \times 10^{-5}$ s was therefore considered acceptable and was used in the simulations.

Penetration was simulated by imposing on the cone penetrometer successive displacement increments. The same rate of penetration is ideally used in computations as in reality, but to reduce computation time, a greater penetration velocity was used in the simulations. This is possible so long as penetration remains quasi-static, so that there is no rate dependence in the value of q_c . Table 4 details the parameters for the MPM analyses reported in this paper.

Table 4. General numerical scheme used for the MPM simulations of cone penetration in sand (after Bisht 2021).

Feature	Implementation
Type of MPM	uGIMP
Time integration	Explicit: $\Delta t = 2 \times 10^{-5}$ s Mass scaling factor: 25
Mesh	Structured irregular grid divided into moving and compressible regions; Q4 element with initially four material points; element size approximately equal to the width of the shear band
Penetration velocity	$v_{\text{cone}} = 0-10$ cm/s for $t \leq 1$ s; 10 cm/s for $t > 1$ s
Initial stress field	Initial vertical stress known; $K0 = 0.45$ assumed
Contact model	Coulomb friction model with $\mu_f = 0.3$
Stress integration algorithm	Explicit with automatic sub-stepping and error control
Objective stress rate and strain measure	Modified kinematic logarithmic rate; Hencky strain
Volumetric locking	Locking not observed
Constitutive model	Loukidis and Salgado (2009) sand model; Parameters calibrated to Ottawa sand used

ρ : density; Δt = time step size; Q4: linear quadrilateral elements; $K0$: coefficient of lateral earth pressure at-rest; mps.: material points; v_{cone} : penetration velocity of cone; and μ_f coefficient of friction.

The grid used to perform the simulations resembles that shown in Figure 1. It has a moving grid region that moves down with the cone penetrometer and a compressible region at the bottom (Woo and Salgado 2015). The nodes at the bottom of the compressible grid do not move, but those above them do. To capture shear bands that develop near the cone base and cone shaft, the smallest element size was chosen to be roughly equal to the shear band width observed in sands (e.g., Alshibli and Hasan 2008; Alshibli and Sture 1999; Desrues and Viggiani 2004; Salgado et al. 2017; Tehrani et al. 2017).

4.3 Validation using calibration chamber tests

The calibration chamber with a viewing window to enable digital image correlation (DIC) analysis of penetration tests was used to perform two cone penetration tests in dense samples subjected to two different levels of vertical effective stress.

The chamber, shown in Figure 4, is a half-cylindrical calibration chamber with a diameter D_c of 1680 mm and a height of 1200 mm. The tests were performed under BC3 calibration chamber boundary conditions (Ghionna and Jamiolkowski 1991; Salgado et al. 1998) by using an inflatable air-rubber bladder at the top of the sample and rigid lateral walls. Three cameras with a resolution of 5 megapixels (SV5M10 complementary metal-oxide semiconductor CMOS cameras, EPIX, Buffalo Grove, Illinois) were used to take images during testing (GalvisCastro et al. 2019; Salgado et al. 2016; TovarValencia et al. 2018).



Figure 4. DIC calibration chamber at COFFEE, Purdue University: front view, showing viewing windows.

Figure 5 shows a comparison of measured q_c with the q_c values computed using MPM for two values of vertical effective stress at the level of the cone. The MPM simulations capture the gradual rise of q_c from the time the cone penetrometer enters the soil, which is also observed in the real experiment, and also the plateau that forms in the q_c versus depth plot once boundary effects are no longer a factor. The experiments have not been repeated for confirmation, but the comparisons of the plots from the

MPM simulation with those obtained from the calibration chamber test are encouraging.

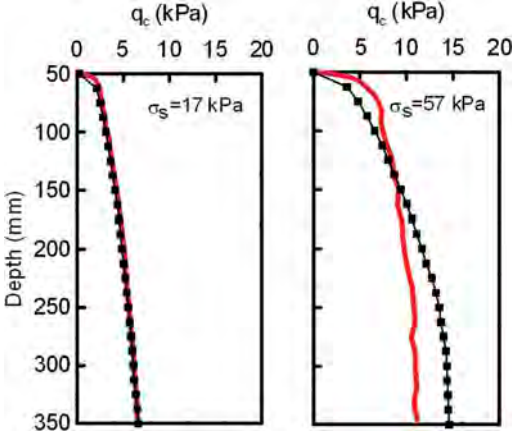


Figure 5. Comparison of MPM simulations of cone penetration tests in a calibration chamber with the results of those tests (modified after Bisht 2021).

What a DIC calibration chamber enables us to do that a regular calibration chamber does not is the measurement of displacement fields. Figure 6 shows a comparison of the horizontal and vertical displacement increments measured using a DIC analysis of images collected during a small downward move of the cone penetrometer to those computed using MPM. The comparison shows that MPM can effectively capture displacement fields around the advancing cone penetrometers in addition to also approximating closely the cone resistance values.

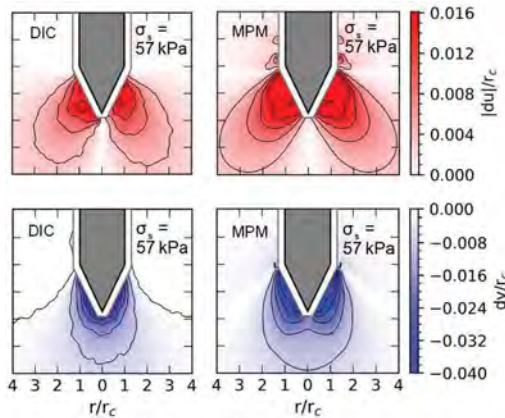


Figure 6. Comparison of vertical and horizontal displacement increments $-du$ and dv – obtained from DIC analysis of the chamber test and MPM simulations of the same test (modified after Bisht 2021).

5 CONE PENETRATION IN CLAY

5.1 Formulation

Simulation of cone penetration in clay requires a coupled, hydro-mechanical, effective stress analysis. Such an analysis allows the calculation of effective stress and pore pressure everywhere in the soil domain as the penetration progresses. It is accomplished in the analysis discussed here using a single material point to represent both the soil matrix and water and an explicit scheme to solve the governing equations, which are in terms of the velocity of the soil matrix and the velocity of water as the primary variables (Bisht et al. 2021b). Incompressibility constraints in the soil matrix are resolved using the non-linear B-bar method, and pore pressures are computed at element centers.

A coupled formulation can be used to handle penetration under partial drainage conditions. Undrained conditions need not be assumed. If we do assume undrained conditions, a simplification of the governing equations is possible. The governing equations are derived from consideration of momentum of the water, momentum of the soil matrix, and interaction of the soil particles and water though a drag resistance between the two due to a relative velocity.

5.2 Validation

The MPM formulation has been validated using, among other benchmarks, the one-dimensional consolidation theory of Terzaghi (1943). We show that here for illustration of the quality of the analysis framework, but point readers to Bisht et al. (2021b) for a more extended discussion of the accuracy and robustness of the numerical schemes.

Figure 7(a) shows a soil wall with height equal to 1.0 m and width equal to 0.075 m. An MPM grid was superposed on the wall. The grid is a structured regular grid with linear quadrilateral (Q4) elements with dimensions $0.025 \text{ m} \times 0.025 \text{ m}$. Each element contained four material points initially. The Young's modulus E of the soil is 10,000 kPa, its Poisson's ratio is 0.3, soil particle density is 2.67 ton/m^3 , the initial porosity is 0.4, and the hydraulic conductivity is 10^{-3} m/s . The density of water is 2.67 ton/m^3 and its bulk modulus is 2.2 GPa. An initial pore pressure of 10 kPa was assigned to the soil. A fixed boundary condition was applied at the bottom, and roller boundaries restricting horizontal movement were applied to the sides. Impermeable boundary conditions were applied at the bottom boundary and the two side boundaries. The consolidation test was performed by applying a 10 kPa traction at the top surface and allowing the water to drain from the top. A fixed time step size equal to $1 \times 10^{-5} \text{ s}$ was used in the MPM simulation of the compression of the soil wall.

Figure 7(b) shows that the coupled MPM formulation closely matches the results obtained using the traditional Terzaghi solution.

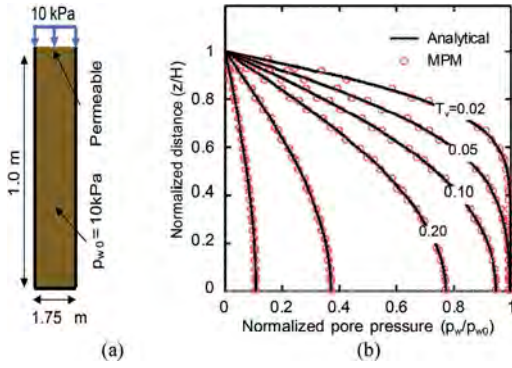


Figure 7. One-dimensional consolidation test: (a) slide of soil undergoing 1D consolidation; and (b) a comparison of the results obtained using the coupled MPM formulation and Terzaghi’s solution after (Bisht et al. 2021b).

5.3 Simulation of a real CPT in clayey soil

We use the two CPTs performed by Landon (2007), which were located approximately 10 m apart, to test the MPM formulation for clay. The cone resistances measured in these two tests at a depth of 9.6 m were approximately 580 kPa and 730 kPa. Soil samples were collected from several depths. Based on testing done on these samples, the soil state at a depth of 9.6 m was estimated to be defined by an initial vertical effective stress $\sigma'_{v0} = 100$ kPa, initial vertical total stress $\sigma_{v0} = 175$ kPa, initial horizontal effective stress $\sigma'_{h0} = 65$ kPa, and overconsolidation ratio $OCR = 2.2$. The groundwater level was at a depth of 1.7 m. The hydraulic conductivity varied from 10^{-10} to 10^{-9} m/s.

The constitutive model used in the simulations is that of Chakraborty et al. (2013). The model contains a total of 22 parameters, most of which, as in the case of the sand model discussed earlier, can be determined through simple inspection and curve fitting of equations to data obtained from routine laboratory tests. The analyses were performed using the calibrated values of Boston Blue Clay (“BBC”) that are given in Chakraborty et al. (2013), except that strain-rate independence is assumed because the problem is quasi-static.

Figure 8 shows both space and material point discretization of the simulations. The default four material points per elements were used. The same general approach followed for the grid in the analysis of cone penetration in sand was repeated for clay. A structured irregular grid with both a moving and a compressible mesh zone was used to discretize the domain. A standard cone with diameter $d_c = 35.7$ mm and cone tip height $h_c = 30.9$ mm (apex angle = 60°) was assumed. Axisymmetric conditions were assumed, and thus only half the cone was discretized.

The goal of the analysis was not to produce the entire history of penetration from the ground

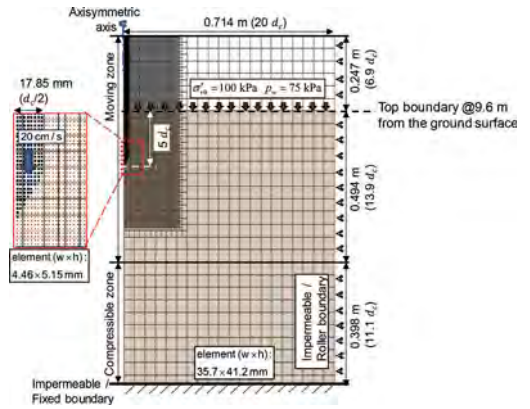


Figure 8. Grid and material point discretization for simulation of cone penetration at a depth of 9.6 m for the cone penetration tests of Landon (2007) (after Bisht et al. 2021b).

surface, but penetration just into the clay layer. Accordingly, the initial position of the cone for the analysis was $5d_c$ below the upper boundary of the clay layer, which is at a depth of 9.6 m from the ground surface.

The soil was discretized using a mesh of dimensions $20d_c$ in width by $25d_c$ in height. The mesh was built with linear quadrilateral elements, each initially containing 2×2 material points.

Figure 9 shows the results of the MPM simulation compared to the two values measured in each CPT sounding at a depth of 9.6m. The comparison is very encouraging.

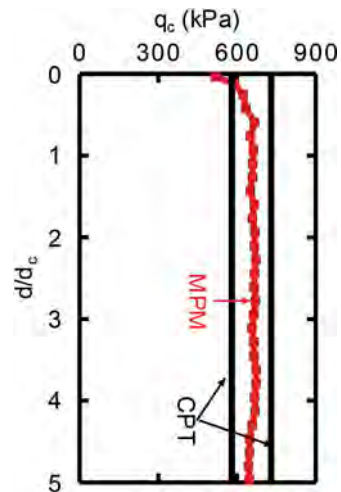


Figure 9. Comparison of cone resistance q_c , during a penetration path $5d_c$ long, with the values measured in two CPT soundings (after Bisht et al. 2021b).

6 IMPLICATIONS FOR FUTURE OF CPT INTERPRETATION

6.1 Importance of MPM in future development of CPT interpretation approaches

This paper has shown that MPM, combined with realistic constitutive models, is capable of accurate predictions of cone resistance in both sandy and clayey soils. What does that mean for CPT interpretation in the future? It depends on how far in the future, and it depends on what type of interpretation we are pursuing.

6.2 Limitation of MPM in the present and in the near term

At present, MPM with finite-size material points, and even, to a lesser degree, with material points that are actual points, is computationally expensive if accurate, realistic simulations are desired. It is important to understand that much faster simulations can be done, and can be found in the literature, but not with the level of discretization required for accuracy. At the time of this writing, simulation of an entire CPT starting from the ground surface is cost-prohibitive in an engineering design setting. However, cloud computing is expected to ease the computational burden significantly in the next several years.

This means that routine application of MPM to simulate entire soundings and the richness of interpretation that would result from that lies in the more distant future. However, it is entirely possible to compute cone resistance locally. For example, if the interest is in a specific layer with a certain soil existing with a certain state, then that is a simulation that is practically possible to perform. The computations done earlier for a clay layer illustrate this.

The other use of MPM is to perform simulations ahead of time for various combinations of soil intrinsic and state variables, and then use the results of these simulations to derive correlations of cone resistance with these variables or to feed them to AI tools. There are two types of relationships that can be developed: direct and indirect relationships.

Indirect relationships constitute the basic tool for pure CPT interpretation: from q_c and other measurements made during a CPT, obtain the values of the soil state variables. Direct relationships allow you to obtain estimates of quantities of direct interest in design, such as unit shaft and base resistance of a pile or liquefaction resistance from cone resistance and any other CPT measurements.

6.3 Indirect interpretation of CPT results

In indirect CPT interpretation methods, we are interested in evaluating soil state from CPT measurements. The thinking is somewhat akin to that of solving a system of equations (Salgado 1993). If there are enough equations, the unknown variables

can be determined. The “equations” in this case are whatever relationships are available between the knowns (q_c and any other measurement) and the unknowns. The unknowns are, in sands, variables such as the relative density or void ratio, the effective stress state and soil fabric. In other words, the unknowns would be state variables. The relationships would be equations developed based on MPM simulations between cone resistance and the state variables. Parameters in these equations would be the soil intrinsic variables, those related to factors like mineralogy, particle size distribution, and the like, as well as critical state parameters. Intrinsic variables would be determined from routine laboratory tests.

Perhaps the greatest impact of the availability of reliable MPM simulation capabilities will be on interpretation in clay. Relationships already exist relating q_c to relative density and lateral effective stress, for example, in sands (Salgado and Prezzi 2007). However, interpretation of CPT results in clay has remained linked to a Tresca-linked view of clay, with relationships between q_c and s_u instead of between q_c and void ratio, effective stress and fabric. In these traditional relationships, a cone factor N_k is defined to relate q_c to s_u , but how should s_u be defined in such a relationship? Should it be that obtained under triaxial compression, triaxial extension or simple shear loading? Additionally, somewhat awkward relationships must be resorted to relating N_k to a rigidity index defined in terms of a modulus and a shear strength that are again not defined. An interpretation method leading to the values of state variables would be preferable.

6.4 Direct interpretation of CPT results

Direct interpretation occurs in a design application context, instead of a soil mechanics or soil characterization context. To develop a direct CPT method, it is necessary that the soil response for the specific design problem can be correlated with q_c and/or other CPT measurement. If the design problem can be itself simulated numerically, we have an entirely science-based correlation that can be used in design. Otherwise, the correlation will be semi-empirical, as liquefaction potential assessment methods must still be. Table 5 contains three of the most important design problems to which the CPT is routinely applied. Foundation loading can already be effectively simulated using the finite element method to settlement levels of interest in design (see, e.g., Han et al. 2017; Loukidis and Salgado 2011; Salgado et al. 2017). MPM can be used for problems in which significant mesh distortion will render FEM analyses not feasible. Liquefaction cannot as yet be simulated. The main obstacle is the unavailability of a constitutive model that can properly simulate the soil response under repeated cycling, so methods will for now and in the near future remain semi-empirical.

Table 5. Direct interpretation of CPT results.

Design problem	Target variables	Basis of relationships
Shallow foundation design	Limit unit bearing capacity qb_L ; settlement w in service	Computational simulations using MPM or FEM
Deep foundation design	Ultimate unit base resistance qb_{ult} ; limit unit shaft resistance qs_L	Computational simulations using MPM or FEM
Liquefaction potential assessment	Cyclic resistance ratio CRR	Semi-empirical because liquefaction cannot yet be accurately simulated

7 CONCLUSIONS

The main purpose of this paper was to review our ability to simulate the cone penetration process. For realistic simulation of cone penetration in both sand and clay, it is necessary to have (1) realistic, robust constitutive models; (2) realistic, robust constitutive model stress integration schemes; and (3) accurate, efficient, robust numerical schemes for integration of the governing equation for the cone penetration process. The paper focused on prong 3 of the simulation framework: the use of the u-GIMP MPM formulation to simulate the penetration process.

MPM replaces Gauss points in Lagrangian FEM formulations by material points. The material points are not affixed to the finite element constituting the mesh or grid into which a body is discretized but rather can move through the grid, even crossing elements. The material points in fact are the discretization of the body, whereas the grid is the discretization of space.

There are certain consequences from this fundamental difference between the two methods. Two of the most consequential are: (1) integration is not as accurate as in FEM; (2) some techniques used in FEM to avoid pathologies, such as volumetric locking, are not effective in MPM; (3) because the grid can always be reset between computation time increments, mesh distortion does not impact calculations, and MPM simulations can progress to very large displacement levels.

The paper illustrated some of the validation exercises that the MPM computational framework discussed here has been subjected to and successfully passed. These validations have shown that accurate cone penetration simulations are possible. The impact of this capability is yet to come. In the future, the ability to accurately, realistically simulate cone penetration and other processes involved in the direct or indirect interpretation of CPT results will lead to high-quality interpretation methods. Other factors in interpretation, such as spatial variability of

soil state variables and soil type, will also be better taken into account with the more advanced command of the mechanics of cone penetration.

REFERENCES

- Alshibli, K. A. & Hasan, A. 2008. Spatial variation of void ratio and shear band thickness in sand using X-ray computed tomography. *Géotechnique* 58(4): 249–257.
- Alshibli, K. A. & Sture, S. 1999. Sand Shear Band Thickness Measurements by Digital Imaging Techniques. *Journal of Computing in Civil Engineering* 13(2): 103–109.
- Bardenhagen, S. G., Brackbill, J. U., & Sulsky, D. 2000. The material-point method for granular materials. *Computer Methods in Applied Mechanics and Engineering* 187(3–4): 529–541.
- Bardenhagen, S. G., Guilkey, J. E., Roessig, K. M., Brackbill, J. U., Witzel, W. M., & Foster, J. C. 2001. An improved contact algorithm for the material point method and application to stress propagation in granular material. *CMES - Computer Modeling in Engineering and Sciences* 2(4): 509–522.
- Belytschko, T. B. & Kennedy, J. M. 1978. Computer models for subsurface simulation. *Nuclear Engineering and Design* 49(1–2): 17–38.
- Bisht, V. 2021. Cone penetration analysis using the Material Point Method. Purdue University.
- Bisht, V. & Salgado, R. 2018. Local transmitting boundaries for the generalized interpolation material point method. *International Journal for Numerical Methods in Engineering* 114(11): 1228–1244.
- Bisht, V., Salgado, R., & Prezzi, M. 2021.a. Simulating penetration problems in incompressible materials using the material point method. *Computers and Geotechnics* Elsevier Ltd 133(December 2019): 103593.
- Bisht, V., Salgado, R., & Prezzi, M. 2021.b. Material Point Method for Cone Penetration in Clays. *Journal of Geotechnical and Geoenvironmental Engineering* 147(12): 1–16.
- Bisht, V., Salgado, R., & Prezzi, M. 2021.c. Simulating penetration problems in incompressible materials using the material point method. *Computers and Geotechnics* 133: 103593.
- Chakraborty, T., Salgado, R., & Loukidis, D. 2013. A twosurface plasticity model for clay. *Computers and Geotechnics* 49(765): 170–190.
- Courant, R., Friedrichs, K., & Lewy, H. 1967. On the Partial Difference Equations of Mathematical Physics. *IBM Journal of Research and Development* 11(2): 215–234.
- Desrués, J. & Viggiani, G. 2004. Strain localization in sand: an overview of the experimental results obtained in Grenoble using stereophotogrammetry. *International Journal for Numerical and Analytical Methods in Geomechanics* 28(4): 279–321.
- Galvis-Castro, A. C., Tovar-Valencia, R. D., Salgado, R., & Prezzi, M. 2019. Effect of loading direction on the shaft resistance of jacked piles in dense sand. *Geotechnique* 69(1).
- Ghionna, V. N. & Jamiolkowski, M. 1991. A critical appraisal of calibration chamber testing of sands. *Proc., 1st Int. Symp. on Calibration Chamber Testing* Elsevier, Amsterdam, The Netherlands 13–39.
- Han, F., Salgado, R., Prezzi, M., & Lim, J. 2017. Shaft and base resistance of non-displacement piles in sand. *Computers and Geotechnics* 83: 184–197.

- Hardin, B. O. & Richart, J. F. E. 1963. Elastic Wave Velocities in Granular Soils. *Journal of the Soil Mechanics and Foundations Division* 89(1): 33–65.
- Hughes, T. J. R. 1980. Generalization of selective integration procedures to anisotropic and nonlinear media. *International Journal for Numerical Methods in Engineering* 15(9): 1413–1418.
- Iaconeta, I., Larese, A., Rossi, R., & Oñate, E. 2019. A stabilized mixed implicit Material Point Method for non-linear incompressible solid mechanics. *Computational Mechanics* Springer Berlin Heidelberg 63(6): 1243–1260.
- Kardani, M., Nazem, M., Carter, J. P., & Abbo, A. J. 2015. Efficiency of high-order elements in large-deformation problems of geomechanics. *International Journal of Geomechanics* 15(6): 04014101.
- Kellezi, L. 2000. Local transmitting boundaries for transient elastic analysis. *Soil Dynamics and Earthquake Engineering* 19(7): 533–547.
- Landon, M. M. 2007. Development of a non-destructive sample quality assessment method for soft clays.
- Loukidis, D. & Salgado, R. 2009. Modeling sand response using two-surface plasticity. *Computers and Geotechnics* Elsevier Ltd 36(1–2): 166–186.
- Loukidis, D. & Salgado, R. 2011. Effect of relative density and stress level on the bearing capacity of footings on sand. *Geotechnique* 61(2): 107–119.
- Lubliner, J. 2008. *Plasticity Theory*. Dover Publications, INC.
- Nazem, M., Carter, J. P., Sheng, D., & Sloan, S. W. 2009. Alternative stress-integration schemes for large deformation problems of solid mechanics. *Finite Elements in Analysis and Design* 45(12): 934–943.
- Nazem, M., Sheng, D., & Carter, J. P. 2006. Stress integration and mesh refinement for large deformation in geomechanics. *International Journal for Numerical Methods in Engineering* 65(7): 1002–1027.
- Of, N. & Yu, L. A. Y. B. H. S. 2000. of S Teady C One P Enetration. *Manager* (July): 594–605.
- Salgado, R. 1993. Analysis of Cone Penetration Resistance in Sand. University of California, Berkeley.
- Salgado, R. 2012. The mechanics of cone penetration: Contributions from experimental and theoretical studies. *Geotechnical and Geophysical Site Characterization 4* CRC Press, Porto de Galinhas, Brazil 131–153.
- Salgado, R. & Bisht, V. 2021. Advances in the solution of geotechnical boundary-value problems. *Computers and Geotechnics* Elsevier Ltd 138(July): 104183.
- Salgado, R., Han, F., & Prezzi, M. 2017. Axial resistance of nondisplacement piles and pile groups in sand. *Rivista Italiana di Geotecnica* 51(4): 35–46.
- Salgado, R., Lyamin, A. V., Sloan, S. W., & Yu, H. S. 2004. Two and Three-dimensional Bearing Capacity of Foundations in Clay. *Geotechnique* Ice Virtual Library 54(5): 297–306.
- Salgado, R., Mitchell, J. K., & Jamiolkowski, M. 1997. CAVITY EXPANSION AND PENETRATION RESISTANCE IN SAND By R. Salgado, Associate Member, ASCE., *Journal of Geotechnical and Geoenvironmental Engineering* 123(April): 344–354.
- Salgado, R., Mitchell, J. K., & Jamiolkowski, M. 1998. Calibration chamber size effects on penetration resistance in sand. *Journal of Geotechnical and Geoenvironmental Engineering* 124(9): 878–888.
- Salgado, R. & Prezzi, M. 2007. Computation of cavity expansion pressure and penetration resistance in sands. *International Journal of Geomechanics* 7(4): 251–265.
- Salgado, R. & Randolph, M. F. 2001. Int. J. Geomech. 2001.1:175–192. *International Journal of Geomechanics* 1(2): 175–192.
- Salgado, R., Tovar, R. D., Tehrani, F. S., Castro, A. G., Han, F., & Prezzi, M. 2016. Effect of surface roughness on the shaft resistance of non-displacement piles embedded in sand. *Geotechnique* 66(5): 386–400.
- Schreyer, H. L., Sulsky, D., & Chen, Z. 1994. A particle method for history-dependent materials. *Computer Methods in Applied Mechanics and Engineering* 118: 179–196.
- da Silva, M. V., Krabbenhoft, K., Lyamin, A. V., & Sloan, S. W. 2011. Rigid-plastic large-deformation analysis of geotechnical penetration problems. *13th International Conference of the International Association for Computer Methods and Advances in Geomechanics (IACMAG)* 42–47.
- Sloan, S. W. & Randolph, M. F. 1982. *Numerical prediction of collapse loads using finite element methods*. *International Journal for Numerical and Analytical Methods in Geomechanics*.
- Sołowski, W. T. & Sloan, S. W. 2015. Evaluation of material point method for use in geotechnics. *International Journal for Numerical and Analytical Methods in Geomechanics* 39(7): 685–701.
- Teh, C. I. & Houlsby, G. T. 2009. An analytical study of the cone penetration test in clay. *Geotechnique* 41(1): 17–34.
- Tehrani, F. S., Han, F., Salgado, R., & Prezzi, M. 2017. Laboratory study of the effect of pile surface roughness on the response of soil and non-displacement piles. *Geotechnical Frontiers 2017* American Society of Civil Engineers, Reston, VA 256–264.
- Terzaghi, K. 1943. *Theoretical Soil Mechanics*. John Wiley & Sons, Inc., Hoboken, NJ, USA.
- Tovar-Valencia, R., Galvis-Castro, A., Salgado, R., & Prezzi, M. 2018. Effect of surface roughness on the shaft resistance of displacement model piles in sand. *Journal of Geotechnical and Geoenvironmental Engineering* 144(3).
- Wallstedt, P. C. & Guilkey, J. E. 2008. An evaluation of explicit time integration schemes for use with the generalized interpolation material point method. *Journal of Computational Physics* 227(22): 9628–9642.
- Wang, B., Vardon, P. J., Hicks, M. A., & Chen, Z. 2016. Development of an implicit material point method for geotechnical applications. *Computers and Geotechnics* Elsevier Ltd 71: 159–167.
- Wang, D., Randolph, M. F., & White, D. J. 2013. A dynamic large deformation finite element method based on mesh regeneration. *Computers and Geotechnics* Elsevier Ltd 54: 192–201.
- Woo, S. I. & Salgado, R. 2015. Bounding surface modeling of sand with consideration of fabric and its evolution during monotonic shearing. *International Journal of Solids and Structures* Elsevier Ltd 63: 277–288.
- Woo, S. I. & Salgado, R. 2018. Simulation of penetration of a foundation element in Tresca soil using the generalized interpolation material point method (GIMP). *Computers and Geotechnics* Elsevier Ltd 94: 106–117.

Practical use of shear wave velocity measurements from SCPTU in clays

M. Long

University College Dublin (UCD), Ireland

ABSTRACT: The main objective of this paper is to promote use of shear wave velocity (V_s) measurements from SCPTU testing as a complement to standard CPTU data. Recent developments in the technique are described. Uncertainties in the methods have been well researched and several methods have been proposed to deal with these uncertainties. Nonetheless V_s measurements seem reliable in isotropic soil conditions. V_s profiles for a range of soft to firm clays world-wide are presented. Clear links between these profiles are identified based on fundamental soil properties. Stiff overconsolidated clays do not follow the same patterns due to pure stress anisotropy and their fissured nature. Correlations between V_s and CPTU data and with a variety of soil properties can be very powerful. However these correlations should ideally be local and only applied to other soils and areas with great caution. An exception might be for correlation between V_s and preconsolidation stress p_c' . Use of SCPTU data to help assess sample disturbance and for the prediction of settlement of footings is described. Some future outlooks including dealing with anisotropy are discussed.

1 INTRODUCTION

Shear wave velocity (V_s) is a fundamental measurement in all solids for example steel, concrete, wood, soil and rock (Mayne, 2000). Because of this broad range of application, V_s values are an attractive means of characterising a range of natural geomaterials. Water is not able to tolerate shear waves. Therefore measurements in soil are not influenced by the presence of groundwater (unlike P-waves).

Over the last decades, V_s measurements have gained popularity in geotechnical engineering practice. Advances in cost effective and efficient methods of determination of V_s focused attention on this parameter, which originally was mainly used for seismic hazard assessment or dynamic analyses. However, its use has been extended to general site characterisation studies, ground movement analyses for tunnels and excavation problems, determination of strength and compressibility parameters by empirical correlation, prediction of the behaviour of deep and shallow foundations, assessment of sample disturbance effects and in the quality control of ground improvement schemes among other applications.

V_s can be measured by a wide range of intrusive and non-intrusive methods, see L'Heureux and Long (2017) for example. In this paper the focus will be on the use of the seismic piezocone test (SCPTU) for V_s measurement.

The paper will deal with some basics on shear waves including shear wave anisotropy. The measurement technique will be briefly described together with some recent developments in the method. Uncertainties in the measurement technique will be

considered. The meaning of numerical V_s values will be discussed and typical V_s profiles for various clays will be presented and compared.

Use of V_s profiles for site characterisation will be described. Correlations between V_s and other SCPTU measurements and with a range of soil properties will be considered. An emphasis on estimating preconsolidation stress from V_s . Finally use of V_s for sample disturbance assessment and for prediction of settlement of shallow foundations will be outlined.

The paper will focus on clay soils only (with some comparison made with peat). It will not deal with earthquake problems such as liquefaction.

It is stressed that the objective of the paper is to promote increasing use of SCPTU V_s measurements as a complement, not as a replacement, to other CPTU measurements. The author supports the suggestion of Mayne et al. (2009), in their Key Note lecture to the 17th ICSMGE in Alexandria, who proposed that in site characterisation studies the standard approach should be in the use of the SCPTU (or seismic dilatometer, SDMT) as up to five separate measurements are captured at each depth tested.

2 SOME BASIC CONSIDERATIONS

2.1 Shear waves

Engineer's interest in V_s determination has largely been driven by the need to obtain values of the small strain shear modulus (G_{max}), as this is an important parameter for a range of geotechnical design applications. This usually involves strains of 10⁻⁴ to 10⁻³ % and less.

According to elastic theory G_{\max} may be calculated from the shear wave velocity using the following equation:

An example for the well-researched Italian clay site at Augusta (saline area) is shown on Figure 1. The materials below 15 m comprise a medium stiff, overconsolidated (overconsolidation ratio, OCR = 2 to 6) Pleistocene marine clay with low to medium plasticity (Lo Presti et al., 1998). V_{s-vh} values from seismic dilatometer (SDMT) and downhole testing are very similar but they are some 100 m/s less than the cross-hole V_{s-hv} values.

For simplicity in this paper the SCPTU measurement will be denoted as V_s unless otherwise stated.

$$G_{\max} = \rho V_s^2 \quad (1)$$

where: G_{\max} is the shear modulus (in Pa), V_s is in m/s, and ρ is the total mass density (in kg/m³).

It is important to remember that for practical use, the G_{\max} value needs to be reduced to give the strain level relevant to a particular problem. This point will be addressed later.

2.2 Anisotropy of shear wave velocity

Anisotropy of shear wave velocity/stiffness may be significant in many clays. This is particularly the case for overconsolidated materials. Butcher and Powell (1995) and others have suggested that to distinguish between shear wave velocities with different propagation and polarisation directions, subscripts can be used to denote these. For example V_{s-hc} denotes a vertically propagating, horizontally polarised shear wave velocity such as would be measured in a downhole or SCPTU test. Similarly V_{s-hv} or V_{s-hh} would be measured in cross-hole testing.

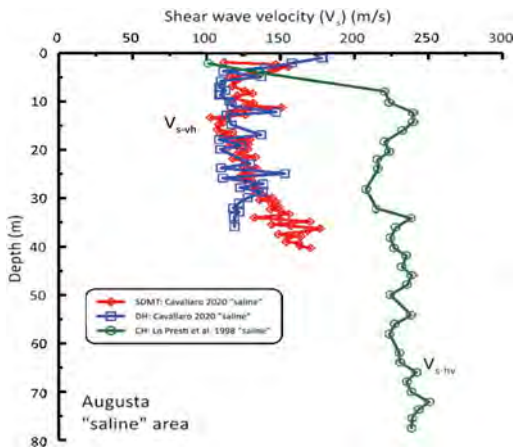


Figure 1. Anisotropy of shear wave velocity for August (saline area) research site in Italy. Data replotted from Lo Presti et al. (1998) and Cavallero (2020).

An example for the well-researched Italian clay site at Augusta (saline area) is shown on Figure 1. The materials below 15 m comprise a medium stiff, overconsolidated (overconsolidation ratio, OCR = 2 to 6) Pleistocene marine clay with low to medium plasticity (Lo Presti et al., 1998). V_{s-vh} values from seismic dilatometer (SDMT) and downhole testing are very similar but they are some 100 m/s less than the cross-hole V_{s-hv} values.

For simplicity in this paper the SCPTU measurement will be denoted as V_s unless otherwise stated.

3 SCPTU MEASUREMENT TECHNIQUE

3.1 Traditional approach

The SCPTU was first introduced in 1984 at the University of British Columbia, see Rice (1984), Campanella et al. (1986) and Robertson et al. (1986). Some schematics to illustrate the test set-up are shown on Figure 2.

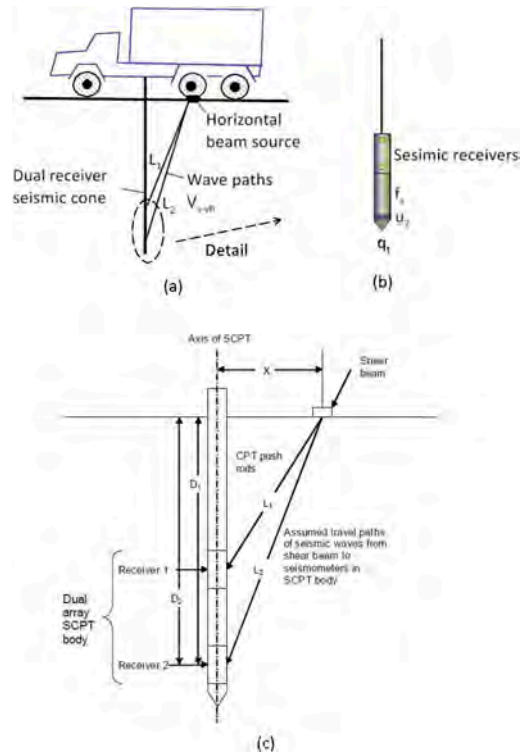


Figure 2. Set-up for CPTU test (a) typical test arrangement (Powell, 2005), (b) details of cone (Mayne, 2000) and (c) schematic for V_s determination (Butcher et al., 2005).

Ideally the test should be carried out according to ASTM (2019) or ISO (2014). Some detailed guidance for the execution of the test is given by Butcher et al. (2005). A standard cone penetrometer is

equipped with one to three horizontally aligned seismic sensors. Originally one sensor was used but most modern equipment has two sets of sensors comprising three component geophones. Butcher and Powell (1996) discuss some problems associated with a single sensor SCPTU. Some commercial companies successfully use equipment with one accelerometer instead of a geophone.

Recordings are made during a pause in the cone penetration typically every 0.5 m. The seismic signals are generated by striking a horizontal beam which is coupled to the ground, usually by the weight of the testing vehicle. Hammers of mass about 10 kg are typically used. The beam should be aligned parallel to the axis of the receivers. Assuming straight ray paths V_s is determined by (Figure 2):

$$V_s = \frac{L_2 - L_1}{t_2 - t_1} \quad (2)$$

where: t_2 and t_1 are the shear wave travel time from source to receiver

Several methods exist for picking the shear wave arrival time such as manually picking the first arrival time, the first major cross-over method or by use of cross correlation. In a dual array seismic cone, the wave traces from each of the two sensors can be used to get the “true interval” travel time between the sensors. Many authors (Lunne et al., 1997b) have stressed the advantage of the “true interval” set-up stating that it gives more accurate results than the “pseudo interval” method where only one sensor is used. A particular advantage is the same source signal, rather than two successive blows, is used in the calculations.

Similar techniques are used in offshore SCPTU testing, see for example Peuchen et al. (2002), Looijien et al. (2017) or Lunne et al. (2013) with the signal being produced by different techniques such as using a seismic cap (Campanella et al., 1986), hydraulic underwater shear wave box (de Lange et al., 1990) or underwater hammers (Paoletti et al., 2013) or the twin hammers of the PROD system (Nguyen et al., 2015).

3.2 SDMT

The seismic dilatometer (SDMT) is the combination of the standard flat dilatometer (DMT) with a similar seismic module for measuring V_s as employed in the SCPTU (Marchetti et al., 2008, Marchetti, 2015). The SDMT employs two geophones spaced 0.5 m apart and therefore allows a more accurate “true- interval” two-receiver test configuration.

3.3 Recent developments in techniques

Typically modern dual sensors are spaced at between 0.5 m and 1.0 m. The system used by the Norwegian Public Roads Administration allows the

sensors to be set at either 0.5 m or 1.0 m (Valsson et al., 2020).

Typically V_s measurements are made at 0.5 to 1 m intervals, the latter often corresponding to rod breaks. Although the process is more time consuming and expensive, McGillivray and Mayne (2004), (McGillivray and Mayne, 2008), Mayne (2005b) and others advocate the use of frequent interval SCPTU (or SDMT) with measurements taken every 0.2 m. An example of such a set of readings compared to conventional single sensor measurements from the famous Treporti test embankment, Venice are shown on Figure 3 (McGillivray and Mayne, 2004). The site is underlain by a complex mixture of silts, sands and clays (Simonini et al., 2007). These data clearly demonstrates that enhanced depth resolution can be achieved with this technique.

Mayne and McGillivray (2008), McGillivray and Mayne (2008), Ku and Mayne (2012), Ku et al. (2013a) and Ku et al. (2013b) introduce the development of continuous interval seismic piezocone testing (CiSCPTU). Here V_s is measured at continuously during cone penetration using a specially developed autoseis source. The system employs an electro-mechanical auto hammer to deliver impact type seismic waves that are continuously recorded while the device is penetrating. As well as producing a detailed V_s profile, the significant advantage of this system is that there is no halting in penetration during the SCPTU procedure and therefore no effect on the resulting q_t , f_s , and u_2 readings.

Examples from this system are also given by Agaiby et al. (2016) and Mayne and Woeller (2015).

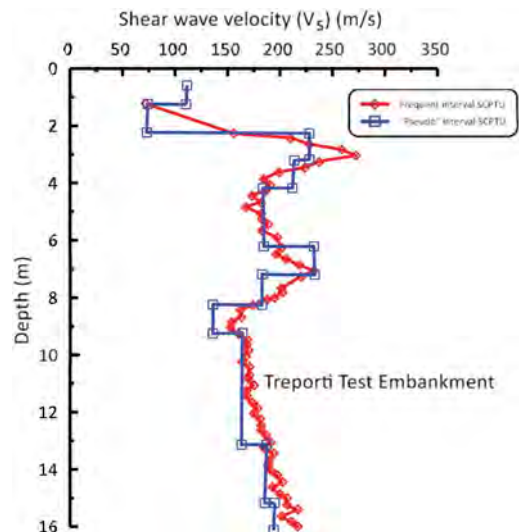


Figure 3. Frequent interval and “pseudo” interval SCPTU from Treporti test embankment (McGillivray and Mayne, 2008).

3.4 Uncertainties in measurements

In engineering practice it is often commonplace to provide a single V_s profile versus depth for a specific location to the design engineer with no description of the uncertainty involved (Stolte and Cox, 2020). There are two types of uncertainty associated with SCPTU measurements, aleatory variability and epistemic uncertainty (Hallal and Cox, 2019).

Aleatory variability is connected to spatial variability of the ground across the site area and can be dealt with by performing multiple tests across a site with perhaps the “gaps” in the data filled by another geophysical technique such as electrical resistivity tomography (ERT).

An epistemic uncertainty refers to the deficiencies by lack of knowledge or uncertainty. Some epistemic uncertainties associated with dual-receiver SCPTU testing are as follows (Peuchen et al., 2020, Stolte and Cox, 2020, Styler and Weemees, 2016, Parasie et al., 2022):

- choice of signal source,
- uncertainties related to timing,
- lateral source offset distance,
- choice of testing interval,
- vertical depth control,
- assumption of isotropic ground conditions,
- assumption of straight-line ray path of the signal,
- identification of signal arrival time,
- external noise (expressed as signal to noise ratio.SNR),
- near field effects especially at shallow depths (< 5m) e.g. from surface waves or acoustic reflections,
- conversion of signal arrival time to shear wave velocity,
- wave interference due to presence of rods/ penetrometer.

In offshore SCPT testing some additional uncertainties could be considered (Peuchen and Gomez Meyer, 2021) such as:

- sea wave interference effects,
- influence of the physical seabed frame used to support the measuring devices (particularly over the top 5 m of a profile),
- ambient noise.

With respect to the lateral distance between the source and the receiver it would seem that if the distance is too great the wave form may be closer to that of V_{s-hh} rather than the conventional V_{s-vh} (Personal communication P.W. Mayne). ASTM (2019) suggests the lateral source offset should be in the range 1 m to 6 m. Hallal and Cox (2019) suggest that this distance is limited to a maximum of 1.5 m.

Hallal and Cox (2019) suggest that ideally the testing interval should be less than 1 m and that

issues with data reduction may occur if there is a stiff layer close to the ground surface.

The length of the wave path between the source and receiver is often assumed to be a straight line (ASTM, 2019). Alternatively the refracted wave path method has been proposed (Joh and Mok, 1998, Kim et al., 2004). This technique is based on refraction caused by stiffness differences between layers. Bang et al. (2014) propose an improvement on this system which they term the mean refracted wave path method.

Much work has been done on assessing different ways of obtaining shear wave travel times and converting these data into shear wave velocity profiles, see for example Baziw (1993), Baziw (2002) Pidlisecky and Haines (2011), Stolte and Cox (2020) or Valsson et al. (2020).

In engineering practice, for example in seismic response analyses, upper and lower bound estimates of V_s versus depth are often used to account for epistemic uncertainty (Stolte and Cox, 2020). However this approach has recently been criticised especially where uncertainty in V_s is assumed to be depth independent (Teague and Cox, 2016). Several researchers, e.g. Garofalo et al. (2016) have shown that V_s uncertainty is more pronounced nearer to the surface than with depth.

Stolte and Cox (2020) provide a suggested means of quantifying the epistemic uncertainty by involving various wave travel time and velocity analysis methods. These authors also state that, although the conventional single V_s profile may be sufficient for design engineers, any site report should clearly state the assumptions that were made and should report on how the wave travel time was obtained and the report should detail the actual results so the engineer can check the resulting V_s values.

Parasie et al. (2022) suggest a technique for estimating an “uncertainty budget” for V_s/G_{max} based on an inventory of items similar to those listed above. They give an example of two cases for SCPTU testing in overconsolidated clay and dense sand and determine that the uncertainty budget in both cases is reasonable.

To end this section on a positive note it has been found that, despite the uncertainties discussed above, there have been many published accounts of V_s measurements where different systems were used by different operators but returned very similar output. This is particularly the case for sites which are underlain by relatively homogenous, isotropic materials. More care needs to be taken in interpreting data from non-homogenous or layered or highly anisotropic soils. The example shown on Figure 4 for the well characterised Fucino site in Italy. The site is underlain by a thick deposit of soft cemented clay (Soccodato, 2003).

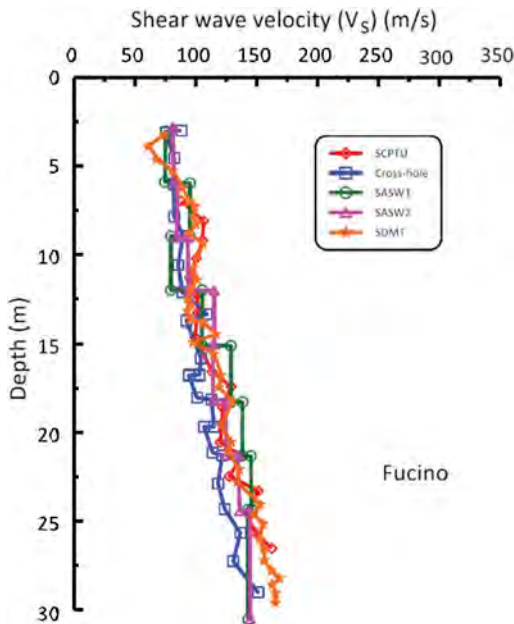


Figure 4. V_s profiles for Fucino site, Italy. Data from Burghignoli et al. (1991), Foti et al. (2006) and Soccodato (2003).

V_s measurements by SCPTU, SDMT, cross-hole and SASW (spectral analysis of surface waves) all give similar results, certainly for the purposes of an engineering type analysis.

Table 1. V_s values for clay soil classification.

Material	NIBS/EN	Poulos (2021)
	V_s (m/s)	V_s (m/s)
Very soft clay	< 100	85 - 105
Soft clay	{100 to	106 - 135
Medium stiff clay	180}	136 - 185
Stiff clay	180 - 360	186 - 275
Very stiff clay	360 - 800	276 - 365

4 SHEAR WAVE VELOCITY VALUES

Before looking at V_s profiles from various countries in detail it is worth considering the possible meaning/classification of numerical V_s values. For seismic assessments the average V_s over the top 30 m of a site ($V_{s,30}$) is often considered.

Both the US (NIBS, 2003) and European (EN, 2004) guidelines quote the same range of V_s values for site classification as summarised on Table 1.

Recently for general engineering classification Poulos (2021) suggested the range of values for site classification also given on Table 1.

The range of values and their allotted meaning is very similar in both cases. For the purposes of this paper an upper bound V_s value for stiff to very stiff clays of 350 m/s will be considered, and all plots will be drawn where possible with this as the maximum value on the x-axis. Similarly the value $V_s = 100$ m/s will be considered

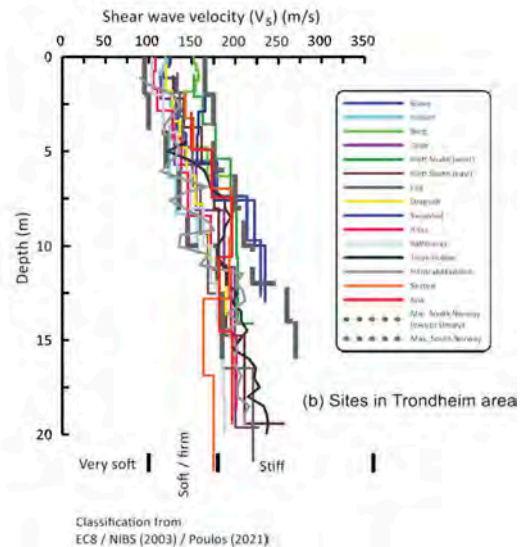
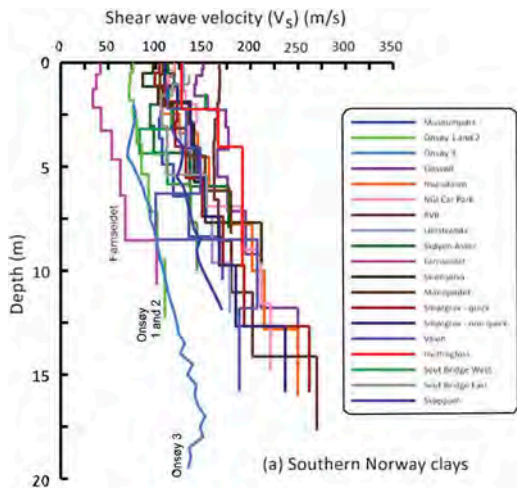


Figure 5. V_s values for Norwegian clays (a) south Norway clays and (b) clays from Trondheim area. Data from L'Heureux and Long (2017) with additional data from Paniagua et al. (2017), L'Heureux et al. (2019) and Dahl and Haugen (2022).

as the upper bound for very soft clays for illustration purposes.

These values need to be treated with caution and can be misleading as will be described later.

5 TYPICAL VS PROFILES FOR CLAYS

5.1 Norwegian clays

A summary of all the available V_s data for Norwegian clays is given on Figure 5, with sites from South-East Norway shown on Figure 5a and those from Mid-Norway/Trondheim area on Figure 5b. The data is mostly taken from L'Heureux and Long (2017) with some additional data as indicated.

Some of the data was obtained using the MASW method (multichannel analysis surface waves) technique. As has been shown in the above paper and elsewhere, the results do not seem to be affected by the technique used or the directions of propagation and polarisation of the waves. This is likely to be due to the largely isotropic nature of these materials.

All the Southern Norway sites show a very similar trend between V_s and depth and differ only in the value of V_s close to the surface. Teachavorasinskun and Lukkunaprasit (2004) found a similar pattern for soft Bangkok clay and they expressed the relationship in the form:

$$V_{sz} = V_{sg} + mz \quad (3)$$

where:

$V_{sz} = V_s$ at any depth z (m/s)

$V_{sg} = V_s$ close to the ground surface (m/s)

m = slope of the line of V_s versus depth (units m/s.m)

Some exceptions are the very soft, high water content and organic, clays at Onsøy and especially Farrisøidet which show much lower values of V_s . In general the values increase from about 125 m/s near the surface to 225 m/s at 20 m depth classifying the materials as soft becoming medium stiff to stiff with depth (Table 1) consistent with other measurements on the soils. For example anisotropically consolidated undrained triaxial compression (CAUC) tests on the clay from the NGTS (Norwegian GeoTest Site) at Tiller-Flotten show undrained shear strength (su) values increasing from about 25 kPa near the surface to about 115 kPa at 20 m depth (L'Heureux et al., 2019).

Data for the Trondheim and Mid-Norway sites show similar values to those from Southern Norway.

The data fits in a very tight band within the limits for the Southern Norway clays. The fact that the soils have similar values is not surprising given the similar depositional and stress history and mineralogy of the sediments.

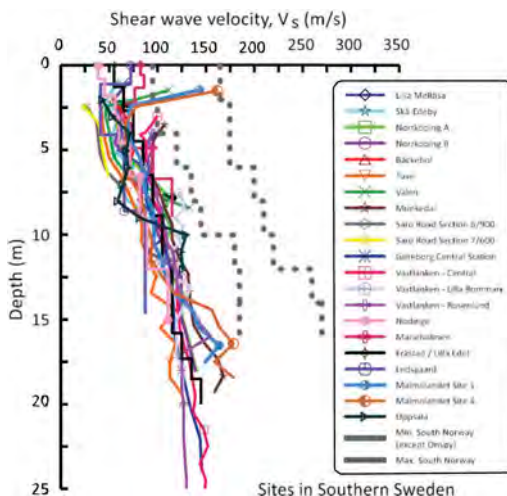


Figure 6. V_s values for Swedish clays. Data from Long et al. (2017) with additional data from Kania et al. (2000), (Dannewitz et al., 2005), Comina et al. (2017) and Granskär (2018).

5.2 Southern Swedish clays

A summary of all the available data from southern Sweden is shown on Figure 6. These data are taken from Long et al. (2017) augmented with additional data as shown.

The data are in general very similar and fall into a relatively narrow band with V_s values typically increasing from 50 m/s at the surface to about 125 m/s at 20 m depth. A similar pattern to the Norwegian data can be seen with the values gradually increasing with depth. However the measured values are significantly less than those from Norway. Also the slope of the Swedish profiles with depth are not as steep as those of the Norwegian sites. These lower values are compatible with the higher water content, greater organic content and lower unit weight and lower silt content of the Swedish clays compared to the Norwegian sediments as will be explored later.

The range of V_s values encountered suggest that the materials are very soft becoming soft to firm (Table 1), again consistent with the results of other testing.

5.3 Clays from Finland

Only limited data is available for V_s profiles from sites in Finland. SCPTU data has been published for the soft clay sites at Perniö, Lempäälä and Masku from southern Finland. These are shown on Figure 7. Two profiles from each site are shown and in general they are very similar.

The profiles shown on Figure 7 are compared to the range of values for Swedish clays from

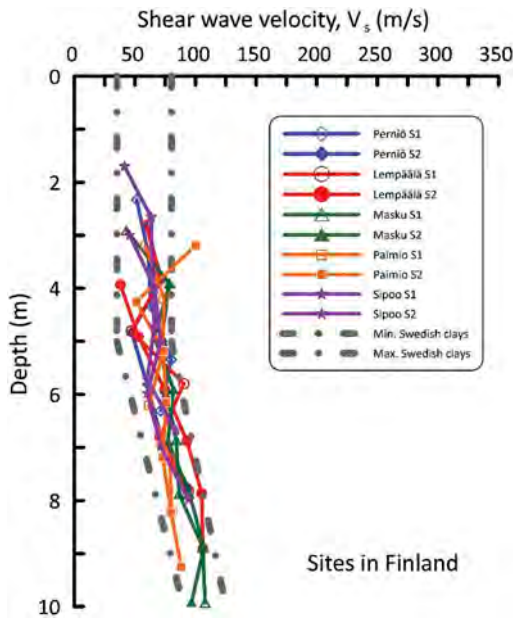


Figure 7. V_s values for Finnish clays (Di Buò et al., 2016, Di Buò et al., 2018, Di Buò et al., 2019).

Figure 6. Overall the range of values measured for the sites in Finland are very like those from Sweden and fall within the range of values measured for the Swedish clays. One possible reason leading to consistent V_s versus depth profiles is to be found in the similarities between the basic clay properties (water content, bulk density and plasticity) (Long and D’Ignazio, 2020).

5.4 Eastern Canadian clays

A compilation of some Eastern Canadian data is shown on Figure 8. Note the geology of the Eastern Canadian area is complex and a more detailed discussion of SCPTU data in this area has recently been published by (Salsabili et al., 2022). The profiles chosen here correspond to well-known geotechnical research sites.

Many of the profiles fall within the bounds of the southern Sweden sites. An exception is the profile from the Quyon Landslide site and perhaps the City of Ottawa data.

5.5 Peats

Trafford and Long (2020) developed a small light-weight probe for measuring the shear wave velocity in peat. The motivation was to allow testing on site where it would not be easy to gain access with traditional SCPTU equipment.

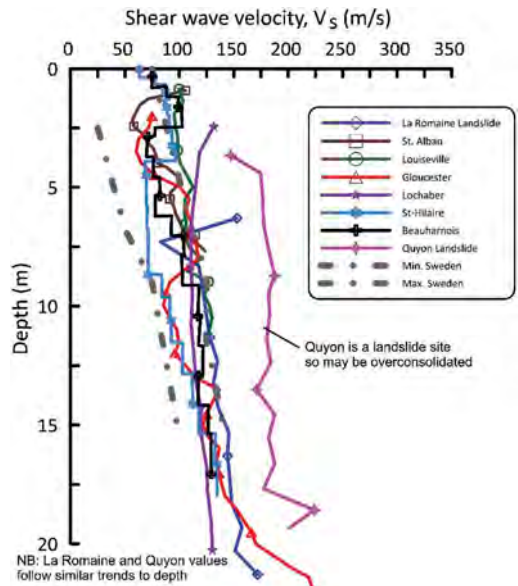


Figure 8. V_s profiles for Eastern Canadian sensitive clays Data from Bouchard et al. (2017), Lefebvre et al. (1994), Leroueil et al. (2003), Mayne et al. (2019), Fabien-Ouellet et al. (2014), Elbeggio et al. (2021) and Agaiby (2018).

The device is very similar to the “pseudo interval” SCPTU described above. V_s measurements, together with parallel water content measurements, for four peat sites in four different countries are show on Figure 9. Water content values are often in the range 1000% to 2000%. Not surprisingly the V_s values are very low, typically 15 m/s. There seems to be a clear trend of lower V_s corresponding to the highest water content.

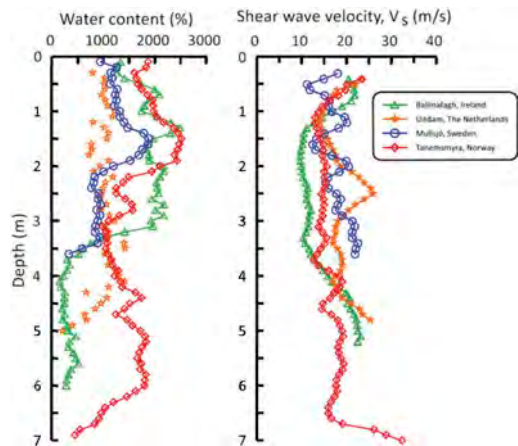


Figure 9. Water content and V_s profiles for four peat sites from four countries (x-axis ranged changed from earlier figures).

5.6 London clay

Perhaps most well characterised stiff clay in the world is London Clay (Hight et al., 2003). Some profiles for V_{s-vh} from SCPTU and other testing in London Clay are shown on Figure 10. Due to the stiffness of the clay and the presence of stiff “clay- stone” bands the tests often need to be terminated at relatively shallow depths. The SCPTU data for the Bradwell B nuclear power station, measured by In Situ Site Investigations Ltd., and reported by LessiCheimariou et al. (2019) are particularly interesting as the tests were able to penetrate to the base of the London clay due to use of a technique of continuing the tests in grouted up boreholes once the original tests were terminated.

On Figure 10 the V_s profiles for soft to medium stiff southern Norwegian clays and stiff to very stiff London clay. Intuitively one would expect the London clay V_s values to be much higher than those of the Norwegian soils. However, as can be seen, the range of values recorded are more or less identical.

The reason for the low values in the London clay is likely to be linked to the fissured nature of these soils (Hight et al., 2003) and due to pure stress anisotropy with the horizontal propagating waves passing along layers of higher stiffness (Butcher and Powell, 1996, Piriyaikul and Haegeman, 2008).

However it is clear that correlations derived for example between V_s and s_u at one location or for one specific soil type need to be applied only with great caution to another soil type.

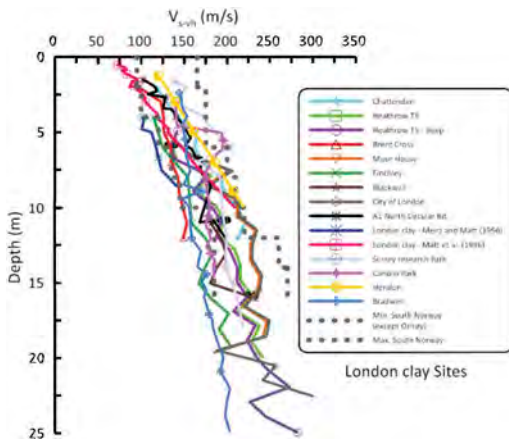


Figure 10. Comparison of V_{s-vh} values for London Clay and range for South Norway clays (L'Heureux and Long, 2017).

London clay data from Powell and Butcher (1991), Butcher and Powell (1995), Gordon et al. (1996), Matthews et al. (1996), Menzies and Matthews (1996), Hight et al. (2003), Hight et al. (2007), Clayton (2011) and Lessi-Cheimariou et al. (2019)

5.7 Other UK stiff overconsolidated clays

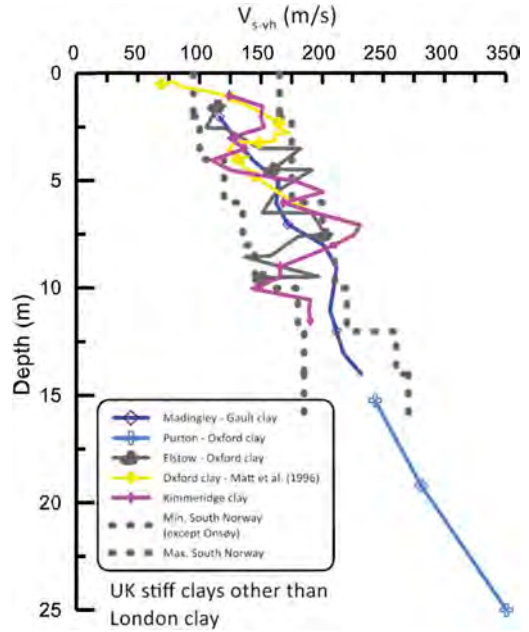


Figure 11. V_{s-vh} values for other UK stiff overconsolidated clays (other than London clay). Data from Butcher and Powell (1995), Hosseini-Kamal et al. (2014), Bates and Philips (2000) and Matthews et al. (1996).

Data for UK stiff clays other than London clay are shown on Figure 11. A picture similar to that of London clay emerges with surprisingly low V_{s-vh} values for these stiff to hard heavily overconsolidated materials. Again the values are similar to those of the South Norway soft to firm clays. Many of these materials have very high V_{s-hh} values and it is likely that the low V_{s-vh} values are due to stress anisotropy and possibly also due to fissuring of the materials.

5.8 Comparison/link between various clay types

Given the consistence of the V_s profiles for different areas it is worth considering the basic engineering properties of the clays in an attempt to identify the links between the V_s values.

According to Leroueil and Hight (2003) and Hardin (1978) the empirical equation describing the influence of the controlling factors on G_{max} (and V_s) can then be written as follows:

$$G_{max} = SF(e)(\sigma'_v \sigma'_h)^n p_a^{(1-2n)} \quad (4)$$

where: S is a dimensionless parameter characterising the considered soil; F(e) is a void ratio function; σ'_v and σ'_h are the vertical and horizontal effective stresses respectively; n is a parameter indicating the influence of stress; and p_a is atmospheric pressure.

Table 2. Summary of material properties for selected study sites. w = water content, Ip = plasticity index, Org. = organic content OCR = overconsolidation ratio, St = fall cone sensitivity. Main references Gundersen et al. (2019), L'Heureux et al. (2019), Wood (2016), Di Buò et al. (2019) and Trak et al. (1980).

Site	w (%)	Clay (%)	Ip (%)	Org. (%)	OCR	St
Onsøy 3	40-80	50-70	25-50	2.5-4	1.1-2.0	5-8
Tiller-Flotten	30-50	45-70	8-20	Very low	1.5-2.0	up to 350
Göteborg CS	60-90	70-90	27-40	2-5	1.5-2.0	12-30
Pernjö	80-110	50-90	30-40	1-2	1.5-2.0	40-60
St. Alban	60-90	45-81	5-30	0.9	2.2	14-22
Peat	1000-2000	Very low	n/a	90-100	Very low	n/a

A summary of the key properties of the clays from well characterized test sites in Norway, Sweden, Canada and Finland are given on Table 2, together with some typical properties of peat. Two sites from Norway were chosen namely the NGTSSites at Onsøy and Tiller-Flotten.

The Tiller-Flotten site is characteristic of many Norwegian clays and is significantly different from the other sites under study. These Norwegian sites have relatively lower water content and plasticity and higher density (1.7 – 1.9 Mg/m³ compared to 1.6 – 1.7 Mg/m³) than the Canadian, Finnish and Swedish sites.

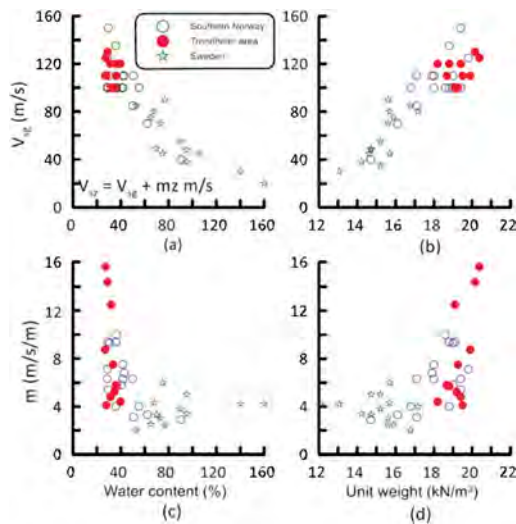


Figure 12. Coefficients V_{sg} and m (Equation 3) as a function of water content and unit weight for sites in Norway and Sweden.

Also Tiller-Flotten has very low organic content compared to the other sites. The Onsøy site parameters are much closer to those of the Swedish, Finnish and Canadian sites. All sites under consideration have similar clay content and stress history.

In order to explore this further, the coefficients V_{sg} and m in Equation 3 are plotted against average water content (w) and unit weight (γ) for each site (over the interval where V_s data is available) on Figure 12 (L'Heureux and Long, 2017, Long et al., 2017). It can be seen that both parameters decrease with increasing w and increase with increasing (γ) as would be expected. The trend between the parameters is reasonably good and these relationships could therefore be used for first order estimates of V_s or for controlling site measurements.

6 USE OF V_s IN SOIL BEHAVIOUR TYPE CHARTS

Robertson (1990) introduced the well-known soil behaviour charts based on normalised cone resistance (Q_t), normalised sleeve friction (F_r) and the pore pressure parameter (B_q)

$$Q_t = \frac{q_t - \sigma_{v0}}{\sigma_{v0}'} \quad (5)$$

$$F_r = \frac{f_s}{q_t - \sigma_{v0}} \quad (6)$$

$$B_q = \frac{u_2 - u_0}{q_t - \sigma_{v0}} \quad (7)$$

where:

q_t = corrected cone end resistance

f_s = sleeve friction

u_2 = pore pressure measured behind cone

u_0 = ambient pore pressure

σ_{v0}/σ_{v0}' = total/effective initial vertical stress

Later Robertson et al. (1995) proposed a complementary SCPTU soil behaviour chart based on Q_t and normalised small strain shear modulus (G_{max}/q_t). This chart was intended mostly for identifying “unusual” soils such as highly compressible sands, cemented and aged soils and clays with either high or low void ratio.

Robertson (2015) suggested that $I_G = G_{max}/q_t$ can be considered to be a small strain rigidly index as it relates small strain stiffness to a measure of soil strength. He proposed a new chart relating Q_{tn} to I_G which could be used to identify soils with microstructure such as cementation/bonding or aging. Note Q_{tn} is an update to Q_t using a variable stress exponent (Robertson, 2009).

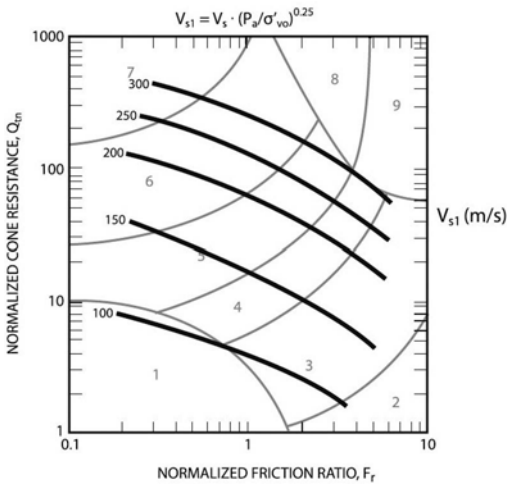


Figure 13. Contours of normalised shear wave velocity superimposed on the normalized $Q_{tn} - Fr$ soil behavior type chart (Robertson, 2009).

Based on 20 years' experience of SCPTU tests in California combined with results from the literature Robertson (2009) also developed a series of contours of normalised shear wave velocity (V_{sn}) and superimposed these on a base of the $Q_{tn} - Fr$ chart as shown on Figure 13. The soils involved were mostly of Holocene age unbonded silica-based soils which tended to plot in the central part of the chart. Some older Pleistocene age soils plot toward the upper right-hand part.

$$V_{sn} = \frac{V_s}{\left(\frac{\sigma_{vm}}{\rho_a}\right)^n} \quad (8)$$

Robertson (2009) and others have chosen the exponent n in Equation 8 = 0.25 and have used the expression V_{s1} for V_{sn} . Ku and Mayne (2013) and Moon and Ku (2016a) and others have pointed out that $n = 0.25$ is based on limited laboratory data on clean quartz and silica sands and suggested n is chosen on site or area specific conditions.

Several authors have suggested that the CPTU u_2 measurement is perhaps the most reliable of the normal three sets of data collected (Lunne et al., 2018). Therefore, as V_s is also relatively easy to measure reliably in isotropic material, it seems logical to attempt to develop a characterisation chart based on these two data sets.

On Figure 14 V_{sn} data are plotted against $\Delta u / \sigma'_{v0}$ ($=u_2 - u_0 / \sigma'_{v0}$) for some Norwegian and UK soft soils.

Here n was chosen to be = 0.5. A tentative division can be made between the lightly overconsolidated material ($OCR < 2$) and the moderately overconsolidated soils ($OCR > 3$).

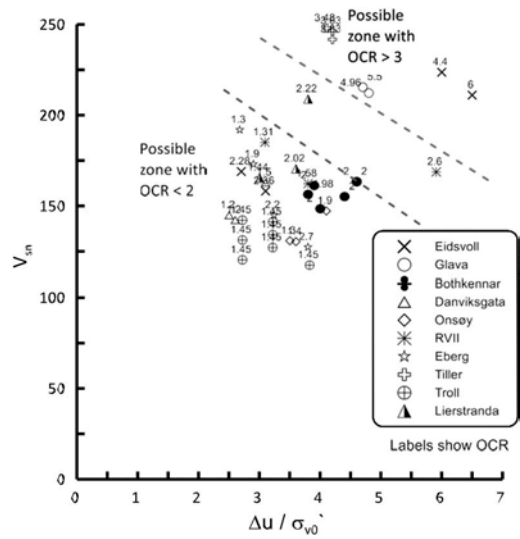


Figure 14. V_{sn} versus $\Delta u / \sigma'_{v0}$ for some Norwegian and UK soft clays. Adapted from Long and Donohue (2010).

Although there appears to be some promise in the use of the charts shown on Figure 13 and 14 and other similar charts, it is felt that some more work, and some more data, is needed to bring these into civil engineering practice.

It is also stressed that these charts are designed to complement the more well-known CPTU soil behaviour charts and not to replace them.

7 CORRELATION BETWEEN V_s AND OTHER SCPTU MEASUREMENTS

Various researchers have studied relationships between CPTU parameters and V_s in clayey soils. These studies have explored relationships between in situ V_s and various parameters such as CPTU tip resistance (q_c), corrected tip resistance (q_t), cone net resistance (q_{net}), sleeve friction (f_s), pore pressure parameter (B_q), effective stress (σ'_v), water content (w) and void ratio (e).

Many empirical relationships between V_s and these CPTU parameters have been published. For example L'Heureux and Long (2017) summarise 21 such relationships for clayey soils. Since the publication of the 2017 paper the author is aware of at least ten further newly developed relationships. These include those by Holmsgaard et al. (2016) for silty soils in Denmark, Shahri and Naderi (2016) for clay soils in south-west Sweden, Zhang and Tong (2017), Zou et al. (2017), Tong et al. (2018) and Duan et al. (2019a) all for Jiangsu clays in China, McGann et al. (2015) for silty soils in Christchurch.

New Zealand and Salsabili et al. (2022) for post-glacial sediments in Southern Québec. In addition Ahmed (2017) and Karray and Hussien (2017) derived generalised relationship for a variety of soils.

Robertson (2015) suggests that even though q_t and V_s are controlled by the same factors there is no unique correlation between q_t and V_s . However it should be possible to obtain a reasonable relationship if the database used is limited to soils of similar mineralogy, stress history, age and cementation.

An example from the Skatval site in Mid-Norway is shown on Figure 15 (Paniagua et al., 2017). Data from this site was not included in the original Norwegian clay database of L'Heureux and Long (2017). However the correlation developed by these authors, as follows on Equation 9, fits very well with the measured data for this new site.

$$V_s = 8.35(q_{net})^{0.22}(\sigma_{v0}')^{0.357} \quad (9)$$

In contrast the relationship developed for Southern Swedish clays by Shahri and Naderi (2016), given in Equation 10, significantly underestimates the measured V_s values

$$V_s = 3.839(q_t)^{0.5151}(1 + B_q)^{0.174} \quad (10)$$

The message here is that very good correlations can be developed between CPTU parameters and V_s but these should be used locally and they should only be used with great care for soil types other than those for which they were intended.

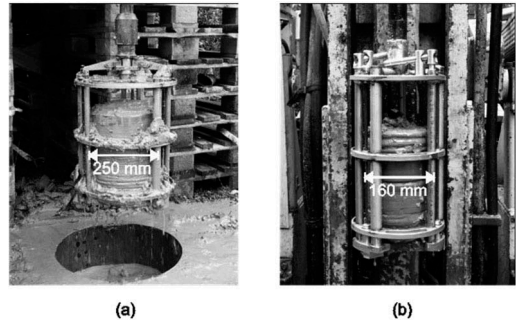


Figure 16. (a) Sherbrooke block sampler and (b) mini-block sampler. Image from (Emdal et al., 2016).

8 CORRELATION BETWEEN V_s AND SOIL PROPERTIES

8.1 General

Much work has been done in the past in correlating V_s with various soil properties derived from laboratory testing. An important consideration is that, for the correlation to be reliable, the quality of the soil samples must be very high. To that end in this paper soil samples extracted by high quality samplers such as the Sherbrooke block (Lefebvre and Poulin, 1979), the mini-block sampler (Emdal et al., 2016) (Figure 16) or the Laval sampler (La Rochelle et al., 1981) only are used.

It is also important that the laboratory tests and the derivation of the resulting parameters is carried out in a consistent manner.

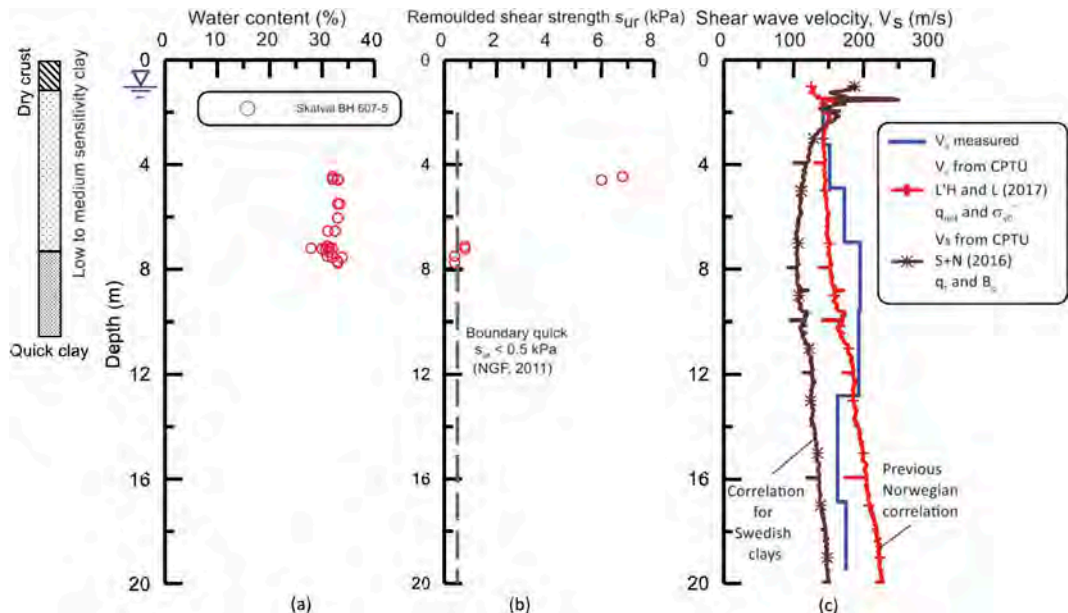


Figure 15. Skatval site Norway – predicted and measured V_s .

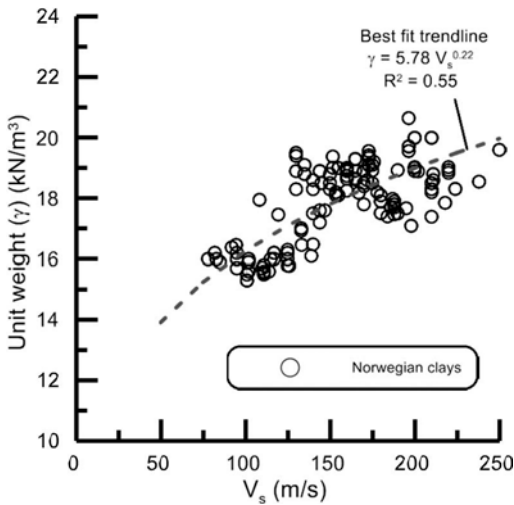


Figure 17. Unit weight versus V_s for Norwegian clays. Data from L'Heureux and Long (2017).

8.2 Unit weight from V_s

An important relationship between geophysical parameters and soil index parameters is that between V_s and unit weight (γ). Various authors such as Mayne (2007) and Moon and Ku (2016a) have developed relationships between V_s and γ using a world-

wide database of soil tests. They have shown how the resulting relationship will depend amongst other factors on soil type, in situ stress and plasticity.

Different equations are suggested for different soil types and the fit between the measured and predicted data can be improved by normalisation of V_s or by introduction of additional parameters such as the plasticity index (I_p) into the relationships. Although these relationships are very useful it is perhaps more worthwhile to develop local correlations. An example of such a correlation for Norwegian clays is shown in Figure 17.

8.3 Undrained shear strength from V_s

Similar to V_s -CPTU relationships much work has been done on deriving empirical relationships between V_s and undrained shear strength s_u . L'Heureux and Long (2017) summarise 16 such relationships. Since the publication of the 2017 paper the author is aware of at least four other publications on the topic by Powell et al. (2016), Moon and Ku (2016b), Duan et al. (2019a) and Duan et al. (2019b).

Undrained shear strength has no unique value but depends on the age of the sample, test type, rate of loading and other factors. Therefore comparisons can only be made on results of tests carried out on exactly the same manner.

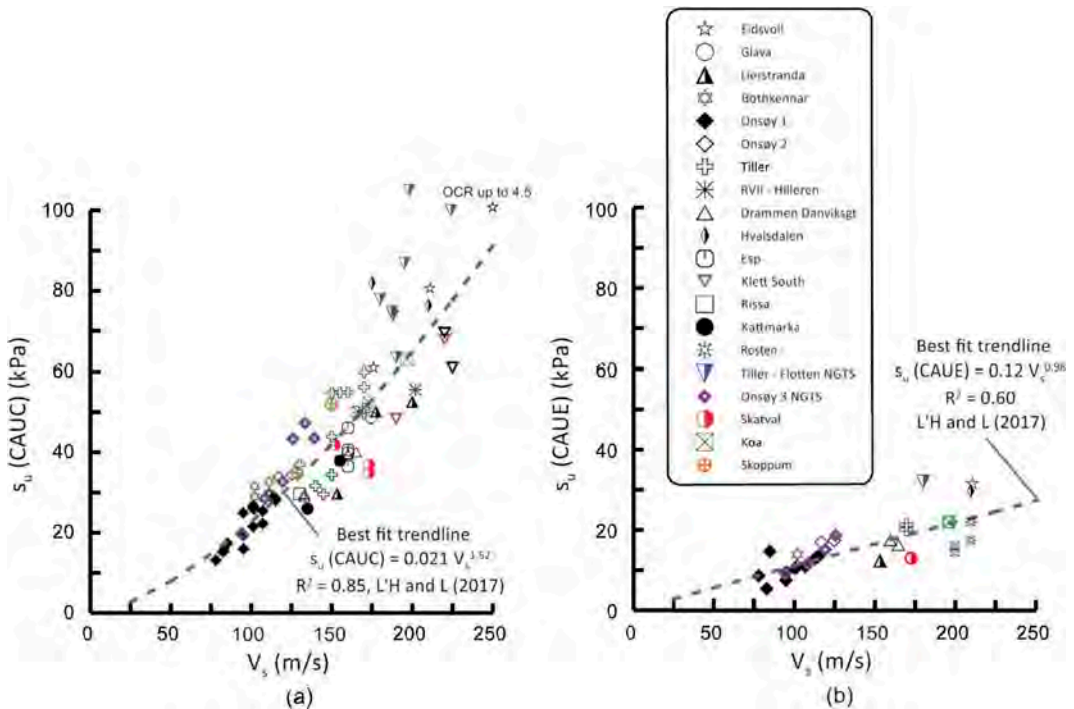


Figure 18. Norwegian clay relationship between s_u and V_s for (a) CAUC tests and (b) CAUE tests. Original 2017 data from L'Heureux and Long (2017) is in black and white font. Recent data is in colour font. Recent data is from Gundersen et al. (2019), L'Heureux et al. (2019), Paniagua et al. (2017) and Dahl and Haugen (2022).

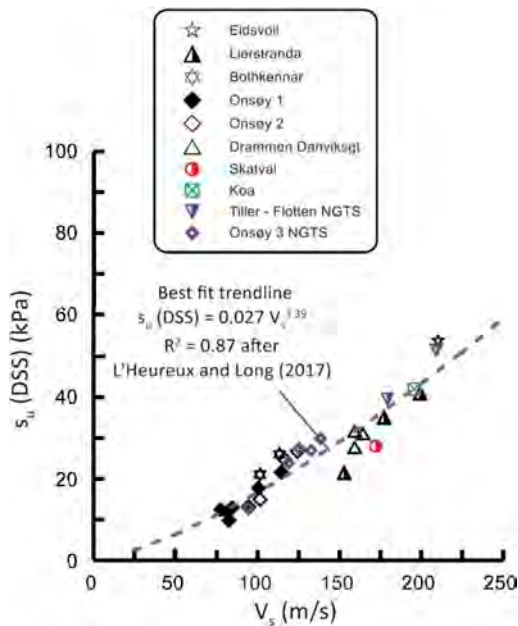


Figure 19. Norwegian clay relationship between s_u and V_s for DSS tests. Original 2017 data from L'Heureux and Long (2017) is in black and white font. Recent data is in colour font. Recent data is from Gundersen et al. (2019), Long et al. (2019) and Paniagua et al. (2017).

In Norway it is common practice to carry out triaxial testing after the sample has been first consolidated anisotropically to the best estimate of its in situ stress. Shearing can subsequently be by compression (CAUC tests) or by extension (CAUE tests).

The s_u values obtained from CAUC and CAUE triaxial tests on high quality samples of Norwegian clay are plotted against in situ shear wave velocity in Figure 18a and 18b respectively. A similar set of data for direct simple shear tests (DSS) are shown on Figure 19.

The "best fit" empirical relationship derived in the 2017 study by L'Heureux and Long (2017) is also shown on Figure 18 and 19. The data used in the 2017 study, which was used to derive the empirical relationships, is shown in black and white font. New data available since the 2017 study are shown in colour. It can be seen that in all three cases the new data fit the old relationships very well and it can be concluded that the 2017 relationships still apply.

A similar set of CAUC data but in this case for various world-wide clays is shown on Figure 20. All the samples were of high quality as described above.

In this case the 2017 relationship for Norwegian clays does not work and in fact would underestimate the measured s_u .

The clear message here is that these V_s - s_u correlations can be very powerful and useful but they

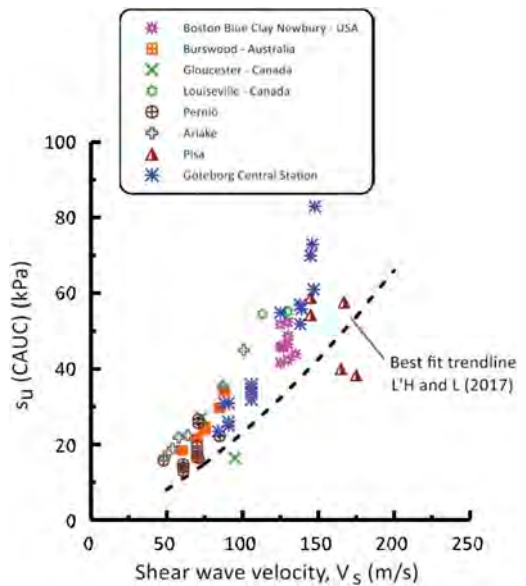


Figure 20. Relationship between s_u and V_s for CAUC tests on world-wide clays for testing on high quality samples. Data is from Landon (2007), Tanaka et al. (1998), Tanaka et al. (2001), Di Buò et al. (2019), Lo Presti et al. (2003) and Wood (2016).

should only be used for the test type and materials for which they were originally derived and they should only be applied to other materials/other test types with great caution.

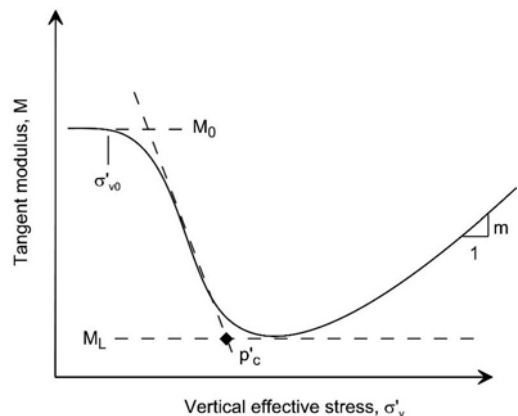


Figure 21. Classical Janbu plot of 1D compression stiffness versus effective stress.

8.4 Preconsolidation pressure from V_s

In this and the following sections V_s measurements are compared to the classical 1D compression parameters often used in Scandinavian practice (Janbu, 1963, Janbu, 1969). The classical Janbu plot of 1D compression stiffness against stress is shown

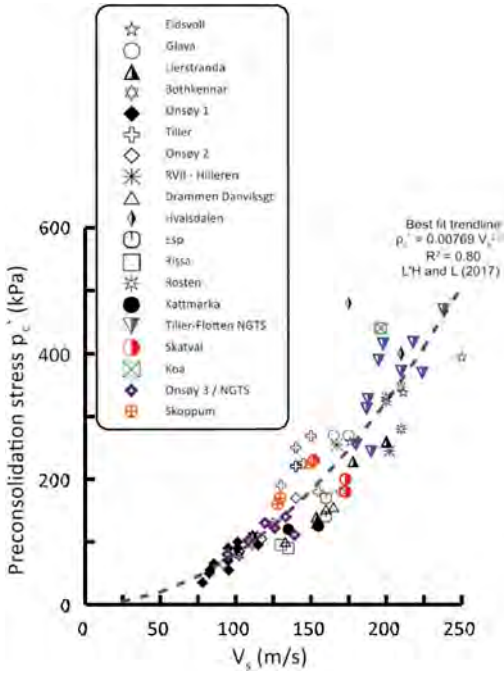


Figure 22. Norwegian clay relationship between p'_c and V_s . Original 2017 data from L'Heureux and Long (2017) is in black and white font. Recent data is in colour font. Recent data is from Gundersen et al. (2019), L'Heureux et al. (2019), Paniagua et al. (2017) and Dahl and Haugen (2022).

on Figure 21. Janbu (1963) used the resistance concept to interpret one dimensional consolidation in an oedometer test. He defined the tangent modulus (or the constrained modulus), M , as the ratio of the change in stress ($\Delta\sigma'$) to the change in strain ($\Delta\varepsilon$) for a particular load increment, i.e.:

$$M = \frac{\Delta\sigma'}{\Delta\varepsilon} \quad (11)$$

As for su above high quality data preconsolidation stress (p'_c) for Norwegian clays published by L'Heureux and Long (2017) has been augmented by more recent data (Figure 22). Again, as found for su , the recent data fit the 2017 correlations very well and support the idea that local V_s correlations based on high quality data can be very powerful.

The relationship derived for Norwegian clays is tested against data for high quality samples of Swedish clay on Figure 23. It can be seen that there is a reasonable relationship between the two parameters for Swedish clay but the data falls above the line derived for Norwegian clay.

At the 2017 International Workshop on Landslides in Sensitive Clays (IWLSC) in Trondheim,

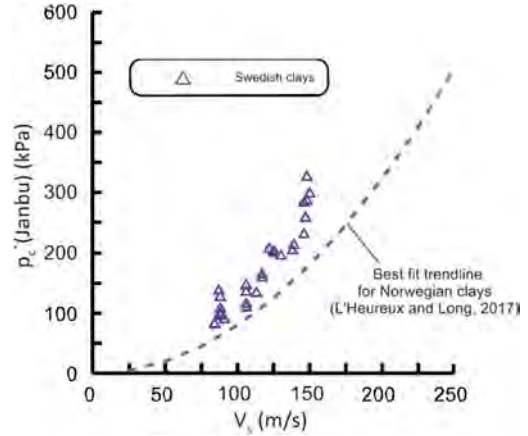


Figure 23. Swedish clay relationship between p'_c and V_s . Data from Wood (2016).

Norway, Professor Guy Lefebvre of the University of Sherbrooke suggested to the author that plots similar to that on Figure 22 and Figure 23 could be made more universal by normalising the V_s value by effective stress. This seems a logical suggestion given the clear differences in the basic properties of the two soil types as demonstrated on Table 2.

Data from various countries, where high quality block sample data were available, are shown on Figure 24a. The V_s data were normalised using Equation 8 with a stress exponent n chosen to = 0.5. Various other exponents, including $n = 0.25$, were also trailed but no difference in the output was found. Full details of this process are given in a companion paper to this conference by Long and L'Heureux (2022).

The normalisation by effective stress appears to be unsuccessful in unifying the data.

To take the stress history of the materials into account the measured V_s data have been normalised by the preconsolidation stress (p'_c) on Figure 24b. As can be seen on Figure 24b this form of normalization As for su above high quality data preconsolidation stress (p'_c) for Norwegian clays published by L'Heureux and Long (2017) has been augmented by more recent data (Figure 22). Again, as found for su , the recent data fit the 2017 correlations very well and support the idea that local V_s correlations based on high quality data can be very powerful. was very successful in harmonising the fifteen sets of data. All fifteen profiles are very similar and show an average V_{snp} value of about 96 m/s. Taking this average V_{snp} value the following equation can be obtained to relate V_s and p'_c .

$$p'_c = 0.0108V_s^2 \quad (12)$$

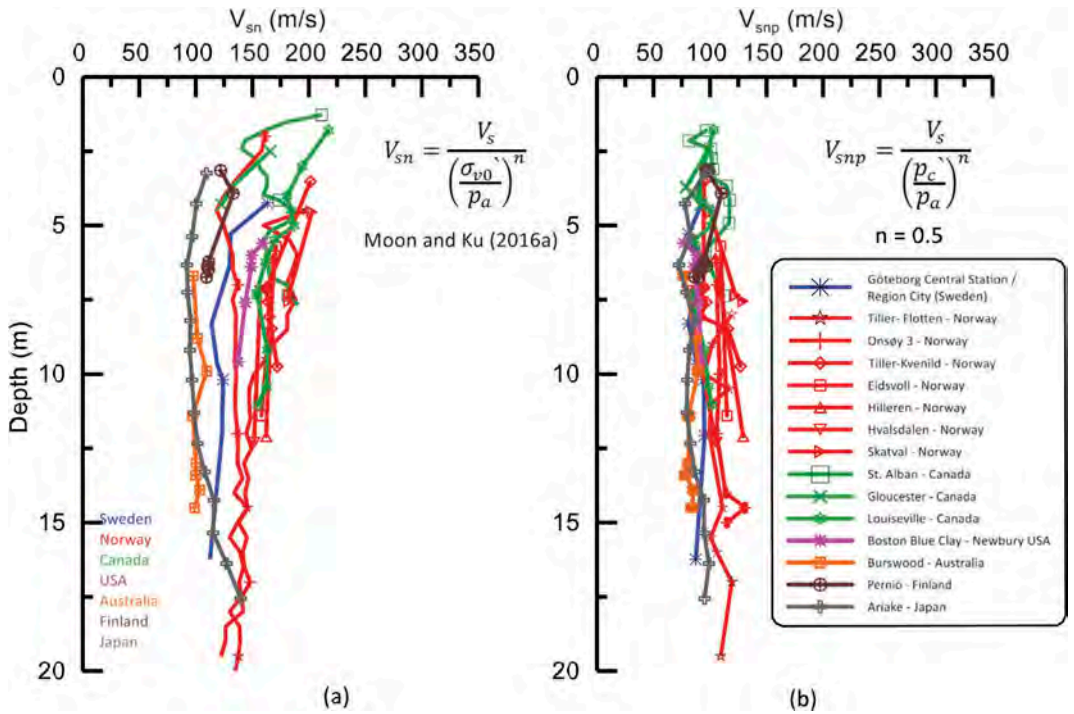


Figure 24. Normalised V_s profiles (a) by vertical effective stress and (b) preconsolidation stress. Data from Wood (2016), Gundersen et al. (2019), L’Heureux et al. (2019), (L’Heureux and Long, 2017), (Paniagua et al., 2017), Landon (2007), Tanaka et al. (1998), Tanaka et al. (2001) and Di Buò et al. (2019).

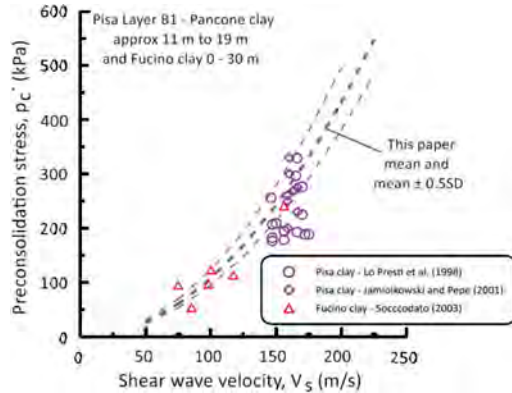


Figure 25. Italian clay relationships between p_c' and V_s trialed against formulae derived in this paper. Data from Lo Presti et al. (1998), Jamiolkowski and Pepe (2001) and Soccodato (2003).

This form of power equation supports and justifies some previous similar empirical equations that have been developed. These include the general relationship developed by Mayne et al. (1998) as shown on Equation 13, that derived for Norwegian marine clays by L’Heureux and Long (2017) (Equation 14) and by Duan et al. (2019a) for Jiangsu clays in China (Equation 15).

$$p_c' = 0.106V_s^{1.47} \quad (13)$$

$$p_c' = 0.00769V_s^{2.009} \quad (14)$$

$$p_c' = 0.1097V_s^{1.3575} \quad (15)$$

Equation 12 is trialed against data for two Italian clays on Figure 25. The mean relationship together with those representing ± 0.5 times the standard deviation are shown. Italian data was not included in the original derivation in Figure 24. The Fucino clay data fits the proposed relationship very well. The fit is reasonable for the complex Pancone clay found beneath Pisa Tower.

8.5 Other one-dimensional consolidation parameters from V_s

Relationships have also been proposed between V_s and other 1D consolidation parameters, for example M_0 and ML (Figure 21). Such data for Perniö clay from Finland and Göteborg Central Station clay from Sweden are compared to relationships for Norwegian clays (L’Heureux and Long, 2017) on Figure 26. In both cases there is a clear relationship between the parameters but the previously published Norwegian clay relationships would underestimate

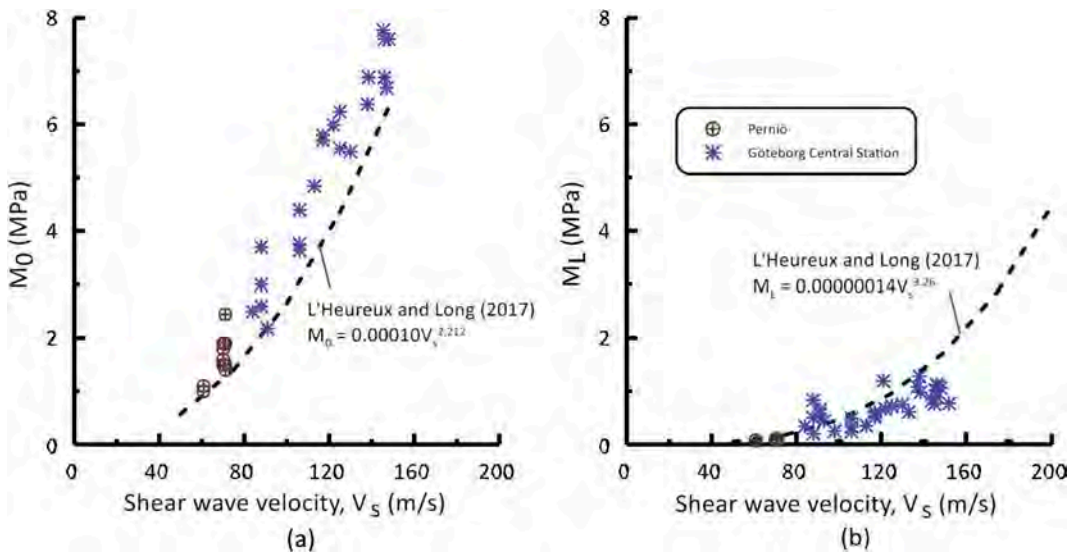


Figure 26. Relationship between (a) M_0 and (b) M_L versus V_s for Swedish (Wood, 2016) and Finnish (Di Buò et al., 2019) clays.

and overestimate respectively the values for Finnish and Swedish clays.

9 USE OF V_s FOR SAMPLE DISTURBANCE ASSESSMENT

Various authors have studied the use of shear wave velocity measurements to assess sample disturbance effects. The overall idea is to compare in situ $V_{s,0}$ as measured by SCPTU for example, to V_s measured on soil samples. Some examples of this work, specifically on clay soils, include that of Landon et al. (2007), Ferreira et al. (2011), Ramsey (2020), Gu et al. (2021) and Long et al. (2021). Other authors have used a combination of V_s and suction measurements to assess sample disturbance, e.g. Donohue and Long (2010) and Horng et al. (2010).

Landon et al. (2007) developed a series of criteria for assessing sample disturbance based on the ratio of V_s measured on the sample (in unconfined conditions) to that of the in situ V_s (e.g. from seismic piezocone, SCPTU). However these criteria were based on tests on low sensitivity, relative high water content and high plasticity clays from Onsøy, Norway, Newbury, USA and Burswood, Australia. The specific guidelines and criteria for assessing sample disturbance from this work is summarised on Table 3. They are compared to the well known method of Lunne et al. (1997a) which involves measuring the change in void ratio relative to the initial void ratio ($\Delta e/e_0$) when consolidating a sample back to its in situ stress in the lab.

It is important to note that Landon's criteria were primarily intended to provide a quick technique for

assessing sample disturbance and to act as a rapid screening tool for assessing sample disturbance prior to advanced laboratory testing. This is of particular concern in offshore site investigations given the cost of these investigations and the need to maximise data quality. They were not intended to replace the more rigorous techniques.

Table 3. Sample quality designation (SQD) from Landon et al. (2007) and (Lunne et al., 1997a).

SQD	Lunne et al. with OCR 1-2 $\Delta e/e_0$	Lunne et al. with OCR 2-4 $\Delta e/e_0$	Sample quality (SQ)
SQ1	0.6	< 0.03 0.04	Very good/excellent
SQ2	0.6	0.04-0.07 0.03-0.05	Good to fair
SQ3	0.35-0.6	0.07-0.14 0.05-0.10	Poor
SQ4	< 0.35	> 0.14 > 0.10	Very poor

The sample disturbance assessment criteria of Landon et al. (2007) are tested against recently derived data from three Norwegian sites on Figure 27. The data are plotted in the form of $V_{s,0}/V_{s,insitu}$ against $\Delta e/e_0$ obtained from CAUC or CAUE tests or CRS tests on Figures 27a and 27b. The sample shear wave velocity was measured using bender elements at zero confining stress ($V_{s,0}$).

For both plots it can be seen that although the data under study here is classified as either SQ1 or

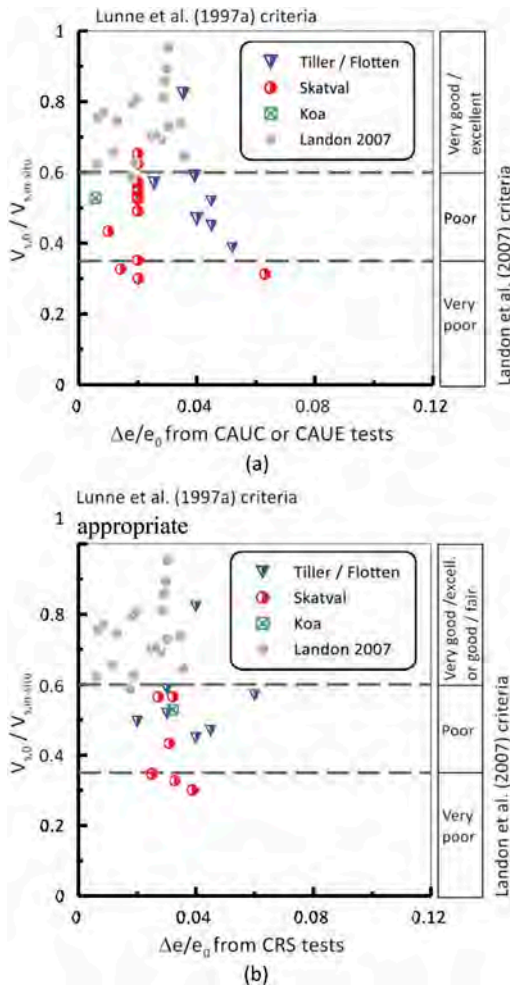


Figure 27. Comparison of shear wave velocity ratio and normalised void ratio for (a) CAUC and CAUE tests and (b) CRS tests. Data from Landon (2007), L'Heureux et al. (2019), Paniagua et al. (2017) and Long et al. (2021).

SQ2 by the criteria of Lunne et al. (1997a) consistent with the observations of the stress – strain and stress path plots, it falls well below that of the data of Landon (2007) and would be classified as “poor” according to the latter criteria.

The clays at Tiller-Flotten, Skatval and Koa differ significantly from those studies by Landon (Table 2). These clays have lower water content, lower plasticity and higher sensitivity compared to Landon’s clays.

Valsson et al. (2020) and Dahl and Haugen (2022) carried out similar studies on low sensitivity but high plasticity Onsøy clay and low plasticity sensitive clay from Skoppum. Their results are not directly comparable with those presented here as the bender element tests were carried out after the samples had been consolidated to the best estimate of the in situ stress. Nonetheless their conclusion were similar

to those found here in that the low plasticity clay from Skoppum showed a significant discrepancy between the field and laboratory tests whereas the results for Onsøy were similar for both techniques.

It is concluded that the criteria Landon et al. (2007) are too strict for the materials under study here. It is suggested that a lower $V_{s,0}/V_{s,insitu}$ limit of 0.35 (compared to 0.6) might be more appropriate for low plasticity sensitive clays considered here. However insufficient data exists here to give a definitive recommendation.

10 USE OF V_s FOR SETTLEMENT PREDICTION

Several researchers have used V_s measurements for the purpose of estimating settlement of foundations. The technique has mostly been used for foundations in sandy soils, e.g. Lehane et al. (2008) but has also been used in soft clay Mayne (2000) and Omar et al. (2011) and soft clayey silt (Mayne, 2005a). Small strain shear modulus (G_{max}) can be calculated directly from V_s (Equation 1). For the ground beneath foundations the strains will be larger and therefore the G_{max} value needs to be adjusted downwards to be compatible with the actual strains encountered.

Perhaps the most common technique for this purpose is the use of the hyperbolic stiffness degradation formula suggested by Fahey and Carter (1993) as follows

$$\frac{G}{G_{max}} = 1 - f \left(\frac{\tau}{\tau_{max}} \right)^g \quad (16)$$

where τ and τ_{max} are the applied shear stress and shear strength respectively and f and g are fitting parameters. The ratio τ/τ_{max} is analogous to the inverse of factor of safety. Values of $f = 1$ and $g = 0.3$ appear to give reasonable estimates for unstructured and uncemented geomaterials and provide a general fit to experimental data (Mayne et al., 2009).

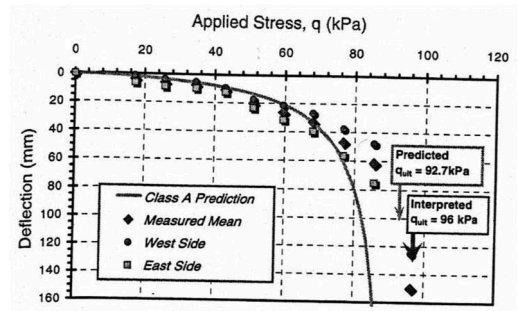


Figure 28. Prediction of settlement of footing on soft silt using V_s (Mayne, 2005a).

Some details for the Class “A” footing response prediction on a trial structure founded on soft silt (known locally as “sleech”) in Belfast, Northern Ireland are shown in Figure 28. Mayne (2005a) used the measured V_s values (Lehane, 2003) and the stiffness degradation formula describe in Equation 16 above to obtain a Class “A” estimate of the footing settlement. It can be seen that the predicted and measured data are in good agreement, especially to an applied stress of about 80 kPa, at which point the onset of bearing capacity failure occurs.

11 FUTURE OUTLOOKS AND CHALLENGES TO SOLVE

Despite significant developments in the equipment, data acquisition systems and the cumulative experience gained over the past 35 years since the introduction of the SCPTU some significant challenges remain to be solved. Perhaps of these the most significant are (Personal communication from Nico Parasie, Fugro):

- measurement uncertainty,
- spatial variability/aleatory uncertainty,
- anisotropy.

Issues related to measurement uncertainty have been well researched and are dealt with in Section 3.2 above.

11.1 Spatial variability

Spatial variability issues, in sites with widely varying ground conditions, can only be dealt with by carrying out a relatively large number of tests or by introducing another technique to “fill the gaps” between the SCPTU testing.

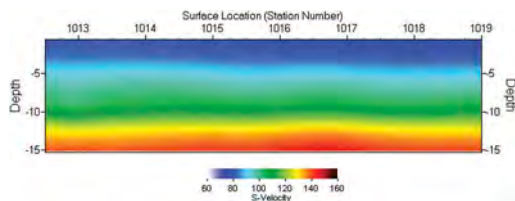


Figure 29. 2D stiffness profile for Onsøy 2 site in Norway. Image courtesy of Dr. Shane Donohue, UCD. Note horizontal and vertical scales the same.

An example of such an approach would be to combine SCPTU with a surface wave technique such as MASW. A 2D stiffness profile for the highly uniform Onsøy 2 site in Norway is shown on Figure 29. This profile was produced by “continuous” MASW where a streamer of geophones mounted on wooden blocks were pulled along and repeated hammer shots were imparted to produce regular seismic signals. The resulting series of 1D profiles were then combined to produce the image.

For offshore investigations a recent development has been to produce images similar to that on Figure 29 using fibre optic/distributed acoustic sensing (DAS) techniques, see for example (Trafford et al., 2021).

Another option is to combine SCPTU with ERT as mentioned above.

11.2 Anisotropy

A significant input in the design of engineering systems such as retaining walls and piles subject to lateral loading is the horizontal ground stiffness. In particular for large monopiles, used for example in offshore wind turbine construction, the behaviour of the system is heavily dependent on the horizontal ground stiffness at small strain. A technique for obtaining such input parameters from SCPTU has been described by McAdam et al. (2020) based on work in the PISA project. Wang et al. (2022) have proposed a simple rotational spring model for the design of laterally loaded rigid piles in sand with V_s as a key input parameter.

Strictly speaking the required input parameter in these cases is V_{s-hh} . Unfortunately SCPTU yields V_{s-vh} . In uniform relatively homogenous softer soils V_{s-hh} and V_{s-vh} have the same values. However for more overconsolidated soils this is not always the case as has been illustrated above for example for UK stiff clays and some Italian clays.

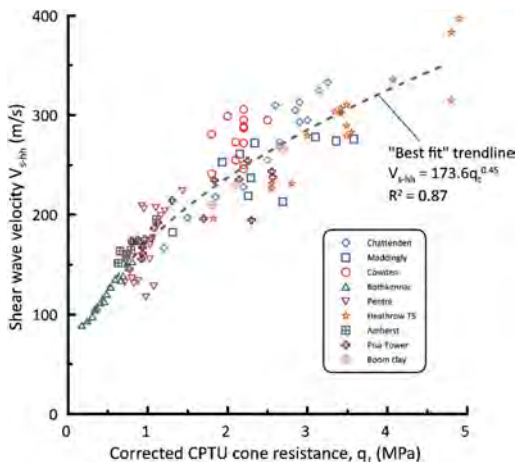


Figure 30. V_{s-hh} versus q_t . Data from Powell and Butcher (2004) and Powell et al. (2016) augmented with additional data from Lo Presti et al. (2003), Jamiolkowski and Pepe (2001), DeGroot and Lutenegeger (2003) and Ku and Mayne (2014).

Powell and Butcher (2004) and Powell et al. (2016) have studied the relationship between corrected cone resistance (q_t) and the various in situ derived shear moduli G_{vh} , G_{hv} and G_{hh} using a database of high quality tests. These authors found

that q_t is most strongly influenced by horizontal stiffness and stress in the ground. They proposed that G_{hh} or V_s -hh could therefore be obtained from correlation with q_t .

The data presented by these authors, augmented by some additional results, are plotted using shear wave velocity rather than shear modulus on Figure 30. It can be seen that the relationship between the two parameters is very good and the resulting “best fit” power function has a good R^2 value of 0.87. As previously suggested by Powell et al. (2016), a suggestion for future work is therefore that V_s -vh is obtained from SCPTU and V_s -hh is obtained from the same test by correlation with q_t .

12 CONCLUSIONS

The main objective of this paper was to summarise the practical and useful application of V_s measurements from SCPTU testing. The intention is to promote the use of SCPTU testing and to highlight the application of V_s data as a compliment to standard CPTU data in future studies and practical projects. It is not intended that V_s measurements replace standard CPTU data. Some conclusions from this work are as follows:

- V_s is a fundamental measure in all solids. Therefore it is an attractive way of characterising a wide range of geomaterials.
- Use of V_s has gained popularity in recent times due to developments in geophysical testing systems and analytical methods.
- Application of the SCPTU testing technique is well covered in guidelines and codes of practice.
- Some descriptions of the equipment used have been given together with some recent developments in the technique including the frequent interval testing and continuous interval testing.
- Uncertainties in the methods have been well researched and understood and several methods have been proposed in the literature suggesting ways of dealing with these uncertainties.
- Despite these uncertainties V_s measurements seem repeatable in isotropic soil conditions using a variety of techniques and methods.
- V_s profiles for sites in southern Norway, mid Norway, Sweden, Finland, Canada and peat have been presented. These data often fall in tight bands.
- There appears to be clear links between these profiles depending on fundamental soil properties such as water content, density, plasticity and also stress history. This has resulted in tentative soil behaviour type charts involving V_s being proposed. This approach seems promising but further work is required on the development and application of these charts.

- An important exception to this is data for stiff overconsolidated clays, such as the UK stiff clays / London clay. For these soils the V_s -vh values are unexpected low. This is due to the natural stress anisotropy and also partially due to the fissured nature of the materials.
- V_s -CPTU correlations can be very powerful. New data for the same soil type in the same area fit the older correlations very well. However these correlations may not work for other areas. Therefore correlations should ideally be locally developed and only applied to other soils and areas with great caution.
- A similar finding was made for soil properties such as s_u and M_0 where once again strong correlations can be developed but these correlations may not apply to other areas
- An exception might be for correlation between V_s and preconsolidation stress p_c' where it seems that high quality data from several areas may fit the same trend.
- SCPTU data can also be used to assess sample disturbance effects by comparing in situ V_s values to measurements made on samples. However it would seem that previously published assessment criteria derived for relatively high plasticity clays may not apply to low plasticity clays.
- V_s has been successfully used to directly predict settlement of footings on clays.
- Some future outlooks include further work on understanding test uncertainties and anisotropy. It is suggested that for future studies V_s -vh could be obtained from SCPTU and V_s -hh by correlation with q_t .

ACKNOWLEDGMENTS

The work presented here largely comes from long term collaboration between the author and colleagues in the Norwegian Geotechnical Institute (NGI), and the Norwegian University for Science and Technology (NTNU). In particular the author is grateful to Jean-Sebastien L'Heureux, Priscilla Paniagua and Tom Lunne.

John Powell of BRE/Geolabs has been very helpful in providing ideas and data in particular with respect stiff overconsolidated clays.

From the academic world Professors Paul Mayne of Georgia Tech and Barry Lehane of the University of Western Australia (UWA) were both very helpful in providing ideas and guidance and in sharing data.

Several colleagues in the geotechnical industry including Nick Ramsey, Joek Peuchen and Nico Parasio of Fugro, Darren Ward and Louisa Dhimitri of In Situ Site Investigation Ltd. and Joe Hobbs of Lankelma Ltd. provided useful data and guidance.

REFERENCES

- Agaiby, S. S. (2018) Advancements in the interpretation of seismic piezocone tests in clays and other geomaterials. PhD Thesis, School of Civil and Environmental Engineering, Georgia Institute of Technology.
- Agaiby, S. S., Cargill, E., Ku, T. & Mayne, P. W. (2016) Continuous-interval seismic piezocone testing in Piedmont residuum. IN Lehane, B. M., Acostamartínez, H. E. & Kelly, R. B. (Eds.) *5th International Conference on Geotechnical and Geophysical Site Characterisation (ISC'5)* Gold Coast, Australia, Australian Geomechanics Society.
- Ahmed, S. A. (2017) Correlating the shear wave velocity with the cone penetration test. *2nd World Congress on Civil, Structural, and Environmental Engineering (CSEE'17)*. Barcelona, Spain.
- ASTM (2019) Standard test methods for downhole seismic testing, ASTM D7400-19. West Conshohocken, PA, USA, ASTM International.
- Bang, E.-S., Cho, S.-J. & Kim, D.-S. (2014) Mean refracted ray path method for reliable downhole seismic data interpretations. *Soil Dynamics and Earthquake Engineering- Elsevier Press*, 65.
- Bates, C. R. & Philips, D. R. (2000) Multi-component seismic surveying for near surface investigations: examples from central Wyoming and southern England. *Applied Geophysics*, 22, 257–272.
- Baziw, E. J. (1993) Digital filtering techniques for interpreting seismic cone data. *Journal of Geotechnical Engineering ASCE*, 119, 98–108.
- Baziw, E. J. (2002) Derivation of seismic cone interval velocities utilizing forward modeling and the downhill simplex method. *Canadian Geotechnical Journal*, 39, 1181–1192.
- Bouchard, S., Ali, H., Leboeuf, D., Leroueil, S. & Cascante, G. (2017) Dynamic properties of sensitive clay deposits. IN Thakur, V., L'heureux, J.-S. & Locat, A. (Eds.) *2nd International Workshop on Landslides in Sensitive Clays (IWLSC), Chapter 15 in Landslides in Sensitive Clays, Advances in Natural and Technological Hazards Research 46*. Trondheim, Norway, Springer International Publishing AG.
- Burghignoli, A., Cavalera, L., Chieppa, V., Jamiolkowski, M., Mancuso, C., Marchetti, S., Pane, V., Paoliani, P., Silvestri, F., Vinale, F. & Vittori, E. (1991) Geotechnical Characterization of Fucino Clay. *10th European Conference for Soil Mechanics and Foundation Engineering (ECSMFE)*. Firenze, Italy, Balkema, Rotterdam.
- Butcher, A. P., Campanella, R. G., Kaynia, A. M. & Massarsch, K. R. (2005) Seismic cone downhole procedure to measure shear wave velocity - a guideline. ISSMGE TC10: Geophysical Testing in Geotechnical Engineering. ISSMGE Bulletin April 2015 issue.
- Butcher, A. P. & Powell, J. J. M. (1995) The effects of geological history on the dynamic stiffness in soils. *XIth European Conference on Soil Mechanics and Foundation Engineering (ECSMFE)*. Copenhagen, Danish Geotechnical Society (DGF).
- Butcher, A. P. & Powell, J. J. M. (1996) Practical considerations for field geophysical techniques used to assess ground stiffness *Proceedings of the Conferences on Advances in Site Investigation Practice* London, U.K., Thomas Telford London.
- Campanella, R. G., Robertson, P. K. & Gillespie, D. (1986) Seismic cone penetration tests. *Use of In-Situ Tests in Geotechnical Engineering, ASCE GSP 6*, 116–130.
- Cavallaro, A. (2020) The use of Cone Penetration Tests (CPT) for the study of the dynamic characteristics of the soils. *2020 IMEKO TC-4 International Conference on Metrology for Archaeology and Cultural Heritage*. Trento, Italy.
- Clayton, C. R. I. (2011) Stiffness at small strain: research and practice. *Géotechnique*, 61, 5–37.
- Comina, C., Krawczyk, C. M., Polom, U. & Socco, L. V. (2017) Integration of SH seismic reflection and Love-wave dispersion data for shear wave velocity determination over quick clays. *Geophysical Journal International*, 210, 1922–1931.
- Dahl, M. & Haugen, E. (2022) Evaluation of selected procedures for estimating shear wave velocity with SCPTu and bender element. *20th International Conference on Soil Mechanics and Geotechnical Engineering (ICSMGE)*. Sydney, Australia, International Society for Soil Mechanics and Geotechnical Engineering (ISSMGE).
- Dannewitz, N., Eriksson, H., Mattsson, H., Larsson, R. & Holm, G. (2005) Utvecklingsprojekt 11357 - sismisk kontrollmetod för kc-pelare - slutrapport 2005-05-31.
- De lange, G., Rawlings, C. G. & Willet, N. (1990) Comparison of shear moduli from offshore seismic cone tests and resonant column and piezoceramic bender element laboratory tests. *Society of Underwater Technology (SUT)*, 16, 13–20.
- Degroot, D. J. & Lutenecker, A. J. (2003) Geology and engineering properties of Connecticut valley varved clay. IN Tan, T. S., Phoon, K. K., Hight, D. W. & Leroueil, S. (Eds.) *In Characterization and Engineering Properties of Natural Soils: Proceedings of the International Workshop*. Singapore A.A. Balkema, Rotterdam.
- DI buò, B., D'ignazio, M., Selänpää, J., Haikola, M., Länsivaara, T. & Di sante, M. (2019) Investigation and geotechnical characterisation of Perniö clay, Finland. *AIMS Geosciences*, 5, 591–616.
- DI buò, B., D'ignazio, M., selänpää, J. & Länsivaara, T. (2016) Preliminary results from a study aiming to improve ground investigation data. *17th Nordic Geotechnical Meeting, NGM 2016, Reykjavik*. Reykjavik, Iceland.
- DI buò, B., Selänpää, J., Länsivaara, T. & D'ignazio, M. (2018) Evaluation of existing CPTu-based correlations for the deformation properties of Finnish soft clays. IN Hicks, M. A., Pisanò, F. & Peuchen, J. (Eds.) *CPT18*. Delft, The Netherlands.
- Donohue, S. & Long, M. (2010) Assessment of sample quality in soft clay using shear wave velocity and suction measurements. *Géotechnique*, 60, 883–889.
- Duan, W., Cai, G., Liu, S. & Puppala, A. J. (2019a) Correlations between shear wave velocity and geotechnical parameters for Jiangsu clays of China. *Pure and Applied Geophysics*, 176, 669–684.
- Duan, W., Cai, G., Liu, S., Puppala, A. J. & Chen, R. (2019b) In-situ evaluation of undrained shear strength from seismic piezocone penetration tests for soft marine clay in Jiangsu, China. *Transportation Geotechnics*, 20, 100253.
- Elbeggo, D., Ethier, Y., Dubé, J. S. & Karray, M. (2021) Critical Insights in laboratory shear wave

- velocity correlations of clays. *Canadian Geotechnical Journal*, Accepted manuscript.
- Emdal, A., Gylland, A., Amundsen, H. A., Kåsin, K. & Long, M. (2016) The mini-block sampler. *Canadian Geotechnical Journal*, 53, 1235–1245.
- EN (2004) EN ISO 1998-1:2004: Eurocode 8: Design of structures for earthquake resistance - Part 1: General rules, seismic actions and rules for buildings European Committee for Standardisation (CEN), Brussels, Belgium.
- Fabien-ouellet, G., Fortier, R. & Giroux, B. (2014) Joint acquisition and processing of seismic reflections and surface waves in a sensitive clay deposit in the Outaouais region (Québec), Canada. IN L'heureux, J.-S., Locat, A., Leroueil, S., Demers, D. & Locat, J. (Eds.) *Advances in Natural and Technological Hazard Research 36, From Geoscience to Risk Management, 1st International Workshop on Landslides in Sensitive Clays (IWLSC)*. Québec, Springer.
- Fahey, M. & Carter, J. P. (1993) A finite element study of the pressuremeter in sand using a nonlinear elastic plastic model. *Canadian Geotechnical Journal*, 30, 348–362.
- Ferreira, C., Vianna Da Fonseca, A. & Nash, D. F.T. (2011) Shear wave velocities for sample quality assessment on a residual soil. *Soils and Foundations - Japanese Geotechnical Society*, 51, 683–692.
- Foti, S., Lancellotta, R., Marchetti, D., Monaco, P. & TOTANI, G. (2006) Interpretation of SDMT tests in a transversely isotropic medium. IN Failmezger, R. A. & Anderson, J. B. (Eds.) *Second International Conference on the Flat Dilatometer*. Washington, D.C., USA.
- Garofalo, F., Foti, S., Hollender, F., Bard, P. Y., Cornou, C., Cox, B. R., Dechamp, A., Ohrnberger, M., Verron, V., Sicilia, D., Teague, D. & Vergnault, C. (2016) Interpacific project: Comparison of invasive and non-invasive methods for seismic site characterization. Part II: Intra-comparison between surface wave and borehole methods. *Soil Dynamics and Earthquake Engineering - Elsevier Press*, 82, 241–254.
- Gordon, M. A., Clayton, C. R. I., Thomas, T. C. & Matthews, M. C. (1996) The selection and interpretation of seismic geophysical methods for site investigation. *Proceedings of the Conferences on Advances in Site Investigation Practice* London, U.K., Thomas Telford London.
- Granskär, J. (2018) Evaluation of SCPT-surveys as method for accessing dynamic modulus, MSc Thesis Luleå University of Technology, Department of Civil, Environmental and Natural Resources Engineering.
- Gu, X., Jiang, W., Qian, J., Huang, M. & Shen, P. (2021) Sampling disturbance evaluation based on the shear wave velocity measured in laboratory and field tests. *6th International Conference on Geotechnical and Geophysical Site Characterisation (ISC'6)*. Budapest, Hungarian Geotechnical Society.
- Gundersen, A. S., Hansen, R. C., Lunne, T., L'heureux, J.-S. & Strandvik, S. O. (2019) Characterization and engineering properties of the NGTS Onsøy soft clay site. *AIMS Geosciences*, 5, 665–703.
- Hallal, M. M. & Cox, B. R. (2019) Theoretical evaluation of the interval method commonly used for downhole seismic testing. *ASCE Geo-Congress 2019: 8th International Conference on Case Histories in Geotechnical Engineering*. Philadelphia, Penn., USA, American Society of Civil Engineering, Reston, Va.
- Hardin, B. O. (1978) The nature of stress – strain behaviour for soils. In *Proceedings ASCE Speciality Conference on Earthquake Engineering and Soil Dynamics, Pasadena, California*.
- Hight, D. W., Gasparre, A., Nishimura, S., Minh, N. A., Jardine, R. J. & Coop, M. R. (2007) Characteristics of the London clay from the Terminal 5 site at Heathrow Airport. *Géotechnique*, 57, 3–18.
- Hight, D. W., Mcmillan, F., Powell, J. J. M., Jardine, R. J. & Allenou, C. P. (2003) Some characteristics of London Clay. IN Tan, T. S., Phoon, K. K., Hight, D. W. & Leroueil, S. (Eds.) *Proceedings International Workshop on Characterisation and Engineering Properties of Natural Soils*. Singapore, Balkema, Rotterdam.
- Holmsgaard, R., Ibsen, L. B. & Nielsen, B. N. (2016) Interpretation of seismic cone penetration testing in silty soil. *Electronic Journal of Geotechnical Engineering, EJGE*, 21, 4759–4479.
- Hornig, V., Tanaka, H. & Obara, T. (2010) Effects of sampling tube geometry on soft clayey sample quality evaluated by nondestructive methods. *Soils and Foundations Japanese Geotechnical Society*, 50, 93–107.
- Hosseini-Kamal, R., Coop, M. R., Jardine, R. J. & Brosse, A. (2014) The post-yield behaviour of four Eocene-to-Jurassic UK stiff clays. *Géotechnique*, 64, 620–634.
- ISO (2014) ISO 19901-8: International Organization for Standardization, Petroleum and Natural Gas Industries -Specific Requirements for Offshore Structures – Part 8: Marine Soil Investigations. Geneva, ISO/CEN.
- Jamiolkowski, M. & Pepe, M. C. (2001) Vertical yield stress of Pisa clay from piezocone tests. *Journal Geotechnical and Geoenvironmental Engineering, ASCE*, 127, 893–897.
- Janbu, N. (1963) Soil compressibility as determined by oedometer and triaxial tests. *Proceedings of the 3rd European Conference on Soil Mechanics and Foundation Engineering*. Wiesbaden, Germany, Deutsche Gesellschaft für Erd-und Grundbau e.V.
- Janbu, N. (1969) The resistance concept applied to deformations of soils. *Proceedings of the 7th International Soil Mechanics and Foundation Engineering Conference*. Mexico City, A.A. Balkema, Rotterdam.
- Joh, S. H. & Mok, Y. J. (1998) Development of an inversion analysis technique for downhole testing and continuous seismic CPT. *Journal of the Korean Geotechnical Society*, 14, 95–108.
- Kania, A., Madshus, C. & Zackrisson, P. (2000) Ground vibration from high-speed trains: prediction and counter measure. *Journal Geotechnical and Geoenvironmental Engineering, ASCE*, 126, 531–537.
- Karray, M. & Hussien, M. N. (2017) Shear wave velocity as a function of cone penetration resistance and grain size for Holocene-age cemented soils: a new perspective. *Acta Geotechnica*, 12, 1129–1158.
- Kim, D. S., Bang, E. S. & Kim, W. C. (2004) Evaluation of various downhole data reduction methods to obtain reliable V_s profile. *ASTM Geotechnical Testing Journal*, 27, 585–597.
- Ku, T. & Mayne, P. W. (2012) Frequent-interval SDMT and continuous SCPTu for detailed shear wave velocity profiling in soils. *Geotechnical Engineering Journal of the SEAGS & AGSSEA*, 43, 34–40.

- Ku, T. & Mayne, P. W. (2013) Evaluating the in situ lateral stress coefficient (K0) of soils via paired shear wave velocity modes. *ASCE Journal of Geotechnical and Geoenvironmental Engineering*, 139, 775–787.
- Ku, T. & Mayne, P. W. (2014) Stress history profiling in soils using OCD–G0 anisotropy relationship. *Proceeding Institute of Civil Engineers, Geotechnical Engineering*, 167, 476–490.
- Ku, T., Mayne, P. W. & Cargill, E. (2013a) Continuous-interval shear wave velocity profiling by auto-source and seismic piezocone tests. *Canadian Geotechnical Journal*, 50, 382–390.
- Ku, T., Weemees, I., Cargill, E., Mayne, P. W. & Woeller, D. (2013b) Post-processing continuous shear wave signals taken during cone penetrometer testing. *ASTM Geotechnical Testing Journal*, 36, 1–11.
- L'heureux, J.-S., Lindgård, A. & Emdal, A. (2019) The Tiller-Flotten research site: Geotechnical characterisation of a sensitive clay deposit. *AIMS Geosciences*, 5, 831–867.
- L'heureux, J.-S. & Long, M. (2017) Relationship between shear wave velocity and geotechnical parameters for Norwegian clays. *Journal of Geotechnical and Geoenvironmental Engineering ASCE*, 04017013–1 – 04017013–20.
- La Rochelle, P., Sarraih, J., Tavenas, F., Roy, M. & Leroueil, S. (1981) Causes of sampling disturbance and design of a new sampler for sensitive soil. *Canadian Geotechnical Journal*, 18, 52–66.
- Landon, M. E. (2007) Development of a non destructive sample quality assessment method for soft clays. *PhD Thesis, Department of Civil and Environmental Engineering, University of Massachusetts, Amherst*. PhD Thesis, Department of Civil and Environmental Engineering, University of Massachusetts, Amherst.
- Landon, M. E., De Groot, D. J. & Sheahan, T. C. (2007) Nondestructive sample quality assessment of a soft clay using shear wave velocity. *ASCE Journal of Geotechnical and Geoenvironmental Engineering*, 133, 424–432.
- Lefebvre, G., Beloueuf, D., Rahhal, M. E., Lacroix, A., Warde, J. & Stokoe, K. H. (1994) Laboratory and field determinations of small-strain shear modulus for a structured Champlain clay. *Canadian Geotechnical Journal*, 31, 61–70.
- Lefebvre, G. & Poulin, C. (1979) A new method of sampling in sensitive clay. *Canadian Geotechnical Journal*, 16, 226–233.
- Lehane, B. M. (2003) Vertically loaded shallow foundations on soft clayey silt. *Institution of Civil Engineers Journal of Geotechnical Engineering*, 156, 17–26.
- Lehane, B. M., J.P., D. & Schneider, J. A. (2008) Settlement prediction for footings on sand. IN BURNS, S. E., Mayne, P. W. & Santamarina, J. C. (Eds.) *Deformation Characteristics of Geomaterials*. Atlanta, Georgia, IOS Press, Amsterdam.
- Leroueil, S., Hamouche, K., Tavenas, F., Boudali, M., Locat, J., Virely, D., Roy, M., La Rochelle, P. & Leblond, P. (2003) Geotechnical characterisation and properties of a sensitive clay from Québec. IN Tan, T. S., Phoon, K. K., Hight, D. W. & Leroueil, S. (Eds.) *Proceedings International Workshop on Characterisation and Engineering Properties of Natural Soils*. Singapore, Balkema, Rotterdam.
- Leroueil, S. & Hight, D. W. (2003) Behavior and properties of natural soils and soft rocks. IN Tan, T. S., Phoon, K. K., Hight, D. W. & Leroueil, S. (Eds.) *Proceedings International Workshop on Characterisation and Engineering Properties of Natural Soils*. Singapore, Balkema, Rotterdam.)
- Lessi-Cheimariou, A., Tromans, I., Hadlow, N., Floyd, M. & Pateman, J. (2019) A novel technique for deep seismic cone tests in challenging ground conditions. *2019 SECED Conference - Earthquake risk and engineering towards a resilient world*. Greenwich, London, Society for Earthquake and Civil Engineering Dynamics.
- Lo Presti, D. C. F., Jamiolkowski, M. & Pepe, M. (2003) Geotechnical characterization of the subsoil of Pisa Tower IN Tan, T. S., Phoon, K. K., Hight, D. W. & Leroueil, S. (Eds.) *In Characterization and Engineering Properties of Natural Soils: Proceedings of the International Workshop*. Singapore A.A. Balkema, Rotterdam.
- Lo Presti, D. C. F., Pallara, O., Maugeri, M. & Cavallaro, A. (1998) Shear modulus and damping of a stiff marine clay from in situ and laboratory tests. IN Robertson, P. K. & Mayne, P. W. (Eds.) *Proceedings 1st. International Conference on Geotechnical Site Characterisation*. Atlanta, Georgia, Balkema, Rotterdam.
- Long, M. & D'ignazio, M. (2020) Shear wave velocity as a tool for characterising undrained shear strength of Nordic clays. *18th Nordic Geotechnical Meeting*. Helsinki, Finland (Conferece held virtually January 2021), IOP Conf. Series: Earth and Environmental Science 710 (2021) 012008.
- Long, M. & Donohue, S. (2010) Characterisation of Norwegian marine clays with combined shear wave velocity and CPTU data. *Canadian Geotechnical Journal*, 47, 709–718.
- Long, M. & L'heureux, J.-S. (2022) Shear wave velocity - SCPTU correlations for sensitive marine clays. *5th International Symposium on Cone Penetration Testing (CPT'22)* Bologna, Italy.
- Long, M., L'heureux, J.-S., Fiskvik Bache, B. K., Lund, A. K., Hove, S. E., Sødal, K. G., Amundsen, H. A., Nordal, S. & Montafia, A. (2019) Site characterisation and some examples from large scale testing at the Klett quick clay research site. *AIMS Geosciences*, 5, 344–389.
- Long, M., Paniagua, P. & L'heureux, J.-S. (2021) Assessing sample disturbance in low plasticity sensitive clays using shear wave velocity. *6th International Conference on Geotechnical and Geophysical Site Characterisation (ISC'6)*. Budapest, Hungarian Geotechnical Society.
- Long, M., Wood, T. & L'heureux, J.-S. (2017) Relationship between shear wave velocity and geotechnical parameters for Norwegian and Swedish sensitive clays. IN Thakur, V., L'heureux, J.-S. & Locat, A. (Eds.) *2nd International Workshop on Landslides in Sensitive Clays (IWLSC), Chapter 6 in Landslides in Sensitive Clays, Advances in Natural and Technological Hazards Research 46*. Trondheim, Norway, Springer International Publishing AG.
- Looijien, P., Cooper, A. G. & Doan, D. H. (2017) Seismic cone testing using seafloor drill technology. *79th EAGE Conference and Exhibition*. Paris, France, European Association of Geoscientists and Engineers (EAGE).

- Lunne, T., Berre, T. & Strandvik, S. (1997a) Sample disturbance in soft low plasticity Norwegian clay. IN Almeida, A. (Ed.) *Symposium on Recent Developments in Soil and Pavement Mechanics*. Rio de Janeiro, Balkema, Rotterdam.
- Lunne, T., Kelleher, P. J., Banimahd, M., Degroot, D. J., Nguyen, H. Q. & Senders, M. M. (2013) Offshore site characterisation of small strain modulus using a seabed drilling system. *Offshore Technology Conference, Houston, Texas*.
- Lunne, T., Robertson, P. K. & Powell, J. J. M. (1997b) *Cone Penetration Testing in Geotechnical Practice*, Blackie Academic and Professional, London.
- Lunne, T., Strandvik, S., Kåsin, K., L'heureux, J.-S., Haugen, E., Urucci, E., Veldhuijzen, A., Carlson, M. & Kassner, M. (2018) Effect of cone penetrometer type on CPTU results at a soft clay test site in Norway. IN Hicks, M. A., Pisanó, F. & Peuchen, J. (Eds.) *CPT18*. Delft, The Netherlands.
- Marchetti, D. (2015) Applications and Recent Developments of the Flat Dilatometer (DMT) and Seismic Dilatometer (SDMT). *XVIIth European Conference on Soil Mechanics and Geotechnical Engineering (ECSMGE)* Edinburgh, Scotland, Thomas Telford Ltd.
- Marchetti, S., Monaco, P., Totani, G. & Marchetti, D. (2008) In situ tests by seismic dilatometer (SDMT). *From Research to Practice in Geotechnical Engineering, A Geotechnical Special Publication Honoring John H. Schmertmann*. ASCE Geoinstitute.
- Matthews, M. C., Hope, V. S. & Clayton, C. R. I. (1996) The use of surface waves in the determination of ground stiffness profiles. *Institution of Civil Engineers Journal of Geotechnical Engineering*, 119, 84–95.
- Mayne, P. W. (2000) Enhanced geotechnical site characterization by seismic piezocone penetration tests. *Invited lecture, Fourth International Geotechnical Conference*, . Cairo University, Egypt.
- Mayne, P. W. (2005a) Class “A” footing response prediction from seismic cone tests. IN Di Benedetto, H., Doanh, T., Geoffroy, H. & Sauzéat, C. (Eds.) *3rd International Symposium on Deformation Characteristics of Geomaterials*. Lyon, France, Swets and Zeitlinger, Lisse.
- Mayne, P. W. (2005b) Keynote: Integrated ground behavior: in-situ and laboratory tests. IN Di Benedetto, H., Doanh, T., Geoffroy, H. & Sauzéat, C. (Eds.) *International Symposium on Deformation Characteristics of Geomaterials*. Lyon, Taylor and Francis.
- Mayne, P. W. (2007) *Cone Penetration Testing: A Synthesis of Highway Practice*, National Cooperative Highway Research Program Synthesis 368. Washington, D.C., Transport Research Board, National Cooperative Highway Research Program.
- Mayne, P. W., Cargill, E. & Miller, B. (2019) Geotechnical characteristics of sensitive Leda clay at Canada test site in Gloucester, Ontario. *AIMS Geosciences*, 5, 390–411.
- Mayne, P. W., Coop, M. R., Springman, S. M., Huang, A. B. & Zornberg, J. G. (2009) Geomaterial behavior and testing - Keynote lecture. IN Hamza, M. (Ed.) *17th International Conference on Soil Mechanics and Geotechnical Engineering (ICSMGE)*. Alexandria, Egypt, Millpress/IOS Press Rotterdam.
- Mayne, P. W. & McGillivray, A. V. (2008) Improved shear wave measurements using autoseis sources. *Deformational Characteristics of Geomaterials*. Amsterdam, The Netherlands, Millpress/IOS Press.
- Mayne, P. W., Robertson, P. K. & Lunne, T. (1998) Clay stress history evaluated from seismic piezocone tests. IN Robertson, P. K. & Mayne, P. W. (Eds.) *Proceedings 1st. International Conference on Geotechnical Site Characterisation*. Atlanta, Georgia, Balkema, Rotterdam.
- Mayne, P. W. & Woeller, D. J. (2015) Advances in seismic piezocone testing. *XVIIth European Conference on Soil Mechanics and Geotechnical Engineering (ECSMGE)* Edinburgh, Scotland, Thomas Telford Ltd.
- Mcadam, R. A., Byrne, B. W., Houlsby, G. T., Beuckelaers, W. J., Burd, H. J., Gavin, K. G., Igoe, D. J. P., Jardine, R. J., Martin, C. M., Muir Wood, A., Potts, D. M., Gretlund, J. S., Tarborda, D. M. G. & Zdravkovic, L. (2020) Monotonic laterally loaded pile testing in a dense marine sand at Dunkirk. *Géotechnique*, 70, 986–998.
- McGann, C. R., Bradley, B. A., Taylor, M. L., Wotherspoon, L. M. & Cubrinovski, M. (2015) Applicability of existing empirical shear wave velocity correlations to seismic cone penetration test data in Christchurch New Zealand. *Soil Dynamics and Earthquake Engineering - Elsevier Press*, 75, 76–86.
- McGillivray, A. V. & Mayne, P. W. (2004) Seismic piezocone and seismic flat dilatometer tests at Treporti. IN Viana Da Fonseca, A. & MAYNE, P. W. (Eds.) *2nd International Conference on Geotechnical and Geophysical Site Characterisation, ISC'2*. Porto, Millpress.
- McGillivray, A. V. & Mayne, P. W. (2008) An automated seismic source for continuous-push shear wave velocity profiling with SCPT and frequent-interval SDMT. IN Huang, A. B. & Mayne, P. W. (Eds.) *3rd International Conference on Geotechnical and Geophysical Site Characterization - ISC'3*. Taipei, Taylor and Francis, London.
- Menzies, B. & Matthews, M. C. (1996) The continuous surface wave system: a modern technique for site investigation. *Special Lecture at the Indian Geotechnical Conference*. Madras, Geotechnical Data Systems (GDS), Egham, Surrey, UK.
- Moon, S.-W. & Ku, T. (2016a) Development of global correlation models between in situ stress-normalized shear wave velocity and soil unit weight for plastic soils. *Canadian Geotechnical Journal*, 53, 1600–1611.
- Moon, S.-W. & Ku, T. (2016b) Empirical estimation of soil unit weight and undrained shear strength from of shear wave velocity measurements. IN Lehane, B. M., Acosta-Martínez, H. E. & Kelly, R. B. (Eds.) *5th International Conference on Geotechnical and Geophysical Site Characterisation (ISC'5)* Gold Coast, Australia, Australian Geomechanics Society.
- Nguyen, H. Q., Degroot, D. J., Meidani, M., Vanneste, M. & Lunne, T. (2015) Measurement and interpretation of downhole seismic probe data for estimating shear wave velocity in deep-water environments. IN MAYER, V. (Ed.) *International Symposium on Frontiers in Offshore Geotechnics (ISFOG III)*. Oslo, Norway, CRC Press.
- Nibs (2003) National Institute of Building Sciences/Building Seismic Safety Council - National Earthquake Hazard Reduction Program - Recommended provisions for seismic regulations for new buildings and other structures (Federal Emergency Management Agency

- 450). *Part 1: Provisions*. Washington, DC, Building Seismic Safety Council.
- Omar, M. N., Abbiss, C. P., Taha, M. R. & Nayan, K. A. M. (2011) Prediction of long-term settlement on soft clay using shear wave velocity and damping characteristics. *Engineering Geology*, 123, 259–270.
- Paniagua, P., L'heureux, J.-S., Carroll, R., Kâsin, K., Sjursen, M. & Amundsen, H. A. (2017) Evaluation of sample disturbance of three Norwegian clays. *19th International Conference on Soil Mechanics and Geotechnical Engineering (ICSMGE)*. Seoul, South Korea.
- Paoletti, L., Mouton, E. & Liposcak, I. (2013) Comparison of underwater MASW, seismic CPT and downhole methods offshore Croatia IN Coutinho, R. Q. & Mayne, P. W. (Eds.) *Proceedings 4th. International Conference on Geotechnical and Geophysical Site Characterisation (ISC'4)* Recife, Brazil, September 2012.
- Parasie, N., Franken, T. & Peuchen, J. (2022) Assessment of seismic cone penetration testing for small strain shear modulus. *5th International Symposium on Cone Penetration Testing (CPT'22)* Bologna, Italy.
- Peuchen, J., De Ruijter, M. R., Hospers, B. & Assen, R. L. (2002) Shear wave velocity integrated in offshore geotechnical practice. *SUT-OSIG-02-379 Society of Underwater Technology Conference*. London, UK (2002), Society of Underwater Technology.
- Peuchen, J. & Gomez Meyer, E. (2021) Geo-intelligence from databases of offshore in situ tests in public domain. *6th International Conference on Geotechnical and Geophysical Site Characterisation (ISC'6)*. Budapest, Hungarian Geotechnical Society.
- Peuchen, J., Kaltekis, K., Klein, M., Murali, M., Van Erp, F. C. W. & Hicks, M. A. (2020) Characteristic values for geotechnical design of offshore monopiles in sandy soils – case study. In(ed.): proceedings (pp. - 1892–1901). . IN Westgate, Z. (Ed. *4th International Symposium on Frontiers in Offshore Geotechnics (ISFOG 2020)*. Deep Foundations Institute.
- Pidlisecky, A. & Haines, S. S. (2011) Bayesian approach for determining velocity and uncertainty estimates from seismic cone penetrometer testing or vertical seismic profiling data. *Canadian Geotechnical Journal*, 48, 1061–1069.
- Piriyakul, K. & Haegeman, W. (2008) Anisotropic shear wave velocity of overconsolidated Boom clay. IN Huang, A. B. & Mayne, P. W. (Eds.) *3rd International Conference on Geotechnical and Geophysical Site Characterization - ISC'3*. Taipei, Taylor and Francis, London.
- Poulos, H. G. (2021) Use of shear wave velocity for foundation design. *Geotechnical and Geological Engineering*, Published online October 2021.
- Powell, J. J. M. (2005) Session report: Technical session 1c: In situ testing. *Proc. 16th International Conference on Soil Mechanics and Geotechnical Engineering*. Osaka, Balkema, Rotterdam.
- Powell, J. J. M. & Butcher, A. P. (1991) Assessment of ground stiffness from field and laboratory tests *In Proceedings Xth ECSMFEE*. Firenze, Rotterdam, Balkema.
- Powell, J. J. M. & Butcher, A. P. (2004) Small strain stiffness assessments from in situ tests. IN Viana Da Fonseca, A. & Mayne, P. W. (Eds.) *2nd International Conference on Geotechnical and Geophysical Site Characterisation, ISC'2*. Porto, Millpress.
- Powell, J. J. M., Dhimitri, L., Ward, D. & Butcher, A. P. (2016) Small strain stiffness assessment from in situ tests - revisited. IN Lehane, B. M., Acosta-Martínez, H. E. & Kelly, R. B. (Eds.) *5th International Conference on Geotechnical and Geophysical Site Characterisation (ISC'5)* Gold Coast, Australia, Australian Geomechanics Society.
- Ramsey, N. (2020) Optimising Geotechnical Engineering Models (GEMs). IN S., H., S., P. & R., G. (Eds.) *Advances in Offshore Geotechnics. Lecture Notes in Civil Engineering, Vol 92*. Singapore, Springer.
- Rice, A. H. (1984) The seismic cone penetrometer. Master of Science, Civil Engineering, University of British Columbia, Vancouver, B.C.
- Robertson, P. K. (1990) Soil classification using the cone penetration test. *Canadian Geotechnical Journal*, 27, 151–158.
- Robertson, P. K. (2009) Interpretation of cone penetration tests - a unified approach. *Canadian Geotechnical Journal*, 46, 1337–1355.
- Robertson, P. K. (2015) Comparing CPT and V_s liquefaction triggering methods. *ASCE Journal of Geotechnical and Geoenvironmental Engineering*, 141, 04015037–1–04015037–10.
- Robertson, P. K., Campanella, R. G., Gillespie, D. & Rice, A. (1986) Seismic CPT to measure in situ shear wave velocity. *Journal of Geotechnical Engineering ASCE*, 112, 791–803.
- Robertson, P. K., Sasitharan, S., Cunning, J. C. & Segoo, D. C. (1995) Shear wave velocity to evaluate flow liquefaction. *ASCE Journal Geotechnical Engineering*, 121, 262–273.
- Salsabili, M., Saeidi, A., Rouleau, A. & Nastev, M. (2022) Development of empirical CPTu- V_s correlations for post-glacial sediments in Southern Quebec, Canada, in consideration of soil type and geological setting. *Soil Dynamics and Earthquake Engineering - Elsevier Press*, 154.
- Shahri, A. A. & Naderi, S. (2016) Modified correlations to predict the shear wave velocity using piezocone penetration test data and geotechnical parameters: a case study in the southwest of Sweden. *Innov. Infrastruct. Solut., Springer*, 1:13.
- Simonini, P., Ricceri, G. & Cola, S. (2007) Geotechnical characterization and properties of Venice lagoon heterogeneous silts. IN Tan, T. S., Phoon, K. K., Hight, D. W. & Leroueil, S. (Eds.) *Proceedings 2nd International Workshop on Characterisation and Engineering Properties of Natural Soils ("Natural Soils 2006")*. Taylor and Francis Group, London.
- Soccodato, F. M. (2003) Geotechnical properties of Fucino clayey soil. IN Tan, T. S., Phoon, K. K., Hight, D. W. & Leroueil, S. (Eds.) *In Characterization and Engineering Properties of Natural Soils: Proceedings of the International Workshop*. Singapore A.A. Balkema, Rotterdam.
- Stolte, A. C. & Cox, B. R. (2020) Towards consideration of epistemic uncertainty in shear-wave velocity measurements obtained via seismic cone penetration testing (SCPT). *Canadian Geotechnical Journal*, 57, 48–60.
- Styler, M. A. & Weemee, I. (2016) Evaluating and reporting uncertainty in downhole shear wave velocities. *3rd International Conference on Performance-based Design in Earthquake Geotechnical Engineering*.

- Vancouver, Canada, International Society for Soil Mechanics and Geotechnical Engineering, London, UK.
- Tanaka, H., Hamouche, K. K., Tanaka, M., Watabe, Y., Leroueil, S. & Fournier, I. (1998) Use of Japanese sampler in Champlain Sea clay. IN Robertson, P. K. & Mayne, P. W. (Eds.) *Proceedings 1st. International Conference on Geotechnical Site Characterisation*. Atlanta, Georgia, Balkema, Rotterdam.
- Tanaka, H., Locat, J., Shibuya, S., Soon, T. T. & Shiwakoti, D. R. (2001) Characterisation of Singapore, Bangkok and Ariake clays. *Canadian Geotechnical Journal*, 38, 378–400.
- Teachavorasinskun, S. & Lukkunaprasit, P. (2004) A simple correlation for shear wave velocity of soft Bangkok clays. *Géotechnique*, 54, 323–326.
- Teague, D. P. & Cox, B. R. (2016) Site response implications associated with using non-unique V_s profiles from surface wave inversion in comparison with other commonly used methods of accounting for V_s uncertainty. *Soil Dynamics and Earthquake Engineering - Elsevier Press*, 91, 87–103.
- Tong, L., Che, H., Zhang, M. & Li, H. (2018) Review of shear-wave velocity prediction equations based on piezocone penetration test data: example from Yangtze River floodplain deposits at Nanjing, Jiangsu Province, China. *Quarterly Journal of Engineering Geology and Hydrogeology*, 51, 229–246.
- Trafford, A., Donohue, S., Ellwood, R., Godfrey, A. & Wacquier, L. (2021) The application of distributed acoustic sensing for shallow marine investigations - an intertidal case study. *Near Surface Geoscience 2021 (NSG'21): The 27th European Meeting of Environmental and Engineering Geophysics*. Bordeaux, France (and Online), European Association of Geoscientists & Engineers (EAGE).
- Trafford, A. & Long, M. (2020) Relationship between shear wave velocity and undrained shear strength of peat *ASCE Journal of Geotechnical and Geoenvironmental Engineering*, 146, 04020057–1 - 04020057–10.
- Trak, B., La Rochelle, P., Tavenas, F., Leroueil, S. & Roy, M. (1980) A new approach to the stability analysis of embankments on sensitive clays. *Canadian Geotechnical Journal*, 17, 526–544.
- Valsson, S. M., Dahl, M., Haugen, E. & Degago, S. A. (2020) Estimating shear wave velocity with the SCPTU and bender element. *18th Nordic Geotechnical Meeting*. Helsinki, Finland (Conferece held virtually January 2021), IOP Conf. Series: Earth and Environmental Science 710 (2021) 012017.
- Wang, H., Lehane, B. M., Bransby, M. F., Askarinejad, A., Wang, L. Z. & Y., H. (2022) A simple rotational spring model for laterally loaded rigid piles in sand. *Marine and Structures*, Inpress.
- Wood, T. (2016) On the small strain stiffness of some Scandinavian soft clays and impact on deep excavations, PhD thesis Department of Civil and Environmental Engineering, Chalmers University of Technology, Göteborg, Sweden. *Department of Civil and Environmental Engineering, Chalmers University of Technology, Göteborg, Sweden*. Göteborg, Sweden, Chalmers University of Technology.
- Zhang, M. & Tong, L. (2017) New statistical and graphical assessment of CPT-based empirical correlations for the shear wave velocity of soils. *Engineering Geology*, 226, 184–191.
- Zou, H., Liu, S., Cai, G., Puppala, A. J. & Bheemasetti, T. V. (2017) Multivariate correlation analysis of seismic piezocone penetration (SCPTU) parameters and design properties of Jiangsu quaternary cohesive soils. *Engineering Geology*, 228, 11–38.

Invited papers



Taylor & Francis

Taylor & Francis Group

<http://taylorandfrancis.com>

Uncertainties associated with CPT data acquisition

R. Soage Santos
Orsted, London, UK

ABSTRACT: Cone penetration test (CPT) and piezocone penetration test (CPTU) are the dominant in situ testing techniques for soil investigations. CPT/CPTU data is used directly in design or used to derive geotechnical properties for design of infrastructure. Occasionally, acquired CPT/CPTU data exhibit anomalies which can cause uncertainties about use in geotechnical design. Consequently, it is very important to understand, and when possible, minimize the uncertainty associated to CPT/CPTU measurements so these can be considered in planning, design, and installation of infrastructure. The practical challenges associated to the quantification of uncertainty and the difficulties of its standardization are discussed. A comprehensive review of uncertainty contributors associated to CPT/CPTU measurements is provided. This document discusses and proposes a standardization approach that combines performance-based cone classification system based on calibration data, with a method-based approach to control and minimize the uncertainty contributions rising from execution of CPT/CPTU.

1 INTRODUCTION

The cone penetration test and piezocone penetration test (CPT/CPTU) are the most dominant in situ testing technique for soil investigations. CPT/CPTU provide valuable input for safe and economical design of many structures and therefore, assessing the representativeness of the CPT/CPTU results is essential.

This document broadly reviews the challenges related to the assessment of CPT/CPTU results quality. Most often, the CPT provides reliable data with depth, particularly the independent parameters q_c (cone resistance), f_s (sleeve friction), and u_2 (pore pressure). Occasionally, acquired CPT/CPTU data exhibit anomalies which can cause uncertainties about applicability in geotechnical design of offshore structures. Peuchen *et al.* 2020 provides detailed examples of data anomalies and discusses how to avoid them.

CPT/CPTU are among the most fundamental datasets used to define soil layers and infer parameters for safe geotechnical design of infrastructure and is often used directly in design of foundations (for instance pile capacity calculations). Thus, it is very important to understand the quality and therefore the uncertainties associated to CPT/CPTU results that are to be applied in design. The term uncertainty of measurement intends to express the doubt regarding the validity/representativeness of the results. Quantification of uncertainty is very important, because ignoring uncertainty may result in the choice of non-optimal geotechnical design and decision making which could lead to costly and unsafe infrastructure development. Understanding

uncertainty is even more important when using the CPT/CPTU measurements directly in design. Note that additional uncertainty is introduced when inferring geotechnical parameters from CPT/CPTU data. Additional uncertainties associated to data interpretation is out of the scope of this document.

The objective of this document is to propose a way forward for maximizing the quality and representativeness of the CPT/CPTU results by controlling and reducing of the uncertainties.

Before proposing a new approach and methodology, it is necessary to understand and review potential sources of uncertainty (uncertainty contributors) and previous standardization efforts aimed to control and minimize uncertainty. The following sections will review standardization efforts and discusses the challenges associated to standardization.

2 CPT/CPTU STANDARDS

2.1 *Development in requirements*

There have been several documents describing requirements and recommendations for the cone penetration test. Before 1980s only cone penetrometers without pore pressure measurements were included. But, in later years the CPTU, or piezocone, has also been covered. In 1977 the Society of Soil Mechanics and Foundation Engineering (ISSMFE) issued a document that included recommendations regarding cone geometry and provided some requirement to precision: *The precision to be obtained should not be*

worse than the larger of the following values: 5 % of the measured value or 1 % of the measuring range of the sensor used. Later documents have left out such references to the measuring range.

The Swedish Geotechnical Society Guideline in 1993 (SGF, 1993) introduced the concept of accuracy classes where the requirements were related to what the results were to be used for. ASTM released, in 1979, the first CPT standard published by a national standardization institute. ASTM did not embrace the accuracy class approach but just included reference to estimates of precision of cone resistance (q_c) and sleeve friction (f_s). Later updates in ASTM 5778-12 (ASTM, 2012) and ASTM 5778-20 (ASTM, 2020) followed the same approach providing estimates of expected precision for q_c , f_s , and u_2 and providing requirements for the calibration errors expressed as maximum allowable errors as percentage of full-scale output (FSO).

In 2012, the first CPT/CPTU standard was published by an international standardization institution. ISO 22476-1:2012 (ISO 2012) opted for an application class scheme, defining four classes for given soil profiles and the use of CPT results. Each application class specifies minimum accuracy requirements for q_c , f_s , and u_2 with an associated degree of uncertainty. In the ISO standard for Marine Soil Investigations 19908-1:2014 (ISO 2014) a simplification was made to accommodate offshore practice resulting in three application classes.

2.2 Present status

Two principal CPT/CPTU standards widely used are ISO 2012 and ASTM 2020. While the overall procedural approach is rather aligned between these two standards, there are still some fundamental differences regarding the uncertainty requirements of the CPT/CPTU results.

ISO 2012 and ISO 2014 propose a performance-based approach to classify CPT/CPTU results into application classes defined by limiting values of accuracy. Thus, these standards express the uncertainty requirements in terms of accuracy: *“If all possible sources of errors are added, the minimum accuracy of the recorded measurements should be better than the largest of the values given in Table 1. The uncertainty analysis should include internal friction, errors in the data acquisition, eccentric loading, temperature (ambient and transient) effects, pore pressure effects in gaps below and above the friction sleeve, and dimensional errors.”*

While the statement has the right intention it is challenging to implement in practice. Using the term accuracy implies the knowledge of the true value. It is not possible, to prove and document, with 100% confidence, how accurate the CPTU measurements are, since the true values are not known. The standard provides little guidance as to how errors and accuracy can be calculated. In practice, identifying and quantifying ‘all possible sources of error’ is

near impossible and this presents a fundamental problem with the demonstration of compliance.

The ASTM, 2020, approach avoids the intrinsic difficulties associated with expressing requirements in terms of uncertainty, by expressing requirements in terms of repeatability or precision. ASTM, 2020 states: *“There are little direct data on the precision of this test method, in particular because the natural variability of the ground”* and merely provides informative and generic estimates of the precision of q_c , f_s and u_2 from experience in uniform deposits. ASTM, 2020 clearly attempts to mitigate or diminish the uncertainty associated with the CPT/CPTU measurements by providing procedural requirements regarding the calibration of cone penetrometer in a laboratory environment and sets minimum requirements for the precision of q_c , f_s and u_2 in relation to a series of potential sources of uncertainty, although omits some important contributors. The most obvious omission is the requirement for the minimum uncertainty (or precision) of the reference source used in calibration. ASTM, 2020 states: *“In cases where higher level of precision is required, stricter calibration requirements would be required”* however not further advice is provided regarding the cases where higher precision is required or how to make the calibration requirements stricter. In summary ASTM, 2020, focuses on providing requirements for the calibration of cone penetrometers and for field methodology but does not provide requirements for assessing performance in the field.

None of these standards provide unequivocal guidelines on how to evaluate data quality. They only discuss some of the factors that could influence the data quality. A number of methods are used throughout the industry, and the approaches vary from company to company. This makes it very difficult to compare the quality of CPT/CPTU results from various systems and providers and creates difficulty for geotechnical practitioners, who may often need to take conservative judgements for design. The practical challenge related to this topic is setting up robust and detailed guidelines for the assessment of data quality of a performed test more or less immediately upon completion of the CPTU, so it can be repeated if necessary.

2.3 Present challenges using standards

Recent publications discussed in depth the difficulties of using ISO 2012 and ISO 2014 to assess the quality of CPT/CPTU results (Peuchen and Terwindt 2014 and 2015, Lunne et al 2017). The main difficulty arises from the definition of application class and the lack of procedural detail for the classification of CPT/CPTU results in practise. The vague nature of the recommendations opens up for different interpretation and can cause contractual disputes. Some of the practical questions that CPT/CPTU data providers and users are facing are listed here:

- How to determine and document that a certain Application Class can be obtained before the start of field work, for instance in the tender phase?
- Regarding the CPTU parameter accuracy requirements: is it an absolute requirement that all three parameters (q_c , f_s and u_2) shall fulfill the limiting values given in Table 1? Should the main emphasis be given to the measured parameters, which are most crucial for the interpretation methods?
- ISO 2012 Annex D, clause D2.1 refers to zero readings before and after a test: For CPTU's, a first attempt at recommendations for limiting values is to follow the minimum accuracy according to the applications given in Table 1. How reliable are the zero readings before and after for this evaluation? How does cleaning of the cones etc. play a role?
- What is the overall best approach for the evaluation of the resulting Application Class after a test has been completed?
- If a test is evaluated to be in a lower Application Class than required in the project specifications, how shall the results be treated in the definition of representative parameters for design?
- From a client's point of view: Which Application Classes and default values are reasonable to require in the project specifications? What is achievable in which conditions?

3 CHALLENGES ASSOCIATED WITH THE QUANTIFICATION OF UNCERTAINTY

The term uncertainty of measurement intends to express the doubt regarding the validity of the results. It follows, from the discussions in previous sections, that a detailed and robust methodology for the quantification of the uncertainty associated with CPT/CTU profiles is desired and necessary to resolve the challenges associated with the assessment of quality. Unfortunately, the quantification of measurement uncertainty for CPT/CPTU results is not trivial.

The formal definition of the term uncertainty of measurement is, in accordance with the International Vocabulary of Metrology (VIM:2012), as follows: "non-negative parameter characterizing the dispersion of the quantity values being attributed to a measurand, based on the information used". ISO/IEC Guide 98-3:2008 adopt the use of uncertainty of measuring in the operational sense. This is to avoid the previous issues associated to terms like accuracy and error, which implies by definition the true value needs to be known in order to calculate accuracy.

ISO/IEC Guide 98-3:2008 and JCGM 100:2008 provides guidance for the estimation of uncertainty of measurement. Measurement uncertainty comprises, in general, many components or uncertainty contributors. The combined standard uncertainty of a

measurement can be expressed as the positive square root of the sum of the uncertainty contributors. The expanded standard uncertainty can then be used to express the probability or level of confidence of the estimations of uncertainty by using a coverage factor.

Some of the uncertainty contributors may be evaluated by "Type A" evaluation of measurement uncertainty. Where the statistical distribution of the quantity values from series of repeated measurements under the same conditions are compared against a reference and can be characterized by standard deviations. Other uncertainty contributors may be evaluated by "Type B", which are evaluations based on scientific judgement considering probability density functions based on experience, theoretical modelling, manufacturers specifications or other information.

It is not possible to apply "Type A" approach to field measurements given the difficulties associated in finding a perfectly uniform site that removes soil variability from the uncertainty equation. In addition, the uncertainties may also depend on the soil type, and this make this approach unpractical.

Peuchen and Terwindt (2014, 2015) proposed a model that applies a "Type B" evaluation of uncertainty of CPT/CPTU profiles. Their work really represents an in-depth evaluation of the factors that can influence the various measurements during a CPTU. The analyses of uncertainties are based on input parameters found in literature, own investigations, some general knowledge on transducers, etc. The uncertainty analysis proposed becomes rather subjective and hazy when weighting coefficients are applied to the uncertainty calculation model for representing poor operational procedures and adverse soil conditions. Peuchen and Terwindt concluded that the approach proposed can be considerable conservative and that further studies were required.

In current practice the implementation of "Type B" evaluations for estimating the uncertainty of CPTU measurements is cumbersome and inevitably involves making conservative assumptions to fill the gap of knowledge regarding the uncertainty distributions of certain components. An added challenge is to reach consensus between all sectors, contractors, design engineers, consultants, certifiers, and researchers may have different interest from enterprises involve in manufacturing or those involve in the distribution of services.

Modelling uncertainty using a "Type B" is difficult to implement without adding excessive conservatism. It requires deep knowledge on the behaviour of each particular measurement system and this in turn requires substantial research from geotechnical practitioners, equipment operators and manufacturers. In particular research effort is required to gain sufficient understanding on:

- Development of standard methodologies and requirements to test and measure the behavior of

a particular cone penetrometer design to minimize or eliminate subjective judgement when selecting uncertainty probability distributions and sensitivity coefficients.

- Development of an unambiguous methodology for reporting uncertainty probability distribution and sensitivity coefficients.

In summary, modelling uncertainty using a “Type B” evaluation can be a viable option for determining uncertainty of CPTU measurement, further maturation and consensus for calculation methodologies are required, before this approach can be incorporated into a standardization document.

4 CHALLENGES ASSOCIATED WITH STANDARDISATION

ISO Working Groups are responsible for the development of standardisation documents. Working groups are generally composed by technical experts and delegates appointed by the national standardisation participating in the standard. The main objective of a working group is delivering the minimum requirements to minimise the level of uncertainty associated to results and to deliver sufficient methodology descriptions to ensure consistent and repeatable results.

Working Groups are generally composed by diverse experts with different areas of competence and with specific experience on the local practise in their countries. Generally, the most important challenge is reaching agreement and consensus within the working group to ensure that the draft standard document is supported by the majority of countries during the balloting stages. Reaching consensus often requires long discussions, preparation and revision of formulations, datasets and evidence to demonstrate the scientific or operational rigor of a position or opinion.

Whenever possible, requirements should be expressed in terms of performance criteria, leaving maximum flexibility to technical development and innovation.

An important consideration for the Working Group is to use clear and concise language, well define terminology, clear unambiguous requirements to reduce the possibility of multiple interpretations. In this regard the provision of informative material in the form of examples, explanations and figures is very valuable to improve understanding and ease implementation.

Working Groups must consider the needs and the challenges from the industry and reach stakeholders to ensure key objectives, needs and challenges are served. During preparation of the standard the Working Group must take into consideration the cost of implementation of the standard in the industry against the value added and ensure, that the new requirements are practical and cost effective. Finally,

the extent of the implementation period must be considered to ensure that the industry is able to react to requirement changes. In this regard Working Groups have often to consider the standard document as “work in progress” and consider a staged approach particularly when large changes in requirements are needed.

5 UNCERTAINTY CONTRIBUTORS

Whether a series of equations for quantifying the uncertainty associated with the CPT/CPTU measurements are formulated, or whether a series of effective testing methodology requirements are established to minimise the level of uncertainty, it is fundamental to start by mapping out the potential sources of uncertainty and classifying their relative weight on the overall CPT/CPTU quality.

The tables presented below shows the main uncertainty contributors associated to CPT/CPTU results grouped into three categories. Tables provide a subjective qualitative assessment of the impact on uncertainty, as function of the maximum cone resistance registered in the test. Additional commentary describing the contributors and the potential mitigation measures are included. Table 1A describes contributors associated with the measurement system; Table 1B lists the contributors linked to testing methodology (including procedure, equipment and operator dependency) and Table 1C presents the contributors intimately associated the effects, caused by the interaction between cone penetrometer and soil, during the penetration phase.

From the varied list of uncertainty contributors, it is clear, that the measuring system uncertainties are easier to measure with robust laboratory testing procedures. Soage Santos *et al.* (2022) discuss in detail the quantification of calibration uncertainty.

The uncertainties associated with testing methodology are described in detail in recent publications (Peuchen and Terwindt, 2014, Lunne *et al.* 2017, Kardan *et al.* 2016). Testing methodology related uncertainties can be minimised or fully removed by implementing best practise guidance and prescriptive procedures.

Uncertainties associated with the effects derived from cone penetrometer-soil interaction are more difficult to measure and control. The most important contribution to uncertainty during testing is temperature variations. The importance of temperature changes is widely discussed in literature (Boylan, 2008, McCallum, 2010, Peuchen, 2014). Transient temperature gradients resulting from frictional heat during cone penetration and from thermal flux through push rods causes heating of a cone penetrometer. Temperature-induced drift under in situ stress and axial loading is without a doubt the larger error contributor on CPTU results. Figure 1 shows an example of the magnitude of the drift and the behavior of the measurement system when a cone is

Table 1A. Uncertainties associated with the CPT/CPTU measurement system.

Uncertainty contributors	Potential impact to uncertainty of CPT/CPTU results			Comments	Potential mitigation
	Profiles with $q_c < 1\text{MPa}$	Profiles with $1 < q_c < 3\text{MPa}$	Profiles with $q_c > 3\text{MPa}$		
Reference	High	Medium to high	Medium to high	Refers to the measurement of uncertainty or the reference used for the calibration of a sensor. The reference uncertainty should be several times lower than the instrument that is under calibration.	Introduction of a robust standard procedure for calibration of cone penetrometers. Definition of standard methodology for type A evaluation of uncertainty (in accordance with ISO/IEC Guide 98-3:2008 and JCGM 100:2008 recommendations) specific for the calibration of cone penetrometers under laboratory conditions
Reproducibility	High	Medium to high	Medium to high	Refers to the extent, to which consistent results are obtained when an experiment is repeated under a set of different conditions	
Repeatability	High	Medium to high	Medium to high	Refers to the closeness of successive measurements when carried out under as set repeatability conditions	
Resolution	High	Medium to high	Medium to high	Refers to the ability of a measurement system to detect small changes. The resolution indicates the smallest change in the measurand that a measurement system can detect.	
Zero drift	High	Medium to high	Medium to high	Refers to the difference in the measurement at zero load or pressure before and after applying a load or pressure increment	
Interpolation	High	Medium to high	Medium to high	Refers to the difference of the values given by the calibration interpolation equation and the actual measurements taken during the calibration	
Reversibility	High	Medium to high	Medium to high	Refers to the difference between two separate measurements taken at the same point, the first is taken during a series of increasing measurement values, and the other during a series of decreasing measurement values	
Apparent load transfer	High	Medium to high	Medium to high	Refers to the undesired influence experienced by a sensor caused by another sensor. For instance, when in compression type cone penetrometers sleeve friction strain gauge perceives changes, when the cone resistance sensor is loaded or vice versa.	
Normalised net area ratio	High	Medium to high	Medium to high	Applying a correct net area ratio for cone resistance corrections is of importance specially in clays. Best practise recommendations suggest the determination of net area ratio in a pressure cell during calibration. It should be noted that the net area ratio varies with applied pressure and there is some variance along the measurement range.	
Dimensions and geometry	High	Medium to high	Medium	CPT/CPTU measurements are highly dependent on geometry and deviation from the standard recommended geometries will compromise the representativeness of the results. In addition, cone resistance and sleeve friction are reported in units of pressure thus the uncertainty associated to the determinations of cone and sleeve friction area will have an important impact on the CPTU reported measurements	

Table 1B. Uncertainties associated with testing methodology.

Uncertainty contributors	Potential impact to uncertainty of CPT/CPTU results	Profiles with $q_c < 1\text{MPa}$	Profiles with $1 < q_c < 3\text{MPa}$	Profiles with $q_c > 3\text{MPa}$	Comments	Potential mitigation
Temperature	High	High	Medium to high	Medium	Changes in temperature will affect the results of the test due to sensors do not readily compensate for transient temperature changes. Prior to testing, the penetrometer should be brought to a stable temperature as close as possible to the expected ground temperature. This is particularly important when the penetrometer temperature is significantly higher or lower than the ground temperature.	Introduction of robust methodology, equipment and reporting requirements to prevent or minimise the error caused by these potential contributors.
Zeroing	High	High	Medium to high	Medium	Loads caused by trapped soil, or any other loads influencing the cone (handling, embedment in soil) can result in offsets being wrongly introduced while zeroing the measurement system and adding unnecessary uncertainty to CPTU datasets. In addition, unrepresentative zero reference values are likely to penalise the cone performance assessment after testing by comparing reference readings before and after the test	
Saturation	High	High	Medium to high	Medium	Gas or air trapped in the pressure chamber will cause delays in the sensor response (sluggish response) resulting in unrepresentative data. The pore pressure data will be invalid. This has a direct impact on the representativeness of the cone resistance, as cannot be corrected for pore pressure effects. Careful selection of filter elements, saturation fluid and saturation method are required to minimize the adverse effects on uncertainty.	
Rate of penetration	High	High	Medium to high	Medium	CPT/CPTU measurements are highly dependent on the penetration rate and deviations from the standardised rates will compromise the representativeness of the results.	
Placement of CPT rig at ground surface	Medium-high	Medium-high	Medium	Low-medium	The weight of the CPT rig can cause changes in the natural stresses in the ground. Placement of the weight need to be considered to avoid influencing the soil to be tested.	
Stops in penetration	Medium	Medium	Low to medium	Low	May cause adherence of soil to cone penetrometer body and thus false increase in cone resistance and sleeve friction. The acceleration and deceleration required for starting and stopping a test will inevitably cause local change in cone sensor readings	

Table 1C. Uncertainties associated with effects caused by cone penetrometer-soil interaction.

Uncertainty contributors	Potential impact to uncertainty of CPTU results	Profiles with $q_c < 1\text{MPa}$	Profiles with $1 < q_c < 3\text{MPa}$	Profiles with $q_c > 3\text{MPa}$	Comments	Potential mitigation
Temperature	High	Medium to high	Medium	Medium	Frictional heat developed during penetration can be significant and the consequence is large drifts will occur during testing. This is perhaps the most important source of uncertainty	Introduction of additional sensors to monitor temperature and bending changes and applied sound correction methods based on laboratory studies. Introduction of robust methodology, equipment and reporting requirements to prevent or minimise the error caused by these potential sources
Loss on saturation	High	Medium to high	Medium	Medium	It is sometimes difficult to maintain filter saturation during testing, particularly when pushing through a desiccated crust or through dilatant soils. Loss of saturation leads to sluggish pore pressure response and reliable fluid pressure data may not be consistently obtained. In instances testing approach need to be adjusted, for example by applying predrilling through a partially saturated soil to avoid losing saturation before reaching the saturated zone.	
Dimensions and geometry	Medium to high	Medium	Low to medium	Low to medium	As discussed, early variations dimensions and geometry of a cone can significantly contribute to uncertainty. Even when the dimensions and geometry are well known at the commencement of a test, the high frictional forces, and the abrasive nature of some soil types of my cause small variations on cone penetrometer dimensions and therefore affect the results. This is most likely to occur in sandy profiles and will have a significant effect on soft and loose sediments underlying the sand layer.	
Bending	Medium	Low to medium	Low	Low	During penetration the cone can be subjected to bending moments. This influence is generally small for q_c and f_s (error $< 10\text{kPa}$ and $< 1\text{kPa}$ respectively) for cone penetrometers using double bridge strain gauge.	
Inclination	Medium	Low to medium	Low	Low	Control of inclination is of particular importance contributor to depth uncertainty. In addition, larger inclination will affect the cone resistance and sleeve friction readings. Cone resistance can be affected significantly (10%) in anisotropic soils when inclinations exceed 30 degrees	
Soil trapped or adhered	Low to medium	Low	Low	Low	Trapped soil and dirt on gaps and seals can cause undesirable resistance that will impact the measurements specially when testing soft clays. Soils can also stick to the cone penetrometer surfaces effectively increasing the projected area and providing overestimates of q_c and f_s .	

submerged into a water bath at different temperatures in laboratory conditions.

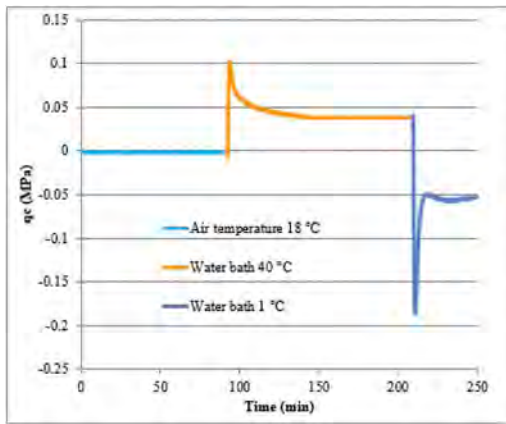


Figure 1. Example of verification data for temperature influence.

Additional uncertainty is introduced when inferring geotechnical parameters from CPT/CPTU data. These additional uncertainties associated with data interpretation is out of the scope of this document. Powell and Dhimitri, 2022 provide detailed discussion and advice for avoiding introduction of undesired uncertainty when deriving geotechnical parameters from CPT/CPTU results.

6 RECOMMENDED WAY FORWARD

The implementation of a rigid performance-based approach for quantifying CPT/CPTU uncertainties using modelling techniques (“Type B” uncertainty analysis) is complex and not fully developed. Modelling uncertainty requires maturation and large amount of research effort. Peuchen and Terwindt 2014 work has shown good potential for the application of this type of analysis, but currently it is not considered a feasible approach in practise as discussed in section 3. In this section a recommended methodology for standardising quality control is proposed.

There is ample opportunity to improve the overall quality of the CPT/CPTU results by implementing standard requirements with the objective of minimising the sources of uncertainties presented in Table 1. Different approaches can be followed to target the three main uncertainty groups:

1. Performance-based approach: Uncertainty analysis (Type A) to quantify uncertainty on measuring systems.
2. Method-based approach. Provide unequivocal procedures and equipment specifications to reduce uncertainty caused by operator and equipment bias.

3. Technological enhancement: Incorporating new technology that facilitates deeper understanding of the uncertainties rising from soil-equipment interaction.

6.1 Application of uncertainty analysis to cone penetrometer calibration results

The uncertainty contributions intrinsically associated to the CPT/CPTU measurement system can be better understood and quantified by conducting a series of well design and robust procedures for the calibration of cone penetrometers. Uncertainty analysis “Type A” is applied to the calibration results, allowing systematic quantification of the cone penetrometer ability to produce repeatable results under laboratory conditions.

Requirements for calibration of cone penetrometers and verification of cone penetrometers and uncertainty calculations are incorporated in (draft) standards published by ISO, particularly ISO/DIS 22476-1:2021 and ISO/DIS 19901-8:2022. The use of uncertainty analysis on calibration results implies the departure from the existing application class type approach and the inevitable implementation challenges discussed earlier. Instead, a series of “cone penetrometer classes” can be established using limiting values that defines the minimum uncertainty requirements to satisfy a given cone class. This provides a cone penetrometer classification framework that allows transparent comparison between systems, regardless of manufacturer or supplier. And facilitates the selection of cone penetrometers to match the project and design sensitivity requirements.

Calibration uncertainty analysis and performance indicators based on verification tests defines the best cone class that a particular system can obtain under laboratory conditions. Soage Santos *et al.* 2022 describes this scheme in some detail and provides example of the results.

6.2 Improving and controlling quality by implementation of testing methodology requirements

Most of the uncertainties associated to testing methodology (listed in Table 1B) can be greatly reduced by prescribing detailed methodologies and equipment requirements. For instance, zeroing the cone penetrometer acquisition system is critical. If zeroing is performed while the cone penetrometer is undergoing temperature changes or when the cone is embedded or covered in soil, the cone will experience significant drifts affecting the representativeness of the data. Thus, clear requirements regarding temperature stability and presence of undesired loads while zeroing the measurement system are necessary.

Significant uncertainty, up to 4% on cone resistance, can rise from using the default areas (cone

design areas) in the conversion of force to pressure measurements rather than the actual measured areas. This can be readily prevented by ensuring that cone geometry is measured in a calibration laboratory and monitored in the field. Powell and Lunne 2005 and Powell et al. 2021 showed the impact of cone dimensions and geometry on CPTU results.

While CPT/CPTU measurement systems are generally reliable and robust, experience shows that every single component of the CPT/CPTU measurement system may deteriorate, suffer damage, or experience drifts during operations (transport, system set up or testing). Consequently, it is imperative to monitor the integrity of the system during field operations. A diagnostic check scheme can be introduced to classify the CPT/CPTU test results.

Reference readings and output stability are non-subjective diagnostic checks that can be measured and quantified. For instance, observed differences of reference readings taken before and after a test will indicate if the measuring system has experienced a drift during the penetration or retraction of the cone from the ground. The absolute difference of values observed can be used for classifying the CPTU results in accordance with prescribed limits to assign a “performance category” to the test.

CPT/CPTU “performance categories” does not provide quantification the uncertainty of a particular test but allows identification of results that may have been affected by equipment malfunction or procedural error. Certain CPT/CPTU applications, like the characterisation of soft clays for foundation design, may require highly representative and repeatable results and consequently better performance is required. The CPT/CPTU category scheme can accommodate this by defining allowable limits for a given soil profile or for a range of soil conditions. In order to avoid potential conflicts caused by interpretation, the soil categories can be linked to prescribed ranges of cone resistance, for example profiles showing $q_c < 1\text{MPa}$ can be used instead of using terms like “Very soft to firm clays”.

It is important to highlight those changes such as ambient temperature, ambient pressure, the presence of dirt in the cone seals and adhesion of clayey soils can cause reference readings differences, that are not directly related to the changes that the measurement system may have experienced in the ground. For a performance category scheme to work as intended, it is fundamental, that reference readings are taken under similar conditions every time so that a meaningful comparison can be made. This challenge can be addressed by the incorporation of very clear testing methodology requirements.

Not all the uncertainty contributors associated to test methodology can be easily quantified and included in a CPT/CPTU performance classification scheme due to the impossibility to quantify them. However, qualitative assessment of test performance is very valuable and relevant information to the

users and interpreters of the CPT/CPTU datasets. The introduction of rigid reporting requirements for capturing qualitative performance assessment can be a suitable approach to deal with this challenge. Some examples of qualitative performance observations are listed below:

- Information related to the responsiveness of sensor to soil changes
- Pore pressure sluggish responses
- Sleeve friction or cone resistance insensitivity caused by dirt trapped in cone seals and gaps.
- Pore water pressure cavitation effects experienced during testing
- Qualitative indication of the soil disturbance caused by the seabed frame or drilling activities

Draft ISO/DIS 22476-1:2021 and ISO/DIS 19901-8:2021 capture quality monitoring by means of test categories, as discussed above, and provide highly detailed normative procedures ranging from field operations preparations to test termination and reporting activities.

6.3 *Improving and controlling uncertainty by encouraging technological development*

The uncertainty contributors resulting from the effects of the interaction between cone penetrometer and soil (see Table 1C) are especially challenging to quantify, control or correct. The introduction of additional technical requirements targeted to reduce and understand the uncertainty caused by the development of temperature variations and bending moment during testing will be greatly beneficial to improve the quality of CPT/CPTU results, especially in unfavourable soil profiles (i.e., dense sands, stiff to hard clays and interbedded soils profiles). Temperature changes of 10 degrees are not uncommon in unfavorable soils (i.e., Dense sands) and can cause drifts on q_c in the order of 300kPa, which is a very large error when trying to characterize a clay unit underlying a dense sand unit.

Laboratory verification tests, designed to measure how temperature or bending moment variations affects the performance of q_c , f_s and u_2 sensors can be introduced. Performance indicator limiting values (expressed in terms of kPa/°C and kPa/N) can be included as part of the cone classification scheme described in section 6.2 such that cone penetrometer classes are defined by the combination of the uncertainty associated to the calibration and the test verification results.

Further, the inclusion of temperature sensors in cone penetrometers can additionally provide valuable information on sensor performance during field testing. As the effect of temperature changes on a particular cone design can be measured under laboratory conditions it is relatively straight forward to develop correction algorithms based on the variations of temperature recorded by the temperature

sensor. The application of this technology can greatly reduce the uncertainty of CPT/CPTU results in unfavourable conditions where temperature changes dominate the uncertainty of the results.

Draft ISO/DIS 22476-1:2022 and ISO/DIS 19901-8:2022 introduces a cone penetrometer class that requires the inclusion of a temperature sensor. This clearly promotes technological development targeting the reduction of the uncertainties caused unavoidable temperature changes during testing in unfavourable conditions. It should also be noted that the required presentation of results of the ISO verifications covers the influences of temperature and bending on the parameters q_c , f_s , and u .

7 SUMMARY AND CONCLUSIONS

CPT/CPTU provide fundamental input for safe and economical design of many structures. Assessing the representativeness of the CPT/CPTU results is essential. Consequently, it is important to understand, and when possible, minimize the uncertainty associated to CPT/CPTU measurements, so these can be considered in planning, design, and installation of infrastructure.

The practical challenges associated to the quantification of uncertainty and the difficulties of its standardization have been discussed in depth in this document.

Uncertainty contributors associated to CPT/CPTU measurements have been categorized into three main groups: (1) Uncertainties associated with the measuring system, (2) Uncertainties resulting from testing methodology (including procedure, equipment and operator dependency) and (3) Uncertainties intimately associated with the effects caused by the interaction between cone penetrometer and soil. This classification of uncertainty contributors allows proposing a standardization approach that addresses each group with a combination of performance-based and method-based requirements, aiming to control and minimize the uncertainty contributions rising from execution of CPT/CPTU.

Uncertainties associated with the measurement system can be reduced by the introduction of a detailed calibration and verification procedures and prescribed methodology for uncertainty quantification. This also enables the development of a performance-based cone penetrometer class scheme. The approach allows for easy comparison of cone penetrometers, regardless of manufacturer or supplier, and assists the appropriate selection of cone penetrometer for specific applications.

Uncertainties resulting from test methodology can be addressed by implementing a quality monitoring scheme defining test categories based on quantitative performance indicators such as reference readings differences and output stabilities. In addition, detailed normative procedures ranging from field operations preparations to test termination and

reporting activities will also improve repeatability and representativeness of the results.

Uncertainties intimately associated the effects caused by the interaction between cone penetrometer and soil are often unavoidable. The introduction of new technology that allows measurement of these uncertainties and enables the development of suitable corrections improving the quality and therefore the overall certainty of the CPT/CPTU measurements even in unfavourable conditions.

ACKNOWLEDGEMENTS

The author would like to thank his colleagues at ISO 19901-8 work group, Tom Lunne, Joek Peuchen, Tim Carrington for sharing their knowledge and for the challenging and fruitful technical discussions that greatly influenced the opinions expressed in this document. Special thanks go to Gülin Yetginer for her amazing work keeping the group working as a team with a focus on reaching consensus and delivering a much-improved draft standard document. Further, the author would like to acknowledge the valuable support and input received from all the members of the ISO 22476-1 workgroup, special thanks go to Håkan Garin, Kees-Jan van der Made, Marius Tremblay, Kristoffer Kåsin, Diederick Bouwmeester and Wouter Vervaele. Last but not least thanks to John Powell and Tom Lunne for providing moral and technical support and for sharing their vast experience and knowledge.

REFERENCES

- ASTM International, 2012. *ASTM D5778-12 Standard Test Method for Electronic Friction Cone and Piezocone Penetration Testing of Soils*. West Conshohocken: ASTM International.
- ASTM International, 2020. *ASTM D5778-20 Standard Test Method for Electronic Friction Cone and Piezocone Penetration Testing of Soils*. West Conshohocken: ASTM International.
- Boylan, N., Mathijssen, F., Long, M. and Molenkamp, F. 2008. Cone penetration testing of organic soils. Proceedings, *Baltic Geotechnical Conference, September. Gdansk, Poland*.
- International Organization for Standardization, 2008. *ISO/IEC Guide 98-3:2008 Uncertainty of Measurement – Part 3: Guide to the Expression of Uncertainty in Measurement (GU:1995)*. Geneva: ISO.
- International Organization for Standardization. 2012. *Geotechnical investigation and testing – Field testing – Part 1: Electrical cone and piezocone penetration tests, International Standard ISO 22476-1:2012. (With Technical Corrigendum 1, January 2013)*. Geneva: International Organization for Standardization.
- International Organization for Standardization, 2014. *ISO/DIS 19901-8:2021 Petroleum and Natural Gas Industries - Specific Requirements for Offshore Structures – Part 8: Marine Soil Investigations*. Geneva: ISO.
- International Organization for Standardization, 2021. *ISO/DIS 22476-1:2021 Geotechnical Investigation and*

- Testing – Field Testing – Part 1: Electrical Cone and Piezocone Penetration Test*. Geneva: ISO.
- International Organization for Standardization, 2022. *ISO/DIS 19901-8:2022 Petroleum and Natural Gas Industries - Specific Requirements for Offshore Structures – Part 8: Marine Soil Investigations*. Geneva: ISO.
- ISSMFE International Society for Soil Mechanics and Foundation Engineering, 1977. Report of the subcommittee on standardization of penetration testing in Europe, Appendix A, recommended standard for the cone penetration test (CPT). *Proceedings of the ninth international conference on soil mechanics and foundation engineering*, Tokyo.
- JCGM. 2008 Joint Committee for Guidelines in Metrology. *Evaluation of measurement data_ Guide to expression of uncertainty in measurements* JCGM 100: 2008.
- JCGM. 2012 Joint Committee for Guidelines in Metrology. *International vocabulary of metrology – Basic and general concepts and associated terms (VIM)*. JCGM 200: 2012.
- Kardan C., Viking k., Nik L., Larsson S., 2016. *Influence of operator performance on quality of CPTu results*. 17th Nordic Geotechnical Meeting. Challenges in Nordic Geotechnics. Reykjavik.
- Lunne, T., Santos, R. Brink Clausen, J. & Powell, J.J.M. 2017. *Guidelines for Use of CPTU Application Classes According to ISO 19901-8: (2014)*. In: Society For Underwater Technology Offshore Site Investigation and Geotechnics Committee, ed. *Offshore Site Investigation and Geotechnics: Smarter Solutions for Future Offshore Developments: Proceedings of the 8th International Conference 12-14 September 2017*, Royal Geographical Society, London, UK: Volume 2. London: Society for Underwater Technology, pp. 300–307.
- McCallum, A. Barwise, A. Soage Santos, R. (2010). *CPT in polar snow-equipment and procedures*, 2rd International Symposium on Cone Penetration Testing CPT10: 2010 – Huntington Beach, California.
- Peuchen, J., Santos, R., Yetginer, A.G., Eckart, W.S., Carrington, T.M. & Lunne, T. 2020. *CPT data showing anomalies – assessment and potential postprocessing*. In Z. Westgate (ed.). *4th International Symposium on Frontiers in Offshore Geotechnics (ISFOG 2020): proceedings* (pp. 1026–1035). Deep Foundations Institute.
- Peuchen, J. & Terwindt, J., 2014. *Introduction to CPT accuracy*. In 3rd International symposium on cone penetration testing CPT14: May 12-14 (2014). Las Vegas, Nevada.
- Peuchen J and Terwindt J. (2015). *Measurement uncertainty of offshore Cone Penetration Tests*. Proc. ISFOG 15 Frontiers in Offshore Geotechnics III – Meyer (Ed.) © 2015 Taylor & Francis Group,
- Powell JJM and Lunne T. (2005). *A comparison of different sized piezocones in UK clays*. Proc. XVIth ICSMGE, Osaka, September 2005. Vol. 2, pp729–734.
- Powell JJM and Dhimitri L. and Ward, D. (2021). *The friction sleeve measurement in CPTU-Does size matters? – A new study*. 6th International Conference on geotechnical and geophysical site characterization. Budapest.
- Powell JJM and Dhimitri L. (2022). *Watch out for the use of global correlations and “blackbox” interpretation of CPTU data*. 5th International Symposium on Cone Penetration Testing CPT’22. Bologna.
- Soage Santos R., Gomez Meyer E, Peuchen J., Yetginer G., Lunne T., Carrington T., 2022. *Calibration of cone penetrometers according to International Organization for Standardization requirements*. 5th International Symposium on Cone Penetration Testing CPT’22. Bologna.
- Swedish Geotechnical Society (1993) “*Recommended Standard for Cone Penetration testing*”. SGF Report 1:93, June 15 1992.

CPT equipment: Recent advances and future perspectives

D.J. White

University of Southampton, UK

ABSTRACT: The basic configuration of the cone penetrometer test (CPT) has remained constant for half a century since the electric piezocone became widespread in the 1970s and the dimensions and test protocols were standardized soon after. The results of a conventional CPT performed today might be indistinguishable from a test conducted at the same location in 1972, aside from improved data logging and presentation. This discussion reflects on advances in CPT and other penetrometer equipment presented at this conference and in the recent literature, and presents discussion points to be considered during the event. Two general observations emerge: (i) advances in instrumentation, sensing and mechanical engineering have created a vast range of variations on the conventional CPT, providing excitement for technologists, researchers and a small subset of users; (ii) the conventional CPT is heavily standardized, commoditized and automated, and is progressively replacing the SPT in onshore practice. The result is a dispersion of practice: the majority of civil engineers base their ground characterization on a durable 1970s technology, updated with automation and improved data quality, while a minority are enjoying exploration of non-standard innovations – with mixed levels of impact. This conference provides a chance for us to (i) reflect where our activities sit in this spectrum, (ii) enjoy learning about recent advances, and (iii) debate how we will characterize the ground in another 50 years.

1 INTRODUCTION

1.1 Purpose and scope of this discussion paper

I was invited by the organisers of this conference to prepare a presentation for the start of the discussion session on the subject of CPT and other penetrometer equipment. This written contribution is to provide a record of the presentation in advance, and the presentation is intended to set the scene for a productive discussion.

The paper draws on the manuscripts presented at this event related to penetrometer equipment, as well as recent literature on the subject, and I have also tried to draw in wider context from the civil engineering industry, and other relevant industries, to give context to the drivers of CPT equipment developments.

The discussion that follows sets current developments in the context of the history of the CPT. This short contribution cannot comprehensively cover the full history and range of this technology, which is properly described by other keynote and review papers such as Broms & Flodin (1988), Lunne et al. (1997), Lunne (2012) and Massarch (2014).

Many of the advances described in the papers of CPT'22 are non-mainstream – relating to specialized modifications or applications of the CPT – so this review is a journey mainly through the exotic. However, there are contributions that provide incremental

but useful improvements to traditional CPT equipment, which are suited to widespread adoption.

1.2 Elements of penetrometer equipment

To review advances in CPT equipment it is useful to define a baseline starting point, which is taken by defining a ‘conventional’ CPT. Also, it is useful to divide CPT equipment into the various functional elements of the test and examine the advances in each. Table 1 lists the adopted set of functional elements.

Table 1. Functional elements of CPT equipment.

Element	Description
Delivery	How the CPT equipment reaches the site location (at the soil surface)
Deployment	How the CPT advances into the subsoil, to the test location
Sensing	The instrument types and measurements taken during the test
Motion	The applied movement during the test
Scale	The size of the instrument

For the baseline case of the conventional CPT, these functional elements are shown in Figure 1. They are essentially unchanged since the 1970s,

when standard dimensions and penetration rates emerged from early standardization work.

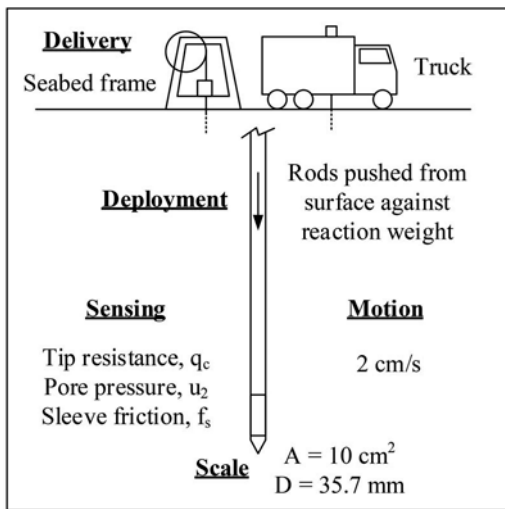


Figure 1. Conventional CPT systems – onshore and offshore.

2 CPT EQUIPMENT ADVANCES

2.1 Introduction

The following sub-sections discuss advances related to each functional element. The advances that feature in this review are summarized in Figure 2, which can be compared to the baseline of Figure 1. However, Figure 2 is not an exhaustive record of CPT equipment innovations, and many more can be found in the earlier CPT and ISOPT/ESOPT conferences.

2.2 Delivery

For *delivery* to onshore sites, early CPT rigs were mounted on rugged vehicles and today's fleets of commercial CPT rigs includes large and small wheeled or tracked vehicles, driven by people sat in a driving seat.

Recent onshore *delivery* advances have eliminated the wheels and tracks and in some cases the driver, to allow CPT testing in situations where these may not be used. This may, for example, be due to (i) extremely soft ground (e.g. tailings or marsh), (ii) hostile locals (e.g. for military trafficability assessments) or (iii) the lack of oxygen (e.g. on Mars) (Figure 3).

Uncrewed and remote-controlled onshore CPT delivery systems that have been trialled include aerial drones (Baez et al. 2020) and uncrewed wheeled or tracked vehicles (e.g. Scholz et al. 2014, Olmedo & Lipsett 2020). These technologies allow soil consistency assessments in wetlands, agricultural land and tailings ponds (Figure 3a-c). Robotic vehicles with advanced manipulators are widely used in agriculture

for sowing, weeding and harvesting, and these carry soil condition sensors. It is a simple extension to add a penetrometer system to these vehicles. Interplanetary landers have also conducted penetrometry.

For *delivery* to offshore underwater sites, the remote-controlled CPT vehicle is not as esoteric as onshore. Trials of ROV-mounted CPT systems were reported in the early 1980s by Geise & Kolk (1983) and the GeoROV CPT system (Edmunds 2014) has found widespread use as a lightweight seabed penetrometer system over the past decade (Figure 3d).

During an ROV-based CPT test, the crew is above the apparatus, on the vessel that the unit is tethered to. A logical extension, aligned with trends in other offshore survey technologies, is for the crew to remain on land, and the vessel to be uncrewed. Autonomous (or uncrewed) surface vessels are now used for geophysical surveys, and an uncrewed geotechnical survey is a realistic prospect.

Compared to sampling operations, penetrometer testing is easier to perform in an uncrewed situation due to the complexity of sample handling and storage. Penetrometer testing will therefore be a central element of future uncrewed geotechnical surveys, both offshore and onshore. This likely increase in reliance on penetrometry is a driver of more advanced test types, as discussed in Section 2.5, to replace the reduction in data if sampling is eliminated or reduced.

2.3 Deployment

2.3.1 Introduction

For *deployment* of the cone penetrometer into the subsoil, a conventional onshore CPT rig usually has a hydraulic pushing system, with rods of 2.5–3.0 m length, that are connected after each push by the operator. Some offshore systems use coiled rods (e.g. Power & Geise 1994, Meunier et al. 2004), or a robotic drilling system (e.g. Kelleher & Randolph 2005). The vertical reaction force is provided by the vehicle weight, sometimes supplemented by ground anchors, or by the skirts of a suction-type foundation on the base of the unit (e.g. Boggess & Robertson 2010).

Advances in deployment of the penetrometer fall into two primary categories: (i) techniques to speed-up the deployment process and (ii) techniques to reduce the vertical required reaction force and therefore increase the potential depth of penetration.

2.3.2 Speeding up deployment

In this conference, Storteboom et al. (2022a) describe a new trademarked 'SingleTwist' rod connection system, which allows a long CPT string to be compactly stored and quickly assembled by robotics (Figure 4a). The rods are held together with a flexible ball joint, for storage on a reel, but require only 1/6th of a turn to become rigidly connected for deployment. The ball joint connection

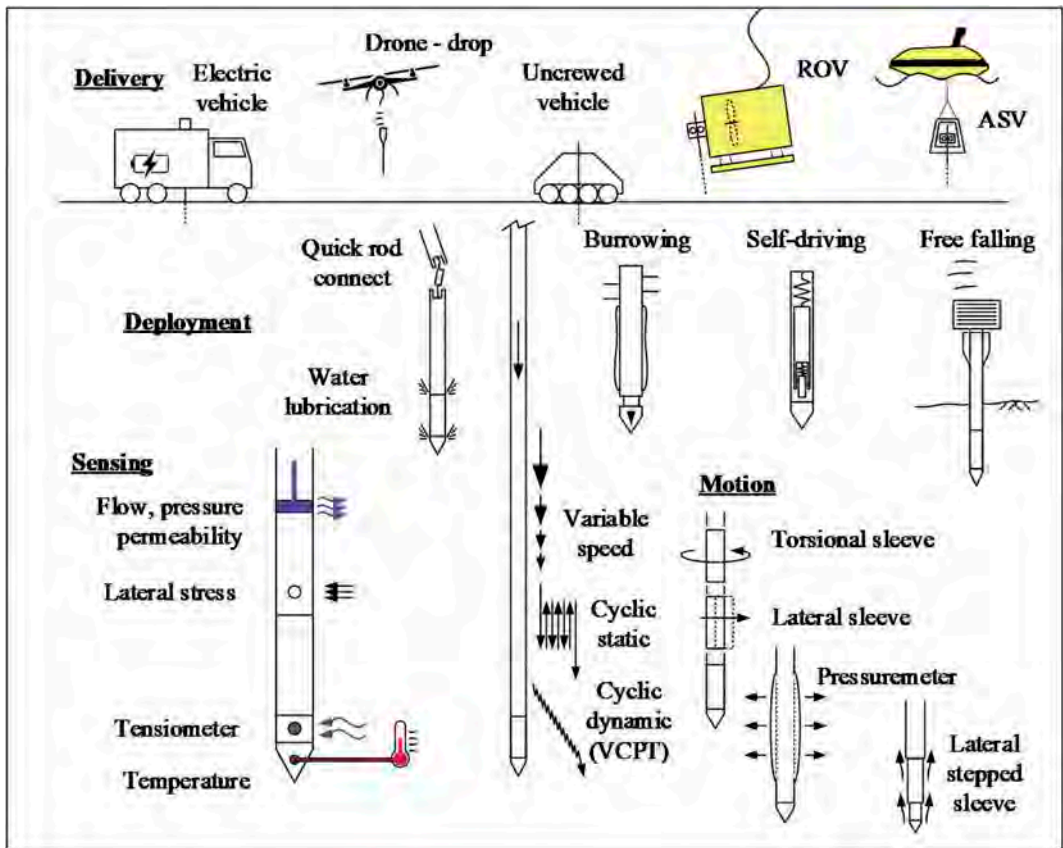


Figure 2. CPT equipment advances: selected from this conference and recent literature – as discussed in Section 2.

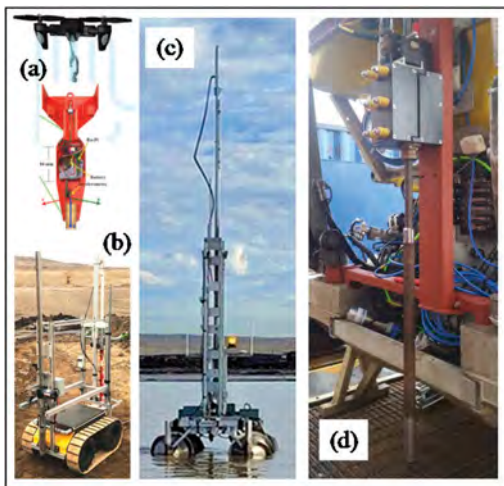


Figure 3. Advances in *delivery* of CPT equipment: uncrewed vehicles, (a) aerial (Baez et al. 2020), (b) land (Olmedo & Lipsett 2016), (c) land/water (HELIX25: www.copperstonetech.com) and (d) underwater (ROVcone www.bluefieldgeo.com).

features a protected data cable running through the joint.

An alternative speed-up technique, which also removes the need for any vertical reaction force, is to use a free-falling penetrometer (FFP). These systems are gaining wide use in research for shallow seafloor characterization (e.g. Stark et al. 2009, Steiner et al. 2014, Stark 2016) and their interpretation methods are evolving in parallel with free falling anchor research (Chow et al. 2017). Commercial FFP systems are also used for deepwater soft soils, sometimes with combined free-falling and static push test stages (e.g. Young et al. 2011).

In this conference, Kang et al. (2022) present sea trials in a relatively lightweight FFP, weighing 38 kg (Figure 4c). Studies such as this demonstrate how a self-contained low cost FFP data system (e.g. Randolph et al. 2018) allows multiple rapid CPTs to be performed.

However, these studies, and others (e.g. Stephan et al. 2015, Peuchen et al. 2017) show the challenge of achieving sufficient penetration in sands to reach the depth required for typical designs – such as assessing trenchability for cable route surveys. FFP penetration



Figure 4. Advances in deployment of CPT equipment: (a) SingleTwist™ connectors (Storteboom et al. 2022a), (b) water lubrication (Yetginer-Tjelta et al. 2022), (c) free falling system (Kang et al. 2022) and (d) self-driving system (HP³ Spohn et al. 2018).

of up to 15-20 m is reported in soft clays by the ‘CPT stinger’ (Jeanjean et al. 2012). However, the reported trials in sandy or stiff clay soils have achieved only 1–3 m penetration in some situations, even with a heavy 250-500 kg FFP unit. The challenge of achieving sufficient penetration may be exacerbated in dilatant sands by the undrained response. This effect also complicates the data interpretation, due to the change in drainage conditions relative to a standard CPT as well as the viscous rate effect (White et al. 2018). The depth range can be extended by a static push unit in the FFP (e.g. Jeanjean et al. 2012, Peuchen et al. 2017). This approach requires the embedment from the initial free fall stage to provide sufficient reaction.

2.3.3 Reducing reaction force, raising depth range
Twin advances of a lighter CPT system and an increased depth range can be achieved through methods that reduce or eliminate the external force required to push the rods through the ground.

A simple modification to reduce the pushing force that can form an addition to a conventional CPT system is a lubrication system to inject water or drilling mud around the rods (e.g. Jefferies & Funegard 1983).

In this conference, Yetginer-Tjelta et al. (2022) report a systematic investigation into different methods of water injection at the tip and rods of a seafloor CPT system (Figure 4b). This was part of a long term campaign on the Dogger Bank in the North Sea, with more than 500 CPTs. These improvements to the equipment have led to an

approximate doubling of the depth achieved, including penetration through sands with $q_c > 100$ MPa.

2.3.4 Bypassing reaction force: Self-burrowing

An alternative to eliminating rod friction is to eliminate the rods themselves, and transform the CPT unit into a burrowing robot. Setting aside questions of navigation and power, this concept relies on the sleeve friction to provide a reaction force to overcome the cone tip resistance. Natural burrowers such as razor clams, earthworms and roots have been used as bio-inspiration for robots that could evolve into a rod-free CPT (e.g. Winter et al. 2014, Tao et al. 2020, Naclerio et al. 2021). Martinez et al. (2020) show that a roughened sleeve with a length-diameter ratio of $L/D = 4-6.5$ is required in dense sands – the most difficult conditions – to provide the required reaction.

An additional strategy to ease burrowing is to reduce the tip resistance by fluidizing the soil ahead of the robot, or in dry sand by aerating it. The approach has been successfully demonstrated in the laboratory by a steerable robot using an externally-provided air supply to fluidise the soil ahead (Naclerio et al. 2021).

The rise of robotics has led to many proposals for burrowing robots to be used across civil engineering applications. Perhaps self-burrowing CPTs will feature in future versions of this conference.

2.3.5 Bypassing reaction force: Self-driving

An alternative to self-burrowing is self-driving, in which the CPT is advanced by a driving mechanism that is incorporated within the machine itself. This concept was adopted by the Heat Flow and Physical Properties Package (HP³) of the Insight Mission that took a lander to Mars during 2018.

The HP³ system featured a CPT-like ‘Mole’ device, 400 mm long, 27 mm in diameter, with a mass of 860 g. The Mole was designed to pull a 5m-long Science Tether into the subsoil to a depth of 3 – 5m (Spohn et al. 2018, Kromer et al 2019) (Figure 4d).

The driving mechanism was designed to achieve 0.1-1mm of set per blow, at a rate of 0.28 blows/sec. Laboratory trials show this probe self-driving to 5 m depth in a sandy Mars-simulant soil of crushed basalt sand. Comparisons with conventional CPTs in the same bed showed that penetration at around 20 mm/min was possible in soil with $q_c \sim 1$ MPa (Spohn et al. 2018, Wippermann et al. 2020).

However, attempts to penetrate the surface of Mars were unsuccessful, despite the Mole operating correctly. The probe failed to overcome the initial penetration resistance of the shallowest few centimetres and created a wide hole around the probe. This prevented the shaft resistance on the Mole from providing resistance against the hammer recoil, contributing to the failure to penetrate. Despite various attempts over a period of two years, the Mole remained stuck in a shallow open hole on the surface

of Mars (Spohn et al. 2021). Despite these difficulties on Mars, the project demonstrates the feasibility of self-burial by a CPT-like device using an internal hammer system.

2.4 Sensing

2.4.1 Introduction

The *sensing* on a conventional cone comprises primarily the three CPT parameters, tip and sleeve resistance, and pore pressure (i.e. q_c , f_s and u_2) with additional measurements of depth and tilt. The seismic piezocone test also provides measurements of shear wave velocity, V_s , at discrete depths.

A wide range of additional sensors have been incorporated within the cone, some of which are illustrated in Figure 2, based on contributions to this conference and other recent publications. These are discussed under the following headings of (i) mechanical, (ii) hydraulic and (iii) thermal.

2.4.2 Advances in mechanical sensing

It is well recognized that the fundamental strength and stiffness properties of a soil, in whatever constitutive framework is considered, do not uniquely correlate with the three basic cone parameters. This uncertainty can be reduced by taking one or more further mechanical readings, such as normal or shear stress values, by testing with a modified instrument equipped with additional sensors. These additional sensors are commonly mounted in further sleeves behind the conventional single friction sleeve.

For example, Isaev et al. (2022) describe in this conference a lateral stress cone, which is equipped with three pairs of lateral total stress and pore pressure sensors in successively larger diameter sleeves (Figure 5a). This type of ‘lateral stress cone’ provides data ‘on-the-fly’ (i.e. during steady penetration) that is analogous to a dilatometer or three points on a pressuremeter expansion curve. Correlations are explored to link these measured stresses, via their ratios or differences, to the in situ stress state and OCR.

A similar theme of multiple sleeves was proposed by DeJong & Frost (2002), using different values of roughness. In this case the multi-sleeve approach allows rough and smooth interface strengths to be measured, and the CPT sleeve to be tailored to the interface for which a design friction is required. By measuring sleeve friction at two positions, a new normalized friction parameter related to the degradation of friction can be calculated, and used as a fourth non-dimensional CPT parameter, to augment Q_t , F_r and B_q . This multi-friction parameter, MFP, allows the conventional range of CPT soil classification charts (e.g. Robertson 2009) to be supplemented by an extra chart using a derivative of MFP (Hebeler et al. 2018).

Friction sleeve data is sometimes treated with caution, due to potential unreliability from two

sources: (i) errors in measuring the applied shear stress due to load leakage through the seals and/or low load cell sensitivity in subtraction cones and (ii) variations in the applied shear stress due to the sleeve roughness or minor differences in diameter or alignment of the sleeve. A review of these difficulties is presented in this conference by McConnell & Wassenaar (2022), who describe a new cone with improved load cell design to overcome these limitations and provide more reliable friction sleeve data in soft soils.

2.4.3 Advances in hydraulic sensing

Multiple contributions to this conference focus on the reliable measurement of hydraulic properties. Lunne et al. (2022) report on a revival of multiple pore pressure measurements – a review of early data that used the u_1 (tip and face) and u_3 (top of sleeve) sensors, alongside the conventional u_2 (shoulder). They show that normalized parameters using the difference or ratio between u_1 and u_2 can provide a reasonable correlation with OCR on a site-by-site basis, but the correlation with the conventional Q_t remains stronger.

One of the difficulties with CPT pore pressure data is the potential for unreliability due to poor saturation of the sensor filter element, air trapped elsewhere in the tip and cavitation. In this conference, Rocchi et al (2022) describe a new device that can be used to rapidly assure the saturation of a piezocone tip (Figure 5b). This device is used to test the saturation level by applying an impulse of pressure to the sensor, and then checking Skempton’s B-value for the response.

Saturation is especially important when performing CPTs in unsaturated soils, where negative pore pressures are to be measured. In this conference, Tarantino et al. (2022) describe the development of a Tensiocone – a CPT attachment incorporating a high capacity tensiometer (HCD). They describe the laboratory validation of a new adapter that sits between the cone tip and friction sleeve, equipped with a surface-mounted tensiometer. Field trials did not show agreement between in situ tensiometers and the tensiocone measurements. This was traced to a cross-sensitivity between CPT axial load and tensiometer reading, which will be rectified in a new design of the sensor.

A further development of hydraulic measurement using the CPT is to impose a flow of water from the tip or shaft of the cone, and measure the associated pressure, in order to determine the local permeability. This adaptation is analogous to the conventional constant head borehole flow test (Hvorslev 1951). A similar adaptation has been applied to the pressuremeter, by withdrawing the device to create a test ‘well’ and applying controlled flow (Ratnam et al. 2001).

Gundersen et al. (2022), in this conference, describe trials using a ‘flow cone’ equipped to release water through a porous sleeve located

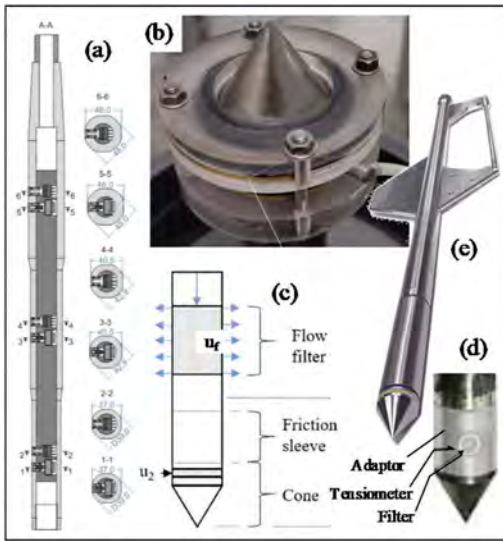


Figure 5. Advances in sensing on CPT equipment: (a) Tensiometer (Tarantino et al. 2022), (b) saturation verification (Rocchi et al. 2022), (c) the ‘flow cone’ (Gundersen et al. 2022), (d) Tensiometer adaptor (Tarantino et al. 2022) and (e) a parallel thermal probe element (www.datem.co.uk).

1.23 m above the shoulder of the cone, which is also equipped with pressure measurement (Figure 5c). Tests are reported from NGI’s Halden test site, which comprises of silt. In these conditions, the sleeve measurement indicates an excess pore pressure remaining from the cone penetration process, and the dissipation response at the porous sleeve is used to infer the soil permeability. Prior studies using the same device at a sand site reported by Gundersen et al. (2019), show accurate direct measurement of permeability through constant head or falling head tests at the sleeve.

2.4.4 Advances in thermal sensing

CPTs are usually equipped with a temperature sensor within the tip, which can be used to check for temperature-induced drift of any sensors, and to also indicate the ground temperature – which may feature a step change at the depth of the water table.

More advanced use of the temperature data is described by Vardon et al. (2018, 2019). They describe the use of passive temperature responses to evaluate the thermal conductivity of the soil surrounding the CPT. The passive approach relies on the dissipation of heat generated by the penetrometer-soil friction during the installation process. This is a simplification of the active approach, which was developed earlier for geophysical research, which relies on an internal heating element to provide a pulse of heat that is recorded at other locations along the device. This type of ‘thermal needle probe’ can involve a thin extension from the front of a conventional CPT, or a parallel thinner element behind the friction sleeve, such as the example shown in Figure 5e produced by Datem.

These advances in the use of CPTs for thermal measurements reflect new markets related to ground heat energy systems and buried cables for offshore wind. Both of these applications relate to the energy transition and are rapidly growing markets.

2.5 Motion

2.5.1 Introduction

The *motion* in a conventional CPT is continuous penetration, usually at a rate of 2 cm/s, with intermittent pauses for rod changes or dissipation phases.

There have been many attempts to expand this motion through different speeds, patterns and directions of movement, some of which are the subject of papers in this conference. Changes in the pattern of vertical movement are made possible by advanced drive systems, which allow specific patterns of movement or load to be applied to the top of the cone rods. Meanwhile, modern miniature robotic technology has allowed miniature actuators to be incorporated in sleeve elements located behind the cone tip. This allows elements to be displaced relative to the main cone rod, with the corresponding soil response measured. The extensions can be summarized as follows:

1. Novel vertical movement: (i) different speeds, (ii) large amplitude cycles, (iii) small vibratory cycles;
2. Separate elements for other movements: (iv) expansion – i.e. the cone-pressurimeter, (v) rotation or (vi) lateral translation

Recent contributions to each of these test variations are briefly discussed below.

2.5.2 Variations in the vertical movement

Studies of large-amplitude cyclic CPTs – with vertical movement by several cone diameters – were prompted by similar testing of flow-round penetrometers (such as the T-bar or ball). For these devices, the cyclic penetration process is symmetric, with soil flowing in reverse around the protrusion. Cyclic T-bar or ball penetrometer tests provide a measure of soil sensitivity (e.g. Randolph 2004).

For a CPT, cyclic vertical movement may lead to a hole opening beneath the CPT, but if this does not occur the process can be similarly symmetric. Regardless of the flow at the cone tip, the cyclic movement on the friction sleeve also provides data that can support estimates of sensitivity or the degradation of friction on piles (e.g. Hebler et al. 2005, Diambra et al. 2014, Shonberg et al. 2019).

Small amplitude high-frequency vertical cycles can also be applied concurrent with the standard installation push. This type of test and device is known as a Vibro-CPT (VCPT) or Vibropiezococone

(e.g. McGillivray et al. 2000, Jorat et al. 2014, Al-Sammarraie et al. 2018). These vibrations can be imposed by an oscillating mass attached to the rods, or by control of the hydraulic actuator. VibroCPT installations typically feature 10-15 Hz vibrations on top of the standard 2 cm/s penetration, creating a vibratory amplitude on the order of 1 mm at the cone tip. Due to rod compression, accelerometer data from the tip is double integrated to find the tip motion.

The simplest interpretation of the VCPT is as the reduction ratio between q_c in a VCPT and an adjacent conventional CPT. This has been used as an indicator of liquefaction potential (e.g. McGillivray et al. 2000). In this conference, Al-Sammarraie et al. (2022) describe recent VCPT studies that have investigated more detailed interpretation of the q_c response within individual VCPT cycles. The aim is to link the measured response to pile-soil interaction models used for vibratory pile driving.

In softer soils, a further variation in vertical movement is to apply varying rates of penetration, altering the rate in steps – a so-called ‘twitch’ test (House et al. 2001, Randolph & Hope 2004, Silva et al. 2006). This test provides a basis to estimate the consolidation coefficient, albeit taking approximately the same time as a conventional dissipation test. However, a further benefit is that twitch results provide a ratio between the slow (drained) and fast (undrained) resistance, which can be linked to strength, stiffness or state (e.g. OCR) parameters (Schneider et al. 2007, Suzuki & Lehane 2015, Dienstmann et al. 2017, White et al. 2018, Mo et al. 2020).

Penetrometer tests that span a range of motion rates and also involve periods of cyclic movement and dissipation periods allow a wide range of soil strengths to be mapped out (e.g. Chow et al. 2019). These tests can mimic the loading history applied by infrastructure to the ground. The results may therefore be suitable for scaling to the changing capacity of a foundation system under ‘whole life’ loading (e.g. Zhou et al. 2020, Gourvenec 2020).

2.5.3 Pressuremeter elements

The earliest example of an additional actuated element combined with the CPT is the cone pressuremeter. Early studies using a pressuremeter incorporated above the cone led to interpretation solutions that focused on the cyclic and unloading stages, acknowledging that the initial penetration of the cone will have disturbed the in situ stress state (e.g. Houlsby & Withers 1988, Withers et al. 1989, Bellotti et al. 1989, Ferreira & Robertson 1992, Bolton & Whittle 1999, Whittle & Liu 2013).

Recently the cone pressuremeter has found new usage in relation to offshore wind, for the determination of soil stiffness for monopile foundations (e.g. Whittle et al. 2017). In this conference Vinco & Sachetto (2022) describe a new cone pressuremeter

system designed particularly to verify the results of ground improvement activities (Figure 6a). For this application the system must be small, portable and suited to use within existing buildings, and requires only a low penetration force and depth capability. This system uses water as the control fluid, in common with another recently-developed pressuremeter described by Lopes dos Santos et al. (2019).

These new systems could support wider adoption of the cone-pressuremeter, taking advantage of the use of unload-reload loops and the unloading phase to gather strength and stress-strain or stiffness degradation curves from the measured data. It has also been demonstrated that pressuremeter tests can include large numbers of constant pressure-amplitude cycles, which may allow insights into the cyclic response, that can be translated into lateral p-y response models (e.g. Briaud et al. 1984, Lopes dos Santos 2020).

2.5.4 Torsional or lateral motion elements

Miniaturization of electromechanical systems allows actuators to be located within the cone sleeve. This allows concepts such as a torsional (t- θ) sleeve element (Frost & Martinez 2013, Figure 6b) and a laterally-moving p-y-type element (Diambra et al. 2022, in this conference, Figure 6c). These concepts offer the potential to provide more detailed soil characterization, by measuring load-

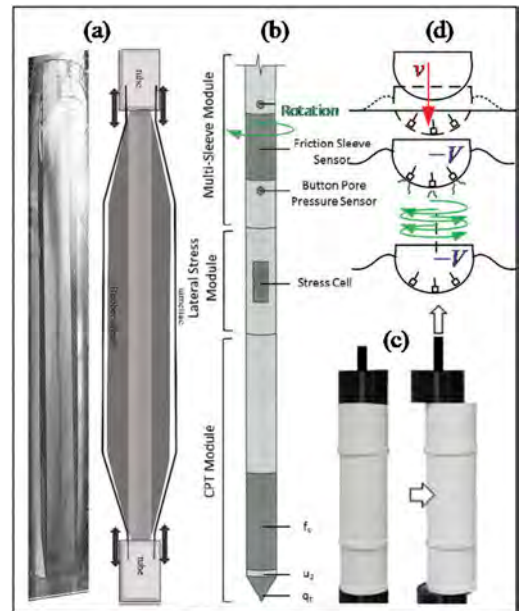


Figure 6. Advances in *motion* during CPT-type testing: (a) pressuremeter module (Vinco & Sachetto 2022), (b) Torsional sleeve (Frost & Martinez 2013), (c) lateral (p-y) sleeve (Diambra et al. 2022) and (d) rotational shallow penetrometer tests (White et al. 2022).

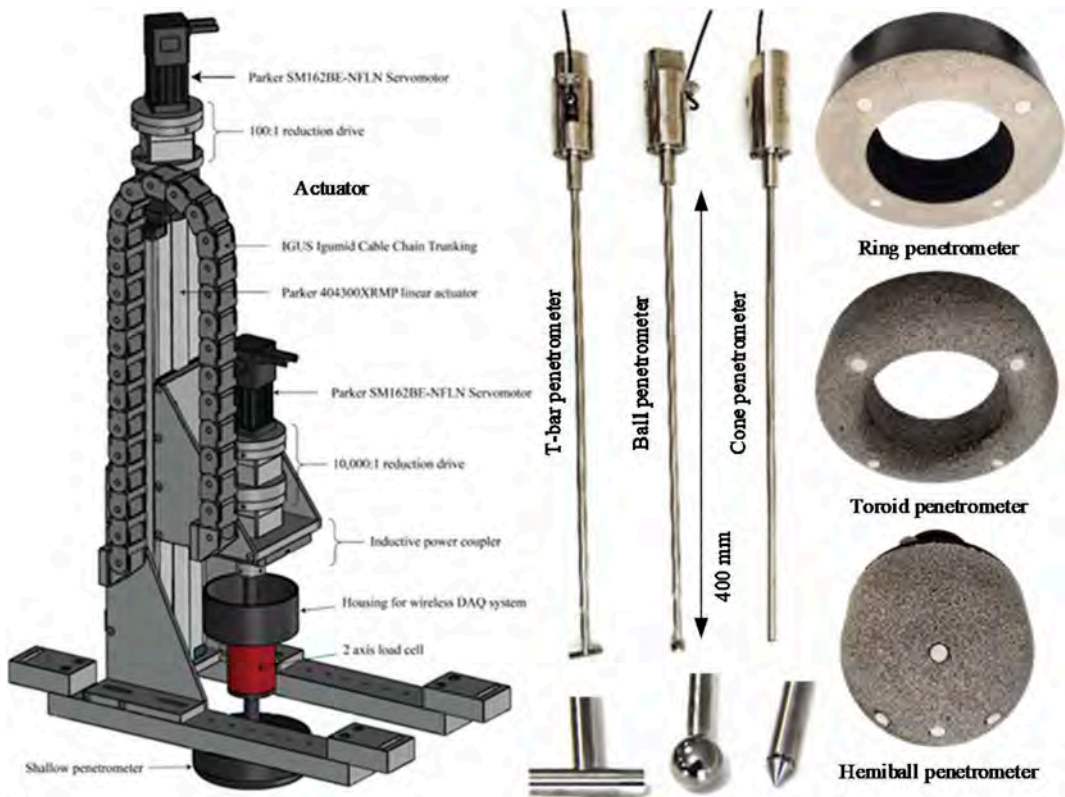


Figure 7. Shallow penetrometer system – a combination of CPT, T-bar and ball strength profiling tools and the shallow ring, toroid and hemiball devices for near-surface soil strength, interface strength and consolidation property measurement (White et al. 2022).

displacement responses for modes of soil deformation that are different to the cylindrical expansion of the pressuremeter.

For example, laboratory torsional shear tests indicate differences in the rate of pore pressure generation compared to axial shearing. Meanwhile, lateral deformation is more closely linked to pile p-y loading than cylindrical expansion. These locally-actuated sleeve concepts remain to be proven beyond trial prototype devices, but such robotic cones (or ROBOCONES, to use the term coined by Diambra et al. 2022) could create exciting possibilities for complex in-situ tests.

The introduction of more complex dual-directional actuation in a penetrometer test has been successful for shallow devices, such as the ring, toroid and hemiball penetrometers. These tests involve penetration of the device by a fraction of a diameter, followed by phases of dissipation (on clay soils) and rotation (Figure 6d).

In this conference, we present test execution and interpretation procedures for a rotational penetrometry system that has been used for more than 300 tests over the past 6 years, including for

several commercial projects (White et al. 2022). The system features electromechanical drives with feedback control, so a vertical load can be maintained while the device rotates and settles. Drained and undrained interface strength parameters, as well as consolidation properties, are derived from the tests.

3 HOW DOES CPT EQUIPMENT ADVANCE?

3.1 *Are equipment advances led by new ideas?*

This discussion and the wider CPT'22 conference feature numerous advances in CPT equipment, some of which will influence future practice, and many of which will not. So this closing part of the discussion offers some views on how the CPT equipment used in practice becomes more advanced. Hopefully this will prompt the sharing of wider views during the conference, and I look forward to learning from these.

The last equipment example discussed above – rotational testing using shallow penetrometers (Figure 7) – is an example that I have been heavily

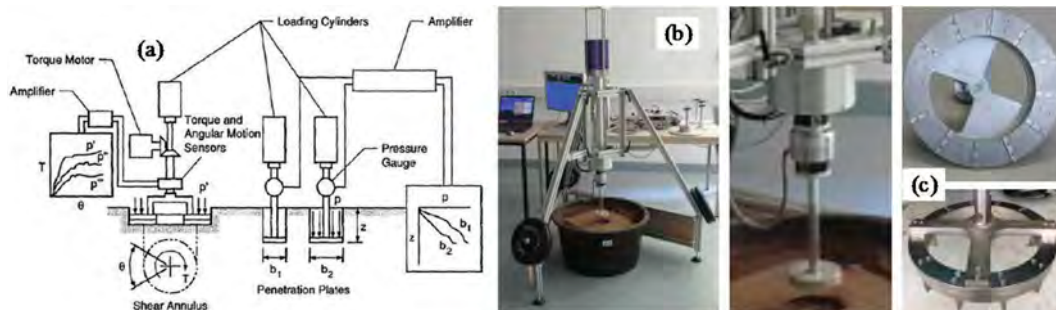


Figure 8. The bevameter – the original shallow penetrometer? (a) Bevameter principles (Bekker 1969), (b) Laboratory Bevameter system (Apfelbeck et al. 2011), (c) Shear plates for torsional Bevameter tests (top: Apfelbeck et al. 2011, bottom: Kim et al. 2021).

involved in, so I will use this as a living case study of an advance that might or might not have a future life.

These shallow penetrometers emerged from research at UWA at a time when we were heavily focused on seabed pipelines, and their friction on the seafloor. Centrifuge model testing of short pipeline elements was being used to assess design friction coefficients (White & Gaudin 2008). This led to the idea of a ‘pipe-like’ in situ test, but using rotation to allow longer distances of interface sliding. Prof. Mark Randolph and I proposed this concept as Dr Yue Yan’s PhD topic and she developed the shallow penetrometer concept (Yan 2013). Dr Sam Stanier took the topic further in the RIGSS Joint Industry Project, with close support from industry, and co-supervising Dr Mark Schneider’s PhD on this topic. The devices worked well, we devised rigorous interpretation methods, and the devices appeared to meet an industry need.

But was this type of test a new idea? It turns out not. After the PhD studies and the RIGSS JIP were completed, we discovered parallel research in the world of terramechanics and agriculture that involved a similar type of test – the bevameter (Bekker 1969, Wong 2010). This device was developed in the 1950s and resembles the ring penetrometer and the torsional plate penetrometer (Watson & Randolph 1998).

A bevameter test involves penetration and rotation of a ring-shaped device, with the pressure-sinkage and torque-rotation results being used to characterize the soil for assessment of trafficability (Figure 8). Bevameters have been developed for attachment to lunar landers and Mars rovers (Bekker 1969, Apfelbeck et al. 2011, Edwards et al. 2017). Their interpretation is rarely rooted in the same soil mechanics principles as are familiar for CPTs and our shallow penetrometers, but the test concept is similar.

So – shallow penetrometers might deserve to be counted as an advance, but they are not a new idea. The message is perhaps that (i) a new idea may

create an advance but (ii) there may be plenty of old ideas that we are yet to develop into a suitable form that can be brought into the geotechnical market.

3.2 Are equipment advances led by new markets?

3.2.1 Introduction

The shallow penetrometer story leads to the question of markets for advances in penetrometer testing. Many of the advances reviewed in this paper target a particular market that requires additional information from a penetrometer test – through an additional *sensor* or *motion* stage. Or, the advances relate to a new market where conventional *delivery* and *deployment* methods are unsuited.

The offshore engineering examples discussed below illustrate three market pulls that have supported recent penetrometer equipment advances.

3.2.2 High temperature high pressure pipelines

The emergence of high temperature high pressure (HTHP) seabed pipelines around 20 years ago led to an increased focus on near-surface seabed strength. Engineered lateral buckling schemes for HTHP pipelines require reliable estimates of the embedment and the subsequent axial and lateral soil resistance (Bruton et al. 2007).

This market led to innovations such as miniature box-core-based CPT, T-bar and ball penetrometer systems (Low & Randolph 2010, Puech et al. 2010) and the shallow penetrometer systems (Yan et al. 2010, Boscardin & DeGroot 2015, White et al. 2017). These devices are designed to characterize only the shallowest half metre or so of the seafloor, by conducting tests in box core samples. There is a particular emphasis on remoulded properties, which control pipeline embedment, and interface strength, which controls axial pipeline friction.

3.2.3 Subsea power cables

The offshore wind industry has created a major market for cable route surveys, which has

similarities with the on-bottom pipeline survey market. However, a particular feature of subsea cable design is the importance of thermal properties. The thermal insulation created by the trench backfill can have a strong influence on the cable rating and operating temperature (Dix et al. 2017).

A response to this market has been the development of new in situ thermal tests, that can be integrated within a conventional CPT-based route survey. Some of these devices (e.g. Figure 5e) use the violin bow-type design of thermal probe that has been used by the earth science community for studying heat flow from the deep earth into the oceans (e.g. Lister 1979). Once again – the idea is not new, but the concept has recently entered geotechnical survey practice in response to a market pull.

Another approach to a thermal measurement is the passive thermal CPT (T-CPT) system, which is easily added to a standard cone test. In this test the decay of the heat developed by the penetration process is used to infer the thermal conductivity. This simplicity has allowed the T-CPT to rapidly enter geotechnical survey practice.

A further driver for adoption of the T-CPT is the evidence that thermal conductivity measurements from samples are biased compared to in situ data. A review of hundreds of in situ and ex situ thermal conductivity measurements by Vardon et al. (2019) showed that the thermal conductivity measured in laboratory tests is consistently lower than in situ data. This is attributed to slight de-saturation and a reduction in density of the samples (Vardon et al. 2019).

3.2.4 *Project acceleration: Reliance on in situ data*

A further example of a market pull that is motivating advances in CPT equipment, is the need to accelerate the maturation of projects, from planning to operation. This is linked to the energy transition, with wind projects aiming for faster progression from planning or final investment decision (FID) to the beginning of energy production, compared to oil and gas projects.

As an illustration, offshore wind projects in Europe typically take 7-10 years to progress from initial planning to operation and in China the process is compressed into 2-4 years. In the past, major oil and gas projects often had a longer timeline than European offshore wind, and also a smaller footprint to survey.

The rest of the world needs to approach Chinese rates of project maturation if net zero targets are to be met. DNV (2021) predict a global wind capacity of 5.9 TW by 2050, which will require around a quarter of a million turbines to be installed in the next 30 years, with the annual rate of installation increasing by a factor of 10 compared to now.

One method to compress the project timeline is to increase the use of in situ geotechnical test data for determining design parameters. This can eliminate or reduce the importance of the period required for

samples to reach the testing laboratories, be tested, and an interpreted set of design parameters be generated.

If in situ testing takes a larger role in determining design parameters, then there is a strong market pull for new types of in situ test, or extensions of the CPT, which can explore the detailed aspects of soil response that are conventionally determined from laboratory testing – such as cyclic behaviour, and stiffness parameters.

This market pull has created the driver for cyclic and small strain components of CPT-type tests such as the seismic CPT, the VCPT, the cone-pressurimeter and the locally-actuated lateral and torsional sleeves. The ability to determine thermal properties in situ, rather than relying on laboratory tests, also allows compression of the project timeline.

3.3 *Are equipment advances led by new technology?*

A final driver of equipment advances is the emergence of new technologies across mechanical and electronic engineering, as well as new types of vehicle. Over the past twenty years, the emergence of low cost sensors, data acquisition systems, actuators and communication technologies have permitted new types of sensor and testing protocol to be devised. Miniaturization has allowed additional equipment to be packed into the shaft of the CPT.

Also, the low cost and wide availability of mechatronic devices has opened up and democratized the process of equipment development. Small companies or individuals can now prototype sensors and devices that could previously only be produced and trialled by major organisations.

Massarch (2014), in his comprehensive review of the CPT, past and present, discussed a future in which sensors are so cheap that the device can be left in situ after the penetration test. This idea opens up the possibility that penetration tests are not a snapshot of the ground condition at a moment in time, but implant a sensor in the ground, that continues to operate, relaying back the condition of the ground through the life of the surrounding infrastructure. The boundary between in situ testing and field monitoring thus becomes blurred.

Automation technology also means that the execution of a CPT is becoming an ‘office job’. In this conference, Storteboom et al. (2022b) describe a new hybrid CPT truck that operates using battery when on site. A carousel system automatically connects the CPT rods so the operator has minimal mechanical activities to perform. Storteboom et al. (2022b) report that “*the workplace of the CPT operator is turned into an office environment*”. They describe an improvement in working conditions, reduced absenteeism and higher productivity.

A final example of emerging technology is the digital environment used to hold and process CPT data, and the integration of this into the geotechnical design workflow and the digital model of the resulting construction. The geotechnical survey industry in the UK was an early adopter of standardized data formats, through the AGS standard, which is named after the Association of Geotechnical and Geoenvironmental Specialists, who are custodians of the standard. Version 1 of this data format was released in 1992, and version 4.1.1 is the current edition (AGS 2022).

The AGS format is widely used in the UK and worldwide, and improves the workflow and assurance of geotechnical data, as well as simplifying the sharing and public release of geotechnical data. For example, the Crown Estate (England and Wales) requires wind farm operators to release survey data to the Marine Data Exchange portal. This data commonly takes the form of reports, but for geotechnical in situ testing the data is often held in the AGS format, where it can be rapidly assimilated into other software for wider use.

A common software platform for storing and interpreting in situ data is gINT, which is owned by the Bentley software house. Bentley also own PLAXIS, and the two programs have growing interface capabilities. A consequence of this connectivity from raw CPT data to geotechnical numerical modelling software is that there is a single digital workflow from site measurements to design output.

This connectivity can be used to allow more rapid progression from survey to construction. It can also eliminate the human attention given to geotechnical data that is often held dear in our discipline. For example, the progression of data through factual reporting, interpretive reporting and ground model development involves detailed evaluation and thought processes that support geotechnical risk analysis, as well as design parameter choices.

On the other hand, we could take the counter view, which is that a smooth processing pipeline from in situ data towards design will liberate geotechnical specialists. We can spend more time assessing the information created by the data, rather than passing data between spreadsheets and different types of software.

3.4 *Equipment advances: Does standardisation help or hinder?*

Standardisation of the CPT emerged in the 1970s and has more recently been set out in various international standards produced by the ISO, CEN and others (e.g. ISO 2012, 2014).

Many advances in CPT equipment remain ‘within standard’, such as methods for efficient deployment of the rod string or improvements to load cells or data transfer. However, many advances in penetrometer equipment are ‘non-standard’,

which creates difficulties when clients wish to assure data quality or set contract specifications and develop a competitive supplier market.

Two key challenges are therefore faced by developers of any new equipment that deviates from the standards:

1. *The need for a specification:* a test specification is required to define and allow assurance that any testing is conducted according to an appropriate procedure, agreed between client and contractor. A hierarchy of specification types, listed by the strength of their basis, might be: (i) a publication by the system developers, (ii) a guideline emerging from a Joint Industry Project, or developed with a verification agency, (iii) a guideline developed more openly by an industry technical committee or association (e.g. CFMS, CIRIA and the ISSMFE have supported guidelines on in situ testing) (iv) a recommended practice or standard produced by an international standards body (e.g. ISO, CEN, API).

In practice, procedures generally evolve upwards through this hierarchy over a period of perhaps a decade – as seen by the procedures adopted for flow-round penetrometers that have now reached ISO 19901-8.

2. *The need for market competition.* A second challenge facing proponents of an advance in penetrometer equipment is that new test types will rarely be specified by clients if there is only one supplier. This places developers of new equipment in the difficult position of requiring a competitor to come into existence in order for demand to be created. This situation does not apply to equipment advances that are ‘within standard’, since the specification is unaffected.

However, using the example of the shallow penetrometers for a final time, research funding for the RIGSS JIP from owners/operators was conditional on more than one contractor also being part of the project, in order to ensure that a competitive supply chain could emerge.

The heading for this final sub-section was perhaps a little frivolous. Standards are invariably beneficial for industry and should not hinder innovation. However, innovators of new ‘non-standard’ in situ test equipment need to be prepared to address the two challenges set out above. Developing reliable equipment that offers a technical benefit over standard test methods will not necessarily lead to industry adoption. Time and effort must be spent ‘socialising’ the technology among the community of practice, for example at events like this conference. It is then necessary to develop open guidance and specifications for execution and interpretation of non-standard tests. Finally, it might even be necessary to support open competition in the marketplace to avoid the technology being from a sole source.

4 CONCLUDING COMMENTS

The basic configuration of the cone penetrometer test (CPT) has remained constant for around 50 years. This discussion has reviewed recent advances in penetrometer equipment presented in this conference and elsewhere, considering separately the (i) delivery, (ii) deployment, (iii) sensing and (iv) motion aspects of the penetrometer test.

It is evident that new innovations in instrumentation, electronics and mechanical engineering have created a vast range of variations on the conventional CPT equipment. In some cases these advances provide a small but widespread improvement in penetrometer testing, such as improved rod connection systems, hybrid-powered CPT trucks and better saturation and calibration systems. In other cases the advances are more ambitious, aiming to incorporate new sensors and motion systems within a penetrometer, to allow new types of measurement to be incorporated in the testing process.

The result is a dispersion of practice: the majority of civil engineers base their ground characterization on a durable 1970s technology, updated with automation and improved data quality, while a minority are enjoying exploration of non-standard innovations – with mixed levels of impact.

This discussion, and the wider conference, is an opportunity to reflect, learn and debate how we will characterize the ground in another 50 years.

ACKNOWLEDGEMENTS

I am grateful for the kind invitation by the CPT'22 organising committee to present this discussion paper. In relation to the shallow penetrometer research, I acknowledge the support for that work from the RIGSS JIP (Fugro, Total, Woodside and Shell), as well as the collaboration with Dr Sam Stanier, Dr Henning Mohr, Prof. Mark Randolph and Dr Mark Schneider.

This review has also been supported by the EPSRC Offshore Renewable Energy Supergrid Hub (grant EP/S000747/1) and by the EPSRC grant EP/W006235/1 (ROBOCONE – intelligent robotics for next generation ground investigation and design – PI Dr Andrea Diambra). All opinions and any mistakes or misrepresentations are my own.

REFERENCES

AGS (2022) Electronic transfer of geotechnical and geo-environmental data, AGS4 Edition 4.1.1 – March 2022 Publ. Association of Geotechnical and Geoenvironmental Specialists

Al-Sammarraie D., Kreiter S., Kluger M.O., Goodarzi M. & Morz T. (2022) VCPT: an in situ soil investigation method to validate the vibratory pile-soil interaction models. Proc. 5th Int. Symposium on Cone Penetration Testing (CPT'22). Bologna. (this conference).

Al-Sammarraie D., Kreiter S., Stahler M.O., Goodarzi M. & Morz T. (2018) New vibratory cone penetration device for in-situ measurement of cyclic softening. International Symposium on Cone Penetration Testing, 2018.

Apfelbeck M., Kuß S., Rebele B., Schäfer B. (2011) A systematic approach to reliably characterize soils based on Bevameter testing. Journal of Terramechanics, 48(5):360–371

Baez V.M., Shah A., Akinwande S., Jafari N.H. & Becker A.T. (2020) Assessment of soil strength using a robotically deployed and retrieved penetrometer. IEEE/RSJ International Conference on Intelligent Robots and Systems (IROS) pp. 7324–7329, doi: 10.1109/IROS45743.2020.9341424.

Bekker, M.G. (1969) Introduction to Terrain-Vehicle Systems. University of Michigan Press, Ann Arbor, Mich.

Bellotti, R., Ghionna, V., Jamiolkowski, M., Robertson, P. K. & Peterson R.W. (1989) Interpretation of moduli from self-boring pressuremeter tests in sand. Géotechnique 39(2):269–292.

Boggess, R. and Robertson, P.K. (2010) CPT for soft sediments and deepwater investigations. International Symposium on Cone Penetration Testing, CPT'10. 2:127–136.

Bolton, M. D. & Whittle, R. W. (1999) A non-linear elastic/perfectly plastic analysis for plane strain undrained expansion tests. Géotechnique, 49(1):133–141.

Boscardin A.G. & Degroot D.J. (2015) Evaluation of a toroid for model pipeline testing of very soft offshore box core samples Frontiers in Offshore Geotechnics III – Proc. 3rd Int. Symp. on Frontiers in Offshore Geotech., ISFOG 2015. 363–368.

Briaud, J. L., Riner, K. B. & Ohya, S. (1984) Cyclic pressuremeter tests for cyclic lateral loads. Offshore Technology Conference, Houston. doi:10.4043/4678-MS

Broms, B.B. & Flodin, N. (1988) History of soil penetration testing. International symposium on penetration testing, ISOPT 1, 1:157–220.

Bruton D., Carr M. & White D.J. (2007) The influence of pipe-soil interaction on lateral buckling and walking of pipelines: the SAFEBUCK JIP. Proc. 6th Int. Conf. on Offshore Site Investigation and Geotechnics, London. 133–150.

Chow S.H., O'Loughlin C.D., White D.J. & Randolph M.F. (2017) An extended interpretation of the free-fall piezocone test in clay. Géotechnique. 67(12):1090–1103

Chow S.H., O'Loughlin C.D., Zhou Z., White D.J. & Randolph M.F. (2020). Penetrometer testing in a carbonate silt to explore changes in soil strength. Géotechnique 70(12):1160–1173

DeJong, J.T. and Frost, J.D. (2002). A multi-friction sleeve attachment for the cone penetrometer. ASTM Geotechnical Testing Journal, 25(2):111–127

Diambra A., Ciavaglia F., Harman A., Dimelow C., Carey J. & Nash D. F. T. (2014). Performance of cyclic cone penetration tests in chalk. Geotechnique Letters, 4 (3):230–237

Diambra A., Creasey J., Leonet J., Conn A., Ibraim E., Mylonakis G., White D.J., Cerfontaine B., Gourvenec S.M. & Igoe D. (2022) Concept design of a new CPT module for direct in situ measurement of p-y soil responses. Proc. 5th Int. Symposium on Cone Penetration Testing (CPT'22). Bologna. (this conference).

Dienstmann, G.; Schnaid, F.; Maghous, S.; Dejong, J.T. (2017). Piezocone penetration rate effects in transient

- gold tailings. *Journal of Geotechnical and Geoenvironmental Engineering*, ASCE. 04017116-1
- Dix, J.K., Hughes, T.J., Emeana, C.J., Pilgrim, J.A., Henstock, T.J., Gernon T.M., Thompson, C.E.L. & Vardy, M.E., (2017) Substrate controls on the life-time performance of marine HV cables. *Proc. 8th Int. Conf. Offshore Site Investigations and Geotechnics*. Society for Underwater Technology. 88–108.
- DNV (2021) Energy transition outlook. DNV, Hovik.
- Edmunds J. (2014) Gaining traction. *Offshore Engineer Magazine*. 3 February 2014.
- Edwards M.B., Dewoolkar M.M., Huston D.R. & Creager C. (2017) Bevameter testing on simulant Fillite for planetary rover mobility applications. *J. Terramechanics*, 70:13–26
- Ferreira, R.S. & Robertson, P.K. (1992) Interpretation of undrained self-boring pressuremeter test results incorporating unloading. *Can. Geotechnical J.*, 29:918–928.
- Frost J.D. & Martinez A. (2013) Multi-sleeve axial-torsional-piezo friction penetration system for sub-surface characterization. *Proc. 18th Int. Conf. on Soil Mech. and Geotech. Eng. (18th ICSMGE)*. Paris, France, 1:527–530.
- Geise, J.M. & Kolk, H.J. (1983). The use of submersibles for geotechnical investigations. *Proc. Submarine Technology, The Design and Operation of Underwater Vehicles*, Paper 7.3, London, Society for Underwater Technology.
- Gourvenec S.M. (2020) Whole-life geotechnical design: What is it? What's it for? So what? And what next?: Keynote. In *Proc. 4th Int. Symp. on Frontiers in Offshore Geotechnics*. Deep Foundations Institute. 206–246.
- Gundersen A.S., Carotenuto P., Lunne T., Walta A. & Sparrevik P.M. (2019) Field verification tests of the newly developed flow cone tool—In-situ measurements of hydraulic soil properties. *AIMS Geosciences*, 5 (4):784–803.
- Gundersen A.S., Lunne T., Stelzer R., Blaker O, Tucker G. W. & Krogh L. (2022) Flow cone – new CPTU add-on module trialed in Halden silt. *Proc. 5th Int. Symposium on Cone Penetration Testing (CPT'22)*. Bologna. (this conference).
- Hebeler, G.L., Frost, D.J., Schneider, J.A. & Lehane, B.M. (2005). Cyclic friction piezocone tests for offshore applications. *Int. Symp. on Frontiers in Offshore Geotech.* 967–972.
- Hebeler, G.L., Martinez A. & Frost J.D. (2018) Interface response-based soil classification system. *Canadian Geotech. J.*, 55(12):1795–1811.
- Houlsby, G.T. & Withers, N.J. (1988) Analysis of the cone pressuremeter test in clay. *Géotechnique*, 38 (4):575–587.
- House, A.R., Oliveira, J.R.M. and Randolph, M.F. (2001) Evaluating the coefficient of consolidation using penetration tests. *Int. J. Physical Modelling in Geotechnics*, 1 (3): 17–26.
- Hvorslev, M. J. (1951) Time lag and soil permeability in ground-water observations. *US Army Corps of Engineers, Waterways Experiment Station Bulletin No. 36*, Mississippi, USA.
- Isaev O.N., Sharafutdinov R.F. & Zakatov D.S. (2022) Determination of natural stress state parameters for clay soils by using 3LSU-CPTU penetrometer. *Proc. 5th Int. Symposium on Cone Penetration Testing (CPT'22)*. Bologna. (this conference).
- ISO (2012). ISO 22476-1:2012: Geotechnical investigation and testing - Field testing - Part 1: Electrical cone and piezocone penetration test. International Standardisation Organisation
- ISO (2014). ISO 19901-8:2014: Petroleum and natural gas industries - Specific requirements for offshore structures - Part 8: Marine soil investigations. International Standardisation Organisation [a 2022 edition is currently under international ballot]
- Jeanjean, P., Spikula, D. & Young, A. (2012). Technical vetting of free-fall cone penetrometer. *Proc. Int. Conf. on Offshore Site Investigation and Geotechnics*, London, UK. 179–186
- Jefferies M.G. & Funegard E. (1983). Cone penetration testing in the Beaufort Sea. *Proc Conference on Geotechnical Practice in Offshore Eng.*, Austin, Texas, ASCE, 220–243
- Jorat, M. E., Mörz, T., Schunn, W., Kreiter, S., Moon, V., & de Lange, W. (2014). Geotechnical Offshore Seabed Tool (GOST): a new cone penetrometer. *Proc. 3rd International Symposium on Cone Penetration testing*. 207–215
- Kang H., Kwon O., Shin C., Seo J. & Jang I. (2022). Development of free fall cone penetration testing system. *Proc. 5th Int. Symposium on Cone Penetration Testing (CPT'22)*. Bologna. (this conference).
- Kelleher, P. J. & Randolph, M. F. (2005) Seabed geotechnical characterisation with a ball penetrometer deployed from the Portable Remotely Operated Drill. *Int. Symp. on Frontiers in Offshore Geotechnics I*, Perth, Australia. 365–371
- Kim, J.T., Im, D.U., Choi, H.J., Oh, J.W., Park, Y.J., (2021) Development and performance evaluation of a bevameter for measuring soil strength. *Sensors* 21, 1541
- Krömer O., Scharringhausen M., Fittock M., Tsakyridis G., Wippermann T., Witte L., Grott M., Knollenberg J., Spohn T., Krause C., Hudson T.L., Lichtenheldt R., Grygorczuk J., & Wisniewski L. (2019) Design details of the HP³ mole onboard the InSight mission. *Acta Astronautica*. 164:152–167
- Lister, C.R.B., (1979) The pulse-probe method of conductivity measurement, *Geophys. J. Royal Astr. Soc.*, 57:451–461
- Lopes dos Santos, A. & Dupla, J-C & Canou, J & Droniuc, N. (2019). Laboratory validation of an innovative mono-cell pressuremeter probe: test procedures and first results. *Proc. XVII European Conference on Soil Mechanics and Geotechnical Engineering*. Reykjavik, Iceland. 8pp.
- Lopes dos Santos A. (2020). Determination of soil shear modulus at low strain level using an innovative pressuremeter probe: Application to cyclic pile design. Dissertation presented for the degree of Doctor of Université Paris-Est.
- Low, H.E. & Randolph, M.F. (2010). Strength measurement for near-seabed surface soft soil using manually operated miniature full-flow penetrometer. *ASCE Journal of Geotechnical and Geoenvironmental Engineering* 136:1565–1573.
- Lunne, T., Robertson, P.K. & Powell, J.J.M. (1997). *Cone Penetration Testing in Geotechnical Practice*, Blackie Academic/London, Routledge, New York: 312 p.
- Lunne, T. (2012). The CPT in offshore investigations – a historic perspective. *Geomechanics and Geoengineering: An International Journal*. 2(2):75–101.
- Lunne T., Ghanekar R., Tucker G.W., Santos R. & Krogh L. (2022) The revival of multiple pore pressure

- measurements in the Cone Penetration Test. Proc. 5th Int. Symposium on Cone Penetration Testing (CPT'22). Bologna. (this conference).
- Martinez A., DeJong, J.T., Jaeger, R. & Khosravi A. (2020). Evaluation of self-penetration potential of a bio-inspired site characterization probe by cavity expansion analysis. *Canadian Geotech. J.*, 57(5):706–716.
- Massarsch K.R. (2014) Cone Penetration Testing – A Historic Perspective. Proc. 3rd International Symposium on Cone Penetration Testing. 97–134
- McConnell A. & Wassenaar E. (2022) An innovative new 3 MPa CPT – to detect and measure very small f_s values. Proc. 5th Int. Symposium on Cone Penetration Testing (CPT'22). Bologna. (this conference).
- McGillivray, A., Casey, T., Mayne, P. W. & Schneider, J. A. (2000) An electro-vibrocone for site-specific evaluation of soil liquefaction potential. Proc. Geo-Denver 2000, Innovations and Applications in Geotechnical Site Characterization.
- Meunier, J., Sultan, N., Jegou, P. & Harmegnies, F. (2004) First tests of Penfeld: a new seabed penetrometer. Proc. 14th Int. Offshore & Polar Eng. Conf., Toulon, France, 338–345
- Mo, P-Q, Gao, X-W, Yang, W, Yu, H-S. (2020) A cavity expansion-based solution for interpretation of CPTu data in soils under partially drained conditions. *Int J Numer Anal Methods Geomech.* 44:1053–1076.
- Naclerio, N.D., Karsai, A., Murray-Cooper M., Ozkan-Aydin Y., Aydin E., Goldman D.I. & Hawkes E.W. (2021) Controlling subterranean forces enables a fast, steerable, burrowing soft robot. *Science Robotics* 6:55 eabe2922.
- Olmedo, N.A. & Lipsett, M.G. (2016) Design and field experimentation of a robotic system for tailings characterization. *J. Unmanned Vehicle Systems* 4 (3):169–192.
- Peuchen J., Looijens P. & Stark N. (2017) Offshore characterisation of extremely soft sediments by free fall penetrometers. Proc. Int. Conf. on Offshore Site Investigation and Geotechnics. Society for Underwater Technology. 370–377
- Power P. & Geise J. (1994) Offshore soil investigation techniques and equipment for the next century. Proc. of the Int. Conf. on Behaviour of Offshore Structures, BOSS'94, Boston, 1:97–109
- Puech, A., Orcozo-Calderón, M. and Foray, P. (2010). Mini T-bar testing at shallow penetration. Int. Symp. on Frontiers in Offshore Geotechnics II, Perth, Australia. 305–310.
- Randolph, M.F. (2004). Characterisation of soft sediments for offshore applications. 2nd Int. Conf. on Site Characterization, Rotterdam, The Netherlands, 1:209–232.
- Randolph, M.F., Stanier, S.A., O'Loughlin, C.D., Chow, S. H., Bienen, B., Doherty, J.P., Mohr, H., Ragni, R., Schneider M.A., White D.J., Schneider J.A. (2018) Penetrometer equipment and testing techniques for offshore design of foundations, anchors and pipelines. Invited keynote Lecture. Proc. 4th Int. Symp. on Cone Penetration Testing, CPT '18. Delft. 3–24.
- Randolph, M. F., and Hope, S. N. (2004) Effect of cone velocity on cone resistance and excess pore pressure. Proc. Int. Symp. On Engineering Practice and Performance of Soft Deposits, Yodogawa Kogisha Co. Ltd., Osaka, Japan, 147–152.
- Ratnam S., Soga K., Mair R.J., Whittle R.W. & Tedd P. (2001) Permeability measurement using the self-boring pressuremeter. Proc. Int. Conf. on In Situ Measurement of Soil Properties and Case Histories, Bali, Indonesia. 667–672.
- Rocchi I., Tonni L., Gottardi G. & Marcolongo M. (2022) Experimental procedure for checking the saturation degree of piezocone tips. Proc. 5th Int. Symposium on Cone Penetration Testing (CPT'22). Bologna. (this conference).
- Schneider J.A., Lehane B.M. & Schnaid F. (2007) Velocity effects on piezocone measurements in normally and over consolidated clays. *International Journal of Physical Modelling in Geotechnics.* 7:23–34
- Scholz C., Göttinger M., Hinck S., Möller K. & Ruckelshausen A. (2014) Automatic soil penetrometer measurements and GIS-based documentation with the autonomous field robot platform BoniRob. 12th Int. Conf. of Precision Agriculture.
- Shonberg A., Harte M., Tucker G. Rattley M. & Gibbs P. (2019) Innovative use of the CPT to assess the in situ degradation of an offshore overconsolidated clay. Proc. Offshore Technology Conference. Paper OTC29414.
- Silva, M. F., White, D. J., and Bolton, M. D. (2006) An analytical study of the effect of penetration rate on piezocone tests in clays. *Int. J. Numerical & Analytical Methods in Geomechanics* 30(6):501–527.
- Spohn T., Grott M., Smrekar S.E., Knollenberg J., Hudson T. L., Krause C., Müller N., Jänchen J., Börner A., Wippermann T., Krömer O., Lichtenheldt R., Wisniewski L., Grygorczuk J., Fittock M., Rheershemius S., Sprowitz T., Kopp, E., Walter I., Plesa A. C., Breuer D. & Morgan, P. (2018) The Heat Flow and Physical Properties Package (HP3) for the InSight mission. *Space. Sci. Rev.*, 214, 96
- Spohn T., Hudson T.L., Witte L., Wippermann T., Wisniewski L., Kediziora B., Vrettos C., Lorenz R.D., Golombek M., Lichtenfeld R., Grott M., Knollenberg J., Krause C., Fantinati C., Nagihara S., & Grygorczuk J. (2021) The InSight HP³ mole on Mars: Lessons learned from attempts to penetrate to depth in the Martian soil. Submitted to *Advances in Space Research*. On arXiv, ref. arXiv:2112.03234
- Stark N., Hanff H., & Kopf A. (2009) Nimrod: a tool for rapid geotechnical characterization of surface sediments. *Sea Technology.* 50(4):2230–2235.
- Stark N. (2016) Geotechnical site investigation in energetic nearshore zones: opportunities & challenges. Keynote lecture. Int. Conference on Geotechnical and Geophysical Site Characterisation 5. 69–80
- Steiner A., Kopf A.J., L'Hereux J-S., Kreiter S. Stegmann S., Hafidason H. & Moerz T. (2014). In situ dynamic piezocone tests in natural clayey soils – a reappraisal of strain-rate corrections. *Canadian Geotechnical Journal.* 51(3): 272–288.
- Stephan S., Kaul N., & Villinger, H. (2015). Validation of impact penetrometer data by cone penetration testing and shallow seismic data within the regional geology of the southern north sea. *Geo-Marine Letters.* 35(3): 203–219.
- Storteboom O., Woollard M. & Allen B. (2022a) Increased safety and productivity for seabed Cone Penetration Test using the SingleTwist™ with ROSON. Proc. 5th Int. Symposium on Cone Penetration Testing (CPT'22). Bologna. (this conference).
- Storteboom O., Woollard M. & Ooms B. (2022b) Sustainability in CPT practice: hybrid CPT track-truck. Proc. 5th Int. Symposium on Cone Penetration Testing (CPT'22). Bologna. (this conference).

- Suzuki Y., & Lehane B.M. (2015) Cone penetration at variable rates in kaolin–sand mixtures. *International Journal of Physical Modelling in Geotechnics* 15(4): 209–219.
- Tao J., Huang S., Tang Y. (2020) SBOR: A minimalistic soft self-burrowing-out robot inspired by razor clams. *Bioinspiration and Biomimetics*. 15, 055003.
- Tarantino A., Capotosto, Bottaro F., Bellio M. & Gallipoli D. (2022) Tensiocone: a cone penetrometer with the facility to measure negative pore-water pressure. Proc. 5th Int. Symposium on Cone Penetration Testing (CPT'22). Bologna. (this conference).
- Vardon P.J., Baltoukas D. & Peuchen, J. (2018) Thermal Cone Penetration Test (T-CPT). In Proc. 4th International Symposium on Cone Penetration Testing. 649–655.
- Vardon P.J., Baltoukas D. & Peuchen J. (2019) Interpreting and validating the thermal cone penetration test (T-CPT). *Géotechnique*, 69(7): 580–592.
- Vinco G. & Sabetto M. (2022) New portable pressiocone system for carrying out CPT & FDP tests. Proc. 5th Int. Symposium on Cone Penetration Testing (CPT'22). Bologna. (this conference).
- Watson, P.G. & Randolph, M.F. (1998). Torsional vane and plate load tests. Proc. International Conference Centrifuge '98, Rotterdam, Netherlands. 1: 167–173.
- White D.J. & Gaudin C. (2008) Simulation of seabed pipe-soil interaction using geotechnical centrifuge modelling. Proc. 1st Asia-Pacific Deep Offshore Technology Conference, Perth, Dec 2008. 28pp.
- White D.J., Stanier S.A., Schneider M., O'Loughlin C.D., Chow S.H., Randolph M.F., Draper S.D., Mohr H., Morton J.P., Peuchen, J., Chow F.C., Fearon R. & Roux A. (2017) Remote intelligent geotechnical seabed surveys – technology emerging from the RIGSS JIP. Proc. Int. Conf. Offshore Site Investigation & Geotechnics. SUT, London. 1214–1222
- White D.J., O'Loughlin C.D., Chow S.H. & Stark N. (2018) Interpretation of free fall penetrometer tests in sands: An approach to determining the equivalent static resistance. Proc. 4th Int. Symp. on Cone Penetration Testing. 695–701.
- White D.J., Stanier S.A. & Mohr H. (2022) Characterisation of near-surface sediments using a blend of vertical and shallow rotational penetrometers. Proc. 5th Int. Symposium on Cone Penetration Testing (CPT'22). Bologna. (this conference).
- Whittle R., & Liu L. (2013). A method for describing the stress and strain dependency of stiffness in sand. Proc. 18th Int. Conf. on Soil Mechanics and Geotechnical Eng. Paris.
- Whittle R., Palix E., & Donaghy D. (2017). The influence of insertion process on determining the stiffness characteristics of chalk, using pre-bored, self-bored and pushed pressuremeters. Proc. 8th Int. Conf. on Offshore Site Investigation & Geotech. London Soc. for Underwater Tech. 308–315.
- Winter A.G., Deits R.L.H., Dorsch D.S., Slocum A.H. & Hosoi A.E. (2014) Razor clam to roboclam: Burrowing drag reduction mechanisms and their robotic adaptation. *Bioinspiration and Biomimetics*. 9, 036009.
- Withers N.J., Howie J., Hughes J.M.O. & Robertson P.K. (1989) Performance and analysis of cone pressuremeter tests in sands. *Géotechnique* 39(3): 433–454
- Wippermann T., Hudson T.L., Spohn T., Witte L., Scharringhausen M., Tsakyridis G., Fittock M., Krömer O., Hense S., Grott M., Knollenberg J. & Lichtenheldt R. (2020) Penetration and performance testing of the HP3 Mole for the InSight Mars mission. *Planetary Space Science*. 181, 104870
- Wong J.Y. (2010) Theory of ground vehicles. 4th Edition. Wiley, New York.
- Yan Y., White D.J. & Randolph M.F. (2010) Investigations into novel shallow penetrometers for fine-grained soils. Proc. 2nd Int. Symp. on Frontiers in Offshore Geotechnics. Perth. 321–326
- Yan Y. (2013) Novel methods for characterising pipe-soil interaction forces in situ in deep water. PhD thesis, University of Western Australia
- Yetginer T.I., Bodtker S., Rose M., Lunne T., Meyer V. & Duffy C. (2022) Development of an enhanced CPT system for Dogger Bank. Proc. 5th Int. Symposium on Cone Penetration Testing (CPT'22). Bologna. (this conference).
- Zhou Z., O'Loughlin C.D. & White D.J. (2020) The changing strength of carbonate silt: Parallel penetrometer and foundation tests with cyclic loading and reconsolidation periods. *Canadian Geotechnical Journal* 57 (11):1664–1683.

Non-deterministic interpretation and applications of CPT testing data

M. Uzielli

*Department of Civil and Environmental Engineering, University of Florence, Italy
Georisk Engineering S.r.l., Florence, Italy*

ABSTRACT: The evolution of geotechnical design codes towards reliability-based and probabilistic concepts, the growing global awareness towards risk management for engineered and natural systems, and the global digital transition are steering geotechnical research and practice towards non-deterministic and data-centric approaches to geotechnical characterization and design. The quasi-continuity and high repeatability of CPT measurements inherently endow this testing method with a central role in the momentous shift in paradigm. This paper contributes principles and selected examples which exemplify the nature and use of non-deterministic CPT-based methods for geotechnical site characterization, design, and geohazards risk management. Current cautions and limitations to the development, dissemination, and implementation of these methods are arguably surmountable and provide stimulating opportunities for a collective effort on the part of the CPT community to meet the evolving requirements and trends in geotechnical practice, research, and education.

...ἔοικα γοῦν τούτου γε συμκρῶ τιμι αὐτῷ τούτῳ σοφώτερος εἶναι, ὅτι ἂ μὴ οἶδα οὐδὲ οἶομαι εἰδέναι.

"... I seem, then, in just this little thing to be wiser than this man at any rate, that what I do not know I do not think I know either."

- Plato, Apology

1 LEVERAGING THE UNAVOIDABLE

"As far as laws of mathematics refer to reality, they are not certain; and as far as they are certain, they do not refer to reality."

- Albert Einstein, "Geometry and experience" (1921)

The variability in testing data and derived design parameters is a distinctive trait of the geotechnical discipline with respect to other engineering disciplines which deal with artificial materials. Measured properties effectively vary due to the natural heterogeneity and complexity of soils, which are generated and continuously modified by natural geologic and geomorphologic processes. In-situ effects due to stress state and stress history lead to spatially variable measurements even for compositionally homogeneous deposits. The spatial and temporal variability of geotechnical properties can be especially appreciated in the results of geophysical testing and geotechnical in-situ testing, which involve larger volumes of soils than laboratory tests. Moreover, the same test conducted at the same spatial location may produce different results due to the temporal variability of the natural environment (e.g., seasonal fluctuations in water content,

groundwater level, etc.) and to imperfect measurement capability. Some degree of inaccuracy and imprecision is always present in testing operations.

The variability in measured values thus stems from inherent soil variability and measurement uncertainty. When transposed in quantitative engineering analyses, these variabilities result in uncertainty. When representative values are calculated from measured data (e.g., the mean value over a depth interval), additional statistical estimation uncertainty arises from the limited number of values used to calculate these values. Moreover, when testing data are used to calculate engineering design parameters, a further source of uncertainty is introduced due to transformation models which are always approximate and imperfect models of the physical world.

Given the evident existence of considerable uncertainties in geotechnical engineering, the question arises as to "whether" and "how" to address them. The complete neglect of uncertainty is unacceptable from both the ethical and technical viewpoints. Failing to acknowledge the existence and relevance of uncertainty would imply that basic geotechnical notions and geotechnical code prescriptions are not adhered to, since these do address uncertainty (either implicitly or explicitly, as discussed later). This paper focuses on how the geotechnical discipline has evolved from the primordial "deterministic" paradigm, in which the modeling of uncertainty is implicit, to the currently trending "non-deterministic" paradigm, in which uncertainties are modelled, processed, and reported explicitly, and is continuing to evolve towards a "data-centric"

mode which fosters the synergy between engineering judgment and the increased availability of data, facilitating the treatment of uncertainty in characterization and design.

Through a specific focus on cone penetration (CPT) testing, this paper attempts to provide examples from research and case-study applications of the pivotal role of CPT testing in accompanying the geotechnical discipline towards an emerging non-deterministic and data-centric paradigm. Far from aiming to provide a structured theoretical treatment of non-deterministic and data-centric approaches and from contributing an exhaustive review of available examples, this contribution wishes to spark both an interest and the willingness, on the part of researchers and practitioners, to contribute proactively to the continued development, refinement, promotion, and dissemination of uncertainty-based and data-centric methods relying on CPT. Lastly, it aims to stimulate a constructive discussion focusing on how some current aspects requiring attention actually represent opportunities for the further refinement of methods for interpretation and use of CPT results in characterization and design.

While this paper advocates the increased use of non-deterministic, data-centric methods, it wishes to convey the awareness that such methods largely rest on the broad shoulders of the ingenious, pioneering deterministic methods which have laid the foundations of the geotechnical discipline, and which have nurtured its growth and evolution.

2 A HISTORY OF CHANGE

"The quest for certainty blocks the search for meaning. Uncertainty is the very condition to impel man to unfold his powers."

- Erich Fromm

The concepts of "determinism" and "non-determinism" stem from the fundamental question regarding the cause behind the occurrence of events, which has engaged philosophers in the East and West since ancient times. The deterministic approach prevailed over the stochastic approach in the technical community for many centuries. In the past decades, led by the high-energy physics community and facilitated by advancements in statistical-probability theory, enhanced data analysis capabilities, and increased computational power, the non-deterministic approach has replaced the deterministic one in many scientific and technical disciplines, and is progressively gaining momentum in others, including geotechnical engineering. Moreover, improved data collection technologies and computational power increasingly advocate the adoption of approaches making use of big data, which can further boost the performance of non-deterministic approaches. While a brief account of the transition from the deterministic to the non-deterministic and

data-centric paradigm is provided below, readers are referred to Baecher & Christian (2003), Phoon (2020) and Tang & Phoon (2021) for further insights into the philosophical, conceptual, and operational evolution of the geotechnical discipline.

2.1 *The past: The illusion of certainty*

Geotechnical engineering, as all engineering disciplines, originated and developed speaking the deterministic language, in which uncertainties are neither modelled, processed, nor reported explicitly, but are lumped together and represented implicitly in design methods, for instance through factors of safety. Numerous research contributions and real-world cases continue to provide new evidence that deterministic approaches are prone to overestimating or underestimating the performance of geotechnical systems because they are unable to parameterize the "real" complexity in soil-structure systems and the inevitable approximation in the models used to obtain design parameters from testing data. For instance, neglecting to model the spatial variability of design parameters prevents the identification of relevant failure modes (e.g., non-symmetric failure modes foreseeable even in presence of symmetric foundations and axial loading conditions, see Figure 1).

Overconservatism and unconservatism are both to be avoided: while the first entails the excessive use of resources to attain a target level of performance, the second, more seriously, fails to achieve performance and can result in failures which bring human and economic losses.

2.2 *The present: Embracing uncertainty*

In the context of engineering disciplines, the adjective "non-deterministic" refers to a broad range of methods and techniques relying most frequently – but not exclusively – on statistical and probability theory.

The development of ingenious approaches based on concepts such as reliability-based and performance-based analysis and design, along with increased computational power and efficiency, have allowed civil engineering to embark on the evolution from the primordial deterministic paradigm towards the non-deterministic one. The latter is characterized by the explicit consideration of uncertainty. The adoption of the non-deterministic approach allows to exploit powerful mathematical tools such as statistics and probability to model, process, and report uncertainties quantitatively.

While all engineering disciplines originated within the deterministic framework, geotechnical engineering has been delayed in initiating its transition, probably due to the greater inherent difficulty in quantifying and modelling its uncertainties. The geologic environment is made up of two- or even three-phase natural materials and is thus inherently

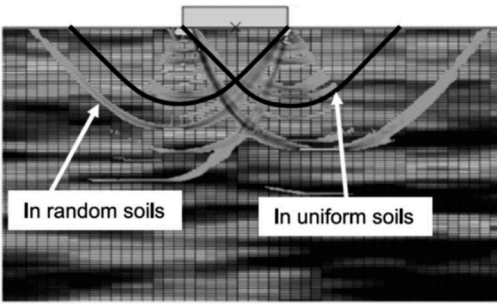


Figure 1. Comparison of failure modes for a surficial footing on uniform and spatially variable soils (from Li et al. 2014).

more complex and less easily characterized and modelled than structural materials such as steel, concrete, or timber. Nonetheless, in the past decades seminal research contributions and increased computational power have fostered and accelerated the development of non-deterministic methods.

The progressive shift towards non-deterministic methods is perhaps the most distinctive trait behind the development of evolutionary geotechnical design codes which are based on statistical, probabilistic, and performance-based concepts and which are gradually replacing the traditional deterministic design codes. Notable examples are Eurocode 7, Eurocode 8, the AASHTO (American Association of State Highway and Transportation Officials) LRFD Bridge Design Specifications, CHDBC (Canadian Highway Bridges Design Code), and JSHB (Japanese Specifications for Highway Bridges). The adoption of the non-deterministic paradigm enables the conceptual and formal harmonization between geotechnical and structural design, thus contributing to enhanced homogeneity and effectiveness in the design of soil-structure systems. Embracing non-determinism for geotechnical practice is no longer a choice in many parts of the world and is becoming less and less so at a global level. Despite the above, the transition to the non-deterministic paradigm is far from complete.

2.3 The future: Data meets knowledge

The momentous global process of digital transition which characterizes our time brings unprecedented possibilities. A new “data-centric” paradigm is emerging involving the synergy between the increased availability of data, evolutionary approaches such as machine learning, and expert engineering judgment (e.g., Phoon 2020). Such paradigm is extremely well-suited to synergize with non-deterministic approaches in defining the new identity of the geotechnical discipline.

Comprehensive compendia of literature estimates of uncertainties in soil parameters are available in the geotechnical literature (e.g., Uzielli et al. 2007; ISSMGE 2021). However, most estimates refer to

total uncertainty. Prior to the introduction of the data-centric paradigm, soil property statistics determined from total uncertainty analyses could only be applied reliably to the specific set of site conditions, measurement techniques and procedures, and correlation models for which the design soil properties were derived. The site-specificity of variability parameters had thus constituted a long-standing limitation and an obstacle to the diffusion of non-deterministic approaches. A main strength of the data-centric paradigm thus lies in the provision of quantitative probabilistic methods to allow the integration between site-specific data collected for a given project and “big indirect data”, i.e., existing data of any type collected from past stages of the same project or past projects at the same site, neighboring sites, or beyond.

The progressive surge of the data-centric paradigm is arguably entwined with the increasing centrality of the Bayesian approach in geotechnical engineering. Bayesian statistical analyses, differently from “frequentist” statistical analyses, provide analysts with the tools to update a “prior” probability model through the availability of new evidence (e.g., data observations) to obtain a “posterior” model. This approach is particularly suited for the geotechnical engineering discipline, in which it is often necessary to supplement site- and case-specific data (or aprioristic engineering judgment) with data from other sites, or to update characterization and design values as new data become available. The use of Bayesian methods in the data-centric approach promises to be useful in circumventing the limitations of site-specificity of geotechnical variability estimates, and in actually leveraging the availability of “indirect” data from other sites (see, e.g., the outcomes of Project DeepGeo at <http://yo-1.ct.nust.edu.tw/jge/files/articlefiles/v16i2202106031836319463.pdf>). The data-centric paradigm arguably provides the natural evolution of the geotechnical discipline, provided that researchers and practitioners are provided with the necessary simple knowledge required to correctly interact with data (Tang & Phoon 2021).

“Data-centric” and “non-deterministic” are not synonymous. While the data-centric approach does not imply *per se* resorting to non-deterministic methods, the former clearly fosters the latter. Increased data numerosity increases the applicability, meaningfulness, and reliability of non-deterministic techniques. Many statistical and probabilistic analyses, for instance, rely on the availability of sufficient quantities of data, and the level of confidence of their outputs increases with increasing numerosity of data samples. As the quantity and quality of data are expected to continue to increase over time, failing to proactively confer further centrality to the data-centric approach in both geotechnical research and practice would be nothing short of a wasted huge opportunity.

2.4 *In medio stat virtus*

In their illuminating treatment of geotechnical uncertainty, Baecher & Christian (2003) opined that a hybrid approach involving both deterministic and non-deterministic methods is “proper to the geotechnical engineering discipline”. This statement is increasingly and fully supported by a conspicuous, growing corpus of research and real-world applications, in which some aspects of a specific geotechnical analysis can be sufficiently well-described deterministically for practical purposes, while for others it is *convenient* to describe and model phenomena and variables as if they behaved, at least to some degree, in a random manner. A typical example is found in the quantitative modeling of spatial variability of soil properties, which is often pursued through the decomposition of data into a deterministic trend and a fluctuating, supposedly random component. The hybrid approach is fully compatible with the data-centric paradigm since the availability of more and better data is beneficial to both deterministic and non-deterministic analyses.

3 THE COMPETITIVE ADVANTAGES OF CPT TESTING

CPT testing has long been known to surpass other in-situ testing methods with respect to the high numerosity, quasi-continuity, and accuracy of its measurements. Moreover, CPT testing is highly standardized. Such features endow this testing method with several relevant “competitive advantages” in the light of the emerging data-centric, non-deterministic approach to geotechnical site characterization, geotechnical design, and geohazards risk analysis.

The small measurement interval which is unique to CPT testing among in-situ testing methods results in significantly higher data numerosity, i.e., in a higher number of measurements obtained for any given depth interval. Sample numerosity plays a decisive role in the applicability and significance of non-deterministic analyses. In most general terms, higher data numerosity is beneficial at least in terms of: (a) reduced statistical uncertainty; (b) improved modelling of inherent spatial variability and estimation of spatial averaging effects; and (c) improved estimation of transformation uncertainty. Ultimately, increased data numerosity contributes to the optimization of cost-performance optimization in geotechnical characterization and design by reducing the likelihood of unconservatism and the degree of over-conservatism. Data-centric approaches relying on machine learning also enhance their performance (when not outright requiring) large data sets. Phoon et al. (2021) opined that CPT data is the only practical source of data for data-driven site characterization (DDSC).

The concepts of testing repeatability and accuracy is related to measurement uncertainty. The latter is due to equipment, procedural-operator, and random testing effects. Previous research (e.g., Kulhawy & Trautmann 1996) indicates that CPT testing repeatability is higher in comparison to that pertaining to other testing methods. Peuchen & Terwindt (2014) provided an extensive insight into CPT measurement uncertainty and affirmed that piezocone testing is closest to an ideal penetration tool than any other in-situ testing method. In principle, high accuracy is desirable in non-deterministic analyses because low epistemic measurement uncertainty contributes to a lower total uncertainty. High standardization allows more stringent control on testing data quality. Peuchen & Parasie (2019) highlighted the ongoing technical and normative activities aimed at the continued pursuit of high CPT testing standardization.

The innumerable possible ramifications stemming from these virtuous attributes of CPT testing do not allow their exhaustive enumeration. Selected examples are provided in the following among the many ingenious available in the geotechnical literature.

4 NON-DETERMINISTIC CPT-BASED SITE CHARACTERIZATION

“Exploring the unknown requires tolerating uncertainty.”

- Brian Greene

Non-deterministic approaches have been proposed for fundamental activities related to CPT-based geotechnical site characterization including soil behavior classification, stratigraphic profiling, and spatial variability modeling. Selected examples are presented in the following, and readers are referred to Cao et al. (2017) for a more comprehensive treatment of such topic.

4.1 *Soil behavior classification*

CPT testing is frequently used for soil behavior classification through approaches which link the quantitative measurements of the mechanical resistance to cone penetration to likely corresponding soil types. The association between mechanical resistance and soil type is pervaded by significant uncertainties stemming from in-situ state effects (e.g., cementation, overconsolidation), by the inter-site and intra-site variability in compositional and mechanical properties of soils, and by the complexity of soil behavior.

CPT-based soil behavior classification methods routinely used in geotechnical practice are overwhelmingly deterministic. While their use worldwide and in many different soil and site conditions attests to their high performance, these methods are inherently unable to quantify explicitly the degree of uncertainty in their outputs. Methods for the non-deterministic CPT-based soil classification have nonetheless been made

available in the geotechnical literature since many years. Zhang & Tumay (2003) proposed the probabilistic region estimation method. Such approach provides a depth-wise profile of the probability that a set of CPT measurements (more specifically, cone resistance and friction ratio) correspond to cohesive-, intermediate-, or cohesionless-behavior soil type (see Figure 2).

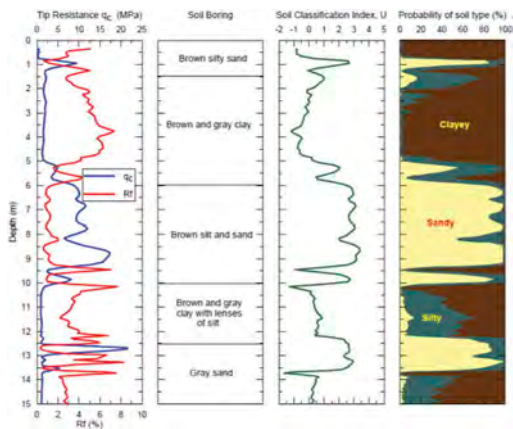


Figure 2. Non-deterministic depth-wise soil behavior classification (Zhang & Tumay 2003).

4.2 Stratigraphic profiling

Stratigraphic profiling is one of the main applications of CPT testing. Such process involves the identification of interfaces between soil units which can be considered sufficiently homogeneous and/or significant for specific purposes. Reliable stratigraphic profiling is also relevant to geotechnical design. For example, in CPT-based pile design, the identification of a stratigraphic interface between a layer with low bearing capacity and one with high bearing capacity and stiffness is fundamental in the definition of design pile length. Cone resistance in layered soil is affected not only by the layer currently being traversed but also by the underlying and, under certain conditions, overlying layers, depending on the position of the cone relative to such layers.

Several non-deterministic approaches for CPT-based stratigraphic profiling have been proposed. Wang et al. (2019), for example, developed a Bayesian unsupervised learning approach for automatic layer detection and soil classification with an explicit quantification of uncertainty, using CPT-based parameters (i.e., normalized sleeve friction F_R and normalized cone resistance Q_t) commonly used in the well-established soil behavior classification system by Robertson (1990). Figure 3 provides a visual representation of the approach, highlighting the capability of the method to simultaneously provide both soil

behavior type and stratigraphic profiling from CPT testing data.

4.3 Spatial variability modeling

In-situ testing typically reveals that engineering properties of geomaterials vary spatially both in the horizontal and vertical directions (most often with higher variability in the latter case due to layering- and stress-related effects). In absence of geological, geomorphological, or geotechnical macro-discontinuities (e.g., layer interfaces) which should be accounted for by separating data by homogeneous soil units through stratigraphic profiling and soil behavior classification, soil properties (as parameterized, for instance, in CPT data) can be expected to vary gradually in conformity with the conceptual principle stated by Leibniz (1704) by which “*tout va par degrés dans la nature, et rien par saut*” (“everything occurs gradually in nature, and nothing by jumps”). Spatial variability can never be estimated with full precision and accuracy at any scale, from the micro-scale to the macro-scale, due to the finite number of tests and measurement uncertainty.

The importance of the quantitative modeling of spatial variability is increasingly acknowledged in research and practice as: (1) it is necessary for the conduction of simulation-based analyses based on techniques such as random field modeling; (2) it allows the spatial interpolation of in-situ testing measurements and of derived parameters and the quantification of uncertainties in interpolation estimates at unsounded locations, thereby providing support in the planning and integration of geotechnical investigation campaigns and optimizing their cost-performance ratio; (3) allows the quantitative estimation of the spatial averaging effect, by which the effects of variability on geotechnical design can be rationally calibrated with respect to the spatial extension of geotechnical structures (typically, pile foundations).

Multiple approaches and techniques have been used to the purpose of geotechnical spatial variability modeling. In many of these techniques, variability is often modeled most efficiently through the integration between deterministic and non-deterministic approaches, i.e., through the decomposition of data into a trend which is expressed deterministically (for instance through a polynomial function) and a fluctuating component, which is assumed to be a random variable, and which is investigated using statistical, probabilistic, geostatistical, and random field theory among others.

Regardless of the specific technique used, CPT is particularly suited for the modeling of spatial variability because of its small measurement interval, which allows, jointly with its high testing repeatability, more reliable estimation of small-scale variability in the vertical direction with respect to other in-situ testing methods. Moreover, higher data numerosity reduces statistical uncertainty in non-deterministic analyses such as the modeling of semivariograms for the modeling of spatial correlation.

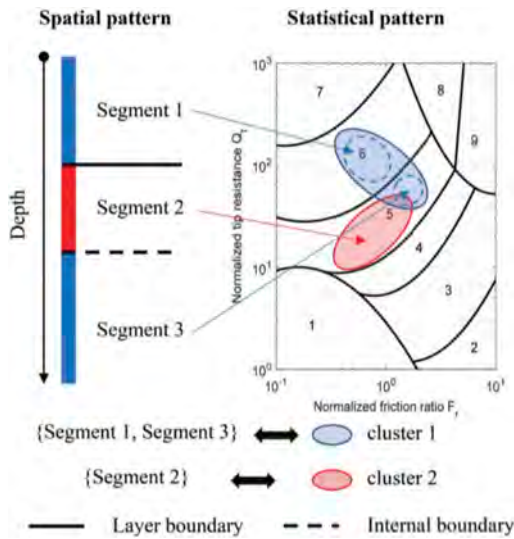


Figure 3. Statistical clustering for non-deterministic stratigraphic profiling (from Wang et al. 2021).

5 NON-DETERMINISTIC CPT-BASED GEOTECHNICAL DESIGN

Non-deterministic approaches are available for the utilization of CPT data in geotechnical design, both in the derivation of design parameters and in design methods. As shown in the following selected examples, such approaches allow improved and more rational calibration and assessment of the performance of geotechnical design. Readers are referred to Tang & Phoon (2021) for a more comprehensive insight into geotechnical transformation uncertainty.

Engineering models which relate in-situ and laboratory testing measurements to geotechnical design parameters, whether theoretical, empirical, experimental, or a combination thereof, are always approximate simplifications of physical soil-structure systems. Geotechnical models are thus invariably affected by bias (which relates to the model's precision) and/or dispersion (which refers to the model's accuracy). Empirical correlations have been made available to estimate numerous geotechnical design parameters from CPT testing results. Lunne et al. (1997) tabulated comparatively the degree of applicability of a wide range of in-situ testing methods to the estimation of geotechnical parameters, assessing that CPT testing overall outperformed other methods. Robertson & Cabal (2015) tabulated the perceived applicability of piezocone testing to the estimation of soil parameters for coarse-grained and fine-grained soils (Table 1), once again assessing the overall utility of CPT for geotechnical parameter estimation.

Table 1. Perceived applicability of CPTU for deriving soil parameters (from Robertson & Cabal 2015).

Parameter	Coarse	Fine
Relative density	2-3	-
State parameter	2-3	-
Young's and shear moduli	2-3	2-4
Overconsolidation ratio	5	1
Undrained strength	-	1-2
Coefficient of consolidation	3-4	2-3
Peak friction angle	2-3	4
In-situ stress ratio	5	2
Small-strain shear modulus	2-3	2-4
1-D Compressibility	2-3	2-3
Sensitivity	-	2
Permeability	3-4	2-3

Note: 1=high; 2=high to moderate; 3=moderate; 4=moderate to low; 5=low.

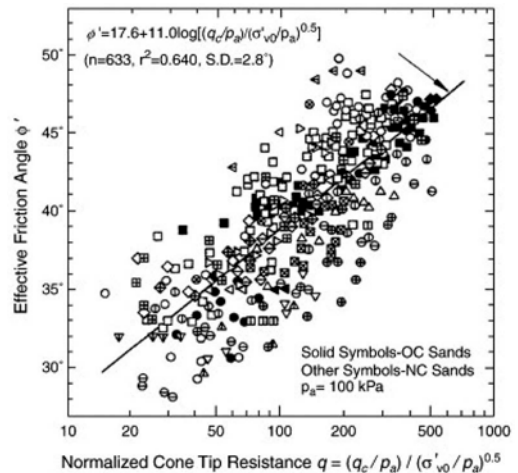


Figure 4. Source data and deterministic correlation for estimating friction angle from CPT (Kulhawy & Mayne 1990).

In the light of the non-deterministic insight into CPT testing, the “degree of perceived applicability” could be related conceptually to the reliability of the transformation models, i.e., to the magnitude of transformation uncertainty. However, this qualitative assessment can hardly be translated into quantitative probabilistic formulations which can be seamlessly used in new geotechnical design codes. Available CPT-based correlations are overwhelmingly deterministic. They are typically obtained as “best-fit”, central tendency models from scattered data, and are thus amenable to an “intermediate” degree of conservatism.

An example of the transition to non-deterministic CPT-based estimation of geotechnical parameters is

related to the estimation of effective friction angle of sands from stress-normalized cone resistance. Figure 5 shows the data used by Kulhawy & Mayne (1990) to develop their well-known deterministic model

$$\phi' = 11.0 \cdot \log_{10}(q_{t1}) + 17.6 \quad (1)$$

While goodness-of-fit statistics (typically, the coefficient of determination R^2) or descriptive second-moment dispersion statistics (e.g., standard deviation, variance) are provided together with the regression model in best-practice cases such as this one, these are in principle not sufficient to allow the model-based estimation of properties for different levels of conservatism. Moreover, the statistical distribution of data around the best-fit model cannot be characterized statistically beyond second-moment description.

Uzielli & Mayne (2019) proposed a probabilistic transformation model using a high-quality database comprising CPT and triaxial tests. The logarithmic formulation

$$\phi' = p_1 \cdot \ln(q_{t1}) + p_2 \quad (2)$$

has the same ease of practical applicability as the previous deterministic model while allowing the estimation of ϕ' for varying levels of conservatism (i.e., for different probabilities of exceedance P_{exc}) by varying model coefficients p_1 and p_2 as shown in Table 2. Figure 5 plots the curves corresponding to probabilities of exceedance 0.05, 0.50, 0.75, and 0.95 of effective friction angle in comparison with the deterministic model by Kulhawy & Mayne (1990). While the performance of the deterministic methods is overall comparable to the probabilistic method for a “median” probability of exceedance, it is apparent that the latter allows the fuller exploitation of the experimental dataset. It is also apparent that the deterministic model does not refer uniformly to a probability of exceedance for increasing values of q_{t1} . Thus, the degree of conservatism in the deterministic model is not established univocally.

The transition to a data-centric paradigm can further enhance the quality and utility of new-generation geotechnical transformation models. Site-specific data are typically sparse and incomplete. The geotechnical discipline has adapted to this fact by providing transformation models which are

Table 2. Coefficients of the logarithmic CPT-based model for the estimation of friction angle for various probabilities of exceedance (Uzielli & Mayne 2019).

P_{exc}	0.95	0.75	0.50	0.05
p_1	4.27	4.00	3.81	1.70
p_2	18.1	20.3	22.2	35.1

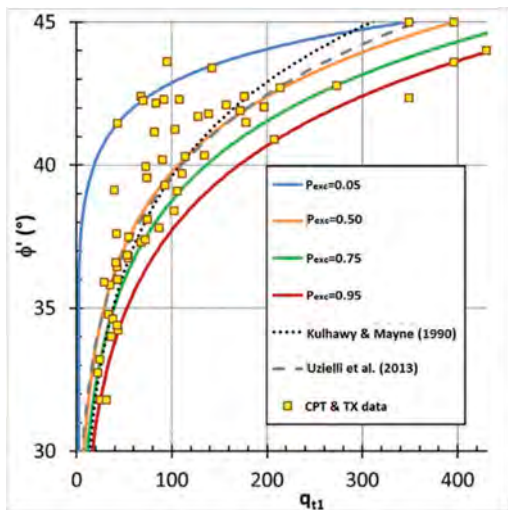


Figure 5. Comparison of probabilistic (Uzielli & Mayne 2019) and deterministic (Kulhawy & Mayne 1990) models for the estimation of effective friction angle from stress-normalized cone resistance.

founded on data from multiple sites. While geotechnical engineers are trained to operate the transition between “indirect” data (i.e., from other sites) to “direct” (i.e., local) data by applying transformation models and assessing the results critically using engineering judgment, non-deterministic approaches based on the data-centric paradigm allow an improved synergy between indirect and direct data. Through Bayesian approaches relying on the data-centric paradigm, it is possible to quantify the reliability of indirect data with respect to direct data and to provide a “hybrid” transformation model which relies on both datasets, and in which the weight of the “indirect” model is determined on the basis of objective criteria such as the “similarity” between indirect sites and the target site, e.g., in terms of soil types. For example, Ching et al. (2021) used a hierarchical Bayesian modelling framework to apply hybridization to the estimation of undrained strength of clays from CPT testing. Figure 6 illustrates indirect site-specific models as well as the hybrid model for the target site-specific model. Ellipses represent the uncertainties associated with the respective models, which are quantified explicitly.

An increasing set of non-deterministic CPT-based design methods are also available in the geotechnical literature. Cai et al. (2021) provided a framework for the CPT-based calculation of axial pile capacity in spatially variable soil. The study relied on the simulation of CPT profiles through random field modeling and on the statistical-based calculation of pile capacity for varying target levels of conservatism. Figure 7 provides a comparative visual representation of simulated profiles of cone resistance at preset

spatial separation distances within the design site for smaller and larger horizontal correlation distances. Random field modeling also allows to refer explicitly to the scale of fluctuation, thus allowing the quantification of the spatial averaging effect by which the influence of the variability in soil properties is smoothed out along the shaft. The rigorous inclusion of the spatial averaging effect contributes to calibrating the effect of inherent soil variability and to reconstruct rationally the degree of conservatism in design to its target level. CPT testing data are particularly suited for simulation purposes because of the higher reliability in the estimation of vertical spatial variability parameters stemming from the quasi-continuity of measurements in comparison to other in-situ testing methods.

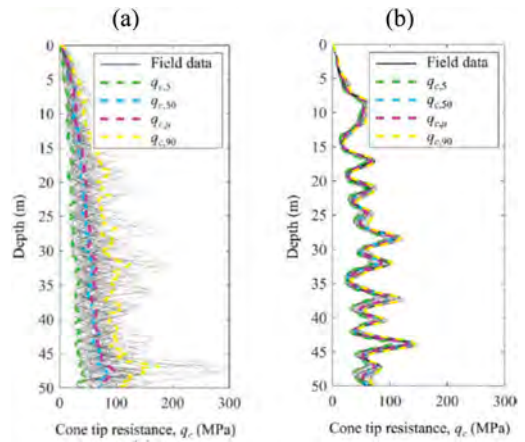


Figure 7. Simulation of horizontal site-scale variability of cone tip resistance for: (a) lower; and (b) higher horizontal correlation distance (adapted from Cai et al. 2021).

6 NON-DETERMINISTIC CPT-BASED GEORISK ANALYSIS

In-situ testing results are frequently used in the increasingly relevant contributions of geotechnical engineering to geohazards risk analysis. Methods have been made available for various hazards and related phenomena including the prediction of triggering of seismic liquefaction, seismically induced soil densification, lateral spreading, and slope stability, among others. The prediction of seismic liquefaction triggering has arguably received most attention. Numerous simplified liquefaction evaluation approaches based on the results of in-situ tests (SPT, CPT, DMT, seismic testing) have been made available over the past decades. Among these, CPT-based methods have been shown to provide significant advantages over others due to: (a) the capability to detect thin layers; (b) the repeatability of measurements; (c) the relative speed and economy.

As in all ramifications of the geotechnical discipline, deterministic methods for liquefaction assessment have preceded non-deterministic methods chronologically and are still today predominant even though literature findings increasingly indicate that non-deterministic methods provide multiple significant advantages. First, they allow users to define liquefaction boundary curves for target levels of conservatism, thereby contributing to cost-performance optimization with respect to the vulnerability and value of elements at risk in a specific area. Second, they explicitly include uncertainties in the estimation of the parameters and models used to estimate seismic demand and soil resistance parameters. Third, they allow a more realistic and physics-based modelling and treatment of geotechnical phenomena. The latter point can be well exemplified by the following.

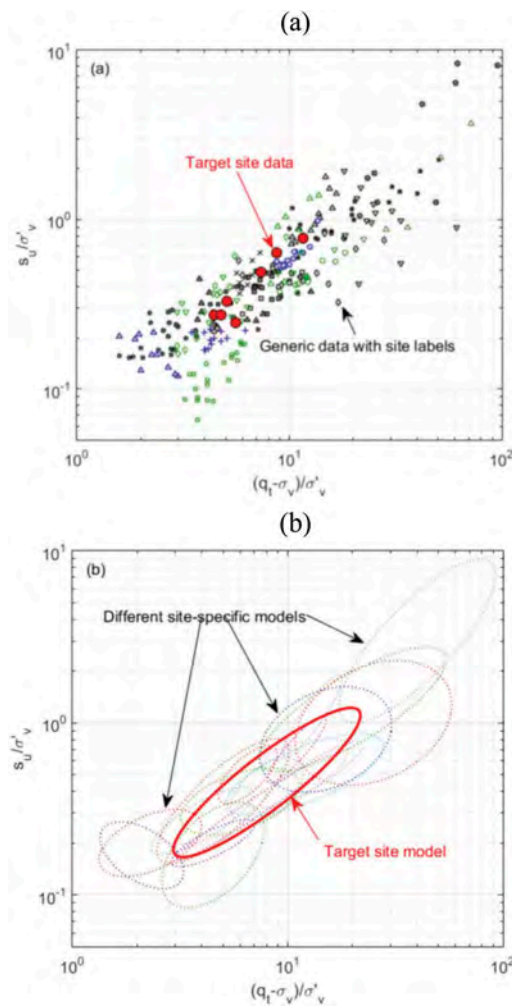


Figure 6. Hybridization of direct and indirect data-driven models for undrained strength from CPT: (a) target site and generic data; (b) resulting site-specific and target site models (Ching et al. 2021).

A vast bulk of research and experimental evidence indicates that seismic liquefaction typically occurs in loose or medium-density, saturated cohesionless soils, while high-plasticity, fine grained soils are inherently “non-liquefiable” due to the relevance of the cohesive component of shear strength. A fundamental step in the implementation of simplified CPT-based methods lies in the assessment of inherent soil liquefiability. Such methods are developed from databases pertaining to soils which are expected to be inherently liquefiable based on prior knowledge, and are thus applicable solely to such soils, i.e., the calculation of the cyclic resistance ratio CRR, which parameterizes the cyclic resistance of soils to liquefaction, is pursued solely at depths corresponding to soils preliminarily assessed to be liquefiable. The applicability of simplified methods must be assessed depth-wise, as stratigraphic profiles can be very heterogeneous in terms of soil types and can include both liquefiable and non-liquefiable soil.

All simplified CPT-based liquefaction evaluation methods include quantitative approaches to the depth-wise assessment of the liquefiability or non-liquefiability of soils. Such assessment typically relies on the definition of deterministic threshold values of the soil behavior classification index I_c (typically varying between 2.4 to 2.6 among methods) which provide a strict boundary between liquefiable and non-liquefiable layers. The assessment resulting from the adoption of deterministic thresholds is invariably binary, i.e., a set of CPT measurements corresponds to either a “fully liquefiable” or “fully non-liquefiable” measured soil volume interval. The hypothesis of an abrupt discontinuity between non-liquefiability and full liquefiability is hardly compatible with well-established geotechnical knowledge and evidence by which liquefiability can be expected to decrease gradually with increasing percentage of fines in a soil. Incidentally, the non-binary effect of varying fines content is already included in simplified methods through the calculation of fine-sand equivalent stress-normalized cone resistance (usually denoted by $q_{c1N,cs}$), which takes continuous (albeit usually inferiorly and superiorly bounded), values, but does not intervene in the preliminary assessment of liquefiability. Moreover, calculated values of I_c are pervaded by uncertainty stemming from measurement depth offset effects, layering effects, and uncertainty in measurements of q_c and f_s . The progressive variation of the degree of liquefiability should be accounted for quantitatively.

Non-deterministic approaches to susceptibility evaluation can contribute to improving deterministic methods. Maurer et al. (2017) proposed deterministic and probabilistic correlations relating I_c to liquefaction susceptibility as defined by four well-established published criteria. Figure 8 shows the respective liquefaction susceptibility probability curves. Such curves, if duly integrated into existing deterministic

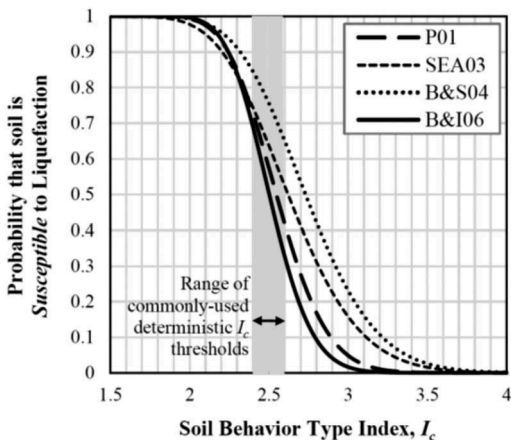


Figure 8. Probability of liquefaction susceptibility as a function of the soil behavior type index (from Maurer et al. 2017).

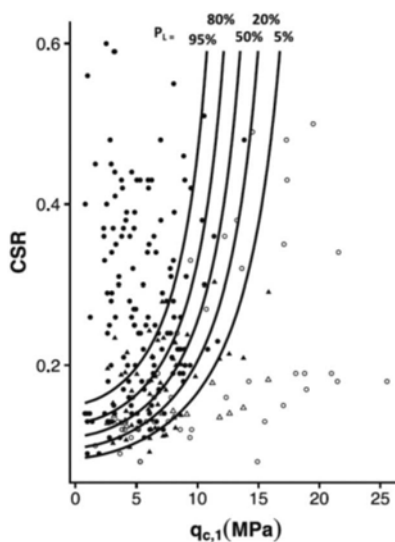


Figure 9. Probabilistic liquefaction boundaries (Schmidt & Moss 2021).

methods, could provide a useful means to quantify liquefiability as a continuous (as opposed to binary) variable and to partially circumvent the limitations which are inherent to deterministic approaches.

“Fully” non-deterministic CPT-based approaches, mostly relying on Bayesian methods for the prediction of liquefaction triggering, are available in the geotechnical literature and are being increasingly used in practice. In comparison with deterministic approaches which provide a single liquefaction boundary curve, these allow the selection of liquefaction boundaries for varying degrees of conservatism while accounting explicitly for uncertainties. Figure 9 provides an example of probabilistic

liquefaction boundaries for varying probability levels as calculated from normalized cone resistance using the approach proposed by Schmidt & Moss (2021). This approach addresses and processes uncertainties in the parameters used in the estimation of cyclic resistance and cyclic stress, as well as uncertainties stemming from intra-event correlation in loading variables and differences in event sample sizes.

Non-deterministic methods can also be used to spatialize the outputs of deterministic simplified CPT-based methods. For example, Guan & Wang (2022) developed a probabilistic method for characterizing the horizontal spatial distribution of the deterministically calculated cyclic resistance ratio, cyclic stress ratio, and factor of safety against liquefaction in data from CPT soundings using Bayesian compressive sampling and Monte Carlo simulation. The method relies on the generation of random field samples and allows the modeling and quantification of spatial variability, interpolation uncertainty, and model uncertainty. Example outputs of the methods include spatial distributions of statistics of the factor of safety resulting from the interpolation of deterministic values obtained at 6 CPT sounding verticals. Figure 10a refers to the mean values of the factor of safety calculated from 10,000 realizations of random fields, while Figure 10b plots the spatial distribution of the coefficient of variation, which provides a quantitative measure of the level of uncertainty in the spatialized values of the factor of safety.

The availability of quantitative measures of uncertainty associated with interpolated values provides a fundamental advantage over deterministic characterization methods, at least because: (1) the parameter is defined probabilistically for direct use in reliability-based methods; and (2) it becomes

possible to assess where estimation uncertainty exceeds thresholds of tolerability/acceptability, thus providing direct indications for the conduction of supplementary tests. The visual representation of the spatial variability of the interpolation estimates of the factor of safety allows rational decision-making regarding possible supplementary investigations.

7 TURNING CAUTIONS INTO OPPORTUNITIES

The adoption and implementation of methods such as those presented in the previous sections should never occur in absence of engineering judgment and geotechnical knowledge. Cautions should be adopted at all stages of CPT-based analyses to ensure the geotechnical significance and formal correctness of the quantitative procedures relying on uncertainty modeling. This paper argues that current cautions can be successfully addressed through synergies between research and practice.

7.1 Interpretation in layered soils.

Previous studies explored the problem of cone penetration in layered soils analytically (e.g., Yu 2006) or experimentally, either in calibration chambers (e.g., Tehrani et al. 2017) or centrifuges (e.g., Mo et al. 2017). Some of these studies define “sensing distance” as the distance from a layer interface at which the cone resistance first starts changing because the cone is approaching it, and “development distance” the distance from a layer interface at which the cone resistance ceases to be affected by the interface as it moves away from it.

A further complication is given by the fact that the three fundamental CPT parameters pertain to different depths and to different volumes of soil. This fact stems from the physical geometry of the cone and by the inherent differences between the volumes of soils and the physical phenomena affecting cone resistance, sleeve friction, and pore pressure. These three measurements, involving different volumes of soil during penetration. Theoretical modeling of cone penetration has shown that such extent may depend on cone size, geometry, and soil type and stiffness. Thus, the volumes of soil involved in cone tip resistance and sleeve friction measurements are variable. The existence of a measurement depth offset between cone resistance, sleeve friction, and pore pressure is well-known. Approaches relying on statistical techniques such as cross-correlation have been proposed and are implemented in widely used commercial CPT interpretation software.

While CPT measurements ultimately reflect the true mechanical behavior of the in-situ soil volume in terms of its resistance to cone penetration, they do not provide fully reliable information if data are not corrected for layering effects, and measurement

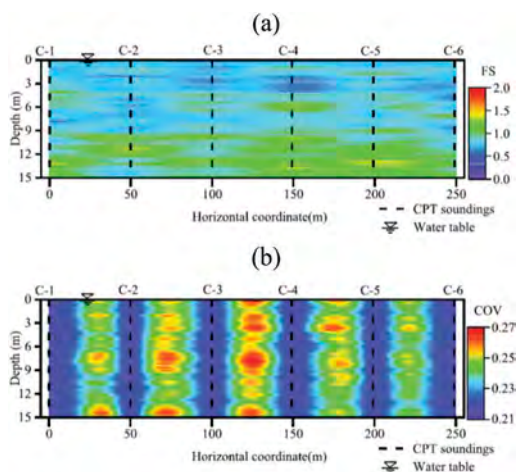


Figure 10. Example statistical outputs of the horizontal spatialization of the factor of safety against liquefaction: (a) mean; (b) coefficient of variation (from Guan & Yang 2022).

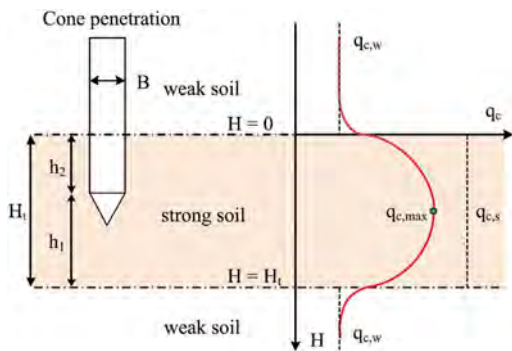


Figure 11. Schematic of cone penetration in multilayered soils: strong soil embedded in weak soils (Mo et al. 2017).

offset prior to being used for stratigraphic profiling, soil classification, and in the calculation of geotechnical design parameters. This is because depth-wise measured values do not correspond to the true values at the same depth. CPT-based approaches relying on the depth-wise processing of measurements should in principle be preceded by a pre-processing of data to account for layering effects and for the inherent depth offset between measurements. If such pre-processing is not conducted, these approaches will be pervaded by additional epistemic uncertainty, however sophisticated they may be. The magnitude of the epistemic uncertainty related to layering effects and depth offset tend to increase with stratigraphic complexity.

Despite the inherent complexity in physical phenomena involving cone penetration in layered soils, studies such as those mentioned above have provided ingenious analytical models for the estimation of sensing distance and development distance and for the correction of raw measurement data. The development of efficient algorithms for the translation of the results of these studies into software applications provides a stimulating challenge and an opportunity for considerable improvement in the significance of CPT data interpretation for routine implementation in non-deterministic methods for geotechnical site characterization and design. Operating in the light of the non-deterministic paradigm provides an ideal scenario as uncertainties in the “true” values of CPT measurements in layered profiles can be expressed explicitly.

7.2 Improved quantification of measurement uncertainty

The separation of the components of total uncertainty may prove to be a complex process depending on the quality and quantity of data from a specific case. The relative contribution of total uncertainty is also highly case-specific, and depends on site conditions and inherent spatial variability, and degree of

equipment and procedural control in testing data. Geotechnical uncertainty models are typically additive (e.g., Phoon & Kulhawey 1999). The magnitude of individual uncertainty components can thus be estimated in reverse-mode, i.e., by subtracting known uncertainty terms from the total uncertainty which is observed. Consistent approaches to the quantification of measurement uncertainty would result in the availability of more reliable parameterization of measurement uncertainty, leading to more confident subtractive-mode implementation of uncertainty models to estimate aleatory and other epistemic uncertainties from total uncertainty. To this purpose, Peuchen & Terwindt (2014) advocated the development of a shared, less ambiguous glossary (e.g., “repeatability” is strictly not synonymous to “accuracy”) and the compilation of a reference measurement uncertainty dataset from real cases (as opposed to “ideal” cases referring to unrealistically controlled conditions).

7.3 Upgrading of geotechnical correlations

While new, non-deterministic transformation models yielding design properties from CPT data such as the ones presented in this paper are progressively being made available, the vast majority of geotechnical correlations (including CPT-based correlations) remain deterministic. The full migration of the geotechnical discipline to the non-deterministic paradigm cannot prescind from the upgrading of geotechnical correlations to formats which are compatible with new paradigms. This could be aided by, for instance, through: (a) specific and systematic focus of new research on the development of non-deterministic correlations; and (b) a collective effort on the part geotechnical researchers and practitioners to contribute existing data for the non-deterministic reformulation of existing literature correlations.

8 CONCLUDING REMARKS

This paper has hopefully provided a meaningful insight into the possible benefits of non-deterministic methods for the interpretation of CPT data and its utilization in many and diverse aspects of geotechnical engineering. It has also aimed to highlight the inherent competitive advantage of CPT over other in-situ testing methods in meeting the demands of the new non-deterministic, data-centric paradigm of the geotechnical discipline.

The progressive migration of geotechnical design codes towards non-deterministic formats and the ever-strengthening global digital transition indicates that embracing and implementing such paradigm in practice is no longer a choice for the geotechnical community at large, but rather a beneficial, convenient obligation. Providing students, practitioners, and researchers with sufficient theoretical knowledge and practical tools to understand and implement

non-deterministic methods and approaches is a necessity. ISSMGE TC304 “Engineering Practice of Risk Assessment & Management” recently exerted a formidable effort resulting in a state-of-the-art report containing a conspicuous bulk of quantitative estimates of inherent variability parameters as well as statistics for geotechnical design model factors, random field parameters of geotechnical properties, statistics for transformation uncertainties, and characteristic values of geotechnical parameters for use in non-deterministic design methods.

To further exploit the opportunities offered by the global digital revolution and improved measurement technologies, and to meet the requirements of evolutionary design codes, the geotechnical community must persist in the transition towards the data-centric approach, which is fully compatible with the non-deterministic paradigm. To facilitate and stimulate this transition, new geotechnical databases providing high-quality, validated information are made publicly available. An example database including CPT testing outputs is the ISSMGE TC304 database – 304dB at <http://140.112.12.21/issmge/tc304.htm>. This paper wishes to encourage the CPT community to actively contribute to this database.

The surge of data-driven approaches does not undermine the central role of geotechnical expertise and engineering judgment. Rather, new engineering paradigms and technological evolutions now require that geotechnical engineering judgment also rely on skills allowing the comprehension of uncertainties and the enhanced analysis of the data which geotechnical testing provides. A modern geotechnical engineering education would thus greatly benefit from structured training in statistical and probabilistic methods, specifically including Bayesian approaches, along with data analysis and machine learning methods. Current practitioners could receive these contents through high-quality professional development initiatives. On the academic side, geotechnical researchers focusing on non-deterministic and data-centric methods should continue striving to make their promising findings increasingly accessible through open-source sharing, free software, and on an improved communication skills to allow a more immediate comprehension of new findings on the part of the geotechnical community at large. ISSMGE-related initiatives focusing on these topics could be disseminated through structured protocols with academia and professional bodies.

The translation of non-deterministic mathematical frameworks of varying complexity and sophistication into practically utilizable executables for the interpretation of CPT data may further foster the transition of the geotechnical community towards cost-performance optimization in geotechnical site characterization, design, and in the analysis and management of georisks, in full accordance with current global trends aimed at sustainability, circularity, and community participation.

REFERENCES

- Baecher, G.B. & Christian, J.T. 2003. *Reliability and statistics in geotechnical engineering*. New York: John Wiley & Sons.
- Box, G. E. P., Luceño, A. & del Carmen Paniagua-Quiñones, M. 2009. *Statistical Control By Monitoring and Adjustment*. John Wiley & Sons.
- Cai, Y., Bransby, F., Gaudin, C. & Uzielli, M. 2021. A framework for the design of vertically loaded piles in spatially variable soil. *Computers and Geotechnics* 134. DOI: 10.1016/j.compgeo.2021.104140
- Cao, Z., Wang, Y. & Li, D. 2017. *Probabilistic approaches for geotechnical site characterization and slope stability analysis*. Springer. ISBN: 978-3-662-52914-0.
- Ching, J., Wu, S. & Phoon, K.K. 2021. Constructing quasi-site-specific multivariate probability distribution using hierarchical Bayesian model. *Journal of Engineering Mechanics*, ASCE. DOI: 10.1061/(ASCE)EM.1943-7889.0001964.
- Einstein, A. 1921. “Geometry and experience”. Address to the Prussian Academy of Sciences in Berlin, January 27th, 1921.
- Guan, Z. & Wang, Y. 2022. CPT-based probabilistic liquefaction assessment considering soil spatial variability, interpolation uncertainty and model uncertainty. *Computers & Geotechnics* 141. DOI: 10.1016/j.compgeo.2021.104504.
- ISSMGE – Technical Committee TC304 “Engineering Practice. 2021. *State-of-the-art review of inherent variability and uncertainty in geotechnical properties and models*.
- Kulhawy, F.H. & Mayne, P.W. 1990. *Manual on estimating soil properties for foundation design*. EPRI Report EL-6800, Electric Power Research Institute.
- Kulhawy, F.H. & Trautmann, C.H. 1996. Estimation of in-situ test uncertainty. In C.D. Shackelford, P.P. Nelson and M.J.S. Roth (eds.), *Uncertainty in the Geologic Environment: From Theory to Practice*, ASCE Geotechnical Special Publication No. 58: 269–286.
- Leibniz, G.W. 1704. *Nouveaux essais* IV, 16, 12.
- Li, J., Tian, Y. & Cassidy, M.J. 2014. Failure mechanism and bearing capacity of footings buried at various depths in spatially random soil *J. Geotech. Geoenviron. Eng.*, ASCE. DOI: 10.1061/(ASCE)GT.1943-5606.0001219.
- Maurer, B.W., Green, R.A., van Ballegooy, S. & Wotherspoon, L. 2017. Assessing liquefaction susceptibility using the CPT soil behavior type index. *Proceedings of the Third International Conference on Performance-Based Design in Earthquake Geotechnical Engineering – PBDIII*, Vancouver, July 16-19.
- Mo, P.-Q., Marshall, A.M. & Yu, H.-S. 2017. Interpretation of cone penetration test data in layered soils using cavity expansion analysis. *J. Geotech. Geoenviron. Eng.*, ASCE. DOI: 10.1061/(ASCE)GT.1943-5606.0001577.
- Peuchen, J. & Terwindt, J. 2014. Introduction to CPT accuracy. *Proceedings of the 3rd International Symposium on Cone Penetration Testing*, Las Vegas.
- Peuchen, J. & Parasie, N. 2019. Challenges for CPT accuracy classes. *Proceedings of the XVII ECSMGE-2019, Geotechnical Engineering foundation of the future*, Reykjavik. ISBN 978-9935-9436-1-3. DOI: 10.32075/17ECSMGE-2019-0049

- Phoon, K.-K. & Kulhawy, F.W. 1999. Characterisation of geotechnical variability. *Canadian Geotechnical Journal* 36: 612–624.
- Phoon, K.-K. 2020. The Story of Statistics in Geotechnical Engineering. *Georisk: Assessment and Management of Risk for Engineered Systems and Geohazards*. DOI: 10.1080/17499518.2019.1700423.
- Phoon, K.-K., Ching, J. & Shuku, T. 2021. Challenges in data-driven site characterization. *Georisk: Assessment and Management of Risk for Engineered Systems and Geohazards*. DOI: 10.1080/17499518.2021.1896005.
- Robertson, P.K. 1990. Soil classification using the cone penetration test. *Canadian Geotechnical Journal* 27:151–158.
- Robertson, P.K. & Cabal, K.L. 2015. *Guide to Cone Penetration Testing for Geotechnical Engineering* – 6th Edition. Gregg Drilling & Testing, Inc.
- Schmidt, J. & Moss, R. 2021. Bayesian hierarchical and measurement uncertainty model building for liquefaction triggering assessment. *Computers & Geotechnics* 132, 103963. DOI: 10.1016/j.compgeo.2020.103963.
- Tang, C. & Phoon, K.-K. 2021. *Model uncertainties in foundation design*. CRC Press, Boca Raton. DOI: 10.1201/9780429024993.
- Tehrani, F.S., Arshad, M.I., Prezzi, M. & Salgado, R. 2017. Physical modeling of cone penetration in layered sand. *J. Geotech. Geoenviron. Eng.*, ASCE. DOI: 10.1061/(ASCE)GT.1943-5606.0001809.
- Uzielli, M., Lacasse, S., Nadim, F. & Phoon, K.-K. 2007. Soil variability analysis for geotechnical practice. Keynote paper, In T.S. Tan, K.K. Phoon, D. W. Hight & S. Leroueil (eds.), *Proceedings of the 2nd International Workshop on Characterisation and Engineering Properties of Natural Soils*. Singapore, November 29 – December 1, 2006. The Netherlands: Taylor & Francis.
- Uzielli, M., and P. W. Mayne. 2019. “Probabilistic assignment of effective friction angles of sands and silty sands from CPT using quantile regression.” *Georisk: Assessment and Management of Risk for Engineered Systems and Geohazards* 13(4): 271–275. DOI:10.1080/17499518.2019.1663388
- Yu, H.-S. 2006. The first James K. Mitchell lecture in situ soil testing: From mechanics to interpretation. *Geomech. Geoeng.: An Int. J.*, 1(3),165–195.
- Zhang, Z. & Tumay, M.T. 2003. Non-traditional approaches in soil classification derived from the cone penetration test. In G.A. Fenton & E. H. Vanmarcke (eds.), *Probabilistic Site Characterisation at the National Geotechnical Experimentation Sites*, ASCE Geotechnical Special Publication No. 121: 101–149.

Combined use of CPT & DMT: Background, current trends and ongoing developments

P. Monaco

University of L'Aquila, L'Aquila, Italy

ABSTRACT: This paper aims to introduce and stimulate the discussion on the use of CPT & DMT and on the potential of their mutual integration for enhanced site characterization and geotechnical design. It provides a brief overview of background information, current trends and ongoing developments on the combined use of CPT & DMT testing. Specific issues addressed in the paper include: (a) CPT-DMT comparisons and inter-relationships; (b) derivation of soil parameters from combined CPT & DMT data; (c) applications based on combined CPT & DMT data.

1 INTRODUCTION

The use of in-situ testing for geotechnical site characterization has continued to expand over the past few decades, gaining an increasing role over the traditional practice based on drilling and sampling for laboratory testing. Often today in-situ tests represent the major part of a site investigation, particularly in geomaterials that are difficult to sample and test using conventional methods (e.g., sands, tailings, semi-liquid soils). Mayne et al. (2009) summarized the key advantages of in-situ tests: (a) they can be done relatively quickly as compared with laboratory tests, (b) results are available immediately, (c) large numbers of data are obtained, and (d) vertical and lateral variability can be assessed over the site.

In this context, the cone/piezcone penetration test (CPT/CPTu) and the flat dilatometer test (DMT) have proven to be particularly efficient and expedient for routine site investigations. In fact: (a) both are direct-push probes, which do not need a borehole for advancement, (b) multiple measurements are collected from a single sounding, (c) the data are obtained digitally and can be accessed for use immediately after completion of the sounding or even in real-time during advancement of the probe, (d) their instrumental accuracy is high, unlike “older” techniques such as the standard penetration test (SPT), (e) technological upgrades, such as additional sensors or full automation (e.g., Medusa DMT, Marchetti et al. 2019), can be easily implemented.

The use of direct-push in-situ tests providing multi-measurements was emphasized by Mayne et al. (2009) as a more efficient approach to geotechnical site characterization. Particularly beneficial and versatile is their “hybrid” configuration that combines the

advantages of full-displacement penetrometer probes with downhole geophysics (seismic piezocone SCPTu, seismic dilatometer SDMT), capable to provide information on soil behavior from the small to the large-strain range.

A single SCPTu sounding provides up to five independent measurements: the basic CPTu measurements (cone resistance q_t , sleeve friction resistance f_s , pore pressure u_2), the shear wave velocity V_S , and information on soil consolidation/permeability parameters if dissipation tests are performed by monitoring the u_2 decay with time (e.g., time to reach 50% degree of consolidation, t_{50}). A single SDMT sounding provides a comparable number of independent measurements: the basic DMT pressure measurements (A , B and optional C corrected to p_0 , p_1 , p_2 respectively), the shear wave velocity V_S , as well as the compression wave velocity V_P when using the SPDMT configuration equipped with two pairs of receivers for S- and P-wave (Amoroso et al. 2020), and information on soil consolidation/permeability parameters if dissipation tests by monitoring the A -pressure decay with time are performed (e.g., reference time in the A -decay curve, t_{flex}).

For these reasons, Mayne et al. (2009) suggested that the SCPTu and SDMT direct-push tests should serve as the basis for the minimum required level of effort in routine and daily site investigation practices by the profession, in order that adequate amounts and sufficiently different types of data are collected for a given project. These data are complemented with sampling and laboratory testing.

The CPT and the DMT have in common the same equipment for insertion (push rig, rods) and a similar range of soil type applications (clays, silts, sands). Both tests are utilized in site investigations to obtain

information on stratigraphy, soil types and parameters to be used with general or dedicated design methods. However, each test has advantages and limitations and may prove more adequate in specific applications. E.g., the CPT is commonly used for pile design and liquefaction assessment, the DMT generally provides good predictions of settlements of shallow foundations.

In common practice, the CPT is often the preferred primary in-situ test, supported by a much larger consolidated use. On the other hand, the DMT can provide distinctive contributions in a routine site investigation: (1) information on stress history, which has a dominant influence on soil behavior; (2) being an in-situ pressure-displacement test, the DMT results are more closely related to “working strain” soil stiffness than penetration tests.

Some questions that may arise are then: are the two in-situ tests equivalent? Is one test (CPT or DMT alone) self-standing and sufficient for exhaustive geotechnical site characterization? Are there any advantages in the combined use of CPT & DMT?

One notable emerging trend (Marchetti 2015, Marchetti & Monaco 2018) is the increasing diffusion in site investigation practice of a “multi-parameter/multi-test” approach, based on the combination of CPT & DMT. This approach benefits, besides from the multiple measurements provided by a single CPT or DMT sounding, also from the combination of the different measurements obtained from nearby CPT and DMT soundings. Examples of application of a multi-parameter/multi-test approach based on the combined use of CPT & DMT are illustrated in this paper, aiming to stimulate the discussion on the potential of the mutual integration of these two in-situ tests for enhanced site characterization and geotechnical design. The terms ‘CPT’ and ‘DMT’ are herein intended in a general sense, referring to any equipment configurations (i.e., CPT(u), SCPT(u); DMT, SDMT, Medusa (S)DMT).

2 CPT-DMT CORRELATIONS

Interrelationships between CPT & DMT parameters can be helpful to expand and improve correlations and applications by using existing experience and databases from one test and extrapolating to the other (Robertson 2012).

Robertson (2009a) reviewed published records of data from nearby CPT and DMT soundings, as well as existing correlations for geotechnical parameters, in an effort to identify possible intercorrelations. The key in this approach was the recognition that, since the main DMT interpreted parameters are normalized, they should be correlated with normalized CPT parameters. Correlations were tentatively established between the three “intermediate” DMT parameters, i.e., the material index I_D , the horizontal stress index K_D and the dilatometer modulus E_D (Marchetti 1980), and the CPT normalized cone resistance Q_{t1} ,

normalized friction ratio F_r and Soil Behavior Type (SBT) Index I_c , defined as follows:

$$I_D = \frac{p_1 - p_0}{p_0 - u_0} \quad (1)$$

$$K_D = \frac{p_0 - u_0}{\sigma'_{v0}} \quad (2)$$

$$E_D = 34.7(p_1 - p_0) \quad (3)$$

$$Q_{t1} = \frac{q_t - \sigma_{v0}}{\sigma'_{v0}} \quad (4)$$

$$F_r = \left[\frac{f_s}{(q_t - \sigma_{v0})} \right] 100(\%) \quad (5)$$

$$I_c = \left[(3.47 - \log Q_{t1})^2 + (\log F_r + 1.22)^2 \right]^{0.5} \quad (6)$$

where p_0 = corrected first DMT pressure reading, p_1 = corrected second DMT pressure reading, q_t = corrected cone resistance, f_s = sleeve friction resistance, u_0 = pre-insertion in situ equilibrium pore pressure, σ_{v0} = in situ total vertical stress, σ'_{v0} = in situ effective vertical stress.

Robertson (2009a) explained that in most of the available published records the DMT K_D is normalized by σ'_{v0} as in the original formulation (Eq. 2) proposed by Marchetti (1980). Therefore, the CPT cone resistance Q_{t1} was normalized by σ'_{v0} in a consistent manner, i.e., assuming the exponent for stress normalization $n = 1$, as originally proposed by Robertson (1990), although currently used updated formulations (e.g., Robertson 2009b) refer to a normalized cone resistance Q_m that uses a variable n :

$$Q_m = \left[\frac{(q_t - \sigma_{v0})}{p_a} \right] \left(\frac{p_a}{\sigma'_{v0}} \right)^n \quad (7)$$

where p_a = atmospheric pressure in same units as q_t and σ_v , n = stress exponent that varies with SBT I_c (for $n = 1$, $Q_m = Q_{t1}$).

In addition, stress normalization for K_D is a debated issue. Robertson (2009a, 2015) suggested that a more complex normalization for K_D , similar to Q_m , would likely be more appropriate, especially in sands, and future CPT-DMT correlations could use more suitable normalized parameters. However, for typical stress levels in geotechnical engineering of about 65-200 kPa (i.e., ≈ 4 -20 m) the normalization method has little influence on the normalized parameters, hence updated CPT-DMT correlations using a different normalization may not change significantly. On the other hand, Marchetti (2015) remarked that a linear increase with depth of the DMT p_0 (i.e., a nearly constant K_D calculated using $n = 1$) is observed to large depths at

various test sites. In contrast, the increase of the CPT q_t with depth is generally less than linear, corresponding to $n < 1$. Such a different trend was attributed by Marchetti (2015) to the fact that the DMT blade, having a rectangular cross section with a width/thickness ratio ≈ 6 , is less affected by arching than a conical probe, resulting in a more linear trend of p_0 with depth which justifies $n = 1$ for K_D .

The preliminary set of average CPT-DMT correlations proposed by Robertson (2009a) is:

$$I_D = 10^{(1.67-0.67I_c)} \quad (8)$$

When $I_c \leq 2.60$ (i.e., for sand-like soils):

$$K_D = \frac{0.144Q_{t1}}{[10^{(1.67-0.67I_c)}]} \quad (9a)$$

When $I_c > 2.60$ (i.e., for clay-like soils):

$$K_D = \beta(Q_{t1})^{0.95} + 1.05 \quad (9b)$$

$$E_D/\sigma'_{v0} = 5Q_{t1} \quad (10)$$

where the constant β varies with soil sensitivity ($0.30 < \beta < 0.7$), with an average value $\beta = 0.3$.

The correlations for I_D , K_D (Eqs 8, 9a, 9b) depend on soil type, reflected in the CPT index I_c , which is a function of both Q_{t1} and F_r . These correlations are shown in Figure 1 in the form of contours of DMT I_D , K_D on the CPT normalized SBT chart $Q_{t1} - F_r$.

The relationship between DMT I_D and CPT I_c (Eq. 8) was established considering that both parameters are used to identify soil type. It is noted that I_D , likewise I_c , is a parameter reflecting the mechanical soil behavior, not a soil classification index based on real grain size distribution (Marchetti 1980). Robertson & Wride (1998) suggested that $I_c = 2.60$ can be assumed as an approximate boundary between sand-like and clay-like soils. Based on Eq. 8, $I_c = 2.60$ corresponds roughly to $I_D \approx 1$. In a general sense, CPT and DMT results are drained in sand-like soils ($I_c \leq 2.60$, $I_D > 1$) and undrained in clay-like soils ($I_c > 2.60$, $I_D < 1$). The correlation for K_D (Eqs 9a, 9b) can be sensitive to the cut-off $I_c = 2.60$ when CPT data fall close to the boundary between clay-like and sand-like soils. DMT results in the transition region of silt-mixture soils may also be influenced by partial drainage.

Robertson (2015), based on additional pairs of CPT & DMT (e.g., Togliani et al. 2015), suggested a more simplified link between CPT Q_{t1} and DMT K_D , I_D for young uncemented soils (i.e., soils with little or no microstructure):

$$Q_{t1} = (1.5 \log I_D + 7.5)I_D K_D \quad (11)$$

The (smoother) contours of DMT K_D corresponding to Eq. 11 are also plotted in Figure 1 (red dashed lines) on the CPT normalized SBT $Q_{t1} - F_r$ chart.

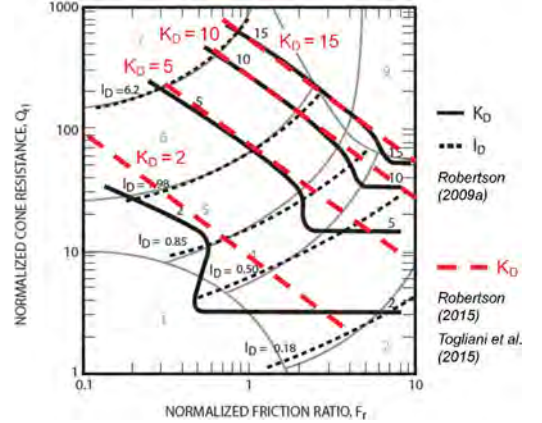


Figure 1. Contours of DMT K_D , I_D on the CPT normalized SBT $Q_{t1} - F_r$ chart for young uncemented soils (from Robertson 2017).

To stimulate a discussion on this topic, it is worth recalling what was observed by Robertson (2009a, 2015), i.e., the proposed CPT-DMT correlations are approximate and influenced by variations in in-situ stress state, soil density, stress and strain history, age, cementation, soil sensitivity. These correlations are unlikely to be unique for all soils, but they may form a framework for possible future refinements. Moreover, they may provide further insight into possible future correlations for the DMT with other geotechnical parameters and design applications, since the CPT has a somewhat more extensive theoretical background compared to the DMT, as well as a larger database of documented case histories for certain applications (e.g., liquefaction assessment). Marchetti (2011) recognized that procedures helpful for extracting as much information as possible from the field data represent a precious contribution since soil information is vital for the determination of reliable soil parameters for design, but costly to obtain. Correlations interconnecting CPT & DMT are useful in that translation formulas permit: (1) the use of interpretation methods or charts developed for one test with the results of the other test, (2) converting a database available for one test to a database for the other test. However, Marchetti (2011) stressed that intrinsic limits exist to the accuracy of the CPT-DMT translations, which, despite further refinements, are bound to remain of an approximate nature. These limits are mostly due to the different sensitivity to stress history

of the representative normalized CPT and DMT parameters, as will be discussed in the following.

A different theoretical approach for establishing interrelationships between the CPT and the DMT in soft clays has been explored by Mayne (2016), Ouyang & Mayne (2017, 2018) and earlier studies, based on a CPT-DMT compiled database in clays that progressively expanded over the years.

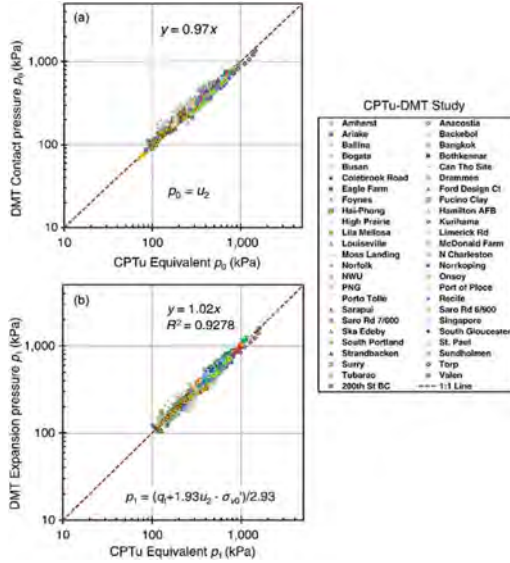


Figure 2. Comparison of DMT and CPTu-equivalent pressures p_0 (a) and p_1 (b) for 49 clays (adapted from Ouyang & Mayne 2018).

Mayne (2016) and Ouyang & Mayne (2017) established a theoretical nexus between CPTu readings (q_t and u_2) and DMT pressures (p_0 and p_1) based on spherical cavity expansion solutions for undrained penetration of both probes in soft clays. This nexus would permit an exchange of interpretations between the two tests, offering a complementary extension of methodologies. Data from paired sets of CPTu-DMT results in a variety of clays were used to support and validate the theoretical links. The net cone resistance, q_{net} , defined as:

$$q_{net} = q_t - \sigma_{v0} \quad (12)$$

was linked to the DMT pressure readings p_0 , p_1 by the following relationship:

$$q_{net} = 2.93p_1 - 1.93p_0 - u_0 \quad (13)$$

Ouyang & Mayne (2018) further expanded this concept and suggested that q_t and u_2 measured from

the CPTu can be utilized to duplicate equivalent DMT pressures p_0 and p_1 , and vice versa, according to the relationships:

$$p_0 = u_2 \quad (14)$$

$$p_1 = \frac{(q_t - 1.93u_2 - \sigma'_{v0})}{2.93} \quad (15)$$

Eq. 14 is in agreement with earlier studies (Mayne & Bachus 1989, Mayne 2006) that found the p_0 from DMT very similar to the pore pressures u_2 measured by CPTu in intact clays and clayey silts. Figure 2 shows a good agreement between the pressures p_0 , p_1 measured by DMT and their CPTu-equivalent p_0 , p_1 estimated by Eqs 14 and 15, based on 49 paired CPTu-DMT data sets in a variety of natural soft to firm clays and silts worldwide, having an overconsolidation ratio OCR between 1 to 2.5.

The approach proposed by Ouyang & Mayne (2017, 2018) is valid only for undrained penetration conditions, which are generally accepted to occur for both CPTu and DMT in low permeability clays at a standard penetration rate of 20 mm/s. The approach could be invalidated in intermediate permeability soils, such as silts, where drainage conditions may be different. The CPTu readings q_t and u_2 are taken during penetration (at time $t = 0$), whereas the DMT readings p_0 and p_1 are obtained at approximately $t = 15$ s and $t = 30$ s after penetration respectively, hence some pore pressure dissipation may have occurred prior to obtaining the DMT readings.

3 CPT VS. DMT DATA COMPARISONS

3.1 Sensitivity to stress history of DMT vs. CPT

The horizontal stress index K_D is a key parameter obtained from DMT interpretation. K_D reflects cumulatively various stress history effects (overconsolidation, aging, in-situ horizontal earth pressure, K_0), as summarized by Marchetti (2010).

Numerous researchers have observed that the DMT K_D is considerably more sensitive than the CPT cone resistance q_c in monitoring compaction in the field. The higher sensitivity of the DMT to stress history is confirmed by comparisons CPT-DMT in controlled calibration chamber (CC) testing conditions. Jamiolkowski & Lo Presti (1998), in CC tests in Ticino sand, found the DMT K_D much more sensitive to stress-strain history (including aging-like effects) than the CPT q_c . Lee et al. (2011) investigated the effects of stress history on CPT and DMT in CC testing on 40 large specimens of Busan sand having different relative density D_r and OCR in the range 1 to 8. The overconsolidation produced an almost negligible increase in the normalized cone resistance $q_c / (\sigma'_{v0})^{0.5}$ (Figure 3a), but a substantial increase in K_D (Figure 3b). It appears

that, while the normalized q_c reflects essentially D_r , and only to a minor extent OCR ,

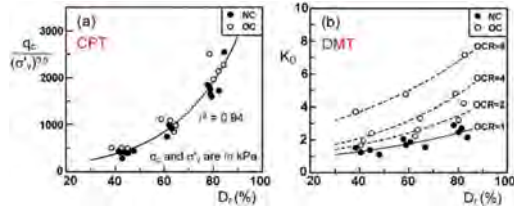


Figure 3. Effect of stress history on (a) normalized q_c from CPT, and (b) K_D from DMT in CC testing on Busan sand (modified from Lee et al. 2011).

K_D reflects not only D_r , but also stress history effects. The higher reactivity of K_D to OCR indicated by Figure 3, in agreement with other available experiences, implies that to the same normalized q_c may correspond different values of K_D (Marchetti 2016). In Figure 3a the coefficient of determination r^2 close to 1 for data points of any OCR suggests poor ability of the normalized q_c to distinguish OC from NC sands, hence estimating OCR from CPT alone appears problematic. This example supports the necessity of a multi-parameter/multi-test approach based on both DMT & CPT for estimating OCR in sand, as will be discussed in the following.

3.2 Soil parameters estimated from DMT vs. CPT

Many indirect correlations exist between DMT and CPT results, since both tests are used to estimate various geotechnical parameters.

The DMT interpretation is commonly based on the original correlations developed by Marchetti (1980) for “textbook” soils, although several updates, reviewed by Marchetti et al. (2001), have been proposed. Among the various parameters obtained from DMT, the 1-D constrained modulus M (M_{DMT}) is the most generally appreciated. According to Marchetti (1980) M_{DMT} is obtained from E_D (Eq. 3), which links soil stiffness to the p_0 and p_1 measured during membrane expansion (a “mini load test”), corrected as a function of I_D (soil type) and K_D (OCR). Several favorable comparisons in terms of both M_{DMT} vs. reference M and DMT-predicted vs. measured settlements have shown that, in general, M_{DMT} is a reasonable estimate of the “operative” or “working strain” modulus.

Numerous correlations have been proposed to estimate the constrained modulus M from CPT in various soil types. Typically, M is obtained by multiplying the cone resistance (q_c or q_t), or the net cone resistance ($q_t - \sigma_{v0}$), by an empirical coefficient α which depends on soil type and other soil properties, and may vary in a rather large range (e.g., 1 to 10).

Comparisons of moduli M estimated from DMT vs. CPT have been published by several authors. As an example, Amoroso et al. (2022a) compared the

depth profiles of M estimated from DMT and CPTu before/after ground improvement with Rammed Aggregate Piers (RAP) in silty and sandy soils at the Bondeno test site, Italy. In natural soils they found a rather good agreement between M estimated from DMT (Marchetti 1980) and from CPTu using the correlations proposed by Robertson (2009b), as shown in Figure 4, while other CPT-based correlations (Lunne & Christophersen 1983, Senneker et al. 1988) provided M equal to about half the values of M obtained from DMT and from Robertson (2009b). The agreement between the latter two methods is not surprising. In fact, the development of the CPT correlations for M by Robertson (2009b) was partly “guided” by the author’s correlations between normalized DMT and CPT parameters (Robertson 2009a), based on the recognition that M estimated from DMT has often been shown to provide excellent estimates of settlement (e.g., Monaco et al. 2006). However, Figure 4 also shows that in treated soils, using the same correlations, the increase in M from DMT was found much more evident than the increase in M from CPTu, suggesting higher ability of M_{DMT} to reflect the benefit of soil treatment.

As to the undrained shear strength (s_u) in clay, available comparisons of s_u from DMT vs. other tests at well-documented sites have often found that the depth profiles of s_u estimated from DMT (Marchetti 1980) plot in an intermediate position, in particular in between the s_u profiles obtained from CPT(u) assuming variable values of the cone bearing capacity factor (N_k or N_{kt}). An example is shown in Figure 5 (Marchetti et al. 2022), where the s_u values obtained in Fucino clay by Medusa DMT are compared with the s_u from CPT(u) and from other tests.

Comparisons CPT-DMT are also available in terms of pore pressure index and consolidation/drainage parameters inferred from dissipation tests. The DMT, though non provided with a pore pressure sensor as the CPTu, permits to determine the pre-insertion in-situ equilibrium pore pressure u_0 in sand and to discern layers of different permeability based on the closing pressure p_2 . As described by Marchetti et al. (2001), in sand $p_2 \approx u_0$, while in clay $p_2 > u_0$ due to some excess pore pressure induced by penetration persisting at the time of the p_2 measurement. The pore pressure index U_D (Lutenegger & Kabir 1988) is defined as:

$$U_D = \frac{(p_2 - u_0)}{(p_0 - u_0)} \quad (16)$$

The parameter U_D is the DMT equivalent of the pore pressure ratio B_q from CPTu:

$$B_q = \frac{(u_2 - u_0)}{(q_t - \sigma_{v0})} \quad (17)$$

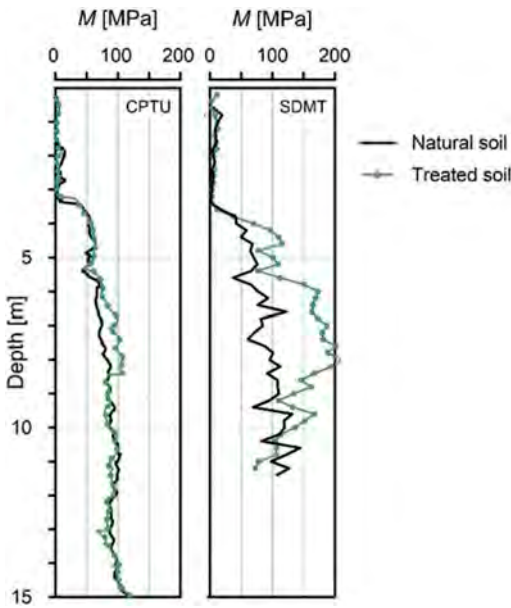


Figure 4. Comparison of constrained moduli M estimated from CPTu (Robertson 2009b) and SDMT (Marchetti 1980) in natural and treated soils at the Bondeno test site (modified from Amoroso et al. 2022a).

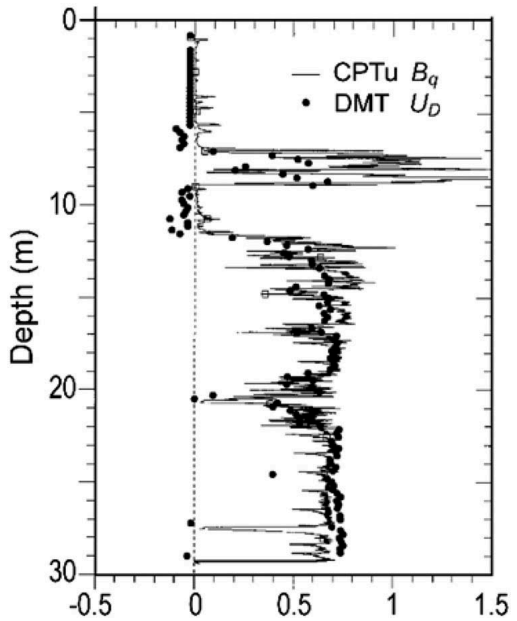


Figure 6. Comparison of U_D from DMT and B_q from CPTu (Benoit 1989, from Marchetti et al. 2001).

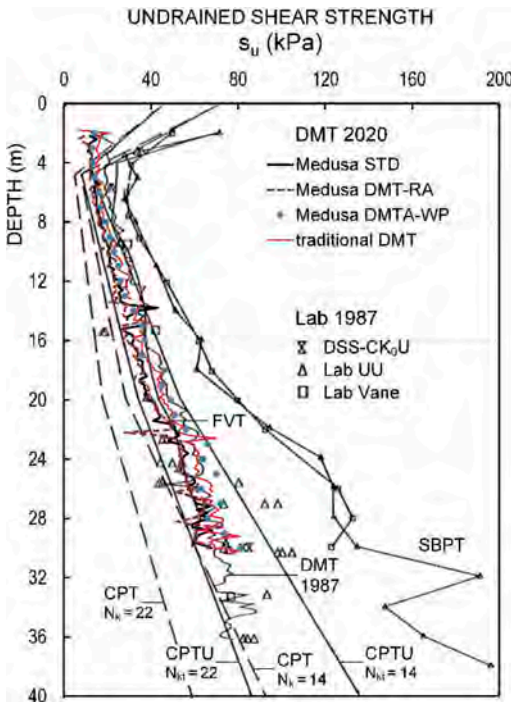


Figure 5. Comparison of profiles of the undrained shear strength s_u from standard/Medusa DMT, CPT/CPTu and other in-situ and laboratory tests (data from Burghignoli et al. 1991) at Fucino-Telespazio (Marchetti et al. 2022).

Similar to B_q , U_D may help delineate soil stratigraphy, particularly in highly stratified deposits. In free-draining soils $U_D \approx 0$, in non free-draining soils $U_D > 0$. The example in Figure 6 (Benoit 1989) shows a good agreement between DMT U_D and CPTu B_q .

The use of the DMT in intermediate soils (silty sands, silts, sandy silts) is being increasingly Monaco et al. (2014) as part of an extensive investigated (Schnaid et al. 2016, 2018). Monaco et al. (2021) presented preliminary results of tests carried out using the Medusa DMT adopting variable pressurization and penetration rates in intermediate soils in the Po river valley, Italy, combined with CPTus at variable penetration rates. In these soils, the highly accurate and repeatable time-for-reading facility of the Medusa DMT permitted to identify some trends in the variation of DMT pressure measurements in response to variable-rate testing conditions, i.e., a slower penetration/pressurization rate ‘shifts’ the interpretation towards drained behavior, while a faster penetration/pressurization rate ‘shifts’ the interpretation towards undrained behavior. In sand, a fully drained response was found for any penetration/pressurization rate. U_D appears as a suitable independent parameter to discern between drained, undrained or partially drained soil behavior and may be usefully combined with I_D to obtain some ‘soil behavior type’. Ongoing research investigates the potential of combining variable-rate Medusa DMT and CPTu tests as an innovative approach for characterizing the in-situ behavior of intermediate soils.

The DMT is also used to estimate in-situ consolidation/permeability parameters by means of

dissipation tests. Differently from CPTu, the decay with time monitored by the DMT is not that of the pore pressure, but of the total contact A -pressure. This involves lack of worry over desaturation or poor saturation of a porous element, which may affect the u_2 measurement in CPTu dissipation tests. The Medusa DMT technology, which permits to acquire up to 3 repeated A -pressure readings per second, has extended the range of soil types in which A -dissipations are feasible from low permeability soils (clays, silty clays) to intermediate permeability soils (silts, silty sands).

4 DERIVATION OF SOIL PARAMETERS BY COMBINED USE OF CPT & DMT

4.1 Estimating OCR in sand from DMT & CPT

The combined use of DMT & CPT may provide estimates of the OCR in sand. Marchetti et al. (2001) suggested to use the ratio between the constrained modulus from DMT M_{DMT} and the cone resistance q_c from CPT as an indicator OCR in sand:

$$M_{DMT}/q_c = 5 - 10 \text{ in NC sands} \quad (18a)$$

$$M_{DMT}/q_c = 12 - 24 \text{ in OC sands} \quad (18b)$$

The above preliminary indications were based on available CPT-DMT data before/after compaction of sand fills (e.g., Jendebly 1992), where M_{DMT}/q_c was found to increase with the overconsolidation achieved by compaction, combined with data from CC research and from other tests.

The possibility to estimate OCR in sand by the combined use of DMT and CPT was investigated by Monaco et al. (2014) as part of an extensive experimental study carried out at the Treporti Test Site, Venice, Italy. At this site, a full-scale cylindrical trial embankment (40 m diameter, 6.7 m height, applied pressure 106 kPa) was built and monitored from the beginning of its construction until its complete removal, four years later. Using same-depth values of M_{DMT} and q_t obtained in sand layers from paired DMT and CPTu soundings carried out at the times when reference “imparted OCR ” were known, i.e. at end-of-construction and post-removal, Monaco et al. (2014) derived the correlation (Figure 7):

$$OCR = 0.0344(M_{DMT}/q_t)^2 - 0.4174(M_{DMT}/q_t) + 2.2914 \quad (19)$$

Using the same data set, Monaco et al. (2014) also constructed a correlation $OCR-K_D$ based only on DMT. However the $OCR-K_D$ correlation is not

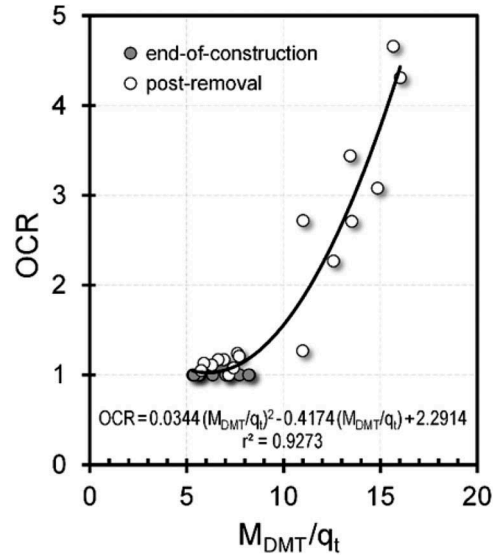


Figure 7. Correlation $OCR-M_{DMT}/q_t$ in sands obtained from paired DMT-CPTu data at the Treporti trial embankment test site (modified from Monaco et al. 2014).

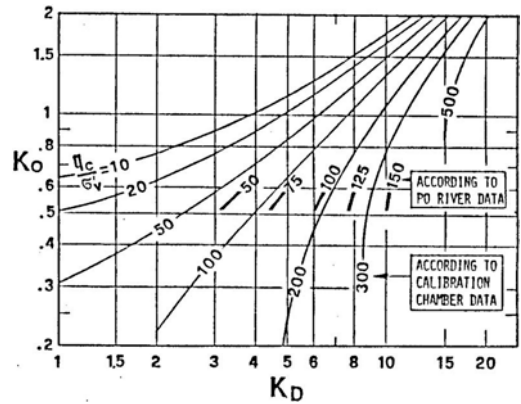


Figure 8. Chart for evaluating $K_0 = f(K_D, q_c/\sigma'_v)$ proposed by Marchetti (1985).

unique, but likely depending also on the relative density D_r . In fact, going back to the CC results shown in Figure 3b (Lee et al. 2011), it can be deduced that for a given D_r , there is a one-to-one correspondence between K_D and OCR values (i.e., a vertical line having constant D_r in the diagram intersects each OCR curve for a unique K_D value), but if D_r is not constant the same OCR may result from a different combination of K_D and D_r . Hence a given K_D may be due either to a low D_r , and a high OCR , or to a high D_r , and a low OCR . In order to separate the D_r effect from the OCR effect, i.e., to pinpoint the right OCR, D_r pair and then to estimate

OCR , the normalized q_c (Figure 3a) is also necessary to provide an indication of D_r on the horizontal axis. Hence both q_c and K_D would be needed to estimate OCR in sand, i.e., CPT alone or DMT alone are insufficient. The $OCR-K_D$ correlation by Monaco et al. (2014) works well at the Treporti test site where it was calibrated because in these sands D_r is almost uniform, but it may not work at sites where D_r is variable. Based on CC tests on Busan sand samples having different D_r and OCR , Choo et al. (2015) proposed a correlation to estimate OCR in sand based on K_D and D_r , with D_r also estimated from DMT, hence using only DMT data. This $OCR-K_D$ correlation needs to be calibrated for each specific sand.

The $OCR-M_{DMT}/q_t$ correlation (Eq. 19) by Monaco et al. (2014), based on both DMT and CPTu data, appears to have more general validity and may provide broad OCR estimates in different sands. Additional research is encouraged to investigate the dependency of the correlation $OCR-M_{DMT}/q_t$ on D_r , stress level and possibly sand type.

4.2 Estimating K_0 in sand from DMT & CPT

Similar considerations may be extended to the estimation of K_0 in sand. The $K_0 - q_c - K_D$ chart in Figure 8, elaborated by Marchetti (1985), is probably the first example of combined use of CPT & DMT. The chart permits to estimate K_0 once q_c and K_D are known. Figure 8 shows, besides the continuous curves obtained from CC tests, an additional scale for q_c/σ'_v based on 25 data points in Po river sand, where an average value $K_0 = 0.55$ was estimated.

Baldi et al. (1986) enriched such $K_0 - q_c - K_D$ chart with additional CC work and converted it into the following equations:

$$K_0 = 0.376 + 0.095K_D - 0.0017q_c/\sigma'_{v0} \quad (20a)$$

$$K_0 = 0.376 + 0.095K_D - 0.0046q_c/\sigma'_{v0} \quad (20b)$$

Eq. 20a was determined as the best fit of CC data, obtained on pluviated artificial sand, while Eq. 20b was obtained by modifying the last coefficient to predict “correctly” K_0 for the natural Po river sand.

Marchetti et al. (2001) recommended using Eqs 20a and 20b (Baldi et al. 1986) with the following values of the last coefficient: -0.002 in “freshly deposited” sand, -0.005 in “seasoned” sand. In this way, the influence of OCR on K_0 is incorporated by the choice of the last coefficient, which involves appreciable subjectivity (e.g., a sand could be assumed as “fresh” if $K_D = 1-2$, “seasoned” if $K_D = 5-6$).

Choo et al. (2015), based on CC testing on Busan sand, proposed a correlation to estimate K_0 in sand from DMT only, but similarly to OCR this correlation requires specific calibration for different sands.

Based on the CC data set by Baldi et al. (1986), Hossain & Andrus (2016) proposed to estimate K_0 in sand by use of the following correlation:

$$K_0 = 0.72 + 0.456 \log OCR + 0.035K_D - 0.194 \log(q_c/\sigma'_v) \quad (21)$$

in which the influence of OCR on K_0 is explicitly taken into account. Eq. 21 could be used in combination with OCR estimated by Eq. 19.

All the above considerations imply that the challenging task of estimating OCR and K_0 in sands requires a multi-parameter/multi-test approach, based on the combined use of DMT and CPT.

5 APPLICATIONS BASED ON COMBINED USE OF CPT & DMT DATA

5.1 Use of DMT & CPT in monitoring ground improvement

Several comparisons of pre-post CPT & DMT executed for monitoring ground improvement are available. Various studies have found the increase in M_{DMT} after soil treatment approximately twice the increase in q_c . For instance, Jendebay (1992) found an increase of the ratio M_{DMT}/q_c from $\approx 5-12$ pre-compaction to $\approx 12-24$ post-compaction of a loose sand fill (Figure 9a). Bałachowski & Kurek (2015) found the mean increase in M_{DMT} after vibroflotation of sand about 2.3 times higher than the corresponding increase in q_c and an increase of M_{DMT}/q_c from $\approx 2-10$ pre-compaction to $\approx 10-24$ post-compaction (Figure 9b). Amoroso et al. (2022a, b), using paired DMT and CPTu data before/after ground improvement with Rammed Aggregate Piers (RAP) at the Bondeno test site, found a similar trend of the ratio M_{DMT}/q_t (Figure 10), consistent with the observed increase in M_{DMT} higher than M from CPTu in treated soils (Figure 4). This evidence suggests that the DMT is more sensitive to stiffness variations as a consequence of the increase in horizontal stress produced by soil treatment, as reflected by the increase in K_0 (and OCR), also shown in Figure 10. Similar pre-post comparisons were reported by Amoroso et al. (2018). The finding that compaction (a sort of “imparted overconsolidation”) increases both M_{DMT} and q_c , but M_{DMT} at a faster rate, inspired the use of the ratio M_{DMT}/q_c as a “proxy” of OCR , as previously discussed.

5.2 Liquefaction assessment based on DMT & CPT

The use of the DMT for liquefaction assessment is receiving increasing attention. Much of the interest on the development of simplified methods based on the DMT K_D derives from its high sensitivity to stress history, besides to other factors (e.g., D_r , K_0 , aging) that

influence liquefaction resistance. Numerous researchers (e.g., Pyke 2003, Leon et al. 2006 and many others) have pointed out that past stress-strain history (overconsolidation, aging) is likely to have a much greater effect on increasing liquefaction resistance than penetration resistance.

Simplified methods for estimating the cyclic resistance ratio (CRR) based on DMT K_D have been proposed over the years, including the most recent by Monaco et al. (2005), Tsai et al. (2009), Robertson (2012), Marchetti (2016), Chiaradonna & Monaco (2022) shown in Figure 11 (valid for magnitude $M = 7.5$ and clean uncemented sand).

All these methods have in common a strong link with CPT-based methods in their origin, in an effort to relate in some way to the field performance database that provides a vast experimental validation for current methods based on CPT, but is currently limited for DMT-based methods.

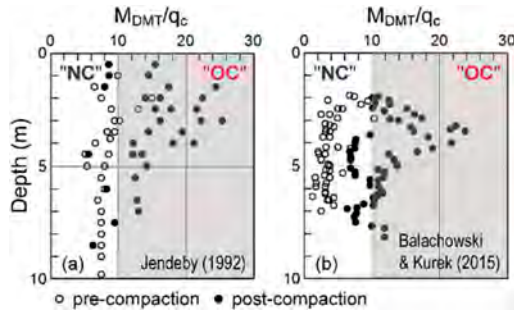


Figure 9. Ratio M_{DMT}/q_c before-after compaction of sand fills/deposits: data from (a) Jendebly (1992), (b) Balachowski & Kurek (2015).

The $CRR-K_D$ curve by Monaco et al. (2005) was obtained by translating “consensus” CPT (and SPT) curves, namely the CPT curve by Robertson & Wride (1998), using the relative density D_r as intermediate parameter. This approach is inevitably affected by some uncertainty in estimating D_r from the in-situ tests. Differently, Tsai et al. (2009) obtained a $CRR-K_D$ curve by translating “consensus” CPT (and SPT) curves, again Robertson & Wride (1998) for CPT, by using direct correlations between the CPT normalized clean sand equivalent cone resistance and the DMT K_D , established using data from paired CPT-DMT soundings at five saturated loose sand sites in Taiwan that experienced liquefaction.

Using a similar approach, independently, Robertson (2012) re-elaborated the CPT-DMT data set collected by Tsai et al. (2009) and proposed, for young uncemented sands ($I_D > 1.2$ and $2 < K_D < 6$), an average relationship between the normalized clean sand equivalent cone resistance $Q_{m,cs}$, defined as:

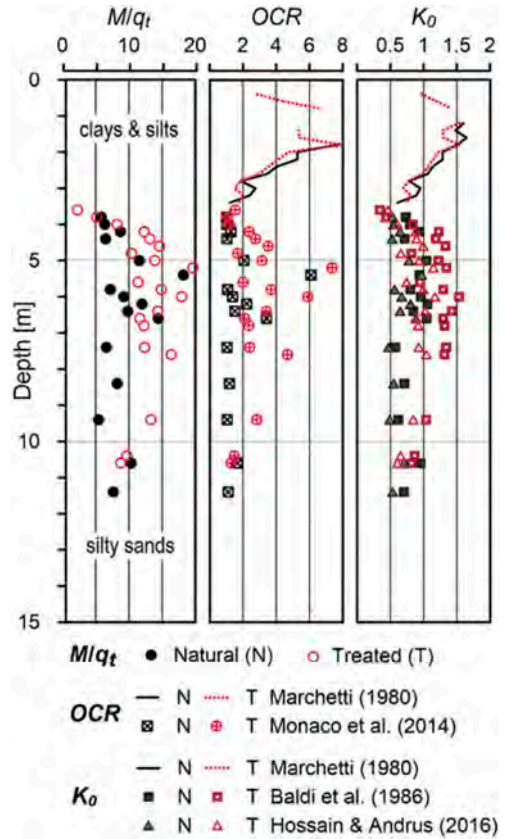


Figure 10. Profiles of M_{DMT}/q_c , OCR and K_0 obtained from combined DMT-CPTu data in natural and treated soils at the Bondeno test site (modified from Amoroso et al. 2022b).

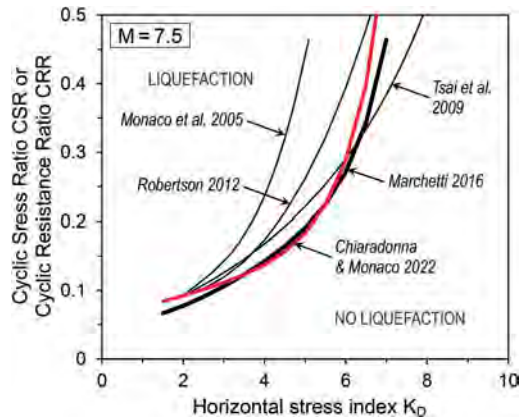


Figure 11. Recent $CRR-K_D$ correlations for clean sand.

$$Q_{m,cs} = K_c \cdot Q_m \quad (22)$$

where K_c = correction factor for fines content estimated using I_c , and the DMT K_D :

$$Q_{m,cs} = 25K_D \quad (23)$$

Based on Eq. 23, Robertson (2012) converted the Robertson & Wride (1998) $CRR-Q_{m,cs}$ curve into a $CRR-K_D$ curve. Later Marchetti (2016) obtained a new $CRR-K_D$ curve by combining the same Eq. 23 with the CPT curve by Idriss & Boulanger (2006).

Chiaradonna & Monaco (2022) proposed an update of the $CRR-K_D$ curve adopting the CPT-based framework by Boulanger & Idriss (2014). Using the CPT-DMT data set by Tsai et al. (2009), considering only CPT data having I_c between 1.5 and 2.6, a direct correlation was established between K_D and the clean sand equivalent cone resistance q_{c1Ncs} defined according to Boulanger & Idriss (2014):

$$q_{c1Ncs} = q_{c1N} + \Delta q_{c1N} \quad (24)$$

where q_{c1N} is the normalized cone resistance and Δq_{c1N} accounts for the effect of fines content.

Despite the dispersion, the data set (Figure 12) is well described by a linear trend with a slope of 20. Figure 12 also shows a second data set from the Scortichino site, Italy, where both CPT and SDMT data were available (Tonni et al. 2015), which is better interpreted by a linear trend with a slope of about 30. Based on this limited data, Chiaradonna & Monaco (2022) adopted an average coefficient of 25:

$$q_{c1Ncs} = 25K_D \quad (25)$$

which is compatible with Eq. 23 by Robertson (2012), also used by Marchetti (2016). By substituting Eq. 25 into the $CRR-q_{c1Ncs}$ curve by Boulanger & Idriss (2014), a new $CRR-K_D$ curve was obtained.

Average CPT-DMT correlations such as Eq. 23 (Robertson 2012) and Eq. 25 (Chiaradonna & Monaco 2022) may be useful to convert CPT- into DMT-based liquefaction triggering curves. On the other hand, the example in Figure 12 suggests that the $q_{c1Ncs} - K_D$ relationship varies from one site to another, presumably as a consequence of the higher sensitivity of K_D to stress history. Two sites may have similar q_{c1Ncs} , but different K_D depending on different stress history (Marchetti 2016). This implies that q_{c1Ncs} and K_D do not contain equivalent information, and may also explain in part the high dispersion of the CPT-DMT correlations (Marchetti 2015). Robertson (2015), recognizing the higher sensitivity of K_D to factors that cause soil microstructure (stress and strain history, age, cementation/bonding), suggested using the $Q_{m,cs} - K_D$ relationship to assess microstructure, noting that in young uncemented sands generally $Q_{m,cs} > 16 K_D$, while soils with significant microstructure tend to have $Q_{m,cs} < 16 K_D$.

In perspective, the DMT could offer a valuable integration to current methods for liquefaction assessment based on CPT, SPT or V_s , also given the

general recommendation towards the use of “redundant” correlations based on different in-situ techniques/parameters. The main drawbacks of current DMT-based methods are: (1) lack of any correction factor for the fines content, and (2) limited experimental validation based on field performance data from real earthquakes. Ongoing research is attempting to fill these gaps. The implementation of an adequate case-history database for validation of the DMT-based approach could support the introduction of more consistent liquefaction triggering curves, considering also the fines content influence.

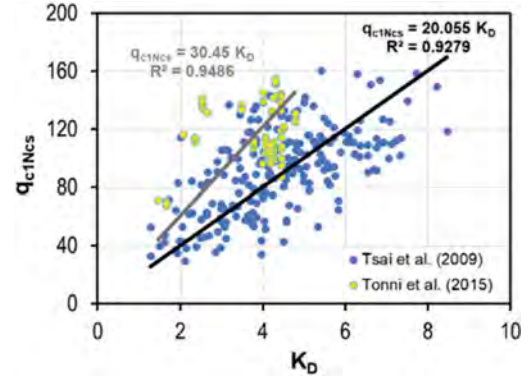


Figure 12. Relationship $q_{c1Ncs} - K_D$ from published CPT-DMT data records at two test sites (Chiaradonna & Monaco 2022).

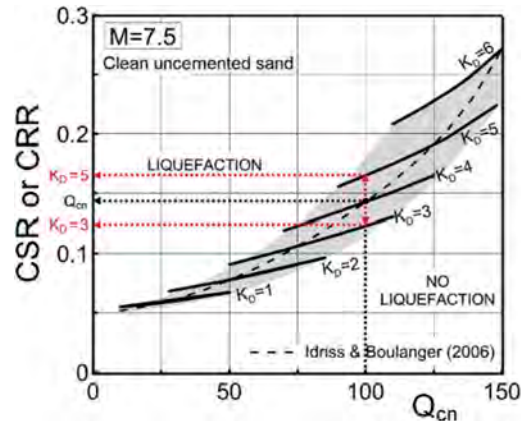


Figure 13. Correlation for estimating CRR based on both DMT & CPT for clean sand (modified from Marchetti 2016).

Besides the $CRR-K_D$ curve, Marchetti (2016) also proposed a method to estimate CRR based on the combined use of DMT & CPT (Figure 13), aiming to complement the higher sensitivity of K_D to stress history with the much larger field performance support of CPT-based methods. The conceptual framework is the

following: (1) estimate CRR using a “consensus” CPT liquefaction curve; (2) increase (shift upwards) the CRR predicted by CPT if K_D is high, reduce it (shift downwards) if K_D is low. As an example, Figure 13 for a normalized cone resistance $Q_{cn} = 100$ and $K_D = 3$ provides $CRR = 0.125$ (i.e., lower than predicted by the dashed CPT curve), while for the same $Q_{cn} = 100$ and $K_D = 5$ the chart provides $CRR = 0.17$ (i.e., higher than predicted by CPT). The method proposed by Marchetti (2016) for estimating CRR from both DMT & CPT is another example of multi-parameter/multi-test approach. It is expectable that an estimate based on two measured independent parameters could be more accurate than an estimate based on just one parameter.

6 PROPER MATCHING OF CPT & DMT DATA

One specific issue that arises when using any interpretation or design approach that requires the combination of CPT & DMT results is the proper matching of corresponding data. In fact, the CPT measurements are taken every 10-20 to 50 mm, whereas the DMT pressure readings are taken every 200 mm. Data from paired CPT & DMT soundings shall be matched at respective elevations. Care must be adopted even when nearby soundings are carried out at the same ground elevation, particularly in non uniform, highly stratified deposits.

Comparisons between individual same-depth values from nearby CPT & DMT profiles often show considerable scatter due to variations in soil stratigraphy and consistency, hence adjacent data from the same depth may not always represent the same soil. Sand deposits are often characterized by high variability in grain size distribution and D_r , then plots of individual data points from nearby CPT & DMT may show large scatter. The profiles of q_t may also differ slightly from those of adjacent DMT since the CPT senses soil slightly ahead and behind the cone tip (up to 15 cone diameters, depending on soil strength, stiffness and in-situ effective stresses, Ahmadi & Robertson 2005). The DMT appears to be less influenced by soil layers ahead and behind since the probe is stopped and the membrane expanded in horizontal direction. Hence, in interbedded soils the CPT may be influenced by adjacent soil layers somewhat more than the DMT (Robertson 2009a).

Any comparison between adjacent CPT & DMT should be done in terms of the near continuous profiles with depth, so that any variation in soil stratigraphy can be identified from the profiles. It is also common to compare values obtained at the same depth within relatively uniform sections of a deposit. As an example, at the highly stratified Treporti test site (Monaco et al. 2014) the paired CPTu-DMT data, including the data pairs $M_{DMT} - q_t$ shown in Figure 7, were carefully selected by retaining only pairs from uniform soil layers of significant thickness to avoid any possible mismatching of data.

In general, the following matching criteria may be adopted: (1) match paired CPT & DMT profiles

accounting for respective ground elevations, if not coincident; (2) correct both CPT & DMT test depths for inclination; (3) select soil type (e.g., sand-like, $I_c \leq 2.60$ and $I_D > 1$, or clay-like, $I_c > 2.60$ and $I_D < 1$) and possibly depth range of interest; (4) identify “visually” or by cross-correlation of representative parameters (e.g., q_t and M_{DMT}) corresponding soil layers in CPT & DMT profiles, to detect any depth misalignment offset; (5) identify soil layers having a reasonable thickness (e.g., in which at least two DMT readings are present) and relatively uniform CPT & DMT parameters; (6) use average values of CPT & DMT parameters in each layer. It would be desirable that the matching algorithm is implemented in software tools, although some visual inspection and judgment may be still needed.

7 CONCLUDING REMARKS

Direct-push in-situ tests such as the CPT and the DMT, particularly in their powerful seismic configurations, have proven to be remarkably expedient in geotechnical site investigations. Recent experience highlights an increasing awareness of researchers and practitioners that an adequate site investigation for a given project cannot rely solely on one isolated testing technique, delineating the trend of expanding diffusion of a multi-parameter/multi-test approach in site investigation practice.

The CPT and the DMT can be effectively combined to obtain more accurate information on stratigraphy and stress history of soil deposits, more reliable estimates of soil parameters (e.g., OCR and K_0 in sand) and for various design applications (e.g., monitoring ground improvement, liquefaction assessment). Moving towards an in-situ multi-parameter/multi-test approach appears a logical trend. In this respect, the availability of the DMT stress history parameter K_D is important not only “per se”, but also in combination with parameters obtained from CPT.

Each test has advantages and limitations. The CPT is often used more than the DMT, especially for smaller projects, being faster and less expensive (no pauses of penetration are required for obtaining the measurements, as for the DMT). However, the DMT has been shown to be more sensitive to stress history, which has a dominant influence on soil behavior. Hence, their mutual integration could helpfully merge the respective advantages and counterbalance their limitations. For instance, the CPT could be used for a “screening” of the site on a large scale, the DMT at locations of particular relevance for the project. Adjacent CPT & DMT at selected locations should be planned. The increase in time and cost of a site investigation program including paired CPT & DMT soundings can be efficiently optimized considering that both tests can share the same insertion rig and rods, and even the same cable when using the Medusa DMT (i.e., only the probe connected to the

bottom rod needs to be changed). Such “redundancy” would be largely compensated by substantial increase in soil information.

Interrelationships between CPT & DMT can be used to expand and improve correlations and applications by using experience and databases from one test and extrapolating to the other test. The accumulation and sharing of paired data sets from companion series of CPT & DMT soundings at well-documented and benchmark test sites is a desirable address for future research and practice.

ACKNOWLEDGEMENTS

Special thanks to Peter K. Robertson for sharing his updates on CPT-DMT correlations. Thanks to Diego Marchetti, Sara Amoroso, Anna Chiaradonna for their helpful suggestions, to Gianfranco Totani and Giovanni Bosco for the shared experience on in-situ testing. Grateful thanks to Silvano Marchetti for his constant and bright guidance over many years.

REFERENCES

- Ahmadi, M.M. & Robertson, P.K. 2005. Thin layer effects on the CPT q_c measurement. *Can. Geotech. J.* 42(9): 1302–1317.
- Amoroso, S., Comina, C. & Marchetti, D. 2020. Combined P- and S-Wave Measurements by Seismic Dilatometer Test (SPDMT): A Case History in Bondeno (Emilia Romagna, Italy). *Geotech. Testing J.* 43(2): 383–393.
- Amoroso, S., Garcia Martinez, M.F., Monaco, P., Tonni, L., Gottardi, G., Rollins, K.M., Minarelli, L., Marchetti, D. & Wissmann, K.J. 2022a. Comparative study of CPTU and SDMT in liquefaction prone silty sands with ground improvement. *J. Geotech. Geoenviron. Eng.* (accepted) [http://dx.doi.org/10.1061/\(ASCE\)GT.1943-5606.0002801](http://dx.doi.org/10.1061/(ASCE)GT.1943-5606.0002801)
- Amoroso, S., Martínez, M.F., Tonni, L., Gottardi, G., Monaco, P., Rollins, K.M., Minarelli, L., Marchetti, D. & Wissmann, K.J. 2022b. Monitoring ground improvement by Rammed Aggregate Piers using a combined CPTU and SDMT approach at a silty sand liquefaction-prone site in Emilia-Romagna. *Proc. 5th Int. Symp. Cone Penetration Testing CPT'22, Bologna*, 8-10 June 2022.
- Amoroso, S., Rollins, K.M., Monaco, P., Holtrigter, M. & Thorp, A. 2018. Monitoring Ground Improvement Using the Seismic Dilatometer in Christchurch, New Zealand. *Geotech. Testing J.* 41(5): 946–966.
- Bałachowski, L. & Kurek, N. 2015. Vibroflotation Control of Sandy Soils. In S. Marchetti, P. Monaco & A. Viana da Fonseca (eds), *Proc. 3rd Int. Conf. Flat Dilatometer DMT'15, Rome*, 14-16 June 2015, 185–190.
- Baldi, G., Bellotti, R., Ghionna, V., Jamiolkowski, M., Marchetti, S. & Pasqualini, E. 1986. Flat Dilatometer Tests in Calibration Chambers. *Proc. Spec. Conf. Use of In Situ Tests in Geotech. Eng. In Situ '86, Blacksburg*, 431–446.
- Benoit, J. 1989. Personal communication to S. Marchetti.
- Boulanger, R.W. & Idriss, I.M. 2014. CPT and SPT liquefaction triggering procedures. *Report No UCD/GCM-14/01*, University of California at Davis.
- Burghignoli, A., Cavallera, L., Chiappa, V., Jamiolkowski, M., Mancuso, C., Marchetti, S., Pane, V., Paoliani, P., Silvestri, F., Vinale, F. & Vittori, E. 1991. Geotechnical characterization of Fucino clay. *Proc. 10th Eur. Conf. Soil Mech. Found. Eng., Florence*, 26-30 May 1991, 1: 27–40. Rotterdam: Balkema.
- Chiaradonna, A. & Monaco, P. 2022. Assessment of liquefaction triggering by seismic dilatometer tests: comparison between semi-empirical approaches and non-linear dynamic analyses. *Proc. 20th Int. Conf. Soil Mech. Geotech. Eng., Sydney*, 1-5 May 2022.
- Choo, H., Lee, W., Lee, C., Kim, Y.-S. & Lee, M.-J. 2015. Perception of Overconsolidated States of Coarse-Grained Soils Using DMT Results. In S. Marchetti, P. Monaco & A. Viana da Fonseca (eds), *Proc. 3rd Int. Conf. Flat Dilatometer DMT'15, Rome*, 14-16 June 2015, 205–212.
- Hossain, M.A. & Andrus, R.D. 2016. At-Rest Lateral Stress Coefficient in Sands from Common Field Methods. *J. Geotech. Geoenviron. Eng.* 142(12): 06016016.
- Idriss, I.M. & Boulanger, R.W. 2006. Semi-empirical procedures for evaluating liquefaction potential during earthquakes. *Soil Dyn. Earthquake Eng.* 26(2-4): 115–130.
- Jamiolkowski, M. & Lo Presti, D.C.F. 1998. DMT research in sand. What can be learned from calibration chamber tests. *1st Int. Conf. Site Characterization ISC '98, Atlanta*, 19-22 April 1998 (oral presentation).
- Jendeby, L. 1992. Deep Compaction by Vibrowring. *Proc. Nordic Geotech. Meeting NGM-92, Aalborg*, 1: 19–24.
- Lee, M.J., Choi, S.K., Kim, M.T. & Lee, W. 2011. Effect of stress history on CPT and DMT results in sand. *Eng. Geol.* 117(3-4): 259–265.
- Leon, E., Gassman, S.L. & Talwani, P. 2006. Accounting for Soil Aging When Assessing Liquefaction Potential. *J. Geotech. Geoenviron. Eng.* 132(3): 363–377.
- Lunne, T. & Christophersen, H.P. 1983. Interpretation of cone penetrometer data for offshore sands. *Proc. 15th Annual Offshore Technology Conf.*, 181–188.
- Lutenegger, A.J. & Kabir, M.G. 1988. Dilatometer C-reading to help determine stratigraphy. *Proc. Int. Symp. Penetration Testing ISOPT-1, Orlando*, 1: 549–554. Rotterdam: Balkema.
- Marchetti, D., Monaco, P., Amoroso, S. & Minarelli, L. 2019. In situ tests by Medusa DMT. *Proc. XVII Eur. Conf. Soil Mech. Geotech. Eng., Reykjavik*, 1-6 September 2019.
- Marchetti, D., Monaco, P., Totani, G., Totani, F. & Amoroso, S. (2022). Comparisons CPT-DMT in soft clay at Fucino-Telespazio GeoTest site. *Proc. 5th Int. Symp. Cone Penetration Testing CPT'22, Bologna*, 8-10 June 2022.
- Marchetti, S. 1980. In Situ Tests by Flat Dilatometer. *J. Geotech. Eng. Div.* 106(GT3): 299–321.
- Marchetti, S. 1985. On the Field Determination of K_0 in Sand. *Proc. 11th Int. Conf. Soil Mech. Found. Eng., San Francisco*, 5: 2667–2673. Rotterdam: Balkema.
- Marchetti, S. 2010. Sensitivity of CPT and DMT to stress history and aging in sands for liquefaction assessment. *Proc. 2nd Int. Symp. Cone Penetration Testing CPT'10, Huntington Beach*, 9-11 May 2010.
- Marchetti, S. 2011. Discussion of “CPT-DMT Correlations” by P.K. Robertson. *J. Geotech. Geoenviron. Eng.* 137(4): 441–442.
- Marchetti, S. 2015. Some 2015 Updates to the TC16 DMT Report 2001. In S. Marchetti, P. Monaco & A. Viana da

- Fonseca (eds), *Proc. 3rd Int. Conf. Flat Dilatometer DMT'15, Rome*, 14-16 June 2015, 43–65.
- Marchetti, S. 2016. Incorporating the Stress History Parameter K_D of DMT into the Liquefaction Correlations in Clean Uncemented Sands. *J. Geotech. Geoenviron. Eng.* 142(2): 04015072.
- Marchetti, S. & Monaco, P. 2018. Recent Improvements in the Use, Interpretation, and Applications of DMT and SDMT in Practice. *Geotech. Testing J.* 41(5): 837–850.
- Marchetti, S., Monaco, P., Totani, G. & Calabrese, M. 2001. The Flat Dilatometer Test (DMT) in Soil Investigations – A Report by the ISSMGE Committee TC16. Official version approved by ISSMGE TC16 reprinted in R. A. Failmezger & J.B Anderson (eds), *Proc. 2nd Int. Conf. Flat Dilatometer, Washington D.C.*, 2-5 April 2006, 7–48.
- Mayne, P.W. 2006. Interrelationships of DMT and CPT Readings in Soft Clays. In R.A. Failmezger & J. B Anderson (eds), *Proc. 2nd Int. Conf. Flat Dilatometer, Washington D.C.*, 2-5 April 2006, 231–236.
- Mayne, P.W. 2016. Evaluating effective stress parameters and undrained shear strengths of soft-firm clays from CPTu and DMT. *Australian Geomech. J.* 51(4): 27–55.
- Mayne, P.W. & Bachus, R.C. 1989. Penetration Pore Pressures in Clay by CPTU, DMT, and SBP. *Proc. 12th Int. Conf. Soil Mech. Geotech. Eng., Rio de Janeiro*, 291–294. Rotterdam: Balkema.
- Mayne, P.W., Coop, M.R., Springman, S.M., Huang, A.B. & Zornberg, J.G. 2009. Geomaterial behavior and testing. *Proc. 17th Int. Conf. Soil Mech. Geotech. Eng., Alexandria*, 5-9 October 2009, 4: 2777–2872. Amsterdam: IOS Press.
- Monaco, P., Amoroso, S., Marchetti, S., Marchetti, D., Totani, G., Cola, S. & Simonini, P. 2014. Overconsolidation and Stiffness of Venice Lagoon Sands and Silts from SDMT and CPTU. *J. Geotech. Geoenviron. Eng.* 140(1): 215–227.
- Monaco, P., Marchetti, S., Totani, G. & Calabrese, M. 2005. Sand Liquefiability Assessment by Flat Dilatometer Test (DMT). *Proc. 16th Int. Conf. Soil Mech. Geotech. Eng., Osaka*, 4: 2693–2697. Rotterdam: Millpress.
- Monaco, P., Tonni, L., Amoroso, S., Garcia Martinez, M.F., Gottardi, G., Marchetti, D. & Minarelli, L. 2021. Use of Medusa DMT in alluvial silty sediments of the Po river valley. *Proc. 6th Int. Conf. Geotech. Geophys. Site Characterisation ISC'6, Budapest*, 26-29 September 2021.
- Monaco, P., Totani, G. & Calabrese, M. 2006. DMT-predicted vs observed settlements: a review of the available experience. In R.A. Failmezger & J.B Anderson (eds), *Proc. 2nd Int. Conf. Flat Dilatometer, Washington D.C.*, 2-5 April 2006, 244–252.
- Ouyang, Z. & Mayne, P.W. 2017. Spherical cavity expansion nexus between CPTu and DMT in soft-firm clays. *Proc. 19th Int. Conf. Soil Mech. Geotech. Eng., Seoul, 17-22 September 2017*, 631–634.
- Ouyang, Z. & Mayne, P.W. 2018. Effective stress parameters of clays from DMT. *Geotech. Testing J.* 41(5): 851–867.
- Pyke, R. 2003. Discussion of “Liquefaction Resistance of Soils: Summary Report from the 1996 NCEER and 1998 NCEER/NSF” by T.L. Youd et al., *J. Geotech. Geoenviron. Eng.* 129(3): 283–284.
- Robertson, P.K. 1990. Soil classification using the cone penetration test. *Can. Geotech. J.* 27(1): 151–158.
- Robertson, P.K. 2009a. CPT-DMT Correlations. *J. Geotech. Geoenviron. Eng.* 135(11): 1762–1771.
- Robertson, P.K. 2009b. Interpretation of cone penetration tests – a unified approach. *Can. Geotech. J.*, 46(11): 1337–1355.
- Robertson, P.K. 2012. The James K. Mitchell Lecture: Interpretation of in-situ tests – some insights. In R. Coutinho & P.W. Mayne (eds), *Proc. 4th Int. Conf. Geotech. Geophys. Site Characterization, Porto de Galinhas*, 1: 3–24.
- Robertson, P.K. 2015. Soil Behavior Type using the DMT. In S. Marchetti, P. Monaco & A. Viana da Fonseca (eds), *Proc. 3rd Int. Conf. Flat Dilatometer DMT'15, Rome*, 14-16 June 2015, 243–250.
- Robertson, P.K. 2017. DMT-CPT Correlations. *Prof. Silvano Marchetti Memorial Session on In-Situ Testing, 19th Int. Conf. Soil Mech. Geotech. Eng., Seoul, 17-22 September 2017* (oral presentation).
- Robertson, P.K. & Wride, C.E. 1998. Evaluating cyclic liquefaction potential using the cone penetration test. *Can. Geotech. J.* 35(3): 442–459.
- Schnaid, F., Belloli, M.V.A., Odebrecht, E. & Marchetti, D. 2018. Interpretation of the DMT in silts. *Geotech. Testing J.* 41(5): 868–876.
- Schnaid, F., Odebrecht, E., Sosnoski, J. & Robertson, P.K. 2016. Effects of test procedure on flat dilatometer test (DMT) results in intermediate soils. *Can. Geotech. J.* 53(8): 1270–1280.
- Senneset, K., Sandven, R., Lunne, T., By, T. & Amundsen, T. 1988. Piezocone Tests in Silty Soils. *Proc. Int. Symp. Penetration Testing ISOPT-1, Orlando*, 2: 955–966. Rotterdam: Balkema.
- Togliani, G., Calzolari, L. & Menghini, A. 2015. Governolo & Gonzaga (Mantua, Italy) Experimental Sites: In situ Test comparison. In S. Marchetti, P. Monaco & A. Viana da Fonseca (eds), *Proc. 3rd Int. Conf. Flat Dilatometer DMT'15, Rome*, 14-16 June 2015, 259–270.
- Tonni, L., Gottardi, G., Amoroso, S., Bardotti, R., Bonzi, L., Chiaradonna, A., d’Onofrio, A., Fioravante, V., Ghinelli, A., Giretti, D., Lanzo, G., Madiati, C., Marchi, M., Martelli, L., Monaco, P., Porcino, D., Razzano, R., Rosselli, S., Severi, P., Silvestri, F., Simeoni, L., Vannucchi, G. & Aversa, S. 2015. Interpreting the deformation phenomena triggered by the 2012 Emilia seismic sequence on the Canale Diversivo di Burana banks. *Rivista Italiana di Geotecnica* 49 (2):28–58 (in Italian).
- Tsai, P.-H., Lee, D.-H., Kung, G.T.-C. & Juang, C.H. 2009. Simplified DMT-Based Methods for Evaluating Liquefaction Resistance of Soils. *Eng. Geol.* 103(1-2): 13–22.

Technical papers

Session 1: Equipment and procedures



Taylor & Francis

Taylor & Francis Group

<http://taylorandfrancis.com>

Incorporation of SH source wave parameter “SH Polarization” within DST seismic trace characterization

Erick Baziw & Gerald Verbeek

Baziw Consulting Engineers Ltd., Vancouver, Canada

ABSTRACT: Downhole Seismic Testing (DST) is an important geotechnical testing technique for site characterization that provides low strain in-situ interval shear wave velocity estimates, which are fundamental design parameters for static and dynamic soil analysis. A challenging problem in DST is to obtain an accurate assessment or characterization of the quality of the acquired seismic data, which is then used to guide the analysis process to obtain the most accurate interval velocity values. The characterization process is referred to as Seismic Trace Characterization (STC). STC derives various independent parameters of the acquired seismic data at a particular depth, which are then fused together into a single classification. To date Baziw Consulting Engineers has identified five STC independent parameters. These five parameters are the linearity estimates from the polarization analysis, the cross correlation coefficient of the full waveforms at the particular depth and the preceding depth, a uniquely developed parameter referred to as the signal shape parameter, the signal-noise-ratio and the peak symmetry differential, which provides insight into the skewing or time shifting of the peak source wave response. This paper outlines a newly identified seismic trace feature that is independent of the parameters listed above. This new parameter is SH Polarization (SHP), which quantifies the desired polarization of the generated source on the horizontal plane compared with particle motion generated on the vertical plane.

1 INTRODUCTION

The fundamental goal of Downhole Seismic Testing (DST) is to obtain accurate estimates of low strain ($<10^{-5}$) shear (V_s) and compression (V_p) wave velocities. These velocities are directly related to the various soil elastic constants, such as the Poisson's ratio, shear modulus, bulk modulus and Young's modulus. These parameters form the core of mathematical theorems to describe the elasticity/plasticity of soils and they are used to predict the soil response (settlement, liquefaction or failure) to imposed loads. Accuracy in the estimation of these two in-situ velocities is of paramount importance because their values are squared during the calculation of the soil elastic constants. In DST a seismic source wave is generated at the ground surface, and one or more downhole seismic receivers are used to record this wave at predefined depths. From these recorded seismic traces arrival times are estimated and corresponding interval velocities calculated.

Baziw Consulting Engineers (BCE) has invested considerable resources into the characterization of DST traces (Baziw and Verbeek 2016, 2017, and 2018) to address three fundamental concerns. 1) What is the quality of the acquired seismic data sets? 2) What signal processing techniques can be applied to improve the signal-to-noise ratio (SNR) of

the seismic data? And 3) What is the appropriate confidence level in the calculated interval velocities estimates? Over time work in addressing these three concerns has resulted in the standardization of a DST post data processing methodology, which has proven highly accurate and reliable. Currently quality assessment through Seismic Trace Characterization (STC) relies upon five independent parameters (Baziw and Verbeek 2016, 2017 and 2018):

- Parameter 1: the linearity estimates (LIN) the linearity or rectilinearity from polarization analysis. The LIN trace metric quantifies the correlation between X, Y and Z axis responses. The linearity approaches unity when the rectilinearity is high and approaches zero when the rectilinearity is low. Linearity values nearing 1.0 identify seismic recordings that have highly correlated responses and strong directionality, the quality of the data set with a high linearity value can be considered good. Lower linearity values on the other hand indicate lower quality traces.
- Parameter 2: the Cross Correlation Coefficient (CCC) of the full waveforms at the particular depth and the preceding depth. The CCC trace metric gives an indication of the similarity between the two waves being correlated when

deriving relative arrival times. CCC values approaching 1.0 indicate that the two waveforms are highly correlated. CCC values approaching 0 indicate very poor correlation.

- Parameter 3: the Signal Shape Parameter (SSP). The SSP trace metric quantifies the deviation of the shape of the frequency spectrum from an ideal bell shape. SHP values approaching 1.0 indicate that the frequency has a desirable bells shape. SHP values approaching 0 indicates that the frequency spectrum deviates significantly from the desired bell shape.
- Parameter 4: the Peak Symmetry Differential (PSD) trace metric facilitates the identification of traces whose peak source wave responses have been significantly skewed due to measurement noise or source wave reflection interference. The “peak symmetry” error assessment is also carried out on the adjacent peaks and/or troughs if the amplitude exceeds 70 % of that for the peak response. Traces with low PSD value are of a lesser quality and require more attention during analysis.
- Parameter 5: Signal to Noise Ratio (SNR). The SNR trace metric is solely provided to quantify what portion of the spectral content of the recorded seismogram resides within the desired source frequency spectrum irrespective of source wave distortions such as near-field effects, reflections, refractions, and “dirty sources”.

As part of the post analysis of the seismic traces these parameters are then converted into a STC grade ranging from A to F where A is highly desirable and F is unacceptable without corrective action. Next they are used as a guide for the data analysis and seismic signal processing (Baziw and Verbeek, 2018). A central part of this processing is the source wave Signature Feature Isolation (SFI) to clearly identify the source wave in the seismic trace by applying an exponential decay function to the remainder of the trace. This can be performed in three different ways:

- ASD or Automatic Signal Decay, where the program identifies the absolute maximum amplitude on all trace under analysis and then applies the decay function on either side of that feature.
- GSD or Guided Signal Decay, where the user identifies a specific feature for the traces under analysis and then applies the decay function on either side of that feature.
- ISD or Individual Signal Decay, where the user identifies a specific feature for each trace under analysis and then applies the decay function on either side of that feature on that particular trace.

The analysis process can then be visualized as outlined in Figure 1.

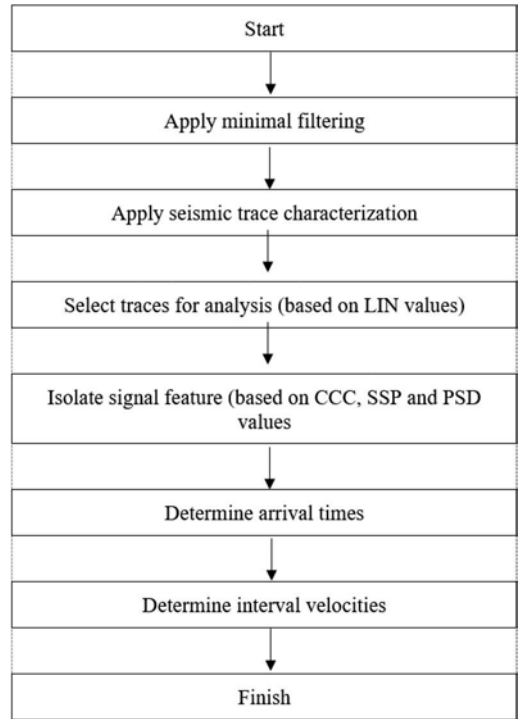


Figure 1. DST data processing flow chart incorporating STC parameters.

In this paper, the preliminary implementation and mathematical details of a new STC parameter is outlined. This new parameter, the so called SH Polarization (SHP), quantifies the desired polarization of the generated source on the horizontal plane compared with particle motion generated on the vertical plane.

2 STC PARAMETER SH POLARIZATION (SHP)

Seismic sources are designed to generate either compression (P), vertically polarized shear (SV) waves or horizontally polarized (SH) shear waves. Figure 2 illustrates the compression and shear source waves impacting upon a triaxial seismic sensor package. As it is shown in Figure 2, the P-wave’s particle motion is in the same direction as the raypath, the SH waves particle motion is perpendicular to the raypath and is parallel to the horizontal ground surface, while the SV wave’s particle motion is also perpendicular to the raypath, but along the vertical normal to the raypath.

P or SV waves generate four outgoing waves when impacting an interface (reflected SV and P waves and transmitted SV and P waves). In contrast, SH waves have the desirable property of only generating one reflected and one transmitted SH at an interface. This results in considerably simplified seismic data sets. A popular SH source is the well-known

hammer beam (ASTM, 2017). The hammer-beam consists of applying a hammer blow laterally to the sides of special designed plates fixed at the surface.

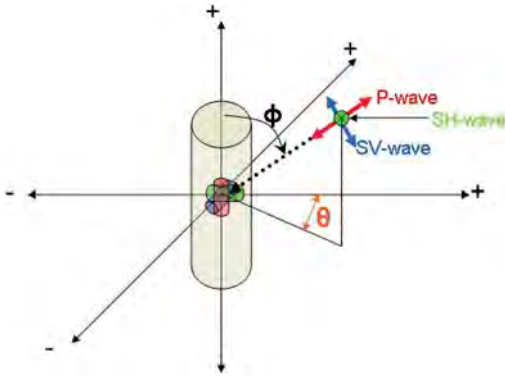


Figure 2. Source P, SV, and SH body waves impacting upon a triaxial sensor package.

The new STC parameter SHP quantifies and applies a grade [A to F] to how closely the measured SH wave seismic traces adhere to the desired polarization of the shear wave on the horizontal plane. The SHP algorithm can be summarized as follows, assuming that a triaxial (x, y and z axes) seismic trace has been recorded.

1. Apply a minimal filter (200 Hz low pass) to the acquired SH source wave.
2. Determine time index, t^* , where the maximum absolute amplitude of the full waveform ($\rho(t) = \sqrt{x^2(t) + y^2(t) + z^2(t)}$) occurs.
3. Establish a time window T which is defined as $t^* - \Delta t$ to $t^* + \Delta t$ where $\Delta t = 30\text{ms}$.
4. Over the established time T calculate the energy of the full waveform, E_p , and the energy of the particle motion on the X-Y plane E_{xy} ($xy(t) = \sqrt{x^2(t) + y^2(t)}$).
5. Calculate energy ratio $ER = E_{xy}/E_p$.
6. Assign a SHP rank based upon calculated ER value as outlined in Table 1.

Table 1. SHP rank and description.

ER Numeric Value [0-1]	SHP Rank [A-F]	STC Description
0.8 to 1.0	A	very good to good
0.65 to 0.8	B	good to acceptable
0.5 to 0.65	C	acceptable to questionable
0.3 to 0.5	D	questionable to unacceptable
< 0.3	F	unacceptable

The SHP rankings outlined in Table 1 are preliminary values. These values will be adjusted and refined as a greater number DST seismic traces are processed.

3 IMPLEMENTATION OF SHP STC PARAMETER ON REAL DATA SETS

The first and second real data sets outlined in this section were acquired by Perry Geotech Limited located in Tauranga, New Zealand. Figure 3 illustrates a SH source wave DST vertical seismic profile (x, y and z axis responses) of SH DST seismic data acquired on the Left Side (LS) of the seismic probe, while Figure 4 shows the VSP of data acquired on the Right Side (RS) of the seismic probe. The STC parameters for the LS and RS are outlined in Tables 2 and 3, respectively.

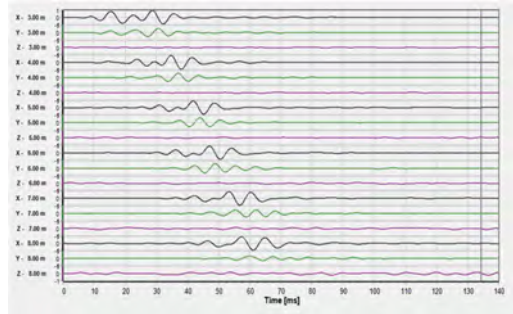


Figure 3. Data Set 1 – real data set. VSP of data acquired on LS of seismic probe (200Hz low pass filter applied).

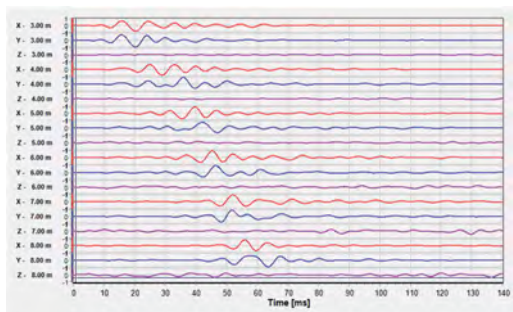


Figure 4. Data Set 1 – real data set. VSP of data acquired on right side of seismic probe (200Hz low pass filter applied).

As is evident from Tables 2 and 3 the data sets from the LS and RS have low STC values of ‘D’s and ‘F’s (predominantly due to low LIN values), but with high SHP rankings. This suggests that the acquired seismic traces have the desirable polarization on the horizontal plane, but will require preferable axis

Table 2. STC parameters for LS for Data Set 1.

Depth [m]	LIN [0-1]	SSP [0-1]	CCC [0-1]	PSD [0-1]	SNR [0-1]	STC [A-F]	SHP [A-F]
3	0.68	0.54	0	0.86	0.71	N/A	A
4	0.71	0.77	0.69	0.81	0.86	D	A
5	0.59	0.71	0.96	0.73	0.88	D	A
6	0.44	0.70	0.99	0.74	0.91	D	A
7	0.60	0.75	0.96	0.57	0.97	D	A
8	0.88	0.80	0.96	0.59	0.92	D	B

Table 3. STC parameters for RS for Data Set 1.

Depth [m]	LIN [0-1]	SSP [0-1]	CCC [0-1]	PSD [0-1]	SNR [0-1]	STC [A-F]	SHP [A-F]
3	0.77	0.76	0	0.89	0.54	N/A	A
4	0.30	0.77	0.77	0.94	0.88	D	A
5	0.21	0.63	0.80	0.82	0.84	F	A
6	0.46	0.65	0.87	0.77	0.88	D	A
7	0.53	0.69	0.93	0.93	0.98	D	A
8	0.34	0.73	0.85	0.97	0.96	D	B

selection (in this case the X axis) given the LIN values. The SHP rankings give added confidence in the ability to isolate SH responses and derive accurate interval velocities after SFI implementation.

Table 4 outlines the estimated LS and RS interval velocities and corresponding spread. As is shown in Table 4 there is overall high correlation between the LS and RS results (desired values should be $\leq 10\%$ spread), with only the estimated values for the depth interval 3.0m to 4.0m showing a spread slightly above 10%.

The second data set is another example where the LS and RS have again low STC values of ‘D’s and ‘F’s (but now due to low PSD values) and high SHP rankings.

Table 4. Estimated LS and RS interval velocities.

Depth [m]	Depth Interval Velocity			
	LS [m/s]	RS [m/s]	Avg. [m/s]	Spread ¹ [%]
0.0-3.0	182.4	204.1	193.3	5.6
3.0-4.0	150.4	122.2	136.3	10.3
4.0-5.0	129.4	141.5	135.5	4.5
5.0-6.0	171.3	164.6	168	2.0
6.0-7.0	151.4	141.4	146.4	3.4
7.0-8.0	214.5	239.5	227	5.5

¹ The spread is defined as $\frac{1}{2} \times (\text{LS Interval Velocity} - \text{RS Interval Velocity}) / \text{Avg. Interval Velocity}$

For this data set Figure 5 illustrates a vertical seismic profile (x, y and z axis responses) of SH DST seismic data acquired on the Left Side (LS) of the seismic probe, while Figure 6 shows the VSP of data acquired on the Right Side (RS) of the seismic

probe. The STC parameters for the LS and RS are outlined in Tables 5 and 6, respectively.

The SHP rankings suggest that the acquired seismic traces have desirable polarization on the horizontal plane, but will require signal feature isolations based upon the LIN and SSP (LS) and PSD (RS) values.

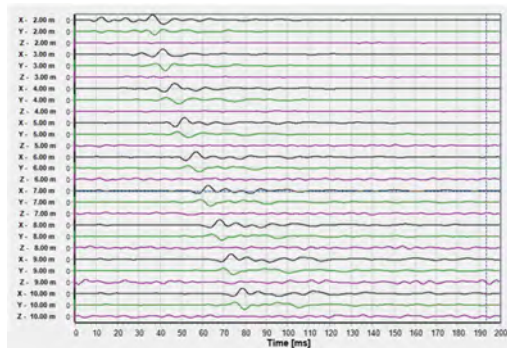


Figure 5. Data Set 2 – real data set. VSP of data acquired on LS of seismic probe (200Hz low pass filter applied).

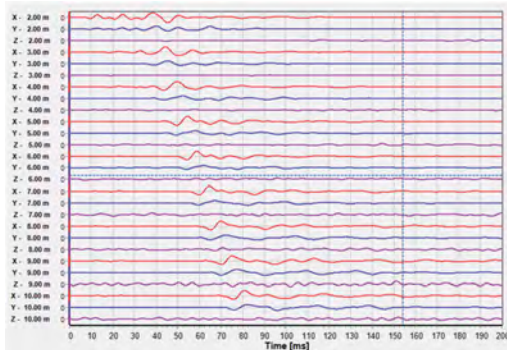


Figure 6. Data Set 2 – real data set. VSP of data acquired on RS of seismic probe (200Hz low pass filter applied).

Table 5. STC parameters for LS for Data Set 2.

Depth [m]	LIN [0-1]	SSP [0-1]	CCC [0-1]	PSD [0-1]	SNR [0-1]	STC [A-F]	SHP [A-F]
2	0.83	0.65	0.62	0.6	0.95	N/A	A
3	0.8	0.79	0.71	0.89	0.97	D	A
4	0.81	0.67	0.88	0.7	0.98	B	A
5	0.77	0.7	0.95	0.58	0.93	B	A
6	0.76	0.63	0.96	0.8	0.97	D	A
7	0.71	0.58	0.97	0.98	0.98	D	B
8	0.75	0.55	0.99	0.96	0.98	D	B
9	0.76	0.5	0.98	0.89	0.98	D	B
10	0.79	0.53	0.98	0.86	0.98	D	A
11	0.78	0.54	0.98	0.86	0.98	D	B
12	0.84	0.55	0.98	0.84	0.98	D	B

Table 6. STC parameters for RS for Data Set 2.

Depth [m]	LIN [0-1]	SSP [0-1]	CCC [0-1]	PSD [0-1]	SNR [0-1]	STC [A-F]	SHP [A-F]
2	0.79	0.58	0.58	0.77	0.98	N/A	A
3	0.88	0.66	0.81	0.77	0.98	B	A
4	0.83	0.69	0.88	0.92	0.98	B	A
5	0.81	0.63	0.92	0.01	0.98	F	A
6	0.8	0.63	0.97	0.01	0.98	F	B
7	0.81	0.55	0.96	0.01	0.98	F	B
8	0.82	0.54	0.98	0.01	0.98	F	B
9	0.84	0.48	0.98	0.01	0.98	F	C
10	0.83	0.58	0.98	0.2	0.98	F	B
11	0.84	0.51	0.99	0.51	0.98	D	B
12	0.84	0.54	0.98	0.65	0.98	D	B

Table 7. Estimated LS and RS interval velocities for Data Set 2.

Depth [m]	Depth Interval Velocity		Avg. [m/s]	Spread ¹ [%]
	LS [m/s]	RS [m/s]		
0.0-2.0	103.1	106.5	119.1	0.8
2.0-3.0	120.8	117.4	135.85	0.7
3.0-4.0	134.0	137.7	171.45	0.7
4.0-5.0	179.1	163.8	173.85	2.2
5.0-6.0	160.7	187	158.55	3.8
6.0-7.0	157.7	159.4	171.2	0.3
7.0-8.0	173.9	168.5	176.35	0.8
8.0-9.0	174	178.7	175.6	0.7
9.0-10.0	180.4	170.8	172.8	1.4
10.0-11.0	166.2	179.4	148.1	1.9
11.0-12.0	143.8	152.4	119.1	1.5,

1 The spread is defined as $\frac{1}{2} \times (\text{LS Interval Velocity} - \text{RS Interval Velocity}) / \text{Avg. Interval Velocity}$

Table 7 outlines the estimated LS and RS interval velocities and corresponding spread for Data Set 2. As is shown Table 7 there is overall very high correlation between the LS and RS results.

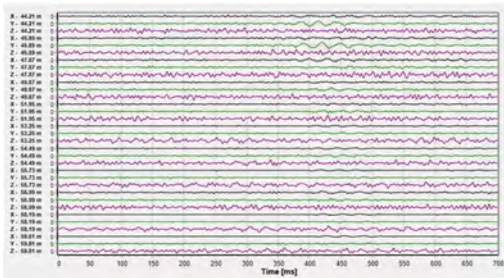


Figure 7. Data Set 3 – real data set. VSP of data acquired on LS of seismic probe (200Hz low pass filter applied).

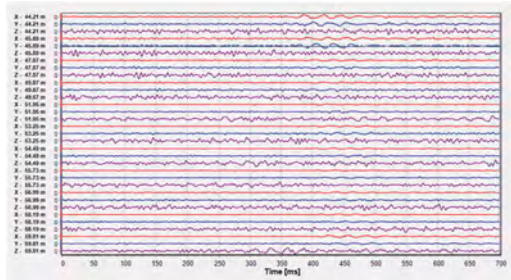


Figure 8. Data Set 3 – real data set. VSP of data acquired on RS of seismic probe (200Hz low pass filter applied).

Table 8. STC parameters for LS for Data Set 3.

Depth [m]	LIN [0-1]	SSP [0-1]	CCC [0-1]	PSD [0-1]	SNR [0-1]	STC [A-F]	SHP [A-F]
44.2	0.87	0.33	0.9	0.89	0.89	N/A	C
45.9	0.85	0.27	0.97	0.34	0.94	D	C
47.9	0.68	0.41	0.95	0.36	0.8	D	D
49.9	0.76	0.46	0.88	0.94	0.81	D	D
51.9	0.51	0.46	0.62	0.01	0.83	F	F
53.2	0.82	0.53	0.47	0.01	0.79	F	F
54.4	0.82	0.55	0.84	0.01	0.81	F	D
55.7	0.63	0.59	0.75	0.64	0.82	F	F
56.9	0.39	0.54	0.97	0.01	0.77	F	F
58.9	0.57	0.51	0.65	0.49	0.79	F	F
59.8	0.87	0.53	0.26	0.85	0.76	F	F

Table 9. STC parameters for RS for Data Set 3.

Depth [m]	LIN [0-1]	SSP [0-1]	CCC [0-1]	PSD [0-1]	SNR [0-1]	STC [A-F]	SHP [A-F]
44.2	0.72	0.37	0.92	0.63	0.88	N/A	C
45.9	0.78	0.31	0.96	0.83	0.91	D	C
47.9	0.62	0.56	0.95	0.25	0.79	D	D
49.9	0.43	0.5	0.87	0.69	0.86	D	F
51.9	0.73	0.48	0.73	0.01	0.89	F	F
53.2	0.71	0.51	0.89	0.45	0.73	F	F
54.4	0.7	0.52	0.72	0.01	0.8	F	F
55.7	0.63	0.5	0.46	0.94	0.7	F	F
56.9	0.75	0.52	0.53	0.28	0.8	F	F
58.9	0.71	0.59	0.89	0.52	0.51	D	F
59.8	0.73	0.14	0.92	0.42	0.86	D	D

The third data set demonstrates that for a data set with poor STC and SHP values it is (generally) not possible to obtain accurate SH interval velocity estimates. Figures 7 and 8 illustrate the LS and RS traces for a real data set acquired during an offshore DST investigation. The STC parameters are outlined in Tables 8 and 9, respectively.

The combination of very poor STC and SHP values strongly suggests that it is not possible to isolate source wave response by implementing SFI. And therefore this data set was indeed dropped and not analyzed. This shows the importance of having these parameters available in real-time during data acquisition to ensure that the collected data is useful and can be used to derive interval velocities.

4 CONCLUSIONS

Downhole Seismic Testing (DST) is an important geotechnical testing technique which provides estimates of low strain ($<10^{-5}$) shear and compression wave velocities, but there is a need for a widely accepted seismic trace characterization (STC) methodology of the acquired data.

In the past BCE had identified five independent STC parameters (linearity estimates from the polarization analysis, the cross correlation coefficient of the full waveforms at the particular depth and the preceding depth, the signal shape parameter, the signal-noise-ratio and the peak symmetry differential). In this paper, the mathematical and implementation details of a new STC parameter have been outlined. This new parameter, denoted as SHP, quantifies the desired polarization of a horizontally generated shear wave on the horizontal plane compared with particle motion generated on the vertical plane. SH source waves should have negligible particle motion along the vertical axis.

As illustrated in this paper, the initial assessment of the SHP STC parameter when processing real data sets is very promising, although it is fully expected that the SHP ranking will be refined once the parameter has been applied to additional data sets.

In addition the authors intend to develop an approach to incorporate the SHP ranking into the post-processing methodology for seismic data

REFERENCES

- ASTM (American Standards and Testing Methods). 2017. D7400: Standard Test Methods for Downhole Seismic Testing. ASTM Vol. 4.09 Soil and Rock (II): D5877–latest.
- Baziw, E. 2002. Derivation of Seismic Cone Interval Velocities Utilizing Forward Modeling and the Downhill Simplex Method. *Can. Geotech. J.*, 39(5),1181–1192.
- Baziw, E., and Verbeek, G. 2016. Frequency spectrum “bell-curve” fitting as a component of SCPT interval velocity accuracy assessment. 5th International Conference on Geotechnical Site Characterization (ISC-5). September 5- 9, 2016. Queensland – Australia. Australian Geomechanics Society, 1431–1436.
- Baziw, E., and Verbeek, G. 2017. Quality Assessment of Seismic Data Sets and the Impact on Interval Velocity Estimates in DST. Presented and published in the proceedings of the DFI 42nd Annual Conference on Deep Foundations. October 24-27, 2017 - New Orleans, USA.
- Baziw, E. and Verbeek, G. 2018. The use of seismic trace characterization to guide the analysis of DST results to obtain more accurate soil parameters. presented and published in the DFI 43rd Annual Conference on Deep Foundations conference proceedings. October 24-27, 2018 - Anaheim, CA.

Methodology for obtaining true cone bearing estimates from blurred and noisy measurements

Erick Baziw & Gerald Verbeek

Baziw Consulting Engineers Ltd., Vancouver, Canada

ABSTRACT: Cone penetration testing (CPT) is an important and widely used geotechnical *in-situ* test for assessing soil properties and mapping soil profiles. CPT consists of pushing at a constant rate an electronic cone into penetrable soils and recording the resistance to the cone tip or cone bearing (q_m). These values (after correction for the pore water pressure to get q_t) are utilized to characterize the soil profile along with measured sleeve friction and pore pressure. The q_m measurements can have significant fluctuations when penetrating sandy, silty gravelly soils, resulting in “high” peaks due to interbedded gravels and stones and “low” peaks due to softer materials or local pore pressure build-up. Furthermore, the q_m values are blurred and/or averaged which results in the inability to identify thin layers and the distortion of the soil profile characterization. Baziw Consulting Engineers has invested considerable resources in addressing these two q_m measurement challenges. The q_mKF algorithm was developed to address the additive measurement noise. In this case the dynamics of q_m are modeled within a state-space mathematical formulation and a Kalman filter is then utilized to obtain optimal estimates of q_m . The q_mHMM algorithm implements a hidden Markov model smoother so that true cone bearing are obtained from the averaged/blurred q_m values. This paper outlines the integration of the q_mKF and q_mHMM algorithms and demonstrates the performance first with test bed simulations (to show the functionality of the algorithm) and then through the analysis of various actual q_m data sets.

1 INTRODUCTION

1.1 Cone bearing measurements

The Cone Penetration Test (CPT) is a geotechnical in-situ tool which is utilized to identify and characterize sub-surface soils (Lunne et al., 1997; Robertson, 1990; ASTM D6067, 2017). In CPT a cone penetration rig pushes the steel cone vertically into the ground at a standard rate and data are recorded at regular intervals during penetration. The cone has electronic sensors to measure penetration resistance at the tip (q_m) and friction in the shaft (friction sleeve) during penetration. A CPT probe equipped with a pore-water pressure sensor is called a piezo-cone (CPTU cones). For piezo-cones with the filter element right behind the cone tip (the so-called u_2 position) it is standard practice to correct the recorded tip resistance for the impact of the pore pressure on the back of the cone tip. This corrected cone tip resistance is normally referred to as q_t . The distortions which effect the cone tip measurements are two-fold: 1) the cone tip resistance are smoothed/averaged (Boulanger and DeJong, 2018; Baziw and Verbeek, 2021a) where cone tip values measured at a particular depth are affected by values above and below the depth of interest, and 2) the cone bearing measurements are susceptible to anomalous peaks and troughs due to the

relatively small diameter cone tip penetrating sandy, silty and gravelly soils (Baziw and Verbeek, 2021b).

1.2 Cone bearing smoothing/averaging

The measured cone resistance at a particular depth is an averaged/smoothed measurement of the true values q_v above and below the depth of interest (Boulanger and DeJong, 2018; Robertson, 1990; Baziw and Verbeek, 2021a, 2021b). Mathematically the measured cone tip resistance q_m is described as (Baziw and Verbeek, 2021a)

$$q_m(d) = \sum_{j=1}^{60 \times \left(\frac{d_c}{\Delta}\right)} w_c(j) \times q_v(\Delta_{qm} + j) + v(d) \quad (1)$$

$$\Delta_{qm} = (d - \Delta_{wm}), \Delta_{wm} = 30 \times \left(\frac{d_c}{\Delta}\right)$$

where

- d the cone depth
- d_c the cone tip diameter
- Δ_{qm} the q_m sampling rate
- $q_m(d)$ the measured cone tip resistance
- $q_v(d)$ the true cone tip resistance (prior to pore water pressure correction)

$w_c(d)$ the $q_v(d)$ averaging function
 $v(d)$ additive noise, generally taken to be white with a Gaussian pdf

In equation (1) it assumed that w_c averages q_v over 60 cone diameters centered at the cone tip. Boulanger and DeJong (Boulanger and DeJong, 2018) outline how to calculate w_c below (after correcting the equation for w_l (Baziw and Verbeek, 2021a)):

$$w_c = \frac{w_1 w_2}{\sum w_1 w_2} \quad (2a)$$

$$w_1 = \frac{C_1}{1 + \left| \left(\frac{z'}{z'_{50}} \right)^{m_z} \right|} \quad (2b)$$

$$w_2 = \sqrt{\frac{2}{1 + \left(\frac{q_{t,z'}}{q_{t,z'=0}} \right)^{m_q}}} \quad (2c)$$

where:

z' the depth relative to the cone tip normalized by the cone diameter

z'_{50} the normalized depth relative to the cone tip where $w_1 = 0.5 C_1$

The cone penetration averaging function w_c for varying $q_{t,z'}/q_{t,z'=0}$ ratios is illustrated in Figure 1.

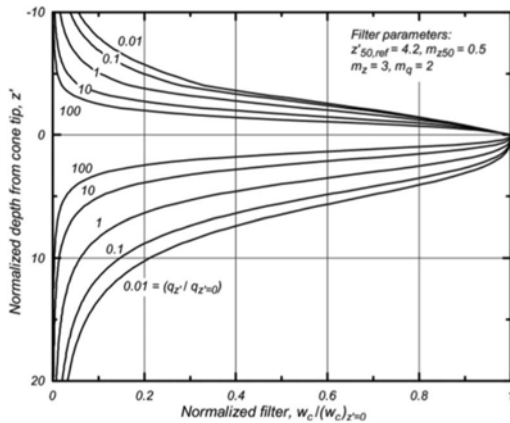


Figure 1. Schematic of thin layer effect for a sand layer embedded in a clay layer (Boulanger and DeJong, 2018).

1.3 Cone bearing measurement noise

The smoothed/averaged cone bearing measurement q_m given by eq. (1) can also contain sharp anomalous and spurious peaks and troughs (Lunne, Robertson and Powell, 1997)

These anomalous and spurious cone bearing measurements are due to the relatively small diameter cone tip penetrating sandy, silty and gravelly soils. As illustrated in Figure 2, the “high” peaks

result from the penetration of interbedded gravels and stones and the “low” peaks results from the penetration of softer materials or local pore pressure build-up. Figure 3 illustrates an example of a cone bearing profile which contains significant anomalous/spurious q_m data from approximate depths 10m to 18m and 22m to 30m. There is also significant pore pressure variability at these depths.

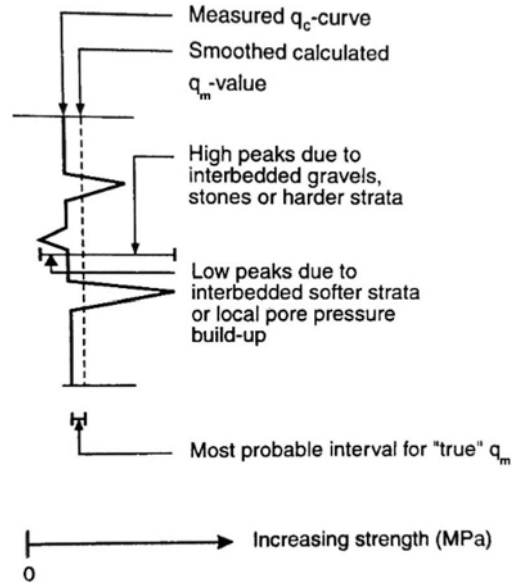


Figure 2. Schematic of anomalous/spurious cone bearing data (after Mortensen and Sorensen, 1991).

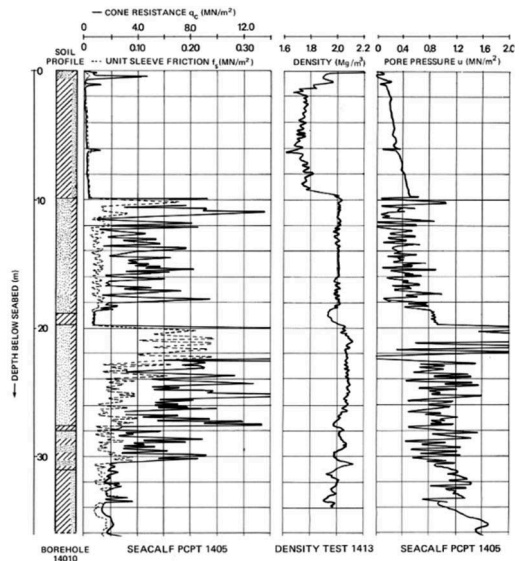


Figure 3. Combined results of piezocone test and nuclear density test at Gullfaks C in the North Sea (Tjelta et al. 1985).

2 FILTER FORMULATION

2.1 $qmHMM$ algorithm formulation

The initial algorithm developed by Baziw and Verbeek (2021a) (the so called $q_mHMM-IFM$) to address the smoothing/averaging of cone bearing measurements (eq. (1)) combined a Bayesian recursive estimation (BRE) Hidden Markov Model (HMM) filter with Iterative Forward Modelling (IFM) parameter estimation in a smoother formulation. The $q_mHMM-IFM$ provided estimates of the true q_v values from the measured blurred values. In recent modifications and enhancements of the $q_mHMM-IFM$ it was possible to drop the IFM portion of the algorithm. This was predominantly accomplished by refining the HMM filter parameters.

The HMM filter (also termed a grid-based filter) has a discrete state-space representation and has a finite number of states (Arulampalam et al., 2002). In the HMM filter the posterior PDF is represented by the delta function approximation as follows:

$$p(x_{k-1}|z_{1:k-1}) = \sum_{i=1}^{N_s} w_{k-1|i, k-1}^i \delta(x_{k-1} - x_{k-1}^i) \quad (3)$$

where x_{k-1}^i and $w_{k-1|i, k-1}^i$, $i = 1, \dots, N_s$, represent the fixed discrete states and associated conditional probabilities, respectively, at time index $k-1$, and N_s the number of particles utilized. In the case of the q_mHMM algorithm the HMM discrete states represent possible q_v values where

Table 1. HMM filtering algorithm.

Step	Description	Mathematical Representation
1	Initialization (k=0) – initialize particle weights.	e.g., $w_k^i \sim 1/N_s$, $i = 1, \dots, N_s$ (4)
2	Prediction - predict the weights.	$w_{k i, k-1}^j = \sum_{j=1}^{N_s} w_{k-1 k-1}^j p(x_k^j x_{k-1}^j)$ (5)
3	Update - update the weights.	$w_{k k}^j = \frac{w_{k i, k-1}^j p(z_k x_k^j)}{\sum_{j=1}^{N_s} w_{k i, k-1}^j p(z_k x_k^j)}$ (6)
4	Obtain optimal minimum variance estimate of the state vector and corresponding error covariance.	$\hat{x}_k \approx \sum_{i=1}^{N_s} w_{k k}^i x_k^i$ & (7)
5	Let k = k+1 & iterate to step 2.	$P_{\hat{x}_k} \approx \sum_{i=1}^{N_s} w_{k k}^i (x_k^i - \hat{x}_k)(x_k^i - \hat{x}_k)^T$

In the above equations it is required that the likelihood pdf $p(z_k|x_k^j)$ and the transitional probabilities $p(x_k^j|x_{k-1}^j)$ be known and specified.

maximum, minimum and resolution values are specified. The HMM governing equations are outlined in Table 1.

The q_mHMM algorithm implements a BRE smoother. BRE smoothing uses all measurements available to estimate the state of a system at a certain time or depth in the q_v estimation case (Arulampalam et al., 2002; Baziw and Verbeek, 2021a; Gelb, 1974). This requires both a forward and backward filter formulation. The forward HMM filter (\hat{q}_k^F) processes measurement data (q_m) above the cone tip ($j = 1$ to $30 \times (\frac{d_c}{\Delta})$) in (1)). Next the backward HMM filter (\hat{q}_k^B) is implemented, where the filter recurses through the data below the cone tip ($j = 30 \times (\frac{d_c}{\Delta})$ to $60 \times (\frac{d_c}{\Delta})$) in (1)) starting at the final q_m value. The optimal estimate for q_v is then defined as

$$\hat{q}_k^v = (\hat{q}_k^F + \hat{q}_k^B)/2 \quad (8)$$

where the index k represents each q_m measurement.

In both the forward and backward HMM filter formulation a bank of discrete q_v values ($i = 1$ to N) varying from low (q_{iL}) to high (q_{iH}) and a corresponding q_t resolution q_{iR} is specified. The required number of fixed grid HMM states is given as $N_s = (q_{iH} - q_{iL})/q_{iR}$. In Table 1 the notation of the states x^i is mapped to q^i to reflect the bank of q_t values.

In the q_mHMM forward and backward filter formulation the transitional probabilities (i.e., $p(x_k^i|x_{k-1}^j)$ or $p(q_k^i|q_{k-1}^j)$ for each HMM state (i.e., discrete cone tip, q^i) is set equal due to the fact that there is equal probability of moving from a current cone tip value to any other value between the range q_{iL} to q_{iH} . The likelihood PDF $p(z_k|q_k^i)$ in the HMM filter outlined in Table 1 is calculated based upon an assumed Gaussian measurement error as follows:

$$p(z_k|q_k^i) = \frac{1}{\sqrt{2\pi\sigma}} e^{\left[\frac{(q_c(d) - z_k^i)^2}{2\sigma^2} \right]} \quad (9)$$

where σ^2 is the variance of the measurement noise. Baziw and Verbeek (2021a) outline the details of the q_mHMM algorithm forward and backward filter formulation.

2.2 $qmKF$ algorithm formulation

The Kalman Filter (Gelb, 1974) is an optimal (least squares) recursive filter which is based on state-space formulations of physical problems. Application of this filter requires that the physical problem be modified by a set of first order differential equations which, with initial conditions, uniquely define the system behaviour. The filter utilizes knowledge

Table 2. KF governing equations.

Description	Mathematical Representation
System equation	$x_k = F_{k-1}x_{k-1} + G_{k-1}u_{k-1}$ (10)
Measurement equation	$z_k = H_k x_k + v_k$ (11)
State estimate extrapolation	$\hat{x}_{k k-1} = F_{k-1}\hat{x}_{k-1 k-1}$ (12)
Error cov. extrapolation	$P_{k k-1} = F_{k-1}P_{k-1 k-1}F_{k-1}^T$ (13)
Measurement extrapolation	$G_{k-1}Q_{k-1 k-1}G_{k-1}^T$ (14)
Innovation	$\hat{z}_k = H_{k-1}\hat{x}_{k k-1}$ (15)
Variance of innovation	$\Delta_k = z_k - \hat{z}_k$ (15)
Kalman gain matrix	$S_k = H_k P_{k k-1} H_k^T + R_k$ (16)
State estimate update	$K_k = P_{k k-1} H_k^T (S_k)^{-1}$ (17)
Error covariance update	$\hat{x}_{k k} = \hat{x}_{k k-1} + K_k \Delta_k$ (18)
	$P_{k k} = [I - K_k H_k] P_{k k-1}$ (19)

In (10) and (11) v_k and u_k are *i.i.d* Gaussian zero mean white noise processes with variances of Q_k and R_k , respectively (i.e., $v_k \sim N(0, R_k)$ and $u_k \sim N(0, Q_k)$).

of system and measurement dynamics, assumed statistics of system noises and measurement errors and statistical information about the initial conditions.

Table 2 outlines the KF governing equations. In Table 2 x_k denotes the state to be estimated, F_{k-1} denotes the state transition matrix which describes the system dynamics, u_{k-1} the process or system noise (model uncertainty), G_{k-1} describes the relationship between x_k and u_{k-1} , and H_k the relationship between the state and the available measurement (measured cone resistance q_m). The KF can be applied to problems with linear time-varying systems and with non-stationary system and measurement statistics. The KF can be implemented for estimation, smoothing and prediction.

The motivation of implementing the KF for the optimal removal of spurious cone bearing measurements is that it can use any number, combination and sequence of external measurements. For example, it is envisioned measurements from the vane shear test undrained strength could be incorporated within $q_m KF$ algorithm based upon empirical correlations. Furthermore, it also fits into our goal of implementation of data fusion techniques into CPTU and SCPT.

Baziw and Verbeek (2021B) present a thorough outline of the $q_m KF$ algorithm. For completeness, the KF state and measurement equations are described below.

2.3 System model

To specify the $q_m KF$ systems equations in the standard KF state-space form, the following states need to be defined

$$\begin{bmatrix} x_1 \\ x_2 \\ x_3 \end{bmatrix} \equiv \begin{bmatrix} q_m \text{ conebearingposition} \\ q_m \text{ conebearingvelocity} \\ q_m \text{ conebearingacceleration} \end{bmatrix} \quad (20)$$

The discrete system equation (eq. (10)) is given as

$$\begin{bmatrix} x_{1k+1} \\ x_{2k+1} \\ x_{3k+1} \end{bmatrix} = \begin{bmatrix} 1 & \Delta & \Delta^2/2 \\ 0 & 1 & \Delta \\ 0 & 0 & a_w \end{bmatrix} \begin{bmatrix} x_{1k} \\ x_{2k} \\ x_{3k} \end{bmatrix} + \begin{bmatrix} 0 \\ 0 \\ b_w \end{bmatrix} u_k \quad (21)$$

where Δ is the q_m sampling rate and a_w and b_w are the defining parameters of a first order Gauss-Markov (GM) process. The GM process describes the cone bearing acceleration and w_k is white Gaussian noise with zero mean and unit variance.

2.4 Measurement model

Currently two synthesized measurements are incorporated into the $q_m KF$ algorithm: 1) The best fit seventh degree polynomial to the q_m profile and 2) Output after applying a fourth order low pass frequency filter to the q_m profile. At a later date it is envisioned that additional measurements could be incorporated into the $q_m KF$ algorithm as previously described.

$$\begin{bmatrix} z_1 \\ z_2 \end{bmatrix} \equiv \begin{bmatrix} \text{seventh order polynomial best fit} \\ \text{output after applying low pass filter} \end{bmatrix} \quad (22)$$

A best fit 7th degree polynomial is made to the q_m measurements every 1m to 1.4 m depth increment (allowed to be refined by investigator based upon data under analysis) so that the anomalous and spurious peaks and troughs are minimized. This polynomial is then fed into the $q_m KF$ algorithm as a measurement. The order of the polynomial and depth increment were selected due to the averaging/blurring of the q_m measurements where it would be highly unlikely that there would be greater than 6 turnings¹ in a 1m to 1.4m depth increment. This assumption was tested with extensive test bed simulation.

A 4th order 250Hz to 300 Hz (allowed to be refined by investigator based upon data under analysis) Butterworth low pass frequency filter is applied to the q_m measurements measurement so that the anomalous and spurious peaks and troughs are minimized even further. This 250Hz low passed frequency filtered trace is then fed into the $q_m KF$ algorithm as a measurement.

¹ The maximum number of turnings of a polynomial function is always one less than the degree

3 IMPLEMENTATION OF Q_MHMM AND Q_MKF ALGORITHMS

3.1 Test bed simulation

The performance of the q_mHMM and q_mKF algorithms were evaluated by carrying out challenging test bed simulations. This section outlines one of those simulations.

Figure 4 illustrates a simulation of thin bed layering (0.2m) where there is alternating true q_v values of 30MPa and 90MPa (light grey trace) interbedded within a 50 MPa background layer. As is shown in Figure 3 there is a resulting oscillation averaged/smooth q_m trace (black trace) with no sharp peaks or troughs. The output (black dotted trace) of the q_mHMM algorithm is also illustrated in Figure 4. It shall be obvious that the q_mHMM algorithm performed well as the derived q_v' values closely matched the originally specified q_v values.

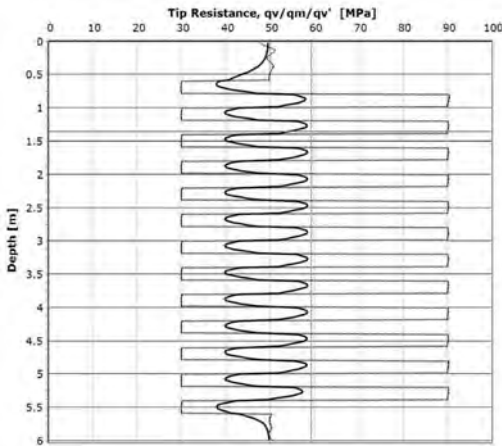


Figure 4. Simulated true cone bearing measurements q_v (light grey trace) and corresponding averaged/blurred q_m (black trace) measurements. The q_mHMM estimated q_v' trace (black dotted trace) is superimposed upon the true cone bearing values.

Figure 5 illustrates the simulated q_m data of Figure 4 (black) with additive noise to represent anomalous/spurious q_m data (red trace). The spurious data was simulated with Gauss-Markov process noise (Baziw and Verbeek, 2021b) with a variance of 60 and time constant of 0.1. The simulated Gauss-Markov noise then had a 250Hz high pass filter applied.

Figure 6 illustrates the estimated q_v (black dotted) trace from the q_mHMM algorithm after processing the output of the q_mKF algorithm (blue trace) of Figure 5. Superimposed on these traces is the true q_v (light grey) trace of Figure 4. As is evident from Figure 6, the combination of the q_mKF and q_mHMM

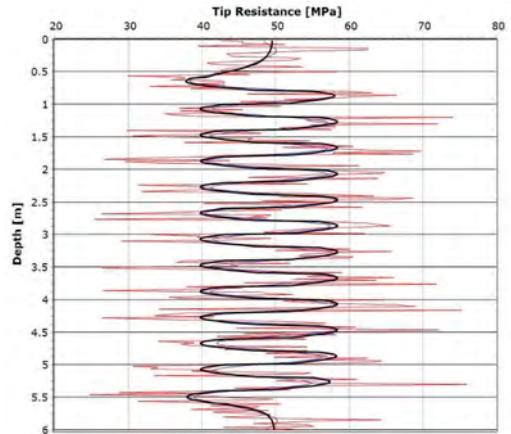


Figure 5. Simulated cone bearing averaged/blurred q_m (black trace) of Figure 3, spurious q_m trace (red trace) feed into the q_mKF algorithm, and the q_mKF algorithm output (blue trace).

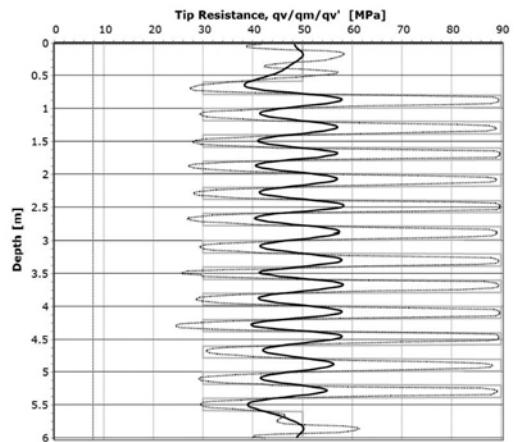


Figure 6. Simulated true cone bearing measurements q_v (light grey trace) and corresponding averaged/blurred q_m (black trace) measurements. The q_mHMM estimated q_v' trace (black dotted trace) is superimposed upon the true cone bearing values.

algorithms results in obtaining impressive estimates of true q_v values from challenging q_m data sets.

3.2 Real data examples

After extensive test best analysis, the q_mKF and q_mHMM algorithms were evaluated implemented on real data sets. Figures 7a, 7b and 7c show q_m profiles acquired by Perry Geotech Limited located at Tauranga New Zealand. It is clear from the results presented in these figures that the effect of averaging/

smoothing of the true q_v values (eq. (1)) can result in a significant reduction in the recorded peaks of q_v values, which may very well impact the design based on the CPT data. The q_mKF and q_mHMM algorithms significantly minimize or undo this effect.

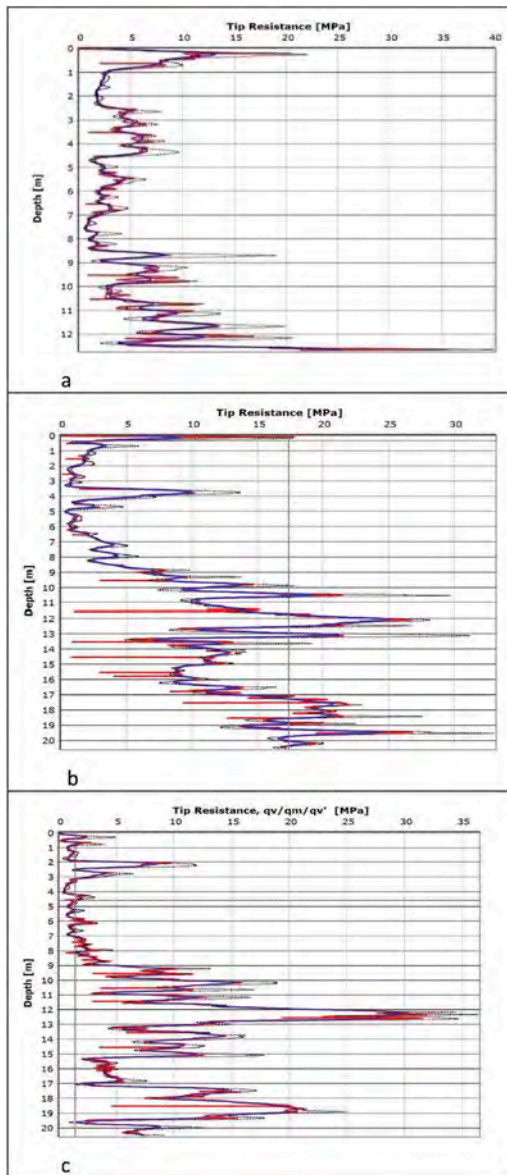


Figure 7. Real data sets. q_m (red trace), output from q_mKF (blue trace) and q_mHMM estimated q_v trace (black dotted trace).

4 CONCLUSIONS

The q_mKF and q_mHMM algorithms outlined in this paper can effectively minimize the anomalous and spurious peaks and troughs to provide a more accurate depth profile of the cone tip resistance.

By applying these algorithms CPT will provide a more realistic soil behavior profile and also allow for more accurate identification of thin layers. In turn it will provide more accurate input data for any design process that uses the CPT results as direct input.

REFERENCES

- ASTM D6067/D6067M – 17 (2017), “Standard Practice for Using the Electronic Piezocone Penetrometer Tests for Environmental Site Characterization and Estimation of Hydraulic Conductivity”, ASTM Vol. 4.09 Soil and Rock (II): D5877-latest.
- Arulampalam, M.S., Maskell, S., and Clapp, T. 2002. A tutorial on particle filters for online nonlinear/non-Gaussian Bayesian tracking. *IEEE Transactions on Signal Processing*, vol. 50, no. 2, 174–188.
- Baziw, E. and Verbeek, G. 2021a. Cone Bearing Estimation Utilizing a Hybrid HMM and IFM Smoother Filter Formulation. Accepted for publication within the *International Journal of Geosciences (IJG) Special Issue on Geoscientific Instrumentation, Methods and Data Systems*.
- Baziw, E. and Verbeek, G. 2021b. Implementation of Kalman Filtering Techniques for Filtering CPT Cone Bearing Measurements. Accepted published in the *DFI 46th Annual Conference on Deep Foundations conference proceedings*. October 12-15, 2021 - Las Vegas, NV.
- Boulanger, R.W. and DeJong, T.J. 2018. Inverse filtering procedure to correct cone penetration data for thin-layer and transition effects. *Proc., Cone Penetration Testing 2018*, Hicks, Pisano, and Peuchen, eds., Delft University of Technology, The Netherlands, 25–44.
- Gelb, A. (1974). *Applied Optimal Estimation* (4th Edition). Cambridge, Mass: MIT Press.
- Lunne, T., Robertson, P.K., and Powell, J.J.M. 1997. *Cone penetrating testing: in geotechnical practice*. Taylor & Francis.
- Robertson, P.K. 1990. Soil classification using the cone penetration test. *Canadian Geotechnical Journal* 27 (1), 151–158.
- Robertson, P.K. 1990. Soil classification using the cone penetration test. *Canadian Geotechnical Journal* 27 (1), 151–158.
- Tjelta, T. I., Tiegies, A.W.W., Smits, F.P., Geise, J.M., and Lunne, T. 1985. In-Situ Density Measurements by Nuclear Backscatter for an Offshore Soil Investigation. *Proc. Offshore Technology Conference*, Richardson Texas, Paper No 40917

Evaluation of parameters inducing desaturation of a piezocone: Saturation liquid viscosity and exposure to dry sand

G. De Backer, R.D. Verastegui-Flores, W. Vervaele, L. Vincke & K. Haelterman
Department of Mobility and Public Works, Flemish Government, Ghent, Belgium

ABSTRACT: Several CPTU tests were performed in both ideal and adverse conditions at a test site in Zwijnaarde. The influence of exposure to unsaturated soils was examined by holding well-saturated piezocones in dry sand for several minutes without a protective rubber membrane. After the exposure to dry sand, penetration was performed from the ground level through the unsaturated and saturated subsoil. These tests show suboptimal pore pressure measurements, compared to the tests under ideal circumstances, regardless of the duration of the exposure to dry sand. Results reveal that, in adverse conditions, the densely packed sandy top layer, rather than the exposure to dry sand, has contributed to the desaturation of the piezocones. The impact of the viscosity of the saturation liquid on pore pressure quality was studied by performing tests with a 50 and 100 cSt silicone oil. Under ideal circumstances, the viscosity does not play a role in terms of quality of the pore pressure measurements. However, in adverse conditions, results showed a better performance for a silicone oil with 100 cSt viscosity.

1 INTRODUCTION

The repeatability of CPTU parameters has been evaluated in many research studies. Generally a reasonably good repeatability is found for pore water pressure measurements, provided good saturation is achieved and maintained, even when performed with equipment from different manufacturers, as described by e.g. Paniagua et al. (2021), Lunne et al. (2018), Powell et al. (2005). Although dynamic pore water pressure measurements might be a reliable parameter, it is known that many aspects can influence these measurements, such as the element location, design and volume of ports, the type and degree of saturation of the fluids, cavitation of the element fluid system, resaturation lag time, depth and saturation of soil during testing (ASTM 2012). The importance of properly saturating a piezocone sensor has been elaborately documented in literature (e.g. Lunne et al. 1997, ISO 22476-1:2012, ASTM 2012). The need for de-airing the saturation liquid in a vacuum chamber has often been emphasized.

In our daily practice, we experience that even well-saturated piezocones may produce poor pore water pressure measurements, if penetration is started above the groundwater level. This is generally avoided by executing a pre-drilling. However, the problem still occurs in cases where the groundwater level is not exactly known or where the groundwater is to be found at considerable depth. In these situations in presence of unsaturated soils we noticed that the penetrometers seem to be quite prone to desaturation.

In this paper, the influence of the viscosity of the silicone oil on the quality of the pore water pressure measurements is evaluated. Also the influence of exposure to unsaturated soils is evaluated by holding the penetrometer several minutes in dry sand.

2 TEST SITE IN ZWIJNAARDE

The test site in Zwijnaarde is located in the south of Ghent, Belgium. The subsoil consists of Quaternary sand layers, with small sublayers of sandy silt to silt, as can be seen in Figure 1. The Quaternary layers have a thickness of approximately 17 m. With a depth of 15 m, all CPTUs in this testing campaign were performed in the Quaternary layers.

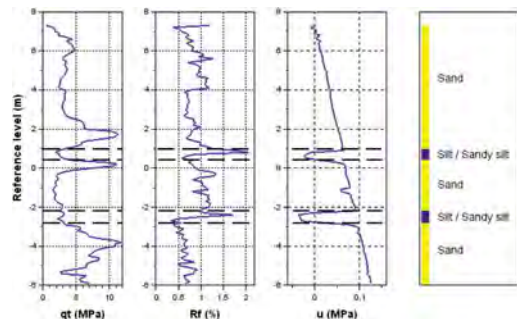


Figure 1. CPTU-data and soil classification.

In the sandy layers, the measured pore water pressures equal the hydrostatic pressure, since the sand is permeable. When passing through the silty layers a drop in the pore water pressure can be noticed in Figure 1. This reduction in pore water pressure is noticed for all pore pressure measurements and is caused by dilative behavior of the dense silt layers, when being sheared during penetration. Although the tests are performed in a small area, there are some spatial variations, both in terms of level and magnitude of the peak cone resistance in the sand layers as well as in the occurrence of the small silt layers, causing pressure drops in the pore pressure measurements.

3 TEST CAMPAIGN AND CONE PENETROMETER DATA

The test campaign took place from March to April 2020. All tests were carried out within an area of 10 by 25 m with a distance of approx. 1 m between two neighboring test points. Four identical piezocones from the same manufacturer were used. The piezocones are of the compression type.

The pore pressure is measured at the u_2 location, which is just above the conical part. A silicone oil, with varying viscosity, was used as saturation fluid.

An overview of the piezometer characteristics is given in Table 1.

Table 1. Cone penetrometer data.

Cone type		Compression
Ac		10 cm ²
Filter type		HDPE - 10 micron
Capacity*	q_c	75 MPa
	f_s	1 MPa
	u_2	2 MPa
Saturation fluid		Silicone oil

* Nominal values – penetrometers calibrated according to EN ISO 22476-1 2012 class 2

The same saturation procedure has been used for all tests, according to EN ISO 22476-1 (2012). The silicone oil was de-aired in a vacuum chamber together with the filters for a duration of at least 24 hours. In a next step, the cone tip was filled with de-aired silicone oil using a syringe. Thereafter, the cone was assembled with a pre-saturated filter and placed back in the vacuum chamber for at least 2 hours at vacuum followed by 20 minutes at atmospheric pressure before removing and covering it with a protective rubber membrane.

4 TEST PROGRAM

4.1 Exposure to dry sand

To examine the impact on desaturation, well-saturated piezocones were kept in a bucket with dry

sand for a certain time interval before executing a CPTU test. The piezocones were protected with a rubber membrane which was removed right before entering a bucket of dry sand. The dry sand is known as ‘Mol Sand’, characterized by a median particle diameter D_{50} of 0.2 mm and a uniformity coefficient $UC = D_{60}/D_{10}$ of 1.6. Four different time intervals were considered: 5 min, 15 min, 30 min and 60 min.

Immediately after exposure to dry sand, CPTU tests were performed over a depth of 15 m. The results of these pore pressure measurements in adverse conditions are evaluated and compared with CPTU tests performed in the same test field, however, this time starting from the saturated subsoil (ideal conditions). To achieve this, these CPTUs were initiated from a pre-drilled borehole of a depth of 1.5 m. PVC tubes along the shaft prevented collapse of the borehole. The piezocone filters were covered with a rubber membrane directly after saturation. Water was added to the drilling hole, while descending the piezocone in the borehole. The additional water dissipated entirely in the sandy top layers before penetration through the saturated subsoil started. The CPTUs performed according to best practices are referred to as tests under ideal circumstances. Adverse conditions in the present research refers to exposure to dry sand, absence of the protective rubber membrane and no pre-drilling.

4.2 Viscosity

The standard saturation liquid, as recommended by the piezocone manufacturer, is a silicone oil with a viscosity of 50 cSt, combined with a filter with a 10 μ m pore diameter. In order to decrease desaturation, a more viscous silicone oil of 100 cSt was also used to saturate the piezocone. Similar CPTU tests were carried out as with the 50 cSt liquid.

Table 2 gives an overview of the parameters that were varied in relation to the number of tests performed.

Table 2. Test program.

Parameter	Tested values	Number of tests
Viscosity	50 cSt	12
	100 cSt	12
Duration in dry sand	0 min*	9
	5 min**	4
	15 min	4
	30 min	3
	60 min	4

* Zero minutes in dry sand corresponds to ‘ideal circumstances’.

** For one test the duration was 7 min instead of 5 min.

4.3 Evaluation criteria

All pore pressure measurements were evaluated and divided into 4 quality categories: good, fair, mediocre and poor. Evaluation criteria were: similarity to the hydrostatic pressure line and speed of response of the sensor.

Based on a borehole measurement, the water table is at about 7.3 m above sea level, which corresponds to 1.5 to 1.7 m depth. At a depth of 15 m a short dissipation test was conducted for all soundings, resulting in a slightly lower water table. Pore pressure measurements show this slight shift in hydrostatic line too at approximately 0 to 1 m reference level, where a small silty layer occurs. For this reason, an upper and lower hydrostatic line is drawn in all pore water pressure figures, indicated by $u_{0,u}$ and $u_{0,l}$ respectively.

Figure 2 shows an example of pore pressure measurements for each category. The blue dashed line represents a good measurement as it coincides well with the hydrostatic pressure lines and shows a quick response after a pressure drop, as can be seen at e.g. a level of 6.5 m. Some small peaks above the hydrostatic pressure can be noticed between level -3 and -5 m. Unfortunately, there are no cohesive soils at the test site that would generate large and sustained positive pore pressures which would facilitate the evaluation of the sensor response. The pore pressure drops in Figure 2 are not the result of a drop in penetration speed. A constant speed of 2 cm/s was achieved, using a continuous sounding technique. However, the drops agree well with the occurrence of small silty layers in the corresponding CPT-profile.

The green dotted line represents a ‘fair’ pore pressure measurement. Slightly slow response is noticed after a pressure drop, for instance at around 5 m and -0.5 m. However, it still rejoins the good measurement line. The red dotted line shows the ‘mediocre’ results, for which the sensor shows even slower response and a larger deviation from the hydrostatic line.

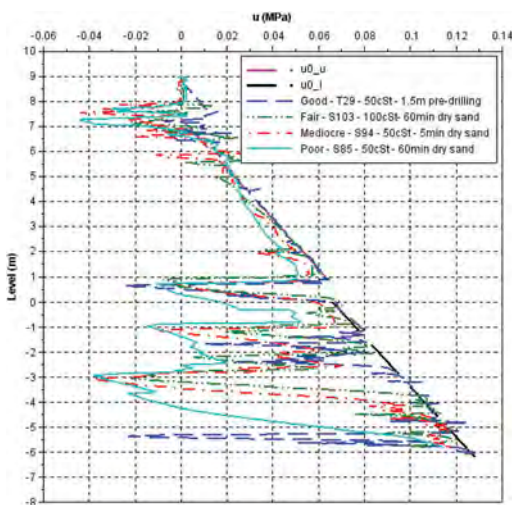


Figure 2. Examples of 4 quality categories of pore pressure measurements versus reference level.

For the ‘poor’ measurements, in Figure 2 indicated with a light blue solid line, a clear sluggish response is noticed and it is impossible to determine the hydrostatic line from the pore pressure measurements.

5 TEST RESULTS

5.1 Comparison of measured data

Figure 3 shows the measured cone resistance q_c , sleeve friction f_s and pore water pressure u_2 for all tests, grouped according to their pore pressure quality category. The reference level is based on the depth measurements corrected for inclination and elevation.

As expected, all tests performed under ideal circumstances show good pore pressure measurements. Remarkably in this group, one outlier has been 60 minutes in dry sand and still shows no clear signs of desaturation. This is not the case for the other tests that have been a certain time in dry sand without the protection of a rubber membrane.

Although not the purpose of this study, it is worthwhile to have a look at the q_c and f_s measurements as well. For the top layers the repeatability of q_c is generally quite good. The values of f_s show more scattering. Larger variations for f_s compared to q_c are also found in literature (Paniagua et al. 2021, Lunne et al. 2018). Some anomalies also drew our attention: S112 (cone 2) and T59 (cone 3) show lower q_c and f_s values, whereas T31 and S94 (both cone 4) give higher f_s values. It is unclear what might have caused these anomalies. Since the pore water pressure measurements don’t seem to be affected, they were not excluded from the analysis.

Note that the less reliable pore pressure measurements cannot be attributed to a single underperforming piezocone, since all 4 piezocones showed very similar pore pressure measurements in ideal circumstances and because no correlation was observed between any pore pressure quality category and a particular piezocone.

5.2 Viscosity

Since all tests with zero exposure to dry sand produced good pore pressure measurements, regardless of the viscosity of the silicone oil, it can be stated that the viscosity has no influence on the results, if they are performed under ideal circumstances.

However, when the piezocone is exposed to dry sand and subjected to relatively high suction pressures during shearing, it seems that the viscosity does play a role. Based on the results depicted in Figure 4, it is likely that a 100 cSt viscosity might withstand better to desaturation than a 50 cSt viscosity. However, the results should be interpreted with caution given the relatively small number of tests. Further research is to

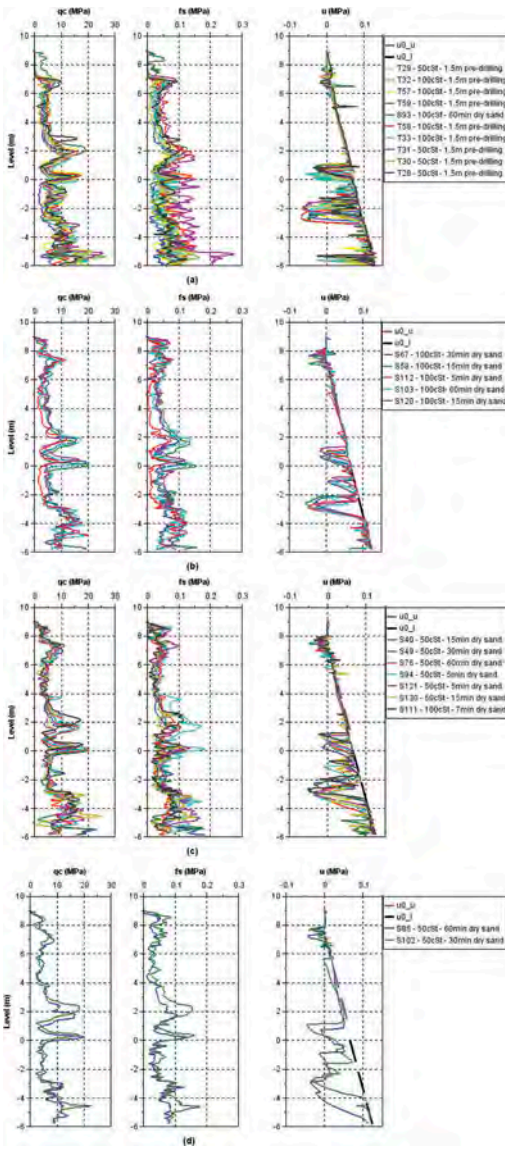


Figure 3. Measured q_c , f_s and u grouped by quality category based on the pore pressure measurements (a) good, (b) fair, (c) mediocre and (d) poor.

be carried out to better understand the advantages and possible drawbacks of using a more viscous silicone oil.

5.3 Exposure to dry sand

The impact on the quality of the pore pressure measurements as a function of the time of contact with dry sand is presented in the bubble plots of

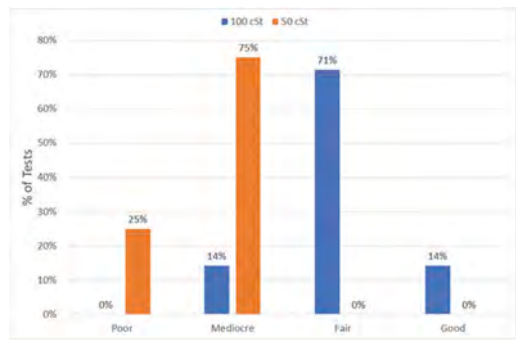


Figure 4. Percentage of tests under adverse conditions as a function of pore pressure quality categories for 100 cSt and 50 cSt viscosity of silicone oil.

Figure 5 for both silicone oil viscosities, 50 cSt and 100 cSt.

Each bubble shows the number of tests for a certain combination of pore pressure quality category and number of minutes in dry sand. One would expect a descending trendline showing decreasing quality in the pore pressure measurements for increasing minutes in dry sand. However, this is not the case, especially not for the plot with 100cSt. There is no clear relation between pore pressure quality and contact duration in dry sand. Only zero minutes in dry sand results in an obvious link with good quality measurements.

During pore water pressure observation tests in dry sand, no or very small suction pressures - smaller than the measurement accuracy- were measured. On the other hand, significant negative pore water pressures were observed going from -30 to -50 kPa during penetration for the tests in adverse conditions. For this reason, it seems likely that the negative pressures, occurring shortly after penetration, have been more detrimental to the saturation of the piezocone than the static contact with dry sand. At small depth fairly high q_c values are registered (up to approx. 10 MPa), indicating a high relative density of the sand layer. This sand dilates during penetration and it mobilizes negative pore pressures. This might explain why the contact time in dry sand seems not to be decisive on the quality of the pore pressure measurement and moreover, it might explain why the outlier (CPTU S93), which remained 60 minutes in contact with dry sand, still produced good pore pressure measurements. During penetration this test experienced rather small q_c values (max. 6.5 MPa) just above the water table and consequently small suction pressures were measured (up to -15 kPa), which is in the same order of magnitude as for the other tests producing good results.

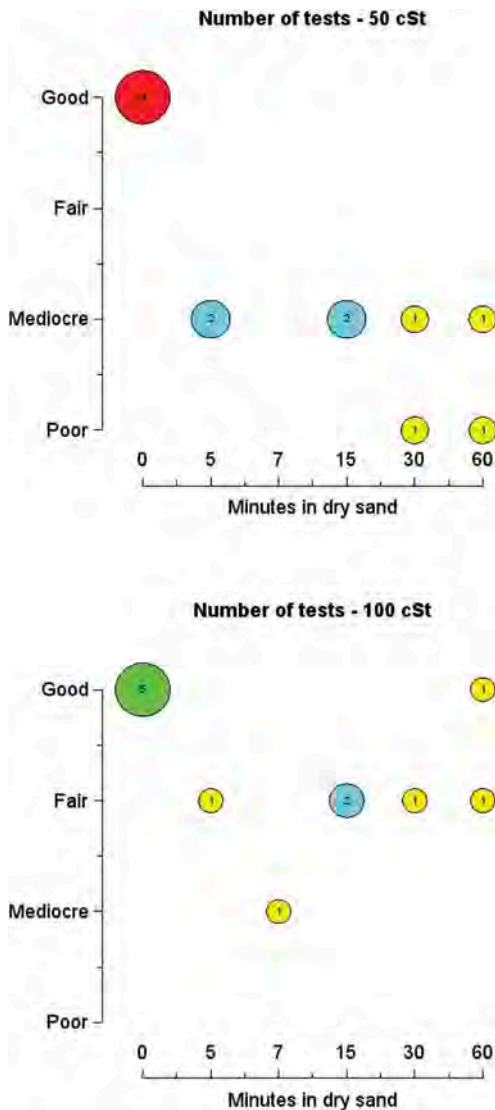


Figure 5. Pore pressure quality category in relation to the exposure to dry sand for 50 cSt and 100 cSt silicone oil.

6 CONCLUSIONS

Twenty-four CPTUs were performed at the test site in Zwijnaarde in both 'ideal' and 'adverse' circumstances in order to compare pore pressure measurements.

The tests have been performed for two different values of viscosity of the saturation liquid, i.e. 50 and 100 cSt. The results showed that, under optimal conditions, good pore pressure measurements are observed, regardless of the viscosity. However, in adverse conditions, the results suggest that cone

penetrometers saturated with 100 cSt silicone oil might withstand better to desaturation compared to those saturated with 50 cSt silicone oil. Further research is to be carried out to evaluate the impact of the viscosity of the silicone oil on desaturation.

The influence of exposure to unsaturated soils was simulated by holding initially well-saturated piezocones in contact with dry sand for several minutes. During their exposure to dry sand the piezocones were not protected by a rubber membrane. All but one piezocones showed clear signs of desaturation during penetration, even when exposed briefly to dry sand. Since no or very small suction pressures were generated during the pore pressure observation tests in dry sand, it is likely that mainly the negative pressures, associated with dilation during penetration of the sandy top layer, have adversely impacted the saturation rather than the exposure to dry sand. In a subsequent study it would be interesting to separate the effect of exposure to dry sand and initial penetration through the unsaturated dense sandy layer, by also performing a pre-drilling for the penetrometers exposed to dry sand.

ACKNOWLEDGEMENTS

The authors would like to thank David Fraeyman and Andy Fraeyman for preparing and performing all field tests and for their valuable contribution in optimizing the execution process.

REFERENCES

- ASTM D5778–12 2012. Standard Test Method for Performing Electronic Friction Cone and Piezocone Penetration Testing of Soils, ASTM International. www.astm.org.
- ISO 2012. Geotechnical investigation and testing – Field testing – Part 1: Electrical cone and piezocone penetration tests, International Standard ISO 22476-1.
- Lunne T., Robertson P.K. & Powell J.J.M. 1997. *Cone Penetration Testing in geotechnical practice*. Taylor & Francis Ltd. ISBN 0 419 23750 X.
- Lunne T., Strandvik S., Kåsin K., L'Heureux J.-S., Haugen E., Uruci E. & Kassner M. 2018. Effect of cone penetrometer type on CPTU results at a soft clay test site in Norway. *Proceedings of the 4th International Symposium on Cone Penetration Testing CPT 2018*: 417–422. Delft.
- Paniagua P., Lunne T., Gundersen A., L'Heureux J.-S. & Kåsin K. 2021. CPTU results at a silt test site in Norway: effect of cone penetrometer type. *IOP Conf. Ser.: Earth Environ. Sci.* 710 012010.
- Peuchen, J. & Terwindt J. 2014. Introduction to CPT accuracy. *Proceedings of the 3rd International Symposium on Cone Penetration Testing*, Las Vegas, Nevada, USA.
- Powell, J.J.M. & Lunne, T. 2005. A comparison of different piezocones in UK clays. *Proceedings of ISSMGE Conference*, Osaka.

Large diameter cone penetrometers: What is an appropriate location for the transition to the rod diameter?

D.A. de Lange, T.A. van Duinen & D.J. Peters

Deltares, Delft, The Netherlands

ABSTRACT: 15 cm² cone penetrometers are typically pushed to depth by means of 10 cm² rods. Therefore, a transition in diameter will be present at a certain distance from the cone shoulder. Although the standards give a requirement for the position of this transition, cone penetrometer configurations that don't meet this requirement are often preferred by CPT sounding companies and are being used in practice. This raises a dilemma. In order to fuel discussion, a first step was made by performing two series of 9 CPTs with different penetrometer geometries. The effects of the penetrometer designs on the measured quantities were investigated. From a preliminary analysis of the results no systematical differences between the different penetrometers were observed. When these preliminary findings are better understood and validated, the standards can be updated.

1 INTRODUCTION

From perspective of a CPT sounding company it is beneficial to have a system that has enough resistance against breakage of the pushing rods and allows deep penetration without the need of an excessive load. For Dutch practice, most commonly utilized cone penetrometers have a projected base area of 10 cm² (diameter, $D = 3.6$ cm) or 15 cm² ($D = 4.4$ cm). However, in general similar pushing rods are used for both cone types, which implies the need for a transition from the wider penetrometer to the smaller pushing rods in case of a 15 cm² cone penetrometer. According to NEN-EN-ISO 22476, the lowest point of the transition should be at least $11.2D$ ($= 49$ cm) above the cone shoulder. In practice, however, we notice that companies do prefer and use configurations in which the transition is much closer to the cone shoulder (± 23 cm or about $5D$). The main reason for this deviation from the standards is reduction in required force to reach depth, as the configuration acts like a friction reducer. Further, smaller inclination deviations are observed with a 15 cm² cone compared to a 10 cm² cone. Therefore, it is understandable that CPT sounding companies prefer such a system over systems that meet the standards.

These observations lead to the following questions:

1. What are the effects of the penetrometer configuration on cone resistance, q_c , sleeve friction, f_s , and/or pore water pressure?

2. What was the basis for the requirements in the testing standards?

Some companies refer to Powell & Lunne (2005) and claim that the measured quantities are hardly affected by the shorter distance from shoulder to transition. Powell and Lunne discuss tests in UK clays, utilizing 15 cm² piezocones with sleeve areas of 200 and 300 cm². They conclude there is little difference in results between the different sleeve areas. However, the distances from shoulder to transition are not mentioned. Heijnen (1972) presents extensive field research on the shape of the cone penetrometer (10 cm²), as different results in q_c were observed from a "Dutch mantle cone" and a "straight electrical cone" in sands. Heijnen concluded that a reduction in diameter behind the cone might influence q_c significantly, but that such effects also rapidly decrease with distance from the cone shoulder. Interestingly, no significant differences were observed between a "straight" cone (constant diameter over full length) and a cone with a reduced diameter from 10 cm above the cone "tip" ($2.8D$). However, we believe that such conclusions should be treated with caution due to natural variability of the subsoil and measurement uncertainty.

Most likely, the basis for the requirements in NEN-EN-ISO 22476 are the classical analytical solutions for the bearing capacity of footings, like the Prandtl-wedge. The size of the failure wedge is typically a function of the friction angle of the soil and can extend to great distances from the cone

shoulder, e.g. Figure 1. However, this seems to contradict with the pile base shape factors from NEN 9997-1+C2, see Figure 2. For instance, in case of a 15 cm² cone with 10 cm² rods ($D_{eq}/d_{eq} = 1.5$), only $H \geq 2D$ is required to become comparable with a fully straight pile concerning the tip resistance in sands.

From above findings it might be expected that the different configurations of the 15 cm² cone as we come across in the field will not significantly influence q_c . However, it is important to validate this with empirical evidence. Further, the potential influence on the friction readings is less clear so far, as the penetrometer geometry also might affect the horizontal soil stresses around the sleeve. Deltares proposed a series of CPTs using 15 cm² cone penetrometers having the transition at different distances from the shoulder. This paper discusses the test details, results, and the next steps required to solve this issue.

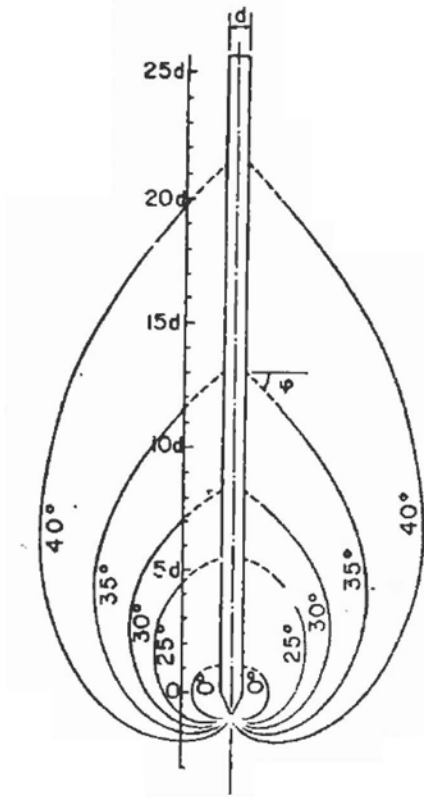


Figure 1. Logarithmic spirals (Van Mierlo & Koppejan 1952).

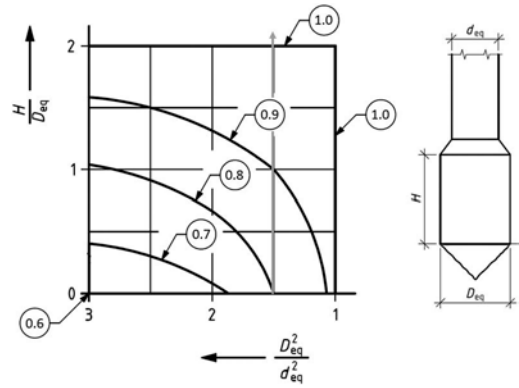


Figure 2. Pile base shape factor β for piles in sand (NEN 9997-1+C2).

2 MATERIALS AND METHODS

Two test series were performed in April and December 2021. In total 18 CPTs were executed at a green field, that has been empty for years, adjacent to the Deltares campus, Delft, The Netherlands. Four different 15 cm² penetrometer configurations have been used. Configurations A and B do meet the requirements of NEN-EN-ISO 22476 with respect to the location of the transition, while configurations C and D don't. The cone dimensions are given in Figure 3 and Table 1. As can be observed, the area and the location of the friction sleeve was near identical for all penetrometers. All penetrometers were manufactured by the same company and all tests were executed by the same company. The locations and the order of the CPTs are given in Figure 4. E.g. "A2" refers to penetrometer type A and the second CPT of the test series. The target penetration level was 25 m below surface level for all tests, passing through Holocene clay and peat deposits and Pleistocene sand. Pore water pressures were not measured.

Table 1. Penetrometer characteristics.

	A	B	C	D
Penetrometer	cm	cm	cm	cm
Shoulder – transition distance	52	52.5*	31.5	19
Sleeve – transition distance	34	34.5*	13.5	1
Transition length	1	-	5	8

* Distance to friction reducers is given.

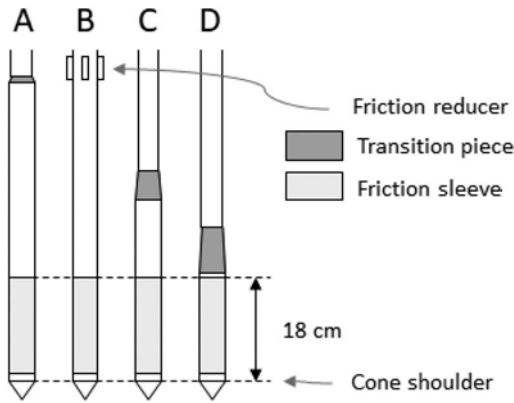


Figure 3. Schematization of utilized 15 cm² penetrometers.

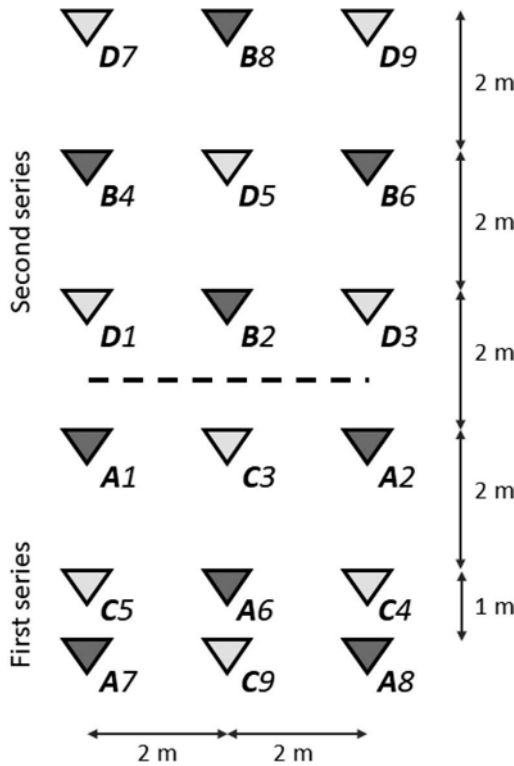


Figure 4. CPT locations and order.

3 PRELIMINARY RESULTS

The results are presented in Figures 5-14. Total cone inclinations of about 1° to 3° were measured at final depth. Therefore, interference between the tests are excluded. Figure 5 shows the q_c -profiles from all type-A tests to indicate the inherent variability. The results of the central CPT are emphasized. Figure 6 also presents the results of this central CPT, but now with respect to the results of all type-C tests. Similar plots are given for f_{ss} , see Figures 7-8. q_c - and f_s -profiles as

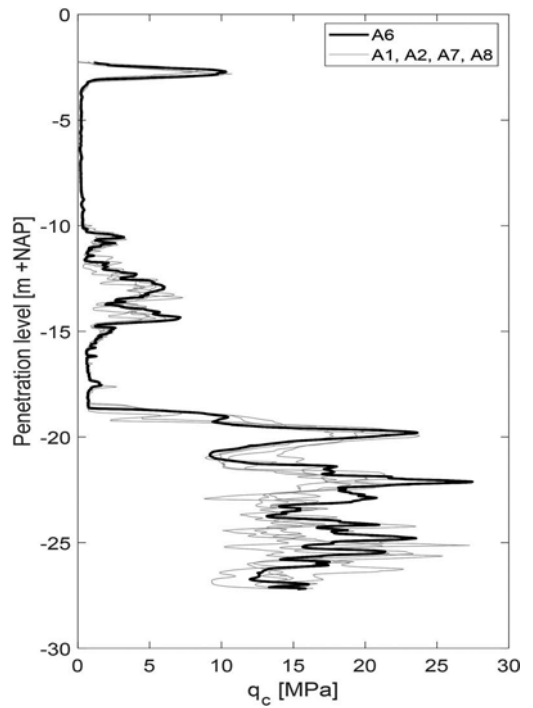


Figure 5. Results from A6 with respect to other type A results.

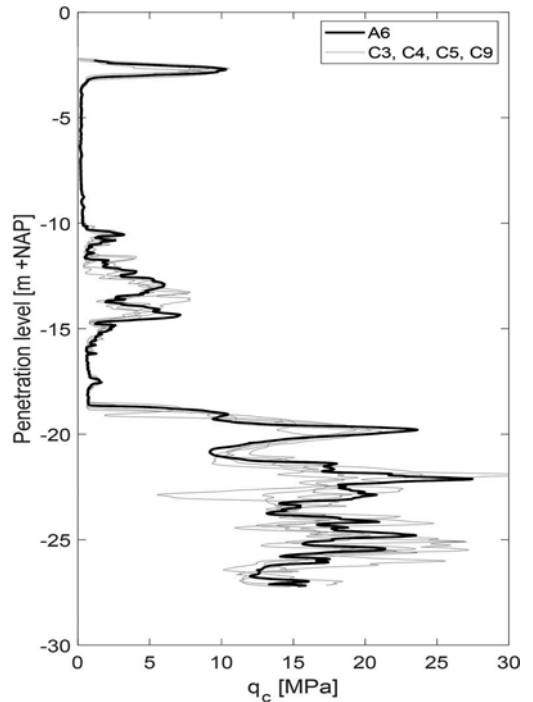


Figure 6. Results from A6 with respect to type C results.

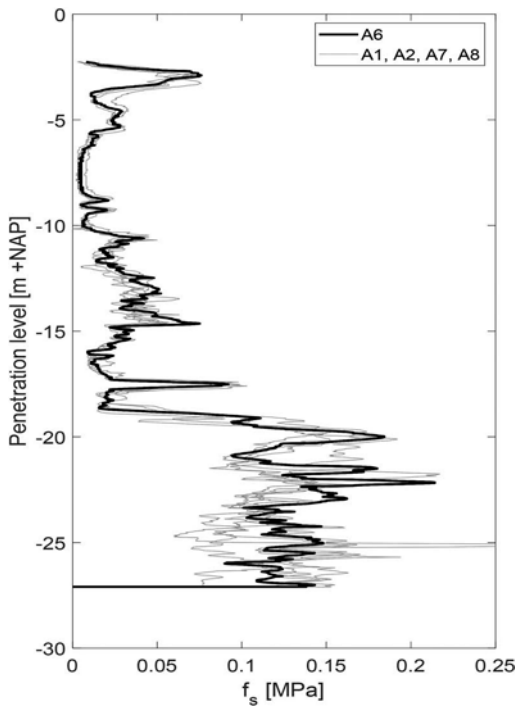


Figure 7. Results from A6 with respect to other type-A results.

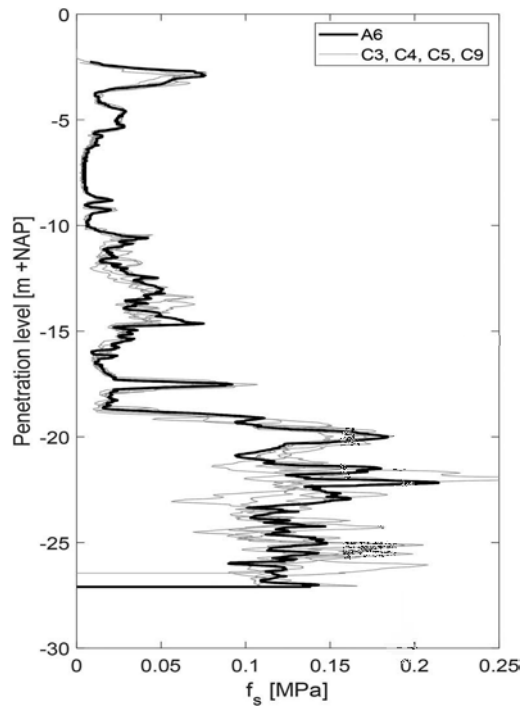


Figure 8. Results from A6 with respect to type-C results.

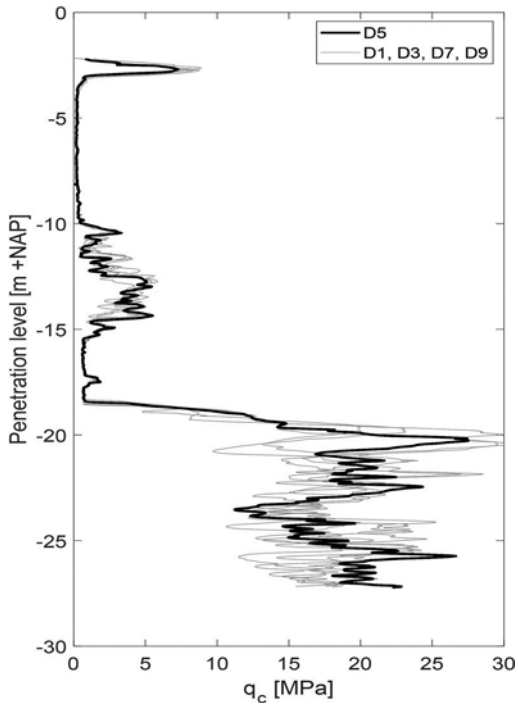


Figure 9. Results from D5 with respect to other type D results.

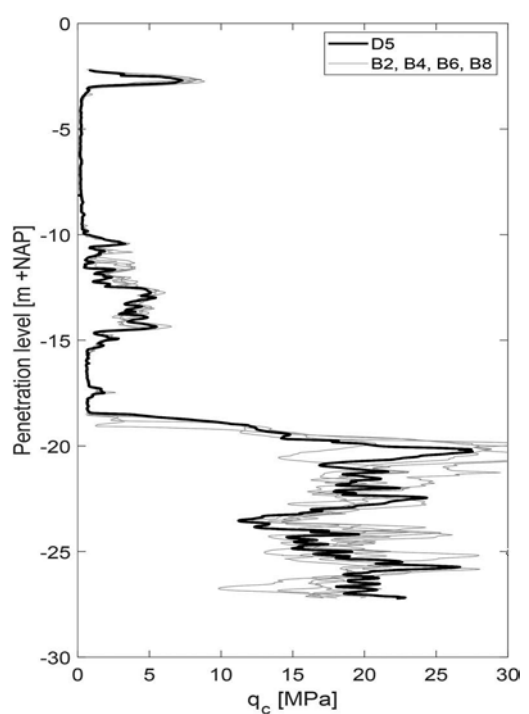


Figure 10. Results from D5 with respect to type B results.

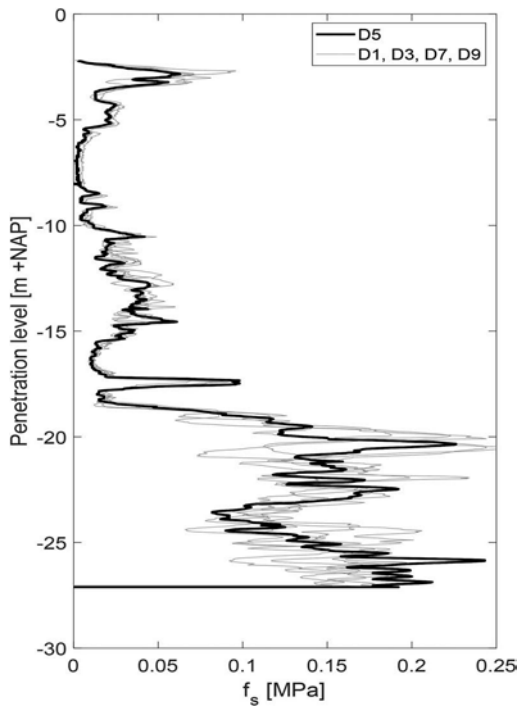


Figure 11. Results from D5 with respect to other type D results.

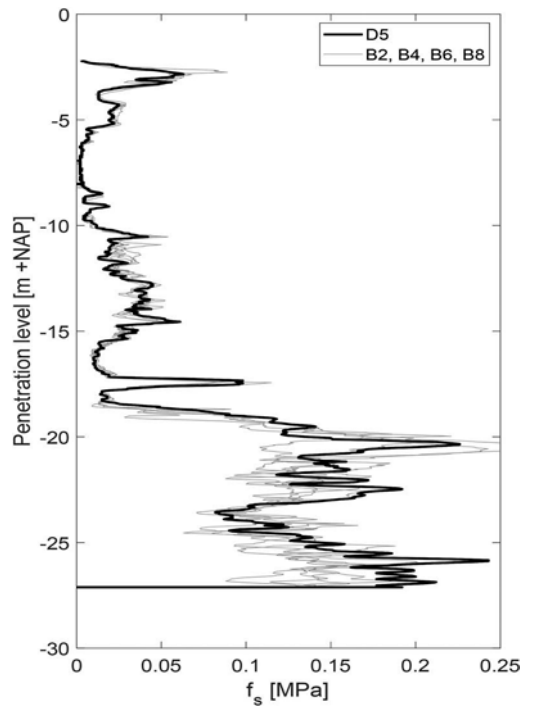


Figure 12. Results from D5 with respect to type B results.

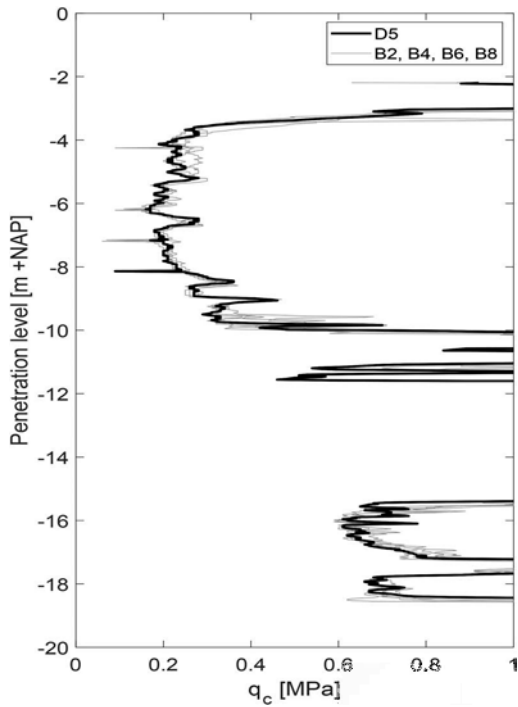


Figure 13. Results from D5 with respect to type B results (zoomed in on the soft Holocene layers).

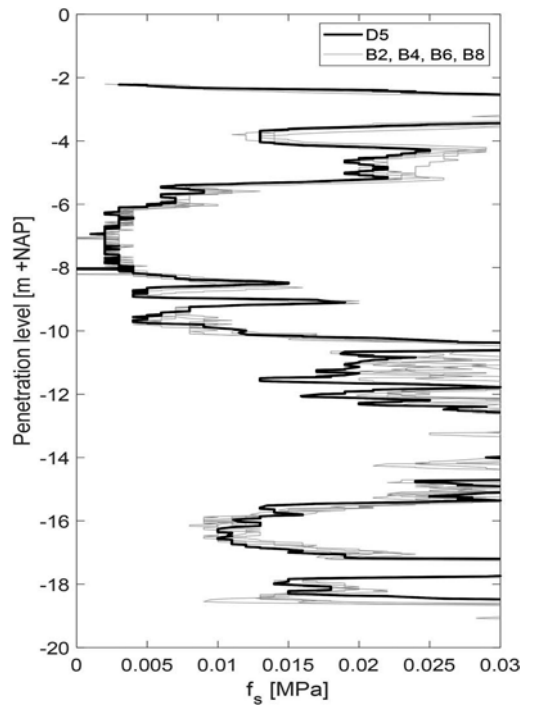


Figure 14. Results from D5 with respect to type B results (zoomed in on the soft Holocene layers).

being measured during the second test series are given in Figures 9-14. From the results, no systematical differences were observed, neither for q_c nor f_s , neither in clay nor peat nor sand.

4 CONCLUDING REMARKS

In practice, different penetrometers with large cone diameter are used, several of which don't meet the requirements of the standards. A range has been tested in the presented first investigation. The location of the diameter transition ranged from 4.4 to 12 times D from the cone shoulder. From a preliminary analysis of the results no systematical differences were observed. This is an important finding. As a first next step, the results can be analyzed in more detail. Further, we foresee the need to consult archives and involved people to understand the background and motivation of the adopted standards. In order to achieve a broader basis and have a better statistical support of present results, tests should be repeated at other locations, in other soil types. For better understanding of the mechanisms, a combination of numerical (e.g. MPM) and physical modelling can be applied. Lastly, should you want to contribute, any relevant information from your side is more than welcome! Please contact the corresponding author.

ACKNOWLEDGEMENTS

The authors would like to acknowledge Gouda Geo-Equipment for making the different cone penetrometers available, Inpijn Blokpoel Ingenieurs for execution of the CPTs and Delft University of Technology for allowing us to use their land for this first investigation.

REFERENCES

- Heijnen, W.J. (1972). De vorm van de elektrisch sondeerconus. *Verhandelingen Fugro Sondeersymposium 1972*: 17–27 (in Dutch).
- NEN-EN-ISO 22476-1:2012 en Geotechnical investigation and testing - Field testing - Part 1: Electrical cone and piezocone penetration test.
- NEN 9997-1+C2:2017 Geotechnical design of structures - Part 1: General rules (in Dutch).
- Powell, J.J.M. & Lunne, T. (2005). A comparison of different sized piezocones in UK clays. *Proceedings of the 16th International Conference on Soil Mechanics and Geotechnical Engineering*: 729–734.
- Van Mierlo, W.C. & Koppejan, A.W. (1952). Lengte en draagvermogen van heipalen. *Bouw 19-1-1952, no. 3*: 1–11 (in Dutch).

Issues related to piezocone sleeve friction measurement accuracy in soft sensitive clays

B. Di Buò & M. D'Ignazio

Tampere University / Ramboll Finland Oy, Tampere, Finland

T. Lämsivaara & M. Haikola

Tampere University, Tampere, Finland

ABSTRACT: Over the past decades, the piezocone testing has been increasingly adopted for field investigation as it offers a quick and cost-effective methodology for subsoil profiling and geotechnical parameters estimation. Although the piezocone testing has revealed good applicability worldwide, difficulties are encountered in complex soil conditions, such as soft sensitive clays. One of the key issues in such soils is represented by the poor quality of the sleeve friction (f_s) measurement due to inaccuracy and poor resolution of the sleeve sensor. This paper investigates the influence of f_s data quality on soil parameters determination with particular emphasis on the soil behavior type (SBT) chart classification. The field investigation was conducted in a soft sensitive clay site located in Finland using two different penetrometers: a standard piezocone and an advanced piezocone characterized by enhance accuracy sleeve friction sensor. Results show that the use of high-resolution piezocone plays a key role in soft clays to avoid misleading soil type classification.

1 INTRODUCTION

1.1 Cone penetration testing (CPT)

Cone Penetration Testing (CPT) is a fast and reliable means of conducting subsurface investigation for soil profiling, site characterization and geotechnical parameters evaluation. Since the first introduction of the mechanical probe in 1930s, the equipment has been significantly improved by adding porous filters and transducers, obtaining the modern electronic piezocones (CPTu). Nowadays, the traditional piezocone testing provides three independent readings with depth: the cone tip resistance (q_c), the sleeve friction (f_s), and the excess pore water pressure (u_2) measured behind the cone tip (u_2). The q_c value should be corrected (q_t) to consider the pore pressure acting behind the shoulder. This correction is significant in soft to stiff clayey soils (Jamiolkowski et al. 1985, Robertson and Campanella 1988, Lunne et al. 1997).

The data provided by piezocone test is generally characterized by high precision and accuracy. The sensor accuracy is the difference between the target and the measured value while the precision refers to the degree of reproducibility of a measurement. These aspects are summarized in Figure 1.

Another aspect that plays a key role in data quality is the sensor resolution which is the smallest detectable incremental change that can be measured.

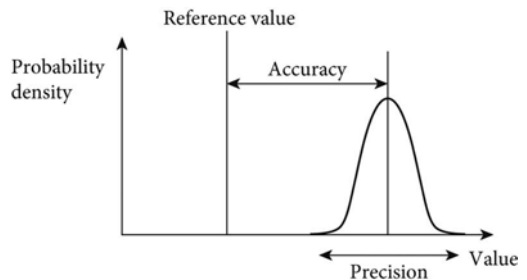


Figure 1. Accuracy and precision definition (source Wikipedia).

This is crucial in soft sensitive clays as the value of f_s is generally very low (<1 kPa).

The equipment available on the market are characterized by different features such as dimensions, tolerances, and sensor accuracy. However, all the specifications, technical requirements, and test procedures are outlined in the European Standards (EN-ISO 22476-1) and American Standards (ASTM D5778 - 20). All these aspects are extensively discussed by (Lunne et al. 1997). Although several piezocones can be employed for CPTu testing, it is fundamental to choose the appropriate equipment to obtain high-quality and reliable data, especially in soft sensitive clays. As an example, studies conducted by

Tampere University (Di Buò et al. 2016, Di Buò 2020) have revealed that standard penetrometers are not suitable to correctly measure f_s in Finnish soft soil, which negatively affects the data interpretation and the accuracy of soil profiling as the small variability of f_s throughout the entire deposit cannot be detected. Moreover, the f_s is fundamental for the soil classification based on the Soil Behavior Type (SBT) chart proposed by Robertson (1990) or for the assessment of a number of geotechnical parameters, such as the soil sensitivity (Mayne 2014). Despite the importance of the f_s data, its correct measurement is still considered one of the main challenges in soft sensitive clays.

This paper presents the CPTu test results obtained from a soft sensitive clay test site located in Pohja, Southern Finland. The soundings have been performed using a “standard” probe and a penetrometer characterized by enhanced sensor accuracy and resolution, herein after referred to as “advanced”. The results are analyzed and compared, pointing out the influence of f_s measurement on the SBT classification and the improvements that can be obtained using high accuracy sensors. The main goal of the study is to investigate the influence of the piezocone sensor accuracy on the soil interpretation, rather than a comparison between cone manufacturers.

1.2 Equipment

The two penetrometers adopted in this study were provided by two different manufacturers. Both cones are characterized by 60° apex angle, 10 cm² base and 150 cm² sleeve area. The first one, referred to as “standard”, has been largely used for site investigation in Finnish soft clays as detailed by Di Buò et al. (2020): it consists of an electronic instrumented probe with a nominal range of 7.5 MPa, which is particularly suitable for soft soils investigation. The second, referred herein after as “advanced”, is characterized by a nominal range of 50 MPa and higher accuracy compared to the previous cone. This cone has been used at the Pohja site as an attempt to overcome the issues related to the f_s measurement previously discussed. The technical features of both piezocones are summarized in Table 1. The enhanced accuracy of the advanced penetrometer is the result of the embedded sensors type and their configurations. In particular, the q_c and f_s load cells are characterized by four strain gauges wired into a Wheatstone bridge configuration. The bridge is compensated with four modules: two for the material elastic modulus temperature compensation, one for the zero-offset correction and the last one for zero-offset temperature compensation. The Wheatstone Bridge circuit consists of two simple series-parallel arrangements of resistances connected between a voltage supply terminal and ground producing zero voltage difference between the two parallel branches when balanced. It has two input terminals and two output terminals consisting of four resistors configured in a diamond-like arrangement. This configuration allows for high accuracy in the parameter

Table 1. Technical features of the piezocones.

Standard penetrometer				
	q_c	f_s	u_2	Inclination
Maximum capacity	7.5 MPa	0.15 MPa	2 MPa	20°
Accuracy	0.2% (15 kPa)	0.7% (1 kPa)	0.25% (5 kPa)	0.5°
Advanced penetrometer				
	q_c	f_s	u_2	Inclination
Maximum capacity	50 MPa	1.6 MPa	2.5 MPa	20°
Accuracy	0.01% (5 kPa)	0.0025% (0.04 kPa)	0.0015% (0.04 kPa)	0.5°

measurement. Similarly, the u_2 sensor consists of a silicon piezoresistive load cell in Wheatstone bridge configuration.

1.3 Test site

The Pohja site locates on the southern coast of Finland along the railway line connecting the cities of Helsinki and Turku. The ground elevation is around 9 m above current sea level and the overall topography is flat. However, on a wider scale, the site locates in a valley surrounded by shallow hills with bedrock outcrops. The Pohja site subsoil consists of about 1.5 m thick dry crust layer overlaying a soft slightly consolidated clay layer. Below, silty and sandy layers are encountered. The bedrock is located at depth of 14 m. The water content decreases with depth, from 130% between 2m and 4m till reach 60% at about 7.5 m depth. The natural water content exceeds the liquid limit throughout the entire deposit. Plasticity index is 30–60 and sensitivity, defined as the ratio between intact (s_u) and remoulded undrained shear strength ($s_{u,rem}$), varies between 40 and 60 below the dry crust layer. The undrained shear strength evaluated by the fall cone (FC) test is 7 kPa under the dry crust layer and increases linearly with depth reaching 12 kPa at the depth of 7.5 m. The geotechnical properties of Pohja clay are shown in Figure 2.

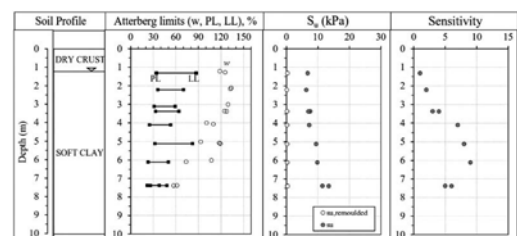


Figure 2. Index properties of Pohja clay.

2 CPTU DATA ANALYSIS

2.1 CPTu soundings

A total of three CPTu soundings are performed, two of them obtained from the advanced piezocone and one representative vertical from the standard cone. The main purpose herein is to investigate the impact of the sensor accuracy in the measurement readings. The same testing procedure has been adopted for both penetrometers. An initial pre-drilling is made to avoid pushing the cone into the dry crust layer which may cause the desaturation of the porous stone. Prior to CPTu sounding, the cone is placed into the hole filled with water for temperature balancing. Then, the apparatus is pushed into the soil at a standard rate of penetration of 20 mm/s till reaching the coarse layer (≈ 7 m). The measured q_c has been further corrected to account for the pore water pressure acting behind the cone as follows:

$$q_t = q_c + u_2(1 - a) \quad (1)$$

where a is the net cone area ratio provided by the manufacturer after the calibration process. The soundings are conducted using a ceramic filter element replaced after each test. The saturation is ensured by submerging the cone tip into a silicon oil bath in a vacuum device.

Results illustrated in Figure 3 indicate the presence of a homogeneous clay layer from 1 m to 7 m depth followed by interlayers of silts and sands. It is worth observing that both piezocones provide nearly identical response in terms of q_t and u_2 while f_s measurements made using the standard cone are characterized by poor accuracy and low resolution. In particular, higher f_s values are measured by the standard cone (>4 kPa) while the advanced cone indicates f_s values lower than 1 kPa. Even though this difference may seem neglectable, the total error is significant, and it has a great impact in the SBT classification as soil parameter estimation as discussed later.

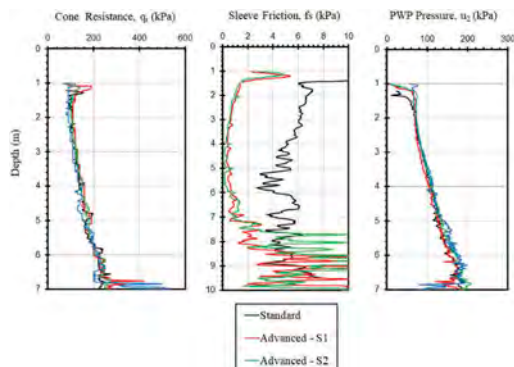


Figure 3. CPTu soundings at Pohja site.

2.2 Soil Behavior Type (SBT) chart

Since its first introduction, the CPT has been widely used for soil profiling and classification. Several authors have proposed classification charts that link the CPT parameters (q_t and f_s) to the soil type (Bege-mann 1965, Robertson et al. 1986, Robertson 1990). Among them, the soil behavior type (SBT) chart proposed by Robertson et al. 1986 has become quite popular. It identifies 12 types of soil based on the q_t and f_s values. This approach is mainly based on classifying the soil based on the in-situ behavior which depends on the strength, stiffness and compressibility. In contrast, the unified soil classification system (USCS) does not provide any information on the mechanical behavior as it is based on the grain-size distribution and plasticity. However, in most cases, both approaches agree fairly well as detailed by Molle (2005). The SBT chart has been further improved introducing the normalized parameters:

$$Q_t = \frac{q_t - \sigma_{v0}}{\sigma'_{v0}} \quad (2)$$

$$F_r = \frac{f_s}{q_t - \sigma_{v0}} \times 100 \quad (3)$$

$$B_q = \frac{u_2 - u_0}{q_t - \sigma_{v0}} \quad (4)$$

where Q_t is the normalized cone tip resistance, F_r is the normalized friction ratio, σ_{v0} is the total overburden vertical stress, σ'_{v0} is the vertical effective stress, u_0 is the hydrostatic pore water pressure. The normalized SBT (SBTn) chart is more reliable as it takes into account the influence of the in-situ stress in the soil classification which is particularly important when the sounding is performed at great depths. The charts are illustrated in Figure 4.

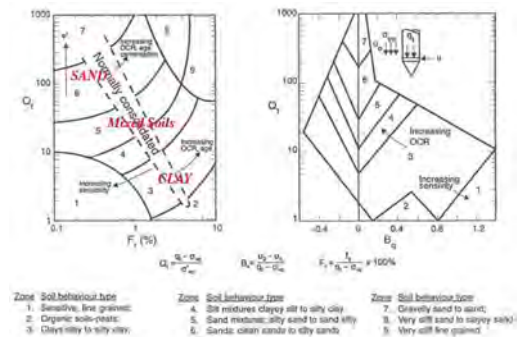


Figure 4. Normalized SBT chart proposed by Robertson 1990.

More recently, Robertson et al. (1998) introduced a normalized cone parameter with a variable stress exponent (n), defined as:

$$Q_{tn} = \left[\frac{q_t - \sigma_{v0}}{p_a} \right] \left(\frac{p_a}{\sigma'_{v0}} \right)^n \quad (5)$$

$$n = 0.38(I_c) + 0.05 \left(\frac{\sigma'_{v0}}{p_a} \right) - 0.15 \quad (6)$$

where p_a is the atmospheric pressure (≈ 100 kPa) and I_c is the SBT index first introduced by Jeffries and Davies (1993) and further modified by Robertson (1990) as:

$$I_c = \sqrt{(3.47 - \log Q_i)^2 + (\log F_r + 1.22)^2} \quad (7)$$

The normalized SBT chart is shown in Figure 5 with the indication of the I_c values for the different soil type regions.

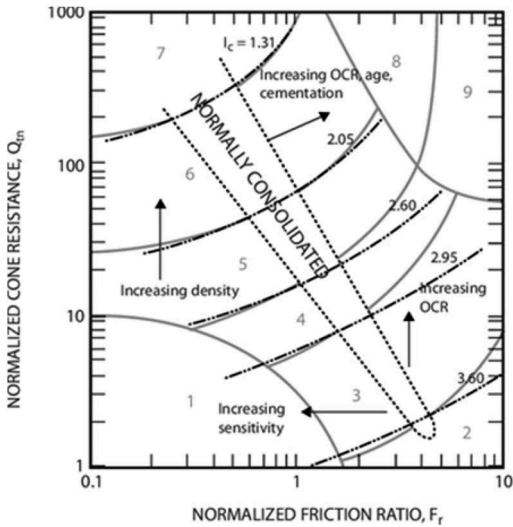


Figure 5. Contours of I_c on a normalized soil behavior type (SBTn) chart (Robertson 1990).

Recently, Robertson (2016) proposed an updated version of the SBT chart to capture the contractive-dilative soil behavior (Figure 6).

In this study, the original SBT chart proposed by Robertson (1990) is taken into account as the main purpose is to evaluate the soil sensitivity instead of the contractive-dilative soil behavior. It is worth observing that soft sensitive clay region is located at the bottom left of the Q_{tn} and F_r chart, or in the bottom right of the $Q_t - B_q$ chart (Figures 7, 8, and 9). Clearly, the correct evaluation of the f_s is fundamental for a correct evaluation of the SBT. To investigate this aspect, the CPTu soundings performed with the two penetrometers have been assessed separately for soil classification by using

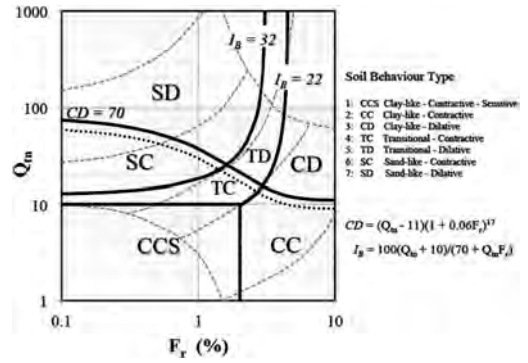


Figure 6. Proposed updated SBTn chart based on Q_{tn} - F_r (Robertson 2016).

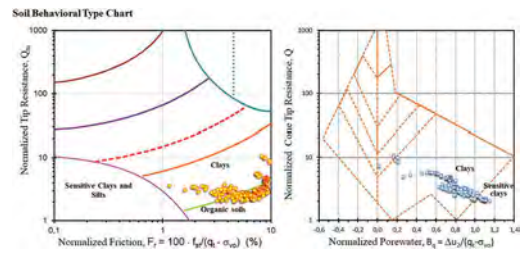


Figure 7. Soil behavior type (SBTn) chart based on standard CPTu cone data.

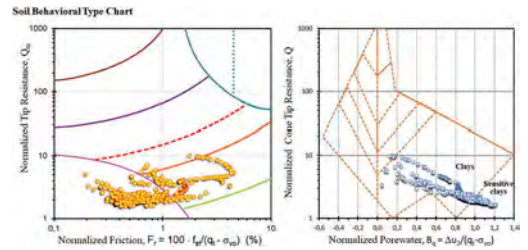


Figure 8. Soil behavior type (SBTn) chart based on the S-1 sounding (advanced cone).

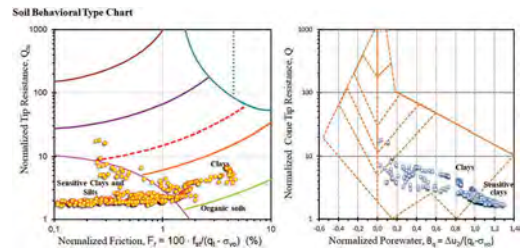


Figure 9. Soil behavior type (SBTn) chart based on the S-2 sounding (advanced cone).

the SBTn charts. Results are presented in Figures 7,8, and 9. As expected, in the $Q_m - F_f$ chart, the data obtained using the advanced cone fall almost entirely in the sensitive clay region while the data points provided by the standard cone fall between the clay and organic clay regions. The reason for this lies obviously in the overestimation of f_s from the standard cone which negatively affected the SBT evaluation. In contrast, the $Q_m - B_q$ chart provides more reliable SBT classification in both cases, even though most of the standard cone data points appear to fall in the clay region.

3 SENSITIVITY EVALUATION BASED ON CPTU DATA

In addition to the SBT classification, the f_s is used in a number of correlations for soil parameters estimation. Several authors (Schmertmann 1978, Robertson and Campanella 1988, Lunne et al. 1997, Robertson 2006) tried to obtain the soil sensitivity based on f_s or the normalized friction ratio (FR). From a theoretical point of view, it is reasonable to correlate the f_s data with the remoulded shear strength ($s_{u,rem}$) obtained from the fall cone test. As shown in Figure 10, the f_s measurement provided by the advanced cone fits fairly well with the $s_{u,rem}$ data (Figure 10) while the standard cone does not catch the trend.

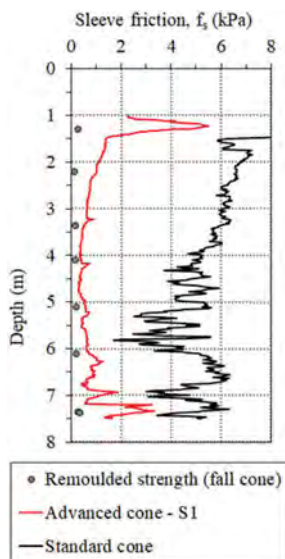


Figure 10. Comparison between the remoulded shear strength ($s_{u,rem}$) measured from the fall cone test and the sleeve friction from CPTu soundings.

4 DISCUSSION AND CONCLUSIONS

The presented study investigated the influence of the sleeve friction f_s measurement accuracy and resolution on the interpretation of piezocone data in soft sensitive clays. The study is limited to a single test site located in Pohja, Southern Finland. It has been shown that in these soils f_s values are significantly low (<1 kPa) and, therefore, the sleeve sensor should have sufficient resolution to perform accurate measurements. As shown for the Pohja site, traditional piezocones with f_s resolution >1 kPa may provide misleading results, thus inducing to an incorrect classification of the soil type based on the SBT charts. Moreover, the f_s appears to be a key parameter for a reliable estimation of the soil remoulded strength and sensitivity. Therefore, when performing CPTu soundings in soft sensitive clays, it is highly suggested to adopt suitable piezocone equipment with accurate and precise sleeve friction sensor for a reliable and robust data interpretation.

The use of high-accuracy site investigation equipment is a key aspect for geotechnical risk assessment in soft sensitive clay areas. This aspect is relevant in relation to detection of sensitive clay layers that may trigger progressive failure during e.g. excavation works, or, as often observed in Norway or Canada, may induce large landslides because of human activity in the area or by other natural phenomena.

REFERENCES

- ASTM, D. 3441, 1986. Standard test method for deep quasistatic, cone and friction-cone penetration tests of soils: 414–419.
- Lunne, T., Robertson, P.K. & Powell, J.J.M. 1997. Cone penetration testing in geotechnical practice. London, Spon Press. 312p
- Di Buò, B. 2020. Evaluation of the Preconsolidation Stress and Deformation Characteristics of Finnish Clays based on Piezocone Testing. PhD Thesis, Tampere University, Tampere, Finland. ISBN 978-952-03-1468-2
- Di Buò, B., D'Ignazio, M., Selänpää, J. & Lämsivaara, T. 2016. Preliminary results from a study aiming to improve ground investigation data. *Proceedings of the 17th Nordic Geotechnical Meeting*: 187–197.
- Di Buò, B., Selänpää, J., Lämsivaara, T., & D'Ignazio, M. 2018. Evaluation of existing CPTu-based correlations for the deformation properties of Finnish soft clays. In *Cone Penetration Testing 2018* (pp. 185–191). CRC Press.
- Jefferies, M.G., & Davies, M.P. 1993. Use of CPTu to estimate equivalent SPTN 60. *Geotechnical Testing Journal*, 16(4), 458–468.
- ISO, E. 22476-1, 2009. Geotechnical investigation and testing. Field testing. Part, 1.
- Jamiolkowski, M., Ladd, C.C., Germaine, J.T. & Lancellotta, R. 1985. New developments in field and laboratory testing of soils. *Proceedings of the 11th Int. Conf. on Soil Mech. and Found. Engineering*, San Francisco, Vol. 1, pp. 57–153.

- Robertson, P.K. 1990. Soil classification using the cone penetration test. *Canadian Geotechnical Journal*, 27(1), 151–158.
- Robertson, P.K. 2009. Interpretation of cone penetration tests—a unified approach. *Canadian Geotechnical Journal*, 46(11), 1337–1355.
- Robertson, P.K. 2016. Cone penetration test (CPT)-based soil behaviour type (SBT) classification system - an update. *Canadian Geotechnical Journal*, 53(12), 1910–1927.
- Robertson, P.K., and Campanella, R.G. 1988. Guidelines for geotechnical design using CPT and CPTU. University of British Columbia, Vancouver, Department of Civil Engineering, *Soil Mechanics Series*, 120.
- Robertson, P.K., & Wride, C.E. 1998. Evaluating cyclic liquefaction potential using the cone penetration test. *Canadian geotechnical journal*, 35(3), 442–459.
- Schmertmann, J. H. 1978. Guidelines for cone penetration test: performance and design (No. FHWA-TS-78-209). United States. Federal Highway Administration.
- Selänpää, J., Di Buò, B., Haikola, M., Lämsivaara, T., & D'Ignazio, M. 2018. Evaluation of existing CPTu-based correlations for the undrained shear strength of soft Finnish clays. In *Cone Penetration Testing 2018* (pp. xxx–xxx). CRC Press.
- Zhang, G., Robertson, P. K., & Brachman, R. W. 2002. Estimating liquefaction-induced ground settlements from CPT for level ground. *Canadian Geotechnical Journal*, 39(5), 1168–1180.

Flow cone – new CPTU add-on module trialled in Halden silt

A.S. Gundersen, T. Lunne, R. Stelzer & Ø. Blaker
Norwegian Geotechnical Institute

G.W. Tucker & L. Krogh
Ørsted

ABSTRACT: Hydraulic conductivity is an important soil parameter for design of shallow foundation concepts for offshore wind, and there is a need for a new tool that can measure this parameter in a reliable way. A new module has been developed that can be mounted behind a standard piezocone test (CPTU) probe. Water can be injected in a controlled manner into the CPTU equipment and flow out into the surrounding soil through a filter an offset behind the friction sleeve, while water pressure (u_f) is measured by a transducer mounted in the filter itself. During penetration of the CPTU probe, water flows out at a constant rate, while u_f is measured in addition to CPTU parameters q_c , f_s and u_2 . At desired depth intervals penetration can be stopped and either a dissipation test or constant flow rate test can be carried out to determine hydraulic conductivity.

Hydraulic fracture tests can be performed in low permeability soils, where water flow is used to induce a vertical crack in the soil. The vertical crack is then allowed to close while pore pressure is monitored, from which the closing pressure can be determined and subsequently used to determine the in-situ K_0 -condition.

This paper describes a series of hydraulic conductivity tests and a hydraulic fracture test carried out at one of Norway's recently established geotechnical test sites, a silt dominated site in Halden. Several tests were successfully carried out and the results were benchmarked against hydraulic conductivity as measured by falling head tests in standpipes and laboratory tests. In general, the results compared well to credible benchmarking tests, showing a promising potential for this tool.

1 INTRODUCTION

Hydraulic conductivity (k) and coefficient of earth pressure at rest (K_0) are required parameters for a wide range of geotechnical engineering problems, including design of shallow foundation solutions for offshore wind. However, these parameters are challenging to measure accurately, both in-situ and in the laboratory. The purpose of the flow cone add-on module is to measure hydraulic conductivity in sands but trial testing at the Halden silt site suggests a wider range of application for the tool. This paper presents results from cone penetration testing, dissipation testing and hydraulic fracture testing in Halden silt, including current interpretation methodology for flow cone dissipation data in low permeability soils.

2 HALDEN SITE

The site is located close to the city Halden in a recreational park, Rødsparken. A silty, clayey sand constitutes the topsoil and extends down to about 4.5-5.0 m below ground level (Unit I), being generally loose to medium dense, with some organic material.

The normally consolidated clayey silt layers below (Units II and III) extend down to about 15-16 m below ground level (bgl) in the southwest corner of the site. The silt is uniform and structureless to mottled, with primary bedding and laminations almost absent due to bioturbation. Units II and III contain similar amounts of quartz (40%), plagioclase (30%), feldspar (12%), clay minerals and mafic minerals (amphibole). Classification and in-situ tests suggest that the silt becomes sandier closer to the deeper soil unit, which consists of a low to medium strength clay (Unit IV). The clay unit has a slightly laminated structure, with occasional shell fragments and drop stones (Blaker et al., 2019).

3 OVERVIEW OF TESTS

This paper presents a range of laboratory and in-situ tests as part of the assessment of flow cone results. To facilitate easy reading, Table 1 is included providing a general overview of benchmark tests and flow cone tests, number of tests carried out, nomenclature and depth ranges.

Table 1. Overview of benchmark tests and flow cone tests.

Equipment	Test type	Number of tests	Test abbreviation	Location IDs	Test IDs	Depth range	Comments
Oedometer	Constant head*	22	Oedometer	-	-	4.5-18.7 m bgl	Benchmark tests
Triaxial	Constant head	13	Triaxial	-	-	5.3-14.6 m bgl	Benchmark tests
Standpipe	Falling head	10	HA-SLT	1 to 5	1 to 2	6-15 m bgl	Benchmark tests
CPTU	Cone penetration	1	HA-CPTU	-	-	2-18 m bgl	Benchmark test
Flow cone	Cone penetration	4	HA-FCPTU	1 to 4	-	2-18 m bgl	
Flow cone	Dissipation	13	HA-FCPTU	1 to 4	1 to 4	6-15 m bgl	
Flow cone	Hydraulic fracture	1	HA-FCPTU	4	5	16.41 m bgl	

*Hydraulic conductivities at zero axial strain (back-extrapolated along the linear e-log(k) line)

4 BENCHMARK TESTS

4.1 Oedometer and triaxial tests

Constant-head hydraulic conductivity tests were conducted at different stress levels during a selected number of oedometer tests and during the consolidation stage of several triaxial tests (Sandbækken et al., 1986, Berre, 1982). Hydraulic conductivity was determined by flowing de-aired water through the specimens. Values from oedometer tests represent hydraulic conductivity at zero axial strain (i.e., at a void ratio comparable to in-situ conditions). Values from triaxial test specimens represent the hydraulic conductivity at the in-situ effective stress state (i.e., after consolidation and some subsequent change in void ratio).

4.2 In-situ falling head tests

Ten in-situ falling head tests (slug tests) were conducted in parallel with flow cone testing at five corresponding depths. The excess pore pressure from standpipe installation could dissipate for 24 hours before falling head tests were initiated by pouring clean tap water into the standpipes. Figure 1 illustrates pressure heads with velocity and best fit linear regression lines, showing good repeatability for all tests except the tests 15 m bgl, which may be explained by a small gap between the standpipe and surrounding soil for test HA-SLT-5-1.

For interpretation of hydraulic conductivity, the velocity method was preferred over time lag method due to its simplicity and independence of piezometric level (Chapuis, 2012). From the slope, m_v , of the linear regression lines in Figure 1, the hydraulic conductivity, k , was determined using Equation (1), refer to Daniel (1989) for further details, where A is the internal cross-sectional area of the standpipe and L and D are the length and diameter of the well screen, respectively.

$$k = \frac{A * \ln\left(\frac{L}{D} + \sqrt{1 + \left(\frac{L}{D}\right)^2}\right)}{m_v \left(2\pi L - 2.8D * \ln\left(\frac{L}{D} + \sqrt{1 + \left(\frac{L}{D}\right)^2}\right)\right)} \quad (1)$$

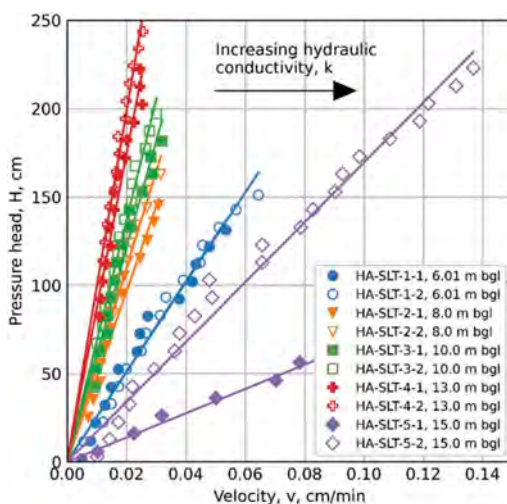


Figure 1. Pressure head with velocity from in-situ falling head tests. Measured results and best fit linear regression lines.

5 EQUIPMENT AND PROCEDURES

The flow cone is a standard cone penetrometer paired with a custom-built hydraulic module, see Figure 2 (Gundersen et al., 2019). The hydraulic module consists of a bronze filter offset behind the cone sleeve and a control system at ground surface. The control system handles data acquisition and provides flow rate control by means of a linear step motor driving a piston. Parameters such as ambient pressure, system pressure, water pressure inside filter (u_f) and flow rates are recorded. During cone

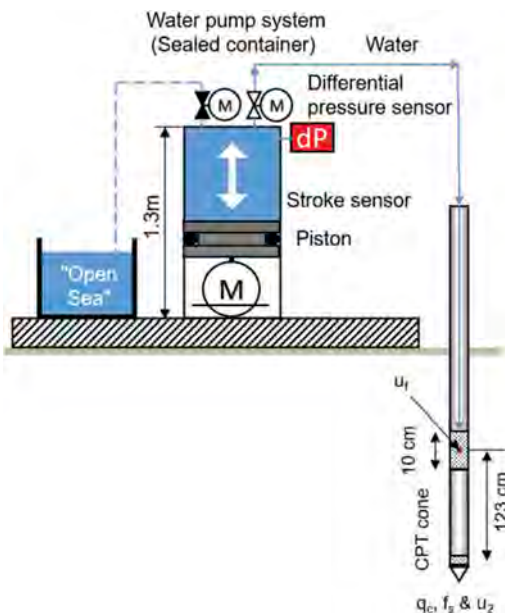


Figure 2. Equipment and setup of the flow cone (Gunder- sen et al., 2019). The offset between u_2 and u_f measurements is 123 cm.

penetration, water flows into the surrounding soil through the filter at a constant rate while u_f is measured in addition to cone resistance (q_c), sleeve friction (f_s) and pore pressure (u_2). The purpose of water flow during cone penetration in low permeability soils is to maintain filter saturation and prevent filter clogging. At desired depths penetration can be stopped and either a dissipation test, constant flow rate test or hydraulic fracture test can be conducted.

A hydraulic fracture test is performed by inducing a crack in the soil by water flow for subsequent monitoring of pore pressure decay. The test is intended for low permeability soils with $K_0 < 1$, meaning that the in-situ horizontal stress is lower than the vertical, and thus a vertical crack is expected to initiate first. To split the soil, a sufficiently high flow rate must be applied. At Halden, 30 ml/min was selected based on previous experience from testing in soft clays. The vertical crack closes when the pore pressure equals the soil pressure normal to the crack, and the basis for K_0 derivation is that this soil pressure is equal to the in-situ total horizontal stress, σ_{h0} (Bjerrum and Andersen, 1972).

All tests at Halden were carried out using a standard 10 cm² Geotech Nova cone with acoustic data transmission from probe to user interface, with standard penetration rate of 20 mm/s \pm 5 mm/s. In total, 13 dissipation tests were carried out to a target 75 % dissipation of initial excess pore pressure where all CPTU parameters were logged including u_f .

6 MEASURED AND DERIVED PARAMETERS

6.1 Cone penetration tests

Figure 3 illustrates the corrected cone resistance (q_c), sleeve friction (f_s) and pore pressures (u_2 & u_f) with depth below ground level corrected for inclination. The figure includes results from a standard CPTU (HA-CPTU), suggesting that a constant flow rate of 5 ml/min during cone penetration, which was selected based on previous experience, has negligible effect on the standard cone penetration measurements (i.e., q_c , f_s , and u_2).

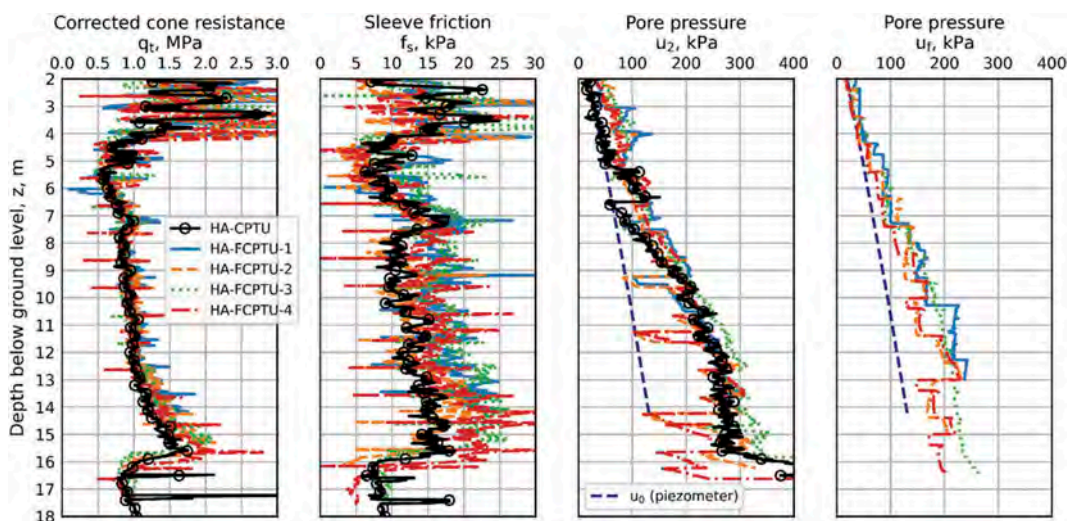


Figure 3. Corrected cone resistance, q_c , sleeve friction, f_s , pore pressure behind cone shoulder, u_2 , and pore pressure, u_f , with depth.

6.2 Pore pressure dissipation tests

Figures 4 and 5 illustrate the measured pore pressures u_2 and u_f with square root of time. Most of the tests in Figure 4 exhibit dilative behavior (non-monotonic), which is consistent with previous dissipation tests conducted at the Halden site (Carroll and Paniagua, 2018). The pore pressure, u_f , generally exhibits a monotonic decrease with time but a small delay in pore pressure decay is evident in Figure 5.

The square root method proposed by Sully et al. (1999) was used to determine hydraulic conductivity from u_2 -dissipation data, back-calculating the initial pore pressure, assuming an initial linear relationship between pore pressure and square root of time.

Rigidity index ($I_r = G/s_u$) and constrained modulus (M) are required for estimating hydraulic conductivity from flow cone dissipation tests. Teh and Houlsby (1991) showed that I_r influences the plastic failure zone around the cone tip during penetration and hence the associated stresses and pore pressures. Carroll and Paniagua (2018) interpreted u_2 -dissipation results from Halden using I_r based on advanced laboratory testing and conservative undrained shear strength. In addition, two methods proposed by Krage et al. (2014) were examined, Method-A and Method-B. The latter compared the best with advanced laboratory data and has thus been applied. Method-B rigidity index is calculated using Equation (2), where G_{max} is the small strain shear modulus and σ_{v0} and σ'_{v0} are the in-situ total and effective vertical stress, respectively.

$$I_r = 0.26 \left(\frac{G_{max}}{\sigma'_{v0}} \right) \left(\frac{1}{0.33 \left[0.33 \left(\frac{q_t - \sigma_{v0}}{\sigma'_{v0}} \right) \right]^{0.75}} \right) \quad (2)$$

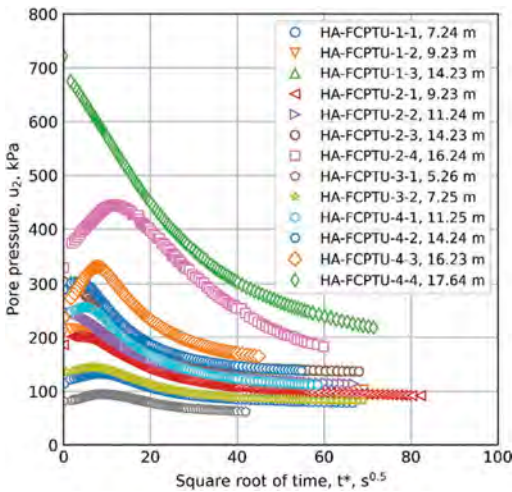


Figure 4. Measured pore pressure u_2 with square root of time.

Best estimate values of G_{max} , σ_{v0} , σ'_{v0} and M found in Blaker et al. (2019) were used as basis for interpretation of hydraulic conductivity. Input of corrected cone resistance in Equation 2 was derived from linear interpolation of the results presented in Figure 4.

As part of proposing an interpretation methodology for u_f -dissipation, triple element CPTU results from Halden were reviewed. This review suggested that the initial excess pore pressure, $u_{f,i}$, is primarily caused by the cone penetration itself, not the input water flow of 5 ml/min. On this basis, it was concluded that the Teh and Houlsby (1991) framework for location 10 radii behind the cone shoulder could be used to estimate the hydraulic conductivity. Figures 6 and 7 show the head ratio with dimensionless time factor for u_2 -dissipation and u_f -dissipation using the framework by Teh and Houlsby (1991). The figures show a good fit to the shape of the theoretical solutions, which is discussed further in Section 7.

6.3 Hydraulic fracture test

One hydraulic fracture test was conducted 16.41 m below ground level, the result of which is illustrated in Figure 8. The figure shows measured pore pressure with velocity (i.e., how quickly the pore pressure decays). The pressure at which the crack closes was estimated to 2240 cm. Based on piezometric level from stand-pipe falling head tests and an average soil unit weight of 19.2 kN/m^3 , this yields a K_0 value of 0.44, which falls within the expected K_0 -range (0.4 to 0.65) for the Halden site.

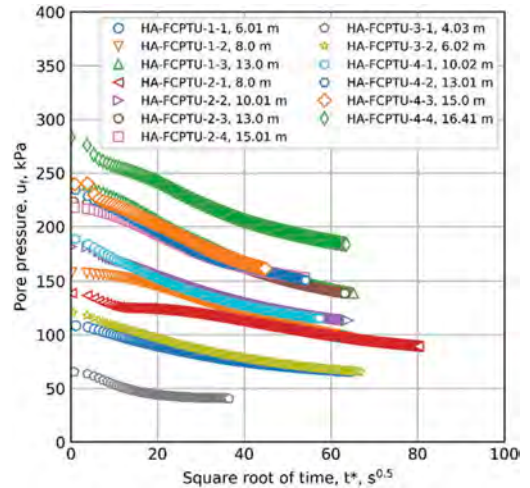


Figure 5. Measured pore pressure u_f with square root of time.

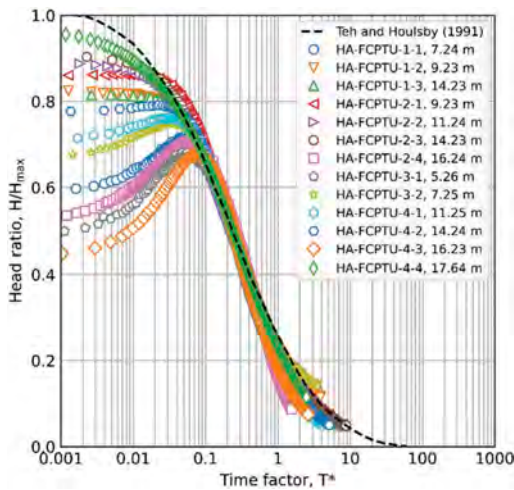


Figure 6. Pore pressure, u_2 , head ratio with dimensionless time factor proposed by Teh and Houlsby (1991).

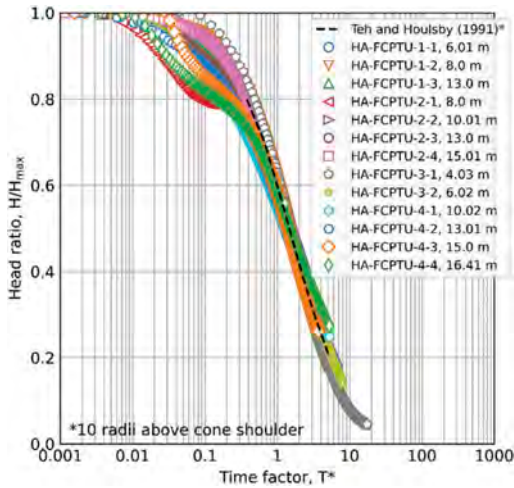


Figure 7. Pore pressure, u_1 , head ratio with dimensionless time factor proposed by Teh and Houlsby (1991).

7 DISCUSSION AND COMPARISON

Figure 9 illustrates the hydraulic conductivities from benchmark tests (oedometer, triaxial and in-situ falling head tests) and flow cone u_2 -dissipation and u_1 -dissipation tests with depth. Oedometer and in-situ falling head tests generally present the highest and lowest hydraulic conductivities, respectively. The difference may be explained by the oedometer values being picked at zero axial strain with presumably higher void ratio than in-situ conditions. For the in-situ falling head tests, a concern is filter clogging during installation, causing reduced water injection area and lower calculated hydraulic conductivities. Other aspects of the in-situ falling head tests involve soil disturbance, stress changes, transient

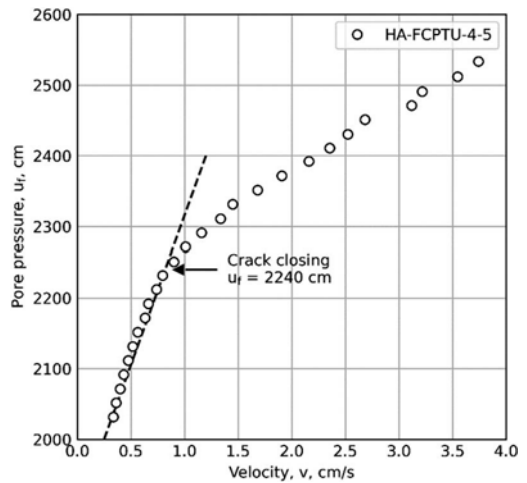


Figure 8. Pore pressure, u_1 , with rate of change in pore pressure, velocity, including discontinuous interpretation line.

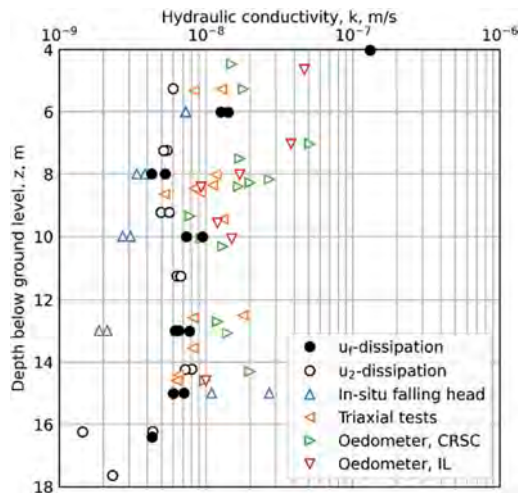


Figure 9. Hydraulic conductivity from benchmark tests and flow cone tests with depth.

consolidation, variations in piezometric level, shape factor, etc.

Hydraulic conductivities from u_2 -dissipation and u_1 -dissipation show good agreement with triaxial test results, especially from 10 m to 15 m bgl. It is evident from Figure 9 that u_2 -dissipation and u_1 -dissipation tests can identify the main soil layering i.e., the clay below 16 m bgl and the sand 4 m bgl presenting significantly lower and higher hydraulic conductivities, respectively, as expected.

Except for falling head and u_2 -dissipation results below 14.5 m bgl, in-situ tests show good repeatability. In contrast, oedometer results show some scatter which may be due to disturbance during sampling and sample handling having significant influence on the results due to small sample size.

Distribution of excess pore pressures around the cone tip and shoulder are generally more complex than alongside friction sleeve and CPTU rods. Based on Teh and Houlsby (1991) it is expected that flow patterns for u_f are predominantly radial and more repeatable compared to u_2 . With pure radial flow, the influence of filter size is expected to be negligible, however this should be investigated for confirmation.

The laboratory and in-situ tests differ in that for laboratory tests, de-aired water was used for hydraulic conductivity testing, while clean tap water was used for in-situ tests. For future in-situ testing water with properties as in the field should be used. In addition, the laboratory tests gave vertical hydraulic conductivity while horizontal consolidation properties dominate in-situ dissipation, suggesting hydraulic conductivity anisotropy ratio close to one at Halden.

The proposed interpretation methodology for flow cone hydraulic conductivity requires input of rigidity index and constrained modulus, which may be unknown or difficult to determine. The impact of these parameters on the estimated hydraulic conductivity should be further investigated.

From the testing at Halden it is evident that the effect of water flow during cone penetration is pore pressure build-up. However, the influence of 5 ml/min of water flow on the excess pore pressure was negligible compared to that from cone penetration itself. It is suggested that flow rate be determined based on experience and equations from Gundersen et al. (2019) to produce project specific hydraulic heads. It is considered most important to avoid flow rates yielding excessive hydraulic heads and thereby zero effective stresses in the soil surrounding the u_f -filter also leading to significant soil disturbance and/or erosion.

The determined K_0 -value from hydraulic fracture test compares well with the general trend presented in Blaker et al. (2019). However, more tests should be carried out before conclusions can be drawn on the appropriateness of K_0 -determination using flow cone module.

8 SUMMARY AND CONCLUSIONS

The flow cone is a standard cone penetrometer paired with a custom-built hydraulic module including a pressure transducer inside a porous cylindrical filter located an offset behind the friction sleeve and was trialled at the Halden silt site. Pore pressure development with time was measured at two locations, behind cone shoulder, u_2 , and 1.23 m behind cone shoulder, u_f . The majority of u_2 dissipation plots suggest dilative behavior and a square root of time method was used to correct the initial pore pressure.

Hydraulic conductivity from flow cone dissipation (u_2 , u_f), in-situ falling head and constant head oedometer and triaxial tests were compared. u_f dissipation presents best repeatability, whereas in-situ falling head tests and constant head oedometer tests yielded the lowest and highest values of hydraulic conductivity respectively. Due to the larger volume of soil and greater height of

the triaxial test specimen, the hydraulic conductivity measurements made on these specimens are generally expected to be more reliable. Results from flow cone dissipation and constant head triaxial tests compare well. These observations present a confident potential of the proposed methodology for u_f dissipation, which is based on classical uncoupled solution for undrained cone penetration and subsequent pore pressure dissipation. However, further studies should be carried out to fully verify the proposed interpretation methodology, also considering the influence of rigidity index, compressibility, filter size, soil disturbance and general soil behavior.

One hydraulic fracture test was conducted in the clay unit at Halden resulting in a coefficient of earth pressure at rest that compares well with the general trend from literature.

ACKNOWLEDGEMENTS

This work was funded by Ørsted and in part the Norwegian Research Council. The authors are grateful to many of their colleagues for valuable discussions and greatly appreciate the high-quality work by NGI field investigation group with Kristoffer Kåsin, Stig Bjørnsvik and Don Terje Christiansen as main contributors.

REFERENCES

- Berre, T. (1982) Triaxial Testing at the Norwegian Geotechnical Institute. *Geotechnical Testing Journal*, 5, 3–17.
- Bjerrum, L. & Andersen, K. H. (1972) In-situ measurements of lateral pressures in clay. *European Conference on Soil Mechanics and Foundation Engineering*, 5. Madrid 1972. *Proceedings*. Madrid, Sociedad Española de Mecánica del Suelo y Cimentaciones.
- Blaker, Ø., Carroll, R., Paniagua Lopez, A. P., Degroot, D. J. & L Heureux, J.-S. (2019) Halden research site: geotechnical characterization of a post glacial silt.
- Carroll, R. & Paniagua, P. (2018) Variable rate of penetration and dissipation test results in a natural silty soil. *Cone Penetration Testing 2018*. CRC Press.
- Chapuis, R. P. (2012) Predicting the saturated hydraulic conductivity of soils: a review. *Bulletin of engineering geology and the environment*, 71, 401–434.
- Daniel, D. E. (1989) In situ hydraulic conductivity tests for compacted clay. *Journal of Geotechnical Engineering*, 115, 1205–1226.
- Gundersen, A. S., Carotenuto, P., Lunne, T., Walta, A. & Sparrevik, P. (2019) Field verification tests of the newly developed flow cone tool—In-situ measurements of hydraulic soil properties.
- Krage, C., Broussard, N. & Dejong, J. (2014) Estimating rigidity index (IR) based on CPT measurements. *Proceedings of the 3rd International Symposium on Cone Penetration Testing, Las Vegas, Nev.*
- Sandbækken, G., Berre, T. & Lacasse, S. (1986) Oedometer testing at the Norwegian Geotechnical Institute. *Consolidation of soils: Testing and evaluation*. ASTM International.
- Sully, J. P., Robertson, P. K., Campanella, R. G. & Woeller, D. J. (1999) An approach to evaluation of field CPTU dissipation data in overconsolidated fine-grained soils. *Canadian geotechnical journal*, 36, 369–381.
- Teh, C. & Houlsby, G. (1991) An analytical study of the cone penetration test in clay. *Geotechnique*, 41, 17–34.

Estimating in-situ frozen loamy soil viscosity from CPT

O.N. Isaev

Gersevanov Research Institute of Bases and Underground Structures (NIIOSP), “Research Center of Construction” JSC, Moscow, Russia

ABSTRACT: Viscosity is used for calculation of settlements and deformations of frozen loamy soils and ice caused by viscous flow at constant speed under action of long-term loads. A method for determining the viscosity coefficient of frozen loamy soil by CPT was developed. Experimental studies by CPT were carried out in a quasi-static mode (a series of short tests at low well-controlled speeds) and in a step-increasing relaxation-creeping mode (a series of penetrometer stabilizations in which the penetrometer and the speed of its penetration gradually decreased). Comparative data «unit cone resistance q_c – velocity of penetration v_c » were analyzed using mathematical statistics methods. For frozen loamy soil, a generalized regression equation $q_c = M(v_c)^m$ was established. Parameters M and m are calculated based on empiric equations, depending on the soil temperature. Viscosity values obtained by uniaxial compression CPT were compared. As a result of statistical analysis, an empirical transition coefficient between them was established.

1 INTRODUCTION

Permafrost soils (Roman 2002, Khrustalev 2005) occupy 25% of the world dry land: 65% in Russia, 50% in Canada, 60% in Alaska, 65% in Mongolia and 22% in China. They possess special physical and mechanical properties due to ice. If permafrost soils are frozen during construction and operation, settlements of foundations must be determined taking into account the developing plastic deformations (flow) of ice.

The flow rate is calculated based on the viscosity coefficient. It is determined by the laboratory test for uniaxial compression with an increasing stepwise load in accordance with the Standard (GOST 12248.9-2020). There exist other laboratory methods for the viscosity coefficient to be determined: in-plane shear method (Pekarskaya 1963), “ball” method (Maslov 1984), multi-plane shear device (Recommendations 1989), ball stamp (Roman & Kotov 2013, Roman & Kotov 2016) and viscometer (Ter-Martirosyan & Ermoshina 2019). They have not been widely used yet. In-situ methods have not been used until recently.

Laboratory methods have some disadvantages: soil under natural stress cannot be tested; soil samples are often damaged when drilling out. As a result, reconsolidation is required before testing; extra work is also required (drilling to select samples; transportation, storage and preparation of samples for testing). When drilling out samples of

frozen soils, their original temperature can be disturbed and soils may thaw.

The paper proposes a method for determining the viscosity coefficient of frozen loamy soils by CPT.

2 EXPERIMENTAL AND THEORETICAL PREREQUISITES FOR DETERMINING THE VISCOSITY COEFFICIENT OF FROZEN SOILS BY CPT

When testing plastic-frozen loamy soils with a temperature of $-0.3 \dots -0.1$ °C, Ladanyi (1976) revealed that cone resistance q_c versus the velocity of penetration v_c is perfectly described by the power law

$$q_c = q_c^0 (v_c/v_c^0)^m = M(v_c)^m \quad (2.1)$$

where q_c^0 and v_c^0 = coordinates of a point on the cross-plot $q_c(v)$; $M = q_c^0/(v_c^0)^m$ = empirical parameter; $m < 1$ – nonlinearity parameter. If $v_c^0 = 1$ ($M = q_c^0$) and $q_c^0 = 1$ ($M = 1/(v_c^0)^m$) the formula (2.1) takes a simpler form $q_c = q_c^0 (v_c)^m$.

Let us assume that the thickness of the frozen soil compression zone under the cone is approximately (generally, compression zone has more complex dependence on penetrometer diameter) equal to one

tenth of its diameter. Then the relative velocity of penetration $\dot{\varepsilon}_c$ is equal to

$$\dot{\varepsilon}_c = v_c / (0.1d_c), \quad (2.2)$$

where d_c = cone diameter.

The relationships $\tau(\dot{\gamma})$ and $\sigma(\dot{\varepsilon})$ are mostly non-linear in frozen soils and ice. Viscosity coefficients η_τ and η_σ depend on the applied load during creeping. The rheological equations for shear and compression stresses are $\tau = \eta_\tau(\tau)\dot{\gamma}$ and $\sigma = \eta_\sigma(\sigma)\dot{\varepsilon}$. Such viscosity is characteristic for bodies possessing structural strength. This viscosity is sometimes referred to as structural viscosity. Such bodies include frozen soil and ice.

Let us consider cone penetration into a nonlinear viscous body with a variable viscosity coefficient η . The rheological equation is as follows

$$q_c = \eta_c(q_c)\dot{\varepsilon}_c, \quad (2.3)$$

where η_c = conditional viscosity coefficient of soil in CPT. Using (2.1) and (2.2) – $\dot{\varepsilon}_c/\dot{\varepsilon}_c^0 = (q_c/q_c^0)^{1/m}$. Let us change this equation to (2.3)

$$q_c = \left[\frac{\dot{\varepsilon}_c^0}{q_c^0} \left(\frac{q_c}{q_c^0} \right)^{\frac{1-m}{m}} \right]^{-1} \dot{\varepsilon}_c \quad (2.4)$$

Thus, the conditional viscosity coefficient in CPT will be

$$\eta_c = \left[\frac{\dot{\varepsilon}_c^0}{q_c^0} \left(\frac{q_c}{q_c^0} \right)^{\frac{1-m}{m}} \right]^{-1}. \quad (2.5)$$

Taking into account that $\dot{\varepsilon}_c^0 = v_c^0 / (0.1d_c)$ and $M = q_c^0 / (v_c^0)^m$, the equation (2.5) is as follows:

$$\eta_c = \left[\frac{v_c^0}{0.1d_c q_c^0} \left(\frac{q_c}{q_c^0} \right)^{\frac{1-m}{m}} \right]^{-1} = 0.1d_c (M)^1 (q_c)^{m-1} \quad (2.6)$$

Using (1.1) and (2.2) - (2.5) can be $\eta_c(v_c)$ or $\eta_c(\dot{\varepsilon}_c)$

$$\eta_c(v_c) = \left[\frac{v_c^0}{0.1d_c q_c^0} \left(\frac{M(v_c)^m}{q_c^0} \right)^{\frac{1-m}{m}} \right]^{-1} = 0.1d_c M (v_c)^{m-1}, \quad (2.7)$$

$$\eta_c(\dot{\varepsilon}_c) = 0.1d_c M (v_c)^{m-1} = (0.1d_c)^m M (\dot{\varepsilon}_c)^{m-1}. \quad (2.8)$$

Let us take the uniaxial viscosity coefficient η_{uc} as a reference value. The condition of equality of the viscosity coefficients for uniaxial compression η_{uc} and CPT η_{CPT} is

$$\eta_{uc} = \eta_{CPT} = \psi \eta_c, \quad (2.9)$$

where ψ - empirical transition coefficient (further - transition coefficient).

Thus, in order to determine the viscosity coefficient from CPT η_{CPT} , it is enough to determine the transition coefficient ψ . The following problem is discussed further.

3 GENERAL DESCRIPTION OF SOILS. EQUIPMENT AND METHODS FOR EXPERIMENTAL STUDIES

CPT was performed in-situ and in the laboratory (refrigeration chamber). Permafrost soils were tested in-situ: loams, sandy loams and clays – less frequently; soil temperature $T = -0.2 \dots -2.1$ °C; moisture content $w = 12 \dots 38$ %; massive and thin-layered cryogenic texture; ice inclusions up to 1-4 mm. Artificially frozen loams were tested in the laboratory, $T = -1.1$ and -2.2 °C, $w = 21$ %.

A penetrometer with a friction sleeve, Ø35.6 mm (Ryzhkov & Isaev 2016) and a temperature sensor in a cone (to measure soil temperature T) was used. In-situ tests were carried out in a quasi-static mode and a stepwise stabilization mode.

The quasi-static mode involved the procedure of penetrometer stopping and holding until it froze into soil. The penetrometer is then tested by performing a series of short pushes of the penetrometer was performed at different velocities $v_c = 3 \cdot 10^{-4} \dots 2$ m/min. To prevent the effect of soil heterogeneity on the test results, high and low velocities were alternated.

Stepwise stabilization (relaxation-creep) mode – the test is also performed after stopping and holding until it froze into soil. However, it differs from the quasi-static in that the penetrometer is tested by performing a series of stepwise increasing stabilizations. The stabilization of the penetrometer at the step was carried out by supplying oil to the hydraulic jacks which push the penetrometer. The given value q_c having been obtained, the supply of oil was stopped and the stabilization mode started. The load acting on the penetrometer and its velocity (as a result of relaxation-creep of the surrounding soil) gradually decreased and the intensity decreased as well, $v_c = 2 \cdot 10^{-5} \dots 0.6$ m/min.

The quasi-static mode was used in the refrigeration chamber. The velocity of penetration was set by regulating the speed of the screw press on which the lever was dropped, $v_c = 10^{-6} \dots 0.08$ m/min.

The study procedure was as follows.

Stage 1: The test results were divided into statistical samples of data pairs « $q_c - v_c$ » depending on their mode and soil temperature.

Stage 2: An approximation (1.1) was used for each statistical sample; M and m were determined; sampled values of the correlation coefficient ρ , determination coefficient R^2 and theoretical correlation ratio R were determined as well; the degree of linearization of the experimental data in the coordinates « $\ln q_c \sim \ln v_c$ » was visually evaluated.

Stage 3: The effect of the test mode and soil temperature on M and m was assessed. Statistical analysis was performed; the regression equations applicable for M and m to be determined by temperature T were specified; M and m , ρ , R^2 and R were also determined.

Stage 4: The conditional viscosity coefficient in CPT η_c and the viscosity coefficient obtained during uniaxial compression tests η_{uc} were compared; the transition coefficient $\psi = \eta_{uc}/\eta_c$ was determined. The values of η_{uc} were taken from the books on laboratory data for uniaxial compression tests. The values of η_c were taken based on the generalized results of CPT under the quasi-static mode – in accordance with the empirical equations (see stage 3). The compared pairs of values η_{uc} and η_c had the same values of T and ε_c .

Stage 5: The effect of various factors on the transition coefficient ψ was studied (cone resistance q_c , velocity of penetration v_c , relative speed of soil deformation $\dot{\varepsilon}_c$, soil temperature modulus $|T|$, compressive stresses under uniaxial compression σ , soil type). Regression equations were calculated.

Stage 6: Two-stage verification of the proposed method for determining η_{uc} from CPT data was carried out. The first stage was based on the data used in the previous stages. The second stage was based on the new comparative data used on the experimental site.

4 RESULTS AND ANALYSIS OF EXPERIMENTAL STUDIES

The total number of data pairs « $q_c - v_c$ » – over 400. Typical cross-plots are shown in Figure 4.1.

Statistical analysis has shown that q_c versus (v_c) is described by the power equation (2.1); a high degree of data linearization in the coordinates « $\ln q_c \sim \ln v_c$ » is revealed (Figure 4.1). The values of R have been as follows: 0.76 ... 0.98 for in-situ tests under the quasi-static mode, 0.89 ... 0.98 under stepwise stabilization, 0.92 ... 0.94 under laboratory conditions. The cross-plot of q_c versus (v_c) is described by a single curve

(2.1) without an inflection point on the plot « $\ln q_c \sim \ln v_c$ » if $T = -0.2 \dots -2.2$ °C and $v_c = 10^{-6} \dots 4 \cdot 10^{-2}$ m/min.

Figure 3.2 makes it possible to conclude that M possesses great variability and depends on the test mode and soil temperature. Its value is slightly higher under stepwise stabilization than when tested under the quasi-static mode. The difference in M values during in-situ and laboratory tests is due to the fact that the soil is permafrost in the first case, and it is artificially frozen in the second case. This obviously led to its decompaction and decrease in strength. In addition, the difference in soil moisture and dispersion also affected. A linear relationship has been established

$$M = a_M T + b_M, \quad (4.1)$$

where a_M and b_M = empirical coefficients, for in-situ tests under the quasi-static mode $a_M = -10.07$ and $b_M = 5.060$.

Due to soil strength increase, M increases when temperature decreases. Extrapolation of the straight lines $M(T)$ for all test modes illustrates that the straight lines intersect approximately in one point which shows the initial temperature of soil freezing. When loamy soils are in a thawed state - $M = 6.57 \dots 7.58$ for the temperature range of the onset of freezing (-0.15 ... -0.25 °C).

The nonlinearity coefficient m is less variable, $m < 1$. With the temperature decrease m decreases, i.e. the nonlinearity of the equation (1.1) increases since ice-cement content and rheology of soil increase. The value of m hardly depends on the test mode and soil type. Temperature T has the greatest effect on it. Figure 4.2.b illustrates that the experimental values of $m(T)$ obtained for various modes and test conditions can be described by the general linear relationship

$$m = a_m T + b_m \quad (4.2)$$

where a_m and b_m = empirical coefficients, for the general linear relationship $a_m = 0.0235$ and $b_m = 0.1280$, for in-situ tests in the quasi-static mode $a_m = 0.0184$ and $b_m = 0.1217$.

The correlation coefficient ρ between m and T is 0.59 for the total statistical sample. This can be considered acceptable, since it takes into account the large heterogeneity of the data included in it. Substituting (4.1) and (4.2) in (2.7) and (2.8), the conditional viscosity coefficient η_c can be as follows:

$$\eta_c(v_c) = 0.1 d_c (a_M T + b_M) (v_c)^{a_m T + b_m - 1}, \quad (4.3)$$

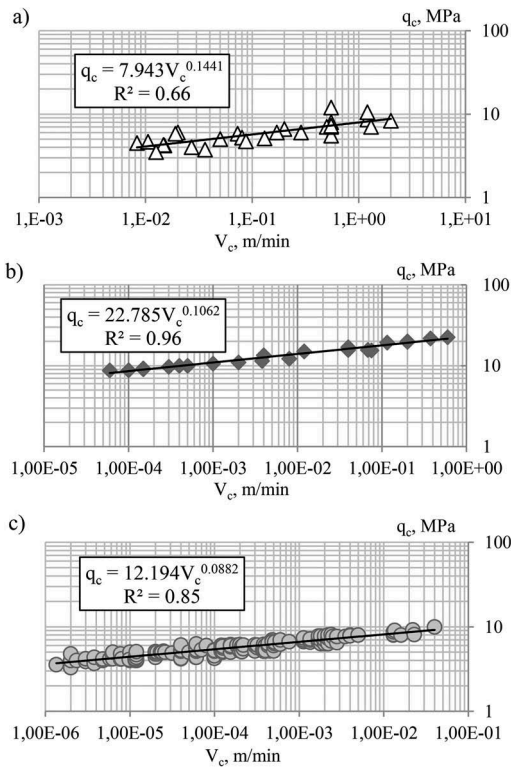


Figure 4.1. “ $v_c - q_c$ ” diagrams: in-situ tests under a quasi-static mode, $T = -0.2\text{ }^\circ\text{C}$ (a); in-situ tests under stepwise stabilization, $T = -1.0\text{ }^\circ\text{C}$ (b); laboratory tests in a refrigeration chamber under the quasi-static mode, $T = -1.1\text{ }^\circ\text{C}$ (c).

$$\eta_c(\dot{\epsilon}_c) = (0.1d_c)^{a_m T + b_m} (a_m T + b_m) (\dot{\epsilon}_c)^{a_m T + b_m - 1}. \quad (4.4)$$

For in-situ tests in the quasi-static mode (4.3) and (4.4) are as follows:

$$\eta_c(v_c) = 0.1d_c(-10.07T + 5.060)(v_c)^{0.0235T - 0.8720} \quad (4.3.a)$$

$$\eta_c(\dot{\epsilon}_c) = (0.1d_c)^{0.235T + 0.1280} (-10.07T + 5.060) (\dot{\epsilon}_c)^{0.0235T - 0.8720} \quad (4.4.a)$$

According to (2.7), the conditional viscosity coefficient of thawed loamy soils η_c is as follows for the temperature range of the onset of freezing (thawed state):

$$\eta_c(v_c) \approx 0.7d_c(v_c)^{-0.87}. \quad (4.4.b)$$

The viscosity coefficients of frozen loamy soils obtained after uniaxial compression tests η_{uc} (data taken from the books, Table 4.1) and η_c evaluated by the formula (4.4.a) depending on $\dot{\epsilon}_c$ and T have been compared.

The transition coefficient $\psi = \eta_{uc}/\eta_c$ was used for correlation. The influence of various factors on ψ was studied: cone resistance q_c , velocity of penetration v_c , relative speed of soil deformation $\dot{\epsilon}_c$, soil temperature modulus $|T|$, stresses under uniaxial compression σ , loamy soil type. The values of $|T|$, $\dot{\epsilon}_c$ and σ were taken after uniaxial compression tests; v_c was evaluated by the formula (1.2); q_c – by the formula (1.1); M and m – by the formulas (3.1) and (3.2).

Analysis of the results presented in Table 4.2 and in Figure 4.3 makes it possible to conclude the following.

The greatest influence on ψ is exerted by q_c and T , the relationship is nonlinear. The linkage is strong or very strong. The influence of v_c , $\dot{\epsilon}_c$ and σ on the coefficient ψ is very weak. The influence of the soil type (loam, clay loam, sandy loam) is insignificant – the points referring to experimental data for different soils do not meet any definite patterns.

Empirical equations for the viscosity coefficient of frozen loamy soil under uniaxial compression based on CPT data were proposed

Table 4.1. Comparison of viscosity coefficients (η_{uc}) and (η_c) obtained after uniaxial compression tests (data taken from the books) and calculated by the formula (4.4.a).

Soil type	$T, \text{ }^\circ\text{C}$	$\sigma, \text{ MPa}$	$\dot{\epsilon}, \text{ min}^{-1}$	$\psi = \eta_{uc}/\eta_c$	n	Uniaxial compression tests after
Loam W=31...38 %	-7.9...-1.7	0.25...0.50	$2.5 \cdot 10^{-5} \dots 2.4 \cdot 10^{-4}$	0.002...0.129	4	Tsytoovich 1973
Sandy loam W=12...13 %	-6.0...-0.9	0.25...0.50	$1.5 \cdot 10^{-5} \dots 1.3 \cdot 10^{-4}$	0.015...0.105	5	Tsytoovich 1973
Clay loam W=23	-3.0	1.20	$1.0 \cdot 10^{-3}$	0.017	1	Roman 2002
Clay loam	-3.0	0.40...0.80	$1.3 \cdot 10^{-8} \dots 6.6 \cdot 10^{-10}$	0.045...0.071	5	Grechishchev 1963

Notes: T – soil temperature; σ – stress under uniaxial compression; $\dot{\epsilon}$ – speed of flow under uniaxial compression; n – number of comparative data pairs

Table 4.2. Statistical analysis of various factors influencing the coefficient ψ for frozen loamy soils.

Parameter	Statistical indicators			Regression equation	Linkage
	ρ	R^2	R		
q_c	0.61	-	-	$\psi = -0.0004q_c + 0.0632$	Average
	-	0.81	0.90	$\psi = 0.0618e^{-0.018q_c}$	Strong
	-	0.86	0.93	$\psi = 0.3299q_c^{-0.860}$	Very strong
v_c	0.12	-	-	Linear	Very weak
	-	0.0093	0.096	Exponential	
	-	0.058	0.24	Power	
\hat{e}_c	0.12	-	-	Linear	Very weak
	-	0.0093	0.096	Exponential	
	-	0.058	0.24	Power	
$ T $	0.77	-	-	$\psi = -0.01 T + 0.10$	Strong
	-	0.85	0.92	$\psi = 0.1945e^{-0.531 T }$	Very strong
	-	0.68	0.82	$\psi = 0.1653 T ^{-1.552}$	Strong
σ	0.14	-	-	Linear	Very weak
	-	0.0001	0.01	Exponential	
	-	0.00005	-	Power	

Notes: ρ – sample correlation coefficient; R^2 – sample determination coefficient; R – theoretical correlation ratio

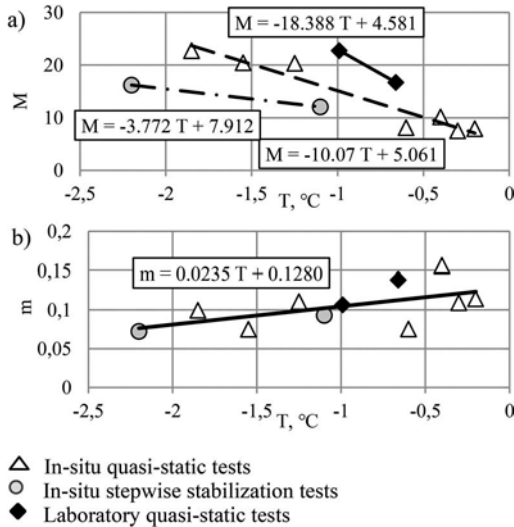


Figure 4.2. Diagrams of $M(T)$ and $m(T)$ after in-situ and laboratory CPT data.

$$\eta_{CPT(q)} = \psi_q \eta_c, \quad (4.5)$$

$$\eta_{CPT(T)} = \psi_T \eta_c \quad (4.6)$$

where ψ_q and ψ_T = empirical coefficients;
 $\psi_q = 0.330q_c^{-0.860}$, $\psi_T = 0.195e^{-0.531|T|}$.

Experimental verification of (4.5) and (4.6) was carried out in two stages by calculations and statistical analysis of the ratios $\eta_{CPT(q)}/\eta_{uc}$ and $\eta_{CPT(T)}/\eta_{uc}$.

The data from Table 4.1 were used at the first stage. The value of η_c in (4.5) and (4.6) was evaluated by (4.3.a). Figure 4.4 shows the histograms of these ratios. The analysis showed that the statistical data were close for $\eta_{CPT(q)}$ and $\eta_{CPT(T)}$. Taking into account the influence of a large number of factors, they can be considered quite acceptable.

At the second stage, verification was carried out by direct comparative tests on the experimental site. The viscosity coefficients of plastic-frozen clay loam calculated from CPT data were compared with the coefficients ψ_q and ψ_T obtained after direct tests for uniaxial compression η_{cu} . The CPT procedure was done next to a deep pit where uniaxial compression tests were carried out. $T = -0.6 \dots -0.7$ °C, $w = 17.9 \dots 18.2$ %, ice content $0.1 \cdot v_c = 3.1 \cdot 10^{-4} \dots 2$ m/min, $q_c = 4.1 \dots 8.5$ MPa. Figure 4.5 shows that the coefficient ψ_T is more accurate – $\eta_{CPT(T)}/\eta_{uc} = 0.75$ and ψ_q - less accurate – $\eta_{CPT(q)}/\eta_{uc} = 0.44$. The medians Me of the ratios $\eta_{CPT(q)}/\eta_{uc}$ and $\eta_{CPT(T)}/\eta_{uc}$ actually coincide with their mean values, i.e. the values are significant. Experimental verification has shown that the transition coefficient ψ_T evaluated by (4.6) makes it possible to determine the viscosity coefficient of frozen loamy soil under uniaxial compression by CPT data with sufficient accuracy for practical use.

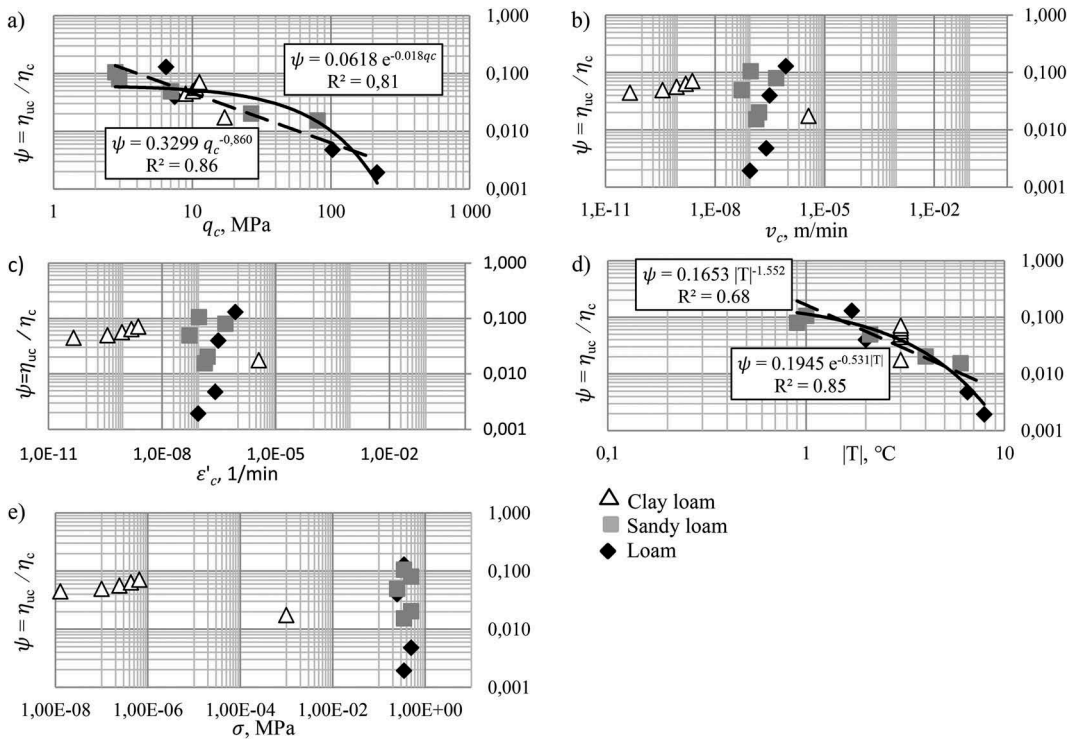


Figure 4.3. The effect of various factors on ψ (cone resistance q_c (a), velocity of penetration v_c (b), relative speed of soil deformation $\dot{\epsilon}_c$ (c), soil temperature modulus $|T|$ (d), compressive stresses under uniaxial compression σ (e).

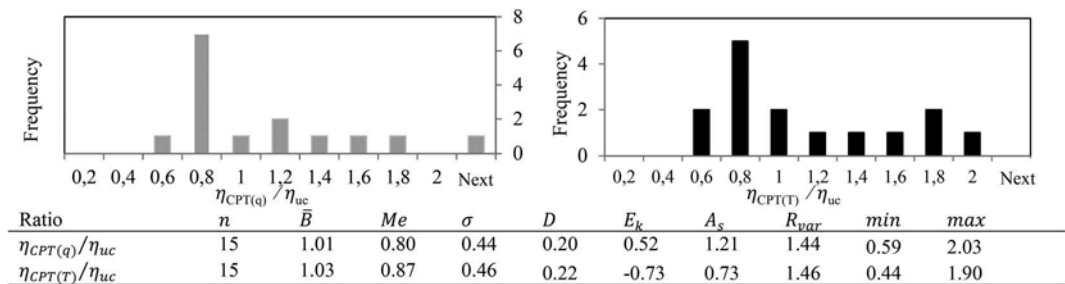
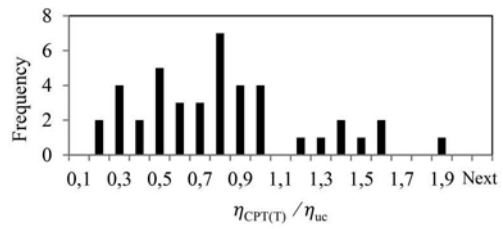
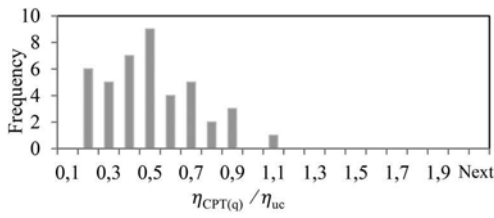


Figure 4.4. Histograms of ratios $\eta_{CPT(q)}/\eta_{uc}$ and $\eta_{CPT(T)}/\eta_{uc}$ (η_{uc} is taken from Table 4.1).

5 CONCLUSIONS

At present, laboratory methods are the only ones used to determine the viscosity coefficient of frozen soil. The uniaxial compression test is the one which is preferred. Proposed is the method to determine the viscosity coefficient of frozen loamy soils from CPT data. CPT can be performed in the quasi-static or relaxation-creeping modes. The method is based on the power equation of cone resistance versus velocity of penetration. The studies have resulted in power-law

regression equations to be obtained. The effects of the CPT mode and soil temperature on soil parameters have been studied. Empirical relationships have been established to determine the transition coefficient from the conditional viscosity coefficient under CPT to the viscosity coefficient under uniaxial compression. Thus, soil resistance to CPT and soil temperatures exert the greatest influence on the transition coefficient. Experimental verification of the method has shown its applicability in practice.



Ratio	<i>n</i>	\bar{B}	<i>Me</i>	σ	<i>D</i>	<i>E_k</i>	<i>A_s</i>	<i>R_{var}</i>	<i>min</i>	<i>max</i>
$\eta_{CPT(q)}/\eta_{uc}$	42	0.44	0.44	0.23	0.052	-0.43	0.39	0.89	0.11	1.00
$\eta_{CPT(T)}/\eta_{uc}$	42	0.75	0.72	0.41	0.171	-0.07	0.67	1.64	0.18	1.81

Figure 4.5. Histograms of ratios $\eta_{CPT(q)}/\eta_{uc}$ and $\eta_{CPT(T)}/\eta_{uc}$ (direct comparative tests).

Notes: $\eta_{uc(q)}$ and $\eta_{uc(T)}$ - viscosity coefficient evaluated by formulas (4.5) and (4.6); *n* - number of statistical sample data; \bar{B} - mean values; *Me* - median; σ - standard of deviation; *D* - dispersion; *A_s* - asymmetry; *E_k* - kurtosis; *R_{var}* - range of variation; *min* - minimum value; *max* - maximum value.

REFERENCES

- GOST 12248.9-2020. Soils. Strength and Deformability Parameters of Frozen Soils Determined by Uniaxial Compression. (rus).
- Grechishchev, S. E. 1963. Creeping of Frozen Soils in a Difficult Stress State. Collection of Papers "Strength and Creep of Frozen Soils". Sib. Dept. of Academy of Sciences of the USSR/ (rus) Publ. House of the Academy of Sciences of the USSR, 1963. (rus).
- Khrustalev, L. N. 2005. Fundamentals of Geotechnics in Permafrost: Textbook. - M.: Publ. House of Moscow State University, - 542 pp (rus).
- Ladanyi, B. 1976. Use of static penetration test in frozen soils. Canad. Geotech. J., Vol.13 p.p. 95–110.
- Maslov, N. N. 1984. Physical and Technical Theory of Loamy Soils Creep in Construction Practice. –M.: Stroyizdat – 176 pp. (rus).
- Pekarskaya, N. K. 1963. Shear Strength of Frozen Soils with its Dependence on Temperature. M. Publ. House of the Academy of Sciences of the USSR – 108 pp. (rus)
- Recommendations for Soil Creep and Consolidation to be determined by Laboratory Tests/PNIIS - M.: Stroyizdat, 1989, 64 pp. (rus).
- Roman, L.T. 2002. Mechanics of Frozen Soils. - M.: MAIK "Nauka/Interperiodica" - 426 pp. (rus).
- Roman, L.T. & Kotov, P. I. 2013. Viscosity of Frozen Soils determined with a Ball Stamp. Earth Cryosphere, vol. XVII, №4, P. 30–35. (rus).
- Roman, L.T. & Kotov, P. I. 2016. Viscosity of Frozen and Thawing Soils. "OFMG". №1. P.16–19. (rus)
- Ryzhkov, I.B. & Isaev, O.N. 2016. Cone Penetration Testing of Soils in Geotechnics. Stockholm, Sweden: Bokforlaget Efron & Dotter AB, 408 p.
- Ter-Martirosyan, A.Z. & Ermoshina, L.S. 2019. Experience in determining viscosity of soil on the basis of experimental studies. IOP Conference Series: Materials Science and Engineering, 687 (4), DOI: 10.1088/1757-899X987/4/044039.
- Tsytoich, N. A. Mechanics of Frozen Soils. –M.: Vysshchaja Shkola, 1973. – 448 pp. (rus).

Determination of natural stress state parameters for clay soils by using 3LSU-CPTU penetrometer

O.N. Isaev, R.F. Sharafutdinov & D.S. Zakatov

Gersevanov Research Institute of Bases and Underground Structures (NIIOSP), "Research Center of Construction" JSC, Moscow, Russia

ABSTRACT: The article presents the results of experimental studies on the use of lateral stress measurements by using the LS-module (includes full and pore pressure sensors) of 3LSU-CPTU penetrometer to determine the parameters of the natural stress state (NSS) of clay soils (the coefficient of lateral pressure at rest K_o , the effective pre-compaction stress POP , the over-compaction stress σ'_c , the overconsolidation ratio OCR , the natural total σ_{ho} and effective σ'_{ho} horizontal stress in the soil). In experiments, the LS-module with three pairs of sensors located in areas with different diameters ($\varnothing 37$ mm, $\varnothing 41$ mm and $\varnothing 45$ mm) was used. The results of a statistical analysis of the relationships between LS-module (twenty-six direct and derived types were considered) and NSS parameters of clay soils are presented. It is shown that K_o , OCR , σ'_{ho} in the soil is determined with the greatest accuracy.

1 INTRODUCTION

The efficiency of using CPT is higher when using penetrometers with additional sensors and devices (Burns & Mayne 1998, Lunne et al. 2004, Ryzhkov I. B. & Isaev 2016). For example, a penetrometer with a lateral stress module (LS-module), includes full and pore pressure sensors. These penetrometers have been developed and investigated since the 1980s (Campanella et al. 1990, Howie et al. 2014, Huntsman et al. 1986, Bayne & Tjelta 1987, Sully & Campanella 1990, Sully & Campanella 1991, Takesue & Isano 2001). However, according to the Lunne et al. (2004), «the lateral stress cone is still not a tool that has found practical use». In the USSR and Russia, until recently, they have not been developed or investigated.

Modern powerful software geotechnical platforms (PLAXIS, MIDAS GTS, Z-Soil, etc.) are using numerical methods. Knowledge of natural stress state parameters of soils is required as initial data of numerical calculations.

The paper presents the results of experimental studies on the use of lateral stress measurements by using the LS-module of 3LSU-CPTU penetrometer to determine the parameters of the natural stress state (NSS) of clay soils (the coefficient of lateral pressure at rest K_o , the effective pre-compaction stress POP , the over-compaction stress σ'_c , the over-consolidation ratio OCR , the natural total σ_{ho} and effective σ'_{ho} horizontal stress in the soil). Studies to determine the natural pore pressure in soil u_0 are described in detail in Isaev et al. (2020a) paper.

2 INVESTIGATED SOILS, EQUIPMENT AND TEST PROCEDURE

The main physical and mechanical properties of clay soils are given in Table 1. Stiff clay and firm-stiff loam were studied. Soils lay at a depth of 3.5-41.7 m. Tests were carried out at experimental sites in Moscow.

Table 1. Properties of clay soils.

Soil	ρ , g/cm ³	e , d.q.	I_p , d. q.	I_b , d.q.	C , kPa	φ , °	E_s , MPa
Stiff clay	1.77	1.17	0.45	0.18	57	20	25
Firm-stiff loam	2.00	0.65	0.14	0.36	10	22	10

The following parameters were calculated and defined: natural (hydrostatical) pore pressure in the soil u_0 , over-compaction stress σ'_c , effective pre-compaction stress $POP = \sigma'_c - \sigma'_{vo}$, overconsolidation ratio $OCR = \sigma'_c / \sigma'_{vo}$, coefficient of lateral pressure at rest $K_o = \sigma'_{ho} / \sigma'_{vo}$, natural total σ_{vo} and effective $\sigma'_{vo} = \sigma_{vo} - u_0$ vertical stress in the soil, natural total σ_{ho} and effective σ'_{ho} horizontal stress in the soil.

The σ'_c , POP , OCR parameters were determined by the methods of Casagrande (1936) and Becker et al. (1987) by laboratory tests in compression

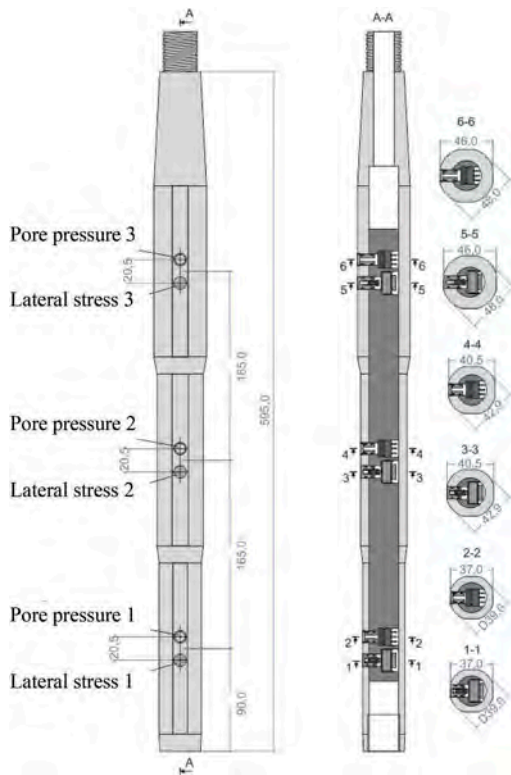


Figure 1. General schematic of LS-module.

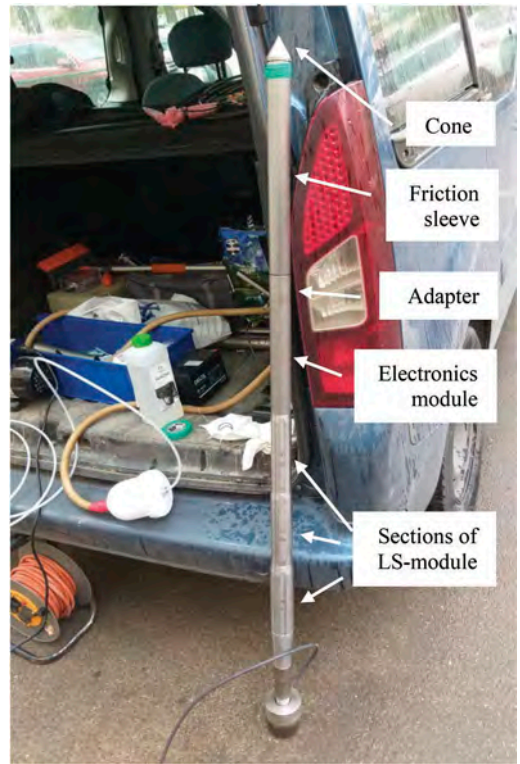


Figure 2. 3LSU-CPTU penetrometer general assembly.

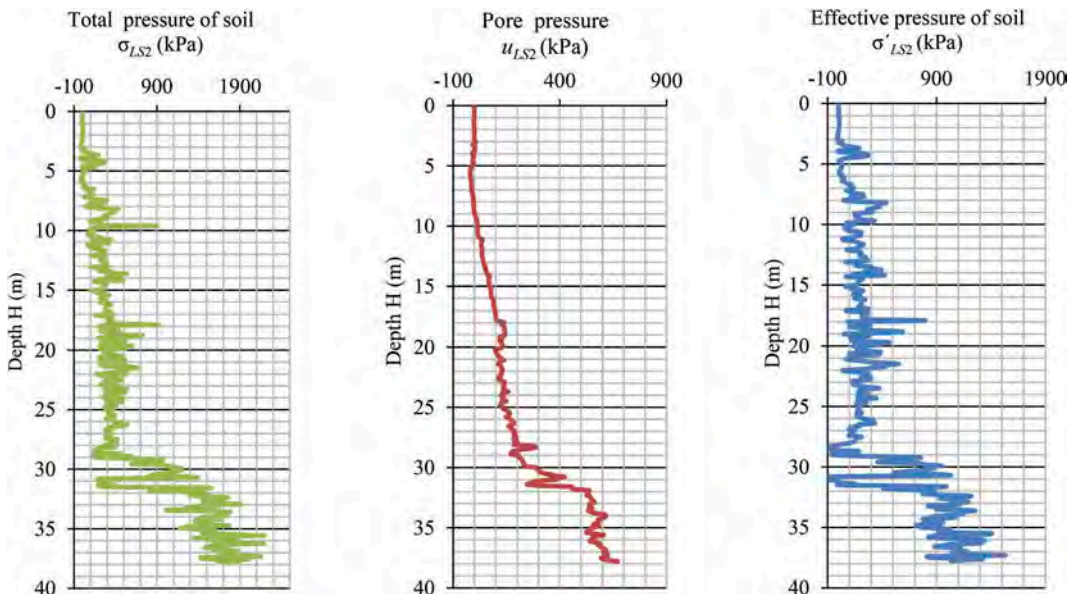


Figure 3. Example of σ_{LS} , u_{LS} , σ'_{LS} profiles with a layer of stiff clay at Moscow (Isaev et al. 2020b)

instruments. The results of both methods were averaged. Coefficient K_o was calculated by Meyerhof (1976) formula, coefficient – by Jaky (1944):

$$K_o = K_o^{nc} OCR^\alpha = (1 - \sin \varphi) OCR^\alpha \quad (1)$$

where φ – angle of internal friction; $\alpha = 0.5$ - degree index.

The σ'_{ho} value was calculated using the formula

$$\sigma'_{ho} = K_o \sigma'_{vo} \quad (2)$$

Tests were carried out using 3LSU-CPTU probe. It was developed and manufactured jointly by NIIOSP and USM-Engineering (Isaev et al. 2020b). It included two modules (Figure 1, 2) – the CPTU main (lower) module with a cone and friction sleeve and 3LSU additional (upper) module with lateral sensors of soil pressure and pore pressure. Above the modules was a unit with electronics, above it there was a push rod. The main module had $\varnothing 35.7$ mm. The 3LSU-module included three pairs of sensors located in cylindrical sections of $\varnothing 37$ mm, $\varnothing 41$ mm and $\varnothing 45$ mm. When the probe was pushed, total ($\sigma_{LS1}, \sigma_{LS2}, \sigma_{LS3}$), pore ($u_{LS1}, u_{LS2}, u_{LS3}$) and effective ($\sigma'_{LS1} = \sigma_{LS1} - u_{LS1}, \sigma'_{LS2} = \sigma_{LS2} - u_{LS2}, \sigma'_{LS3} = \sigma_{LS3} - u_{LS3}$) pressures were measured by pairs of sensors (pore pressure and lateral stress) №1, №2, №3 on the lateral module surface.

Studies were carried out in several stages.

First stage. Listing and NSS parameterization. Six parameters were selected: $K_o, POP, \sigma'_c, OCR, \sigma_{ho}, \sigma'_{ho}$. Listing and LS-module parameterization. Nine direct parameters ($\sigma_{LS1}, \sigma_{LS2}, \sigma_{LS3}; u_{LS1}, u_{LS2}, u_{LS3}; \sigma'_{LS1}, \sigma'_{LS2}, \sigma'_{LS3}$) and seventeen combined parameters ($\sigma_{LS3}/\sigma_{LS1}, \sigma_{LS2}/\sigma_{LS1}, \sigma_{LS3}/\sigma_{LS2}; u_{LS3}/u_{LS1}, u_{LS2}/u_{LS1}; I_{D13} = \Delta\sigma_{LS13}/\Delta\sigma_{LS1U}, I_{D12} = \Delta\sigma_{LS12}/\Delta\sigma_{LS1U}; K_{D1} = \Delta\sigma_{LS1U}/\sigma'_{vo}, K_{D2} = \Delta\sigma_{LS2U}/\sigma'_{vo}, K_{LS1} = \sigma_{LS1}/\sigma_{vo}, K_{LS2} = \sigma_{LS2}/\sigma_{vo}, K_{LS3} = \sigma_{LS3}/\sigma_{vo}; K'_{LS1} = \sigma_{LS1}/\sigma'_{vo}, K'_{LS2} = \sigma_{LS2}/\sigma'_{vo}, K'_{LS3} = \sigma_{LS3}/\sigma'_{vo}; E_{D13} = R_1\Delta\sigma_{LS13}/\Delta R_{13}, E_{D12} = R_1\Delta\sigma_{LS12}/\Delta R_{12}$) were investigated.

Where $\Delta\sigma_{LS12} = \sigma_{LS2} - \sigma_{LS1}, \Delta\sigma_{LS13} = \sigma_{LS3} - \sigma_{LS1}, \Delta\sigma_{LS1U} = \sigma_{LS1} - u_0; \Delta\sigma_{LS2U} = \sigma_{LS2} - u_0; \Delta R_{12} = R_2 - R_1, \Delta R_{13} = R_3 - R_1; R_1, R_2, R_3$ = radius of LS-module in the areas where the sensors are located 1, 2, 3.

The NSS and LS-module parameters for each comparative test were combined into one data group. 19 comparative data groups were compiled.

Second stage. Correlation data mining, determination of the strength of statistical linkage between NSS and LS-module parameters of the clay soils. The value and statistical significance of the sample correlation index ρ was determined. Assessment of the presence of nonlinear significant statistical relationships.

Third stage. Regression data analysis for strength correlations. Approximation of data by linear and

nonlinear (exponential, logarithmic, polynomial, power-law) function. Selection of dependencies with maximum correlation coefficient ρ , theoretical correlation relation R , coefficient of determination R^2 . The strength of the statistical relationship (for ρ and R) was estimated in accordance with Chaddock-Snedecor scale.

Fourth stage. Comparison of NSS parameters obtained by standard (direct) methods and calculated using LS-module parameters (based on regression equations). Estimation of the accuracy of determining the parameters of the NSS by empirical dependencies.

Statistical analysis was performed using IBM SPSS Statistics and MS Excel software.

3 RESULTS AND ANALYSIS OF EXPERIMENTAL STUDIES

Tables 2 and 3 summarize the experimental data for LS-module and NSS parameters of clay soils. Table 4 give the correlation matrix of ρ for statistical relationship between LS-module and NSS parameters of clay soils.

Table 2. Generalized LS-module measurement results of clay soils.

$\sigma_{LS1}/\sigma'_{LS1}/u_{LS1}$, kPa	$\sigma_{LS2}/\sigma'_{LS2}/u_{LS2}$, kPa	$\sigma_{LS3}/\sigma'_{LS3}/u_{LS3}$, kPa
254 ... 1657	84 ... 1879	67 ... 2090
42 ... 1576	88 ... 1409	42 ... 1706
-17 ... +215	-20 ... +670	-15 ... +383

Table 3. Generalized NSS parameters of clay soils.

σ'_c , kPa	OCR, d.q.	POP, kPa	K_o , d.q.	σ'_{ho} , MPa
140 ... 2400	2.9 ... 12.7	77 ... 1938	0.93 ... 2.23	0.06 ... 0.72

Regression data analysis showed that the empirical data can be approximated with approximately equal accuracy by linear and nonlinear regression equations (the difference between ρ and R in almost all cases is less than 5%).

Analysis of Table 4 allows to note the following.

1. For σ'_c the highest degree of correlation ($\rho = 0.61 \dots 0.68$) was revealed with $\sigma_{LS1}, \sigma'_{LS1}, \sigma_{LS2}, \sigma'_{LS2}, \sigma_{LS3}, \sigma'_{LS3}$ (Figure 4). In other cases, it is less. For factors of the combined type, it is mainly statistically insignificant. With an increase in σ'_c , the values of σ_{LS} and σ'_{LS} also increase, but with little change in intensity ($\Delta\sigma'_c/\Delta\sigma_{LS} = 0.5 \dots 0.8$ and $\Delta\sigma'_c/\Delta\sigma'_{LS} = 0.7 \dots 0.8$), which weakly depends on the diameter of the module.

- For OCR the highest degree of correlation strength ($\rho = -0.56 \dots -0.60$) was revealed with the parameters of the combined type $\sigma_{LS2}/\sigma_{LS1}$, I_{D13} , K_{D2} , E_{D12} (Figure 5). As the OCR increases, the parameter values decrease. The relationship with most of the other parameters is statistically insignificant.
- For K_o the highest degree of correlation strength ($\rho = -0.58 \dots -0.64$) was revealed with the parameters of the combined type K_{D2} , $\sigma_{LS2}/\sigma_{LS1}$ and K'_{LS2} (Figure 6). With their increase, the value of K_o decreases. In other cases, the relationship is insignificant.
- The correlation between σ_{ho} and LS-module parameters is the strongest. The maximum correlation ($\rho=0.91 \dots 0.95$) was found for σ_{LS1} , σ'_{LS1} , σ_{LS2} , σ'_{LS2} , σ_{LS3} , σ'_{LS3} (Figure 7).

Table 4. Correlation matrix of ρ for statistical relationship between LS-module and NSS parameters.

LS-module parameters	Natural stress state (NSS) parameters					
	σ'_c	OCR	POP	K_o	σ'_{ho}	σ_{ho}
σ_{LS1}	0.66	-0.39	0.48	-0.34	0.92	0.95
u_{LS1}	0.03	-0.47	-0.10	-0.47	0.29	0.35
σ'_{LS1}	0.68	-0.35	0.51	-0.30	0.93	0.95
σ_{LS2}	0.59	-0.45	0.40	-0.42	0.88	0.93
u_{LS2}	0.51	-0.44	0.32	-0.41	0.82	0.86
σ'_{LS2}	0.61	-0.45	0.43	-0.41	0.89	0.93
σ_{LS3}	0.61	-0.44	0.43	-0.39	0.89	0.94
u_{LS3}	0.57	-0.43	0.38	-0.39	0.86	0.90
σ'_{LS3}	0.62	-0.43	0.44	-0.39	0.89	0.93
$\sigma_{LS3}/\sigma_{LS1}$	0.25	-0.48	0.11	-0.45	0.51	0.56
u_{LS3}/u_{LS1}	0.51	-0.43	0.36	-0.38	0.75	0.80
$\sigma_{LS2}/\sigma_{LS1}$	0.17	-0.60	0.01	-0.59	0.49	0.56
u_{LS2}/u_{LS1}	0.51	-0.43	0.36	-0.38	0.75	0.80
$\sigma_{LS3}/\sigma_{LS2}$	0.01	0.14	0.04	0.16	-0.06	-0.09
I_{D13}	0.23	-0.51	0.09	-0.49	0.01	0.11
K_{D1}	-0.50	-0.04	-0.43	-0.10	-0.55	-0.53
E_{D13}	0.38	-0.48	0.21	-0.46	0.66	0.70
I_{D12}	-0.37	-0.16	-0.43	-0.20	-0.22	-0.18
K_{D2}	-0.23	-0.60	-0.32	-0.64	0.02	0.11
E_{D12}	0.19	-0.56	0.03	-0.54	0.50	0.59
K'_{LS1}	-0.07	0.04	-0.04	-0.01	-0.11	-0.10
K'_{LS2}	-0.33	-0.54	-0.38	-0.58	-0.14	-0.07
K'_{LS3}	-0.06	-0.48	-0.15	-0.50	0.14	0.20
K_{LS1}	-0.39	-0.43	-0.42	-0.49	-0.23	-0.16
K_{LS2}	-0.40	-0.48	-0.45	-0.54	-0.23	-0.16
K_{LS3}	-0.29	-0.35	-0.32	-0.39	-0.17	-0.12

The degree of strength of the statistical relationship (Chaddock-Snedecor scale):

	- the relationship is statistically insignificant
	- $\rho = 0.3-0.5$
	- $\rho = 0.5-0.7$
	- $\rho = 0.7-0.9$
	- $\rho = 0.9-0.99$

The relationship can be approximated by linear equations of the form $y = kx$ or $y = kx + b$. For σ_{LS1} , their plots actually overlap and pass through the origin of coordinates. For other lateral pressures, the line plots are also quite close to each other. With an increase in σ_{ho} , the values of these LS-module parameters increase with little change in intensity ($\Delta\sigma_{ho}/\Delta\sigma_{LS} = 0.4 \dots 0.5$ and $\Delta\sigma_{ho}/\Delta\sigma'_{LS} = 0.5 \dots 0.6$).

A weaker relationship with the results of measurements by pore pressure sensors and the combined parameters obtained on their basis. The exception is u_{LS1} , for which it is not statistically significant. This is probably due to the fact that, in comparison with the soil adjacent to the probe, the change in pore pressure with time has less inertia – as the friction sleeve passes along the soil layer, before the u_{LS1} sensor approaches it, the pore pressure has time to change significantly. Additional effects on u_{LS1} do not occur, because the cone with the friction clutch and the u_{LS1} section have approximately the same diameter.

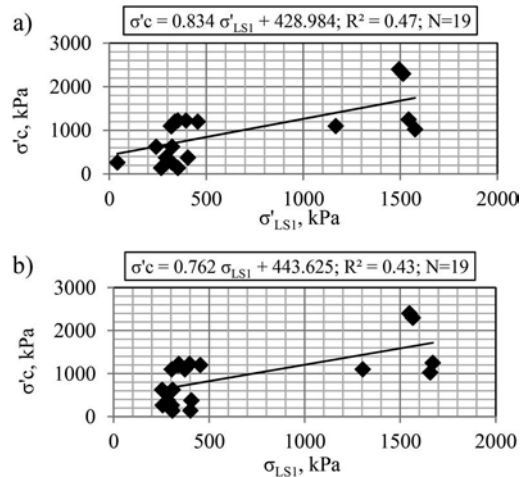


Figure 4. Regression analysis of relationship between over-compaction stress σ'_c , and LS-module parameters σ'_{LS1} (a) and σ_{LS1} (b).

With other LS-module parameters of the combined type, the relationship is much weaker. For most of them it is statistically insignificant.

- The nature and strength of the statistical relationship σ'_{ho} with LS-module parameters are generally similar to that for σ_{ho} .
- The correlation between POP and LS-module parameters is not statistically significant, except for σ_{LS1} ($\rho=0,48$).

For strong correlations, regression equations were calculated. The verification of their applicability was

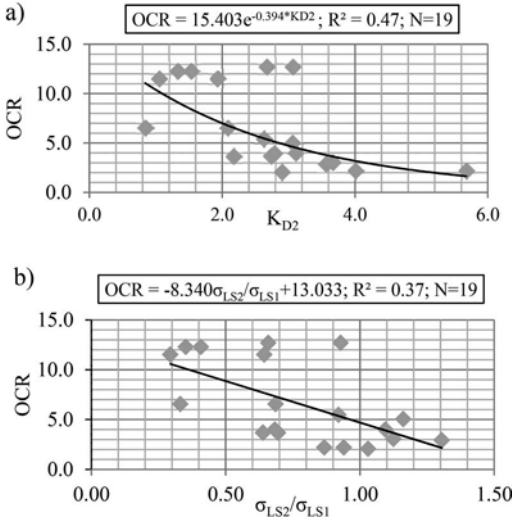


Figure 5. Regression analysis of relationship between overconsolidation ratio OCR and LS-module parameters K_{D2} (a) and $\sigma_{LS2}/\sigma_{LS1}$ (b).

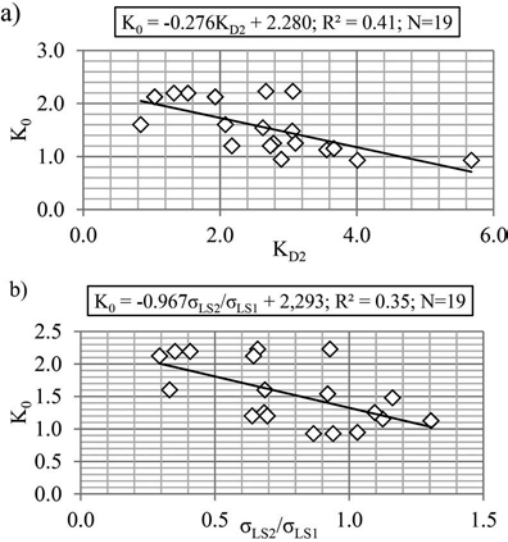


Figure 6. Regression analysis of relationship between coefficient of lateral pressure at rest K_0 and LS-module parameters K_{D2} (a) and $\sigma_{LS2}/\sigma_{LS1}$ (b).

carried out by analyzing the ratios of the calculated (according to the regression equations) to the reference values of NSS parameters (Table 5): σ'_{ce}/σ'_c , OCR_e/OCR , K_{oe}/K_o , σ_{hoe}/σ_{ho} , $\sigma'_{hoe}/\sigma'_{ho}$.

\bar{B} = mean; Me = median; σ = standard deviation; $V_\sigma = \sigma/\bar{B}$ = variability index; e = subscript, means that parameter is calculated according to the regression equation

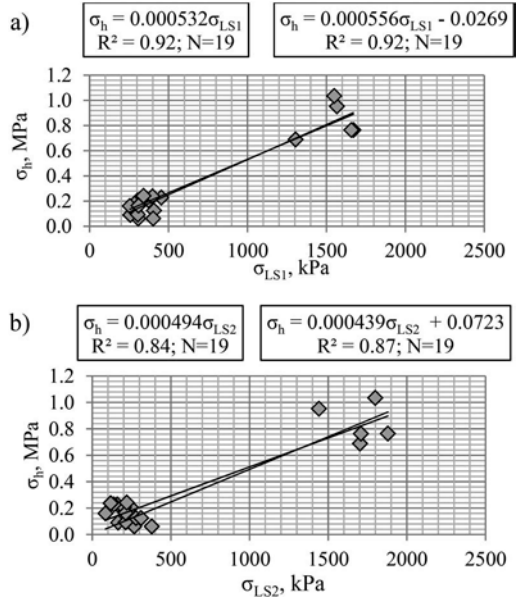


Figure 7. Regression analysis of relationship between natural total horizontal stress in the soil σ_{ho} and LS-module parameters σ_{LS1} (a) and σ_{LS2} (b).

Table 5. Verification the accuracy of regression relationships.

Ratio	Regression equation	Ratio statistics			
		\bar{B}	Me	σ	V_σ
$\frac{\sigma'_{ce}}{\sigma'_c}$	$\sigma'_{ce} = 0.834\sigma'_{LS1} + 428.984$	1.56	1.12	1.32	0.85
	$\sigma'_{ce} = 0.762\sigma_{LS1} + 443.625$	1.60	1.09	1.39	0.86
$\frac{OCR_e}{OCR}$	$OCR_e = 15.403e^{-0.394 * KD2}$	1.11	1.04	0.50	0.45
	$OCR_e = -8.341 \frac{\sigma_{LS2}}{\sigma_{LS1}} + 13.033$	1.29	0.98	0.68	0.53
$\frac{K_{oe}}{K_o}$	$K_{oe} = -0.276K_{D2} + 2.280$	1.05	1.06	0.24	0.23
	$K_{oe} = -0.967 \frac{\sigma_{LS2}}{\sigma_{LS1}} + 2.293$	1.07	0.99	0.28	0.26
$\frac{\sigma_{hoe}}{\sigma_{ho}}$	$\sigma_{hoe} = 0.000556\sigma_{LS1} - 0.0269$	1.18	0.99	0.63	0.54
	$\sigma_{hoe} = 0.000439\sigma_{LS2} + 0.0723$	1.23	0.98	0.74	0.60
$\frac{\sigma'_{hoe}}{\sigma'_{ho}}$	$\sigma'_{hoe} = 0.000334\sigma_{LS1} + 0.0472$	1.18	0.92	0.61	0.51
	$\sigma'_{hoe} = 0.000354\sigma'_{LS1} + 0.0480$	1.16	0.92	0.58	0.50

Regression equations for determining: σ'_c – give unsatisfactory mean ($\bar{B}=1.56\dots1.60$) and variability ($V_\sigma = 0.85\dots0.86$); OCR , σ_{ho} and σ'_{ho} – give relatively satisfactory mean ($\bar{B}=1.11\dots1.29$) and great variability ($V_\sigma = 0.45\dots0.60$); K_o – give good mean ($\bar{B}=1.05\dots1.07$) and satisfactory variability ($V_\sigma = 0.23\dots0.26$).

In order to improve the accuracy of determining OCR and σ'_{ho} , the possibility of their estimation based on the regression equations obtained for K_o (Table 5) was investigated.

Formula (1) can be transformed to the form $OCR = [K_o / (1 - \sin \varphi)]^{1/\alpha}$. Substituting into it from the Table 5 regression equation $K_o(K_{D2})$, you can obtain semiempirical equation in form $OCR(K_{D2}, \varphi)$. If we substitute the regression equation for K_o from the Table 5 into the expression $\sigma'_{ho} = K_o \sigma'_{vo}$, we obtain a semiempirical equation $\sigma'_{ho}(K_{D2}, \sigma'_{vo})$. Both semiempirical equations are shown in the Table 6.

Verification and assessment of the applicability of semiempirical equations were performed (Table 6). For this purpose, the statistics of the ratios OCR_e / OCR and $\sigma'_{hoc} / \sigma'_{ho}$ were calculated for the new equations and compared with the previous statistics given in Table 5.

Comparative analysis showed that semiempirical equations, compared to regression ones, have less variability (coefficient of variation V_σ is 2 times less). Therefore, they allow more precise definition of OCR and σ'_{ho} .

Table 6. Verification the accuracy of semiempirical relationships.

Ratio	Regression equation	Ratio statistics			
		\bar{B}	Me	σ	V_σ
$\frac{OCR_e}{OCR}$	$OCR_e = \left[\frac{-0.967 \frac{\sigma_{LS2}}{\sigma_{LS1}} + 2.293}{1 - \sin \varphi} \right]^2$	1.12	0.88	0.57	0.21
$\frac{\sigma'_{hoc}}{\sigma'_{ho}}$	$\sigma'_{hoc} = (-0.276 K_{D2} + 2.280) \sigma'_{vo}$	1.05	1.07	0.25	0.23

\bar{B} = mean; Me = median; σ = standard deviation; $V_\sigma = \sigma / \bar{B}$ = variability index; e = subscript, means that parameter is calculated according to the semiempirical equation

Thus, for preliminary geotechnical calculations, parameters of the natural stress state of stiff clay and firm-stiff loam according to the LS-module measurements are recommended to be determined using the following equations:

$$K_o = -0.276 K_{D2} + 2.280 \quad (3)$$

$$OCR = \left[\left(-0.967 \frac{\sigma_{LS2}}{\sigma_{LS1}} + 2.293 \right) / (1 - \sin \varphi) \right]^2, \quad (4)$$

$$\sigma'_{ho} = (-0.276 K_{D2} + 2.280) \sigma'_{vo}, \quad (5)$$

where $K_{D2} = (\sigma_{LS2} - u_0) / \sigma'_{vo}$ = normalized total soil pressure on lateral surface of LS-module second section; σ_{LS1} and σ_{LS2} = total soil pressures on lateral surface of LS-module first and second sections; $\sigma'_{vo} = \sigma_{vo} - u_0$ = effective vertical stress in the soil, u_0 = natural pore pressure in soil; φ = angle of internal friction.

Equations (3) - (5) have features.

- They are valid only if the coefficient of lateral pressure at rest K_o is determined by formula (1).
- Calculations by equations require knowledge of the soil pressure on the lateral surface, both of the first and second sections of the LS-module (σ_{LS1} and σ_{LS2}). In this case, the diameters of the first and second sections should be $\varnothing 37$ mm and $\varnothing 41$ mm.
- All equations contain not direct measurements of pressures σ_{LS1} and σ_{LS2} , but their normalized (combined) values (K_{D2} , $\sigma_{LS2} / \sigma_{LS1}$).

4 CONCLUSIONS

The paper shows that the parameters of the natural stress state of clay soils can be determined through the use of tests by penetrometer with cylindrical lateral stress module (LS-module).

It is recommended to use LS-module with two sections with different diameters. For section diameters $\varnothing 37$ mm and $\varnothing 41$ mm, empirical dependences are proposed to determine coefficient of lateral pressure at rest K_o , overconsolidation ratio OCR and effective horizontal stress in the soil σ'_{ho} .

REFERENCES

- Bayne J.M. & Tjelta T.I. 1987. Advanced cone penetrometer development for in-situ testing at Gulfaks C. In Proceedings of the 19th Offshore Technology Conference, Richardson, Texas, USA, pp. 531–540.
- Becker, D.B., Crooks, J.H.A., Been K. & Jefferis, M.G. 1987. Work as criterion for determining in-situ & yield stresses clays // Can Geotech. J. №24, pp. 549–594.
- Burns S.E. & Mayne P.W. 1998. Penetrometers for Soil Permeability and Chemical Detection. Funding provided by NSF and ARO issued by Georgia Institute of Technology Report No GIT-CEEGeo-98-1, July 1998. Georgia Institute of Technology. 144 p.
- Campanella R.G., Sully J.P., Greig J.W. & Jolly G. 1990. Research and development of a lateral stress piezocone. Transportation Research Record. No. 1278, pp. 215–224.
- Casagrande, A. 1936. The determination of the preconsolidation load and its practical significance. Proc. First Intern. Conf. on Soil Mech. & Found. Eng. Cambridge, pp. 60–64.
- Howie J.A., Campanella R.G. & Rivera Cruz I. 2014. Evaluation of the UBC lateral stress module. Proceedings of the 3rd International Symposium on Cone Penetration Testing, Las Vegas, USA. pp. 497–505.
- Huntsman S.R., Mitchell J.K. & Klejbuk L.W.Jr. 1986. Shinde S.B. Lateral stress measurement during cone penetration. Proceedings of the Conference of Use of In-Situ Tests in Geotechnical Engineering, Blacksburg, VA, USA. pp. 617–634.
- Isaev O.N., Sharafutdinov R.F. & Zakatov D.S. 2020a. 3LSU-CPTU dissipation soil test of long duration // «JSC Research Center of Construction» Gazette. № 3 (26), pp. 50–62.

9. Isaev O.N., Sharafutdinov R.F., Zakatov D.S., Baukov A.Y., Pavlov S.V. & Kamenev A.A. 2020b. 3LSU-CPTU electronic lateral stress cone penetrometer. *Geotechnics*, Vol. XII, No. 1, pp. 60–72.
10. Lunne T., Robertson P.K. & Powell J.J.M. 2004. *Cone penetration testing in geotechnical practice*. Spon Press, London and New York. 312 p.
11. Meyerhof G.G. 1976. Bearing capacity and settlement of pile foundations // *Journal of Geotechnical Engineering*, ASCE. V. 102. GT3, pp. 197–228.
12. Ryzhkov I.B. & Isaev O.N. 2016. *Cone penetration testing of soils in geotechnics*. Stockholm, Sweden: Bokforlaget Efron & Dotter AB. 385 p.
13. Sully J.P. & Campanella R.G. 1990. Measurement of lateral stress in cohesive soils by full-displacement in-situ test methods. *Transportation Research Record*. 1278, pp. 164–171.
14. Sully J.P. & Campanella R.G. 1991. Effect of lateral stress on CPT penetration pore pressures // *Journal of Geotechnical Engineering*, ASCE. No. 117(7), pp. 1082–1088.
15. Takesue K., Isano T. 2001. Development and application of a lateral stress cone. *Proceedings of the International Conference on In-situ Measurement of Soils Properties and Case Histories*, Bali, India. pp. 623–629.
16. Jaky J. 1944. Anyugalmi nyomas tenyezoje (The coefficient of earth pressure at rest) // *Magyar Mernok es Epitesz Egylet Kozlonye (Journal for Society of Hungarian Architects and Engineers)*. October, pp. 355–358.

Towards correlating seabed penetrometer and chirp sonar measurements

R. Jaber & N. Stark

Virginia Tech, Blacksburg, VA, USA

ABSTRACT: Cone Penetration Testing (CPT) and seabed coring represent key methods to determine geotechnical properties offshore. Physical testing is typically combined with geophysical surveying, i.e., chirp sonar sub-bottom profilers, and results are qualitatively related to extrapolate geotechnical properties between physical test locations. Literature suggests that more quantitative relationships can be established between geotechnical properties and geoacoustic responses. However, specific correlations are still rare, and correlating frameworks are often complex and in need of additional parameters. This study attempts to explore correlations between geotechnical properties measured using a portable free fall penetrometer (PFFP) and determined from soil samples and chirp sonar at a frequency of 8-12 kHz. Preliminary results focusing on fine-grained sediments using data collected in the York River, Virginia, USA suggest relations between sediment properties using PFFP measurements and geoacoustic properties using chirp measurements and laboratory testing.

1 INTRODUCTION

The development of coastal infrastructure and offshore renewable energy, scour and erosion prediction and assessment, as well as naval applications require a thorough understanding of seabed sediment properties (Harris et al. 2008). In-situ geotechnical testing such as Cone Penetration Testing (CPT), soil sampling, and core extraction are typically relied on to determine geotechnical seabed properties (Saleh & Rabah 2016). Geophysical methods provide high-resolution bathymetry, sub-surface soil strata mapping, seabed morphology, and even estimates of sediment properties (Ballard 2017). The ability of geophysical methods to survey large areas of the seabed efficiently have contributed significantly to the knowledge and understanding of the seabed (Saleh & Rabah 2016, Jackson & Richardson 2007). The development of more robust frameworks that utilize penetrometer testing for the calibration of geophysical tools to derive geotechnical properties with high accuracy and reliability from geophysical surveying while reducing the need for physical testing and coring has the potential to increase efficiency and decrease costs in offshore site investigation, as well as provide more geotechnical data during scour and erosion monitoring.

Several studies examined the integration of acoustic and geotechnical testing, towards better soil characterization, scour assessment, and direct correlations between geotechnical properties and acoustic measurements (Wang & Stewart 2015, Pecknold & Osler 2011, Harris et al. 2008, Osler et al. 2006, Bull et al. 1998). Most correlations between geotechnical properties and acoustics evolved from empirical approaches

(Harris et al. 2008) to geoacoustic models that investigate the theory of sound propagation using direct or indirect methods (Ballard 2017, Hamilton 1980). Geoacoustic parameters such as acoustic impedance, reflection coefficient, backscatter intensity, index of impedance, and others have been related to geotechnical soil properties such as porosity, particle size and bulk density. However, specific geoacoustic frameworks readily available and including geotechnical soil properties particularly from in-situ testing are still rare, and often hampered by the need for and sensitivity to multiple input parameters which may be difficult to obtain (Pecknold & Osler 2011). Challenges also include the spatial variability of seabed stratification on the order of centimeters which obscures field calibration and validation (Jackson & Richardson 2007).

This study makes an attempt to relate portable free fall penetrometer measurements (PFFP) and chirp sonar sub-bottom profiling at 8-12 kHz towards a direct correlation between penetrometer tests and geoacoustic response for seabed site investigation. With regards to geoacoustic properties, this study focuses on acoustic impedance and the reflection coefficient.

2 METHODS & SURVEY LOCATIONS

Data was collected in the York River estuary, Virginia, USA, with water depths ranging from ~ 2 m to ~ 7.5 m. For this article, a cross-transect was chosen that started at 37°20'23.15"N 76°37'52.35"W and ends at 37°20'44.75"N 76°37'0.16"W (Figure 1), featuring predominately fine-grained sediments.

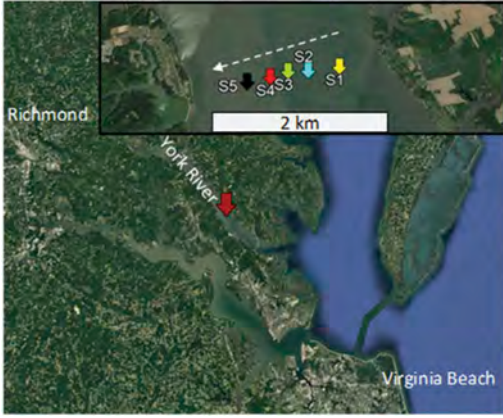


Figure 1. The investigated cross-shore transect in the York River estuary indicated by the red arrow with the five stationary stations (S1-S5) along the station indicated by the different colors (Map data: Google, SIO, NOAA, U.S Navy, NGA, GEBCO).

The chirp sonar was installed at the side of the boat with its head approximately 30 cm under water. The entire transect was measured with the chirp sonar with longer stationary recordings at five specific locations (S1-S5) along the transect (Figure 1). The PFFP was deployed from the same vessel simultaneously to chirp sonar surveying at locations S1-S5. Five PFFP deployments were conducted per location. Box core samples of ~ 30 cm length below seabed surface were recovered at the same locations.

Chirp sonar data was collected using a firmware data acquisition software. The chirp sonar was operated at an 8-12 kHz sweep in low energy mode to focus on sediments in the upper < 10 m of the estuary bed (Stratabox HD manual 2016). The chirp sonar sends sound signals into the water column, which then penetrate the seabed. The intensity of the signal reflected at different soil layers varies based on the different soil layer properties and interfaces with different geoacoustic properties. It should be noted that chirp sonars are typically deployed for deeper soil stratigraphy investigations, while the work presented here explores the deployment of chirp sonar to investigate top-surface sediments at a sediment depth < 1 m in line with the depth of interest for sediment dynamics as well as with the PFFP penetration depth.

Portable free fall penetrometers (PFFP) are a rapid in-situ investigation tool of the uppermost seabed layers (Randolph 2016). PFFP results have evolved from rapid seabed characterization to detection of soil layering, characterization of geotechnical sediments, mapping of sediment type, and more quantitative site characterization (Stark & Wever 2009, Stoll & Akal 1999). The PFFP was used in this study to estimate quasi-static bearing capacity ($qsbc$) and undrained shear strength (s_u) of seabed surface sediments. The specific lightweight instrument enabled multiple tests per location in a rapid manner and simultaneously to

the chirp sonar surveying. The data processing from the measured PFFP deceleration to estimate $qsbc$ and s_u followed the concept presented by, e.g., Aubeny and Shi (2006) and Albatal and Stark (2017) and as discussed by Stark and Ziotopoulou (2017) for the PFFP used. A detailed description can be found in those publications, amongst others. In this paper, the $qsbc$ calculations utilizes logarithmic and power law expressions for strain rate correction factors (Steiner et al. 2014; Stark and Ziotopoulou 2017).

Box core samples were tested in the geotechnical laboratory for grain size analysis, laboratory miniature vane shear, water content, and bulk density using ASTM D1140, D4648, D2216, and D7263 respectively. Porosity was measured from the core samples and deduced from phase relationships using water content.

2.1 Acoustic impedance from sediment samples

The results of porosity and bulk density were used to calculate the expected acoustic impedance $Z = \rho_b c_b$, and reflection coefficient RF based on LeBlanc et al.'s (1992) approach summarized in the equations below:

$$c_b = \left(\frac{1}{\beta_b} + \frac{4\mu}{3} \right)^{0.5} \quad (1)$$

$$\beta_b = \beta_w n + \beta_g (1 - n) \quad (2)$$

where c_b is the compressional wave velocity, β_b is the bulk compressibility of water, ρ_b is the bulk density of sediment, μ is the bulk modulus of rigidity, β_g is the grain compressibility, $\beta_g = \beta_R \beta_w$ taken as $4.85E-11 \text{ m}^2$, n is the soil porosity, β_w is the compressibility of bottom water, and β_R is the grain compressibility relative to bottom water. The bulk modulus of rigidity can be estimated using:

$$\mu = \mu_o \left(\frac{\rho_b}{\rho_w - 1} \right)^\eta \quad (3)$$

where μ_o is the rigidity constant taken as $5E-7 \text{ N/m}^2$, ρ_w is the density of water, and η is an arbitrary exponential power constant, taken as 1.

The reflection coefficient can then be calculated:

$$RF = \frac{Z - Z_w}{Z + Z_w} \quad (4)$$

where Z_w is the impedance of water (ρ_w/β_w)^{1/2}, taken as $1.53E06 \text{ kg/m}^2\text{s}$ and Z is the acoustic impedance of seabed sediments.

At each of the stationary sites, the chirp sonar recorded the same location for a few minutes.

The recordings were saved in segy format files and were read and processed in a MATLAB code that displays the variation in the signal amplitude envelope (without phase information) with seabed depth. The multiple reflection approach suggested by Bull et al. (1998) was then tested to calculate the reflection coefficient of the seafloor using the amplitude and the two-way travel time of the primary seabed reflector and the first multiple of the seabed reflector as shown in the formula below:

$$RF = \frac{TWT_m A_m}{TWT_p A_p} \quad (5)$$

where TWT_m is the two-way travel time of the first multiple of the seabed reflector, A_m is the amplitude of the first multiple seabed reflector, TWT_p is the two-way travel time of the primary seabed reflector, A_p is the amplitude of the primary seabed reflector. The acoustic impedance of the sediments can then be calculated from the reflection coefficient results using Eq. 4. The reflection coefficient was calculated after applying a moving average of the trace range amplitudes to account for local noise variations.

3 RESULTS

The chirp sonar measurements along the measured transect as derived from the manufacturer software is shown in Figure 2 with S1-S5 highlighted. In the following sections, results from the stationary chirp recordings, PFFP deployments, and soil testing of core samples collected at sites S1 through S5 are presented.

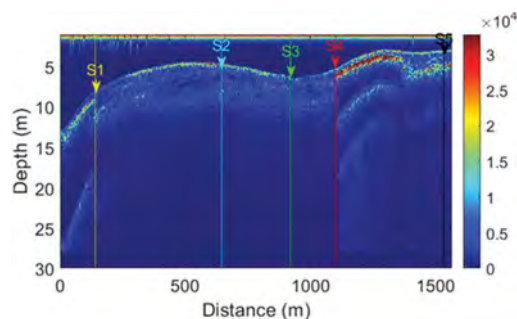


Figure 2. Depiction of chirp sonar backscatter intensity (as relative digital number) along the cross-transect at York River, VA. The five different locations surveyed are marked by the arrows with annotations S1-S5.

3.1 Chirp sonar

The porosity varied slightly with a minimum and a maximum of 0.74 and 0.83 at sites S2 and S4, respectively (Table 1). The bulk density ranged between a minimum of 1.21 g/cm³ and a maximum

of 1.69 g/cm³ at sites S3 and S5, respectively. Hence, following LeBlanc et al. (1992) (Eqs. 1-4), the lowest acoustic impedance Z and reflection coefficient RF based on sediment properties predicted from the core samples are 1.9E+06 kg/m²s and 0.11 at S3 respectively, and the highest are 2.3E+06 kg/m²s and 0.2 at S5, respectively (Table 1).

Table 1. Sediment geotechnical and acoustic properties for sites S1-S5.

Site	n	ρ_b (g/cm ³)	Z (kg/m ² s)	RF
S1	0.78	1.28	2.0E+06	0.13
S2	0.74	1.54	2.2E+06	0.18
S3	0.81	1.21	1.9E+06	0.11
S4	0.83	1.46	2.0E+06	0.15
S5	0.75	1.69	2.3E+06	0.20

Table 2 shows the Z and RF derived from the chirp sonar following the approach by Bull et al. (1998) (Eq. 5) for sites S1-S5. The presented ranges account for variability observed during the stationary measurements. It should be noted that “stationary” still included some boat motion within the range of a single anchor line.

Table 2. Acoustic impedance and reflection coefficient results from the chirp sonar.

Site	Z (kg/m ² .s)	RF
S1	3.6-4.6E+06	0.40-0.50
S2	3.7-8.5E+06	0.42-0.70
S3	3.2-4.6E+06	0.35-0.50
S4	1.9-6.0E+07	0.85-0.95
S5	4.6-9.8E+06	0.50-0.73

The reflection coefficients estimated ranged from 0.35 up to 0.73 for all sites, except for S4, where the results seem to be drastically higher than the rest of the sites. The acoustic impedance varied between 3.2E+06 kg/m²s and 9.8E+06 kg/m²s, except for S4 also where the results reached up to 6.0E+07 kg/m²s. No clear reason for the observations at S4 was found. It may be hypothesized that gas was present in the sediment from biogenic processes, but due to a lack of data to confirm or reject the hypothesis, chirp results at S4 will be rejected from further analysis.

3.2 PFFP results

A representative deceleration profile for each of the five sites (S1-S5) along the transect is shown in

Figure 3. A maximum deceleration (dec) of ~ 3.5 g was recorded for sites S1, S4 and S5 and a higher maximum deceleration of ~ 5.7 and 7.5 g was recorded for sites S2, and S3, respectively. The increase in deceleration with depth at sites S1, S4, and S5 seems gradually linear compared to a steeper increase at S2 with some irregularities observed in the profile between 20-30 cm. The deceleration profile at S3 can be divided into two layers, an upper softer layer (above ~ 40 cm), and a stiffer lower layer (below ~ 40 cm).

The maximum deceleration was then used to calculate the maximum $qsbc$ and s_u using strain rate parameters k and β ranging from 0.1 to 0.15, and 0.035 to 0.085, respectively (Chow et al. 2017, Steiner et al. 2014). Cone factor (N_{kt}) values typically reported for CPT in fine-grained sediments range between 4 and 20 (Robertson & Cabal 2015). Mayne & Peuchen (2018) reported N_{kt} ranging from 8 to 25 based on a database composed of 62 clays. Therefore, cone factors of 12.3 and 10 were chosen for this study based on the values reported by Mayne & Peuchen (2018) for offshore normally consolidated clay and sensitive clays, respectively.

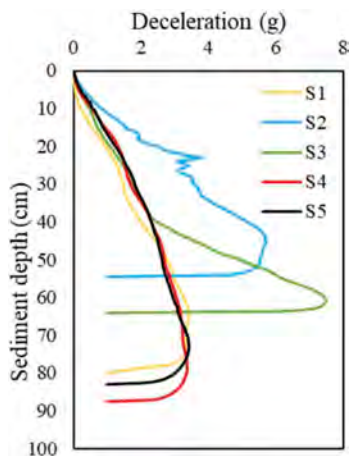


Figure 3. Deceleration and $qsbc$ -depth profiles for sites S1-S5. Different colors represent the different sites.

4 DISCUSSION

Based on LeBlanc et al. (1992) and others, these values suggest sediments coarser than sand, and thus, represents not only a mismatch to the estimates obtained from sediment samples, but also with expectations based on literature. The difference between both reflection coefficients varied between a factor of 2 and 4. However, no consistent factor was obvious, likely indicating that

the multiple approach adopted by Bull et al. (1998) might not be applicable. A reason for this may be the local water depth. Warner (1990) initially introduced this approach for deep water investigations, and Bull et al. (1998) applied it to water depths of ~ 9 m. The water depth along the tested transect reached only ≤ 7.5 m. Also, multiples are only clearly visible at some of the target locations when revisiting the initial output (Figure 2). This necessitates the need to explore different processing methods to calculate the reflection coefficient, likely utilizing phase information that were not collected here for simplification, or to investigate the application of an inverse model as suggested by Wang & Stewart (2015). However, it should be noted that despite the mismatch in Z and RF between the geoacoustic properties estimated using the chirp measurements and those estimated from sample testing, both seem to follow a similar trend with respect to the different locations. For instance, sites S2 and S5 record the highest reflection coefficients while sites S1 and S3 record the lowest, as reported by both measurement methods. This supports further evidence for the expected response of the chirp sonar backscatter intensity based on differences in sediment properties; however, also highlights limitations of the Bull et al. (1998) approach to accurately derive Z and RF for the shallow water – shallow penetration conditions encountered here.

Table 3 summarizes the main results of the PFFP, represented by the maximum dec , $qsbc$, and s_u along with the chirp and laboratory testing results represented by one of the geoacoustic properties, RF . The multiple $qsbc$ and s_u results reported per site correspond to the different strain rate correction methods, parameters, and cone factors used.

The variation in the $qsbc$ values at each site based on the different k and β reaches up to ~ 10 kPa, with the variations becoming more significant at large deceleration values (e.g. S2 and S3). The power-law equation for the strain rate correction with β of 0.085 always seem to give the lowest $qsbc$ result. Similarly, the undrained shear strength values seem to vary between 0.3 up to 0.9 kPa with the largest variations reported at sites S2 and S3. Sediment strength was relatively consistent towards the estuary banks (S1, S4, and S5) and higher and more variable in the center of the estuary (S2 and S3). The significant difference of S4 observed in the chirp sonar was not reflected in the PFFP. Acoustic methods are highly sensitive to gas, while gas content would be expected to decrease sediment strength, the threshold for detection may be higher.

Table 3. PFFP results (dec, q_{sb}, s_u), chirp and sample testing results (RF) at the five sites (S1-S5) for different strain rate parameters and cone factors.

Site	k/β	dec (g)	q _{sb} (kPa)	s _u N _{kr} -12.3	s _u N _{kr} -10	RF- chirp	RF- sample
S1	0.1	3.4	24.1	2.0	2.4	0.45	0.13
	0.15		22.1	1.8	2.2		
	0.035		24.6	2.0	2.5		
	0.085		19.5	1.6	2.2		
S2	0.1	5.7	40.2	3.3	4.0	0.56	0.18
	0.15		36.9	3.0	3.7		
	0.035		41.1	3.3	4.1		
	0.085		32.1	2.6	3.2		
S3	0.1	7.5	53.3	4.4	5.3	0.43	0.11
	0.15		49.3	4.0	4.9		
	0.035		54.5	4.4	5.5		
	0.085		43.7	3.6	4.4		
S4	0.1	3.4	24.2	2.0	2.4	-	0.15
	0.15		22.3	1.8	2.2		
	0.035		24.7	2.0	2.5		
	0.085		19.5	1.6	2.0		
S5	0.1	3.4	24.3	2.0	2.4	0.62	0.20
	0.15		22.4	1.8	2.2		
	0.035		24.8	2.0	2.5		
	0.085		19.6	1.6	2.0		

Focusing on S1 and S5 showing similar PFFP profiles with soft sediments (Figure 3 and Table 3), significant differences were noted in the chirp sonar (Figure 1 and Table 2), and similarly, differences were noted in the sediment cores' bulk density and porosity (Table 1). This may suggest that those slight variations in porosity ($n = 0.75$ and $n = 0.78$) affect the geoacoustic response noticeably, particularly when considering the possibility of abundant gas content), but may not affect the sediment strength, and thus, the PFFP to the same degree.

Location S3 suggested an overall higher sediment strength based on the maximum values throughout the penetration; however, matched the observations at S1 and S5 up to a penetration depth of 40 cm. As sediment cores were only obtained to a penetration depth of 30 cm and the method applied to estimate Z and RF from the chirp sonar bases on surface layer reflection, a discussion of PFFP vs. chirp sonar for S3 may be included in the discussion of S1 and S5. Then, S3 matches well with S1, and S5 strikes as an outlier (Table 3). Revisiting Figure 3 reveals that S5 shows stronger reflections and variability with multiple stronger reflectors within the top meters of the seabed. Similar to S4, the presence of gas may be hypothesized. Additionally, the shallower water depth approaches the systems minimum, possibly also affecting the chirp response.

Finally, location S2 suggested an increased sediment strength for the entire PFFP penetration depth over all other deployment locations, and indeed,

a higher reflection coefficient RF was suggested from the sediment samples and confirmed by the chirp sonar (Table 3).

Despite the limited variability in the seabed sediments, results seem to suggest certain trends between sediment strength and reflection coefficient, as measured by the PFFP and the chirp sonar. This encourages further work that would follow-up on current findings and address limitations and shortcomings mentioned here. This mainly includes considering different soil types, layered systems, and comparisons at different sediment depths. Additionally, it includes exploring reasons behind the mismatches observed between the RF results based on the chirp and sample testing and exploring different processing methods that are better suited for shallow water depths.

5 CONCLUDING REMARKS

This paper investigates the relations between reflection coefficients and acoustic impedance predicted from sediment samples and observed from chirp sonar measurements with portable free fall penetrometer (PFFP) testing along a transect crossing the York River estuary characterized by fine sediments. The presented data set is a small excerpt of a larger data set that includes many different seabed sediment characteristics. A limitation of the presented data set is the limited variability of the seabed sediments. Nevertheless, the data suggests that locations of increased sediment strength (S2 with an undrained shear strength estimated of up to 4.1 kPa within the uppermost meters of the seabed surface) also featured lower porosity suggesting a higher reflection coefficient which was confirmed by the chirp sonar measurements. It should be noted that this trend was visible even with the limited sediment variability of lower undrained shear strength sites reaching up to 2.5 kPa within the upper meter of the seabed surface. However, the data also revealed the need for further considerations such as: i) Which sediment depths or sediment depth ranges should results be compared at? ii) Related to i), how should layering be addressed then? iii) The effects of gas content on geotechnical properties versus geoacoustic properties. iv) Possible limitations regarding water depth in which chirp sonar is deployed in. v) What is the sensitivity of the PFFP and the chirp sonar to different sediment properties? These questions will be addressed further in follow-on work.

ACKNOWLEDGEMENTS

The authors of the paper would like to thank the National Science Foundation (NSF) through grant CMMI-1751463 and the Naval Research Lab through grant N00173-19-1-G018 for funding this work. The authors would also like to thank Grace

Massey, Cristin Wright and Liz Smith for their help in data collection, and Joe Calantoni and Jesse McNinch for valuable discussions of the topic.

REFERENCES

- Albatal, A. & Stark, N. 2017. Rapid sediment mapping and in situ geotechnical characterization in challenging aquatic areas. *Limnology and Oceanography: Methods*, 15(8), 690–705.
- ASTM D4648M. 2016. Standard Test Methods for Laboratory Miniature Vane Shear Test for Saturated Fine-Grained Clayey Soil. West Conshohocken, PA; ASTM International.
- ASTM D1140. 2017. Standard Test Methods for Determining the Amount of Material Finer than 75- μm (No. 200) Sieve in Soils by Washing. West Conshohocken, PA; ASTM International
- ASTM D2216. 2019. Standard Test Methods for Laboratory Determination of Water (Moisture) Content of Soil and Rock by Mass. West Conshohocken, PA; ASTM International.
- ASTM D7263-2021. Standard Test Methods for Laboratory Determination of Density and Unit Weight of Soil Specimens. West Conshohocken, PA; ASTM International.
- Ballard, M. S. & Lee, K. M. 2017. The acoustics of marine sediments. *Acoust. Today*, 13(3), 11–18.
- Bull, J. M., Quinn, R., & Dix, J. K. 1998. Reflection coefficient calculation from marine high resolution seismic reflection (Chirp) data and application to an archaeological case study. *Marine Geophysical Researches*, 20(1), 1–11.
- Chow, S. H., O’Loughlin, C. D., White, D. J., & Randolph, M. F. 2017. “An extended interpretation of the free-fall piezocone test in clay.” *Géotechnique*, 67 (12), 1090–1103.
- Hamilton, E. L. 1980. Geoacoustic modeling of the sea floor. *The Journal of the Acoustical Society of America*, 68(5), 1313–1340.
- Harris, M. M., Avera, W. E., Abelev, A., Bentrem, F. W., & Bibee, L. D. 2008. Sensing shallow seafloor and sediment properties, recent history. *Proc. of Oceans 2008*, Quebec City, September 15-18, 1-11.
- Jackson, D. R., & Richardson, M. D. 2007. *High-frequency seafloor acoustics, The Underwater Acoustics Series*, Springer, New York.
- LeBlanc, L. R., Mayer, L., Rufino, M., Schock, S. G., & King, J. 1992. Marine sediment classification using the chirp sonar. *The Journal of the Acoustical Society of America*, 91(1), 107–115.
- Mayne, P. W. & Peuchen, J. 2018. CPTu bearing factor Nkt for undrained strength evaluation in clays. Proc. of *Cone Penetration Testing 2018 (CPT’18)*. Delft, Netherlands, June 21-22, 2018.
- Osler, J, Furlong, A. & Christian, H. 2006. Acoustic sensing techniques for the shallow water environment: inversion methods and experiments. *2nd Workshop on Experiments Acoustic Inversion Techniques for Assessment of the Shallow Water Environment*, Ischia, ITALY.
- Pecknold, S. & Osler, J. C. 2011. Sensitivity of acoustic propagation to uncertainties in the marine environment as characterized by various rapid environmental assessment methods. *Ocean Dynamics*, 62(2), 265–281.
- Randolph, M.F. 2016. New tools and directions in offshore site investigation. *Australian Geomechanics*, 51(4), 81–92.
- Robertson, P.K. & Cabal, K.L. 2015. Guide to cone penetration testing-6th Edition. Gregg Drilling and Testing Inc, Signal Hill.
- Saleh, M. & Rabah, M. 2016. Seabed sub-bottom sediment classification using parametric sub-bottom profiler. *NRIAG Journal of Astronomy and Geophysics*, 5(1), 87–95.
- Stark, N. & Wever, T.F. 2009. Unraveling subtle details of expendable bottom penetrometer (XBP) deceleration profiles. *Geo-Marine Letters*, 29(1), 39–45.
- Stark, N., & Ziotopoulou, K. 2017. Undrained shear strength of offshore sediments from portable free fall penetrometers: theory, field observations and numerical simulations. Proc. of Offshore Site Investigation Geotechnics 8th International Conference, Society for Underwater Technology, South Kensington, 391–399.
- Steiner, A., Kopf A. J., L’Heureux J. S., Kreiter S., Stegmann S., Haflidason H. & Moerz T. 2014. In situ dynamic piezocone penetrometer tests in natural clayey soils-a reappraisal of strain-rate corrections. *Canadian Geotechnical Journal*. 51: 272–288.
- Stoll, R. D. & Akal, T. 1999. XBP - tool for rapid assessment of seabed sediment properties. *Sea Technology*, 40(2), 47–51.
- SyQwest 2016. StrataBox HD Chirp Operations and Maintenance Manual. <http://www.syqwestinc.com/products/sub-bottom-profilers/stratabox> (June 5, 2019).
- Wang, J. & Stewart, R. 2015. Inferring marine sediment type using chirp sonar data: Atlantis field, Gulf of Mexico. *Society of Exploration Geophysicists*, 2385–2390.
- Warner, M. 1990. Absolute reflection coefficients from deep seismic reflections. *Tectonophysics*, 173(1-4), 15–23.

Development of free fall cone penetration testing system

Hyoun Kang, Osoon Kwon, Changjoo Shin, Jungmin Seo, Insung Jang & Man Dong-Woo
Korea Institute of Ocean Science & Technology, Busan, Korea

ABSTRACT: For the rigorous design of offshore structures, the geotechnical characteristics of the seabed ground should be rigorously investigated, in the deep water, seabed ground surveys are complex equipment and costly. Free fall type ground survey equipment that can acquire a simple and comparatively accurate ground is developed when only the characteristic investigation of the shallow depth ground such as the submarine pipeline, the submarine cable burial is the main concern. In this study, FFCPT was developed. Based on behavior results of numerical model simulation for FFCPT, it was manufactured. Water depth was obtained using pressure sensor and penetrated depth was estimated by the double integration of acceleration signal. In addition, we can verify vertical penetration at real field test of FFCPT using 2axis of inclinometer. So, the results of the seabed type offshore CPTu experiment and the developed model were compared and the performance was evaluated.

Keywords: FFCPT (cone penetration testing system), tip resistance, sleeve friction, pore pressure

1 INTRODUCTION

Recently, various types of equipment that are operated underwater have been developed. Among them, it is very important to characterize the seabed ground for the movement of equipment. However, there is not much technology of the equipment to understand the characteristics of the seabed ground, size of the equipment is large, and It takes a very complicated process to identify the characteristics of the seabed ground. The Free-Fall cone penetration testing system (FFCPT) has been developed as a tool for the rapid environmental assessment of seabed and water column properties for anti-submarine warfare and mine counter measure operations

The FFCPT makes direct measurements of geotechnical properties of the seabed. It has the same scaling factors as a conventional pushed cone penetrometer, but with a larger diameter to house the instrumentation and power supply. It is designed to free-fall into the seabed and to survive impacts with rock, if and when that happens. It consists of a nose cone instrumented with geotechnical sensors, power supply, electronics, and tail pressure sensor. It measures acceleration and dynamic sediment pore pressure as a function of depth of penetration into the seafloor. The FFCPT also records hydrostatic pressure, to monitor its descent velocity during free-fall, and optical backscatter for the detection of the water-

sediment interface which is particularly helpful on high porosity fluid-mud seabed.

CPT(Cone Penetration Test) is the most accurate field survey method to measure the strength and characteristics of the ground in the field. In the ocean, CPT(Cone Penetration Test) are conducted in a variety of ways.

In this study, compared to the equipment used on land, it is relatively easy to carry in the marine field, A Free Fall Cone Penetration Testing System-(FFCPT) was developed to obtain accurate ground data(tip resistance, friction resistance). and the characteristics of the seabed ground were identified by the sea trials.

In addition, the depth of subsea ground and ground data were finally compared with the results of the seabed type offshore cone penetration test and Free Fall Cone Penetration Testing System in the same area to assess performance.

2 SITE CONDITIONS AND INVESTIGATION

In this study, experiments were conducted in Gunsan, located on the west coast of South Korea, as shown in Figure 1.

As shown in Figure 2, the feasibility of the experimental location was evaluated by the seabed type offshore cone penetration test subsea survey results, and the subsea ground survey results were shown.



Figure 1. Test site location map.

The water depth is about 1.0 meter at low tide and about 8.0 m at high tide. The prevailing current velocity is 1.59 m/sec at maximum and 0.80 m/sec at minimum. The seafloor at the test site consists of roughly 8.0 meter of clayey silt or sandy clay underlain by medium silty sand. As shown in Figure 2, the characteristics of the ground as a distribution map.

3 DEVELOPMENT OF FFCPT

FFCPT should not be disturbed by power or communication line, in order to increase penetration force during freely falling. Therefore, all parts such as power source, electronic board, sensors, etc. must be installed in body of the FFCPT except recovery wire.

Figure 3 is the canister for electronic part is made of aluminum alloy to have a light weight and buoyancy compared to the rod and cone probe which are made of iron. Since the center of buoyancy is set to be 0.6m upper than the center of mass, the flip-over motion of FFCPT can be prevented during free fall.

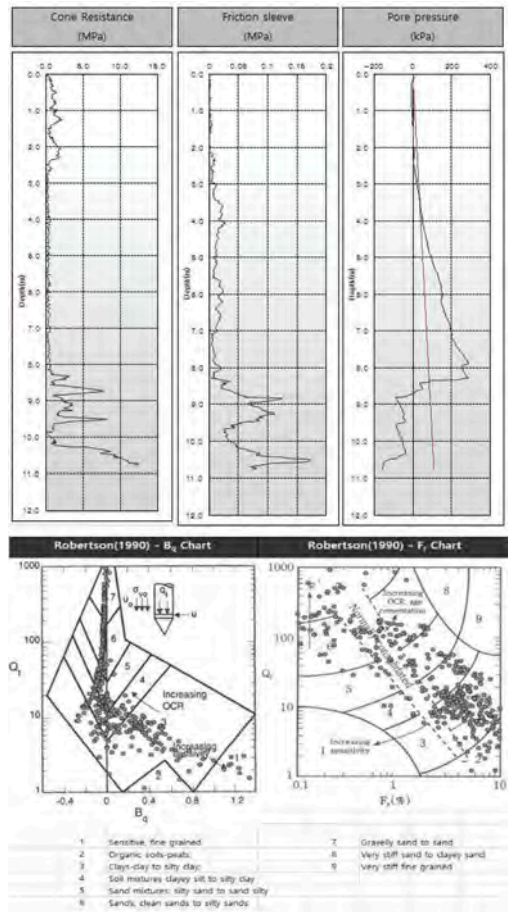


Figure 2. Result of test site location.

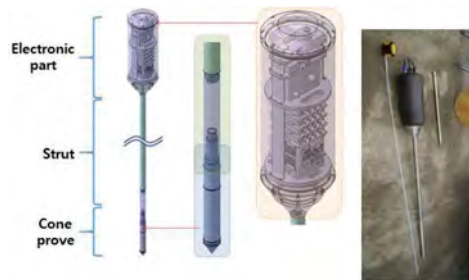


Figure 3. Configuration of FFCPT.

Several sensors and electronic parts such as DAQ, battery, etc. are embedded as shown in Figure 4(a). To obtain these signals, NI crio for DAQ was applied. Estimation of the penetration depth of FFCPT using acceleration is the fundamental data for ground characteristics analysis, so dedicated

equipment that can accurately measure it is required. In addition, the acceleration signal and other sensor signals require time synchronization. For this purpose, a dedicated module for vibration measurement and a DC-type acceleration were used, and when other sensor signals were input, time synchronized measurements were performed based on the acceleration signal. A 2-axis inclinometer is installed for tracking the underwater free fall motion. The pressure sensor was applied to check the water depth at the test point. It is manufactured so that it can operate continuously for more than 8 hours after power on using large-capacity battery. According to Newton's Law, the underwater terminal speed just before impact is calculated by integration of the obtained acceleration.

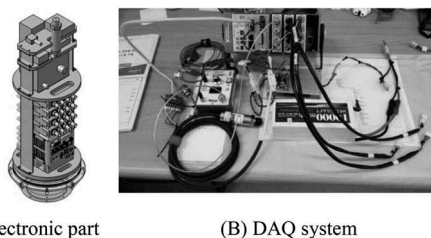


Figure 4. Detailed design of electronic part in the FFCPT.

4 TESTING METHODS AND RESULTS

4.1 Testing methods

Figure 5 is the an experiment was conducted to obtain subsea ground data (cone tip resistance, friction resistance) using the developed FFCPT

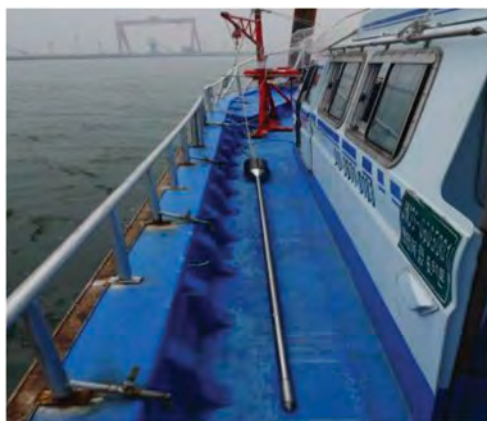


Figure 5. FFCPT.

Figures 6 and 7 are the FFCPT with a length of 4m and weight of 38kg was placed on a moving crane and dropped freely in sea 20m deep. In order to verify the

performance of the developed FFCPT, free fall experiments were repeated five times and data were obtained.



Figure 6. Drop test of FFCPT_1.



Figure 7. Drop test of FFCPT_2.

4.2 Result of test

In this study, subsea ground characteristics data (cone tip resistance, friction resistance) were obtained using the developed FFCPT (Free Fall Cone Penetration Testing System).

As shown in Table 1, the final penetration depth was 0.21 m, 0.24 m, 0.26 m, 0.22 m and 0.49 m, and the average was 0.28 m.

Table 1. Result of test.

	Final penetration depth(m)	Cone resistance(MPa)	friction resistance(MPa)
FFCPT-1	0.21	0.0048~5.2755	0.0~0.0153
FFCPT-2	0.24	0.0006~4.8709	0.0~0.0118
FFCPT-3	0.26	0.0141~5.3009	0.0~0.0114
FFCPT-4	0.22	0.0131~4.2026	0.0~0.0116
FFCPT-5	0.49	0.0006~2.5260	0.0~0.0115

4.2.1 Result of FFCPT-1

Figure 8 is the final penetration depth of FFCPT-1 was 0.21m and ground data (cone tip resistance, friction resistance) values were measured. The results of the experiment were shown as follows

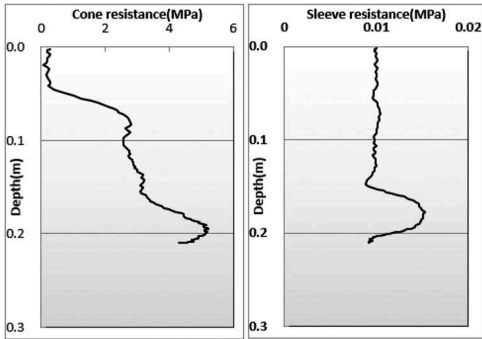


Figure 8. Result of FFCPT-1.

Figure 8 is the distribution range of cone tip resistance was measured in the range of 0.0048 to 5.2755MPa, and the distribution range of the friction resistance was measured in the range of 0.0000 to 0.0153MPa. As a result of the experiment, from 0m to 0.1m, it is judged as Clay silt to silty clay, and up to 0.2m, it is judged as Silty sand to sandy silt.

4.2.2 Result of FFCPT-2

Figure 9 is the final penetration depth of FFCPT-1 was 0.24m and ground data (cone tip resistance, friction resistance) values were measured. The results of the experiment were shown as follows.

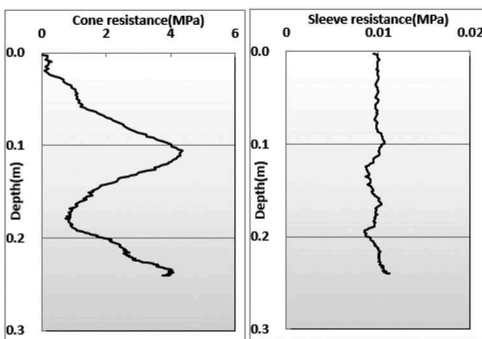


Figure 9. Result of FFCPT-2.

Figure 9 is the distribution range of cone tip resistance was measured in the range of 0.0006 to 4.8709MPa, and the distribution range of the friction resistance was measured in the range of 0.0000 to 0.0118MPa. As a result of the experiment, from 0m to 0.1m, it is judged as Silty sand to sandy silt, from

0.1m to 0.18m, it is judged as Clay silt to silty clay, and up to 0.25m, it is judged as Silty sand to sandy silt.

4.2.3 Result of FFCPT-3

Figure 10 is the final penetration depth of FFCPT-1 was 0.26m and ground data (cone tip resistance, friction resistance) values were measured. The results of the experiment were shown as follows.

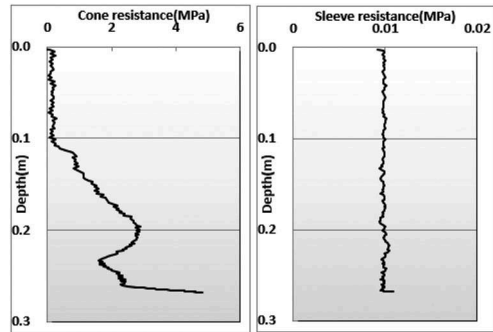


Figure 10. Result of FFCPT-3.

Figure 10 is the distribution range of cone tip resistance was measured in the range of 0.0141 to 5.3009MPa, and the distribution range of the friction resistance was measured in the range of 0.0000 to 0.0114MPa. As a result of the experiment, from 0m to 0.2m, it is judged as Silty sand to sandy silt, and up to 0.27m, it is judged as Clay silt to silty clay.

4.2.4 Result of FFCPT-4

Figure 11 is the final penetration depth of FFCPT-1 was 0.22m and ground data (cone tip resistance, friction resistance) values were measured. The results of the experiment were shown as follows

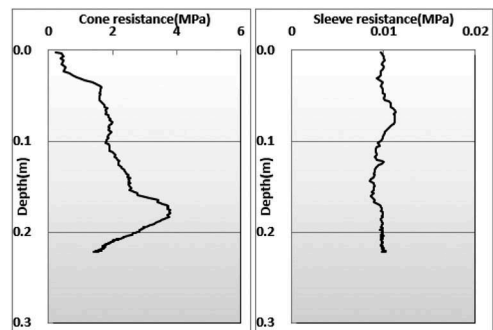


Figure 11. Result of FFCPT-4.

Figure 11 is the distribution range of cone tip resistance was measured in the range of 0.0131 to 4.2026MPa, and the distribution range of the friction resistance was measured in the range of 0.0000 to

0.0116MPa. As a result of the experiment, from 0m to 0.17m, it is judged as Clays-clay to silty clay, and up to 0.22m, it is judged as Silty sand to sandy silt.

4.2.5 Result of FFCPT-5

Figure 12 is the final penetration depth of FFCPT-1 was 0.49m and ground data (cone tip resistance, friction resistance) values were measured. The results of the experiment were shown as follows.

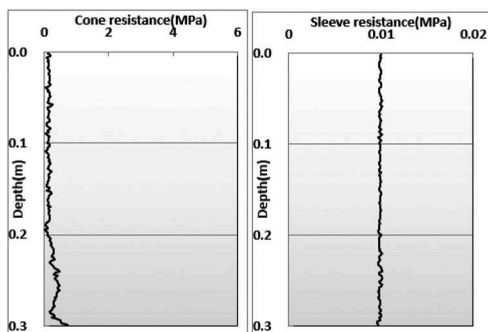


Figure 12. Result of FFCPT-5.

Figure 12 is the distribution range of cone tip resistance was measured in the range of 0.0006 to 2.5260MPa, and the distribution range of the friction resistance was measured in the range of 0.0000 to 0.0115MPa. As a result of the experiment, from 0m to 0.3m, it is judged as Clays-clay to silty clay.

5 CONCLUSIONS

FFCPT was developed to obtain seabed geotechnical properties conveniently. After the FFCPT falls under water and impacts on seabed ground, the device acquires the geotechnical properties during penetration. It is very important to secure the penetration depth because the equipment measures the properties according to the penetration depth. Sea-trial free-fall test was performed.

Analysis of this study, subsea ground characteristics data were obtained using the developed FFCPT. The analysis results are as follows.

The final penetration depth was 0.21 m, 0.24 m, 0.26 m, 0.22 m and 0.49 m, and the average was 0.28 m. This is judged not to penetrate more than 0.49m because it is not deep water and it is light weight of ffcpt.

FFCPT1-5 are the distribution range of cone tip resistance was measured in the range of 0.0006 to 5.3009MPa, and the distribution range of the friction resistance was measured in the range of 0.0000 to 0.0153MPa.

According to the comparative analysis of the seabed type offshore cone penetration test and FFCPT, it was difficult to accurately compare the

locations of the test sites because it was judged that there was a gap of up to 5 to 10 meters due to the movement of the ship.

Due to the following conclusions, it is deemed necessary to estimate the appropriate depth of water in future field experiments. In addition, it is deemed necessary to increase the weight of the FFCPT even if the depth of the water is not deep enough to improve the final penetration depth.

Through this study, the basis of underwater behavior analysis of the FFCPT for seabed penetration was secured. If this equipment is improved and apply to obtain the ground characteristics in deep seabed, it is expected to be used very conveniently at low cost.

ACKNOWLEDGMENT

This research was supported by the project “Development of the support vessel and systems for the offshore field test and evaluation of offshore equipments (PM62241)” funded by Korea Institute of Ocean Science & Technology(KIOST).

REFERENCES

- [1] Changjoo Shin, Sung Gyu Won, OSoon Kwon, In Sung Jang, Jung-min Seo, Hyoun Kang, 2019. Estimation of Ground Penetration Depth for Underwater Free Fall Cone Penetration Tester. Proceeding of Korean Marine Robot Technology Society, Seoul, South Korea, 62–64.
- [2] By John Osier, Arnold Furlong, Harold Christian “The Integration of the Free Fall Cone Penetrometer(FFCPT) with the Moving Vessel Profiler (MVP) for the Rapid Assessment of Seabed Characteristics”, “International hydrographic review”, Vol. 7 No. 3, 2006, 46–47
- [3] Evans and Ashley D., “Hydrodynamics of mine impact burial,” Naval Postgraduate School, 2002.
- [4] John Osler, Arnold Furlong, Harold Christian and Mike Lamplugh, “The integration of the free fall cone penetrometer(FFCPT) with the moving vessel profiler-(MVP) for the rapid assessment of seabed characteristics,” The International Hydrographic Review, vol. 7(3), pp. 45–53, 2006.
- [5] Koumoto, T et al., “Theory and practice of the fall cone test”, Vol. 51, No. 8, 2001, pp.701–712
- [6] Kurt Seifert and Oscar Camacho, “Implementing position algorithms using accelerometers,” Freescale Semiconductor Application Note, AN3397, 2007
- [7] McCarty JL, Carden HD, 1962. Impact characteristics of various material obtained by an acceleration-time history technique applicable to evaluating remote targets. NASA technical report(NASA-TN-D-1269), University of Texas at Austin.
- [8] Stegmann, Sylvia et. al., “Design of a modular, marine free-fall cone penetrometer”, Sea Technology, Vol. 47, No. 2, 2006, pp.1–27.
- [9] Stegmann, Sylvia et. al., “Initial Results of a new Free Fall-Cone Penetrometer (FF-CPT) for geotechnical in situ characterisation of soft marine sediments”, Vol. 86, No. 3, 2006, pp.1–199.
- [10] Sung-Chul Lee, 2008. A study on the Estimation on Undrained Shear Strength and Preconsolidation Pressure

Using N-Value Obtained from Standard Penetration Test, Graduate School of Korea Maritime University.

- [11] Sylvia Stegmann, Tobias Morz and Achim Kopf, "Initial results of a new free fall-cone penetrometer for geotechnical in-situ characterization of soft marine sediments," *Norwegian Journal of Geology*, 86(3), pp. 199–208, 2006.
- [12] Yanli Yang, Yanfei Zhao, Dali Kang, 2016. Integration on acceleration signals by adjusting with

envelopes. *Journal of Measurements in Engineering*, 4(2),117–121.

- [13] Youngshin Consultant, [Online] (Updated 2010) Available at:<http://www.piletest.net/product_3_2_4.html> [Accessed July 2019].

The Integration of the Free Fall Cone Penetrometer-(FFCPT) with the Moving Vessel Profiler (MVP) for the Rapid Assessment of Seabed Characteristics

Evaluation of statistical fluctuation of measured data from nuclear density cone penetrometer

Muthusamy Karthikeyan

Surbana Jurong Consultants Pte Ltd, Singapore

ABSTRACT: This paper describes research conducted to investigate the statistical fluctuation and interpret the density profiles obtained by a nuclear-density cone penetrometer (ND-CP). The laboratory results show that the amount of fluctuations present in the ND-CP measurements can be approximated by Normal or Gaussian distribution. The coefficient of variation for RI count and BG count data's is 2.4% and 15.1% respectively. The moving-average technique has been employed for the measured raw data at different time intervals in order to reduce the statistical fluctuation. It was found that the error due to the statistical fluctuation in ND-CP measurement is less than 1% if an averaging span of 10 cm is used. The raw data obtained from the field results when averaged over 10cm depth shows that the cone profile count distribution trend is not distorted or deformed compared to the original raw data, which means the loss of information about the density through the filtering is negligible. This averaging is necessary to smooth the measured wet density profile. Therefore, the ND-CP measurements are averaged over a span of 10cm depth to minimize the statistical fluctuations.

1 INTRODUCTION

The in-situ wet density of soil can be measured reliably using Nuclear-Density Cone Penetrometer (ND-CP) (Shibata et al., 1993; Karthikeyan et al., 2001; 2004; Tan et al., 2004; Dasari et al., 2006 and Karthikeyan et al., 2007; Karthikeyan and Tan, 2008; Rui et al. 2013). Most of the earlier researchers mentioned above have focused on the effectiveness of the ND-CP in determining the soil properties for settlement analysis, evaluation of liquefaction potential of sandy deposits and determination of the strength of sub-soil after ground improvement. Recently, the ND-CP was used to characterize a reclaimed land (Karthikeyan et al., 2004, Dasari et al., 2006 and Karthikeyan et al., 2007).

Natural deposits laid down under water are often layered. Sometimes, these layers can be identified by changes in the density of soil. The ND-CP measurement is affected by the measuring volume and if this volume is occupied by layers of different densities, then the relationship between the observed count rate and true wet densities become correspondingly more complex (Karthikeyan and Tan, 2008). As the measuring volume of the ND-CP traverses through this soil with changing density, the count rate measured corresponds to a measurement of some composite material. If the ND-CP is used to characterize soil with greater heterogeneity, for example, a fill made of lumps, the interpretation of the exact nature of such lumpy fill is more complex. As the density and

thickness of each layer change, the ND-CP measurements will produce a pattern that changes correspondingly. An ability to interpret this signature is essential to the profiling of such soil, which is a major challenge. Any measurement based on observing the radiation emitted in nuclear decay is subject to some degree of statistical fluctuation. These inherent fluctuations represent an unavoidable source of uncertainty in all nuclear measurements and often can be the predominant source of imprecision or error. To account for uncertainty in cone measurement, knowledge of the uncertainties should be understood. In this paper, results from an experimental investigation will be presented to investigate the statistical fluctuation and interpret the density profiles obtained by a nuclear-density cone penetrometer (ND-CP) so as to improve the interpretation of the actual soil profile.

2 DESCRIPTION OF NUCLEAR-DENSITY CONE PENETROMETER (ND-CP)

Figure 1 shows major components of a ND-CP. The lower part of the cone houses various sensors to measure the usual cone parameters, namely, cone resistance (q_c), sleeve friction (f_s) and pore pressure (u_2). The size of the lower part conforms to the standards recommended by the International Society for Soil Mechanics and Foundation Engineering (ISSMFE, 1989) for cone penetration testing and ASTM Standard D 5778. The diameter of the cone is

35.6 mm and the apex angle is 60°. The base area of the cone is 10 cm² and the area ratio, *a*, is equal to 0.75 which is determined from calibration measurement at the laboratory (the effort to eliminate the adverse effects of friction sleeve and unequal cone tip). A porous ceramic filter is located just behind the cone tip. The total length of the shaft housing the sensors is 258 mm. After this, the shaft tapers outwardly at an angle of 15°. The tapered portion of the shaft is 49 mm long, above which the shaft has a constant diameter of 48.6 mm and extends for a total length of 896 mm. This upper part houses the radioisotope source, the detector, and a preamplifier

The ND-CP uses gamma-ray as the source. Gamma rays interact with soil predominantly depending on the level of the energy. The Compton scattering is predominant within an energy range of 600 keV and 1.2 MeV, and is a function of the material density. If the detector is designed to measure only the incoming photons within the range described, then the incoming photons are a function of the density of the material only. The gamma ray source used in the construction of the ND-CP is a Cesium (Cs137) isotope with a half-life of 37.6 years, and the detector is sodium iodide activated with thallium (NaI (TI)) scintillator mounted on a photomultiplier tube. The length of the NaI scintillation detector is 10.2 mm. The separation distance between the source and center of gamma detector is 255 mm. The ND-CP is pushed into the soil layer at a rate of approximately 1 - 2 cm/sec and cone resistance (*qc*), sleeve friction (*fs*), pore pressure (*u*), radioisotope (RI) count are recorded continuously.

The intensity of the radioisotope sources used in these cones is very low compared to the radioisotopes used in medical equipment that pose problems to human health. However, it is still necessary to take precautionary measures to avoid radiation exposure in humans by wearing a lead apron and also by frequent monitoring of radiation exposure using a radiation meter (Dasari et al., 2006).

In using the ND-CP, it is the net above the background (BG) radioisotope count that is used. Thus, a separate reading of this BG count has to be taken either immediately prior or after the test. The

detailed description and working procedure of ND-CP have been discussed by Karthikeyan (2005), Dasari et al. (2006), Karthikeyan et al. (2007) and Karthikeyan & Cisy (2019).

2.1 Procedure for processing the ND-CP results

Current design of the ND-CP requires two probing for every single measuring point, one probing to obtain the background (BG) count of naturally occurring gamma photons and another probing to measure the actual nuclear density (RI) count. The background count is measured using a dummy cone, in which only the detector is placed to measure the naturally occurring gamma photons. This natural radioactive (background) count is a type of noise which must be subtracted from the count measured to give the actual nuclear density measurement. To determine the wet density and water content of soil, the measured raw data needs to be processed for the final profiles through the following steps: (i) depth corrections (ii) noise suppression or elimination (iii) statistical fluctuations and averaging of measured RI cone data. Figure 2 also shows the flow chart for processing of measured RI cone data. The detailed procedures for processing of measured RI cone data will be discussed subsequently in the following section.

2.1.1 Depth corrections

As stated earlier, the upper part of the RI cone houses the radioisotope source, the detector and a preamplifier. The lower part of the cone houses various sensors to measure the usual cone parameters, namely cone resistance, pore pressure and the sleeve friction. Therefore, it is important to correct the measurement of the different sensors reading into the same depth level as the other parameters to ensure proper characterization of soil layers. Therefore, the following depth correction needs to be carried out for raw data for further interpretations. If the measurement center for a RI cone is considered at the cone resistance sensor (load cell), then the other sensors readings are corrected accordingly, for example, the depth of sleeve friction, pore pressure, RI count, BG count are raised about 0.11 m, 0.04 m, 0.60 m and 0.36 m, respectively. The distances are based on the function of the cone design.

2.1.2 Noise suppression or elimination

In several practical cases, it is possible that the depth-meter reading could be affected by either delayed response or disturbing inertial effects, caused, for example, by velocity fluctuations (acceleration, vibrations, and so forth). Hence, it will affect the accuracy of RI cone measurement. To avoid this discrepancy in the RI cone results, it is important to measure the RI Count and BG Count in both penetration and uplift stage so that the retardation error can be pointed easily. The “analog recording” of the density–depth profile

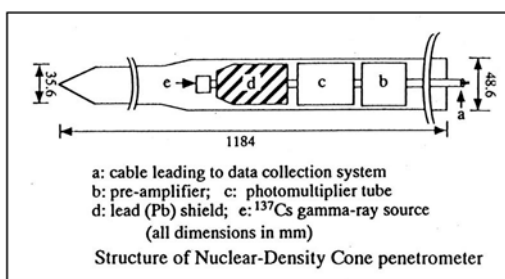


Figure 1. Diagram of Nuclear-Density Cone Penetrometer (ND-CP). (after Shibata et al., 1993 and Dasari et al., 2006).

then will show “retardation hysteresis” loops, which enclose the representative density profile. Figure 3 shows the typical BG count profile measured for both penetration stage and uplift stage profile. From the figure, it can be seen that there is an abnormal behavior observed in the penetration stage measurement due to undesirable shock. These undesirable shocks can be removed by comparing with the uplift stage measurement. Figure 3 illustrates the typical BG count profile after elimination of the undesirable noise.

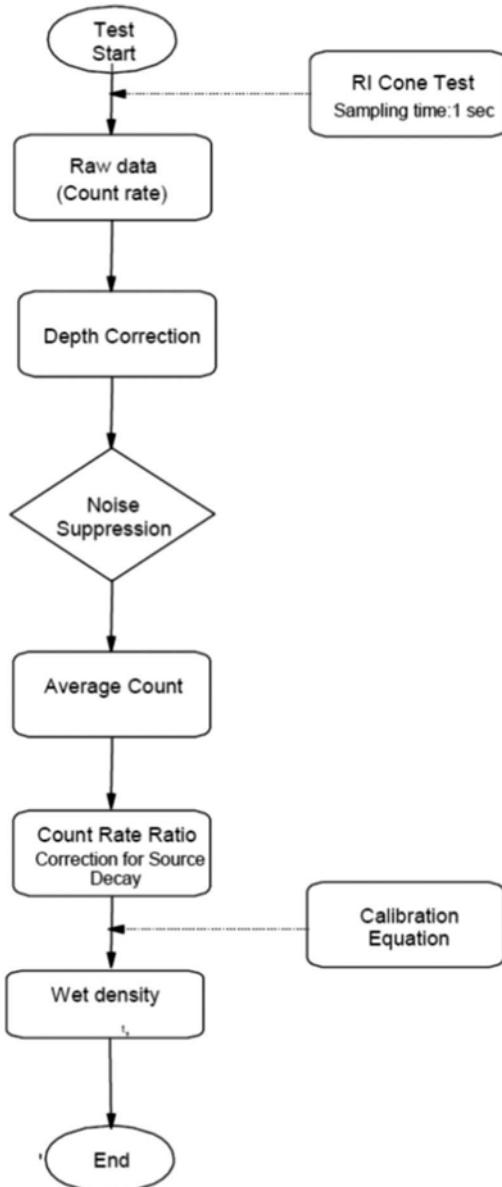


Figure 2. Flow chart for processing the RI cone results.

2.1.3 Averaging of measured RI cone data

Radioactive decay is a random process. Consequently, any measurement based on observing the radiation emitted in nuclear decay is subject to some degree of statistical fluctuation. These inherent fluctuations represent an unavoidable source of uncertainty in all nuclear measurements and often can be the predominant source of imprecision or error (Knoll, 2000). The source-originated fluctuations affect the precision of the RI cone. The error in density/water content due to these fluctuations can be minimized by designing equipment such that the radioactive count is high. Many sources of uncertainties can be reduced with increased sampling and good practices, but due to the nature of geomaterials, inherent uncertainties cannot be eliminated. Inherent uncertainties can be quantified by a statistical analysis. The error can also be minimized by decreasing the statistical fluctuation through filtering data over a short depth. Nobuyama (2000) reported that the RI cone measurement needs to be averaged over a depth in order to reduce the statistical fluctuation. To re-evaluate the statistical fluctuation of RI cone measurement, a laboratory counting experiments is carried out and discussed in the following paragraphs. The understanding of these statistical fluctuations is also important in the interpretation of the ND-CP results for highly heterogeneous soils.

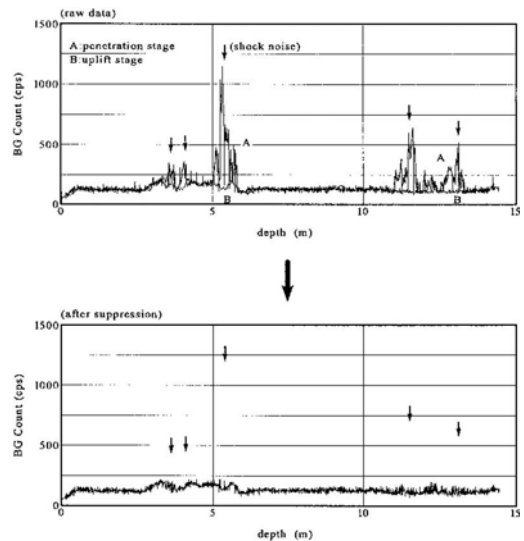


Figure 3. An example of Noise Suppression or Elimination (after Nobuyama, 2000).

3 EXPERIMENTAL SETUP

An experimental setup was designed for studying the statistical fluctuation of wet profile measured by ND-CP. A series of laboratory counting experiment was carried out using the ND-CP under identical conditions. One of the controlling factors is the size of the

laboratory calibration chamber. The density is measured using a source and detector. The signals from the source interact with soil and the modified signals are captured by the detector. The degree of modification of the signals is a function of material property. RI cone measurements (density) are evaluated in an extended volume around the central point of the radioactive source and detector configuration, which is called the “measuring volume”.

Based on the theory of gamma scattering and neutron methods, the “measuring volume” around the source was found to be about 30 cm radius. Karthikeyan and Tan (2008) reported that the maximum radius of the influence zone for ND-CP is 23.6 cm when used in water and it decreases with increasing wet density of the material. It was also established that the ND-CP measurement provides the average wet density of the composite soil within the measuring volume.

Therefore, a stainless-steel chamber with diameter of 700 mm and height of 1000 mm was used for the experiments. This calibration chamber was filled with water and the ND-CP was kept inside at the centre of the calibration chamber to measure the statistical fluctuations of RI Count and BG Count under identical condition.

4 STATISTICAL FLUCTUATION OF ND-CP

Figure 4 shows the typical variations of RI count and BG count data measured in water under ideal condition. There are 121 separate measurements, each taken at a 1 sec interval. When the measurements were being made during the 121 secs, the source of the radiation was ‘steady’. The source of the radiation did not change in its nature. Nevertheless, the number of counts recorded per sec is clearly not constant. This is the statistical nature of ND-CP measurement.

The frequency of occurrence of an error of any given magnitude can be calculated for a given determination by the application of the laws of probability. Various distribution laws are used to relate the magnitude of a deviation from true average and the number of events which experiences that particular deviation. The normal distribution is useful for describing the spread in data occurring in various aspects of nuclear-radiation detection (Price, 1964; and Tsoufanidis, 1995). The extent of the statistical fluctuations about the true mean may be expressed in terms σ , the standard deviation and is approximated by normal distribution (Nobuyama, 2000). The standard deviation is defined as the square root of the scatter data about the mean value. The standard deviation is used commonly to indicate the accuracy with which a sample of a given size can estimate the mean value of test results. The coefficient of variation, COV, is another measure of variability of a sample and is defined as the ratio between the standard deviation and mean value. The COV expresses the magnitude of variability as a fraction or as a percentage of the mean value. This facilitates comparison of data from different samples

because the mean and standard deviation tend to change together, so typically the coefficient of variation remains fairly stable (Snedecor and Cochran, 1989).

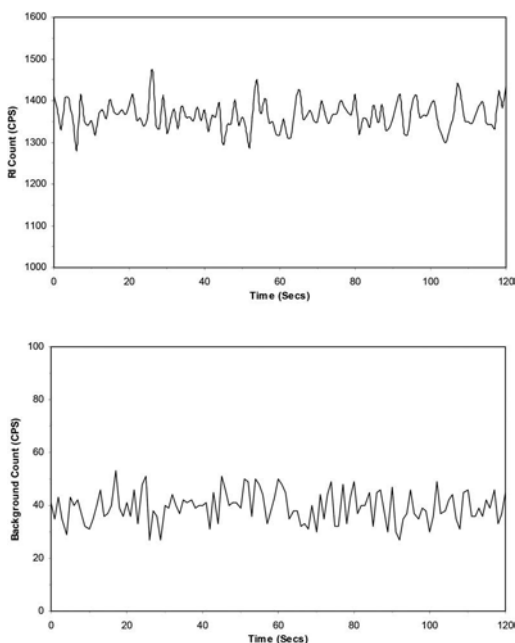


Figure 4. Typical variations of RI Count and BG Count data measured in water under ideal condition.

Figure 5 illustrates the form of normal distribution along with its mean and standard deviation of measured RI count and BG count data. This figure show that the amount of fluctuations present in the ND-CP measurements can be approximated by Normal or Gaussian distribution. It is also noted that the ND-CP measurements fluctuate within the range of \pm (twice of the standard deviation, σ) from its mean value. The coefficient of variation for RI count and BG count data's is 2.4% and 15.1% respectively. Nobuyama (2000) reported that the error could be minimized through filtering the data over a short depth. For this, the moving-average technique has been employed for the measured raw data at different time intervals.

Figure 6 shows the changes in COV for different moving-averaging interval for RI Count and BG count data. From the figures, it can be seen that the COV decreases with increasing moving-average time interval. It is also inferred from Figure 6 that the COV is fairly constant after a moving-average interval of 6 secs to 7 secs. This further confirms that the averaging or filtering of wet density profiles measured by ND-CP is necessary to reduce the statistical fluctuations.

In field test, the ND-CP was pushed into the ground at a rate of approximately 1.5 cm/sec, and thus it will cover a distance of 10 cm within 6 – 7

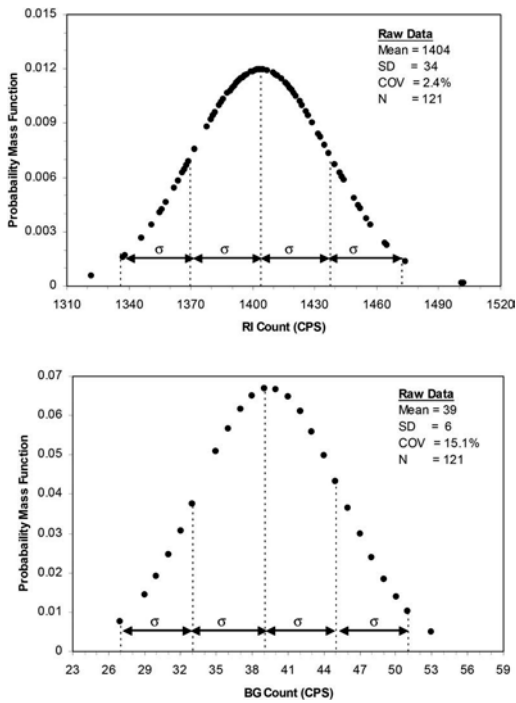


Figure 5. Illustrating the statistical fluctuations of RI Count and BG Count data in the form of normal distribution along with its mean and standard deviation (σ) (a) RI Count (b) BG Count.

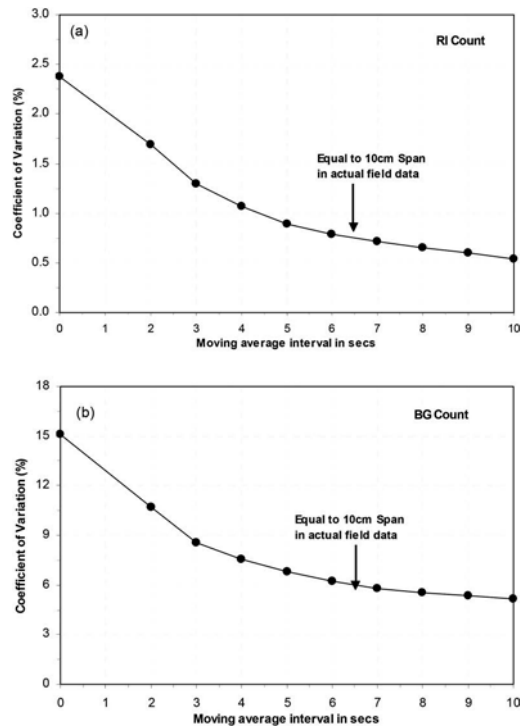


Figure 6. Changes in COV with different moving averaging intervals (a) RI Count (b) BG Count.

secs. While comparing the BG count with RI count in water, the BG count is too small, and it is almost equal to the minimum detectable count of ND-CP. Therefore, if the effect of the BG count is neglected, as can be seen in Figure 6 (a) the error due to the statistical fluctuation in ND-CP measurement is less than 1% if an averaging span of 10 cm is used. This can be also demonstrated using the field results shown in Figure 7 (a) and (b) which were obtained by averaging over 5 cm and 10 cm depths respectively. The raw data are also shown for comparison purpose. As can be seen, when averaged over 10 cm depth, the RI cone profile count distribution trend is not distorted or deformed compared to the original raw data, which means the loss of information about the density and moisture through the filtering is negligible. This filtering is necessary to smooth the density profile. Therefore, the RI cone measurements that are reported subsequently are averaged over a span of 10 cm depth to minimize the statistical fluctuations.

5 CONCLUSIONS

This paper describes research conducted to investigate the statistical fluctuation and interpret the density profiles obtained by a nuclear-density cone penetrometer (ND-CP) so as to improve the

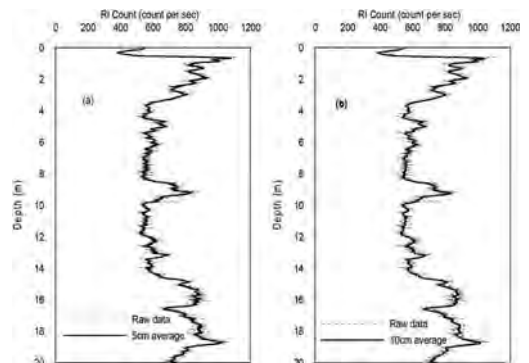


Figure 7. Comparison of measured ND-CP raw data and averaged data (a) 5 cm average span (b) 10 cm average span.

interpretation of the actual soil profile. The laboratory results show that the amount of fluctuations present in the ND-CP measurements can be approximated by Normal or Gaussian distribution. It was also found that the averaging or filtering of wet density profiles measured by ND-CP is necessary to reduce the statistical fluctuations. It was found that the error due to the statistical fluctuation in ND-CP measurement is less than 1% if an averaging span of

10 cm is used. The raw data obtained from the field results when averaged over 10 cm depth shows that the cone profile count distribution trend is not distorted or deformed compared to the original raw data, which means the loss of information about the density through the filtering is negligible. This averaging is necessary to smooth the measured wet density profile. Therefore, the ND-CP measurements are averaged over a span of 10 cm depth to minimize the statistical fluctuations.

REFERENCES

- Dasari, G. R., Karthikeyan, M., Tan, T. S., Mimura, M. and Phoon, K.K., (2006). "In situ evaluation of radioisotope cone penetrometers in clays", *Geotech. Test. J.*, Vol. 29, No. 1, pp. 45–53.
- ISSMFE, (1989). "International reference test procedure for cone penetration test (CPT)", In Report of the ISSMFE Technical Committee on Penetration testing of soils –TC 16, with references to test procedures, Swedish Geotechnical Institute (Linkoping), Information, Vol. 7, pp. 6–16.
- Karthikeyan M. (2005). Application of Radioisotope Cone Penetrometer to characterize a lumpy fill, PhD Dissertation, National University of Singapore, 219p.
- Karthikeyan, M, Dasari, G.R., Tan, T.S., Lam, P.W., Loh, Y.H. Wei, J. and Mimura, M. (2001). "Characterization of a reclaimed land site in Singapore", Proceedings of 3rd International Conference on Soft Soil Engineering, Hong Kong, 6 – 8 December 2001, pp. 587–592.
- Karthikeyan, M., Dasari, G.R. and Tan, T.S., (2004). "In situ characterization of land reclaimed using big clay lumps", *Canadian Geotech. J.*, Vol. 41, No. 2. pp. 242–256.
- Karthikeyan M., Tan T.S., Mimura, M., Yoshimura, M. and Tee C.P. (2007). "Improvements in Nuclear-Density Cone Penetrometer for Non-Homogeneous Soils", *Soils Found.*, Vol. 47 No. 1, pp. 109–117.
- Karthikeyan, M. and Tan, T.S (2008). Profiling of Heterogeneous Soil Using Nuclear-Density Cone Penetrometer. *Geotechnical Testing Journal*, American Society of Testing Materials, Vol.31, No. 6, pp. 513–525.
- Knoll, G.F. (2000). Radiation detection and measurement, Third Edition, John Wiley and Sons, 801p.
- Nobuyama, M. (2000). The result of the RI cone penetration tests. NUS internal report no 6004998/264 submitted by Soil and Rock Engineering Co. Ltd., Japan. 2000.
- Price, W. J. (1964) Nuclear radiation detection. Second Edition, McGraw-Hill Book Company, 430p.
- Rui J, Hino T, Chai J, Hamada, T, Yoshimura, M. (2013). Interpretation of density profile of seabed sediment from Nuclear density cone penetration test results, *Soils and Foundation*, Volume 53, No.5, pp.671–679.
- Shibata, T., Mimura, M. and Shrivastava, A.K., (1993). "RI cone penetrometer experience in marine clays in Japan", Proceedings of the 4th Canadian Conference on Marine Geotechnical Engineering, St. John's Nfld., 27-29 September 1993. Vol. 3, pp.1024–1033.
- Snedecor, G.W and Cochran, W. G. (1989) *Statistical Methods*, 8 ed. Ames: Iowa State Univ. Press.
- Tan, T. S., Karthikeyan, M., Phoon, K. K., Dasari, G. R., and Mimura, M., (2004), "Use of a Radioisotope Cone to characterize a lumpy fill," Proceedings of the Second International Conference on Geotechnical and Geophysical Site Characterization, ISC-2, Porto-Portugal, 19–22 September 2004, Vol. 1, pp. 801–808.
- Tsoufanidis, N. (1995). *Measurement and detection of radiation*, Second Edition Taylor and Francis, 614p. 1995.

On the accuracy and precision of the seismic cone penetration test – a field test study on the seismic source

O. Koreta, A.H. Augustesen & L. Krogh

Ørsted

K. Lundvig & S. Bøtker-Rasmussen

Geo

ABSTRACT: The seismic cone penetration test (SCPT) is one of the most frequently used *in situ* testing methods for deriving the small strain shear modulus. Offshore SCPT results often present large scatter, in particular when data are obtained with different operational setups. No standard or industry consensus exist in terms of requirements to system key characteristics, operational testing procedures, interpretation and the numerical quality control of the traces obtained. Seismic sources currently deployed as part of the offshore industry practice have been developed individually by the various suppliers. This paper presents the findings of an onshore experimental study with the objective to increase the understanding of the influence of the offshore seismic source setup on SCPT results under controlled operational procedures. Accuracy and precision of the SCPT are investigated as part of the study.

1 INTRODUCTION

With the expansion and development of the offshore wind industry, the small strain stiffness (G_{max}) has become a key parameter for offshore wind facility designs, especially for the design of monopile foundations. G_{max} can be derived from laboratory and *in situ* tests.

The seismic cone penetration test (SCPT) is a cost-effective *in situ* technique used to derive G_{max} , through the measurement of the velocity (V_s) of propagating shear waves. The SCPT was initially developed for onshore use with simple beam sources equipped with sledge hammers. In contrast, the offshore seismic sources are complex electro-mechanical systems and the SCPT offshore is associated with additional challenges compared to the onshore source; less control of the source orientation and contact with the seabed (detached sources) and difficulties in isolating the background noise originating from the vessel, umbilical or drill string (source attached to the frame).

The offshore seismic sources are designed and built individually by the suppliers. The main differences between the various offshore applications involve a) method of deployment, b) source characteristics (frequency, energy, geometry, horizontal distance between source and SCPT, orientation, method of contact), c) type of triggers (contact, sensor), d) type and distance between receivers (geophone, accelerometers) e) acquisition system and f) method of interpretation.

Most of the details concerning the listed system parameters are not standardized in ISO (2014).

This implies that the acquisition of SCPT data offshore suffers from a) a significant degree of scatter (Gibbs et al. 2018, Masters et al. 2019), b) challenges to acquire reliable data at large scale c) challenges to replicate results in a consistent manner, d) lack of numerical control and acceptance criteria, e) inefficient operational procedures. Furthermore, a key concern remains the quantification of the measurement uncertainty, i.e. accuracy and precision of the measurements.

An onshore field test study was performed with the key objective to increase the understanding of the influence of the offshore seismic source setup on SCPT results under controlled operational procedures. Furthermore, accuracy and precision were investigated as part of the study. The high-level scope of work compares performance of adjacent SCPTs using an offshore and an onshore seismic source, each with a different frequency content, recorded with the same receivers at the same SCPT location.

As no standard reference test exists for the SCPT, the accuracy cannot be known exactly. However, a series of laboratory (bender element and resonant column testing) and alternative *in situ* (seismic dilatometer, SDMT and multichannel analysis of surface waves, MASW) stiffness measurements were performed to validate and benchmark the SCPT results. This paper presents the background, the test program, and relevant results from the field test study.

2 BACKGROUND

Campanella et al. (1986) presented the SCPT for offshore applications. However, there are no comprehensive studies on the evaluation of accuracy and precision of modern offshore seismic sources. In contrast, extensive studies have been performed in relation to the repeatability of the onshore source (beam) setup (e.g. Rice, 1984, Campanella & Robertson, 1984, Robertson et al., 1986).

Rice (1984) developed a beam source (sledge hammer), with a length between 2-3 m, loaded using a weighted plank such as a CPT rig vehicle. High quality and polarized signals could be achieved to a depth of 30 m without stacking the signals.

Laing (1985) confirmed the results using the source proposed by Rice (1984) and concluded that the beam source produced strong, directional, and repeatable shear waves. The beam source is used nowadays as a common form to generate shear waves (ASTM 2019). As a consequence of preceding literature studies, the beam source is used as benchmark for the results from the offshore source.

Gillespie et al. (1985) and Gillespie (1990) investigated the repeatability of V_s from SCPT through a series of onshore testing at three Norwegian research sites, Onsøy and Drammen (clay sites) and Holmen (sand site). The tests were performed using a beam source, with the same characteristics as described by Rice (1984).

Three adjacent SCPT tests at the clay sites showed agreement within $\pm 5\%$ of the measured V_s . In sand, the V_s was more scattered, visually exceeding a variation of $\pm 10\%$, which was attributed to the variation of cone resistances between adjacent tests.

Gillespie (1990) concluded that ensuring a close contact between source and ground will significantly improve the quality of the signal and subsequently the identification of the arrival times. The error on the V_s was found to be as low as $\pm 2\%$ for a V_s of 200 m/s. The depth control of the test was shown to induce an additional error of up to $\pm 5\%$.

3 TESTING PROGRAM

3.1 Site conditions

The test site is located in a sand pit near Kongensbro west of Aarhus, Denmark. The soil conditions were initially confirmed by a CPT (CPT2) and an adjacent borehole (BH1) to depths of 20 m and 17 m, respectively (Figure 3). The ground water table (GWT) was constantly monitored at a depth of 0.6 m during the test period. The soil comprises of a 0.3 m thick layer of sand fill overlying a medium to coarse medium dense sand to a depth of 11.5 m. The sand is uniformly graded. A layer of marine clay continues to the end of the BH/CPTUs. The CPTUs show uniform soil conditions with some local variations in the cone resistances

Table 1. Summary of soil parameters.

Soil type	Depth	Fines content	Plasticity index	Undrained shear strength	Peak Friction angle
	m	%	%	kPa	°
Sand	0.0-11.5	1-5	-	-	33-39
Clay	11.5-20.0	-	18-28	200-270	-

(Figures 8-9). A summary of classification and strength parameters is provided in Table 1.

3.2 Equipment and test setup

The SCPTs were conducted using Geo's CPT crawler rig with a maximum thrust capacity of 20 tonnes (Figure 1). The 10 cm² seismic module consists of a dual receiver array spaced at 0.5 m distance and equipped with triaxial accelerometers. The SDMT consists of a dual accelerometer dilatometer.

The onshore source is a timber beam with a length of 3.5 m equipped with steel plates at both ends. The two steel hammers (left and right) have each a length of 1 m and a weight of 12.8 kg. The offshore seismic source is a dual-hammer source designed and built by Geo. The total weight is 1300 kg and the sampling frequency is 5000 Hz.

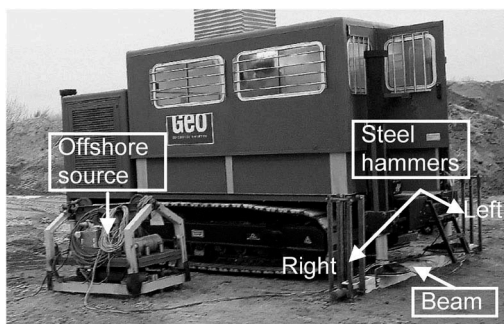


Figure 1. Photo from the field test setup (main configuration).

To obtain comparable testing conditions, both seismic sources were placed with their centers at a distance of 2.6 m from the SCPT (Figure 2). The respective orientations of both sources and hammer directions (left and right) were kept consistent for all tests.

3.3 Test program

The test program comprised three clusters of tests, equally distributed in a 3 m radius around the center (Figure 3). Three SCPT tests were performed for

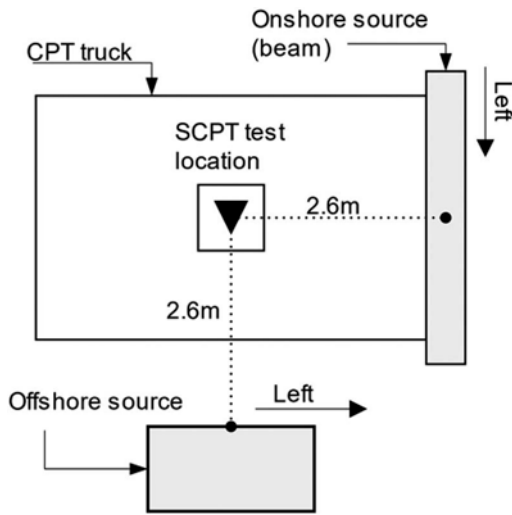


Figure 2. Seismic test setup (main configuration).

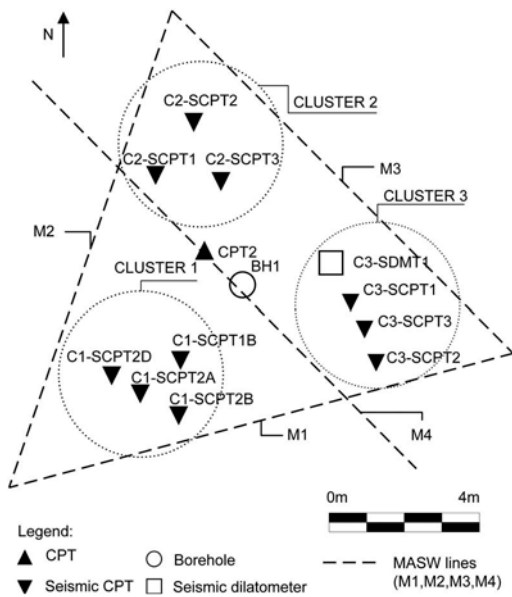


Figure 3. Detailed field test program.

each cluster and the signals were recorded in sequence from both seismic sources. One SDMT test was performed in Cluster 3 and four MASW lines (M1 to M4) were run in a triangular setup within the same area. The target penetration depth for SCPT tests was 15 m. The SCPTs at Clusters 1 and 2 were scheduled for assessing repeatability and reproducibility of the measured V_s . With reference to the tests performed in cluster 2, Figure 4 shows the approaches used for clusters 1 and 2.

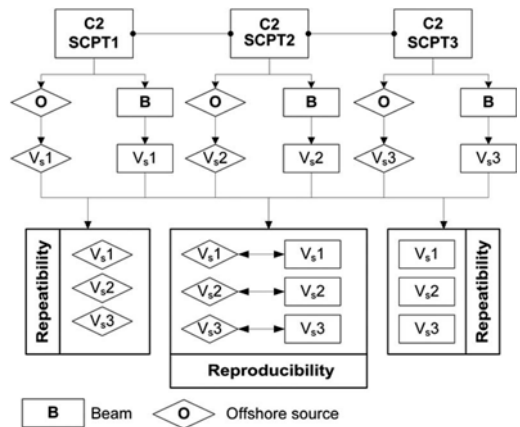


Figure 4. Test program for Cluster 2 illustrating the approach for assessing repeatability and reproducibility.

The repeatability was investigated by comparing results from multiple adjacent SCPT tests from the same source (being either the offshore or onshore beam source). The reproducibility was investigated through variations in the results as a consequence of using two different sources for generating the shear waves (each with a different frequency content) recorded with the same receivers at the same SCPT location.

Two SCPTs in Cluster 3 aimed to investigate the effect of source distance by changing the horizontal distance between the offshore source and the SCPT. Distances of 5 m (C3-SCPT1) and 10 m (C3-SCPT2) were adopted. The remaining test (C3-SCPT3) aimed to investigate the effect of cone size on the SCPT results by using a 15cm² cone. This test was unfortunately aborted after cone refusal on a stone.

Laboratory and other *in situ* (SDMT and MASW) tests were performed for benchmarking the SCPT results. The SDMT was performed using a different set of receivers. A total of 15 bender element (BE) tests (vertically propagating, horizontally polarized waves) were performed in conjunction with isotropically consolidated triaxial tests (CID). The shear wave velocity (V_s) was measured at five different frequencies at the target consolidation stress to estimate the optimal frequency and the peak-to-peak and zero crossing methods were adopted to interpret the traces. In addition, two resonant column (RC) tests were performed.

4 RESULTS

4.1 Quality assessment

The interval V_s has been calculated from left and right shots using traces that met certain quality requirements only. Figure 5 shows an example of a representable signal of acceptable quality. The Seismic Trace Characterization (STC), as proposed by

Baziw & Verbeek (2017), has been performed on all traces to evaluate the quality of the signals. The data quality varies from acceptable (Class C) to very good (Class A). The quality of traces at shallow depth (less than 2 m) has been problematic to unacceptable (Class D, F) for both sources. However, in general a higher signal quality is observed from the beam source compared to the offshore source.

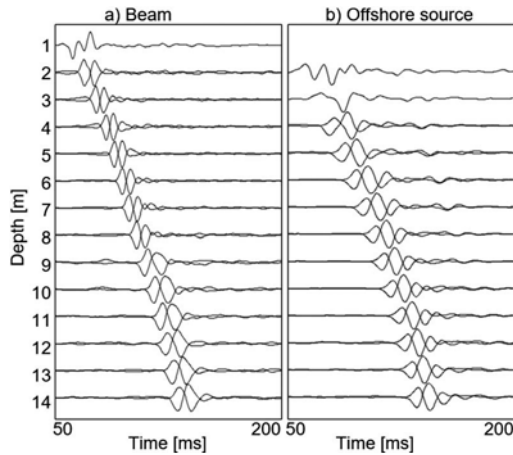


Figure 5. Seismic signals for C2-SCPT3 from both sources.

4.2 Uncertainties

The key input to the determination of V_s includes travel time and travel distance. They are susceptible to uncertainty originating from the specific system characteristics, including sampling frequency, trigger repeatability, data filtering, depth uncertainty, etc.

For a given sampling frequency, the error induced on V_s can theoretically be expressed as a function of V_s and the distance between receivers as presented and demonstrated by Rice (1984). Adopting Rice's approach to the SCPT data in this study, Figure 6a shows that for a sampling frequency of 5 kHz and a distance between receivers of 0.5 m, the error on V_s varies from 4% to 12%. Figure 6b shows that in order to reduce the V_s error to 10% (accuracy requirements according ISO 2014), the sampling frequency must be increased to 6 kHz. Alternatively, the accuracy can be increased by increasing the distance between receivers for the same sampling frequency.

The error induced on V_s due to trigger repeatability has been assessed by comparing the arrival times between stacked and multiple unstacked signals at the same depth. The offset between relative arrival time should be less than 1%, as recommended by ASTM (2019). For the range of measured V_s at the site, the error due to trigger repeatability is assessed to a maximum of $\pm 2\%$. This error is reduced to zero when V_s is calculated from traces generated by the same shot in a dual array setup.

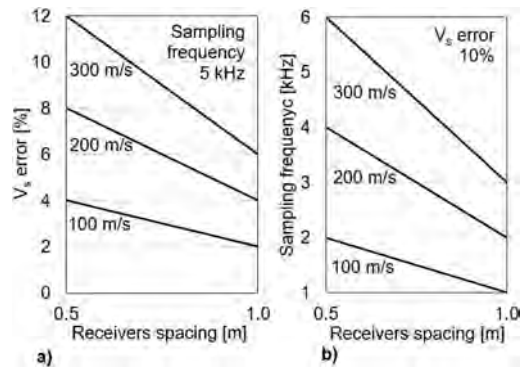


Figure 6. Induced error on V_s as function of sampling frequency, distance between receivers and soil V_s (maximum measured V_s is 300 meter per second, m/s).

Bandpass filters have not been applied on the acquired data. However, the application of filters close to the dominant frequency (60 Hz to 80 Hz for the offshore source) can cause a phase shift and induce an additional error to V_s . The time shift caused by the application of a low pass filter can be estimated based on Rice (1984). For the project presented in this paper, an application of a low pass filter with a cut-off frequency of 60 Hz is expected to induce an error larger than 10% for a V_s equal to 200 m/s.

The depth accuracy of the CPT rig is estimated to be better than 1%. In general, the uncertainty in the depth penetration for push systems is determined with high accuracy.

The uncertainties on V_s related to the interpretation method depend primarily on the data quality and on the assumed travel path. As described by Lunne et al (1997), correction of the travel path due to refraction can have a considerable impact on V_s . According to Laing (1985), the straight-line approximation is satisfactory for calculation of V_s when the angle of travel path is higher than 45° . Hence, for depth shallower than the horizontal source distance, refraction of shear waves along the soil boundaries is likely to occur.

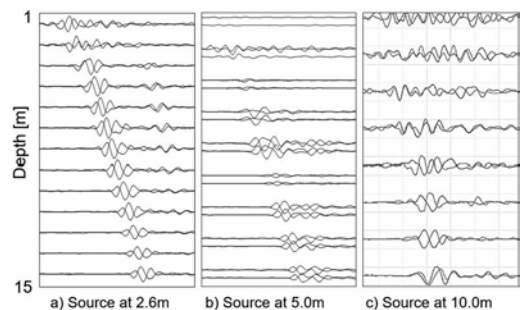


Figure 7. Illustration of seismic traces at Cluster 3, for three considered offshore source distances.

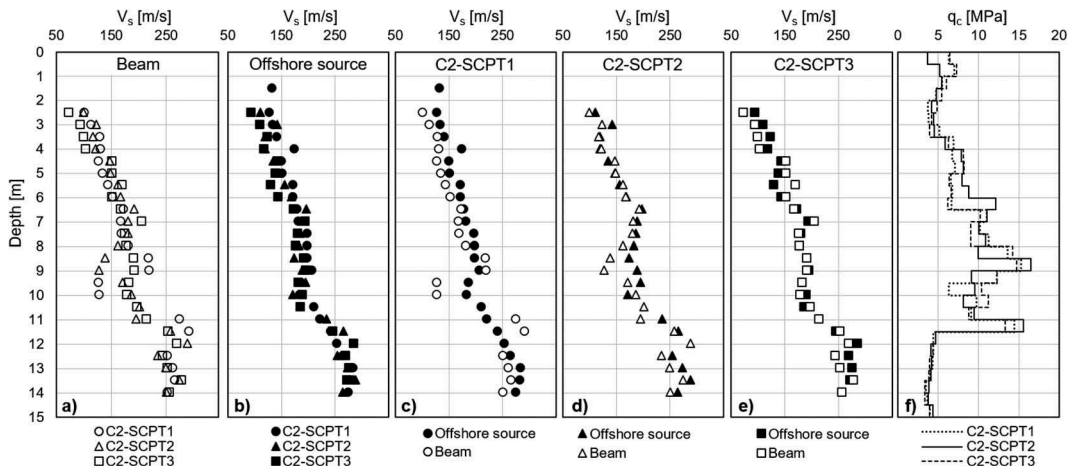


Figure 8. Comparison of the SCPT measured V_s at Cluster 2 between Beam (onshore source) and Offshore source.

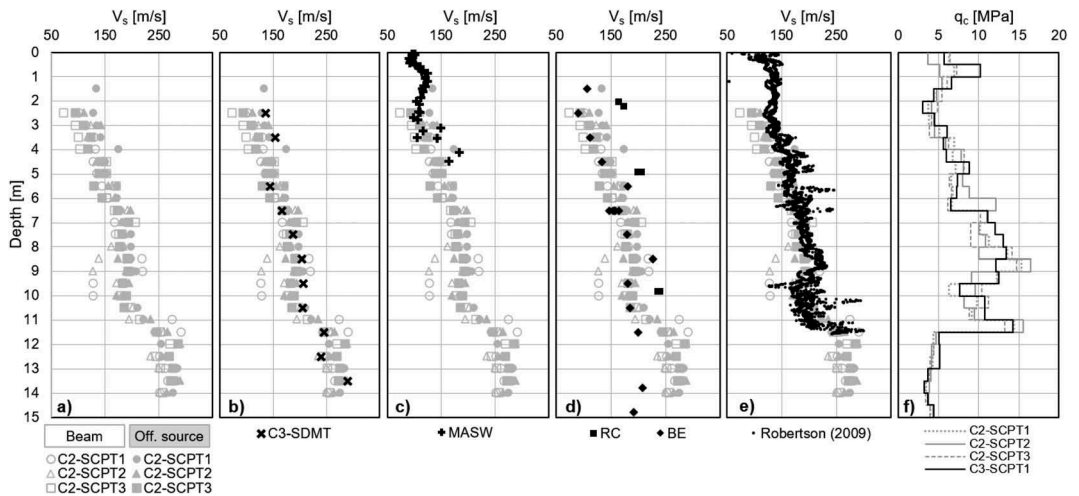


Figure 9. Comparison of the measured V_s at Cluster 2 between SCPT, seismic dilatometer (SDMT), multichannel analyses of surface waves (MASW), bender elements (BE), resonant column (RC), correlation from CPT data using Robertson (2009) correlation.

The impact of the horizontal distance between the seismic source and the SCPT was investigated by placing the offshore source at different distances of 2.6 m, 5.0 m and 10.0 m to the SCPT. Figure 7 shows the signal quality (signal-to-noise-ratio) decreasing with increasing distance. The results are in line with the findings by Rice (1984).

4.3 Repeatability and reproducibility

Figures 8a-f present the comparison of the derived V_s from the different sources for Cluster 2. Figures 8a and b indicates a good repeatability for both sources, with an average coefficient of variation

in V_s of up to $\pm 10\%$. Locally, the variation of certain V_s measurements exceeds $\pm 20\%$ (8–10 m depth). This difference cannot immediately be explained by the data. However, the larger variation in V_s is reflected by correspondingly larger variations in cone resistances (q_c), indicating that differences in V_s from the two sources are likely also reflecting local changes in geology. No obvious differences were observed in the variation in V_s between the sand and the clay. The repeatability of V_s for both clusters is similar and is summarised in Table 2.

The reproducibility of V_s is found reasonable for Cluster 2, with a variation from $\pm 6\%$ to $\pm 11\%$ (Figures 8c-e). The differences observed for the two

sources cannot be attributed to the geology as the tests were performed at the same position. However, the individual travel paths of the shear waves may be subject to local soil variations. Another factor contributing to the reproducibility is the trigger timing. It appeared challenging in the field to run the trigger signal from both sources simultaneously, using the same software. Table 3 presents similar reasonable reproducibility of V_s for both clusters. In general, both repeatability and reproducibility of the sources show an average variation of about $\pm 10\%$.

Figures 9a-f compares SCPT results for Cluster 2 with SDMT, MASW, BE and RC test results as well as V_s based on Robertson (2009).

Table 2. Source repeatability.

Cluster	Beam	Offshore source
	%	%
Cluster 1 (SCPT1 vs SCPT2)	± 9	± 8
Cluster 2 (SCPT1 vs SCPT2 vs SCPT3)	± 10	± 7
Average all tests	± 10	± 8

Table 3. Source reproducibility.

	Cluster 1 SCPT		Cluster 2 SCPT			Average
	1	2	1	2	3	All tests
Sources	%	%	%	%	%	%
Beam vs Off. source	± 11	± 9	± 11	± 6	± 6	± 10

Figure 9b illustrates the results of using a set of different receivers on the SDMT and confirms the assumption that V_s is independent of the recording equipment (receivers), which is in accordance with similar findings from McGillivray & Mayne (2004).

MASW data is uniform and overlaps the SCPTs in the depth range of 1.5 m to 4.5 m. V_s measured from BE test is comparable with SCPT measurements for the sand, whereas the RC tests return higher values. The range of V_s from all measurement are similar and representative of the soil conditions.

5 CONCLUSIONS

The small strain stiffness (G_{max}) has become a key parameter for offshore wind facility designs, especially for the design of monopile foundations. Hence, accurate and precise measurements of G_{max} is important. For

position-specific wind turbine foundation designs, G_{max} is traditionally determined from SCPTs. However, the performance of SCPTs are affected by a number of factors associated with the seismic source and with the operational setup in general. Therefore, the repeatability and reproducibility of offshore SCPTs have been observed to relatively low compared to an onshore setup. The main objective of this study was to obtain an understanding of the impact of the offshore seismic source setup on SCPT results and to understand the challenges with the existing setups and hence shed light on the scatter observed offshore. Therefore, two different sources were used in a sand pit in Denmark. The SCPT results using an offshore source were benchmarked against the SCPT results using an onshore source. The results show that under reasonably controlled operational conditions and when potential sources of errors are taken into account, the SCPTs can be satisfactorily repeated and reproduced with a variation of $\pm 10\%$, using both onshore and offshore sources. Careful preparation and execution of the SCPTs are essential. Especially it is deemed necessary to a) obtain a good contact between the ground and the source, b) orientate the source towards the receivers to maximise the signal amplitude in one direction, and c) position the source horizontally. Furthermore, key system characteristics (sampling frequency, trigger repeatability) play an important role in the accuracy of the measured shear wave velocity.

ACKNOWLEDGMENT

The research presented herein was performed as a Joint Industry Project (JIP) carried out between Ørsted and Geo. The care and effort exerted by both parties during testing are highly appreciated.

REFERENCES

- ASTM D7400 2019. Standard test methods for downhole seismic testing.
- Baziw, E.J. & Verbeek, G. 2017. Quality assessment of seismic data sets and the impact on interval velocity estimates. In *Proceedings of DFI 42nd Annual Conference on Deep Foundations*. Article 2821.
- Campanella, R.G. & Robertson, P.K., 1984. A seismic cone penetrometer to measure engineering properties of soil. In *SEG Technical Program Expanded Abstracts 1984*: 138–141.
- Campanella, R.G., Robertson, P.K. & Gillespie, D. 1986. A seismic cone penetrometer for offshore applications. In *Oceanology*: 479–486.
- Gibbs, P., Pedersen, R.B., Krogh, L., Christopher, N., Sampurno, B. & Nielsen, S.W. 2018. Challenges in marine seismic cone penetration testing. In *Cone Penetration Testing 2018*: 303–308.
- Gillespie, D., Lunne, T. & Campanella, R.G. 1985. Tests with UBC seismic cone at three Norwegian research sites. *Report No. 59040, 1*. NGI.
- Gillespie, D.G., 1990. *Evaluating shear wave velocity and pore pressure data from the seismic cone penetration*

- test (Doctoral dissertation, University of British Columbia).
- ISO 19901-8 2014. Petroleum and natural gas industries - Specific requirements for offshore structures - Part 8: Marine soil investigations.
- Laing, N.L. 1985. *Sources and receivers with the seismic cone test, MASC* (Doctoral dissertation, Thesis, Dept. of Civil Eng., Univ. of British Columbia).
- Lunne T., Robertson P. & Powell J. 1997. *CPT in geotechnical practice*. New York: Blackie Academic.
- Masters, T.A., Juskiewicz, P., Mandolini, A. & Christian, H. 2019. A critical appraisal of the benefits of and obstacles to gaining quality data with offshore seismic CPT and PS logging. In *Offshore Technology Conference*. Article 29485.
- McGillivray, A. & Mayne, P.W. 2004. Seismic piezocone and seismic flat dilatometer tests at Treporti. In *Proc. 2nd Int. Conf. on Site Characterization 2*: 1695–1700.
- Rice, A.H. 1984. *The seismic cone penetrometer* (Doctoral dissertation, University of British Columbia).
- Robertson, P.K. 2009. Interpretation of cone penetration tests—a unified approach. *Canadian geotechnical journal*, 46(11): 1337–1355.
- Robertson, P.K., Campanella, R.G., Gillespie, D. & Rice, A. 1986. Seismic CPT to measure in situ shear wave velocity. *Journal of Geotechnical Engineering*, 112(8): 791–803.

The revival of multiple pore pressure measurements in the cone penetration test

T. Lunne

Norwegian Geotechnical Institute, Oslo, Norway

R.K. Ghanekar

Consultant, Panvel, India

G.W. Tucker, R. Santos & L. Krogh

Ørsted, Denmark

ABSTRACT: In common practice the most usual positioning of the filter location for the piezocone (CPTU) is at the cone shoulder (u_2) which is recommended by ISO 19901-8:2014 and ISO 22476-1:2012. However, these ISO standards allow additionally for pore pressure measurements to be taken at the cone face (u_1) or behind the friction sleeve (u_3). The triple element piezocone (CPTU3) offers a solution whereby measurements of pore pressure can be taken simultaneously at all three locations. By taking these three pore pressure measurements the soil behaviour classification may be enhanced by interpretation in terms of c_h from u_1 , u_2 and u_3 and by correlations to overconsolidation ratio (OCR) and lateral stress ratio (K_0). In this paper the correlations to OCR are explored by establishing a database from historical data as presented in international geotechnical literature.

1 INTRODUCTION

The pore pressure measurement taken using the piezocone (CPTU) can be recorded with depth or as dissipation over time when penetration is paused. The most common pore pressure measurement is behind the cone shoulder (u_2), as preferred by ISO 19901-8:2014 and ISO 22476-1:2012. However, these ISO standards allow additionally for penetration pore pressure measurements to be taken on the cone face (u_1) or behind the cone sleeve (u_3) as shown in Figure 1. The so-called triple element piezocone (CPTU3) was used by several researchers in the 1980s and 1990s but has seen very little use in the last 25 years. The available literature indicates that CPTU3 has considerable potential relative to the standard CPTU including:

- Correction of sleeve friction (f_s) for pore pressure effects
- Increased reliability of assessment of horizontal coefficient of consolidation (c_h) from three sets of dissipation tests
- Evaluation of drainage conditions around the cone – especially for intermediate soils where partial drainage occurs
- Improved layering detection using u_1 compared to u_2

- Enhanced correlations to stress history and in situ horizontal stress

This paper explores the last aspect of correlations to stress history by developing a database from available CPTU3 tests published mainly in the 1980s and 1990s. First a review of the earlier reported use of pore pressures in connection with CPT is made.

2 HISTORY OF PORE PRESSURE MEASUREMENT IN THE CPT/CPTU

Pore pressure measurement during penetration of a probe was introduced in the 1970s (Janbu & Senneset, 1974, Torstensson, 1975, Wissa et al., 1975). The pore pressure probe used by Janbu & Senneset (1974) resembled an electrical cone, with the same area at the base of the cone. The other probes had different geometries and dimensions, but all had cylindrical porous elements. From the beginning, the large potential of such probes was recognised. At that time, CPTs and pore pressure probe tests were performed in adjacent deployments, for instance Janbu & Senneset (1974) used a CPT and in parallel a standard NGI piezometer.

Although Parez et al. (1976) had already developed and used equipment able to measure cone resistance (q_c) and pore pressure simultaneously, it was only in the early 1980s that many researchers

around the world started to use a pore pressure measurement element incorporated in the electrical cone (e.g. Roy et al., 1980, Campanella & Robertson, 1981). Battaglio et al., (1986) presented results from CPTU3 tests carried out in a medium to stiff clay at the Pontida site (Italy). Fugro and McClelland both developed CPTU3 probes in the mid 1980s, see Bayne & Tjelta (1987) and Zuidberg et al. (1988).

Based on CPTU data from several clays with a range of overconsolidation ratio (OCR) values, Robertson et al. (1986) presented a conceptual pore pressure distribution along the length of a penetrating



Figure 1. Pore pressure measurement positions.

cone penetrometer for clays, ranging from normally consolidated to heavily overconsolidated clays (Figure 2). The pore pressure distribution is normalised by in-situ hydrostatic pore pressure (u_0).

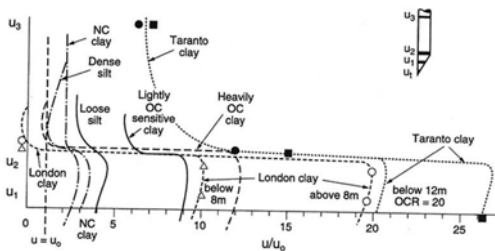


Figure 2. Pore pressure distribution in saturated clays around a penetrating cone based on field measurements (Robertson et al., 1986).

Figure 2 indicates that the pore pressure measured at the tip or face of the cone (u_{1t} or u_{1f} , designated u_{1c} and u_1 respectively on inset of Figure 2) is higher than that measured at u_2 , which again is higher than that measured at u_3 . Figure 2 also illustrates the potential to use relative values of u_{1t} or u_{1f} , u_2 and u_3 to estimate OCR and possibly lateral stress ratio (K_0).

Early studies based on limited data, reported by Sully et al. (1988), Sully & Campanella (1991) and others showed the potential of correlations among Pore Pressure Difference (PPD) = $(u_1 - u_2)/u_0$ vs OCR and

suggested that they will vary with soil type as shown in Figure 3, this was later confirmed by Powell and Lunne (2005).

3 LEARNINGS FROM DATABASE

Based on the potential use of the CPTU3 seen from the literature review, it was decided to collect available data from previously published field test results to

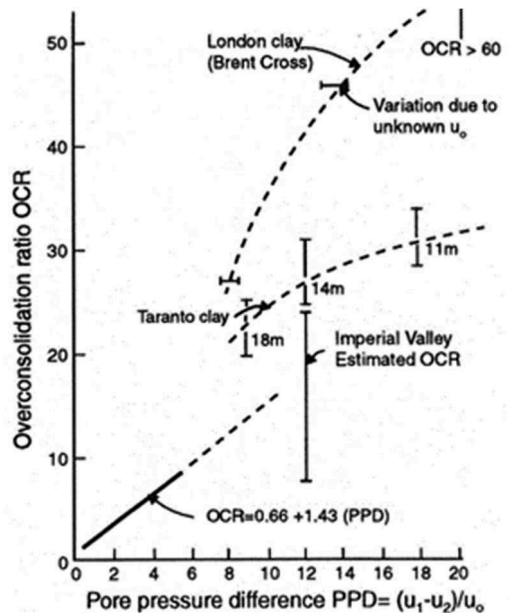


Figure 3. PPD vs OCR for OCR > 10 (Sully et al., 1988).

create a database of pore pressure measurements, index properties and stress history values. The objective of the database was to evaluate reported correlations between the measured pore pressures and reported correlations between geotechnical engineering parameters and parameters derived from pore pressure measurements, referred to hereafter as pore pressure parameters.

The data used to create the database represent a range of clays from Europe and the USA, taken mainly from Chen & Mayne (1994), Larsson & Mulabdic (1991), Sandven (1991), Powell & Lunne (2005), and from unpublished data from offshore soil investigations in the North Sea where NGI was the consultant and some recent NGI projects. When possible, datasets were checked by studying the original source. Uncertain or poor-quality data were removed from the originally prepared database where appropriate.

Altogether, the final database contained 546 datasets from 63 sites (both offshore and onshore). OCR values, based on oedometer tests, are available for

all 63 sites, whereas K_0 values are available from 5 UK and 2 Norwegian clays, mainly based on results of self-boring pressuremeter tests.

Table 1. Details of relevant datasets in final database.

Parameter	u_{1t}	u_{1f}	u_{1f}^*	u_2	u_3
Data points	56	381	36	512	413
Parameter	OCR	K_0			
Data points	313	112			

* Calculated from u_{1t} (as explained later in the paper)

In addition to PPD (defined above) other derived pore pressure parameters utilising u_1 and u_2 , are found in literature:

1. Pore pressure ratio (PPR) = u_1/u_2 (Sully et al., 1988)
2. Excess pore pressure ratio (PPR1) = $(u_1 - u_0)/(u_2 - u_0)$ (Sully et al., 1988)
3. Normalized Pore Pressure Difference (PPSV) = $(u_1 - u_2)/\sigma'_{v0}$

Since the present database contained a reasonably good number of datasets for u_3 also, similar parameters involving u_1 and u_3 , and u_2 and u_3 were also derived. Parameters derived using u_1 and u_2 were designated with suffix 'a', using u_1 and u_3 with suffix 'b' and using u_2 and u_3 with suffix 'c'.

Excellent correlation was found between u_{1t} and u_{1f} (Figure 4). Using this relationship u_{1f} was calculated for 36 datasets where only u_{1t} values were measured. For subsequent analyses

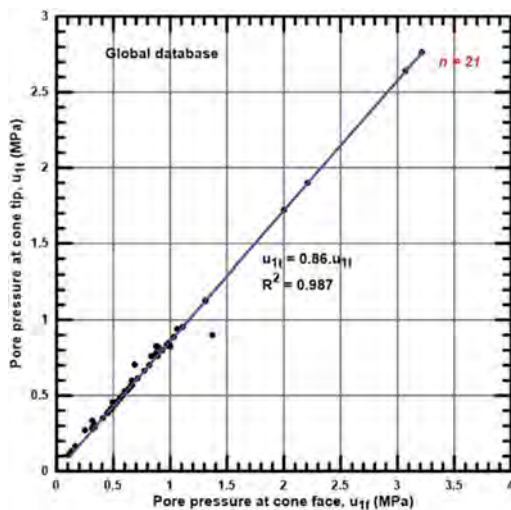


Figure 4. Relationship between u_{1t} and u_{1f} for global data base.

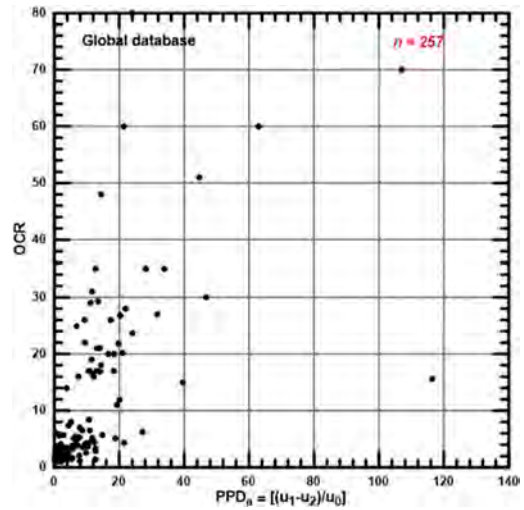


Figure 5. PPDa vs OCR for global data base.

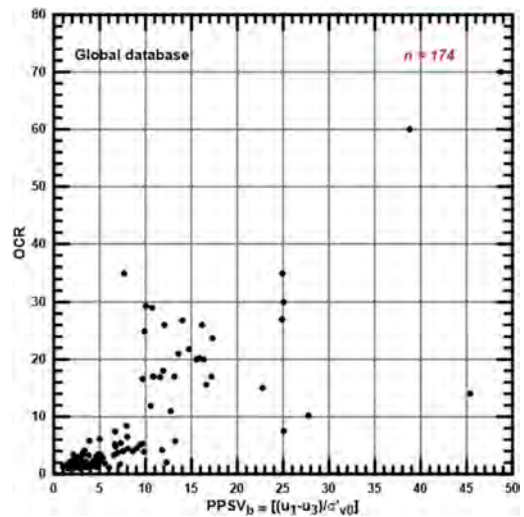


Figure 6. PPSVb vs OCR for global data base.

only u_{1f} was used and for simplicity called u_1 . However, ratios involving u_1 and u_2 , u_1 and u_3 or u_2 and u_3 did not show good correlations when all data were plotted. With reference to Figure 2 this is as expected.

The database contains OCR ranging from 1 to 80, evaluated mainly from oedometer test results. OCR data plotted against PPRa, PPRb and PPRc, and against PPR1a, PPR1b and PPR1c did not show any clear trends. PPDa, PPDb, PPDc, PPSVa, PPSVb and PPSVc showed only a weak trend of increasing with increasing OCR but no clear relationship could be established due to

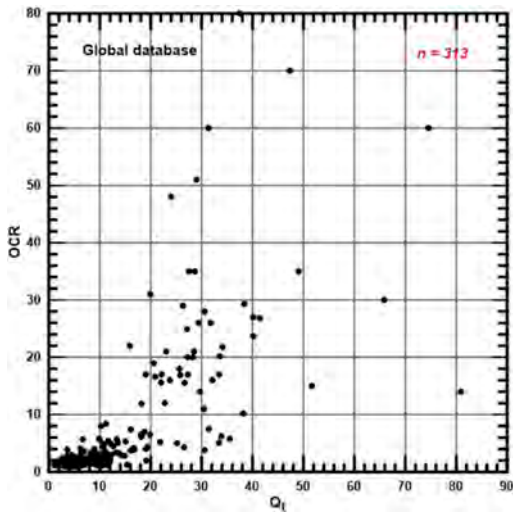


Figure 7. Relationship between Q_t vs OCR for global data base.

very large scatter, as shown by the examples in Figure 5 and 6. Figure 7 shows that the most frequently used correlation between OCR and Q_t ($= (q_c - \sigma_{v0}) / \sigma_{v0}$), also shows a very large scatter where it was not meaningful to fit a trendline.

The findings from the database indicate that it may not be possible to establish a strong correlation between pore pressure parameters and OCR that are valid for all cohesive soils. This status is similar to the correlation factor N_{kt} , the ratio of net cone resistance to undrained shear strength, where after decades of attempts by researchers and industry reported N_{kt} values are still wide ranging. With this example in mind, it will therefore be necessary to establish local correlations between pore pressure parameters and OCR as is commonly the practice for N_{kt} .

4 ATTEMPTS AT LOCAL CORRELATIONS

4.1 General

Two data sets that are believed to be of good and reliable quality have been selected for an illustration of local correlations.

- The glacial till at Cowden, UK, thoroughly tested in the 1990s as documented by Powell and Butcher (2003).
- Two Norwegian moderately overconsolidated stiff marine clays tested by Sandven (1991).

4.2 Glacial till at Cowden

Part of the programme was to carry out new CPTU3 tests at Cowden. However, the pore

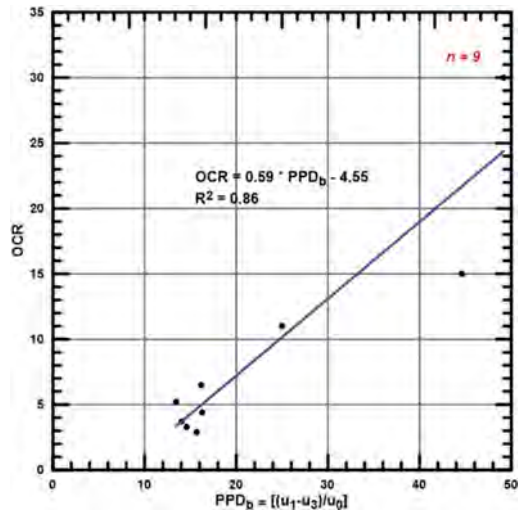


Figure 8. Correlation of PPD_b vs OCR for Cowden glacial till.

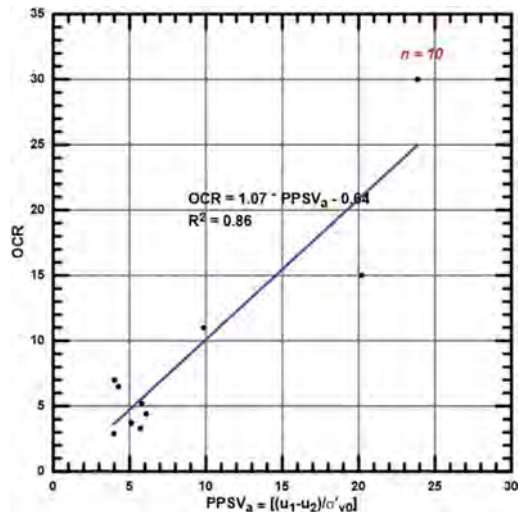


Figure 9. Correlation of PPSVa vs OCR for Cowden glacial till.

pressures measured suffered from unsatisfactory saturation and historic measurements given by Powell and Lunne (2005) were used, since these were considered to be of good quality. Correlations to PPD parameters showed equally good results when based on $u_1 - u_2$ (PPDa) and $u_1 - u_3$ (PPDb). An example of the latter is shown in Figure 8. The same conclusion can be drawn regarding OCR to PPSV where, as an example, PPSVa is shown in Figure 9. All four PPD and PPSV correlations had R^2 values in the range 0.83 - to 0.87.

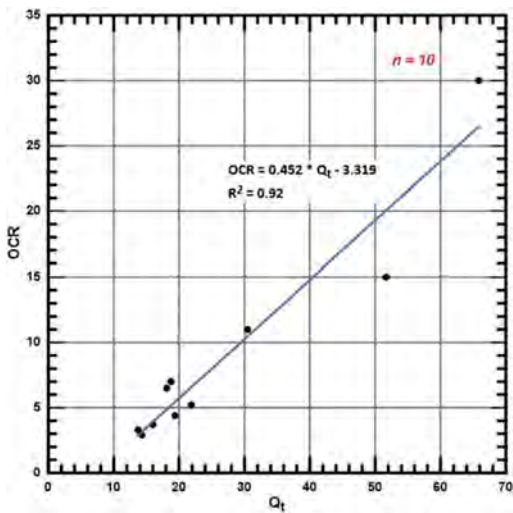


Figure 10. Correlation of Q_t vs OCR for Cowden glacial till.

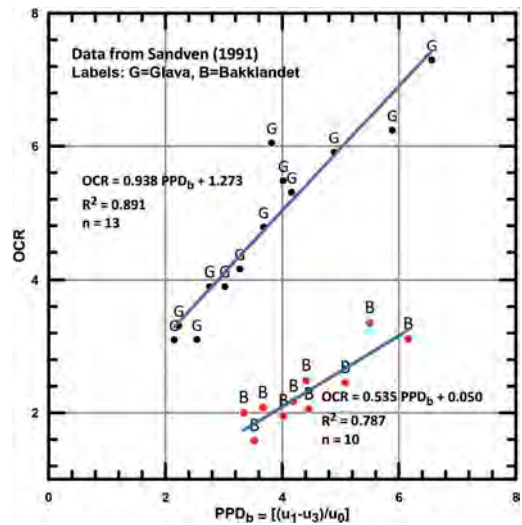


Figure 12. Correlation of PPD_b to OCR for Bakklundet and Glava clays.

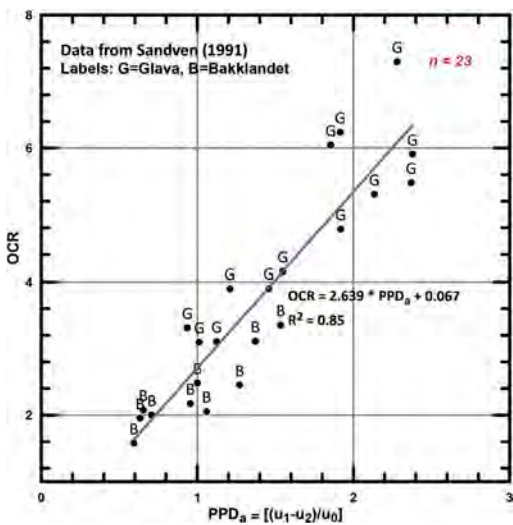


Figure 11. Correlation of PPD_a vs OCR for Bakklundet and Glava clays.

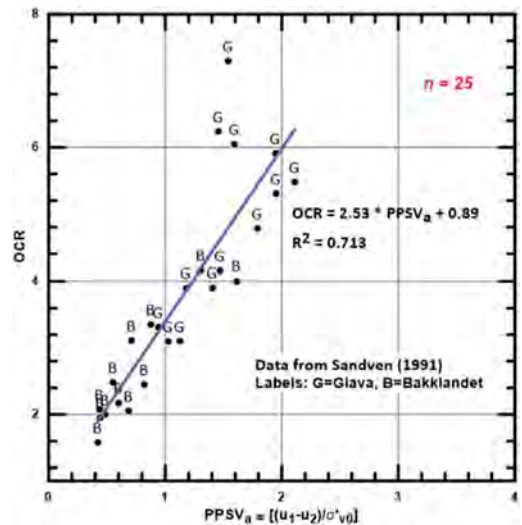


Figure 13. PPSV_a vs OCR for Bakklundet and Glava clays.

Figure 10 shows that the most frequently used correlation between OCR and Q_t is actually showing less scatter, with an R^2 value of 0.92, compared to the PPD and PPSV correlations.

4.3 Trondheim area clays

Sandven reported results of CPTU3 tests from two sites in the Trondheim area of Norway: Glava and Bakklundet. Both sites are described

as moderately overconsolidated stiff marine clays. Figure 11 show that for PPD_a a reasonably good correlation can be found with the Bakklundet data generally plot somewhat lower compared to Glava data. However, when plotting OCR vs PPD_b as shown in Figure 12 the Bakklundet data plot significantly lower compared to Glava data, but both the sites show local and reasonably good linear trends.

In Figure 13 PPSV_a show a reasonably good correlation to OCR, whereas Figure 14 shows that for

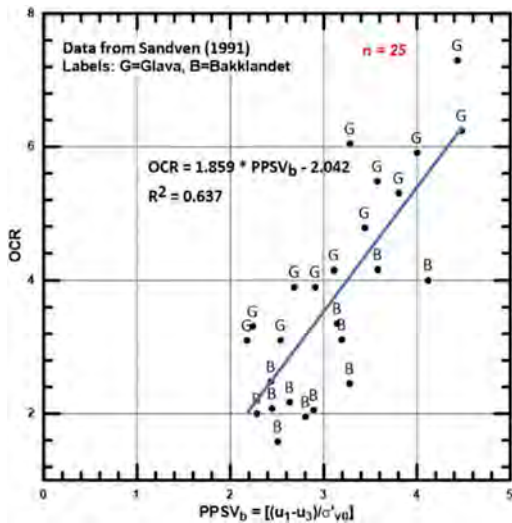


Figure 14. PPSV_b vs OCR for Bakklundet and Glava clays.

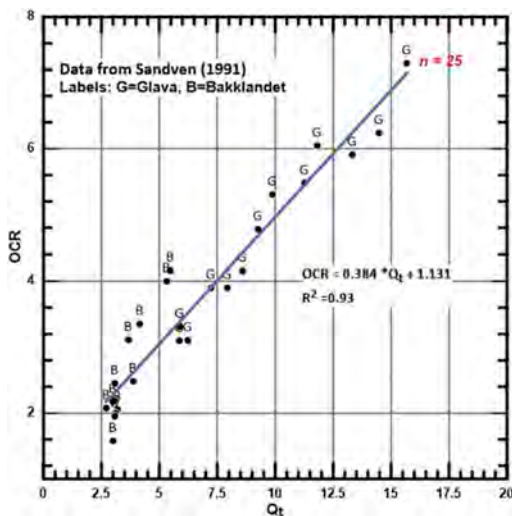


Figure 15. Q_t vs OCR for Bakklundet and Glava clays.

PPSV_b Bakklundet data plot somewhat lower than the Glava data.

Figures 12 and 14 really show that the difference between u_2 and u_3 is much lower for the tests at Bakklundet compared to Glava. Sandven (1991) does not make any comments about this difference.

Figure 15 shows that the correlation that is mostly used for standard CPTUs based on Q_t (e.g. by Lunne et al., 1997) actually gives a better correlation than PPD or PPSV illustrating with this example that there may not be any additional benefit using

CPTU3 OCR correlations compared to correlations with a standard CPTU.

5 DISCUSSION ON CORRELATIONS

The correlation attempts described in this paper are relatively simple.

Since the data base includes soil classification parameters like water content liquid and plastic limits, future work could explore multiparameter regression analyses to see if this can result in any better correlations. Since K_0 estimates are also available at 7 (out of 63) sites, correlations to this parameter could also be explored.

6 SUMMARY AND CONCLUSIONS

Based on geotechnical literature and unpublished material a data base has been established with CPTU3 parameters (q_c , f_s , u_2 , u_1 and u_3) as well as laboratory data giving index parameters and stress history values in terms of overconsolidation parameters. After removing some uncertain data in quality assessment process, the data contain data sets from 63 sites representing a range of clays from Europe and the USA.

The simple correlation study reported in this paper indicates that using all the data available it is not really possible to show any reliable correlation between pore pressure parameters and OCR.

When choosing two sets of local data from the data base (Cowden glacial till and Trondheim area moderately over consolidated marine clays) reasonably good correlations have been found with pore pressure parameters PPD and PPSV. However, for the two sub-data sets even better correlations are obtained when using correlations to Q_t which can be obtained from standard CPTU tests. This indicates that regarding correlations to OCR the inclusion of u_1 and/or u_3 in the CPTU may not improve the accuracy/reliability of the OCR values over the values obtained from standard CPTU.

Other advantages of the CPTU3 relative to the standard CPTU, including results of dissipation tests, are not evaluated in this paper.

ACKNOWLEDGEMENTS

The authors are grateful to the support of Ørsted to give permission to publish this work. The authors would like to thank NGI for the development of the historical database.

REFERENCES

Battaglio, M., Bruzzi, D., Jamiolkowski, M. & Lancellotta, R. 1986. Interpretation of CPTs and CPTUs

- 1st part: undrained penetration of saturated clays. *Field Instrumentation and In-Situ Measurements: Proceedings of the 4th International Geotechnical Seminar, Singapore*: 129–143.
- Bayne, J.M. & Tjelta, T.I. 1987. Advanced cone penetrometer development for in-situ testing at Gullfaks C. *Proceedings of the 19th Offshore Technology Conference, Houston, OTC paper 5420(1)*: 531–540.
- Chen, S.C. & Mayne, P.W. 1994. Profiling overconsolidation ratio by piezocone tests. *National Science Foundation, Report no. GIT-CEEGEO-94-1*.
- Campanella, R.G. & Robertson, P.K. 1981. Applied cone research. *Procs Symp on Cone Penetration Testing and Experience, ASCE, St. Louis*: 343–362.
- Janbu, N. & Senneset, K. 1974. Effective stress interpretation of in situ static penetration test. *Procs of the European Symposium on Penetration Testing, Stockholm, 2:2*: 181–193.
- Larsson, R. & Mulabdic, M. 1991. Piezocone tests in clay. Swedish Geotechnical Institute. *Report no. 42*.
- Lunne, T., Robertson, P.K. & Powell, J. (1997) CPT and piezo-cone testing in geotechnical practice. Textbook: Spon Press, Taylor and Francis Company, London.
- Parez, L., Bachelier, M. & Sechet, B. 1976. Pression interstitielle developpee au fonçage des penetrometres. *Proceedings of the 6th European Conference on Soil Mechanics and Foundation Engineering, Vienna, 1.2*: 533–538.
- Powell, J.J.M. & Butcher, A.P. 2003. Characterisation of a glacial till at Cowden, Humberside. *Workshop, Characterisation and Engineering Properties of Natural Soils*: 983–1020. Singapore, 2002.
- Powell, J.J.M. & Lunne, T. 2005. Use of CPTU data in clays/fine grained soils. *Studia Geotechnica*. XXVII (3 – 4): 29–65.
- Robertson, P.K., Campanella, R.G., Gillespie, D. & Greig, J. 1986. Use of piezometer cone data. *Proceedings of In-Situ 86 Specialty Conference, American Society of Civil Engineers, Blacksburg*: 1263–1280.
- Roy, M., Tremblay, M., Tavenas, F. & La Rochelle, P. 1980. Induced pore pressures in static penetration tests in sensitive clay. *Proceedings of the 44th Canadian Geotechnical Conference, Calgary, Preprint Volume, 11.3.1 to 11. 3.13*.
- Sandven, R. 1990. Strength and deformation properties of fine-grained soils obtained from piezocone tests. PhD thesis, Norwegian Institute of Technology, Trondheim, Norway.
- Sully, J.P., Campanella, R.G. & Robertson, P.K. 1988. Overconsolidation ratio of clays from penetration pore pressures. *Journal of Geotechnical Engineering, American Society of Civil Engineers, 114(2)*: 209–216.
- Sully, J.P. & Campanella, R.G. 1991. Effect of lateral stress on CPT penetration pore pressures. *Journal of Geotechnical Engineering, American Society of Civil Engineers, 117(7)*: 1082–1088.
- Torstensson, B.A. 1975. Pore pressure sounding instrument. *Procs Conference on In Situ Measurement of Soil Properties, American Society of Civil Engineers, Raleigh, 2*: 48–54.
- Wissa, A.Z.E., Martin, R.T. & Garlanger, J.E. 1975. The piezometer probe. *Procs Conf on In Situ Measurement of Soil Properties, ASCE, Raleigh, 1*: 536–545.
- Zuidberg, H.M., ten Hoope, J. & Geise, J.M. 1988. Advances in in-situ measurements. *Procs 2nd International Symposium on Field Measurements in Geomechanics, Kobe, 1*: 279–291.

Comparisons CPT-DMT in soft clay at Fucino-Telespazio GeoTest site

D. Marchetti

Studio Prof. Marchetti, Rome, Italy

P. Monaco & G. Totani

University of L'Aquila, L'Aquila, Italy

F. Totani

Consultant Engineer, L'Aquila, Italy

S. Amoroso

University of Chieti-Pescara, Pescara, Italy

Istituto Nazionale di Geofisica e Vulcanologia, L'Aquila, Italy

ABSTRACT: This paper presents the comparison of results obtained from CPT/CPTU tests carried out in past investigations and from recent DMT tests carried out using the automated Medusa DMT, adopting different test procedures (standard, repeated A -readings, A -reading while penetrating), at the benchmark soft clay test site of Fucino-Telespazio, Italy. In particular, the depth profiles of the undrained shear strength s_u of the Fucino clay obtained from CPT/CPTU interpretation are compared with the s_u profiles obtained from standard DMT and from Medusa DMT using different test procedures, as well as with the s_u values obtained from field vane test (FVT), self boring pressuremeter test (SBPT) and laboratory tests available from past investigations, resulting generally in good agreement.

1 INTRODUCTION

Benchmarking is of significant importance in geotechnical engineering for testing and validating both innovative soil investigation methods and foundation solutions. The growing interest in this topic is documented by the 1st International GeoTest Site Symposium ISGTS, Oslo, 2019, aiming to promote an increasing use of benchmark test sites, selected to ensure simplicity of geotechnical conditions (i.e., relatively homogenous soil deposit) and ease of interpretation (i.e., pre-existing laboratory and field data).

Fucino-Telespazio is a well known benchmark 'GeoTest site' in Italy, constituted by a thick deposit of cemented, homogeneous soft lacustrine clay of high plasticity. The site was extensively investigated at the end of the 1980s by means of several in situ and laboratory tests carried out by various international research groups (Burghignoli et al. 1991). Earlier experimentation with the flat dilatometer (DMT) at this site was carried out in the 1970s, as reported by Marchetti (1980). Subsequently, in 2004-2005 the site was selected for validation of the seismic dilatometer (SDMT, Foti et al. 2006, Marchetti et al. 2008). More recently,

in 2020 the same site was selected for experimentation with the automated Medusa DMT, ideally linking past experience and recent technological developments.

This paper presents the comparison of results obtained at Fucino-Telespazio from cone/piezcone penetration tests (CPT/CPTU) carried out in past investigations and from recent DMT tests carried out using the Medusa DMT equipment (briefly described in the next section) by adopting different test procedures. In particular, the focus in this paper is on the evaluation of the undrained shear strength s_u of the Fucino clay by different test methods.

2 MEDUSA DILATOMETER TEST

The Medusa DMT (Figure 1) is the last-generation, fully-automated version of the DMT. It is a self-contained probe able to autonomously perform dilatometer tests using a blade of standard dimensions without the pneumatic cable, the control unit and the gas tank required in the traditional pneumatic DMT configuration. A motorized syringe, driven by an electronic board powered with

rechargeable batteries, hydraulically expands the membrane to obtain the DMT *A*, *B*, *C* pressure readings, which are acquired and stored automatically at each test depth (typically every 0.20 m). The automatic (volume controlled) hydraulic pressurization of the membrane is highly repeatable and permits to impose a programmable timing (i.e., the recommended standard timing, or different timing corresponding to variable pressurization rates) to obtain the pressure readings. The probe may operate in cableless mode, which is a significant practical advantage in the offshore industry and for deep investigations. An optional electric cable may be used to obtain real-time data during test execution.

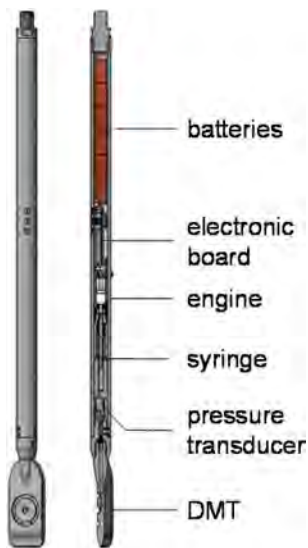


Figure 1. Main components of the Medusa DMT.

The Medusa DMT has several advantages over the traditional DMT equipment in terms of test automation, field productivity and increased accuracy (Marchetti 2018, Marchetti et al. 2019). It also provides the possibility of performing additional measurements, not feasible with the traditional DMT, including continuous measurement of the total horizontal pressure against the membrane with time at a stationary test depth, to obtain information on soil response in terms of fully drained/partially drained/undrained behavior, or during probe penetration, to obtain information on the in-situ stress state. Due to the increased accuracy of pressure measurements and controlled pressurization rate, the Medusa DMT is particularly useful for testing soils which are usually difficult to characterize using common in-situ techniques, such as very soft or even nearly liquid soils (Marchetti et al. 2021), mine tailings and intermediate soils (Monaco et al. 2021).

3 THE FUCINO-TELESPAZIO BENCHMARK TEST SITE

The Fucino-Telespazio test site is located in the Fucino basin, central Italy, about 80 km east of Rome. In 1986 the site was selected as a national benchmark test site and investigated by means of a joint effort of a number of Italian and international research groups. The primary aim of the investigation was to carry out comparative in situ and laboratory tests in a suitable soft clay deposit. The choice fell on the Fucino-Telespazio site due to its marked spatial homogeneity and apparently simple geological history. The site is constituted by a thick deposit of soft, homogeneous, highly structured CaCO_3 cemented clay of lacustrine origin (Fucino clay). The experimental activity, which lasted more than two years (1986-88), was documented in several research reports and papers. In particular, the data shown in this paper are taken from Burghignoli et al. (1991), who presented a comprehensive description of the in situ and laboratory testing program and a detailed geotechnical characterization of the Fucino clay.

The in situ testing program included boreholes with undisturbed sampling, cone/piezcone penetration tests (CPT/CPTU), self boring pressuremeter tests (SBPT), flat dilatometer tests (DMT), field vane tests (FVT), seismic cone tests (SCPT), cross-hole tests (CH), down-hole tests (DH), surface wave tests (SASW) and piezometer measurements.

Laboratory tests were carried out on a large number of undisturbed samples, including determination of index properties, incremental loading (IL) and constant rate of strain (CRS) oedometer tests, unconsolidated undrained (UU), isotropically consolidated drained (CID) and undrained (CIU) triaxial compression tests, direct simple shear tests (DSS-CK₀U), laboratory vane tests (VT), resonant column tests (RC) and cyclic torsional shear tests (CTS).

To minimize the influence of spatial variability of the clay properties, the field investigations were concentrated in an area of $10 \times 40 \text{ m}^2$, to a depth of about 40 m. The superimposed profiles of the cone resistance q_c measured from four CPTs performed at the corners of the area (Figure 2) show a fair homogeneity of the site, both in vertical and horizontal directions: the soil stratigraphy is virtually identical at all test locations, with thin sandy layers identified at the same depths by all tests. Similar results were found in three CPTUs carried out in the same area.

The Fucino clay is characterized by high plasticity (plasticity index *PI* mostly between 40 and 70%, natural water content *w* between 60 and 120%). Despite its relatively recent deposition, the clay is highly structured and cemented. The calcium carbonate

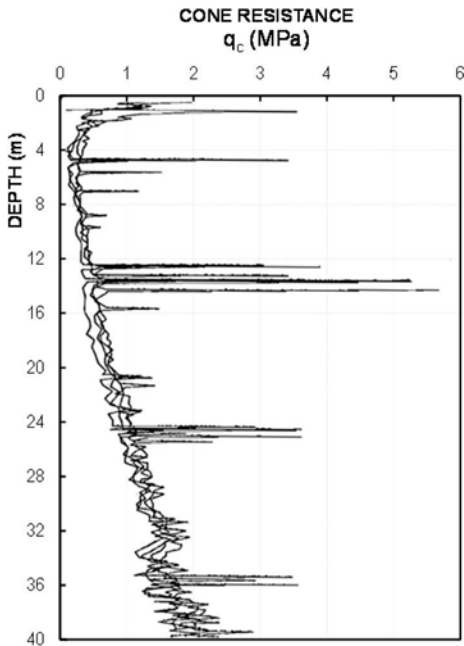


Figure 2. CPT results from past investigations at Fucino-Telespazio (Burghignoli et al. 1991).

CaCO₃ content was found to range between 10 and 30% in the upper 25 m, increasing to an average value of about 60% below this depth. The clay deposit is geologically normally consolidated. However both laboratory and in situ tests indicated a light overconsolidation, which was attributed mostly to diagenetic interparticle bonding due to CaCO₃ cementation. Burghignoli et al. (1991) pointed out that structure and cementation have a dominant influence on stress history, compressibility, consolidation and shear strength properties of the Fucino clay.

4 MEDUSA DMT TESTS AT THE FUCINO-TELESPAZIO BENCHMARK TEST SITE

An experimental program at the Fucino-Telespazio test site, including three Medusa DMT soundings and one traditional pneumatic DMT sounding carried out using the SDMT equipment, was completed in September 2020. All soundings were performed at close mutual distance, to a depth of 30 m.

The Medusa DMT soundings were carried out using three different test procedures (see Monaco et al. 2022 for details), which differ essentially for the technique adopted for measuring the *A*-pressure.

4.1 Standard DMT procedure (STD)

The STD procedure is the same procedure of the traditional pneumatic DMT test. As soon as the

test depth is reached, the penetration is stopped and the DMT test cycle starts. The activated motorized syringe gradually increases the hydraulic pressure to the membrane. When the internal oil pressure equals the external soil pressure, the membrane lifts-off from its seat and starts to expand laterally. When the membrane has expanded of 0.05 mm at its centre, the *A*-pressure is recorded. After the *A*-reading, the motorized syringe continues to increase the pressure until the membrane displacement at the centre equals 1.10 mm. At this instant the second pressure reading *B* is recorded. As soon as the *B*-reading is obtained, the motorized syringe starts decreasing the oil pressure. If the *C*-pressure reading is requested, the motorized syringe applies a gradual and controlled depressurization after the *B*-reading and the membrane slowly returns to its initial position against the sensing disc. At the instant in which the contact reactivates, the corresponding pressure is recorded as the *C*-pressure reading. In the STD procedure the pressurization rate is regulated by the motorized syringe so that the *A*-pressure reading is obtained 15 s after start of pressurization and the *B*-pressure reading 15 s after the *A*-pressure reading, in accordance with existing standards of the pneumatic DMT (ASTM D6635-15, ISO 22476-11:2017(E)). The *C*-reading is typically obtained 30 s after start of depressurization following the *B*-reading.

4.2 DMT repeated *A*-readings procedure (DMT-RA)

The DMT-RA procedure differs from the STD procedure only in the first part of the measurement sequence, before membrane expansion, while the *B*- and *C*-pressure readings are taken exactly in the same way. As previously described, in the STD procedure the *A*-reading is taken when the membrane centre has expanded horizontally 0.05 mm against the soil, replicating exactly the same procedure implemented in the traditional pneumatic DMT test. The motorized syringe of the Medusa DMT, driven by the electronic board, is also able to maintain the membrane in equilibrium with negligible horizontal displacement of the membrane. The DMT-RA procedure makes use of this capability. The initial stage of the DMT test cycle with the DMT-RA procedure, before penetrating to the next test depth, consists in maintaining the membrane in equilibrium with the soil pressure. This state is obtained with very rapid pressure corrections operated by the motorized syringe, with negligible membrane displacement. In this situation the membrane is in equilibrium at 0.05 mm distance from the sensing disc. When the new test depth is reached, the test cycle starts ($t = 0$) and repeated sequential *A*-readings are taken with time during the rapid pressure corrections of the motorized syringe, monitoring the total horizontal soil pressure against the membrane with time. All the

sequential A -readings are obtained without any displacement of the soil, because the blade is advanced to the test depth with the membrane already at 0.05 mm displacement from the sensing disc. Such DMT-RA procedure is characterized by the duration (T_{diss}) of the sequential A -readings taken with time (dissipation), before concluding the DMT test cycle with the standard B and C readings. The parameter T_{diss} is selected and pre-programmed before starting the test cycle, so that the membrane expansion will be activated after the time T_{diss} has elapsed. At Fucino-Telespazio T_{diss} was set equal to 15 s, to comply with the standard timing adopted in the STD procedure. The procedure and timing for taking the B and C readings are the same as in the STD procedure.

4.3 DMT A -reading while penetrating procedure (DMTA-WP)

The capability of the Medusa DMT to maintain the membrane in equilibrium with negligible horizontal displacement enables to obtain continuous measurements of the total horizontal pressure of the soil against the membrane during penetration of the probe. The DMTA-WP procedure consists in performing repeated A -pressure measurements (equivalent to A -pressure reading at $t = 0$ instead of the standard time of $t = 15$ s) recorded during penetration of the Medusa DMT at a constant rate. The sequence of A -readings is generally taken over depth intervals of 1 m, corresponding to the typical length of push rods. Almost all penetrometers require to stop penetration every meter to add a push rod, during which B and C pressure readings may be taken without employing additional time. A constant penetration rate of 20 mm/s, as in the standard test procedure, is generally adopted. The current Medusa DMT equipment does not include instrumentation to measure the penetration depth during the readings. Most penetrometers include an encoder (for CPT measurements) and may output a time versus depth file, helpful for accurately associating the A -readings to the corresponding depth at which they were taken. When such information is missing, the time-depth relation may be estimated assuming an average speed of penetration, estimated by measuring the time for penetrating a 1-meter rod. The average speed and the time from the start of penetration enables to estimate the depth of each A -reading. Although not as accurate as with an encoder, the error is reasonably limited in terms of % error, since each measuring interval is maximum 1 m long.

4.4 Comparison of results obtained by different test procedures

Figure 3 shows the comparison of the results obtained by Medusa DMT using the three different test procedures (STD, DMT-RA, DMTA-WP) and the results obtained by traditional DMT. The test

results obtained from Medusa DMT were processed using the same data reduction and interpretation formulae used for the traditional DMT test (ISSMGE TC16 Report, Marchetti et al. 2001). In particular, Figure 3 shows the depth profiles of the corrected pressure readings p_0, p_1, p_2 (A, B, C corrected with the calibration offsets $\Delta A, \Delta B$ to account for membrane stiffness), as well as of the derived parameters material index I_D and horizontal stress index K_D . For the DMT-RA sounding, the A -pressure reading used in data processing is the last value obtained from the A -dissipation series, i.e. the A -pressure recorded 15 s after start of pressurization. In the processing of data from all soundings the groundwater table was assumed at a depth of 0.60 m below the ground surface, as indicated by the p_2 values observed in the very few thin sand layers.

The profiles of p_0 obtained by Medusa DMT using the three different test procedures are very similar, despite the different techniques adopted for measuring the A -pressure, and in good agreement with the profile of p_0 obtained by traditional DMT.

The profiles of p_1 and p_2 obtained by Medusa DMT (all test procedures) and traditional DMT are nearly coincident. The values of p_1 and p_2 obtained by the DMTA-WP procedure are discontinuous, because in this case the B and C pressure readings are performed at depth intervals of 1 m, instead of 0.20 m as in the STD and DMT-RA procedures.

The profile of the material index I_D , which depends on the difference ($p_1 - p_0$), shows some inconsistency between the values obtained by different test procedures. In particular, the values of I_D calculated from p_0 and p_1 data acquired by the DMTA-WP procedure appear significantly lower than the I_D values provided by the STD and the DMT-RA procedures. This discrepancy could be due to the fact that in the DMTA-WP procedure the A -pressure is measured at $t = 0$ instead of $t = 15$ s, resulting in lower values of the difference ($p_1 - p_0$), and for low I_D values such incongruity is amplified by the logarithmic scale. The values of the horizontal stress index K_D , which depends only on p_0 , do not seem influenced by the adopted test procedure.

5 EVALUATION OF THE UNDRAINED SHEAR STRENGTH FROM CPT/CPTU AND DMT

As described by Burghignoli et al. (1991) and Soccodato (2003), the shear strength characteristics of the Fucino clay were determined by means of a variety of in situ and laboratory tests carried out in the 1987 investigation. In particular, the undrained shear strength s_u was obtained from CPT and CPTU interpretation with the usual relationships, respectively:

$$s_u = \frac{q_c - \sigma_{v0}}{N_k} \quad (1)$$

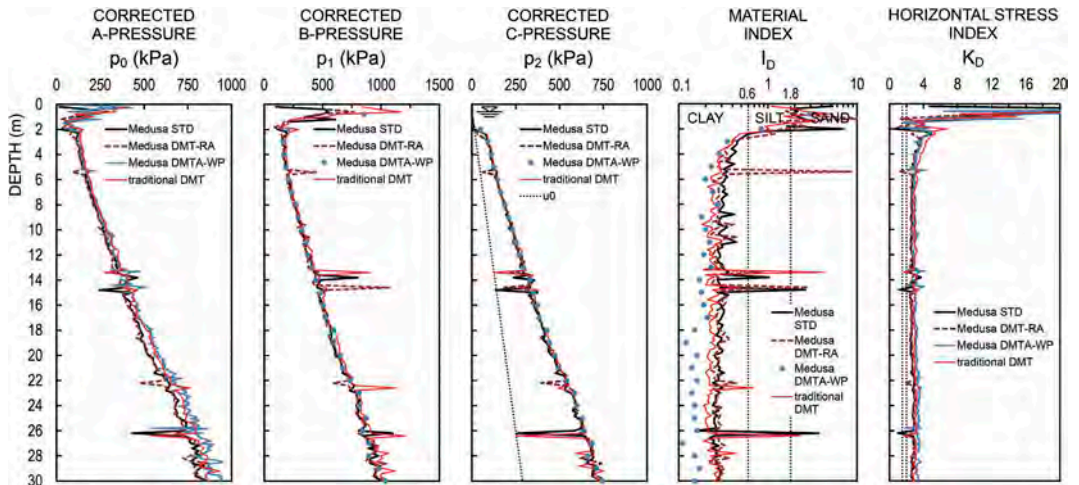


Figure 3. Results obtained by Medusa DMT using different test procedures and by traditional DMT at Fucino-Telespazio.

$$s_u = \frac{q_t - \sigma_{v0}}{N_{kt}} \quad (2)$$

where q_c = cone resistance (CPT), q_t = corrected cone resistance (CPTU), σ_{v0} = total overburden stress, N_k and N_{kt} = cone bearing capacity factors for CPT and CPTU respectively, which were assumed to range between 14 and 22.

The undrained shear strength s_u was estimated from DMT results, both obtained by traditional pneumatic DMT and by Medusa DMT in the 2020 investigation, using the original correlation proposed by Marchetti (1980):

$$s_u = 0.22\sigma'_{v0}(0.5K_D)^{1.25} \quad (3)$$

Figure 4 shows the comparison of the depth profiles of the undrained shear strength s_u obtained at Fucino-Telespazio from different in situ and laboratory tests in past investigations and in the 2020 Medusa DMT campaign. In particular, the s_u profiles from the 1987 investigation shown in Figure 4 (data from Burghignoli et al. 1991) were obtained in situ from several CPT and CPTU tests, field vane tests (FVT), self boring pressuremeter tests (SBPT), DMT tests, and in the laboratory from direct simple shear tests (DSS-CK₀U) and unconsolidated undrained triaxial compression tests (UU) and laboratory vane tests. For CPT and CPTU only the lower- and upper-bound trend lines, corresponding to the average s_u estimated from Eqs. 1 and 2 by assuming N_k and N_{kt} equal to 22 and 14 respectively, are plotted in Figure 4. The values of s_u from FVT in Figure 4 are not corrected for strain rate and anisotropy effects.

Figure 4 shows an overall agreement between the s_u values obtained from different in situ and laboratory tests. With reference to the various field tests results obtained in 1987, Burghignoli et al. (1991)

observed that, below an upper desiccated crust, there is a fair agreement between the s_u values resulting from FVT and DMT. The SBPT provided values of s_u significantly higher than those resulting from other in situ and laboratory tests. Soccodato (2003) suggested that low values of N_k for CPT are needed in order to match the data, while $N_{kt} = 15$ seems to

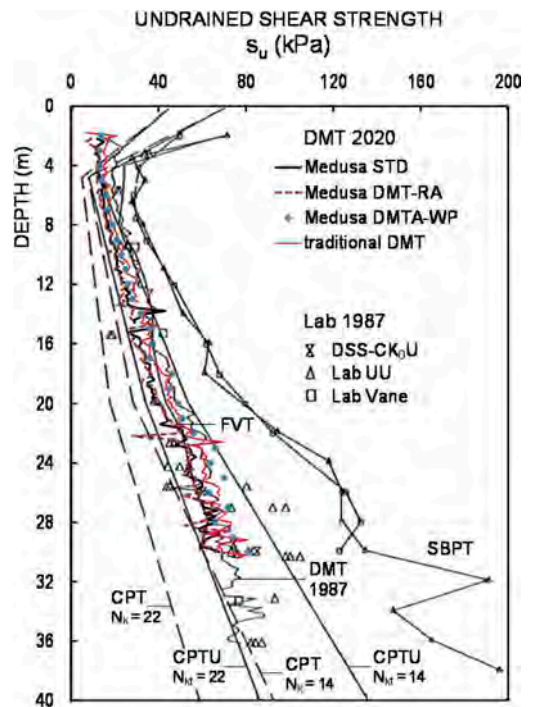


Figure 4. Undrained shear strength s_u at Fucino-Telespazio from recent DMT tests vs. s_u from CPT/CPTU and other in situ and laboratory tests obtained in the 1987 investigation (modified from Burghignoli et al. 1991).

be appropriate for CPTU. As to laboratory tests, the values of s_u resulting from UU and from DSS-CK₀ U tests show a marked increase below a depth of about 25 m, reflecting the increase of CaCO₃ content with depth. This feature is not reflected by the results of the in situ tests with the exception of the SBPT, which provided a different trend of s_u below 24–25 m of depth. Burghignoli et al. (1991) commented that in highly structured soft clays, like the Fucino clay, the results of push-in situ testing techniques, such as CPT/CPTU and DMT, can be hampered by the destructuration of the tested soil induced by the insertion of the probe, which may partially obliterate the effect of diagenetic bonds on the inferred s_u .

In Figure 4 the profiles of s_u estimated by Eq. 3 from the results of the three Medusa DMT tests carried out adopting different test procedures (STD, DMT-RA and DMTA-WP) and from the traditional DMT carried out in the 2020 campaign are superimposed to the profiles obtained by all test methods in past investigations. As already noted with reference to the K_D profiles (Figure 3), which are used to estimate s_u by Eq. 3, the s_u values are not practically influenced by the adopted test procedure. The s_u values obtained from Medusa DMT and the traditional pneumatic DMT are almost coincident, and also in very good agreement with the s_u obtained from DMT tests carried out in 1987. In general, the profiles of s_u obtained from all DMTs plot in between the s_u profiles determined by other in situ and laboratory tests. This finding is in line with previous experience. In fact, as described in the TC16 DMT Report (Marchetti et al. 2001), the s_u estimated from DMT by Eq. 3 has generally been found to be in an intermediate position between the s_u estimated from other tests, as presented by various researchers in different clays (e.g., Nash et al. 1992 at the National Research Site of Bothkennar, UK).

6 CONCLUSIONS

Benchmark GeoTest sites, such as the Fucino-Telespazio soft clay test site, prove to be of paramount importance for testing and validating innovative soil investigation methods. In this respect, the recent experimental program at Fucino-Telespazio with Medusa DMT (the last-generation, fully-automated version of the DMT) could uniquely benefit of the availability of an existing large and consistent data set obtained in past investigations from a variety of high-quality in situ and laboratory tests.

Due to the increased accuracy of pressure measurements and controlled pressurization rate, the Medusa DMT is particularly useful for testing very soft soils, in which the measured pressures are typically very small. Moreover, its technical features permit to implement alternative test procedures (repeated A -readings, A -reading while penetrating), besides the ‘standard’ DMT procedure. The

comparison of the results obtained at Fucino-Telespazio indicate a substantial consistency of measurements provided by Medusa DMT adopting different test procedures and by traditional pneumatic DMT.

The interpretation of Medusa DMT test results in terms of soil parameters takes advantage of the wide experience available for the traditional pneumatic DMT test, and essentially shares the same set of established soil property correlations available in literature. The profiles of s_u obtained from both Medusa DMT and traditional DMT in Fucino clay are found in an intermediate position between the s_u profiles determined by other in situ and laboratory tests, in particular by CPT/CPTU tests. This finding is in agreement with other comparisons of s_u estimated from DMT and from other tests, available from several soft clay test sites.

ACKNOWLEDGEMENTS

This study was part of an activity cofunded by the Start-up & SME Booster Programme from the EIT RawMaterials, funded by the EIT, a body of the European Union supported under the Horizon 2020 research and innovation program.

Telespazio – Fucino Space Centre is gratefully acknowledged for permitting to access the field testing area, as well as for the continuous and friendly support during the Medusa DMT testing program in September 2020.

REFERENCES

- ASTM D6635-15. 2015. Standard Test Method for Performing the Flat Plate Dilatometer. ASTM International, West Conshohocken, PA, USA.
- Burghignoli, A., Cavalera, L., Chieppa, V., Jamiolkowski, M., Mancuso, C., Marchetti, S., Pane, V., Paoliani, P., Silvestri, F., Vinale, F. & Vittori, E. 1991. Geotechnical characterization of Fucino clay. *Proc. 10th European Conf. on Soil Mech. and Foundation Eng., Florence, Italy, 26-30 May 1991*, 1: 27–40. Rotterdam: Balkema.
- Foti, S., Lancellotta, R., Marchetti, D., Monaco, P. & Totani, G. 2006. Interpretation of SDMT tests in a transversely isotropic medium. *Proc. 2nd Int. Conf. on the Flat Dilatometer, Washington D.C., USA, 2-5 April 2006*, 275–280.
- ISO 22476-11:2017(E). 2017. Geotechnical Investigation and Testing – Field Testing – Part 11: Flat Dilatometer Test. International Organization for Standardization, Geneva, Switzerland.
- Marchetti, D. 2018. Dilatometer and Seismic Dilatometer Testing Offshore: Available Experience and New Developments. *Geotech. Testing J.* 41(5): 967–977.
- Marchetti, D., Danziger, F. & Jannuzzi, G.M.F. 2021. Comparison of DMT results using traditional pneumatic equipment and the Medusa DMT in the Sarapuí II soft clay deposit in Brazil. *Proc. 6th Int. Conf. on Geotechnical and Geophysical Site Characterisation ISC’6, Budapest, Hungary, 26-29 September 2021*.

- Marchetti, D., Monaco, P., Amoroso, S. & Minarelli, L. 2019. In situ tests by Medusa DMT. *Proc. 17th European Conf. on Soil Mech. and Geotech. Eng. ECSMGE-2019, Reykjavik, Iceland, 1-6 September 2019*.
- Marchetti, S. 1980. In Situ Tests by Flat Dilatometer. *J. Geotech. Eng. Div.* 106 (GT3): 299–321.
- Marchetti, S., Monaco, P., Totani G. & Calabrese M. 2001. The Flat Dilatometer Test (DMT) in Soil Investigations – A Report by the ISSMGE Committee TC16. *Proc. Int. Conf. on Insitu Measurement of Soil Properties and Case Histories, Bali, Indonesia*, 95–131. Official version approved by ISSMGE TC16 reprinted in *Proc. 2nd Int. Conf. on the Flat Dilatometer, Washington D.C., USA, 2-5 April 2006*, 7-48.
- Marchetti, S., Monaco, P., Totani, G. & Marchetti, D. 2008. In Situ Tests by Seismic Dilatometer (SDMT). *Geotechnical Special Publication (GSP 180), From Research to Practice in Geotechnical Engineering*, 292–311.
- Monaco, P., Marchetti, D., Totani, G., Totani, F. & Amoroso, S. 2022. Validation of Medusa DMT test procedures in Fucino clay. *Proc. 20th Int. Conf. on Soil Mech. and Geotech. Eng., Sydney, Australia, 1-5 May 2022*.
- Monaco, P., Tonni, L., Amoroso, S., Garcia Martinez, M.F., Gottardi, G., Marchetti, D. & Minarelli, L. 2021. Use of Medusa DMT in alluvial silty sediments of the Po river valley. *Proc. 6th Int. Conf. on Geotechnical and Geophysical Site Characterisation ISC'6, Budapest, Hungary, 26-29 September 2021*.
- Nash, D.F.Y., Powell, J.J.M. & Lloyd, I.M. 1992. Initial investigations of the soft clay test site at Bothkennar. *Geotechnique* 42(2): 163–181.
- Soccodato, F.M. 2003. Geotechnical Properties of Fucino Clayey Soil. *Characterisation and Engineering Properties of Natural Soils*, 1: 791–807. Lisse: Swets & Zeitlinger.

An innovative new 3MPa CPT – to detect and measure very small f_s values

A.J. McConnell

Founder of Insitu Geotech Services Pty Ltd (IGS)

E.J.C. Wassenaar

Regional Manager Asia-Pacific at Geomil Equipment B.V.

ABSTRACT: CPT testing of extremely soft soils and tailings materials requires the ability to detect and measure very low q_c values and extremely low f_s values. The former of these can and has been solved by use of low capacity cones with high quality well-calibrated load cells. The latter, detection and measurement of extremely low f_s values is an industry-wide problem, often treated as an “elephant in the room”. This paper describes development of an innovative new CPT cone that the authors believe has largely solved this problem.

1 INTRODUCTION

Insitu Geotech Services (IGS) undertakes much CPT testing in soils and sediments that can be described in everyday terms as “extremely soft”, or even as “ooze”; for clients who are seeking data that permits them to make confident designs.

As a consequence they are almost every day working in an arena where one would aspire to better than Application Class 1 testing quality, if being described according to ISO 22476-1-2012.

To achieve the highest quality that they can in testing these conditions and in satisfying clients they:

- Use known good quality CPT cones. In soft soils these have been previously usually of 25MPa or 10MPa tip capacity.
- Maintain/manage all CPTs meticulously.
- Undertake in-house calibration-checking-recalibration under a very stringent program, as described below.

The IGS calibration program is run in-house because, as you can see from the explanation below, it would be unworkable to contract it out:

- Every cone is calibrated before every job, then recalibrated after the job, each time using the cone’s actual dimensions, not nominal values. If the job runs more than one week, then the cones are changed over with freshly calibrated cones on an approximate 7-day service cycle. All of this is carefully recorded and a calibration-drift-performance type of history is developed for each cone.
- Recalibration data is then always compared to the data from the previous calibration, to cross-check for any significant change.

- And, they take before-vs-after zero-load-drift comparisons, as part of each test’s management.

It’s rigorous, it works, and it’s business as usual, built into the company culture and cost structures.

Following the above approach IGS has been successful in regard to the ability to defensibly and repeatably measure very low q_c values, and to be as good as reasonably achievable at measuring f_s values.

2 LIMITATION RE MEASURING VERY SMALL SLEEVE FRICTIONS

In regard to f_s though, they have run up against the “industry normal” limitation in measuring very small sleeve frictions; a limitation that is associated with the design of normal Compression Cones.

To help discussion of this, refer to Figure 1 below.

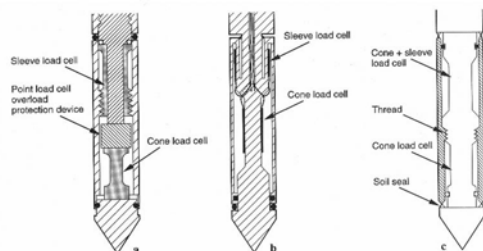


Figure 1. Design of Cone Penetrometers (Lunne et al 1997).

In this paper type (a) is designated as a Compression Cone and type (c) as a Subtraction Cone.

For this discussion, the relevant difference between a Compression Cone and a Subtraction Cone is that:

- A Compression Cone has separate load cells for the tip and the sleeve. Hence these load cells can be sized for the purpose; typically a larger cell for the tip and a smaller load cell for the sleeve.
- A Subtraction Cone has two load cells that must both be of the larger variety. Typically they would be identical or nearly identical. One of these, that just behind the tip, measures the tip load only and the other, above the screwed on connection to the sleeve, measures the combined tip-plus-sleeve load.
- Software subtracts one value from the other to determine the sleeve friction load. Hence a relatively big number is subtracted from another relatively big number to get a smaller number. If calibration of either or both load cells is not precise, or they drift differently during a test or after calibration, one can reasonably expect significant errors in the sleeve values determined this way.

Compression Cones (these authors perceive) were developed in the first instance ostensibly to improve a CPT's ability to measure sleeve friction.

3 THE CURRENT PARADIGM

So this is the current industry-wide paradigm:

- If you want to most accurately measure sleeve friction, you must use a Compression Cone.

In support of this statement that this is the current paradigm, refer (Robertson et al 2015), as follows:

For accurate sleeve resistance measurements in soft sediments, it is recommended that cones have separate (compression) load cells.

And in support of something that follows in this paper, quoting from the same document as above, the following paragraph, referring now to Compression Cones:

f_s measurements, in general, will be less accurate than tip resistance, q_c , in most soft fine-grained soils.

The problem is that, in extremely soft or ooze-like soils, this “in general expected lower accuracy” in f_s typically ends up meaning no f_s measurement at all, or something too low to be credible.

4 EXPLANATION – WHY VERY SMALL SLEEVE FRICTIONS ARE ELUSIVE

4.1 A simple explanation – referring to Figure 1

- In a Compression Cone, the sleeve has to move slightly to permit it to apply load to the friction sleeve load cell.
- Dirt seals behind the friction sleeve resist this slight movement and use up some of the force applied by soil friction to the friction sleeve.
- Hence a noticeable error occurs if this applied force is very low (as it will be in extremely soft materials).

If one is testing stronger materials then it's not a significant issue at all, but if one is testing extremely soft material it becomes a problem.

Until recently this limitation was typically handled as an “elephant in the room”, not talked about much, but rather agonisingly hanging around in the shadows in the background of CPT testing.

But it's become a pretty big deal for organisations like IGS that nowadays do much testing in extremely soft or ooze-like soils; and for their clients.

4.2 References to this problem by others

This issue was discussed at CPT'14 in a paper (Santos et al 2014) where the authors ascribed the problem to the friction in sleeve seals and presented an example sleeve calibration showing the difference in load cell readings compared to applied load (Figure 2a) without friction sleeve seals, and (Figure 2b) with seals.

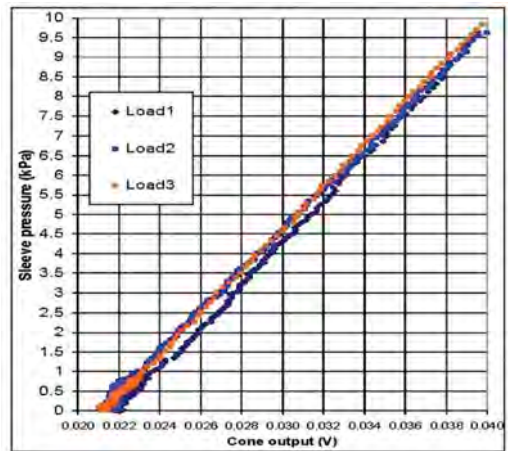


Figure 2(a). Sleeve calibration with no seals (Santos et al 2014).

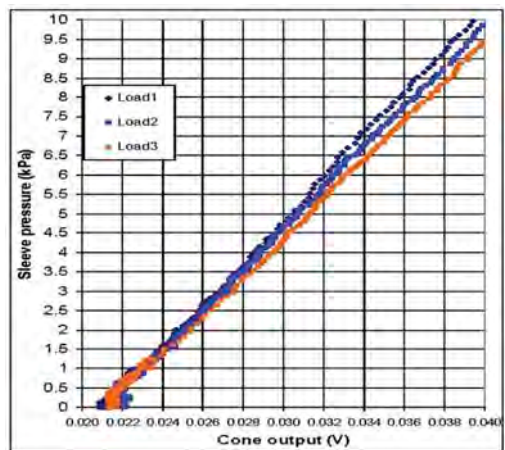


Figure 2(b). Sleeve calibration with seals (Santos et al 2014).

Those authors discussed an innovative spring-loaded (preloaded) sleeve seal design to attempt to solve the problem. This has/had been taken up by A.P. van den Berg for their cone design.

The issue was again mentioned in a paper at the 2021 Mine Waste and Tailings Conference, (Entezari et al 2021). In that paper, the authors were discussing limitations in the use of CPT data to determine the fines content of extremely soft oil sands tailings.

In that paper, for the analysis they were undertaking, many data points were “*screened out in order to remove data where the soil-sleeve friction was less than internal o-ring (sic) friction*”.

This meant discarding a good deal of their data.

5 IGS WANTED A SOLUTION – NOT AN EXCUSE OR ANOTHER COMPROMISE

IGS wanted a solution, so talked at length to their supplier/partner Geomil as to what this might entail. They then jointly conceived and funded an atypical design as a trial.

The conversation and thinking went as follows:

- a) As described in Section 4, Compression Cones have friction sleeves that must move a small amount to be able to register an f_s reading.
- b) The sleeves of Subtraction Cones do not have to move more than a minuscule amount to register friction load. But they have the historically-deemed problem of having to subtract one big number from another big number to get a small one, as discussed in Section 3.
- c) As one solution, would it be possible to develop a Subtraction Cone with unusually high quality and sensitive load cells, and to calibrate these very rigorously to help overcome the problem in subtracting a big number from a big number?
- d) And would it be possible to design for much lower cone capacity overall, hence making the two big numbers smaller, further reducing the problem?
- e) And would it be possible to make the load cells more responsive than normal, by adopting different construction materials for the elastic bases on which the cells’ strain gauges would be fixed?

Of course this would all comprise a significant paradigm shift, compared to the existing one. Reiterating here: *If you want to most accurately measure sleeve friction, you must use a Compression Cone.*

Some heart was taking in the knowledge that Fugro’s very sensitive Fibre Optic Cone, announced at the prototype stage via a paper (Looijen et al 2018) at CPT’18 in Delft, also designed for testing soft materials, is a Subtraction Cone with unusually sensitive load cells; in principle the same idea.

So IGS and Geomil talked more and eventually Geomil made a first small run of special cones to the agreed design. In accord with (c) and (d) above, they opted for a cone size of 15cm² and tip capacity of

only 3MPa; this being adequate for the testing of extremely soft materials that were/are the target.

And, in accordance with (e) above they opted for a special alloy base for the load cells, giving a physical strain gauge response approximately 300% greater than it would be for a conventional steel base.

Of course, also in accordance with (c) above, IGS has adopted the same calibration regime discussed in Section 1, with the enhancement of using dead weights for the application of load to the tip and sleeve for (at the moment) the bottom approximate 6% of loading; ie up to ~0.17MPa on the tip and ~11.5kPa on the sleeve. Planning is that in the future IGS will go full-range with the dead weights. At present they are using a very sensitive calibrated load cell of just 5kN capacity for the remainder of the range.

6 HIGH HOPES AND EXPECTATIONS

Because of high hopes for these cones, IGS has set a policy in place that, to the extent possible, they will calibrate these cones to achieve the accuracy outcomes proposed by the new draft international standard ISO/DIS 22476-1 criteria for Class 1+ cones.

To date that objective is looking good. A full IGS calibration for one of these cones is shown on the last page of this paper.

In other words, these cones, under these rigorous calibration processes, are pretty remarkable by current measures.

Of course calibration is just one aspect of a CPT. How have these cones behaved in the field?

7 FIELD TRIALS

IGS has had several 3MPa cones in operation now for a few months, in one place testing very soft natural soils and in other places testing ooze-like tailings sediments. The results are satisfying, demonstrating:

- a) Ability to repeatably detect, measure and record very low q_c values – say 10kPa and even below.
- b) Ability to repeatably detect, measure and record very low f_s values that make sense when compared to the q_c values being measured – say 1kPa and even below.

Figure 3 below, shows the improved response to sleeve friction compared to what was previously possible.

Laboratory tests on samples taken from this coal tailings dam site showed the materials tested (in the test plot “troughs”) to have:

- 37% fine sand, 51% silt size, 12% clay size.
- Liquid Limit 34%, Plasticity Index 9%, Moisture Content 40.5% (ie in liquid phase).
- Soil Particle Density (“SG”) 1.52t/m³.

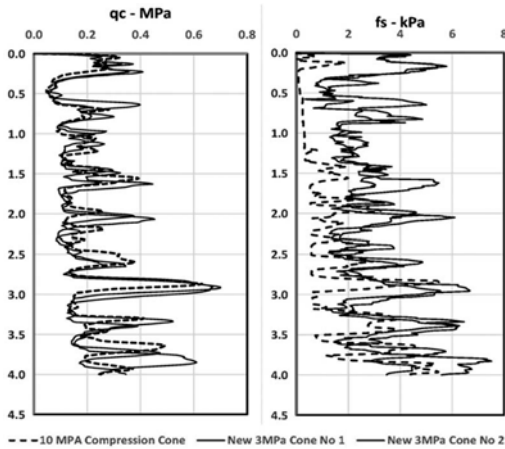


Figure 3. Q_c and f_s plots – new 3MPa cone vs 10MPa Compression Cone – tests by IGS – plotted to 4.0m depth for relevance.

All the tests undertaken with these new cones show the ability to measure very low q_c and a much improved response in regard to sleeve friction.

8 CPT-BASED SOIL BEHAVIOUR TYPE (SBT)

Data from the tests shown in Section 7 have been processed using the computer software CPeT-IT v.3.0 – CPT Interpretation Software (Ioannides 2007) to plot CPT-based Soil Behaviour Type using the classification system proposed by Robertson (2016). Plots are shown below as Figures 4(a) and (4(b)).

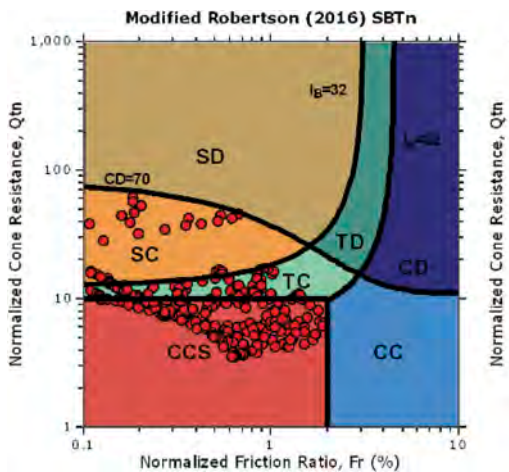


Figure 4(a). SBT to 3.2m from 10MPa Compression Cone.

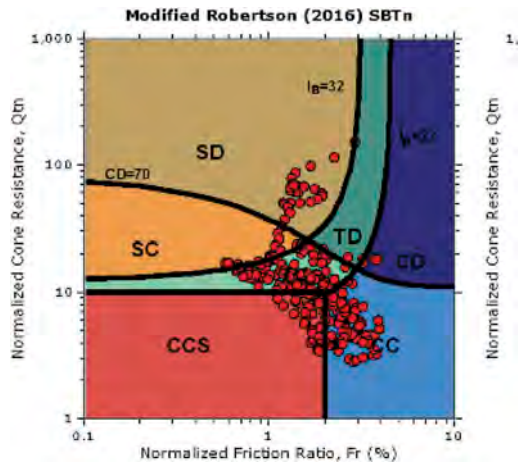


Figure 4(b). SBT to 3.2m from the new 3MPa Cone.

- CCS: Clay-like – Contractive – Sensitive
- CC: Clay-like – Contractive
- CD: Clay-like – Dilative
- TC: Transitional – Contractive
- TD: Transitional – Dilative
- SC: Sand-like – Contractive
- SD: Sand-like - Dilative

The data from the new 3MPa cones interpret SBT that is significantly different to that from the 10MPa Compression Cone.

9 FIELD TRIALS - ZERO-LOAD-OFFSETS

The CPT industry/profession is passionate on the issue of comparing “before-vs-after” zero-load-offset values as a method of determining/monitoring:

- the quality and actual condition of a cone itself, and
- the quality of a test that has been undertaken.

IGS’s cone history recording system will one day allow a report on the reliability of this dependence on zero-load-offsets; a quantified study to support the passion (or otherwise).

In the meantime however it is acknowledged that this is an accepted field indicator of the quality of a test undertaken, so monitoring and recording these zero-load-offsets is part of IGS’s every-test practice.

The new draft ISO/DIS 22476-1 relies heavily on this parameter in determining test quality, called “Test Category”, with different Categories/qualities numbered A to D in the draft; A being the highest quality.

Under the draft standard, one decides the Test Category by:

- a) the Class of cone used and
- b) the drift/difference in the before-vs-after zero-load-offset values.

In the draft standard, a before-vs-after drift/difference of less than 15kPa for the tip, combined with less than 2kPa drift/difference for the sleeve, categorises the test as Class A, the highest test quality classification.

This typically involves measuring the after-test-offsets once the cone has been cleaned and reassembled after testing. It cannot be a value extracted from the completed test's data file, as this immediately-after value is likely to be influenced by dirt in seals and gaps after cone extraction.

Figures 5(a) and 5(b) below show sets of before-vs-after drift/difference data from the first three IGS jobs, using two of these new 3MPa cones.

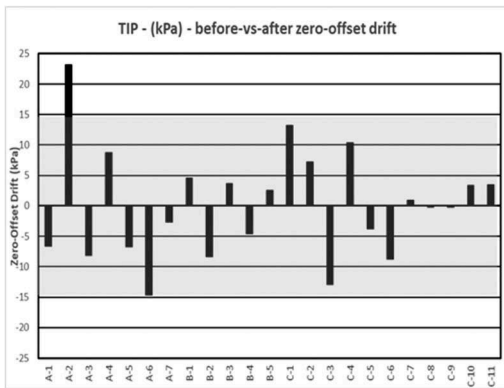


Figure 5(a). Before-vs-After Tip Zero-Load-Offsets -23 tests by IGS (grey shaded band is +/- 15kPa).

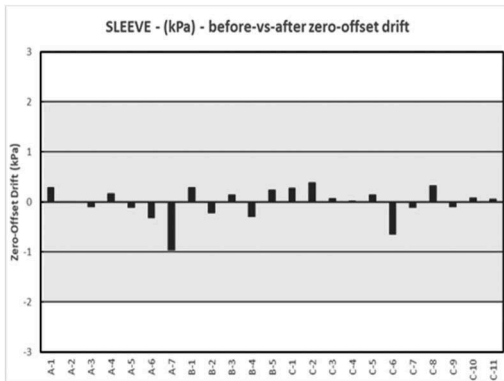


Figure 5(b). Before-vs-After Sleeve Zero-Load-Offsets -23 tests by IGS (grey shaded band is +/- 2kPa).

The data shows that, except for one test, all of these tests undertaken using the 3MPa cones have experienced drift/difference of less than the designated 15kPa for the tip, and all achieved better than 2kPa for the sleeve.

The single test that fell outside 15kPa for the tip was the second test ever made using one of these cones and the before-vs-after monitoring process in

that instance had not been undertaken cautiously – transient temperature shift was a possible cause of that aberration – remember that these are all very small numbers.

By the time of the CPT'22 Conference IGS's database will be more comprehensive.

10 TRANSIENT TEMPERATURE EFFECTS

Transient temperature effect is a matter that IGS takes seriously in all of their testing. Their default testing procedures do what is reasonably possible to minimise these effects during all stages of a test.

The new 3MPa cones are each fitted with a temperature sensor and IGS is currently developing a plot format for these cones that will include temperature along with the usual parameters of q_c , f_s and u .

The work has not yet been done; however we anticipate that these new cones may stabilise more quickly than conventional cones due to the use of the special alloy instead of steel in the load cell bases.

By the time of the CPT'22 Conference we authors expect to be able to report on this aspect of these new 3MPa cones.

11 SUMMARY AND CONCLUSIONS

Measurement of extremely low sleeve friction (f_s) values during CPT testing is an industry-wide problem, often treated as an “elephant in the room”.

This paper describes the development of an innovative new CPT cone that the authors believe has largely solved this problem.

The solution has involved shifting of the paradigm, that “*if you want to most accurately measure sleeve friction, you must use a Compression Cone*”. This solution involved the use of a Subtraction Cone design.

The solution also involved development of more-responsive-than-conventional load cells using a special alloy for the load cell base, rather than steel.

So far the new CPT, calibrated and managed as described in this paper, is meeting or exceeding the authors' expectations.

REFERENCES

- Entezari, I., T. Boulter, S. McGregor, & J. Sharp (2021). Machine Learning to Estimate Fines Content of Tailings Using Gamma Cone Penetration Test. *Australia: Proc AusIMM Mine Waste And Tailings Conference*.
- Ioannides, (2007) CPeT-IT CPeT-IT v.3.0 – CPT Interpretation Software. (Online). Available: <http://geologismiki.gr/products/cpet-it>
- Looijen, P., N. Parasie, D. Karabacak & J. Peuchen (2018) Fibre optic cone penetrometer. *The Netherlands: Proc CPT'18*.
- Lunne, T., P.K Robertson & J.J.M Powell (1997). *Cone Penetration Testing In Geotechnical Practice*.

Robertson P. K. & K.L. Cabal (2015) *6th Edition Guide to Cone Penetration Testing for Geotechnical Engineering*.
 Robertson P. K. (2016) Cone penetration test (CPT)-based soil behaviour type (SBT) classification system – an

update. *Canadian Geotechnical Journal* 53, 12, December 2016.
 Santos R.S., A. Barwise & M. Alexander (2014). Improved CPT sleeve friction sensitivity in soft soils. *Las Vegas, USA, 3rd International Symposium on Cone Penetration Testing*.

CONE IDENTIFICATION AND DIMENSIONS SHEET

3 MPa Special Purpose Piezocone

Note that this cone calibration has been undertaken taking these "actual" dimensions into account:

cone area: 16.22 cm ²	sleeve area: 228.91 cm ²	
---	--	--

NOMINAL TIP

Cone No	AS15CPIPT_S21003
Type	SPECIAL PURPOSE
Tip Area (sq cm)	16
Tip Capacity (MPa)	3
Calibration Date	15 October 2021

MEASURED TIP DIMENSIONS ISO 22476-1:2012 requirements

CD	44.62	critical	43.20	to	44.10	mm
CH	38.50		29	to	38	mm
S	11.74		9	to	12	mm
A	68.00		55	to	65	degrees

actual tip area = 15.22 cm²
deviation = 1.4%

NOMINAL SLEEVE

Cone No	AS15CPIPT_S21003
Type	SPECIAL PURPOSE
Sleeve Area (sq cm)	228
Sleeve Capacity (kPa)	300
Calibration Date	15 October 2021

MEASURED SLEEVE DIMENSIONS ISO 22476-1:2012 requirements

SD-1	44.11	critical	44.02	to	44.37	max 44.2
SD-2	44.11	critical	44.02	to	44.37	max 44.2
SL	165.19		162.3	to	165.3	

actual sleeve area = 228.91 cm²
deviation = 1.7%

PORE PRESSURE

Cone No	AS15CPIPT_S21003
Type	SPECIAL PURPOSE
Piezo Capacity (kPa)	2000
Calibration Date	15 October 2021

CALIBRATED BY: AS

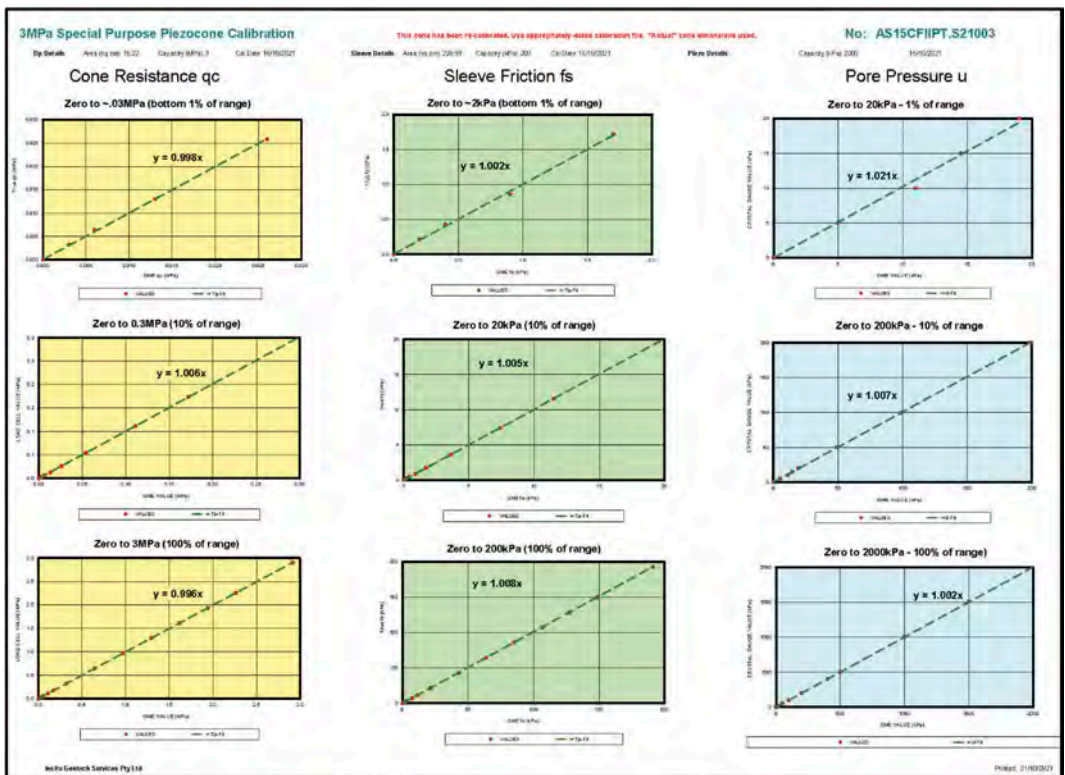
DATE: 15/10/2021

NOTES:

CHECKED BY:

DATE:

NOTES:



Assessment of seismic cone penetration testing for small strain shear modulus

N. Parasie, T. Franken & J. Peuchen

Fugro, Nootdorp, The Netherlands

ABSTRACT: Reliable values of in situ shear modulus at small strain (G_{max}) are important for foundation design, particularly for large investments in offshore wind energy. The seismic cone penetration test (SCPT) method is commonly considered as primary reference for providing G_{max} of soil. The SCPT data acquisition process covers a combination of cone penetration testing and seismic downhole testing. Values of shear wave velocity are correlated with G_{max} . This paper presents a complete inventory of SCPT standard uncertainty components for G_{max} . These components are ranked as Low, Medium or High, indicating relative impact on a combined standard uncertainty budget for derived values of G_{max} . Supplementary discussion is provided based on theory and practice, with suggestions on uncertainty reduction. The focus of the assessment is on conventional SCPT systems, with a hammer impact source at ground surface and a dual-receiver seismic cone penetrometer.

1 INTRODUCTION

The in situ shear modulus at small strain (G_{max}) is one of the important soil parameters for geotechnical design situations for which relatively small displacements are critical to structure performance, for example monopile response to horizontal load is governed by soil stiffness and monopile stiffness. By reducing the uncertainty in soil stiffness, the monopile foundation design can be further optimized.

At this low strain level, the soil response is too small for direct measurement of G_{max} . Therefore, G_{max} is typically derived indirectly from shear wave velocity (v_s) and bulk (mass) soil density (ρ), using $G_{max} = \rho \cdot v_s^2$.

Due to good cost-quality ratio, the seismic cone penetration test (SCPT) is one of the most commonly applied acoustic methods for providing G_{max} of soil. SCPT data acquisition covers a combination of cone penetration testing and seismic downhole testing. SCPT methodology is well documented; examples are ISO 19901-8 (2014), ASTM D7400 (2019) and Campanella & Davies (1994). Styler et al. (2016) provide an excellent overview of 35 years of SCPT experience, including equipment, procedures and interpretation of seismic signals.

SCPT data acquisition provides derived values of ' $v_{s;vh}$ ', where v and h refer to (approximately) vertically downward propagating (v), horizontally polarized (h) shear waves. Hence, G_{max} discussed in this paper is ' $G_{max;SCPT}$ '.

Various publications cover individual uncertainty components for G_{max} derived from SCPT data.

Examples include Gillespie (1990), Howie & Amini (2005), Stolte & Cox (2020), and Styler et al. (2016). This paper provides a complete overview of standard uncertainty (u_i) components for G_{max} (Sections 3 and 4) as basis for a combined standard uncertainty (u_c) budget (Section 5). Supplementary quantification and discussion are provided based on theory and practice, with suggestions on uncertainty reduction.

A clear and complete insight in G_{max} uncertainties is a first step into improving SCPT measurements and consequently providing more accurate G_{max} values for foundation design.

2 PREMISES

This paper uses a Type B evaluation of standard uncertainty (u_i) as defined by ISO (2008). Where a Type A evaluation is obtained from repeated observations, a Type B evaluation is obtained by scientific judgement based on all of the available information on the possible variability of input quantities.

The presented uncertainty assessments consider a conventional SCPT system and two settings for soil conditions (Table 1). Procedure, operator and system design errors are not considered.

The selected SCPT system and procedures comply with ISO 22476-1 (2012), ISO 19901-8 (2014) and ASTM D7400 (2019). It has a polarized hammer impact source at ground surface, with the centre point of the source at

a fixed horizontal offset of 1 m from the initial vertical axis of the push rods of a CPT thrust machine (refer to Section 4.2 for discussion on other source offset distances). A dual-receiver seismic piezocone penetrometer applies, with two sets of 3-component geophones with a centre-to-centre spacing of 1 m (refer to Section 4.3 for discussion on other receiver spacings). The cone penetrometer is stationary for the selected test depth interval and the uncertainty assessments only consider data for the dual-receiver interval. The selected signal sample rate is 3 kHz, with incorporation of pre-trigger data recording. Stacking of 5 to 10 seismic traces is assumed to be applied as standard practice.

Table 1. Soil conditions – two cases.

	Depth	G_{max}	q_c	v_s	ρ
Case	m	MPa	MPa	m/s	kg/m ³
C1 OC clay	4-5	17	~0.65	100	1700
C2 Dense sand	25-26	180	~36	300	2000

OC = overconsolidated q_c = CPT cone resistance

3 INVENTORY OF UNCERTAINTIES

Tables 2 to 4 show u_i components for G_{max} , derived for Cases C1 and C2. The uncertainties are grouped by time/timing components, spatial/ distance components and equipment/setting components. Quantification of the uncertainties is based on values published in literature when available, calculated estimates and/or best-estimate expert assessments (Type B evaluation of u_i).

The 1st column ‘Uncertainty ID’ in the table lists the G_{max} uncertainty components.

The 2nd column ‘Impact’ refers to the influence of the u_i component on G_{max} , expressed as percentage of standard uncertainty (u_i) normalised to the corresponding derived value for G_{max} given in Table 1, i.e. u_i/G_{max} . Tables 2 to 4 use the following categories: L = Low impact with u_i/G_{max} in the range of 0 to 1 %, M = Medium impact with u_i/G_{max} in the range of 1 % to 5 %, and H = High impact with $u_i/G_{max} > 5$ %. Indicators with a ‘?’ are for a best guess uncertainty impact, i.e. more research may be required. The selected ranges for u_i/G_{max} allow focus on understanding and reducing those uncertainties that have M or H impact. About 2/3 of the uncertainly components fall in the L range, 1/6 in the M range and 1/6 in the H range.

The 3rd column ‘Comp.’ stands for ‘Complexity’ and refers to challenges in quantification of an u_i component, rated from Low (L), Medium (M) to High (H) complexity. High complexity items often depend on specific situations or on other u_i

components, which makes them more difficult to quantify and mitigate.

The 4th column ‘Dep.’ Refers to dependencies of u_i components, i.e. primary and secondary uncertainties shown by the IDs in the left column of each table.

The 5th column ‘Notes’ includes items such as brief clarifications of the u_i components, references to literature and/or references to Section 4 for more detailed discussion.

4 SUPPLEMENTARY NOTES

4.1 Ray path between source and receivers

This section provides notes on Uncertainty ID 5 of Table 3. The uncertainties assessed for cases C1 and C2 assume straight-line ray paths between source and receivers. The uncertainties are ranked as High impact.

A straight-line assumption is according to common practice, e.g. ASTM D7400 (2019). This practice should be adequate for relatively homogeneous soil conditions within the immediate zone of the depth interval selected for deriving G_{max} . Soil homogeneity (or otherwise) can be readily interpreted from the location-specific CPT profile acquired as part of the SCPT activities.

Actual ray paths between source and receivers are largely controlled by (1) source offset and depth of receivers discussed in Section 4.2 and (2) soil heterogeneity, particularly layer boundaries with high contrast of acoustic impedance. Travel time errors from interval methods generally diminish with depth, as the angle of incidence of ray paths between source and receivers becomes increasingly vertical and the assumption of a straight line becomes more applicable (Butcher & Powell 1996).

Kim et al. (2004) and Hallal & Cox (2019) illustrated high impact on v_s (and thus G_{max}) with a linear ray path assumption where soil layer boundaries with high impedance contrast are in-between the two sets of receivers. For this situation ASTM D7400 (2019) suggests accounting for refracted ray paths by applying Snell’s law using ray tracing methods (RT), or estimation of shear wave velocities from linear trends per layer with support from CPT profiles using slope-based methods (SM). Kim et al. (2004) provide details for these methods.

4.2 Source offset

This section provides notes on Uncertainty ID 7 of Table 3. Cases C1 and C2 consider a lateral source offset of 1 m. The uncertainties are ranked as Medium impact and Low impact.

ASTM D7400 (2019) suggests a lateral source offset in the range of 1 m to 6 m. In practice, both small and large source offsets have advantages and disadvantages.

Table 2. Uncertainties related to time/timing components.

Uncertainty ID	Impact			Dep.	Notes
	C1	C2	Comp.		
1. Trigger timing	L	M	L	4, 21	ISO 19901-8 (2014) and ASTM D7400 (2019) consider trigger timing. Accurate trigger timing can be obtained in several ways, such as trigger-receiver clock synchronization, or by using a very high signal sample rate. Calculations indicate that trigger timing variability accounts for approximately $u_1/G_{max} = 1\%$ for C1 and $u_1/G_{max} = 3\%$ for C2.
2. Signal latency	L	L	L	-	Signal latency has no influence on interval velocity, as it is a constant within a particular data acquisition system.
3. Arrival time selection	L	L	L	1, 6, 14	Stolte and Cox (2020) indicated that arrival time selection methods (first cross-over, maximum peak, cross-correlation) vary by approximately 0.1 ms if any influence from ground conditions is removed. A measurement error of 0.1 ms implies $u_3/G_{max} = 0.4\%$ for C1 and C2. Presentation of a velocity range for several methods can be useful for insight in sensitivity of arrival time selection.
4. Signal sampling rate	L	L	L	10	ISO 19901-8 (2014) and ASTM D7400 (2019) consider signal sampling rate. For recording of traces the Nyquist sampling theorem must be met, i.e. a sampling rate that is at least twice the maximum source signal frequency. Calculations indicate $u_4/G_{max} = 0.1\%$ for C1 and $u_4/G_{max} = 0.2\%$ for C2. For accurate arrival time selection, the signal should be up-sampled to at least 40 kHz.

Table 3. Uncertainties related to spatial/distance components.

Uncertainty ID	Impact			Dep.	Notes
	C1	C2	Comp.		
5. Ray path between source and receivers	H	H	H	4, 7, 8, 9, 11, 20	Refer to Section 4.1.
6. Signal damping and signal distortion along ray path	M	M	M	3, 4, 10, 11, 14, 15, 21	Howie and Amini (2005) indicated effects of waveform shape, near-field influence, attenuation, frequency content, peak frequency shift and signal widening on arrival time selection methods (first cross-over, maximum peak and cross correlation). For a depth range of 4 m to 10 m, the (collective) uncertainties were estimated to be within 0.2% to 2% of theoretical v_s . This implies $u_6/G_{max} = 0.4\%$ to 4% for C1 and C2.
7. Source offset	M	L	M	5, 8, 11, 20	Refer to Section 4.2.
8. Spacing of receivers	M	M	H	4,5,9, 11,16	Refer to Section 4.3.
9. Spatial position of cone penetrometer relative to source	L	L	H	3,5,7	ISO 22476-1 (2012), ISO 19901-8 (2014) and ASTM D7400 (2019) require determination of vertical position of a cone penetrometer by measurement of penetration length and inclination. Calculations indicate $u_9/G_{max} = 0.7\%$ for C1 and $u_9/G_{max} = 0.1\%$ for C2, based on considerations given by Peuchenand Wemmenhove (2020). Polarization analysis can be applied to estimate relative orientation of the receivers.

For a linear ray path assumption, a source offset in the range 1 m to 4 m will give a relatively small angle of incidence between source and horizontal soil layering. For heterogenous conditions, a source offset closer to the axis of the SCPT push rods is preferred, because the effects of refraction decrease with diminishing source offset (Kim et al. 2004). For penetration depths of less than 5 m, Butcher & Powell (1996) indicate u_7 ranging from approximately 1 % of v_s for

a 1 m source offset to 20 % of v_s for source offsets of > 4 m. These values correspond to $u_7/G_{max} = 2\%$ and $u_7/G_{max} = 44\%$.

For source offsets > 4 m the assumption of linear ray paths should not be applied and refracted ray paths should be accounted for (refer to Section 4.1). The use of larger source offsets can limit near-field effects of refracted waves and improve estimation of interval velocities (Baziw & Verbeek 2014).

Table 4. Uncertainties related to equipment/ setting components.

Uncertainty ID	Impact				Notes
	C1	C2	Comp.	Dep.	
10. Frequency spectra of source and receivers	L	L	M	-	Low impact for C1 and C2 considers that the receivers are capable of recording the source frequency spectrum. Records of the source signature (signal) can be useful for evaluation of frequency spectra.
11. Soil stratigraphy and soil anisotropy	M	M	H	-	Refer to Section 4.4.
12. Imperfect source	L	L	H	15	A hammer source is theoretically seen as a point source creating a perfect pulse signal. In practice, the source has inertia and has a specific geometry; the pulse signal will be imperfect. Gillespie (1990) concludes that source-soil coupling and stacking significantly reduce impact of variations in the source impulse. Isolation of the first arrival peak may be considered during data processing to remove, for example, ringing in the recorded signal.
13. Inertia of push rod and seismic cone penetrometer	L?	L?	H	-	The receivers are fixed in a stiff metal rod instead of fully decoupled points in soil. Resulting uncertainties appear unknown.
14. External noise	H	H	H	-	Cases C1 and C2 consider common levels of external noise. External noise is typically expressed as signal to noise ratio (SNR). Examples for SNR improvement are (1) a more powerful source, (2) SCPT system engines switched-off and (3) selection of day/ time of data acquisition with low external noise conditions related to traffic and/or weather. SNR can be determined by evaluating the magnitude spectrum of external noise recorded from e.g. pre-trigger of the receivers. Filtering for external noise can be applied outside the frequency range of the seismic source signal.
15. Source-soil coupling and decoupling from hold-down mass	L	L	M	11, 12	Depending on source characteristics and source-soil interface, soil degradation can progressively develop with number of hammer strikes. The use of dampers between hold down mass and source is common. Examples for potential improvement include (1) increase of the hold down mass (or vertical force), (2) implement geometry/ material for high shear coefficients at source-soil interface and (3) locally increase ground resistance by surface levelling and/or ground improvement.
16. Receiver characteristics	L	L	L	10	Detrending and demeaning of recorded data can be applied to remove system drift. A systematic error of system drift between receivers is sometimes observed. The cause of this error is unclear, although Styler et.al. (2013) rule out a systematic orientation bias and time-bias between receiver pairs.
17. Receiver-soil coupling	L	L	M	8, 9, 11	SCPTs generally provide good receiver-soil coupling. Soil containing e.g. gravel, cobbles or cemented zones may be unfavourable. ISO 19901-8 (2014) and ASTM D7400 (2019) allow a seismic receiver module with a slightly larger diameter compared to the push rod section below and above the seismic receiver module.
18. A/D conversion of receiver data	L	L	L	4, 10	Cases C1 and C2 assume appropriate design for instrument response, analogue to digital (A/D) conversion, jitter, etc.
19. Near field effects	H	L	H	3,7, 8,9, 10, 12,14	Especially at shallow depths (<5 m), seismic signals can be affected by interference with surface waves, acoustic reflections from ground surface at shallow depth and limited recordable source frequency spectrum.
20. Wave propagation through push rods	L	L	H	5	Acoustic waves through steel push rod are much faster than v_s for soil and therefore pose no problem in interpretation of S-wave arrivals. Decoupling of push rods from the thrust machine (unclamping) may reduce unwanted wave propagation through the push rods.
21. Source signal repeatability	L	L	L	1, 12, 15	Gillespie (1990) mentions time measurement repeatability within 0.05 ms due to varying frequency content of the source. For C1 and C2, this would imply $u_{21}/G_{max} = 0.2\%$. Monitoring of non-normalized traces acquired during SCPT data acquisition can allow removal of any 'bad' traces from the dataset.
22. CPT thrust machine imposes stresses and strains to soil	L?	L	M	-	Uncertainty for G_{max} for C1 depends on soil stratigraphy for depth zone of 0 to 5 m. In general, uncertainty is assessed as Low impact below about 5 m below ground surface.
23. Push rods and cone penetrometer impose stresses and strains to soil	L?	L?	H	-	The soil influence zone is in the order of 0.15 m around the push rod, potentially creating a higher velocity zone. The geometry of this zone typically shows minor dependence on soil conditions. Therefore, uncertainty is assessed as Low impact. Actual uncertainties appear unknown.
24. Velocity to shear modulus conversion	H	H	M	11	Contributing uncertainties include (1) applicability of theoretical model $G_{max} = \rho \cdot v_s^2$, (2) input of soil density ρ and (3) error for v_s (squared). Soil density derived from measurements of (nearby) high quality soil samples can reduce uncertainty compared to CPT/ SCPT based correlations for soil density.

4.3 Spacing of receivers

This section provides notes on Uncertainty ID 8 of Table 3. The uncertainties for Cases C1 and C2 are ranked as Medium impact for a dual-receiver interval of 1 m.

A choice for spacing of receivers typically represents a trade-off for considerations such as practicability, depth resolution and accuracy of G_{max} values (e.g. Gibbs et al. 2018).

Variation in v_s of approximately 2% has been demonstrated by Styler et. al (2013) between receiver pairs spaced 0.5 m and 1 m at a depth of 5 m, corresponding to $u_8/G_{max} = 4\%$ for Case C1.

Ghose (2012) presented results of two field experiments conducted with a seismic cone penetrometer with 7 tri-component accelerometers at 0.25 m spacing. An advantage of multi arrays is that it allows for evaluation of measurements over more multiple spacings within a single CPT push. No evidence for reduction of data quality was observed with 0.25 m receiver spacing compared to larger spacings within the same CPT push. These findings suggest that high accuracy G_{max} data can be obtained with relatively small receiver spacing. For heterogeneous soil, a small depth interval improves G_{max} resolution with depth. On the other hand Gibbs et. al. (2018) mention that an improved resolution with 0.5 m receiver spacing may not compensate for the difficulties in accurately determining the shorter time delay between the traces compared to a system with 1 m spacing of receivers.

Selection of a large depth interval allows ‘averaged’ results for G_{max} , with due consideration of ray paths affected by soil layer boundaries with high impedance contrast (see Section 4.1). SCPT results for a combination of small depth intervals and overlapping large depth intervals within one soil unit can provide insight in G_{max} sensitivity for receiver spacing.

4.4 Soil stratigraphy and soil anisotropy

This section provides notes on Uncertainty ID 11 of Table 4. The uncertainties for Cases C1 and C2 are ranked as Medium impact.

Comments on soil stratigraphy are included in Section 4.1.

Soil anisotropy effects on G_{max} are usually not considered or well understood.

Soil can be represented by an elastic stiffness matrix with three shear components G_{vh} , G_{hv} and G_{hh} , where the subscript h denotes horizontal direction and the subscript v denotes vertical direction. Soil is anisotropic, i.e. the isotropic condition where $G_{vh} = G_{hv} = G_{hh}$ is a theoretical simplification. Cross-anisotropy (axi-symmetric conditions where $G_{vh} = G_{hv} \neq G_{hh}$) is a more realistic representation of in situ soil conditions. Pennington et al. (1997) provide an example for cross-anisotropy affecting G_{max} where $G_{hh} \approx 1.5G_{vh}$. Furthermore Pennington et al.

(1997) highlight cases for clays with azimuthal stress variations where $G_{vh} \approx 1.3G_{hv}$, i.e. the assumption of cross-anisotropy does not apply.

The SCPT method records signals of wave propagation in approximately vertical direction with particle motion in an approximately horizontal plane. This means that G_{max} values derived for SCPTs are largely representative of the G_{vh} component for a simple cross-anisotropic case. Soil heterogeneity, stress conditions and more complex anisotropy can require further attention.

Note that cross-hole seismic testing (e.g. ASTM D4428 2014) can approach the G_{hh} component.

5 COMBINED STANDARD UNCERTAINTY

The uncertainty inventory of Tables 2 to 4 is complete, thus allowing approximate estimates to be made for a combined standard uncertainty (u_c) budget for G_{max} .

A simplified approach by assuming sensitivity coefficients c_i equal to 1, would be to calculate u_c according to $u_c^2 = \sum (c_i u_i)^2$ (ISO 2008), where i refers to the uncertainty IDs of Tables 2 to 4. Approximately average values of the selected uncertainty intervals can be assumed for an initial estimate of u_c : $u_i/G_m = 0.2\%$ for Low impact, $u_i/G_{max} = 2\%$ for Medium impact and $u_i/G_{max} = 7\%$ for High impact. This calculation approach gives $u_c/G_{max} = 14.6\%$ corresponding with $u_c = 2.5$ MPa for Case C1 ($G_{max} = 17$ MPa) and gives $u_c/G_{max} = 12.8\%$ corresponding with $u_c = 23.0$ MPa for Case C2 ($G_{max} = 180$ MPa).

The estimated u_c values seem reasonable for the test method (SCPT) and cases considered.

ACKNOWLEDGEMENTS

The authors are indebted to many dedicated colleagues and gratefully acknowledge Fugro’s persistent commitment to excellence in seismic cone penetration testing. The opinions expressed in this paper are those of the authors. They are not necessarily shared by Fugro.

REFERENCES

- ASTM International, 2014. ASTM D4428/D4428M-14: Standard test methods for crosshole seismic testing. West Conshohocken: ASTM International.
- ASTM International, 2019. ASTM D7400/D7400M-19: Standard test methods for downhole seismic testing. West Conshohocken: ASTM International.
- Bazui E. & Verbeek G., 2014. Identifying critical layers using SCPT and seismic source moveout. In Cone Penetration Testing 2014: Proceedings of the 3th International Symposium on Cone Penetration Testing (CPT14): Las Vegas, Nevada, USA, 12-14 May 2014 (pp. 357–364). CRC Press.

- Butcher, A.P., & Powell, J.J.M., 1996. Practical considerations for field geophysical techniques used to assess ground stiffness. In *Advances in Site Investigation Practice: Proceedings of the International Conference Held in London on 30-31 March 1995*.
- Campanella, R.G. & Davies, M.P., 1994. The seismic piezocone: a practical site investigation tool. In: *Geophysical Characterization of Sites*, ISSMFE, Technical Committee No 10 for XIII ICSMFE, New Delhi, India.
- Gibbs, P., Pedersen, R.B., Krogh, L., Christopher, N., Sampurno, B. & Nielsen, S.W., 2018. Challenges in marine seismic cone penetration testing. In M.A. Hicks, F. Pisanò & J. Peuchen (eds.). *Cone Penetration Testing 2018: Proceedings of the 4th International Symposium on Cone Penetration Testing (CPT18)*: Delft, The Netherlands, 21-22 June 2018 (pp. 303–308). CRC Press.
- Gillespie, D.G., 1990. Evaluating shear wave velocity and pore pressure data from the seismic cone penetration test (Doctoral dissertation, University of British Columbia).
- Ghose, R., 2012. A microelectromechanical system digital 3C array seismic cone penetrometer. *Geophysics*, 77(3), WA99–WA107.
- Hallal, M.M. & Cox, B.R., 2019. Theoretical evaluation of the interval method commonly used for downhole seismic testing. In *Geo-Congress 2019: Engineering Geology, Site Characterization, and Geophysics* (pp. 376–386). Reston, VA: American Society of Civil Engineers.
- Howie, J.A. & Amini, A., 2005. Numerical simulation of seismic cone signals. *Canadian geotechnical journal*, 42(2), 574–586.
- International Organization for Standardization, 2008. *ISO/IEC Guide 98-3:2008 Uncertainty of measurement - Part 3: Guide to the expression of uncertainty in measurement (GUM:1995)*. Geneva: ISO.
- International Organization for Standardization, 2014. *ISO 19901-8:2014 Petroleum and Natural Gas Industries - Specific Requirements for Offshore Structures - Part 8: Marine Soil Investigations*. Geneva: ISO.
- International Organization for Standardization, 2012. *ISO 22476-1:2012 Geotechnical investigation and testing — Field testing — Part 1: Electrical cone and piezocone penetration test*. Geneva: ISO.
- Kim, D.S., Bang, E.S. & Kim, W.C., 2004. Evaluation of various downhole data reduction methods for obtaining reliable Vs profiles. *Geotechnical Testing Journal*, 27(6), 585–597.
- Pennington, D.S., Nash, D.F.T. & Lings, M.L., 1997. Anisotropy of G0 shear stiffness in Gault clay. *Géotechnique*, 47(3), 391–398.
- Peuchen, J. & Wemmenhove, R., 2020. Depth accuracy of data points in marine soil investigation. In Z. Westgate (ed.). *4th International Symposium on Frontiers in Offshore Geotechnics (ISFOG 2020): proceedings* (pp. 1036-1045). Deep Foundations Institute.
- Stolte, A.C. & Cox, B.R., 2020. Towards consideration of epistemic uncertainty in shear-wave velocity measurements obtained via seismic cone penetration testing (SCPT). *Canadian Geotechnical Journal*, 57(1), 48–60.
- Styler, M.A., Weemee, I. & Mayne, P.W., 2016. Experience and observations from 35 years of seismic cone penetration testing (SCPTu). *Proceedings GeoVancouver 2016 (Proc. 69th Canadian Geotechnical Conference, Westin)*.
- Styler, M.A., Woeller, D. & Howie, J.A., 2013. Measuring down-hole shear waves from a vibrating perpetual source during Cone Penetration Testing. In *Canadian Geotechnical Conference: GeoMontreal, No. 442*, Montreal, Canada.

Experimental procedure for checking the saturation degree of piezocone tips

I. Rocchi

Department Environmental Engineering, Technical University of Denmark, Denmark

L. Tonni, G. Gottardi & M. Marcolongo

Department DICAM, University of Bologna, Italy

ABSTRACT: A correct measurement of the water pore pressure is essential to obtain reliable CPT results. Although this has always been a major concern, it still remains a possible relevant source of error in common engineering practice. In addition to usual reasons, such as malfunctioning of the equipment, its poor calibration and/or maintenance, a lack of complete saturation of the piezocone tip can play a major role. In fact, a correct and timely pore pressure measurement relies entirely on the full saturation of the pore pressure system. The variety of saturation fluids and methods that is encountered in practice is a clear evidence of the still existing uncertainties on the most suitable procedure. Furthermore, unless the saturation process is explicitly detailed, its choice is typically left to the contractor and the measurement quality can only be established a posteriori, after the test has been completed. This paper describes a novel experimental equipment that enables quantifying the degree of saturation of the piezocone tip prior to testing. The methodology proposed is inspired to the B-value check, which is routinely used in geotechnical laboratory testing to assess the degree of saturation, e.g. prior to triaxial testing. In addition, it could also be applied after a test, so that it would be possible to assess whether saturation was retained while testing. This promising approach, when extended to different saturation procedures and validated by engineering practice, has the potential to become a relevant benchmark for reliable CPT testing.

1 INTRODUCTION

Piezocone testing in its simplest version, i.e. including independent measurements of cone resistance (q_c), sleeve friction (f_s) and pore pressure (u_2), was established in the eighties and has since gained a leading role in field classification and characterization of soils. Piezocone measurements can be affected by a number of imprecisions, as accurately explained by Sandven (2010). These include, but are not limited to malfunctioning of the equipment, poor calibration and/or maintenance, which are shared with other experimental techniques. However, a lack of complete saturation plays a key role and is specific to CPTU tests. Although this has long since been acknowledged and has been a major concern since the advent of CPTU, it still remains a large source of error in common engineering practice, possibly the most important.

A correct measurement of the pore pressure is essential to obtain reliable CPTU results in terms of both soil profiling and mechanical properties evaluation. In terms of profiling, high quality measurements of pore pressure are particularly important for fine grained materials and intermediate soils, where pore pressure response is crucial to an accurate soil classification, for example using normalized pore pressure parameters as suggested by Schneider et al. (2008).

Furthermore, reliable pore pressure measurements are also important because the correct cone resistance (q_t) is determined as $q_t = q_c + (1 - a)u_2$, where a is the area ratio of the cone, typically between 0.8-0.9. In addition, thin lenses are better detected by sudden variations in the pore pressure readings, as layers ahead of the tip might influence the resistance recorded due to plugging or punch through phenomena (Lunne et al. 1997). Furthermore, high quality measurements are fundamental to provide reliable input parameters. For example, compliance in the measuring system can provide misleading results when assessing consolidation parameters by means of dissipation tests.

Variables such as the (porous) filter element location and design, the volume of the chamber connecting the filter to the pore pressure transducer, the saturation fluid and its degree of saturation, the air entry (i.e. cavitation) value of the system and lag time required for “resaturation”, as well as the depth and saturation of soil during testing, all affect the pore-water pressure measurement during testing (dynamic measurement) and dissipation, upon stopping the advancement of the tip. However, the quality can only be established a posteriori, i.e. after the test has been completed.

This paper describes an innovative approach that allows quantifying the degree of saturation of the

piezocone prior to testing. The methodology proposed uses the pore-pressure parameters proposed by Skempton (1954) and is routinely used in laboratory testing to assess saturation, e.g. prior to triaxial testing. Preliminary laboratory measurements on a given piezocone, filter and saturation fluid under different saturation conditions of the filter are presented to establish whether there is a measurable correlation between the pore pressure coefficient and the saturation degree of a piezocone tip.

2 SATURATION IN LABORATORY TESTING

Saturation of soil pores is of paramount importance in laboratory testing, not simply because the strength and deformability properties may differ considerably between saturated and unsaturated states, but also because any effective stress analysis is developed based on tests results obtained in experimental set ups that rely heavily on this assumption. For example, the consolidation theory formulated by Terzaghi & Fröhlich (1936) is based on the assumption that volumetric strain is solely a result of change in the void ratio, or water content, of the soil, i.e. that the soil grains and water are incompressible and the soil is saturated. While it is possible to calculate the volumetric strain in an oedometer without relying on this assumption, by measuring the change in the height of specimen, this is not in other cases, such as triaxial tests. In this case, the volumetric strain calculated is based on the volume of water entering or leaving a closed hydraulic system connected to the soil specimen. Therefore, any element in this hydraulic system having compressibility higher than the soil specimen (i.e. air bubbles) affects the strain measured as a result of an increment in stress. On the other hand, in a triaxial undrained test the effective stress is calculated as the difference between the applied total stress and the pore pressure measured in a closed system connected to the soil specimen. Based on the pore-pressure coefficients (Skempton 1954)

$$\Delta u = B[\Delta\sigma_3 + A(\Delta\sigma_1 - \Delta\sigma_3)] \quad (1)$$

Where $\Delta\sigma_1$ and $\Delta\sigma_3$ are the changes in the principal stresses, while A and B are the pore-pressure coefficients. Assuming a closed hydraulic system disconnected from the specimen, if the system is not compliant (i.e. infinite stiffness) an isotropic increment of stress, must result in an equal increment in the fluid pressure, which corresponds to the pore pressure in the soil specimen. Compliance may arise from deformability of the hydraulic system, soil grains or the fluid, but typically, it is assumed that the two increments are the same for a saturated soil. In other words, the only relevant source of compliance is assumed to arise from air in the soil pores or elsewhere in the system.

Saturation in triaxial tests is checked based on this principle, by applying an isotropic increment of total

stress (i.e. cell pressure) in undrained conditions and monitoring the response in pore pressure. The ratio between the increment observed in pore pressure and the increment applied in cell pressure (B) is approximately 1 for saturated soils. Since the smaller the ratio, the larger the error in the measurement, standards require to proceed with testing only after having achieved $B = 0.95-0.97$ for sands and $B = 0.97-0.99$ for clays. Because correct pore pressure and volumetric strain measurements rely entirely on the full saturation of the pore pressure system, if the B value is not satisfactory, the pressure of the hydraulic system (i.e. back pressure) is increased maintaining a constant effective stress, so that air bubbles are dissolved and the compressibility of the fluid reduced.

3 SATURATION IN PIEZOCONE TESTING

Table 1 provides an overview of the porous materials and pore size suggested in different standards and used in practice, based on an international survey by DeJong et al. (2007). The great variety of saturation methods and media encountered in engineering practice is a symptom of the uncertainties that still exist on the subject. The most commonly used materials are relatively few. Polypropylene filters have the advantage to be inexpensive and disposable, but have comparably higher compressibility than sintered steel or ceramic filters, which are respectively subject to wear or brittleness on the other hand. The range of the filter pore size is rather wide. In fact, there is one order of magnitude difference in the ranges allowed by ASTM (D5778-12) and EN ISO 22476-1-2012 (i.e. the standard recommended by also the Eurocode7), while several sizes are encountered in practice, where the largest size used is beyond the prescribed ranges.

Table 1. Filter characteristics in piezocones.

Setting	Material	Pore size μm
ASTM Standard D5778-12	Sintered steel or bronze	20-200 μm
	Ceramic Plastic	
EN ISO (EC7) Standard	Sintered steel or bronze	2-20 μm
	Ceramics	
	Porous PVC and HDPE Carborundum	
Current practice*	Sintered steel or brass	10, 50, 80, 120, 150, 250 μm
	Ceramic	
	Plastic	
	Sintered glass beds	

*Data from DeJong et al. (2007).

With regards to the saturation fluid for the filter, both ASTM and Eurocode7 suggest deaired water only if tests are carried out throughout saturated non-dilative (e.g. dense sands) soils. Otherwise, glycerin or similar high viscous fluids are suggested, such as silicon oil. However, according to DeJong et al. (2007) a much wider variety of fluids is used, including hydraulic oil, vegetable oil and water-glycerin mix. While higher viscosity diminishes the risks of cavitation, it is counterproductive with respect to the ability to deair the fluid. Similarly, risks of cavitation reduce with pore size, but saturation is more difficult to achieve due to lower permeability.

Finally, with regards to saturation of the filters, ASTM suggests either applying a 90 kPa vacuum while submerging the filters or boiling them in water, both for at least 4 h. Eurocode7 suggests either applying the filters in a vacuum for 24 h, or boiling them in water for at least 15 min. DeJong et al. (2007) investigated the minimum time requirement and vacuum needed to ensure saturation based on a qualitative assessment of 15-45 μm polypropylene filters. Their cross sections was examined after saturation using different fluids mixed with food coloring. Based on this study, saturation by vacuum requires at least 85 kPa. Glycerin takes at least 4 h to saturate the filters, while water and silicon oil take just above and below 1 h, respectively. In particular, the best performance was obtained with low to intermediate viscosity silicon oil (100-1000 cS).

While a correct functioning of the pore pressure measuring system requires saturation of the filters, this is not sufficient in itself to guarantee good results. Air bubbles may be trapped within the tip threaded hollow (1) as showed in Figure 1, or in the chamber connecting the pore pressure transducer and the filter (2). For this reason, the code of practice suggests specific methods to assemble the tip to ensure saturation. In particular, ASTM suggests assembling the filter onto the piezocone while submerged in the deaired medium used to prepare the elements, flushing all confined areas with fluid to remove air bubbles, before tightening the tip on the piezocone. Eurocode7 also suggests assembling the piezocone while submerged in the de-aired saturation fluid. However, it suggests that saturation of the disassembled piezocone can be carried out either by injection of fluid in the chamber connecting the pressure transducer and the filter or by placing the disassembled piezocone under vacuum for 15-30 min. Alternatively, filter-less piezocones can be employed, where the pressure transducer is in direct contact with the soil by means of a grease-filled slot. This so called “slot-filtered” piezocone does not require a specific saturation procedure. However, it must be ensured that no air is trapped while assembling the tip. Furthermore, because of the higher viscosity of the “saturation fluid” it might be more difficult to ensure that it is deaired.

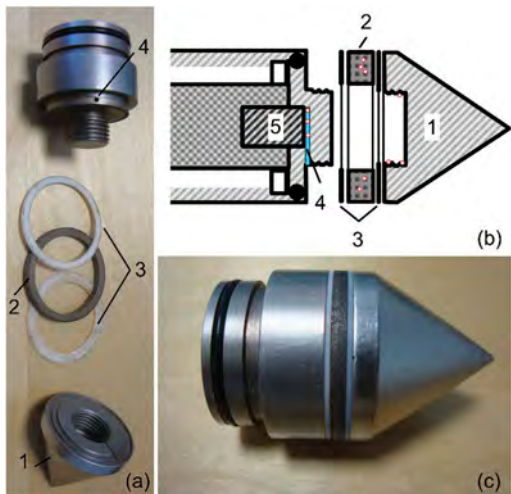


Figure 1. Piezocone tip: (a) disassembled, (b) schematic cross section showing likely location of air bubbles and (c) assembled tip. 1 piezocone tip, 2 porous filter, 3 seals, 4 chamber connecting porous filter to pore pressure transducer and 5 pore pressure transducer.

4 PROCEDURE PROPOSED TO CHECK PIEZOCONES SATURATION

Figure 2a shows a schematic diagram of the device proposed to check the saturation of the piezocone directly on site, whereas the photo of a prototype can be seen in Figure 2b. In essence, the device applies a pressure impulse on the assembled tip through an annular chamber that is placed around the piezocone filter (2 in Figure 2a). The invention is patented by the University of Bologna (Rocchi et al. 2017).

The ratio between the increment recorded by the pore pressure sensor placed inside the piezocone and an independent pressure transducer monitoring the impulse applied, is used to calculate the pore pressure coefficient B . The degree of saturation of the piezocone pore pressure measuring system can then be assessed as a whole, by associating the measured B ahead of testing to the quality of the CPTU test performed. Once the thresholds values for B that guarantee satisfactory results in terms of pore pressure measurements in CPTU tests are established, testing should proceed only if these values are achieved. Otherwise, the tip would be saturated and assembled again, replacing the filter if necessary, until obtaining a satisfactory result (see the flow chart in Figure 3). The test could also be performed at the end of the CPTU so as to assess whether saturation was retained during the test.

5 METHODOLOGY

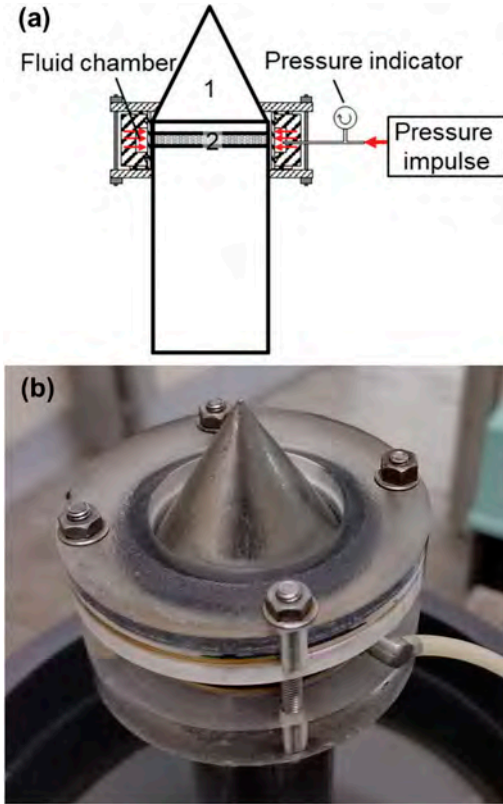


Figure 2. (a) Schematic diagram of the device seen in a cross section, while fitted on the piezocone (side view). 1 Piezocone tip and 2 porous filter. (b) Photograph of the prototype while mounted on a piezocone.

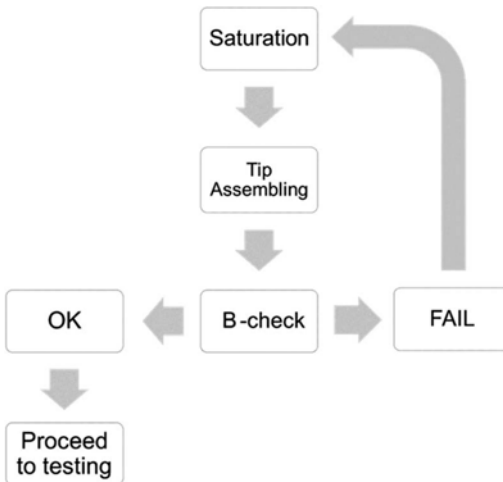


Figure 3. Flow chart of testing procedure including assessment of the pore pressure measuring system saturation.

Three different saturation conditions were investigated on a given piezocone, filter type and saturation fluid. The filter position in the piezocone used was u_2 . Furthermore, the filter was made of 5 μm sintered stainless steel purchased already saturated with a 20 cS silicon oil. The tests were performed at the laboratory floor, i) under ideal saturation conditions as recommended by the standards; ii) partial desaturation induced by pressurizing the filter with air at 85 kPa for 24 h; iii) desaturation by pressurizing the filter with air at 600 kPa for 1 h. Based on the weight loss recorded, which is due to the oil expelled from the filter, the saturation degree was estimated to be 100%, 91% and 3%, respectively. These conditions are therefore subsequently referred to as S, for ideal saturation conditions and LD and HD, for low and high desaturation, respectively. While they clearly do not correspond to the conditions encountered as a result of different saturation procedures they were selected to investigate the widest extent by which the measured B can vary with relevant saturation degrees.

In all cases, ahead of mounting the filter and assembling the cone, the piezocone and the seals were placed under an 85 kPa vacuum in a silicon oil chamber. After 15 min, the vacuum was released and a syringe was used to inject silicon oil in the chamber connecting the pore pressure transducer to the filter (4 in Figure 1), while the piezocone remained submersed. After an additional 15 min under vacuum, the tip was assembled while immersed in silicon oil and tightened. For the tests designated with S only, the assembled cone was subsequently placed under vacuum in the same oil chamber for further 15 min.

Afterwards, the device was positioned onto the cone while the assembled cone was still in the oil chamber so as to ensure hydraulic contact, while applying a small pressure (i.e. <5 kPa). The cone and the device were then removed from the oil chamber and a 50 kPa was applied in the device chamber. Subsequently, the device was used to apply a series of pressure impulses ranging from 50 to 300 kPa. Each impulse of nominally 50 kPa, was applied within a 1 s interval and kept for 30 s before increasing the pressure in the device further. The pore pressure measurements recorded by the piezocone and the device were datalogged continuously during the process.

6 PRELIMINARY RESULTS

Figure 4 shows a set of preliminary results obtained, where it can clearly be seen that the measured pore pressure coefficient B differs for the 3 saturation conditions employed. For each of the conditions investigated, 3 filters were tested. The subsequent results present the average values

measured under each condition, while the error bars indicate the minimum and maximum values recorded. Under each condition, there is a relatively good degree of repeatability, independently of the pressure applied for fully saturated conditions. On the contrary, B increases with the pressure applied for LD because the compliance of the system is reduced, as the pressure increases and air becomes less compressible. As expected, the B values measured for HD are almost zero because of the almost fully desaturated conditions of the filter. However, there is a considerable difference measured at 50kPa for S and LD conditions, even though the saturation degree of the filter is still above 90%. In summary, a strict correlation between the saturation degree of the filters and the pore pressure coefficient B was found.

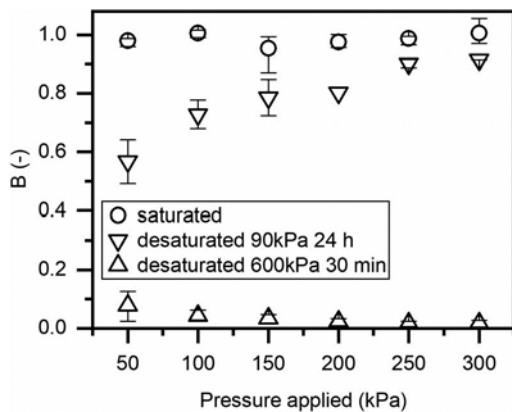


Figure 4. Comparison of pore pressure coefficient measured on piezocone assembled with filters having different degrees of saturation.

7 CONCLUSIONS

The article discusses the still open issues related to poor saturation in piezocone testing and presents an innovative methodology and device, based on a pore-pressure coefficient, that can be used to quantitatively assess saturation before proceeding to testing. This would provide a great advantage as typically the quality of tests can only be assessed

a posteriori. In addition, this measurement can also be applied after carrying out a test so that it would be possible to assess whether saturation was retained.

The preliminary results presented herein demonstrate that there is a strict correlation between the pore pressure coefficient and the saturation conditions of the filter. Based on this proof of concept, the device invented should be validated on other tips and with different saturation degrees of the entire hydraulic system and could be then subsequently employed to investigate the most suitable saturation processes and media. Furthermore, comparison of pore pressure measurements for CPTU performed on a same unit under different conditions as attested by the proposed methodology are recommended to identify threshold values suitable for testing.

REFERENCES

- ASTM D5778-12, 2012. *Standard method for electronic friction cone and piezocone penetration testing of soils*. ASTM International, West Conshohocken, PA.
- DeJong, J.T., Yafate, N.,J., DeGroot, D.J. 2007. Design of a miniature piezoprobe for high resolution stratigraphic profiling. *Geotechnical Testing Journal*, 30(4),1–11.
- EN ISO 22476-1-2012, 2012, *Geotechnical investigation and testing.– Field testing – Part 1: Electrical cone and piezocone penetration testing*. Geneva, Switzerland: ISO.
- Lunne, T., Robertson, P.K., Powell, J.J.M. 1997. *Cone penetration testing in geotechnical practice*. Chapman & Hall, UK.
- Rocchi, I., Tonni, L., Gottardi, G.; University of Bologna. *Device for checking the degree of saturation of a pressure sensor unit of a piezocone and method for performing the check*. Italian patent PCT/IB2017/053104, filed 26/05/2017.
- Sandven, R. 2010. Influence of test equipment and procedures on obtained accuracy in CPTU. In M.A.J. Williams & H. Faure (eds), *Proceedings 2nd international symposium on Cone Penetration Testing, Huntington Beach, CA, USA*. Volume 1: Keynote Lectures, Paper No. KN1
- Schneider, J.A., Randolph, M.F., Mayne, P.W., Ramsey, N. R. 2008. Analysis of factors influencing soil classification using normalized piezocone tip resistance and pore pressure parameters. *Journal of Geotechnical and Geoenvironmental Engineering*, ASCE, 134(11): 1569–1586.
- Skempton, A. 1954. The pore-pressure coefficients A and B. *Geotechnique*, 4, 143–147.
- Terzaghi, K., Fröhlich, O.K. 1936. *Theorie der Setzung von Tonschichte*, Leipzig/Wien Deuticke.

Using penetrometer in situ and in box-core testing to obtain design information for lazy wave riser-soil interaction

O. Safaqah

ExxonMobil, Houston, Texas, USA

H.E. Low, S. Pant & S. Ingarfield

Fugro

M.F. Bransby & M.F. Randolph

Centre for Offshore Foundation Systems, Oceans Graduate School, The University of Western Australia, Australia

Z.J. Westgate

*Department of Civil and Environmental Engineering, University of Massachusetts Amherst, USA
Formerly Fugro*

ABSTRACT: Geotechnical assessment of vertical seabed stiffness during small vertical cycles of riser movement is important for riser fatigue analysis. These stiffness values change both with the amplitude of the cycles (because of non-linear stiffness) but also as the seabed consolidates under the small amplitude loading during long-term operation. To encapsulate both effects in design, a series of site-specific small displacement ball penetrometer testing was conducted both at seabed and in box-core samples on deck during a geotechnical survey for a recent deep water project. The paper describes the cyclic load and displacement controlled in situ testing, the results obtained, and how this data aided design. Of particular note were the long duration cyclic tests which were carried out for sufficiently long so as to not only capture secant stiffness reduction due to remoulding, but also subsequent stiffness increases due to consolidation. This novel test program performed on intact soil (as opposed to reconstituted samples in the laboratory or geotechnical centrifuge) confirms that consolidation hardening can occur in naturally structured near-seabed soils.

1 INTRODUCTION

Subsea risers experience cyclic and axial strain due to environmental and operational loads. These are generally concentrated within the touchdown zone (TDZ), or the zone of the riser which first comes into contact with the seabed. Since operational riser movements are predominantly vertical in the TDZ, the riser response depends on the vertical seabed stiffness. Previous investigations of vertical seabed stiffness concentrated on steel catenary risers (SCRs) which experience large amplitude movements within both the vertical and lateral planes, resulting in seabed softening and trenching (Bridge and Howells, 2007). This has led to the development of non-linear soil models that describe the change in vertical seabed reaction (V, or P) during vertical penetration (z), extraction and re-penetration (e.g. Bridge et al. 2004; Randolph and Quiggin, 2009; Aubeny and Biscontin, 2009; Clukey et al. 2017; see Figure 1). Although there has been significant focus on large amplitude movements, some models have

investigated the hysteretic seabed resistance developed during relatively small riser movements and how the normalized stiffness ($K_{sec} = k_{sec}/N_c s_u$, where $k_{sec} = \Delta P/\Delta z$, N_c is a bearing factor, and s_u is the undrained shear strength) reduces with increasing displacement amplitude.

As compared to the SCR, TDZ movements of a lazy-wave riser (LWR) are several orders of magnitude smaller, in the range of 0.1 to 1% of the riser diameter. These movements may lead to initial seabed softening but are unlikely to lead to significant trenching. Instead, the focus is on the non-linear relationship between seabed stiffness and riser displacement amplitude, with the structural fatigue assessment using equivalent linear-elastic springs (k_{sec}).

Recent data obtained from centrifuge tests in normally consolidated clay (e.g. Hodder et al., 2009; Yuan et al., 2016) suggest that the riser-seabed stiffness could increase or 'harden' with time due to soil consolidation. For overconsolidated clay this consolidation hardening effect on riser seabed stiffness remains uncertain (Clukey et al. 2017). Long-term

consolidation hardening has only been observed in model tests conducted with reconstituted clays or kaolin clay (e.g. Clukey et al., 2005; Hodder et al., 2009, Yuan et al., 2016; Hou et al., 2018) and to the authors' knowledge there is no published model test data on intact soil samples nor is there any existing design framework to incorporate this hardening behavior in a site-specific manner.

This paper reports a series of in situ tests conducted offshore on the seabed and in box cores to support a deep water oil and gas development. The tests were able to take site-specific measurements of cyclic softening and hardening and were used to inform riser design. Recommendations for future testing are made based on the findings.

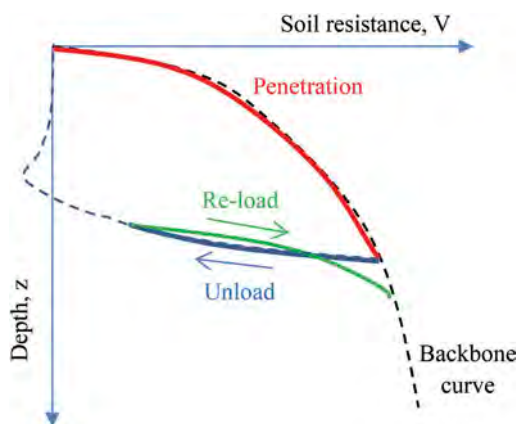


Figure 1. Schematic of cyclic vertical load-penetration response for pipelines and risers.

2 SITE AND DESIGN CONDITIONS

The soil conditions across the project site comprised a thin (5 to 15 cm) drupe of very soft clay with undrained shear strength (s_u) values less than 5 kPa, below which is a soft clay layer with a slight 'crust' with s_u up to 12 kPa, extending down to 0.5 m below the seabed. The strength profile then gradually reduces to normally consolidated conditions (Figure 2).

A conventional geotechnical site investigation campaign was conducted including sampling by piston coring and box coring and in situ testing by T-bar penetrometer. The long term cyclic ball penetrometer tests described here are novel and were performed specifically to support geotechnical design advice regarding operational riser-soil interaction.

During operation, the lazy-wave risers (LWRs) were expected to cycle vertically under small amplitudes ranging from about 0.1% to 1% of the riser diameter. Since high seabed stiffness reduces fatigue life, accurate quantification of the stiffness in the 'crust' layer was key to the riser design and the variation in stiffness throughout their design life was important to quantify.

3 FIELD TESTING

3.1 Overview

The field testing comprised in situ ball penetrometer testing at seabed and on-deck ball penetrometer testing in box core samples. The ball penetrometer tests comprised 'standard' tests (such as monotonic penetration/extraction and large amplitude displacement-controlled cyclic events to measure s_u profiles and sensitivity (S_t), respectively). These were supplemented with novel small amplitude load and displacement-controlled cyclic tests designed to replicate the expected field riser movement. The advantage in the box core and in situ tests is that the 'crust' material is undisturbed, avoiding the challenge of having to recreate field conditions in a laboratory model test set-up. This allowed the in situ soil response to be measured, capturing the effect of soil structure of an overconsolidated clay on changes in stiffness. Another advantage of this approach is that test results were available during the geotechnical campaign, rather than having to wait for sample transport, testing and interpretation as would be required during conventional laboratory ex-situ testing.

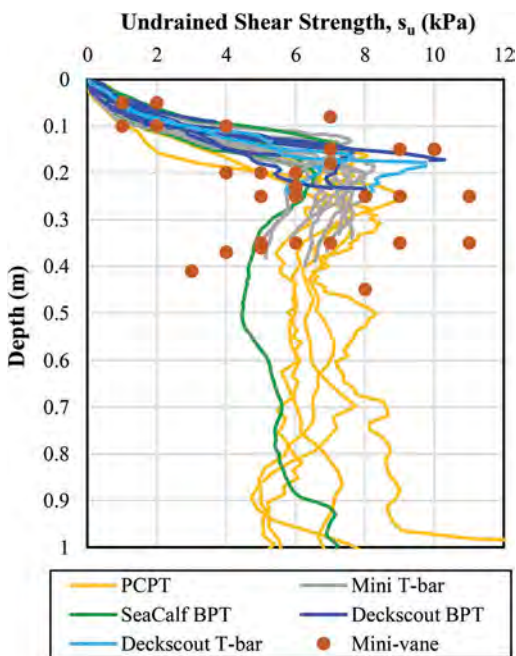


Figure 2. Undrained shear strength profile at site.

3.2 In situ ball penetrometer testing

In situ testing was performed using the Fugro Sea-Calf seabed frame system deployed from the back of a geotechnical drilling vessel (Figure 3). A ball penetrometer of diameter 78 mm (hence projected

base area of 4778 mm²) was pushed with a rod of 25 mm diameter and measurements of penetration resistance, sleeve friction and pore pressure were recorded during the tests.

The cyclic tests involved displacement-controlled cycles of fixed amplitude (typically ranges from ± 0.02 m to ± 0.15 m) conducted at a displacement rate of 0.02 m/s. The cyclic tests started with 30 cycles of large amplitude cyclic displacement (± 0.1 m to ± 0.15 m) to remold the soil, followed by long term (up to 35 hours) small amplitude cyclic displacement (± 0.02 m) to measure the long term cyclic load response.



Figure 3. Fugro SEACALF system.



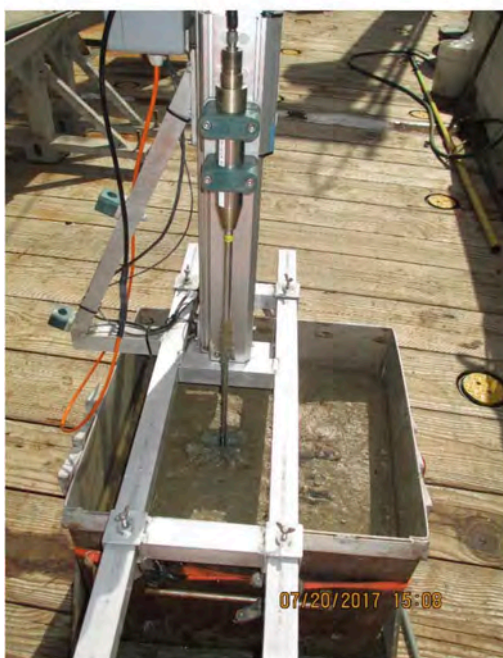
(a)

3.3 In box core ball penetrometer testing

A ball penetrometer of 33 mm diameter was actuated using Fugro's DeckScout system mounted on the top of 0.5 m x 0.5 m x 0.5 m box core on the deck of the drilling vessel (Figure 4).

The tests were started by penetrating the ball monotonically to a target depth at a displacement rate of 200 mm/min, measuring the plastic penetration. The ball was then unloaded until the bearing pressure reached approximately 1 kPa and ready for the start of the test.

The long term cyclic test was then conducted using load control, with load limits set at +11 kPa (maximum value) and approximately 0 kPa (minimum value) for each cycle. The ball penetration rate was about 0.06 mm/min while the extraction rate was about 0.12 mm/min. This difference in displacement rate was an artefact of the testing system, but is not expected to have affected the results. The cycling was continued until no obvious changes in secant loading stiffness were observed, which required up to 8 hours (2600 cycles) of continuous cyclic loading.



(b)

4 RESULTS: IN SITU TESTING

A typical result for the in situ cyclic ball penetrometer test is shown on Figure 5. For each cycle of the test, the secant stiffness (k_{sec}) was calculated using the change in bearing pressure (Δq) from peak to

Figure 4. Fugro DeckScout system showing (a) box core sampler and (b) close up of actuator with miniature ball penetrometer.

trough (and vice versa) and the associated change in penetration (Δz). Figure 6 presents the resulting trend of increasing stiffness (in the loading phase) with cycles, with an approximately 40% increase in stiffness by the end of the test compared to the initial value. The final level of consolidation in the soil for this test was only about 50% based on the normalized time factor ($T = t c_v / D^2$) calculated to be 0.16, where t is the test duration, c_v is the coefficient of consolidation, and D is the ball penetrometer diameter. Further cycling would therefore have likely increased the secant stiffness further, but was not feasible because of vessel time availability.

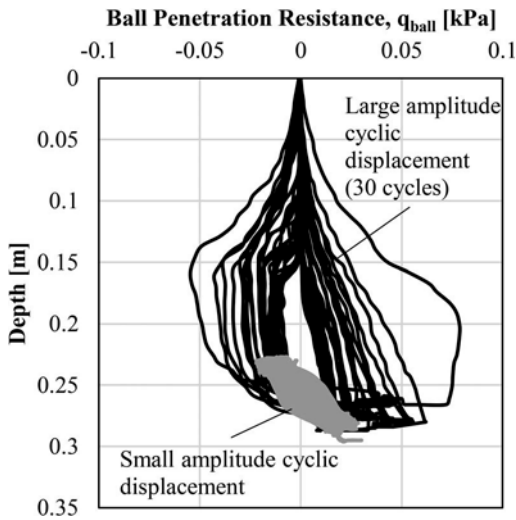


Figure 5. Overall load-penetration response during a long-term cyclic in situ ball penetrometer test.

5 RESULTS: IN BOX CORE TESTING

A typical box core ball penetrometer test result is shown on Figure 7. Because the cycles were load-controlled and the soil stiffness changed during the testing, the cyclic displacement amplitude reduced during the testing as shown in Figure 8a from about 1.2% of ball diameter at the start of the test to about 0.6% of diameter at the end.

As for the in situ testing, for each cycle of the in box core testing the secant stiffness (k_{sec}) was calculated using the change of bearing pressure (Δq) from peak to trough (and vice versa) and the associated change in penetration (Δz). Results are shown in Figure 8b, demonstrating the cyclic hardening behavior resulting in an increase of stiffness of approximately 80%, slightly higher in the loading phase compared to unloading. The normalized time factor $T = 0.72$ for this test is higher than the in situ SeaCalf tests, resulting in increased hardening. However, it replicates the results of similar testing performed in centrifuge model tests (e.g. Hodder et al., 2009, Yuan et al., 2016).

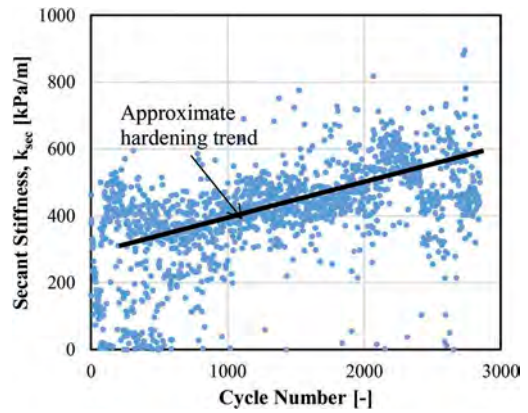


Figure 6. Typical result from a long-term cyclic in situ ball penetrometer test ($\Delta z/D \approx 80\%$).

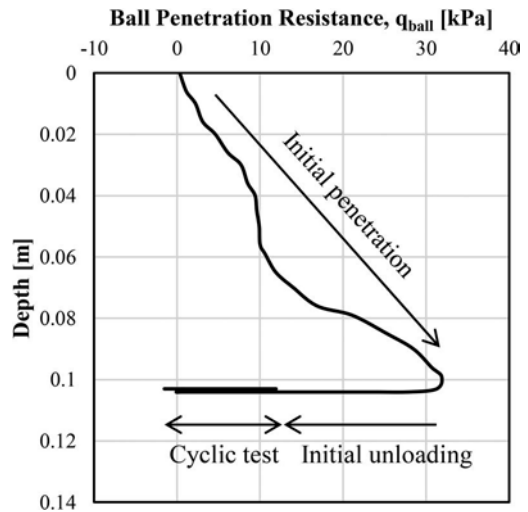
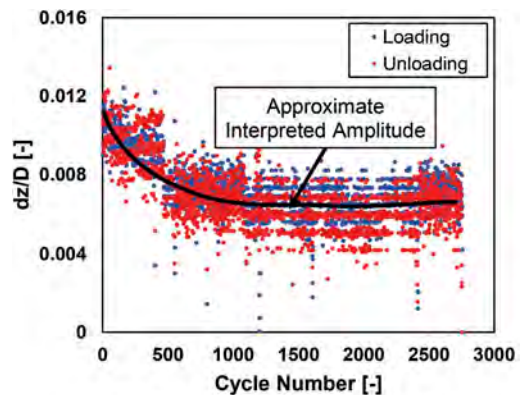


Figure 7. Overall load-penetration response during a long-term cyclic box core ball penetrometer test.



(a) Deduced cycle-by-cycle displacement range

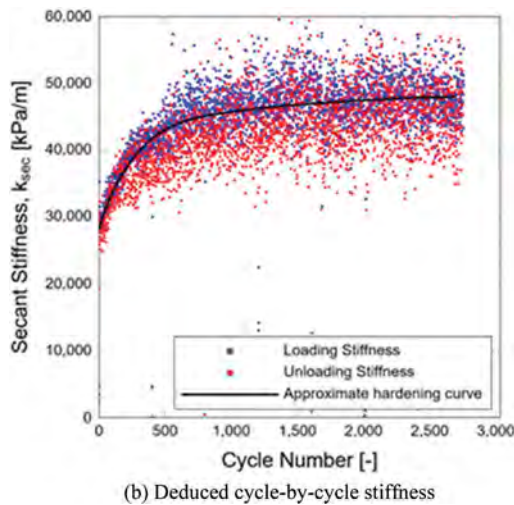


Figure 8. Typical results from a long-term cyclic box core ball penetrometer test

5.1 Measurement quality

Both the in situ SeaCalf and on-deck box core testing were limited by the control mechanism used, which resulted in some variation in cyclic amplitude. For the SeaCalf testing, the displacement-controlled condition resulted in soil consolidating away from the maximum depth range of the ball penetrometer, thus likely not mobilizing the full soil resistance during later downward movements. For the box core testing, the very small amplitude ball movements per cycle, e.g. 0.2 mm at the end of the test, challenged the precision of the displacement measurement system. In both cases, there is significant ‘noise’ in the acquired data. Consequently, long term moving averages were used to smooth out the data to allow the assessment of the evolution of soil stiffness as the tests progressed. Improvements to the testing devices have since been made to reduce this measurement uncertainty for future projects.

6 IMPLICATIONS FOR DESIGN

There remains debate within the subsea riser design community on the appropriateness of incorporating consolidation hardening in riser design (Clukey et al., 2017). The debate currently hinges upon whether cyclic riser response at the seabed is a load-controlled or a displacement-controlled process. For SCRs, the large amplitude vertical (and often lateral) motions of a riser under operational conditions limit the potential for consolidation hardening to occur. This is for two reasons: first, the seabed is continuously being softened and displaced due to the larger riser motions; second, translation of the TDZ both longitudinally and transverse to the original TDZ results in fresh seabed soil being subject to this

cyclic process and therefore limiting the time available for soil to harden. Because of these larger motions and displacement of the seabed soils, SCRs may generally be considered to be displacement-controlled in the TDZ region most subject to fatigue concerns.

For LWRs, however, the cyclic amplitudes in the TDZ are much smaller than for SCRs due the lazy-wave configuration, and the TDZ is therefore less likely to relocate during the design life. The motions of a LWR near the front of the TDZ may be displacement-controlled since they are driven by the translation of movements in the riser initiating at the floating facility. However, further along the TDZ, the upward movements are by definition displacement-controlled, but the downward movement is gravity-controlled, i.e. load controlled, and the resulting cyclic settlement of the riser into the seabed is governed by its on-bottom weight. This is likely to be similar for SCRs towards the ‘back’ (stationary end) of the TDZ where the catenary-induced stress concentration is negligible.

With further understanding of these differences in load and displacement-controlled behavior between SCRs and LWRs, designers can more accurately model the real response, or at minimum consider a conservative approach to fatigue design comprising a high estimate of seabed stiffness. The long-term vertical seabed stiffness of the seabed under loading conditions representative of a LWR, as illustrated through the data presented in this paper, can increase by up to 80% through this consolidation hardening process. Additional cycles of movement and time may have resulted in further increases in secant stiffness.

7 CONCLUSIONS

A geotechnical site investigation performed at a deep water site in soft clay comprised a novel program of cyclic ball penetrometer testing at the seabed (in situ) and in box core samples on deck of the vessel. The tests were performed under displacement-controlled (in situ) and load-controlled (in box core) conditions. The objective of the tests was to assess the potential for consolidation-induced increases in soil strength and resulting vertical seabed stiffness under small amplitude movements and loads which could detrimentally affect the fatigue life of the risers. The data presented confirm that consolidation hardening can occur in undisturbed overconsolidated clay, extending the observations by others for centrifuge and single-gravity model tests in reconstituted and normally consolidated clays.

The results suggest that consolidation hardening may be relevant for lazy-wave riser fatigue analysis, given the potential for long-term small amplitude cyclic movements which occur at a common touchdown zone throughout the riser design lifetime.

ACKNOWLEDGEMENTS

The authors would like to express their appreciation to Fugro and ExxonMobil for allowing publication of this data. The fifth author holds the Fugro Chair, whose support is gratefully acknowledged. Discussions with Professor David White of the University of Southampton (formerly UWA) on consolidation hardening are also acknowledged.

REFERENCES

- Aubeny, C.P. and Biscontin, G., (2009). Seafloor-riser interaction model. *Int. Journal of Geomechanics, ASCE*, 9(3) 133–141.
- Bridge, C., Laver, K., Clukey, E.C., and Evans, T.R. (2004). Steel catenary riser touchdown point interaction model. *Proceedings Offshore Technology Conf.*, OTC16628, Houston, Texas, USA.
- Bridge, C.D. and Howells, H.A., (2007). Observations and modeling of steel catenary riser trenches, *Proceedings of the 17th International Offshore and Polar Engineering Conference*, Lisbon, Portugal, July 1-6, pp. 803–813.
- Clukey, E.C., Haustermans, L. and Dyvik, R. (2005). Model tests to simulate riser-soil interaction effects in touchdown point region. *In International Symposium on Frontiers in Offshore Geotechnics* (pp. 651–658).
- Clukey, E.C., Aubeny, C.P., Zakeri, A., Randolph, M.F., Sharma, P.P., White, D.J., Sancio, R. and Cerkovnik, M. (2017). A perspective on the state of knowledge regarding soil-pipe interaction for SCR fatigue assessments. *In Offshore Technology Conference*. Paper Number: OTC-27564-MS, Houston, Texas, USA.
- Einav, I. and Randolph, M.F. (2005). Combining upper bound and strain path methods for evaluating penetration resistance. *International journal for numerical methods in engineering*, 63(14), pp.1991–2016.
- Fahey, M. and Carter, J.P. (1993). A finite element study of the pressuremeter test in sand using a nonlinear elastic plastic model. *Canadian Geotechnical Journal*, 30(2), pp.348–362.
- Hodder, M., White, D. and Cassidy, M.J. (2009). Effect of remolding and reconsolidation on the touchdown stiffness of a steel catenary riser: guidance from centrifuge modelling. *In Offshore Technology Conference*, OTC-19871-MS, Houston, Texas, USA.
- Hou, Z., Sahdi, F., Gaudin, C., and Randolph, M. (2018). Evolution of riser-soil stiffness in a soil crust layer. *In Vietnam Symposium on Advances in Offshore Engineering* (pp. 130–136). Springer, Singapore.
- Randolph, M.F. and Quiggin, P., (2009). Non-linear hysteretic seabed model for catenary pipeline contact, *Proc. 28th Int. Conf. Ocean, Offshore and Arctic Engineering*, May 31 – June 5, Honolulu, Hawaii, USA.
- Viggiani, G. and Atkinson, J.H. (1995). Stiffness of fine-grained soil at very small strains. *Geotechnique*, 45 (2), 249–265.
- Yuan, F., White, D. J., and O’Loughlin, C. D. (2016). The evolution of seabed stiffness during cyclic movement in a riser TDZ on soft clay. *Geotechnique*, 67(2), 127–137. July 10.1680/jgeot.15.P.161.

Calibration of cone penetrometers according to International Organization for Standardization requirements

R. Soage Santos
Ørsted, London, UK

E. Gómez Meyer & J. Peuchen
Fugro, Nootdorp, The Netherlands

G. Yetginer
Equinor, Stavanger, Norway

T. Lunne
Norwegian Geotechnical Institute, Oslo, Norway

T. Carrington
Fugro, Wallingford, UK

ABSTRACT: Detailed requirements for calibration of piezocone penetrometers are incorporated in standards published by International Organization for Standardization (ISO). The use of these standards can provide input for comparisons of cone penetration test (CPT) systems deployed in practice by means of cone penetrometer classes. It is important that parties specifying or supplying CPT data take note of the implications of the new requirements and the opportunities and benefits of appropriate selection of cone penetrometer classes. In addition, the information available from calibration and verification of a particular cone penetrometer can provide input into estimation of uncertainties of data points in CPT profiles used for design of structures.

This paper focusses on background information about topics considered for development of the ISO requirements. These topics included (1) practical and economical test methods achievable in a calibration laboratory, (2) assessment of differences in exposure conditions applied in the calibration process and site conditions likely to be encountered during actual cone penetration testing, and (3) cone penetrometers that incorporate ancillary sensors and algorithms for reducing the influence of temperature on CPT results.

1 INTRODUCTION

Detailed requirements for calibration of cone penetrometers are incorporated in (draft) standards published by ISO, International Organization of Standardization, particularly ISO/DIS 22476-1:2021 for cone penetration tests (CPT) conducted onshore and nearshore. The same calibration requirements are incorporated in ISO/DIS 19901-8:2021 for CPTs in offshore settings. The use of these standards (hereafter abbreviated to ISO 22476 and ISO 19901) can provide input for comparisons of CPT systems deployed in practice. In addition, the information available from calibration and verification of a particular cone penetrometer can provide input in estimation of uncertainties of data points in CPT profiles used for design of structures.

Earlier versions of ISO 22476 and ISO 19901 (ISO 22476:2012 and ISO 19901-8:2014) considered performance specifications by ‘application classes’, whereby requirements were given for accuracy of in-situ CPT results without detailed step-by-step procedures or method specifications. Application of these performance specifications proved difficult in practice (Lunne et al. 2017, Peuchen & Parasie 2019). For this reason, ISO changed to a method specification, particularly providing detailed requirements for calibration and verification of cone penetrometers in a calibration laboratory. The calibration and verification results provide the required information for assignment of a cone penetrometer to one of multiple ‘cone penetrometer classes’ specified in ISO 22476 and ISO 19901. A further step in method specification is required: monitoring and logging of

acquired test data, followed by assignment of test results in ‘test categories’.

This paper focusses on background information about topics considered for development of the ISO requirements for calibration and verification of cone penetrometers. These topics included (1) practical and economical test methods achievable in a calibration laboratory, (2) assessment of differences in exposure conditions applied in the calibration process and site conditions likely to be encountered during actual cone penetration testing, and (3) cone penetrometers that incorporate ancillary sensors and algorithms for reducing the influence of temperature on CPT results.

ISO 22476 is a draft international standard (DIS). It was published by ISO in June 2021. Where applicable, this paper considers country feedback received for this DIS. Final published version of ISO 22476 and ISO 19901 can differ from the information presented here.

2 CALIBRATION AND VERIFICATION REQUIREMENTS

2.1 Overview

Table 1 presents an overview of calibration and verification requirements for cone penetrometers. The ISO column refers to both ISO 22476 and ISO 19901; ASTM refers to ASTM D5778-20.

Note that the required presentation of results of the ISO verifications covers the influences of temperature and bending on the parameters q_c , f_s , and u . Here, temperature influence is about the internal temperature in the cone penetrometer possibly affecting sensor performance.

The ISO reporting requirements for calibration and verification include assignment of the cone penetrometer to one of the cone penetrometer classes.

Table 1. Overview of calibration and verification requirements for cone penetrometers.

Item	ISO	ASTM
Calibration laboratory*	N	I
Measuring intervals for calibration	N	N
Penetrometer geometry*	N, C, U	N, V
Cone resistance*, q_c	N, C, U	N, C
Sleeve friction*, f_s	N, C, U	N, C
Pore pressure*, u	N, C, U	N, C
Net area ratios*, a and b	N, C	I, C
Temperature, T	-	I, C
Inclination, i	N, C, U	I, C
Influence of ambient temperature*	N, V	N, V
Influence of transient temperature*	N, V	-
Influence of penetrometer bending	N, V	-

C = calibration; I = informative; N = normative; U = uncertainty calculation; V = verification; * = details in sections following; - not covered.

The primary differences between ISO and ASTM are related to (1) detailed requirements for a calibration laboratory, (2) metrological calculation of calibration uncertainties and (3) normative (mandatory) versus informative (recommended) text. It can be noted that a calibration laboratory that invested in calibration and verification apparatus according to ISO 22476 and/or ISO 19901 should be able to provide the normative calibration and verification information according to both ISO and ASTM. The reverse can require additional investment.

2.2 Calibration laboratory

A normative reference to ISO/IEC 17025 provides the basic requirements for the calibration laboratory. ISO/IEC 17025 covers laboratory quality management, including detailed reporting requirements for calibration certificates.

2.3 Measuring intervals for calibration

ISO 22476 and ISO 19901 include normative text with respect to measuring intervals for calibration. For example, a minimum range is specified for inclination. Recommendations (informative) are given for selection of measuring intervals for calibration of q_c , f_s and u .

2.4 Cone resistance and sleeve friction

Calibration for q_c and f_s requires application of a series of axial loading and unloading series to the cone penetrometer, similar to ISO 376:2011. A notable requirement is the logging and supplementary presentation of output values of the penetrometer other than those for q_c or f_s , for the purpose of checking for any unwanted effects of axial loading on output of sensors other than the one selected for calibration.

Estimation of calibration uncertainty is prescribed in detail. Uncertainties cover those related to: (1) reference force, (2) geometry of the cone penetrometer and (3) uncertainties related to force sensor in the cone penetrometer, particularly reproducibility, repeatability, resolution, zero drift, interpolation, reversibility and apparent load transfer from cone to friction sleeve (and vice versa). Calculation equations consider standard uncertainties, combined standard uncertainties and expanded measurement uncertainties defined according to ISO/IEC Guide 99:2007.

Table 2 presents a selection of example output according to ISO requirements.

2.5 Pore pressure and net area ratios

Calibration for pore pressure u takes place with the cone penetrometer in a pressure vessel. A series of increasing and decreasing pressure series are applied.

Table 2. Example summary of laboratory calibration uncertainties for q_c , according to ISO requirements.

F_r [kN]	u_1 [kN]	u_2 [kN]	u_3 [kN]	u_4 [kN]	u_5 [kN]	u_6 [kN]	u_7 [kN]	u_8 [kN]	u_c [kN]	u_c [kPa]	u_{dim} [mm ²]	$u_{c,dim}$ [kPa]	U_{qc} [kPa]
0	0.0150	0.0007	0.0000	0.0000	0.0000	0.0000	0.0000	0.0000	0.0150	14.65	0.3024	14.65	29.31
8	0.0390	0.0006	0.0000	0.0000	0.0004	0.0154	0.0344	0.0000	0.0543	52.96	0.3024	53.01	106.02
16	0.0630	0.0012	0.0012	0.0000	0.0008	0.0064	0.0419	0.0000	0.0759	74.11	0.3024	74.25	148.51
24	0.0870	0.0007	0.0007	0.0000	0.0012	0.0026	0.0453	0.0000	0.0982	95.80	0.3024	96.05	192.10
32	0.1110	0.0004	0.0004	0.0000	0.0016	0.0119	0.0468	0.0000	0.1210	118.13	0.3024	118.48	236.97
40	0.1350	0.0013	0.0013	0.0000	0.0020	0.0182	0.0473	0.0000	0.1442	140.76	0.3024	141.23	282.46
48	0.1590	0.0009	0.0009	0.0000	0.0024	0.0195	0.0482	0.0000	0.1673	163.27	0.3024	163.85	327.70
56	0.1830	0.0027	0.0027	0.0000	0.0028	0.0135	0.0488	0.0000	0.1899	185.34	0.3024	186.04	372.07
64	0.2070	0.0032	0.0032	0.0000	0.0032	0.0028	0.0476	0.0000	0.2125	207.35	0.3024	208.17	416.34
72	0.2310	0.0049	0.0049	0.0000	0.0036	0.0159	0.0474	0.0000	0.2364	230.73	0.3024	231.66	463.31
80	0.2550	0.0045	0.0045	0.0000	0.0040	0.0409	0.0000	0.0000	0.2583	252.10	0.3024	253.15	506.31

F_r : reference force; u_1 : standard uncertainty, reference force; u_2 : standard uncertainty, reproducibility; u_3 : standard uncertainty, repeatability; u_4 : standard uncertainty, resolution; u_5 : standard uncertainty, zero drift; u_6 : standard uncertainty, interpolation; u_7 : standard uncertainty, reversibility; u_8 : standard uncertainty, load transfer; u_c : combined standard uncertainty, calibration; u_{dim} : combined standard uncertainty, cross-sectional area of cone tip; $u_{c,dim}$: combined standard uncertainty, u_c and u_{dim} ; U_{qc} : expanded measurement uncertainty, calibration u_c and u_{dim} ; cross-sectional area of cone tip used for calculation of uncertainties: 1024.74 mm²

The procedure and presentation of results are generally similar to those for q_c and f_s . The estimation of calibration uncertainty considers a reduced number of uncertainties.

Net area ratios a and b for the cone and the friction sleeve are also determined with the cone penetrometer in the pressure vessel. Values of a and b typically show slight pressure dependence. ISO determines these values at $u = 2$ MPa.

2.6 Temperature influence

Verification of a cone penetrometer for temperature influence requires two water-filled baths, one at a temperature of 0 °C and one at 30 °C. The baths are at atmospheric conditions. A prescribed alternating sequence applies for immersion of the cone penetrometer in the two thermostat baths. The cone penetrometer is thus subjected to induced change in ambient temperature as well as transient temperature cycling, see Figure 1. The ‘measured temperature’ shown in Figure 1 refers to temperature measured by a sensor in the cone penetrometer.

The verification procedure specifically allows for optional, explicit correction of force (q_c and f_s) and pressure (u) data for temperature influence. Uncorrected and corrected results must be reported for this case. For example, cone penetrometer class 1+ of ISO 22476 includes requirements for incorporation of a temperature sensor in the cone of the cone penetrometer. The temperature (T) data can then be used for correction of temperature influence on q_c , f_s and u .

Reporting of results is mainly by key performance indicators that relate variation of the parameter of interest (for example q_c) to the temperatures of the water baths and to time.

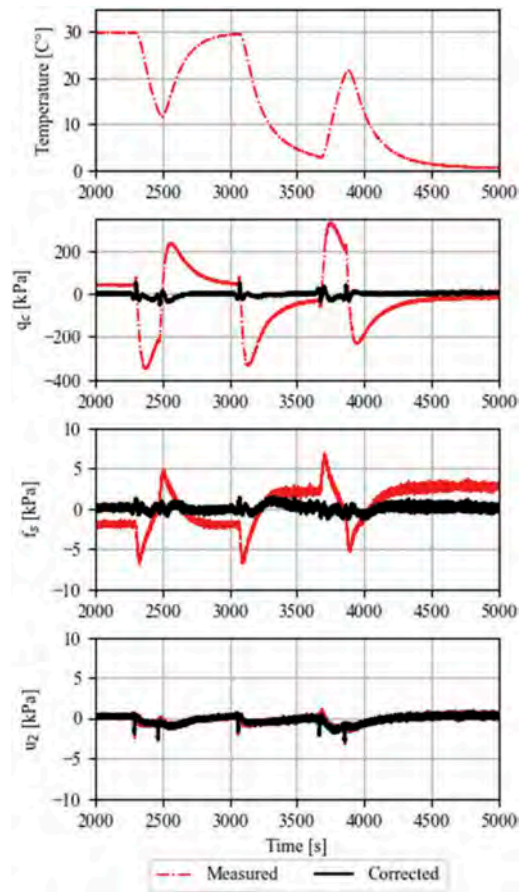


Figure 1. Example of verification data for temperature influence.

3 DISCUSSION

3.1 Use of results

ISO 22476 and ISO 19901 distinguish between (1) records of calibrations and verifications and (2) test report or calibration certificate.

The records include substantial data files, particularly as they include time-based logging files for a logging frequency of ≥ 1 Hz. The logging applies to output of each of the primary sensors of the cone penetrometer, for the durations of the various calibration and verification activities. The records are retained by the calibration laboratory. Inspection of the records can provide valuable information for quality management, particularly if the records are tracked for multiple calibrations of a single cone penetrometer and if the records are compared for multiple cone penetrometers.

A test report or calibration certificate covers a summary of the records. The summary is adequate for use in practice, i.e. understanding the performance of the cone penetrometer at the time of calibration.

3.2 Exposure conditions

Simulated exposure conditions for a cone penetrometer in the calibration laboratory will, inevitably, differ from in situ exposure conditions. Particularly, laboratory calibration and verification consider particular characteristics in isolation, see Table 1.

Laboratory checks would be challenging for assessing the potential influence of in situ exposure conditions, such as (1) ambient and induced stress conditions imposed by soil and water, (2) soil displacement relative to the cone penetrometer, (3) temperature exposure varying from freezing to, say, 60°C , (4) combined and variable axial (compressive and tensile), torsional and moment loading imposed on the cone penetrometer. Common combinations of these influences cannot be readily quantified in a laboratory setting. Robust design and quality monitoring of cone penetrometers remains important (e.g. Peuchen & Terwindt 2014; Peuchen et al. 2020).

ISO 22476 and ISO 19901 capture quality monitoring by means of test categories, as discussed above. This is normative. Additional (informative) guidance and recommendations are also provided.

3.3 Uncertainty calculations

The calibration requirements include prescriptive uncertainty calculations, i.e. a combination of detailed calibration procedures and detailed requirements for calculation of uncertainties. This approach allows easy comparison of cone penetrometers, regardless of manufacturer/ supplier.

The uncertainty calculation approach presented in the ISO standards includes equations that (1) follow metrological principles (ISO, 2008) and premises and (2) apply to the specified laboratory setting. One of

the premises is that the standard uncertainty of the reference, for example the measurement unit for force reference, has much better uncertainty characteristics than the force sensor of the cone penetrometer. If this is not the case, then the results of uncertainty calculations can be dominated by the uncertainty of the reference and will not necessarily reflect the actual laboratory performance of the cone penetrometer. This dominating influence can apply to the top end of the cone penetrometer classes, where requirements for cone penetrometers can approach performance of commonly available reference measurement units.

3.4 Temperature stability of primary sensors

Figure 1 includes an example of temperature correction of q_c by post-processing. The approach for f_s and u would be as for cone resistance.

The case of Figure 1 is for a subtraction-type cone penetrometer equipped with strain-gauge load cells with conventional temperature compensation for ambient temperature influence. This particular cone penetrometer also includes a temperature sensor within the cone penetrometer. The acquired records of temperature (T) data versus time (t) are additional to the primary CPT parameters and at the same frequency. The correction method uses a temperature model that mathematically increases (or reduces) values of q_c . This model is penetrometer-specific and parameter-specific (in this case q_c). The temperature model relies on a polynomial best-fit of q_c and T (and their derivatives in time), derived from the data recorded in the calibration laboratory.

During cone penetration testing, T and q_c are recorded versus t . The temperature model is subsequently applied by post-processing of the complete CPT dataset, such that both uncorrected (raw data) and corrected q_c data are retained.

It can be seen from Figure 1 that significant reduction of temperature influence can be achieved in the laboratory. Robust design of a cone penetrometer and tested algorithms should also achieve significant reduction of temperature influence during actual cone penetration testing under conditions differing from those in the laboratory.

4 CONCLUSION AND RECOMMENDATIONS

The International Organization of Standardization published (draft) standards ISO/DIS 22476-1:2021 and ISO/DIS 19901-8:2021. These documents include detailed requirements for calibration and verification of piezocone penetrometers. These requirements are believed to be practical and economical, nevertheless exceed the extent of calibration activities that represents current (2022) industry practice.

It is recommended that parties supplying CPT data take note of the implications of the new requirements. Furthermore, it is recommended that parties involved in specifying CPTs take note of the

opportunities and benefits, notably by means of appropriate selection of cone penetrometer classes.

Standards tend to follow, not lead, technology developments or widespread application of a particular technology. A technology example for CPTs would be the incorporation of ancillary sensors and algorithms for reducing the influence of temperature on CPT results, now covered by the ISO standards. The resulting standardisation has influenced the cone penetrometer classes introduced in the ISO standards. In turn, the cone penetrometer classes allow easy comparison of cone penetrometers for use in practice, regardless of manufacturer/ supplier.

REFERENCES

- ASTM International, 2020. *ASTM D5778-20 Standard Test Method for Electronic Friction Cone and Piezocone Penetration Testing of Soils*. West Conshohocken: ASTM International.
- International Organization for Standardization, 2007. *ISO/IEC Guide 99:2007 International Vocabulary of Metrology – Basic and General Concepts and Associated Terms (VIM)*. Geneva: ISO.
- International Organization for Standardization, 2008. *ISO/IEC Guide 98-3:2008 Uncertainty of Measurement – Part 3: Guide to the Expression of Uncertainty in Measurement (GU:1995)*. Geneva: ISO.
- International Organization for Standardization, 2011. *ISO 376:2011 Metallic Materials – Calibration of Force-proving Instruments used for the Verification of Uniaxial Testing Machines*. Geneva: ISO.
- International Organization for Standardization, 2014. *ISO/DIS 19901-8:2021 Petroleum and Natural Gas Industries - Specific Requirements for Offshore Structures – Part 8: Marine Soil Investigations*. Geneva: ISO.
- International Organization for Standardization, 2017. *ISO/IEC 17025:2017 General Requirements for the Competence of Testing and Calibration Laboratories*. Geneva: ISO.
- International Organization for Standardization, 2021a. *ISO/DIS 19901-8:2021 Petroleum and Natural Gas Industries - Specific Requirements for Offshore Structures – Part 8: Marine Soil Investigations*. Geneva: ISO.
- International Organization for Standardization, 2021b. *ISO/DIS 22476-1:2021 Geotechnical Investigation and Testing – Field Testing – Part 1: Electrical Cone and Piezocone Penetration Test*. Geneva: ISO.
- Lunne, T., Santos, R. & Brink Clausen, 2017. Guidelines for Use of CPTU Application Classes According to ISO 19901-8: (2014). In: Society For Underwater Technology Offshore Site Investigation and Geotechnics Committee, ed. *Offshore Site Investigation and Geotechnics: Smarter Solutions for Future Offshore Developments: Proceedings of the 8th International Conference 12-14 September 2017, Royal Geographical Society, London, UK: Volume 2*. London: Society for Underwater Technology, pp. 300–307.
- Peuchen, J., Santos, R., Yetginer, A.G., Eckart, W.S., Carrington, T.M. & Lunne, T. 2020. CPT data showing anomalies – assessment and potential postprocessing. In Z. Westgate (ed.). *4th International Symposium on Frontiers in Offshore Geotechnics (ISFOG 2020): proceedings* (pp. 1026–1035). Deep Foundations Institute.
- Peuchen, J. & Parasie, N., 2019. Challenges for CPT accuracy classes. In *Proceedings of the XVII European Conference on Soil Mechanics and Geotechnical Engineering - ECSMGE 2019: geotechnical engineering foundation of the future*. https://www.ecsmge-2019.com/uploads/2/1/7/9/21790806/0049-ecsmge-2019_peuchen.pdf
- Peuchen, J. & Terwindt, J., 2014. Introduction to CPT accuracy. In *3rd International symposium on cone penetration testing CPT14: May 12- 14 (2014)*. Las Vegas, Nevada.

Long-term strength determination of frozen soils by CPT

Ivan Sokolov & Nikolay Volkov
Fugro, Russian Federation

ABSTRACT: Frozen soils show rheological behavior which results in changing mechanical properties in time under applied load. It is highly complicated to determine the long-term strength of a frozen soil. Rheological behavior of frozen soils appears in creep or stress relaxation. This paper presents a new method to measure long-term strength of frozen soils using CPT equipment named Stress Relaxation Test (SRT). Conventional tests are focused on the creep behavior by creating constant loads and measuring strains. The SRT is based on stress relaxation approach by creating constant deformations and measuring stress by a cone. Cone resistance (q_c) would give compression long-term strength, as for sleeve friction (f_s) – shear long-term strength. SRT long-term strength results can be applied directly to pile bearing capacity estimation. A comparison between such estimation and results from a full scale static pile load test is provided in the paper.

1 INTRODUCTION

1.1 *Frozen soil rheological behavior*

The frozen soil shows a rheological behavior under an excess load from structures. In order to describe the degree of rheological behavior, the long-term strength is used which is the resistance of a soil to failure in response to a long-term load application (Tsytoich, 1975). In other words, long-term soil strength corresponds to a stress at and below which no failure takes place within practically observable period of load application. Long-term strength of frozen soils is 5 to 15 times less than instantaneous strength, or resistance to rapid destruction. The key long-term strength characteristics of frozen soil are long-term compressive strength and long-term shear strength over the freezing surface (Sayles, 1968).

There are two ways to evaluate long-term soil strength. The first way is to measure deformation under applied constant load which are high enough to induce non-attenuating creep which results in failure with time or, in another words “deformation vs time”. When several tests are conducted with various loads, the curve “load vs time of failure” is plotted. An asymptote of the curve is interpreted as the ultimate long-term strength.

The second way is to measure the excess stress caused by applied constant deformation. The definition of stress relaxation is given by Vyalov (Vyalov, 1986). It is a process of decrease in stress over time, which is necessary to maintain constant deformation. Stress relaxation

happens due to redistribution of elastic and plastic deformations in time. The relaxation period is one of the most important rheological parameters of frozen soils. It is important to highlight that relaxation period is much shorter (by several orders) compared to after-effect period. This is the main advantage of the proposed new method.

1.2 *S. Vyalov's logarithmic equation application for frozen soil behavior*

The strength of frozen soils decreases over time as a result of the absence of a long-term strength limit for ice, which is a permanent and important component of frozen soil. An accelerated method of testing soils for long-term strength, using a “dynamometric” apparatus shortening the test period was invented by Vyalov. The design of the apparatus provides the application of the load to a soil sample through a dynamometer with fixation of its position and recording of decreasing stress value on it. The logarithmic relaxation equation is used to process the obtained data.

Logarithmic equation of long-term strength:

$$\tau = \frac{\beta}{\ln \frac{t_p+1}{T}} \quad (1)$$

where τ — measured cone resistance or sleeve friction in MPa; t_p — measurement time, s; β , T — the parameters are temperature and strain rate dependent (Vyalov, 1986).

2 CPT APPLICATION FOR LONG-TERM STRENGTH EVALUATION

2.1 CPT in Stress Relaxation Test (SRT) mode

The principle scheme of the dynamometric method is implemented in the Stress Relaxation Test (SRT) of frozen soil by CPT with stabilization. When the cone is deployed on a test depth, the load is kept applied to the soil, exceeding the value of its instantaneous strength, but when the cone penetration is paused like for a dissipation test, the cone is kept loaded (the rods are clamped) and the stress relaxation is recorded. For each individual SRT, a single value of long-term strength of frozen soil is obtained. To be more specific, for data obtained using a cone resistance sensor is the long-term compressive strength of the frozen soil, and for data obtained using a sleeve friction sensor, it is the value of the long-term shear strength. A result of the measurement is the values of the long-term strength of frozen soil were obtained at each depth of the cone SRT deployment.

An example of SRT relaxation curve provided below on Figure 1.

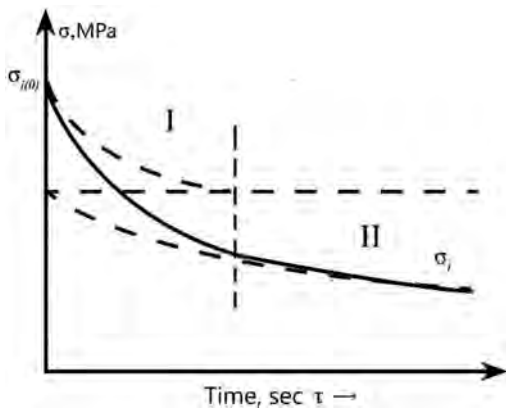


Figure 1. Stress relaxation curve.

During the stress relaxation test, an increase in plastic deformation occurs due to a decrease in the part of elastic deformation keeping the constant value of the total deformation. The proportion change causes the stress relaxation. To evaluate the value of the long-term strength of the soil, the SRT should be performed until a certain point of stress reduction in the sensor, which presents in the stage II of the relaxation curve, Figure 1. In stage I of the relaxation curve, the cone freezes into the soil after penetration pause starts. At this stage besides relaxation some creep happens and contributes some inconsistency to the measured curve. Then the stage II starts when creep contribution is negligible and the curve starts to follow the equation (1) (Sokolov, 2020).

2.2 SRT data processing

To process the SRT results, measurements of stress relaxation at each cone deployment depth are taken into account and processed using the long-term strength equation (1), reduced to the form $y = kx + b$.

$$\frac{1}{\sigma} = \frac{1}{\beta} \cdot \ln(t_p + 1) - \frac{1}{\beta} \cdot \ln T \quad (2)$$

where $y = \frac{1}{\sigma}$; $x = \ln(t_p + 1)$; $k = \frac{1}{\beta}$; $b = -\frac{1}{\beta} \cdot \ln T$

Figure 2 illustrates processing linearized cone resistance data for a SRT. The value of the reliability of the linear approximation of the data in this case is 0.997.

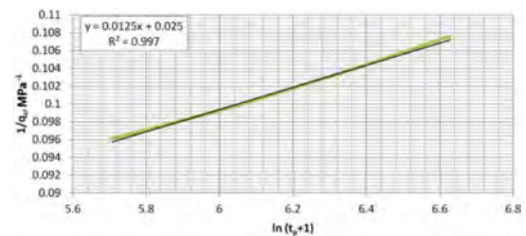


Figure 2. Example of SRT data linearization.

Based on the obtained coefficients $k = 0.0125$ and $b = 0.025$, the coefficients $\beta = 80$, $T = 0.139$ and the equation of long-term compressive strength is defined:

$$\sigma_c(t) = \frac{80}{\ln \frac{t_p + 1}{0.139}} \quad (3)$$

where σ_c — interpreted as the compressive long-term strength of the soil.

Equation (3) allows to calculate a long-term strength value for any period of time. For instance, for 10 days $\sigma_c = 5.1$ MPa and for 100 years $\sigma_c = 3.4$ MPa.

Similarly, based on the sleeve friction sensor data, the obtained value is interpreted as the shear long-term strength of frozen soil.

It is important to set the frame of applicability of Equation (2). The stress relaxation measurements under the tip of the cone were obtained. Successful completion of the test is reached upon condition of the stage II of the relaxation curve is met. The same situation was observed for the sleeve friction sensor. It is assumed that, on the stage I, the cone freezes into the ground, and only after that rheological behavior can be clearly observed on the data, which represents in data curves (q_c and f_s) following the Equation (2).

The field data quality assessment is required to check the applicability of the field data, i.e. if the stage 2 was reached during the test. The field data acquisition software was developed with continuous analysis array of the obtained data using Equation (2). After the stress relaxation test starts, Equation (2) is applied for an interval of the relaxation curve. In the example on Figure 3a, an interval of 100 seconds is used for calculation. The data of 600-700 seconds interval has automatically processed to calculate β , T factors (Figure 3b).

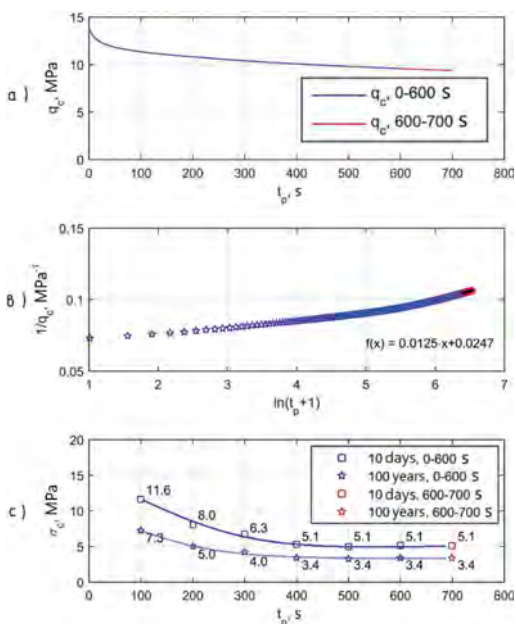


Figure 3. Field iteration processing of the SRT data.

Next, the equation of the long-term strength is derived, as shown above for the formula (3), and the soil long-term strength (σ) is calculated for lifetime period $t_p = 100$ years in seconds. Figure 3c shows values for 100 years (red asterisk), also shows values for 10 days (red square) at the end part of the relaxation curve 600-700 seconds.

This algorithm can be applied to calculate the long-term strength for any part of the collected data. Six previous iterations were performed correspondingly for the sections of the curve for the 1-100 seconds (the First iteration), for the 100-200 seconds (the Second iteration), etc. and displayed in blue, respectively (Figure 3c). Figure 3c shows that, the calculated long-term soil strength values are consistent started from period 400 seconds, and they are equal to 3.4 MPa for lifetime period $t_p = 100$ years and 5.1 MPa for the lifetime period $t_p = 10$ days.

Figure 3a shows slow decreasing of the stress value in the sensor, we suggest that the stress relaxation curve had to reach the stage II starting from 400 second of the test, and follows Equation (3).

Figure 3 illustrates just 7 iterations of the field QA approach, but the data acquisition software adds a new long-term soil strength value every new record of the stress in the sensor (Sokolov, 2020).

3 FIELD DATA APPLICATION

3.1 Pile bearing capacity calculation

The pile bearing capacity (PBC) calculation is based on the long-term soil strength data. The calculation is based on a similar conventional approach, the sequential summation of the values of end bearing and side friction. The difference is that the developed calculation does not use any empirical factors. The calculation is made according to the formula:

$$F_{ui} = \sigma_c \cdot A + \sum \sigma_s \cdot A_{af,i} \quad (4)$$

where σ_c – average compression long-term soil strength; A – pile area; σ_s – average shear long-term soil strength; $A_{af,i}$ – unit side area of the pile.

The calculation is performed for the recorded values of σ_c and σ_s for each measurement of stress relaxation test. The test-time interval t_p is set as 10 days, in the case of a full-scale pile test under a static load, and the life-time interval t_p is 100 years to evaluate the ultimate long-term pile bearing capacity.

Construction site nearby Salekhard was selected to confirm the SRT based results and PBC calculation in frozen soils. On this site, full-scale static pile load tests (SPLT) were carried out. SRT was performed near the tested pile within 2 meter distance (Volkov et al, 2019).

SPLT was conducted in accordance with GOST 5686-2012. The load was applied in 10 steps, each step lasted 1 day and was equal 5 or 10 tons. The last step lasted for 24 hours was $F_H = 55$ tons, the next step $F_H = 60$ tons caused pile failure. GOST 20522-2012 provides equation (5) to calculation the ultimate long-term pile bearing capacity:

$$F_H^H = 0.65 \cdot F_H \quad (5)$$

where F_H^H – ultimate long-term pile bearing capacity; F_H – step load at which the pile failure occurred.

Comparison of PBC calculation results based on SRT with the results on SPLT in frozen ground provided in the Table 1.

The bearing capacity of a driven pile with length of 10.6 m in frozen soil with a time interval of 10 days is about 66 tons (663 kN), and the pile failure occurred at load step of 60 tons. The SRT value differs by 10% from SPLT value. These are very close results. In turn, the calculated SPLT value for 100

Table 1. Comparison of PBC calculation results based on SRT and SPLT.

Time period	10 days		100 years	
	SRT	SPLT	SRT	SPLT
End bearing	446*	—	292	—
Side friction	217	—	117	—
Ultimate	663	550-600	409	357-390

* All values are in kN.

years is equal to 39 tons and the calculated SRT value is about 41 tons (409 kN). The obtained results for 100 years correlate to each other relatively good as well.

3.2 Long-term strength for various soils

The results of σ_c and σ_s measurements were collected from the various sites in Russia where permafrost ground was encountered (Sokolov, 2020). The results were classified with different soil types and averaged to a single value. This allowed to compare them with the recommended values which are commonly used to verify the design values, in particular, R – pile unit end bearing, R_{af} – pile unit side friction (Aksenov, 2001). The comparison of the values is presented in Table 2.

Table 2. Comparison between long-term soil strength measured by SRT (σ_c and σ_s) and recommended values for pile unit end bearing (R) and pile unit side friction (R_{af}).

Soil type	Ice content	σ_c	R	σ_s	R_{af}
		kPa	kPa	kPa	kPa
Lean clay	None	2430	900-1100	69	40-100
	Low	1335	800-950	35	40-100
	Medium	707	400-550	19	40-60
	Rich	517	400-550	21	40-60
Silty clay	None	2228	750-1050	114	40-60
	Low	2179	850-1050	53	40-60
Silty sand	Low	1963	1000-1800	23	50-130
Fine sand	Low	4584	1000-1700	63	50-80
Medium sand	Low	6977	1500	171	50

The results clearly show the influence of the ice content. In lean clay and silty clay σ_c and σ_s decrease if the ice content increases, so as the recommended R and R_{af} . This tendency is confirmed by theoretical studies of the ice content influence on the mechanical properties of the frozen soils.

The influence of the grain size if other conditions being equal, can also be observed for silty, fine and medium sands. An increase of coarse particles gives more resistance to both compression and shear.

4 CONCLUSIONS

Stress Relaxation Test (SRT) of frozen soil by CPT with stabilization was developed based on an accelerated laboratory method of testing soils for long-term strength, using a principle of the “dynamometric” apparatus invented by Vyalov. The logarithmic relaxation equation is used to process the field data.

SRT provides individual values of the long-term strength for frozen ground at a certain depth. Data obtained using a cone resistance sensor is interpreted as long-term compressive strength of the frozen soil (σ_c), and data from sleeve friction sensor – the long-term shear strength (σ_s).

The results on σ_c and σ_s are applicable for calculation of pile bearing capacity in the frozen soil without empirical factors.

The results of σ_c and σ_s on the various sites showed consistency and good relation with the recommended values for pile unit end bearing and pile unit side friction.

REFERENCES

- Aksenov, V. I. 2001. Recommendations for determine the frozen soils strength with a marine type of salinization. FGUP PNIIS, Moscow. – 42 pages (in Russian).
- Sayles, F.H. 1968. Creep of frozen sands, United States Army Corps of Engineers CRREL.
- Sokolov I. 2020. Determination method for strength properties of frozen soils by cone penetration testing. PhD Thesis – Moscow State University, Moscow, 2020 – 149 pages (in Russian).
- Tsytoovich, N. A. 1975. The Mechanics of Frozen Ground, New York, McGraw-Hill, 448 p. ISBN-10: 0070654107
- Volkov N.G., Sokolov I.S., 2019. Estimation of pile bearing capacity in permafrost based on stress relaxation measured by cone penetration testing. Geotechnics, Vol. XI, No. 1, pp. 68–78, <http://dx.doi.org/10.25296/2221-5514-2019-11-1-68-78>.
- Vyalov, S.S. 1986. Rheological Fundamentals of Soil Mechanics, Volume 36, 1st Edition. Publisher: Elsevier. ISBN: 0444600566. 564 pages.

Efficiency examined of hands-free Cone Penetration Testing using the SingleTwist™ with COSON

O. Storteboom & M. Woollard

A.P. van den Berg, Heerenveen, The Netherlands

J. Verhagen

GWR Ingenieursbureau, Rotterdam, The Netherlands

ABSTRACT: The Cone Penetration Test (CPT) cabin as working environment, built on trucks, crawlers or Track-Trucks®, will more and more develop from a workshop into an office. Before, operators were mainly dealing with manual operations to keep the production going. Nowadays and in the future, it can be increasingly expected that time “on board” will be spend on design or other office-related work next to performing CPTs. This paper describes a system that has been designed to support this market development. By integrating the patented SingleTwist™ technology in a CPT cabin with the COSON continuous pushing system, an automatic and hands-free CPT machine is created. The assembly and disassembly of the CPT string takes place fully automatically. This paper describes the efficiency of the SingleTwist™ technology. The City of Rotterdam, the first owner of a Track-Truck with COSON-ST, deployed their system in different projects. One project is chosen to further elaborate on its advantages and experience in practice.

1 INTRODUCTION

Changing requirements and regulations are spurring continuous development of CPT systems. The need for increasing operational efficiency requires systems that can start up more quickly and run without further intervention or control. These systems are expected to have a simple human-machine-interface to monitor the process and receive system alerts in the event of imminent quality loss or maintenance requirements on the equipment or data acquisition system. These expectations focus on obtaining better CPT data, performed in a shorter time and with less effort. Smart and dedicated technology is required to meet these needs. A combination of digital data processing, an accurate system feedback and a simple and robust design delivering excellent quality, safety, long service life and easy maintenance is needed to face the increasing demands.

The answer is “back-to-basics”. The CPT rod, the most simple and robust part of the CPT system, has become the core of a new development. The CPT rod is the connecting link between the measuring cone and the pushing system. More than 90 percent of the time required for a cone penetration test consists of handling the CPT rods. Far reaching efficiency improvements can be found in a creative approach towards these rods. This paper presents the SingleTwist (ST)-technology as the result of such a creative design process. The introduction of this

new technology is preceded by an overview of pushing systems developed over time and is concluded with a description of a practical application. This new insight will ensure a changing working environment inside the CPT cabin: a shift from operator to engineer or from manual to hands-free operations and from manual labor to data processing, assessments and design work.

2 DEVELOPMENT OF CPT PUSHING SYSTEMS

To performing a CPT soil investigation, it is necessary to push a measuring cone into the soil over time. We can see that the development of pushing systems has kept pace with that of measuring cones. The first systems used in the 1930s were suitable for testing with mechanical cones. The power source used was often the operator’s muscle strength, a jack was used for power transmission and the maximum pushing force was limited to 50 kN. With the arrival of the electrical cone in the 1950s, higher demands were also placed on the pushing device. Soil investigation at larger depths required higher pushing forces. A continuous speed also became important and an electrical connection to the cone was required to show measurement data in real time. Due to increasing demands for comfort, the pushing device had to be set up in a closed and conditioned cabin.

The following subsections describe the pushing systems developed at A.P. van den Berg for onshore and offshore soil investigation. The specific A.P. van den Berg trade names are indicated in brackets.

2.1 Onshore CPT pushing systems

The range of pushing systems varies from a single lightweight pushing cylinder for hand carried CPT solutions to heavy duty pushing devices built on trucks and on large crawlers.

2.1.1 Light weight systems

Lightweight CPT systems (HYSON LW) are very suitable for installation in hand carried applications and on light vehicles such as mini crawlers. The pushing system has a single hydraulic cylinder with a maximum pushing capacity of 100 kN. Due to its low weight and small size, it can easily be applied in basements, back yards and on dikes.



Figure 1. HYSON 100 kN in Mini CPT Crawler (left) and Track-Truck with HYSON 200 kN inside the cabin (right).

2.1.2 Heavy duty systems

Heavy-duty CPT pushing systems (HYSON) are very suitable for installation on crawlers (Figure 1) or inside the CPT cabin of a truck or a truck with tracks (Track-Truck®). Stand-alone CPT systems mounted on a frame can be used as a skid system onshore or on a barge or jack-up rig for near-shore applications. The pushing system has two cooperating hydraulic cylinders, which are interconnected by an upper and a lower beam. A maximum pushing capacity of 300 kN is feasible, but it is often limited to 200 kN.

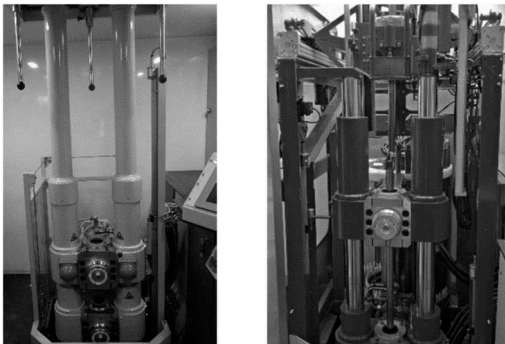


Figure 2. COSON (left) and AUTOCOSON (right) 200 kN inside cabin in CPT vehicle.

2.1.3 Heavy duty continuous systems

The continuous CPT system (COSON, Figure 2) is a further development of the above-described systems with intermittent stroke. In fact, it is a dual pushing system, built on top of each other. This pushing system is equipped with four cooperating hydraulic cylinders, provided with two independently moving hydraulic clamps. This allows a continuous movement of the CPT string when pushed into the soil. The maximum pushing capacity is often limited to 200 kN.

2.2 Heavy duty automatic systems

The continuous CPT system as described above was very suitable for a further automation of the handling of CPT rods (AUTOCOSON, Figure 2). This system consists of a continuous CPT system supplemented with a carousel system that automatically feeds the CPT rods. The cable for data transfer was replaced by light conductors inside the CPT rods for wireless data transfer (Optocone). The automatic pushing system can run a full cone penetration test without intervention of the operator. As a result, the tasks of the operator shift to monitoring and administrative work. In fact, a part of the office work can be prepared or even performed in the CPT cabin.

2.3 Offshore CPT pushing systems

Unlike onshore pushing systems which are used on land or above the water surface, offshore pushing systems are intended to operate under the water level. This imposes special demands on the equipment towards reliability and durability and use of material that are suitable for marine conditions. In offshore CPT systems we can distinguish between wireline systems for use in drill pipes, and seabed systems for performing a CPT from the seabed. Both systems require specific facilities on board of a ship.

3 PATENTED SINGLE TWIST™ (ST) TECHNOLOGY

The fact that being involved with onshore as well as offshore developments can foster cross-fertilization is proven by the development of the SingleTwist (ST) technology. Initially, the ST-technology was developed for the ROSON seabed CPT system. By incorporating the patented folding ST-rods in the seabed system, a compact, safe and easy to handle ROSON-ST is created. Later it turned out that this technology is also suitable for onshore CPT, which has resulted in the development of the COSON-ST. By integrating the patented ST-technology in a CPT cabin with the COSON continuous pushing system, an automatic and hands-free CPT machine is created.

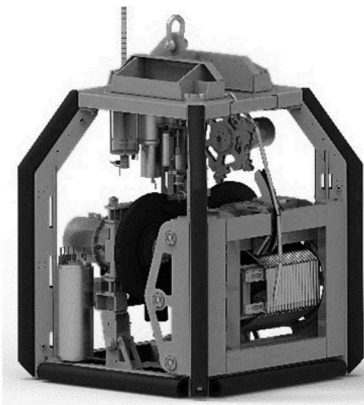


Figure 3. ROSON-ST seabed CPT system.

3.1 *ST-rods: The foldable CPT string*

The ST-rod is the smart element that makes up the CPT string. In the next subsections the interconnection of the ST-rods, the transfer of measurement data through the ST-rods and the storage of ST-rods on the Folder are described more in detail (Figure 4).



Figure 4. Folder (left), storage of the ST-rods, Twister (middle), to connect the ST-rods and data transfer (right).

3.2 *ST-rod connection*

By using a multiple bayonet thread, a strong and reliable connection has been invented that can be quickly fastened and loosened. The most striking external characteristic of the ST-rod connection are three separate threaded areas. Each of these areas covers 1/6th of the circumference of the rod, so that the inner thread of the female part can be directly aligned with the outer thread of the male part. This important feature of a bayonet coupling makes it possible to fix the connection with a very short 1/6 turn. The seven thread runs in combination with the high quality hardened SS material ensure a strong connection with a maximum holding force of 420 kN. At the front end of both the male and female threads a slope is provided, so that the rods slide into each other easily. The optimal design has been obtained with computer-

aided design, strength calculations according to the finite element method and computer aided manufacturing. The theoretical specifications have been confirmed with exhaustive laboratory and field tests.

3.2.1 *ST-rod data transfer*

A CPT rod not only ensures the transfer of the pushing and pulling force, but also the transfer of data. Most common is a connection between cone and data logger by means of a cable. A cable is very reliable, has a large bandwidth for data transfer, can be applied both onshore and offshore, and requires no further supporting equipment. However, the cable is vulnerable especially at rod connections, which must be taken into account particularly when used in automated systems.

The light conductor is a proven technology in CPT and a good option for data transfer. There is no continuous cable running through the rods, which makes handling a lot easier. This is a useful feature especially in automated systems. However, data transfer with light conduction has a limited bandwidth and is not very suitable for an offshore environment.

For data transfer in the ST-system it was decided to use a 4-core flexible cable with a small diameter. Because only digital cones are used, the number of cores can be limited to four. The requirement for applying ST-technology offshore was an important consideration for choosing this cable. To protect the cable it is fully integrated into the ST-rods and the intermediate ball joints at the rod connections. This minimizes the risk of damage. Furthermore, the cable must be able to compensate for the change in length during assembly and release of the ST-rods. This has been solved by using a flexible spiral cable.

3.2.2 *ST-rod storage and maintenance*

The foldable ST-string is stored on a reel called the ST-Folder as shown in Figure 4. The Folder has a diameter of 2 m and is provided with spacers at the circumference. This allows the ST-rods to be precisely positioned in 13 rows. The total storage capacity of the Folder is an ST string of maximum 70 m length. To easily reel up the string, the ST-rods have a length of 350 mm. The Folder is powered by an electric motor. This motor is electronically coupled to the Sprocket wheel, which feeds the ST-string to the pushing system. In this way, the Folder keeps pace with the movements of the pusher. To perform maintenance, the foldable string can be replaced completely or partially. The foldable string is made up of 2.8 m sections that contain eight ST-rods. Connectors on both ends of the cable inside a section allow for the electrical connection between sections.

3.3 *Twister on continuous pushing system*

The Twister (Figure 4) realizes the transition of the foldable ST-string into a solid CPT string. The Twister is mounted on the upper beam of the continuous pusher system (COSON). Both are described in following subsections.

3.3.1 Twister

The purpose of the Twister is to connect and disconnect the ST-rods. Therefore, the Twister is arranged on top of the upper beam of the pusher. The rod to be tightened is hydraulically clamped by the Twister. The other rod that is already part of the CPT string is held by the COSON clamp of the upper beam. As soon as the rods are correctly positioned, an electrically driven rotation of the Twister follows, providing a maximum torque of 350 Nm. To ensure a good connection between two tightened rods, the Twister checks both the rotation angle and the torque. At least an angle of 50° and a torque of 250 Nm must have been reached. The angle and torque are also an indication of the thread quality. If the angle becomes larger in combination with a lower torque, this may indicate wear of the thread.

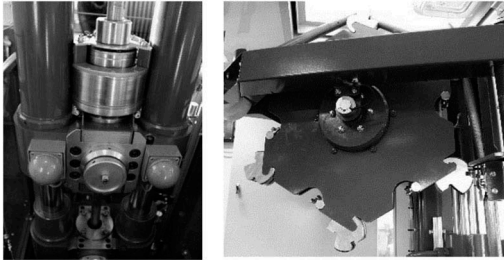


Figure 5. Continuous pushing system (left) and Sprocket, wheel for connection (right).

3.3.2 Continuous pushing system

The continuous pushing system (COSON, Figure 5) is used in the ST-concept, because by using the continuous pusher the Folder can also move continuously, which is an easier process to control adding and removing rods. Furthermore, the small installation height provides sufficient room for a Sprocket wheel on top, without special roof requirements. Finally, the rod length of 350 mm is chosen to match the stroke of the continuous pusher, so each rod is clamped and (un)tightened at the same position by the Twister. The COSON continuous pushing system is a proven technology with a track record of more than 20 years.

3.4 Sprocket wheel for connection

The Sprocket (Figure 5) is the connecting link between the Folder and the Twister. It ensures the correct position of the ST-rods in relation to the Twister. It also ensures the correct feeding speed, so that a smooth cooperation between Folder and Twister is guaranteed. Furthermore, the Sprocket ensures that the rods are pushed together in order to twist them properly. In addition, vice versa that the rods are pulled apart directly after they have been loosened.

3.4.1 Correct positioning, constant speed and smooth twisting of ST-rods

The electrically driven Sprocket is mounted on the static part of the pusher. There are six guiding blocks on the sprocket that precisely position the rods.

Because the Sprocket exerts a constant push or pull load on the string, the average Sprocket rotation speed is exactly the same as the pusher speed. During a CPT the pusher moves at a continuous speed of 15 to 25 mm/sec. During retraction, this movement is non-continuous with an average speed of 70 mm/sec.

For tightening the bayonet coupling of the ST-rods, it is necessary that the seven thread runs are exactly opposite to each other. This is achieved by the constant push load of the Sprocket. The rods to be tightened are pushed together, so a connection is established properly.

3.5 Operation and HMI

The ST-system enables a fully automatic and hands-free CPT cycle. The operator just has to bring the ST-system to the correct condition to start or continue a cycle. This is done with the clear push/pull and speed symbols on the left side of the screen (Figure 6). After positioning, the cycle is started with just one push on the start button. The effect of an action is made visible within this image of the system on the right side of the screen, by changing colours or moving component parts. All movements of the different clamps, the pusher, Twister, Sprocket and Folder can be operated separately. Important process variables are continuously displayed, such as the CPT speed, the angle and torque of tightening rods, the angular position of the sprocket wheel and the oil pressure and temperature. Furthermore, it is possible to set alarm values for the maximum reachable total push load and inclination of the cone.

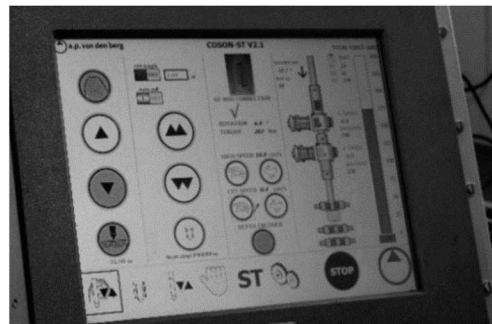


Figure 6. Touch screen for operation and real time presentation CPT data.

4 PRACTICAL APPLICATION

The VLG, the Engineering Department of the City of Rotterdam procured the first COSON-ST pushing system built on a Track Truck. Since

early 2019 the company in the Netherlands has used this CPT system successfully in various projects. For example the company executed more than 300 CPTs on projects in Amsterdam and 32 CPTs and 30 magneto measurements with the Icone Magneto click-on module on a project in Rozenburg (the Netherlands). Their typical workday is filled with two to eight CPTs at multiple locations. One project was selected to share as typical example in the following sections.

Compared with more traditional CPT systems, the VLG confirms that the COSON-ST automated system has removed the causes for physical strain. The operators do not have to lift, guide and screw CPT rods anymore. Secondly, the ST-system is timesaving. Preparation takes less time, as there is no need to raise a hatch and to place an end set including inner casing. The operator just has to prepare and install the Icone. The timesaving in the CPT cycle is mainly achieved during pulling. It is proven that a complete 50 m CPT can be performed approximately ten minutes faster with the COSON-ST with two hydraulic clamps than with the HYSON with one clamp. On top of that, after one push on the button, the operators' hands are free to prepare the next test or perform other (engineering) activities. With the application of thicker CPT rods, 40 mm instead of 36 mm, the risk of buckling and breaking is much smaller and that provides the VLG with a lot of confidence. The company has regularly pushed with a total force of more than 15 tons without any problems, whereas with previous CPT systems the VLG was already on guard with respect to breakage at lower pushing forces. Due to these rods, the time-consuming use of casing for lateral support is also required less often. This all results in an average production of 10 CPTs of 40 m in a working day at one project location. On longer days with favorable conditions, the company has even reached 17 of these CPTs. The maximum CPT depth of 70 m with VLG's CPT string size has also been realized.

The selected project concerned the geotechnical investigation required for the design of new bridges that are part of the Polder path in Schiebroekse polder in Rotterdam, The Netherlands. This is a cycle link between the city of Rotterdam and the Schie nature reserve. Eight CPTs were performed.

4.1 Purpose investigation bridges polder path

The main purpose of performing Cone Penetration Tests was to calculate the load capacity for prefabricated concrete piles, for the determination of the pile lengths and to indicate the preconditions required to prevent the potential bursting.

4.2 Equipment used

The VLG uses the Track-Truck with COSON-ST as a standard in order to execute CPTs, because the



Figure 7. Track-Truck with COSON-ST in the cabin.

working environment is ergonomically optimized and the production rate is increased by at least 10%. In order to build new bridges (part of the Polder path in Schiebroekse polder) in Rotterdam, the CPTs were performed with the Track-Truck with COSON-ST (20 ton CPT truck with tracks) as well. A Track-Truck can run on the highway as an ordinary truck with its tracks retracted. After lowering the tracks, the Track-Truck does not get stuck in soft and hilly terrain such as the location where the new bridges will be built. Inside the cabin of the Track-Truck the COSON-ST pushing system is integrated. This matches with the safety, physical load and efficiency requirements of the VLG, the Engineering practice of the City of Rotterdam. A digital 15 cm² piezocone (Icone) was used as the measuring instrument. The modules Seismic, Conductivity, Magneto and Vane could be used along with the Icone, but additional parameters were not requested in this project.

4.3 Test method

The bearing capacity of the piles has been determined with the help of a D-foundation computer program. The pile point level must be chosen in such a way that the requirements of the NEN EN 9997-1 +C2:2017 Geotechnical design are met. The piles are calculated for pressure load.

4.4 Test results

The CPTs performed with the COSON-ST and 15 cm² Icone for the design of new bridges part of the Polder path in Schiebroekse polder in Rotterdam, The Netherlands, gave a good image of the soil for the foundation advice. An aquifer was found at circa 12 m depth with the 6th and 7th Cone Penetration Test (Figure 8). In this respect, the risk for the development of wells, when digging in the (unfavorable) area at two bridges, has been checked. This check indicates that there is no bursting risk of the soil when excavating for the abutments of these two bridges. The CPTs are used to calculate the bearing capacity of precast concrete piles for a pile level at a depth of 20 m. Of these indicative calculations is the D-Foundations output included in Figure 9.

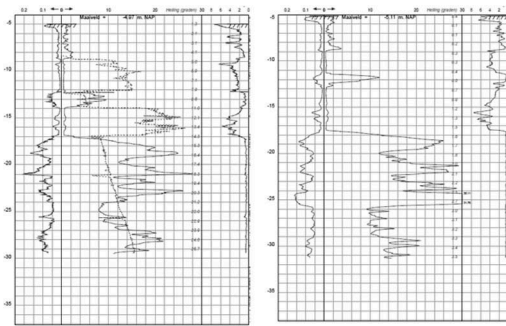


Figure 8. Left: CPT nr. 6 including pore water pressure: showing an aquifer between clay layers at 12 m depth. Right: CPT nr. 7 without pore water pressure: showing an aquifer between clay layers at 12 m depth.

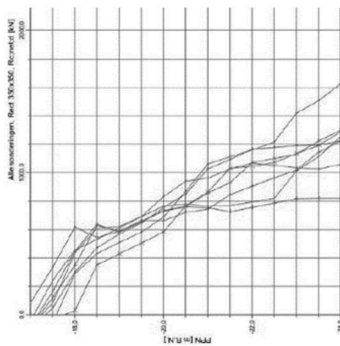


Figure 9. Output D-Foundations indicative calculations piles bearing capacity.

5 CONCLUSIONS

Cone Penetration Testing (CPT) is a recognized and widespread method for efficiently performing in-situ soil surveys, for e.g. foundation advice. Over time, CPT has been improved by integrating digital electronics inside the measuring cone. In addition, the pushing system needed upgrades, because soil investigation is carried out at increasing depths, which requires higher pushing forces. In addition, developments have also focused on operational efficiency and an ergonomically optimized work environment. The CPT cabin as working environment, built on trucks, crawlers or Track-Trucks, will more and more develop from a workshop into an office. The most prominent development is the ability to perform automatic and hands-free CPTs using the patented Single-Twist™- technology with the COSON pushing

system. With a single push of the button, the automatic CPT cycle is completed. The CPT string, with the measuring instrument (cone) fitted at the tip, is pushed into the soil in one continuous movement. This string is built up automatically from a reel with separate, but interconnected, ST-rods.

The so-called COSON-ST has proven to be a robust CPT pushing system providing reliable data about the soil and ensuring the operational efficiency, which is increasingly expected. The COSON-ST has more than proven itself and the VLG feels confident to let the system do its work. VLG experienced a production rate increase of at least 10%. The system works faster than standard CPT pushers, as it can start up more quickly and runs without further intervention or control. It does not require any manpower during the push/pull cycle of a CPT. The operator only has to provide the start/stop signals. Another advantage, which is proven according to VLG, is that the working environment is ergonomically optimized, because manual actions near the moving system are almost unnecessary. Indeed time “on board” is spent on design or other office-related work next to performing CPTs. An additional advantage of the COSON-ST is that the depth range is increased because of the continuous CPT push. CPTs are realized faster and in addition to the already shorter preparation time, this continuous movement results in a faster pushing and pulling process with a higher production rate as a consequence. Furthermore, the ST-rod is designed in such a way that the risk of breakage and the associated downtime and costs are limited.

Based on the input from VLG we can conclude that the COSON-ST is a welcome contribution to the expected change of the working environment inside the CPT cabin. A shift from operator to engineer and from manual operation to data processing and assessment will occur.

In addition to the onshore application described in this paper, the ST-technology can also be used offshore. The ROSON-ST is immediately operational and can perform a CPT fully automatically from the seabed in a very safe and timesaving way.

REFERENCES

- Brouwer, J.J.M. 2007. *In-situ soil testing*. Bracknell: IHS BRE Press.
- Lunne, T, Robertson, P.K., Powell, J.J.M. 1997. *Cone Penetration Testing in Geotechnical Practice*. London: Blackie Academic & Professional.
- Schnaid, F. 2009. *In situ testing in Geomechanics, the main tests*. London, New York: Taylor & Francis.

Sustainability in CPT practice: Hybrid CPT Track-Truck

O. Storteboom & M. Woollard

A.P. van den Berg, Heerenveen, The Netherlands

B. Ooms

BAM Infra Nederland, Gouda, The Netherlands

ABSTRACT: Sustainability in construction is of great importance in government projects, but also of growing concern in the market in general. In this way, earth can be passed on to future generations in a healthy way. A sustainable realization of construction projects, within strict environmental standards, is the reason for companies to invest in electrification of equipment, so without carbon and nitrogen emissions. In terms of CPT, BAM Infra Nederland has taken the world's first hybrid truck with tracks into use early 2021. The heavy 4x4 truck is, while at the project location, electrically powered without emitting harmful substances such as carbon and nitrogen emissions. Both the CPT soil investigation and driving on the tracks are executed completely electrically. On the road, the truck is powered by the usual diesel engine. BAM Infra Nederland has now used the hybrid CPT Track-Truck for various projects. In the paper, experiences from practice are further elaborated and explained.

1 INTRODUCTION

Rising prices of fossil fuels, increasing scarcity of crude oil, and government regulations and policies against diesel and gasoline powered vehicles owing to surging pollution are major factors changing the preference toward alternative fuel powered vehicles. This is a factor boosting the hybrid truck market during the coming years. Moreover, evidence suggests that road transport accounts for more than 50% of the total health impact of air pollution caused due to emissions of harmful gases from vehicles. This is prompting governments and car manufacturers to design and develop alternative solutions to curb transportation emissions. This has led to the development of hybrid technology for automotive, which unlike conventional vehicles, does not consume a large amount of fuel and emits less carbon. Furthermore, increasing automation and usage of machinery to simplify manual work in various industries such as construction, agriculture transportation, mining, and infrastructure, have fuelled the application of hybrid trucks in these sectors. However, the high initial and maintenance costs of hybrid trucks is anticipated to restrain the hybrid truck market (Automotive Team, Hybrid Truck Market, Forecast 2019 -2027). Besides this development, companies more and more want to invest in sustainability.

Towards the CPT market there is more and more a need for sustainable equipment. The hybrid truck with tracks meets this need by performing CPT soil investigation in a sustainable way. In the

next paragraphs the development of onshore CPT pushing systems are described briefly. In paragraph 3 the hybrid Track-Truck is explained and in paragraph 4 experiences from practice are further elaborated.

2 DEVELOPMENT OF ONSHORE CPT PUSHING SYSTEMS

Nowadays, the range of onshore CPT pushing systems varies from a single lightweight pushing cylinder for hand carried CPT solutions to heavy duty pushing devices built on trucks and on large crawlers. With regard to the heavy duty pushing devices the importance of sustainability is increasing

2.1 *Lightweight CPT systems*

Lightweight CPT systems (Figure 1) are very suitable for installation in hand carried applications and on light vehicles such as mini crawlers. The lightweight pushing system has a compact size (165 × 310 mm without anchors) and low weight (only 85 kg) in combination with sufficient pushing capacity to perform a reliable CPT. The 100 kN lightweight pusher is designed to perform in-situ geotechnical soil investigations at locations inaccessible to other equipment, such as basements, back yards, swampy and overgrown land.



Figure 1. Lightweight CPT system (100 kN pusher).



Figure 2. 100 kN pusher in mini CPT crawler.



Figure 3. Truck-Truck with 200 kN pusher inside the cabin.

2.2 Heavy duty systems

Heavy-duty CPT pushing systems are suitable for installation on crawlers or inside the CPT cabin of a truck or a truck with tracks.

The CPT Crawlers (Figure 2) have tracks for better manoeuvrability in rough or soft terrain. The crawler is the only option at sites where the maximum allowed height is limited. Separate carriage is required for transport of the crawler. The truck with tracks (Figure 3) is suitable for soft and hilly terrain where other heavy vehicles get stuck (for more information, see paragraph 3.1).

Stand-alone CPT systems mounted on a frame can be used as a skid system onshore or on a barge or jack-up rig for near-shore applications. The pushing system has two cooperating hydraulic cylinders, which are interconnected by an upper and a lower beam. A maximum pushing capacity of 300 kN is feasible, but in many cases for reasons of maximum vehicle weights, this is limited to 200 kN.

The heavy duty pushing system is powered by the truck PTO or a separate power pack. Hybrid systems with electrical mode are available since the beginning of 2021.

2.3 Heavy duty continuous systems

The continuous CPT system (Figure 8) is a further development of the above-described systems with intermittent stroke. In fact, it is a dual pushing system, built on top of each other. This pushing system is equipped with four cooperating hydraulic cylinders, provided with two independently moving hydraulic clamps. This allows a continuous movement of the CPT string when pushed into the soil. The maximum pushing capacity is often limited to 200 kN.

The continuous pushing system is able to handle 1.000 mm CPT rods. Because of the continuous movement of the CPT string, the cohesion with the surrounding soil is less, so a greater penetration depth can be achieved with the same pushing force.

2.4 Heavy duty automatic systems

The continuous CPT system as described above was very suitable for a further automation of the handling of CPT rods. This system consists of a continuous CPT system supplemented with a carousel system that automatically feeds the CPT rods. The cable for data transfer was replaced by light conductors inside the CPT rods for wireless data transfer.

By integrating the patented ST-technology into a CPT cabin with the continuous pushing system, a fast CPT machine for hands-free operations is created (Storteboom O. et al, 2022). On the vehicle, the workplace of the CPT operator is turning into an office environment. The assembly and disassembly of the CPT string takes place fully automatically with a continuous CPT pusher. The working environment is ergonomically optimized, because less machine work needs to be done. On average the production rate is increased by 20% compared to a standard CPT pusher.



Figure 4. Automatic CPT System.



Figure 5. Small fuel (diesel) tank in the hybrid truck.

3 HYBRID TRACK-TRUCK

3.1 CPT Truck with tracks (*Track-Truck*)

The Track-Truck was invented by A.P. van den Berg and has a record of accomplishment of more than 30 years. With its tracks retracted, the Track-Truck can run on the highway as an ordinary truck. After lowering the tracks, the Track-Truck is in its element in soft and hilly terrain where other heavy vehicles are stuck. The track system reduces the wheel load by 60 to 70%. Manoeuvring the Track-Truck is performed from the driver's cabin or with a remote control from a safe distance. The penetrometer is easily operated via the touch screen, the clear Human-Machine Interface (HMI). A maximum pushing capacity of 200 kN, enables any soil investigation using the cone penetration method.

3.2 Hybrid system

The hybrid truck with tracks integrates a combination of a traditional internal combustion

engine system along with fuel tanks (Figure 5) and an electric propulsion system, which constitutes of an electric motor and battery pack. The 4×4 truck serves as a basis for the truck to which the hybrid part was added.

4 PRACTICAL APPLICATION

BAM Infra Nederland, part of Royal BAM Group, is a leading player in the Netherlands in the field of infrastructure. As a leading company, BAM has formulated ambitious goals in the field of sustainability. These objectives are concentrated around minimizing emissions (up to zero emissions), reducing the use of primary raw materials, the use of renewable energy and encouraging circular construction.

BAM wants to build emission-free. In the field of equipment, BAM is looking for emission-free alternatives. BAM already introduced the world's first electric roller. Beginning of 2021 the hybrid CPT truck on tracks was added to the sustainable fleet (Figure 6).

4.1 *Minimizing emissions*

Conducting soil investigation by a diesel-powered truck on tracks means that the diesel engine must be running to provide power to all drive systems and the CPT measuring system. Although these systems require little power, the diesel engine continuously emits combustion gasses and noise. In urban areas, this is more and more intolerable and limited by strict environmental requirements.

These restrictive conditions open up an opportunity by making soil investigation possible with targeted adjustments. To silence the diesel engine, another energy source must be available. An energy source that is clean at the point of use and produces virtually no noise emission. The most obvious choice is the use of an electro motor capable of driving the hydraulic pumps. Together with a battery pack with sufficient storage capacity for a full day of soil probing, completes this solution.

4.2 *New generation CPT Track-Truck*

A.P. van den Berg was approached by BAM Infra Nederland to develop a CPT Track-Truck as sustainable as possible. The solution is a hybrid variant. The heavy 4×4 truck moves over the road with a clean diesel engine that meets the highest emission requirements. On location, it is electrically powered to carry out soil investigations without emitting harmful substances such as carbon and nitrogen. In addition, the hybrid Track-Truck does its heavy work in a quiet way.

The hybrid system offers the possibility to conduct CPT soil investigations completely emission-free. The Track-Truck is equipped with a 90 kW electric motor that drives a second pump set.



Figure 6. Hybrid CPT Track-Truck.

The pump set provides hydraulic pressure to drive the tracks and to perform the CPT soil investigation. The electric motor is powered by a battery pack with a capacity of 70 kWh. This power is sufficient to perform 9 medium CPTs with a CPT depth of 25 meters and to drive the Track-Truck on the tracks for about 60 minutes. On site it is possible to change the power source for the drive from diesel to electric. With electric drive, the diesel engine can be switched off. In some cases the electric drive is stopped, then the diesel engine will start and automatically switch from electric to diesel. This transition is so smooth that the driven process is not affected by this. If no power is drawn during electric drive, the electric motor switches to an energy-saving mode, where the speed is reduced to 500 rpm. As soon as power is required, the electric motor revs up and energy is almost immediately available. If no power is drawn for a longer period of time, the electric motor switches off manually to save energy. The batteries for the hybrid system (see Figure 11) can be charged at a charging station or with a 3-phase connection with a maximum power of 22 kW. In order to fully charge the battery four to five hours is required. In addition, a small fuel tank is installed in order to drive from and to locations.



Figure 7. Digital cone.



Figure 8. 200 kN continuous pushing system inside cabin of hybrid CPT vehicle.

4.3 Equipment used

The digital cone (Figure 7) measures the four standard parameters: cone tip resistance (q_c), sleeve friction (f_s), pore water pressure (u) and inclination ($I_{x/y}$). The digital cone is mechanically 40% stronger than its analogue predecessor and is at the same time more accurate, more reliable and easier to maintain. Calibration data is stored in the cone itself, so separate data holders such as USB sticks are no longer necessary. Digital cones come with a pre-pressure and seal assembly that reduces cone maintenance.

The continuous pushing system is an advanced CPT system for performing CPTs for soil research. The continuous pushing system is able to push a CPT probe into the soil with a continuous movement and with a maximum capacity of 200 kN (Figure 8). The truck on tracks is a standard 4x4 truck with tracks between the front and rear axle. This provides the Track-Truck with a large load capacity for moving on soft subsoil. The Track-Truck is equipped with a hybrid drive. This means that all functions, except truck driving, can be powered by the diesel engine of the truck or by an electric motor. The electric motor is powered by a battery pack with a capacity of 70 kWh. The hybrid Track-Truck is capable of emission-free CPT and track driving, meeting a zero emissions requirement on site.

4.4 User experience

The hybrid CPT Track-Truck has been used for more than six months by BAM Infra Nederland (Figure 9).



Figure 9. Example of a project in which the hybrid Track-Truck is used.

4.4.1 Test results

The CPT in Figure 10 is an examples of the many CPTs which the BAM has performed in the centre of Amsterdam (The Netherlands). In this specific project 13 CPTs were performed up to a depth of 68m below ground level. The hybrid Track-Truck can enter the centre of Amsterdam without a special environmental exemption. Furthermore it was experienced as much cleaner and quieter when performing the CPTs.

4.4.2 Savings

In the first six months the hybrid Track-Truck has used 3,000 liter of diesel. The traditional Track-Truck used 9,000 liter of diesel, so in total 6.000 liter (67%) is saved. The Hybrid Track-Truck saves on average fifty liter per day, or saves approximately 32,000 kilograms of CO₂ per year.

4.4.3 Sound level

In practice the engine of the Track-Truck is only used on the trips to and from the location. The fact that the engine no longer has to run during CPTs and when moving the tracks lowers the sound level considerably. When moving on tracks and during CPTs it hardly makes any noise when you are outside the cabin. Inside the cabin a lower noise level is experienced of less than 67 dB(A). This could be lowered even more when the insulation is upgraded and special damping techniques are used.

When moving on tracks and during CPTs it hardly makes any noise when you are outside the cabin. Inside the cabin a lower noise level is experienced of less than 67 dB(A). This could be lowered even more when the insulation is upgraded and special damping techniques are used.

4.4.4 CPT soil investigation

The experience regarding the CPT investigation is that the CPT soil investigation results are similar

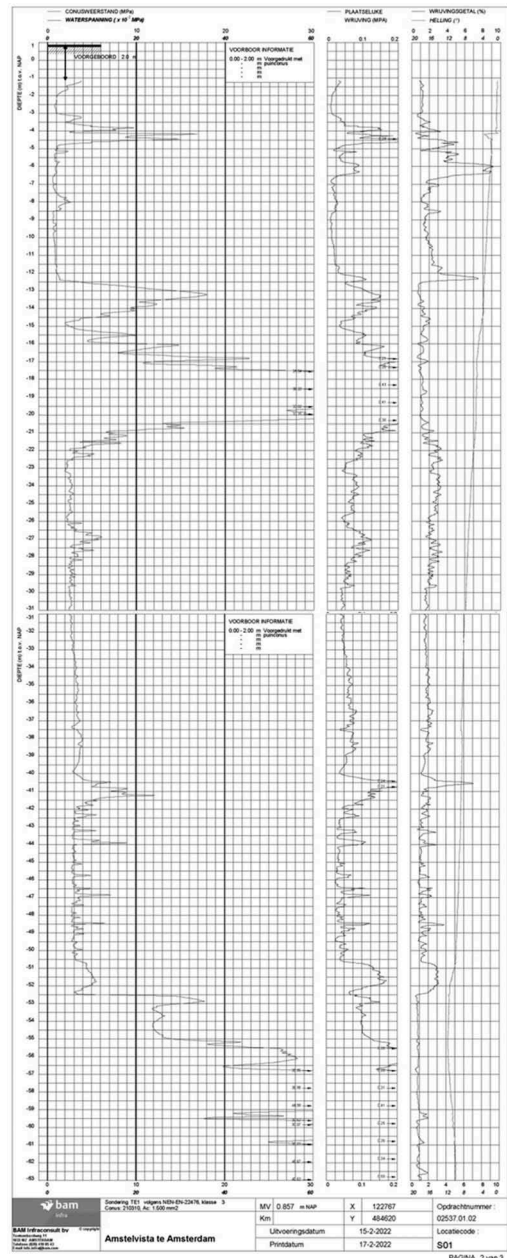


Figure 10. CPT with the hybrid Track-Truck in the centre of Amsterdam.

to the traditional CPTs. There is no difference in pushing capacity, CPT velocity and fast pulling the probe out of the soil. In general, no quality loss is experienced when performing the CPT soil investigation fully electrical.

4.4.5 Hybrid battery

The hybrid battery (Figure 11) and drive are characterized by high operational reliability, ample drive

power and a long service life of 25 years. The safety for users is increased due to less noise and no emission of harmful gases. During times when no power is required from the system, significant savings in fuel consumption are achieved. The electrical system has a modular structure of components, which means that faults can be solved quickly and service can be provided easily. The batteries are charged with a max. capacity of 22 kW via a wall socket or a public charging stations. Experience from the practice show that you can work 1.5 day on a full battery charge.



Figure 11. Batteries for the hybrid system.

5 CONCLUSIONS

A sustainable realization of construction projects, within strict environmental standards, is the reason for companies to invest in electrification of equipment, so without carbon and nitrogen emissions.

In terms of CPT, the hybrid Track-Truck is, while at the project location, electrically powered without emitting harmful substances such as carbon and nitrogen emissions. Both the CPT soil investigation and driving on the tracks are executed completely electrically. On the road, the truck is powered by the usual diesel engine.

The hybrid Track-Truck was launched early 2021. Experiences from practice show that the fuel consumption is lowered by 67%. On daily basis fifty liter is saved and approximately 32,000 kilograms of CO₂ per yearly basis.

The tracks are electrically driven and therefore the sound level is lower compared to fuel driven Track-Trucks. With a full battery charge CPTs can be performed during 1.5 day before the battery needs to be recharged. The experience with regard to CPT soil investigations are more or less similar compared to traditional CPTs.

REFERENCES

- Automotive Team Hybrid Truck Market - *Global Industry Analysis, Size, Share, Growth, Trends, and Forecast 2019 – 2027*
- Brouwer, J.J.M. 2007. *In-situ soil testing*. Bracknell: IHS BRE Press.
- Lunne, T, Robertson, P.K., Powell, J.J.M. 1997. *Cone Penetration Testing in Geotechnical Practice*. London: Blackie Academic & Professional.
- Storteboom, O, Woollard, M. 2022. *Efficiency examined of hands-free Cone Penetration Testing using the Single-Twist with COSON'*.

Elastic soil properties investigated using seismic tests to complement the CPT

O. Storteboom & M. Woollard

A.P. van den Berg, Heerenveen, The Netherlands

J.L. Rangel-Núñez

UAM-Azc and Ingeum Ingeniería, Mexico

ABSTRACT: Seismic tests are performed to investigate the elastic properties of the soil. Elastic soil properties are essential input for the prediction of soil-surface motions related to earthquake excitations and for the design of foundations for vibrating equipment, for the assessment of offshore structure behavior during wave loading and to predict deformations around excavations. To investigate these elastic properties of the soil, seismic tests can be performed. The digital Icone is easily extendable by click-on modules to measure additional CPT parameters. The Icone Seismic module is the instrument to investigate the elastic soil properties. This click-on module is automatically recognized, creating a true plug & play system. It contains three accelerometers to receive left and right shear waves as well as compression waves. The Icone Seismic system can be applied both onshore and offshore and has a 1,000 m water depth rating. In this paper the Icone Seismic system is described. Feedback from onshore fieldwork with the Icone Seismic will highlight the user experience with this approach.

1 INTRODUCTION

Elastic soil properties are essential input for the prediction of ground-surface motions related to earthquake excitation and for the design of foundations for vibrating equipment, for the assessment of offshore structure behavior during wave loading and to predict deformations around excavations. To investigate these elastic properties of the soil, seismic tests can be performed by means of the Icone Seismic system.

The seismic piezocone penetration test (SCPTu) provides multipoint simultaneous measurement of tip resistance (q_T), sleeve friction (f_s), pore pressure (u_2), and compressional and shear wave velocities (V_p and V_s , respectively) following the down-hole geophysical testing strategy, but without using pre-drilling. This type of test has been successfully applied in geotechnical exploration for more than three decades (Lunne et al., 1997; Mayne & Campanella, 2005). Improvements have now been achieved such as using dual seismic sensors to detail the stratigraphy and to perform continuous-interval seismic piezocone tests by semi-continuous wave generation using the autoseis device at the rate of 1 strike/second (Mayne & Woeller, 2015).

In the next paragraphs, the various Icone click-on modules are described with a focus on the seismic module.

2 ICONE AND CLICK-ON MODULES

Since Cone Penetration Testing (CPT) is used for soil investigation, a tremendous development has occurred in the techniques to measure soil parameters. After CPT with the mechanical cone had proven to be very useful, the development of the electrical cone brought a big step forward in ease of use and accuracy. Nowadays the advantages of digital technology are available for further improvements.

2.1 Digital cone

The digital cone or Icone measures the four standard parameters: cone tip resistance (qc), sleeve friction (fs), pore water pressure (u) and inclination (Ix/y). The Icone is mechanically 40% stronger than its analogue predecessor and is at the same time more accurate, more reliable and easier to maintain. Calibration data is stored in the cone itself, so separate data holders such as USB sticks are no longer necessary. Icones come with a pre-pressure and seal assembly that reduces cone maintenance.

2.2 Icone and click-on modules

In the past years, several click-on modules for the Icone were developed and the seismic module is part of it. In this chapter, the following three are



Figure 1. Icone data acquisition concept.

described: the conductivity module (Figure 2), the magnetometer module (Figure 3) and the vane module (Figure 4). The seismic module is described in paragraph 3. All modules except the Icone Vane can be used with a 10 cm² and a 15 cm² Icone. When CPT-data is not required, the click-on modules can also be used with a dummy tip instead.

2.3 Conductivity module

The measurement of electrical conductivity in the subsoil is a function of both the conductivity of the pore water and the soil particles, the first being the dominant factor. With the Conductivity module changes in the concentration of (dissolved) electrolytes are determined without specifying the exact nature of these electrolytes. Therefore, the module facilitates separation of zones with differentiated water content, including determining the water table depth and the thickness of the capillary zone or separation of fresh and salt water carrying soil layers. Another very important application of the conductivity module is detection of (the degree of) contamination in a soil body. Further soil investigation should provide details on the actual contaminants.



Figure 2. Conductivity module with 10 cm² Icone.

2.4 Magneto module

Unknown structures and obstacles, like unexploded ordnance (UXO), are a risk factor in the execution of earthworks. To avoid risks of damage and interruptions of work, these underground elements must be identified and mapped. Most underground structures contain metal such as sheet-piles, ground anchors and pipelines or a combination of metal and concrete, such as

reinforced foundation piles. Power supply cables and above structures have in common that they affect the earth's magnetic field. Using the Magneto module, metal objects in the underground can be detected by interpreting anomalies of the earth's magnetic field.



Figure 3. Magneto module with 10 cm² Icone.

2.5 Vane module

In soft fine-grained soils, the field vane test (FVT) is a popular and effective complement to the CPT. The vane test allows in-situ measurement of the peak, residual and remolded undrained shear strength of soft fine-grained materials, such as clay, silt and mine tailings. The Icone Vane is a digital vane with a downhole motor and torque cell that is used for in-situ measurement and evaluation of shear strength that can be deployed in soft soils where a prediction of the undrained shear strength is required.



Figure 4. Icone Vane (without protection tube).

3 SEISMIC MODULE



Figure 5. Seismic module with 10 cm² Icone.

Seismic tests are performed to investigate the elastic properties of the soil. For this purpose a shear wave (S) or a compression wave (P) is guided into the soil. Elastic soil properties are essential input for prediction of ground-surface motions related to earthquake excitation and for assessment of: foundation design for vibrating equipment, offshore structure behavior during wave loading and deformations around excavations.

3.1 Principles

Elastic soil parameters are determined by measuring the propagation speed of an applied sound wave between two known depths. Mostly this is done by pushing the seismic module into the soil and stopping at 1-meter intervals. During the pause in penetration, a shear or compression wave is generated at surface level and the time required for the wave to reach the seismic sensors is recorded. The time difference between two consecutive seismic tests performed is a measure of the elastic properties of the soil. The following can be calculated as a function of the seismic data (shear and compressional wave velocities, V_s and V_p , respectively) and the soil density (ρ , usually already known), eqs 1 to 6: small strain shear modulus (G_{max}), constrained modulus (M), Poisson's ratio (ν), elasticity modulus (E), bulk modulus (κ) and Lamé's constant (λ).

$$G_{max} = \rho V_s^2 \quad (1)$$

$$M = \rho V_p^2 \quad (2)$$

$$\nu = \frac{2 - (V_p/V_s)^2}{2 \left[1 - (V_p/V_s)^2 \right]} \quad (3)$$

$$E = 2G_{max}(1 + \nu) \quad (4)$$

$$\kappa = \frac{E}{3(1 - 2\nu)} \quad (5)$$

$$\lambda = \frac{E\nu}{(1 + \nu)(1 - 2\nu)} \quad (6)$$

An even faster and more accurate way is to use two seismic modules, which are mounted, at a fixed distance of exactly 0.5 or 1 meter. Since the time difference between two consecutive measurements is approximately 2 ms, a very consistent measurement of the trigger signal is required. This requirement is met by using the same high sensitive sensors for the trigger module and by placing this module in the immediate vicinity of the hammer.

3.2 Data processing and visualizing

Both the Icone Seismic Module as well as the Icone are part of our modular data acquisition concept that

is based on digital data transfer. The system consists of a digital data logger, called Icontrol, and the Ifield software for real-time data presentation. Due to application of digital technology, multiple parameters can be retrieved by several modules. Upon connection, the Icontrol data logger and Ifield software will automatically recognize the specific cone and/or module, so it is a true plug & play system.

The output signals from the seismic sensors are being digitized inside the seismic module and from here transferred to the Icontrol data logger at surface level. After all tests have been performed, the data obtained are then analyzed offline by processing software, determining the propagation speed and corresponding elastic soil parameters for all investigated depth ranges.

4 PRACTICAL EXPERIENCES

Determination of shear wave velocity profiles has been applied to define the stratigraphic profile and to evaluate site effects, *i.e.* dynamic amplification or liquefaction, however, its field of application has now been extended. In fact, it is also applied in arability studies, for the design and control of soil treatment, and lately in the determination of the parameters of advanced constitutive equations. Therefore, it is common in an exploration campaign to determine such a profile, but this is not trivial since there are different methods and, in principle, it is necessary to define which one to use. The definition of the method depends on several factors, namely, experience and mastery of the proper execution and interpretation of the method, the alteration and deformation induced in the subsoil, the degree of heterogeneity, to mention the most important ones. For example, although the seismic refraction method is easy to perform and is a non-invasive technique, its interpretation is not easy, mainly when velocity inversion is present in the subsoil; unfortunately, in geotechnical problems this condition is frequent. Regarding the down-hole, up-hole and cross-hole techniques, it is necessary to take care not to induce an excessive alteration in the subsoil when the borehole is drilled. With respect to the techniques based on the measurement of surface waves, the problem is that the solution is not unique, so the method is very dependent on the experience and the geotechnical information available.

With respect to the seismic piezocone test (sCPTu), it has the advantage that the alteration generated in the subsurface is less than that produced with the conventional down-hole technique or with the suspension-logging test (SLT), since in the latter it is necessary to drill a borehole, where a relaxation is generated and a cake is created around the borehole.

The following are five projects where the shear wave profile was determined. Two of them were

carried out in Mexico City (CDMX) for the design of building foundations, a third for the design of the liquefiable soil deposit improvement system and the remaining two were for the study of tailings dams.

HYSON 100kN installed on a 14t Mercedes-Unimog truck was used in all projects (Figure 6). A 10 cm² piezocone was used with the seismic module (Figure 5). The wave generation system was by means of the lateral strike of a beam.



Figure 6. Equipment used for secondary wave profile determination.

4.1 Building design in CDMX

The urban area of Mexico valley can be divided in three main geotechnical zones: Foothills (Zone I), Transition (Zone II) and Lake (Zone III). In the foothills, or hills, very compact but heterogeneous volcanic soils (*i.e.* tuffs) and lava are found. These materials contrast with the highly compressible soft soils of the Lake Zone. Generally, in between, a Transition Zone is found where clayey layers of lacustrine origin alternate with sandy alluvial deposits erratically distributed. Mexico City is mainly located in the lake zone.

Very soft soil deposits of the lake area, whose average thickness is 30 m, are mainly clayey with alternating hard lenses/layers (a superficial crust and ash, silty sand lenses or thin layers), and they are characterized by an high humidity ($100 < w_n < 900\%$), high plasticity index, ($100 < PI < 500$), large one-dimensional compressibility ($C_{c, max} \approx 10$) and low shear wave velocity ($V_s < 100\text{m/s}$). Those unusual values are produced mainly by the clay microstructure and composition, and the high diatoms content (Rangel et al. 2014).

There are two important factors that affect the design of the foundation of a building in the lake and transition zones of Mexico City, where almost 80% of the buildings are located: earthquakes and regional subsidence. Regarding the first aspect, Mexico City has a high dynamic amplification coefficient, max 25 (Pérez Rocha *et al.*, 2009), therefore, it is necessary to know the velocity law of the subsoil, at least in the strata that amplify the seismic wave, that is, up to 30 and 40 m depth.

4.1.1 Building project 1

The construction of a hotel in the lake area of Mexico City is contemplated, which consists of a 14-story tower and low-rise buildings, both with

a basement. The foundation solution proposed for the tower consists of piles at a depth of 31 m.

Purpose investigation. The main purposes in using the seismic piezocone at this site, was to:

- Determine the soil stratification and dynamic properties.
- Estimate the capacity of piles.
- Determine site spectrum.

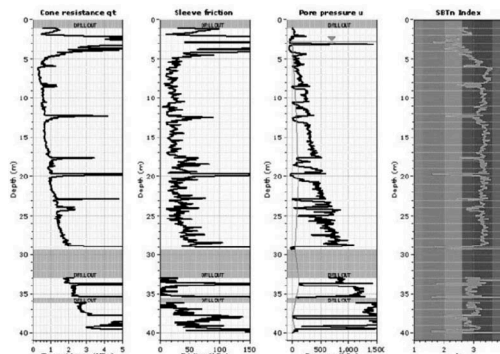


Figure 7. Primary parameters determined with the sCPTu.

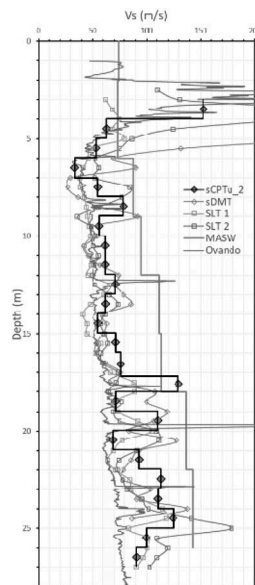


Figure 8. S-wave velocity profile determined with different techniques: sCPTu, sDMT, SLT, MASW and Ovando's correlation.

Results. Because this building is located in an area with significant seismic amplification, part of the exploration campaign was directed to determine the velocity profile of the secondary wave in order to design its foundation. Figure 7 shows a detail of the stratigraphy detected with the sCPTu sounding, which is typical of the Mexico City Lake area, and

Figure 8 shows the secondary wave velocity profile obtained with different techniques: seismic piezocone (sCPTu), seismic dilatometer (sDMT), suspension logging Test (SLT), multi-channel analysis of surface waves (MASW) and an empirical correlation applicable to CDMX deposits (Ovando et. al., 2007). It is observed that all the techniques produce similar results, although the values determined with MASW are almost double those determined with borehole techniques. Likewise, it can be seen that the values obtained with SLT were lower, possibly attributable to the greater alteration that occurs in the soil when drilling, and in general the values determined with sCPTu, sDMT and using Ovando's correlation were very similar.

4.1.2 Building project 2

The project considers the construction of a shopping center and four towers (14, 18, 20 and 22 levels), three for residential use and one for office use, with shared parking basements on a large basement, whose maximum general excavation level is -16.00 m. The project is located in the lake area.

Purpose investigation. The main purposes in using the seismic piezocone at this site, was to:

- Determine the soil stratification and dynamic properties.
- Estimate the capacity of piles.
- Determine site spectrum.

Results. An extensive exploration campaign was carried out including the following techniques: sCPTu, sDMT, Vane Shear Test (VST), Pressuremeter (PMT), Phicometer (PHI), undisturbed sampling and laboratory tests. The geotechnical design model is presented in Figure 9. For the short-term shear strength (s_u), the results of the VST and TX-UU tests were used for the soft soils and the PMT and PHI for the hard soils; for the shaft strength of the piles, the f_s (sCPTu test) and the residual strength determined with VST were used; the piezometric conditions were evaluated from CPTu Δu ; the compressibility moduli to determine the soil long-term behavior were obtained from piezocone correlations and oedometer tests; and finally, the dynamic response was studied from the velocity profile obtained with the sCPTu.

4.2 Subsoil improvement design

An oil refinery will be built in southern Mexico. Due to the high seismicity of the area and the existence of deposits with alluvial and fluvial soil intercalations below the groundwater level, the liquefaction potential is high, for which an improvement of the subsoil is pro-posed, so an exploration campaign has been proposed which includes the determination of S-wave velocity profiles in order to design such improvement. Figure 10 shows a sounding showing typical conditions in the project, where intercalations between soft and frictional soils are observed. Based

on the soil characterization and the design earthquake, an initial liquefaction analysis was carried out to corroborate the liquefaction potential and based on the S-wave velocity profile, the target for the design of the improvement was established, in other words, that profile where liquefaction no longer occurs.

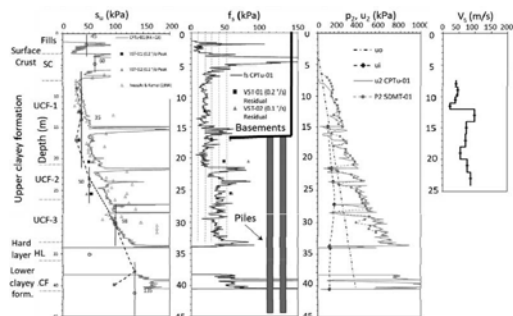


Figure 9. Geotechnical model for design of the site 2.

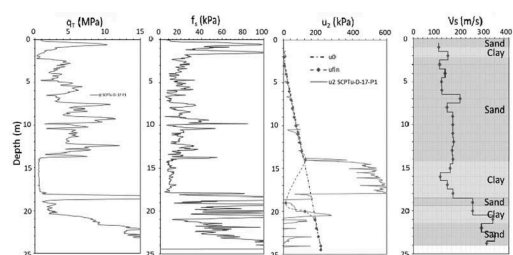


Figure 10. Stratigraphic profile for the subsoil improvement zone.

4.3 Stratigraphic conditions in tailings dams

In the case of tailings dams, where there are very young and heterogeneous deposits, exploration campaigns have been carried out to determine the stratigraphic profile and mechanical parameters with *in situ* tests, since obtaining unaltered samples is difficult in most cases. It highlights the importance of shear wave profiles in conjunction with vane and CPTu Δu tests, in order to carry out dam stability analyses and identify potentially unstable strata (determination of G_{os} , s_u and k). The results obtained in two mines in Mexico are presented below (Figures 11 and 12). It is observed that in all cases the values of the tip resistance q_T oscillate strongly and this gives an idea of the heterogeneity that exists in this type of deposits. This behavior is also observed in the shear velocity profiles, so it is necessary to try to decrease the distance at which the determination of velocity S-wave is made. Also, it is observed that sometimes the value of u_2 is negative, which implies the development of suction. When observing the results of the dissipation tests, it is obtained that the

curves differ from those obtained in natural soils, where it is difficult to obtain the initial value of the pore pressure. All these aspects make it difficult to define the stratigraphic profile and to determine the properties in the field, which is why conducting an exploration campaign in tailings dams is currently a challenge.

An alternative to determining the velocity profile is through correlations. Figure 13 shows the velocity profiles obtained from the sCPTu measurement and the one determined by means of q_T vs V_s correlations, although the correlation provides adequate values, it does not capture the peaks.

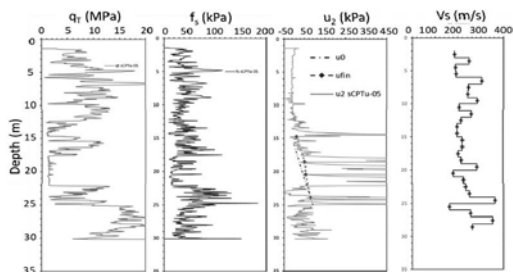


Figure 11. Results of the sCPTu- Δu tests for the case of tailings dam 1.

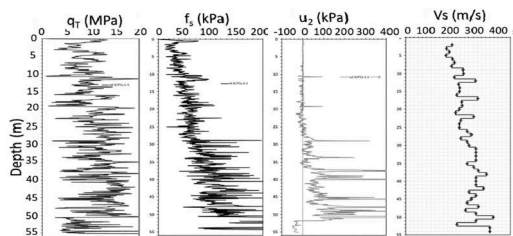


Figure 12. Results of sCPTu tests for the case of tailings dam 2.

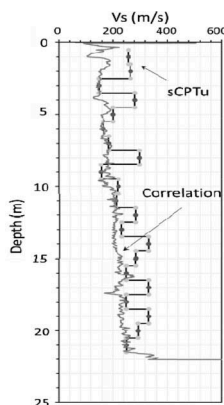


Figure 13. Comparison between the s-wave velocity profiles obtained with the sCPTu and by correlations with q_T ; for the sCPTu-2 borehole in tailings dam 1.

5 CONCLUSIONS

Cone Penetration Testing, as a technique for *in-situ* soil investigation, is a recognized and widespread method for efficiently performing of soil surveys. CPT is in the course of time continuously improved like developments concerning the application of digital electronics inside the cone. The most prominent of these is the ability to easily extend the digital Icone by click-on modules to measure additional parameters. Any module is automatically recognized by the Iconcontrol data logger, creating a true plug & play system.

To investigate elastic properties of the soil, seismic tests can be performed by means of the Icone Seismic system. Four case studies are described where the s-wave velocity profile is determined with the seismic piezocone for the following purposes: foundation design, ground improvement design and tailings dam studies. In the case of foundation design, the velocity profile is used to evaluate the amplification of clay deposits. This is determined with several techniques and it is observed that the procedure with seismic piezocone produces satisfactory results due to the low level of deformation induced during its execution. It is also shown that by combining the sCPTu- Δu techniques with VST it is possible to determine parameters of the geotechnical model for foundation design.

In the case of soil improvement design, based on the velocity profile determined with the seismic piezocone, the liquefaction potential of a soil deposit is evaluated, and then a target velocity profile is proposed for the improvement that no longer generates liquefaction. Finally, examples are presented where the velocity profile is determined for the case of tailings dams in Mexico using correlations and those determined by seismic piezocone, and it is observed that the profiles obtained with correlations are not able to capture the maximum points of the profile.

The seismic module has proven to be an accurate and reliable measuring device, which can be used for different measuring techniques for soil analysis.

REFERENCES

- Lunne, T, Robertson, P.K., Powell, J.J.M. 1997. *Cone Penetration Testing in Geotechnical Practice*. London: Blackie Academic & Professional.
- Mayne, P.W & G. Campanella. 2005. "Versatile Site Characterization by Seismic Piezocone". Proc. 16th Int. Conf. on Soil Mechnc. & Geo. tech Engrg., Osaka, Japan, 2, pp. 721–724.
- Mayne P.W. & D.J. Woeller. 2015. "Advances in seismic piezocone testing", *Geotechnical Engineering for Infrastructure and Development: XVI European Conference on Soil Mechanics and Geotechnical Engineering*, ICE, ISBN 978-0-7277-6067-8.
- Ovando-Shelley E., Ossa A., & Romo M. 2007. "The sinking of Mexico City: Its effects on soil properties and seismic response", *Soil Dynamics and Earthquake Engineering* 27: 333–343
- Pérez Rocha L.E., M. Ordaz, E. Reinoso. 2009. "Interpolación espacial de las amplificaciones dinámicas del terreno", *Ingeniería Sísmica*, 80, pp. 85–112.

Tensiocone: A cone penetrometer with the facility to measure negative pore-water pressure

A. Tarantino & A. Capotosto
University of Strathclyde, Scotland, UK

F. Bottaro & M. Bellio
Tecnopenta S.r.l., Teolo (PD), Italy

D. Gallipoli
Università degli Studi di Genova, Italy

ABSTRACT: CPT sounding initially passes through the vadose zone, that is the zone above the phreatic surface where pore-water pressure is negative and degree of saturation is usually lower than unity. Negative pore-water pressure (suction) significantly affects tip resistance and sleeve friction and lack of knowledge of soil suction in this zone makes CPT data difficult if not impossible to interpret. For the case of Piezocone Cone Penetration Test (CPTU), crossing the vadose zone also exposes the cone tip porous filter to desaturation jeopardising the measurement of positive pore-water pressure once the cone penetrates the saturated zone below the phreatic surface. This paper presents the concept of the Tensiocone, a cone penetrometer with the facility to measure pore-water pressure in both negative and positive range. A first prototype was tested in the laboratory and in the field to investigate one of the major challenges in Tensiocone measurement, that is whether adequate contact can be established between the ground and the tensiometer porous filter during penetration.

1 INTRODUCTION

The Cone Penetration Test (CPT) is a valuable device for characterising soil stratigraphy and estimating soil mechanical properties. The penetrometer is inserted from the ground surface and initially crosses the vadose zone, that is the zone above the phreatic surface where pore-water pressure is negative (suction) and degree of saturation is usually lower than unity. This vadose zone can extend to several meters.

Strength and stiffness of the ground in the vadose zone are significantly affected by suction variations as a result of rainfall and evapotranspiration and so do the tip resistance and sleeve friction. Empirical equations used for characterising soil properties from CPT profiles have been developed from tests conducted in the calibration chamber on soils in dry or saturated states. These equations clearly do not hold for unsaturated soils. Data acquired when crossing the vadose zone are therefore difficult if not impossible to interpret in routine practice.

In recent years, the research groups at the University of New South Wales in Australia (Pournaghiazar et al. 2012; Yang & Russell 2015, 2016) and the University of Oklahoma in the US (Miller et al. 2018; Miller & Collins 2019) have conducted extensive experimental campaigns where CPTs were performed

in calibration chambers on unsaturated soils (by controlling or monitoring suction). This has led to a new generation of semi-empirical equations where soil properties can be inferred from tip resistance and sleeve friction by explicitly considering the influence of suction. However, the use of these equations in routine applications remains a challenge due to the difficulty of measuring suction in the field at depths greater than 1-2m.

The most obvious approach to measure suction during penetration is to provide the penetrometer with a High-Capacity Tensiometer to measure pore-water pressure in the negative range (Tarantino 2002; Marinho et al. 2008). A HCT can also measure pore-water pressure in the positive range and this would enable CPT measurements also in the saturated zone below the phreatic surface. The HCT could offer more accurate measurements than Piezocone Cone Penetration Test (CPTU) because it would not suffer from desaturation when passing through the unsaturated vadose zone (Mondelli et al. 2009; Sandven 2010).

This paper presents the development a new cone penetrometer named ‘Tensiocone’, which incorporates a high-capacity tensiometer for the measurement of pore-water tension during cone penetration. The major challenge with this design is to ensure proper contact between the high air-entry porous filter and the

ground. In laboratory measurements using standing-alone high-capacity tensiometers, a soil paste is interposed between the high-capacity tensiometer and the soil to ensure continuity between water in the soil pores and water in the tensiometer water reservoir. This paste cannot be used on the HCT installed on the penetrometer as it would be taken off as soon as the HCT touches the ground.

2 TENSIOCONE CONCEPT AND DESIGN OF FIRST PROTOTYPE

The concept of the Tensiocone is illustrated in Figure 1. An adaptor is placed between the friction sleeve and the cone tip and incorporates a High-Capacity Tensiometer (HCT) (Tarantino & Mongiovi, 2002). The first prototype presented in this paper was designed without the cone tip and friction sleeve since the aim was to test the pore-water pressure measurement. However, the same adaptor could be easily incorporated into a fully functional cone penetrometer.

The measurement of pore-water pressure is carried out laterally to minimise the stresses on the porous filter compared to the case of a porous filter located on the penetrometer tip. The major challenge with this new instrument is to ensure proper contact between the porous ceramic filter and the ground.

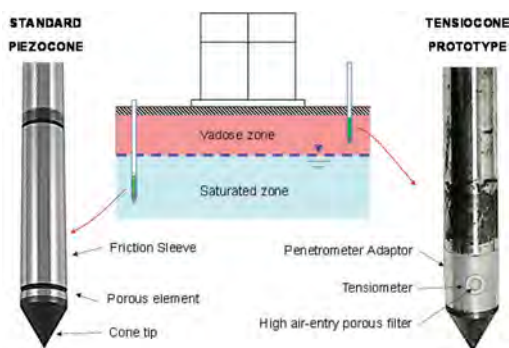


Figure 1. Piezocone and Tensiocone for pore-water pressure measurement below and above the phreatic surface respectively.

2.1 Tensiocone HCT

The HCT is installed horizontally into the adaptor and its size must be kept small in order to maintain the rear electrical connections near the axis of the cone and allow the electrical cables to run through the hollow push rods. Figure 2 shows the design concept for the HCT.

It consists of an integral strain-gauge diaphragm and an extension to support a perforated board with four pins to connect the thin strain-gauge wires to the thick cable wires transferring the signal through the hollow push rods. A high air-entry value porous

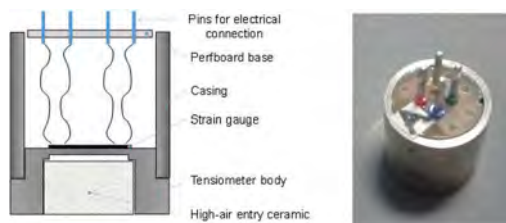


Figure 2. High-Capacity Tensiometer (HCT) installed in the cone penetrometer shaft.

filter (800 kPa) was cut and glued into the HCT using epoxy. The same epoxy was also initially used to fix the tensiometer to the penetrometer adaptor.

2.2 Reliability of HCT measurement

The performance of two tensiocone HCTs was initially tested via simultaneous measurement on a kaolin sample compacted to 300 kPa vertical stress at 30% water content. Measurement was carried out in the suction box described in Tarantino & Mongiovi (2003). The box lid has two holes equipped with O-rings to install the two HCTs. O-rings are also interposed between the annular cylinder hosting the sample and the base and lid respectively to prevent evaporation from inside the suction box. A small air gap was present between the top surface of the sample and the lid.

The two HCTs with an initially dry porous filter were subjected to ‘one-shot’ saturation directly in the saturation chamber by pressuring water to 4 MPa for 5 days. The response of the HCTs was then tested by generating water tension up to cavitation (by wiping the porous filter). Cavitation occurred at the air-entry value of the porous ceramic filter. The HCTs were then placed again in the saturation chamber at 4 MPa for 5 days.

The long-term measurement test is shown in Figure 3. The two HCTs successfully measured the same pore-water tension despite the fluctuations due to water drops condensing on the lid and falling periodically on the sample surface. Cavitation occurred as the 800 kPa air-entry value of the porous filter was approached.

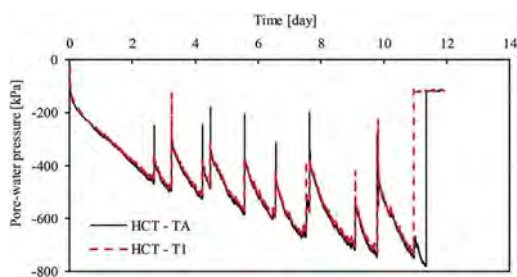


Figure 3. Long term measurement using two High-Capacity Tensiometers installed simultaneously on the same clay sample.

3 TENSIOCONE MEASUREMENT IN MOCK-UP LABORATORY TEST

A series of penetration tests were carried out in samples placed in a mould 100 mm diameter and 150 mm height (Figure 4). A transparent lid was used to seal the upper surface of the sample to avoid evaporation during the test. Two holes were made into the lid; the larger one was used to insert the tensiophone whereas the smaller one was used to install a HCT on the top of the sample to benchmark the measurement by the Tensiocone HCT. The aim of the test was to verify whether adequate contact could be established between the HCT porous and the soil during penetration in the absence of the clay paste typically used in HCT measurements.

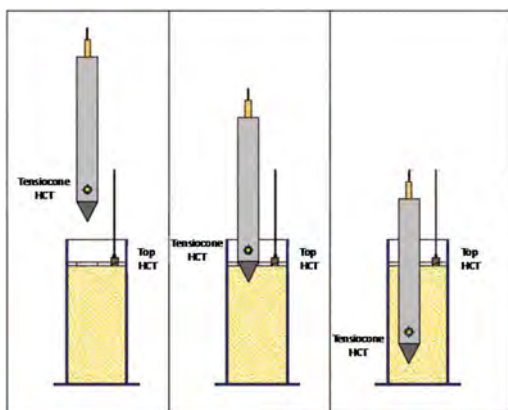


Figure 4. Mock-up scale test to simulate measurement during penetration.

3.1 Lightly compacted sample

The first test was made on a lightly compacted sample, which should represent the worst case scenario (the lower the density, the lower is the radial pressure pushing the soil against the HCT porous filter). The sample was prepared using 80% of coarse fraction (sand) and 20% of fine fraction (Speswhite kaolin clay) humidified at 30% water content calculated with respect to the dry mass of kaolinite clay only (corresponding to 6% overall water content). The two fractions were mixed dry and water was then sprayed over the mix. After mixing, the humidified soil was sealed in a plastic bag for at least 24h for water content equilibration.

In this test, the soil was placed in the mould in a single layer and compacted manually. After closing the mould with the transparent lid, the tensiophone was penetrated for about 100 mm into the sample. Another HCT was installed on the top surface of the sample. To improve the contact between the top HCT and the sample surface, a thin layer of kaolin paste (water content 100%) was interposed between the top HCT and the soil. Figure 5 shows the results of the pore-water

pressure measurements of the two HCTs installed on the tensiophone and top surface respectively.

There was a lowest value of water pressure detected by the tensiophone HCT during penetration. Following penetration, pore-water pressure increased to -550 kPa and equalised to this value. The top HCT equalised to a slightly lower pressure (-560 kPa) therefore showing that adequate contact could be established between the porous ceramic filter of the tensiophone HCT and the sample.

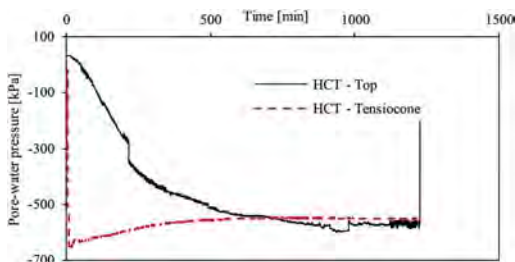


Figure 5. Penetration test on lightly compacted sample (20% clay/ 80% sand).

3.2 Moderately compacted samples

The second part of the experimental program involved moderately compacted samples. Three samples with different coarse/fine fraction ratio and compaction water content were prepared for this purpose. The soil was first humidified and cured for at least 24h in sealed plastic bags and then compacted in three layers inside the mould using a loading frame until reaching the target dry density of 1.4 g/cm^3 .

Figure 6 shows the pore-water pressure measurements during penetration in a sample composed of 80% of sand, 20% of kaolin and humidified at 40% water content calculated with respect to the mass of the fine fraction (corresponding to an overall water content equal to 8%). Similar to the lightly compacted sample, the tensiophone pore-water pressure decreased during penetration and increased once penetration was stopped until achieving equilibrium. The top HCT converged to similar values (the drop at the end of the measurement was due to the loss of contact with the sample).

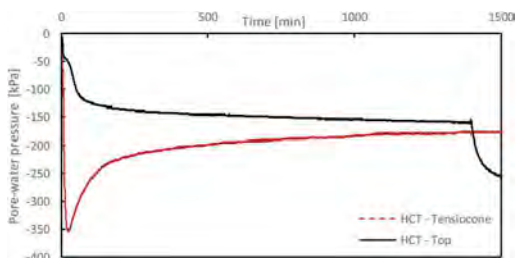


Figure 6. Penetration test on moderately compacted sample (80% sand, 20% kaolin, 40% water content to kaolin dry mass).

4 TENSIOCONE MEASUREMENT IN THE FIELD

The second compacted sample was prepared using only Speswhite kaolin humidified at 32% water content. The as-compacted suction was measured using the top HCT before starting the penetration of the tensiocone. Once the top HCT measurement reached equilibrium, the tensiocone penetration was started. Figure 7 shows the results of the measurement of the pore-water pressure of the two tensiometers during the last part of the tensiocone penetration. Again, once penetration stopped, the measurement of the tensiocone HCT attained the same value recorded by the top HCT.

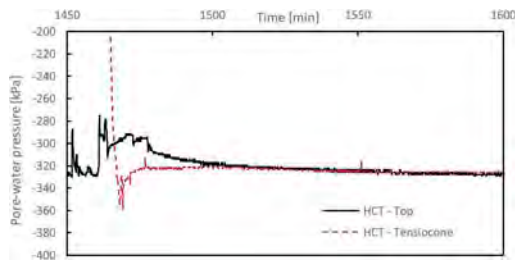


Figure 7. Penetration test on moderately compacted sample (0% sand, 100% kaolin, 32% water content to kaolin dry mass).

The third sample was prepared with 60% coarse fraction and 40% fine fraction. The water content calculated with respect to the dry mass of the fine fraction was 40%, corresponding to an overall water content equal to 16%. The results of this test are shown in Figure 8. The tensiocone pore-water pressure decreased during penetration and then increased up to -145 kPa. This value was markedly different from the top HCT that equalised at about -40 kPa. This discrepancy was also observed in other tests not reported herein.

The reason for such a discrepancy was not due to poor contact between the soil and the HCT porous filter. The pore-water pressure recorded by the tensiocone HCT levelled off suggesting that adequate contact could be established. In fact, if an air gap had formed between the soil and the porous ceramic filter, water from the ceramic filter would have evaporated into the air gap and pore-water pressure would have started declining rapidly over time.

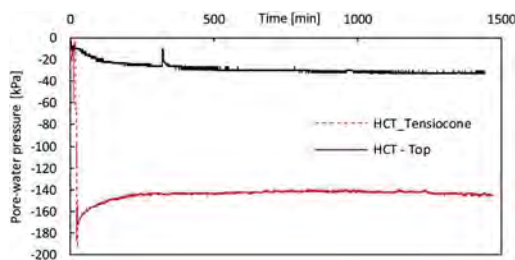


Figure 8. Penetration test on moderately compacted sample (60% sand, 40% kaolin, 40% water content pect to kaolin dry mass).

The tensiocone prototype (only equipped with a lateral HCT) was tested on the crest of the Adige river embankment at about 1 km downriver from the bridge that connects the local railway station to the town of Egna (BZ), Italy. The embankment made of a silty material was instrumented with two series of conventional tensiometers at depths of 1.8 m, 3.25 m, and -4.7 m and depths of -2 m, -3.45 m, and -4.5 m respectively. At the time of the CPT, these tensiometers showed a pore-water pressure profile nearly hydrostatic at depths greater than 3 m (associated with the phreatic surface located at 7m below the embankment crest). These field measurements were aimed to provide a reference to benchmark the measurements by the tensiocone HCT.

The tensiometer installed in the tensiocone was preliminarily saturated for more than 24 hours using a portable saturation chamber (at the constant pressure of 4MPa). The pressure in the saturation chamber was applied via a piston screw pump (Figure 9a). The tensiocone was then removed from the saturation chamber and placed in water for zeroing (Figure 9b). Finally, the tensiocone was removed from water and screwed onto the first push rod. Once removed from water, the porous filter was immediately covered with kaolin paste to prevent cavitation during the short period of time where the HCT remained exposed to air before penetrating the ground (Figure 9c). This kaolin paste was chipped off once the tip started penetrating the embankment.

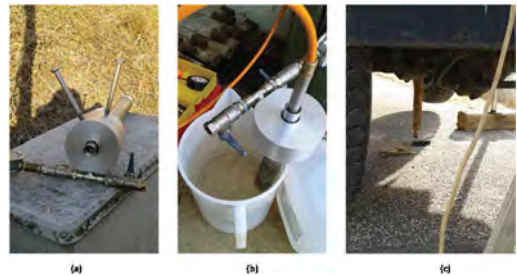


Figure 9. Field test. (a) Tensiocone in the pre-pressurization chamber. (b) Tensiocone in free water before installation. (c) Tensiocone at the onset of penetration.

The pore-water pressure measured at different depths is shown in Figure 10. The thrust system was stopped four times at four different depths. During penetration, pore-water pressure always tended to decrease whereas equilibrium was established in a relatively short time after penetration was stopped. The pore-water pressure levelling off once penetration was stopped was taken as an indication that adequate contact could be established between the ground and the HCT porous filter.

However, the equilibrium values were not consistent qualitatively and quantitatively with a hydrostatic pore-water pressure profile controlled by the phreatic

surface at 7m depth. It was then speculated that the HCT readings were affected by spurious mechanical deformation of the HCT sensing diaphragm. Two types of stresses can influence the measurement, the radial stress due to the ground lateral compression and the axial stresses imposed by the thrust system.

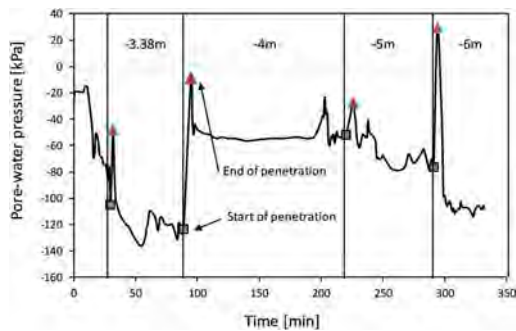


Figure 10. Results of field test.

5 LOADING EFFECTS

To investigate whether the tensiocone HCT readings were affected by spurious mechanical deformation of the sensing diaphragm, the tensiocone was placed in a loading frame. The tensiocone HCT porous filter was air dried for several days so that the HCT should have measured zero-gauge pressure throughout the mechanical axial compression of the tensiocone.

Figure 11 shows the results of the axial loading test. The tensiocone was compressed in steps up to 10 kN (0kN, 2 kN, 5 kN and 10 kN) and then unloaded in steps (10kN, 5 kN, 2 kN and 0 kN). Step duration was 15 seconds. The HCT recorded significant 'false' changes in pressure up to 180 kPa. In the field test, circumferential stresses might have also generated additional spurious readings.

The first HCT prototype was designed as an integral strain gauge diaphragm and any deformation of the HCT body due to the compression of the shaft directly affected the response of the sensing diaphragm. This design is clearly not suitable for the HCT to be incorporated into the tensiocone.

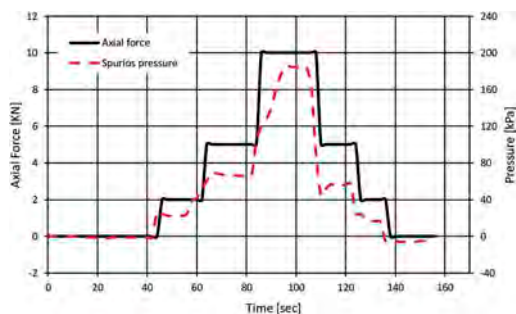


Figure 11. Mechanical effect on the HCT of the first tensiocone prototype.

6 CONCLUSIONS

This paper has presented the concept of the Tensiocone, a cone penetrometer with the facility to measure pore-water pressure in both negative and positive range. A first prototype was tested in the laboratory and the field to investigate one of the major challenges in tensiocone measurement, i.e. whether adequate contact can be established between the ground and the HCT porous filter during penetration.

The clay paste usually applied to the high air-entry porous filter of standing alone HCTs to ensure adequate hydraulic continuity between the pore-water and the water in the HCT reservoir cannot be used in CPT. The measurement of the negative pore-water pressure during penetration has to rely on the contact generated by the radial compression during penetration of the CPT shaft.

Laboratory tests showed that adequate contact could be established even under unfavourable conditions, i.e. high fraction of coarse-grained material (this makes the contact more difficult to achieve) and lower soil density (low radial stresses develop in a lightly compacted sample). The field test also showed that equilibrium could be reached after stopping the penetration, indicating that adequate contact could be established between the penetrometer HCT and the ground in a real case scenario.

However, it was observed that the compression of the shaft induced deformations in the HCT resulting in false pressure readings. This explains the almost random values recorded during the field penetration test and the discrepancy between the suction measured by the tensiocone HCT and the HCT placed at the top of the sample in the laboratory tests. The next challenge in the design of the penetrometer shaft is therefore to isolate mechanically the HCT from the shaft and this will be the focus of future tensiocone design developments.

ACKNOWLEDGEMENTS

The financial contribution of the European Commission to this research through the Marie Curie Industry-Academia Partnership and Pathways Network MAGIC (Monitoring systems to Assess Geotechnical Infrastructure subjected to Climatic hazards) – PIAPP-GA-2012-324426 – is gratefully acknowledged.

REFERENCES

- Marinho, F. A. M., Take, W. A. & Tarantino, A. 2008. Measurement of matric suction using tensiometric and axis translation techniques. In *Laboratory and field testing of unsaturated soils. Geotechnical and Geological Engineering*, 26: 615–631. 10.1007/s10706-008-9201-8.
- Miller, G. & Collins, R. 2019. A method for predicting the influence of matric suction changes on CPT tip resistance. *E3S Web of Conferences* 92: 18005. 10.1051/e3sconf/20199218005.

- Miller, G., Tan, N., Collins, R., Muraleetharan, K. 2018. Cone Penetration Testing in Unsaturated Soils. *Transportation Geotechnics*. 17. 10.1016/j.trgeo.2018.09.008.
- Mondelli, G., De Mio, G., Giacheti, H.L. & Howie, J. A. 2009. The use of slot filter in piezocone tests for site characterization of tropical soils. In M. Hamza et al. (Eds.), *Proceedings of the 17th International Conference on Soil Mechanics and Geotechnical Engineering*. IOS Press. 10.3233/978-1-60750-031-5-973
- Pournaghiazar, M., Russell, A., Khalili, N. 2012. Linking cone penetration resistances measured in calibration chambers and the field. *Géotechnique Letters* 2: 29–35. 10.1680/geolett.11.00040.
- Sandven, R. 2010. Influence of test equipment and procedures on obtained accuracy in CPTU. In Mitchell et al. (eds.), *2nd International Symposium on Cone Penetration Testing*, Huntington Beach, CA, USA, May 2010.
- Tarantino, A. 2002. Panel lecture: direct measurement of soil water tension. In J. F. T. Jucá, T. M. P. de Campos and F. A. M. Marinho (Eds.), *Unsaturated soils: proceedings of the third international conference, UNSAT2002*, vol 3, pp. 1005–1017. Lisse, the Netherlands: A. A. Balkema (Taylor & Francis).
- Tarantino, A. & Mongiòvi, L. 2002. Design and construction of a tensiometer for direct measurement of matric suction. In J. F. T. Jucá, T. M. P. de Campos and F. A. M. Marinho (Eds.), *Unsaturated soils: proceedings of the third international conference, UNSAT2002*, vol. 1, pp. 319–324. Lisse, the Netherlands: A. A. Balkema (Taylor & Francis).
- Tarantino, A. & Mongiòvi, L. 2003. Calibration of tensiometer for direct measurement of matric suction. *Géotechnique* 53(1): 137–141. 10.1680/geot.2003.53.1.137.
- Yang, H-W. & Russell, A. 2015. The cone penetration test in unsaturated silty sands. *Canadian Geotechnical Journal* 53. 10.1139/cgj-2015-0142.
- Yang, H-W. & Russell, A. 2016. The cone penetration test in unsaturated silty sands. *E3S Web of Conferences* 9: 09008. 10.1051/e3sconf/20160909008.

New portable pressiocone system for carrying out CPT+FDP tests

G. Vinco

Geotechnical Engineer, Technical Manager of URETEK SOLUTIONS Group

M. Sacchetto

Geotechnical Engineer, Freelance Consultant

ABSTRACT: Geotechnical investigations in the foundation soil of existing buildings have always been challenging due to limited space and difficult access. URETEK has developed a portable integrated system for simultaneously carrying out a CPT and a pressiometric test with Full Displacement Pressuremeter. The 30 kN thrust penetrometer to be used is very small. The reaction is given by two “microanchors”. The cone is a standard 10 cm² digital memory cone (no cable), capable of measuring qc, fs, U every centimeter. Above the cone there is the FDP equipment with a rubber sheath covered by steel plates and connected, by a tube filled with water, to a device for creating pressure to inflate the sheath and measure pressure-volume curves as in a standard pressiometric test. The pressure-volume device and the depth transducer are connected to a microcomputer that is programmed to carry out CPT+FDP tests in an easy-to-use/user-friendly way.

1 INTRODUCTION

The recovery of existing buildings is the key to building development in Western countries where the population does not grow, and housing standards have long since reached a satisfactory level. Tax incentives and funding introduced by national governments and the European Community have strongly oriented the offer towards systems and solutions that promote the recovery and adaptation of structures to current safety and energy saving standards. Among the various sectors, geotechnics has seen the birth and development of new technologies capable of restoring the mechanical characteristics of the soil of existing foundations with a minimum impact. Injections of expanding resins represent an example of this. It is a technology that can be done in structures in operation by applying a simple and non-invasive process (Dei Svaldi et Al. 2005). The subsequent phase of verification and control of the effectiveness of the injection intervention is carried out by in situ geotechnical tests performed with small portable lightweight equipment, capable of operating in narrow and confined spaces. For the verification of the improvement of the ground following the injection of resins, the use of a small portable penetrometer, called 30-20 (Cestari, 2013) consisting of a falling weight of 0.3 kN which is dropped from a height of 20 cm onto the axis of a battery of rods with a conical tip screwed to the bottom. The vertical fall of the mass makes the cone penetrate the ground for a certain depth. The specific

energy per driving stroke is equal to 60 kJ/ m² and the number of strokes required for the penetration of 10 cm represents the resistance of the ground. Dynamic tests 30-20 are mainly used for a comparison between the cone resistance of the natural soil and the treated soil. Only in particular cases (clean sands), the measured values can be reliably correlated to the geotechnical parameters of resistance and deformability. The success of the consolidation technique with expanding resins, the publication of the design guide and the dissemination of dedicated software have created the increasing need for more precise information on the geotechnical parameters of the treated soils (Manassero et Al.2014). For this reason, the R&D sector of Uretek, a multinational company operating in the consolidation sector with injections of expanding resins, has been involved for some time in the construction of a light and easy-to-use instrument capable of detecting directly with the due accuracy the resistance and deformability of the treated soil.

2 GENERAL DESIGN OF THE EQUIPMENT

Dynamic tests (especially the ones with low energy, like the above mentioned 30-20) are considered reliable only in certain contexts (clean sands or granular soils); therefore, it was decided to design equipment for static tests instead than dynamic, with piezocone CPTU or electrical cone CPTE. In fact, for the CPTU/CPTE are available many correlations that

allow to reliably calculate the geotechnical parameters of the subsoil (Cestari F. 2013). However, the CPTU/CPTE are not deformative tests, but the resistance is measured breaking and displacing the soil, meaning that geotechnical parameters are obtained in an empirical/semi-empirical way and therefore do not give (if not indirectly) parameters related to the deformation and/or the stress history of the subsoil (Robertson P.K. 2009, Robertson P.K., Cabal K.L. 2012).

For this reason, it was chosen from the beginning to couple an FDP (Full Displacement Pressiometer) to the CPTU, so that the penetrometric and pressiometer data could complement each other and provide a more complete picture of the geotechnical characteristics of the subsoil (H.S. Yu et Al., 1996, J. L. Briaud, 1992, J.L. Briaud et Al. 1979, P. Cosentino 2018, Amar S. et. Al. 1991, Robertson, P.K et Al.1983).

The pressiometer is an instrument that, in the standard version with large diameter (60 mm), would require the careful execution of a pre-hole, but at this stage it was decided not to design a rotary drilling machine (albeit of small dimensions) as it would not adhere to the initial targets: portability, low or no impact, speed and ease of use even for operators who are not experienced in drilling and pressiometer testing.

There are few small diameter (36 or 44 mm) FDP systems available on the market, none of which are integrated with a CPTU/CPTE system. All the equipment used so far has been customized (P.E. Failmezger et 2005, A. Drevininkas 2017). The combination of CPT (Cone Penetration Test) and PRESSIOMETER (hence the name PRESSIOCONE) requires to be used with a static penetrometer. The penetrometers that are on the market, although some models are small, are not very suitable for working in contexts where we would like to operate.

Some commercial models are small and can be disassembled with an external power unit but require a considerable effort for setup before each test, being equipment that are not produced in large series they are also relatively expensive.

Furthermore, all the small penetrometers on the market are anchored with augers for the reaction to the thrust, which is almost never feasible in the contexts of confined spaces inside existing buildings.

For these reasons we have opted for the design of a "custom" penetrometer that meets the basic requirements of ease of use, portability, electrical operation, reduced height, anchoring without augers, with a thrust of at least 30 kN and standard driving speed. of 2 cm/s.

3 CHARACTERISTICS OF THE CONE

Although there are cones of reduced diameter (5 cm² with a diameter of about 2.6 cm) we chose to have a standard cone with an area of 10 cm² and

a diameter of 3.56 cm, to have more space for digital electronics and especially for having no problems in interpreting the data (the 10 cm² cones are the most widely used and the correlations are very solid). Therefore, the cone is a custom model that responds to the most recent standards and allows the measurement of q_c , f_s , U ; the design of the cone and electronics leaves the possibility of making a CPTE cone with only the q_c and f_s or a cone equipped with additional sensors (for instance inclinometers, seismic, resistivity, thermal, etc.).

The cone is designed for extremely easy maintenance, with the tip, filter and sleeve that can be removed on site. The filter for the U can be either in sintered metal saturated with deaerated silicone oil or slotted (slot filter) saturated with silicone grease.



Figure 1. Memory piezocone (including battery and electronics).

In order not to have problems related to the management of the cable, given that the passage through the rods would interfere with the pressiometer tube, creating many problems on site, it was decided to design a custom system with memory.

The cone electronics are structured as follows:

- high resolution A/D circuit (24 bits)
- programmable microprocessor
- Large memory capacity and expandable
- high-capacity and small in length
- rechargeable NiMh battery (60 hours of power before recharge)

A great effort was carried out to optimize the power consumption of electronics, for limiting the dimensions of the piezocone (in length), the total length of the piezocone being comparable to most cones without memory. It has been designed to be used (eventually) also with cable, transmitting digital signal.

The test procedures with the memory cone are:

- a. preparation of the cone and connection with a computer or data logger, which is connected to the encoder depth transducer
- b. synchronization of the cone and datalogger and definition of the time $T = 0$; starting from $T = 0$ the cone starts storing all the values of q_c , f_s , U as a function of time (scanning every second or half second) and the data logger the values of depth as a function of time (data logger is connected to the depth transducer)
- c. execution of the test
- d. recovery of the cone
- e. downloading data from the cone and from the datalogger, at this point there are two data matrices, one coming from the cone with all the data as a function of time only, one coming from the datalogger with depth as a function of time.

f. synchronization of the matrices: the matrices are automatically synchronized allowing to have the penetrometric data vs. depth (not only vs. time, with exception of the eventual dissipation tests).

4 FEATURES OF THE FDP PRESSIOMETER

The FDP (Full Displacement) Pressiometer is made of a special rubber sheath coated with six shaped steel plates and mounted on a cylindrical body which has an attachment for the piezocone in the lower part and an attachment for the penetrometer rods in the upper part. The steel lamellae can slide up and down at both ends so to follow the expansion of the sheath.



Figure 2. Sheath and lamellae.

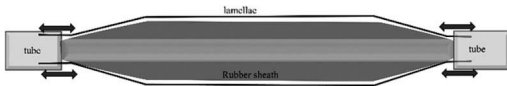


Figure 3. Lamellae sliding inside the tube while the sheath expands.

The length of the sheath and the lamellae is 34 cm, the diameter of the sheath (including the lamellae) is 34 mm, with an internal volume of around 200 cm³ (not inflated), see Figures 2, 3. The pressure gauge, unlike the others on the market, has been designed to be inflated with water instead of nitrogen.

The water, in this prototype, emulsified with oil, is pressurized through a “Rilsan” plastic tube that is placed through the rods; however, we plan to use special sealed rods to avoid using the internal tubing and pressurize directly through the rods.

The sheath is pressurized by a system essentially consisting of a cylinder and a piston which will be driven (in the final version) by a worm screw connected to an electric stepping motor, digitally controlled by the programmed data logger.

Each revolution of the motor corresponds to a movement of the piston and therefore a certain volume, measured with great accuracy.

In the cylinder there is a digital pressure cell connected to the data logger (same device that manages the cone). However, the preliminary trial tests (carried out for designing the pressiometer) have been carried out with a manometer using a preliminary version of the system, not yet automatized and with a manually driven piston and a manometer for measuring the pressure

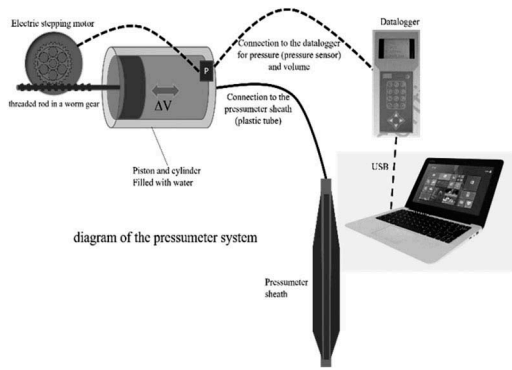


Figure 4. Setup of the FDP system.

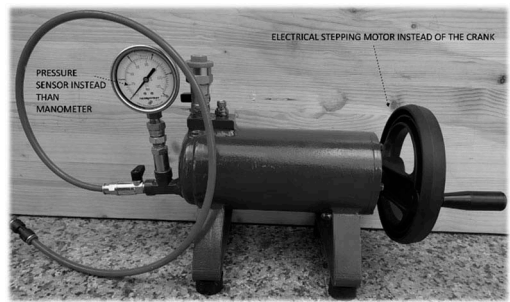


Figure 5. Manual pressurization System and manometer.

The datalogger is programmed not only to manage the test manually, but also to automatically perform some pressiometer test “sequences”.

Each sequence contains a certain number of steps which define time, volume, pressure. In this way it is possible (for instance) to set a preset for a certain automatic sequence for a certain type of soil or to memorize a manual sequence of a test in progress.

This procedure ensures maximum operational flexibility, ease of use even for Users with little or no experience in pressiometer testing and the possibility to manage tests remotely (simply by exchanging remotely the files that define a certain sequence, thus fulfilling the requirements of Industry 4.0).

5 FEATURES OF THE PENETROMETER

The most important feature of the new type of penetrometer, which distinguishes it from all models on the market, will be the anchoring, in relation to the operational context in which the tests will be performed.

In fact, the pressiocone tests will be carried out mainly under the existing foundations, mostly inside buildings, in the not treated soils first and after in treated soils with resins; therefore, it would be impossible to anchor with augers or use ballasted penetrometers.

For this reason, the penetrometer will be anchored with two Microanchors (URETEK, 2017), being small tie rods placed in the foundations after execution of a small hole (26 mm diameter) and fixed with expanding resins; numerous tests have confirmed that two anchors are more than sufficient for a thrust of $30 \div 50$ kN (which will be the maximum thrust obtainable with the penetrometer).

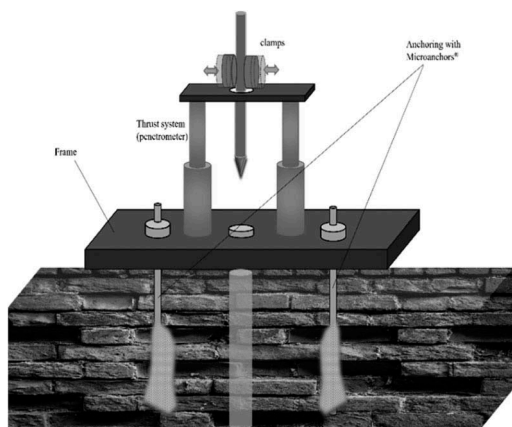


Figure 6. Setup of the penetrometer.

Basically, the new penetrometer consists in a light frame with three holes, a central one for the passage of the pressiocone and two lateral ones for the installation of the two Microanchors for reaction.

The thrust devices (pistons) will be chosen according to the available space and the requested thrust. One more difference with the standard penetrometers will be that the thrust devices will not push the rods from the top of them, but will push dragging the rods laterally, with special clamps, to leave the mouth at the top of the rods free, so better managing the pressiometer tube and for reducing the height (“through spindle”). At the same time with this system any rod of any length can be pushed for any depth without constrains.

6 TRIAL TESTS

At present we have carried out some preliminary trial tests, for testing separately the piezocone, the FDP pressiometer with different types of sheaths and lamellae and the penetrometer; finally, we tested all equipment together.

The field tests have been carried out during summer 2021 in a site (San Felice Extra, north of Verona) where the stratigraphy is gravel and small cobbles embedded in stiff silty clay, as shown in the following graph.

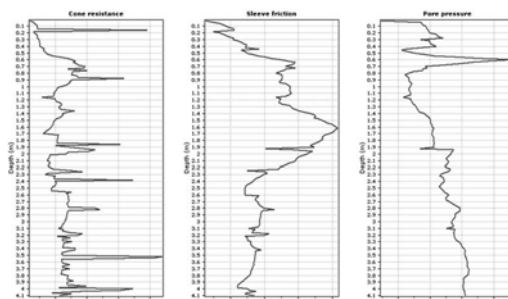


Figure 7. Q_c , f_s , U graph.

The groundwater table in that area is deeper than the maximum depth reached with the tests, (around -4 m) so the U seems not to be significant.

For pushing the pressiocone has been used a prototype of penetrometer, the microanchors have been installed in the natural soil instead than in the foundations.

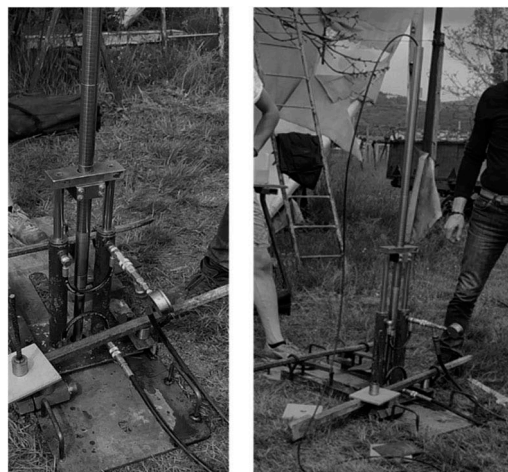


Figure 8. Prototype of the penetrometer, anchored with microanchors.

Before starting the test, a very careful saturation of the system (pressumeter, Rilsan tube, manual pump) has been made with water (emulsified with oil), not to leave any air bubble in the circuit.

The pressiometric tests have been carried out every meter starting from $-1.0 \div -1.5$ stopping the pushing of the rods and making the sheath expand up to the double of the initial volume, sometimes with loops, measuring pressure vs. volume at times $T=0$ (immediately after expansion) and $T=180$ s (180 seconds after).

an example of a pressumeter test graph carried out at -2.5 m is shown below, the two curves show the V - P values at time $T = 0$ and $T = 180$ s

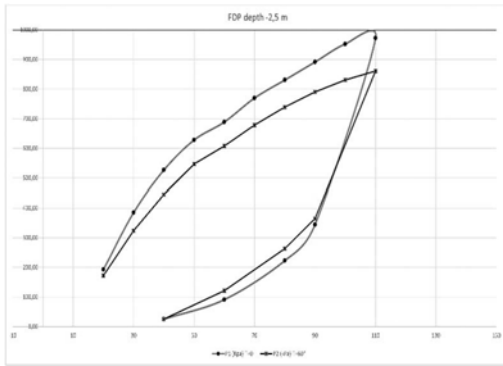


Figure 9. V-P (volume-pressure) graphs at time T = 0 and T = 180 s.

7 CONCLUSIONS

The first results were very encouraging, and all parts of the instrumentation worked properly. Thus, the guidelines for the future development of the instrumentation and for the definition of the test execution procedures were completely outlined: anchoring, preparation, and calibration of the piezocone and of the FDP, programming of the FDP test sequences.

This first phase will be followed in a very short time by comparative validation tests in which tests will be carried out (first in “natural” soils and then in soils treated with resins) with the pressiocone and, at a short distance, comparative tests with standard instrumentation (boreholes with sampling and laboratory tests, with execution of standard pressiometer tests, SPT, Vane Test, execution of CPTU and DMT dilatometric tests).

REFERENCES

- Manassero, Dominijanni, 2014 *Consolidamento dei terreni con resine espandenti – Guida alla progettazione* – McGraw-Hill Education.
- Robertson, P.K., Cabal K.L., 2012 *Guide to Cone Penetration Testing for Geotechnical Engineering*, Gregg Drilling & Testing, Inc., 5th Edition,
- Robertson, P.K., 2009 *Interpretation of Cone Penetration Tests - a unified approach.*, Can. Geotech. J. 46(11): 1337–1355
- A. Drevininkas, M. Manzari, 2017, *Evaluation of Full Displacement Pressuremeter for Geotechnical Investigation in Southern Ontario*, Proceedings GEO OTTAWA 2017
- H.S.Yu, F.Schnaid, I.F.Collins. 1996 *Analysis of Cone Pressuremeter Tests in sands*. Journal Of geotechnical Engineering. Vol.122 Issue 8
- Briaud, J.L., Shields, D.H., 1979, “*A Special Pressuremeter and Pressuremeter Test for Pavement Evaluation and Design*, Geotechnical Testing Journal, ASTM 2: 3
- Briaud, J. L. 1992. *The Pressuremeter*. Taylor & Francis Group plc, London, UK.
- Failmezger, P.E. 2005. *Development of a Robust Push-In Pressuremeter*. Symposium International ISP5/PRESSIO 2005, Ponts & Chaussees, France
- Dei Svaldi, A. Favaretti, M. Paschetto, A. & Vinco, G.2005. *Analytical modelling of the soil improvement by injections of high expansion pressure resin*. In *6th International Conference on Ground Improvement Techniques*; Congress proceedings, Coimbra, 18-19 July 2005: 577–584
- F.Cestari 2013 *Prove Geotecniche in Situ* Flaccovio Editore
- P. Cosentino, A. Shaban, A. Boggs 2018. *Predicting Bearing Ratios of Granular Soils Using Dynamic Cone Penetrometer and Modified PENCEL Pressuremeter Tests* Proceedings IFCEE 2018
- Amar S. et. Al., 1991. *Utilisation des résultats des essais pressiométriques pour le dimensionnement des fondations en Europe, 1ère partie: Pressiomètre Ménard/Pressiomètre auto-foreur*. Rapport du Comité Technique Régional Européen n° 4 Pressiomètres, comitat Français de la Mécanique des Sols et des Fondations, Rotterdam: Balkema,
- Robertson, P.K., Hughes, J.M.O., Campanella, R.G., and Sy, A.,1983. *Design of Laterally Loaded Displacement Piles Using a Driven Pressuremeter*. ASTM STP 835, Kansas City
- URETEK, *Microanchors*, pers.comm.

Characterisation of near-surface sediments using a blend of vertical and shallow rotational penetrometers

D.J. White

University of Southampton, UK

S.A. Stanier

University of Cambridge, UK

H. Mohr

University of Western Australia and MSMT Solutions, Perth, Australia

ABSTRACT: The mechanical properties of near-surface sediments – to a depth of approximately half a metre – are relevant to the design of cables, pipelines and other shallowly-embedded infrastructure, as well as benthic habitat characterisation. For this depth of interest, vertically-pushed penetrometers – such as the cone, T-bar or ball – can be supplemented by shallow rotational devices such as the toroid or hemiball. In this paper, we report vertical and shallow rotational penetrometer test procedures and show results obtained in project conditions on natural soil samples. By combining these different penetrometers, a wider and more reliable set of mechanical properties – spanning strength and consolidation behaviour – can be obtained, compared to conventional practice. The paper concludes with practical advice on testing protocols and interpretation methods to best characterise the shallow seafloor, including the use of novel shallow penetrometers.

1 INTRODUCTION

1.1 *Shallow seabed properties*

The properties of the shallowest half metre of the seabed are relevant to the design of cables, pipelines and other shallowly-embedded infrastructure such as rock dump and scour protection systems, as well as the study of benthic ecosystems. The importance of accurately determining the strength and consolidation properties of the seafloor is emphasized in good practice guidance (e.g. ISO 19901-4, White et al. 2017).

Typical practice to characterize the shallowest seafloor includes (i) box core or drop core sampling, (ii) penetrometer testing from a seabed frame or into a box core and (iii) index testing of samples.

In this paper, we describe how practice can be enhanced by modern vertical and shallow rotational penetrometer testing to determine more accurately the strength and consolidation properties of the seafloor.

1.2 *Novel shallow penetrometer systems*

Shallow penetrometers, which combine vertical movement and rotation about the vertical axis, were first trialled a decade ago, using toroid and hemiball shapes (Yan et al. 2010). Subsequent work includes laboratory studies (e.g. Boscardin & de Groot 2015,

Schneider et al. 2020a) and numerical simulations (Stanier & White 2015, Yan et al. 2017, Schneider et al. 2020b,c). Some of this work formed part of the Remote Intelligent Seabed Surveys (RIGSS) Joint Industry Project (www.rigssjip.com).

2 COMBINED PENETROMETER SYSTEM

2.1 *Actuation system*

A shallow penetrometer test aims to subject the seabed to a loading history that replicates the conditions around infrastructure, and provides a simple basis to interpret fundamental soil properties, including the interface shear strength at the penetrometer surface. The control requirements involve vertical and rotational motion in load-controlled contact with the seabed. These requirements exceed current systems for CPT and T-bar testing, which involve only vertical motion between specified position limits.

A system for vertical and shallow penetrometry must therefore meet the following requirements:

1. Accurate identification of the touchdown point, when the penetrometer contacts the seabed.
2. Control via feedback of the vertical load on the penetrometer, e.g. during a dissipation step.

3. Allow ‘programmable motion control’ so that sequences (e.g. penetration-dissipation-rotation) can be performed without intervention.
4. Allow variable speeds of movement to permit testing over a range of drainage conditions.

An actuator system that meets these requirements was developed as part of the RIGSS Joint Industry Project (Figure 1, Schneider et al. 2020a). The capabilities are summarised as follows:

1. Controlled motion at rates of 0-3 mm/s (vertical) and 0-3 deg/s (rotational), allowing drained and undrained movements in clay and silt soils (drained in sand), with positioning resolution of 0.0125 μm and 9×10^{-6} degrees.
2. Load measurement and control to an accuracy of ± 0.1 N, even on-deck under ship motion – as proven during offshore trials. This force resolution corresponds to less than 0.02 kPa of undrained strength, for the sizes of shallow penetrometer used, so the system accuracy is much better than typical sample variability.
3. A user interface and motion control system allows pre-programmed steps of consolidation (under set vertical load) and/or cyclic rotation.
4. Ruggedised packaging in plastic flight cases allows transport offshore or by plane.

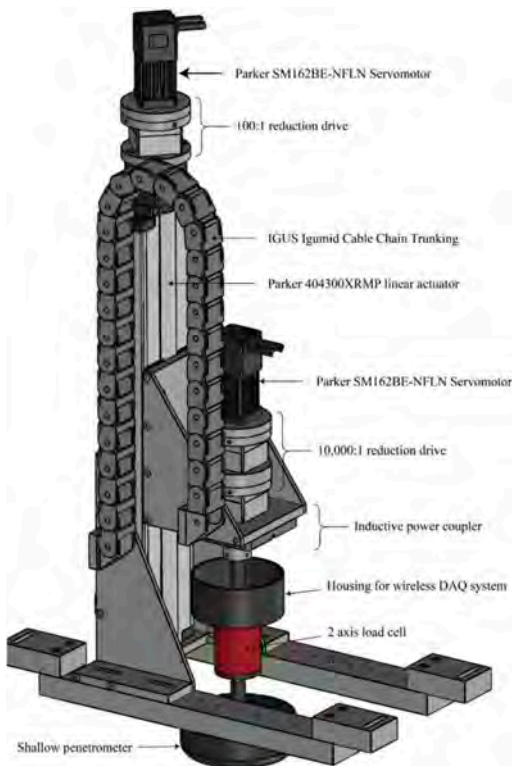


Figure 1. Penetrometer system: vertical and rotational actuation.



Figure 2. Miniature penetrometers: $\varnothing 5 \times 20$ mm T-bar, $\varnothing 10$ mm ball, and $\varnothing 5$ mm cone (MSMT Solutions).

The shallow penetrometer actuator system is capable of operation offshore on deck, in box cores. However, it is equally suited to use in the laboratory, with recovered samples. Both modes have been used.

2.2 Miniature vertical penetrometers

To measure the shallow strength profiles of samples, miniature scaled versions of the conventional cone, ball and T-bar penetrometers are used. These attach via simple fittings to the same actuator, and provide high resolution profiles of shear strength. For the ball and T-bar, remoulded strength is also obtained through a cyclic phase. The penetrometers shown in Figure 2 have replaceable top load cells and were manufactured by MSMT Solutions (Perth, Australia).

2.3 Shallow rotational penetrometers

Three shallow rotational penetrometers are shown in Figure 3: ring and toroid penetrometers of outer diameter, $D_o = 125$ mm, and body width or diameter, $D_b = 25$ mm, and a hemiball with overall diameter, $D = 100$ mm. All penetrometers are roughened by a sand coating and feature embedded pore pressure transducers with porous stones flush with the curved surfaces.

2.4 Sampling and testing location

The penetrometer system mounts onto box cores, or can rest on a frame over a sample. Tests on intact samples can be performed in box cores on deck, or jumbo samples can be extracted from a box core (e.g. in a 250 mm diameter plastic tube) and transported back to the lab for penetrometer testing (Figure 4).

A typical combined testing programme for a single box or jumbo core involves (i) vertical penetrometer tests to assess the strength profile, followed by (ii) one or more shallow penetrometer tests to measure interface strength and near-surface consolidation



Figure 3. Shallow penetrometers: ring, toroid and hemiball.

properties. If insufficient surface area is available, extra shallow penetrometer tests can be performed after scraping away the top layer or on remoulded samples.

3 STRENGTH PROFILING

Example profiles from the miniature vertical penetrometers are shown in Figure 5, for conditions with penetration resistance from 10 to 1000 kPa.

T-bar tests in very soft clay (Figure 5a) resolve the undrained strength, s_{ub} , to $1/10^{\text{th}}$ of a kPa, and are consistent with shallow penetrometer strength data. Miniature cone and T-bar data from undrained penetration in carbonate silt (Figure 5b) show consistent penetration resistance

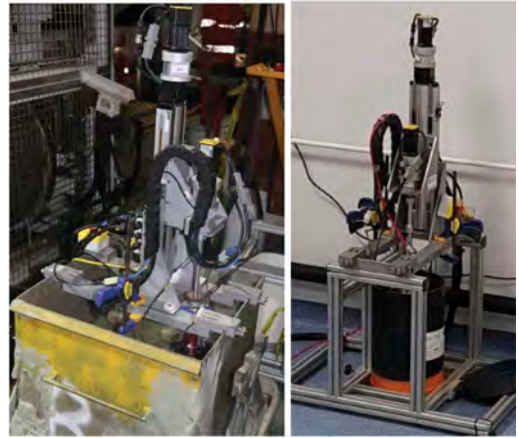


Figure 4. Testing on deck (left) and in the lab (right).

across both instruments, and agreement with standard ($D = 35.7 \text{ mm}$) cone data from a seabed frame system. However, for the sandy silt example (Figure 5c), the initial penetration resistance of the standard cone is lower, perhaps due to near-surface effects on the penetration mechanism, which have minimal influence on the miniature cone.

4 SHALLOW PENETROMETER TESTING

4.1 Typical test procedure

The usual steps of a shallow penetrometer test are illustrated in Figure 6. The steps are described in Table 1, which sets out the control applied to the vertical and rotational axes in each step, the end points of each step and the typical speed or durations

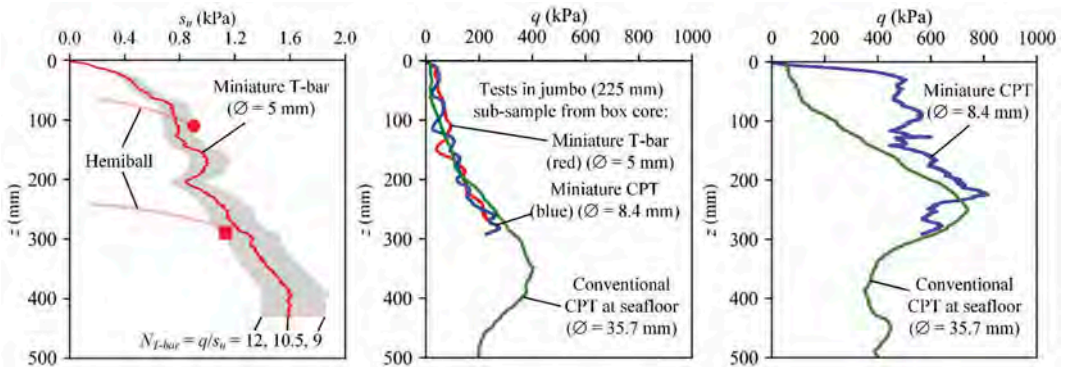


Figure 5. Vertical penetrometer tests in intact seabed samples (i) Clay (ii) Carbonate silt (iii) Carbonate sandy silt.

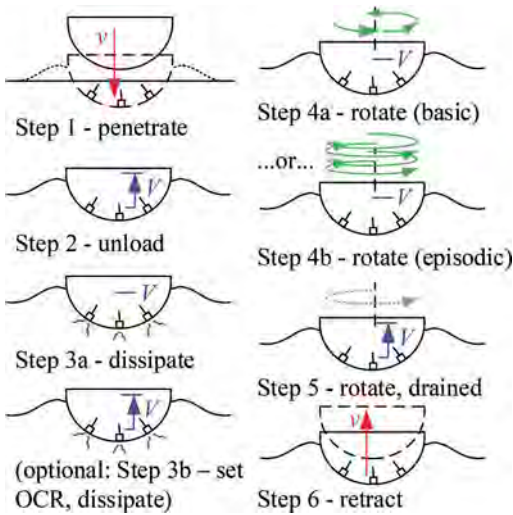


Figure 6. Stages of a shallow rotational penetrometer test.

relevant to testing in soft clay. On sandy soils the periods are more rapid, and the dissipation pauses may not be required. Figure 7 shows typical raw results.

4.2 Typical test results

The usual interpretation procedure for a shallow penetrometer test is set out in Table 2, and the interpreted data is shown in Figure 8. The interpretation methods for soil strength and consolidation parameters are based on bearing capacity theory and dissipation solutions. The interface strength parameters derived from the rotational stages involve a correction for ‘wedging’ effects for the hemiball and toroid devices. Ring penetrometer data does not need this correction.

Ideally, fully undrained and fully drained strengths can be measured, limited by the maximum actuator speed and test duration, respectively, relative to the soil coefficient of consolidation. Regard-

Table 1. Typical shallow penetrometer test procedure.

Step	Step name	Control parameters	Control values (toroid and ring)	Step procedure	Step end point
0	Prepare	Vertical rate, v Rotation rate, $\omega = 0$	$v = 0.5 \text{ mm/s}$	Position penetrometer above test location in sample and drive penetrometer to test start point. Take zero readings from all transducers. Confirm response of pore pressure transducers to hydrostatic head.	Visual check: penetrometer is $\sim 20 \text{ mm}$ above sample surface
1	Penetrate	Vertical rate, v Rotation rate, $\omega = 0$	$v = 0.4 \text{ mm/s}$	Drive penetrometer vertically to $0.5D$ embedment (or until the load cell limit, V_{limit} , is reached). Maximum measured vertical load is captured as V_{max} and used in control of Step 2.	When $w = 0.5D$ or vertical load, $V = V_{limit}$
2	Unload	Vertical load, V Rotation rate, $\omega = 0$	$V = V_{max}/2$	Reduce vertical load on penetrometer by a factor of 2, to $V = V_{max}/2$, (to avoid excessive settlement during rotational stage of test) and hold this load. (Or unload to a specified V to match the applied stress relevant for design).	Move immediately to Step 3
3	Dissipate	Vertical load, V Rotation rate, $\omega = 0$	$V = V_{max}/2$	Hold penetrometer under load of $V = V_{max}/2$, allowing dissipation of excess pore pressure, Δu .	When $\Delta u/\Delta u_{ini} < 0.1$
3b	Set OCR, dissipate	Vertical load, V Rotation rate, $\omega = 0$	$V = (V_{max}/2)/OCR$	(Optional, <i>OCR test option</i>) Reduce vertical load by a specified ratio; repeat pore pressure dissipation. (Consider the OCR range relevant to design when planning tests. If needed, add Step 3b in some tests).	When $\Delta u/\Delta u_{ini} < 0.1$

(Continued)

Table 1. (Cont.)

4	4a	Vertical load, V Rotation rate, ω	Fast-medium-slow, $\Delta\theta = 20$ deg rotation at each speed, $\omega = 0.4, 0.04, 0.004$ deg/s	<i>Basic monotonic test option:</i> Rotate device by a specified angle, at fast, medium and then slow speeds, to measure the undrained (initially) and drained (later) torsional resistance, T .	When $\theta = 60^\circ$
	4b	Vertical load, V Rotation rate, ω	$\omega = \pm 0.4$ deg/s for $\Delta\theta = 20^\circ$ $t_{consol} = 30$ min	<i>Episodic test option:</i> Perform episodes of rotation and consolidation. In each rotation stage turn through a fixed angle at the fast speed, alternating direction between cycles. During consolidation period, t_{consol} , between cycles, maintain vertical load. Typically the response stabilises after ~ 15 episodes.	When the cycles are complete
5	Drained sweep	Vertical load, V Rotation rate, ω	$dV/dt = -V_{max}/(2t_{unload})$ $\omega = 0.004$ deg/s	Rotate penetrometer at constant slow speed while reducing the vertical load to zero over the unloading period, t_{unload} . Typically set $t_{unload} \sim 30$ minutes on clay. This step gives the change in T with V , measuring the friction across a range of normal stresses.	When $V = 0$ (i.e. when the penetrometer lifts away from the sample)
6	Retract	Vertical rate, v Rotation rate, $\omega = 0$	$v = -0.5$ mm/s	Withdraw penetrometer vertically to above the sample surface. Take additional zero readings.	Penetrometer returns to starting position above sample surface

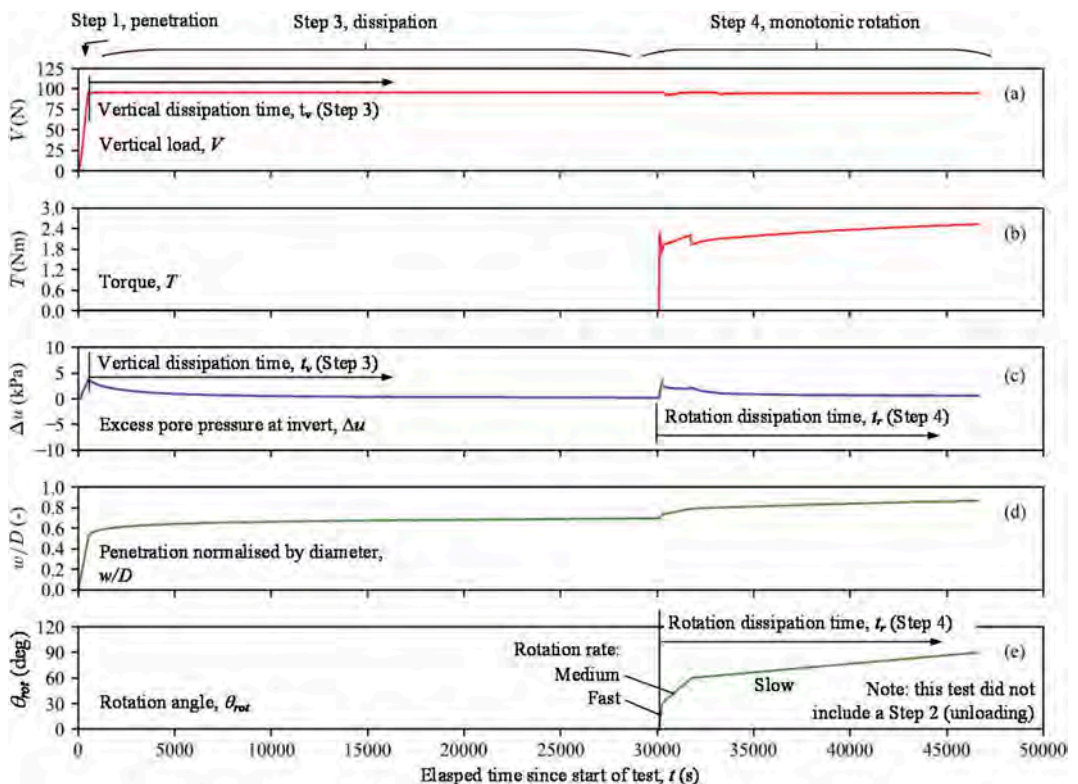


Figure 7. Typical unprocessed results from shallow penetrometer test with a monotonic rotation step (hemiball in soft clay).

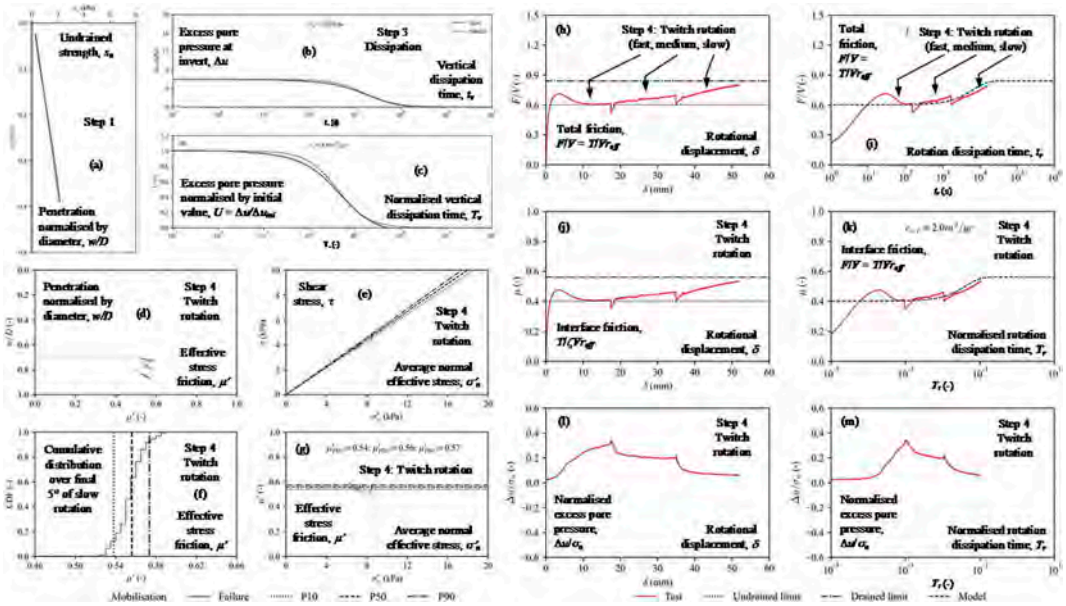


Figure 8. Typical interpreted results from a shallow penetrometer test with a monotonic rotation step (hemiball in soft clay).

less, an effective stress interpretation with a weighted average pore pressure provides effective friction parameters, even if the rotation is undrained or partially drained.

The interpreted results in Figure 8 show the following derived soil parameters: (i) profile of undrained strength, s_u , (sub-figure (a)); (ii) consolidation coefficient during loading path (c); (iii) undrained interface strength (j); (iv) drained interface strength (j); (v) consolidation coefficient for shearing path (k); (vi) effective stress failure envelope (e) and (vii) effective stress friction (as distribution) (g).

5 RESEARCH STUDIES AND PROJECT USAGE

The penetrometer system has been used for >300 tests at the time of writing, for research activities and for commercial projects across three continents. Typical project test programmes have involved 10-20 shallow penetrometer tests spread over 3-4 distinct soil zones, with parallel vertical penetrometer profiling. Reliable and repeatable measurements of interface strength have been obtained for clays, silts and sands. Examples of added project value have included (i) the first ever data on consolidation coefficient at the very near-surface, (ii) better characterization of the consolidation-hardening behaviour from repeated

surface sliding on clay and (iii) more detailed and repeatable measurements of drained and undrained interface strength parameters.

The shallow penetrometers offer an alternative to the low stress interface shear box. In our experience, this test can be unreliable compared to shallow penetrometer tests due to extraneous forces polluting the shear and normal forces measured in the shear box. Further studies into shallow penetrometers, particularly focusing on the ring, are reported by Mohr et al. 2022 and Singh et al. 2022.

6 CONCLUSIONS

Vertical and shallow rotational penetrometer tests together provide a new method to obtain a wider and more reliable set of near-surface seabed mechanical properties compared to conventional practice.

The equipment, procedures and interpretation approach for the new types of shallow penetrometer are now well-established, with the key details summarized in this paper. Drained and undrained interface strength parameters, as well as consolidation properties, can be objectively derived through rapid testing in box cores or samples recovered to the laboratory.

Table 2. Typical shallow penetrometer test interpretation procedure.

Step type	Step name/ Input parameter(s)	Calculated parameter(s)	Calculation approach		Calculation coefficients	
			Ring	Toroid Hemiball		
1	Penetration Vertical load, V	Undrained shear strength, s_u	$s_{um}, k_{su} = f(V(w))$ – use iteration to fit a linear s_u profile ($s_u = s_{um} + k_{su}w$) (Stanier & White 2015) $U = \frac{\Delta u}{\Delta u_{lim}} = \frac{1}{1 + \left(\frac{T_r}{T_{50,v}}\right)^m}$ with time $T_v = \frac{c_v t_r}{D^2}$		N/A	See S&W reference
3	Dissipation Excess pore pressure response, $\Delta u(t_r)$	Consolidation coefficient, c_v (for stress path after vertical penetration)	Plot data and equation of $\Delta u/\Delta u_{int}$ vs. t_r , adjust c_v . Or find $t_{v,50}$ when $\Delta u/\Delta u_{int} = 0.5 \rightarrow c_v = T_{50,v} D^2 / t_{v,50}$ t_v : time since start of dissipation (i.e. start of step 3). $\mu_{ud} = \frac{\sigma_{su}}{\sigma'_v} = \frac{F}{V} = \left(\frac{T_r}{\sigma'_v V_{eff}}\right)_{ud} = \frac{F}{V} = \left(\frac{T_r}{\sigma'_v V_{eff}}\right)_{dr}$ $\mu_{dr} = \mu'_r = \tan \delta = \left(\frac{\sigma_{su}}{\sigma'_v}\right)_{dr} \left(\frac{T_r}{T_{50,v}}\right)^n$ with $T_r = \frac{c_v t_r}{D^2}$		$T_{50,v} = 0.0675$ $m = 1.00$ (Singh et al. 2022)	$T_{50,v}$ and m vary with w/D . See Schneider et al. (2020b)
4, 5	Rotation Vertical load, V Torque, T Total friction, $\mu = T/V$ Excess pore pressure, $\Delta u(t_r)$	Undrained interface friction, μ_{ud} Drained interface friction, μ_{dr} Consolidation coefficient, $c_{v,r}$ (for stress path during rotation)	$\mu = \mu_{dr} - (\mu_{dr} - \mu_{ud})0.5 \left(\frac{T_r}{T_{50,v}}\right)$ with $T_r = \frac{c_v t_r}{D^2}$ Use same method of fitting as described in Step 3. t_r : time since start of rotation (i.e. start of step 4). $\mu' = \left(\frac{\sigma_{su}}{\sigma'_{n,ave}}\right)$ where $\tau_{int} = \frac{T}{A_c}$ and $\sigma'_{n,ave} = \sigma_{n,ave} - \Delta \mu_{ave} = \frac{\zeta V}{A_c} - \beta \Delta u_{pos}$		$\zeta = 1$ $r_{eff} = L + \frac{D^2}{12L} L = \frac{1}{2}(D_o - D_b)$ $T_{50,r} = 0.25$ $n = 0.9$	ζ, τ_{eff}, A_c and $\beta = \frac{\Delta \mu_{max}}{\Delta \mu_{pos}}$ vary with w/D . See Schneider et al. (2020b, c)
		Effective stress envelope, μ'^{-}	$A_c = 2\pi D_b L$ $\beta = \frac{\Delta \mu_{max}}{\Delta \mu_{pos}} \approx 0.7$ for pore pressure at mid radius			

These methods have been developed through >300 tests, supported by theoretical and numerical analysis, and have been applied in several commercial projects.

ACKNOWLEDGEMENTS

We acknowledge support from the RIGSS JIP (Fugro, Total, Woodside and Shell), the EPSRC Offshore Renewable Energy Supergen Hub (grant EP/S000747/1) and Prof. Mark Randolph and Dr Mark Schneider.

REFERENCES

- Boscardin, A.G. & DeGroot, D.J. 2015. Evaluation of a toroid for model pipeline testing of very soft offshore box core samples. Proc. ISFOG2015, Taylor & Francis, London: 363–368.
- ISO 19901-4:2022. Specific requirements for offshore structures — Part 4: Geotechnical design considerations. ISO (draft).
- Mohr H., Stanier S.A. & White D.J. 2022. The ring penetrometer for interface shear testing on sand. Geotechnique. In review.
- Schneider M., Stanier S., White D.J. & Randolph M.F. 2020a. Apparatus for measuring pipe-soil interaction behaviour using shallow ‘pipe-like’ penetrometers. ASTM Geotechnical Testing Journal 43(3): 622–640.
- Schneider M., Stanier S., White D.J. & Randolph M.F. 2020b. Shallow penetrometer tests: theoretical and experimental modelling of the penetration and dissipation stages. Canadian Geotechnical Journal 57(4): 568–579
- Schneider M., Stanier S., White D.J. & Randolph M.F. 2020c. Shallow penetrometer tests: theoretical and experimental modelling of the rotation stage. Can. Geot. J. 57(4):568–579
- Singh V., Mohr H., Stanier S.A. Bienen B. & Randolph M. F. 2022. Characterisation of interface friction strain-rate dependency of soft sediments at low stresses using a ring penetrometer. Geotechnique. In review.
- Stanier, S. & White D.J. 2015. Shallow penetrometer penetration resistance. ASCE J. Geo Geoenv. Eng. 141 (3):04014117
- White D.J., Stanier S.A., Schneider M., O’Loughlin C.D., Chow S.H., Randolph M.F., Draper S.D., Mohr H., Morton J.P., Peuchen, J., Chow F.C., Fearon R. & Roux A. 2017. Remote intelligent geotechnical seabed surveys – technology emerging from the RIGSS JIP. Proc. Int. Conf. OSIG. 1214–1222
- White, D.J., Clukey EC, Randolph MF, Boylan NP, Bransby MF, Zakeri A, Hill AJ, Jaeck C. 2017. The state of knowledge of pipe-soil interaction for on-bottom pipeline design. OTC 27623, Proc. Offshore Technology Conference, Houston.
- Yan Y., White D.J. & Randolph M.F. 2010. Investigations into novel shallow penetrometers for fine-grained soils. Proc. 2nd ISFOG. Perth. 321–326.
- Yan Y., White D.J. & Randolph M.F. 2017. Elastoplastic consolidation solutions for scaling from shallow penetrometers to pipelines. Canadian Geotechnical Journal 54:881–895.

Development of an enhanced CPT system for Dogger Bank

Tor Inge Yetginer-Tjelta
Equinor, Stavanger, Norway

Simon Bøtker-Rasmussen
Geo, Copenhagen, Denmark

Mike Rose
SSE Renewables, Perth, Scotland

Tom Lunne & Vaughan Meyer
NGI, Oslo, Norway

Callum Duffy
Logos Geoservices Ltd, Oxford, UK

ABSTRACT: An enhanced seafloor CPT system has been developed to support completion of the soil investigation campaign for Dogger Bank. This enhanced system has a demonstrable and significant performance increase over standard seafloor CPT systems; capable of pushing through dense sand layers with $q_c > 100$ MPa and through tens of meters of very stiff clays. At Dogger Bank, this enhanced system has enabled CPT penetrations of more than 40 m below seafloor, in soils where standard systems could only average in the twenties. The system enhancement has been achieved through the application and adaption of techniques well known in the geotechnical industry (water lubrication and water injection), but which have never before been combined in an offshore seafloor CPT system. The performance of the enhanced CPT system has enabled a reliance on seafloor CPTs to acquire data to beyond monopile toe depths, therefore removing absolute reliance on boreholes to acquire data at turbine locations and facilitating the fast and efficient development of a geotechnical design basis.

1 INTRODUCTION

A challenge in offshore wind farm development is designing a soil investigation campaign that efficiently and cost effectively provides the geotechnical data required for the design of pile foundations. With many years of gradually applying in situ testing as an active part of building a design basis, it is observed that seafloor CPTs are both efficient and less expensive than boreholes, yet they are often compromised by not being able to penetrate to pile toe depths.

Monopiles are the primary foundation type for the Dogger Bank wind farm development. As outlined in the companion paper (Yetginer-Tjelta et al., 2022), the design of monopiles requires soil data to 40-45 m below seafloor. Furthermore, windfarm layouts are commonly only confirmed late in project execution, necessitating a rapid turnaround from turbine location definition, to the delivery of a geotechnical design basis. Due to these factors, seafloor CPTs would be the preferred solution provided that a penetration to greater than 40m can be achieved.

Soil conditions at Dogger Bank consist mainly of dense to very dense sands and very stiff clays. For these soils, experience has shown that for “standard” seafloor CPTs, refusal frequently happens between 20-30m below seafloor. This is due to the combined effects of high rod friction in the stiff clays and high tip resistance encountered within the dense sand layers, frequently found at the base of Dogger Bank clays, at 25 to 30m below seafloor. Consequently 40+ m penetration cannot be achieved at most locations at Dogger Bank.

The seafloor CPT penetration statistics from the two preliminary soil investigation campaigns in 2010 and 2012 illustrate these factors:

Table 1. Summary of early seafloor CPT penetration depths Dogger Bank.

Year	No. CPTs 1)	Final penetration depth (m bsf)		
		Minimum	Maximum	Average
2010	97	3.8	40.2	22.5
2012	87	8.9	40.1	27.2

Whilst these CPTs provide good data for the development of a ground model, the sub 40m penetrations would not enable standard seafloor CPTs to be relied on as the primary data acquisition tool for monopile design. Therefore, for the purpose of designing the turbine location specific completion soil investigation (SI) campaign, the following options were considered:

- Revisit turbine locations with seafloor CPT refusals of less than ~40m penetration with a drillship and down hole CPTs, or
- Accept high uncertainty on soil conditions below refusal depth and build trust into a good ground model, or
- Attempt to reach deeper with an improved “deep” seafloor CPT system.

Revisiting seafloor CPT refusal locations with a drillship was deemed not acceptable for reasons of cost and time. Whilst the reliance on the ground model below refusal depth was similarly rejected due to the complex geology and reworked soils. Geophysical reflectors were frequently broken and made it difficult and often impossible to follow any layer more than a few hundred meters. Furthermore, the lower sand (base of Dogger Bank) is found between 25-35m; coincident with the seabed multiple of the UHR seismic data. This resulted in very poor confidence for the ground model below this depth since all detailed information on layer thickness and general stratigraphy disappeared in the strong multiple reflection and little details were visible below.

From the above it is clear that development of equipment and procedures for achieving larger penetration with seafloor CPTs was of critical importance to support the efficient and cost-effective delivery of the Dogger Bank completion SI campaign. This became a main objective with the various CPT campaigns in the period 2018-2021. This is further detailed in Sections 3, 4 and 5 below. It became a stepwise approach where trials, results/experience and modifications were considered on a continuous basis.

As outlined by Yetginer-Tjelta et al. (2022), 3D UHRS geophysics in 2019 (and beyond) improved the resolution and capability of the ground model but were not sufficient to replace CPT data as the basis for foundation design.

2 PREVIOUS WORK TO REACH DEEPER PENETRATION

The most common way of increasing penetration is to reduce the friction along the CPT rods. Frequently a friction reducer such as an expanding coupling is used at some distance behind the cone. Thus, the diameter of the hole is expanded and the friction

between the rod and the soil is reduced. According to ISO22476-8: 2012 the friction reducer must be at least 400 mm behind a 10 cm² cone in order not to influence the measured CPTU parameters. Offshore soil investigations with a seafloor rig often use a 15 cm² cone and 10 cm² rods, which gives good results in many cases.

Another way of reducing the rod friction is to inject water or drilling mud at some location above the friction reducer. Jefferies and Funegard (1983) reported such a system and showed that the pushing force can be reduced by up to 50 % (Figure 1). Staveren (1995) reported that in stiff overconsolidated Belgian Boom clay, normal CPTs met refusal at 5 m penetration: using mud injection, up to 62 m penetration could be achieved.

In very dense sand, high cone resistance can be a factor limiting penetration. Bayne and Tjelta (1987) and Yagi et al. (1988) reported designs of cone penetrometers where water could be injected into the soil through channels in the penetrometer tip. The cone design reported by Bayne and Tjelta (1987) was intended to be used to investigate how much skirt penetration resistance in dense dilatant sand could be reduced by water injection. High negative pore pressures and increased effective stresses, resulting in high cone resistance, may be neutralized by adding water during penetration. This cone penetrometer was unfortunately not used in practice. Yagi et al. (1988) used their cone

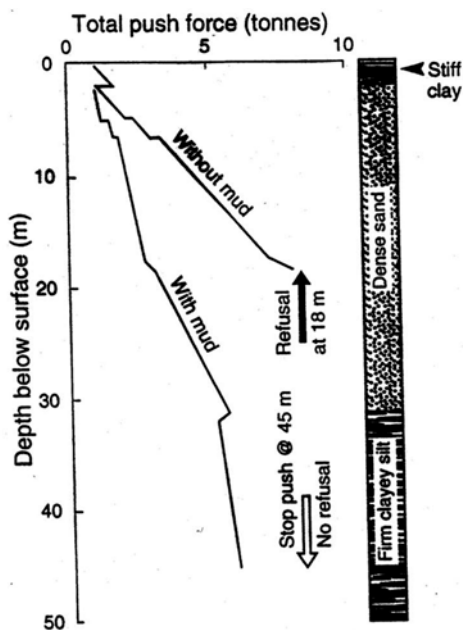


Figure 1. Total cone push force with and without mud injection (adapted from Jefferies and Funegard, 1983).

penetrometer to carry out tests at various effective stresses. They controlled this by adding water or air through the tip during cone penetration.

In summary, for further work at Dogger Bank in 2018 the ideas of rod lubrication and potentially water injection at or around the cone tip were selected for further experimenting.

3 ENHANCED CPTS USING ROD LUBRICATION

A strategic cooperation contract was agreed between the Dogger Bank project and the Danish contractor Geo with the aim to improve seafloor CPT penetration below mudline from being in the low 20m's to anything towards 40m (later changed to 45 m). In 2018 the following modifications were introduced to reach this aim:

1. Increased thrust capacity, i.e. 250 kN net thrust available at seafloor.
2. A rod lubrication system which reduced or eliminated friction accumulation in the stiff clays to enable deeper penetrations in the clays and thus enable more thrust capacity in the dense sand layers at base of Dogger Bank clay units.

These first tests improved the penetration depth below seafloor significantly, from an average of 23 m to approx. 35.8 m, and with several CPTs reaching close to 40 m (target depth at that stage)

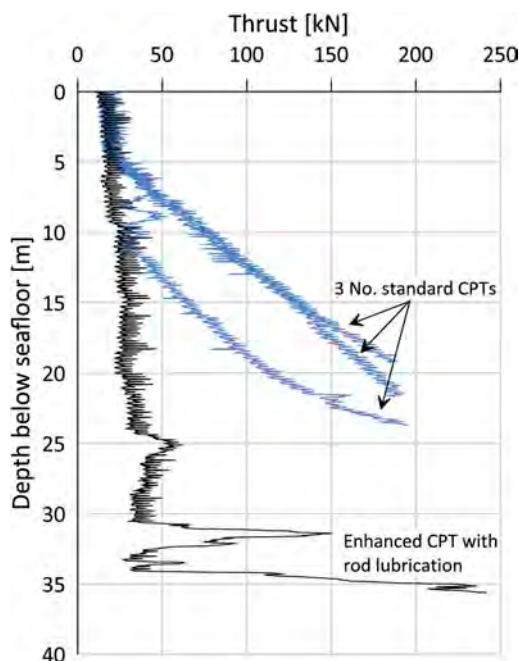


Figure 2. Thrust for Enhanced CPT with lubrication and 3 CPTs with no lubrication.

and one test meeting the target with still 5 kN thrust reserve. Figure 2 shows total thrust curves for 4 CPTs within an area of 110 x 110m with 3 standard CPTs reaching maximum thrust between 19 and 24m whilst one CPT with rod lubrication reached 35.2m including penetration through two dense sand layers.

In addition to thrust, pressure and flow rate of lubrication water are measured. There is a potential for using these parameters in the interpretation of the test results.

4 DIRECT PUSH CPT WITH WATER INJECTION AT TIP, MEASURING THRUST ONLY (DCPT)

From the testing in 2018 (above) it was clear that rod lubrication worked and enabled significantly deeper penetration. It also meant when the dense sand layers were met at about thirty meters depth, only 10-15% of the thrust capacity was spent on reaching this depth (note the relatively constant thrust with depth in mostly clay down to 30m). But some of the sand layers were very dense, with q_c values of more than 100 MPa, and for some locations significantly more than 10-15% of the thrust was required to overcome layered units. Refusal was therefore still frequently encountered in dense sand layers. To deal with locations where several sand layers made the rod lubrication less efficient, and where deeper sand layers added to frequent refusals in the 30 m range, further work took part along two parallel paths.

Firstly, further improvements were made to improve the efficiency of rod lubrication. Many options were tested, including:

- variations in water injection hole diameter and location (radially and axially)
- combination with friction reducers of various thickness and length
- high and low water pressures
- variations in water volume.

Secondly, to improve the penetration of very dense sand layers, water injection at the cone was attempted in different ways. This built on experience gained over many years from projects such as Gullfaks C (Tjelta et al., 1986), Dudgeon suction anchor trials 2013 (unpublished), and the OWA Suction Anchor Trial Installation Campaign 2015 (unpublished) where significant reduction in the penetration resistance of skirts and suction anchors was observed by injecting water at the skirt tip. The effect comes from partly reducing dilation in dense sand, removing dilation completely (and reducing effective stresses) or in some cases probably by flushing away sand particles.

Various geometries of the cone with flushing through the tip, at the face and at the neck were tried, see two examples in Figure 3. These cone types were not instrumented and were named DCPTs (Direct Cone Penetration Test), with the only

recording of penetration resistance being total thrust (a bit like the mechanical cones in the early days of cone testing). Water injection at these positions is expected to have some influence on a measured cone resistance, but nevertheless this system did result in deeper penetration and provided information of what was below the dense sand at which time the water injection can be reduced or halted.



Figure 3. Various cone tips with water flushing for DCPT cones.

Figure 4a shows an enhanced CPT to 45m depth (red curve) in parallel with a non-instrumented cone, DCPT (black curve). At this location it was possible to penetrate both cone types to 45 m (target depth). At many other locations the enhanced CPT met refusal at shallower depth and soil stratigraphy had to be inferred from thrust curves only (Figure 4b provides an example).

What this parallel test in Figure 4a shows is a very good correlation between q_c and thrust when rod friction is kept low and relatively constant. This test (black curve) uses combined rod lubrication and cone water injection.

Figure 4b shows an enhanced CPT meeting refusal due to max thrust and high tip resistance (114 MPa) whilst the DCPT reached 40m without any problem (40m was target depth at this test location), and clearly provides relevant information of soil strength and stratigraphy. For instance, the driveability of large monopiles can be considered feasible since the dense sand layers at 26 and 34m are proven to be relatively thin. When soil stratigraphy is very variable (less homogeneous and/or rod lubrication is less efficient) the thrust/ q_c correlation is less accurate. Although the DCPT system worked well in 2019, some locations had to be covered by drilling and down-hole CPTs. This experience stimulated further development.

5 DCPT WITH MEASUREMENT OF TIP RESISTANCE (iDCPT)

To achieve improved penetration in the very dense sand layers at Dogger Bank (q_c in the range of

100-150 MPa), the S-cone was developed, as shown in Figure 5. This is a cone tip which combines the power of a 5 cm² cone in spearheading into dense sand, combined with large holes for water injection to reduce sand resistance on the face of the cone with enlargement following closely behind the cone tip. The early version of this S-cone was non-instrumented and only thrust was recorded. Later versions of the S-cone are instrumented, with q_c and inclination recorded (named the iDCPT), but due to robustness being prioritised and space limitations associated with water injection, the tool has less accuracy than a standard cone according to ISO specifications. However, as can be observed in Figure 6, where an enhanced CPT and an iDCPT were performed only meters apart; the enhanced CPT met refusal at 24 m whilst the iDCPT using the S-cone penetrated to 45 m. The correlation between q_c from the robust iDCPT and the enhanced CPT is good, and it is seen that the iDCPT provides useful information for layers below the depth of penetration attained by the enhanced CPT.

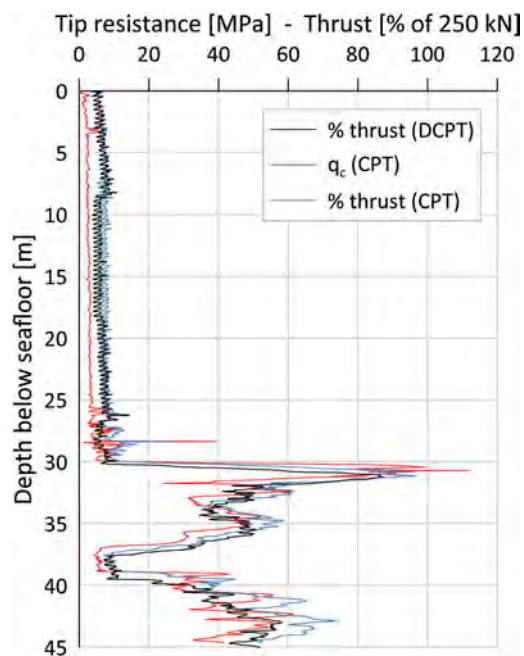


Figure 4. a) Location A (top): Comparisons between normal CPT and DCPT - enhanced CPT and DCPT both penetrate to ca. 45 m; b) Location B (bottom): Enhanced CPT refused at 26 m whilst the DCPT reached 40 m (target depth at the time, could have gone deeper).

The most efficient combination of water injection (pressure and volume), friction reducers and cone shapes may depend on the soil conditions and will invariably include some trial and error in the beginning, but the results speak for themselves (Table 2).

From pre-2018, the average CPT depth has increased from 22m to 44m in an area where dense sand layers dominate below 25-30m. These numbers do not include the iDCPT. A challenge has also been to distribute water in the most efficient way between the rod lubrication and the tip flushing.



Figure 5. Instrumented cone tip used with the iDCPT.

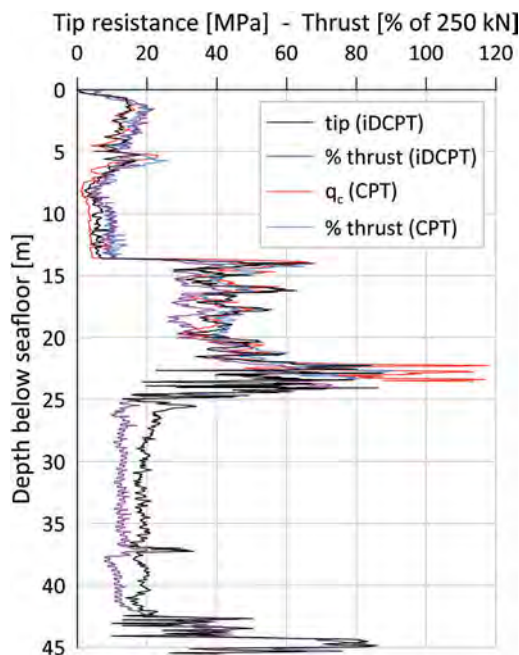


Figure 6. Enhanced CPT and iDCPT.

Table 2. Summary of Seabed CPT penetration depths Dogger Bank.

Year	No. CPTs 1)	Final penetration depth (m bsf)		
		Minimum	Maximum	Average
2010	97	3.8	40.2	22.5
2012	87	8.9	40.1	27.2
CPT equipment enhancements from 2018 onwards				
2019	100	14.3	45.6	38.8
2020	120	7.5	50.3	40.1
2021	98	23.5	58.8	44.5

6 DISCUSSION

The main objective set out at the start of 2018 was to reach sufficient penetration with seafloor CPT testing without the need for drilling and down-hole CPTs.

Two main targets were identified in these early days:

1. Reduce or “eliminate” rod friction to enable deeper penetration and have more thrust capacity available when dense sand layers appeared at base of Dogger Bank formation.
2. Improve the ability to penetrate into and through dense sand layers with tip resistances in excess of 100 MPa.

This objective has been met; seafloor penetration depth to 40-45m is now possible at Dogger Bank at most locations. The importance of this objective goes beyond the operational aspects of seafloor CPTs being more efficient than down hole CPTs in a borehole. It allows for reduced time from confirmed turbine layout to delivery of a geotechnical design basis “by the speed with which the data can be acquired, processed and interpreted to provide geotechnical engineering parameters. This is advantageous for the development of offshore wind farm projects which may have 100 or more WTGs. For the Dogger Bank WTG locations, continuous seafloor CPT data permitted semi-automatic processing and analysis of data and thus:

- 1) Rapid development of geotechnical design profiles (preliminary profiles available in a matter of minutes);
- 2) Early phase monopile driveability predictions for identifying the potential risk of refusal during installation.” quote from companion paper (Tjelta et al 2022)

On a side note, the ability to penetrate into and through dense sand layers with tip resistance in excess of 100 MPa at more than 30m below seafloor is not trivial. It requires a significant reduction of rod friction. In doing so, the combined effect of a friction reducer and water injection as described in this paper is necessary, and it has taken time and efforts to arrive at a geometry

that works. The impact of altered geometry due to extreme wear on all parts in the CPT system complicates the feedback. Figure 7 indicates the changes taking place. Diameter changes, and friction reducers are ripped off by the continuous abrasion from dense quartz sand.



Figure 7. New rod with friction reducer 44mm left and to the right the wear has reduced diameter to 41 mm and in parts of the FR it is ripped off completely.

Outstanding challenges to be addressed are effective lubrication while the CPT string is being built, and effective lubrication in permeable sand layers.

The importance of the following elements has been recognized during the 3-4 years it has taken to develop a fully operational and efficient enhanced seafloor CPT system:

- Friction reduction and ideally removal along the entire rod by a combination of a friction reducer above the friction-sleeve and water injection
- Increased thrust force when stiff clays and dense sand layers are combined, like at Dogger Bank
- The importance of inclination measurement in the cone, both for operational purposes (abort the CPT if becoming excessive or to push deeper to compensate for rod inclination) and for final presentation of results with true vertical depth
- Special measures at the cone tip to tackle extremely dense sand layers with q_c above 100 MPa.

7 SUMMARY AND CONCLUSIONS

A seafloor CPT system with improved (enhanced) capabilities has been developed for the Dogger Bank field investigations in the period 2018-2021. The main

objective of this development was to improve the depth range to more than 40m below seafloor in an environment where average penetration used to be in the low 20m's. This has been achieved through systematic development and adaptation of techniques well known in the geotechnical industry (water lubrication and water injection). However, these techniques have never before been combined in an offshore CPT system to produce a machine capable of pushing through dense sand layers with $q_c > 100$ MPa and very stiff clays. The result has been a 100% increase in CPT penetration depth compared to a few years ago.

This performance enables fast and efficient development of a geotechnical design basis when combined with early boreholes strategically placed in geological units to build a ground model, as discussed in the companion paper (Yetginer-Tjelta et al., 2022).

ACKNOWLEDGEMENTS

The authors are grateful to Dogger Bank Wind Farm for the opportunity to create new solutions in delivering a timely and efficient design basis and for permission to publish. Colleagues in Equinor, SSE, Geo and NGI are acknowledged for their contribution to the development of an enhanced CPT tool and to this paper.

REFERENCES

- Bayne, J.M. and Tjelta, T.I. (1987) "Advanced cone penetrometer development for in situ testing at Gullfaks C". Offshore Technology Conference, Richardson, Texas, Paper No. 5420.
- Jefferies, M.G. and Funegard, A. (1983) "Cone penetration testing in the Beaufort Sea". Proceedings of the Conference on Geotechnical Practice in Offshore Engineering, Austin, Texas, 220-43, American Society of Engineers (ASCE).
- Staveren, M. van (1995) "Advanced deep cone penetration testing and backfilling in overconsolidated clay". Proceedings of the International Symposium on Cone Penetration Testing, CPT '95, Linköping, Sweden, 2, 99-104, Swedish Geotechnical Society.
- Tjelta, T.I., Guttormsen, T.R., Hermstad, J. (1986) "Large-Scale Penetration Test at a Deepwater Site", Offshore Technology Conference, Houston, Texas, May 1986, Paper number OTC.
- Yagi, N., Enoki, M. and Yatabe, R. (1988) "Development of a penetrometer capable of applying pore pressure". Proceedings of the International Symposium on Penetration Testing, ISOPT-1, Orlando, 2, 1051-7, Balkema Pub., Rotterdam.
- Yetginer-Tjelta T.I., De Sordi, J., Caferra, L., Rose, M., Duffy, C., Lunne, T., Blaker, Ø., Strandvik, S. & Meyer, V. (2022). "The role of cone penetration testing in the Dogger Bank offshore wind farm". Proc. 5th Int. Symp. on Cone Penetration Testing, CPT'22, Bologna, Italy, 8-10 June 2022.



Taylor & Francis

Taylor & Francis Group

<http://taylorandfrancis.com>

Session 2: Interpretation



Taylor & Francis

Taylor & Francis Group

<http://taylorandfrancis.com>

CSi – a joint industry project into CPTUs in silty soils

A.H. Augustesen
Ørsted, Denmark

P. Carotenuto, C. Bilici & T. Lunne
Norwegian Geotechnical Institute, Norway

R.C.J. Lindeboom & L. Krogh
Ørsted, Denmark

J. van den Bosch & R. Barth
Fugro, The Netherlands

C. Erbrich & S. Ingarfield
Fugro, Australia

D. Giretti
University of Bergamo, Italy

V. Fioravante
University of Ferrara, Italy

H. Dias
Equinor

M-C Sougla
Vattenfall

A. Barwise
RWE

S. de Wit
Shell

D. Burbury
Scottish Power Renewables

N. Adams
Carbon Trust

ABSTRACT: The CPTU constitutes the main *in situ* offshore investigation tool for geotechnical site characterisation and provision of soil input for the design of wind turbine foundations. CPTUs are typically performed at all foundation positions. Thus, all obtained results of supporting geotechnical *in situ*, model and laboratory testing need to be confidently correlated to the CPTU parameters. Most of the interpretation methodologies available for industry practice consider the soil behaviour around the cone either as fully drained or undrained, and acknowledged and well-proven correlations between CPTU parameters and classification and engineering properties exist for sand and clay. However, for transitional soils, e.g. silty soils, which may exhibit partial drainage during standardized cone penetration, such robust interpretation schemes do not exist. This paper presents the background, the objectives, setup and early field results of a joint industry project into CPTUs in silty soils for developing schemes for planning, execution and interpretation.

1 INTRODUCTION

The Offshore Wind Industry is rapidly expanding across the globe. This expansion leads to the exploration of offshore wind sites that are characterized by thick layers of silty sand and silt mixtures. In contrast to sampling boreholes, CPTUs are performed on all wind turbine positions, which in many cases can be more than 100 positions covering large areas. The CPTU parameters must be confidently correlated to all supporting geotechnical tests to mitigate the following risks: a) site characterization and establishing facility position-specific soil parameters for foundation design, b) choice of foundation concept and relevant design methodologies, c) installation predictions, d) cable design and e) increased project maturation times and site investigation scopes. However, as opposed to sand and clays, the Industry finds it generally challenging to properly identify and capture the behaviour of transitional soil, e.g. silty sand, silts and silt mixtures, with standardized CPTUs. No simple, robust, and standardized testing approaches and interpretation methodologies have been calibrated to these types of soils.

A Joint Industry Project (CSi – CPTUs in Silty soils) is currently being executed within the Carbon Trust Offshore Wind Accelerator programme with the main objective to develop robust guidelines targeting the industry for planning, specification, execution, and interpretation of CPTUs in silty soils. Focus is especially paid to

- Soil classification and mechanical behaviour
 - New and/or revised soil classification and soil behaviour type charts
 - Identification of transition between drainage conditions including rate effects, i.e. of drained to partially drained to undrained conditions
- Correlations to engineering properties
 - Strength and stiffness.
- Guidelines for specifying and executing CPTUs for identifying silty soils and their behaviour.

The project targets mainly silty and transitional soils with low plasticity. This paper presents the background of the CSi project as well as the overall project set-up and early findings from a test site in Halden, Norway.

2 BACKGROUND

CPTUs carried out at a standard constant penetration rate (20 mm/s \pm 5 mm/s according to ISO 2012) generally result in an undrained response in clay and a drained response in sand (Lunne et al. 1997). However, for silty soils partially drained conditions may prevail at the standard penetration rate, see DeJong et al. (2013). Understanding the drainage conditions around the penetrating cone is key to interpret CPTUs in silty soils (correlation with engineering parameters and classification charts).

2.1 Drainage conditions

In recent years the normalized penetration velocity V represents an often-used framework to indicate the drainage conditions around the penetrometer and to demonstrate how CPTU parameters change with penetration rate v , soil properties (horizontal coefficient of consolidation of the soil c_h) and cone penetrometer diameter d , see e.g. Randolph & Hope (2004), Kim et al. (2008) and Schneider et al. (2008). The normalized penetration velocity is defined as:

$$V = \frac{v d}{c_h} \quad (1)$$

For contractive soils and a given cone diameter, the cone shoulder pore pressure u_2 increases, and the cone resistance decreases with increasing V , whereas the opposite may be observed for u_2 for dilative soils (Schneider et al. 2007 and Krage & DeJong 2016). Drained penetration is observed to occur for $V < 0.01-0.3$ and undrained penetration for $V > 20-100$ (Randolph 2004, Bihs 2021). v and d are parameters, which can be fully controlled and specified. Therefore, an accurate determination of c_h is important in the estimation of V . c_h depends on stress history, density and grain composition.

Determination of the operational value of the coefficient of consolidation of the soil is not straight forward, especially not for the more coarse-grained transitional soils. Most of the work to date, numerically and experimentally, is anchored in contractive clay-like soils and undrained conditions.

c_h can be determined from piezocone dissipation tests (PPDT) accounting for partial consolidation during cone penetration, and hence penetration rate, in the interpretation of the tests (DeJong & Randolph 2012). However, for transitional soils, the excess pore pressure measured at the cone shoulder u_2 does not always decay monotonically over time during dissipation and a dilatatory response can be observed. Burns & Mayne (1998) and Paniagua et al. (2016) discuss different approaches to determine t_{50} , the time associated for 50% dissipation, dealing with both standard and non-standard (dilatatory) dissipation curves. Carrol and Paniagua (2018) note that different interpretation methods can lead to significant differences in the estimated t_{50} and hence c_h .

The rigidity index I_r is required to interpret dissipation tests. However, the concept of I_r , developed for fully undrained conditions, may not be appropriate for partially drained conditions. Krage et al. (2014) provide guidance on how to determine I_r .

To overcome some of the challenges with the estimation of c_h , Schnaid et al. (2020) propose a modified version of the normalized penetration velocity depending on v , t_{50} , d and I_r .

CPTUs at variable penetration rates (VRCPTU) are traditionally performed to investigate the drainage conditions around the cone. Even with a robust methodology to estimate V , a link between V and engineering properties and soil classification need to be developed – also for engineering practice.

2.2 Soil classification

Soil behaviour type (SBT) charts, like Robertson (1990) and later updates or Schneider et al. (2008), are often used for classification purposes. The charts are based on standard CPTU geometries and a penetration rate of 20 mm/s.

Research (e.g. Schneider et al. 2008, Bradshaw et al. 2012) and practice support that silty soils can plot on a large range of zones in the SBT charts and thus the SBT charts alone can, at present, not be used to robustly identify grain composition or plasticity for a silt deposit. The reason is that the position in the SBT chart is a function of several parameters, including grain size, plasticity, *in situ* density, stress history and local geological history. Furthermore, partial drainage conditions affect where data plots on the SBT charts (DeJong & Randolph 2012) and use of additional data from dissipation tests and VRCPTUs may aid the identification of silty soils.

2.3 Strength and stiffness

Current practice in the offshore wind industry for assessing silty soils is to apply methods anchored in either clean sand (drained conditions, effective stress approach) or pure clay (undrained conditions, total stress approach).

The relation between cone resistance and the undrained shear strength through the cone factor N_{kt} has been investigated in the literature, e.g. Senneset et al. (1988), Blaker et al. (2019), Naeini & Moayed (2017) and Huang et al. (2021). For the effective stress friction angle Senneset et al. (1988) suggested an approach, which considers pore pressure build-up and is relevant for partially drained conditions. Bihs (2021) reports that both the drained and undrained strength depends on the choice of penetration rate. Senneset et al. (1988), Lunne et al. (1997), Robertson (2009) and Tonni & Simonini (2013) discuss constrained and small strain shear modulus.

Correlations between CPTU parameters and engineering properties are dependent on the quality of the samples tested in the laboratory for calibration purposes. Furthermore, for the strength correlations a unique failure criterion may not exist for undrained shear of especially dilative transitional soils (Blaker & DeGroot 2020). It is complicated to retrieve and prepare intact samples for testing and currently no robust and well-proved criterion for evaluating sample disturbance exists. Sampling and handling of silty samples are thus of importance to the CSi project.

3 CSI PROJECT SETUP

3.1 CSi project scope and approach

The CSi project includes a comprehensive scope of work, see Figure 1, on different scales and platforms to meet the project objectives and to exploit current and new methodologies and hypotheses for addressing the project challenges, cf. Sections 1, 2.

Initial studies in terms of a literature review and a project plan provides the background and detail the other activities. The guidelines, addressing the project objectives, are based on analyses of high-quality factual data gathered in a database. The data are extracted from different sources.

In situ tests, and parallel laboratory tests, will be performed on aged natural silty soils at two complementary onshore test sites (Halden, Norway and Vorne-Putten, the Netherlands). VRCPTUs with different cone sizes, dissipation tests, seismic CPTUs and sampling (the static hydraulic piston sampler and the static gel-push sampler) will be undertaken. The onshore test site data are supplemented by Partners' data from offshore projects across the world as well as data from other silt sites published in the literature, thereby increasing the applicability of the database.

Calibration chamber testing, centrifuge testing and associated standard element laboratory tests complement the onshore test site data by providing test results under well-defined and controlled conditions. Furthermore, they are also relevant for benchmarking to existing interpretation schemes for clean sand. VRCPTUs and dissipation tests are performed at different densities and consolidation stresses with full-scale and miniature cones in unaged non-plastic silty sand and reconstituted clean sands (Fioravante et al. 2022).

A state-of-the-art numerical model will expand the general applicability of the guidelines by validating and extrapolating the design space offered by the experimental data. Furthermore, recommendations with respect to numerical models for predicting CPTUs in transitional soils will be provided. The critical state based Norsand constitutive model along with large-deformation finite element and cavity expansion analyses will be used to calibrate and validate the model based on field, laboratory and model tests (calibration and centrifuge testing).

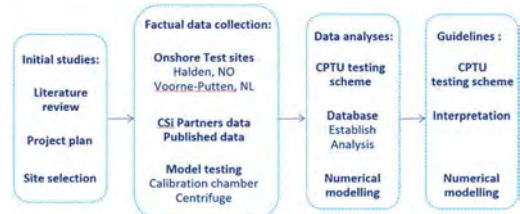


Figure 1. High-level strategy adopted during the CSi project.

3.2 CSi organisation

The CSi project is developed and led by Ørsted in partnership with five other offshore wind developers. The project is run as a discretionary project through the Carbon Trust's Offshore Wind Accelerator programme. The technical activities are managed and executed by the Norwegian Geotechnical Institute (NGI), supported by Fugro and ISMGEO. Selected activities are reviewed by an independent technical review panel to substantiate the developed methodologies. A certification body (DNV) ensures that the outcome is practically, applicable and relevant for industry practice and future standardization. Figure 2 illustrates the CSi organizational setup.

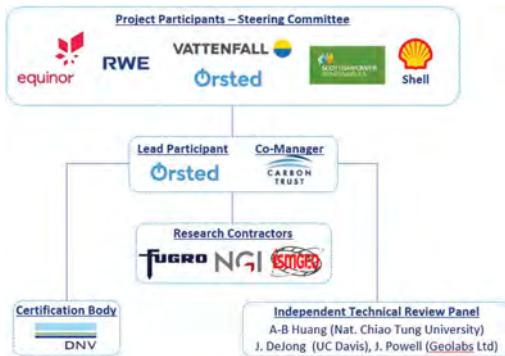


Figure 2. Schematic view of the CSi project setup.

4 FIELD TESTING AT HALDEN, NORWAY

4.1 Test site and test programme

The Halden site is located in southern Norway and is one of five sites within the Norwegian Geo-Test Sites program (NGTS). Extensive geophysical, *in situ* and laboratory testing have been carried out as part of the site characterization (see Blaker et al. 2019) and for subsequent research. Normally consolidated clayey silt is deposited between depths of five and 16 m and divided into two units, Unit II and Unit III, which are homogenous across the site.

The *in situ* testing programme (CPTUs and a borehole) was carried out in September 2021 and is summarized in Table 1 and Figure 3. The CPTUs were performed according to ISO (2012), except that non-standard penetration rates were also adopted. All tests were closely spaced but ensuring no interference with each other.

Efforts were made to ensure good saturation of the filters and cone chamber. At fast rate, the u_2 sensor must respond quickly and at slow rates, it shall ensure accurate measurements due to the small values of excess pore pressures measured. Plastic,

bronze and HPDE filters were used for the 5, 10 and 15 cm^2 cones, respectively. All filters and cones chambers were saturated with silicon oil. The filters were saturated under vacuum and placed in a container of saturation fluid before mobilization and until assembling with the cone. The cone chamber was first saturated with syringes and hereafter left submerged in a chamber with silicon oil along with the filters. Vacuum was also applied for up to 90 minutes for the 5 and 10 cm^2 cones. The penetrometer was assembled in submerged conditions and covered in a rubber membrane. The filters were replaced after each test.

Table 1. In situ testing scope, Halden campaign.

Item	Description
Cones	10 cm^2 single element (u_2) 15 cm^2 dual element (u_1 and u_2) 5 cm^2 single element (u_2)**
Scope per cone	1 CPTU benchmark*, 20 mm/s rate 1 VRCPTU, 0.2 mm/s rate, 2 PPDT 1 VRCPTU, 2.0 mm/s rate, 2 PPDT 1 VRCPTU, 200 mm/s rate, 2 PPDT

* 2 benchmark tests carried out for the 10 cm^2 cone

** Additional scope funded by the NGTS project

*** Dissipation tests (PPDT) as per Figure 3

Attention was also given to monitor the ground water table and thus the hydrostatic pressure (u_0 -profile), since u_0 enters the calculation of e.g. B_q and is the baseline for dissipation tests. The ground water pressure was continuously monitored at four depths by means of standpipes permanently installed at the site, indicating hydrostatic conditions with the water table at 1.85 m depth.

To investigate the drainage conditions around the cone through the normalized penetration velocity V , the chosen penetration rates cover four orders of magnitude (from 0.2 mm/s to 200 mm/s). The aim was to span from drained to undrained response during penetration. Furthermore, three cone sizes were used to investigate the effect of diameter. The u_1 sensor (located at the cone face) was used in addition to u_2 to study the differences in response during both variable rate penetration and during dissipation. The approach of having one long stroke at variable rate per soil unit at each location was preferred to the alternative twitch tests (see e.g. DeJong et al. 2013) because: (a) from VRCPTU tests performed earlier at Halden it was found that after changes in rate or dissipation tests, the length required to build up u_2 was in several cases up to 1.0 m and (b) shorter strokes can be affected by vertical variability and hence are thought to be less robust for future recommendations for offshore site investigations.

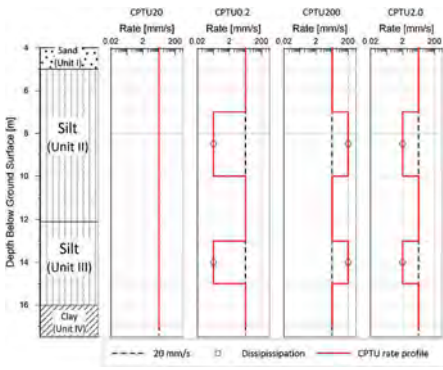


Figure 3. Specified penetration rate profiles for VRCPTUs.

4.2 Test results

Figure 4 shows selected results of standard rate CPTUs and VRCPTUs carried out with the 10 cm² and 15 cm² cones. The penetration rate profiles indicate that the rig accurately controls the speed in all tests.

At depths of 10-12/13m all CPTUs are performed at standard rate. There is generally a good match of q_t , f_s and u_2 between the location with the CPTU at standard rate and the VRCPTU locations for both cones (10 cm² and 15 cm²), respectively, indicating that (a) adjacent locations have similar soil conditions and hence the profiles at different rates and (b) the cones are performing consistently among different

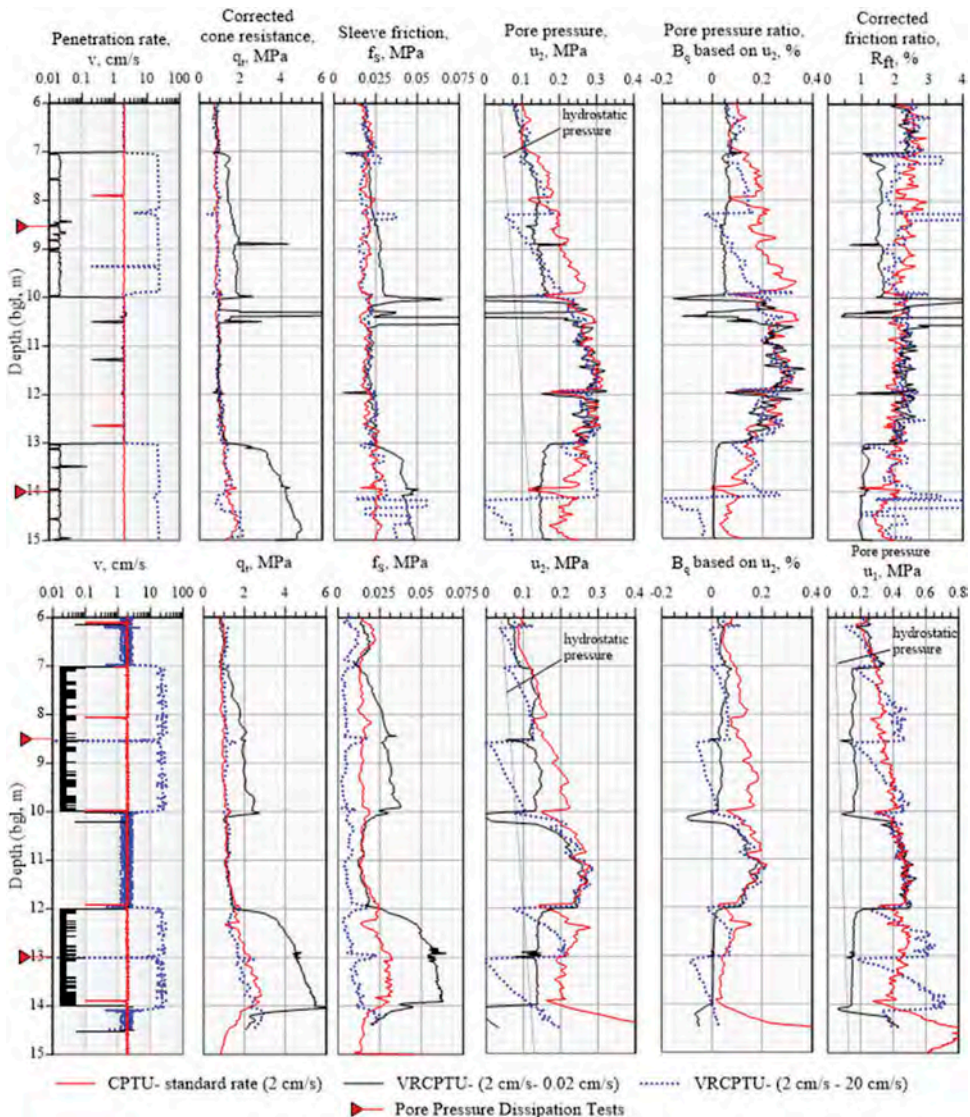


Figure 4. Selected in situ test results, CSi Halden campaign. 10 cm² cone (upper figures) and 15 cm² cone (lower figures).

locations. The long strokes (up to 1.5 m before any stop, cf. Figure 3) allow for a clear identification of the changes in q_t , f_s and u_2 for penetrations at 0.2 mm/s compared to the standard rate. These aspects provide robustness to the VRCPTU interpretation approach.

During penetration at 0.2 mm/s both cones show an increase in q_t and f_s and a reduction in u_2 compared to the tests with standard rate. For example, q_t increases on average from 1.0 MPa to 1.6 MPa and B_q decreases from 0.2 % to 0.05 % for the 10 cm² cone in Unit II. In Unit III, the impact of a slower rate appears more markedly with q_t increasing from 1.5 MPa to 4.2 MPa and B_q decreasing from 0.08% to zero. This may be due to the less plastic and coarser nature of the lower unit.

In contrast, the VRCPTUs at 200 mm/s do not appear to affect q_t or f_s compared to CPTUs at standard rate (though for the 15 cm² cone the entire f_s profile is shifted at the location). Generally, after a prolonged stop in penetration, either for dissipation testing or for change in rate, u_2 increases smoothly and linearly with depth often starting with an abrupt negative increment in the pore pressure. These results will be further scrutinized during the project.

The u_1 profile for the 15 cm² cone shows similar trends to the u_2 sensor for both the highest and lowest rates noting that (a) the drop in pore pressure during slow penetration is more distinct and (b) at high rates u_1 appears to exceed u_2 for the standard rate CPTU after typically 50-70 cm of penetration after having changed rate or after a dissipation test.

Figure 5 shows the results of a representative dissipation test performed with the 15 cm² cone. u_1 decays monotonically over time whereas u_2 exhibits a dilatary response. This response is similar to what has been reported for cases in overconsolidated clays (e.g. Lunne et al. 1997). The effect of this difference on the estimated coefficient of consolidation will be investigated.

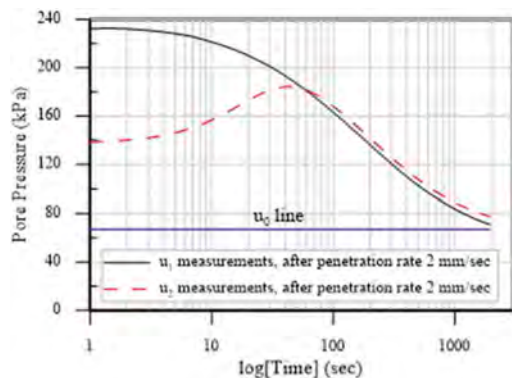


Figure 5. Dissipation test at 8.5 m depth, 15 cm² cone.

5 CONCLUSIONS

Even with the landmark research undertaken over the last decades on CPTUs in silty soils, more research is needed to establish robust guidelines for use in engineering practice. The objective of the Joint Industry Project CSi is to provide such guidelines. The background, objectives, setup, and approach of the CSi project are described in this paper along with some initial results from the Halden test site. Field testing at the Voorne-Putten test site as well as centrifuge and calibration chamber testing are currently being performed in parallel with laboratory testing and numerical modelling. More Partners and Contractors are invited to join the project for the opportunity of investigating more innovative equipment and methods, such as partially drained triaxial testing and selected CPTU add-on sensors. Furthermore, field trials for validating the project outcome are essential and will add to the robustness and broaden the applicability of the project.

ACKNOWLEDGEMENT

The CSi Project is managed through the Carbon Trust's joint industry Offshore Wind Accelerator (OWA) program. The Authors acknowledge the provision of financial and technical support by the following project partners: Ørsted (lead partner), Equinor, Vattenfall, Shell, RWE and Scottish Power Renewables.

REFERENCES

- Bihs, A. 2021. *Investigation of a coarse silt deposit by varied rate CPTU testing*. PhD dissertation, NTNU, Norway.
- Blaker, Ø. & DeGroot, D.J. 2020. Intact, disturbed and reconstituted undrained shear behavior of low-plasticity natural silt. *Journal of Geotechnical and Geoenvironmental Engineering* 146(8): 04020062.
- Blaker, Ø., Carroll, R., Paniagua, P., DeGroot, D. & L'Heureux J.-S. 2019. Halden research site: Geotechnical characterization of a post glacial silt. *AIMS Geosciences* 5(2): 184–234.
- Bradshaw, A.S., Morales-Velez, A.C. & Baxter, C.D.P. 2012. Evaluation of existing CPT correlations in silt. *Geotechnical Engineering Journal of the SEAGS & AGSSEA* 42(1).
- Burns, S.E. & Mayne, P.W. 1998. *Penetrometers for soil permeability and chemical detection*. Georgia Institute of Technology, Report No. GIT-CEEGEO-98-1.
- Carroll, R. & Paniagua, P. 2018. Variable rate of penetration and dissipation test results in a natural silty soil. In Pisano, Hicks & Peuchen (eds) *Cone Penetration Testing (CPT18)*: 205–212. CRC Press/Balkema - Taylor & Francis Group.
- DeJong, J.T. & Randolph, M.F. 2012. Influence of partial consolidation during cone penetration on estimated soil behavior type and pore pressure dissipation measurements. *Journal of Geotechnical and Geoenvironmental Eng.* 138(7): 777–788.

- DeJong, J.T., Jager, R.A., Boulanger, R.W., Randolph M.F. & Wahl, D.A.J. 2013. Variable penetration rate cone testing for characterization of intermediate soils. In Countinho & Mayne (eds) *Geotechnical and Geophysical Site Characterization ISC'4*. London: Taylor & Francis.
- Fioravante, V., Giretti, D., Augustesen, A.H., Lindeboom, R., Krogh, L., Dias, H.F., Sougle, M.C., Barwise, A., de Wit, S. & Burbury, D. 2022. Calibration cone penetration testing in silty soils. In *Cone Penetration Testing (CPT22)*.
- Huang, A-B., Augustesen, A.H., Leth, C.T., Molyneaux, E. D.G & Krogh, L. 2020. A field study in the effects of fines on the interpretation of CPTU. In *Geotechnical and Geophysical Site Characterization ISC'6*: 509–514.
- ISO 22476-1 2012. Geotechnical investigation and testing – Field testing – Part 1: Electrical cone and piezocone test.
- Kim, K., Prezzi, M., Salgado, R. & Lee, W. 2008. Effect of penetration rate on cone penetration resistance in saturated clayey soils. *Journal of Geotechnical and Geoenvironmental Engineering* 134(8): 1142–1153.
- Krage, C.P. & DeJong, J.T. 2016. Influence of drainage conditions during cone penetration on the estimation of engineering properties and liquefaction potential of silty and sandy soils. *Journal of Geotechnical and Geoenvironmental Engineering* 142(11): 4016059.
- Krage, C.P., Broussard, N.S. & DeJong, J.T. 2014. Estimating rigidity index (IR) based on CPT measurements. *3rd International Symposium on Cone Penetration Testing (CPT14)*: 727–735.
- Lunne T., Robertson P. & Powell J. 1997. *CPT in geotechnical practice*. New York: Blackie Academic.
- Naeini, S. & Moayed, R. 2007. Evaluation of undrained shear strength of loose silty sands using CPT results. *International Journal of Civil Engineering* 5(2): 104–117.
- Paniagua, P., Carroll, R., L'Heureux, J.S. & Nordal, S. 2016. Monotonic and dilatatory excess pore water dissipations in silt following CPTU at variable penetration rate. In Acosta-Martinez, Kelly & Lehane (eds), *Geotechnical and Geophysical Site Characterization ISC'5*: 509–514.
- Randolph, M.F. 2004. Characterisation of soft sediments for offshore applications. In *Geotechnical and Geophysical Site Characterization ISC'2*: 209–232 Millpress, Netherlands.
- Randolph, M.F. & Hope, S. 2004. Effect of cone velocity on cone resistance and excess pore pressures. In *IS Osaka-Engineering Practice Performance Soft Deposits*: 147–152.
- Robertson, P.K. 1990. Soil classification using the cone penetration test. *Canadian Geotechnical Journal* 27 (1):151–158.
- Robertson, P.K. 2009. Interpretation of cone penetration tests – a unified approach. *Canadian Geotechnical Journal* 46: 1337–1355.
- Schnaid, F.G., Dienstmann, E., Odebrecht & Maghous, S. 2020. A simplified approach to normalisation of piezocone penetration rate effects. *Geotechnique* 70(7): 630–635.
- Schneider, J.A., Lehane, B.M., & Schnaid, F. 2007. Velocity effects on piezocone tests in normally and over-consolidated clays. *Int. Journal of physical Modelling* 7 (2): 23–34.
- Schneider, J.A., Randolph, M.F., Mayne, P.W., & Ramsey, N.R. 2008. Analysis of factors influencing soil classification using normalized piezocone tip resistance and pore pressure parameters. *Journal of Geotechnical and Geoenvironmental Engineering* 134(11): 1569–1586.
- Senneset K., Sandven R., Lunne T., By T. & Amundsen T. 1988. Piezocone tests in silty soils. In De Ruiter (ed.), *ISOPT-1, Orlando, FL*: 955–966. Rotterdam: Balkema.
- Tonni, L. & Simonini, P. 2013. Shear wave velocity as function of cone penetration test measurements in sand and silt mixtures. *Engineering Geology* 163: 55–67.

Numerical investigation of piezocone dissipation tests in clay: Sensitivity of interpreted coefficient of consolidation to rigidity index selection

A. Barati Nia, D.M. Moug & A.P. Huffman

Department of Civil and Environmental Engineering, Portland State University, Portland, USA

J.T. DeJong

Department of Civil and Environmental Engineering, University of California, Davis, USA

ABSTRACT: Standard methods for interpreting the coefficient of consolidation (c_h) from CPTu dissipation tests require an estimation of the soil's rigidity index ($I_r=G/s_u$). For the Teh & Houlsby numerically derived dissipation solution, the values of shear modulus (G) and undrained shear strength (s_u) were straight forward to specify due to the use of the elastic-perfectly plastic Von-Mises soil constitutive model. However, estimation of appropriate G and s_u values is not as straight forward for field dissipation tests. The objective of this study is to examine the sensitivity of the interpreted c_h to various approaches for estimating I_r . The study is performed with an axisymmetric direct cone penetration model to simulate piezocone dissipation. Simulations are performed with the MIT-S1 constitutive model calibrated for Boston blue clay behavior. Analyses examine how the sensitivity changes for normally to lightly overconsolidated clay, and slightly to strongly anisotropic hydraulic conductivities. The results indicate that c_h interpretation is not highly sensitive to I_r estimation when I_r is within standard values for clay; however, the sensitivity appears to increase as the overconsolidation ratio increases.

1 INTRODUCTION

The piezocone (CPTu) dissipation test is often used as an in situ method to estimate the coefficient of consolidation in the horizontal direction (c_h) and hydraulic conductivity of fine-grained soils. The CPTu dissipation test records excess pore water pressure (Δu) at the cone shoulder (u_2 position) as porewater pressure returns to the hydrostatic condition during a pause in penetration. The dissipation response is primarily controlled by the initial distribution of Δu around the cone and c_h , among other factors.

Various researchers have proposed methods for estimating c_h ; however, the Teh and Houlsby (1991) method remains widely used:

$$c_h = \frac{T^* r^2 \sqrt{I_r}}{t} \quad (1)$$

where T^* is a modified time factor; r is the radius of the piezocone; I_r is the soil rigidity index; and t is the time to a degree of dissipation corresponding to T^* .

The Teh & Houlsby (1991) method was developed with the strain path method and Von-Mises soil model to estimate the initial Δu distribution, then Δu dissipation was modeled with Terzaghi consolidation theory. This method for interpreting c_h uses the square root of

I_r that was empirically determined to closely agree with the model data. The time to reach 50% dissipation at the u_2 position (t_{50}) is often used because it provides sufficient dissipation data without requiring large dissipation times in the field. An example estimation of t_{50} from a CPTu u_2 dissipation curve is shown in Figure 1. For t_{50} , T^* is equal to 0.245.

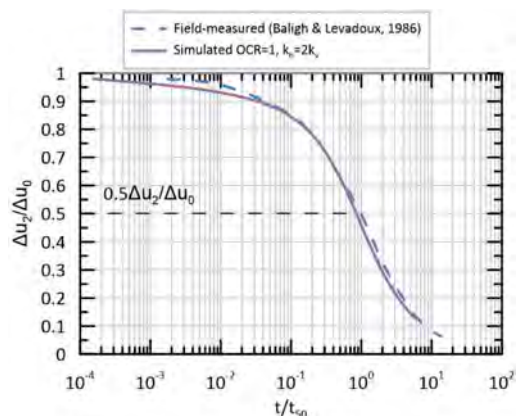


Figure 1. Comparison of a normalized field-measured u_2 dissipation curve in BBC and a simulated curve with MIT-S1 calibrated for BBC.

In addition to Teh & Hously (1991), other methods to interpret c_h from dissipation tests require an I_r value (e.g., Burns & Mayne, 1998, Chai et al., 2012). I_r is the ratio of shear modulus (G) to the undrained shear strength (s_u). Therefore, a single I_r value represents average G and s_u values for the complex loading, strain, and porewater conditions around the penetrating cone. For the Teh and Hously (1991) numerically derived dissipation solution, the values of G and s_u were straightforward to specify due to the use of the elastic-perfectly plastic Von Mises soil constitutive model. However, natural soil behaviors include strain softening, non-linear behavior, and anisotropic strengths. As a result, the selection of appropriate G and s_u values is not straightforward.

There are three standard approaches for estimating I_r : laboratories tests, CPT-based, and empirical relationships. Although laboratory shear testing on intact soil specimens is a direct method to estimate I_r , this approach typically requires the most effort and expense compared to CPT-based and empirical estimates. Accordingly, empirical methods or CPT-based approaches are frequently used to estimate I_r values. Given the various approaches, there remains uncertainty regarding how sensitive interpreted c_h values are to the estimated I_r .

For this study, different methods for estimating I_r will be presented and used to estimate I_r values for Boston blue clay (BBC). The various I_r values will be used to interpret c_h from simulated dissipation tests in normally and lightly overconsolidated BBC and for slightly anisotropic and strongly anisotropic hydraulic conductivities. The interpreted c_h values from the simulations will be compared to the c_h values estimated from assigned model properties.

2 SIMULATED PIEZOCONE DISSIPATION IN BOSTON BLUE CLAY

CPTu dissipation was simulated with the finite difference program FLAC (Itasca, 2019) and the MIT-S1 constitutive model (Pestana & Whittle, 1999). MIT-S1 is a bounding surface plasticity model that can capture the anisotropic undrained strength behavior of clays, which is advantageous for direct cone penetration simulations (Moug et al. 2019). To capture CPTu dissipation, first, undrained steady state penetration was simulated with MIT-S1 calibrated for BBC behavior. The penetration model is a direct axisymmetric model that uses an Arbitrary Lagrangian Eulerian rezoning and remapping algorithm to accommodate large deformations around the penetrating cone. A description of the model and implementation with the MIT-S1 model, including validation for undrained penetration in BBC, is published in Moug et al. (2019). After reaching steady-state stress and porewater pressure conditions, at approximately 25 cone diameters of simulated penetration, penetration is paused and brought to static conditions. Then, Δu

dissipation is simulated to capture the full response around the cone during a CPTu dissipation test.

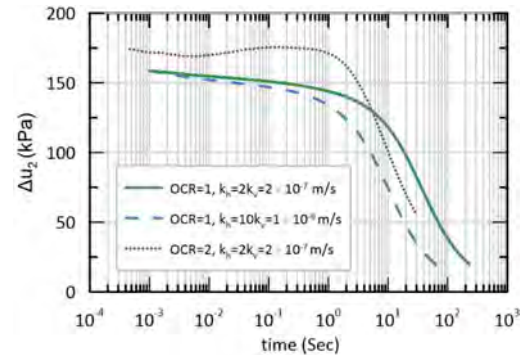


Figure 2. Simulated u_2 dissipation for OCR = 1 with $k_h/k_v = 2$ and 10, and OCR = 2 BBC with $k_h/k_v = 2$.

Simulated u_2 dissipation for normally consolidated BBC is presented in Figure 1 and Figure 2. The initial conditions are vertical effective stress (σ'_{vo}) of 100 kPa, horizontal effective stress of 50 kPa, and hydrostatic porewater pressure of 100 kPa. A summary of these initial conditions and simulation results for undrained penetration are presented in Table 1. The horizontal hydraulic conductivity (k_h) for dissipation is 2×10^{-7} m/s, and is two times larger than the vertical hydraulic conductivity (k_v). Although these values of k_h and k_v are at least an order of magnitude higher than typical values for clayey soils (Kulhawey & Mayne, 1990), the objectives of this study are not compromised since dissipation is simulated from undrained conditions. In Figure 1, the u_2 dissipation curve is normalized by the initial Δu and t_{50} to compare it to a field-measured dissipation test in BBC (Baligh & Levandoux, 1986). The normalized simulated dissipation results in OCR=1 of BBC agree well with the field-measured results.

Table 1. Initial conditions and results for simulated undrained cone penetration in BBC with OCR=1.

	Value
<i>Initial conditions</i>	
Pore pressure, u_0	100 kPa
Vertical effective stress, σ'_{vo}	100 kPa
Horizontal effective stress, σ'_{ho}	50 kPa
<i>Simulated penetration results</i>	
Cone tip resistance, q_t	355 kPa
Pore pressure at the cone shoulder, u_2	259 kPa

3 RIGIDITY INDEX ESTIMATION METHODS

Estimation of c_h relies on estimated I_r values. Because I_r values for natural clay deposits may vary between

50 to 600, the c_h estimation can be different by a factor of up to 4 for a given clay (Schnaid et al., 1997). This variability of I_r may reflect changes due to OCR and PI; however, there may also be differences in I_r values depending on the method used to estimate the value. In the following subsections, different approaches for estimating I_r are briefly introduced and used to obtain I_r values for OCR = 1 BBC.

3.1 Laboratory test approaches

Laboratory testing of intact soil samples is a direct method for estimating I_r . However, uncertainties remain for estimating I_r from laboratory shear tests. s_u depends on initial stress state, loading conditions, loading rate, stress history, degree of fissuring, boundary conditions, etc. For example, one clay tested with isotropically consolidated undrained triaxial compression (CIUC) and anisotropically consolidated undrained triaxial compression (CAUC) will likely yield different s_u between the two tests, reflecting the different initial consolidation conditions. I_r interpreted from CAUC tests was used for several research studies that examined dissipation test interpretation (Krage et al., 2014; Schnaid et al. 1997); however, in practice, CIUC is a more common and simple to perform a test.

I_r values also depend on G estimation. The secant shear modulus at 50% of the yield stress (G_{50}) and 25% of the yield stress (G_{25}) were investigated by Schnaid et al. (1997) for dissipation test interpretation. G_{50} was considered by Schnaid et al. (1997) to reasonably represent the stress and strain levels in the vicinity of the cone.

For estimation of I_r in this study, CIUC and CAUC tests were simulated with single element models in FLAC and the MIT-S1 model calibrated for BBC. The simulated CIUC and CAUC results for deviatoric stress (q) versus deviatoric strain (ϵ_q) are shown in Figure 3. The values of I_r from the stress-strain paths in Figure 3 are summarized in Table 2. The G values for estimating I_r from CIUC and CAUC single element simulations were calculated at

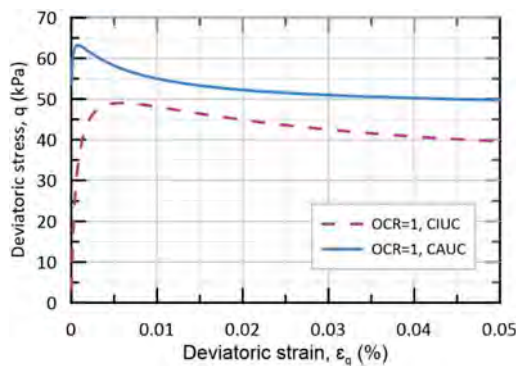


Figure 3. Single element CIUC & CAUC simulations for OCR=1 BBC.

50% of the strain level required to reach the yield stress. Past researchers estimated G at 50% of the yield stress (Keaveny & Mitchell, 1986; Schnaid et al., 1997); however, this approach was overly stiff for the simulated results. This likely reflects sample disturbance effects from obtaining and preparing the sample that are not captured in the simulated response. An examination of published CIUC and CAUC tests for BBC (Landon, 2007) indicated there was about a 35% difference between I_r values estimated with 50% of strain and 50% of stress to yield stress. Consequently, 50% of the strain level to yield stress was considered for G_{50} to calculate I_r values from CIUC and CAUC.

3.2 CPT-based approaches

Several methods have been proposed to estimate I_r values from CPTu test data. These approaches have the advantage that the required data to estimate I_r are collected during the process of performing CPTu dissipation test.

Krage et al. (2014) analyzed a database of CAUC test results with corresponding CPTu data to develop two approaches to estimate I_r . The two approaches are called “method A” (I_{rA}) and “method B” (I_{rB}). Both methods use a functional reduction of G_{max} to approximate G_{50} , where $G_{50}/G_{max} = 0.26$ and G_{max} is estimated from V_s measurements obtained from the seismic CPT profile. Method A estimates s_u from laboratory testing. Consequently:

$$I_{rA} = 0.26 \times \frac{G_{max}}{s_u} \quad (2)$$

Since this relationship was developed with CAUC laboratory test results, the simulated CAUC s_u value was used to estimate I_{rA} for this study.

Method B from Krage et al. (2014) generalizes Method A with a CPT-based approximation of s_u . The estimation of s_u is based on relationships between q_t and OCR (i.e., Chen & Mayne, 1994) and SHANSEP principles of s_u normalization by σ'_{vo} and OCR. The estimation of I_{rB} is:

$$I_{rB} = 0.26 \left(\frac{G_{max}}{\sigma'_{vo}} \right) \left(\frac{1}{0.33 \times \left[\frac{0.33(q_t - \sigma_{vo})}{\sigma'_{vo}} \right]^{0.75}} \right) \quad (3)$$

Using the simulated q_t value from penetration in normally consolidated BBC resulted in OCR < 1. Therefore, the estimation of I_{rB} used OCR = 1 as opposed to the q_t -estimated OCR in the denominator of Equation 3. G_{max} was approximated from MIT-S1 stiffness parameters, which were selected in Moug et al. (2019) to be consistent with shear wave velocity data in BBC (Landon 2007).

Mayne (2001) developed a theory-based estimation of I_r with spherical cavity expansion and critical state soil mechanics (SCE-CSSM):

$$I_r = \exp\left(\frac{q_t - \sigma_{v0}}{q_t - u_2}\right) \times \left(\frac{1.5}{M} + 2.925\right) - 2.925 \quad (4)$$

in which $M = (6\sin\phi')/(3-\sin\phi')$ and ϕ' is the effective friction angle. M was determined from the critical state ϕ' for the MIT-S1 calibration for BBC (Pestana et al., 2002), which resulted in an M value of 1.35.

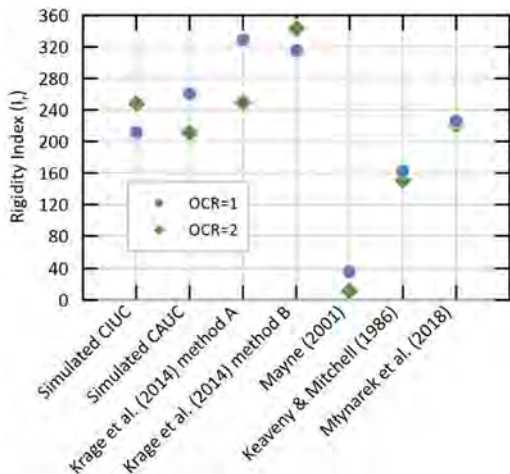


Figure 4. Comparison of I_r values estimated with different methods for OCR=1 and OCR = 2 BBC.

The Mayne (2001) approximation of I_r resulted in a low value of 36. However, it should be noted that this estimate of I_r is relatively sensitive to changes in q_t and u_2 . For example, a 10% increase in q_t results in an I_r value that is four times larger, or a 10% increase in u_2 results in an I_r value that is over 10 times larger than the original estimate.

3.3 Empirical relationships

Empirical relationships are used to estimate I_r from soil index properties and/or OCR. Keaveny & Mitchell (1986) observed that for ordinary clays, I_r increases by decreasing OCR and decreasing plasticity index (PI). Mayne (2001) provided an equation-based estimate of the Keaveny & Mitchell (1986) relationships with:

$$I_r = \frac{\exp\left(\frac{137-PI}{23}\right)}{1 + \ln\left(1 + \frac{(OCR-1)^{3.2}}{26}\right)^{0.8}} \quad (5)$$

The average PI of BBC was reported in Landon (2007) as 20. Therefore, for OCR = 1 BBC, $I_r = 162$ by the Keaveny & Mitchell (1986) estimation.

Młynarek et al. (2018) performed multivariate regression analysis to investigate relationships between I_r and PI, OCR, and liquidity index (LI) for different soil groups such as overconsolidated & aged clay, organic & young clay, aged till and young till. Although the analysis was performed with regionally-limited soils and one of the authors' conclusions was that I_r values and relationships should be regionally developed, the relationship for organic and young clays is included herein for comparison:

$$I_r = 4.73PI - 4.78OCR - 14.04LI + 151.74 \quad (6)$$

For OCR = 1 BBC, a LI of 1.14 was used based on data in Landon (2007), resulting in $I_r = 226$.

3.4 Summary of estimated I_r

A summary of the estimated I_r values for OCR = 1 BBC is provided in Table 2 and Figure 4. Generally, the values are consistent with typical I_r for OCR = 1 clay. The values estimated from single element simulations of CIUC and CAUC tests do not show a large difference: 212 and 261 for CIUC and CAUC, respectively. The I_r values estimated with Krager et al. (2014) methods are comparable between themselves but are larger than the laboratory-estimated values, with $I_{rA} = 329$ and $I_{rB} = 315$. As discussed above, the I_r value estimated with Mayne (2001) results in a notably lower value than the other estimation methods but is sensitive to small changes in q_t or u_2 . I_r estimated with empirical methods yielded values of 162 and 226 for Keaveny & Mitchell (1986) and Młynarek et al. (2018), respectively. These estimates are consistent with typical values for clay; the Keaveny & Mitchell (1986) relationship estimates an I_r value lower than the laboratory-based estimates, while Młynarek et al. (2018) is consistent with the laboratory-based estimates.

Table 2. I_r values for OCR=1 BBC estimated with various methods.

Method	I_r
Simulated CIUC	212
Simulated CAUC	261
Krager et al. (2014) method A	329
Krager et al. (2014) method B	315
Mayne (2001)	36
Keaveny & Mitchell (1986)	162
Młynarek et al (2018)	226

4 INTERPRETED c_h SENSITIVITY TO I_r

c_h values from a simulated CPTu u_2 dissipation test in OCR = 1 BBC are estimated using the various I_r values presented in the previous section and with Equation 1. The dissipation test was performed for BBC with a $k_h/k_v = 2$, representing slightly anisotropic hydraulic conductivity conditions. The simulated u_2 dissipation curve is shown in Figure 2, which has a t_{50} of 32 seconds. The c_h values interpreted from simulated u_2 dissipation ($c_{h,interpreted}$) are compared to c_h values assigned to the cone penetration model ($c_{h,model}$). This comparison is shown in Figure 5.

The range of $c_{h,interpreted}/c_{h,model}$ in Figure 5 is between 0.56 and 1.69 for the various I_r estimation methods. Generally, the sensitivity of $c_{h,interpreted}/c_{h,model}$ to the estimated I_r is low since $c_{h,interpreted}$ is proportional to $\sqrt{I_r}$ in the Teh & Houlsby (1991) relationship. It should be noted that estimating I_r with CIUC or CAUC does not significantly impact $c_{h,interpreted}$ indicating that there may not be a strong advantage of one test condition over the other for this application. Additionally, across the various I_r values, the variability of $c_{h,interpreted}$ appears to be within a typical range due to the variability of soil properties, estimation of t_{50} , and methods for interpreting c_h (e.g., Huffman & Moug, 2022).

5 THE EFFECT OF PERMEABILITY ANISOTROPY AND OCR ON c_h ESTIMATION

The sensitivity of c_h to I_r is further explored by examining dissipation in lightly overconsolidated and highly anisotropic BBC. To this end, u_2 dissipation tests were also performed for OCR = 1 with $k_h/k_v = 10$; and OCR = 2 with $k_h/k_v = 2$. These u_2 dissipation curves are shown in Figure 2. These simulated results show that although the k_h for both OCR = 1 and OCR = 2 models is the same, t_{50} decreases as OCR increases from OCR = 1 to OCR = 2. This may be attributed to a smaller Δu distribution around the penetrating cone as OCR increases and increasing soil stiffness as OCR increases and, therefore, less porewater pressure migration to dissipate the Δu field.

Estimated I_r values for OCR = 2 BBC are compared to those estimated in the previous section for OCR = 1 in Figure 4. Although the differences in I_r among different approaches are still considerable, the differences between OCR = 1 and OCR = 2 for every method are relatively small.

The comparison between $c_{h,interpreted}$ with the various I_r values and $c_{h,model}$ is shown in Figure 5. Comparing the ratio of $c_{h,interpreted}$ to $c_{h,model}$ for OCR = 1 with different hydraulic conductivity anisotropy, the differences between $k_h/k_v = 2$ and 10 across the various I_r estimation methods are similar. The ratio of $c_{h,interpreted}$ to $c_{h,model}$ for $k_h/k_v = 10$ ranged from 0.48 to 1.46. This indicates that c_h estimation using various I_r estimation methods is not strongly affected by hydraulic conductivity anisotropy.

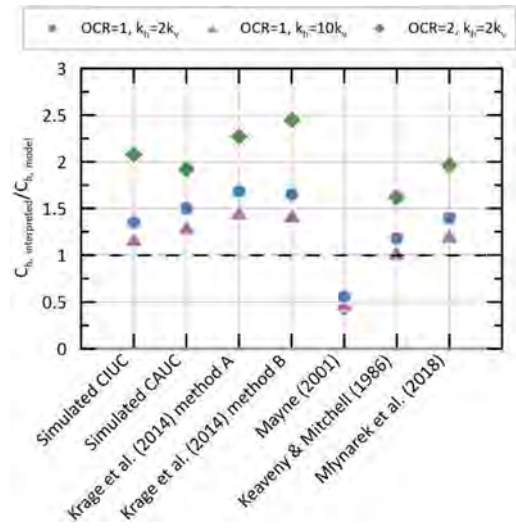


Figure 5. Comparison of c_h estimated from simulated results and different I_r with c_h assigned to the dissipation models for OCR = 1, OCR = 2, and $k_h/k_v = 2$ and 10 BBC.

Comparing $c_{h,interpreted}$ to $c_{h,model}$ for OCR = 1 and OCR = 2, indicates that as OCR increases, the sensitivity of $c_{h,interpreted}$ to estimated I_r increases. The ratios of $c_{h,interpreted}$ and $c_{h,model}$ for OCR = 2 are in some cases twice as large as the ratio for OCR = 1 with the same hydraulic conditions, with the exception of $c_{h,interpreted}$ using the I_r values from Mayne (2001). For OCR = 2 the ratio of $c_{h,interpreted}$ to $c_{h,model}$ ranged from 0.44 to 2.45.

6 CONCLUSIONS

This study examined the sensitivity of CPTu dissipation test interpretation to estimated I_r values. For a given soil, there are various approaches to estimate I_r . Simulated CPTu dissipation tests in BBC were used to examine how the interpreted c_h from CPTu dissipation tests changes with different methods to estimate I_r . c_h was interpreted from simulated u_2 dissipation following undrained cone penetration using the Teh & Houlsby (1991) method, which requires an estimation of I_r . I_r was estimated with several approaches that represent laboratory test-based, CPT-based, and empirical-based approaches. The sensitivity of c_h to various I_r estimations was evaluated for BBC with OCR = 1 with slightly anisotropic hydraulic conductivity, OCR = 1 with strongly anisotropic hydraulic conductivity, and OCR = 2 with slightly anisotropic hydraulic conductivity. Ultimately, interpreted c_h was compared with the modeled c_h to assess the variability of estimated c_h over a range of reasonable I_r values. Although this study was performed for a single soil, it does provide some

insight into the role of I_r estimation on CPTu dissipation test interpretation. The results support the following conclusions:

1. Due to a square root of I_r in the Teh & Houlsby (1991) method (Equation 1), the sensitivity of c_h to I_r is relatively low. For OCR = 1 BBC, the range of I_r estimates was large: between 36 and 329. However, the $c_{h,interpreted}$ values ranged from 0.56 to 1.69 times the $c_{h,model}$ with slightly anisotropic hydraulic conductivity. When the hydraulic conductivity was strongly anisotropic, the $c_{h,interpreted}$ values ranged from 0.48 to 1.46 times $c_{h,model}$. However, it should be noted that c_h interpretation methods may also contribute to discrepancies between $c_{h,interpreted}$ and $c_{h,model}$, in addition to the estimated I_r value.
2. Increasing the OCR from 1 to 2 appeared to result in $c_{h,interpreted}$ values that were increasingly sensitive to the estimated I_r values. Estimated I_r values for OCR = 2 ranged from 11 to 343, and $c_{h,interpreted}$ values were between 0.44 and 2.45 times larger than $c_{h,model}$. The larger discrepancy between $c_{h,interpreted}$ and $c_{h,model}$ for OCR = 2 compared to OCR = 1 may be due to a smaller Δu distribution around the penetrating cone and increased soil stiffness, resulting in faster dissipation and a smaller t_{50} . The smaller t_{50} leads to more sensitivity to I_r even though the range of estimated I_r values was smaller.
3. Minor differences were observed between estimated c_h values using the I_r values from CIUC and CAUC testing in OCR = 1 and OCR = 2 BBC. Because CIUC is considered a more simple test to perform, with further investigation, it may be considered reasonable to estimate I_r values for CPTu dissipation test interpretation.

ACKNOWLEDGEMENTS

Funding for this research was provided by the National Science Foundation (award CMMI-1927557). Any opinions, findings, conclusions, or recommendations expressed in this material are those of the authors and do not necessarily reflect the views of the NSF.

REFERENCES

- Agaiby, S. S., & Mayne, P. W. (2018). Evaluating undrained rigidity index of clays from piezocone data. *Cone Penetration Testing 2018 - Proceedings of the 4th International Symposium on Cone Penetration Testing, CPT 2018, 1985*, 65–71.
- Baligh, M. M., & Levandoux, J.-N. (1986). Consolidation after undrained piezocone penetration. II: Interpretation. *Journal of Geotechnical Engineering*, *112*(7), 727–745. [https://dx.doi.org/10.1061/\(ASCE\)0733-9410\(1986\)112:7\(727\)](https://dx.doi.org/10.1061/(ASCE)0733-9410(1986)112:7(727))
- Burns, S. E., & Mayne, P. W. (1998). Monotonic and dilatatory pore-pressure decay during piezocone tests in clay. *Canadian Geotechnical Journal*, *35*(6), 1063–1073. <https://dx.doi.org/10.1139/cgj-35-6-1063>
- Chai, J., Sheng, D., Carter, J. P., & Zhu, H. (2012). Coefficient of consolidation from non-standard piezocone dissipation curves. *Computers and Geotechnics*, *41*, 13–22. <https://dx.doi.org/10.1016/j.compgeo.2011.11.005>
- Chen, B., & Mayne, P. (1994). Profiling the overconsolidation ratio of clays by piezocone tests. In *Rep. No. GIT-CEGEO-94* (p. 294). <https://scholar.google.com/scholar?hl=en&btnG=Search&q=intitle:Profiling+the+Overconsolidation+Ratio+of+Clays+by+Piezocone+Tests#0>
- Huffinan, A. P. E., & Moug, D. M. (2022). Interpretation of Field-Measured and Simulated Non-Monotonic CPTu Dissipation Tests. *For Proceedings of the 2022 ASCE GeoCongress*.
- Itasca. (2019). *Fast Lagrangian Analysis of Continua* (8.1). Itasca Consulting Group, Inc.
- Keaveny, J. M., & Mitchell, K. (1986). Strength of fine-grained soils using the piezocone. In S. P. Clemence (Ed.), *Use of In situ tests in geotechnical engineering* (pp. 668–685). ASCE.
- Krage, C. P., Broussard, N. S., & Dejong, J. T. (2014). Estimating rigidity index (I_r) based on CPT measurements. *3rd International Symposium on Cone Penetration Testing (CPT14), Teh 1987*, 727–735.
- Kulhawy, F. H., & Mayne, P. W. (1990). Manual on Estimating Soil Properties for Foundation Design. In *Ostigov* (p. 299). https://www.osti.gov/energycitations/product.biblio.jsp?osti_id=6653074
- Landon, M. M. (2007). *Development of a non-destructive sample quality assessment method for soft clays*. University of Massachusetts Amherst.
- Mayne, P. W. (2001). Stress-strain-strength-flow parameters from enhanced in-situ tests. *International Conference on In-Situ Measurement of Soil Properties & Case Histories*, 27–48.
- Młynarek, Z., Wierzbicki, J., & Stefaniak, K. (2018). Rigidity index (I_r) of soils of various origin from CPTu and SDMT tests. *Cone Penetration Testing 2018 - Proceedings of the 4th International Symposium on Cone Penetration Testing, CPT 2018*, 441–446.
- Moug, D. M., Boulanger, R. W., DeJong, J. T., & Jaeger, R. A. (2019). Axisymmetric Simulations of Cone Penetration in Saturated Clay. *Journal of Geotechnical and Geoenvironmental Engineering*, *145*(4), 04019008. [https://dx.doi.org/10.1061/\(asce\)gt.1943-5606.0002024](https://dx.doi.org/10.1061/(asce)gt.1943-5606.0002024)
- Pestana, J. M., & Whittle, A. J. (1999). Formulation of a unified constitutive model for clays and sands. *International Journal for Numerical and Analytical Methods in Geomechanics*, *23*(12), 1215–1243. [https://dx.doi.org/10.1002/\(SICI\)1096-9853\(199910\)23:12<1215::AID-NAG29>3.0.CO;2-F](https://dx.doi.org/10.1002/(SICI)1096-9853(199910)23:12<1215::AID-NAG29>3.0.CO;2-F)
- Pestana, J. M., Whittle, A. J., & Gens, A. (2002). Evaluation of a constitutive model for clays and sands: Part II - Clay behaviour. *International Journal for Numerical and Analytical Methods in Geomechanics*, *26*(11), 1123–1146. <https://dx.doi.org/10.1002/nag.238>
- Schnaid, F., Sills, G. C., Soares, J. M., & Nyirenda, Z. (1997). Predictions of the coefficient of consolidation from piezocone tests. *Canadian Geotechnical Journal*, *34*(2), 315–327. <http://dx.doi.org/10.1139/t96-112>
- Teh, C. I., & Houlsby, G. T. (1991). An analytical study of the cone penetration test in clay. *Geotechnique*, *41*(1), 17–37. <https://dx.doi.org/10.1680/geot.1991.41.1.17>

Correlation of CPT measurements and VibroCore penetration speed for medium, calcareous sands: A case study of the cable route survey at the North Sea

K. Bartczak & G. De Vries

Marine Sampling Holland B.V., The Netherlands

ABSTRACT: The Cone Penetration Test (CPT) is one of the most popular in-situ testing methods used in qualitative and quantitative research of characteristics of the subsurface sediments, both onshore and offshore. In offshore cable route surveys, CPT tests are often accompanied by VibroCoring (VC) boreholes. The article endeavours to verify whether there is a clear correlation between the relative density of cohesion-less soils and the VC penetration characteristics. The research has been based on an offshore site investigation campaign in the North Sea consisting of over 100 CPTs and VCs, supplemented by an extensive laboratory testing program. After a strict selection of locations, around one-fifth of those tests have been utilised in the correlation studies. The ultimate goal of this study was to demonstrate if processing data recorded during VC testing can increase certainty in the prediction of soil's strength parameters.

1 INTRODUCTION

VibroCoring is a technique of extracting a sediment core from the seabed, in which a steel tube with an inner plastic liner is vibrated into the seabed by the action of two counter-rotating eccentric weights driven by an electric- or hydraulic motor. To collect the fieldwork data used in this paper, a slightly modified VibroCorer Viking VKG-6 was used. The corer is characterized by 30 kN of vibrating force, vibrating frequency of 28 Hz, the inside diameter of the core barrel of 96 mm and its net length of 6.0 m. The penetration is measured employing sensors and magnets placed each 5.0 centimetres along the barrel. The data is logged with a frequency of 10 Hz. In common practice, a live view of the current penetration is used to determine if the penetration is properly succeeding and whether it should be already terminated.

This paper poses the question whether records of this data can add value to the data obtained from processing the cores and possibly other tests, such as CPTs, performed at the site. A database of over 100 CPTs and VCs, which were a part of the cable route survey in the North Sea, was utilised in this research. From all the tests, a lot of 33 locations characterised by homogeneous stratigraphy was selected for the studies. The soil profile mainly consisted of calcareous, medium sands in the medium-dense to very dense states. In two groups, there was an underlying clay layer starting at around 4.0 to 4.5 m deep. Field testing of each location comprised of both VC and CPT tests. Correlation of CPT results and relative density was

possible on the grounds of the laboratory testing program, which comprised both standard index tests and advanced testing.

2 EVALUATION OF RELATIVE DENSITY

2.1 Introduction

The chosen 33 locations create a triangle-shaped area around 7×10 km big. Elevation of around one-third of those was between –10 to –20 metres Lowest Astronomical Tide (LAT), while for the other two-thirds, the range was between –25 to –35 metres LAT. The usage of tests with highly varying elevations might be problematic when analysing and correlating the VC and CPT data. As each test starts at a slightly different elevation, using many tests is marked with noise and peaks in data, which affect the latter interpretation. Therefore, the analysis on CPT and VC data sets was made only as a function of depth. To simplify the analysis, the 33 picked locations were divided into seven groups in a manner to obtain the most uniform soil profile in each group.

2.2 Laboratory testing data

The determination of a lab-based Relative Density (RD) profile was made on a selection of lab testing results consisting of 22 minimum and maximum density tests and 161 dry density tests. The resulting mean (and standard deviation) of RD value was

equal to 69% (32%) for all 150 tests, while for the selected locations 73% (33%). The evaluated RD profile is shown in Figure 1 below.

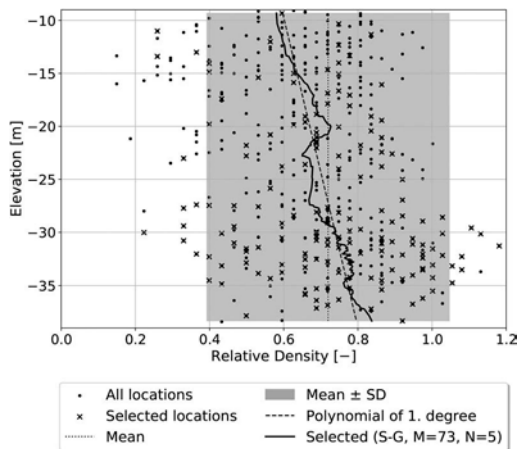


Figure 1. Lab-based relative density in a function of elevation.

For plotting the depth-trend (solid line), the Python implementation (SciPy) of Savitzky-Golay (S-G) Filter (Savitzky & Golay 1964) has been used. For smoothing the VC data presented in the latter part of this paper, a polynomial interpolation algorithm had to be found. The S-G filter has been chosen as the best solution, and the same algorithm was proposed for the lab-based RD to avoid extra noise in further analysis. The window length (M), and the polynomial degree (N), were chosen via an iterative process of minimization values of the cost function, i.e. Mean Square Error (MSE) between the lab data points and smoothed values.

2.3 CPT data

In Figure 2, an average value of CPT-tip resistance is plotted for each of the seven groups. Several correlations for CPT-based RD have been tested to find the best fit with laboratory-based values. The one that provided the best fit was the one proposed for Ticino, Toyoura, Hokkusund Sand (Jamiolkowski, Lo Presti, & Manassero 2003) presented in Equation 1 below.

$$RD(\%) = \frac{100}{C_2} \ln\left(\frac{q_c}{C_0(\sigma'_{vc})^{C_1}}\right), \quad (1)$$

where: $C_0 = 0.175$; $C_1 = 0.500$ and $C_2 = 3.1$.

The fit between the correlation mentioned above and the laboratory-based data (visibly rougher curves) for two selected (and the biggest) groups is shown in Figure 3.

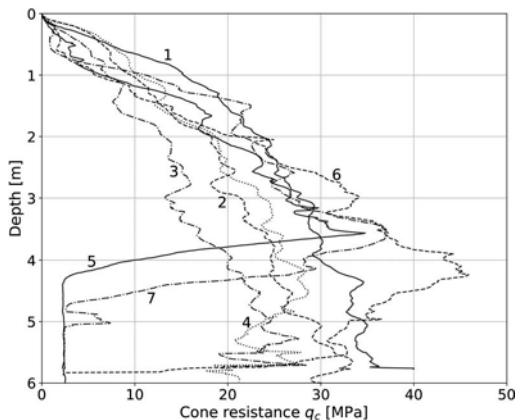


Figure 2. CPT Cone resistance in Depth.

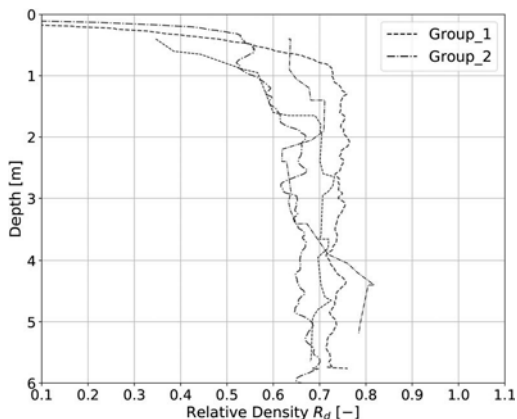


Figure 3. CPT- and LAB-based RD in-depth for two selected groups.

3 VIBROCORE DATA INTERPRETATION

3.1 Data clearing

In these specific soil conditions, the core barrel's full penetration was reached after around 2 minutes of vibrations. The penetration data recording frequency was 10Hz, which gives over 1200 readings per 500 centimetres of penetration on average. As the resolution of depth measurement is 1.67 cm, this means that each centimetre of penetration has been logged 4 times, which results in high accuracy, but also a very high level of noise (penetration readings tend to "jump" up and down by over a dozen of centimetres). Other aspects that induced the need for rigorous data clearing include turning the vibrating motor off and on again in case of an obstacle or penetration hindrance and the free-fall penetration of the barrel when it touches the seabed.

Therefore, VC data had to be cleared from the top 20 centimetres of data classified as unreliable and then filtered according to the steps shown below. The clearing steps explained below correspond to the numbers of VC lines in Figure 4.

1. If the consecutive penetration reading is smaller than the previous one - the previous value is kept and the smaller one ignored. This prevents from appearing of any negative penetration speed values;
2. Exponential Smoothing (Statsmodels.org, Hyndman2018) of penetration readings with dumping factor $\alpha = 0.15$;
3. Applying the Savitzky-Golay Filter (SciPy) with $N = 7$ and M of 53 for VC penetration speed, S_P , above 0.075 m/s and 203 for penetration speed below 0.075 m/s along at least 50 consecutive readings.

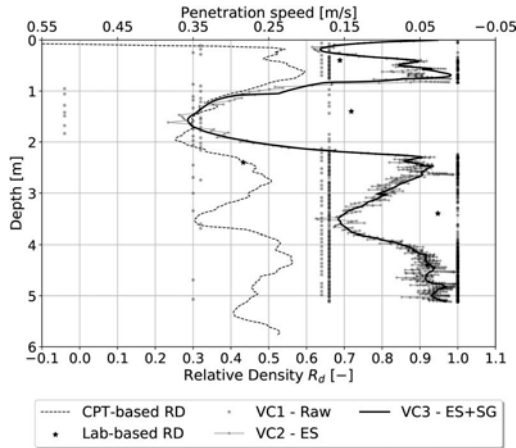


Figure 4. CPT- and LAB-based RD and VC penetration speed in depth - chosen test from Group 3.

The reason for choosing the S-G filter was a trial-and-error process of testing several algorithms with decision criteria including lack of distortion of readings in-depth tendency, and correct depiction of average value at each depth with no severe over or underestimation. In addition, the S-G filter has two convolution coefficients, which iterative customisation allows reducing the MSE between the original data-set and the fitted curve.

3.2 Relationship between CPT-based RD and VC penetration speed

The relationship between the CPT and VC data sets is depicted in Figure 5, where the CPT-based RD and VC penetration speed are plotted together for the chosen group. The correlation between the mean in-depth values of those data sets is measured with Pearson's coefficient, ρ . The correlation studies are based only on the depth range between 0.20 and 5.00

m (3.70 m for the 5th and 7th group because of the underlying clay layer). The statistical relationship measured with the Pearson's coefficient has been summarised in Table 1 below.

Table 1. Correlation studies between CPT-based R_d and VC S_P .

Group	ρ (0.2 – 5.0m)	ρ (0.2 – 1.7m)	ρ (1.7 – 5.0m)
1	-0.59	-0.44	0.44
2	-0.91	-0.68	-0.27
3	-0.73	-0.20	-0.51
4	-0.75	0.04	-0.20
5	-0.68	-0.07	-0.51
6	-0.93	-0.76	-0.63
7	-0.78	-0.63	-0.62
AVG	-0.77	-0.39	-0.33

Based on the correlation studies of VC penetration speed, S_P , and CPT-based RD, R_d , an important conclusion has been drawn that the correlation is not constant in-depth. Although the correlation for the whole penetration dataset bracket together was strong ($\rho = -0.77$), it is not the case when the data is separated. The correlation is better in the upper section, apart from two groups that showed no correlation. In the upper section (until 1.7m of penetration on average), the strong negative correlation is severely affected by an initial uneven penetration speed of a “wavy” nature. Even though the data has been thoroughly cleaned and filtered, the noise generated by vibrations does not allow formulating a clear and undoubtful correlation in each test. The correlation in the bottom section could be improved by introducing an additional parameter, which could be based on, for example, a net surcharge or penetration depth.

3.3 VC-based RD formula

To verify what mechanisms govern VC penetration speed and whether it is possible to correlate it to the non-cohesive soils' RD, physical aspects linking those parameters need to be researched on.

The relationship between the cone tip resistance, q_c , and the relative density, D_r , was initially proposed by Lancellotta (Lancellotta 1983) as shown in Equation 2 below:

$$D_R = A_0 + B_0 \cdot X \quad (2)$$

where: $X = \ln\left[\frac{q_c}{(\sigma'_{v0})^\alpha}\right]$ A_0 , B_0 and α = empirical correlation factors.

It is assumed that the VC-based RD should be formulated in the same way, but with the cone resistance, q_c , replaced by the VC Penetration Resistance q_{VC} . The q_{VC} parameter should depend on the depth of penetration and the penetration speed, which is mainly governed by:

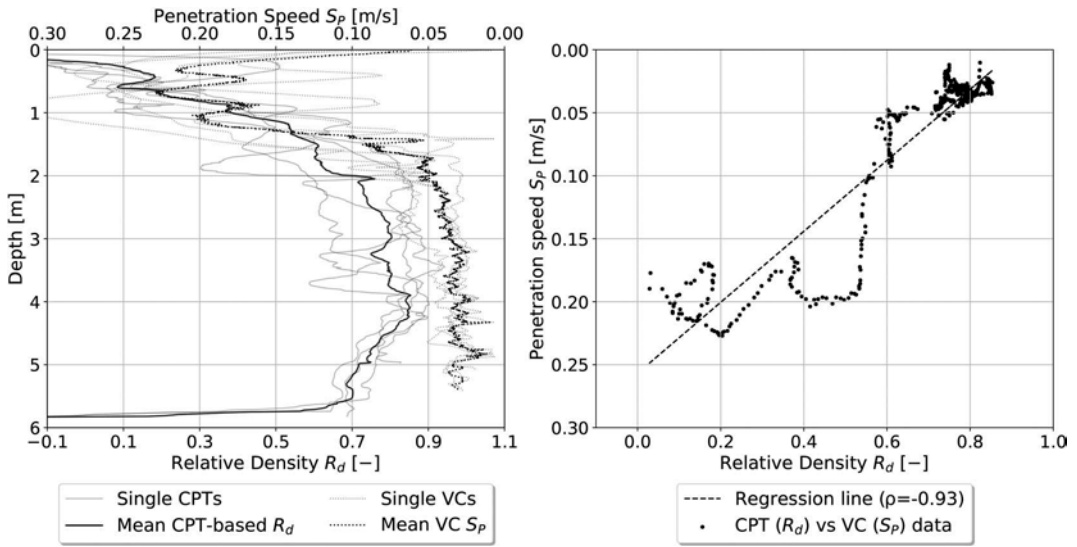


Figure 5. CPT-based Relative Density and VC penetration speed and their correlation in Depth for Group 6.

- Liquefaction susceptibility, which mainly depends on relative density and grain size distribution and uniformity coefficient (Saikia & Chetia 2014);
- Vibrations frequency and intensity;
- Frictional resistance, which depends on the depth of the penetration, angle of friction at the interface between a cohesion-less soil and a steel core barrel, friction coefficient and water content (Mosaddeghi, Hosseini, Hajabbasi, Sabzalian, & Sepehri 2021), is assumed to be constant.

The intensity and frequency of vibrations generated by the motor are approximately constant; however, the vibrations transmitted along the barrel are dumped by the medium surrounding the barrel, i.e. firstly by the water and later the soil. Hence, the deeper the barrel is penetrated, the more vibrations dissipate to the soil above the cutting shoe at the bottom of the barrel, limiting the liquefaction occurrence.

The dependence of penetration resistance, F , on velocity for non-deforming projectiles is represented by the Poncelet equation (Bless, Omidvar, & Iskander 2018), which is a relatively similar problem in physical meaning and is shown below.

$$F = M \cdot \frac{dv}{dt} = A(C\rho v^2 + R) \quad (3)$$

where M is a projectile mass, v is penetration velocity, ρ is the bulk density of sand, C is Poncelet drag, which ranges from 0.7 for loose to 1.1 for dense sand (Bless, Omidvar, & Iskander 2018), R is bearing strength (frictional resistance) that for the core barrel can be estimated with unit skin resistance equation:

$$R = \sum_{i=1}^n A_i \sigma'_h \tan(\delta) = \sum_{i=1}^n L_i \pi d K_s \sigma'_v \tan(\delta) \quad (4)$$

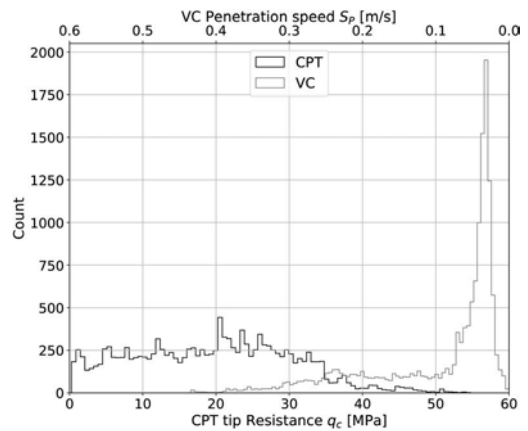


Figure 6. Histograms of q_c and S_p from all 33 tests for depths from 0.20 to 5.00 m.

where L_i is incremental barrel penetration, d is barrel's diameter, K_s is coefficient of earth pressure, δ is angle of friction at interface and σ'_v is effective overburden pressure. Summing up all the relationships listed above, following dependency is proposed:

$$q_{VC} \sim D_2 S_p^2 \cdot f(L_i) + D_3 L_i \sigma'_v \quad (5)$$

where D_2 is a correlation factor and is negative, $f(L_i)$ is a function that links difficulty in liquefying soil beneath the cutting shoe with the depth of penetration, and D_3 is an empirical factor that is positive. For a better understanding of those parameters' relationship, the distributions of the tip resistance and VC penetration speed are plotted in Figure 6.

The distribution of q_c is almost uniform, with approximately the same density in between 0 and 35 MPa. The distribution of penetration speed is

approximately log-normal. Therefore, the penetration speed cannot be incorporated linearly in the equation as the tip resistance is. After substitution of q_{VC} to Equation 2 and a preliminary verification process, which resulted in a few changes to the formula, the following relation is proposed:

$$D_{R,VC} = D_0 + \frac{100}{D_1} \ln \left[\frac{D_2 S_P^2 \cdot f(L_i) + D_3 L_i \sigma_v^{D_4}}{D_5 (\sigma'_v)^{D_6}} \right] \quad (6)$$

where $D_{R,VC}$ is relative density in percents, S_P^2 is VC penetration speed in m/s, $f(L_i)$ is simplified to L_i , i.e. the penetration depth expressed in meters, σ'_v is effective vertical stress in kPa.

The proposed formula has been validated firstly with correlation factors same as in Equation 2, and employing iterative process, the constants were calibrated to the following values: $D_0 = 60, D_1 = 6.2, D_2 = -0.45, D_3 = 0.02, D_4 = 0.2, D_5 = 0.005, D_6 = 0.6$.

4 VC-BASED FORMULA VALIDATION

The formula proposed in the previous section has been tested along with all seven groups. The main problems that appeared in this process, and are limiting the reliability of the results, are as follows:

- The value of D_2 constant should be high to keep the meaning of S_P significant. However, if this value is too high compared to D_3 and D_4 , the value in the logarithm becomes negative. This gives a small threshold of reasonable D_2 values;
- The constant of D_4 had to be introduced to minimise the value second phrase of the nominator - without it, the values of $R_{D,VC}$ in the deeper section of the test were unrealistic;
- There are limitations connected with the fact that S_P is to the power of 2. For low values of penetration speed, it results in practically no influence of S_P values on the computed value of $R_{D,VC}$.

The exemplary results are shown in Figure 7 for the same group as before. The correlation itself has visibly increased, but the accuracy of RD estimations are still very low. The results have been summarised in Table 2 below, analogically to the previous Table 1.

Table 2. Correlation studies between CPT-based R_d and VC-based $R_{D,VC}$.

Group	ρ (0.2 – 5.0m)	ρ (0.2 – 1.7m)	ρ (1.7 – 5.0m)
1	0.72	0.85	-0.64
2	0.94	0.90	0.29
3	0.90	0.84	0.55
4	0.69	0.15	0.14
5	-0.03	0.52	0.79
6	0.97	0.92	0.62
7	0.37	0.71	0.61
AVG	0.65	0.70	0.35

5 SUMMARY

5.1 Conclusions

This study was based on geotechnical data acquired from VC and CPT tests performed at 33 locations, which were divided into 7 groups with very selected, homogeneous stratigraphy consisting of medium-dense to very dense medium sand.

The main conclusion is that the penetration speed, together with the effective vertical stress and penetration depth, is not enough for the precise estimation of the relative density of cohesion-less soil. Studies presented in this paper have shown that there is a strong correlation between VC penetration speed and CPT-based relative density in the upper 1.50 - 2.00 meters of penetration. Furthermore, the Formula 6 provided relative density estimations of the correct order of magnitude and increased correlation in most of the groups. However, the reliability and accuracy of relative density estimation with the usage of VC data is very low and not enough for applications in geotechnical design.

The main aspects negatively affecting the estimations' accuracy are the erratic penetration speed in the upper section (between 0.0 - 1.7 m of depth) and the effects of exponentiation of penetration speed in the bottom section, which gives wrong estimations of relative density. One way of tackling those issues would be to divide the formula into two parts, i.e. one part for the penetration speed above 0.075 m/s and the other part for values below this threshold. Another way would be to incorporate acceleration into the equation instead of penetration speed or reduce the exponent from 2 to a smaller number.

5.2 Limitations

There are several limitations related to the derived correlation factors and formulas:

- Related to the coring technique and its physical meaning:
 - Ignoring the friction of the core barrel in the calculations. The friction raises with penetration and should be incorporated in the calculations in the other way than it is in CPT-based formulas for relative density;
 - The influence of the net surcharge has been calculated in the same way as in CPT-based formula;
- Related to the data processing:
 - The penetration data records have been cleared out of not-significant records. Whether the record is significant or not is up to the engineering judgments, which is ambiguous. Due to the high frequency of VC data logging (10 Hz), the records are noisy; hence, each user would end up with different cleared data sets;

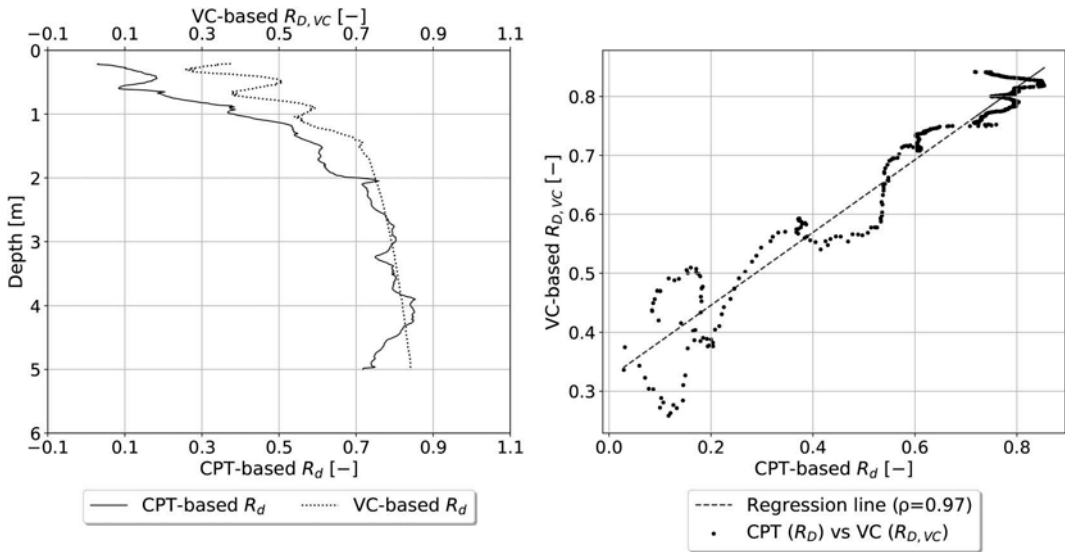


Figure 7. CPT-based Relative Density and VC-based Relative Density and their correlation in depth for Group 6.

- The filtering technique presented in Subsection 3.1 has better performance for tests with penetration time longer than 30 seconds, while for quick sampling, the results are still prone to errors;
- All limitations, which apply to Savitzky-Golay Filter and its SciPy implementation, apply to the results of this analysis as well.

5.3 Recommendations for further research

As concluded above, the topic is promising in terms of increasing certainty in estimations of soil parameters; however, the literature and research on this subject are very limited. Therefore, the following concerns could be further elaborated on:

- The phenomenon of the vibration-induced liquefaction underneath the core barrel and its influence on the penetration speed of the core barrel;
- Studies on relating the relative density not only to the penetration speed but also the acceleration could bring new conclusions on the usage of VC data in the estimation of relative density;
- The relative and absolute error estimation should be incorporated into the correlation studies.
- Calibration of coefficients in the formula relating the VC penetration speed and relative density should be performed more thoroughly. An

optimisation algorithm integrating dynamic Bayesian networks could be of great help in this matter.

REFERENCES

- Bless, S. J., M. Omidvar, & M. Iskander (2018). Poncelet coefficients for dry sand. *AIP Conference Proceedings* 1979(July), 1–6.
- Jamiolkowski, M., D. C. F. Lo Presti, & M. Manassero (2003, jan). Evaluation of Relative Density and Shear Strength of Sands from CPT and DMT. In J. Germaine, T. Sheahan, and R. Whitman (Eds.), *Soil Behavior and Soft Ground Construction*, Reston, VA, pp. 201–238. American Society of Civil Engineers.
- Lancellotta, R. (1983). Analisi di Affidabilità in Ingegneria Geotecnica". In *Atti dell'Istituto di Scienza delle Costruzioni*, Volume 625, Torino. Politecnico di Torino.
- Mosaddeghi, M. R., F. Hosseini, M. A. Hajabbasi, M. R. Sabzalian, & M. Sepehri (2021). Chapter Two - *Epichloë* spp. and *Serendipita indica* endophytic fungi: Functions in plant-soil relations. Volume 165, pp. 59–113. Academic Press.
- Saikia, R. & M. Chetia (2014). Critical Review on the Parameters Influencing Liquefaction of Soils. 3(4), 110–116.
- Savitzky, A. & M. J. Golay (1964). Smoothing and Differentiation of Data by Simplified Least Squares Procedures. *Analytical Chemistry* 36(8), 1639–1643.
- SciPy. Savitzky-Golay filter.

CPT data interpretation for an improved characterization of the paleosol stratigraphy in the Po River Valley, Italy

I. Bertolini, M. Marchi, L. Tonni & G. Gottardi
DICAM Department, University of Bologna, Italy

L. Bruno
Department of Chemical and Geological Sciences, University of Modena, Italy

A. Amorosi
Department of Biological, Geological and Environmental Sciences, University of Bologna, Italy

ABSTRACT: Post-depositional phenomena can produce significant changes in the geotechnical properties of soils. Although the identification of the effect of such phenomena on the soil structure may contribute significantly to the interpretation of the soil mechanical behaviour, their characterization is not routinely carried out in practice. In this context, the novel application of paleosol features in the definition of geotechnical stratigraphic models can result in improved characterization of soil deposits in alluvial sites. Sedimentology uses paleosols (i.e. fossil soils with peculiar geologic properties) as markers for stratigraphic correlations in alluvial areas at large scale. This paper outlines the main properties of these geological objects and investigates the strategies for their identification in cone penetration tests (CPT). The analyses are discussed with reference to boreholes and CPTs data in 3 well documented sites in the Po River Valley (Italy). First, sedimentological identification of paleosols from borehole corings is introduced; then, geotechnical interpretation of CPT is carried out on such a basis, showing how poorly developed paleosols (Inceptisols) found in the investigated sites, are difficult to be identified through CPT logs and how they plot in the well-established Robertson's classification charts.

1 INTRODUCTION

The Po Plain-Adriatic sea system is an elongated basin originated from the Po River catchment. It consists of a > 7km thick Pliocene - Quaternary sedimentary succession, with a 30m-thick Holocene succession that overlies Late Pleistocene deposits. The Holocene depositional history can be investigated through integrated stratigraphic, sedimentological and paleontological analyses. A total of 22 sedimentary facies, grouped into 5 main depositional systems, have been identified in the Po River catchment (Amorosi et al, 2017).

The present work focuses on three locations in the Po Plain, in Province of Ferrara (Figure 1), characterized by well-drained floodplain deposits, which belong to the alluvial plain depositional system. These deposits consist of different mixtures of clay and silt and show peculiar pedogenetic features: paleosols. The investigation started from the description of three continuous corings EM-S3, EM-S1 and EM-S5, located in Gaibana, Dogato and Ostellato, respectively. Then, three CPTU tests, each one performed in proximity to one coring, were analysed.

The stratal architecture of the Holocene succession of the Po coastal plain in Figure 2 shows the spatial distribution of the facies associations along the investigated section. The Holocene deposits, down to a depth between -10 and -20 m a.s.l, consist predominantly of a thick swamp clay succession that grades distally into



Figure 1. Location of the investigated site.

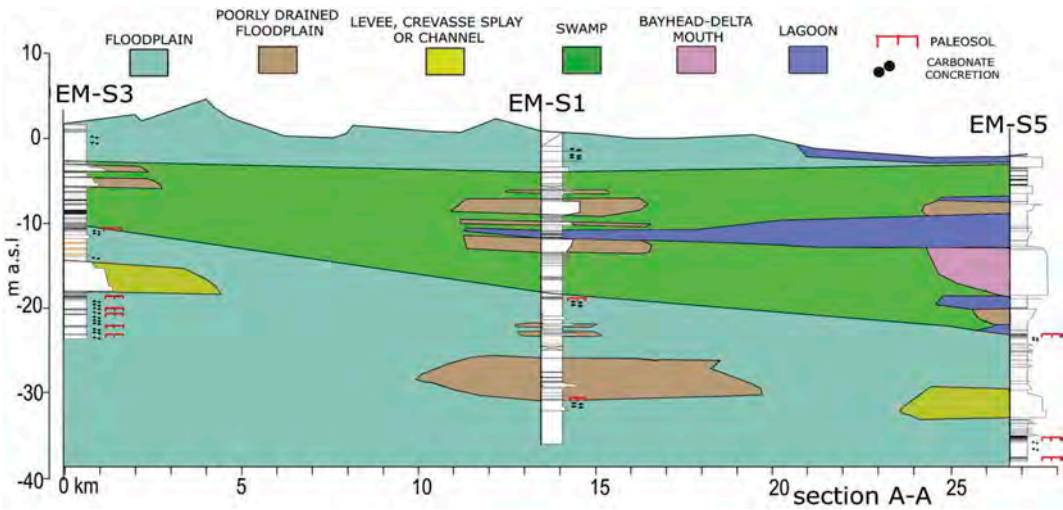


Figure 2. Stratigraphic architecture with indication of the different facies association along section A-A in Figure 1.

lagoonal and bay-head delta deposits. Below the Holocene succession, Pleistocene deposits are predominantly well-drained floodplain silts and clays with subordinate fluvial-channel deposits (Amorosi et al, 2017).

2 PALEOSOL ORIGIN AND DEVELOPMENT

The floodplain facies association is characterized by the presence of paleosols, buried ancient soils formed on a ground surface of the past and subjected to physical, biological and chemical modifications caused by the interactions between soil, atmosphere and vegetation. Their development is strictly connected to fluvial activity which in turn depends on river sediment supply/discharge. A schematic representation of paleosol horizons (A_b , B_k , B_w) development is shown in Figure 3. When fluvial incision takes place in response to eustatic or climatic control, the adjacent interfluvial areas are prevented from river flooding and they experience soil development (paleosol 1 in Figure 3 top). In case of prolonged subaerial exposure, vegetation starts to grow on the top soil, enriching the A_b horizon in organic matter. Moreover, weathering in the vadose zone causes leaching of carbonates from horizon A_b and their precipitation into the underlying B_k , in form of millimetric to centimetric nodules. The horizon B_w is characterized by incipient weathering, while horizon C does not experience pedogenetic modifications. In case of high sediment supply/discharge, fluvial incision is rapidly filled by the transported sediments, and interfluvial areas experience frequent flooding events and crevasse lobe accumulation. Under these conditions, the water table is usually

close to the ground level and then, there is no vadose zone. Due to the fact that river continues to supply new sediments, soil formation is hindered. When the river enters a new stable phase of bed incision, renewed pedogenesis occurs on the interfluvial areas (paleosols 2 and 3 in Figure 3 top).

Holocene paleosols are more discontinuous and immature (Entisols, Amorosi et al., 2014). Paleosol identification is a valid help in the stratigraphic analysis of mud-dominated Late Pleistocene and Holocene deposits. For this reason, they are largely used as regional stratigraphic markers (Amorosi et al, 2017).

3 PALEOSOL IDENTIFICATION

In current practice, paleosols in floodplain deposits can be identified by the physical analysis of core samples (visual inspection). The A_b horizon usually exhibits a darker colour with respect to the illuvial B_k - B_w horizons, due to the higher quantity of organic matter. The B_k horizon typically shows carbonate nodules and often a microstructure created by calcareous cementation between particles. Figure 3 (bottom) shows a typical succession of horizons A_b - B_k - B_w . Considering the results of the pocket penetrometer, represented in Figure 4 for the EM-S3 borehole, it can be observed that A_b (whose top is identified with the paleosol symbol shown in the legend, just below the poorly drained floodplain) shows higher values of pocket penetrometer (PP) due to its overconsolidation state created by aging and pedogenetic processes, while B_k is characterized by medium-high values of PP, as a result of the carbonate accumulation and/or of the calcareous cementation between solid particles. In addition to the visual core inspection, simple

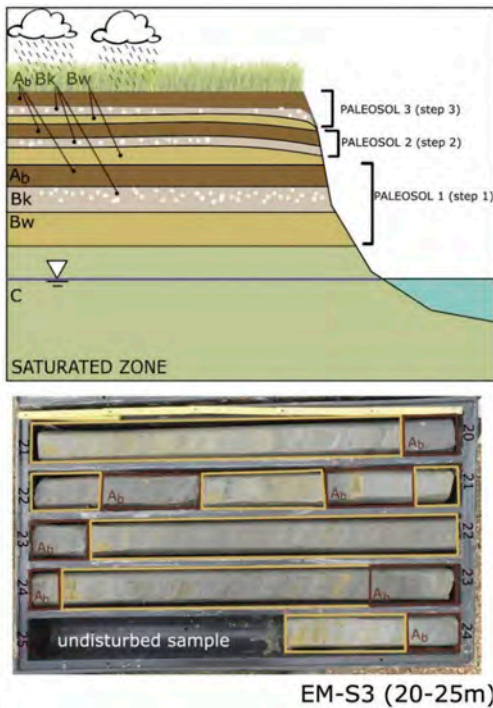


Figure 3. Top: schematic representation of development of paleosol horizons (A_b , B_k , B_w). Bottom: picture of the cores extracted at 20 and 25m depth from EM-S3 borehole.

laboratory tests have been performed in order to control experimental data that characterize the paleosols stratigraphy (Bruno et al, 2020).

In Figure 4, standard characterization tests have been performed on two samples of the A_b horizon of core EM-S3 (11.55m and 19.55m), on one sample of the B_k horizon (12.55m) and two samples of the C horizon (20.55m and 14.35m). The carbonate content showed low values (close to zero) for the A_b samples. The organic content determination confirmed that the highest values belong to the A_b horizon, which is coherent with the presence of a vegetation cover during soil development. An increase in particle grain size was observed from paleosol horizon A_b to B_k at the depth of 11.50-12.50 m. Indeed, the deposition in the B_k horizon of Fe and Mn oxides and the formation of secondary calcite nodules causes the enrichment in coarse grain material (recognized as sand in the laboratory procedure). On the other hand, the plasticity index is greater in the A_b horizon. A likely explanation is accumulation and mineralization of the organic matter and its association with clay minerals (Bruno et al, 2020). Samples from C horizons, not subjected to pedogenic processes, show an organic content close to 2.3%, PI around 16-17%, carbonate content $\sim 20\%$, clay content of $\sim 15\%$ and silt content $\sim 75\%$.

The observations of cores, extracted with a continuous perforating system, and, as additional tool, the results of classification tests carried out in the geotechnical laboratory, are a valuable aid for the identification of paleosol horizons in alluvial deposits. These types of investigations require a significant budget, especially when the study involves large areas. The economic effort, as well as the duration of the investigation campaign, could be significantly reduced by means of other geotechnical in situ tests. To this scope, CPTs, being rapid, cost-effective and widely used in practice, are taken into account as a possible additional investigation method, to be used with the aim of extending punctual information from boreholes to larger areas. In this paper, the application of CPT tests is analysed with respect to determination of the soil stratigraphy deduced from the soil behaviour type index (SBT) (Robertson, 2010). Paleosols are geological horizons with peculiar mechanical behaviour due to micro-structure creation as a consequence of pedogenetic processes and aging. A microstructured soil is characterized by a higher yield stress, peak strength and small-strain stiffness G_o with respect to an ideal soil. At large strain, the soil is subjected to destructuration and it may show a contractive behaviour (Leroueil and Hight, 2003). In order to investigate the effectiveness of this approach, the well-drained floodplain deposits identified in the three CPTU profiles, close to EM-S1, EM-S3 and EM-S5, were plotted on different soil classification charts available in the literature. Firstly, the Robertson (1990) chart was considered (Figure 5). Potentially, CPT-based charts could have the capability of recognizing paleosols since they rely on in situ mechanical behaviour and not directly on soil classification criteria based on grain size distribution and plasticity, such as the USCS (Unified Soil Classification System) (Tonni et al., 2019a, Tonni et al., 2019b). On the normalized Q_r-F_r chart the majority of records belong to SBT zone 3 (clay), on the right side of the normal consolidated central area, characterized by increasing OCR .

Data which have CPT-based SBT in either zone 4 or 5, could reflect the same soil (in terms of grain size), but stiffer, with higher OCR (horizon A_b), or a coarser layer as a consequence of a higher percentage of sand or carbonate nodules (B_k horizons). Similar results can be deduced from the Q_r-B_q charts (lower part of Figure 5), where the majority of the points are located in zone 3 (clay) and, to a lesser extent, in zones 4 (silty mixtures) and 5 (sand mixtures). Points showing SBT 4 and 5 plot around the vertical line $B_q=0$. Comparing these groups of data (SBT 4 and 5) in the Q_r-F_r and Q_r-B_q charts, it can be noticed that a larger amount of points plots into zones 4 or 5 in the Q_r-B_q chart rather than in the Q_r-F_r chart. This likely reflects the presence of a significant silty component in this part of the deposits (see also grain size distribution in Figure 4 of samples EM-S3 and its

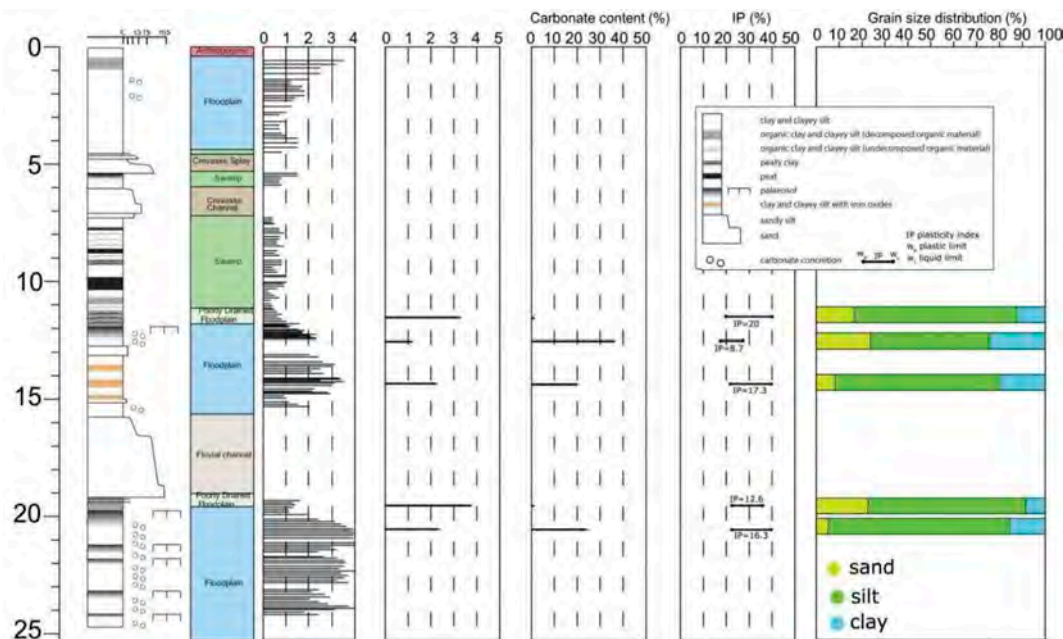


Figure 4. Physical characterization of five soil samples belonging to the continuous coring EM-S3. Two samples (11.55 and 19.55m deep, respectively) belong to horizon A_b; The sample at 12.55m belongs to horizon B_k and the remaining two samples belong to horizon C.

Robertson's chart in Figure 5). These layers can be more effectively detected using the B_q parameter, which captures the dilatant behavior of silts (or paleosols) and the possible occurrence of coarser thin layers, not revealed by F_r . In a recent update of the classification charts, Robertson (2016) suggested to use $CD=70$ line in the Q_m-F_r chart (Figure 5) to recognize microstructured soils. Indeed, the $CD=70$ line should separate contractive from dilatative behaviours and it can be expressed with the following formula:

$$CD = 70 = (Q_m - 11)(1 + 0.06 F_r)^{17} \quad (1)$$

With Q_m normalized cone resistance and F_r normalized friction ratio.

In case of microstructured soils with contractive behaviour at large strains, but due to the increased strength and stiffness for cementation or aging, higher values of Q_m may be recorded. As a result, cemented soils wrongly plot on the dilatative region of the chart. In Figure 5 the majority of the points plots below the boundary line $CD=70$ and only few points, that may show some microstructure, above it. On the Q_m-F_r chart, the modified SBT_n boundaries (black continuous lines) proposed by Schneider et al (2012) have been superimposed on the original SBT_n zones (black dashed lines) by Robertson (1990). The modified contours are based on the Modified Soil Behaviour Index I_B expressed as follows:

$$I_B = 100 \frac{(Q_m + 10)}{(Q_m F_r + 70)} \quad (2)$$

In addition to Robertson's approaches, a different classification system, proposed by Schneider et al (2008) was also taken into account. Its application showed that the investigated soils have a predominantly contractive behaviour, belonging to the clay like contractive soils (CC) and the transitional contractive soils (TC). Schneider et al (2008) also suggests that microstructured soils plot above a line of equation $Q_m = -U_2 + 20$, where U_2 is defined as the ratio between the excess pore water pressure and the effective stress in the point. No points that satisfy this condition were found within the investigated depth. Figure 6 shows the results of the CPTU test performed in close proximity to EM-S5, in terms of corrected cone resistance q_r , f_s and u_2 . Using the sedimentological characterization of facies in core EM-S5, and the SBT classification system, the geological-geotechnical stratigraphy was identified. It can be easily observed that the recognition of the different sedimentary facies starting solely from CPTU classification, in case no geological information is available, is not straightforward, as clearly shown by the comparison between central lagoon, crevasse splay and floodplain deposits. Focusing on the alluvial plain deposit (floodplain), it is interesting at this stage to compare how points plot with depth in the classification charts (Figure 6). The comparison

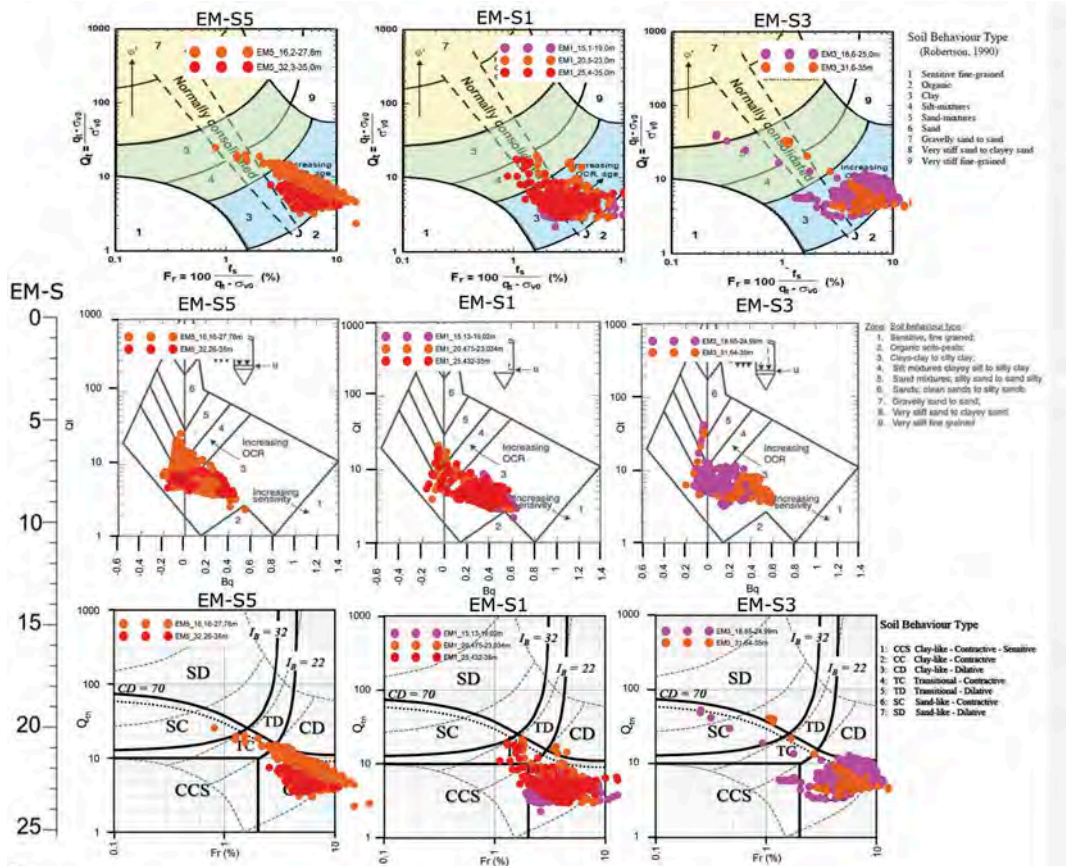


Figure 5. Soil Behaviour Type data plotted in the Robertson (1990) F_r-Q_r , and B_q-Q_r charts and in Robertson (2009) F_r-Q_m chart for the floodplain deposits identified in EM-S5, EM-S1 and EM-S3 boreholes.

suggests that crevasse splay horizons, in particular those at a depth of 18 – 19.5 m and 22.5 – 23 m, show SBT 4 and 5 in almost all types of charts. This is due to the presence of cm-thick sandy layers that characterize this type of facies. On the contrary, the floodplain layers, where paleosol horizons have been identified, plot in SBT zone 4 only on the Q_r-B_q Robertson (1990)'s chart, while the other classification charts recognize them as homogeneous SBT 3. This peculiarity could be justified by the fact that in fine grained soils the B_q parameter is more sensitive than F_r , to the presence of structure variations within thin layers, which cannot be detected through the F_r parameter.

5 CONCLUSIONS

In this paper, it has been shown how CPT data collected in floodplain deposits of the river Po plot on well-known classification charts (Robertson 1990; Robertson, 2009, Schneider et al, 2008).

Although CPTU classification charts proved to be a potential valuable help in the identification of

sedimentary facies in the alluvial Po Plain, they do not provide univocal identification of paleosol horizons without the support of their geological preliminary recognition. This evidence applies to low mature paleosols, peculiar horizons of the floodplain facies subjected in the past to microstructuration for cementation (B_r) or aging (A_b): they do not appear to be easily identified by using only information from cone penetration tests (q_p , f_s , u_2). Integrating the visual inspection of paleosols from cores with basic classification laboratory tests is crucial to a correct geotechnical-geological interpretation, especially in relatively homogeneous, mud-prone alluvial deposits, where sand bodies display strongly lenticular geometries.

The paleosol horizons investigated in this study cannot be identified as microstructured soils in the classification charts available in the literature. This fact is probably a sign of the low maturity of these paleosols (Inceptisols), which only account for relatively short periods of subaerial exposure of the ancient topsoil. Nonetheless, a characteristic feature of paleosol horizons seems to be shown by the Q_r-B_q Robertson's (1990) chart, which

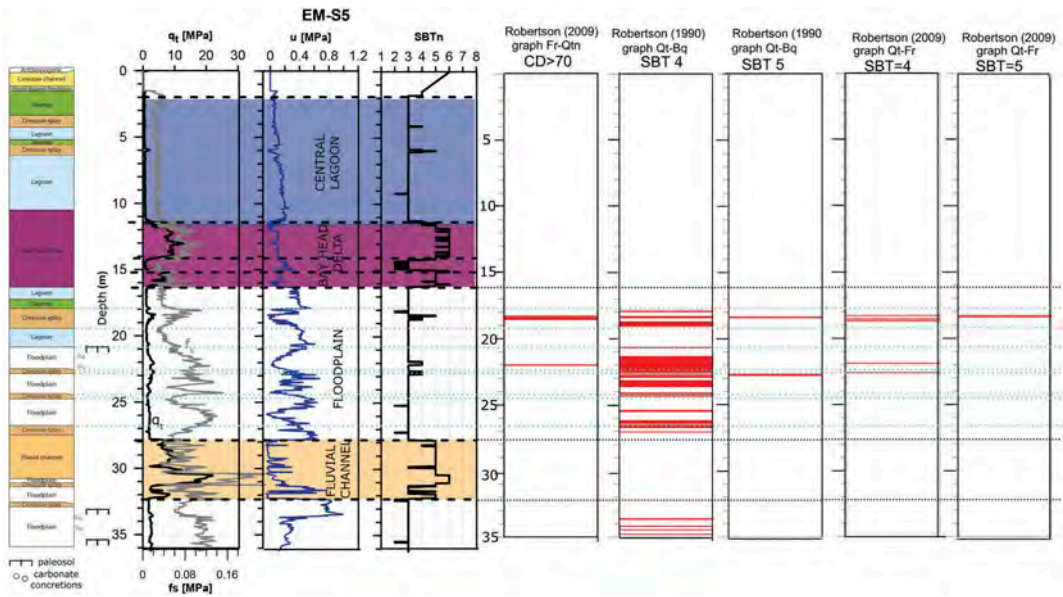


Figure 6. Left side: stratigraphic log of the continuous coring EM-S5. From left to right: corrected tip resistance q_t , sleeve friction f_s , pore water pressure u_2 and soil behaviour type (Robertson, 2009) vs depth of the CPTU performed in close proximity to EM-S5. The final five columns represent with a red line the depth where SBT 4 or 5 have been found in the classification charts.

highlights the presence of SBT 4, where all the other charts provide SBT 3. Further investigations through dilatometer or other in situ tests will be carried out in the next future to expand the results of this study.

REFERENCES

- Amorosi, A., Bruno, L., Campo, B., Morelli, A., Rossi, V., Scarponi, D., Hong, W., Bohacs, K.M, Drexler, T.M. 2017. Global sea-level control on local parasequence architecture from Holocene record of the Po Plain, Italy. *Marine and Petroleum Geology*.
- Amorosi, A., Bruno, L., Rossi, V., Severi, P., Hajdas, I. 2014. Paleosol architecture of a late Quaternary basine margin sequence and its implications for high resolution, non-marine sequence stratigraphy. *Glob. Planet. Change* 112:12–25.
- Bruno L., Marchi M., Bertolini I., Gottardi G., Amorosi A. 2020. Climate control on stacked paleosols in the Pleistocene of the Po Basin (northern Italy). *Journal of Quaternary Science*, vol 35(4): 559–571.
- Leroueil, S. & Hight, D.W. 2003. Behaviour and properties of natural soils and soft rocks. In Tan et al (eds), *Characterization and engineering properties of natural soils*, vol.1.
- Robertson, P.K. 2016. Cone penetration test (CPT)-based soil behaviour type (SBT) classification system-an update. *Canadian Geotechnical Journal*.
- Robertson, P.K. 1990. Soil classification using the cone penetration test. *Canadian Geotechnical Journal*, 27(1): 151–158.
- Robertson, P.K. 2009. Interpretation of cone penetration test-a unified approach. *Canadian Geotechnical Journal*, 46(11): 1337–1355.
- Schneider, J.A., Randolph, M.F., Mayne, P.W., Ramsay, N. R. 2008. Analysis of factors influencing soil classification using normalized piezocone tip resistance and pore pressure parameters, *Journal of Geotechnical and Geoenvironmental Engineering*, 134(11): 1569–1586.
- Schneider, J.A., Hotstream, J.N., Mayne, P.W., Radolph, M. F. 2012. Comparing CPTU Q-F and $Qt-\Delta u/2/6'$ vo soil classification charts. *Geotechnique Letters* 000:1–7.
- Tonni, L., Garcia Martinez, M.F., Maurini, D., Calabrese, L. 2019a. Developing a regional-scale geotechnical model of the north-western Adriatic coastal area (Italy) for urban planning and robust geotechnical design. *Proc. 17th European Conference on Soil Mechanics and Geotechnical Engineering, ECSMGE*.
- Tonni, L., Garcia Martinez, M.F., Rocchi, I. 2019b. Recent developments in equipment and interpretation of cone penetration test for soil characterization. *Rivista Italiana di Geotecnica* 53(1): 71–99.

Application of CPT to the evaluation of permeability in a Po river embankment prone to backward erosion piping

Ilaria Bertolini, Guido Gottardi, Michela Marchi & Laura Tonni
University of Bologna, DICAM, Italy

Agnese Bassi & Alessandro Rosso
Interregional Agency for the Po River, AIPO, Italy

ABSTRACT: Backward erosion piping is one of the most critical issues for the stability of many river embankments worldwide. The article presents results from an extensive geotechnical campaign carried out on a section of the Po river embankments (Italy), prone to backward erosion piping. The aim of the investigations was twofold: firstly, identifying the stratigraphic arrangement of the river system causing favourable conditions for piping occurrence, and secondly determining the permeability of the aquifer and the finer top stratum (blanket) in their undisturbed state, as well as that of the preexisting eroded zone in proximity of the sand boil (i.e. the volume around the exit hole). Indeed, analytical and numerical approaches available in the literature are particularly sensitive to the value of permeability of the aquifer, which should therefore be determined in undisturbed conditions. CPT tests turned out to be suitable and economical to this scope. This study presents an integrated analysis of in situ testing data, collected from boreholes, piezocone test and Lefranc test, aimed at estimating the saturated permeability of the different soil units using different experimental methods and interpretation approaches. A comparison between alternative CPT-based methods and field permeability tests is proposed. A good agreement between the different methods was found, thus suggesting the suitability of CPT for the hydraulic characterization of soils.

1 INTRODUCTION

Backward erosion piping is an internal erosion process which may occur in stratigraphic contexts characterized by a shallow thin clayey layer (“blanket”) overlying a highly permeable stratum (aquifer), where significant seepage flow can develop. Such stratigraphic conditions are typical of alluvial plains where major lowland rivers flow and of delta areas, protected by high-rise embankments. When the water level in the river rises, a high hydraulic head difference may be attained, resulting in an increase of the seepage flow in the aquifer. In such conditions, the water flow may concentrate towards local discontinuities where the hydraulic gradients increase, possibly creating flow exit pipes and the consequent initiation of the backward erosion process. The phenomenon could then progress eroding sand particles at the interface between the aquifer and the blanket, creating at the same time sand boils on the ground surface.

Backward erosion piping is recognized to represent a serious threat to dams and levees. Indeed, this phenomenon typically affects the surroundings of embankments of major lowland rivers in China, USA, and The

Netherlands, among others. A widespread occurrence of sand boils has been also reported for the Danube. In Italy, along the Po River, more than 130 sand boils have been registered and the majority of them (80) reactivate periodically during high-water events (Merli et al., 2015; Aielli et al., 2019; Marchi et al., 2021).

An in-depth understanding of the mechanism and a reliable assessment of piping risk require both the preliminary development of a detailed stratigraphic model of the whole river embankment system and the accurate estimate of soil permeability. The different approaches, either analytical or numerical (e.g. USACE 2000; Sellmeijer et al. 2011; García Martínez et al., 2020), for the modelling of this phenomenon, are indeed based on a careful characterization of the hydraulic properties of soils. As a result, due to the significant extent of the areas to be investigated and to the fact that characterization involves coarse grain soils, field investigations turn out to be the only possible practical approach which can be adopted for the definition of the soil parameters required in the analyses. This paper discusses the determination of soil permeability from CPTU tests carried out in a piping-prone section of the Po river embankments.

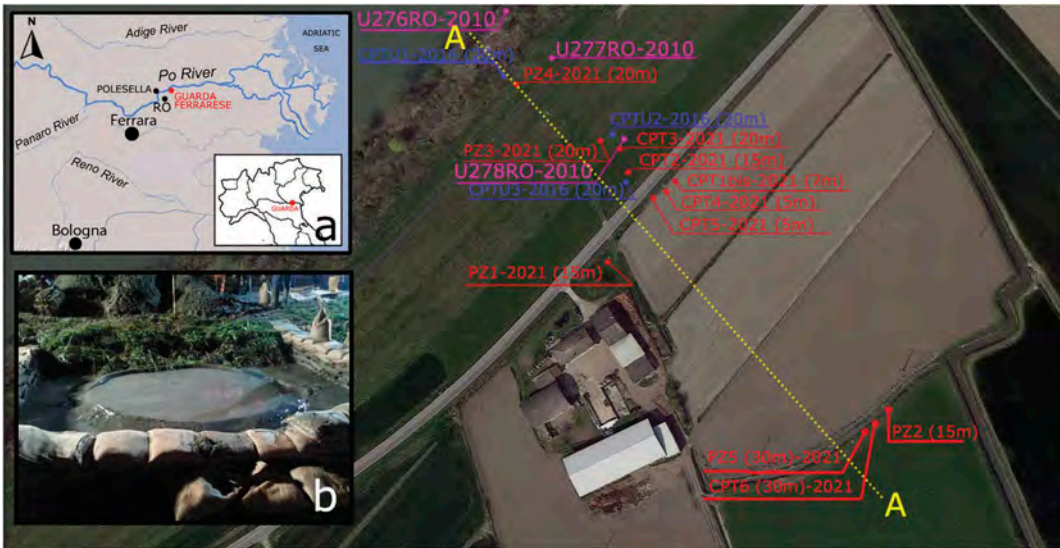


Figure 1. Geographical localization of the investigated site in Guarda Ferrarese (Ro, Italy). In photo 1b, the sand boil reactivation in November 2014 in the investigated river embankment section.

2 THE STUDY AREA

The Po River is the main Italian watercourse. It flows across northern Italy from the Western Alps to the Adriatic Sea near Venice, for an overall length of 650 km. In the last two centuries, the height of Po river embankments has been progressively increased, with the obvious benefit of preventing overtopping while increasing at the same time the susceptibility to piping of the whole area. The higher the water level in the river, the greater the water head difference at the toe of the embankment landside, which, in turn, results in an increase of the probability of sand boil occurrence. In addition, the variation of flood dynamics, induced by climate changes, generates more

recurrent and intense high-water events and consequently further aggravates the problem.

On that account, over the last years local authorities have launched a number of investigation campaigns on the most critical areas, with the aim of mitigating the flood risk connected to backward erosion piping.

This paper is based on the experimental dataset recently collected in one of the most investigated sections of the Po river, located in Guarda Ferrarese (Ferrara province) (Figure 1a). Here, an historical sand boil of remarkable size (the sand volcano reached an external diameter higher than 2.5 m), located landside of the riverbank section, at the bottom of a ditch, reactivates recurrently during high water events.

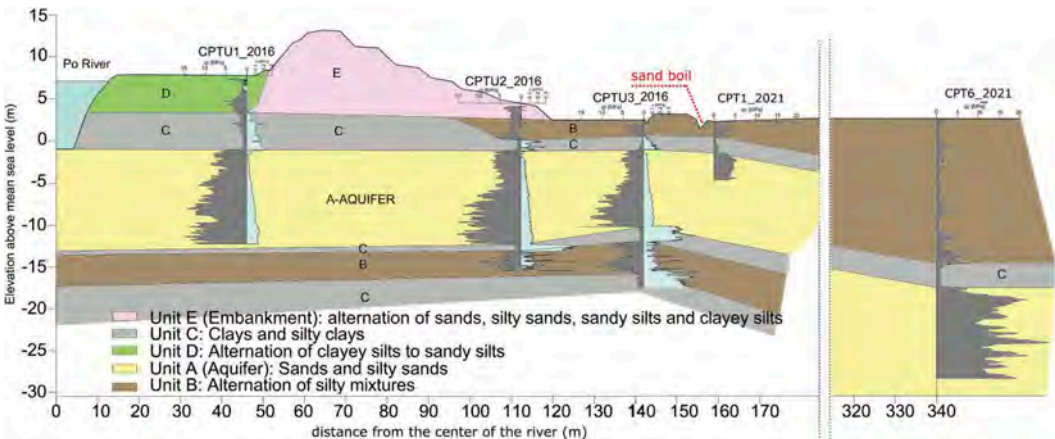


Figure 2. Stratigraphic model of Section A-A in Figure 1, with CPTU log profiles.

3 GEOTECHNICAL INVESTIGATIONS AND STRATIGRAPHIC MODEL

Figure 1 shows the location of the main in situ tests performed in the investigated river embankment section, in three different stages of geotechnical campaigns: in 2010, 2016 and 2021. During the 2016 investigation, dissipation tests have been performed in units B and C, in order to gain a better insight into the permeability characteristics of the subsoil, in terms of the horizontal permeability k_h . In 2021, the geotechnical campaign included continuous coring boreholes with execution of Lefranc permeability tests and SPT. In addition, Casagrande piezometers have been installed in the bored holes to monitor pore water pressures changes in both the confined and the phreatic aquifer (blanket), in relation to the variation of the water level in the river (PZ1, PZ2, PZ3, PZ4 and PZ5 in Figure 1).

The stratigraphic model in Figure 2 shows profiles of the corrected cone resistance (q_c) and the pore pressure (u_2) for the 2016 piezocone tests, which have been interpreted according to the classification framework proposed by Robertson (2009). Samples extracted during borings have been also taken into account to support stratigraphic modelling.

As evident from Figure 2, five different soil units have been identified. Unit A (aquifer) is the sandy layer where the erosion process takes place in case of piping. On the top of this unit, there are the continuous clayey and silty horizons C and B, creating favorable conditions for backward erosion piping initiation and progression. It is worth noting that the thickness of the "blanket" (comprising units B and C) tends to reduce in close proximity to the sand boil, as deduced from CPT1bis (2021) and CPT5 (2021). In particular, the thickness changes from 3.72m to 2.96m moving toward the ditch, being the CPT5 (2021) test closer to the longitudinal axis of the ditch. The reduction of the

blanket thickness approaching the ditch may give a reason for the position of the sand boil. Moreover, the thickness of the lesser permeable unit C, roof of the aquifer, decreases from 1.76m in CPT1bis to 1.2m in CPT5.

Laboratory tests have been carried out on 14 disturbed soil samples collected during borings. Samples have been tested to measure grain size distributions (Figure 3A) and plastic properties of the finer samples (Figure 3B). Unit A (no. 5 samples) turns out to have an average percentage of fine and coarse materials equal to 14% (standard deviation, SD , equal to 16%) and 86% ($SD = 16\%$), respectively. The organic content is extremely low (0.28%) and the carbonate content equal to 10%. Unit C (no.3 samples) and E (no. 2 samples) are dominated by fine-grained soils, with a percentage of clay and silt equal to 52% ($SD = 20\%$) and 60.8% ($SD = 6.5\%$), respectively. Unit B, consisting of an alternation of silty mixtures, is composed of 39% silt and 8% clay, with plasticity index equal to 14% ($SD = 7.8\%$) and organic content 0.72%. The samples of the investigated units B and C are located in the left side of the Casagrande chart (Figure 3) and therefore can be classified as low plasticity silts and clays.

4 DETERMINATION OF THE SATURATED PERMEABILITY

Estimates of the saturated permeability of the different soil units have been first obtained using the well-known CPTU-based empirical correlations proposed by Robertson (2010), given by:

$$1.0 < I_c \leq 3.27: k = 10^{(0.952 - 3.04 I_c)} [\text{m/s}] \quad (1)$$

$$3.27 < I_c \leq 4.0: k = 10^{(-4.52 - 1.37 I_c)} [\text{m/s}] \quad (2)$$

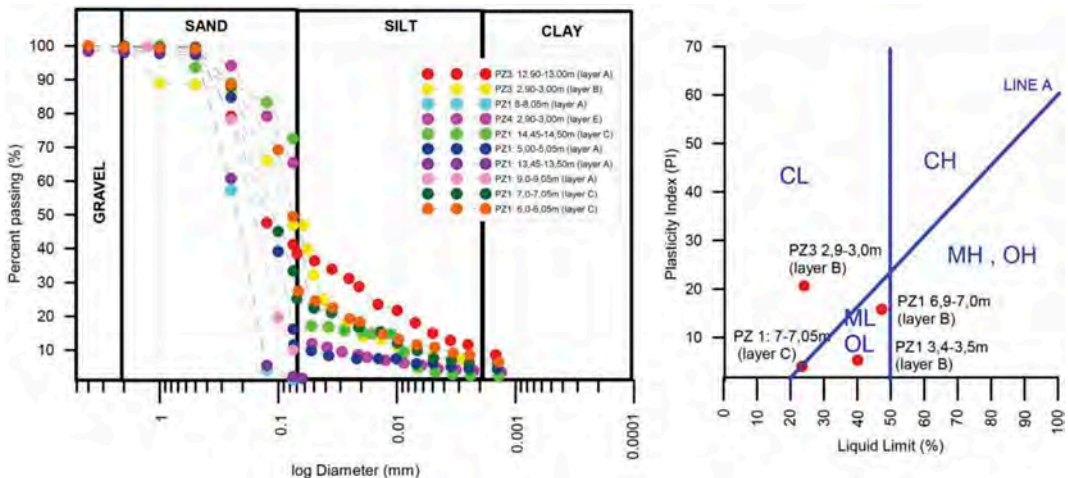


Figure 3. (Left) Particle size distribution of soil samples collected from boreholes; (Right) Soil classification according to the Plasticity Chart.

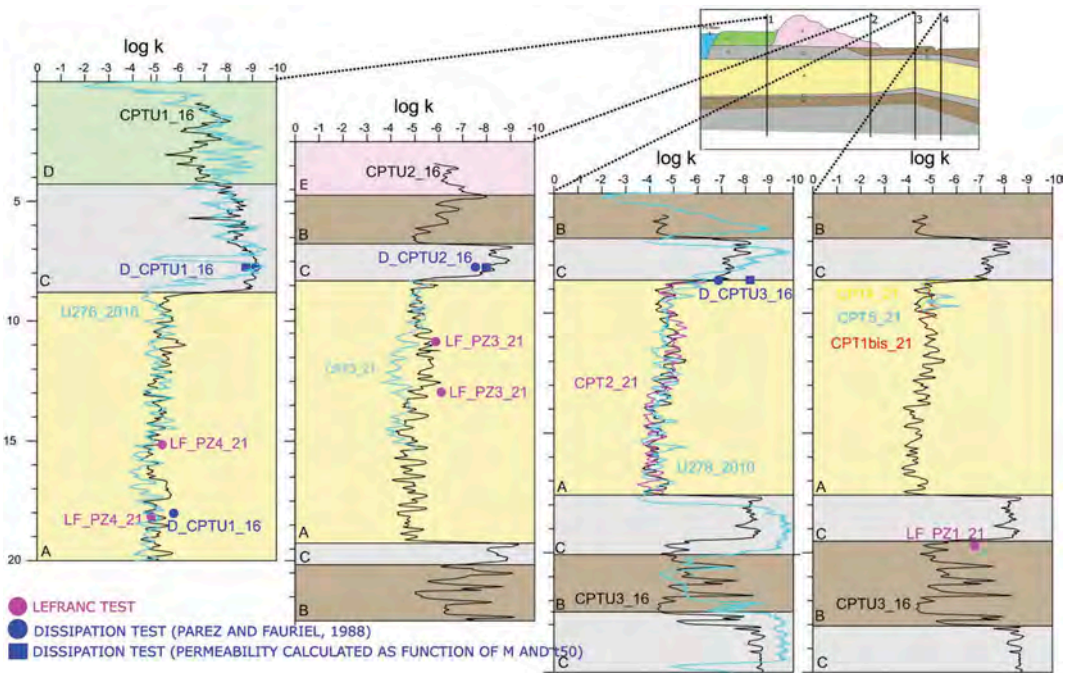


Figure 4. CPTU-based $\log k$ profiles in four different vertical alignments of the investigated river embankment section, in conjunction with permeability data deduced from Lefranc and dissipation tests.

Robertson's correlations are function of I_c , which generally relates well to soil grain size distribution, although this index is mainly intended to identify an in-situ soil behaviour.

The permeability profiles deduced using eqs. (1) and (2) are shown in Figure 4.

In addition, the frequency distributions of $\log(k)$, as deduced from CPTU data, are provided in Figure 5. This

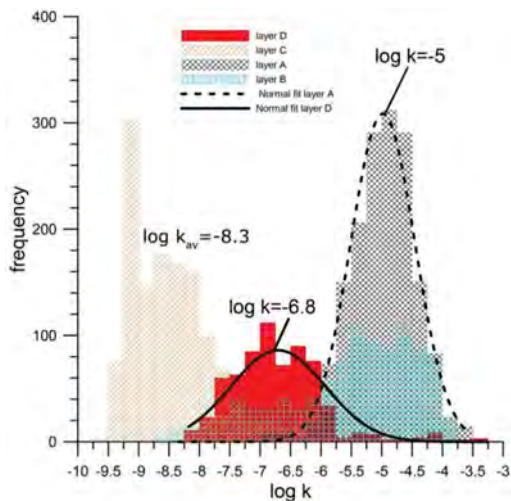


Figure 5. Frequency distribution of permeability data ($\log k$) from CPTU for each soil unit under investigation.

plot shows that the coarser layers A and D exhibit a bell-shaped distribution, typical of a normal distribution, while the heterogeneous unit B, characterized by alternations of silty-sands and sandy-silts, presents a bimodal distribution. In this case, the higher peak is found at $\log(k) = -4.75$ (i.e. $k = 10^{-4.75}$ m/s), typical of silty-sands, whereas the smaller peak corresponds to $\log(k) = -6.8$, consistent with sandy-silts. In unit C, the frequency distribution of $\log(k)$ is asymmetric, with a peak at -9.75 (thus low permeability clay) and mean value equal to -8.3 , the latter value corresponding to a permeability typical of silty-clayey soils. This outcome reflects the fact that unit C is an alternation of clay and silty-clay materials.

The analysis of soil permeability was also developed using no. 7 dissipation tests, carried out in the 2016 CPTU tests. These data have been analysed using two approaches: the well-established Parez and Fauriel (1988) simplified formulation, which provides estimates of the permeability k_h from the time for 50% excess pore pressure dissipation (t_{50}), and the correlation based on the 1D constrained modulus M and the coefficient of consolidation in horizontal direction $c_{h,h}$, according to the following formula:

$$k_h = (c_h \cdot \gamma_w) / M \quad (3)$$

where γ_w is the unit weight of water. In eq. (3), c_h has been approximated according to Robertson (2010):

Table 1. Mean values of soil permeability, as deduced from CPTU interpretation in terms of I_c and Parez and Fauriel (1988) method, and results from Lefranc tests (standard deviation given in brackets).

	Lefranc Test	log k (k in m/s)		Lefranc Test	k (m/s)	
		From dissipation	From CPTU (I_c)		From dissipation	From CPTU (I_c)
A	-6.05 (0.74)	-5.71 (0.38)	-5.04 (0.42)	8.91E-07	1.95E-06	9.12E-06
B	-5.79 (0.22)		-5.99 (0.79)	1.62E-06		1.02E-06
C		-8.33 (0.44)	-8.34 (0.79)		4.68E-09	4.57E-09
D			-6.54 (0.52)			1.62E-07
E			-6.08 (1.20)			1.17E-05

$$h = (1.67 * 10^{-6}) 10^{(1-\log t_{50})} \quad (4)$$

whereas the constrained modulus M has been estimated using the Robertson (2009) formulation, suggested for soils with $I_c > 2.2$ and thus including a wide variety of soils such as sandy silts, silts and clays:

$$M = \alpha_M (q_t - \sigma_{vo}) \quad (5)$$

with

$$\alpha_M = Q_m, \text{ when } Q_m \leq 14 \quad (6)$$

$$\alpha_M = 14, \text{ when } Q_m > 14 \quad (7)$$

being Q_m the stress-normalized corrected cone resistance, as defined in Robertson (2009).

Results from the analysis of dissipation tests are shown in Figure 4. It is worth observing here that the indirect determination of k described above requires a reliable interpretation of dissipation tests, which could be affected by partial drainage effects when performed in predominantly silty sediments (such as unit B). In this case, the estimate of t_{50} and c_h from dissipation tests, using standard approaches, might be somewhat inaccurate (Tonni et al., 2019).

The latest site investigation campaign, performed in 2021, also included n° 7 Lefranc tests (LF). These tests consist in the injection of water by gravity into

a chamber filled with gravel located at the bottom of a borehole and then in the measurement of the water level lowering with time. The permeability can be calculated using information on the geometry of the internal chamber (area, length and diameter) and the measurements of the variable head during the test.

The determination of the permeability by means of Lefranc test is particularly suitable for soils having permeability higher than 10^{-7} m/s, which corresponds to units B and A of the investigated subsoil.

The estimates of k , as obtained from the different methods described above, are all shown in Figure 4. It can be observed that local determination of the permeability, provided by interpretation of dissipation tests or by Lefranc tests, are generally in good agreement with CPTU-based profiles of k predicted using eqs. (1) and (2). As regards the vertical alignment n° 4, located on the right side of the ditch, close to the sand boil, the permeability obtained from the Lefranc test, at 14.5 m in depth, could be only compared with the permeability profile computed from CPTU3_2016, which is the closest piezocone test though located on the opposite side of the road embankment. Table 1 summarizes the average values of permeability obtained from the different methods. The table confirms what previously observed in Figure 4, i.e. that minor differences exist between dissipation-based-values of k and CPTU-based predictions provided by eqs. (1) and (2).

An additional data analysis is provided in Table 2, where the average and the standard deviation of $\log(k)$, as computed from piezocone tests, are reported for

Table 2. Mean values (standard deviation in brackets) of the permeability of each soil unit, as computed from each cone penetration test.

log k (k in m/s)	D	C	A	B	C2	B2	C3	E
CPTU1_2016_Berm	-6.86 (0.52)	-8.48 (0.51)	-5.11 (0.39)					
U277_2010_Crest		-8.57 (0.83)	-5.18 (0.54)	-6.54 (1.07)	-8.57 (1.06)	-5.25 (0.87)	-9.25 (0.29)	-6.08 (1.20)
CPTU02_2016_Outerslope	-6.59 (0.45)	-7.71 (1.22)	-5.06 (0.45)		-8.23 (0.52)	-6.80 (1.07)		
CPTU3_2016_BankToe		-8.48 (0.62)	-4.95 (0.41)	-6.11 (1.03)	-8.94 (0.76)		-8.91 (0.24)	

every soil unit, taking into account the increasing distance of the test from the river course. In this analysis, the fine-grained unit C has been divided into 3 distinct sub-units, namely the upper unit C and the deeper soil units C1 and C2 (see Figure 6). Similarly, the predominantly silty unit B has been divided into the shallowest unit B and the deep unit B2.

The differences in the permeability values within each soil unit appear to be small, thus indicating a substantial homogeneity in the horizontal direction. Such condition facilitates the numerical modelling of the phenomenon (García Martínez et al., 2018).

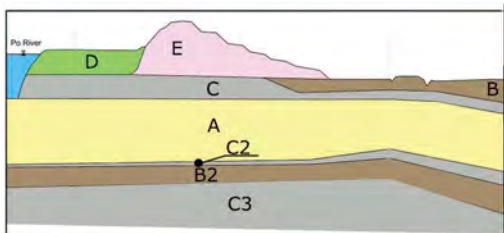


Figure 6. Stratigraphic section of the investigated river embankment with indication of the different soil units specified in Table 2.

In particular, a minor variability is observed between the average values of permeability in the aquifer A. Moving from the centre to the toe of the embankment, a slight increase of k is observed, likely due to a reduction of porosity beneath the embankment due to its self-weight.

5 CONCLUSIONS

The assessment of backward erosion piping susceptibility of river embankment systems requires the accurate estimate of the permeability of the soil units affected by underseepage, irrespective of the approach (numerical or analytical) adopted for the analysis.

In this study, the well-known Robertson's (2010) empirical formulation, providing profiles of the permeability k as a function of the Soil Behaviour Type Index, I_c , has been used to estimate the permeability of an aquifer and the blanket forming the subsoil of a river embankment prone to piping, along the major Italian watercourse. The comparison with alternative determinations of k , based on dissipation tests or Lefranc permeability tests, showed a good agreement between the estimates provided by the different methods.

According to results presented in this paper, cone penetration tests have proven to be a valuable strategy for the definition of the saturated permeability of the soil layers underlying the embankment. The estimation of permeability from I_c results in a continuous profile of k with depth, which appears to be an important added value in comparison with a limited number of local measurements from dissipation or Lefranc tests.

In this study, the use of a few CPTU, performed in different locations of the river embankment section (namely the berm, the crest, the toe of the embankment and in proximity of the sand boil) has provided information on the spatial variability of permeability. A negligible variation of this parameter has been observed, especially for the aquifer. Such an evidence potentially simplifies the analysis of the phenomenon since a unique mean value can be assumed as representative of the permeability of each soil unit.

Such outcomes, though preliminary, appear to be very promising in view of an intensive application of the method for the assessment of piping susceptibility of the river embankments along the mid-lower stretch of the Po.

REFERENCES

- Aielli S., Pavan S., Parodi S., Rosso A., Tanda M.G., Marchi M., Vezzoli G., Pantano A., Losa D., Sirtori M. 2019. Collection and analysis of the reactivation data of the historical sand boils in the po river levees. *Lecture Notes in Civil Engineering*, 17, 327–335.
- García Martínez M.F., Gottardi G., Marchi M., Tonni L. 2018. Modelling a sand boil reactivation in the middle-lower portion of the po river banks. *Numerical methods in geotechnical engineering IX*, 2, 1219–1225.
- García Martínez M.F., Tonni L., Marchi M., Tozzi, S., Gottardi G. 2020. Numerical tool for prediction of sand boil reactivations near river embankments. *Journal of Geotechnical and Geoenvironmental Engineering* 146 (12): 06020023.
- Marchi M., García Martínez M.F., Gottardi G., Tonni L. 2021. Field measurements on a large natural sand boil along the river Po (Italy). *Quarterly Journal of Engineering Geology and Hydrogeology* 54(4): qjehg2020–097
- Merli C., Colombo A., Riani C., Rosso A., Martelli L., Rosselli S., Severi P., Biavati G., De Andrea S., Fossati D., Gottardi G., Tonni L., Marchi M., García Martínez M.F., Fioravante V., Giretti D., Madiái C., Vannucchi G., Gargini E., Pergalani F., Compagnoni M. 2015. Seismic stability analyses of the Po River Banks. *Engineering Geology for Society and Territory 2: Landslide Processes*, 877–880.
- Parez, L. & Fauriel, R. 1988. Le piézocône améliorations apportées à la reconnaissance des sols. *Revue française de Géotechnique*, 44: 13–27.
- Robertson, P.K. 2009. Interpretation of cone penetration tests - a unified approach. *Canadian Geotechnical Journal* 46(11): 1337–1355.
- Robertson, P. K. 2010. Estimating in-situ soil permeability from CPT & CPTu. In: *Proc. 2nd International Symposium on Cone Penetration Testing*. Huntington Beach, California.
- Sellmeijer, H., Lopez de la Cruz, J., van Beek, V., Knoeff, H. 2011. Fine-tuning of the backward erosion piping model through small-scale, medium-scale and IJkdijk experiments. *European Journal of Environmental and Civil Engineering*, 15(8):1139–1154.
- Tonni L., García Martínez M.F., Rocchi I. 2019. Recent developments in equipment and interpretation of cone penetration test for soil characterization. *Rivista Italiana di Geotecnica* 53(1): 71–99.
- USACE. 2000. *Design and Construction of Levees*, U.S. Army Corps of Engineers. Washington, DC.

Dissipation tests to evaluate the equilibrium pore pressure

F.A.B. Danziger, G.M.F. Jannuzzi & A.V.S. Pinheiro

Coppe and Polytechnic School, Federal University of Rio de Janeiro, Brazil

ABSTRACT: Dissipation tests are carried out with two main purposes: the estimation of the horizontal coefficient of consolidation, $c_{h,}$ and the evaluation of the equilibrium pore pressure. Regarding the first case, even in soft clays the duration of the test doesn't need to be more than 40 minutes, in most situations. However, in the latter case a long time is needed to reach equilibrium, even when probes with small diameters are used. The present paper presents results of long-term dissipation tests performed in a soft clay layer, aiming at the decision of executing or not an underpinning of shallow foundations of a damaged warehouse which suffered significant settlements.

1 INTRODUCTION

According to Campanella & Robertson (1988), the pore pressure measurement during the penetration of a probe was carried out for the first time at the beginning of the 1970s, as described by Wissa et al. (1975) and Torstensson (1975). The main purpose of the Wissa et al.'s (1975) probe was to determine flow patterns through dams and pore pressure fluctuations due to waves and tides. However, this could only be achieved after the dissipation of the pore pressures generated during probe installation. Wissa et al. (1975) and Torstensson (1975) realized the enormous potential of the pore pressure measured during penetration, and Torstensson (1975) mentioned the possibility of assessment of the coefficient of consolidation from the time necessary to pore pressure dissipation.

It must be pointed out that Janbu & Senneset (1974) and Schmertmann (1974) also used a pore pressure probe and a Geonor electric piezometer, respectively, to investigate the pore pressure generation during the probe installation.

It is generally accepted that the piezocone was formally born (i.e., the joint measurement of cone resistance, $q_c,$ sleeve friction, $f_s,$ and pore pressure, u) at the beginning of 1980s, from the publication of several papers in the 1981's ASCE Symposium on Cone Penetration Testing and Experience held in St. Louis, and the 1982's II European Symposium on Penetration Testing held in Amsterdam.

Since then, dissipation tests have been used both to estimate the horizontal coefficient of consolidation, $c_{h,}$ and the evaluation of the equilibrium (or hydrostatic) pore pressure.

However, in the latter case, a long time is needed to reach equilibrium when tests are carried out in soft clays, even when probes with small diameters are

used. The present paper presents results of long-term dissipation tests performed aiming at the decision of executing or not an underpinning of a damaged warehouse.

2 DISSIPATION TESTS

2.1 General

Pore pressure dissipation occurs as soon as the probe penetration is halted, even for a simple rod addition in the rod stem. In general, tests are carried out on specific depths of particular interest for the soil investigation. The time for dissipation depends on the coefficient of consolidation and the diameter of the filter, the higher the coefficient of consolidation and the smaller the filter diameter the faster is the dissipation (e.g., Torstensson, 1977). In most soil types and regular piezocone 10 cm² penetrometers, full dissipation can be achieved in less than one hour. However, when tests are performed in soft clays full dissipation may need a few days. Nevertheless, since most methods use t_{50} to evaluate the coefficient of consolidation, in most cases 30–40 minutes of test duration is enough for the estimation of the coefficient of consolidation.

There are some methods to estimate the coefficient of consolidation from dissipation tests (e.g., Torstensson, 1977, Levadoux & Baligh, 1986, Houlsby & Teh, 1988, Danziger et al., 1997). The methods based on the Strain Path Method seem to be more used in practice.

2.2 The evaluation of the equilibrium pore pressure

Some engineering applications require the measurement of the equilibrium pore pressure, both onshore

and offshore. In the offshore case, the verification of the presence of gas on sediments to estimate the safety of pile foundations of platforms was carried out by Lunne et al. (1996). The determination of the so-called “drilling window” for the installation of jetted conductors in clays (e.g., Jeanjean et al., 2015) also requires the equilibrium pore pressure measurement.

In the onshore case, the previously mentioned determination of flow patterns through dams and pore pressure fluctuations due to waves and tides (Torstensson, 1975) are possible applications.

In all those cases, since tests have been performed in clays, the time required for full dissipation is significant, thus probes with small filter diameters have been used. Figure 1 presents pore pressure probes used offshore (Peuchen & Klein, 2011).

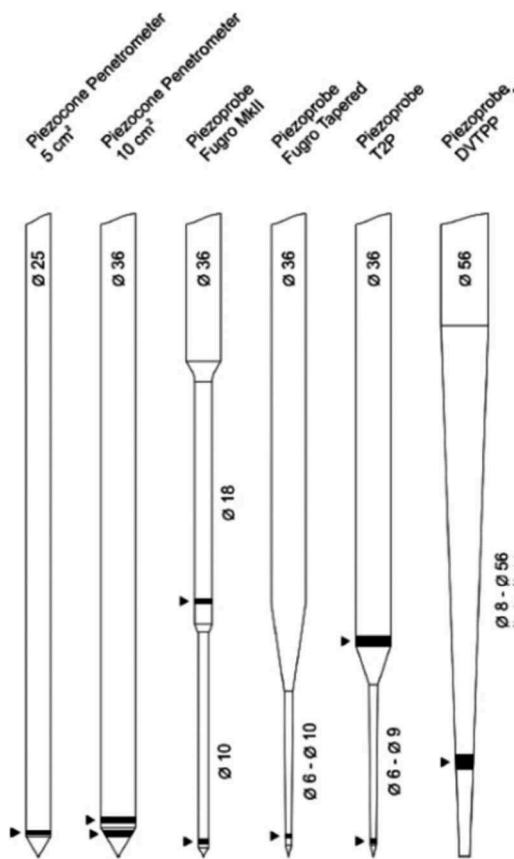


Figure 1. Small diameter pore pressure probes (Peuchen & Klein, 2011).

Another increasing application is the determination of pore pressure equilibrium for tailings dams, however in such cases probes with small filter diameters are not required, because in most cases sandy silts or silty sands constitute the materials to be tested. The time for full dissipation is not significant in those

materials, therefore regular 10 cm² penetrometers may be used.

In all cases, an issue with the measurement of the equilibrium pore pressure is the accuracy of the zero (reference) reading. Any possible variation must be avoided, since significantly influences the reliability of the measurements. A way to solve this issue is to use dual pore pressure penetrometers, which have been adopted by the Federal University of Rio de Janeiro since 1996 on regular basis (Bezerra, 1996, Danziger et al., 1997). The use of two independent pore pressure sensors eliminates any doubts regarding the reliability of the measurements. An example is presented in Figure 2, in which a pore pressure smaller than the hydrostatic (u_0), assumed as the water unit weight multiplied by the distance between the water table position and the tested depth, is verified.

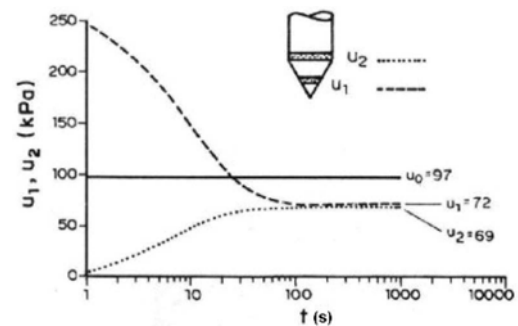


Figure 2. Dissipation test performed on the main Brazilian motorway with a dual pore pressure piezocone (Danziger et al., 1998, Danziger, 2007).

Since the material tested is dilative, the pore pressure u_2 at the onset of dissipation (time $t=0$), measured at the cone shoulder, recorded a negative excess pore pressure, because this position is dominated by the shear stresses. The pore pressure u_1 , measured at cone face, however, recorded a positive excess pore pressure at $t=0$, because this position is dominated by octahedral stresses. After a certain time both u_1 and u_2 record the same pore pressure, below the hydrostatic pressure. If only one sensor was available, doubts regarding the reliability of the measurements would certainly exist, because at that time there was no apparent reason for such an event. However, the measurements carried out triggered an investigation which discovered that a beer factory (not close to the tested site) was taking water from the ground, generating a reduction in pore pressure in depth.

3 THE CASE

A warehouse of an industry in the state of Rio de Janeiro, Brazil, presented serious damages due to

excessive settlements. The warehouse is founded on shallow foundations constructed on an embankment overlying a soft clay layer. The company in charge of the repair wanted to know whether the settlements had already ceased or were still under development. If they had ceased, just repairing the damaged construction would take place, whereas underpinning with deep foundations in addition to repairing the structure would be necessary to significantly reduce further displacements of the structure.

The soil profile from a CPT is presented in Figure 3, where it can be observed an upper embankment until 10.2 m depth, followed by a soft clay layer until 15.0 m depth. The water table is approximately 5.3 m below ground level.

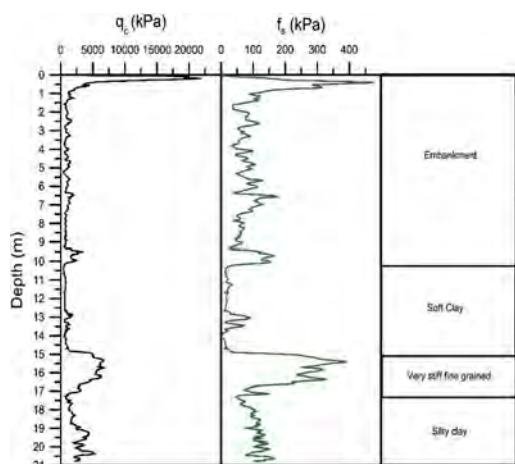


Figure 3. Soil profile.

It was not known whether the consolidation of the clay layer due to the embankment and surcharges on the ground had already ceased or not. Therefore, it was decided to verify whether the pore pressures generated by the loading had dissipated or not, by the measurement of the equilibrium pore pressures at different depths inside the clay material. Since the expected time for full dissipation would be significant, a pore pressure probe with a filter with a smaller diameter than a regular penetrometer (10 cm^2) would be used. The available probe has only one filter, 11.6 mm in diameter, made of sintered bronze (Figure 4), rather than two filters in the piezocone penetrometer routinely used by Coppe/UFRJ.

Since the interest of the measurements was only the soft clay layer, a casing borehole was executed until 8 m depth, which was filled with water. The probe was then inserted into the casing and pushed at a constant rate of 20 mm/s, the standard rate used for piezocone testing. It must be highlighted that: i) although several penetrometers are saturated with fluids like glycerin and silicon oil to keep saturation

when penetration is carried out on unsaturated material, the Coppe/UFRJ procedure is always to saturate the filter with water, following a procedure developed by NGI (Lacasse, 1980) in which vacuum is used; a parallel CPT is then carried out in the unsaturated soil; ii) the pore pressure is recorded during probe lowering inside the casing filled with water, which is then used to check the sensor calibration.

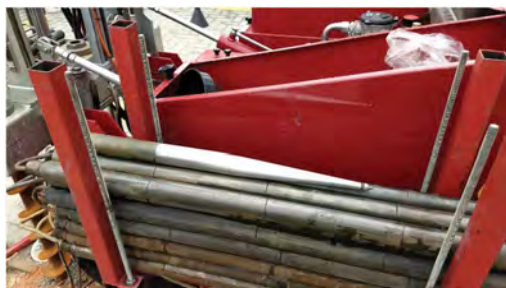


Figure 4. Pore pressure probe used for the determination of equilibrium pore pressure.

The pore pressure probe was pushed to 11.11 m, approximately 1 m below the top of the clay layer, then the dissipation was allowed to occur. The data acquisition system was kept inside a room adjacent to the test site, and the chart pore pressure versus time (in a log scale) was observed, and pictures were sent to the Coppe/UFRJ team, which had returned to the laboratory in Rio de Janeiro, to follow the

Table 1. Dissipation tests performed.

Test	Depth	Duration (day)
1	11.11	5
2	12.11	7
3	13.11	2
4	14.10	1
5	14.85	4



Figure 5. Picture showing a time close to the end of dissipation, 11.11 m test depth.

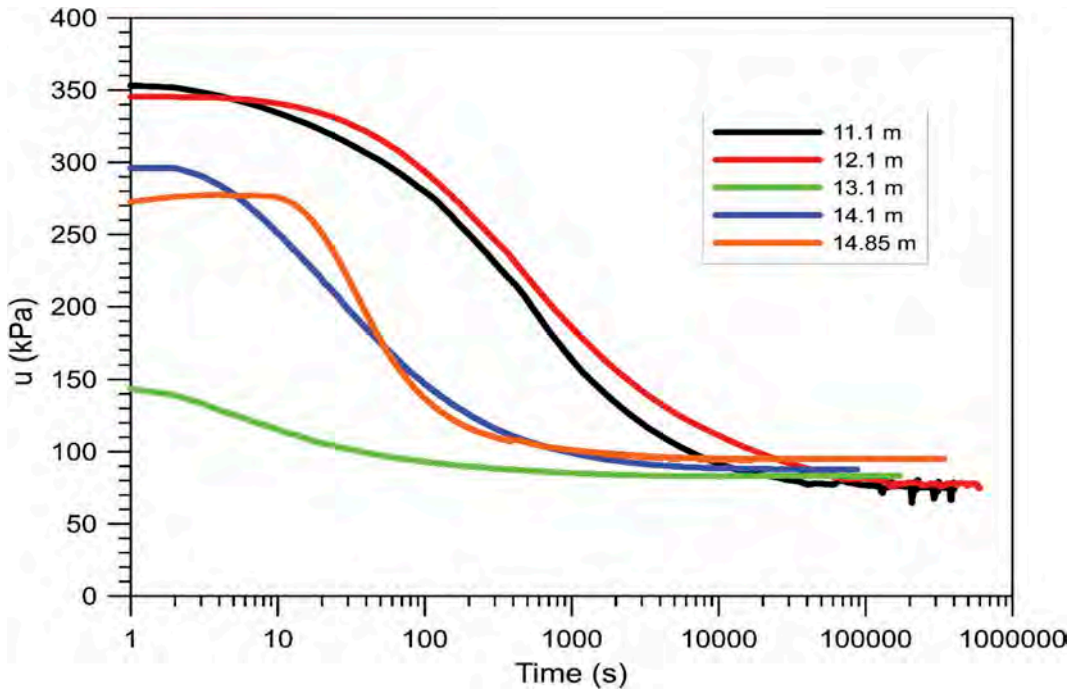


Figure 6. Dissipation tests performed.

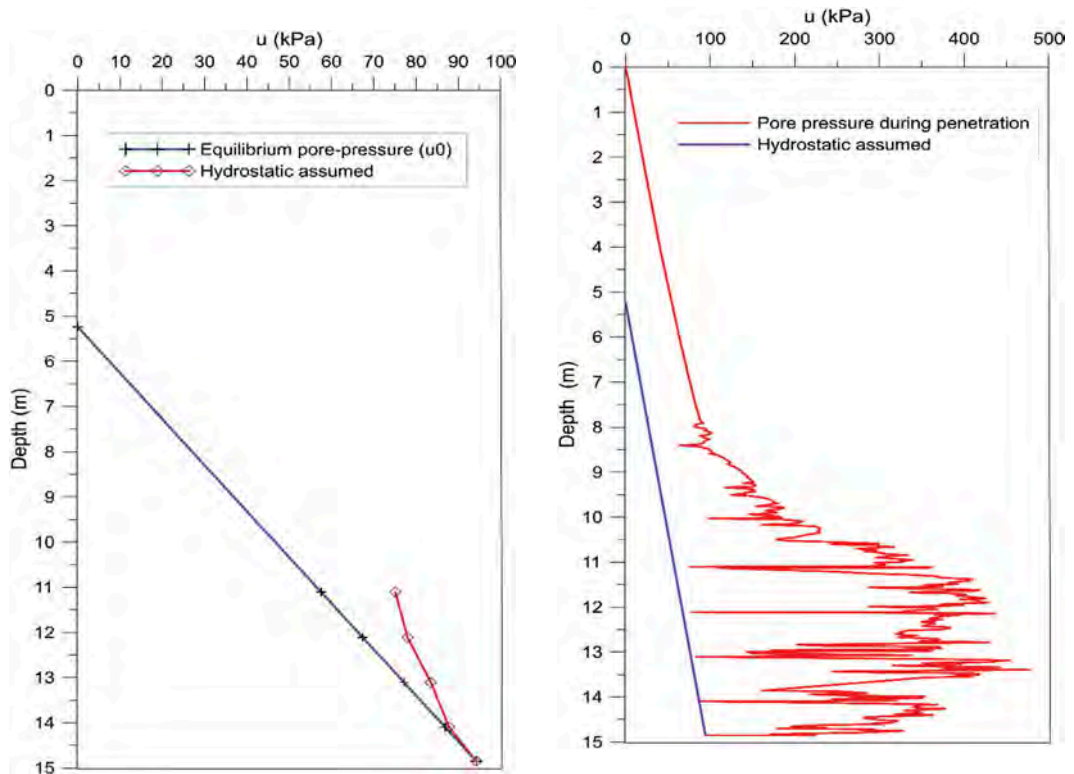


Figure 7. Equilibrium pore pressure versus depth of all tests.

Figure 8. Pore pressure measured during installation and dissipation.

dissipation remotely. Figure 5 shows one of such pictures, in which dissipation was considered almost completed. When this occurred, a member of the team traveled to the test site and pushed the probe to the next depth. Table 1 presents the tested depths and the duration of each test until complete dissipation. Figure 5 presents some oscillations in the final part of the test, which was attributed to loading – unloading activities near the test. Those activities were requested to be interrupted to not disturb the tests, especially in its final part.

Figure 6 presents all dissipation tests, and Figure 7 shows the equilibrium pore pressure versus depth of all tests. The assumed hydrostatic pore pressure, based on the water depth on top of the soft clay, is also shown in the figure. It can be observed that there is still an excess pore pressure in the soft clay, especially in shorter depths.

Figure 8 shows the pore pressure measured during installation (including during lowering the probe inside the 8 m long casing) and the dissipation tests.

Based on the obtained results, it was decided to underpin the shallow foundations of the warehouse.

4 SUMMARY AND CONCLUSIONS

Long-term dissipation tests with a pore pressure probe have been carried out in a soft clay layer. The tests aimed at the evaluation of the equilibrium pore pressure to know whether the soft clay was still under consolidation due to an embankment. A few days were necessary to reach full dissipation, even with the small diameter of the probe (11.6 mm) used. An excess pore pressure was measured in three out of the five tests performed, indicating that the clay was still under consolidation.

Based on these measurements, it was decided that an underpinning of the shallow foundations with deep foundations was necessary, in addition to repairing the damaged warehouse.

REFERENCES

- Bezerra, R.L. (1996). *Third generation of Coppe/UFRJ piezocone penetrometer* (in Portuguese). D.Sc. Thesis, COPPE/UFRJ, Rio de Janeiro.
- Campanella, R.G. & Robertson, P.K. (1988). Current status of the piezocone test - state-of-the-art report. *Proc., ISOPT-1*, Orlando, Vol. 1, pp. 93–116.
- Danziger, F. A. B. (2007). In Situ Testing of Soft Brazilian Soils. *Studia Geotechnica et Mechanica XXXIX*, 5–22.
- Danziger, F.A.B., Almeida, M.S.S. & Sills, G.C. (1997). The significance of the strain path analysis in the interpretation of piezocone dissipation data. *Géotechnique 47, No. 5*, 901–914.
- Danziger, F.A.B., Almeida, M.S.S. & Bezerra, R.L. (1997). Piezocone research at COPPE/Federal University of Rio de Janeiro, 1997. *Proc., Int. Symp. on Recent Developments in Soil and Pavement Mechanics*, Rio de Janeiro, pp. 229–236.
- Danziger, F.A.B., Almeida, M.S.S., Paiva, E.N., de Mello, L.G.F.S. & Danziger, B.R. (1998). The piezocone to determine stratigraphy and soil classification (in Portuguese). *Proc., XI COBRAMSEG*, Brasília, Vol. II, pp. 917–926.
- Houlsby, G.T. & Teh, C.I. (1988). Analysis of the piezocone in clay. *Proc., ISOPT-1*, Orlando, Vol. 2, pp. 777–783.
- Janbu, N. & Senneset, K. (1974). Effective stress interpretation of in situ static penetration test. *Proc., ESOPT*, Stockholm, Vol. 2-2, pp. 181–193.
- Jeanjean, P., Zakeri, A., Al-Khafaji, Z., Hampson, K. Clukey, E. & Liedtke, E. (2015). Geotechnics for wells top-hole section and conductor. *Frontiers in Offshore Geotechnics III – Meyer (Ed.)*, Taylor & Francis Group, London, Vol. 1, pp. 95–128.
- Lacasse, S. (1980). *Procedure for deairing the pore pressure probe in the laboratory*. NGI report 40015-6, Oslo.
- Levadoux, J.N. & Baligh, M.M. (1986). Consolidation after undrained piezocone penetration. I: prediction. *Journal of Geotechnical Engineering, ASCE 112, No. 7*, 707–726.
- Lunne, T., Isa, O.M. & Tan, M. (1996). Shallow gas problem at Duyong B offshore Malaysia. *Proc., 11th Offshore South East Asia Conf.*, Singapore.
- Peuchen, J. & Klein, M. (2011). Prediction of formation pore pressures for top hole well integrity. *Proc., Offshore Technology Conference*, Houston, TX, paper 21301.
- Schmertmann, J.H. (1974). Penetration pore pressure effects on quasi-static cone bearing, q_c . *European Symposium on Penetration Testing*, Stockholm, Vol. 2-2, pp. 345–351.
- Torstensson, B.A. (1975). Pore pressure sounding instrument. *Proc., Specialty Conf. on In Situ Measurement of Soil Properties, ASCE*, Raleigh, Vol. II, pp. 48–54.
- Torstensson, B.A. (1977). The pore pressure probe. *Fjellsprengningsteknikk, Bergmekanikk/ Geoteknikk*, 34.1–34.15.
- Wissa, A.Z.E., Martin, R.T. & Garlanger, J.E. (1975). The piezometer probe. *Proc., Specialty Conf. on In Situ Measurement of Soil Properties, ASCE*, Raleigh, Vol. I, pp. 536–545.

Dynamic characteristics of the soils by Cone Penetration Tests (CPT)

A. Cavallaro

CNR-ISPC, Catania, Italy

ABSTRACT: A geotechnical project requires a site-specific investigation to collect data regarding the sub-surface conditions. Soil explorations must be made to determine the presence and identification of underlying strata, groundwater conditions, types of geomaterials, their depths and thicknesses, and the associated engineering parameters required for geotechnical design. The Cone Penetration Test (CPT) represents one of the most widely used on-site investigation methods in geotechnical engineering. This paper presents some empirical correlations available by Cone Penetration Tests (CPT) for determining the main geotechnical characteristics of soils. Moreover it aims to evaluate the small strain shear modulus by means of empirical correlations based on penetration tests results, CPT, Standard Penetration Tests (SPT) and Flat Dilatometer Marchetti Tests (DMT) or laboratory geotechnical investigations. It is aimed to achieve a better understanding of the obtained geotechnical parameters and the empirical correlations, justifying the investigation effort and enabling reliable input data for advanced dynamic analysis.

1 INTRODUCTION

Currently, CPT static sounding is one of the most popular field study as its specificity provides rich quasi-continuous data at depth. The CPT results enable to infer the soil profile as well as strength and stiffness parameters even at great depths in a cost effective way (Robertson et al., 1986, Kulhawy & Mayne, 1990; Fellenius & Eslami, 2000; Powell & Lunne, 2005; Robertson, 2009; Mayne, 2020).

The results presented in the article add new data to the documented knowledge. The results of field studies and guidelines on the soil of Noto area have been described in previous publications (Cavallaro et al., 2003a, 2003b; Cavallaro & Maugeri, 2003), and the data from soundings are the basis for determining soil parameters (Mayne, 2016) and engineering calculations.

In the light of the above, linking the numerical results of CPT static sounding to the genesis of soil will bring significant benefits to geotechnicians and engineering geologists in terms of data interpretation.

This paper intends to propose a critical evaluation of geotechnical parameters (Cavallaro, 2020) with special attention for small strain shear modulus G_0 .

2 INVESTIGATION PROGRAM AND BASIC SOIL PROPERTIES

The Pliocene Noto deposits of Trubi Formation mainly consist of a medium stiff, over-consolidated

lightly cemented silty-clayey-sand (Cavallaro et al., 2003a; Cavallaro & Maugeri, 2003).

The pre-consolidation pressure σ'_p and the over-consolidation ratio $OCR = \sigma'_p / \sigma'_{v0}$ were evaluated from the 24h compression curves of incremental loading (IL) oedometer tests.

Moreover, Marchetti's flat dilatometer tests (DMT) were used to assess OCR and the coefficient of earth pressure at rest K_0 following the procedure suggested by (Marchetti, 1980).

For depths of about 15 m, DMT results show an OCR from 1 to 4.5 ($K_0 = 0.5 \div 1.0$).

The OCR values inferred from oedometer tests (OCR from 1 to 3) are lower than those obtained from in situ tests.

One possible explanation of these differences could be that lower values of the pre-consolidation pressure σ'_p are obtained in the laboratory because of sample disturbance.

The value of the natural moisture content w_n prevalently range from between 12 - 37 %. Characteristic values for the Atterberg limits are: $w_l = 37 - 69$ % and $w_p = 17 - 22$ %, with a plasticity index of $PI = 15 - 47$ %. The obtained data indicate a low degree of homogeneity with depth of the deposits (Cavallaro et al., 2003b; Cavallaro & Maugeri, 2003).

Shear modulus G and damping ratio D of Noto soil were obtained also in the laboratory by resonant column tests (RCT). These tests were performed on Shelby tube specimens retrieved from Noto site. The Resonant Column/Torsional shear apparatus were used for this purpose.

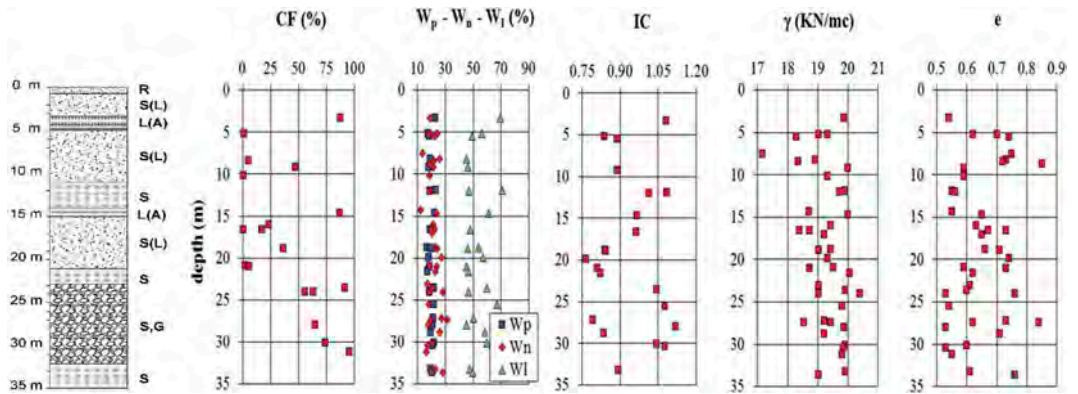


Figure 1. Borehole and index properties of Noto soil; where R: Landfill; S(L): Silty Sand; L(A): Clayey silt; S: Sand; S,G: Sand and Gravel.

3 EVALUATION GEOTECHNICAL PARAMETERS FROM CPT

CPT tests are widely used to investigate the subsoil in order to obtain information on the different physical-mechanical properties of the soils. Empirical laws are therefore available for determining the main geotechnical characteristics of soils.

The following geotechnical parameters have been determined:

- Total unit weight γ ;
- Angle of shear resistance ϕ' ;
- Undrained resistance c_u ;
- Shear modulus G_0 .

It is possible to evaluate the total weight unit γ by empirical correlations of CPT in situ measurement:

- Mayne et al. (2010):

$$\gamma_t = 11.46 + 0.33 \log(z) + 3.1 \log(f_s) + 0.7 \log(q_t) \quad (1)$$

where z = depth [m], f_s = sleeve friction resistance [kN/m^2] and q_t = corrected cone resistance [kN/m^2].

- Robertson & Cabal (2010):

$$\gamma/\gamma_w = 0.27 [\log(R_f)] + 0.36 [\log(q_t/P_a)] + 1.236 \quad (2)$$

where γ_w = water weight unit [kN/m^3], $R_f = (f_s/q_t)$ = friction ratio [-], q_t = corrected cone resistance [kN/m^2] and P_a = atmospheric pressure, expressed in the same unit of measurement of q_t .

- Mayne & Peuchen (2012):

$$a) \gamma_t = 26 - 14/[1 + 0.5 \log(f_s + 1)]^2 \quad (3)$$

$$b) \gamma_t = 12 + 1.5 \ln(f_s + 0.1) \quad (4)$$

for clays and sands.

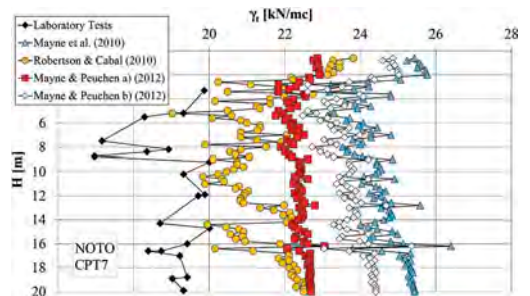


Figure 2. Total unit weight γ by empirical correlations based on CPT.

Figure 2 shows a comparison between the results obtained in the laboratory and those obtained by the empirical relationships proposed.

It is possible to observe that the results obtained are comparable even though the relationship proposed by Robertson & Cabal (2010) is better aligned with the experimental results.

Numerous empirical correlations have been proposed for the determination of ϕ' :

- Meyerhof (1951):

$$\phi' = 17 + 4.49 \ln(q_c) \quad (5)$$

where q_c = cone resistance [kg/cm^2].

- De Beer (1965):

$$\phi' = 5.9 + 4.76 \ln(q_c/\sigma'_{vo}) \quad (6)$$

where σ'_{vo} = effective vertical stress [kg/cm²].

- Dourgunouglu & Mitchell (1975):

$$\phi' = 14.4 + 4.8 \ln(q_c) - 4.5 \ln(\sigma'_{vo}) \quad (7)$$

the terms q_c and σ'_{vo} are expressed in the same unit of measurement [kg/cm²].

- Robertson et al. (1983):

$$\tan \phi' = 1/2.68 [\log(q_c/\sigma'_{vo}) + 0.29] \quad (8)$$

the terms q_c and σ'_{vo} are expressed in the same unit of measurement [kPa].

- Kulhawy & Mayne (1990):

$$\phi' = 17.6 + 11 \log[q_c/(\sigma'_{vo} \cdot \sigma_{atm})] \quad (9)$$

where $\sigma_{atm} = p_a$ = atmospheric pressure, expressed in the same unit of measurement of q_c [kPa].

- Marchetti (1997):

$$\phi' = 28 + 14.6 \log(K_D) - 2.1 [\log(K_D)]^2 \quad (10)$$

where K_D = horizontal stress index by DMT ($q_c/\sigma'_{vo} \approx 33 \cdot K_D$).

- Jefferies & Been (2006):

$$\phi' = \phi_{cv} + 15.84[\log(Q_m)] - 26.88 \quad (11)$$

where ϕ_{cv} = constant volume friction angle and $Q_m = (q_t - \sigma_{vo})/\sigma'_{vo}$ normalized cone resistance.

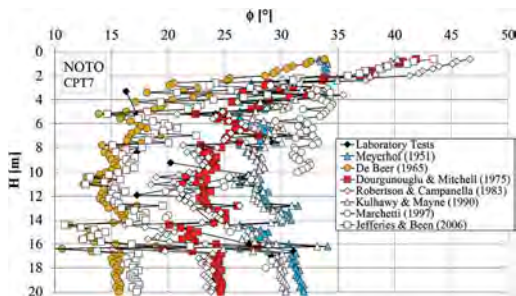


Figure 3. Angle of shear resistance ϕ' by empirical correlations based on CPT.

Regarding the results obtained for the angle of shear resistance ϕ' , reported in Figure 3, it is observed that the values obtained in the laboratory by direct shear tests intersect all the empirical relationships proposed. Probably because these relationships fail to, evaluate correctly the stratigraphic variations of the soil. High values of ϕ' were obtained in correspondence of the most superficial layers where no laboratory data is available. Overall, the Robertson & Campanella (1983) equation seems to approximate better the results of the direct shear tests.

As for the evaluation of the undrained resistance c_u the following empirical expressions were used:

- Lunne et al. (1976):

$$c_u = (q_c - \sigma_{vo})/(20.7 - 0.18 PI) \quad (12)$$

where PI = plasticity index.

- Lunne & Kleven (1981) and Lunne et al. (1997):

$$c_u = (q_c - \sigma_{vo})/N_k \quad (13)$$

where N_k = empirical factor for bearing capacity dependent on depth and opening angle of the penetrometer cone (11 - 19).

Figure 4 shows the c_u values obtained by laboratory tests and empirical correlations. The laboratory data aligns well with the c_u values derived from the correlations. High values of undrained resistance were obtained by the expression of Lunne & Kleven (1981) on the surface layers and at a depth of about 16 m.

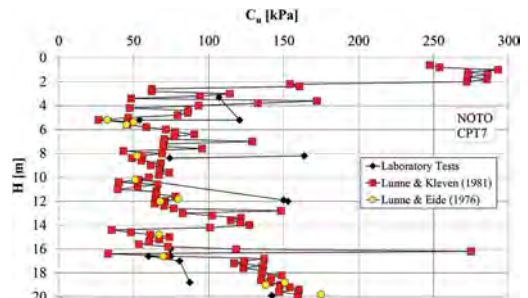


Figure 4. Undrained resistance c_u by empirical correlations based on CPT.

4 EVALUATION G_0 FROM CPT

The small strain shear modulus G_0 can be evaluated by laboratory Resonant Column Tests (RCT) (Capillieri et al., 2014; Castelli et al., 2016a) or in situ by Down Hole tests and SDMT (Castelli et al., 2016b; Cavallaro et al., 2012a, 2012b; Marchetti et al., 2008; Cavallaro

& Grasso, 2021) using the relationships: $G_o = \rho V_s^2$ (where: ρ = mass density) based on theory of elasticity.

An attempt was made to evaluate the small strain shear modulus by means of the following empirical correlations based on penetration tests results, CPT, SPT and DMT or laboratory results available in literature (Figure 5).

- Imai & Tomaichi (1990):

$$G_o = 28 \cdot (q_c)^{0.611} \quad (14)$$

for any soil.

- Mayne & Rix (1993):

$$G_o = \frac{406 \cdot q_c^{0.696}}{e^{1.13}} \quad (15)$$

for clayey strata;

where: G_o and q_c are both expressed in [kPa] and e is the void ratio. Equation (15) is applicable to clay deposits only.

- Simonini & Cola (2000):

$$G_o = 49.2 \cdot (q_t)^{0.51} \quad (16)$$

It is also possible to evaluate the small strain shear modulus using the relation $G_o = \rho \cdot V_s$ by the following equations proposed by Ohta & Goto (1978) and Yoshida and Motonori (1988) for the shear waves velocity V_s :

- Ohta & Goto (1978):

$$V_s = 69 \cdot N_{60}^{0.17} \cdot Z^{0.2} \cdot F_A \cdot F_G \quad (17)$$

where: V_s = shear wave velocity (m/s), N_{60} = number of blow/feet from SPT with an Energy Ratio of 60 %, Z = depth (m), F_G = geological factor (clays = 1.000, sands = 1.086), F_A = age factor (Holocene = 1.000, Pleistocene = 1.303)

- Yoshida and Motonori (1988):

$$V_s = \beta \cdot (N_{SPT})^{0.25} \cdot \sigma'_{v0}{}^{0.14} \quad (18)$$

where: V_s = shear wave velocity (m/s), N_{SPT} = number of blows from SPT, σ'_{v0} = vertical pressure, β = geological factor (any soil=55, fine sand=49).

- Hryciw (1990):

$$G_o = \frac{530}{(\sigma'_v/p_a)^{0.25}} \frac{\gamma_D/\gamma_w - 1}{2.7 - \gamma_D/\gamma_w} K_o^{0.25} \cdot (\sigma'_v \cdot p_a)^{0.5} \quad (19)$$

where: G_o , σ'_v and p_a are expressed in the same unit; $p_a = 1$ bar is a reference pressure; γ_D and K_o are respectively the unit weight and the coefficient of earth pressure at rest, as inferred from DMT results according to Marchetti (1980).

- Jamiolkowski et al. (1995):

$$G_o = \frac{600 \cdot \sigma'_m{}^{0.5} p_a^{0.5}}{e^{1.3}} \quad (20)$$

The Jamiolkowski et al. (1995) method was applied considering a given profile of void ratio.

The values for parameters, which appear in equation (20), are equal to the average values resulting from laboratory tests performed on quaternary Italian clays and reconstituted sands.

Equation (20) incorporates a term, which expresses the void ratio; the coefficient of earth pressure at rest only appears in equation (19). However only equation (19) tries to obtain all the input data from the DMT results.

As regard Noto soil the G_o values obtained with the methods above indicated for CPT and SPT are plotted against depth in Figure 5.

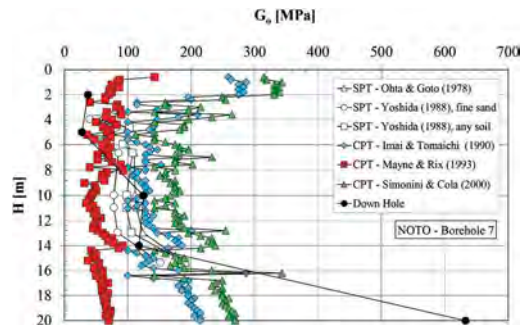


Figure 5. Small strain shear modulus G_o by empirical correlations based on CPT and SPT.

The results obtained show a greater similarity between the G_o results obtained by the empirical correlations proposed for SPT, which, moreover, are quite close together. The G_o values, obtained through the correlation equations proposed for CPT are more dispersed and higher.

The lowest values of the shear modulus are obtained by the equation proposed by Mayne & Rix (1993). Only by the Down Hole test it is possible to identify the rapid increase of G_o at a depth of 20 m in correspondence with some layer characterized by higher mechanical characteristics that both CPT and SPT cannot identify.

The N_{60} values, experimentally determined during SPT, did not show any important variation in the transition zone at depth of 20 m, where the characteristics of the soil change from silty sand to sand and then to sand with gravel.

Standard Penetration Tests were performed at intervals from 1.5 to 3.0 m. The quite large interval used could explain why the thin sand layers were not detected. Consequently, the obtained G_o values, in the transition zone, resulted to be quite low.

Unfortunately, the depth investigated by DMT is not able to intercept the most consistent layers of sand and sand with gravel. However, the method by Hryciw (1990) is the best one to follow the trend of the results obtained from the Down Hole tests, as can be seen in Figure 6.

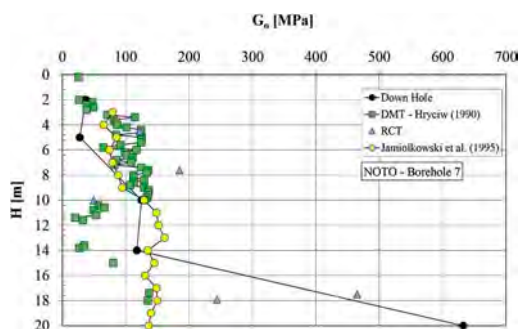


Figure 6. G_o from Down Hole, empirical correlation and RCT.

From a comparison between Figure 5 and Figure 6 all the considered methods show very different G_o values of the Pliocene Noto soil. On the whole, Down Hole seem to provide the most accurate trend of G_o with depth even if the available data are unable to investigate the behavior of the soil for depths greater than 20 m. The method by Jamiolkowski et al. (1995) was applied considering a given profile of void ratio but while guaranteeing continuity of results, it fails to intercept the most consistent layers of sand and sand with gravel.

In Figure 6 the RCT results are also reported. The data obtained also show as the dynamic laboratory tests are able to interpret the G_o trend obtained from the Down Hole test.

Figure 7 reports a comparison between DH test measurements and the corresponding empirical correlations. Since the DH test was performed with an interval of about 5 m, it was necessary to interpolate the intermediate values. From the comparison obtained it is possible to observe a more disordered initial phase in correspondence with the more superficial layers while subsequently a horizontal linear relationship is highlighted with the exception of the depth of 16.20 m.

5 CONCLUDING REMARKS

A site characterization for a possible advanced dynamic response analysis has been presented in this

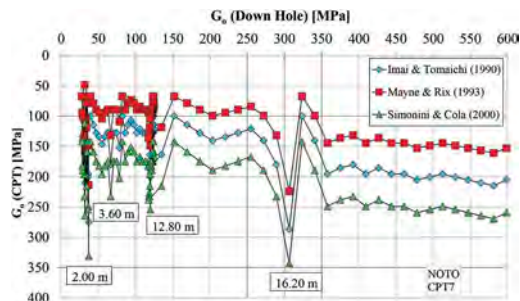


Figure 7. G_o from Down Hole vs G_o by empirical correlation.

paper. On the basis of the data shown it is possible to draw the following conclusions:

- empirical correlations between the small strain shear modulus and penetration test results were used to infer G_o from SPT, CPT, DMT and Down Hole. This comparison clearly indicates that a certain relationship exists between G_o and the penetration test results, which would encourage to establish empirical correlations for a specific site. This approach makes it possible to consider the spatial variability of soil properties in a very cost effective way.
- The values of G_o were compared to those measured with DMT and DH tests. This comparison indicates that some agreement exists between empirical correlations by DMT and DH test.
- relationships like those proposed by Jamiolkowski et al. (1995) seem to be capable of predicting G_o profile with depth only in the initial strata. The accuracy of these relationships could obviously be improved if the parameters, which appear in the equations, were experimentally determined in the laboratory for a specific site.
- Down Hole test only is probably able to investigate correctly the various layers of soil, identifying even the smallest variations in the mechanical characteristics.

REFERENCES

- Capilleri, P., Cavallaro, A. & Maugeri, M., 2014. Static and Dynamic Characterization of Soils at Roio Piano (AQ). *Italian Geotechnical Journal*, vol. XLVIII, no. 2, Aprile - Giugno 2014, Patron Editore, 38-52.
- Castelli, F., Cavallaro, A., Grasso, S. & Ferraro, A., 2016a. In Situ and Laboratory Tests for Site Response Analysis in the Ancient City of Noto (Italy). *Proc. of the 1st IMEKO TC4 Int. Workshop on Metrology for Geotechnics*, Benevento, 17-18 March 2016, 85-90.
- Castelli, F., Cavallaro, A. & Grasso, S., 2016b. SDMT Soil Testing for the Local Site Response Analysis. *Proc. of the 1st IMEKO TC4 Int. Workshop on Metrology for Geotechnics*, Benevento, 17-18 March 2016, 143-148.

- Cavallaro A., Massimino M. R., Maugeri M., 2003a. Noto Cathedral: Soil and Foundation Investigation. *Construction and Building Materials*, no. 17, 2003, 533–541.
- Cavallaro, A., Maugeri, M. & Ragusa, A., 2003b. Small Strain Stiffness from in Situ and Laboratory Tests for the City of Noto Soil. *Proc. of the 3rd International Symposium on Deformation Characteristics of Geomaterials*, Lyon, 22-24 September 2003, 267–274.
- Cavallaro, A. & Maugeri, M., 2003. Site Characterization by In-Situ and Laboratory Tests for the Microzonation of Noto. *Proc. of Symposium on Geotechnical Analysis of Seismic Vulnerability of Monuments and Historical Sites*, Catania, 15 November 2001, Geotechnical Analysis of Seismic Vulnerability of Monuments and Historical Sites, Patron Editor, 2003, Edited by Maugeri M. and Nova R., 237–256.
- Cavallaro, A., Grasso, S., Maugeri, M. & Motta, E., 2012a. An Innovative Low-Cost SDMT Marine Investigation for the Evaluation of the Liquefaction Potential in the Genova Harbour (Italy). *Proc. of the 4th Int. Conf. on Geotechnical and Geophysical Site Characterization*, ISC⁴, Porto de Galinhas, 18-21 September 2012, vol. 1, 2013, 415–422.
- Cavallaro, A., Grasso, S., Maugeri, M. & Motta, E., 2012b. Site Characterisation by in Situ and Laboratory Tests of the Sea Bed in the Genova Harbour (Italy). *Proc. of the 4th Int. Conf. on Geotechnical and Geophysical Site Characterization*, ISC⁴, Porto de Galinhas, 18-21 September 2012, vol. 1, 637–644.
- Cavallaro, A., 2020. Use of CPT for the Study of the Dynamic Properties of the Soils. *Proc. of the IMEKO TC4 International Conference on Metrology for Archaeology a Cultural Heritage*, Trento, 22-24 October 2020, 242–247.
- Cavallaro, A. & Grasso, S., 2021. Small Shear Strain Modulus Degradation by the Seismic Dilatometer Marchetti Tests (SDMTs). *Proc. of the 6th International Conference on Geotechnical and Geophysical Site Characterisation*, Budapest, 26-29 September 2021.
- De Beer, E.E., 1965. Bearing Capacity and Settlement of Shallow Foundations on Sand. *Proc. of the Symposium on Bearing Capacity and Settlement of Foundations*, Duke University, 15–33.
- Dourgunouglu, H.T. & Mitchell, J.K., 1975. Static Penetration Resistance of Soils: I - Analysis. *Proc. of the ASCE Specialty Conference on In-situ Measurement of Soil Parameters*. Raleigh, N.C., 151–171.
- Fellenius, B.H. & Eslami, A., 2000. Soil Profile Interpreted from CPTu Data. *Proc. of the Geotechnical Year 2000*, Asian Inst. of Technology, Thailand, 27-30 November 2000, p. 18.
- Hryciw, R.D., 1990. Small Strain Shear Modulus of Soil by Dilatometer. *JGED, ASCE*, vol. 116, no. 11, 1700–1715.
- Jamiolkowski, M., Lo Presti, D. C. F. & Pallara, O., 1995. Role of In-Situ Testing in Geotechnical Earthquake Engineering. *Proc. of the 3rd Int. Conf. on Recent Advances in Geotechnical Earthquake Engineering and Soil Dynamics*, St. Louis, Missouri, 2-7 April 1995, vol. II, 1523–1546.
- Jefferies, M.G. & Been, K., 2006. Soil Liquefaction - A Critical State Approach. *Taylor & Francis*, 478 pages.
- Kulhawy, F.H. & Mayne, P.W., 1990. Manual on Estimating Soil Properties for Foundation Design. *Report EL-6800, Electric Power Research Institute*, Palo Alto, Ca.
- Lunne, T.J., de Ruiter, J. & Eide, O., 1976. Correlation between Resistance and Vane Shear in Some Scandinavian Soft to Medium Stiff Clays. *Canadian Geotechnical Journal*, 13, 430–441.
- Lunne, T. & Kleven, A., 1981. Role of CPT in North Sea Foundation Engineering. *Symposium on Cone Penetration Engineering Division*, ASCE, 49–75.
- Lunne, T., Robertson, P. & Powell, J., 1997. Cone Penetration Testing in Geotechnical Practice. *Blackie Academic and Professional*, Chapman and Hall.
- Marchetti, S., 1980. In Situ Tests by Flat Dilatometer. *Journal of Geotechnical Engineering*, ASCE, 1980, no. GT3.
- Marchetti, S., 1997. The Flat Dilatometer Design Applications. *Proc. of the 3rd Geotechnical Engineering Conference*, Cairo University, 5-8 January 1997.
- Marchetti, S., Monaco, P., Totani, G. & Marchetti, D., 2008. In Situ Tests by Seismic Dilatometer (SDMT). *From Research to Practice in Geotechnical Engineering*, ASCE Geotech. Spec. Publ. no. 170, New Orleans, 9-12 March 2008.
- Mayne, P.W. & Rix, G.J., 1993. Gmax-qc Relationships for Clays. *Geotechnical Testing Journal*, vol. 16, no. 1, 54–60.
- Mayne, P.W., Peuchen, J. & Bouwmeester, D., 2010. Soil Unit Weight Estimated from CPTu in Offshore Soils. *Frontiers in Offshore Geotechnics II* (Proc. ISFOG 2010, Perth), Taylor & Francis Group, London: 371–376.
- Mayne, P.W. and Peuchen, J., 2012. Unit Weight Trends with Cone Resistance in Soft to Firm Clays. *Geotechnical and Geophysical Site Characterization 4*, vol. 1, CRC Press, London: 903–910.
- Mayne, P.W., 2016. Evaluating Effective Stress Parameters and Undrained Shear Strengths of Soft-Firm Clays from CPTu and DMT. *Proc. of the 5th International Conference on Geotechnical and Geophysical Site Characterization*, ISC 2016, vol. 1, 400, July 2016, 19–39.
- Mayne, P.W., 2020. Use of In-Situ Geotechnical Tests for Foundation Systems. *Proc. Széchy Károly Emlékkonferencia*, no. 402, 12–73 September 2020.
- Meyerhof, G.G., 1951. The Ultimate Bearing Capacity of Foundations. *Geotechnique*, 2, 301–332.
- Ohta, Y. & Goto, N., 1978. Empirical Shear Wave Velocity Equations in Terms of Characteristic Soil Indexes. *Earthquake Engineering and Structural Dynamics*, vol. 6, 1978.
- Powell, J.J.M. & Lunne T., 2005. Use of CPTu Data in Clays/Fine Grained Soils. *Studia Geotechnica et Mechanica*, vol. 27, no. 3-4, 431, 29–66.
- Robertson, P. K., Campanella, R.G. & Wightman A., 1983. SPT-CPT Correlations. *Journal of the Geotechnical Engineering Division*, vol. 108, no. GT 11, 1449–1459.
- Robertson, P.K., Campanella, R.G., Gillespie, D. & Greig J., 1986. Use of Piezometer Cone Data. *In-Situ '86 Use of In-situ testing in Geotechnical Engineering*, GSP 6, ASCE, Reston, VA, Specialty Publication, SM 92, 1263–1280.
- Robertson P. K., 2009. Interpretation of Cone Penetration Tests a Unified Approach. *Canadian Geotechnical Journal*, vol. 46, 435, no. 11, 1337–1355.
- Robertson, P. K. & Cabal, K. L., 2010. Guide to Cone Penetration Testing for Geotechnical Engineering, *Gregg Drilling & Testing*.
- Simonini, P. & Cola S., 2000. On the Use of the Piezocone to Predict the Maximum Stiffness of Venetian Soils. *Journal of Geotechnical and Geoenvironmental Engineering*, vol. 126, no. 4, 378–382.
- Yoshida, Y., and Motonori, I. 1988. Empirical Formulas of SPT Blow-Counts for Gravelly Soils. *Proc. of ISOPT-1*, Orlando (USA).

Validating cone penetration test in partially drained conditions using a simplified numerical modelling method

R.W.L. Chia, Z.Z. Wang & S.H. Goh

Department of Civil and Environmental Engineering, National University of Singapore, Singapore

ABSTRACT: A simplified numerical modelling method, the Press-Replace Method (PRM), is applied to simulate the cone penetration process under conditions that range from fully undrained to fully drained. In this study, rigorous validations of the PRM technique for simulating the cone penetration test were performed. The results for a fully undrained and drained penetration are compared against published information using cone factor solutions. Coupled-consolidation analyses at different cone penetration rates were then carried out for a smooth cone, and the results processed to obtain the dimensionless backbone curves for comparison with published data. The consolidation analyses were further extended to a rough cone subjected to different penetration rates, for which there is little, if any, numerical simulation results reported in the literature. The results and computed backbone curves obtained using the smooth and rough soil-cone interfaces are presented and compared in this paper.

1 INTRODUCTION

The cone penetration test (CPT) is a widely used site investigation tool for the characterization of soil and the estimation of engineering properties through empirical and theoretical correlations. This method of testing provides a continuous profiling of the ground. The cone penetration in a clayey soil would typically be considered as an undrained process, whereas in a sandy soil, it is assumed as a drained process. Probable issues may arise when penetration occurs in intermediate soil layers whereby the penetration process is neither undrained nor drained. The majority of existing theoretical and empirical solutions to determine soil properties are based on the assumption of either a fully undrained or a fully drained condition. As such, partially drained conditions could complicate the interpretation of results.

In this study, finite element analysis is employed to model the penetration process in partially drained conditions, by simulating the penetration at different rates. Experimental studies in the published literature indicate that, when the rate of pore pressure dissipation is faster than the penetration rate, the soil near the cone consolidates during penetration. As a result, a higher tip resistance is expected as compared to undrained conditions (Lehane et al., 2009; Oliveira et al. 2011).

To model the large deformation scenarios like cone penetration, different types of modeling techniques (e.g. Updated Lagrangian, Arbitrary Lagrangian Eulerian (ALE) and Remeshing Interpolation Technique combined with Small-Strain (RITSS)) have been used to overcome the numerical issues

associated with the large distortions of the discretized finite element mesh, many of which require additional subroutines. In this paper, a simplified method, the Press-Replace Method (PRM), is used to simulate the process of cone penetration. PRM can be easily implemented in standard small-strain finite element programs without the need for additional subroutines to execute remeshing or a mesh update.

PRM was first introduced to model suction anchors (Andersen et al 2004), and was refined and employed to model the installation of piles and spudcan (Engin et al., 2015; Sivasithamparam et al., 2015; Wang & Goh, 2018). A preliminary study of cone penetration was conducted by Engin et al. (2015) by comparing cone factors with other published literatures. Paniagua et al. (2014) compared numerical results obtained through PRM with laboratory scale cone penetration experiments. PRM was also used to simulate undrained cone penetration tests by Lim et al. (2018), who validated its performances in stress magnitude, principal stress direction and excess pore pressure against other existing numerical approaches such as LDPE, SSFE and MPM. More recent advances in PRM for cone penetration problems were presented by Paniagua et al. (2021), in which soil stresses and pore pressure measurements of a model scale penetration test with varying penetration rates were compared against the results from PRM back-analyses. However, the study only considered three different orders of penetration rates.

As the application of PRM to simulate cone penetration test in partially drained conditions has not been widely reported in the literature, an attempt to

rigorously validate its performance in partially drained conditions is presented in this paper. This paper first provides a concise summary of PRM and its implementation in the finite-element program PLAXIS 2D. Secondly, results obtained in partially drained conditions will be processed and compared against information from published literatures. Lastly, the influence of different soil-cone roughness on the penetration process under partially drained conditions will be briefly examined.

2 METHODOLOGY

PRM models penetration problems via a displacement control scheme (Engin et al., 2015), in which a prescribed displacement is first applied to the cone shaft to simulate the incremental pressing of the cone into the soil. This is followed by the replacement of that slice of the soil (through which the cone has incrementally penetrated) by the cone material. This systematic ‘press-and-replace’ process is presented in Figure 1. Figure 1 illustrates a standard 36mm diameter cone with some initial embedment. The intended downward incremental movements of the cone are represented by slices below the cone that are set up during the mesh generation process. The thickness of the slices is defined as t_s . Interface elements were added to the sides of these slices to model the interaction between the soil and cone. These interfaces were extended slightly beyond the corners of the slices; these interface extensions help reduce stress fluctuations around the angled corners of the cone. The length of these extensions is defined as $i_{int-ext}$.

The process starts with a prescribed downward displacement u_y ($= 0.1D$, where D is the cone diameter) of the cone over the thickness of one slice t_s (also equal to $0.1D$). This represents a “press” phase. Within the same phase, the interfaces and the interface extensions bounding the cone are activated. Upon completion of this phase, the stress states of the soil elements in the deformed mesh will correspond to those caused by the pressing of the cone over the prescribed incremental depth. In the next phase, the soil material that was originally occupying the slice below the cone (in the preceding phase) will be changed to the cone material, thus making this the “replace” phase. To increase the penetration depth to $0.2D$, the “press” phase is repeated and u_y is increased from $0.1D$ to $0.2D$. As the cone advances downward, the cycle of “press” and “replace” is repeated. Accordingly, more slices must be created for greater penetration depths. To ease calculation time, after the initial “press” phase, successive “press” and “replace” phases can be combined into one phase. Negligible or little difference in the computed cone resistance was observed (Lim, 2017).

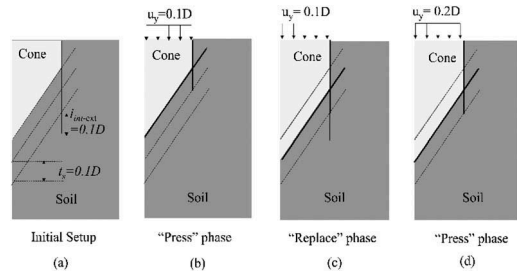


Figure 1. An example of PRM technique for cone penetration; a) Initial Setup, b) First “press” phase c) “replace” phase d) Subsequent “press” phase.

3 NUMERICAL MODELLING

3.1 Model dimensions and soil models

The FEM program used in this study is PLAXIS 2D CONNECT Edition V21. Investigations were carried using a standard cone diameter (D) of 36mm and a tip angle of 60° with an axisymmetric setup. As this paper involves a comparison study using published data from multiple sources (Yi et al., 2012; Sheng et al., 2014; Ceccato et al., 2016; Orazalin et al., 2018) with different model set-ups and assumptions, the following standardized procedures were adopted in all the PRM models of this study for simulating the different cases. These are: 1) As recommended by Engin et al. (2015), $\Delta u_y = t_s = i_{int-ext}$ of $0.1D$ will be adopted; 2) The initial setup begins with a soil body, which is followed by the first “press” that represents the embedment of the cone (Figures 2, 3) When required, the overburden stress in the soil will be modeled using a surcharge loading imposed by a 0.05m thick linear-elastic soil layer with the appropriate unit weight. The model dimensions adopted will follow those reported in the respective source literatures. Key details of these literatures and their soil models are summarized in Table 1. Figure 2 illustrates a typical finite element setup used in this study.

3.2 Soil-cone interface

Interfaces elements were used to model the interaction between the soil and cone surfaces. With each incremental advancement (Δu_y) of the cone, the interface elements bounding the entire penetrometer are activated. Interface elements allow for slippage (relative movement between the cone and the adjacent contacting soil) to occur as the cone displaces downwards.

Separate interface materials were created and assigned to the shaft and cone of the penetrometer. The general properties of the interface materials follow the neighboring soil; however, shear strength properties were varied depending on the desired roughness.

Table 1. Key set-up details of respective literatures used in this study.

Author/ Approach	Soil model Input	Soil-Cone Contact	Soil Properties Input										
			E' (kPa)	λ	κ	ϕ (°)	M	$k(\text{ms}^{-1})$	e_0	K_0	OCR	Overburden stress (kPa)	
Yi et al (2012)/ Updated Lagrangian	Mohr's Cou- lomb Model*	Smooth	0.026 + 380z	-	-	-	23	-	5E-10	-	0.6	1	0
Sheng et al. (2014)/ Updated Lagrangian	Modified Cam-clay model	Smooth	-	0.3	0.05	-	1	1E-7	-	2	0.5	1.394	50
Ceccato et al. (2016)/ Material Point Method	Modified Cam-clay model	Smooth	-	0.205	0.04	-	0.92	1.02E-3 to 1.02E-8 ^	-	1.41	0.68	1	50
Orazalin (2018)/ Lagrangian FEM with an auto- mated pro- cedure for remeshing	Modified Cam-clay model	Smooth	-	0.205	0.04	-	0.92	1.02E-3 to 1.02E-8 ^	-	1.41	0.68	1	50

Note:

E' : effective Young's modulus; ϕ : effective friction angle; λ : virgin compression index; κ : swelling index; z : depth; k : hydraulic conductivity; e_0 : initial void ratio; K_0 : Coefficient of earth pressure at rest; OCR : overconsolidation ratio.

^: Hydraulic conductivity is varied to obtain partial drainage conditions

*: A Drucker-Prager Soil model was adopted in Yi et al. (2012)

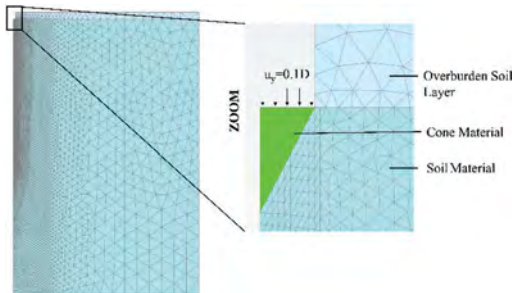


Figure 2. Typical finite element mesh of a first “press” phase with 18,359 elements and 161,903 nodes.

4 RESULTS

4.1 Cone factor comparison for undrained and drained penetration

Using a case study from Yi et al. (2012), preliminary investigations for both undrained and drained conditions were carried out and compared. To achieve an undrained penetration, a penetration rate of 0.0278 m/s is selected (Yi et al., 2012). Similarly, to achieve drained penetration, a slow penetration rate of 1E-10 m/s was used (Yi et al., 2012).

For undrained penetrations, the results are presented in the form of the cone tip factor (N_c), which is calculated as $N_c = (q_c - \sigma_{v0})/s_u$, where q_c is the calculated cone tip resistance from the analysis, s_u is the equivalent undrained shear strength corresponding to the friction angle ϕ or friction coefficient M prescribed in the model, and σ_{v0} denotes the total overburden stress (Lu et al., 2004).

The calculated N_c values from the present PRM analysis are plotted against the normalized cone depth (H/D , where H is the penetration depth and D is the cone diameter), as shown in Figure 3. The results agree well with the data reported by Yi et al. (2012), with a stabilized N_c value of approximately 9. This stabilized N_c value also agrees well with other published solutions (Teh & Houlsby, 1991; Yu et al., 2000; Abu-Farakh et al., 2003; Lu et al., 2004; Walker & Yu, 2006).

For a drained penetration, the cone factor N_q is used for comparison. It is calculated as $N_q = q_c'/\sigma'_{v0}$ (Yu, 2004; Ahmadi et al., 2005), in which q_c' denotes the effective cone resistance obtained from the analysis and σ'_{v0} the effective vertical stress. Figure 4 shows the computed N_q values plotted against the normalized cone depth (H/D). The results obtained from the present PRM analysis agree well with the reported solution from Yi et al. (2012). The stabilized

N_q value of approximately 7.5 also falls within the range of 5 ~ 8 reported in other publications.

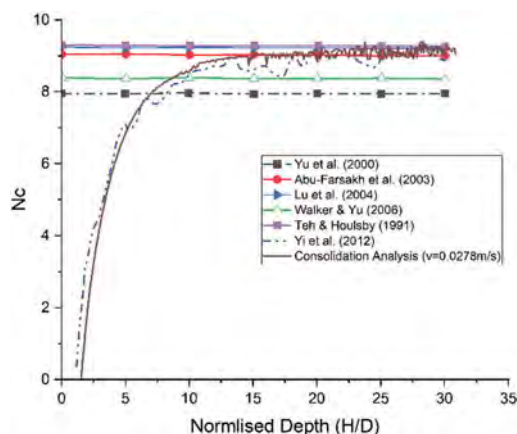


Figure 3. Comparison of calculated N_c with literature (Yi et al., 2012) and published solutions.

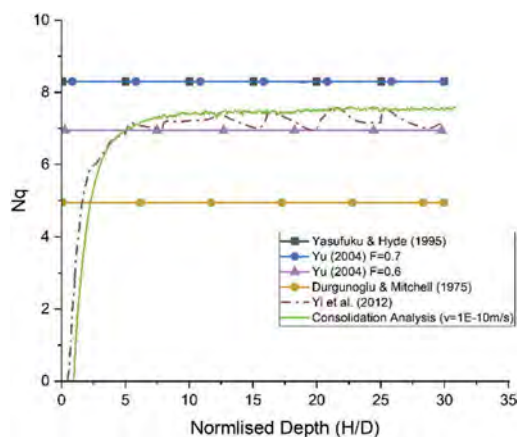


Figure 4. Comparison of calculated N_q with literature (Yi et al., 2012) and other published solutions.

4.2 Consolidation analysis of the penetration process at different cone penetration rates

In this section, the effect of different cone penetration rates is explored and validated. The effect of varying the penetration rates will result in partial drainage conditions (Suzuki and Lehane, 2014). Partial drainage occurs when there is concurrent generation and dissipation of excess pore pressures during the penetration process. In this section, the results from two published numerical case studies are adopted for comparison: (i) Sheng et al. (2014) and (ii) Ceccato et al. (2016) and Orazalin et al. (2018).

For both studies, the modified Cam-clay (MCC) model (Roscoe & Burland, 1968) is adopted to simulate the soil behavior in a more realistic manner.

The penetration rate is represented using the non-dimensional velocity $V (= vD/c_v)$ proposed by Randolph & Hope (2004), in which v , D and c_v denote the cone penetration velocity, cone diameter and the soil's coefficient of consolidation respectively. The c_v value in the MCC model is given by Equation 1, in which e_0 is the initial void ratio, k and σ'_{v0} represents the hydraulic conductivity and effective vertical stress, λ denotes the virgin compression index and γ_w is the unit weight of water.

$$c_v = \frac{k(1 + e_0)}{\gamma_w \lambda} \sigma'_{v0} \quad (1)$$

4.2.1 Comparison with Sheng et al. (2014)

Results obtained using PRM is presented in Figure 5. Sheng et al. (2014) associated an undrained and drained penetration in a soil body (with permeability 10^{-7} m/s) to a penetration rate of $v = 200$ cm/s and $v = 0.0002$ cm/s respectively. Figure 5 plots the variation of the net cone resistance ($q_c - \sigma'_{v0}$) with normalized depth (H/D), in which good agreement was obtained between the results from the PRM analyses and those reported by Sheng et al. (2014) for the drained and undrained penetration conditions.

In the same figure, the results from consolidation analyses at various penetration rates proposed by Sheng et al. (2014) are also shown. At a penetration depth $10H/D$, the net cone resistances of 213 kPa and 137 kPa are achieved for the drained and undrained conditions respectively. Penetration velocities between $v = 200$ cm/s and $v = 0.0002$ cm/s resulted in the net cone resistances falling between the range of 137 to 213 kPa. The results from the various penetration rates were processed, following which the dimensionless backbone curve as illustrated in Figure 6 was obtained. In Figure 6, a normalized cone resistance (q_n) (Randolph & Hope, 2004) is plotted against a normalized penetration rate represented by v/k , where v and k denote the penetration velocity and hydraulic conductivity respectively. Instead of adopting the normalized velocity V proposed by Randolph & Hope (2004), Sheng et al. suggested the use of the normalized term v/k , which provides a more direct relationship that could facilitate the processing of data. The normalized cone resistance q_n is defined as:

$$q_n = \frac{q_c - \sigma'_{v0}}{q_{ref} - \sigma'_{v0}} \quad (2)$$

in which q_{ref} is the reference cone resistance obtained from a fully undrained penetration. From the fitted dimensionless backbone curve of Figure 6, a stabilized q_n value at $v/k = 0.1$ can be obtained for the drained condition. The q_n values predicted by

PRM and Sheng et al (2014) at $v/k = 0.1$ are 1.56 and 1.68 respectively with a 7% difference in value. PRM predicts an undrained penetration response when $v/k > 200,000$ (approximately), whereas a drained behavior is observed when $v/k < 20$ (approximately). For intermediate values of v/k between 20 and 200,000, the effect of partial drainage is observed. A similar behavior was observed in the results of Sheng et al. (2014), for which the best fit curve showed partial drainage occurring between v/k values of 30 and 400,000 (approximately). Overall, there is good agreement between the PRM results and those reported by Sheng et al. (2014) in terms of the q_n values as well as the intermediate values of v/k (indicating partial drainage). For this example, these comparisons affirm the validity of the PRM to predict reasonable results under partial drainage conditions.

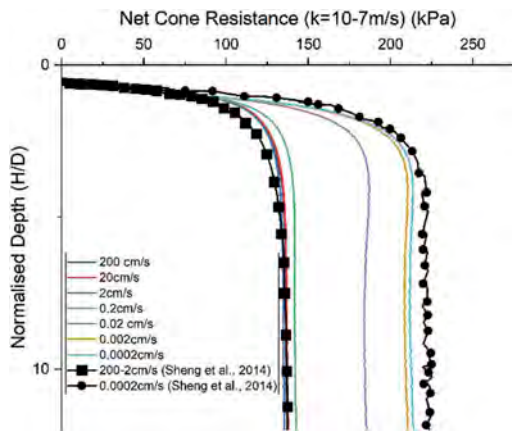


Figure 5. Comparison of undrained and drained net cone resistance between PRM and literature (Sheng et al., 2014).

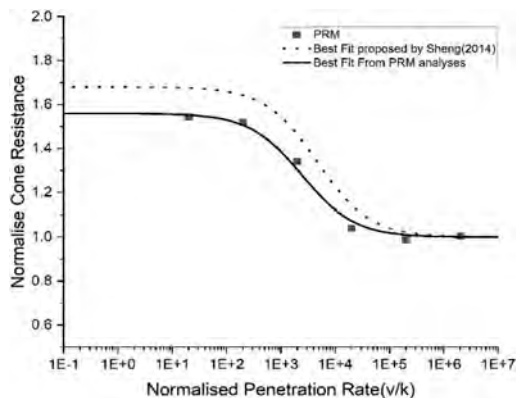


Figure 6. Comparison of dimensionless backbone curve between PRM and literature (Sheng et al., 2014).

4.2.2 Comparison with Ceccato et al. (2016) and Orazalin et al. (2018)

In this section, the PRM results will be studied compared against those reported by Ceccato et al. (2016) and Orazalin et al. (2018). These two published works adopted different numerical techniques to simulate the same cone penetration set-up proposed by Ceccato et al. (2016). Both Ceccato et al. and Orazalin et al. adopted a MCC soil model to capture the soil behavior. However, for simulating the penetration process, Ceccato et al. (2016) used the Material Point Method (MPM), whereas Orazalin et al. (2018) adopted the Lagrangian finite element method with an automated remeshing procedure.

In this section, the normalized net tip resistance ($q_{n.net}$) is plotted against the normalized velocity V (Randolph & Hope, 2004) to obtain the dimensionless backbone curve. The normalized net tip resistance is defined as follows:

$$\text{Normalized Nettip Resistance } (q_{n.net}) = \frac{q_{cnet}}{q_{ref.net}} = \frac{q_c - \sigma_{v0}}{q_{ref} - \sigma_{v0}}$$

Using PRM, the cone penetration at different rates were modeled using consolidation analysis. A comparison of the computed cone resistances for the fast and slow penetration are presented in Figure 7 and Figure 8 respectively. These results plot the total cone resistance against the normalized penetration displacement in an undrained (fast) and drained (slow) penetration. The normalized penetration displacement is defined as the ratio of the penetration displacement to the cone diameter.

Figure 7 shows good agreement between the results reported by Ceccato et al. (2016) and Orazalin et al. (2018), while the PRM an undrained cone resistance which is about 7% higher. The results obtained by Lim (2017) are also plotted. Overall, the PRM results for the undrained response of this particular case study

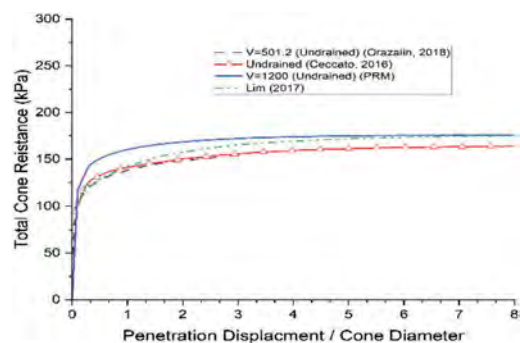


Figure 7. Comparison of calculated total cone resistance with literature (Ceccato et al., 2016; Lim, 2017; Orazalin et al., 2018) in an undrained penetration.

compare favorably with those reported by Orazalin et al. (2018), Ceccato et al. (2016) and Lim (2017).

For a drained penetration, Figure 8 shows that PRM predicts a greater cone tip resistance of 263kPa compared to the MPM value of 210 kPa reported by Ceccato et al. (2016), which is a difference of about 25%. Despite the good agreement observed for the undrained response, the cone tip resistance obtained by Orazalin et al. (2018) for the drained response is about 250kPa, or about 20% higher than the MPM value. For the drained penetration, Orazalin et al.'s results are closer to those obtained using PRM.

The cone resistance results at different penetration rates obtained by Ceccato et al. (2016), Orazalin et al. (2018) and the PRM approach are processed and plotted, in the form of $q_{n,net}$ against the normalized velocity V , to produce the backbone curves shown on Figure 9. This figure shows that the PRM predictions of the normalized tip resistance $q_{n,net}$ are approximately the average of those predicted by Ceccato et al. (2016) and Orazalin et al. (2018).

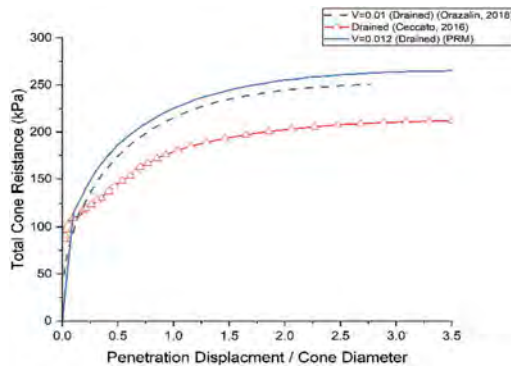


Figure 8. Comparison of calculated total cone resistance with literature (Ceccato et al., 2016; Orazalin et al., 2018) in a drained penetration.

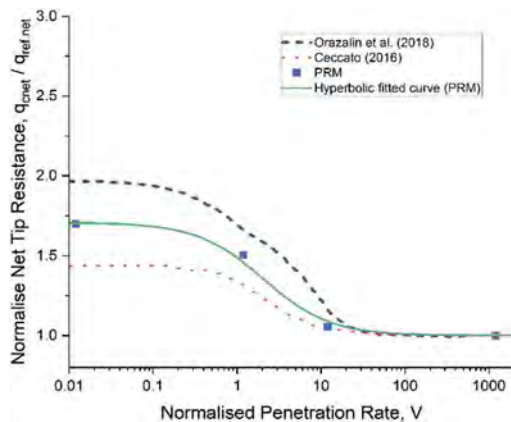


Figure 9. Comparison of dimensionless backbone curve between PRM and literature (Ceccato et al., 2016; Orazalin et al., 2018).

4.3 Effects of cone roughness

This section explores the influence of cone roughness with a case example taken from Yi et al. (2012). Cone roughness affects the stress-transfer interaction between the cone and soil surfaces, and are characterized by the friction angle φ_{int} and cohesion c_{int} assigned to the interface elements.

For this study, the interface cohesion c_{int} is assumed to be negligible, although a small value of 0.001 kPa is used to avoid numerical instability. Hence, the interface friction φ_{int} is the only parameter controlling the interaction between the 2 surfaces. The analyses are performed for φ_{int} values of 0, 8°, 16° and 23° to capture the transition from a perfectly smooth to a fully rough cone-soil contact.

Figure 10 plots the PRM computed undrained and drained responses for the perfectly smooth ($\varphi_{int} = 0^\circ$) and fully rough ($\varphi_{int} = 23^\circ$) interface conditions, in the form of the normalized depth (H/D) against q_c . For both the undrained and drained conditions, a higher q_c value is obtained when $\varphi_{int} = 23^\circ$, the increase being much more significant for the drained response.

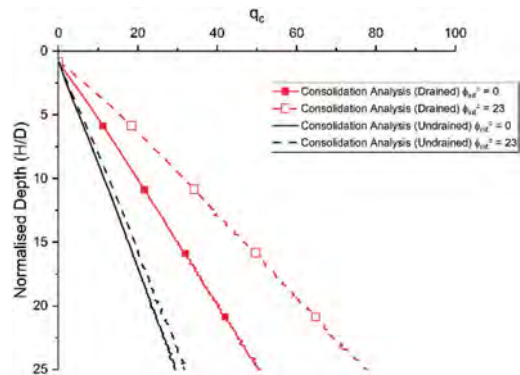


Figure 10. Illustration of cone tip resistance for an undrained and drained penetration, when $\varphi_{int}^o = 0$ and $\varphi_{int}^o = 23$.

Subsequently, PRM analyses are performed for different penetration rates with different values of φ_{int} . The results are summarized and presented in the form of backbone curves obtained by plotting $q_{n,net}$ against V , as shown in Figure 11 for 3 different depths (15H/D, 20H/D, 25H/D). Four distinctive backbone curves may be fitted to the data. These correspond to φ_{int} values of 0, 8°, 16° and 23°, with drained $q_{n,net}$ values of 2.38, 2.90, 3.4, 3.61 respectively. Figure 11 shows that increasing the cone roughness results in higher $q_{n,net}$ values across the whole spectrum of penetration rates. Further studies should be performed to examine the rate of increase of $q_{n,net}$, as well as the absolute cone resistance values (q_c), for different φ_{int} values at different penetration rates. This would provide a better understanding of the relationship between φ_{int} with $q_{n,net}$ and q_c .

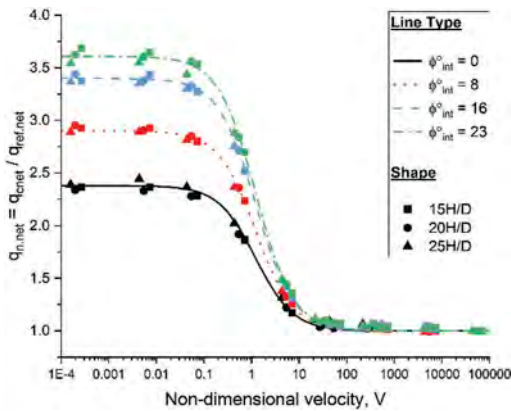


Figure 11. $Q_{n,net}$ against non-dimensional velocity, V , for $\phi_{int} = 0^\circ, 8^\circ, 16^\circ$ and 23° .

5 CONCLUSION

This paper presents a simplified approach, the Press-Replace Method (PRM), for modeling large deformation penetration problems using a small strain finite element program. The PRM approach was used in this paper to model cone penetration in soils under different drainage conditions. This paper compares the PRM predictions against the results of 4 examples taken from the published literature.

The PRM results from drained and undrained penetrations were presented and compared against the published results for the 4 examples (Yi et al., 2012; Sheng et al., 2014; Ceccato et al., 2016; Orazalin et al., 2018). In general, the PRM results (undrained and drained) are close to and within the range obtained by other researchers using different modeling techniques.

The effect of partial drainage was studied and validated in this paper by performing consolidation analysis with different penetration rates. The results, in the form of dimensionless backbone curves obtained by plotting normalized resistances against normalized velocity, compare favorably with those reported by Sheng et al. (2014) and Orazalin et al. (2018). Some discrepancies were observed when compared to the MPM results of Ceccato et al. (2016), which could be due to the use of a different tip geometry.

The effects of cone roughness were also explored in this paper. The results show an increase in q_c and $Q_{n,net}$ values with the interface friction angle ϕ_{int} .

REFERENCES

Abu-Farsakh, M., Tumay, M., & Voyiadjis, G. (2003). Numerical parametric study of piezocone penetration test in clays. *International Journal of Geomechanics*, 3(2), 170–181.

Andersen, K. H., Andresen, L., Jostad, H. P., & Clukey, E. C. (2004, January). Effect of skirt-tip geometry on set-up outside suction anchors in soft clay. In *International Conference on Offshore Mechanics and Arctic Engineering* (Vol.37432, pp. 1035–1044).

Ahmadi, M. M., Byrne, P. M., & Campanella, R. G. (2005). Cone tip resistance in sand: modeling, verification, and applications. *Canadian geotechnical journal*, 42(4), 977–993.

Ceccato, F., Beuth, L., & Simonini, P. (2016). Analysis of piezocone penetration under different drainage conditions with the two-phase material point method. *Journal of Geotechnical and Geoenvironmental Engineering*, 142(12), 04016066.

Durgunoglu, H. T., & Mitchell, J. K. (1975). Static penetration resistance of soils I-analysis. In *Proc. ASCE Conf. In-Situ Measure. Soil Properties* (p.1).

Engin, H. K., Brinkgreve, R. B. J., & Van Tol, A. F. (2015). Simplified numerical modelling of pile penetration—the press-replace technique. *International Journal for Numerical and Analytical Methods in Geomechanics*, 39(15), 1713–1734.

Lehane, B. M., O’loughlin, C. D., Gaudin, C., & Randolph, M. F. (2009). Rate effects on penetrometer resistance in kaolin. *Géotechnique*, 59(1), 41–52.

Lim, Y. X. (2017). *Numerical study of cone penetration test in clays using press-replace method* (Doctoral dissertation, National University of Singapore (Singapore)).

Lim, Y. X., Tan, S. A., & Phoon, K. K. (2018). Application of press-replace method to simulate undrained cone penetration. *International Journal of Geomechanics*, 18(7), 04018066.

Lu, Q., Randolph, M. F., Hu, Y., & Bugarski, I. C. (2004). A numerical study of cone penetration in clay. *Géotechnique*, 54(4), 257–267.

Oliveira, J. R., Almeida, M. S., Motta, H. P., & Almeida, M. C. (2011). Influence of penetration rate on penetrometer resistance. *Journal of Geotechnical and Geoenvironmental Engineering*, 137(7), 695–703.

Orazalin, Z. Y., & Whittle, A. J. (2018). Realistic numerical simulations of cone penetration with advanced soil models. In *Cone Penetration Testing 2018* (pp. 483–489). CRC Press.

Paniagua, P., Nordal, S., & Engin, H. K. (2014). Back calculation of CPT tests in silt by the Press-Replace technique.

Paniagua, P., Nordal, S., Emdal, A., Engin, H. K., & Kim, Y. (2021, May). Back-Calculation of Stresses and Pore Pressures Around a Penetrating Cone in Silt. In *International Conference of the International Association for Computer Methods and Advances in Geomechanics* (pp. 260–267). Springer, Cham.

Randolph, M., & Hope, S. (2004). Effect of cone velocity on cone resistance and excess pore pressures. *Proc. 1st Int. Symp. on Engineering Practice and Performance of Soft Deposits, Osaka*, 147–152.

Roscoe, K., & Burland, J. B. (1968). On the generalized stress-strain behaviour of wet clay. In *Engineering Plasticity, Cambridge University Press*, 535–609

Sheng, D., Kelly, R., Pineda, J., & Bates, L. (2014). Numerical study of rate effects in cone penetration test. In *3rd international symposium on cone penetration testing* (pp. 419–428).

Sivasithamparam, N., Engin, H. K., & Castro, J. (2015). Numerical modelling of pile jacking in a soft clay. In *Computer Methods and Recent Advances in Geomechanics: Proceedings of the 14th International Conference of International Association for Computer Methods and Recent Advances in Geomechanics, 2014 (IACMAG 2014)* (pp. 985–990). Taylor & Francis Books Ltd.

Suzuki, Y., & Lehane, B. (2014). Field observations of CPT penetration rate effects in Burswood clay. In *3rd International Symposium on Cone Penetration Testing*

- (pp. 403–410). International Symposium on Cone Penetration Testing.
- Teh, C. I., & Houlsby, G. T. (1991). An analytical study of the cone penetration test in clay. *Geotechnique*, 41(1), 17–34.
- Walker, J., & Yu, H. S. (2006). Adaptive finite element analysis of cone penetration in clay. *Acta Geotechnica*, 1(1), 43–57.
- Wang, Z. Z., & Goh, S. H. (2018). Spudcan installation and post installation behaviour in soft clay: The press-replace method. In *Numerical Methods in Geotechnical Engineering IX* (pp. 1503–1510). CRC Press.
- Yasufuku, N., & Hyde, A. F. L. (1995). Pile end-bearing capacity in crushable sands. *Géotechnique*, 45(4), 663–676.
- Yi, J. T., Goh, S. H., Lee, F. H., & Randolph, M. F. (2012). A numerical study of cone penetration in fine-grained soils allowing for consolidation effects. *Géotechnique*, 62(8), 707–719.
- Yu, H. S., Herrmann, L. R., & Boulanger, R. W. (2000). Analysis of steady cone penetration in clay. *Journal of Geotechnical and Geoenvironmental Engineering*, 126(7), 594–605.
- Yu, H. S. (2004). The First James K. Mitchell Lecture In situ soil testing: from mechanics to interpretation. *Geomechanics and Geoengineering: An International Journal*, 1(3), 165–195.

Cone penetration testing to constrain the calibration process of a sand plasticity model for nonlinear deformation analysis

A. Chiaradonna

University of L'Aquila, L'Aquila, Italy

T.J. Carey

The University of British Columbia, Vancouver, Canada

K. Ziotopoulou & J.T. DeJong

University of California at Davis, Davis, USA

ABSTRACT: A reliable prediction of liquefaction-induced damage typically requires nonlinear deformation analyses with an advanced constitutive soil model calibrated to the site conditions. The calibration of constitutive models can be performed by relying primarily on a combination of commonly available properties and empirical or semi-empirical relationships, on laboratory tests on site-specific soils, on in-situ penetration tests, or a combination thereof. Chiaradonna et al. (2022) described a laboratory-based calibration approach of the PM4Sand constitutive model and evaluated the prediction accuracy against the response of a centrifuge experiment of a submerged slope. This paper addresses an alternate calibration approach in which the PM4Sand model is calibrated using centrifuge in-situ CPT data. The model performance for the resulting calibration is evaluated against the centrifuge experimental data and prior simulations from Chiaradonna et al. (2022). In this case, the CPT-based calibration resulted in more accurate estimations of the dynamic response and permanent displacements.

1 INTRODUCTION

A reliable prediction of liquefaction-induced damage usually requires performing nonlinear deformation analyses by adopting advanced constitutive soil models. Constitutive model calibration protocols have been developed to guide the selection of parameters, firstly driven by the goal to reproduce the soil element behavior as observed in laboratory element tests and, if tests are not available, against the broader body of data and engineering relationships in the literature. For larger scale experiments, the use of in-flight miniature Cone Penetration Tests (CPT) in centrifuge testing has provided system level soil properties and better definition of soil conditions before and after any applied shaking (Kim et al. 2016; Khosravi et al. 2018; Moug et al. 2019; Darby et al. 2019; Carey et al. 2020). Darby et al. (2019) used CPT soundings collected prior to multiple shaking events to define liquefaction triggering correlations in a centrifuge experiment. The cyclic resistance for the investigated sand in the experiment was lower than that inferred from case history-based liquefaction triggering correlations. Data from in-flight miniaturized CPTs strongly constrain several soil parameters, e.g., relative density D_R , and were therefore useful to define model calibration parameters.

Chiaradonna et al. (2022) modelled the dynamic response of a centrifuge experiment consisting of a submerged 10-degree slope of a poorly graded clean sand at a D_R of 63% (Carey et al. 2022a). Shaking was imposed by applying a 1 Hz at the base of the model container. CPTs were pushed using a 10 mm cone in the experiment prior to and following shaking, but were not considered in the calibration performed by Chiaradonna et al. (2022).

The critical state compatible, stress ratio-based, bounding surface plasticity constitutive model PM4Sand (Boulanger & Ziotopoulou 2017), implemented in the commercial finite-difference platform FLAC (Itasca, 2016) was adopted in the simulations. The primary input parameters of the model are the apparent relative density (D_R), the shear modulus coefficient (G_o), and the contraction rate parameter (h_{po}). A laboratory-based calibration was defined on the results of undrained cyclic direct simple shear tests performed on reconstituted samples (Humire et al. 2022). The simulation of the centrifuge test by adopting the laboratory-based calibration reasonably simulated the pore pressure and acceleration time histories, while the permanent horizontal displacements were overpredicted by a factor of three (Chiaradonna et al. 2022).

In this paper, the aforementioned simulation was revisited by calibrating PM4Sand parameters using the cone tip resistance as measured in the centrifuge by Carey et al. 2022a. The D_R is the target value of 63%, which was verified through a pre-shaking cone penetration test (Carey et al. 2022a). The soil behavior at small strains (i.e., G_0) was estimated by the measured cone tip resistance through the application of several literature relationships, whose efficacy was verified against the shear moduli based on the measured shear wave velocity. The cyclic resistance ratio (CRR), which is primarily controlled by the contraction rate parameter (h_{pc}) in PM4Sand, was estimated through the normalized cone tip resistance measured in the experiment and the CPT-based empirical triggering liquefaction chart by Boulanger & Idriss (2014).

The comparison between simulated and experimental soil response is made to verify that in-flight CPT testing in the centrifuge experiments properly measures the cyclic strength of soils. In addition, the comparison between the CPT-based calibration and the calibration based on cyclic laboratory tests performed by Chiaradonna et al. (2022) is also discussed.

2 EXPERIMENTAL PROGRAM

2.1 Overview of centrifuge test

A 14 m-high submerged embankment with a 10-degree slope constructed with a uniform profile of sand was tested in a rigid container at 40g using the 9-m radius centrifuge at the Center for Geotechnical

Modeling located at the University of California, Davis (Figure 1). The soil was a clean poorly graded sand, hereafter called 100A sand (Sturm 2019). The physical properties of the 100A sand are $e_{min} = 0.579$, $e_{max} = 0.881$, $D_{50} = 0.18\text{mm}$, $C_u = 1.68$, and $G_s = 2.62$. The embankment was dry-pluviated to a target $D_R = 63\%$, overlying a dense sand layer ($D_R > 90\%$) of the same soil. The model was saturated with methylcellulose pore fluid that had a viscosity that was 40x that of water (40 CSt).

Instrumentation within the model included pore pressure transducers and accelerometers, which enabled monitoring the coupled excess porewater pressures and acceleration responses. Piezoceramic bender element pairs were placed at two depths in the model to measure the shear wave velocity. Measurements were performed at 1 g and at 40 g, before and after shaking, for a total of 6 measurements. The processing of bender element time histories is reported by Carey et al. (2021). Horizontal displacement time-histories were measured using high-speed videos of the deforming embankment's cross-section recorded through the transparent side walls of the model container and GEOPIV image analysis software (Carey et al. 2022a).

The ground motion sequence included four shaking motions, all of which included a linear ramp to the maximum acceleration, a hold at the maximum acceleration for a certain number of cycles, and a non-linear decay. All motions had a prototype frequency of 1 Hz but varied in their number of cycles and amplitude of the hold cycles. Further details about the motion are given by Carey et al. (2022a, b). Herein the system response to the motion shown in

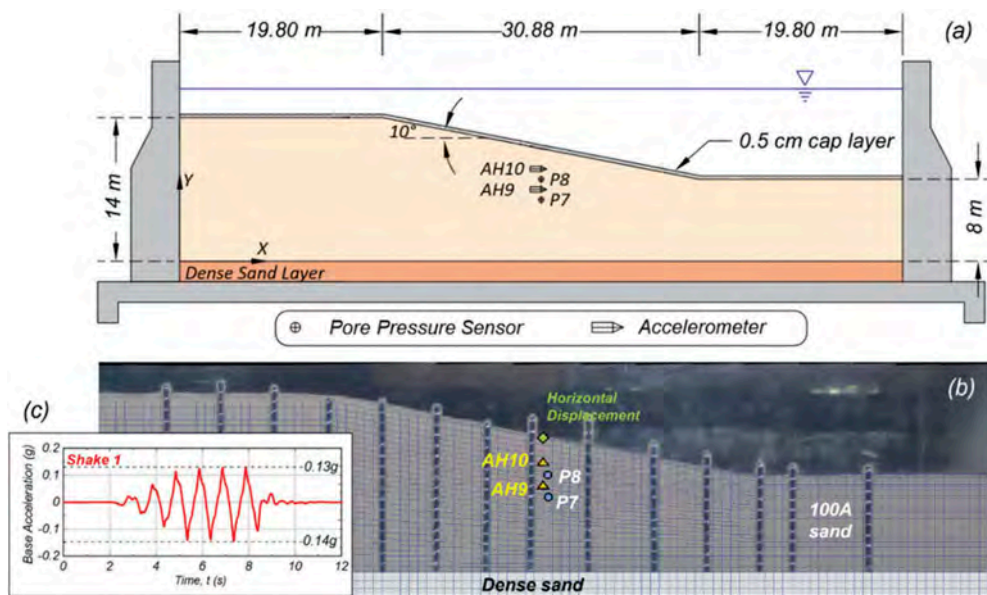


Figure 1. (a) Cross-section of the centrifuge model with accelerometers and porewater pressure sensors (length in prototype scale); (b) FLAC numerical grid used in the simulations overlaid on a photo of the centrifuge model test cross-section; and (c) recorded input motion from the centrifuge experiment used in this study.

Figure 1c with a maximum acceleration of 0.14g is analyzed. For brevity, only the shallowest sensors of the mid-slope array were analyzed (Figure 1a,b).

2.2 Experiment characterization using a CPT

A 10 mm-diameter cone penetrometer was pushed before and after the completion of the ground motion sequence. Cones were pushed into the soil 457 mm at the model scale at a penetration rate of 1 cm/s using a hydraulic actuator (Carey et al. 2022a). Figure 2a presents the CPT profile prior to shaking, measured in the upper bench of the slope.

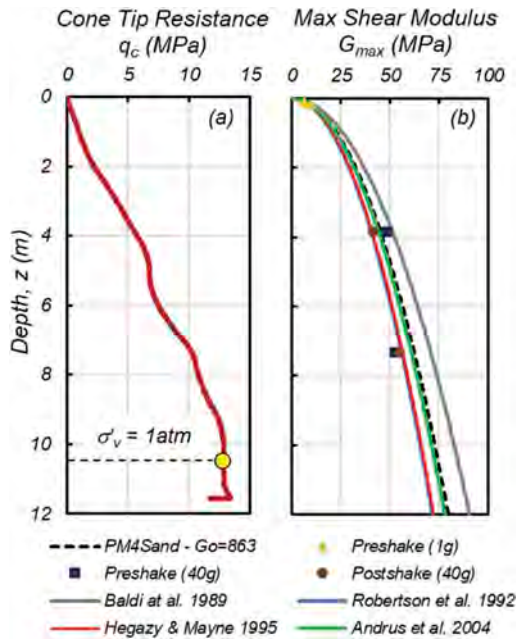


Figure 2. (a) CPT sounding measured prior to the start of the shaking sequence; and (b) comparison of G_{max} values based on bender elements in the model test with predicted G_{max} profiles from literature.

Shown in Figure 2a is the pre-shake CPT penetrated to depths that exceeded an overburden stress of 1 atm. Hence, the depth of 10.45 m corresponds to an overburden effective stress of 1 atm and the cone tip resistance, referred to as q_{c1} , was 12.8 MPa. The q_{c1} measurement was sufficiently deep to avoid shallow penetration effects in the model (Kim et al. 2016; Sawyer 2020) and was used to calculate the normalized corrected cone tip resistance, q_{c1N} , as defined by Boulanger & Idriss (2014), which was rounded to 126.0 for the considered case. Since the considered soil has a fines content equal to zero, the 'equivalent clean sand' normalized and corrected cone tip resistance, q_{c1Ncs} , is also 126.0.

3 ESTIMATION OF MODULUS AND CRR

3.1 Estimation of small-strain shear modulus

The shear wave velocity measurements made prior to and following the shaking event were used to calculate the small strain shear modulus, with the values shown in Figure 2b. The small-strain shear modulus at the depth of the atmospheric pressure, $G_{max,1}$, was calculated according to $G_{max,1} = \rho V_{S1}^2$, where ρ is the soil saturated density of 1,958 kg/m³ at the $D_R = 63\%$.

Several literature relationships expressing the normalized shear wave velocity, V_{S1} , as a function of the cone tip resistance measured in sands were selected and applied using q_{c1N} and are given in Table 1. The laws are expressed by an exponential function:

$$V_{S1} = m q_{c1N}^n \quad (1)$$

where m and n are the coefficients listed in Table 1. The vertical profile of G_{max} as a function of the mean effective stress, p' , is expressed as:

$$G_{max} = G_o P_a \left(\frac{p'}{P_a} \right)^{0.5} \quad (2)$$

where P_a is the atmospheric pressure (101.3 kPa) and G_o is the shear modulus coefficient calculated by imposing $G_{max} = G_{max,1}$ in Eq. (2) for an effective vertical stress, σ'_v , equal to the atmospheric pressure (Table 1). The mean effective stress, p' is related to the depth, z , as follows:

$$p' = \left(\frac{1+K_0}{2} \right) \sigma'_v = \left(\frac{1+K_0}{2} \right) \gamma' z \quad (3)$$

where K_0 is the coefficient of earth pressure at rest, assumed equal to 0.5, and γ' is the unit weight of the submerged soil. Eq. (2) can be expressed as a function of the depth. As evident in Figure 2b, the bender element-based G_{max} values were generally consistent with the predicted G_{max} profiles.

Table 1. Considered $V_{S1} - q_{c1N}$ relationships.

Relationship	m	n	V_{S1}	G_o
	m/s		m/s	
Baldi et al. 1989	110	0.13	206	964
Robertson et al. 1992	60.3	0.23	183	762
Hezagy & Mayne 1995	72.8	0.192	184	769
Andrus et al. 2004	62.6	0.231	191	830

3.2 Estimation of the cyclic resistance ratio

The estimation of the CRR for the 100A sand was obtained through the normalized cone tip resistance q_{c1Ncs} and the CPT-based triggering liquefaction relationship developed by Boulanger & Idriss (2014), as shown in Figure 3. For the q_{c1Ncs} of 126.0, the CRR was equal to 0.186.

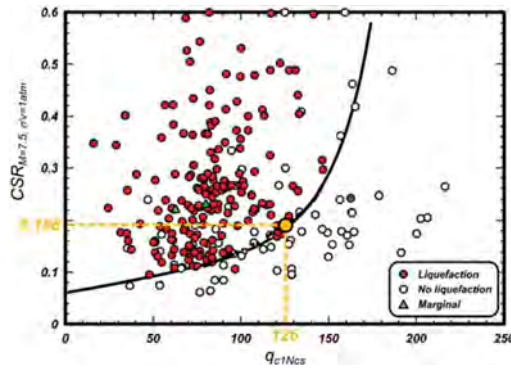


Figure 3. Estimation of CRR from the CPT-based liquefaction triggering curve by Boulanger & Idriss (2014).

4 PM4Sand CALIBRATION

The PM4Sand model calibration based on the experimental CPT data is referred to as “CPT calibration”. The calibration focused on defining the three primary input parameters, D_R , G_o , and h_{po} . The secondary parameters were left to their default values (Boulanger & Ziotopoulou 2017). Specifically, D_R was set to 63%, controlled by the centrifuge test design, and G_o was set to 863, the average of the upper (964) and lower (762) bounds of the G_o relationships in Table 1. The h_{po} parameter of 0.21 was iteratively calibrated via single element undrained cyclic stress-controlled direct simple shear (DSS) simulations until a satisfactory match between the Cyclic Stress Ratio (CSR) and CRR of 0.186 was reached for a triggering criterion of 3% shear strain in 15 cycles.

Figure 4 illustrates CSR versus number of cycles to liquefaction for a 3% single amplitude shear strain triggering criterion for the “CPT calibration”. This curve is generated from a series of single element DSS simulations using the calibrated PM4Sand primary variables, subjected to a range of CSRs. Experimental points as measured through cyclic DSS tests (green points) for two different overburden effective vertical stresses are also plotted for reference. The data for a $\sigma'_{vo} = 50$ kPa were used as the dataset for the laboratory-based calibration (“Lab calibration”) in Chiaradonna et al. (2022).

The cyclic strength at 15 cycles is 0.186 for the “CPT calibration” and 0.133 for “Lab calibration”, implying that the soil resistance to liquefaction as

estimated by the in-situ CPT is 1.4 times higher than that measured by direct simple shear tests.

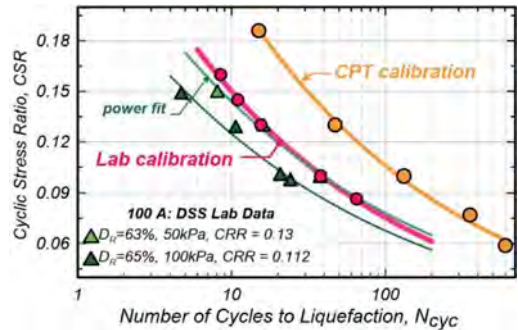


Figure 4. Cyclic resistance curves used in the simulations (CPT calibration) vs calibration based on direct simple shear data (Lab calibration) and experimental data.

5 NUMERICAL SIMULATION RESULTS

The centrifuge test was numerically simulated with the finite difference program FLAC (Itasca, 2016). The geometry of the analysis domain was based on the centrifuge prototype dimensions (Figure 1a). The discretized domain is shown in Figure 1b, with further details available in Chiaradonna et al. (2022).

The predicted and observed time histories of the horizontal displacement at the surface of the mid-slope (Figure 1b) are shown in Figure 5. The experimental trend exhibits a progressive accumulation of displacements, with a final permanent value of 7 cm.

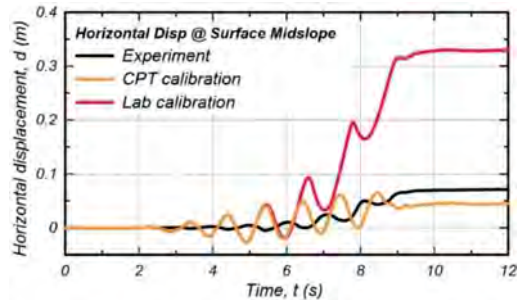


Figure 5. Comparison of horizontal displacement measured at the surface of the embankment slope and numerical simulations from the CPT and Lab calibrations.

The magnitude of the displacement oscillations per cycle is relatively minor, resulting in a clear ratcheting of downslope displacement. The CPT calibration predicted displacements that were practically identical to the experiment with a permanent horizontal displacement was 5 cm. The oscillations in displacements for the CPT calibration are larger compared to the

experiment and predict a dynamic upslope movement. For context, the lab calibration-based simulation predicted significantly higher displacements, with the accumulation primarily occurring during the last two cycles of shaking at full acceleration amplitude and during the decay.

The agreement between the experimentally measured and CPT Calibration simulation of the mid-slope displacement also extended to the global deformation patterns across the centrifuge experiment. This is evident in Figure 6 where contours of horizontal displacement of the experiment are presented. The magnitude and spatial distribution of the displacement field is nearly identical.

While the agreement of the displacement fields is central for performance-based design, examining the pore pressure and acceleration time histories as well as the response spectra at the mid-slope during shaking, is also insightful. Figure 7 presents the pore pressure and acceleration time histories of the upper two locations on the mid-slope. The pore pressure generation time histories for P7 and P8 show different patterns of accumulation, as well as different residual values at the end of shaking. Excess pore pressure ratio, r_u , peaks in P7 are better captured by the “Lab calibration” compared to the “CPT calibration”. The experiment reached an r_u of 1 after several cycles, while the simulation did not. However, at the end of shaking both the experimental and the CPT calibration simulation have a r_u value less than about 0.7, implying that resedimentation and re-establishment of the effective stress profile has been partially taking place.

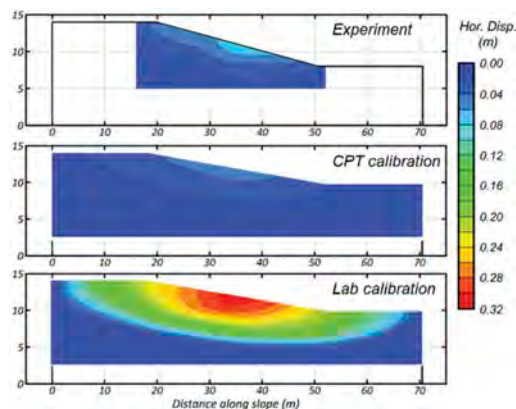


Figure 6. Contour fields of displacement from the shake measured in the centrifuge experiment, and the numerically predicted contours using the CPT and Lab PM4Sand calibrations.

The acceleration time histories between the measured experimental response and the CPT calibration simulation are nearly identical for the lower AH9 accelerometer, time history, and in the first part of the AH10 time history. However, later in the AH10 time

history the predicted accelerations in the simulation are lower. These trends are also evident in the clear agreement in the spectral acceleration plots for AH9, with show consistency across all periods. For AH10 the higher spectral acceleration at the predominant period of 1 Hz is evident. For periods less than 0.7 s, spectral accelerations are better captured better by the “Lab calibration” due to the dilation spikes in the time histories of acceleration; however, these high frequencies have a minor contribution to the overall movement of the embankment.

The agreement in deformation, acceleration, acceleration response spectra, and excess porewater pressure trends stand in clear contrast to the trends for the “Lab Calibration” simulation. As evident in Figures 6 and 7 the displacements that accumulate near the end and after shaking are significantly larger at the mid-slope surface and throughout much of the model. The primary reason for these differences is attributed both (1) to the lower cyclic resistance ratio (CRR) of the laboratory data which contributes to an early onset of liquefaction and its associated deformations, and (2) the continuing deformation after the end of shaking due a high excess pore pressure.

6 DISCUSSION

The numerical simulation presented in this paper demonstrates the utility and value of CPT measurements in centrifuge experiments. Simulations based on a CPT-based calibration of the PM4Sand constitutive model provided a very satisfactory match to the observed system level responses. Past parametric investigations by Chiaradonna et al. (2022) had shown that a CRR higher than the one obtained from DSS tests would likely justify the observed responses.

However, that study was inconclusive as to whether the higher in-situ CRR was an artifact of arching or sloping ground conditions or that in general the DSS data in this case had misrepresented the in-situ centrifuge conditions. The present study demonstrated that the CPT measurements provided a significantly improved characterization of the cyclic resistance of the centrifuge model and thus a more successful validation of the response, particularly with respect to displacements.

Future work will investigate the (i) influence of other contributing factors such as 3D effects and arching, (ii) effect of sloping ground conditions on cyclic strength, and (iii) reasons between the discrepancy of the DSS-based CRR and the CPT-based CRR.

7 CONCLUDING REMARKS

This paper addressed the calibration of a critical state compatible, stress ratio-based, bounding surface plasticity constitutive model aiming at

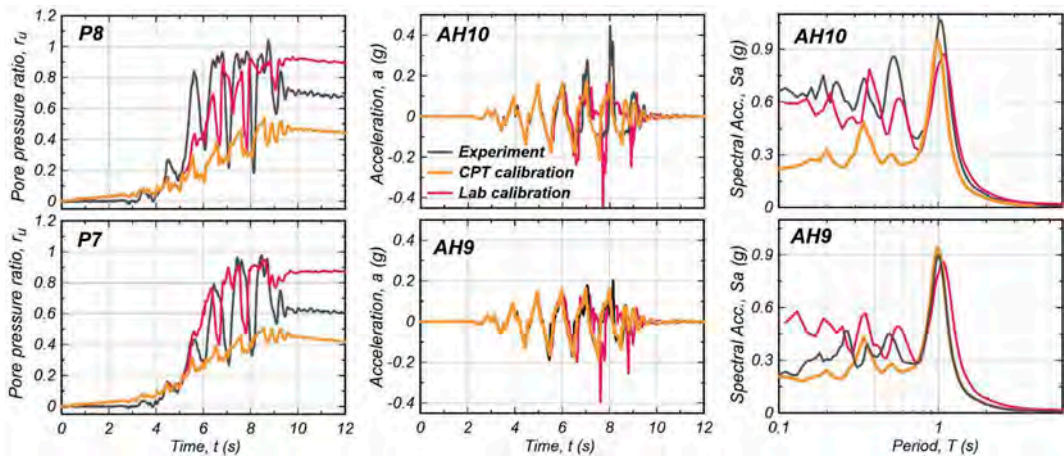


Figure 7. Comparison of the measured experimental and numerically simulated responses for ‘CPT Calibration’ vs. ‘Lab Calibration’. Results are for the select sensors (Figure 1) in terms of porewater pressure ratio, acceleration time histories, and response spectra (5% damping).

numerically simulating the dynamic behavior of a poorly-graded sand slope. While deficiencies in the horizontal displacement prediction were highlighted by a calibration obtained from cyclic laboratory tests (Chiaradonna et al. 2022), the use of CPT data as a calibration basis produced a better prediction of both displacements and accelerations. The reliability of the simulation can be ascribed mainly to two principal reasons: (i) the cyclic strength of the soils is directly estimated by combining the measured cone tip resistance of the soil tested in centrifuge with the CPT-based triggering liquefaction chart, and (ii) the small-strain shear modulus is well reproduced by the applied literature relationships for clean sands. This study strengthens the importance of in-flight CPT measurements in centrifuge tests and represents a step forward in the calibration of advanced constitutive models using measurements from in-situ CPT tests. Further applications to available centrifuge tests with different relative densities and gradation of soils will be performed to generalize the obtained results.

ACKNOWLEDGEMENTS

The National Science Foundation (NSF) provided funding for this work (Grant No. CMMI-1916152) and for the Natural Hazards Engineering Research Infrastructure (NHERI) centrifuge facility at UC Davis (Grant No. CMMI-1520581). Any opinions, findings, and conclusions, or recommendations expressed in this material are those of the author(s) and do not necessarily reflect those of the NSF. The lead author was supported by the U.S. Fulbright Scholar Program.

REFERENCES

- Andrus, R.D., Piratheepan, P., Ellis, B.S., Zhang, J. & Juang, C.H. 2004. Comparing liquefaction evaluation methods using penetration- V_s relationships. *Soil Dyn. Earthq. Eng.* 24: 713–721.
- Baldi, G., Bellotti, R., Ghionna, V., Jamiolkowski, M. & Lo Presti, D.C.F. 1989. Modulus of sands from CPTs and DMTs. *Proc. 12th Int. Conf. on Soil Mech. and Found. Eng., Rio de Janeiro, 13–18 August 1989*. Vol. 1: 165–170. Rotterdam: Balkema.
- Boulanger, R.W. & Idriss, I.M. 2014. *CPT and SPT liquefaction triggering procedures*. Report No UCD/GCM-14/01, University of California at Davis, California, USA.
- Boulanger, R.W. & Ziotopoulou, K. 2017. *PM4Sand (Version 3.1): A sand plasticity model for earthquake engineering applications*. Technical Report No. UCD/CGM-17/01, Center for Geotechnical Modeling, University of California, Davis.
- Carey, T.J., Chiaradonna, A., Love, N., DeJong, J.T., Ziotopoulou, K., Martinez, A. 2021. *Effect of soil gradation on the response of a submerged slope when subjected to shaking –centrifuge data report for TJC01*. Report No. UCD/CGM-21/03, University of California at Davis, California, USA.
- Carey, T.J., Chiaradonna, A., Love, N., Wilson, D.W., Ziotopoulou, K., Martinez, A. & DeJong, J.T. 2022a. Effect of soil gradation on embankment response during liquefaction: a centrifuge testing program. *Soil Dyn. Earthq. Eng.* (Under review).
- Carey, T.J., DeJong, J.T., Ziotopoulou, K., Martinez, A. & Chiaradonna, A. 2022b. The effects of gradation on the dynamic response of sloping ground. *Proc. 20th Intern. Conf. on Soil Mech. & Geotech. Eng., Sydney, 1–5 May 2022* (Accepted).
- Carey, T.J., Gavras, A. & Kutter, B.L. 2020. Comparison of LEAP-UCD-2017 CPT Results. In *Model Tests and Numerical Simulations of Liquefaction and Lateral Spreading*: 117–129. Cham: Springer.

- Chiaradonna, A., Ziotopoulou, K., Carey, T.J., DeJong, J.T. & Boulanger, R.W. 2022. Dynamic Behavior of Uniform Clean Sands: Evaluation of Predictive Capabilities in the Element- and the System-Level Scale. *GeoCongress 2022, Charlotte, 20–23 March 2022* (Accepted paper).
- Darby, K.M., Boulanger, R.W., DeJong, J.T. & Bronner, J.D. 2019. Progressive Changes in Liquefaction and Cone Penetration Resistance across Multiple Shaking Events in Centrifuge Tests. *J. Geotech. Geoenviron. Eng.*, ASCE 145(3).
- Hegazy, Y.A. & Mayne, P.W. 1995. Statistical correlations between VS and cone penetration data for different soil types. *Proc. 1st International Symposium on Cone Penetration Testing, CPT '95, Linköping, 4-5 October 1995*, 2: 173–178.
- Humire, F., Ziotopoulou, K. & DeJong, J.T. 2022. Evaluating shear strain accumulation of sands exhibiting cyclic mobility behavior. *Proc. 20th Intern. Conf. on Soil Mech. and Geotech. Eng., Sydney, 1–5 May 2022* (Accepted paper).
- Itasca 2020. FLAC – Fast Lagrangian Analysis of Continua, Version 8.1. Minneapolis, MN: Itasca Consulting Group.
- Kamai, R., & Boulanger, R.W. (2011). Characterizing localization processes during liquefaction using inverse analyses of instrumentation arrays. *Meso-Scale Shear Physics in Earthquake and Landslide Mechanics*, 219–238.
- Khosravi, M., Boulanger, R.W., DeJong, J.T., Khosravi, A., Hajjalilue-Bonab, M. & Wilson, D.W. 2018. Centrifuge modeling of cone penetration testing in layered soil. In Geotechnical Special Publication 290, S. J. Brandenberg and M. T. Manzari (eds.); *Proc. Geotechnical Earthquake Engineering and Soil Dynamics V, Austin, 10–13 June 2018*.
- Kim, J.H., Choo, Y.W., Kim, D.J. & Kim, D.S. 2016. Miniature cone tip resistance on sand in a centrifuge. *J. Geotech. Geoenviron. Eng.*, ASCE 142 (3).
- Moug, D.M., Price A.B., Bastidas, A.M.P., Darby, K.M., Boulanger, R.W. & DeJong, J.T. 2019. Mechanistic Development of CPT-Based Cyclic Strength Correlations for Clean Sand. *J. Geotech. Geoenviron. Eng.*, ASCE 145(10).
- Robertson, P.K., Woeller, D.J. & Finn, W.D.L. 1992. Seismic CPT for evaluating liquefaction potential. *Canadian Geotechnical Journal* 29: 686–695.
- Sawyer, B.D. 2020. *Cone penetration testing of coarse-grained soils in the centrifuge to examine the effects of soil gradation and centrifuge scaling*. Master's Thesis. UC Davis.
- Sturm, A.P. 2019. *On the Liquefaction Potential of Gravelly Soils: Characterization, Triggering and Performance*. PhD Dissertation. UC Davis.

Probabilistic delineation of soil layers using Soil Behavior Type Index

S. Collico & M. Arroyo

Universidad Politécnica de Cataluña, Barcelona, Cataluña, Spain

M. DeVincenzi, A. Rodriguez & A. Deu

Igeotest s.l. Figueres, Cataluña, Spain

ABSTRACT: CPTu-based soil profiling has become a key component in the geotechnical design process. However, this is an interpretative process, affected by the inherent variability of soil properties, measurement noise and subjective heuristics. These are difficult to communicate to other interpreters or, even for the same interpreter, to transfer across profiles. A semi-automated tool for CPTu data interpretation is presented as an aid in this interpretation process. A probabilistic-based algorithm is employed to elicit the implicit heuristics in CPTu-based soil profiling and facilitate transference. Univariate normal distributions fit Soil Behavior Type Index data. Soil class boundaries, taken from a conventionally accepted chart, are sequentially activated with user-specified refinement. Thin layers under cone resolution are merged using well-established criteria. An application to CPTu records on finely interlayered deltaic deposits is illustrated, in which output delineations resulting from different analyst choices are compared among themselves and with one based on core description.

1 INTRODUCTION

Differentiation of ground units by means of stratigraphic profiling is a key step of site characterization for geotechnical design. Among all the in-situ tests, Cone Penetration Tests CPTu are widely employed for layer's identification based on the soil response to the probe. An aid for CPTu postprocessing results is given by Soil Behavior Type (SBT) charts (Douglas & Olsen, 1981; Robertson, 1990, 2009) that allow every reading to be classified. Analysts can then establish boundary layers by inspecting the profile of soil class assignment derived from these charts.

This is an interpretation task, and as such is strongly affected by analyst knowledge, experience and heuristics. The interpretation process followed is sometimes difficult to explain and might appear arbitrary and be a subject of disputes if other parties are involved. Even if that is not the case, the same analyst may find it difficult to ensure coherence of interpretation across different soundings of a site.

As an example, when a thin silt layer (e.g., 20-30 cm) is embedded in two thick sand units, the analyst, based on his experience, may or may not consider relevant the presence of such layer. An additional and more sensitive issue arises when dealing with multiple CPTu sounding records and the so called cross-site variability (Zhang et al., 2004). Layer's identification, by accounting for information of different locations, is an even more complex process since both

vertical and horizontal inherent variability and measurements errors, that might differ during each test, intervene. Therefore, such lack of transparency and not methodical process of layers' identification, should be addressed.

Different probabilistic methodologies have addressed the problem of stratigraphic profiling based on CPTu. Some works (Jung et al., 2008; Wang et al., 2013) put the focus on the basic classification scheme applied. They point that generally established soil class boundaries are inherently inaccurate to derive site-specific soil profiling and address this issue by updating the classification scheme according to site-specific observations.

Another line of thinking is the one that enable the integration geological unit's information to CPTu data (Depina et al., 2016; Krogstad et al., 2018). These works employ SBT charts only as a reference template, and CPTu soil class assignment refers to geological units identified from retrieved core samples and/or previous studies.

This work follows a different line of thinking and it is based on a more modest approach, mainly oriented for practical use. SBT charts— here Robertson, (2009) —are considered as conventionally accepted template for soil classification with given (not uncertain) class boundaries. The probabilistic approach is applied only to assess inherent variability and measurements error of CPTu readings. The probabilistic parameters introduced are then oriented to quantify the degree of internal coherence of each

identified layer, and, at the same time, eliciting analyst heuristics and interpretation criteria.

The tool fits a univariate normal distribution to interpret data originated from one or various CPTu probes, which are gradually plotted on Robertson (2009) chart, identifying soil units in a probabilistic manner. Class boundaries are sequentially activated with user-specified refinement. Thin layers (layers below a specified minimum thickness resolution) are assessed through a practical merging scheme. This work applies the methodology previously proposed by Collico et al., (2020) to Robertson, (2009) SBT chart. In Collico et al., (2020), a bivariate normal distribution approach was applied to fit CPTu observations on Robertson, (1990) SBT chart. The flexibility of such work is here exploited to fit Soil Behavior Type Index observations according to Robertson, (2009) class boundaries.

As illustrated section 2, the proposed methodology consists of three main parts: a probabilistic model to CPTu data; a staged classification procedure and an option for automated thin layer consolidation.

2 METHODOLOGY

2.1 Soil behavior type index I_C

Among all SBT charts, one of the most popular is the Robertson (2009) chart (Figure 1). Based on the work of Douglas & Olsen, (1981) and Jefferies & Davies (1991), Robertson (2009) highlighted how Robertson (1990) class boundaries could approximate by a concentric circle whose radius can be defined by a unified parameters denoted as soil behavior class index I_C which combine both normalized CPTu parameters as:

$$I_C = \left[(3.47 - \log(Q_m))^2 + (\log(F_R) + 1.22)^2 \right]^{0.5} \quad (1)$$

with:

$$Q_m = \left[(qt - \sigma_{v0}) / p_a \right] (p_a / \sigma'_{v0})^n \quad (2)$$

$$n = 0.381I_C + 0.05(\sigma'_{v0} / p_a) - 0.15 \quad (3)$$

where $n \leq 1$ is a soil-type dependent exponent which normalizes for the effect of stress level on tip resistance.

Robertson (2009, 2016) highlighted that despite being a single-valued index, by including the stress exponent n , I_C based soil delineation might provide more useful information on soil behavior than one based on Robertson (1990) classes.

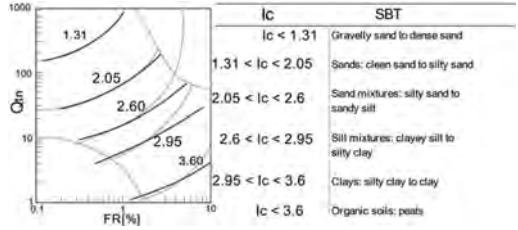


Figure 1. Soil Behavior Type chart based on Soil behavior Type Index I_C .

2.2 Statistical model for CPTu data

When plotting CPTu observations classified by SBT, inherent variability and measurements errors, generate some data scatter (Figure 2). In this study a univariate normal distribution is fitted to SBT data of a given stretch of CPTu:

$$f(I_{C_i}) = \frac{1}{\sigma_{I_C} \sqrt{2\pi}} \exp\left(-\frac{1}{2} \frac{(I_{C_i} - \mu_{I_C})^2}{\sigma_{I_C}^2}\right) \quad (4)$$

with μ_{I_C} , σ_{I_C} mean and standard deviation of I_C data sample. An example of 3D representation of fitted univariate normal distribution for a 5m I_C profile (Figure 2b) is reported in Figure2b. The area of color, under the density function, indicate the extent of an interval pre-established representative data interval. As explained below, the interplay between this interval and SBT class boundaries is exploited to obtain a systematic procedure for layer identification.

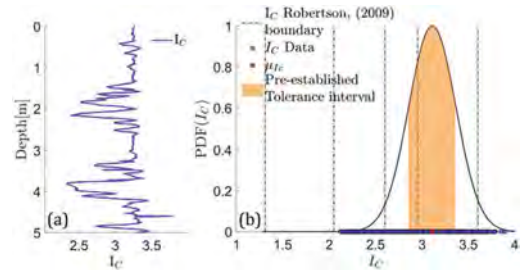


Figure 2. a) Synthetic I_C record. b) Corresponding univariate distribution and pre-established representative interval plotted on Robertson (2009) chart.

2.3 Class assignment criteria

Once the CPTu SBT values corresponding to a particular stretch are fitted to a univariate normal distribution, the fitted data will be assigned to the soil class in which the distribution mean is found. Two user-specified acceptance thresholds (i.e.,

model parameters) are used to divide the CPTu record into different stretches:

- Noise-threshold parameter, $P(\sigma_{I_c})$
- Class-mixture tolerance parameter, m

The meaning of these two parameters is rather intuitive. The P parameter (Figure 2b), expressed in term of standard deviations, establishes the width of the representative data sample interval ($P = \mu_{I_c} \pm \sigma_{I_c}$). It is introduced to account for the possibility of extreme values of I_c within the dataset (e.g., shelly inclusions in clays). As an example, by considering a value of $P = 2$, the representative interval would contain 95% of the underlying data and 5% will be considered as noise.

The class-mixture tolerance parameter m is introduced so that the user can modulate the relevance of the underlying classification system in the soil profiling exercise. The value of m is defined as the area proportion of specified representative interval that is allowed to cross soil class boundaries. In other word, the m value explicit how strictly adhered to are pre-established class boundaries when the CPTu is subdivided into layers. Parameter m expresses the degree of belief on the underlying classification adopted.

2.4 Classification levels

The original Robertson (2009) chart introduces six different soil classes. In some circumstances simpler classifications might appear more suitable to the analyst. This possibility has been enabled in this work introducing a staged classification procedure, in which SBT-based classifications of progressive refinement are introduced sequentially.

The coarser level uses a dual classification, distinguishing only between:

- Clay-like behavior (C-L)
- Sand-like behavior (S-L)

These two soil classes, representative of undrained and drained response for C-L and S-L respectively, are identified by the I_c boundary value 2.6 (Figure 3), (Robertson 2009). That boundary is here onwards designed as a primary boundary. A second, more refined, level of classification introduces a soil-mixture class to account for partially drained soil response to the cone probe, along with a sand-like and clay-like classes. The boundaries separating these three classes (Figure 3) are designed as secondary boundaries. Finally, the most refined classification level introduces all six soil classes of the original Robertson, (2009) proposal. The limits between them and here designated as tertiary boundaries.

The analyst might choose directly a particular classification level or might run sequentially through all levels.

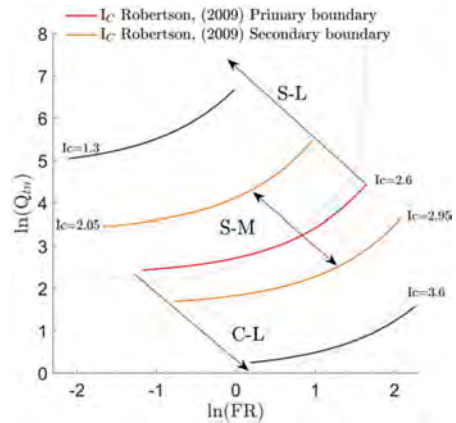


Figure 3. Class boundary at first and second staged classification on Robertson (2009) chart.

2.5 Thin layer treatment

Any semi-automated analysis of CPTu records is liable to end identifying thin layers (e.g., thinner than 20 cm). It is well recognized that the cone diameter employed limits the ability of CPTu to resolve thin layers, as the measured cone tip resistance is affected by both development and sensing distances (Boulangier & Dejong, 2018). Due to those two limits, the measured soil resistance does not coincide with that of the material at the tip location, i.e., measured soil resistance in absence of both development and sensing distances. Therefore, the cone is only able to unambiguously identify layers above a minimum layer resolution of 150- 200 mm. A simplified practical approach to deal with this difficulty is to merge layers below the minimum thickness with adjacent ones of similar soil behavior type (Ganju et al. 2017).

This strategy is also adopted here, with details slightly dependent on the classification level selected. At the first and second refinement levels thin layers are merged based on the closeness on mean value of I_c . At the third level, when using the full (Robertson, 2009) classification chart, the situation is analogous to that of Ganju et al. (2017) and the same auxiliary criteria based on class groupings are applied.

2.6 Single CPTu analysis workflow

The main workflow steps are reported in Figure 4. The analyst has to feed in a CPTu record to analyze and select the level of classification, minimum layer resolution and the P and m values. The code can then start analyzing the CPTu input record by selecting a segment of CPTu data pairs long enough (e.g., 10 points) to fit an initial PDF (I_c). The PDF(I_c) is then updated by adding the next CPTu data point, moving downwards through the record. Such updating allows the I_c density to move on the SBT line until the representative interval (given by P) surpasses any class boundaries by a larger proportion than that allowed

by m . At that time, data that fed the univariate density are assigned to the identified layer, whose soil class is assigned depending on location of the mean value of the univariate distribution. The procedure resumes by analyzing the next segment in the CPTu record until all the record is analyzed (Figure 4). An example of layer identification is depicted in Figure 5 for a synthetic I_c profile and $P = 1.5$ and $m = 0$ using a first level (binary) classification.

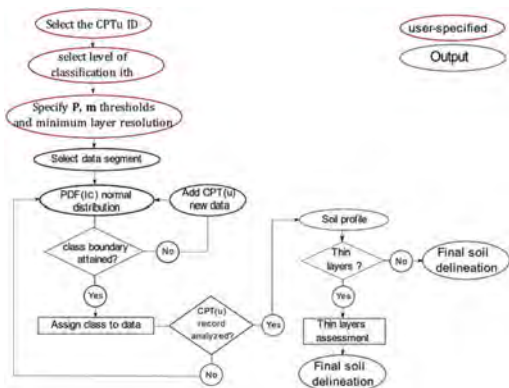


Figure 4. General workflow of single CPTu analysis.

2.7 Multiple CPTu analysis

The same methodology can be applied to multiple CPTu records. The aim is to identify common layers at different locations according to a pre-established depth correspondence criterion between the records. This may just be a hypothesis of layers parallel to the ground level, or following a linear trend throughout the site or any other criteria.

Once selected the depth criterion, the univariate density is now initialized by $n_{CPT(u)}$ length (initial data segment) data points, with $n_{CPT(u)}$ number of CPTu records analyzed (Figure 6a). The univariate density is then updated by $n_{CPT(u)}$ data (one for each sounding record analyzed) until the boundary condition is attained according to P and m threshold (Figure 6b). After stoppage, to ensure that identified layers belong to the same soil type, data assigned to the layer for each CPTu sounding is analyzed separately, and n_{CPTu} univariate density distributions are computed. A common soil layer is identified only if the n_{CPTu} mean values are within the same class boundaries, (Figure 6b). The procedure then resumes until all the CPTu records are analyzed.

Qualitative considerations on layer lateral continuity may be then inferred depending on thickness of identified common layers and relative distance of CPTu locations. As an example, if a thick common soil layers is identified and the relative distance of C-

PTu locations is less than typical value of horizontal scale of fluctuation (e.g., 40 – 80m, Phoon & Kulhawy 1999) lateral continuity could be assumed.

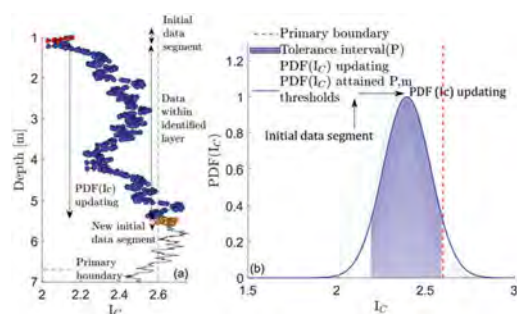


Figure 5. General workflow of single CPTu analysis.

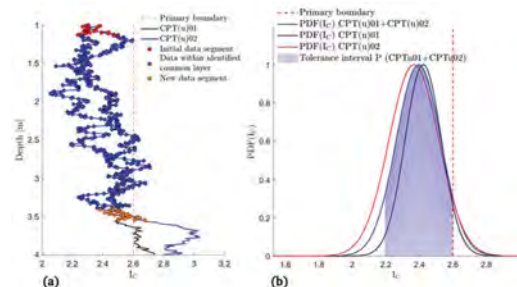


Figure 6. Common layer identification by employing two CPTu sounding record.

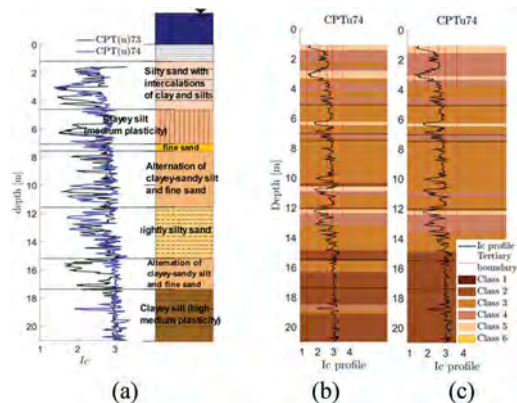


Figure 7. Layer delineation a) from core sample inspection. From CPTu using all SBT classes with b) $P = 1.8$; $m = 0.05$. c) $P = 1$; $m = 0.2$.

3 ILLUSTRATIVE EXAMPLE

3.1 Case study

The proposed methodology is tested on CPTu records obtained at Barcelona harbor (Spain). Two adjacent CPTu sounding profiles (CPTu74, CPTu73), each up to 21m depth from seabed surface (Figure 7) are analyzed. An independently established soil layer profile was available for the site, which was derived from cores retrieved at the same location where CPTu74 was performed. Laboratory samples were retrieved each 5 m depth and core description followed UNE-EN ISO 14688-1 from which a detailed soil profile was derived. The boundaries identified (Figure 7a) carried significant uncertainty due to the complex structure and strong heterogeneity of the site. The layering of Figure 7a was directly checked against cone results. For each layer, CPTu74 data were assigned to one of the six classes of Robertson (2009). Percentages of I_C data are reported in Table 1. Up to 15.5 it is evident how core-based layers are mainly composed by soil-mixture class (class 3 and 4 of Robertson, 2009). However, a significant heterogeneity is evident within each layer.

3.2 Case study-single CPTu record

The procedure previously described was applied to the CPTu74 record. The P and m model parameters were varied to try to match the core-based delineation. A third staged delineation was initially selected due to the detailed core-based description. By considering $P=1.8$ (e.g., about 92% representative interval) and 5% threshold mixture, all core-based boundaries (except one at 17.4 m depth) were identified (Figure 7). However, several additional layers were detected as expected from the results in (Table 1). To illustrate the effect of varying the fitting control parameters, the same record is reanalyzed using the $m=0.2$ value and $P=1$ (i.e., representative interval of about 68%) (Figure 7c). The parameters of the reanalysis result in a simpler profile, but it is noticeable that the layers disappearing are not simply the thinner ones (e.g., at 6 m depth) but others (e.g., at 19 m depth) that were less statistically contrasted with their neighbors.

An alternative route to profile simplification is to use a coarser classification level. This is explored in Figure 8a, b using the same CPTu74 record and maintaining the same control

parameters as in (Figure 7b). Most boundaries established by core inspection are recovered by the binary classifier, whereas that is not the case for the second level profile. It is interesting to observe how the coarser binary classification results in very fast layer alternance in the first 14 m, Figure 8a whereas the introduction of the “mixtures” class results in a rather homogenous profile (Figure 8b).

This result is also clear when another CPTu is analyzed using the same control parameters (Figure 9). Comparing the different profiles obtained, the analyst can decide which set of choices (classification level, P and m values) results in the level of detail that is more meaningful for engineering design process. Once the analyst heuristics are thus elicited, they can be systematically applied at all site locations.

3.3 Multiple CPTu records

As an example of simultaneous analysis, the two CPTu records discussed above were considered. Based on previous study on this area a depth correspondence criterion parallel to the seabed surface was selected. By assuming the same P and m value, 2D cross sections for three different level of classifications are reported in Figure 10. For identified common layers, lateral continuity was assumed due to the relatively close distance between CPTu (e.g., about 50 m). At first level 15% of data was classified as S-L, 59% as C-L, and 26% corresponded to “not common” layers. Increasing the classification refinement level at every profile the continuity between different site investigation points is reduced. Using second and third level classifications, the percent of data in “not common” layers increase to 40% and to 58%, respectively.

Table 1. Percent of soil class data within each geological unit.

Depth	SBT1	SBT2	SBT3	SBT4	SBT5	SBT6
[m]	%	%	%	%	%	%
1-5.1	-	2	34	43	21	-
5.1-7.05	-	1.5	68.9	13.8	15.8	-
7.05-7.5	-	-	56.6	43.4	-	-
7.5-12.05	-	15	63	15	6	-
12.05-15.5	-	30	31	29	10	-
15.5-17.4	-	68	22	3	7	-
17.4-21	-	83.3	13.6	2.7	1.4	-

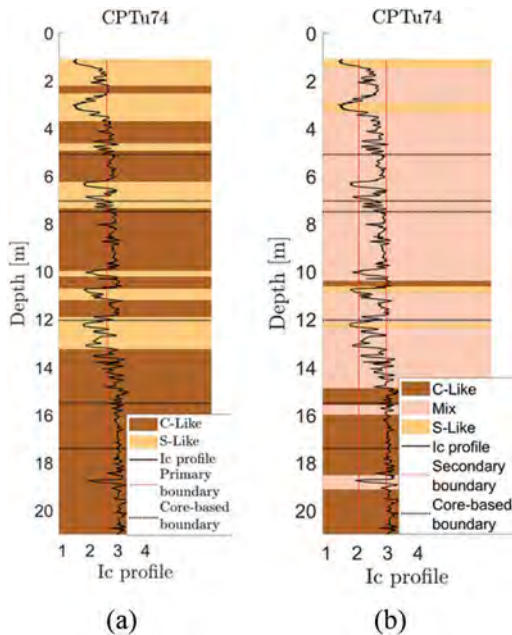


Figure 8. CPTu profile layering resulting from $P=1.8$; $m=0.05$ a) using a first level classification b) using a second level classification.

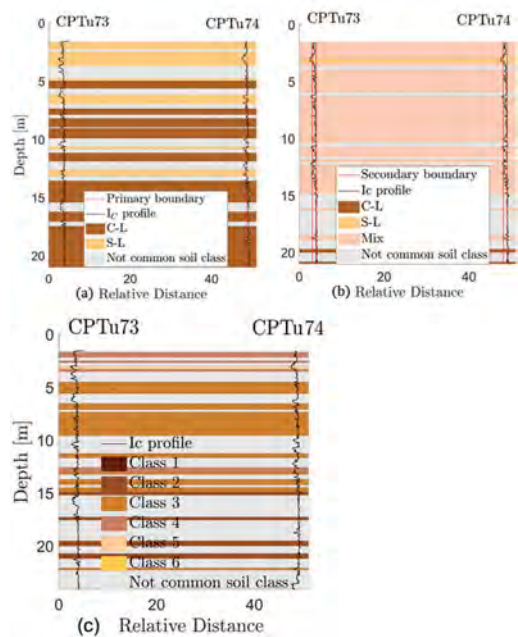


Figure 10. a) Soil delineation at second staged classification for $P=1.86$; $m=0.05$ b) Soil delineation at third staged classification for $P=1.8$; $m=0.05$.

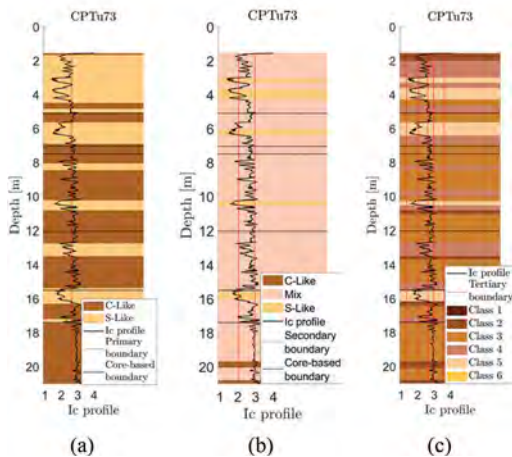


Figure 9. Soil delineation for $P=1.8$; $m=0.05$ for CPTu73; a) first level classification. b) second level classification. c) third level classification..

4 CONCLUSION

This work describes a novel probabilistic procedure for soil delineation based on CPTu sounding records aiming to facilitate communication in the process of layer delineation. Subjective heuristics, applied within CPTu records interpretation, are elicited and quantified facilitating consensus in the soil

delineation process. The proposed methodology is application to multiple CPTu records to help discern continuous layering. Although the method has been illustrated using SBT it is easily adaptable to any other chart-based classification procedure (Collico et al. 2020).

REFERENCES

Boulanger, R. W., & Dejong, J. T. (2018). Inverse filtering procedure to correct cone penetration data for thin-layer and transition effects. *Cone Penetration Testing 2018 - Proceedings of the 4th International Symposium on Cone Penetration Testing, CPT 2018*, 25–44.

Collico, S., Devincenzi, M., & Rodriguez, A. (2020). Semi-automated probabilistic soil profiling using CPTu. *6th INTERNATIONAL CONFERENCE ON GEOTECHNICAL AND GEOPHYSICAL SITE CHARACTERISATION*.

Depina, I., Le, T. M. H., Eiksund, G., & Strøm, P. (2016). Cone penetration data classification with Bayesian Mixture Analysis. *Georisk*, 10(1), 27–41. <http://dx.doi.org/10.1080/17499518.2015.1072637>

Douglas, B. J., & Olsen, R. S. (1981). *SOIL CLASSIFICATION USING ELECTRIC CONE PENETROMETER, October 1981*, 209–227.

Jefferies, M., & Davies, M. (1991). Soil Classification by the cone penetration test: Discussion. *Can. Geotech. J.*, 28, 173–176.

Jung, B. C., Gardoni, P., & Biscontin, G. (2008). Probabilistic soil identification based on cone penetration tests.

- Geotechnique*, 58(7), 591–603. <http://dx.doi.org/10.1680/geot.2008.58.7.591>
- Krogstad, A., Depina, I., & Omre, H. (2018). Cone penetration data classification by Bayesian inversion with a Hidden Markov model. *Journal of Physics: Conference Series*, 1104(1). <http://dx.doi.org/10.1088/1742-6596/1104/1/012015>
- Phoon, K. K., & Kulhawy, F. H. (1999). Characterization of geotechnical variability. *Canadian Geotechnical Journal*, 36(4), 612–624. <http://dx.doi.org/10.1139/t99-038>
- Robertson, P. K. (1990). Soil classification using the cone penetration test. *Canadian Geotechnical Journal*, 27(1), 151–158. <http://dx.doi.org/10.1139/t90-014>
- Robertson, P. K. (2009). Interpretation of cone penetration tests — a unified approach. *Canadian Geotechnical Journal*, 46(11), 1337–1355. <http://dx.doi.org/10.1139/t09-065>
- Robertson, P. K. (2016). *Cone penetration test (CPT) - based soil behaviour type (SBT) classification system — an update*. 1927(July), 1910–1927.
- Robertson, P. K., & Wride, C. E. F. (1998). *Evaluating cyclic liquefaction potential using the cone penetration test*.
- Uzielli, M., Vannucchi, G., & Phoon, K. K. (2015). Random field characterisation of stress-normalised cone penetration testing parameters. *Risk and Variability in Geotechnical Engineering*, 1, 3–20. <http://dx.doi.org/10.1680/ravige.34860.0001>
- Wang, Y., Huang, K., & Cao, Z. (2013). *Probabilistic identification of underground soil stratification using cone penetration tests*. 776(May), 766–776.
- Zhang, L., Asce, M., Tang, W. H., Asce, H. M., Zhang, L., & Zheng, J. (2004). *Reducing Uncertainty of Prediction from Empirical Correlations*. May, 526–534.

Clustering analysis to improve total unit weight prediction from CPTu

S. Collico & M. Arroyo

Department of Civil and Environmental Engineering (DECA), Universidad Politecnica de Cataluña, Barcelona, Spain

M. DeVincenzi, A. Rodriguez & A. Deu

Igeotest s.l. Figueres, Spain

ABSTRACT: Accurate estimates of soil unit weight are fundamental for correctly post process CPTu data and making use of Soil Behavior Type-based classification systems. Soil-specific and global regressions have been proposed for this purpose. However, soil-specific correlation might pose a problem of pertinence when applied at new sites. On the other hand, global correlations are easy to apply, but generally carry large systematic uncertainties. In this context, this work proposes a data clustering technique applied to geotechnical database aiming to identify hidden linear trends among dimensionless soil unit weight and normalized CPTu parameter according to some unobservable soil classes. Global correlations are then revisited according to such data subdivision aiming to improve accuracy of soil unit weight prediction while reducing transformation uncertainty. A new probabilistic criterion for soil unit weight prediction is also obtained. The potential benefits of the proposed procedure are illustrated with data from a Llobregat delta site (Spain).

1 INTRODUCTION

CPTu interpretation is almost always based on stress normalized cone readings. For instance, soil classification charts (Robertson, 1990; Been & Jefferies, 2006; Schneider et al., 2008) use stress normalized tip resistance, friction and excess pore pressure parameters. Total soil unit weight γ_t is thus a necessary input in any CPTu interpretation exercise.

Soil unit weight is measured on undisturbed samples from boreholes. Such samples are not always available, particularly for granular soils and/or in early stages of site investigation. As a simpler alternative, total soil unit weight can be estimated indirectly from piezocone and seismic piezocone readings. In the last decades several proposals have been presented to achieve this purpose (Mayne, 2009; Mayne et al., 2010; Robertson & Cabal, 2010; Mayne, 2014; Lengkeek, 2018).

These proposals are all based on empirical regression using databases in which cone readings are paired with soil unit weight measurements. A trade-off typically arises between coverage (the scope of the original soil database) and precision (the predictive power of the regression). Global regressions, usually described as applicable to soils with a "normal" or common mineralogy, are widely applicable but less precise than regressions developed only for a certain class of soil (i.e., soil specific). On the other hand, soil specific regressions are more difficult to

apply at a particular site because they have less coverage and require a previous soil classification step, which may introduce additional uncertainty. One possible way out of this problem is to develop soil-specific regressions for unit weight using a global database that is segmented into soil classes for regression purposes. How to define those classes?

In this work we employ a Gaussian Mixture Model (a.k.a., GMM) technique to identify hidden classes in a global database described by Mayne, (2014) with the purpose of establish more accurate regressions. GMM have been previously applied to CPTu data analyses (Depina et al., 2016; Krogstad et al., 2018) to identify soil classes for stratigraphic delineation. In those studies, a Bayesian perspective was introduced, as having the possibility of updating the stratigraphic groups as more information was gathered was deemed essential. In the present work a fixed database is considered and therefore the Bayesian updating aspect has been omitted.

A key step of applying such data clustering technique is to express the reference database, including soil unit weight and CPTu data, as a multivariate normal distribution before GMM is applied. To this end we use a methodology laid out by Ching et al., (2014), to rationally account for predictor co-dependence and to establish or revise correlations between different variables.

In what follow, key steps to construct valid multivariate distribution are reported followed by a brief

description of finite Gaussian Mixture Models. In the results section, an example of data subdivision and assignment to identified hidden classes is reported using dimensionless soil unit weight and normalized CPTu parameters. Existing correlations are re-examined using the new soil classes and a new one is proposed.

2 METHODOLOGY

2.1 Setting up a multivariate distribution

Ching et al., (2014) and Phoon & Ching, (2018) proposed a systematic cumulative transform procedure to build standard multivariate normal distributions for multivariate databases. Such approach is adopted in this study to treat the Mayne, (2014) database.

Essentially the steps involved are:

1. For a given set of selected observations $\underline{\Omega}$ (e.g., $\underline{\Omega} = [\Omega_1, \Omega_2]$ with $\Omega_1 = [n \times 1]$ and n number of observations) define marginal distributions Ω_i for each of the component variates in the database;
2. Transform the different marginals into standardized normal distributions \mathbf{X}_i
3. Assume that transformed observations $\mathbf{X} = [\mathbf{X}_1, \mathbf{X}_2]$ follow a multivariate normal distribution $f(\mathbf{X})$;
4. Obtain a random sample from $f(\mathbf{X})$, and transform it back to the non-normalized space, obtaining the simulated set $\underline{\Omega}_{sim}$
5. Check by inspection the overlap between $\underline{\Omega}_{sim}$ and $\underline{\Omega}$.

A key step in the procedure is the definition of marginal distributions for the different variates in the database (in this case dimensionless soil unit weight and normalized CPTu parameters). Lognormal distributions have been frequently used in geotechnical applications (Phoon & Kulhawy, 1999). The lognormal is included in the Johnson system of distributions (Ching et al., 2014), which has three main families: the lognormal system S_L , the bounded system S_B and unbounded system S_U . Choosing between the whole system of Johnson distributions offers versatility while maintaining the interesting property of having analytical expressions to transform into standard normal variables and back (Ching et al. 2014).

The selection of an appropriate Johnson distribution for a particular dataset is based on the first four moments of a sampling distribution (George & Ramachandran, 2011). Examples of Johnson distributions fitted to different variates of the Mayne, (2014) global database are given in (Figure 1).

2.2 Multivariate as a gaussian mixture

The multivariate distribution that represents the database might be conceived as a combination of several

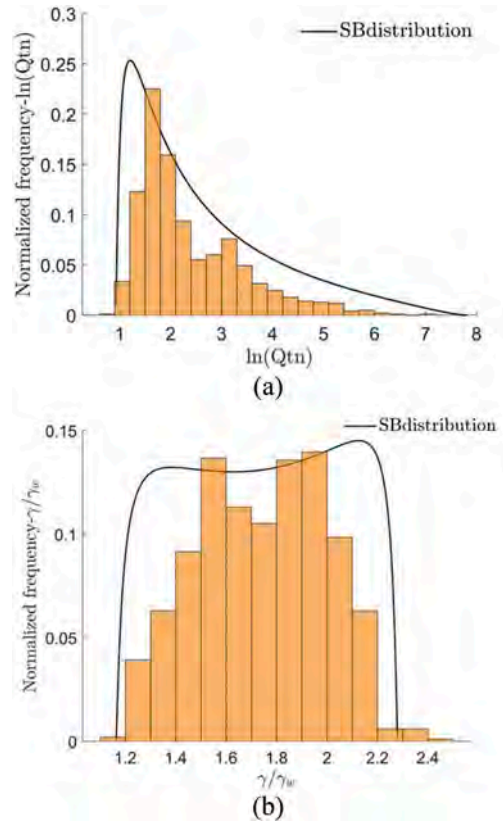


Figure 1. Fitting Johnson probability density function to a) $\ln(Q_m)$; b) γ_i/γ_w data of Mayne, (2014) database.

underlying components (the hidden classes that we are trying to identify). This is formalized using a Gaussian Mixture Model, (Depina et al., 2016; McLachlan & Peel, 2000), that expresses the transformed -standardized- multivariate distribution as a linear combination of K multivariate gaussians:

$$f(\underline{x}_i|\zeta) = \sum_{j=1}^K \pi_j \phi_j(\underline{x}_i|\Theta_j) \quad (1)$$

Each ϕ_j represents a component of the mixture and is a multivariate normal probability density function with the same structure as $f(\mathbf{X})$. Therefore, each component has its own statistical parameters, denoted by Θ_j . In our case they include a vector of means and a covariance matrix (i.e., $\mu_j, \underline{\Sigma}_j$). The collection of all the Θ_j is denoted by $\underline{\Theta}$. Each component has a weight π_j (proportion of data assigned to ϕ_j); weights are chosen so that they add up to one and are collected in a vector $\underline{\Pi} = (\pi_1, \dots, \pi_K)$. $\zeta =$ collection of all the unknown parameters of the mixture model (i.e., $[\Theta; \underline{\Pi}]$).

Depending on the values that ζ finally takes each observation x_i would have a certain probability p_{ij} of belonging to a particular component ϕ_j .

Gaussian Mixture analysis consists of estimating the most probable ζ , $\hat{\zeta}$. This is generally done through the Expectation-Maximization (EM) algorithm (Samé et al., 2011; Huang et al., 2017; Liu et al., 2019) which alternates an expectation step in which observations are assigned exclusively to a particular gaussian component and a maximization step, in which the log-likelihood function for the incomplete dataset is maximized.

The concept of GMM could be also formulated in a Bayesian framework, by integrating prior knowledge $p(\zeta)$ and observations $\underline{\Omega}$ to obtain posterior estimates of ζ . Due to lack of previous studies, this work only applies GMM. For more detailed information about the Bayesian formulation, analysis about optimal number of hidden classes to consider and most plausible normalized CPTu parameters to be considered, the reader is referred to Collico, (2021).

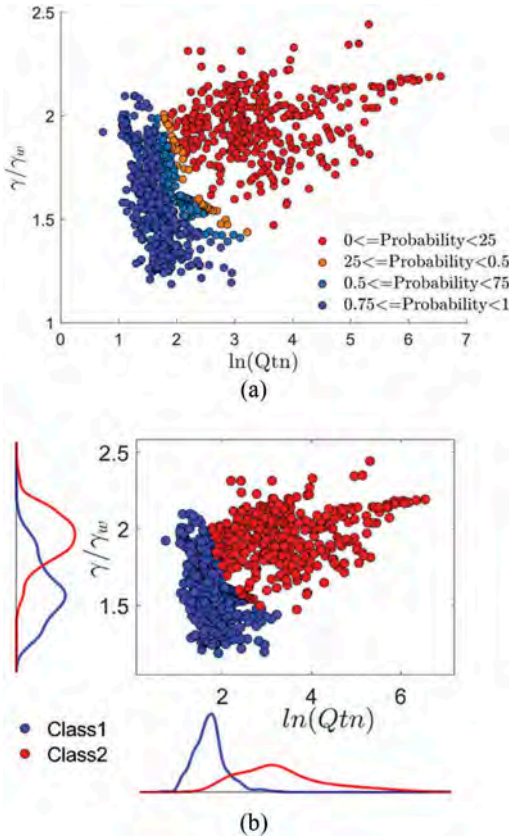


Figure 2. A) Assigned probability of belonging to component 1 of the GMM b) Scatter and marginal distributions of observations for the two hidden classes identified.

3 RESULTS

3.1 Cluster definition and analysis

There are six variates in the Mayne, (2014) database. To illustrate the methodology proposed in a simple setting, we consider only two of them, namely dimensionless unit weight γ_t/γ_w and normalized tip resistance, $\ln(Q_{tn})$. After fitting a bivariate distribution to all the data pairs $\gamma_t/\gamma_w - \ln(Q_{tn})$ we run the expectation-maximization algorithm to identify a GMM with two components.

An example illustrating the probabilities of data belonging to a particular component of the Gaussian mixture is given in Figure 2a. Clustering is based on such probabilities. A simple choice is to assign data to the component in which they have the largest probability of belonging. For two components this is equivalent to enforcing a probability threshold of 0.5 as clustering criteria. The result of doing so in this case is reported in Figure 2b, while statistics for the two clusters in the $\underline{\Omega}$ space are reported in Table 1.

To understand the meaning of this newly identified soil classes, the clustered data is plotted in Soil Behavior Type charts (Robertson, (2016); Schneider et al. (2008) (Figure 3). Results show that the first hidden class identified is dominated by Clay-Like-Contractive soils (C - C, Figure 3a), while the second hidden correlation identified is represented by a wider range of conventional soil types.

Table 1. Covariance matrix and mean vector of $\gamma_t/\gamma_w - \ln(Q_{tn})$ hidden classes identified.

Class	Mean	Covariance
1	μ_{γ_t/γ_w}	$\mu_{\ln(Q_m)}$
	1.59	1.71
2	μ_{γ_t/γ_w}	$\mu_{\ln(Q_m)}$
	1.95	3.32

	γ_t/γ_w	$\ln(Q_{tn})$
Class 1	0.04	-0.036
Class 2	-0.036	0.125
Class 1	0.025	0.04
Class 2	0.04	0.94

3.2 Generating cluster-based correlations

The clustered data can be used to generate new correlations. Such correlations need not be based on the same restricted subset of the global database that was used to generate the clustering. For instance, we use here correlations that follow a template proposed by Mayne, et al., (2010) (i.e., $\gamma_t = a + b \cdot \log(z) + c \cdot \log(f_s) + d \cdot \log(q_t)$). Results in terms of coefficient of determination, R^2 and regression standard error, σ_{eT} are reported in Table 2, while regression coefficients are reported in Table 3. The standard error, after GMM subdivision, is at least 13% smaller than the one of global database. The coefficient of determination R^2 is also smaller for the clusters than for the global database. These effects are particularly strong for Hidden class 2.

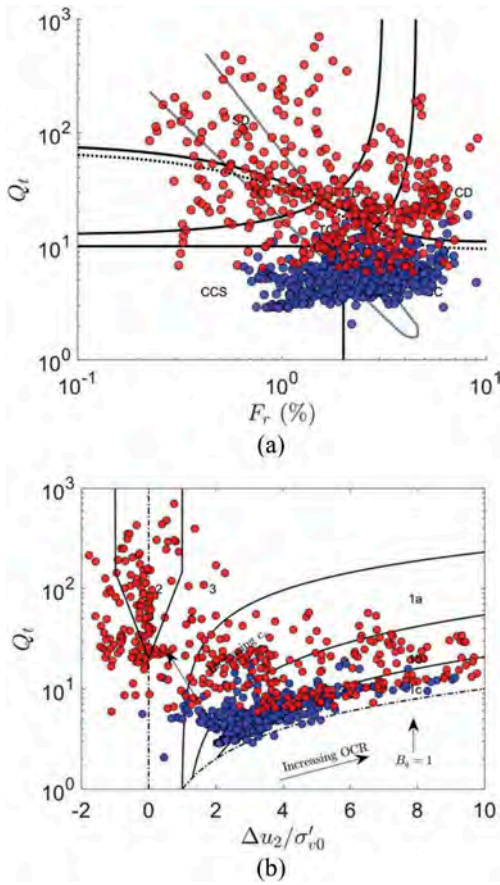


Figure 3. Scatter plot of data belonging to each hidden cluster identified on SBT charts: a) Robertson, (2016); b) Schneider et al., (2008).

Table 2. Coefficient of determination and regression standard error before and after database subdivision.

	R^2	σ_{er}
Global	0.66	1.44
Hidden class 1	0.6	1.25
Hidden class 2	0.39	1.22

However, those comparisons are somewhat misleading, as the statistics are computed using different observations. The improvement of predictive strength after clustering is more clearly identified through a cross-validation procedure. To this end we run a simulation exercise in which we randomly selected 85% of the data in each cluster and used them to fit cluster specific correlations, as well as a global one in which no cluster distinction was made. Then we applied those correlations, to the remaining 15% of the dataset -the validation data. The sum of squared residuals $||SS_{res}||$ was

computed at each trial, for each one of the correlations (global, cluster 1, cluster 2). 500 such simulations were performed. Results, reported in Figure 4 for both Hidden classes, highlight the benefit of the GMM as the distribution of error norms is clearly shifted towards lower values.

Table 3. Coefficient of the regression for linear form of Mayne (2010) after BMA subdivision.

	a	b	c	d
Global	8.78	-0.67	2.24	1.457
Class1	-0.78	-4.2	7.77	-0.57
Class2	15.34	0.052	0.02	1.94

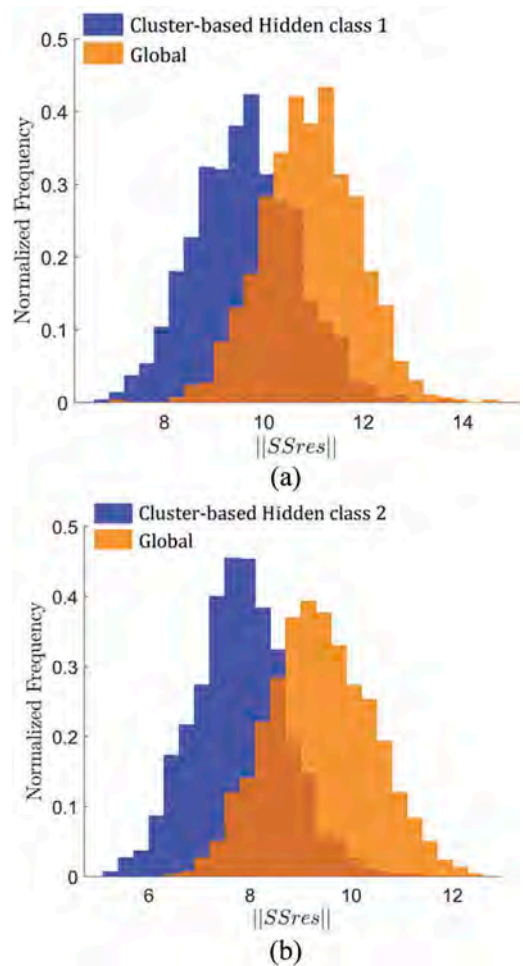


Figure 4. Cross validation of revisited regression and comparison with global literature correlation for a) Hidden class 1. B) Hidden class 2.

3.3 Application to new sites: Decision boundary

To assign CPTu observations at a new site to a cluster, we use the (non-normalized) Robertson, (1990) SBT chart. Plotting the clustered data in that chart we apply discriminant analysis (Ghojogh & Crowley, 2019) to establish a user-friendly separation criteria for new CPTu observations. The decision boundary (Figure 5) obtained takes the shape of a quadratic in Robertson (1990) chart. This boundary line between the two clusters has the following expression:

$$2.37 + [0.2\ln(R_f) - 1.58\ln(q_t)]^2 \pm \sigma_{\text{boundary}} = 0 \quad (2)$$

with σ_{boundary} systematic uncertainty associated with decision boundary ($\sigma_{\text{boundary}} = 0.13$).

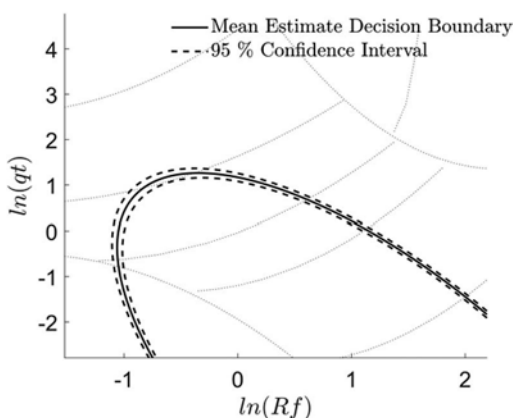


Figure 5. Mean estimate and 95% Confidence Interval of decision boundary.

3.4 Illustrative example

The cluster-based correlations just developed are now applied to results of a particular CPTu campaign performed at a Llobregat site (SW Barcelona-Spain). Several infrastructures have been developed around this site during the last decades, requiring extensive onshore-nearshore geotechnical investigation. Along with in-situ investigation, laboratory tests were performed on selected sub-samples from undisturbed Shelby tubes recovered every 5m in each borehole. For this study we consider data from 20 CPTu and 44 total soil unit weight measurements. More detail on this campaign is given by Deu et al., (2021).

All the CPTu data were plotted on Robertson graph, showing that the site is dominated by silty soils. Then each CPTu observation was assigned to class 1 or 2 according to the mean value of the decision boundary (Figure 6a). Most of the data were assigned to Hidden class 2.

The cluster-based correlation was applied to the 20 CPTu data and the results are plotted in (Figure 6b), indicating the mean and spread of the predicted values.

The same is done using the global correlation, obtained using the whole database, without clustering. Summary results are also presented in Table 4. They include the

Table 4. Statistics of mean value of total unit weight prediction.

	μ_{γ_t}	$\sigma_{\mu_{\gamma_t}}$
Global correlation	17.47	0.48
Cluster-based correlation	18.1	0.42
Laboratory	19.45	0.66

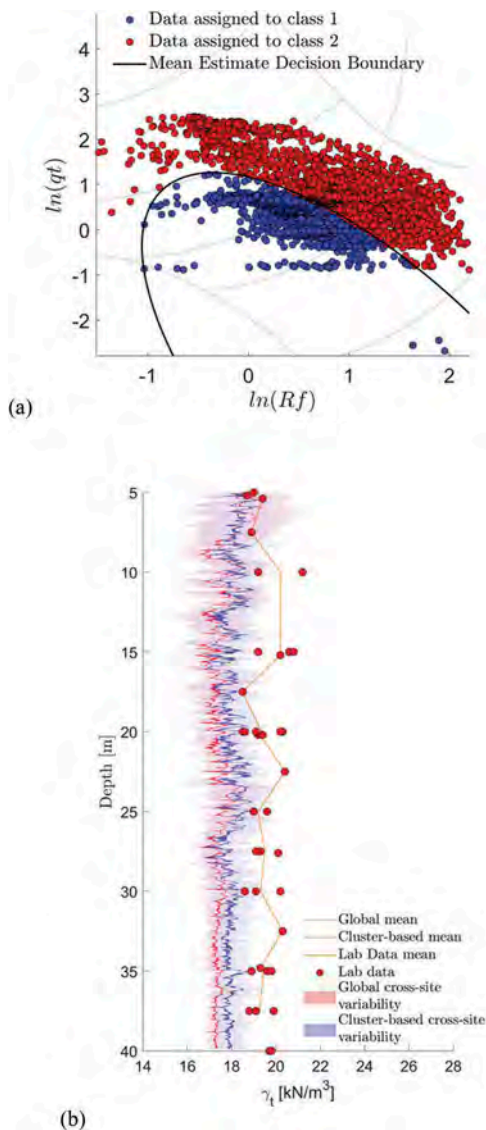


Figure 6. A) CPTu data assigned to class 1 and class 2 according to the proposed criterion. b) Profile of total unit weight prediction for cluster-based and global correlations and laboratory observations.

overall predicted mean estimate as well as the standard deviation of the means evaluated at different depths.

The cluster-based correlation clearly exhibits an improvement of total unit weight prediction at the site (Figure 5b), when compared global correlation. It has a lower dispersion and its mean is closer to that of the laboratory measurements. It is clear, however, that even the cluster-based correlation underestimates the laboratory mean. There are several possible explanations for this discrepancy. One is that samples of silty soils generally tend to be densified upon sampling (Lim et al. 2018). The other is that the reference database is somewhat scarce in the silt area were most datapoints in the example lie (compare Figures 6a and 3a).

4 CONCLUSION

This study describes a first attempt to apply GMM clustering to geotechnical database.

The clustering technique has been applied in a space parametrized by dimensionless soil unit weight and normalized cone tip resistance, assuming the existence of two unobserved classes, selected at 50% probability. One of emerging hidden classes can be associated to Clay-Like-Contractive class, while the second is representative of a wide range of soil types. Assignment of new data to the hidden classes is based on a discriminant line generated on non-normalized SBT charts (Robertson, 1990). CPTu data subdivision according to such classes has been shown to increase the predictive strength of correlations. This has been illustrated using a correlation template from Mayne et al., (2010) in which unit weight is predicted from shaft friction, depth and tip resistance.

Beyond the particular application explored here, the technique presented here may prove useful to improve accuracy and precision of empirical CPTu based correlations established using global databases.

REFERENCES

Ching, J., Phoon, K., & Chen, C. (2014). Modeling piezocone cone penetration (CPTU) parameters of clays as a multivariate normal distribution. 91(July 2012), 77–91.

Collico, S., (2021). Geotechnical characterization of marine sediments via statistical analysis (Unpublished doctoral dissertation). Universidad Politècnica de Catalunya (UPC), Barcelona, Spain.

Depina, I., Le, T. M. H., Eiksund, G., & Strøm, P. (2016). Cone penetration data classification with Bayesian Mixture Analysis. *Georisk*, 10(1),27–41. <https://doi.org/10.1080/17499518.2015.1072637>

Deu, A., Martí X., Peña S., Tarragò D., Gens A., & Devincenzi, M. (2021) DMT, CPTU and laboratory tests comparison for soil classification and strength parameters of deltaic soft soils in Barcelona Port, Proceedings of the 6th International Conference on Site Characterization ISC-6 Budapest

George, F., & Ramachandran, K. M. (2011). Estimation of parameters of johnson's system of distributions. *Journal*

of Modern Applied Statistical Methods, 10(2),494–504. <https://doi.org/10.22237/jmasm/1320120480>

Ghojogh, B., & Crowley, M. (2019). Linear and Quadratic Discriminant Analysis: Tutorial. 4, 1–16. <http://arxiv.org/abs/1906.02590>

Huang, T., Peng, H., & Zhang, K. (2017). Model selection for Gaussian mixture models. *Statistica Sinica*, 27(1),147–169. <https://doi.org/10.5705/ss.2014.105>

Krogstad, A., Depina, I., & Omre, H. (2018). Cone penetration data classification by Bayesian inversion with a Hidden Markov model. *Journal of Physics: Conference Series*, 1104(1). <https://doi.org/10.1088/1742-6596/1104/1/012015>

Lengkeek, H. J. (2019). CPT based unit weight estimation extended to soft organic soils and peat. January 2018.

Lim GT, Pineda JA, Boukpeti NA, Fourie AN, Carraro JA. Experimental assessment of sampling disturbance in calcareous silt. *Géotechnique Letters*. 2018 Sep;8(3):240–7.

Liu, Y., Ye, L., Qin, H., Ouyang, S., Zhang, Z., & Zhou, J. (2019). Middle and Long-Term Runoff Probabilistic Forecasting Based on Gaussian Mixture Regression. *Water Resources Management*, 33(5),1785–1799. <https://doi.org/10.1007/s11269-019-02221-y>

Mayne, P.W., Peuchen, J., & Bouwmeester, D. (2010). Soil unit weight estimation from CPTs. 2nd International Symposium on Cone Penetration Testing, 2 (May),8. <https://doi.org/10.1201/b10132-41>

Mayne, P. W. (2014). Interpretation of geotechnical parameters from seismic piezocone tests. 3rd International Symposium on Cone Penetration Testing (CPT'14), 47–73.

Mayne, Paul W, Coop, M. R., Springman, S. M., & Zornberg, J. G. (2009). Geomaterial behavior and testing. Proceedings of the 17th International Conference on Soil Mechanics and Geotechnical Engineering: The Academia and Practice of Geotechnical Engineering, 5, 2777–2872.

McLachlan, G. J., & Peel, D. (2000). Finite mixture models. John Wiley & Sons.

Phoon, K. K., & Ching, J. (2018). Risk and Reliability in Geotechnical Engineering. In *Risk and Reliability in Geotechnical Engineering*. <https://doi.org/10.1201/b17970>

Phoon, Kok Kwang, & Kulhawy, F. H. (1999). Characterization of geotechnical variability. *Canadian Geotechnical Journal*, 36(4),612–624. <https://doi.org/10.1139/t99-038>

Robertson, P. K. (1990). Soil classification using the cone penetration test. *Canadian Geotechnical Journal*, 27(1),151–158. <https://doi.org/10.1139/t90-014>

Robertson, P. K. (2016). Cone penetration test (CPT) - based soil behaviour type (SBT) classification system — an update. 1927(July), 1910–1927.

Robertson, P. K., & Cabal, K. L. (2010). Estimating soil unit weight from CPT. May.

Samé, A., Chamroukhi, F., Govaert, G., & Akin, P. (2011). Model-based clustering and segmentation of time series with changes in regime. *Advances in Data Analysis and Classification*, 5(4),301–321. <https://doi.org/10.1007/s11634-011-0096-5>

Schneider, J. A., Randolph, M. F., Mayne, P. W., & Ramsey, N. R. (2008). Analysis of factors influencing soil classification using normalized piezocone tip resistance and pore pressure parameters. *Journal of Geotechnical and Geoenvironmental Engineering*, 134(11),1569–1586. [https://doi.org/10.1061/\(ASCE\)1090-0241\(2008\)134:11\(1569\)](https://doi.org/10.1061/(ASCE)1090-0241(2008)134:11(1569))

Combining CPTU and UMASW to characterise Irish offshore deposits

M. Coughlan

*School of Civil Engineering, University College Dublin, Belfield, Dublin, Ireland
SFI Research Centre for Applied Geosciences (iCRAG), Ireland
Gavin and Doherty Geosolutions Ltd., Dublin, Ireland*

A. Trafford, M. Long & S. Donohue

*School of Civil Engineering, University College Dublin, Belfield, Dublin, Ireland
SFI Research Centre for Applied Geosciences (iCRAG), Ireland*

S. Corrales

APEX Geophysics, Gorey, Wexford, Ireland

ABSTRACT: The north Irish Sea is earmarked for the development of several offshore wind farms. The complex Quaternary history of this area has resulted in a legacy of geotechnically challenging deposits, including heterogeneous glacial deposits, soft sediments and gas-charged sediments. Multichannel Analysis of Surface Waves (MASW) is commonly used onshore to produce shear wave velocity (V_s) profiles and is increasingly being used offshore (UMASW). When used in tandem with *in-situ* Cone Penetration Testing (CPTU) profiles it is a powerful tool for characterising offshore deposits. UMASW profiles were obtained from sites across the north Irish Sea coincident with CPTU profiles. V_s profiles from UMASW show good agreement with CPTU parameters in a range of geological settings. The purpose of this paper is to present a characterisation of geological deposits using a combined approach of CPTU and UMASW. By doing so the aim is to further develop classification charts that can give reliable characterisations of offshore deposits by combining non-invasive geophysical techniques and traditional CPTU.

1 INTRODUCTION

1.1 Background

The use of the Multichannel Analysis of Surface Waves (MASW) technique is used extensively in onshore geotechnical investigations, providing a profile of shear wave velocity (V_s) against depth. Additional geotechnical parameters, such as the small strain stiffness (G_{max}), can be derived using this V_s profile and subsequently used as input for foundation design. Typically, measurement of G_{max} requires high-quality undisturbed samples for laboratory-based testing, which are challenging to acquire and only measure discrete sampling locations. In this way, *in-situ* geophysical testing like UMASW offers a rapid method of measuring the bulk response of undisturbed sediment (Long & Donohue, 2007). When combined with other *in-situ* testing, such as Cone Penetration Testing (CPTU), V_s profiles derived from the Underwater MASW (UMASW) have been shown to be powerful complementary tools in characterising marine sediments (e.g. Long & Donohue, 2010) and in offshore geotechnical site investigations (Long et al., 2020).

The north Irish Sea has experienced a complicated geological history comprising of ice-sheet advance and retreat coupled with marine transgression and complex sea-level rise (e.g. Scourse et al., 2021; Ward et al., 2016). As a result, glacial deposits have been deposited on bedrock, which in turn are overlaid by marine sediments that are known to host shallow gas (Coughlan et al., 2019). These geological conditions create a number of potential geohazards and geotechnical constraints that may inhibit the extensive development of offshore wind planned for the area (Coughlan et al., 2020; Guinan et al., 2020).

Shear wave velocity (V_s) profiles were acquired using the UMASW technique from a number of locations where CPTU data existed. This paper presents V_s and CPTU data in order to characterise challenging ground conditions, such as heterogeneous glacial deposits and soft marine sediments hosting shallow gas.

1.2 Site location and description

The study area is outlined in Figure 1. In this area UMASW data were collected at 19 locations, corresponding with locations where previous geotechnical

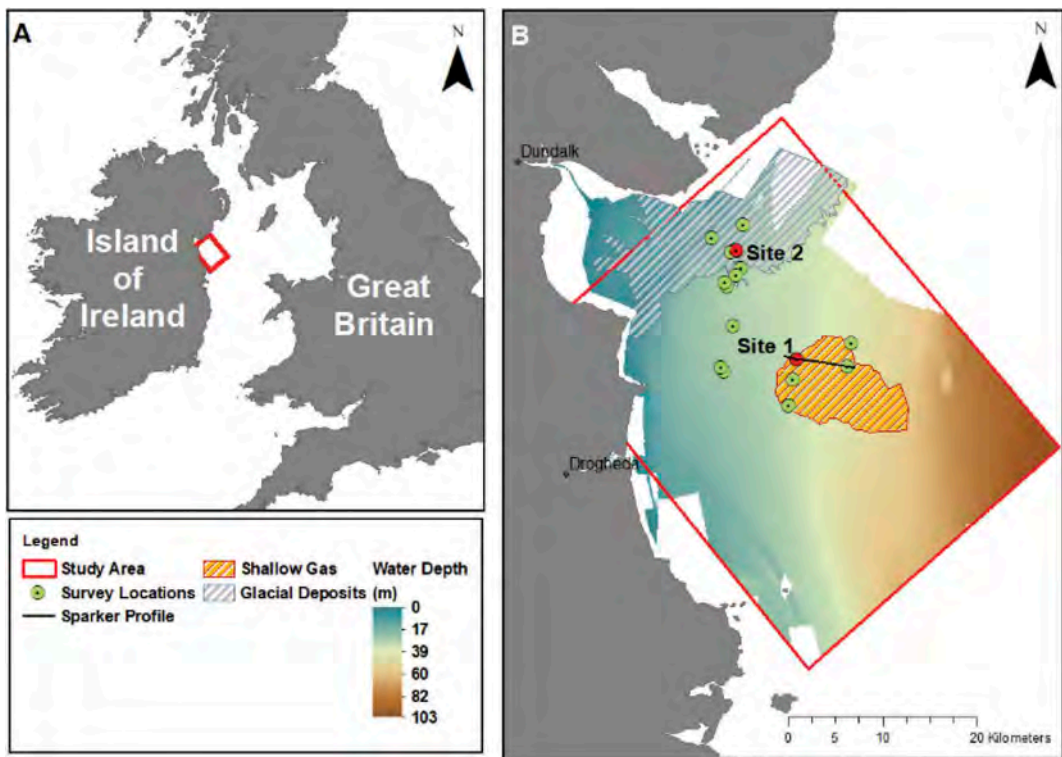


Figure 1. Study area map with data site locations. Areas of shallow gas and glacial deposits are from Coughlan et al. (2020).

data had been acquired. The data presented in this paper were obtained at 2 locations representing differing geological conditions: soft sediments with shallow gas (Site 1) and glacial deposits (Site 2). Site 1, located in an area known as the Western Irish Sea Mud Belt (WIMSB: Belderson, 1964). Coughlan et al. (2019), identified four stratigraphic units. These consist of a basal subglacial (lodgement) till emplaced by the Irish Sea Ice Stream (ISIS) as it advanced across the area, underlain by irregular bedrock. As the ISIS retreated during deglaciation, ice-proximal outwash gravels, sands and silts were deposited in a glaciomarine to glaciolacustrine. As deglaciation continued, the area became increasingly ice-proximal and dark muddy sands were deposited in a glaciomarine to marine environment. Finally, Holocene marine muds varying in thickness lie above an erosive horizon marking the base of the Holocene (Woods et al., 2019), and form the contemporary seabed. These Holocene sediments are known to host shallow gas (Coughlan et al., 2021; Yuan et al., 1992).

At Site 2, to the north and north-west, the Holocene muds and silts thin out and coarsen to sands with the underlying glacial units out- and sub-cropping at the seafloor. In the vicinity of Dundalk Bay, a large arcuate moraine ridge is evidence of a readvance of the Irish Ice Sheet eastward (Callard et al., 2019). This feature is correlated with ice

margins mapped onshore and is likely correlative to the Clogher Head and/or Killard Point Stadial, both of which are exposed in onshore sections, in a period spanning 18.2 to 16.5 ka BP (McCabe et al., 2005).

2 MATERIALS AND METHODS

2.1 Cone Penetration Testing (CPTU)

CPTU data was acquired in the study area in 2014 onboard the *RV Celtic Explorer*, using the University of Bremen developed Geotechnical Offshore Seabed Tool (GOST) system. The hardened stainless steel cone tip had a cross-sectional area of 5 cm² and sleeve area of 75 cm² recording tip resistance, sleeve friction and differential pore pressure with a sampling frequency of ~30 Hz, resulting in a vertical resolution of ~2 mm with a maximum tip resolution of 0.06 MPa and a range up to 120 MPa. The GOST system has an operational weight of between 2 and 8 tonnes depending on the addition of weighted plates for extra stability. It has 8 tonnes of hydraulic push power with variable hydraulic pressure of 0-20 MPa. Exact control on push velocity during penetration allows for data to comply to the highest international including DIN 4904 and ISO 22476-1:2012

requirements. The interface was a digital one of industrial RS485 BUS using direct A/D converting of a measured variable with overvoltage and reverse protection. Raw CPTU data were calibrated using standard methods according to (Lunne et al., 1997).

2.2 Underwater Analysis of Surface Waves (UMASW)

UMASW data were acquired as part of the Developing Site Investigation Methodologies and Constraint Mapping Products for Offshore Renewable Energy (DeSIRE) Survey in 2020. The set-up comprised two Geometrics Model DHA-7 bay cables, each consisting of 24 hydrophones moulded onto the receiver cable, that was deployed onto the seabed from a main vessel (*Ocean Navigator*) using a smaller auxiliary vessel (*Fionn MacCumhaill*). Hydrophone spacing on the cable was 3.125 m and it was attached to a mooring weight at the *Ocean Navigator* end, whilst a clump weight deployed by the *Fionn MacCumhaill* secured it at the other end. The *Fionn MacCumhaill* also acted as a gunboat for the seismic source, which comprised a Sercel 12 cu.in. Mini G. Gun, allowing for shots to be taking at different positions along the cable (McGrath et al., 2016).

Processing of UMASW data involved the Fourier transform of time series shot data to produce phase velocity (c) – frequency (f) intensity plots, often referred to as dispersion curves images. The method relies on the dispersive nature of surface waves where different frequencies sample different depths within the ground travelling at different velocities.

Surfseis software developed by the Kansas Geological Survey was used for the processing and analysis of the surface wave data (Park et al., 1999, 2007). Once the surface wave response has been isolated and the high semblance curve picked the software carries out a least squares inversion of the data to produce a 1D V_s profile. The UMASW data were processed using a default 10-layer variable thickness model based on the input picked dispersion curves. These parameters are routinely used to give a good approximation of the seismic layer thickness and resulting V_s profile. The frequency content resolved

from the dispersion curves defines both the upper and lower depth limits of the inversion process (Figure 2). The shallowest resolvable depth is approximately 1/3 to 1/2 of the maximum phase velocity wavelength (c/f). The maximum resolvable depth is defined in the same way by the minimum phase velocity wavelength. In this instance the range of reliable V_s values is typically between 3 and 25 m.

3 RESULTS

3.1 Site 1

CPTU and UMASW for Site 1 is shown in Figure 3. The data show 2.5 m to 5 m of a Very Soft clayey silt (Unit 1) overlying a Soft to Firm clay layer to circa. 18 m (Unit 2). At 18 m there is a transition to a Firm to Stiff clayey Silt/sandy Silt (Unit 3), with a corresponding drop in u_2 . The transition from the base of Unit 2 into Unit 3 at Site 1 correlates with the presence of shallow gas as determined by seismic sparker profiles in Coughlan et al. (2019) and Figure 4.

During the acquisition of seismic sparker profiles the presence of shallow gas, predominantly contained within the Holocene fine-grained sediments, results in high acoustic reflectivity at the top of the gas unit. This reduces the signal to noise ratio manifesting itself as acoustic turbidity within the gas and acoustic blanking below the gas. These effects result in a lower resolution of the underlying units, reducing the ability to identify and pick horizons from the seismic profiles. (e.g. Judd and Hovland, 1992; Tóth et al., 2014). In the DeSIRE study area, shallow gas had previously been mapped by Coughlan et al. (2019, 2021; Figure 1).

The division between Unit 1 and 2 is most clear from the u_2 data, where the pore pressure picks up in the clay but can also be seen from the change in slope of the q_t and f_s profiles. The division between units 2 and 3 is clear from all 3 sets of CPTU data. As the cone penetrates from the clay to the more coarse material, q_t increases, f_s (and R_f) reduces and u_2 drops back towards the hydrostatic value.

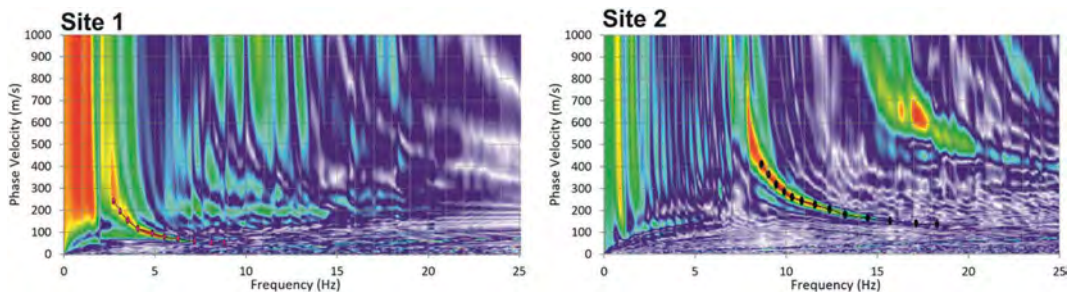


Figure 2. Dispersion curves produced in 45 m water depth at Site 1 and Site 2 in 25 m water depth.

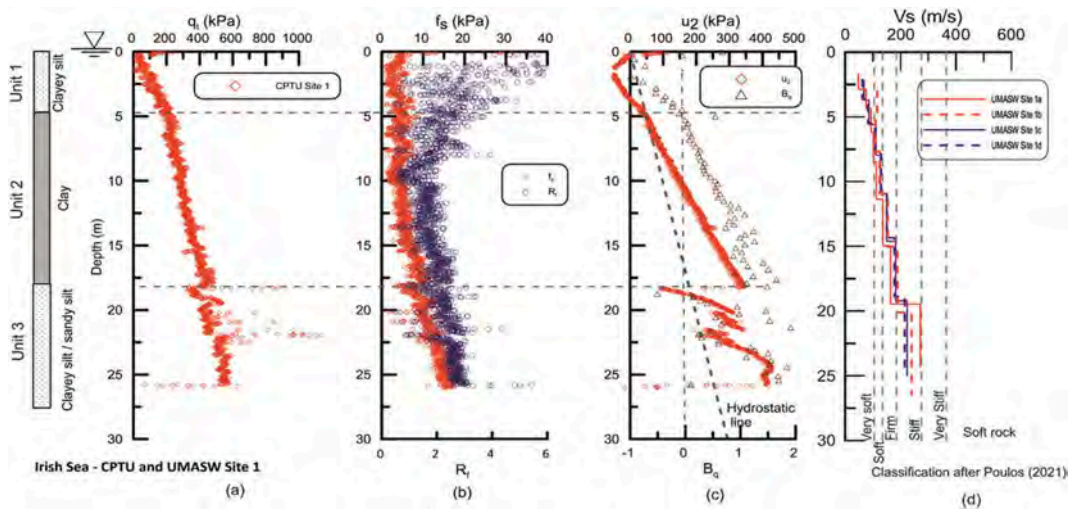


Figure 3. CPTU data for Site 1 is presented in the form of (a) corrected tip resistance (q_t), (b) sleeve friction (f_s) and friction ratio (R_f) and (c) pore pressure generated in the u_2 filter position and normalised pore pressure parameter (B_q) versus depth (Lunne et al., 1997). In addition the parallel UMASW profiles for Site 1 are shown in (d).

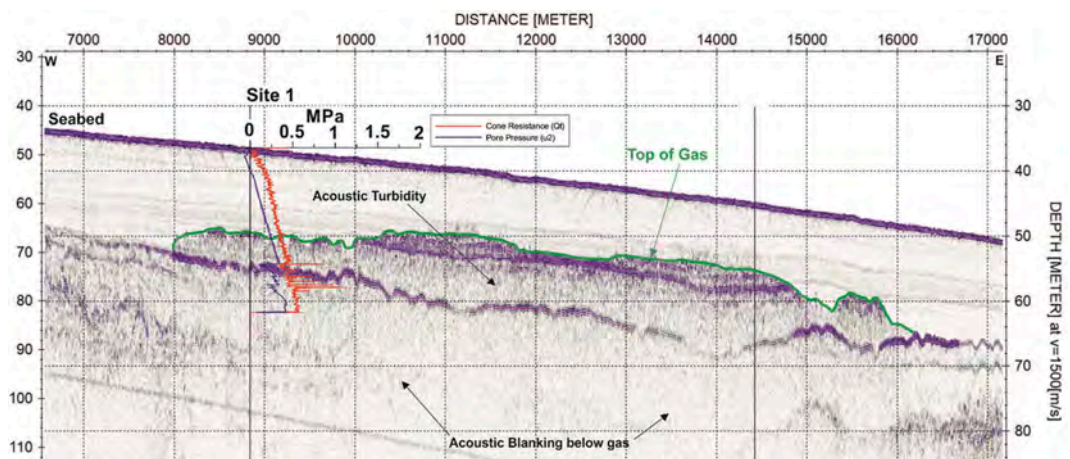


Figure 4. Seismic profile for line highlighted in Figure 1 (see Coughlan et al. (2019) for further details).

The UMASW profiles (Figure 3d) are consistent with the CPTU data, correlating well with the q_t values. The profile identifies Very Soft sediments ($< 100\text{m/s}$) to the base of Unit 1 at c. 5 m increasing from Soft to Firm to Stiff ($100 - 180\text{ m/s}$) at the base of Unit 2 at c. 18 m. Unit 3 corresponds to Stiff material ($>180\text{ m/s}$) below this depth. Stiffness designations according to the classification system proposed by Poulos (2021).

The Robertson et al. (1986) soil behaviour type chart (SBT) for Site 1 is shown on Figure 5 and is consistent with the findings presented above. Both the B_q/q_t and R_f/q_t components of the chart work well for this case. The data for the upper 5 m of the sediment (Unit 1) is close to the boundaries of the

charts but suggests that the material is an organic-type material. The 5 m to 18 m clay sediment (Unit 2) is classified correctly as a sensitive fine-grained material or a clay. Finally, the deeper material (Unit 3) is classified as either a clay or a silty clay.

3.2 Site 2

Data for Site 2 is shown on Figure 6. Only limited CPTU data is available here as no f_s and u_2 data were recorded. The q_t values confirm that the material is highly competent with q_t values increasing rapidly with depth up to a value of about 18 MPa with refusal at 3.25 m. However, the UMASW data was

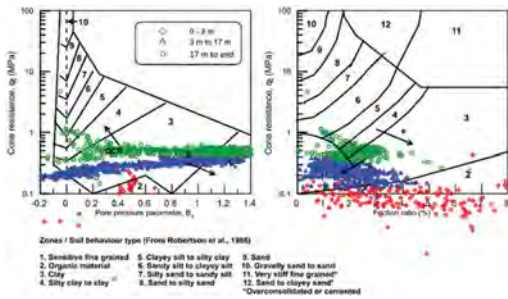


Figure 5. Soil behaviour type classification for Site 1 CPTU data (from Robertson et al., 1986).

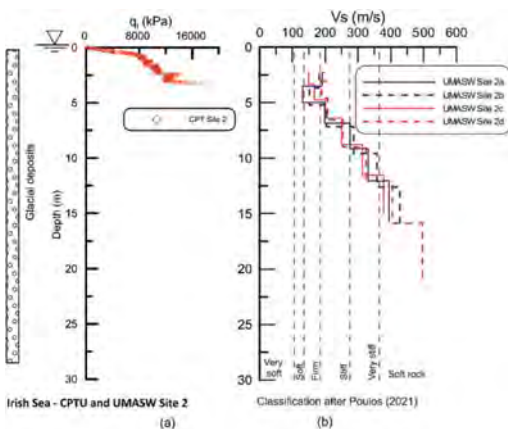


Figure 6. CPTU data for Site 2 is presented in the form of (a) tip resistance (q_t) (Note the different x-axis scales from Figure 3). In addition, the corresponding UMASW profile is shown in (b).

able to resolve data to c. 15 m. The classification system proposed by Poulos (2021) suggests the material designation as increasing Firm, through Stiff and Very Stiff to Hard with depth.

4 CONCLUSIONS

The area of the north Irish Sea studied here exhibits a lateral variability of complex deposits, which are potentially challenging to the deployment of offshore renewable energy infrastructure such as foundations. These deposits include soft, fine-grained Holocene sediments, gas-charged sediments, and heterogeneous glacial deposits. Previous efforts at CPTU data acquisition in these sediments had mixed results, with limited penetration in particular in glacial deposits. The use of SBT based on Robertson et al. (1986) is considered suitable here due to the relatively shallow depths and nature of the sediment known in the area. Future work will include comparison with updated charts (e.g. Robertson, 2016) and cross-

checking across profiles and with available lab data.

In this study the UMASW technique was successfully applied across this variety of geological conditions and a range of water depths from 17 to 45 m, obtaining reliable V_s profiles to c. 25 mbsb. The two sites presented in this paper highlight the presence of soft Holocene sediments with shallow gas (Site 1), as well as glacial deposits (Site 2).

UMASW proved effective at Site 2 in characterising heterogeneous glacial deposits at depths below CPTU refusal. At Site 1 MASW showed good correlation with CPTU to similar depths, however both methods were ineffective in determining the presence of shallow gas, which was identified using seismic sparker profiles. V_s and CPTU profiles show good agreement and can be used to develop classification charts for offshore deposits in complex geological areas.

The UMASW application is shown to be a proven method of providing geotechnical parameters for sub-seabed characterisation. When used in combination with other complimentary methods such as CPTU and seismic reflection a more robust ground model can be delivered.

ACKNOWLEDGEMENTS

This project was carried out at the SFI Centre of Research in Applied Geoscience (iCRAG) with funding from the Geological Survey of Ireland (GSI) as well as the Sustainable Energy Authority of Ireland (SEAI) under their Research, Development and Demonstration Funding Programme 2019 (Award: 19/RDD/411). Dr. Mark Coughlan is funded under an Irish Research Council Enterprise Partnership Scheme Postdoctoral Fellowship (EPSPD/2020/109) and in part by a research grant from Science Foundation Ireland (SFI) under Grant Number 13/RC/2092, with support from Gavin and Doherty Geosolutions Ltd and the Geological Survey of Ireland (GSI). The authors would like to thank Tony Lombard, Ian Sharkey (Apex Geophysics) and Eoin Grimes (Irish Commercial Charter Boats) for their skill and support in acquiring UMASW data. CPTU data was acquired onboard the RV Celtic Explorer (CE14001: Developing Geotechno-stratigraphies), which was funded through the Marine Institute Ship-time Programme and the Sustainable Energy Authority of Ireland (SEAI) Ocean Energy Research and Development Programme 2014 (Award: OCN 00016).

REFERENCES

Belderson, R. H. (1964). Holocene sedimentation in the western half of the Irish Sea. *Marine Geology*, 2, 147–163.
 Callard, S. L., Plets, R., Cooper, A., Long, A., Kelley, J., Belknap, D., Edwards, R., Quinn, R., & Jackson, D. (2019). The evolution of a submerged glacial and

- deglacial landscape from east Ireland (Dundalk Bay and Carlingford Lough). *International Union for Quaternary Research*.
- Coughlan, M., Long, M., & Doherty, P. (2020). Geological and geotechnical constraints in the Irish Sea for offshore renewable energy. *Journal of Maps*, 16(2), 420–431. <https://doi.org/10.1080/17445647.2020.1758811>
- Coughlan, M., Roy, S., O'Sullivan, C., Clements, A., O'Toole, R., & Plets, R. (2021). Geological settings and controls of fluid migration and associated seafloor seepage features in the north Irish Sea. *Marine and Petroleum Geology*, 123. <https://doi.org/10.1016/j.marpetgeo.2020.104762>
- Coughlan, M., Wheeler, A. J., Dorschel, B., Long, M., Doherty, P., & Mörz, T. (2019). Stratigraphic model of the Quaternary sediments of the Western Irish Sea Mud Belt from core, geotechnical and acoustic data. *Geo-Marine Letters*, 39(3), 223–237.
- Guinan, J., McKeon, C., O'Keefe, E., Monteys, X., Sacchetti, F., Coughlan, M., & Nic Aonghusa, C. (2020). INFOMAR data supports offshore energy development and marine spatial planning in the Irish offshore via the EMODnet Geology portal. *Quarterly Journal of Engineering Geology and Hydrogeology*, 54, qjgeh2020-033. <https://doi.org/10.1144/qjgeh2020-033>
- Judd, A. G., & Hovland, M. (1992). The evidence of shallow gas in marine sediments. *Continental Shelf Research*, 12(10), 1081–1095.
- Long, M., & Donohue, S. (2007). In situ shear wave velocity from multichannel analysis of surface waves (MASW) tests at eight Norwegian research sites. *Canadian Geotechnical Journal*, 44(5), 533–544. <https://doi.org/10.1139/t07-013>
- Long, M., & Donohue, S. (2010). Characterization of Norwegian marine clays with combined shear wave velocity and piezocone cone penetration test (CPTU) data. *Canadian Geotechnical Journal*, 47(7), 709–718. <https://doi.org/10.1139/T09-133>
- Long, M., Trafford, A., McGrath, T., & O'Connor, P. (2020). Multichannel analysis of surface waves (MASW) for offshore geotechnical investigations. *Engineering Geology*, 272, 105649. <https://doi.org/10.1016/j.enggeo.2020.105649>
- Lunne, T., Robertson, P. K., & Powell, J. J. M. (1997). *Cone Penetration Testing In Geotechnical Practice*. Blackie Academic & Professional.
- McCabe, A. M., Clark, P. U., & Clark, J. (2005). AMS C dating of deglacial events in the Irish Sea Basin and other sectors of the British – Irish ice sheet. *Quaternary Science Reviews*, 24, 1673–1690. <https://doi.org/10.1016/j.quascirev.2004.06.019>
- McGrath, T., Long, M., O'Connor, P., Trafford, A., & Ward, D. (2016). Multichannel Analysis of Surface Waves (MASW) Offshore Geotechnical Investigations. In A.-M. & K. Lehane (Eds.), *Proceedings of the 5th Int. Conf. on Geotechnical and Geophysical Site Characterisation (ISC'5)* (pp. 911–916). Australian Geomechanics Society.
- Park, C. B., Miller, R. D., & Xia, J. (1999). Multichannel analysis of surface waves. *GEOPHYSICS*, 64(3), 800–808. <https://doi.org/10.1190/1.1444590>
- Park, C. B., Miller, R. D., Xia, J., & Ivanov, J. (2007). Multichannel analysis of surface waves (MASW) - Active and passive methods. *Leading Edge (Tulsa, OK)*, 26(1), 60–64. <https://doi.org/10.1190/1.2431832>
- Poulos, H. G. (2021). Use of shear wave velocity for foundation design. *Geotechnical and Geological Engineering, in press*.
- Robertson, P. K. (2016). Cone penetration test (CPT)-based soil behaviour type (SBT) classification system — an update. *Casndian Geotechnical Journal*, 53(12), 1910–1927. <https://doi.org/10.1139/cgj-2016-0044>
- Robertson, P. K., Campanella, R. G., Gillespie, D., & Greig, J. (1986). Use of Piezometer Cone data. *ASCE Speciality Conference In-Situ '86: Use of In-Situ Testing in Geotechnical Engineering*. American Society of Engineers (ASCE), 1263–1280.
- Scourse, J. D., Chiverrell, R., Smedley, R., Small, D., Burke, M., Saher, M., Van Landeghem, K., Duller, G. A. T., Ó Cofaigh, C., Bateman, M., Benetti, S., Bradley, S. L., Callard, S. L., Evans, D., Fabel, D., Mc Carron, S., Medialdea, A., Moreton, S., Ou, X., ... Clark, C. (2021). Maximum extent and readvance dynamics of the Irish Sea Ice Stream and Irish Sea Glacier since the Last Glacial. *Journal of Quaternary Science*, 1–25. <https://doi.org/10.1002/jqs.3313>
- Tóth, Z., Spieß, V., & Jensen, J. (2014). Seismo-acoustic signatures of shallow free gas in the Bornholm Basin, Baltic Sea. *Continental Shelf Research*, 88, 228–239. <https://doi.org/10.1016/j.csr.2014.08.007>
- Ward, S. L., Neill, S. P., Landeghem, K. J. J. Van, Scourse, J. D., Bradley, S. L., & Uehara, K. (2016). Sensitivity of palaeotidal models of the northwest European shelf seas to glacial isostatic adjustment since the Last Glacial Maximum. *Quaternary Science Reviews*, 151, 198–211. <https://doi.org/10.1016/j.quascirev.2016.08.034>
- Woods, M. A., Wilkinson, I. P., Leng, M. J., Riding, J. B., Vane, C. H., Lopes dos Santos, R. A., Kender, S., De Schepper, S., Hennissen, J. A. I., Ward, S. L., Gowing, C. J. B., Wilby, P. R., Nichols, M. D., & Rochelle, C. A. (2019). Tracking Holocene palaeostratification and productivity changes in the Western Irish Sea: A multi-proxy record. *Palaeogeography, Palaeoclimatology, Palaeoecology*, 532, 109231. <https://doi.org/https://doi.org/10.1016/j.palaeo.2019.06.004>
- Yuan, F., Bennell, J. D., & Davis, A. M. (1992). Acoustic and physical characteristics of gassy sediments in the western Irish Sea. *Continental Shelf Research*, 12(10), 1121–1134.

Cone factor from CPTU tests in very soft clays at the east of Mexico's valley

J.M. De La Rosa R. & F.A. Flores López

Ingenieros Geotecnistas Mexicanos. S.C., México.

ABSTRACT: From the results obtained during an exploration campaign, the correlation between CPTU resistance and the undrained shear strength of soft clays at the valley of Mexico, is evaluated in this paper. This campaign consisted of 50 piezocone penetration tests, 50 soil sampling borings and laboratory tests carried out on more than 300 undisturbed soil samples recovered along 10 square kilometers. The samples were tested by means of unconfined compression and unconsolidated undrained triaxial compression tests. The correlation of the determined undrained shear strength and the experienced CPTU results was evaluated and the empirical cone factor (Nkt) was determined for all tests. The main innovation lies in the fact that for the eastern zone of the Valley of Mexico, the geotechnical characterization is not abundant and there are information gaps for this and other design parameters.

Keywords: CPTU, Nkt, Undrained shear strength, Valley of Mexico

1 INTRODUCTION

1.1 *Origins of Mexico's valley*

Mexico City is located on a lacustrine plain in the Basin of Mexico that occupies an approximate area of 9,600 km² and is located at 2,250 m above sea level. This basin remained open (exoreic) until 700,000 years ago, when extensive volcanic activity formed the Sierra de Chichinautzin, which closed the basin (Mooser, 1963) and obstructed drainage to the Balsas River. For this reason, the water was stored and gave rise to several lakes. At the foot of the mountains and due to the sudden change in the slopes of the rivers, large alluvial deposits of highly variable composition and cross-stratification are located, evidence of an erosive dynamic due to periods of intense rain. This area of the city was enabled as a flood control zone through the creation of artificial lagoons causing surface depressions by pumping. Texcoco Project (1969). The soils found in this zone correspond to very soft and saturated lacustrine clays, subject to a regional subsidence process due to the extraction of water by deep pumping. The use of CPTU is a common option to know the stratigraphic sequence for the determination of settlements magnitude.

Currently, the urban development of the city has been pushing towards the east, driven by a new airport under construction which was canceled three years ago. However, during its execution this project triggered the infrastructure needs of the area, so it is necessary to expand the knowledge about its geotechnical characterization. This situation makes this publication necessary and useful.

2 BACKGROUND

2.1 *Empirical cone factor*

The many existing formulations to correlate Cone penetration tip resistance (q_c) from CPT/CPTU, results with the undrained shear strength of clays (S_u) are summarized in many publications. Most of those investigations found S_u linearly proportional with the corrected tip resistance of the cone as shown in equation (1):

$$S_u = \frac{q_c - \sigma_{v0}}{Nkt} \quad (1)$$

Where,

- S_u : Undrained shear strength.
- q_c : Tip resistance of the cone/piezocone.
- σ_{v0} : Total overburden pressure.
- Nkt: Empirical cone factor.

2.2 *Previous research and typical values*

Most of the research aimed at estimating the value of (Nk) that correlates CPT/CPTU with S_u . Variation ranges has been estimated between 11 and 19 by Lunne & Kleven (1981) for normally consolidated Scandinavian marine clays, also Jorss (1998) estimated values ranging from 15 to 20 for marine y boulder clays, respectively. Mexico City's clays present Nk values between 5 and 11, according to Santoyo et al. (1989). Some values range between 5 and 28 for different types of soils, according to Chen (2001) and

Gebre-selassie (2003). Also, Ovando (2011) related $S_u = q_c/N_k$ with N_k values of 13 for Mexico City. Typically, N_k is between 10 and 18, with an average of 14 (Robertson & Cabal, 2015). The marine clays of the Gulf of Mexico present N_k values between 12 and 20, according to Cruz et al. (2019).

2.3 Geotechnical input information

2.3.1 Field exploratory survey

Based on the dimensions of the project structures, a geotechnical exploration campaign was executed to define the stratigraphic profile, from which the laboratory program was planned. The exploration campaign consisted of boreholes between 25 and 50 m deep (SPT/SHB mixed, SM and piezocone tests, CPTU), in addition to a surface exploration campaign, consisting of 150 open-pit wells (PCA), 100 plate load Tests (PP) and strategically located piezometric stations.



Figure 1. Location of SM boreholes.

The exploratory drilling was carried out according to the corresponding ASTM standard, in the case of mixed SM drilling, the SPT technique was combined with the selective recovery of undisturbed samples using a thin-walled tube (Shelby) and the Electronic Friction Piezocone Test was performed using a digital equipment that complies with the ASTM D5778-20 standard and that allows the measurement of resistance to tip penetration (q_c), lateral friction (f_s) and pore pressure behind de cone (u_2).

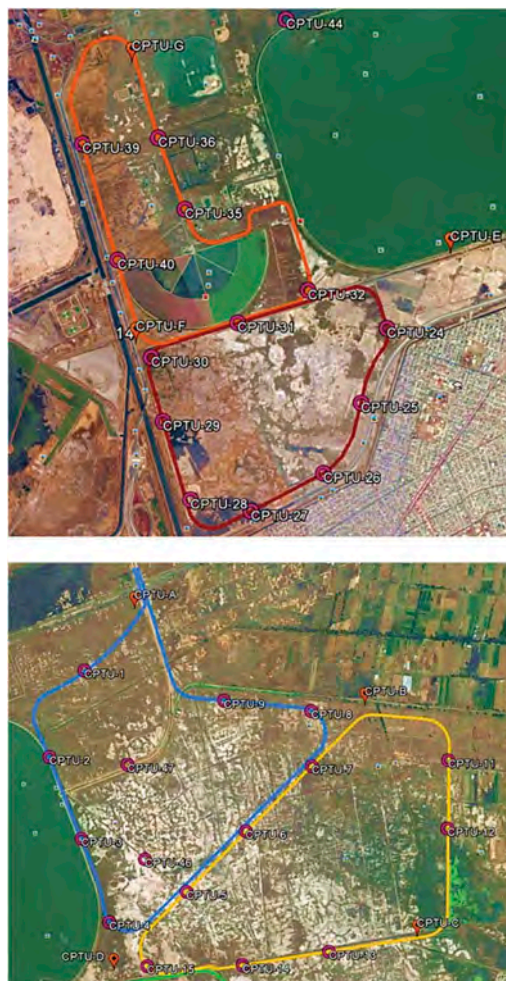


Figure 2. Location of CPTU tests.

2.3.2 Laboratory tests

All the samples obtained in the exploration work were macroscopically identified and classified both in the field and in the laboratory, according to the Unified Soil Classification System. Tests

were carried out to determine the following index properties: Natural water content (150 to 400%). Limits of consistency (liquid limit, plastic limit) and plasticity index (100 to 300%). Grain size analysis. Percentage of fines (90 to 100%). Relative specific weight and density of solids (2.30 in average, maximum of 2.65 and minimum of 2.15).

The mechanical properties were determined based on the following tests: Unconfined compression shear resistance. Triaxial compression test UU with determination of Young's Modulus (E). Triaxial compression test CU. Compressibility in one-dimensional consolidation tests.

2.4 Analysis of parameters

The fulfillment of the objective for geotechnical characterization is not easy due to the variability of the results obtained in the field and laboratory tests. Another difficulty that causes uncertainty in representative soil results is the considerable size of the study area and the relatively large distances between boreholes and measurement points. To achieve a satisfactory description of the properties and stratigraphic characteristics of the subsoil, the use of descriptive statistics tools was used. In the next section, the analysis criteria and selection of parameters used are presented.

2.5 Criteria for quantitative analysis and variability of the parameters

By having a soil property measured repeatedly, we get a data set called a "data sample" that can be analyzed quantitatively using statistical parameters. For the values obtained in the project, although there are many parameters that can be estimated, the following were evaluated: Mean, median, mode, variance, standard deviation.

The analysis of variability of the soil properties was graphically complemented by means of a histogram calculating its corresponding probability distribution in order to select the data to be considered to describe the geotechnical parameters.

3 RESULTS OBTAINED

3.1 Mechanical properties

Based on the analysis of variability and the selection of representative values, the results of the CPTU tests on site and the laboratory results were correlated. For this project, the results obtained from the electrical cone (tip resistance) are more representative, since the SPT tests

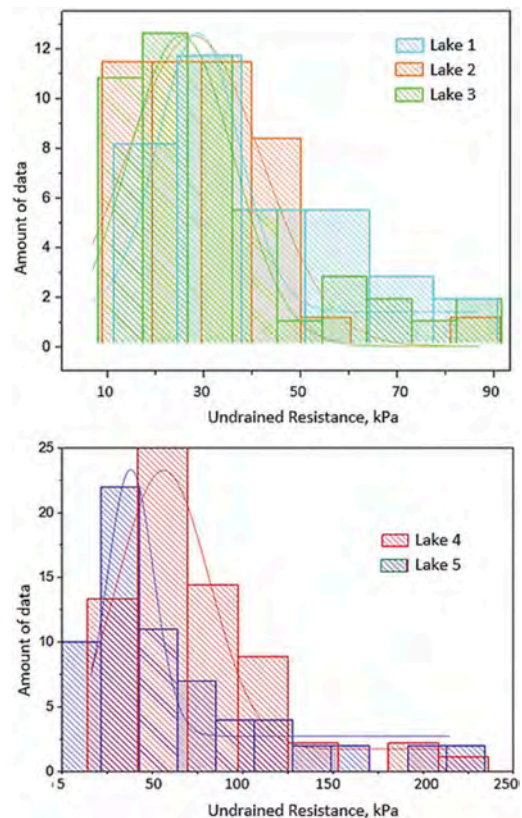


Figure 3. Histogram of simple and triaxial compressive strength UU and its normal probability function.

mostly obtained the number of blows N equal to zero, which does not provide relevant data for characterization purposes. The histogram of all the correlated data was generated and the normal logarithmic probability distribution function that best fit the measured values was obtained (Figure 3). Figure 4 shows the results obtained by correlating the tip resistance with the laboratory results for the UU resistance of the soils, where a linear increase can be seen as a function of depth, it is also observed that there is more variation near the soil surface associated with the surface crust.

Figure 5 shows the average values of Undrained Resistance obtained in the laboratory and Tip Penetration Resistance, obtained on site for all samples.

3.2 Cone factor values

Once the corresponding analyzes had been carried out and the results obtained in the field and laboratory correlated, the average values of

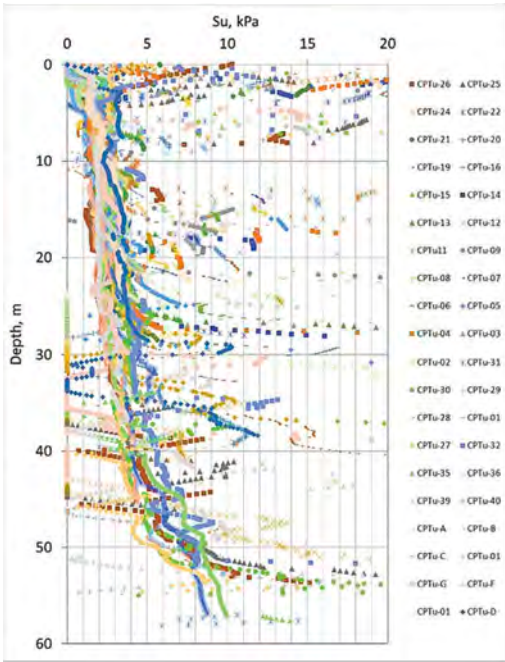


Figure 4. Undrained resistance obtained by correlating laboratory tests and electrical cone results.

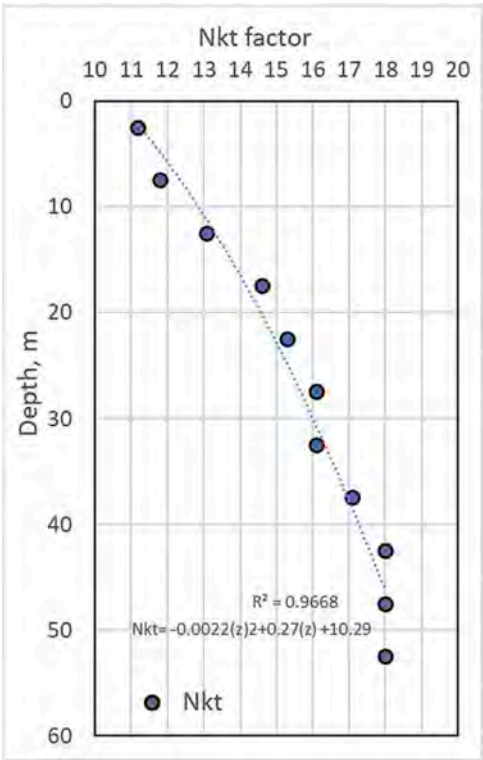


Figure 6. Average Cone Factor Nkt, depending on the depth range analyzed.

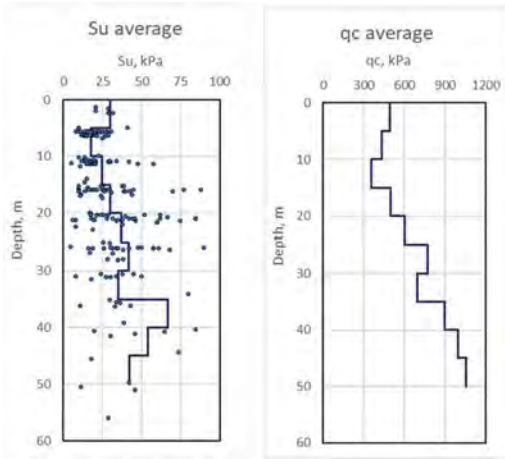


Figure 5. Average values of Soil Undrained Resistance (Su) and Tip Penetration Resistance along the explored depth for all samples.

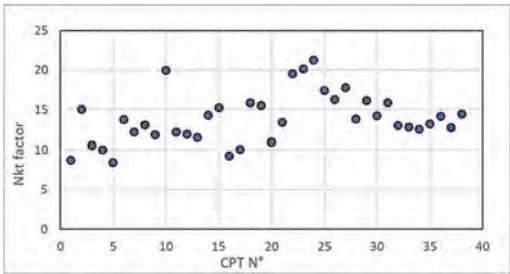


Figure 7. Average Cone Factor Nkt, for each CPTU analyzed.

Nkt, shown in Figure 7, were obtained for the 38 most representative CPTU. The results obtained range between 8 and 21 with an average of 14; while Figure 6 shows the average Nkt values obtained by depth range every five meters, also for the 38 most representative CPTU.

4 DISCUSSION AND CONCLUSIONS

4.1 Variability of results

The results obtained during the analysis for this research, indicate that in 87% of the cases, the cone factor Nkt is between 10 and 20, **with an average of 14** of the 12,500 data analyzed, the maximum value found was 25 and the minimum 7. Figure 6 shows a progressive variability of the Nkt factor as a function of depth during the first 25 meters of depth, with

values between 11 and 16, while for greater depths a stabilization around values higher than the average is observed (16 to 19). Figure 8 shows the variability analysis between the proposed cone factor Nkt average and the results from the direct correlation of the Tip Resistance (qc) and the laboratory UU resistance (Su). Excluding the values obtained near the surface, due to what is mentioned in section 3.1, an $R = 86\%$ is obtained in the adjusted regression line.

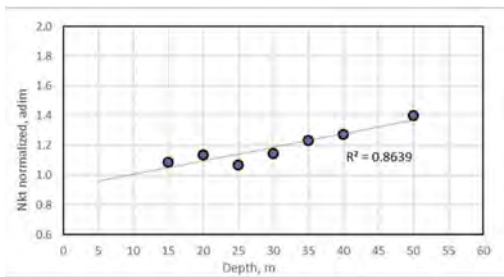


Figure 8. Nkt average/correlated vs depth.

The variability of Nkt shown in Figure 6 with respect to depth is due in part to clay samples obtained with water contents between 50% and 450%. For extreme cases, sample recovery becomes challenging and results in non-representative samples. This variability as function of depth is a typical behavior for marine clays, and the lacustrine nature of the virgin, high-salinity clays to the east of the valley is consistent with this trend.

4.2 Future lines of research

In addition to the results obtained so far, there is sufficient data to establish correlations between Su and Index properties. Data consist of Atterberg limits from 500 samples and elastic Young's modulus from 200 samples.

4.3 Current trends in the valley of Mexico

The current trends among the predominant players of Mexican geotechnics can be observed with a tendency to promote the use of automated equipment to control the driving speed of the tip with the valid argument that there is some relevant variation between the parameters obtained in an automated way by comparing them with those derived from rudimentary field estimates, such as the most common practice of drawing division marks of predetermined length on the drilling rods and maneuvering the drill so that the guide adapts to the required speed of penetration.

In addition, the application spaces for nationally produced equipment have decreased because, although they comply with ASTM or

similar standards, they do not usually include temperature and verticality sensors, which have proven necessary to guarantee the quality of the results obtained.

These trends, point to a less widespread use of the electric cone due to the costs involved in this modernization, as well as more accurate results in cases where this technique is applied. However, these improvements are unlikely to replace or lessen the need for laboratory testing, while the main objective of using the electric cone will remain unchanged: to determine the stratigraphic sequence in previously explored areas where the stratigraphy is partially known in advance.

ACKNOWLEDGMENTS

In this section we express our gratitude to the geotechnical team of the company CONSULTORIA INTEGRAL EN INGENIERÍA, who carried out much of the supervision of the field and laboratory work, as well as the collection and primary processing of the information obtained. Also, in a special way to the COMISION NACIONAL DEL AGUA, as the government dependency responsible for the project from which the analyzed data was obtained.

REFERENCES

- Carrillo, N. et al. 1969. Proyecto Texcoco. Secretariat of Finance and Public Credit of Mexico.
- Chen, C. 2001. Evaluating undrained shear strength of Klang clay from Cone penetration test, In: International Conference on In Situ Measurement of Soil Properties and Case Histories, Parahyangan Catholic University of Indonesia.
- Cruz, D. et al. 2019. Los suelos marinos de la Sonda de Campeche y Litoral Tabasco, Golfo de México. XVI Panamerican Conference on Soil Mechanics Geotechnical Engineering in the XXI Century: Lessons learned and future challenges.
- Gebreselassie, B. 2003. Experimental, analytical and numerical investigations of excavations in normally consolidated soft soils, PhD thesis, University of Kassel.
- Jörß, O. 1998. Erfahrungen bei der Ermittlung von cu-Werten mit der Hilfe von Drucksondierungen in bindigen Böden, Geotechnik, 21.
- Lunne, T. & Kleven, A. 1981. Role of CPT in North Sea Foundation Engineering, In: Symposium on Cone Penetration Engineering Division, ASCE.
- Mooser, F. 1963. Historia tectónica de la Cuenca de México: Boletín de la Asociación Mexicana de Geólogos Petroleros.
- Ovando, E. 2011. Some geotechnical properties to characterize Mexico City Clay, 14th Pan-American Conference on Soil Mechanics and Geotechnical Engineering.
- Robertson, P. & Cabal, K. 2015. Guide to Cone Penetration Testing for Geotechnical Engineering. Gregg drilling, 6th edition.
- Santoyo, E. et al. (1989). El cono en la exploración geotécnica. México: TGC Geotecnia.

Piezocone testing in Nordic soft clays: Comparison of high-quality databases

M. D'Ignazio & B. Di Buò

Tampere University, Tampere, Finland
Ramboll Finland Oy, Tampere, Finland

T. Länsivaara

Tampere University, Tampere, Finland

J.S. L'Heureux & P. Paniagua

Norwegian Geotechnical Institute, Trondheim, Norway

J. Selänpää

Destia Oy, Tampere, Finland

ABSTRACT: Soft and sensitive clays are widespread in Scandinavia. Piezocone correlations for Norwegian clays have been previously proposed based on high-quality block samples from several sites. Recently, a large database of Finnish soft clays was compiled by Tampere University from piezocone measurements as well as high-quality laboratory tests on specimens from large tube samples. Finnish and Norwegian clays exhibit some differences in terms of basic properties. Norwegian clays show lower water content, lower organic content, higher silt content and lower plasticity than the clays from Finland. This may be linked to the source of the materials, their depositional and post-depositional processes that in turn impact on the mechanical behaviour.

This paper aims to compare piezocone Norwegian and Finnish data with focus on strength and stress history. The database trends are compared for relevant engineering parameters. The data and its variability are critically discussed considering differences in geological history, basic properties, sampling techniques and disturbance.

1 INTRODUCTION

Piezocone (CPTU) testing is one of the most reliable site investigation tools in soft clays, as it has proven repeatability of measurements and can be used to detect soil layering and derive a large number of geotechnical parameters (e.g., Lunne et al. 1997a, Robertson 2009, Di Buò 2019). During cone penetration, the standard CPTU equipment measures cone tip resistance q_c , sleeve friction f_s and excess pore pressure above the cone tip u_2 .

The use of CPTU is widespread in Norway, regardless of the project size. CPTU correlations for Norwegian clays derived from high-quality laboratory data on block samples (Karlsrud et al. 2005, Paniagua et al. 2019) have been in use for nearly two decades. On contrary, CPTU testing is still on the rise in Finland, where weight soundings, dynamic penetration testing and field vane testing are among the most preferred site investigation tools. This is mainly a consequence of the lack of local correlations as well as limited experience by the operators. Nevertheless, in recent years the Tampere University (TUNI) has

carried out studies on CPTU testing and correlations in Finnish soft clays (Di Buò et al. 2016, Di Buò et al. 2018, Selänpää et al. 2018, Di Buò 2020, Di Buò et al. 2020, Selänpää 2021). The calibration database includes testing on large tube samples retrieved with a Laval-type tube sampler developed by Tampere University (Di Buò et al. 2019). Both the Norwegian and the Finnish databases include laboratory index tests, constant-rate-of-strain (CRS) oedometer tests, undrained triaxial compression (CAUC) and extension tests (CAUE) and direct simple shear tests (DSS).

The scope of this paper is to compare the Norwegian and Finnish clay data to better understand how the basic clay properties impact on the CPTU response in these clays. The database trends are compared for two key engineering parameters, i.e. undrained shear strength and overconsolidation ratio. The observations in terms of cone factors and calibration coefficients are critically discussed, considering differences in basic properties, geological history, sampling techniques and features of the databases.

2 GEOLOGICAL HISTORY OF NORDIC CLAYS

A detailed study on the geological formation of fine-grained sediments in Finland was conducted by Gardemeister (1975). Fine-grained soil sediments in Finland originated in the late Pleistocene, during the retreat of the continental ice sheet in the Weichselian ice age (11,700 years ago). The entire Scandinavian region was covered by a large ice sheet named Fenno-Scandian that spread out from the Scandinavian Mountains to Northwest Russia, UK, and The Netherlands. The stratigraphy of Finnish soil deposits is the result of a series of processes that occurred at the end of the last glacial period when the Fenno-Scandian ice sheet retreated and during the Holocene (i.e. c. last 10,000 years ago). The glacier meltwater accumulated between the front of the ice sheet and the southern shores, giving rise to what currently is the Baltic Sea. This area underwent four environmental stages in the postglacial progression of the Baltic basin, known as Baltic Ice Lake, Yoldia Sea, Ancylus Lake, and Littorina Sea. (Gardemeister 1975)

Despite the extensive studies conducted on this topic, the process of the formation of the Baltic Sea is not completely clear. Its connection with the Atlantic Ocean during the different phases made the salinity vary with location, depth, and time. The complex origin and development of this area may explain the different geotechnical properties characterizing the clay deposits located in Finland and Sweden compared with the Norwegian ones. The Baltic Ice Lake originated during the retreat of the Weichselian glacier, when meltwater accumulated and formed a freshwater lake. At this stage, the connections with the North Sea and the Atlantic Ocean were closed because the ground on the entire depression rose faster than the sea level. However, a short connection with the sea across central Sweden occurred during the Yoldia Sea stage. At the early stage, the depositional environment was still characterized by low salinity owing to the heavy water flow from the continental ice sheet. The salinity increased after 200 years of the ingression of salt water, creating the condition for a brackish depositional environment. Afterward, the isostatic uplift of the Baltic basin closed the connection with the Atlantic Ocean and the Yoldia Sea turned into Ancylus Lake. This stage lasted until a new connection with the North Sea was established owing to the continuous rising of the water level of Ancylus Lake, forming the Littorina Sea. Finally, the continuous land rise made the connection with the Ocean shallower, thus creating the conditions for the formation of the current Baltic Sea, which is characterized by brackish water. (Gardemeister 1975)

It is evident that the combination of the sea water intrusion and freshwater flow from the melting glacier created a heterogeneous depositional environment characterized by variable salinity content. Although the salt leaching process is considered as the main factor explaining the high sensitivity of Scandinavian marine clays, further studies are needed for Finnish clays.

3 EVALUATION OF ENGINEERING PROPERTIES OF CLAY FROM CPTU

3.1 CPTU parameters

Engineering properties of clays are derived from both measured and normalized CPTU parameters. Among these:

- Normalized cone resistance $Q_t = (q_t - \sigma_v) / \sigma'_v$
- Normalized excess pore pressure $Q_u = (u_2 - u_0) / \sigma'_v$
- Normalized effective cone resistance $Q_e = (q_t - u_2) / \sigma'_v$
- Pore pressure ratio $B_q = (u_2 - u_0) / (q_t - \sigma_v)$

where q_t is the corrected cone tip resistance, σ_v is the total overburden vertical stress, σ'_v the vertical effective stress, u_2 the pore pressure measured above the cone tip, u_0 the in-situ pore pressure.

In addition, $(q_t - \sigma_v)$, $(u_2 - u_0)$ and $(q_t - u_2)$ are commonly referred to as q_{net} , Δu and q_e , respectively.

3.2 Overconsolidation ratio

The over-consolidation ratio (OCR) is defined as the ratio of effective preconsolidation stress σ'_p and the vertical effective stress σ'_v . Several authors verified the dependence of σ'_p and OCR on the cone tip resistance and excess pore pressure parameters, with σ'_p and OCR increasing with increasing q_{net} , σ_u , q_e and Q_t , Q_u , Q_e respectively. (e.g. Chen and Mayne 1996, Lunne et al. 1997, D'Ignazio et al. 2019).

In practice, the relationship between σ'_p and q_{net} is the most used (Equation 1). The relationship between OCR and Q_t is used in the same way as (Equation 2):

$$\sigma'_p = k(q_t - \sigma_v) = kq_{net} \quad (1)$$

$$OCR = k \frac{q_t - \sigma_v}{\sigma'_v} = k \frac{q_{net}}{\sigma'_v} = kQ_t \quad (2)$$

where k is an empirical parameter. Similar equations are found in the literature for Δu , q_e and Q_u , Q_e . An average value of $k \approx 0.32$ is suggested by Chen and Mayne (1996) based on statistical analysis of piezocone-oedometer data involving a variety of different clays. D'Ignazio et al. (2019) found k in the range 0.15-0.5 for clays with OCR $\approx 1-5$. Paniagua et al. (2019) found $k = 0.20-0.75$ for Norwegian clays, while Di Buò (2019) suggested $k = 0.28$ with coefficient of variation (COV) ≈ 0.1 for Finnish soft clays.

3.3 Undrained shear strength

The net cone resistance q_{net} is related to the undrained shear strength s_u by means of the cone factor N_{kt} as:

$$s_u = \frac{q_{net}}{N_{kt}} \quad (3)$$

Similarly, Δu and q_e are related to s_u by means of the cone factors $N_{\Delta u}$ and N_{ke} respectively as:

$$s_u = \frac{\Delta u}{N_{\Delta u}} \quad (4)$$

$$s_u = \frac{q_e}{N_{ke}} \quad (5)$$

For low OCR offshore and onshore clays, Low et al. (2010) reported $N_{kt} = 8.6-15.3$ and $N_{\Delta u} = 3.3-8.8$ for triaxial compression (CAUC) and $N_{kt} = 11-20$ and $N_{\Delta u} = 4.8-11.9$ for field vane test (FVT). Paniagua et al. (2019) found $N_{kt} = 5-16$ and $N_{\Delta u} = 5-10$ for CAUC in onshore Norwegian clays with OCR less than 6. Paniagua et al. (2019) further observed $N_{ke} \approx 1,5-10$ for CAUC decreasing with increasing B_q . Selänpää (2021) suggested $N_{kt} = 9.1$, $N_{\Delta u} = 7.7$, and $N_{ke} = 4.5$ with COV ≈ 0.1 for CAUC in Finnish soft lightly overconsolidated clays. D'Ignazio & Lehtonen (2021) observed $N_{\Delta u} \approx 11$ for FVT in a soft organic sulphate rich lightly overconsolidated clay from Finland. D'Ignazio et al. (2020) found $N_{kt} = 20-32$ (CAUC) for an overconsolidated North Sea clay with OCR $\approx 4-20$, with N_{kt} increasing with increasing OCR.

4 HIGH-QUALITY CLAY DATABASES

4.1 Norway

The Norway CPTU database is presented in detail by Paniagua et al. (2019). The database consists of 61 high-quality block samples data points collected from 17 Norwegian clay sites located all over the country. For these points, both CPTU and laboratory measurements are available. The laboratory tests were carried out on specimens obtained from large diameter ($\varnothing 250$ mm) block samples and mini-block ($\varnothing 150$ mm) Sherbrook samples (Emdal et al. 2016). For Norwegian clays, block samples seem to ensure higher quality than the more traditional $\varnothing 54$ mm or $\varnothing 72$ mm piston samples (e.g., Lunne et al. 2006, L'Heureux et al. 2018).

The database includes laboratory index tests, constant-rate-of-strain (CRS) oedometer tests, anisotropically consolidated undrained triaxial compression (CAUC) and extension tests (CAUE) and direct simple shear tests (DSS).

Sample quality was assessed according to the Lunne et al. (1997b) criterion based on the normalized change in void ratio $\Delta e/e_0$ from CAUC tests. Data points fall within sample quality categories "Very good to excellent" and "Good to fair".

Soil properties were measured from specimens collected down to a maximum depth of 22 m. The clay properties cover a wide range of plasticity index, with I_p varying between 4 (low plastic) and 49 (very high plastic), a wide range of water content ($w = 28-72\%$), a wide range of sensitivity (S_t) values

($S_t = 2-240$). The OCR ranges from 1 to 6, while the clay content varies between 21 and 65%.

4.2 Finland

The Finland TUNI's CPTU database is summarized in the works carried out by Di Buò (2019), with focus on preconsolidation stress, and Selänpää (2021), with focus on undrained shear strength. Data was collected from 5 test sites located in Southern Finland. Both CPTU and laboratory measurements are available from the test sites.

The laboratory tests were carried out on specimens obtained from large diameter ($\varnothing 132$ mm) Laval-type sampled designed by Tampere University and presented in detail by Di Buò et al. (2019). Some of the tests were performed on specimens obtained from a mini-block ($\varnothing 150$ mm) Sherbrook sampler (Emdal et al. 2016).

The database includes laboratory index tests, n.99 constant-rate-of-strain (CRS) oedometer tests, n. 17 anisotropically consolidated undrained triaxial compression (CAUC) and n. 14 extension tests (CAUE), n. 14 direct simple shear tests (DSS) and n. 14 field vane tests (FVT).

Sample quality was assessed according to the Lunne et al. (1997b) criterion based on the relative void ratio change at reconsolidation $\Delta e/e_0$ from CAUC as well as CRS tests. CAUC data points from $\varnothing 132$ mm samples fall within sample quality categories "Very good to excellent", while the CRS data points and fall within "Very good to excellent" and "Good to fair" sample quality categories.

Soil properties were measured from specimens collected down to a maximum depth of 9 m. The clay properties cover a plasticity index I_p varying between 16 (low-medium plastic) and 59 (very high plastic), a wide range of water content ($w = 66-127\%$), a wide range of sensitivity (S_t) values ($S_t = 16-98$). The OCR ranges from 1 to 2, while the clay content varies between 40 and 100%.

5 COMPARISON OF CPTU DATABASES OF NORWEGIAN AND FINNISH CLAYS

5.1 Overconsolidation ratio

Figures 1, 2 and 3 show plots of OCR versus the normalized values of cone resistance Q_p , pore pressure Q_u and effective cone resistance Q_e . The plots suggest a well-defined trend line for the Finland data, while the Norway data appears to be characterized by higher scatter.

Even though the uncertainty associated with OCR for Finnish clays appears to be lower than that for the Norwegian clays, it must be noted that the Finland data is obtained from 5 sites all located in the Southern part of the country; while the Norwegian data is collected from 17 sites spread all over the country,

where areas might have undergone different geological histories. However, the OCR range of the Finland data (OCR = 1-2) is lower than that of the Norway data (OCR = 1-7). For $OCR < 2$, the mean trends of the two databases appear to be consistent, despite the larger scatter in the Norway data. Consistency is also found between the OCR based on mini-block samples and Ø132 mm samples of Finnish soft clays.

The coefficient k of Equation 2 is ≈ 0.3 in Figure 1 for Finnish clays. Such a value is often assumed in practice in absence of site-specific oedometer tests.

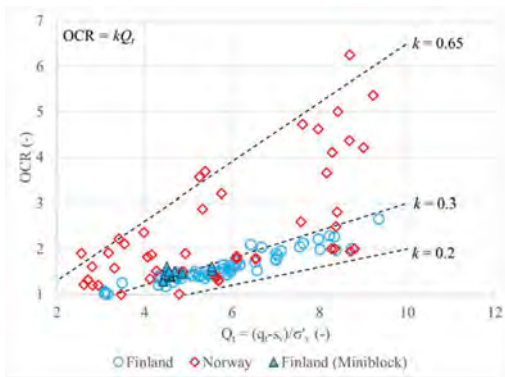


Figure 1. OCR vs Q_c .

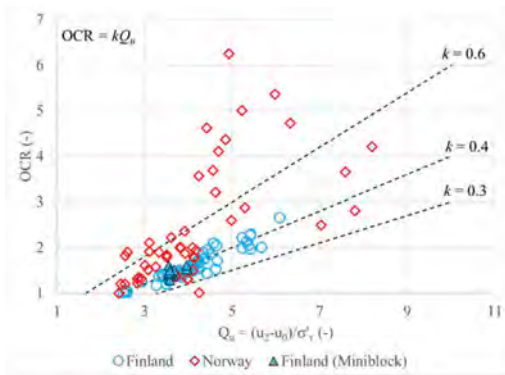


Figure 2. OCR vs Q_u .

Data in Figures 1, 2 and 3 show a remarkable variability of the calibration coefficients, particularly for the Norwegian database. Figure 4 shows the variation of k ($=OCR/Q_c$) with plasticity index (I_p). The coefficient k appears to vary as a function of plasticity, decreasing with increasing I_p . Such a trend could not be observed when treating the two databases separately. Nevertheless, for $I_p < 20\%$, the data from Finland is consistent with measurements at larger I_p .

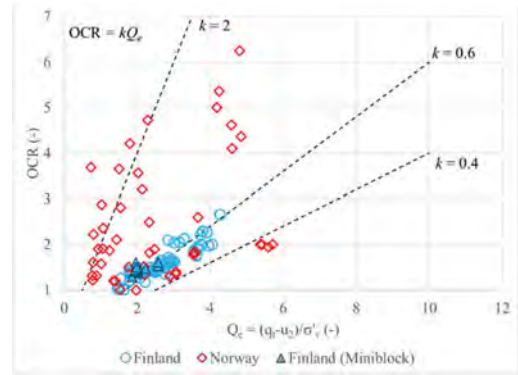


Figure 3. OCR vs Q_e .

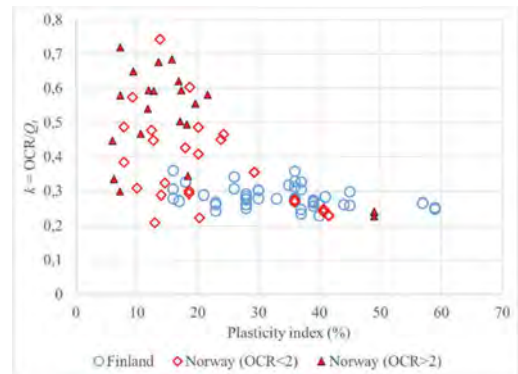


Figure 4. $K = OCR/Q_c$ vs plasticity index.

5.2 Undrained shear strength

The undrained shear strength from triaxial CAUC tests (s_{uC}) is taken as a reference and used for comparison of the Finland and Norway databases.

Figures 5, 6 and 7 illustrate the variation of s_{uC} with q_{net} , Δu and q_e respectively. The s_{uC} from Finnish clay deposits is generally lower than that of Norwegian clays. It must be noted that the sampling depths are limited to 9 m below ground level for the Finland data, while depths reach up to 22 m for the Norway data. Therefore, the deeper samples in the Norway database experienced larger stress relief than the samples from Finland. Nevertheless, for the depth range 0-9 m, s_{uC} of Norwegian clays is in the range 26-62 kPa, while s_{uC} of Finnish clays is 12-24 kPa. One possible explanation for this is the variation of OCR with depth. As shown in Figure 8, the range of OCR is larger for the Norwegian data. Given that s_u increases with increasing OCR (e.g. D'Ignazio et al. 2016, Selänpää 2021), this explains the higher strength of Norwegian clays at shallow depths.

The cone factor values for Norwegian and Finnish clays are discussed in detail by Paniagua et al. (2019)

and Selänpää (2021). Cone factors N_{kt} , N_{Au} and N_{ke} present some variability as illustrated in Figures 5, 6 and 7. As for the OCR, the variability appears to be the lowest for the Finland data. The variability of cone factors for Norwegian clays was discussed by Karlsrud et al. (2005) and Paniagua et al. (2019). These studies suggested a dependency of cone factors on OCR and lightly on index properties, although the proposed correlations are characterized by a non-negligible scatter.

Figure 9 presents the variation of the normalized CAUC strength s_{uC}/σ'_v with OCR. In agreement with previous analyses, the Finland data shows overall a well-defined trend and a lower scatter. For $OCR < 2$, the normalized s_{uC}/σ'_v of Finnish clays appears to be higher than that of the Norwegian clays, with the Miniblock samples data from Finland showing slightly higher values than the Laval Ø132 mm samples. This may result from the fact that the lower OCR points in the Norway database are observed at greater depths than in the Finnish database (Figure 8). This may be an indicator of the stress dependency of the normalized shear strength of clays.

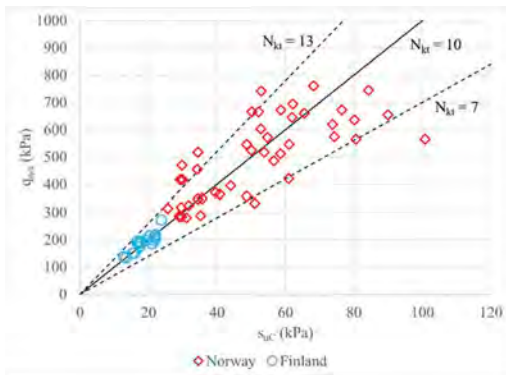


Figure 5. Q_{net} vs s_{uC} .

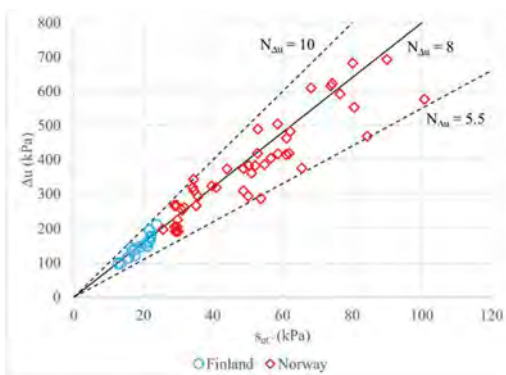


Figure 6. Δu vs s_{uC} .

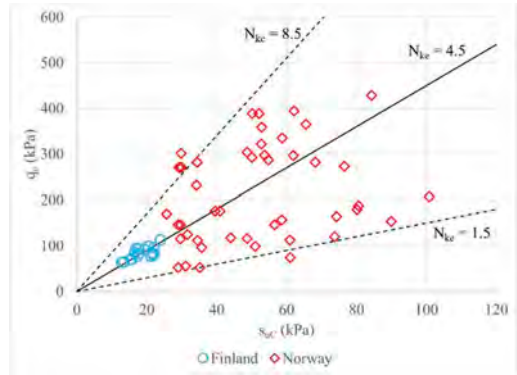


Figure 7. Q_c vs s_{uC} .

Karlsrud & Hernandez-Martinez (2013) and Paniagua et al. (2019) discussed how the variability of Norwegian clays in Figure 9 may be captured by the variability of water content. Considering that the Finland data is characterized by higher water content, this may further support the results of these studies.

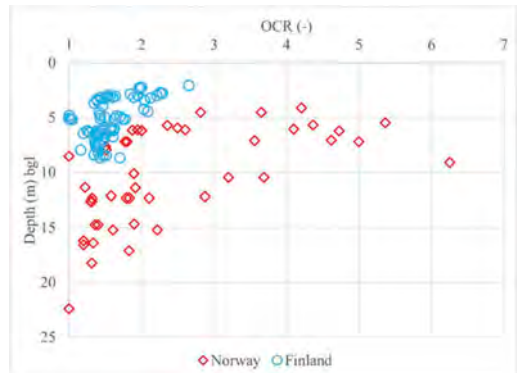


Figure 8. OCR vs depth.

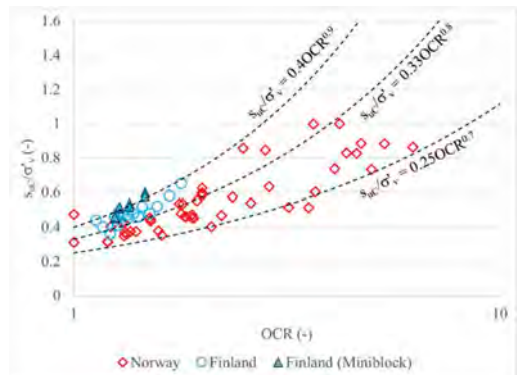


Figure 9. s_{uC} vs OCR.

6 DISCUSSION AND CONCLUSIONS

This study has compared two high-quality clay databases from Finland and Norway. Both databases include piezocone (CPTU) measurements and laboratory testing from different sites. Laboratory specimens were mainly retrieved from large diameter block sampler (Norway) and large diameter Laval-type tube sampler (Finland). Constant-rate-of-strain (CRS) oedometer tests results and undrained triaxial compression (CAUC) tests were used as reference tests to compare the overconsolidation ratio (OCR) and undrained shear strength from triaxial compression tests (s_{uC}) and their trends with respect to CPTU parameters.

The study showed that the shear strength of Finnish clays is lower than that of Norwegian clays. This is mainly due to the stress histories of the soils, i.e., the OCR of Finnish clays is generally lower when comparing samples from the same depth interval.

The larger scatter in both OCR and s_{uC} observed for the Norwegian data might be related to the fact that the Finnish data is collected from 5 sites all located in Southern Finland, while the Norwegian database comprises 17 sites spread all over Norway, where areas might have experienced different depositional histories and relative fall of sea level. Furthermore, the Finnish data has been collected using the same piezocone and sampling equipment for all sites, while the Norwegian data has been acquired over a period of 30+ years using different equipment. Even though data has been collected according to best practice, differences in measured CPTU parameters may be observed when using different cones (Lunne et al. 2018).

Future research shall focus on the mineralogy of clays. Mineral composition can have a large effect on the flocculation potential and building of strength of the soil (e.g. Torrance 2014). Depositional and post-depositional processes for both countries are also important aspects to investigate in depth. For a more thorough comparison, it is recommended to add data from Central and Northern Finland to the Finnish database.

REFERENCES

Chen, B.S., & Mayne, P.W. 1996. Statistical relationships between piezocone measurements and stress history of clays. *Canadian Geotechnical Journal*, 33(3), 488–498.

Di Buò, B. 2020. Evaluation of the Preconsolidation Stress and Deformation Characteristics of Finnish Clays based on Piezocone Testing. PhD Thesis, Tampere University, Tampere, Finland. ISBN 978-952-03-1468-2

Di Buò B., D'Ignazio M., Selänpää J. & Länsivaara T. 2016. Preliminary results from a study aiming to improve ground investigation data. *Proceedings of the 17th Nordic Geotechnical Meeting*: 187–197.

Di Buò, B., Selänpää, J., Länsivaara, T., & D'Ignazio, M. 2018. Evaluation of existing CPTu-based correlations for the deformation properties of Finnish soft clays. In *Cone Penetration Testing 2018* (pp. 185–191). CRC Press.

Di Buò, B., Selänpää, J., Länsivaara, T. & D'Ignazio, M. 2019. Evaluation of sample quality from different sampling methods in Finnish soft sensitive clays. *Canadian Geotechnical Journal*, 56(8), 1154–1168.

Di Buò, B., D'Ignazio, M., Selänpää, J., Länsivaara, T., & Mayne, P. W. 2020. Yield stress evaluation of Finnish clays based on analytical piezocone penetration test (CPTu) models. *Canadian Geotechnical Journal*, 57(11), 1623–1638.

D'Ignazio, M., Phoon, K.K., Tan, S.A., & Länsivaara, T.T. 2016. Correlations for undrained shear strength of Finnish soft clays. *Canadian Geotechnical Journal*, 53(10), 1628–1645.

D'Ignazio, M., Lunne, T., Andersen, K. H., Yang, S., Di Buò, B., & Länsivaara, T. 2019. Estimation of preconsolidation stress of clays from piezocone by means of high-quality calibration data. *AIMS Geosciences*, 5(2); 104–116.

D'Ignazio, M., Andersen, K. H., Engin, H. K., Sivasithamparam, N., Jostad, H. P & Yetginer, G. 2020. Interpretation of piezocone tests in overconsolidated clays using SHANSEP. *International Symposium on Frontiers in Offshore Geotechnics (ISFOG) 2020*, Austin, Texas

D'Ignazio, M., & Lehtonen, V. 2021. Using SHANSEP for verification of unreliable piezocone data in clays. In *IOP Conference Series: Earth and Environmental Science* (Vol. 710, No. 1, p. 012011). IOP Publishing.

Emdal, A., Gylland, A., Amundsen, H.A., Kåsin, K., & Long, M. 2016. Mini-block sampler. *Canadian Geotechnical Journal*, 53(8), 1235–1245.

Gardemeister, R. 1975. On engineering-geological properties of fine-grained sediments in Finland. Dissertation. Technical Research Center of Finland, Building Technology and Community Development, Publication 9. 91 p.

Karlsrud, K., Lunne, T., Kort, D.A., & Strandvik, S. 2005. CPTU correlations for clays. In *Proceedings of the international conference on soil mechanics and geotechnical engineering*, Vol. 16 (2), AA Balkema.

Karlsrud, K., & Hernandez-Martinez, F.G. 2013. Strength and deformation properties of Norwegian clays from laboratory tests on high-quality block samples. *Canadian Geotechnical Journal*, 50(12), 1273–1293.

L'Heureux, J. S., Gundersen, A. S., D'Ignazio, M., Smaavik, T., Kleven, A., Rømoen, M., ... & Hermann, S. 2018. Impact of sample quality on CPTU correlations in clay—example from the Rakkestad clay. In *Cone Penetration Testing 2018* (pp. 395–400). CRC Press.

Low, H. E., Lunne, T., Andersen, K. H., Sjørusen, M. A., Li, X. & Randolph, M. F. 2010. Estimation of intact and remoulded undrained shear strengths from penetration tests in soft clays. *Géotechnique*, 60(11), 843–859.

Lunne, T., Robertson, P.K. & Powell, J.J.M. 1997a. Cone penetration testing in geotechnical practice. London, Spon Press. 312p

Lunne, T., Berre, T., & Strandvik, S. 1997b. Sample disturbance effects in soft low plastic Norwegian clay. In *Proceedings of the Conference on Recent Developments in Soil and Pavement Mechanics*, Rio de Janeiro, Brazil, Rotterdam: Balkema, 81–102.

Lunne, T., Berre, T., Andersen, K. H., Strandvik, S., & Sjørusen, M. 2006. Effects of sample disturbance and consolidation procedures on measured shear strength of soft marine Norwegian clays. *Canadian Geotechnical Journal*, 43(7), 726–750.

Lunne, T., Strandvik, S., Kåsin, K., L'Heureux, J. S., Haugen, E., Uruci, E., ... & Kassner, M. 2018. Effect of cone penetrometer type on CPTU results at a soft clay test

- site in Norway. In *Cone Penetration Testing 2018*, 417–422, CRC Press.
- Paniagua, P., D'Ignazio, M., L'Heureux, J. S., Lunne, T. & Karlsrud, K. 2019. CPTU correlations for Norwegian clays: an update. *AIMS Geosciences*, 5, 82–103.
- Robertson, P.K. 2009. Interpretation of cone penetration tests —a unified approach. *Canadian Geotechnical Journal*, 46 (11), 1337–1355.
- Selänpää, J. 2021. Derivation of CPTu Cone Factors for Undrained Shear Strength and OCR in Finnish Clays. PhD Thesis, Tampere University, Tampere, Finland. ISBN 978-952-03-2156-7.
- Selänpää, J., Di Buò, B., Haikola, M., Länsivaara, T., & D'Ignazio, M. 2018. Evaluation of existing CPTu-based correlations for the undrained shear strength of soft Finnish clays. In *Cone Penetration Testing 2018*. CRC Press.
- Torrance, J. K. 2014. Chemistry, sensitivity and quick-clay landslide amelioration. In *Landslides in Sensitive Clays*, 15–24. Springer, Dordrecht.

Prediction of resilient modulus of cohesive subgrade soils from CPTU data using polynomial neural networks

Wei Duan

College of Civil Engineering, Taiyuan University of Technology, Taiyuan, China
School of Transportation, Southeast University, Nanjing, China

Zening Zhao

School of Transportation, Southeast University, Nanjing, China

Guojun Cai*

School of Transportation, Southeast University, Nanjing, China
School of Civil Engineering, Anhui Jianzhu University, Hefei, China

Anhui Wang

China Construction Industrial & Energy Engineering Group Co., Ltd., Nanjing, China

Ruifeng Chen

School of Transportation, Southeast University, Nanjing, China

Anand J. Puppala

Zachry Department of Civil and Environmental Engineering, Texas A&M University, USA

Songyu Liu

School of Transportation, Southeast University, Nanjing, China

Surya Sarat Chandra Congress

Zachry Department of Civil and Environmental Engineering, Texas A&M University, USA

ABSTRACT: Although various empirical models have been proposed to predict the resilient modulus (M_r) from laboratory test parameters, less effort has been made in developing reliable empirical models using piezocone penetration test (CPTU) data. Moreover, the prediction accuracy of the existing empirical models is not high enough. In the present study, a novel empirical model was proposed to predict the M_r from CPTU data based on the polynomial neural network. To this end, a comprehensive database comprising 16 different sites in Jiangsu province, China, was firstly compiled, which contains 124 sets of M_r , cone tip resistance (q_c), sleeve friction (f_s), pore water pressure (u_2), moisture (w), and dry density (γ_d) values at the in-situ stress condition. Taking the in-situ M_r values as reference values, three empirical models were developed using the group method of data handling (GMDH) neural network. The results show that proposed GMDH model 3 (GMDH method) with the input parameters of q_c , f_s , w , and γ_d can accurately predict the M_r . The obtained specific expressions for prediction of M_r further prove the reliability of the GMDH model. Overall, the new GMDH method can more accurately predict the M_r of subgrade soil and guide engineering practice.

1 INTRODUCTION

The properties of subgrade soils are the key contents in the design and performance of a pavement structure (Liu et al., 2016; Ghorbani et al., 2020). Among these properties of dry density, moisture content, stress state, the resilient modulus (M_r), and so on, the M_r is

an important index that describes the nonlinear stress-strain behavior of soil materials with respect to repeated traffic loading. The definition of M_r can be expressed as the ratio of the repeated deviator stress to the recoverable axial strain. The most usually used method to determine such property of M_r is using the repeated load triaxial test with a closed loop servo

*Corresponding author
DOI: 10.1201/9781003308829-49

pneumatic loading system (AASHTO, 1993; NCHRP, 2004). However, most of the results from laboratory tests generally run into difficulties: size limitations, disturbance, and actual maintenance effects (Duan et al, 2019). Instead, the in situ tests can provide more direct and accurate results, thus, several attempts were made to determine and understand the behavior of resilient modulus property based on different soil properties (Mohammad et al. 2002; Tarawneh et al. 2014; Liu et al., 2016; Heidariapanah et al., 2017; Ghorbani et al. 2018).

In fact, some empirical correlations between M_r and other test indices such as undrained shear strength, unconfined compressive strength, and California Bearing Ratio (CBR) has been established. Additionally, the in situ testing indices are also very well-received when related the indices to M_r . Among these in situ tests, the cone penetration test (CPT), especially for the piezocone penetration test (CPTU) is treated as the most accurate method that have the advantage of near-continuous, repeatable measurements that provide a detailed profile of the subsurface soil layers (Ghorbani et al. 2018). The past studies have confirmed that the M_r is a function of CPT measured parameters (cone tip resistance (q_c), sleeve friction (f_s)), moisture content (w), applied stress and confining pressure (Mohammad et al., 2007). several empirical correlations have been proposed that related to M_r to soil properties, stress states, and CPT testing indices (Mohammad et al. 2002; Liu et al. 2016; Ghorbani et al., 2020). However, the it appears that most prior studies suggested the empirical correlations may be limited to site-specific conditions due to rather selective and limited in-situ data obtained from only a few sites. Moreover, the studies related to CPTU indices are very limited (Liu et al. 2016; Ghorbani et al., 2020).

With recent advances in computational software and hardware (Zhao et al., 2021a), the use of the artificial neural network (ANN) method as a statistical regression technique to approximate input-output relationships in geotechnical engineering has gained impetus for its ability to effectively deal with the complex relationships in recent years (Juang et al., 1999; Zhao et al., 2021b). However, the major drawback of ANN is that the detected dependencies are hidden in the ANN structure, and the correlations are often not expressed intuitively (Duan et al., 2021a). The group method of data handling (GMDH) type neural network is a polynomial neural network that using a powerful identification technique to model complex relationships between multiple variables (Moayed et al., 2017). Hence, in the present study, the GMDH model is proposed for predicting M_r based on these parameters of cone tip resistance (q_t), sleeve frictional resistance (f_s), dry density (γ_d) and moisture (w).

In this present study, the feasibility of the GMDH algorithm to predict the M_r of cohesive subgrade soils has been conducted. Details of the development of various GMDH-type network models for in-situ

M_r evaluation have been presented. A comparison of the predictions from the existing empirical correlations are presented in detail. Salient findings and conclusions are shown based the above results and analysis.

2 GMDH ALGORITHM

The GMDH algorithm an inductive self-organizing approach to estimate black-box models with an unknown correlation between variables. The kernel of GMDH is to build an analytical function in a feed-forward network based on a quadratic node transfer function and use regression technique to determine the coefficients of partial quadratic polynomials (Duan et al. 2021a). Assume y_i and \hat{y}_i represent the actual output and predicted outputs of GMDH neural network, respectively.

For a given input vector $x_i = [x_{i1}, x_{i2}, \dots, x_{im}]^T$, $i = 1, 2, \dots, M$, the mathematical relationship between the input and the output variables of GMDH neural network can be simplify expressed by a system of partial quadratic polynomials consisting of only two variables (neurons) as

$$\hat{y} = G(x_i, x_j) = a_0 + a_1x_i + a_2x_j + a_3x_ix_j + a_4x_i^2 + a_5x_j^2 \quad (1)$$

The coefficients of each quadratic function (G) can be obtained for an optimal fit for the output in the input-output data pairs. The optimal fit is based on the least root mean square error (RMSE) described as:

$$RMSE = \sqrt{\frac{1}{M} \sum_{i=1}^M (\hat{y}_i - y_i)^2} \quad (2)$$

The purpose of GMDH neural network is to determine the coefficient a_i in Eq. (1) to minimize the RMSE by regression techniques. A number of partial descriptions are formed based on all possibilities of obtaining the output variable from two independent variables to construct the regression polynomial that best fits the dependent observations (y_i , $i = 1, 2, \dots, M$). The normal equations can be solved using the least squares method as follows:

$$\mathbf{a} = (\mathbf{A}^T \mathbf{A})^{-1} \mathbf{A}^T \mathbf{Y} \quad (3)$$

where $\mathbf{a} = [a_0, a_1, a_2, a_3, a_4, a_5]^T$ is the vector of unknown coefficients of the quadratic polynomial in Eq. (1); $\mathbf{Y} = [y_1, y_2, y_3, \dots, y_M]^T$ is the vector of output values from observation. The best estimation of the coefficients in Eq. (1) from the whole set of M data triples can be determined through the Eq. (3).

3 DATABASE

3.1 Site description

Geotechnical investigations were conducted in Jiangsu Province, China and sixteen (16) different test sites are investigated and considered in this study as shown in the Figure 1. The geological formations of Quaternary clays mainly contain Marine, Yangtze River Delta, Floodplain of Long River, Floodplain of Abandoned Yellow River, Lagoon of Lixia River and Lagoon of Taihu Lake. Based on the previous analysis, the subsoil profile in these test sites mainly clay deposits.

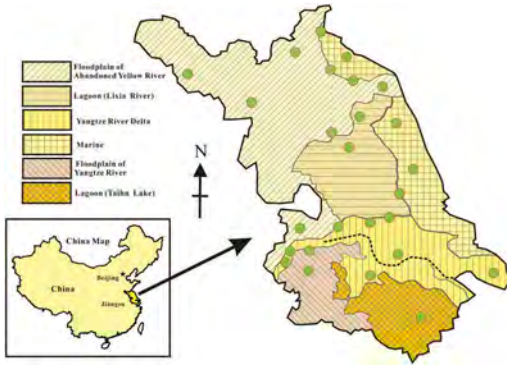


Figure 1. Location of the testing sites.

3.2 Laboratory tests and field CPTU tests

Based on the soil samples from the testing sites, laboratory tests were performed to obtain the w , γ_d and M_r properties. The resilient modulus tests were conducted on the soil samples by repeated load triaxial tests. The CPTU soundings have been conducted at the adjacent locations near the boreholes where the soil samples were collected to ensure the predicted M_r value with the in-situ stress level. In the next section, the CPTU technique along with representative profile is presented.

CPTU field tests were conducted using a light-weight truck with a 20-ton-capacity hydraulic system, which is in accordance with international standards (Lunne et al., 1997; ASTM D5778, 2012; Duan et al., 2021b). The sizes of the CPTU probe are as follows: The section area of the cylindrical cone penetrometer is 10 cm^2 with a tip angle of 60° , the surface area of the friction cylinder is 150 cm^2 . The penetration rate was set as 20 mm/s , and nearly continuous data were produced at intervals of about 50 mm . Compared with CPT, the pore pressure can be measured simultaneously and the ground water table (GWT) can be identified based on CPTU test. Based on the test results, the GWT value varied with the range of 0.4 m to 4.5 m . Figure 2 shows a typical profile of the SCPTU sounding. Thus, a database of 124 data sets

including q_c , f_s , w , γ_d and M_r is compiled and used for the following analysis.

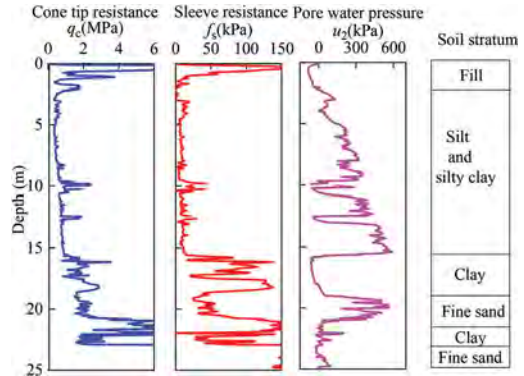


Figure 2. Typical profiles of piezocone penetration test.

4 CONSTRUCTION OF GMDH MODELS

4.1 GMDH models development

The data points can be separated into three subsets in the ratios of 7:2:1 for training, testing, and validation. Actually, the subsets of testing and validation are always merged into one. Thus, the data sets separated with a ratio of 7:3 for the training and testing (including validating), respectively. Of the 124 data sets, 87 data points were randomly selected for the training while 37 data points were used only for validating the developed models. In the present study, four variables (q_c , f_s , w , γ_d) were considered to demonstrate the prediction ability of the GMDH network. Three categories are considered as follows: i) w , γ_d ; ii) q_c , f_s ; iii) q_c , f_s , w , γ_d . The relative root mean square error (RRMSE), absolute fraction of variance (R^2) are utilized for the performance evaluation of GMDH models.

4.2 GMDH models results

The values of the RRMSE, and R^2 for each model are listed in Table 1. It can be observed that all developed GMDH models have shown relative good performance. Comparing the performance of model 1 using soil indices from laboratory tests, the predicted performance has been improved using the CPT parameters based on the results of model 2. The CPT parameters seems to be more useful in predicting M_r values. From the perspective of performance evaluation, model 3 was found to be the best among other GMDH models. This is not surprise because the input parameters are comprehensive and GMDH has strong predictive ability. Thus, the accuracy of predictions can be consistently improved if more indices are involved in the GMDH model.

Table 1. Performance of GMDH models in predicting M_r in testing dataset.

Model	Inputs	RRMSE	R^2
1	w, γ_d	0.5571	0.6896
2	q_c, f_s	0.4730	0.7762
3	q_c, f_s, w, γ_d	0.1314	0.9827

Based on the analysis, the specific equations are presented subsequently.

1) Model 1

$$M_r = 140.9416 - 8.3239\gamma_d - 2.3476\omega + 0.02757\omega \cdot \gamma_d + 0.3018\gamma_d^2 + 0.01661\omega^2 \quad (4)$$

2) Model 2

$$M_r = 9.7980 + 386.2597f_s - 0.5083q_c + 65.5731q_c \cdot f_s - 1902.9274f_s^2 + 2.0608q_c^2 \quad (5)$$

3) Model 3

$$M_r = 27.5607 + 0.7400X_2 - 4.3630\gamma_d + 0.02173\gamma_d \cdot X_2 - 0.001522X_2^2 + 0.1606\gamma_d^2 \quad (6-1)$$

$$X_2 = 2.8207 + 0.3640X_1 + 89.3235f_s + 2.08785f_s \cdot X_1 + 0.003977X_1^2 - 26.5075f_s^2 \quad (6-2)$$

$$X_1 = 44.5084 - 1.1459\omega + 21.8014q_c - 0.09932q_c \cdot \omega + 0.009240\omega^2 - 1.6703q_c^2 \quad (6-3)$$

Taking model 2 as an example, the targeted values (scatter points in red) and predicted curved surface values (colored) using Eq. (5) is shown in Figure 3. It can be observed that the data points of targeted values are closed to the curved surface and they are uniformly distributed on both sides of the predicted curved surface, indicating the ease and practicability of the GMDH model using CPT parameters (q_c, f_s). Thus, under the condition that the accuracy requirement is satisfied, model 2 can be chosen as an option for its simplicity, whereas model 3 is a better choice when high precision is required.

The points scatter of predicted (calculated by GMDH model 3 along with model 1 and model 2) versus targeted ψ values has further demonstrated the accuracy of resilient modulus evaluation using

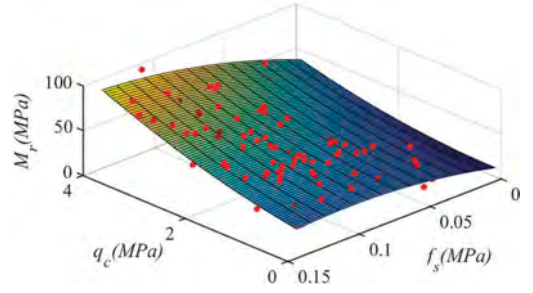


Figure 3. Correlation of M_r with q_c and f_s using GMDH model 2.

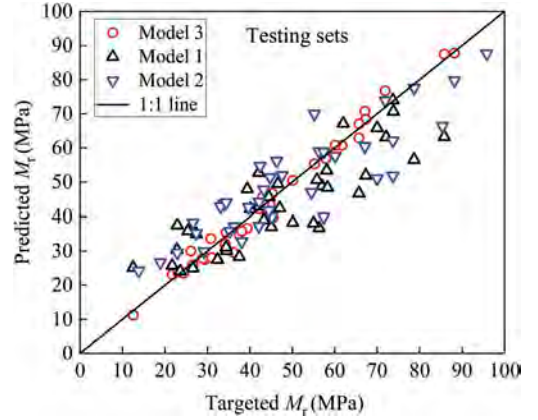


Figure 4. Comparison between targeted M_r and predicted M_r .

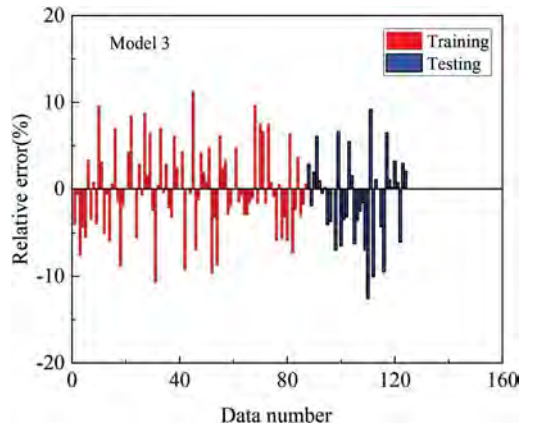


Figure 5. Variation in the relative errors obtained from GMDH method (Model 3).

GMDH model 3 (Figure 4). Compared with model 1 and 2, the predicted points by GMDH model 3 are closer (near 1:1 line) to those targeted values. Thus, the GMDH model 3 was considered as the GMDH method for predict the resilient modulus of subgrade

soils. Overall, the predicted values by the GMDH models are smaller than the targeted values, which will lead to conservative engineering design.

Figure. 5 Plots the relative errors (defined as the percentage difference between the GMDH predicted and the targeted values) for the training and testing sets. Observably, most of the GMDH estimations of the data patterns for model 3 fell within $\pm 12\%$ of the targeted values. Overall, it is feasible to apply GMDH method to evaluate the resilient modulus of subgrade soils.

5 CONCLUSIONS

In this study, the feasibility of GMDH polynomial neural networks in modeling a regional database containing Quaternary clay from different geologic formations in Jiangsu province, China. Three GMDH models using all or part of the parameters including M_r at the in-situ stress condition, CPTU indices (q_c, f_s), and laboratory indices (w, γ_d).

The relative good prediction results are obtained from all GMDH models and it is confirmed that the GMDH is capable of effectively capturing the non-linear relationships. The most significant advantage for GMDH is that specific expressions can be given in predicting geotechnical parameters. Among three types of GMDH models, model 3 including q_c, f_s, w and γ_d is selected as the GMDH method for its high accuracy.

ACKNOWLEDGEMENTS

The majority of the work presented in this paper was funded by the National Key R&D Program of China (Grant No. 2020YFC1807200), the National Natural Science Foundation of China (Grant No. 52108332, No. 41877231, and No. 42072299), and the Project of Nanjing Construction System Science and Technology(Ks2153). The financial supports are greatly acknowledged.

REFERENCES

American Association of State Highway and Transportation Officials (AASHTO). Guide for design of pavement structures. Washington, D. C., 1993.
 Duan, W., Cai, G., Liu, S., Puppala, A.J. & Chen, R. 2019. In-Situ Evaluation of Undrained Shear Strength from Seismic Piezocone Penetration Tests for Soft Marine

Clay in Jiangsu, China. *Transportation Geotechnics* 20:100253.
 Duan, W., Congress, S.S.C., Cai, G., Liu, S., Dong, X., Chen, R. & Liu, X. 2021a. A hybrid GMDH neural network and logistic regression framework for state parameter-based liquefaction evaluation. *Canadian Geotechnical Journal* online.
 Duan, W., Congress, S. S. C., Cai, G., Puppala, A. J., Dong, X., & Du, Y. 2021b. Empirical Correlations of Soil Parameters based on Piezocone Penetration Tests (CPTU) for Hong Kong-Zhuhai-Macau Bridge (HZMB) Project. *Transportation Geotechnics*, 100605.
 Ghorbani, B., Sadrossadat, E., Bazaz, J. B., & Oskooei, P. R. 2018. Numerical ANFIS-based formulation for prediction of the ultimate axial load bearing capacity of piles through CPT data. *Geotechnical and Geological Engineering*, 36(4), 2057–2076.
 Ghorbani, B., Arulrajah, A., Narsilio, G., Horpibulsuk, S., & Bo, M. W. 2020. Hybrid Formulation of Resilient Modulus for Cohesive Subgrade Soils Utilizing CPT Test Parameters. *Journal of Materials in Civil Engineering*, 32(9), 06020011.
 Heidaripanah, A., Nazemi, M., & Soltani, F. 2017. Prediction of resilient modulus of lime-treated subgrade soil using different kernels of support vector machine. *International Journal of Geomechanics*, 17(2), 06016020.
 Liu, S., Zou, H., Cai, G., Bheemasetti, T. V., Puppala, A. J., & Lin, J. 2016. Multivariate correlation among resilient modulus and cone penetration test parameters of cohesive subgradesoils. *Engineering Geology*, 209, 128–142.
 Lunne, T., Robertson, P.K. & Powell, J.J.M. 1997. *Cone Penetration Testing in Geotechnical Practice*. CRC Press, London.
 Mohammad, L. N., Herath, A., Abu-Farsakh, M. Y., Gaspard, K., & Gudishala, R. 2007. Prediction of resilient modulus of cohesive subgrade soils from dynamic cone penetrometer test parameters. *Journal of Materials in Civil Engineering*, 19(11), 986–992.
 National Cooperative Highway Research Program (NCHRP), 2004. *Guide for Mechanistic Empirical Design of New and Rehabilitated Pavement Structures. Part 2, Design Inputs*. Final Rep. No. NCHRP 1-37A, Washington, D.C.
 Tarawneh, B., & Nazzal, M. D. 2014. Optimization of resilient modulus prediction from FWD results using artificial neural network. *Periodica Polytechnica Civil Engineering*, 58(2), 143–154.
 Zhao, Z., Duan, W. & Cai, G. 2021a. A novel PSO-KELM based soil liquefaction potential evaluation system using CPT and Vs measurements. *Soil Dynamics and Earthquake Engineering* 150: 106930.
 Zhao, Z., Congress, S.S.C., Cai, G. & Duan, W. 2021b. Bayesian probabilistic characterization of consolidation behavior of clays using CPTU data. *Acta Geotechnica* 1–18.

Effect of sand bio-cementation on cone tip resistance: A numerical study

M.El Kortbawi, K. Ziotopoulou & J.T. DeJong
University of California, Davis, CA, USA

D.M. Moug
Portland State University, Portland, OR, USA

ABSTRACT: Understanding the effect of soil cementation on cone measurements is important for the identification of naturally cemented soil deposits and for the verification of soil improvement achieved by various forms of artificial cementation, including bio-cementation. This paper presents the results of an effort to connect cone tip resistances with fundamental, constitutive level, bio-cementation-induced changes in soil behavior. To this end, a direct axisymmetric cone penetration model using the Mohr-Coulomb constitutive model and grid rezoning and remapping algorithms is used to model cone penetration in bio-cemented sands. By connecting the results of cone penetration simulations in a Mohr-Coulomb material to real data and established relationships, this work will guide selection of equivalent strength properties of these challenging materials. More specifically, the apparent cohesion, peak friction angle, dilation angle, and small-strain shear modulus within the Mohr-Coulomb constitutive model are varied parametrically across a reasonable range of parameter values informed by past laboratory, bench-scale, and centrifuge tests. Results show that cone penetration resistance in bio-cemented sands is mostly influenced by the interconnected apparent cohesion and the small-strain shear modulus, while other parameters play a secondary role.

1 INTRODUCTION

The cone penetration test (CPT) is a widely used field test for soils in subsurface explorations due to its ability to provide continuous information on the stratigraphy, and to be correlated to physical and engineering properties of the subsurface strata (e.g., Robertson & Campanella 1983, Lunne et al. 1997, Robertson 2016). While the CPT has been mostly used for the characterization of sands and clays, it may also be used for the identification of naturally cemented soils deposits (e.g., Puppala et al. 1995, Roy 2008) and artificially cemented and improved soils, including bio-cemented ones (e.g. Gomez et al. 2018, Darby et al. 2019).

Bio-cementation is a relatively new ground improvement technique in which microorganisms present in the soil are stimulated under specific conditions to precipitate calcite which coats and bridges soil particle contacts. The artificially precipitated calcite is analogous to natural cementation and can be considered as a proxy for naturally cemented sands (e.g., DeJong et al. 2006, DeJong et al. 2010). To date, the characterization of bio-cemented sands and, similarly, naturally cemented sands in the field remains a challenging task due to difficulties in sampling and its high cost.

Classification and characterization approaches for bio-cemented sands developed to date have been

primarily derived through empirical analyses of field data obtained in cemented soils, although some full scale 1-g and reduced scale centrifuge modeling data are also available. Therefore, the CPT has been proposed as a field test able to overcome the limitations of sampling and to provide direct indications of the presence of the cementation in the field. In general, the cone tip resistance and the shear wave velocity both increase with cementation, which suggests the development of a framework relating these two parameters as an indicator of possible cementation. Currently, such a framework is not available for the interpretation of the CPT data and their correlation to soil strength parameters for bio-cemented sands.

This paper presents the results of an effort to connect cone tip resistances with fundamental, constitutive level, bio-cementation-induced changes in soil behavior. To this end, a direct axisymmetric cone penetration model using the Mohr-Coulomb constitutive model and grid rezoning and remapping algorithms (Moug 2017) is used to model cone penetration in bio-cemented sands. By connecting the results of cone penetration simulations in a Mohr-Coulomb material to real data and established relationships, this work will guide selection of equivalent strength properties of these challenging materials. More specifically, the apparent cohesion, peak friction angle, dilation angle,

and small-strain shear modulus within the Mohr-Coulomb constitutive model are varied parametrically across a reasonable range of parameter values informed by past laboratory, bench-scale, and centrifuge tests.

The axisymmetric penetration model is briefly introduced, followed by a summary of the equivalent Mohr Coulomb input parameters. Simulation results are presented, interpreted, and compared against a published soil behavior type chart as well as experimental data from a reduced scale centrifuge model test. Conclusions pertaining to the validity of the proposed framework and the results are drawn.

2 NUMERICAL INVESTIGATION

2.1 Axisymmetric penetration model

The axisymmetric model presented in Figure 1 simulates the steady-state penetration of a standard 10 cm² (3.57 cm-diameter) cone into the soil column. Boundary conditions are imposed for a soil flowing into the bottom of the model upwards relative to a fixed cone. Mohr-Coulomb interface elements are applied at the interfaces between the cone and soil to represent an interface roughness factor of 0.60, which is the ratio of the interface friction angle to the soil friction angle. Stresses and Mohr-Coulomb material properties are initialized for a “wished-in-place” condition at the depth of interest. Initial stress conditions correspond to an at-rest K_0 condition and a fully drained penetration is simulated. The cone penetration is velocity-controlled at the gridpoints across the top boundary. The right radial boundary is far enough from the cone to avoid any boundary effects and is thus defined as an infinite elastic boundary. The bottom boundary is sufficiently far from the cone’s zone of influence to maintain the prescribed in-situ stress conditions. Large deformations are handled with a user-implemented Arbitrary Lagrangian-Eulerian (ALE) algorithm which performs grid rezoning and remapping during the cone penetration. Penetration is simulated until a steady state penetration resistance is achieved (Moug et al. 2019), which is approximately 25 cone diameters of penetration.

2.2 Input parameters and calibration

The application of bio-cementation treatment to sands, as well as the geologic-time scale process where sand is gradually cemented, induce changes in the stiffness and strength. While difficult to characterize in the field, coupling the simulated cone tip resistance in a Mohr-Coulomb type of material and established relationships can guide the selection of equivalent strength parameters for these challenging geomaterials. The Mohr-Coulomb constitutive model was selected because it defines a failure envelope with a cohesion intercept and a peak friction angle which can be representative of bio-cemented sands. More broadly, it is a simple

model with few parameters and nicely describes a broad range of responses without unnecessary complexities. Based on numerous bench-scale and large-scale experiments on bio-cemented sands, a linear relationship between the “apparent” cohesion (c) and the change in shear wave velocity (ΔV_s) was developed to estimate the value of cohesion from the measured post-cementation in-situ V_s (El Kortbawi et al., under review).

$$\Delta V_s = 18.9c \quad (1)$$

where ΔV_s = the change in shear wave velocity in m/s and c = the “apparent” cohesion in kPa.

Following an extensive literature review on bio-cemented sands (e.g., Nafisi et al. 2019, Nafisi et al. 2020, Wu et al. 2020) and using the above empirical relationship, the values for the input parameters in Table 1 was defined.

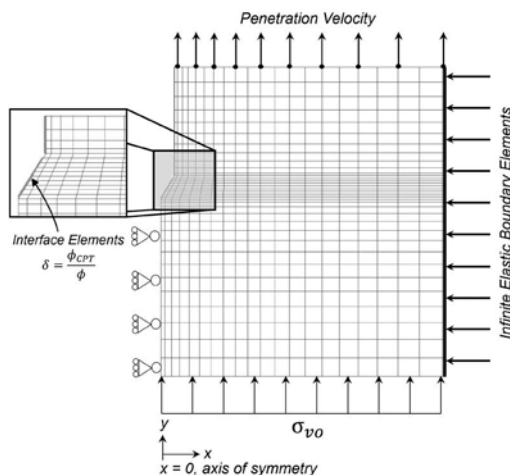


Figure 1. Geometry and boundary conditions of the numerical cone penetration model (Moug, 2017).

Table 1. Variables for parametric study.

Variable	Tested values
Cohesion, c (kPa)	0, 10, 20
Friction angle, ϕ (degrees)	30, 35
Dilation angle, ψ (degrees)	0, 10
“Functional” shear modulus, G_{sec} (kPa)	Based on the relationship between ΔV_s and cohesion
Confining stress, σ_{v0} (kPa)	35, 100

Due to the large strains around the penetrating cone, the small-strain shear modulus (G_{max}) as an input model parameter does not reflect the complex deformations and strain softening in the plastic region near the cone tip which would result in an overestimation of the cone tip resistance (Teh & Houlsby 1991, Lu et al. 2004). Therefore, a reduction factor is applied to G_{max} (where $G_{max} = \rho V_s^2$ and ρ is the density) to account for the shear modulus softening and a secant shear modulus (G_{sec}) is used, where $G_{sec} = G_{max}/F$ and $F = 0.15 c + 3$ based on a calibration process and comparison of simulated cone penetration with experimental results (El Kortbawi et al., under review). The chosen initial V_s ($V_{s,ini}$) values normalize with respect to the varying confining stresses of 35 and 100 kPa, hence the results of these simulations are examined in absolute terms such as q_c instead of incremental terms (Δq_c).

The input to each set of simulations is summarized in Tables 2 and 3 for the confining stresses of 35 and 100 kPa, respectively.

Table 2. Simulation input parameters for $\sigma'_{vo} = 35$ kPa.

	Cohesion (kPa)		
	0	10	20
$V_{s,ini}$ (m/s)	150	150	150
ΔV_s (m/s)	0	189	378
Reduction factor F	3	4.5	6
G_{sec} (kPa)	12,750	43,149	78,262

Table 3. Simulation input parameters for $\sigma'_{vo} = 100$ kPa.

	Cohesion (kPa)		
	0	10	20
$V_{s,ini}$ (m/s)	200	200	200
ΔV_s (m/s)	0	189	378
Reduction factor F	3	4.5	6
G_{sec} (kPa)	22,667	56,814	93,783

3 RESULTS

The focus of the subsequent analyses and illustrations is the cone tip resistance q_c . Open and closed symbols correspond to confining stresses of 35 and 100 kPa, respectively. Circle and square symbols correspond to friction angle of 30 and 35 degrees, respectively. Figure 2a presents the variation of the absolute q_c with an increasing shear stiffness (proportional to V_s according to $G_{max} = \rho V_s^2$), friction angle, and confining stress at a dilation angle

of 0° . Figure 2b illustrates the change in q_c with the change in V_s due to the presence of a cohesion (Eq.1) for the given combinations of stress states and friction angles. Figure 2c illustrates the effect of the confining stress on q_c by normalizing it according to $Q_t = (q_t - \sigma_{vo})/\sigma'_{vo}$. Collectively, these figures confirm that: (1) the cone tip resistance increases considerably with the increase in the cementation level, (2) the change in q_c is due to the changes in cementation only, and (3) the ‘‘cemented’’ friction angle may have an effect on the increase in q_c but to a lesser extent than the shear stiffness.

Figure 3 Presents the variation of the tip resistance as a function of the confining stress with varying strength parameters, cohesion from 0 to 20 kPa, and friction angle from 30 to 35 degrees. Circle and

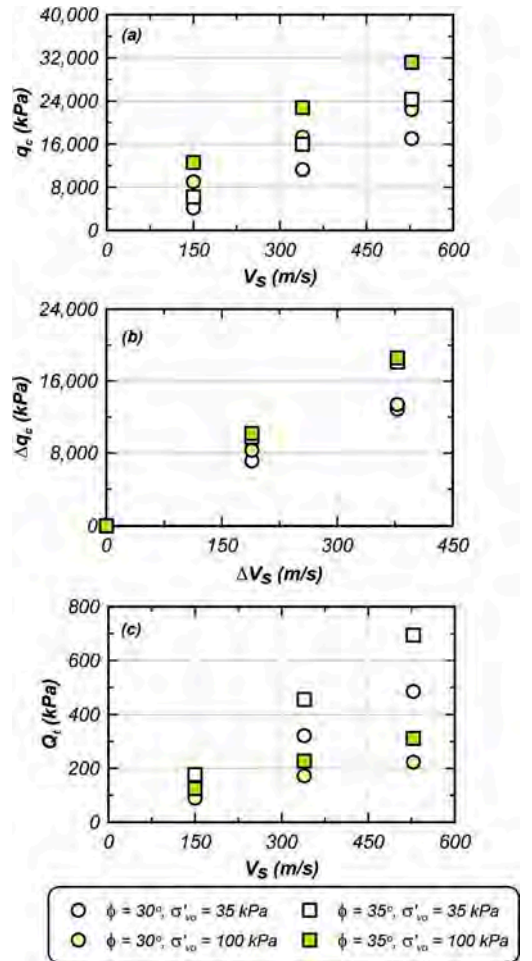


Figure 2. (a) Variation of q_c as a function of V_s , (b) variation of Δq_c with varying ΔV_s , and (c) variation of normalized Q_t as a function of V_s , for varying ϕ of 30° and 35° and different confining stresses at ψ of 0° .

square symbols correspond to friction angles of 30 and 35 degrees, respectively, whereas the shading corresponds to increasing the cohesion from 0 to 20 kPa.

Similar to Figure 2, a positive trend exists between q_c and σ'_{vo} where the following observations are made: (1) for $\sigma'_{vo} = 35$ kPa, q_c for $c = 20$ kPa is around 4 times the q_c for $c = 0$ kPa, whereas for a higher $\sigma'_{vo} = 100$ kPa, this ratio decreases to 2.5 times regardless of the friction angle, (2) for $c = 0$ kPa, q_c for $\sigma'_{vo} = 100$ kPa is around twice the q_c for $\sigma'_{vo} = 35$ kPa, whereas for $c = 20$ kPa, this ratio decreases to 1.3 times regardless of the friction angle, and (3) for $\sigma'_{vo} = 35$ kPa, q_c for $\phi = 35^\circ$ is around 1.5 times q_c for $\phi = 30^\circ$ whereas for $\sigma'_{vo} = 100$ kPa this ratio slightly decreases to 1.4 times, regardless of the cohesion. These observations suggest that: (1) cohesion is the major contributor to the enhanced tip resistance, followed by the confining stress, and then followed by the friction angle, and (2) the effect of the cementation is more significant at low confining stress.

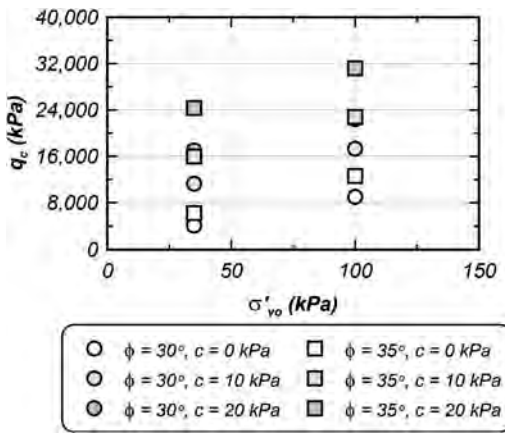


Figure 3. Variation of q_c as a function of σ'_{vo} for varying ϕ and c at ψ of 0° .

Figure 4 Incorporates, in addition to the cohesion, friction angle and confining stress, the effect of the dilation angle ψ . Figures 4a and 4b correspond to $\phi = 30^\circ$ and 35° , respectively, and the diamond and triangle symbols correspond to a ψ of 0° and 10° , respectively. The results show that the increase in the dilation angle leads to a larger cone tip resistance, due to stronger dilation of the soil which in turn results in a higher resistance of the soil to shearing. The q_c with a $\psi = 10^\circ$ (a limit for bio-cemented sands suggested by the literature e.g., Wu et al. 2020) is 3 to 4 times higher relative to q_c with a $\psi = 0^\circ$, depending on the strength parameters with this ratio increasing for a higher confining stress (σ'_{vo} of 100 kPa).

The current state of practice uses previously established charts for the interpretation of CPT data

and classification of soils which include cemented sands. As the change in shear stiffness plays a major role in the behavior of bio-cemented sands and cemented sands in general, the small-strain shear modulus G_{max} and the stress-normalized cone tip resistance Q_t can be correlated to guide the soil behavior type and extend it to these cemented soils. Figure 5a presents the simulation results for the different scenarios. In addition to the simulation results from this work, experimental data obtained from cones pushed in a bio-cemented specimen in a centrifuge model (Darby et al. 2019) are plotted. Several levels of cementation were established by the experimentalists targeting light, moderate, and heavy cementation levels. The datapoints from the cones pushed in treated sands plot reasonably within the region corresponding to soils with “ageing cementation”, with few datapoints plotting close to the “uncemented” region due to their light level of cementation (Darby et al. 2019). Specimens with higher levels of cementation follow the trend discussed earlier. Moreover, Figure 5a shows that the simulation results for $\sigma'_{vo} = 35$ kPa fall within the range of the experimental data from Darby et al. (2019) with a similar confining stress of 35 kPa, hence validating the proposed approach.

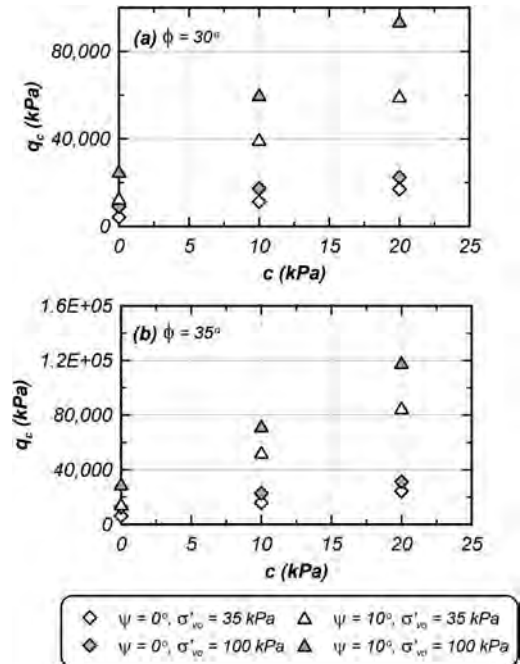


Figure 4. Variation of q_c as a function of c for varying ψ and σ'_{vo} at, (a) ϕ of 30° , and (b) ϕ of 35° .

The CPT-based classification chart according to Q_t and G_o/q_t is reproduced in Figure 5b and the simulation and experimental results are overlaid.

Figure 5b shows a reasonable agreement between the expected soil behavior from the input parameters (i.e., uncemented sands with zero cohesion versus cemented sands with nonzero cohesion) and the suggested soil behavior from the chart. For example, the simulations with $c = 0$ kPa plot in the “sand” behavior type on the chart as expected for a cohesionless uncemented sand. Similarly, the simulations with $c > 0$ kPa plot in the region corresponding to soils with “ageing cementation” on the chart. Moreover, the aforementioned relative magnitude of Q_t and G_o/q_t between the cemented sands and the uncemented sand is also evident on the soil classification chart.

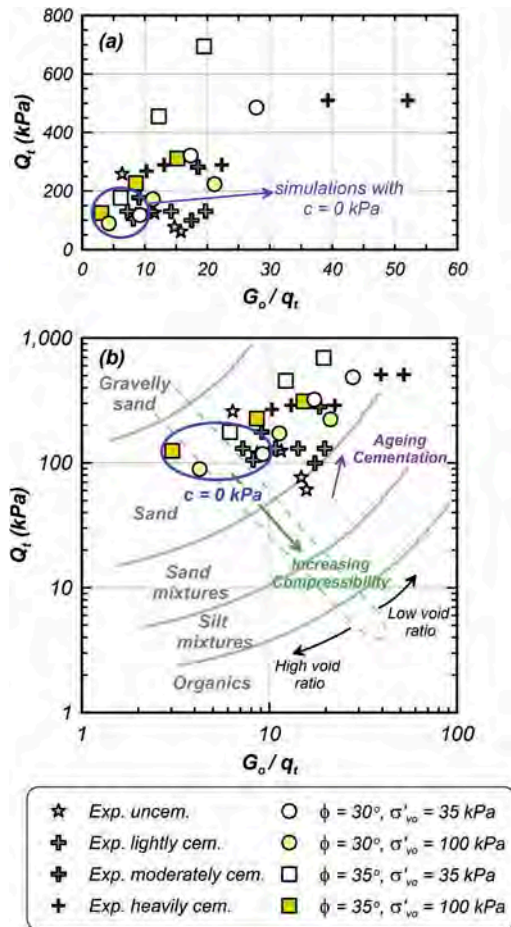


Figure 5. Soil classification chart based on normalized cone resistance and small-strain shear modulus, reproduced from Lunne et al. (1997), and overlaid with simulation results from this work and experimental data from the centrifuge test from Darby et al. (2019).

The results suggest that as cohesion increases, i.e., the level of cementation precipitated at the particle contacts increases, the soil moves vertically

towards a higher normalized tip resistance and laterally to a higher normalized stiffness. When other parameters remain constant, increasing the friction angle results in a larger q_c , hence the soil moves vertically towards a higher normalized tip resistance but horizontally towards a smaller normalized stiffness due to the normalization with q_c .

4 CONCLUDING REMARKS

The cone penetration test has been commonly used in soils to indicate the soil behavior type and to assess the soil’s resistance in bearing capacity and liquefaction mitigation applications. Its use can be extended to bio-cemented or cemented sands. Some limitations are associated with pushing cones in cemented sands, such as the inability of the cone to detect light cementation (equivalent to calcite content less than 3%) and the destructive nature of the test to any pre-existing cementation in the soil. However, it is still a common and valuable test able to provide proxies of the expected soil behavior and its degree of cementation in the absence of more viable exploration methods.

In this paper, a parametric study on the input parameters to an axisymmetric cone penetration model for sands was presented in the context of its application to bio-cemented sands. The numerical model implemented the Mohr-Coulomb constitutive model which was used to estimate equivalent “cemented” strength parameters. Although the Mohr-Coulomb constitutive model prescribed constant strength parameters to strain-dependent soil conditions, the approximation with a “functional” shear modulus allows the model to reasonably predict the elastic-plastic behavior of bio-cemented soils in the failure zone near the cone tip. The input parameters varied in this paper are the cohesion, friction angle, dilation angle, and confining stress. The results were analyzed in terms of cone tip resistance, and the study confirmed that it increased with increasing the level of cementation, and suggested that the cohesion value is the main contributor to this improvement in the soil resistance. The dilation and friction angles also affect the soil’s resistance but to a lesser extent. Simulation results were also compared to experimental data from CPTs pushed in bio-cemented sands and to previously established soil behavior type charts for “unusual” soils. The simulation results fell within the range of the experimental data and they both plotted in the “ageing cementation” region of the chart. Hence the proposed framework appears reasonable to estimate the soil’s strength and overcome the challenges in sampling cemented sands.

Oftentimes, considerable effort is put into the selection of input parameters for numerical models. The above observations related to the effect of input parameters on the cone tip resistance are insightful for prioritizing the choice of input parameters and

can be potentially used to guide parameter selection for numerical models, based on CPT data, to represent cemented materials in numerical simulations.

The ranges of input parameter values used in this study reflect the typical ranges found in the literature for lightly and moderately bio-cemented sands. The trends presented here may be cautiously extrapolated to reasonably higher strength parameters and confining stresses; however, the relative magnitudes may warrant further exploration.

In the developing field of bio-cemented sands, numerical models that are validated and calibrated against existing data can be leveraged to populate and synthesize data that are not yet available. While some approximations such as the estimation of the cohesion value and the reduced secant shear modulus are made herein, the numerical model is still a valuable tool to, in the first stage, study the sensitivity of the results to input parameters and, in the second stage, synthesize data needed to develop correlations between these various parameters. El Kortbawi et al. (under review) extend this work to develop a correlation between the cone tip resistance and the cohesion in order to implement it in a plasticity constitutive model for bio-cemented sands.

Adding to the importance of the CPT in indicating the behavior of the present soil, it can and should be a preferred method for post-cementation verification in the field. The CPT can thus serve as a tool in the design of ground improvement methods and in the QA/QC of the final improvement, especially in the field of bio-cementation ground improvement techniques.

ACKNOWLEDGMENTS

This material is based upon work primarily supported by the National Science Foundation (NSF) under NSF Award Number EEC-1449501. Any opinions, findings and conclusions, or recommendations expressed in this material are those of the author(s) and do not necessarily reflect those of the NSF. The authors are grateful to Professor R. W. Boulanger for discussions and insights that set the framework of this work in its original stages.

REFERENCES

- Darby, K., Hernandez, G., DeJong, J. T., Boulanger, R. W., Gomez, M. G., & Wilson, D. W. (2019). Centrifuge model testing of liquefaction mitigation via microbially induced calcite precipitation. *Journal of Geotechnical and Geoenvironmental Engineering*, 145(10).
- DeJong, J. T., Mortensen, B. M., Martinez, B. C., & Nelson, D. C. (2010). Bio-mediated soil improvement. *Ecological Engineering*, 36(2), 197–210.
- DeJong, J. T., Fritzsche, M. B., & Nüsslein, K. (2006). Microbially induced cementation to control sand response to undrained shear. *Journal of Geotechnical and Geoenvironmental Engineering*, 132(11), 1381–1392.
- El Kortbawi, M., Moug, D. M., Ziotopoulou, K., DeJong, J. T., Boulanger, R. W. (under review). Application of an axisymmetric cone penetration model to bio-cemented sands. *Journal of Geotechnical and Geoenvironmental Engineering*.
- Gomez, M. G., DeJong, J. T., & Anderson, C. M. (2018). Effect of bio-cementation on geophysical and cone penetration measurements in sands. *Canadian Geotechnical Journal*, 55, 1632–1646.
- Lu, Q., Randolph, M. F., Hu, Y., & Bugarski, I. C. (2004). A numerical study of cone penetration in clay. *Géotechnique*, 54(4), 257–267.
- Lunne, T., Robertson, P. K., & Powell, J. J. M. (1997). *Cone penetration testing in geotechnical practice*.
- Moug, D. M. (2017). *Axisymmetric cone penetration model for sands and clays*. Doctoral Dissertation, University of California, Davis.
- Moug, D. M., Price, A. B., Parra Bastidas, A. M., Darby, K. M., Boulanger, R. W., & DeJong, J. T. (2019). Mechanistic development of CPT-based cyclic strength correlations for clean sand. *Journal of Geotechnical and Geoenvironmental Engineering*, 145(10).
- Nafisi, A., Mocelin, D., Montoya, B. M., & Underwood, S. (2019). Tensile strength of sands treated with microbially induced carbonate precipitation. *Canadian Geotechnical Journal*, 57, 1611–1616.
- Nafisi, A., Montoya, B. M., & Evans, T. M. (2020). Shear Strength Envelopes of Biocemented Sands with Varying Particle Size and Cementation Level. *Journal of Geotechnical and Geoenvironmental Engineering*, 146(3).
- Puppala, A. J., Acar, Y. B., & Tumay, M. T. (1995). Cone penetration in very weakly cemented sands. *Journal of Geotechnical Engineering*, 121(8), 589–600.
- Robertson, P. K. (2016). Cone penetration test (CPT)-based soil behaviour type (SBT) classification system — an update. *Canadian Geotechnical Journal*, 53, 1910–1927.
- Robertson, P. K., & Campanella, R. G. (1983). Interpretation of cone penetration tests. *Canadian Geotechnical Journal*, 20(4), 1–81.
- Roy, D. (2008). Coupled use of cone tip resistance and small strain shear modulus to assess liquefaction potential. *Journal of Geotechnical and Geoenvironmental Engineering*, 134(4), 519–530.
- Teh, C. I., & Houlsby, G. T. (1991). An analytical study of the cone penetration test in clay. *Géotechnique*, 41(1), 17–34.
- Wu, S., Li, B., & Chu, J. (2020). Stress-dilatancy behavior of MICP-treated sand. *International Journal of Geomechanics*, 21(3), 04020264. [https://doi.org/10.1061/\(asce\)gm.1943-5622.0001923](https://doi.org/10.1061/(asce)gm.1943-5622.0001923).

A data-driven approach to predict shear wave velocity from CPTu measurements

I. Entezari & J. Sharp

ConeTec Group, Burnaby, British Columbia, Canada

P.W. Mayne

Georgia Institute of Technology, Atlanta, Georgia, USA

ABSTRACT: The use of machine learning modelling to predict shear wave velocity (V_S) from piezocone penetration tests (CPTu) is presented. A large dataset of paired V_S -CPTu data ($n = 104,054$) compiled from seismic piezocone (SCPTu) soundings completed in a wide variety of soil types with various stress histories and geological environments was used to develop machine learning models to directly estimate V_S from CPTu data. The impact of soil microstructure on the results was investigated and separate models were developed to predict V_S in cemented and uncemented soils. The results of machine learning models outperformed the existing widely used CPT-based relationships to predict V_S .

1 INTRODUCTION

Shear wave velocity (V_S) is an important property of geomaterials and is widely used to evaluate the dynamic and elastic properties of soils in geotechnical design. V_S measurements provide the fundamental stiffness of the ground in terms of the small-strain shear modulus (G_o), specifically: $G_o = \rho V_S^2$, where $\rho = \gamma_t/g_a$ = soil total mass density, γ_t = soil total unit weight, and g_a = gravitational acceleration constant.

V_S measurements can be obtained using a variety of test methods. The value of V_S can be measured in the laboratory using high quality undisturbed samples and special equipment (resonant column, bender elements), which is costly and restricted to a limited number of samples. In-situ measurements of V_S are preferable to preserve site-specific conditions and minimize errors due to sampling disturbance and stress release.

In-situ measurements of V_S can be obtained through downhole and crosshole tests, seismic piezocone tests (SCPTu), spectral analysis of surface waves (SASW), and multichannel analysis of surface waves (MASW). SCPTu method is often preferred as it is a rapid and cost-effective technique to measure in-situ wave velocities in conjunction with CPTu parameters, including cone tip resistance (q_t), sleeve friction (f_s), and dynamic porewater pressure (u_2) in a single direct push sounding.

Although performing site-specific testing is the preferred method to determine shear wave velocity, several empirical relationships have been developed to estimate V_S from the basic CPTu for lower risk

projects. When actual measurements of V_S are not practical, estimates can still provide useful additional information. Existing empirical CPT relationships for V_S have been developed using statistical approaches. This paper explores the use of a data-driven approach via machine learning modelling to predict V_S from CPTu. Machine learning requires little or no priori assumptions to be considered and thus are more flexible than statistical models.

The development dataset used in this study is comprised of V_S -CPTu data pairs from ConeTec SCPTu soundings collected from 2017 to early 2021. The soundings have been completed in a wide variety of soil types with various stress histories and are from geological environments around the world. The dataset is tested with a random forest algorithm to develop a model for the prediction of V_S from CPTu data. The results of the machine learning models are compared to empirical equations proposed by Mayne (2006) and Robertson (2009). Furthermore, the impacts of soil microstructure and cementation on estimated V_S results are discussed and separate models are developed for the categories of uncemented and cemented soils.

2 BACKGROUND

2.1 Seismic Piezocone Tests (SCPTu)

The SCPTu is similar to the CPTu probe with the addition of one or more geophones or accelerometers located behind the cone tip. As shown in Figure 1, the equipment required to perform SCPTu includes the

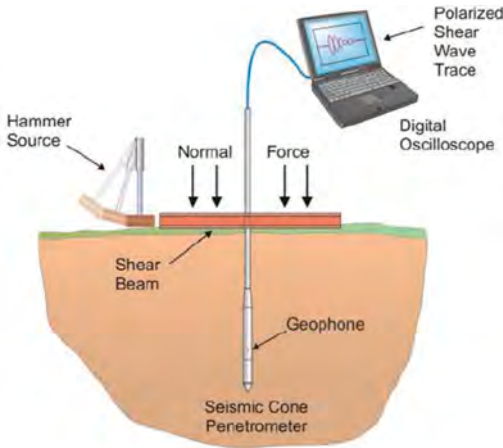


Figure 1. Schematic of seismic CPTu equipment.

seismic source on the ground surface, seismic sensors behind the cone probe, a data-acquisition system, and a data recording trigger circuit (Styler et al. 2016).

The seismic testing is conducted at selected depth intervals (typically every 1m), while the penetrometer is pushed into the ground. The shear waves are generated by striking a horizontal beam pressed firmly against the ground. Paired left-and right-strikes are used to define either the first arrival time of shear waves, or first crossover, or both. V_S is calculated using the difference in arrival times of the shear wave traces between the source and geophone at two successive depths. The SCPTu has several advantages including correlated V_S and CPTu results, the capability to do deep tests, the ability to measure compression wave velocity (V_P), and availability of soil property interpretations based on small-strain rigidity index ($I_G = G_o/q_{net}$, where q_{net} is cone net tip resistance).

2.2 Existing CPT relationships

Relationships between CPT data and V_S have been studied previously by various researchers. Hegazy & Mayne (1995) developed various expressions to estimate V_S using parameters including tip resistance (q_c), sleeve friction (f_s), vertical effective stress (σ'_{vo}), and in-situ void ratio (e) for Quaternary clays, sands, and mixed soils. Various relationships have also been proposed by Piratheepan (2002) for the estimation of V_S based on tip resistance (q_c), sleeve friction (f_s), vertical effective stress (σ'_{vo}), depth (z), and soil behaviour type index (I_c) for Holocene clays, sands, and other soils. Mayne (2006) showed a relationship where the V_S is a function of the sleeve friction (f_s) for Quaternary soils. Another correlation developed by Andrus et al. (2007) for Holocene and Pleistocene soils is based on tip resistance (q_t), depth (z), soil behaviour type index (I_c), and a time factor depending on the soil

age. Robertson (2009) also developed a generalized soil relationship where V_S is a function of net tip resistance ($q_{net} = q_t - \sigma_{vo}$), total vertical stress (σ_{vo}), atmospheric pressure (σ_{atm}), and soil behaviour type index (I_c). An overview on some of the CPT relationships to predict V_S has been provided in Wair et al. (2012).

In this study, the estimated V_S results from the machine learning models are compared to the results obtained by the empirical expressions proposed by Mayne (2006) and Robertson (2009), shown in Equations 1 and 2, respectively:

$$V_s = 118.8 \log(f_s) + 18.5 \quad (1)$$

$$V_s = [(10^{0.55I_c + 1.68})(q_t - \sigma_{vo})/\sigma_{atm}]^{0.5} \quad (2)$$

where V_S is in m/s in both equations, f_s is in kPa in Eq. 1, and σ_{atm} is in same units as q_t and σ_{vo} in Eq. 2.

2.3 Impact of soil microstructure

The existing empirical correlations developed for interpretation of CPT results have been generally developed using silica-based uncemented soils with little or no microstructure (Robertson 2016). Therefore, caution should be exercised when CPT based relationships are used in soils with microstructure. According to Robertson (2016), the empirical parameter, K_G^* , can be used to determine whether soils are cemented or not. K_G^* is calculated as $(G_o/q_{net})(Q_{tn})^{0.75}$ (Robertson 2016), where Q_{tn} is the normalized tip resistance. Soils with K_G^* of less than 330 are likely young and uncemented with little or no microstructure, while soils with K_G^* of greater than 330 can be classified as cemented and microstructured soils.

The cemented versus uncemented soils are considered in this study for the evaluation of the performance of the machine learning model. Furthermore, individual models are developed specifically for uncemented and cemented soils.

3 DESCRIPTION OF DATASET

To investigate the potential of a data-driven approach to estimate V_S from CPTu data, a dataset of paired V_S -CPTu data was compiled using ConeTec's geospatial database. The database was queried to find the relevant information that resulted in 14,855 SCPTu tests worldwide with more than 248,500 V_S -CPTu data pairs. For this study, soundings collected after 2016 were selected in order to only utilize modern tests with increased quality control. Procedural changes in ConeTec's SCPTu methodology yielded slightly higher accuracy in V_S measurements due to signal enhancement and signal

stacking after this date (Styler & Weemeees 2016). Consequently, the dataset was reduced to 104,809 V_S -CPTu data pairs from 7171 independent SCPTu soundings worldwide. Most of the soundings are from North America, with additional contributions from various sites in South America, Australia, Europe, and Asia. To pair the CPTu parameters with V_S measurements at a given depth, the median of CPTu parameters over a window size equal to the V_S depth interval was calculated. Only depth intervals equal to or less than 1 m were considered to minimize variations due to potential soil heterogeneity. The CPTu parameters paired with V_S included corrected tip resistance (q_t), sleeve friction (f_s), porewater pressure (u_2) and depth (z) at each V_S measurement. Additional parameters including normalized tip resistance (Q_{tn}), normalized friction ratio (F_r), normalized porewater pressure (B_q), net tip resistance (q_{net}), total stress (σ_{vo}), and effective stress (σ'_{vo}) as well as small-strain shear modulus (G_o), small-strain rigidity index (I_G), and K_G^* were also calculated.

Calculation of a number of these parameters required the soil unit weight (γ). The machine learning model based on corrected tip resistance (q_t), sleeve friction (f_s), porewater pressure (u_2) and depth (z) developed by Entezari et al. (2021) was used to estimate unit weight at each depth. The measured equilibrium pore pressure profile of each SCPTu sounding, combined with the estimated unit weight profile, was used to determine in-situ vertical stresses.

Data points with net tip resistance (q_{net}) of less than 100 kPa were screened out to remove fluid-like tailings from the dataset. Also, data points with sleeve friction (f_s) of less than 1 kPa were screened out in order to remove data where the soil-sleeve friction was less than internal o-ring friction. The final dataset used included 104,054 V_S -CPTu data pairs. Table 1 lists the summary statistics of the paired dataset.

Table 1. Summary statistics of the V_S -CPTu dataset.

	Min	Max	Mean
V_S (m/s)	9	1000	251
q_t (MPa)	0.1	94.1	8.4
f_s (kPa)	1.0	1577	117.6
u_2 (kPa)	-87.2	5489	245.0
z (m)	0.3	129.6	17.3
σ'_{vo} (kPa)	0.1	2185	215.4

Total number of data pairs = 104,054.

3.1 Soils with microstructure

The plot of normalized tip resistance (Q_{tn}) versus small-strain rigidity index (I_G) for the dataset is shown in Figure 2. Accordingly, 63,740 data points

fall in the young and uncemented soils category (soils with little or no microstructure), where K_G^* is less than 330 (green points in Figure 2). Another 40,314 data points fall in the cemented soils category (soils with microstructure), where K_G^* is greater than 330 (blue points in Figure 2).

3.2 Training and test datasets

The dataset was split into training and test sets. The training set was used to calibrate the model whereas the test set was used to evaluate the model performance. The data collected from 2017 to 2019 was used as the training set and data collected in 2020 and early 2021 provided the test set. This allows for an unbiased performance evaluation of the model (a blind test) where the potential errors due to variation in stress histories and geological environments are taken into account. The number of paired V_S -CPTu data points for the training and test sets are listed in Table 2.

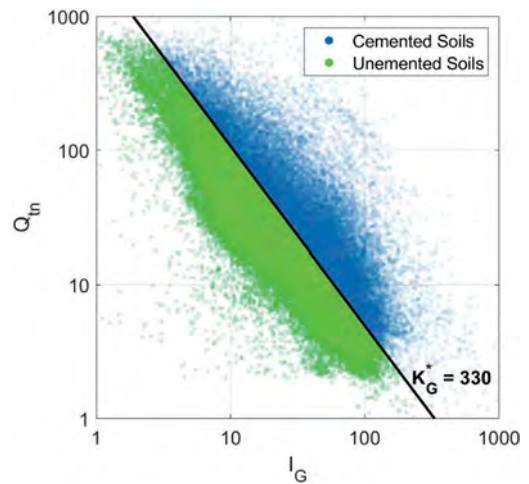


Figure 2. The dataset plotted in the Q_{tn} - I_G chart.

Table 2. Number of data pairs in the training and test sets.

	All	Uncemented	Cemented
Training set	73,010	45,386	27,624
Test set	31,044	18,354	12,690

4 MACHINE LEARNING MODELLING

Machine learning models acquire information from prior data, allowing the computers to discover predictive rules applicable for future data. Machine learning models are generally data-hungry and need large

datasets for training. In general, as more data become available, the more accurate and robust the predictions become. Machine learning is widely used in numerous disciplines and has gained interest in geotechnical engineering. Example applications of machine learning for CPT interpretations can be found in Erzin & Ecemis (2016), Reale et al. (2018), Wang et al. (2019), Erharter et al. (2021), Rauter & Tschuchnigg (2021), and Entezari et al. (2020, 2021).

In this study, the random forest algorithm (Breiman 2001) was employed to calibrate CPTu data to V_S measurements. It is one of the most widely used machine learning algorithms for classification and regression tasks. Random forest is an ensemble of several decision trees and thus overcomes the shortcomings of traditional decision trees, predominantly overfitting. The models here were trained using four input parameters including corrected tip resistance (q_t), dynamic porewater pressure (u_2), sleeve friction (f_s), and depth (z).

4.1 Performance evaluation

The performance of the random forest models is evaluated using the properties of the cumulative distribution function (CDF) of errors on the test set. The error is calculated as the discrepancy between the measured V_S from SCPTu and predicted V_S from the random forest models. The 50th percentile in the CDF is taken as the bias of the prediction. Assuming the errors follow a normal distribution, the CDF values at 15.9% and 84.1% correspond to ± 1 standard deviation. The average of the two CDF values at 15.9% and 84.1% is considered as the overall error of the model.

To compare the performance of the machine learning models to existing CPTu expressions, similar performance evaluation is performed on the test set using the predicted V_S obtained from the equations proposed by Mayne (2006) and Robertson (2009).

5 RESULTS

5.1 All-soils model

An all-soil model was developed using the random forest model trained with all data points in the training set. The relationship between measured V_S from SCPTu and the estimated V_S from the random forest model is shown in Figure 3. This relationship is shown for the test set. The R^2 of the model on the test set was observed to be 0.58. The error analysis using CDF of errors showed that the bias and error of the estimated results are -8.5 and 49.5 m/s, respectively. The bias -8.5 m/s means that random forest model overestimates the measured V_S by 8.5 m/s overall. The error of 49.47 m/s means that 68.2% of the estimated V_S values fall within ± 49.5 m/s of the measured V_S from SCPTu testing.

The performance of the model was also assessed on uncemented and cemented soils. When only uncemented soils were considered in the test set, the bias and error of the estimated V_S results are -23.4 and ± 34.8 m/s, respectively. For cemented soils, the bias and error of the estimated V_S were observed to be 27.2 and ± 62.8 m/s, respectively.

5.2 Uncemented and cemented soils models

Using the uncemented and cemented soil categories in the training set, two separate models were developed for the estimation of V_S in these types of soils. Figure 4 shows the relationship between the SCPTu measured and random forest predicted V_S for the fraction of the test set in uncemented soils. As can be seen, the correlation between estimated and measured V_S significantly improved compared to the all-soils model shown in Figure 3 (R^2 of 0.79 compared to 0.58). The bias and error of the estimated results were observed to be 0.6 and 28.2 m/s, respectively.

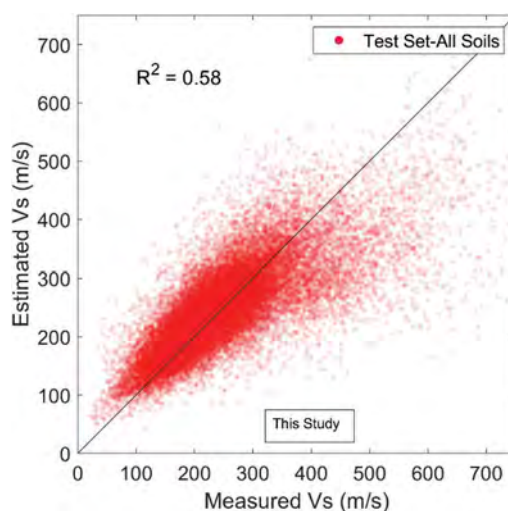


Figure 3. Relationship between measured and random forest estimated V_S on the test set using all soils.

Evidently, the random forest model is far better able to model the relationship between V_S and CPTu parameters in uncemented soils, compared to the all-soil scenario.

The results of the random forest model developed for cemented soils are also shown in Figure 4. The bias and error were observed to be -12.3 and 54.1 m/s, respectively. Compared to the all-soil model, this model performs better on cemented soils, but the bias and error are still high. This is presumably because microstructure can have a variety of impacts on CPTu parameters. Thus, the learnt relationship between V_S and CPTu parameters in

cemented soils of the training set may not be applicable on the cemented soils of the test set.

5.3 Existing relationships

Figure 5 shows the relationships between the estimated V_S calculated using the methods of Mayne (2006) and Robertson (2009) with the measured V_S using SCPTu on the test set. For the Mayne (2006) model, the bias and error were observed to be 12 and 68.6 m/s, respectively, when error assessment was done on all soils. When only uncemented soils were considered, the bias and error were dropped to -7.2 and

52.5 m/s, respectively. The bias and error were calculated to be 51.1 and 82.8 m/s, respectively, on cemented soils.

In case of Robertson (2009) model, the bias and error were 21.5 and 64.3 m/s, respectively, on all soils in the test set. The bias and error were observed to be -6.1 and 50.3 m/s, respectively, for uncemented soils, compared to 69.2 and 57.8 m/s for cemented soils. Overall, it can be seen that these expressions perform better on uncemented soils, as expected. A summary of model performances is presented in Table 3. It should be noted that no limits were applied to the two existing methods because the intent was to compare the results to those obtained from the random forest models developed using a wide range of soil types. Limiting the range of applicable data to be used in the existing methods would be prudent and may result in a better average correlation and error.

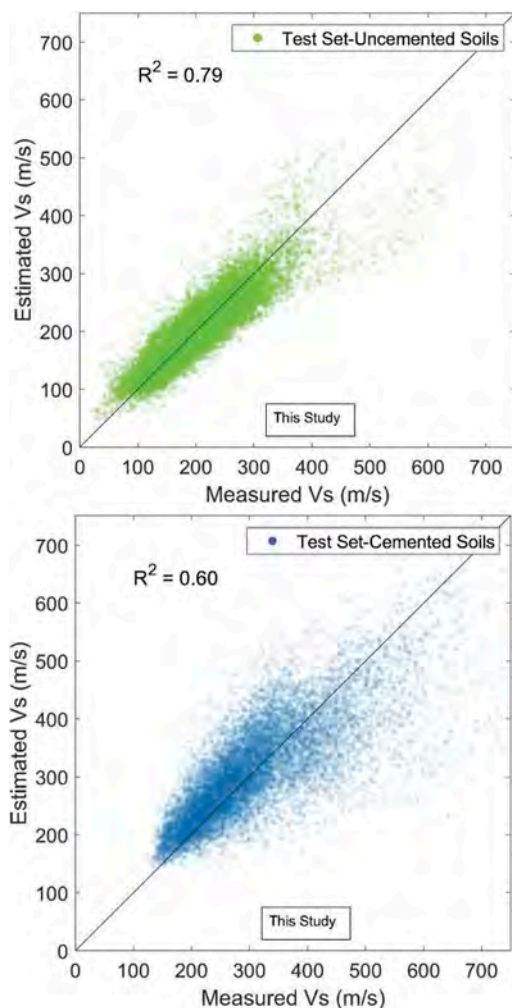


Figure 4. Relationships between measured and random forest estimated V_S of the uncemented (top) and cemented soils (bottom) in the test set when separate models were trained using uncemented and cemented soils in the training set.

Table 3. Performance of different models.

Model	Bias±Error (m/s)		
	All Soils	Uncemented	Cemented
RF-All Soils	-8.5±49.5	-23.4±34.8	27.2±62.8
RF-Uncemented	NA	0.6±28.2	NA
RF-Cemented	NA	NA	-12.3±54.1
Mayne (2006)	12.0 ±68.6	-7.2±52.5	51.1±82.8
Robertson (2009)	21.5 ±64.3	-6.1±50.3	69.2±57.8

5.4 Example SCPTu V_S profile

An example SCPTu profile of V_S estimated using the random forest models developed in this study is shown in Figure 6. The estimated V_S values from the expressions of Mayne (2006) and Robertson (2009), as well as the measured V_S profile, are displayed along with the results of this study. The SCPTu sounding is from 2020 and is thus part of the test set. As evident, both all-soils and uncemented models are in agreement with the measured V_S . The uncemented model, however, shows less fluctuations and a better performance compared to the all-soils model. Both of these models appear to outperform the Mayne (2006) and Robertson (2009) models. The analysis of K_G^* revealed that the soils are uncemented for the whole profile except for depth ranges between 3.5-9 m and 15-17.5 m.

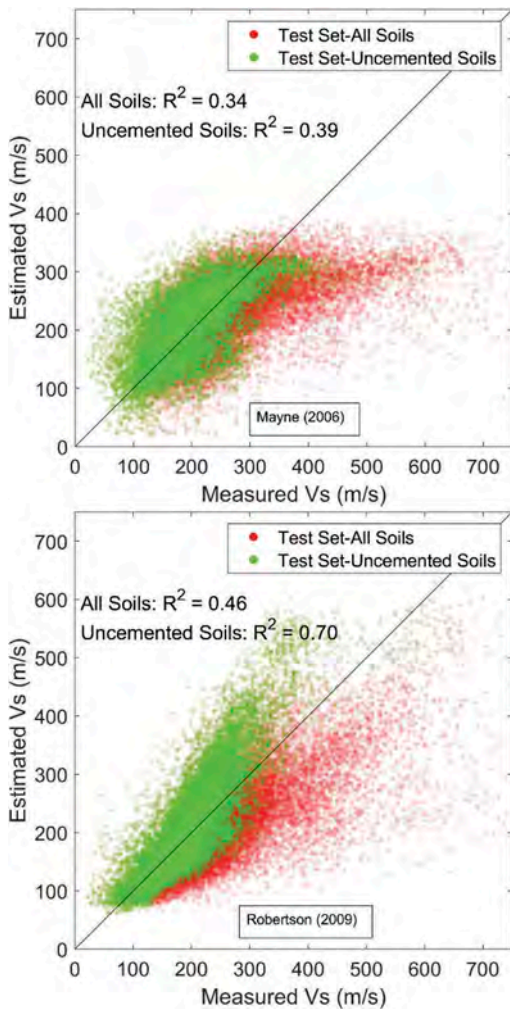


Figure 5. Relationships between measured vs. estimated V_S using Mayne (2006) (top) and Robertson (2009) (bottom) methods.

6 DISCUSSION

In practice, a priori information on the soil micro-structure is required in order to be able to employ soil-specific models developed in this study to estimate V_S (uncemented and cemented soils models). Determining the soils categories based on K_G^* is not practical without knowing V_S . Therefore, information on soil categories should be available from other sources such as previous SCPTu testing in the region under investigation or information on the geology of soils.

When such information is not available, the results of this study showed that the developed all-soils model performs better than the Mayne (2006) and Robertson (2009) models when CPTu is pushed in regions with both cemented and uncemented soils.

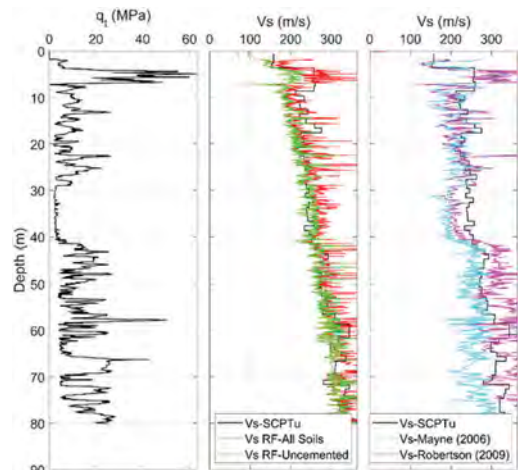


Figure 6. Example profile of V_S estimated from models developed in this study and existing relationships.

When a priori information on soil categories is available, the soil-specific models developed in this study could lead to better results than the all-soils model and the equations proposed by Mayne (2006) and Robertson (2009).

In future work, the dataset compiled in this study will be used to investigate the potential of machine learning algorithms to classify and identify cemented and uncemented soils from CPTu parameters. However, K_G^* of 330 as a threshold to distinguish cemented from uncemented soils has been determined empirically and may not be an absolute metric.

In addition to the models developed and presented in this paper, random forest models were trained by adding normalized tip resistance (Q_n), normalized friction ratio (F_r), normalized porewater pressure (B_q), and effective stress (σ'_{vo}) to the input variables, but no significant improvements were observed.

7 CONCLUSIONS

Machine learning models using a random forest algorithm were developed to directly predict V_S from CPTu data. A dataset of paired V_S -CPTu data compiled from 7171 SCPTu soundings completed at various sites with a wide variety of soil types, stress histories, and geological environments was used to develop machine learning models. Results showed that the all-soils model developed using random forest algorithm can estimate V_S with ± 49.5 m/s error. The model developed for uncemented soils showed a significant improvement and could predict V_S with ± 28.2 m/s error. The model developed for cemented soils achieved an accuracy of ± 54.1 m/s. All the developed machine learning models outperformed the studied existing relationships from literature. Although actual measurement of V_S is always

preferable, it appears to be more crucial when dealing with soils that have microstructure. The models developed are from a very large dataset compiled from SCPTu soundings from various geological regions and are therefore considered to be robust, however engineering judgement should always be exercised when using any empirical statistics or models.

REFERENCES

- Andrus, R.D., Mohanan, N.P., Piratheepan, P., Ellis, B.S., and Holzer, T.L. 2007. Predicting shear wave velocity from cone penetration resistance, *Proc. 4th Intl. Conf. on Earthquake Geotech. Engrg.*, Thessaloniki, Greece.
- Breiman, L. 2001. Random forests. *Machine Learning*, 45(1): 5–32.
- Entezari, I., McGowan, D., and Sharp, J. 2020. Tailings characterization using cone penetration testing and machine learning, *Proc. Tailings & Mine Wastes 2020*, University of British Columbia, Vancouver, 695–704.
- Entezari, I., Sharp, J., and Mayne, P.W. 2021. Soil unit weight estimation using the cone penetration test and machine learning, *Proc. GeoNiagara 2021*, Niagara Falls, Canada.
- Erharter, G.H., Oberhollenzer, S., Fankhauser, A., Marte, R., and Marcher, T. 2021. Learning decision boundaries for cone penetration test classification, *Computer-Aided. Civil & Infrastructure Eng.* 1: 1–15.
- Erzin, Y. & Ecemis, N. 2016. The use of neural networks for the prediction of cone penetration resistance of silty sands. *Neural Comput. Appl.* 28: 727–736.
- Hegazy, Y.A. & Mayne P.W. 1995. Statistical correlations between VS and cone penetration data for different soil types. *Proc. CPT '95*, Linkoping, Sweden, Vol. 2: 173–178.
- Mayne, P.W. 2006. In-situ test calibrations for evaluating soil parameters. *Proc. Characterization and Engineering Properties of Natural Soils II*, Singapore, Vol. 3: 1601–1652.
- Piratheepan, P. 2002. Estimating shear wave velocity from SPT and CPT data. *MSc Thesis*, Clemson University.
- Rauter, S. & Tschuchnigg, F. 2021. CPT data interpretation employing different machine learning techniques. *Geosci. J.* 11(7), 265.
- Reale, C., Gavin, K., Librić, L., Jurić-Kačunić, D. 2018. Automatic classification of fine-grained soils using CPT measurements and Artificial Neural Networks. *Adv. Eng. Inform.* 36: 207–215.
- Robertson, P.K. 2009. Interpretation of cone penetration tests – a unified approach, *Can. Geotech. J.* 46 (11):1337–1355.
- Robertson, P.K. 2016. Cone penetration test (CPT)-based soil behaviour type (SBT) classification system-an update. *Can. Geotech. J.* 53: 1910–1927.
- Styler, M.A. & Weemees, I. 2016. Quantifying and reducing uncertainty in down-hole shear wave velocities using signal stacking. *Proc. ISC'5, Gold Coast, Australia.*
- Styler M.A., Weemees, I., Mayne, P.W. 2016. Experience and observations from 35 years of seismic cone penetration testing (SCPTu), *Proc. GeoVancouver 2016*: www.cgs.ca
- Wair, B.R., DeJong, J.T., and Shantz, T. 2012. *Guidelines for Estimation of Shear Wave Velocity*. PEER Rept. 2012/08, Pacific Earthquake Engineering Research Center, Berkeley, CA: 95 p.
- Wang, H., Wang, X., Wellmann, J.F., Liang, R.Y. 2019. A Bayesian unsupervised learning approach for identifying soil stratification using cone penetration data. *Can. Geotech. J.* 56: 1184–1205.

Interpretation and comparison of CPT derived soil properties to static and cyclic laboratory tests on unique fine-grained soils in Western Washington and Oregon

B. Exley, A. Pynch, J. Jacoby & B. Thunder
Haley & Aldrich, Inc., USA

ABSTRACT: CPT interpretation methods are evaluated against laboratory and in-situ methods to identify and evaluate the soil properties of multiple non-textbook soil deposits located in Western Washington and Oregon. These deposits include unique glacially overridden soils which are widespread in the Puget Sound region, as well as younger soils which vary widely in depositional history and stress history.

The glacially overridden deposits can be very thick and are heavily overconsolidated, often showing signs of fissures and slickensides when they are fine-grained, with SPT blowcounts frequently much larger than $N=100$ in coarse grained deposits. Based on the CPTs included in this paper, the fine-grained overconsolidated materials are typically identified by the CPT as sand-like and dilative, and generally have I_c values between 2.0 and 2.6 despite frequently having index properties which classify the soils as stiff to hard high plasticity clay. This paper documents the characteristics of these soils to facilitate identification of them by the CPT.

Additionally, the correlated strength, preconsolidation pressures, and cyclic resistance of the younger fine-grained soils are evaluated against laboratory testing methods. This includes documenting a site in Beaverton, Oregon with several CPTs paired with constant rate of strain consolidation laboratory tests and both monotonic and cyclic direct simple shear tests in the fine-grained Missoula Flood Deposits as part of a study on the susceptibility of the silt to liquefaction or cyclic softening.

1 INTRODUCTION

Western Washington and Oregon each consist of soil conditions which generally do not fall under the classical soils. The Puget Sound Lowlands in Western Washington generally are a deep basin that has been glacially overridden several times, with the most recent occurring approximately 15,000 years ago during the Vashon Stade of the Fraser glaciation (Booth & Goldstein, 1994). The glacially overridden soils were subjected to approximately 5,000 feet of ice (Easterbrook 1969), resulting in very dense and very hard soil deposits that engineers generally do not attempt to push CPTs in.

Holocene age deposits tend to be interlayered due to depositional environment and frequently consist of relatively silty sands or low plasticity silts. These characteristics generally make them difficult to collect and test using high quality undisturbed samples. When silt-rich, these soils do not behave like classical sand-like or clay-like materials.

2 GLACIALLY OVERRIDDEN SOILS

2.1 *Fine-grained material*

The glacially overconsolidated fine-grained soils in the Puget Sound Lowlands are known to widely vary in strength due to the presence of blocky texture and slickensides in zones. However, when intact, they exhibit significant strength and stiffness. Unfortunately, the soils are also brittle and easily sheared due to the rotary action of a pitcher barrel when undisturbed sampling is attempted. Accordingly, being able to reliably estimate the soil properties using the CPT presents significant value where the soils are intact. However, initial Soil Behavior Type screening tools generally describe the soils as having a more coarse-grained behavior than would be measured by traditional index testing.

This trend has been observed on multiple sites, with observed tip resistances in the fine-grained material often about 100 tsf or more with SBT index values of approximately 2 to 2.2. Documented on

Figure 1 are three CPT sounding results from a site which was located along Interstate 405 south of Bellevue, Washington (Site 1). Three CPTs were pushed into a likely glacially overconsolidated fine-grained material. However, the materials had lower q_t values than previously mentioned, ranging from about 50 to 75 tsf. The I_c index was generally about 2.2.

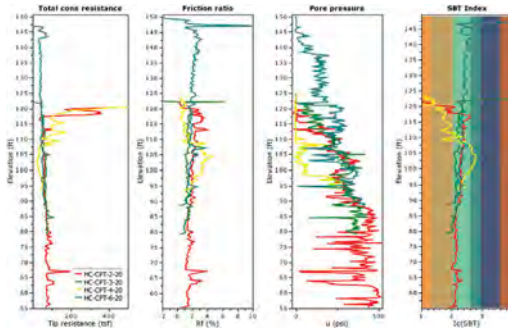


Figure 1. Site 1 basic CPT results.

The CPTs were advanced near existing borings which had index testing completed on the samples that identified the fine-grained soil as a high-plasticity clay (CH). A qualitative screening of the sounding shows large positive excess pore pressure values with B_q values generally between 0.3 and 0.5. Evaluating the soil type using a technique which considers pore pressure response (Schneider 2008), the CPT correctly identifies the material as a clay. An example of this interpretation is shown on Figure 2 for HC-CPT-2-20.

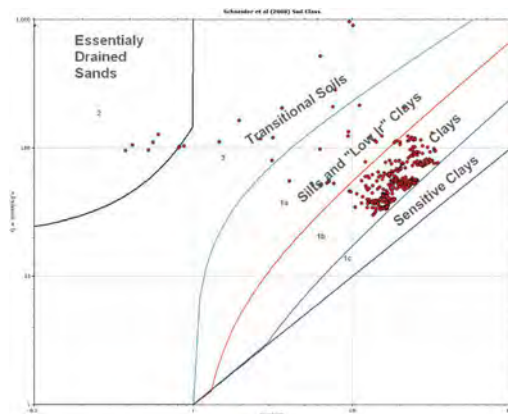


Figure 2. Example schneider plot interpretation of HC-CPT-2-20.

Correctly identifying the material as a clay facilitates the use of appropriate methods to estimate

design properties. The use of the modified Norwegian Institute of Technology (NTH) method (Ouyang & Mayne 2019) results in an interpreted friction angle of approximately 35 degrees, which is consistent with the results of consolidated undrained triaxial tests on undisturbed samples of similar clays in the region. This friction angle can then be used to refine the estimated preconsolidation pressure, resulting in a refined estimate as documented in Mayne and Miller (2021).

3 SUSCEPTIBILITY TO LIQUEFACTION OR CYCLIC SOFTENING OF RECENTLY DEPOSITED FINE-GRAINED SOILS

As previously noted, the Holocene aged fine-grained soils in the Pacific Northwest are commonly silt-rich with relatively low plasticity, and are characterized as “transitional” soils when using the SBT Index. This causes significant difficulties for consultants in identifying whether the material has a “sand-like” or “clay-like” behavior when subjected to cyclic loading. These soils do not consistently identify with an $I_c > 2.6$, further confounding identification of them through traditional filtering methodology when assessing sand-like behavior. An in-depth study of these soils in the Pacific Northwest has been completed and is documented by the Oregon Department of Transportation (Dickenson et. al 2021). The study includes a publicly accessible database that is being continually updated with new data. Currently, the database includes over 300 cyclic tests targeted at evaluating the response of these silty materials to cyclic loading. In general, their findings show that the materials do not exhibit the significant degradation of shear stiffness and strengths that sands do as the porewater pressure increases. Gingery (2014) showed that, for sands with relative densities of less than 40%, sands tend to exhibit post-liquefaction accumulation of shear strains per cycle of approximately 2% per cycle. Conversely, while silts do accumulate shear strains during cyclic loading, the accumulated shear strain per cycle is typically much smaller. For example, a sample of the Columbia River Silt with a PI = 1 and an OCR = 1 accumulates approximately 0.7% shear strain per cycle for single amplitude shear strains larger than 3% (Dickenson et. al 2021). Further, unlike sands, these soils do not tend to show the large loss of strength following cyclic loading which imposes large pore pressure ratios (R_u) or single amplitude shear strains larger than 3%. Accordingly, the term “liquefaction” is misleading when used to describe response to cyclic loading of these soils. Documented herein is a case study of Willamette Silt encountered in Beaverton, Oregon (Site 2) with evaluation of the cyclic resistance of those soils relative to traditional liquefaction triggering methods.

Site 2 is a well-documented site that has had 19 CPTs advanced through the soil profile, as well as 21 traditional SPT borings and 24 test pits. In support of a recent seismic assessment of the site, several CPTs and borings were advanced (included in the totals above), the latter of which included undisturbed

samples used for advanced laboratory testing. The samples were collected and extruded using methods generally consistent with those recommended by Ladd & DeGroot (2003), including cutting and delaminating the soil from the tube to minimize sample disturbance during preparation of the sample for testing. In addition to index testing, constant rate of strain (CRS) consolidation testing, static direct simple shear testing (DSS), and cyclic direct simple shear testing (CDSS) was completed. The DSS and CDSS tests were completed using a SHANSEP type testing methodology to explicitly evaluate the effects of overconsolidation on the samples and attempt to overcome some of the impacts of sample disturbance that may have occurred during testing.

Fill materials, if encountered, ranged between approximately 2 and 15 feet thick and generally consisted of either reworked native silty/clayey soils or imported gravels. More significant thicknesses of fill were encountered on the south end of Site 2 in proximity to Cedar Mill Creek. Materials interpreted as native alluvium generally consisted of very soft clays underlying thicker fills in proximity to Cedar Mill Creek. The generally silty Missoula Flood deposits were encountered in all of the explorations near the surface or at depths of up to approximately 35 feet below ground surface (bgs) underlying fill and alluvium. All of Haley & Aldrich's explorations encountered high- to low-plasticity clay interpreted to be the Hillsboro Formation underlying the Missoula Flood deposits at approximately 22 to 75 feet bgs. All the explorations terminated in materials interpreted as the Hillsboro Formation down to approximately 101.5 feet, the maximum depth explored. While the layering is generally consistent across the site, there is significant intra-deposit variation across the site. Therefore, the assessment of an individual CPT is presented to simplify the case study. However, the results were broadly applicable across the site.

The basic results of CPT-6 are presented on Figure 3. The I_c index in the fine-grained soils is on average about 2.5. Interestingly, the index appears to be insensitive to index properties of the soils, however the pore pressure ratio was more responsive to transitions between silt and clay.

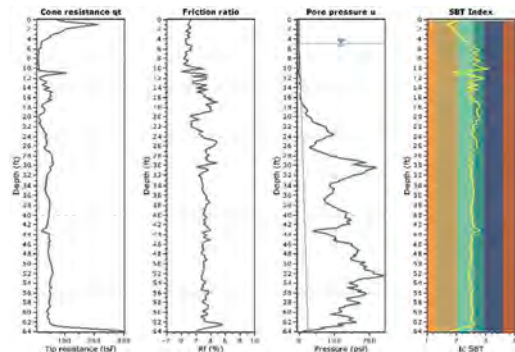


Figure 3. Site 2 basic CPT results for WHQ CPT-6.

For a preliminary evaluation of the susceptibility to liquefaction of the fine-grained soils encountered at the project site, we used Bray & Sancio (2006) criteria based on soil index tests. According to the findings in Bray & Sancio (2006), the amount and type of clay minerals in the soil best indicate liquefaction susceptibility, which can be quantified by PI and the ratio of water content and liquid limit (w_c/LL). Based on the available soil index tests for the project site, 9 out of 22 samples (41%) tested in the depth range of 5 to 55 feet bgs are considered to be susceptible or moderately susceptible to liquefaction by the Bray & Sancio (2006) criteria.

The use of a typical I_c cut-off for the transition between sand-like and clay-like behavior of 2.6 would result in analyzing most of the profile as a sand, calculating a magnitude 7.5 normalized cyclic resistance ratio ($CRR_{7.5}$) of approximately 0.15. However, as noted, Dickenson et. al and others have observed that these materials behave in a manner more similar to clays. An assessment of the profile using a methodology similar to that presented by Idriss & Boulanger (2006) results in an improved assessment of the soil's response to cyclic loading.

3.1 Overconsolidation ratio profiling

The use of the generalized expression for stress history (Agaiby & Mayne 2019) with dependency on I_c did not adequately reflect the laboratory test results. This is due to the insensitivity of the I_c index to changes in soil type in these soils. Agaiby & Mayne presented alternative relationships to estimate the exponent m' on D_{50} and fines content. However, these generally did not provide consistent differentiation between the silts and clays, and a relationship associated with B_q was observed. As such, a modified m' exponent was developed as a function of the pore pressure ratio. The preconsolidation pressure was estimated according to Equations 1 and 2, which are modifications of the methods presented by Agaiby & Mayne (2018):

$$\sigma'_p = 0.33(q_{net})^{m'} \left(\frac{\sigma_{atm}}{100} \right)^{1-m'} \quad (1)$$

$$m' = 1 - \frac{0.28}{1 + (B_q/0.05)^{25}} \quad (2)$$

The resulting overconsolidation ratios calculated for CPT-6 are presented on Figure 4, with nearby CRS results from nearby borings. There was a general trend on the site that the clays had significantly larger OCR's than the silts and sands, which is reflected in the reduction of OCR with the drop in B_q that reasonably fits the trends observed in the lab tests. Some differences in elevation of the transitions between silts and clays is expected between the borings and the CPT. This likely explains the depth offset between the CPT predicted OCR for B7-S6 and B9-S12. This trend was observed in other CPTs as well.

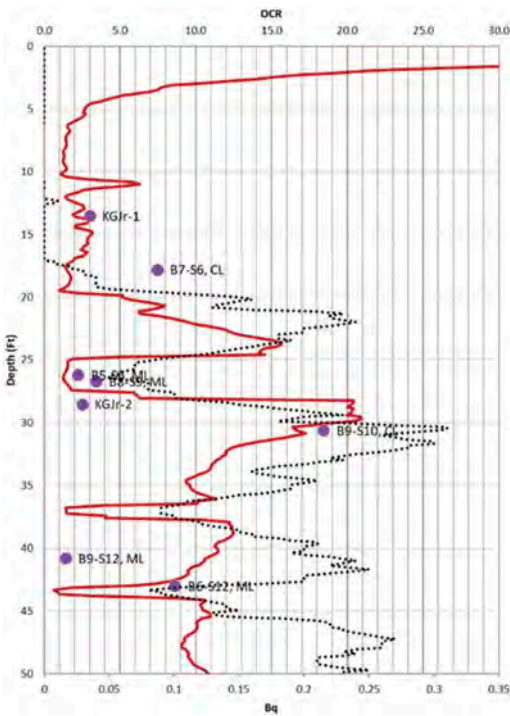


Figure 4. OCR profile for WHQ CPT-6.

3.2 Shear strength profiling

The undrained shear strength of the materials can be calculated using critical state soil mechanics for the appropriate stress path (Mayne 2005). The effective stress friction angle can be calculated by the modified NTH method (Ouyang & Mayne 2018). Equation 3 can be used to calculate the undrained shear strength for the direct simple shear (DSS) stress path. When calculating the undrained shear strength, it was found that using a $\Lambda=0.7$ works well for these silty soils.

$$\left(\frac{S_u}{\sigma_{vo}}\right)_{DSS} \approx 0.5 \sin \Phi' OCR^{\Lambda} \quad (3)$$

The laboratory test results from DSS testing for depths between 10 and 30 feet deep are presented on Figure 5. Figure 6 provides a comparison of the CPT derived properties with the laboratory-based model fit.

3.3 Cyclic resistance profiling

Dickenson et. al (2021) presents the cyclic resistance ratio (CRR) of silts in the Pacific Northwest according to Equation 4, where N is the number of cycles:

$$\frac{CSR}{OCR^{0.8}} = a \times N^{-b} \quad (4)$$

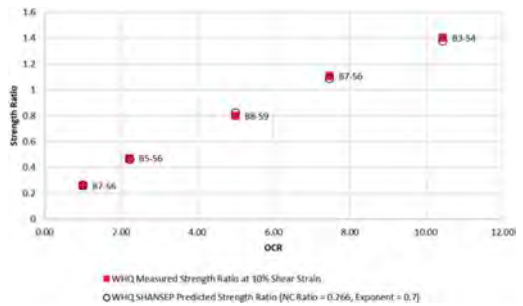


Figure 5. DSS undrained shear strength ratios.

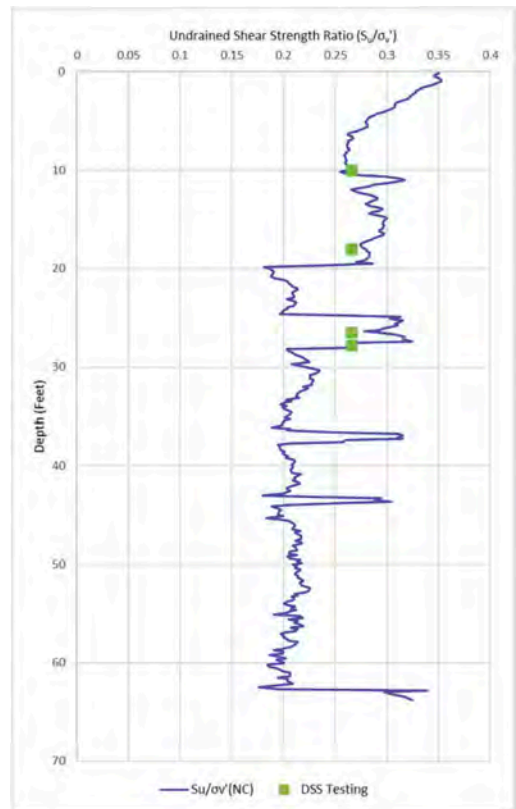


Figure 6. CPT-6 calculated normally consolidated shear strength ratios compared to lab test model fit.

The “a” coefficient can be described as a function of the normally consolidated undrained shear strength ratio. Using model parameters of $a = 0.8 * S_u / \sigma_v' = 0.213$ and $b = 0.15$ results in a reasonable fit for the soils as tested for a single amplitude shear strain of 3%, as shown on Figure 7. The model fit may be increased by approximately 0.05 for larger shear strain amplitudes up to approximately 7%. The model fit results in a CRR at 30 cycles equivalent to 50% of the undrained shear strength, which can be used in

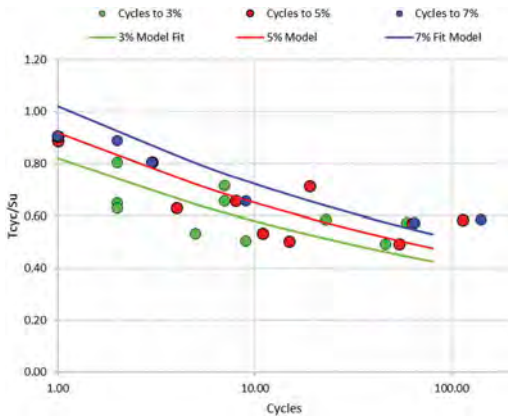


Figure 7. Cyclic shear strain accumulation as a function of undrained shear strength and number of cycles.

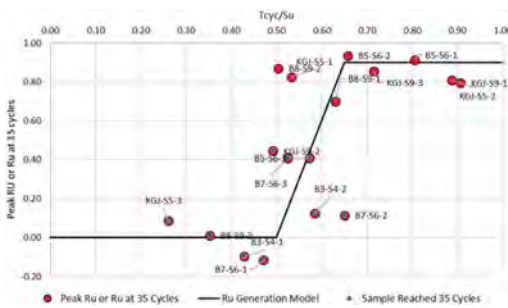


Figure 8. Peak R_u generation normalized to shear strength and cyclic loading.

combination with the values presented in Figure 6 to develop a $CRR_{7.5}$ profile. This fit is less than the $CRR = 0.8 * S_u$ recommended by Idriss and Boulanger (2006) for clays, but results in a significantly larger CRR than the sand-like behavior presented previously for soils that are overconsolidated. This reduction may be due to the use of SHANSEP-like testing methodology to directly control the sample OCR, resulting in a loss of the in-situ soil stiffness.

The “a” coefficient is generally less than the coefficients presented by Dickenson et. al for other soils in the Pacific Northwest. This is consistent with observations that under cyclic loading these soils tend to generate more excess pore pressures than most of the silts in the Pacific Northwest database, with max R_u values of approximately 0.9, as shown on Figure 8, suggesting the silts on Site 2 are more sand-like than many other silts in the region.

When the CRR is exceeded, resulting in an R_u greater than 0.8, the post cyclic shear strength was approximately 50% of the undrained shear strength.

4 CONCLUSIONS

When evaluating the behavior of glacially overconsolidated soils in Western Washington, it has been shown that penetration of the CPT through the overconsolidated fine-grained soils of the Puget Sound Lowlands can be readily accomplished. When evaluating those soils, practitioners should consider the use of Schneider plots to facilitate identification of fine-grained soils that may otherwise not be identified by SBT.

Additionally, the assessment of cyclic resistance ratios of transitional soils in the Pacific Northwest is documented. The soils generally have an I_c less than 2.6, resulting in most practitioners using sand-like liquefaction assessment methods. This significantly underestimates the soils cyclic resistance ratio. Classic liquefaction behavior was not observed in any of the cyclic laboratory tests in soils associated with an I_c index as low as 2.2. I_c values generally ranged from 2.3 to 2.6 for depths in the soils tested with plasticity index values as low as 5.

A methodology was presented to assess the cyclic resistance to cyclic softening of the transitional soils that is consistent with other soils in the Pacific Northwest that can be used in combination with existing stress history and shear strength profiling techniques. Further refinement to OCR profiling methods in soils other than clay would be beneficial. An example of such refinement would be the development of a unified approach which provides a theoretical framework for both drained and undrained materials, which also addresses the impact of site-specific shear strength parameters in a consistent manner.

REFERENCES

- Agaiby, S.S. & Mayne, P.W. 2019. CPT evaluation of yield stress profiles in soils. *Journal of Geotechnical and Geoenvironmental Engineering* 145(12).
- Booth, D.B. & Goldstein, B. 1994. Patterns and processes of landscape development by the Puget lobe ice sheet. *Washington Division of Geology and Earth Resources* 80: 207–218.
- Bray, J.D. & R.B. Sancio 2006. Assessment of the liquefaction susceptibility of fine-grained soils. *Journal of Geotechnical and Geoenvironmental Engineering*, 132(9), pp.1165–1177.
- Dickenson, S.E., Khosravifar, A., Beaty, M., Bock, J., Moug, D., Schlechter, S., & Six, J. 2021. Cyclic and post-cyclic behavior of silt-rich, transitional soils of the Pacific Northwest; a database for geo-professionals in practice and research. Salem, OR: Oregon Department of Transportation.
- Easterbrook, D.J. 1969. Pleistocene chronology of the Puget Lowland and San Juan Islands, *Washington. Geological Society of American Bulletin* 80: 2273–2286.

- Gingery, J.R. 2014. Effects of liquefaction on earthquake ground motions. Doctoral Dissertation, UC San Diego.
- Idriss, I. M. & Boulanger, R. W. (2008). Soil liquefaction during earthquakes. *Monograph MNO-12*, Earthquake Engineering Research Institute: Oakland, CA
- Ladd, C.C & DeGroot D.J. 2003. Recommended practice for soft ground site characterization: Arthur Casagrande Lecture. *Proc. of the 12th Panamerican Conference on Soil Mechanics and Geotechnical Engineering* 1:3–57. Cambridge, MA.
- Mayne, P.W. 2005. Integrated ground behavior: in-situ and lab tests. H.D Benedetto, T. Doanh, H. Geoffroy, & C. Sauzeat (eds), *Deformation Characteristics of Geomaterials* 155–180; London, UK; Taylor and Francis Group plc.
- Mayne, P.W. & Miller, B. 2021. Analytical solutions for evaluating CPTu soundings in overconsolidated Hartford clay. ISC-6 Paper 100.
- Ouyang, Z. and Mayne, P.W. 2018. Effective friction angle of clays and silts from piezocone. *Canadian Geotechnical Journal* 55(9): 1230–1247.
- Robertson, P.K. & Cabal, K.L. 2015. Guide to Cone Penetration Testing for Geotechnical Engineering 6th Edition. Singal Hill, CA: Gregg Drilling & Testing, Inc.
- Schneider, J.A., Randolph, M.F., Mayne, P.W. & Ramsey, N.R. 2008. Analysis of factors influencing soil classification using normalized piezocone tip resistance and pore pressure parameters. *Journal Geotechnical and Geoenvironmental Engineering*. 134 (11): 1569–1586. Gingery (2014)

Evaluation of cyclic softening potential using CPTu and assessment with cyclic triaxial test results: A case study

K. Fakharian, M. Bahrami & M. Kashkooli

Department of Civil & Environmental Engineering, Amirkabir University of Technology, Tehran, Iran

H. Vaezian & T. Bahrami

Pars GeoEnviro Inc., Tehran, Iran

ABSTRACT: An extensive geotechnical investigation was performed on an oil terminal site located in a seismically active field. Combination of *in situ* and laboratory tests were performed including Piezocone Penetration Tests (CPTu), some of which were adjacent to the borehole locations, providing a detailed stratigraphic soil profile and different physical and mechanical parameters. In this paper, the application of the CPTu test for analyzing cyclic liquefaction is evaluated and discussed. Both “liquefaction” and “cyclic softening” potentials are evaluated depending on the magnitude of I_c factor. A clayey silt layer was identified having an I_c factor of about 2.5 between 12 and 19 m of depth. The average q_c of this layer was 6 MPa and friction ratio (RF) was 2.5. The induced pore pressure, u , was measured between 300 to 1800 kPa from 12 to 19 m of depth. The equivalent SPT counts from correlations with CPT were 15 while the real SPT counts were about 50 or higher. According to CPT data, the factor of safety of liquefaction was calculated having an average of 0.56 for a 0.49g earthquake with $M=7$. Undisturbed samples were taken from the layer onto which cyclic undrained liquefaction tests were carried out. The results, however, revealed that specimens were resisting the cyclic liquefaction with sufficiently high factor of safety. The soil classification in the laboratory showed that the soil was clay and not silty clay. Detailed analyses and interpretations are carried out to find out the reasons of the differences between CPTu correlations and real response of the specimens to cyclic loading. The results show that modifications might be required at times in interpretations of soil classification as well as liquefaction potential evaluation for soils at the borderline of low plasticity clay and silty clay.

1 INTRODUCTION

Liquefaction can be defined as a loss of strength and stiffness in soils, divided into “cyclic liquefaction” and “cyclic softening” categories. The terms “sand-like” and “clay-like” were introduced to refer to soils whose stress-strain behavior under undrained monotonic and cyclic loading is similar to that of sands and clays, respectively (Boulanger & Idriss 2004). Soils like gravels, sands, and very low plasticity silts that are recognized as “sand-like” can experience some level of cyclic liquefaction. However, the term “clay-like” is reserved for clay and plastic silts which can experience cyclic softening (Robertson 2009).

Developing high positive pore pressure under undrained cyclic loading can reach the “sand-like” soil at the state of zero effective stress causing a condition under which the initial soil structure is lost, and large deformations occur. Alongside the size and duration of the imposed cyclic loading, *in situ* state parameters and soil structure, including relative density, effective confining stress, age, fabric, and

cementation, affect “sand-like” soil response to the cyclic liquefaction (Robertson 2009). Generally, loose, young, uncemented “sand-like” soil is known to be highly susceptible to cyclic liquefaction. In contrast, “clay-like” soils do not reach zero effective stress due to the developed pore pressure under the same undrained cyclic loading condition. In “clay-like” soil, the buildup pore pressure is controlled by key features, including *in situ* state, sensitivity, age, fabric, and cementation. Soft normally to lightly overconsolidated and sensitive clays are considered to tolerate significant shear strains. They are susceptible to cyclic softening that cause lateral and vertical deformations.

Monotonic and cyclic undrained loading tests data show that soil transition from sand-like to clay-like behavior appears over fine-grained soils on a fairly narrow range of plasticity indices (Boulanger & Idriss 2006). To distinguish between fine-grained soils that may exhibit sand-like behavior versus clay-like behavior, researchers have developed several criteria. The Chinese criteria have been widely for evaluating the liquefaction susceptibility of silts

and clays (Boulanger & Idriss 2006). Based on Atterberg limits for those reported data from sites in China, Seed & Idriss (1971) categorized clayey soils having less than 15% finer than $5 \mu\text{m}$, $LL < 35$, and $w_c > 0.9 LL$ as vulnerable to severe strength loss as a result of earthquakes (Seed 1982). Andrews & Martin (2000) reviewed a few case histories, concluding that soils are susceptible to liquefaction if they have 10% finer than $2 \mu\text{m}$ and $LL < 32$. Soils are not susceptible to liquefaction if they have 10% finer than $2 \mu\text{m}$ and $LL > 32$. Further study is required for soils that meet one, but not both, of these criteria (Andrews & Martin 2000). Bray et al. (2004) provided new liquefaction criteria for soils containing significant fine contents. The criteria are considered fine-grained soils with plastic index, $PI < 12$ and $w_c > 0.85 LL$ as susceptible to liquefaction. Boulanger & Idriss (2006) suggested that for practical purposes, fine-grained soils exhibit clay-like behavior if they have $PI \geq 7$. If a soil plots as CL-ML, the PI criterion may be reduced to $PI \geq 5$. Fine-grained soils that do not meet these criteria should be considered sand-like liquefiable, unless appropriate *in situ* and laboratory testing have shown otherwise (Bray et al. 2004).

The most common CPT-based classification systems are based on behavior characteristics and are often referred to as a soil behavior type (SBT) classification (e.g., Robertson, 1990). The SBT charts are behavior-based descriptions, while the general soil classification is textural-based (Robertson 2016). The charts proposed by Robertson (1990) and the present update (Robertson 2009) have become very popular, in which cone resistance, q_c , and sleeve resistance, f_s , are normalized to account for *in situ* stress level with depth. Since then, many CPT soil behavior type charts have been developed (e.g., Jefferies & Davies 1993, Ramsey 2002, Schneider et al. 2012). Robertson & Wride (1998) had suggested that $I_c = 2.6$ was an approximate boundary between soils that were either more sand-like or more clay-like. The Robertson SBTn chart works well in ideal soils but can be less effective in structured soils. The term “ideal soil” describe soils with little or no microstructure that are predominately young and uncemented. The term “structure” is used to describe features either at the deposit scale, macrostructure, e.g., layering and fissures, or at the particle scale, microstructure, e.g., bonding and cementation (Robertson 2016). Older natural soils tend to have some microstructure due to the post-deposition. Many researchers have contributed to developing the CPT-based models to evaluate liquefaction based on cyclic liquefaction case histories that were limited to predominately silica-based ideal soils (e.g., Robertson & Wride 1998). The updated method proposed by Robertson (2009) is the most widely used method to assess the potential for liquefaction. The method was initially developed for clean sands and it proposed a unified approach, in which two sets of equations are created for sand-like and clay-like behavior in liquefaction.

An industrial site on northern shorelines of Gulf of Oman was lately developed where boreholes and CPTu tests were carried out. At a small zone of this site near sea, the CPTu tests identified a clayey silt to silty clay with I_c factor of slightly below 2.5 (average of 2.497). The Robertson classification chart used correlations of the sand-like soil with $I_c < 2.5$ for this layer and concluded that this layer is highly liquefiable with a factor of safety, $FS = 0.54$ for the 0.49 g peak ground acceleration, PGA, of the field. This is while SPT correlations indicate a much greater $FS = 0.9$ to 1, also assuming that the soil is sand-like. Cyclic triaxial tests were carried out on undisturbed specimens revealing that the soil is not liquefiable.

In this paper, the geotechnical condition of the site is characterized presenting the CPTu and SPT data along with blow count profile of a precast concrete pile driven in this zone. The soil classification results from CPTu data and soil sampling and lab data are compared and attempts are made to account for the contradictions between CPTu data and other methods.

2 STUDY SITE

2.1 Location and morphology

The study site is located near Jask in Hormozgan Province, southern Iran, on the northern shorelines of Gulf of Oman. The site is approximately 300 m away from sea. This area is located in the Zagros orogenic zone and generally consists of marl, sandstone, and silty/clayey sediments. The site area is situated in a seismically active zone. The PGA with a return period of 475 years is estimated equal to 0.49g on the basis of a site-specific seismology study carried out by Pars GeoEnviro Consulting Engineers.

2.2 Geotechnical conditions

An extensive geotechnical investigation was performed at the study site. A combination of *in situ* and laboratory tests were carried out including Piezocone Penetration Tests, CPTu, some of which were adjacent to the borehole locations, providing a detailed stratigraphic soil profile and different physical and mechanical parameters. Total of 12 CPTu points as well as 6 boreholes were considered for the geotechnical investigation objectives.

Subsurface layers across the site mostly consist of cohesive soil containing clay and silty clay, and non-cohesive soil containing silty sand to sandy silt. After processing all data from field exploration, *in situ* tests including CPTu and SPT, as well as lab tests, the site area has been divided into three main zones in terms of geotechnical characteristics and subsoil conditions as shown for BH5. Zone b, which is the focus of this paper, mainly consists of a 6 m thick layer from

non-plastic silt and sand categorized as medium dense to dense starting from ground surface; underneath this layer, a layer consisting of plastic lean clay is located down to depth of around 12 m and categorized as firm stiff to stiff. Third layer starts from depth 12 m and extends down to the end of investigated BHs and CPTs consisting of clay and silty clay with PI=10-11; this layer is categorized as very stiff.

In most locations across the site, there has been a good compatibility between geotechnical data obtained from borehole sampling and the ones obtained on the basis of CPTu processed data and soil classification charts. However, in Zone b in which two CPTu tests as well as one borehole were executed, some incompatibilities are observed, especially between the results from CPT6 and BH5. BH5 which was continuously drilled down to 20 m is located adjacent to CPT6 penetrating to 19.1 m. Below 11 m, incompatibilities were more severely observed in classification, equivalent SPT numbers, and most significantly, liquefaction/cyclic softening potential analyses.

3 CPT DATA INTERPRETATIONS

3.1 Soil classification

Among proposed SBT charts on the basis of CPT data, the updated unified approach by Robertson (2009) is employed. The effective overburden stress is used to normalize tip and sleeve friction resistances as Q_t and F_r , as shown in Eqs. 1 and 2, respectively.

$$Q_t = \left[\frac{q_t - \sigma_{v0}}{\sigma'_{v0}} \right] \quad (1)$$

$$F_r = \left[\frac{f_s}{q_t - \sigma_{v0}} \right] 100\% \quad (2)$$

where q_t is CPT corrected cone resistance, $q_t = q_c + u_2 (1-a)$. The “a” is net area ratio of the cone determined from laboratory calibration for the cone, with a typical value between 0.7 and 0.85, f_s is CPT sleeve friction, σ_{v0} and σ'_{v0} are *in situ* total and effective vertical stresses, respectively. The primary ground water table is evaluated from site observations and rechecked from drilled adjacent borehole as 5 m from the surface at the CPT location. Figure 1 also shows the recorded data of CPT6 in Zone “b”. Profile of soil behavior classification based on Robertson (2009) method is plotted next to the CPT data alongside of the profile of soil classification from laboratory test.

The data points scattering over the Q_t - F_r chart are plotted in Figure 2. The soil layering according to CPT classification are three layers: Layer I: the top 5 m can be categorized as “clean sand to silty sand”, Layer II: between 5 to 12 m, dominantly “clay to silty clay”, and Layer III: between 11 to 19.5 m, classified as “silt mixtures, clayey silt to silty clay”. Layer III is categorized as a transition layer in the SBT chart. To further evaluate and verify the classification, another chart proposed by Eslami & Fellinius (1997) was attempted as shown in Figure 3.

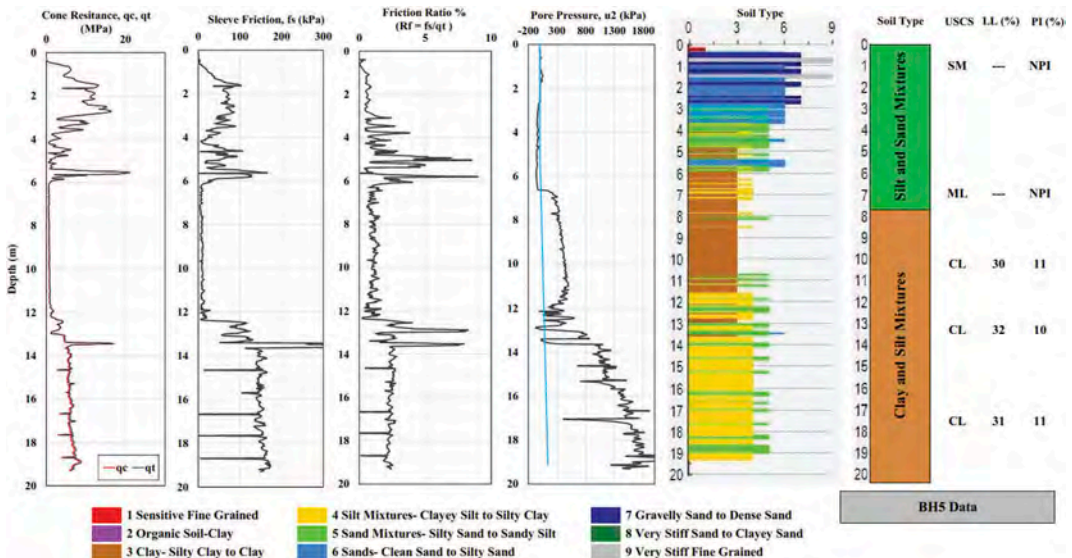


Figure 1. CPT6 cone resistance, sleeve friction, friction ratio, and pore pressure profile accompanied by soil classification profile based on Robertson (2009) and soil classification based on laboratory tests on adjacent borehole BH5.

Considering plotted data on Figures 2 and Figure 3, the two proposed classification SBT charts show an accumulation of points over 12 to 19 m representing by red squares. The accumulation of points is mainly categorized as clayey silt to silty clay over the SBT chart proposed by Robertson (2009) on Figure 2. These points have I_c value close to the suggested boundary, $I_c=2.6$, distinguishing between sand-like or clay-like behavior by Robertson & Wride (1998). The proposed boundary $I_c=2.6$ is the approximate boundary between soils that can be either claylike or sandlike, however, it is not always a good fit, except for predominately young uncemented, and normally consolidation soils referred to as ideal soil (Robertson, 2016). Also, the other CPTu tests performed at the site in different locations show the existence of this behavior type layer which is recognized as a transition layer between sand-like and clay-like behavior.

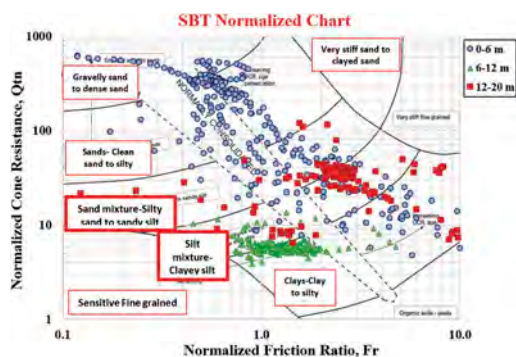


Figure 2. Scattered data points on Qt-Fr soil behavior type chart proposed by Robertson (2009) for CPT6.

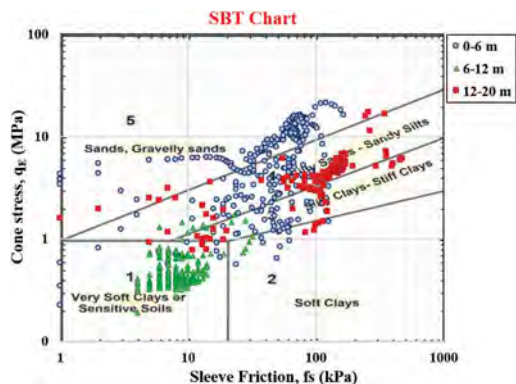


Figure 3. Scattered data points on q_e - f_s classification chart proposed by Eslami & Fellenius (1997) for CPT6.

3.2 Liquefaction & cyclic softening

A procedure suggested by Robertson & Wride (1998) is used to evaluate the potential for cyclic softening and cyclic liquefaction. The procedure used the basic methodology, developed by Seed & Idriss (1971), calculating cyclic stress ratio, CSR, induced by the earthquake, and cyclic resistance ratio, CRR of the soil. If $CSR > CRR$, then liquefaction can occur. The proposed procedure estimates CRR based on the “sand-like” or “clay-like” classification, separated by the defining boundary of $I_c=2.6$. The updated procedure is well established by Robertson (2009).

To get an outlook of the potential for cyclic liquefaction, Robertson (2009) presented a SBT Qt-Fr chart by defining “dilative” and “contractive” zones as a guide. Figure 4 shows the plotted data points over the chart for CPT6. The I_c boundaries of 2.5 and 2.7 are plotted with dashed lines. The red dots of the layer 12-20 m are dominantly in the transition zone and some points slightly below 2.5. The plots indicate that the points are at the “dilative” zone of the chart.

In all assessments, the earthquake magnitude, M , is estimated 7 with PGA equal to 0.49 g. Figure 5 shows the profile of safety factors for cyclic liquefaction for sand-like soil classification and cyclic softening for claylike soil classification with depth. The calculations demonstrate that the soil beneath the performed location has potential for either of the cyclic liquefaction and cyclic softening. In layers with clay-like behavior, $I_c > 2.7$, green points, FS is approximately around 0.73 in cyclic softening. While in sand-like layers, $I_c < 2.5$, red points; I_c between 2.5 and 2.7, yellow points, the average safety factor against cyclic liquefaction is 0.56.

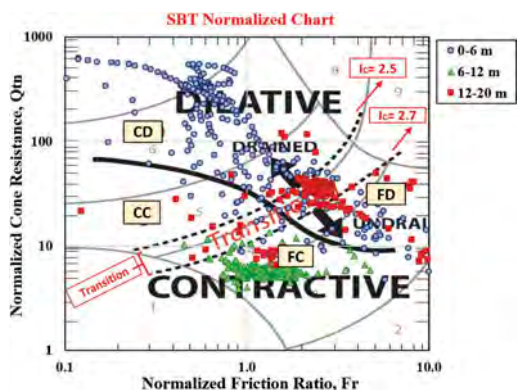


Figure 4. Data points on soil behavior type chart proposed by Robertson (2009) for CPT6.

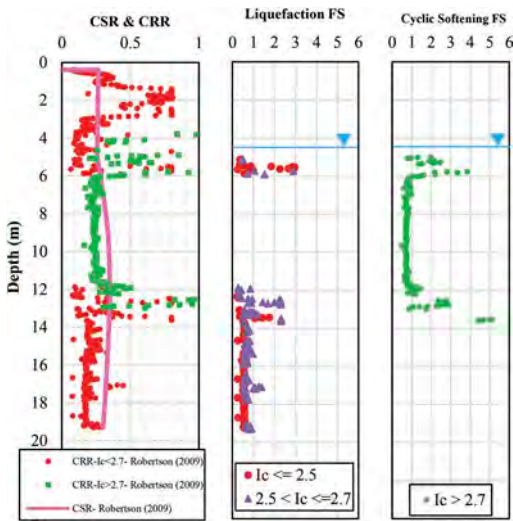


Figure 5. Liquefaction analysis of layers at location of CPT6; “liquefaction: is for sand-like ($I_c < 2.5$) and transition zone ($2.5 < I_c < 2.7$); “cyclic softening” is for clay-like ($I_c > 2.7$).

4 COMPARISON WITH BOREHOLE SAMPLES

4.1 Atterberg limits and classification

The results of Atterberg Limits tests performed according to ASTM D-4318 shows that a thick plastic layer is situated with $PI = 10-11$ extended between 12 to 20 m (Figure 1). CPTu results show that in this layer, silt mixtures containing clayey silt to silty clay are dominant. According to I_c value, this layer is located in sand-like zone as far as classification is concerned ($I_c \leq 2.6$). It seems that lab testing shows more dominant clayey soil than CPT classification.

SPT test was carried out with intervals of 2 m in soil layers as well. N-SPT obtained from SPT test in BH5 is shown in Figure 6. In addition, N-SPT is estimated from available correlations proposed by Robertson (2012) as well as Jefferies and Davies (1993) based on CPTu test results, as shown (Figure 6). Comparing actual SPT number with correlated values from CPT shows that in upper 6 m sand, there is fairly good compatibility between SPT and CPTu data; in deeper depths consisting of clay, N-SPT values from SPT test are somewhat greater than values correlated from CPTu down to 10 m within the firm clayey layer. Below this, the N-SPT from the tests is significantly higher than CPT correlation, highlighting a very stiff layer. The blow count data of a 400 mm precast concrete square pile is also plotted in Figure 6 versus depth to further validate the soil stratification. Good correlations exist in layers I and II, while the blow counts rapidly reached 20 blows per 100 mm penetration and beyond and pile driving was stopped. The blow count record further confirm the trend of N-SPT counts rather than N-SPT correlated from CPT.

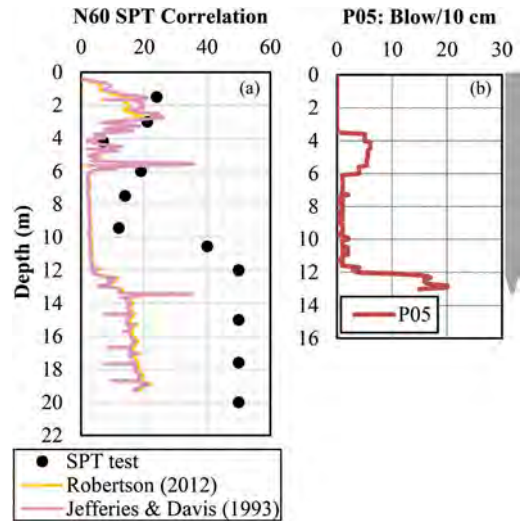


Figure 6. Comparison between direct results and correlated results: (a) N-SPT from actual SPT test and correlated from CPT, (b) blow count values from actual pile tests program.

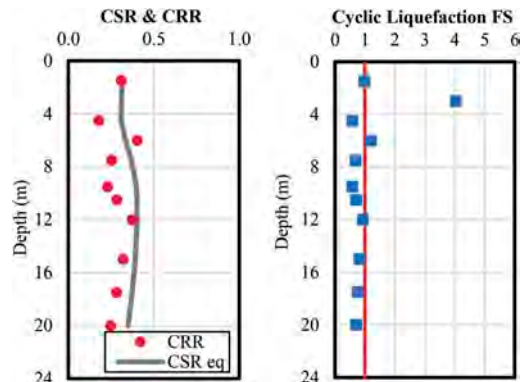


Figure 7. Assessments of liquefaction: (a) CSR values from SPT numbers based on Youd et al. (2001) and CRR values based on Seed & Idriss (1971), (b) factor of safety against liquefaction.

An evaluation of liquefaction is also performed based on SPT results according to the method proposed by Youd et al. (2001). The SPT-based assessments for cyclic liquefaction is presented in Figure 7. The results show that both CPT and SPT confirm the probability of liquefaction occurrence in the layer at the depth of 12 to 20 m. However, SPT-based assessment generally shows higher FS values close to unity.

4.2 Cyclic triaxial tests

The liquefaction resistance could be evaluated using undrained cyclic triaxial tests with two-way, symmetrical loading in compression and extension (Yang & Sze, 2011). For the mode of cyclic mobility, the usual

approach is to define failure criterion as the point that is accompanied by the occurrence of 5% double-amplitude (DA) axial strain (Toki et al., 1986; Ishihara, 1996).

A series of cyclic triaxial tests were carried out for the assessment of liquefaction and cyclic softening occurrence of the 3rd layer. An undisturbed sample extracted from depth 12 m was studied by cyclic triaxial test. Assuming peak ground acceleration of $a_{max}=0.49g$, the average stress for liquefaction triggering was calculated equal to $CSR=0.37$ based on the method proposed by Seed & Idriss (1971). After saturating the soil sample and being consolidated under $\sigma_{3c}=120$ kPa, cyclic deviatoric stress considering $CSR=0.37$ varying in the range of ± 100 kPa has been applied on the sample. The results show that no sign of failure exist (Figure 8). For an earthquake with $M=7$, according to Boulanger & Idriss (2004), the number of cycles equivalent to an earthquake for triggering liquefaction is 25 for clay-like soil samples. Figure 8 shows that at cycle No. 1000, DA axial strain is equal to 3.4%, which is much less than the proposed criterion. Thus, although CPTu correlated results for assessing cyclic liquefaction shows high risk of cyclic softening at the layer between depth of 12 and 20 m, the performed triaxial test shows no evidence of liquefaction under assumed seismic condition.

5 CONCLUSIONS

The layer between 12 to 19 m is classified using two classifications systems as clayey silt to silty clay.

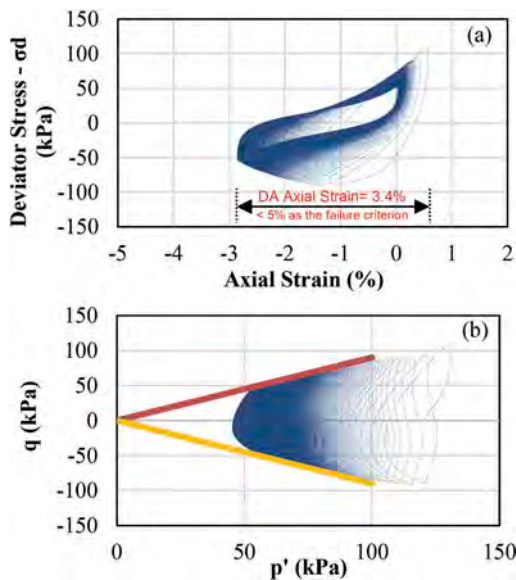


Figure 8. Cyclic triaxial test results at the end of 1000th cycle: (a) loops of deviator stress/axial strain, (b) Effective stress paths on Cambridge p' - q diagram.

The lab testing on the specimens classified the soil as CL with $PI=10-11$ and relatively high shear strength under cyclic loading. The SPT N-value is greater than the N-value correlated with q_c . CPTu results show very high induced pore-water pressure for the subject layer even up to 1800 kPa, therefore, the layer is highly compressible. This is while the SBC has recognized the soil as dilative. Cyclic triaxial test confirm that soil is not liquefiable even after 25 cycles.

It looks like that an I_c value of slightly below and above 2.5 mandated using “cyclic liquefaction” correlations of CPTu. This is while the soil is in fact clay-like and “cyclic softening” correlations should have been used instead. When the soil is classified at the transition zone, special cares are required in adopting correlations with CPTu data to evaluate liquefaction.

REFERENCES

- Andrews, D. C. A., & Martin, G. R. 2000. Criteria for liquefaction of silty soils. *Proc., 12th World Conf. on Earthquake Engineering*, 1–8.
- Begemann, H. K. 1965. The friction jacket cone as an aid in determining the soil profile. *Proc. 6th Int. Conf. on SMFE*, 1, 17–20.
- Boulanger, R., & Idriss, I. 2004. Evaluating the potential for liquefaction or cyclic failure of silts and clays. *Center for Geotechnical Modeling, Dept. of Civil and Environmental Engineering, Univ. of California*, Davis, California, USA.
- Boulanger, R. W., & Idriss, I. M. 2006. Liquefaction Susceptibility Criteria for Silts and Clays. *Journal of Geotechnical and Geoenvironmental Engineering*, 132 (11),1413–1426.
- Bray, J. D., Sancio, R. B., Riemer, M. F., & Durgunoglu, T. 2004. Liquefaction susceptibility of fine-grained soils. *Proc., 11th Int. Conf. on Soil Dynamics and Earthquake Engineering and 3rd Int. Conf. on Earthquake Geotechnical Engineering*, 1, 655–662.
- Douglas, B. J., & Olsen, R. 1981. Soil classification using electric cone penetrometer. *Symp. on Cone Penetration Testing and Experience, Geotech. Eng. Div.*, 209–227.
- Eslami, A., & Fellenius, B.H. 1997. Pile Capacity by direct CPT and CPTu methods applied to 102 case histories. *Canadian Geotechnical Journal*, 886–898.
- Ishihara, K. 1996. Soil behaviour in earthquake geotechnics. *Oxford: Clarendon Press*.
- Jefferies, M. G., & Davies, M. P. 1993. Use of CPTU to estimate equivalent SPT N 60. *Geotechnical Testing Journal*, 16(4),458–468.
- Ramsey, N. 2002. A calibrated model for the interpretation of cone penetration tests (CPTs) in North Sea quaternary soils. *Offshore Site Investigation and Geotechnics' Diversity and Sustainability. Proceedings of an International Conference of offshore Site Investigation and Geotechnics*, PP. 341–356. London, UK.
- Robertson, P.K. 2009. Performance based earthquake design using the CPT. *Conference on PBD in Earthquake Geotechnical Engineering*, Tokyo.
- Robertson, P.K. 2009. Interpretation of cone penetration tests - A unified approach. *Canadian Geotechnical Journal*, 46(11), 1337–1355.

- Robertson, P.K. 2016. Cone penetration test (CPT)-based soil behavior type (SBT) classification system - An update. *Canadian Geotech. Journal*, 53(12),1910–1927.
- Robertson, P.K. 1990. Soil classification using the cone penetration test. *Canadian Geotechnical Journal*, 27 (1),151–158.
- Robertson, P.K., Wride, C.E. 1998. Evaluating cyclic liquefaction potential using the cone penetration test. *Discussion 1. Canadian Geotec. Journal*, 37(1), 442–458.
- Schneider, J.A., Hotstream, J.N., Mayne, P.W., & Randolph, M.F. 2012. Comparing CPTU Q–F soil classification charts. *Géotechnique Letters*, 2(4),209–215.
- Seed, H.B., & Idriss, I.M. 1971. Simplified procedure for evaluating soil liquefaction potential. *Journal of the Soil Mechanics and Foundations Division*, 97(9), 1249–1273.
- Seed, H.B. 1982. Ground motions and soil liquefaction during earthquakes. *Earthquake Engineering Research Institute*, Berkeley, California, USA.
- Toki, S., Tatsuoka, F., Miura, S., Yoshimi, Y., Yasuda, S., & Makihara, Y. 1986. Cyclic undrained triaxial strength of sand by a cooperative test program. *Soils Found.* 26, No. 3, 117–128.
- Yang, J., & Sze, H.Y. 2011. Cyclic behaviour and resistance of saturated sand under non-symmetrical loading conditions. *Géotechnique*, 61:1,59–73.
- Youd, T.L., Idriss, I.M., Andrus, R.D., Arango, I., Castro, G., Christian, J.T., Dobry, R., Finn, W.D.L., Harder, Jr. L.F., Hynes, M.E., Ishihara, K., Koester, J. P. Liao, S.S.C., Marcuson III, W.F., Martin, G.R., Mitchell, J.K., Moriwaki, Y., Power, M.S., Robertson, P.K., Seed, R.B., & Stokoe, K.H. II. 2001. Liquefaction Resistance of Soils: Summary Report from the 1996 NCEER/NSF Workshops on Evaluation of Liquefaction Resistance of Soils. *Journal of Geotechnical and Geoenvironmental Engineering*, 127 (10), pp. 817–833.

Application of integrated Game Theory-optimization subground stratification (-IGTOSS) model to Venetian Lagoon deposits

M.S. Farhadi & T. Länsivaara

*Faculty of Built Environment, Department of Civil Engineering, TERRA Research Center
Tampere University, Tampere, Finland*

L. Tonni

*Department of Civil, Chemical, Environmental and Materials Engineering (DICAM)
University of Bologna, Bologna, Italy*

ABSTRACT: The geographical and geological spatial variabilities raise challenges for geotechnicians to devise globally applicable subground stratification models working based on cone penetration testing (CPT). Recently, a novel CPT-based stratification and classification model was proposed in Tampere University, Finland. It combines the soil behavior type (SBT) classification chart proposed by Robertson (1990) with a novel integrated Game Theory-optimization subground stratification model (denoted herein as RIGTOSS). The model has already been verified based on few test sites results from Taiwan and the U.S. Therefore, in this paper, the RIGTOSS model is developed further, and it is evaluated based on the stratification profiles provided by CPT experts for the Venetian Lagoon deposits. The test site has been selected because of high variability of CPT measurements and the thin transient soil layers in the area. The results indicated comparable stratification profiles from the developed model(s) and the profiles by experts, derived based on field and laboratory tests.

1 INTRODUCTION

Stratifying and classifying the soil behavior type (SBT) based on loads of sampling and laboratory testing can be currently in conflict with the sustainable design of a project. Furthermore, it may not finally lead to a desirable stratification-classification profile due to the probable discontinuities and soil disturbances in sampling. This problem is more challenging in highly variable and stratified soils. Then the thin transient layers may not be determined accurately. A solution can be sought in the advantageous continuous measurements of cone penetration test (CPT). Although, there are already challenges in the interpretation of the CPT measurements, and consequently in stratifying soils based on them.

In the past, much investigation has triggered the SBT classification and stratifying soils based on the CPT measurements. Several SBT classification charts have been successfully proposed based on data sets from around the world (Douglas 1981, Robertson 1990, Schneider et al. 2012, Eslami et al. 2017); although, in several studies, their applicability has been criticized for several soil types and geographical regions (Ricceri et al. 2002, Gylland et al. 2017). Besides, stratification models have

been recently appealed to researchers, and several models have been proposed (Wang et al. 2013, Ching et al. 2015, Wang et al. 2019). They often recognize strata based on computing a consistency factor among the succeeding CPT measurements in depth. A probable problem of this approach has been with the recognition of thin strata. There have been recent improvements, though. On the other hand, several methods are proposed which seek the change points in the succeeding CPT measurements, as the boundaries of strata. They may discover the thin strata better, compared to the former approach. Following the latter approach, a novel model is proposed in Tampere University, Finland, named herein integrated Game Theory-optimization subground stratification (-IGTOSS) model (Farhadi & Länsivaara 2021).

The -IGTOSS model has been previously combined with the classification chart proposed by Robertson (1990), so called RIGTOSS. In this study, it is developed further, and applied to the CPTu ('-u' indicates the pore water pressure measured in CPT) measurements at the highly nonhomogeneous deposits of the Venetian lagoon, Italy. Herein, the modified model is explained briefly, and the resulting stratification profiles of the site are compared with the ones suggested by experts.

2 STRATIFICATION MODEL

The basics of the utilized stratification model are described in (Farhadi & Lämsivaara, 2021). In general, the proposed model consists of the following steps:

1. Importing and interpreting CPTu measurements
2. Denoising interpreted measurements
3. Stratifying and classifying soils based on integrated Game Theory-soil classification charts
4. Illustrating stratification profile

In the Game Theory model, the previously optimized parameters are utilized herein as well. The steps 1 and 3 are briefly explained below.

2.1 Classification charts and data interpretation

The previously published model contained only the F_r - Q_t Robertson SBT classification chart (1990). It is developed in this study, and currently, three other CPTu-based classification charts are implemented in the model. Hence, the modified model consists of:

- a. RIGTOSS_{Fr-Qt} (sub)model: stratification based on the F_r - Q_t classification chart, proposed by Robertson (1990).
- b. RIGTOSS_{Bq-Qt} (sub)model: stratification based on the B_q - Q_t classification chart, proposed by Robertson (1990).
- c. SIGTOSS_{Fr-Qt} (sub)model: stratification based on the F_r - Q_t classification chart, proposed by Schneider et al. (2012).
- d. SIGTOSS_{(Δu2/σ'v0)-Qt} (sub)model: stratification based on the $(\Delta u_2/\sigma'_{v0})$ - Q_t classification chart, proposed by Schneider et al. (2012).

The initial R/S letters of the mentioned (sub)models names represent either of the employed charts proposed by Robertson (1990) or Schneider et al. (2012).

In the classification charts, several normalized parameters are used, which are interpreted from the CPTu measurements as:

- Normalized cone tip resistance, Q_t :

$$Q_t = \frac{q_n}{\sigma'_{v0}} = \frac{q_t - \sigma_{v0}}{\sigma'_{v0}} \quad (1)$$

- Friction ratio, F_r :

$$F_r = \frac{f_s}{q_n} \times 100 = \frac{f_s}{q_t - \sigma_{v0}} \times 100 \quad (2)$$

- Pore pressure ratio, B_q :

$$B_q = \frac{\Delta u_2}{q_n} = \frac{u_2 - u_0}{q_t - \sigma_{v0}} \quad (3)$$

- Normalized excess pore pressure, $\Delta u_2/\sigma'_{v0}$, which equals $B_q Q_t$;

where, q_n is the net corrected cone tip resistance, σ'_{v0} is effective vertical stress, q_t is total corrected cone tip resistance, σ_{v0} is total vertical stress, f_s is sleeve friction, u_2 is pore pressure measured at the cone shoulder, u_0 is the in-situ pore pressure prior to cone penetration, and Δu_2 is the excess pore pressure measured at the cone shoulder in penetration. As generally utilized, q_t is the corrected measured cone tip resistance, q_c , based on water content and unequal end effect of the piezometer: $q_t = q_c + u_2(1-a)$, where, a is the cone area ratio.

For computation of the in-situ vertical effective stress, σ'_{v0} , unit weight of soil, γ , is computed based on the equation by Robertson & Cabal (2010), which provides a continuous profile in depth:

$$\frac{\gamma}{\gamma_w} = 0.27 [\log R_f] + 0.36 \left[\log \left(\frac{q_t}{p_a} \right) \right] + 1.236 \quad (4)$$

where, friction ratio, R_f , equals $(f_s/q_t) \times 100$, γ_w is the unit weight of water in same unit as γ , and p_a is the atmospheric pressure in the same unit as for q_t .

2.2 Digitized classification charts

In order to implement the charts in computations, different equations have been fitted to the boundary lines of each classification chart. The fitted equations for the F_r - Q_t chart of Robertson (1990) is previously published in Farhadi & Lämsivaara (2021). The fitted equations for the other used charts are presented in Figures 1-3.

In Figure 1, the SBT zones in the B_q - Q_t chart of Robertson (1990) are defined as:

1. Sensitive, fine-grained soils
2. Organic soils and peat
3. Clays (clay to silty clay)
4. Silt mixtures (silty clay to clayey silt)
5. Sand mixtures (sandy silt to silty sand) or cemented soil
6. Sand (silty sand to clean sand)
7. Sand to gravelly sand
8. Sand (clayey sand to 'very stiff' sand)
9. Very stiff, fine-grained, overconsolidated

Note that the SBTs of 8 and 9 only exist in the F_r - Q_t chart, not in the B_q - Q_t chart.

Figures 2-3 illustrate the classification charts proposed by Schneider et al. (2012) and the fitted equations to the boundary lines. In these two charts, the SBTs are defined as:

1a. Low- I_R clays ($I_R = G/S_u$; where, I_R , G and S_u represent rigidity index, shear modulus, and undrained strength, respectively)

1b. Clays

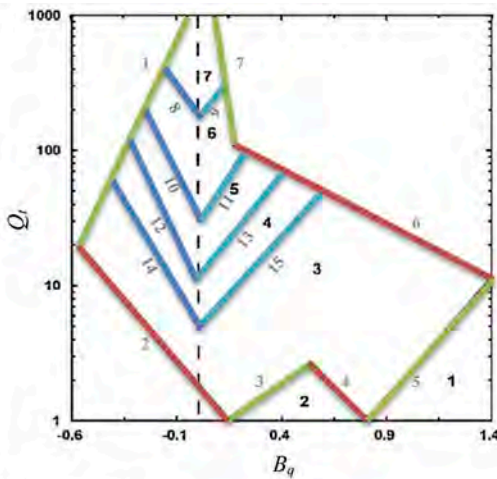
1c. Sensitive clays

3. Silts and transitional soils

2. Essentially drained sands and sand mixtures

3 TEST SITE

The data of the CPTu measurements are derived from a long-lasting project in the Venetian lagoon basin, Treporti test site, Italy. The importance of studying the Treporti site originated from the regional land subsidence in 1970s, and designing submersible gates to protect Venice from recurrent flooding in 1990s. There exist predominantly Pleistocene silty sediments of the Venetian lagoon basin with a high variability of strata (Tonni & Gottardi 2019), which can be a challenging soil condition to stratify.

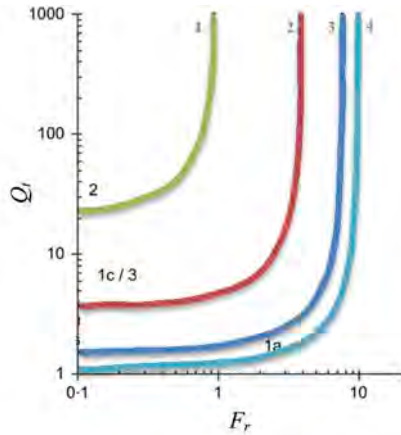


Line	Equation
1	$y = 3.2658x + 3.1106$
2	$y = -1.8182x + 0.2643$
3	$y = 1.0551x + 0.1487$
4	$y = -1.6003x + 1.2965$
5	$y = 1.7339x - 1.4019$
6	$y = -0.8139x + 2.1723$
7	$y = -10.361x + 3.8844$
8	$y = -2.2189x + 2.2501$
9	$y = 2.0043x + 2.2281$
10	$y = -3.3930x + 1.4843$
11	$y = 2.3345x + 1.4666$
12	$y = -3.3298x + 1.0567$
13	$y = 1.8446x + 1.0468$
14	$y = -2.7551x + 0.6999$
15	$y = 1.6359x + 0.6958$

* y and x stand for $\log(Q_t)$ and B_q , respectively.

Figure 1. The equations fitted to the boundary lines of the B_q - Q_t classification chart proposed by Robertson (1990). The boundary lines numbers are shown in grey.

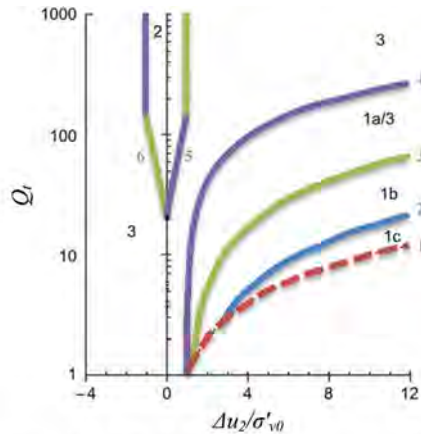
A sandy loading bank was constructed for studying the compressibility behavior of silty deposits at the site. For details of the Treporti site refer to Tonni & Gottardi (2011). Several CPTu tests were performed before and after construction of the loading



Line	Equation
1	$y = (-2.599x + 0.0003) / (x^4 + 2.418x^3 + 2.189x^2 - 1.176x - 0.0124)$
2	$y = (-327.7x^3 + 6481x^2 - 9851x + 3617) / (x^3 + 13580x^2 - 17150x + 5389)$
3	$y = (-7.102x + 6.555) / (x^4 + 8.338x^3 + 10.15x^2 - 46.84x + 27.2)$
4	$y = (-524.4x^2 - 237.6x + 848.7) / (x^4 + 814.3x^3 + 4563x^2 - 13510x + 8155)$

* y and x stand for $\log(Q_t)$ and F_r , respectively.

Figure 2. The equations fitted to the boundary lines of the F_r - Q_t classification chart proposed by Schneider et al. (2012). The boundary lines numbers are shown in grey.



Line	Equation
1	$y = (7861x^2 + 29940x - 44390) / (x^4 - 33.84x^3 + 2694x^2 + 73050x - 4572)$
2	$y = (1296x - 2062) / (x^3 - 33.7x^2 + 1041x + 769)$
3	$y = (601.3x - 739.8) / (x^3 - 26.6x^2 + 493.9x - 255.2)$
4	$y = (598.1x - 578.3) / (x^3 - 22.55x^2 + 382.3x - 299.3)$
5	$y = -0.7734x + 1.364$
6	$y = 0.8438x + 1.312$

* y and x stand for $\log(Q_t)$ and $\Delta u_2/\sigma'_{v0}$, respectively.

Figure 3. The equations fitted to the boundary lines of the $(\Delta u_2/\sigma'_{v0})$ - Q_t classification chart proposed by Schneider et al. (2012). The boundary lines numbers are shown in grey.

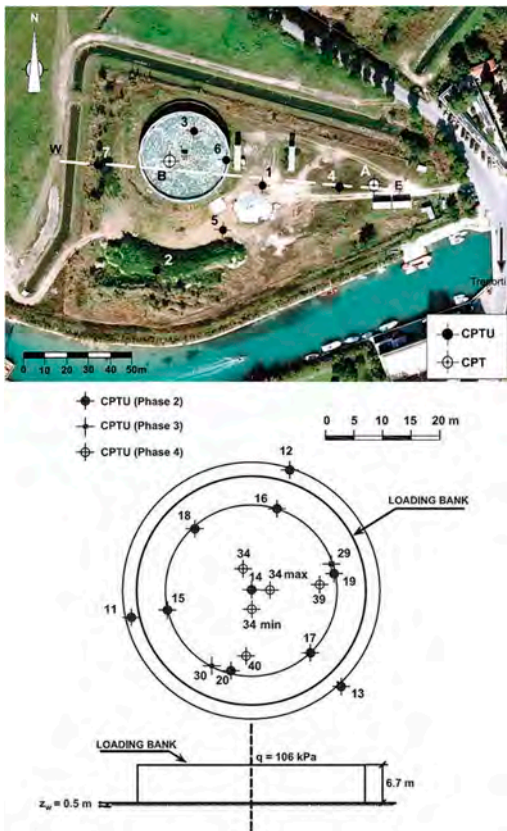


Figure 4. Location of CPTu tests at Treporti test site (TTS), from Tonni & Gottardi (2011). The diameter of the loading bank is 40 m.

bank. In this study, the CPTu measurements before the bank construction are utilized, which are indicated as ‘Phase 2’ in Figure 4.

4 RESULTS AND DISCUSSION

4.1 Stratification profiles

The (R/S)IGTOSS models were applied to nine CPTu measurements: CPTu 11-CPTu 19.

In the first step, data were imported into the model and were interpreted.

In the second step, the interpreted data were denoised using the locally estimated scattered smoothing (LOESS) method. The results of the smoothing for the four interpreted parameters of test CPTu14 (performed at the center of the loading bank) are presented in Figures 5a-5d. As can be observed, the benefit of the smoothing has been denoising the outliers (for instance, the abrupt large fluctuations at depths of 10-17 m), such that the general trends of variations would be preserved.

The solid lines in Figures 5f-5i show the identified SBT versus depth after using directly the classification charts of F_r-Q_i and B_q-Q_i by Robertson (1990) and F_r-Q and $(\Delta u_2/\sigma'_{v0})-Q$ by Schneider et al. (2012), respectively. It can be observed that the succeeding data points are highly variable on the charts and too many SBTs/strata are identified. Thus, it may be really challenging for a geotechnician to decide on the number of strata and their boundary depths in highly heterogeneous soils, such as in the Venetian lagoon. In this regard, (R/S)IGTOSS models facilitate the stratification procedure. Their resulting stratification profiles (illustrated with colored contours) for the test CPTu14 can be compared with the profiles resulting from direct use of classification charts in Figures 5f-5i. In the colored stratification profiles, the tone of colors varies from blue to yellow; where yellow means the highest probable SBT, and vice versa. Then, it is observed that after applying the (R/S)IGTOSS models, less strata can be detected generally.

Figure 5j illustrates the distribution of all CPTu measurements points on the used classification charts. As observed, especially in the F_r-Q classification chart of Schneider et al. (2012), numerous points are located out of the boundary lines of the chart, indicated by $SBT='f'$ in Figure 5h. They may result from different factors, such as uncertainties in measurements, interpretation methods and parameters, or incompatibility of the chart with the soils at the Treporti site. However, Figures 5f-5i unveil that after application of (R/S)IGTOSS models, a large number of the data points close to the boundary lines have been regarded within the zones. It evidences that the model considers the proximity of the succeeding points in detecting strata.

4.2 Spatial variability of sediments

Figure 6 illustrates the highly horizontal variability of deposits in the Venetian lagoon for tests CPTu11, CPTu12 and CPTu13, located around the perimeter of the loading bank. Although the (R/S)IGTOSS models have identified the strata based on each CPTu (Figures 6b-6m), it is still challenging to find similar layers with almost the same boundary depths at the test site. This is due to the highly spatial variability of soils at the Treporti site.

4.3 Comparison of classification charts

Despite the spatial variability of deposits at the Treporti site, and highly alternation of different grain-sized sediments, Gottardi & Tonni (2005) reported the following strata (as illustrated in Figures 5e and 6a):

- very soft silty clay, from ground level to 2 m in depth,

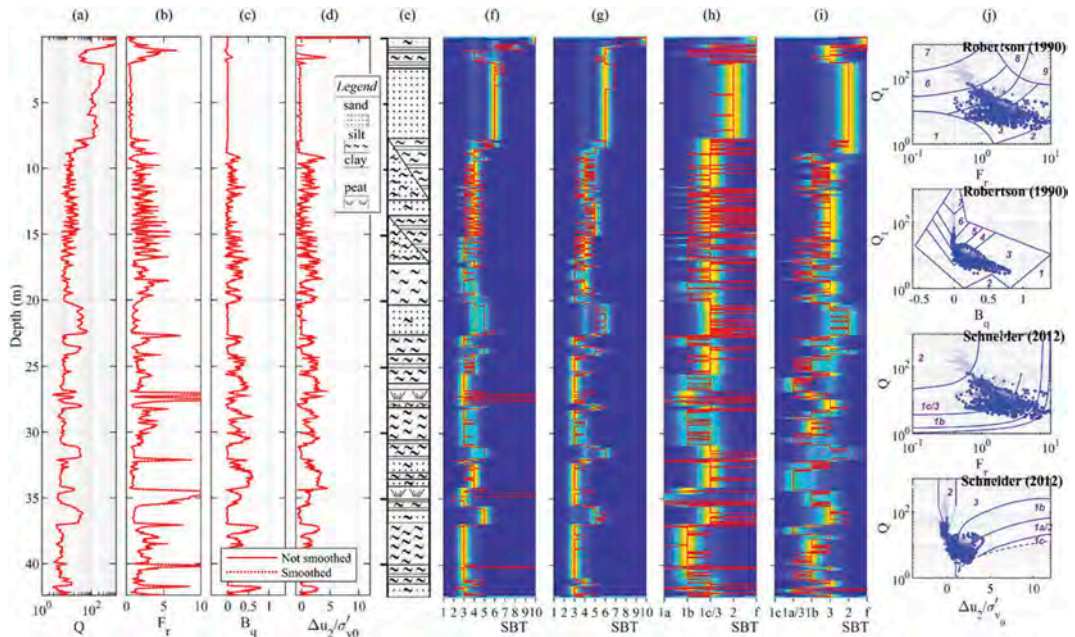


Figure 5. Illustration of CPTu measurements, experts stratification profile, RIGTOSS and SIGTOSS stratification profiles, and distribution of CPTu measurements on classification charts, for test CPTu14: a-d) smoothed versus unsmoothed interpreted CPTu parameters, e) expert-based stratification reported for Treporti site (Tonni & Gottardi 2011), f-i) directly chart-based stratification profile, presented by solid line, versus the profiles by the RIGTOSS_{Fr-Q}, RIGTOSS_{Bq-Q_t}, SIGTOSS_{Fr-Q} and SIGTOSS_{(Δu_v/σ'_{v0})-Q} models, respectively, and, j) distribution of measurements points on the classification charts (the color of data points gets darker with depth). In (R/S)IGTOSS stratification profiles, SBTs of '10' and 'f' mean that the data points located out of the boundaries of the classification charts.

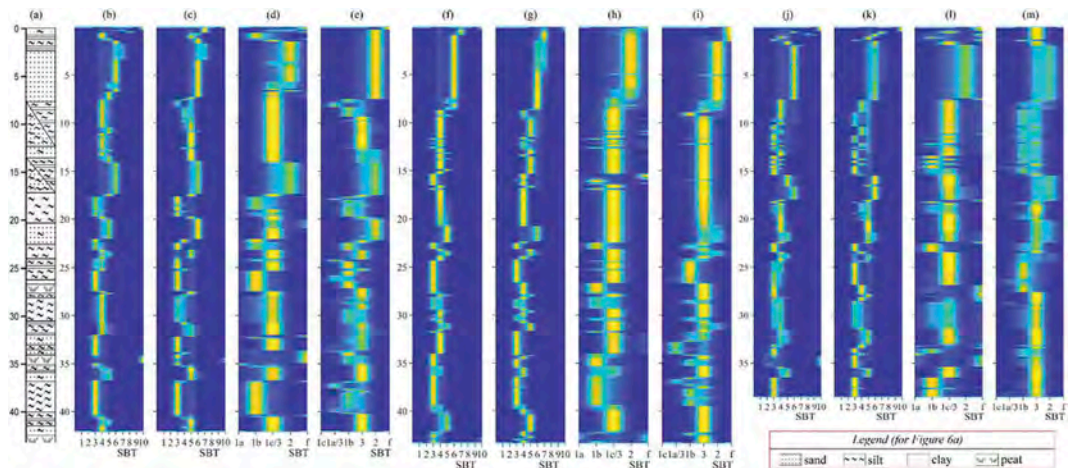


Figure 6. The expert-based stratification profile (a) by Tonni & Gottardi (2011) compared with the profiles from RIGTOSS and SIGTOSS models for tests: b-e) CPTu11, f-i) CPTu12, and, j-m) CPTu13. Every four profiles, i.e. a-e, f-i, and j-m, are derived from RIGTOSS_{Fr-Q_t}, RIGTOSS_{Bq-Q_t}, SIGTOSS_{Fr-Q} and SIGTOSS_{(Δu_v/σ'_{v0})-Q}, respectively.

- medium-fine sand (to approximately 8 m in depth),
- silt with thin layers of sandy to clayey silt, from 8 to 20 m in depth,
- dense clean sand (interbedded within the silty unit, though not everywhere),
- silty sand,
- alternate layers of silty sand, sandy silt, and clayey silt, with occasional presence of peat, at depths greater than 24 m.

Figures 5-6 indicate highly variable behaviour of soil at depths less than 2 m. However, they are

mostly silt, or silty clays, which is almost similar to the observation of Gottardi & Tonni (2005).

At the depth range of approximately 2-8 m, an almost homogeneous layer is identified with SBT of 6, that means sand (silty sand to clean sand) according to the Robertson chart, and based on the Schneider et al. chart, SBT is 2, that means essentially drained sands and sand mixtures. Although the SBT from two charts are almost similar, the thickness of the layer based on each chart is a little different. For example, Figure 6h shows SBT of 2 from surface to approximately 7.5 m deep, while Figure 6f indicates SBT of 6 for 1-8.5 m deep.

From 8 to 40 m in depth, highly variable deposits are identified. Their SBTs based on the Robertson charts are 3 or 4 and at some depths it is 5. Generally, they range from clay/silty clays to sandy silts/silty sands. On the other hand, the chart by Schneider et al. (2012) indicates almost all SBT classes from 1b to 3, which means from clays and sensitive clays to drained sands and sand mixtures. Therefore, using each chart leads to different profiles of stratigraphy. Such observations may lead to the necessity of a site-specific classification chart, such as the B_q-F_r chart by Ricceri et al. (2002).

5 CONCLUSIONS

In this study, a stratification-classification model is modified and employed for the highly variable deposits of Venetian lagoon, Treporti site, Italy. The model classified soil behavior based on four classification charts. It was observed that the model was capable of stratifying highly variable deposits. Generally, the obtained stratification profiles have been comparable with the profile provided by experts, which have been not only based on CPTu tests, but also based on the field and experimental tests.

The differences between the model and experts stratification profiles originate from numerous factors, such as the incompatibility of the classification charts with the testing site condition, uncertainties in measurements, or different criteria in classifying soils in contrast to those of the available classification charts.

ACKNOWLEDGEMENTS

The study was supported partly by a grant from Tekniikan Edistämissäätiö for the first author.

REFERENCES

- Ching, J., Wang, J.-S., Juang, C.H. & KU, C.-S. 2015. Cone penetration test (CPT)-based stratigraphic profiling using the wavelet transform modulus maxima method. *Canadian Geotechnical Journal* 52: 1993–2007.
- Douglas, B. 1981. Soil classification using electric cone penetrometer. Symp. on Cone Penetration Testing and Experience, Geotech. Engrg. Div., 1981. ASCE, 209–227.
- Eslami, A., Alimirzaei, M., Aflaki, E. & Molaabasi, H. 2017. Deltaic soil behavior classification using CPTu records—Proposed approach and applied to fifty-four case histories. *Marine Georesources & Geotechnology* 35: 62–79.
- Farhadi, M.S. & Lämsivaara, T. 2021. Development of an integrated game theory-optimization subgroup stratification model using cone penetration test (CPT) measurements. *Engineering with Computers*: 116. <https://doi.org/10.1007/s00366-020-01243-0>
- Gottardi, G. & Tonni, L. 2005. The Treporti test site: Exploring the behaviour of the silty soils of the Venetian lagoon. *Proceedings of the 16th International Conference on Soil Mechanics and Geotechnical Engineering, 2005*. IOS Press: 1037–1040.
- Gylland, A.S., Sandven, R., Montafia, A., Pfaffhuber, A.A., Kåsin, K. & Long, M. 2017. CPTU classification diagrams for identification of sensitive clays. *Landslides in Sensitive Clays*: 57–66. Springer.
- Ricceri, G., Simonini, P. & Cola, S. 2002. Applicability of piezocone and dilatometer to characterize the soils of the Venice Lagoon. *Geotechnical & Geological Engineering* 20: 89–121.
- Robertson, P.K. 1990. Soil classification using the cone penetration test. *Canadian Geotechnical Journal* 27: 151–158.
- Robertson, P.K. & Cabal, K. 2010. Estimating soil unit weight from CPT. *2nd International Symposium on Cone Penetration Testing, 2010*: 2–40.
- Schneider, J.A., Hotstream, J.N., Mayne, P.W. & Randolph, M.F. 2012. Comparing CPTU Q-F and $Q-\Delta u_2/\sigma'_{v0}$ soil classification charts. *Géotechnique Letters* 2: 209–215.
- Tonni, L. & Gottardi, G. 2011. Analysis and interpretation of piezocone data on the silty soils of the Venetian lagoon (Treporti test site). *Canadian Geotechnical Journal* 48: 616–633.
- Tonni, L. & Gottardi, G. 2019. Assessing compressibility characteristics of silty soils from CPTU: lessons learnt from the Treporti Test Site, Venetian Lagoon (Italy). *AIMS Geosci* 5: 117–144.
- Wang, H., Wang, X., Wellmann, J.F. & Liang, R.Y. 2019. A Bayesian unsupervised learning approach for identifying soil stratification using cone penetration data. *Canadian Geotechnical Journal* 56: 1184–1205.
- Wang, Y., Huang, K. & Cao, Z. 2013. Probabilistic identification of underground soil stratification using cone penetration tests. *Canadian Geotechnical Journal* 50: 766–776.

Application of two novel CPTu-based stratification models

M.S. Farhadi & T. Länsivaara

*Faculty of Built Environment, Department of Civil Engineering, TERRA Research Center
Tampere University, Tampere, Finland*

J.S. L'Heureux & T. Lunne

Norwegian Geotechnical Institute, Geotechnics and Natural Hazards, Oslo, Norway

ABSTRACT: Two novel CPTu-based stratification models are applied to the measurements at four Norwegian sites, including a broad range of soil behavior types (SBTs). The two models, called RIGTOSS and SIGTOSS, are developed based on the recently proposed integrated Game Theory-optimization subground stratification (-IGTOSS) model. The RIGTOSS model includes two submodels classifying the SBTs based on either the F_r - Q_t or B_q - Q_t charts by Robertson (1990); and similarly, the SIGTOSS model includes two submodels classifying the SBTs based on either the F_r - Q_t or $(\Delta u_2/\sigma'_{v0})$ Q_t charts by Schneider et al. (2012). The resulting stratification profiles of the four submodels were compared with the ones provided by experts, derived from extensive field and experimental testing. Similarity was observed and the results are promising. Differences at this stage can be attributed to incompatibility of the classification charts with the Norwegian soils and more specifically soil heterogeneities at the Øysand test site.

1 INTRODUCTION

A significant advantage of cone penetration test is the continuity of measurements in depth. This valuable feature can contribute to a better understanding of subground, which may not be obtained only from sampling. As an example, it can lead to one of the main applications of CPTu testing, which is the stratification and classification of the soil behaviour type (SBT). Currently, the stratification-classification needs combining CPTu measurements with experimental and probably other field tests. However, it is desirable to stratify and classify soils only based on the CPTu measurements, which is targeted in this study.

The CPTu-based stratification-classification has been extensively investigated. Initially, a generally applicable method was sought to classify soils based on the CPTu measurements, which resulted into several classification charts (Robertson 1990, Schneider et al. 2012, Eslami et al. 2017). Despite the breakthroughs, the observed inaccuracies of the charts for different sites have left the question open, and researchers are still proposing soil-type- or site-specific classification charts (Ricceri et al. 2002, Gylland et al. 2017). However, using only the classification charts could not provide accurate stratification profiles while they represented largely high number of strata especially in highly variable soils. Therefore, several researchers focused on combining

classification charts with computational methods for stratifying soils based on CPTu measurements (Ching et al. 2015, Wang et al. 2019, Shuku et al. 2020).

In Tampere university, Tampere, Finland, a novel CPT-based stratification-classification model, named -IGTOSS here, is proposed integrating several computational models: a Game Theory model, the evolutionary Grey Wolf Optimizer (GWO) and the classification chart proposed by Robertson in 1990 (Farhadi & Länsivaara 2021). It was previously evaluated based on several CPTu tests in Taiwan and the US. In this study, the model is developed further including three other SBT classification charts. Then, it is applied to several CPTu tests from Norway containing a broad range of SBTs.

2 -IGTOSS MODEL

2.1 Normalized CPTu parameters

The utilized normalized parameters interpreted from the CPTu measurements are (Schneider et al. 2012):

- i) Normalized cone tip resistance, Q_t :

$$Q_t = \frac{q_n}{\sigma'_{v0}} = \frac{q_t - \sigma_{v0}}{\sigma'_{v0}} \quad (1)$$

ii) Friction ratio, F_r :

$$F_r = \frac{f_s}{q_n} \times 100 = \frac{f_s}{q_t - \sigma_{v0}} \times 100 \quad (2)$$

iii) Pore pressure ratio, B_q :

$$B_q = \frac{\Delta u_2}{q_n} = \frac{u_2 - u_0}{q_t - \sigma_{v0}} \quad (3)$$

iv) Normalized excess pore pressure, $\Delta u_2/\sigma'_{v0}$, which equals $B_q Q_t$;

where, q_n is the net corrected cone tip resistance, σ'_{v0} is the effective vertical stress, σ_{v0} is the total vertical stress, q_t is the total corrected cone tip resistance, f_s is sleeve friction, u_2 is the pore pressure measured at the cone shoulder, u_0 is the in-situ pore pressure prior to cone penetration, and Δu_2 is the excess pore pressure measured at the cone shoulder in penetration. As generally utilized, q_t is the measured cone tip resistance, q_c , corrected based on water content and unequal end effect of the piezometer: $q_t = q_c + u_2(1-a)$, where, a is the cone area ratio.

2.2 Developed stratification model

The basics of the stratification model are described in Farhadi & Lämsivaara (2021). In this study, it has been developed further containing three other classification charts. A concise flowchart of the modified model is presented in Figure 1.

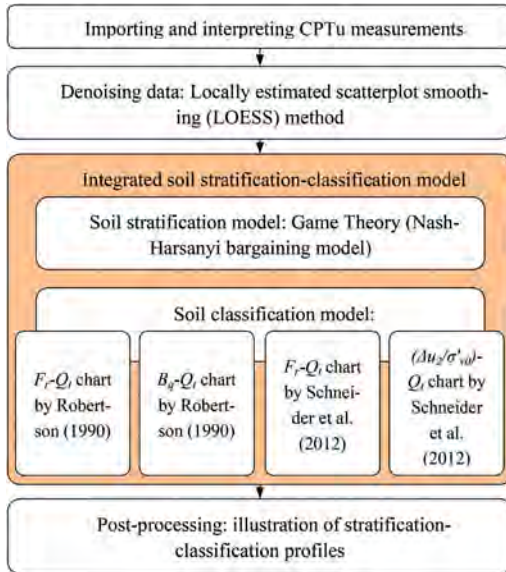


Figure 1. Concise flowchart of the proposed (R/S)ITGOSS model(s).

As illustrated in Figure 1, in the *first step*, the CPTu data are imported and interpreted. A constant soil unit weight, γ , for the whole depth of cone penetration is used to interpret Q_t , F_r , B_q and $\Delta u_2/\sigma'_{v0}$.

In the *second step*, the interpreted data is smoothed using a spatial regression method, called locally estimated scatterplot smoothing (LOESS). 1% of data is used as the spatial regression range.

In the *third step*, the integrated stratification-classification model specifies the strata boundaries depths, using a Game Theory model, as described in Farhadi & Lämsivaara (2021). Then, the SBT is determined from a classification chart, in each of the following submodels:

- RIGTOSS $_{F_r-Q_t}$ based on the F_r-Q_t chart by Robertson (1990),
- RIGTOSS $_{B_q-Q_t}$ based on the B_q-Q_t chart by Robertson (1990),
- SIGTOSS $_{F_r-Q_t}$ based on the F_r-Q_t chart by Schneider et al. (2012),
- SIGTOSS $_{(\Delta u_2/\sigma'_{v0})-Q_t}$ based on the $(\Delta u_2/\sigma'_{v0})-Q_t$ chart by Schneider et al. (2012).

The introductory R or S letters in the names of the RIGTOSS and SIGTOSS models indicate the utilized classification charts.

In the charts by Robertson (1990), the SBTs are defined as:

- Sensitive, fine-grained
- Organic soils - peats
- Clays - clay to silty clay
- Silt mixtures - clayey silt to silty clay
- Sand mixtures-silty sand to sandy silt
- Sands, clean sand to silty sand
- Gravelly sand to sand
- Very stiff sand to clayey (heavily overconsolidated or cemented) sand
- Very stiff fine-grained

In the charts by Schneider et al. (2012), the SBTs are defined as:

- Low- I_R clays ($I_R = G/S_u$; where, I_R , G and S_u represent rigidity index, shear modulus, and undrained strength, respectively)
- Clays
- Sensitive clays
- Silts and transitional soils
- Essentially drained sands and sand mixtures

In the *final step*, the identified SBTs of the strata are plotted three-dimensionally with colored contours, as explained in Farhadi & Lämsivaara (2021).

The interested readers may contact the first author for the MATLAB code; which will be probably described further in a separate paper in future.

3 TEST SITES

The developed (R/S)ITGOSS models are applied to the CPTu data from four sites in Norway (Figure 2):



Figure 2. Location of the test sites in Norway (provided by MATLAB, hosted by Esri, and Google Earth Pro).

Table 1. Soil properties of the test sites, in brief (Blaker et al. 2019, Gundersen et al. 2019, Quinteros et al. 2019, and L'Heureux et al. 2019).

Property	Halden		Onsoy		Øysand		T-F*	
	min	max	min	max	min	max	min	max
w_n^{**} (%)	20	35	45	65	12	33	30	53
γ (kN/m ³)	18.3	20.8	15	19	13	23	16.8	19.1
FC (%)	15	99						
CC (%)	2	17	45	68	0	18	40	70
LL (%)	27.5	37.5	46	77			27	53
I_p (%)	6	13	25	50			7	29
S_r			5	19			0	360
OC (%)			30	50				
SC (g/L)			8	36			2	3

* T-F stands for Tiller-Flotten.

** w_n : natural water content; γ : unit weight; FC : fines content; CC : clay content; LL : liquid limit; I_p : plasticity index; S_r : sensitivity; OC : organic content; and SC : salt content.

a silt site at Halden, a soft clay site at Onsoy, a medium dense sand site at Øysand, and a quick clay site at Tiller-Flotten (L'Heureux & Lunne 2019).

The Halden site consists of a natural fjord marine deposit including mostly a low plasticity silt. A majority of bulky angular grains was observed at the scanning electron microscope (SEM) test: 41% quartz and 42% feldspar (Carroll & Paniagua 2018). Water table was 2.5 m below the surface. Further soil properties for all sites are presented in summary in Table 1.

The Onsoy site consists of a marine clay deposit with similar behaviour as that observed in Canada, Japan, Southeast Asia, Sweden, and Finland. The site has a thick layer of uniform very soft to soft clay.

The Øysand site consists of a 20 m thick glacio-fluvial mostly sandy deposit. The site includes several strata of gravelly sand (fluvial deposit), fine silty sand (deltaic soils), and clay-and-silt. The sand layer includes fine to medium uniform sand, predominantly of quartz minerals, some plagioclase and micas.

The Tiller-Flotten site consists of marine and glaciomarine sediments with a thick layer of sensitive clay from 8 m below terrain.

4 RESULTS AND DISCUSSION

4.1 Denoising data

Figure 3 shows the interpreted smoothed F_r , Q_t , B_q and $\Delta u_2/\sigma'_{v0}$ parameters for tests HALC19 and HALC20. It can be observed that the major variations are preserved after smoothing, and the minor sharp variations are smoothly approximated. Thus, the smoothing rarely impacts the resulting stratification profile while the model finds the strata boundaries

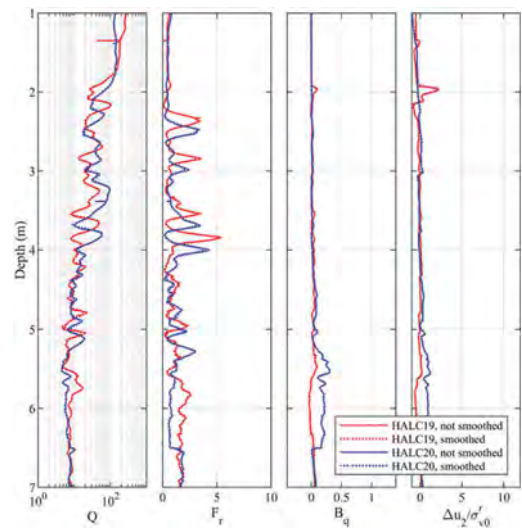


Figure 3. Illustration of the smoothing impact on the parameters interpreted from the CPTu tests at the Halden site.

mostly based on the large change points. However, most importantly it removes the outliers in data, such as those caused by stopping the cone penetration.

4.2 Stratification-classification profiles

4.2.1 Halden

Figure 4 illustrates the stratification-classification profiles for test HALC19.

Figures 4a-4d show that the interpreted parameters look similar before and after smoothing; although, several abrupt changes are removed. For

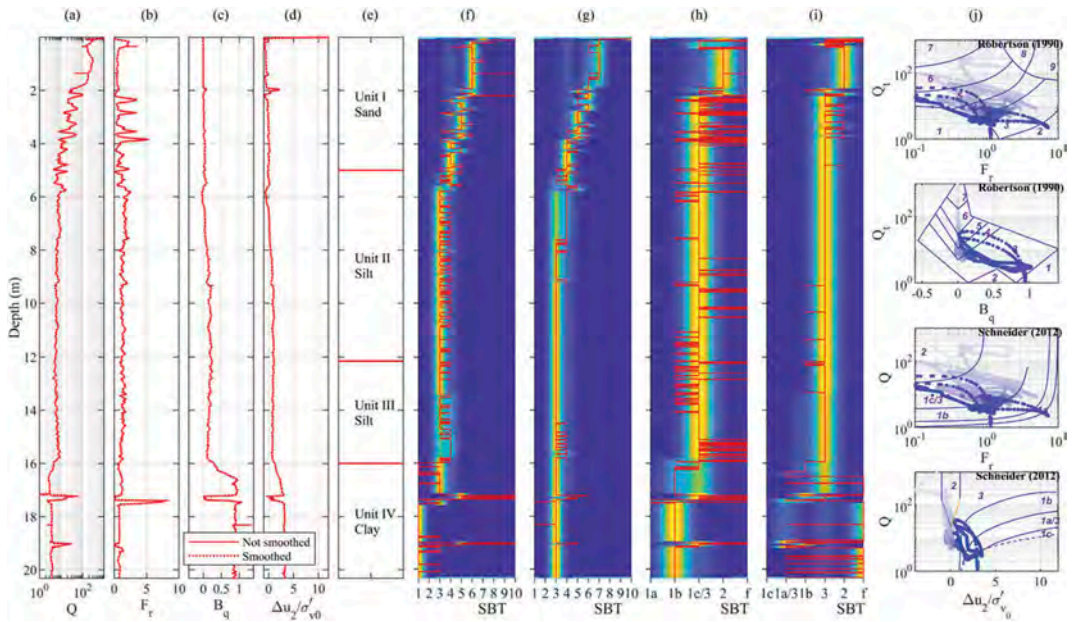


Figure 4. Illustration of CPTu measurements, experts stratification profile, RIGTOSS and SIGTOSS stratification profiles, and distribution of CPTu measurements on classification charts, for test HALC19, from Halden investigation site: a-d) smoothed versus unsmoothed interpreted CPTu parameters, e) expert-based stratification reported for Halden site (Blaker et al. 2019), f-i) directly chart-based stratification profile, presented by a solid line, versus the profiles provided by the RIGTOSS $_{Fr-Q_t}$, RIGTOSS $_{Bq-Q_t}$, SIGTOSS $_{Fr-Q_t}$ and SIGTOSS $_{(\Delta u_2/\sigma'_{v0})-Q_t}$ models, respectively, and, j) distribution of measurements points on the classification charts (the color of data points gets darker with depth). In (R/S)IGTOSS stratification profiles, SBTs of '10' and 'f' mean that the data points located out of the boundaries of the classification charts. [In profiles, the yellow color shows higher probability of the SBT.].

example, in Figure 4a, two sudden changes at approximate depths of 0.5 and 1.4 m are removed after smoothing.

Figure 4e illustrates the experts' judgement based on the in-situ and laboratory tests performed by Norwegian Geotechnical Institute (NGI). Four main soil deposits are identified: a loose to medium dense silty clayey sand from 0 to 5 m (Unit I), two clayey silt layers with the same geologic origin and almost the same material (Units II and III), and a deeper unit consisting of medium stiff clay (Unit IV) (Blaker et al. 2019).

In Figures 4f-4i, the solid lines show the stratification profiles after using directly the classification charts. A large number of thin layers can be identified with dissimilar SBTs, compared with the (R/S) IGTOSS contoured profiles (Figures 4f-4i) and the experts' profile (Figure 4e). The identification of numerous strata originates from the location of the CPTu measurements points on a classification chart; which may be located close to the SBT boundary lines, but on different sides.

The colour-contoured profiles in Figures 4h-4i show that the SIGTOSS $_{Fr-Q_t}$ and SIGTOSS $_{(\Delta u_2/\sigma'_{v0})-Q_t}$ models indicate three thick strata. However, the RIGTOSS $_{Fr-Q_t}$ and RIGTOSS $_{Bq-Q_t}$ models indicate approximately 5 thick strata

(Figures 4f-4g). Thinner layers can be observed with different probabilities at these thick strata.

Figure 4j illustrates the location of the CPTu measurements on the classification charts. The colour of the points gets darker with depth. They show the variability of the soil at the Halden site. In addition, comparing them with Figures 4f-4i showed that the (R/S)IGTOSS profiles are correctly determined.

4.2.2 Onsøy

Figure 5 shows the (R/S)IGTOSS results for tests ONSC19, ONSC20, and ONSC21, performed at the south-east corner of the Onsøy site. The distances between their locations were less than 2.1 m.

Figures 5a-5d indicate the impact of the smoothing method, and an appropriate repeatability of CPTu tests; although, the ONSC20 measurements deviate from the other two tests at some depths.

Comparing Figures 5e with two sets of Figures 5f-5i and 5j-5m indicates a generally appropriate similarity in recognizing the soil type as clay; although, the strata identified by experts are more than the strata identified by the (R/S)IGTOSS models. On the other hand, several thin layers are identified by the (R/S)IGTOSS models.

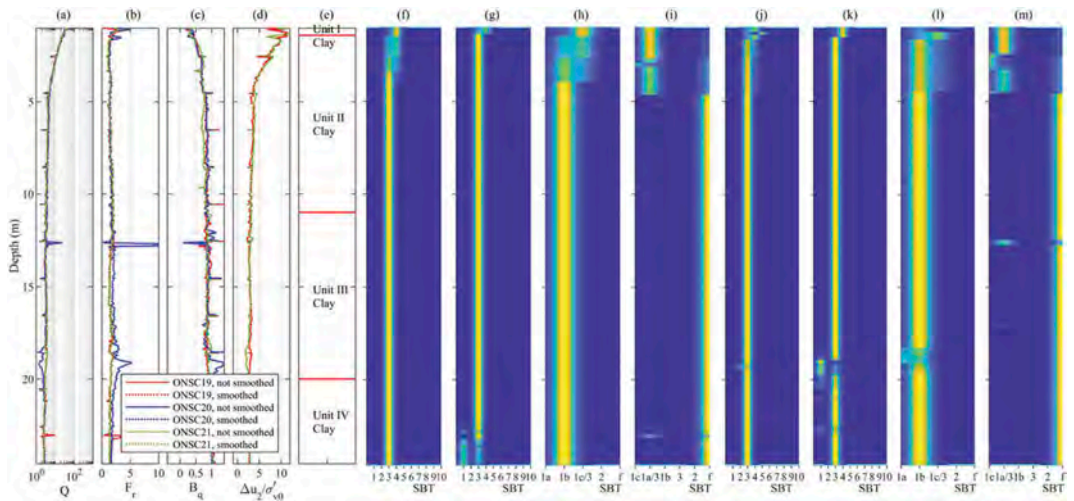


Figure 5. Comparison of the CPTu measurements at the Onsøy test site: a-e) smoothed and unsmoothed measurements of tests ONSC19, ONSC20, and ONSC21, f-i) respectively, RIGTOSS $_{Fr-Q_t}$, RIGTOSS $_{Bq-Q_t}$, SIGTOSS $_{Fr-Q_t}$ and SIGTOSS $_{(\Delta u_2/\sigma'v_0)-Q_t}$ profiles for ONSC19, and, j-m) respectively, RIGTOSS $_{Fr-Q_t}$, RIGTOSS $_{Bq-Q_t}$, SIGTOSS $_{Fr-Q_t}$ and SIGTOSS $_{(\Delta u_2/\sigma'v_0)-Q_t}$ profiles for test ONSC20.

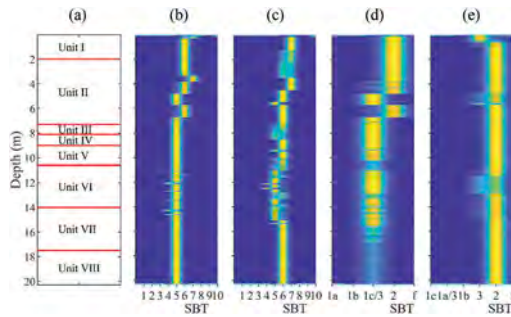


Figure 6. Comparison of (a) experts' stratification profile with the (b) RIGTOSS $_{Fr-Q_t}$, (c) RIGTOSS $_{Bq-Q_t}$, (d) SIGTOSS $_{Fr-Q_t}$ and (e) SIGTOSS $_{(\Delta u_2/\sigma'v_0)-Q_t}$ models profiles, for test OYSC40, Øysand site. In the experts' profile, Unit I is sand (silty, fine; layers and seams of medium to coarse sand), Unit II is sand (fine to coarse, gravelly), Unit III is sand (fine, traces of organic material), Unit IV is sand (fine to medium, silty), Unit V is sand (medium to coarse, gravelly), Unit VI is sand (fine to medium, silty), Unit VII is silt (sandy, clayey), and Unit VIII is sand (fine to medium, silty) (Quinteros et al. 2019).

4.2.3 Øysand

Figure 6 shows the experts' stratification profile (Quinteros et al. 2019) compared with the (R/S)IGTOSS profiles for test OYSC40. The experts recognized several strata of sandy soils for the whole depth, except for Unit VII, which is mainly silty. Similarly, the (R/S) IGTOSS models identified mostly sand mixtures; except SIGTOSS $_{Fr-Q_t}$ that identified silts and transitional soils, i.e. SBT=3, but at depths different from Unit VII. In general, the strata boundaries recognized by the models differ significantly from the experts'

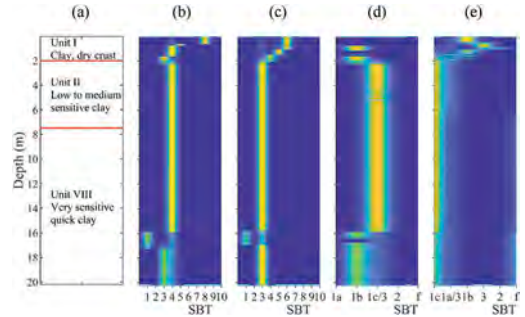


Figure 7. Comparison of (a) experts' stratification profile with the (b) RIGTOSS $_{Fr-Q_t}$, (c) RIGTOSS $_{Bq-Q_t}$, (d) SIGTOSS $_{Fr-Q_t}$ and (e) SIGTOSS $_{(\Delta u_2/\sigma'v_0)-Q_t}$ models profiles, for test TILC17, Tiller-Flotten site (L'Heureux et al. 2019).

judgement at Øysand; although, the SBT characterization is quite similar.

4.2.4 Tiller-Flotten

Figure 7 compares the SBT profiles by the experts (L'Heureux et al. 2019) and (R/S)IGTOSS models for test TILC17. It is interesting that only the SIGTOSS $_{(\Delta u_2/\sigma'v_0)-Q_t}$ model has clearly recognized the sensitive clays. Albeit, in the SIGTOSS $_{Fr-Q_t}$ model the SBT has been mainly either 1c, sensitive clay, or 3, i.e. silts and transitional soils. Besides, the RIGTOSS model could not recognize the sensitive clays, i.e. SBT = 1, well; however, it found them as clays or silt mixtures. Further, it can be observed that the strata change depths are recognized differently by the models and the experts.

4.2.5 Comparison of classification charts

Comparing the RIGTOSS_{Fr-Qt} and RIGTOSS_{Bq-Qt} profiles in Figures 4-7 for each test, indicates almost similar stratification profiles. However, differences can be due to the different numbers of SBT zones on the classification charts, and different interpreted parameters used in each of them.

Similarly, comparing the SIGTOSS_{Fr-Qt} and SIGTOSS_{($\Delta u_2/\sigma'_{v0}$)-Qt} profiles in Figures 4-7 indicates almost similar profiles with respect to the strata boundaries depths; but the SBT differences are visible. Besides, data points may be located out of the boundaries of the SIGTOSS_{($\Delta u_2/\sigma'_{v0}$)-Qt} chart, i.e. SBT='f' in the profiles. This may originate from several factors, such as the incompatibility of the chart with the Norwegian soils, using different interpretation methods in this study in contrast to the ones used in Schneider et al. (2012), and the small zone of '1c' on the chart.

Figures 4-7 indicated that judging based on the Schneider's chart might have advantage over using the Robertson chart for the Norwegian fine-grained soils; although, it can be confusing to differentiate clays from silts based on the Schneider's chart.

On the other hand, comparing the RIGTOSS and SIGTOSS profiles, less strata are determined based on the charts proposed by Schneider et al. (2012), while they include less SBT zones. Then, it may affect the precision of stratification and the recognized number of strata; which can be observed in Figures 5 and 6, as examples.

5 CONCLUSIONS

A stratification-classification model by Farhadi & Länsivaara (2021) is developed further in this study to include different CPTu-based soil classification charts. The developed models are applied to four Norwegian soils. As observed, the stratification profiles of the models are comparable with the profiles presented by experts –which resulted from extensive field and laboratory experiments. However, there are still differences between them, principally originating from:

- using different soil classification viewpoints or parameters implemented in the available classification charts,
- incompatibility of the used classification charts with the Norwegian soils, especially for fine-grained soils, and,
- spatial variability of soils, resulting into almost different stratification profiles for the CPTu tests performed close to each other.

In addition, it was observed that the CPTu measurements points may be located out of the bounds of the Schneider's $\Delta u_2/\sigma'_{v0} - Q$ chart, which could be

caused by the incompatibility of the chart with the Norwegian soils.

ACKNOWLEDGEMENT

The authors acknowledge the support from Norwegian GeoTest Sites infrastructure (NGTS) for access to data. The study was also supported partly by Tekniikan Edistämissäätiö (Finnish Foundation for Technology Promotion), Grant No. JNR. 8375, for the first author.

REFERENCES

- Blaker, Ø., Carroll, R., Paniagua Lopez, A.P., Degroot, D. J. & L'Heureux, J.-S. 2019. Halden research site: geotechnical characterization of a post glacial silt. *AIMS Geosciences* 5(2): 184–234. doi: 10.3934/geosci.2019.2.184.
- Carroll, R. & Paniagua, P. 2018. Variable rate of penetration and dissipation test results in a natural silty soil. *Cone Penetration Testing 2018*. CRC Press.
- Ching, J., Wang, J.-S., Juang, C.H. & Ku, C.-S. 2015. Cone penetration test (CPT)-based stratigraphic profiling using the wavelet transform modulus maxima method. *Canadian Geotechnical Journal* 52(12): 1993–2007. <https://doi.org/10.1139/cgj-2015-0027>.
- Eslami, A., Alimirzaei, M., Aflaki, E. & Molaabasi, H. 2017. Deltaic soil behavior classification using CPTu records—Proposed approach and applied to fifty-four case histories. *Marine Georesources & Geotechnolgy* 35: 62–79. doi: 10.1080/1064119X.2015.1102185.
- Farhadi, M.S. & Länsivaara, T. 2021. Development of an integrated game theory-optimization subground stratification model using cone penetration test (CPT) measurements. *Engineering with Computers*. <https://doi.org/10.1007/s00366-020-01243-0>.
- Gundersen, A., Hansen, R., Lunne, T., L'Heureux, J.-S. & Strandvik, S.O. 2019. Characterization and engineering properties of the NGTS Onsøy soft clay site. *AIMS Geosciences* 5: 665–703. doi: 10.3934/geosci.2019.3.665.
- Gylland, A.S., Sandven, R., Montafia, A., Pfaffhuber, A.A., Kåsin, K. & Long, M. 2017. CPTU classification diagrams for identification of sensitive clays. *Landslides in Sensitive Clays*. Springer.
- L'Heureux, J.-S., Lindgård, A. & Emdal, A. 2019. The Tiller–Flotten research site: Geotechnical characterization of a very sensitive clay deposit. *AIMS Geosciences* 5(4): 831–867. doi: 10.3934/geosci.2019.4.831.
- L'heureux, J.-S. & Lunne, T. 2020. Characterization and engineering properties of natural soils used for geotesting. *AIMS Geosciences* 6(1): 35–53. doi: 10.3934/geosci.2020004.
- L'Heureux, J.-S., Carroll, R., Lacasse, S., Lunne, T., Strandvik, S.O., Degago, S., Instanes, A., Nordal, S. & Sinitsyn, A. 2017. New Research Benchmark Test Sites in Norway. *Geotechnical Frontiers 2017*.
- Quinteros, S., Gundersen, A., L'Heureux, J.-S., Carraro, A.H. & Jardine, R. 2019. Øysand research site: Geotechnical characterisation of deltaic sandy-silty soils. *AIMS Geosciences* 5(4): 750–783. doi: 10.3934/geosci.2019.4.750

- Ricceri, G., Simonini, P. & Cola, S. 2002. Applicability of piezocone and dilatometer to characterize the soils of the Venice Lagoon. *Geotechnical & Geological Engineering* 20: 89–121. doi: 10.1023/A:1015043911091.
- Robertson, P.K. 1990. Soil classification using the cone penetration test. *Canadian Geotechnical Journal* 27(1): 151–158. <https://doi.org/10.1139/t90-014>.
- Schneider, J.A., Hotstream, J.N., Mayne, P.W. & Randolph, M. F. 2012. Comparing CPTU Q–F and Q– $\Delta u_2/\sigma_{v0}'$ soil classification charts. *Géotechnique Letters* 2(4): 209–215. <https://doi.org/10.1680/geolett.12.00044>.
- Shuku, T., Phoon, K.-K. & Yoshida, I. 2020. Trend estimation and layer boundary detection in depth-dependent soil data using sparse Bayesianlasso. *Computers and Geotechnics* 128, 103845. <https://doi.org/10.1016/j.compgeo.2020.103845>.
- Wang, H., Wang, X., Wellmann, J.F. & Liang, R.Y. 2019. A Bayesian unsupervised learning approach for identifying soil stratification using cone penetration data. *Canadian Geotechnical Journal* 56(8): 1184–1205. doi: 10.1139/cgj-2017-0709.

Numerical simulation of CPT in sands using DeltaSand and Hardening Soil models

M. Fetrati

MARUM–Center for Marine Environmental Sciences, University of Bremen, Bremen, Germany

V. Galavi

Deltares, Delft, The Netherlands

M. Goodarzi

*MARUM–Center for Marine Environmental Sciences, University of Bremen, Bremen, Germany
COWI A/S, Hamburg Branch Office, Germany*

S. Kreiter

MARUM–Center for Marine Environmental Sciences, University of Bremen, Bremen, Germany

T. Mörz

*MARUM–Center for Marine Environmental Sciences, University of Bremen, Bremen, Germany
Geo-Engineering.org GmbH, Bremen, Germany*

ABSTRACT: In this paper, Hardening Soil model with small-strain stiffness (HSsmall) and DeltaSand model are used as constitutive soil models to simulate the Cone Penetration Test (CPT) using the Material Point Method (MPM). Both models are formulated within the double hardening framework, in which independent yield surfaces represent mechanical behavior of soil under deviatoric and volumetric loadings. DeltaSand is a new advanced state-dependent constitutive model in which the relative density is incorporated in the formulation to represent the mechanical behavior of soil under deviatoric and volumetric loading in different stresses and relative densities. The numerical simulations are compared with CPTs in Cuxhaven Sand in a calibration chamber. Both constitutive soil models are compared with each other and DeltaSand is found to be capable to capture the soil behavior during quasi-static CPT.

1 INTRODUCTION

The Cone Penetration Test (CPT) is a widespread tool in both onshore and offshore for soil characterization, (Lunne 2010) due to repeatability, accuracy, and simplicity. Simulating CPT, as a mean to further interpret and understand the CPT results, is challenging because of the large deformation near the cone and complex behavior of soil under various type of loading. Different numerical approaches have been used to simulate CPT, considering the large deformation calculations, such as the Particle Finite Element Method in Geomechanics (G-PFEM) (Monforte *et al.* 2017, 2018, Schweiger & Hauser 2021, Carbone *et al.* 2022), Finite Difference Method (FDM) (Moug *et al.* 2019), Finite Element Method (FEM) (Goodarzi *et al.* 2018), Discrete Element Method (DEM) (Khosravi *et al.* 2020), and the Material Point Method (MPM) (Ghasemi *et al.* 2018,

Martinelli & Galavi 2021). Each of these approaches has its pros and cons. For instance, investigation of the interactions of the soil particles with each other and with the cone is possible through DEM simulation in a precise manner. However, a high number of particles and, followed by that, a significant amount of time is required for a realistic boundary value problem. FEM has the ability to model realistic boundary value problems and lower computational time but suffers from mesh distortion in the simulation of large deformation problems. On the other hand, MPM discretizes the continuum medium in material mass points and has the ability to simulate large deformations' problems without mesh distortion. MPM utilization in different geotechnical problems is comparatively new (Coetzee *et al.* 2005, Zabala & Alonso 2011, Solowski & Sloan 2015, Goodarzi & Rouainia 2017, Ghasemi *et al.* 2018, Galavi *et al.* 2019).

In addition to the numerical approach to simulate CPT, employing an appropriate constitutive soil model to predict the soil behavior in different soil states is indispensable. Various soil models have been used to predict the soil behavior in CPT simulations, such as Mohr-Coulomb (Huang *et al.* 2004), Drucker-Prager (Susila & Hryciw 2003), Hardening Soil (HS) (Tolooiyan & Gavin 2010), and Hypoplastic with intergranular strain (Fan *et al.* 2018). However, either they need recalibration for different relative densities or face several issues pertaining to the numerical stability.

In this paper, the Material Point Method, along with Hardening Soil model with small-strain stiffness (HS-small) and DeltaSand model (Galavi 2021), is used. The latter model is a new advanced state-dependent constitutive soil model, which is an elasto-plastic constitutive model formulated based on the double hardening framework. The simulation outcomes are compared with CPT tests in the MARUM Calibration Chamber (MARCC) in order to evaluate the capability of the new constitutive model in capturing the soil response throughout the simulation of CPT.

2 NUMERICAL MODEL

2.1 MPM formulation

The benefits of combined point-based and mesh-based strategies in MPM is the avoidance of mesh distortion and collecting the history of simulation in material points. (Sulsky *et al.* 1994).

The entire domain of the problem is covered by computational mesh similar to FEM. Additionally the continuum body is divided into a set of Material Points (MPs), which can relocate in the whole computational mesh contrary to the fixed position of Gaussian integration points within elements in FEM.

In the material point method, the momentum balance equations are solved in the computational mesh nodes, and constitutive equations and mass conservations are solved in MPs. The required information for solving balance equations in the mesh is transferred from MPs to the degrees of freedoms at nodes in the beginning of each calculation step. After solving the balance equations at nodes, the position of MPs, acceleration, and velocity at the MPs will be updated. The computational grid does not store any permanent information; therefore, all nodal data are discarded at the end of each calculation step.

A contact algorithm is employed to model the frictional contact between the cone and the soil. In order to enhance the precision of the contact algorithm and simulate the cone penetration into the soil, the moving mesh concept (Al-Kafaji 2013) is utilized here. In this concept, the deformable mesh is located between the fixed boundary and the moving mesh part, adjusting its dimensions with time. The refined mesh at the contact will always stay around the cone in this concept.

In standard MPM, MPs inside elements are used as integration points. Therefore, the accuracy of the integration depends on the location and numbers of MPs. The Gauss integration method, in contrast, utilizes a fixed number of integration points in a perfectly suited location to obtain accurate integration similar to FEM (Beuth & Vermeer 2013). Beuth *et al.* (2007) suggested a combination of both integration methods to mitigate stress oscillations in elements due to MPs crossing between elements. This is based on an assumption that stresses of MPs in a fully-filled linear element are identical, and therefore, stress calculation and integration can be performed on one Gauss Point in the elements. This numerical scheme leads to less computational effort than the standard material point integration (Martinelli & Galavi 2021). This mixed integration method is used in this study.

In problems in which the inertia effect is insignificant, mass scaling can reduce the computational cost by scaling the density. This scheme increases the time step size by a factor of \sqrt{MS} :

$$\Delta t_{critical}^{MS} = \frac{L_{min}}{\sqrt{E/MS \times \rho}} = \sqrt{MS} \times \Delta t_{critical} \quad (1)$$

where Δt_{crit} is the critical time step; L_{min} is the smallest element length; E is young modulus; ρ is density, and MS is the mass scaling factor. Sensitivity analysis is required to determine the amount of mass scaling factor such that it does not lead to inaccurate results. More information about the MPM formulation can be found in (Martinelli & Galavi 2021).

2.2 Constitutive soil models

This paper uses two constitutive soil models, HS-small and DeltaSand, to model the cone penetration into the soil. The list of parameters for the HS-small model and their values for the Cuxhaven sand for different relative densities are given in Table 1 and 2.

The full description of HS-small model can be found in (Benz 2007). The parameters of the HS-small model are calibrated for the Cuxhaven Sand based on laboratory experiments (Kluger 2014). Since the state dependency is not implemented in the HS-small model, unrealistically high dilation during shearing might occur. The maximum dilation angle is, therefore, decreased to stop unrealistic volume increase during extensive deformations (Martinelli & Galavi 2021).

DeltaSand captures the soil behavior under volumetric and deviatoric loading in different soil states (Galavi 2021). Deviatoric, volumetric, and tension cut-off yield surfaces are incorporated in the model. The deviatoric part in DeltaSand includes three deviatoric yield surfaces such that two of which are implemented to reproduce the cyclic behavior of sands. An extended Marsouka-Nakai criterion

Table 1. Description of HS-small model parameters.

parameters	Units	Description
E_{50}^{ref}	[kPa]	The secant stiffness from triaxial test when the ratio of deviatoric stress to the deviatoric stress at failure is 0.5
E_{oed}^{ref}	[kPa]	The tangent stiffness obtained from oedometer tests
E_{ur}^{50}	[kPa]	Unloading/reloading stiffness
ν_{ur}	[-]	Unloading/reloading Poisson's ratio
φ'	[°]	Effective friction angle
c'	[kPa]	Effective cohesion
ψ	[°]	Dilation angle
m	[-]	Rate of stress dependency in stiffness behavior
$\gamma_{0.7}$	[-]	Shear strain at which the shear modulus decreases to almost 70% of its initial value
G_0^{ref}	[kPa]	Shear stiffness at small strains
R_f	[-]	Failure ratio q_f/q_d (ratio of deviatoric stress at the failure to an asymptotic value of deviatoric stress)

Table 2. HS-small model parameters.

parameters	Units	Relative Densities (%)			
		83.48	85.63	86.85	92.53
E_{50}^{ref}	[kPa]	83000	85500	86500	92500
E_{oed}^{ref}	[kPa]	83000	85500	86500	92500
E_{ur}^{50}	[kPa]	249000	256500	259500	277500
ν_{ur}	[-]	0.2	0.2	0.2	0.2
φ'	[°]	41.4	41.7	41.8	42.4
c'	[kPa]	1	1	1	1
ψ	[°]	0.01	0.01	0.01	0.01
m	[-]	0.439	0.432	0.429	0.411
$\gamma_{0.7}$	[-]	0.00012	0.00011	0.00011	0.00011
G_0^{ref}	[kPa]	116700	118200	119000	122900
R_f	[-]	0.896	0.893	0.891	0.884

(Matsuoka & Nakai 1974) is used for the deviatoric yield surfaces. The hardening-softening rule that is used in this model is given in Eq. (2):

$$\sin \varphi'_{mob} = \sin \varphi'_i + \frac{\varepsilon_q^p f_d(e)}{A + \varepsilon_q^p} \left(\sin \varphi'_{cv} - \sin \varphi'_i \right) \quad (2)$$

where $f_d(e)$ is a function to connect the hardening-softening rule to the current void ratio; φ'_i and φ'_{cv} are initial effective and critical friction angles, respectively; A is a parameter to control plastic stiffness.

The volumetric section of DeltaSand is an elliptical yield surface with an associated flow rule. This yield surface is expressed as follows:

$$f_v = \frac{q^2}{M_v} + p'^2 - p_c^2 \quad (3)$$

where q and p' are Von Mises deviatoric stress and mean effective stress, respectively; p_c is effective pre-consolidation stress; M_v is a shape factor that is acquired from a 1D consolidation loading. A full explanation of the constitutive relations of the DeltaSand model can be found in (Galavi 2021).

2.3 The schematization of CPT in the calibration chamber

The calibration chamber was developed in the Marine Engineering Geology working group of the Center for Marine Environmental Sciences (MARUM), University of Bremen (Fleischer *et al.* 2016, Stähler *et al.* 2018). MARCC samples have a diameter of 30 cm and a height of 55 cm. A piezocone with a diameter of 12 mm is used in the chamber. This chamber has the capability of conducting the tests under “BC5” boundary conditions (Fleischer *et al.* 2016).

The numerical model geometry used as equivalent to MARCC BC5 (simulated field boundary condition) is shown in Figure 1. BC5 presumes that the specimen is in an infinite soil volume with known horizontal stiffness (Kluger *et al.* 2021). The ratio of chamber diameter to cone diameter in the numerical model is 125 for field conditions to avoid boundary effects. A thin layer of 5 cm is modeled with a linear elastic material to simulate the vertical effective stresses in experiments. Vertical effective stress equals 200 kPa, and the K_0 value is 0.45 as it was in the laboratory experiments. Due to the symmetry of the geometry, a 2D axisymmetric material point formulation (Galavi *et al.* 2019) is employed. The meshes are fine near the cone, and their size increase as they get close to the far-field boundary. Quadrilateral elements are used in all simulations.

The mini-cone is modeled as a rigid body that penetrates into the soil under drained condition with a prescribed velocity of 2 cm/s like in the laboratory experiments. The initial position of the cone is below the soil surface, and it is pushed into the soil until it reaches a steady-state for measuring the cone resistance q_c . The contact friction angle of 15 degrees is chosen as the cone surface is smooth (Al-Mhaidib 2005). At the beginning of the simulations, the MPs' positions are defined uniformly in rectangular clusters in the whole domain. This uniform distribution is independent of the elements' size and type. In order to avoid the formation of unrealistic empty elements, the number of material points was chosen so that they fill all elements throughout the penetration.

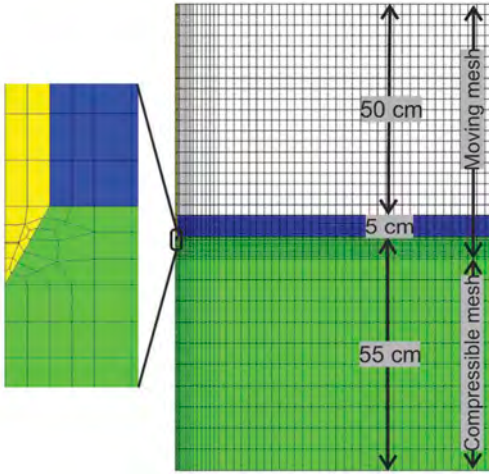


Figure 1. Schematic illustration of the model geometry. Yellow: cone, green: soil, blue: elastic layer as a surcharge.

3 RESULTS

3.1 Calibration of DeltaSand

Prior to the simulation of CPT in the calibration chamber, the parameters of the DeltaSand model for Cuxhaven sand were obtained from experiments. The oedometer tests with four relative densities and triaxial tests with three relative densities are used to cover medium-dense to dense sand samples (Kluger 2014). In this study, the kinematic hardening parts of the model, implemented in the model to capture the mechanical behavior of soil under cyclic loadings, were ignored. Therefore, only parameters related to the isotropic hardening parts of the model are calibrated and presented here. A brief description of DeltaSand parameters is presented in Table 3. The calibration procedure was conducted using the SoilLab feature of PLAXIS (Plaxis 2021). The results of the calibration are depicted in Figure 2 and Figure 3, and the final set of parameters is given in Table 4. Detailed explanations and steps for calibrating the DeltaSand model are represented in (Galavi 2021).

3.2 Simulation results vs. laboratory tests

In this section, the capabilities of the constitutive soil models are shown by comparing the numerical outcomes with laboratory test results. The same geometry, boundary conditions, number of elements, number of material points are used for comparing the constitutive soil models. The steady-state cone resistance was reported here obtained from averaging the values of cone resistances for depths between 18-32 cm, similar to the experiments.

Table 3. DeltaSand parameters.

parameters	Unit	Description
J_G^{ref}	[-]	Reference elastic stiffness
n	[-]	Power stiffness parameter
h_s	[stress]	Hardness parameter
C_{oed}	[-]	Oedometer parameter
α	[-]	Parameter to control peak friction angle
β	[-]	Parameter to control volumetric behavior
A_{mat}	[-]	Plastic stiffness parameter
e_{min}	[-]	Minimum void ratio
e_{crit}	[-]	Critical void ratio
e_{max}	[-]	Maximum void ratio
φ'_{cv}	[°]	Friction angle in constant volume
G_{ratio}^*	[-]	Ratio of stiffness in small strains to medium strains
γ_r	[-]	Reference shear strain at $G_{ratio} = 0.722$

$$*G_{ratio} = G_0/G$$

Table 4. Set of parameters used in all numerical simulations.

J_G^{ref}	n	h_s	C_{oed}	α	β	A_{mat}	e_{min}
[-]	[-]	[MPa]	[-]	[-]	[-]	[-]	[-]
920	0.3	30	1.1	1.65	0.95	0.016	0.47
e_{crit}	e_{max}	φ'_{cv}	G_{ratio}	γ_r			
[-]	[-]	[°]	[-]	[-]			
0.8	0.85	32	5	0.0001			

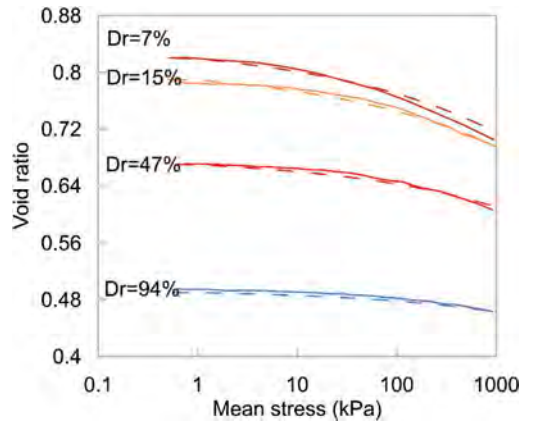


Figure 2. Simulation and experimental results of oedometer tests on loose to dense sand (Solid lines: experiment; dashed lines: simulations).

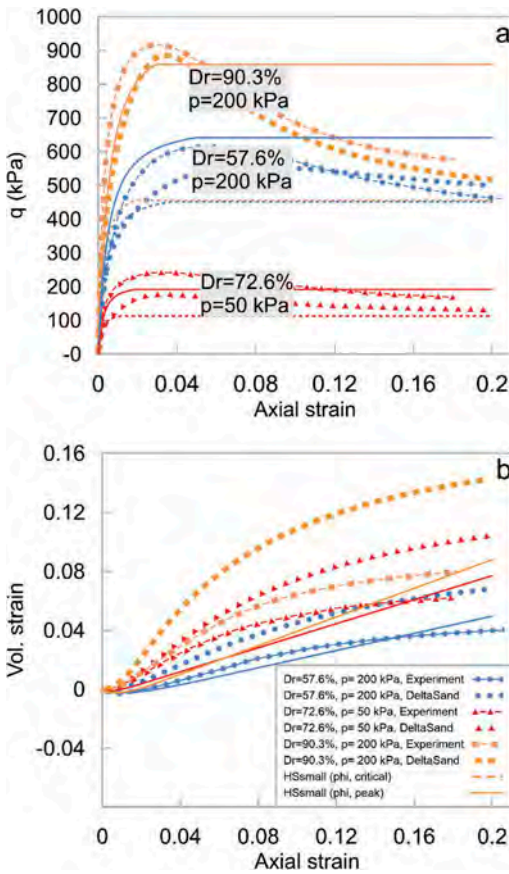


Figure 3. Simulation (DeltaSand and HSSmall) and experimental results of drained monotonic triaxial tests on medium dense and dense sand.

3.2.1 DeltaSand constitutive model

A sensitivity analysis to identify the optimum mesh size was conducted for DeltaSand. The results of simulations for fine, medium-fine, and coarse mesh

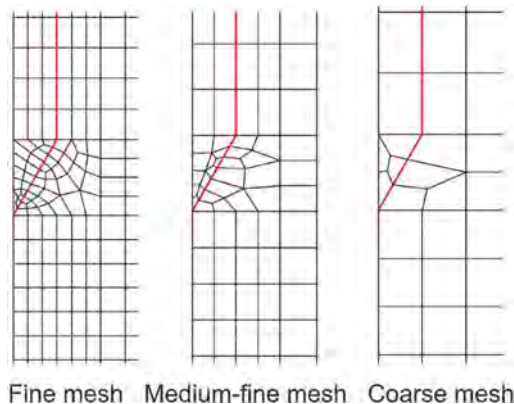


Figure 4. Different mesh size adjacent to cone.

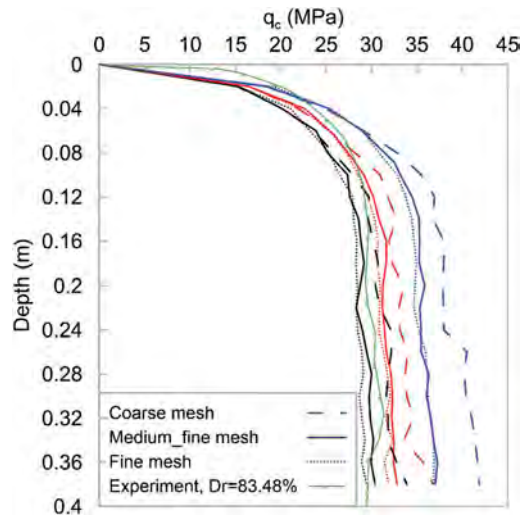


Figure 5. Mesh size effect on q_c - Dr results (Black: $Dr = 83.48\%$, red: $Dr = 86.85\%$, and blue: $Dr = 92.53\%$).

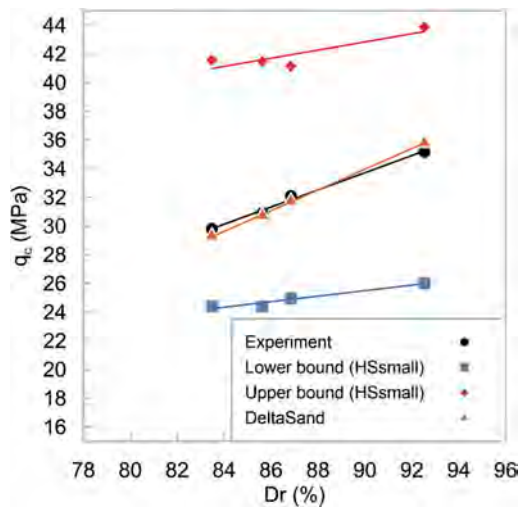


Figure 6. Comparison of experimental and numerical results using DeltaSand and HSSmall model (Upper bound obtained using ϕ_{peak} and lower bound using $\phi_{critical}$ in HSSmall model).

were compared to each other. The obtained averaged q_c regarding depths between 18-32 cm for fine and coarse mesh are within 2% and 5% of the ones obtained with fine mesh. The number of elements for coarse mesh is 929 and for medium-fine and fine mesh are 2463 and 3680, respectively. The average element size exactly beneath the tip for coarse mesh is 4 mm and for medium-fine and fine mesh are 1.7 mm and 1.1 mm, respectively. Therefore, the medium-fine is an optimum choice for analysis, considering that the results do not differ tremendously

from the ones obtained from finer mesh. Moreover, using medium-fine mesh is computationally more efficient. Figure 4 shows different mesh sizes adjacent to the cone. Figure 5 illustrates the results of q_c in different depth for different mesh sizes. Besides, the experiment result for relative density 83.48% is included in this figure.

Figure 6 illustrates the $q_c - D_r$ curve for both numerical and experimental data under BC5 condition. The obtained results with DeltaSand match well with the experimental data. A set of parameters is used for all relative densities, which demonstrates the capability of DeltaSand.

3.2.2 HS-small constitutive model

The input parameters for HS-small model are calibrated based on relative density for the Cuxhaven sand and were presented in Table 2 and Figure 3. Figure 3 represents the calibration results based on two different friction angles- peak and critical friction angles are shown by solid and dashed lines, respectively. Figure 6 compares the obtained $q_c - D_r$ curve from numerical modeling with laboratory tests under the BC5 condition. Contrary to the DeltaSand model, the Hardening Soil has no state-dependent parameter. It should be noted that the simulations are run with two different friction angles, the critical friction angle as lower bound and the peak friction angle upper bound, while other parameters are constant. The experimental data are located between the lower and upper bound numerical simulations. Another shortcoming of the HS-small soil model is that different sets of parameters have to be used for each relative density.

4 CONCLUSION

In this study, the cone penetration in a small volume calibration chamber MARCC was simulated using two different constitutive soil models, namely Hardening Soil with small-strain stiffness and DeltaSand.

Prior to simulations, material parameters were calibrated for both constitutive soil models based on the laboratory tests. The results showed that DeltaSand can capture the sand behavior better than the HSsmall.

The result of simulations showed that the DeltaSand model can capture the soil behavior around the cone for different relative densities with one set of parameters. Simulating CPT with HS-small soil models, however needs recalibration of material parameters for different relative densities and neither calibration of the model at peak strength nor at critical state strength could reproduce the experimental results for a complex problem like CPT. Moreover, the effect of element size on simulation outcomes was analyzed in this study. The simulations showed that the mesh size has a negligible effect on the results for fine and medium-fine meshes, while a coarse mesh can affect the results.

ACKNOWLEDGMENT

The authors would like to acknowledge the support of the project “VCPTu2PDA”, FKZ: 03EE3025A by the Federal Ministry for Economic Affairs and Energy (BMWi) and the MARUM—Center for Marine Environmental Sciences, University of Bremen. The help and assistance of Geo-Engineering.org GmbH, RWE Renewables GmbH, Deltares and COWI A/S as project partners are also greatly appreciated.

REFERENCES

- Al-Kafaji, I. K. J. (2013) *Formulation of a Dynamic Material Point Method (MPM) for Geomechanical Problems*, University of Stuttgart.
- Al-Mhaidib, A. I. (2005) ‘Shearing rate effect on interfacial friction between sand and steel’, in *The Fifteenth International Offshore and Polar Engineering Conference*.
- Benz, T. (2007) *Small strain stiffness of soils and its consequences*. Universität Stuttgart.
- Beuth, L., Benz, T., Vermeer, P. A., Coetzee, C. J., Bonnier, P. and Van Den Berg, P. (2007) ‘Formulation and validation of a quasi-static material point method’, in *Proceedings of the 10th international symposium on numerical methods in Geomechanics (NUMOG)*, Rhodes, Greece, pp. 189–195.
- Beuth, L. and Vermeer, P. A. (2013) ‘Large deformation analysis of cone penetration testing in undrained clay’, *Installation effects in geotechnical engineering*. Taylor & Francis Group London.
- Carbonell, J. M., Monforte, L., Ciantia, M. O., Arroyo, M. and Gens, A. (2022) ‘Geotechnical particle finite element method for modeling of soil-structure interaction under large deformation conditions’, *Journal of Rock Mechanics and Geotechnical Engineering*. Elsevier.
- Coetzee, C. J., Vermeer, P. A. and Basson, A. H. (2005) ‘The modelling of anchors using the material point method’, *International journal for numerical and analytical methods in geomechanics*. Wiley Online Library, 29(9), pp. 879–895.
- Fan, S., Bienen, B. and Randolph, M. F. (2018) ‘Stability and efficiency studies in the numerical simulation of cone penetration in sand’, *Geotechnique Letters*, 8(1), pp. 13–18. doi: 10.1680/jgele.17.00105.
- Fleischer, M., Kreiter, S., Mörz, T. and Huhndorf, M. (2016) ‘A small volume calibration chamber for cone penetration testing (CPT) on submarine soils’, in *Submarine Mass Movements and their Consequences*. Springer, pp. 181–189.
- Galavi, V. (2021) ‘DeltaSand: A state dependent double hardening elasto-plastic model for sand: Formulation and validation’, *Computers and Geotechnics*, 129(April 2020). doi: 10.1016/j.compgeo.2020.103844.
- Galavi, V., Martinelli, M., Elkadi, A., Ghasemi, P. and Thijssen, R. (2019) ‘Numerical simulation of impact driven offshore monopiles using the material point method’, *Proceedings of the XVII ECSMGE - Geotechnical Engineering foundation of the future*, (September). doi: 10.32075/17ECSMGE-2019-0758.
- Ghasemi, P., Calvello, M., Martinelli, M., Galavi, V. and Cuomo, S. (2018) ‘MPM simulation of CPT and model calibration by inverse analysis’, *Cone Penetration Testing 2018 - Proceedings of the 4th International*

- Symposium on Cone Penetration Testing, CPT 2018*, pp. 295–301.
- Goodarzi, M. and Rouainia, M. (2017) ‘Modelling Slope Failure Using a Quasi-static MPM with a Non-local Strain Softening Approach’, *Procedia Engineering*. Elsevier B.V., 175, pp. 220–225. doi: 10.1016/j.proeng.2017.01.015.
- Goodarzi, M., Stähler, F. T., Kreiter, S., Rouainia, M., Kluger, M. O. and Mörz, T. (2018) ‘Numerical simulation of cone penetration test in a small-volume calibration chamber: The effect of boundary conditions’, in *Cone Penetration Testing 2018*. CRC Press, pp. 309–315.
- Huang, W., Sheng, D., Sloan, S. W. and Yu, H. S. (2004) ‘Finite element analysis of cone penetration in cohesionless soil’, *Computers and Geotechnics*, 31(7), pp. 517–528. doi: 10.1016/j.compgeo.2004.09.001.
- Khosravi, A., Martinez, A. and DeJong, J. T. (2020) ‘Discrete element model (DEM) simulations of cone penetration test (CPT) measurements and soil classification’, *Canadian Geotechnical Journal*, 57(9), pp. 1369–1387. doi: 10.1139/cgj-2019-0512.
- Kluger, M. O. (2014) *Hypoplastizität: Von der Parameterbestimmung bis zur numerischen Modellierung eines Cuxhavener Sandes*. Universität Bremen.
- Kluger, M. O., Kreiter, S., Stähler, F. T., Goodarzi, M., Stanski, T. and Mörz, T. (2021) ‘Cone penetration tests in dry and saturated Ticino sand’, *Bulletin of Engineering Geology and the Environment*. Bulletin of Engineering Geology and the Environment, (2006). doi: 10.1007/s10064-021-02156-y.
- Lunne, T. (2010) ‘The CPT in offshore soil investigations—a historic perspective’, *Proc. CPT*, 10, pp. 71–113.
- Martinelli, M. and Galavi, V. (2021) ‘Investigation of the Material Point Method in the simulation of Cone Penetration Tests in dry sand’, *Computers and Geotechnics*. Elsevier Ltd, 130(November), p. 103923. doi: 10.1016/j.compgeo.2020.103923.
- Matsuoka, H. and Nakai, T. (1974) ‘Stress-deformation and strength characteristics of soil under three different principal stresses’, in *Proceedings of the Japan Society of Civil Engineers*, pp. 59–70.
- Monforte, L., Arroyo, M., Carbonell, J. M. and Gens, A. (2017) ‘Numerical simulation of undrained insertion problems in geotechnical engineering with the Particle Finite Element Method (PFEM)’, *Computers and Geotechnics*, 82, pp. 144–156. doi: 10.1016/j.compgeo.2016.08.013.
- Monforte, L., Arroyo, M., Carbonell, J. M. and Gens, A. (2018) ‘Coupled effective stress analysis of insertion problems in geotechnics with the particle finite element method’, *Computers and Geotechnics*. Elsevier, 101, pp. 114–129.
- Moug, D. M., Boulanger, R. W., DeJong, J. T. and Jaeger, R. A. (2019) ‘Axisymmetric Simulations of Cone Penetration in Saturated Clay’, *Journal of Geotechnical and Geoenvironmental Engineering*, 145(4), p. 04019008. doi: 10.1061/(asce)gt.1943-5606.0002024.
- Plaxis (2021) ‘PLAXIS 2D Manual’. Bentley Systems.
- Schweiger, H. F. and Hauser, L. (2021) *Numerical Simulation of CPT with the Clay and Sand Model (CASM) Including Effects of Bonding, Lecture Notes in Civil Engineering*. Springer International Publishing. doi: 10.1007/978-3-030-64514-4_11.
- Sołowski, W. T. and Sloan, S. W. (2015) ‘Evaluation of material point method for use in geotechnics’, *International Journal for Numerical and Analytical Methods in Geomechanics*. Wiley Online Library, 39(7), pp. 685–701.
- Stähler, F. T., Kreiter, S., Goodarzi, M., Al-Sammarraie, D., Stanski, T. and Mörz, T. (2018) ‘Influences on CPT-results in a small volume calibration chamber’, in *Proceedings of China-Europe Conference on Geotechnical Engineering*, pp. 730–733.
- Sulsky, D., Chen, Z. and Schreyer, H. L. (1994) ‘A particle method for history-dependent materials’, *Computer methods in applied mechanics and engineering*. Elsevier, 118(1–2), pp. 179–196.
- Susila, E. and Hryciw, R. D. (2003) ‘Large displacement FEM modelling of the cone penetration test (CPT) in normally consolidated sand’, *International Journal for Numerical and Analytical Methods in Geomechanics*, 27(7), pp. 585–602. doi: 10.1002/nag.287.
- Tolooiyan, A. and Gavin, K. (2010) ‘Finite element analysis of the CPT for design of bored piles’, in *2nd International Symposium on Cone Penetration Testing, Huntington Beach, CA, USA*.
- Zabala, F. and Alonso, E. E. (2011) ‘Progressive failure of Aznalcóllar dam using the material point method’, *Géotechnique*. Thomas Telford Ltd, 61(9), pp. 795–808.

CPT calibration in centrifuge: Effect of partial saturation on cone resistance

V. Fioravante

Department of Engineering, University of Ferrara, Italy

D. Giretti

Department of Engineering and Applied Science, University of Bergamo, Italy

E. Dodaro, C.G. Gragnano & G. Gottardi

Department of Civil, Chemical, Environmental and Materials Engineering, University of Bologna, Italy

ABSTRACT: When dealing with unsaturated soil conditions, the influence of matric suction on cone tip resistance of the soil above the ground water table is typically neglected in engineering practice, with consequent possible misinterpretation of soil features. In the last decades, various researchers have investigated the influence of suction on cone resistance for sands, whilst still little is known for silty materials, whose contribution can be significant and extended for many meters above the groundwater table. Such issue is especially relevant for compacted earth structures, like river embankments, typically made of a heterogeneous mixture of intermediate soils. With the aim of providing a contribution and stimulating its correct implementation into geotechnical practice, a set of miniature piezocone tests have been carried out in a centrifuge on both saturated and partially saturated silty sand models. The interpretation of CPT results is discussed, highlighting the effect of partial saturation on cone tip resistance.

1 INTRODUCTION

Due to its reliability and time and cost effectiveness, the cone penetration test (CPT) represents a valuable tool for continuous stratigraphy profiling and geotechnical soil properties estimation. Most of the existing approaches for analyzing CPT results are based on fully saturated or dry conditions, for which interpretation methods are well established and have a solid theoretical background (Robertson and Campanella 1983a, b; Lunne et al. 1997; Mayne 2007; Robertson 2009). However, in several cases CPT soundings may cross a vadose zone, conventionally extended from the ground level to the water table, where partially saturated soil states are very likely to occur. Thus, a reliable interpretation of CPT data in unsaturated soil layers is of pivotal importance for the design, optimization and management of the engineering works interacting with soils at shallow depths (e.g. foundations, road pavements) or influenced by infiltration, evapo-transpiration and transient groundwater flow, such as river embankments, earth dams or backfill of retaining walls.

As observed by Yang and Russell (2016), for an accurate analysis of CPT results in partially saturated soils, the in-situ stress state needs to be accurately evaluated, taking into account the variations with depth of the matric suction and the effective degree of saturation of soils. In the current practice, instead, the

contribution of suction to the effective stress is frequently neglected, due to difficulties in assessing the in-situ moisture content and in obtaining a reliable pore water pressure distribution, often resulting in excessively conservative design approaches and in the incorrect evaluation of soil features (Russell and Khalili 2006). Various studies have been recently carried out to gain insights on the influence of unsaturated conditions on CPT data, mostly limited to sandy soils (Hryciw and Dowding 1987; Bolton et al. 1999; Russell et al. 2010; Pourmaghiazar et al. 2013; Jarast and Ghayoomi 2018), all showing evidence that the cone penetration resistance, q_c , can be significantly increased by suction. Conversely, limited research has been carried out on CPTs in unsaturated silty materials (Silva and Bolton 2005; Tan 2005; Yang and Russell 2016), due to the intrinsic complexity related to partial drainage, occurring during penetration at the standard rate of 20 mm/s (Paniagua et al. 2014), and to the microfabric of intermediate soils. Most of these studies have been performed on reconstituted samples, under the controlled laboratory environment of calibration chambers or centrifuges, in order to eliminate the typical uncertainties related to soil heterogeneity and parameters estimation, while only few field tests have been performed so far to evaluate the effect of soil moisture content on the cone resistance, q_c (Lehane et al. 2004; Collins and Miller 2014; Giacheti et al. 2019). The

present paper aims at contributing to a better understanding of the effect of matric suction on CPT results interpretation. For this purpose, a set of piezocone tests have been carried out on a compacted mixture of sand and finer material in the 240 g-ton geotechnical centrifuge facility at the Experimental Institute for Geotechnical Modelling (Italian acronym: ISMGEO) of Seriate (Bergamo, Italy), in both saturated and partially saturated conditions. The use of monitoring sensors allows to clearly define the pore pressure distribution of the models under different water table depths. Furthermore, implications of using various assumptions on the calculation of the effective stress states during penetration, starting from matric suction measures, are preliminarily discussed and CPT calibration in the centrifuge is attempted.

2 EXPERIMENTAL CAMPAIGN

2.1 Equipment, tested material and test procedure

A scheme of models tested is presented in Figure 1. The testing soils are Ticino sand (TS, Baldi et al., 1982, 1986, Fioravante, 2000, Jamiolkowski et al., 2003, Fioravante & Giretti, 2016) and Pontida clay (PON, Ventini et al. 2021). TS is a coarse to medium, uniform silica sand, of alluvial origin, mainly composed by angular grains; PON is a low plasticity kaolinitic clayey silt, deposited in a post-glacial lake environment. The overall experimental campaign has been performed considering different mixtures of TS and PON. However, in this contribution, only the results of a test carried out on a mixture of 85% by weight of TS and 15% by weight of PON are discussed. The main physical properties of the mixture, obtained from an accurate laboratory characterization, are listed in Table 1. In particular, the minimum and maximum dry density have been obtained following ASTM 4254 - Method A (2016) and ASTM D1557 - 12e1 (2012) - Modified Proctor method, respectively. Figure 2 compares the grain size distribution of TS, PON and the mix.

Table 1. Main physical properties of the mixed soil 85% TS+15%PON.

SOIL	G_s	d_{50}	C_U	C_C	$\gamma_{d,min}$	$\gamma_{d,max}$
		mm	-	-	kN/m ³	kN/m ³
85%TS+15% PON	2,695	0,499	13,2	10,9	13,92	18,15

The ISMGEO miniaturized piezocone used in the tests has a diameter $d = 11.3$ mm and a total cone area of 100.3 mm². It incorporates a 60° cone tip with a load cell to measure tip forces up to 9.8 kN and a 36.9 mm long shaft, which connects to an upper

section containing a second 9.8 kN load cell, used to measure tip resistance plus sleeve friction. In addition, the cone has a 35-bar capacity Druck PDCR pressure transducer for interstitial pressure measurements. Physical models were reconstituted in layers of prescribed height to obtain a 1g dry density of 90% of $\gamma_{d,max}$ and using an initial water content of about 17%. The container was a cylindrical box, 400 mm in diameter. With a ratio D/d (D is the container diameter) equal to about 36, boundary side effects were minimized. During the reconstitution, pore pressure transducers (ppts M, P, Q, N, R) and tensiometers (tens 1, 2, 3) were embedded in the model at prescribed heights (Figure 1) and at a distance of 50 mm from the box axis. Once the total height was achieved, the soil saturation was completed applying to the model a continuous vacuum pressure of about -70 kPa for 12 hours. Then a rigid frame which holds a linear displacement transducer to monitor

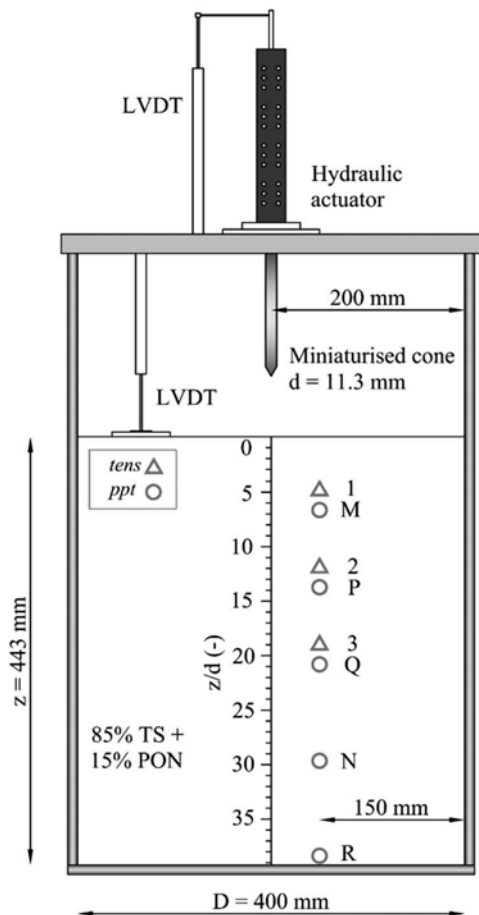


Figure 1. Sketch of the cylindrical strongbox containing details of geometry, transducers and in-flight miniature probe.

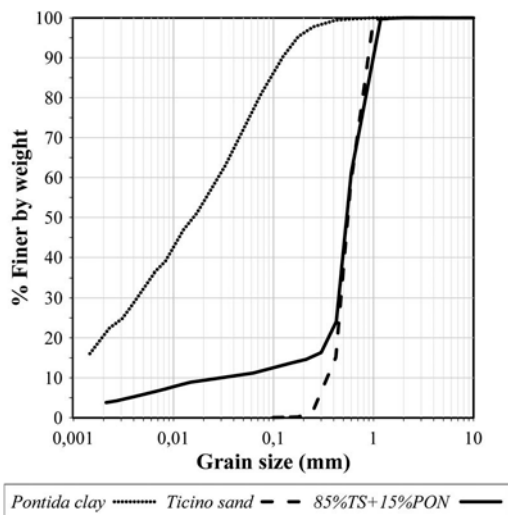


Figure 2. Grain size distribution of the tested soils.

the soils surface settlement, the miniaturized piezocone and the actuator was fixed to the top of the container.

The container was loaded onto the centrifuge and accelerated to the target (50g at the soil surface). After the in-flight consolidation, a first CPTU was carried out in the central axis of the model. At the end of penetration, the penetrometer was lifted, the centrifuge was stopped, the equipment was moved 70 mm from the original position and the model was re-accelerated. When the pore pressure equilibrium was achieved again, as identified by real-time pore pressure monitoring data, an outflow was imposed to the soil model by opening a hydraulic valve placed at the bottom of the cylindrical box. The outflow was interrupted when the water table reached almost mid depth. Following pore pressure stabilization, a second CPTU was carried out in a model partially saturated in the upper part and saturated below, with matric suction and pore pressure data continuously recorded. It has to be noticed that, due to settlement induced by saturation, centrifuge accelerations and desaturation of the model, the soil sample underwent a progressive increase in density, with an average void index value equal to 0.480 (at the beginning of the test in saturated conditions) and to 0.475 (at the beginning of the test in partially saturated conditions).

3 CENTRIFUGE TEST RESULTS

The data recorded during the piezocone advancement in both fully saturated soil conditions (continuous lines) and with the phreatic surface below the ground level (dotted lines) are presented in Figure 3. To take into account the progressive mobilization of the cone resistance from the free model surface (Schmertmann, 1978), the data registered in the first

10 d of penetration from the ground level were removed (Gui and Bolton 1998). The plot shows the variation with the dimensionless depth (i.e. the ratio between penetration depth, z , and cone diameter, d) of the sleeve friction resistance, f_s , and of the corrected cone tip resistance, q_t , this latter expressed as:

$$q_t = q_c + u_2(1 - a) \quad (1)$$

where q_c is the measured cone tip resistance, $a = 0.785$ is the net area ratio, determined from laboratory calibration, and u_2 is the pore pressure generated during cone penetration and measured just behind the cone. In addition, the pore pressure values measured by ppts (in the positive range) and tensiometers (both in positive and negative ranges) are also plotted, with circles and triangles, respectively, together with u_2 data. The dimensionless depth of the water level has been determined from the measures of the ppt placed at the bottom of the

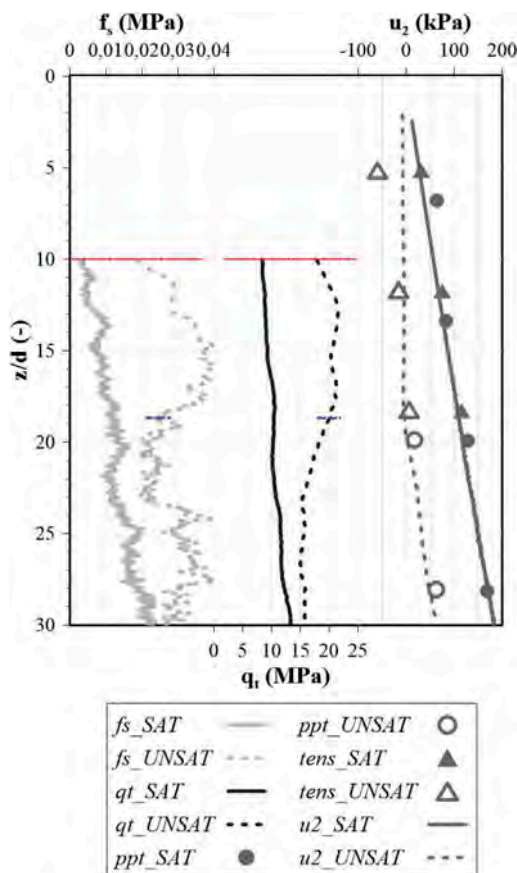


Figure 3. Variation with the dimensionless depth, z/d , of the sleeve friction resistance, f_s , of the pore pressure generated during cone penetration, u_2 , together with the pore pressure measurements (circles and triangles) and of corrected cone tip resistance, q_t .

model; for the test in unsaturated conditions, its value, $z/d_{w,UNSAT}$ is equal to 18.7 and is drawn in bold hatched line (Figure 3).

The ppts and tensiometers monitoring data fit quite well the u_2 measured during penetration, showing a hydrostatic distribution of pore pressures in the positive range of values in both experiments (*SAT* and *UNSAT*) and a less than hydrostatic distribution in the unsaturated area (*UNSAT* model), highlighting that the process of lowering the water table led to a hydraulic equilibrium of pore pressure in the saturated soil area also for the unsaturated test. On the other hand, distributions of q_t and f_s show significant differences between the two tests, i.e. higher cone tip resistance and sleeve friction in the area where desaturation occurred, where the suction effect is clearly tangible. It should be noticed that, since the cone tip and sleeve friction resistances vary with the relevant overburden stress for the same material, the CPT data plotted in Figure 3 require a stress normalization for a proper interpretation and comparison of resistance profiles.

4 STRESS NORMALIZATION

Stress conditions are significantly different in the two tests. The change in the water table depth, in fact, leads to a variation of the saturation level and produces suction states in the partially saturated soil in the *UNSAT* experiment and subsequent effects on the test results. At least two independent stress state variables should be considered for an accurate description of the relevant soil behaviour (i.e. Morgenstern, 1979; Fredlund et al., 2012); however, it is also well known that the most commonly used CPT charts and correlations are based on a single-valued effective stress approach. To show the implications of adopting a single-valued effective stress approach, the Bishop's effective stress equation (1959) for unsaturated soils has been here used, such as:

$$\sigma' = (\sigma - u_a) + S_r(u_a - u_w) \quad (2)$$

with $(\sigma - u_a)$ being the net stress, S_r the degree of saturation and $(u_a - u_w)$ the matric suction. For such test interpretation, it is therefore required the knowledge of the distribution of S_r and of $(u_a - u_w)$, typically not readily available in traditional engineering applications. Two different assumptions have been thus made here, with a first simplified case (*UNSAT,1*) considering a hydrostatic distribution of pore pressure above the groundwater line and a constant degree of saturation equal to 0.5, while a second case (*UNSAT,2*) aims at representing the experimental conditions closely, with a matric suction distribution determined on the base of tensiometer measurements and a variable degree of saturation, provided by the water retention curve obtained from physical soil properties through the procedure suggested in Aubertin et al. (2003). For both cases, the calculated values of total stress, σ_v , and effective stress,

σ'_v , the pore pressure, u_0 , and the degree of saturation are plotted with dimensionless depth in Figure 4. Considering a constant 0.5 value of the degree of saturation (*UNSAT,1*), a noticeable increase in the effective stress distribution is produced. Instead, due to the significant percentage of sand in the tested material, the degree of saturation tends to rapidly reduce with the increase of matric suction (absolute) values, evidencing in case *UNSAT,2*, a limited impact on the effective stress as calculated with equation (2). It is now possible to try to determine general trends in the soil response to CPT advancement.

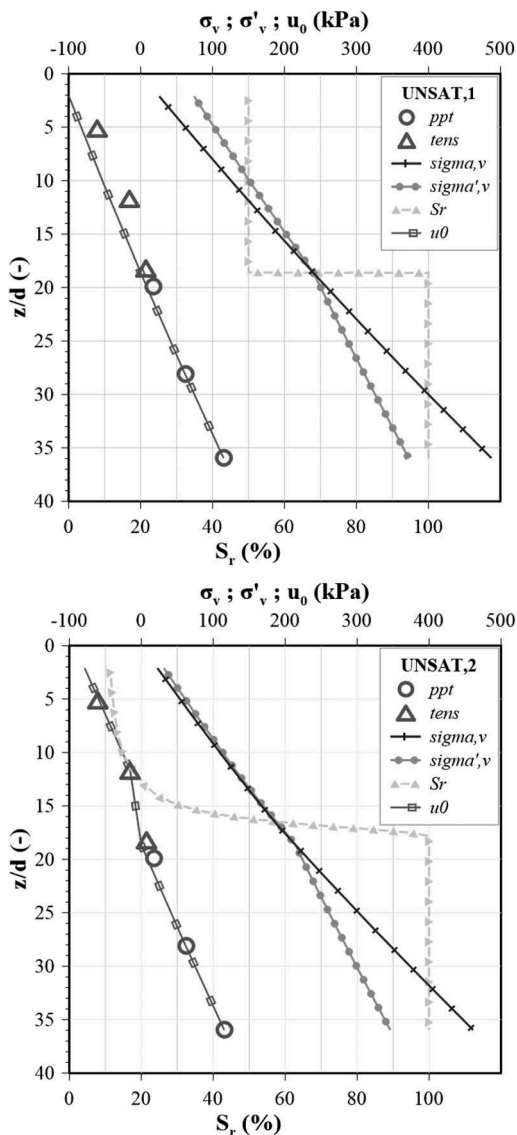


Figure 4. Calculated values of total, σ_v , and effective, σ'_v , stresses acting on vertical direction, pore pressure, u_0 , and degree of saturation, S_r , are plotted with dimensionless depth, z/d , under a simplified assumption (*UNSAT,1* top graph) and based on tensiometer data (*UNSAT,2* bottom graph).

According to Robertson's (2009) very popular unified approach, the normalized cone resistance, Q_m , and the Soil Behavior Type index, I_{cn} , are calculated using a stress exponent, n , that varies with soil type and stress level. Specifically:

$$Q_m = \left(\frac{q_t - \sigma_v}{p_{a2}} \right) \left(\frac{p_a}{\sigma'_v} \right)^n \quad (3)$$

$$I_{cn} = \left[(3.47 - \log Q_m)^2 + (\log F + 1.22)^2 \right]^{0.5} \quad (4)$$

$$n = 0.381(I_{cn}) + 0.05 \left(\frac{\sigma'_v}{P_a} \right) - 0.15 \quad (5)$$

$$F = f_s / [(q_t - \sigma_v)] \quad (6)$$

where p_a and p_{a2} are reference pressures in the same units of q_c , σ_v and σ'_v , while F is the normalized friction ratio. Results obtained from the present CPT tests performed before (*SAT*) and after (*UNSAT*) the water table lowering are plotted in Figure 5, in terms of Q_m and I_{cn} , considering both the simplified (*UNSAT,1*) and the more accurate (*UNSAT,2*) assumptions for the calculation of stress conditions (see Figure 4). Considering the test conducted in fully saturated conditions (*SAT*), values of Q_m and I_{cn} tend to be relatively constant with depth and typical of sandy materials, in good agreement with Robertson's approach.

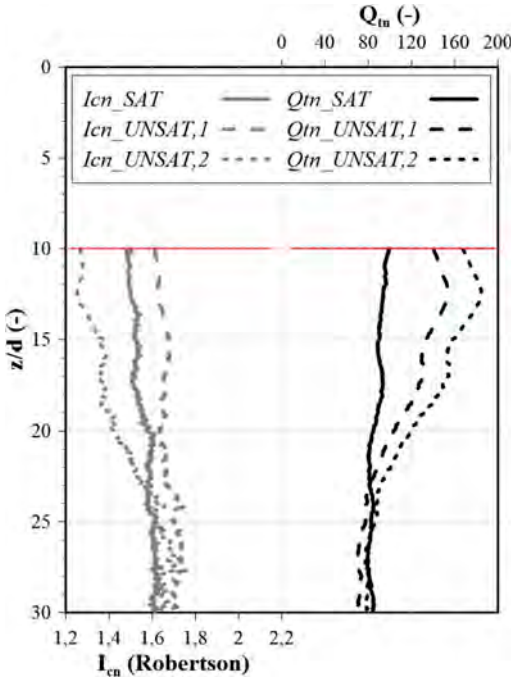


Figure 5. Variation with the dimensionless depth, z/d , of the normalized cone resistance, Q_m , and the Soil Behavior Type index, I_{cn} , calculated using the stress exponent, n .

However, for the test performed after the water table lowering, significant variations can be found in the values of Q_m when comparing the advancement in the saturated versus the unsaturated zones. For dimensionless depths lower than $z/d_{w,UNSAT}$ (18.7), none of the two assumptions on the effective stress and saturation degree provide uniform Q_m profiles, despite the material is essentially the same in the two experiments, showing higher normalized cone resistances in the unsaturated with respect to the saturated zone. Indeed, below the water table, the assumption based on monitoring data (*UNSAT,2*) tends to produce similar values to the test performed in fully saturated conditions, rather than for the case of a simplified assumption (*UNSAT,1*). Analogous observations can be done for the I_{cn} data, always within the range of sandy materials (1.31 – 2.05), but with substantial differences between the saturated and the unsaturated zones.

Hence, adopting a single-valued effective stress approach for stress normalization to interpret the CPT data in the unsaturated zone appears to be not fully reliable.

5 CONCLUSIONS

Results from small-scale laboratory tests, which included CPT execution with pore pressure and suction measurements in a centrifuge environment, have been presented herein. The experiments described are referred to a soil mixture, made of mainly coarse-grained particles with a limited fine fraction, tested under different saturation conditions. In fact, the only variation in the two presented cases was related to their water table depth, either at almost the ground surface or at a lower level, obtained through a dewatering process. Monitoring sensors, pore pressure transducers and tensiometers, located along the model depth, played an essential role in determining the soil suction distribution above the water table and in identifying the hydraulic equilibrium reached at the end of the outflow phase. Data measured during cone penetration tests (f_s , q_t and u_2), before and after the dewatering process, show only limited differences in the saturated zones, further reduced by adopting the stress normalization of Robertson's unified approach.

On the other side, when comparing cone penetration data measured in the unsaturated versus the saturated zones, substantial differences in the selected stress-normalized results (Q_m and I_{cn}), regardless of the assumption on suction and saturation degree profiles above the water table, can be detected. Therefore, from the data presented herein, it would appear that the effect of partial saturation on cone tip resistance provided by the matric suction is not duly taken into account by simply applying a stress normalization by the Bishop's equation for unsaturated soils. In other terms, it seems that the combined use of a single effective stress variable (as typically assumed when more specific information on

unsaturated soil behavior is lacking) with the standard CPT charts and correlations cannot produce a similarly reliable data interpretation. Additional investigations, including the use of other materials, are clearly required to better define such critical issue.

ACKNOWLEDGMENT

This research was funded under the scheme for “Research Projects of National Relevance” (in Italian: Progetti di Ricerca di Rilevante Interesse Nazionale-PRIN), Bando 2017, grant number 2017YPMBWJt, promoted by the Italian Ministry of Education, University and Research (in Italian: Ministero dell’Istruzione, dell’Università e della Ricerca-MIUR).

REFERENCES

- ASTM D1557-12e1. 2012. Standard Test Methods for Laboratory Compaction Characteristics of Soil Using Modified Effort (56,000 658 ft-lbf/ft³ (2,700 kN-m/m³)). ASTM International, West Conshohocken, PA.
- ASTM D4254-16. 2016. Standard test methods for minimum index density and unit weight of soils and calculation of relative density. ASTM International, West Conshohocken, PA
- Aubertin, M., Mbonimpa, M., Bussière, B. & Chapuis, R.P. 2003. A model to predict the water retention curve from basic geotechnical properties. *Canadian Geotechnical Journal*. 40: 1104–1122.
- Baldi, G., Bellotti, R., Ghionna, V., Jamiolkowski, M. & Pasqualini, E. 1982. *Design parameters for sand from CPT. Proc. 2nd European Symposium on Penetration Testing*. Amsterdam: 425-432.
- Baldi, G., Bellotti, R., Ghionna, N., Jamiolkowski, M. & Pasqualini, E. 1986. Interpretation of CPTs and CPTU's. *2nd Part. Proc. 4th International Geotechnical Seminar*. Nanyang Technological Institute, Singapore: 143–156.
- Bishop, A. W. 1959. The principle of effective stress. *Teknisk Ukeblad*. 106(39): 859–863.
- Bolton, M.D., Gui, M.W., Garnier, J., Corte, J.F., Bagge, G., Laue, J. & Renzi, R. 1999. Centrifuge cone penetration tests in sand. *Géotechnique*. 49(4): 543–552.
- Collins, R. & Miller, G.A. 2014. Cone penetration testing in unsaturated soils at two instrumented test sites. *Proc. 6th International Conference on Unsaturated Soils*. Sidney, Australia: 1489-1494.
- Fioravante, V. 2000. Anisotropy of small strain stiffness of Ticino and Kenya Sands from seismic wave propagation measured in triaxial testing. *Soils and Foundations*. 40(4): 129–142.
- Fioravante, V. & Giretti, D. 2016. Unidirectional cyclic resistance of Ticino and Youyora sands from centrifuge cone penetration tests. *Acta Geotechnica*. 11(4): 953–968.
- Fredlund, D.G., Rahardjo, H., & Fredlund, M.D. 2012. *Unsaturated soil mechanics in engineering practice*. New York: John Wiley & Sons.
- Giacheti, H., Rodrigues, R., Bezerra, R. & Rocha, B. 2019. Seasonal influence on cone penetration test: An unsaturated soil site interpretation. *Journal of Rock Mechanics and Geotechnical Engineering*. 11(2): 361–368.
- Gui M. W. & Bolton M. D. 1998. Geometry and scale effects in CPT and pile design, *Proc. 1st International Conference on Geotechnical Site Characterization*. Atlanta, Georgia: 1063–1068.
- Hryciw, R.D. & Dowding, C.H. 1987. Cone penetration of partially saturated sands. *Geotechnical Testing Journal*. 10 (3): 135–141.
- Jamiolkowski, M.B., Lo Presti, D.C.F., & Manassero, M. 2001. Evaluation of Relative Density and Shear Strength from CPT and DMT. *ASCE Geotechnical Special Publication*. 119: 201–238.
- Jarast, P. & Ghayoomi, M. 2018. Numerical modeling of cone penetration test in unsaturated sand inside a calibration chamber. *International Journal of Geomechanics*. 18 (2).10.1061/(ASCE)GM.1943-5622.0001052.
- Lehane, B.M., Ismail, M.A. & Fahey, M. 2004. Seasonal dependence of in situ test parameters in sand above the water table. *Géotechnique*. 54(3): 215–218
- Lunne, T., Robertson, P.K. & Powell, J. 1997. *Cone penetration testing in geotechnical practice*. London: Blackie Academic and Professional.
- Mayne, P.W. 2007. *Cone penetration testing. A synthesis of highway practice*. Washington, D.C.: Transportation Research Board.
- Morgenstern, N. R. 1979. Properties of compacted soils, *Proc. 6th Pan American Conference on Soil Mechanics and Foundation Engineering*. Lima, Peru. 3: 349–354.
- Paniagua, P. & Nordal, S. 2015. Influence of variable rates of penetration on silt behavior and its SBT classification. *Proc. 15th Pan-American Conference on Soil Mechanics and Geotechnical Engineering*. Buenos Aires, Argentina: 509-516.
- Pournaghiazar, M., Russell, A.R. & Khalili, N. 2013. The cone penetration test in unsaturated sands. *Géotechnique*. 63(14): 1209–1220.
- Robertson, P.K. 2009. Interpretation of cone penetration tests - A unified approach. *Canadian Geotechnical Journal*. 46 (11): 1337–1355.
- Robertson, P.K., and Campanella, R.G. 1983a. Interpretation of cone penetration tests. Part I: Sand. *Canadian Geotechnical Journal*. 20(4): 718–733.
- Robertson, P.K., and Campanella, R.G. 1983b. Interpretation of cone penetration tests. Part II: Clay. *Canadian Geotechnical Journal*. 20(4), 734–745.
- Russell, A.R., and Khalili, N. 2006. On the problem of cavity expansion in unsaturated soils. *Computational Mechanics*. 37(4): 311–330.
- Russell, A.R., Pournaghiazar, M. & Khalili, N. 2010. Interpreting CPT results in unsaturated sands. *Proc. 2nd International Symposium on Cone Penetration Testing*. Huntington Beach, USA.
- Schmertmann, J.H. 1978. Guidelines for Cone Penetration Test (Performance and Design). *U.S. Department of Transportation, Federal Highway Administration*. Report FHWA-TS-, Washington: 787–209.
- Silva, M. & Bolton, M. 2005. Interpretation of centrifuge piezocone tests in dilatant, low plasticity silts. *Proc. of International Conference on Problematic Soils*. Cyprus, Greece.
- Tan, N.K. 2005. Pressuremeter and cone penetrometer testing in a calibration chamber with unsaturated Minco Silt. *PhD dissertation*. University of Oklahoma.
- Ventini, R., Dodaro, E., Gragnano, C.G., Giretti, D., & Pirone, M. 2021. Experimental and numerical investigations of a river embankment model under transient seepage conditions. *Geosciences*. 11(5), 192.
- Yang, H. & Russell, A.R. 2016. Cone penetration tests in unsaturated silty sands. *Canadian Geotechnical Journal*, 53(3): 431–444.

Calibration cone penetration testing in silty soils

V. Fioravante

University of Ferrara, Italy

D. Giretti

University of Bergamo, Italy

T. Lunne & P. Carotenuto

Norwegian Geotechnical Institute, Norway

A.H. Augustesen, R. Lindeboom & L. Krogh

Ørsted, Denmark

H. Dias

Equinor

M.-C. Sougle

Vattenfall

A. Barwise

RWE

S. de Wit

Shell

D. Burbury

Scottish Power Renewables

ABSTRACT: The Offshore Wind Industry's rapid expansion across the globe requires geotechnical modeling of sites that are often characterized by layers of silty sand and silt mixtures. The CPTU is the main *in situ* offshore investigation tool for defining the ground conditions and for establishing facility position and soil parameters for foundation design, but no simple and robust methodologies exist for characterizing transitional soils. This paper presents some results of CPTUs carried out in a large calibration chamber and in a centrifuge aimed at contributing to the development of guidelines for planning, specification, execution, and interpretation of CPTUs in transitional soils.

1 INTRODUCTION

After the installation of the first Offshore Wind Farm in Denmark in 1991, the Offshore Wind Industry (OWI) has been increasing exponentially in Europe and recently also in new markets such as the US East Coast and the Asia-Pacific Countries.

Soil modelling and spatial mapping for the design and installation of foundations for offshore wind turbines is generally based on the combined and staged use of seismic surveys, piezocone penetration testing (CPTU) and boreholes with soil sampling. However, in many regions where the OWI is expanding, layers of transitional soils, i.e. neither clean sand nor clay,

are unexpectedly encountered and not predicted by the CPTU interpretation. This is mainly due to the lack of robust methodologies for characterizing silty sand and silt mixtures based on CPTU, as existing correlations between CPTU parameters and classification and engineering properties have been developed for sand and clay. Consequently, the cost and risk of developing offshore wind farms in these regions are high.

The goal of the CSi – CPTU in silty soils – Joint Industry Project is ultimately to develop guidelines for set-up, execution and interpretation of CPTUs in silty soils, see Augustesen et al. (2022). This goal is pursued by a combination of research activities including

in situ testing, numerical modelling and using a significant number of CPTUs, carried out in a large calibration chamber and in a geotechnical centrifuge at the ISMGEO laboratory (Italy, Baldi et al. 1982, Baldi et al. 1986).

With the main aim of highlighting the impact of fines content on soil strength and stiffness, the tests are carried out on a clean sand and on the sands mixed with non-plastic fines to obtain 15% and 30% fines content (grain size < 0.063 mm). Some of the preliminary results of the calibration chamber and centrifuge tests are presented in this paper, together with a brief description of the testing apparatuses and procedures.

2 TESTING SOIL AND PROGRAM

2.1 Ticino Sand and Ticino Filler

The sand and silty sand used for the experimentation are Ticino Sand (TS) and Ticino Filler (TF). TS is a clean silica sand used extensively in the past for calibration chamber, centrifuge and laboratory tests (Baldi et al. 1982, 1986, Fioravante 2000, Jamiolkowki et al. 2003, Fioravante & Giretti 2016). The batch used for the CSI project is named TS11, which is a natural, coarse to medium clean sand, with principal components of quartz (36% by weight), feldspar (40%), mica (11%). TF is the natural flour obtained by sieving the coarser fraction of Ticino sand and has similar mineralogical composition (21% quartz, 47% feldspar, 16% mica).

Optical microscope analysis evidenced that in both materials quartz is mainly present in sub-angular, equidimensional grains, feldspars are in both round and prismatic form, while micas are in lamellae. A diffractometric study shows that the mineralogical composition of the two materials is compatible with dominant origin from metamorphic rocks. Stereo microscope observations denote a type of transport that is relatively low in energy and of short duration, compatible with poorly worked sand.

Grain size distribution of TS11 and TF is shown in Figure 1. Table 1 lists the main index properties.

In this paper the preliminary results of tests carried out on clean TS11 and on a mix of TS11 and TF characterized by 15% FC (MIX15%) are discussed, see Figure 1 and Table 1. The minimum and maximum void ratios reported in Table 1 were measured according to the method proposed by Knudsen et al. (2020), validated for silty sand with FC as high as 14%.

2.2 Test program and procedure

Tables 2 and 3 provide the main characteristics of the calibration chamber (CC) and centrifuge (CCC) models discussed in this paper. The values of void ratio e , relative density D_R and dry unit weight γ_d refer to the end of consolidation. The test layout is sketched in Figure 2. All the models were normally consolidated.

The tests on clean TS11 were meant to assess if CC and CCC cone penetration tests were comparable with each other and with previous studies carried out using TS and the same facilities. In addition, they were aimed at validating the use of the centrifuge as a calibration tool of CPTUs in sandy soils. Indeed, centrifuge CPTUs have the advantage, with respect to calibration chamber tests, of giving a q_c -profile over a wide range of vertical stress, rather than a single q_c value associated to the specific level of the applied stress of a single sample. This is under the condition that the effects of rigid boundaries and scale effects are minimised. In addition, CCC models are smaller and a test requires few days compared to about two weeks for a CC test. If validated, CCC CPTUs can be extensively used to explore the effect of variable density, fine content, stress level, over-consolidation ratio on the penetration resistance.

2.2.1 The ISMGEO calibration chamber

The calibration chamber specimens are 1.4 m high and 1.2 m in diameter. The CC is a flexible-wall chamber and it can impose four different boundary conditions (BC):

- BC1: constant vertical and horizontal stresses, $\sigma_v = \text{const}$ and $\sigma_h = \text{const}$;
- BC2: zero vertical and horizontal strains, $\Delta\varepsilon_v = \Delta\varepsilon_h = 0$;
- BC3: constant vertical stress and zero horizontal strain, $\sigma_v = \text{const}$ and $\Delta\varepsilon_h = 0$;
- BC4: constant horizontal stress and zero vertical strain, $\sigma_h = \text{const}$ and $\Delta\varepsilon_v = 0$.

Two cells enclose the specimen. This allows obtaining a zero average lateral strain boundary condition by keeping the pressure in the outer cell equal to the pressure, developed by the specimen, in the inner cell. Vertical and horizontal stresses can be applied independently in a controlled manner to the boundaries of the sample. Vertical stresses are applied to the specimen through a piston (positioned at the bottom of the chamber) raised by pressured water and the horizontal stresses are applied by the pressure of water surrounding the specimen.

Table 1. Grain size and index properties of testing soils.

		TS11	TF	MIX15%
D_{60}	[mm]	0.49	0.098	0.43
D_{50}	[mm]	0.46	0.075	0.38
D_{10}	[mm]	0.32	0.009	0.028
U_c	[-]	1.53	11	15.4
G_s	[-]	2.695	2.772	2.721
$*\gamma_{d,max}$	[kN/m ³]	16.18	-	18.03
$*\gamma_{d,min}$	[kN/m ³]	13.05	-	13.93
e_{min}	[-]	0.634	-	0.48
e_{max}	[-]	1.026	-	0.916

* Knudsen et al. (2020)

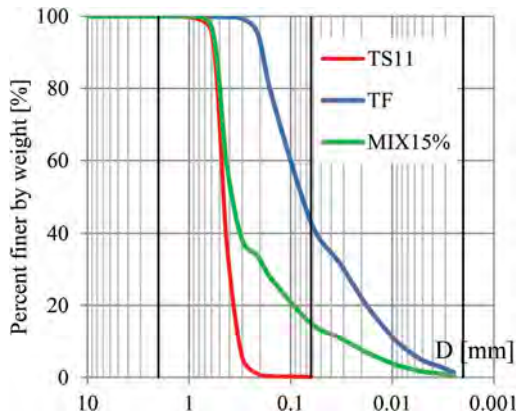


Figure 1. Grain size distribution of TS11, TF and MIX15%.

Table 2. CC Test Program.

test	Soil	D_R (%)	σ'_v (kPa)	e (-)	γ_d (kN/m ³)	V^*
1	TS11	48	50	0.84	14.39	V1&V2
2		49	200	0.83	14.41	V1&V2

* V1 = 20 mm/s, V2 = 100 mm/s

Table 3. CCC Test Program (N=63).

test	Soil	D_R (%)	σ'_v (kPa)	e (-)	γ_d (kN/m ³)	V^*
3	TS11	43	50-180	0.86	14.22	V1
4		44		0.85	14.26	V2
9	MIX15%	53	60-220	0.7	15.85	V1
11		53		0.7	15.85	V2

* V1 = 20 mm/s, V2 = 100 mm/s

The CC specimens are enclosed at the sides and base by a membrane, sealed at the top around an aluminium plate, which confines the specimen and transfers the thrust of the chamber piston from the specimen to a top lid. A 120 mm diameter hole is present in the centre of the lid; by changing the sealing hollow bush it is possible to press devices of different sizes into the specimen.

The loading frame, which counteracts the vertical load transferred to the lid during the compression of the specimen, also holds the hydro-mechanical press which pushes the test devices into the chamber during penetration tests. A hollow jack mounted inside the loading frame is used to counteract the vertical load; it is automatically controlled by a closed loop system, which equalizes the compression force in real time and allows to keep the lid position fixed and independent

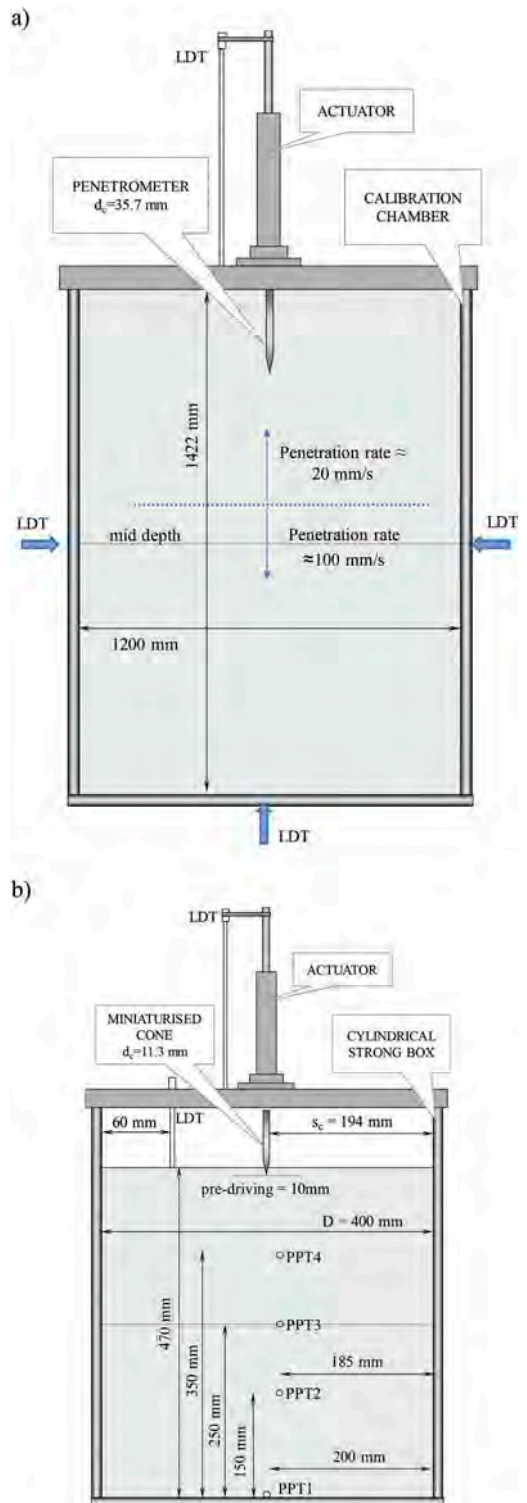


Figure 2. CC (a) and CCC (b) models.

from the frame deformations. Thus the specimen deformation can be monitored by measuring the chamber piston displacement.

The penetration probes used during the tests is a standard piezocone 35.7 mm in diameter, with a total area of 10 cm² and an apex angle of 60°. Two load cells measure the tip resistance and the lateral friction, independently; a pressure transducer measures the pore water pressure behind the tip (u_2).

The CC specimens were reconstituted in 15 strata using the undercompaction method (Ladd, 1978). Hereafter, they were saturated through an upwards flow of deaerated water and then by application of a back pressure. Reaching a Skempton B-value equal or larger than 0.95, the specimens were consolidated by applying the target vertical and horizontal stresses. To allow for comparison with the centrifuge tests, during which a rigid strong box houses the models and prevents the development of horizontal strains, the BC3 condition was adopted in the CC. In consequence, horizontal effective stresses imposed in CC were calibrated during the consolidation step to avoid radial deformations. A standard rate ($V1 = 20$ mm/s) was adopted in the upper part of the specimen and the maximum velocity possible for the loading system ($V2 = 100$ mm/s) in the lower part, see Figure 2a.

2.2.2 The ISMGEO geotechnical centrifuge

The ISMGEO geotechnical centrifuge is a beam centrifuge made up of a symmetrical rotating arm with a diameter of 6 m, a height of 2 m, a width of 1 m, and a nominal radius of about 2.2 m to the model base (Baldi et al.1988, Fioravante et al. 2021). The miniaturised piezocone used for the tests has a diameter $d_c = 11.3$ mm, an apex angle of 60° and a sleeve friction of 11 mm in diameter and 37 mm in length. One load cell measures the cone resistance and another one measures the cone resistance plus the shaft friction, up to forces of 9.8 kN. A pressure transducer is installed behind the tip for interstitial pressure measurements (u_2).

The centrifuge specimens are 470 mm high and 400 mm in diameter and were reconstituted at 1g using the undercompaction method within a rigid strong box. They were saturated under vacuum using deaerated water and subjected in flight to an acceleration field of 63 g imposed at mid depth (geometrical scaling factor $N = 63$). The scaling factor and the angular velocity adopted allowed to obtain a vertical stress of about 50 kPa at a depth of 120 mm from ground surface (which is the depth at which the cone resistance q_c is no more affected by top boundary effects) and of 200 kPa at a distance of 150 mm from the container bottom (depth beyond which q_c can be affected by the rigid bottom boundary); 50 kPa and 200 kPa are the vertical effective stresses imposed in the calibration chamber (tests N. 1 and 2 in Table 2).

The CCC boundary conditions are: $D/d_c = 35$, where D is the internal diameter of the container and $s_c/d_c = 17$, where s_c is the distance between the CPT and the side wall. These values are sufficiently large

to minimise any scale effects on the results (Bolton et al. 1999). The ratio of the cone diameter to the mean particle size is $d_c/D_{50} \approx 25$ for TS11 and $d_c/D_{50} \approx 30$ for MIX15%. CCC models were instrumented with pore pressure transducers (PPT in Figure 2), located at the base to monitor the water table and at three relevant depths of penetration, at a distance of one cone diameter from the penetration axis.

For each test condition two penetration rates were adopted; a standard rate $V1 = 20$ mm/s and a higher rate $V2 = 100$ mm/s (both velocities properly scaled).

3 TEST RESULTS

3.1 CPTUs in clean TS11

The results of the tests discussed in this section are shown in Figure 3 and were obtained from soil models of clean TS11 reconstituted at a relative density D_R slightly lower than 50%. In Figure 3 the corrected cone resistance q_t is plotted as a function of the vertical effective stress σ'_v . The tests are numbered according to Tables 2 and 3. The black and white squares represent the representative q_t measured in the CC specimens (Tests 1 and 2). For each CC test, two q_t values are plotted: one is the average value measured in the upper half of the model, with the probe penetrating at the standard rate $V1$; the second value refers to the faster rate $V2$ adopted in the lower half of the model. The black and grey lines in Figure 3 are the q_t profiles measured in the CCC (Tests 3 and 4). The vertical effective stresses in the centrifuge models are computed referring to: i) the average soil unit weight at the end of the in-flight consolidation, ii) the depth of the water table (estimated from PPT measurements) and iii) the acceleration field distortion. Figure 3 also shows the q_t profile (dashed line) estimated using the equation of Jamiolkowski et al. (2003). This allows to express the cone resistance as function of the vertical effective stress and relative density, using correlation coefficients calibrated by the Authors for Ticino sand and accounting for the saturation effects. It is worth noting that the correlation was calibrated on the base of CC tests carried out using the same apparatus employed for the present experimentation. For the centrifuge tests, the u_2 profiles, compared with the hydrostatic lines derived from the PPT measures, are given in Figure 4.

The centrifuge test results show that the soil models were rather homogeneous and the tests are repeatable, as the two q_t profiles are almost superimposed. The penetration was, as expected, drained for both penetration rates, see Figure 4. A very good agreement between CC and CCC results can also be observed, see Figure 3. In addition, the measured cone resistance is very well described by the correlation proposed by Jamiolkowski et al. (2003). This is considered an important result, as it demonstrates that CC and CCC give comparable CPT results, which are also consistent with previous studies carried out using TS and the same facilities; these data

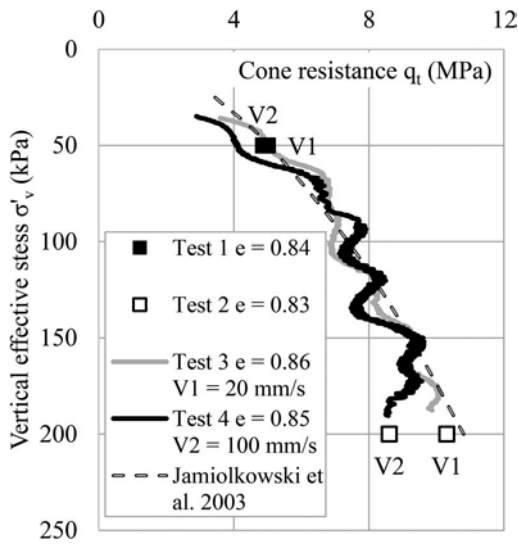


Figure 3. Centrifuge (solid lines) and Calibration Chamber (squares) CPTUs on TS11 - cone resistance q_t .

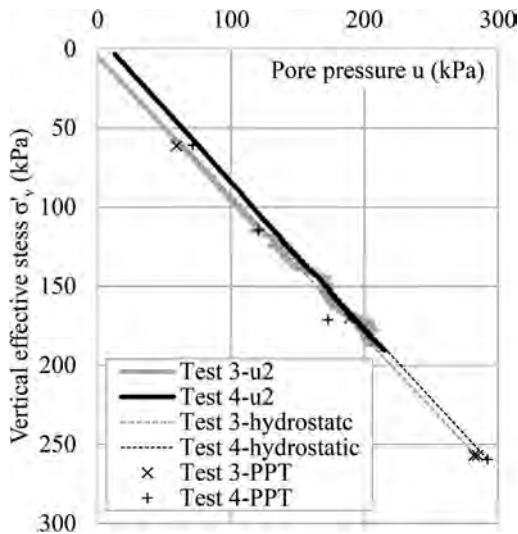


Figure 4. Centrifuge CPTUs on TS11 - PPT measures, hydrostatic line, pore pressure u_2 .

are used as benchmark for the following testing stages and, in the first instance, used to evaluate the effect of 15% FC on the cone resistance, for the same relative density and stress state.

3.2 CPTUs in MIX15%

Two centrifuge tests (9 and 11 in Table 3) on MIX15% were carried out using the same test conditions as those of tests 3 and 4, i.e. similar relative density (about 50%), stress range and penetration rate. Test 9 was carried out using the standard rate V1; test 11 was

run at V2. Figures 5 and 6 show the results. Inspecting the u_2 profiles (Figure 6), the penetration appears to be practically drained irrespective of the penetration rate, similar to the results on TS11.

However, as to the effect of FC on the penetration resistance (Figure 5), MIX15% had a penetration resistance about 40% lower than TS11, even though the void ratio is higher and the relative density is lower for TS11 compared to MIX15% (see Table 3). It's worth noting that drained and undrained triaxial tests on reconstituted samples indicate a shearing resistance angle at critical state of 36° and 35° for TS11 and MIX15%, respectively. On the other hand, the two materials proved to have different volumetric behavior during shearing. The results of 4 drained triaxial tests carried out on medium dense TS11 and MIX15% samples are shown in Figure 7, in the void ratio e - mean effective stress p' and in the stress deviator $q - p'$ plane. All the samples were reconstituted in strata at medium density (similar to the CC and CCC specimens, see Table 2 and 3) and were K_0 -consolidated under a vertical stress of 50 and 200 kPa. While MIX15% manifested a contractive behavior, TS11 dilated.

In general, the cone penetration resistance q_t of an uncemented and unaged soil depends on the material properties and the state of the soil (stress level and density). The state of the soil governs the direction of volumetric strains, (dilation or contraction) during shearing, which, in turns, controls the stress increment around the tip. Consequently, a dilative soil will develop a larger stress increment around the tip and will oppose larger resistance to penetration than a contractive material, as observed for TS11 and MIX15%.

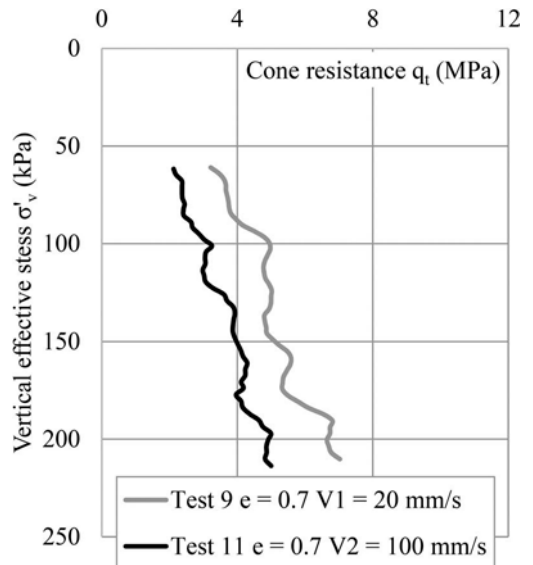


Figure 5. Centrifuge CPTUs on MIX15% - cone resistance q_t .

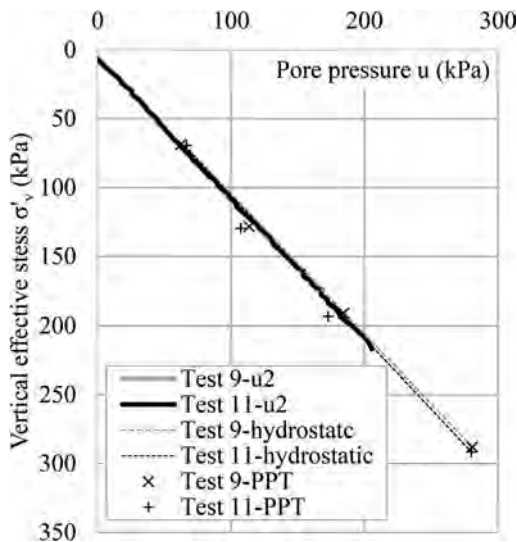


Figure 6. Centrifuge CPTUs on MIX15% – PPT measures, hydrostatic line, pore pressure u_2 .

4 CONCLUSIONS

A very good agreement between results of CC and CCC CPTUs in clean TS11 was observed and the measured cone resistance is very well described by the correlation proposed by Jamiolkowski et al. (2003).

The sand mixed with none plastic silt experiences a drop of cone resistance in the centrifuge, which cannot be attributed to effect of partial drainage during penetration, as the measured u_2 profile is straight and coincident with the hydrostatic line and no excess pore pressures developed neither at the standard penetration rate nor during the faster penetration.

The drop of cone resistance is attributed to contractive behaviour of the silty sand at the test density and stress in contrast with the dilative behaviour of the clean sand.

The centrifuge has proved to be a reliable CPT calibration tool in clean sand, alternative to the calibration chamber, with the advantage of providing a continuous cone penetration resistance profile over a wide range of stress level in significantly less time. If a good agreement between centrifuge and calibration chamber results will be gained also for the MIX15%, the centrifuge alone will be employed in a further stage of experimentation, during which 10 additional calibration CPTUs will be carried out on a mix of TS11 and TF characterized by 30% FC (MIX30%). Samples will be reconstituted varying soil density and overconsolidation ratio and will be tested varying the penetration rate. The calibration CPTUs and the complementary laboratory tests will be interpreted in the frame of CSi project with the final goal of contributing to

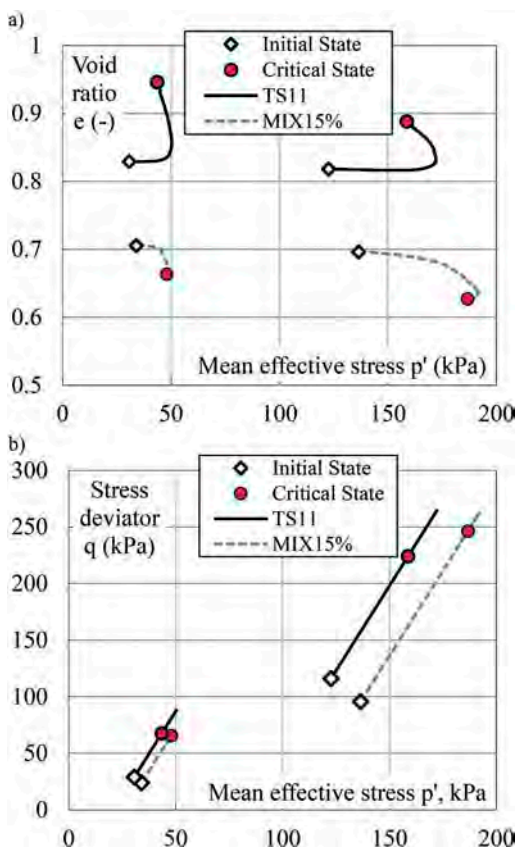


Figure 7. Drained triaxial tests on TS11 and MIX15%: a) e - p' plane; b) q - p' plane.

the development of acknowledged, simple and robust guidelines for specification, execution and interpretation of CPTUs in silty soils/silt mixtures.

ACKNOWLEDGMENTS

The CSi Project is managed through the Carbon Trusts's joint industry Offshore Wind Accelerator (OWA) program. The Authors acknowledge the provision of financial and technical support by the following project partners: Ørsted (lead partner), Equinor, Vattenfall, Shell, RWE and Scottish Power Renewables.

REFERENCES

- Augustesen, A.H., Carotenuto, P., Bilici, C., Lunne, T., Lindeboom, R.C.J., Krogh, L., van den Bosch, J., Barth, R., Erbrich, C., Giretti, D., Fioravante, V., H. Dias, H., Sougle, M-C., Barwise, A., de Wit, S., Burbury, D., Adams, N. 2022. CSi – a joint industry project into CPTUs in silty soils. Submitted for publication in the Proceedings of CPT'22.

- Baldi, G., Bellotti, R., Ghionna, V., Jamiolkowski, M. and Pasqualini, E. 1982. Design parameters for sand from CPT. Proc. ESOPT 2, Amsterdam.
- Baldi, G., Bellotti, R., Ghionna, N., Jamiolkowski, M. and Pasqualini, E. 1986. Interpretation of CPTs and CPTU's, 2nd Part. Proc 4th International Geotechnical Seminar, Nanyang Technological Institute, Singapore, 143–156.
- Baldi, G., Belloni, G., Maggioni, W. (1988). The ISMES Geotechnical Centrifuge. In *Centrifuge 88*, Paris, Corté J. F. Ed., Balkema, Rotterdam, 45–48.
- Bolton, M.D., Gui, M. W., Garnier, J., Corte, J. F., Bagge, G., Laue, J. & Renzi, R. (1999). Centrifuge Cone Penetration Tests in Sand. *Geotechnique*, 49(4), 543–552.
- Fioravante, V. 2000. Anisotropy of small strain stiffness of Ticino and Kenya Sands from seismic wave propagation measured in triaxial testing. *Soils and Foundations*, Vol. 40, No.4, 129–142.
- Fioravante, V. & Giretti, D. 2016. Unidirectional cyclic resistance of Ticino and Toyoura sands from centrifuge cone penetration tests. *Acta Geotechnica*, 11:953, doi:10.1007/s11440-015-0419-3.
- Fioravante, V. Giretti, D., Airoldi, S., Moglie J. 2021. Effects of seismic input, fine crust and existing structure on liquefaction from centrifuge model tests. *Bulletin Of Earthquake Engineering*, vol. 19, p. 3807–3833, ISSN: 1570-761X, doi: 10.1007/s10518-021-01139-4.
- Jamiolkowski, M.B., Lo Presti, D.C.F., Manassero, M. 2003. Evaluation of Relative Density and Shear Strength from CPT and DMT. *Soil Behavior and Soft Ground Construction*, Ladd Symposium, MIT, Cambridge Mass. Geotechnical Special Publication No. 119, ASCE, Reston, Virginia, pp. 201–238.
- Knudsen, S., Powell, J.J.M, Lunne, T., Thomsen, N.V., Krogh, L., Barwise, A. 2020. Development of new robust procedures for the determination of maximum and minimum dry densities of sand. Submitted to ISFOG2020.
- Ladd, R.S. 1978. Preparing tests specimens using under-compaction. *Geotechnical Testing Journal*, GTJODJ, 1(1), 16–23.

Comparison between coefficients of consolidation from CPTu and laboratory tests for Guaratiba's soft soil, Rio de Janeiro, Brazil

M.M. Freire, M.E.S. Marques & M.C. Tassi
Military Institute of Engineering, Rio de Janeiro, Brazil

L.A. Berbert
Prodec Consultoria, Rio de Janeiro, Brazil

ABSTRACT: This paper presents a discussion about vertical (c_v) and horizontal (c_h) coefficients of consolidation of Guaratiba's very soft clay, located at the lowlands of the West Zone of Rio de Janeiro city, Brazil. Due to the thickness of the deposit, high compressibility of the clay, and low undrained strength, the settlement stabilization, even with vertical drains, are known to take of about 30 months to occur at these lowlands. Thus it is essential to know c_v , c_h and c_h/c_v relationship in order to predict when settlement stabilization will occur. The variability of c_v and c_h values is very high, probably due to the wide range of organic matter, sand lenses and the sand content throughout the soft soil deposit. The aim of the paper is to compare these values of coefficients of consolidation obtained from the dissipation tests and from the consolidation tests and to discuss an approach to determine them for design considering their variability.

1 INTRODUCTION

Vertical (c_v) and horizontal (c_h) coefficients of consolidation are used to predict settlement evolution with time, and are essential for the design of embankments over soft soils, mainly when vertical drains are used.

Coefficients of consolidation are estimated from dissipation tests, carried out at a prestabilished depth of CPTu, from CRS and incremental consolidation tests, consolidation on triaxial tests and from field monitoring. They are related to permeability (k), which is a parameter that, for soils, has a range of values on the order of about 10^6 m/s. This parameter depends on several factors as: diameter, distribution, shape, texture and mineral composition of particles; flow and fluid type; soil structure; water content; void ratio and temperature.

Thus, it does not come as a surprise that the values from field monitoring, field tests and laboratory are different, due to:

- The boundary conditions are very different in the field, where lateral deformations exist, and in the laboratory consolidation test, where the deformation is unidirectional;
- The occurrence of sand lenses in the field, reducing the stabilization time, a fact that is not reproduced in the laboratory;
- Secondary consolidation takes place in the field and is disregarded in the analysis of field data.

Permeability ratio (k_h/k_v) is used for the estimate of c_h or c_v , but regardless of the type of test, for very soft, very organic soils, there is a wide range of consolidation coefficient values obtained for these deposits.

This paper presents a discussion about coefficients of consolidation values from dissipation tests and consolidation tests carried out at a very soft organic clay deposit of Rio de Janeiro city.

2 SITE DESCRIPTION

The site is located at Guaratiba, a neighborhood area of increasing population density in the city of Rio de Janeiro, Brazil (Figure 1), limited on one side by the coastal massifs and on the other side by the ocean.

The area of the site is 1.5 km² and the thickness of the soft soil in the deposit reaches 13.5 m. The water table is coincident with ground level, and the site is under water at the rainy season.

The geotechnical investigation consisted of 98 boreholes with Standard Penetration Test carried out in order to map clay thickness. After that, 15 geotechnical investigation clusters (see Figure 2) were implemented: 15 CPTu with 41 pore-pressure dissipation tests, 15 undisturbed Shelby samples, 40 oedometer consolidation tests, field vane tests, characterization and mineralogy tests.

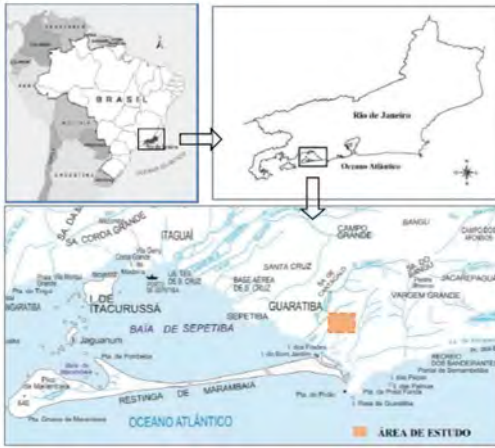


Figure 1. Site localization.

Some geotechnical characteristics of the clay are: natural water content values vary from 50% to 150%; the plasticity index is between 62% and 103%; initial void index vary from 1.51 to 3.65; organic matter content from 1.74% to 13.3% and the undrained strength is in the range of 9 to 36 kPa. The compression ratio, $C_c/(1+e_0)$, vary from 0.27 to 0.51, preconsolidation pressure from 23 to 50 kPa and OCR values from 1.07 to 3.34. All those characteristics indicate a very compressible clay.

From macro-drainage projects in this region, conducted by the city of Rio de Janeiro, the embankments must level up to 3m in order to avoid floods. The work schedule of embankment construction over soft soils city is directly related to vertical (c_v) and horizontal consolidation (c_h) values, which are in the order of $2-3 \times 10^{-8} \text{ m}^2/\text{s}$ at the West Zone of Rio de Janeiro, under normally consolidated stresses.

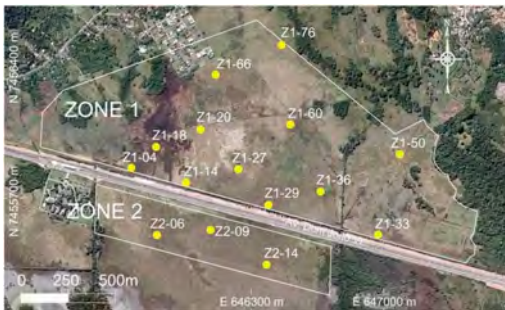


Figure 2. Geotechnical investigation clusters.

3 LABORATORY AND CPTU TESTS RESULTS

The main tests used to determine the coefficient of consolidation are laboratory consolidation test

and dissipation field tests carried out with a CPTu.

From dissipation tests, c_h values can be obtained from Equation 1, proposed by Houslyby and Teh (1988):

$$c_h = \left(\frac{T_h \times R^2 \times \sqrt{Ir}}{t} \right) \quad (1)$$

where:

T_h – Time Factor;

R – Piezocone Radius;

Ir – Rigidity Index (G/S_u);

G – Shear modulus

S_u – Undrained strength

t – Dissipation Time/Period.

In order to obtain c_v values from c_h values of CPTu tests, it is necessary to obtain the permeability ratio (k_h/k_v) as follow.

$$c_h = \left(\frac{k_h}{k_v} \right) c_v \quad (2)$$

Conventional and special oedometer tests were carried out on Sarapuí organic soft clay, located at Guanabara Bay, 60 km from Guaratiba (Coutinho, 1976; Lacerda et al., 1977, 1995). These tests were carried with radial drainage in order to obtain c_h . The c_h/c_v relationship obtained was between 1.0 and 2.0 at normally consolidated range, which is typical for very soft clays, as shown in Table 1, for worldwide deposits. Thus, the permeability ratio used for design in engineering practice for the soft clay deposits of Rio de Janeiro City has been 1.5.

Table 1. Ranges of possible field values of permeability ratio of soft clay deposits (Jamiolkowski et al. 1985).

Nature of clay	K_h/k_v
No macrofabric, or only slightly developed macrofabric, essentially homogeneous deposits	1.0 to 1.5
From fairly well to well developed macrofabric, e.g. sedimentary clays with discontinuous lenses and layers of more permeable material	2.0a4.0
Varved clays and other deposits containing embedded and more or less continuous permeable layers	3.0 to 15.0

In order to obtain laboratory c_h of Guaratiba, from consolidation tests, the samples were rotated 90° from its original in situ position. Using this procedure, c_v values were obtained, as shown in the schema of Figure 3, from 10 HS samples and c_h from 10 VS samples, using square root of time method proposed by Taylor, as shown in Table 2.

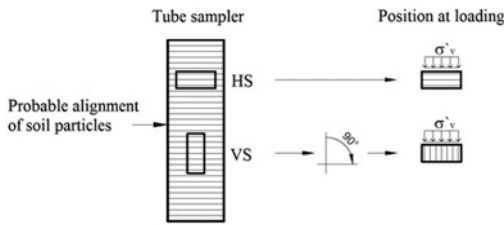


Figure 3. Sampling details.

Since the effective stress at the top of the clay deposit was very low, consolidation tests loading began at 3.0 kPa, with load increment ratio equal to one ($\Delta\sigma/\sigma = 1$), and at vertical effective stress of 100 and 200 kPa the samples were at the normally consolidated range. From average values, c_h/c_v was in the order of 1.2 for Guaratiba clay (Berbert, 2016). Thus, it was possible to estimate from $c_h = 1.2 c_v$, the values of c_h for another set of 20 consolidation tests carried out on HS samples.

Table 2. C_h and c_v from consolidation tests at normally consolidated range.

Vertical	Depth (m)	Stress (kPa)	C_h	C_v	C_h	C_v	K_h/k_v
			(VS)	(HS)	AV	AV	
			(x10 ⁻⁸ m ² /s)				
Z1-27	3	100	2.3	1.9	1.8	1.6	1.2
		200	1.4	1.3			
	5	100	2.1	1.3	1.6	1.3	1.3
		200	1.2	1.3			
	7	100	2.3	3.0	2.2	2.9	0.8*
		200	2.0	2.7			
Z1-18	1,5	100	4.4	8.4	3.8	5.5	0.7*
		200	3.3	2.5			
	3,5	100	3.6	2.5	3.1	2.3	1.3
		200	2.5	2.0			
Z1-29	2	100	2.6	2.9	2.2	2.7	0.8*
		200	1.8	2.6			
	6	100	2.3	1.6	2.1	1.8	1.1
		200	1.9	2.1			
Z1-36	3	100	2.3	1.4	2.1	1.3	1.6
		200	1.9	1.2			
	7	100	2.1	1.9	2.2	1.7	1.3
		200	2.3	1.4			
Z1-60	4	100	7.2	4.7	4.9	3.7	1.3
		200	2.6	2.6			

* K_h/k_v assumed=1

From CPTu dissipation tests, the c_h at normally consolidated range was obtained from Equation 3 (Jamiolkowski et al. 1985):

$$c_h(nc) = \left(\frac{C_r}{C_c} \right) c_h(oc) \quad (3)$$

where $c_h(oc)$ at overconsolidated range was obtained from equation (1) and C_r/C_c was 0.15. Table 3 shows results of c_h values from both tests.

Table 3. The c_h values from consolidation tests and CPTu tests at normally consolidated range.

Vertical	Depth (m)	C_v (HS) x 1.2	C_h (VS)	C_h (CPTu)*
		(x10 ⁻⁸ m ² /s)		
Z1-04	3	3.5	-	-
	5	83.3**	-	-
Z1-14	2	3.4	-	17.3
	6	1.4	-	6.3
	8	1.5	-	-
Z1-18	1,5	-	3.8	-
	3,5	-	3.1	-
Z1-20	3	3.0	-	2.9
	4,7	-	-	2.3
	3	-	1.8	2.5
Z1-27	5	-	1.6	3.1
	7	-	2.2	6.1
	2	-	2.2	16.7
	4	-	-	7.0
Z1-29	6	-	2.1	8.7
	8	-	-	10.1
	10	2.1	-	13.1
Z1-33	2	3.7	-	-
	5	1.6	-	-
Z1-36	3	-	2.1	5.0
	7	-	2.2	-
Z1-50	2	4.9	-	-
Z1-60	4	-	4.9	-
Z1-66	3	2.7	-	-
Z1-76	3	1.6	-	-
	5	2.1	-	-
	4	1.6	-	3.7
	6	-	-	3.1
Z2-06	7	1.68	-	-
	8	-	-	6.2
	10	2.28	-	4.7
	3	-	-	3.7
Z2-09	5	1.68	-	5.7
	7	2.28	-	6.8
Z2-14	2	1.56	-	11.8
	4	1.68	-	6.2

* CPTu values at normally consolidated range

** not considered

Sample Z1-04 at 5m had a high c_v value. A possible cause of this high value is the fact that this sample had the lowest initial void index, natural moisture and organic matter value.

4 DISCUSSION

Guaratiba clay is a little less compressible than most clays from the western region of Rio de Janeiro City

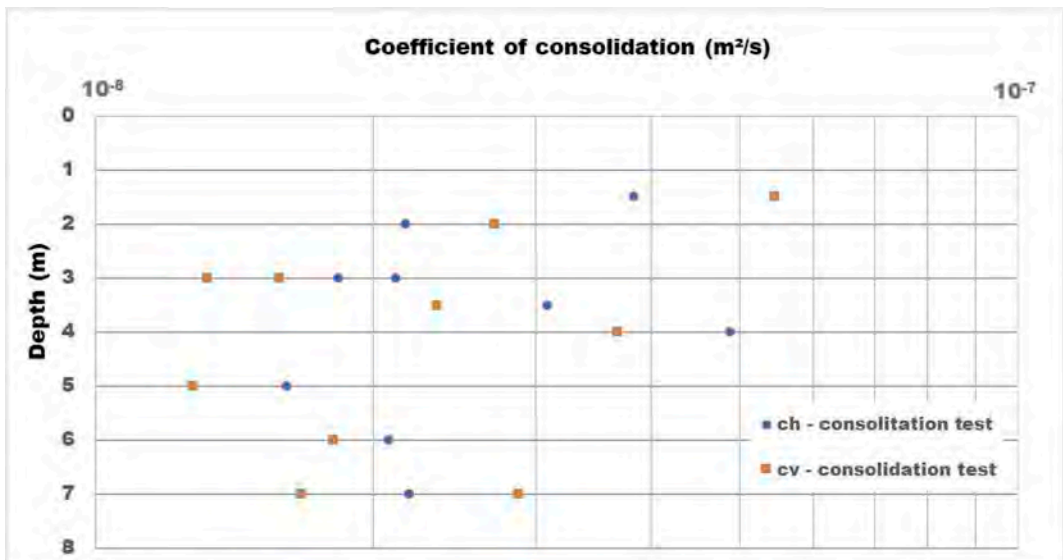


Figure 4. c_v and c_h values from consolidation tests at normally consolidated range.

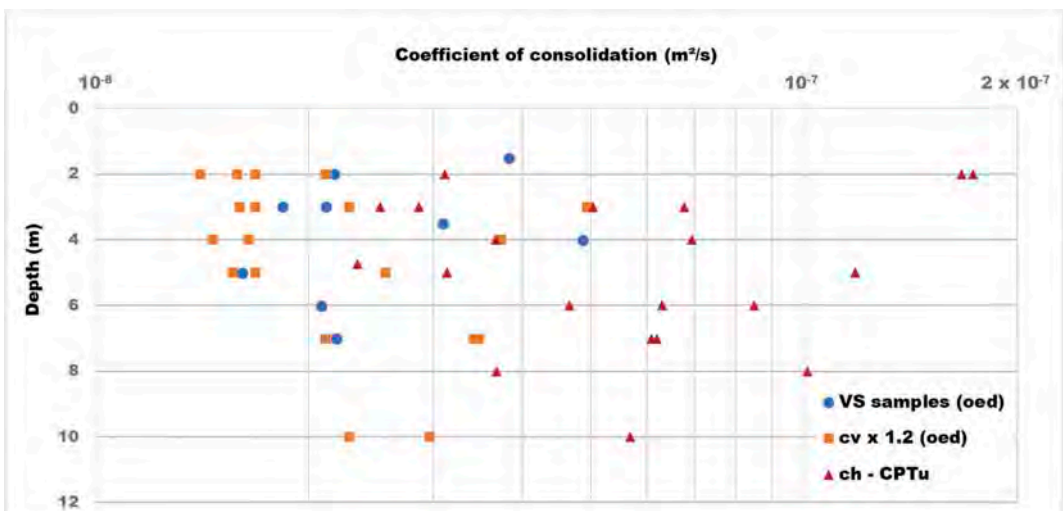


Figure 5. c_h values from consolidation tests and dissipation tests at normally consolidated range.

and also less plastic. However, the values of c_v and c_h of Guaratiba clay are inside the range of the c_v values obtained for western region Rio de Janeiro clays for the normally consolidated range: $10^{-9} \text{ m}^2/\text{s}$ to $2 \times 10^{-7} \text{ m}^2/\text{s}$ for Recreio and Barra da Tijuca clays (Almeida and Marques, 2013). From consolidation tests, it is not possible to obtain a specific range for c_v or c_h , but the majority of data shows higher c_h , at a certain depth as shown in Figure 4.

Figure 5 shows c_h results from CPTu compared with laboratory consolidation tests. It seems that CPTu values are higher than laboratory tests, which

could be attributed to sample disturbance, since sampling those very compressible clays is very difficult.

Almeida and Marques (2013) showed that the great variability of c_h values is not uncommon for Rio de Janeiro clays, and the difference between c_v values from laboratory data and field instrumentation can be as high as 10.

5 CONCLUSIONS

This paper showed the comparison between c_v and c_h values at normally consolidated range from special

consolidation tests and CPTu tests. These parameters are important to obtain settlement prediction with time, thus essential for deadlines of earthworks.

The c_h values from CPTu tests and from consolidation tests (HS and VS samples) are inside the wide range of magnitude of values of Rio de Janeiro clays.

However, the variation of values makes it difficult to adopt a c_h value for design. In this case, which c_h or c_v is recommended for the practice? Average values does not seem adequate, since it could underestimate the deadlines of the work. It is suggested to choose a value that meets most cases, considering that the work schedule could be adjusted depending on field monitoring.

Therefore, together with field and laboratory tests, field instrumentation is necessary to monitor the work.

REFERENCES

- Almeida, M. S. S. & Marques, M. E. S. 2013. *Design and performance of Embankments on very soft soils*. Londres. 228p.
- Berbert, L.A. 2016. *Evaluation of vertical and horizontal consolidation coefficients of soft soil deposit aiming settlements prevision of infrastructure works* (in Portuguese). M.Sc. Dissertation, Transportation Engineering Program, Military Institute of Engineering, Rio de Janeiro, 182 p.
- Jamiolkowski, M. & Ladd, C. C. & Germaine, J. T. & Lancellotta, R. 1985. *New developments in field and laboratory testing of soils*. In: Proc. XI ICSMFE. San Francisco, 1985. v.1, p. 57–153.
- Rosa, A. C. & Marques, M.E.S. 2019. *Estimative of coefficient of consolidation from piezocone dissipation tests* (in Portuguese). GEOSUL 2019. Joinville, Santa Catarina, Brazil.
- Santos, H.M.C. 2004. *Physical, chemical, mineralogical and geotechnical characterization of gleissolos of baixadas de Jacarepaguá, Guaratiba and Santa Cruz – from the city of Rio de Janeiro* (in Portuguese). D.Sc. Thesis, Department of Geology, Federal University of Rio de Janeiro, CCMN, Rio de Janeiro.
- Houlsby, G. T. & TEH, C. I. 1988. *Analysis of the piezocone in clay. Proceedings of the International Symposium on Penetration Testing, ISOPT-1, Orlando, 2, Balkema Pub., Rotterdam: 777–783.*
- Coutinho, R. Q. 1976 *Consolidation characteristics from radial drainage tests on a soft Clay of Fluminense Lowlands* (in Portuguese). Master's Thesis – COPPE/UFRJ, Rio de Janeiro.
- Lacerda, W. A. & Almeida, M. S. S. & SANTA MARIA, P. E. L. & Coutinho, R. Q. 1995. *Interpretation of radial consolidation tests. Proceedings of the International Symposium on Compression and Consolidation of Clayey Soils*, Yoshikuni, Kusabe (eds), Hiroshima, Japan, Vol. 2, 1091–1096. Rotterdam: Balkema.
- Lacerda, W. A. & Costa Filho, L. M. & Coutinho, R. Q. & duarte, A. R., 1977. *Consolidation characteristics of Rio de Janeiro soft clay*. Proceedings of Conference on Geotechnical Aspects of Soft Clays, Bangkok, 231–244.

Quantitative modelling of spatial variability of piezocone data from Venice lagoon silty soils

G. Gottardi, M. Ranalli & L. Tonni

Department of Civil, Chemical, Environmental and Materials Engineering, DICAM, Alma Mater Studiorum, University of Bologna, Italy

M. Uzielli

Department of Civil and Environmental Engineering, DICEA, University of Florence, Italy
Georisk Engineering S.r.l., Florence, Italy

ABSTRACT: As geotechnical research and design codes rely increasingly on probabilistic approaches, site characterization should also be conducted in the light of the explicit quantification of the uncertainty and spatial variability in soil properties. This paper provides a practical case-study application of spatial variability analysis of piezocone data obtained at a test site in the Lagoon surrounding the historic city of Venice, in North-Eastern Italy, where unusually dense and regularly spaced CPT test data were available. Empirical semivariograms are calculated for cone resistance, sleeve friction, and porewater pressure, along with the soil behavior classification index obtained from these measurements at a set of reference measurement depths. A number of theoretical semivariogram models are fitted comparatively and best-fit models are selected based on objective criteria and subjective judgment. Characteristic semivariogram parameters, providing information on correlation distance and small-scale variability, are retrieved. Modeling options are explained and results are analyzed and assessed critically.

1 INTRODUCTION

The definition of subsoil properties for engineering purposes is a difficult task due to the indetermination in geotechnical data which is employed in the characterization process. Such indetermination can be ascribed to both the soils and the investigators. Soils are natural materials, which are formed and continuously modified by complex geological processes, as discussed in detail by Hight & Leroueil (2003). The variety and complexity of such processes result in physical heterogeneity and, consequently, in the spatial and temporal variability of quantitative parameters. In any type of real-world geotechnical problem, moreover, it is impossible to obtain exhaustive values of data at every desired point because of practical and economical constraints. The testing methods by which such data are obtained are always imperfect and non-repeatable to some degree. Moreover, if measured parameters require transformation for use in geotechnical analyses and design, they are to serve as inputs to transformation models which, whether theoretical, empirical or experimental, are invariably incapable of perfectly replicating the complexity of the physical world. A steadily increasing bulk of research and experience, not to mention the uncertainty-based

character of evolutionary design codes based on limit-state design and reliability analysis, attest to the relevance of indetermination in geotechnical data and models, and of the importance of considering its effects on characterization and design.

In the technical literature, the terms variability and uncertainty are often employed interchangeably. Here, variability is defined as an observable manifestation of heterogeneity of one or more physical parameters and/or processes, while uncertainty pertains to the modeler's state of knowledge and strategy, and reflects the decision to recognize and address the observed variability in a qualitative or quantitative manner. Inherent soil variability describes the variation of properties from one spatial location to another within a soil mass. Such variability is parameterized quantitatively by aleatory uncertainty. Epistemic uncertainty, on the contrary, stems from the investigator's invariably limited information, imperfect measurement and modelling capabilities.

In investigating the spatial variability of a geotechnical property, both aleatory and epistemic uncertainties are addressed, as both contribute to the uncertainty which is modelled, processed, and reported. The aim of this paper is to provide a practical case-study of characterization of spatial variability of

the mechanical properties of soils as parameterized by piezocone data from a site located near the historical city of Venice, in North-Eastern Italy. Spatial variability analysis is performed through the calculation of empirical semivariograms and the subsequent fitting of theoretical semivariogram models.

2 TEST SITE DESCRIPTION

The Venetian lagoon is underlain by about 800 m of Quaternary deposits which originated from alternate phases of continental and marine sedimentation associated to marine regressions and transgressions occurred over the last 2 million years. Over the last forty years, the upper 100 m sediments of the Venetian lagoon have been thoroughly investigated, in relation to the regional land subsidence (e.g. Ricceri & Butterfield, 1974) as well as the foundation design of the submersible gates intended to protect the historical city of Venice against recurrent flooding (e.g. Simonini et al., 2007). These sediments have proven to be highly heterogeneous and stratified in a continuous alternation of slightly overconsolidated and predominantly silty sediments, ranging from medium-fine sands (SP-SM) with sub-angular grains to silts (ML) and very silty clays (CL). Coarse sediments are predominantly composed of silicates and carbonates, whilst silts and silty clays, which originated from mechanical degradation of sands, display a content of clay minerals (illite with minor quantities of chlorite, kaolinite and smectite) never exceeding 20% in weight. Generally, cohesive soils are slightly overconsolidated due to aging or oxidation.

A representative test site of such heterogeneous and stratified subsoil was located outside Treporti, a historical fishermen's village on the Cavallino coast line facing the North Eastern lagoon. At this site an extensive research program was recently carried out by the Italian Universities of Padova, Bologna and l'Aquila, with the aim of better understanding the behavior of such heterogeneous sediments. The research program, consisting of a detailed geotechnical characterization through in-situ tests, continuous-coring boreholes and high-quality laboratory tests, also included the construction and the subsequent gradual removal of a full-scale, 6.5 m high and 40 m in diameter, vertical-walled cylindrical test bank, in conjunction with a very detailed monitoring system of subsoil strains and pore water pressures (Tonni & Gottardi, 2011, 2019).

The extensive experimental program carried out in Treporti included no. 24 piezocone tests. The campaign was conducted in four phases, in relation to the different loading conditions associated to the presence of the bank. Figure 1 shows a plan of the area together with the location of CPTU tests.

The 'first phase' of the in-situ testing campaign, including no. 7 piezocone tests located throughout the selected area, was intended to give an initial description of the test site subsoil, with specific



Figure 1. Treporti CPTU test site.

reference to the detection of the most compressible soil layers.

A very detailed 'second phase' testing program was then performed just on the subsoil beneath the test bank to be built. All the second phase tests, numbered from 11 to 20, were located within a - 45 m diameter circular area. They were lined up along three diameters, splitting the circular area in three 120° identical slices, and placed on two concentric circumferences, inner (D=30 m) and outer (D=45 m) with respect to the loading bank (D=40 m). All tests were pushed as deep as possible, depending on the maximum available thrust, typically to about 42 m.

In addition to the main investigation program, two further testing phases were carried out. Immediately after the loading bank construction, the 'third phase' was performed from top of the bank, whereas a final 'fourth-phase' testing campaign was launched after the loading bank removal. The aim was to examine the stress-history effect on the soil mechanical properties along a number of verticals already investigated in both the pre-bank and post-bank construction phases (Tonni & Gottardi, 2009).

Due to the importance of ensuring the quality of the dataset in terms of homogeneity of loading conditions, only testing data from the first and second phases were used in this analysis. Typical piezocone log profiles of Venetian subsoil are reported in Figure 2, showing the corrected cone resistance q_c and the pore pressure u of CPTU tests located along the W-E cross section. Profiles of CPTU 6 and CPTU 14, located approximately 7-8 m north from the selected alignment, are superimposed on the same plot.

The figure clearly shows the high stratification and marked horizontal spatial variability of stratigraphy, which are typical features of Venetian lagoon subsoil. Indeed, while piezocone log profiles provide immediate evidence of a well-defined, 6-7 m thick top layer of silty sand, the underlying, dense alternation of thin layers of sandy and clayey silts is significantly variable from one location to another. The continuous

horizontal variation of the soil stratigraphy is particularly evident in the pore pressure logs, where u rarely follows up the hydrostatic level, often falls below it, but never develops high Δu values, typical of pure normally consolidated or slightly overconsolidated clays. A potentially more compressible fine-grained unit, which is mainly composed of silts, can be detected in the CPTU profiles from 7-8 m to 20 m depth. However, the thickness of such silty unit is clearly not constant throughout the whole test site area, as it is often interbedded with a clean sand layer of variable thickness. Soil heterogeneity and high degree of interbedding make the analysis of field data rather difficult.

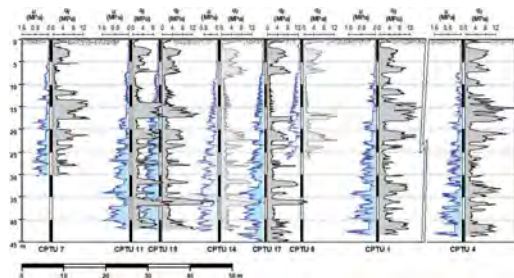


Figure 2. Typical soil profile of Venetian subsoil at Treporti site.

3 SPATIAL VARIABILITY ANALYSIS

3.1 Spatial correlation analysis of CPTU data

Spatial variability can be investigated quantitatively using several approaches. Semivariogram-based modeling ranks among the most widely used due to its close relationship with geostatistical kriging interpolation. Semivariogram-based modeling accommodates weakly (but not necessarily strongly) stationary data sets, i.e., data presenting spatial trends, provided that spatial correlation depends on measurement spacing but is independent of specific measurement location. The empirical absolute semivariogram of a dataset is computed as

$$\gamma(h) = \frac{1}{2N(h)} \sum_{(i,j)|h_{ij}=h} (\zeta_i - \zeta_j)^2 \quad (1)$$

where $N(h)$ is the number of data pairs sampled at locations separated by a spatial distance h (hereinafter referred to as lag distance), ζ_i and ζ_j are the data values at the i^{th} and j^{th} locations, respectively.

Calculating empirical semivariance by Eq. (1) for different lag distances allows quantification of the magnitude and variation of spatial correlation with lag distance. Small $\gamma(h)$ values are representative of high spatial correlation, while high $\gamma(h)$ values attest for low correlation.

The quantitative parameterization of spatial correlation given by the empirical semivariogram includes both aleatory uncertainty (given by the measurable scatter in the parameters of interest) and epistemic uncertainty (comprising measurement error and inherent variability at sub-measurement interval scale). The analysis was performed in a pseudo-3D approach, which means estimating the spatial variability only in the horizontal planes at nominal analysis depth, ranging from 1m to 40m below ground surface at 1-meter intervals. This approach requires the availability of an exceptional database in terms of the number of CPTU verticals at different distances from each other, within the area to be analysed.

In practice, the calculation of empirical semivariograms relies on the establishment of a lag tolerance, both on distance (by accepting data pairs which separation distance is acceptably close to the nominal lag distance) and direction (by allowing a preset degree of deviation from the nominal direction between two sampled locations). The reason for the acceptance of such tolerances (which should not be too large in order to avoid the introduction of excessive distortion and bias) lies in the opportunity to have a greater number of pairs, which results in a more statistically reliable semivariogram structure. In order to identify an optimum lag interval (in terms of regularity and accuracy of empirical semivariance values), a parametric analysis on Δh was carried out. In particular, empirical semivariograms with lag intervals of 5 m, 10 m and 15 m were calculated at each analysis depth and for all three CPTU test parameters; namely: tip resistance q_t , sleeve friction f_s , and induced pore pressure u_2 . In all cases, the distance tolerance \hat{h} was set equal to one half the lag interval Δh (Isaaks & Srivastava 1990), i.e. =2.5 m, 5 m and 7.5 m, respectively. Thus, all data points are considered at least once, with no redundancies at any lag distance value. An intermediate lag interval of $\Delta h=10$ m (with an associated lag tolerance $\hat{h}=5$ m) was deemed to be the most suitable, since it is small enough to preserve the inherent variability of semivariance while providing a clearer structure of spatial correlation than smaller lag intervals.

Example empirical semivariograms, pertaining to q_t at analysis depth of 27 m and calculated for the three different values of lag spacing, are shown in Figure 3. In the plots, for each estimated semivariance value (black points), the corresponding number of contributing data pairs is indicated. The calculation sample numerosity makes it possible to assess the reliability of each semivariance value (with larger $N(h)$ ensuring lower statistical uncertainty in calculated semivariance).

3.2 Modelling of empirical spatial variability

The fitting of suitable semivariogram models to empirical semivariograms is a fundamental step in the quantitative modelling of soil spatial variability

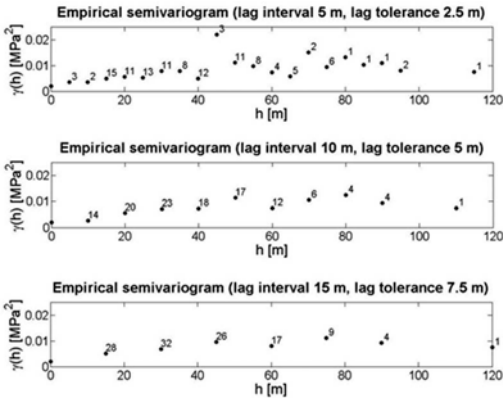


Figure 3. Empirical semivariogram of q_t at 27 m depth, for different values of lag interval and lag tolerance.

using geostatistical approaches... Numerous semivariogram models are available in the literature (e.g., Isaaks & Srivastava 1990). Among the most widely used models are the *spherical*, *exponential*, and *Gaussian* models, characterized by the following equations, respectively:

$$(S)\gamma(h) = \begin{cases} C \left[1.5 \frac{h}{a} - 0.5 \left(\frac{h}{a} \right)^3 \right] + C_0 & |h| \leq a \\ C + C_0 & |h| > a \end{cases} \quad (2)$$

$$(E)\gamma(h) = C \left[1 - \exp\left(-\frac{3h}{a}\right) \right] + C_0 \quad (3)$$

$$(G)\gamma(h) = C \left[1 - \exp\left(-\frac{3h^2}{a^2}\right) \right] + C_0 \quad (4)$$

where C_0 is the semivariogram nugget, $C + C_0$ is the sill (i.e., the maximum value of semivariance), and a is the range (i.e., the lag distance at which semivariance attains the sill value).

The *spherical model* displays a linear behavior at short lag distances; subsequently, it flattens and reaches the sill at a . The *exponential model* and the *Gaussian model* instead approach their sill value asymptotically. For these models, the range a is defined as the lag distance at which the semivariogram value attains 95% of the sill value. Like the spherical model, the *exponential model* is linear at very small lag distances but reaches the sill value more gradually. The *Gaussian model*, instead, shows a parabolic behaviour near the origin, and is characterized by an inflection point.

The three models served as candidates in the analysis of spatial correlation of CPTU parameters within the Treporti site. The choice of the semivariogram model reflects the user's assessment regarding

the structure (model), magnitude (sill), spatial extent (range), and level of epistemic uncertainty (measurement uncertainty and small-scale variability), respectively, of spatial correlation. Such an assessment is based on a combination of objective approaches (provided by the possible use of regression techniques) and subjective belief (e.g., manual fitting, critical assessment of results of regression).

The quantification of the semivariogram nugget is not a univocal procedure. Operationally, the assignment of a semivariogram nugget should rely on the user's "backward extrapolation" of a best-fit semivariogram model to zero-lag distance. In practice, this procedure provides reliable results only if reliable empirical semivariance values are available for small lag distances. This is arguably not the case with the Treporti data sets. Consequently, in order to provide a consistent and conservative criterion for estimating semivariogram nuggets, it is necessary to resort to existing knowledge regarding the phenomena contributing to the nugget effect. The piezocone test is known to have one of the lowest total measurement errors among in-situ test in current practice (Uzielli 2008). CPTU measurement error represents a combination of several sources of variability and cannot generally be evaluated in routine geotechnical analysis. It is thus necessary, in most, to refer to literature approaches and values of measurement uncertainty. The latter is most often parameterized by the coefficient of variation of measurement uncertainty (COV_m). Based on the above, nuggets were tentatively calculated as:

$$C_0 = \frac{1}{2} COV_m^2(\xi) \cdot \xi_N^2 \quad (5)$$

in which

$$\xi_N = m(\xi) + 3 \cdot s(\xi) \quad (6)$$

is a "characteristic" conservative estimate of the CPTU parameter ξ of interest. Comprehensive tables of measurement uncertainty parameters for laboratory and in-situ testing are available in Uzielli (2008). Kulhawy & Trautmann (1996) reported COV_m of measurement uncertainty for q_c and f_s in CPTU testing as $COV_m(q_c)=0.07$ and $COV_m(f_s)=0.12$. Gauer et al. (2002) estimated the COV_m of measurement uncertainty for u_2 at $COV_m(u_2)=0.07$. The corrected cone tip resistance q_t is not measured directly but is obtained from q_c and u_2 by the model given in corrected cone tip resistance model. Assuming that q_c and u_2 are independent and statistically uncorrelated parameters, the COV_m of measurement uncertainty of q_t can be approximated using the following additive model:

$$COV_m(q_t) = \sqrt{COV_m^2(q_c) + COV_m^2(u_2)} \quad (7)$$

The standard deviation of measurement uncertainty can be expressed by inverting the definition of the coefficient of variation:

$$\sigma_m(\xi) = E(\xi) \cdot COV_m(\xi) \quad (8)$$

Assigning a constant value to a coefficient of variation implies the acceptance of the fact that the standard deviation varies proportionally with the expected value of the parameter. As q_c , f_s and u_2 generally increase with overburden stress (i.e., with depth) in homogeneous soil layers, measurements at greater depths are assumed to be less precise and accurate than measurements taken at shallow depths. This hypothesis is consistent with piezocone practice, as deeper measurements potentially suffer from the undesirable effects of inclination, elastic compression of rods, filter obstruction, etc. Such effects hinder the accuracy and precision of testing results, ultimately increasing measurement uncertainty. The characteristic value in ξ_N was taken as the arithmetic mean $m(\xi)$ of an extended data sample (comprising measurements pertaining to the depth interval defined by the nominal analysis depth \pm a depth tolerance, established at 0.10 m to account for possible measurement offsets) increased by 3 sample standard deviations $s(\xi)$ of the same data sample.

Fitting of semivariogram models was performed on empirical semivariograms for each parameter and for each analysis depth, for a total of 120 fitting operations. With the exception of the assignment of semivariogram nuggets as previously described, the fitting procedure was carried out manually, with no implementation of numerical optimization techniques. It is well known that manual semivariogram fitting is preferable over automatized fitting (e.g. Isaaks & Srivastava 1990; Journel & Huijbregts 1978). With the aim of obtaining the best possible adjustment to the empirical data, the three models were tested comparatively: semivariogram model parameters a , C_0 and C were varied subjectively, and the goodness-of-fit of the resulting semivariance values was assessed qualitatively. In the latter process, a greater weight was awarded to the adherence of theoretical models to empirical values at small lag distances, which result in a greater number of data pairs and are thus more reliable than those pertaining to large lag distances.

Despite the typical lack of complete regularity and noted in most of the calculated empirical semivariograms, the overall qualitative assessment of the goodness-of-fit fit of semivariogram models was at least satisfactory. For illustrative purposes, best-fit cases of spherical, exponential and Gaussian models are shown in Figure 4. These cases refer to q_t at depth 32 m, u_2 at depth 29 m and f_s at depth 27 m.

Figure 5 illustrates instead numerical tables with, for each analysis depth, the best-fit semivariogram model (S: spherical; G: Gaussian; E: exponential), best-fit semivariogram parameters (range a ; nugget

C_0 ; sill C_0+C) and relative nugget $C_0/(C_0+C)$, for q_t , f_s and u_2 .

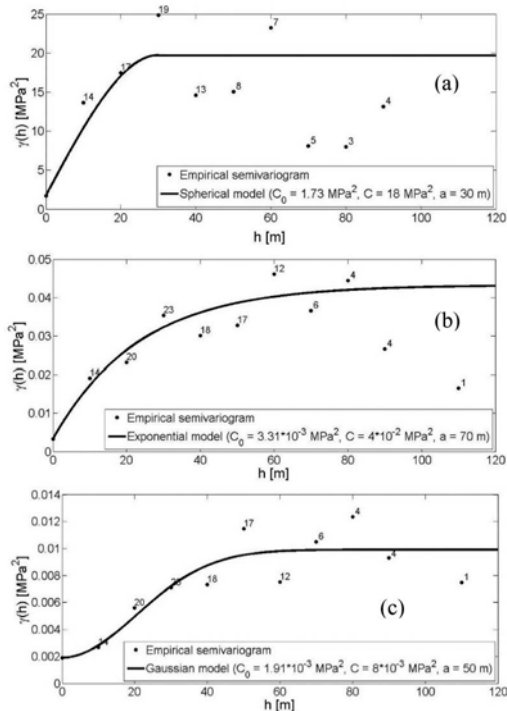


Figure 4. Semivariogram models fitting to the empirical semivariograms of q_t at 32 m (a), of u_2 at 29 m and of f_s at 27 m.

A number of observations can be drawn regarding the best-fit semivariogram models and their respective parameters. The most frequent best-fit model was found to be the spherical model. Concerning the range a , neither a relationship between the values relative to q_t and f_s at each analysis depth, nor a particular depth-wise trend is identified for either parameter. CPTU parameters q_t and f_s show instead a quite strong correlation regarding the nugget term C_0 . More specifically, a positive statistical correlation (quantitatively parameterized by a linear correlation coefficient of 0.7) between the C_0 values of q_t and those of f_s was noted. For these two parameters, C_0 shows a proportional increase with depth. This is at least partly a consequence of the calculation method adopted for C_0 , which partially relies on the definition of a characteristic value which is related to second-moment sample statistics. As both q_t and f_s tend to increase with depth due to in-situ stress effects, it may be expected that increasing sample statistics would induce the above noted correlation. Comparative examination of the relative nugget values showed that the contribution of measurement error and small-scale variation to spatial variability is more relevant (approximately by one order of magnitude) for f_s than for q_t and u_2 . This observation is consistent with the well-known fact that sleeve friction

q_t											
z[m]	BFM	a [m]	C_0 [MPa ²]	C_0+C [MPa ²]	$C_0/(C_0+C)$	z[m]	BFM	a [m]	C_0 [MPa ²]	C_0+C [MPa ²]	$C_0/(C_0+C)$
1	E	30	8.67E-03	2.59E-01	3.35E-02	21	G	70	1.03E+00	8.03E+00	1.28E-01
2	E	30	3.59E-01	2.26E+00	1.59E-01	22	S	10	7.70E-01	1.77E+00	4.35E-01
3	E	1	3.63E-01	3.63E-01	1.00E+00	23	E	1	1.88E-02	1.88E-02	1.00E+00
4	G	50	2.69E-01	1.57E+00	1.72E-01	24	S	40	5.73E-01	3.57E+00	1.60E-01
5	S	30	2.31E-01	1.13E+00	2.05E-01	25	G	70	2.74E-02	5.74E-02	4.77E-01
6	E	30	6.82E-01	5.18E+00	1.32E-01	26	G	60	4.97E-02	2.30E-01	2.16E-01
7	G	40	8.87E-01	4.89E+00	1.82E-01	27	S	20	3.12E-01	1.51E+00	2.06E-01
8	S	20	1.14E-01	1.26E+00	9.04E-02	28	S	30	9.09E-01	7.91E+00	1.15E-01
9	G	80	6.58E-02	2.07E+00	3.19E-02	29	S	10	3.52E-02	4.02E-02	8.76E-01
10	G	80	1.23E-01	2.62E+00	4.69E-02	30	G	50	3.07E-01	3.31E+00	9.29E-02
11	G	40	8.14E-02	6.81E-01	1.10E-01	31	S	20	6.04E-01	7.10E+00	8.51E-02
12	G	50	4.73E-01	1.05E+01	4.51E-02	32	S	30	1.73E+00	1.97E+01	8.75E-02
13	S	30	8.37E-02	5.34E-01	1.57E-01	33	G	80	1.50E+00	3.15E+01	4.76E-02
14	G	60	7.49E-01	1.67E+01	4.47E-02	34	G	60	5.80E-01	1.06E+01	5.48E-02
15	S	60	1.69E+00	3.57E+01	4.72E-02	35	S	20	1.67E+00	1.12E+01	1.12E-01
16	S	30	1.57E+00	2.16E+01	7.30E-02	36	S	30	2.19E+00	2.72E+01	8.06E-02
17	S	40	1.47E+00	2.15E+01	6.84E-02	37	S	20	1.65E+00	1.97E+01	8.42E-02
18	S	50	1.45E+00	1.95E+01	7.47E-02	38	E	1	2.19E-01	2.19E-01	1.00E+00
19	S	50	3.98E-02	1.40E-01	2.85E-01	39	G	60	6.96E-02	1.90E-01	3.67E-01
20	S	30	9.88E-02	8.99E-01	1.10E-01	40	S	20	1.48E-01	6.98E-01	2.12E-01

f_s											
z[m]	BFM	a [m]	C_0 [MPa ²]	C_0+C [MPa ²]	$C_0/(C_0+C)$	z[m]	BFM	a [m]	C_0 [MPa ²]	C_0+C [MPa ²]	$C_0/(C_0+C)$
1	S	20	1.46E-05	3.96E-05	3.69E-01	21	E	1	2.17E-04	2.17E-04	1.00E+00
2	S	20	1.58E-05	5.58E-05	2.83E-01	22	S	50	1.39E-04	2.19E-04	6.34E-01
3	E	1	2.63E-05	2.63E-05	1.00E+00	23	E	1	4.28E-05	4.28E-05	1.00E+00
4	E	1	1.84E-05	1.84E-05	1.00E+00	24	G	70	1.67E-04	3.67E-04	4.55E-01
5	S	10	1.81E-05	2.51E-05	7.21E-01	25	S	20	2.29E-05	5.79E-05	3.96E-01
6	S	60	3.13E-05	1.11E-04	2.81E-01	26	G	80	4.98E-05	1.50E-04	3.32E-01
7	S	20	6.17E-05	1.02E-04	6.07E-01	27	G	50	1.91E-03	9.91E-03	1.93E-01
8	S	20	1.79E-05	8.29E-05	2.16E-01	28	E	1	4.42E-04	4.42E-04	1.00E+00
9	S	70	5.51E-05	7.05E-04	7.81E-02	29	S	10	6.28E-05	1.63E-04	3.86E-01
10	G	90	8.22E-05	8.82E-04	9.32E-02	30	G	100	9.78E-05	4.48E-04	2.18E-01
11	G	30	1.55E-05	4.55E-05	3.40E-01	31	S	10	1.13E-04	5.63E-04	2.01E-01
12	G	50	3.85E-05	1.89E-04	2.04E-01	32	E	20	3.34E-04	1.53E-03	2.18E-01
13	S	30	2.82E-05	2.53E-03	1.12E-02	33	G	40	7.96E-04	5.30E-03	1.50E-01
14	G	70	2.00E-04	1.80E-03	1.11E-01	34	G	60	2.42E-03	2.84E-02	8.51E-02
15	S	70	2.35E-04	1.84E-03	1.28E-01	35	S	20	3.78E-03	1.38E-02	2.75E-01
16	S	80	1.63E-04	1.06E-03	1.53E-01	36	S	30	3.44E-04	1.29E-03	2.66E-01
17	E	30	1.70E-04	8.20E-04	2.07E-01	37	S	50	4.41E-04	2.54E-03	1.74E-01
18	G	70	1.41E-04	7.91E-04	1.78E-01	38	S	10	1.94E-04	4.44E-04	4.37E-01
19	G	70	8.27E-05	2.83E-04	2.93E-01	39	S	10	6.85E-05	7.85E-05	8.73E-01
20	S	60	2.10E-05	4.10E-05	5.13E-01	40	S	10	4.18E-04	1.12E-03	3.74E-01

u_2											
z[m]	BFM	a [m]	C_0 [MPa ²]	C_0+C [MPa ²]	$C_0/(C_0+C)$	z[m]	BFM	a [m]	C_0 [MPa ²]	C_0+C [MPa ²]	$C_0/(C_0+C)$
1	S	20	2.79E-05	6.28E-04	4.44E-02	21	S	40	2.65E-04	2.56E-03	1.03E-01
2	S	10	3.02E-06	3.90E-05	7.73E-02	22	S	40	2.40E-04	1.24E-03	1.93E-01
3	S	80	3.18E-06	1.52E-05	2.10E-01	23	S	40	1.76E-03	4.26E-03	4.13E-01
4	S	10	5.67E-06	1.07E-05	5.31E-01	24	E	20	9.29E-04	1.29E-02	7.18E-02
5	S	10	1.32E-05	1.03E-04	1.28E-01	25	S	10	1.94E-03	5.44E-03	3.57E-01
6	G	50	3.90E-05	6.39E-04	6.10E-02	26	G	60	2.57E-03	3.26E-02	7.89E-02
7	G	50	2.54E-05	2.05E-04	1.24E-01	27	E	40	4.67E-03	5.47E-02	8.54E-02
8	S	80	3.79E-04	1.44E-02	2.63E-02	28	S	40	1.10E-03	8.60E-03	1.28E-01
9	G	40	2.91E-04	3.79E-03	7.68E-02	29	E	70	3.31E-03	4.33E-02	7.65E-02
10	S	80	3.59E-04	7.36E-03	4.88E-02	30	E	50	4.03E-03	7.40E-02	5.44E-02
11	S	30	5.08E-04	4.51E-03	1.13E-01	31	S	40	3.23E-03	4.02E-02	8.03E-02
12	E	50	4.85E-04	7.69E-03	6.31E-02	32	S	40	2.88E-03	5.29E-02	5.45E-02
13	E	40	6.08E-04	7.81E-03	7.79E-02	33	G	50	5.06E-03	1.05E-01	4.81E-02
14	S	30	7.54E-04	1.38E-02	5.48E-02	34	G	70	6.22E-03	1.06E-01	5.85E-02
15	S	30	9.37E-04	1.54E-02	6.07E-02	35	S	10	3.40E-03	8.40E-03	4.05E-01
16	E	50	9.09E-04	1.39E-02	6.53E-02	36	S	30	1.97E-03	3.00E-02	6.56E-02
17	S	30	1.37E-03	2.14E-02	6.41E-02	37	S	10	6.78E-03	1.37E-01	4.96E-02
18	E	40	1.56E-03	2.16E-02	7.25E-02	38	S	50	5.94E-03	6.59E-02	9.01E-02
19	E	30	1.32E-03	1.63E-02	8.10E-02	39	S	40	4.57E-03	3.26E-02	1.40E-01
20	S	20	2.03E-03	2.80E-02	7.23E-02	40	S	20	7.32E-03	6.23E-02	1.17E-01

Figure 5. Best fit semivariogram models and parameters for q_t , f_s , and u_2 .

measurements are affected by a larger measurement uncertainty.

4 CONCLUSIONS

This paper has illustrated the background concepts and operational details of the analysis of spatial correlation of CPTU parameters measured at the Treporti site through semivariogram-based modelling. Despite the particularly high stratigraphic complexity of the site, the inspection of output characteristic parameters of best-fit semivariogram models provided interesting qualitative and quantitative correspondences with

well-established knowledge regarding the degree of spatial correlation and the magnitude of measurement uncertainty in cone resistance, sleeve friction, and pore pressure measurements.

Aside from their inherent utility in describing spatial correlation structures, the analyses performed herein could serve as inputs to two categories of analyses aimed at non-deterministic geotechnical site characterization; namely: geostatistical kriging and random field modelling. In the first case, semivariogram model parameters serve as direct inputs to geostatistical kriging methods, specifically in the calibration of coefficients in the linear kriging interpolation methods. In the second case, model parameters can be used to estimate scales of fluctuation, which are necessary for the definition of random fields. Both approaches are cost-efficient means in providing estimates of soil properties at unsampled locations and to parameterize the associated uncertainty for seamless inclusion in rapidly developing statistical and probabilistic geotechnical methods.

REFERENCES

- Hight, D.W. & Leroueil, S. 2003. Characterization of soils for engineering purposes. *Characterization and engineering properties of natural soils*, Volume I, Tan et al. Eds, Balkema Publishers.
- Isaaks, E.H. & Srivastava, R.M. 1990. *An introduction to applied geostatistics*. Oxford University Press, New York.
- Journel, A.G. & Huijbregts, C.J. 1978. *Mining geostatistics*. Academic Press, Inc.
- Kulhawy, F.H. & Trautmann, C.H. 1996. Estimation of in-situ test uncertainty. *Uncertainty in the Geologic Environment: From Theory to Practice*, Geotechnical Special Publication No. 58: 269–286. New York: ASCE.
- Ricceri, G. & Butterfield, R. 1974. An analysis of compressibility data from a deep borehole in Venice. *Geotechnique*, 24(2), pp. 175–192.
- Simonini, P., Ricceri, G., and Cola, S. 2007. Geotechnical characterization and properties of the Venice lagoon heterogeneous silts. In Proc. 2nd International Workshop on Characterization and Engineering Properties of Natural Soils, Singapore, 29 November – 1 December 2006, pp. 2289–2327. London: Taylor & Francis.
- Tonni, L. & Gottardi, G. 2009. Partial drainage effects in the interpretation of piezocone tests in Venetian silty soils. In Proc. *17th Int. Conf. on Soil Mech. & Geot. Eng.*, Alexandria, Egypt, 5-9 October 2009, Vol. 2, pp. 1004–1007.
- Tonni, L. & Gottardi, G. 2011. Analysis and interpretation of piezocone data on the silty soils of the Venetian lagoon (Treporti test site). *Canadian Geotechnical Journal* 48(4): 616–633.
- Tonni, L. & Gottardi, G. 2019. Assessing compressibility characteristics of silty soils from CPTU: lessons learnt from the Treporti Test Site, Venetian Lagoon (Italy). *Aims Geosciences* 5 (2): 117–144.
- Uzielli, M. 2008. Statistical analysis of geotechnical data. Keynote paper, *Proceedings of the 3rd International Conference on Site Characterization*, Taiwan, April 1-4, 2008. The Netherlands: Taylor & Francis.

Thin-layer detection from the cone resistance rate of change

H.B. Hammer

Dr.techn. Olav Olsen AS, Trondheim, Norway

S. Nordal

Norwegian University of Science and Technology (NTNU), Norway

J.-S. L'Heureux & H. Skrede

Norwegian Geotechnical Institute (NGI), Norway

ABSTRACT: True determination of soil parameters for thin clay layers in sand or silts from CPTU measurements is challenging. Cone resistance in thin layers is influenced by the surrounding layers resulting in unrepresentative measurements. Measurements should be corrected for this effect prior to interpretation of parameters. Such correction requires accurate information about the thickness of the thin layer. Previous studies have shown that the pore pressure parameter of the CPTU may not properly identify the layer interfaces for thin clay layers in sand. In this study a “cone resistance rate of change” parameter is suggested for thin-layer interface detection. Results from recently performed physical experiments at NTNU as well as from prior studies are used to evaluate the ability of this parameter to detect thin layers of clay in sand. The parameter appears to detect layer interfaces with good accuracy, even for layers with thickness as thin as the cone diameter. The results suggest that the approach may estimate layer thickness quite well and aid towards efficient correction of cone resistance to achieve more realistic soil parameters for thin clay layers in sand.

1 INTRODUCTION

The near-continuous measurements of CPTU parameters cone resistance (q_c , q_t), pore pressure (u_2) and skin friction (f_s) provide great details of the subsurface. The combined response of these parameters can be used for characterization of materials for thick homogenous sediments. Close to layer interfaces and in thin layers the measurements may be significantly influenced by multiple materials simultaneously. Accurate characterization and interpretation of geotechnical parameters of thin layers requires correction of these effects, which in turn depends on the layer thicknesses. It is therefore important to obtain detailed information of the layer interfaces. The u_2 parameter may not provide accurate measurement of the thickness of such thin clay layers (Hird et al. 2003, van der Linden et al. 2018, Hammer et al. *in press*).

This study assesses the possibility of detecting layer interfaces from cone resistance measurements based on its rate of change. Layering between different combinations of sand and clay layers are assessed from physical experiments. There are complex relations between the mechanical properties of different materials and the measured cone resistance. However, the

evaluations in the current study relies exclusively on the cone resistance measurements and soil type (i.e., sand or clay), rather than the geotechnical parameters of the soils.

2 TRANSITION AND THIN-LAYER EFFECTS

Values of the cone resistance that only reflect a single, homogenous material is labeled the *characteristic* cone resistance of the material. Close to a layer interface between different materials, the measured cone resistance may deviate from the characteristic cone resistance. This is due to factors such as the cone geometry and difference in stiffness and strength between the materials. The distances of transition effects in the materials are labeled sensing- and developing distance, as illustrated in Figure 1 (a).

In a thin layer, where the layer thickness is less than the sum of the sensing- and developing distance of the thin layer, the extreme value will not equal the characteristic cone resistance, known as *thin-layer effects*. An example of this is illustrated in Figure 1 (b). The characteristic cone resistance in thin layers can be estimated through correction factor, K_H (Youd & Idriss 2001):

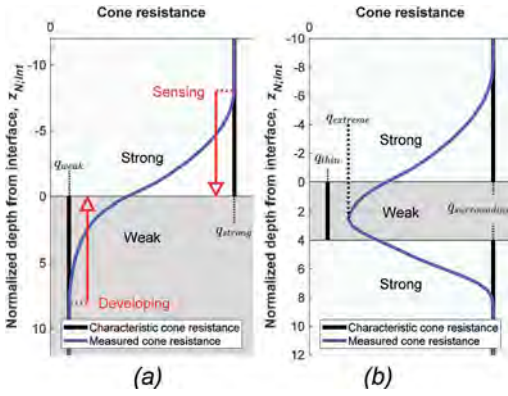


Figure 1. Illustration of transition- and thin-layer effects for (a) a two-layered composition and (b) a three-layered composition.

$$q_{thin} = K_H \cdot q_{extreme} \quad (1)$$

Values of K_H is less than or equal 1 in thin weak layers, e.g., Figure 1(b). For the opposite case, in thin strong layers, values are greater or equal 1. Factors of K_H are proposed for thin sand layers in clay (i.e., thin strong layers) based on field data and experiments. It is however a lack of proposed correction factors for thin weak layers.

The proposed correction factors are typically dependent on the thin layer thickness compared to the cone diameter (H/d_c) and the contrast between the characteristic cone resistance of the thin layer and the surrounding layers (i.e., $q_{thin}/q_{surrounding}$). More advanced methods of thin layer corrections have been proposed, most noticeably the inverse filtering procedure (Boulangier & DeJong 2018).

3 CONE RESISTANCE RATE OF CHANGE

The cone resistance is in this study presented against the depth of the cone tip (z) normalized on the cone diameter (d_c):

$$z_N = \frac{z}{d_c} \quad (2)$$

The depth is furthermore referenced to the depth of a layer interface (z_{int}):

$$z_{N:int} = \frac{z - z_{int}}{d_c} \quad (3)$$

The subscript of the cone resistance measurement type is omitted in this study. I.e., the symbol q is used rather than q_c or q_t . The latter is the corrected cone resistance for pore pressure due to unequal area effects. Each measurement of q can be labeled with and index

i , i.e., q_i . These values have a corresponding measurement depth z_i , where values of depth are increasing with increasing indices.

Assuming a constant characteristic cone resistance for each layer, such as for the examples in Figure 1, the derivate of the measured cone resistance is expected to reflect the transition effects. The derivate can be expressed as the change of measured cone resistance over the distance between measurements. The derivate of q becomes:

$$\left(\frac{\Delta q}{\Delta z_N} \right)_i = \frac{q_{i+1} - q_i}{z_{i+1} - z_i} \cdot d_c \quad (4)$$

The unit of this parameter is given in units of stress, e.g., MPa.

Hammer et al. (in press) proposed a normalized parameter of cone resistance rate of change, q'_i , defined as $\Delta q/\Delta z_N$ divided by the average cone resistance between the two depths:

$$\begin{aligned} q'_i &= \left(\frac{\Delta q}{\Delta z_N} \right)_i \cdot \frac{1}{0.5 \cdot (q_{i+1} + q_i)} \\ &= \frac{q_{i+1} - q_i}{z_{i+1} - z_i} \cdot \frac{2 \cdot d_c}{q_{i+1} + q_i} \end{aligned} \quad (5)$$

An advantage of normalizing the derivative of the average measurement is an increased emphasize on transition effects in weak materials. This parameter showed promise for detecting interfaces for thin clay layers.

The procedure of Boulangier & DeJong (2018) consisted of three main components, where the first two corrects measurements of cone resistance for thin layer effects. The last component attempts to correct for transition effects. Profiles corrected for thin-layer effects are evaluated based on the rate of change to identify and approximate sharp transition (i.e., interfaces). The resistance rate of change was defined as:

$$m_i = \ln \left(\frac{q_{i+1}}{q_i} \right) \cdot \frac{d_c}{z_{i+1} - z_i} \quad (6)$$

Interfaces was in the study determined primarily based on whether the values of m (calculated from cone resistance profiles corrected for thin-layer effects) were greater than 0.1.

Both q' and m are parameters describing the relative change in cone resistance over normalized distances (Δz_N). The two parameters are compared for various relations of q_{i+1}/q_i over one cone diameter distance ($\Delta z_N = 1$) in Figure 2. The parameter m is for this situation represented with f_1 while f_2 represents q' . Two additional relationships are added for comparison, f_3 and f_4 , these represent $\Delta q/\Delta z_N$ normalized on q_i and q_{i+1} respectively. From this it is evident that there is

a negligible difference between q' and m for small relative changes, q_{i+1}/q_i . Due to the numerical advantages of computing the function f_1 rather than f_2 , the parameter m is used in this study for the cone resistance rate of change. Each measurement of m_i is assigned to the average depth between z_i and z_{i+1} . Note that if the distances between measurements are approximately constant, this only results in a change the reference depth.

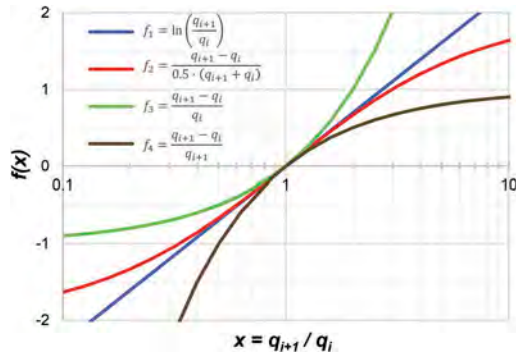


Figure 2. Different measurements of cone resistance rate of change.

The advantages of the cone resistance rate of change m compared to the derivative $\Delta q/\Delta z_N$ is highlighted through an example of one of the physical experiments from de Lange (2018). Figure 3 presents values of q together with calculated values of m and $\Delta q/\Delta z_N$. The soil sample has thin alternating clay and sand layers of $H=3.2d_c$ between two sand layers. Three measurements of the same sample were performed with the sample exposed to a surcharge load of 25, 50 and 200 kPa.

The two primary advantages of m compared to $\Delta q/\Delta z_N$ are firstly the apparent independency on the stress level, as observed from the figure. Secondly, values of m appear to reach extreme values at constant distances to the layer interfaces. The second advantage will be explored in chapter 5.

4 DATA FROM PHYSICAL EXPERIMENTS

4.1 Experiments

The normalized cone resistance rate of change was applied to measurements from physical experiments on layered sand and clay. The aim to determine its ability to detect layer interfaces as well as characterize thin-layer- and transition effects. Results of recent experiments performed at NTNU are evaluated together with multiple studies from literature. A list of all references of the experiments evaluated in this study is presented in Table 1.

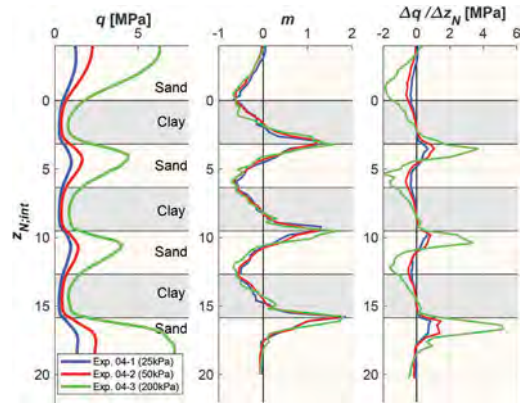


Figure 3. Example of values of m compared to $\Delta q/\Delta z_N$. Measurements from de Lange (2018), containing multiple thin clay and sand layers of thicknesses of $H=3.2d_c$ between sand layers. The names of the series indicate the applied surcharge.

The physical experiments are performed on constructed samples of layered sands and clays in chambers. Preparation methods and material properties of sands and clays vary between the different experiments. In general, the sands in the created samples are described as clean, uniform, and homogenous. Clay layers are also homogenous and primarily described as soft. The relations between the material properties and the measured cone resistance are not evaluated in this study.

The CPT probes used in all experiments have 60° apex while the cone diameters are varying from 1 to 3.6 cm. The diameter size (rounded in millimeters) of the different experiments are shown in Table 1.

The results of Hammer (2020) and Skrede (2021) are corrected for unequal area effects, however, the differences in thin clay layers were found to be neglectable. The measurements from literature are primarily not corrected for unequal area effect.

Table 1. Physical experiments of cone penetration in calibration chambers of layered sands and clays evaluated in this study.

Reference	Materials	d_c [cm]
van der Berg (1994)	Sand, clay	3.6
Teh et al. (2010)	Sand, clay	1
Mlynarek et al. (2012)	Sand, clay	3.6*
Tehrani et al. (2017)	Sand	3.2
van der Linden et al. (2018)	Sand, clay	2.5
de Lange (2018)	Sand, clay	2.5
Wang (2019)	Clay	1
Hammer (2020)	Sand, clay	3.6
Skrede (2021)	Sand, clay	3.6

* Probe properties were not found, a standard size (10cm^2) is assumed

4.2 Results from chamber tests at NTNU

The problem of thin clay layers in sand has been studied through large scale physical experiments in a CPTU chamber at NTNU (Norwegian University of Science and Technology) in Trondheim during the last two years. Samples were constructed in a chamber of 1.2 m diameter and 1 to 2.2 m height. Multiple cases of varying thin-layer thickness were tested at varied stress states. Details on the experiments and results are presented in the MSc theses Hammer (2020) and Skrede (2021). A combined six sample cases were constructed and tested in the two studies, named E1 - E6.

4.3 Results from literature

Multiple studies have been performed on physical experiments of cone penetration in layered sand and/or clays. The experiments that are found to be relevant for this study are summarized in Table 1. The cone resistance measurements of these studies were digitized from figures in a detailed manner. Depth measurements were converted to the normalized depth of the cone tip below a layer interface ($z_{N;int}$). The measurements from literature were interpolated at $0.3d_c$ intervals since the actual intervals between measurements are unknown. For a standard cone with area 10 cm^2 this corresponds to measurements each 1 cm.

5 RESULTS

5.1 Sand

The profiles of two experiments with dense over loose sand from Tehrani et al. (2017) are presented in Figure 4 (top). Minimum values of m coincide with the layer interface with values of -0.2 and -0.3. The study defined sensing lengths of $5.1d_c$ for both experiments, reflecting approximately the distance from where m changes sign to the layer interface. Developing distances were defined as $2.2d_c$ and $2.4d_c$, respectively.

Figure 4 (bottom) show the opposite layering, i.e., loose sand over dense sand. The maximum values of m for the two experiments were 0.5, these values occur at a distance $1-2d_c$ prior to the layer boundary. Sensing distances were described as $2.8 d_c$ and $3 d_c$, respectively, while developing distances were $3.8 d_c$ and $3.9 d_c$.

5.2 Clay

Transition effects between clay layers was evaluated in the study of Wang (2019). Results of experiments with stiff clay over soft clay are presented in the top of Figure 5. Values of m decrease only from a distance of about $1d_c$ prior to the layer interface. The transition towards the characteristic cone resistance of the soft clay layer (i.e., the developing length) appear to be over about $4-6d_c$.

Results of experiments with soft over stiff clay are shown in Figure 5 (bottom). Sensing distance is for this layering case about $1d_c$ as well, while the developing distance appear to be about $2d_c$.

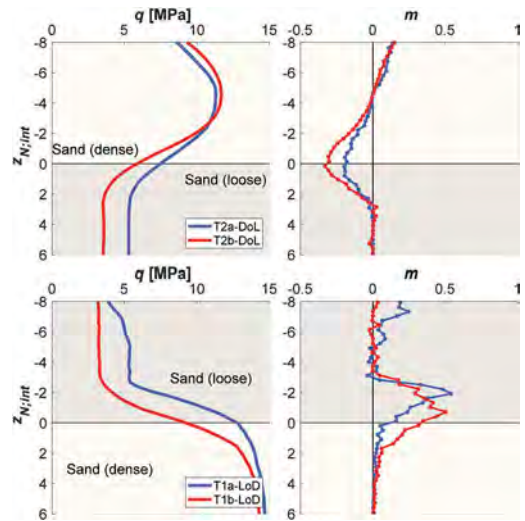


Figure 4. Q and m profiles for layered sand, experiments of Tehrani et al. (2017). Top: dense over loose sand. Bottom: Loose over dense sand.

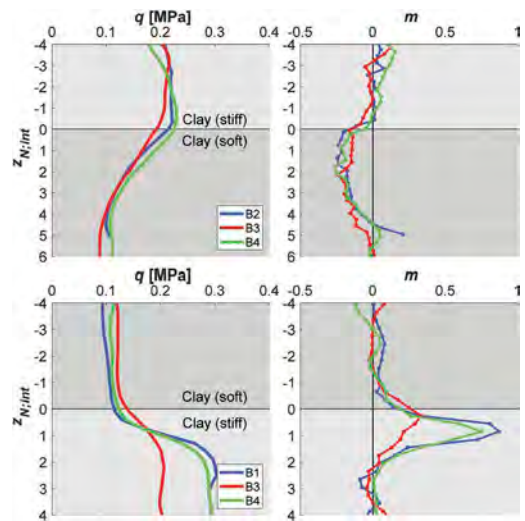


Figure 5. Q and m profiles for layered clay, experiments from Wang (2019). Top: stiff over soft clay. Bottom: soft over stiff clay.

5.3 Sand and clay

Various studies have included experiments on thick layers of sand and clay. These include van der Berg (1994), Teh et al. (2010), Mhynarek et al. (2012), van der Linden et al. (2018) and Skrede (2021). Four of these are presented in Figure 6 for a thick sand layer over clay. Three of the q -profiles are increasing until $2-3d_c$ distance to the interface due to the proximity to the top surface of the sample. This causes greater uncertainty in the interpretation of sensing distance. An approximation of the sensing distance may be $2-3d_c$ for these three

measurements and $5-6d_c$ for Mlynarek et al. (2012). Extreme values of the m -profiles were between -0.8 and -0.6 , reached within $1d_c$ of the actual layer boundary.

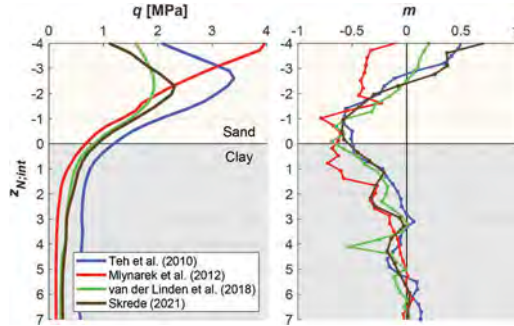


Figure 6. Q and m profiles for two-layered samples of sand over clay from multiple studies.

The opposite layering is presented in Figure 7. Similar to the two-layered clay in section 5.2, the clay layers exhibit a very short sensing distance of about $1d_c$. The contrast (i.e., ratio) between the characteristic cone resistance of the bottom sand layer and the clay layer varies from 25 to 100. The developing distance displayed in the sand layer appear to be approximately $3d_c$. Extreme values of the m -profiles vary from 2.6 to 4.4 and occur at the layer interface.

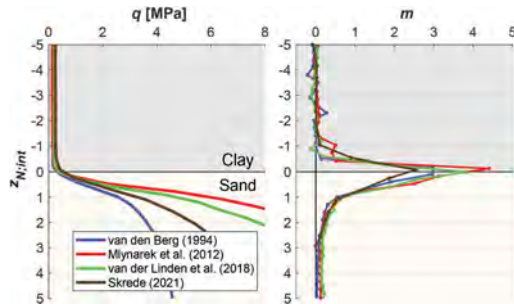


Figure 7. Q and m profiles for two-layered sand and clay from multiple studies. Top: sand over clay. Bottom: clay over sand.

5.4 Thin clay layer in sand

Measurements from NTNU experiments E2 (Hammer 2020) and E5 (Skrede 2021) of thin clay layers with thickness $0.56-2.2d_c$ are presented in Figure 8. The characteristic cone resistance of the sand layers were about 10 times that of the clay layer. The m -profiles for the three different layer thicknesses primarily have extreme values for the top transition of between -0.6 and -0.5 . These occur very close to the clay layer interface. Extreme values of m for the bottom transition occur $0-1d_c$ below the bottom interface. The extreme values decrease with

decreasing layer thickness. Sensing and developing distances in the sand can be approximated to $2-3d_c$ and $2d_c$, respectively.

5.5 Multiple thin sand and clay layers

Numerous experiments on samples with multiple thin sand and clay layers of equal thickness is presented in the study of de Lange (2018). Here, three of these are presented. The first is the “exploratory test 4” presented in Figure 3 with thicknesses $3.2d_c$. Figure 9 and Figure 10 present respectively “soil model 02” with layer thicknesses $1.6d_c$ and “soil model 08” with layer thicknesses $0.8d_c$. Both the experiment with thicknesses $3.2d_c$ and $1.6d_c$ reaches extreme values of m very close to or at the interfaces. Extreme values of m prior to clay layers and sand layers are respectively about -0.6 and $1-1.8$. For the sample with layer thicknesses $0.8d_c$ the values of m are significantly lower than the other two experiments. However, the shape of the m -profile is largely the same and extreme values of m correspond to interfaces fairly well.

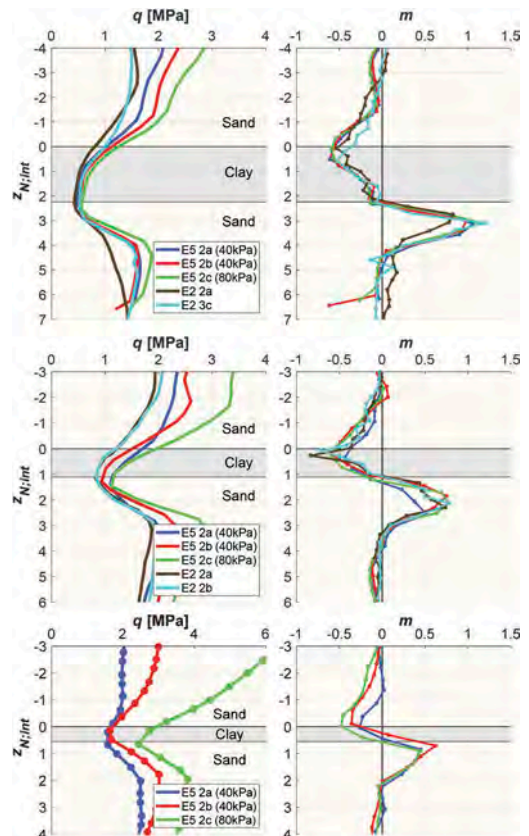


Figure 8. Q and m profiles for thin clay layers in sand. Experiments from Hammer (2020) and Skrede (2021). Top: $H=2.2d_c$. Middle: $H=1.1d_c$. Bottom: $H=0.56d_c$ (each measurement point is marked with dots).

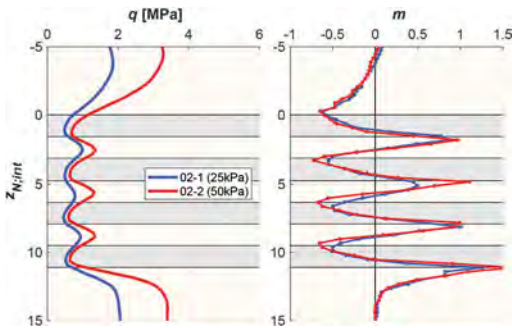


Figure 9. Q and m profiles for multiple thin layers of sand and clay, $H=1.6d_c$. Experiments from de Lange (2018).

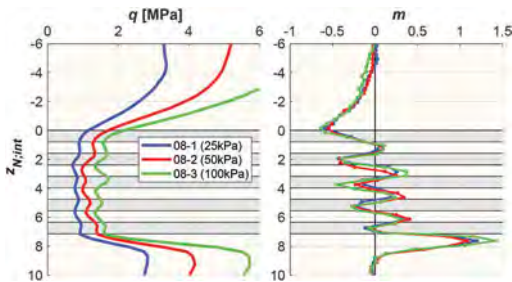


Figure 10. Q and m profiles for multiple thin layers of sand and clay, $H=0.8d_c$. Experiments from de Lange (2018).

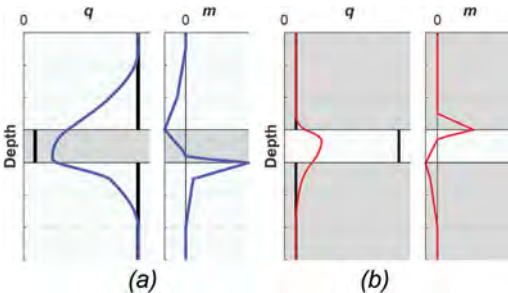


Figure 11. Illustration of the expected thin-layer effects in (a) a thin clay layer embedded in sand and (b) a thin sand layer embedded in clay. Black lines are the characteristic cone resistance.

6 DISCUSSION

6.1 Sensing and developing lengths

It is evident from the experiments that the sensing and developing distances of sand and clay are significantly different. While penetration in sands exhibit an almost equal sensing- and developing distances, there are large differences in clays. In clays, the sensing distance appear to typically be about one cone diameter in front of the cone tip, while the developing distance are up to six times the amount. This difference is considered to be

key in understanding the thin-layer effects acting in sand and clays. Figure 11 illustrates the expected thin-layer effects in (a) a thin clay layer in sand and (b) a thin sand layer in clay due to the difference in sensing and developing distances.

6.2 Layer interface detection

Based on the studied experiments, layer interfaces between sand and clay may be interpreted based on representative extreme values of m . The top interface of clay layers can be approximated at a depth with an extreme value of m less than -0.4 . For layers with small contrast in characteristic cone resistance, such as the two-layered sand/ or clay, a value of about -0.2 can indicate a layer interface. A bottom interface of a clay layer may be interpreted at the depth where the parameter m reaches an extreme positive value of at least 0.5 .

7 CONCLUSIONS

A cone resistance rate of change parameter shows promising possibilities to detect layer interfaces between sand and clays. The parameter additionally yields useful information on transition effects. It allows for efficient interpretation of layer boundaries and may even detect layers as thin as the cone diameter. The use of the parameter for interface detection depends on a significant contrast in characteristic cone resistance between layers. Testing on field data is needed to look deeper into the possibilities and the limitations for this method of layer interface detection in naturally formed deposits.

REFERENCES

- Boulangier, R., & DeJong, J. 2018. Inverse filtering procedure to correct cone penetration data for thin-layer and transition effects. *Proceedings of the 4th International Symposium on Cone Penetration Testing (CPT'18)*, Delft, 21-22 June.
- de Lange, D.A. 2018. *CPT in Thinly Layered Soils* (J. van Elk & D. Doornhof, Eds.; No. 1209862-006-GEO-0007).
- Hammer, H.B. 2020. *Physical experiments on CPTU thin-layer effects of thin clay layers embedded in sand* (Master's thesis). Norwegian University of Science and Technology (NTNU), Trondheim, Norway. 11250/2689484
- Hammer, H.B., Nordal, S. and L'Heureux, J.-S. In press. Detection of thin clay layers in sand using a standard CPTU probe. *20th International Conference on Soil Mechanics and Geotechnical Engineering (ICSMGE)*, Sydney, 1-5 May.
- Hird, C., Johnson, P., & Sills, G. 2003. Performance of miniature piezocones in thinly layered soils. *Geotechnique*, 53(10),885-900. 10.1680/geot.2003.53.10.885
- Młynarek, Z., Gogolik, S., & Póltorak, J. 2012. The effect of varied stiffness of soil layers on interpretation of CPTU penetration characteristics. *Archives of civil and*

- mechanical engineering*, 12(2),253–264. 10.1016/j.acme.2012.03.013
- Teh, K. L., Leung, C. F., Chow, Y.K. & Cassidy, J. 2010. Centrifuge model study of spudcan penetration in sand overlying clay. *Géotechnique*, 60(11),825–842. 10.1680/geot.8.P.077
- Tehrani, F.S., Arshad, M. I., Prezzi, M., & Salgado, R. 2017. Physical modeling of cone penetration in layered sand. *Journal of Geotechnical and Geoenvironmental Engineering*, 144 (1).10.1061/(ASCE)GT.1943-5606.0001809
- Skrede, H. 2021 *CPTU-detection of thin clay layers in sand* (Master's thesis). Norwegian University of Science and Technology (NTNU). Trondheim, Norway.
- van den Berg, P. 1994. *Analysis of soil penetration*. (Doctoral dissertation, Delft University of Technology).
- van der Linden, T.I., De Lange, D.A., & Korff, M., 2018. Cone Penetration Testing in Thinly Inter-Layered Soils. *Geotechnical Engineering*. 10.1680/jgeen.17.00061
- Wang, Y. 2019. *Centrifuge Modelling and Numerical Analysis of Penetrometers in Uniform and Layered Clays*. (Doctoral dissertation, The University of Western Australia). 10.26182/5d14603a91815
- Youd, T.L. and Idriss, I.M. 2001. Liquefaction resistance of soils: summary report from the 1996 NCEER and 1998 NCEER/NSF workshops on evaluation of liquefaction resistance of soils. *Journal of Geotechnical and Geoenvironmental Engineering*, ASCE, 127(4),297–313. 10.1061/(ASCE)1090-0241(2001)127:4(297)

Recalculation of in-situ CPTu in intermediate soils using G-PFEM

L. Hauser, S. Oberhollenzer, A. Gharehaghajlou, H.F. Schweiger & R. Marte

Institute of Soil Mechanics, Foundation Engineering and Computational Geotechnics, Graz University of Technology, Graz, Austria

C. Fabris

Geoconsult ZT GmbH, Puch bei Hallein, Austria

ABSTRACT: Piezocone penetration in intermediate soils is often associated with partially drained behaviour which has to be taken into account when interpreting the results. As part of the research project PITS, the effect of partial drainage on in-situ testing in postglacial silty deposits in Austria is investigated by means of in-situ testing campaigns, laboratory testing and numerical simulations. The present work presents a numerical recalculation of in-situ CPTu, carried out with different penetration velocities in a silty soil layer at the test site Rhesi near lake Constance, using the application G-PFEM. The results agree reasonably well with the in-situ measurements considering the given heterogeneity of the soil layer and suggest that partial drainage occurs during the penetration process.

1 INTRODUCTION

The interpretation of piezocone testing (CPTu) in intermediate soils is a challenging task considering the fact that standard testing with a penetration velocity, v , of 2 cm/s often takes place under partially drained conditions. This has been shown, e.g. by Paniagua *et al.* (2013) on the basis of small-scale experiments where local drainage around the cone tip was observed. Therefore, specific approaches have been developed to quantify partial drainage at normalized penetration velocities (Randolph and Hope, 2004; Schnaid *et al.*, 2020) and to account for this effects when deriving parameters, such as the coefficient of consolidation (DeJong and Randolph, 2012), from CPTu data.

The research project PITS, initiated at TU Graz in cooperation with the Federal Chamber of Architects and Chartered Engineering Consultants, aims to improve the characterization of postglacial silty deposits in Austria by means of in-situ testing addressing, inter alia, the effect of partial drainage.

The present work focusses on the numerical recalculation of CPTu tests carried out in a silty layer, where partially drained behaviour is observed, with penetration velocities of 0.5 and 2 cm/s. First, the in-situ testing campaign and the numerical model are outlined. Then, the results of the recalculations are presented and discussed highlighting the partially drained behaviour during penetration.

2 IN-SITU TESTING CAMPAIGN

As part of the ongoing research project PITS a comprehensive in-situ testing campaign was carried out at test site Rhesi, located in the forelands of the river Rhine near lake Constance in Austria. CPTu tests with different penetration velocities of 0.1, 0.5, 2 and 10 cm/s were carried out along with dissipation tests at different depths using u_1 and u_2 probes. Additionally, soil samples were recovered for laboratory testing and seismic flat dilatometer tests (SDMT) were performed. Figure 1 shows the obtained profiles of q_t , f_s , u_1 and u_2 over depth for the penetration velocities of 0.5 and 2 cm/s. For the following numerical study, layer L2, characterized by sand-silt alterations, is of main interest and a 0.5 m thick sublayer located at a depth of around 11.3 to 11.8 m is selected for recalculation. According to EN ISO 14688-1, the sublayer is classified as sa' cl' Si. Overall, the in-situ results show a clear scatter due to the sand-silt alterations. However, the calculated mean and median values of q_t , f_s , u_1 and u_2 are in good agreement for the considered sublayer. A shear wave velocity of around 170 m/s was measured at the considered depth and a friction angle of 30° results from direct shear testing.

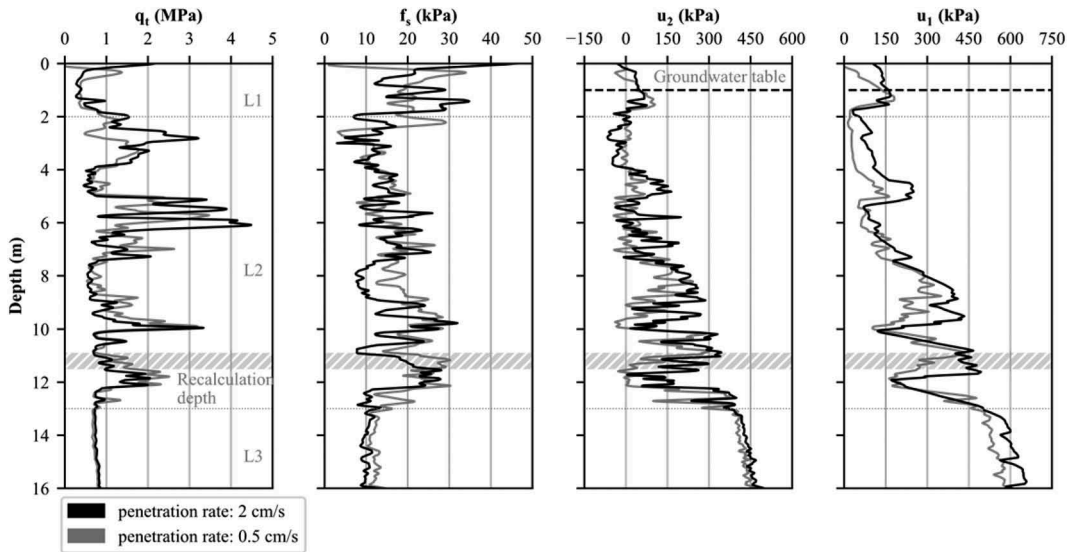


Figure 1. In-situ measurements (q_t , f_s , u_1 , u_2) over depth at test site Rhesi; depth used for the numerical recalculation marked at 11.5 m below the ground surface.

3 NUMERICAL MODEL

The numerical simulation of cone penetration testing is a challenging task involving large displacements and deformations of the soil around the penetrometer, nonlinear material behaviour and frictional contact between the ideally rigid cone and the deformable soil. Advanced numerical methods have already been successfully applied to model cone penetration (Ciantia *et al.*, 2016; Ceccato *et al.*, 2016; Sheng *et al.*, 2009; Yuan *et al.*, 2019). For the present work, the application G-PFEM (Carbonell *et al.*, 2022), an implementation of the Particle Finite Element Method (PFEM) developed for modelling large deformation problems in geotechnics within the framework Kratos (Dadvand *et al.*, 2010), is used.

3.1 G-PFEM

In the PFEM, a given boundary value problem is solved performing frequent remeshing of critical regions of the integration domain which is treated as a cloud of particles carrying all information. At the beginning of a time step, particles/nodes may be added or removed in certain regions. Subsequently, the boundaries of the domain are defined and the mesh is created which is used for solving the computation step by means of the Finite Element Method (FEM). Finally, an updated cloud of nodes/particles is obtained at the end of the time step (Oñate *et al.*, 2011). Large deformations of the domain can be treated efficiently as excessive mesh distortion is avoided, however, at the cost of increased computational effort. A stabilized, mixed formulation of the quasi-static linear momentum and mass balance

equations in an Updated Lagrangian manner is used in connection with low equal order approximations (linear triangular elements) of the displacement and pore pressure fields. Additionally, the determinant of the deformation gradient is introduced as a nodal variable (Monforte *et al.*, 2017b). Constraints due to frictional contact between cone and soil, according to a Coulomb friction law, are enforced using a penalty method. Also, no water flow normal to the contact interface is allowed as the rigid body is impervious. The interested reader is referred to Monforte *et al.* (2017a) and Carbonell *et al.* (2022) for a more detailed outline of the application G-PFEM.

For the present study, the Clay and Sand Model (CASM), a non-associated elastoplastic model proposed by Yu (1998), is used allowing for a flexible definition of the yield surface geometry by means of the model parameters r and n . For particular combinations of r and n the surfaces of the Original Cam Clay model (OCCM) and the Modified Cam Clay model (MCCM) may be obtained as shown in Figure 2. Adapted to finite strains according to Monforte *et al.* (2015), the model features the hyperelastic model by Housley (1985) with the modified swelling index κ^* and the shear modulus G . Coupling of volumetric and deviatoric response is not considered, thus, the parameter α equals zero. The classical critical state hardening rule is adopted according to which the preconsolidation pressure evolves with plastic volumetric strain depending on κ^* and the modified compression index λ^* . The implemented version of the CASM and its extension for structured material as well as the FD_MILAN model have already been used in connection with G-PFEM for modelling cone penetration (Hauser

and Schweiger, 2021; Monforte *et al.*, 2021; Oliynyk *et al.*, 2021).

3.2 CPTu model

The penetration process is modelled in 2D as an axisymmetric problem consisting of a rectangular, deformable soil domain (measuring 2.2 m in height and 1 m in width) and a rigid cone with 15 cm² base area and a tip angle of 60°. Overburden pressure is applied on top of the domain while the lateral and lower boundaries are fixed in normal direction (see Figure 3). Initially, the probe is already inserted in the soil and the downwards movement of the rigid body starts from there. A constant initial stress field is applied assuming weightless soil and the stationary values of q_t , f_s , u_1 and u_2 are reached after an initial transient phase of roughly 10 radii of penetration. The initial mesh, the contact stiffness and the criteria for mesh refinement were chosen based on previous studies (Hauser and Schweiger, 2021).

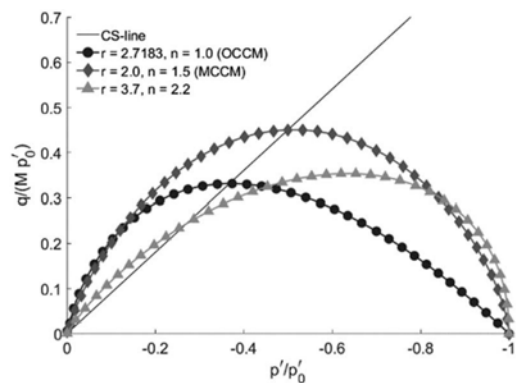


Figure 2. CASM yield surfaces for different combinations of r and n in the q - p' space normalized with respect to respective preconsolidation pressure p'_0 .

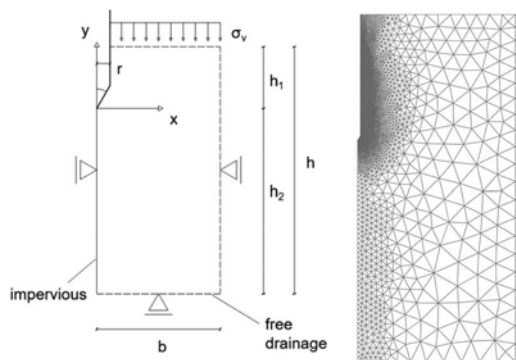


Figure 3. Axisymmetric model and refined mesh during penetration.

4 RESULTS OF THE RECALCULATION

The recalculation was performed for a 0.5 m thick sub-layer at an average depth of 11.55 m leading to the constant initial stress field defined through $\sigma'_v = 128$ kPa, $\sigma'_h = 64$ kPa and $u_0 = 110$ kPa with K_0 being 0.5. For this study, the yield surface of the CASM is assumed to be a MCC ellipse ($r = 2$, $n = 1.5$) since no experimental evidence for an alternative, more suitable choice of r and n is available. This results in an associated flow rule which influences the pore pressure development. However, the effect of a non-associated flow rule is not addressed in this study. The overconsolidation ratio (OCR) is equal to 1. G_0 is calculated from V_s for a density of 1.83 g/cm³ and a ratio $G_0/G = 5$ is used to estimate the shear modulus at working strains, G , of 10600 kPa. Marchetti and Monaco (2018) suggest a similar value of around 4.2 for G_0/G for a clayey silt at a site in Italy. Assuming uncoupled volumetric and deviatoric behaviour in the hyperelastic model ($\alpha = 0$), κ^* is determined in such a way that a Poisson's ratio of 0.2 is obtained for the initial mean stress and the given G . Eventually, λ^* is defined through the ratio $\lambda^*/\kappa^* = 4$. The parameter set, as summarized in Table 1, yields an undrained shear strength of 39 kPa which is obtained from a numerically simulated triaxial compression test for the given initial stress state. A contact friction angle of 9° at the interface between penetrometer and soil is used which proved to be a reasonable assumption in previous studies (Hauser *et al.*, in press).

Table 1. Material parameters for the numerical recalculation of a silty layer at a depth of 11.55 m at test site Rhesi.

γ [kN/m ³]	ϕ [°]	r [-]	n [-]	OCR [-]
0	30	2	1.5	1
κ^* [-]	G [kPa]	α [-]	λ^* [-]	K_0 [-]
0.0061	10600	0	0.0244	0.5

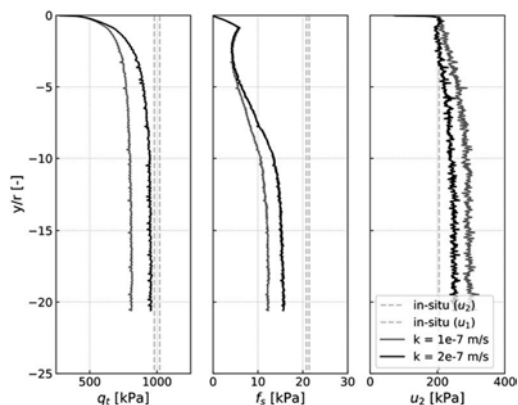


Figure 4. Results of the recalculation of q_t , f_s , u_2 over normalized depth compared to the in-situ tests executed for $v = 2$ cm/s with a u_1 and u_2 piezocone, respectively.

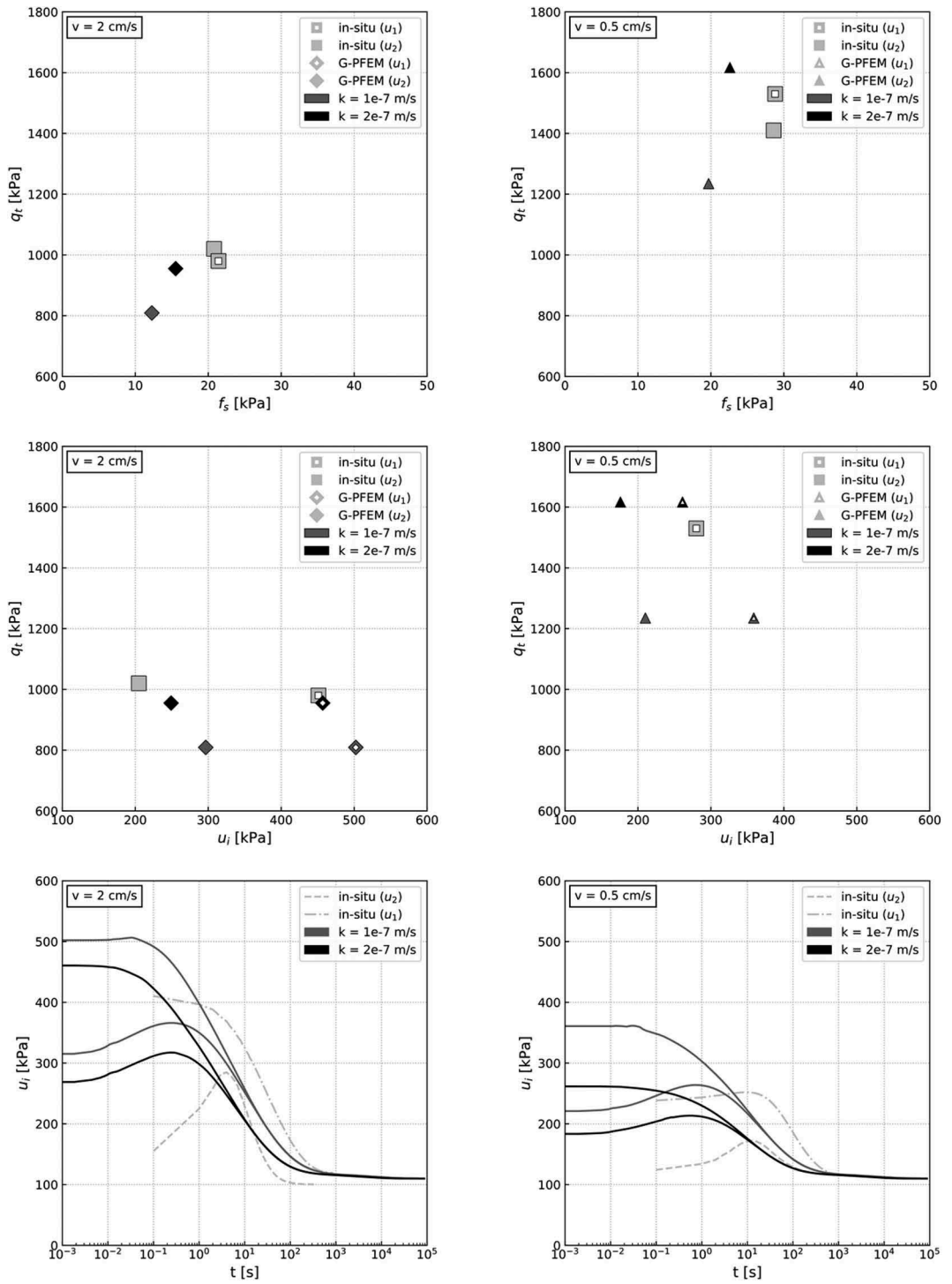


Figure 5. Comparison of in-situ measurements (square markers and dashed lines) and numerical recalculations for penetration velocities of 0.5 and 2 cm/s as well as permeabilities of 1×10^{-7} and 2×10^{-7} m/s in terms of q_t , f_s , u_1 , u_2 and pore pressure dissipation curves. Note that the in-situ u_2 pressure for $v = 0.5$ cm/s is not available for comparison.

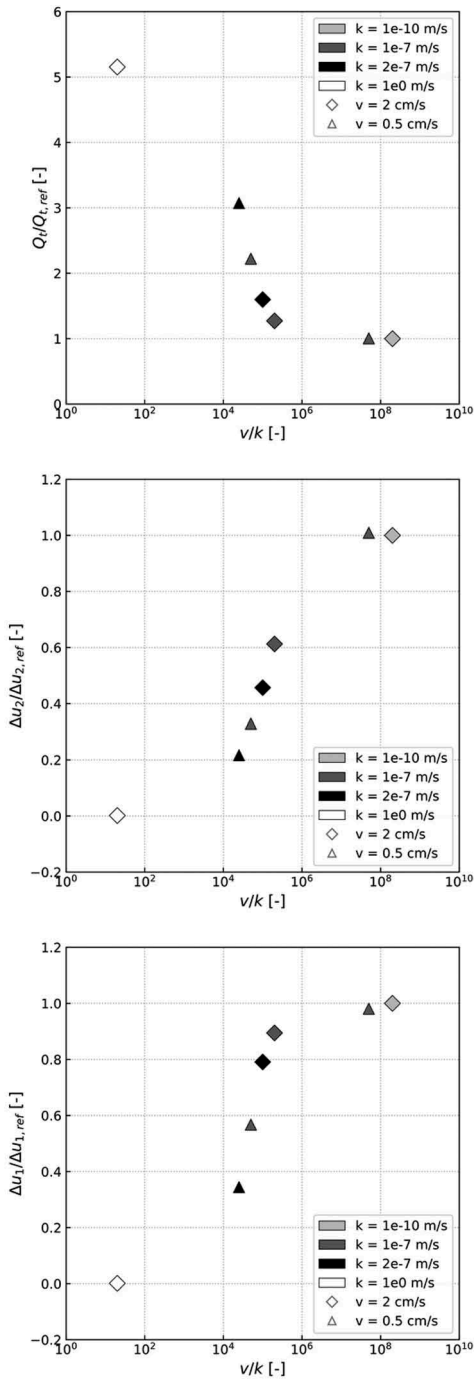


Figure 6. Tip resistance Q_t and excess pore pressures Δu_1 and Δu_2 normalized with respect to the undrained tip resistance $Q_{t,ref}$ and the undrained excess pore pressures $\Delta u_{1,ref}$ and $\Delta u_{2,ref}$, respectively over the penetration velocity v normalized by the permeability k (Sheng *et al.*, 2014).

Recalculations were carried out for the penetration velocities of 0.5 and 2 cm/s as well as for isotropic permeabilities equal to $1 \cdot 10^{-7}$ and $2 \cdot 10^{-7}$ m/s. The results are presented in Figure 5 comparing the in-situ and the recalculated q_t , f_s , u_1 , u_2 along with the pore pressure dissipation curves. Thereby, the numerical results for q_t , f_s , u_1 , u_2 are obtained from the penetration curves as the average between 16 and 17 radii of penetration (see Figure 4) while the in-situ values represent the average over the considered 0.5 m thick sublayer. As expected, the lower permeability $k = 1 \cdot 10^{-7}$ m/s leads to more “undrained like” behaviour, resulting in lower q_t , f_s and higher u_1 , u_2 as well as longer dissipation times, compared with the higher permeability $k = 2 \cdot 10^{-7}$ m/s. However, better agreement between the in-situ results and the recalculations, in terms of q_t , f_s , u_1 , u_2 , is reached for $k = 2 \cdot 10^{-7}$ m/s as both penetration velocities match the in-situ results reasonably well. Numerically, the dissipation curves at the u_1 and u_2 position tend to coincide after around 10 to 12 s which is not the case for the in-situ measurements. For $k = 1 \cdot 10^{-7}$ m/s, the recalculated dissipation curves lie between the in-situ ones, however, the initial pore pressure is significantly higher.

For $k = 2 \cdot 10^{-7}$ m/s, the dissipation time and the initial pore pressures are reduced suggesting better agreement with the in-situ measurements in terms of initial pore pressure. Additional calculations with permeabilities of $1 \cdot 10^{-10}$ m/s and $1 \cdot 10^0$ m/s were performed in order to obtain fully undrained and fully drained references cases.

5 DISCUSSION

The recalculations employing the higher permeability of $2 \cdot 10^{-7}$ m/s appear to match the in-situ q_t , f_s , u_1 and u_2 best for the two considered penetration velocities. In case of faster penetration (2 cm/s) the numerical response is slightly more “undrained like” compared to the in-situ measurements while the response is rather on the drained side for slower penetration (0.5 cm/s). The difference between the in-situ and the recalculated dissipation curves is more pronounced as the pore pressure at the u_1 position decays significantly faster compared to the in-situ measurement. However, considering the heterogeneity of the layer and the fact that the in-situ curves for u_1 and u_2 originate from two different tests, carried out in close proximity and at roughly the same depth with the u_1 and u_2 probe, respectively, the overall behaviour, especially the non-monotonic decrease of the u_2 pressure, is properly reproduced by the numerical model. Also, anisotropic permeability was not considered in the present numerical study.

The recalculated CPTu quantities appear to be sensitive to the considered range of penetration

velocities and permeabilities suggesting partially drained behaviour. Figure 6 shows the tip resistance Q_t and the excess pore pressures Δu_1 and Δu_2 normalized with respect to the undrained reference $Q_{t,ref}$, $\Delta u_{1,ref}$ and $\Delta u_{2,ref}$, respectively, plotted against the penetration velocity normalized by the permeability (Sheng *et al.*, 2014). Therefore, the undrained calculation for $v = 2$ cm/s and $k = 1 \cdot 10^{-10}$ m/s is used as reference case. Compared to the undrained reference, the tip resistance increases by a factor of 3 for $v = 0.5$ cm/s and $k = 2 \cdot 10^{-7}$ m/s and by a factor of more than 5 for the drained case. Similarly, Δu_1 decreases by a factor of up to 2.8 and Δu_2 by a factor of up to 5 with respect to the maximum undrained pressure suggesting that the shape of the pore pressure bulb changes with drainage condition. Also, the recalculated tests lie within the proposed range for partial drainage, i.e., $2 \cdot 10^1 < v/k < 2 \cdot 10^6$ (Sheng *et al.*, 2014).

6 CONCLUSION

The numerical recalculation of in-situ CPTu, performed in a silty postglacial deposit in Austria, confirmed that partial drainage governs the penetration process as the obtained q_t , f_s , u_1 and u_2 are highly sensitive to the considered range of penetration velocities and soil permeabilities. Overall, the numerical results match the in-situ measurements reasonably well for the considered 0.5 m thick sub-layer, which is, to a certain degree, heterogeneous due to the presence of alternating thin layers of sand and silt. Hence, the dissipation behaviour could not be reproduced as accurately as q_t , f_s , u_1 and u_2 resulting in faster dissipation of pore pressure at the u_1 position compared to the in-situ results. Nevertheless, the study demonstrates that the application G-PFEM is capable of modelling cone penetration under partially drained conditions in a realistic way.

ACKNOWLEDGEMENT

The authors acknowledge the financial and logistical support provided by the Austrian Research Promotion Agency and the Federal Chamber of Architects and Chartered Engineering Consultants.

REFERENCES

- Carbonell, J.M., Monforte, L., Ciantia, M.O., Arroyo, M. and Gens, A. (2022), "Geotechnical particle finite element method for modeling of soil-structure interaction under large deformation conditions", *Journal of Rock Mechanics and Geotechnical Engineering*.
- Ceccato, F., Beuth, L., Vermeer, P.A. and Simonini, P. (2016), "Two-phase Material Point Method applied to the study of cone penetration", *Computers and Geotechnics*, Vol. 80, pp. 440–452.
- Ciantia, M.O., Arroyo, M., Butlanska, J. and Gens, A. (2016), "DEM modelling of cone penetration tests in a double-porosity crushable granular material", *Computers and Geotechnics*, Vol. 73, pp. 109–127.
- Dadvand, P., Rossi, R. and Oñate, E. (2010), "An Object-oriented Environment for Developing Finite Element Codes for Multi-disciplinary Applications", *Archives of Computational Methods in Engineering*, Vol. 17 No. 3, pp. 253–297.
- DeJong, J.T. and Randolph, M. (2012), "Influence of Partial Consolidation during Cone Penetration on Estimated Soil Behavior Type and Pore Pressure Dissipation Measurements", *Journal of Geotechnical and Geoenvironmental Engineering*, Vol. 138 No. 7, pp. 777–788.
- Hauser, L. and Schweiger, H.F. (2021), "Numerical study on undrained cone penetration in structured soil using G-PFEM", *Computers and Geotechnics*, Vol. 133, p. 104061.
- Houlsby, G.T. (1985), "The use of a variable shear modulus in elastic-plastic models for clays", *Computers and Geotechnics*, Vol. 1 No. 1, pp. 3–13.
- Marchetti, S. and Monaco, P. (2018), "Recent Improvements in the Use, Interpretation, and Applications of DMT and SDMT in Practice", *Geotechnical Testing Journal*, Vol. 41 No. 5, p. 20170386.
- Monforte, L., Arroyo, M., Carbonell, J.M. and Gens, A. (2017a), "Numerical simulation of undrained insertion problems in geotechnical engineering with the Particle Finite Element Method (PFEM)", *Computers and Geotechnics*, Vol. 82, pp. 144–156.
- Monforte, L., Arroyo, M., Gens, A. and Carbonell, J.M. (2015), "Integration of elasto-plastic constitutive models in finite deformation: An explicit approach", in Oñate, E., Owen, D.R.J., Peric, D. and Chiumenti, M. (Eds.), *Computational Plasticity XIII Fundamentals and Application: Proceedings of the XIII International Conference on Computational Plasticity*, International Center for Numerical Methods in Engineering (CIMNE), Barcelona, Spain, pp. 398–406.
- Monforte, L., Carbonell, J.M., Arroyo, M. and Gens, A. (2017b), "Performance of mixed formulations for the particle finite element method in soil mechanics problems", *Computational Particle Mechanics*, Vol. 4 No. 3, pp. 269–284.
- Monforte, L., Gens, A., Arroyo, M., Mánica, M. and Carbonell, J.M. (2021), "Analysis of cone penetration in brittle liquefiable soils", *Computers and Geotechnics*, Vol. 134, p. 104123.
- Oliynyk, K., Ciantia, M.O. and Tamagnini, C. (2021), "A finite deformation multiplicative plasticity model with non-local hardening for bonded geomaterials", *Computers and Geotechnics*, Vol. 137, p. 104209.
- Oñate, E., Idelsohn, S.R., Celigueta, M.A., Rossi, R., Martí, J., Carbonell, J.M., Ryzhakov, P. and Suárez, B. (2011), "Advances in the Particle Finite Element Method (PFEM) for Solving Coupled Problems in Engineering", in Oñate, E. and Owen, D.R.J. (Eds.), *Particle-based methods: Fundamentals and applications*, *Computational Methods in Applied Sciences*, Vol. 25, Springer, Dordrecht, London, pp. 1–49.
- Paniagua, P., Andò, E., Silva, M., Emdal, A., Nordal, S. and Viggiani, G. (2013), "Soil deformation around a penetrating cone in silt", *Géotechnique Letters*, Vol. 3 No. 4, pp. 185–191.

- Randolph, M.F. and Hope, S. (2004), "Effect of cone velocity on cone resistance and excess pore pressures", *Proceedings of the IS Osaka - Engineering Practice and Performance of Soft Deposits*, pp. 147–152.
- Schnaid, F., Dienstmann, G., Odebrecht, E. and Maghous, S. (2020), "A simplified approach to normalisation of piezocone penetration rate effects", *Géotechnique*, Vol. 70 No. 7, pp. 630–635.
- Sheng, D., Kelly, R., Pineda, J. and Lachlan, B. (2014), "Numerical study of rate effects in cone penetration test", Las Vegas, Nevada, USA.
- Sheng, D., Nazem, M. and Carter, J.P. (2009), "Some computational aspects for solving deep penetration problems in geomechanics", *Computational Mechanics*, Vol. 44 No. 4, pp. 549–561.
- Yu, H.S. (1998), "CASM: a unified state parameter model for clay and sand", *Int. J. Numer. Anal. Meth. Geomech.*, Vol. 22, pp. 621–653.
- Yuan, W.-H., Zhang, W., Dai, B. and Wang, Y. (2019), "Application of the particle finite element method for large deformation consolidation analysis", *Engineering Computations*, Vol. 36 No. 9, p. 370.

Full-flow CPT tests in a nearshore organic clay

S. Hov

GeoMind, Stockholm, Sweden

Norwegian Geotechnical Institute, Trondheim, Norway

K. Borgström

GeoMind, Stockholm, Sweden

P. Paniagua

Norwegian Geotechnical Institute and Norwegian University of Science and Technology, Trondheim, Norway

ABSTRACT: The T-bar is a full-flow CPT with a larger probe surface area compared with the conventional CPT probe. The tip has the shape either of a ball or as an upside-down T, a so-called T-bar. The term ‘full-flow’ comes from the assumption that the earth ‘flows’ around the tip, which is a realistic assumption for soils with extremely low undrained shear strength. This paper presents a case study where a large number of T-bar tests have been performed in a nearshore organic clay with high water content and very low undrained shear strength. The test site is located in Stockholm, Sweden, where planned land reclamation and capping of contaminated top soils are challenging from a stability perspective due to the low strength of the soil. T-bar tests were thus performed to characterise the shear strength profile of the soil in detail, especially at shallow depths where sampling was difficult and the shear strength values were under 5 kPa. A N-factor relating the net cone resistance (q_{net}) and the undrained shear strength of the soil (c_u) was evaluated based on T-bar measured parameters and direct simple shear tests and undrained triaxial tests on samples taken at greater depths. This allowed to estimate shear strength profiles with depth. For all tests, both the penetration and extraction cone resistance were measured, and a good correlation was obtained between this ratio and the soil sensitivity measured in the laboratory. In addition, the sensitivity was correlated to the organic content of the clay. These correlations were found to be OCR-dependent. Further, cyclic tests were performed, and their results were correlated with the remoulded shear strength values. This facilitated mapping of the soil conditions across the site.

1 INTRODUCTION

Conventional CPT tests have long been used in all types of soil to interpret strength characteristics. In extremely soft clays the penetration resistance is however very small, and hence full-flow penetration tests was developed during the late 1990s, mainly for offshore applications (Stewart & Randolph, 1994; Randolph, 2004). The full-flow probe has the shape of a ball or a upside-down ‘T’ in order to increase its probe area and hence the penetration resistance.

The probe area is normally enlarged 10 times compared to conventional CPT tests. As the full-flow probe is mounted on conventional CPT probe, only replacing the tip, the probe area is 10 times larger than the drilling rod. This gives several advantages in extremely soft soils:

- The penetration resistance is 10 times higher, i.e. the measurement uncertainties originating from the load cell decrease

- The correction of overburden stress and pore pressure measurements are one tenth, i.e. they are almost negligible
- The resistance can be measured during penetration and extraction, giving additional data on soil type and behaviour

This paper presents a case study where full-flow CPT tests have been performed nearshore as part of a land reclamation project. An old industrial area, located in the northeastern part of central Stockholm, is undergoing residential development. Highly contaminated soils are also planned to be capped, i.e. a fill layer is placed on the seabed to minimize dispersion of contamination. The soil consists of extremely soft organic clay and gyttja, and hence the filling is challenging from a stability perspective. The full-flow CPT tests were performed to obtain high-quality detailed strength properties, especially in the upper part of the soil. In addition, the area had local variation due to earlier unknown works such as dredging, and hence mapping of the nearshore area

was important. The full-flow CPT tests was shown to be an excellent method to quickly map the area, as a complement to sampling and laboratory testing.

2 BACKGROUND

2.1 Previous work on full-flow CPT tests

The full-flow CPT tests have been used during the last 20 years for field applications (e.g., Yafraite *et al.*, 2009; Peuchen & Terwindt, 2016; Nakamura *et al.*, 2009; Boylan *et al.*, 2011; Schaeffers & Weemes, 2012), as well as in laboratory tests including centrifuge tests (Almeida *et al.*, 2011; Levacher *et al.*, 2016; Sahdi *et al.*, 2014). In addition, the full-flow test has been analysed theoretically by e.g. Randolph & Andersen (2006) and Zhu *et al.* (2020).

In Sweden, a research project on sensitive clays on land was performed around 10 years ago (Larsson *et al.*, 2014; Åhnberg & Larsson, 2012). The purpose was to investigate cyclic strength degradation of highly sensitive and quick clays.

Randolph (2004), DeJong *et al.* (2010) and Lunne *et al.* (2011) provide excellent all-inclusive description of the method.

2.2 Correction of tip resistance

Similar as for the conventional CPT test, the measured tip resistance is corrected by overburden stress and measured pore pressure. This corrected tip resistance (q_{net}) is calculated by Eq. 1 (DeJong *et al.*, 2010):

$$q_{net} = q_c - [p_o - u_2(1 - a)] \frac{A_s}{A_p} \quad (1)$$

where q_c = measured tip resistance; p_o = total vertical overburden stress; u_2 = measured pore pressure, a = area ratio, A_s = area of rod; and A_p = tip area. This equation assumes that the soil ‘flows’ around the probe and applies a vertical stress on the upper surface. As the ratio $A_s/A_p \approx 0.1$, the effect of overburden stress and pore pressure is one tenth of that for conventional CPT tests. It is thus often negligible.

2.3 Evaluation of shear strength

The undrained shear strength (c_u) is calculated as:

$$c_u = \frac{q_{net}}{N_{Tbar}} \quad (2)$$

Usually, site specific calibrations are recommended, however, the N_{Tbar} factor normally is found to be around 10-13 (Lunne *et al.*, 2011; DeJong



Figure 1. The Iskyrometer (top left), column penetration test (top right) and T-bar used in this study (bottom). The T-bar was $\varnothing 40$ mm and width 250 mm (tip area 10,000 mm²). The drilling rod is $\varnothing 36$ mm (area $\sim 1,000$ mm²). Sources: Kallstenius (1961), Massarsch (2014), Geotech (2019).

et al., 2010). It is found to be dependent on soil type, sensitivity and rate of strain softening.

According to theoretical studies by Randolph & Andersen (2006) the N_{Tbar} is in the range 11-13, not noticeably dependent on strength anisotropy if the average strength is used. For cyclic tests, i.e. several cycles of penetration and extraction over an interval, a remoulded strength can be interpreted with a N_{Tbar} varying between 10.5-15.

Larsson *et al.* (2014) studied 13 different Swedish soils and found that N_{Tbar} was highly dependent on the soil’s plasticity, in particular its liquid limit. A range between ~ 7 for low-plastic soils to ~ 16 for high-plastic soils were found.

2.4 Comparison with similar tests

Although the shape of the T-bar probe is unique, there are two other penetration tests which are remarkably similar. The ‘Iskyrometer’ was developed by the Swedish Geotechnical Institute during the 1930s for soft clays. The Iskyrometer consists of two foldable wings which are folded during penetration and unfolded when extracted where the extraction resistance is measured. Calibration of shear strength was done by comparing extraction resistance, fall cone test and in situ vane tests, and a N-factor of around 10-15 was found, dependent on both sensitivity and organic content (Kallstenius, 1961).

The Iskyrometer is no longer in use but was supposedly the origin for the column penetration tests which is used as a quality control of dry deep mixing columns. For this application, a N-factor of 10 is used (Axelsson, 2001), but this has undergone surprisingly little research.

Photographs of the Iskymeter, the column penetration and T-bar probe are shown in Figure 1. Notably, the Iskymeter, the standard dimension column penetration test and the full-flow CPT have equal probe areas, i.e. 10,000 cm². The N-factor for interpretation of shear strength is also similar.

2.5 Extraction ratio

The extraction ratio for full-flow CPT tests, i.e. ratio between penetration (q_m) and extraction (q_{out}) resistance is often used to interpret the soil's sensitivity. For low sensitive soils, the ratio is typically 0.6-0.8 decreasing to around 0.3 for highly sensitive soils (DeJong *et al.*, 2010).

3 SITE AND METHODS

3.1 Soil profile

Figure 2 shows a typical soil profile in one of the boreholes with a water depth of ~18 m. The sediments consist of clayey gyttja from seabed down to appr. 10 m depth. From around 10 m the soil is categorised as clay. As the organic content and water content decreases with depth, the density increases.

The plastic limit is normally not determined in Swedish engineering practice. Instead, only the liquid limit is used for empirical correlations, including silt and organic content. Figure 3 shows values of liquid limits vs. organic content from tests on the soil profile shown in Figure 1. This correlation allows a simple mapping of soil type only by liquid limit values.

3.2 Execution of the field work

The nearshore area had limited water depths, and all tests and sampling were done using a pontoon with supporting legs as a stable working platform. A total of around 30 T-bar tests were performed in an area of around 400x500 m. However, only a few is presented herein due to limited space. Around half was done with data acquisition also during extraction, and a few was performed with cyclic tests.

All T-bar tests were performed with the drilling rod within a casing to prevent excess deflection of the rod. Divers attached the T-bar probe under the casing, and also noted the time of penetration into seabed.

Sampling was done using the standard Swedish piston sampler (50 mm and 60 mm diameter).

3.3 Laboratory tests

A total of around 40 samples were retrieved. Routine analyses, i.e. bulk density, natural water content, liquid limit and intact and remoulded shear strength with fall cone (FC) tests were performed on all samples.

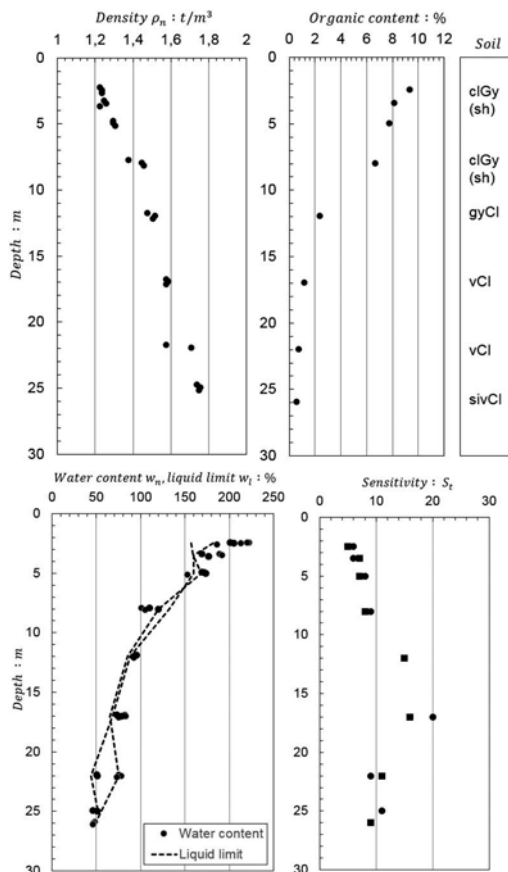


Figure 2. Typical soil profile (water depth ~18 m). cl = clay, gy = gyttja, sh = shales, v = varved, si = silt. Soil classification according to EN ISO 14688-1 and -2.

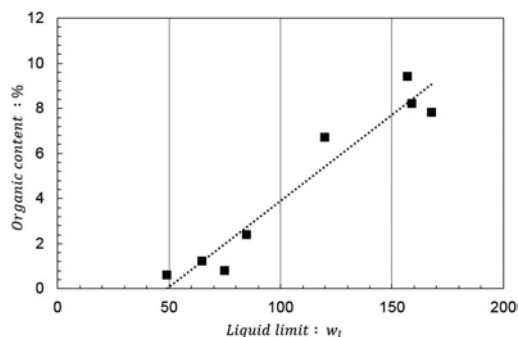


Figure 3. Liquid limit vs. organic content on samples from borehole shown in Figure 1.

On selected samples, CRS oedometer, direct simple shear (DSS) and triaxial compression and extension tests were performed.

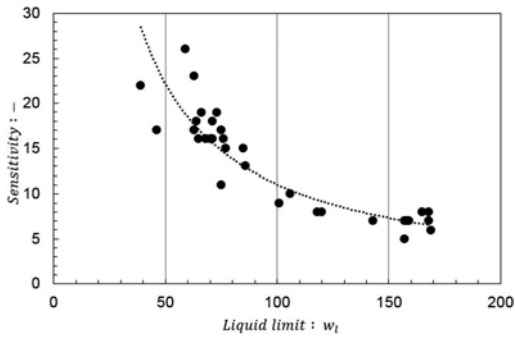


Figure 4. Liquid limit vs. sensitivity on all samples.

4 RESULTS

4.1 Evaluation of undrained shear strength

The strength anisotropy is larger for silty clay than organic clay and gyttja. It was thus decided to calibrate the N_{Tbar} against the undrained direct simple shear strength (c_u^{DSS}). This eliminates any anisotropy effects in the penetration tests as it is done in a stratigraphy of both organic and silty clay (example in Figure 2). Interpreting the c_u^{DSS} is also normal practice for conventional CPT tests in Sweden.

Trials of correlating q_{net} with strengths from FC and DSS tests were done using several soil parameters, however, the N_{Tbar} was found to be best expressed as a function of the liquid limit. Notably, the liquid limit reflects the type of soil, its organic content and sensitivity (Figure 3 and 4). The following expression was evaluated:

$$N_{Tbar} \approx 5 + 10 \times w_L \quad (3)$$

w_L is here given in decimal form. A typical example of a strength profile with depth is shown in Figure 5. Here, Equations 1–3 gives strength values similar to FC and DSS tests. The figure also shows c_u^{DSS} calculated by empirical correlations with preconsolidation stress from CRS oedometer tests and c_u^{DSS} (Hov *et al.*, 2021). Figure 5 also shows results from triaxial tests at shallow depths, although these were not used for interpretation of the T-bar tests.

As seen in the figure, the strengths are extremely low just below the seabed, in practice zero at seabed, but increasing with around 1.2 kPa/m. By correlating the T-bar tests with laboratory data on greater depths, it is thought that a strength extrapolation towards the seabed is realistic. The T-bar tests seemed to confirm this. Obviously, strengths evaluations from full-flow tests are more certain than conventional CPT test due to the larger tip resistance, thus reducing the measurement uncertainties.

For normal ranges of liquid limits for inorganic clays, i.e. liquid limits around 40–80%, the N_{Tbar} varies between ~ 10 and ~ 13 . These values are similar to those found by Larsson *et al.* (2014), Nakamura *et al.* (2009), Randolph & Andersen (2006) and others.

For higher values of liquid limits, i.e. organic clays and gyttja, the N_{Tbar} is up to ~ 20 according to Equation 3. This is in the same range as reported for tests in peat (e.g., Long & Boylan, 2012; Boylan *et al.*, 2011).

4.2 Evaluation of sensitivity

The extraction resistance was measured for several of the T-bar tests. An example is given in Figure 6 where both the extraction (q_{out}) and penetration (q_{in}) resistance is shown. The q_{out} is consistently lower than q_{in} , as expected, due to the remoulding occurring around the probe.

Figure 7 plots all extraction ratios (q_{out}/q_{in}) vs. sensitivity values from laboratory FC tests where T-bar tests and sampling were done in the same location. The ratios varies between 0.45 and 0.9, decreasing with increasing sensitivity. This is in the same range as reported by e.g. DeJong *et al.* (2010) for low sensitive soils.

There is a clear correlation between the two variables, despite the relative small variation in sensitivity. This relationship is also seen in e.g. Yafrate *et al.* (2009). The correlation is however OCR-dependent (the OCR in the OC area is around 1.2–3).

4.3 Evaluation of remoulded shear strength

Cycles were performed in an attempt to correlate the penetration resistance with the remoulded strength measured in the laboratory (using FC tests). Cycles over 1 m intervals are shown in Figure 6, and a detailed resistance plot of the upper cycle is shown in Figure 8. This cycle was performed in clayey gyttja with a water content of 150–200%. A clear decrease in both penetration and extraction resistance is seen for each cycle.

Figure 9 plots the average penetration resistance (q_{in}) for each cycle vs. number of cycles. It seems that after 5–7 cycles, the decrease in resistance seems to level off. This is similar to the findings from e.g. Yafrate *et al.* (2009).

The measured remoulded undrained shear strength in the laboratory was 1.1 kPa. The N-factor in the clayey gyttja was thus evaluated to:

$$N_{Tbar,rem} \approx 35 \quad (4)$$

It should be noted that cycles were performed in a very limited number of locations, so the dependency of plasticity, sensitivity or OCR has not been evaluated.

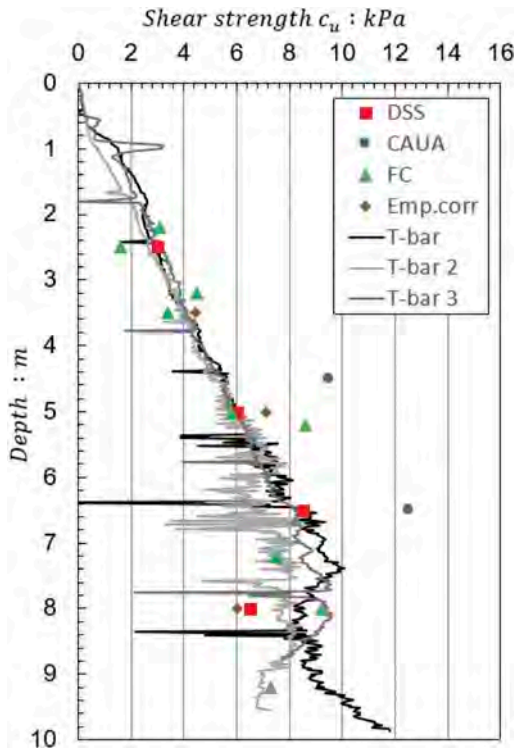


Figure 5. Typical example of evaluated strength by Eqs. 1-3 plotted together with results from laboratory tests. Strength “Emp.corr” is based on empirical correlations with the preconsolidation stress σ'_c from CRS oedometer tests; $c_u^{DSS} \approx (0.125 + 0.205 \times w_L) \times \sigma'_c$ for OCR=1,0-1,3 (Hov *et al.*, 2021).

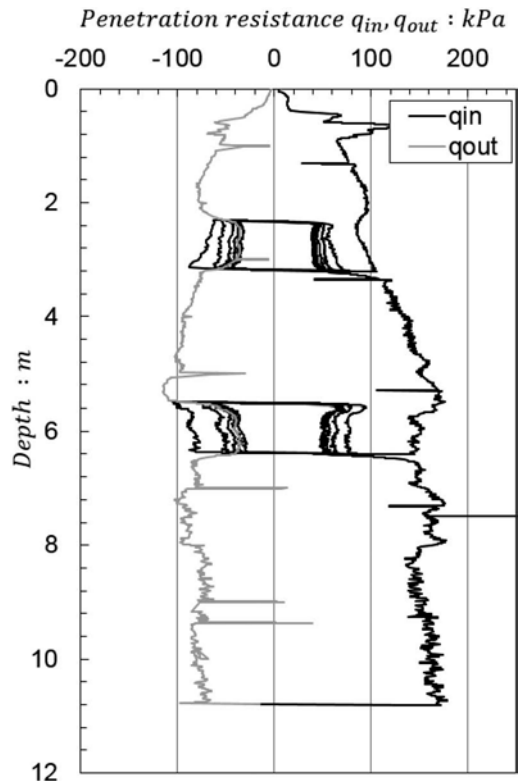


Figure 6. Typical example of penetration and extraction resistance in one T-bar test. Two sets of cycles were performed during penetration.

5 DISCUSSION

The T-bar tests were shown to be very useful for this type of project. The two main benefits were: a) detailed analyses of undrained shear strength in the upper part of the deposit, i.e. for strengths which in practice increases from zero, and b) a rough mapping of soil conditions by analysing the extraction ratio.

The very low strengths are difficult to measure with conventional CPT probes due to the large measurement uncertainty. In addition, sampling of such low strength sediments is very difficult, and in practice impossible with the Swedish piston sampler as it is dependent on soil resistance when coring (the coring is done by rotation of the drilling rods, but the outer part of the sampler is kept still using the soil resistance).

The use of T-bar tests showed that the strength increases almost linearly from zero at seabed. This was valuable information for stability evaluation of

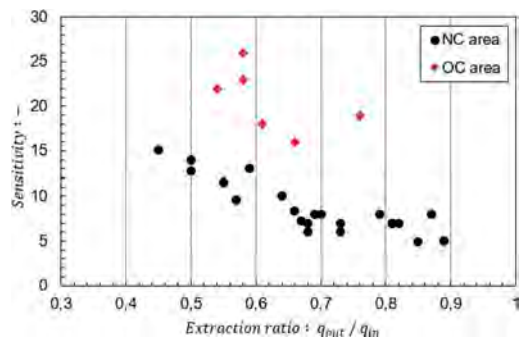


Figure 7. Values of sensitivity from laboratory tests (fall cone) and evaluation extraction ratio (example given in Figure 6).

the planned capping of the contaminated areas and filling for land reclamation.

The rough mapping of soil conditions was possible using the correlations between extraction ratio, sensitivity, liquid limit and organic content.

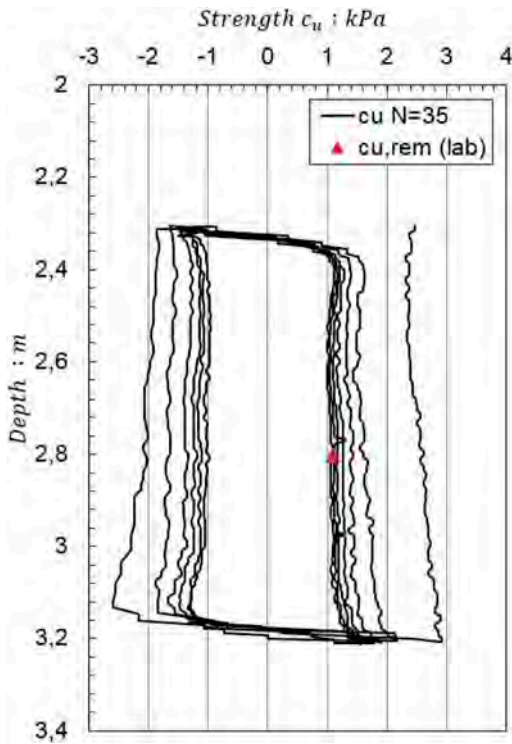


Figure 8. Example of cyclic test (upper cycle shown in Figure 6). Shear strength evaluated using $N = 35$. Negative strength is shown for extraction to make the figure more readable.

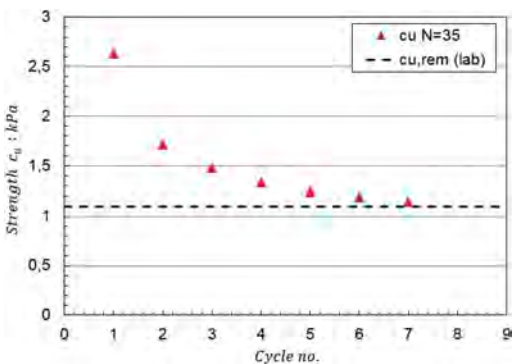


Figure 9. Measured strength using $N=35$ and remoulded strength from FC tests for cycle shown in Figures 7 and 8.

6 CONCLUSIONS

This paper presents a nearshore case study where a large number of T-bar tests have been performed.

The sediments consisted of organic clay and gyttja. The following conclusions are drawn:

- The T-bar test is a useful testing equipment for soils with extremely low shear strengths,
- The N-factor was evaluated to vary between ~ 10 and ~ 20 ,
- The N-factor increases with increasing plasticity (i.e. liquid limit),
- A good correlation was obtained between the extraction ratio and sensitivity,
- A N-factor of around 35 was found for cyclic tests to evaluate the remoulded shear strength.

REFERENCES

- Almeida, M.S., Oliviera, J.R., Motta, H.P., Almeida, M.C. & Borges, R.G. (2011). CPT and T-bar penetrometers for site investigation in centrifuge tests. *Soils and Rocks*, 34(1), pp. 79–88.
- Axelsson, M. (2001). Deep stabilisation with lime-cement columns – methods for quality control [In Swedish]. *Swedish Deep Stabilization Research Centre*, Report 8.
- Boylan, N., Long, M. & Mathijssen, F.A.J.M. (2011). In situ strength characteristics of peat and organic soil using full-flow penetrometers. *Can. Geotech. J.* 48, 1085–1099.
- DeJong, J., Yafrate, N., DeGroot, D., Low, H.E. & Randolph, M. (2010). Recommended practice for full-flow penetrometer testing and analysis. *Geotechnical Testing Journal*, Vol. 33, No. 2.
- EN ISO 14688-1 and -2. Geotechnical investigation and testing Part I and II. International Standard.
- Geotech (2019). CPT Geotech Nova – T-bar full-flow sounding equipment.
- Hov, S., Prästings, A., Persson, E., Larsson, S. (2021). On empirical correlations for normalised shear strengths from fall cone and direct simple shear tests in soft Swedish clays. *Geotech Geol Eng* 39, 4843–4854.
- Kallstenius, T. (1961). Development of two modern continuous sounding methods. *Proc. 5th Int. Conf. on Soil Mech. and Found. Eng.*, Vol. 1, pp. 475–480.
- Larsson, R., Åhnberg, H. & Schälin, D. (2014). T-bar tests in soft and sensitive Swedish clays. *Proc. 3rd Int. Symp. on CPT*, Las Vegas, pp. 449–458.
- Levacher, D., Razakamanatsoa, A., Gupta, R. & Katsumi, T. (2016). Comparative su measurements with vane shear and T-bar testing on soft soils in laboratory. *15th Asian Reg. Conf. on Soil Mech. and Geoth. Eng.*, JGS, pp. 465–468.
- Lunne, T., Andersen, K., Low, H.E., Randolph, M. & Sjørsen, M. (2011). Guidelines for offshore in situ testing and interpretation in deepwater soft clays. *Can. Geotech. J.* 48, 543–556.
- Long, M. & Boylan, N., (2012). In-situ testing of peat – a review and update on recent developments. *Geotech. Eng. J. of SEAGS & AGSSEA*, Vol. 43, No. 4, pp. 41–55.
- Massarsch, R. (2014). Cone penetration testing – A historic perspective. *Proc. 3rd Int. Symp. on CPT*, Las Vegas, pp. 97–134.
- Nakamura, A., Tanaka, H. & Fukasawa, T. (2009). Applicability of T-bar and ball penetration tests to soft clayey grounds. *Soils and Foundation*, Vol. 49, No. 5, 729–738.

- Peuchen, J. & Terwindt, J. (2016). Critical appraisal of T-bar penetration tests. *Geot. and Geoph. Site Characterisation*, pp. 351–356.
- Randolph, M. & Andersen, K. (2006). Numerical analysis of T-bar penetration in soft clay. *ASCE Int. J. of Geom.*, 6(6), 411–420.
- Randolph, M. (2004). Characterisation of soft sediments for offshore applications. Keynote lecture. *Proc. 2nd Int. Conf. Site Characterisation*, Porto, Vol. 1, pp. 209–231.
- Sahdi, F., Gaudin, C., White, D. & Boylan, N. (2014). Interpreting T-bar tests in ultra-soft clay. *Int. J. of Phys. Mod. In Geot.*, 14(1), 13–19.
- Schaeffers, J. & Weemees, I. (2012). Comparison of in-situ shear strength measurement techniques of soft clay. *20th Vancouver Geotechnical Society Symposium*, Soft Ground Engineering, Vancouver (BC).
- Stewart, D.P. & Randolph, M.F. 1994. T-bar penetration testing in soft clay. *J. Geot. Eng. Div.*, ASCE, 120(12), 2230–2235.
- Yafrate, N., DeJong, J., DeGroot, D. & Randolph, M. (2009). Evaluation of remoulded shear strength and sensitivity of soft clay using full-flow penetrometers. *ASCE J. Geot. Geoenv. Eng.*, Vol. 135, No. 10.
- Zhu, B., Dai, J. & Kong, D. (2020). Assess the effects of loading rate and interface roughness on T-bar penetration resistance. *Soils and Foundations*, 60, pp. 266–273.
- Åhnberg, H. & Larsson, R. (2012). Degradation of undrained shear strength due to dynamic actions and large strains. Swedish Geotechnical Institute, Report 75, Linköping.

Bayesian supervised learning of 2D subsurface soil stratigraphy using limited cone penetration tests with consideration of uncertainty

Yue Hu

Department of Civil and Environmental Engineering, National University of Singapore, Singapore

Yu Wang

Department of Architecture and Civil Engineering, City University of Hong Kong, Hong Kong, China

ABSTRACT: Cone penetration tests (CPT) have been widely used for soil stratification in geotechnical site investigation for decades. However, due to time and budget limits, the layout of CPT sounding at a specific project site is often sparse, leading to significant interpolation uncertainty in the development of subsurface soil 2D cross-section, particularly at locations without CPT measurements. Such development is often combined with empirical classification criteria, which further introduce model uncertainty to soil stratification. These uncertainties may pose great risks to the geotechnical engineering practice. A Bayesian supervised learning method is presented in this paper for probabilistic soil stratification in a 2D cross-section using limited CPT. The proposed method can not only automatically stratify soils in a 2D cross-section from limited CPT soundings, but also can properly quantify the associated uncertainties. Complete 2D CPT data cross-section is firstly learned from limited number of 1D CPT profiles using Bayesian supervised learning. The associated interpolation uncertainty is modelled numerically using non-parametric random field simulation based on the results of Bayesian supervised learning. Parametric autocorrelation function of CPT data along either vertical or horizontal direction is not needed. A probabilistic model is also developed to account for the model uncertainty of an empirical soil behavior type classification chart. The interpolation uncertainty and soil classification model uncertainty are then evaluated simultaneously in a Monte Carlo simulation framework. A simulated data example is used for illustration. The results suggest that the proposed method performs well.

1 INTRODUCTION

Subsurface soil stratification is an indispensable element in geotechnical engineering as required for geotechnical designs and analyses. However, due to time and budget limits, the layout of site investigation points is often sparse, leading to significant challenge and uncertainty in the development of 2D subsurface soil stratigraphy which is frequently adopted in geotechnical analysis. In engineering practice, such development is often combined with an empirical soil classification system, which inevitably introduce additional model uncertainty to soil stratification. These uncertainties may pose great risks to the geotechnical designs, analyses, and construction process (e.g., Clayton 2001; Mayne 2007). It is therefore necessary to properly evaluate the uncertainties associated with 2D subsurface soil stratification.

Cone penetration tests (CPT) have been widely used for soil stratification in geotechnical site investigation. It can be used to classify subsurface soils, identify stratification, and quantify associated uncertainty in a single sounding (e.g., Robertson 1990;

Wang et al. 2013). When interpreting 2D vertical soil cross-section using CPT, interpolation between adjacent CPT profiles or stratigraphy should be performed. However, direct 2D interpolation using conventional geostatistical methods is difficult because of the limitation of CPT soundings number and the spatially varying soil layer boundaries which render the soil properties in the 2D cross-section highly non-stationary (e.g., Wang et al. 2019). In this case, it is even more challenging to reasonably tackle the interpolation uncertainty quantification associated with the 2D subsurface stratigraphy. On the other hand, CPT-based soil classification relies on empirical soil classification charts to transform the continuous CPT measurements to discrete soil behavior type (SBT). Note that these charts rely on a series of deterministic SBT classification boundaries which are developed from site investigation data globally. These classification charts might not provide consistent results at a specific site and introduce model uncertainty when used locally (e.g., Boulanger & Idriss 2014; Maurer et al. 2019). How to incorporate the model uncertainty of SBT classification

boundaries in the CPT-based 2D soil stratification remains unsolved.

To address the abovementioned challenges, a Bayesian supervised learning method is proposed to interpret 2D subsurface soil stratigraphy from limited CPT with explicit evaluation of both interpolation uncertainty and SBT chart model uncertainty. The proposed framework is introduced in the following section and then illustrated using a simulated example.

2 THE PROPOSED METHOD

The proposed framework is based on a Monte Carlo simulation (MCS) and comprises of three components. First, SBT index I_c of CPT data is firstly interpolated in the concerned 2D cross-section from limited CPT using a Bayesian supervised learning algorithm in a non-parametric manner. The interpolation uncertainty is quantified automatically during learning process and then modelled by I_c random field simulation based on the learning outcome. Second, a probabilistic SBT chart is developed by adapting an empirical chart to consider the model uncertainty using which random samples of SBT chart with random classification boundaries are drawn. Third, each random field sample of I_c is matched with a random sample of SBT chart to produce a Monte Carlo sample of SBT cross-section with soil stratigraphy. Statistical analysis is then performed on the generated Monte Carlo samples. Both uncertainties are evaluated simultaneously under MCS. The three components are introduced in the following three subsections, respectively.

2.1 Bayesian supervised learning with random field simulation

The full I_c data variability in the concerned 2D cross-section are learned from the profiles of limited CPT. In the context of the Bayesian supervised learning, 2D data matrix \mathbf{F} (e.g., I_c data matrix of a 2D cross-section), which is spatially varying along coordinates x_1 and x_2 (e.g., depth direction and horizontal direction), has a dimension of $N_{x_1} \times N_{x_2}$. Mathematically, \mathbf{F} is expressed as a weighted summation of a series of orthonormal 2D basis functions (e.g., Zhao et al. 2018; Hu et al. 2020; Wang et al. 2020&2021):

$$\mathbf{F} = \sum_{t=1}^{N_{x_1} \times N_{x_2}} \mathbf{B}_t^{2D} \omega_t^{2D} \quad (1)$$

in which \mathbf{B}_t^{2D} is the t -th 2D basis function, while ω_t^{2D} is the weight coefficients of \mathbf{B}_t^{2D} . Discrete wavelet transform may be selected to construct \mathbf{B}_t^{2D} (e.g., Donoho et al. 2006). Note that for compressible images (e.g., spatially correlated CPT data cross-section), most ω_t^{2D} have negligibly small values

except for a limited number of non-trivial ones. Therefore, the \mathbf{F} may be reconstructed approximately if those non-trivial weight coefficients can be identified and estimated using sparse measurements \mathbf{Y} (e.g., CPT profiles data at limited locations), which is a sub-matrix of \mathbf{F} with a dimension of $M_{x_1} \times M_{x_2}$ ($M_{x_1} \ll N_{x_1}$, $M_{x_2} \ll N_{x_2}$). The relation between \mathbf{Y} and ω_t^{2D} is expressed as:

$$\mathbf{Y} = \sum_{t=1}^{N_{x_1} \times N_{x_2}} \mathbf{A}_t^{2D} \omega_t^{2D} \quad (2)$$

in which \mathbf{A}_t^{2D} is the sub-matrix of \mathbf{B}_t^{2D} with a dimension of $M_{x_1} \times M_{x_2}$. \mathbf{A}_t^{2D} just reflects the measured elements in \mathbf{B}_t^{2D} . Equation 2 enables those non-trivial coefficients to be learned through maximum likelihood estimation under a Bayesian framework (e.g., Tipping 2001). The learned weight coefficient vector is denoted as $\hat{\omega}^{2D}$. After derivation, it is found that the posterior distribution of $\hat{\omega}^{2D}$ given measurement data follows a multivariate Student's t distribution, with the mean vector and covariance matrix expressed as (e.g., Zhao et al. 2018; Hu et al. 2020):

$$\begin{aligned} \mu_{\hat{\omega}^{2D}} &= \mathbf{H}V_{tr} = (\mathbf{J} + \mathbf{D})^{-1}V_{tr} \\ \mathbf{COV}_{\hat{\omega}^{2D}} &= \frac{d_n \mathbf{H}}{c_n - 1} = \frac{d_n (\mathbf{J} + \mathbf{D})^{-1}}{c_n - 1} \end{aligned} \quad (3)$$

in which \mathbf{J} is a matrix with element $J_{t,s} = tr[\mathbf{A}_t^{2D} (\mathbf{A}_s^{2D})^T]$, ($t, s = 1, 2, \dots, N_{x_1} \times N_{x_2}$). “ tr ” represents trace operation in linear algebra. \mathbf{D} is a diagonal matrix with diagonal elements $D_{t,t} = \alpha_t$ ($t = 1, 2, \dots, N_{x_1} \times N_{x_2}$) in which α_t are non-negative parameters to be determined by a maximum likelihood algorithm (e.g., Tipping, 2001). V_{tr} is a $N_{x_1} \times N_{x_2}$ vector with element $V_{tr}(t) = tr[\mathbf{Y} (\mathbf{A}_t^{2D})^T]$. $c_n = M_{x_1} \times M_{x_2} / 2 + c$; $d_n = d + (\|\mathbf{Y}\|_2^2 - \mu_{\hat{\omega}^{2D}}^T \mathbf{H}^{-1} \mu_{\hat{\omega}^{2D}}) / 2$. c and d are non-negative small constants to achieve an uninformative prior in the Bayesian formulation. Due to the compressibility of \mathbf{F} , only those N_a ($N_a \ll N_{x_1} \times N_{x_2}$) non-trivial coefficients need to be estimated, and the rest are zeroed out. Therefore, in Equation 3, the $\mu_{\hat{\omega}^{2D}}$ is reduced to an $N_a \times 1$ vector and $\mathbf{COV}_{\hat{\omega}^{2D}}$ is reduced to an $N_a \times N_a$ matrix for simplicity.

Given the learning results in Equation 3, random samples of $\hat{\omega}^{2D}$ can be generated through eigen decomposition (e.g., Hu et al. 2019; Hu and Wang 2020):

$$\hat{\omega}^{2D} = \mu_{\hat{\omega}^{2D}} + \sum_{i=1}^{N_a} \mathbf{U}_i \sqrt{\lambda_{\hat{\omega}^{2D}}^i} Z_i \quad (4)$$

in which U_i is the i -th eigen-vector of the covariance matrix $\mathbf{COV}_{\hat{\omega}^{2D}}$; $\lambda_{\hat{\omega}^{2D}}$ is the i -th eigenvalue of $\mathbf{COV}_{\hat{\omega}^{2D}}$; Z_i is a set of independently and identically distributed standard Gaussian random variables. Using Equation 4, random vectors $\hat{\omega}^{2D}$ can be generated readily through realizations of Z_i . After that, extensive RFS of the approximated 2D data $\hat{\mathbf{F}}$ (e.g., I_c data 2D cross-section) are subsequently reconstructed by substituting the random vectors $\hat{\omega}^{2D}$ into Equation 1 as below:

$$\hat{\mathbf{F}} = \sum_{i=1}^{N_u} \mathbf{B}_i^{2D} \hat{\omega}_i^{2D} \quad (5)$$

Each generated 2D RFS indicates a possible outcome of Bayesian supervised learning. The ensemble directly reflects the interpolation uncertainty.

2.2 Probabilistic SBT chart

The empirical I_c – based SBT chart summarized in Table 1 was developed from a global soil database compiling CPT data obtained predominately within limited depths (e.g., Robertson 1990; Robertson & Wride 1998). It is expected that the SBT chart might not provide accurate classification and introduce model uncertainty when used locally at a specific project site. In other words, those empirical I_c classification boundaries (e.g., see Table 1) can vary from site to site (e.g., Boulanger & Idriss 2014; Maurer et al. 2019). To consider the model uncertainty, a probabilistic I_c – based SBT classification chart is developed. The five SBT classification boundaries (i.e., 1.31, 2.05, 2.6, 2.95, 3.6) listed in Table 1 are denoted as B1 to B5 and modelled as five Gaussian random variables, respectively. The mean values of B1 to B5 are taken as their original values, as summarized in the second column of Table 2. According to literature (e.g., Boulanger & Idriss 2014; Maurer et al. 2019) on I_c data variability, a set of standard deviation (SD) values for B1 to B5 is suggested in this study, as summarized in the third column of Table 2. SD of B1, B2 and B5 are taken as 0.1, while the SD of B3 and B4 are taken as 0.05. The probabilistic SBT chart allows for the varying nature of I_c – based classification criteria at different local sites. Extensive random samples of classification boundaries can be generated by repetitively sampling B1 to B5, leading to random samples of SBT chart. Each random sample is a possible state of the uncertain SBT classification chart and will randomly match with one RFS of I_c data cross-section for classification and stratification purposes.

2.3 Statistical analysis of Monte Carlo simulation

By pairing 2D I_c RFS with a random sample of SBT chart, each point in that 2D cross-section can

be mapped, leading to a 2D SBT cross-section. After repeating the process N_B times with different combination of 2D I_c data RFS and SBT chart random samples, N_B 2D SBT cross-sections are generated. Each SBT cross-sections serves as a possible state of subsurface soil stratigraphy given limited CPT. Statistical analysis is then performed for those N_B SBT cross-sections. The probability of soil at a given point (x_1, x_2) being mapped to a specific SBT, e.g., $\text{SBT}=t$ ($t=2, 3, \dots, 7$), can be calculated as (e.g., Hu and Wang 2020):

$$p(\text{SBT}_{x_1, x_2} = t) = \frac{N_{x_1, x_2}^t}{N_B} \times 100\% \quad (6)$$

in which N_{x_1, x_2}^t is the number of SBT values at point (x_1, x_2) that equal to t . Equation 6 quantitatively measures how likely the soil at a point (x_1, x_2) is classified as any one of the six SBT. The SBT with the highest probability is taken as the most likely SBT at the point (x_1, x_2). Similarly, the most likely SBT cross-section is obtained. In addition, the classification uncertainty is quantified by the SD of SBT samples at a given point. The higher the SD, the higher the uncertainty. Similarly, an SD cross-section can be calculated which reflects the pattern of uncertain region in the 2D cross-section. The SD cross-section directly assesses the reliability of soil stratigraphy.

3 ILLUSTRATIVE EXAMPLE

To illustrate the proposed framework, a simulated geological cross-section example is provided in this section. As shown in the Figure 1a, a 2D vertical cross-section is simulated. Four soil types exist in this cross-section, i.e., clay, silt mixtures, sand mixtures and sand, which correspond to SBT values of 3 to 6, respectively. Spatial variability of I_c data in each soil layer is generated using assumed random field model. The random field parameters used (e.g., mean μ_{I_c} , standard deviation σ_{I_c} , correlation lengths along horizontal direction λ_h and vertical direction λ_v) are summarized in Table 3. An exponential correlation structure is adopted in this simulation. The simulated 2D I_c data cross-section is shown by colormap in the Figure 1b. The I_c data cross-section is a 128×256 matrix with resolution of 0.1m for both directions. It is regarded as a geological setting at a specific site. Note that the complete I_c data cross-section is usually not available in engineering practice. This example is just for illustration and validation purposes. Suppose that six (i.e., $M=6$) CPT soundings are conducted within the cross-section, as denoted by black dash lines (e.g., M1-M6) in Figure 1. I_c data profiles of M1-M6 are shown in Figure 2. These six 1D I_c data

profiles are used as input to interpret the soil stratigraphy under the proposed framework.

After constructing the \mathbf{Y} matrix in Equation 2 from data profiles of M1-M6, the Bayesian supervised learning is implemented. Then $N_B=500$ 2D RFSs of I_c data are generated from the learning results. Four examples of I_c cross-section are shown by colormap in Figure 3. Each plot in Figure 3 is a possible interpolation of I_c data in this 2D cross-section from six CPT soundings. No parametric correlation structure is needed for the learning process. Next, $N_B=500$ random SBT classification charts are generated from the probabilistic SBT classification boundary model. Note that a Gaussian random variable ranges from negative infinity to positive infinity. To mitigate the overlapping problem, the Gaussian probability density functions (PDF) for B1-B5 are truncated respectively to a range of mean \pm three standard deviation, as summarized in the fourth column of Table 2.

By randomly pairing a RFS of I_c data cross-section with one random sample of SBT chart,

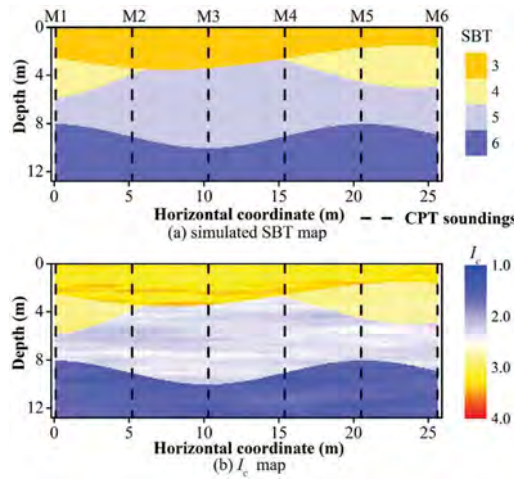


Figure 1. Simulated geological cross-section (a) and I_c data (b) in a 2D cross-section.

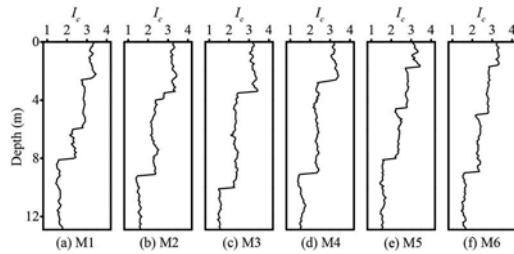


Figure 2. I_c profiles of six CPT soundings.

a Monte Carlo sample of 2D SBT cross-section is obtained. After repeating this procedure 500 times, $N_B=500$ SBT cross-sections are obtained. Four

examples of SBT cross-sections are shown in Figures 4a-4d. These four 2D SBT cross-sections correspond respectively to the four RFS of 2D I_c data shown in Figure 3 mapped with random sample of SBT charts shown above each subplot of Figure 4. Note that each of these SBT cross-section indicates a possible soil stratigraphy.

Using $N_B=500$ Monte Carlo samples of 2D SBT cross-section, statistical analysis is performed using Equation 6. The most likely SBT cross-section is shown in the Figure 5a. In the most likely SBT cross-section, four SBT (i.e., SBT3-6) are presented, which is consistent with the underlying true stratigraphy. The original soil zone boundaries are shown by black solid lines for comparison. Note that the most likely SBT cross-section is generally comparable to the underlying true one, although the soil zone boundaries are not perfectly learned due to interpolation uncertainty and model uncertainty in SBT chart. The uncertainties can be evaluated simultaneously through SD of $N_B=500$ SBT cross-sections, as shown in Figure 5b. It is found that the bright areas with high uncertainty are generally consistent with the underlying true boundaries (i.e., the black solid lines). The results in Figure 5b suggest that the underlying true soil zone boundaries can be approximated based on the SD of N_B SBT cross-sections. The proposed framework performs reasonably well in the interpretation of 2D soil stratigraphy and uncertainty quantification, given only six CPT soundings.

Table 1. I_c – based SBT classification chart (after Robertson 1998).

Range of SBT index I_c	SBT ID	SBT description
$I_c < 1.31$	7	Gravelly sand to dense sand
$1.31 < I_c < 2.05$	6	Sands: clean sand to silty sand
$2.05 < I_c < 2.60$	5	Sand mixtures: silty sand to sandy silt
$2.60 < I_c < 2.95$	4	Silt mixtures: clayey silt to silty clay
$2.95 < I_c < 3.60$	3	Clays: silty clay to clay
$I_c > 3.60$	2	Organic soil: peats

Table 2. Probabilistic model of the I_c – based SBT classification boundaries.

Boundaries	Mean	SD	Range
B1	1.31	0.1	[1.01, 1.61]
B2	2.05	0.1	[1.75, 2.35]
B3	2.6	0.05	[2.45, 2.75]
B4	2.95	0.05	[2.8, 3.1]
B5	3.6	0.1	[3.3, 3.9]

4 EFFECT OF SOUNDING NUMBER

To investigate the effect of CPT soundings number M on the proposed framework, an additional scenario with $M=25$ CPT soundings is discussed. Those 25 CPT are performed with equal space in the 2D cross-section of illustrative example (i.e., see Figure 1). Following the same procedures as described above, $N_B=500$ Monte Carlo samples of 2D SBT cross-section are obtained. The most likely SBT cross-section in this scenario is shown in Figure 6a. The approximated soil stratigraphy in this scenario becomes more accurate. The quantified uncertainty also shrinks significantly, as shown in the Figure 6b. Those thin bright area with high uncertainty is in good agreement with boundary

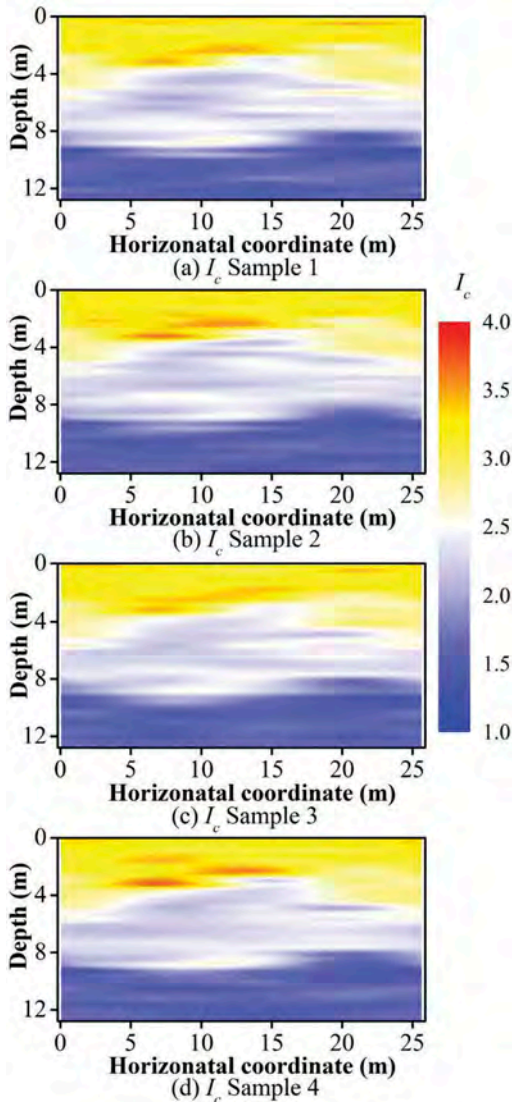


Figure 3. Four examples of 2D I_c data RFS.

locations. The proposed method is data-driven and features fine scale spatial variability to the interpolation result when M increases.

5 CONCLUSIONS

A novel Monte Carlo simulation (MCS) – based framework was proposed in this paper for interpreting soil stratigraphy in a 2D cross-section from

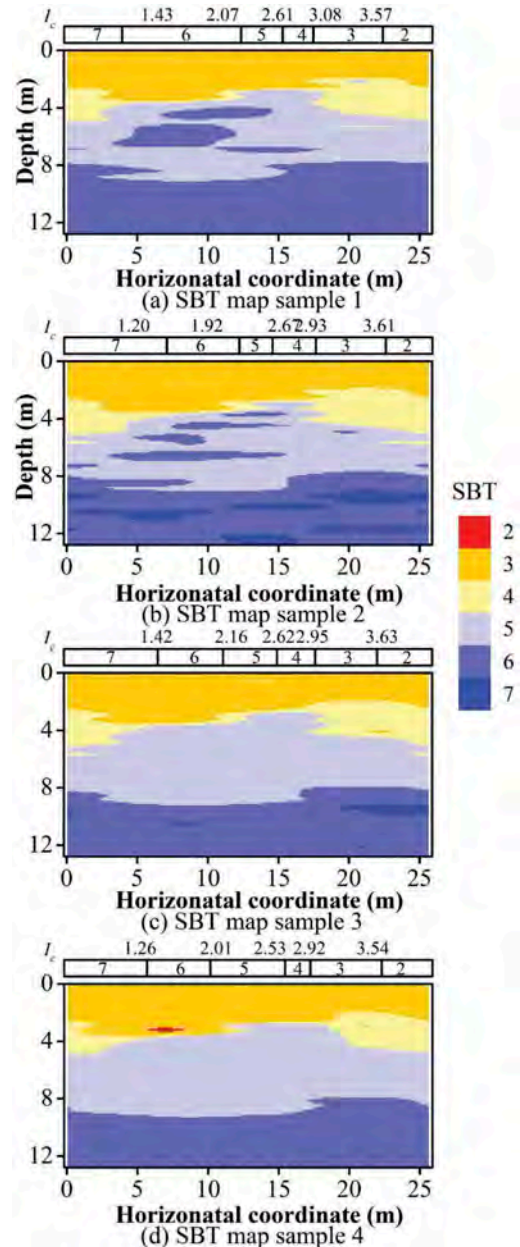


Figure 4. SBT cross-sections for the four I_c samples in Figure 3.

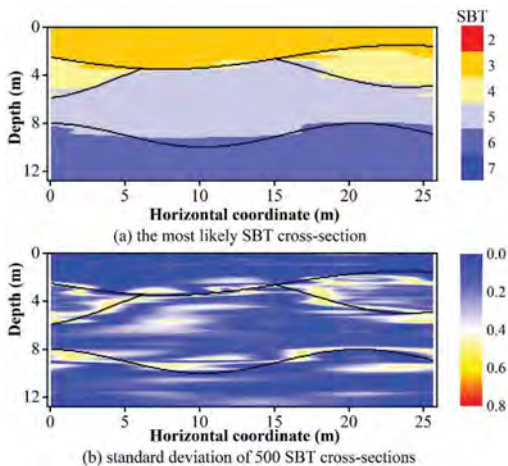


Figure 5. Statistics of generated SBT cross-sections when $M=6$: (a) the most likely SBT cross-section; (b) standard deviation of 500 SBT cross-sections.

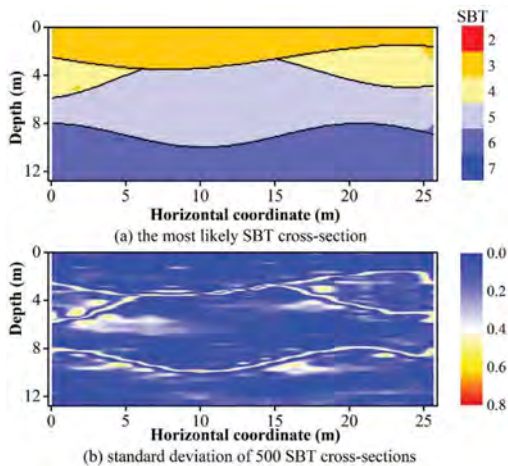


Figure 6. Statistics of generated SBT cross-sections when $M=25$: (a) the most likely SBT cross-section; (b) standard deviation of 500 SBT cross-sections.

Table 3. Random field parameters for the simulated 2D I_c cross-section.

Layer	μ_{Ic}	σ_{Ic}	λ_h (m)	λ_v (m)
Layer1	3.2	0.1	15	1
Layer2	2.8	0.07	30	2
Layer3	2.3	0.1	20	1.5
Layer4	1.5	0.1	25	1.8

limited cone penetration tests (CPT) with consideration of uncertainty. Complete CPT data cross-section was learned from limited CPT soundings via

Bayesian supervised learning. The associated interpolation uncertainty was modelled by non-parametric random field simulation based on the learned results. A probabilistic soil behavior type (SBT) chart was developed for incorporating the model uncertainty in the empirical chart. The interpolation uncertainty of I_c data and model uncertainty in SBT chart were considered simultaneously under MCS. Key equations and detailed implementation procedures were provided. Numerical example was illustrated and showed that the proposed method performed reasonably well. Sensitivity study suggested that the proposed method was data-driven. As the number of CPT soundings increased, the most likely SBT cross-section became accurate and associated interpolation uncertainty reduced significantly.

ACKNOWLEDGEMENTS

The work described in this paper was supported by grants from the Research Grants Council of the Hong Kong Special Administrative Region, China (Project Nos. CityU 11213119 and CityU 11202121). The financial supports are gratefully acknowledged.

REFERENCES

- Boulangier, R., & Idriss, I. 2014. CPT and SPT based liquefaction triggering procedures. *Report No. UCD/CGM.-14, 1*.
- Clayton, C. R., Matthews, M. C., & Simons, N. E. 1995. *Site investigation: a handbook for engineers*. Blackwell Science.
- Donoho, D., Maleki, A. & Shahram, M. 2006. Wavelab 850. Software Toolkit for Time-Frequency Analysis. *Stanford University*.
- Hu, Y., Zhao, T., Wang, Y., Choi, C., & Ng, C. W. W. 2019. Direct Simulation of Two Dimensional Isotropic or Anisotropic Random Field from Sparse Measurement using Bayesian Compressive Sampling. *Stochastic Environmental Research and Risk Assessment*, 33(8-9), 1477–1496.
- Hu, Y., Wang, Y., Zhao, T., & Phoon, K. K. 2020. Bayesian supervised learning of site-specific geotechnical spatial variability from sparse measurements. *ASCE-ASME Journal of Risk and Uncertainty in Engineering Systems, Part A: Civil Engineering*, 6(2), 04020019.
- Hu, Y., & Wang, Y. 2020. Probabilistic soil classification and stratification in a vertical cross-section from limited cone penetration tests using random field and Monte Carlo simulation. *Computers and Geotechnics*, 124, 103634.
- Maurer, B., Green, R., van Ballegooy, S., & Wotherspoon, L. 2019. Development of region-specific soil behavior type index correlations for evaluating liquefaction hazard in Christchurch, New Zealand. *Soil Dynamics and Earthquake Engineering*, 117, 96–105.
- Mayne, P. W. 2007. *Cone penetration testing*. Transportation Research Board.
- Robertson, P. 1990. Soil classification using the cone penetration test. *Canadian Geotechnical Journal*, 27 (1), 151–158.

- Robertson, P., & Wride, C. 1998. Evaluating cyclic liquefaction potential using the cone penetration test. *Canadian Geotechnical Journal*, 35(3),442–459.
- Tipping, M. E. 2001. Sparse Bayesian learning and the relevance vector machine. *Journal of machine learning research*, 1(Jun), 211–244.
- Wang, Y., Huang, K., & Cao, Z. 2013. Probabilistic identification of underground soil stratification using cone penetration tests. *Canadian Geotechnical Journal*, 50 (7),766–776.
- Wang, Y., Zhao, T., Hu, Y., & Phoon, K. K. 2019. Simulation of random fields with trend from sparse measurements without detrending. *Journal of Engineering Mechanics, ASCE*, 145(2), 04018130.
- Wang, Y., Hu, Y., & Zhao, T. 2020. CPT-based subsurface soil classification and zonation in a 2D vertical cross-section using Bayesian compressive sampling. *Canadian Geotechnical Journal*, 57(7),947–958.
- Wang, Y., Hu, Y. & Phoon, K.K., 2021. Non-parametric modelling and simulation of spatiotemporally varying geo-data. *Georisk: Assessment and Management of Risk for Engineered Systems and Geohazards* (published online), <https://doi.org/10.1080/17499518.2021.1971258>.
- Zhao, T., Hu, Y., & Wang, Y. 2018. Statistical interpretation of spatially varying 2D geo-data from sparse measurements using Bayesian compressive sampling. *Engineering Geology*, 246, 162–175.

Estimation of constrained modulus from CPT measurements in case of Holocene sands

Zsombor Illés, István Kádár, Gábor Nagy, András Mahler & László Nagy
Budapest University of Technology and Economics, Budapest, Hungary

ABSTRACT: In case of major projects there are numerous measurements which provide a sufficient set of data to determine characteristic values based on statistical methods. In the current paper Cone Penetration Test (CPT), oedometer and Flat Dilatometer Test (DMT) results are analyzed. Constrained or oedometric modulus is one of the most important deformation parameters, which has a key role in settlement estimation. There are various recommendations to derive E_{oed} from CPT tip resistance values. Three of these recommendations are compared with the results of the oedometer tests and the correlation used in case of DMT measurements.

Keywords: Constrained modulus, CPT, Tip-resistance, DMT, Normally-consolidated layers

1 INTRODUCTION

1.1 *Measurements and methods*

Several Cone Penetration Tests were conducted at a site in South-Central Hungary near the Danube. The probes penetrated until the depth of 20 - 40 meters. Altogether 32 CPTs were analyzed, penetrating at least to the depth of 25 - 26 m, until the bottom of Holocene layers; clay, sand, and gravel. Below that, over-consolidated late Miocene (Pannon) layers were found.

Different methods are evaluated for estimating constrained modulus from cone penetration resistance of the CPT measurements in the article. These three methods are the following: Sanglerat (1972), Lunne and Christoffersen (1983) and Eslaamizaad and Robertson (1996).

Furthermore, laboratory soil identification and oedometric tests were also carried out. In addition, there is a possibility to compare Cone Penetration and Flat Dilatometer Test (DMT) results.

1.2 *Geology and stratigraphy of the site*

The project site is located in South-Central Hungary. It used to be the flood plain of the river Danube until the construction of a dike system. During the previous phases of the industrial compound's construction, the extracted soil was placed on the current site as a backfill. The fill material consists of fine sands, less often silty sands, mostly grey-yellow silty clay and lean clay, and medium sands. The landfill includes

construction waste as well. Its thickness varies between 3.5-5.5 m.

Alluvial deposits are generated during periods of high-water level when a predominantly suspended fine matter settles to the surface of the floodplain. It is composed of lean clay mixed with firm-stiff organic matter, and its thickness is approximately 0.7 m.

As described by Kádár and Nagy (2018), below the alluvial deposit, there is eolian sand (transported by wind). The rounded particles are in the size range of silt and fine sands; the layer has a thickness of 5.0 m. It is followed by fluvial sand containing fine, medium, coarse and gravelly sands over a thickness of 5.3 m. It abruptly turns into gravelly sands and gravel; it forms a 10.0 m thick gravel terrace. Both the in-situ measurements, CPT and DMT, and the oedometric compressions, are evaluated up to the base of the gravelly sand layer. In this study, the eolian and fluvial sands are treated as one layer.

2 SOIL CLASSIFICATION AND LABORATORY MEASUREMENTS

2.1 *Evaluation of CPT measurements*

The CPT measurements were conducted according to MSZ EN ISO 22476-1:2013.

The CPT-based soil behavior of the layers; landfill, lean clay, silty sand and gravelly sand are presented in Figure 1. A CPT-based normalized soil behavior chart was suggested by Robertson (1990) and updated by Robertson (2009). The parameters used are summarized in Robertson (2016).

The stratification of the area was defined according to traditional geotechnical soil identifications and CPT measurements. The layers appearing at the CPT logs are presented in Figure 1. One dot is one layer in one CPT. According to normalized cone resistance (Q_{tn}) and normalized friction ratio (F_r), the top layer, landfill, is classified as silty sand and sand. The lean clay is regarded as clay, silty clay and sandy silt. This layer is not present in all the CPTs. The layers of eolian and fluvial sands (Kádár and Nagy, 2018) are classified as silty sand and sand, while the last normally consolidated layer is sand. The four layers are not overconsolidated as they more or less fall in the diagonal of the diagram.

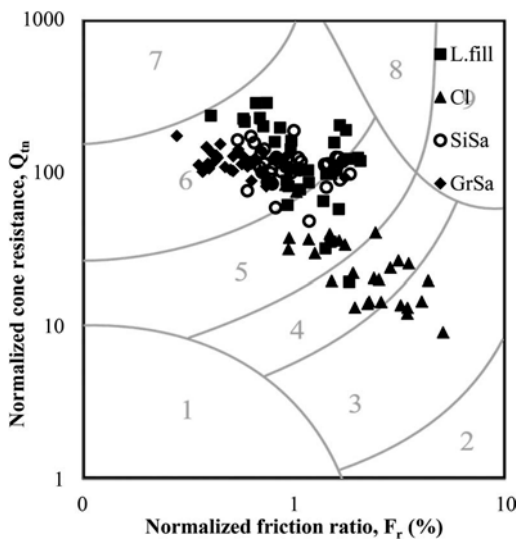


Figure 1. Classification of the layers according to Robertson (2009).

Each layers' parameters obtained by CPT are summarized in Tables 1-4, tip resistance (q_c), skin friction (f_s) and friction ratio (R_f). To each of the three parameters, minimum, maximum, average, standard deviation and coefficient of variation are defined.

Table 1. CPT parameters of the landfill.

Parameter	q_c [MPa]	f_s [MPa]	R_f [%]
No. of samples	33	33	33
Average	10.08	102.30	1.38
Min	2.11	36.58	0.28
Max	22.95	252.76	3.15
Std.	5.55	54.03	0.66
Co.V.	0.55	0.53	0.48

Table 2. CPT parameters of the lean clay.

Parameter	q_c [MPa]	f_s [MPa]	R_f [%]
No. of samples	26	26	26
Average	2.69	53.52	2.65
Min	0.29	1.60	0.90
Max	7.73	89.53	6.50
Std.	1.37	16.22	1.30
Co.V.	0.51	0.30	0.49

Table 3. CPT parameters of the silty sand.

Parameter	q_c [MPa]	f_s [MPa]	R_f [%]
No. of samples	32	32	32
Average	17.09	170.28	1.02
Min	8.77	74.22	0.52
Max	24.79	309.02	1.83
Std.	3.47	71.21	0.38
Co.V.	0.20	0.42	0.37

Table 4. CPT parameters of the gravelly sand.

Parameter	q_c [MPa]	f_s [MPa]	R_f [%]
No. of samples	33	33	33
Average	23.64	126.19	0.67
Min	16.76	68.75	0.27
Max	30.86	234.51	2.99
Std.	3.23	34.66	0.49
Co.V.	0.14	0.27	0.73

The landfill and the lean clay CPT parameters have a higher coefficient of variation than the sandy layers.

2.2 Evaluation of DMT measurements

On the test site 11 DMT soundings penetrated to different depth. The flat dilatometer was developed in the 1980s by Silvano Marchetti. Shear strength parameters of the soils such as undrained shear strength (c_u), and friction angle (φ), can be derived. One of the most helpful information that DMT measurements can derive is related to the soil layers' stress history. Overconsolidation ratio (OCR), and coefficient of lateral earth pressure (K_0) can be determined in the case of sands, in which sampling would be difficult (Marchetti et al. 2001).

In this paper, constrained modulus is estimated by DMT measurements, which is the key parameter for settlement calculation.

Two corrected readings (p_0 and p_1) are obtained by the flat dilatometer, from these, material index (I_D), horizontal stress index (K_D), and dilatometer

modulus (E_D) are calculated. Vertical drained constrained modulus M_{DMT} can be determined according to Eq. (1) (Marchetti, 1980) as:

$$M_{DMT} = E_D \cdot R_M(K_D, I_D) \quad (1)$$

where R_M is a correction primarily depending on the stress history (K_D).

2.3 Oedometer tests

To test the stress-strain relationship and the consolidation parameters of each layer oedometer tests were carried out according to MSZE CEN ISO/TS 17892-5:2010 standard. Undisturbed samples were tested with 0-100-200-400-600 kPa, it was a usual practice to load, unload and reload the samples; a common load path was 0-2-23-45-100-2-100-200-400 kPa.

A linear assumption was used between each load step according to Eq. (2).

$$E_{oed} = \frac{\Delta\sigma_{ef}}{\Delta\varepsilon} = \frac{\Delta\sigma_{2,ef} - \Delta\sigma_{1,ef}}{\varepsilon_2 - \varepsilon_1} \quad (2)$$

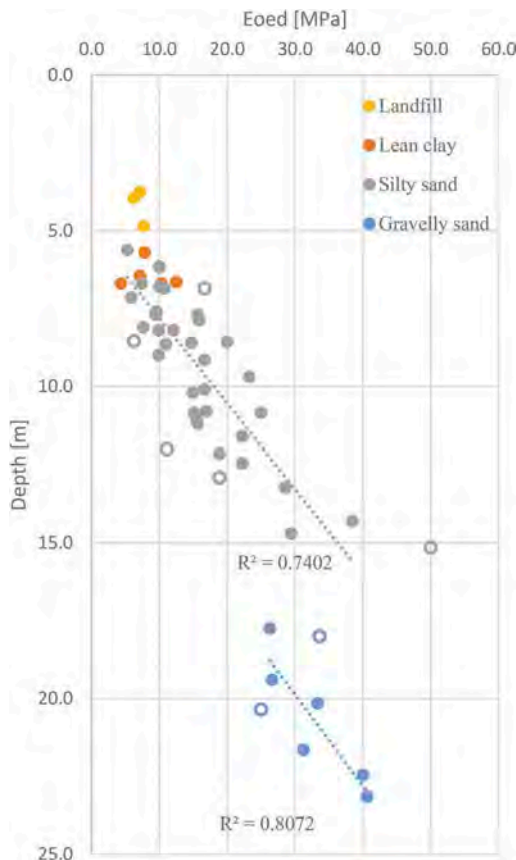


Figure 2. Different layers oedometric modulus and the depth of the samples.

The results of the oedometric tests and the depth from where the samples were extracted are presented in Figure 2. the modulus is related to the stress state as well as the depth.

In the case of the silty sand layer, the following correlation can be derived between the depth and oedometric modulus:

$$E_{oed} = 3.64 \cdot z - 18.42 \quad (3)$$

While in case of the gravelly sand layer, a different correlation can be made:

$$E_{oed} = 3.43 \cdot z - 38.14 \quad (4)$$

The linear correlations (Eq. 2.-3.) describe the connection between depth and oedometric modulus well.

3 METHODS USED TO DERIVE THE CONSTRAINED MODULUS

3.1 Sanglerat method

The Cone Penetration Testing (CPT) sounding was developed in the Netherlands in the 1930s. It was used to investigate the layers' penetration resistance for pile foundation design. A key parameter for settlement calculation is the restrained modulus (M). Buisman (1940) proposed the following correlation between the tip resistance and oedometric modulus in case of cohesionless soils (sands):

$$M = 1.5 \cdot q_c \quad (5)$$

1.5 multiplier in Eq. (5) was replaced to α_m by Sanglerat (1972):

$$M = \alpha_m \cdot q_c \quad (6)$$

The values for the coefficient in the case of cohesive soils were also defined and presented by Sanglerat (1972), later synthesized by Kumala Sari et al. (2017). According to Figure 1. the landfill is classified as "silts of low plasticity", although it is very heterogenic, and a high percentage of construction waste can be found in it. According to Figure 1. and laboratory identification tests, the lean clay layer is considered a "clay of low plasticity", while the last two layers of silty sand gravelly sand are regarded as "sands".

3.2 Lunne and Christophersen method

Most correlations between CPT results and the drained constrained modulus (M) refer to the tangent modulus, as found from oedometer tests. The reference value of M is typically based on the effective vertical stress σ'_{v0} (Lunne et al. 1997).

Lunne and Christoffersen (1983) reviewed the available (at that time) calibration chamber test results and made the following recommendations to estimate M in case of normally consolidated uncemented silica sands:

$$M = 4 \cdot q_c \quad \text{for } q_c < 10 \text{ MPa} \quad (7)$$

$$M = 2 \cdot q_c + 20 \text{ (MPa)} \quad \text{for } 10 < q_c < 50 \text{ MPa} \quad (8)$$

$$M = 120 \text{ MPa} \quad \text{for } q_c > 50 \text{ MPa} \quad (9)$$

They also included overconsolidated sands in their studies and made rough estimates for them as well.

3.3 Eslaamizaad and Robertson method

Based on the assessment of extensive calibration tests on quartz sand (Baldi et al. 1986; Fioravante et al. 1991). Eslaamizaad and Robertson (1996) proposed an alternative method to estimate M from CPT data.

The method presents a correlation incorporating normalized cone resistance and normalized vertical effective stress in the form of:

$$M = k_M \cdot p_a \left(\frac{\sigma'_{v0}}{p_a} \right)^n \quad (10)$$

where:

n : stress exponent equal to 0.200 for normally consolidated sands, and 0.128 for overconsolidated sands.

p_a : atmospheric pressure. in the same units as σ'_{v0} , M and q_c .

k_M : is a dimensionless modulus number which can be determined using Figure 3. based on normalized cone penetration resistance (q_c/p_a) and estimated overconsolidation ratio (OCR).

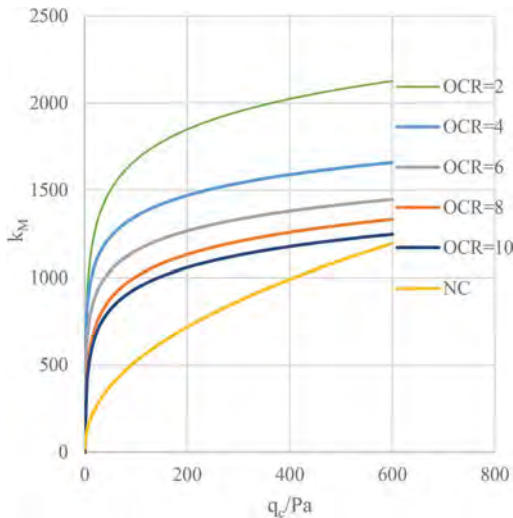


Figure 3. Consolidation modulus number of sand as a function of cone resistance and OCR (Eslaamizaad and Robertson, 1996).

The k_M functions of different OCRs' are estimated by digitalizing the figure in Lunne et al. (1997). The estimated functions are the following:

$$NC = 61.66 \cdot \left(\frac{q_c}{p_a} \right)^{0.4634} \quad (11)$$

$$OCR 2 = 510.45 + 252.69 \ln \left(\frac{q_c}{p_a} \right) \quad (12)$$

$$OCR 4 = 558.56 + 172.06 \ln \left(\frac{q_c}{p_a} \right) \quad (13)$$

$$OCR 6 = 396.68 + 164.20 \ln \left(\frac{q_c}{p_a} \right) \quad (14)$$

$$OCR 8 = 163.71 + 182.77 \ln \left(\frac{q_c}{p_a} \right) \quad (15)$$

$$OCR 10 = 142.53 + 172.72 \ln \left(\frac{q_c}{p_a} \right) \quad (16)$$

The method has the advantage that prior knowledge of relative density is not required (Lunne et al. 1997). When Eslaamizaad and Robertson (1996) compared the estimated values against the ones measured in the calibration chamber, they were between 75% and 125%. Later the M values are provided for each layer in Figure 5; the ones estimated according to Eslaamizaad and Robertson (1996) are divided by 1.25.

4 EVALUATION OF THE RESULTS

4.1 Vertical soil profile

The 32 CPTs average, minimum and maximum tip resistance (q_c) are presented in a vertical profile (Figure 4). The average cone resistance (q_c) was used for the calculation of restrained modulus (M) by Sanglerat (1972), Lunne and Christoffersen (1983) and Eslaamizaad and Robertson (1996) methods.

There are lower and upper limits for cohesive soils (landfill and lean clay). The eodometric moduli of each layer measured on undisturbed samples in the laboratory are also shown in Figure 4. Eodometric (E_{oed}) and constrained (M) modulus are the same mechanical parameters. If it was measured in the laboratory, the E_{oed} abbreviation is used, while if it is estimated from field measurements, CPT and DMT, M is allocated.

The layers' thickness in Figure 4. is just the average of the 32 CPTs. It happens that sometimes an oedometric or DMT test falls below or above the assigned stratum.

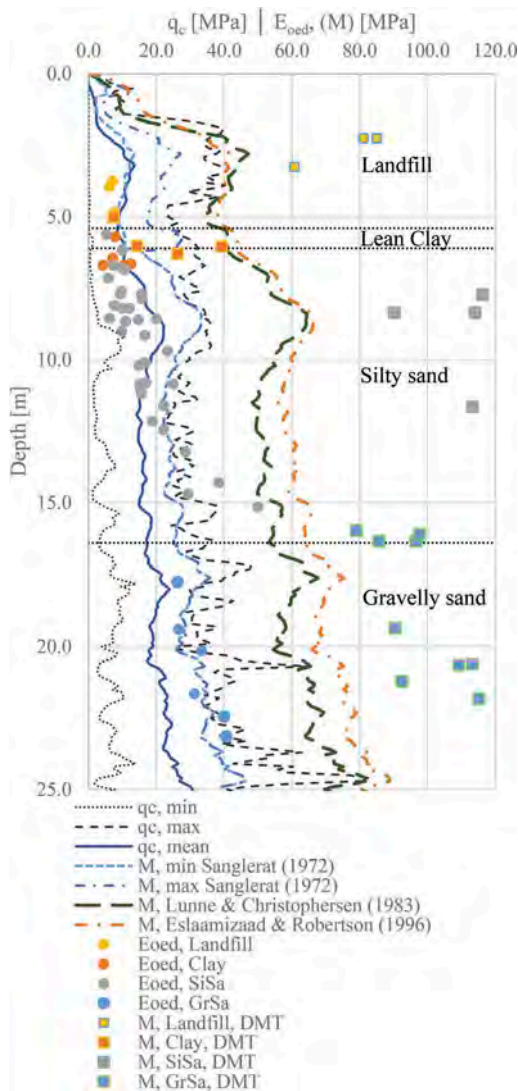


Figure 4. Soil strata with CPT values, estimated constrained (M), measured oedometric (E_{oed}) moduli.

In the upper two strata (landfill and lean clay) the oedometric moduli measured in the laboratory seem to agree with the minimum value estimated by Sanglerat (1972). In the top layer, constrained modulus derived from DMT measurements are way higher, than the results of other methods. The local inhomogeneity is probably also playing a part in the extreme DMT results. The scatter of the measurements is not really concerning as no foundation will be built in landfill. The moduli estimated by DMT measurements in lean clay spread between the other methods based on CPT. In the lower two strata of silty sand and gravelly sand, the results of oedometer tests distribute around the values estimated by the Sanglerat (1972)

method (Figure 4, Table 5.). However, the results of the oedometric test vary with depth, Figure 2. Eq. 2-3.

Table 5. Constrained modulus of silty sand and gravelly sand.

Parameter	Silty sand		Gravelly sand	
	E_{oed}	$M_{Sang.}$	E_{oed}	$M_{Sang.}$
No. of samples	33	102	6	85
Average	15.59	25.56	33.03	33.48
Min	5.30	15.78	26.31	25.99
Max	38.46	33.64	40.63	46.08
Std.	7.44	3.44	6.26	4.71
Co.V.	0.48	0.13	0.19	0.14

In lower two strata the DMT measurements result in a higher constrained modulus (Figure 4.) as the methods proposed by Lunne and Christophersen (1983) and Eslaamizaad and Robertson (1996).

4.2 Different soil layers

The estimated constrained moduli by different methods for each layer are summarized in Figure 5. From the applied methods Lunne and Christophersen (1983) and Eslaamizaad and Robertson (1996) were calibrated against tests of silica sand, their capability to estimate soil parameters in cohesive soils is questionable. It is assumed that DMT measurements give a better prediction of constrained modulus as CPT measurements (Marchetti, 2015) for two main reasons: (i) blades cause penetration distortions lower than axy-cylindrical probes, (ii) modulus by a mini load test relates better to a modulus than a penetration resistance.

This is supported by many case studies such as the Sunshine Skyway Bridge in Florida (Schmertmann, 1998), where the constrained modulus from back calculation was closes by the DMT measurements. It is also common to use the DMTs as a calibration for CPT sounding, Jacksonville Power Plant reported by Schmertmann (1998) and a project in Bucharest (Poenu et al., 2021).

The correlation between CPT and DMT data was analyzed in the top layer of the silty-sand, regarded as eolian sand, Figure 6.

Only 4 DMT and CPT test results for a single sub-layer, 47 measurement pairs are analyzed. The CPT data is averaged to be compared with a DMT measurement. R^2 value greater than 0.7 indicates that the linear correlation describes the investigated parameters with sufficient accuracy. The following equation is on the border of the criteria, where: q_c and the constant is in MPa, so as the obtained M_{DMT} result.

$$M_{DMT} = 5.87 \cdot q_c + 92 \quad (17)$$

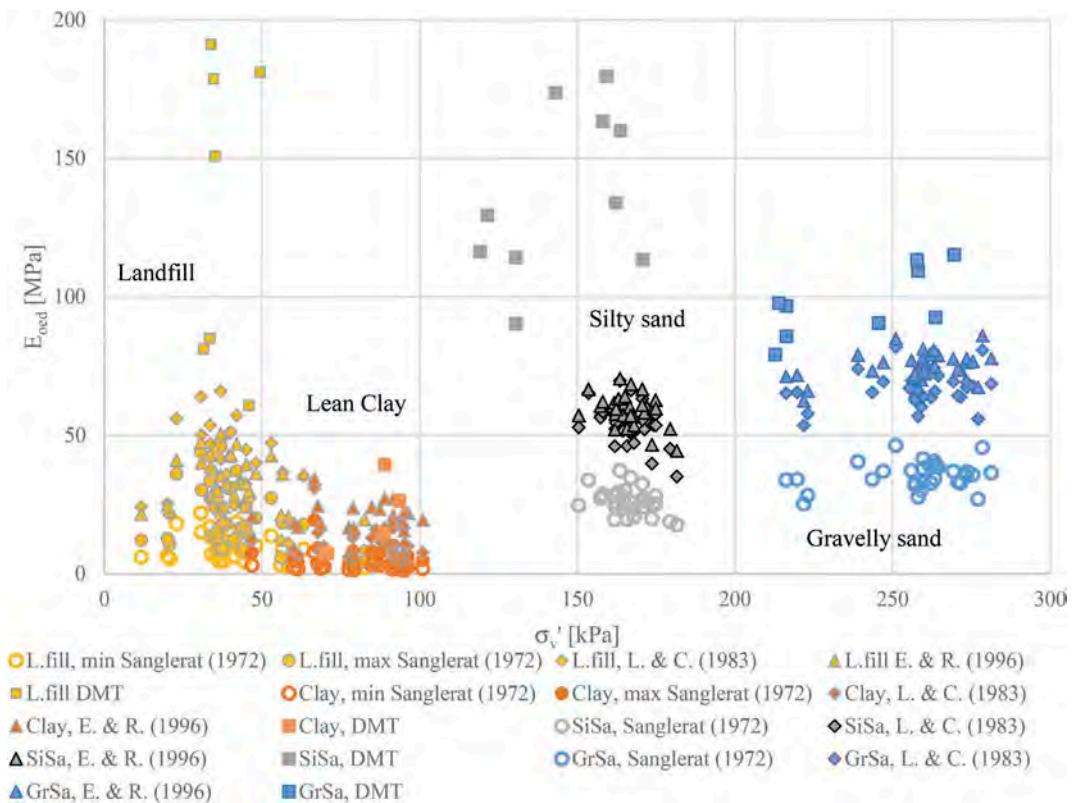


Figure 5. Constrained modulus of the layers (landfill, lean clay, silty sand and gravelly sand).

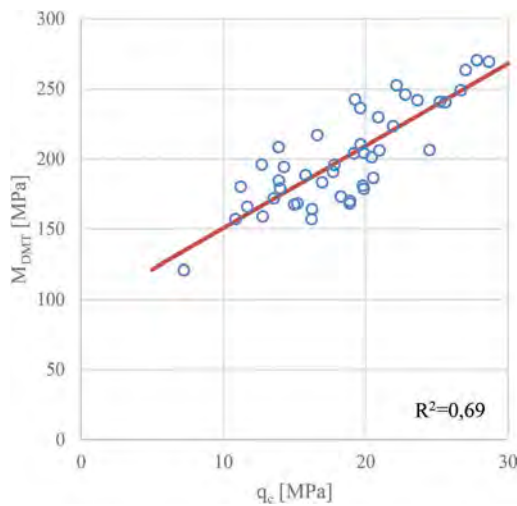


Figure 6. Correlation between q_c and M_{DMT} for Eolian sand layer.

5 CONCLUSIONS

According to Table 5, the constrained moduli estimated by the Sanglerat (1972) method correlates well with the measured ones in the laboratory by oedometer.

The calculated oedometric modulus values have a linear correlation with depth (Figure 2, and Eq. 3-4).

The dilatometer disturbs the soil less than the CPT, so more realistic constrained modulus can be estimated, which is way higher than the results of investigated correlations (Eslaamizaad and Robertson, 1996; Lunne and Christoffersen, 1983) Figure 4-5.

A simple linear connection (Eq. 17) is derived between the cone resistance of CPT and the constrained modulus estimated by DMT in case of the upper eolian layer of silty sand (Figure 6). It corresponds to the mean value, in case of design the characteristic value must be used.

REFERENCES

- Baldi, G., Belotti, R., Ghionna, N., Jamiolkowski, M., Pasqualini, E., 1986. Interpretation of CPT and CPTU; 2nd part: drained penetration of sands., in: Fourth International Geotechnical Seminar., Singapour., pp. 143–156.
- Buisman, K., 1940. Grondmechanica. Uitgeverij Waltman, Delft, Netherlands.
- Eslaamizaad, S., Robertson, P.K., 1996. Cone penetration test to evaluate bearing capacity of foundation in sands, in: 49th Canadian Geotechnical Conference. Presented at the 49th Canadian Geotechnical Conference, St. John's, Newfoundland, pp. 429–438.
- Fioravante, V., Jamiolkowski, M., Tanizawa, F., Tatsuoka, F., 1991. Results of CPTs in Toyoura quartz sand, in: Symposium on Calibration Chamber Testing. Presented at the Symposium on Calibration Chamber Testing, Elsevier, Potsdam, Germany, pp. 135–146.
- Kádár, I., Nagy, L., 2018. Comparison of determination of oedometric modulus based on CPT and laboratory testing in case of pleistocene sand layers. *ce/papers* 2, 683–688. <https://doi.org/10.1002/cepa.749>
- Kumala Sari, P., Sari, T., Mochtar, N., Yogyakarta, D., 2017. Consolidation parameters evaluation of cohesive soils in Lianganggam, Kalimantan Indonesia using CPT data. *International Journal of Current Research* 9, 58509–58513.
- Lunne, T., Christoffersen, H.P., 1983. Interpretation of cone penetrometer data for offshore sands. *Offshore Technol. Conf.*; (United States) 1.
- Lunne, T., Powell, J.J.M., Robertson, P.K., 1997. *Cone Penetration Testing in Geotechnical Practice*. CRC Press.
- Marchetti, S., 2015. Some 2015 Updates to the TC 16 DMT Report 2001, in: DMT '15 3rd Int. Conf. on the Flat Dilatometer. Presented at the DMT '15 3rd Int. Conf. on the Flat Dilatometer, Rome, Italy, p. 23.
- Marchetti, S., 1980. In Situ Tests by Flat Dilatometer. *ASCE Jnl GED* 106, 299–321.
- Marchetti, S., Monaco, P., Totani, G., Calabrese, M., 2001. The Flat Dilatometer Test (DMT) in soil investigation, in: A Report by the ISSMGE Committee TC16, *Encyclopedia of Earth Sciences Series. T*, Washington D.C., p. 41. https://doi.org/10.1007/978-3-319-73568-9_174
- MSZ EN ISO 22476-1:2013, 2013. Geotechnical investigation and testing. Field testing. Part 1: Electrical cone and piezocone penetration test (ISO 22476-1:2012).
- MSZE CEN ISO/TS 17892-5:2010, 2010. Incremental loading oedometer test.
- Poenaru, A., Bilcu, A., Meirosu, A., Saidel, T., Batali, L., 2021. In situ and laboratory soil investigations. Correlations between different parameters specific to Bucharest area. Presented at the ISC'6, Budapest, p. 10.
- Robertson, P.K., 2016. Cone penetration test (CPT)-based soil behaviour type (SBT) classification system — an update. *Can. Geotech. J.* 53, 1910–1927. <https://doi.org/10.1139/cgj-2016-0044>
- Robertson, P.K., 2009. Interpretation of cone penetration tests — a unified approach. *Can. Geotech. J.* 46, 1337–1355. <https://doi.org/10.1139/T09-065>
- Robertson, P.K., 1990. Soil classification using the cone penetration test. *Can. Geotech. J.* 27, 151–158. <https://doi.org/10.1139/t90-014>
- Sanglerat, G., 1972. *The penetrometer and soil exploration: interpretation of penetration diagrams theory and practice*, 2nd enlarged ed. ed, *Developments in geotechnical engineering*. Elsevier, Amsterdam Oxford New York.
- Schmertmann, J.H., 1998. *Dilatometers Settle In*. Civil Engineering ASCE 4.

Evaluation of complex CPTu dissipation tests of B.E.S.T.

E. Imre

BGK, HBM EKIK, Óbuda University, Budapest, Hungary

M. Hegedűs

BME, Budapest, Hungary

Apostol Brc, Budapest, Hungary

L. Bates & S. Fityus

University of Newcastle, Newcastle, Australia

ABSTRACT: The u_2 complex pore water pressure dissipation tests made in NC-LOC sandy soils at the Bolivian test site were evaluated with the variants of a mathematically precise, automatic method in the function of the testing time. The identified c became near constant and its error became small after a so called minimum testing time $t_{\min} < t_{50}$ depending on the variant. The traditional t_{50} method failed in some cases since the tests were with types I, II, III, V and t_{50} varied from 4s to a value being larger than 15 min (not measured).

1 INTRODUCTION

The pore water pressure dissipation tests of B.E.S.T were started to be evaluated by using the well-known t_{50} method and some suggested methods.

The complex dissipation tests were made in NC-LOC sandy soils, the t_{50} varied from 4s to an unknown value being longer than 15 min (in tests with $t_{\max} < t_{50}$), therefore, the t_{50} method failed in some cases.

By using the suggested methods, the evaluation was made in the function of the testing time for all tests. The c identified from truncated tests became near constant with t after a minimum testing time $t_{\min} < t_{50}$.

2 MATERIALS AND METHODS

2.1 The tests

The B.E.S.T. site is about 40 m wide and 100 m long. The geotechnical conditions of the site have been investigated using conventional in-situ and laboratory methods at each single pile location (Figure 1). The following in-situ tests have been performed: SPT, SCPTU (with dissipation tests), SDMT, PMT, SASW and REMI geophysical tests. Each borehole and field test is identified with the letter of its designated test pile.

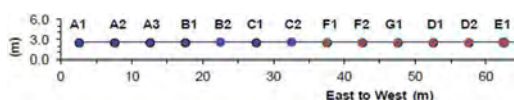


Figure 1. Dissipation test locations.

2.2 Geology and soil profile

The city of Santa Cruz de la Sierra lies in the southern part of the Amazonas. The geology of the area is characterized by a Paleozoic (250 million years old) sedimentary basin.

The soils of interest are quaternary. The main agent is the Piray River and its tributaries, which past meandering over the area has resulted in a sedimentation-erosion-sedimentation process and a geological profile dominated by fine to medium sands with intermittent layers of clay or clayey sand. Due to the compressible soils, even light buildings need to be supported on piles.

The groundwater table at the site is situated seasonally between the ground surface and about 0.5 m depth.

Sandy/plastic soils had negative/positive excess pore water pressure during penetration and dissipation, which indicates the soil types. The upper about 10 to 20 m part of the profile consists of LOC clays, silts, sands, in various combination and thickness.

In the pore water pressure profile (Figure 2) four plastic layers 1 to 4 with positive excess pore water pressure were isolated between the following depths: 2.5 to 5.0 m; 11 to 15 m; 15 to 17 m; below 22 m, resp. Sand-silt is found among the plastic layers.

The measured u_2 dissipation curves (Figures 2 to 3) were with types I, II, III, V, (Sully et al, 1999). The t_{50} varied between 4 s and $t_{50} > 15$ min. A crust was likely found in layer 1, indicated by the larger t_{50} values (Figure 2.).

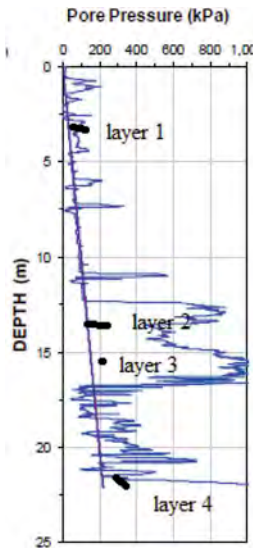


Figure 2. Dissipation tests in plastic soil layers 1 to 4.

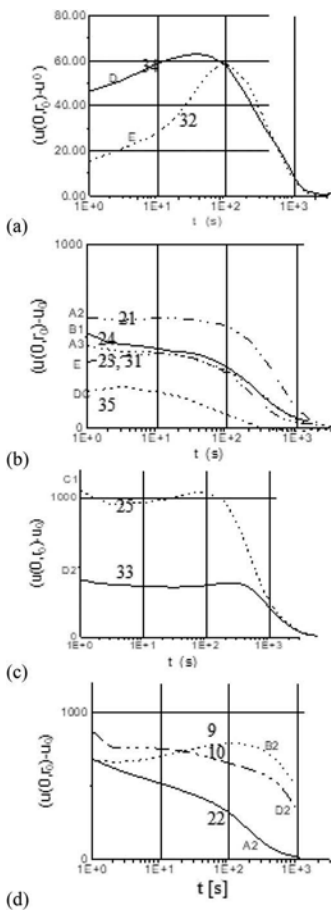


Figure 3. (a) to (d): Dissipation curves in layer 1 to 4. In the same layer both monotonic, non-monotonic curve may occur.

Table 1. Dissipation test list, depth, notation, t_{50} .

	Layer 2			Layer 4		
	depth [m]	sign	t_{50} [s]	depth [m]	sign	t_{50} [s]
A2	13,6	21	190	22,0	22	120
A3	13,6	23	220			
B1	13,3	24	250			
B2				22,5	9	> 850
D2				22,0	10	> 720s
DC	12,8	35	450	20,3	36	4

Table 2. Dissipation test list, depth, notation, t_{50} .

	Layer 1			Layer 3		
	depth [m]	sign	t_{50} [s]	depth [m]	sign	t_{50} [s]
C1				15,17	25	1020
D2	2,7	34	500	15,63	33	550
E1	2,3	32	500			

Table 3. Comparing c [cm²/s] from various methods, $t = t_{max}$.

z [m]	c [cm ² /s] with method			
	t_{50} method	k=1, fast	slow	
21	13.6	0.02 to 0.13	0.6	0.42
22	22.0	0.03 to 0.42	1.8	1.2
24	13.3	0.01	0.6	0.48
36	20,3	negative (sand)	54	4.8
9	22.5	shorter than t_{50}	0.15	0.06
10	22,0	shorter than t_{50}	0.18	0.12

2.3 The evaluation methods

The one-point model fitting (Teh-Houlsby, 1988; Lunne et al. 1992) requires time of t_{50} and I_r which is difficult to assess (Mayne, 2007).

The one-point model fitting (at t_{50} cannot handle more than one initial condition (if $t_{50} < 50$ s, and if the dissipation is starting from less than u_0 values). The reliability of the identified c is not tested.

The suggested evaluation methods imply (i) an automatic and mathematically precise non-linear inverse problem solution, (ii) some initial condition identification methods which can be used in partly drained penetration, (iii) some reliability testing.

The methods are depending on r_1 but its value can be taken into account using a model law, resulted from the derived time factor T (see App.).

The newer methods (“fast” and “slow”) are based on the mathematically precise Least Squares fitting of a new consolidation model, with different initial condition identification.

In the “slow” method, the first 1..200 terms of the analytical solution (large numerical work) are used, with some pre-elaborated, parametric shape functions. In the “fast” method, the first few (1.. k) terms are used (small numerical work) for both the monotonic ($k = 1$) and the non-monotonic (1.. $k > 1$) time variation of the pore water pressure.

The c values were identified at testing times $t = 0,3$ min; $t = 0,5$ min; $t = 5$ min besides at $t = t_{max}$. Since only one case (test 24) was a “real time” evaluation in the sense, that the evaluation was made after each measured data sampled generally in every second, the results of this work are approximate. It can also be noted that the LS merit function related to the slow method has several minima, the fast method has a unique distinct minimum for $k = 1$, can be quasi-degenerated, with large error for $k = 3$ (see Figure 4).

3 RESULTS

3.1 Evaluation using maximum testing time

According to the results (Table 3), the c values identified with the various methods as earlier (Imre et al, 2018). The fast methods gave larger c by about a factor of 1.5 than the slow methods. The one-point t_{50} method gave smaller c by generally about factor of 10 to 30 depending on Ir . The fast $k=1$ method usually gave distinct solution, a worse fit, a faster decay, and thus a higher c value than the slow method.

3.2 Evaluation of truncated tests, monotonic data

According to the results (see Figures 5 to 7, Tables 4 to 6), the $c - t$ functions generally decreased for the fast method, and was generally constant for the slow method. The identified c became generally about constant at a minimum testing time t_{min} except in one case (test 21). The $t_{min} < t_{50}$ was met for the slow method in every case, the t_{min} was shorter or longer than the t_{50} time for the fast methods. The fast $k=3$ method gave better fit but too large parameter error.

3.3 Evaluation of truncated tests with complex data

According to the results shown in Figures 8 to 10, Tables 7 - 8, at the initial – non– monotonic – part of the tests, the parameter error was high and c changed. The identified c became about constant and the error dropped at a minimum testing time t_{min} .

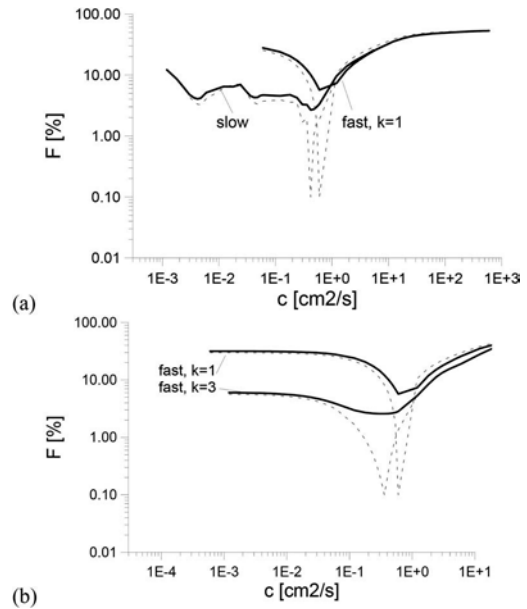


Figure 4. Deepest section of the LS merit function, Test 21. (a) Slow method, several minima, distinct minimum for $k = 1$. (b) The minimum is quasi-degenerated, with large error for $k = 3$.

Table 4. Test 24, $c - t$, slow and fast method, $t_{50} = 6,1$ min.

testing time [min]	c [cm ² /s] with method		
	fast $k = 1$	slow	fast $k = 3$
0,3	1,8	0,48	6
0,5	1,2	0,12	6
5	0,6	0,54	0,6
52	0,6	0,48	0,24

Table 5. Test 21, $c - t$, slow and fast method, $t_{50} = 3,2$ min.

testing time [min]	c [cm ² /s] with method		
	fast $k = 1$	slow	fast $k = 3$
0,33	3,00	0,42	1,80
0,50	1,80	0,30	6,00
3,33	1,20	0,60	0,60
23,50	0,60	0,42	0,36

Table 6. Test 22, $c - t$, slow and fast method, $t_{50} = 2$ min.

testing time [min]	c [cm ² /s] with method		
	fast $k = 1$	slow	fast $k = 3$
0,33	5,40	1,80	6,00
0,50	4,20	1,20	6,00
3,33	1,80	1,20	1,80
18,00	1,80	1,20	1,80

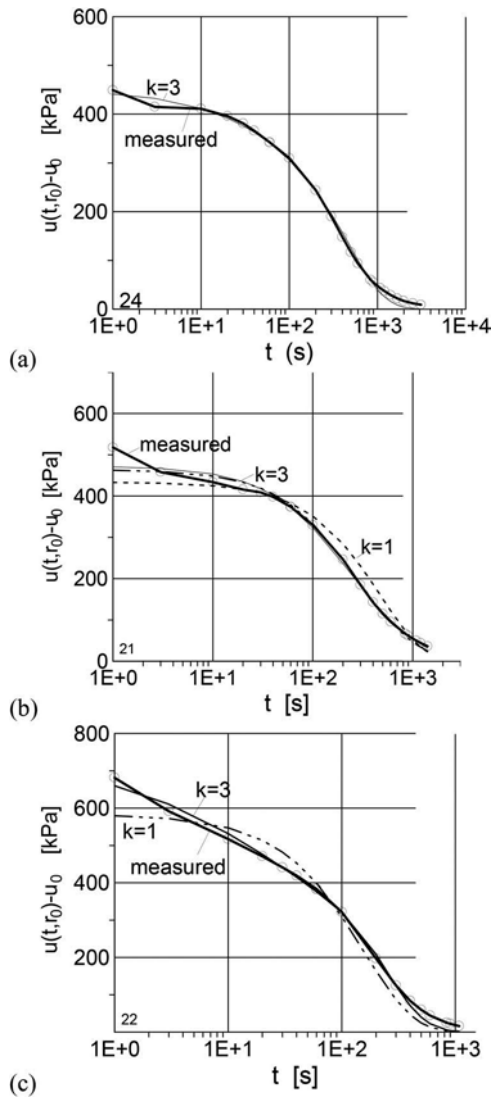


Figure 5. Monotonic curves, measured and fitted data. (a) Test 24, the dissipation test in layer 2 at B1. (b) Test 21 in layer 2 at A2. (c) Test 22 in layer 4 at D2.

Table 7. Complex test 34, c with t , $k=1$ to 3, $t_{50} = 8,3$ min.

testing time [min]	c [cm ² /s] with method		
	fast $k=1$	slow	fast $k=3$
0,33	1.80	4.80	3.60
0,50	1.20	4.20	3.00
4,00	0.12	1.20	1.20
60,00	0.18	0.60	0.60

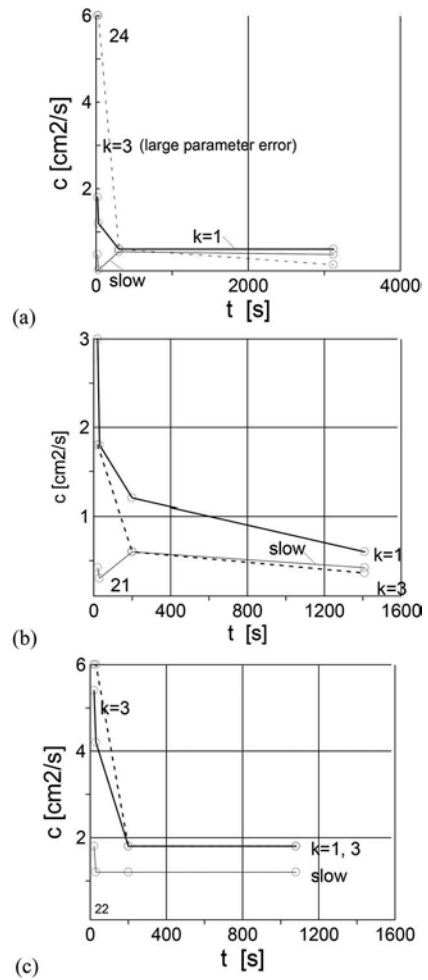


Figure 6. The c - t function. (a) Test 24, layer 2 at B1, $t_{50} = 250$ [s]. (b) Test 21, layer 2 at A2, $t_{50} = 190$ [s]. (c) Test 22, layer 4 at A2, $t_{50} = 120$ [s].

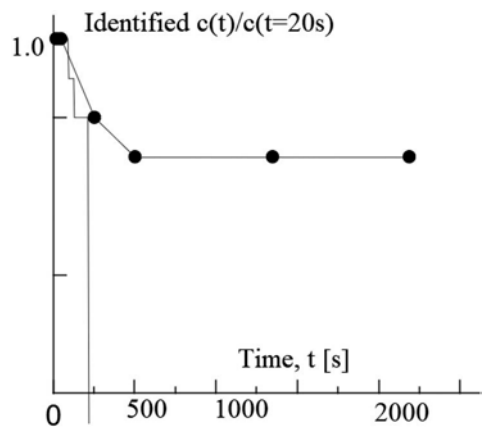


Figure 7. "Real-time" evaluation, $k = 1$. Test 24. (see Figure 6(a).).

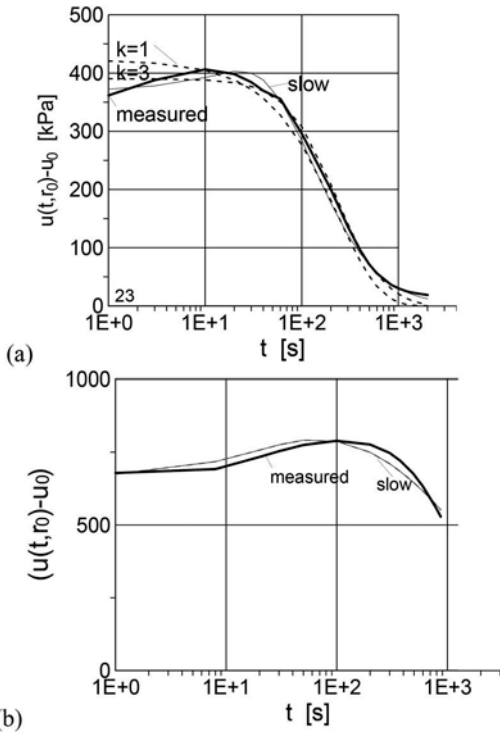


Figure 8. Complex dissipation curves, measured and fitted data. (a) Test 23, layer 2 at A3. (b) Test 9, layer 4 at B2.

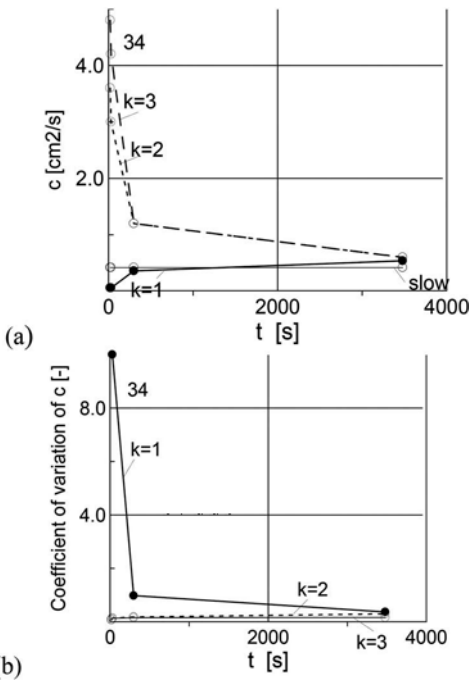


Figure 9. Complex dissipation tests. Test 34, layer 1, D2, $t_{50} = 500$ [s]. (a) Function $c-t$. (b) Coefficient of variation $C_v(c)-t$.

The $t_{min} < t_{50}$ was met for the slow method and the fast $k=1$ method in general.

The tests 9 and 10 – made on a more plastic soil layer, being shorter than t_{50} –, and test 36 – made in sand with fully negative excess pore water pressure – were successfully evaluated with similar results.

4 DISCUSSION

4.1 The effect of filter position

The $c - t$ function was determined for the monotonic dissipation tests of the Bothkennar soft clay measured after undrained penetration, in filter positions E to A with the fast $k=1$ method (Imre et al, 2010). The $c - t$ function was about constant in fps E, in filter position D it became about constant at a minimum testing time $t_{min} \sim 30$ min which was less than $t_{50} \sim 90$ min (Figure 11, Table A-1).

In the present study, after partly drained penetration, in fps u_2 (\sim fps D and C), the t_{min} was the smallest and less than t_{50} in every case for the slow method only. For the fast methods, t_{min} was less than t_{50} in about half of the cases. The minimum testing time t_{min} can be assessed precisely from real-time evaluation. Further research is suggested on this.

4.2 Complex dissipation of LOC soils

According to Figure 3, in the same layers both monotonic, non-monotonic curves occurred. Type I and II curves are commonly understood results from normally consolidated (NC) and lightly over-consolidated (LOC) clays, type III to V are attributed to heavily over-consolidated (HOC) soils.

Some recent studies (Lim, 2019, Figure 11) revealed that „Extremely fine mesh around the cone penetrometer made possible to study dissipation curves from very closely spaced stress points. It is found that type I, II and III curves are all possible outcomes from NC and LOC soils.”

4.3 Initial condition and space domain

The suggested methods are based on r_1 , valid after undrained penetration. The one-point t_{50} method gave smaller c by about factor of 10 to 30 than the suggested methods. The difference can probably be attributed to the due to undrained value $r_1 = 37r_0$.

The c identified can be modified for other r_1 using the model law (see the App.) but no values are available to r_1 valid in (partly) drained penetration. Further research on is needed (Osman, 2021).

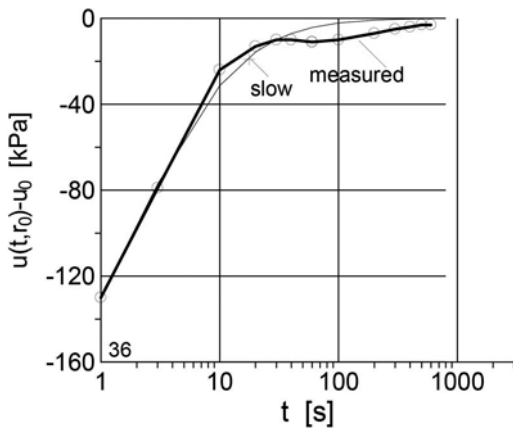


Figure 10. Dissipation test in sand (DC, test 36).

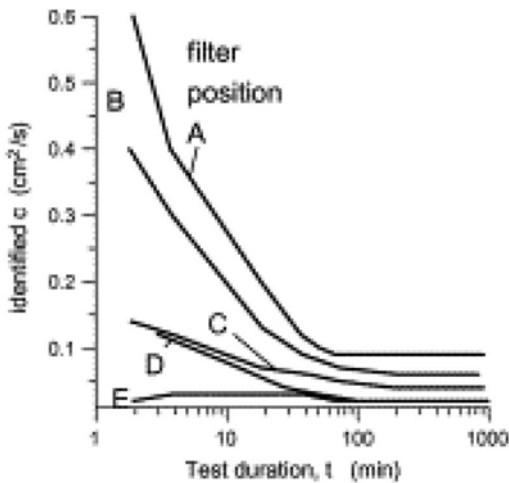


Figure 11. Variation of the uncorrected c with test duration τ .

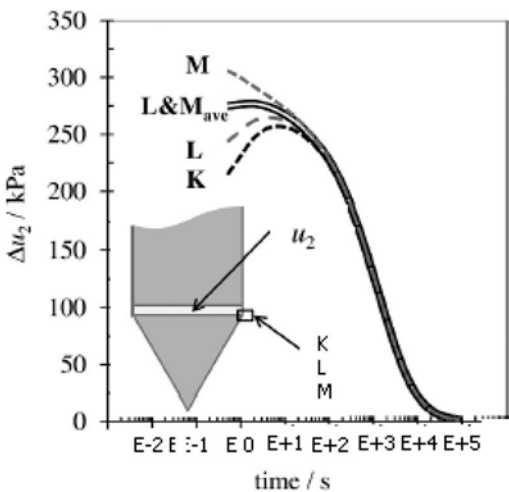


Figure 12. Shape issues.

Table 8. Test 23, Function c - t , (slow:0,6), $t_{50} = 4$ min.

testing time [min]	fast method			
	k = 1		k = 3	
	c [cm ² /s]	Cv(c)	c [cm ² /s]	Cv(c)
0,33	0,06	18,66	4,20	0,11
0,50	0,06	11,27	3,00	0,12
3,33	1,20	0,30	1,20	0,11
33,50	1,20	0,31	0,60	0,16

5 SUMMARY, CONCLUSION

5.1 The evaluation results

In the present study, the complex dissipation curves of B.E.S.T. test site, measured in filter position u_2 , were evaluated in the function of the testing time t .

(1) The c identified with the various methods (t_{50} and the newer) using the long test data ($t = t_{\max}$) showed similar pattern as in previous research. Some complex or short tests were impossible to be evaluated with the t_{50} method.

(2) Truncated tests ($t < t_{\max}$), were evaluated with the newer methods with various elapsed time values. Generally (with one exception), at a minimum testing time t_{\min} , the identified c became about constant, the error of c became as small as in the long tests. The t_{\min} was always smaller than t_{50} for the slow method, and sometimes for the fast methods even in the case of the complex shaped, short tests.

5.2 Summary, conclusions

The c was identified with various methods only in a few elapsed times. It became generally constant after a minimum testing time t_{\min} , which was always smaller than t_{50} for the slow method but only in half of the cases for the fast methods with various k .

It follows that - by evaluating in real time with the fast methods -, the c can be determined theoretically earlier than t_{50} . More than one method is suggested to be used for the evaluation since the solution of the fast $k=1$ method is unique only. The slow method is suggested to be applied for the evaluation only in a few elapsed times, due to the large numerical work.

Previous research indicates that t_{\min} can be the shortest in filter position u_3 (Imre et al 2010) due to the one-dimensional state. Further research is suggested on the real time evaluation, on the t_{\min} in various filter positions and on partly drained penetration (to assess initial and boundary condition).

ACKNOWLEDGEMENT

The help of Professor Peter Roberson in data suggestion is greatly acknowledged.

REFERENCES

- Baligh, M. M. 1986. Undrained deep penetration, II. pore pressures. *Geotechnique*, 36(4): 487–503.
- Imre, E.; Rózsa, P.; Bates, L.; Fityus, S. 2010. Evaluation of monotonic and non-monotonic dissipation test results. *Computers and Geotechnics*, 37, Issues 7–8, 885–904.
- Imre, E.; Schanz, T.; Bates, L.; Fityus, S. 2018: Evaluation of complex and/or short CPTu dissipation tests. Cone Penetration Testing 2018: *Proc. of the 4th International Symposium on Cone Penetration Testing*. CRC Press, 351–357.
- Lunne, T., Robertson P.K. and Powell, J.J.M 1992. *Cone penetration testing*, Blackie Academic & Professional.
- Lim, Y X; Tan, S A; Kok-Kwang Phoon 2019 Interpretation of horizontal permeability from piezocone dissipation tests in soft clays. *Computers and Geotechnics*, 107. 189–200.
- Sully, J.P., Robertson, P.K., Campanella, R.G., Woeller, D.J. 1999. An approach to evaluate field CPTu dissipation data in overconsolidated fine-grained soils. *CGJ*. 36: 369–381.
- Teh, C.I. and Houlsby, G.T. 1988. Analysis of the cone penetration test by the strain path method. *Proc. 6th Int. Conf. on Num. Meth. in Geomechanics, Innsbruck*. 1:397–400.
- Osman, A. 2021. Modelling of penetrometers. Dissipation test workshop ISC6. Sept. 26th 2021, personal communication.

APPENDIX - SUGGESTED MODEL/MODEL LAW

Consolidation model

The system of differential equations, new boundary conditions, for pore water pressure u for displacement v and the suggested time factor T (Imre et al 2010):

$$E_{oed} \frac{\partial}{\partial r} \frac{1}{r} \frac{\partial}{\partial r} (rv) - \frac{\partial u}{\partial r} = 0 \quad (1)$$

$$-\frac{k}{\gamma_v} \frac{1}{r} \frac{\partial}{\partial r} \left(r \frac{\partial u}{\partial r} \right) + \frac{\partial}{\partial t} \frac{1}{r} \frac{\partial}{\partial r} (rv) = 0 \quad (2)$$

$$u(t, r)|_{r=r_1} = 0, \quad \frac{\partial u(t, r)}{\partial r} \Big|_{r=r_1} = 0 \quad (3)$$

$$v(t, r)|_{r=r_1} \equiv v|_{r_1} > 0, \quad v(t, r)|_{r=r_1} \equiv 0 \quad (4)$$

$$T = \frac{ct}{(r_1 - r_0)^2} \quad (5)$$

where v is displacement, r is space coordinate, t is time. k is permeability, γ_v is unit weight of water, E_{oed} is oedometric modulus, J_n and Y_n are Bessel functions, c is coefficient of consolidation, the λ_i , μ_i and C_i ($i=1..k$) depend on the space domain (r_0 and r_1) and the initial condition, T time factor.

The value of r_1 and initial condition can be determined by the strain path theory using the rigidity index I_r , the OCR, friction angle and rate of penetration (Figure A-1, Baligh 1986).

Model law

In this section the use of the model law is presented on some examples, regarding the evaluation of the

monotonic data of Bothkennar clay (fast model, first term solution, $k=1$).

If the evaluation is made assuming $r_1 = 37r_0$ – valid in filter position E but using data of various filter positions, – then from the identified c , the “correct” value of r_1 can be back-calculated with the “ c formula”:

$$r_{1,2} = \sqrt{\frac{c_2}{c_1}} (r_{1,1} - r_0) + r_0 \quad (6)$$

According to the results (Table A-1), the back-computed r_1 values varies from $37r_0$ to $17r_0$ as the sensor positions changes from E to A. As a comparison, the value of r_1 with the strain path prediction of Baligh 1986 varies from $22-23r_0$ to $37r_0$.

The r_1 can be computed on the basis of the measured dissipation times with the “ t formula”:

$$r_{1,2} = \sqrt{\frac{t_2}{t_1}} (r_{1,1} - r_0) + r_0. \quad (7)$$

using the r_1 value valid for filter position E. According to the results (Table A-1), the back-computed r_1 values vary from $37r_0$ to $18r_0$ as the sensor positions changes from E to A.

Table A-1. The r_1 from identified c and measured t_{50} values.

Identified c [cm ² /s]	computed	Measured	computed
	r_1/r_0	t_{50} (min)	r_1 [cm]
A	0.09	17,0	18.74
B	0.06	20,8	29.92
C	0.04	25,5	48.28
D	0.02	36,0	58.74
E	0.02*	36,0*	64.75*

* considered as reference value

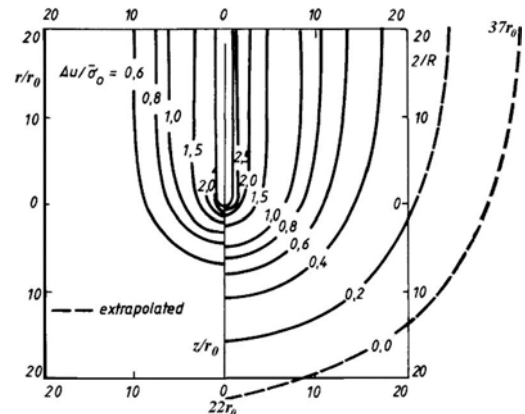


Figure A-1. The zero pore pressure line r_1 (after Baligh, 1986). Left and right: bilinear and hyperbolic modelling. $I_r=150$.

Simulation of CPT penetration in sensitive clay

J. Isaksson

*Chalmers University of Technology, Sweden
NCC AB, Sweden*

J. Yannie

NCC AB, Sweden

M. Karlsson & J. Dijkstra

Department of Architecture and Civil Engineering, Chalmers University of Technology, Sweden

ABSTRACT: This paper presents the results from numerical simulations of CPTu penetration in a natural clay combining the SCLAY1S constitutive model with a large deformation Finite Element framework including a coupled deformation and porewater pressure formulation. The hierarchical model formulation of SCLAY1S captures many features of a natural sensitive clay, such as the evolving anisotropic strength-stiffness response, as well as the degradation of the initial bonding. A sensitivity analysis is performed varying the overconsolidation ratio (OCR), bonding and anisotropy, also the hydraulic conductivity (hence, c_v) of the clay. The findings indicate that some soil properties (the c_v and OCR) impact both the normalised cone resistance Q_c and the generation of excess porewater pressures. In contrast the sensitivity S_f of soft soils primarily affects Q_c . In the current work it seems that the effects of the inherent and stress induced (from CPT penetration) anisotropy is not detected using these normalised plots.

1 INTRODUCTION

The cone penetration test is a widely used method to perform geotechnical site investigation, by continuous measuring of the cone resistance, the sleeve friction, and in case of the piezocone (CPTu) the generated excess porewater pressures, during the penetration into a soil. This allows the mapping of a deposit to be performed in a time-effective manner with a high resolution (Lunne et al. 1997). Further soil characterisation can be performed using classification systems based on statistical correlations of normalised CPTu results against borehole data, see e.g. Robertson (2016) and Schneider et al. (2008). Due to the continuous measurement of the soil response, the CPTu is a great tool to detect differences in the response between and within soil layers by relying on a contrast in hydro-mechanical properties, e.g a change in hydraulic conductivity, overconsolidation ratio or sensitivity (brittleness).

Another approach to establish the relation between soil properties and CPTu response is to use numerical modelling where a prescribed change of a model parameter of a given constitutive model leads to a change in CPTu response. This approach is becoming increasingly more attainable with the ongoing developments for numerical analyses. Three modelling aspects that are necessary for accurate simulation

of CPTu penetration are (i) the capability of the Finite Element (FE) code to deal with large deformations (ii) the adequate coupling of deformations and the generation/dissipation of excess porewater pressures (iii) a constitutive model that incorporates the complex features of natural soils.

A number of numerical methods able to simulate the kinematics of CPTu penetration in FE have been reported, among others the Arbitrary Lagrangian Eulerian method (Berg et al. 1996, Walker & Yu 2006), Material Point Method (Ceccato et al. 2016), Geotechnical Particle Finite Element Method (Hauser & Schweiger 2021, Monforte et al. 2021), and remeshing procedures (Hu & Randolph 1998, Orazalin & Whittle 2018, Mahmoodzadeh et al. 2014). In some cases the effects of CPT penetration are captured in an Updated Lagrangian framework (Yi et al. 2012, Konkol & Bałachowski 2018, Mahmoodzadeh et al. 2014).

Some of the studies (Ceccato et al. 2016, Monforte et al. 2021, Yi et al. 2012, Konkol & Bałachowski 2018, Mahmoodzadeh et al. 2014, Orazalin & Whittle 2018) also incorporates a coupled stress formulation enabling the study of partial drainage during penetration. Constitutive models able to describe advanced soil features such as brittleness (Monforte et al. 2021) and anisotropy (Hauser & Schweiger 2021, Orazalin & Whittle 2018) has also been incorporated to simulate CPTu penetration.

This paper builds upon those previous studies by implementing SCLAY1S in a fully coupled Eulerian Finite Element (FE) framework. Subsequently, the relation between the CPTu response and different soil properties is investigated. The model parameters varied, include the hydraulic conductivity (k), the sensitivity of the soil (S_t), the fabric anisotropy and the overconsolidation ratio (OCR).

2 NUMERICAL MODEL

Natural features of soft clay, such as breakage of initial bonding and fabric anisotropy, are captured by the SCLAY1S constitutive model (Koskinen et al. 2002) and (Karstunen et al. 2005). The elasto-plastic model originates from the Modified Cam Clay (MCC) constitutive model (Roscoe & Burland 1968), in addition to the volumetric hardening of MCC, SCLAY1S also incorporates rotational hardening and gradual degradation of bonding due to plastic strains in the soil. In short, the evolution of the initial anisotropy and degradation of strength is controlled by volumetric plastic strains and deviatoric plastic strains in the hardening law. The model is hierarchical, i.e. an appropriate choice of model parameters leads to the (de-) activation of the model features that capture (evolution of) anisotropy and destructuration. Hence, in its simplest form the model formulation becomes identical to MCC.

For the current work, the SCLAY1S model was implemented in the Tochnog Professional (Rodde-man 2021) finite element framework that is able to handle large deformations by using an Eulerian description with a fixed mesh, where the solution fields for the stress, material velocity and other state variables of the calculation are advected through the domain. Penetration of the CPTu into the soil is performed with the moving boundary method proposed by Dijkstra et al. (2011). Initially, the cone is considered to be outside of the calculation domain, i.e. above the soil surface, and the desired stress state and other state variables required for the model are prescribed to establish the initial state in the model. The numerical penetration is then performed by defining a geometric entity representing the CPTu and prescribing the penetration velocity v to all nodes in this geometry while simultaneously expanding the geometry downwards with the same penetration velocity.

The axisymmetric nature of the problem is exploited using a 2D simplification where the horizontal soil movement and groundwater flow is prevented perpendicular to the axis of symmetry. The geometry and boundary conditions of the numerical model are presented in Figure 1. The initial stress state is prescribed by the vertical effective stress (σ_v'), initial porewater pressure (u_0) and the initial earth pressure coefficient (K_0). Horizontal movement is prevented at the far right boundary while keeping the porewater pressure constant to u_0 , hence

allowing for groundwater flow across the boundary. At the bottom boundary, vertical groundwater flow and soil movement is prevented. The top boundary of the domain is modelled with a prescribed vertical load that is in equilibrium with the total vertical stress (σ_v) and is equal to the sum of σ_v' and the initial porewater pressure u_0 . The increase in stress due to the weight of the soil in the domain is set to be zero to create a uniform soil domain.

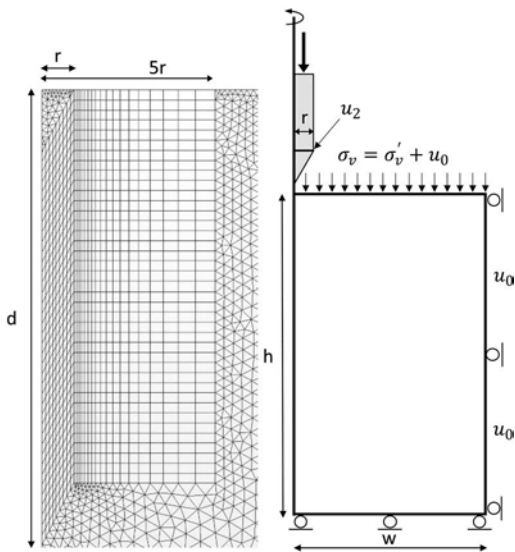


Figure 1. Boundary conditions and mesh in the region close to the penetrating CPTu.

All simulations presented in the study were performed using a 60 cone with a diameter (d) of 0.036 m corresponding to a radius (r) of 0.018 m. The height of the domain h was set to two times the penetration depth and the width w was set to $40r$, to prevent numerical disturbance related to boundary effects. A structured quadrilateral mesh (see Figure 1) was required in the location of the penetrating cone to ensure geometrical compatibility between the mesh and the penetrating cone that is prescribed with a geometry entity. Quadrilateral elements were used in a region extending 5 cone radii (r) from the axis of symmetry. The rest of the domain is filled with unstructured triangular elements. In total, the model contains 1789 quadrilateral elements and 3579 triangular, both with first order shape functions. All simulations in this paper were performed with a penetration rate v of 0.02 m/s down to a final penetration depth of $20d$. The porewater pressure presented in this study was extracted from a position right above the cone shoulder corresponding to the u_2 position. The cone resistance q_c was calculated from the total force needed to push the inclined cone tip downwards divided by the area of the cone. The net

cone resistance q_{net} was calculated by subtracting the initial vertical stress σ_{v0} from the cone resistance q_c .

Table 1. Model parameters used to investigate the effect of drainage conditions on the CPTu response.

Symbol	Parameter	Value
σ_v'	Vertical effective stress [kPa]	109
u_0	Initial porewater pressure [kPa]	70
$K0$	Initial earth pressure coefficient [-]	0.61
OCR	Overconsolidation ratio [-]	1.02
e_0	Initial void ratio [-]	1.41
λ	Virgin compression index [-]	0.205
κ	Swelling/recompression index [-]	0.044
ν	Poisson's ratio	0.3
M	Slope of CSL line [-]	0.9
χ_0	Initial amount of bonding [-]	0
a	Rate of destructuration [-]	0
b	Rate of destructuration due to deviator strain [-]	0
α_0	Initial anisotropy [-]	0
ω	Rate of rotation [-]	0
ω_d	Rate of rotation due to deviator strain [-]	0

3 VARIATION OF HYDRAULIC CONDUCTIVITY

Initially, the effect of the drainage conditions on the CPTu response was studied using a MCC model formulation, by varying the hydraulic conductivity k in the range 5.510^{-3} m/s and 1.110^{-8} m/s. An isotropic hydraulic conductivity was used in all performed simulations. All the model parameters used in the numerical study are presented in Table 1 and are based on those derived for kaolin clay, as used for the numerical studies of the CPTu in Mahmoodzadeh et al. (2014). The normalised penetration velocity V is used to define the current drainage conditions for quasi-static penetration problems, as it enables the comparison between various test conditions. V is defined as:

$$V = \frac{vd}{c_v} \quad (1)$$

where v is the penetration rate, d is the diameter of the CPT cone and c_v is the vertical consolidation coefficient of the soil.

$$c_v = \frac{k_v(1 + e_0)\sigma'_{v0}}{\lambda\gamma_w} \quad (2)$$

The normalised penetration velocity helps to correct for experimental scaling conditions by linking the penetration velocity and size of the object and soil

volume (drainage lengths) to the properties of the soil such as the vertical effective stress σ'_{v0} , initial void ratio e_0 , stiffness λ and the hydraulic conductivity (via the vertical consolidation coefficient c_v).

DeJong & Randolph (2012) proposed a backbone curve of both the net cone resistance and excess porewater pressure normalised with the corresponding undrained value based on the result from seven different studies investigating the change in response for the CPTu under different drainage conditions and confining stress p . Mahmoodzadeh & Randolph (2014) also proposed a backbone curve based on a series of centrifuge test of CPTu penetration in kaolin clay. The net cone resistances are normalised with the results from the undrained penetration simulation and are presented in Figure 2. Whereas, the results for the normalised excess porewater pressure are presented in Figure 3. Both figures also show the two proposed backbone curves.

The transition of the simulated net cone resistance from the undrained to the intermediate and drained state are in good agreement with both backbone curves. The relative magnitude of the net cone resistance in the drained state, however, is considerably larger when compared to the proposed backbone curves. As this study is with equal strength in the soil as in the element near the interface, the contact between the CPTu and the soil can be considered rough. Monforte et al. (2021) performed an additional sensitivity study on the impact of the interface roughness on the CPTu simulations. The normalised net cone resistance for the rough interface ($\phi = 19$) increased with about 40 % from the smooth interface (included in Figure 2). In contrast, the normalised excess porewater pressure response is not greatly affected by the interface formulation. Looking at Figure 2 the results from this study fit in between the smooth and the rough interface response reported by Monforte et al. (2021).

The normalised excess porewater pressure from this study is slightly shifted compared to the other studies (Figure 3). This is due to the presence of some numerically locked-in porewater pressures in a single element near the cone shoulder, i.e. at the u_2 position and is most prominent for very low hydraulic conductivities corresponding to a practically undrained state with normalised penetration velocities above 50. The porewater pressure presented herein, are unsmoothed and taken from the u_2 position and is considered to be accurate when looking at the relative change in response between the analyses in the sensitivity study.

4 CPTU IN SOFT CLAYS

The numerical investigation into the impact of soil properties on the CPTu penetration in soft (sensitive) clays was performed starting from a normally consolidated and isotropic reference state without

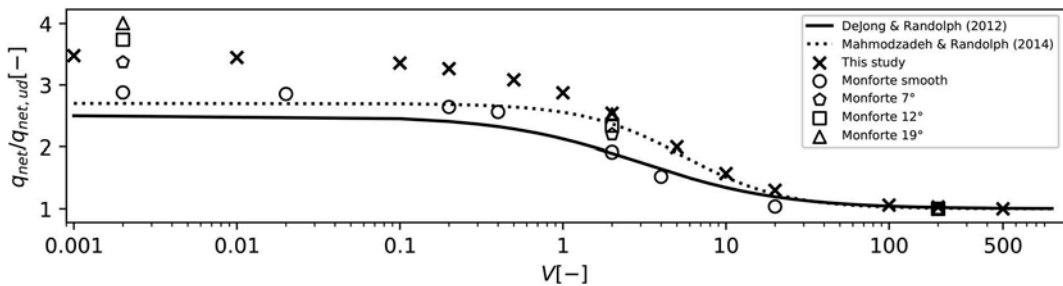


Figure 2. Normalised cone resistance over normalised penetration rate. Comparison between results from this study and Mahmoodzadeh & Randolph (2014) and DeJong & Randolph (2012). Results from Monforte et al. (2021) is included to indicate the effect of interface properties on the CPTu response.

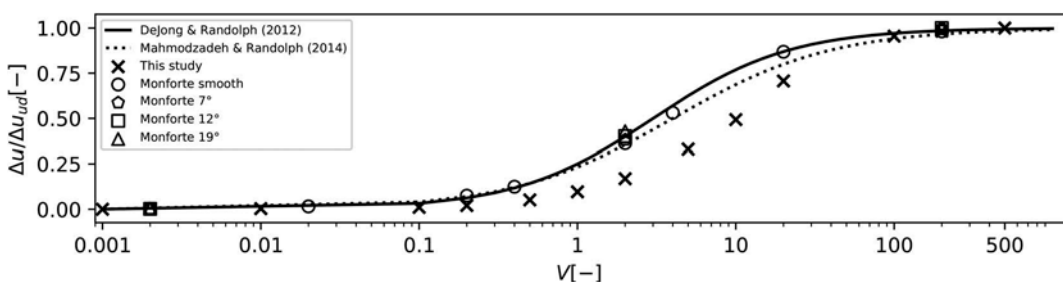


Figure 3. Normalised excess porewater pressure over normalised penetration rate. Comparison between results from this study and Mahmoodzadeh & Randolph (2014) and DeJong & Randolph (2012). Results from Monforte et al. (2021) is included to indicate the effect of interface properties on the CPTu response.

Table 2. Parameters used for investigation of the CPTu response in soft clays.

Symbol	Parameter	Value
OCR	Overconsolidation ratio [-]	1.2, 1.5, 1.8
χ_0	Initial amount of bonding [-]	2, 5, 10, 20, 50
a	Rate of destructuration [-]	6
b	Rate of destructuration due to deviator strain [-]	0.4
α_0	Initial anisotropy [-]	0.352
ω	Rate of rotation [-]	10
ω_d	Rate of rotation due to deviator strain [-]	0.374

initial bonding, using a normalised penetration velocity of $V=200$ for the CPTu. First, the impact of OCR on the soil response was investigated by increasing the OCR in three increments from 1.02 to 1.8. The brittleness of the soil was also investigated by varying the SCLAY1S state parameter for destructuration χ_0 between 0 (no initial structure) and 50 (clay with a high sensitivity). Although this parameter is closely related to the sensitivity of the soil it should not be considered to be similar. Finally, the impact of fabric anisotropy on the

CPTu response was studied by introducing an initially inclined yield surface, that evolves with deviatoric and volumetric strains, in the model formulation. Table 2 presents the range of the SCLAY1S parameters used. The rate parameters and anisotropy α_0 are assumed based on Gras et al. (2017) for natural clays, whilst keeping the original parameters from the kaolin clay. This ensures consistency of model parameters between simulations. Although this approach captures the soft soil features found in natural clays, the dataset does not represent a natural clay deposit.

Robertson (1990) proposed a classification system based on the normalised cone resistance Q_t and pore pressure ratio B_q , where

$$Q_t = \frac{q_{net}}{\sigma'_{v0}} \quad (3)$$

$$B_q = \frac{\Delta u}{q_{net}} \quad (4)$$

The Q_t is the relation between the net cone resistance from the CPTu measurements and the initial effective vertical stress. B_q is the excess porewater

pressure divided by the net cone resistance. This classification system is shown in Figure 4 with the results from the present numerical study. The arrows that annotate the data points correspond to each model parameter and are showing the direction of the normalised CPT response when the parameter is increased in the numerical analysis. Distinct trends for each parameter are clearly identified and are in good agreement with trends proposed by Robertson (1990), for both S_t and OCR .

The numerical results are also presented in the classification chart (Figure 5) originally proposed by Schneider et al. (2008), which is based on Q_t and the excess porewater pressure (Δu) normalised with the initial vertical effective stress (σ'_{v0}). The impact of changing S_t , OCR and c_v indicates clear trends that are in good agreement with the response suggested by Schneider et al. (2008). The effect of fabric anisotropy α only shows limited impact on the results. The results only slightly changed, due to the lower Q_t and excess porewater pressures when compared to the isotropic model results.

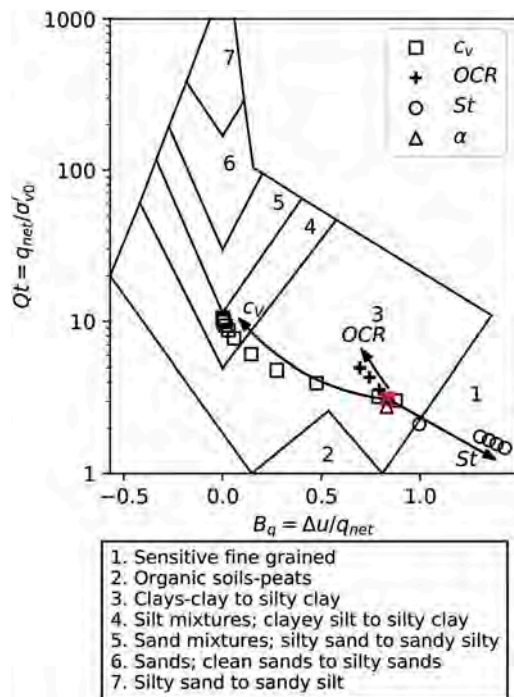


Figure 4. The effect on CPTu response from changing the consolidation coefficient c_v ; overconsolidation ratio OCR ; sensitivity S_t and considering fabric anisotropy α in the characterisation chart for CPTu proposed by Robertson (1990).

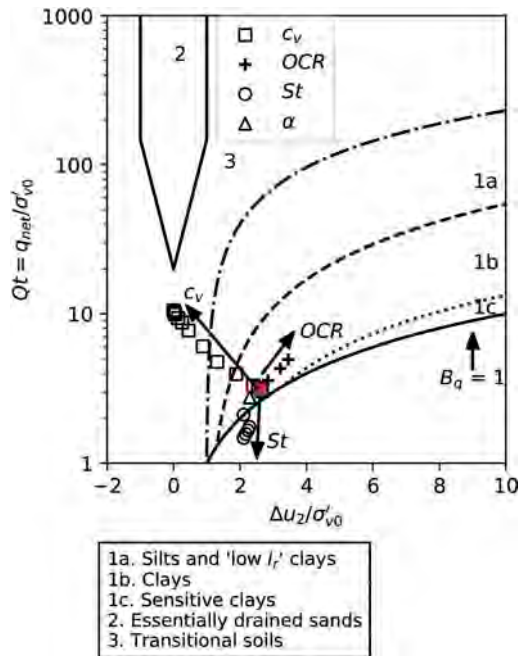


Figure 5. The effect on CPTu response from changing consolidation coefficient c_v ; overconsolidation ratio OCR ; sensitivity S_t and considering fabric anisotropy α in the characterisation chart for CPTu proposed by Schneider et al. (2008).

5 CONCLUSIONS

This paper presents the results from a series of CPTu simulations using a large deformation Finite Element framework in which partial consolidation during penetration is considered by linking the material deformations to the coupled response of porewater flow. An Eulerian framework, in which the mesh is fixed and the soil is able to move independently of the mesh, has been used, to avoid mesh distortions from large deformations associated with the CPTu penetration. The SCLAY1S model is implemented for these analyses, as it captures the evolving anisotropic strength-stiffness response, as well as the degradation of the initial bonding present in natural sensitive clays.

In the first part of the paper the effect of different drainage conditions is quantified and the overall trend compares well with prior work. Further studies need, however, to be conducted to improve the accuracy of the calculated porewater pressures at the shoulder of the CPTu. Extending the study to also include the response on the friction sleeve of the CPTu could further expand the conclusions of this study.

The impact of features that are fundamental to soft soils, i.e. hydraulic conductivity, OCR , sensitiv-

ity and anisotropy, on the CPTu response have been investigated in a hierarchical manner. The following can be concluded after integrating the results in the CPTu classification charts:

- Increasing the hydraulic conductivity leads to an increase in normalised penetration resistance while the normalised excess porewater pressure is decreasing.
- Increasing the OCR is associated with an increase in both the normalised cone resistance and the normalised excess porewater pressure.
- Increasing S_t leads to a considerable decrease in the normalised cone resistance while leaving the normalised excess porewater pressure nearly unaffected
- The simulated CPTu response is practically unaffected by soil anisotropy.

The conclusions of this study are in good agreement with suggestions from Robertson (1990) and Schneider et al. (2008) for the anticipated response from a change in c_v , OCR and S_t . Hence, the results of this study contribute to the interpretation of the widely used classification charts, by linking it to the fundamental features of natural soils.

The extensive empirical evidence used to establish the relation between CPT and soil characteristics is in good agreement with the numerical results, increasing the confidence in the ability to accurately simulate penetration into soft soils with the proposed numerical method. Finally, the numerical simulations should be validated further against in-situ CPTu data.

ACKNOWLEDGEMENTS

The authors acknowledge the financial support provided by SBUF (Development fund of the Swedish construction industry, grant 13614) and BIG (Better Interaction in Geotechnics, grant A2019-19, from the Swedish Transport Administration)

REFERENCES

Berg, P., R. Borst, & H. Huétnik (1996). An eulerean finite element model for penetration in layered soil. *International Journal for Numerical and Analytical Methods in Geomechanics* 20, 865–886.

Ceccato, F., L. Beuth, P. Vermeer, & P. Simonini (2016). Two-phase material point method applied to the study of cone penetration. *Computers and Geotechnics* 80, 440–452.

DeJong, J. & M. Randolph (2012). Influence of partial consolidation during cone penetration on estimated soil behavior type and pore pressure dissipation measurements. *Journal of Geotechnical and Geoenvironmental Engineering* 138 (7), 777–788.

Dijkstra, J., W. Broere, & O. Heeres (2011). Numerical simulation of pile installation. *Computers and Geotechnics* 38, 612–622.

Gras, J., N. Sivasithamparam, M. Karstunen, & J. Dijkstra (2017). Strategy for consistent model parameter

calibration for soft soils using multi-objective optimisation. *Computers and Geotechnics* 90, 164–175.

Hauser, L. & H. Schweiger (2021). Numerical study on undrained cone penetration in structured soil using g-pfm. *Computers and Geotechnics* 133, 104061.

Hu, Y. & M. Randolph (1998). A practical numerical approach for large deformation problems in soil. *International Journal for Numerical and Analytical Methods in Geomechanics* 22, 327–350.

Karstunen, M., H. Krenn, S. Wheeler, M. Koskinen, & R. Zentar (2005). Effect of anisotropy and destructuretion on the behavior of murro test embankment. *International Journal of Geomechanics* 5(2), 87–97.

Konkol, J. & L. Baachowski (2018). Large deformation modelling of cpt probing in soft soil—pore water pressure analysis. In M. A. Hicks, F. Pisanò, and J. Peuchen (Eds.), *Proceedings of the 4th International Symposium on Cone Penetration Testing (CPT'18)*, London, pp. 371–376. CRC Press.

Koskinen, M., M. Karstunen, & S. Wheeler (2002). Modelling destructuretion and anisotropy of a natural soft clay. In Mestat (Ed.), *Proc., 5th European Conf. Numerical Methods in Geotechnical Engineering*, Paris, pp. 11–20. Presses de l'ENPC/LCPC.

Lunne, T., P. Robertson, & J. Powell (1997). *Cone penetration testing in geotechnical practice*. New York: E & FN Spon/ Routledge.

Mahmoodzadeh, H. & M. Randolph (2014). Penetrometer testing: Effect of partial consolidation on subsequent dissipation response. *Journal of Geotechnical and Geoenvironmental Engineering* 140 (6), 04014022.

Mahmoodzadeh, H., M. Randolph, & D. Wang (2014). Numerical simulation of piezocone dissipation test in clays. *Geotéchnique* 64 (8), 657–666.

Monforte, L., A. Gens, M. Arroyo, M. Mánica, & J. Carbonell (2021). Analysis of cone penetration in brittle liquefiable soils. *Computers and Geotechnics* 134, 104123.

Orazalin, Z. & A. Whittle (2018). Realistic numerical simulations of cone penetration with advanced soil models. In M. A. Hicks, F. Pisanò, and J. Peuchen (Eds.), *Proceedings of the 4th International Symposium on Cone Penetration Testing (CPT'18)*, London, pp. 483–489. CRC Press.

Robertson, P. (1990). Soil classification using the cone penetration test. *Canadian Geotechnical Journal* 27, 151–158.

Robertson, P. (2016). Cone penetration test (cpt)-based soil behaviour type (sbt) classification system — an update. *Canadian Geotechnical Journal* 53, 1910–1927.

Roddeman, D. (2021). Tochnog professional user's manual, october 21. <https://www.tochnogprofessional.nl/manuals/user/user.pdf>. Accessed: 2021- 10-21.

Roscoe, K. & J. Burland (1968). On the generalized stress-strain behaviour of wet clay. In *Engineering plasticity*, Cambridge Univ. Press, Cambridge U.K., pp. 553–609.

Schneider, J., M. Randolph, P. Mayne, & N. Ramsey (2008). Analysis of factors influencing soil classification using normalized piezocone tip resistance and pore pressure parameters. *Journal of Geotechnical and Geoenvironmental Engineering* 134(11), 1569–1586.

Walker, J. & H. S. Yu (2006). Adaptive finite element analysis of cone penetration in clay. *Acta Geotechnica* 1, 43–57.

Yi, J. T., S. H. Goh, F. Lee, & M. Randolph (2012). A numerical study of cone penetration in fine-grained soils allowing for consolidation effects. *Geotéchnique* 62 (8), 707–719.

A CPT-based method for estimation of undrained shear strength of sands and transitional soils

K. Kaltekis & J. Peuchen

Fugro, Nootdorp, The Netherlands

ABSTRACT: This paper presents a practical approach for developing a site-specific CPT-based method for monotonic undrained shear strength (s_u) in sands and transitional soils, using results of laboratory undrained triaxial compression (CU) tests on reconstituted and undisturbed specimens as reference. The methodology includes use of net cone resistance values normalised to vertical effective stress, a procedure for pairing of CPT data with CU test results, and definition of a practical failure criterion for deriving s_u from CU test data. The presented approach is particularly useful for application in offshore wind, where the economics of wind farm development favour performing only a single cone penetration test (CPT) per wind turbine location. This setting drives development of CPT-based methods for key geotechnical parameters for foundation design.

1 INTRODUCTION

The characterisation of undrained behaviour of sands and transitional soils (e.g. silty sands, low plasticity silts) is important for large foundations subject to significant short-duration loading and cyclic loading. Therefore, undrained shear strength (s_u) of sands and transitional soils is an important geotechnical parameter that can be used (i) as direct input in calculation models for fully undrained modelling, and (ii) for defining a reference for normalisation of cyclic soil parameter values.

This study presents a practical framework for developing a site-specific CPT-based method for s_u in sands and transitional soils, using results of laboratory undrained triaxial compression (CU) tests on reconstituted and undisturbed specimens as reference. The methodology includes use of (1) net cone resistance values (q_n , defined as $q_n = q_c + (1 - a)u_2 - \sigma_v$, where q_c is cone resistance, a is net area ratio, u_2 is pore pressure at the cylindrical extension above the base of the cone and σ_v is vertical total stress) normalised to vertical effective stress (σ'_v), (2) a procedure for pairing of CPT data with CU test results, and (3) definition of a practical failure criterion for deriving s_u from CU test data.

The approach outlined in this paper is particularly useful for application in offshore wind, where the economics of wind farm development can dictate performing only a single cone penetration test (CPT) per wind turbine location. This setting drives development of CPT-based methods for key geotechnical parameters for foundation design.

This paper includes an example of the site-specific approach, using input data taken from two wind farm sites offshore Netherlands, namely the Hollandse Kust (west) site and the Hollandse Kust (noord) site (Figure 1, HKW and HKN respectively). The input data are in the public domain, as per the European INSPIRE (2018) directive for spatial information.

2 DATABASE

2.1 Geological setting

The HKW site and the HKN site are located in the southern North Sea. Water depths are typically between 15 m and 34 m relative to LAT.

The sites comprise Quaternary deposits with a predominantly sandy sedimentary profile with occasional clay layers associated with internal channelling (RVO, 2019; RVO, 2020). Sands are mainly fine and medium with occasional coarse size in some of the soil units. The sites have been subject to evolution throughout the Pleistocene and the Holocene. Sediments and processes from these time periods dominate the geological framework. Geological formations present at the two sites within the top 50 m below seafloor include (from older to younger) Yarmouth Roads, Eem, Naaldwijk and Southern Bight. These geological formations show no evidence of cementation. Figure 2 illustrates a microscopic photograph of a typical sand sample from the HKW site.



Figure 1. Locations of HKW and HKN sites.



Figure 2. Microscopic photograph of a typical unwashed sand sample from the HKW site.

2.2 CPT data

The available CPT data were acquired according to ISO (2014). The data are available in digital tabular format and include piezocone CPTs and seismic piezocone CPTs performed in both non-drilling mode (direct push from seafloor) and drilling mode (vessel drilling, downhole push) deployment.

2.3 CU data

The database includes results of CU tests performed according to ISO 17892-9:2018, using reconstituted specimens, prepared by moist reconstitution, and undisturbed specimens. Reconstituted specimens were prepared based on estimated in situ density. Other specimen density considerations are described below (section titled ‘data pairing’). It is generally

recognised that reconstituted specimens may give lower shear strength than undisturbed specimens (Hoeg et al., 2000).

The specimens were recompressed to the estimated in situ stress conditions, using conventional back pressures for specimen saturation. No pre-cycling was applied. Recompression conditions were either isotropic or anisotropic, depending on the estimated in situ stress state ($K_0 = 1$ for isotropic stress state and $K_0 \neq 1$ for anisotropic stress state, where K_0 is coefficient of earth pressure at rest).

Database screening was applied, considering soil type and laboratory specimen homogeneity. Soil type was assessed based on sample description, review of particle size distribution and Atterberg limits. Particularly for undisturbed test specimens of transitional soil, specimens containing interbedded or non-uniform material, distinct strata/layer changes or gravel were excluded from further analysis because they can adversely affect undisturbed sample quality and test processing results for a premise of a homogeneous laboratory test specimen.

The screened database includes laboratory results from 33 CU tests on reconstituted soil specimens (26 in sand and 7 in transitional soil) and 5 CU tests on undisturbed soil specimens in transitional soil. The specimen test depths ranged from 2 m to 38 m below seafloor. Table 1 presents classification parameters for the database used. Figure 3 presents results of two typical triaxial tests from the database, one in sand and one in transitional soil.

Table 1. Classification parameters.

Parameter	Sand	Transitional soil
D_r (%)	55-110	35-85
FC (%)	1-8	20-80
CC (%)	-	3-24
C_u (-)	1.5-3.8	5.3-80
D_{50} (mm)	0.17-0.35	0.02-0.15
quartz content (%)	85-100	84-95
particle shape	subangular to well rounded	subangular to rounded

Notes: Transitional soil = (very) silty sand, clayey sand, low plasticity (clayey, sandy) silt; D_r = relative density; FC = fines content; CC = clay content; C_u = coefficient of uniformity; D_{50} = particle diameter where 50 % of the dry mass of soil has a smaller particle diameter

It is generally inconsistent and impractical to use peak deviator stress as a criterion for deriving s_u for dense dilative soils such as many of the ones in the database used for this study. In dilative specimens, large negative pore pressures develop until the end of the test (to about 20 % axial strain; see blue line in bottom plot of Figure 3) or until cavitation occurs.

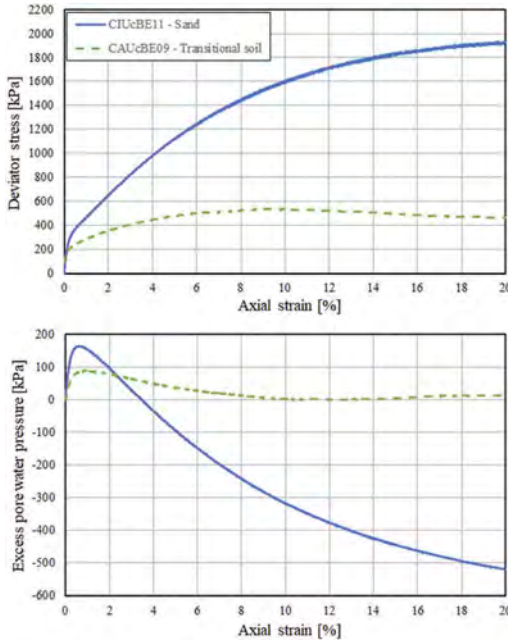


Figure 3. Example of typical triaxial test results from the database (applied back pressures: CIUcBE11 – Sand: 1291 kPa; CAUcBE09 – Transitional soil: 687 kPa).

Cavitation depends on the back pressure applied to the triaxial test specimen. Sufficiently high back pressure should be applied to test specimens that are expected to exhibit dilative behaviour while shearing. It should be noted that large negative pore pressures can be sustained in a laboratory setting with controlled application of (high) back pressure, but are typically not observed during cone penetration. All tests of the database had a back pressure which was at least equal to the hydrostatic pressure at the depth point of each test specimen.

Common criteria were reviewed for deriving s_u from the CU data, i.e. peak deviator stress, peak stress ratio, peak pore pressure, zero excess pore pressure and limiting strain (refer to Brandon et al. (2006) for background information on the various criteria for interpretation of s_u). Peak stress ratio was selected as the most practically useful and most consistent criterion across the database. Therefore, this paper defines s_u at $(\sigma'_1/\sigma'_3)_{max}$, where σ'_1 and σ'_3 are the effective principal stresses.

2.4 Data pairing

Pairing of CPT data (q_n) with CU test results considered the following:

- Laboratory test data were considered as primary, because of single data points versus CPT profiling data;

- Selection of CPT values for comparison with the laboratory data from reconstituted soil specimens focused on estimation of an equivalent in situ relative density D_r of the reconstituted soil specimen based on (1) specimen density and (2) estimated values for minimum and maximum (index) dry densities:

$$D_r = (e_{max} - e)/(e_{max} - e_{min}) \quad (1)$$

where e_{max} is maximum index void ratio, e_{min} is minimum index void ratio and e is specimen void ratio. Selection of values for e_{min} and e_{max} included assessment of laboratory test results per soil unit, per soil type and site-wide;

- Final selection of D_r involved some engineering judgement, particularly for transitional soil specimens, since the estimation of D_r inevitably involves significant uncertainty, which increases with increase of percentage fines. The uncertainty in the selected values for e_{min} and e_{max} should also be noted, particularly since there are various test methods commonly used in the industry that can give significant differences, especially for the maximum (index) dry density (Lunne et al., 2019). The equivalent value of q_n was then back-calculated based on the following equation by Kulhawy & Mayne (1990):

$$q_n = 350 \cdot D_r^2 \cdot P_a^{0.5} \cdot \sigma'_v{}^{0.5} - \sigma_v \quad (2)$$

where P_a is atmospheric pressure;

- Selection of CPT values for comparison with the laboratory data from undisturbed soil specimens focused on CPT-borehole proximity, use of CPT data showing the lower q_n values and relatively high values of soil behaviour type index I_c , thereby accounting for the expected bias in selection of the laboratory test specimens, and allowance for small (< 1 m) depth offsets between nearby CPT and sample borehole locations.

3 CPT-BASED METHOD

The approach to estimate continuous profiles of s_u involved analysis of the relationship between derived values of s_u and q_n , normalised to effective vertical stress σ'_v . This led to a bi-linear relationship that is presented in Figure 4 and Equation 3:

$$\frac{s_u}{\sigma'_v} = \begin{cases} 0.0096 \cdot \frac{q_n}{\sigma'_v} - 0.4823, & \text{for } \frac{q_n}{\sigma'_v} \geq 124 \\ 0.703 & , \text{for } \frac{q_n}{\sigma'_v} < 124 \end{cases} \quad (3)$$

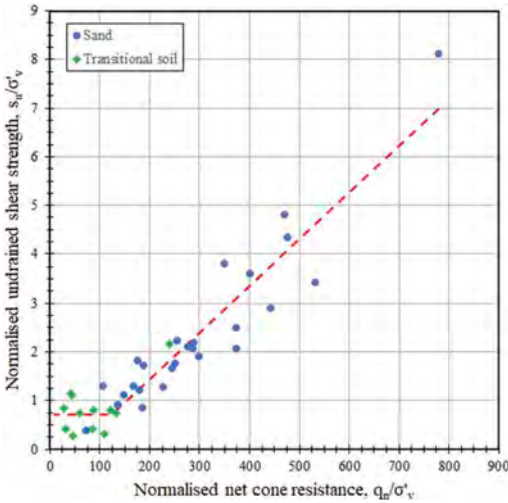


Figure 4. Undrained shear strength derived from in CU tests on sand and transitional soil as a function of net cone resistance.

Comments on Equation 3 are as follows:

- A best fit relationship based on linear least squares regression was considered for values of $q_n/\sigma'_v \geq 124$ based on paired sets of data in sand ($n = 26$, $R^2 = 0.87$, S.E. = 0.59);
- A constant value of s_u/σ'_v for values of $q_n/\sigma'_v < 124$ considering a mean value for s_u/σ'_v within this range, the wide scatter and the absence of a significant trend ($R^2 = 0.38$) between s_u and q_n in transitional soil;
- The method is robust and allows for development of continuous profiles of s_u in sand and transitional soil based solely on input from CPT data, though it is noted that for transitional soil engineering judgement has been applied;
- CPT parameter uncertainty for strongly layered soil will be higher than for uniform soil (Peuchen and Terwindt, 2015). Note also that CPT results are influenced by uncertainty related to undrained, partially drained or drained conditions during cone penetration, particularly in transitional soil with drainage conditions influenced by factors such as soil constituents and (post-)depositional settings. Any of these conditions may apply (DeJong and Randolph, 2012);
- The method covers medium dense to very dense normally consolidated to slightly overconsolidated silty to clean sands and sandy silts;
- Derived values of s_u in sand correspond to values for cone factor N_{kt} ranging between 85 and 176 for the range $q_n/\sigma'_v \geq 60$, which represents more than 95 % of the q_n/σ'_v values in sand across the wind farm sites;
- Derived values of s_u in transitional soil correspond to values for cone factor N_{kt} ranging between 28 and 107 for the range $20 \leq q_n/\sigma'_v \leq 75$, which represents more than

95 % of the q_n/σ'_v values in transitional soil across the wind farm sites;

- Derived values of s_u are in good agreement with the scatter of derived values presented in Andersen (2015).

4 DISCUSSION AND CONCLUSIONS

The method, in combination with an equivalent method for clays, enables derivation of continuous s_u profiles at any CPT location within a given site. This is particularly useful for offshore wind farm developments where one or multiple CPTs are performed per wind turbine location without availability of location-specific laboratory data. Soil behaviour type (i.e. sand, transitional soil or clay behaviour) can be distinguished directly from CPT with application of general or site-specific limits of soil behaviour type indices such as I_c or I_B (Robertson, 2016). Figure 5 presents an example profile from the HKW site.

Equation 3 can be applied with appropriate modifications to produce design profiles of characteristic values of s_u for use in foundation design calculations. To this purpose, the modifications would need to consider at least the following (ISSMGE, 2021):

- Calculation model and its specified principles;
- Limit state and mobilised zone of ground;
- Loading regime and field drainage conditions;
- Transformation uncertainty of derived values to characteristic values;
- Statistical evaluation accounting for statistical fitting uncertainties within the given dataset.

For the horizontal portion of the bi-linear relationship (i.e. the cut-off value for $q_n/\sigma'_v < 124$, see Equation 3), the following particular considerations also apply for selection of characteristic values:

- A probable low value for s_u/σ'_v should be used for slightly overconsolidated soil that would be in the order of magnitude for conventional clays;
- Allowance should be made for *overestimation* of s_u derived from undisturbed transitional soil specimens due to sample disturbance and subsequent reduction of water content during reconsolidation that can lead to soil phase transformation from contractive to dilative (Andersen, 2015).

The method appears robust for two particular sites at the North Sea. The two sites include multiple geological units and multiple soil types; further optimisation should be feasible by differentiation on the basis of geological unit and soil type. Soil type differentiation can consider CPT-based soil behaviour type indices, with confirmation by index sample data that can easily be acquired in an offshore laboratory, such as particle size distribution and particle shape by image analysis (ISO, 2006). Further differentiation may also allow wider application of CPT-based methods.

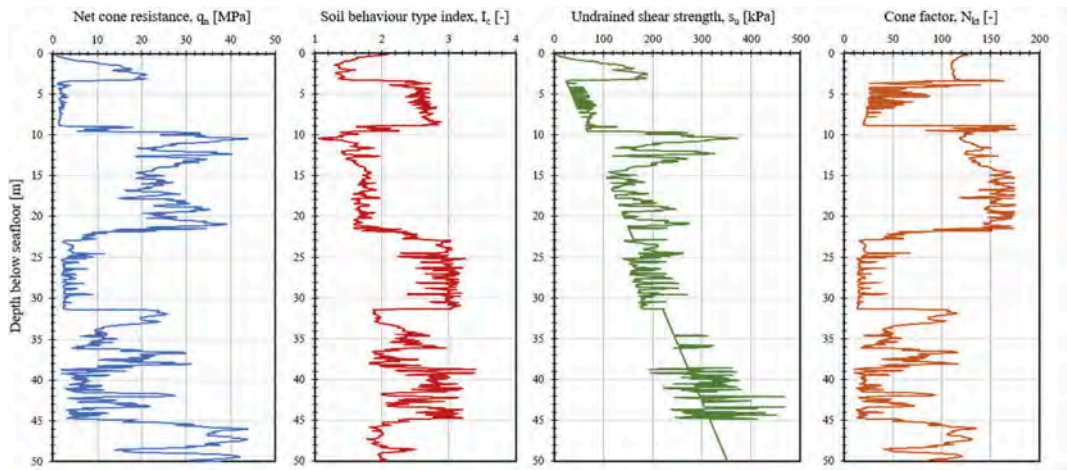


Figure 5. Example profile of s_u from the HKW site comprising three soil types (i.e. sand, transitional soil and clay). Supplementary profiles of q_n , I_c and N_{kt} are also displayed. Soil type is distinguished based on I_c ($I_c < 2.05$: Sand, $2.05 < I_c < 2.6$: Transitional soil, $I_c > 2.6$: Clay). Note that in clay a CPT-based correlation, similar to Equation 3, was used.

Various advanced regression algorithms can be trialled in order for the optimum results to be obtained in terms of statistical evaluation of datasets, including opportunities for potentially making better use of the data by means of automated advanced data analytics such as machine learning and big data.

REFERENCES

- Andersen, K.H. 2015. Cyclic soil parameters for offshore foundation design. *The 3rd McClelland Lecture. Frontiers in Offshore Geotechnics III, ISFOG'2015*, Meyer (Ed). Taylor & Francis Group, London. Proc., 5–82.
- Brandon, T.L., Duncan, J.M. & Rose, A.T. 2006. Drained and undrained strength interpretation for low-plasticity silts. *Journal of Geotechnical and Geoenvironmental Engineering* 132(2): 250–257.
- Hoeg, K., Dyvik, R. & Sandbækken, G. 2000. Strength of undisturbed versus reconstituted silt and silty sand specimens. *Journal of Geotechnical & Geoenvironmental Engineering* 126 (7): 606–617.
- INSPIRE Infrastructure for Spatial Information in Europe. 2018. Available from <https://inspire.ec.europa.eu/>.
- International Organization for Standardization. 2006. *ISO 13322-2:2006 Particle size analysis - image analysis methods - part 2: dynamic image analysis methods*. Geneva: ISO.
- International Organization for Standardization. 2014. *ISO 19901-8:2014 Petroleum and Natural Gas Industries – Specific Requirements for Offshore Structures – Part 8: Marine soil investigations*. Geneva: ISO.
- International Organization for Standardization. 2018. *ISO 17892-9:2018 Geotechnical Investigation and Testing - Laboratory testing of Soil - Part 9: Consolidated triaxial compression test on water saturated soils*. Geneva: ISO.
- International Society of Soil Mechanics and geotechnical engineering (ISSMGE) – Technical Committee TC304 ‘Engineering Practice of Risk Assessment and Management’. 2021. *State-of-the-art review of inherent variability and uncertainty in geotechnical properties and models*.
- Kulhawy, F.H. & Mayne, P.W. 1990. *Manual on estimating soil properties for foundation design*. Electric Power Research Institute (EPRI), Palo Alto, California, 1 vol. (EPRI Report; EL-6800).
- Lunne, Knudsen, S., Blaker, Ø., Vestgården, T., Powell, J.J. M., Wallace, C.F., Krogh, L., Thomsen, N.V., Yetginer, A.G. & Ghanekar, R.K. 2019. Methods used to determine maximum and minimum dry unit weights of sand: Is there a need for a new standard?. *Canadian Geotechnical Journal* 56(4): 536–553.
- Peuchen, J. & Terwindt, J. 2015. Measurement uncertainty of offshore cone penetration tests. *Frontiers in Offshore Geotechnics III, ISFOG'2015*, Meyer (Ed). Taylor & Francis Group, London. Proc., 1209–1214.
- Robertson, P.K. 2016. Cone penetration test (CPT)-based soil behaviour type (SBT) classification system – an update. *Canadian Geotechnical Journal* 53: 1910–1927. Published at www.nrcresearchpress.com/cgj on 14 July 2016.
- RVO Netherlands Enterprise Agency. 2019. *Report - Geological Ground Model HKN – Fugro*. Available at <https://offshorewind.rvo.nl/file/view/55040046/Report+-+Geological+Ground+Model+HKN+-+Fugro>.
- RVO Netherlands Enterprise Agency. 2020. *Report - Geological Ground Model HKW – Fugro*. Available at <https://offshorewind.rvo.nl/file/view/55040628/Report+-+Geological+Ground+Model+HKW+-+Fugro>.

Comparison of frozen soil strength characteristics by cone penetration and triaxial compression testing

Daniil Lagosha

Lomonosov Moscow State University, Russian Federation

Ivan Sokolov & Nikolay Volkov

Fugro, Russian Federation

ABSTRACT: The paper provides comparison of field and laboratory tests of permafrost soil. Electrical resistivity and temperature piezocone penetration tests (RTCPTu) were carried out in the area of sporadic distribution of permafrost. RTCPTu detected islands of permafrost at depth more than 10 meters. Based on this information, undisturbed samples of warm permafrost soils with massive cryogenic structure and thick ice lenses (up to 10 cm) were collected using CPT equipment with a direct push soil sampler (MOSTAP) mounted instead of cone. The samples were kept in frozen condition and transported to the soil lab, where physical properties and triaxial compression tests were carried out. The CPT results included the characteristics of long-term frozen soil strength such as σ_c – the long-term cone resistance and σ_n – the net long-term cone resistance. The results of triaxial tests provided the characteristics of peak strength: σ_1 – the maximum vertical stress and $\sigma_1 - \sigma_3$ – deviator stress at failure. The frozen soil samples were cleared from ice lenses since it is not possible to test them with thick ice lenses. The results of CPT and triaxial testing showed fairly similar values, when the cone measured resistance in frozen soil with massive cryogenic structure. When the cone was located near ice lenses, the net long-term cone resistance appeared to be much lower compared to deviator stress. This observation is in line with conventional theory on physics of ice which states that ice has near-zero long-term strength. The obtained results clearly show the value and advantage of CPT in permafrost (in-situ testing) compared with triaxial compression testing (laboratory). The properties of frozen soil in-situ may significantly differ from properties of frozen soil in a sample. This must be considered for designing civil structures on permafrost.

1 INTRODUCTION

Conventional geotechnical drilling and sampling of permafrost is a challenging problem due its vulnerability. Frozen soils with high ice content at a temperature near freezing point may be easily disturbed due to frictional heating, drilling fluid, ice brittleness and other factors. CPT on permafrost is a maturing technology which has been successfully applied recently. A great benefit would be to use CPT equipment together with direct push soil sampling which is commonly used for non-frozen soils. This combination of CPT and frozen soil sampling was successfully tested in the city of Novy Urengoy, West Siberia, Russia in 2019.

The site is located in Novy Urengoy, Russia. The soils of the site were investigated on a depth of more than 25 m using field and laboratory tests. Retrospectively the site is located in the northern part of the West Siberian plain in the river basin, where accumulation of lake-alluvial sediments took

place. The surface relief is flat due to urban construction. Site soils are represented by clays (from sandy to silty) and sands, rarely peat. In some areas, there are permafrost soils from a depth of 9-15 meters.

The roof of permafrost soils is marked at different depths under the structures on this site. Moreover, there is the complete absence of frozen rocks on some parts of the site. So, there are uneven settlements of structures, which lead to theirs deformation and formation of cracks in them, causing the emergency condition of structures.

The site was located in the basements of two residential buildings (Figures 1, 2). The height of the basements is less than 2 meters. There are many continuous sewer and heating pipes inside, complicating the tests. Thus, site conditions did not permit the using of a heavy vehicle-based cone penetration unit or other commonly used field methods using large-sized equipment.

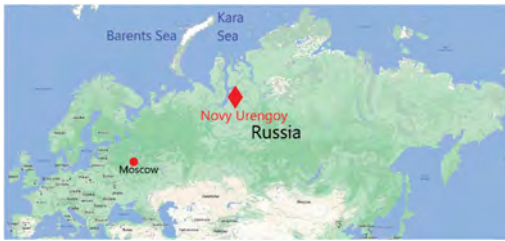


Figure 1. Map location area – Novy Urengoy, Russia.



Figure 2. Site view.

2 FIELD TESTS OF PERMAFROST - CPT

2.1 CPT performing

To perform cone penetration tests (CPT) with measuring of conductivity, temperature and pore pressure RTCPTu, a special small-sized unit with a nominal penetration force of 150 kN was used (Figure 3).

CPT was carried out in two modes: continuous (a constant rate-controlled penetration) and “with stabilization” of the cone (similar to “dissipation” test but rods are kept clamped). The second mode when q_c is measured is also called stress relaxation test, which carried out in a frost layer of the soil to investigate the relaxation behaviour of permafrost.

The stress relaxation test allows to obtain the soil strength parameters similar to those of the continuous type test, but instead of the values of first type test, stabilized second type test values of the cone and at the friction sleeve resistance (q_{cs} , MPa and f_{ss} , MPa) are obtained. Based on the results of the stress relaxation test, it is calculated the long-term strength of the soil under the cone (σ_c , MPa) and on the friction sleeve (σ_s , MPa). In moving of a cone, the soil is loaded by a value more than the instantaneous strength. When a cone stops moving, it is fixed and the stress relaxation is recorded. The values are recorded until the readout parameters stabilize.

Correlation of the listed parameters for frozen soils is as follows:

- for the cone resistance: $q_{cv} > q_{cs} > \sigma_c$ is always observed, and $q_{cv} = q_{cs}$ (0 sec) at the same CPT point and at the same depth;



Figure 3. Map location area – Novy Urengoy, Russia.

- for the friction sleeve resistance: can be $f_{sv} \approx \approx < f_{ss}$ and $f_{sv} > f_{ss}$, but f_{sv} and f_{ss} are always more than σ_s .

Cone penetration tests in velocity mode were executed at 2 cm/s for maximum depths up to 30 m, including tests in cone stabilization mode. They were performed to a depth of 25 m below the ground surface. Temperature and stress relaxation measurements were mostly made at the depth of permafrost spreading: from 7-9 m to 25 m with intervals of 1 m at 9-11 m and 2-5 m at 11-25 m. Frozen soil temperature measurements confirmed the presence of frozen soils at the site. The tests were carried out in July-August 2019. Measured temperatures in the frozen soils ranged from -0.9 to -0.1°C.

2.2 MOSTAP soil sampling

Soil sampling was performed with a MOSTAP direct push soil sampler (Robertson, 2014) from the CPT unit. A total of 13 soil sampling points were executed on the site. Sampling was carried out very close to the CPT points, at a distance of 1-2 m, for reliable correlation of the results of testing and sampling and minimal influence of soil variability factor. In total, 146 samples were taken, of which 110 of them were unfrozen and 36 of them were frozen (Figure 4). It is worth to emphasize that the sampling of frozen soils using the MOSTAP technology was carried out for the first time.

In this paper, frozen clay was considered as the object of researching. It was chosen due to the fact that it was the cause of uneven sedimentation at the site. It was also of scientific interest to research the strength characteristics of the frozen soil areas with thick ice lenses.

Considering frozen soil layer was investigated well by both sampling and cone penetration testing. The temperature of the investigated soil varies from -0.3 to -0.11°C. It is deposited from a depth of 10 m. Sampling was carried out at a depth of

10-15 m. 11 samples were taken. Within this layer, 16 points of CPT were executed in the velocity mode and 45 stress relaxation tests in the stabilization mode of the cone. Out of this number of tests, values for analysis were selected from 8 points. All the CPT points with stress relaxation tests were located very close to the frozen soil sampling points - at a distance of 1-2 m.



Figure 4. Part of investigated frozen soil, sampled by MOSTAP.

3 LABORATORY TESTS OF PERMAFROST – TRIAXIAL COMPRESSION TESTING

3.1 *Specimens preparing*

Various characteristics of the composition and properties of investigated soils were determined in the field laboratory. According to their results, the soil can be characterized as frozen clay from silty to sandy, with ice from well-bonded, no excess ice to thick ice inclusions, non-saline, from very stiff to soft.

To determine the strength characteristics of the investigated soil by triaxial test, specimens were made of selected samples of frozen clay. Soil samples with a massive cryogenic structure were tested in a triaxial compression apparatus to ensure that the homogeneity condition of the specimen was met.

Specimen preparation for the test was carried out in a special room with the maintenance of negative temperature (cryogenic chamber). The specimens cut from the frozen samples had a cylinder shape with a height (h) to diameter (d) ratio of 2:1 (70 mm: 35 mm) (Figure 5).

3.2 *Performing tests and theirs results*

The chamber and the counter-pressure system of the triaxial apparatus chamber supplying the fluid to the stamps, and the holes in the stamps were filled with a special liquid with a negative freezing temperature by raising the pressure in the counter-pressure system with complete displacement of air bubbles. The triaxial tests were executed in the consolidated-undrained mode without pore pressure measurements. The investigated soil was in the frozen state, so it was not possible to measure pore pressure.

In this case to determine the strength of the soil in full stresses, it was measured by the peak of the stress deviator. The specimen is broken by applying a vertical loading with the pressure in the chamber



Figure 5. Example of a test soil specimen in cross-section and longitudinal section.

previously reached and the drainage blocked. Kinematic test mode was used: vertical loading is applied with a given constant rate of deformation of the specimen. The rate of specimen loading was 0.02 mm/minute.

Soil temperature during triaxial tests is -1°C . This is the highest subzero temperature that can be maintained in the apparatus to keep specimens in frozen state. In the natural soil conditions, their temperature is close to the freezing start temperature and to zero - from -0.3 to -0.1°C , which is technically extremely difficult to assign in the device today. The tests lasted from 11 to 21 hours. The consolidation time of the samples was 4 hours. The confining stress in the triaxial device was within 280-300 kPa.

Of the executed five tests, it can be highlighted two “paired” tests, i.e. performed on specimens taken from one sampling point and one depth interval, and one “unpaired” test. Therefore, all specimens were aged for 1 day and tested under identical consolidation and loading conditions, so the “paired” tests could be compared to each other.

Figures 6 and 7 show the results of triaxial tests. Specimens No. 2-5 exhibited a brittle behaviour,

specimen No. 1 exhibited a ductile behaviour (Figure 7). “Paired” specimens No. 1 and No. 2, No. 3 and No. 4 showed quite close peak strength to each other: 697 and 679 kPa; 989 and 935 kPa, respectively. The results are repeatable and confirm the validity of the testing procedure.

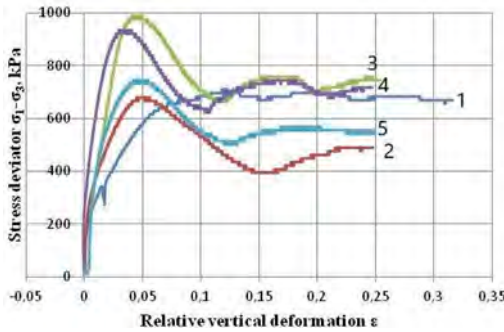


Figure 6. The graph of deviator stress dependence on vertical axial deformation.

It should be noted that fracturing time of specimens No. 1 and No. 2 was quite close - 15 and 13 hours, respectively. At the same time, specimens No. 3 and No. 4 had two times more different fracturing times - 7 and 16 hours. However, in both cases the values of stress peak deviator in “paired” specimens are quite close.

The vertical stresses σ_1 and deviators at fracture of specimens $\sigma_1 - \sigma_3$ obviously have the same patterns. The values of σ_1 and $\sigma_1 - \sigma_3$ range from 0.96 to 1.28 MPa and from 0.68 to 0.94 MPa, respectively.



Figure 7. A frozen soil sample after the triaxial test and its failure character.

4 COMPARISON CPT AND TRIAXIAL TESTS RESULTS

4.1 Mechanism of tests

The triaxial tests simulated natural soil conditions similar to the stress relaxation tests performed by cone penetration testing.

The mechanism of these tests is quite similar. In the triaxial compression device, the stamp transmits vertical stress to the specimen, and the fluid filling the chamber space makes all-round pressure on the specimen, allowing the stress-strain state of the tested soil in the natural conditions to be remake as much as possible (Figure 8b).

When executing the stress relaxation test by CPT, the cone is penetrated directly into the soil to the depth of the investigation, stopping at that depth. As a result, the soil mass makes all-round compression of the investigated soil layer from all sides, and the cone, similarly to the stamp in the triaxial apparatus, assigns vertical stress at a constant rate of deformation. In addition, CPT is sensitive to transient zones of the soil mass (changes in soil type) and soil variability, such as ice lenses, due to the influence zone of the cone (Figure 8a).

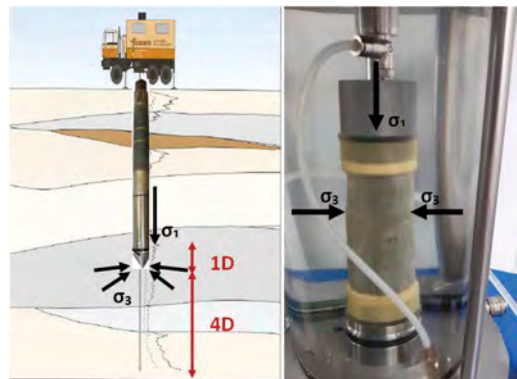


Figure 8. Mechanism of the main stresses in the test method of: a) CPT and zone of influence of the cone; b) triaxial compression.

The principle of the major stresses in both test methods is similar, but it is necessary to consider factors that will reflect the difference between the results obtained by them. These factors are:

- ground temperature;
- geometric shape of the stamp/cone;
- soil variability;
- stress-strain state of the soil.

As a result of the performed tests and their processing the following strength characteristics were obtained:

- by CPT method:
 - cone resistance q_c ;
 - long-term cone resistance σ_c ;
 - net long-term cone resistance σ_n ;
- by triaxial compression method:
 - vertical stress at specimen failure σ_1 ;
 - stress deviator at specimen failure (peak soil strength) $\sigma_1 - \sigma_3$.

The cone resistance of the soil q_c in this paper is taken equal to the corrected cone resistance values

$$q_t = q_c - (1 - a)u_2 \quad (1)$$

where a - base area coefficient of the cone, u_2 - pore pressure (Lunne et al., 1997), i.e. pore pressure in frozen soils is not considered. Consequently, $q_t = q_c$.

From the values of q_c obtained from direct measurements, it was obtained the values of the long-term cone resistance σ_c . For this purpose, it was used the method of calculating this parameter based on the dynamometric method of Vyalov (1986).

This method of measuring stress relaxation helps in evaluating the long-term strength of the soils which serve as the basement of the structure. Processing application of stress relaxation curves obtained in the field tests with the help of the described equation makes it possible to obtain values of long-term strength of soil at a given depth. The validity of application of this equation is confirmed by researches of Vyalov (1986), Volkov and Sokolov (2018; 2019; 2020).

4.2 Comparison of the results

Based on the obtained values of the long-term cone resistance σ_c , the values of the net long-term cone resistance of the soil σ_n were obtained by:

$$\sigma_n = \sigma_c - \sigma_{vo} \quad (2)$$

where σ_{vo} - overburden stress (Lunne et al., 1997).

To compare the results of the strength characteristics investigation of the investigated soil, the values of σ_c and σ_1 and as well σ_n and $\sigma_1 - \sigma_3$ were taken and their dependence on the depth of the investigation was plotted (Figures 9, 10).

As a result of the analysis it should be paid attention to the following:

1. The pattern of σ_1 and $\sigma_1 - \sigma_3$ values growth with depth is clearly traced, similar to the pattern of the long-term cone resistance of the soil.
2. The values of σ_c obtained at the depth of investigated soils vary from 0.25 to 1.15 MPa. It should be noted the increase of long-term cone resistance of the soil with increasing the depth of investigation.

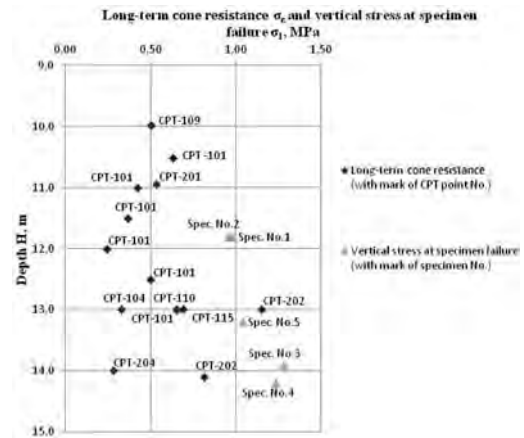


Figure 9. The graph of long-term cone resistance and vertical stress at triaxial test failure of specimen dependence on depth.

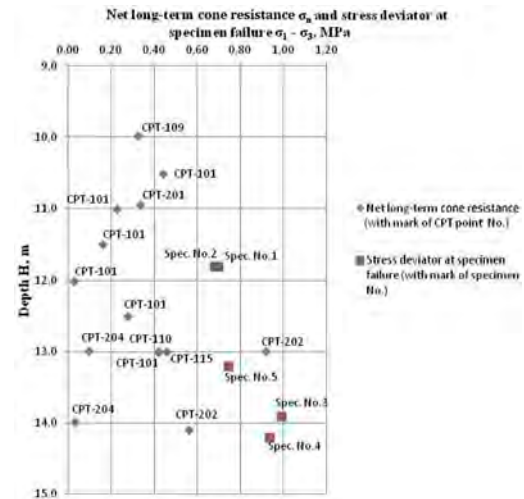


Figure 10. The graph of net long-term cone resistance and stress deviator at triaxial test failure of specimen dependence on depth.

3. The values of σ_n change from 30 to 920 kPa. A higher net long-term cone resistance with increasing depth is also noted.
4. Minimum values of σ_n (30 kPa) are close to zero. This indicates the presence of ice lenses in the zone of cone influence. Such frozen soils are characterized by low bearing capacity during long-term loading application.
5. The maximum values of σ_n (0.56-0.92 MPa) and σ_c (0.82-1.15 MPa) obtained by CPT correlate well with stress deviators (0.7-1.0 MPa) and vertical stress (0.96-1.3 MPa) in failure of specimens tested by triaxial compression. These values were observed in frozen soils with massive cryogenic

structure, which was confirmed by sampling. In addition, frozen soil samples were tested in the triaxial apparatus with exactly this cryogenic structure to meet the condition of sample homogeneity.

6. The temperature of the triaxial tests is -1°C . This is the highest subzero temperature that can be maintained for high-temperature frozen specimens in triaxial testing. In the natural soil conditions, their temperature is close to the freezing start temperature and to zero - from -0.3 to -0.1°C , which is technically extremely difficult to create in the device today. As it is known, when the temperature of frozen soil decreases, its strength increases. Perhaps that is why the values of the results of triaxial tests are correlated with the maximum values of CPT.

Thus, the results of cone penetration and triaxial testing show fairly similar results in the case of a massive cryogenic structure of soil. Determining the strength in frozen soil with lensed cryogenic structure is currently an important question. There is not yet a consistent method for such determination. In this case, CPT revealed that in frozen high-temperature ice-rich clays, the long-term strength

over time when the load is applied will tend to small values, close to zero.

REFERENCES

- Lunne T., Robertson P.K., Powell J.J. 1997. Cone penetration testing in geotechnical practice. Publishing house of the Spon Press, London and New York.
- Robertson, P.K., and Cabal, K.L. 2014. Guide to Cone Penetration Testing for Geotechnical Engineering, 6th Edition, Signal Hill, California: Gregg Drilling & Testing, Inc.
- Sokolov I. 2020. Determination method for strength properties of frozen soils by cone penetration testing. PhD Thesis – Moscow State University, Moscow (in Russian).
- Volkov, N., Sokolov, I. & Jewell, R. 2018. CPT Testing in Permafrost. Proceedings 4th International Symposium on Cone Penetration Testing / N. Volkov [and etc.] // – CPT'18. – Netherlands, Delft – 2018. – pp. 1258–1268.
- Volkov N.G., Sokolov I.S., 2019. Estimation of pile bearing capacity in permafrost based on stress relaxation measured by cone penetration testing. *Geotechnics*, Vol. XI, No. 1, pp. 68–78.
- Vyalov, S.S. 1986. *Rheological Fundamentals of Soil Mechanics*, Volume 36, 1st Edition. Publisher: Elsevier.

Fincone: A study on the use of CPT in soft sensitive clays

T. Lämsivaara

Tampere University, Tampere, Finland

B. Di Buò

Tampere University/Ramboll Finland Oy, Tampere, Finland

J. Selänpää

Tampere University/Destia, Tampere, Finland

M. Knuuti & M. Haikola

Tampere University, Tampere, Finland

ABSTRACT: The paper presents the results of a recent study on the application of CPTU on soft sensitive Finnish clays. An extensive field and laboratory investigation program was carried out, including 9 test sites of which 5 were studied in more detail. In each of the test sites, a minimum of 4 CPTU soundings, 2-3 field vane test with a new type of down hole vane, sampling with a newly developed large diameter tube sampler and an extensive laboratory investigation program were carried out. Transformation models were developed to estimate the undrained shear strength, preconsolidation stress, and constrained modulus for the over consolidated region. In addition, new information about anisotropy of Finnish clays were obtained. In general, the CPTU tests proved to be very reliable with very good repeatability. However, the measurement of sleeve friction proved to be somewhat problematic for the very soft and sensitive clays studied.

1 INTRODUCTION

Until 2010, the use of CPTU had not gained wide popularity in Finland. Attempts made in the 90's to assess the undrained shear strength of Finnish soft clays with the CPTU had not been very successful mainly due to accuracy problems related to the low undrained shear strength (s_u) values for both the CPTU and the field vane tests used as reference. As the problems with the field vane test became clearer (Mansikkamäki, 2015), a need to find better solutions became obvious.

Based on this background Research Centre Terra at Tampere University started together with the Finnish Transport Agency a comprehensive study to establish reliable correlations to estimate s_u and preconsolidation stress (σ'_p) of soft clays, and to promote the use of CPTU in Finland. To achieve these goals, an extensive field and laboratory investigation program was carried out at 9 test sites. This paper gives an overview of the project, describing the test sites, field, and laboratory work executed, and the correlations and other results found during the study.

2 TESTING PROGRAMME

The CPTU tests included tests with two different probes, i.e., a sensitive cone and a high-capacity cone with a maximum cone resistance of 7.5 MPa and 75 MPa respectively. Both cone types have a standard 60° apex tip, with a cross-sectional area (A_c) of 10 cm² and a sleeve area (A_s) of 150 cm². The filter element for measuring the pore-water pressure is located at the shoulder, above the cone tip (u_2).

In addition, seismic and resistivity modules were used. A minimum of 4 soundings were performed at each site. In addition to CPTU tests, field vane tests were carried out with a new type of down hole vane, characterized by measuring system and torque motor located right above the vane, to overcome problems related to rod friction (Selänpää et al. 2018). Comparative test with standard type of up-hole devices were carried out at some of the sites.

To ensure high quality undisturbed samples for the laboratory tests, a new sampler was developed (Di Buò et al. 2019). The sample resembles the SGI type of Laval sampler, with a cutting wire and possibility to feed air/water to avoid suction during withdrawing.

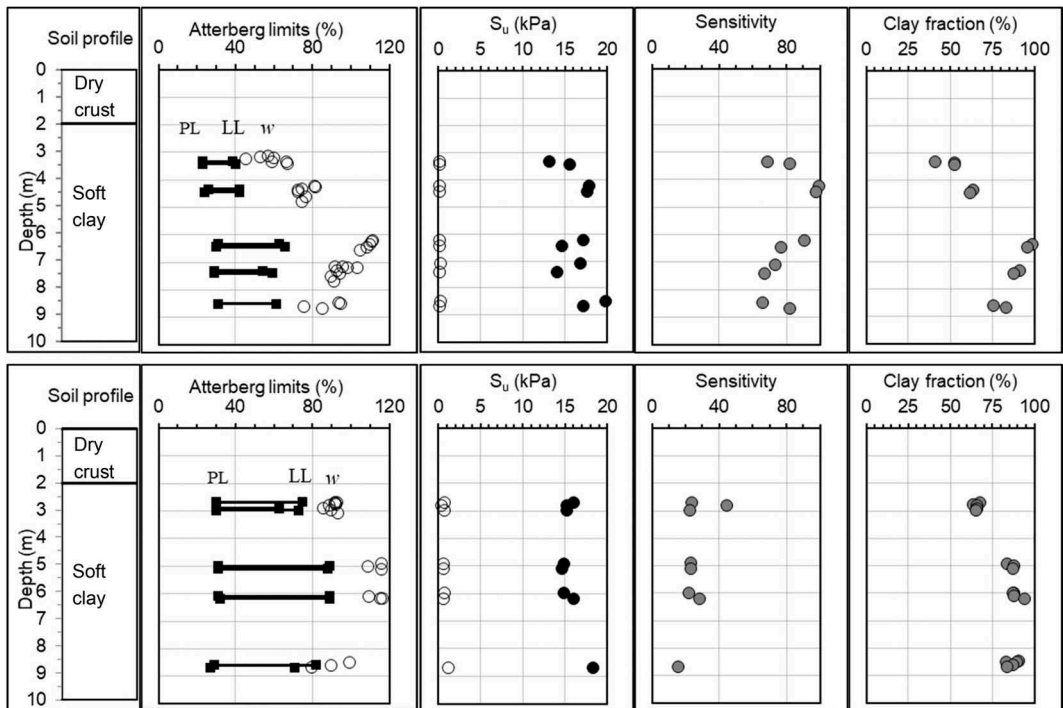


Figure 1. Index properties and undrained shear strength for Paimio (upper figure) and Sipoo (lower figure) test sites.

The sample is though somewhat smaller in size, having an internal diameter of 131 mm. Another difference is that the samples are stored in the sampling tubes that can be pressurized to keep the in-situ stress conditions.

The laboratory tests included classification tests, CRS oedometer tests, triaxial compression and extension tests and direct simple shear (DSS) tests. All tests have been conducted in accordance with appropriate standards when available.

3 TEST SITES

Field and laboratory investigations have been carried out altogether in 9 different sites, i.e., in Perniö, Masku, Paimio, Sipoo, Lempäälä, Murro, Kotka, Joensuu and Pohja. The five foremost have been the main testing sites in calibration of cone factors and are presented here in more detail.

The Perniö test site is located on the southwestern coast of Finland, about 140 km west of the city of Helsinki. The soil stratigraphy of the deposit includes a 1–1.5 m thick dry crust underlain by 8–9 m thick, soft clay layer; silt and stiff sandy layers can be found at a greater depth. The groundwater table is located at 1 m depth.

The Masku test site is located at the southwestern coast of Finland, near the city of Turku. The soil stratigraphy includes a 1.5 m thick weathered clay

crust, followed by an 8 m thick, soft clay layer. The groundwater table is located at 1.2 m depth.

The Paimio test site is also located close to the city of Turku. The stratigraphy consists of a 2 m thick clay crust overlaying an 8 m thick, soft clay layer. The groundwater table is located at 0.8 m depth.

The Sipoo site is situated 30 km north of the city of Helsinki. The deposit consists of a homogeneous soft clay layer between 2 and 9 m depth and a 2 m thick dry crust layer. The groundwater table is located at 1 m depth.

The Lempäälä test site is located close to the city of Tampere. The soil stratigraphy consists of a 1–1.5 m thick dry crust layer, followed by 1–1.5 m of organic soil underlain by a soft sensitive low-plastic clay layer. The groundwater table is located at 0.6 m depth.

All sites are characterized by low s_u values and high water content (w), usually above the liquid limit (LL). The clays are thus very sensitive and their remolded shear strength values obtained by the fall cone test are generally below 0.5 kPa for Perniö, Paimio and Lempäälä sites, and close to unity for Sipoo and Masku sites.

The index properties and the intact (black) and remolded (white) undrained shear strength obtained from the fall cone test, of the clays for Paimio representing highest sensitivity (S_r) and Sipoo representing lowest S_r are presented in Figure 1. Typically for

the clays with lower plasticity index PI , the w is much higher than the LL , resulting in high liquidity index (LI), which correlates strongly with S_r .

4 QUALITY OF DATA

In general, the repeatability of the CPTU tests was found very good. As an example, the coefficient of variation (COV) values for corrected cone tip resistances and pore pressure measurements varied between 0.026 – 0.060 and 0.023 – 0.106 respectively between different sites (Knutti & Lämsivaara 2019 a, b). However, for the sleeve friction measurements, the resolution was too low for the very soft sensitive clay sites, in which the measured values generally were below 5 kPa (COV values in the range 0.15 -0.30). In Figure 2 results from four tests carried out using the sensitive cone and one with the high-capacity cone are presented from Paimio test site. As can be seen, the four corrected tip resistance measurements are very similar, while the one using the high-capacity cone is giving somewhat lower values. This observation was generally made in all test sites. It should be noted that the high-capacity cone had not been calibrated especially to low values. The too low resolution is clearly visible on the sleeve friction graph.

While the pore pressure measurements for the two types of cones were performed with same kind on transducers having the same accuracy, the minor differences that can be seen between the different pore pressure measurements are related to the preparation works and actual measurements, not to the equipment.

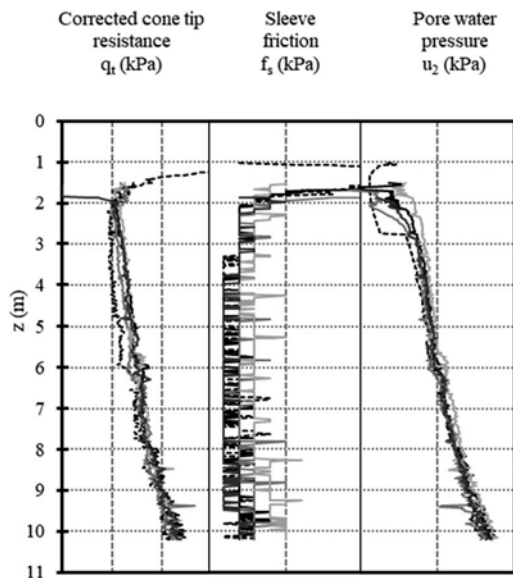


Figure 2. CPTU results from Paimio test site. Results from four sensitive cone measurements are presented with solid lines, while the results from one high-capacity cone measurement are given by a black dotted line.

The new down-hole field vane device showed better consistency and repeatability than traditional up-hole devices. The COV values for the down hole field vane test varied in between 0.04 and 0.23 between different sites, with an average of 0.14 for 88 tests. When the tests are performed with care, and casing is used for the up-hole device, the two methods gave very similar results for intact clay, although there was a slight tendency to higher values for the down-hole device. However, for the remolded undrained shear strength the down-hole device clearly yielded lower values, closer to values obtained with the fall-cone.

The quality of the undisturbed soil samples was mainly evaluated based on the criteria proposed by Lunne et al. (1997). Accordingly, sample quality is classified as “very good to excellent”, “good to fair”, “poor”, and “very poor”. In Figure 3 the sample quality found for CRS oedometer tests are presented as change of void ratio versus depth. The same sampler types are indicated by equal marker shapes while different shades are used for the various sites. As can be seen, most of the samples fall into categories “very good to excellent” and “good to fair”. The poor results for the TUT sampler at Lempäälä site is explained by it being the first site where the new sampler was tested, and all procedures were not in order at the beginning. However, as the procedures were optimized mostly “very good to excellent” quality samples were obtained. Results from laboratory test obtained from samples classified as poor or very poor have not been used in the calibrations. As reported by Di Buò et al. (2019), the sample quality did not suffer from a storage time of two years.

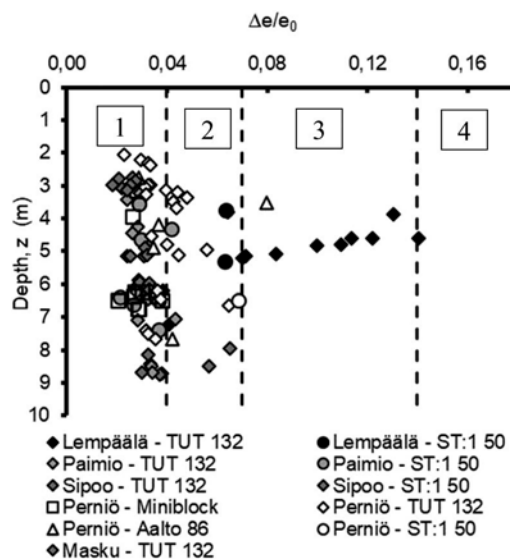


Figure 3. Sample quality according to the Lunne criteria (1997), 1 – very good to excellent, 2 – good to fair, 3 – poor, 4 -very poor.

5 TRANSFORMATION MODELS

5.1 Evaluation based on SCE-CSSM

Di Buò et al. (2020) and Di Buò (2020) studied the possibilities of the hybrid spherical cavity expansion – critical state soil mechanics (SCE-CSSM) framework by Mayne (1991) and Chen and Mayne (1994), and the modified SCE-CSSM solution (Agaiby 2018) for the determination of σ'_p / OCR . It can be concluded that for low sensitivity (St) clays both solutions gave a relatively good match, but as St increased the modified solutions performed much better. Another general finding of the study is that the friction angle values needed in the solutions can be seen more as curve fitting values rather than true values. To get good correlation to laboratory based σ'_p values, the used friction angle values needed to be clearly higher than those observed in the laboratory.

Based on the above theoretical framework Di Buò et al. (2020) and Di Buò (2020) proposed simplified transformation models based on average operational values, calibrated those based on the entire data, and finally suggested five equations for evaluating σ'_p in Finnish clays. Out of those five the following two are herein suggested as the primary transformation models:

$$\sigma'_p = 0.28(q_t - \sigma_{vo}) \quad (1)$$

$$\sigma'_p = 0.39(u_2 - u_o) \quad (2)$$

The outcome of Eq. (1) and (2) are presented in Figure 4 in comparison to CRS oedometer based σ'_p values for Paimio and Sipoo test sites.

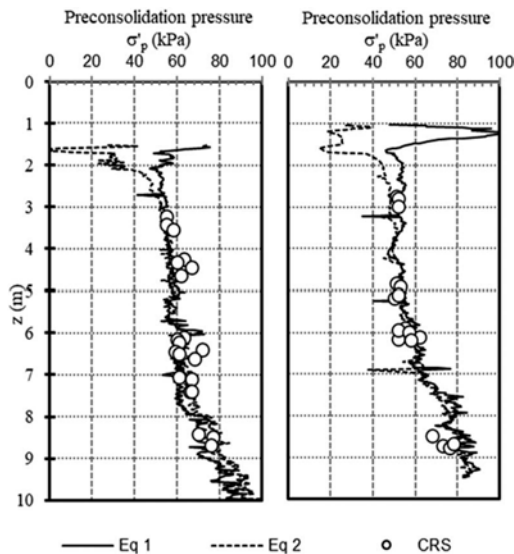


Figure 4. Values of σ'_p evaluated using Equations (1) and (2) in comparison to CRS test results.

It could further be noted, that for Equation (1), the low sensitivity clays indicated generally a lower multiplier than 0.28, while for high sensitivity clays a higher multiplier were generally found. All clays had an OCR generally below 2.

5.2 Evaluation based on index properties

After discussing various theories Selänpää (2021) studied the influence of index properties and pore pressure ratio (B_q) to the cone factors. The main goal was to determine the best practical transformation models for determination of undrained shear strength. Cone factors were determined in relation to different shearing modes (tests) for undrained (triaxial) compression ($s_{u\ comp}$), undrained (triaxial) extension ($s_{u\ ext}$), direct simple shear (DSS) (test) ($s_{u\ DSS}$), measured field vane ($s_{u\ FV\ meas}$) and corrected field vane ($s_{u\ FV\ corr}$) undrained shear strength. Field vane measurements were corrected as a function of liquid limit according to Helene-lund (1977). In general, it can be concluded that best correlations were found for $s_{u\ comp}$ as the triaxial compression test revealed to be the most reliable test with lowest scatter. For the $s_{u\ FV\ corr}$ Selänpää suggested that the N_{kt} and $N_{\Delta u}$ cone factors would depend on PI and the N_{ke} cone factor on B_q . The two previous proposed $s_{u\ FV\ corr}$ equations are as follows:

$$s_{u\ FV\ corr} = \frac{(q_t - \sigma_{vo})}{0.126 \cdot PI + 11.793} \quad (3)$$

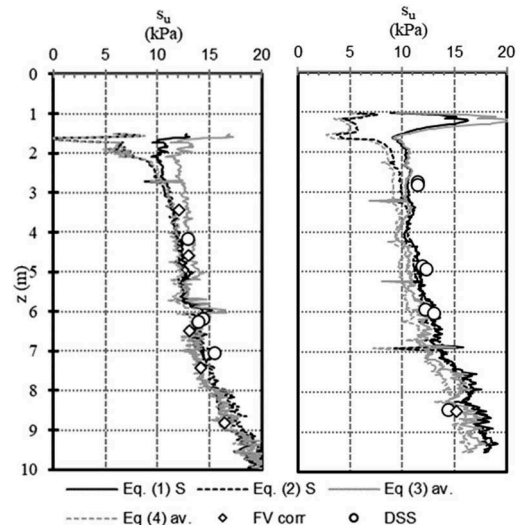


Figure 5. Values of s_u evaluated using Equations (3) and (4) and (1) and (2) applying the SHANSEP approach in comparison to field vane and DSS test results for Paimio (left) and Sipoo (right) test sites.

$$s_{u\text{ FV corr}} = \frac{(u_2 - u_o)}{0.064 \cdot PI + 10.279} \quad (4)$$

In Figure 5 the results of Equations (3) and (4) are compared with $s_{u\text{ FV corr}}$ and $s_{u\text{ DSS}}$ data for Paimio and Sipoo test sites using average PI values. To compare the different approaches by Di Buò (2020) and Selänpää (2021), values determined using Equations (1) and (2) applying the SHANSEP to estimate s_u is applied. Accordingly, s_u can be determined from:

$$s_u = S \cdot \sigma'_{vo} \cdot OCR^m \quad (5)$$

For the parameters S and m values reported by D'Ignazio et al. (2016) with $S = 0.244$ and $m = 0.763$, are used.

For the Sipoo test site, only one good quality field vane test was achieved, so the comparison is primarily to DSS test results. As can be seen from Figure 5, all equations performed quite well for the Paimio site. For the Sipoo test sites, the estimation is also good, although some minor underprediction might be indicated by the $s_{u\text{ DSS}}$ values in the upper part.

6 SOME OTHER FINDINGS

6.1 SBT charts

For all test sites the soil behaviour type (SBT) was evaluated based on the normalized SBT charts by Robertson (1990). A general finding was that although the clays were in general sensitive, the classification charts indicated them with very few exceptions as clays, rather than sensitive clays. For the chart based on the normalized friction ratio this can at least partly be explained by the low accuracy of the sleeve friction measurements as discussed before. However, neither the chart based on the normalized porewater ratio succeeded in identifying the sensitive clay layer while the values in

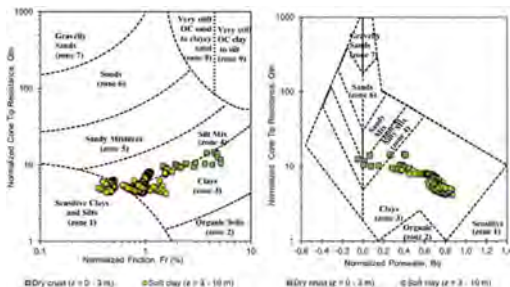


Figure 6. Soil behavior type (SBT) according to Robertson (1990) for the sensitive Paimio clay (Di Buò, 2020).

practise never plotted on the zone for sensitive clays. The SBT charts for Paimio site, with a high sensitivity of the clay ($S_t = 60\text{...}100\%$) is presented in Figure 6 (Di Buò, 2020).

6.2 Anisotropy of s_u

The anisotropy of s_u for Finnish clays was studied systematically for the first time. The anisotropy ratios were determined by comparing the peak undrained strength values of respective tests corresponding to the different shear modes, irrespective of the shear strain values (Selänpää 2021). The ratio $s_{u\text{ ext}}/s_{u\text{ comp}}$ varied between 0.52-0.70, with a slight tendency to increase with plasticity and/or water content. The average value for the ratio is 0.615. Similarly, the ratio $s_{u\text{ DSS}}/s_{u\text{ comp}}$ varied between 0.56-0.72, with a slight tendency to increase with water content. The average value for the ratio is 0.64. What is notable is the very small difference between $s_{u\text{ ext}}$ and $s_{u\text{ DSS}}$ values.

6.3 Constrained modulus for OC region

Di Buò et al. (2018) and Di Buò (2020) evaluated different approaches to determine the constrained modulus M_o for the overconsolidated region. As the value for M_o is quite sensitive to sample quality, the correlations generally showed a rather high scatter. However, a simple approach relying on the relatively accurate determination of σ'_p proved to provide a pragmatic solution giving consistent values. The σ'_p for high quality samples of soft Finnish clays is reached approximately at a vertical strain of 4%. Therefore, the value of M_o can be evaluated by firstly using transformation models as in Equations (1) and (2) to evaluate the σ'_p , and then divide the σ'_p value with 0.04 to obtain the M_o . As example such an approach for the pore pressure based Equation (2) yielded a COV value of 0.21 between CRS and CPTU based M_o values.

6.4 Additional modules

In all test sites investigations were also conducted using two additional modules connected directly behind the cone, namely the seismic (S) and resistivity (R) modules. In general, two tests were performed for each site using both modules, showing good repeatability.

The shear wave velocity values varied between 40-110 m/s. The measured electrical conductivity values ranged from about 50 up to 300 mS/m, correlating highly with pore water salinity.

7 CONCLUSIONS AND FUTURE DEVELOPMENTS

In the FINCONE project the application of CPTU was studied for soft sensitive Finnish clays. Comprehensive testing, including high quality sampling, extensive laboratory program and down hole field

vane in addition to the CPTU was performed altogether on 9 test sites, of which 5 were studied in more detail. Based on the achieved database transformation models were developed to evaluate σ'_p , s_u and M_ρ . Moreover, information about the anisotropy of Finnish clays were achieved for the first time. In addition, shear wave velocity and resistivity data were obtained from the S- and R-modules of the used CPTU equipment.

The CPTU data proved to be very reliable with good repeatability. However, the sleeve friction measurements suffered from too low resolution for the very low values. Some doubts were also raised about their accuracy. The resulting transformation models proved to work well for studied soft clays. It should though be noted that the clays are rather similar in nature, with low OCR and generally high water and clay content.

In the future, the aim is to broaden the range of studied soils to silty soils and fine sands and develop further transformation models for them. In addition, CPTU based soil characterization as well as determination of deformation properties for the normally consolidated will be studied. Some early results of the former are also presented in this conference (Farhadi et al. 2022).

ACKNOWLEDGEMENTS

The guidance of late Professor Rolf Sandven in the early phases of the project is highly acknowledged and remembered with warmth.

The guidance of Professor Paul Mayne and his warm hospitality during the visiting periods for the second and third author contributed highly to their studies and is very much acknowledged.

The financial support of the Finnish Transport Agency and Tampere University is highly appreciated in carrying out the study.

REFERENCES

- Agaiby, S. 2018. Advancements in the interpretation of seismic piezocone tests in clays and other geomaterials. Doctoral dissertation, School of Civil & Environmental Engineering, Georgia Institute of Technology, Atlanta.
- Chen, B.S., and Mayne, P.W. 1994. Profiling the overconsolidation ratio of clays by piezocone tests. Rep. No. GIT-CEEEO-94, 1
- Di Buò, B. 2020. Evaluation of the Preconsolidation Stress and Deformation Characteristics of Finnish Clays based on Piezocone Testing. PhD Thesis, Tampere University, Tampere, Finland. ISBN 978-952-03-1468-2
- Di Buò, B., D'Ignazio, M., Selänpää, J., Länsivaara, T. & Mayne, P. W., 2020. Yield stress evaluation of Finnish clays based on analytical piezocone penetration test (CPTU) models. In: Canadian Geotechnical Journal. 57, 11, p. 1623–1638 16 p.
- Di Buò, B., Selänpää, J., Länsivaara, T., & D'Ignazio, M. 2018. Evaluation of existing CPTU-based correlations for the deformation properties of Finnish soft clays. In Cone Penetration Testing 2018 (pp. 185–191). CRC Press.
- Di Buò, B., Selänpää, J., Länsivaara, T., and D'Ignazio, M. 2019. Evaluation of sample quality from different sampling methods in Finnish soft sensitive clays. Canadian Geotechnical Journal, 56(8): 1154–1168.
- D'Ignazio, M., Phoon, K.K., Tan, S.A., & Länsivaara, T.T. 2016. Correlations for undrained shear strength of Finnish soft clays. Canadian Geotechnical Journal, 53(10), 1628–1645.
- Farhadi, M.S, Länsivaara, T. & Tonni, L. 2022 a). Application of integrated Game Theory-optimization subground stratification (-IGTOSS) model to Venetian Lagoon deposits. Submitted. CPT22. Bologna.
- Farhadi, M.S, Länsivaara, T, L'Heureux, J.S & Lunne, T. 2022 b). Application of two novel CPTu subground stratification models. Submitted. CPT22. Bologna.
- Helenelund, K. V. 1977. Methods for reducing undrained shear strength of soft clay. In Swedish Geotechnical Institute, Proceedings (No. Report No. 3 Proceeding).
- Knuuti, M. & Länsivaara, T. 2019 a). Variation of Measured CPTu Data. Proceedings of the 7th International Symposium on Geotechnical Safety and Risk (ISGSR). Ching, J., Li, D-Q. & Zhang, J. (eds.). Singapore: p. 164–169 6 p.
- Knuuti, M. & Länsivaara, T. 2019 b). Variation of CPTu-based transformation models for undrained shear strength of Finnish clays. In: Georisk. 13, 4, p. 262–270 9 p.
- Lunne, T., Berre, T., and Strandvik, S. 1997. Sample disturbance effects in soft low plastic Norwegian clay. In Symposium on Recent Developments in Soil and Pavement Mechanics.
- Mansikkamäki, J. 2015. Effective stress finite element stability analysis of an old railway embankment on soft clay. PhD thesis, Department of Civil Engineering, Tampere University of Technology, Tampere, Finland.
- Mayne, P.W. 1991. Determination of OCR in clays by piezocone tests using cavity expansion and critical state concepts. Soils and foundations, 31(2): 65–76.
- Robertson, P.K. 1990. Soil classification using the cone penetration test. Canadian Geotechnical Journal, 27(1), 151–158.
- Selänpää, J., Di Buò, B., Haikola, M., Länsivaara, T., & D'Ignazio, M. 2018. Evaluation of existing CPTU-based correlations for the undrained shear strength of soft Finnish clays. In Cone Penetration Testing 2018 (pp. xxx–xxx). CRC Press.
- Selänpää, J. 2021. Derivation of CPTu cone factors for undrained shear strength and OCR in Finnish clays. PhD Thesis, Tampere University, Tampere, Finland.

CPT-based unit weight estimation extended to soft organic clays and peat: An update

H.J. Lengkeek

*Delft University of Technology, Delft, The Netherlands
Witteveen+Bos, Deventer, The Netherlands*

R.B.J. Brinkgreve

*Delft University of Technology, Delft, The Netherlands
Bentley Systems, Delft, The Netherlands*

ABSTRACT: Various CPT-based correlations exist for the unit weight of natural soils. One such correlation includes organic soils Lengkeek et al. (2018). This correlation is presented as a framework where the coefficients can be optimized and is based on predominantly Class 2 CPT records. This publication uses an expanded database which includes additional pairs of predominantly Class 1 CPT records selected from Holocene deposits in the Netherlands, on mineral clays, organic clays and peats. This results in a more extensive database and an improved CPT-based unit weight correlation for the whole range of soil types, which is proposed to replace the existing correlation. In addition, a specific unit weight correlation for peats is presented.

1 INTRODUCTION

1.1 Automated processing of CPTs

Cone penetration testing (CPT) has become increasingly popular as the preferred in-situ test method as it can be used for soil classification, estimation of geotechnical parameters and use in empirical methods. With the increase of automated processed CPT data in engineering (Brinkgreve, 2019), it is critical to have an accurate estimation of soil unit weight as this is the first and most important step in geotechnical parameter determination. This is particularly relevant for organic soils which are often not included in existing CPT-based parameter determination methods.

1.2 Organic soils

Organic soils are formed during the decomposition of dead organic substances i.e., remnants of plants and animals. This process takes place in different ways, mainly through bacterial activity, intensified by oxygen and temperature. Another type of sediment with a highly variable organic content are the floodplain sediments, which are deposited when streams at high water overflowed natural embankments. The peat areas and deposits of organic soils occur to a large extent in the northern parts of the world.

To date, most published research on CPT application is on mineral soils. Existing CPT-based correlations for mineral clays do not capture the behavior of soft

organic clays and peats well compared to other soils. The properties of peats have been investigated and extensively published, i.e. Den Haan and Kruse (2007), (Mesri and Ajlouni, 2007). However, limited attention has been devoted to the whole range of slightly organic clay to peat, and how this relates to CPT measurements. These organic soft soils are frequently present within the Holocene deposits in the Netherlands and in other deltaic areas worldwide. Organic soft soils are characterized by a low unit weight and high compressibility. Organic soft soils can be identified by a high organic content and high CPT friction ratio. In contrast to other soft soils, the strength is not necessarily low.

1.3 Aim of this publication

By combining soil properties obtained from laboratory testing with CPT results, layer-, site- or region-specific correlations can be obtained between CPT measurement data and geotechnical properties of the soil. When automating the interpretation of CPTs, it is preferable to have a direct and reliable relation between the measurements and the soil unit weight. With a more reliable in-situ derived estimation of unit weight, the effect of human interference is limited to a minimum. Moreover, because many soil properties (and thus the applicable correlations) depend on the stress level, it is paramount to have an indication of the stress profile over the depth. For this purpose, the use of lookup tables such as those found in textbooks is not preferable. The aim of this publication is twofold:

- To validate and improve the CPT-based unit weight correlation (Lengkeek et al., 2018) for the whole range of soils.
- To present additional insight in relations between index properties and CPT measurements for organic soils.

1.4 Research approach and databases

The 2018 database includes the sample unit weight and Class 2 CPTs (ISO22476-1, 2012) of Holocene and Pleistocene sedimentary deposits in the Netherlands. This database is used for the initial unit weight correlation and includes all soil types, however mainly mineral soils.

The 2021 database follows from soil investigations from various dike reinforcement projects across the Netherlands. This database includes classification laboratory tests and Class 1 CPTUs of mainly Holocene organic clays and peats. The CPT data is taken from the same depth as the samples, with a maximum allowable distance between borehole and CPT of 1 meter. These soil investigations are performed in the period 2010-2020.



Figure 1. Overview of 57 CPT-borehole pair locations in the Netherlands.

The Dutch Water Authorities requires that all new soil investigations be performed according to a dedicated protocol for dikes, summarized in a standardized STOWA Excel sheet (www.helpdesk

water.nl). The CPTs are standardized in GEF format. These standardized formats are very useful and efficient to set up a comprehensive database. An overview of the locations and number of CPT-borehole pairs is presented in Figure 1. The total number of undisturbed samples is 464, the number of CPT pairs is 233 of which 211 include the unit weight, 136 include organic content and 109 include specific gravity. The data of this research is available in the Delft University of Technology repository and published in Lengkeek (2022).

2 UNIT WEIGHT CORRELATION

2.1 Soil type categories

The selected classification method for organic fine-grained soils is based on the FHWA system. Sand (coarse grained soils) are classified based on the sample identification description. The FHWA classification system, based on organic content measured by the Loss on ignition (N), consists of the following soil categories:

- mineral fine-grained soils: $N \leq 3\%$.
- mineral fine-grained soils with organic matter: $3 < N \leq 15\%$.
- organic fine-grained soils: $15 < N \leq 30\%$.
- peats: $N > 30\%$.

The classification results for the 2021 database with organic soils are presented in Table 1. The names of the soil categories in the graphs are shortened for practical reasons. For samples where the organic content is unknown, the classification is based on the unit weight; Peat: $\gamma_{sat} \leq 12$, Organic clay: $12 < \gamma_{sat} \leq 14$, Clay with organic matter: $14 < \gamma_{sat} \leq 17$, Clay, mineral: $\gamma_{sat} > 17$, all in kN/m^3 .

Table 1. Classification results for organic soil types: average organic content, range of unit weight and specific gravity per soil type in the 2021 database.

Results:	N_{mean}	γ_{sat}	G_s
Soil type	(%)	(kN/m^3)	(-)
Peat	79	10.1 - 13.1	1.4 - 2.0
Organic Clay	22	11.6 - 14.0	1.9 - 2.4
Clay (org.matter)	8	12.4 - 19.2	2.3 - 2.7
Clay (mineral)	2	15.6 - 20.0	2.6 - 2.7

2.2 Updated CPT-based unit weight correlation

The updated CPT-based unit weight correlation is based on the combined database. The 2018 database mainly consists of mineral soils whereas the 2021 database mainly consists of organic soils. The combined database allows for a validation and improvement of the correlation for unit weight. The CPT-based unit weight correlation of Lengkeek et al. (2018) is shown in Equation (1). The correlation is

based on the corrected cone resistance q_t and friction ratio R_f , which are both normalized by a reference value. The reference unit weight, here 19.5 kN/m³, is the value when q_t equals $q_{t,ref}$. The updated variables based on the combined database of 427 pairs are presented in Table 2.

$$\gamma_{sat} = \gamma_{sat,ref} - \beta \cdot \frac{\log\left(\frac{q_{t,ref}}{q_t}\right)}{\log\left(\frac{R_{f,ref}}{R_f}\right)} \quad (1)$$

Herein:

$\gamma_{sat,ref}$ is the reference unit weight at which the cone resistance is constant regardless of R_f .

$q_{t,ref}$ is the reference cone resistance at which the unit weight is constant regardless of friction ratio.

$R_{f,ref}$ is the reference friction ratio at which the apex of all lines of equal unit weight is located.

β is the fit factor, which is a measure for the inclination of the equal unit weight contours.

Table 2. Updated parameters for unit weight correlation.

Parameter	Value	Unit
$\gamma_{sat,ref}$	19.5	kN/m ³
$q_{t,ref}$	9.0	MPa
$R_{f,ref}$	20	%
β	2.87	

Figure 2 presents all measured data per soil type combined with the lines of equal unit weight [10, 21] kN/m³. The results are plotted on the SBT template of Robertson (2010). From this figure it can be concluded that the lines of equal unit weight are well aligned with the orientation of SBT zone boundaries. Coarse grained soils, SBT=5 and higher correspond to a unit weight of 18 to 21 kN/m³. The variation in unit weight for fine soils is much larger.

Figure 3 shows the measured unit weight versus the predicted unit weight using the improved correlation. The points are subdivided in the database categories [Peat; Organic Clay; Clay with organic matter; Mineral Clay; Sand]. These database categories are based on the laboratory classification. From this graph it can be seen that the trend follows the 1:1 line very well. The scatter is larger for lower unit weights and organic soils; however, for peats the results are close to 10 kN/m³, which is also the minimum value as applied.

Figure 4 presents an example of a CPT with clay, peat and sand layers, including the unit weight according to Equation 1. The unit weight from the laboratory tests are respectively 12.6 to 15.0 kN/m³ in the upper 2m clay, 10.3 kN/m³ for the peat layer and 19.5 kN/m³ for the underlain sand layer.

The performance of the improved correlation can be expressed in statistical parameters such as the coefficient of determination (R^2) and the standard deviation

on regression (S_y) and the slope of the trendline through the origin [x =measured, y =predicted]. The comparison with other existing correlations Mayne (2014), (Robertson and Cabal, 2010, Lengkeek et al., 2018) is presented in Table 3. The R^2 and S_y comply to Ordinary Least Squares (OLS) regression with free intercept. The slope complies to regression through the origin and is a measure for the bias of the trend in Figure 3. From this comparison it can be concluded that the new correlation performs better for all statistical parameters. The 2018 correlation results in slightly different values which validates the use it.

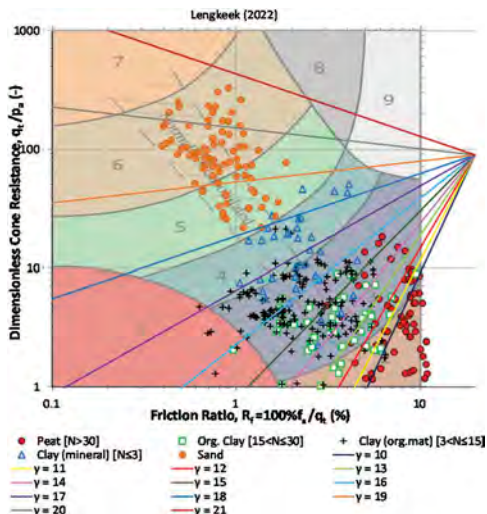


Figure 2. Unit weight measurements and lines of equal unit weight of the improved correlation, presented on top of Robertson (2010) SBT template.

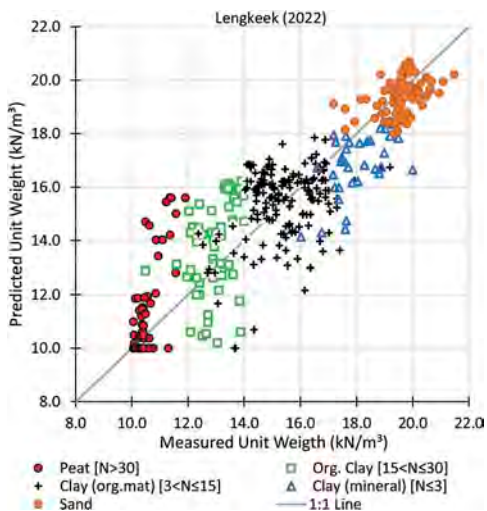


Figure 3. Measured versus predicted unit weight based on the improved correlation.

Table 3. Comparison of statistical results of multiple correlations for the whole range of soils.

Method	R ²	S _y	OLS slope [y:x]	slope through origin [y:x]
Improved correlation	0.80	1.32	0.84	1.00
Lengkeek (2022)				
Lengkeek (2018)	0.79	1.33	0.80	1.00
Robertson & Cabal (2010)	0.25	1.46	0.26	1.06
Mayne (2014)	0.12	1.68	0.20	1.03

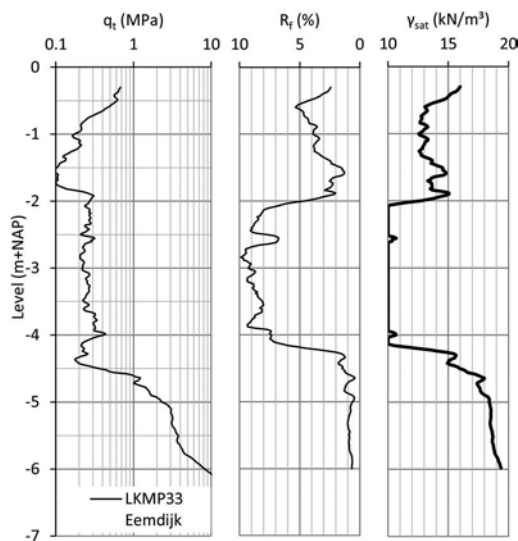


Figure 4. CPT results and unit weight according to equation 1 for a CPT from Eemdijk, the Netherlands.

3 CPT-BASED CORRELATIONS FOR ORGANIC SOILS

3.1 Introduction

The pairwise established database of classification test results and CPT measurements allows for comparison of properties of organic soils and additional insight in relations. In this section three graphs with organic content and index properties are presented as well as three graphs with CPT-based correlations.

For each graph the results and the confidence intervals are plotted in the graphs and the statistical parameters are shown in the title. The subcategories are indicated in the legend. The regression is applied to all samples as one group and not per soil type.

Correlations for each soil category would result in a lower coefficient of determination and limit any reliable correlation to an average value and standard deviation per soil type.

3.2 Correlations with organic content

Figure 5 presents the organic content versus the water content and was first published by Mitchell and Soga (2005). This correlation provides a first estimate of the organic content for any soil which is expected to be organic. The data shows an increase of organic content with water content up to N=90 which is considered as a physical upper bound. The bi-linear fit performs better than the correlation by Mitchell and Soga (2005), which is based on less data.

Figure 6 presents the specific gravity versus the organic content. The results confirm the empirical relation as published by Den Haan and Kruse (2007). Once the organic content is known, the specific gravity and ultimately the unit weight can be estimated.

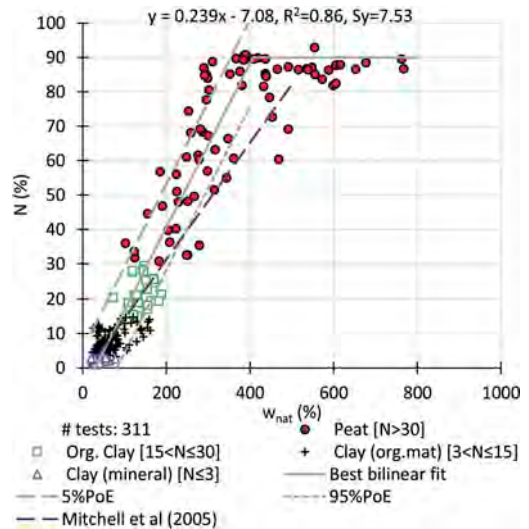


Figure 5. Organic content versus natural water content, for organic to mineral soils. Best bi-linear fit: $N = \min[90\%, 0.239 w_{nat} - 7.08]$ with standard deviation $S_y = 7.53$.

Figure 7 presents the unit weight versus the organic content. This figure is the basis for the secondary criteria for classification of organic soils based on the unit weight. The variation is more than that for the specific gravity correlation as the unit weight is not just a unique soil property but also a state parameter depending on the preloading and stress level.

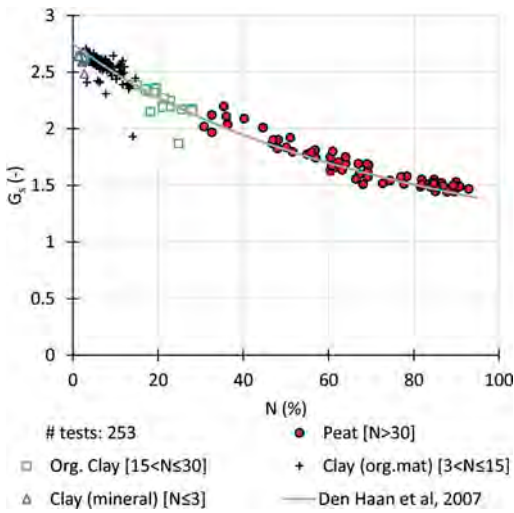


Figure 6. Specific gravity versus organic content, for organic to mineral soils. The standard error on regression (S_y) is 0.082 and coefficient of determination (R^2) is 0.97.

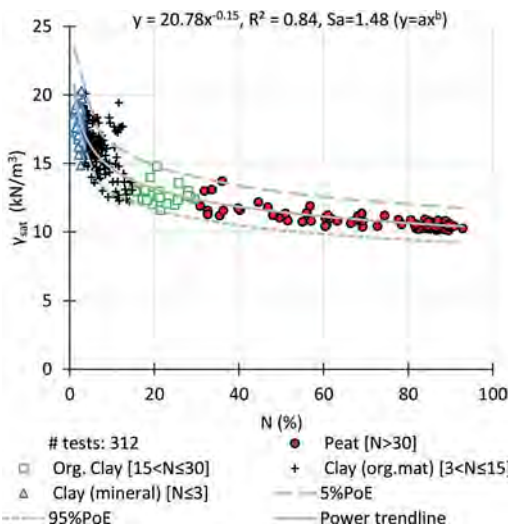


Figure 7. Saturated unit weight versus organic content, for organic to mineral soils. The best power function fit is: $\gamma_{sat} = 20.8N^{-0.153}$ with standard deviation $S_a=1.48$ (for $y=a \cdot x^b$).

3.3 CPT-based correlations

Figure 8 presents the unit weight of soils that are classified as peat and the correlation is shown in Equation (2). This figure illustrates a linear relation where the range is [10, 12] kN/m³, the R^2 is moderate and the $S_y=0.265$ kN/m³. This correlation is only applicable with prior knowledge of the soil type and cannot be used for organic clays. The accuracy is however better than Equation (1).

$$\gamma_{sat,peat} = 0.000685 \cdot q_t + 10.1 \quad (2)$$

Where $\gamma_{sat,peat}$ is the saturated unit weight of peat in (kN/m³) and q_t is the corrected cone resistance in (kN/m²).

Figure 9 presents the specific gravity versus the friction ratio. Figure 10 presents the organic content versus the friction ratio. Both correlations confirm that the unique soil properties are reasonably correlated with the friction ratio with a high R^2 . However, the large variation S_y makes these correlations less useful in practice.

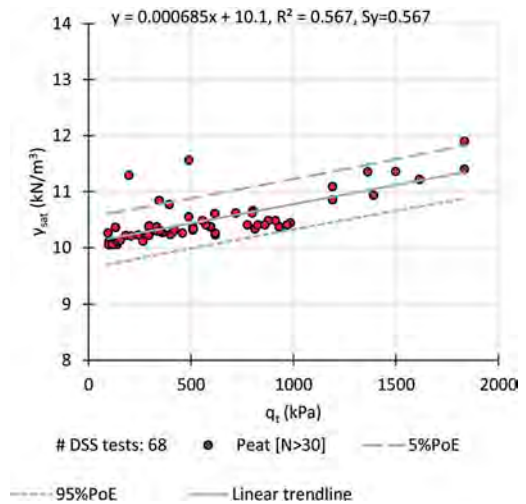


Figure 8. Saturated unit weight versus CPT corrected cone resistance, for soils classified as peat.

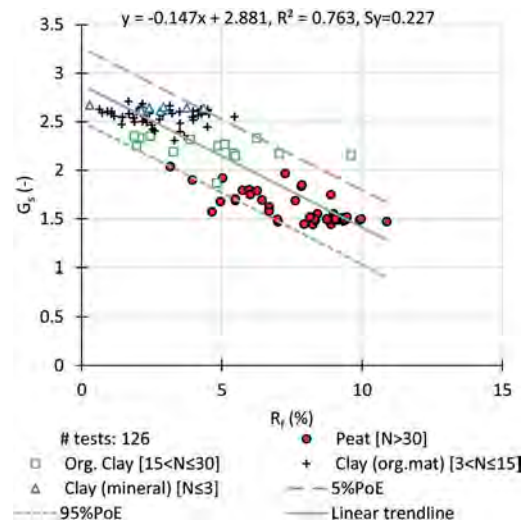


Figure 9. Specific gravity versus CPT friction ratio, for organic to mineral soils. The subcategories are indicated in the legend. The best linear fit is: $G_s = -0.147R_f + 2.88$ with standard deviation $S_y=0.227$.

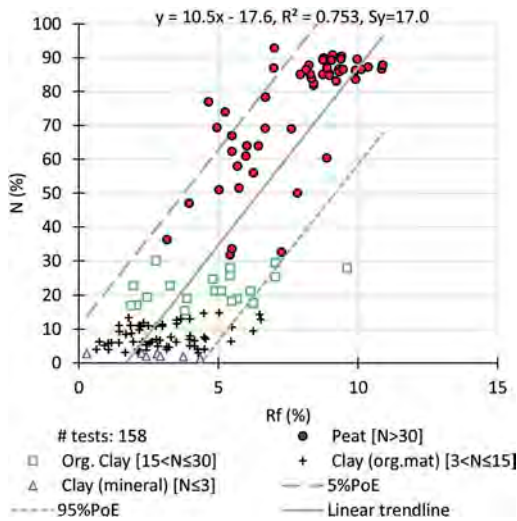


Figure 10. Organic content versus CPT friction ratio, for organic to mineral soils. The subcategories are indicated in the legend. The best linear fit is: $N = 10.5R_f - 17.6$ with standard deviation $S_y = 17.0$.

4 CONCLUSIONS AND RECOMMENDATIONS

The pairwise established database of classification test results and CPT measurements provides valuable insight into the properties of organic soils as well as new and updated correlations.

The existing unit weight correlation is validated and improved by the extension of the 2018 database with organic soils resulting in 427 pairs. The statistical parameters of the improved CPT-based unit weight correlation are compared with existing correlations and show better performance. The advantage of the improved correlation shown in equation 1 is that it can be applied for organic soils and mineral sedimentary soils. This is useful for SBT classifications which include stress correction. Specifically, for soils which are classified as peat, equation 2 can be used with even higher accuracy.

The 2021 database confirms existing relations between the organic content and other index parameters. Furthermore, the organic content and specific gravity can be correlated to the CPT friction ratio. Both correlations confirm that the unique soil properties are reasonably correlated with the friction ratio.

The correlations allow for establishing prior estimates where no laboratory tests are available. The disadvantage of this approach is that it increases inherent variation along the trend and the possibility that site specific units are biased to the trendline.

The confidence interval and standard deviation are provided to account for such bias. For final estimates of soil parameters, it is recommended to combine these correlations with sampling and testing of site-specific geological units.

In general, it is highly recommended to perform CPTs adjacent to boreholes, select pairs of high-quality laboratory tests according to a standardized protocol (STOWA). This will allow for new or improved correlations which will improve prior estimates.

ACKNOWLEDGEMENTS

The authors would like to thank the POVM, established in 2015 by Water Authorities in the Netherlands, who initiated and financed “Eemdijkproef”.

This work is part of the “Perspectief” research programme All-Risk with project number P15-21, which is (partly) financed by NWO Domain Applied and Engineering Sciences.

REFERENCES

- Brinkgreve, R. B. J. 2019. Automated Model And Parameter Selection: Incorporating Expert Input into Geotechnical Analyses. *Geo-Strata—Geo Institute of ASCE*, 23, 38–45.
- Den Haan, E. J. & Kruse, G. A. M. 2007. Characterisation and engineering properties of Dutch peats. *Characterisation and engineering properties of natural soils*, 3, 2101–2133.
- ISO22476-1 2012. Geotechnical Investigation and Testing - Field Testing - Part 1: Electrical Cone and Piezocone Penetration Test. International Organization for Standardization.
- Lengkeek, H. J. 2022. CPT-based classification and correlations for organic soils. *4TU.ResearchData*.
- Lengkeek, H. J., De Greef, J. & Joosten, S. 2018. CPT based unit weight estimation extended to soft organic soils and peat. *4th International Symposium on Cone Penetration Testing (CPT'18)*. Delft.
- Mayne, P. W. 2014. Interpretation of geotechnical parameters from seismic piezocone tests. *Proceedings, 3rd International Symposium on Cone Penetration Testing*.
- Mesri, G. & Ajlouni, M. 2007. Engineering Properties of Fibrous Peats. *Journal of Geotechnical and Geoenvironmental Engineering*, 133, 850–866.
- Mitchell, J. K. & Soga, K. 2005. Fundamentals of Soil Behavior 3rd ed., JohnWiley & Sons. Inc. *Foundation failure*.
- Robertson, P. K. 2010. Soil behaviour type from the CPT: an update. *2nd international symposium on cone penetration testing, USA*.
- Robertson, P. K. & Cabal, K. L. 2010. Estimating soil unit weight from CPT. *2nd International symposium on cone penetration testing*.

CPT-based classification of soft organic clays and peat

H.J. Lengkeek

Delft University of Technology, Delft, The Netherlands
Witteveen+Bos, Deventer, The Netherlands

R.B.J. Brinkgreve

Delft University of Technology, Delft, The Netherlands
Bentley Systems, Delft, The Netherlands

ABSTRACT: An updated CPT-based classification system of organic clays and peat is proposed based on an extensive pairwise established database of classification tests and CPT measurements. This new classification system is proposed to supplement the existing dimensionless q_t/p_a -Rf-chart of Robertson (2010). The Robertson (2010) dimensionless classification system is selected for refinement because it appears to perform better than normalized systems for peats with very low stresses (<20 kPa). A combination with Robertson (2009 and 2016) is possible in cases where a stress normalization cut-off is used.

1 INTRODUCTION

1.1 *Application of CPTs in dike projects*

To successfully plan, design and construct a geotechnical project, various types of investigative techniques to obtain sufficient geotechnical information are required. Geotechnical field investigations generally comprise boreholes with sampling and in-situ cone penetration tests, performed with a friction cone penetrometer (CPT) or with a piezocone penetrometer (CPTU).

The use of CPTs in the design of dikes in the Netherlands has increased over the years. On a typical dike project, CPTs are performed typically every 100m along the center line and supplemented with 3 CPTs and 1 borehole along a cross section every 200m. The number of CPTs is typically 5 times greater than the number of boreholes. This is due to the relative costs and the increased possibilities associated with the use of CPTs.

1.2 *CPTs in organic soils*

Cone penetration testing has become increasingly popular as the preferred in-situ test method as it can be used for soil classification, estimation of geotechnical parameters and use in empirical methods. The initial soil texture-based classifications were based on direct measurement of cone resistance (q_c) and sleeve friction (f_s) e.g. Begemann (1965). The current CPT-based classification systems are based on behavior characteristics and are often referred to as

a Soil Behavior Type (SBT) classification. These classification systems include pore pressure measurements from CPTU tests and the shear wave velocity from SCPT tests, e.g. Robertson (2016). Examples of CPT based empirical methods can be found in the Eurocode (EN1997-1, 2005, EN1997-2, 2007), where the cone resistance is used for the estimation of soil strength. In addition, there is a wide range of publications on CPT based estimation of geotechnical parameters. A comprehensive overview can be found in Kulhawy and Mayne (1990), (Lunne et al., 2002, Mayne, 2014).

To date, most published research in the field of CPT application is on mineral soils. Existing CPT-based correlations for mineral clays do not properly capture the behavior of organic clays and peats compared to other soils. The properties of peats have been investigated and extensively published, i.e., Den Haan (1997), (Mesri and Ajlouni, 2007). However, limited attention has been devoted to the whole range of slightly organic clay to peat, and how this relates to CPT measurements. These organic soils are frequently present within the Holocene deposits in the Netherlands and in other deltaic areas worldwide. Organic soils are characterized by a low unit weight and high compressibility. Organic soils can be identified by a high organic content and high CPT friction ratio. In contrast to other soft soils, the shear strength is not necessarily low.

1.3 *Aim of this publication*

The aim of this publication is to improve the applicability of CPTs for organic soils. To achieve

this, results from soil investigations from dike reinforcement projects across the Netherlands have been collected. CPTs and boreholes that were performed in proximity of each other have been selected. The laboratory tests results and CPT measurements were taken at the same level, paired, and processed into a regional database. In this paper an improvement for CPT based classification systems for organic soils is proposed.

1.4 Research approach and databases

This research combines an existing database (Lengkeek et al., 2018) and a new compiled database for organic soil properties, referred to as the 2021 database. The 2018 database includes the sample unit weight and Class 2 CPTs of Holocene and Pleistocene sedimentary deposits in the Netherlands. An overview of the locations and number of CPT-borehole pairs is presented in Figure 1.

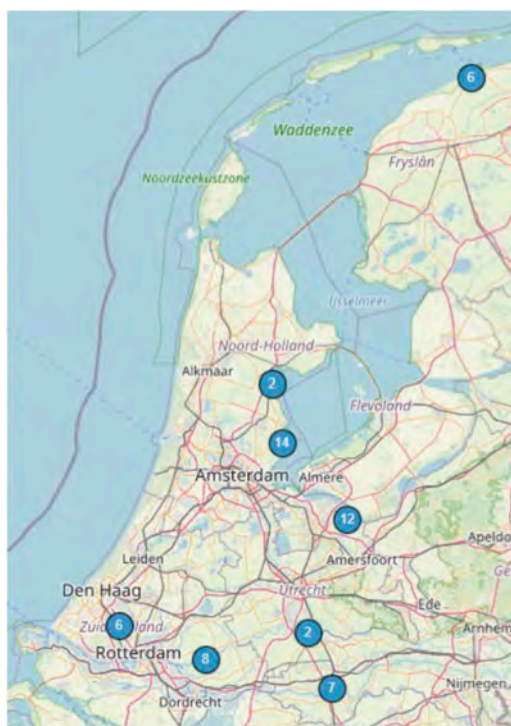


Figure 1. Overview of 57 CPT-borehole pair locations in the Netherlands.

The 2021 database includes soil investigations from various dike reinforcement projects across the Netherlands. The 2021 database includes classification laboratory tests and Class 1 CPTs of Holocene organic clays and peats. The CPT data is taken from the same level as the samples, with a maximum allowable distance between borehole and CPT of 1 meter. These soil investigations were performed in the period

2010-2020. Recently, the Dutch Water Authorities required that all new soil investigations be performed according to a dedicated protocol for dikes, summarized in a standardized STOWA Excel sheet (www.helpdeskwater.nl). The CPTs are standardized in GEF format. These standardized formats are very useful and efficient to set up a comprehensive database. The data of this research is available in the Delft University of Technology repository and published in Lengkeek (2022).

2 CLASSIFICATION OF ORGANIC SOILS

2.1 Laboratory classification

Existing classification systems are based on geomorphology, topography, chemical properties, botanical origin, genetic processes, or physical characteristics. From a geotechnical engineering perspective, the physical characterization is the most relevant. Several classification systems for organic soils are used in various countries and are based on similar grounds. In many cases, a certain degree of humification Von Post (1922) is used for the classification of peat, together with the normal geotechnical parameters, such as water content, Atterberg limits, organic content, bulk density etc. Understanding the stratification and properties in a soil profile is made easier if the geological history and the environmental conditions at deposition of the sediments are known.

Examples of classifications for geotechnical engineering can be found in Landva et al. (1983), (NEN5104, 1989, Huang et al., 2009, ISO14688-1, 2017, ISO14688-2, 2017, Von Post, 1922). Both the term ‘organic content’ and ‘ash content’ are used to identify organic soils. The classification systems differ, in particular for organic content in the range [20,50] %, where peats and organic clays overlap.

2.2 CPT-based classification methods

CPT-based classification methods provide two-dimensional charts for soil type classification based on the CPT measurements. These charts were developed through direct correlation between the CPT data and the corresponding soil type determined from adjacent borings. The initial soil texture-based classifications were based on direct measurement of cone resistance and sleeve friction (Begemann, 1965, Schmertmann, 1978).

Robertson et al. (1986) developed a non-normalized soil behavior-based classification, initially with 12 zones. In Robertson (2010) this is updated to 9 zones based on dimensionless cone parameters (q_t/p_a , R_f) and the non-normalized SBT-index I_{SBT} . Robertson (1990) presented the normalized soil behavior classification for 9 zones based on the linear normalized cone parameters (Q_{t1} , F_r , B_q). The soil behavior type index I_{c1} is added to this in Robertson and Wride (1998). In (Robertson, 2009,

Zhang et al., 2002) the classification system SBT_n is adjusted with a variable stress exponent n and non-linear normalized cone resistance Q_{tn} and nonlinear SBT-index I_{cn} .

Since 1990, more CPT soil behavior-type charts have been developed including (Been and Jefferies, 1993, Eslami and Fellenius, 1997, Schneider et al., 2008). In Robertson (2016) a modified SBT classification system is presented with 7 zones and charts based on Q_{tn} versus the small-strain rigidity index I_G and versus the normalized pore pressure U_2 . Furthermore, a new hyperbolic shaped modified SBT-index I_B is introduced.

Existing CPT based classifications generally relate to mineral soils which are present worldwide. The major disadvantage of existing CPT based classification methods is that the classification of organic soils is inaccurate. In many cases a peat layer is classified as clay (SBT=3) instead of organic material (SBT=2). Furthermore, it does not distinguish between peats and organic clays. Engineering of dike projects in the Netherlands, where peat is often present, is therefore mostly based on local experience or the non-stress normalized q_t/p_a -Rf chart of Robertson (2010). CPTUs are generally performed; however, the pore pressure classification charts are not used due to the presence of gas in organic soils, which causes a reduced and unreliable pore pressure response.

2.3 Organic soil type categories

The 2021 database includes classification tests according to different standards and systems (NEN, EN, ISO). The organic content is measured for most samples. The fine grained soils are classified according to one system: FHWA (Huang et al., 2009). The FHWA classification system is based on the organic content measured by the loss on ignition (N) and consists of the following soil categories:

- mineral fine-grained soils: $N \leq 3\%$.
- mineral fine-grained soils with organic matter: $3 < N \leq 15\%$.
- organic fine-grained soils: $15 < N \leq 30\%$.
- peats: $N > 30\%$.

For samples where the organic content is unknown, the classification is based on the unit weight; Peat: $\gamma_{sat} \leq 12$, Org.Clay: $12 < \gamma_{sat} \leq 14$, Clay (org.mat): $14 < \gamma_{sat} \leq 17$, Clay (mineral): $\gamma_{sat} > 17$, all in kN/m^3 .

3 UPDATED SBT ZONES FOR ORGANIC SOILS

3.1 Stress normalization

The samples of the combined database (2018 and 2021) are taken from 0.5 to 15m depth and effective vertical stresses in the range of 5 to 150 kPa. For situations with the presence of peat layers and high-water

tables, stresses are sometimes less than 20 kPa at 10m depth. Therefore, care should be taken with CPT-based classifications that include stress normalization, as illustrated in the following example.

A peat layer below a dike with a high stress level of about 100 kPa is originally classified as SBT=2 (Robertson, 2010) and SBT_n=2 (Robertson, 2009), but the same peat layer beside the dike with a low stress of 20 kPa moves up to SBT_n=3 and will be classified as clay. This second classification is not correct as the soil type is the same, but only the stress state is different. Consequently, the soil profiling beside the dike can be incorrect, and the wrong parameters will be appointed to this layer. In this example, the normalized cone resistance Q_{tn} is 5 times higher than Q_t . These high stress corrections are not included in the international databases where most of the stresses are typically in the range of 50 to 300 kPa.

Particularly for dike projects there is a second argument not to apply a large stress correction. The peat layers beside the dike are generally over-consolidated by an OCR of 2, due to a combination of water level changes and aging. The same peat layer below the dike, which has been raised periodically, is only slightly over-consolidated. As the cone resistance is related to the preconsolidation stress more than the vertical effective stress, the actual stress correction should be about 2 to reflect the state properties.

The proposed adjustments to the SBT charts, as will be presented in the next paragraphs, are valid for the non-stress normalized SBT chart (Robertson, 2010) and the stress-normalized SBT chart (Robertson, 2009) with the application of the stress normalization cut-off $C_n \leq 2$.

3.2 Proposed SBT adjustment

This paragraph presents the adjustment to the SBT classification for organic soils, such as those encountered in deltaic areas in the Netherlands. The results from the combined database are plotted on the (Robertson, 2010) template in Figure 2. The soil categories consist of the categories in Table 1, including one category for sand.

The data coincides to a large extent with SBT zones, which is expected for the mineral soils. A few datapoints coincide with SBT=1 (sensitive soils) and no points coincide with SBT=7, 8 and 9. Soils of SBT=7 can be present in Pleistocene sand deposits and gravelly deposits, which are present along the river Meuse in the South of the Netherlands. Soils of SBT=8 and 9 are not expected in a deltaic area up to 15 m depth.

There are major differences in SBT=2 and 3, where a significant amount of organic soils plot in SBT=3. The performance results based on the existing Robertson (2010) classification of organic fine-grained soils are presented in Table 2. It is concluded that most of the organic soils, including most of the peats, plot in

SBT=3 ($I_c \leq 3.6$). The performance is about the same for I_{cn} based on stress normalization including $C_n \leq 2$. Without the C_n cut-off almost all points plot outside of SBT=2.

Table 1. CPT results of 2018 and 2021 database.

Soil type	average		range	
	q_t (MPa)	R_f (%)	q_t (MPa)	R_f (%)
Peat [N>30]	0.5	7.8	0.1 - 1.8	3.2 - 11.0
Org. Clay [15<N≤30]	0.4	3.8	0.1 - 0.9	1.0 - 9.6
Clay (org.mat) [3<N≤15]	0.6	2.5	0.1 - 2.1	0.6 - 6.5
Clay (mineral) [N≤3]	1.7	2.4	0.2 - 5.1	1.1 - 4.6
Sand	10.2	0.9	2.2 - 33.1	0.4 - 1.9

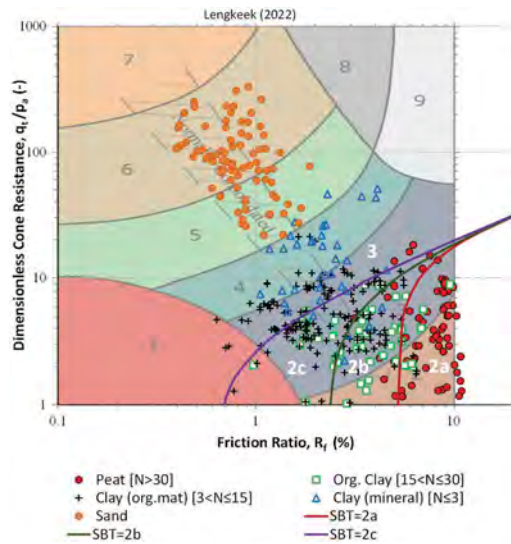


Figure 2. 2018 and 2021 database results and proposed SBT adjustment for organic soils, presented on top of Robertson (2010) SBT template.

Table 2. Performance results for organic soils based on existing Robertson (2010) SBT classification. Percentage is number of samples per category plotted in a SBT zone.

SBT zone: Soil type	SBT2 ($I_c > 3.6$)	SBT3,4 ($I_c \leq 3.6$)
Peat [N>30]	35%	65%
Org. Clay [15<N≤30]	21%	79%
Clay (org.mat) [3<N≤15]	6%	94%
Clay (mineral) [N≤3]	0%	100%

Table 3. Performance results for organic soils based on proposed adjustments to Robertson (2010) SBT classification.

SBT zone: Soil type	SBT=2a	SBT=2b	SBT=2c	SBT=3, 4
Peat [N>30]	78%	15%	1%	4%
Org. Clay [15<N≤30]	16%	42%	40%	2%
Clay (org.mat) [3<N≤15]	3%	22%	38%	37%
Clay (mineral) [N≤3]	0%	11%	3%	86%

The proposed adjustment is that SBT=2 and part of SBT=3 are redefined and split up into SBT=2a (Peat), 2b (Organic Clay) and 2c (Mineral Clay, with organic matter). No adjustments are proposed to the boundaries between SBT=3, 4 and higher. This is also not possible as this database does not distinguish between silts and clays due to the lack of Atterberg limits tests. Most of the classified points plot in the correct SBT zone when using the proposed adjustment, although there is still some overlap with the adjacent SBT zones. The selection of the boundaries is determined by maximizing the group of positives and minimizing the number of false positives and false negatives.

In addition, the boundaries are selected to separate over-consolidated organic soils from over-consolidated plastic clays, such as Pot clay (Pleistocene) and Boom clay (Oligocene) encountered in the Netherlands. The maximum cone resistance occasionally measured in peats at high stress levels is about 2 MPa. This results in a rather sharp transition from SBT=2a to SBT=3. The new boundaries are extended to a friction ratio of 20%, which is occasionally measured in peats at low stress levels.

The performance results are presented in Table 3. It is concluded that majority (78%, 86%) of the classified points in SBT=2a, 3, 4 are correct. For SBT=2b and 2c, it is concluded that a significant number of points plot in the adjacent SBT zone but still the largest subgroup (38%, 42%) complies with the proposed SBT zone. The number of false positives outside of the adjacent SBT zones is less than 5%.

The formulation for the new proposed boundaries is shown in Equation (1). The parameter values are shown in Table 4.

$$q_t/p_a = a(R_f - R_{f,min})^b \quad (1)$$

Figure 3 presents a CPT according to the adjusted classification system. From the borehole and samples, the following layers are identified: organic clay from surface, soft clay with organic material

Table 4. Parameter values for boundaries of proposed adjustments to Robertson SBT (2010) and SBTn (2009) classification.

SBT & SBTn boundary:			
Parameter	SBT=2a	SBT=2b	SBT=2c
a (-)	8.0	5.2	4.7
b (-)	0.50	0.62	0.64
$R_{f,min}$ (%)	5.2	2.3	0.60

(-1.5 m NAP), peat (-2.0 m NAP), sand (-4.3 m NAP). The layers are well captured except that based on the CPT classification an intermediate layer is shown between the peat and sand layer, which is likely a transition effect.

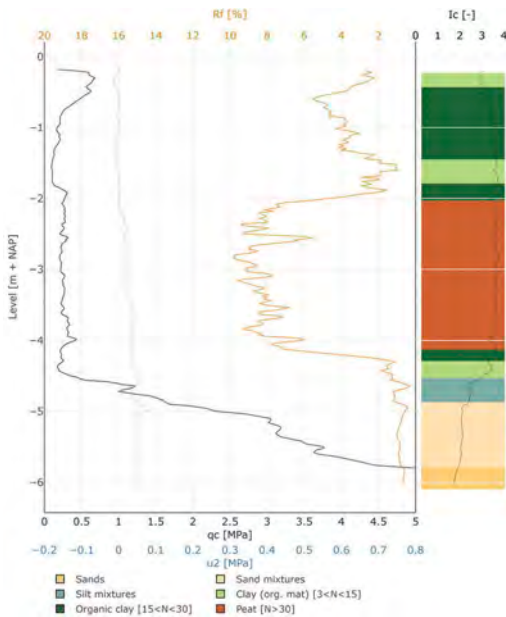


Figure 3. CPT LKMP33 at Eemdijk the Netherlands classified with the proposed system to include soils.

The proposed boundaries are optimized such that they can also be applied as adjustment to (Robertson, 2009, Robertson, 2016), in combination with a stress normalization cut-off equal to $C_n \leq 2$. The parameters in Equation 1 are replaced by Q_{tm} and F_r . These boundaries for organic soils do not apply if there is no stress normalization cut-off applied. The results of the 2021 database are plotted in Figure 4 on top of the combined 2009 and 2016 template. In this figure $C_n=1.7$ is applied in line with recommended practice by (Boulanger and Idriss, 2016). The mineral clays and sands are not included, as not all stresses required for normalization are known. Most

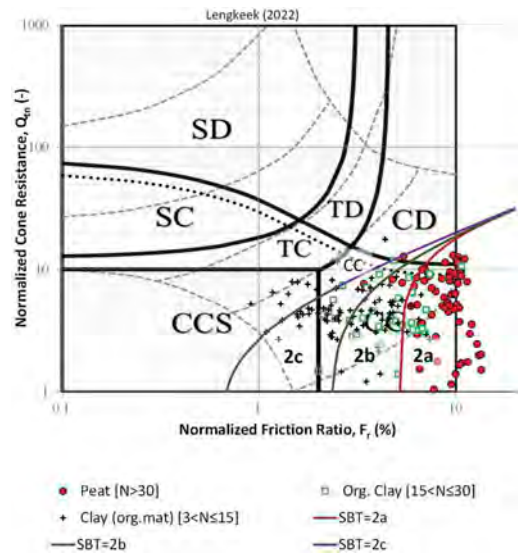


Figure 4. 2021 database results and proposed SBT adjustment for organic soils, presented on top of Robertson (2009 & 2016) SBT template.

points plot in the CC category, contractive clays, although quite some points plot in the CCS, contractive clays sensitive, category which is larger than the SBT=1 (2009) category. A few points plot in the CD category, dilative clays. Those points correspond to the organic soils with high stresses or large over-consolidation.

4 CONCLUSIONS AND RECOMMENDATIONS

This publication presents the challenges in CPT-based classification of organic soils. One of the challenges is that the identification and estimation of unit weight for organic clays and peats from CPT data is often in accurate using existing methods.

The coarse grained and fine-grained soils classified as mineral soils correspond well with existing SBT classifications. The organic soils, classified according to the FHWA method, do not match well with the SBT classification. In the proposed adjustment to Robertson (2010), SBT=2 (Organic soils) and SBT=3 are redefined and split up into SBT=2a (Peat), SBT=2b (Organic Clay) and SBT=2c (Mineral Clay with organic matter). The classification is based on data pairs up to 15 m depths and 150 kPa vertical effective stresses. The new SBT zones can also be applied in the SBTn classifications by Robertson (2009) and (Robertson 2016) in combination with a $C_n=1.7$ as stress normalization cut-off.

In general, it is highly recommended to perform CPTs adjacent to boreholes, select pairs of high-quality laboratory tests according to a standardized protocol (STOWA). The pairwise established 2021 database of classification test results and CPT

measurements provides valuable insight in the properties of organic soils and an improved classification system.

ACKNOWLEDGEMENTS

The authors would like to thank the POVM, established in 2015 by Water Authorities in the Netherlands, who initiated and financed the “Eemdijkproef”.

This work is part of the “Perspectief” research programme All-Risk with project number P15-21, which is (partly) financed by NWO Domain Applied and Engineering Sciences.

REFERENCES

- Been, K. & Jefferies, M. G. 1993. *Towards systematic CPT interpretation*, Thomas Telford Publishing.
- Begemann, H. K. 1965. The friction jacket cone as an aid in determining the soil profile. *Proc. 6th Int. Conf. on SMFE*, 1, 17–20.
- Boulanger, R. W. & Idriss, I. M. 2016. CPT-Based Liquefaction Triggering Procedure. *Journal of Geotechnical and Geoenvironmental Engineering*, 142, 04015065.
- Den Haan, E. J. 1997. An overview of the mechanical behaviour of peats and organic soils and some appropriate construction techniques. *Conference on Recent Advances in Soft Soil Engineering*, 5-7 March 1997, Kuching, Serawak. Geodelft.
- EN1997-1 2005. Eurocode 7: Geotechnical design - part 1: General rules. European Committee for Standardization.
- EN1997-2 2007. Eurocode 7: Geotechnical Design - Part 2: Ground investigation and testing. European Committee for Standardization.
- Eslami, A. & Fellenius, B. H. 1997. Pile capacity by direct CPT and CPTu methods applied to 102 case histories. *Canadian Geotechnical Journal*, 34, 886–904.
- Huang, P.-T., Patel, M., Santagata, M. C. & Bobet, A. 2009. Classification of organic soils. Joint Transportation Research Program, Indiana Department of Transportation and Purdue University, West Lafayette, Indiana,.
- ISO14688-1 2017. Geotechnical investigation and testing - Identification and classification of soil - Part 1: Identification and description. International Organization for Standardization.
- ISO14688-2 2017. Geotechnical investigation and testing - Identification and classification of soil - Part 2: Principles for a classification. International Organization for Standardization.
- Kulhawy, F. H. & Mayne, P. W. 1990. Manual on estimating soil properties for foundation design.; Electric Power Research Inst., Palo Alto, CA (USA); Cornell Univ., Ithaca, NY (USA). Geotechnical Engineering Group.
- Landva, A. O., Korpjiaakko, E. O. & Pheaney, P. E. 1983. Geotechnical Classification of Peats and Organic Soils. In: Jarrett, P. M. (ed.) *Testing of Peats and Organic Soils*. West Conshohocken, PA: ASTM International.
- Lengkeek, H. J. 2022. CPT-based classification and correlations for organic soils. *4TU.ResearchData*.
- Lengkeek, H. J., De Greef, J. & Joosten, S. 2018. CPT based unit weight estimation extended to soft organic soils and peat. *4th International Symposium on Cone Penetration Testing (CPT'18)*. Delft.
- Lunne, T., Powell, J. J. M. & Robertson, P. K. 2002. *Cone Penetration Testing in Geotechnical Practice*, CRC Press.
- Mayne, P. W. 2014. Interpretation of geotechnical parameters from seismic piezocone tests. *Proceedings, 3rd International Symposium on Cone Penetration Testing*.
- Mesri, G. & Ajlouni, M. 2007. Engineering Properties of Fibrous Peats. *Journal of Geotechnical and Geoenvironmental Engineering*, 133, 850–866.
- NEN5104 1989. Classificatie van onverharde grondmonsters (In Dutch), Classification of unconsolidated soil samples. Nederlands Normalisatie-instituut.
- Robertson, P. K. 1990. Soil classification using the cone penetration test. *Canadian Geotechnical Journal*, 27, 151–158.
- Robertson, P. K. 2009. Interpretation of cone penetration tests — a unified approach. *Canadian Geotechnical Journal*, 46, 1337–1355.
- Robertson, P. K. 2010. Soil behaviour type from the CPT: an update. *2nd international symposium on cone penetration testing, USA*.
- Robertson, P. K. 2016. Cone penetration test (CPT)-based soil behaviour type (SBT) classification system — an update. *Canadian Geotechnical Journal*, 53, 1910–1927.
- Robertson, P. K., Campanella, R. G., Gillespie, D. & Greig, J. 1986. Use of piezometer cone data. *Use of in situ tests in geotechnical engineering*. ASCE.
- Robertson, P. K. & Wride, C. E. 1998. Evaluating cyclic liquefaction potential using the cone penetration test. *Canadian Geotechnical Journal*, 35, 442–459.
- Schmertmann, J. H. 1978. Guidelines for cone penetration test: performance and design. United States. Federal Highway Administration.
- Schneider, J. A., Randolph, M. F., Mayne, P. W. & Ramsey, N. R. 2008. Analysis of Factors Influencing Soil Classification Using Normalized Piezocone Tip Resistance and Pore Pressure Parameters. *Journal of Geotechnical and Geoenvironmental Engineering*, 134, 1569–1586.
- Von Post, L. 1922. Sveriges Geologiska Undersöknings torvinventering och några av dess hittills vunna resultat (In Swedish). SGU peat inventory and some preliminary results. 36.
- Zhang, G., Robertson, P. K. & Brachman, R. W. I. 2002. Estimating liquefaction-induced ground settlements from CPT for level ground. *Canadian Geotechnical Journal*, 39, 1168–1180.

Shear wave velocity – SCPTU correlations for sensitive marine clays

M. Long

School of Civil Engineering, University College Dublin (UCD), Ireland

J.-S. L'Heureux

Norwegian Geotechnical Institute (NGI), Trondheim, Norway

ABSTRACT: The purpose of this paper is to encourage the use of the seismic cone penetrometer (SCPTU) in soil characterisation studies. There has been an increase in use of shear wave velocity (V_s) data in geotechnical engineering. This has been prompted by improvements in measurement and analytical systems. A significant advantage, as is confirmed here, is that V_s can be measured easily and repeatedly by several different techniques in the sensitive marine clays under consideration here. Here the focus is on the derivation of preconsolidation stress (p_c') from V_s . A rational method of determining a V_s/p_c' relationship is outlined with resorting to empirical data analysis. The proposed relationship is shown to work well for Canadian sensitive clay data as has been shown previously for Norwegian and Swedish clays

1 INTRODUCTION

There has been increasing recent use of shear wave velocity (V_s) measurements in geotechnical engineering practice. This has been driven by advances in cost effective and efficient methods of determination of V_s . Traditionally V_s measurements were used for seismic and dynamic analyses. However, they are being increasingly used for site characterisation studies, determination of soil parameters, foundation settlement analyses, assessment of sample disturbance and in the quality control of ground improvement schemes.

This paper focuses on the use of V_s values to provide first order estimates and quality control checking of some geotechnical properties of sensitive marine clays. Unfortunately, it has been shown that different forms of the correlation equations have been developed in different areas. It appears that local correlations are necessary for satisfactory use of the technique as demonstrated for example by L'Heureux and Long (2017), Duan et al. (2019) or Elbeggo et al. (2021). In this paper data for clays in eastern Canada will be examined and compared with similar clays in Norway and southern Sweden. The marine clays of these three countries have similar properties and share a comparable geological depositional environment.

The V_s profiles and basic soil properties in these areas will be studied to investigate any systematic differences and links between the V_s measurements. Focus will be then placed on use of V_s to determine the important preconsolidation stress (p_c') parameter. It is hoped that that this work can lead to a unification of these important practical relationships.

2 V_s MEASUREMENTS

2.1 *Invasive methods*

Geophysical methods can be divided into two categories: invasive and non-invasive. Common invasive methods include down-hole logging, cross-hole logging, suspension logging, seismic dilatometer (SDMT) and the seismic cone penetration test (SCPTU). In Scandinavia and Canada most invasive testing is done with the SCPTU.

A standard CPT is equipped with one or more seismic sensors. The seismic signals are only recorded during pauses in penetration, commonly every 0.5 or 1.0 m. A horizontal beam coupled to the ground surface by the weight of the testing vehicle is the source of the seismic energy. The beam is struck on end with a hammer to generate shear waves. V_s is determined from the travel-time differences along the assumed travel path length for receiver depth.

2.2 *Non-invasive methods*

Of available non-invasive geophysical methods, perhaps that most widely used in Scandinavia and Canada is the multichannel analysis of surface waves (MASW) technique. This technique was introduced in the late 1990s by the Kansas Geological Survey (Park et al., 1999). This method utilises the dispersion property of surface waves for the purpose of V_s profiling. Some further details on the use and validation of the MASW technique in Norwegian clays can be found in L'Heureux and Long (2017).

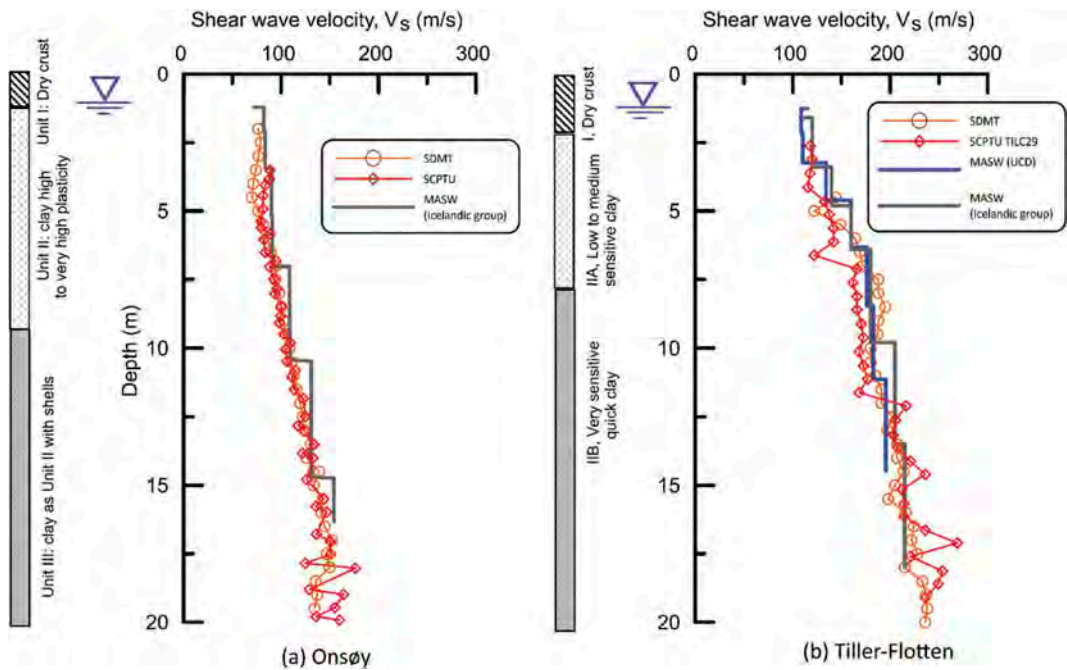


Figure 1. (a) V_s profiles Onsøy site. Data from Gundersen et al. (2019) and Icelandic group MASW from Ólafsdóttir et al. (2019) and (b) Tiller-Flotten. SDMT and SCPTU No TILC29 data from L’Heureux et al. (2019) and MASW from Icelandic Group from Ólafsdóttir et al. (2019).

2.3 Comparison of V_s measurements using different techniques

Between 2016 and 2019, NGI and its partners established five National GeoTest Sites (NGTS) in Norway for testing and verifying innovative soil investigation methods and foundation solutions (L’Heureux et al., 2017). Two of the sites at Onsøy and Tiller-Flotten are underlain by soft sensitive marine clays. The soils at Tiller-Flotten can be classified as quick below a depth of about 8 m using laboratory Swedish fall cone data. V_s profiles have been made with several techniques at these two sites, see Figures 1a and 1b.

The profiles from SCPTU, SDMT and MASW at the two sites are very similar. The V_s values at Onsøy are significantly less than those at Tiller-Flotten. The reasons for this will be explored below.

3 V_s PROFILES FROM NORWAY, SOUTHERN SWEDEN AND EASTERN CANADA

Several V_s profiles from a series of selected sites in Norway are shown on Figure 2a. The sites are from several areas of the country including southern Norway, the area around Trondheim and northern Norway. Measurements were made using a variety of techniques as discussed above. In general the V_s profiles are very similar and show V_s increasing approximately linearly with depth from about 125 m/s at the

surface to about 225 m/s at 20 m depth. The Tiller-Flotten data falls within this general trend. An exception to the trend is the data from Onsøy where the values of V_s are significantly lower though they do show a clear tendency for an increase with depth.

A similar set of data from Southern Sweden is shown on Figure 2b. Again all values are very similar but here they are much lower than the Norwegian measurements with V_s increasing from some 50 m/s near ground level to 125 m/s at 20 m depth. In fact the Swedish data is very similar to the Onsøy profile.

A compilation of available Eastern Canadian data is shown on Figure 3. Many of the profiles fall within the bounds of the Southern Sweden sites. An exception is the profile from the Quyon Landslide site and perhaps the City of Ottawa data.

4 COMPARISON OF PROPERTIES OF CLAYS FROM THE THREE COUNTRIES

A summary of the key properties of the clays from the three countries is given on Table 1. For this purpose typical sites have been chosen, namely Göteborg Central Station from Southern Sweden, St. Alban from Eastern Canada as well as the two NGTS sites at Onsøy and Tiller-Flotten from Norway.

The Tiller-Flotten site (and generally many of the Norwegian sites) are significantly different from the other sites.

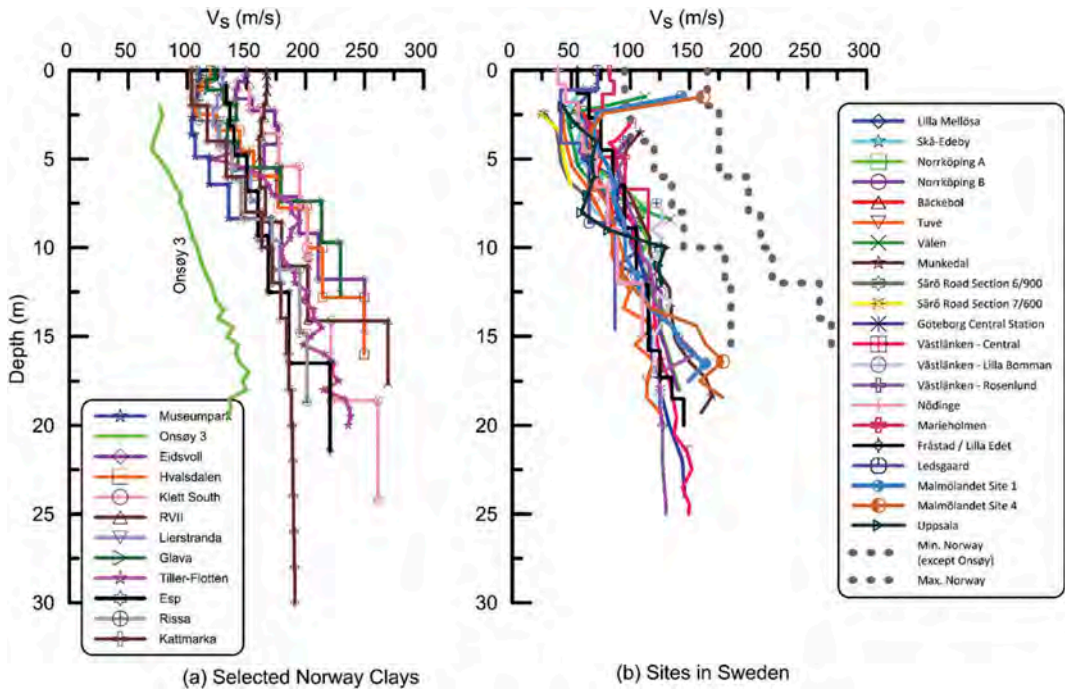


Figure 2. (a) V_s profiles for selected Norwegian sites. Data from L’Heureux and Long (2017) and this paper and (b) for Swedish clays from Long et al. (2017) and Long and D’Ignazio (2020).

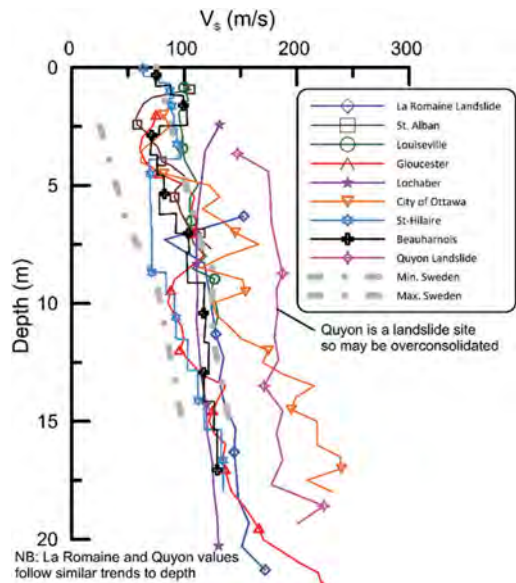


Figure 3. V_s profiles for Eastern Canadian sensitive clays. Data from Bouchard et al. (2017), Lefebvre et al. (1994), Leroueil et al. (2003), Mayne et al. (2019), Fabien-Ouellet et al. (2014), Motazedian et al. (2011), Elbeggo et al. (2021) and Agaiby (2018).

These Norwegian sites have relatively lower water content and plasticity and higher density ($1.7 - 1.9 \text{ Mg/m}^3$ compared to $1.6 - 1.7 \text{ Mg/m}^3$) than the Canadian and Swedish sites. Also Tiller-Flotten has very low organic content compared to the other sites. The Onsey site parameters are much closer to those of the Swedish and Canadian sites. All sites under consideration have similar clay content and stress history.

Table 1. Summary of material properties for the study sites: w = water content, I_p = plasticity index, Org. = organic content OCR = overconsolidation ratio, S_t = fall cone sensitivity. Main references Gundersen et al. (2019), L’Heureux et al. (2019), Wood (2016) and Trak et al. (1980).

Site	W (%)	Clay (%)	I_p (%)	Org. (%)	OCR	S_t
Onsey	40-80	50-70	25-50	2.5-4	1.1-2.0	5-8
Tiller-Flotten	30-50	45-70	8-20	Very low	1.5-2.0	up to 350
Göteborg CS	60-90	70-90	27-40	2-5	1.5-2.0	12-30
St. Alban	60-90	45-81	5-30	0.9	2.2	14-22

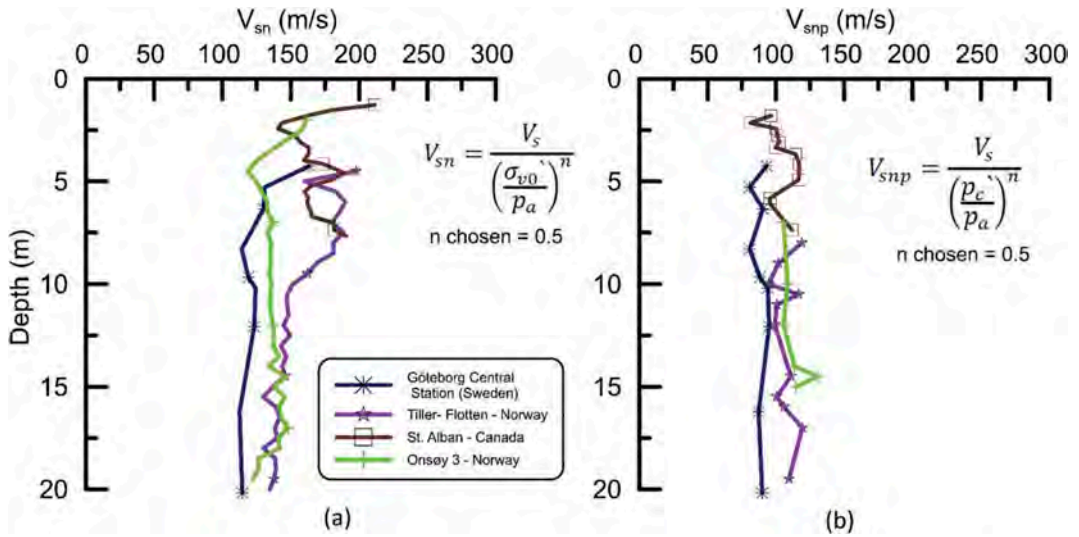


Figure 4. Normalised V_s profiles (a) by vertical effective stress and (b) preconsolidation stress.

5 NORMALISATION OF V_s VALUES

5.1 Normalisation by vertical effective stress

According to Hight and Leroueil (2003) and Hardin (1978) the controlling factors on V_s are primarily functions of soil density, void ratio, and effective stress, with secondary influences including soil type, age, depositional environment, cementation and stress history. It is logical then to attempt to harmonise the V_s profiles by normalising them with respect to in situ vertical effective stress (σ_{v0}). Here the normalised parameter V_{sn} is determined from as follows:

$$V_{sn} = \frac{V_s}{\left(\frac{\sigma_{v0}}{p_a}\right)^n} \quad (1)$$

Mayne et al. (1998), Robertson (2009) and others have chosen $n = 0.25$ based mostly on laboratory data on silica sands. Here a value of 0.5 has been chosen. Data from the four selected study sites normalised as above are plotted against depth on Figure 4a. Although the normalisation brings the values from the four study sites closer together there are still significant differences between the values especially those of Tiller-Flotten and St. Alban below about 4 m. The value of n was altered but no improvements in the relationships were observed.

5.2 Normalisation by preconsolidation stress

To take the stress history of the materials into account the measured V_s data have been normalised by the preconsolidation stress (p_c') on Figure 4b. A form of normalisation very similar to that expressed in Equation 3 has been used as follows:

$$V_{s2} = \frac{V_s}{\left(\frac{p_c'}{p_a}\right)^{0.5}} \quad (2)$$

Unfortunately, as is well known, p_c' can be heavily influenced by sample disturbance effects and by the method used to determine p_c' from the measured oedometer tests data. To deal with the issue of sample disturbance the sites have been chosen where very high quality samples are available. Data from Sherbrooke block or mini-block samples were available for all four sites. The Casagrande (1936) technique was used to determine p_c' at three of the sites with the Janbu (1969) approach being used for the Göteborg Central Station site. No correction has been applied to the p_c' data. The reported values have been used and compared directly to V_s measurements at the same depth.

As can be seen on Figure 4b this form of normalisation was very successful in harmonising the four sets of data. All four profiles are very similar and show an average V_{snp} value of about 100 m/s. Taking this average V_{snp} value the following equation can be obtained to relate V_s and p_c' .

$$p_c' = 0.01 V_s^2 \quad (3)$$

This form of power equation supports and justifies some previous similar empirical equations that have been developed. These include the general relationship developed by Mayne et al. (1998) as shown on Equation 4, that derived for Norwegian marine clays by L'Heureux and Long (2017) (Equation 5) and by Duan et al. (2019) for Jiangsu clays in China (Equation 6)

$$p_c' = 0.106 V_s^{1.47} \quad (4)$$

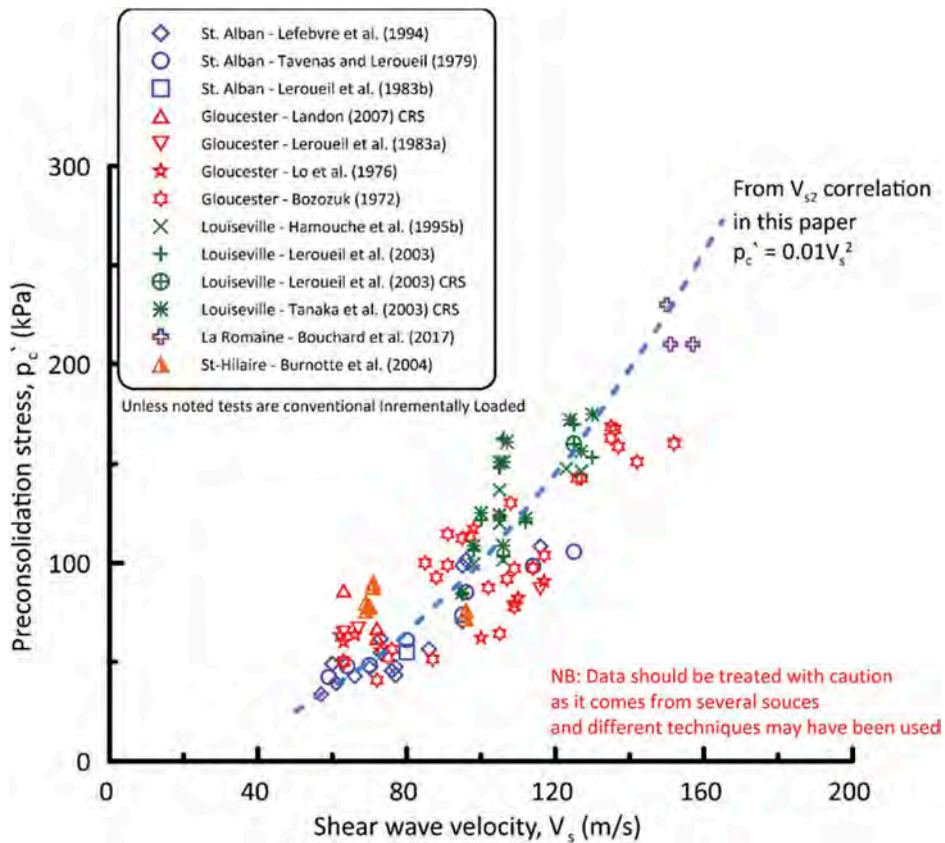


Figure 5. Relationship between V_s and p_c' for Eastern Canada clays. Data from Lefebvre et al. (1994), Tavenas and Leroueil (1979), Leroueil et al. (1983b), Landon (2007), Leroueil et al. (1983a), Lo et al. (1976), Bozozuk (1972), Hamouche et al. (1995), Leroueil et al. (2003), Tanaka et al. (2003), Bouchard et al. (2017) and Burnotte et al. (2004).

$$p_c' = 0.00769V_s^{2.009} \quad (5)$$

$$p_c' = 0.1097V_s^{1.3575} \quad (6)$$

6 V_s - P_c' RELATIONSHIP FOR EASTERN CANADA CLAYS

Available V_s and parallel p_c' data for Eastern Canada clays is shown on Figure 5. This data should be treated with caution as it comes from several sources and it is possible different sampling techniques, testing techniques and methods of deriving p_c' may have been used. The data is shown merely to illustrate the application and usefulness of Equation 5 and suggests further work on this approach is well warranted.

7 CONCLUSIONS

The purpose of this paper was to highlight some advantages in the use of V_s values in soil characterisation studies and to therefore encourage the use of the

SCPTU device. The particular focus here was the derivation of p_c' from V_s data for sensitive marine clays. It was shown that despite V_s profiles for marine clays from different countries being often different, normalisation by p_c' harmonises the different profiles. A rational method, without resorting to empirical correlations, is outlined for the derivation of a formula which relates V_s and p_c' . The derived formula is tested successfully on a set of data for Canadian marine clays. More sites should be included in the relationship shown on Figure 4b to study the likely variation in the values determined.

REFERENCES

- Agaiby, S. S. (2018) Advancements in the interpretation of seismic piezocone tests in clays and other geomaterials. PhD Thesis, School of Civil and Environmental Engineering, Georgia Institute of Technology.
- Bouchard, S., Ali, H., Leboeuf, D., Leroueil, S. & Cascante, G. (2017) Dynamic properties of sensitive clay deposits. IN Thakur, V., L'Heureux, J.-S. & Locat, A. (Eds.) *2nd International Workshop on Landslides in Sensitive Clays (IWLSC)*.

- Bozozuk, M. (1972) The Gloucester test fill. PhD Dissertation, Department of Civil Engineering, Purdue University, West Lafayette, IN, 184.
- Burnotte, F., Lefebvre, G. & Grondin, G. (2004) A case record of electrosmotic consolidation of soft clay with improved soil-electrode contact. *Canadian Geotechnical Journal*, 41, 1038–1053.
- Casagrande, A. (1936) The determination of the pre-consolidation load and its practical significance. *Proceedings of the 1st International Soil Mechanics and Foundation Engineering Conference*. Cambridge, Massachusetts.
- Duan, W., Cai, G., Liu, S. & Puppala, A. J. (2019) Correlations between shear wave velocity and geotechnical parameters for Jiangu clay of China. *Pure and Applied Geophysics*, 176, 669–684.
- Elbeggio, D., Ethier, Y., Dubé, J. S. & Karray, M. (2021) Critical Insights in laboratory shear wave velocity correlations of clays. *Canadian Geotechnical Journal*, Accepted manuscript.
- Fabien-Ouellet, G., Fortier, R. & Giroux, B. (2014) Joint acquisition and processing of seismic reflections and surface waves in a sensitive clay deposit in the Outaouais region (Québec), Canada. *1st International Workshop on Landslides in Sensitive Clays (IWLSC)*. Québec, Springer.
- Gundersen, A. S., Hansen, R. C., Lunne, T., L'heureux, J.-S. & Strandvik, S. O. (2019) Characterization and engineering properties of the NGTS Onsøy soft clay site. *AIMS Geosciences*, 5, 665–703.
- Hamouche, K., Leroueil, S., Roy, M. & Lutenerger, A. J. (1995) In situ evaluation of K_0 in eastern Canada clays. *Canadian Geotechnical Journal*, 32, 677–688.
- Hardin, B. O. (1978) The nature of stress – strain behaviour for soils. In *Proceedings ASCE Speciality Conference on Earthquake Engineering and Soil Dynamics, Pasadena, California*.
- Hight, D. W. & Leroueil, S. (2003) Characterisation of soils for engineering purposes. IN Tan, T. S., Phoon, K. K., Hight, D. W. & Leroueil, S. (Eds.) *Proceedings International Workshop on Characterisation and Engineering Properties of Natural Soils*. Singapore, Balkema, Rotterdam.
- Janbu, N. (1969) The resistance concept applied to deformations of soils. *Proceedings of the 7th International Soil Mechanics and Foundation Engineering Conference*. Mexico City, A.A. Balkema, Rotterdam.
- L'heureux, J.-S., Lindgård, A. & Emdal, A. (2019) The Tiller-Flotten research site: Geotechnical characterisation of a sensitive clay deposit. *AIMS Geosciences*, 5, 831–867.
- L'heureux, J.-S., Lunne, T., Lacasse, S., Carroll, R., Strandvik, S. O., Ozkul, Z., Instanes, A., Sinitsyn, A., Degago, S. A. & Nordal, S. (2017) Norway's National GeoTest Site Research Infrastructure (NGTS). *19th International Conference on Soil Mechanics and Geotechnical Engineering (ICSMGE)*. Seoul.
- L'heureux, J.-S. & Long, M. (2017) Relationship between shear wave velocity and geotechnical parameters for Norwegian clays. *Journal of Geotechnical and Geoenvironmental Engineering ASCE*, 04017013-1 – 04017013-20.
- Landon, M. E. (2007) Development of a non destructive sample quality assessment method for soft clays. *PhD Thesis, Department of Civil and Environmental Engineering, University of Massachusetts, Amherst*. PhD Thesis, Department of Civil and Environmental Engineering, University of Massachusetts, Amherst.
- Lefebvre, G., Beloueuif, D., Rahhal, M. E., Lacroix, A., Warde, J. & Stokoe, K. H. (1994) Laboratory and field determinations of small-strain shear modulus for a structured Champlain clay. *Canadian Geotechnical Journal*, 31, 61–70.
- Leroueil, S., Hamouche, K., Tavenas, F., Boudali, M., Locat, J., Virely, D., Roy, M., La Rochelle, P. & Leblond, P. (2003) Geotechnical characterisation and properties of a sensitive clay from Québec. IN Tan, T. S., Phoon, K. K., Hight, D. W. & Leroueil, S. (Eds.) *Proceedings International Workshop on Characterisation and Engineering Properties of Natural Soils*. Singapore, Balkema, Rotterdam.
- Leroueil, S., Samson, L. & Bozozuk, M. (1983a) Laboratory and field determination of preconsolidation pressures at Gloucester. *Canadian Geotechnical Journal*, 20, 477–490.
- Leroueil, S., Tavenas, F., Samson, L. & Morin, P. (1983b) Preconsolidation pressure of Champlain clays, Part 2, Laboratory determination. *Canadian Geotechnical Journal*, 20, 803–816.
- Lo, K. Y., Bozozuk, M. & Law, K. T. (1976) Settlement analysis of the Gloucester test fill. *Canadian Geotechnical Journal*, 13, 339–354.
- Long, M. & D'ignazio, M. (2020) Shear wave velocity as a tool for characterising undrained shear strength of Nordic clays. *18th Nordic Geotechnical Meeting*. Helsinki, Finland (Conferece held virtually January 2021), IOP Conf. Series: Earth and Environmental Science 710 (2021) 012008.
- Long, M., Wood, T. & L'heureux, J.-S. (2017) Relationship between shear wave velocity and geotechnical parameters for Norwegian and Swedish sensitive clays. *2nd International Workshop on Landslides in Sensitive Clays (IWLSC)*.
- Mayne, P. W., Cargill, E. & Miller, B. (2019) Geotechnical characteristics of sensitive Leda clay at Canada test site in Gloucester, Ontario. *AIMS Geosciences*, 5, 390–411.
- Mayne, P. W., Robertson, P. K. & Lunne, T. (1998) Clay stress history evaluated from seismic piezocone tests. IN Robertson, P. K. & Mayne, P. W. (Eds.) *Proceedings 1st. International Conference on Geotechnical Site Characterisation*. Atlanta, Georgia, Balkema.
- Motazedian, D., Hunter, J. A., Pugin, A. & Crow, H. (2011) Development of a Vs30 (NEHRP) map for the city of Ottawa, Ontario, Canada. *Canadian Geotechnical Journal*, 48, 458–472.
- Ólafsdóttir, E. A., Bessason, B., Erlingsson, S., L'heureux, J.-S. & Bazin, S. (2019) Benchmarking of an open-source MASW software using data from three Norwegian GeoTest Sites. *17th European Conference on Soil Mechanics and Geotechnical Engineering (ECSMGE)*. Reykjavik, Iceland.
- Park, C. B., Miller, D. M. & Xia, J. (1999) Multichannel analysis of surface waves. *Geophysics*, 64, 800–808.
- Robertson, P. K. (2009) Interpretation of cone penetration tests - a unified approach. *Canadian Geotechnical Journal*, 46, 1337–1355.
- Tanaka, H., Shiwakoti, D. R. & Tanaka, M. (2003) Applicability of SHANSEP method to six different natural clays using triaxial and direct shear tests. *Soils and Foundations*, 45, 43–55.
- Tavenas, F. & Leroueil, S. (1979) Clay behaviour and the selection of design parameters. *7th European Conference on Soil Mechanics and Foundation Engineering (ECSMFE)*. Brighton, UK.
- Trak, B., La Rochelle, P., Tavenas, F., Leroueil, S. & Roy, M. (1980) A new approach to the stability analysis of embankments on sensitive clays. *Canadian Geotechnical Journal*, 17, 526–544.
- Wood, T. (2016) On the small strain stiffness of some Scandinavian soft clays and impact on deep excavations, PhD thesis Department of Civil and Environmental Engineering, Chalmers University of Technology, Göteborg, Sweden.

A simplified method to incorporate the benefits of microstructure for cyclic liquefaction analyses using the SCPT

K. Lontzetidis

CMW Geosciences, New Zealand

P.K. Robertson

Gregg Drilling Inc., USA

D.J. Morton

CMW Geosciences, New Zealand

ABSTRACT: Cyclic liquefaction resistance of sand deposits can increase due to microstructure that results from several factors, such as aging and bonding. Available empirical correlations, using either SPT, CPT or shear wave velocity (V_S) data, were derived from cyclic liquefaction case histories that considered very young Holocene-age, essentially normally consolidated, unbonded, silica-based soils that may not apply to soils with significant microstructure. Seismic CPT (SCPT) data can be used to identify soils with significant microstructure, since both aging and bonding tend to increase the small-strain stiffness (reflected in the measured V_S) significantly more than they increase the large-strain strength of a soil (reflected in the CPT penetration resistance). Hence, for a given soil, both age and bonding tend to increase V_S more than the larger-strain cone resistance, all other factors (such as, in situ stress state, density, etc.) being constant. The normalized rigidity index (K_G) has been proposed (Robertson, 2016) as a parameter, that combines V_S and normalized CPT tip resistance (Q_m), to detect and quantify the presence of microstructure. This paper presents and discusses a suggested method to quantify the increased resistance to cyclic liquefaction due to microstructure by utilizing K_G . Results will be presented from older soil deposits in New Zealand well as compare the results with existing correlations that account for “aging”.

1 INTRODUCTION

Over the last 40 years, since the first simplified method to assess soil liquefaction potential was proposed by Seed and Idriss (1971), empirical methods have evolved to improve the reliability of predicting liquefaction triggering. Empirical correlations are based on either standard penetration test (SPT), cone penetration test (CPT) or shear wave velocity (V_S) data. The CPT is now the most commonly used in-situ test to evaluate liquefaction potential in liquefaction-prone areas. The main advantages of the CPT are the continuous and repeatable measurements that provide a detailed profile of the soil, as well as major developments in CPT-based liquefaction prediction methods that have occurred over recent years (e.g., Boulanger and Idriss 2014). A limitation of all liquefaction prediction methods is that they have been derived from cyclic liquefaction case histories that consider very young Holocene-age, essentially normally consolidated, unbonded, silica-based soils. Correlation of results from those case histories can therefore be conservative when applied to older or bonded soils. Pleistocene-aged soils (>12,000 years)

are considered to have a low risk of cyclic liquefaction (Youd and Perkins, 1978). Several researchers have worked to quantify the influence of the age on liquefaction potential through laboratory and in-situ testing (e.g., Seed 1979; Troncoso et al. 1988, Arango and Miguez 1996; Arango et al. 2000; Robertson et al. 2000; Lewis et al. 2004, Lewis et al. 1999; Hayati and Andrus 2008).

The objective of this paper is to investigate an alternative method to estimate the potential positive effects of either age or bonding of a soil by utilizing the normalized rigidity index (K_G) proposed by Robertson (2016). Seismic CPT (SCPT) data from early to late Pleistocene-age soils in New Zealand (NZ) are used to evaluate the proposed method. The results using the proposed method are compared with another method also utilising seismic CPT data.

2 PREVIOUS STUDIES

Several researchers have established correlations between the age of a soil and the increase in liquefaction resistance (e.g., Seed (1979); Troncoso et al.

(1988); Lewis et al. (1999) Arango et al. (2000) Lewis et al. (2004) Leon et al. (2006) Hayati and Andrus (2008). Results show that there is an increase in liquefaction resistance with increasing soil age.

Andrus et al. (2009) proposed a ratio of the measured to estimated V_s (MEVR) to quantify the increase in resistance to cyclic loading of older soils. Saftner et al. (2015) presented a summary of past relationships, in terms of a Strength Gain Factor K_{DR} , for resistance to cyclic loading and age (Figure 1) and proposed a new relationship to account for geologic age by evaluating data from explosive compaction tests.

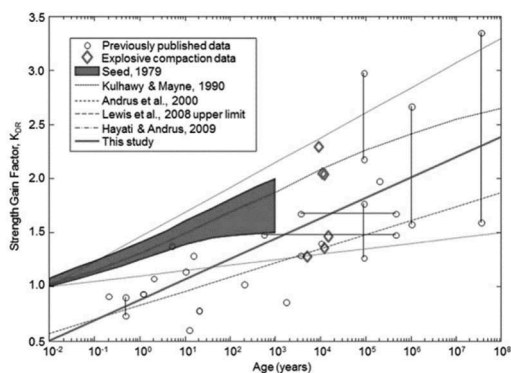


Figure 1. Relationship between strength gain factor (K_{DR}) and soil age based on data from explosive compaction tests and previous studies (After Saftner et al. 2015).

One limitation of a correction based on geologic age, it that past liquefaction events can modify the behavior of a soil so that its ‘behavior age’ is not the same as its geologic age. Hence, a correction based on behavior characteristics may have wider application.

3 MICROSTRUCTURE

Eslaamizaad and Robertson (1996) showed that it is possible to identify soils with significant microstructure (due to age, bonding or unusual mineralogy) using the SCPT based on a link between the ratio of small strain shear modulus (G_o), net cone resistance (q_n) and the normalized cone resistance (Q_{tn}), since both aging and bonding tend to increase the small-strain stiffness (G_o) significantly more than they increase the large-strain strength of a soil (reflected in Q_{tn}). Hence, for a given soil, both age and bonding tend to increase the small-strain shear wave velocity (V_s) more than the larger-strain cone resistance, all other factors (in situ stress state, etc.) being constant.

Robertson (2015) modified slightly the equation proposed by Schneider and Moss (2011) to identify

soil microstructure. This was done by extending the link between the CPT and the V_s using the empirical parameter, K_G defined by:

$$K_G = (G_o/q_n) (Q_{tn})^{0.75} \quad (1)$$

where G_o is in same units as q_n , Q_{tn} is dimensionless, and K_G is essentially a normalized rigidity index.

Most of the existing empirical correlations developed for the interpretation of CPT results are predominantly based on experience in silica-based soils with little or no microstructure (e.g., Robertson 2009; Mayne 2014). Hence, if soils have $K_G < 330$, the soils are likely young and unbonded (i.e., have little or no microstructure) and can be classified as ‘ideal’ soils (unstructured) where most traditional CPT-based empirical correlations for liquefaction prediction likely apply. Soils with $K_G > 330$ tend to have significant microstructure, and the higher the value of K_G , the more microstructure is likely present. Hence, if a soil has $K_G > 330$, the soils can be classified as ‘structured’ soils where traditional generalised CPT-based empirical liquefaction prediction correlations may have less reliability and where local modification may be needed. The influence of increasing microstructure on in situ soil behavior is often gradual, and any separating criteria can be somewhat arbitrary. Data suggests that very young unbonded soils tend to have K_G values closer to 100, whereas soils with some microstructure (e.g., early Pleistocene-age) tend to have K_G values closer to 330. As will be shown later, soils with $K_G < 330$ tend to have little or no microstructure where empirical CPT-based liquefaction prediction correlations tend to provide good estimates of soil behavior.

4 STUDY AREA

4.1 Site description

The Ruakura site comprises an area of approximately 177 ha and is located at the intersection of Silverdale Road and Ruakura Road, in Hamilton, New Zealand. The land use has generally remained unchanged from agricultural practices since at least 1974 (circa). There are a few buildings/structures, which have occupied the land to service the agricultural operations (i.e., sheds, water tanks). The natural topography of the site is typically flat with minor undulations from historic stream channels. The elevation of the site ranges from RL 40.0 m to RL 42.0 m.

4.2 Geology

The published geological map (Edbrooke, 2005, Figure 2) indicates that most of the site is underlain by late Pleistocene-age river deposits of the Hinuera Formation (12,000-27,000yr) consisting of cross-bedded pumice sand, silt, and gravel with interbedded peat

(2Qa). Early to mid-Pleistocene-age river and igneous deposits of the Walton Group (27,000-2,000,000y) extend into the western part of the site and comprise a sequence of ignimbrites and tephra from several sources and fine-grained volcanoclastic alluvium (eQa). The north-eastern part of the site is indicated to be underlain by Holocene-age swamp deposits and peat of the Tauranga Group (0-12,000y), consisting of soft, dark brown to black, organic mud, muddy peat and woody peat with minor overbank sand, silt, and mud swamp deposits (Q1a).

Based on site specific CPT data, the mean I_c values for each geological formation are 1.9 for the Tauranga Group, 1.8 for the Hinuera Formation and 2.7 for the Walton Group.

4.3 Geotechnical investigation

Several phases of geotechnical investigation have been undertaken within the site over recent years. It was recognised that the soils at Ruakura are unlikely to fit the historical liquefaction database used to develop most empirical liquefaction prediction techniques due to:

1. The geologic age of the deposits found in parts of the site are older (Pleistocene-age) than the database (Holocene-age).
2. The Hinuera deposits are composed of unusual mineralogy (pumice) compared to the historical data base (silica-based soils).

The latest investigation included twenty-two (22) SCPTs. Factual data from those tests are presented in various geotechnical reports prepared by CMW. The SCPTs were undertaken to support the liquefaction analysis as well as to check for increased resistance to cyclic liquefaction of soils due to their age.

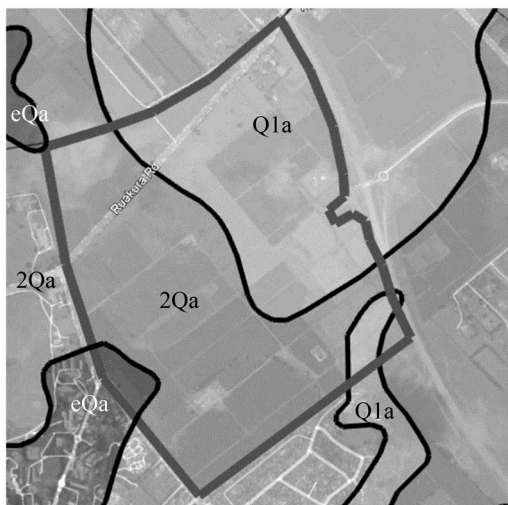


Figure 2. Geological map of the Ruakura site.

5 CORRELATION BETWEEN THE STRENGTH GAIN FACTOR AND K_G

Andrus et al. (2009) and Hayati and Andrus (2009) suggested a method using MEVR, to account for soil aging on the resistance to cyclic loading (CRR) using CPT and V_s results. Based on laboratory and field cases, they proposed a deposit resistance factor (strength gain factor, K_{DR}) to correct for age using:

$$K_{DR} = 1.08MEVR - 0.08 \quad (2)$$

to correct the cyclic resistance ratio, CRR_K due to the age of the deposit:

$$CRR_K = CRR_{CPT} \times K_{DR} \quad (3)$$

where CRR_{CPT} is the CPT-based CRR from case histories for young Holocene-age deposits. The measured V_s is computed from in-situ distance and travel time measurements using the SCPT and the estimated V_s can be obtained for sands by the following equation:

$$V_{s1,E} = 62.6(Q_{tn,cs})^{0.231} \text{ m/s} \quad (4)$$

where $V_{s1,E}$ is the estimated shear-wave velocity corrected for overburden pressure and $Q_{tn,cs}$ is the normalized clean sand equivalent cone resistance.

Hayati and Andrus (2009) showed that the MEVR approach is based on a reference age of about 23 years for $V_{s1,E}$ which was considered a representative average age for the liquefaction case history database. Many of the liquefaction cases are associated with deposits that have a “behavioral age” (the time since the last critical disturbance or liquefaction event) not more than 100 years. Previous liquefaction (or even ground improvement implementation) is assumed to be a critical disturbance event when the grain-to-grain contacts were damaged and reformed.

A similar approach has been proposed by Robertson (2015) using the Schneider and Moss (2011) empirical parameter K_G following a similar measured to estimated K_G ratio defined by

$$MEK_G = K_{G,M} / K_{G,E} \quad (5)$$

where $K_{G,M} = K_G$ based on measured values of V_s and q_t , and $K_{G,E} = 200$ is the estimated average value for very young (~23 years), unbonded soils. Based on the definition of K_G [Eq. (1)], the MEK_G ratio is insensitive to changes in CPT q_t and $Q_{tn,cs}$ due to aging. Since q_t has been shown to be

relatively insensitive to aging and/or light bonding, it is reasonable to assume that,

$$MEK_G = MEVR^2 \quad (6)$$

The advantage of using MEK_G is that it does not require the calculation of an estimated V_s , which has an associated uncertainty, especially in soils that are not clean sands. Hence, a similar approach can be applied using MEK_G instead of $MEVR$ and apply Eqs. (2) and (6) to estimate the strength gain factor, K_{DR} .

6 DATA USED TO ESTIMATE SOIL MICROSTRUCTURE

The locations of the most recent twenty-two SCPTs undertaken as part of the project investigation are shown in Figure 3.

At each test location, shear wave velocity (V_s) measurements were undertaken at 1m intervals vertically. The CPT cone resistance data was then averaged over a depth of 0.5m above and below the relevant V_s measurement depth. From the V_s data and soil density (averaged within 1m zone), the maximum shear modulus (G_o) was calculated using the following.

$$G_o = \rho (V_s)^2 \quad (7)$$

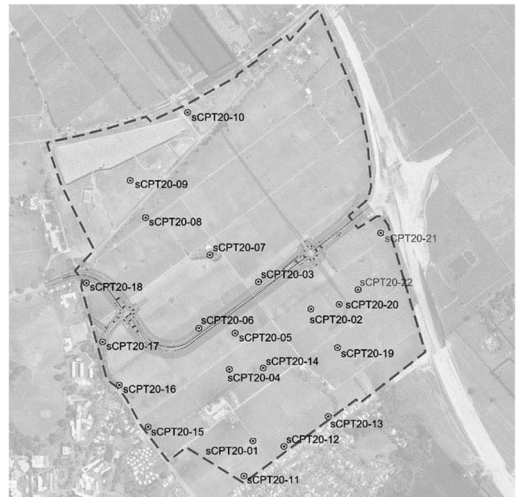


Figure 3. Site plan showing the locations of the SCPTs.

where ρ is the soil density in kg/m^3 .

Compiling the CPT data, the net cone resistance (q_n) and the normalized cone resistance (Q_m), were calculated using the following two equations.

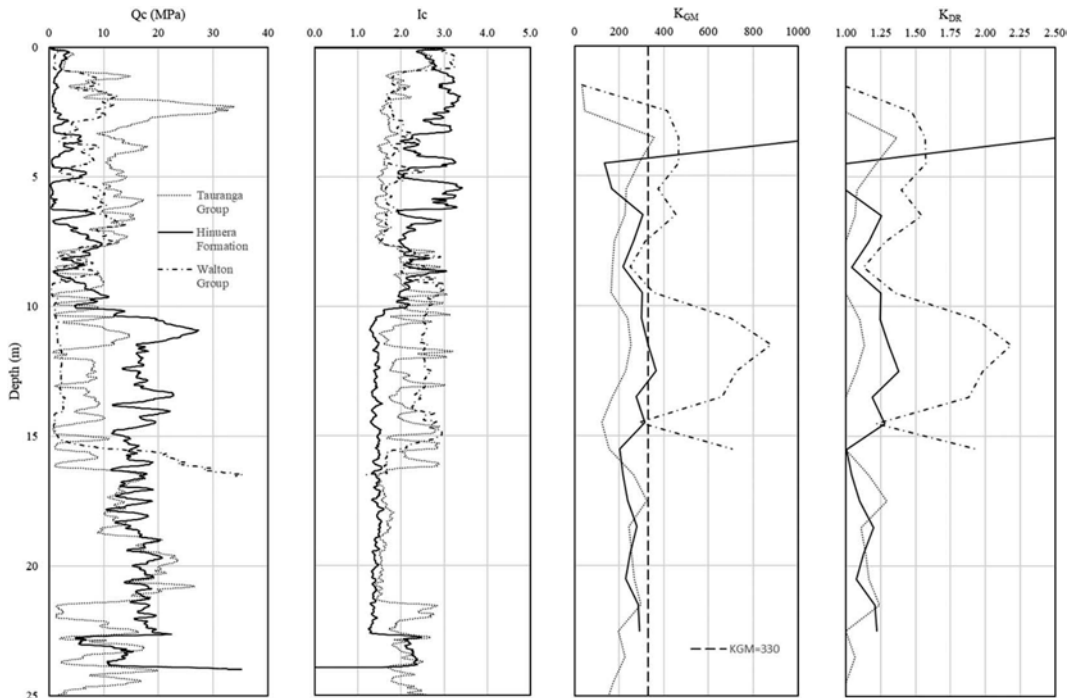


Figure 4. Typical examples of in-situ test results and the calculated values of K_{GM} and K_{DR} .

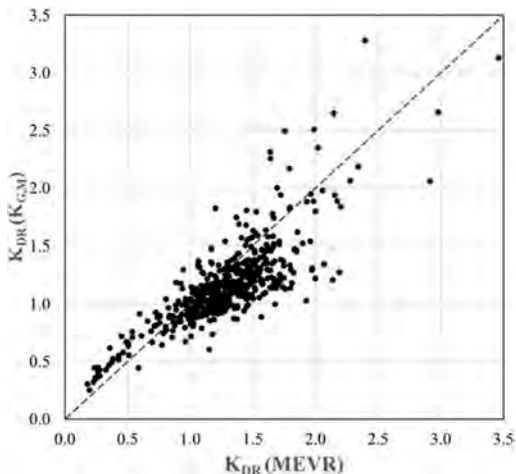


Figure 5. Comparison of the K_{DR} calculated using MEVR and $K_{G,M}$.

$$q_n = q_t - \sigma_{vo} \quad (8)$$

$$Q_{tn} = \left(\frac{q_t - \sigma_{vo}}{P_{a2}} \right) \left(\frac{P_a}{\sigma'_{vo}} \right)^n \quad (9)$$

where q_t is the corrected cone resistance, σ_{vo} the vertical total stress, P_a and P_{a2} are reference pressures (100kPa), σ'_{vo} is the effective vertical stress and n is the stress exponent that varies with I_c (Robertson & Cabal 2015).

Based on the above methodology, a set of small strain shear modulus (G_o), net cone resistance (q_n) and normalized cone resistance (Q_{tn}) data points were calculated at 1m depth intervals. By utilizing equation 1, the measured normalized

rigidity index (K_{GM}) was then calculated. Finally, by combining equations 2, 5 and 6, the strength gain factor (K_{DR}) was calculated using the following equation.

$$K_{DR} = 1.08 \sqrt{K_{G,M}/K_{G,E}} - 0.08 \quad (10)$$

And since $K_{G,E} = 200$ for very young (~23 years), unbonded soils, this is simplified to:

$$K_{DR} = 1.08 \sqrt{K_{G,M}/200} - 0.08 \quad (11)$$

Equation 11 presents the strength gain factor K_{DR} , as a function of the measured normalized rigidity index $K_{G,M}$. without the need to calculate a reference V_s value.

Figure 4 presents the results from three typical SCPTs, one for each geological formation encountered in the area, together with the calculated profiles of measured normalized rigidity index (K_{GM}) and the strength gain factor (K_{DR}). Figure 4 illustrates that the average K_{DR} value increases with the geological age of the soil deposits.

Figure 5 presents a comparison of K_{DR} values calculated by Andrus et al., 2009 using MEVR with those using $K_{G,M}$ as proposed in this study. This shows that the $K_{G,M}$ method estimates a K_{DR} value that is on average 10% lower than that using the MEVR method. It is also noted that at shallow depths, the K_{DR} values calculated from $K_{G,M}$ are higher than those calculated using MEVR, while this trend decreases with depth.

Figure 6 shows the cumulative frequency distribution of K_{DR} from each method ($K_{G,M}$ and MEVR) for

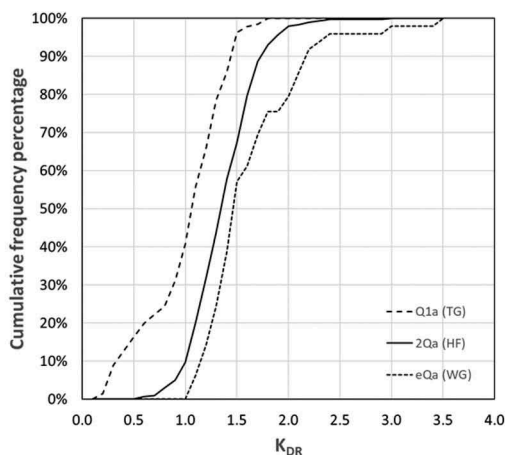
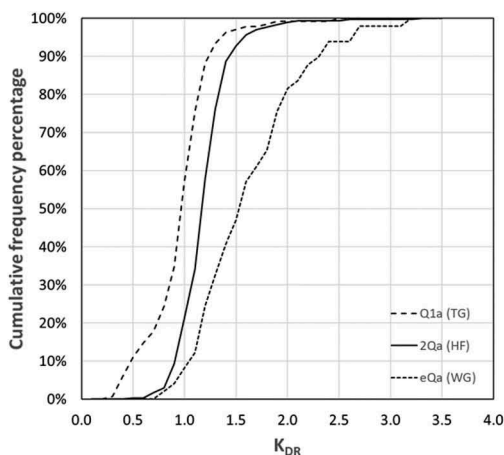


Figure 6. Comparison of the results of the K_{DR} , calculated using the proposed $K_{G,M}$, and MEVR for each of the three geological formations.

each of the three geological formations. The results indicate that the Holocene-age deposits of the Taurangi Group (Q1a), indicate little or no microstructure with 50th percentile $K_{DR}(K_{G,M}) = 1.0$, and $K_{DR}(MEVR) = 1.1$. The slightly older Hinuera Formation (2Qa) indicates some microstructure with 50th percentile $K_{DR}(K_{G,M}) = 1.2$ and $K_{DR}(MEVR) = 1.3$. The older Walton Group (eQa), indicates more microstructure with 50th percentile $K_{DR}(K_{G,M}) = K_{DR}(MEVR) = 1.5$. These results plot at the low range of the values presented in Saftner et al. 2015 (Figure 1) for the age of the Hinuera (2Qa) and Walton Group (eQa).

7 CONCLUSIONS

As part of the geotechnical investigation for the Ruakura Development in New Zealand a number of geotechnical investigation campaigns have been undertaken that included 22 SCPTs to support liquefaction analysis and to evaluate the increased resistance of older soils to cyclic loading.

This paper presents an alternate method to quantify the increased resistance to cyclic loading of soils due to microstructure, which can be readily implemented utilising SCPT data.

The results of the strength gain factor K_{DR} , by the proposed method using the normalised rigidity index, compare well with results using the MEVR.

The proposed method returns a rather low increase in resistance to liquefaction compared to other methods (see Figure 1).

REFERENCES

- Andrus, R. D. and Hayati, H. 2009. Updated Liquefaction Resistance Correction Factors for Aged Sands, *J. Geotech. Geoenviron. Eng.*, 135(11),1683–1692.
- Andrus, R. D., Hayati, H., and Mohanan, N. P. 2009. Correcting liquefaction resistance of aged sands using measured to estimated velocity ratio *J. Geot. Geoenv. Eng.*, 135(6),735–744.
- Arango, I., Lewis, M. R., and Kramer, C. 2000, Updated liquefaction potential analysis eliminates foundation retrofitting of two critical structures, *Soil Dynamics Earthquake Eng.*, Elsevier Limited, 20: 17–25.
- Arango, I., and Miguez, R. E. 1996, Investigation of the seismic liquefaction of old sand deposits, *Report on Research, Bechtel Corporation*, National Science Foundation Grant No. CMS-94-16169, San Francisco, CA.
- Boulanger, R. W., and Idriss, I. M., 2014, CPT and SPT based liquefaction triggering procedures, *Rep. No. UCD/CGM-14/01, Center for Geotechnical Modeling, Dept. of Civil and Environmental Engineering, College of Engineering, Univ. of California, Davis, CA*, 138.
- Bwambale, B., Andrus R. D., and Cubrinovski, M., 2017, Influence of age on liquefaction resistance of Holocene alluvial and marine soils in Christchurch and Kaiapoi, New Zealand, *PBD III Earthquake Geotechnical Engineering*, Vancouver.
- Clayton, P. J., de Graaf K. L., Yong I., and Green, R. A., 2019, Comparison of assessments of liquefaction potential in selected New Zealand pumiceous soils, *Earthquake Geotechnical Engineering for Protection and Development of Environment and Constructions*.
- Clayton, P. J., and Johnson, J. T., 2013, Liquefaction resistance and possible aging effects in selected Pleistocene soils of the Upper North Island, *Proc. 19th NZGS Geot. Symposium*.
- Clayton, P. J., Tilsley, S. C., Bastin, S. H., and Green, R. A., 2017, Case study in the use of paleoliquefaction techniques to investigate liquefaction potential of Waikato soils for the Hamilton section of the Waikato expressway, *Proc. 20th NZGS Geotechnical Symposium*.
- Clayton, P. J., Yong, I., and Wotherspoon, L., 2017, Case study in the use of shear wave velocity techniques to investigate liquefaction potential of Waikato soils for the Hamilton section of the Waikato expressway, *Proc. 20th NZGS Geotechnical Symposium*
- Edbrooke, S. W., 2005, Geology of the Waikato area, *Institute of Geological and Nuclear Sciences*, Lower Hutt, New Zealand.
- Eslaamizaad, S., and Robertson, P. K. 1996, Seismic cone penetration test to identify cemented sands, *Proc. 49th Canadian Geotechnical Conf.*, St John's, Newfoundland, Canadian Geotechnical Society (CGS), 1, 352–360.
- Hayati, H., and Andrus, R. D. 2008, Liquefaction potential map of Charleston, South Carolina based on the 1886 earthquake, *Journal of Geotechnical and Geoenvironmental Eng.*, 134(6) DOI:10.1061/(ASCE)1090-0241(2008)134:6(815).
- Hayati, H., Andrus, R.D., 2009, Updated liquefaction resistance correction factors for aged sands, *J. Geotech. Geoenviron. Eng.* 135 (11), 1683–1692.
- Leon, E., Gassman, S.L., and Talwani, P., 2006, Accounting for Soil Aging when Assessing Liquefaction Potential, *J. of Geotechnical and Geoenvironmental Eng.*, 132 (3), 363–377.
- Lewis, M. R., Arango, I., Kimball, J. K., and Ross, T. E. 1999, Liquefaction resistance of old sand deposits, *Proc., 11th Panamerican Conf. on Soil Mechanics and Geotechnical Engineering*, Foz do Iguassu, Brazil: 821–829.
- Lewis, M. R., McHood, M. D., and Arango, I. 2004, Liquefaction evaluations at the Savannah River Site, A Case History, *Proc., Fifth Int. Conf. on Case Histories in Geotechnical Engineering*, New York, NY.
- Mayne, P. W. 2014, Interpretation of geotechnical parameters from seismic piezocone tests, *3rd Int. Symp. on Cone Penetration Testing*, CPT14, Gregg Drilling & Testing, CA.
- Robertson, P. K. 2009, Interpretation of Cone Penetration Tests—A unified approach, *Can. Geotech. J.*, 46 (11),1337–1355.
- Robertson, P. K. 2015. Comparing CPT and Vs Liquefaction Triggering Methods, *Journal of Geot. and Geoenvironmental Engineering*, ASCE, 141 (9):04015 037,10.1061.
- Robertson, P. K. 2016. Cone penetration test (CPT)-based soil behavior type (SBT) classification system —an update, *Can. Geotech. J.* 53: 1910–1927.
- Robertson, P. K. and Cabal, K. L. 2015, Guide to Cone Penetration Testing for Geotechnical Engineering, 6th edition, Gregg Drilling & Testing, Inc.
- Robertson, P. K., Wride, C. E. (Fear), List, B. R., Atukorala, U., Biggar, K. W., Byrne, P. M., Campanella, R. G., Cathro, D. C., Chan, D. H., Czajewski, K., Finn, W. D. L., Gu, W. H., Hammamji, Y., Hofmann, B. A., Howie, J. A., Hughes, J., Imrie, A. S.,

- Konrad, J.-M., Küpper, A., Law, T., Lord, E. R. F., Monahan, P. A., Morgenstern, N. R., Phillips, R., Piché, R., Plewes, H. D., Scott, D., Segó, D. C., Sobkowicz, J., Stewart, R. A., Watts, B. D., Woeller, D. J., Youd, T. L., and Zavodni, Z. 2000, The CANLEX project: summary and conclusions, *Canadian Geotechnical Journal*, 37: 563–591.
- Saftner, D.A., Green R.A., and Hryciw, R. D., 2015, Use of explosives to investigate liquefaction resistance of aged sand deposits, *Engineering Geology* 199: 140–147.
- Schneider, J. A., and Moss, R. E. S. 2011, Linking cyclic stress and cyclic strain-based methods for assessment of cyclic liquefaction triggering in sands, *Geotech. Lett.*, 1, 31–36.
- Seed, H. B. 1979, Soil liquefaction and cyclic mobility evaluation for level ground during earthquakes, *Journal of the Geotechnical Eng. Div.*, 105(2): 201–255
- Seed, H. B., and Idriss, I. M. 1971, Simplified procedure for evaluating soil liquefaction potential, *J. Soil Mech. and Found. Div.*, 97(9), 1249–1273.
- Troncoso, J., Ishihara, K., and Verdugo, R. 1988, Aging effects on cyclic shear strength of tailing materials, *Proc., Ninth World Conf. on Earthquake Engineering*, Vol. III: 121–126.
- Youd, T. L., and Perkins, D. M., 1978, Mapping of liquefaction induced ground failure potential, *J. Geotech. Engrg. Div.*

Classification of Miocene deposits using CPT data

A. Makra

GR8 GEO, Athens, Greece

H. Kim

DL E&C Co. Ltd, Seoul, South Korea

ABSTRACT: Soil classification based on CPT data is commonly carried out using classification charts which link the type of soil behaviour to the measured tip resistance, sleeve friction and pore water pressure. These charts have been successful in interpreting soil behaviour in young, saturated, uncemented soil deposits but often diverge from observations in samples in older deposits. The geotechnical investigation conducted for the 1915 Çanakkale bridge included 20 offshore boreholes with 18 adjacent CPT soundings conducted downhole that penetrated several meters into Miocene-age sediments. This paper investigates those data sets and proposes a modified chart for the classification of the Miocene deposits accounting for their microstructure. The proposed modification is useful for classifying Miocene deposits in similar geological settings through the performance of CPTs.

1 INTRODUCTION

Cone Penetration Testing (CPT) is a very common in situ sounding tool used to collect geotechnical data at sites. The CPT provides a cost-efficient, fast and reliable method to obtain continuous soil profiles. The basic idea of the test is that a standardized cone is pushed into the ground at a constant penetration rate while the tip resistance, sleeve friction and pore water pressure are measured.

Several methods of soil classification have been developed to correlate CPT data to soil characteristics (Schmertmann 1978, Robertson 1990, 2009, Schneider 2008, Robertson 2016). Unlike the most common soil classification systems [ASTM D2487 (USCS), BSCS BS 5930] that are based on the physical properties of soils such as grain size distribution and plasticity index, CPT classification methods are based on behaviour characteristics and are generally described as Soil Behaviour Type (SBT) classification systems (Robertson 2016).

These CPT based classification charts have proven to be very efficient in predicting soil type in young (Quaternary) soil deposits. However, older soils with significant microstructure often require site specific modifications to the classification charts so that the effect of the microstructure on the CPT data is properly reflected in the SBT classification system (Robertson 2016).

Although the existing CPT database is extensive for younger and softer deposits, fewer data exist for

Miocene sediments because the high stiffness and strength of the deposit typically precludes significant CPT penetration. This lack of data has limited the development of a globally accepted approach for interpretation of CPT data in Miocene sediments. However, evolutions in CPT techniques increasingly allow for achieving greater penetration in stiffer soils. An early interpretation of the ground profile in these stiffer soils using CPT based SBT classification systems can be very useful, especially at an early stage of project development.

In the 1915 Çanakkale bridge project area, a significant number of CPT soundings were conducted onshore, nearshore and offshore in combination with geophysical surveys, boreholes and other geotechnical in situ tests (SPT, wireline logging, etc.) and extensive laboratory testing.

In addition to seabed CPTs, the down-hole mode was adopted for offshore CPTs to be able to collect data from relatively stiff and competent materials. In contrast to onshore and seabed CPT testing where the cone is continuously pushed from the surface to refusal, down-hole CPTs are conducted within a borehole with typically 1.5 to 3.0m stroke lengths. Upon completion of the CPT, the portion penetrated by the cone is drilled out and the borehole is continued with either a subsequent CPT test or sampling (Figure 1).

In the 1915 Çanakkale Bridge project, down-hole CPTs were continuously advanced with drill outs to the depth where the material became too stiff for

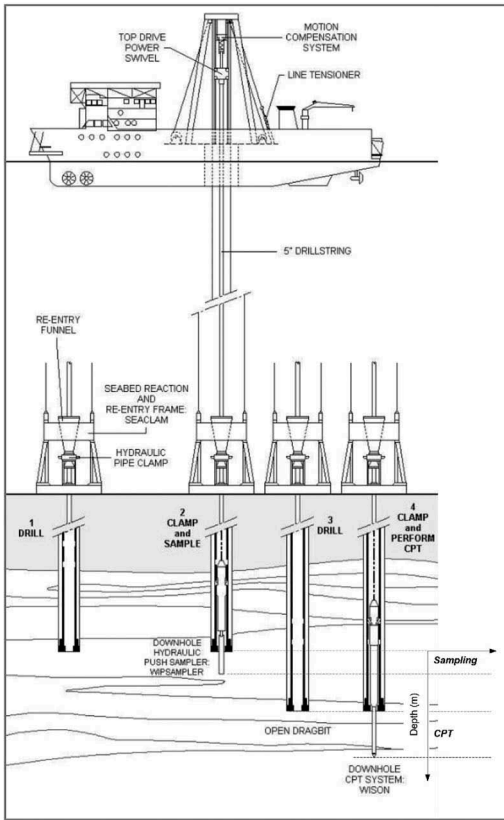


Figure 1. Procedures for drilling, push sampling and CPT testing (modified after ISSMGE 2005).

CPT testing. Thus, a significant CPT data set of Miocene soils was collected from the site.

The identification of the Miocene deposits was primarily based on the interpretation of the geophysical survey data, which were also confirmed by borehole data. When CPT data associated with the Miocene deposits were interpreted, the classification based on the Robertson (2009, 2016) charts shown on Figures 2 and 3 was inconsistent with the observations and laboratory data obtained from borehole core samples - probably due to the significant microstructure of the Miocene. For instance, the CPT data obtained from Miocene mudstone were expected to fall within Zone 9: Very Stiff Fine Grained and CD: Clay like Dilative based on Robertson (2009, 2016) (Figures 2 and 3, respectively), but many CPT data points plotted outside of Zone 9, displaying a different trend. Thus, site-specific modifications of the chart were required for the Miocene sediments. This paper proposes a modified Robertson classification chart that can be used for the classification of fine grained heavily over-consolidated Miocene mudstones using CPT data based on the data set from the 1915 Çanakkale bridge project.

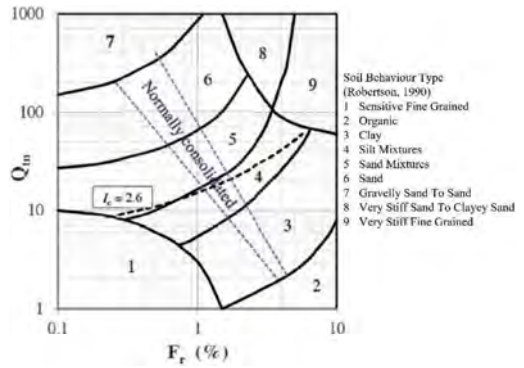


Figure 2. CPT Classification Chart from Robertson (2009).

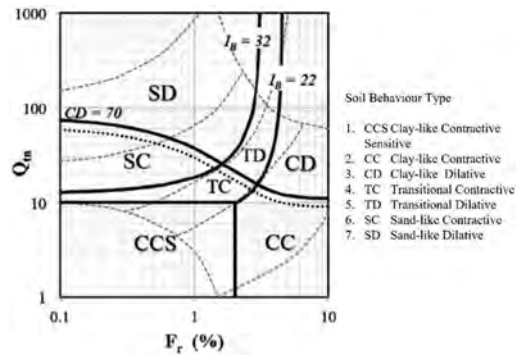


Figure 3. CPT classification chart from Robertson (2016).

2 FRAMEWORK

The 1915 Çanakkale bridge is located between Gelibolu in East Thrace and Lapseki on the Biga Peninsula (Troas). The site investigation was conducted by Fugro (Fugro 2018a, b) and consisted of extensive geological, geophysical and geotechnical investigations. CPTs were performed onshore, nearshore and offshore. Although the onshore CPTs penetrated only a few meters into the upper (typically weaker) Miocene layers before experiencing refusal, offshore CPT using down-hole mode allowed for the continuation of testing beyond initial refusal and the collection of data deeper within harder strata. Although down-hole CPTs are discontinuous and require additional care in the execution and processing of the test results, they are an efficient method to collect CPT data in deeper strata or below a very stiff/dense layer where seabed CPTs would have refused. Offshore CPTs using down-hole mode are the main source of CPT data in Miocene units presented in this paper. Boreholes were drilled adjacent to the CPT locations to facilitate the interpretation and integration of the geotechnical data. The boreholes progressed with continuous sampling

in the soil layers and rotary core drilling in the rock and the samples were immediately processed at the site and onboard laboratories to minimize sample disturbance and to expedite data availability. In several of these explorations, after the completion of drilling, P-S wireline logging was conducted (Fugro 2018a).

3 RESULTS AND DISCUSSION

The bedrock of the project site consists of Miocene sedimentary rock of the Çanakkale formation, composed primarily of mudstones and sandstones with few siltstone, marl and limestone layers of limited thickness. The top of the Miocene geologic unit was initially interpreted from geophysical data and then refined locally by borehole and CPT data (Figure 4). The Miocene deposits are of the same origin as the overlying younger (Holocene and Pleistocene) layers, complicating the visual distinction between the stratigraphic units. Thus, the top of Miocene bedrock in the boreholes was identified based on the degree of cementation, structure (bedding, fissures) and strength of the material.

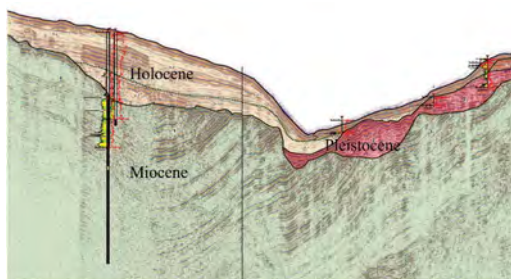


Figure 4. Geophysical and geotechnical cross section, Çanakkale Strait, Offshore, (Fugro 2018a).

CPT data were acquired only in Miocene mudstones with occasional thin sandstone interlayers. The CPT equipment was not able to penetrate through thick sandstone layers. The top of Miocene was characterized by a sudden increase in tip resistance, followed by increases in friction ratio and pore water pressure. Figure 5 presents typical tip, sleeve friction and pore water pressure traces of CPT data in Miocene mudstones. The tip resistance generally ranges between 5MPa and 25MPa and the friction ratio from 1.5 to 6%, with the lower friction ratio (less than 2%) corresponding to the thin sandstone interlayers.

Figure 6 shows CPT data collected from the Miocene deposit plotted on the Robertson (2009, 2016) classification charts. Most of the CPT data are plotted within Zones 4 and 5 of the chart as per Robertson (2009) and TD and CD as per Robertson (2016). However, the Zones 4 and 5 are described as having a mainly drained behaviour and being primarily

coarse grained (Zone 4: Silt mixtures, Zone 5: Sand mixtures, refer to Figure 2 and Figure 6a). The TD and CD are described as dilative and mainly transitional material with smaller portion in the clay-like and sand-like range. Note that these descriptions showing the soil behaviour do not properly reflect the expected behaviour of the Miocene deposit.

A small fraction of the data (about 20%) are plotted within Zone 3 which corresponds to clays. CPT data plotted within Zone 3 are mostly located close to the boundary between Quaternary and Miocene deposits where the stiffness of mudstones/clays is low (*i.e.*, less than a few hundred kilopascals).

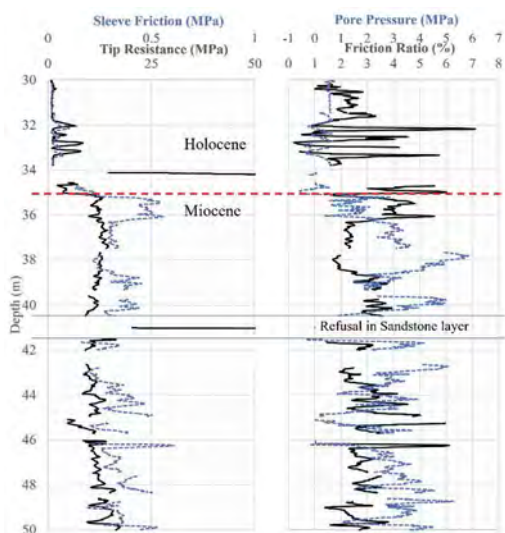


Figure 5. Typical CPT trace of Holocene and Miocene deposits from the European Tower explorations (CPT ID: ET-5).

Laboratory tests performed on mudstone samples showed fines contents exceeding 80% and an average plasticity index (PI) of 45, which is classified as fat clay (CH) per ASTM D2487. Based on the geotechnical descriptions of the boreholes with consolidation and strength tests (uniaxial compressive and UU triaxial strength values), the Miocene mudstones are lightly lithified, fresh, overconsolidated, with strengths ranging from extremely weak (<1MPa) to very weak (1-5MPa) rock per ISRM (2007) recommendations or hard clay (>0.2MPa) per the ASTM soil classification system.

Although the Miocene mudstone is classified as CH per USCS, the CPT classification chart incorrectly suggests that the material displays sandlike behaviour due to its relatively high normalized tip resistance caused by the effects of cementation and aging as well as overconsolidation.

Figure 7 shows a comparison of the CPT data from Holocene clayey deposits with the data from Miocene mudstones in the offshore European side of the Çanakkale bridge project. The CPT data from two deposits show that whilst the normalized friction ratios are similar, the normalized tip resistances are much higher in the Miocene deposits. As shown on Figure 7a, b, the CPT data obtained from Holocene deposits fall within Zone 3 (clay and clay-like contractive), and CC (Clay-like Contractive) and CCS (Clay-like Contractive Sensitive). Although the classification of Miocene deposits using the CPT data were inconsistent with sample descriptions and laboratory tests, the SBT classification using CPT data for the Holocene clayey deposits is consistent with the borehole and laboratory data, both of which indicate the Holocene deposit to be a soft to firm, near-normally consolidated clay.

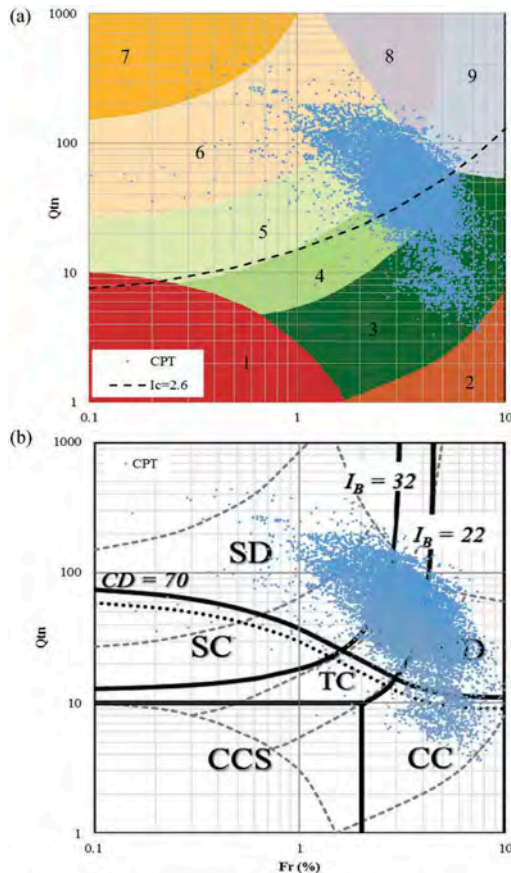


Figure 6. CPT data from the Miocene deposit on (a) Robertson (2009) and (b) Robertson (2016) Classification Charts, (Data obtained from Çanakkale Strait, Offshore European and Anatolian Towers).

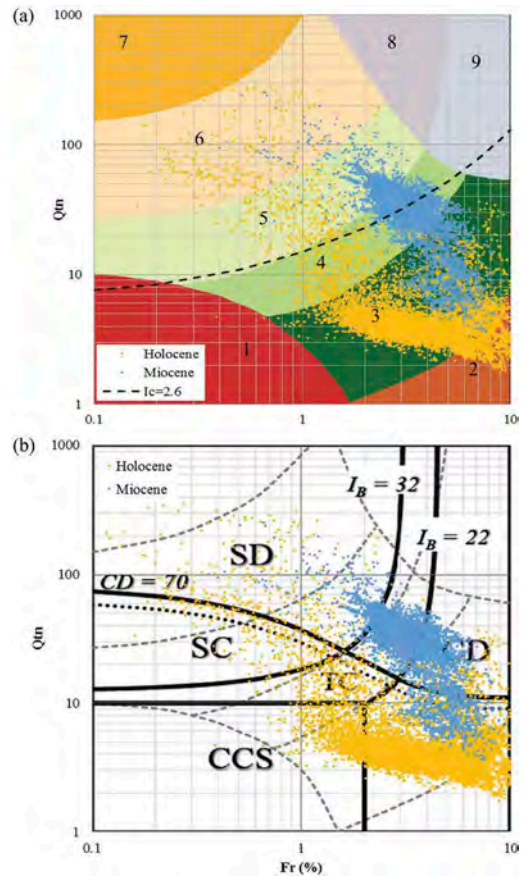


Figure 7. CPT data from Miocene and Holocene deposits on (a) Robertson (2009) and (b) Robertson (2016) Classification Charts, (Data obtained from Çanakkale Strait, Offshore European and Anatolian Towers).

Since Miocene age deposits are expected to have microstructure related to aging and cementation or other post-depositional processes, the microstructure of the sediments around the 1915 Çanakkale bridge was assessed following the recommendations of Robertson (2016) which relate microstructure to the normalized tip resistance (Q_m), the small strain stiffness (G_0) and the net cone tip resistance ($q_n = q_t - \sigma_v$). Robertson (2016) introduces a modified normalized small strain rigidity index K_G^* defined as:

$$K_G^* = \left(\frac{G_0}{q_n} \right) (Q_m)^{0.75} \quad (1)$$

Young, uncemented soils tend to have K_G^* values ranging between 100 and 330, while soils with significant microstructure tend to have K_G^* values

exceeding 330 (Robertson 2016). The small strain stiffness of the Miocene deposits was measured using seismic CPT and wireline logging data.

Figure 8 presents the normalized tip resistance (Q_{tm}) versus small-strain rigidity index (I_G) plot for Holocene, Pleistocene and Miocene deposits in the Çanakkale bridge area. The plotted data in the figure are from the European and Anatolian Tower explorations and cover a range of depths between 5 and 50m to represent the various ground units (Holocene, Pleistocene and Miocene) and changes in stiffness. The plot was made using representative small strain stiffness values corresponding to measured shear wave velocities and associated normalized tip resistances taken from the representative value of measured tip resistances within the same sublayer where the shear wave velocity was measured (about 1m above and below the depth where the shear wave velocity was measured).

Based on Figure 8, Holocene soils appear to have little or no microstructure while the Pleistocene and Miocene deposits likely have significant microstructure. Hence, classifying these sediments requires adjustments to the SBT classification systems proposed by Robertson (2009, 2016) to account for microstructure.

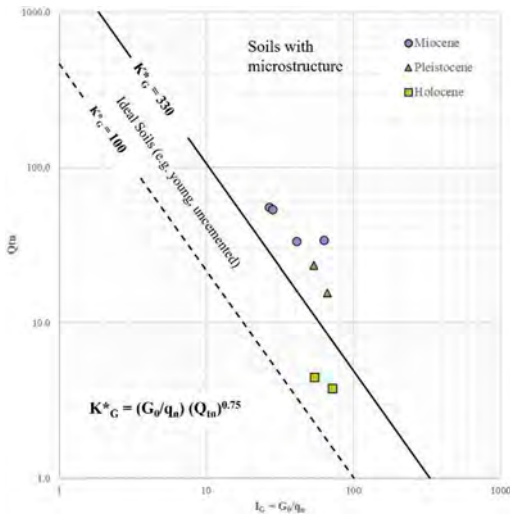


Figure 8. $Q_{tm} - I_G$ chart to identify soils with microstructure per Robertson (2016).

The CPT data obtained from the Miocene deposit are characterized by: normalized tip resistances between 25 and 100MPa and normalized friction ratios between 2% and 5% (Figure 6). Thus, a new Zone associated with the Miocene mudstones on the Q_{tm} versus F_r (%) plot is proposed by modifying Robertson (2009) chart. Basically, the modified zone from SBT classification that corresponds to Miocene

mudstones extends Zone 9 into Zones 4 and 5 with a normalized friction ratio of 2% and higher. In addition, the zone also covers small portions of Zones 6 and 8 bounded by F_r (%) of 2% and Q_{tm} of 200. The newly proposed Miocene Zone represents the CPT data collected from the Miocene mudstones at the site.

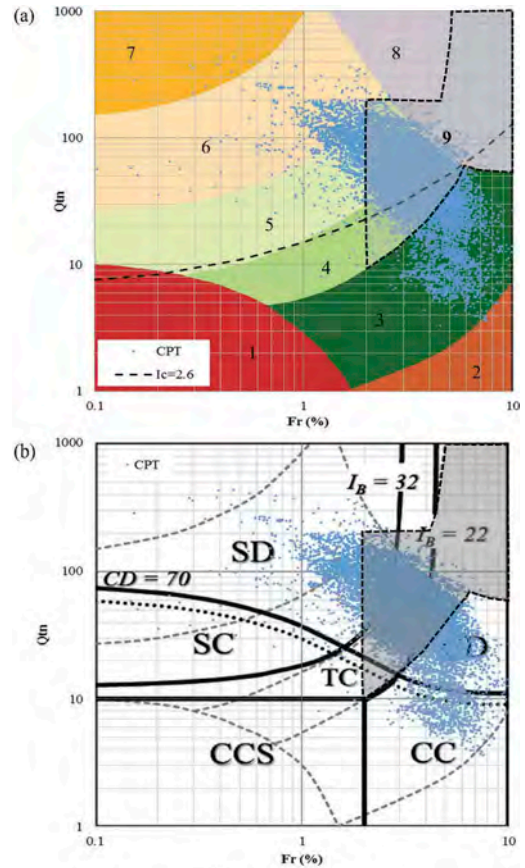


Figure 9. Proposed Modification of the (a) Robertson (2009) and (b) Robertson (2016) Classification Charts for Miocene Deposits.

4 SUMMARY AND CONCLUSION

A Modified Soil Behaviour Type (SBT) classification is proposed to identify Miocene fine-grained deposits on the Q_{tm} versus F_r (%) chart based on the CPT data obtained from the 1915 Çanakkale bridge project. The Miocene deposits were identified through the performance of geophysical surveys, and boreholes drilled adjacent to CPT soundings. The subsurface stratigraphy interpreted from the geophysical survey is in good agreement with borehole data, which enabled delineation of CPT data within

the Miocene deposits. The use of down-hole mode CPT allowed for the collection of significant data set from the Miocene deposits.

While the Robertson charts have proven to be effective for young uncemented soils, modifications appear to be warranted for sediments with significant microstructure.

Within Miocene mudstones, inconsistencies were noted between the soil classification of samples and those interpreted from CPT charts typically where the CPT data plot in zones of the soil classification charts that are described as primarily coarse-grained. Based on a comparison of the CPT data with the cores and samples collected within the Miocene deposit, the materials characterized by friction ratios greater than about 2% that plot within these zones are mostly fine-grained and appear to display mainly undrained responses during cone penetration. For this study, the Robertson (2009) chart has been modified to delineate Miocene deposit with friction ratios greater than 2 percent as fine-grained. Similar modifications are expected to be applicable in similar geological settings where fine-grained intermediate geomaterials are present and are weak enough to permit meaningful penetration by commonly used CPT equipment. The finding from this study should facilitate the classification of similar deposits especially when CPT soundings are performed at an early project stage prior to conducting boreholes.

REFERENCES

- ASTM. 2011. D2487-11. Standard practice for classification of soils for engineering purposes (Unified Soil Classification System). ASTM International
- British Standards Institution 2015 BS 5930:2015 Code of practice for ground investigations. London: BSI.
- International Society of Soil Mechanics and Geotechnical Engineering Technical Committee 1 (ISSMGE TC1) 2005. Geotechnical & geophysical investigations for offshore and nearshore developments. International Society for Soil Mechanics and Geotechnical Engineering.
- Fugro 2018a. 1915 Çanakkale bridge site characterization report. Prepared for DLSY JV. Çanakkale: Fugro
- Fugro 2018b. 1915 Çanakkale bridge engineering parameters report. Prepared for DLSY JV. Çanakkale: Fugro
- International Society of Rock Mechanics (ISRM) 2007. The complete ISRM Suggested Methods for rock characterization, testing and monitoring: 1974–2006. In: Ulusay R, Hudson JA (eds) Suggested Methods prepared by the Commission on Testing Methods, International Society for Rock Mechanics, compilation arranged by the ISRM Turkish National Group. Ankara: Kozan Ofset.
- Robertson, P.K. 1990. Soil classification using the cone penetration test. *Canadian Geotechnical Journal*, 27(1): 151–158
- Robertson, P.K. 2009. Interpretation of cone penetration tests – a unified approach. *Canadian Geotechnical Journal*, 46(11): 1337–1355.
- Robertson, P.K. 2016 Cone Penetration Test (CPT)-Based Soil Behaviour Type (SBT) Classification System—An Update. *Canadian Geotechnical Journal*, 53(12): 1910–1927
- Schmertmann, J.H. 1978. Guidelines for CPT: performance and design. Report FHWA-TS-78-209. Washington DC: Federal Highway Administration.
- Schneider, J.A., Randolph, M.F., Mayne, P.W., and Ramsey, N.R. 2008. Analysis of factors influencing soil classification using normalized piezocone tip resistance and pore pressure parameters. *Journal of Geotechnical and Geoenvironmental Engineering, ASCE*, 134(11): 1569–1586

On the interpretation of piezocone dissipation testing data in clay

F.M. Mántaras

Geoforma Engenharia Ltda, Brazil

F.S. Pereira

University of Western Australia, Australia

E. Odebrecht

State University of Santa Catarina, Brazil

Geoforma Engenharia Ltda, Brazil

F. Schnaid

Federal University of Rio Grande do Sul, Brazil

ABSTRACT: Piezocone dissipation tests are routinely used to estimate the *in situ* coefficient of consolidation (c_h). This is achieved either by extracting a single point of the dissipation curve (usually, the time for 50% dissipation, t_{50}) or by adjusting a theoretical solution to the experimental data. Results from a piezocone investigation carried out in the Holocene clay deposit of Tubarão are reported and interpreted to evaluate the accuracy of existing procedures to estimate c_h . Explicit recommendations on how to curve fit dissipation curves and use the first and second derivatives to estimate t_{50} are presented. Validation of the proposed method is provided from field tests reaching up to 75% dissipation. The proposed method does not require accurate measurements of equilibrium pressure and relies less on engineering judgment when compared to reference procedures. Furthermore, the method performed reasonably well with a shorter dissipation time (40% dissipation).

1 INTRODUCTION

The coefficient of consolidation (c_h) can be measured in laboratory from oedometer tests or assessed from *in situ* test results, preferably from piezocone dissipation tests. In the case of piezocone data, evaluation of c_h is based on the variation in pore pressure with time and interpretation rely either on one-dimensional cavity expansion (Vésic, 1972; Torstensson, 1977; Randolph & Wroth, 1979; Burns & Mayne, 1998) or two-dimensional strain path method (Levadoux & Baligh, 1986; Baligh & Levadoux, 1986; Teh & Houlsby, 1991). Both monotonic and dilatatory soil response can be modelled in this type of approach, being the Teh & Houlsby method (1991) the standard for monotonic pore pressure dissipation response and the Burns & Mayne method (1998) the alternative for dilatatory response.

The procedure for assessing c_h from dissipation tests is based on a series of straightforward recommendations that requires plotting normalized excess pore pressure ($U = (u_t - u_0)/(u_i - u_0)$), against time on a log and/or \sqrt{t} scale, where u_t is the pore pressure at time t and u_0 is the *in situ* equilibrium pore pressure (Lunne et al, 1997). Albeit the procedure is apparently simple to apply, there

are uncertainties in assessing both the initial pore pressure u_i and the equilibrium *in situ* pore pressure u_0 . Reliable measurement of the equilibrium *in situ* pore pressure, essential to the interpretation of c_h , is not always straightforward to obtain and requires considerable engineering judgment in many applications. In clays, the pore pressure generated in a piezocone test can be allowed to dissipate to the equilibrium value to assess the *in situ* equilibrium pore pressure but this can take hours and makes the use of the piezocone economically unfeasible for routine engineering applications. In cases such as coastal and nearshore investigation, tests are affected by tide variations and piezometer measurements have to be interpreted to estimate average equilibrium pressures. In man-made structures such as tailing-retention dams the determination of phreatic surface location is influenced by pond location, anisotropic permeability of deposits, boundary flow conditions, permeable layers, among other factors (e.g. Vick, 1983). Furthermore, equilibrium pore pressure will be higher than hydrostatic pressure in the presence of artesian flow or in soil layers undergoing consolidation, and lower than hydrostatic pressure in the presence of downward flow (Robertson & Cabal, 2008).

Due to uncertainties in defining u_0 , the time for 50% dissipation of excess pore pressure (t_{50}) may be in error and so is the estimated value of c_h . To partially overcome this problem, a recommendation is made to adjust the complete dissipation curve to obtain the best global value of the horizontal coefficient of consolidation, instead of matching just a single point (usually 50%) of the recorded dissipation (e.g. Lunne et al. 1997). The present paper extends this view by deriving the equation used to curve fitting the measured pore pressure data. Once this is accomplished, the slope of the derivate at the minimum point is zero and corresponds to t_{50} . The time t_{50} can then be used in the interpretation of the value of c_h using standard methods.

A polynomial equation was shown to best-fit the theoretical solutions of Teh & Houlsby (1991) and Burns & Mayne method (1998), and the derivative of the function is easily computed. Since the equilibrium *in situ* pore pressure is no longer required to calculate the percentage of dissipation, one of the uncertainties in deriving c_h is eliminated.

These concepts have been applied to two long duration dissipation tests carried out in the Holocene clay deposit of Tubarão. Results show excellent agreement between the reference and polynomial curve fitting methods in assessing c_h . The polynomial fitting method was shown to provide reasonable estimates of c_h even for lower degree of dissipation.

2 THEORETICAL BACKGROUND

The proposed method was first presented in Mántaras et al. (2014) and consists on curve fitting the field pore pressure measurements to estimate t_{50} . The fitting generates a standard curve that can be useful in interpolating a set of pore pressure values to define a function that is smooth and comes close to the measured data. Once the function is selected and the curve fitting is completed, the function's first derivative is calculated and the minimum point of the function where the slope is zero is identified. In the second derivate this point is zero. These two points (zero slope in the first derivate and zero in the second) correspond to the point of inflection of the normalized dissipation curve and define the theoretical value of t_{50} .

This simple mathematical procedure captures the essence of physical models developed for the interpretation of piezocone dissipation data. Verification, justification, and reasoning is given through mathematical derivation of the solutions proposed by Teh & Houlsby (1991). A polynomial equation is used to curve fit the data, with the actual mathematical expression (degree) defined by the minimum r^2 . First and second derivatives correspond to the point of inflection of the normalized dissipation curve and define the theoretical value of t_{50} .

Basic arguments introduced by Mántaras et al. (2014) are re-stated here before discussing the applicability of the proposed approach to piezocone

dissipation tests. The method's mathematical reasoning was also verified against a theoretical solution for dilatatory response (Burns & Mayne, 1998), which is available in Mántaras et al., 2014. As dilatatory response is not in the scope of this paper, the derivation is not presented here.

Teh & Houlsby (1991) method: From a theoretical perspective, the strain path method was used to demonstrate that dissipation curves are not unique because the initial pore pressure distribution is highly sensitive to the value of I_r (Baligh, 1985). This prompted the normalization of test data by means of dimensionless time factor T^* , as introduced by Teh & Houlsby (1991):

$$T^* = \frac{c_h t}{r^2 \sqrt{I_r}} \quad (1)$$

where r is the probe radius, t the dissipation time (normally adopted as t_{50}), I_r the rigidity index ($= G/S_u$) and G the shear modulus. A constant I_r is used in the solution although in fact the value of the shear modulus depends on the shear strain amplitude, which is shown by strain path calculations to vary in a complex manner around a 60° penetrometer.

Excess pore pressure in the soil generated during penetration of the piezocone can be expressed as a negative function distribution for the probe radial distance, with no excess pore pressure at an infinite distance from the cone face. The rate of decay can be conveniently represented using approximate numerical algorithms, thus offering a means of implementing data on a spreadsheet. Exponential and logarithm equations for matching the data have been proposed by Mayne (2001), Chung (2014) and others (Fig. 1). The logarithm equation proposed by Mayne (2001) to fit the data is:

$$u_2^* \cong (0.85 + 10T^*)^{-0.45} - 0.08 \quad (2)$$

In a logarithmic time scale, the variable T^* is replaced by $10^{(x-3)}$:

$$u_2^* \cong \left(0.85 + 10 \cdot 10^{(x-3)}\right)^{-0.45} - 0.08 \quad (3)$$

The derivative of the function with respect to the variable x is expressed as:

$$\frac{du_2^*}{dx} \cong \frac{-4.5}{[0.85 + 10^{(x-2)}]^{1.45}} \cdot 10^{(x-2)} \cdot \ln(10) \quad (4)$$

Alternatively, a polynomial expression is used to facilitate the mathematical treatment of the differentiation. Expression (4) could be accurately represented by an x^{th} degree polynomial, providing means of fitting both monotonic and dilatatory soil response.

$$u_2^* = a_0 + a_1x + a_2x^2 + a_3x^3 + \dots + a_nx^n \quad (5)$$

The first and the second derivatives from equation (5) can be easily obtained:

$$\frac{du_2^*}{dx} = a_1 + 2 \cdot a_2 \cdot x^1 + 3 \cdot a_3x^2 + 4 \cdot a_4x^3 + \dots + n \cdot a_n \cdot x^{(n-1)} \quad (6)$$

$$\frac{ddu_2^*}{ddx} = 2 \cdot a_2 + 6 \cdot a_3x^1 + 12 \cdot a_4x^2 + \dots + n \cdot (n - 1) \cdot a_n \cdot x^{(n-2)} \quad (7)$$

Equation 6 represents the slope of pore pressure dissipation in log scale and can be differentiated to obtain the inflection point of the $u_2^* \times T^*$ curve (Fig. 2).

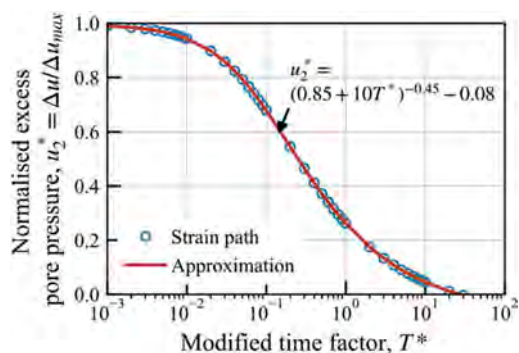


Figure 1. Teh & Houlsby solution (1991) and approximation with logarithmic equation from Mayne (2001).

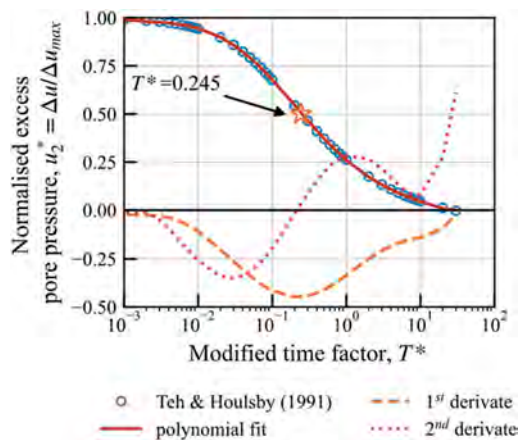


Figure 2. 1st and 2nd derivatives of Teh & Houlsby (1991) solution.

In the analysis, the program is instructed to graph the curve to check the compatibility of the measured data with the superimposed curve, as well to plot the first and second derivatives to calculate t_{50} . The minimum value of the polynomial first derivate corresponds to a time factor $T^*=0.245$ which is the theoretical value calculated by Teh & Houlsby (1991).

It is then concluded that the mathematical approach of adjusting the complete dissipation curve, followed by the determination of t_{50} from the first and second derivatives, is the simplest and most consistent way to obtain the best global value of the coefficient of consolidation, c_h .

3 TESTING PROGRAM

The testing program was performed at the Experimental Testing Site located in the delta of Tubarão river in the Southern Coast of Brazil. Comprehensive site investigation comprising seismic piezocone, field vane shear tests, dilatometer tests and standard penetration tests has been carried out to identify soil type and stratigraphy (e.g. Mántaras et al., 2015). Sediments in the upper 20m are predominantly normally consolidated, formed during the last 8000 years in the Holocene period after the most recent glaciation (Odebrecht & Schnaid, 2018; Schnaid & Odebrecht, 2015; Lunne et al. 2014). Below a depth of 6m the clay layer has an average plasticity index (PI) of 55% (Schnaid et al., 2016).

A standard 10cm² piezocone (CPTu) with pore pressure measurement on the shoulder just above the cone face (u_2) was used in the testing program. Tests were carried out according to ASTM D5778 (2012) standards. Figure 3 shows the penetration test results obtained from the piezocone penetration test at the Tubarão Site. The clay layer from 7 to 13m is relatively homogeneous, with occasional lenses of silty sand. After tests measurements show that the water level fluctuates around 1m below the ground surface.

The penetration test was halted at the target depths of 10 and 13m, where the soil is normally consolidated. Up to 1.5h was allowed for pore pressure dissipation to obtain at least 75% of dissipation. Table 1 summarizes the piezocone test program.

4 RESULTS

The normalized field excess pore pressure dissipation curves for the tests CPTu_10m and CPTu_13m are presented in Figure 4. The clay is normally consolidated, exhibiting monotonically decreasing dissipation curves.

The monotonic excess pore pressure dissipations were evaluated by best fitting the complete dissipation curves using the Teh & Houlsby (1991) method. The theoretical fitting provides good matching with the experimental dissipation over the complete pore pressure monotonic decay for both tests, and consequently, the interpreted c_h values are considered as reference

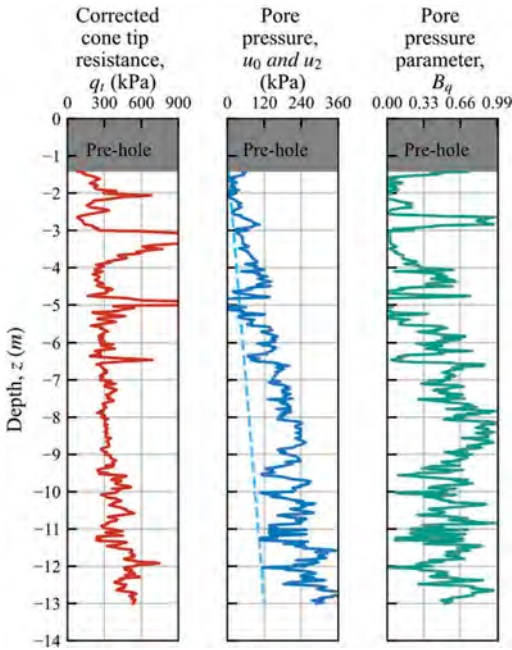


Figure 3. Results from piezocone penetration test at Tubarão Experimental Testing Site: (a) corrected cone tip resistance, q_t (b) pore pressure, u_0 and u_2 and (c) pore pressure parameter, B_q .

Table 1. Test program at the Tubarão clay site

Dissipation test name	Depth (m)	Test time (s)	Degree of dissipation at end of test ($1 - \Delta u / \Delta u_{max}$)
CPTu_10m	10.00	3700	0.78
CPTu_13m	13.00	5470	0.75

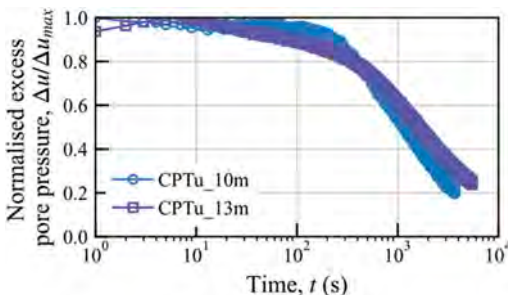


Figure 4. Dissipation test at 10 and 13m depth.

for the Tubarão Site. The horizontal coefficient of consolidation evaluated by the model was $7.79E^{-7}m^2/s$ and $4.10E^{-7}m^2/s$ for 10m and 13m depth respectively, assuming the rigidity index was 100 (Odebrecht & Schnaid, 2018).

The polynomial fitting method was used to compute t_{50} from tests CPTu_10m and CPTu_13m. First, the measured piezocone pore pressure dissipation data were best fitted with a polynomial equation of 8th degree in the logarithm of time plot. The first and second derivate were then computed to obtain the inflection point, which correspond to t_{50} , as discussed in section 2. Figure 5 illustrates the application of the polynomial fitting method to obtain t_{50} from tests CPTu_10m and CPTu_13m.

The c_h values evaluated from t_{50} extracted from the polynomial method fall within the range of values calculated with the reference method. For the tests performed at 10m depth, c_h was $7.32E^{-7}m^2/s$, whereas for the test carried out at 13m, c_h was $4.55E^{-7}m^2/s$. This represents a difference of less than ~10% between methods for both tests.

This set of complete dissipation tests shows that the proposed mathematical fit provides estimates of c_h that compares well with values from the existing theoretical solutions, enhancing the confidence in the proposed method. The polynomial fitting method has the advantage of being independent of an accurate measurement of the equilibrium pressure and relying less in engineering judgement in fitting the data with theoretical solutions, which introduces uncertainties in the estimation of c_h .

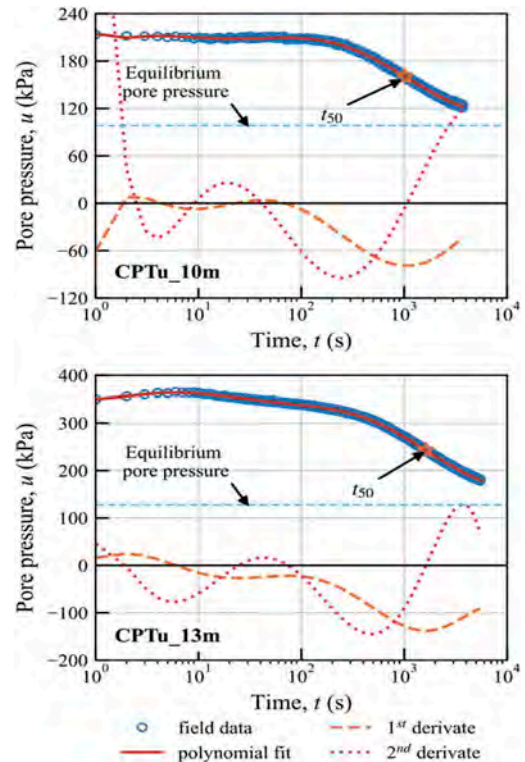


Figure 5. Application of the polynomial fitting method for tests CPTu_10m and CPTu_13m.

5 INCOMPLETE PIEZOCONE DISSIPATION TESTS

Previous interpretation was centered in complete dissipation tests where the degree of dissipation was greater than 75%. It is then necessary and economically convenient to evaluate incomplete CPTu dissipation tests where c_h values are estimated for early degrees of dissipation. Previous researchers have already considered the alternative of interpreting incomplete dissipation test (e.g. Schnaid et al, 1997; Krage et al, 2015), because significant time savings allow for more pore pressure dissipation tests in a site investigation plan.

The predictive approach proposed to estimate t_{50} , and therefore c_h , from measured cone dissipation tests was similar to the one described by Krage et al. (2015). The polynomial function was fitted to each dissipation test using truncated data sets from 40 to 70% dissipation. The optimal fitting equation was then derived to estimate t_{50} for each set of partial dissipation data, which was then used to estimate c_h ($c_{h,est}$). For data set truncated at dissipation degree less than 50%, a point simulating equilibrium pore pressure in a very long time ($t=100,000s$; $u_2=u_0$) was added to obtain a polynomial equation with a realistic dissipation like shape. An example is provided in Figure 6, where the fitted equation for test CPTu_13m truncated at 40% of dissipation is shown. The polynomial equation fits well the dissipation field data up to 40% dissipation but diverges after, as expected, since the data for dissipation higher than 40% was not used to derive the polynomial equation. Despite this, $c_{h,est}$ was $3.21E^{-7}m^2/s$, representing a difference of only 22% when compared to the reference value.

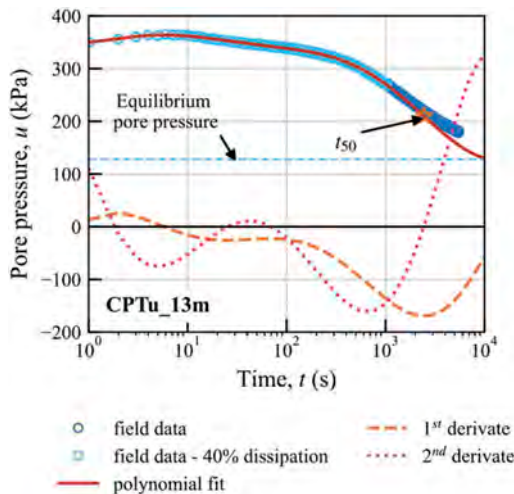


Figure 6. Application of the polynomial fitting method for tests CPTu_13m truncated at 40% of dissipation.

The percentage error ratio for $c_{h,est}$ was calculated as the numerical difference between predicted and

reference c_h ($c_{h,ref}$), normalized by $c_{h,ref}$, and expressed as percent, $[(c_{h,est} - c_{h,ref}) / c_{h,ref}]$. The $c_{h,ref}$ is the one obtained from the complete available data interpreted using the reference method. Figure 7 shows the percentage error ratio against truncated data sets at different degrees of dissipation.

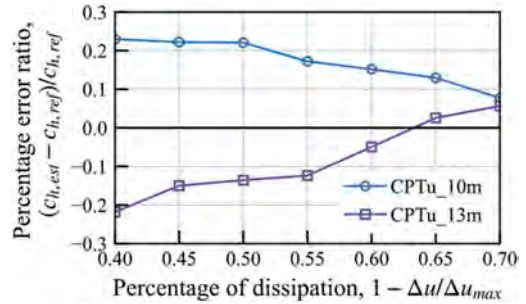


Figure 7. Percentage error ratio against truncated data sets from 40 to 70% dissipation for tests CPTu_10m and CPTu_13m.

The percentage error ratio to $c_{h,ref}$ is less than 25% in all cases and less than 20% in most cases, even with only 40% dissipation of excess pore pressure. It is worth recalling that the I_r value has a direct effect on the estimated absolute value of c_h (e.g. Keaveny & Mitchell 1986, Houlsby & Wroth 1991, Robertson et al. 1992, Schnaid et al. 1997, Mayne, 2001) and the uncertainty in selecting an appropriate I_r value exceeds the uncertainty in predicting t_{50} results once dissipation test exceeds 40%. The method seems to have potential to reduce the required time in field to estimate c_h , although further validation is required.

6 CONCLUSIONS

This paper presents an alternative method for t_{50} computation by fitting the piezocone pore pressure dissipation curve with a polynomial equation. Explicit recommendations are given for the fitting technique, including using the first and second derivatives to calculate t_{50} . The proposed method has the advantage of being independent of the equilibrium pore pressure measurement and requiring less engineering judgement. Furthermore, the proposed method seems to provide c_h estimates within 25% accuracy from incomplete dissipation test halted after only 40% dissipation (in respect to the c_h using a complete dissipation test and reference method).

REFERENCES

ASTM. (2012). "Standard Test Method for Electronic Friction Cone and Piezocone Penetration Testing of Soils." ASTM D5778-12, West Conshohocken, PA.

- Baligh, M. M.; Levadoux, J-N. (1986). "Consolidation after undrained piezocone penetration II: Interpretation." *J. of Geotechnical Engineering*, 10.1061/(ASCE)0733-9410(1986)112:7(727)
- Burns, S. E.; Mayne P. W. (1998). "Monotonic and Dilatory pore-pressure decay during piezocone tests in clay." *Canadian Geotechnical Journal*, 35(6),1063–1073.
- Chung, S. G., Kweon, H. J., and Jang, W. Y. (2014). "Hyperbolic fit method for interpretation of piezocone dissipation test." *J. of Geotechnical and Geoenvironmental Engineering*, 10.1061/(ASCE)GT.1943-5606.0000967, 251–254.
- Houlsby, G.T., and Wroth, C.P. (1991). "The variation of shear modulus of a clay with pressure and overconsolidation ratio." *Soils and Foundations*, 31(3),138–143.
- Keaveny, J., and Mitchell, J. K. (1986). "Strength of fine-grained soils using the piezocone." *Proc., Use of in Situ Tests in Geotechnical Engineering*, ASCE, Reston, VA, 668–685.
- Krage, C. P., DeJong, J. T., and Schnaid, F. (2015). "Estimation of the Coefficient of Consolidation from Incomplete Cone Penetration Test Dissipation Tests". *J. of Geotechnical and Geoenvironmental Engineering*, 10.1061/(ASCE)GT.1943-5606.0001218.
- Levadoux, J-N.; Baligh, M. M. (1986). "Consolidation after undrained piezocone penetration I: Prediction". *J. of Geotechnical Engineering*, 10.1061/(ASCE)0733-9410(1986)112:7(707).
- Lunne, T.; Robertson, P. K.; Powell, J. J. M. (1997). *Cone Penetration Testing in Geotechnical Practice*. Blackie, Melbourne, Australia.
- Lunne, T.; Yang, S.; Schnaid, F. (2014). "CPT Interpretation." *Proc., 3th International Symposium on Cone Penetration Testing, Las Vegas*, 145–164.
- Mántaras, F. M.; Odebrecht, E.; Schnaid, F. (2014). "On the Interpretation of Piezocone Dissipation Testing Data." *Proc., 3th International Symposium on Cone Penetration Testing, Las Vegas*, 315–322.
- Mántaras, F. M.; Odebrecht, E.; Schnaid, F. (2015). "Using piezocone dissipation test to estimate the undrained shear strength in cohesive soil." *Canadian Geotechnical Journal*, 52(3),318–325.
- Mayne, P.W. (2001). "Stress-Strain-Strength-Flow Parameters from Enhanced In-Situ Tests." *Proc., International Conference on In-Situ Measurement of Soil Properties and Case Histories, Bali, Indonesia*, 27–48.
- Odebrecht, E; Schnaid, F. (2018). "Assessment of the stress history of Quaternary clay from piezocone tests." *Soils and Rocks*, 41(2),179–189.
- Randolph, M.F.; Wroth, C.P. (1979). "An analytical solution for the consolidation around a driven pile". *International Journal for Numerical and Analytical Methods in Geomechanics*, 3(3),217–229.
- Robertson, P.K.; Cabal, K.L. (2008). "Guide to cone penetration testing for geo-environmental engineering". Gregg Drilling & Testing Inc.
- Schnaid, F.; Sills, G.C.; Soares, J.M.; Nyirenda, Z. (1997). "Predictions of the coefficient of consolidation from piezocone tests." *Canadian Geotechnical Journal*, 34 (2),143–159.
- Schnaid, F.; Odebrecht, E. (2015). "Challenges in the Interpretation of the DMT in Tailings." *Proc., 3th International Conference on the Flat Dilatometer, Rome*.
- Schnaid, F.; Odebrecht, E.; Sosnoski, J.; Robertson, P.K. "Effects of test procedure on flat dilatometer test (DMT) results in intermediate soils." *Canadian Geotechnical Journal*, 53(8),1270–1280.
- Teh, C. I.; Houlsby, G. T. (1991). "An analytical study of the cone penetration test in clay." *Géotechnique*, 41 (1),17–34.
- Torstensson, B. A. (1977). "Time-dependent effects in the field vane test". *Proc., International symposium of soft clay, Bangkok*, 387–397.
- Vick, S. G. (1983). *Planning, Design, and Analysis of Tailings Dams*. Wiley, New York.

Determination of fine-grained soil parameters using an automated system

I. Marzouk & F. Tschuchnigg

Graz University of Technology, Institute of Soil Mechanics, Foundation Engineering and Computational Geotechnics, Graz, Austria

F. Paduli, H.J. Lengkeek & R.B.J. Brinkgreve

Delft University of Technology, Delft, The Netherlands

ABSTRACT: Performing numerical analysis successfully depends on several factors. One of the most important factors is determining the constitutive model parameters correctly. It is often the case that these parameters are determined based on limited soil data. Using in-situ tests for determining these parameters has several advantages such as minimal disturbance of the soil and lower cost compared to laboratory tests. However, it is not possible to determine soil parameters directly from in-situ tests results. Thus, empirical correlations are required for interpreting soil parameters. Generally, several correlations exist for the same parameter, which will lead to calculating several values for the same parameter. An ongoing research project focuses on formulating an automated parameter determination (APD) framework that uses a graph-based approach to identify constitutive model parameters based on in-situ tests. This is achieved by using two spreadsheets as an input, one for parameters and the other for equations (correlations used to calculate parameters). Based on these two spreadsheets, the system generates paths between the parameters and calculates the value(s) for each individual parameter. So far, the research project focused on determining the parameters for coarse-grained soil based on cone penetration test (CPT) results. Due to the fact that the system was set up in a modular and adaptable way, it is possible to expand the system to accommodate more soil types and in-situ tests. It is the aim of the research project to increase the reliability of the parameters values (required to perform numerical analysis) determined from in-situ tests. This paper focuses on expanding the current framework to determine parameters for fine-grained soil. By using the two spreadsheets as an input, the system successfully calculates the value(s) for fine-grained parameters. Further validation, dealing with several values for each parameter, determining the accuracy of derived parameters and expanding the system to accommodate other in-situ tests and types of soils are part of ongoing research.

1 INTRODUCTION

There are several reasons that make the use of numerical analysis preferable compared to the traditional methods. One of the main advantages is the level of detail that can be obtained in several geotechnical engineering problems such as soil-structure interaction Brinkgreve (2019). Several factors influence the success of the numerical analysis. One of the most important factors is determining the constitutive model parameters properly. The main challenge in determining these parameters is the limited available soil data. It is often the case that these parameters need to be defined based on experimental tests (e.g., triaxial and oedometer tests) which are not always available in all projects.

On the other hand there are in-situ investigations, where the cone penetration test (CPT) is one of the most popular in-situ tests as it is quick and often used in soil profiling and estimating soil parameters. Moreover, CPT has other advantages such as minimal

disturbance of the soil and lower cost compared to laboratory tests. The main disadvantage of the interpretation of in-situ tests is that parameters cannot be determined directly from the results of the tests as the laboratory tests. However, a number of empirical relationships exist that link soil parameters to in-situ tests results, it is often the case that several relationships exist to determine the same parameter, which lead to a wide range of values for the parameter of interest. The reason for this variation is mainly related to the fact that these relationships are not applicable for all situations (e.g., specific soil types). In literature, several guides exist dealing with the interpretation of CPT such as Kulhawy & Mayne (1990), Lunne, Robertson, & Powell (1997), Mayne (2014) and Robertson (2015).

An ongoing research project focuses on creating an automated parameter determination (APD) system to determine constitutive model parameters based on in-situ tests. The framework relies on a graph-based approach that uses some of the characteristics of graph

theory. The project aims to create a transparent and an adaptable parameters determination framework. Transparency is achieved by illustrating how the available information is used to compute parameters and adaptability is achieved by allowing the users of the system to incorporate their knowledge and experience into the system. Van Berkom et al. (2022) illustrated the determination of parameters for coarse-grained soils based on CPT data. This paper extends the framework presented in Van Berkom et al. (2022) by including parameters for fine-grained soils.

The 2nd section briefly describes the APD framework, while the 3rd section presents selected empirical relationships used to determine parameters for fine-grained soils. In the 4th section, the output of the APD for a simple example is illustrated. In the final section the conclusions of this study are summarized.

2 AUTOMATED PARAMETER DETERMINATION (APD) FRAMEWORK

2.1 Framework

The framework consists of several modules that are connected together. A schematic representation of the modules is shown in Figure 1. CPT raw data, in Geotechnical Exchange Format (GEF) are imported to the first module (GEF Reader). Afterwards the CPT measurements (cone resistance q_c , sleeve friction f_s & porewater pressure readings u_2) are passed to the second module (CPT layer interpretation). The second module determines the SBT based on Robertson (2010) modified non-normalized SBT chart and stratifies the CPT profile into several layers sharing the same SBT. For each layer, the average of the CPT measurements (q_c , f_s & u_2) within this layer is computed. The averaged CPT measurements are used by module 3 (Layer state), to determine the state of all layers (overconsolidation ratio OCR and coefficient of earth pressure K_0). The output of modules 2 and 3 is transferred to module 4, where the parameters are connected with the equations (correlations) and the parameters of interest are calculated. In the final module, parameters calculated in module 4 are converted to constitutive model parameters. The system is built in the programming language Python.

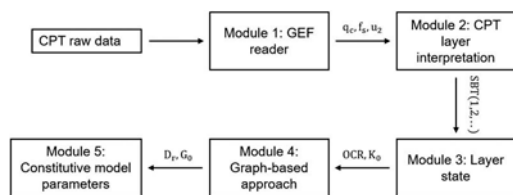


Figure 1. Schematic representation of the parameter determination modules.

The paper focuses on the output of module 4 at a specific depth. The layering process is not considered (modules 2 and 3) in this contribution. Moreover, the paper only presents the determination of fine-grained soil parameters (output of module 4) without the transition to constitutive model parameters (module 5).

Table 1. SBT zones according to Robertson (2010).

Zone	Soil Behaviour Type (SBT)
1	Sensitive fine-grained
2	Clays – organic soil
3	Clays: clay to silty clay
4	Silt mixtures: clayey silt & silty clay
5	Sand mixtures: silty sand to sandy silt
6	Sands: clean sands to silty sands
7	Dense sand to gravelly sand
8	Stiff sand to clayey sand (overconsolidated)
9	Stiff fine-grained (overconsolidated)

2.2 SBT interpretation

Robertson (2010) modified non-normalized SBT chart is used to classify the CPT profile. This SBT chart is based on dimensionless cone resistance, (q_c/p_a), where p_a is the atmospheric pressure and friction ratio (R_f in percent, $R_f = f_s/q_c$ 100%). The chart consists of 9 different zones, each corresponding to a different soil behaviour type (Table 1). At each depth, q_c and R_f are used to access the chart and determine the SBT for this depth. As a result, this module is used to distinguish between fine and coarse-grained soils.

2.3 Graph-based approach

The graph-based approach used in APD is described in detail in Van Berkom et al. (2022) and illustrated in Figure 2. The idea is to create links between source parameters (CPT raw data) via intermediate parameters to destination parameters (final soil or model parameters). Based on a given set of correlations, the system will create all the paths (chains of correlations) that provide the link from the source parameters all the way to the destination parameters and the system will calculate the destination parameter values from the input values of the source parameters (CPT data).

In the APD framework, the terms ‘correlation’, ‘formula’, ‘equation’, ‘rule of thumb’ is replaced by the term ‘method’. This general term is used as parameters could be determined based on several ways (e.g., tables and charts) (Van Berkom et al. (2022)). The system must link the methods and parameters that share a relationship. As an example, a method to compute the coefficient of earth pressure at rest according to Jaky (1944) is defined as follows, $K_0 = 1 - \sin(\phi')$, where K_0 is the coefficient of earth pressure at rest and ϕ' , is the effective internal friction angle of the soil. The system must identify

the input and output for this method (the output is K_0 and the input is ϕ'). Consequently, links connecting these parameters should be generated.

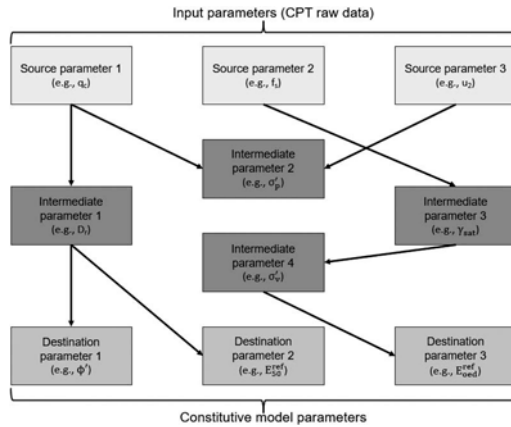


Figure 2. Graph-based approach implemented in APD.

2.4 Generating the graph

As shown in the previous subsection, the relationships between methods and parameters are defined by the output and input(s) of different methods. The parameters and methods are considered as external inputs to the system. The system requires two input files: methods and parameters. Users of the system may extend the standard database of methods and parameters provided with the system. The system connects the methods and parameters together, and computes the intermediate and destination parameters. Two different spreadsheets in comma-separated values (CSV) format corresponding to parameters and methods are used to generate the graph.

Each of the two CSV files has special properties. The methods CSV file requires the following properties, *method_to*, *formula*, *parameters_in*, *parameters_out*, *validity* and *reference*. Each of these unique properties need to be provided by the user in a CSV file. Taking the coefficient of earth pressure at rest method presented in the previous subsection as an example, *method_to* would present the name of the method, in this case it might be *method_to K₀*. In the field of *formula*, the equation should be defined, $1 - \sin(\phi')$. *Parameters_in* implicitly states the input for this method, ϕ' . Similar to *parameters_in*, the output of the method is stated in the field of *parameters_out*, K_0 . The validity field specifies the applicability of different methods. Some methods are applicable for all types of soils, other methods are only valid for coarse-grained soils and others are only suitable for fine-grained soils. As shown in Table 1, the SBT is based on Robertson (2010) modified non-normalized SBT chart. In that sense, the validity is defined in terms of SBT. If the

method is only valid for silt, the validity would be SBT(4). Regarding the method of coefficient of earth pressure at rest, the validity would be SBT(1234567). The reference field is an optional argument, where the user could state the author of the method (e.g., Jaky_1944).

The parameters CSV file requires the following properties, *symbol*, *value*, *unit*, *constraints*, and *description*. All of the parameters that have been used in the methods CSV files (in the fields of *formula*, *parameters_in* and *parameters_out*) must be defined in the parameters CSV file. The notation of the parameter (which was used in the methods CSV file) is stated in the *symbol* field (e.g., u for porewater pressure). In case the user wants to fix a value for a parameter (e.g., unit weight of water), the *value* field is used for this purpose. The *unit* field is an optional argument where the user could specify the unit of the parameter. It is highly recommended to provide the unit for all parameters to avoid unit conversion mistakes (e.g., using q_c in MPa in a method that requires q_c in kPa). Lower and upper bounds could be applied to parameters through the *constraints* field. Any computed value lower than the lower bound or higher than the upper bound would be discarded for the given parameter. The *description* field is an optional argument, where the user could define the parameter (e.g., OCR is the over-consolidation ratio).

By formulating the two CSV files (methods and parameters) as described, the system imports the two files and forms links between the methods and parameters (*parameters_in* & *parameters_out*) that are related together. The output of this procedure is a graph showing the links between all the defined parameters and methods. Moreover, the computed values for different parameters are shown on the graph. The current version of APD contains more than 100 methods.

3 SELECTED CPT FINE-GRAINED SOIL CORRELATIONS

A standard validated database for methods and parameters has been compiled and is continuously updated and improved. However, users are responsible for validating the outcome of the system, even if they used the provided standard database. Users still need to apply their geotechnical experience and knowledge to the outcome. Nevertheless with limited geotechnical knowledge, the system should result in reasonable values for different parameters. In this section, some methods for different fine-grained soil parameters are presented. These methods and parameters are used to generate the graph in the following section.

3.1 Unit weight

The calculation of the total unit weight (γ_t) is required to compute the total and effective vertical

stress, that are important in many correlations between CPT results and soil parameters. The selected correlations for estimating the unit weight in the APD system are:

$$\bullet \gamma_t = \gamma_w [0.27[\log R_f] + 0.36[\log(q_t/p_a)] + 1.236] \quad (1)$$

by Robertson & Cabal (2010), where γ_w is the unit weight of water and q_t is the corrected cone resistance (defined as $q_t = q_c + (1 - a) \times u_2$, where a is the cone tip net area ratio).

$$\bullet \gamma_t = 19 - 4.12 \left[\frac{\log(\frac{\delta}{q_t})}{\log(\frac{30}{R_f})} \right] \quad (2)$$

by Lengkeek, de Greef, & Joosten (2018).

$$\bullet \gamma_t = 26 - \frac{14}{1 + [0.5 \log f'_s + 1]^2} \quad (3)$$

by Mayne (2014).

3.2 Stress history

The stress history is often represented by the over-consolidation ratio ($OCR = \frac{\sigma'_p}{\sigma'_v}$, where σ'_p is the pre-consolidation stress and σ'_v is the effective vertical stress). The selected correlations for estimating OCR in the APD system are:

$$\bullet OCR = \frac{\sigma'_p}{\sigma'_v} = \frac{0.33(q_t - \sigma_v)^{m'}}{\sigma'_v} \quad (4)$$

by Mayne et al. (2009), where σ_v is the total vertical stress and m' is the yield stress exponent that increases with fines content and decreases with mean grain size. Mayne (2017) proposed determining m' from CPT material index I_c as follows:

$$- m' = 1 - \frac{0.28}{1 + (\frac{8I_c}{2.65})^{25}}, \text{ where } I_c \text{ is determined by an iterative process Robertson (2009) based on normalized cone parameter } (Q_m) \text{ with variable stress exponent } (n) \text{ that varies with } I_c. \quad (5)$$

$$\bullet OCR = 0.33 \times Q_m \quad (5)$$

by Kulhawy & Mayne (1990) and Robertson (2009), where:

$- Q_m = \frac{q_t - \sigma_v}{p_a} / (\frac{p_a}{q_t})^n$, where p_a is in the same units as q_t and σ_v ,

$$- n = 0.381(I_c) + 0.05(\frac{\sigma'_v}{p_a}) - 0.15 \leq 1.0$$

$$- I_c = \sqrt{(3.47 - \log Q_m)^2 + (\log F_r + 1.22)^2}$$

3.3 Strength parameters

The following correlation is used to determine the effective friction angle (ϕ') in the APD system:

$$\phi' = 29.5B_q^{0.121}(0.256 + 0.336B_q + \log(Q_t)) \quad (6)$$

by Mayne et al. (2009), where B_q is the normalized porewater pressure ($B_q = (u_2 - u_0)/(q_t - \sigma_v)$) and Q_t is the normalized cone resistance ($Q_t = \frac{q_t - \sigma_v}{\sigma'_v}$). The valid range for this correlation ϕ' is $0.1 \leq B_q \leq 1.0$ and $20 \leq \phi' \leq 45$.

3.4 Stiffness parameters

The 1-D constrained tangent modulus, M is used to estimate settlements. The following correlation is used to determine the constrained modulus in the APD system:

$$M = \alpha_M(q_t - \sigma_v) \quad (7)$$

Robertson (2009) suggested an approach based on I_c to determine α_M as follows:

- When $I_c > 2.2$:

$$\alpha_M = Q_m \text{ (if } Q_m < 14)$$

$$\alpha_M = 14 \text{ (if } Q_m > 14)$$

- When $I_c < 2.2$:

$$\alpha_M = 0.03[10^{(0.55I_c + 1.68)}]$$

4 DETERMINING FINE-GRAINED SOIL PARAMETERS

In this section, an example of the output of the system is presented. The methods CSV file used for this example, contains the correlations presented in the previous section, as well as other formulas used to compute some intermediate parameters (e.g., methods to calculate q_t, B_q, R_f, Q_t). The parameters CSV file includes all the parameters defined in the methods CSV file.

The system imported a CPT GEF file and determined the SBT at each depth. The interpreted SBT at

each depth is shown in Figure 3. For generating the graph, a CPT measurement at a depth of 10 m ($z = 10$ m) was chosen (Figure 3). This measurement has the following properties, $q_c = 1015.5$ kPa, $f_s = 31.5$ kPa and $u_2 = 351.6$ kPa. The ground water level (GWL) is located at 6 m below the ground level. The cone tip net area ratio is provided in the CPT GEF file as 0.85 ($a = 0.85$).

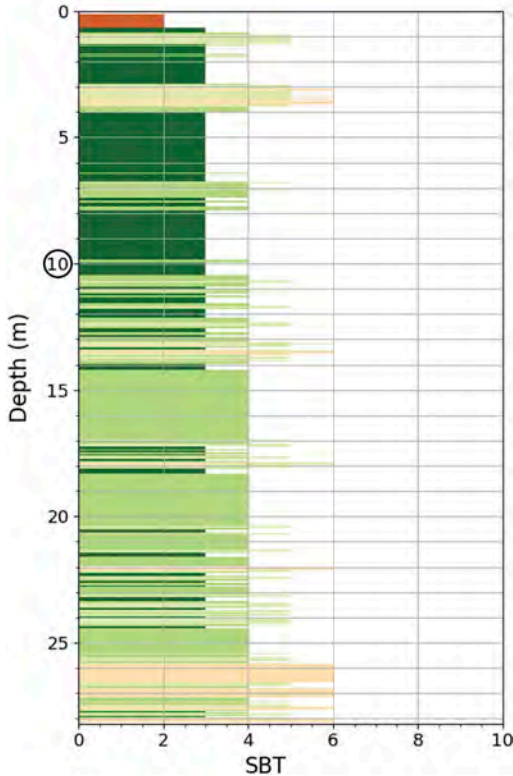


Figure 3. Interpreted SBT at each depth.

The unit weight of water (γ_w) is defined as 10 kN/m³. The atmospheric pressure (p_a) corresponds to 100 kPa. The interpreted SBT is 3, therefore, the soil type at this depth is clay (according to Table 1). The generated graph is shown in Figure 4.

The graph consists of green and blue nodes. The green nodes correspond to parameters, while the blue nodes correspond to methods. The arrows between different entities (parameters and methods) within the system. The arrows have a defined direction (going from a parameter to a method or from a method to a parameter).

Focusing on the unit weight of the soil (γ_{sat} located at the lower left corner in Figure 4), it is clear that three methods contribute to γ_{sat} . The methods correspond to the three correlations presented in the previous section, where $method_to_gamma_sat_1$ is Equation 1, $method_to_gamma_sat_2$ is Equation 2 and $method_to_gamma_sat_3$ is Equation 3. Three values were computed respectively as, 17.33, 16.25 and 17.09 kN/m³. Moving to OCR (located at the lower right corner in Figure 4), two methods contribute to OCR, where $method_to_OCR_1$ corresponds to Equation (4) and $method_to_OCR_2$ corresponds to Equation (5). Two values were computed respectively as 2.14 and 2.18. The friction angle (ϕ_{hip} located at the lower part in Figure 4) is obtained by only one method ($method_to_phi_{hip}$) corresponding to Equation (6). The friction angle was computed as 30.99. Similar to the friction angle, the constrained modulus (M_{CPT} located at the right-hand side of the graph in Figure 4) is obtained by only one method ($method_to_MCPT$) corresponding to Equation 7. The constrained modulus was computed as 5903 kPa.

As discussed in Equation 4, I_c , Q_m and n are determined through an iterative process. This iterative process requires the knowledge of the total and effective vertical stress. As a result, an initial

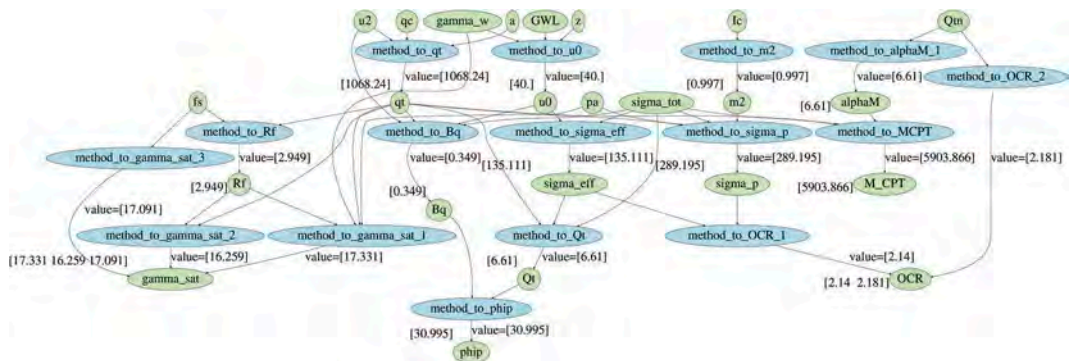


Figure 4. An example of a graph.

estimate for the unit weight is required to compute these parameters. In that sense, Equation 1 is used to compute an initial value for the unit weight, which in turn, is used to calculate the total stress (σ_{tot} in Figure 4), effective stress, I_c , Q_m and n . Consequently, it might be noticed from Figure 4 that Q_m and I_c (located at the top right corner in 4) are used directly as source parameters because they were calculated in a previous step internally before the graph was generated. Therefore, Equations 2 and 3 are only used to compute γ_{sat} for comparison purposes and they do not influence the calculation of the total and effective stress. As the system is formulated in an adaptable way, the user can decide which correlation for the unit weight to be used for the initial estimate for the total, effective stress and for the calculation of I_c , Q_m and n .

5 CONCLUSIONS

This paper is an extension to the automated parameter determination system presented in Van Berkom et al. (2022). The previous section presented proof of concept where a graph-based approach was used to calculate parameters for fine-grained soil. The presented system is transparent, flexible, and adaptable where the users can incorporate their experience and knowledge into the system by extending the standard database of methods and parameters provided with the system. The research project aims to increase the confidence in the parameters values (required to perform numerical analysis) determined from in-situ tests.

Figure 4 presented a simple example where a limited number of methods were used. In case of using several methods, this will lead to a scatter for the computed parameters. Dealing with this scatter and determining which approach is more suitable for choosing a specific value from the range of the computed values is part of an ongoing research. In addition, other SBT charts (e.g., Robertson (2009)) normalized SBTn chart and Robertson (2016) SBT chart) are added to the system. Moreover, the compiled correlations database is continuously validated, updated and the output of different correlations is compared to laboratory tests results whenever they are available. Correlations for calculating typical fine-grained soil parameters (e.g., plasticity index, PI , liquid limit, LL , compression index, C_c and swelling index, C_s) were also added to the database. Furthermore, the connection between soil parameters and constitutive model parameters is to be established. The database includes several correlations

between soil parameters and Plaxis Hardening Soil model with small-strain stiffness (HSsmall) (Benz (2007)). This is one of the main aspects of the research project as it will allow the transition from the CPT measurements to constitutive model parameters that could be used directly for numerical analysis.

REFERENCES

- Benz, Thomas (2007). *Small-strain stiffness of soils and its numerical consequences*. Ph. D. thesis, University of Stuttgart, Germany.
- Brinkgreve, R.B.J. (2019). Automated model and parameter selection. *Geostrata*, 41–47.
- Jaky, J. (1944). The coefficient of earth pressure at rest. In Hungarian (a nyugalmi nyomás tenyezője). *J. Soc. Hung. Eng. Arch. (Magyar Mernok es Epitesz-Egyelet Kozlonye)*, 355–358.
- Kulhawy, F.H. & Mayne, Paul (1990). Manual on Estimating Soil Properties for Foundation Design.
- Lengkeek, H. J., de Greef, J., & Joosten, Stan (2018). CPT based unit weight estimation extended to soft organic soils and peat. *Cone Penetration Testing 2018*.
- Lunne, Tom, Robertson, P., & Powell, John (1997). Cone Penetration Testing in Geotechnical Practice. *Soil Mechanics and Foundation Engineering 46*.
- Mayne, Paul (2014). Interpretation of geotechnical parameters from seismic piezocone tests. *Proceedings, 3rd International Symposium on Cone Penetration Testing (CPT14, Las Vegas) 102*, 47–73.
- Mayne, Paul (2017). Stress History of Soils from Cone Penetration Tests. *Soils and Rocks 40*, 203–216.
- Mayne, Paul, Coop, M, Springman, Sarah, Huang, An-Bin, & Zornberg, Jorge (2009). State-of-the-art paper (SOA-1): geomaterial behavior and testing.
- Robertson, P. (2009). Interpretation of cone penetration tests – A unified approach. *Canadian Geotechnical Journal 46*, 1337–1355.
- Robertson, P.K. (2010). Soil Behaviour Type from the CPT: An Update. *2nd International Symposium on Cone Penetration Testing, Huntington Beach 2*, 575–583.
- Robertson, P.K. (2015). Guide to cone penetration testing for geotechnical engineering. *Proceedings, 3rd International Symposium on Cone Penetration Testing (CPT14, Las Vegas)*.
- Robertson, P.K. & Cabal, K.L. (2010). Estimating soil unit weight from CPT. *2nd International Symposium on Cone Penetration Testing, Huntington Beach*.
- Robertson, P. K. (2016). Cone penetration test (CPT)-based soil behaviour type (SBT) classification system — an update. *Canadian Geotechnical Journal 53*(12).
- Van Berkom, I.E., Brinkgreve, R.B.J., Lengkeek, H.J., & De Jong, A.K. (2022). An automated system to determine constitutive model parameters from in situ tests. *Proceedings of the 20th International Conference on Soil Mechanics and Geotechnical Engineering, Sydney 2022. To be published*.

Undrained shear strength of clays from piezocone tests: A database approach

P.W. Mayne

Georgia Institute of Technology, Atlanta, GA, USA

J. Peuchen

Fugro, Nootdorp, The Netherlands

ABSTRACT: Deriving undrained shear strength of clays from piezocone tests (CPTU) suits the use of a database approach, particularly because good correlations are expected on the basis of theoretical correspondence. Benefits of a database approach include a minimal environmental footprint and field schedule shortening, primarily because of reduced borehole sampling and laboratory testing focused on verification rather than development of comprehensive site-specific data sets. This paper expands on the classic expression $s_u = q_{net}/N_{kt}$ where s_u is a reference undrained shear strength obtained by laboratory testing, q_{net} is the net cone resistance and N_{kt} is a cone bearing factor that is noted to decrease with increasing values of CPTU pore pressure ratio B_q . The database includes CPTU results and high-quality laboratory triaxial compression tests from 70 different clay deposits, of which 8 represent new case studies. The clays are allocated to 5 main categories: (a) soft-firm offshore; (b) soft-firm onshore; (c) soft sensitive; (d) stiff overconsolidated intact; and (e) stiff fissured clays. Organic clays and cemented clays are excluded.

1 INTRODUCTION

When a geotechnical exploration discovers that clay forms all or a portion of the subsurface environment, the magnitude of the undrained shear strength (s_u) parameter is generally sought for input into calculation models involving ground stability, particularly related to shallow foundations, pilings, and slopes. Undrained shear strength can also be important for transitional soils and sands, where combinations of geometry and loading rate can lead to undrained soil response.

Undrained shear strength is not a unique property of clays but affected by many variables, including mode of shearing, rate of loading, shear direction, initial stress state, failure criterion and other factors (Mayne 2008). This paper expands on the most common expression $s_u = q_{net}/N_{kt}$ where s_u is a reference undrained shear strength, q_{net} is net cone resistance and N_{kt} is a cone bearing factor according to classical bearing capacity theory. Values of N_{kt} can be obtained from analytical, theoretical, or numerical solutions, such as those based on limit plasticity, cavity expansion, finite elements, and strain path method. Well over 50 solutions are available for N_{kt} (e.g., Lunne, et al. 1997; Yu & Mitchell 1998; Col-reavy 2016; Agaiby 2018).

Here, an empirical database approach is considered for N_{kt} . The database approach uses data from high quality piezocone penetration test (CPTU) results matched at the same elevations as high quality samples subjected to laboratory testing.

2 DATABASE PARAMETERS

2.1 Triaxial compression tests

The reference undrained shear strength was defined as a triaxial compression mode, designated s_{uc} :

- Derived value (Eurocode 7) of s_{uc} from laboratory tests on Class 1 samples (ISO 22475-1:2006);
- Anisotropically-consolidated undrained triaxial compression tests (CAUC or CK₀UC) according to ISO 17892-9:2018 or equivalent; Note for fissured clays, often only CIUC tests were available;
- Recompression to the estimated in-situ stress conditions, using conventional back pressures for specimen re-saturation;
- $s_{uc} = 1/2(\sigma_1 - \sigma_3)_{max}$ defined as failure criterion or $(\sigma_1'/\sigma_3')_{max}$ as failure criterion when $(\sigma_1 - \sigma_3)$ provides no distinct maximum (Ladd & DeGroot 2003; Lade 2016), where σ_1' and σ_3' are the effective principal stresses.

2.2 Piezocone penetration tests

For the CPTU (ISO 22476-1:2012), three separate measurements are obtained: (a) corrected cone resistance, q_t ; (b) sleeve friction, f_s ; and (c) pore pressure, u_2 . These measurements are acquired at depth intervals of between 10 mm and 50 mm during a constant vertical push rate of 20 mm/s.

For each elevation, values of q_{net} and pore pressure ratio B_q were derived:

- $q_{net} = q_t - \sigma_{vo}$, where σ_{vo} = total vertical overburden stress;
- $B_q = \Delta u_2 / q_{net}$, where $\Delta u_2 = u_2 - u_0$ and u_0 = hydrostatic pressure.

Of further note, f_s can be used to provide an evaluation of the soil unit weight (γ) needed in the calculation of σ_{vo} (Mayne et al. 2010a, 2010b; Mayne & Peuchen 2012). Consequently, all three readings (q_t , f_s , u_2) are utilized in the assessment of s_{uc} of clays.

3 TRIAXIAL - PIEZOCONE DATABASE

A total of 62 natural clays that were subjected to CAUC lab testing ($n = 407$) provided the initial basis for this study (Mayne 2014). The majority of clays were deposited in a marine environment, although a few were lacustrine or alluvial or deltaic in origin. A few sensitive clays were originally formed as sediments in salt-water and later exposed to leaching by freshwater.

The clay sites were classified into 5 separate groups (Mayne & Peuchen 2018), including: (a) 17 offshore clays that were normally-consolidated (NC) to lightly-overconsolidated (LOC); (b) 29 onshore clays that were also NC - LOC, (c) 6 soft sensitive clays; (d) 5 intact overconsolidated clays (OC); and (e) 5 fissured OC clays.

From the database approach, the trend of the relationship for evaluating N_{kt} is presented in Figure 1

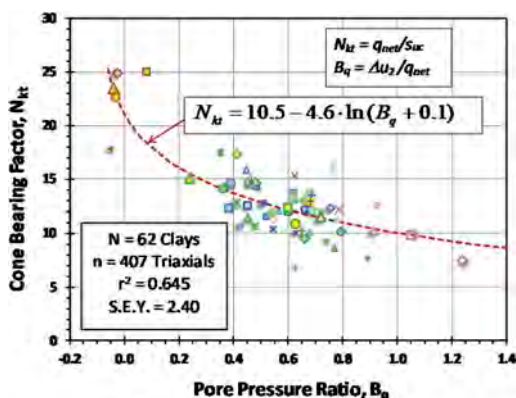


Figure 1. Trend of N_{kt} with B_q (Mayne & Peuchen 2018).

and expressed by Equation 1 (Mayne & Peuchen 2018) for values of $B_q > -0.1$:

$$N_{kt} = 10.5 - 4.6 \cdot \ln_e(B_q + 0.1) \quad (1)$$

Comments are as follows:

- An advantage of this approach over many other solutions for N_{kt} is that the CPTU provides all the necessary input;
- The methodology covers a wide range of clays showing $B_q > -0.1$, including soft to firm to stiff clays which vary from sensitive to insensitive, and intact to fissured;
- The approach does not apply to organic or cemented clays.

Since the initial database findings, a number of new case studies have become available that permit a validation of Equation 1. Herein, triaxial and CPTU data from 8 clays from Europe, Asia, and North America are presented. Three sites are from offshore locations and five clays are onshore deposits.

4 NEW CASE STUDIES

4.1 Luva, Norwegian sea

Luva is an offshore gas reserve located in 1300 water depth of the Norwegian sea. The site consists of very soft plastic clays having sensitivities in the range of 2 to 5. Index testing indicates a natural water content $w_n \approx 65\%$ to 75% , liquid limit $w_L \approx 70\%$, plastic limit $w_P \approx 29\%$, and plasticity index $I_p \approx 41\%$ (Lunne et al. 2014). Series of consolidation tests indicate that the site has not been mechanically overconsolidated, showing yield stress ratios ($YSR = \sigma_p'/\sigma_{vo}'$) in the general range of 1.2 to 1.7, primarily due to ageing.

Figure 2 shows q_t and u_2 with depth below the seafloor, pore pressure ratio B_q , and derived profile of s_{uc} from the N_{kt} relationship. In the last graph, the CPTU results are shown in comparison with 42 CAUC triaxial tests with good agreement.

4.2 Sipoo, Finland

Sipoo is located about 30 km north of Helsinki. The site consists of a homogeneous soft clay deposit between 2 and 9 m depth and water table near the surface (DiBuò et al. 2019). Index tests on the clay include: $w_n = 101 \pm 12\%$, $w_L = 79 \pm 10\%$, $w_P = 30 \pm 1\%$, $I_p = 50 \pm 9\%$, and clay fraction $CF = 79 \pm 11\%$. Laboratory CRS consolidation tests give a mean $YSR = 1.76$ and sensitivity by laboratory fall cone ranges from 15 to 44 with a mean $S_t = 25 \pm 8$.

Results from a representative CPTU at Sipoo are shown in Figure 3. The CPTU-evaluated profiles of s_{uc} compare well with the four laboratory CAUC test values on high-quality samples taken from the site.

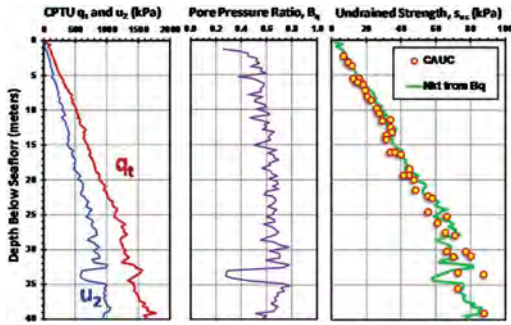


Figure 2. Profiles in clay at offshore Luva site, Norwegian Sea (data from Lunne et al. 2014).

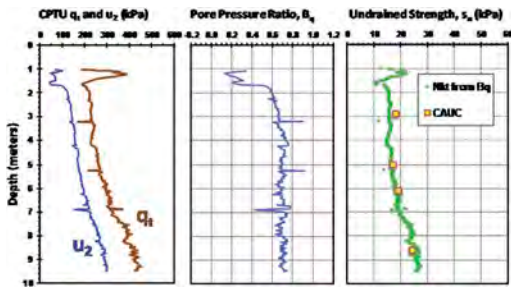


Figure 3. Profiles at Sipoo soft clay test site, Finland (data from DiBuò et al. 2019).

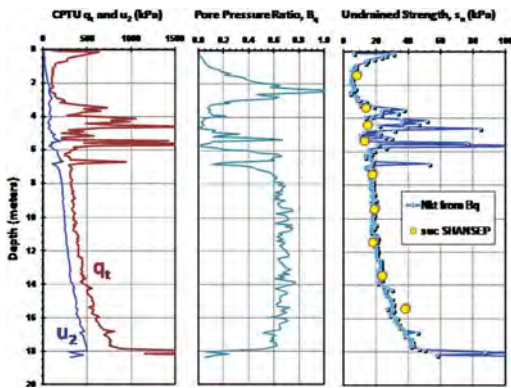


Figure 4. Profiles in soft clay at Saga, Japan (data from Hossain & Chai 2014).

4.3 Saga, Japan

The Saga TB site is located at the south of Japan next to the Ariake Sea. The upper 4 to 5 m is comprised of sandy silty clay while the underlying 12 m is a silty clay. Groundwater is encountered at a depth of 0.6 m.

Figure 4 shows profiles from a representative CPTU at the site (Hossain & Chai 2014). Nine consolidation tests on this clay indicated a mean

YSR = 1.83. Mean values of laboratory index parameters include: $w_n = 107 \pm 20 \%$, $w_L = 88 \pm 20 \%$, $w_P = 38 \pm 4 \%$, and $I_p = 54 \pm 13 \%$.

Using the aforementioned consolidation data and normalized undrained strength ratios from triaxial compression tests on Saga clay reported by Samang and Miura (2005), a profile of undrained shear strength was developed using the SHANSEP method (Ladd & DeGroot 2003). Figure 4 shows the comparison of the laboratory reference profile of s_{uc} in very good agreement with the CPTU derived values.

4.4 Tiller-Flotten, Norway

Tiller-Flotten near Trondheim, Norway serves as the experimental grounds involving quick clay research (L'Heureux et al. 2019). Groundwater is subjected to drawdown so that the hydrostatic pressure is considerably lower than normal.

Figure 5 shows a representative piezocone sounding (Mayne et al. 2019). The uppermost 2.5 m of soil is interpreted as a dry/desiccated layer of stiff over-consolidated sandy clay. Beneath this crust, throughout the sounding depths up to 30 m lies a soft fine-grained soil. The clay is extremely sensitive to quick from approximately 7.5 m below the surface (sensitivity > 100). In the quick clay zone below 7 m depth, typical index parameters are $w_n = 45 \%$, $w_L = 35 \%$, $w_P = 20 \%$, and $I_p = 15 \%$, with $CF \approx 45 \%$.

Figure 5 shows very good agreement from the CPTU-derived s_{uc} values with those obtained from 7 benchmark CAUC series on high-quality block samples.

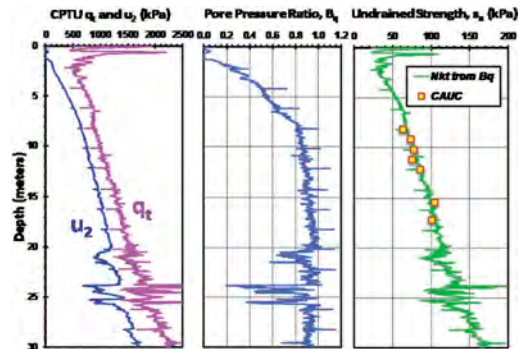


Figure 5. Profiles in highly sensitive clay at Tiller-Flotten research site, Norway (data from L'Heureux et al. 2019).

4.5 Sainte-Monique, Canada

Locat et al. (2015) detail the results of ground investigations for a major landslide involving firm to stiff sensitive nearly normally-consolidated plastic grey silty clay. The site is located some 130 km northeast of Montreal near the Nicolette River. Index tests show $56 \leq w_n \leq 77\%$, $53 \leq w_L \leq 65 \%$, $28 \leq I_p \leq 40\%$, $72 < CF$

< 85%, and liquidity index $1.1 \leq LI \leq 1.4$. Sensitivities derived from fall cone indicate $39 \leq S_t \leq 55$. Laboratory consolidation tests gave YSR between 0.9 and 1.2.

Figure 6 shows the piezocone profile in an undisturbed area outside of the limits of the landslide. The high value of B_q gives a low value of N_{kt} which in turn compares well with two CAUC and three CIUC triaxial tests performed on undisturbed samples.

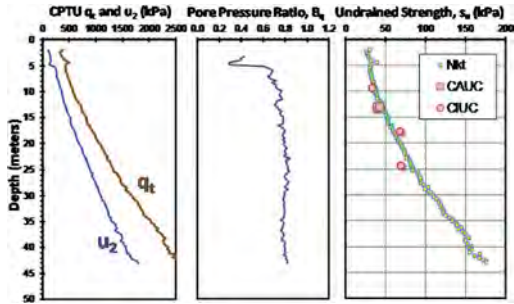


Figure 6. Profiles in sensitive clay at Sainte Monique, Quebec (data from Locat et al. 2015).

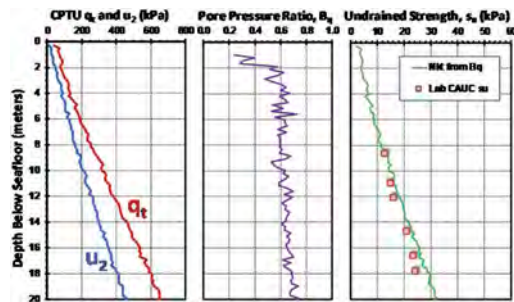


Figure 7. Profiles in soft plastic clay at Liwan offshore site, South China Sea (data from Palix et al. 2013).

4.6 Liwan, South China Sea

A deepwater geotechnical investigation was performed at the Liwan 3-1 offshore site in the Pearl River Mouth Basin of the South China Sea involving geophysics, sampling, piezocones, T-bars, vane, dissipation tests, and advanced laboratory testing (Palix et al. 2013). The site is underlain by soft highly-plastic clays. Liquid limits decrease from 130 % at seafloor to 80 % at 10 m below seafloor, with corresponding I_p going from 85 % to 50 % over the same depth interval. Clay fractions range between 25 to 50 %. Natural water contents vary from over 200 % at seafloor to about 90 % at 20 m depth. Measurements of calcium carbonate content range from 6 % to 25 %.

Figure 7 shows a piezocone profile and the corresponding and reasonable profiles of s_{uc} from the representative CPTU sounding and 6 CAUC triaxial tests.

4.7 Martin's Point Bridge, United States

A field case study with CPTU soundings in natural overconsolidated intact clays of the Presumpscot Formation is presented using data from Martin's Point Bridge, near Portland, Maine (Hardison & Landon 2015). The general stratification of the site (Figure 8) consists of a shallow organic silt layer underlain by stiff OC Presumpscot clay that extends from depths to 2 to 14 m and overlies glacial outwash sand and bedrock.

Shelby tube samples of the clay were collected at the site from different elevations and tested for index properties, consolidation parameters, and triaxial strength characteristics. The results of laboratory index testing on the clay gave an average unit weight $\gamma = 16.5 \text{ kN/m}^3$, natural water contents $w_n \approx 30$ to 40 %, liquid limits in the range of $20 \leq w_L \leq 45$ %, and plasticity indices (I_p) between 10 and 20 %. Sensitivities derived from field vane and fall cone were generally in the range of 2 to 9.

The groundwater table is located at a depth of 2 m. The stress history profile was determined by a series of 13 constant-rate-of-strain (CRS) consolidation tests that showed YSRs decreasing from 11 at 2 m depth to YSR = 3 at 14 m depth.

A total of 15 CAUC triaxial tests were performed, including both recompression and SHANSEP type methods (Ladd & DeGroot 2003). The derived profile of s_{uc} from the CPTU is presented in Figure 8 with values increasing from about 35 to 100 kPa in the deposit and shown to be in reasonably good agreement with the triaxial series.

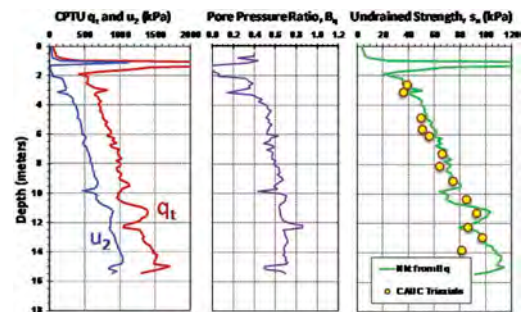


Figure 8. Profiles in firm OC clay at Martin's Point Bridge, Maine (data from Hardison & Landon 2015).

4.8 Offshore Denmark

This case study considers the Danish sector of the North Sea. The site has a water depth of about 45 m and includes about 3 m of Holocene sands which are underlain by hard Pleistocene age clays of the Doggerbank formation. Laboratory index tests on the clay indicate mean values: $w_n = 34$ %, $w_L = 49$ %, $I_p = 27$ % and $\gamma = 19.4 \text{ kN/m}^3$. Calcium

carbonate contents average 19 % for the clay. Consolidation tests indicate the clay to be overconsolidated with YSR decreasing from about 9 to 4 in the depth interval from 3 to 15 m below the seafloor.

Figure 9 shows low B_q values averaging 0.08, the N_{kt} - B_q algorithm gave a high mean value of $N_{kt} = 21$ for the clay and the corresponding profile of s_{uc} compares reasonably with the values from only two CAUC tests on undisturbed samples from the site.

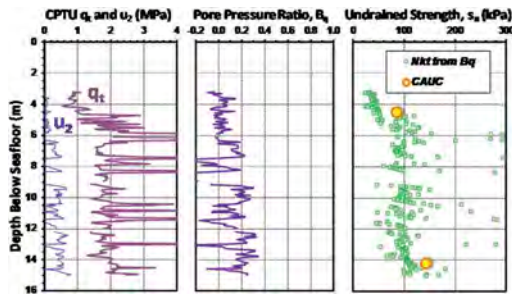


Figure 9. Profiles in stiff fissured OC Doggerbank clay at Danish offshore site.

5 CONCLUSIONS

The empirical methodology considers cone bearing factor ($N_{kt} = q_{net}/s_{uc}$) as a function of pore pressure ratio ($B_q = \Delta u_2/q_{net}$). The underlying database includes statistical analyses of 407 CAUC triaxial tests performed on 62 different clay deposits that were also field tested by CPTU.

The general trend shows N_{kt} varying from as high as 30+ for stiff fissured overconsolidated clays to low values of around 6 for soft sensitive and quick clay deposits. Generally, N_{kt} decreases with B_q .

Eight new case studies are presented showing the reasonableness and reliability of the earlier-derived methodology for assessing undrained strength of clays from piezocone penetration tests. Triaxial compression tests (CAUC, CK_0UC , and occasionally CIUC) on high-quality undisturbed samples were used as the benchmark reference tests. The final tally for the database now includes CPTU data from 70 clay sites with a total of 497 triaxial compression tests that provide the benchmark values of s_{uc} .

REFERENCES

- Agaiy, S.S. (2018). Advancements in the interpretation of seismic piezocone tests in clays and other geomaterials. *PhD dissertation*, Civil & Environmental Engineering, Georgia Institute of Technology, Atlanta, GA: 923 p.
- Colreavy, C. (2016). Use of piezoball penetrometers for measuring shear strength and consolidation characteristics of soft soil. *PhD dissertation*, Centre for Offshore Foundation Systems, Univ. of Western Australia, Perth: 304 pages.
- DeGroot, D., Lunne, T. and Tjelta, T.I. (2011). Recommended best practice for geotechnical site characterization of cohesive offshore sediments. *Frontiers in Offshore Geotechnics II* (Proc. ISFOG, Perth), Taylor & Francis Group, London: 33–57.
- DiBuò, B., D'Ignazio, M., Selänpaä, J., Lämsivaara, T. and Mayne, P.W. (2019). Yield stress evaluation of Finnish clays based on analytical CPTu models. *Canadian Geotech. Jour.* 57 (11): 1623–1638; doi:10.1139/cgj-2019-0427.
- Hardison, M.A. and Landon, M.L. (2015). Correlation of engineering parameters of the Presumpscot formation to SCPTU. *Report No. ME 15-12*, prepared by Univ. of Maine for Maine DOT, Augusta, 394 p.
- Hossain, J. and Chai, J. (2014). Estimating coef. of consolidation and hydraulic conductivity from piezocone test results. *Geomechanics and Engineering* 6 (6): 577–592.
- Hong, S.J., Lee, M.J., Kim, J.J. and Lee, W.J. (2010). Evaluation of undrained shear strength of Busan clay using CPT. *Proc. 2nd Intl. Symp. on Cone Penetration Testing*, Vol. 2 (Huntington Beach, CA), Omnipress: 313–320.
- ISO (International Organization for Standardization) 2012. Geotechnical investigation and testing – Field testing – Part 1: Electrical cone and piezocone penetration tests, International Standard ISO 22476-1:2012. (with technical corrigendum 1, January 2013). Geneva.
- Karlsruh, K., Lunne, T. and Brattlien, K. (1996). Improved CPTU interpretations based on block samples. *Proc. Nordic Geotechnical Meeting*, Reykjavik, Paper 3.4: 195–201.
- Knappett, J.A. and Craig, R.F. (2012). *Craig's Soil Mechanics, 8th Edition*, Spon Press, Taylor & Francis Group, London: 570 pages.
- L'Heureux, J.-S., Lindgård, A. and Emdal, A. (2019). The Tiller-Flotten research site: geotechnical characterization of a very sensitive clay deposit. *AIMS Geosciences* Volume 5, 4: 831–867
- Ladd, C.C. and DeGroot, D.J. (2003). Recommended practice for soft ground site characterization. *Soil & Rock America 2003*, Vol. 1 (Proc. 12 PCSMGE, MIT), Vertag Glückauf, Essen: 3–57.
- Lade, P.V. (2016). *Triaxial Testing of Soils*, John Wiley & Sons, Ltd, Chichester, UK: 402 p.
- Locat, A., Leroueil, S., Fortin, A., Demers, D. and Jostad, H.P. (2015). The 1994 landslide at Sainte-Monique, Quebec: geotechnical investigation. *Canadian Geotechnical Journal* 52 (4): 490–504.
- Low, H.E., Lunne, T., Andersen, K.H., Sjørnsen, M.A., and Randolph, M.F. (2010). Estimation of intact and remoulded undrained shear strengths from penetration tests in soft clays. *Geotechnique* 60 (11): 843–859.
- Lunne, T., Christoffersen, H.P. and Tjelta, T.I. (1985). Engineering use of piezocone data in North Sea clays. *Proc. ICSMFE*, Vol. 2, San Francisco, 907–912.
- Lunne, T., Robertson, P.K. and Powell, J.J.M. (1997). *Cone Penetration Testing in Geotechnical Practice*, Routledge-Taylor & Francis Group, London: 352 p.
- Lunne, T. (2010). The CPT in offshore soil investigations - a historic perspective. *Geomechanics & Geoengineering*, Vol. 7 (2): 75–101.
- Lunne, T., Andersen, K.H. and Yang, S.L. (2014). Undrained shear strength for deep water field development in the Norwegian Sea. *Proceedings. 5th International Workshop on CPTU and DMT in soft clays and organic soils*, Polish Committee of Geotechnics, Poznan: 213–228.

- Mayne, P.W. (2008). Piezocone profiling of clays for maritime site investigations. *Geotechnics in Maritime Engineering*, Vol. 1 (Proc. 11th Baltic Sea Geotechnical Conference, Gdansk), Polish Committee on Geotechnics: 333–350.
- Mayne, P.W., Peuchen, J., and Bouwmeester, D. (2010a). Unit weight evaluation from CPT. *Proceedings, 2nd Intl. Symposium on Cone Penetration Testing (CPT'10)*, Vol. 2, Huntington Beach, California: 169–176.
- Mayne, P.W., Peuchen, J., and Bouwmeester, D. (2010b). Soil unit weight estimated from CPTu in offshore soils. *Frontiers in Offshore Geotechnics II* (Proc. ISFOG, Perth), Taylor & Francis Group, London: 371–376.
- Mayne, P.W. and Peuchen, J. (2012). Unit weight trends with cone resistance in soft to firm clays. *Geotechnical and Geophysical Site Characterization 4*, Vol. 1 (Proc. ISC-4, Pernambuco), CRC Press, London: 903–910.
- Mayne, P.W. (2014). Development of an automated methodology for evaluation of undrained shear strength of offshore clays from piezocone penetration tests. *Report I22931* by Georgia Tech Research Corp. (Project No. 2006U94) to Fugro, The Netherlands: 192 p.
- Mayne, P.W., Peuchen, J. & Baltoukas, D. (2015). Piezocone evaluation of undrained strength in soft to firm offshore clays. *Frontiers in Offshore Geotechnics III*, Vol. 2 (ISFOG, Oslo), Taylor & Francis, London: 1091–1096.
- Mayne, P.W. & Peuchen, J. (2018). Evaluation of CPTU N_{kt} cone factor for undrained strength of clays. *Cone Penetration Testing 2018* (Delft), CRC: 423–429.
- Mayne, P.W., Paniagua, P., L'Heureux, J-S., Lindgård, A., and Emdal, A. (2019). Analytical CPTu model for sensitive clay at Tiller-Flotten, Norway. *Proc. XVII European Conf on Soil Mechanics & Geotech Engrg. (ECSMGE)*: Paper 0153, Reykjavik, Icelandic Geotechnical Society: www.issmge.org.
- Palix, E., Chan, N., Yangrui, Z. and Haijin, W. (2013). Liwan 3-1: How deep water sediments from South China Sea compare with Gulf of Guinea sediments. *Proceedings, Offshore Technology Conference*, Houston, Texas, OTC Paper 24010, Vol 2, 1101–1108.
- Paniagua, P., L'Heureux, J-S., Carroll, R., Kåsin, K. and Sjørusen, M. (2017). Evaluation of sample disturbance of three Norwegian clays. *Proc. Intl. Conf. on Soil Mechanics and Geotechnical Engineering*, Seoul, 481–484. www.issmge.org
- Powell, J.J.M. & Quarterman, R.S.T. (1988). The interpretation of cone penetration tests in clays with particular reference to rate effects. *Penetration Testing 1988*, Vol. 2 (Proc. ISOPT-1, Orlando), Balkema, Rotterdam: 903–909.
- Robertson, P.K. 2009. Interpretation of cone penetration tests: a unified approach. *Canadian Geotechnical Journal* 46 (11): 1337–1355.
- Samang, L., Miura, N. and Sakai, A. (2005). Geotechnical properties of soft cohesive lowland soils deposited in Saga Airport Highway, Japan. *Media Komunikasi Teknik Sipil*, Vol. 13 (3): EDISI XXXIII: 19–35
- Schnaid, F. (2009). *In Situ Testing in Geomechanics: The Main Tests*. CRC Press, Taylor & Francis Group, London, 352 pages.
- Yu, H.S. and Mitchell, J.K. (1998). Analysis of cone resistance: review of methods. *Journal of Geotechnical and Geoenvironmental Engineering* 124 (2): 140–149.

Evaluating geoparameters of Maine sensitive clay by CPTU

P.W. Mayne

Georgia Institute of Technology, Atlanta, GA USA

P. Paniagua

Norwegian Geotechnical Institute and Norwegian University of Science & Technology, Trondheim, Norway

B. Di Buò

Tampere University, Tampere, Finland

S.S. Agaiby

Cairo University, Giza, Egypt

ABSTRACT: Using two sets of analytical solutions for CPTU in clays, a suite of theoretically-consistent geoparameters is shown to be in good agreement with independent laboratory and field test results obtained on sensitive Presumpscot clay in Portland, Maine, USA. Fall cone tests indicate a mean sensitivity of $S_t \approx 37$. Values of undrained rigidity index (I_R), undrained shear strength (s_u), and yield stress ratio (YSR) are provided by a modified spherical cavity expansion-critical state hybrid model while an effective stress limit plasticity solution is utilized to assess the effective friction angle of the sensitive clay at both peak strength [Φ' at q_{max}] and also at maximum obliquity [Φ' at $(\sigma_1'/3)_{max}$]. A CPTU screening method that uses three simplified equations for YSR helps to identify that the clay is sensitive.

1 INTRODUCTION

1.1 Falmouth Bridge, Maine

A geotechnical investigation for a new bridge along state highway route 26/100 at the northern portion of Portland, Maine, USA was performed by the University of Maine for the Maine Department of Transportation (Hardison & Landon 2015). The site is located to the east of Interstate I-95 and underlain by sensitive clays of the Presumpscot Formation and in close proximity to prior landslides along the Presumpscot River in the community of Westbrook (Devin & Sandford 2000), as shown by Figure 1.

The subsurface exploration for the Portland-Maine bridge included soil test borings, drive sampling, undisturbed sampling, seismic piezocone penetration test (SCPTU) soundings, and various series of laboratory tests (Langlais 2011). A detailed summary of the geotechnical data and results is provided by Hardison & Landon (2015).

1.2 Interpretation of CPTU in clays

The interpretation of CPTU in clays often relies on empirical correlations and simple statistical trends, although theoretical formulations also play a role. In

this paper, two sets of analytical closed-form solutions are utilized so that a consistent and rational assessment is made for stress history and shear strength, both in terms of effective stress parameters (i.e., friction angle, Φ') and total stress analysis (i.e. undrained shear strength, s_u).

The yield stress, or preconsolidation stress (σ_p') is presented in terms of the normalized yield stress ratio: $YSR = \sigma_p' / \sigma_{v0}'$. Conventionally, results from one-dimensional consolidation tests are taken at various elevations to develop the profile of YSR with depth in clays. Herein, a modified spherical cavity expansion-critical state soil mechanics (SCE-CSSM) hybrid model for CPTU in clays provides three YSR profiles, as well as a measure of undrained rigidity index ($I_R = G/s_u$), where G is the shear modulus.

2 CONE PENETRATION TESTS

2.1 Piezocone soundings

The CPTU provides three continuous readings with depth: (a) cone tip resistance, q_t ; (b) sleeve friction, f_s ; and (c) penetration porewater pressure, u_2 . The standard rate of advancement is 20 mm/s, although the use of variable rate CPTU soundings have been revealed



Figure 1. Locations of bridge site and landslide in soft sensitive Presumpscot clay, Portland, Maine, USA.

to provide an effective method to characterize silts, mixed soils, and mine tailings that exhibit partially-drained behavior.

2.2 Seismic piezocone testing

The addition of a set of geophones to the standard penetrometer allows for downhole geophysical testing, most often at the 1-m rod breaks. A horizontal seismic source or autoseis unit is used to generate horizontally-polarized shear waves that are propagated vertically with depth. The profile of shear wave velocity (V_s) is used to obtain the small-strain shear modulus ($G_0 = G_{max}$) via elastic theory:

$$G_{max} = \rho_t \cdot V_s^2 \quad (1)$$

where $\rho_t = \gamma_t / g_a =$ total soil mass density, $\gamma_t =$ total soil unit weight, and $g_a =$ acceleration constant.

A representative SCPTU at the Portland-Maine Bridge site showing q_t , f_s , u_2 , and V_s in sensitive soft clay is presented in Figure 2.

2.3 CPTU parameters

It is convenient to express the CPTU results as net readings: (1) net cone resistance: $q_{net} = q_t - \sigma_{vo}$; (2) excess porewater pressure: $\Delta u = u_2 - u_0$; and (3) effective cone resistance: $q_E = q_t - u_2$; where σ_{vo} = total vertical overburden stress, u_0 = equilibrium porewater pressure; and $\sigma_{vo}' = \sigma_{vo} - u_0 =$ effective overburden stress.

Furthermore, several normalized and dimensionless CPTU parameters can be defined: $Q = q_{net} / \sigma_{vo}'$, $U = \Delta u / \sigma_{vo}'$, and $F_r (\%) = 100 \cdot f_s / q_{net}$. Note that the first three of these parameters are inter-related via: $U = Q \cdot B_q$.

An update to the normalized Q is now provided with a variable exponent that depends upon soil type, termed Q_m . Details are provided by Robertson (2009) and Robertson & Cabal (2015).

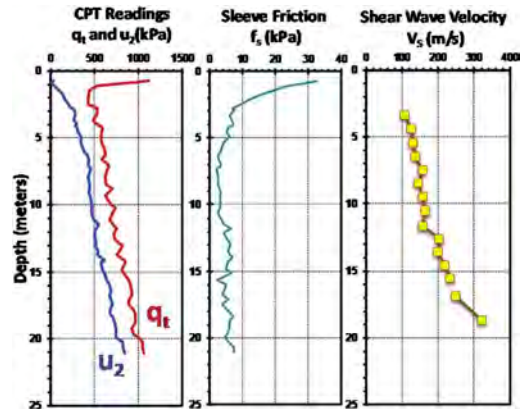


Figure 2. Profiles of q_t , f_s , u_2 , and V_s from SCPTU at Route 26/100 bridge site in Portland, Maine (data from Hardison & Landon 2015).

3 GEOPARAMETERS FROM CPTU

The evaluation of soil engineering parameters from CPTU is often addressed using empirical correlations and/or statistical trends derived from prior databases. As a result, some of the obtained values of the geoparameters are inconsistent with each other, or not well-matched well amongst each other, since they are assessed independently.

In this paper, the following geoparameters are assessed theoretically using two analytical solutions: (a) effective stress friction angle (Φ') at both q_{max} and $(\sigma_1' / \sigma_3')_{max}$; (b) rigidity index, I_R ; (c) undrained shear strength, s_u ; and (d) yield stress ratio $YSR = \sigma_p' / \sigma_{vo}'$. Thus, their values are obtained in a consistent and rational manner. Moreover, independent laboratory reference data on recovered soil samples are shown to be comparable with the CPTU evaluations.

3.1 Index parameters of clay

Laboratory index tests on the sensitive Presumpscot clay at the Portland-Maine site indicated: natural water content: $w_n = 43.6 \pm 7.3\%$, liquid limit: $LL = 42.1 \pm 6.9\%$, plasticity index: $PI = 17.5 \pm 5.6\%$, liquidity limit: $LI = 1.13 \pm 0.34$; and specific gravity of solids: $G_s = 2.78$. Measured unit weights gave a mean of $\gamma_t = 1.74 \text{ kN/m}^3$, while natural water contents using G_s and $S = 1$ indicated a value of around 18.4 kN/m^3 .

3.2 Soil behavior type

For soil classification by CPTU, it is common to utilize soil behavior type (SBT) charts. Hardison & Landon (2015) discuss the use of SBT that rely on Q-F and Q- B_q diagrams (Robertson & Cabal 2015). For the CPTU data at Portland-Maine Bridge, the

Q-F charts primarily indicate a zone 3 soil type (clays to silty clays), with an intermingling of zone 1 (sensitive soils), as shown in Figure 3. For the Portland CPTU data, the Q-B_q chart fails to find sensitive clays, as presented in Figure 4.

A SBT chart by Schneider et al. (2012) uses Q and U to identify soil types. This approach seems to better recognize sensitive clays, as shown in Figure 5.

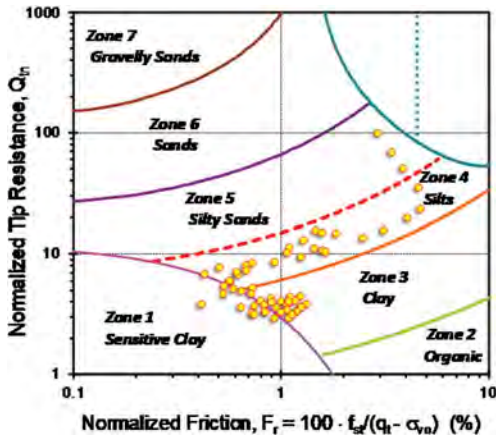


Figure 3. Portland-Maine CPTU data in Q-F soil behavior chart.

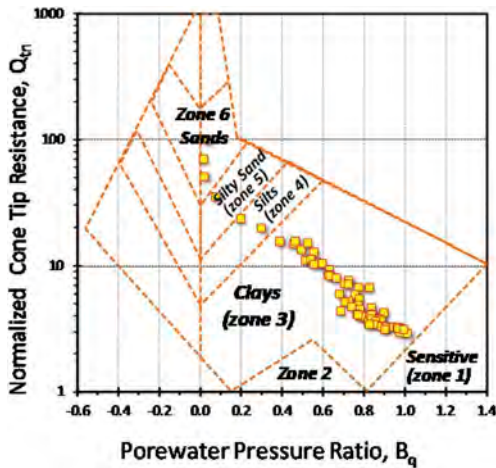


Figure 4. Portland-Maine CPTU data in Q-B_q soil behavior chart.

In fact, clay sensitivities (S_t) measured by lab fall cone range from 9 to 268 at the Portland bridge site. Based on the guidelines discussed by Holtz et al. (2011), the clay classifies as medium to highly sensitive below depths of 6 m where $S_t > 8$, as evidenced by Figure 6.

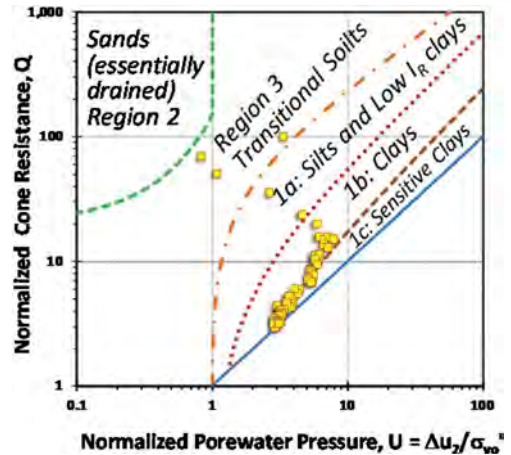


Figure 5. Portland-Maine CPTU data in Q-U soil behavior chart.

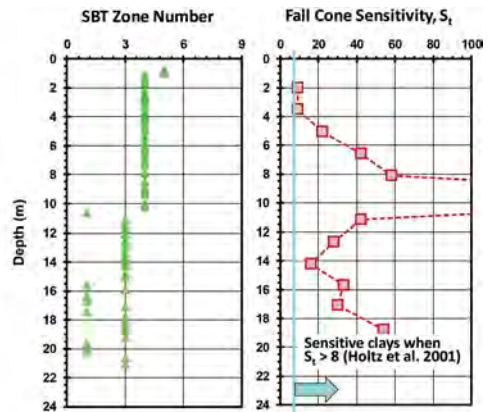


Figure 6. Profiles of SBT zone number from Q-F chart and clay sensitivity for Presumpscot clay at Portland-Maine site.

3.3 Screening for sensitive clays by CPTU

In addition to SBT charts for identification of sensitive soils, a simple CPTU screening can be used, as detailed elsewhere (Agaiby & Mayne 2018, 2021; Mayne et al. 2019).

For “regular” clays that are inorganic and insensitive, the following applies:

$$0.60q_E \approx 0.33q_{net} \approx 0.54 \Delta u_2 \quad (2)$$

For sensitive clays, the following hierarchy applies:

$$0.60q_E < 0.33q_{net} < 0.54 \Delta u_2 \quad (3)$$

For the CPTU at Portland-Maine Bridge, Figure 7 shows that the hierarchy from (3) applies, thus identifying sensitive soft clay at depths below 6 m.

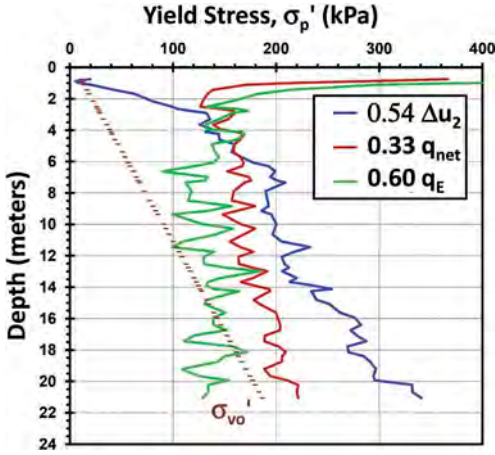


Figure 7. CPTU screening hierarchy to identify sensitive clays at Portland-Maine site.

3.4 Friction angle of sensitive Presumpscot clay

The effective stress friction angle (Φ') is a fundamental property of soil and an important parameter for stability analysis, foundation design, and numerical FEM simulations.

For the landslide investigation near Route 26/100, Devin & Sandford (2000) presented triaxial compression test data on soft sensitive Presumpscot clay. Figure 8 shows CK_0UC triaxial stress paths for a NC specimen, indicating a value of $\Phi'_1 = 30^\circ$ at peak strength, while at later stages of shearing, a value of $\Phi'_2 = 30^\circ$ is obtained at maximum obliquity (M.O.), defined when $(\sigma_1/\sigma_3)_{max}$ occurs.

To obtain Φ' in sensitive clays from CPTU, the Norwegian Institute of Technology (NTH, now NTNU) developed an effective stress limit plasticity solution for assessing Φ' in all soil types (Janbu & Senneset 1974; Senneset et al. 1989; Sandven et al 2016). The expression for the case where $c' = 0$ and undrained

penetration ($\beta = 0$) can be expressed:

$$Q = \frac{\tan^2(45^\circ + \phi'/2) \cdot \exp(\pi \cdot \tan \phi') - 1}{1 + 6 \cdot \tan \phi' (1 + \tan \phi') \cdot B_q} \quad (4)$$

Since iteration is required, an approximate inversion to express Φ' directly in terms of CPTU parameters Q and B_q has been devised for the following ranges: $0.05 \leq B_q < 1.0$ and $18^\circ < \Phi' < 45^\circ$ (Mayne 2007):

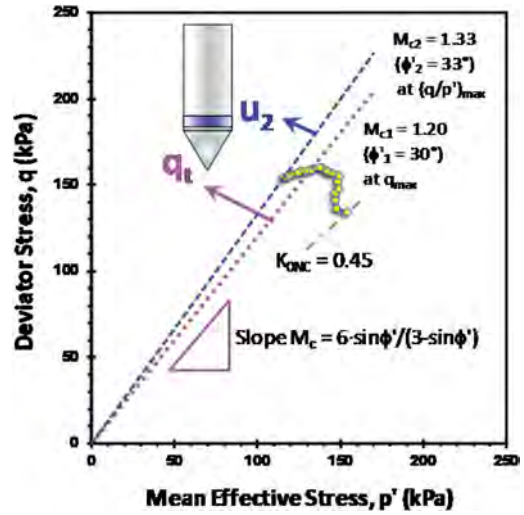


Figure 8. Triaxial stress path for Presumpscot clay at landslide site in Portland, Maine (data from Devin & Sandford 2000).

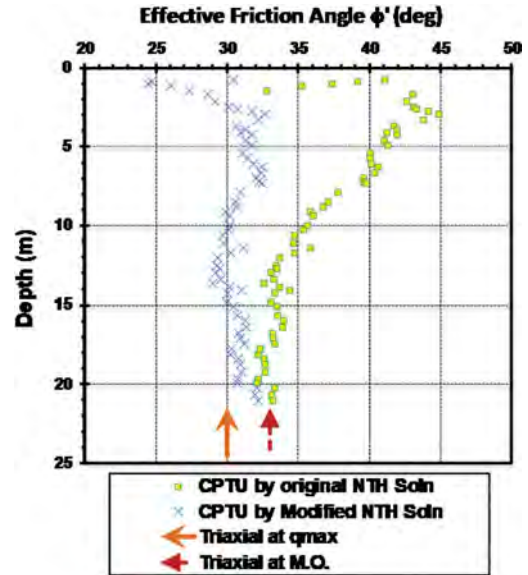


Figure 9. Profiles of Φ'_1 and Φ'_2 from CPTU using NTH solutions.

$$\Phi' = 29.5^\circ \cdot B_q^{0.121} \cdot [0.256 + 0.336 \times B_q + \log_{10} Q] \quad (5)$$

The value of Φ' corresponding to large strains or maximum obliquity is obtained with this original

NTH solution. Figure 9 shows the profile of Φ'_2 with depth and that a value of $\Phi'_2 \approx 33^\circ$.

To obtain the value of Φ'_1 at q_{\max} , a modified NTH solution is implemented (Sandven et al. 2016; Ouyang & Mayne 2019). In this case, Q in (4) is replaced with Q' that includes stress history:

$$Q' = Q/\text{YSR}^\Lambda \quad (6)$$

where $\text{YSR} = \sigma'_p / \sigma'_{vo}$ = yield stress ratio. The exponent Λ can be theoretically calculated as $\Lambda = 1 - C_s/C_c$ where C_c = compression index and C_s = swelling or recompression index, however, more often is assigned as a value $\Lambda \approx 0.7$ to 0.8 for insensitive clays and $\Lambda \approx 0.95$ to 1.0 for sensitive and quick clays (Ouyang & Mayne 2019).

At the Route 26/100 Falmouth Bridge site in Portland, Maine, the trend of YSR with depth from CRS consolidation tests indicates:

$$\text{YSR} \approx 5.12 \cdot z^{-0.508} \quad (7)$$

where z = depth (meters). The CRS results will be presented later in the paper.

Adopting $\Lambda = 0.95$ for soft sensitive Presumpscot clay and using Q' from (6) in (5), the profile of Φ'_1 with depth is shown in Figure 9. From depths between 8 to 20 m, the CPTU value more or less agrees with the CK_0UC value $\Phi'_1 = 30^\circ$.

3.5 Rigidity index

The undrained rigidity index is defined as $I_R = G/s_u$ where G = shear modulus and s_u = undrained shear strength. The difficulty here is that the magnitude of G ranges greatly, from a very high value at the nondestructive range at G_{\max} to a low value at failure (G_f) corresponding to peak strength.

In many instances, empirical correlations for estimating I_R are used. A UC-Berkeley method developed from triaxial tests on clays by Keaveny & Mitchell (1986) relates I_R with plasticity index (PI) and YSR, for which an approximate expression is available (Mayne 2007).

$$I_{R50} \approx \frac{\exp[(137 - PI)/23]}{1 + \ln_e \left[(\text{YSR} + 1)^{3.2} / 26 + 1 \right]^{0.8}} \quad (8)$$

which applies when: $10 < \text{PI} < 50$ and $\text{YSR} < 10$. For the range of PI at Portland-Maine Bridge ($9 < \text{PI} < 28$), this indicates an $120 < I_R < 250$.

A UC-Davis approach uses results from SCPTU to obtain a mobilized stress level based value of I_R

at 50% strength. In this case, I_{R50} is obtained from:

$$I_{R50} = \frac{1.81 \cdot G_{\max}}{(q_{\text{net}})^{0.75} (\sigma'_{vo})^{0.25}} \quad (9)$$

where G_{\max} , q_{net} , and σ'_{vo} are all in same units. At the Portland, Maine site, this approach gives a range: $148 < I_R < 260$.

A spherical cavity expansion - critical state soil mechanics (SCE-CSSM) model for CPTU in sensitive clays provides the direct assessment of I_R (Agaiby & Mayne 2018):

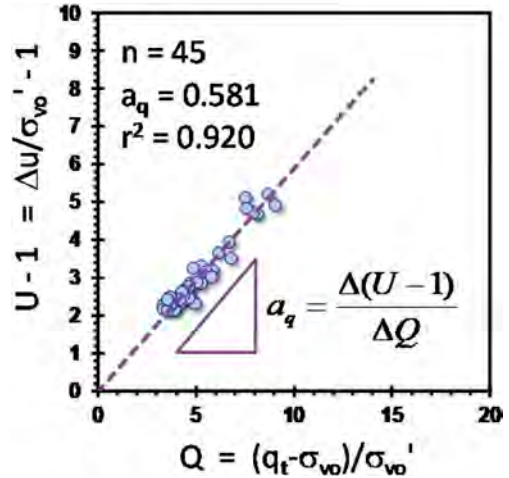


Figure 10. Plot of $U-1$ versus Q to obtain slope parameter a_q for evaluating rigidity index of Presumpscot clay.

$$I_R = \exp \left[\frac{1.5 + 2.925 \cdot M_{c1} \cdot a_q}{M_{c2} - M_{c1} \cdot a_q} \right] \quad (10)$$

where $M_c = 6 \cdot \sin \phi' / (3 - \sin \phi')$ is the frictional parameter in Cambridge q - p' space and a_q is obtained as the slope of $(U-1)$ versus Q . The value of M_{c1} corresponds to Φ'_1 at q_{\max} while M_{c2} is associated with Φ'_2 at large strains.

For the Portland site, a slope parameter $a_q = 0.581$ is obtained, as shown in Figure 10. Using the corresponding values of $M_{c1} = 1.20$ and $M_{c2} = 1.33$ gives a calculated $I_R = 266$.

The three approaches for I_R are presented in Figure 11. The upper bounds for the UCB and UCD methods imply that $I_R = 266$ from SCE-CSSM solution is reasonable.

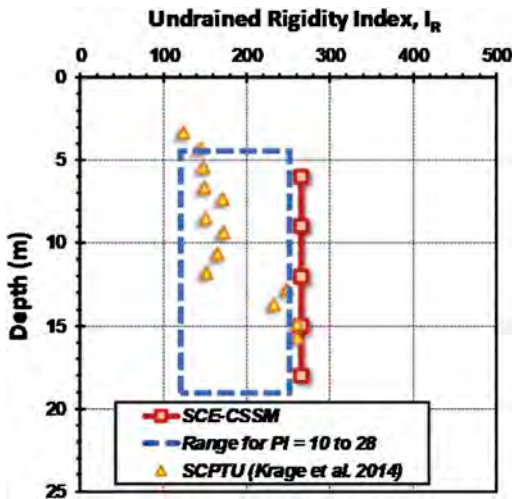


Figure 11. Undrained rigidity index profiles at Portland site.

3.6 Yield stress ratio at Portland-Maine site

The SCE-CSSM provides three expressions for YSR in clays that are functions of either Q or U, as well as both Q and U (Di Buò, et al. 2019):

$$YSR = 2 \cdot \left[\frac{Q/M_{c1}}{1.95 + 0.667 \cdot \ln_e I_R} \right]^{1/\Lambda} \quad (11)$$

$$YSR = 2 \cdot \left[\frac{U - 1}{0.667 \cdot M_{c2} \cdot \ln_e I_R - 1} \right]^{1/\Lambda} \quad (12)$$

$$YSR = 2 \cdot \left[\frac{Q - (M_{c1}/M_{c2}) \cdot (U - 1)}{1.95 \cdot M_{c1} + (M_{c1}/M_{c2})} \right]^{1/\Lambda} \quad (13)$$

The input parameters of Q and U, together with $M_{c1} = 1.20$, $M_{c2} = 133$, $\Lambda = 0.95$, and $I_R = 266$ are used to generate three profiles of YSR. The associated yield stresses (σ_p') are consistent and shown to be in good agreement with CRS consolidation tests on undisturbed samples from the site, as seen in Figure 12a.

3.7 Undrained shear strength

For the Portland, Maine site, a series of constant volume direct simple shear (DSS) tests were performed (Langlais 2011). These results can be converted to an equivalent triaxial compression mode (CK₀UC) via a simple relationship that depends on Φ' (Mayne 2008):

$$s_{uDSS}/s_{uc} = 0.65 \quad (14)$$

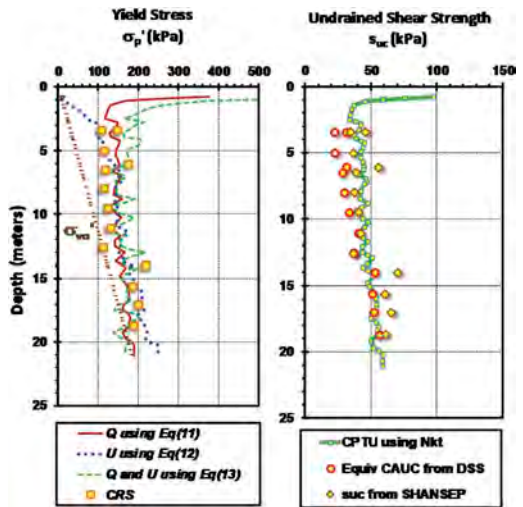


Figure 12. Profiles of yield stress and undrained shear strength for sensitive Presumpscot clay in Portland, Maine (reference lab data from Hardison & Landon 2015).

Alternatively, a SHANSEP type approach can be used where (Hardison & Landon 2015):

$$s_{uc} = S \cdot YSR \wedge \sigma_{vo}' \quad (15)$$

where $S = 0.33$ and $\wedge = 0.95$. Here, the results of the CRS consolidation tests provide the YSR.

For the CPTU, the undrained shear strength is a triaxial compression mode such that:

$$S_{uc} = q_{net}/N_{kt} \quad (16)$$

where N_{kt} is a cone bearing factor obtained from SCE theory (Vesic 1977):

$$N_{kt} = 4/3 \cdot (\ln_e I_R + 1) + \pi/2 + 1 \quad (17)$$

For a value of $I_R = 266$, the calculated bearing factor is $N_{kt} = 11.35$.

All three evaluations of s_{uc} for soft sensitive clay at Portland are presented in Figure 12b with reasonable agreement shown for all profiles.

4 ADDITIONAL CASE STUDIES

These analytical CPTU solutions have also been successfully applied to a number of other sensitive clays, including Finland (Di Buò, et al. 2019), Norway (D'Ignazio, et al. 2019; Mayne et al. 2019), USA (Mayne & Benoit 2020), and Canada (Agaiby & Mayne 2018; Agaiby et al. 2021).

5 CONCLUSIONS

Two sets of analytical solutions for CPTU in soft sensitive clays are applied to a case study involving the Presumpscot Formation in Portland, Maine. A consistent and theoretical assessment is made for the geoparameters of the clay, including effective stress friction angle (Φ' at q_{\max} and Φ' at M.O.), rigidity index (I_R), undrained shear strength (s_{uc}), and yield stress ratio (YSR). The values from these closed-form solutions are in general agreement with results from laboratory testing on undisturbed samples, including CRS-type consolidation tests, triaxial compression tests, and direct simple shear. A simple means for screening to identify sensitive clays from “regular” insensitive and inorganic clays is also presented.

ACKNOWLEDGMENTS

The first author extends appreciation to ConeTec Group of Burnaby, BC for providing funds to Georgia Tech on in-situ research activities.

REFERENCES

- Agaiby, S.S. and Mayne, P.W. 2018. Interpretation of piezocone penetration and dissipation tests in sensitive Leda Clay at Gloucester Test Site. *Canadian Geotech. Journal*, 55(12): 1781-1794; <http://dx.doi.org/10.1139/cgj-2017-0388>.
- Agaiby, S.S. and Mayne, P.W. 2021. CPTU identification of regular, sensitive, and organic clays towards evaluating preconsolidation stress profiles. *AIMS GeoSciences* 7 (4): 553–573.
- Agaiby, S.S., Mayne, P.W., and Greig, J. 2021. CPTU screening method to identify soft sensitive clays in Canada. *Proceedings GeoNiagara: 74th Canadian Geotechnical Conference*, Paper ID 118, Canadian Geotech Society.
- Di Buò, B., D’Ignazio, M., Selänpää, J., Lämsivaara, T. and Mayne, P.W. 2019. Yield stress evaluation of Finnish clays based on analytical CPTu models. *Canadian Geotech. Jour.* 57 (11): 1623–1638; doi.org/10.1139/cgj-2019-0427
- Devin, S.C. and Sandford, T.C. 2000. Shear strength of sensitive clay slopes in Maine. *Proceedings Slope Stability 2000*, GSP 101 (GeoDenver) ASCE, Reston, Virginia: 114–128.
- D’Ignazio, M., Lindgård, A. and Paniagua, P. 2019. *Soil Parameters in Geotechnical Design, Report SP8*, prepared by Norwegian Geotechnical Institute (NGI) for the Norwegian Research Council, Oslo: 70 p.
- Hardison, M.A. and Landon, M.L. 2015. Correlation of engineering parameters of the Presumpscot formation to the seismic cone penetration test. *Technical Report 15-12* prepared by University of Maine, Advanced Structures and Composites Center, submitted to Maine Dept. of Transportation, Augusta: 394 pages.
- Holtz, R.D., Kovacs, W.D. and Sheahan, T.C. 2011. *An Introduction to Geotechnical Engineering*, 2nd Edition, Pearson, Upper Saddle River, NJ: 853 p.
- Janbu, N., and Senneset, K. 1974. Effective stress interpretation of in situ static penetration tests. *Proceedings of the 1st European Symposium on Penetration Testing*, Vol. 2, Swedish Geotechnical Society, Stockholm: 181–193.
- Keaveny, J. and Mitchell, J.K. 1986. Strength of fine-grained soils using the piezocone. *Use of In-Situ Tests in Geotechnical Engineering* (Proc. In-Situ’86, Blacksburg), GSP 6, ASCE, Reston, Virginia: 668–685.
- Krage, C.P., Broussard, N.S., & DeJong, J.T. 2014. Estimating rigidity index based on CPT measurements. *Proceedings of the 3rd International Symposium on Cone Penetration Testing*, Las Vegas: 727–735. www.usucger.org
- Langlais, N.D. 2011. Site characterization using the seismic piezocone in Presumpscot clay and correlations to engineering parameters, *MS Thesis*, ID 1569, Civil Engineering Department, The University of Maine: 249 pages.
- Mayne, P.W. 2007. *NCHRP Synthesis 368: Cone Penetration Testing*, Transportation Research Board, Washington, DC: 118 p. www.trb.org
- Mayne, P.W. 2008. Piezocone profiling of clays for maritime site investigations. *Geotechnics in Maritime Engineering*, Vol. 1 (Proceedings, 11th Baltic Sea Geotechnical Conference, Gdansk), Polish Committee on Geotechnics: 333–350.
- Mayne, P.W., Paniagua, P., L’heureux, J-S., Lindgård, A., and Emdal, A. 2019. Analytical CPTu model for sensitive clay at Tiller-Flotten site, Norway. *Proc. XVII ECSMGE: Geotechnical Engineering Foundation of the Future*, Paper 0153, Reykjavik, Icelandic Geot. Society: www.issmge.org
- Mayne, P.W. and Benoît, J. 2020. Analytical CPTU models applied to sensitive clay at Dover, New Hampshire. *Journal of Geotechnical & Geoenvironmental Engineering* 146 (12) DOI: 10.1061/(ASCE)12GT.1943-5606.0002378
- Ouyang, Z. and Mayne, P.W. 2019. Modified NTH method for assessing effective friction angle of normally consolidated and overconsolidated clays from piezocone tests. *Journal of Geotechnical & Geoenvironmental Engineering* 145(10), [doi.org/10.1061/\(ASCE\)GT.1943-5606.0002112](https://doi.org/10.1061/(ASCE)GT.1943-5606.0002112)
- Robertson, P.K. 2009. Interpretation of cone penetration tests: a unified approach. *Canadian Geot. J.* 46 (11): 1137–1355.
- Robertson, P.K. and Cabal, K. 2015. *Guide to Cone Penetration Testing for Geotechnical Engineering*, 6th edition, Gregg Drilling, Signal Hill, CA: 140 pages.
- Sandven, R., A. Gylland, A. Montafia, K. Kåsin, A. A. Pfaffhuber, and M. Long. 2016. In-situ detection of sensitive clays, Part II: Results. *Proc., 17th Nordic Geotechnical Meeting: Challenges in Nordic Geotechnic*, Icelandic Geotechnical Society, Reykjavik: 113–123.
- Schneider, J.A., Hotstream, J.N., Mayne, P.W. and Randolph, M.F. (2012). Comparing CPTu Q-F and $Q-\Delta u_2/\sigma_{vo}$ soil classification charts. *Geotechnique Letters*, Vol. 2 (4): 209–215.
- Senneset, K., Sandven, R., and Janbu, N. 1989. Evaluation of soil parameters from piezocone tests. *Transportation Research Record* 1235, National Academy Press, Washington, DC: 24–37.
- Vesic, A.S. 1977. *NCHRP Synthesis 42: Design of Pile Foundations*, Transportation Research Board, National Academies Press, Washington, DC: 68 p.

CPTU evaluations in Appalachian Piedmont residual sandy silts

P.W. Mayne

Georgia Institute of Technology, Atlanta, GA, USA

E. Cargill

ConeTec Group, Richmond, VA, USA

ABSTRACT: Results from recent piezocone testing are compared with a statistical set of 22 prior CPTU soundings at the Opelika National Geotechnical Experimentation Site in Alabama. The site is underlain by residua comprised of fine sandy silts of the Appalachian Piedmont geologic province in the eastern USA. The cone resistance and sleeve friction from a 2016 CPTU compare well with the mean values from previous soundings while the porewater pressure readings are similar yet different because of a drop in the groundwater table from 2 m to 10 m over the period of study. Evaluations of the effective friction angle and yield stress from CPTU in residual soils are presented and compared with benchmark values obtained from laboratory triaxial and consolidation test results. Most interestingly, as the soil is intermediate with about 50-50 silt and sand, both undrained and drained penetration give more or less the same results.

1 INTRODUCTION

Since 70% of the Planet Earth is covered by oceans, most soils are formed originally as marine sediment. As a consequence, the majority of geotextbooks and research studies have focused on the interpretation of in-situ and laboratory tests involving water-borne deposits. It is estimated that approximately 5% of soils globally are found to be residual type, formed by the in-place disintegration and weathering of parent bedrock (USDA 2021), thus the evaluation of geoparameters in residua has been less well understood and quantified.

In this paper, results from piezocone penetration tests (CPTU) in residual sandy silts at a national test site in the southeastern USA are presented and interpreted. Of specific interest, the interpretation of effective stress parameters (c' and ϕ') and yield stress profile (σ_p') with depth provide the main focus.

When standard CPT soundings are performed at 20 mm/s, the results are considered *undrained* in clays, whereas in sands the response is taken as *drained* (Lunne et al. 1997). For silts, however, it is unclear whether the data are undrained or drained, or more likely in the regime of *partially-drained* behavior (DeJong, et al. 2012; Holmsgaard et. al. 2016; Blaker et al. 2019).

2 APPALACHIAN PIEDMONT RESIDUUM

The Appalachian Piedmont geologic province extends along the eastern USA ranging from Alabama to New Jersey, as shown in Figure 1. In addition to the surficial

extent, the Piedmont lies beneath younger sediments of the Atlantic Coastal Plain deposits. Moreover, the Piedmont serves as an important source of crushed stone, aggregate, and sands from quarries, as well as provides the natural foundation bearing material for buildings, bridges, and highway pavements for major urbanized centers, including Atlanta/GA, Greenville/SC, Columbia/SC, Raleigh/NC, Charlotte/NC, Richmond/VA, Washington/DC, Baltimore/MD, and Philadelphia/PA.



Figure 1. Extent of Appalachian Piedmont in eastern USA.

Primary rock types include gneiss and schist of Precambrian Z-age that were later intruded by granitic rocks of Paleozoic age. Residual soils commonly form as very fine sandy silts (ML, MH) to very silty fine sands (SM) and a dual system (ML-SM) has been used in a modified form of the Unified Soil Classification System.

A generalized profile of the residual and saprolitic soil and rock types is presented in Figure 2. In the

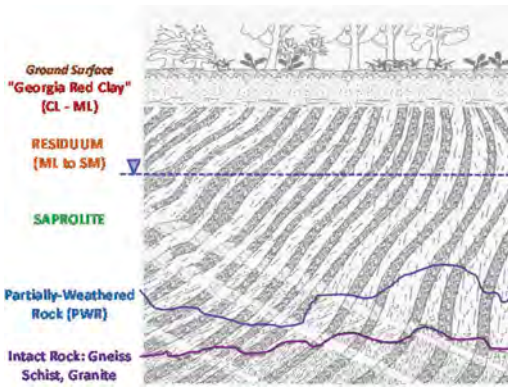


Figure 2. Generalized soil-rock profile in Piedmont geology.

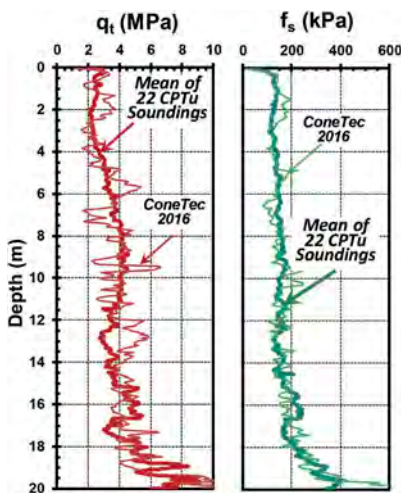


Figure 3. Comparison of mean q_t and f_s profiles from 22 CPTU series (2009 vintage) with 2016 sounding at Opelika test site.

southern Piedmont, saprolitic residuum is called *partially-weathered rock* (PWR) when the standard penetration test (SPT) values exceed 100 blows per foot (bpf), whereas in the northern Piedmont, the term *decomposed rock* is used and defined when SPT values exceed 60 bpf.

2.1 Opelika test site, Alabama

Some three decades ago, six national geotest sites were established with federal funding in the continental USA (Benoît & Lutenegeger 2000).

The Opelika test site in Alabama is situated in the Piedmont geology and serves as research grounds for laboratory, in-situ, geophysical, and full-scale foundation studies (Vinson & Brown 1997; Mayne et al. 2000; Mayne & Brown 2003; Anderson et al. 2019). The site

is approximately 150 hectare, owned by the Alabama Dept. of Transportation, and managed by Auburn University.

2.2 CPTU soundings at Opelika NGES

During the period from around 1995 to approximately 2000, many CPTU soundings were conducted at the Opelika NGES by several research groups and commercial testing firms (Mayne & Brown 2003). A statistical summary of some 22 CPTUs at the site are reported by Mayne et al. (2009), as shown by Figure 3. At the time of those series of soundings, the groundwater table was generally found to be around 2 to 3 m deep (Anderson et al. 2019).

In 2016, two new CPTUs were conducted by ConeTec Group as part of a new research program on energy piles (Atalay 2019). Results from one of these soundings is superimposed on the q_t and f_s profiles in Figure 3, showing very good overall agreement in these profiles in magnitudes while also displaying some local variations within the residual soil profile due to differential weathering.

Penetration porewater pressures at the shoulder position (u_2) in the Piedmont residuum is often negative below the groundwater table (Finke et al. 2001), as evident in Figure 4. The 2016 CPTU reading is also shown and differs in that the water table was considerably lower ($z_w \approx 10$ m), as detailed by Anderson et al. (2019).

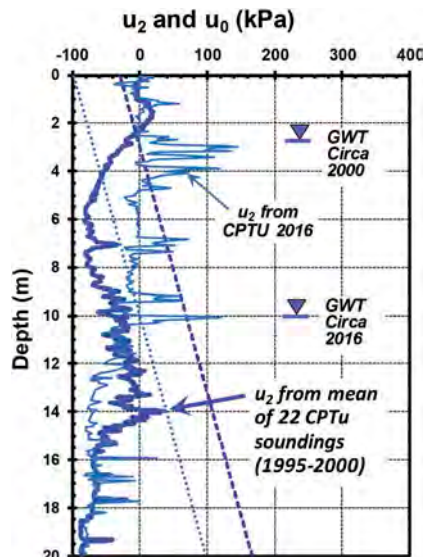


Figure 4. CPTU porewater pressure readings in fine sandy silt at Opelika test site.

2.3 Groundwater effect on CPTU

The depth to groundwater governs the equilibrium porewater pressure (u_0) and may affect the CPTU readings. Of interest here too is that the soils may be either dry, partially- or fully-saturated due to capillarity, since partially saturated soils may occur in the vadose zone between the ground surface and groundwater.

In some reported studies involving groundwater tables and partially saturated soils, the CPTU readings can show differences at seasonal changes due to matrix suction, partial or full capillarity, desiccation, and rainfall (e.g., Lehane et al. 2004; Huffman et al. 2015; Giaceti et al. 2019). In fact, for CPT in residual clayey sands derived from sandstone, Giaceti et al. (2019) showed changes in q_t and f_s in the upper 4 m while less differences at greater depths. Lehane et al. (2004) had two test areas at the same site, one with eucalyptus trees and one in an open area. The CPTU soundings in the open area did not show seasonal changes, while those in the treed area did. Huffman showed some seasonal changes in CPTU readings at a silty site in Oregon.

However, the q_t and f_s profiles at Opelika do not show significant differences in the 2000 and 2016 profiles of cone and sleeve resistances, despite the large changes in groundwater levels.

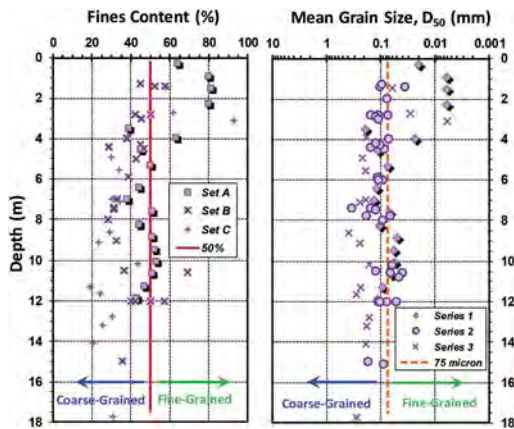


Figure 5. Fines content and mean grain size at Opelika.

3 GEOCHARACTERIZATION OF PIEDMONT

In this section, selected CPTU interpretations in Piedmont residuum at Opelika will be compared with laboratory results.

3.1 Laboratory testing of residuum

An extensive set of drive samples and undisturbed tube samples were collected for laboratory testing. The

lab program included: index testing, grain size, one-dimensional consolidation, triaxial compression, resonant column, direct shear, and permeability (Vinson & Brown 1997).

Results from mechanical analyses using sieves of recovered samples are presented in Figure 5. The measured fines content (FC) and mean grain size (D_{50}) are shown with depth to 16 m. It is evident that the soil particle sizes are at the threshold demarcation between fine-grained soils and coarse-grained soils, i.e. $D_{50} = 0.075$ mm corresponding to the US No. 200 sieve.

The fines content has a mean value $FC = 44\%$ ($n = 63$), thus the dual symbol ML-SM is seen appropriate for the fine sandy silts to silty fine sands. Average liquid limits and plasticity indices were 46% and 8%, respectively, although many specimens test as non-plastic (Mayne & Brown 2003). Natural water contents typically range between 20 and 40% in the upper 16 m, yet specifically for the earlier set of data, the mean $w_n = 29.9 \pm 6.2\%$ ($n = 26$) that dropped to $w_n = 25.7 \pm 7.0\%$ ($n = 37$) in 2016, presumably due to the groundwater drop.

Due to the closure of a nearby marble quarry some 4 km from the site in 2014, the groundwater has now begun a recovery toward its former regime (Anderson et al. 2019).

3.2 Yield stress profiles in Piedmont residuum

Consolidation tests on undisturbed samples from the site are reported by Hoyos & Macari (1999). Figure 6 shows the interpreted profile of yield stress (σ_p') and yield stress ratio ($YSR = \sigma_p'/\sigma_{v0}'$) from this test series. Assuming that full capillarity occurs in the overburden, a drop in the groundwater table to 20 m and subsequent rise to a depth of 3 m could explain the apparent preconsolidation stress caused by changes in effective stress at the Opelika site (Mayne 2013).

For CPTU, a generalized first-order evaluation of σ_p' is made from (Mayne et al. 2009):

$$\sigma_p' = 0.33 q_{net}^{m'} \text{ [units of kPa]} \quad (1)$$

where m' is an exponent that varies with soil type: $m' = 1.0$ (clays), 0.9 (organic soils), 0.85 (silts), 0.80 (silty sands), and 0.72 (clean quartzitic sands). For the fine sandy silts of the Piedmont geology, a value of 0.83 has been found suitable (Mayne 2013). The profile agrees well with the values from one-dimensional consolidation tests, as evident from Figure 6. The value of m' has also been related to mean grain size (D_{50}), fines content (FC), and material index (I_c), as detailed by Agaiby & Mayne (2019).

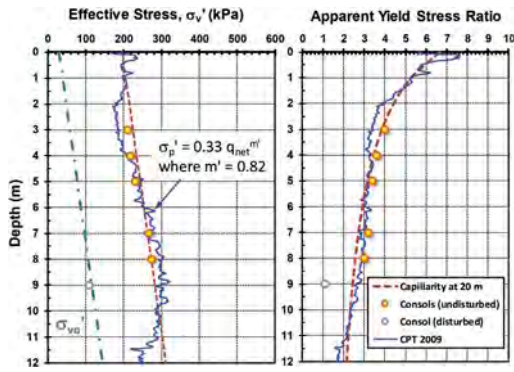


Figure 6. Yield stress and YSR at Opelika test site.

3.3 Triaxial friction angle of Piedmont soils

A total of 23 triaxial compression tests were performed on tube samples taken from the site (Vinson & Brown 1997; Brown & Vinson 1998). A summary of these tests is presented in Figure 7 giving an overall effective stress envelope represented by the Mohr-Coulomb parameters: $c' = 0$ and $\phi' = 35.5^\circ$.

At each sample depth, several CIUC type triaxials were conducted where the confining stresses were applied either at the in-situ overburden, or approximately half or about double the effective overburden.

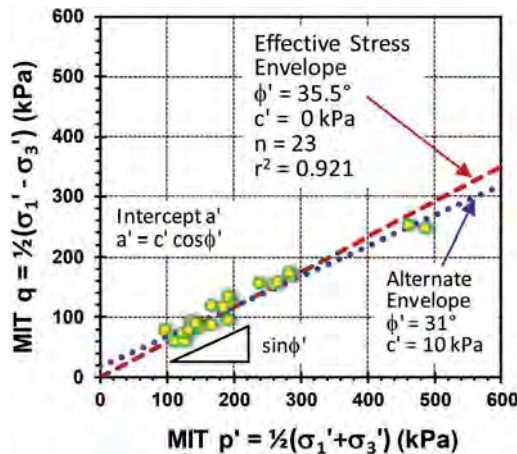


Figure 7. Summary triaxial tests at Opelika test site.

Consequently, an evaluation of the secant effective friction angle at six depths is made in Figure 8. Values of ϕ' ranged from 33.5° to 37.1° .

4 CPTU EVALUATION OF FRICTION ANGLE

For CPTU in silts, it is not initially clear whether the evaluation should be drained, undrained, or intermediate, such as partially-drained (DeJong et al.

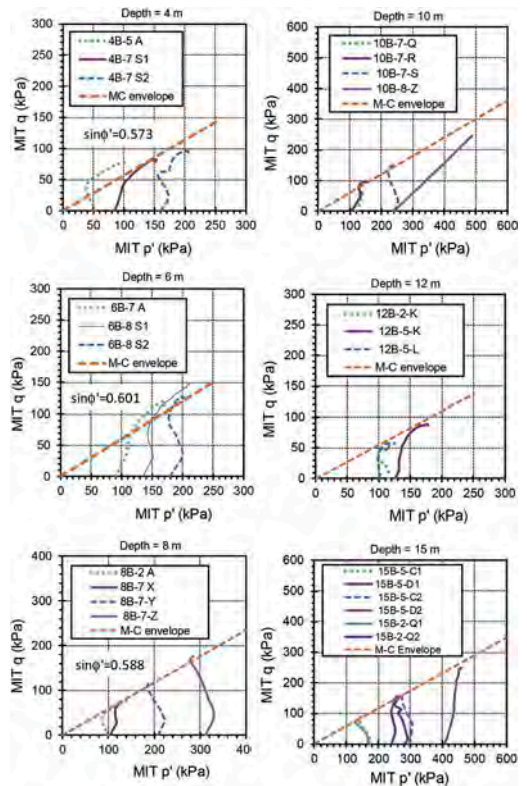


Figure 8. Triaxial results for various depths at Opelika.

2012; Holmsgaard et al. 2016; Bihs et al. 2018). This is a major conundrum for CPTU interpretation in Piedmont fine sandy silts.

4.1 CPTU evaluation of ϕ' in sands

At the standard rate of 20 mm/s, CPTU in clean sands is considered drained response. Various methods for evaluating ϕ' from CPTU in sands are available (Ching et al. 2017) including an approach from Robertson & Campanella (1983):

$$\phi' = \arctan[0.1 + 0.38 \cdot \log_{10}(q_t/\sigma_{v0}')] \quad (2)$$

A method based on corrected CPT chamber tests from Kulhawy & Mayne (1990):

$$\phi' = 17.6^\circ + 11.0^\circ \cdot \log_{10}[(q_t/\sigma_{atm})/(\sigma_{v0}'/\sigma_{atm})^{0.5}] \quad (3)$$

where $\sigma_{atm} \approx 1 \text{ bar} = 100 \text{ kPa}$. A modified form of this is given by Robertson & Cabal (2015):

$$\phi' = 17.6^\circ + 11.0^\circ \cdot \log_{10}(Q_{tn}) \quad (4)$$

where $Q_{tn} = (q_{net}/\sigma_{atm})/(\sigma_{vo}'/\sigma_{atm})^n$ is a normalized net cone tip resistance that has a variable exponent that ranges from about 1 in clays to 0.75 in silts to around 0.5 in sands.

For the Opelika CPTU, the various normalized cone resistance parameters (q_t/σ_{vo}' , q_{t1} , Q , Q_{tn}) are shown in Figure 9a. It can be stated that these profiles are quite similar.

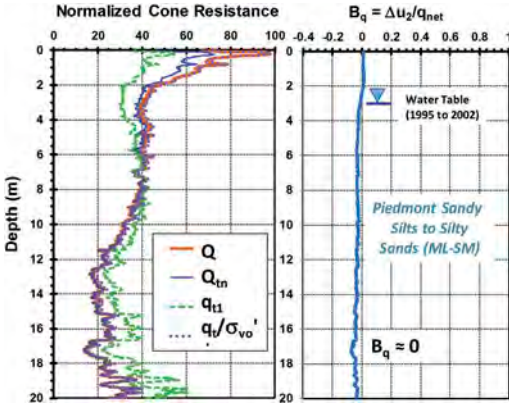


Figure 9. Normalized CPTU parameters at Opelika: (a) cone resistance; (b) porewater pressure ratio.

In fact, a recent study of 27 sands and silty sands that were sampled undisturbed using special freezing methods and/or gel samplers confirmed the relationships given by both (3) and (4) by comparison with laboratory triaxial compression tests ($n = 63$) and field CPTU (Uzielli & Mayne 2019).

4.2 CPTU evaluation of ϕ' in clays

At the standard CPTU rate of 20 mm/s in clays, response is taken to be undrained, corresponding to no volumetric strains (DeJong et al. 2012). Clays are identified when the CPT index $I_c \geq 2.95$ (Robertson & Cabal 2015). In consideration of clayey silts, a value of $I_c > 2.6$ is often taken to be “undrained” response.

A limit plasticity solution developed at the Trondheim Institute of Technology (NTH) for CPTU evaluation of ϕ' under undrained conditions is available from Senneset et al. (1989) that relates Q to ϕ' and B_q :

$$Q = \frac{\tan^2(45^\circ + \phi'/2) \cdot \exp(\pi \cdot \tan \phi') - 1}{1 + 6 \cdot \tan \phi' (1 + \tan \phi')} \cdot B_q \quad (5)$$

An approximation for ϕ' is expressed directly as a function of Q and B_q for the following ranges: $0.05 \leq B_q < 1.0$ and $18^\circ < \phi' < 45^\circ$ (Mayne 2007):

$$\phi' = 29.5^\circ \cdot B_q^{0.121} \cdot [0.256 + 0.336 \cdot B_q + \log_{10} Q] \quad (6)$$

In fact, data on over 105 different clays tested under both triaxial compression and CPTU have been calibrated to show they give comparable ϕ' values (Ouyang & Mayne 2018).

4.3 CPTU evaluation of ϕ' in fissured geomaterials

For the case where $B_q < +0.05$, eqn (6) is not valid and results from CPTUs at Opelika show $B_q \approx 0$, in fact, technically the B_q values are negative and average around -0.02 to -0.05 , as evidenced by Figure 9b. Negative porewater pressures are often recorded in fissured geomaterials, such as stiff over-consolidated clays (Mayne et al. 1990), but also observed in residual soils (Schneider et al. 2001; Finke et al. 2001).

From a measurement viewpoint, Campanella & Robertson (1988) showed the u_2 readings in a stiff clay were either slightly negative or slightly positive depending on the specific filter element, and thus u_2 can be affected by the thickness, width, and actual location of the porous element. Furthermore, studies by DeJong et al. (2007) show that type of fluid (water, oil, glycerine, silicone), its viscosity, and degree of saturation play a role in porewater pressure measurements during CPTU. Of final note, the NTH solution cannot handle negative B_q (Sandven 1990).

As such, a value of $B_q = 0$ is assumed at Opelika for CPTU at standard rates of 20 mm/s. An approximation for (5) when $B_q = 0$ can be expressed (Ouyang & Mayne 2019):

$$\phi' = 8.18^\circ \cdot \ln_c(2.13 \cdot Q) \quad (7)$$

4.4 Effective ϕ' from I_c relationship

Using the database on 27 undisturbed sands and silty sands, a relationship was also found between ϕ' and CPT material index, I_c (Mayne 2020):

$$\phi' = 53.0^\circ - 6.9^\circ I_c \quad (8)$$

for values of $I_c \leq 2.6$.

The profile of I_c at Opelika is presented in Figure 10 showing the intermediate geomaterial more or less follows the threshold value of $I_c = 2.60$ to 11 m depth.

4.5 CPTU evaluation of ϕ' in Piedmont silts

The above 4 drained equations [i.e., (2), (3), and (4)] one undrained method [i.e., eqn (7)], and CPT index

expression [i.e., eqn (8)] are all applied to the mean CPTU data at Opelika, as shown in Figure 11. Interestingly, all 5 methods approximately agree with each other. Moreover, all CPT expressions agree well and provide comparable profiles to the effective friction angles obtained from the lab triaxial compression test series. This likely only occurs for this very silty fine sand to very sandy silt because of its high fines content (average FC = 44%) and material index at the undrained-drained border of $I_c = 2.60$, since the mean value of index $I_c \approx 2.7$ for this site.

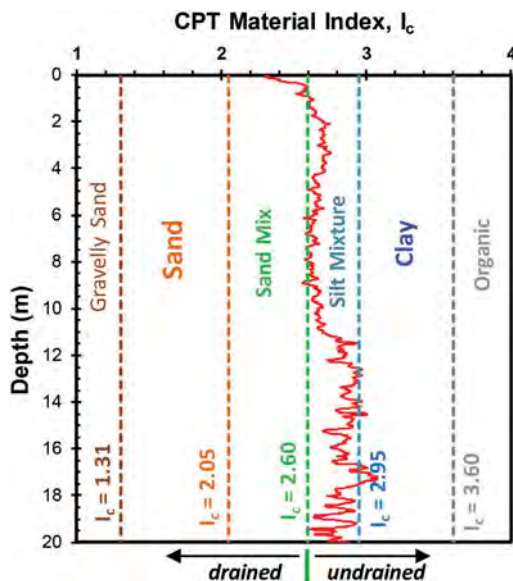


Figure 10. Profile of CPT material index at Opelika.

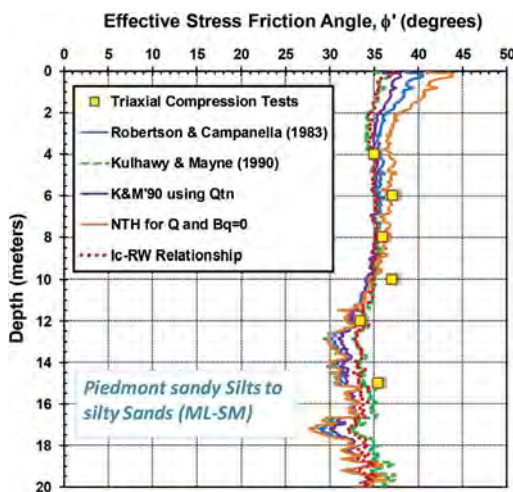


Figure 11. Profile of effective friction angle from five CPTU expressions in comparison with triaxial results on natural Opelika sand-silt mixture.

5 CONCLUSIONS

Interpretation of CPTU in residual soils is complicated by their mixed constituency of clay, silt, sand, and rock particles, as well as considerations of partially drained, fully-drained, and undrained behavior, particularly at the standard rate of 20 mm/s. Nevertheless, success was shown for CPTU in residual silts and sands (ML-SM) at the Opelika national test site, located within the Appalachian Piedmont geologic province in eastern USA. Specifically, a means to profile the yield stress ratio (YSR) from a generalized approach that uses net cone resistance and an exponent $m' = 0.82$. Moreover, a surprising agreement is found in the assessment of effective friction angle ϕ' by use of both drained and undrained CPTU equations that compare well with series of triaxial compression tests.

ACKNOWLEDGMENTS

Thanks to Dr. Fikret Atalay for sharing recent lab data from Opelika NGES, Alabama.

REFERENCES

- Agaiby, S.S. and Mayne, P.W. 2019. CPT evaluation of yield stress in soils. *Journal of Geotechnical & Geoenvironmental Engineering* 145 (12): doi:10.1061/(ASCE)GT.1943-5606.0002164.
- Anderson, J.B., Montgomery, J., Jackson, D., Kiernan, M. and Shi, C. 2019. Auburn University national geotechnical experimentation site in Piedmont residuum. *AIMS GeoSciences* 5(3): 645–664. DOI: 10.3934/geosci.2019.3.645
- Atalay, F. 2019. Engineered transition zone systems for enhanced heat transfer in thermo-active foundations. *PhD Dissertation*, Civil & Env. Engineering, Georgia Institute of Technology, Atlanta GA: 221 pages.
- Benoit, J. and Lutenegeger, A.J., editors 2000. *National Geotechnical Experimentation Sites*. GSP 93, ASCE, Reston, Virginia: 397 pages.
- Bihs, A., Nordal, S., Long, M., Paniagua, P. and Gylland, A. 2018. Effect of piezocone penetration rate on the classification of Norwegian silt. *Cone Penetration Testing 2018*, (Proc. CPT'18, Delft), CRC Press, Taylor & Francis, London: 143–149.
- Blaker, Ø., Carroll, R., Paniagua, P., DeGroot, D.J. and L'Heureux, J-S. 2019. Halden site: geotechnical characterization of a post glacial silt *AIMS GeoSciences* 5 (2): 184–234.
- Brown, D.A. and Vinson, J. 1998. Comparison of strength and stiffness parameters for a Piedmont residual soil. *Geotechnical Site Characterization*, Vol. 2 (Proc. ISC-1, Atlanta), Balkema, Rotterdam: 1229–1234.
- Campanella, R.G. and Robertson, P.K. 1988. Current status of the piezocone test. *Penetration Testing 1988*, Vol. 1 (Proc. ISOPT, Orlando), Balkema, Rotterdam: 93–116.
- Ching, J., Lin, G-H., Chen, J-R. and Phoon, K-K. 2017. Transformation models for effective friction angle and relative density calibrated based on generic database of coarse-grained soils. *Canadian Geot. J.* 54 (4): 481–501.

- DeJong, J.T., Yafrate, N.J. and DeGroot, D.J. 2007. Design of a miniature piezoprobe for high resolution stratigraphic profiling, *ASTM Geotech. Testing J.* 30 (4): 1–13.
- DeJong, J.T., Jaeger, R.A., Boulanger, R.W., Randolph, M. F. and Wahl, D. 2012. Variable penetration rate cone testing for characterization of intermediate soils. *Geotechnical and Geophysical Site Characterization 4*, Vol. 1 (Proc. ISC-4, Recife), Taylor & Francis, London: 25–42.
- Finke, K.A., Mayne, P.W. & Klopp, R.A. 2001. Piezocone penetration testing in Atlantic Piedmont residuum. *Journal of Geotechnical & Geoenvironmental Engineering* 127 (1): 48–54.
- Giacheti, H.L., Bezerra, R.C., Rocha, B.P. and Rodrigues, R.A. 2019. Seasonal influence on cone penetration test: an unsaturated soil site example. *Journal of Rock Mechanics & Geotechnical Engineering* 11: 361–368.
- Holmsgaard, R., Nielsen, B.N. and Ibsen, L.B. 2016. Interpretation of cone penetration testing in silty soils conducted under partially drained conditions. *Journal of Geotechnical and Geoenvironmental Engineering* 142 (1) ASCE: 04015064. [https://doi.org/10.1061/\(ASCE\)GT.1943-5606.0001386](https://doi.org/10.1061/(ASCE)GT.1943-5606.0001386)
- Hoyos, L.R. & Macari, E.J. 1999. Influence of in-situ factors on dynamic response of Piedmont residual soils. *ASCE Journal of Geotech. & Geoenvironmental Engrg* 125 (4), 271–279.
- Huffman, J.C., Martin, J.P. and Stuedlein, A.W. 2015. Assessment of reliability-based serviceability: Limit state procedures and full-scale loading tests. *Proceedings, Fifth International Symposium on Geotechnical Safety & Risk (5th ISGSR, The Netherlands)*, IOS Press, Rotterdam: 313–319.
- Lehane, B.M., Ismail, M.A. and Fahey, M. 2004. Seasonal dependence of in-situ test parameters in sand above the water table. *Geotechnique* 54 (3): 215–218.
- Lunne, T., Robertson, P.K. and Powell, J.J.M. 1997. *Cone Penetration Testing in Geotechnical Practice*, EF Spon/Routledge, Taylor & Francis Group, London: 418 p.
- Mayne, P.W., Kulhawy, F.H., and Kay, J.N. 1990. Observations on the development of pore water pressures during piezocone penetration in clays, *Canadian Geotechnical Journal* 27 (4): 418–428.
- Mayne, P.W. & Brown, D.A. 2003. Site characterization of Piedmont residuum of North America. *Characterization and Engineering Properties of Natural Soils*, Vol. 2, Swets and Zeitlinger, Lisse: 1323–1339.
- Mayne, P.W. 2007. *NCHRP Synthesis 368: Cone Penetration Testing*, Transportation Research Board, Washington, DC: 118 p. www.trb.org
- Mayne, P.W., Coop, M.R., Springman, S., Huang, A-B., and Zornberg, J. 2009. State-of-the-Art Paper (SOA-1): Geomaterial behavior and testing. *Proc. 17th Intl. Conf. Soil Mechanics & Geotechnical Engineering*, Vol. 4 (ICSMGE, Alexandria), Millpress/IOS Press Rotterdam: 2777–2872.
- Mayne, P.W. 2013. Evaluating yield stress of soils from laboratory consolidation and in-situ cone penetration tests. *Sound Geotechnical Research to Practice*, (Proc. GeoCongress, San Diego, GSP 230), ASCE, Reston/VA: 406–420.
- Mayne, P.W. 2020. The 26th Széchy Lecture: Use of in-situ geotechnical tests for foundation systems. *Proceedings of the Széchy Károly Emlékkonferencia*, published by the Hungarian Geotechnical Society, Budapest: 12–73.
- Ouyang, Z. and Mayne, P.W. 2018. Effective friction angle of clays and silts from piezocone penetration tests. *Canadian Geotechnical Journal* 55 (9): 1230–1247.
- Ouyang, Z. and Mayne, P.W. 2019. Modified NTH method for assessing effective friction angle of normally consolidated and overconsolidated clays from piezocone tests. *Journal of Geotechnical & Geoenvironmental Engineering* 145(10), doi:10.1061/(ASCE)GT.1943-5606.0002112
- Robertson, P.K. and Cabal, K. 2015. *Guide to Cone Penetration Testing for Geotechnical Engineering*, 6th edition, Gregg Drilling, Signal Hill, CA: 140 pages.
- Sandven, R. 1990. Strength and deformation properties of fine-grained soils obtained from piezocone tests. *PhD Dissertation*, Dept. of Civil Engrg., Norwegian Institute of Technology, Trondheim: 605 pages.
- Schneider, J.A., Peuchen, J., Mayne, P.W., and McGillivray, A.V. 2001. Piezocone profiling of residual soils. *Proc. Intl. Conf. on In-Situ Measurement of Soil Properties & Case Studies*, Bali, Indonesia: 593–598. www.uscger.org
- Senneset, K., Sandven, R., and Janbu, N. 1989. Evaluation of soil parameters from piezocone tests. *Transportation Research Record* 1235, National Academy Press, Washington, DC: 24–37.
- United States Department of Agriculture (USDA) 2021, Natural Resources Conservation Service, Washington, DC: https://www.nrcs.usda.gov/wps/portal/nrcs/detail/wa/soils/?cid=nrcs144p2_036333
- Uzielli, M. and Mayne, P.W. (2019). Probabilistic assignment of effective friction angle of sands and silty sands from CPT using quantile regression. *Georisk: Assessment & Management of Risk for Engineered Systems and Geohazards* 13(4): Taylor & Francis, London: 272–275. DOI: 10.1080/17499518.2019.1663388
- Vinson, J.L. & Brown, D.A. 1997. Site characterization of the Spring Villa geotechnical test site and a comparison of strength and stiffness parameters for a Piedmont residual soil, *Report No. IR-97-04*, Highway Research Center, Harbert Engineering Center, Auburn University, AL: 385 p.

Soil unit weight prediction from CPTs for soils and mining tailings

T. Menegaz & E. Odebrecht

University of Santa Catarina State, Joinville, Santa Catarina, Brazil

H.P. Nierwinski

Federal University of Santa Catarina, Joinville, Santa Catarina, Brazil

F. Schnaid

Federal University of Rio Grande do Sul, Porto Alegre, Rio Grande do Sul, Brazil

ABSTRACT: An accurate estimation of the total unit weight (γ_t) of soils and mining tailings is a requirement for several geotechnical engineering applications. In the interpretation of CPT testing data, the value of γ_t is needed for the evaluation of both the total and effective stresses, as well as in the accurate determination of subsequent parameters. Current methods for determining γ_t based CPT data have been developed for a wide range of natural soils where the specific gravity of solids (G) generally ranges from 2.5 to 2.7. However, a large gap exists for soils or mining tailings where G is often higher, such as in the case of bauxite and zinc. This paper presents a compilation of results of CPT tests, and laboratory measurements of specific gravity of solids and total unit weight on bauxite and zinc mine tailings. The application of the literature methodologies was evaluated for this database and the statistical coefficient of determination (r) was presented, which is determined between the measured value and the value estimated by the correlations

1 INTRODUCTION

An adequate geotechnical investigation is necessary for the understanding of soil behavior. Laboratory and field data are generated, which allow the designer to predict the behavior of the studied soil, offering more security for project development. According to Lunne, Robertson & Powell (1997), field and laboratory tests complement each other; however, field tests have some attractions. One of these is the cone penetration test (CPT) or piezocone test (CPTu), which is conducted by driving a set of steel rods and a conical point into the ground with the aid of a reaction system mounted on the ground surface. The following quantities are continuously measured in this test: tip resistance (q_c), lateral friction (f_s), and generated pore pressure (u). Combining these values also makes it possible to determine two parameters used to evaluate the soil behavior, namely the friction ratio (R_f) and the pore pressure parameter (B_q). The literature presents several correlations for obtaining geotechnical parameters from CPTu test results (Kulhawy & Mayne (1990); Schmertmann (1978); Teh & Houlsby (1991); Larsson & Mulabdic (1991)). However, one of the essential information in the interpretation of the test is the value of the natural soil unit weight.

The methods presented in the literature for determining γ_t from the results of the cone test use the tip

resistance (q_t), the lateral friction (f_s), and also the value of the shear wave velocity (v_s) through the soil. These methods consist of empirical formulations developed from natural soil databases, encompassing a range of specific gravity of solids (G) values, usually ranging from 2.5 to 2.7 (MAYNE, 2007). Some specific proposals seek to address organic soils, for G values ranging from 1.45 to 2.33 (LENGKEEK *et al* 2018). However, considering the extensive applicability of cone tests, encompassing both soft soil deposits and mining tailings, there is a need to evaluate correlations for estimating soil unit weight for wider ranges of specific gravity of solids values, for which the correlations available in the literature may present limitations.

In this context, the present study compiles and organizes a database of cone tests and laboratory tests, encompassing bauxite and zinc mining tailings soils with a specific gravity of solids values above the average of natural soils. The aim is to verify the applicability of existing specific weight estimation relationships and verify which method best adapts to these data. The study will be based on statistical analysis with the help of the statistical software R Studio®, where the value of Pearson correlation coefficient (r), determined between the measured value and the estimated value of specific weight, will be evaluated. The

Pearson correlation coefficient (r) represents the linear association between two random variables. Usually, the analysis is made by graphical representation of the relation of data, using a scatter diagram. This coefficient varies from -1 to +1 and indicate the tendency of one variable to increase or decrease with the other variable, respectively (PATTEN & NEWHART, 2017; ZHOU *et al* 2016). In this paper, the Pearson correlation coefficient (r) is used to verify the relation between the measured soil unit weight and the estimated value by literature correlations.

1.1 Methods for estimating the natural soil unit weight

There are several proposals in the literature for determining the natural soil unit weight (γ_t); among them, we can mention Robertson & Cabal (2010), Mayne & Peuchen (2012) and Mayne (2014). To develop the correlation proposed by Robertson & Cabal (2010), as can be seen in Equation 1, experiments and correlations between wave velocity and soil unit weight were combined (MAYNE, 2007), along with relationships between unit weight and DMT test results (MARCHETTI, 1980). Thus, Robertson & Cabal (2010) developed approximate contours of unit weight values as a function of dimensionless parameters of resistance (q_t/σ_{atm}) and lateral friction ($R_f = f_s/\sigma_{atm}$).

$$\gamma_t/\gamma_w = 0.27 [\log R_f] + 0.36 [\log(q_t/\sigma_{atm})] + 1.236 \quad (1)$$

where R_f = friction ratio x 100%; q_t = corrected tip resistance; γ_w = water unit weight (kPa); and σ_{atm} = atmospheric pressure (kPa).

Robertson & Cabal (2010) also point out that the vast majority of soils present a specific gravity of solids (G) in the range of 2.5 to 2.7. For soils with G outside this range, some interference may occur in the proposed correlation given by the previous equation, so they proposed Equation 2, where the value of G is introduced.

$$\gamma_t/\gamma_w = [0.27[\log R_f] + 0.36[\log(q_t/\sigma_{atm})] + 1.236]G/2.65 \quad (2)$$

As for Mayne & Peuchen (2012), the authors' first evaluation consisted of relating the unit weight of the materials with the respective plasticity index, verifying a tendency of reduction of the specific weight with the increase of the plasticity of the material. As the plasticity index is not obtained using the cone test, the authors investigated and

identified a relationship between the plasticity index and the ratio between the tip resistance and the depth, denominated m_q ($m_q = q_t/z$). Analyses were performed and two equations were obtained (Equations 3 and 4).

$$\gamma_t = \gamma_w + m_q/8 \quad (3)$$

$$\gamma_t = 0.636(q_t)^{0.072}(10 + m_q/8) \quad (4)$$

A differentiated methodology is proposed by Mayne (2014) to estimate the soil unit weight through CPTu test results, relying only on the relationship of specific weight with the lateral cone friction (f_s) measurements. The proposed equation is presented by Equations 5 and 6.

$$\gamma_t = 26 - (14/1 + [0.5 \cdot \log(f_s + 1)]^2) \quad (5)$$

$$\gamma_t \approx 12 + 1.5 \ln(f_s + 1) \quad (6)$$

2 DATABASE

In order to achieve the research objective, a database of geotechnical investigation results was analyzed. The database is formed by 197 observations resulting from investigations in 4 different Brazilian bauxite and zinc deposits. The items surveyed in the database were based on the definition of the main parameters to be used in the statistical analysis to apply existing correlations, thus making it possible to verify their performance with the compiled data. The data for bauxite and zinc mining tailings are presented, by depth range, in Tables 1 and 2, respectively.

Table 1. Bauxite mining tailings database – parameters variation.

Depth (m)	γ_t (kN/m ³)	q_t (MPa)	f_s (kPa)	G	R_f
1 – 4.75	13.48 – 20.43	0.03 – 0.99	0.5 – 13.36	2.39 – 3.36	0.26 – 14.48
5 – 10	14.48 – 21.45	0.03 – 2.0	0.79 – 17.49	2.85 – 3.22	0.48 – 3.58
11 – 15	16.44 – 20.44	0.39 – 0.95	4.48 – -23.29	2.88 – 3.14	0.68 – 3.63
16 – 20	15.58 – 20.26	0.73 – 1.95	6.82 – 19.11	2.98 – 3.14	0.93 – 2.74

Table 2. Zinc mining tailings database – parameters variation.

Depth (m)	γ_t (kN/m ³)	q_t (MPa)	f_s (kPa)	G	R_f
1 – 5	11.27 – 13.58	0.03 – 0.22	0.14 – 2.57	3.28 – 3.35	0.28 – 1.56
6 – 12	12.6 – 14.3	0.22 – 1.10	1.77 – 16.99	3.29 – 3.37	0.5 – 1.62

3 VERIFICATION OF EXISTING METHODS IN LITERATURE

In this step of the study, the methods present in the literature for natural soils as presented in step 1.1 were used to estimate the soil unit weight, comparing the result obtained by applying the formulations with the values defined in the results of geotechnical tests.

Together with the database formed with the parameters for the analysis of correlations between CPT and CPTu tests, the equations were entered into the Excel software spreadsheet. Each of the correlations was entered in a column, sorted by author and year of development, starting from the oldest to the most recent.

In order to make an evaluation between the values calculated by the correlations of the methods and the unit weight values present in the results of the geotechnical tests, the software R Studio® was used as a statistical tool.

Table 3. Verification of methods with bauxite mining tailings.

Method	Equation	r value
Robertson & Cabal (2010)	Equation 1	0.2
Robertson & Cabal (2010)	Equation 2	0.42
Mayne & Peuchen (2012)	Equation 3	0.2
Mayne & Peuchen (2012)	Equation 4	0.22
Mayne (2014)	Equation 6	0.3

Table 4. Verification of methods with zinc mining tailings.

Method	Equation	r value
Robertson & Cabal (2010)	Equation 1	0.79
Robertson & Cabal (2010)	Equation 2	0.78
Mayne & Peuchen (2012)	Equation 3	0.43
Mayne & Peuchen (2012)	Equation 4	0.64
Mayne (2014)	Equation 6	0.85

The use of Pearson correlation coefficient (r) was chosen to evaluate if those two variables, the measured specific weight and, the estimated specific weight, are related to each other. Furthermore, it is intended to analyze which method demonstrates to have more compatibility with each soil type evaluated. For each type of studied soil and correlations graphs were generated. The results of the analyses are presented by soil type in Tables 3 and 4, being bauxite tailings and zinc, respectively.

The bauxite mining tailings were the first to be analyzed, bringing the strongest correlation value, the method of Robertson & Cabal (2010), in Equation 2, with an $r = 0.42$. This equation presents in its formulation the coefficient of specific gravity of solids (G). And the weakest correlation occurred in two equations of different methods, the first by Robertson & Cabal, Equation 1, and the second by Mayne & Peuchen (2012), Equation 4, presenting an $r = 0.2$. The graphs with the strongest and weakest correlations are illustrated in Figures 1 and 2.

For zinc mining tailings, the results were more positive when compared to bauxite mining tailings. For the Mayne (2014) method, the strongest correlation was obtained, being $r = 0.85$. However, not all results were above $r = 0.7$. Mayne

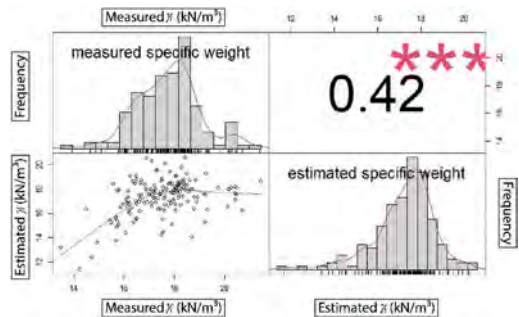


Figure 1. The strongest correlation in bauxite mining tailings.

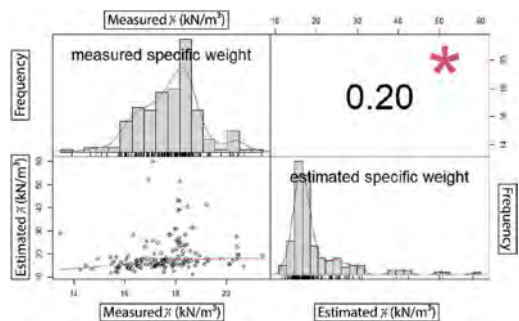


Figure 2. The weakest correlation in bauxite mining tailings.

and Peuchen (2012), in Equation 4, presents the weakest result among all, where $r = 0.43$. The graphs with the strongest and weakest correlations are presented in Figures 3 and 4.

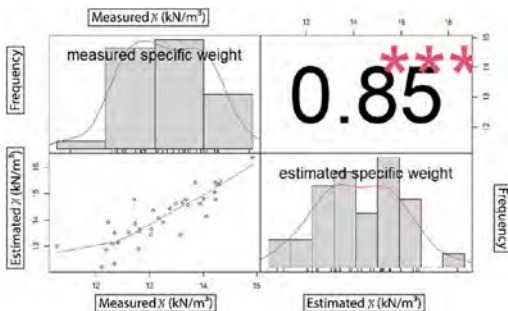


Figure 3. The strongest correlation in bauxite mining tailings.

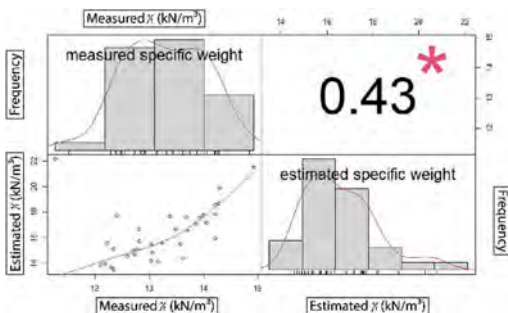


Figure 4. The weakest correlation in bauxite mining tailings.

4 CONCLUSIONS

This paper sought to assemble a database of Brazilian mining tailings soils for verification of methods present in the literature for natural soils.

Through this study, it was possible to define which method in the literature for natural soils best suited the mining tailings data in the database.

The Pearson correlation coefficient (r) values between the measured data and the data calculated by the methods indicated that some of the methods offered a positive result when using the database, but in most cases the results showed that there is a need to generate a new equation that encompasses a range of soils with actual specific gravity of solids values varying more than just the range for normal soils (2.5 to 2.7).

REFERENCES

- Lengkeek, H. J.; De Greef, J.; Joosten, S. (ed) 2018. CPT based unit weight estimation extended to soft organic soils and peat. *Cone Penetration Testing 2018*: 389–394.
- Lunne, T; Robertson P. K.; Powell, J.J.M. (ed) 1997. *Cone Penetration Testing*. London: Blackie Academic & Professional.
- Mayne, P. W. (ed) 2007. *Cone Penetration Testing*. Washington, DC: The National Academies Press.
- Mayne, P. W.; Peuchen, J.; Bowmeester, D. (ed) 2010. Unit weight trends with cone resistance in soft to firm clays. *Geotechnical and Geophysical Site Characterization: Proceedings of the 4th International Conference on Site Characterization ISC-4*: 903–910.
- Mayne, P.W. (ed) 2014. Interpretation of geotechnical parameters from seismic piezocone tests. *Proceedings, 3rd International Symposium on Cone Penetration Testing*: 47–73.
- Robertson, P. K.; Cabal, K.L. (ed) 2010. Estimating soil unit weight from CPT. *2nd International Symposium on Cone Penetration Testing*: 2 – 40.
- Robertson, P. K.; Cabal, K.L. (ed) 2014. *Guide to Cone Penetration Testing for Geotechnical Engineering*. California: Gregg Drilling & Tests Inc.
- Patten, M.L.; Newhart, M. (eds) 2017. *Understanding Research Methods*. London: Routledge.
- Zhou, H.; Zhihong, D.; Xia, Y.; Fu, M. (ed) 2016. A new sampling method in particle filter based on Pearson correlation coefficient. *Neurocomputing 216*: 208–215.

Use of DMT and CPTU to assess the G_0 profile in the subsoil

Z. Młynarek

University of Life Sciences, Poznań, Poland

J. Wierzbicki

Institute of Geology, Adam Mickiewicz University, Poznań, Poland

P. Monaco

University of L'Aquila, L'Aquila, Italy

ABSTRACT: The subject of this article is the analysis of the relationship between G_0/M_{DMT} and K_D , where G_0 is the small strain shear modulus, while M_{DMT} and K_D are respectively the constrained modulus and the horizontal stress index determined from DMT tests. This relationship allows to determine a profile with depth of G_0 from standard DMT test results, useful when data from non-seismic DMT investigations are available. The analysis was based on a large amount of data for a wide range of soils of different origins in Poland. The dataset included OC and NC loams, silts, medium sands, silty sands and fine sands. The overconsolidation ratio (OCR) was estimated from CPTU and DMT tests. The obtained empirical G_0/M_{DMT} vs. K_D relationships were compared with the correlations established by Marchetti et al. (2008) for different soil types. To account for the significant influence of overconsolidation, an original empirical relationship between G_0/σ'_p and K_D , where σ'_p is the preconsolidation stress, was determined based on data from all investigated fine-grained soils.

1 INTRODUCTION

Recent achievements of research on in-situ testing allow to determine a wide range of soil parameters necessary for geotechnical design of a planned investment. The piezocone (CPTU) and flat dilatometer (DMT) tests take up a special position in these investigations. In the group of geotechnical parameters sought for design of foundations of many engineering structures, the parameters related to soil stiffness, such as the small strain shear modulus G_0 and the constrained modulus M , play an important role. The CPTU and DMT tests are particularly convenient for determining the profiles with depth of these moduli in the subsoil. In particular, the seismic piezocone (SCPTU) and the seismic dilatometer (SDMT) tests permit to determine the in-situ depth profile of G_0 from the measured shear wave velocity V_s . The cost of these techniques, however, is higher than the standard non-seismic CPTU and DMT tests, which are preferred in many practical cases. In absence of V_s measurements, G_0 can be estimated from the results of a standard DMT using the empirical correlations proposed by Marchetti et al. (2008). The use of such correlations must be accompanied by the awareness that many independent variables affect the quality of the assessment of the G_0 modulus. It is generally accepted that the quality of a geotechnical parameter depends on two factors: (1)

the quality of the testing technique (Młynarek 2010), and (2) the parameter variability, related to subsoil properties (Lacasse & Nadim 1994). The analysis of the influence of the latter group of factors on the correlation between G_0 and the horizontal stress index K_D from DMT, with particular emphasis on the preconsolidation effect, is the subject of this paper.

2 LOCATION AND BASIC GEOLOGICAL SETTING OF THE TEST SITES

The research was carried out at five test sites located in Poland (Figure 1), four in the area covered by the Late Pleistocene glaciation and one in the impact zone of periglacial processes in the Pleistocene. Two sites, Kaźmierz and Lipno, are located within the Weichsel glaciation, ended about 15,000 years ago. The near-surface geological formations are dominated by loam and glacial sands over 12 m thick. In the subsurface zone loams are mainly originated from melt-out facies and characterized by low preconsolidation. They rest on loams of the lodgement facies with a higher degree of preconsolidation (Kaźmierz site). The clay fraction in glacial clays does not exceed 25%. They are dominated by the sand fraction, even up to 70%. The sites of Jarocin and Koźmin are located in the Riss glaciation zone, in the



Figure 1. Location of the test sites.

foreground of the Weichsel glaciation line. Here the dominant soils are loams of the lodgement facies, characterized by a high (> 10%) calcium carbonate content, a sand fraction lower than the loams of the Weichsel glaciation and an increase (up to 40%) in the silt fraction. These clays are often called ‘grey loams’ for their characteristic grey-brown color. The Łañcut site is located in the zone of loess covers and loess-like silts. These soils were originated in the Middle and Late Pleistocene as extensive covers of aeolian silty sediments, deposited in the foreland of the Pleistocene ice sheet. The particle size distribution is very homogeneous and characterized by 60-70% of silt fraction and about 20% of sand fraction. A characteristic feature of the loess covers is the frequent occurrence of carbonate cementation, which causes a quasi-preconsolidation effect (Młynarek et al. 2013).

3 ESTIMATE OF *OCR* FROM CPTU AND DMT

The stress history of soil deposits is commonly assessed based on the overconsolidation ratio (*OCR*) or the preconsolidation stress (σ'_p). Profiles with depth of these parameters at the investigated sites were obtained from CPTU and DMT data.

Based on CPTU test results, the *OCR* was estimated using the relationship (Wierzbicki 2010):

$$OCR_{CPTU} = 5.68 \ln Q_t - 15.64 \quad (1)$$

where Q_t = normalized cone resistance.

The original formula by Marchetti (1980) was used to estimate the *OCR* from DMT:

$$OCR_{DMT} = (0.5K_D)^{1.56} \quad (2)$$

where K_D = horizontal stress index.

The *OCR* profiles obtained from CPTU and DMT were used to qualify the investigated soil deposits as normally consolidated (NC) or overconsolidated (OC). The *OCR* was found to vary between 1 to 11.

The comparison of *OCR* depth profiles estimated from CPTU and DMT at two representative sites is shown in Figures 2 and 3, along with the profiles of measured and interpreted parameters obtained from CPTU (corrected cone resistance q_t , friction ratio R_f , pore pressure u_2) and from DMT (corrected pressure readings p_0 and p_1 , material index I_D). A relatively large difference between the *OCR* estimated from CPTU and DMT is found at the Kaźmierz site in loam

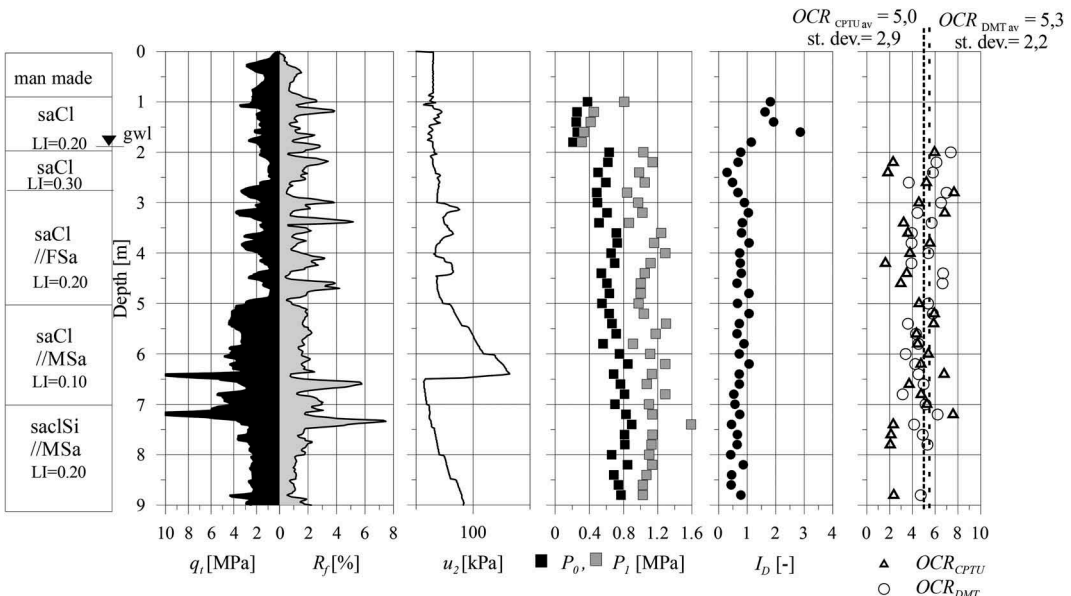


Figure 2. CPTU and DMT test results and estimated *OCR* profiles in loam at Kaźmierz test site (*LI* = liquidity index, saCL = sandy loam, saclSi = fluvioglacial silt, MSa = fluvioglacial sand).

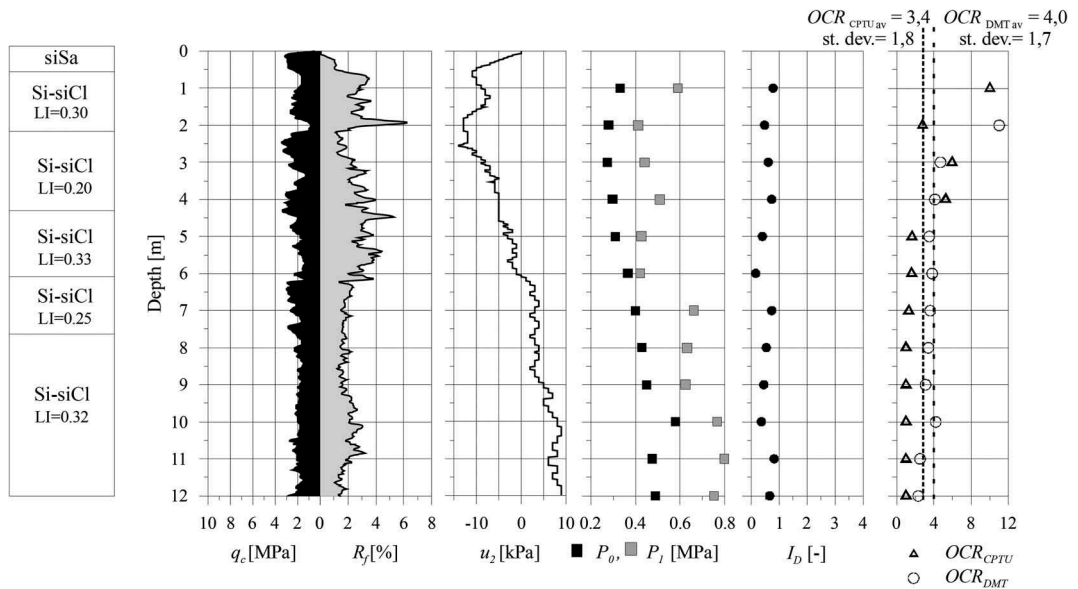


Figure 3. CPTU and DMT test results and estimated OCR profiles in loess at Łañcut test site (LI = liquidity index, Si-siCl = loess, siSa = fluvial sand).

and sandy loam (Figure 2), particularly in correspondence of thin sand layers. However the mean values of the OCR from DMT and CPTU for the entire subsoil profile do not differ significantly (level of confidence interval of statistical analysis $\alpha = 0.05$). The average values over the 9 m investigated depth show a limited standard deviation. The loess deposit at the Łañcut site (Figure 3) is composed of silty clay and silt with homogeneous macrostructure. The OCR estimated from CPTU and DMT are similar, and their average values over the 12 m investigated depth do not differ significantly from the statistical point of view.

4 ASSESSMENT OF THE CORRELATION BETWEEN G_0 AND DMT PARAMETERS

Marchetti et al. (2008) investigated the experimental interrelationship between small strain and working strain stiffness using SDMT. They identified a relationship between the ratio G_0/M_{DMT} and K_D having the functional form shown by Equation 3:

$$\frac{G_0}{M_{DMT}} = f(K_D) \quad (3)$$

where G_0 = small strain shear modulus obtained from the measured shear wave velocity V_S as $G_0 = \rho \cdot V_S^2$ (ρ = soil density), M_{DMT} = constrained modulus and K_D = horizontal stress index obtained from standard DMT interpretation (Marchetti 1980). Based on data obtained from 34 sites, in a variety of soil types, Marchetti et al. (2008) proposed distinct correlations for clay, silt and sand (Figure 4).

The correlations formulated by Marchetti et al. (2008) were taken as a reference for the comparative analysis with the experimental data obtained in this study. A total number of 989 SDMT test results, obtained from soil deposits of different origin, macrostructure and OCR , were analyzed. The analysis of the relationship written in the form of Equation 3 was carried out considering the following soil groups, corresponding to the soil classification adopted by the Polish Standards (1986): clay (clay fraction > 30%); sandy loam (clay fraction = 10-20%, sand fraction 50-90%); loam; silt (clay fraction 10-20%, silt fraction 30-60%); fine/medium sand; fine/silty sand.

Figure 5 shows the datapoints $G_{0(m)}/M_{DMT}$ vs. K_D obtained for all soil groups, where $G_{0(m)}$ is intended as the G_0 determined from V_S measured by SDMT. Figure 5 confirms the conclusions formulated by Marchetti et al. (2008): (i) a functional correlation exists between the ratio G_0/M_{DMT} and K_D ; (ii) a correlation between these variables should be constructed for specific groups of soils, at least distinguishing between fine and coarse-grained soils; (iii) these correlations are affected by the pre-consolidation effect, which can be defined by σ'_p or OCR .

These findings prove that it is necessary to analyze the relationship between $G_{0(m)}/M_{DMT}$ and K_D in selected soil groups. Figures from 6 to 11 illustrate, for each soil group: (a) the relationship between $G_{0(m)}/M_{DMT}$ and K_D , compared with the equations proposed by Marchetti et al. (2008) for similar soil types (Figure 4); (b) the comparison between $G_{0(m)}$ obtained from measured V_S and $G_{0(c)}$ calculated according to Marchetti et al. (2008).

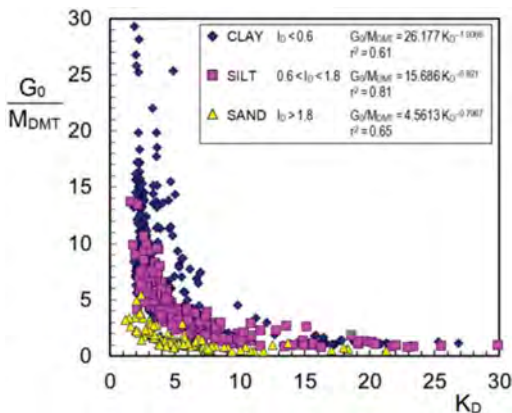


Figure 4. Relationship between the ratio G_0/M_{DMT} and K_D according to Marchetti et al. (2008) (from Monaco et al. 2009).

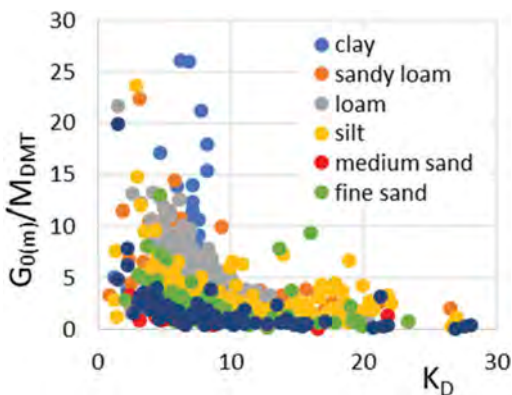


Figure 5. Relationship between the ratio $G_{0(m)}/M_{DMT}$ and K_D in different soil types from all investigated sites.

Figure 6 refers to clay. The $G_{0(m)}/M_{DMT}$ vs. K_D datapoints (Figure 6a) from the investigated sites (OC clay) plot higher than the correlation proposed by Marchetti et al. (2008) for clay. The moduli $G_{0(m)}$ obtained from the measured V_S differ significantly from the moduli $G_{0(c)}$ calculated according to Marchetti et al. (2008), particularly for the higher values of $G_{0(m)}$, while for low $G_{0(m)}$ the values of $G_{0(c)}$ and $G_{0(m)}$ are closer to the 1:1 correlation line (Figure 6b). The same effect was found by Młynarek et al. (2013) comparing the constrained moduli M from DMT and CPTU tests for Pliocene OC clays. The best-fit relationship for the $G_{0(m)}/M_{DMT}$ vs. K_D datapoints in Figure 6a is given by Equation 4:

$$\frac{G_{0(m)}}{M_{DMT}} = 342.75 K_D^{-1.861} R^2 = 0.6102 \quad (4)$$

Figure 7 refers to sandy loam. The $G_{0(m)}/M_{DMT}$ vs. K_D datapoints (Figure 7a) plot relatively close to the correlations proposed by Marchetti et al. (2008) for clay and silt. The moduli $G_{0(m)}$ (Figure 7b) are very similar to the moduli $G_{0(c)}$ calculated according to Marchetti et al. (2008) for clay. Again, the lower values of $G_{0(m)}$ and $G_{0(c)}$ lie near the 1-1 correlation line. The best-fit relationship for the $G_{0(m)}/M_{DMT}$ vs. K_D datapoints in Figure 7a is given by Equation 5:

$$\frac{G_{0(m)}}{M_{DMT}} = 48.785 K_D^{-1.284} R^2 = 0.7341 \quad (5)$$

Figure 8 refers to loam. The $G_{0(m)}/M_{DMT}$ vs. K_D datapoints (Figure 8a) plot slightly higher than the correlations proposed by Marchetti et al. (2008) for clay and silt. Accordingly, the moduli $G_{0(m)}$ (Figure 8b) slightly differ from the moduli $G_{0(c)}$ estimated according to Marchetti et al. (2008) for clay. The best-fit relationship for the $G_{0(m)}/M_{DMT}$ vs. K_D datapoints in Figure 8a is given by Equation 6:

$$\frac{G_{0(m)}}{M_{DMT}} = 50.096 K_D^{-1.114} R^2 = 0.6603 \quad (6)$$

Figure 9 refers to silt. The $G_{0(m)}/M_{DMT}$ vs. K_D datapoints (Figure 9a) plot rather close to the correlation proposed by Marchetti et al. (2008) for silt. The moduli $G_{0(m)}$ (Figure 9b) are similar to the moduli $G_{0(c)}$ calculated according to Marchetti et al. (2008) for silt. The best-fit relationship for the $G_{0(m)}/M_{DMT}$ vs. K_D datapoints in Figure 9a is given by Equation 7:

$$\frac{G_{0(m)}}{M_{DMT}} = 22.608 K_D^{-0.608} R^2 = 0.7083 \quad (7)$$

Figure 10 refers to fine/medium sand. The $G_{0(m)}/M_{DMT}$ vs. K_D datapoints (Figure 10a) plot very close to the correlation proposed by Marchetti et al. (2008) for sand. The moduli $G_{0(m)}$ (Figure 10b) are very similar to the moduli $G_{0(c)}$ calculated according to Marchetti et al. (2008) for sand. The best-fit relationship for the $G_{0(m)}/M_{DMT}$ vs. K_D datapoints in Figure 10a is given by Equation 8:

$$\frac{G_{0(m)}}{M_{DMT}} = 8.7499 K_D^{-1.283} R^2 = 0.7684 \quad (8)$$

Figure 11 refers to fine/silty sand. The $G_{0(m)}/M_{DMT}$ vs. K_D datapoints (Figure 11a) plot very close to the

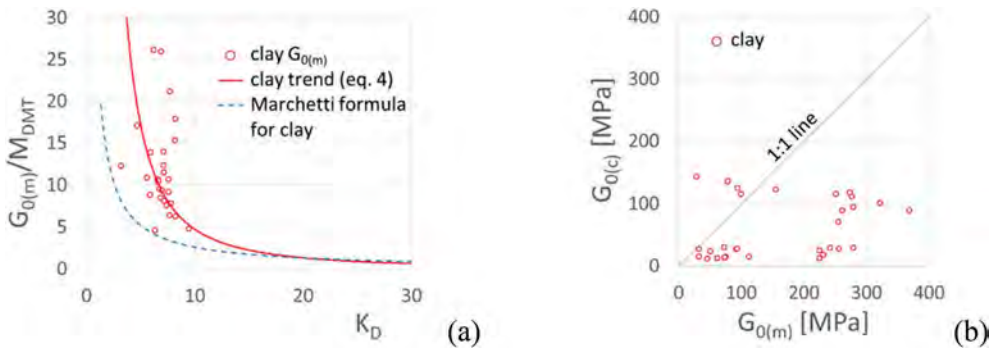


Figure 6. (a) Relationship between $G_{0(m)}/M_{DMT}$ and K_D in clay. (b) Comparison between $G_{0(m)}$ obtained from measured V_S and $G_{0(c)}$ calculated according to Marchetti et al. (2008) for clay.

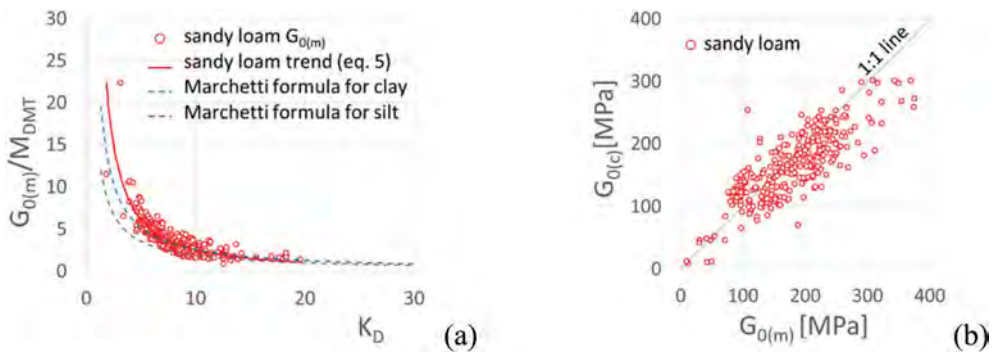


Figure 7. (a) Relationship between $G_{0(m)}/M_{DMT}$ and K_D in sandy loam. (b) Comparison between $G_{0(m)}$ obtained from measured V_S and $G_{0(c)}$ calculated according to Marchetti et al. (2008) for clay.

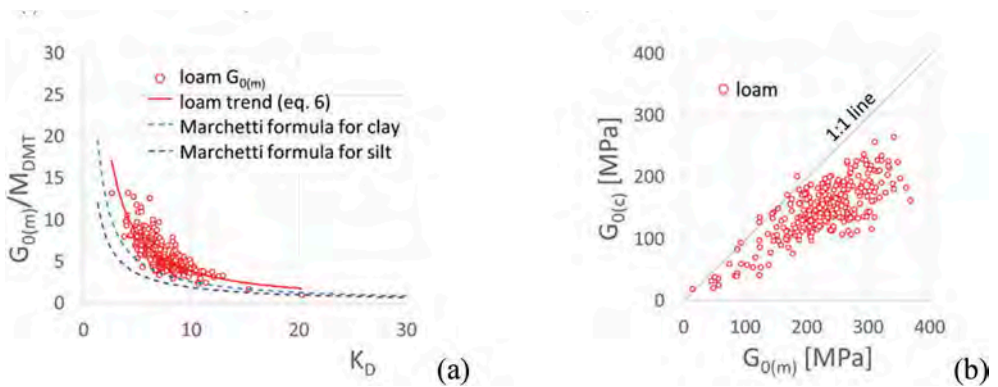


Figure 8. (a) Relationship between $G_{0(m)}/M_{DMT}$ and K_D in loam. (b) Comparison between $G_{0(m)}$ obtained from measured V_S and $G_{0(c)}$ calculated according to Marchetti et al. (2008) for clay.

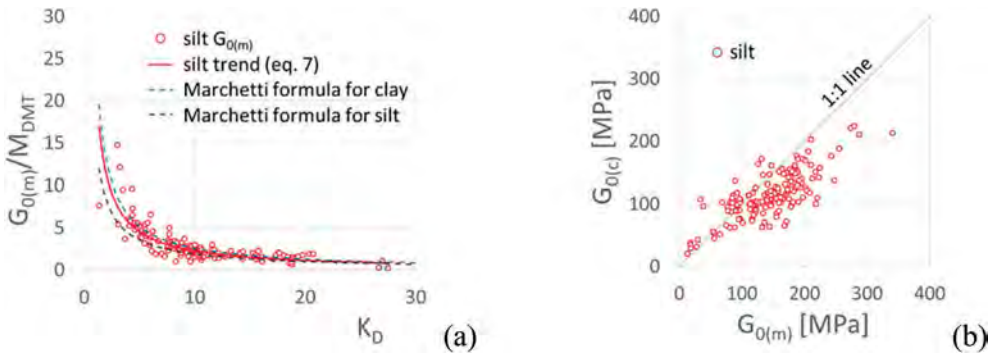


Figure 9. (a) Relationship between $G_{0(m)}/M_{DMT}$ and K_D in silt. (b) Comparison between $G_{0(m)}$ obtained from measured V_S and $G_{0(c)}$ calculated according to Marchetti et al. (2008) for silt.

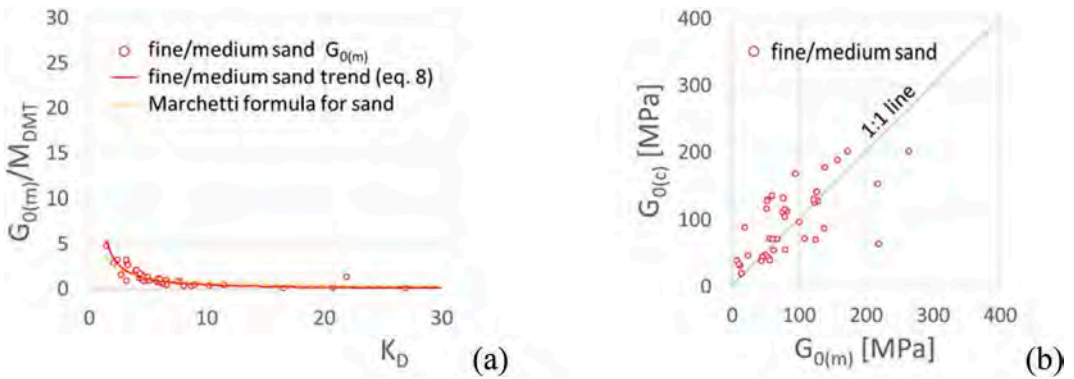


Figure 10. (a) Relationship between $G_{0(m)}/M_{DMT}$ and K_D in fine/medium sand. (b) Comparison between $G_{0(m)}$ obtained from measured V_S and $G_{0(c)}$ calculated according to Marchetti et al. (2008) for sand.

correlations proposed by Marchetti et al. (2008) for silt and for sand. The moduli $G_{0(m)}$ (Figure 11b) are very similar to the moduli $G_{0(c)}$ calculated according to Marchetti et al. (2008) for sand. The best-fit relationship for the $G_{0(m)}/M_{DMT}$ vs. K_D datapoints in Figure 11a is given by Equation 9:

$$\frac{G_{0(m)}}{M_{DMT}} = 16.716K_D^{-1.184} R^2 = 0.6582 \quad (9)$$

The lowest values of the coefficient R^2 , obtained for clay ($R^2 = 0.6102$) and for fine/silty sand ($R^2 = 0.6582$), are very similar to those found by Marchetti et al. (2008) in clay and sand (Figure 4). Possibly in these soils the assessment of the $G_{0(m)}/M_{DMT} - K_D$ relation is affected by local variability in grain size distribution and macrostructure at the various sites.

Due to the significant impact of overconsolidation on the functional shape of the relationship $G_{0(m)}$ vs.

K_D in cohesive soils, a new correlation was established in which $G_{0(m)}$ was normalized by the preconsolidation stress σ'_p . The value of σ'_p was determined from the OCR estimated from DMT.

Figure 12 shows the $G_{0(m)}/\sigma'_p$ vs. K_D datapoints obtained from the tested soils belonging to the group of cohesive soils (sandy loam, loam, clay and silt). The two areas denoted as A and B, that plot far away from the general $G_{0(m)}/\sigma'_p - K_D$ trend line, are related to fissured clays and cemented silts. These soils need a separate interpretation. The best-fit relationship for the $G_{0(m)}/\sigma'_p$ vs. K_D datapoints in Figure 12 is given by Equation 10:

$$\frac{G_{0(m)}}{\sigma'_p} = 1548K_D^{-1.058} R^2 = 0.6703 \quad (10)$$

This correlation has a satisfactory statistical evaluation and, in principle, could be applied to all cohesive soils to estimate G_0 based on K_D .

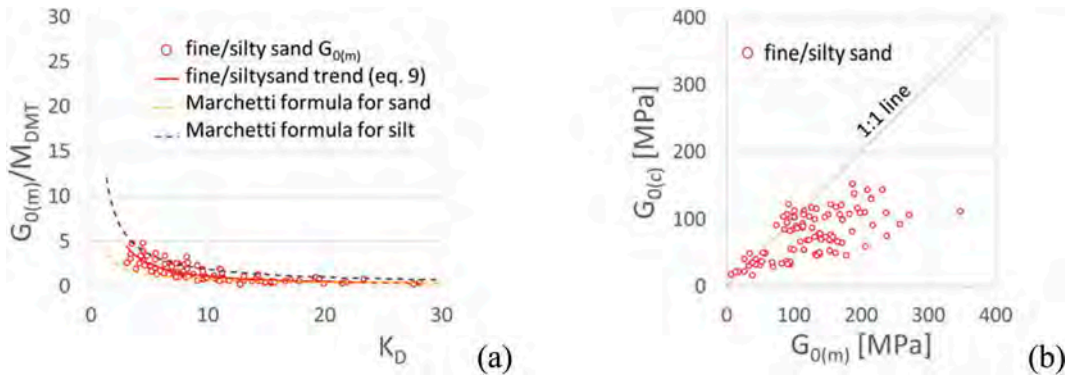


Figure 11. (a) Relationship between $G_{0(m)}/M_{DMT}$ and K_D in fine/silty sand. (b) Comparison between $G_{0(m)}$ obtained from measured V_S and $G_{0(c)}$ calculated according to Marchetti et al. (2008) for sand.

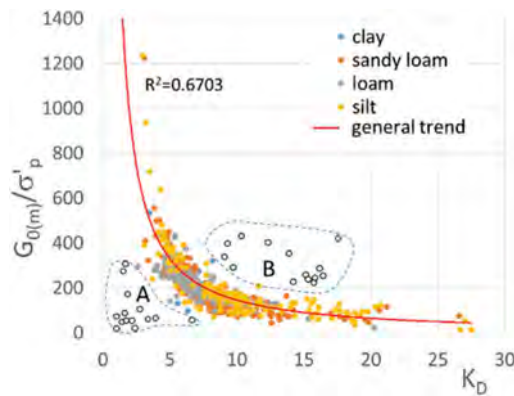


Figure 12. Relationship between $G_{0(m)}/\sigma'_p$ and K_D for sandy loam, loam, clay and silt.

5 CONCLUSIONS

The obtained research results allow to formulate the following general conclusions.

- In the construction of the correlation $G_0/M_{DMT} = f(K_D)$ it is necessary to take into account soil type, with a general distinction between cohesive and non-cohesive soils. This fully confirms the concept by Marchetti et al. (2008).
- Overconsolidation has a significant influence on the functional form of the $G_0/M_{DMT} = f(K_D)$ relationship. For the examined OC loams, especially for clays, the Marchetti et al. (2008) correlations require some correction. Grain size of the soil and overconsolidation are significant. On the other hand, a satisfactory agreement between the G_0 measured and calculated according to Marchetti et al. (2008) was found for medium/fine sands and silts, and in general for NC soils (low K_D).
- The proposed $G_{0(m)}/M_{DMT} = f(K_D)$ correlations have a high statistical significance and may prove useful to determine a continuous profile with

depth of G_0 in soils of different origin based on standard DMT test results.

- Fissured clays and cemented soils require a separate extensive analysis and interpretation.
- The relationship $G_{0(m)}/\sigma'_p = f(K_D)$ can be considered very promising for practical purposes, because it allows to determine G_0 for the whole set of OC cohesive soils.

REFERENCES

- Lacasse, S. & Nadim, F. 1994. Reliability issues and future challenges in geotechnical engineering for offshore structures. *Proc. 7th Int. Conf. on Behaviour of Offshore Structures*, Cambridge MA, USA, 1: 1–48. Amsterdam: Elsevier.
- Marchetti, S. 1980. In Situ Tests by Flat Dilatometer. *J. Geotech. Eng. Div.* 106(3): 299–321.
- Marchetti, S., Monaco, P., Totani, G. & Marchetti, D. 2008. In Situ Tests by Seismic Dilatometer (SDMT). *Geotech. Spec. Publ. GSP 180, From Research to Practice in Geotechnical Engineering*: 292–311.
- Młynarek, Z. 2010. Quality of In-Situ and Laboratory Tests Contribution to Risk Management. *Proc. 14th Danube European Conf. on Geotech. Eng.*, Bratislava, Slovakia.
- Młynarek, Z., Wierzbicki, J. & Stefaniak, K. 2013. Deformation characteristics of overconsolidated subsoil from CPTU and SDMT tests. *Proc. 4th Int. Conf. on Geotechnical and Geophysical Site Characterization*, Porto de Galinhas, Brazil, 18–21 September 2012, 2: 1189–1193. London: Taylor & Francis Group.
- Monaco, P., Marchetti, S., Totani, G. & Marchetti, D. 2009. Interrelationship between small strain modulus G_0 and operative modulus. *Performance-Based Design in Earthquake Geotechnical Engineering – from Case History to Practice, Proc. IS-Tokyo 2009*, Tsukuba, Japan, 15–17 June 2009, 1315–1323. London: Taylor & Francis Group.
- Polish standards. 1986. Building soils, Nomenclature, classification and description. PN-86/B-02480.
- Wierzbicki, J. 2010. Evaluation of subsoil overconsolidation by means of in situ tests at the aspect of its origin. *Scientific dissertations No. 410*, University of Life Sciences in Poznań Publishing, Poland, 181–182 (in Polish).

Physical and numerical modelling of T-CPT for mechanisms of penetration and heat transfer

P.Q. Mo & L. Gao

China University of Mining and Technology, Xuzhou, China

H.S. Yu

University of Leeds, Leeds, UK

X.L. Tao

Jiangsu Vocational Institute of Architectural Technology, Xuzhou, China

Q.Z. Ma

CCCC-FHDI Engineering Co., Ltd. GuangZhou, China

ABSTRACT: Thermal-Cone Penetration Test (T-CPT) is proposed as a new type of in-situ soil testing method for estimations of both mechanical and thermal properties of soil layers. Physical modelling of T-CPT is conducted in this study to obtain the effects of soil density, penetration depth and heating duration on the penetration resistance and thermal responses. Discrete Element Method (DEM) is then adopted to simulate the processes of penetration, heating and cooling, for investigations of penetration induced stress and temperature distributions in the surrounding soil. The measurements of thermal responses are analyzed to validate the simulation and to evaluate the interpretation method for thermal properties. The results could be used as a benchmark for further analyses of mechanisms of penetration and heat transfer. The interpretation method for T-CPT data is to be developed to improve the performance, with implications to utilization of geothermal energy.

1 INTRODUCTION

Utilization of geothermal energy has become one of the most important and practicable approaches for solving energy shortage with rapidly growing demand and environmental problems (EIA 2009; Capareda 2019). Geothermal energy pile, serving as a new type of pile foundations to extract and/or inject heat into ground at shallow depths using heat carrier medium in heat exchanger piles, can provide majority of required heating/cooling energy, save energy costs, and reduce fossil fuel demand and carbon footprint (Rotta Loria and Laloui 2017; Sani et al. 2019). However, the measurements and determinations of thermal properties are crucial to the evaluation of geothermal energy in the soil profile and the estimation of heat amount to be extracted or injected into the soil layers (Loveridge et al. 2015). Thermal cone penetration test (T-CPT) is a new in-situ testing method based on the traditional cone penetration test, by introducing additional temperature sensors and/or heating elements, which aims to simultaneously measure both mechanical

and thermal responses of the probe during penetration (Akrouch et al. 2016; Vardon et al. 2019; Mo et al. 2021). As a convenient in-situ testing technique, the T-CPT avoids the sampling disturbance for laboratory tests and overcomes the defects of high cost and long testing time of in-situ thermal response test. This tool is useful and convenient in practical applications by inserting the probe into certain depths and conducting thermal tests during the pause of penetration. It is of great significance to the development and utilization of geothermal energy.

In order to look insight into the macro-micro penetration and thermal mechanisms of T-CPT, a type of T-CPT probe and its testing method are proposed in this study to measure the thermal responses of both heating and cooling stages after certain penetration depths. The penetration and heat conduction of T-CPT are then simulated using discrete element method, with investigation of soil movement, force chain and penetration resistance during probe pushing. The thermal responses during heating and cooling are also examined to evaluate the heat transfer mechanisms and the interpretation methods.

2 PHYSICAL MODELLING OF T-CPT

2.1 Physical model and penetrometer of T-CPT

This study attempts to conduct physical modelling of T-CPT, to develop a new type of in-situ CPT based testing method and to investigate the relations between soil properties and penetration and temperature responses. The testing system is assembled by the container with soil, penetrometer, actuator and data acquisition, as shown in the schematic of Figure 1a. This model with 1 m cubic size is small enough to conduct full-size (36 mm diameter) penetration tests without introducing significant boundary effects. A T-CPT penetrometer is proposed in this study, by installing a section with heating elements behind the traditional standard CPTu module (Figure 1b). The heat section is embedded between two insulation sections, and three temperature sensors are equipped at different locations in the heat and insulation sections.

The soil used in the experiments is typical sand in Xuzhou, China, with an average diameter of $d_{50} = 0.5$ mm, uniformity coefficient of $c_u = 2.44$, and curvature coefficient of $c_c = 1.05$. The thermal properties are measured by Hot Disk Analyser at CUMT, giving that thermal conductivity $k = 1.15$ W/m/K and specific heat capacity $c = 850$ J/kg/K.

The probe is pushed at various depths (i.e. $z = 180, 360, 540$ mm) for heating and cooling tests, and the heating periods are designed with 60, 120, 300, and 600 s, to investigate the effects of stress condition and heating time. Temperature sensors are also embedded in the soil at various locations to obtain the temperature distributions during heating and cooling. Note that the physical model is a full-scale model with limited boundary effects, and thus the scale effect for mechanical and thermal measurements should be negligible.

2.2 Results of penetration

The results of cone tip resistance in soils with different relative density are presented in Figure 2. The two tests in dense sand with relative density of 80 % provide comparable developments of penetration resistance, validating the repeatability of the testing method. The maximum q_c is reached at a magnitude of 1 MPa after a depth of about 180 mm, which is 5 times of probe diameter. This surface influence zone is relatively larger, owing to the stress gradient and the low stress condition without surcharge. The changes of tip resistance after 360 mm of penetration are presumably attributed to the inhomogeneous soil layers and the approximating bottom boundary. The loose sample, with relative density around 50 %, generally shows 40 % smaller cone tip resistance.

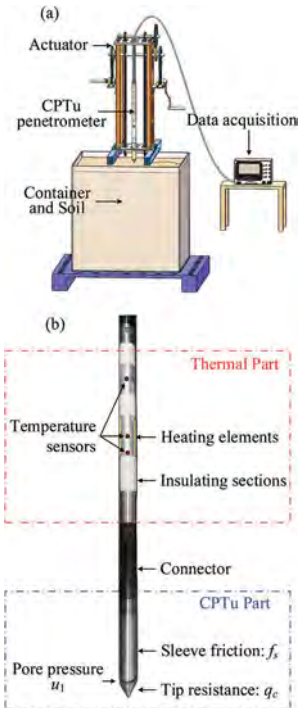


Figure 1. Physical model for T-CPT and design of penetrometer.

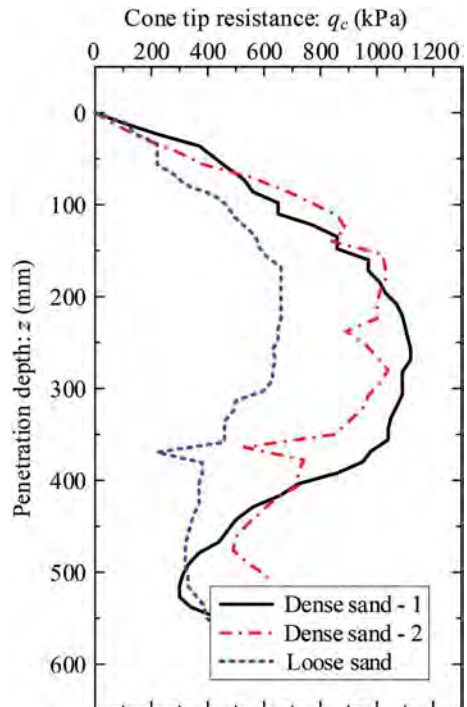


Figure 2. Cone tip resistance against penetration depth.

2.3 Results of heating and cooling

The heating and cooling tests are conducted following the pause of penetration. The temperature responses of three sensors installed in the probe during the heating for 600 s in dense sand and the subsequent cooling are described in Figure 3a. The temperature of Sensor 1, which is located at the center of heating elements, rises to 58 °C at 600 s, whereas the increase for Sensor 2 (at side of heating elements) is less than 25 °C. The Sensor 3 is mounted in the insulation section, which is less affected by the heating elements. However, the gradual increase of 8 °C is attributed to heat conduction through soil. Both measurements from Sensor 1 and Sensor 2 can be directly used for interpretation of soil thermal properties.

The temperature response of soil is depicted in Figure 3b, based on the three embedded temperature sensors at a similar depth with the heating elements of the probe. The radial distances to the center of probe is 20, 40, and 60 mm, respectively. It is clear to notice that the trends of temperature change are similar to the probe sensors, whereas the curves are more gradual, and the peak appears later with longer distance for heat transfer. It also shows the magnitude of temperature distribution around the probe at

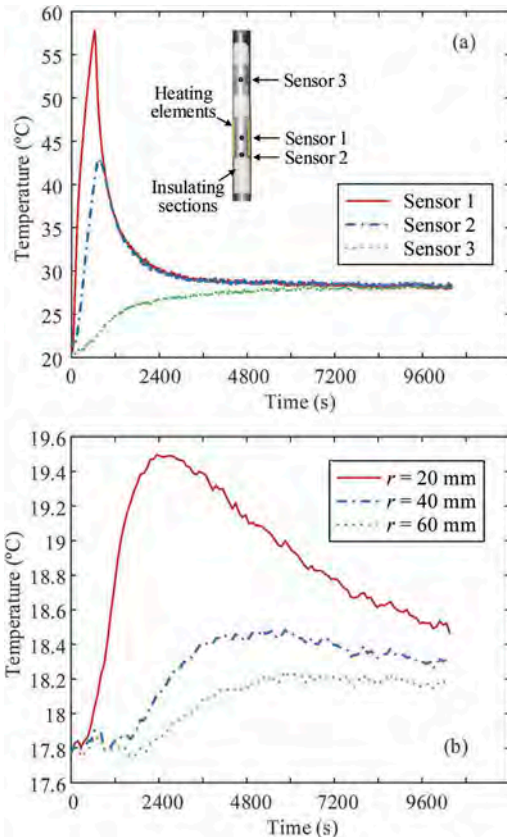


Figure 3. Temperature responses of sensors in probe and soil.

a given moment during heating and cooling, contributing as an important benchmark for numerical and theoretical calculations.

The results of Sensor 1 in dense sand, with various penetration depth (i.e. $z = 10, 20, 30R$, R is probe radius) and different heating duration ($t_{\text{heat}} = 60, 120, 300, 600\text{s}$) are systematically analyzed. Similar trends are obtained, and the traditional interpretation method of ASTM (2014) and Vardon et al. (2019) gives an average estimation of thermal conductivity with $k_{\text{pred}} = 1.27\text{W/m/K}$, which is 10% overestimation comparing to the calibrated 1.15W/m/K from elementary tests. This indicates that the proposed T-CPT penetrometer and testing procedure with limited heating and cooling durations need to be applied with an improved interpretation method based on further investigation of mechanisms of penetration and heat transfer.

3 DEM SIMULATION OF T-CPT

3.1 Mechanical and thermal properties of soil sample

To investigate the mechanisms of penetration and heat transfer of T-CPT, the testing processes with penetration, heating and cooling are simulated using three-dimensional Discrete Element Method (DEM). The soil is prepared to mimic the Ottawa 20-30 sand, with an average diameter of $d_{50} = 0.725$ mm, uniformity coefficient of $c_u = 1.13$, and curvature coefficient of $c_c = 1.01$. Cubic samples with side length of 13 mm are created using about 5800 spherical particles for triaxial tests, to verify its mechanical behaviour. In order to maintain a similar initial void ratio with $e_0 = 0.650$ before shearing, isotropic consolidation tests under different confining pressures are conducted by setting corresponding frictional coefficient between particle contacts. Considering the calculation efficiency and accuracy, the finish of consolidation is defined by the following criterions according to Zhao et al. (2020):

$$\beta_f = \frac{\sum_{B_j \in V} \left| \sum_{c \in B_j} (f_j^c + f_j^b) \right|}{2 \sum_{c \in V} |f^c|} \leq 0.002 \quad (1)$$

$$\gamma_f = \frac{|p' - \sigma_0|}{\sigma_0} \leq 0.04 \quad (2)$$

$$\delta_f = \frac{q}{p'} \leq 0.04 \quad (3)$$

where β_f = unbalanced force ratio, f_j^c and f_j^b = total contact force and body force of the j^{th} particle, f^c = contact force; γ_f = error of mean stress, σ_0 = designed confining pressure, p' = mean stress of particle assembly; and δ_f = ratio of deviatoric and mean stresses, q = deviatoric stress of particle assembly.

The consolidated samples under confining pressure of 0.1 MPa, 2.0 MPa, and 3.5 MPa are adopted to conduct undrained triaxial shear tests with a constant strain rate of 0.08 %/s. The particle-particle friction coefficient is 0.3, and both normal and shear contact stiffnesses are set as 3×10^2 kPa, using linear elastic contact model. The results of triaxial shear tests show that the critical states of samples are reached with large shear strain for $\varepsilon_1 > 30\%$, and the ultimate stress ratios lead to the estimation of internal friction angle with $\phi_{cs} = 21.5^\circ$. The softening phenomenon after peak stress ratio is more obvious for sample with lower confining pressure, and the dilation is restrained under high stress condition, which indicating the reasonability of the mechanical properties of the granular material.

The thermal properties of soil samples in this study are calibrated by elementary tests for one-dimensional heat conduction. The unit thermal resistance T_c in DEM model is defined by the following heat transfer relationship between two contacted particles:

$$\Delta T \cdot n_i = T_c \cdot L \cdot q_i \quad (4)$$

where ΔT = temperature difference between particles, n_i = direction of heat transfer, L = distance between particle centers, q_i = heat flux of unit length. The thermal dilation is also considered to include the thermal effects on stress-strain behaviour of granular material, by defining a linear relation with:

$$\Delta R = \alpha \cdot R \cdot \Delta T \quad (5)$$

where α = coefficient of linear expansion, R = radius of particle, and ΔR = temperature induced change of particle radius.

Taking $\alpha = 2 \times 10^{-7} \text{ K}^{-1}$ for silicon sand, soil samples with over 10,000 particles and identical particle size distributions are calibrated to examine the variation of heat conductivity against samples with different unit heat resistance and void ratio. Figure 4a presents the stabilized temperature field after 600 s of heat conduction with a constant temperature gradient of 1 K/cm. The results of heat conductivity varying with unit heat resistance and void ratio are shown in Figure 4b, which also serve as a benchmark for the design of thermal properties of granular material.

3.2 Numerical model of T-CPT

According to the axisymmetric model, a quarter model with 90° sector is adopted in this study, while the soil parameters are calibrated through the aforementioned elementary tests. To minimize the calculation time for a physical model of T-CPT, the soil samples with radius of 42 mm and height of 45 mm are prepared as previous

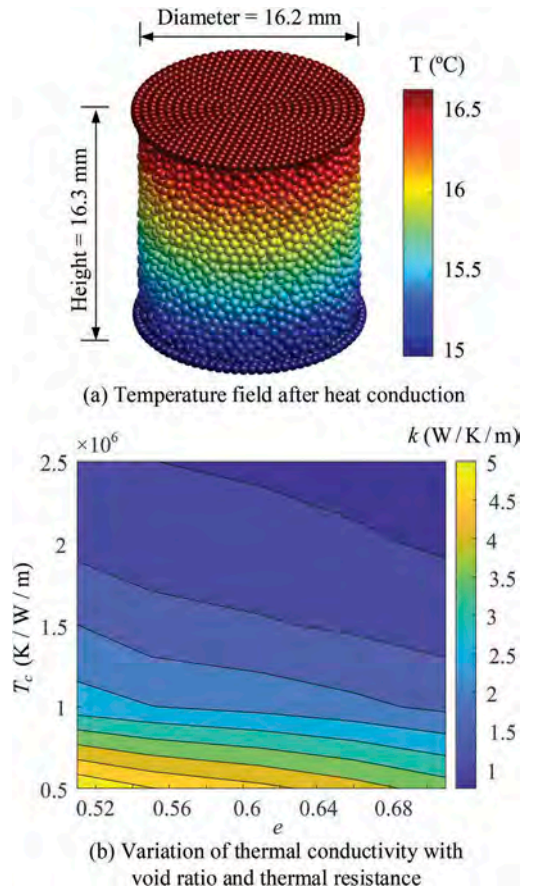


Figure 4. Results of one-dimensional thermal conduction for calibration of thermal properties.

sections, whereas the outer particles (i.e. distance to center larger than 21 mm) are expanded uniformly to reduce the total particle number to around 55,000. The soil samples are initially consolidated by gravity and then compressed with an overburden pressure of 200 kPa, resulting an average initial void ratio of $e_0 = 0.614$. The particle density is 2650 kg/m^3 , and frictional coefficient between particles is again set as 0.3.

A penetrometer with diameter of 6 mm and apex angle of 60° is modelled for T-CPT tests, with a proportion of 1/6. The frictional shaft is set behind the cone shoulder with a length of 5 mm, and the heating section is in coincidence with the frictional shaft. To evaluate the scale effect, the ratio of probe diameter and average particle size is approximately 8.3, and the ratio of sample size to probe size is larger than 14 to reduce the boundary effect. The penetration is conducted at a constant velocity of 20 mm/s, and the total penetration depth is about 36 mm. The initial temperature field is set as 20°C , and the heating and cooling processes are simulated after the pause of penetration. According to the

calibration chart of Figure 4b, the unit thermal resistance is set as 2.5×10^6 K/W/m, giving an equivalent thermal conductivity of $k = 1.1$ W/m/K. The specific heat capacity is 960 and 460 J/kg/K for probe and soil, respectively. The heat power is 0.04 W, due to the scaled heating element in the miniaturized probe. The heating period lasts for 60 s and the subsequent cooling stage is longer than 420 s. The numerical results of penetration and heat transfer are described in the following sections. With these results, the soil distortion, mechanical developments and heat transfer during penetration, heating and cooling are clear to understand the T-CPT mechanisms, which could contribute to the interpretation of T-CPT data in practical applications.

3.3 Results of penetration

The normalized cone tip resistance q_c / σ'_{v0} against normalized penetration depth z/B is shown in Figure 5. The penetration resistance increases with depth, and tends to reach a relative constant magnitude with 18 times of initial vertical stress after a transition zone with a depth of 2.5 times probe diameter.

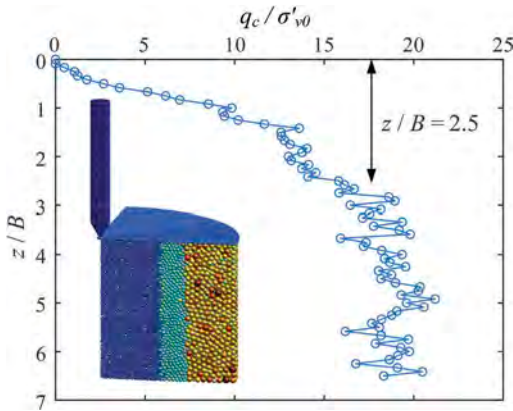


Figure 5. Normalized cone tip resistance during penetration.

The penetration induced soil stress distributions at various penetration depths (i.e. $z/B = 2, 4, 6$) are described in Figure 6 for both radial and vertical stress fields. It is clear to notice that the stress distribution around the penetrometer is mainly developed adjacent to the cone tip. Comparing to the development of radial stress, the degradation of vertical stress is generally concentrated in vertical directions below the cone face. Apart from the growing penetration induced stresses, the influence zone is also increased with penetration depth. The results of stress fields provide the meso-scale information of penetrometer-soil interaction, along with the force chain distributions and evolution during penetration.

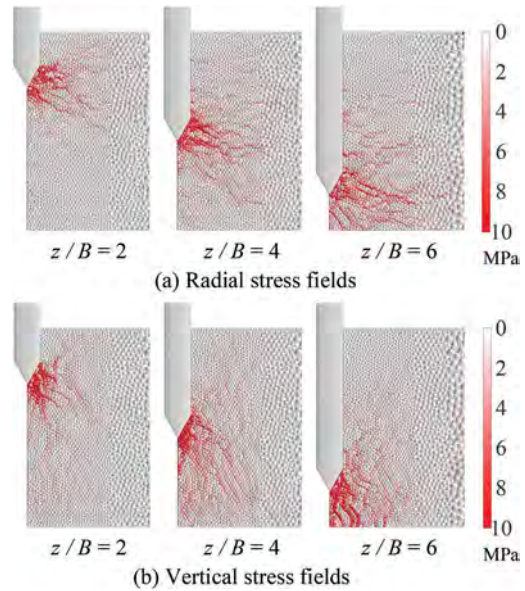


Figure 6. Results of one-dimensional thermal conduction for calibration of thermal properties.

3.4 Results of heat transfer

During the heating and cooling stages after the pause of penetration at $z/B = 6$, the heat flux is transferred from heating element embedded in the probe to the surround soil through heat conduction. The temperature fields at various heating and cooling periods are depicted in Figure 7, showing the evolution of heat conduction. It is obvious to see that the heat transfer in soil is mainly in a spherical profile, owing to the relatively small size of heating element. The contours shown in Figure 7 also describe the influence zone of heating. After 60 s of heating, the surrounding soil with a size of probe diameter is affected by notable temperature change (i.e. 1°C). The size of this influence zone increases with time through heat conduction, while the magnitude of temperature dissipates during the cooling stage.

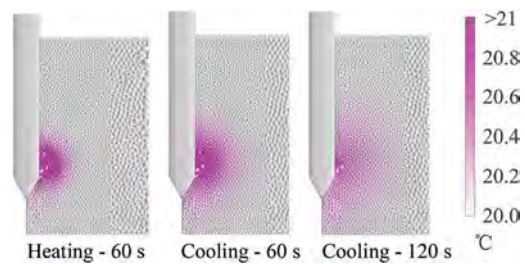


Figure 7. Results of one-dimensional thermal conduction for calibration of thermal properties.

The measurements of temperature in the probe are obtained at both heat section and insulation section, as presented in Figure 8a. The blue curve indicates the temperature at the center of heating element, which rises to 34.9 °C at 60 s of heating and reduces significantly in the following cooling stage. The element at the heat insulation section is hardly affected, while limited temperature change (<0.8 °C) is induced by the heat transfer from heated soil.

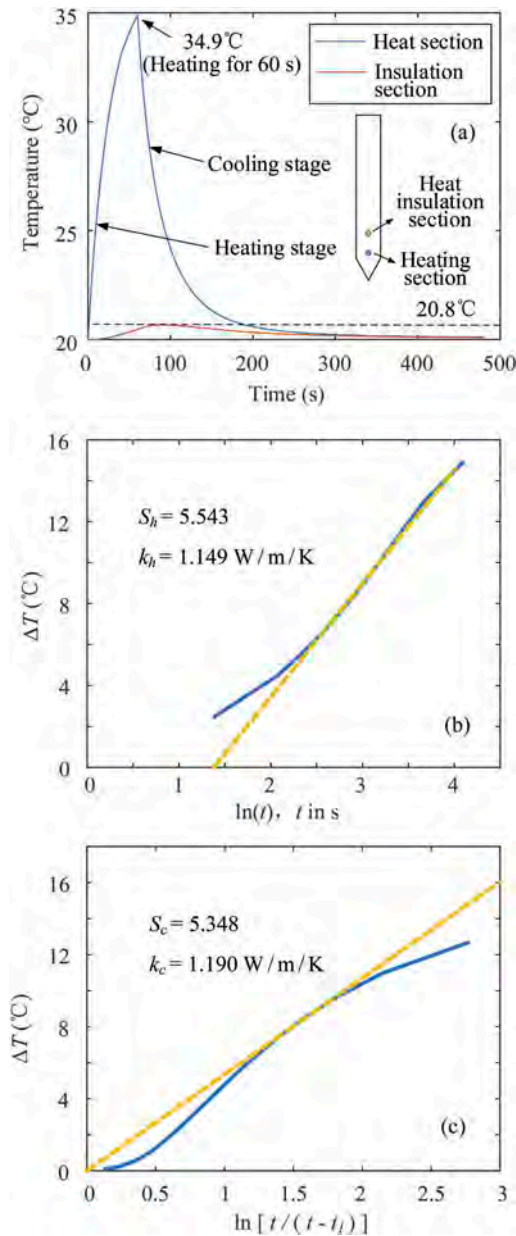


Figure 8. Results of one-dimensional thermal conduction for calibration of thermal properties.

The interpretation of temperature response is shown in Figure 8b and 8c, based on the methods of Vardon et al. (2019) for both heating and cooling stages. Although the heat power is relatively small and the heat transfer in granular material is complex, the back-calculated heat conductivity is not far from the input value of $k = 1.1\text{W/m/K}$. The heating data gives the predicted magnitude of heat conductivity $k_h = 1.149\text{W/m/K}$, with 4.5 % of overestimation. Additionally, the error is larger for cooling data, resulting in $k_c = 1.19\text{W/m/K}$, even though the cooling stage lasts for over 400 s. It may be contributed to the boundary effect, since the side and bottom boundaries are not far enough from the cone and they are set as adiabatic. Note that these differences may be attributed to the material properties, especially from the mechanical aspects. Detailed investigation is to be conducted to promote the simulation of penetration and heat transfer and thus to improve the interpretation method with limited heating and cooling time in further studies.

4 CONCLUSIONS

Physical modelling and DEM simulation of T-CPT are conducted in this study to investigate the mechanisms of penetration and heat transfer. A type of T-CPT probe with both temperature sensors and heating elements is proposed, together with its testing method for heating and cooling after a pause of penetration. Apart from the measurement of penetration resistance, the thermal responses of sensors in the probe and soil are obtained to examine the temperature changes and heat conduction during heating and cooling stages. The existing interpretation method is shown to overestimate the thermal conductivity of soil. DEM model is later validated to simulate the processes of T-CPT, after calibration of thermal properties of granular material. The distributions and evolutions of stresses and temperature in soil are presented to illustrate the meso-scale mechanisms of penetration and heat conduction. The simulated thermal responses are analyzed to validate the numerical method, and to evaluate the existing interpretation method. The results of this study are important to understand the mechanisms of probe-soil interactions, which could contribute to the further developments of T-CPT and its testing and interpretation methods.

ACKNOWLEDGEMENT

The authors would like to acknowledge financial supports from National Natural Science Foundation of China (Grant No. 51908546, Grant No. 52178374), China Postdoctoral Science Foundation (Grant No. 2020T130699), and Key University Science Research Project of Jiangsu Province (Grant No. 20KJA560003).

REFERENCES

- Akrouch, G.A., Briaud, J.L., Sanchez, M. & Yilmaz, R. 2016. Thermal cone test to determine soil thermal properties. *J. Geotech. Geoenviron. Engng.* 142(3): 04015085.
- ASTM. 2014. *D5334-14: Standard test method for determination of thermal conductivity of soil and soft rock by thermal needle probe procedure*. West Conshohocken, PA, USA: ASTM International.
- Capareda, S.C. 2019. *Introduction to Renewable Energy Conversions*. CRC Press. DOI: 10.1201/9780429199103.
- EIA. 2009. *Renewable Energy Consumption and Electricity Preliminary Statistics 2008*.
- Loveridge, F., Olgun, C.G., Brettmann, T. & Powrie, W. 2015. Group thermal response testing for energy piles. *Eur. Conf. Soil Mech. Geotech. Eng.*, vol. XVI.
- Mo, P.Q., Ma, D.Y., Zhu, Q.Y. & Hu, Y.C. 2021. Interpretation of heating and cooling data from thermal cone penetration test using a 1D numerical model and a PSO algorithm. *Computers and Geotechnics* 130: 103908.
- Rotta Loria, A.F. & Laloui, L. 2017. Thermally induced group effects among energy piles. *Géotechnique* 67(5): 374–393.
- Sani, A.K., Singh, R.M., Amis, T. & Cavarretta, I. 2019. A review on the performance of geothermal energy pile foundation, its design process and applications. *Renewable and Sustainable Energy Reviews* 106: 54–78.
- Vardon, P.J., Baltoukas, D. & Peuchen, J. (2019). Interpreting and validating the thermal cone penetration test (T-CPT). *Géotechnique* 69(7): 580–592.
- Zhao, S.W., Zhao, J.D. & Guo, N. 2020. Universality of internal structure characteristics in granular media under shear. *Physical review. E* 101(1–1).

Soil stratigraphy from seismic piezocone data and multivariate clustering in alluvial soil deposits: Experience in the Lower Tagus Valley region

F. Molina-Gómez, D. Cordeiro, C. Ferreira & A. Viana da Fonseca

CONSTRUCT-GEO, Faculdade de Engenharia da Universidade do Porto (FEUP), University of Porto, Portugal

ABSTRACT: The identification of soil stratigraphy at a given site is crucial for geotechnical analysis and design. This study addresses the delineation of soil stratigraphy from seismic piezocone penetration test (SCPTu) measurements. For this purpose, SCPTu data from an experimental site in the Lower Tagus Valley region (close to Lisbon) were compiled. Soil stratigraphy was obtained by applying a multivariate clustering approach using the direct measurements reported by SCPTu. The hierarchical clustering results were compared against the soil behaviour index profile. Moreover, the differences/similarities obtained from multivariate clustering were validated by contrasting statistical results against the visual description of samples collected in the experimental site at Lower Tagus Valley using advanced sampling techniques; namely, Gel-Push sampler. The main findings showed that the clustering approach implemented herein detects and groups soil layers with similar soil behaviour types, allowing delineating the soil stratigraphy in multilayer alluvial soil deposits.

1 INTRODUCTION

The identification of soil stratigraphy is one of the main concerns for the characterisation of soils deposits. A realistic identification of the soil variability in depth reduces the failure probability of geotechnical structures. The cone penetration test (CPT) and its enhanced versions provide reliable identification of soil multi-layering due to its simultaneous measurements. Hence, soil stratigraphy can be assessed using CPT data by correlating in situ measurements with parameters inferred by applying a strong theoretical background.

Although no samples are recovered in CPT sounding, the large number of data from this type of testing allows identifying the soil stratigraphy. Therefore, such data can be interpreted by statistical methods. Hegazy & Mayne (2002); Liao & Mayne (2007); Molina-Gómez, Viana da Fonseca, Ferreira, Sousa, & Bulla-Cruz (2021) applied cluster analysis approaches to delineate the stratigraphy in different types of soil deposits. In these studies, the authors compared their statistical analyses against soil behaviour index profiles, originally proposed by (Robertson 1990). Such a comparison showed a good fitting between results, validating the applicability of clustering for delineating the soil stratigraphy.

This study addresses the delineation of soil stratigraphy from seismic piezocone (SCPTu) measurements by applying the clustering approach proposed by Molina-Gómez, Viana da Fonseca, Ferreira, Sousa, & Bulla-Cruz (2021). The SCPTu measurements were carried out in an experimental site

located at Lower Tagus Valley, south of Portugal. Embedded layers of sandy and clayey soils with an alluvial origin from the Tagus River compose such an experimental site (Viana da Fonseca, Ferreira, Ramos, & Molina-Gómez 2019). Besides, in such a site, high-quality undisturbed samples were collected using an advanced sampling technique—the Gel-Push (GP) sampler. The visual observation of these samples confirmed the detected stratigraphy from the multivariate clustering.

2 DESCRIPTION OF THE CLUSTERING APPROACH

In this study, the agglomerative hierarchical clustering approach proposed by Molina-Gómez, Viana da Fonseca, Ferreira, Sousa, & Bulla-Cruz (2021) was applied. Such an approach comprises the following phases: (i) selection of the data and identification of variables; (ii) standardisation of the variables; (iii) computation of the distance (or similarity) matrix; (iv) application of clustering technique; (v) selection of the cut level of the dendrogram, associated with the best partition, for defining the number of clusters; (vi) interpretation of cluster results; and (vii) validation by comparison against soil behaviour type profiles. Besides, it includes a comparison against visual examination of high-quality undisturbed samples collected using the GP sampler, as a novel validation in such a clustering approach. The clustering procedure adopted for this study is described following.

For the data standardisation, the Zscore method was adopted, as suggested by Hegazy & Mayne (2002):

$$Z_{ij} = \frac{x_{ij} - \bar{x}(X_j)}{s(X_j)} \quad (1)$$

where Z_{ij} is the standardised value, x_{ij} is the SCPTu measurement at a certain depth of the SCPTu variable, X_j is the SCPTu variable of each profile, $\bar{x}(X_j)$ is the average of the SCPTu variable and $s(X_j)$ is the standard deviation of the SCPTu variable.

The distance among pairs of objects is represented by a matrix $D_{(n \times n)}$ (Härdle & Simar 2015). Equation 2 describes the matrix distance, D , that contains measures of similarity among the n objects, where $d_{i,j}$ are the distances between the measurements of SCPTu variables.

$$D = \begin{bmatrix} d_{1,1} & d_{1,2} & \cdots & \cdots & \cdots & d_{1,n} \\ \vdots & d_{2,2} & \ddots & & & \vdots \\ \vdots & \vdots & d_{3,2} & \ddots & & \vdots \\ \vdots & \vdots & \vdots & d_{4,2} & \ddots & \vdots \\ d_{n,1} & d_{n,2} & \cdots & \cdots & \cdots & d_{n,n} \end{bmatrix} \quad (2)$$

Nowadays, there are different similarity measurements, including Euclidean distance, Manhattan distance, Pearson, cosine and power (Johnson & Wichern 2007). Härdle & Simar (2015) claimed that no specific rule or theory is available on which to base the choice of similarity measurements. In this study, Euclidean distance was used to compute the matrix D of piezocone data, as recommended by (Liao & Mayne 2007). Such a method estimates the geometric distance—based on the Pythagorean theorem—of two observations in a multidimensional space. Equation 3 describes the Euclidean distance of two observations, where k is the number of variables and i is the variable index.

$$d(P, Q) = d(Q, P) = \sqrt{\sum_{i=1}^k (q_i - p_i)^2} \quad (3)$$

Starting with the matrix D (see Equation 2) an iterative procedure takes place to join/grouping the most similar classes and update matrix D , which ends when all data is grouped in a particular cluster (Bulla-Cruz, Lyons, & Darghan 2021). The iterations are carried out according to a specific aggregation criterion. In this study, the complete linkage method was applied. The algorithm of complete linkage distance is:

$$d(R, P + Q) = \max\{d(R, P), d(R, Q)\} \quad (4)$$

where $P + Q$ are clustered measurements of SCPTu variables and R is a possible new group.

The best-known result of a Hierarchical Classification is a graphical representation—dendrogram. The quality of SCPTu data grouping (i.e. the number of clusters) can be assessed by comparing the number of soil classes identified by the soil behaviour type (SBT) chart proposed by (Robertson 1990). Afterwards, such a number is validated by the Average Silhouette Method (Rousseeuw 1987). The Average Silhouette Method computes the average silhouette of observations for different numbers of clusters (K), indicating K_{opt} value as the maximum average silhouette over a range of possible values for a different number of clusters.



Figure 1. Experimental site map and location of the investigation points.

As before noticed, the underlying mathematics of cluster analysis is simple to implement. However, it requires extensive calculations because of the large amount of data. Therefore, all computations were conducted in RStudio, which is a free integrated environment for statistical programming and graph plotting (Molina-Gómez, Bulla-Cruz, & Darghan 2019).

3 EXPERIMENTAL SITE

Within the scope of two research projects on soil liquefaction developed in the CONSTRUCT-GEO research centre of FEUP, a vast site characterisation campaign was carried in an experimental site in the Lower Tagus Valley (south of Portugal). The site characterisation comprised the definition of liquefaction risk by micro-zonation maps (Saldanha, Viana da Fonseca, & Ferreira 2018). This geotechnical test site is located in the municipalities of Vila Franca de Xira and Benavente, covering a zone with 14683 ha area and 50.8 km perimeter. In situ tests for geotechnical characterisation were performed at specific locations, referenced as site investigation points (SI). Figure 1 shows the map and SI locations within the experimental site.

For this study, SI15 was selected since there advanced sampling techniques were implemented for collecting high-quality samples for the first time in Portugal (Molina-Gómez, Viana da Fonseca, Ferreira, Ramos, & Cordeiro 2021). The groundwater level in SI15 was identified at about 2.5 m depth. Moreover, in this point, an SCPTu was carried out. Shear wave velocities (V_S) were measured at each 0.50 m depth. The values of cone resistance (q_c), sleeve friction (f_s) and pore-water pressure generated during cone penetration (u_2) were averaged each ± 0.25 m depth (ranges of 0.5 m), considering the depth of the V_S measurements, to compare the SCPTu data profiles. Figure 2 presents the SCPTu profiles and the averaged values in the specific depths of V_S measurements at SI15.

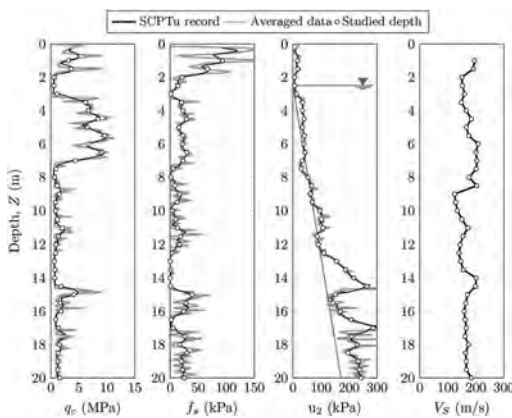


Figure 2. SCPTu profiles at SI15.

The SCPTu data were analysed using the software Cliq v.3.0. The analyses were carried out based on the unified approach proposed by Robertson (1990), which includes the classification of soil behaviour type (SBT) zones according to the soil behaviour type index (I_c). I_c computation considers the following procedure:

$$Q_t = \frac{q_t - \sigma_{v0}}{\sigma'_{v0}} \quad (5)$$

$$Fr = \left(\frac{f_s}{q_t - \sigma'_{v0}} \right) 100\% \quad (6)$$

$$I_c = \left[(3.47 - \log Q_t)^2 + (\log Fr + 1.22)^2 \right]^{0.5} \quad (7)$$

where q_t is the cone resistance corrected for pore water effects ($q_t = q_c + u_2(1 - a)$); a is the cone area ratio; σ_{v0} is the current in situ total vertical stress; σ'_{v0} is the current in situ effective vertical stress.

Figure 3 presents the interpretation of the soil profiles in terms of soil type chart. Classification results indicate that the soil profile at SI-15 has five different soil types, which are characteristic of soil deposits in the Lower Tagus Valley from the Quaternary (Ferreira, Viana da Fonseca, Ramos, Saldanha, Amoroso, & Rodrigues 2020).

The soils of the experimental site appear in zones 3, 4, 5 and 6, thus typically behave as 'clay to silty clay', 'clayey silt to silty clay', 'silty sand to sandy silt' and 'clean sand to sand to silty sand', respectively. Points located in Zone 1 were not considered for defining the number of clusters because there is not a well-defined characterisation for these soil types; that is, out-of-range zones with $I_c = \infty$. Based on the above consideration, the clustering of SI15 can be performed considering four groups.

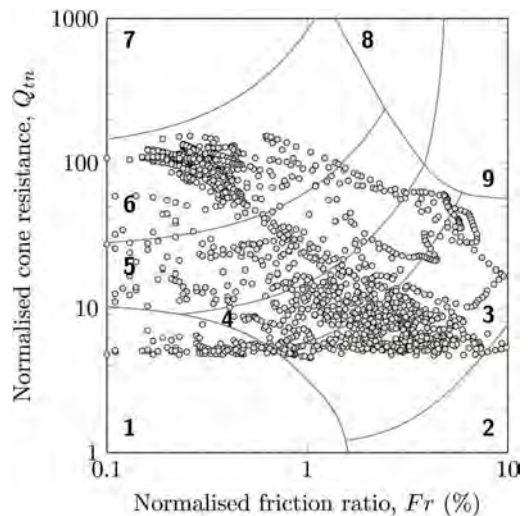


Figure 3. Results of soil classification type.

4 ADVANCED SAMPLING

The collection of high-quality samples is critical to obtain representative test results for soil characterisation in the laboratory (Ferreira, Viana da Fonseca, & Nash 2011). A typical sampling campaign involves the following stages: drilling, sampler insertion, sampler retrieval, tube sealing, transport, soil extrusion, sample storage and preparation for element testing (Hight 2000). Nowadays, sampling processes are conducted using diverse techniques, such as hydraulically activated push tubes, rotary devices and freeze sampling, where the freezing method is the most expensive (Viana da Fonseca & Pineda 2017).

In this research, an advanced sampling technique developed by the Japanese geotechnical company Kiso-Jiban Consultants, to develop a method able to

replace freezing techniques. There are four different variations of GP: GP-Rotary, GP-Drilling, GP-Triple, and GP-Static. In this study, the GP-Static (GP-S) was implemented. This sampling device uses a hydraulic activated fixed-piston and follows the same principle of the Osterberg-type sampler.

On the other hand, the GP is an advanced sampling technique, which uses a viscous polymer gel to collect high-quality undisturbed samples. The gel use, as the main innovation for soil sampling, afforded the name for this technique. The gel must be prepared at a 1 vol% concentration ratio of the viscous polymer in clean water (Mori & Sakai 2016). The purpose of using the viscous gel is to significantly reduce the friction between the sample and walls liner during both the insertion of the sampler into the ground and during the sample extrusion in the laboratory (Viana da Fonseca, Ferreira, Molina-Gómez, & Ramos 2019). Besides, the rheological properties of the polymer gel allow preserving the soil structure of the collected samples.

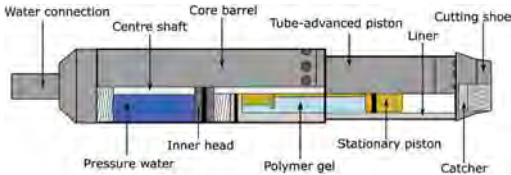


Figure 4. Schematic of GP sampler components (Molina-Gómez, Ferreira, Ramos, & Viana da Fonseca 2020).

Unlike conventional hydraulic activated fixed-piston, the GP-static device includes three pistons: (i) the stationary piston, (ii) the sampling tube-advancing piston, and (iii) the core-catcher activating piston. At the maximum performance, the GP sampler can collect samples with 71 mm diameter and 1 m length. However, according to the soil type to be sampled, the device can suffer damages in the cutting shoe (Molina-Gómez, Viana da Fonseca, Ferreira, Ramos, & Cordeiro 2021). Details about the performance and quality sampling using the GP sampler are provided in Molina-Gómez, Ferreira, & Ramos (2020). Figure 4 schematises the components of the GP-Static sampler.

The GP sampling was carried out in four boreholes located at about 5 m distance to the SCPTu sounding. During the experimental campaign, a total of 14 GP samples were collected at the SI15 location. The sampling depths were selected considering suitable layers for liquefaction assessment by element testing in the laboratory. The liquefiable layers were defined by detecting zones with $I_c < 2.6$. Figure 5 illustrates the sampling depths for each technique. Moreover, in Figure 5, the sampling depths are contrasted against the averaged soil behaviour index profile of SI15.

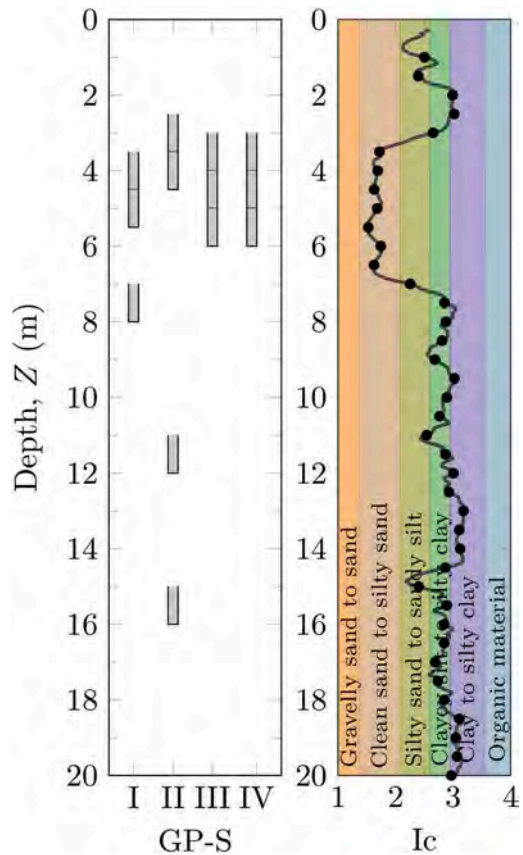


Figure 5. Sampling depths for each advanced technique and averaged soil behaviour index profile at SI15.

5 ANALYSIS OF RESULTS

A cluster analysis in terms of the depth (Z) and using the standardised data recorded at SI15 by the four channels of SCPTu (e.g. q_c , f_s , u_2 , V_S) was carried out. Liao & Mayne (2007) used normalised data to define the soil stratigraphy by applying a multivariate approach (e.g. Q_t and Fr parameters). However, Molina-Gómez, Viana da Fonseca, Ferreira, Sousa, & Bulla-Cruz (2021) obtained a better grouping using standardised raw data instead of standardised normalised data. These authors showed that the differences between clustering were because of the uncertainties associated with the in situ stress-state assessment, which depends on the unit weight (γ). Nevertheless, γ is a physical property that differs according to the CPT correlation applied, although the literature reports several correlations to estimate such a physical parameter, such as Mayne, Peuchen, & Bouwmeester (2010), Robertson & Cabal (2010), Lengkeek, de Greef, & Joosten (2018).

In this study, only the clusters with at least two continuous measurements are considered soil layers, as suggested by Liao & Mayne (2007). Hence, a minimum layer thickness of 1.0 m was defined. Clusters with points without a continuous group of data (single points) were considered as lenses or transition zones (Hegazy & Mayne 2002). The cluster analysis was conducted for obtaining four groups, which correspond to different soil behaviour types or layers previously identified in Figure 3. Such a number of groups was compared against the results of the Average Silhouette Method, which allows estimating the optimum number of clusters, K_{opt} . Figure 6 shows $K_{opt} = 4$, validating the selection of the number of clusters based on the SBT criterion.

Figure 7 presents the dendrogram obtained from the cluster analysis of SCPTu data. This dendrogram shows the clustering of all depths and the distances between the aggregate clusters. A distance of about 5 defined four clusters, which correspond to the layers composing the soil stratigraphy of the studied zone.

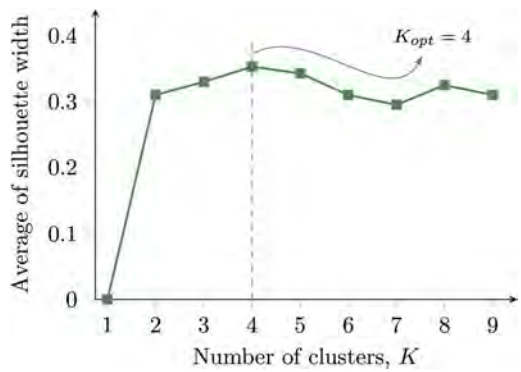


Figure 6. Estimation of the optimum number of clusters.

In addition, Figure 7 indicate the SBT zone of each cluster through a comparison against the I_c profile and high-quality samples.

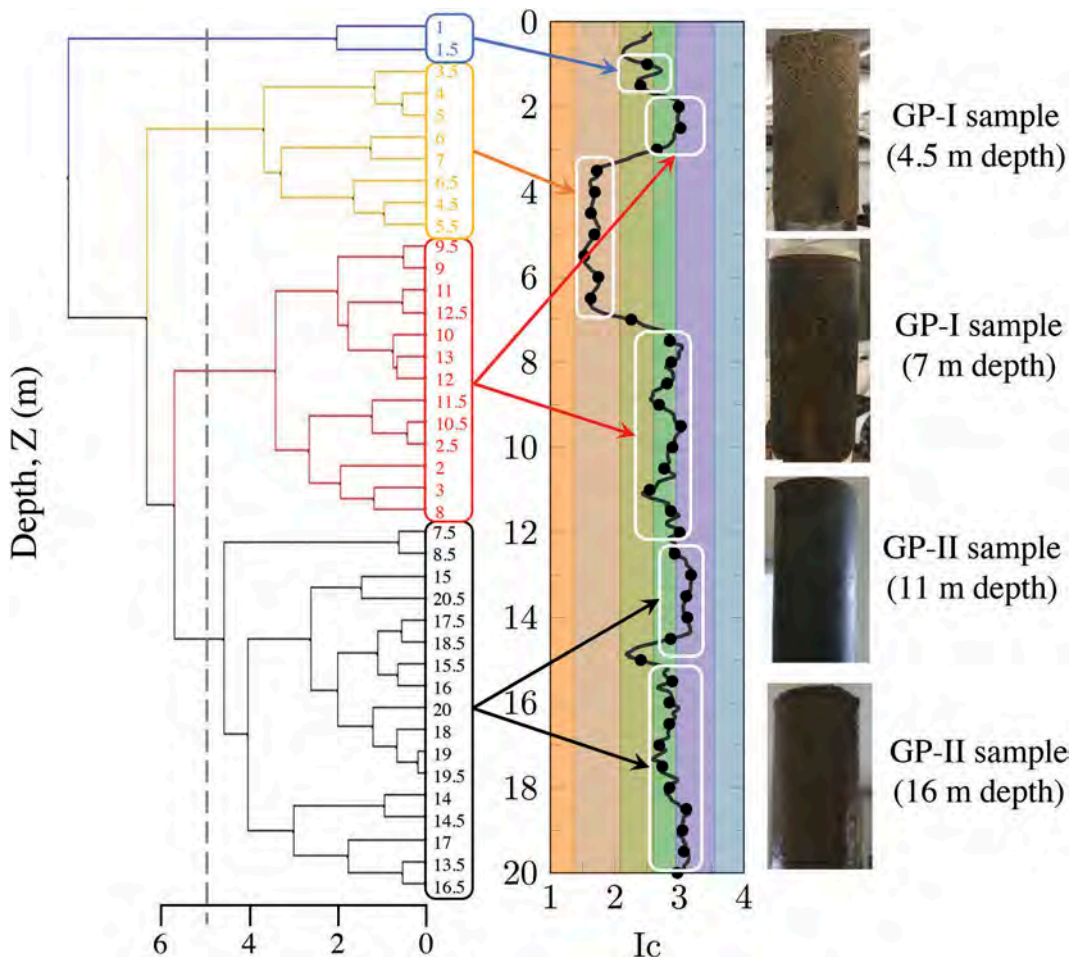


Figure 7. Soil stratigraphy of SI15 inferred from cluster analysis and comparisons between dendrogram against I_c profile and high-quality samples.

layers that behave as 'silty sand to sandy silt' (1 m to 1.5 m depth), 'clean sand to sand to silty sand' (3 m to 7 m depth), 'clayey silt to silty clay' (2 m to 3 m depth and 8 m to 14.5 m depth) and 'clay to silty clay' (12.5 m to 14.5 m depth and 15.5 m to 20 m depth). Besides, two transitional layers composed of soils that behave as 'silty sand to sandy silt' were identified at 7.5 and 15 m depth.

On the other hand, Figure 7 shows photographs of GP samples collected at representative depths of the layers identified in the cluster analysis (e.g. 4.5 m, 7 m, 11 m and 16 m depth). A visual examination in the laboratory of GP samples supported cluster results; that is, the sample collected at 4.5 m depth is a sand, the sample collected at 7 m depth corresponds to a silt mixture, and the samples collected at 11 m and 16 m depth are clay with different content of granular particles.

The simultaneous comparisons between dendrogram, I_c profile and high-quality GP validated the implementation of the clustering approach to define the soil stratigraphy and detect interlayers from SCPTu data. Therefore, the clustering approach proposed herein provided a reliable data grouping for defining soil stratigraphy of alluvial soil deposits of the Lower Tagus Valley—a region with high inter-layering. Moreover, this clustering approach can be applied to other datasets from other experimental sites using raw data from the four parameters of the SCPTu. This information provides a method that allows defining soil layers with similar properties and behaviour, useful in the design of geotechnical structures.

6 CONCLUSION

In this paper, a hierarchical clustering approach for defining the soil stratigraphy from SCPTu data at a site investigation point located in the Lower Tagus Valley (south of Portugal) has been applied. The approach comprises a complete-linkage algorithm, formulated in RStudio, which used the Euclidean distance of standardised SCPTu measurements (q_c , f_s , u_2 and V_s). The method is objectively capable of classifying similar groups of data in the soil profile, delineating different layer boundaries and soil transitions. The statistical results were validated by comparing the dendrogram against the I_c profile and visual examination of high-quality samples collected using the GP sampler. These comparisons are the main contribution of this study since they confirmed the correspondence between the defined stratigraphy (clusters) with the soil behaviour type and soil composing the soil layers. Therefore, this clustering approach can be applied to other datasets from other experimental sites using raw data from the four parameters of the SCPTu.

ACKNOWLEDGEMENTS

This work was also financially supported by UIDB/04708/2020 and UIDP/04708/2020 of CONSTRUCT – Institute of R&D in Structures and Construction funded by the national funds through the FCT/MCTES (PIDDAC). The first author acknowledges the Portuguese Foundation for Science and Technology (FCT) for the support through SFRH/BD/146265/2019 grant.

REFERENCES

- Bulla-Cruz, L. A., L. Lyons, & E. Darghan (2021). Complete-Linkage Clustering Analysis of Surrogate Measures for Road Safety Assessment in Roundabouts. *Revista Colombiana de Estadística* 44(1), 91–121.
- Ferreira, C., A. Viana da Fonseca, & D. F. T. Nash (2011). Shear wave velocities for sample quality assessment on a residual soil. *SOILS AND FOUNDATIONS* 51(4), 683–692.
- Ferreira, C., A. Viana da Fonseca, C. Ramos, A. S. Saldanha, S. Amoroso, & C. Rodrigues (2020). Comparative analysis of liquefaction susceptibility assessment methods based on the investigation on a pilot site in the greater Lisbon area. *Bulletin of Earthquake Engineering* 18, 109–138.
- Härdle, W. K. & L. Simar (2015). *Applied Multivariate Statistical Analysis* (4 ed.). Springer Berlin Heidelberg.
- Hegazy, Y. & P. W. Mayne (2002). Objective site characterization using clustering of piezocone data. *Journal of Geotechnical and Geoenvironmental Engineering* 128, 986–996.
- Hight, D. W. (2000). Sampling Methods: Evaluation of Disturbance and New Practical Techniques for High Quality Sampling in Soils. In *7 Congresso Nacional de Geotecnia*, Porto.
- Johnson, R. A. & D. W. Wichern (2007). *Applied Multivariate Statistical Analysis* (6 ed.). Pearson Education International.
- Lengkeek, A., J. de Greef, & S. Joosten (2018). CPT based unit weight estimation extended to soft organic soils and peat. In *Cone Penetration Testing IV: Proceedings of the 4th International Symposium on Cone Penetration Testing (CPT'18)*, Delft, The Netherlands, pp. 389–394. Taylor & Francis Group.
- Liao, T. & P. W. Mayne (2007). Stratigraphic delineation by three-dimensional clustering of piezocone data. *Georisk* 1, 102–119.
- Mayne, P., J. Peuchen, & D. Bouwmeester (2010). Soil unit weight estimation from CPTs. In *2nd International Symposium on Cone Penetration Testing*.
- Molina-Gómez, F., L. Bulla-Cruz, & E. Darghan (2019). Profiles analysis as a modality of repeated measures for comparing grain size distributions in granular bases. *Measurement: Journal of the International Measurement Confederation* 146, 930–937.
- Molina-Gómez, F., A. Viana da Fonseca, C. Ferreira, C. Ramos, & D. Cordeiro (2021). Novel sampling techniques for collecting high-quality samples: Portuguese experience in liquefiable soils. In *6th International Conference on Geotechnical and Geophysical Site Characterization, ISC'6*, Budapest, pp. paper 115.

- Molina-Gómez, F., C. Ferreira, & A. Ramos, C. Viana da Fonseca (2020). Performance of gel-push sampling in liquefiable soils. *Géotechnique Letters* 10, 256–261.
- Molina-Gómez, F., A. Viana da Fonseca, C. Ferreira, F. Sousa, & L. A. Bulla-Cruz (2021). Defining the soil stratigraphy from seismic piezocone data: A clustering approach. *Engineering Geology* 287, 106111.
- Mori, K. & K. Sakai (2016). The gp sampler: a new innovation in core sampling. In Lehane, Acosta-Martínez, and Kelly (Eds.), *Geotechnical and Geophysical Site Characterisation 5*, pp. 99–124. Australian Geomechanics Society.
- Robertson, P. K. (1990). Soil classification using the cone penetration test. *Canadian Geotechnical Journal* 27, 151–158.
- Robertson, P. K. & K. L. Cabal (2010). Estimating soil unit weight from CPT. In *2nd International Symposium on Cone Penetration Testing*, Huntington Beach, CA, USA.
- Rousseeuw, P. J. (1987). Silhouettes: A graphical aid to the interpretation and validation of cluster analysis. *Journal of Computational and Applied Mathematics* 20, 53–65.
- Saldanha, A. S., A. Viana da Fonseca, & C. Ferreira (2018). Microzonation of the liquefaction susceptibility: case study in the lower Tagus valley. *Geotecnia* 142, 07–34.
- Viana da Fonseca, A., C. Ferreira, F. Molina-Gómez, & C. Ramos (2019). Collection of high-quality samples in liquefiable soils using new sampling techniques. In *Proceedings of the XVII ECSMGE-2019*, pp. paper 014.
- Viana da Fonseca, A., C. Ferreira, C. Ramos, & F. Molina-Gómez (2019). The geotechnical test site in the greater lisbon area for liquefaction characterisation and sample quality control of cohesionless soils. *AIMS Geosciences* 5, 325–343.
- Viana da Fonseca, A. & J. Pineda (2017). Getting high-quality samples in ‘sensitive’ soils for advanced laboratory tests. *Innovative Infrastructure Solutions* 2, 34.

Undrained strength from CPTu in brittle soils: A numerical perspective

L. Monforte, M. Arroyo & A. Gens
CIMNE-UPC, Barcelona, Spain

ABSTRACT: Static liquefaction of soils that have a brittle undrained response (hydraulic fills, mine tailings or sensitive clays) may lead to sudden failures of large consequence. Given the importance of undrained failure, obtaining precise estimates of peak and residual yield strength is important. The CPTu plays a major role in the geotechnical characterization of these geomaterials and so do CPTu-based estimates of undrained strength. Most of the methods available for CPTu-based estimation of undrained strength are empirical, based on correlation with other laboratory or field tests. When such correlations are established difficulties appear due to variable disturbance affecting the reference laboratory samples and parasitic effects, such as unaccounted for partial drainage during penetration or unknown side friction, affecting the cone results. Such difficulties are not present when using numerical simulation. The paper builds upon a series of CPTu simulations using a model able to represent brittle undrained failure. Confounding factors such as partial drainage and cone side friction are systematically varied to examine their effect on the results. The results are then employed to examine the performance of several empirical methods frequently employed to obtain peak and residual strength from CPTu.

1 INTRODUCTION

Some geomaterials (hydraulic fills, mine tailings or sensitive clays) may exhibit undrained softening upon shearing (static liquefaction): a drastic decrease of the effective mean stress and mobilized undrained shear strength. Static liquefaction is a brittle response that may lead to catastrophic sudden failures, often associated with loss of life and major environmental impact (Gens, 2019). The identification and characterization of these materials is therefore of paramount importance.

The extraction of good-quality samples of these loose/soft soils is challenging and in situ tests are essential for their characterization (Been, 2016; Gens 2019). The interpretation of CPTu soundings in these brittle materials is not always straightforward, particularly as their permeability does frequently result in partly drained conditions (Schnaid, 2021). Nevertheless, several correlations are in use to relate cone metrics and peak and residual undrained shear strength in brittle soils.

Numerical simulation of CPT may offer new insights of the mechanisms during insertion, leading to more reliable interpretation techniques. To this end, Monforte et al (2021) reported a parametric analysis employing the Particle Finite Element method (PFEM) in which several materials with different idealized materials of variable undrained brittleness were considered in the simulation of CPTu. The analysis also assessed the effect of drainage conditions and interface friction angle on cone metrics. In this

work we exploit the simulation database of Monforte et al (2021) to assess several cone interpretation techniques frequently employed in current practice to infer undrained strength.

2 NUMERICAL DATABASE

2.1 Simulation method

Numerical simulations (Monforte et al, 2021) have been carried out by means of G-PFEM (Geotechnical Particle Finite Element Method), specially designed for the analysis of problems involving the penetration of rigid structures into fluid-saturated soil masses (Monforte et al, 2017, 2018).

The cone has standard dimensions and is assumed rigid. CPT symmetry allows for an axisymmetric model. The stress state is set up by prescribing a vertical stress of 96 kPa at the top boundary and of 56 kPa at the radial boundary, i.e. a K_0 value of 0.58. The CPT is advanced by 30 diameters into the soil attaining a steady state in all the simulated records.

2.2 Materials simulated

The soil is described by a version of the Clay and Sand Model (CASM) (Yu, 1998; Manica et al. 2021; Arroyo & Gens, 2021). Common constitutive parameters for all cases examined are reported in Table 1. Materials with different brittleness index are obtained by modifying the geometry of the yield surface (shape

parameter, n , and spacing ratio, r), see Table 2. Because of these choices all the simulated materials share the same normal compression line, but their critical state line has different positions on the compression plane. In undrained conditions, all materials share the same peak undrained shear strength, whereas the residual undrained shear strength varies (Table 2).

Example triaxial responses after anisotropic (K_0) consolidation are reported in Figure 1. In undrained conditions, after reaching the peak, deviatoric stresses reduce due to strain softening; material A is the most brittle whereas material H is almost insensitive.

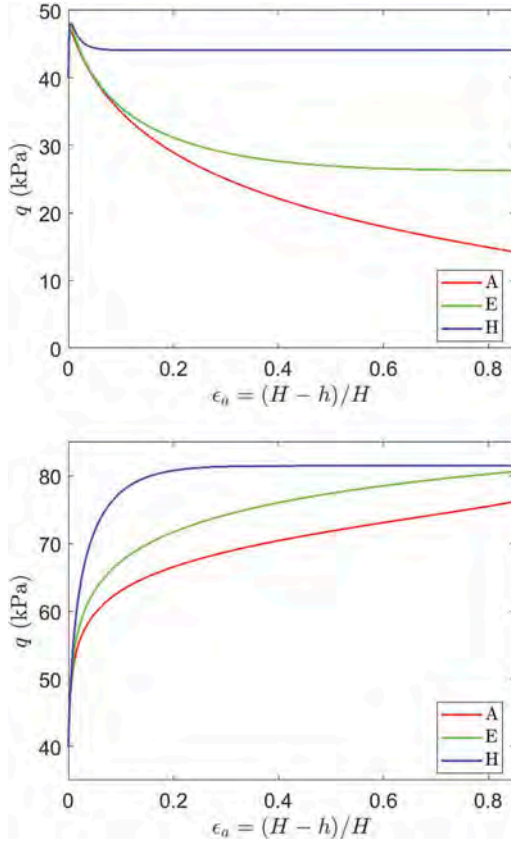


Figure 1. K0 triaxial compression behavior of materials A, E and H: undrained loading, top, and drained loading, bottom.

2.3 Parametric study

For every CASM material, the parametric analysis presented below examines the effect of drainage conditions and soil-cone interface friction angle. Drainage conditions are controlled through permeability values, which have been varied between 10^{-9} m/s and 10^{-3} m/s. To avoid clutter most results below are only presented for three values: 10^{-8} m/s (fully undrained), 10^{-6} m/s (partly drained) and 10^{-3} m/s (fully drained).

The interface friction angles employed ($\delta = 0, 7^\circ, 12^\circ$ and 19°) correspond to interface efficiencies, $\tan(\delta)/\tan(\phi)$, between 0 and 0.74, since the soil friction angle is 24° .

Currently, manufactured average roughness, R_a , for CPTu friction sleeves may lie between $0.65\mu\text{m}$ and $0.15\mu\text{m}$ (EN ISO 22476-1), in a range that aims to approach the roughness that may be later acquired upon use. For fine grained soils the resulting normalized roughness (R_a/D_{50}) will typically vary in the range (10^{-3} to 10^{-1}) that has been experimentally shown (Subba Rao et al. 2000; Eid et al. 2014) to result on interface efficiency between 0.3 and 0.9. On this basis the higher values of interface friction in the parametric study would be representative of testing on clays and fine silts, whereas the lower values would be more representative for testing on coarser silts and sands.

Table 1. Constitutive parameters common for all materials.

κ	λ	M	G (kPa)	K_0	e_0	OCR
0.016	0.053	0.98	3000	0.58	1	1

Table 2. Constitutive parameters varied.

Material	n	r	S_u^{peak} (kPa)	S_u^{res} (kPa)	Ψ
A	10	12	23.5	6.9	0.093
E	8	4	23.8	13.2	0.052
H	4	2	24	22.1	0.026

3 SIMULATION RESULTS AND CLASSIFICATION CHARTS

Figure 2 reports the results in two classification charts proposed by Robertson (1991; 2016). The 1991 chart is expressed using the following normalized parameters

$$Q_{l1} = \frac{q_t - \sigma_v}{\sigma'_{v0}} \quad B_q = \frac{u_2 - u_0}{q_t - \sigma_v} \quad (1)$$

whereas the 2016 chart is expressed using the following normalized parameters

$$Q_m = \left(\frac{q_t - \sigma_{v0}}{p_a} \right) \left(\frac{p_a}{\sigma'_{v0}} \right)^n F_r = \frac{f_s}{q_t - \sigma_v} \quad (2)$$

where n is an index, which is ultimately dependent on Q_m and F_r , and is established by iteration.

In the B_q vs Q_l classification graph the dominant effect is that of permeability. The undrained simulations have always $B_q > 0.5$, those drained have $B_q = 0$ and the partly drained ones lie in between. For impermeable materials brittleness plays also a significant

role, with material A (most brittle) generating the larger pore pressures. Interface friction has no systematic effect. According to this chart Material A will classify as sensitive, fine grained, if impermeable, as clay to silty clay if partly drained and as a silt mixture if fully drained.

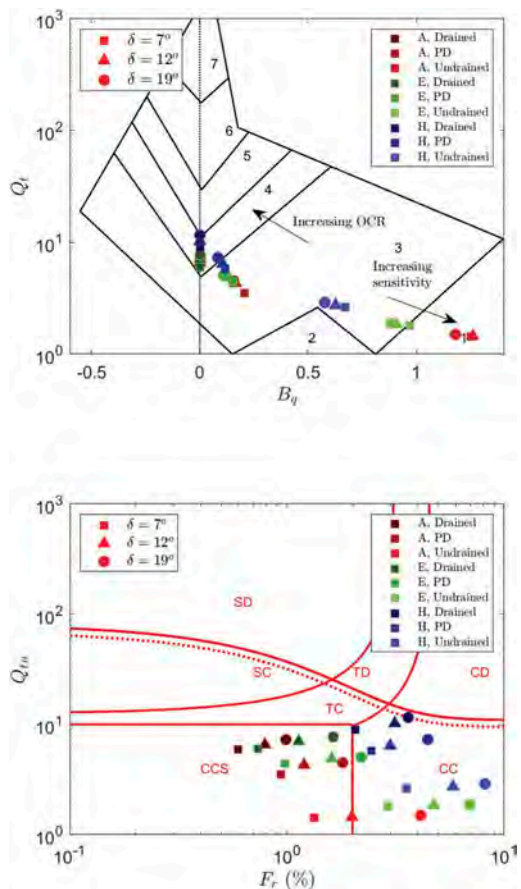


Figure 2. Results of the analyses of CPTu test with different permeabilities and interface friction angles plotted on classification charts. Above: Robertson 1991. Below: Robertson 2016. The marker color indicates undrained brittleness; marker shape indicates side friction values; marker hue indicates permeability. PD = Partly drained.

In the F_r vs Q_{tm} classification graph all numerical results plot in the “contractive” zone, which is correct as none of the CASM materials were dilatant in shear. For material A most simulated results fall into the “sensitive” zone (CCS), which seems correct. However, this is also the case for material E if partly or fully drained, which seems excessive. There is also some disagreement with the graph when the effect of permeability is considered. Results for all materials and interface frictions shift upwards as permeability is increased. Although this is in line with the trend in the graph, even the fully drained material would

classify as “clay-like” and be expected to behave in an undrained manner under CPTu. Finally, it is noticeable how changes on interface friction result in significant shifts along the F_r axis for the same brittleness and permeability.

4 PEAK UNDRAINED SHEAR STRENGTH

4.1 Cone factors

One of the most frequent and important applications of the CPTu is to obtain estimates of peak undrained strength. The dominant approach uses empirically determined cone factors, that relate cone measurements and undrained strengths. Cone factors based on tip resistance and excess pore pressure are defined as

$$N_{kt} = \frac{q_t - \sigma_v}{s_u} \quad N_{\Delta u} = \frac{u_2 - u_0}{s_u} \quad (3)$$

It has been stressed many times (e.g. Mayne & Peuchen, 2018) that for this approach to make sense the target undrained strength of the correlation should be clearly specified. Peak undrained strengths measured on triaxial compression after anisotropic (K_0) consolidation are adopted here as a target, in line with previous work (e.g. Karlsrud et al. 2005). Another important factor (Lunne et al. 1997) is sample disturbance, as it will affect the laboratory values employed in correlations. Poor sample quality will typically decrease the undrained peak strength measured on the laboratory and thus increase empirically determined cone factors.

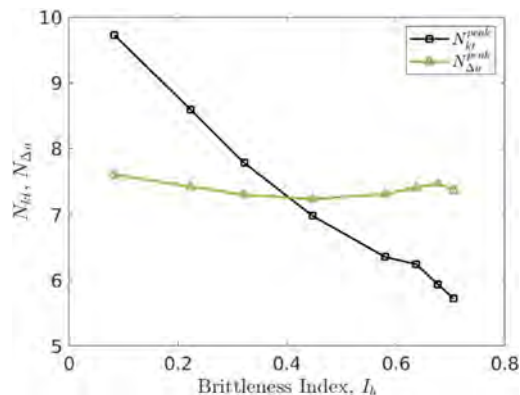


Figure 3. Cone factors for peak undrained strength in terms of the brittleness for smooth, undrained simulations.

Figure 3 reports the cone factors in terms of the brittleness index for smooth, undrained simulations. The tip resistance cone factor N_{kt} is far more variable than the pore pressure cone factor $N_{\Delta u}$, something well in line with empirical observations (Lunne et al. 1997). Furthermore, the values of $N_{\Delta u}$ obtained from

these undrained smooth simulations cluster around the value 7.5, well supported by experimental work on Norwegian clays (Paniagua et al. 2019).

The advantage of $N_{\Delta u}$ as a more stable factor disappears when partial drainage is introduced in the picture (Figure 4). Excess pore pressure reduces and the cone factor required to recover peak undrained strength reduces accordingly. The effect of interface friction on this trend appears to be relatively small. The more realistic frictional simulations result on slightly smaller $N_{\Delta u}$ than the empirical average, something that may be explained by a small amount of sampling disturbance.

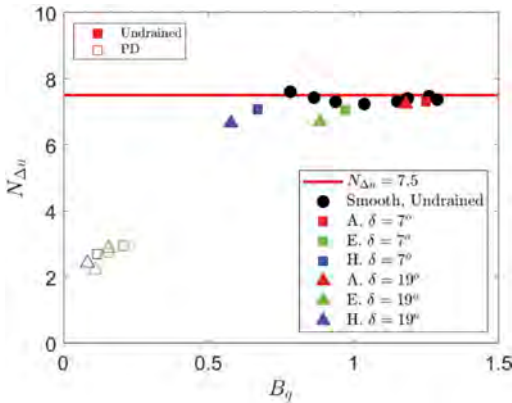


Figure 4. Simulation results and relations from literature between cone factor $N_{\Delta u}$ and pore pressure parameter B_q .

The variability of N_{kt} is sometimes accounted for using B_q as an auxiliary variable (Lunne et al. 1997; Mayne & Peuchen, 2018). Figure 5 presents the results for frictional undrained and partly drained simulations in that format. The results suggest that the higher cone factors that are sometimes obtained at low B_q may be related to partial drainage. For fully undrained cases, it is also noteworthy that the cone factors for the less brittle material H are only slightly below the value ($N_{kt} = 12$) that empirical studies assign to clays of moderate to low sensitivity (Low et al. 2010). As material brittleness is increased the simulated N_{kt} cone factors reduce. The reduction observed is steeper than what data from general databases, such as that of Mayne & Peuchen (2018) would suggest. This difference is likely to be the result of increased sampling damage for the more brittle soils, something also borne out by the steeper decrease that was observed by Lunne et al (1997), using a more restricted dataset of higher sampling quality.

As noted by Karlsrud et al (2005) a relation between N_{kt} and B_q mediated by $N_{\Delta u}$ is just implied by their definition. According to the results just presented the undrained CASM simulations should then be fitted by

$$N_{kt} = \frac{N_{\Delta u}}{B_q} = \frac{7.5}{B_q} \quad (4)$$

Which is closely correct for the undrained results and far off the mark for partially drained cases (Figure 6).

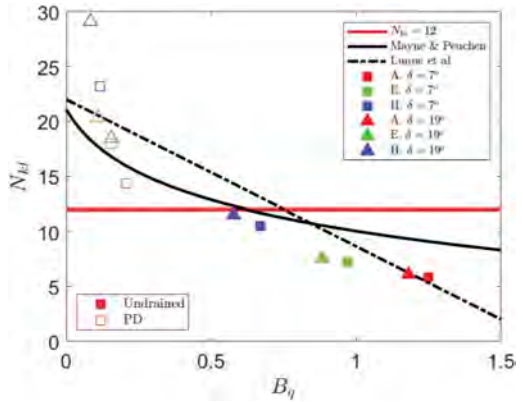


Figure 5. Simulation results and relations from literature between cone factor N_{kt} and pore pressure parameter B_q .

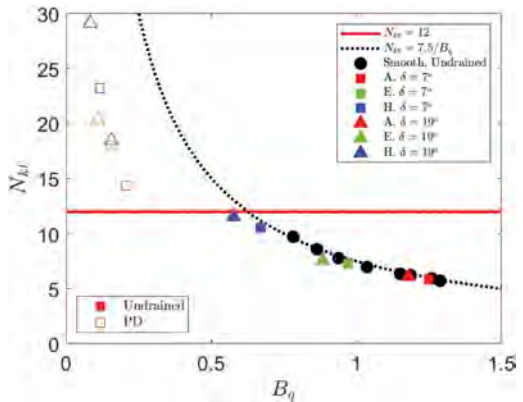


Figure 6. Simulation results and relations from literature between cone factor N_{kt} and pore pressure parameter B_q .

4.2 Case-history based correlations

Olson & Stark (2003) back-analyzed case history data of flow liquefaction failures to obtain estimates of stress normalized undrained peak (yield) strength which were then correlated with the results of CPT. This correlation reads

$$\frac{S_{\mu}^{pk}}{\sigma_{v0}} = 0.205 + 0.0143 q_{c1} \pm 0.04 \quad (5)$$

$$q_{c1} = q_c \frac{1.8}{0.8 + \left(\frac{\sigma'_v}{p_u}\right)} \quad (6)$$

where the tip and corrected tip resistance q_{c1} are expressed in MPa. The simulated CPT results lie in the range 0.14 to 1.14 q_{c1} for which the correlation predicted upper bound of normalized peak strength is 0.21, only slightly below the input value.

5 RESIDUAL UNDRAINED SHEAR STRENGTH

5.1 Sleeve friction

Empirical observations of the close similitude of sleeve friction to residual undrained strength in clay as measured by vane tests or laboratory test on remolded soil are frequent (Lunne et al. 1997; Robertson, 2010). This can be simply expressed as

$$\frac{S_u^{res}}{\sigma'_{v0}} \approx \frac{f_s}{\sigma'_{v0}} \quad (7)$$

Figure 7 reports the normalized friction sleeve resistance of PFEM simulations in terms of the normalized residual undrained shear strength predicted by CASM; results are plotted for undrained and partly drained conditions. For high interface friction angles and undrained conditions, Equation (7) holds, and the friction sleeve is approximately equal to the residual undrained shear strength. For lower interface friction angles the tangential stress acting on the friction sleeve is lower than the residual undrained shear strength and Equation (7) becomes highly conservative. The importance of sleeve roughness for this correlation is thus clearly demonstrated. Interestingly, the effect of partial drainage is small for the more brittle material A, but large for the less brittle H.

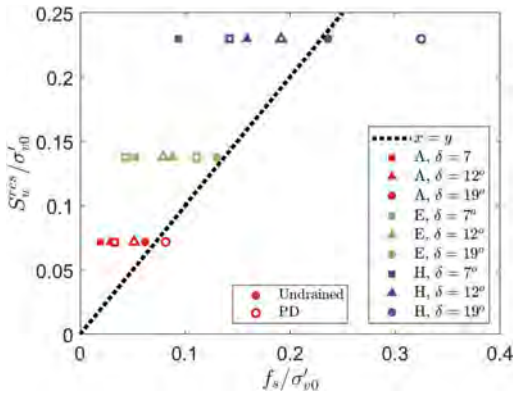


Figure 7. Residual undrained strength and side friction. All results correspond to practically undrained tests.

5.2 Case-history based correlations

Case-history back-analysis by Olson & Stark (2002) in which post-liquefaction geometry was considered led to another correlation of residual undrained strength with corrected tip resistance q_{c1} . Again, the correlation obtained has very little sensitivity to q_{c1} in the range covered by our simulations and the predicted stress normalized residual (liquefied) undrained strength is practically constant. This is interesting, as the stress normalized residual strength is controlled by CASM material parameters and also constant for a given material type. The simulation results are above the recommended limits, but, for the most brittle material A, well within the values supporting the correlation (Figure 8). This comparison is unaffected by partial drainage or sleeve friction values. It is also worth mentioning that although material A is brittle, CASM has been fitted to represent even more brittleness when back-analyzing liquefaction failures (Arroyo & Gens, 2021; Mánica et al. 2021). Despite that Olson & Stark (2002) upper bound might still be somewhat conservative.

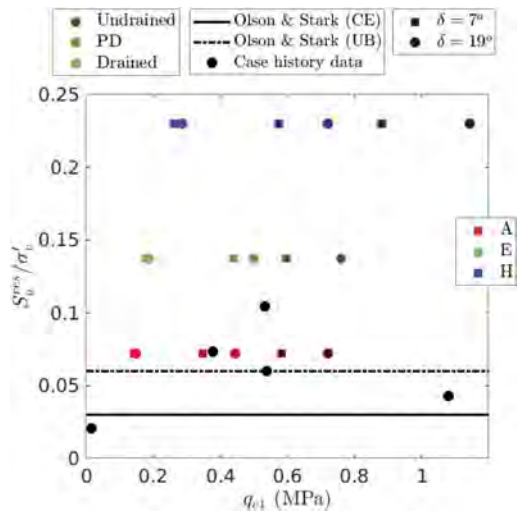


Figure 8. Comparison of the numerical results with case-history based correlation of Olson & Stark (2002).

Robertson (2010, 2021) also proposed correlations between residual undrained shear strength and cone metrics based on case history data. For materials with soil behavior type (SBT) index, $I_c > 3$ it is recommended to use the relation -discussed above with sleeve friction. For materials with SBT $I_c < 3$ a different relation was proposed. The soil behavior type index, I_c is defined as

$$I_c = \left((3.43 - \log Q_m)^2 + (\log F_r + 1.22)^2 \right)^{0.5} \quad (8)$$

The relation with undrained strength is based on $Q_{m,cs}$ a corrected, “clean sand equivalent”, value of normalized cone resistance Q_m . This correction is given by:

$$Q_{m,cs} = K_c Q_m \quad (9)$$

The correction factor K_c is itself also dependent (through fifth-order polynomials) on I_c .

Robertson relations (2010, 2021) are plotted in Figure 9 alongside the results for the fully drained simulations, which were the only ones resulting on $I_c < 3$. The relations are postulated as lower bounds and the simulation results plot above them, except for a datapoint that represents high mobilized interface friction for soil H, which is almost non-brittle. For the higher brittleness case A, which is likely more similar to the soils in the database, the degree of conservatism implied by the relation does not appear excessive.

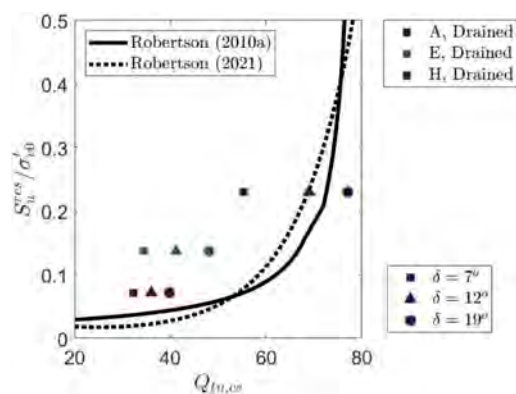


Figure 9. Comparison of numerical results with Robertson (2010, 2021) correlations for normalized residual undrained strength. The marker color indicates undrained brittleness; marker shape indicates side friction values; marker hue indicates permeability.

6 CONCLUSIONS

The ability to simulate CPTu response using realistic geometry and constitutive models is still relatively recent. If exploited systematically it will open a way to reduce the relatively large uncertainty that hinders empirically based correlations, by identifying which parasitic factors may be playing a role in some datasets and/or suggesting ways to adapt general correlations to the local soil characteristics.

This has been illustrated here for the case of soils with a brittle undrained response. The results indicate that partial drainage is a major factor when selecting cone factors for $s_{u,pk}$. They also suggest that, when aiming for undrained residual strength, Olson & Stark

(2002) proposals are more robust than Robertson (2010, 2021), as these are more sensitive to the possibility of partial drainage and -for fine grained soilsto the state of the cone-soil interface. Still, these results are based on a limited set of simulations and would require confirmation from more systematic parametric analyses.

ACKNOWLEDGMENTS

The authors acknowledge financial support from the Spanish Ministry of Economy and Competitiveness, through the “Severo Ochoa Programme for Centres of Excellence in R&D” (CEX2018-000797-S).

REFERENCES

- Arroyo, M. & Gens, A. 2021. Computational analyses of Dam I failure at the Corrego de Feijao mine in Brumadinho, Final Report; available at <http://www.mpf.mp.br/bmg/salade-imprensa/docs/2021/relatorio-final-cinme-upc-1>
- Been, K. 2016. Characterizing mine tailings for geotechnical design. *Australian Geomechanics*, 51(4), 59–78.
- Gens, A. 2019. Hydraulic fills with special focus on liquefaction. *Proceedings of the XVIII European Conference on Soil Mechanics and Geotechnical Engineering*.
- Eid, H. T., Amarasinghe, R. S., Rabie, K. H. & Wijewickreme, D. 2014. Residual shear strength of fine-grained soils and soil–solid interfaces at low effective normal stresses. *Canadian Geotechnical Journal*, 52(2), 198–210.
- EN ISO 22476-1. 2012. Geotechnical investigation and testing. Field testing. Electrical cone and piezocone penetration test
- Karlsrud, K., Lunne, T., Kort, D. A. & Strandvik, S. 2005. CPTU correlations for clays. In *Proceedings of the 16th international conference on soil mechanics and geotechnical engineering* (pp. 693–702). IOS Press.
- Lunne, T., Robertson, P. K. & Powell, J. J. 1997. Cone penetration testing in geotechnical practice. CRC Press.
- Low, H. E., Lunne, T., Andersen, K. H., Sjørnsen, M. A., Li, X., & Randolph, M. F. 2010. Estimation of intact and remoulded undrained shear strengths from penetration tests in soft clays. *Géotechnique*, 60(11), 843–859.
- Mánica, M. A., Arroyo, M., Gens, A. & Monforte, L. 2021. Application of a critical state model to the Merriespruit tailings dam failure. *Proceedings of the Institution of Civil Engineers - Geotechnical Engineering*, 1–15.
- Mayne, P. W. & Peuchen, J. 2018. Evaluation of CPTU Nkt cone factor for undrained strength of clays. In *Cone Penetration Testing 2018* (pp. 423–429). CRC Press.
- Monforte, L., Arroyo, M., Carbonell, J.M. & Gens, A. 2017. Numerical simulation of undrained insertion problems in geotechnical engineering with the particle finite element method (PFEM). *Computers and Geotechnics*. 82:144–156.
- Monforte, L., Arroyo, M., Carbonell, J.M. & Gens, A. 2018. Coupled effective stress analysis of insertion problems in geotechnics with the particle finite element method. *Computers and Geotechnics*. 101:114–129.
- Monforte, L., Gens, A., Arroyo, M., Mánica, M. & Carbonell, J.M. 2021. Analysis of cone penetration in brittle liquefiable soils. *Computers and Geotechnics*. 134:104123.

- Olson, S. M. & Stark, T. D. 2002. Liquefied strength ratio from liquefaction flow failure case histories. *Canadian Geotechnical Journal*, 39(3), 629–647.
- Olson, S. M. & Stark, T. D. 2003. Yield strength ratio and liquefaction analysis of slopes and embankments. *Journal of Geotechnical and Geoenvironmental Engineering*, 129(8), 727–737.
- Paniagua, P., D'Ignazio, M., L'Heureux, J.-S., Lunne, T., Karlsrud, K. 2019. CPTU correlations for Norwegian clays: an update. *AIMS Geosciences* 2019, 5(2): 82–103
- Robertson, P. K. 1991. Soil classification using the cone penetration test: Reply. *Canadian geotechnical journal*, 28(1), 176–178.
- Robertson, P.K. 2010. Evaluation of flow liquefaction and liquefied strength using cone penetration test. *Journal of Geotechnical and Geoenvironmental Engineering*.136 (6): 842–853.
- Robertson, P. K. 2016. Cone penetration test (CPT)-based soil behaviour type (SBT) classification system—an update. *Canadian Geotechnical Journal*, 53(12), 1910–1927.
- Robertson, P.K. 2021. Evaluation of flow liquefaction and liquefied strength using cone penetration test: an update. *Canadian Geotechnical Journal*. In press.
- Schnaid, F. 2021. The Ninth James K. Mitchell Lecture: On the Geomechanics and Geocharacterization of Tailings. *Int. Conf. On Site Charact.*, Budapest.
- Subba Rao, K. S., Allam, M. M., & Robinson, R. G. 2000. Drained shear strength of fine-grained soil–solid surface interfaces. *Proceedings of the Institution of Civil Engineers-Geotechnical Engineering*, 143(2), 75–81.
- Yu, H.S. 1998. CASM: a unified state parameter model for clay and sand. *International Journal for Numerical and Analytical methods in Geomechanics*. 22: 621–653.

Assessment of deltaic soil behavior classification using AUT: GMD database regarding CPTu records

Mohammad H. Naghibi, Abolfazl Eslami & Sara Heidarie Golafzani

Department of Civil and Environmental Engineering, Amirkabir University of Technology (AUT), Tehran, Iran

ABSTRACT: Cone penetration tests (CPT and CPTu) are unique geotechnical in-situ tools for soil behavior classification (SBC). Identification and classification of subsurface marine layers help geotechnical engineers analyze, design, and monitor. Thus, a significant database of 398 cases was collected from 58 sites in 18 countries with CPTu soundings, and soil profiling obtained by direct boring and laboratory testing, namely AUT: CPTu&GMD (Amirkabir University of Technology): Geo-Marine CPTu Database. Furthermore, diverse essential parameters such as normalized cone resistance q_c , friction ratio R_f , soil behavior type index I_{SBT} are available at 0.1 m intervals. CPTu-based classification methods were subdivided into three generations, and several methods for marine deposits were examined utilizing 57 case studies from the AUT: CPTu&GMD. The results indicated that directly incorporating all three parameters of q_c , f_s , and u_2 is recognized to be more accurate than utilizing mathematical relationships, which reduces uncertainties and increases accuracy in identifying subsurface layers.

1 INTRODUCTION

Projects constructed in marine environments such as nearshore, offshore and onshore are mainly accompanied by particular foundations suitable for the superstructure regarding the available site soil deposits.

Furthermore, characterizing the subsurface layers in such environments is accompanied by limitations and difficulties heightening the effect of the embedded uncertainties in geotechnical designs. Accordingly, the projects in these areas are highly important, and care should be taken in their designs. Otherwise, irreversible damages will happen, leading to a decrease in the infrastructure's stability, limited or prohibited utilization, and an increase in the projects' preservation costs due to the ambiguities in subsoil depiction. Therefore, identifying and classifying the subsurface marine layers is crucial and assists geotechnical engineers in analyzing, designing, monitoring, and maintaining civil projects. Geotechnical studies are the first and most critical step in construction because they enable the geotechnical engineer to make appropriate decisions based on this information while minimizing existing uncertainties (Eslami et al., 2019).

Identification of subsurface layers is frequently accomplished through laboratory, nondestructive (NDT), and in-situ tests. Laboratory tests have limitations, including intact sample preparation, sample size, sample transport and storage, accurate site stress modeling for laboratory conditions and information discontinuity, and in-depth measurements, and their effects will be more crucial in marine

environments. NDT tests lack the necessary precision to determine soil profiles (Eslami et al., 2019, Randolph and Gourvenec, 2017).

Furthermore, the development of geotechnical engineering has led to widespread in-situ testing by standardized penetrometers. The cone and piezocone penetration tests (CPT and CPTu) are some of the most remarkable geotechnical in-situ tools for soil behavior classification (SBC) due to rapid application, accuracy, providing continuous records in-depth, and the possibility of implementation in marine areas. Due to inherent soil uncertainty, measurement, and modeling errors, classifying soils in marine environments by the CPTu test becomes more important. Thus, the application of CPT and CPTu databases can significantly improve the validation and evaluation process and increase the reliability in geotechnical engineering (Eslami et al., 2017, Eslami & Fellenius, 2004, Robertson, 2010). Accordingly, a significant database of 398 cases was collected from 58 sites in 18 countries with adjacent CPTu soundings, namely Amirkabir University of Technology: CPTu and Geo-Marine Database, or AUT: CPTu&GM database. This database consists of offshore, onshore, nearshore, and riverine areas, with the most recorded cases being from Europe, the United States of America, and China. Soil profiling was obtained via direct boring and laboratory testing in this database. Moreover, for all cases, several parameters such as normalized cone resistance Q_c , friction ratio R_f , soil behavior type index I_{SBT} are available at 0.1 m intervals.

Researchers have presented numerous diagrams to identify and classify the behavior of subsurface layers using CPT and CPTu test results. Considering that each diagram is developed based on different databases, the accuracy of each diagram changes. As a result, this research attempted to measure the accuracy of several most common diagrams. The diagrams are compared proportionally to the type of soil, based on 57 case studies of AUT: CPTu&GMD, which will lead to the presentation of a model, allowing geotechnical engineers to select diagrams appropriate to the type of soil available the site to identify the behavior of subsurface layers.

2 AMIRKABIR UNIVERSITY OF TECHNOLOGY: GEO-MARINE-CPTu DATABASE; AUT: CPTu&GMD

The compiled marine database comprises CPTu test records and soil profiles from boreholes drilled within their vicinity. The records include 398 cases from 58 sites and 18 countries, mainly in the United States, Europe, China, and New Zealand. The gathered sites in the database belong to onshore sites near the shoreline about 21%, nearshore sites located in waters less than 30 meters deep around 26%, offshore sites located in waters deeper than 30 meters nearly 15%, and riverine sites roughly 38%. This database contains approximately 10000 meters of soil profiles and covers a wide range of marine deposits, including clay, sensitive, sand-gravel, over-consolidated clay, and mixed or deltaic soils.

In addition to the CPTu records digitized each 10 cm in-depth and the soil profiles from boreholes, other parameters used via soil behavior classification (SBC) diagrams are also determined using available correlations. Figure 1 shows the details of the AUT: CPTu&GM database in a flowchart.

3 ANALYSES AND ASSESSMENT

In this study, soil behavioral classification diagrams are classified into three generations based on the results of the CPTu test. First-generation (basic-generation) diagrams, such as diagrams of Douglas and Olsen (1981), Campanella et al. (1985) and, Robertson (2010), use only two parameters out of the three parameters obtained from the piezocone test, along with mathematical equations, for soil classification. The cone tip resistance q_c and sleeve friction f_s are the two parameters usually used. Second-generation (middle-generation) diagrams, such as diagrams of Robertson (1990), Jefferies and Davies (1993), Eslami & Fellenius (1997), and Eslami (2019), apply all three parameters of cone tip resistance, sleeve friction, and excess pore water pressure, as well as mathematical equations, to identify subsurface layers. Moreover, Eslami et al. (2015) diagram, which directly uses the three

mentioned parameters without mathematical equations to identify soil, is a third-generation (advanced-generation) diagram since using no mathematical relationships reduces the uncertainties. The use of mathematical relationships is the main difference between the second-generation and the third-generation diagrams. This study aims to assess the performance of seven common SBC diagrams belonging to the three mentioned generations, including 1-Douglas and Olsen (1981), 2-Campanella et al. (1985), 3-Robertson (1990) (Q_t - B_q), Robertson (2010), 4-Jefferies and Davies (1993), 5-Eslami & Fellenius (1997), 6-Eslami et al. (2015) 7-Eslami (2019), using 57 cases from the AUT: CPTu&GM Database. The investigated cases are from 16 countries worldwide as follows: USA: 10 logs, China: 5 logs, Canada: 3 logs, New Zealand: 3 logs, Italy: 3 logs, Norway: 3 logs, Poland: 3 logs, Finland: 3 logs, Sweden: 3 logs, Ireland: 3 logs, Brazil: 3 logs, England: 3 logs, Japan: 3 logs, Portugal: 3 logs, Australia: 3 logs, Turkey: 3 logs.

Additionally, all four types of sites in the database AUT: CPTu&GMD have been evaluated, including 15 Onshore, 20 Nearshore, 4 Offshore, and 18 Riverine cases.

Fifty-seven mentioned cases include 1420 meters of CPTu soundings and soil descriptions from drilling boreholes. Their frequency is such that it consists of 117 meters of sensitive soil, 98 meters of clay, 1135 meters of mixed or deltaic soil, 54 meters of sand and gravel, and 16 meters of over-consolidated soil. Figure 2 demonstrates the distribution of investigated deltaic soils in different SBC charts.

The accuracy of each diagram in predicting each soil type forms the evaluated areas, i.e., clay, sensitive, deltaic (mixed), overconsolidated, and sand-gravel, and has been calculated in percentage according to Equation 1.

$$SR = \left(\frac{L'}{L} \right) \times 100 \quad (1)$$

Where SR is the success rate; L' is the total length of correctly identified soil profiles regarding a specific soil type; L is the total length of investigated profiles concerning a particular soil type.

According to Figure 3, each diagram's statistical evaluation results are displayed separately on a radar chart. The radar diagram contains five axes regarding the considered soil types. Axes are calibrated from 0% to 100%. These values indicate the desired diagram's accuracy in identifying the soil associated with each axis.

As shown in Figure 3, identifying sensitive soils has improved with the advent of second-generation diagrams that use all three parameters q_c , f_s , and u_2 and mathematical equations for soil classification.

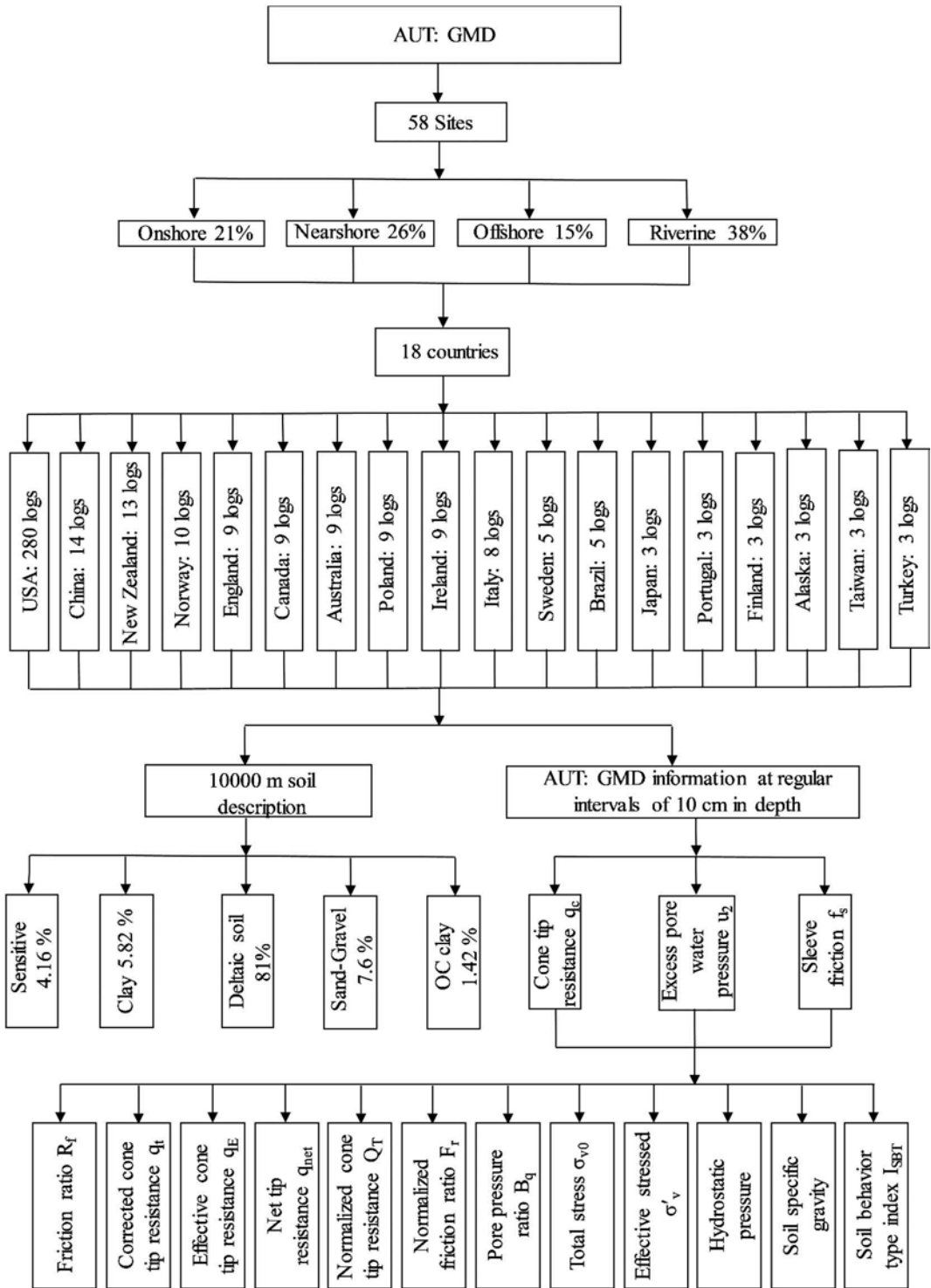


Figure 1. The details of AUT: CPTu&GMD database.

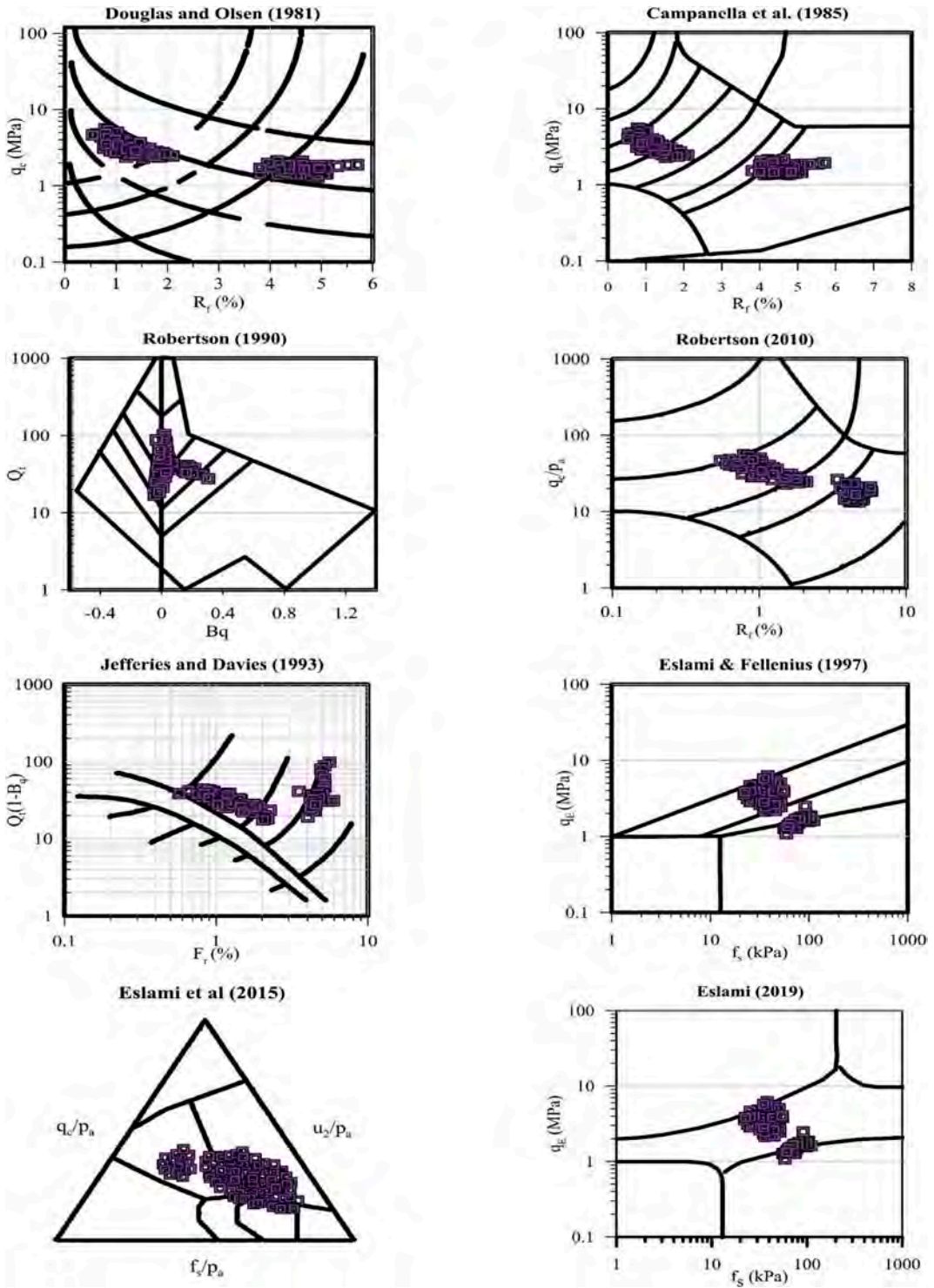


Figure 2. Deltaic soils of AUT: CPTu&GMD on different charts.

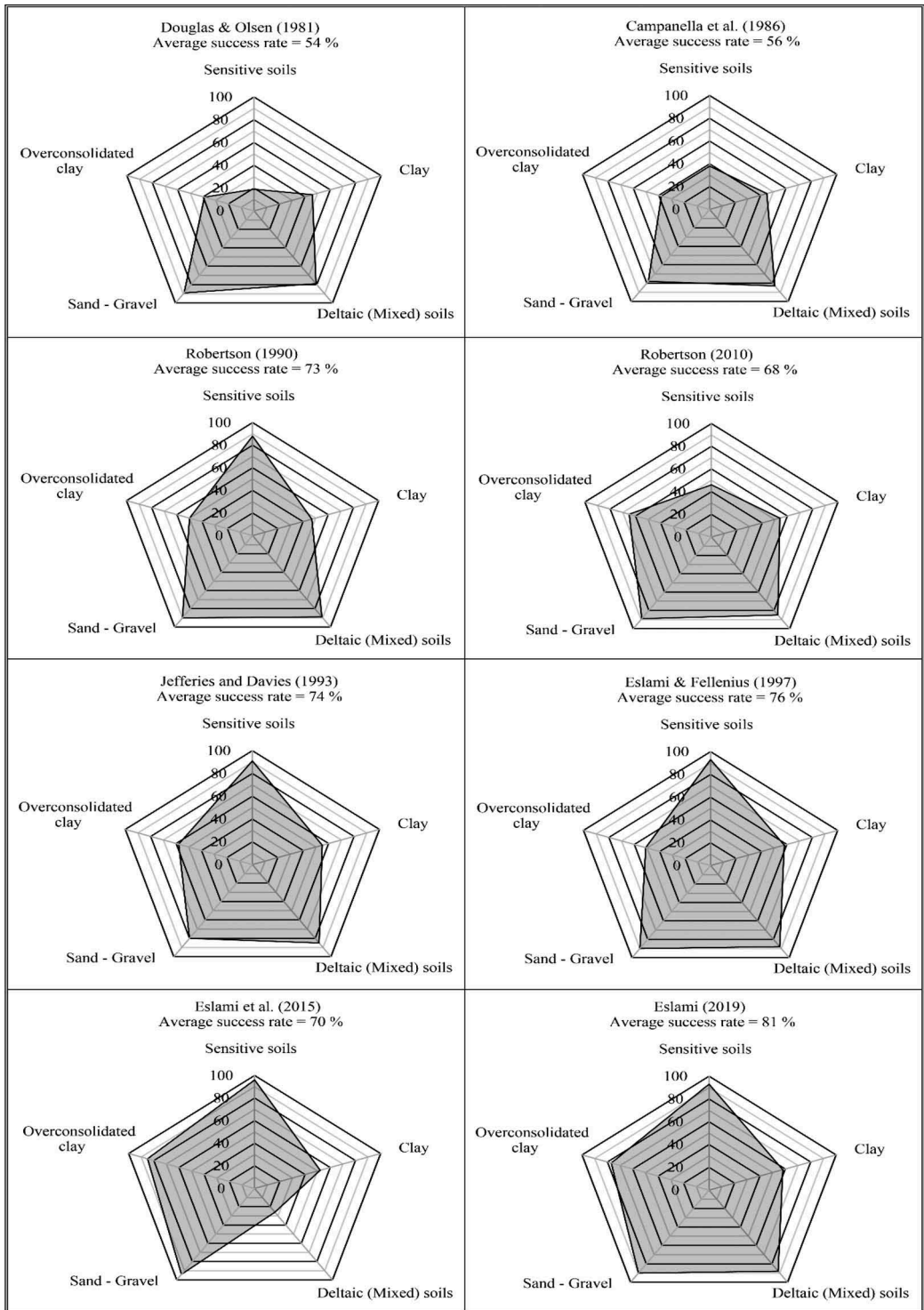


Figure 3. The performance assessment of each SBC diagram for the investigated database.

The Douglas and Olsen (1981) and Campanella et al. (1985) diagrams, i.e., the first-generation of the charts, showed a low accuracy in identifying sensitive soils. However, this accuracy has reached more than 80 percent by applying second-generation diagrams. Although this trend continued until the Eslami & Fellenius (1997) diagram showed more than 90% success in identifying sensitive soils, the Robertson (2010) chart has shown a low accuracy in identifying sensitive layers due to using a pattern similar to the first-generation diagrams and not using the excess pore water pressure parameter. That shows the essential role of the excess pore water pressure parameter in identifying sensitive soil. The Eslami & Fellenius (1997), Eslami et al. (2015) and, Eslami (2019) diagrams were able to identify sensitive soils with more than 90% accuracy.

Due to the low cone tip resistance of silts and normally consolidated clays, it seems this parameter plays a minor role in distinguishing clay from silt. The diagrams now mainly use sleeve friction and excess pore water pressure parameters for this purpose. Therefore, it is more challenging to identify clay than the other four soil types for diagrams. However, the maximum accuracy is about 60%, which belongs to Jefferies and Davies (1993), Eslami & Fellenius (1997), and Eslami (2019) charts. Except for Eslami (2019) diagram, other diagrams of the first and second generations identify overconsolidated clay with less than 60% accuracy. The Eslami (2019) diagram has characterized overconsolidated clay with about 77% accuracy. Although the highest accuracy is for the third-generation chart of Eslami et al. (2015), it has identified a success rate of 85% overconsolidated clay. Douglas and Olsen (1981), Campanella et al. (1985), Robertson (1990) ($Q_t - B_q$), Robertson (2010), and Jefferies and Davies (1993) diagrams identify mixed or deltaic soils with an accuracy of 80 to 90 percent. While the Eslami et al. (2015) diagram detects these soils with less than 20% success, Eslami & Fellenius (1997) and Eslami (2019) diagrams have an accuracy of over 90% for this purpose. First and second-generation diagrams identify layers of sand gravel with 80 to 90 percent accuracy, and only the third-generation chart does so with over 90% success.

4 CONCLUSIONS

Marine deposits are mainly problematic soils due to their formation process, and their characterization increases the reliability of geotechnical designs in onshore and offshore structures. Accordingly, the AUT: CPTu&GMD was compiled, and 57 cases were selected, including offshore, onshore, and riverine sites, to assess the performance of SBC diagrams classified as first, second, and third generations according to their simplifications and assumptions.

The investigated diagrams were 1-Douglas and Olsen (1981), 2-Campanella et al. (1985), 3-Robertson (1990) ($Q_t - B_q$), Robertson (2010), 4-Jefferies and Davies (1993), 5-Eslami & Fellenius (1997), 6-Eslami et al. (2015), 7-Eslami (2019). Five soil types, i.e., sensitive soils, clay, mixed or deltaic soils, overconsolidated clay, and sand-gravel, were considered to assess the performance of SBC diagrams in predicting the marine soil types.

Results indicated that the accuracy of the diagrams changes with the variation of soil type. Also, assessed diagrams are adequately accurate in identifying deltaic soils, especially diagrams that use all three parameters of q_c , f_s and, u_2 for soil classification. Eventually, Eslami et al. (2015) chart directly implements all three CPTu records, i.e., q_c , f_s , and u_2 , which reduces uncertainties in soil behavioral classification instead of applying mathematical correlations and was more suitable for classifying deltaic soils for the investigated database.

REFERENCES

- Douglas, B. Soil classification using electric cone penetrometer. Symp. on Cone Penetration Testing and Experience, Geotech. Engrg. Div., 1981. ASCE, 209–227.
- Eslami, A., Alimirzaei, M., Aflaki, E. & Molaabasi, H. 2017. Deltaic soil behavior classification using CPTu records—Proposed approach and applied to fifty-four case histories. *Marine Georesources & Geotechnology*, 35, 62–79.
- Eslami, A. & Fellenius, B. H. 1997. Pile capacity by direct CPT and CPTu methods applied to 102 case histories. *Canadian Geotechnical Journal*, 34, 886–904.
- Eslami, A., Moshfeghi, S., Molaabasi, H. & Eslami, M. M. 2019. *Piezocene and Cone Penetration Test (CPTu and CPT) Applications in Foundation Engineering*, Butterworth-Heinemann.
- Heidarie Golafzani, S., Eslami, A. & Jamshidi Chenari, R. 2020. Probabilistic Assessment of Model Uncertainty for Prediction of Pile Foundation Bearing Capacity; Static Analysis, SPT and CPT-Based Methods. *Geotechnical and Geological Engineering*, 38, 5023–5041.
- Jefferies, M. & Davies, M. 1991. Soil classification by the cone penetration test: Discussion. *Canadian Geotechnical Journal*, 28, 173–176.
- Randolph, M. & Gourvenec, S. 2017. *Offshore geotechnical engineering*, CRC press.
- Robertson, P. K. 1990. Soil classification using the cone penetration test. *Canadian geotechnical journal*, 27, 151–158.
- Robertson, P. K. Soil behaviour type from the CPT: an update. 2nd International symposium on cone penetration testing, 2010. Cone Penetration Testing Organizing Committee, 575–583.
- Robertson, P. K. & Cabal, K. Estimating soil unit weight from CPT. 2nd International Symposium on Cone Penetration Testing, 2010. 2–40.
- Robertson, P. K., Campanella, R. G., Gillespie, D. & Greig, J. Use of piezometer cone data. Use of in situ tests in geotechnical engineering, 1986. ASCE, 1263–1280.

A review of methods for estimating undrained brittleness index from the CPT

Y. Narainsamy & S.W. Jacobsz

University of Pretoria, Pretoria, South Africa

ABSTRACT: The Cone Penetration Test (CPT) is a useful tool for soil profiling due to its near continuous data measurements, low cost and repeatability. When conducting designs or safety evaluations of slopes, it is often of interest to understand the undrained response of the soil at large strains. This behaviour can be defined in terms of the Undrained Brittleness Index (I_B) which relates the yield undrained shear strength to the steady state undrained shear strength. Over time, a number of field case histories where strain softening during undrained shear was deemed to have occurred have been assessed, and a relationship between corrected tip resistance and I_B was proposed (Sadrekarimi, 2014). A quick clay test site and a silt test site in Norway included in a recently published open access geotechnical database were assessed. It was found that the method proposed by Sadrekarimi (2014) underestimated the I_B for both the quick clay and silt test sites. It was also noted that there are some limitations with a popular screening method for identifying soils susceptible to strength loss during undrained shear.

1 INTRODUCTION

1.1 Cone Penetration Testing

The Cone Penetration Test (CPT) is a useful tool for soil profiling. It provides near continuous data measurements, repeatable results, is cost effective and tests can be conducted relatively quickly. When designing and conducting safety evaluations of slopes and embankments, it is often useful to understand the undrained response of the soil at large strains. This is important as soils which exhibit strain softening (contractive) behaviour will have a lower strength than soils which exhibit strain hardening (dilative) behaviour. This state is sometimes represented using the state parameter ψ as suggested by Been & Jefferies (1985). The state parameter is the difference in void ratio between the current void ratio and the void ratio at steady state, at the same effective confining stress.

However, the state of the soil simply describes the tendency for contraction or dilation at large strains. For many problems it is of more value to know the extent of the expected contraction, if any. Soils which exhibit a rapid reduction in undrained shear strength are referred to as brittle soils and an example of such behaviour can be seen in Figure 2. Brittle failure mechanisms are of particular concern as failure can initiate rapidly as was seen in the 2019 Feijão tailings dam failure (Robertson et al., 2019). One method of quantifying the brittleness of a soil is to use the Undrained Brittleness Index. The objective of this paper is to investigate the performance of the CPT-based method proposed by Sadrekarimi (2014) on predicting the Undrained Brittleness Index for

soils at two test sites in Norway: a quick clay test site and a silt test site.

1.2 Undrained Brittleness Index (I_B)

The Undrained Brittleness Index (I_B) was initially proposed by Bishop (1971), and is used to define a relationship between the yield and steady state undrained shear strength of a soil and is shown in Equation 1.

$$I_B = \frac{s_u(\text{yield}) - s_u(\text{steady state})}{S_u(\text{yield})} \quad (1)$$

where $s_u(\text{yield})$ is the yield undrained shear strength and $s_u(\text{steady state})$ is the steady state undrained shear strength. These parameters are shown visually in Figure 2. I_B ranges from 0 to 1, with $I_B = 1$ indicating complete loss of shear strength, i.e. a highly contractive response, while $I_B = 0$ indicates no loss of strength with strain. Note that the undrained brittleness index should not be confused with the modified soil behaviour type index I_B which is used by some researchers (e.g. Robertson, 2016).

2 REVIEW OF EXISTING RELATIONSHIPS

2.1 CPT correlations

Due to the large deformations and stresses induced during CPT probing, it is common to pursue empirical relationships between geotechnical parameters

and measured responses from the CPT. In one such study, a large database of 600 laboratory shear tests were reviewed. An attempt was then made to relate the yield and steady state undrained shear strengths to the corrected tip resistance (q_{c1}), based on field case histories where undrained shearing was believed to have occurred (Sadrekarimi, 2014). As part of this study, a relationship between I_B and q_{c1} was also identified.

When analysing the field case histories, the yield and undrained shear strengths were determined based on results of static limit equilibrium back analyses (Olson, 2001; Muhammad, 2012). The characteristic yield undrained shear strength was determined by varying the shear strength in the soil zones deemed susceptible to strength loss during undrained shear until a factor of safety against failure of 1.0 was calculated using Spencer's method (Spencer, 1967). Drained shear strengths were assumed to be mobilized in the zones above the phreatic surface (i.e. material zones deemed not to be susceptible to strength loss during undrained shear). The liquefied or steady state undrained shear strength was either determined using a simplified force diagram approach with kinematic considerations or a rigorous limit equilibrium approach considering the final failure geometry, depending on the available information. The corrected tip resistance measured in the field was then related to I_B in the form of a screening method as shown in Equation 2.

$$I_B = 0.882 - 0.053q_{c1} \pm 0.06 \quad (2)$$

where q_{c1} is the corrected cone tip resistance as determined using the equations described by Kayen et al. (1992). Upon review of the field case history database used to develop the relationship, it becomes clear that a biased dataset was used (i.e. the dataset only includes data from sites where strain softening was deemed to have occurred and therefore does not include material that strain hardens).

2.2 Open access geotechnical databases

With the rapid advancement of technology and the ease of global communication, there has been a recent development to populate and maintain open access geotechnical databases. Two such databases are: the Premstellar Geotechnik and Norwegian GeoTest Site databases. The former includes hundreds of CPT tests results and associated indicator tests (Oberhollenzer et al., 2021), and the latter is described in more detail below. It is expected that more open access geotechnical databases will be developed and maintained in the future.

3 ANALYSIS

3.1 NGTS test sites

In 2017 the Norwegian Geotechnical Institute (NGI) established the Norwegian GeoTest Sites (NGTS). The objective of the NGTS was to develop test sites that could be used for testing and verifying innovative soil investigation methods, as well as facilitate research activities relating to soil behaviour and foundation design (L'Heureux et al., 2017). The NGTS comprise five test sites in different soils, all located in Norway as shown in Figure 1.

A unique aspect of the NGTS is that the field and laboratory test data have been made publicly available through the Datamap web based application (Doherty et al., 2018). In addition to the NGTS data, data from the Australian National Field Testing Facility (NFTF) is also included on the Datamap application. Although six test sites were included in the combined NGTS and NFTF database, only two contained sufficient information for use in this study. These two sites are discussed in further detail below.



Figure 1. Location of the NGTS test sites.

3.2 The Tiller-Flotten test site

The Tiller-Flotten geotechnical test site is located in Trondheim in Norway. The site consists of a 50 m thick marine deposit of sensitive clay (L'Heureux et al., 2019). Due to the glacial history of the area, the clays are overconsolidated, with an OCR between 1.5 and 3.0. A rigorous CPTu field testing regime was conducted and Anisotropically Consolidated Undrained Compression (CAUC) triaxial tests were conducted on high quality Sherbrooke block samples obtained from boreholes adjacent to the CPTu test locations. The water table is located between 1 and 2 m below ground level and the pressure distribution is approximately hydrostatic to 5.5 m whereafter the pressure build-up is sub-hydrostatic.

The clays have a bulk unit weight of 18 kN/m^3 and are split into two sub-profiles as shown in Figure 4. Unit IIA extends from 2 m below surface to 7.5 m below surface and comprises clay of medium sensitivity and Unit IIB extends from depths greater than 7.5 m and comprises clay of extreme sensitivity. Results from the CAUC triaxial tests, shown in Figure 2, indicate brittle behaviour which is expected of a sensitive clay.

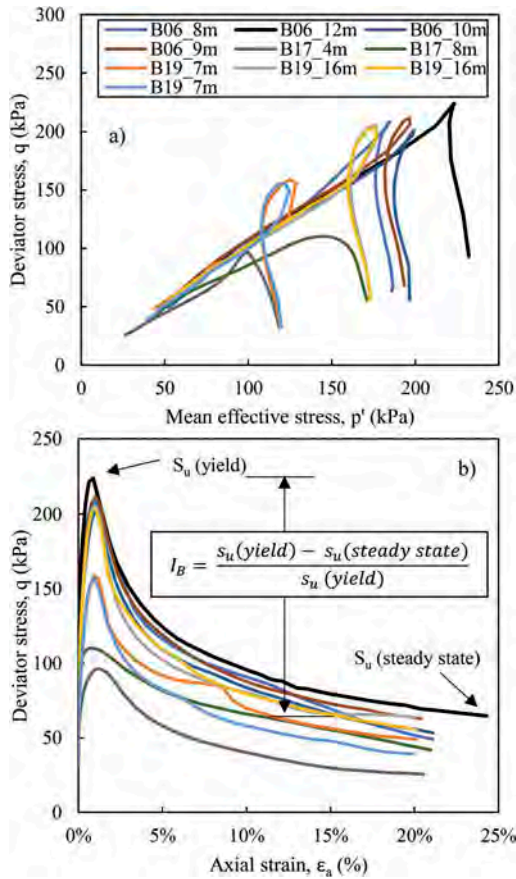


Figure 2. Triaxial test results on the Sherbrooke samples from the Tiller-Flotten test site.

3.3 The Halden test site

The Halden geotechnical test site is located approximately 120 km south of Oslo in Norway. The site consists of a 10 to 12 m thick deposit of fjord-marine, low plasticity clayey silt (Blaker et al., 2019). The silts are normally consolidated and the water table is located 2 m below surface with a hydrostatic profile in the silt layer, changing to sub-hydrostatic in the underlying clays. As with the Tiller-Flotten site, a rigorous CPT_u field testing regime was conducted and CAUC triaxial tests were conducted on high quality Sherbrooke block samples obtained from boreholes adjacent to the CPT_u test locations.

The silts have a bulk unit weight of 19 kN/m^3 and are split into two sub-profiles as shown in Figure 5: Unit II which extends from 5 m below surface to 12 m below surface; and Unit III which extends from 12 m below surface to 16 m below surface. Units II and III are regarded as the same material with the same geologic origin and were separated simply based on the results from the indicator tests which indicated that the silt becomes sandier in the lower Unit III. Results from the CAUC triaxial tests are shown in Figure 3. With the exception of the sample obtained at 9 m depth from borehole 1 (B01_9m) which showed strain softening behaviour, all the other samples showed strain hardening behaviour.

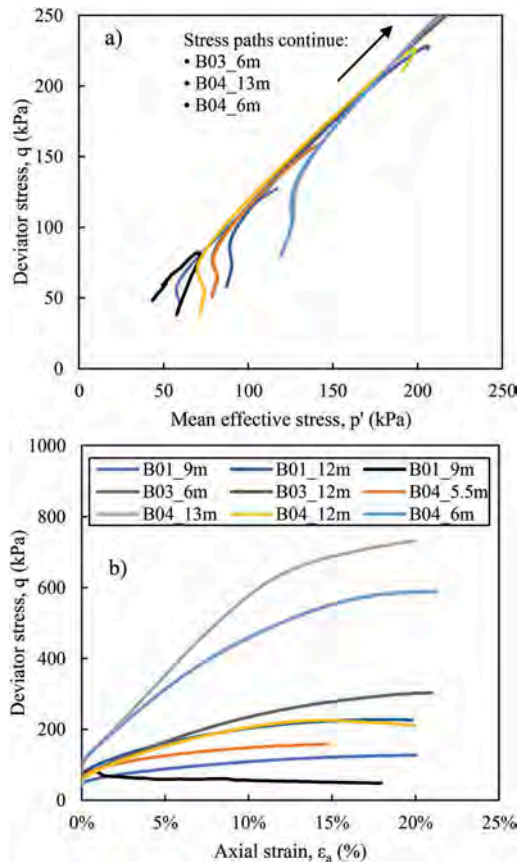


Figure 3. Triaxial test results on the Sherbrooke samples for the Halden test site.

3.4 Analysis of CPT data

The raw CPT data obtained from the database were processed using version 3.6.2.6 of the CPeT-IT software package developed by Geologismiki (Geologismiki, 2021). When analysing CPT data, it is important to note that the load cells which measure the sleeve friction and tip resistance are geometrically offset on the cone. Therefore, to correct the data such that the

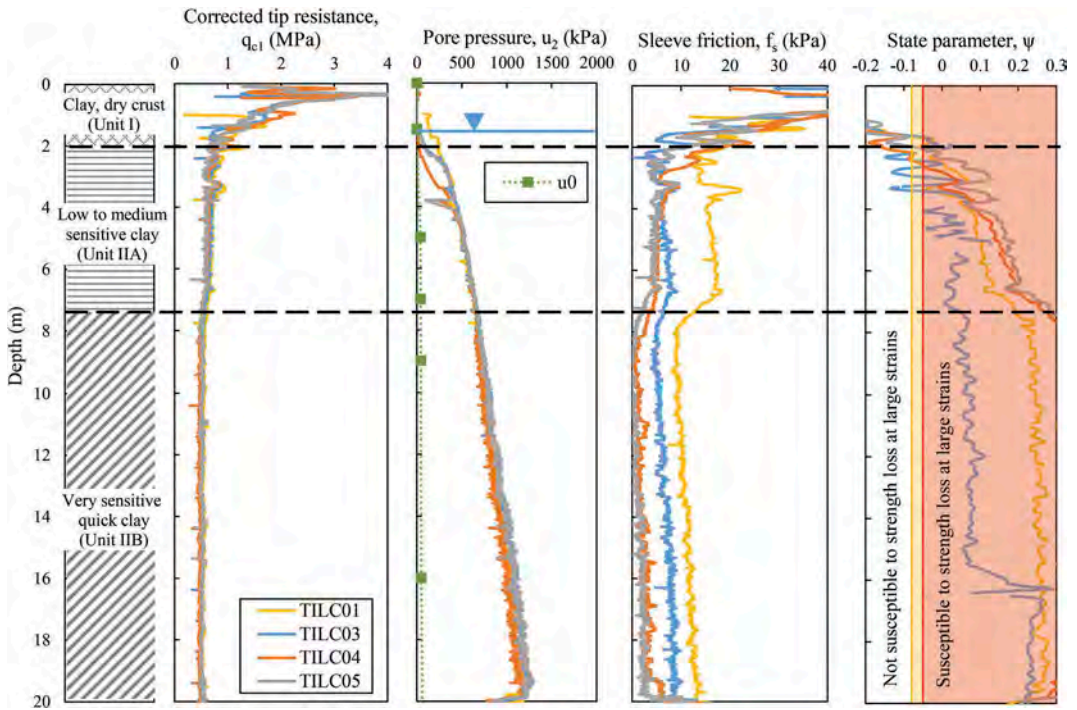


Figure 4. CPT data for selected probes at the Tiller-Flotten quick clay reference site (after L'Heureux et al., 2019).

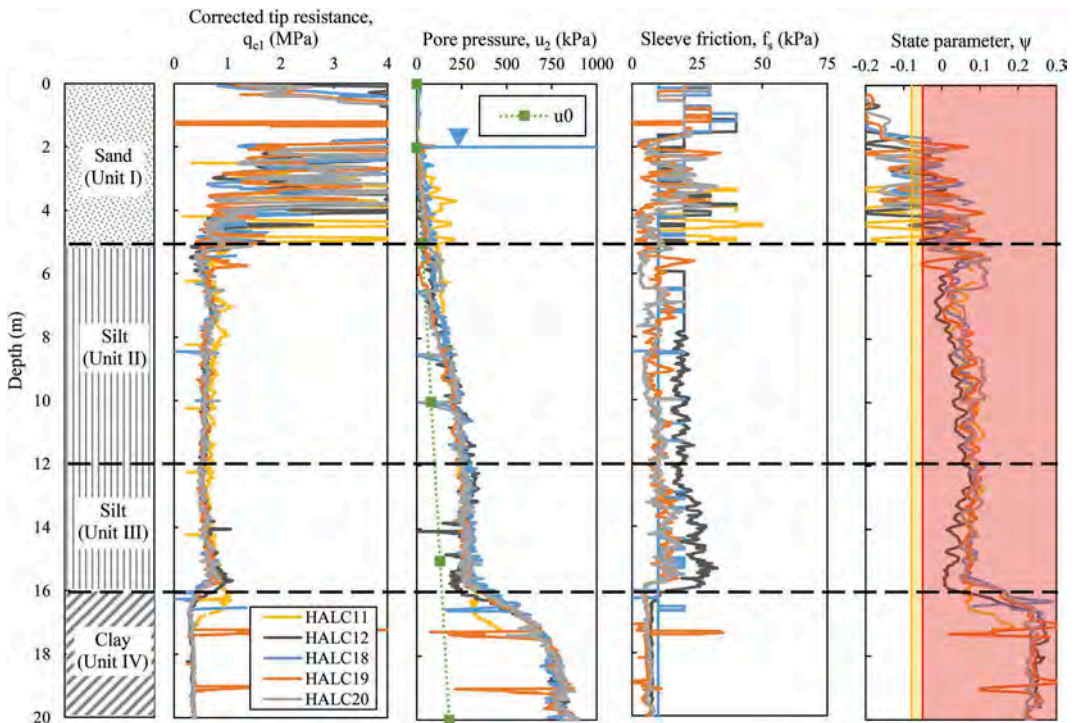


Figure 5. CPT data for selected probes at the Halden silt reference site (after Blaker et al., 2019).

measured cone resistance and sleeve friction can be compared at the same depth, a vertical shift is applied. This shift distance is a function of the physical location of the sleeve friction and load cell as well as the rigidity of the soil. The Cross Correlation Function (CCF), as proposed by Jaksa et al. (2002) was used for this assessment. The interpreted CPT data for the Tiller-Flotten and Halden test sites are shown in Figure 4 and Figure 5, respectively. Based on the soil behaviour index I_c as proposed by Robertson & Wride (1998) and the pore pressure ratio Bq , it was deemed that the probing through the Tiller-Flotten clay and Halden silt was predominantly undrained. It is therefore appropriate to assess the CPT data in terms of undrained hydraulic conditions.

3.5 Susceptibility to strength loss during undrained shear

Several methods have been proposed to estimate the state of the soil, specifically with regard to the undrained behaviour at large strains. One such method is a screening method proposed by Plewes et al. (1992) where the state parameter (ψ) of the soil is estimated. The method is referred to as a screening method as the state parameter is estimated based only on CPT data and some limitations have been identified (e.g. Torres-Cruz, 2021; Narainsamy et al., 2022). For this assessment, the original implementation of the Plewes method was used. Material with $\psi > -0.05$ was assumed to be susceptible to strength loss at large strains during undrained shear, material with $\psi < -0.08$ was considered not susceptible to strength loss at large strains. A transition zone was defined where $-0.08 < \psi < -0.05$. These limits are commonly used in research and practice (e.g. Jefferies & Been, 2015).

Applying the screening method to the NGTS site results in the ψ with depth charts shown in Figure 4 and Figure 5. Figure 4 clearly shows the Tiller-Flotten clay as susceptible to strength loss at large strains and this correlates well with the observed response from the triaxial data (Figure 2). Figure 5 also shows the Halden silt as susceptible to strength loss at large strains. However this does not correlate well with the observed response from the triaxial data (Figure 3). This emphasises the screening nature of the Plewes method and that more advanced methods may need to be considered in practice.

3.6 Summary of test data analysed

A summary of the test data assessed is shown in Table 1. For the Tiller-Flotten clay site, a total of 10 triaxial tests and 5 CPT tests were assessed. An average q_{c1} of 0.55 MPa and I_B of 0.71 was determined. For the Halden silt site, a total of 9 triaxial tests and 5 CPT tests were assessed, and an average q_{c1} of 0.63 MPa and I_B of 0.05 was determined.

Table 1. Summary of data analysed.

Test site	Tiller-Flotten	Halden
Material	Marine clay	Clayey silt
No of triaxial tests	10	9
Type of test	CAUC	CAUC
Undrained response	Strain softening	Strain hardening
No of CPT soundings	5	5
Susceptible to strength loss at large strains?*	Yes	Yes
Average q_{c1} (MPa)	0.554	0.633
Average I_B	0.713	0.050

* according to the Plewes et al. (1992) screening method

4 RESULTS

The I_B determined from the CAUC triaxial test results, and the average q_{c1} determined from the CPT tests for the Tiller-Flotten clay and Halden silt are shown in Figure 6. Also plotted on Figure 6 are the case histories investigated by Olson (2001) and Muhammad (2012), as well as the relationship proposed by Sadrekarimi (2014). It was found that for the Tiller-Flotten clay, the proposed relationship provided a reasonable estimate of the I_B . However, the Halden silt plots much lower. This is due to the fact that the proposed relationship is simply a function of the corrected tip resistance and not any laboratory test data. Since the Halden silt exhibited strain hardening behaviour during undrained shear in triaxial compression, the material shows no brittleness.

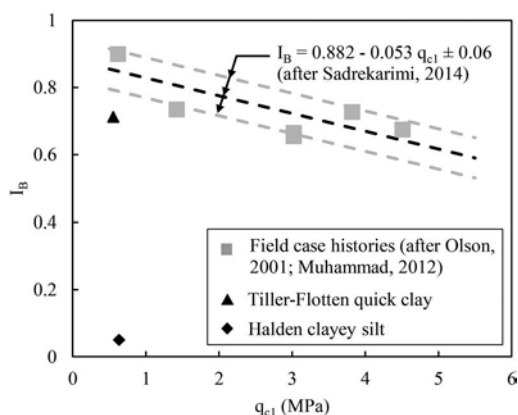


Figure 6. Results from this study compared to previously published data.

This over-estimation of the I_B for a strain-hardening material is expected as the empirical relationship was derived based on field case histories where only strain softening material was involved (i.e. it was a biased database). Care therefore needs

to be taken when using the Plewes screening method, as well as when using the relationship proposed by Sadrekarimi (2014), ensuring that they are applied to materials similar to those from which they were derived and validated against.

5 CONCLUSIONS

CPT and triaxial data from two NGTS research test sites were assessed: the Tiller-Flotten quick clay site and the Halden silt site. A strain softening screening assessment was performed, and the undrained brittleness index was determined for both sites. The following was found:

1. The Plewes et al. (1992) screening method identified that the Halden silt material is contractive at large strains. However, with the exception of one test, the results from the triaxial tests indicated dilative behaviour. Care therefore needs to be taken when using this method to assess soils susceptible to strain softening behaviour during undrained shear.
2. The relationship proposed by Sadrekarimi (2014) between corrected tip resistance (q_{c1}) and undrained brittleness index (I_B) was found to overestimate the undrained brittleness index for both the Halden silt and the Tiller-Flotten clay. This method should therefore only be used as a screening method and a more rigorous assessment is recommended when assessing the undrained brittleness index using the CPT.

ACKNOWLEDGEMENTS

The authors gratefully acknowledge GeoLogismiki for providing an educational licence for the CPeT-IT CPT interpretation software.

REFERENCES

Been, K., & Jefferies, M. G. 1985. A state parameter for sands. *Géotechnique*, 35(2), 99–112.

Bishop, A. W. 1971. Shear strength parameters for undisturbed and remolded soil specimens. *Roscoe Memorial Symp.*, 3–58.

Blaker, Ø., Carroll, R., Paniagua Lopez, A. P., DeGroot, D. J., & L Heureux, J.-S. 2019. Halden research site: geotechnical characterization of a post glacial silt, *AIMS Geosciences*, 5(2), 184–234.

Doherty, J. P., Gourvenec, S., Gaone, F. M., Pineda, J. A., Kelly, R., O’Loughlin, C. D., & others. 2018. A novel web based application for storing, managing and sharing geotechnical data, illustrated using the national soft soil

field testing facility in Ballina, Australia. *Computers and Geotechnics*, 93, 3–8.

Geologismiki. 2021. CPET-IT. Retrieved from <http://www.geologismiki.gr/Products/CPeT-IT.html>

Jaksa, M. B., Kaggwa, W. S., & Brooker, P. I. 2002. An improved statistically based technique for evaluating the CPT friction ratio. *Geotechnical Testing Journal*, 25(1), 61–69.

Jefferies, M., & Been, K. 2015. *Soil liquefaction: a critical state approach*, 2nd Ed. CRC press.

Kayen, R. E., Mitchell, J. K., Seed, R. B., Lodge, A., Nishio, S., Coutinho, R., & others. 1992. Evaluation of SPT, CPT, and shear wave-based methods for liquefaction potential assessment using Loma Prieta data. *Proc., 4th Japan-US Workshop on Earthquake-Resistant Des. of Lifeline Fac. and Countermeasures for Soil Liquefaction*, 1, 177–204.

L’Heureux, J.-S., Lindgård, A., & Emdal, A. 2019. The Tiller-Flotten research site: Geotechnical characterization of a very sensitive clay deposit, *AIMS Geosciences*, 5(4), 831–867.

L’Heureux, J. S., Carroll, R., Lacasse, S., Lunne, T., Strandvik, S. O., Degago, S., & others. 2017. New Research Benchmark Test Sites in Norway. *In Geotechnical Frontiers 2017*, 631–640.

Muhammad, K. 2012. *Case history-based analysis of liquefaction in sloping ground*. PhD Thesis, University of Illinois.

Narainsamy, Y., Jacobsz, S., Geldenhuys, L., & Hörtkorn, F. 2022. A review of liquefaction potential screening in engineering practice. *Proc. 20th Int. Conf. on Soil Mechanics and Geotech. Eng.* Sydney.

Oberhollenzer, S., Premstaller, M., Marte, R., Tschuchnigg, F., Erharter, G. H., & Marcher, T. 2021. Cone penetration test dataset Premstaller Geotechnik. *Data in Brief*, 34, 106618.

Olson, S. M. 2001. *Liquefaction analysis of level and sloping ground using field case histories and penetration resistance*. PhD Thesis, University of Illinois.

Plewes, H. D., Davies, M. P., & Jefferies, M. G. 1992. CPT based screening procedure for evaluating liquefaction susceptibility. *Proc. of the 45th Canadian Geotech. Conf.*, Toronto, 4, 1–9.

Robertson, P. K., & Wride, C. E. 1998. Evaluating cyclic liquefaction potential using the cone penetration test. *Canadian Geotechnical Journal*, 35(3), 442–459.

Robertson, P. K., de Melo, L., Williams, D. J., & Wilson, G. W. 2019. *Report on the expert panel on the technical causes of the failure of the feijão dam 1*.

Robertson, P. K. 2016. Cone penetration test (CPT)-based soil behaviour type (SBT) classification system—an update. *Canadian Geotechnical Journal*, 53(12), 1910–1927.

Sadrekarimi, A. 2014. Effect of the mode of shear on static liquefaction analysis. *Journal of Geotechnical and Geoenvironmental Engineering*, 140(12), 4014069.

Spencer, E. 1967. A method of analysis of the stability of embankments assuming parallel inter-slice forces. *Géotechnique*, 17(1), 11–26.

Torres-Cruz, L. A. 2021. The Plewes Method: a Word of Caution. *Mining, Metallurgy & Exploration*, 1–1

A comparative study on CPTu-based soil classification methods: Case studies

T.D. Nguyen & P.S. Khin

VNU Vietnam Japan University, Hanoi, Vietnam

Q.N. Pham

Vietnam Petroleum Institute, Hanoi, Vietnam

A.T. Vu

Le Quy Don Technical University, Hanoi, Vietnam

ABSTRACT: This paper presents a comparative study on the applicability of three CPTu-based soil classification charts, namely, Robertson's normalized (SBTn) chart (Robertson 2009), Eslami-Fellenius (EF)'s non-normalized chart (Eslami and Fellenius 1997) and Robertson's non-normalized (SBT) chart (Robertson 2010). A well-monitored database of CPTu data at six study sites of different geological conditions was used for the analyses. It is found from the study that when the effective stress (σ'_{v0}) is small, typically smaller than 150 kPa, the EF's and Robertson's SBTn charts results in similar soil types obtained from visual classification procedure (VCP) whereas the Robertson's SBT chart results in similar or slightly coarser soil types. When the σ'_{v0} becomes larger, the Robertson's SBTn chart still results in soil types well matched with those obtained from the VCP but both the non-normalized charts tend to result in coarser soil types. This feature of the non-normalized charts is more pronounced in stiff clayey or dense sandy soils.

1 INTRODUCTION

The CPTu is one of the most versatile and useful field tests in soil investigation and one of its main applications from the test results is soil classification. In the literature, the Robertson's normalized soil behaviour type (SBTn) chart (Robertson 1990, 2009) is the most popularly recommended one. Besides, Eslami-Fellenius (E-F)'s method (Eslami and Fellenius 1997, Fellenius 2021) is also a good alternative. The key difference in input parameters for Robertson's SBTn and E-F's charts is that only basic measurements of the test are required for the E-F's chart whereas effective vertical stress (σ'_{v0}) is additionally required for the Robertson's SBTn chart. In many cases, exact value of soil density and in-situ pore pressure (u_0) (and therefore the effective stress) are not available, the Robertson's SBTn chart is therefore less effective in real-time classification (Fellenius 2021).

To facilitate the real-time application to soil classification, Robertson (2010) introduced an updated non-normalized chart (SBT) initially proposed by Robertson et al. (1986) that requires only basic measurements but stressed that this updated non-normalized chart could give reasonable result in the range of effective stress from 50 to 150 kPa.

Robertson (2010) and Robertson and Cabal (2015) recommended that in general the normalized chart (Robertson 1990, 2009) provide more reliable identification of SPT than the non-normalized chart.

The CPTu has been an indispensable field test in soil investigation for nearshore and offshore wind farms projects along the coast of Vietnam these days. The applicability of the charts to new geological conditions, especially to onshore and offshore sites, is merit to be investigated.

This paper presents a comparative study on the applicability of the Robertson's SBTn chart (Robertson 2009), Robertson's non-normalized chart (Robertson 2010) and E-F's chart (Eslami-Fellenius 1997, Fellenius 2021). For this, CPTu data from four onshore sites in Vietnam and Korea and two offshore sites in the East Sea (Vietnam) are used for analyses.

2 EXPERIMENTAL TEST SITES

2.1 Test site location

In this study, CPTu test results from six study sites of different geological conditions are brought into analyses. The abbreviated names and locations of the sites are given in Table 1, which are graphically illustrated

Table 1. Name and location of the test sites.

No.	Site name	Condition	Longitude	Latitude	Location
1	VSIP	Onshore	106° 42' 8.98" E	20° 54' 52.21" N	Hai Phong Province, Vietnam
2	KC	Onshore	105° 43' 44" E	21° 3' 22.92" N	Hanoi, Vietnam
3	TPP	Onshore	106° 12' 55.54" E	20° 5' 55.29" N	Nam Dinh Province, Vietnam
4	MOC	Onshore	128° 54' 14.25" E	35° 5' 5.8" N	Busan City, Korea
5	PVN1	Offshore	108° 20' 56.63" E	10° 12' 41.36" N	East sea, Vietnam
6	PVN2	Offshore	108° 48' 09.69" E	07° 55' 24.40" N	East sea, Vietnam

in Figure 1. The first three test sites, namely, Vietnam Singapore Industrial Park (VSIP), Kim Chung Residential Complex (KC), and Nam Dinh Thermal Power Plant (TPP), are located in the Red River delta, Vietnam. A research program on consolidation characteristics of clayey soils has been conducted recently by the first author at the sites in which CPTu and elaborate soil sampling for laboratory tests were conducted.

The fourth site, namely, Myeongji Ocean City (MOC), is located in the Nakdong River Estuary of Nakdong River delta, West of Busan city, Korea. The CPTu and soil sampling at the site were conducted by the first author some years ago in a research program on bearing capacity of driven pile foundation (Kim et al. 2012).

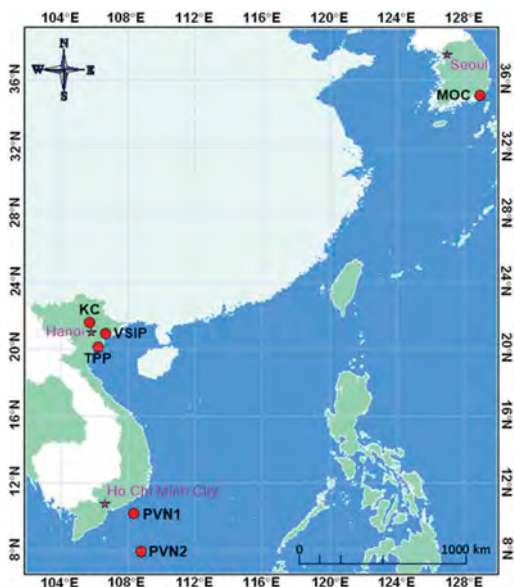


Figure 1. Location of the test sites.

The last two sites, namely, PVN1 and PVN2 are located in the East Sea of Vietnam (Figure 1). The CPTu with soil sampling and other field tests were elaborately conducted by Fugro for PetroVietnam (PVN) in an investigation program for building drill rigs at the sites. The water depth at the two sites was

measured using a combination of electronic sensor and echo sounder and the average value at the PVN1 and PVN2 sites was 56.3 m and 119.9 m, respectively.

2.2 CPTu tests

For the first three test sites (VSIP, KC, TPP), the CPTu was carried out using a piezocone of 10 cm² cross-sectional area with a filter mounted at the cone shoulder (u₂ position). The test was performed following procedures recommended in the ASTM 5778 – 20 (2020) standard. The key research objective at the sites was on consolidation characteristics of the clayey soils thus the CPTu was carried out in upper clayey and silty soil layers only. The CPTu at MOC site was carried out using a piezocone of 15 cm² with also the measurement of pore pressure at the cone shoulder (u₂ position).

At the offshore test sites, drilling operations were carried out through a motion compensated Fugro Offshore Drilling Rig over a moon pool in the centre of the vessel. On the other hand, sampling was conducted through the open-centre bit using Wison BHA and collars, which facilitated umbilical piston, push and hammer sampling operations. The CPTu was conducted using Fugro's Downhole Wison system with a cone of 10 cm² base area, 60° apex, 150 cm² cylindrical sleeve, and a filter at cone shoulder to measure u₂. The rate of penetration during testing was kept between 20 mm to ± 5 mm per second throughout the 3.0 m continuous stroke.

Although analyses were fully carried out for the six test sites, typical analysis results from only four sites, namely, VSIP, MOC, PVN1, and PVN2, will be presented in detail due to limited allowance of space.

2.3 Soil profiles

Soil layers at each site were carefully classified based on results from physical tests in the lab with the support of visual classification procedures (VCP) from boring records (e.g., soil sample from the SPT sampler) at the site. Figure 2 shows soil layers and basic soil properties at the four sites. To facilitate the evaluation later, soil layers in each site were simply named from L1 to Ln downwards as shown in the figure.

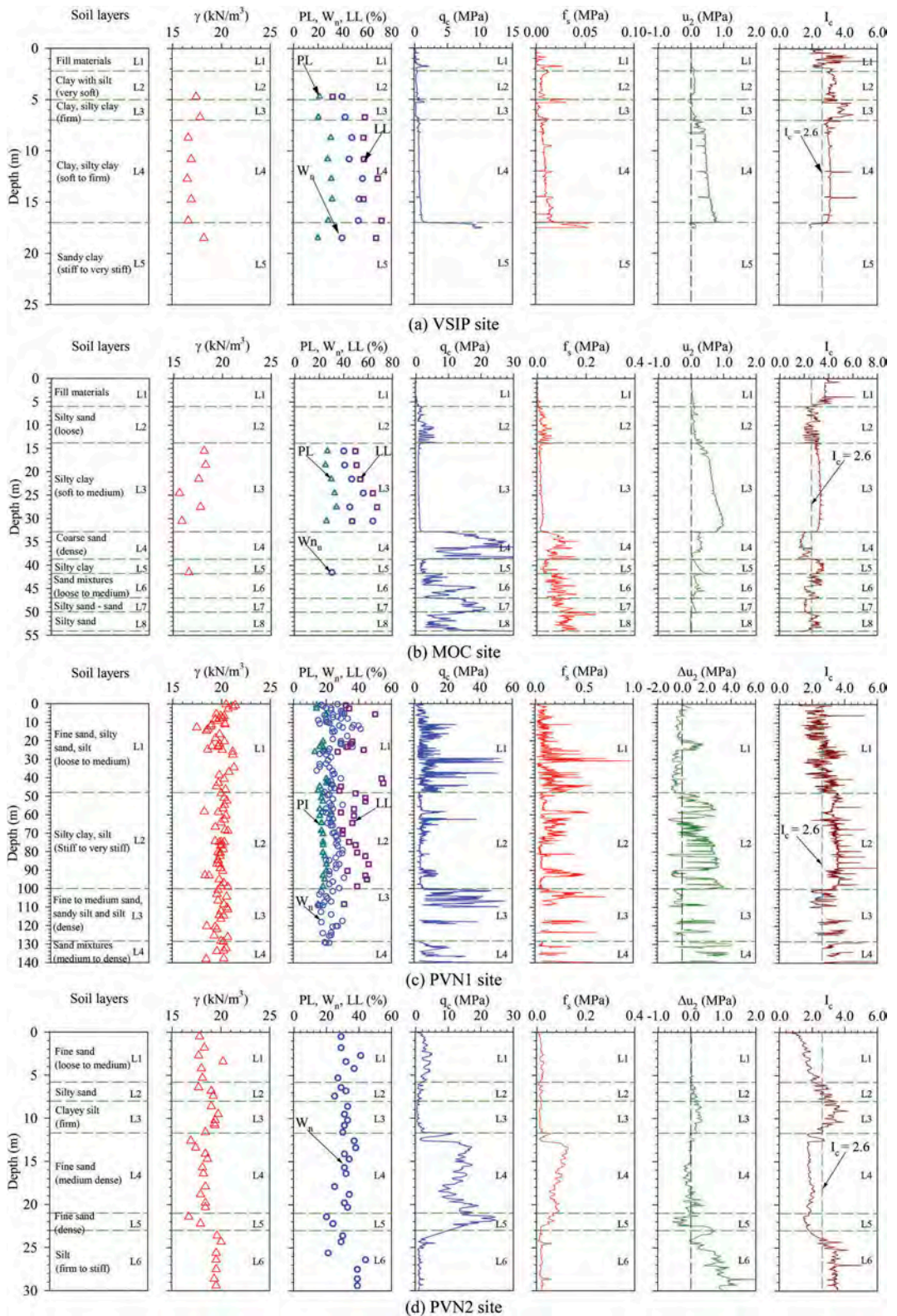


Figure 2. Soil profiles at the study sites.

At the the VSIP site, the CPTu was carried out in soft to firm clay layers up to the depth of 17 m (Figure 2(a)). At the MOC site, the CPTu was carried out up the sandy gravel layer (at 55.0 m) (Figure 2(b)), and thus both sandy and clayey soil types are available for analyses.

At the PVN1 site, the soil profile (up to the depth of 140 m) consists of many alternate sub-layers of silty clay, clayey silt, sandy silt and silty sand; however, the soil profile might be broadly divided into four main layers as shown in Figure 2(c). At the PVN2 site, the soil profile (up to the depth of 30.0 m) consists of 6 layers of both clayey and sandy soil types as shown in Figure 2(d).

Figure 2 also shows the cone resistance (q_c), sleeve friction (f_s), pore water pressure (u_2) and excess pore water pressure (Δu_2) diagrams, and soil behavior type index (I_c) (Roberson 2009) from the CPTu at the study sites. It is interesting to note from q_c and u_2 diagrams that the soil layers can easily be identified and are well matched with the classification from physical parameters profile shown in Figure 2. Note that the Δu_2 value of some sandy layers was negative (e.g., 24.0 – 48.0 m at PVN1 and 15.0 – 23.0 m at PVN2). This unusual characteristic is typically found in sandy deposits in offshore environment due to the cavitation phenomenon (Lunne et al. 1997).

The soil behavior type index (I_c) also helps to classify the soil profiles well. For example, at the depths of 0.4 to 17.6 m (VSIP site), 13.8 to 32.8 m (MOC site), 48.0 to 100.0 m (PVN1 site) the I_c is pronouncedly larger than 2.6, indicating that the layers are clayey soils. The index value of other layers is mostly equal or less than this boundary value, indicating the layers are silty to sandy soils.

3 SOIL CLASSIFICATION RESULTS

3.1 Influence of effective stress

The influence of effective stress to soil behaviour type has been discussed extensively in many studies (e.g., Robertson 1990, 2009) and it is examined through the case studies herein. It is found from the cases that when the effective stress is less than about 150 kPa the E-F's and Robertson's normalized (SBTn) charts provide rather similar soil types for both clayey soil and sandy soil, however the Robertson's non-normalized (SBT) chart tends to indicate similar or slightly coarser grained soil types compared with those from the normalized chart. As an example, Figure 3 shows the three charts applied to layer L4 (silty clay) at the VSIP site. As shown, both E-F's and Robertson's SBTn charts indicate that soil in this layer is clay to silty clay and is well matched with results from lab test results and VCP but the Robertson's SBT chart indicates that the soil is more likely silt mixtures (clayey silt & silty clay). Similar finding is found for the upper layers at the six sites (i.e., the effective stress is relatively small). Note that the parameters of the charts are as follows: the effective cone stress $q_E = q_t - u_2$, where $q_t = q_c + (1-a)u_2$; the normalized cone resistance $Q_m = [(q_t - \sigma_{v0})/p_a] (p_a/\sigma'_{v0})^n$, the normalized friction ratio $F_r = [f_s/(q_t - \sigma_{v0})]100\%$, the sleeve friction ratio: $R_f = 100(f_s/q_c)$.

When the effective stress becomes larger, the influence of effective stress becomes more pronounced and especially the E-F's chart also tends to indicate slightly coarser soil type compared with that obtained from the lab test results and VCP, and from Robertson's SPTn chart. For instant, Figure 4 shows a comparison of classified soil types from the charts applied to layer L4 (stiff to very stiff silty clay – silt)

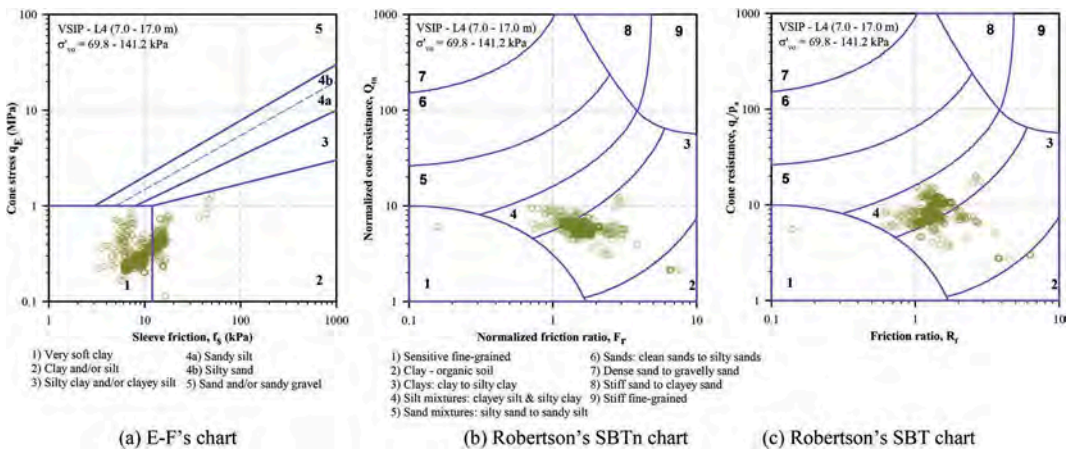


Figure 3. Soil classification charts for layer 4 at VSIP site.

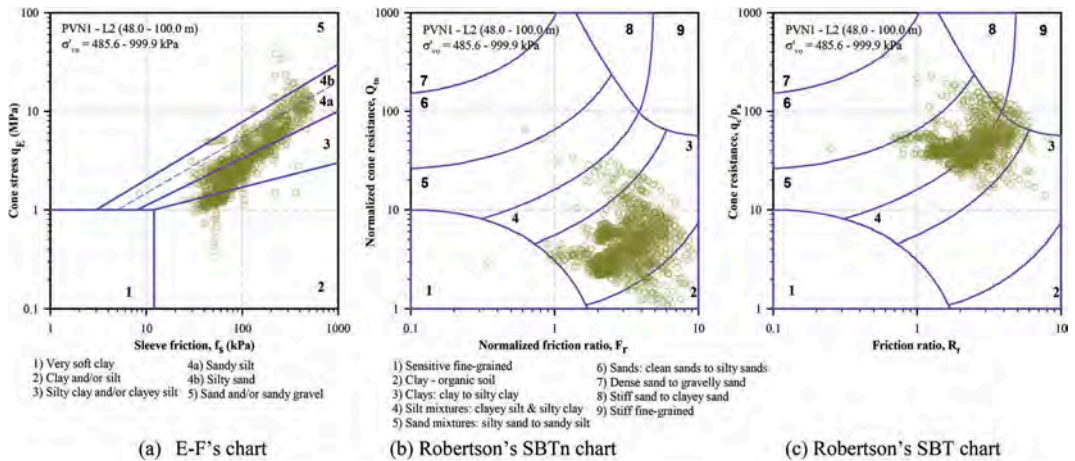


Figure 4. Soil classification charts for layer 2 at PVN1 site.

at PVN1 site. The figure indicates that the Robertson's SBTn chart results in similar soil types obtained from the lab test results and VCP whereas the EF's and Robertson's SBT charts indicate soil types that are likely silt to silty sand. Besides the influence of effective stress, the discrepancy in this case may also be attributed to the stiffness of this soil layer since the soil layer is stiff to very stiff. The discrepancy is found less pronounced in soft to firm silty clayey soil even at relatively large effective stress (e.g., for the layers L3 and L5 at MOC site).

3.2 Influence soil types

It is known that in a normally consolidated, homogeneous clay layer, the cone resistances (q_c or q_t)

typically increases linearly with the increase in vertical effective stress (σ'_{v0}). However, in a homogeneous sand layer, the resistances increase nonlinearly with the increase in the effective stress. This is why the stress exponent (n) is applied to the normalized cone resistance (Q_{tn}) and n is often 1.0 for clayey soils and less than 1.0 for sandy soils. The non-normalized classification charts (e.g., E-F's and Robertson's SBT ones) do not take into account this characteristic.

Figure 5 shows an example of the charts applied to layer L4 (medium dense fine sandy) at PVN2 site. The figure indicates that at relatively small vertical effective stress and medium dense condition, the three charts result in similar soil types and they well match with the soil type obtained from the VCP.

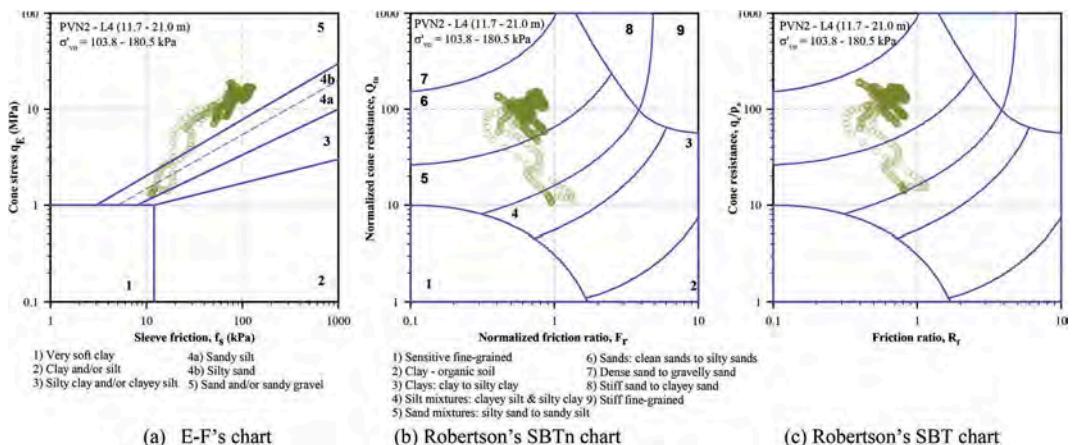


Figure 5. Soil classification charts for layer 4 at PVN2 site.

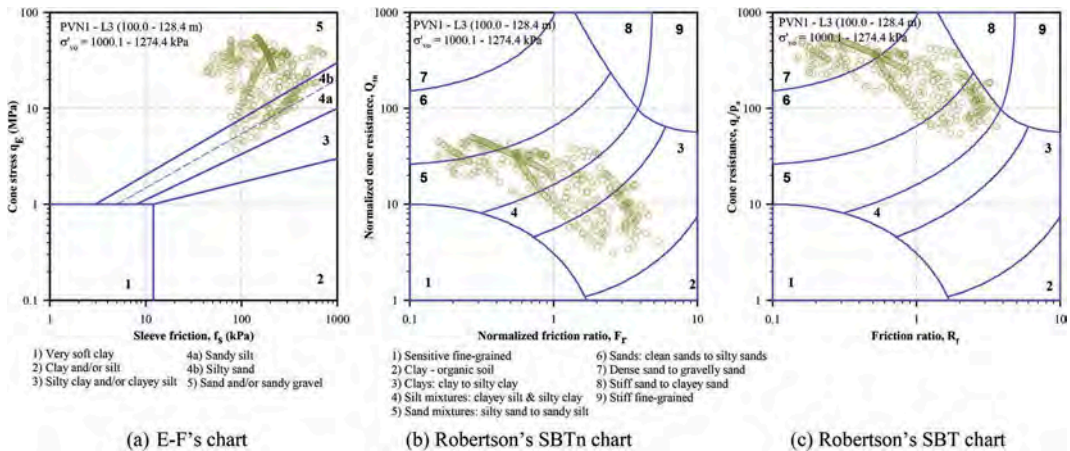


Figure 6. Soil classification charts for layer 3 at PVN1 site.

Similar finding is obtained from layers L1 & L2 at PVN2 site, L2 at MOC site, L1 at PVN1 site.

When the depth (i.e., the effective stress) becomes larger the influence sandy soil type to the effectiveness of the charts becomes more pronounced. For example, Figure 6 shows a comparison of soil types obtained from the three charts applied to layer L3 (dense, fine to medium sand with sandy silt & silt) at PVN1 site. It is very clear from the figure that the Robertson's SBTn chart results in soil types matched relatively well with the results from the VCP whereas the two non-normalized charts indicate rather coarser soil types. Similar finding was found from layers L4, L6, L7, L8 at MOC site.

influenced by large effective stress and sandy soil type as discussed above.

4 CONCLUSIONS

This paper presents a comparative study on the applicability of the three CTPu-based soil classification charts, namely, Robertson's normalized (SBTn) chart, Eslami-Fellenius (E-F)'s non-normalized chart and Robertson's non-normalized (SBT) chart. CPTu data in association with soil sampling at six sites from different geological conditions were used for the analyses. The following key conclusions are drawn from the study.

- 1) when the effective stress is less than about 150 kPa the E-F's and Robertson's normalized (SBTn) charts provide rather similar soil types for both clayey soil and sandy soil, however the Robertson's non-normalized (SBT) chart tends to indicate similar or slightly coarser grained soil types compared with those from the normalized chart. When the effective stress becomes larger the influence of the stress becomes more pronounced, and especially the E-F's chart also tends to indicate slightly coarser soil type compared with that obtained from the lab test results and VCP and from Robertson's SPTn chart. This indicates that the non-normalized charts tend to result coarser soil types than the actual soil types when the effective stress is large enough.
- 2) The characteristic of indicating coarser soil types from the non-normalized charts becomes more pronounced in sandy soils, especially dense sands at large depths.
- 3) From the analysis results in this study, it might be concluded that the Robertson's normalized chart is most reliable among the three charts.

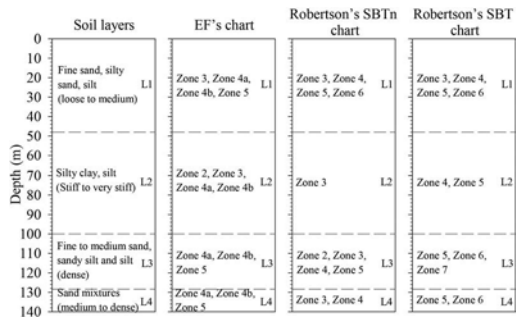


Figure 7. Comparison of soil profiles of soil types from the charts at PVN1 site.

Figure 7 shows a typical comparison of soil types obtained from the lab test results and VCP and from the three classification charts. For simplicity, in each main layer, soil types from the charts are simply noted by zone numbers that data points fall on. It is clear from the figure classified soil types are

ACKNOWLEDGEMENT

The authors would like to thank PVI and PVN for their kind permission of use of data at the two off-shore sites.

REFERENCES

- ASTM 5778 – 20 (2020). Standard test method for electronic friction cone and piezocone penetration testing of soil. ASTM International.
- Eslami, A., Fellenius, B. H. (1997). Pile capacity by direct CPT and CPTu methods applied to 102 case histories. *Canadian Geotechnical Journal*, 34(6),886–904.
- Fellenius, B.H. (2021). *Basics of foundation design* (Jan 2021 ed.). Electronic edition.
- Kim,S.R., Chung, S.G., Nguyen, T.D. and Fellenius, B. H. (2012). Design for settlement of pile groups by the unified design method – A case history. *Geotechnical Special Publication* No. 227, ASCE, pp. 545–567.
- Lunne, T., Robertson, P.K. and Powell, J.J.M. (1997). Cone penetration testing. Blackie Academic & Professional.
- Robertson, P. K (2009). Interpretation of cone penetration tests - a unified approach. *Canadian Geotechnical Journal*, 46(11),1337–1355.
- Robertson, P.K. (2010). Soil behavior type from the CPT: An update. *The 2nd International symposium on Cone Penetration Testing*, CPT'10, Huntington Beach, CA, USA.
- Robertson, P.K. and Cabal, K.L. (2015). *Guide to cone penetration testing for geotechnical engineering* (6th ed). Gregg Drilling & Testing, Inc.
- Robertson, P.K., Campanella, R.G., Gillespie, D. and Greig, J. (1986). Use of piezometer cone data. *In-Situ '86 – Use of In-situ testing in Geotechnical Engineering*, GSP 6, ASCE, pp. 1263–1280.

Characterization of young sediments using CPTu and Medusa SDMT

S. Oberhollenzer, L. Hauser, F. Brand, R. Marte & H.F. Schweiger

Institute of Soil Mechanics, Foundation Engineering & Computational Geotechnics, Graz University of Technology, Graz, Austria

D. Marchetti

Studio Prof. Marchetti, Rome, Italy

S. Pfeifer

illwerke vkw AG, Bregenz, Austria

ABSTRACT: Piezocone penetration tests (CPTu) and seismic flat dilatometer tests (SDMT) present costand time-efficient insitu investigation techniques for onshore as well as offshore projects. Since soil sampling is often related to a strong soil disturbance in fine-grained sediments, parameter identification is frequently based on insitu measurements in combination with correlations. As shown in previous studies, correlations are more difficult to develop in silt-dominated sediments. To overcome this problem, the research project PITS (parameter identification using insitu tests in silts), was launched by Graz University of Technology in cooperation with the Federal Chamber of Architects and Chartered Engineering Consultants. To investigate the influence of time effects (age) and microstructure on the load-settlement behaviour of normally to slightly underconsolidated sediments, deposits younger than 50 years have been investigated at the water storage reservoir Raggal (Austria) using CPTu as well as Medusa SDMT. Both probes were pushed first through the water and subsequently into the sediments by means of a stand-alone pushing device, where the testing setup was installed on a floating pontoon. In order to prevent buckling of the penetration rods, additional casing tubes (along the water) were used. In a last step, soil sampling was executed using the CPT-Ranger system by Geomil. To characterize and quantify the sediments microstructure, shear wave velocities determined insitu by means of SDMT ($V_{S,SDMT}$) are compared with measurements on reconstituted soil samples using bender elements ($V_{S,BE}$). Ratios $V_{S,BE}/V_{S,SDMT} \approx 1$ indicate the presence of no or moderate soil microstructure. On the other hand, postglacial deposits of similar grain size distribution are characterized by smaller $V_{S,BE}/V_{S,SDMT}$ ratios, indicating a higher microstructure.

1 INTRODUCTION

1.1 Motivation

Fine-grained sediments define the soil layering of various basins and valleys within Alpine regions. Many of these basins and valleys were formed during several glacial periods and remained as lakes after the melting. Over thousands of years they have been filled by mainly fine-grained sediments. Therefore, such (geologically) young soils are often characterized by a high groundwater table and are generally in a normally consolidated or slightly under consolidated state. In the area of Salzburg or Bregenz it was observed that such sediments often present unexpected low settlements under static loading on shallow foundations. On the other hand, it was observed that dynamic loads introduced by heavy construction measures (e.g. soil improvement measures, jet grouting) can lead to significant settlements. One possible explanation for this observation might be related to microstructural bonds

within the grain-to-grain matrix, which lead to an increase in strength and stiffness (Leroueil 1992). At the same time, they can easily be destroyed due to heavy construction measures or non-adequate soil sampling techniques. On the other hand, insitu tests and especially seismic measurements (e.g. seismic piezocone penetration test SCPTu or seismic flat dilatometer test SDMT) are becoming increasingly popular to quantify and characterize microstructure (Robertson 2016).

To gain an improved understanding of structure in postglacial deposits by means of insitu tests Graz University of Technology in cooperation with the Federal Chamber of Architects and Chartered Engineering Consultants initiated the research project PITS (parameter identification using insitu tests in silts).

1.2 Aim

The present paper tries to investigate how aging can influence the development of microstructure.

Therefore, young sediments with an age of approximately 50 years deposited in the water storage reservoir Raggal (Austria) have been investigated using CPTu, SDMT and laboratory tests (e.g. oedometer, bender element).

Based on the comparison of shear wave velocities, determined insitu (Medusa SDMT) and in the laboratory on reconstituted samples (bender element), the degree of microstructure could be quantified and is further compared with measurements of post-glacial (older) sediments.

2 INSITU TESTS

2.1 Piezocone penetration test - CPTu

The piezocone penetration test (CPTu) is a widely used insitu test for soil classification and parameter identification. During test execution, a cone with a cross-section area equal to 10 or 15 cm² is pushed under constant penetration rate (2 cm/s) into the soil using a pushing device (e.g. truck, rig or demountable systems). Simultaneously, the tip resistance q_c , sleeve friction f_s and dynamic pore water pressure u_i are measured continuously over depth. The measurement of the pore water pressure is usually performed above the cone at position u_2 . Alternatively, the pore water pressure can be measured directly at the cone (position u_1). Normalized parameters can be calculated based on insitu measurements and further used for soil classification (using soil behavior type chart) or in combination with correlations to identify soil parameters.

2.2 Seismic Medusa flat dilatometer test - Medusa SDMT

The flat dilatometer is an insitu soil testing equipment developed by Professor Silvano Marchetti in the late 1970s (Marchetti 1980). A steel blade – containing a thin, expandable, circular steel membrane mounted on one side – is pushed into the soil on a constant penetration rate equal to 2 cm/s. The blade is connected to a pneumatic electrical cable running through the penetration rods, up to a control unit at surface. In the standard testing procedure, the penetration is stopped every 20 cm. When performing a classic DMT, the membrane is inflated with gas to obtain two pressure readings at defined deformations of the membrane: the A-pressure (center of the membrane deforms 0.05 mm) and B-pressure (center of the membrane deforms 1.10 mm). A third pressure reading, the C-pressure (closing pressure), can optionally be taken by slowly deflating the membrane soon after B until it returns to position A.

The Medusa dilatometer (Medusa DMT) is a self-contained, fully automated version of the flat dilatometer, able to autonomously perform dilatometer tests without the pneumatic cable and gas tank.

A motorized syringe, driven by an electronic board powered with rechargeable batteries, hydraulically expands the membrane to obtain the A, B and C pressure readings, which are acquired and stored automatically at each test depth (Marchetti 2014).

Since the test execution is performed automatically, the influence of operators can be reduced significantly, alternative timing of measurements become feasible and repeated A-pressure readings can be carried out accurately.

The seismic flat dilatometer is a combination of the flat dilatometer (or Medusa DMT) with the seismic module for measuring the shear wave velocity V_S behind the blade. The seismic module is a cylindrical element situated above the DMT blade and equipped with two receivers fixed at a vertical distance of 0.50 m. The measurements are commonly performed at depth intervals equal to 50 cm while stopping the penetration procedure. The shear wave source – located at the ground surface or in the present case at the lake floor bottom – generally consists of a S-hammer which strikes horizontally a rectangular steel plate pressed against the soil. The generated shear wave first reaches the upper receiver, then, after a delay, the lower receiver. The seismograms acquired by the two receivers, amplified and digitized at depth, are transmitted to a computer at the surface for real-time interpretation of V_S (Marchetti et al. 2008).

3 TEST SITE WATER STORAGE RAGGAL

3.1 General information

The water storage reservoir Raggal (see Figure 1), located in the western part of Austria, is operated by the energy operator *illwerke vkw* and is part of the hydropower plant *Oberstufe Lutz*. Due to natural sedimentation, about 50,000 m³ of material are deposited within the storage every year. To prevent blockage of important water intake points and to pass the annual inflow of sediments through the dam, these sediments are regularly removed near the dam using a dredger (see Figure 1).

3.2 Investigation

In a first step, the thickness of the sediments was investigated by means of echo soundings. The excavation works on the one hand and the location of insitu tests on the other hand have been designed/defined based on the latter. With increasing distance from the dam, the flow velocity rises and the deposited sediments become coarser. This relationship could be confirmed based on aerometer and sieve analyses on soil samples, recovered from the reservoir. In the front third of the water reservoir - where the finest sediments are deposited - *illwerke vkw* carried out excavation works during our investigation campaign. In order not to hinder the excavation work and to ensure all safety regulations, the insitu tests

were carried out approximately 300m behind the concrete-dam (see Figure 1). Based on echo soundings it could be ensured to investigate sediments of approximately 20 m thickness. All insitu tests were carried out starting from a floating pontoon within a rectangular area of approximately 10 x 5 m to ensure the comparability of test results (see Figure 1).

The insitu campaign consisted of piezocone penetration tests (CPTu) with pore water pressure measurements at position u_1 and u_2 , seismic Medusa flat dilatometer tests (Medusa SDMT) and soil sampling by means of CPT-Ranger. All tests were executed in collaboration with the companies mjp ZT GmbH and Studio Prof. Marchetti.



Figure 1. Water reservoir Raggal: Overview and location test site.

4 TEST EXECUTION

4.1 Floating pontoon and pushing device

Since the reservoir was filled with water during test execution, all insitu tests were executed from the floating pontoon presented in Figure 2a (which is usually used for sediment transportation). The construction is composed of four air-filled steel boxes (two boxes each side), connected by three 2.8m long IPE300 profiles. The external dimensions and weight of the barge amount to 10 m x 8 m and 13 tons respectively. The mobile stand-alone system by Geomil (Fox-150) was used as pushing device for all insitu tests. Thereby, a separate power pack, driven by a petrol motor, powers the Fox-150 hydraulically. In order to avoid any tilting during test execution, it was tried to fix the penetration device on the floating-pontoon center. In a first step, HEA profiles were clamped onto the IPE300 profiles. Subsequently, the “stand-alone system” was attached to the (longitudinal assigned) HEA profiles using two GEWI bars (see Figures 2b and 2d). Free areas were covered by wooden constructions to ensure work safety during test execution (see Figures 2e and 2f). Finally, the floating

pontoon was moved to the desired position using a motorboat and additionally fixed at the shore using four steel cables (see Figure 2g).

4.2 Piezocone penetration test and seismic Medusa flat dilatometer test

The water depth and the thickness of the sediment deposits were approximately 7 m and 20 m respectively during test execution. In order to prevent any buckling of penetration rods along the water section, additional casing tubes (with a slightly larger inner-diameter than the outer diameter of the pushing rods) were used to increase the cross-section and moment of resistance. In a first step, CPTu or SDMT probes were lowered to the lake floor bottom ensuring an embedment depth of approximately 2 m. Afterwards, casing tubes were lowered by using the stand-alone system. Once the casing tubes reached the lake bottom (sediment top surface) the penetration process was continued by means of pushing rods. Consequently, casing tubes were installed along the water section only. Due to the buckling problem and the limited weight of the pontoon, the sediments were investigated down to a depth of approximately 15 m. After reaching the final testing depth, first the casing tubes and subsequently the penetration rods were pulled back.

To determine the shear wave velocity, the S-hammer shown in Figure 3a was designed and built in cooperation with Studio Prof. Marchetti and Behensky. The shear wave is triggered using a 45kg drop-weight. Since water does not allow the transmission of shear waves, the S-hammer was lowered from the floating pontoon to the lake bottom using two winches (see Figures 3b and 3c). During the lowering procedure, additional casing tubes were continuously attached to the head of the structure to verify its position. A rope was used to lift and release the 45kg drop weight from the floating pontoon (see Figure 3c). The shear wave velocity was determined at 50 cm intervals.

4.3 Soil sampling and laboratory testing

In a final step, soil sampling for laboratory testing was executed in 5 depth levels using the CPT-Ranger system. All recovered samples (length = 50 cm, diameter = 7 cm) were carefully transported to Graz University of Technology and further investigated at the geotechnical laboratory. The sediments were characterized with respect to their particle size distribution, Atterberg limits, natural density, natural water content and oedometer stiffness. Furthermore, the shear wave velocity of reconstituted soil samples was determined at different insitu stress levels using bender element tests within a triaxial cell. All reconstituted soil samples were artificially mixed considering the insitu density and water content.

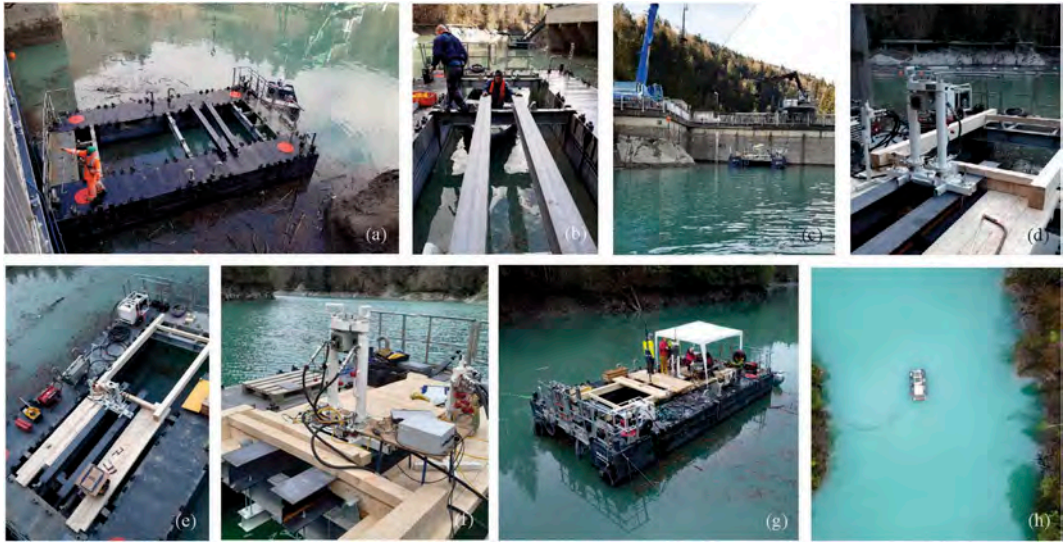


Figure 2. Test execution: Floating pontoon and pushing device.

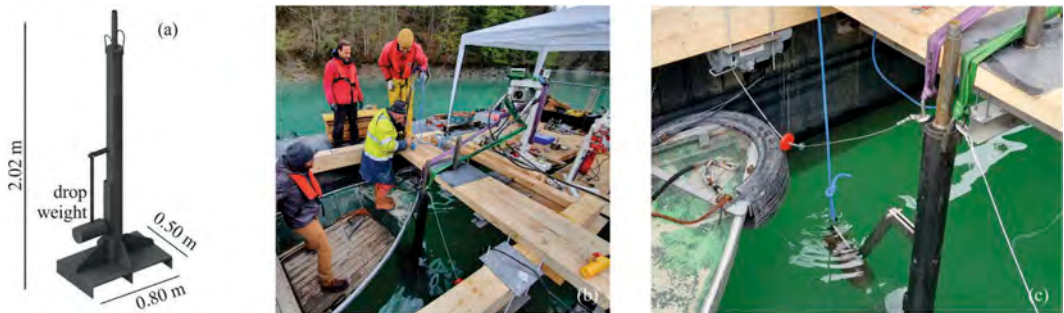


Figure 3. Test execution: Seismic measurements.

5 RESULTS

5.1 *In situ and laboratory results*

The sedimentation history of the water reservoir Raggal is composed of a sequence of fine and coarse-grained layers. As shown in Figure 4, these sand-silt alterations are characterized by an erratic distribution of CPTu measurements over depth (lithology L1). The tip resistance q_c and sleeve friction f_s vary between 0.7 - 3.5 MPa and 5 - 50 kPa respectively. The measured pore water pressure u_2 corresponds to the hydrostatic (insitu) pore water pressure u_0 within sand-dominated layers and rises ($u_2 > u_0$) with higher fines content. This varying trend is also reflected by DMT intermediate parameters I_D ($= 0.4 - 5$), K_D ($= 0.5 - 6$) and E_D ($= 0.5 - 12$ MPa) in Figure 4.

The soil behaviour type index I_C – based on Robertson 1990 – classifies the sediments as “silty

sand to sandy silt” and “clay to silty clay” (see Figure 4d). The DMT classification system according to Marchetti (1980) is based on the material behaviour index I_D and leads to a similar result (“silty sand to sand” and “clayey to sandy silts”).

In a second step, all recovered soil samples have been classified based on their particle size distribution and Atterberg limits according to EN ISO 14688-1 and ASTM 2487-11 (USCS). The particle size distribution of five depths is presented as a bar chart in Figure 5a (red = clay, green = silt, blue = sand). It is evident that sections with increased sand content are represented by higher I_D (DMT) and lower I_C (CPTu) values. On the other hand, four soil samples - classified as clayey, sandy silts (cl' sa' Si) according to EN ISO 14688-1 - have been recovered within fine-grained sections. These sediments present a fines content ($< 0,075\text{mm}$) larger than 90 % and are classified as organic silts (OL, OH) based on USCS (see Figure 5c). Due to their high organic

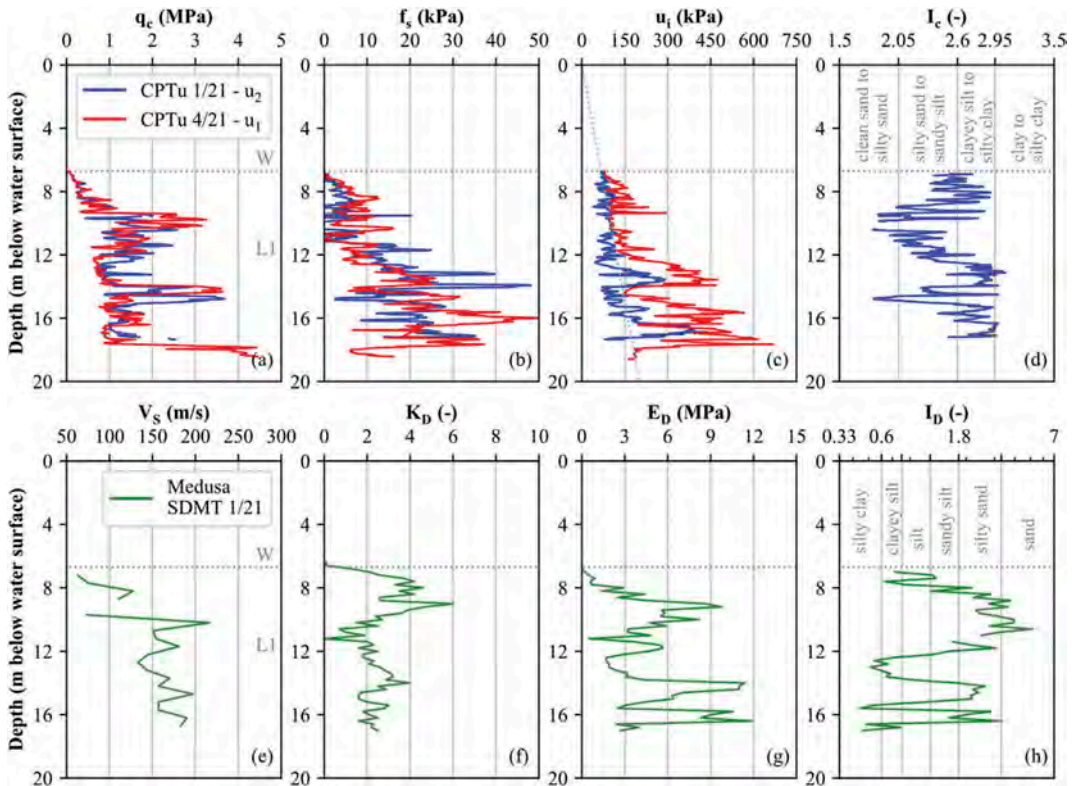


Figure 4. CPTu and SDMT results: (a) tip resistance q_c , (b) sleeve friction f_s , (c) dynamic pore water pressures u_1 and u_2 , (d) soil behaviour type index I_c , (e) shear wave velocity V_s , (f) horizontal stress index K_D , (g) dilatometer modulus E_D and (h) material behaviour index I_D .

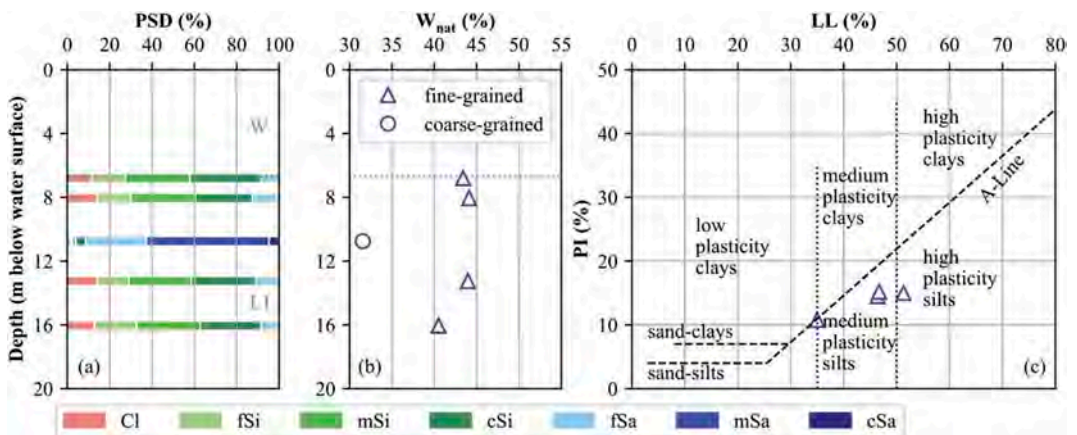


Figure 5. Laboratory results: (a) particle size distribution PSD, (b) natural water content w_{nat} and (c) Atterberg limits.

content (2-3 %), all points are situated below the A-line within the Casagrande diagram.

A small insitu density ($\rho_d \approx 1.2 \text{ g/cm}^3$, $\rho_{sat} \approx 1.75 \text{ g/cm}^3$) and a high natural water content $w_{nat} > 40 \%$ was expected and furthermore

determined within fine-grained (under-consolidated) layers. Nevertheless, it should be noted that natural water contents decrease and insitu densities increase with increasing particle size distribution.

5.2 Microstructure

The insitu shear wave velocity $V_{S,SDMT}$ determined by means of Medusa SDMT is presented in Figure 4e. As described earlier in section 4.1 for CPTu and DMT measurements and intermediate parameters, also the shear wave velocity is strongly influenced by the particle size distribution. Thereby, layers of higher sand-content are characterized by higher V_S values.

In order to quantify the degree of microstructure, bender element tests were performed in a second step on reconstituted soil samples using a triaxial device. It is important to note that material of soil samples recovered at -6.8 m, -8.1 m, -13.3 m and -16.1 m (all characterized by a similar particle size distribution as shown in Figure 5a) was used for this experimental approach. After a K_0 -consolidation, the shear wave velocity was determined for different insitu stress levels. The bender element results are shown in Figure 6a by blue triangles and are compared with SDMT results. Thereby, a regression (grey dotted) line - which goes through fine-grained sections where soil sampling was executed - is used for comparison. Based on the ratio $V_{S,BE}/V_{S,SDMT}$ it is evident that shear wave velocities determined in the laboratory by means of bender elements ($V_{S,BE}$) and in situ using Medusa SDMT ($V_{S,SDMT}$) are in good agreement. Since $V_{S,SDMT}$ and $V_{S,BE}$ differ only slightly, it can be assumed that the investigated sediments within the reservoir Raggal are characterized by no or moderate microstructure.

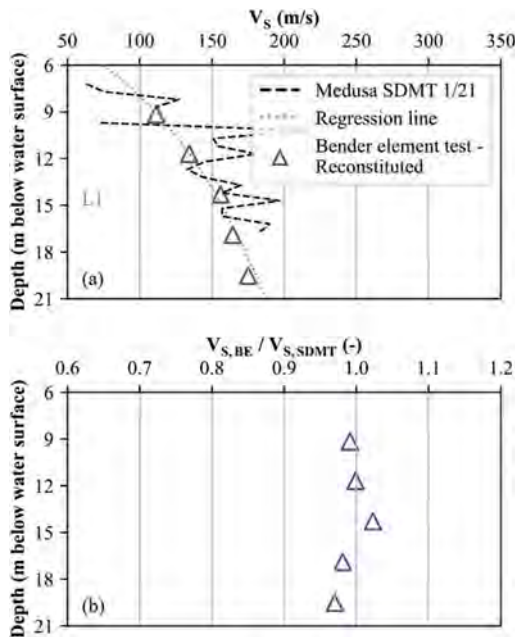


Figure 6. Shear wave velocity V_S : Comparison of SDMT and bender element tests.

6 CONCLUSION

Alpine regions are often characterized by basin landscapes, which were filled by fine-grained sediments after the last glacial period. These (normally to slightly under-consolidated) sediments often show small settlements under static loading, leading to the assumption that they might be characterized by a microstructure. Various authors (e.g. Robertson 2016) showed that structured soils present a higher shear wave velocity compared to unstructured (ideal) soils. The present paper investigated whether and to what extent young sediments, deposited in the water storage reservoir Raggal, are characterized by microstructure. In a first step CPTu, Medusa SDMT and soil sampling was performed from a floating pontoon using a mobile pushing device. The investigated sediments are composed of sand-silt alternations and are characterized by a small insitu density and a high water content $w_{nat} > 40\%$. In a second step bender element tests were performed on reconstituted soil samples and compared with the SDMT results. It was shown that shear wave velocities determined on reconstituted soil samples are in good agreement with SDMT results ($V_{S,BE}/V_{S,SDMT} \approx 1$), indicating no or little microstructure. Within the research project PITS, similar investigations have been performed in older sediments (e.g. rhine valley, basin of Salzburg) too. In these cases $V_{S,BE}/V_{S,SDMT}$ ratios were significantly smaller than 1, indicating a stronger microstructure in postglacial deposits. The present contribution showed that $V_{S,BE}/V_{S,SDMT}$ ratios are a potential indicator to quantify and characterize soil microstructure.

REFERENCES

- ASTM D2487-11. 2011. Standard Practice for Classification of Soils for Engineering Purposes (Unified Soil Classification System).
- EN ISO 14688-1. 2019. Geotechnical investigation and testing – Identification and classification of soil.
- Leroueil, S. 1992. A framework for the mechanical behavior of structured soils, from soft clays to weak rocks. In *Proceedings, US-Brazil NSF Geotechnical Workshop on Applicability of Classical Soil Mechanics Principles to Structured Soils*, Belo Horizonte, pp. 107–128.
- Marchetti, S. 1980. In Situ Tests by Flat Dilatometer. *J. Geotech. Eng. Div.* 106(GT3): 299–321.
- Marchetti, D. 2014. Device comprising an automated cableless dilatometer. *U.S. Patent* 8,776,583, filed July 29, 2011, issued July 15, 2014.
- Marchetti, S., Monaco, P., Totani, G., and Marchetti, D. 2008. In Situ Tests by Seismic Dilatometer (SDMT). In *From Research to Practice in Geotechnical Engineering*, Geotech. Spec. Publ. GSP 180, 292–311. American Society of Civil Engineers, Reston, VA, USA.
- Robertson, P.K. 1990. Soil classification using the cone penetration test. *Canadian Geotechnical Journal*, 27(1): 151–158.
- Robertson, P.K. 2016. Cone penetration test (CPT)-based soil behaviour type (SBT) classification system — an update. *Canadian Geotechnical Journal*, 53: 1910–1927.

PFEM modeling of CPTu tests in saturated structured soils

Kateryna Oliynyk

School of Science and Engineering, University of Dundee, Dundee, UK

Department of Civil and Environmental Engineering, University of Perugia, Perugia, Italy

Matteo O. Ciantia

School of Science and Engineering, University of Dundee, Dundee, UK

Claudio Tamagnini

Department of Civil and Environmental Engineering, University of Perugia, Perugia, Italy

ABSTRACT: The conventional interpretation of CPTu tests is typically based on empirical and semi-empirical correlations based on very crude descriptions of soil behavior, such as the total stress approach coupled with the Terzaghi-Rendulic pseudo-3d consolidation theory for modeling the time evolution of excess pore water pressure. The aim of this work is to show that a more rational interpretation of the coupled deformation and flow processes occurring in the soil during a CPTu test is possible by resorting to the numerical solution of the relevant governing equations, incorporating a realistic constitutive model for the soil. In order to deal with the large displacements and deformations induced by the cone penetration, the Particle Finite Element Method code G-PFEM, recently developed for geomechanical applications, has been used for this purpose. A key feature of the present work is the use of a finite deformation version of a non-associative isotropic hardening plasticity model for structured geomaterials - the FD_Milan model. The model is equipped with a *structure-related* internal variable which provide a macroscopic description of the effects of structure in natural, fine-grained soils. In order to deal with strain localization, typically observed in structured geomaterials upon yielding, the model has been equipped with a non-local version of the hardening laws, which has demonstrated capable of regularizing the pathological mesh dependence of classical FE solutions in the post-localization regime. A number of PFEM simulations of CPTu tests on a soft structured natural clay has been performed in order to assess the effects of the initial bond strength and permeability on the predicted results of the test, as well as on the spatial distributions of accumulated plastic strains, internal variables and excess pore water pressures. The results obtained represent a promising step towards a more rational interpretation of the CPTu tests in structured geomaterials and for their use in the calibration of advanced soil models.

1 INTRODUCTION

The Cone Penetration Test (CPT) is a widely used investigation tool for the characterization of both coarse-and fine-grained soils, for its simplicity, reliability and its relatively low cost. The development of the piezocone, featuring piezometers for the measurement of pore water pressure p_w at different positions on the cone tip, has significantly improved the capabilities of this site investigation tool - now referred to as CPTu test - and opened the way for a more rational interpretation of the test results.

The conventional interpretation of CPT tests is currently based on empirical and semi-empirical correlations, the last based on very crude descriptions of soil behavior, such as the adoption of a total stress approach. The excess pore pressure measurements in CPTu tests are typically used to

identify fine-grained soils (where Δp_w are large) from coarse-grained soils (where Δp_w are small or negligible), or to measure the soil coefficient of consolidation from pore pressure dissipation stages, where the tip advancement is stopped.

The aim of this work is to show that a more rational interpretation of the coupled deformation and flow processes occurring in the soil during a CPTu test is possible by resorting to the numerical solution of the relevant governing equations for the penetration process, and by adopting a realistic constitutive model for the soil. In early attempts to simulate the CPT test with the ALE-FE method, the extreme deformations imposed to the soil by the penetration of the piezocone have represented a substantial difficulty, due to strong mesh distortions which resulted in significant loss of accuracy or loss of convergence at relatively small penetration depths.

An effective alternative to the FEM which has proven to be quite efficient in simulating the cone penetration process is the Particle Finite Element Method (PFEM, Oñate et al. 2011). The PFEM shares many similarities with the updated Lagrangian approach of non-linear FEM, but it is capable of handling the problem of severe mesh distortion by a frequent mesh re-triangulation and h -adaptive refinement, using very efficient algorithms based on extended Delaunay tessellation. The nodes of the spatial discretization - performed with low-order linear triangles or tetrahedra - are treated as material particles, the motion of which is tracked during the numerical simulation. Applications of PFEM to the modeling of CPTu tests have been reported, *e.g.*, by Monforte et al. (2017), Monforte et al. (2018), Monforte et al. (2021), Hauser and Schweiger (2021) and Carbonell et al. (2022).

As far as modeling CPTu tests in clays is concerned, most of the works cited have been carried out adopting the classical MCC model for the soil. Although this critical state model is capable of capturing the essential features of soft, lightly overconsolidated clays, it fails to reproduce the behavior of natural structured clays, characterized by the presence of intergranular bonds of various origin. To investigate the effects of bonding on the soil response to the piezocone advancement, in this work the isotropic hardening elastoplastic model for natural, structured soils proposed by Nova and co-workers (Tamagnini et al. 2002, Nova et al. 2003) has been extended to finite deformations adopting a multiplicative decomposition of the deformation gradient into elastic and plastic parts (see, *e.g.*, Borja & Tamagnini 1998). The finite deformation plasticity model thus obtained - referred to in the following as the FD_Milan model - has been implemented in a geomechanics-oriented PFEM code (G-PFEM, Monforte et al. 2017) and has been used in this work to simulate CPTu tests in a relatively soft natural clay.

The remainder of the paper is as follows. A brief overview of the FD_Milan model is provided in Sect. 2, while the details of the CPTu simulations program are given in Sect. 3. A selection of the results obtained in the PFEM simulations is presented in Sect. 4. Sect. 5 provides the main concluding remarks and suggestions for further studies.

2 THE FD_MILAN MODEL

2.1 Local version

The FD_Milan model is a non-associative, isotropic hardening finite-deformation plasticity model for structured soils and weak rocks, developed by Oliynyk et al. (2021) based on the multiplicative decomposition of the deformation gradient and on the adoption of a suitable free energy function to describe the elastic response of the material. Its

evolution equations in the spatial setting are briefly summarized here:

$$\dot{\boldsymbol{\tau}} = \mathbf{a}^e(\mathbf{d} - \mathbf{d}^p) \text{ (hyperelastic eq.)} \quad (1)$$

$$\mathbf{d}^p = \dot{\gamma} \frac{\partial \mathbf{g}}{\partial \boldsymbol{\tau}} \text{ (flow rule)} \quad (2)$$

$$\dot{P}_s = \dot{\gamma} \rho_s P_s (\hat{V} + \zeta_s \hat{D}) \text{ (hardn. law for } P_s) \quad (3)$$

$$\dot{P}_t = -\dot{\gamma} \rho_t P_t (|\hat{V}| + \zeta_t \hat{D}) \text{ (hardn. law for } P_t) \quad (4)$$

subjected to the Kuhn-Tucker complementarity conditions:

$$f(\tau, P_s, P_t) \leq 0 \quad \dot{\gamma} \geq 0 \quad \dot{\gamma} f(\tau, P_s, P_t) = 0 \quad (5)$$

In the above equations, $\boldsymbol{\tau}$ and $\dot{\boldsymbol{\tau}}$ are the Kirchhoff stress and its Jaumann objective rate; \mathbf{d} is the rate of deformation tensor; \mathbf{d}^p is the plastic rate of deformation tensor; \mathbf{a}^e is the spatial hyperelastic tangent stiffness of the material; $\dot{\gamma}$ is the plastic multiplier; f and g are the yield function and the plastic potential, respectively (see Oliynyk et al. 2021 for details); P_s and P_t are internal variables; the functions

$$\dot{\gamma} \hat{V} = \dot{\gamma} \text{tr} \left(\frac{\partial \mathbf{g}}{\partial \boldsymbol{\tau}} \right) \quad \dot{\gamma} \hat{D} = \dot{\gamma} \sqrt{\frac{2}{3}} \left\| \text{dev} \left(\frac{\partial \mathbf{g}}{\partial \boldsymbol{\tau}} \right) \right\|$$

are the plastic volumetric and deviatoric rates of deformation; and ρ_s , ζ_s , ρ_t and ζ_t are material constants.

The first internal variables P_s (*preconsolidation pressure*) accounts for the hardening/softening effects due to volumetric and deviatoric plastic strains. The second, P_t (*bond strength*), quantifies the effects of material structure (fabric and bonding). A representation of the yield surface in the Kirchhoff stress invariants space $P:Q$, highlighting the role of the internal variables, is given in Figure 1.

For $\zeta_s = 0$, eq. (3) reduces to the classical volumetric hardening law of critical state soil mechanics. Plastic volumetric compaction produces an increase of P_s while plastic dilation is accompanied by a reduction of P_s .

A positive value of the bond strength P_t results in an expansion of the elastic domain in stress space. On the positive part of the P axis, the isotropic yield stress in compression is increased by a quantity $P_m = kP_t$, with k a material constant. On the negative axis, the vertex of the yield surface is displaced from the origin of the stress space to $P = -P_t$. Therefore, the structured material possesses a true cohesion and a non-negligible tensile strength. The region in the stress space contained between the actual yield surface (full black line in Figure 1) and

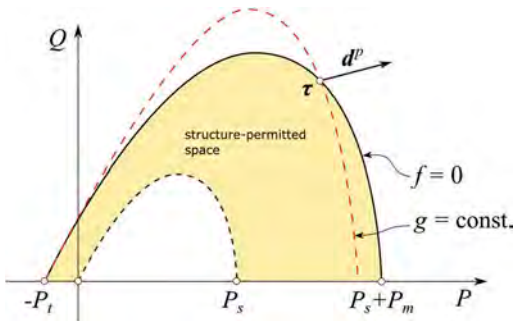


Figure 1. Yield surface and plastic potential of the FD_Milan model.

the intrinsic yield surface of the unstructured material (with $P_t = P_m = 0$, black dashed line in Figure 1), represents the so-called *structure-permitted space*, which is accessible only by the combined effects of fabric and intergranular bonding. As a consequence of the microstructural rearrangement of the soil fabric and the concurrent breakage of intergranular bonds, the structure of the material is progressively destroyed. From a macroscopic point of view, this process induces a progressive reduction of P_t with increasing accumulated plastic deformations. This process is described by the hardening law of eq. (4), in which the RHS is always negative. The final asymptotic value for P_t is zero (full destructuration): the bond-permitted space reduces to zero and the yield surface coincides with the intrinsic yield surface.

2.2 Non-local version

In order to provide a characteristic length scale to the constitutive equation, to regularize the numerical solution in presence of strain localization phenomena, the integral non-local approach of Oliynyk et al. (2021) has been adopted, in which the internal variables P_s and P_t are treated as non-local, spatially averaged quantities over a neighborhood Ω of the material point. The size of this neighborhood is controlled by a material constant ℓ_c , called *characteristic length*.

Let us rewrite the hardening laws (3) and (4) in the following equivalent integrated form:

$$P_s = P_{s0} \exp\{\rho_s(-E_v^p + \xi_s E_s^p)\} \quad (6)$$

$$P_t = P_{t0} \exp\{-\rho_t(N_v^p + \xi_t E_s^p)\} \quad (7)$$

where E_v^p , E_s^p and N_v^p are three strain-like internal variables, whose evolution equations are provided by:

$$\dot{E}_v^p = \dot{\gamma} \hat{V} \quad \dot{E}_s^p = \dot{\gamma} \hat{D} \quad \dot{N}_v^p = \dot{\gamma} |\hat{V}| \quad (8)$$

and P_{s0} and P_{t0} represent the initial values of the internal variables. Once E_v^p , E_s^p and N_v^p are chosen as alternative state variable, their values can be spatially averaged in a neighborhood Ω of each material point $x = \phi(X, t)$ at time t . The spatial averages are computed numerically by the following expressions:

$$\bar{A}(x_i) = \frac{1}{\sum_{x_j \in \Omega} w(x_i, r_{ij})} \sum_{x_j \in \Omega} w(x_i, r_{ij}) A(x_j) \quad (9)$$

where the symbol A stands for one of the variables E_v^p , E_s^p or N_v^p . In eq. (9), $r_{ij} = \|x_j - x_i\|$ is the distance between points located at x_j and x_i , and w is a suitable weighting function, for which the expression proposed by (Galavi & Schweiger 2010):

$$w(x, r_{ij}) = \frac{r_{ij}}{\ell_c} \exp\left\{-\left(\frac{r_{ij}}{\ell_c}\right)^2\right\} \quad (10)$$

has been adopted. The scalar quantity ℓ_c appearing in eq. (10) is a material constant providing the length scale sought after. Once the non-local quantities \bar{E}_v^p , \bar{E}_s^p and \bar{N}_v^p are known, the stress-like internal variables P_s and P_t are computed by eqs. (6) and (7).

3 SIMULATION PROGRAM

In the PFEM simulations of CPTu tests, a standard piezocone, with radius $R = 1.78$ cm and a cone tip angle of 60° is inserted in a calibration chamber with radius $B = 0.45$ m and height $H = 1.05$ m, filled with a fully saturated clay. The problem has been assumed as axisymmetric. A sketch of the problem geometry along with some snapshots of the spatial adaptive PFEM discretization at 3 different tip advancement depths is given in Figure 2.

The piezocone is wished-in-place at an initial depth $z_0 = 0.25$ m and then displaced downwards at a constant penetration speed of 2.0 cm/s, up to a depth $z = z_0 + 20R$. The piezocone tip and its lateral surface are modeled as rigid, impervious surfaces, and a smooth contact interface with the soil is adopted. Given the relatively small dimensions of the calibration chamber, the self weights of the pore water and of the soil have been ignored. The initial pore water pressure has been assumed uniform and equal to zero.

The material constants adopted in the simulations have been obtained by calibrating the model on the available experimental data for the Osaka clay (Adachi et al. 1995) and are reported in Table 1. The

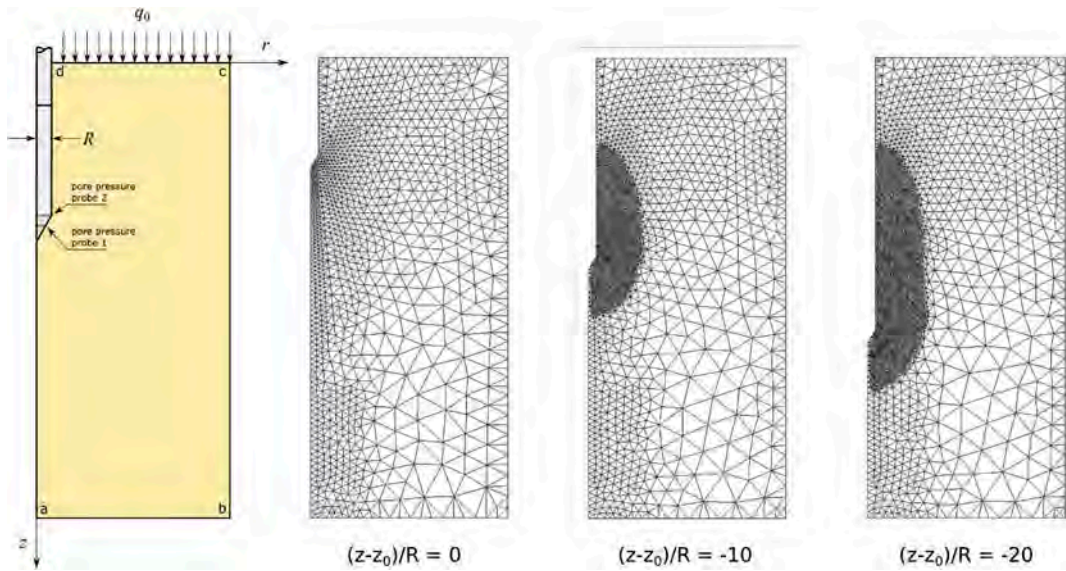


Figure 2. Problem geometry and spatial discretizations at 3 different tip advancement depths.

Table 1. Sets of material constants adopted in the CPTu test simulations (see Oliynyk et al. 2021 for details on the meaning of each constant).

$\hat{\kappa}$	G_0	α	P_{ref}	$M_{f,c}$	α_f	μ_f	$M_{g,c}$
(-)	(MPa)	(-)	(MPa)	(-)	(-)	(-)	(-)
1.82	3.0	0.0	5.0	1.1	0.75	1.50	1.1
α_g	μ_g	ρ_s	ρ_t	ζ_s	ζ_t	k	ℓ_c
(-)	(-)	(-)	(-)	(-)	(-)	(-)	(mm)
0.75	1.5	8.33	15.0	0.0	3.0	5.0	5.0

flow rule has been assumed as associative, so the plastic potential coincides with the yield function.

All the PFEM simulations have been performed as fully coupled hydromechanical problems, adopting the mixed $u-\Theta-p_w$ formulation of Monforte et al. (2017). The bottom and lateral surfaces of the calibration chamber have been assumed as rigid, impervious and perfectly rough boundaries. At the top surface of the soil body a uniform normal pressure $q_0 = 100$ kPa and a constant pore water pressure $p_w = 0$ have been imposed. Consistently with these boundary conditions, the initial Cauchy effective stress in the soil mass has been assumed axisymmetric, with components $\sigma_z = 100$ kPa and $\sigma_r = K_0 \sigma_z$ and $K_0 = 0.5$. The initial value of P_s has been set to 120 kPa.

4 SELECTED RESULTS

Six simulations have been performed considering 4 different hydraulic permeabilities, k_h , in the range $1.0e-9$ to $1.0e6$ m/s, and 3 different initial values for

the bond strength, P_{t0} , from 0 to 60 kPa. With these initial conditions and the material properties listed in Tab. 1 the apparent peak undrained strength $c_{u,p}$ of the soil ranges from 41 to 106 kPa.

The effects of the initial degree of bonding are shown in Figures 3 and 4. The simulations reported have been performed with $k_h = 1.0e-9$ m/s. For such a low permeability value, the penetration process occurs in almost undrained conditions. Figure 3 shows the profiles, relative to the cases of P_{t0} equal to 0, 30 and 60 kPa, of net cone resistance, q_n and excess pore water pressures computed at the cone base ($\Delta p_{w,2}$) and at the cone tip ($\Delta p_{w,1}$) as a function of the normalized penetration depth $Z = (z - z_0)/R$.

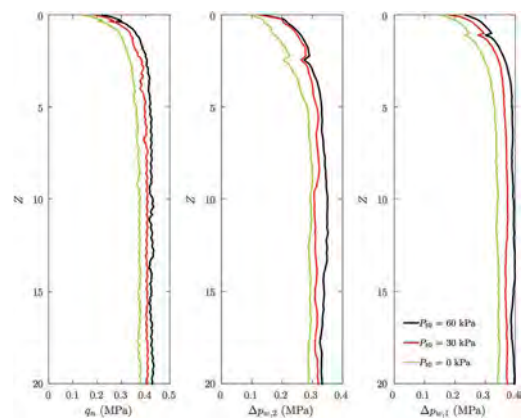


Figure 3. Profiles of net cone resistance, excess pore pressure $\Delta p_{w,2}$ and $\Delta p_{w,1}$ for different initial values of bond strength P_{t0} and $k_h = 1.0e-9$ m/s.

After an initial transient stage up to $Z = 5$, all the profiles reach a stationary state up to the final value of the penetration $Z = 20$. It can be observed that the stationary values of q_n , $\Delta p_{w,1}$ and $\Delta p_{w,2}$ increase with increasing P_{10} : the higher is the initial structure of the soil, the higher are the cone resistance and the excess pore pressures developed during the cone advancement.

Figure 4 shows a comparison of the contour maps of E_s^p , P_s , P_t and $\Delta p_{w,1}$ for the two extreme cases of $P_{10} = 0$ and 60 kPa. In the unstructured soil, the plastic zone around the piezocone extends by about $3R$ around the shaft and the cone, with contour lines following the shape of the penetrating device. In the structured soil, on the other hand, the observed pattern of plastic shear deformations is much more irregular and show the presence of localized shear zones which originate at about $3R$ below the cone tip and bend upwards as the cone advances. The presence of shear localization is most likely due to the softening behavior associated to soil destructuration. In both cases, the preconsolidation pressure P_s is only slightly affected by the penetration process, due to the virtually undrained nature of the soil deformation. In the structured soil, the contour map of P_s highlights the presence of a region of decreasing P_s , located at the boundary of the plastic region, where plastic dilatancy is occurring. The contour map of the bond strength for the structured soil clearly indicates that, in most of the plastic region around the piezocone, the destructuration process is almost complete. Yet, the presence of structure maintains a non-negligible effect on both the cone tip resistance and the spatial distribution of the pore water pressures, as shown in the contour maps of p_w .

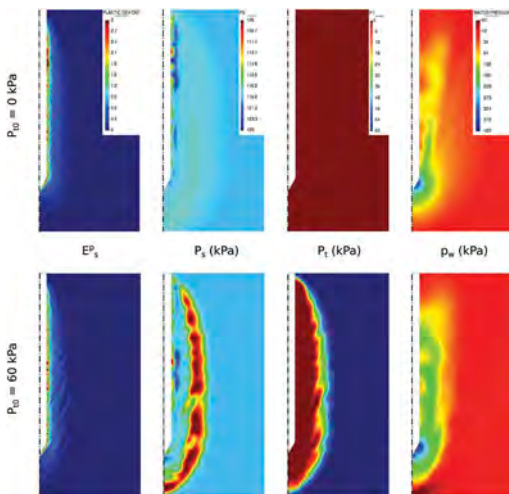


Figure 4. CPTu tests results: contour maps of E_s^p , P_s , P_t and p_w at the maximum penetration depth, for $P_{10} = 0$ kPa (top) and $P_{10} = 60$ kPa (bottom).

The effects of soil permeability on the predicted CPTu results are shown in Figure 5, reporting the profiles of q_n , $\Delta p_{w,1}$ and $\Delta p_{w,2}$ with Z for the four k_h values considered. From the figure, the impact of the soil permeability on the computed excess pore pressures at the two piezometers locations is immediately apparent. In the simulation with the highest permeability value the soil deforms in almost drained conditions, with a maximum Δp_w of about 50 kPa at the position of the piezometer no. 1. The maximum Δp_w are obtained at both piezometers for the lowest K_h value ($1.0e-9$ m/s), and only slightly smaller values of excess pore water pressure are registered at piezometer no. 2 for the next to smallest permeability. This value of k_h ($1.0e-8$ m/s) appears to mark the transition from fully undrained to partially drained soil response.

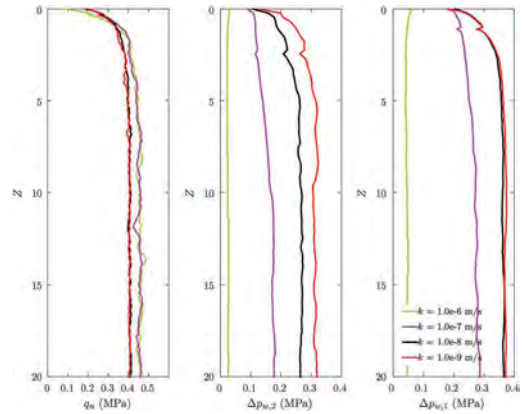


Figure 5. Profiles of net cone resistance, excess pore pressure $\Delta p_{w,2}$ and $\Delta p_{w,1}$ for different soil permeabilities and $P_{10} = 30$ kPa.

As expected, the q_n profiles show a larger cone resistance in the “drained” case, as compared to the “undrained” one, with the two intermediate cases profiles remaining close to the two extremes. Surprisingly, the difference between the different profiles of q_n is not very large, being on average around 13%.

The contour maps of E_s^p in Figure 6 and of E_s^p , P_s , P_t and p_w in Figure 7, for the two limiting cases of the smallest and highest permeability values adopted, indicate that, apart from the large differences observed in the final pore water pressure fields, the collapse mechanisms around the advancing cone tip is fundamentally different in the two cases. In the “undrained” case, the plastic region around the advancing piezocone is quite large, extending for about $6R$ both vertically, below the cone tip, and horizontally from the piezocone axis. The plastic zone is characterized by a complex pattern of accumulated volumetric and deviatoric plastic deformations, with clearly visible bands of localized shear and volumetric deformations. On the other hand, in

5 CONCLUDING REMARKS

The results of this preliminary study appear consistent with the observed CPTu profiles in similar soils and demonstrate that the soil response to the penetration of the piezocone in CPTu tests can actually be modeled quantitatively in a rational and computationally efficient way. The quality of the results obtained depends crucially on the capability of the constitutive model adopted to capture the essential features of the soil response during the penetration process. The FD_MILAN model presented in this work appears particularly well suited in this respect for a wide range of natural geomaterials, ranging from natural clays to porous soft rocks. The multiplicative plasticity model recently proposed by Oliynyk & Tamagnini (2020), based on the breakage mechanics, can represent a possible alternative for coarse-grained soils with crushable grains and collapsible weak rocks. The numerical simulations, performed with different initial bond strengths and soil permeabilities, show that the coupled non-linear PFEM model is capable of capturing: a) the development of plastic deformations induced by the advancement of the cone tip; b) the destructuration associated with plastic deformations; c) the space and time evolution of pore water pressure during the test. A characteristic of the plastic deformations pattern in presence of structure is the appearance of shear bands below the cone tip which propagate laterally as the tip advances and remain stationary thereafter. This feature is most likely associated to the softening mechanism induced by soil destructuration, as described by the FD_MILAN model. These results represent a promising step towards a more rational interpretation of the CPTu tests in structured geomaterials and for their use in the calibration of advanced soil models. The extension of the proposed model to incorporate thermal coupling effects (see, e.g., Tamagnini and Ciantia 2016) will allow the interpretation of T-CPTu tests, which represent a promising development for the thermal characterization of soils in the design of low-enthalpy energy geotechnical structures.

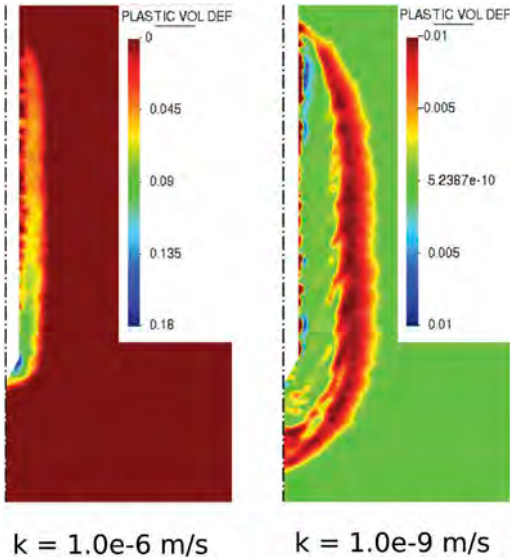


Figure 6. Contour maps of E_p^p for the maximum and minimum permeabilities considered.

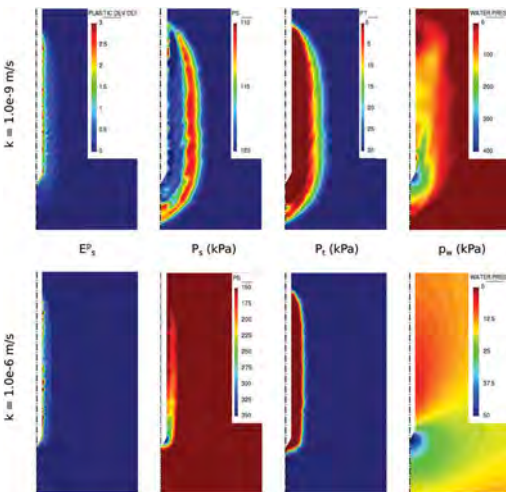


Figure 7. CPTu tests results: contour maps of E_p^p , P_s , P_t and p_w at the maximum penetration depth, for the minimum (top) and maximum (bottom) permeabilities considered.

the “drained” case, the penetration mechanism is more similar to a “punching” process, with a much smaller and homogeneous plastic zone around the cone tip and shaft. This certainly has a major effect on the stress distribution in the soil, which could explain the relatively modest differences registered in the stationary values of q_n in the two cases.

REFERENCES

- Adachi, T., F. Oka, T. Hirata, T. Hashimoto, J. Nagaya, M. Mimura, & T. B. S. Pradhan (1995). Stress-strain behavior and yielding characteristics of Eastern Osaka clay. *Soils and Foundations* 35(3), 1–13.
- Borja, R. I. & C. Tamagnini (1998). Cam-clay plasticity, part III: Extension of the infinitesimal model to include finite strains. *Comp. Meth. Appl. Mech. Engng.* 155, 73–95.
- Carbonell, J. M., L. Monforte, M. O. Ciantia, M. Arroyo, & A. Gens (2022). Geotechnical particle finite element method for modeling of soil-structure interaction under large deformation conditions. *J. of Rock Mech. Geotech. Engng.*, <http://dx.doi.org/10.1016/j.jrmge.2021.12.006>.

- Galavi, V. & H. F. Schweiger (2010). Nonlocal multilaminate model for strain softening analysis. *International Journal of Geomechanics* 10(1), 30–44.
- Hauser, L. & H. F. Schweiger (2021). Numerical study on undrained cone penetration in structured soil using pfpem. *Computers & Geotechnics* 133, 104061.
- Monforte, L., M. Arroyo, J. M. Carbonell, & A. Gens (2018). Coupled effective stress analysis of insertion problems in geotechnics with the particle finite element method. *Computers & Geotechnics* 101, 114–129.
- Monforte, L., J. M. Carbonell, M. Arroyo, & A. Gens (2017). Performance of mixed formulations for the particle finite element method in soil mechanics problems. *Computational Particle Mechanics* 4(3), 269–284.
- Monforte, L., A. Gens, M. Arroyo, M. Manica, & J. M. Carbonell (2021). Analysis of cone penetration in brittle liquefiable soils. *Computers and Geotechnics* 134.
- Nova, R., R. Castellanza, & C. Tamagnini (2003). A constitutive model for bonded geomaterials subject to mechanical and/or chemical degradation. *Int. J. Num. Anal. Meth. Geomech.* 27(9), 705–732.
- Oliyynyk, K., M. O. Ciantia, & C. Tamagnini (2021). A finite deformation multiplicative plasticity model with non-local hardening for bonded geomaterials. *Comp. & Geotechnics* 137.
- Oliyynyk, K. & C. Tamagnini (2020). Finite deformation hyperplasticity theory for crushable, cemented granular materials. *Open Geomechanics* 2, 1–33.
- Oñate, E., S. R. Idelsohn, M. A. Celigueta, R. Rossi, J. Marti, J. M. Carbonell, P. Ryzhakov, & B. Suárez (2011). Advances in the particle finite element method (pfem) for solving coupled problems in engineering. In *Particle-Based Methods*, pp. 1–49. Springer.
- Tamagnini, C., R. Castellanza, & R. Nova (2002). A Generalized Backward Euler algorithm for the numerical integration of an isotropic hardening elastoplastic model for mechanical and chemical degradation of bonded geomaterials. *Int. J. Num. Anal. Meth. Geomech.* 26, 963–1004.
- Tamagnini, C. & M. O. Ciantia (2016). Plasticity with generalized hardening: constitutive modeling and computational aspects. *Acta Geotechnica* 11(3), 595–623.

Effect of the scatter between CPTU measured parameters in soil classification

P. Paniagua

Norwegian Geotechnical Institute & Norwegian University of Science & Technology, Trondheim, Norway

J.-S. L'Heureux

Norwegian Geotechnical Institute, Trondheim, Norway

ABSTRACT: Using piezocones from different manufacturers may yield different results even if the equipment complies with international standards. This causes problems when soil investigation contractors, using different cones, operate in the same area, and especially on the same project. Studies done in soft clay, sand, silt, and quick clays from different Norwegian sites show that repeatability for the cone resistance measurements and penetration pore pressure is good and that it has improved from one cone type to another. However, the scatter in the measured sleeve friction, and hence the friction ratio, is still very significant. Here, an attempt is made to qualitatively describe the impact of the scatter in the soil classification based on CPTU parameters. The most common soil classification charts are used to illustrate this scatter.

1 INTRODUCTION

Performing piezocone tests (CPTU) with cone penetrometers from different manufacturers may give different results even though the equipment is aligned with international standards. Previous studies (Lunne et al. 1986, Gauer et al. 2002, Powell & Lunne 2005, Tigglemann & Beukema 2008, Lunne 2010, Cabal & Robertson 2014 Lunne et al. 2018) have shown that all three measured parameters, cone resistance q_c , friction sleeve f_s and pore pressures u_2 , could vary significantly, and in particular for f_s , depending on the equipment used.

Recent advances in electronics and cone design have been incorporated in the design of the new cones and motivated further field testing. The establishment of the Norwegian GeoTest Sites (NGTS) (L'Heureux & Lunne 2019) has given the opportunity to different companies to do testing at the silt (Paniagua et al. 2021), sand (NGI 2020), quick clay (Lindgård et al. 2019) and soft clay (Lunne et al. 2018) sites. In general, after these tests, it was observed that the measured u_2 and q_c (or corrected cone resistance, q_t) showed little variation between different cone types, while the f_s measurement gave relatively large scatter between different cone types. Then, the question that arises is how much this scatter in the CPTU parameters influence further treatment of the data like for example soil classification based on CPTU.

The present article investigates the impact of varying CPTU equipment and its scatter on the most common CPTU soil behaviour charts. The paper focuses on the effect of the scatter between different types of

piezocones. Further analyses regarding the statistical distribution of scatter with depth and between piezocones for each site is done in Lindgård et al. (2018), Lunne et al. (2018), Paniagua et al. (2020) and NGI (2020).

2 METHODOLOGY

Two relevant CPTU data sets selected at the NGTS study sites in Norway have been chosen for this study. The data sets selected correspond to the ones giving the largest scatter between them, i.e., the maximum (data in red in the figures) and minimum (data in blue in the figures) values. In other words, the selected data sets come from the cones which provide extreme profile results. The difference between the two data sets presented here are measured in terms of its CPTU parameters q_t , u_2 and f_s , and then the data was plotted in terms of the classification systems presented in this paper.

The data sets are then plotted in the soil classification charts proposed by Robertson (1990), Schneider et al. (2008) and Senne set et al. (1989). The data plotted in the soil classification charts has been filtered to represent just the layer where the main soil material for the site is to be found.

It should be clarified that the discussion about the validity of the soil classification charts mentioned above for Norwegian soil conditions is out of the scope of this study. Therefore, it is assumed that the soil classification charts may represent fairly well the soil types studied in the present paper.

The observations presented here assume that the requirements and recommendations given in ISO 22476-1:2012 (Geotechnical investigation and testing - Field testing - Part 1: Electrical cone and piezocone testing) and Norwegian Geotechnical Society (NGF) Guideline No. 5 (2010) are followed. Some of these are:

- Zero readings to be taken before and after each test with the cone penetrometer at a temperature as close as possible to ground temperature.
- It is important to wait until the readings have stabilized before taking zero readings.
- The thrust machine shall push the rods so that the axis of the pushing force is as close to vertical as possible.
- The pore pressure measurement system shall be saturated to give good pore pressure response during penetration.
- For deep CPTUs, it is important to correct the penetration length for inclination effects.
- Recommended minimum distance between a CPT and adjacent boreholes is 2 m.

2.1 Test sites

The NGTS sites selected for the present study are well portrayed in the following publications and are shortly described as follows:

- *Tiller-Flotten quick clay* (L'Heureux et al. 2019): The site consists of thick marine clay deposit of a low to medium sensitivity (1-7,5 m) deposit over a high sensitivity (quick) clay (7,5-20 m depth).
- *Onsøy soft clay* (Gundersen et al. 2019): The site consists of a high plasticity marine clay (1--8 m depth), a medium plasticity clay (8--13 m depth) and a high plasticity clay (13-20m).
- *Halden silt* (Blaker et al. 2019): The silt layer varies between 5-15 m and consists of a uniform marine natural silt.
- *Øysand sand* (Quinteros et al. 2019): The site consists of fluvial and deltaic gravelly-sandy-silt sediments with a gravelly sand layer from 0-14 m, a silt layer from 14-17,5 m depth and a sand layer down to 20 m depth.

2.2 Derived CPTU parameters studied

The soil classification charts are a combined representation of the in-situ behaviour characteristics of the soil under a CPTU. The CPTU might be able to measure up to seven independent parameters like cone resistance, q_c , friction sleeve, f_s , pore pressure, u_2 , shear wave velocity, V_s , and when performing dissipation tests, the time for 50% consolidation, t_{50} , in situ pore pressure, u_o , and hydraulic gradient, i .

Usually the most common parameters (i.e., q_c , f_s and u_2) are normalized to be represented in soil classification charts. Before normalization, the parameter q_c is corrected for unequal pore pressure effects by

the formula $q_t = q_c + a(1-u_2)$, where the parameter a relates the cross-sectional area of the shaft and projected area of the cone.

Robertson (1990) relates the normalized parameters Q_t , B_q and F_r , noted as normalized cone resistance, pore pressure parameter and normalized friction ratio, respectively.

Schneider et al. (2008) and Senneset et al. (1989) make use of some of the normalized parameters (i.e., Q_t and B_q) and relate them to either $\Delta u/\sigma_{vo}'$ for Schneider et al (2008) or q_t for Senneset et al. (1989).

3 RESULTS

The main observations for all sites are given and discussed below. However, due to space limitation focus will mainly be given to the results obtained at the Halden and Onsøy sites, and some specific observations for Tiller-Flotten and Øysand. The complete figures for Tiller-Flotten and Øysand can be sent to the interested readers upon request to priscilla.paniagua@ngi.no.

3.1 Tiller-Flotten quick clay site

The testing of eight different cones from five CPTU manufacturers) showed less variability for the u_2 parameter. The q_t value showed a larger variability than u_2 but lower than f_s (Lindgård et al. 2018). In fact, there are more uncertainties associated to the f_s value since some of the cone types gave good repeatability for f_s readings, while some show relatively large variation.

The following observations were made at Tiller-Flotten:

- For the Robertson (1990) Q_t - B_q plot, the data sets with largest variability all fall in the same soil behaviour type “clay-sensitive” clays. This observation is valid no matter where the largest scatter is in the CPTU parameters.
- For Robertson (1990) Q_t - F_r plot, when the variability focuses in f_s , the data plots in two neighbouring areas (sensitive clay and the limit sensitive clay-clay). When the variability appears in the q_t or u_2 value, then the data plots in the same soil type, however, with a tendency to cover opposite areas in the same or neighbouring soil types.
- For Schneider et al. (2008) (Q_t - $\Delta u/\sigma_{vo}'$) chart and Senneset et al. (1989) (q_t - B_q) chart, no clear difference is observed between the data sets showing largest scatter, for q_t and u_2 parameters. The quick clay is classified as sensitive clay (1c) in Q_t - $\Delta u/\sigma_{vo}'$ plot and over the soft to very soft clay area in the q_t - B_q plot. However, the variation in f_s for Senneset et al. (1989) shows that the soil can be classified as stiff clay-silt.

3.2 Onsøy soft clay site

Seven different cone penetrometers from five manufacturers were used in the comparative testing program and

it was concluded that u_2 was the parameter that showed better repeatability, followed by q_t which generally varies somewhat more (Lunne et al. 2018). Some of the cone types give good repeatability for f_s readings, while some show relatively large variation.

When looking at the derived CPTU parameters in the soil classification charts, the following aspects are observed (see Figure 1):

- In Q_t - B_q and Q_t - F_r charts from Robertson (1990), the soil type is classified in soil types 1 and 3 (sensitive clay-clay) independently of the scatter in any of the CPTU parameters. However, for Q_t - F_r chart, when the scatter is in the u_2 and f_s parameter, the data moves also towards a soil type 2 (organic soils).
- Regarding the charts of Schneider et al. (2008) (Q_t - $\Delta u/\sigma_{vo}$) and Senneset et al. (1989) (q_t - B_q), no difference is observed between the data sets showing largest scatter, for q_t and u_2 parameters. The clay is classified as clay (1b)-sensitive clay (1c) in Q_t - $\Delta u/\sigma_{vo}$ plot and soft-very soft clay in q_t - B_q plot. However, the variation in f_s for Senneset et al. (1989) shows that the soil can be classified as fine silt-medium clay.

3.3 Halden silt site

After testing five different cone penetrometers on this site, it was concluded that u_2 and q_t showed good repeatability between the measurements, while f_s gave the largest variation (Paniagua et al. 2020).

Figure 2 presents the CPTU data sets that give the largest scatter for each of the CPTU parameters in the soil classification charts. Observations made are as follow:

- In the chart Q_t - B_q from Robertson (1990), the soil type is classified in soil types 3 and 4 (silty clay-silt mixtures) independently of the scatter in any of the measured CPTU parameters. However, for Q_t - F_r chart, when the scatter is in the f_s parameter, the data mainly plots in two different soil types (either type 3 or 4). A similar observation applies when the scatter is in the q_t parameter but does not apply when the scatter is in the u_2 parameter.
- For the other charts relating Q_t - $\Delta u/\sigma_{vo}$ (Schneider et al. 2008) and q_t - B_q (Senneset et al. 1989), no difference is observed (i.e., both CPTU data sets plot on top of each other in roughly the same soil types: silt (1a)-transitional soils (3) and silt-fine silt, respectively. An exception is observed when the scatter is in u_2 for the Schneider et al. (1998) plot, where the data sets tend to move to neighbouring soil types (one to soil type 3 and the other one to soil type 1a).

3.4 Øysand sand site

The CPTU parameters from nine cone penetrometers types tested showed results more dependent on the

varying soil conditions for the site. Quinteros et al. (2019) explained this as consequence of the depositional history of the site and the influence of the deltaic foreset beds dipping at an angle of 20-25 degrees. By adjusting the CPTU results in depth, the sand layers appeared to be more homogenous. The relative variation in q_t and u_2 was small and for all practical purposes negligible. However, sleeve friction results showed a large scatter between the different cone types. The variation in sleeve friction also seemed to increase with depth.

Comparison of CPTU data from Øysand on the soil classification charts leads to the following observations:

- In Q_t - B_q and Q_t - F_r charts from Robertson (1990), the soil type is mainly classified from soil types 4 to 7 (silt mixtures to gravelly sand) independently of the scatter in any of the measured CPTU parameters.
- A similar observation applies for the charts of Schneider et al. (2008) (Q_t - $\Delta u/\sigma_{vo}$) and Senneset et al. (1989) (q_t - B_q), where no difference is observed between the data sets showing largest scatter. The deposit is classified as transitional soils (type 3)-sands (type 2) in Q_t - $\Delta u/\sigma_{vo}$ plot and from silt to sand/hard stiff soil in the q_t - B_q plot.

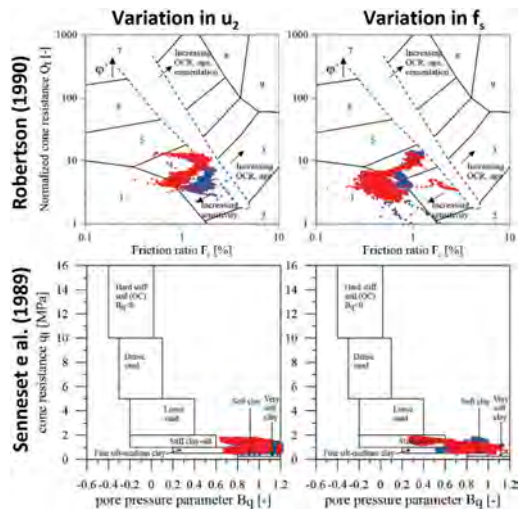


Figure 1. Two CPTU data sets from Tiller-Flotten plotted in two classification charts for two CPTU parameters showing extreme values (min-blue and max-red).

4 DISCUSSION AND CONCLUSION

Generally, previous research on NGTS sites has shown that the measured u_2 shows less variation for one cone type to another while, while q_t shows somewhat larger variation and f_s the largest variation. F_r shows much larger variation compared to B_q .

Therefore, this study has investigated the impact of using CPTU data from different cone types or manufacturers and its influence on the interpretation

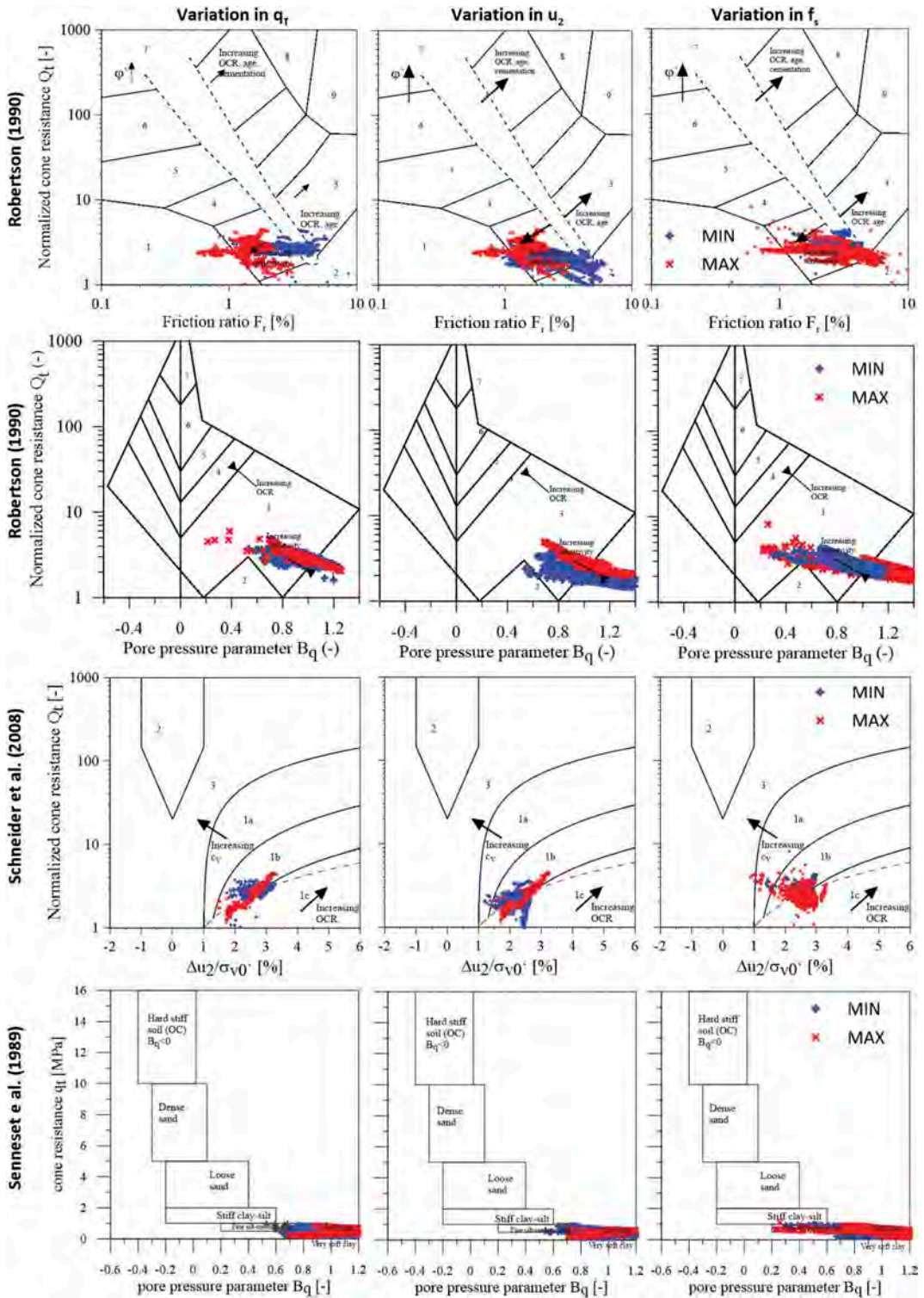


Figure 2. Two CPTU data sets from Onsoy plotted in the different classification charts for each of the CPTU parameters showing extreme values (min and max).

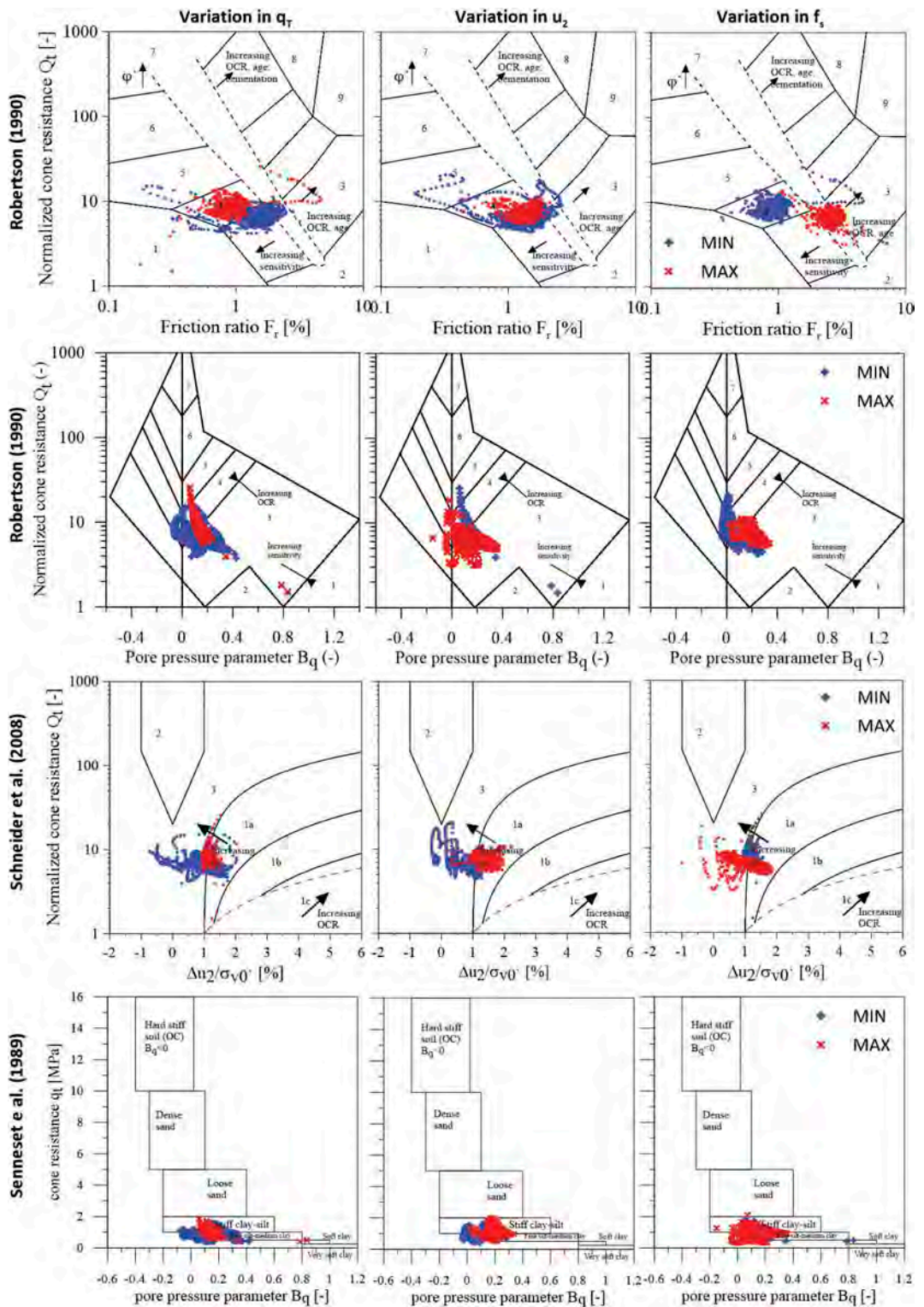


Figure 3. Two CPTU data sets from Halden plotted in the different classification charts for each of the CPTU parameters showing extreme values (min and max).

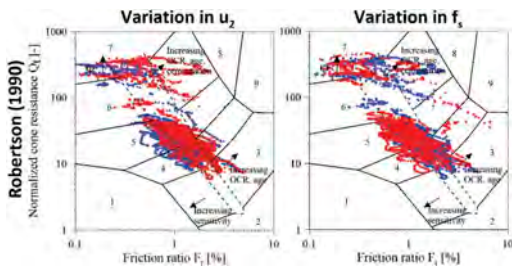


Figure 4. Two CPTU data sets from Øysand plotted in two classification charts for two CPTU parameters showing extreme values (min-blue and max-red).

of soil behavior. The most common soil classification charts have been used in four different soil types.

In general, soil behavior charts using pore pressure measurement and/or derived parameters involving u_2 seem to show less variability in soil classification between the different charts and all soil types. A similar trend is also observed for the cone resistance. In other words, the variation of u_2 and q_t between data sets for a defined soil type do not seem to give a different soil classification in the charts studied here.

The previous observation does not apply when using charts based on sleeve friction measurements. This was highlighted for the Halden silt when the classification chart involved a parameter derived from f_s . It seems that the variation in f_s for Tiller-Flotten clay and Onsøy clay does not have such a strong impact in the classification of the material using the different charts. This seems to also apply for Øysand sand, however, the observations for this site could be influenced by the natural variability of the deposit and therefore it is difficult to conclude.

Finally, due to the large uncertainties with the f_s readings, one should be careful using this parameter, and F_r , when interpreting soil parameters for design. Since the measured u_2 appear to frequently be the most reliable parameters it should be used in addition to q_t for deriving soil parameters.

ACKNOWLEDGEMENTS

-To the Research Council of Norway for funding the Norwegian GeoTest Site project (No. 245650/F50) and the master student Erika Solem for her assistance in plotting the data during the summer 2021.

REFERENCES

- Blaker Ø, Carroll R, Paniagua P, DeGroot D & L'Heureux J-S 2019 Halden research site: geotechnical characterization of a post glacial silt AIMS Geosciences 5 184–234.
- Cabal K & Robertson P 2014 Accuracy and Repeatability of CPT Sleeve Friction Measurements Proc. CPT'14 Las Vegas 271–79
- Gauer P, Lunne T, Mlynarek Z, Wolynski W & Croll M 2002 Quality of CPTu -Statistical analyses of CPTu data from Onsøy NGI Report No.: 20001099-2 Oslo
- Gundersen AS, Hansen RC, Lunne T, L'Heureux JS, Strandvik SO 2019 Characterization and engineering properties of the NGTS Onsøy soft clay site. AIMS Geosciences 5 665–703.
- ISO 2012 Geotechnical investigation and testing – Field testing – Part 1: Electrical cone and piezocone penetration tests International Standard ISO 22476-1: 2012
- L'Heureux J-S & Lunne T 2019 Characterization and Engineering properties of Natural Soils used for Geotesting AIMS Geosciences 5 940–59.
- L'Heureux JS, Lindgård A, Emdal A 2019 The Tiller-Flotten research site: Geotechnical characterization of a sensitive clay deposit. AIMS Geosciences 5 831–867
- Lindgård A, Gundersen A, Lunne T, L'Heureux J-S, Kåsin K, Haugen E, Emdal A, Carlson M, Veldhuizen A & Uruci E 2019 Effect of cone type on measured CPTU results from Tiller-Flotten quick clay site Proceedings Geoteknikkdagen 2018 Oslo 38.1–15
- Lunne T 2010 The CPT in Offshore Soil Investigation – a historic perspective Proc. CPT'10 Los Angeles 71–113.
- Lunne T, Eidsmoen T, Gillespie D & Howland J D 1986 Laboratory and field evaluation on cone penetrometers Proceedings of ASCE Specialty Conference In Situ'86: Use of In Situ Tests in Geotechnical Engineering Blacksburg ASCE 714–29
- Lunne T, Strandvik S, Kåsin K, L'Heureux J-S, Haugen E, Uruci E and Kassner M 2018 Effect of cone penetrometer type on CPTU results at a soft clay test site in Norway. Cone Penetration Testing IV: Proc CPT 2018 Delft 417–22
- NGF 2010 Guideline for execution of CPTU tests Guideline No. 5 Norwegian Geotechnical Society [in Norwegian]
- NGI 2020 Impact of cone penetrometer type on measured CPTU parameters at 4 NGTS sites: silt, soft clay, sand, and quick clay. NGI report 20160154-21-R.
- Paniagua P, Lunne T, Gundersen A., L'Heureux JS, Kåsin K 2021 CPTU results at a silt test site in Norway: effect of cone penetrometer type. in IOP Conference Series: Earth and Environmental Science. IOP Publishing,
- Powell J & Lunne T 2005 A comparison of different piezocones in UK clays Proc. 16th International Conf on Soil Mechanics and Geotechnical Engineering Osaka 729–34
- Quinteros S, Gundersen A, L'Heureux JS, Carraro A, Jardine R 2019 Øysand research site: Geotechnical characterization of deltaic sandy-silty soils. AIMS Geosciences 5 750–783.
- Robertson PK 1990 Soil classification using the cone penetration test. Canadian Geotechnical Journal, 27: 151–158.
- Schneider JA, Randolph MF, Mayne PW & Ramsey N 2008. Analysis of factors influencing soil classification using normalized piezocone tip resistance and pore pressure parameters. J. Geotech. Geoenv. Eng 134 (11) 1569–1586.
- Senneset K, Sandven R & Janbu N. 1989. Evaluation of soil parameters from piezocone tests. Transp Research Record 1235, Nat Acad Press, Washington D.C 24–37
- Tiggemann L & Beukema H 2008 Sounding Ring Investigation Proc. ISC-3 Taiwan 757–62

Evaluation of shear wave velocity profiles in alluvial and deltaic soils using a CPT database

J. Paredes & F. Illingworth

Subterra, Ecuador

ABSTRACT: A seismic piezocone SCPTu database from Guayaquil (EC), consisting of Holocene alluvial and estuarine deltaic soil deposits, is evaluated in this document through V_s mapping when comparing more than 600 CPTu profiles and 45 seismic downhole testing locations. Shear wave velocity downhole measurements were used to adjust CPT-based V_s estimates and compared with cone resistance values. A suitable fit is observed between Robertson (2009a) calculation and downhole measurements, but it tends to over-estimate by 20-30% in soft clayey soils. An age correction factor as a function of normalized s_u/σ'_v ratio has been determined for clayey soils while a V_s - q_t correlation is provided for clays and all soils. A V_{s30} map has been developed based on proposed shear-wave velocity calibration.

1 INTRODUCTION

The alluvial plain and estuarine deltaic deposit of Guayaquil, located on the Ecuadorian coast, correspond geologically to the Holocene age. The stratigraphy usually includes layers of soft to firm clayey soils interbedded with loose sands susceptible to liquefaction in the top 30 meters. It is common to find organic soil, peat and sensitive clay in the estuarine deltaic area. Neighboring the city, stands the Chongón-Colonche Mountain Range that favors the existence of colluvial soils in the north and west area, so there are also soil profiles with high impedance contrast.

In most of these special cases of geotechnical behavior, local standards recommend site-specific response analysis (SRA), where measurement of shear-wave velocity (V_s) profiles results relevant. In addition, V_{s30} criterion is used for site seismic classification, thus V_s profile constitutes an important input for most Guayaquil construction projects.

In 2014, Vera presented a detailed geotechnical characterization of the Guayaquil soils, studying their static and dynamic response. In that research, a geotechnical zoning map was implemented, in which estuarine deltaic geotechnical zones and alluvial zones were identified, according to the geological context and the geotechnical framework. The database used in that study, includes mainly geotechnical information from boreholes, laboratory tests, geophysics estimates and CPT measurements in at least 14 sites locations. The applied methodology was plausible, because until recent, the common practice in Guayaquil for geotechnical research consisted mainly of boreholes, and for measuring V_s , the usual

practice was to execute geophysical exploration (e.g., multichannel analysis of surface wave and microtremors array measurement). However, SCPTu has also been performed in the last few years, thus, it is convenient to analyze an updated database that includes these CPTs and downhole measurements.

Therefore, this paper synthesizes an existing Guayaquil metro area soundings database with emphasis on CPT and downhole tests, carried out in an effective area of 450 km². By comparing existing CPT-based V_s estimates with downhole measurements or correlating cone tip resistance with shear-wave velocity, it is possible to develop equations that allow estimating V_s values more accurately than with conventional estimations, while capturing local behavior of Guayaquil alluvial and estuarine deltaic soil deposits. This analysis is appropriate because in geotechnical research of unconventional soils, it is always advisable to calibrate the geotechnical parameters estimated from the CPT, with measurements obtained in other in situ and laboratory tests (Mayne, 2007b; Robertson, 2012).

Therefore, this paper proposes analyze: 1) a correlation between downhole V_s measured values and those estimated according to Robertson (2009a), as a function of normalized undrained shear strength (s_u ratio), 2) a V_s - q_t correlation for clays and 3) a simplified geotechnical zoning of Guayaquil and the surrounding area through V_{s30} using V_s calibrated values.

This research goes in the same line of the theoretical framework proposed by Andrus et al. (2007), where an age correction factor was encountered. Besides, follows the sense of previous investigations, in which correlations have proposed between CPT measurements and V_s in different types of soils

(Robertson & Campanella, 1983; Baldi et al., 1989; Mayne & Rix, 1995; Hegazy & Mayne, 1995; Robertson, 2009a).

With the obtained results, it will be possible to have a more accurate and cost-efficient tool for seismic classification and site response analysis, than traditional geophysical methods.

2 DATABASE CHARACTERISTICS

All CPTu soundings conducted by Subterra between 2012 and 2020 were registered into an ArcGIS map. For each test, the following characteristics were noted: coordinates, year, total depth, rigid stratum depth, among others. Then, soundings from several geotechnical companies were compiled and a geotechnical exploration campaign was implemented based exclusively on CPTu tests distributed in different sectors of Guayaquil, especially towards the northeast and south of the city, where information available was scarce at the moment.

The total database consisted of 1432 soundings which includes 615 (42.9%) CPTs and 817 (57.1%) boreholes. From the 615 CPTs, 38 were exclusively carried out for this study. Downhole V_s profiles have been measured in 45 CPTs (SCPTu) at 36 different sites, as illustrated in Figure 1. Regarding timeline, 77% of the soundings were carried out after year 2010, while 91% after year 2000. Explored depths range between 2.3 m (shallow rock) and 145.2 m (avg. =

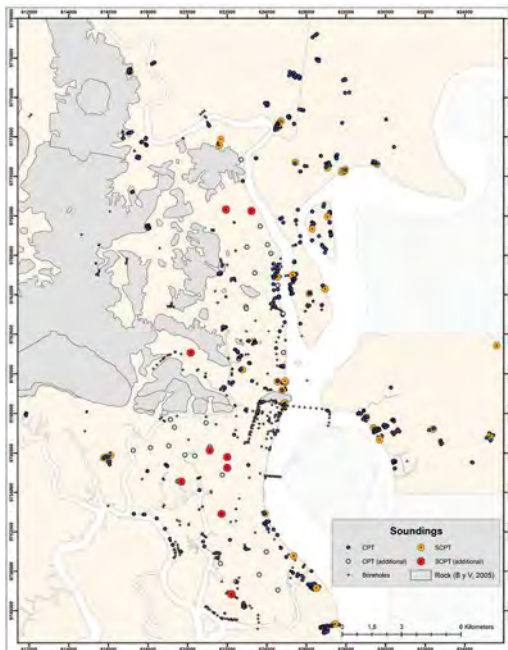


Figure 1. Guayaquil database sounding locations. Rock outcrop (Benítez & Vera, 2006).

27.7 m and $\sigma = 12.0$ m). In addition, 63% of soundings have a depth greater than 24 m, while 83% have a depth greater than 16.5 m.

Geotechnical zoning has been evaluated considering several geotechnical parameters from such database (e.g., average I_c and undrained shear strength every 5 meters, liquefaction potential), in order to have a complete and true understanding of Guayaquil soils. The work of Paredes (2020) can be reviewed for a thorough analysis of Guayaquil geotechnical zoning.

Considering only the 615 CPTs, average total depth is 23.5 m, with a standard deviation of 8.2 m (95% of CPTs underwent refusal conditions). The rigid stratum has been detected at an average depth of 22 m.

3 SHEAR-WAVE VELOCITY EVALUATION

In situ testing was executed with a standard 10 cm² cone, compression type, and 150 cm² sleeve friction. The pore pressure filter (u_2 position) is made out of bronze, and saturated with silicone oil. The piezocone is pushed at 2 cm/s with a 15-ton Pagani TG-63 equipment recording measurements every cm. A seismic module with two triaxial series of geophones is adapted behind the cone for recording shear-wave time arrival every meter.

An initial database filter of shear-wave measurements was applied to discard signals with poor amplitude or profiles located in unfavorable testing conditions like partially flooded ground surface, where contact area between seismic source and ground surface deemed inappropriate for obtaining a clear V_s profile. Thus, 733 downhole seismic readings between 2 and 25 m deep were compiled for this study. Shear-wave velocity values ranged between 50 and 390 m/s (avg. 120 m/s).

3.1 Calibration factor

Seismic CPT has been performed in Guayaquil and the surrounding area since 2014 and it was notable throughout the years that Robertson (2009a) V_s estimate, which is based on vast experience of normalized SBTn chart considering uncemented Holocene and Pleistocene-age soils, tends to over-estimate shear-wave velocity by 20-30% in soft clayey soils, both in estuarine and alluvial zones. However, a good overall trend in the soil profile was always observed if a correction factor was applied to the estimate. As an example, Figure 2a to Figure 2c illustrate several V_s downhole profiles (red dots) and corresponding CPT-based V_s .

There appears to be some scattering when analyzing CPT- V_s pairs, primarily due to the difference between depth interval measurements where readings are taken (e.g., 1 cm for CPT and 1 m for V_s). Thus, data has been filtered based on standard deviation of CPT index I_c (σ_{I_c}), limiting random variability. Also, shallow downhole readings may lack some quality at times due to short time arrivals and thus,

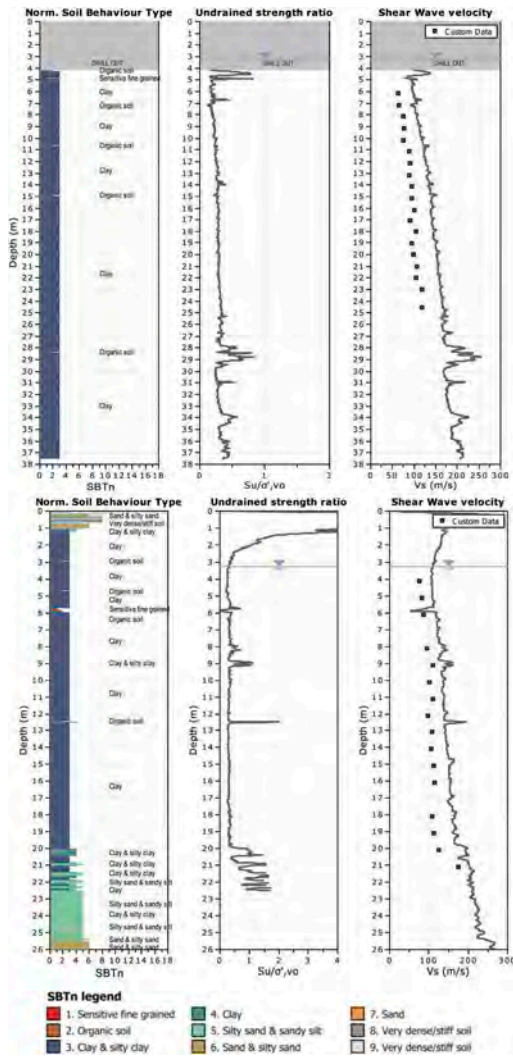


Figure 2a. SBTn (Robertson), s_{u-rat} , V_s downhole and estimated profiles, from two Guayaquil soundings located in estuarine zone.

greater percentage errors. Reason why only data pairs at depths greater than 5 m have been considered in every filtered trend analysis presented in this paper.

A calibration coefficient was calculated for each one-meter avg. CPT-based V_s and downhole V_s measurement. Given a strong relation was initially observed with estimated normalized shear strength ratio ($s_{u-rat} = s_u/\sigma'_{vo}$), measurements were filtered by $\sigma_{ic} < 0.10$, $I_c > 2.6$ and $s_{u-rat} < 2$, the latter two corresponding to clayey soils. Undrained shear strength was calculated from F_r -based N_{kt} factor (Robertson 2012).

Figure 3 shows a simplified regression analysis performed on 324 pairs to calculate correction factor (μ_{vs}) in clays and transitional soils given by:

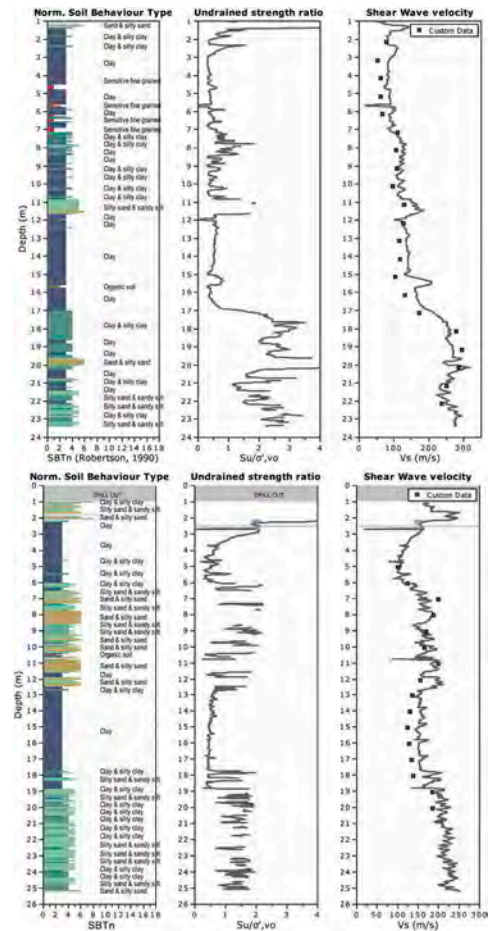


Figure 2b. SBTn (Robertson), s_{u-rat} and V_s profiles, in alluvial zone of Samborondón and Guayaquil.

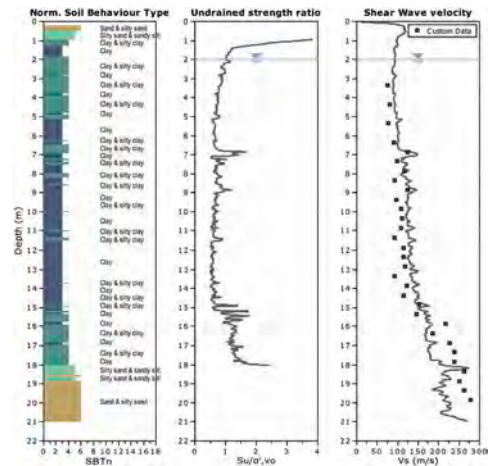


Figure 2c. SBTn (Robertson), s_{u-rat} , V_s downhole and estimated profile, from Durán sounding.

$$\mu_{vs} = \frac{V_{s\text{-measured}}}{V_{s\text{-Robertson}}} = 0.38 \left(s_u / \sigma'_v \right) + 0.60 \quad (1)$$

For sandy soils with $I_c < 2.6$, μ_{vs} ranged between 0.8 and 1.2, with an average value of 0.98. More research is necessary in order to evaluate an accurate calibration factor in these soils. Thus, shown database correction from Figure 3 does not apply for sandy soils.

Robertson (2009a) database included Holocene and Pleistocene soils while 25% higher estimates have been reported for Pleistocene soils. Andrus et al., (2007) even proposed a correction factor as function of deposit age. Therefore, it would be reasonable for Guayaquil soils deposits, where shallow layers date mainly from the Holocene, that estimated values are slightly higher than those measured. However, for deeper soil layers with a higher degree of consolidation (older soils with signs of cementation), Robertson's estimate fits better, and in some cases an underestimation is also observed. This apparent underestimation could be related to cementation that tends to increase V_s (Schneider, et al 2004), while resistance to penetration captures to a lesser extent the effects of age and cementation (Robertson, 2012). The correction factor applies best for a ratio s_u/σ'_v between 0.2 and 1.5, yielding a coefficient that varies between 0.6 and 1.18.

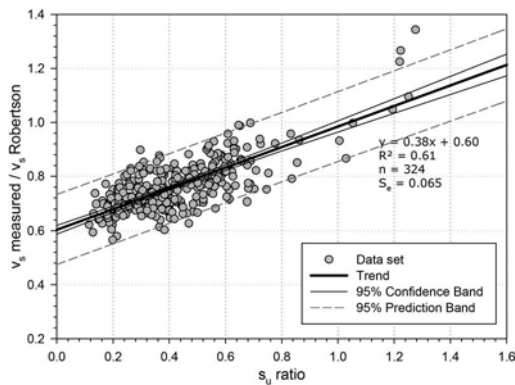


Figure 3. V_s calibration factor as a function of normalized $s_u/\sigma'_v < 2$ ($I_c > 2.6$, $\sigma_{1c} < 0.10$).

3.2 V_s - q_t regression

Two statistical regression analyzes were performed to further evaluate the existing database: one with 733 CPT- V_s pairs (all data) including different geo-materials, and another with 388 resulting from filtering by $I_c > 2.6$ and $q_t < 8$ MPa with low heterogeneity average intervals ($\sigma_{1c} < 0.15$), at depths greater than 5 m. The observed trend between V_s and q_t for Guayaquil is presented in Figure 4.

As expected, a higher R^2 value is obtained from filtered data by avoiding values with considerable lenses across one-meter intervals. Guayaquil clay

deposits are generally homogeneous compared to sandy layers which are rather intercalated throughout the profile, being apparent a better trend when filtering for $I_c > 2.6$. Considering both datasets, a general V_s - q_t trend is proposed in the following expression:

$$V_s = a(q_t)^b \quad (2)$$

where, cone resistance q_t is in MPa, V_s in m/s and regression variables are

$$\text{clay: } a = 117.67, b = 0.49 \quad (n = 388, R^2 = 0.85)$$

$$\text{alldata: } a = 112.82, b = 0.35 \quad (n = 733, R^2 = 0.75)$$

A similar equation has been presented by Mayne and Rix (1995) from 31 natural clay sites. Clays varied from intact to fissured materials with wide ranges of plasticity, sensitivity and OCR. Variables provided in this paper, corresponding to Equation (2) are $a = 133.06$, $b = 0.63$.

The filtered proposed V_s - q_t correlation shows an excellent correspondence in clays, especially for $q_t < 2$ MPa. When including all data, at $q_t > 2$ MPa, V_s - q_t trend is much lower than that filtered.

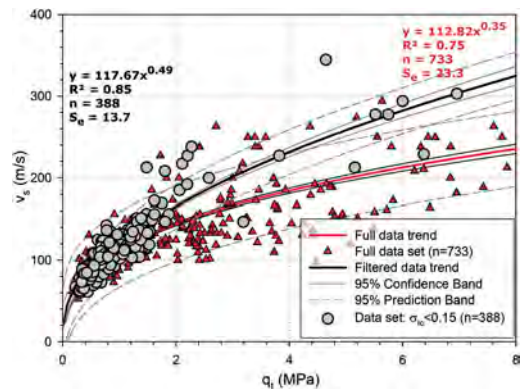


Figure 4. Correlation between shear-wave velocity and cone tip resistance in Guayaquil.

3.3 V_{s30} mapping

On an effort to consolidate previous findings, a V_{s30} map has been developed for Guayaquil based on 615 CPTs. It is plausible to apply Equation (2) for clay in soft homogeneous clayey soils with $I_c > 2.4$ and $q_t < 2$ MPa, while correction factor from Equation (1), limited by 1.18, for the rest of clayey soils with $I_c > 2.4$.

With regards to V_s values for sandy material, since the database is relatively limited, it would seem appropriate to, conservatively, correct Robertson (2009a) equation by a coefficient μ_{vs} of 0.85 for

contractive shallow sands and 0.95 for dilating sands, although the latter could certainly be 20% higher. Yet a correction value of 0.90 for sandy material $I_c < 2.4$ was employed. Figure 5 shows Guayaquil V_{s30} map by applying iterative finite difference interpolation methodology in ArcGIS.

Given that 25% and 66% of CPTs underwent refusal conditions at more than 30 and 20 meters deep, respectively, V_s estimate was extrapolated from those estimated in deepest layers, provided that refusal conditions were effectively present. So, V_{s30} values are rather conservative in these cases.

4 CONCLUSIONS

The presence of geotechnical profiles with special characteristics is very common in the alluvial plain and estuarine deltaic deposit of Guayaquil. For a better understanding of the variation of geotechnical parameters, a database has been compiled with geotechnical information obtained in recent years, consisting of 1432 soundings, with an average depth of 27.7 m. This database has 615 CPTs, from which 45 V_s downhole profile have been obtained while the relationship with CPT has been analyzed, in order to consolidate results through a map of V_{s30} , and for its extended use in the construction projects of the city.

A V_s correction factor for calibrating Robertson (2009a) estimate has been obtained through a direct proportionality with s_u ratio in soils with index I_c (SBTn) > 2.4 . The proposed correction ranges between 0.6 and 1.18, for s_u ratio < 1.5 . Furthermore, a V_s - q_t

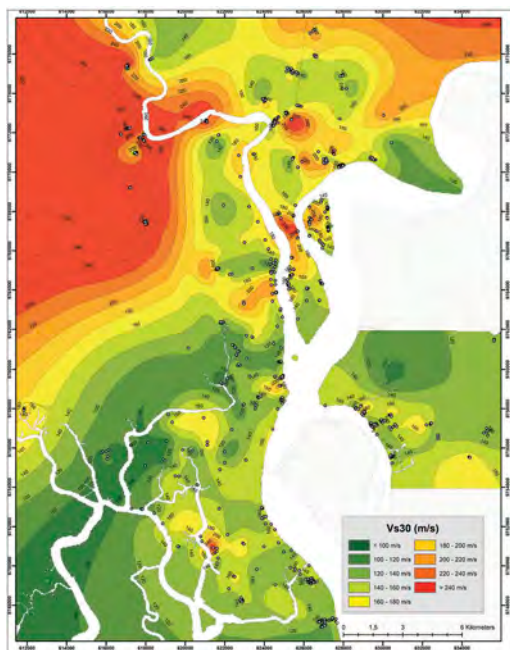


Figure 5. Guayaquil V_{s30} Map.

correlation is proposed for Guayaquil soft homogeneous clays with $q_t < 2$ MPa.

In Guayaquil, local standards require SRA in most projects where soil profiles with special features are encountered. One of the most important input parameters in this type of analysis is V_s profile. Traditionally, geophysics is used to determine this seismic parameter. However, the accumulated experience and proposed equations will allow using a more efficient and accurate methodology when downhole testing or geophysical methods are not available.

REFERENCES

- Andrus, R., Mohanan, N., Piratheepan, P., Ellis, B., & Holzer, T. (2007). (s.f.). Predicting shear-wave velocity from cone penetration resistance. *Proceedings of Fourth International Conference on Earthquake Geotechnical Engineering*. Thessaloniki, Greece, 25–28, June 2007. Paper No. 1454.
- Baldi, G., Bellotti, R., Ghionna, V., Jamiolkowski, M. & Lo Presti, D. (1989). Modulus of sands from CPTs and DMTs, *Proc. 12th International Conference on Soil Mechanics and Foundation Engineering, Vol. 1*, 165–170.
- Benítez, S., & Vera, X. (2006). *Estudio Geológico de la ciudad de la ciudad de Guayaquil. Informe final de Investigación y Estudio del comportamiento dinámico del subsuelo*. IIFIUC, Universidad Católica Santiago de Guayaquil.
- Hegazy, Y. & Mayne, P. (1995). Statistical correlations between V_s and cone penetration data for different soil types, *Proc., International Symposium on Cone Penetration Testing, CPT '95*, Linköping, Sweden, 2, Swedish Geotechnical Society, 173–178.
- Mayne, P., & Rix, G. (1995). Correlations Between Shear Wave Velocity and Cone Tip Resistance in Clays. *Soils & Foundations Vol. 35, No. 2*, 107–110.
- Mayne, P. (2007b). Invited Overview Paper: In-situ test calibrations for evaluating soil parameters, *Characterization & Engineering Properties of Natural Soils, Vol. 3* (Proc. IS-Singapore), Taylor & Francis Group, London: 1602–1652.
- Paredes, J. (2020). Evaluación de parámetros geotécnicos de los depósitos de suelos ubicados en la llanura aluvial y en el complejo deltaico estuarino de Guayaquil. *Master's Thesis. Escuela Superior Politécnica del Litoral (ESPOL)*, Guayaquil, Ecuador.
- Robertson, P., & Campanella, R. (1983). Interpretation of Cone Penetration Tests. Part I: sand, *Canadian Geotechnical Journal*, 20(4), 477–486.
- Robertson, P. (2009a). Interpretation of cone penetration tests – a unified approach. *Canadian Geotechnical Journal* 46, 1337–1355.
- Robertson, P. (2012). Interpretation of in situ tests - some insights. *J.K. Mitchell lecture, Proceedings of ISC'4*, (pp. 3–24). Recife, Brazil.
- Schneider, J., McGillivray, A., & Mayne, P. (2004). Evaluation of SCPTu intra-correlations at sand sites in the Lower Mississippi River valley, USA, *Geotechnical & Geophysical Site Characterization, Vol. 1*, (Proc. ISC-2, Porto), Millpress, Rotterdam, 1003–1010.
- Vera, X. (2014). Seismic Response of a Soft, High Plasticity, Diatomaceous Naturally Cemented Clay Deposit. *Doctoral Thesis. University of California, Berkeley*.

Upscaling 1 500 000 synthetic CPTs to voxel CPT models of offshore sites

J. Peuchen & W. van Kesteren
Fugro, Nootdorp, The Netherlands

V. Vandeweyer & S. Carpentier
TNO, Utrecht, The Netherlands

F. van Erp
RVO – Netherlands Enterprise Agency, Utrecht, The Netherlands

ABSTRACT: In 2020, the Dutch government published 1 500 000 synthetic CPT profiles for use in development of the Hollandse Kust (west) Wind Farm Zone, offshore Netherlands. The scale of this approach was novel at that time and possibly first-ever. The synthetic CPT profiles were derived from a training data set of 122 actual CPTs and ultra-high-resolution (UHR) seismic reflection traces, using machine learning by a convolutional neural network. The synthetic CPT profiles were limited to positions along the 162 UHR survey track lines (2D) and were limited to cone resistance to a depth of 50 m below seafloor. The UHR track lines were spaced at about 400 m. This paper explores upscaling the synthetic CPT approach to voxel (3D) models and adding (S)CPT-based parameters such as shear modulus at small strain G_{max} . Future added-value is expected from post-2020 improvements seen in seismic reflection data resolution, attribute extraction and neural network architecture.

1 INTRODUCTION

Reducing ground risk is important for the development of an offshore wind farm. This requires understanding of the geological and geotechnical conditions to depths in the order of 30 m to 100 m below seafloor (BSF), depending of type of support structure for the wind turbines.

The understanding of ground risk is typically expressed by a ground model or multiple ground models (ISO 2021). These models typically rely on integrated interpretation of geological information, geophysical (UHR and UUHR multichannel seismic reflection) data and geotechnical data (particularly cone penetration tests, CPTs).

Since the 1990's, there has been increasing focus on deriving geotechnical properties directly from geophysical data using methodologies developed in the oil and gas industry (e.g. Nauroy et al. 1998). More recently, trials were made with synthetic CPTs and geotechnical properties generated by interpolating CPT data between investigated locations (Forsberg et al., 2017) and using statistical methods and multi-attribute regression through an artificial neural network (Sauvin et al. 2019). The general approach is covered by ISO 19901-10 Marine Geophysical Investigations (ISO 2021).

This paper describes the status quo for 2020 and explores future opportunities for upscaling the

synthetic CPT approach. The status quo is presented by an example in the public domain (www.offshorewind.nl): the Hollandse Kust (west) Wind Farm Zone, HKW WFZ (Figure 1), offshore Netherlands (Fugro 2020a and 2020b). HKW WFZ data acquisition, data analysis and advice were largely completed in 2019 and 2020. The 1 500 000 synthetic CPT profiles were generated at no schedule impact. DNV GL (2020) sees this cutting edge development as '*a huge step forward in terms of project area overview with respect to geotechnical site conditions and also as a valuable tool to improve and understand the correlation between future geological, geophysical and geotechnical investigations.*'

2 HOLLANDSE KUST (WEST) WIND FARM ZONE

The site for the HKW WFZ is located approximately 53 km from the Dutch coast, covering an area of roughly 176 km² in water depths ranging from 18 m to 36 m LAT.

Ground model input mainly included:

- Geological information;
- Geophysical data: multibeam echosounder, side scan sonar, magnetometer, sub-bottom profiler and 2D-UHR single channel and multi-channel



Figure 1. Location of the future Hollandse Kust (west) Wind Farm Zone.

- seismic reflection data. The data were acquired according to a draft version of ISO (2021);
- Geotechnical data acquired from 57 boreholes with sampling and cone penetration testing (CPT) to a maximum depth of 90 m below seafloor (BSF), 122 seafloor CPTs to a maximum depth of 56 m BSF, 30 seafloor seismic cone penetration test to maximum depth of 56 m BSF, and laboratory testing. The data were acquired according to ISO (2014).

The acquired geophysical and geotechnical data were integrated into a traditional quasi-3D ground model, with seismic reflections tied to geotechnical boundaries derived from seafloor CPT and borehole information (Figure 2). The ground model comprised eight geological soil units, each having a distinct seismic character and spatial distribution.

Figure 2 provides cross sections that illustrate how the traditional ground model was enhanced by 1 500 000 synthetic CPT (cone resistance) profiles and associated error predictions to 50 m below seafloor (Carpentier et al. 2021). The presented cross section has a length of 11 500 m with 4 actual CPTs and about 9000 synthetic CPTs to a depth of 50 m.

The HKW WFZ synthetic CPT profiles were derived from a training data set of 122 actual CPTs and ultra-high-resolution seismic reflection traces, using machine learning by a convolutional neural network. The synthetic CPT profiles were limited to positions along the 162 UHR survey track lines (2D). The UHR track lines were spaced at about 400 m.

Figure 3 shows example checks on predictions. In general, the predicted and measured net cone resistance values showed reasonably good agreement, particularly in the upper 20 m BSF. Below 20 m, prediction was more trend-type. In addition, a trend-type prediction also applies to transitional and strongly layered (<1 metre scale) soil. It can be concluded that the prediction quality for the synthetic CPTs is such that added value can be derived to enhance the general ground model. The HKW WFZ prediction quality is inadequate for geotechnical design.

Reasons for the observed trend-type predictions include data conditioning, resolution of 2D-UHR seismic reflection data and limitations in refinement of the interpreted geological units. Data conditioning was applied by down sampling the CPT data to align

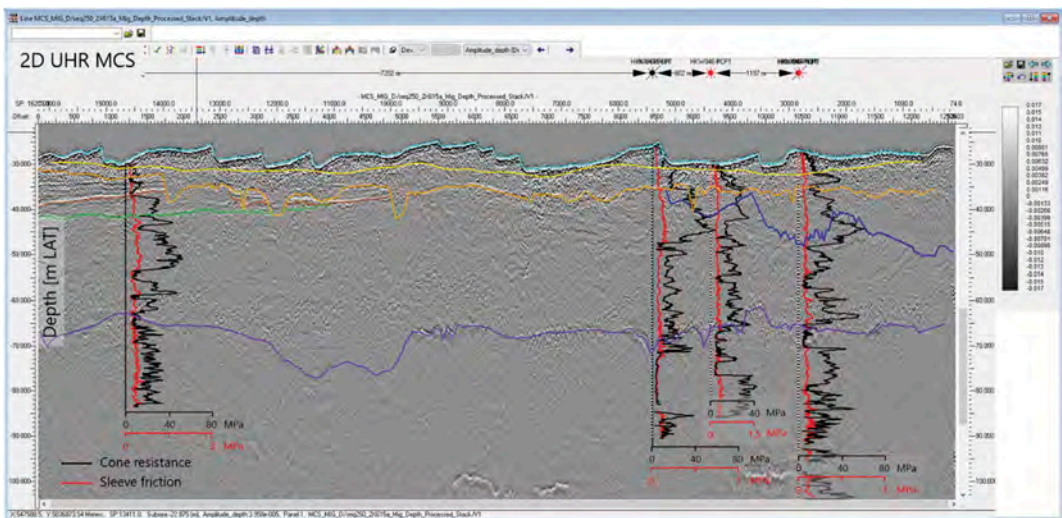


Figure 2a. Example of integrated interpretation of 2D-UHR multi-channel seismic line, aligning geophysical horizon interpretation to identified geotechnical boundaries from seafloor CPT and borehole data.

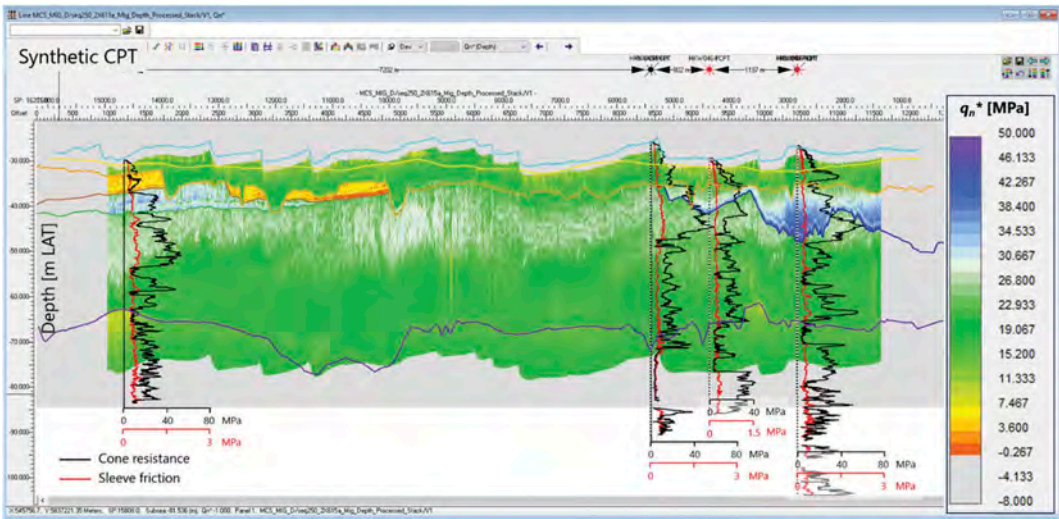


Figure 2b. Predictions of cone resistance (q_n^*) from 2D-UHR seismic (colors ranging from orange to purple) plotted together with measured cone resistance (black traces) and sleeve friction (red traces). See Figure 2a for comparison.

with vertical resolution of the 2D-UHR seismic data (i.e. sample rate of 0.1 m for prediction input versus 0.02 m as measured). Down sampling reduces net cone resistance effects of soil layering. The resolution of the 2D-UHR seismic data decreases with depth. This also affects the ability to identify additional geological units. This effect becomes more pronounced below approximately 20 m BSF.

As expected, training of the convolutional neural network showed decreasing prediction accuracy with increasing lateral distance between the seafloor CPT location and the nearest seismic trace along the 2D-UHR line. This is particularly significant where the correlation distance for spatial soil variability is less than the distance between the seafloor CPT location seismic trace selected for training.

Figures 3 and 4 illustrate prediction quality by means of a quality indicator per geological unit. It can be seen that the lower limits of the quality indicator can provide statistical values for q_n^* that fall outside credible ranges for these specific soils.

3 UPSCALING

3.1 Opportunities for future added value

The following opportunities for upscaling are discussed:

- Enhanced geophysical interpretation
- Improved data pairing for training
- Impact of technology developments
- Predictions for multiple parameters
- Voxel model by geo-statistics
- Voxel model by 3D geophysics

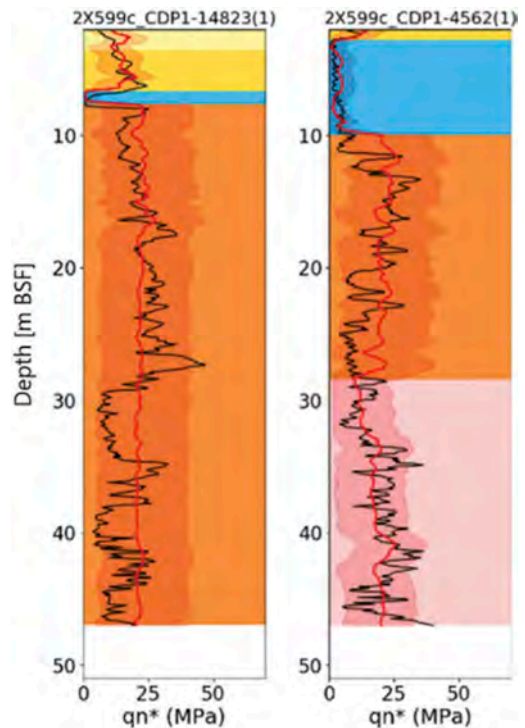


Figure 3. Comparison of actual net cone resistance (black line) versus synthetic net cone resistance (red line). The red halo represents the interval in which predictions are likely to fall (5th and 95th percentiles of the error misfit). Other colour infills indicate geological units.

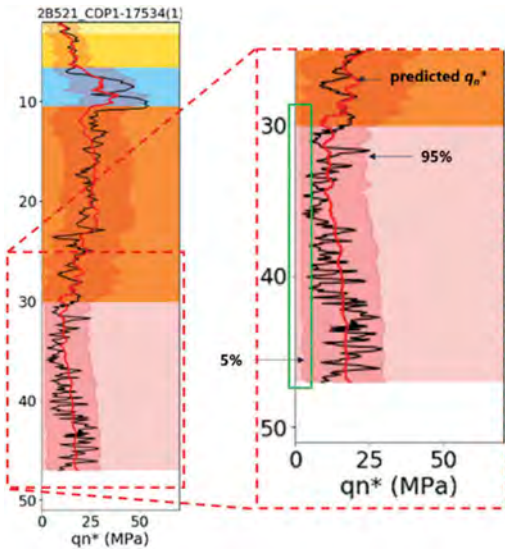


Figure 4. Statistical values for q_n^{**} that fall outside credible ranges (green box).

The opportunities can be considered individually. However, combinations are expected to lead to a step change in added value.

The following sections discuss potential opportunities for a time window of 2020 to 2025.

3.2 Enhanced geophysical interpretation

Figure 2b indicates that the synthetic CPTs can allow for further refinement of the geological model. This, in turn, helps steering future, turbine-specific geotechnical data acquisition, increasing safety and cost-efficiency.

For example, light green colours can be seen between approximately 40 m and 50 m LAT. These strength insights (i.e. trends in net cone resistance) may justify refining the geological model at this depth, by assigning a new geological soil unit to encompass these geotechnical conditions. It should be noted that this potential additional geological soil unit could not be identified from ‘regular’ seismic data (e.g. seismic amplitudes) alone. The example also indicates that synthetic CPT results (1) can give further insight into potential soil heterogeneity, (2) may aid in identifying areas of higher geotechnical uncertainty and (3) can identify where geotechnical conditions deviate from regional trends.

3.3 Improved data pairing for training

Quality of input data is important for success of machine learning.

Attention should be given to accuracy of spatial positions of paired data derived for actual CPT locations and seismic reflection data points: the

closer the better. Particularly, logging of spatial trajectories of deep CPTs should be considered, compared to conventional assumptions for a vertical CPT. Seismic reflection survey should consider specific positioning of the source(s) and specific positioning of multiple points along the streamer(s). This is particularly important for situations where correlation distance for soil spatial variability is limited.

Mitigation options for pairing of spatially distant data can include point-specific matching checks and adjustments, using marker points in the profiles.

3.4 Impact of technology developments

For marine geophysics, significant technology developments are taking place, with high potential for added value in de-risking for ground conditions. For geophysical data acquisition, these include improvements in acoustic sources and streamer control. For processing methodology, notable improvements include de-ghosting algorithms, multiple removal algorithms and velocity models). These improvements will result in opportunities for very high resolution data and high quality seismic attributes.

Fast developments are taking place in neural network architecture. Technology developments for marine soil investigation (CPTs, other in situ testing and laboratory testing) are expected to be ‘incremental’, i.e. at a slow pace compared to marine geophysics and neural network architecture.

3.5 Predictions for multiple parameters

The HKW WFZ choice for synthetic profiles for cone resistance is obvious: input cone resistance data are accurate (Peuchen & Terwindt 2015) and typically show good correlation with geological units and other geotechnical parameters. Shear modulus at small strain G_{max} is another candidate for synthetic predictions. Comments for G_{max} are as follows:

- G_{max} is an important parameter for geotechnical design of monopiles used for support of offshore wind turbines;
- G_{max} is a low-strain soil parameter. Seismic reflection data are also low-strain and good predictive capability would seem obvious;
- Good predictive capability may be impeded by higher uncertainties (compared to CPT cone resistance) for actual G_{max} profiles (Parasie et al. 2022) required for training a neural network. Actual G_{max} values are typically derived from seismic cone penetration tests. These tests rely on time and distance measurements. Data processing requires estimates of input soil density. Premises include theories on acoustic wave propagation and assumptions about heterogeneous soil behaviour as an isotropic elastic medium.

3.6 Voxel model by geo-statistics

Commonly (2022), visualisation of a ground model is by means of 2D cross sections and 2D charts, i.e. in pixels. In some cases, 3D visualisation (e.g. Figure 5) is implemented, allowing interpretation in terms of voxels. Voxel data are typically generated by geo-statistics on a soil-unit basis. Synthetic CPTs can enhance this approach.

An important consideration is the volume of data. Can the information be made available within tight schedules required for energy transition? Can it be easily assessed for decision making?

3.7 Voxel model by 3D geophysics

ISO 19901-10 Marine Geophysical Investigations (ISO, 2021) covers acquisition of 3D UHR seismic reflection data. Currently (2022), acquisition of these data in the foundation zone (upper 100 m BSF) is performed only for occasional offshore wind sites, with some indications of growth in applications of this technology. The availability of 3D UHR seismic reflection data in combination with generation of synthetic geotechnical parameters has the potential for a step-change in voxel ground models and associated added value to offshore developments.

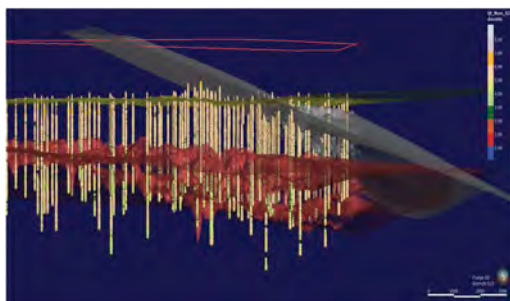


Figure 5. Excerpt of 3D HKW WFZ model in Leapfrog (Seequent, 2021) software.

ACKNOWLEDGEMENTS

We acknowledge the valuable assistance of and fruitful discussions with the Netherlands Enterprise Agency (RVO) during the HKW WFZ project. The primary data used and presented in this paper can be retrieved through www.offshorewind.rvo.nl.

REFERENCES

Carpentier, S., Peuchen, J., Paap, B., Boullenger, B., Meijninger, B., Vandeweyer, V., Van Kesteren, W. & Van Erp, F. (2021). Generating synthetic CPTs from

marine seismic reflection data using a neural network approach. In *Second EAGE Workshop on Machine Learning*, 8-9 March 2021.

DNV GL (2020). Hollandse Kust (west) Wind Farm Zone, Review of Geotechnical Report, Synthetic CPT Profiles (Document No. CR-SC-DNVGL-SE-0190-05500-0 Synthetic CPT Profiles Rev.0, date 6 November 2020 to Rijksdienst voor Ondernemend Nederland).

Forsberg, C.F., Lunne, T., Vanneste, M., James, L., Tjelta, T.I., Barwise, A., Duffy, C. (2017) Synthetic CPTs from Intelligent Ground Models based on the Integration of Geology, Geotechnics and Geophysics as a Tool for Conceptual Foundation Design and Soil Investigation Planning. *Offshore Site Investigation and Geotechnics 2017 conference proceedings – smarter solutions for future offshore developments*, London, UK, 12-14 September 2017 (Volume 1, pp. 1254–1259). Society of Underwater Technology.

Fugro. (2020a). Geological Ground Model – Hollandse Kust (west) Wind Farm Zone – Dutch Sector North Sea (Document No. P904711/06, issue 3, dated 12 May 2020 to Rijksdienst voor Ondernemend Nederland).

Fugro (2020b). Geotechnical Report – Synthetic CPT profiles - Hollandse Kust (west) Wind Farm Zone – Dutch Sector North Sea (Document No. P904711/08, issue 3, dated 14 October 2020 to Rijksdienst voor Ondernemend Nederland).

International Organization for Standardization. (2014). *Petroleum and natural gas industries – specific requirements for offshore structures – part 8: marine soil investigations*. (ISO 19901-8:2014). <https://www.iso.org/standard/61145.html>.

International Organization for Standardization. (2021). *Petroleum and natural gas industries - specific requirements for offshore structures – part 10: marine geophysical investigations*. (ISO 19901-10:2021). <https://www.iso.org/standard/77017.html>.

Leapfrog. (2021). [Software]. Seequent. <https://seequent.com/products-solutions/leapfrog-geo/>.

Nauroy, J.F., Colliat, J.L., Puech, A., Kervadec, J.P. and Meunier, J. (1998). GEOSIS: integrated approach of geotechnical and seismic data for offshore site investigations. In P.K. Robertson & P.W. Mayne (eds.). *Geotechnical site characterization: proceedings of the first international conference on site characterization – ISC'98, Atlanta, Georgia, USA, 19-22 April 1998* (Vol.1, pp. 497–502). Balkema.

Parasie, N., Franken, T and Peuchen J. (2022). Assessment of seismic cone penetration testing for small strain modulus. In *5th International Symposium on Cone Penetration Testing, CPT '22, Bologna, Italy, 8-10 June 2022*.

Peuchen, J. and Terwindt, J. (2015). Measurement uncertainty of offshore Cone Penetration Tests. In Meyer, V. (ed.) *Frontiers in Offshore Geotechnics III: proceedings of the Third International Symposium on Frontiers in Offshore Geotechnics (ISFOG 2015), Oslo, Norway, 10-12 June 2015*. Boca Raton: CRC Press, pp. 1209–1214.

Sauvin, G., Vanneste, M., Vardy, M.E., Klinkvort, R.T. and Forsberg, C.F. (2019). Machine Learning and Quantitative Ground Models for Improving Offshore Wind Site Characterization. *Offshore Technology Conference, Houston, USA, 6-9 May 2019, OTC Paper 29351*.

Automated CPT interpretation with a Convolutional Neural Network

M. Pippi, R. Vink & J. Haasnoot

CEMS Crux Engineering MicroServices BV, Amsterdam, The Netherlands

S. Bersan

CRUX Engineering, Amsterdam, The Netherlands

ABSTRACT: Cone Penetration Tests are widely used in the Netherlands, due to their ease of execution in the Dutch delta deposits and their relatively low cost. As the amount of performed CPTs increases, an automated soil interpretation becomes more and more relevant. Attempts to automate soil classification have been done in the past, but the empirical formulas commonly used do not always provide a satisfactory interpretation for engineering purposes. Besides that the soil type is often not interpreted correctly, there is also the problem that the classification is provided for each measurement (every 2 centimeters) and no strategy is provided to aggregate those tiny layers. This paper shows how a data driven approach can yield better results than the traditional empirical methods. A machine learning model is presented which is based on a Convolutional Neural Network. The Neural Network has been trained on 1800 pairs of CPTs and boreholes that met the condition of being less than 6 meters apart. An algorithm based on the theory of signals is applied to the classification given by the model to group measurements into soil layers. The paper explains the theory behind the model, shows a comparison with the soil classification given by the Robertson correlation and shows how the model can be used in the geotechnical practice.

1 THE DATA

1.1 *Open source data*

In the past decades the Netherlands have been able to perform and store a large amount of soil investigation. Part of this data have been made available to everyone by the no-profit organization TNO through the website DINOLOket (TNO, 2021).

Since 2020, the organization BRO (Basis Registratie Ondergrond) is responsible for the management of the National Data Repository. Every type of soil investigation that is performed for a project financed by the public administration must be registered and stored in the national database.

The reasons behind this approach is given by the fact that making soil investigation available to everyone will improve the estimation of the subsurface and therefore reduce the risks related to incorrect modelling of the soil. Figure 1 give an overview of the CPTs that are available on DINOLOket (these are indicated as brown dots).

1.2 *Data format*

Before the year 2000 the output of the cone penetration test was available in a digital form according to a customer specific format. This seemed to be an ideal situation, as the customers would get the output

in the format they asked for. However, the result was that there was still a number of formats, which were hard to be interchanged thus being a hindering for a sustainable storage of these data.

The variation in formats lead to waste of time and the related costs are estimated to amount to at least NLG 600000 or Euro \approx 270000 a year (price level 1999).

This situation induced the development of a standard format: the GEF (Geotechnical Exchange Format). The characteristic and requirements of the format are specified in the document “Geotechnical Exchange Format for CPT-data” (CUR, 2006).

1.3 *Parsing of the data*

In order to be able to read and use the data in a program, it has first to be parsed. For this task an open source Python library, *pygef*, has been developed. The library is able to read gef formats of CPTs and boreholes and store their content into a *DataFrame* object. The library provides also a traditional way to classify a CPT: via the Robertson (Robertson, 2010) or Been & Jefferies (Been, K., & Jefferies, M. G. 1992) classification methods. The Roberson classification method provided by the Python library has been used for the validation metrics of the model presented in this paper.



Figure 1. Map of CPTs available in Dinoloket (TNO, 2021).

2 THE CEMS MODEL

2.1 Data-driven iteration

A data-driven approach, in a country where so much open source data is available, seems to be the best way to proceed. In order to train the model roughly 49000 CPTs and 40000 boreholes were checked, from which 1800 pairs met the condition of being less than 6 meters apart. These have been used as labeled data for the first model training. The model is retrained periodically whenever new data are available that meet the condition of being not more than 6 metres apart.

2.2 Decision factors

Machine learning is often beneficial with high dimensional data. In this case, the amount of data dimensions is relatively low. When training powerful ML models, like Neural Networks (Multi Layer Perceptron architecture) or Gradient Boosting Trees, on this data, we see comparable results with each other. The results are quite reasonable, but they do not reflect the decision factor of a geotechnical engineer.

An essential part of the decision making is based on the location where the CPT is taken. And when a CPT, for instance, is taken at sea, they can tell by the curve of the line that a certain layer consists of seashells.

If we want a model to be able to take the same decision factors into account as a human does, the model needs to be able to make decision based on the same information.

2.3 Model architecture

The model is based on a Neural Network architecture with convolutional layers that can apply feature extraction on the input signal (Sassi, A. et al., 2019). The model is enhanced with location-based embedding, in this way the model could learn its own location embedding and could learn the probabilities of soil type conditional on a certain location. Furthermore, most of the bore-hole data show that layers consist of multiple soil components in variable percentages. Therefore we should predict the total soil distribution per layer.

In Figure 2 an example of the result of the model is shown. The model predicts the soil distribution over the depth. Qualitatively the predictions of the model seem very reasonable and align with a geotechnical mapping.

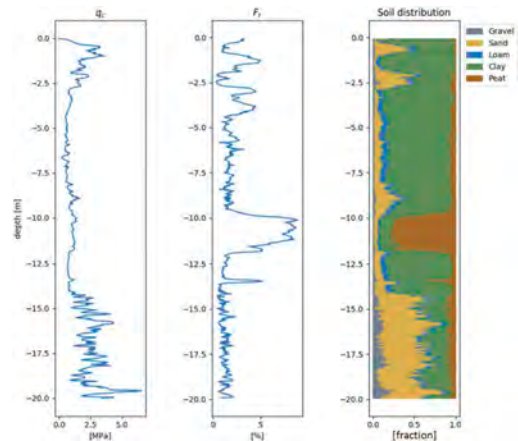


Figure 2. Example result of the CPT interpretation model.

2.4 Location embedding

From the 1800 pairs, 48 location clusters were created by applying K-means algorithm on the location data.

In Figure 3 the locations of the clusters are indicated on the map of the Netherlands. The colors represent a similarity measure between the clusters based on the cosine similarity. Clusters close to each other on the color scale are likely to have similar soil distributions.

Besides comparing the clusters by similarity, we can also run inference for the embedding by nullifying the features. Intuitively this can be regarded as the soil classification you would expect if you only know the location and not considering the information in the CPT. Figure 4 shows the biases that can be applied per location.

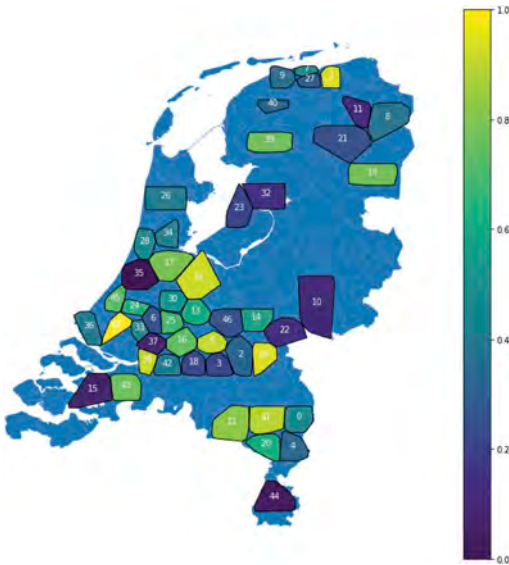


Figure 3. Location clusters.

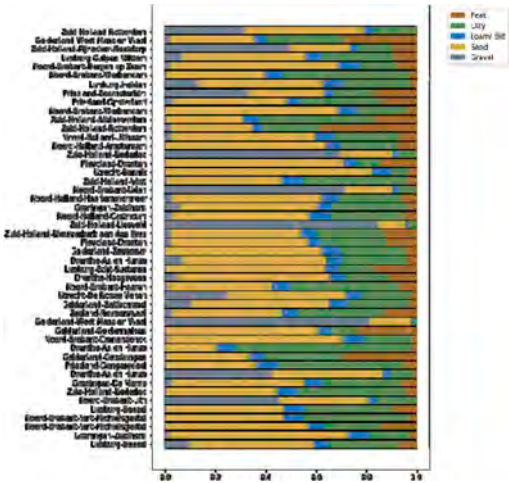


Figure 4. Biases per location.

3 VALIDATION METRICS

3.1 Training metrics

When training a machine learning model usually we have “ground truth labels” being binary True or False, i.e. $y \in (0,1)$. However, the soil labels are never 0 or 1 but they are distributions. Every layer contains different volumetric percentages of soil components, but the sum of all volumes adds up to 1.

For this reason the metrics used to train the model are the Kullback-Leibler divergence (Van Erven, T., & Harremos, P., 2014) and the Wasserstein distance (Hou, L et al., 2016).

3.2 Comparison with Robertson

Comparing the outputs of the model with Robertson requires some translation. Robertson does not predict a soil distribution, but assigns soil types, e.g. ‘Silt mixtures: clayey silt & silty clay’ and ‘Sand mixtures: silty sand & sandy silt’. To be able to make a comparison these classification were transformed into a soil class {Gravel, Sand, Loam, Clay, Peat}.

3.3 A simple validation

A simple way of doing a validation is by looking at precision and recall scores (F1 score) by transforming the probability distributions to main soil classes. In Table 1 the F1 scores are shown, where 0 is a bad prediction and 1 would be a perfect prediction. The column “Support” indicates the number of soil layers with that type of soil as the main type.

Table 1. F1 scores.

Soil type	Support	Robertson	KL-divergence	Wasserstein
Gravel	3731	0.15	0.15	0.1
Sand	137998	0.86	0.83	0.85
Loam	0	0	0	0
Clay	91523	0.64	0.7	0.67
Peat	21398	0.37	0.57	0.74

This comparison is not accurate since a lot of information is lost if we reduce a distribution to a number by taking the mode. If we look at the loam soil type, we can observe that this validation does not consider its prediction. Loam is almost always a subtype in soil layers so it will never come out as the main soil, making it seem that no model can predict this class.

3.4 A better validation: Error distribution

Since we are talking about probabilities, the error distributions show the error margins. In the tables below the Mean Absolute Error (MAE) per soil type is reported. We consider the absolute errors on two subsets of the test set.

Table 2. Precision based absolute errors (lower is better).

Soil type	MAE Robertson	MAE KL-divergence	MAE Wasserstein
Gravel	0.77	0.29	0.22
Sand	0.23	0.31	0.22
Loam	0.93	0.05	0.06
Clay	0.35	0.29	0.3
Peat	0.56	0.28	0.37

Table 3. Recall based absolute errors.

Soil type	MAE	MAE	MAE
	Robertson	KL-divergence	Wasserstein
Gravel	0.18	0.24	0.17
Sand	0.22	0.29	0.2
Loam	0.14	0.04	0.05
Clay	0.44	0.34	0.35
Peat	0.3	0.23	0.22

A subset where the true distribution has non-zero probability for that class can intuitively be regarded as *recall*. A subset where the models assign a significant probability to that class $P(y) > 0.025$ can intuitively be regarded as *precision*.

4 THE GROUPING ALGORITHM

4.1 The motivation

The output of the model is a prediction given for each measurement of the CPT. Although this is probably the most accurate representation of the soil stratigraphy, it is impossible to use 1000+ layers in the traditional software, hence we need to group these tiny layers into macro layers. This is done using an algorithm that is based on considering the CPT measurement a signal.

4.2 The theory

The measured cone resistance and friction ratio are signals and as such we can assume that they follow a Gaussian distribution, as shown in Figure 6.

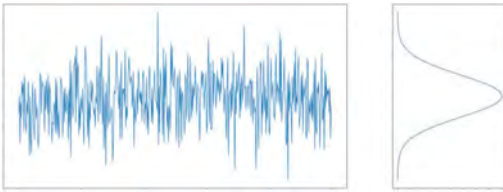


Figure 5. Gaussian signal.

The likelihood of this signal is determined by:

$$L(X_t, \mu, \sigma) = \prod_{t=1}^n P(x_t | \mu, \sigma)$$

If we consider the signal in Figure 6, the likelihood of two sub-signals coming from two Gaussians, separated by change point τ , is higher than

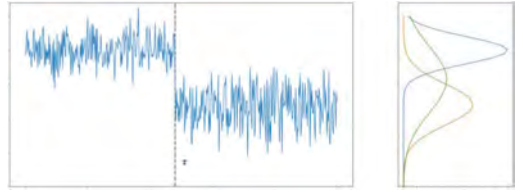


Figure 6. Two Gaussian signals with changepoint τ .

the likelihood of the whole signal coming from one Gaussian.

This observation can be turned into an optimization problem. We search for the minimal negative likelihood by adding new change points τ_i for every point

K in the signal. To prevent having change points at every data point, we introduce a penalty λ .

$$\min \sum_{i=1}^{k+1} [-L(x_{t-1}, x_t)] + \lambda$$

4.3 Final result

Applying the grouping algorithm to the prediction of the model results in a manageable amount of soil layers. By changing the penalty λ we can choose to have more or less layers. A higher penalty will generate less layers, a lower value will generate more layers, as illustrated in Figure 7.

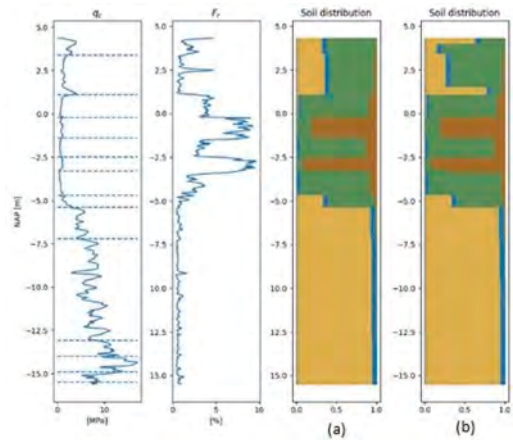


Figure 7. Influence of the penalty parameter on the discretization into soil layers. Fig (a): penalty=2; Fig (b): penalty=1.

5 USAGE OF THE CEMS MODEL

5.1 Web API

The model can be accessed with a HTTPS call via a web REST API, if using the language Python the library *requests* could be used to make the call. In this way the users can incorporate the prediction of the model in their own workflow. The documentation of the REST API can be found on the website (CEMS, 2022). Please note that authentication is needed when using the model, visit the CEMS website at <https://cemsbv.nl/> to learn how to get access.

5.2 Examples

As the soil interpretation is often the first step of a geotechnical design, this building block can be used in many geotechnical applications. So far the CPT interpretation tool has been used in a number of applications including: pile design, levee assessment and improvement, prediction of vibrations induced by the installation of sheet piles.

In case of levees, the model is used to automatically generate longitudinal lithological profiles along the levee as the one shown in Figure 8. These projects often involve a lot of soil investigation which is otherwise difficult to visualize.

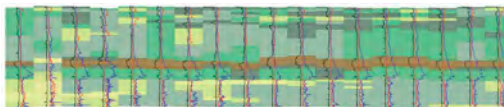


Figure 8. Example of geotechnical longitudinal profile.

Moreover, the automated soil classification can be combined with the geometry of the dike to build calculation files for stability calculations. In the example in Figure 9 the results of soil investigation on the crest and at the toe of the dike have been automatically combined with Lidar measurements of the ground surface and bathymetry data.

5.3 Conclusions

A CPT interpretation based on data proved to be better than empirical formulations. The gain in terms

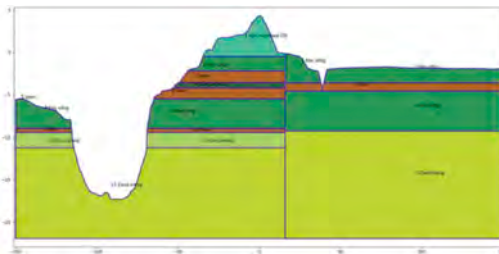


Figure 9. Example of input for a levee stability calculation.

of time when using it in an automated process for geotechnical design is considerable.

The model has been trained only on Dutch soil data. Even though it would probably still give a reasonable prediction outside of the Netherlands, it cannot apply any biases for the location. Future development could include the expansion of the geographical limits of the model, by including CPTs and boreholes from other countries and the definition of location biases and clusters based on expert knowledge.

REFERENCES

- TNO Geologische Dienst Nederland, DINoloket, <https://www.dinoloket.nl/>, last visited 19-11-2021
- CUR, 2006. GEOTECHNICAL EXCHANGE FORMAT FOR CPT-DATA Version: 1, 1, 2
- Hou, L., Yu, C. P., & Samaras, D. 2016. Squared earth mover's distance-based loss for training deep neural networks. arXiv preprint arXiv:1611.05916.
- Van Erven, T., & Harremoës, P. (2014). Rényi divergence and Kullback-Leibler divergence. *IEEE Transactions on Information Theory*, 60(7), 3797–3820.
- Robertson, P. K. 2010. Soil behaviour type from the CPT: an update. In 2nd International symposium on cone penetration testing (Vol.2, pp. 575–583). Cone Penetration Testing Organizing Committee.
- Been, K., & Jefferies, M. G. 1992. Towards systematic CPT interpretation. In *Predictive soil mechanics: Proceedings of the Wroth Memorial Symposium held at St Catherine's College, Oxford, 27-29 July 1992* (pp. 121–134). Thomas Telford Publishing
- Sassi, A., Brahimi, M., Bechkit, W., & Bachir, A. 2019. Location embedding and deep convolutional neural networks for next location prediction. In 2019 IEEE 44th LCN symposium on emerging topics in networking (LCN symposium) (pp. 149–157). IEEE.
- CEMS, Nuclei website, <https://crux-nuclei.com/api/gef-model/ui/>, last visited 14-01-2022

Watch out for the use of global correlations and “black box” interpretation of CPTU data

J.J.M. Powell

Geolabs Limited, Watford, UK

L. Dhimitri

In Situ Site Investigations Ltd, UK

ABSTRACT: Many people interpret soil properties from CPTU measurements based on correlations embedded in software packages without ever questioning the validity of those correlations. This could be termed the ‘black box’ approach! This paper aims to show how dangerous this can be but also the power of the CPTU in helping to show the variations in soil properties within profiles. Based on correlations properties can be both over and under-estimated, which can of course result in both unsafe design and over design. Too often one correlation must be used to derive a soil property required in another correlation, further compounding the potential for errors. A range of sites will be examined with a range of soils varying from very soft clays and silts to stiff clays, sands and soft rocks.

1 INTRODUCTION

The Cone Penetration Test (CPT) or Cone Penetration Test with pore water pressure measurement (CPTU) is almost certainly the most widely used in-situ test both onshore and offshore. Its equipment and operation are well standardised (ISO 22476-1 and ASTM D5778). If these standards are followed and the necessary quality checks are performed, then reliable measured results should be easily obtained and can then be used to derive estimates of the geotechnical parameters to assist the geotechnical design. This is when problems start. Most of the interpretations are semi-empirical in nature and over the years many correlations have been published, linking the measured CPT/U data to the required soil properties. Many people interpret soils from CPTU based on these correlations, which have also been embedded in various software packages without ever questioning their validity. Unfortunately, this is being increasingly done and could be termed the ‘black box’ approach!

Clients are forcing/encouraging CPT contractors to derive soils properties without providing any additional input. It should be acknowledged that these derivations might be guesses, not even best estimates.

Processing of CPT/U raw data starts from converting voltages to engineering units, plotting the results on soil behaviour type charts and ends on generating

all possible soils properties. This is an easy electronic process even without proper user input.

This paper aims to show how dangerous data processing without the proper input can be and how knowledge is required on reliable interpretations. But it also shows how if done with care, the power of the CPTU in determining the variations of soil properties is still so very worthwhile. Based on correlations, properties can be both over and under-estimated, which can of course result in both unsafe design and over-design. Too often one correlation must be used to derive a soil parameter required in another correlation. To further confuse the situation, some of the derived parameters are obtained by using values from other derived/ guessed parameters, adding more errors. It is not intended to mention correlations by name, but to point out the problems that can occur if outputs from software are taken without any user interaction. The packages used are commercially available. No pre-selection of correlations has been made.

For this purpose, 18 commercial sites and 14 test bed sites, which include 100s of CPTUs with a maximum depth of 40m have been studied. Different soils examined vary from very soft to stiff clays, silts, sands and soft rocks. Data cannot be presented for all the sites, but the conclusions are drawn based on all the data that the authors have reviewed. Guidance and advice will be given where possible.

2 SOFTWARE DERIVATION

2.1 Parameters

Some of the geotechnical parameters that can be derived from CPTU test results by using various correlations published in the literature and incorporated into various software packages are listed in Table 1.

Table 1. List of possible parameters to derive from correlations available in the literature.

Parameters	Symbols	Unit
Relative Density	D_r	%
Undrained Shear Strength	s_u	kPa
Water Content	w_c	%
SPT number	N_{60}	-
Shear Wave Velocity	v_s	m/s
Unit weight	γ	kN/m
Small Strain Shear Modulus	G_0	MPa
Small Strain Youngs Modulus	E_0	MPa
Constrained Modulus	M	MPa
Coefficient of volume change	m_v	m^2/MN
Compression Index	C_c	-
Overconsolidation Ratio	OCR	-
Friction Angle	ϕ'	°
Effective Cohesion	c'	kPa
Sensitivity	St	-
Coefficient of Lateral Earth Pressure	K_0	-
Rigidity Index	I_r	-
Hydraulic Conductivity	k (k_h and k_v)	m/s

The process of deriving all geotechnical parameters from CPTU results after gathering the measured data from site, which consists of cone resistance q_c , sleeve friction f_s , and porewater pressure u_2 starts with generating the corrected cone resistance, q_t and friction ratio, R_f through very simple calculations which involve measured results

only. At this phase of data processing Soil Behaviour Type, SBT can be plotted on one of the charts available based on q_c/q_t and R_f .

To derive more soil properties, it is nearly always necessary to have information on groundwater conditions, GWL and density/unit weight, γ to establish total and effective vertical stresses, σ_{v0} and σ'_{v0} , to derive pore pressure ratio, B_q and other normalized parameters, Q_t and F_R .

Information about GWL from the CPTU can only be obtained if full dissipation tests are run and this is seldom done. Hence, guessed GWL must be used as an input to the software if the client cannot supply any information from monitoring it on site. Regarding γ more details are given in the following section.

2.2 Unit weight/ density (γ) and water content (w_c)

When γ is derived from the equations available in the literature and found in many software packages q_c , f_s , and specific gravity of solids, G_s are required to run these calculations. One of the correlations require also shear wave velocity, V_s which is one of the parameters that will be discussed later in the paper.

In Figure 1 are shown some examples of derived γ which are compared with laboratory γ . A significant and consistent underestimation of γ for the glacial till at Cowden (Powell & Butcher, 2002) in England and the silt at Lierstranda (Lunne, 2002) in Norway can be observed. The same behaviour was present at 2 other till sites and 2 more silty clay sites.

In the same figure results from the London clay site at Canons Park (Powell et al., 2003) are also included. Again, derived γ profiles are on the low side of the measured profile. One of the correlations is giving results on the opposite direction of the measured. This pattern of results was apparent for all 5 London clay sites investigated by the authors and was similar in other heavily overconsolidated and aged clay sites. Underestimation is not always the case. γ results for the soft clay at Cran (Shields et al.,

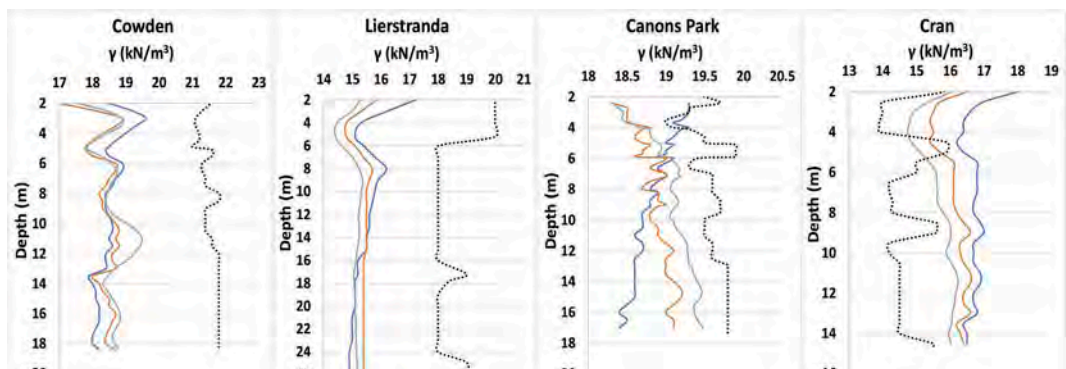


Figure 1. Examples of underestimated and overestimated γ derived from various correlations in use.

1996), in France are highly overestimated, as can be seen from the last graph in Figure 1.

Some packages give also w_c as an output parameter. As might be expected, these results tend to be mirror images of the density profiles using a selected G_s .

2.3 Relative Density (D_r)

When considering sand then D_r is often a desired parameter. In order to derive D_r from CPTU results, q_c , q_t , σ_{v0} and σ_{atm} are typically necessary input. Figure 2 shows results from the sand site at Dunkirk (McAdam et al., 2020), which is partially placed and partially natural deposit. The wide range of derived D_r results after using some of the correlations available in the software is worrying. Generally, underestimation is seen at shallower depths and overestimation at deeper depths. Incorporating the correct γ values and the correct GWL, will significantly improve the results and better define the two layers that comprise this site. The second graph in Figure 2, shows derived D_r before and after compaction of a sand fill. Four different correlations

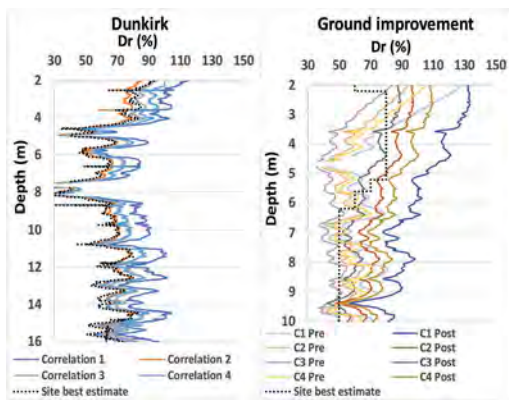


Figure 2. Examples of derived D_r in sands showing under and overestimation of site best estimate values.

available in the specialist software are used to derive D_r , noted in the figure as C1, C2, C3 and C4 Pre and Post, respectively. Once again, the wide range of results, especially those being highly overestimated after compaction is worrying.

2.4 Overconsolidation Ratio (OCR)

When considering OCR or alternatively yield stress, CPTU is known to be a powerful tool to profile it. Some correlations can estimate OCR based on q_t , u_2 , Δu , σ_{v0} , σ'_v and σ_{atm} . Some others require ϕ' and G_0 , which on the other hand require q_c , q_t and/or Q_t and γ . The long list of measured and derived parameters to estimate OCR makes its calculation prone to errors. It is worth mentioning, that OCR is the parameter with the largest number of correlations available.

Figure 3 shows results from some of the sites studied and it can be observed that the shape of the profiles generally follows the sites best estimate. However, the absolute values vary considerably. From all the results we have processed, one of the correlations consistently gives the same results of OCR around 1 for all ground conditions and soil types!

Looking into more details, for the glacial till at Cowden some of the profiles match well with the site best estimates, especially below 22m, where OCR increases. There are results from correlations that highly overestimate OCR, which are not correct. The first attempt for Cowden was done using the default value of γ set up in the specialist software. The second analysis of the results was carried out using the true γ of 22kN/m^3 . Using the correct γ rather than the software generated values for this site, improves the derived OCR results, especially for correlation 6 which is now closer to the best estimate site characteristic values. Although, it is worth mentioning that two of the correlations that seem to not agree are both based on porewater pressure.

At a London Clay site in Canons Park the results presented in this Figure show significant underestimation compared to the site best estimated values,

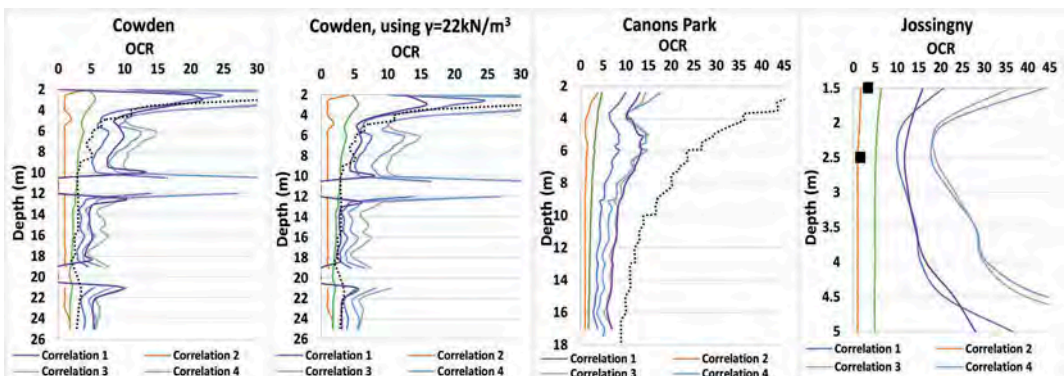


Figure 3. Examples of derived and site best estimate OCR results for 4 sites comprising glacial till, London clay and clayey sand.

although in most cases generated graphs have the correct shape, with values being reduced with depth.

Things can go very wrong indeed, a clayey sand site in Jossingny (Shields et al., 1996), shows unrealistic overestimation as seen in Figure 3.

Using these correlations without questioning the applicability of them in certain soil conditions is seen to give wildly wrong results. Uniform sites (like Cowden) have been examined to show that some correlations respond to changes in OCR caused by erosion. However, what happens if the geology changes, as well? Turning back to the examples above and many more results that authors reviewed for the purpose of this paper, it is not uncommon that a value of around 1 is derived for the full profile-raising concerns on applicability of this specific correlation.

OCR is one of the parameters most influenced by the GWL. Even 1m of GWL change can affect the predicted OCR results from as little as 5% for stiff clays to as high as 45% for soft clays. Therefore, correlations involving GWL as input parameter should be avoided when this information is not accurate.

2.5 Standard Penetration Test (SPT) N Value

The SPT, love it or hate is still one of the widely used in-situ tests worldwide. It has been said that “the best way to get reliable N values is from correlations with CPTU”. The correlations available use q_c , Soil Behaviour Type Index, I_c and σ_{atm} to calculate N. Figures 4 and 5 show CPTU derived SPT profiles and compare them to the in-situ measured SPTs. Four different sites in England are chosen as representative examples, which include the London Clay site of Heathrow Terminal 5 (Hight et al., 2002b) and three commercial sites in Glasgow, Hull and Hemel Hempstead of mixed glacial deposits, silt mixtures underlain soft clay and silt underlain Chalk, respectively.

For London clay at T5, it can be seen that although the generated scattered CPTU profile has almost the same shape, it is below the in-situ measured profile.

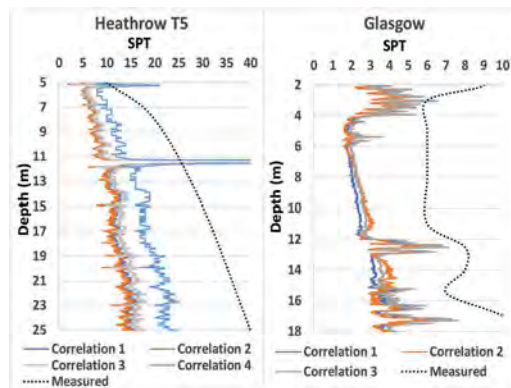


Figure 4. Examples of derived SPT profiles in London and soft clay showing under and overestimation of measured values.

This pattern has been observed on many other clay sites studied, including the soft clays in Glasgow.

However, on two sites presented in Figure 5 results are over and underestimated, in sandy layers and in clayey layers, respectively. Regarding soft rocks, in the second graph below are shown the Chalk results, where in the upper meters in the very weathered Chalk, all SPT profiles seem to agree well. When penetrating through competent Chalk there is a greater difference, with derived results being higher than the measured ones.

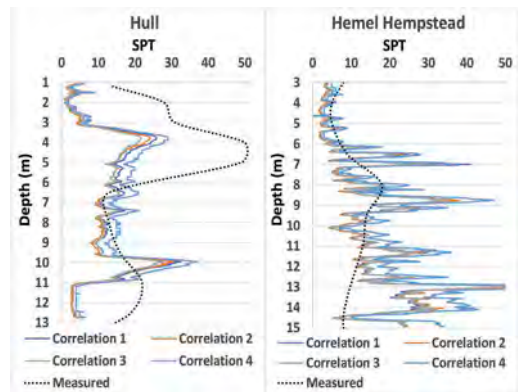


Figure 5. Examples of derived SPT profiles in other soils.

An interesting observation for silt layers from all the studied sites (two also included in Figures 5, the silt layer 6-9.5m in Hull results and 2-6m in Hemel Hempstead results) indicates that measured and derived results show a better agreement in this soil type.

2.6 Shear wave velocity (V_s) and Small Strain Stiffness (G_0)

When V_s and G_0 are considered, it is needed to ensure that anisotropy in the ground is not ignored. This affects the strength and the stiffness of the soils. Results generated from standard geophysical tests, which are typically referred to as downhole and crosshole can be different because of anisotropy. There is a less common crosshole test that allows a third orientation of stiffness to be considered (Butcher & Powell, 2004). As a result, is not enough to know what is being measured, but also which measured direction (vertical or lateral) is the most appropriate for design. For clarity, the following subscripts have been added to V and G to define the orientation of the values: vh for downhole tests and seismic cone, hv for standard crosshole tests and hh for results in a true horizontal plane. The importance of V_s and G_0 means that these parameters are widely desired and therefore derived from measured CPTU results.

Their derivation involves q_t , f_s , σ_{v0} and γ . In the following graphs, derived results are compared with the measured ones from seismic cone tests and are noted as V_{vh} . Figure 6 presents results from four sites, with different geology.

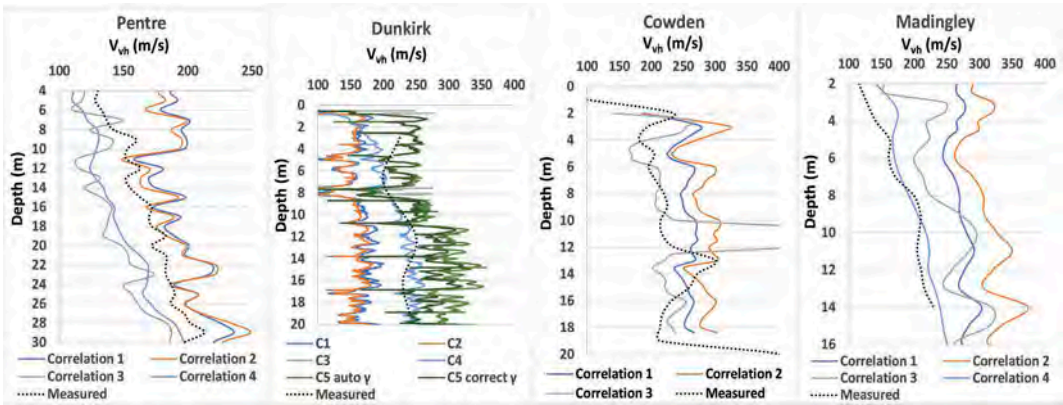


Figure 6. Comparison between measured and derived V_{vh} results in clay sit, sand, glacial till and stiff clay.

Pentre (Lambson et al., 1993) represents a clayey silt site, where the measured V_{vh} profile fall in between the derived one.

For the sands at Dunkirk, which show the largest scatter of derived results the measured V_{vh} profile falls towards the upper bound of the derived values. For the glacial till deposits at Cowden the measured V_{vh} falls towards the lower bound of derived profiles. Although the scatter here is not as large as the one observed for Dunkirk, below 16m derived V_{vh} are overestimated. Furthermore, big differences between are also seen for the stiff clays in Madingley (Butcher & Lord, 1993). Surprisingly, the greatest differences noticed are when deriving V_{vh} from the correlation which is suggested to work best in clays. This indicates that even if some correlations are recommended for one soil type, big differences can still be present. Does this mean that soil type is not the only limitation to the applicability of some correlations?

However, overestimation is not always the case. Figure 7 shows results from very stiff clays in Banbury and dense sands in Machynlleth, where derived V_{vh} are significantly lower than the measured one.

The behaviours seen in Figures 6 and 7 for V_{vh} are also noticed for derived and measured G_{vh} , Figure 8.

The results patterns for G_{vh} match those of Powell (2017) using a wider range of correlations, with the measured values for normally and lightly overconsolidated soils resulting in between derived ones. Meanwhile, the measured G_{vh} for heavily overconsolidated clays fall in the lower bound of derived results.

Derivations of G_{vh} is generally linked to CPTU data. However, derived V_{vh} and γ can be used to calculate G_{vh} . In this case, even if V_{vh} is realistic G_{vh} could have errors for incorrect γ . Results from Dunkirk support this. The G_{vh} profile generated from the software is closer to the site measured profile when correct γ is used. This again shows the importance of accurate input parameters to derive more parameters. Powell and Butcher (2004) and later Powell et al. (2016) suggested that it was the horizontal stresses and stiffnesses that influence q_t and that q_t correlates better with G_{hh} . This idea is further supported by

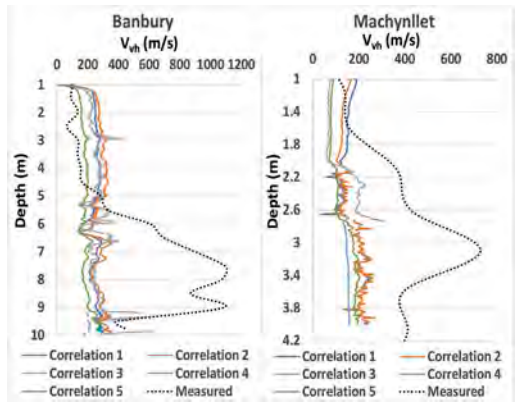


Figure 7. Examples of underestimated derived V_{vh} results.

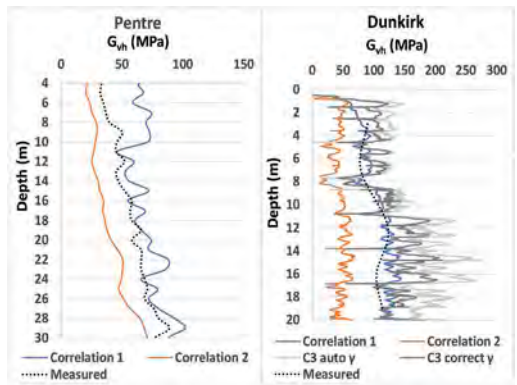


Figure 8. Examples of derived and measured G_{vh} profiles.

Long (2022) who, using the same and additional data suggests that V_{hh} correlates better to q_t than V_{vh} does.

2.7 Other parameters

Undrained shear strength, s_u is highly affected by the choice of cone factor, N_{kt} . This is the principal

problem, although γ and GWL should ideally be known. Some of the software can generate N_{kt} values. Great care must be taken when this is done. It has been found on the studied sites that it can lead to under and overestimation of s_u . Values of N_{kt} should ideally be selected by the designers based on past experiences and the shear test types required, for example compression, extension or simple shear.

Another problem is the assessment of coefficient of lateral earth pressure, K_0 . Correlations exist and are incorporated into software, as well. But, realistic assessment of K_0 from CPTU is still extremely weak and should be treated with great caution.

Another parameter that needs to be treated with growing awareness is permeability (hydraulic conductivity), k , which is widely required for settlement calculations as an input parameter in design software. k from CPTU is a rough guide of possible values for each SBT, giving lower and upper bounds. The importance of dissipation tests to estimate coefficient of consolidation, c_v is crucial. c_v is acceptable when dissipations are carried out below GWL. When GWL is unknown, dissipation tests need to run to equilibrium.

3 DISCUSSIONS AND CONCLUSIONS

In this paper has been suggested that the use of software to process CPTU results into geotechnical information should be done with care. Although these packages perform the mathematical calculations correctly, they are often used with too little basic information, experience and/ or knowledge.

It has been shown that many of the embedded correlations are not suitable for ALL soil types.

In addition, the following points can be made:

- Correct γ and GWL can improve the results of many derived geotechnical parameters;
- Derived parameters obtained based on other previously derived parameters should be avoided;
- Different correlations can give very different derived parameters for the same soil type;
- Sometimes agreements between measured and derived parameters have been found to be purely fortuitous. Two incorrectly derived parameters appearing to give a correct answer, this is worrying!

Correlations used in similar soil types are valuable, as are site specific ones. Parameter profile shape is often promising, but the absolute values between correlation vary wildly.

Can we find correlations that use soil type in terms of I_c as input parameter? It looks unlikely.

Why derive parameters that can be easily measured, like V_{vh} . However, site specific correlation can be useful for example, between q_t and measured V_{vh} from SCPTU, when used with other CPTUs on a site.

The importance of linking CPTU parameters with results from quality laboratory tests cannot be overstressed if efficiency in design is to be achieved.

Correlations can be very useful but should only be used when all influences in their derivation are understood.

Finally, always revisit processing when site specific information becomes available and site-specific correlations are established. They are far from foolproof. Soils properties should be treated with caution if they are derived without basic input information.

REFERENCES

- ASTM D5778-12. 2012. Standard Test Method for Performing Electronic Friction Cone and Piezocone Penetration Testing of Soils. *ASTM International*. West Conshohocken, PA.
- Butcher, A.P. & Powell, J.J.M. 1995. The effects of geological history on the dynamic stiffness in soils. *Proc. 11th ECSMFE*. 1: 27–36.
- Butcher, A.P. & Lord, J.A. 1993. Engineering properties of Gault clay in and around Cambridge, UK. *Geotechnical Engineering of Hard rocks – Soft soils*. 1: 405–416. Balkema.
- Hight, D.W., McMillan, F., Powell, J.J.M., Jardine, R.J. & Allenou, C.P. 2002a. Some characteristics of London clay. *Characterisation and Engineering Properties of Natural soils*, eds Tan et al. 2: 851–908.
- Hight, D.W., Paul, M.A., Barras, B.F., Powell, J.J.M., Nash, D.F.T., Smith, P.R., Jardine, R.J. & Edwards, D. H. 2002b. The characterization of the Bothkennar clay. *Characterisation and Engineering Properties of Natural soils*, eds Tan et al. 1: 543–598.
- ISO 22476-1:2012. Geotechnical investigation and testing: Field testing Part 1: Electrical cone and piezocone penetration test.
- Lambson, M.D., Clare, D.G., Senner, D.W.F. & Semple, R.M. 1993. Investigation and interpretation of Pentre and Tilbrook Grange soil conditions. *In Large scale pile tests in clay (editor J Clarke)*. Thomas Telford: 134–196.
- Lacasse, S. & Lunne, T. 2002. Engineering Properties of Lean Lierstranda Clay. *Proc. Intl Symp Coastal Engineering in Practice, Yokohama September 2000*. 2: 177–186.
- Long, M., 2022. Practical use of shear wave velocity measurements from SCPTU in clays. *Proc. CPT'22, June 2022*.
- McAdam, R.A., Byrne, B.W., Housley, G.T., Burd, H.J., Gavin, K.G., Igoe, D.J.P., Jardine, R.J., Martin, C.M., Potts, D.M., & Zdravković, L. 2020. Monotonic laterally loaded pile testing in a dense marine sand at Dunkirk. *Géotechnique*. 70 (11): 986–998
- Mokkelbost, K.H., Lunne, T. & Powell, J.J.M. 2000. Semi empirical design procedures for foundation design. Proc Nordic Geotechnical Conference
- Powell, J.J.M. & Butcher, A.P. 2002. Characterisation of a glacial clay till at Cowden, Humberside. *Characterisation and Engineering Properties of Natural soils*, eds Tan et al. 2: 983–1020.
- Powell, J.J.M., & Butcher, A.P. 2004. Small Strain Stiffness assessments from in situ tests. *Proc. ISC2 Porto*. 17171722.
- Powell, J.J.M., Butcher, A.P. and Pellew, A. 2003. Capacity of driven piles with time – implications for re-use. *Proc XIIIth ECSMFE*. Prague August 2003. 2: 335–340.
- Powell, J.J.M., Dhimitri, L., Ward, D. & Butcher, A.P. 2016. Small strain stiffness assessments from in situ tests – revisited. *Proc. 5th Intl Conf on Geotechnical and Geophysical Site Characterization ISC'5 Gold Coast*.
- Shields, C.H., Frank, R., Mokkelbost, K.H. & Denver, H. 1996. Design fourfold. *Ground Engineering*. 29 (2): 22–23.

New methods for assessing Plasticity Index and Low-strain Shear Modulus in fine-grained offshore soils

N. Ramsey

Fugro Australia Marine Pty. Ltd., Perth, Western Australia, Australia

K.K. Tho

Fugro Singapore Marine Pte. Ltd., Singapore

ABSTRACT: This paper introduces a new method for predicting Plasticity Index, PI, directly from CPT data. Plasticity Index values predicted using the new method have been designated “PI_{CPT}” to emphasise their CPT-based origin. The new PI_{CPT} method has, in turn, enabled a new method of assessing Low Strain Shear Modulus, G_{\max} , to be proposed, based on a well-established equation published by Viggiani & Atkinson (1995). As an additional benefit, the predicted PI_{CPT} profiles have proven very useful as a simple means of identifying soil-type variations and layer boundaries. This paper presents details of the new formulae that have been developed to estimate PI_{CPT} and G_{\max} , the database that has been used to calibrate the formulae, and the results that have been obtained. Some limitations of the method are presented and discussed, as well as some of the benefits.

1 INTRODUCTION

This paper introduces new methods for estimating PI and G_{\max} directly from CPT data, in fine-grained offshore soils. The new method for estimating PI is also shown to be a simple means of differentiating soil-type variations and layer boundaries.

This paper presents details of the formulae that have been developed, the database that has been used to calibrate the formulae and the results that have been obtained. Some limitations of the method and some discussion on the additional benefits are also presented.

2 DATABASE AND SELECTED SITE DETAILS

2.1 General

The PI database used for this paper comprises approximately 200 PI measurements taken at more than a dozen sites. The sites were purposely chosen to be from a variety of geological environments, and to provide data with a range of plasticity. The majority of the sites comprised predominantly silica soils, but one site comprised high plasticity carbonate silt. The chosen sites were also widely distributed geographically, and from a range of water depths.

The CPT data were gathered by four different geotechnical contractors, using cones made by three different manufacturers. Most of the tests were performed with standard piezocones with projected tip areas of

10 cm² or 15 cm² cones; but, at one site a cone with a projected tip area of 5 cm² cone was used.

Several sites in the database included G_{\max} measurements from Resonant Column (RC), Bender Element (BE) or Seismic Cone (SCPT) tests.

Four sites have been selected for more detailed presentation and discussion of PI and G_{\max} predictions. These sites were chosen because, together, they covered a wide range of plasticity index and liquidity index. At all four sites, the CPTs and sampling boreholes were performed in close proximity, and G_{\max} measurements had been made via RC and/or BE testing. One site also included SCPT measurements.

General details of the soil conditions at the four selected sites are presented in Table 1.

Table 1. General details of site conditions.

Site Name	Plasticity Symbols	~PI ~OCR		Notes
		%	-	
A	CI-CH	15-40	5-10	
B	CI	10-20	1.5-10	
C	CVH-CEH	55-75	1-2	
D	MH	15-25	1-3	Carbonate

The ranges of soil conditions at the selected sites, are also considered representative of the ranges in the database.

3 ASSESSING PI FROM CPT DATA

3.1 General

The general form of the proposed formula for predicting Plasticity Index from CPT (PI_{CPT}) data is presented in Equation 1:

$$PI_{CPT} = \frac{C_1 * R_{ft} * (1 + B_q)^{C_3}}{(0.33 * Q_t)^{C_2}} \quad (1)$$

where R_{ft} is the ratio of sleeve friction, f_s , to total cone resistance, q_t ; B_q is the ratio of excess pore-water pressure, Δu , to net cone resistance, q_{net} ; and Q_t is the ratio of q_{net} to in-situ vertical effective stress, p'_0 .

Although, Equation 1 is essentially an empirical formula, it is based on some well-established concepts. The basic premise of the formula is that friction ratio is primarily affected by the soil's mineralogy, stress history and lateral effective stress. So, by removing the effect of stress history and lateral effective stress, the friction ratio becomes primarily affected only by the soil's mineralogy, which is manifested in terms of the measured Plasticity Index.

As both B_q and Q_t are strongly influenced by stress history, it would seem reasonable that both these parameters could be used to try and reverse the effects of stress history on the measured skin friction. Reversing the effects of effective lateral stress is more challenging, as the B_q parameter is not significantly influenced by lateral effective stress – as may be observed in normally consolidated clay, where B_q can be almost constant over several tens of metres. At first glance, Q_t might also seem to fall into this category. However, it may be remembered that mechanically induced Overconsolidation Ratio, OCR, may be written in terms of the current effective vertical stress and an additional vertical effective stress, Δp that has been removed at some point in time (Equation 2). Hence, as the Q_t parameter is normalised by the current vertical effective stress, it will tend to reduce gradually with depth, if Δp in the soil-layer is constant and greater than zero.

$$OCR = (p'_0 + \Delta p) / p'_0 \quad (2)$$

Initial attempts to assess appropriate coefficients were encouraging, as it was clear that the general trends of measured PI values were being correctly predicted. However, when low values of the C_1 coefficient were chosen, it was necessary to use relatively high C_2 and C_3 coefficients, which made the predicted PI very sensitive to small changes in B_q and Q_t . Whereas when high values of the C_1 coefficient were chosen, it was not possible to choose C_2

and C_3 coefficients that gave consistently acceptable agreement with the measured data. Therefore, an iterative approach was used to optimise the C_1 , C_2 and C_3 coefficients, using the following criteria:

- When viewed on an overall basis, a clear majority of measured PI values, in the database, should be reasonably close to corresponding PI_{CPT} values.
- When viewed on an individual-site basis, a clear majority of measured PI values, should be reasonably close to, and follow the trends of, corresponding PI_{CPT} values.

Based on the two criteria above, a best fit was achieved using C_1 , C_2 and C_3 coefficients of 17.5, 0.31 and 1.2 respectively, as shown in Equation 3.

$$PI_{CPT} = \frac{17.5 * R_{ft} * (1 + B_q)^{1.2}}{(0.33 * Q_t)^{0.31}} \quad (3)$$

where both R_{ft} and PI_{CPT} are percentage-values, in accordance with standard industry practice. Consequently, from now on, PI_{CPT} will be presented, and used, as a percentage.

3.2 Direct comparisons

Figure 1 presents a combined plot of measured PI values plotted directly against automatically picked corresponding PI_{CPT} values, from all the sites. Automatic picking was used to avoid unconscious human bias influencing the picked values. Only values that were clearly inconsistent were removed – for example where a measured PI value was close to a soil-type boundary, but where the CPT data clearly indicated a different boundary elevation.

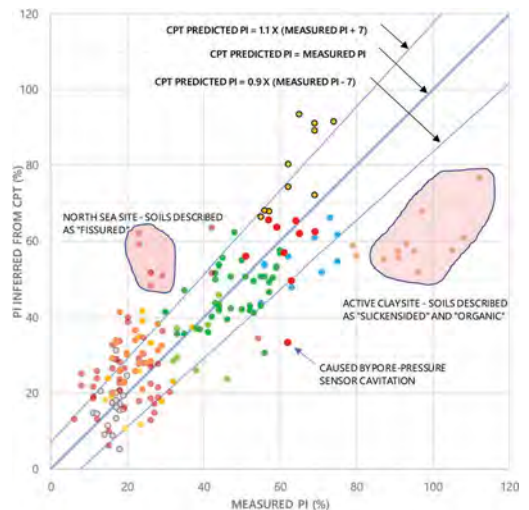


Figure 1. Comparison of all measured PI and PI_{CPT} values.

Figure 1 confirms that, overall, measured PI values, in the database, are reasonably close to corresponding predicted PI_{CPT} values – and when the error is greater than the ranges shown, there is often a clear and identifiable reason. For example:

- a) As shown on Figure 1, extremely high plasticity active clays, often including soil descriptors such as “slickensided” or “organic” tend to be underpredicted.
- b) Strongly structured soils tend to be more difficult to predict. In the example shown on Figure 1, the soils were described as “fissured”, and PI_{CPT} values were greater than measured PI values. However, it is considered possible that PI_{CPT} could over-predict or under-predict measured PI in strongly structured soils.
- c) It is well known that a coarse inclusion, such as a piece of coarse gravel in a fine-grained matrix, can cause temporary variations in both pore-water pressure and sleeve friction – and these variations can lead to erroneous PI_{CPT} predictions. The example highlighted in Figure 1 was caused by an inclusion that was observed in the corresponding soil sample.

3.3 Example sites

3.3.1 General

The section presents comparisons of measured PI and PI_{CPT} at four selected sites. It may be noted, however, the consistency of agreement shown for these four sites is considered typical of the consistency observed at other sites in the database. Even at the “slickensided” site, highlighted in Figure 1, a reasonably consistent difference between predicted and measured values was observed, suggesting the error was systematic rather than random.

3.3.2 Site A

Figure 2 presents a simplified soil profile (based on the adjacent sampling borehole log) to illustrate the interbedded nature of this site. Even so, it may be seen that the predicted PI_{CPT} profile is in good agreement with measured PI values. Furthermore, if $PI_{CPT} \geq 7\%$ is used to define fine-grained soils, the PI_{CPT} profile can be seen to provide a simple means of differentiating fine-grained and coarse-grained soil - and soil-type variations and layer boundaries.

3.3.3 Site B

This site was chosen because of the relatively low Plasticity Index and the relatively large number of measurements. It may be seen from Figure 3 that the predicted PI profile is in good agreement with the measured values. For example, where the measured PI values are uniform in the upper 20 metres, the predicted PI profile is uniform. Below 20 metres there is more variability in the measured PI values, and this is also seen in the predicted profile. Finally, the decrease in measured PI values below 40 metres is also observed in the predicted PI profile (although there is some variability).

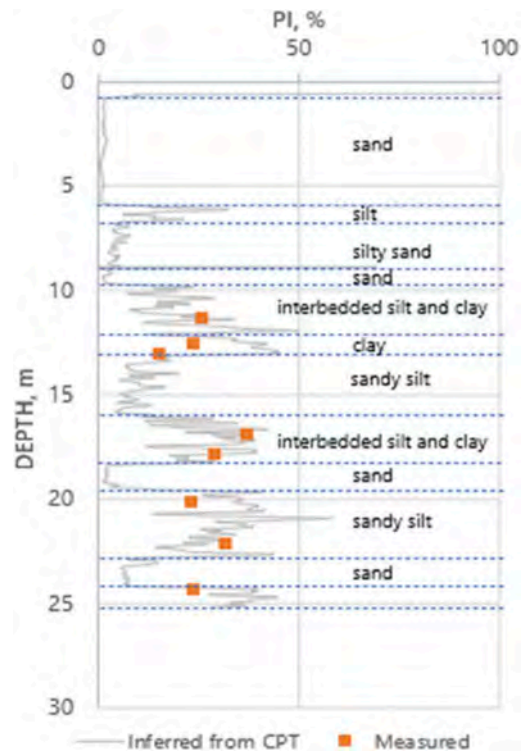


Figure 2. Site A – Measured and inferred PI versus depth.

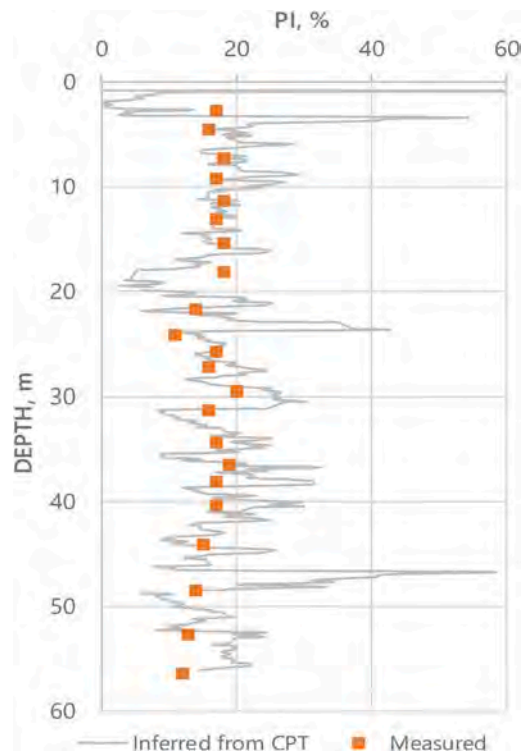


Figure 3. Site B – Measured and inferred PI versus depth.

3.3.4 Site C

This site was chosen because of its very high to extremely high plasticity. As shown in Figure 4, the PI_{CPT} profile generally slightly underpredicts the measured PI values; but, at some locations, the difference was greater, for example in the range 30–40 metres. It is notable, however, that in this depth range, “organic staining” was included in the corresponding soil descriptions. This might suggest the greater differences were caused by locally higher organic content. Although, no direct organic content measurements were made on the corresponding samples – it is notable that organic contents in the same soil unit, at the same site, did indicate local variations in organic content.

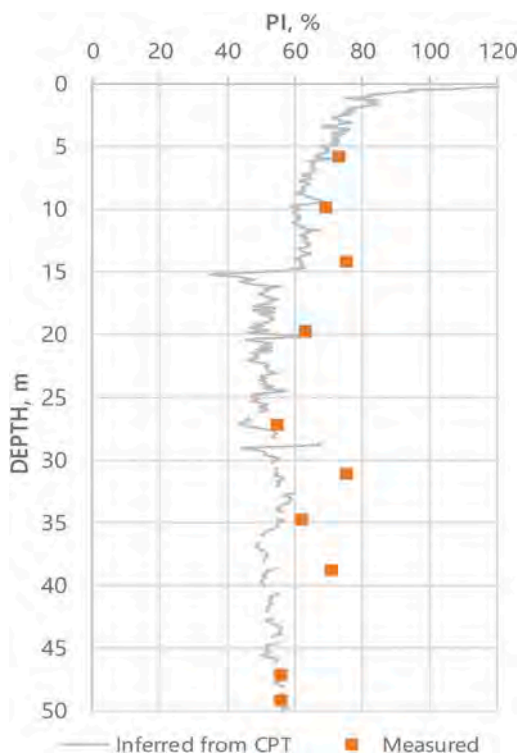


Figure 4. Site C – Measured and inferred PI versus depth.

3.3.5 Site D

This site was chosen because it comprised high plasticity carbonate silt. The agreement between predicted and measured PI values at this site was better than expected. However, we would not consider it wise to assume that a similar level of agreement would be achieved at all carbonate silt/clay sites.

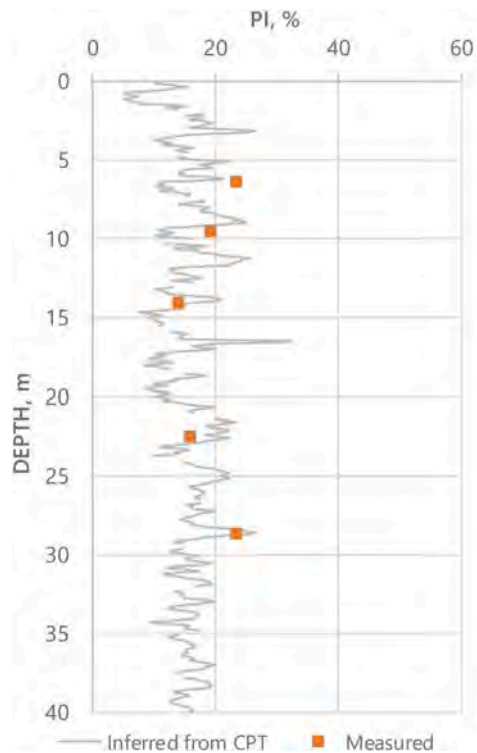


Figure 5. Site D – Measured and inferred PI versus depth.

3.4 Discussion

Generally, the predicted PI_{CPT} values are in good agreement with measured data, at the sites within the database, provided the soils are not organic or significantly structured. However, obviously, the ability to make reliable predictions is highly dependent on the reliability of the input data. Consequently, the following potential sources of error must be avoided or taken into account when interpreting the results:

- Errors in cone zero measurements – particularly the friction sleeve zero measurement.
- Errors in friction sleeve measurements caused by temperature effects – for example when the cone has passed through very dense sand.
- Cone dimensions – particularly friction sleeve dimensions - that are outside the allowable tolerances given in ISO 19901-8 (2014).
- Cone measurements that do not achieve ISO 19901-8 (2014) Application Class 1 limits.
- Incorrect calculation of q_t , q_{net} , R_{ft} and Q_t .
- Sleeve friction measurements not suitably corrected for friction sleeve area effects (Ramsey, 2022).

An additional benefit of the PI_{CPT} formula was that it proved useful for defining the boundaries

between fine-grained and coarse-grained soils. Based on the sites investigated, it also appeared to predict the thickness and plasticity of interbedded layers reasonably reliably.

A further benefit of being able to predict PI, reasonably reliably, is that it enables PI to be explicitly included in G_{max} assessments based on CPT data – and this aspect is discussed in the next section.

4 ASSESSING LOW-STRAIN SHEAR MODULUS USING CPT DATA

4.1 General

The new method for assessing G_{max} directly is an adaptation of the well-established G_{max} formula published by Viggiani & Atkinson (V&A) in 1995, and shown in Equation 4:

$$\frac{G_0}{p_r} = A \left(\frac{p'}{p_r} \right)^n R_0^m \quad (4)$$

where, G_0 is equivalent to G_{max} (kPa), R_0 is equivalent to OCR, p_r is a reference stress (equal to 1 kPa), p' is the mean effective stress (kPa) and 'A', 'n' and 'm' are coefficients that depend on Plasticity Index (%).

The advantage of the V&A (1995) formula over most popular CPT-based methods of assessing G_{max} , is that it explicitly accounts for the principal factors that influence G_{max} , which are OCR, p' and PI. So, as the PI_{CPT} formula can now be used to estimate PI, all the required V&A (1995) input factors can now be directly estimated from CPT data, using Equation 5:

$$G_{max} = p_r * A(PI_{CPT}) * \left[\frac{p'}{p_r} \right]^{n(PI_{CPT})} * OCR^{m(PI_{CPT})} \quad (5)$$

Further details of the methods used to calculate the input factors are discussed in the next sections; followed by profiles comparing predicted and measured G_{max} values, at the four selected sites.

4.2 Estimating the A, n and m coefficients

In the Viggiani & Atkinson (1995) paper, the coefficients 'A', 'n' and 'm' are graphically related to PI (%), and lines that "indicate only the general trends of the data" are annotated on explanatory graphs. Nevertheless, V&A's general trend lines have been used as the basis for the formulae proposed in this paper, which are presented in Equations 6 to 8:

$$A(PI_{CPT}) = 10^{(3.52 - 0.022 * PI_{CPT})} \quad (6)$$

$$n(PI_{CPT}) = 0.27 + 0.35 * \log(PI_{CPT}) \quad (7)$$

$$m(PI_{CPT}) = 0.17 + 0.002 * PI_{CPT} \quad (8)$$

Equations 7 and 8 generate 'n' and 'm' coefficients that are similar to the "general trends" lines shown by V&A (1995). Whereas Equation 6 generates 'A' coefficients that lie slightly below V&A's "general trends" line, because doing so produced a better overall fit with the measured G_{max} values in our database.

4.3 Assessing OCR from CPT data

OCR is one of the key input parameters in Equation 5. Various formulae for predicting OCR from CPT data were assessed, including a new formula that accounted for plasticity. However, it was concluded that the formula presented in Equation 9 (Kulhawy & Mayne, 1990) and illustrated in Figure 6, provided reasonable agreement between predicted and measured OCR values. It is notable that the four data points lying significantly below the "1 to 1" line, in Figure 6, were measured in soils that were considered to have been desiccated by sub-aerial exposure. This is considered to suggest that the yield stress ratio may be underpredicted when the yield stress has increased due to desiccation rather than being mechanically induced – and is, therefore, a limitation on the accuracy of G_{max} predictions made using the new method.

$$OCR_{CPT} = Q_t/3 \quad (9)$$

4.4 Assessing mean effective stress from CPT data

Mean effective stress has been calculated using the Equation 10:

$$p' = (1 + 2 * K_o)/3 * p'_0 \quad (10)$$

where K_o is the lateral earth pressure at rest, and p'_0 is the current in-situ vertical effective stress.

K_o has been calculated using Equation 11, using the approach proposed by Mayne & Kulhawy (1982) and assuming an angle of internal friction of 30° (which is considered sufficiently accurate for the intended purpose):

$$K_o = 0.5 * (OCR_{CPT})^{0.5} \quad (11)$$

The preferred method for estimating current in-situ vertical effective stress, p'_0 , is to use laboratory data from nearby sampling boreholes. However, if

no local data are available, then there are published relationships for assessing submerged unit weight from CPT data, such as Robertson & Cabal (2010).

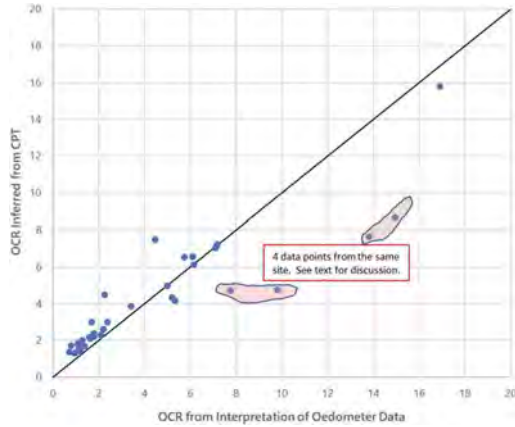


Figure 6. Comparison of predicted and interpreted OCR.

4.5 Comparisons between predicted and measured G_{max} values

4.5.1 General

The four examples that follow are comparisons between predicted and measured G_{max} values at the same four sites, as the PI comparisons.

4.5.2 Site A – G_{max} predictions

Figure 7a) illustrates that the laboratory measurements and SCPT measurements were in good agreement with the predicted G_{max} profile, at this interbedded sand, silt and clay site.

4.5.3 Site B – G_{max} predictions

Figure 7b) presents predicted and measured G_{max} values from Site B. At this, there was initially poor agreement between predicted and measured values. However, on closer inspection, the laboratory test specimens had been consolidated to the estimated vertical effective stress, rather than the mean effective stress. After accounting for this discrepancy, the predicted values are much closer to the measured values, albeit systematically higher. The difference is considered likely to be due to correction errors.

4.5.4 Site C – G_{max} predictions

Figure 7c) indicates very good agreement between predicted and measured G_{max} values, which might seem surprising given that the PI_{CPT} profile at this site was consistently underestimated (see Figure 4). However, at high PI, the $A(PI_{CPT})$ and $n(PI_{CPT})$ coefficients become less sensitive to changes in PI, which probably explains the good agreement.

4.5.5 Site D – G_{max} predictions

The predicted G_{max} profile is in good agreement with the three of the four measured values at this high plasticity carbonate silt site. The reasons for the discrepancy with the lowest laboratory measured value is not completely clear. However, local zones of higher cementation were observed at this site, so it is considered possible that the laboratory test was affected by a locally higher degree of cementation.

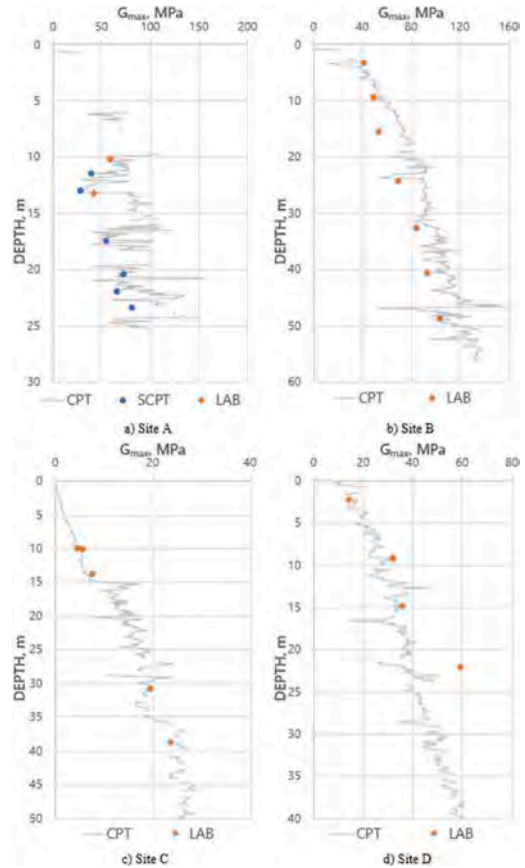


Figure 7. Comparison of predicted and measured G_{max} values.

4.6 G_{max} discussion

- Generally, the new method of predicting G_{max} directly from CPT data, is considered to provide good predictions of G_{max} values at the sites within our database. However, the initial lack of agreement between predicted and measured values at Site B, highlights the need to ensure that any corresponding laboratory tests are consolidated appropriately. Also, as the method is dependent on reliable PI_{CPT} predictions, the same potential sources of error, discussed in Section 3.4, need to be avoided, or taken into

account, when processing the results. Finally, potential errors caused by inaccurate OCR predictions in sub-aerially exposed soils, should be taken into account.

5 CONCLUSIONS AND RECOMMENDATIONS

- A new method of prediction PI values directly from CPT data is proposed. Generally, the predicted PI_{CPT} values are in good agreement with measured PI values in the database.
- An additional benefit of the predicted PI_{CPT} profiles is that the profiles can be used as a simple means of differentiating soil-type variations and layer boundaries.
- A limitation of the proposed new method for predicting PI_{CPT} is that the quality of the predictions is dependent on high quality CPT measurements. Fortunately, this limitation can be mitigated by ensuring all tests are performed with cones that comply with the tolerances and accuracies specified in ISO 19901-8 (2014) for Class 1 testing.
- The new PI_{CPT} formula has enabled a new method for predicting G_{max} to be proposed, based on a well-established equation proposed by Viggiani & Atkinson (1995).
- The predicted G_{max} values are in good agreement with measured G_{max} values in the database.

- The limitations of the proposed new method for predicting G_{max} , are generally similar to the limitations of the new PI_{CPT} method - with the addition of potential errors caused by inaccurate OCR predictions in sub-aerially exposed soils.

REFERENCES

- ISO. 2014. *Petroleum and natural gas industries - specific requirements for offshore structures - Part 8: marine soil investigations*, International Standard ISO 19901-8: 2014.
- Kulhawy, F.H. & Mayne, P.W. 1990. *Manual on estimating soil properties for foundation design*. EPRI Report EL6800, Electric Power Research Institute, Palo Alto.
- Mayne, P.W. & Kulhawy, F.H. 1982. Ko-OCR relationships in soil. *Journal of the Geotechnical Engineering Division*, 108(6), pp.851–872.
- Ramsey, N. 2022. The effects of cone geometry and testing deployment on CPT measurements - practical examples in a normally consolidated deep-water clay. *Proceedings of the 20th International Conference on Soil Mechanics and Geotechnical Engineering*, Sydney, Australia.
- Robertson, P.K. & Cabal, K.L. 2010. Estimating unit weight from CPT. *Proceedings of the 2nd International Symposium on Cone Penetration Testing*, CPT'10, Huntington Beach, CA, USA.
- Viggiani, G. & Atkinson, J.H. 1995. Stiffness of fine-grained soil at very small strains. *Géotechnique*, 45 (2), pp.249–265.

Cone penetration testing and interpretation in the holds of two ore-carrying vessels

N. Ramsey
Fugro, Australia

ABSTRACT: This paper provides details of two in-situ testing programmes performed to assess ore properties in the holds of ore carrying vessels. The first case comprised CPTs in the hold of an iron-ore carrying vessel - at both the ports of loading and discharge – enabling assessment of the ore properties after loading and the changes caused by the voyage. The second case comprised two CPTs and one Seismic Dilatometer Test (SDMT) in the hold of a coal carrying vessel shortly after loading – enabling assessment of the coal properties after loading, and direct comparison of CPT and SDMT interpretations.

1 INTRODUCTION

Ore-liquefaction can be caused by cyclic loading induced by ship-motions. If liquefaction occurs, the ore may lose most, if not all, its inter-particle frictional strength and may flow like a viscous fluid. If flow does occur, one potential consequence is an irredeemable lateral shift in the ship's centre of gravity – a shift that could have potentially catastrophic consequents.

This paper presents details of two high-quality in-situ testing programmes that were performed in the holds of ore carrying vessels, to provide reference information for ore liquefaction and stability assessments. Full details of these assessments are beyond the remit of this paper. However, opportunities to perform in-situ tests on ore mounds in ships' holds are rare – so, it is hoped that the data and interpretations, presented herein, will be of interest to the geotechnical community.

2 PROJECT DETAILS

2.1 Case 1 – iron-ore

2.1.1 Fieldwork

The fieldwork was performed in two phases. Phase 1 comprised, three CPTs at the port of loading and Phase 2 comprised three CPTs at the port of discharge. Each test was performed from the top of the ore mound to the base of the mound. The tests were performed on an approximate one-metre grid, so the maximum separation between any test was approximately two metres.

As may be seen in Figures 1 and 2, different CPT rigs were used at the ports of loading and discharge. However, similar Class 1 piezocones were used at both sites.



Figure 1. CPT equipment at iron-ore port of loading.



Figure 2. CPT equipment at iron-ore port of discharge.

2.1.2 Iron-ore CPT results

Reference CPT data, for the iron ore mound, are presented on Figure 3 (port of loading) and Figure 4 (port of discharge). The test data are generally consistent at

the port of loading (except for some variability in CPT NP2 in the upper 2.5 m). In contrast, significantly more variability is apparent at the port of discharge – in particular, the sleeve-friction measurements are significantly higher. The measured pore-water pressure values were negligible, indicating fully drained behaviour at both ports.

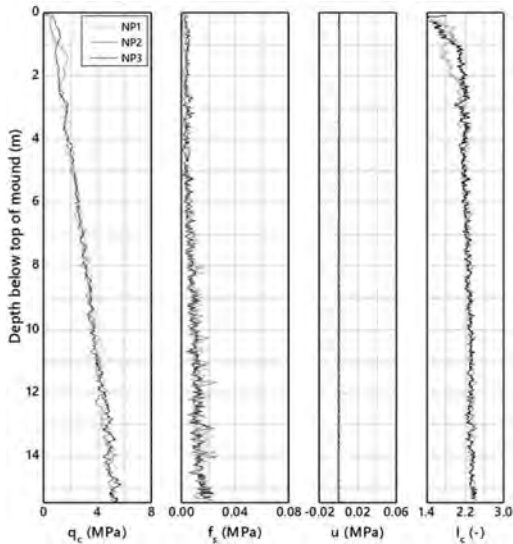


Figure 3. Case 1 – CPT data – Iron-ore port of loading.

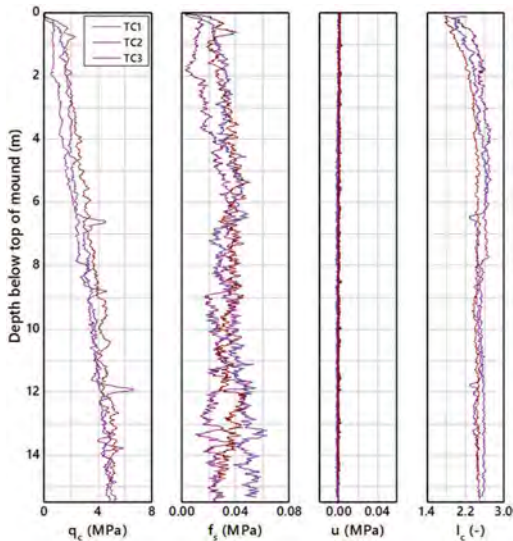


Figure 4. Case 1 – Basic CPT data – Iron-ore port of discharge.

2.2 Case 2 – coal

2.2.1 Fieldwork

The fieldwork was performed shortly after the ship was loaded. The fieldwork comprised CPTs at two locations, approximately 7.6 m apart. CPT PK1 was performed on the top-centre of the coal mound, whilst CPT PK2 was performed closer to the edge of the coal mound. A Seismic Dilatometer (SDMT) test was performed approximately 1.6 m from CPT PK1. Dilatometer measurements were made at 2 m intervals and shear-wave measurements at 4 m intervals.

Figure 5 Illustrates that some preparation of the coal mound was considered necessary to enable the testing rig to be installed in a safe and stable manner. For operational reasons, the test programme was performed at night (Figure 6).



Figure 5. Coal mound at port of loading.



Figure 6. CPT and SDMT equipment on coal mound.

2.3 Coal – CPT results

Reference CPT data are presented on Figure 7. CPT PK1 indicates high variability of cone resistance within the upper seven metres of testing. This is considered likely to be a product of the initial mound levelling works, as the results for CPT PK2 (where less preparation was performed) were highly

variable only in the upper two metres. Beneath the highly variable zones, both CPTs indicated a steady trend of increasing cone tip resistance. Localised peaks of cone resistance below the upper variable zone, are considered likely to be caused by the presence of larger coal fragments. Pore-water pressure values were generally negligible, except between 6-7 m in CPT PK1. This zone of measurable pore pressure was considered likely to be due to a localised zone of higher water and fines contents.

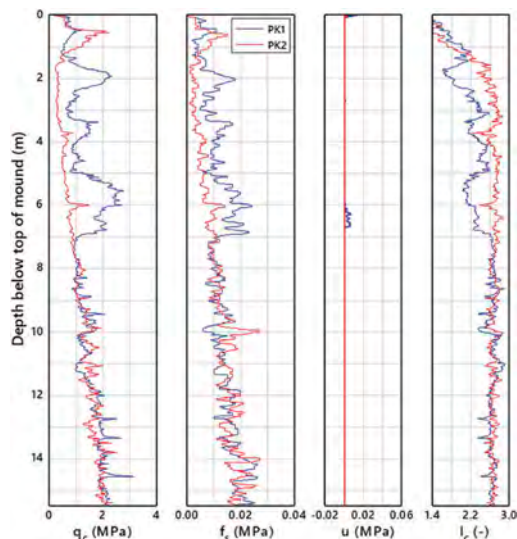


Figure 7. Case 2 - Basic CPT data – Coal port of loading.

3 INTERPRETATIONS

3.1 General

In each case, the average bulk density of the ore, in the ships hold, was calculated as the ratio of the volume of the ore mound (surveyed using a laser-scanning technique), and the mass of ore deposited into the hold during loading.

In each case, maximum and minimum dry density values were provided by the Client, so exact details of the methods are unavailable for this paper. However, it is understood that maximum dry density assessments were based on a standard “Proctor” approach, and minimum dry density assessments were made using a funnel-type approach.

3.2 Case 1 – iron-ore

The CPT results were used to infer density and void ratio profiles at the port of loading and the port of discharge. Changes in these profiles, caused by the ship’s movements during sailing,

could then be inferred by comparing corresponding results.

3.2.1 Iron-ore reference data

- Average dry density, $\rho_{dry} = 1.94 \text{ Mg/m}^3$
- Maximum dry density, $\rho_{d \max} = 2.66 \text{ Mg/m}^3$
- Minimum index dry density, $\rho_{d \min} = 1.76 \text{ Mg/m}^3$
- Particle density, $PD = 3.96 \text{ Mg/m}^3$

3.2.2 Methodology for inferring relative and dry density profiles

The average dry density profile in the ore-mound was inferred using a three-step iterative process.

Step 1 – infer nominal relative density profiles from the CPT data

Step 2 - use the maximum and minimum dry density data to convert the nominal relative density profiles to equivalent dry density profiles.

Step 3 – iterate until the inferred relative density and dry density profiles are plausible and the average inferred dry density is the same as the average dry density (calculated from survey measurements of the mound volume and the measured weight of the loaded ore).

The formulae used to perform these calculations are discussed in the following section.

3.2.3 Density and void ratio calculations

Relative Density, D_r , is an estimate of the state of material packing, relative to reference maximum and minimum values. Relative density is defined as:

$$D_r (-) = (e_{max} - e) / (e_{max} - e_{min}) \quad (1)$$

Based on testing in a large calibration chamber, Baldi et al. (1986) published the generic formula presented in Equation 1, for estimating the nominal relative density of silica sands.

$$D_r(-) = \left(\frac{1}{C_2} \right) \ln \left(\frac{q_c}{C_0 * (\sigma_m^{C_1})} \right) \quad (2)$$

The C_0 , C_1 and C_2 coefficients that provided the best agreement for Ticino sand are summarised in Table 1. These values were used as a starting point for assessments of the iron-ore mound at the port of

Table 1. Summary of coefficients used to estimate relative density profiles in the iron-ore mound.

Material	C_0	C_1	C_2	K_0
Ticino Sand	181	0.55	2.61	0.4
Iron-ore	118	0.55	2.61	0.4

loading. It was concluded that plausible profiles could be obtained simply by changing the C_0 coefficient, as shown in Table 1.

Dry density was calculated using Equation 3:

$$\rho_d (\text{Mg/m}^3) = \frac{\rho_{d \max} * \rho_{d \min}}{(1 - D_r) \cdot \rho_{d \min} + D_r \cdot \rho_{d \max}} \quad (3)$$

Void ratio and volumetric strain profiles were calculated using Equations 4 and 5, respectively. The results are presented on Figure 9, together with the change in volumetric strain between the ports of loading and discharge.

$$\text{Void ratio } e(-) = \frac{PD}{\rho_d} - 1 \quad (4)$$

$$\text{Volumetric strain, } \varepsilon_v(\%) = \frac{e - e_0}{1 + e_0} * 100 \quad (5)$$

Figure 8 presents composite profiles of inferred nominal relative density, dry density, and void ratio. Although the profiles tend to be relatively consistent below approximately 8 m depth, there is much more variability in the upper material. To enable clearer identification of trends, the void ratio data were averaged over 1 m increments. Figure 9 presents the results of this averaging process, in terms of predicted void ratio, change in void ration and volumetric strain. It may be seen that the trends are much clearer in Figure 9. In particular the average volumetric strain profile indicates a steady reduction in

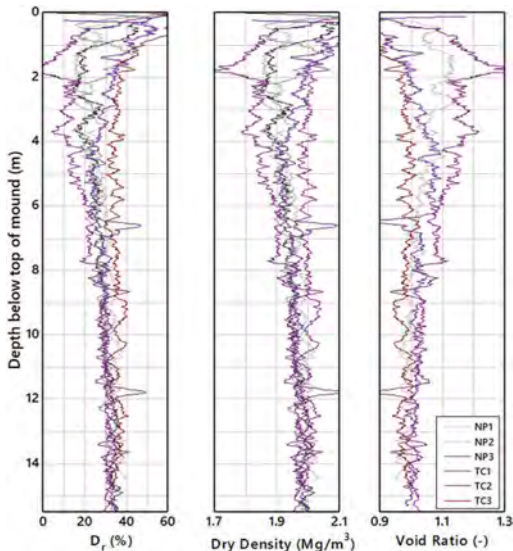


Figure 8. Inferred relative density, dry density, and void ratio profiles at the ports of loading and discharge.

volumetric strain, from greater than 4 % in the upper metre, reducing to less than 1% below 4 m. Of course, the magnitude of these inferred changes was dependent on the metocean conditions encountered during the ship's voyage. Discussion on these aspects is, however, beyond the remit of this paper.

Although the profiles presented on Figures 8 and 9 are inferred, it is interesting to note that the average inferred volumetric strain is in excellent agreement with the average volumetric strain calculated from detailed surveys of the ore-mound geometries at the ports of loading and discharge.

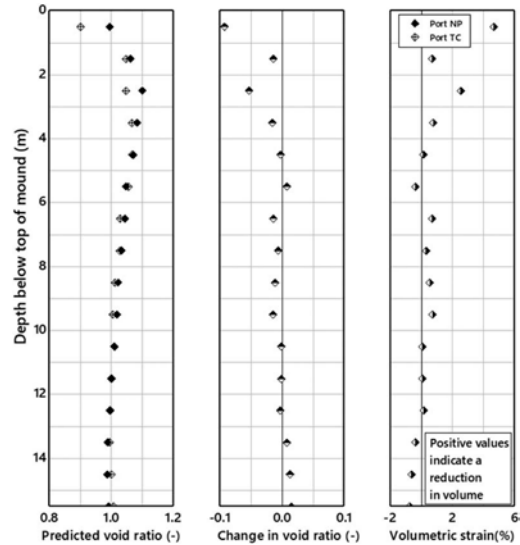


Figure 9. Changes in void ratio and volumetric strain incurred between ports of loading and discharge.

3.3 Case 2 – coal

3.3.1 General approach

The objectives of the testing at the port of loading were to assess density and stiffness variations in the coal, shortly after loading in the ship's hold. The CPT data were used to infer dry density profiles using the same three step approach used for the iron-ore. The CPT data were also used to infer low-strain shear stiffness, G_{\max} , and constrained modulus profiles, to enable for comparison with profiles estimated using the SDMT data.

3.3.2 Coal reference data

- Average dry density, $r_{\text{dry}} = 0.95 \text{ Mg/m}^3$
- Maximum dry density, $r_{d \max} = 1.05 \text{ Mg/m}^3$
- Minimum dry density, $r_{d \min} = 0.71 \text{ Mg/m}^3$
- Particle density, $PD = 1.37 \text{ Mg/m}^3$

3.3.3 Density and void ratio calculations

As for the iron-ore, it was found that the general form, given in Equation 2, could be adapted for use

in the coal mound. However, in the case of the coal mound, all three coefficients were changed in order to infer plausible profiles. The C_0 , C_1 and C_2 coefficients that provided the best agreement are summarised in Table 2.

Table 2. Summary of coefficients used to estimate relative density profiles in the coal mound.

C_0	C_1	C_2	K_o
17	0.4	3.9	0.4

Inferred profiles of relative density, dry density and void ratio are presented on Figure 10.

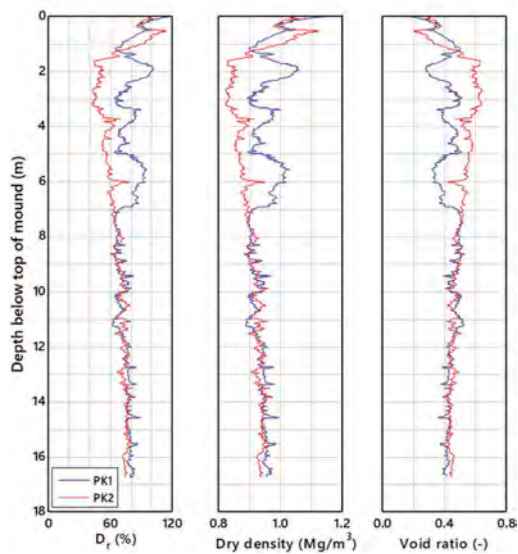


Figure 10. Inferred relative density, dry density, and void ratio profiles at the port of loading.

3.3.4 Constrained modulus calculations

Constrained Modulus, M , was inferred from the SDMT measurements using Equation 6 (Marchetti et al., 2001).

$$M = 0.85 * 34.7 * (P_1 - P_0) / 1000 \quad (6)$$

Baldi et al (1986) developed a correlation for estimating M in silica sands (for a vertical strain of approximately 0.1%) by comparing one-dimensional compression results with cone resistance data measured in a calibration chamber (Baldi, 1985). The correlation, which is presented in Equation 7, considers cone resistance, q_c , in-situ stress conditions, σ'_m , and over-consolidation ratio, OCR:

$$M = C_0 * p_a * \left(\frac{\sigma'_m}{p_a} \right)^{C_1} * OCR^{C_2} * \exp(C_3 * Dr) * q_c \quad (7)$$

The original coefficients published by Baldi et al. (1986) are presented in Table 3, together with the coefficients that provided better agreement with M values inferred from the SDMT measurements.

Table 3. Summary of coefficients used to estimate constrained modulus in the coal mound.

Material	C_0	C_1	C_2	C_3
Baldi et al (1986)	14.48	-0.116	0.313	-1.123
Coal mound	5.4	-0.116	0.313	-0.4

The right-hand graph on Figure 11 presents M , profiles results of both CPT and SDMT interpretations – it is considered that there is acceptable agreement over whole profile.

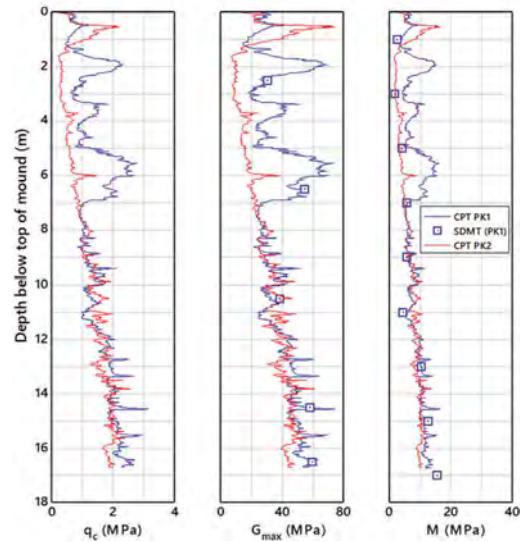


Figure 11. Inferred G_{max} and M profiles at the port of loading.

3.3.5 Low-strain shear modulus calculations

Direct measurements of shear wave velocity were performed during the SDMT testing adjacent to Test PK1. Low-strain shear modulus, G_{max} , values between individual test locations were then calculated using Equation 8:

$$G_{max} = \rho_{bulk} * v_s^2 \quad (8)$$

Equations for estimating G_{max} from cone data were also published by Baldi et al. (1986). However, in the case of the coal mound, it was found that acceptable agreement with the SDMT G_{max} measurements could be obtained simply by increasing the C_0 coefficient in the Baldi et al. (1986) Constrained Modulus equation, by a factor of 4.5 - as shown in Equation 9.

$$G_{max} = 24.3 * p_a * \left(\frac{\sigma'_m}{p_a} \right)^{-0.116} * OCR^{0.313} * \exp(-0.4 * D_r) * q_c \quad (9)$$

The results of the G_{max} interpretations, which are presented on the middle graph on Figure 11, indicate good agreement between the CPT interpretations and the SDMT measurements.

4 DISCUSSION AND CONCLUSIONS

- 1) As expected, ore properties were inferred to vary much more in the upper part of the ore-mound, with variability gradually reducing with depth.
- 2) A general trend of increasing nominal relative density with depth was inferred in all tests. This would be expected, as the standard "high-energy air-pluviation" method used to load the ore vessels would inevitably lead to more compactive effort being applied to materials at greater depths.
- 3) It was possible to obtain good agreement between material properties inferred from CPT data, and material properties inferred from survey data and the weight of material loaded into the ships' holds.
- 4) As expected, the CPT measurements implied that vessel-movement induced densification occurred from the top of the iron-ore mound downwards.
- 5) The consistent increase in sleeve friction noted at in the iron-ore mound at the port of discharge, was considered to suggest that there had been a wave-induced increase in K_o . However, as no testing was performed to quantify any change in K_o , a constant value of K_o was assumed in the calculations. This is considered a potential source of error in the post-voyage calculations of relative density (and hence dry density and void ratio).
- 6) No significant zones of pore pressure were measured at the ports of loading. This was interpreted

to suggest that there had been no significant tendency of the ores to saturate at the base immediately after loading.

- 7) Good agreement between stiffness properties inferred from CPT data and equivalent properties inferred from SDMT results could be obtained by making ore-specific amendments to published correlations.

REFERENCES

- Baldi et al. (1985) Laboratory validation of in-situ tests. Published by the Italian Geotechnical Society (AGI) on the occasion of the ISSMFE Golden Jubilee
- Baldi, G., Bellotti, R., Ghionna, V. N., Jamiolkowski, M. & Pasqualini, E. 1986. Interpretation of CPTs and CPTUs. Part II: Drained Penetration of Sands, Proc. 4th International Geotechnical Seminar on Field Instrumentation and In-situ Measurements, Nanyang Tech Inst. Singapore.
- Marchetti S., Monaco P., Totani G. & Calabrese M. 2001. The Flat Dilatometer Test DMT. in soil investigations - A Report by the ISSMGE Committee TC16, IN SITU 2001, International. Conference on in-situ Measurement of Soil Properties, Bali, Indonesia

SYMBOLS AND ABBREVIATIONS

CPT	Cone Penetration Test (with pore-pressure measurements)
D_r	nominal relative density (%)
e	void ratio (-)
e_0	initial void ratio (-)
f_s	CPT measured sleeve friction (MPa)
G_{max}	low-strain shear modulus (MPa)
I_c	Soil behaviour type index (-)
K_o	Coefficient of earth pressure at rest (-)
M	secant constrained modulus (MPa)
OCR	overconsolidation ratio
p_a	reference stress equal to 98.1 kPa
PD	particle density of ore (Mg/m^3)
P_0	corrected dilatometer pressure reading when the membrane first breaks away from the seating.
P_1	corrected dilatometer reading when the membrane movement is 1.1 mm away from the seating.
p_o'	effective overburden pressure (kPa)
q_c	CPT measured cone resistance (MPa)
SDMT	Dilatometer test with shear-wave measurements
u	CPT measured pore-water pressure (MPa)
v_s	measured shear wave velocity in soil (m/s)
ρ_{dry}	dry density of soil (Mg/m^3)
ρ_{bulk}	bulk density of soil (Mg/m^3)
$\rho_{d max}$	maximum dry density (Mg/m^3)
$\rho_{d min}$	minimum dry density (Mg/m^3)
σ'_m	mean effective stress at test depth (kPa)

Suction influence on CPT and DMT for some Brazilian tropical soils

B.P. Rocha

Federal Institute of São Paulo (IFSP), Advanced Campus of Ilha Solteira, Brazil

R.A. Rodrigues & H.L. Giacheti

Department of Civil and Environmental Engineering, São Paulo State University (Unesp), Brazil

ABSTRACT: Suction plays an important role in geotechnical engineering practice since it influences the mechanical behavior of unsaturated soils. Interpretation of in situ test data at unsaturated soil sites must consider both spatial and seasonal variability, especially in strength and stiffness parameters. This paper presents and discusses CPT and DMT performed at different seasons at two sites with tropical sandy soils. CPT and DMT data were interpreted considering the influence of soil suction. Suction was estimated from water content profiles and soil water retention curves (SWRC). Failure to consider the effect of soil suction in the site investigation of unsaturated soils can lead to inappropriate soil classification as well as significant and unconservative overestimates of geotechnical parameters.

1 INTRODUCTION

Site characterization can be defined as the process of identifying the geometry of relatively homogeneous zones and developing index, strength, and stiffness properties for the soils within these zones. Some *in-situ* testing methods can be used as an alternative to the traditional approach of drilling, sampling, and laboratory testing.

Many geotechnical works (e.g., shallow foundations, embankments, and slopes) are performed on unsaturated deposits. Suction increases the shear strength and stiffness of these soils (Alonso *et al.* 1990). Such influence on the geotechnical soil behavior is well understood based on laboratory tests, however they are expensive and time-consuming since it involves undisturbed soil sampling.

In-situ tests, such as the cone penetration (CPT) and the flat dilatometer (DMT) tests allow combining stratigraphic logging with specific measurements, which is a modern approach available for site characterization and could be used to improve the site characterization in unsaturated soils. Only few studies deal with in situ test interpretation in unsaturated soils, as well as the influence of soil suction in the interpretation (Lehane *et al.* 2004; Pournaghiazar *et al.* 2013; Lo Presti *et al.* 2018; Giacheti *et al.* 2019; Rocha *et al.* 2021).

This paper presents and discusses the influence of soil suction on CPT and DMT carried out in two unsaturated tropical soil sites from Brazil. CPTs, DMTs and water content profiles were determined in

different periods of the year. The tests data are presented and interpreted considering the soil-water retention curves (SWRC). Soil suction influence was incorporated to the effective stress following Bishop's (1959) equation to interpret the in-situ tests data.

2 BACKGROUND

Interpretation of in-situ tests usually assumes pore pressure equal to zero in unsaturated soils. Therefore, the total stress (σ_v) is assumed to be equal to the effective stress (σ_v'). Moreover, the interpretation does not consider the suction contribution to the effective stress.

Soil suction should be incorporated into the interpretation of in-situ tests on unsaturated soils. Suction can be incorporated into effective stress following Bishop (1959), when σ_v' is defined by Equation 1:

$$\sigma_v' = \sigma_v + \chi(u_a - u_w) \quad (1)$$

where χ is the effective stress parameter, u_a is the pore air pressure and u_w is the pore water pressure. Soil suction is the difference between u_a and u_w . χ is equal to 1 for saturated soils and 0 for dry soils, and it can be assumed to be equal to the degree of saturation (S_r) (Öberg & Sällfors 1997; Robertson *et al.* 2017).

The interpretation of CPT data starts by calculating the normalized cone resistance (Q_m) (Eq. 2).

$$Q_m = \left(\frac{q_t - \sigma_v}{p_a} \right) \left(\frac{p_a}{\sigma_v'} \right)^n \quad (2)$$

where σ_v is the total stress, σ_v' is the effective stress, p_a is the atmospheric reference pressure in the same unit as q_c and σ_v , $(q_c e \sigma_v)/p_a$ is the dimensionless net cone resistance, $(p_a/\sigma_v)^n$ is the stress normalization factor, and n is the stress exponent that relates q_c to σ_v' and can be defined in power law relationships defined according to Robertson (2009). The stress exponent (n) is 1.0 for most fine-grained soils, and ranges from 0.5 to 0.9 for coarse-grained soils.

Similar approach can be used to interpret DMT in unsaturated soils. DMT data interpretation begins by determining three intermediate parameters: material index (I_D – Eq. 3), horizontal stress index (K_D – Eq. 4), and dilatometer modulus (E_D – Eq. 5).

$$I_D = (p_1 - p_0)/(p_0 - u_0) \quad (3)$$

$$K_D = (p_0 - u_0)/\sigma_v' \quad (4)$$

$$E_D = 34.7(p_1 - p_0) \quad (5)$$

where p_0 is the corrected first reading, p_1 is the corrected second reading, and u_0 represents the pre-insertion in-situ equilibrium pore pressure.

Lutenegger (1988) reported little change in the I_D profile and a decrease in the K_D and E_D profiles with a reduction in soil suction. So, since the soil suction influences DMT interpretation, it should be incorporated into K_D and E_D values. Soil suction can be incorporated in the σ_v' to calculate the K_D value. However, effective stress is not included in Equation 5. In this way, Equation 6 (Janbu 1963) was used to incorporate soil suction into the E_D value.

$$E_D = K_E p_a \left(\frac{\sigma_v'}{p_a} \right)^n \quad (6)$$

where n is a stress exponent (0.5 for coarse-grained soils), K_E is the modulus number and p_a is the reference pressure assumed equal to 100 kPa.

Two steps were used to determine the measured E_D values without and with considering the soils suction:

- K_E was calculated by Equation 6 considering the soil suction value in the σ_v' by Equation 1.
- The normalized E_D value was calculated by Equation 6 considering K_E previously defined and, assigning soil suction equal to zero to calculate σ_v' .

Such approaches allow soil suction to be incorporated into the interpretation of CPT and DMT data. Suction can be incorporated in σ_v' by using χ and soil suction based on the water content profiles and soil-water retention curves (SWRC). That was used by Giacheti *et al.* (2019) and Rocha *et al.* (2021) and

provided a better CPT and DMT data interpretation for unsaturated soils.

3 STUDY SITES

3.1 Unesp and USP research sites

The Unesp research site are in the city of Bauru, state of São Paulo. The soil at the site is an unsaturated red clayey fine sand with high porosity. It is classified as a soil from SM Group in the Unified Soil Classification System (USCS). The top 13 m is a colluvium soil overlaying a residual soil derived from the weathering of sandstone. The colluvium soil has lateritic soil behavior (LA'). The groundwater level was not found up to 30 m deep.

The USP research site are also located on the central part of São Paulo state in the São Carlos city, which are around 150 km apart from Unesp - Bauru research site. The site profile is a saprolitic sandstone residual soil layer covered by a lateritic clayey sand (LA') layer (6 m thick colluvial soil - Cenozoic sediment) (Machado and Vilar 1998). A 0.2 to 0.5 m thick layer of pebbles separates the Cenozoic Sediment layer from the residual soil. Both layers are classified as a soil from SC Group by USCS. The groundwater level varies seasonally between 9 and 12 m below the ground surface. Table 1 shows typical values for the grain size distribution, void ratio (e), dry unit weight (γ_d), unit weight of solids (γ_s) and consistency limits (w_{LL} and w_{LP}) for both sites.

Table 1. Physical indexes, grain size distribution and USCS classification for the soils from each site.

	Unesp	USP
e	0.65 – 0.81	0.60 – 1.05
γ_d (kN/m ³)	14.8 – 16.5	12.5 – 16.6
γ_s (kN/m ³)	26.5 – 26.9	27.1 – 27.5
Sand (%)	78 – 83	60 – 69
Silt (%)	4 – 8	5 – 14
Clay (%)	12 – 17	17 – 28
w_{LL} (%)	17 – 23	39 – 45
w_{LP} (%)	non-plastic	19 – 25
USCS	SM	SC

3.1.1 Previously performed laboratory tests

Drying soil-water retention curves (SWRCs), oedometer and triaxial tests were carried out on undisturbed soil samples collected from each site. Samples were collected at 1, 3 and 5 m depth for Unesp, and 2, 5 and 8 m depth for USP. The laboratory test campaigns were carried out to study the influence of soil suction on soil strength and stiffness parameters. The main purpose of the laboratory investigation was to assess the influence of suction on the soil behavior.

The SWRCs were obtained using the suction-plate, pressure-chamber, and filter-paper. The results for the tested samples were adjusted according to the van Genuchten (1980) equation. Triaxial compression and oedometer tests were performed on saturated and non-saturated samples. Controlled suction tests were carried out by imposing the desired suction according to axial translation technique (Hilf 1956). Figure 1 and 2 presents the SWRCs for Unesp and USP sites, respectively. The suction effects in the cohesion intercept (c) and preconsolidation stress (σ'_p) are presented in Table 2 for Unesp site and in Table 3 for USP site. The air entry value is very low for the soils from both sites as can be seen in the SWRCs. They are typical sandy soils curves in that most of the water is extracted by a small change in soil suction. The interpretation of soil suction influence on preconsolidation and cohesion intercept combined with SWRC allows to define two regions in SWRCs for Unesp (Figure 1) and for USP sites (Figure 2).

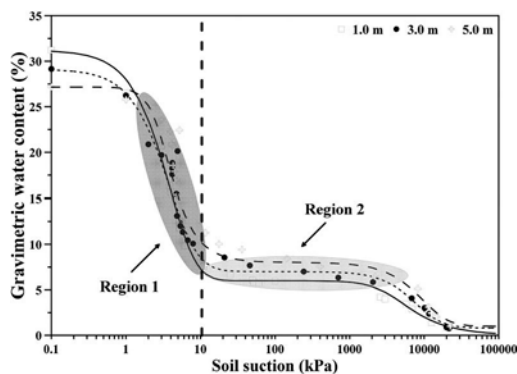


Figure 1. Soil-water retention curves for the soil samples collected at 1.0, 3.0 and 5.0 m depths for Unesp site (adapted from Fernandes *et al.* 2017).

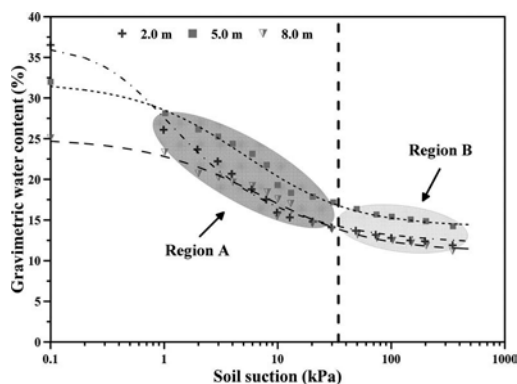


Figure 2. Soil-water retention curves for the soil samples collected at 2.0, 5.0 and 8.0 m depths for USP site (adapted from Machado 1998).

For the Unesp site, water content values higher than 6 to 7% (Region A) the cohesion intercept and preconsolidation stress values were slightly affected. However, the opposite occurs for water content lower than 6 to 7% (Region B). It is noted that in this region of the curves, a slight variation in water content can substantially affect soil suction.

Table 2. Cohesion (c) and preconsolidation stress (σ_p) for different depths and soil suctions for Unesp site (adapted from Fernandes *et al.* 2017).

Suction (kPa)	c (kPa)			σ_p (kPa)		
	1 m	3 m	5 m	1 m	3 m	5 m
0	0	1.2	5.3	30	36	69
50	3	6.5	10.3	77	135	176
100	-	-	-	108	163	205
200	11	13.4	24.2	140	200	221
400	16	21.5	28.3	176	221	229

Similar behavior can be observed for USP site. c and σ_p values are slightly influenced by soil suction for water content higher than 15 to 16%, i.e., Region A of SWRCs (Figure 2). In Region B, both c and σ_p vary markedly with suction, for water content values below 15 to 16% (Figure 2). In this region a slight variation in water content substantially modifies soil suction.

Table 3. Cohesion intercept and preconsolidation stress for different depths and soil suctions for USP site (adapted from Machado 1998).

Suction (kPa)	Cohesion intercept (kPa)			Preconsolidation stress (kPa)		
	2m	5m	8m	2m	5m	8m
0	0	10.5	26.9	41	122	171
40	14.9	26.7	44.6	-	-	-
50	-	-	-	150	181	291
80	21.1	29.6	57.6	-	-	-
100	-	-	-	189	207	310
120	23.1	36.1	51.9	-	-	-
160	30.1	43.9	53.4	-	-	-
300	-	-	-	316	331	351
400	-	-	-	430	-	461

3.1.2 Previously performed in-situ tests

CPTs and DMTs were previously performed in both sites to study the effect of the unsaturated condition on the interpretation of these tests. Water content profiles (Figure 3) and soil water retention curves (Figure 1 and Figure 2) were employed to evaluate such effects.

Figure 3a presents the average water content profiles obtained for the wet and the dry seasons at the Unesp site, while Figure 3b shows moisture content profiles measured between 2014 and 2017 for the USP site. It can be seen in Figure 3a (Unesp site) that there is a significant variation in water content up to 4 m depth, where the soil interacts with the atmosphere, and decreases with increasing depth. The water content in the soil down to 4 m depth is lower than 7% in the dry season and vary from 7% to 10% in the wet season. It can be observed in Figure 3b (USP site) that March/2016 was the period with higher water content and October/2017 was the lowest at the end of the dry season.

It is important to point out that there are trees in both sites. The extraction of water via the roots of the trees during the dry season brought the degree of saturation to approximately 30-40% and, consequently, high values of soil suction (Lehane *et al.* 2004; Giacheti *et al.* 2019; Rocha *et al.* 2021).

Giacheti *et al.* (2019) presented and discussed CPT data to illustrate the seasonal variability for the Unesp site. Soil suction significantly influenced CPT data up to a depth of 4 m at the Unesp site. Rocha *et al.* (2021) presented and discussed the influence of soil suction on DMTs carried out at the USP site. Both papers incorporated soil suction into σ_v' by using χ and soil suction (Eq. 1), as estimated from the degree of saturation and SWRCs, respectively, for better interpretation of CPT and DMT data.

3.2 CPT, DMT and soil sampling

Two campaigns were performed in 2019 at the Unesp site, one in the wet season (April) and one in the dry season (September). Two CPTs, two DMTs and one soil sampling were carried out for each campaign. Two in situ testing campaigns were also carried out at the USP site (March/2016 and October/2017). Three CPTs

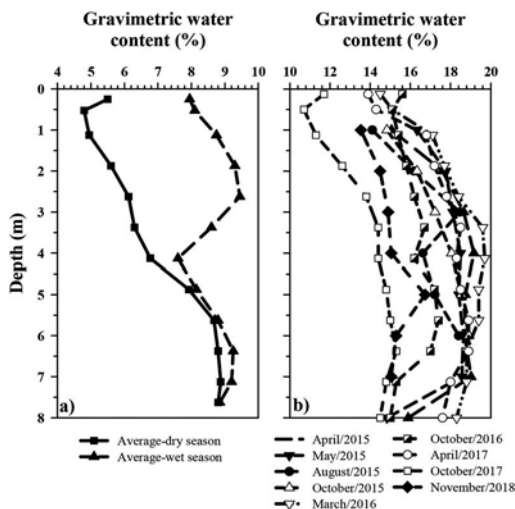


Figure 3. Water content profiles for (a) Unesp and (b) USP sites (adapted from Rocha *et al.* 2021; Giacheti *et al.* 2019).

and one soil sampling were conducted for each campaign. A multi-function penetrometer (150 kN thrust capacity) was used to perform the in situ tests. Soil sampling was carried out from ground surface up to 8.0 m depth by using a helical auger to collect samples every 0.75 m to determine the water content profile.

3.3 CPT and DMT at the Unesp site

Figure 4 and Figure 5 presents the difference between CPTs and DMTs carried out under different water content conditions in terms of average q_c and f_s (Figure 4) and average I_D , K_D and E_D (Figure 5). The data show the soil suction influence on CPT and DMT up to approximately 5 m depth in the, mainly on the q_c , K_D and E_D . Such behavior can be explained from SWRCs (Figure 1). The water content values determined in April/2019 are greater than 6% and tend to be in Region A in the SWRCs (Figure 1), while the water content values determined in September/2019 are lower than 6% and tend to be in Region B of the SWRCs (Figure 1). In Region A of the curve, water content varies greatly with slight variation in suction, and the opposite trend occurs in Region B, where suction values vary significantly with little variation in water content.

Soil suction was incorporated in σ_v' by Equation 1 to improve CPT and DMT interpretation. The estimated soil suction was defined from water content profiles (Figure 4a and Figure 5a) and the SWRCs (Figure 1). It was found that soil suction values can be higher than 1 MPa up to 5 m depth in the September/2019 campaign. Khalili & Khabbaz (1998) highlighted that soil suction varies from 0 to 600 kPa for most practical applications in geotechnical engineering. An average suction value equal to 300 kPa was used in this analysis. χ was assumed to vary linearly with the degree of saturation (S_r) for the Unesp site (Robertson *et al.* 2017; Giacheti *et al.* 2019; Rocha *et al.* 2021). Table 4 presents the average χ parameter for each test campaign and the assumed soil suction value obtained from Figure 1 and Table 1.

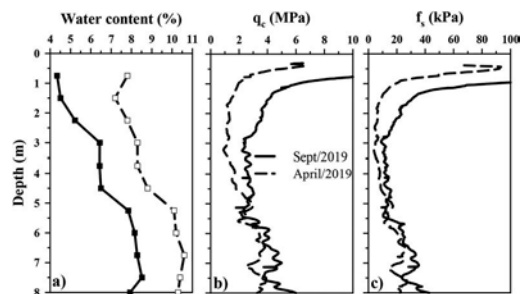


Figure 4. Average q_c , f_s and water content profiles from each test campaign for the Unesp site.

Table 4. Assumed values for χ and soil suction for each test campaign - The Unesp site.

	χ	Soil suction (kPa)
April 2019	0.38	8
Sept/2019	0.25	300

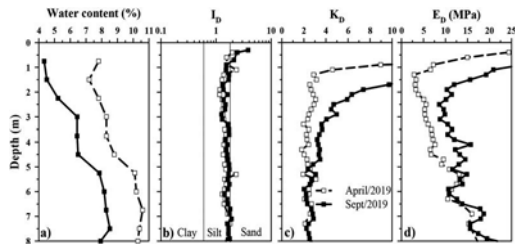


Figure 5. Average I_D , K_D , E_D and water content profiles from each test campaign for the Unesp site.

Figure 6 and Figure 7 showing, respectively, the profiles of Q_{tn} and of K_D and E_D were elaborated without considering the soil suction influence, following *item 2* presented earlier in this paper. The stress exponent (n) was assumed equal to 0.70 for both saturated and unsaturated conditions to determine Q_{tn} for the Unesp site. When the suction values from each test campaign were incorporated into the effective stresses, the average profiles of Q_{tn} , K_D and E_D were similar and equivalent to the profiles without soil suction.

3.4 CPT at the USP site

Figure 8 shows the water content profiles and average q_c and f_s determined for March/2016 and October/2017 campaigns. It is interesting to note in this figure that the variation in soil suction was significant up to approximately 6 m depth.

These differences can be explained by the SWRCs and water content profiles (Figure 2 and Figure 8a). CPTs carried out in March/2016 tend to be in Region A, and October/2017 CPTs in Region B. The estimated soil suction values are lower for March/2016 (water content values higher than

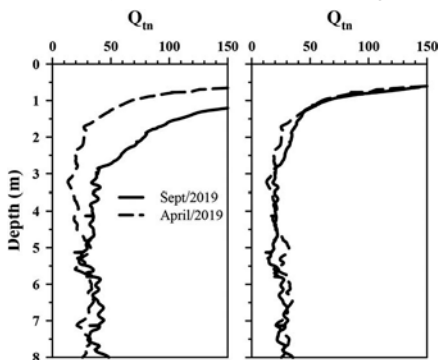


Figure 6. Average Q_{tn} profiles (a) without and (b) with incorporating soil suction for the Unesp site.

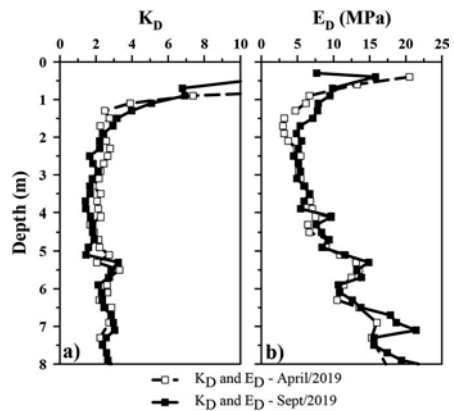


Figure 7. (a) K_D and (b) E_D , considering soil suction influence on σ'_v for the Unesp site.

15.6% - Region A) and higher for October/2017 (water content values lower than 15.3% - Region B).

The CPT interpretation starts from normalized cone resistance (Q_{tn}) calculation by Equation 2. The soil suction was incorporated into σ'_v following Equation 1. Table 5 presents the average χ parameter for both campaigns and the assumed soil suction value determined by Figure 2 and Table 1. The stress exponent (n) was assumed equal to 0.97 to calculate Q_{tn} for both saturated and unsaturated conditions. All Q_{tn} profiles from each campaign are similar (Figure 9) when the soil suction is included in effective stresses (Eq. 1 and Table 5).

Table 5. Assumed values for χ and soil suction for each test campaign - The USP site.

	χ	Soil suction (kPa)
March/2016	0.65	10
October/2017	0.42	150

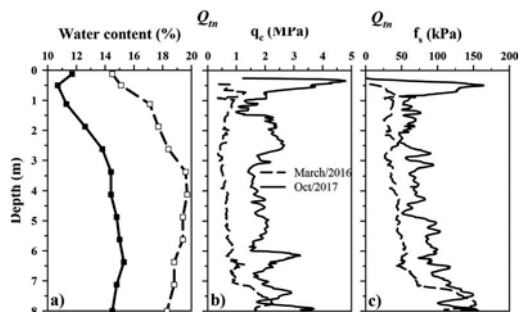


Figure 8. Water content and average CPT profiles from each campaign for the USP site.

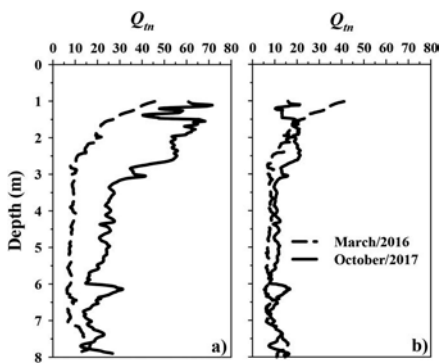


Figure 9. Average Q_m profiles incorporating soil suction for the USP site.

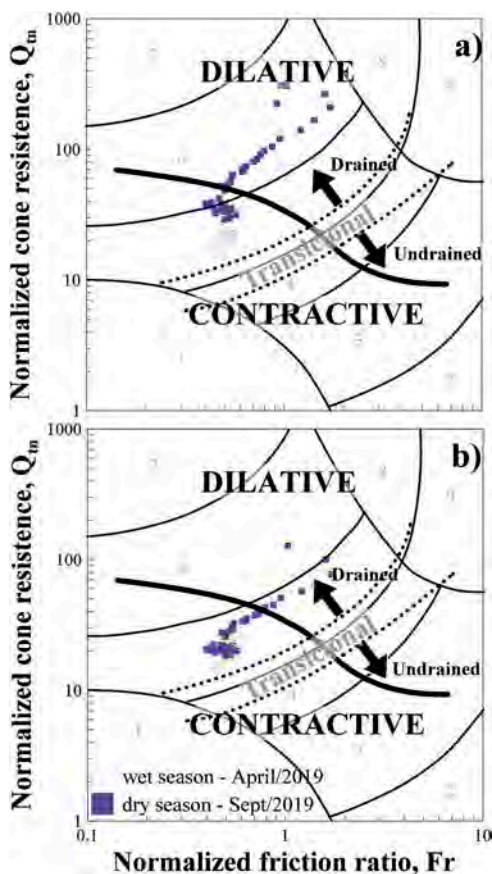


Figure 10. Average CPT data from both wet and dry seasons plotted on the Robertson (2009) classification chart (a) without and (b) with consideration of soil suction into σ_v' .

4 CPT CLASSIFICATION AND SOIL SUCTION

The influence of suction on CPT classification was evaluated for the Unesp site. Figure 10 presents the

average CPT data to the depth of 5 m (active zone) plotted on the CPT classification chart (Robertson 2009) with and without incorporating soil suction into σ_v' . It can be seen in this figure that all CPT data are plotted in the drained penetration zone, which is an appropriate classification for this soil type in unsaturated condition (Yang & Russell 2016).

It can be seen in Figure 10a that when soil suction is not included in σ_v' , the soil is classified predominantly as sands (zone 6) during the dry season (high suction) and as sand mixtures (zone 5) during the wet season (low suction). Figure 10a also indicates that the soil is more contractive during the wet season, while it is more dilative during the dry season. When a suction value equal to 300 kPa was incorporated into σ_v' , the soil behaves in the same way as during the wet season (low suction), i.e., contractive sand mixtures (Figure 10b). This agrees with the dispersant-free particle size distribution curve (Table 1), as well as the change in soil volume during shear (Fernandes *et al.* 2017).

5 CONCLUSIONS

The data presented show the influence of seasonal variation in water content and soil suction profiles and how they influence soil behavior CPT and DMT data are significantly influenced by soil suction. In general, the effects of suction are more pronounced for lower soil densities and confining stresses. It was observed that soil suction significantly influenced CPT data up to a depth of 6 m at the USP site and up to 5 m depth for the Unesp site. The same behavior was also observed for the DMT for the Unesp site.

The effective stress approach allows soil suction to be considered into CPT and DMT data interpretation. The influence can be incorporated in σ_v' by using χ and soil suction based on the water content profiles and SWRC. Such approach provides a better CPT and DMT interpretation for unsaturated soils.

ACKNOWLEDGMENTS

The authors thank the São Paulo Research Foundation, FAPESP (2015/17260-0 and 2017/23174-5), the National Council for Scientific and Technological Development, CNPq (308895/2015-0 and 436478/2018-8) and the Coordination for the Improvement of Higher Education Personnel, CAPES, for the first author scholarship.

REFERENCES

Alonso EE, Gens A, Josa A (1990) A constitutive model for partially saturated soils. *Geotechnique* 40: 405–430. <http://dx.doi.org/10.1680/geot.1990.40.3.405>

- Bishop AW (1959) The principle of effective stress. *Teknisk Ukeblad* 106:859–863
- Fernandes JB, Rocha BP, Rodrigues RA, Giacheti HL (2017) Strength and Stiffness Parameters of an Unsaturated Tropical Soil. 2nd PanAmerican Conference on Unsaturated Soils. <https://dx.doi.org/10.1061/9780784481707.044>
- Giacheti HL, Bezerra RC, Rocha BP, Rodrigues RA (2019) Seasonal influence in CPT: an unsaturated soil site example. *Journal of Rock Mechanics and Geotechnical Engineering* 11(2):361–368. <https://dx.doi.org/10.1016/j.jrmge.2018.10.005>
- Hilf JW (1956) *An investigation of pore-water pressure in compacted cohesive soils*. Ph.D. thesis, Faculty of the Graduate, School of the University of Colorado
- Janbu N (1963) Soil compressibility as determined by oedometer and triaxial tests. In: *Proc. of European conference on soil mechanics and foundation engineering, vol 1*. pp 19–25. Deutsche Gesellschaft für Erd-und Grundbau, Wiesbaden, Germany.
- Khalili N, Khabbaz MH (1998) A unique relationship for the determination of the shear strength of unsaturated soils. *Géotechnique* 48(5): 681–687.
- Lehane BM, Ismail MA, Fahey M (2004) Seasonal dependence of in situ test parameters in sand above the water table. *Geotechnique* 54(3): 215–218. <https://dx.doi.org/10.1680/geot.2004.54.3.215>
- Lo Presti D, Stacul S, Meisina C, Bordoni M, Bittelli M (2018) Preliminary validation of a novel method for the assessment of effective stress state in partially saturated soils by cone penetration tests. *Geosciences* 8(1):1–13. <https://dx.doi.org/10.3390/geosciences8010030>
- Lutenegger AJ (1988) Current status of the Marchetti dilatometer test. In: *Proc. of ISOPT-1 penetration testing: special lecture, vol 1*, pp 137–155. Balkema, Rotherdam.
- Machado SL, Vilar OM (1998) Unsaturated soils shear strength: laboratory tests and expedite determination. *Solos e Rochas* 21(2):65–78 (in Portuguese)
- Marchetti S (1980) In situ tests by flat dilatometer. *Journal of Geotechnical Engineering* 106: 299–321
- Marchetti S, Monaco P, Totani G, Calabrese M (2001) The Flat Dilatometer Test (DMT) in soil investigations: a report by the ISSMGE TC Committee 16. In: *Proceedings of the international conference on in situ measurement of soil properties and case histories*. Parahyangan Catholic University, Bandung, Indonesia, pp 95–132.
- Morais TSO, Tsuha CHC, Bandeira No LA, Singh RM (2020) Effects of seasonal variations on the thermal response of energy piles in an unsaturated Brazilian tropical soil. *Energy Build* 216:109971. <https://dx.doi.org/10.1016/j.enbuild.2020.109971>
- Öberg AL, Sällfors G (1997) Determination of shear strength parameters of unsaturated silts and sands based on the water retention curve. *Geotechnical Testing Journal* 20(1): 40–48. <https://dx.doi.org/10.1520/GTJ11419J>
- Pournaghiazar M, Russell AR, Khalili N (2013) The cone penetration test in unsaturated sands. *Geotechnique* 63 (14):1209–1220. <https://dx.doi.org/10.1680/geot.12.P.083>
- Robertson, PK (2009) Interpretation of cone penetration tests e a unified approach. *Canadian Geotechnical Journal* 46(11): 1337–1355.
- Robertson PK, Fonseca AV, Ulrich B, Coffin J (2017) Characterization of unsaturated mine waste: A case history. *Canadian Geotechnical Journal* 54(12): 1752–1761. <https://dx.doi.org/10.1139/cgj2017-0129>
- Rocha BP, Rodrigues RA, Giacheti HL (2021) The Flat Dilatometer Test in an Unsaturated Tropical Soil Site. *Geotechnical and Geological Engineering*. <https://dx.doi.org/10.1007/s10706-021-01849-1>
- van Genuchten MT (1980) A closed form equation for predicting the hydraulic conductivity of unsaturated soils. *Soil Science Society of America Journal* 44(5):892–898. <https://dx.doi.org/10.2136/sssaj1980.03615995004400050002x>

Study of SPT-CPT and DP-CPT correlations for sandy soils

M.D. Santos

Department of Civil Engineering, Federal University of Espirito Santo, Vitória, Brazil

Department of Civil Engineering, COPPE, Federal University of Rio de Janeiro, Rio de Janeiro, Brazil

K.V. Bicalho

Department of Civil Engineering, Federal University of Espirito Santo, Vitória, Brazil

ABSTRACT: Field penetration tests are widely used in geotechnical engineering for site investigation. The most common in-situ penetration tests are: the Standard Penetration Test (SPT), the Cone Penetration Test (CPT), and the Dynamic Probing (DP). Since there are limitations on their test methodologies and equipment, equations that can describe the relationship between their data are important in geotechnical engineering. This study presents a review of SPT-CPT and CPT-DP correlations for sandy soils, and discusses the uncertainties involved in some previously published correlations in literature. It is also recommended adjustments accounting for variations in soil properties input. Linear regression and residual analysis were carried out in several experimental data sets from different sandy soils and locations. The observed sandy soils' heterogeneity implies in the need of correlations obtained at a regional level. Thus, this study does not aim to exhaust the subject about in situ penetration tests correlations, but rather to recommend and stimulate the critical evaluation and use of previously published correlations and those that will be formulated in the future

1 INTRODUCTION

Site investigation is one of the most important aspects of the preliminary design or viability studies of the geotechnical structures' safety evaluation. Field penetration tests are widely used in geotechnical engineering for site investigation and prediction of bearing capacity and settlement for foundation design. The most common in-situ penetration tests are: the Standard Penetration Test (SPT), the Cone Penetration Test (CPT), and the Dynamic Probing (DP). Since there are limitations on their test methodologies and equipment, equations that can describe the relationship between their data are important in geotechnical engineering.

The Standard Penetration Test (SPT) is a simple and relatively low-cost test routinely used to subsoil investigation in a variety of ground conditions. SPT execution involve the driving of a sampler in the soil, by the repetitive hit of a standard hammer loose in free fall. The SPT test result is known as N-value (N_{SPT} or N_{60} when corrected to a hammer energy efficiency of 60% as recommended by the ISSMFE (1989). In addition to energy efficiency calculation, other corrections are recommended in the literature in order to reduce the spatial and depth variability of the N-Values (Sitharam & Samui 2007).

The Cone Penetration Test (CPT) obtains the soil tip resistance (q_c) and sleeve friction (f_s) by the

pushing of a 60° conical tip with a 20mm/s velocity. Although the CPT does not recover samples in depth like the SPT, CPT data are near-continuous with theoretical background (Robertson 2009). In the piezocone test (CPTu) is also possible to obtain the pore pressure in depth and dissipation tests can be performed do obtain the permeability in situ of materials.

The Dynamic Probing test (DP) determines indirectly the soil resistance by the blow count necessary to prospect the equipment. Therefore, the execution of DP test is similar to the SPT test, in which a hammer is loose in free fall and the blows are counted during the prospection. The DP is usually used as a complementary test to the SPT test, in verification of compacted fills. The blow count can be transformed to a tip resistance (q_d) using the Dutch Formula, which considers the Law of conservation of energy: the soil resistance must be proportional to the initial potential energy, before the free falling. The ISSMFE (1989) recognizes four types of DP equipment, which differs in the hammer mass, drop height, stem and tip characteristics. Thus, there are the Dynamic Probing Light (DPL), the Dynamic Probing Medium (DPM), the Dynamic Probing Heavy (DPH) and the Dynamic Probing Super Heavy (DPSH).

Empirical correlations between CPT and SPT results commonly relate the ratio of the CPT tip resistance (q_c , q_t) and SPT blow count N_{60} , to

particle/grain size information (mean particle size D_{50} or fines content) (Robertson 1990, Santos & Bicalho 2017), soil behavior (Jefferies & Davies 1993, Mayne 2006), or a constant value for certain soil types (Robertson 1990).

This paper investigates correlations between the SPT-CPT and DP-CPT results obtained in Brazilian sandy soils. These correlations allow the evaluation and expansion of data, minimizing complementary campaigns which could be onerous and long standing. Thus, correlations of this type are useful in civil and geotechnical engineering and were studied by many researchers, as Schmertmann (1970), Martins & Miranda (2003) and Souza *et al.* (2012). Nonetheless, as correlations are empirical it is important to highlight some of their limitations: they are applicable only in similar conditions in which they were elaborated, as test standard and soil type; and statistical treatment must be consistent. In this paper, empirical correlations were obtained using linear regression with the verification of the residue's normality. In SPT-CPT correlation the influence of variation of relative density (DR) and depth were also investigated.

2 MATERIALS AND METHODS

SPT-CPT and CPT-DP results empirical correlations were obtained for sandy soils in the metropolitan region of Grande Vitória (GV-ES), located in the state of Espírito Santo (ES), Brazil. The region is geologically characterized by a sedimentary formation attributed to the action of transgression and regression of the sea level during the Quaternary Period. Therefore, soils of the area are composed of marine heterogeneous sediments, with variable relative density. (Castello & Polido 1988, Souza *et al.* 2005).

Tests were driven in shallow subsoil stratum, with depth up to 6m in the saturated zone. The soil was identified as clean quartz sands, presenting angular and sub-angular grain shape, with less than 5% of fines ($< 0.074\text{mm}$), mean particle size between 0.3 and 0.7mm, and relative density varying from loose to dense.

Correlations were developed applying linear regression in N_{60} , q_c and q_d data. SPT and CPT tests were carried out by Brazilian standard proceeding's: ABNT NBR 6484:2020 and ABNT NBR 12069:1991 (mechanical CPT were used). There is not a standard to the DP test in Brazil. So, it was used a modified DPL and DPSH recommended by ISSMFE (1989).

N_{SPT} were corrected to a 60% energy (N_{60}) considering a Brazilian SPT 75% efficiency as follows:

$$N_{60} = \frac{N_{SPT} \cdot 75}{60} = 1,25 \cdot N_{SPT} \quad (1)$$

The influence of depth was also investigated in SPT-CPT correlations, as soils in greater depth are more confined and may affect the blow count. This correction transforms N_{60} in to $(N_{60})_1$, in which the effective stress is corrected to 1 atm by:

$$(N_{60})_1 = C_N \cdot N_{60} \quad (2)$$

where C_N is the correction coefficient for the confinement, in this paper adopted equal to Liao & Whitman (1986) method, valid for normal consolidated sands and presented in Equation 3. It was considered a sand's bulk density of 20 kN/m³ and water table level at 1.5m.

$$C_N = \sqrt{100/\sigma'_v} \quad (3)$$

The blow count obtained in DPL and DPSH tests were transformed to tip resistance (q_d) using the Dutch Formula presented in Equation 4, with M the hammer's mass, H the fall height, N the blow count obtained in DP test, A the tip probe area, s the penetrated length, g the gravity acceleration and M' the stems' mass.

$$q_d = \left(\frac{M \times g \times H \times N_s}{A \times s} \right) \left(\frac{M}{M + M'} \right) \quad (4)$$

SPT-CPT data correlation was written as $q_c = K_c N_{60}$, while DP-CPT correlation was written $q_c = K_e q_d$ (i.e., $K_c = q_c/N_{60}$ and $K_e = q_c/q_d$. N_{60} unit is given in blows/300mm while q_d and q_c are given in MPa).

To form $q_c \times N_{60}$ data pairs, q_c was taken between the depth of $z + 150$ and $z + 450$ mm, to be compared to the last 300mm which N_{SPT} represents. DP data were registered in situ for each 20 cm, while the CPT results were registered for every 25 cm. Thus, data pairs were taken considering the medium of results of a tested meter.

To verify if the correlations are consistent, with a normal distribution of the residue's as required in the Quadratic Least Squares, graphical and hypothesis tests were carried out using the R software. Residues indicates data's natural variation, analytically defined in Equation 5:

$$r_i = y_i - \mu_i \quad (5)$$

Where r_i is the ordinary residue, y_i is the observed data and μ_i is the estimated value in a regression.

To investigate the desired normal distribution of residues, a graphical approach using histogram was carried out. Results are satisfactory if the histogram is symmetrical as illustrated in Figure 1.

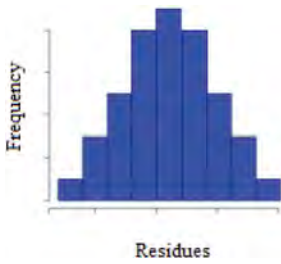


Figure 1. – Histogram example of data presenting normal distribution.

The hypothesis tests were carried out using the Kolmogorov-Smirnov test, which considers the following hypothesis:

- H_0 : data follow a normal distribution
- H_1 : data does not follow a normal distribution

Hypothesis H_0 can be validated if the test result (D_{KS}) is less than the critical value D'_{KS} given in Equation 6, for n number of observations. On contrary, if D_{KS} is higher than D'_{KS} , the normal distribution of residues can be rejected with 1α confidence. In this study, α was adopted equal a 0,05 (95% confidence, which means that the results are in the interval of 95 of 100 observations).

$$D'_{KS} = \frac{1.36}{\sqrt{n}} \quad (6)$$

3 RESULTS AND DISCUSSION

3.1 SPT-CPT data correlations

Considering 34 data pairs of N_{60} and q_c obtained in GV-ES sands, the linear regression was determined and presented in Figure 2, the coefficient of determination value (R^2) was found to be 85%. The $K_c = 0.44$ for GV-ES sandy soils is in reasonable agreement with the coefficient values found by Folque (1976) where K_c varies from 0.4 to 0.45; Ajayi & Balogun (1988) where $K_c = 0.44$; Acka (2002) where $K_c = 0.47$; and Mayne (2006) where $K_c = 0.438$. However, note that Acka (2002) studied soils with strong cementation, characteristic not observed in GV-ES sands. The sand relative density influence could not be observed in the correlations between CPT and SPT results for the investigated sand in the tested site (Figure 2). Cubrinovski & Ishihara (1999) added the mean particle size D_{50} in their empirical correlation between N -value and sand relative

density values. D_{50} in this study ranges from 0.2 mm to 0.6 mm. K_c values tend to increase with the D_{50} (Santos & Bicalho 2017).

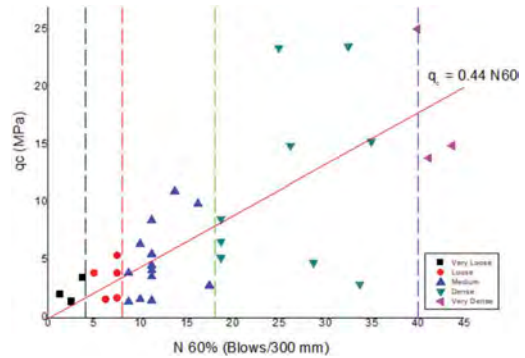


Figure 2. CPT–SPT data correlation and $q_c \times N_{60}$ dispersion graphic.

Figure 3 presents the graphical approach to verify the residues' distribution. Although the histogram is not perfectly symmetrical as required, D_{KS} was found to be 0.19, once to a sample size of 34 $D'_{KS} = 0.23$, $D_{KS} < D'_{KS}$ and the normal distribution of residues could be verified. This means that $K_c = 0.44$ can be classified as a strong coefficient with 95% confidence by the Kolmogorov-Smirnov test.

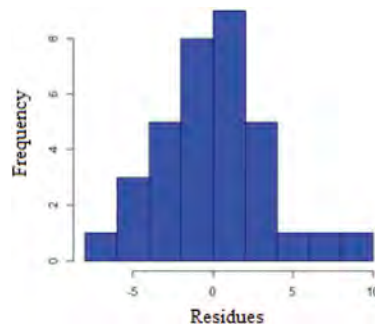


Figure 3. – Residues' histogram for $q_c \times N_{60}$ correlation.

Note that in Figure 2 N_{60} were classified by the relative density (DR) using the intervals from ABNT NBR 6484:2020, in which GV-ES sands were found varying from loose to very dense. Table 1 presents the variation of K_c in terms of DR values suggested by the Brazilian standards ABNT NBR 6484 (2020).

Souza *et al.* (2012) observed that K_c is higher in very loose sands and decreases in very dense sands. The tendency of decreasing K_c with the increasing DR

Table 1. Variation of K_c values in terms of DR values.

DR	N_{SPT} interval*	K_c
	Blows	Blows/300mm
Very loose	≤ 4	0.84
Loose	5 – 8	0.49
Medium	9 – 18	0.42
Dense	19 – 40	0.44
Very Dense	> 40	0.43

* ABNT NBR 6484 (2020).

could not be observed in GV-ES sands, as K_c slightly varies from loose do very dense sands. It was worth to mention that $K_c = 0.84$ for very loose sands was found in a sample of 4 data pairs, and the coefficient must be used with caution, once the sample size is small.

Table 2 shows the result of the nonparametric Kolmogorov-Smirnov hypothesis test for each DR interval investigated herein. As $D_{KS} < D'_{KS}$ in all cases, all coefficients shown in Table 1 can be classified as strong with 95% confidence. Exception is for dense soils, where D_{KS} is higher than D'_{KS} and a normal distribution of residues can be rejected with a 95% confidence. For very dense soil, D_{KS} is very close to D'_{KS} and the normal distribution of residues can be classified as questionable. Thus, specially in this two cases, the indicated K_c in Table 1 should be used with wariness.

Table 2. $K_c \times DR$ – Residue’s analysis.

DR	D_{KS}	D'_{KS}
Very loose	0.25	0.68
Loose	0.22	0.61
Medium	0.13	0.35
Dense	0.97	0.45
Very Dense	0.75	0.78

Table 3 shows results of K_c for each tested meter. In both data treatments (N_{60} and $(N_{60})_1$) it was not possible to confirm a clear tendency of decreasing or increasing K_c with depth. For this purpose, authors suggest that depths greater than 6.3 m must be investigated.

Worth to mention that Schmertmann (1970) and Sanglerat (1972) suggest that the SPT-CPT correlation should be independent of depth. Naime & Fiori (2002) suggest that the independence with depth is valid only in young soils, but K_c decreases with depth in mature soils.

Table 3. Variation of K_c with depth (m).

Depth	$K_c (N_{60})$	$K_c (N_{60})_1$
m	Blows/300mm	Blows/300mm
1.3	0.58	0.29
2.3	0.20	0.14
3.3	0.30	0.23
4.3	0.16	0.13
5.3	0.37	0.33
6.3	0.56	0.53

3.2 DP-CPT data correlations

For correlations between 66 data pairs of q_c and q_d , obtained using CPT and DP tests, respectively, the coefficient $K_c = q_c/q_d$ was found to be 2.34 ($R^2 = 93\%$). Dispersion graph and histogram are presented in Figure 4 and 5 bellow, in which normality could not be verified:

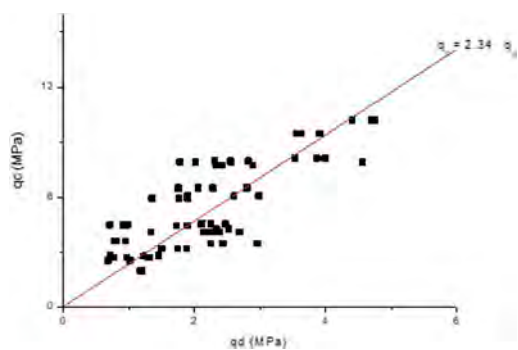


Figure 4. – Dispersion graph for $q_c \times q_d$ correlation.

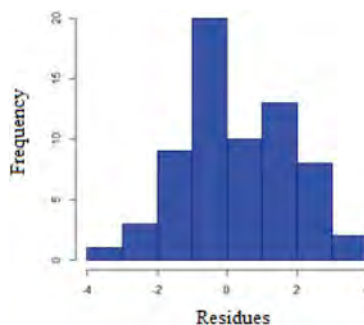


Figure 5. – Residues' histogram for $q_c \times q_d$ correlation.

The Kolmogorov-Smirnov hypothesis test returned a D_{KS} of 0.18. For a 66 sample size, D'_{KS} is 0.17. As $D_{KS} \approx D'_{KS}$ and the normality of residues is questionable. Therefore, the correlation must be used with caution.

Gadeikis *et al.* (2010) recommend a K_e between 1.3 to 2.25 using the DPSH, while Czado & Pietras (2012) found this coefficient between 0.5 to 2.3 using the DPH. Thus, although there is a doubt in the consistency of GV-ES found K_e , its value is similar to those observed in the published literature on this topic.

Waschkowski (1983) suggests that $K_e = 1.0$ ($q_d = q_c$), which was not verified in this study. Similar results were reported by Viana da Fonseca (1996), and the equivalency must be valid only in homogeneous soils, which is not the case of GV-ES sands.

On the other hand, the researchers believe that the blow counts from the DP tests should be corrected to an international reference like is done in SPT, as some energy losses can occur during the test, like in friction, sonorous and thermic energy. This correction should be made before applying the Dutch Formula, as it considers the potential energy before the free fall of the hammer. In this way, the effect of different types of DP and standards would be minimized in the DP results.

4 CONCLUSIONS

This paper presented SPT-CPT and CPT-DP correlations for sandy soils located in the region of Grande Vitória – ES, composed of marine heterogeneous sediments, with variable relative density values.

SPT-CPT correlations were in form of $K_c = q_c / N_{60}$. The GV-ES K_c was found to be 0.44. This value is similar to those found in literature (Folque (1976), Ajayi & Balogun (1988), Mayne (2006)). The linear regression was validated once the residues could be classified in a normal distribution.

It was not possible to find a clear tendency of variation of K_c with relative density as suggested in Souza *et al.* (2012), as well as it was found that K_c does not have a clear dependency with depth variation. This last observation is also found in Schmertmann (1970) and Sanglerat (1972).

CPT-DP results correlation was presented in form of $K_e = q_c / q_d$. The value of K_e around 2.34 was observed for the investigated sands from GV-ES. Although this value is similar to those found in literature (Gadeikis *et al.* 2010, Czado & Pietras 2012), by means of the histogram and Kolmogorov-Smirnov hypothesis test the normal distribution of residues are questionable, and the correlation must be used with caution.

Waschkowski's (1983) suggests that $K_e = 1.0$, but it was not verified to GV-ES sands. It can be observed that supposedly $K_e = 1.0$ is valid only in homogeneous soils. And, it may be recommended that the blow count from the DP data be corrected to an international reference value as applied to the SPT data. This correction must adjust the blow

counts considering that are many sources of energy loss during the fall of the hammer, as losses by friction, sound, and thermic energy.

The correlations presented in this study are valid for sandy soils located in the region of Grande Vitória-ES, Southwest Brazil. It is important to recognize that empirical correlations are limited for the soil type, tests conditions and data treatment. It is always recommended a critical evaluation of previously published correlations.

ACKNOWLEDGEMENTS

The authors would like to acknowledge the Brazilian agency CAPES for financial support. The second author acknowledges support from the Brazilian agency CNPq for the research grant called scientific productivity fellowship.

REFERENCES

- ABNT – ASSOCIAÇÃO BRASILEIRA DE NORMAS TÉCNICAS. NBR 12069. 1991. Solo – Ensaio de penetração de cone in situ (CPT). Rio de Janeiro, ABNT. (in Portuguese)
- ABNT – ASSOCIAÇÃO BRASILEIRA DE NORMAS TÉCNICAS. NBR 6484. 2020. Solo – Sondagens de simples reconhecimento com SPT – Método de Ensaio. Rio de Janeiro, ABNT (in Portuguese)
- Acka, N. 2002. Correlation of CPT-SPT data from the United Arab Emirates. *Engineering Geology* 67, pp. 219–231.
- Ajayi, L.A.; Balogun, L.A. 1988. Penetration testing in tropical lateritic and residual soils - Nigerian experience. *Penetration Testing - 1988. Proceedings ISOPT-1, Orlando, Vol. 1*, pp. 315–328. Ed. De Ruitter. A.A. Rotterdam: Balkema.
- Castello, R.R., Polido, U.F. 1988. Sistematização geotécnica dos solos quaternários de Vitória, ES. *Anais do Simpósio sobre Depósitos Quaternários das Baixadas Litorâneas Brasileiras: Origem, Características Geotécnicas e Experiências de Obras, Associação Brasileira de Mecânica dos Solos, Rio de Janeiro. Tema 3. (In Portuguese)*.
- Czado, B., Pietras, J.S. 2012. Comparison of the cone penetration resistance obtained in static and dynamic fields tests. *AGH Journal of Mining and Geoengineering*. v.36, n.1.
- Cubrinovski, M. & Ishihara, K. 1999. Empirical correlation between SPT N-value and relative density for sandy soils. *Soils and Foundations*, 39(5): 61–71
- Folque, J. 1988. Modernas tendências nas técnicas de ensaio em Mecânica dos Solos. *Informação Técnica - ICT, Geotecnia ITG15. LNEC, Lisboa*.
- Gadeikis, S. Zarzoujus, G. Urbaitis, D. 2010. Comparing CPT and DPSH in Lithuanian soils. In: 2nd International Symposium on Cone Penetration Testing, Huntington Beach, CA, USA. Volume 2ee: Technical Papers, Session 3: Applications, 3–22.
- ISSMFE - International Society for Soil Mechanics and Foundation Engineering. 1989. Report of the ISSMFE - Technical Committee on Penetration Testing of Soils - TC 16. Reference to Test Procedures CPT-SPT-DP-WST. Swedish Geotechnical Institute Information, n. 7.

- Jefferies, M., Davies, M. 1993. Use of CPTu to Estimate Equivalent SPT N60, *Geotechnical Testing Journal* 16, no. 4 pp. 458–468.
- Liao, S. S. C., & Whitman, R. V. 1986. Overburden Correction Factors for SPT in Sand. *Journal of Geotechnical Engineering*, 112(3),373–377.
- Martins, J.B., Miranda, T.F.S. 2003. Ensaio de Penetração nos Solos Graníticos da Região Norte de Portugal. *Alguns Correlações*. Portugal. (in Portuguese).
- Mayne, P.W. 2006. In situ test calibrations for evaluating soil parameters. Overview paper, characterization and engineering properties of natural soils II (proc. Singapore Workshop).
- Naime, R., Fiori, A.P. 2002. Variações nas razões qc/N na região de Passo Fundo, devido a fatores geológicos-ambientais. *Acta Scientiarum Maringá*, v. 24, n. 6, pp. 1819–1824. (in Portuguese)
- Robertson, P.K.1990. Soil classification using the cone penetration test. *Canadian Geotechnical Journal*, 27 (1), pp. 151–158.
- Robertson P.K. 2009. Interpretation of cone penetration tests - A unified approach. *Canadian Geotechnical Journal* 46 (11), pp. 1337–1355N.
- Sanglerat, G. 1972. *The Penetrometer and Soil Exploration*, Amsterdam, London, New York: Elsevier Publishing Company.
- Santos, MD & Bicalho, KV. 2017. Proposals of SPT-CPT and DPL-CPT correlations for sandy soils in Brazil. *Journal of Rock Mechanics and Geotechnical*. V. 9. n.6. pp. 1152-1158
- Schmertmann, J.H. 1970. Static cone to compute settlement over sand. *Journal Soil Mechanics and Foundations Division*, ASCE, v. 96, n. SM3, pp. 1011–1043.
- Sitharam, T.G., Samui, P. 2007. Geostatistical modelling of spatial and depth variability of SPT data for Bangalore. *Geomechanics and Geoengineering*. 2 (4). 307–316.
- Souza, C.R. de G., Suguio, K., Oliveira, A. M. dos S., Oliveira, P.E. de. 2005. Quaternário do Brasil. *Associação Brasileira de Estudos do Quaternário*, ed. Holos, São Paulo, Brasil, p. 102–104. (In Portuguese).
- Souza, J.M.S., Danziger, B.R., Danziger, F.A.B. 2012. The Influence of the Relative Density of Sands in SPT and CPT Correlations. *Soils and Rocks*, São Paulo, v. 35, pp. 99–113.
- Viana da Fonseca, A.J.P. 1996. *Geomecânica dos solos residuais do granito do Porto. Critérios para dimensionamento de fundações directas*. Tese de Doutorado. Faculdade de Engenharia da Universidade do Porto, Portugal. (in Portuguese).
- Waschkowski, E. 1983. *Le Pénéromètre Dynamique*. Bulletin de Liaison des Laboratoires des Ponts et Chaussées, n.125, pp. 95–103.

Correlation between SPT and CPT tests in liquefiable deposits

Rashid Shahgholian, Cristiana Ferreira & António Viana da Fonseca

CONSTRUCT-GEO, Faculty of Engineering of University of Porto, Porto, Portugal

ABSTRACT: Cone penetration test (CPT) started being used for soil investigation almost four decades after the standard penetration test (SPT). Despite their differences, both tests estimate the resistance of the soil against penetration of a probe. Although it is expected that the results of these tests are comparable and directly correlated, different driving mechanisms (static versus dynamic), sensitivity, type and frequency of measured parameters, operational errors, among others, compromise such correlations. In addition, the diverse nature of soils in terms of grain size, packing and fabric, shear strength, permeability, and other soil characteristics also limit the derivation of a unique correlation between CPT and SPT. Many authors have studied these in situ tests, recognizing that such correlation would be valuable, as it would enable the use of design methods and other libraries of correlations available for each individual test. A variety of formulas and charts has been proposed in the literature to describe this relationship, which demonstrates that this is a complex, not a global and simply predictable correlation. In this research, some of the most usual CPT-SPT relations are evaluated for a large dataset of field measurements from a pilot site on liquefiable soils, near Lisbon in Portugal. The extensive analysis of these data showed that the application of previously established, tested, and published correlations, available in the literature for specific sites, requires great care. One of the requirements is the verification of applicability, by comparison between the type of soils under study and those in the literature. Specific correlations for each geological condition must be defined before making engineering estimations based on correlated parameters.

1 INTRODUCTION

Comparison between the results of different geotechnical tests in a site is essential for a correct estimate of the geotechnical parameters of the soil profile. The Standard Penetration Test (SPT) and the Cone Penetration Test (CPT) are two of the most common site characterization techniques, which have advantages and weaknesses over each other. Besides, the literature shows that these tests have different libraries of formulas and relations behind. Correlation of these two tests has a history over seventy years and extensive research indicates there is not a unique relation between them, which may result from the fact that these penetration tests are differently influenced by various factors, including geological conditions, available machinery and tools, operator skills, etc. The application of the empirical equations and charts available in the literature needs to be performed with great care; a certain level of similarity should be assured between the site and the region from which the empirical correlations were developed.

2 METHODOLOGY

Recent investigations on the assessment of liquefaction hazard around Lisbon, in Portugal, were combined

with previous geotechnical studies, namely for the construction of a motorway at the same region, providing a valuable geotechnical data bank. The site is located in the Greater Lisbon region, in the municipalities of Vila Franca de Xira and Benavente, on the left bank of the river Tagus. Boreholes with SPT adjacent to CPT tests were carried out along 9 km of the motorway alignment as shown in Figure 1. More details are available in Ferreira et al. (2020).

In order to correlate the SPT and CPT results, the closest (in plan) CPT point to each SPT borehole was selected, defining a SPT-CPT pair (Figure 1). As a result, techniques such as the inverse distance weighted average method (Zhao & Cai, 2015) is not used. In the present case of a heterogeneous environment, such as recent sedimentary deposits, condensing the CPT records to define the soil profile can be particularly challenging.

In fact, the choice of the size of the averaging window and its adjustment in terms of the most appropriate depth leads to considerable variation in the results. Even relying on just “averaging” may have negative influence over correlation because it neglects the fact that CPT records are influenced by the stiff layers in front of the tip, even before its penetration. As Figure 2 schematically shows, tip resistance and sleeve resistance at the same recording of the CPT correspond to adjacent (not identical)

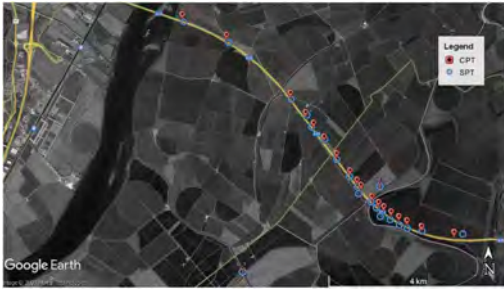


Figure 1. Selected SPT and CPT locations for this study.

depths. On the other hand, the influence of transition zones is considered to be the same for both the CPT and SPT tests. In addition, most researchers believe that the presence of interbedded thin layers will decrease the correlation of the N values and q_c (after Zhao & Cai, 2015).

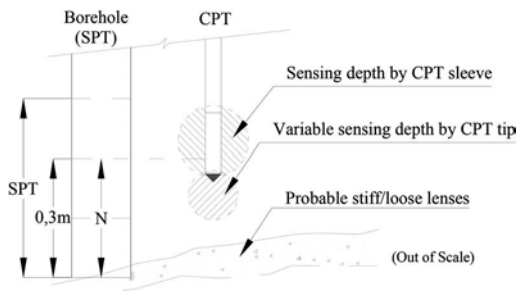


Figure 2. Mismatch of the measuring zone of SPT, with tip resistance and sleeve resistance of CPT.

In this research, CPT values (q_c and f_s) are averaged over the same 30 cm interval of each SPT record, following Jefferies & Davies (1993). Although CPT probe senses ahead of its tip, it is not a clear mechanism to be involved in calculation of equivalent CPT exactly over the same 30 cm depth of the SPT.

To eliminate the influence of non-equal end effects, q_t is used instead of q_c in this study (Campanella et al., 1982).

SPT test results, N_{SPT} , are assumed to correspond to N_{60} , since the energy ratio measured in Portuguese SPT testing campaigns is typically 60%. The corrections to the SPT records including rod length, borehole diameter and effective overburden stress have been applied to the measured SPT values, for obtaining the normalized SPT values, $(N_1)_{60}$.

A total of 285 SPT-CPT pairs of data have been compiled out of the 21 boreholes and their adjacent CPT profiles. The maximum measurement depth reaches 26.5 meters, while the majority of the measurements correspond to depths lower than 21 meters.

The tested soils have been classified according to the soil behavior type index (SBT) (Robertson & Wride, 1998); while samples mainly classified as “clay”, nothing belongs to the “gravel”. The classes suggested by Cubrinovski *et al.*, (2019) are adopted in this research. Unified soil classifications, based on laboratory grading tests are only available for two boreholes (named SI1 and SI7).

In this paper, some of the correlations between CPT and SPT tests available in the literature are presented and discussed (Table 1). Selected SPT-CPT correlations were applied to the existing database to evaluate their performance. Finally, the overall trend of the available data bank is presented and discussed.

Table 1. Some categories of correlation between CPT and SPT.

Reference	SPT	CPT	Other	Eq.
Jefferies & Davies 1993	N_{60}	q_c	I_c	3
Lunne et al. 1997	N_{60}	q_c/p_a	I_c	4
Robertson 2012	N_{60}	q_c/p_a	I_c	5
Shahien & Albatal 2014	N_{60}	q_c/p_a	I_c	6
Robertson et al. 1983	N_{60}	q_c/p_a	D_{50}	7
Shahri et al., 2014	N_{60}	q_c/p_a	D_{50}	8
Kulhawy & Mayne 1990	N	q_c/p_a	D_{50}	9
Kulhawy & Mayne 1990	N	q_c/p_a	FC	10
After Ahmed et al., 2014	N_{55}	q_c/p_a	FC	11
After Shahien & Albatal 2014	N	q_c/p_a	FC	12
*	N	q	-	-

* Numerous authors (see Shahri et al., 2014 & Zhao et al., 2015)

3 BACKGROUND ON SPT-CPT CORRELATIONS

3.1 Ratio methods

Shahri et al. (2014) cited forty formulas that were developed between 1959 and 2003. Similar set of formulas is cited by Zhao & Cai (2015). The appearance of these formulas is either $n = q_c/N$ or $n = (q_c+f_s)/N$, which do not differ considerably since sleeve friction (f_s) rarely reaches more than 10% of the tip resistance (q_c). Depending on the soil type, it is shown that usually $0.1 < n < 1$ MPa, although higher values have also been reported or shown in the literature. By normalizing q_c with atmospheric pressure $P_a = 101$ kPa, the dimensionless domain of n would be $1 < n < 10$.

Schmertmann (1978) believed that $n=4$ is generally acceptable for most soils; sensitive clays are an exception, because SPT in sensitive clays approaches to zero and n increases significantly. The range of n is also approved by many recent researches, namely Akca

(2003), Shahri et al. (2014), Jarushi et al. (2015) and Aral & Gunes (2017) among others. Akca (2003) reported occasionally very high n-values in his research that may be caused by specific (and less frequent) soil conditions, such as cementation, higher density layers, shell fragments, gravels, and other heterogeneities.

Recent research confirms the domain of variation of n but there is considerable scatter in the measurements (Aral & Gunes, 2017). Asci et al. (2015) also reported a trend of n for SPT values below 13, but as SPT values increase, the trend completely differs.

Besides the ratio method, Zhao & Cai (2015) proposed two other correlation categories between SPT and CPT measurements: “function methods” which are more advanced expressions considering more than just the ratio, usually based on statistical analyses but ignoring soil properties; and, “soil parameter methods” which directly address these properties in the correlations.

3.2 Function methods

Referring to the investigation by Jefferies & Davies (1993), SPT is related to the tip resistance and soil behavior type index (I_C). Equations 1 and 2 show the expressions for I_C according to Robertson & Wride (1998) and Jefferies & Davies (1993), respectively.

$$I_c = \sqrt{[3.47 - \log(Q_n)]^2 + [1.22 + \log(F_r)]^2} \quad (1)$$

$$I_c = \sqrt{[3 - \log(Q \times (1 - B_q))]^2 + [1.5 + 1.3 \times \log(F_r)]^2} \quad (2)$$

In these equations, Q and Q_n are normalized tip resistance. F_r is normalized friction resistance and B_q is pore pressure ratio in CPT test.

The correlation proposed by Jefferies & Davies (1993) is shown in Equation 3. Lunne et al. (1997) proposed a small modification to the same formula (Eq. 4).

$$N_{60} = \frac{q_c \text{ (MPa)}}{0.85 \times (1 - \frac{I_c}{4.75})} \quad (3)$$

$$N_{60} = \frac{\left(\frac{q_c}{p_a}\right)}{8.5 \times (1 - \frac{I_c}{4.6})} \quad (4)$$

Robertson (2012) found that the above listed equations under-predict N_{60} in some clays. He proposed the modified formula as in Equation 5. Shahien & Albatal (2014) found these equations do not fit their data bank so they developed Equation 6 for silty sand deposits in Nile Delta.

$$\frac{\left(\frac{q_c}{p_a}\right)}{N_{60}} = 10^{(1.1268 - 0.2817 \times I_c)} \quad (5)$$

$$\frac{\left(\frac{q_c}{p_a}\right)}{N_{60}} = \frac{0.26 \times e^{8.22 \times (1 - \frac{I_c}{4.5})}}{\left(\frac{q_c}{p_a}\right)^{0.65}} \quad (6)$$

Although all these formulas show the correct trend of the measurements, scatter of the real measurements is considerable. It demonstrates that other factors also play a relevant role in the correlation. One of those factors may be the difference between crushable and non-crushable grains (Ahmed et al., 2014). In natural deposits with different mixture of these components, the measurements would not easily obey a single formula. This shows the importance of geotechnical similarity between sites when using the literature correlations. To apply these properties in correlation equations, various attempts have already been made leading to the third group of correlations, based on geotechnical indexes.

3.3 Soil parameter methods

3.3.1 Grain size

Grain size distribution plays a significant role in both SPT and CPT test results. Robertson et al., (1983) presented a graph showing that $n=q_c/N$ increases as D_{50} increase. These kind of correlations are mathematically formulated, as in Equations 7-9 (Shahri et al., 2014). Other similar formulas are cited by Shahien & Albatal (2014) and Ahmed et al. (2014). Non-unique formulas for n as a function of D_{50} indicates that n is influenced by more than just D_{50} .

$$\frac{\left(\frac{q_c}{p_a}\right)}{N_{60}} = 7.735 \times (D_{50})^{0.28} \quad (7)$$

$$\frac{\left(\frac{q_c}{p_a}\right)}{N_{60}} = 6.53 \times (D_{50})^{0.26} \quad (8)$$

$$\frac{\left(\frac{q_c}{p_a}\right)}{N} = 5.44 \times (D_{50})^{0.26} \quad (9)$$

3.3.2 Fines content (FC)

In some cases, SPT and CPT results can be best correlated according to the fines content (Shahri et al. (2014) and Shahien & Albatal (2014)). Equations 10-12 are samples from the collection.

3.3.3 Correlation based on other parameters

Other correlations regarding D_r , V_s , both the D_{50} and I_c , etc., have been studied as well. Available data bank does not cover all the required parameters with sufficient number of data points so they are not covered in this text.

$$\frac{\left(\frac{q_c}{p_a}\right)}{N} = 4.25 - \frac{FC \%}{41.3} \quad (10)$$

$$\frac{\left(\frac{q_c}{p_a}\right)}{N_{55}} = 4.7 - 0.05 * FC \% \quad (11)$$

$$0 \leq N < 10 :$$

$$\frac{\left(\frac{q_c}{p_a}\right)}{N} = 0.0026 \times FC^2 - 0.263 \times FC + 12.34$$

$$10 \leq N < 30 : \quad (12)$$

$$\frac{\left(\frac{q_c}{p_a}\right)}{N} = 0.00085 \times FC^2 - 0.12 \times FC + 8.733$$

$$30 \leq N, FC \leq 20 :$$

$$\frac{\left(\frac{q_c}{p_a}\right)}{N} = 0.001 \times FC^2 - 0.059 \times FC + 5.59$$

4 RESULTS AND DISCUSSIONS ON THE PERFORMANCE OF SPT-CPT CORRELATIONS

4.1 Ratio of the CPT/SPT values

Figure 3 Shows the scatter plot of the arithmetic average over CPT records versus SPT values. The records of the borehole SPT S208 and its relevant CPT measurements, CPT2, appeared as outliers so these were omitted here. In order to organise the database and narrow down the correlation, Cubrinovski *et al.*, (2019) ranges over SBT were used as the boundaries of different groups of soil. Critical SBT boundaries from their point of view are: 1.3, 1.8, 2.1 and 2.6, also adopted by Ferreira *et al.* (2020).

Scatter of the measurements seems reasonable as coarse materials (low SBT values) have higher q_r and vice versa but the trend, even in each sub-group, is not so clear. Frequent measurements have fallen outside the proposed boundaries as well.

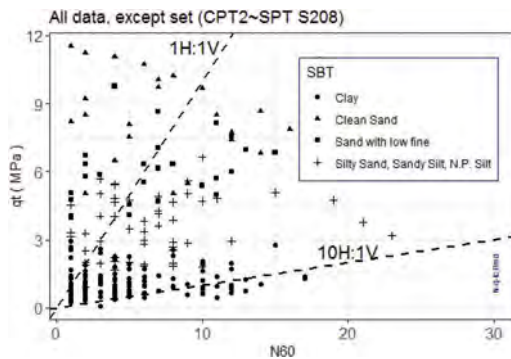


Figure 3. Relation between q_r and N_{60} .

4.2 Correlation between SPT and I_c (Soil behavior type index from CPT)

Figure 4 presents the scatter plot of measurements versus I_c . The distribution of the measurements do not follow even complicated relations as Equations 3-5.

4.3 Correlation between SPT and CPT based on D_{50} (grain size)

Grain size distribution is only available for boreholes S11 and S17. It refers to 48 cases out of 285 in this database. Figure 5 shows the measurements, which do not follow the trends proposed in the literature.

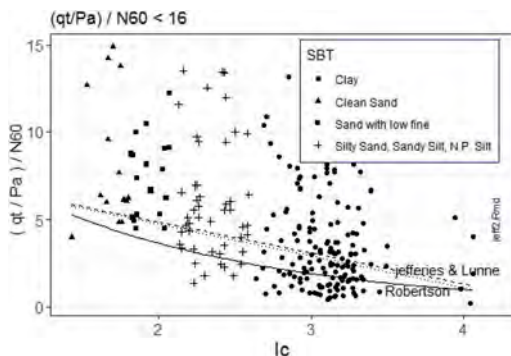


Figure 4. Scatter of the data using Equations 3-5.

4.4 Relation of SPT and CPT based on fines content

Based on the fines content (FC), different correlations of SPT and CPT tests are suggested in the literature. Figure 6 shows that the measurements from

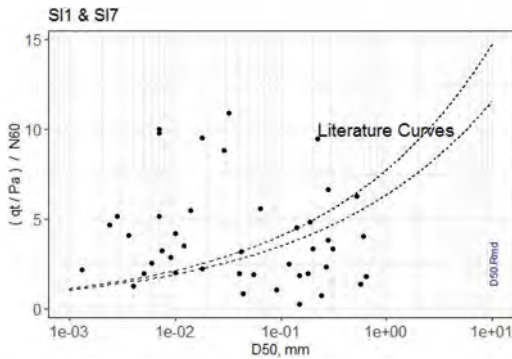


Figure 5. Measured data and published curves in literature (mean grain size, D_{50} , obtained from sieve analysis).

this database do not follow the trend suggested by Kulhawy & Mayne (1990).

4.5 The best-fit correlation between SPT and CPT for the current data bank

The most suitable graphs to represent the correlation between CPT and SPT in this site are presented in Figure 7. In this figure, the clean sand equivalent of CPT records is used, which is normalized for the effective overburden pressure ($q_{1N,cs}$) (Boulanger & Idriss 2014). The figure shows $q_{1N,cs}/(N1)_{60}$ versus $(N1)_{60}$ for different groups of soils according to SBT index and Cubrinovski *et al.*, (2019) classification.

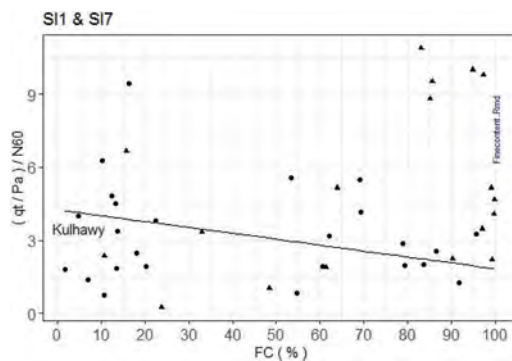


Figure 6. CPT-SPT ratio vs. laboratory fines content and comparison with a literature proposal.

The trends show a variance, which may be related to the mismatch of the CPT and SPT profiles, due to the occasional large distances between the CPT and SPT locations in plan. Variation of the soil properties including grain size distribution, relative density, fines content, variations in cementation etc., may also have some effect; however, parts of those effects are

implemented in the normalized parameters as $q_{1N,cs}$. An important aspect of these graphs is that none of the boreholes has been removed, even the ones that appeared as outliers in previous plots. Figure 7a shows the best fitted curve for sandy soils while silty soils (Figure 7b) show an acceptable trend as well. Figure 8 shows for any specific value of SPT, clean sand has the maximum value of $q_{1N,cs}/(N1)_{60}$; as the fines content increases, this index decreases. Similar trends can be observed for different soil classes. It is clear that for finer non-liquefiable soils ($I_c > 2.6$), the correlation scatter increases considerably. However, the number of available data points in some of the best-fitted groups is not very large; more populated data banks should be checked to show how general such trends are. Other soil classifications may lead to different trends.

In sum, based on the current data, this approach should only be applied to granular non-plastic soils.

5 CONCLUSIONS

Different scatter plots of the available SPT-CPT data set were prepared, and trends were compared with the most common correlations published in the literature. In most cases, the current data does not follow the published correlations. The characteristics of each site, which are embedded in its corresponding correlation equation, restrict its validity to the most similar sites. The existence of a wide range of different correlation proposals is demonstrative that a universal correlation cannot yet be formulated.

Even though the current data bank compiles results by different geotechnical companies over a large period of time (since 2004), the scatter in the graphs shown in Figure 7 evidence clear trends of the measurements, providing an adequate level of confidence in the available data.

Some of the difficulties of correlation between CPT and SPT profiles may be caused by the procedure adopted to condense CPT values over SPT depths. Non-negligible distances in plan between the CPT locations and the nearby SPT were found to have negative influence over the correlation.

All the samples from different boreholes generically follow the trend defined for the relevant soil class, which means that the proposed trends include all data points, since none has been considered as outlier. The trends in coarse granular materials are clearer than at higher I_c classes. However, since this research focused on the characterization of liquefiable deposits, the obtained trends are within the relevant range of applicability. The standard rule of thumb that granular soils show higher values of $n (=q_n/N)$ is confirmed in the proposed correlations.

These correlation trends should be controlled with measurements in other liquefiable sites to assess whether these correspond to general relations or are just a result of the geological and geotechnical

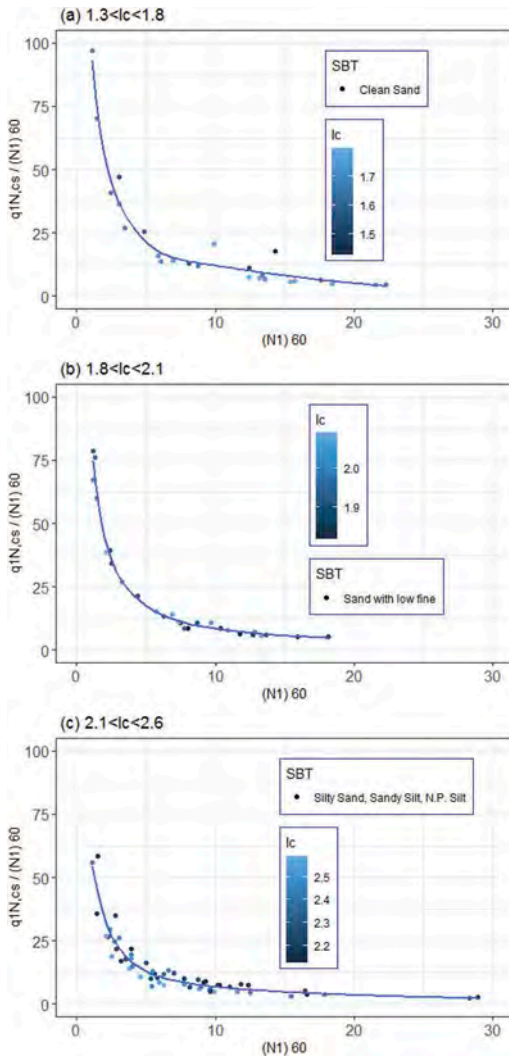


Figure 7. SPT-CPT correlation for different classes of soil.

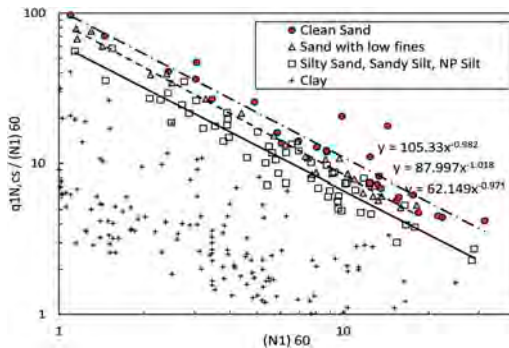


Figure 8. SPT-CPT correlation for different soil classes (in log scale).

characteristics of this specific site. However, based on this research, it can be concluded that this approach to the SPT-CPT correlation is applicable in granular non-plastic soils, such as liquefiable soil deposits.

ACKNOWLEDGEMENTS

The first author has received funding from FCT (Portuguese Foundation for Science and Technology) in the form of the 2021.07363.BD. This work was also financially supported by UIDB/04708/2020 and UIDP/04708/2020 of CONSTRUCT - Institute of R&D in Structures and Construction, funded through FCT/MCTES (PIDDAC).

REFERENCES

- Ahmed, S. M., Agaiby, S. W. and Abdel-Rahman, A. H. (2014) 'A unified CPT-SPT correlation for non-crushable and crushable cohesionless soils', *Ain Shams Engineering Journal*. Faculty of Engineering, Ain Shams University, 5(1), pp. 63–73. doi: 10.1016/j.asej.2013.09.009.
- Akca, N. (2003) 'Correlation of SPT-CPT data from the United Arab Emirates', *Engineering Geology*, 67(3–4), pp. 219–231. doi:10.1016/S0013-7952(02)00181-3.
- Aral, I. F. and Gunes, E. (2017) 'Correlation of Standard and Cone Penetration Tests: Case Study from Tekirdag (Turkey)', in *IOP Conference Series: Materials Science and Engineering*, p. 9. doi: 10.1088/1757-899X/245/3/032028.
- Asci, M. *et al.* (2015) 'Correlation of SPT-CPT Data from the Subsidence Area in Gölçük, Turkey', *Soil Mechanics and Foundation Engineering*, 51(6), pp. 268–272. doi: 10.1007/s11204-015-9288-x.
- Boulanger, RW, Idriss, IM (2014). CPT and SPT based liquefaction triggering procedures. Report No. UCD/CGM-14/01. Center for Geotechnical Modeling, University of California, Davis. 134 pp.
- Campanella, R. G., Gillespie, D. and Robertson, P. K. (1982) 'Pore pressures during cone penetration testing.', *Penetration testing. Proc. 2nd European symposium, Amsterdam, 1982, Vol 2*, (May), pp. 507–512.
- Cubrinovski, M. *et al.* (2019) 'System response of liquefiable deposits', *Soil Dynamics and Earthquake Engineering*, 124(May 2018), pp. 212–229. doi: 10.1016/j.soildyn.2018.05.013.
- Ferreira, C., Viana da Fonseca, A., Ramos, C., Saldanha, Ana Sofia, Amoroso, S., Rodrigues, C. (2020) 'Comparative analysis of liquefaction susceptibility assessment methods based on the investigation on a pilot site in the greater Lisbon area', *Bulletin of Earthquake Engineering*. Springer Netherlands, 18(1), pp. 109–138. doi: 10.1007/s10518-019-00721-1.
- Jarushi, F., Alkaabim, S. and Cosentino, P. (2015) 'A new correlation between SPT and CPT for various soils', *International Journal of Environmental, Chemical, Ecological and Geophysical Engineering*, 9(2), pp. 101–107.
- Jefferies, M. G. and Davies, M. P. (1993) 'Use of CPTu to Estimate Equivalent SPT N60', *Geotechnical Testing Journal*, *GTJODJ*, 16(4), pp. 458–468. doi: 10.1520/gtj10286j.

- Kulhawy, F. H. and Mayne, P. W. (1990) *Manual on Estimating Soil Properties for Foundation Design*, Ostigov. http://www.osti.gov/energycitations/product.biblio.jsp?osti_id=6653074.
- Lunne, T., Robertson, P. K. and Powell, J. J. M. (1997) *Cone Penetration Testing in Geotechnical Practice*, BLACKIE ACADEMIC & PROFESSIONAL.
- Robertson, P. K. (2012) 'Interpretation of In-situ Tests - Some Insights', in *Proceedings of the Fourth International Conference on Site Characterization*. Recife, Brazil, pp. 1–22.
- Robertson, P. K., Campanella, R. G. and Wightman, A. (1983) 'SPT-CPT correlations', *ASCE Journal of Geotechnical Engineering*, 109(11), pp. 1449–1459. doi: 10.1061/(ASCE)0733-9410(1983)109:11(1449).
- Robertson, P. K. and Wride, C. E. (Fear) (1998) 'Evaluating cyclic liquefaction potential using the cone penetration test: Discussion', *Canadian Geotechnical Journal*, 35, pp. 442–459. <http://www.nrcresearchpress.com/doi/10.1139/t99-102>.
- Schmertmann, J. H. (1978) *Guidelines for cone penetration test performance and design*. FHWA-TS-78-209.
- Shahien, M. M. and Albatat, A. H. (2014) 'SPT-CPT Correlations for Nile Delta Silty Sand Deposits in Egypt', in *3rd International Symposium on Cone Penetration Testing*. Las Vegas, Nevada, USA, pp. 699–708.
- Shahri, A. A., Juhlin, C. and Malemir, A. (2014) 'A reliable correlation of SPT-CPT data for southwest of Sweden', *Electronic Journal of Geotechnical Engineering*, 19 E, pp. 1013–1032.
- Zhao, X. and Cai, G. (2015) 'SPT-CPT Correlation and Its Application for Liquefaction Evaluation in China', *Marine Georesources and Geotechnology*, 33(3), pp. 272–281. doi: 10.1080/1064119X.2013.872740.

CPTU-detection of thin clay layers in sand: Results from calibration chamber tests

H. Skrede

Norwegian Geotechnical Institute (NGI), Norwegian University of Science and Technology (NTNU), Norway

H.B. Hammer

Dr.techn. Olav Olsen AS, Norway

S. Nordal

Norwegian University of Science and Technology (NTNU), Norway

J.-S. L'Heureux

Norwegian Geotechnical Institute (NGI), Norway

ABSTRACT: The detection of thin clay layers (i.e. ≤ 20 cm) is challenging for all conventional geotechnical field investigations techniques, including high quality CPTU tests. During the last two years, a research program has been carried out in the geotechnical laboratory at NTNU in Trondheim. The work aims to identify possibilities and limitations in detecting thin clay layers and assess their properties using the CPTU tool. Tests were run in a pressurized chamber where thin horizontal clay layers of both pottery clay and natural, sensitive clay were embedded in a homogenous, medium dense sand. Both a standard piezocone (10 cm^2) and a mini-piezocone (5 cm^2) have been utilized. The results show to what degree the CPTU response in thin layers is influenced by the surrounding sand, and how this influence in practice may lead to serious overestimation of shear strength in thin layers. In addition, the effect of depth-offset of measurements in connection with soil type characterization was evaluated.

1 INTRODUCTION

Analyses of past landslides along the coast of Norway have shown that thin clay layers in sandy shoreline deposits often act as a sliding plane (L'Heureux et al. 2010). An example of a landslide that caused fatalities with these characteristics is the Finneidfjord landslide, which occurred in 1996 (Longva et al. 2003). The clay layers may be so thin (i.e. < 20 cm) that even high quality survey techniques, alike the CPTU, struggle to detect the layers.

This is the background of an ongoing research program at NTNU. A large-scale pressurized model testing facility has been set up and samples are built-in with clay layers of various thicknesses embedded in sand. CPTU-soundings are conducted on chamber samples with the aim of determining if thin layers can be properly identified, and to which degree it is possible to determine the properties of these layers. This article will mainly focus on the executed laboratory experiments and the most important results.

Similar research on the topic has been conducted by e.g. van der Linden et al. (2018) and de Lange

et al. (2018), with main focus on liquefaction potential and pile resistance.

2 METHODOLOGY

In the research program at NTNU, six experiments have so far been conducted (E1-E6). Each experiment consists of constructing a chamber sample, pressurizing it, performing soundings on the chamber sample followed up by excavation with supplementary laboratory testing of soil properties. Clay type, layer thicknesses and stress levels have been systematically varied during the experimental program. This chapter describes the methodology in general, for further details it is referred to MSc theses of Skrede (2021) and Hammer (2020).

Chamber samples were built into a testing chamber of about 1.5 meter height, using reinforced concrete cylinders (sewage manhole rings) with an internal diameter of 1.2 meter. In the base of the chamber an outlet was installed to allow for regulation of the water level. A pore pressure sensor was installed on the outlet.

The bottom 10 cm of the chamber was filled with gravel, covered by a filter cloth. This allowed for an evenly distributed in and outflow of water across the chamber cross-section during the building procedure, preventing interior channelling in the sand. Above the filter cloth a first sand layer of 10 cm was built in. Pressure cells of the Geokon 3500-3 model were placed on top, four horizontally and one vertically (Figure 1). The cells were calibrated by inserting them into a special designed casing and imposing air pressure within the casing. Unfortunately, the cells suffered from some sensitivity drift. This was dealt with by correcting the data linearly from start to end.

The sand used in the chamber came from Kvål, with a d_{50} of 0.492 mm; C_u of 4.24; and e_{min} and e_{max} of respectively 0.502 and 0.873. Two types of clays were used in the tests. The first clay was an industrially made kaolin pottery clay (K148 by Sibelco) delivered in bricks (31x11x12cm³). The second clay type was a natural sensitive clay extracted from 8 to 10,5 meters depth at Flotten, a Norwegian Geo-Test Site, sampled by using a mini-block sampler providing cylindrical samples with 16 cm diameter (Emdal, et al. 2016).

All the pottery clay bricks had almost identical properties. The very sensitive, quick clay extracted from Flotten, is well-documented based on-site investigations reported by L'Heureux et al. (2019). The key properties of the clays are presented in Table 1.

The procedure of constructing sand layers aimed at a homogeneous, medium densely packed sand (relative density $D_r \sim 40-60\%$) in order to resemble a natural sand deposit. Details about the procedures are found in the MSc theses (Hammer, 2020; Skrede, 2021).

In all experiments except the last, pottery clay was utilized. From each brick of pottery clay a specimen was cut to a preferred dimension with a thread saw. Several specimens were then laid together side by side and carefully clamped to form a clay "unit". The purpose of uniting several specimens was to make the clay layer wide enough to act as if it was a continuous horizontal layer. It was still made with limited horizontal extension and did not cover the entire cross section of the chamber partly to save material, but primarily to allow water to flow vertically in the chamber during sample construction and testing.

In the last experiment (E6) mini-blocks (diameter of 16 cm) of natural sensitive clay from Flotten were utilized. Assemblance of units proved to be feasible also for the quick clay but required considerable precision and careful execution. Each clay layer was designed and placed so that the CPTU soundings would be close to the centre of the clay unit as illustrated in strength

*Rough, values based on range of results around 8-10 m depth.

Figure 2 (layer set-up for tests E1-3 and E5).

Two penetrometers were utilized, firstly a standard sized (10 cm²) NOVA-probe from GeoTech AB with a measurement frequency of about 1Hz. Secondly a mini electrical probe (5 cm²) with an approximate measurement frequency of 8Hz that was kindly made

Table 1. Properties of pottery clay and clay from Flotten.

Parameter	Symbol	Pottery clay	Natural clay*	Unit
Water content	w	~24	~45	%
Liquid Limit	w _L	32.7	~28-33	%
Plastic limit	w _p	18.8	~20	%
Plasticity index	I _p	13.9	~8-13	%
Liquidity index	I _L	0.4	~2.4	-
Sensitivity	S _t	~2.5	50-350	-
Undrained shear	s _{u,CAUC}	27.5	~75	kPa

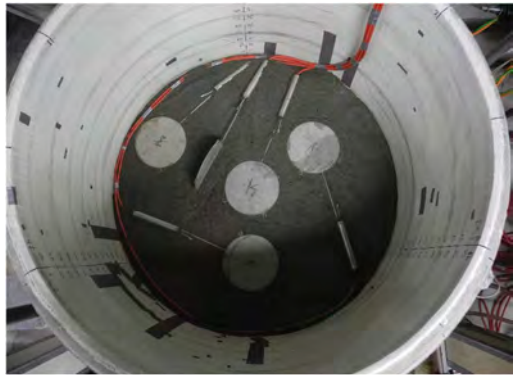


Figure 1. Pressure cell arrangement.

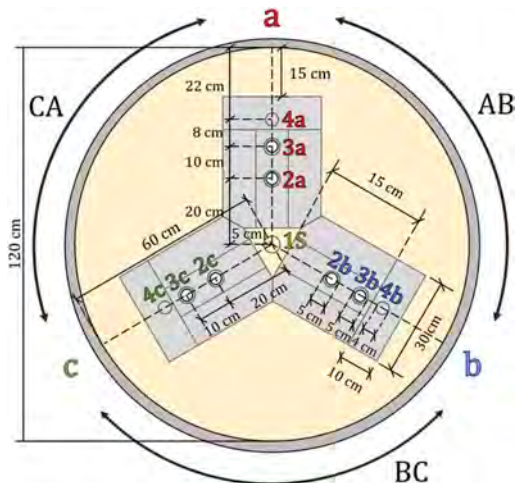


Figure 2. Cross-section of chamber with dimensions of both the clay set-up from experiment 1-3 and 5; and of the overlying metal disc with its 10 soundings holes (1S, 2a-4c). Each of the 3 clay units shown here in grey are built from 4 specimens cut from bricks of pottery clay.

available from Geomil Equipment B.V. This probe was exclusively used in the last experiment (E6). The rate

of penetration was set to 15 mm/s for all experiments to increase the spatial resolution, thus providing more continuous curves, still operating in accordance with European standard (EN ISO 22476-1:2012).

Further details about the chamber sample set-ups, and about how the signal processing was done to increase precision are found in the master's thesis (Skrede, 2021).

To simulate stress states at larger depths, the surface of the chamber samples was subjected to an over-

burden load. The vertical stresses were imposed by a circular metal disc pushed down by three airbellows fastened to an upper supporting metal framework, see Figure 3.

The chamber was designed with ten possible positions for CPTU testing. Three in-line holes were placed in 3 radial sectors 120 degrees apart, denoted sectors a, b, c. The centre hole is referred to as the S position. The holes were in addition numbered from the centre as 1,2,3 and 4. Thus position 1S is in centre while 4c is closest to the concrete wall in sector c. The reference system is shown in Figure 2. Multiple test positions were used for each chamber sample, these were divided into two rounds consisting of "primary soundings" and "secondary soundings". The primary soundings consisted of tests with significant distance to walls and previously tested positions. These were thus considered to reflect undisturbed soil. Secondary soundings were run after the primary soundings in neighbouring positions as reserve for validation, though the measurements reflect disturbed soil.

For each chamber sample, after CPTU testing, a meticulous excavation phase followed, where lab tests were conducted on both the clay and the sand to analyse the soil profile for density and strength.

3 THEORETICAL BACKGROUND

3.1 Stress state in chamber – The silo effect

The stress level in the chamber was influenced by the silo effect or the arching effect caused by vertical shear stresses on the wall. The formula by Janssen (1895) was used with effective stress parameters, Equation (1), to quantify the effect. The decay length, l , was estimated using the given surcharge, q ; and the earth pressure cells at the base, to determine the stress $\sigma'_v(z)$ over the height of the chamber.

$$\overline{\sigma'_v(z)} = \gamma' l + e^{-\frac{z}{l}}(q - \gamma' l) \quad (1)$$

3.2 CPTU-parametrizations

The conventional procedure to classify soils from CPTU results is to normalize the corrected tip resist-

ance, q_t , the sleeve friction, f_s , and the pore pressure, u_2 with respect to in-situ stress. This provides the normalized tip resistance, Q_t , the normalized friction ratio, F_r , and the pore pressure ratio, B_q ; In Equations (2)-(4) q_n is the net cone resistance, see Equation (5).

$$Q_t = \frac{q_n}{\sigma'_{v,0}} \quad (2)$$

$$F_r = \frac{f_s}{q_n} \cdot 100\% \quad (3)$$

$$B_q = \frac{\Delta u_2}{q_n} \quad (4)$$

$$q_n = q_t - \sigma_{v,0} \quad (5)$$



Figure 3. The overburden loading framework on the chamber. Above: the actuator and the probe fixed to a framework.

To estimate the undrained shear strength, s_u , in the clay layers, the empirical relations suggested by Karlsrud et al. (2005) have been used, see Equations (6)-(8). The cone factors, N_i , in these formulas are based on OCR, S_t and I_p . These parameters were estimated for each specimen by using interpolated data from the Flotten site report (L'Heureux et al. 2019).

$$s_{u,kt} = \frac{q_n}{N_{kt}} \quad (6)$$

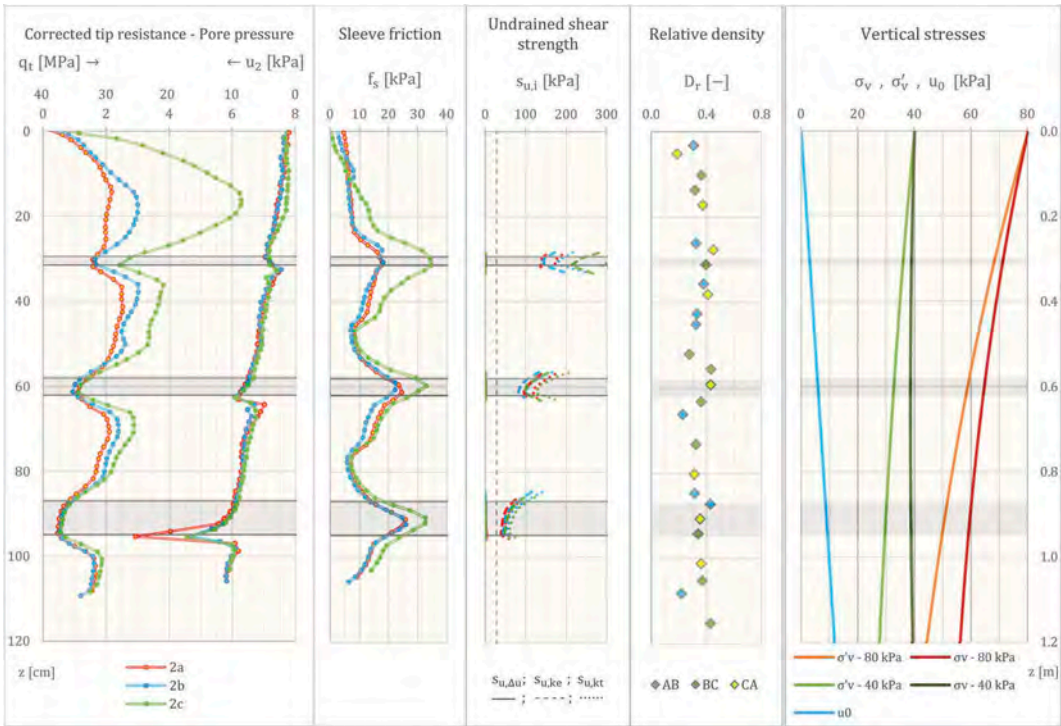


Figure 4. Experiment 5. Left: CPTU-measurements. Mid: Shear strength estimations for the clay layers, note that $s_{u,\Delta u}$ is approximately zero for all layers. Right: Sand density samples results and estimated stress distributions.

$$s_{u,\Delta u} = \frac{\Delta u_2}{N_{\Delta u}} \quad (7)$$

$$s_{u,ke} = \frac{q_t - u_2}{N_{ke}} \quad (8)$$

4 RESULTS

4.1 Soundings from experiment 5

The results of experiment 5 (Figure 4) illustrates typical trends that unveiled upon penetrating clay layers interbedded in sand. The clay layer thicknesses were respectively 2, 4 and 8 cm from the top. The surcharge was set to 40 kPa for soundings in holes 2a and 2b, 80 kPa for 2c. These were the primary soundings, while secondary soundings were performed in the number 3 holes. The latter are not presented in this figure.

The u_2 -measurements were depth-shifted to account for the distance between the position of the pore pressure sensor and the cone tip (the depth of q_t), while f_s was corrected to the end of the sleeve closest the tip, see ch. 5.2 for

explanation. The sample preparation was quite successful in experiment 5 with a fairly constant relative density, D_r , in the sand over the depth of the chamber. Comparing various tests, it is confirmed that q_t varies considerably with relative density and stress level.

4.2 Normalized profiles

To study the variation of q_t through layers of varying thicknesses, a compilation of q_t -profiles is shown in Figure 5. The depth has been normalized with respect to the cone diameter, d_c . The q_t -profiles in the graphs are indexed X-Y-Z for respectively experiment number; surcharge on top of chamber sample in kPa; and sounding hole. The colour of the profiles is according to the surcharge level, with primary and secondary soundings respectively solid and dashed. The jagged appearance of the mini-cone profiles is due to the different approach used in post data treatment for the mini cone. The profiles include a penetration through a 36 cm high pottery clay unit as a reference for the characteristic tip resistance, q_t^{char} , of the pottery clay (E4-40-3b). Here q_t^{char} is defined as the expected tip resistance in an infinitely thick layer for the specific stress level.

5 DISCUSSIONS

5.1 The thin layering effect

To what degree the measured q_t in the thin layers is higher than q_t^{char} depends on the ratio of the layer thickness over the cone diameter, H/d_c , and on the contrast between q_t^{char} in the clay and the tip resistance in the sand. The effect H/d_c is shown in Figure 5 where the mini-cone profiles from E6:4b and 4c have equal sensing- and developing depths compared to the standard-cone profile 1S, when normalized. The “depth terms”, sensing- and developing depths, denote respectively the distance ahead of an interface where q_t is influenced by the next layer; and the distance after the interface q_t retain influence from the previous layer.

The test results show that the q_t -profiles through interbedded layers are not symmetric, as the developing- and sensing distances are different for the upper and lower interface of each clay layer, as apparent in Figure 4 and Figure 5. The characteristics of q_t -profiles during transitions thus have some degree of uniqueness, which then might be used in an attempt to back-calculate layer thicknesses and q_t^{char} .

The tip resistance approaches the characteristic value asymptotically with increasing interbedded layer thicknesses. This implies that calculated s_u based on Equation (6) and (8) provide overestimations of the “true s_u ” (i.e. s_u based on triaxial CAUC-test) whenever the developing depth is not surpassed. As to illustrate, overestimation magnitudes (with reference to calculated extremal value) are listed for all experiments on pottery clay in Table 2. The table does in addition include the magnitude of underestimation when calculated s_u is based on Equation (7), which is a consequence of the excess pore pressure build-up never approaching the characteristic value. From the reference test (E4-40-3b), the developing depth of q_t was about 5-5.3 d_c (18-19 cm) after the interface.

Table 2. The ratios between the extremal value of the CPTU- s_u -parametrizations within a clay layer compared to the “true s_u ” of the clay, presented for different clay layer thicknesses. For $s_{u,kt}$ and $s_{u,ke}$ the ratio of overestimation is presented, while for $s_{u,\Delta u}$ the ratio of underestimation is presented.

Layer thickness	2 cm	4cm	8cm	12 cm
$s_{u,kt, \text{min}}/s_u$	6.3-10.5	2.3-4.6	1.4-2.1	1.1
$s_{u,ke, \text{min}}/s_u$	5.0-7.7	2.0-3.5	1.3-1.7	0.9-1.0
$s_u/s_{u,\Delta u, \text{max}}$	80-125	35-65	4-25	1.8-3.4

5.2 Depth offset

During penetration through thin layers of clay, all CPTU-parameters starts to approach their characteristic value, yet these approaches are “cancelled” upon closing in on the second interface. As measurements are saved as data points versus time, the measurements from the pore pressure sensor are actually made about 1 cone diameter behind the cone tip. This means that the extremal value of u_2 is saved at a different depth than the extremal value of q_t , consequently lowering the extremal value of the pore pressure ratio, B_q , see Figure 6. For the soundings on the natural sensitive clay (E6-1S;4b;4c), the effect of correcting the depth-offset altered the B_q extremal value up to 0.15. Moreover, due to the short distances of excess pore pressure build-up in thin layers, B_q never approach levels which are close to the reference values, requiring extra care upon interpreting CPTU.

Accounting for the depth-offset is more complicated for the sleeve friction measurements, as each measurement is the product of stresses working on the entire friction sleeve. Therefore, it can be stated that the sleeve’s length entails a smoothing effect, making it a component of less depth accuracy and maybe relevance regarding transitions. However, from the experiments, a consistent pattern is apparent: As the probe transits from the sand to the clay the sleeve friction increases drastically when the front end of the sleeve hits the original level of the interface (prior to deformation), whereupon it is decreasing (ref. E4-40-3b). Due to this phenomenon f_s may turn out to be quite useful for identifying thin layers of clay embedded in sand. However, this part is associated with great uncertainty as field measurements of f_s can be rather high in sand, while low in clay, and in addition, f_s varies a lot with probe types. Consequently, this aspect requires further research.

With regards to the previous paragraph, the choice of depth correction for f_s is not obvious. Upon correcting the data points upwards on the sleeve, the extremal magnitude of F_r is smoothed with respect to both lower and upper bounds, making a distinction between materials more difficult (Figure 7). Ironically and conceptually incorrect, the greatest magnitude of F_r is reached if no corrections are made at all.

In conclusion, depth-offset has a big impact on the classification parametrizations during transitions, greatly impacting the identification of the materials

and the layer thicknesses. It should however be underlined that offset corrections do not influence s_u -estimations except for $s_{u,ke}$ with a negligible magnitude.

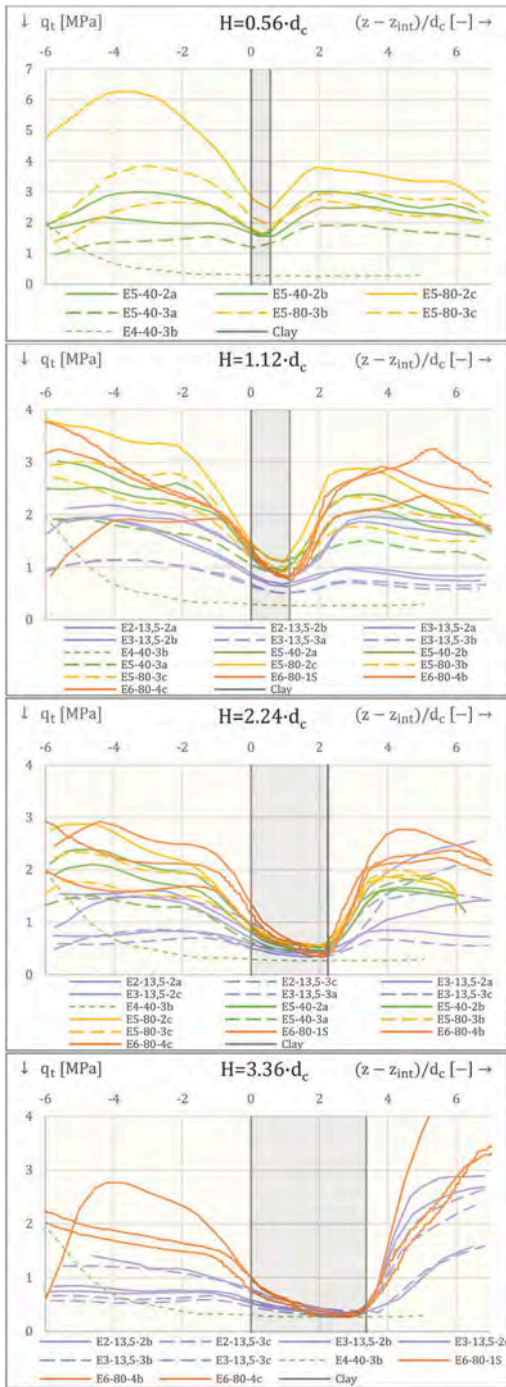


Figure 5. Rotated tip resistance profiles of penetration of clay layers (surface towards left, chamber base towards right), normalized with respect to the cone diameters. The thicknesses of the layers penetrated by respectively the standard cone and the mini-cone were 2, 4, 8 and 12 cm; and 2.8, 5.7 and 8.5 cm. Soundings in natural sensitive clay are marked with orange (E6).

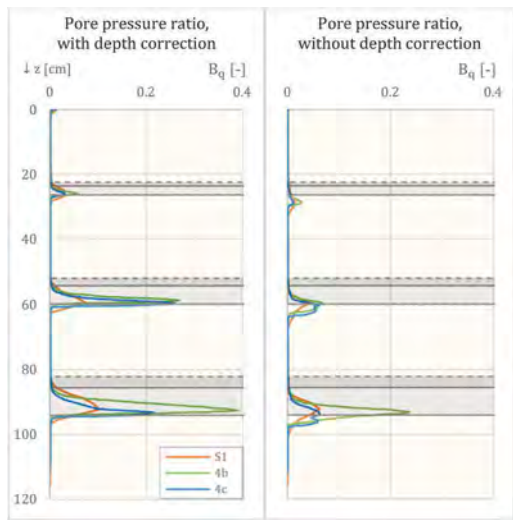


Figure 6. Relative difference of B_q when depth-offset is corrected (left), and not corrected (right) (E6-1S;4b;4c).

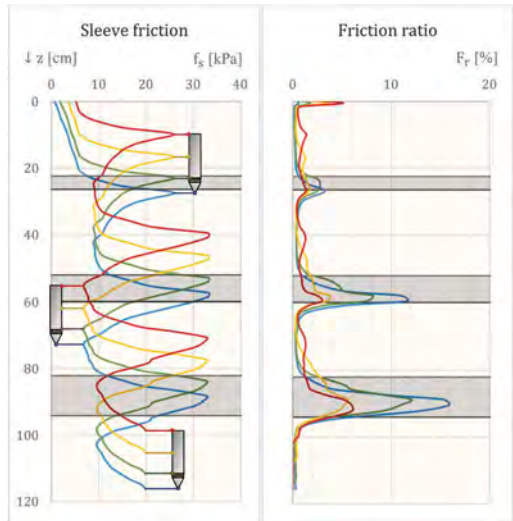


Figure 7. Left: Profile with f_s -readings (E6-1S) not corrected with respect to depth offset (blue) and profiles adjusted for different positions on the friction sleeve. Right: Resulting F_f -graphs based on data from the graphs in the left profile.

6 CONCLUSIONS

Thin, weak and possibly sensitive interbedded clay layers are not easily detected as characteristic reference values are not reached before the cone leaves the layer. In this respect, depth correction proves to be very important for the magnitude of the normalized ratios F_f .

and B_q . Furthermore, calculations of s_u based on the correlations $s_{u,k1}$ and $s_{u,ke}$ will lead to overestimation of s_u as the recorded tip resistance does not approach the characteristic tip resistance of the thin layer. Likewise, calculation of s_u based on the correlation $s_{u,\Delta u}$ will lead to severe underestimation due to the small excess pore pressure build-up in thin layers.

ACKNOWLEDGEMENTS

The authors would like to acknowledge everyone who have contributed to this research program, mainly lab staff at NTNU. We are grateful to NGI for financially aiding the program and to Geomil Equipment for generously lending the mini-cone to the research.

REFERENCES

- Emdal, A., Gylland, A., Amundsen, H.A., Kåsin, K., Long, M. 2016. Mini-block sampler. *Canadian geotechnical journal*, 53(8):1235–1245. Link
- Hammer, H.B. 2020 *Physical experiments on CPTU thin-layer effects of thin clay layers embedded in sand: With analysis-and possible correction of cone resistance in layered profiles*. M.Eng. Master Thesis. Faculty of Civil Engineering, Norwegian University of Science and Technology (NTNU). Lin.
- Janssen, H.A. 1895. Versuche über Getreidedruck in Silozellen. *Zeitschrift des Vereins deutscher Ingenieure*. 39 (35):1045–1049. Link
- Karlsrud, K., Lunne, T., Kort, D.A., Strandvik, S. 2005. CPTU correlations for clays. In *Proceedings of the international conference on soil mechanics and geotechnical engineering*, 2005, Osaka, 16:693–702. Link
- de Lange, D.A., Terwindt, J. and van der Linden, T.I. 2018. CPT in thinly inter-layered soils. Paper presented at the Cone Penetration Testing 2018: *Proceedings of the 4th International Symposium on Cone Penetration Testing (CPT'18)*, 21-22 June, 2018, Delft, The Netherlands. Link
- L'Heureux, J. S., Hansen, L., Longva, O., Emdal, A., & Grande, L. O. 2010. A multidisciplinary study of submarine landslides at the Nidelva fjord delta, Central Norway, - Implications for the assessment of geohazards. *Norwegian Journal of Geology*, Vol 90: 1–20. Trondheim, ISSN 029-196X. Link
- L'Heureux, J.S., Lindgård, A., Emdal, A. 2019. The Tiller-Flotten research site: Geotechnical characterization of a very sensitive clay deposit. *AIMS Geosciences*, 5(4):831–867. Link
- Longva O., Janbu N., Blikra L.H., Bøe R. 2003. The 1996 Finneidfjord Slide: Seafloor Failure and Slide Dynamics. In: Locat J., Mienert J., Boisvert L. (eds.), *Submarine Mass Movements and Their Consequences. Advances in Natural and Technological Hazards Research, vol 19*. Springer, Dordrecht. Link
- Skrede, H. 2021 *CPTU-detection of thin clay layers in sand: Results from calibration chamber testing*. M.Eng. Master Thesis. Faculty of Civil Engineering, NTNU. Link
- van der Linden, T.I., De Lange, D.A., & Korff, M. 2018. Cone Penetration Testing in Thinly Inter-Layered Soils. *Geotechnical Engineering*. Link
- European committee for standardization. 2012. *Geotechnical investigation and testing: Field testing: Part 1: Electrical cone and piezocone penetration test*. EN ISO 22476-1: 2012.

Determination of hydraulic conductivity using HPT & CPTu

M. Slowiok, S. Oberhollenzer & R. Marte

Institute of Soil Mechanics, Foundation Engineering & Computational Geotechnics, Graz University of Technology, Graz, Austria

T. Freudenthaler

mjp ZT GmbH, Saalfelden, Austria

ABSTRACT: In geotechnical engineering insitu tests are becoming increasingly popular to determine the hydraulic conductivity of soils. Direct push methods such as piezocone penetration test CPTu or the hydraulic profiling tool HPT allow characterizations along a linear profile. The determination of hydraulic conductivity with HPT is an alternative to CPTu for drained and partially drained conditions. Thereby, water is continuously injected from a small screened port at the probe into the soil. Based on the required pressure to inject the water into the soil and the constant flow rate, the hydraulic permeability can be determined for a certain range of drainage conditions. The present article compares HPT and CPTu results with slug tests, executed at different test sites in a wide range of grain size distributions. Based on this comparison, a new correlation was elaborated for HPT which enables an improved characterization of hydraulic conductivity.

1 INTRODUCTION

The hydraulic conductivity K of soils is an important soil parameter for a wide range of geotechnical problems (e.g. excavations in combination with dewatering works). In order to determine K , the fluid velocity v and the hydraulic gradient i can be used based on Darcy's law. Hydraulic conductivity can vary between approximately ten orders of magnitude ($K = 10^{-2} - 10^{-12}$ m/s) and is strongly influenced by the grain size distribution, density, void ratio and anisotropy. Furthermore, it was shown earlier that the horizontal hydraulic conductivity can become up to ten times larger compared to the vertical one in sediment deposits (Boley 2019).

In the laboratory, the vertical hydraulic conductivity K_v is determined based on permeameter tests with constant or variable pressure head. In general, the quality of sampling has a great influence on the determined permeability. On the other hand, direct push (DP) methods are time- and cost-efficient alternatives, which became more popular over the last decades. Especially piezocone penetration tests (CPTu) enable a determination of K based on the soil behavior type index I_c or dissipation tests. Thereby, the determined permeability - in contrast to the laboratory tests - is a combination of the horizontal and vertical one. The hydraulic profiling tool (HPT) represents an alternative investigation technique and enables a continuous characterization over depth. Thereby, water is injected under constant rate into

the subsoil. Based on the required pressure to ensure constant flow, K can be determined based on correlations, which were often calibrated based on slug-tests (and might rely therefore on site-specific data).

In the present article different insitu & laboratory tests are compared with reference to the hydraulic conductivity. The main focus is related to direct push methods (HPT, CPTu) in order to characterize their application limits. In a final step, a new correlation to determine K is elaborated for HPT based on additional slug tests.

Four test sites, carried out within Austria (state Salzburg), represent the basis of the present work. The investigation program includes CPTu, HPT, slug-tests and additional laboratory tests. All applied methods (insitu & laboratory tests) are described in the following section.

2 APPLIED METHODS

2.1 Piezocone penetration test (CPTu)

The piezocone penetration test (CPTu) represents a widely used direct push technique for soil characterization. Thereby, a penetrometer is pushed at constant rate (equal to 2 cm/s) into the subsurface. Simultaneously, the tip resistance q_c , sleeve friction f_s & dynamic pore water pressure u_t are measured at the cone continuously over depth. The friction ratio $R_f = f_s/q_t$ (%) can be used as a first indicator for

characterizing the soil behavior type. Thereby, the corrected cone resistance q_t is defined as

$$q_t = q_c + u_2(1 - a) \quad (1)$$

where a is the area ratio of the cone and u_2 is the dynamic pore water pressure measured behind the tip. The cones used for all field investigations present a cross-section area equal to 15 cm² and the porewater pressure was measured at position u_2 .

The hydraulic conductivity can (mainly) be determined based on two approaches: The first method is based on the soil behavior type classifications and provides a continuous K -profile over depth. These classifications can be estimated based on the soil behavior type index I_c (Robertson & Wride 1998).

$$I_c = \left[(3,47 - \log Q_m)^2 + (\log F_r + 1,22)^2 \right]^{0,5} \quad (2)$$

where Q_m is the normalized cone resistance

$$Q_m = [(q_t - \sigma_v)/p_a](p_a/\sigma'_{v0})^n \quad (3)$$

with the total vertical stress σ_{vo} and the effective vertical stress σ'_{vo} and the normalized friction ratio F_r

$$F_r = [(f_s/q_t - \sigma_{v0})]100 \% \quad (4)$$

The soil behavior type index I_c is defined by the radius of concentric circles within the soil behavior type diagram according to Robertson (2010). Higher I_c values represent soils with higher fines content & lower hydraulic conductivity. The empirical correlation to characterize the hydraulic conductivity in m/s based on I_c is shown in equations 5 and 6:

$$\text{When } 1.00 < I_c < 3.27 \quad K = 10^{(0,95 - 3,04 I_c)} \quad (5)$$

$$\text{When } 3.27 < I_c < 4.00 \quad K = 10^{(-4,52 - 1,37 I_c)} \quad (6)$$

The second approach to determine the hydraulic conductivity is based on CPTu-dissipation tests, measuring the pore water pressure decay after stopping the penetration process. The dissipation process is mainly governed by the horizontal coefficient of consolidation, defined as:

$$K_h = (c_h \gamma_w)/M \quad (7)$$

where K_h represents the horizontal hydraulic conductivity, M the 1D constrained modulus at the insitu stress level and γ_w the unit weight of water. In order to back-calculate K_h , c_h & M must be calculated using existing correlations. Based on Teh & Houlsby (1991) or Robertson et al. (1992) c_h (m²/s) can be calculated based on t_{50} (time for 50 % of excess pore water dissipation).

$$c_h = 1.50 (1.67 * 10^{-6}) 10^{(1 - \log t_{50})} \quad (8)$$

for 15 cm² piezocones.

The constrained modulus M can also be determined based on Robertson (2009) using:

$$M = \alpha_M (q_t - \sigma_{v0}) \quad (9)$$

when $I_c > 2.20$:

$$\alpha_M = Q_m \quad \text{when } Q_m \leq 14 \quad (10)$$

$$\alpha_M = 14 \quad \text{when } Q_m > 14 \quad (11)$$

2.2 Hydraulic Profiling Tool (HPT)

The Hydraulic Profiling Tool belongs to the direct push methods too. A probe is pushed into soil under constant penetration rate equal to 2 cm/s. Simultaneously, water is injected at constant flow rate via a small port at the side of the probe. A pressure sensor inside the probe (near the outlet) records the required injection pressure while flow remains constant. Based on the ratio between flow rate and pressure the hydraulic conductivity can be estimated in combination with correlations. In a first step the measured pressure p_{tot} is corrected by the atmospheric pressure p_{atm} and the piezometric pressure p_{piezo} . The piezometric pressure can be calculated based on dissipation tests for selected depths.

$$p_{corr} = p_{tot} - p_{atm} - p_{piezo} \quad (12)$$

In this study two approaches (McCall & Christy (2010), Borden et al. (2021)) are used to calculate the hydraulic conductivity.

The first (empirical) correlation according to McCall & Christy (2010) was calibrated based on slug tests:

$$K_h = 3.53 \cdot 10^{-6} [21.14 \ln(Q/0.15P_{corr}) - 41.71] \quad (13)$$

It should be noted that the approach according to McCall & Christy (2010) is limited to K -values between $2.65 \cdot 10^{-4}$ and $3.53 \cdot 10^{-7}$ m/s.

The enhanced correlation according to Borden et al. (2021) considers Q (mL/min), P_{corr} (kPa) and additionally the penetration rate v (mm/s) as well as probe diameter d (mm),

$$K_h = 7.13 \cdot 10^{-6} \frac{0.12 v d^2 + 0.12 Q}{(0.15 P_{corr})^{1.02}} \quad (14)$$

In addition, the HPT tool offers the measurement of electrical conductivity (EC) using a four-point Wenner array near the tip of the probe. Based on this measurement qualitative estimations regarding the permeability are possible. An increased electrical conductivity is an indicator for a higher fines content and lower hydraulic conductivity.

2.3 Direct Push Slug Test (DPST)

Slug tests are a reliable and cost-efficient technique to determine the permeability of soils insitu. First, an excess porewater pressure is created artificially, before measuring the drop in porewater pressure over time.

The change in water head can be created by adding or removing water within the rods. In our case, the slug test was performed using direct push equipment. After pushing the penetration rod into the desired depth, the penetration procedure is stopped and a filter body (4/8 mm gravel) is created by pulling the rods about 50 cm. While pulling the rods, a lost tip remains in the soil and the filter material is poured through the rod to create a filter length equal to 50 cm.

When the filter section is created, a water head is applied by filling a defined volume of water into the penetration rods. Afterwards, the pressure drop is recorded over time by a sensor. In each depth at least two slug tests were performed and analyzed in combination with the software-package SlugIn (IGME) by using the interpretation methods according to Cooper et al. (1967), Hvorslev (1951) and Bouwer-Rice (1976).

2.4 Laboratory test with constant pressure head and grain-size analysis

At two test sites additional soil sampling was executed using the CPT-Ranger system. The recovered samples present a diameter d and height h equal to 6 cm and 50 cm respectively. Each sample was trimmed down to $d = 5$ cm and $h = 12$ cm to enable permeameter tests. The tests were carried out with a constant pressure head of $\Delta h = 3.6$ m. Consequently, the vertical hydraulic conductivity can be calculated based on the measured discharge Q over time t , the hydraulic gradient $i = \Delta h / \Delta l$ and cross-section area A .

$$K_v = \frac{Q \Delta l}{A \Delta h t} \quad (15)$$

Furthermore, the grain-size distribution was analyzed for each soil sample in order to enable classifications based on Chapuis (2012).

3 TEST SITES

Insitu tests and additional soil sampling was carried out at four test sites within the state of Salzburg, Austria. The investigated soils at Flachau (TS1), Siggerwiesen (TS2), Bruck/Großglocknerstraße (TS3) and Salzburg (TS4) are characterized by a wide range of different grain size distributions (see Figure 1).

Test site 1 (TS1) mainly consists of coarse-grained deposits which are interrupted by silty layers. For TS2 Siggerwiesen (SIG) the subsoil is composed of a heterogeneous aquifer which is followed by a low permeable silty fine sand. The top layer (0-6m) at TS3 is classified as peat and is underlain by sand-silt mixtures. The fourth testing site is situated close to the main train station of Salzburg. The subsoil conditions are characterized by 3 main lithologies: sandy gravel (0-4m), sand-silt alterations (4-9m) and clayey silts (9-25m).

CPTu and HPT-soundings were carried out at all four test sites. Additional slug tests were carried out at three depth levels on each site. At TS3 and TS4 additional soil sampling (for permeameter tests and determination of grain size distribution) was executed.

4 RESULTS

CPTu and HPT measurements (q_t , R_f , EC , P_{corr}) are presented for the different test sites in Figure 1. A low corrected tip resistance q_t and high friction ratio R_f represent fine-grained layers. As mentioned earlier, fine grained sections, presenting a low permeability, are characterized by a high electrical conductivity EC and high P_{corr} values.

TS1 – Flachau consists of a fine-grained layer between 2 and 3 meters, which can be detected based on q_t , R_f , EC and P_{corr} . A second silt-dominated lens follows between 5 and 6 meters. The lower aquifer (6-10m) presents low friction ratios R_f and small P_{corr} values, indicating a high permeability.

At *TS2 – Siggerwiesen* backfill material is present between 0 and 4 meters which is followed by a silty fine sand layer with increasing fines content.

The subsoil at *TS3 – Bruck/Großglocknerstraße* consists of a peat layer within the first 5 meters, followed by sand mixtures. Within the top layer, the friction ratio R_f amounts to approximately 10 %. On the other hand, HPT pressures P_{corr} indicate rather high permeabilities within this layer. The following sandy section (7 – 20m) presents increased q_t , and small R_f values. P_{corr} & EC present a rising trend over depth.

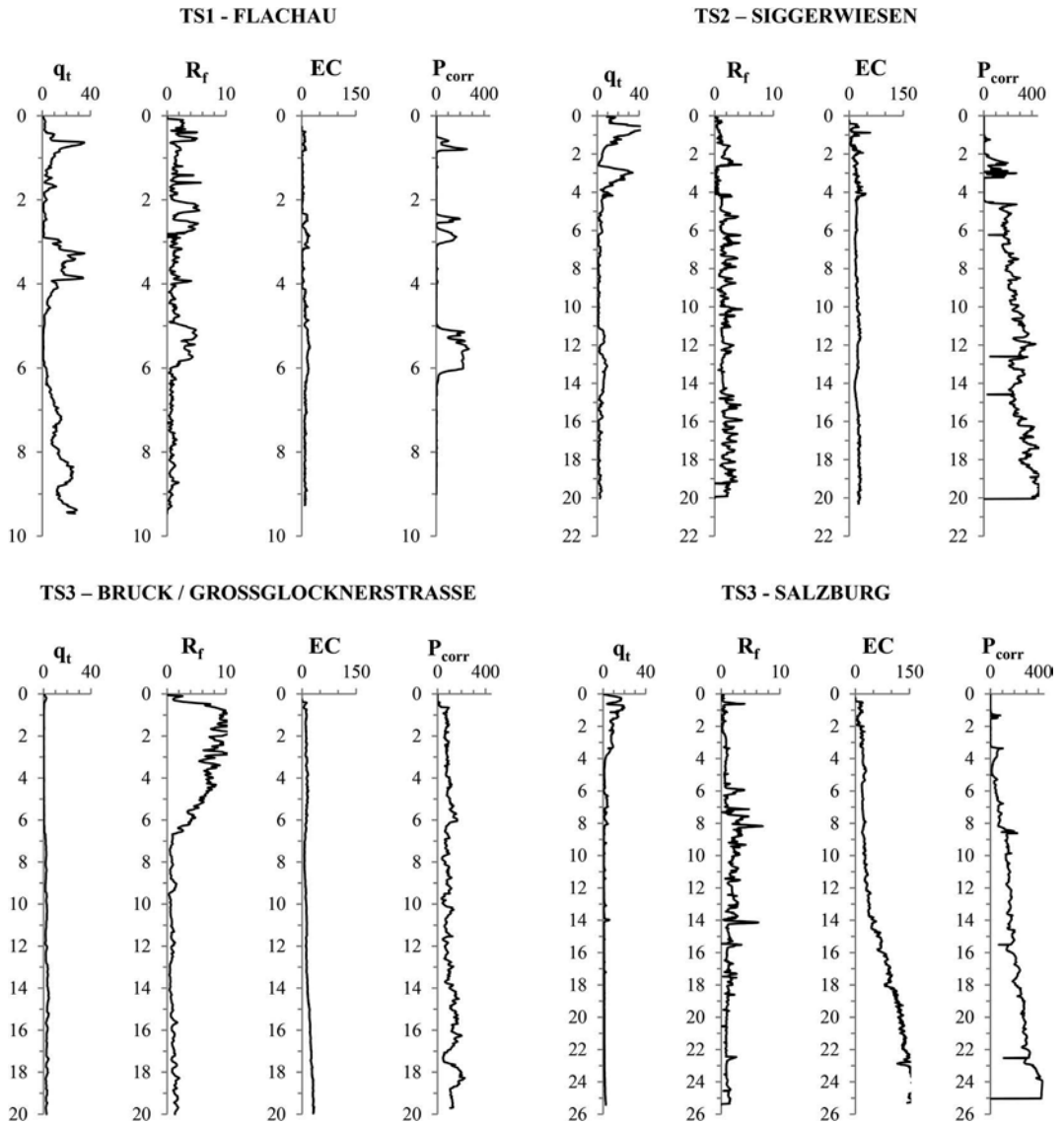


Figure 1. Results from Direct Push stratigraphic profiling over depth (m) – tip resistance q_t (MPa), friction ratio R_f (%), electrical conductivity EC (mS/m) & corrected HPT pressure P_{corr} (kPa).

The subsoil at *TS4 – Salzburg* is composed of backfill material within the upper 4 meters. The fine-grained “Salzburger Seeton” (9 to 25m) is characterized by a small q_t and increased R_f , EC - as well as P_{corr} -values.

In a second step the hydraulic conductivity was evaluated based on CPTu (I_c , dissipation test), HPT, slug tests and laboratory tests (permeameter test, grain-size distribution). Figure 2 presents the determined K values based on different interpretation techniques as well as test sites. A continuous K profile over depth can be evaluated from CPTu (I_c) and HPT data. Selective permeability tests in certain depths complement the test program and are used for comparison.

For *TS1 – Flachau* hydraulic conductivity based on I_c yields to the lowest results. Both HPT-correlations lead to similar results within the same order of magnitude. Slug tests are evaluated based on Hvorslev (1951). The latter results are situated between CPTu (I_c , dissipation test) and HPT results. The slug tests identify the impermeable lens in 5 meter depth. However, the sensitivity of the different tests differ strongly. Slug test data verify the soil layering and are situated between CPTu and HPT results.

At *TS2 – Siggerwiesen* the high permeable aquifer in a depth of 4 meters is recognized by all methods. The fine grained layer from 4 to 20 m indicates low permeability for both CPTu methods. The slug tests

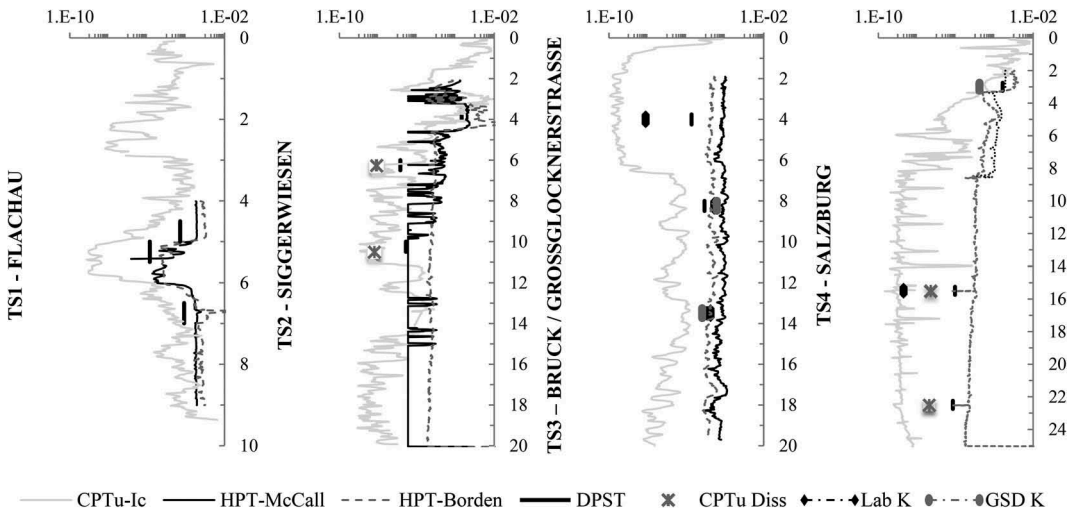


Figure 2. Hydraulic conductivity K (m/s) from different approaches over depth (m) – cone penetration test soil behavior type index $CPTu-I_c$, Hydraulic Profiling Tool HPT , Direct Push Slug Test $DPST$, cone penetration dissipation test $CPTu Diss$, Laboratory permeameter test $Lab K$ & Grain Size Distribution correlation $GSD K$.

suggest a higher permeability whereas McCall & Christy (2010) HPT approach reach the lower K limit.

The continuous readings of $TS3 - Bruck/Großglocknerstraße$ yields to similar trends: $CPTu-I_c$ results lead to the lowest and both HPT -correlations lead to the highest hydraulic conductivity values. The organic layer within the upper 5 meters present a high scatter in K (up to five orders of magnitude). For the lower silty sand layer, the scatter becomes smaller.

At $TS4 - Salzburg$ the same trend (between $CPTu$ and HPT results) is given. Again, the difference in K rises in fine-grained layers. Within the so-called “Salzburger Seeton” slug tests indicate a higher permeability, whereas laboratory and $CPTu$ (dissipation, I_c) results lead to smaller conductivities.

In order to investigate the scatter in K , all insitu and laboratory results are compared within Figure 3. The scatter was evaluated considering the soil behavior type index I_c . To enable a comparison, the data from $CPTu$ and HPT was assigned over an interval equal to 50 cm meters using the median. Vice versa “punctual” K measurements (e.g. dissipation test) were assigned to a median I_c .

As shown in Figure 3, with increasing fine-content the difference in K rises strongly. For small I_c values (indicating coarse-grained material) the variation of the different interpretation techniques is approximately one order of magnitude. As mentioned above, HPT -correlations yield the upper K -end, whereas K values based on $CPTu-I_c$ mark the lower K -end. For sand-silt mixtures the discrepancy increases. This trend continues with increasing fines-content, where HPT -correlations reach the end of applicability. $CPTu$ dissipation,

$CPTu-I_c$ and laboratory results indicate rather low hydraulic conductivity within this section.

In the last step, existing HPT correlations where evaluated. McCall & Christy (2010) suggested for their correlation a lower K limit of $3.5 \cdot 10^{-7}$ and a higher K limit equal to $2.7 \cdot 10^{-4}$ m/s. Their logarithmic approach (see Figure 4) was calibrated

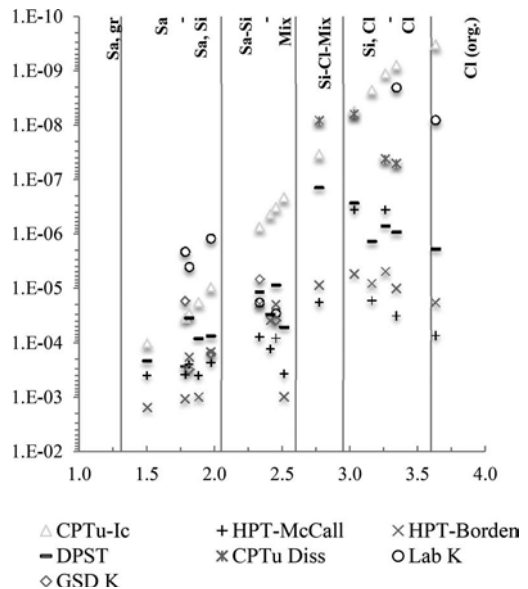


Figure 3. Hydraulic conductivity K (m/s) vs. Soil Behavior Type Index I_c (-).

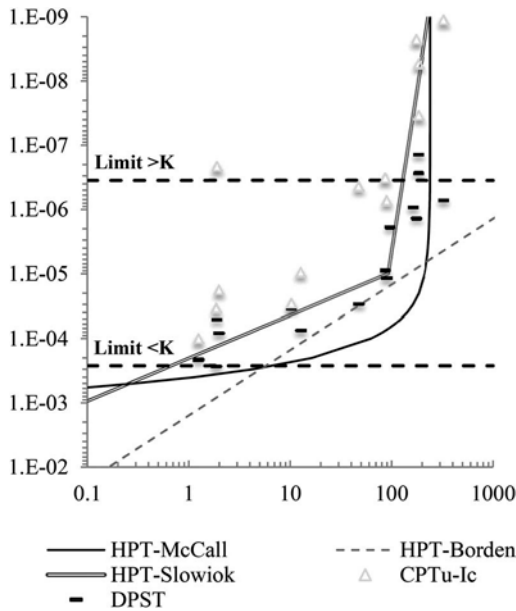


Figure 4. HPT correlations in comparison with slug test and CPTu-Ic in K (m/s) vs. P_{corr} (kPa) space.

based on slug tests and exhibits an asymptote for high P_{corr} . At the low K end permeability changes strongly along a small range of P_{corr} values. On the other hand, Borden et al. (2021) defines a straight line within the K - P_{corr} space. In comparison with the available slug test and CPTu- I_c data, the correlation according to McCall & Christy (2010) is in good agreement with the results. It should be noted, that for P_{corr} values between 10 and 100, the correlation leads to rather high permeabilities. On the other hand, Borden et al. (2021) leads to significantly (unrealistic) high results.

In order to achieve a better agreement with our test results two best-fit curves were defined. The new correlation is based on a potential function which is further subdivided:

$$K_h = 1.65 * 10^{-8} (Q/P_{corr})^{10}$$

when $1.36 < Q/P_{corr} < 1.90$ (16)

$$K_h = 6.53 * 10^{-6} (Q/P_{corr})^{2/3}$$

when $1.90 < Q/P_{corr} < 259.00$ (17)

5 SUMMARY

The objective of this study was to compare and evaluate different insitu and laboratory tests in order to estimate the hydraulic conductivity. Based on investigations at 4 test sites, it was shown that direct push techniques (CPTu, HPT and Slug test) lead to realistic K -results and are reproducible. In addition, it was shown that different investigation techniques present a stronger scatter with increasing fines content. Here, K -values from CPTu- I_c mark the lower boundary, whereas K -values from HPT-correlations mark the upper boundary. It was proven, that existing HPT correlations (McCall & Christy 2010, Borden et al. 2021) should only be used between $K = 1 \cdot 10^{-6}$ and $5 \cdot 10^{-4}$ m/s, which is for many geotechnical projects (e.g. dikes, dewatering) sufficient. Both HPT correlations are realistic representations to determine K by Q/P_{corr} . In addition a new HPT correlation was presented.

REFERENCES

- Boley, Conrad. 2019. Handbuch Geotechnik. Grundlagen – Anwendungen - Praxiserfahrungen. Springer Fachmedien Wiesbaden: Springer Vieweg
- Borden, Robert C., Cha, Ki Young, Liu, Gaisheng. 2021. A Physically Based Approach for Estimating Hydraulic Conductivity from HPT Pressure and Flowrate. In Ground water 59 (2).
- Bouwer, Herman & Rice, R. C. 1976. A slug test for determining hydraulic conductivity of unconfined aquifers with completely or partially penetrating wells. In Water Resour. Res. 12 (3): 423–428.
- Chapuis, Robert P. 2012. Predicting the saturated hydraulic conductivity of soils: a review. In Bull Eng Geol Environ 71 (3): 401–434.
- Cooper, Hilton H., Bredehoeft, John D., Papadopoulos, Istavros S. 1967. Response of a finite-diameter well to an instantaneous charge of water. In Water Resour. Res. 3 (1): 263–269.
- Hvorslev, M. J. 1951. Time lag and soil permeability in ground water observations. Vol. 36.
- IGME. SlugIn 1.0. Slug Test Analysis Software. Version 1.0: Instituto Geologico y Minero de Espana (IGME).
- McCall, W. & Christy, T. M. 2010. Estimating Formation Hydraulic Conductivity (K) from HPT Q/P Ratios (abstract). Proceedings of the 2010 North American Environmental Field Conference. Socorro.
- Robertson, P. K., Sully, J. P., Woeller, D. J., Lunne, T., Powell, J. J. M., Gillespie, D. G. 1992. Estimating coefficient of consolidation from piezocone tests. In Can. Geotech. J. 29 (4): 539–550.
- Robertson, P. K. & Wride, C. E. 1998. Evaluating cyclic liquefaction potential using the cone penetration test. In Can. Geotech. J. 35 (3): 442–459.
- Robertson, P. K. 2009. Interpretation of cone penetration tests — a unified approach. In Can. Geotech. J. 46 (11): 1337–1355.
- Robertson, P. K. 2010. Estimating in-situ soil permeability from CPT & CPTu. 2nd International Symposium on Cone Penetration Testing.
- Teh, C. I. & Houlsby, G. T. 1991. An analytical study of the cone penetration test in clay. In Géotechnique 41 (1): 17–34.

DEM-FDM coupling simulation of cone penetration tests in a virtual calibration chamber

Y. Song, X.Q. Gu & J. Hu

Tongji University, Shanghai, China

ABSTRACT: We performed numerical simulation of the cone penetrating process with discrete element method (DEM) coupled with finite difference method (FDM) to investigate the mechanics of granular soil interacted with a cone penetrometer. The efficacy of particle size amplification method to estimate soil physical indexes has yet to be established and it was validated in this work. The effects of cone-particle chamber size, confining stress and sand modulus on cone tip resistance are analyzed. The results show that the effect of confining stress is consistent with the empirical relationship and the cone tip resistance correlates positively with the number of particles contacting with the cone penetrometer. Furthermore, the distribution of radial stress agrees well with the cavity expansion theory that a nearly linear relation between cone tip resistance and radial stress near the cone penetrometer can be observed.

1 INTRODUCTION

Cone penetration testing can be used for soil classification, determination of soil physical and mechanical parameters, evaluation of pile bearing capacity and liquefaction site discrimination (Yu & Mitchell, 1998). Till now, the relationship between tip resistance and soil parameters is established mainly through bearing capacity theory, cavity expansion theory, finite element simulation or cone penetration calibration chamber test. Chen & Juang (1996), Sokolovskii (2016) proposed a formula to calculate the cone probe coefficient based on the bearing capacity theory and developed an empirical relationship to determine the volumetric strain. The bearing capacity theory fulfill the equilibrium equation and yield criterion, however the kinematics and initial stress state around the penetrometer are disregarded, and the stiffness and compressibility of soil are not carefully accounted. The resulting prediction of cone tip resistance could be spurious. Compared with the bearing capacity theory, the cavity expansion theory not only considers the elastic deformation of soil during penetration, but also considers the plastic deformation, which leads to a simple and accurate solution (Chen & Abousleiman, 2012 and Chen et al., 2019). However, the cavity expansion theory suffers from several shortcomings. For example, the influence of penetration rate and pore water pressure is not considered. Yi (2012) used finite element method to analyze soil deformation around penetrometer with different penetration rates. Finite element simulation requires complex constitutive

models to simulate the stress-strain characteristics of sand, and the large distortion of finite element mesh of the soil near the cone-tip does not guarantee legitimate numerical results. The indoor calibration chamber test may present different results due to the size effect than those from the in-situ test (Wesley,1998). Therefore, the model size effect needs to be investigated cautiously in this regard.

In this work, the discrete element method coupled with finite difference method is used to simulate the cone penetration test, which can effectively analyze cone penetrator-soil interaction mechanics while considering the large deformation characteristics of soil near the cone-tip. In order to consider the shape effect of sand particles, the rolling-resistant linear contact model is used in the simulation. The contact parameters were calibrated in accordance with the triaxial drainage testing result. Effects of different contact parameters on soil properties were briefly discussed and pertinent suggestions were given for the choice of model parameters.

2 COUPLED DEM-FDM SIMULATION SCHEME

2.1 Cone penetration test model

Discrete element method (DEM) is a numerical method calculating the behavior of a large number of particles by computing the trajectories of each particle with Newton's law of motion (Cundall & Strack,1979). It is widely used for conducting down-scaled numerical experiments on virtual sand samples

(Arroyo et al., 2011; Butlanska et al, 2014; Gu et al., 2015). It is advantageous in studying geomechanics by offering both macroscopic and microscopic information of sands compared with traditional numerical methods based on continuum mechanics. While due to the demanding requirement of computational resources, its application on full scale analysis is uninviting. In contrast, finite difference method (FDM) is able to solve the governing equation in a speedy manner while the large deformation of the soil near the cone-tip cannot be handled and the fabric evolution of microstructures can hardly be obtained. Therefore, a DEM and FDM coupling scheme, which can effectively take advantage of the merits of both methods, is appealing for simulating cone penetration testing. In this study, we adopt well recognized software PFC3D for DEM modeling of the near field sand and FLAC3D for FDM modeling of both the cone penetrometer and the far field domain. The coupling of these two is realized via the equilibrium of the interface of the neighboring domains of DEM and FDM.

The schematic of the cone penetration test model is shown in Figure 1a, where the cylindrical ground consists of the inner cylinder and the outer hollow cylinder. The inner cylinder is modeled by DEM containing 79,590 spheres and the hollow cylinder is modeled by FDM containing 50,000 elements. The adopted dimensions of the model are as follows: the diameter of the model domain (D_c) is 752 mm, the height of the soil model (H) is 432 mm, the radius of the inner cylinder (D_1) is 288 mm. As shown in the Figure 1b, the rigid cone penetrometer is modeled by FDM consisting of a frictionless cone rod of diameter (d_c) 35.6 mm, a frictional cone with an inclination of 60° and a frictional sleeve of length (h_c) 32.6 mm. In the simulation, we prescribe a penetrating speed of 0.1 m/s during the entire penetration. In order to ensure that the boundary conditions are consistent with that in the in-situ test, we adopted the boundary conditions suggested by Salgado et al., 1998: the horizontal boundary is prescribed by constant stress, the upper boundary is stress free and the bottom is displacement free.

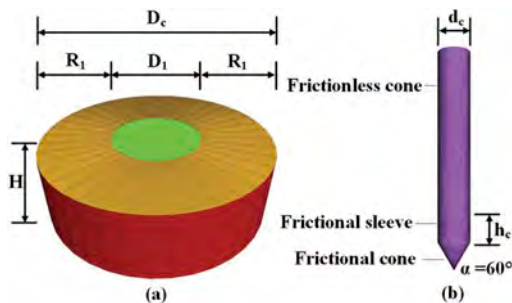


Figure 1. The numerical calculation model of the cone penetration test.

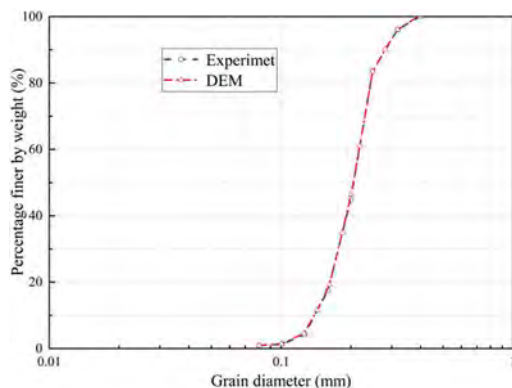


Figure 2. Grain size distribution.

2.2 DEM parameter calibration

In order to realize the faithful constitutive behavior of sands modeled by the discrete particle assembly, the contact parameters were calibrated by comparing them with the triaxial compression test. Note that we adopt the rolling-resistant linear contact model in the DEM simulation to account for the irregular shape of sand particles. The rolling-resistant linear contact model consists of three parts: linear normal and tangential force-displacement relations and a linear rotational constitutive relation. The particle assembly was generated by the radius expansion method to emulate the particle size distribution of Fontainebleau sand measured in the physical test (Bolton et al., 1999), as shown in Figure 2. First, 16,160 proportionally smaller non-overlapping particles were generated in a $4.5 \times 4.5 \times 9 \text{ mm}^3$ cuboid, and then multiplied by the radius expansion coefficient to gradually expand to the target particle size. The DEM model and FDM model of the triaxial compression simulation for calibrating DEM physical parameters are shown in the Figure 3. The FDM model consists 50,000 elements and the Mohr-Coulomb model is adopted as the soil constitutive relation with its parameters listed in Table 1. The strain-controlled loading with a constant speed of 10^{-6} m/s is applied in the axial direction and the uniform confining pressure of 100 kPa is applied to the circumferential direction for both PFC3D and FLAC3D models.

In the DEM simulation, the particle assembly was generated to attain the relative density $Dr=70\%$ which is comparable to physical samples. Typical ranges of contact law parameters suggested by Gu et al. (2020) were first adopted, e.g. contact stiffness, rolling resistance and contact friction. The contact parameters were further fine-tuned to reconcile the DEM simulation result with that from the FDM simulation, which is deemed to be the true constitutive relation of the soil.

Figure 4 Shows the deviatoric stress-strain relations and volumetric strain-axial strain relations for the triaxial drained test with confining stress of 100 kPa from both DEM and FDM simulations. It can be seen that the

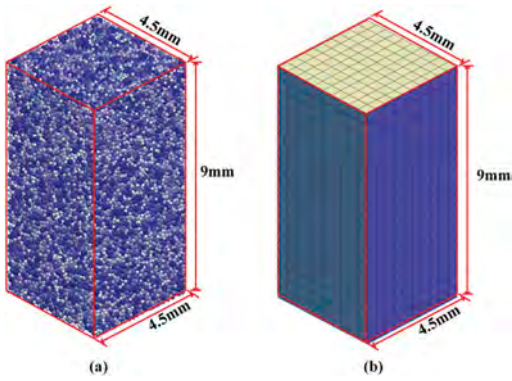


Figure 3. 3D triaxial compression test model for calibrating DEM parameters: (a) PFC3D model and (b) FLAC3D model.

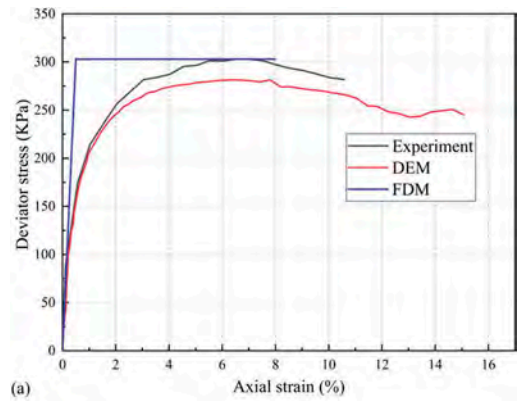
DEM and FDM simulation results (Seif et al., 2010) agree to a satisfactory extent for the dense sample. The calibrated parameters are presented in Table 1.

Table 1. Physical parameters in simulations.

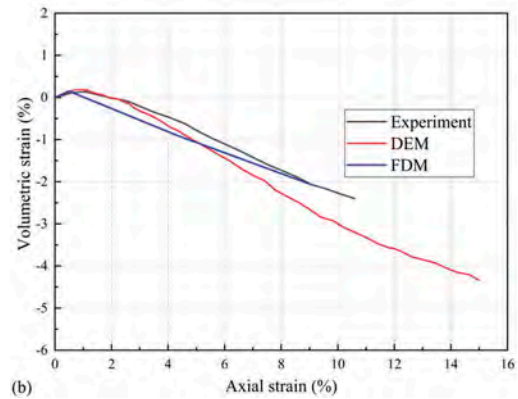
Parameters	Value
Normal and tangential stiffness of cone rod	1.0×10^{10} N/m
Friction coefficient of cone rod	0.2
Normal and tangential stiffnesses of side walls of calibration chamber	1.0×10^{10} N/m
Side wall friction coefficient of calibration chamber	0
Particle stiffness coefficient	6.0×10^8 N/m ²
Stiffness ratio of particle	0.25 ks/kn
Particle friction coefficient	0.33
Rolling resistance coefficient of particles	0.8
Particle density	2650 kg/m ³
Young's modulus in FDM	60.6 MPa
Internal angle of friction in FDM	37.04
Dilation angle in FDM	6.94

3 NUMERICAL SIMULATION AND RESULT ANALYSIS

In order to improve the efficiency of discrete element simulation, the particle size amplification method was used to reduce the number of particles, and the calibrated parameters for the DEM simulation were adopted to honor the true stress-strain relationship (Yan & Dong, 2011). In this study, the particle expansion ratio was chosen to be 35. The simulation result of the cone penetration calibration chamber test with confining stress of 100 kPa is shown in Figure 5. As shown in the figure, the cone tip resistance as well as the number of particles contacting the cone penetrometer clearly progresses along two stages: growth stage and stable stage. During the initial growth stage, the contact



(a) Deviator stress versus axial strain.



(b) Volumetric strain versus axial strain.

Figure 4. 3D triaxial compression test result: (a) deviator stress versus axial strain and (b) volumetric strain of the sample versus axial strain.

number of cone tip particles increases continuously in parallel with the cone tip resistance. When the normalized penetration h/d_c depth reaches 2, the cone tip resistance tends to be stable and the average value is about 8.5 MPa, where h is the penetration depth. The results imply that the microscale and macroscale features are highly correlated and the tip resistance could serve as an indicator of the microstructural characteristics of granular soil.

Particle size amplification method increases the simulation efficiency substantially by reducing the number of particles contacting with the cone tip, while the number of contacting particles and the soil near the cone-tip structure may change. In the following, we show the simulation results considering different sizes of the cone penetrometer to validate the efficacy of the particle size amplification method. Figure 6a shows the evolution of the tip resistance with the normalized penetration depth, with two cone penetrometer sizes and the fixed dimension of the coupling model, i.e. $d_c/D_{50}=4.89$ and 3.81 with D_{50} denoting the mean particle diameter determined from the amplified particle size distribution. It shows that the average tip resistance for $d_c/D_{50}=4.89$ and 3.81 are 7.45 MPa and 7.23 MPa

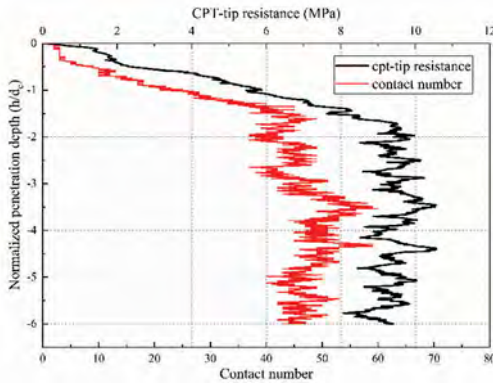


Figure 5. Simulation results of cone penetration test with confining stress of 100 kPa.

respectively. The results indicate that the particle size amplification method with a careful selection of the amplification ratio would not hinder the prediction of tip resistance.

To investigate the size effect of the DEM domain, we conducted simulations with different D_1 and constant R_1 . The results are shown in Figure 6b. It shows

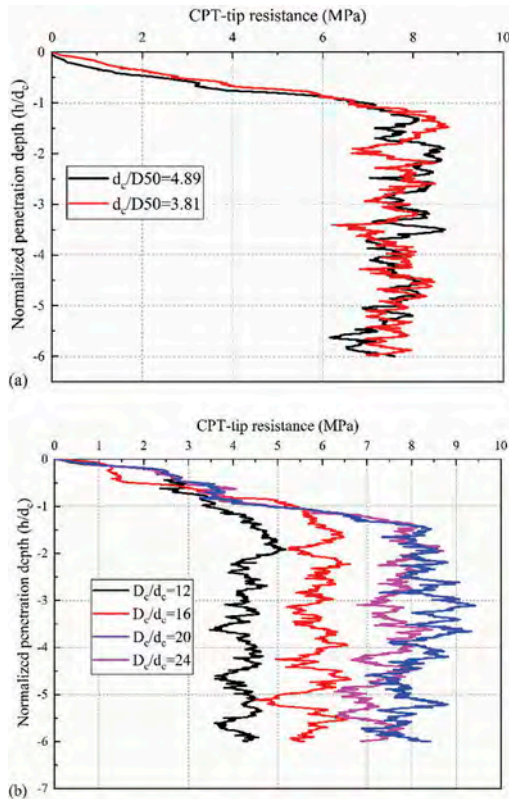


Figure 6. Analysis of the size effect of the model: (a) different cone penetrometer sizes and (b) different coupling model sizes.

that there is a threshold of D_c/d_c under which the tip resistance increases with the size of the DEM domain and beyond which no obvious size effect can be observed.

The soil constitutive behavior depends on the inter particle contact stiffness. To investigate its effect, simulations with two inter particle stiffness were conducted while keeping other parameters the same as in Table 1. Figure 7a shows the variation of radial stress along with the normalized distance r/R , where r is the distance from the center of the cone and R is the radius of the cone. As shown in Figure 7a, the radial stress decreases monotonically to the confining stress, i.e. 100 kPa, as the normalized distance increases. With the increase of the inter particle stiffness, the cone tip resistance increases due to the stiffer behavior of soil.

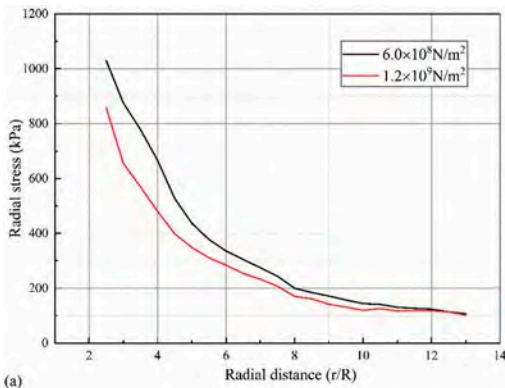
Figure 7b shows the variation of radial stress with the normalized distance under three different confining stresses 50 kPa, 100 kPa and 200 kPa. As shown in Figure 7b, the radial stress decreases monotonically from the cone neighborhood to the outer boundary with all three confining stresses. It is shown that the differences of the radial stresses under different confining stresses are significant especially at the neighborhood of the cone penetrometer. To reconcile the DEM-FDM simulation with in situ CPT testing, attention should be paid on the confining stress prescribed at the outer boundary.

The relationship between the stable tip resistance and the radial stress of the cone tip at $r/R = 2.5$ was also investigated and shown in Figure 8. The results show that there is a good linear relationship between the tip resistance and the tip radial stress ($r/R = 2.5$) under different simulation conditions, which agrees well with the cavity expansion theory (Randolph et al. 1994).

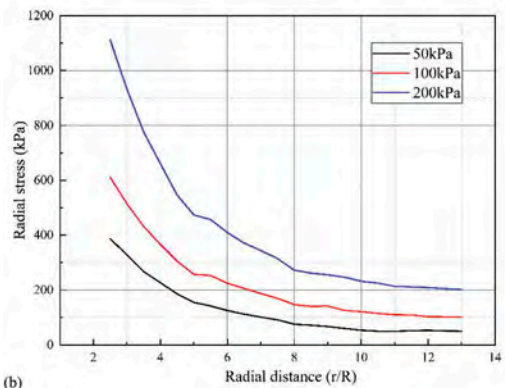
4 DISCUSSION AND OUTLOOK

In this work, we modeled the cone penetrate testing with a DEM-FDM coupling approach. The micro-contact parameters in DEM are calibrated by comparing the triaxial compression simulation results based on DEM and FDM. The size effect of the particle amplification method was analyzed, and the influence of contact stiffness and confining stress was investigated. The main findings of this study can be summarized as follows:

- The DEM-FDM coupling method is a promising and efficient simulation method investigating cone penetration mechanics from both macroscopic and microscopic perspectives.
- The particle size amplification method is capable of further increasing simulation efficiency substantially without undermining the accuracy of the prediction of cone tip resistance, with a cautious selection of the amplification ratio.



(a)



(b)

Figure 7. Factors influencing radial stress distribution of cone tip: (a) soil modulus, (b) confining pressure.

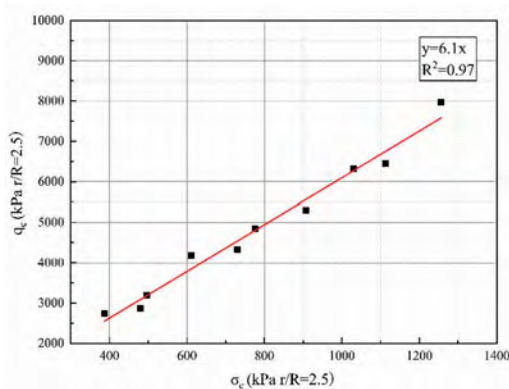


Figure 8. The relationship between cone tip resistance and cone tip radial stress ($r/R = 2.5$).

(c) The effects of contact stiffness and confining stress on the stress field in the soil and cone tip resistance are considerable and attention should be paid on them for emulating the in-situ cone penetration testing.

(d) The cone tip resistance and the radial stress around the cone from DEM-FDM simulation manifests a linear relation, which agrees well with the cavity expansion theory.

REFERENCES

- Arroyo, M., Butlanska, J., Gens, A., Calvetti, F. & Jamiolkowski, M. 2011. Cone penetration tests in a virtual calibration chamber, *Geotechnique* 61(6): 525–531.
- Bolton, M.D., Gui, M.W., Garnier, J., Corte, J.F., Bagge, G., Laue, J. & Renzi, R. 1999. Centrifuge cone penetration tests in sand, *Geotechnique* 49(4): 543–552.
- Butlanska, J., Arroyo, M., Gens, A. & O’Sullivan, C. 2014. Multi-scale analysis of cone penetration test (CPT) in a virtual calibration chamber, *Canadian Geotechnical Journal* 51(1): 51–66.
- Chen, H., Li, L., Li, J. & Wang, H. 2019. Stress transform method to undrained and drained expansion of a cylindrical cavity in anisotropic modified cam-clay soils, *Computers and Geotechnics* 106: 128–142.
- Chen, J.W. & Juang, C.H. 1996. Determination of drained friction angle of sands from CPT, *Journal of Geotechnical Engineering* 122(5): 374–381.
- Chen, S.L. & Abousleiman, Y.N. 2012. Exact undrained elasto-plastic solution for cylindrical cavity expansion in modified Cam Clay soil, *Geotechnique* 62(5): 447–456.
- Cundall, P.A. & Strack, O.D.L. 1980. Discussion: a discrete numerical model for granular assemblies, *Geotechnique* 30(3): 331–336.
- Gu, X., Hu, J. & Huang, M. 2015. K0 of granular soils: a particulate approach, *Granular Matter* 17(6): 703–715.
- Gu X., Zhang J. & Huang X. 2020. DEM analysis of monotonic and cyclic behaviors of sand based on critical state soil mechanics framework. *Computers and Geotechnics* 2020, 128: 103787.
- Randolph, M.F., Dolwin, R. & Beck, R. 1994. Design of driven piles in sand, *Geotechnique* 44(3): 427–448.
- Salgado, R. 1998. Calibration chamber size effects on penetration resistance in sand, *Journal of Geotechnical and Geoenvironmental Engineering* 124(9).
- Seif El Dine, B., Dupla, J.C., Frank, R., Canou, J. & Kazan, Y. 2010. Mechanical characterization of matrix coarse-grained soils with a large-sized triaxial device, *Canadian Geotechnical Journal* 47(4): 425–438.
- Sokolovskii, V.V. 2006. *Statics of granular media*. London: Pergamon Press.
- Wang, D., Bienen, B., Nazem, M., Tian, Y., Zheng, J., Pucker, T. & Randolph, M.F. 2015. Large deformation finite element analyses in geotechnical engineering, *Computers and Geotechnics* 65: 104–114.
- Wesley, L.D. 2002. Interpretation of calibration chamber tests involving cone penetrometers in sands, *Geotechnique* 52(4): 289–293.
- Yan, W.M. & Dong, J. 2011. Effect of particle grading on the response of an idealized granular assemblage, *International Journal of Geomechanics* 11(4): 276–285.
- Yi, J.T., Goh, S.H., Lee, F.H. & Randolph, M.F. 2012. A numerical study of cone penetration in fine-grained soils allowing for consolidation effects, *Geotechnique* 62(8): 707–719.
- Yu, H.S. & Mitchell, J.K. 1998. Analysis of cone resistance: review of methods, *Journal of Geotechnical and Geoenvironmental Engineering* 124(2).

Data-driven soil profile characterization using statistical methods and artificial intelligence algorithms

R.L. Spacagna

CNR IGAG Area della Ricerca Roma 1, Montelibretti (Roma), Italy

A. Baris, L. Paoella & G. Modoni

University of Cassino and Southern Lazio, Cassino, Italy

ABSTRACT: CPT soil profile interpretation represents a fundamental aspect for subsoil stratigraphic reconstruction of complex geological contexts. In some situations, the soil profile may not exhibit evident boundary changes, making the interpretation more difficult. This crucial aspect plays a key role in the layers boundaries discontinuities identification and the construction of bi-dimensional and three-dimensional geotechnical models. In this paper, CPT and boreholes are used to calibrate and validate a massive and automated site characterization by combining statistical tools and artificial intelligence algorithms (AI). The procedure is applied in the complex stratigraphic context of Terre del Reno (Italy). The proposed data-driven analysis allows to combine the geological and geotechnical knowledge of the subsoil in an efficient and automatic way based on site-specific data, obtaining reliable and indispensable results for the construction of a robust and coherent geotechnical model of the subsoil.

1 INTRODUCTION

One of the subsoil stratigraphic reconstruction challenges is to identify homogeneous soil layers characterized by a different behaviour response. The detection of the strata boundaries represents a crucial aspect in the construction of two-dimensional and three-dimensional geotechnical models. The development of the data-driven analysis and the increasing availability of digitized geo-databases allow to improve the current methodologies to obtain an effective and extensive site characterization, providing a less subjective interpretation of the subsoil data (Phoon *et al.*, 2021).

The main studies rely on statistic and probabilistic approaches based on the cone penetration test (CPT) data (Phoon *et al.* 2003, Facciorusso & Uzielli 2004, Uzielli 2008, Wang *et al.* 2013, Paoella *et al.* 2019, Shuku *et al.* 2020). The continuous measurements of soil parameters allow a statistical treatment for the identification of lithological discontinuities and the reconstruction of the stratigraphic profiles (Lo Presti *et al.* 2009). For this purpose, the CPT-based soil behaviour type index (Ic), and the correspondent soil behaviour type (SBT), are used to delineate soil boundaries (Robertson 2016).

This work developed a data-driven methodology for the subsoil stratigraphic reconstruction combining statistical tools and artificial intelligence algorithm (AI). The proposed procedure is applied to the complex

stratigraphic context of Terre del Reno (Italy), extensively affected by seismic liquefaction phenomenon during the May 2012 earthquake sequence (Fioravante *et al.* 2013). From the geodatabase of the Emilia Romagna Region, 102 pairs of CPT and boreholes were selected to calibrate and validate the method. The CPT profiles are analyzed, and the homogeneous layers are identified following statistical methods based on the spatial variability analysis of the measured parameters. Each statistically homogeneous layer is associated with the stratigraphic information extrapolated from closer boreholes, according to the Unified Soil Classification System (USCS). From the previous results, an artificial classifier is trained, and the automatic classification procedure of soil profile is tested on a complementary subset of data.

The proposed data-driven analysis combines the geological and geotechnical knowledge of the subsoil in an efficient and automatic way, based on site-specific data, to obtain reliable and indispensable results for the construction of a robust and coherent geotechnical model of the subsoil.

2 METHODOLOGY

The proposed approach aims to define a methodology for the subsoil stratigraphic recognition, applicable at the urban scale. In practice, this operation is based on the interpretation of a considerable amount of data

coming from different sources. The most diffused approach is to combine the borehole logs stratigraphy and Cone Penetration Test results in a deterministic way with a consequent subjectivity of the interpretation of available data.

The increasing availability of site-specific data collected, digitized and stored in the geodatabase allows to improve, even automatically, the consolidated methodologies for interpretation of subsoil data.

This procedure, summarized in Figure 1, provides a stratigraphic interpretation model applicable to all available surveys in the analyzed area, combining information from different investigation tests. In particular, the proposed methodology identifies the main lithologies from borehole log stratigraphies, the layer discontinuities from the sectioning statistical test of the CPT profiles and the automated stratigraphic classification of each statistically homogeneous layer from AI.

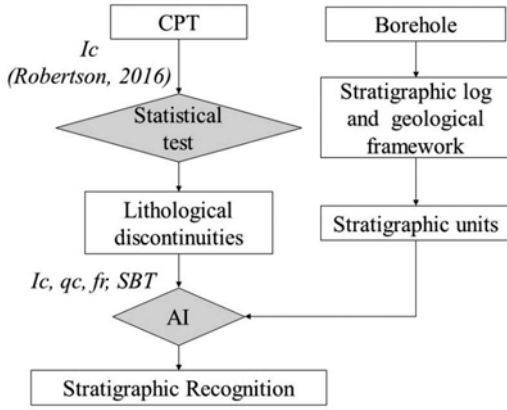


Figure 1. Proposed methodology for the subsoil stratigraphic recognition.

2.1 Definition of stratigraphic units

The definition of the main stratigraphic units detectable in the study area requires a detailed geological, hydrogeological, geomorphological and sedimentological framework.

The stratigraphic reference units for the selected case study are defined by combining the information from the geological framework and the borehole log stratigraphy. The detail of the stratigraphic model, its extension and stratigraphic classification are strictly related to the typology of the performed analysis (i.e. subsidence, liquefaction, design of structures and infrastructures). Therefore, the model (depth and thickness of the strata) and the stratigraphic units are defined according to the analyzed phenomenon (i.e., for a liquefaction risk assessment, the liquefiable layers).

2.2 Soil boundaries discontinuities

The homogeneous soil layers within the CPT profiles are identified based on the soil behaviour type index I_c (Robertson, 2016). The automatic procedure provides an accurate interpretation of the CPT tests considering the spatial correlation of the considered values along with the vertical profile.

This statistical test verifies the equality of the means and the variance of two subsets of data, according to the procedure shown in Figure 2. The two subsets of data (namely Ω_1 and Ω_2 , with size respectively equal to n_1 and n_2 , average \bar{Q}_1 and \bar{Q}_2 , and variance σ_1^2 and σ_2^2) are identified along with the vertical CPT profile with a moving window W_{d_0} divided by d_0 . The T ratio (Equation 1) and the intra-class correlation coefficient ρ_I (Equation 2) are calculated along with the vertical CPT profile.

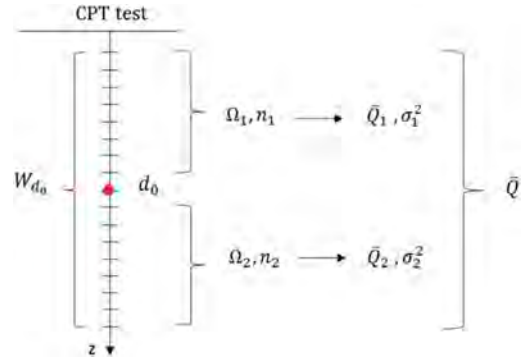


Figure 2. Definition of the two subsets of relevant parameters along the vertical axis of CPT test (from Spacagna et al, 2015).

$$T = \frac{\bar{Q}_1 - \bar{Q}_2}{\gamma_w} \sqrt{\frac{n_1 n_2}{n_1 + n_2}} \quad (1)$$

Where:

$$\gamma_w = \frac{n_1}{n_1 + n_2 - 1} \sigma_1^2 + \frac{n_2}{n_1 + n_2 - 1} \sigma_2^2 \quad (2)$$

$$\sigma_1^2 = \frac{1}{(n_1 - 1)} \sum_{i=1}^{n_1} (Q_i - \bar{Q}_1)^2 \quad (3)$$

$$\sigma_2^2 = \frac{1}{(n_2 - 1)} \sum_{i=1}^{n_2} (Q_i - \bar{Q}_2)^2 \quad (4)$$

$$\rho_I = \frac{\gamma_b^2}{\gamma_b^2 + \gamma_w^2} \quad (5)$$

Where:

$$\gamma_b^2 = \frac{1}{n_1 + n_2 - 1} \sum_{i=1}^{n_1+n_2} (Q_i - \bar{Q})^2 \quad (6)$$

where \bar{Q} is the average of the data Q_i belonging to the window w_{d_0} , with $i=1,2, \dots, (n_1+n_2)$.

To define the window w_{d_0} , the geostatistical approach proposed by Spacagna *et al.* (2015) suggests to calculate the one-dimensional experimental variogram of the variable (Chilès & Delfinet 2012), with a lag equal to the minimum distance of measured point, following the Equation 7.

$$\gamma(h) = \frac{1}{2N(h)} \sum_{i=1}^{N(h)} (z(i) - z(i+h))^2 \quad (7)$$

where $z(i)$ is the value of the considered variable at a location, $z(i+h)$ is the value of the variable at the distance h , and $N(h)$ is the number of couples of points with a distance equal to h . This spatial correlation of the variable is modelled with a theoretical function. In the present study, the spherical model (Chilès & Delfinet 2012) is adopted to interpolate the spatial correlation (Equation 8).

$$\gamma(h) = \begin{cases} C \left(\frac{3}{2} \frac{h}{a} - \frac{1}{2} \frac{h^3}{a^3} \right) & 0 \leq h \leq a \\ C & h > a \end{cases} \quad (8)$$

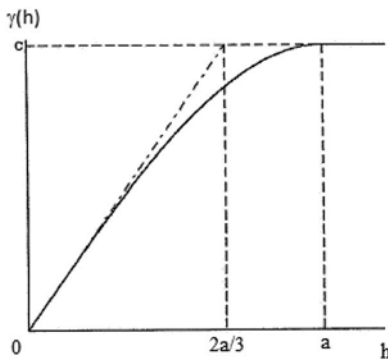


Figure 3. Spherical variogram.

In general, the variogram $\gamma(h)$ is an increasing function with the distance h . The model introduces two parameters. The *sill* C describes the level of spatial variability, and the *range* a represents the maximum distance at which spatial correlation is observed.

The amplitude of w_{d_0} used for the statistical test is defined as a ratio of the range a . The T ratio and ρ_I are calculated for each point d_0 , implementing two new vertical profiles. The higher values of T ratio and ρ_I correspond to a change of behaviour of the CPT-based parameters Ic.

The critical value of the parameter T ratio (t_c) is evaluated considering the 90% confidence interval of the T ratio distribution and is calculated following Equation 9.

$$t_c = \mu_{Tratio} \pm 1,65 \sigma_{Tratio} \quad (9)$$

where μ_{Tratio} and σ_{Tratio} are respectively mean and standard deviation of the distribution of the T ratio values along the vertical profile. The depth to which T ratio values fall outside the confidence interval represents a change of behaviour along the CPT profile.

The critical value of ρ_{Ic} is calculated following the Equation (10) proposed by Herzagy, Mayne, and Rouhani (1996).

$$\rho_{Ic} = \mu_{\rho_I} + 1,65 \sigma_{\rho_I} \quad (10)$$

where μ_{ρ_I} and σ_{ρ_I} are respectively the mean and standard deviation of the distribution of the ρ_I values along the vertical profile. The depth to which ρ_I values are higher than ρ_{Ic} represents a change of behaviour along the CPT profile.

The transition between two different homogeneous layers is assumed at the d_0 depth points which both critical conditions occur simultaneously.

The described algorithm is implemented with open-source R software (R Core Team, 2021).

2.3 Stratigraphic recognition with AI

In the proposed methodology, the stratigraphic recognition, basically the attribution at each statistically homogeneous layers the correspondent stratigraphic unit, is automatically carried out with artificial intelligence (AI), studying the underlying relation between cone penetration tests information and stratigraphic properties. Reale *et al.* (2018) proposed an automatic classification of fine-grained soils using CPT measurements and Artificial Neural Network. Ching, Wu & Phoon (2020) and Ching *et al.* (2020) proposed a Hierarchical Bayesian Model (HBM) to construct transformation models for soil and rock properties.

The algorithms are trained comparing the outcomes derived from couples of CPT-boreholes considered spatially correlated, providing a complementary description of the subsoil. The CPT-borehole distance has been chosen based on the analysis of the spatial

structure of cone tip resistance in the horizontal direction. A measure of the spatial correlation is the scale of fluctuation, representing the maximum distance over which the points are significantly related (Chilès & Delfinet, 2012).

The calibration procedure is structured as follows: first, the couples of complementary CPT and boreholes are extracted from the geodatabase; once CPT profiles are processed, to each statistically homogeneous layer is associated the stratigraphic unit reported in the complementary borehole; last, the CPT output parameters and their correspondent stratigraphic recognition are used to train, test and validate various algorithms.

The artificial classifier characterized by the highest efficiency is selected and applied to automatically assign the stratigraphic units to the remained sectioned cone penetration test profiles distributed over the studied area.

3 CASE STUDY

The Terre del Reno municipality is located in the southern Po river plain in the Emilia Romagna region (Italy). The area was struck by an intense seismic sequence associated with compression fault ruptures in 2012. The main shock of May 20th 2012 (M_w 6.1) produces extensive liquefaction phenomena due to subsoil composition, geologic history and the shallow depth of the groundwater table (Fioravante et al. 2013). The municipality covers an area of 51 km², along a former branch of Reno River and is divided into three main districts: Sant'Agostino, San Carlo and Mirabello (Figure 4a).

The San Carlo area is characterized by a complex stratigraphic context due to the depositional history of the Reno river, highlighted by the significant number of liquefactions induced damages (Figure 4b). The calibration of the methodology has been carried out by analyzing the entire available geodatabase on the territory. However, in this work, the stratigraphic recognition is limited to the San Carlo area.

3.1 Definition of stratigraphic units in the municipality of the Terre del Reno

The subsoil of San Carlo is characterized by a relatively recent geologic history, an intensive depositional sequence of the Reno river and a shallow groundwater table (Figure 4c). The depositional activity of the river left superficial layers of loose sand with a thickness of a few meters. In the same period, the population constructed artificial levees mixing sand with silt to regulate the fluvial regime and limit flooding. The urban area is mainly built near those paleo-channel and paleo-levees.

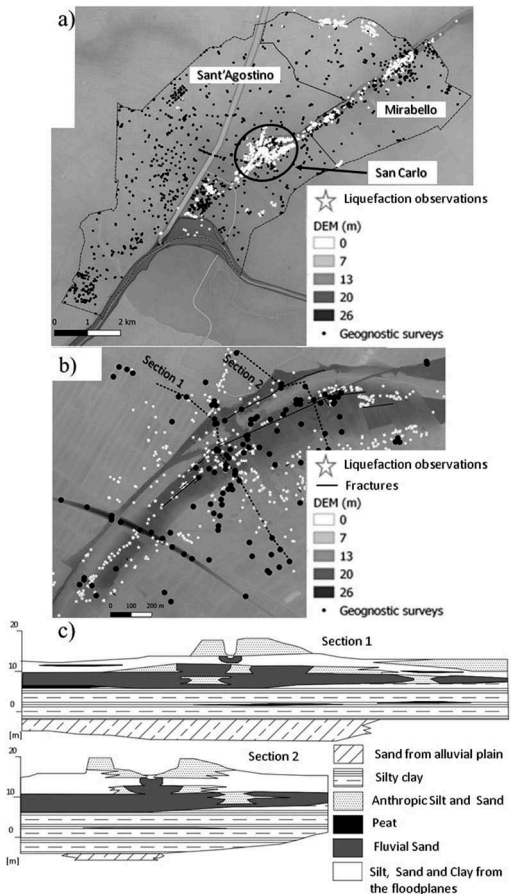


Figure 4. A) Terre del Reno municipality b) San Carlo district, c) Geological sections (adapted from Calabrese *et al.*, 2012).

The deepest layers are constituted of sediments deposited by Apennine and Alpine rivers, interspersed with marine accretion. These alternated processes are ruled by the regression and progression of the Adriatic Sea in the upper Pleistocene-Holocene (Romeo 2012).

The territory of Terre del Reno is covered by around 1700 geognostic surveys, highlighted in Figure 4a. The definition of the stratigraphic units has been carried out analyzing the description reported in 252 boreholes logs distributed all over the municipality. From the geological and sedimentological characterization, four stratigraphic units have been identified in the upper 20 m of the subsoil:

- Unit #1: silt, silty clay, clayey silt;
- Unit #2: sandy silt, silty sand;
- Unit #3: fine and medium clean sand;
- Unit #4: clay, organic clay, organic material.

3.2 CPT profiles processing

The soil boundaries discontinuities recognition has been applied to the district of San Carlo. In the selected area, there is a high density of surveys (Figure 4b). For 369 investigation tests distributed over an area of 3 km², the available boreholes and cone penetration tests reach 82.5%. In particular, the mechanical CPT correspond to 35.5% and the electrical ones to 32% of the total.

The implemented tool provides automatic sectioning of CPT profiles into statistically homogeneous layers.

An example of sectioned CPT profile is shown in Figure 5. From the CPT parameters, the I_c profile is computed. The statistical parameters T_{ratio} and ρ are calculated, and the critical thresholds are estimated. The horizontal dashed lines identify the transition between two different homogeneous layers.

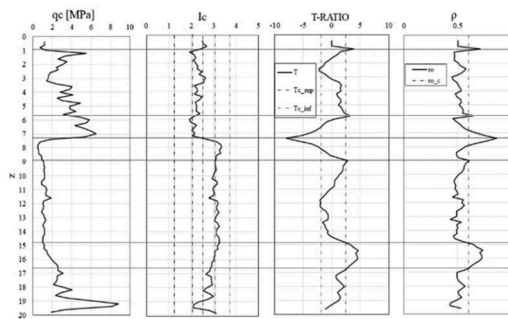


Figure 5. Example of sectioned CPT profile.

For each stratum, the following parameters are computed:

- the Soil Behaviour Type SBT,
- the mean and standard deviation of the I_c values,
- the mean and standard deviation of the friction ratio, FR, defined as ratio between sleeve friction and cone resistance.

3.3 Training and application of the artificial intelligence algorithm

At this stage, information reported in boreholes and sectioned CPT must be cross-correlated to perform an automatic stratigraphic recognition. The calibration of the artificial intelligence algorithm has been performed comparing the outcomes derived from couples of CPT-borehole considered spatially correlated. Due to the complex stratigraphic context in the investigated area of Terre del Reno (Fe), each CPT profile has been considered representative of a circular area having a radius equal to 30 m. This distance has been chosen because the cone tip resistance of the selected site is characterized by

a correlation length equal to $\Theta = 16.5$ m in the horizontal direction and a scale of fluctuation $\delta = 33$ m, representing the maximum distance over which the points are significantly related.

All boreholes located in the defined distance are classified as complementary of the cone penetration tests. The total number of couples CPT-boreholes is equal to 132, but 30 have been deleted due to the poor quality and reliability of the subsoil description. The remaining 102 pairs constitute the starting point for the calibration of the algorithm. The sectioned CPT and the complementary boreholes have been compared.

Besides the output sectioning CPT parameters, at each statically homogeneous layer has been attributed the stratigraphic unit recognized in the complementary boreholes. These parameters are the input values for the calibration of a classifier capable to identify the corresponding stratigraphic unit.

The choice of the algorithm involves the estimation of the efficiency between 32 different artificial classifiers, implemented in the *Classification Learner APP* available in MATLAB R2021b, with a 10 folds cross-validation procedure (Stone 1974). This procedure is suggested to avoid overfitting and to estimate the accuracy obtained within the 10 iterations. Cross-validation divides the dataset into 10 folders of the same size: 9 folders are used to train the classifier while one is used to validate it. This procedure is iterated 10 times, training and testing each folder. The best classifier is a linear discriminant, characterized by an efficiency equal to 81.6%. Linear Discriminant Analysis (LDA) has been proposed by Fischer in 1936. It consists in finding the hyperplane projection that minimizes the interclass variance and maximizes the distance between the projected means of the classes.

In Figure 6a is shown the efficiency of the algorithm to classify the four units, attributing the percentage of success and misclassification. The positive prediction is expressed as Positive Predicted Values (PPV), and the negative classification is expressed as False Discovery Rates (FDR).

Figure 6b consist in a report showing a summary of prediction results of the mutual classification between classes, the grey cells correspond to the PPV and the sum of the remaining elements along the columns is equal to the FDR. For example, the first column summarizes the detail of the layers automatically classified as Unit #1: truly classified in 75.4% of occurrences; Unit #2 has been mistaken with Unit #1 in 15.8% of manifestations; Unit #1 has been attributed to the real Unit #3 in 1.2% and in the remaining 7.6%, Unit #4 has been classified as Unit #1. In particular, the mutual misclassification between sands and clays never occurs. Furthermore, the lower PPV values are associated with Units #1 (silt, silty clay, clayey silt) and #2 (sandy silt, silty sand), located in the upper 10 m of the subsoil and characterized by a complex geological history.

a)

		Predicted Unit			
		1	2	3	4
PPV	1	75.4%	74.9%	83.2%	92.9%
	FDR	24.6%	25.1%	16.8%	7.1%

b)

		Predicted Unit			
		1	2	3	4
True Unit	1	75.4%	7.3%	1.7%	6.2%
	2	15.8%	74.9%	15.1%	0.9%
	3	1.2%	17.4%	83.2%	0.0%
	4	7.6%	0.4%	0.0%	92.9%

Legenda:

- 1: silt, silty clay, clayey silt;
- 2: sandy silt, silty sand;
- 3: fine and medium clean sand;
- 4: clay, organic clay, organic material.

Figure 6. Efficiency of the proposed LDA algorithm.

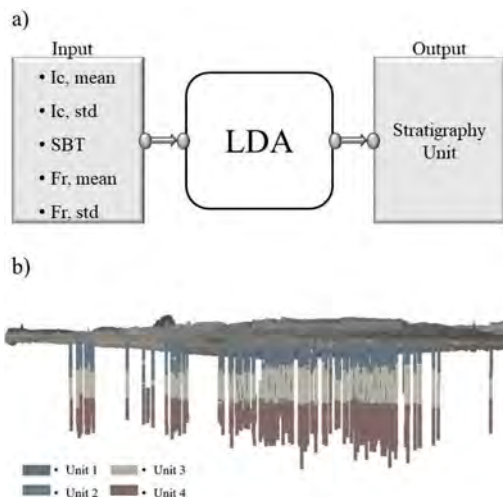


Figure 7. a) Input parameters and output for the selected LDA algorithm and b) application on the surveys disseminated all over the area.

Once the effectiveness was ascertained, the algorithm (Figure 7a) was applied to the remaining cone penetration tests, obtaining the stratigraphic

recognition of the surveys disseminated on the investigated area (Figure 7b).

4 CONCLUSION

This work aims to propose a methodology for subsoil stratigraphic reconstruction based on the most diffused geotechnical survey, combining statistical tools and artificial intelligence algorithms. In particular, the proposed methodology identifies the layer discontinuities from the sectioning statistical test of the CPT profiles, the main lithologies from borehole log stratigraphies, and the automated stratigraphic classification of each statistically homogeneous layer from AI. The procedure has been implemented and validated in the complex geological context of the alluvial plain of Terre del Reno in Italy, characterized by a large geodatabase. The automatized methodology is easily replicable in other contexts for the stratigraphic recognition of the subsoil on a large scale, providing a valid tool for several applications as liquefaction risk analysis at an urban scale on structure and infrastructure (Paoletta *et al.* 2021, Baris *et al.* 2021, Modoni *et al.* 2019) and subsidence study (Spacagna *et al.* 2020, Spacagna & Modoni, 2018). The data-driven analysis provides reliable and indispensable results for the construction of a robust and coherent geotechnical model of the subsoil. The next step concerns the interpolation of the stratigraphic surfaces to obtain a complete reconstruction of the subsoil.

REFERENCES

- Baris, A., Spacagna, R.L., Paoletta, L., Koseki, J. and Modoni, G. 2021. Liquefaction fragility of sewer pipes derived from the case study of Urayasu (Japan). *Bull. Earthquake Eng.* 19, 3963–3986. <https://doi.org/10.1007/s10518-020-00957-2>
- Calabrese, L., Martelli, L., Severi, P. 2012. Stratigrafia dell'area interessata dai fenomeni di liquefazione durante il terremoto dell'Emilia (maggio 2012). *Atti 31° Convegno GNGTS*, Potenza, 20-22 novembre 2012, sess. 2.2, 119–126.
- Chilès, JP. & Delfiner, P. 2012. *Geostatistics: modeling spatial uncertainty*. 2nd edn. Wiley, Hoboken, p 726. ISBN 978-0-470-18315-1.
- Ching, J., Phoon, K. K., Ho, Y. H. and Weng, M. C. 2020. Quasi-site-specific Prediction for Deformation Modulus of Rock Mass. *Canadian Geotechnical Journal*. doi:10.1139/cgj-2020-0168.
- Ching, J., Wu, S. and Phoon, K. K. 2020. Constructing QuasiSite-specific Multivariate Probability Distribution Using Hierarchical Bayesian Model. *Journal of Engineering Mechanics*, under review computing. R Foundation for Statistical Computing, Vienna, Austria.
- Facciorusso, J. & Uzielli, M. 2004. Stratigraphic profiling by cluster analysis and fuzzy soil classification from mechanical cone penetration tests. *Proc. ISC-2 on*

- Geotechnical and Geophysical Site Characterization, Porto*. Vol. 1, Millpress, 905–912.
- Fioravante, V. et al. 2013. Earthquake geotechnical engineering aspects: the 2012 Emilia Romagna earthquake (Italy). *Seventh international Conference on Case Histories in Geotechnical Engineering*, April 29 th – May 4th, 2013. Chicago (US).
- Fisher, R. A. 1918. The correlation between relatives on the supposition of mendelian inheritance. *Trans. R. Soc. Edinb.* 53: 399–433.
- Herzagy, Y., Mayne, P., Rouhani, S. 1996. Geostatistical assessment of spatial variability in piezocone tests. Uncertainty in geologic environment: from theory to practice (GSP 58), *ASCE*, New York, 254–268.
- Lo Presti, D., Meisina, C. and Squeglia, N. 2009. Applicazione delle prove penetrometriche statiche nella ricostruzione del profilo stratigrafico. *Rivista Italia di Geotecnica*.
- MATLAB 2021. *version R2021a*. Natick, Massachusetts: The MathWorks Inc.
- Modoni G., Spacagna R.L., Paoletta L., Salvatore E., Rasulo A., Martelli L., 2019. Liquefaction risk assessment: lesson learned from a case study. *Earthquake Geotechnical Engineering for Protection and Development of Environment and Constructions*. CRC Press. <https://doi.org/10.1201/9780429031274>
- Paoletta, L., Spacagna, R.L., Chiaro, G. and Modoni, G. 2021. A simplified vulnerability model for the extensive liquefaction risk assessment of buildings. *Bull. Earthquake Eng.* 19, 3933–3961. <https://doi.org/10.1007/s10518-020-00911-2>
- Paoletta, L., Salvatore, E., Spacagna, R.L., Modoni, G., Ochmański, M. 2019. Prediction of liquefaction damage with artificial neural networks. *Earthquake Geotechnical Engineering for Protection and Development of Environment and Constructions - Proceedings of the 7th International Conference on Earthquake Geotechnical Engineering*, pp. 4309–4316
- Phoon, K. K., S. T. Quek, and P. An. 2003. “Identification of Statistically Homogeneous Soil Layers Using Modified Bartlett Statistics.” *Journal of Geotechnical and Geoenvironmental Engineering*, ASCE 129 (7): 649–659.
- Phoon, K.K., Ching, J. and Shuku, T. 2021. Challenges in data-driven site characterization, Georisk: Assessment and Management of Risk for Engineered Systems and Geohazards. DOI: 10.1080/17499518.2021.1896005.
- R Core Team. 2021. R: A language and environment for statistical.
- Reale, C., Gavin, K., Librić, L. and Jurić-Kaćunić D. 2018. Automatic classification of fine-grained soils using CPT measurements and Artificial Neural Networks. *Advanced Engineering Informatics*, Volume 36, Pages 207–215, ISSN 1474-0346. <https://doi.org/10.1016/j.aei.2018.04.003>.
- Robertson, P. K. 2016. “Cone Penetration Test (CPT)-Based Soil Behaviour Type (SBT) Classification System – An Update.” *Canadian Geotechnical Journal* 53 (12): 1910–1927
- Shuku, T., Phoon, K. K. and Yoshida, I. 2020. “Trend Estimation and Layer Boundary Detection in Depth-dependent Soil Data Using Sparse Bayesian Lasso.” *Computers and Geotechnics* 128: 103845.
- Spacagna, R.L., Modoni, G., Saroli, M. 2020. An Integrated Model for the Assessment of Subsidence Risk in the Area of Bologna (Italy) *Lecture Notes in Civil Engineering* 2020, 40, pp. 358–368
- Spacagna, R.L., Modoni, G. (2018) GIS-Based Study of Land Subsidence in the City of Bologna. In: Ottaviano E., Pelliccio A., Gattulli V. (eds) *Mechatronics for Cultural Heritage and Civil Engineering. Intelligent Systems, Control and Automation: Science and Engineering*, vol 92. Springer, Cham. https://doi.org/10.1007/978-3-319-68646-2_10
- Spacagna R.L., de Fouquet, C., Russo, G. 2015. Interpretation of CPTU tests with statistical and geostatistical methods. *ISGSR2015 Geotechnical Safety and Risk V T. Schweckendiek et al. (Eds.)* © 2015 The authors and IOS Press. 13-16 October 2015
- Stone, M. 1974. Cross-validatory choice and assessment of statistical predictions. *Journal of the Royal Statistical Society: Series B (Methodological)*, 36(2),111–133. <https://doi.org/10.1111/j.2517-6161.1974.tb00994.x>
- Uzielli, M. 2008. Statistical analysis of geotechnical data. *3rd International Symposium on Geotechnical and Geophysical Site Characterization*, Huang and Mayers (Eds.), 173–193, Taipei, Taiwan, 1-4 april 2008.
- Wang, Y., Huang, k. and Cao, Z. 2013. Probabilistic identification of underground soil stratification using cone penetration tests. *Can. Geotech. J.* 50: 766–776.
- Wang, Y., Huang, K. and Cao, Z. 2013. Probabilistic Identification of Underground Soil Stratification Using Cone Penetration Tests. *Canadian Geotechnical Journal* 50 (7): 766–776.

Capability of seismic CPTu and DMT in assessing propagation velocity of body waves: A comparative study

S. Stacul, D. Lo Presti & N. Nenci
University of Pisa, Pisa, Italy

F. Fiera & M. Perini
Geo-Energizers Snc, Cascina (Pisa), Italy

D. Marchetti
Studio Prof. Marchetti s.r.l., Rome, Italy

E. Pagani & M. Siviero
Pagani Geotechnical Equipment s.r.l., Calendasco (Piacenza), Italy

ABSTRACT: The paper shows the geotechnical characterization of a soft clay test site by means of laboratory testing. Such a test site was established in the campus of the Department of Biology of the University of Pisa at about 1.6 km from the Leaning Tower square. The main (but not exhaustive) scope of the present research activity was to compare the propagation velocity of body waves as obtained from various seismic techniques. A preliminary site characterization, based on both laboratory and in situ tests, was carried out. In situ testing consisted of a preliminary CPTu, three boreholes with four high quality Osterberg-type undisturbed sampling, cross-hole, surface seismic reflection test named Multichannel Analysis of Reflection Waves (MARW). Laboratory tests consisted of soil classification (Atterberg Limits and grain size distribution), incremental loading oedometer tests (OE), direct shear tests (DS) and resonant column tests (RC). Moreover, Pagani seismic piezocone and Marchetti seismic dilatometer were used for the assessment of the propagation velocity of body waves.

1 INTRODUCTION

The capability of seismic piezocones (SCPTu) and seismic Marchetti dilatometers (SDMT) in determining the propagation velocity of body waves is the final objective of the present research activity. For such a purpose, a test site was selected in Pisa. This site is in a campus of the University of Pisa, namely the Department of Biology (Figure 1).



Figure 1. Test site layout.

The in-situ characterization consisted of a preliminary CPTu, boreholes (with undisturbed sampling), cross-hole (CH) and surface seismic tests (i.e. SH re-flection test as Multichannel Analysis of Reflection Waves - MARW). A direct stratigraphy was inferred from borehole S1.

The in-situ characterization was carried out by:

- Geoservizi snc (CPTu)
- Geo-Energizer snc (surface seismic test: MARW)
- Servizi Geologici S.a.s. Morbin F. & C. (boreholes S1, S2, S3)
- SolGeo Srl (Cross-hole. Borehole S2 was used as source, the other two as receivers)

The laboratory test results were carried out on four high-quality Osterberg-type samples. In particular, the results of laboratory classification (Atterberg Limits and grain size distribution), incremental loading oedometer tests (OE), direct shear tests (DS) and resonant column tests (RC) are shown. The recommendations of the Italian Geotechnical Society – AGI were mainly followed in performing laboratory tests (AGI, 1994). Anyway, these recommendations mainly conform to the ASTM standards that were preferred in case of discrepancies.

Table 1 shows the identification number of each sample, the sampling depth, as well as types and number of tests that were performed. Some samples were apparently non-homogeneous; therefore, classification and RC tests were carried out by considering different portion of the samples. The water table was located at a depth of three meter from ground level when the samples were retrieved.

Table 1. Laboratory testing program.

Sample	Depth	Grain Size	Atterberg	DS	OE	RC
	m	#	#	#	#	#
C1	4.5-5.0	1	1	1	1	1
C2	8.5-9.0	4	4	1	1	2
C3	19.5-20.0	1	1	1	1	1
C4	26.5-27.0	3	3	1	1	2

This paper mainly deals with in situ seismic measurements. Laboratory tests are shown but not discussed or compared with in situ test results, except data coming from RC tests.

2 LABORATORY CHARACTERIZATION

2.1 Physical characteristics

Tables 2 and 3 summarize the physical characteristics of the tested samples. In particular, the natural and dry unit weight are reported. As for the unit weight, the mean and the standard deviation are reported. Moreover, the natural water content, the liquid limit and the plasticity index are shown. Percentages of grain size classes and USCS classification (ASTM D2487-17e1, 2017) are eventually reported.

Figure 2 shows the grain size distribution curves. According to the laboratory test results the presence of silt mixtures seems to prevail at various depths.

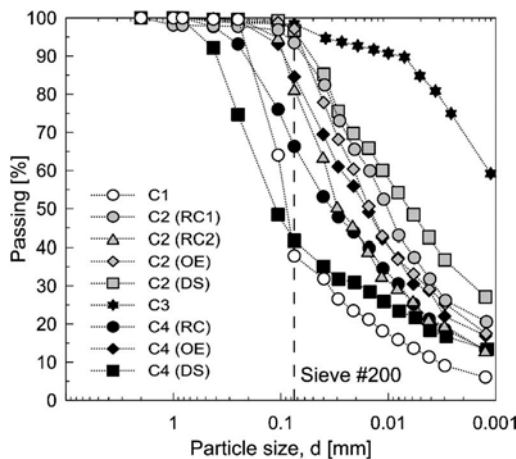


Figure 2. Grain size distribution curves.

Only at a depth of about 20 m a fat clay was identified from classification tests.

2.2 Oedometer and direct shear tests

Tables 4, 5 and 6 summarize the parameters as obtained from incremental loading oedometer tests.

Table 2. Soil classification.

Sample	Depth	Sand	Clay	Pass. #200	USCS
	m	%	%	%	
C1	4.5-5.0	62.12	7.38	37.88	Silty sand
C2(DS)	8.5-9.0	3.33	31.31	96.67	Silt
C2(RC)	8.5-9.0	6.52	23.14	93.48	Silt
C2(RC)	8.5-9.0	18.71	15.8	81.29	Silt clay with sand
C2(OE)	8.5-9.0	2.87	20.98	97.13	Silt
C3	19.5-20.0	1.57	68.49	98.43	Fat clay
C4(DS)	26.5-27.0	58.28	14.93	41.72	Silty Clayey sand
C4(RC)	26.5-27.0	33.66	15.6	66.34	Sandy lean clay
C4(OE)	26.5-27.0	15.44	19.13	84.56	Lean clay with sand

Table 3. Physical characteristics.

Sample	Depth	γ_n	γ_s	w_n	w_L	PI
	m	kN/m ³	kN/m ³	%	%	%
C1	4.5-5.0	18.63 ± 0.28	14.29 ± 0.60	31.52 ± 1.69	N.A.	N.A.
C2(DS)	8.5-9.0	18.31 ± 0.11	13.75 ± 0.15	33.15 ± 0.87	38	4
C2(RC)	8.5-9.0	18.24	13.66	31.75	38	3
C2(RC)	8.5-9.0	18.19	13.66	30.85	34	7
C2(OE)	8.5-9.0	19.32	14.5	31.96	35	3
C3	19.5-20.0	16.14 ± 0.33	10.46 ± 0.60	54.6 ± 4.02	75	45
C4(DS)	26.5-27.0	19.14 ± 0.15	16.08 ± 0.02	19.61 ± 0.93	24	11
C4(RC)	26.5-27.0	19.85	16.55	18.88	29	16
C4(OE)	26.5-27.0	20.43	16.66	21.96	34	18

γ_n : natural unit weight; γ_s : dry unit weight; w_n : natural water content; w_L : liquid limit; PI: plasticity index.

Compressibility parameters are shown in Tables 4 and 5, while the hydraulic parameters in Table 6. The results from oedometer tests confirm what already observed as for the soil classification. The sample at the depth of 20 m exhibits a much greater compressibility and a permeability reduced of about two orders of magnitude. The coefficient of primary consolidation was computed by using both Taylor (1948) and Casagrande (1936) methods. Anyway, in the case of specimens containing more silts the interpretation of the settlement-time curve was clearer

Table 4. Oedometer tests results.

	Depth	σ'_{v0}	OCR	e_0	$M(\sigma'_{v0})$
Sample	m	kPa	-	-	MPa
C1	4.5-5.0	68.8	2.0	0.78	4
C2	8.5-9.0	102.9	1.31	0.85	4
C3	19.5-20.0	151.84	1.13	1.80	2
C4	26.5-27.0	218.27	1.20	0.61	11

σ'_{v0} : effective geostatic stress; OCR: overconsolidation ratio; e_0 : void index; M: oedometric modulus.

Table 5. Compressibility parameters from OE.

	Depth	Cr	Cc	Cs	$C\alpha\epsilon(\sigma'_{v0})$
Sample	m	-	-	-	-
C1	4.5-5.0	0.034	0.226	0.024	1.5E-03
C2	8.5-9.0	0.037	0.258	0.045	9.5E-04
C3	19.5-20.0	0.148	0.587	0.175	5.1E-03
C4	26.5-27.0	0.030	0.15	0.033	7.3E-04

Cr: recompression index; Cc: compression index; Cs: swell index; $C\alpha\epsilon$: coefficient of secondary consolidation.

Table 6. Hydraulic parameters from OE.

	Depth	$C_v(\sigma'_{v0})$	$k(\sigma'_{v0})$
Sample	m	cm^2/s	cm/s
C1	4.5-5.0	3.78E-02	8.4E-07
C2	8.5-9.0	9.21E-03	2.2E-07
C3	19.5-20.0	1.14E-04	5.5E-09
C4	26.5-27.0	2.9E-02	2.7E-07

C_v : coefficient of primary consolidation, k : permeability. γ_n : natural unit weight; γ_s : dry unit weight; w_n : natural water content; w_L : liquid limit; PI: plasticity index.

with the Taylor method than with the Casagrande approach. Therefore, only the results obtained by the Taylor approach are shown. Obviously, the secondary consolidation coefficient was inferred from the semi-log Casagrande representation as slope of the secondary compression branch of the curve.

In the normally consolidated range, the constrained modulus exhibits the typical linear trend with the increase of the consolidation pressure. Only for the C3 sample a decrease of M until the pre-consolidation pressure was observed. The secondary compression coefficient increases, as expected until the applied pressure is 1.5 – 2.0 times the pre-consolidation pressure. On the other hand, the permeability linearly decreases with the applied pressure in a log scale, as usually. Differences between the clay sample (C3) and the other are evident in terms of both compressibility and hydraulic parameters.

Also, direct shear tests were carried out on the four high-quality Osterberg-type samples. For each sample, three specimens were tested in the direct shear box. The applied consolidation pressures were selected to include the best estimate of the in situ vertical effective stress.

Differences between sample C3 and the others were evident in terms of strength parameters. As a first estimate at peak, sample C3 exhibits a cohesion of about 5 kPa and an angle of shear resistance of about 20° whilst other samples have an apparent cohesion of about 2 kPa and an angle of shear resistance of about 30°. At large displacements the apparent cohesion is almost zero while the angle of shear resistance decreases to about 17° for the C3 sample. For the other samples, the angle of shear resistance remains almost constant. Moreover, except for the C3 sample, the others exhibit a certain curvature of the strength envelope.

2.3 Shear stiffness and damping ratio

RC tests were carried out according to ASTM D4015-15e1 (2015). Figures 3 and 4 respectively show the normalized shear modulus and the damping

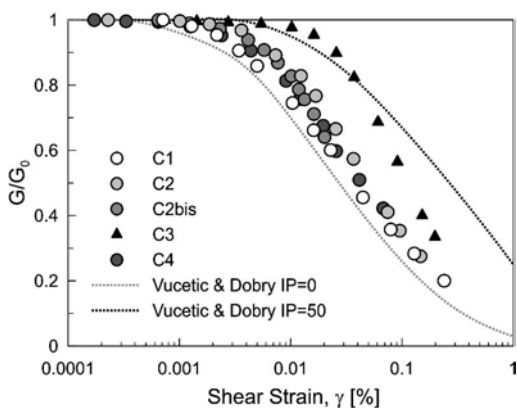


Figure 3. Normalized shear modulus vs. shear strain from RC.

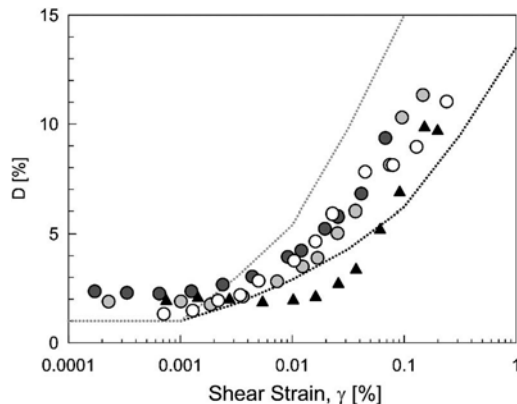


Figure 4. Damping ratio vs. shear strain from RC tests.

ratio as inferred from RC tests vs. the log of the shear strain. The reference curves, that have been suggested by Vucetic and Dobry (1991) for non-plastic soils and for soils with a PI of 50%, are also shown.

The influence of the PI on the RC results is confirmed even though a certain discrepancy is seen for high plasticity soils between the experimental results and the suggested curves. The small strain shear modulus typically ranges in between 36 and 40 MPa while the last specimen of the C4 sample gave an initial shear modulus as high as 90 MPa. The specimens were iso-tropically consolidated at the best estimate of the in situ vertical effective stress.

3 IN SITU TESTS

3.1 CPTu and DMT tests

Figures 5, 6 and 7 respectively show, in a standard format, the results of CPTu (ASTM D5778-20, 2020) and DMT tests (ASTM D6635-15, 2015). In particular, Figure 6 shows the modified SBTn (I(B)) profile (Robertson, 2016, 2021). Figure 8 shows the stratigraphic profile as inferred from borehole S1. Boreholes S2 and S3 were both core destruction surveys. As a preliminary comment, the indirect stratigraphic profiles from CPTu and DMT exhibit some differences. This point should be discussed in the light of laboratory test results, which is beyond the scope of this paper.

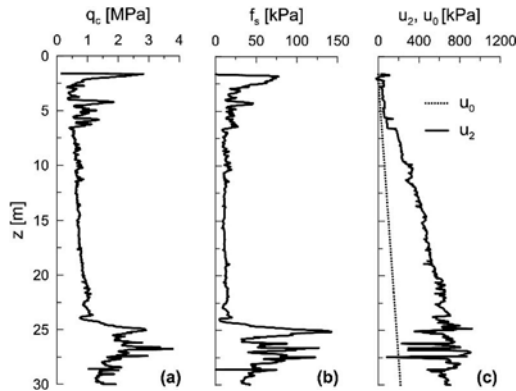


Figure 5. CPTu test results: (a) tip resistance; (b) sleeve friction; (c) pore pressure.

3.2 Body waves propagation velocities via different techniques

Reflection technique is based on recording time elapsing between the instant an elastic impulse is generated from the surface, reflected from a deep lithological interface and raised back to the surface.

In this sense, reflection exploits seismic impedance contrast between different materials and its advantage is the ability to penetrate underground with accuracy.

MARW is an innovative seismic technique based on 1D simplification of classical reflection survey. Advantages of this technique derive in acquiring a single Common Depth Point (CDP) or Common Shot Gather (CSG). Dataset is subsequently analyzed through a regular processing flow to derive a vertical seismostratigraphy. This method reaches its greatest effectiveness in lithological domains characterized by slopes less than 15° .

Figure 9 represents the acquisition geometry of MARW survey. For this test 96 high sensitivity 4.5 Hz horizontal geophones connected to a 96 channels 24 bit Do.Re.Mi SARA Electronic Instruments Seismograph were employed. The energy source consisted of a 12 Kg sledgehammer transversely hitting (three times to increase S/N ratio) a wooden plate placed in B1 position.

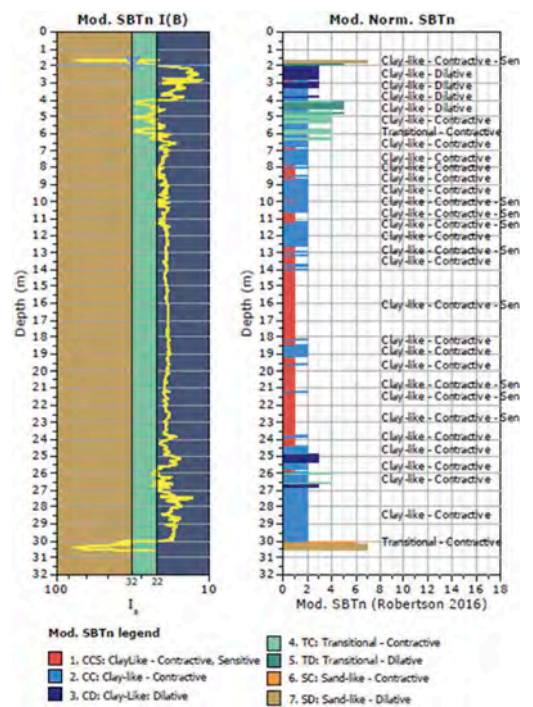


Figure 6. Modified Soil Behaviour Type (SBTn) from CPTu.

A very accurate data processing has been used to increase reflected events visibility: trace normalization, gain recovery (AGC), band pass filter, predictive deconvolution, muting first break, FX deconvolution, NMO correction.

Figure 10 shows from left to right: a) processed CSG before velocity analysis; b) the semblance (which shows velocity values consistent with reflection events); c) time stack trace (repeated four times); d) depth converted stack trace.

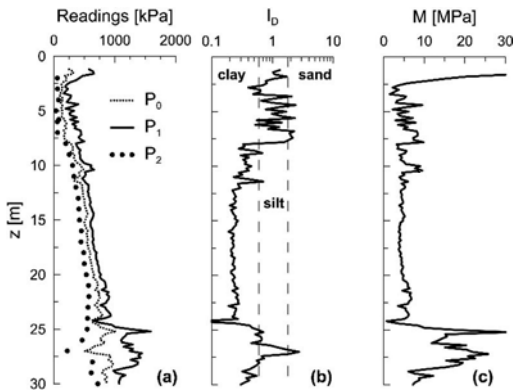


Figure 7. DMT test results: (a) readings; (b) material index; (c) constrained modulus.

Samples	Depth (m)	Graphic Log	Material Description
	0-2	Clay mixtures - Man-made ground	Clay mixtures - Man-made ground
	2-4	Medium stiff and stiff silty clay (brown)	Medium stiff and stiff silty clay (brown)
	4-5	Clayey and sandy silt (brown)	Clayey and sandy silt (brown)
	5-6	Silty sand (gray)	Silty sand (gray)
	6-7	Silty clay (brown-gray)	Silty clay (brown-gray)
Sample C1	7-8	Sandy silt (gray)	Sandy silt (gray)
	8-9	Sandy lens (gray)	Sandy lens (gray)
	9-10	Sandy silt (gray)	Sandy silt (gray)
	10-11	Clay (gray)	Clay (gray)
	11-12	Silty clay, clay	Silty clay, clay
Sample C2	12-13	Organic silty clay	Organic silty clay
	13-14	Clay, silty clay (gray)	Clay, silty clay (gray)
	14-15	Silt-sand mixtures	Silt-sand mixtures
	15-16	Clay, silty clay (gray)	Clay, silty clay (gray)
	16-17	Clay (gray), sandy lens	Clay (gray), sandy lens
	17-18	Clay, fat clay (gray)	Clay, fat clay (gray)
Sample C3	18-20	Clay, fat clay (gray)	Clay, fat clay (gray)
	20-22	Clay, silty clay (gray)	Clay, silty clay (gray)
	22-24	Clay, silty clay (brown)	Clay, silty clay (brown)
	24-26	Stiff clay (gray/green)	Stiff clay (gray/green)
Sample C4	26-28	Clay, silty clay (gray/brown)	Clay, silty clay (gray/brown)
	28-30	Clay (gray)	Clay (gray)

Figure 8. Stratigraphic profile from borehole S1.

Due to limitations related to acquisition geometry, the accuracy of depth and velocity values is progressively reduced beyond depths of about 60 m.

Alongside the geophones array two in-hole seismic tests (Cross-Hole) were carried out.

Cross-hole geophysical surveys consist of direct measurements, at various depths, of longitudinal (P



Figure 9. Seismic reflection survey geometry (MARW).

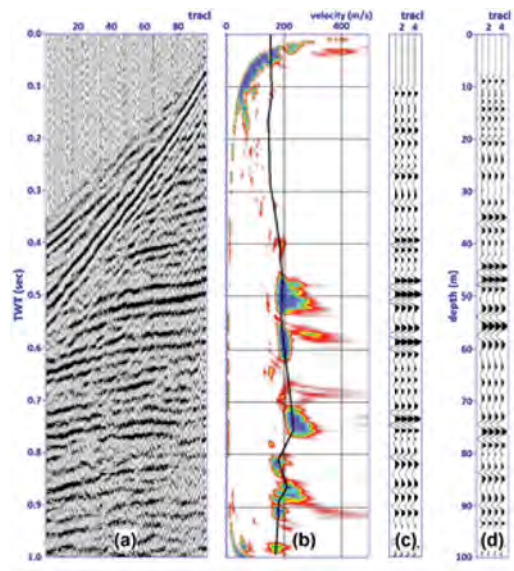


Figure 10. Seismic reflection survey results (MARW).

waves) and transverse (S waves) propagation times between two or more holes along horizontal trajectories. Travel-times, along with distances between source and receiver points, allow defining seismic wave velocity of investigated soils. The CH tests were carried out using central hole (S2) for positioning of transmitting sources and S1 and S3 holes for simultaneous acquisition by means respective receivers (P and S). Therefore, it was possible to verify the subsoil homogeneity of the survey area. A “Sparker” generator was employed to create compression waves while a “GEOS” transducer produced vertical polarized shear waves (instruments, both source and receivers, used for cross-hole survey was by Solgeo s.r.l.). Record of signals (Figure 11) was made by means of two different types of transducers to receive P and S waves respectively.

Pre-amplified hydrophones were employed to receive P waves and pre-amplified 28 Hz AVG geophones (Amplified Vertical Geophone) for S waves. Acquisitions were carried out with 1 m vertical constant intervals by a 2x16Bit MCHA-GP sampler. Signals were acquired with a 100 kHz frequency sampling for S-waves and 200 kHz for P-waves (record length 100 ms). First arrival times were manually picked through a PC interface. Velocities was simply calculated by operating the distance/times ratio. A preliminary inclinometric survey was carried out to define hole deviation from vertical direction through simultaneous measurement of inclination and

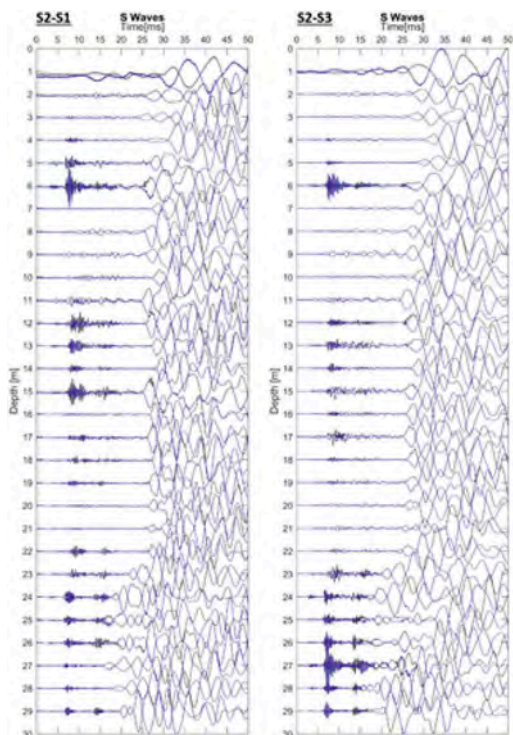


Figure 11. Cross-Hole records (S2-S1 left; S2-S3 right).

orientation. All three holes showed contained inclinations ranging between 10 and 20 cm.

Seismic piezocone consisted of a standard cone (10 cm² area) measuring tip resistance, sleeve friction, dynamic pore pressure and inclination. The piezocone was pushed by means of a Pagani TG73 – 150 penetrometer. The seismic module of SCPT was equipped with two 3D accelerometers. The relative distance between the accelerometers was 0.5 m. Therefore, two waveforms were recorded for each hit by the data acquisition system. The source consisted of a manual hammer (5 kg) hitting a wooden plate. Test interpretation was carried out by means of the cross-correlation method and the true interval method.

The SDMT is the combination of the Flat Dilatometer with an add-on seismic module for measuring the shear wave velocity (Marchetti et al., 2008) and optionally also the compression wave velocity. The seismic module is an instrumented steel rod placed just above the DMT blade and equipped with two receivers spaced 0.5 m. When a shear or compression wave is generated at surface, it first arrives to the upper receiver, then, after a delay, to the lower receiver. The wave traces of the two receivers are amplified and digitized at depth and transmitted to the computer at surface. The software processes the signals and evaluates the arrival delay, providing a real time interpretation of the wave velocity. True interval method is used for evaluating the propagation velocity of body waves. Figure 12 compares the body waves propagation

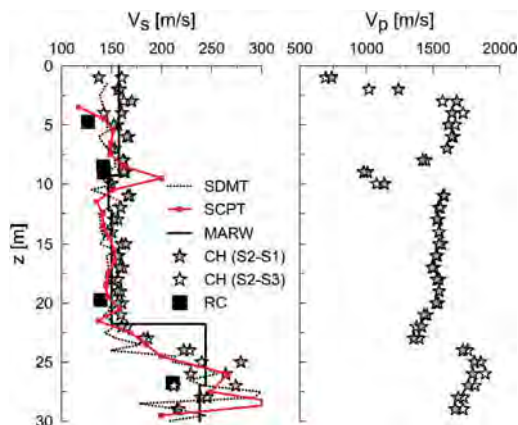


Figure 12. Vs profiles inferred by various techniques.

velocity as inferred from different in situ and laboratory tests. The Figure shows a very satisfactory agreement among the different testing methods. Moreover, laboratory testing well compared to in situ measurements.

4 SUMMARY AND CONCLUSIONS

The paper gives preliminary information about a test site that has been selected for establishing the precision and accuracy of available seismic methods in measuring the propagation velocity of body waves. At this stage we have a preliminary comparison between MARW, CH, SDMT and SCPT. This activity will continue, and we intend to invite other producers of seismic piezocone to participate into this research. As for the S waves the comparison among various techniques is very good. As for the P waves (less important for engineering applications), it is possible to confirm that below the water table (as already observed by various researchers) V_p is almost constant and equal to the propagation velocity in water. On the other hand, only CH test was capable of giving an estimate of V_p .

ACKNOWLEDGEMENTS

We acknowledge the contribution to the investigations given by Geoservizi snc, Geo-Energizer snc, SolGeo Srl and Servizi Geologici S.a.s. Morbin F. & C. These people were very professional and making possible the establishment of such a test site.

REFERENCES

- AGI 1994. Raccomandazioni sulle prove geotecniche di laboratorio. Associazione Geotecnica Italiana.
- ASTM D4015-15e1 2015. Standard Test Methods for Modulus and Damping of Soils by Fixed-Base Resonant

- Column Devices, ASTM International, West Conshohocken, PA, www.astm.org.
- ASTM D6635-15 2015. Standard Test Method for Performing the Flat Plate Dilatometer, ASTM International, West Conshohocken, PA, www.astm.org.
- ASTM D2487-17e1 2017. Standard Practice for Classification of Soils for Engineering Purposes (Unified Soil Classification System), ASTM International, West Conshohocken, PA, www.astm.org.
- ASTM D5778-20 2020. Standard Test Method for Electronic Friction Cone and Piezocone Penetration Testing of Soils, ASTM International, West Conshohocken, PA, 2020, www.astm.org.
- Casagrande, A. 1936. The Determination of the Pre – Consolidation Load and its Practical Significance, *Proc. 1st ICSMFE, III, D – 34*: 60–64. Harvard University Cambridge, Mass.
- Marchetti, S., Monaco, P., Totani, G., Marchetti, D. 2008. In Situ Tests by Seismic Dilatometer (SDMT). Proceedings. From Research to Practice in Geotechnical Engineering, ASCE Geotech. Spec. Publ. No. 180 (honoring J.H. Schmertmann): 292–311.
- Robertson, P. K. 2016. Cone penetration test (CPT)-based soil behaviour type (SBT) classification system—an update. *Canadian Geotechnical Journal*, 53(12): 1910–1927.
- Robertson, P. 2021. Personal communication to D. Lo Presti.
- Taylor, D.W. 1948. *Fundamentals of Soil Mechanics*, John Wiley and Sons.
- Vucetic, M. & Dobry, R. 1991. Effect of Soil Plasticity on Cyclic Response. *Journal of Geotechnical Engineering*, 117: 89–107.

Bayesian estimation of small-strain shear modulus from offshore CPT tests in the North Sea

B. Stuyts & C. Sastre Jurado

OWI-Lab, Vrije Universiteit Brussel, Brussels, Belgium
UGent, Ghent, Belgium

D. Gomez Bautista & A. Kheffache

OWI-Lab, UGent, Ghent, Belgium

ABSTRACT: The rapid expansion of offshore wind energy requires accurate and cost-effective site characterisation. The dynamic response of offshore wind turbine structures installed on monopile foundations strongly depends on the stiffness of the subsoil where the small-strain shear modulus governs the behaviour during operational loading. Direct measurement of the small-strain shear modulus with the seismic CPT (S-PCPT) is increasingly performed offshore. However, the additional cost associated with this test leads to incomplete data coverage. In the past, correlations between cone tip resistance and small-strain shear modulus have been developed for onshore conditions. The increasing availability of offshore site data has allowed a unique dataset of over 2000 small-strain shear modulus measurements from S-PCPT to be created for North Sea soil units. The comparison of the small-strain shear modulus inferred from the S-PCPT data to the corresponding cone tip resistance allows recalibration of the existing correlations. This paper proposes a Bayesian approach to update the correlation model for sands proposed in the literature based on the developed dataset for offshore conditions in the North Sea.

1 INTRODUCTION

1.1 Applications of small-strain shear modulus in geotechnical design

For offshore wind monopile foundations, the design is mainly driven by the fatigue limit state (FLS) (Maes et al. 2016) and is no longer dominated by the ultimate limit state (ULS) which was traditionally the design driver in offshore Oil & Gas platform geotechnical design. An accurate assessment of the fatigue life of the foundation monopile requires the assessment of non-linear soil response which shows a strong dependence on strain level (Zuccarino et al. 2019).

While dynamic soil properties and strain dependence of the shear modulus have traditionally been researched mostly in the context of earthquake engineering (Idriss and Boulanger 2008), the need for accurate foundation response models for monopile foundations has seen a renewed interest in the characterisation of these properties for marine soils in areas with low seismic activity.

Recent design methods for lateral foundation response of offshore monopiles in stiff clay (Byrne et al 2020) and sand (Burd et al. 2020) make use of the small-strain shear modulus as a governing soil parameter. The improved accuracy of the foundation response models has been demonstrated based on in-situ monitoring data (Stuyts et al. 2020).

1.2 Offshore measurement of small-strain shear modulus

Quantifying the small-strain shear modulus (G_{max}) is usually done through in-situ measurements although bender element testing on reconstituted samples can also be performed. Due to the lack of direct access to the seabed, onshore techniques such as cross-hole measurements and surface wave measurements are rarely performed.

Seismic PCPT tests (S-PCPT) are the dominant offshore measurement techniques. Figure 1 shows a sketch of the measurement system. A seismic source at the mudline emits shear waves into the soil which propagate downward with a velocity V_s governed by the mechanical properties of the soil mass. A dual geophone setup is preferred nowadays. The difference in arrival times between the two geophones can be derived by examining the cross-correlation between the two signals. The receiver offset (Δz) divided by the difference in arrival time (Δt) then provides an estimate of the shear wave velocity (V_s). The shear wave velocity can be converted to a small-strain shear modulus when the density of the soil (ρ) is known (Equation 1).

$$G_{max} = \rho \cdot V_s^2 \quad (1)$$

In recent years, the P-S suspension logging technique has been increasingly used offshore (Masters et al. 2019) but the empirical correlation proposed here is based exclusively on S-PCPT measurements.

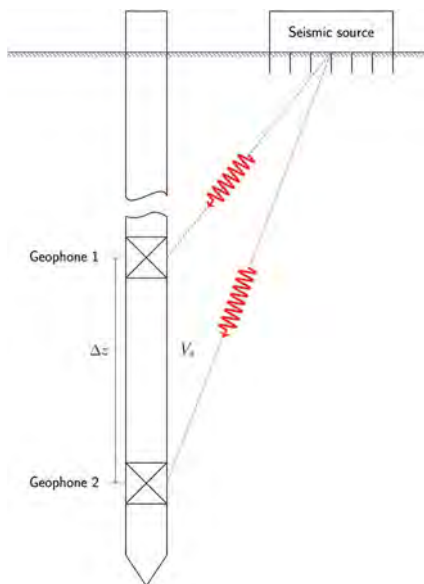


Figure 1. Sketch of S-PCPT measurement system.

2 EXISTING G_{MAX} CORRELATIONS

Because the S-PCPT test is relatively more expensive than a conventional PCPT test, shear wave measurements are generally not available at every foundation location. Instead, several authors have sought to correlate shear wave velocity with conventional PCPT measurements to allow derivation of site-specific stiffness parameters. These studies are based on onshore measurement campaigns where PCPT test data are compared to shear wave velocity measurements at locations where both data types are available.

The mostly widely used correlation for uncemented silica sands was developed by Rix & Stokoe (1991) based on calibration chamber measurements and the results of PCPT, S-PCPT and cross-hole tests. Equation 2 shows the dependence of the small-strain shear modulus on the cone tip resistance and the vertical effective stress level.

$$\left(\frac{G_{max}}{q_c}\right)_{ave} = \alpha \left(\frac{q_c}{\sqrt{\sigma'_{vo}}}\right)^\beta \quad (2)$$



Figure 2. Geospatial distribution of S-PCPT tests.

where the small-strain shear modulus G_{max} , the cone tip resistance q_c and the vertical effective stress σ'_{vo} are given in kPa. The coefficients $\alpha = 1634$ and $\beta = -0.75$ are suggested by the authors.

Several other empirical correlations exist in the literature (Hegazy and Mayne 2006). Most of these correlations were obtained using regression methods (i.e., least squares fitting) that do not directly quantify the uncertainties of predictions. To overcome this issue, the Bayesian framework can be adopted, as it provides the probability distribution of the model parameters instead of a single best estimate. In addition, the Bayesian framework allows further updating as additional data becomes available during future offshore campaigns.

In this paper, the principle of Bayesian updating of the parameters of the correlation between cone resistance and small-strain shear modulus will be outlined based on the aforementioned model proposed by Rix & Stokoe (1991).

3 NORTH SEA G_{MAX} DATASET

3.1 Data sources

A comprehensive dataset of shear wave velocity and small-strain shear modulus of offshore North Sea soils was assembled in the context of research on monopile response back-analysis. Table 1 shows the data compiled for four areas in the Belgian and Dutch sector of the North Sea. The coordinates of the S-PCPT test locations are shown in Figure 2.

The geology of the Borssele area and the Belgian offshore area shows a layered profile with a surface

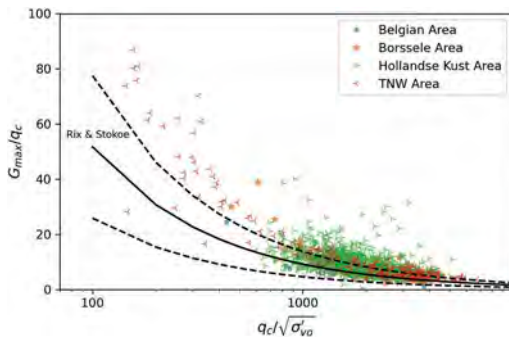


Figure 3. Overview of available data on clean sands and the correlation proposed by Rix & Stokoe. The valid range of the correlation is represented by the dashed lines.

layer of holocene/pleistocene sand overlying a tertiary clay formation which dips towards the northeast. In the Hollandse Kust area, mainly cohesionless sediments are found, with channel features leading to lateral variability of the deposits. Finally, the area north of the Wadden Islands has softer soils at the surface, which are classified as peat based on the normalized Robertson chart (Robertson and Cabal 2015). A summary of the available measurement and its classification following the the normalized Robertson chart is shown in Table 1.

This work will focus on clean sands (SBT_n zone 6) since this is the soil type the correlation was initially developed for. In Figure 3 the data are plotted according to the normalisation suggested by Rix & Stokoe (1991). Although the data confirms the general trend suggested by the authors the bias towards conservative estimates is clear and some data fall outside the valid range of this correlation.

4 BAYESIAN UPDATING

4.1 Introduction

Bayesian theory treats uncertainty as degrees of belief and it allows to combine information from multiple sources for the purpose of updating prior knowledge given new information. From a geotechnical point of view, the Bayesian method follows the same logic as the observational method (originally proposed by Terzaghi) and as a result it is a powerful basis for inference (Baecher 2017).

The core of Bayesian methods is the *Bayes' Rule*. It says that a hypothesis (i.e., parameters to be inferred) expressed as probabilities can be modified (i.e., updated) by observational information according to the conditional probability (*likelihood*) of those observations were a certain hypothesis true or not. If a hypothesis is denoted as H , Bayes' Rule can be written in a "friendly form" (Equation 3).

$$P(H|data) \propto P(data|H) \cdot P(H) \quad (3)$$

where:

- $P(H|data)$ is the *posterior*, the updated probability based on having made certain observations;
- $P(data|H)$ is the *likelihood* of the data;
- $P(H)$ is the *prior*, the probability before seeing the data which reflects prior knowledge.

As more observational data are introduced, uncertainties can be reduced through updating the mean values and decreasing the variance of our hypothesis.

4.2 Probabilistic model

When applied to the derivation of small-strain shear modulus from PCPT measurements, the multiplier α and exponent β in Equation 2 are the principal parameters to be updated by computing posterior distributions using Bayesian inference.

By taking the logarithm of Equation 2, a linear regression model can be used to model the relation between G_{max} and q_c (Equation 4).

$$\log_{10} \left(\frac{G_{max}}{q_c} \right) = \log_{10}(\alpha) + \beta \cdot \log_{10} \left(\frac{q_c}{\sqrt{\sigma'_{v0}}} \right) \quad (4)$$

where the slope is the coefficient β and $\log_{10} \alpha$ the intercept which will be noted by α' .

The dependent variable $\log_{10}(G_{max}/q_c)$ is denoted by y and the independent variable $\log_{10}(q_c/\sqrt{\sigma'_{v0}})$ by x . Then, the linear regression model can be written in a probabilistic manner as in Equation 5 (Gelman et al. 1995).

$$y \sim \mathcal{N}(\mu = \alpha' + \beta \cdot x, \varepsilon) \quad (5)$$

in other words, the dependent variable y is assumed to follow a normal distribution with a linear trend as mean (μ) and a standard deviation (ε). An error term (ε) is used to model the mismatch between the model and the actual data.

After applying Bayes' rule Equation 5 is the likelihood of the data. Following the Bayesian method, prior distributions need to be assumed for the unknowns parameters, to compute the term $P(H)$ from Equation 3. Standardization was performed on the left- and right-hand side of Equation 4. Standardization consists of subtracting the mean from the data and dividing by the standard deviation. One advantage of standardizing the data is that the same weakly informative priors can always be used without having to think about the scale of the data. A common choice is to assume normal distributions as priors for the intercept and slope and a HalfCauchy prior for the error term.

Table 1. S-PCPT data sources.

Project site	Locations	Measurements	No. of measurements per soil type					
			2	3	4	5	6	7
Hollandse Kust Area	85	2016	1	37	114	333	1484	47
Borssele Area	8	60	0	2	8	11	31	8
TNW Area	15	282	44	0	0	11	224	3
Belgian Area	7	85	0	20	42	8	10	5
Total	115	2443	45	59	164	364	1749	63

- 2 Organic soils-peats
- 3 Clays: clay to silty clay
- 4 Silt mixtures: clayey silt to silty clay
- 5 Sand mixtures: silty sand to sand silty
- 6 Sands: clean sands to silty sands
- 7 Gravelly sand to sand

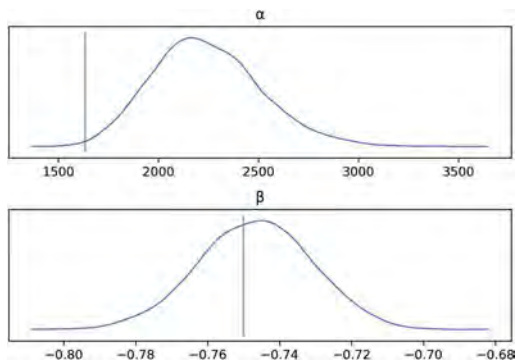


Figure 4. Computed posterior distribution of correlation model coefficients. The proposed values by Rix & Stokoe are represented by vertical grey lines.

5 PROBABILISTIC RECALIBRATION OF G_{MAX} CORRELATION FOR COHESIONLESS SOILS

The probabilistic models were built using PyMC3, a Python package for Bayesian modelling based on Markov Chain Monte Carlo algorithms (Salvatier et al. 2016). The result of a Bayesian analysis is a posterior distribution, not a single value but a distribution of plausible values given the data and the proposed model and there are many methods for computing the posterior distribution. Here, the posterior was estimated numerically using an algorithm from the Markov Chain Monte Carlo (MCMC) family, known as No-U-Turn Sampler (NUTS) (Hoffman et al. 2014).

The posterior distribution of the inferred parameters α and β can be visualized in Figure 4. The results show that the exponent of -0.75 suggested by Rix & Stokoe applies well to the data. However, the multiplier of 1634 suggested based on the calibration chamber dataset needed to be substantially increased for the North Sea dataset. The statistics of these parameters are summarized in Table 2. The mean and standard deviation are shown as well as the 95% Highest-

Table 2. Statistics of α and β from MCMC.

Parameter	Mean	Standard deviation	95% HPD
α	2241	272	[1711, 2761]
β	-0.747	0.016	[-0.778, -0.715]

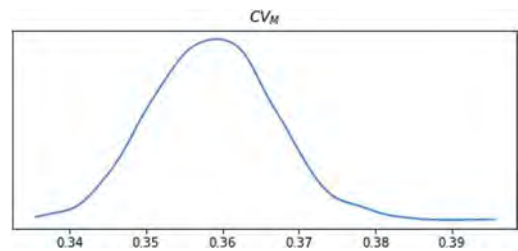


Figure 5. Computed posterior distribution of the model error represented by the coefficient of variation.

Posterior Density (HPD) interval. The 95% HPD is the shortest interval containing the true value of the parameter in question with a probability of 0.95.

Transformation uncertainty which is basically the data scatter about the transformation model can be expressed quantitatively by means of the coefficient of variation (Phoon and Kulhawy 1999). This uncertainty will be noted by CV_M and can be visualised by sampling from the posterior distributions as shown in Figure 5. Transformation uncertainty follows a narrow distribution showing a modal value about 36%.

Finally the inferred model is shown in Figure 6. The average model that fits the data was represented by a black solid line. Note that the most probable value is given by the mode of the posterior. In this case, the mean is a good approximation since the posterior of both coefficients showed a Gaussian shape (Figure 4). This model leads to an improvement in the model bias of 28%. This means that the distribution of the ratio of

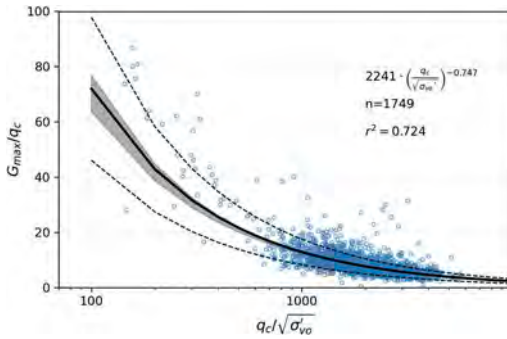


Figure 6. Recalibrated correlation model based on North Sea data: average and standard deviation.

predicted to measured G_{max} shifts closer to unity (the original Rix & Stokoe correlation showed a bias of 0.65).

The dashed lines in Figure 6 represent the average standard deviations of the model prediction based on the average CV_M equals to 0.36. The impact of the *statistical uncertainty* of the correlation model is represented by the semitransparent grey band to illustrate the 95% HPD. Both errors, statistical and transformation uncertainties are not constant, increasing when the ratio $q_c/\sqrt{\sigma'_{vo}}$ decreases. Indeed, for shallow layers, less data is available and noise in the data (e.g. due to waves propagating down the cone rod interfering with the shear wave propagating through soil) introduces more scatter in the small-strain shear modulus measurements. It is therefore possible to conclude that the model does not provide accurate predictions when the ratio $q_c/\sqrt{\sigma'_{vo}}$ is lower than 1000 approximately.

6 CONCLUSIONS AND RECOMMENDATIONS

This paper presents the results of Bayesian inference to recalibrate the correlation model between cone resistance and small-strain shear modulus suggested by Rix & Stokoe (1991). This recalibration is based on a dataset of 1749 small-strain modulus measurements with the S-PCPT for North Sea sands.

The results show that the exponent suggested by Rix & Stokoe is largely confirmed by the assembled dataset. However, the multiplier α needs to be substantially increased as the original Rix & Stokoe correlation underestimates the small-strain shear modulus for nearly all cases. The recalibrated model provided in Equation 6.

$$\left(\frac{G_{max}}{q_c}\right)_{ave} = 2241 \left(\frac{q_c}{\sqrt{\sigma'_{vo}}}\right)^{-0.747} \quad (6)$$

with a coefficient of variation of the prediction error of 0.36.

The average model is useful in obtaining a best estimate of the small-strain shear modulus. The uncertainty on the estimate of G_{max} can be assessed thanks to the coefficient of variation and by assuming a normal distribution. The provided statistics can be used as a basis for a reliability analysis for e.g. lateral pile response. The effect of the uncertainty on G_{max} on the natural frequency estimate could thus be quantified.

Following the Bayesian updating philosophy, the reported statistics of the model coefficients can be used to build priors distribution for further calibration of the model when new project-specific information becomes available.

ACKNOWLEDGEMENTS

The authors would like to acknowledge the support of the Belgian Ministry of Economic Affairs through the ETF project WINDSOIL project. The support of VLAIO through the De Blauwe Cluster SBO SOILT-WIN project is also acknowledged.

The geotechnical data from the Dutch offshore wind farms (RVO.nl) was used under a Creative Commons license.

REFERENCES

- Baecher, G. B. (2017). Bayesian thinking in geotechnics. In *Geo-Risk 2017*, pp. 1–18.
- Burd, H. J., D. M. Taborda, L. Zdravković, C. N. Abadie, B. W. Byrne, G. T. Houlsby, K. G. Gavin, D. J. Igoe, R. J. Jardine, C. M. Martin, et al. (2020). Pisa design model for monopoles for offshore wind turbines: application to a marine sand. *Géotechnique* 70(11), 1048–1066.
- Byrne, B. W., G. T. Houlsby, H. J. Burd, K. G. Gavin, D. J. Igoe, R. J. Jardine, C. M. Martin, R. A. McAdam, D. M. Potts, D. M. Taborda, et al. (2020). Pisa design model for monopiles for offshore wind turbines: application to a stiff glacial clay till. *Géotechnique* 70(11), 1030–1047.
- Gelman, A., J. B. Carlin, H. S. Stern, & D. B. Rubin (1995). *Bayesian data analysis*. Chapman and Hall/CRC.
- Hegazy, Y. A. & P. W. Mayne (2006). A global statistical correlation between shear wave velocity and cone penetration data. In *Site and geomaterial characterization*, pp. 243–248.
- Hoffman, M. D., A. Gelman, et al. (2014). The no-u-turn sampler: adaptively setting path lengths in hamiltonian monte carlo. *J. Mach. Learn. Res.* 15(1), 1593–1623.
- Idriss, I. M. & R. W. Boulanger (2008). *Soil liquefaction during earthquakes*. Earthquake Engineering Research Institute.
- Maes, K., A. Iliopoulos, W. Weijtjens, C. Devriendt, & G. Lombaert (2016, August). Dynamic strain estimation for fatigue assessment of an offshore monopile wind turbine using filtering and modal expansion algorithms. *Mechanical Systems and Signal Processing* 76-77, 592–611.
- Masters, T. A., P. Juskiewicz, A. Mandolini, & H. Christian (2019). A critical appraisal of the benefits

- of and obstacles to gaining quality data with offshore seismic cpt and ps logging. In *Offshore Technology Conference*. OnePetro.
- Phoon, K.-K. & F. H. Kulhawy (1999). Evaluation of geotechnical property variability. *Canadian Geotechnical Journal* 36(4), 625–639.
- Rix, G. J. & K. H. Stokoe (1991). Correlation of initial tangent modulus and cone penetration resistance. In *Calibration chamber testing*. New York: Elsevier, pp. 351–362.
- Robertson, P. & K. L. Cabal (2015). Guide to Cone Penetration Testing. Technical report.
- Salvatier, J., T. V. Wiecki, & C. Fonnesbeck (2016). Probabilistic programming in python using pymc3. *PeerJ Computer Science* 2, e55.
- Stuyts, B., W. Weijtjens, C. Devriendt, H. Versteede, & C. V. Haute (2020). Monopile lateral response calibration from insitu monitoring data. In *4th International Symposium Frontiers in Offshore Geotechnics*, pp. 3557. Deep Foundations Institute.
- Zuccarino, L., A. D. Morandi, & O. Luca (2019). Dynamic properties of offshore sands. In *OTC-29590-MS*. Offshore Technology Conference.

Factors influencing $CPT_U N_{kt}$ for marine clay in Singapore reclaimed land

C. Tanaka, M. Angeles & J.Y. Wong
Arup Singapore Pte. Ltd., Singapore

ABSTRACT: Cone penetration tests with porewater pressure measurements (CPT_U) are extensively adopted in Singapore due to the presence of soft soils from the young deposits of the Kallang Formation. The most prominent member of this formation is the soft Singapore marine clay, which can be present in thicknesses of up to 50m. Singapore is a relatively small island, and as such, over the past few decades has embarked on numerous reclamation projects to increase land to support their growing economy and population. Therefore, significant data in reclaimed land overlying soft deposits is available, especially in the east of Singapore. This has presented the opportunity to review the factors that influences N_{kt} in the marine clay located within this area. N_{kt} plays a significant role in the evaluation of the undrained shear strength (c_u), which is often derived from site-specific calibrations. This paper summarizes the CPT_U results carried out in reclaimed land to the east of Singapore. It discusses the calibration of N_{kt} with other site data, and proposes a range of N_{kt} to be adopted in this location.

1 INTRODUCTION

Reclamation works have been carried out in the east of Singapore in phases, starting with the original reclamation scheme throughout the 1970's and 1980's. Subsequently, further lands were reclaimed for the development of airport infrastructure from the late-1980's till early 2000's, forming the land as it is seen today as shown in Figure 1. Ground improvement works were also conducted to improve the soft marine clay in most of the reclaimed site. A series of site investigation (including CPT_U and boreholes) were carried out on site along the course of the reclamation and ground improvement works to understand the geological conditions and strength of the ground. This paper presents the interpreted undrained shear strength (c_u) results from CPT_U carried after all ground improvement works had been completed, post 2014. It compares the c_u values obtained at two different locations across the site (Location A and B, Figure 1). It also presents a calibration exercise of N_{kt} while drawing correlations to the site history.

2 SITE HISTORY AND GEOLOGY

The site locations A and B were reclaimed in different phases as part of reclamation works that took place from 1992 to 2005 where 2,000 ha of land were reclaimed by placing 272 million m^3 of granular fill in seawater with a depth up to 15m (Bo et al. 2005). This was done in various ways, including direct dumping, hydraulic filling and sand spreading.

Direct dumping was utilized at deeper waters of 6m to 8m, while hydraulic filling was utilized for shallower depths of 2m to 6m.

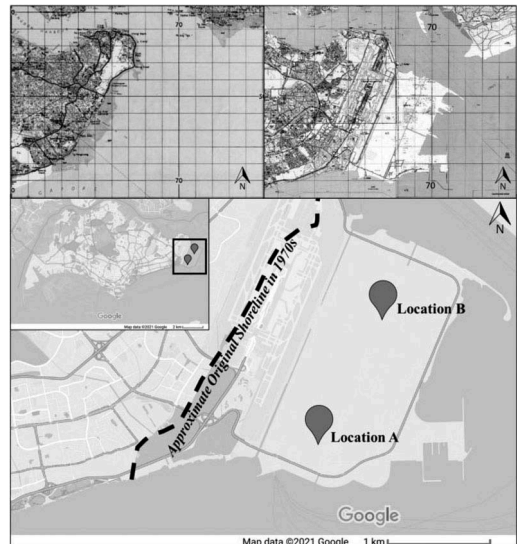


Figure 1. Singapore topography maps in 1970s (top left) and 2010s (top right) and Location of site (bottom).

As the reclaimed site was underlain by 50m of soft marine clay, prefabricated vertical drains (PVD) coupled with surcharging were proposed to accelerate consolidation of the underlying deposits during

Table 1. Summary of site works at Locations A and B.

	Location A	Location B
Reclamation Period ¹	Phase 1A: 1992 to 1997	Phase 1B: 1993 to 1999
Reclamation Method ¹	For sites from -5mCD to -10mCD: Direct Dumping from bottom opening barges then hydraulic filling by cutter suction dredgers Others: Hydraulic filling by cutter suction dredgers	Hydraulic filling by cutter suction dredgers
Ground Improvement History	No known post-reclamation ground improvement	Post reclamation 1993 to 1999: PVD installed at square grids of 1.5 m/ 1.7 m with surcharging of minimally 18 months ¹ Land preparation for future development 2014 to 2018: PVD installed at square grids of 1.0 m/ 1.2 m with surcharging of minimally 6 months

¹Note: Choa (1995)

reclamation works from 1992 to 2005 (Choa et al. 2001) and post reclamation works from 2014 to 2019. A summary of reclamation and known ground improvement history across the two locations can be found in Table 1.

Extensive site investigations have been carried out post ground improvement for land preparation for future development from 2015 to 2020. More than 2000 CPT_U and 1000 boreholes were conducted on site to understand the post-improvement conditions as shown in Figure 2.

The site investigation show the ground conditions across the site are highly variable due to the multiple reclamation methods. Generally, the site consists of approximately 10m to 15m of thick reclamation fill underlain by 5m to 40m of Kallang Formation, followed by the stiff deposits of the Old Alluvium. The most prominent member of the Kallang formation is the soft marine clay, with thickness varying from 20m and 40 m at Locations A and B, respectively as shown in Figure 3.

Site investigations carried out includes in-situ tests: CPT_U and vane shear tests (VST) and laboratory tests: Triaxial unconsolidated undrained tests (UU) and one dimensional Oedometer tests. These tests are used to determine the undrained shear strength of the ground. From the site investigation, the Marine clay has varying consolidation states as discussed in Chapter 5.

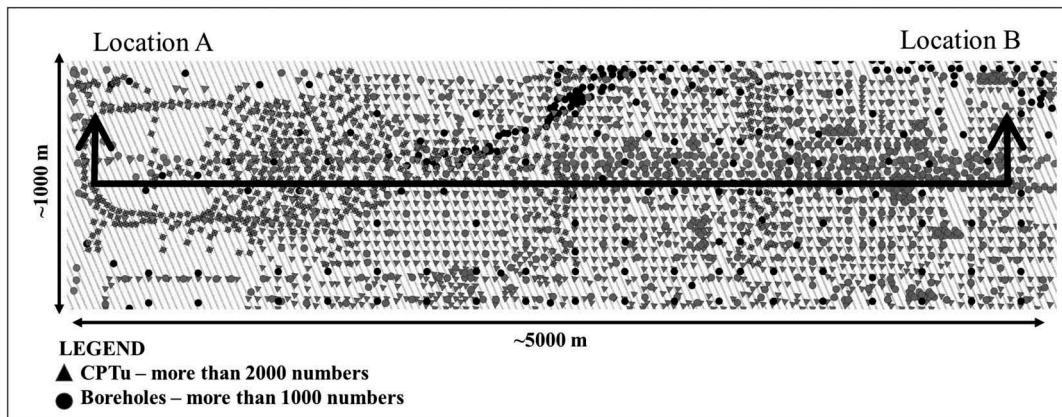


Figure 2. Site investigation plan.

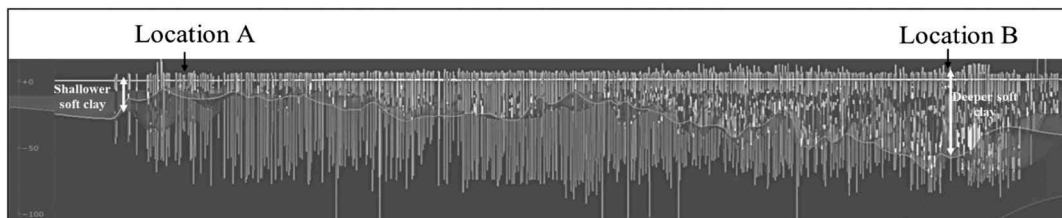


Figure 3. Geological long section.

3 UNDRAINED SHEAR STRENGTH INTERPRETATION OF CPT_U

The undrained shear strength (c_u) of the soil from CPT_U is derived using standard correlation (Lunne et al 2002):

$$c_u = (q_t - \sigma_v) / N_{kt} \quad (1)$$

where:

q_t = corrected cone resistance based on the measured pore pressure; σ_v = total overburden stress; and N_{kt} = empirical cone factor.

The corrected cone resistance (q_t), is calculated from the measured cone resistance (q_c) through the formula

$$q_t = q_c + (1 - a)u_2 \quad (2)$$

where a = net area ratio of 0.8 to 0.82; and u_2 = pore pressure measured just behind the cone.

Various studies have been conducted to determine the range of N_{kt} values as shown in Table 2. It is observed that a wide range of values have been recommended depending on the varying soil conditions and locations.

Theoretical studies have also related the N_{kt} value to plasticity index (I_p). Singapore Marine Clay properties at this location have been extensively studied by Bo et al (2000), and a N_{kt} correlation is proposed based on plasticity index of the clay where:

$$N_{kt} = 23.8 - 0.263I_p \quad (3)$$

With a typical I_p of 40% for the marine clay across the site as seen in Figure 4, an N_{kt} value of approximately 14 is recommended.

According to Bo et al. (2000), the N_{kt} will decrease with increasing I_p although studies by Aas et al. (1986) suggest that N_{kt} will increase with increasing I_p ; La Rochelle et al. (1988) did not find any correlation between N_{kt} and I_p .

Table 2. N_{kt} recommendations from literatures.

N_{kt} range	Type of Soil	Reference
10 – 15	Normally Consolidated Clay	De Ruiter (1982)
15 – 20	Under-Consolidated Clay	De Ruiter (1982)
15 – 21	Lightly Over-Consolidated Singapore Marine Clay	Dobie (1988)
9 – 17	Clay with PI = 33% – 45%	Lunne et al. (2005)

With the varying range of recommended N_{kt} values, calibration with site-specific undrained shear strength data were utilised for more accurate interpretation of the cone factor. The undrained shear strength data was obtained from the measured uncorrected field VST, Laboratory Triaxial UU test, as well as correlation with one-dimensional oedometer tests pre-consolidation pressure ($0.22 P_c'$).

4 CONSOLIDATION STATE OF CLAY

The consolidation state of the ground is determined by comparing the in-situ and laboratory c_u with the empirical normally consolidated (NC) line with respect to existing ground level. The NC line is derived through the formula by Mesri (1975),

$$c_u = 0.22\sigma_v' \quad (3)$$

where σ_v' = effective overburden stress with respect to existing ground level.

In general terms, the c_u that falls below the NC line is considered as under-consolidated with respect to existing ground level, while those that lie above are considered over-consolidated with respect to existing ground level.

5 OBSERVATIONS OF N_{KT} VALUES

5.1 Comparison of CPT_U c_u data with VST, UU and Oedometer test data

The undrained shear strength interpreted from various in-situ and laboratory tests for Locations A and B are summarised in Figures 5 and 6, respectively. Interpretations using N_{kt} of 14 and 20 at the two locations are plotted for comparison.

For Location A, N_{kt} value of 14 appears to over-estimate the CPT_U c_u data as most of the c_u data from the other tests fall below the CPT_U c_u data as shown in Figure 5a. N_{kt} value of 20 better correlates with the other site investigation data as shown in Figure 5b.

For Location B, N_{kt} value of 20 appears to under-estimate the CPT_U c_u data as most of the c_u data from the other tests lies above the CPT_U c_u data as shown in Figure 6a. N_{kt} value of 14 appears to better correlate with the other site investigation data as shown in Figure 6b.

5.2 Comparison of CPT c_u data with NC line

As indicated in Table 1, at Location A, there is not known post reclamation ground improvement

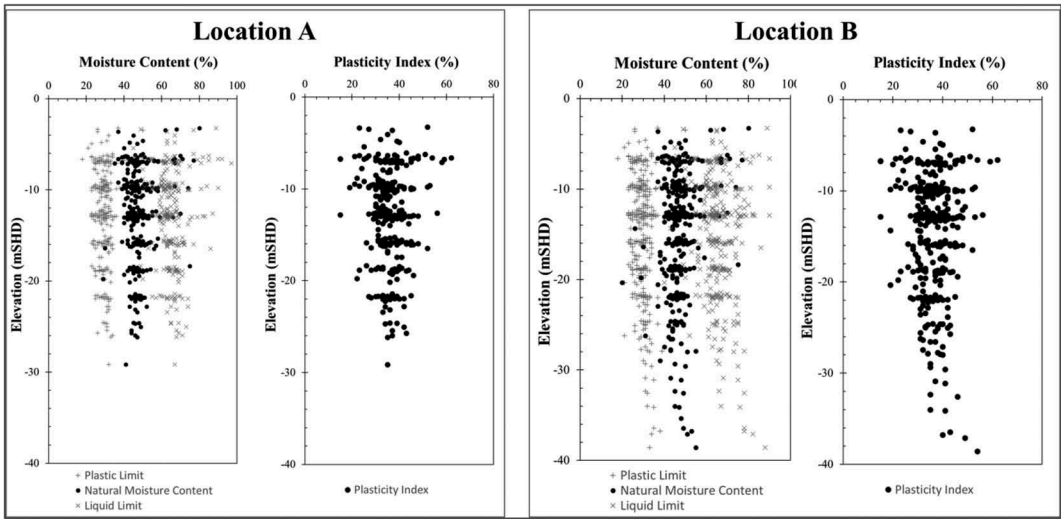


Figure 4. Atterberg limits at locations A and B.

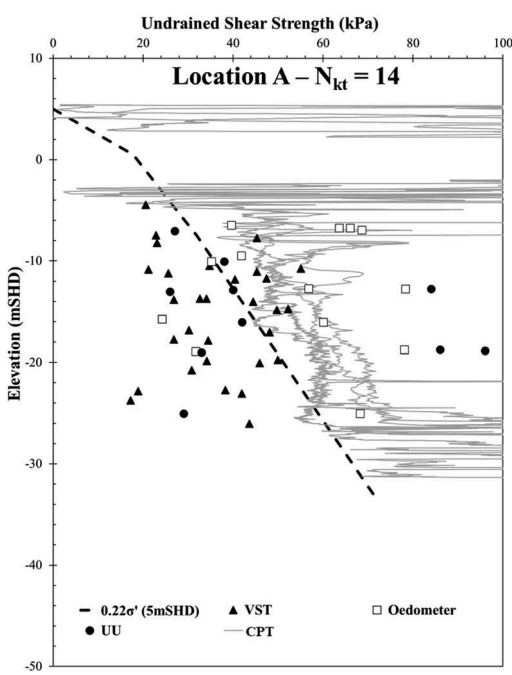


Figure 5a. Location A - c_u plot for $N_{kt} = 14$.

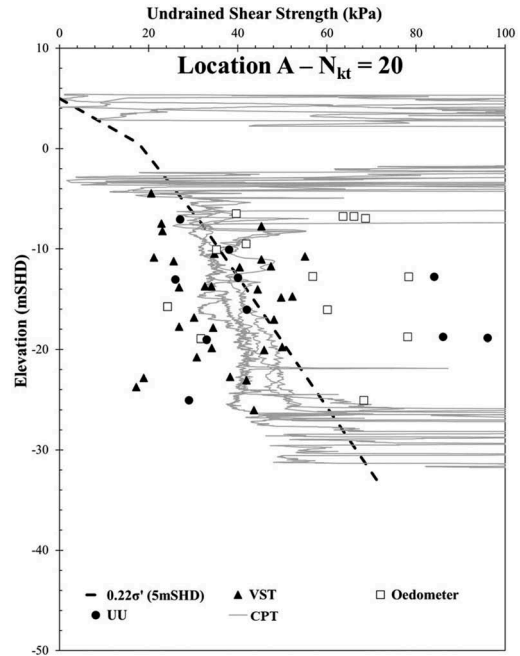


Figure 5b. Location A - c_u plot for $N_{kt} = 20$.

works been carried out. Based on Terzaghi consolidation theory, the marine clay is still undergoing consolidation from the reclamation filling carried out to form the site's current ground level. This is in line with interpreted CPT c_u with higher N_{kt} where the CPT c_u data falls below the NC line.

On the other hand, at Location B, two rounds of extensive ground improvement works were carried out. By Terzaghi consolidation theory, the marine clay is expected to be at least in normally consolidated state or over-consolidated. This is in line with interpreted CPT c_u with lower N_{kt} where the CPT c_u data lies above the NC line.

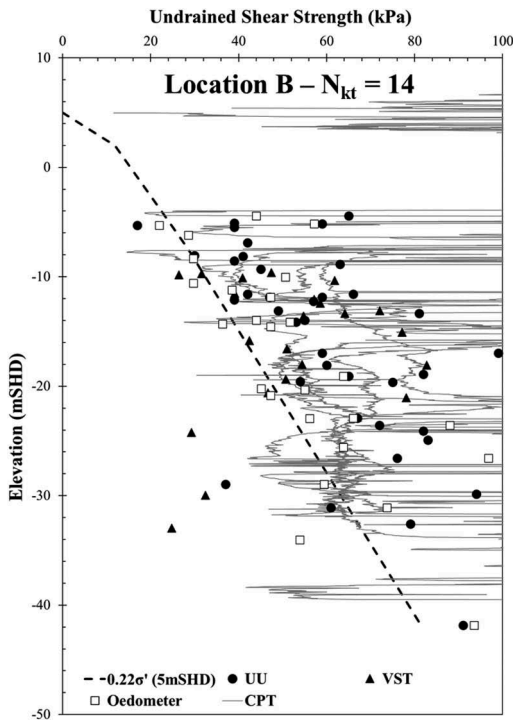


Figure 6a. Location B - c_u plot for $N_{kt} = 14$.

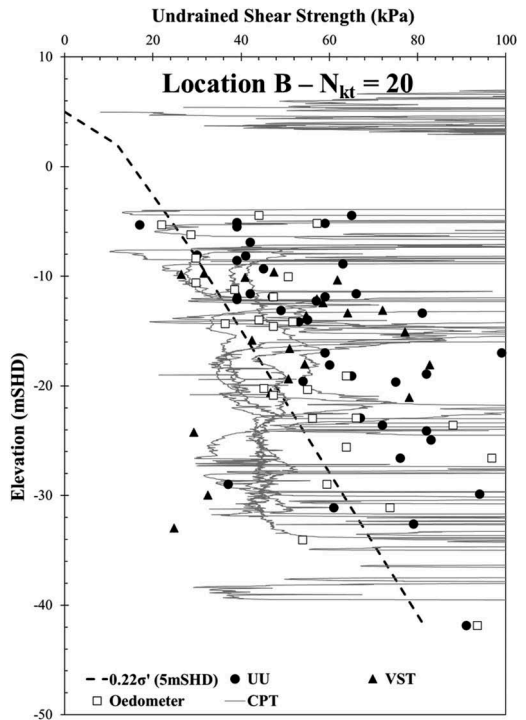


Figure 6b. Location B - c_u plot for $N_{kt} = 20$.

6 CONCLUSION

This paper has presented CPT_U data obtained from two different areas (Location A and B), located within the same site, but with different reclamation and ground improvement histories.

The CPT_U data was used to determine c_u via standard correlations (Lunne,2002). The paper has highlighted that the empirical factor N_{kt} has significant influence in the determination of c_u . Therefore, this paper has presented an N_{kt} calibration exercise by comparing the interpreted c_u from CPT_U with other geotechnical tests, including in-situ vane shear tests, laboratory Triaxial unconsolidated undrained tests and one dimensional Oedometer tests.

The calibration exercise showed that for Location A, which is under-consolidated to existing ground level, an N_{kt} value closer to 20 provides consistency with the c_u obtained from the in-situ and laboratory tests data as well as with its site history. For location B, an N_{kt} value closer to 14 was selected on the same basis.

The N_{kt} values between 14 (Location B) to 20 (Location A) recommend based on a site-specific data calibration is consistent with the general range recommended in other available literature and publications (Lunne,2002).

Based on the N_{kt} variability presented, a site-specific calibration is recommended for derivation of c_u , especially when c_u is critical for the geotechnical design (e.g., assessment of long-term settlements or excavations schemes), and when the site has varying consolidation history, such as the one presented in this paper.

REFERENCES

- Aas G., Lacasse S., Lunne T., and Hoeg K. 1986. Use of in situ tests for foundation design on clay. *Proceedings of the ASCE Specialty Conference*: 1–30
- Bo, M. W., Chang, M. F., Arulrajah, A., & Choa, V. 2000. Undrained shear strength of the Singapore marine clay at Changi from in-situ tests. *Geotechnical Engineering*, 31(2).
- Bo, M. W., Chu, J., & Choa, V. 2005. The Changi east reclamation project in Singapore. *Elsevier Geo-Engineering Book Series* 3: 247–276. Elsevier.
- Campanella, R. G., RG, C., & PK, R. 1982. Pore pressures during cone penetration testing.
- Choa, V. 1995. Changi east reclamation project. In *Compression and consolidation of clayey soils*: 1005–1017.
- Choa, V., Bo, M. W., & Chu, J. 2001. Soil improvement works for Changi East reclamation project. *Proceedings of the Institution of Civil Engineers-Ground Improvement* 5(4): 141–153.
- Chu, J., Bo, M. W. & Arulrajah, A. 2009. Reclamation of a slurry pond in Singapore. *Proceedings of the Institution of Civil Engineers-Geotechnical Engineering* 162 (1): 13–20.

- De Ruiter, J. 1982. The static cone penetration test: State-of-the-art report. *Proc. of the Second European Symposium on Penetration Testing, Amsterdam, May 1982* 2:389–405
- Dobie, M. J. D. 1988. A study of cone penetration tests in the Singapore marine clay. *International Symposium on penetration testing; ISOPT-1. 1*: 737–744.
- La Rochelle, P., Zebdi, M., Leroueil, S., Tavenas, F., & Virely, D. 1988. Piezocone tests in sensitive clays of eastern Canada. *International Symposium on penetration testing; ISOPT-1. 1*: 831–841.
- Lee, S. L., Karunaratne, G. P., Yong, K. Y., Tan, S. A., & Tan, T. S. 1989. Soft clay properties in a layered clay-sand reclamation.
- Lunne, T., Randolph, M. F., Chung, S. F., Andersen, K. H., & Sjørsen, M. 2005. Comparison of cone and T-bar factors in two onshore and one offshore clay sediments. *Frontiers in Offshore Geotechnics (Proc. ISFOG, Perth)*: 981–989.
- Lunne, Tom, John JM Powell, and Peter K. Robertson. Cone penetration testing in geotechnical practice. CRC Press, 2002.

Parameters affecting the CPT resistance of reconstituted sands

Y. Tian & B.M. Lehane

The University of Western Australia, Perth, WA, Australia

ABSTRACT: Despite the popularity of the Cone Penetration Test, uncertainty remains regarding the stress level dependence of q_c in a sand of constant relative density, the effect of the mineralogy and the effect of saturation. This paper provides greater clarity on these effects by presenting results from a large series of drained cone penetration tests performed under controlled conditions in a laboratory pressure chamber. The experiments involve dry and fully saturated silica and carbonate sands placed at a number of relative densities (D_r) and tested at different stress levels and overconsolidation ratios. The observations are compared with existing relationships proposed between q_c and D_r and highlight the approximate nature of such relationships.

1 INTRODUCTION

The relative density (D_r) of coarse-grained soils is usually assessed indirectly from correlations with in-situ test parameters due to the difficulties in obtaining undisturbed samples of these materials. The relationship between CPT cone resistance (q_c) and D_r has been assessed from experiments in laboratory-based pressure chambers that involved CPTs in reconstituted sand samples prepared to a range of D_r values and stress states. The relationships generally employ the following format:

$$D_r = C_1 \ln[q_{c1N}/C_2] \quad (1a)$$

$$q_{c1N} = [(q_c/p_{atm})/(\sigma'/p_{atm})^n] \quad (1b)$$

where q_{c1N} = stress normalized cone resistance; C_1 and C_2 are empirical constants, p_{atm} = atmospheric pressure (100 kPa), n = stress level exponent (typically between 0.5 and 0.7) and σ' = effective stress at the level of the cone tip.

The value of σ' adopted is typically the vertical effective stress (σ'_v) in normally consolidated deposits and the mean effective stress (p') in overconsolidated deposits. The use of p' in overconsolidated deposits reflects the dependence of q_c on the in-situ horizontal effective stress (σ'_h) illustrated by Houlsby & Hitchmann (1988). Popular relationships in the form of Equation (1) proposed by Lunne & Christoffersen (1983) and Baldi et al. (1986) respectively are:

$$D_r = 0.34 \ln[q_{c1N}/16] \quad (2)$$

where $\sigma' = \sigma'_v$ and $n = 0.71$

$$D_r = 0.38 \ln[q_{c1N}/23] \quad (3)$$

where $\sigma' = p'$ and $n = 0.55$

To allow for shallow penetration effects, which are important at geotechnical centrifuge scale, Lehane et al. (2022) used results from over 70 centrifuge tests in range of normally consolidated silica sands to propose the following relationship:

$$D_r = 0.31 \ln[q_{c1N}/(19 \tanh(az/d_c))] \quad (4a)$$

where $\sigma' = \sigma'_v$, $n = 0.7$, z = depth, d_c = diameter of the cone penetrometer and a is assessed from an initial approximate estimate of D_r :

$$a = 0.66 \exp(-2.5D_r) \quad (4b)$$

Kulhawy & Mayne (1990) recognized the importance of ageing, overconsolidation ratio (OCR) and sand compressibility and proposed:

$$D_r = \{(q_{c1N}/(305C_F)) OCR^{-0.18} C_{age}^{0.5}\}^{0.5} \quad (5)$$

where $n = 0.5$; C_F = compressibility factor between 0.91 & 1.09 (higher value for more compressible sand) and $C_{age} = 1.2 + 0.05 \log [t/100]$, where t is the time in years.

This paper presents a re-assessment of these correlations using a new series of pressure chamber tests conducted at the University of Western Australia (UWA). These tests were initially performed to test the general applicability of Equation (4) derived from centrifuge CPT data. The test series was subsequently expanded to examine the effect of sand mineralogy (by comparing q_c data in a silica and carbonate sand), sand saturation level (dry and fully saturated) and overconsolidation ratio (hence σ'_h). The test results allow general conclusions to be drawn regarding the relationship between q_c and D_r for reconstituted sands.

2 TEST PROGRAMME

2.1 Test setup

A schematic diagram of the calibration chamber test is shown in Figure 1. The soil sample is created by pluviation of the sand into a cylindrical chamber, which is then loaded vertically to the desired vertical effective stress via a rigid top plate. This plate has circular openings to allow for penetrometer access to the sand. The vertical effective stress is applied by a hydraulic jack and is monitored by a load cell while the cone is driven into the sample at a constant speed by the actuator located on the steel frame. The maximum imposed vertical effective stress imposed in the experiments described here is 75kPa. The walls of the chamber are rigid and a flexible Teflon sheet is bonded to the inner wall to minimize friction.

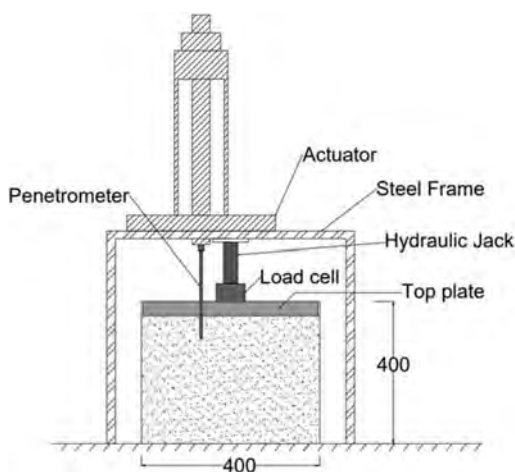


Figure 1. Schematic of the calibration chamber test.

2.2 Sample preparation

Sand samples are prepared in calibration chambers by pluviation. A sand hopper is fitted on two rails which enables it to move both horizontally and vertically. A constant drop height is maintained during the preparation of uniform sand while the hopper cycles in the horizontal direction. Different relative densities are achieved by varying the horizontal travelling speed, the drop height and the sieve situated at the bottom of the hopper.

Two types of sand are used in this study namely (i) UWA sand, which is a fine silica sand that is sourced commercially and has been tested extensively at the University of Western Australia (UWA) and (ii) Ledge Point carbonate sand, which is obtained from a sand dune near Ledge Point, Western Australia. Properties of the two types of sand are listed in Table 1. A miniature cone with the diameter (d_c) of 7mm is employed for the tests described here. The corresponding d_c/D_{50} ratio is in excess of 20 for both sands, as recommended by Bolton et al. (1999) to avoid particle size effects.

Table 1. Properties of sands used in the tests.

Sand	D_{50}		e_{max}	e_{min}	ϕ'_{cs}
	(mm)	Specific gravity			
UWA silica sand	0.18	2.67	0.78	0.50	33°
Ledge Point carbonate sand	0.21	2.76	1.17	0.78	35°

* e_{max} and e_{min} are the void ratio limits and ϕ'_{cs} is the critical state friction angle of the sand

2.3 Test conducted

Over 80 CPTs were conducted in the two sands placed in 12 chambers at a variety of relative densities and consolidated to three vertical effective stress levels (25, 50 and 75kPa). The effects of the degree of saturation (S_r) and overconsolidation ratio (OCR) in silica sand were also examined. A summary of the scope of testing is provided in Table 2, noting that many CPTs were repeated to assess variability and repeatability. Additionally, CPTs were performed to assess if the proximity of the boundary to the penetrometer had an influence on the q_c values measured.

2.4 Boundary effect

Initial trials were conducted to assess if the planned distance of a penetrometer installation location to the chamber boundary (s) influenced the tip resistance.

The steady state q_c values recorded at $\sigma'_v = 50$ kPa in medium dense and dense UWA silica sand at 8, 12 and

Table 2. Summary of the tests conducted.

Sand	D_r	σ'_v		S_r	OCR	$q_{c1N,avg}$
		(kPa)				
UWA	0.1	25, 50, 75		1	1	28
Silica	0.63	25, 50, 75		0	1	118
Sand	0.97	25, 50, 75		0	1-4	283
	0.8	50		1	1	200
Ledge Point	0.06	25, 50, 75		1	1	37
carbonate sand	0.67	25, 50, 75		0	1	163
	0.95	25, 50, 75		0	1	469

27 cone diameters (d_c) from the chamber wall are presented on Figure 2. It is evident that q_c values increased close to the chamber wall at both D_r values when the s/d_c value was less than about 12 and that there is a slightly greater relative effect of the boundary influence in the denser sand. Bolton et al. (1999) found a very similar result in centrifuge CPTs conducted in a circular strongbox, observing no significant increase in q_c due to the proximity of the boundary for silica sand with $D_r=81\%$ at s/d_c ratios in excess of 11. All CPT data reported in the following correspond to test results recorded at $s/d_c > 12$.

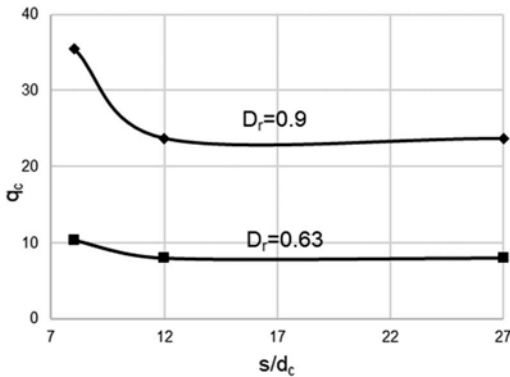


Figure 2. Influence of normalized proximity to rigid chamber boundary (s/d_c) in medium dense and dense UWA silica sand.

It is of interest to note that q_c values recorded at $s/d_c=8$ in Ledge Point carbonate sand were identical to those recorded at $s/d_c=12$ and 27. This reduced boundary influence may arise due to the higher compressibility of the carbonate particles.

3 TEST RESULTS

3.1 Normally consolidated dry silica sand

Typical results obtained during penetration of a 7 mm diameter cone in a pressure chamber are shown in Figure 3(a). These were measured in three separate normally consolidated UWA sand samples with different

D_r values but the same vertical effective stress of 50 kPa. It is seen that the q_c values in dry silica sand increase up to a penetration depth of about $5d_c$ but stabilize thereafter at values of about 2.5 MPa and 8 MPa in the very loose and medium dense silica samples respectively. Evidence from other chamber tests indicated that the slight reduction of q_c with depth seen for these samples is associated with a modest reduction in D_r with depth in these particular samples and is not related to reduced vertical effective stress due to the potential presence of side friction. It should be noted that the very loose sand was water-pluviated and the

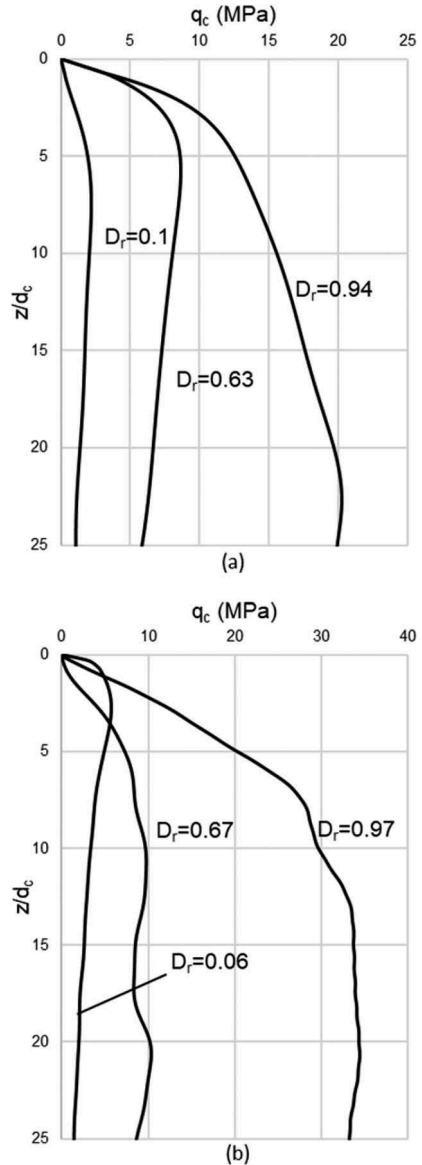


Figure 3. q_c profiles measured at $\sigma'_v=50$ kPa at three relative density values for (a) UWA Silica sand (b) Ledge Point Carbonate sand.

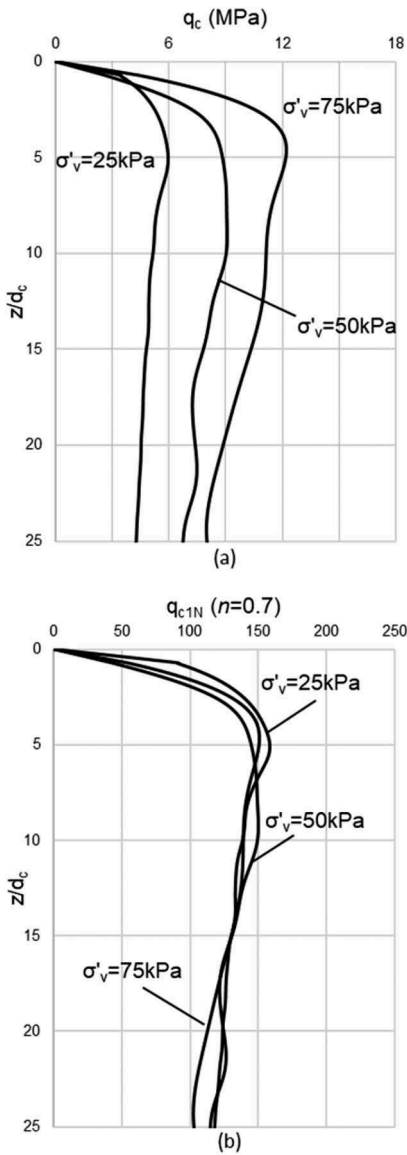


Figure 4. Tip resistance in medium dense UWA silica sand ($D_r=0.63$) under three stress levels: (a) q_c in MPa, (b) q_c normalized.

reducing trend of q_c with depth in this sample indicates that this process resulted in slightly looser sand at depth.

It is also seen on Figure 3(a) that q_c values in dense silica sand increase with depth and do not tend to a steady state until a penetration depth of about 15-20 d_c . This trend is typical of that shown by other tests in dense silica sand. Normalized depths, z/d_c , required to develop steady state conditions in carbonate sand are lower than for silica sand, as seen on Figure 3b. The influence of stress level on the q_c value in a medium dense sample ($D_r=0.63$) is illustrated on

Figure 4. It is evident that, while the steady state q_c value increases with the vertical effective stress in the sample (σ'_v), q_c is not linearly proportional to σ'_v . This tendency is typical of sands and is reflected by the 'n' exponent in the normalized cone resistance, q_{c1N} (Equation 1b). It is shown on Figure 4(b) that the data from the three stress levels are unified when q_{c1N} is plotted using $n=0.7$. Data from all 36 CPTs conducted in normally consolidated UWA silica sand were compiled to find a best fit relationship in the form of Equation (1). The following relationship was found to predict measured D_r values to within 10%.

$$D_r = 0.357 \ln[q_{c1N}/21] \quad (6)$$

where $\sigma' = \sigma'_v$ and $n = 0.7$

Equation (6) is compared with Equation (4) on Figure 5 which was derived independently for the same sand from an extensive series of centrifuge CPTs performed over a larger stress range (from 5 kPa to 330kPa). The plotted centrifuge q_c values correspond to those at the steady state when the hyperbolic tangent term in Equation (4a) is unity. Very good agreement between both data sets is observed, particularly in loose and medium dense sand. The reason for the higher steady state q_c values recorded in dense sand in the centrifuge compared to those in the chamber tests at the same stress levels is under investigation.

Equation (6) is also compared with Equation (2) and (3) in Figure 6, which have previously been proposed for normally consolidated silica sand. Equation (2) has been adjusted to correspond with a stress exponent (n) of 0.7 at the average stress level used in the chamber test of 50kPa to facilitate this comparison. It is evident that agreement is very good between all three equations for $D_r < 0.7$. However, Equation (6) implies greater q_c values in very dense UWA sand, which were also found the centrifuge CPTs.

3.2 Normally consolidated dry carbonate sand

Typical q_c profiles measured in normally consolidated Ledge Point carbonate sand are shown in Figure 3b. A comparison with the silica sand data on Figure 3a indicates higher q_c values are developed in the carbonate sand at the same density and stress level; this trend reflects higher friction angles of the carbonate particles. The q_c profiles in the carbonate samples also tended to show greater fluctuations or 'peakiness', which is attributed to the samples' greater compressibility. Regression analyses of the calibration chamber data indicated a best fit stress level exponent (n) of 0.7, as for the silica sand and the following best fit relationship:

$$D_r = 0.37 \ln[q_{c1N}/30] \quad (7)$$

where $\sigma' = \sigma'_v$ and $n = 0.7$

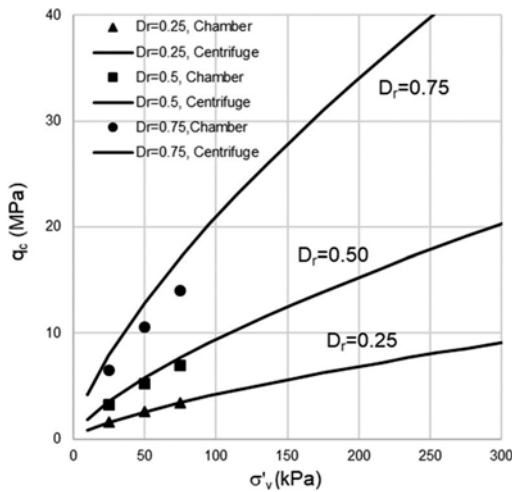


Figure 5. Comparison of q_c relationship with D_r and σ'_v predicted by Equations (4) and (6) for UWA silica sand (for steady state conditions).

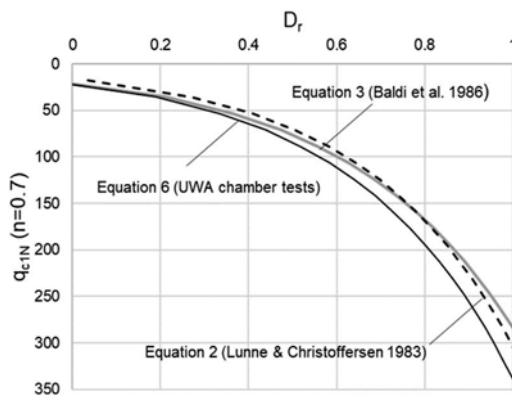


Figure 6. Comparison of normalized q_c relationship with D_r predicted by Equations (2), (3) and (6) for normally consolidated silica sand.

Equation (7) is compared with Figure 7 with Equation (6) derived from the calibration chamber data in UWA silica sand. This comparison illustrates the relative magnitudes of q_c values in the two sand types. Equation (5) is also compared with Equation (6) and (7). A stress level of 50 kPa (which was the mean used in the chamber tests) was assumed to enable Equation (5) to be plotted on this figure as this equation employs a stress level exponent of 0.5. In addition, recommended compressibility factors (C_F) of 0.91 and 1.09 were adopted for the silica and carbonate sands respectively. It is evident from the comparison that general agreement is observed between Equation (5) and Equations (6) and (7) both in terms of the trend with D_r and the relative magnitudes of normalised cone resistance.

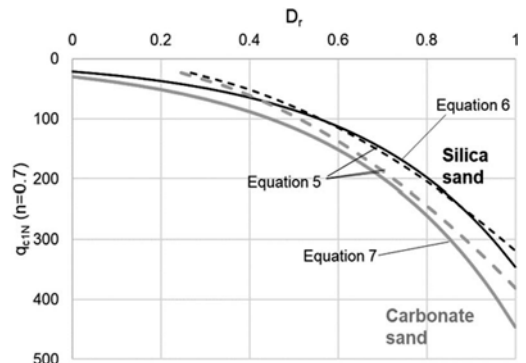


Figure 7. Comparison of relationships derived for silica and carbonate sand (Equation 6 and 7) with Equation (5) proposed by Kulhawy & Mayne (1990).

3.3 Overconsolidated dry silica sand

Five CPTs were conducted in dense silica sand ($D_r = 0.97$) at σ'_v values of 75 kPa, 50 kPa and 25 kPa after the samples had been pre-loaded to either 100 kPa or 75 kPa. Figure 8a shows the normalized tip resistance calculated using σ'_v and indicates that this-normalized value increases with OCR. Figure 8b plots the same data but uses σ'_h to normalize the q_c value for stress level, defined here as:

$$q_{c1N,h} = \left[(q_c / p_{atm}) / (\sigma'_h / p_{atm})^{0.7} \right] \quad (8)$$

where σ'_h was estimated from the following expression of Mayne & Kulhawy (1982) using the friction angles (ϕ) given in Table 1:

$$\sigma'_h = (1 - \sin \phi_{cs}) OCR^{\sin \phi_{cs}} \sigma'_v \quad (9)$$

It is seen that the data at all OCRs are unified on Figure 8b, confirming the suitability of employing σ'_h to normalize the cone resistance proposed by Houlsby & Hitchman (1988). It is notable, however, that $q_{c1N,h}$ continues to increase with depth and did not appear to reach a steady state value.

Values of relative density predicted by Equations (3) and (5), which are intended for use in sands at all OCRs, are compared with the measured relative density in Table 3. It is seen that both equations over-estimate D_r and that the degree of over-estimation increases with OCR. Further studies are ongoing at UWA to investigate q_c trends in overconsolidated sands.

3.4 Effect of saturation

The q_c values measured in dry and fully saturated ($S_r = 0$ and 1) silica sand at a relative density of

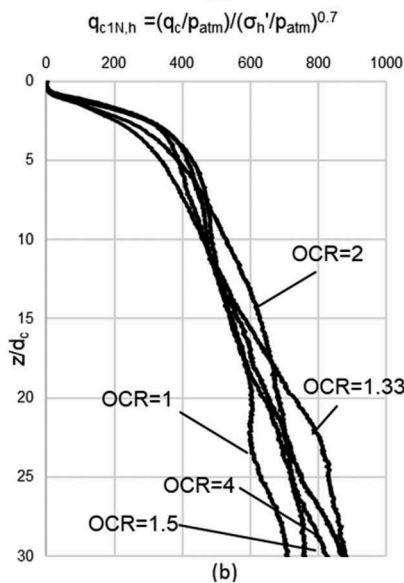
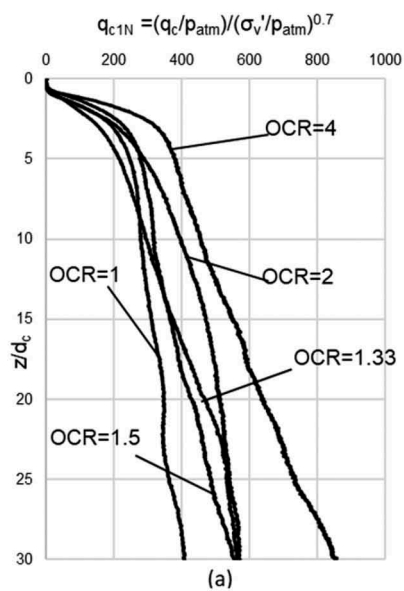


Figure 8. Tip resistance in overconsolidated dense silica sand: (a) normalized by vertical effective stress; (b) normalized by horizontal effective stress.

0.8 are compared on Figure 9. This figure also plots q_c profiles measured at cone penetration rates between 0.1mm/s and 1.0mm/s. It is evident that q_c values, given experimental inaccuracies, are essentially identical in all cases. Additional CPTs performed in loose carbonate sand prepared at $S_r=0$ and $S_r=1$ also showed no dependence of q_c on S_r . These findings contrast with centrifuge data reported by Giretti et al. (2018) who found higher q_c values in dry carbonate sand compared with saturated sand and suggest that the higher

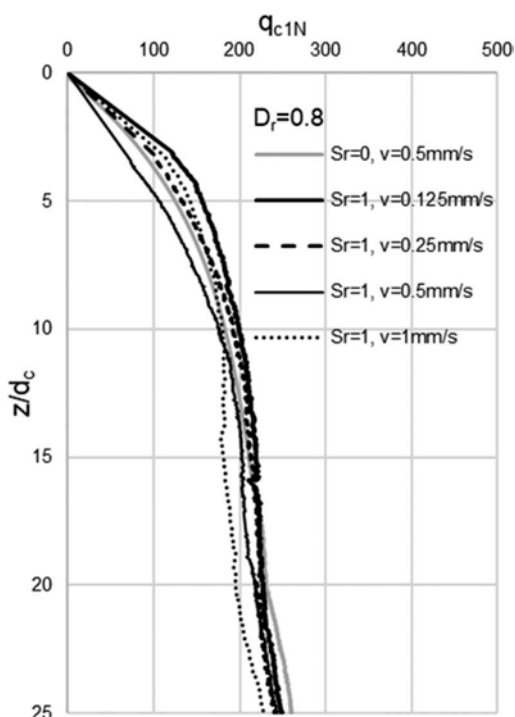


Figure 9. Normalized tip resistance in dry and fully saturated silica sand ($D_r=0.8$) under various penetration rate.

Table 3. Performance of Equations (3) and (5) in dense silica sand.

$D_{r,meas}$	OCR	σ'_v (kPa)	$D_{r,calc}$	
			from Equation(3)	from Equation(5)
0.97	1	75	1.06	1.00
	1.33	75	1.14	1.09
	1.5	50	1.10	1.07
	2	50	1.16	1.13
	4	25	1.19	1.19

* $D_{r,calc}$ values quoted are the average predicted values

values arise due to dry crushed carbonate particles forming a slightly enlarged cone base area on the cone for $S_r=0$ tests. Jamialkowski et al. (2003) also found slightly lower q_c values in saturated sand, which is not evident on Figure 9 for UWA sand.

4 CONCLUSIONS

Over 80 CPTs were performed in calibration chambers at UWA to study the effect on q_c of stress level, mineralogy, overconsolidation ratio and degree of saturation. Relationships between

stress normalized end resistance (q_{c1N}) and relative density (D_r) are developed for UWA silica sand and Ledge Point carbonate sand. These are shown to be generally consistent with previously published correlations indicating that the relationship between q_{c1N} and D_r is relative insensitive to a sand type of given mineralogy. The testing programme highlighted the need for further studies into the development length of the CPT in dense sands and the cone resistance in overconsolidated dense sand.

ACKNOWLEDGEMENT

The first Author acknowledges the financial support through an Australian Government Research Training Program (RTP) Scholarship.

REFERENCES

- Baldi, G., Bellotti, R. & Ghionna, V., 1986. Interpretation of CPTs and CPTUs, Part II: Drained Penetration in Sands. In Proc. of 4th International Geotechnical Seminar on Field Instrumentation and In Situ Measurements, Singapore.
- Bolton, M.D., Gui, M.W., Garnier, J., Corte, J.F., Bagge, G., Laue, J. & Renzi, R., 1999. Centrifuge cone penetration tests in sand. *Géotechnique*, 49(4), pp.543–552.
- Giretti, D., Been, K., Fioravante, V., & Dickenson, S., 2018. CPT calibration and analysis for a carbonate sand. *Géotechnique*, 68(4),345–357.
- Houlsby, G.T. & Hitchman, R., 1988. Calibration chamber tests of a cone penetrometer in sand. *Geotechnique*, 38 (1),pp.39–44.
- Jamiolkowski, M., Lo Presti, D.C.F. & Manassero, M., 2003. Evaluation of relative density and shear strength of sands from CPT and DMT. In *Soil behavior and soft ground construction* (pp. 201–238).
- Kulhawy, F.H. & Mayne, P.W., 1990. Manual on estimating soil properties for foundation design (No. EPRI-EL-6800). Electric Power Research Inst., Palo Alto, CA (USA); Cornell Univ., Ithaca, NY (USA). Geotechnical Engineering Group.
- Lehane, B., Zania, V., Chow, S. & Jensen, M., in press., 2022. “Interpretation of centrifuge CPT data in normally consolidated sands”. (under final review), *Geotechnique*.
- Lunne, T. & Christoffersen, H.P., 1983, May. Interpretation of cone penetrometer data for offshore sands. In *Offshore Technology Conference*. OnePetro.
- Mayne, P.W. & Kulhawy, F.H., 1982. Ko-OCR relationships in soil. *Journal of the Geotechnical Engineering Division*, 108(6),pp.851–872.

Practical experience with cone penetration in frozen soils

N.G. Volkov & I.S. Sokolov

GEOINGSERVICE (Fugro Group), Moscow, Russia

R.A. Jewell

Fugro GeoConsulting, Brussels, Belgium

ABSTRACT: This paper summarizes recent practical experience with CPT investigations at several permafrost sites in Russia. Some of the investigations were performed in unconventional conditions such as with ice cover, in a crawl space, or from a jack-up platform. All CPT measurements used a cone equipped with a temperature sensor to confirm the subzero temperature of frozen soil. Stress relaxation tests were performed in ice-rich permafrost soils to investigate long-term soil strength in both compression and shear. Sampling of frozen soil using direct push techniques was achieved at two sites.

1 INTRODUCTION

Frozen soil has ice content and exhibits rheological behavior, meaning the stress-strain behaviour and mechanical properties change with time. The failure of frozen soil under long-term loading is important for design. The long-term soil strength (the resistance of a soil to failure in response to a long-term load application) is a key parameter in the engineering of frozen ground (Vyalov, 1986). Long-term soil strength can be considered in terms of two main components: the long-term soil strength in compression (σ_c), important for pile end bearing (q_p), and the long-term soil strength in shear (σ_f), important for pile unit side friction (f_p).

Cone penetration testing (CPT) in frozen ground provides valuable data on frozen conditions and soil properties. Both temperature and porewater pressure sensors are required for testing in permafrost (a TCPTU test). Temperature measurement is similar to pore pressure dissipation testing. Penetration is paused and the variation of temperature with time is measured to determine the asymptote. A Stress Relaxation Test (SRT) can be performed at the same time, recording the variation of cone resistance (q_c) and sleeve friction (f_s) with time, for the cone clamped in place. This provides an estimate for the long-term strength in compression (σ_c) and shear (σ_f) (Sokolov, 2020). An SRT test does not increase the time or cost, and data processing can be fully automated for results to be obtained in the field.

2 PRACTICAL EXAMPLES OF SITES WITH CPT IN FROZEN GROUND

Nine cases of TCPTU testing in the Russian Arctic from 2014 to 2021 are listed below. The sites involve a range of permafrost conditions (Figure 1):

1. 2014 – Labytnangy Civil Infrastructure
2. 2015 – Vorkuta Railroad
3. 2016 – Salekhard College
4. 2017 – Ob Gulf, Arctic LNG2
5. 2018 – Ob River, Salekhard Bridge
6. 2019 – Novy Urengoy, Civil Infrastructure
7. 2021 – Kruzenshtern Gas Field, Yamal
8. 2021 – Dikson Area, Kara Sea
9. 2021 – Norilsk river, Talnakh Bridge

The findings from this testing include:

- Frozen sand at -6°C was successfully tested with CPT equipment;
- Up to 62 m of continuous penetration through permafrost was achieved without predrilling;
- Ground ice is generally not found to be critical for cone penetration in permafrost;
- CPT refusal is generally caused by the soil density rather than ice content or soil temperature.

Four of these cases (1-4) were presented at the CPT'18 conference (Volkov et al, 2018). A description for the five sites (5-9) tested between 2018 and 2021 is given below.

2.1 Ob river, Salekhard bridge

TCPTU tests were performed at the Salekhard Bridge site located in the Russian Arctic, some

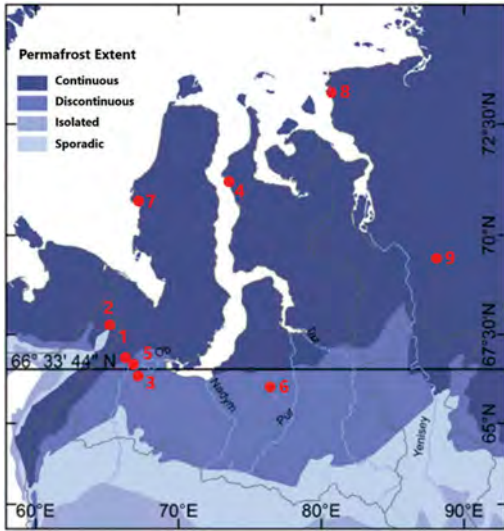


Figure 1. Permafrost sites in Siberia, Russia with CPT investigations (for numbers see description in the text).

160 km upstream from the Ob River estuary (Figure 1, site #5). Three zones at the site of the Ob River bridge are the left bank, the right bank, and the river bed itself. The site is located in a cold region characterized by discontinuous permafrost (Figure 1). The average annual air temperature in the Salekhard area is -5.7°C . The CPT tests were performed during winter January-March 2018 when the Ob River was covered by ice. One CPT was performed to refusal on the right bank and achieved a depth 62 m (with no predrilling). The frozen state of the soil (permafrost) was confirmed by measuring temperature and collecting samples of frozen ground from the adjacent geotechnical borehole. The above is considered to be a record depth for continuous CPT penetration in permafrost.

An interesting observation was made from the CPTs on the left bank. The river formed a talik at this location (an unfrozen soil strata below or near to a river). Due to this talik, part of the soil depth penetrated was frozen and part of it not. This provided an opportunity to compare the same soil horizon in both a frozen and non-frozen state. Although it is generally known that cone resistance in frozen ground is higher compared with the same unfrozen ground, all other conditions being equal, these tests provided a direct quantitative comparison. The cone resistance in the unfrozen sand varied between 8 and 35 MPa, in the frozen sand between 12 and 54 MPa. The refusal depth was similar both in frozen and non-frozen sand and varied between 25 and 30 m.

The CPT data were interpreted to provide soil parameters and associated analysis. For pile design, impact Soil Resistance to Driving (SRD) and Blow Count analyses were completed and axial pile

bearing capacity and uplift capacity were estimated, for locations characterized by both unfrozen and frozen soil conditions. The results compared favourably with subsequent full scale pile tests at the site for both static load capacity and pile drivability.

2.2 Novy Urengoy, Civil infrastructure

In the summer of 2019, TCPTU tests with direct push sampling were performed from a crawl space under a civil apartment complex in Novy Urengoy, Western Siberia (Figure 1, site #6).

The structure, supported by piles driven to 10 m below ground level, was experiencing gradual differential settlement due to unknown reasons. It was assumed that settlement was due to insufficient pile bearing capacity. However, the steps taken to increase pile bearing capacity did not stop the settlement. CPT testing was then applied to investigate in more detail the insitu soil conditions between and below the piles. The depth of cone penetration was 30 m, comfortably exceeding the pile length.

Frozen soil was detected at some locations at a depth 11 m (Figure 2). Distinctive peaks of high values in cone resistance and low values in sleeve friction and electric conductivity were interpreted as ice lenses. Some of these ice lenses are highlighted in Figure 2, as an example.

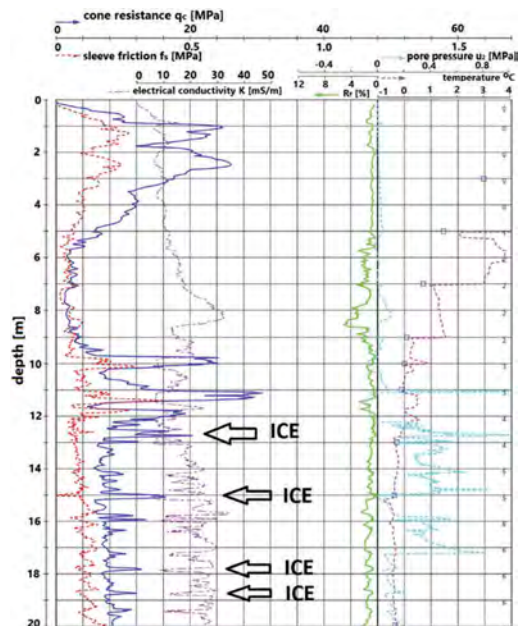


Figure 2. CPT profile in frozen soil at Novy Urengoy.

A direct push probe was then used to collect samples of the frozen soil, using a regular MOSTAP sampler with 35 mm inner diameter (Robertson,

2014). The collected samples confirmed the presence of frozen soil with ice lenses of thickness up to 10 cm (Figure 3). The frozen soil was tested in the laboratory and was found to have a high density that would not compress significantly due to thawing (Table 1). Rather, the thickness of ice lenses were such that significant differential settlement would be expected from gradually melting ground ice.



Figure 3. Frozen soil samples with ice lenses collected by direct push sampler mounted on CPT press at Novy Urengoy.

Table 1. Physical and strength properties of the tested soil.

Parameter	Value		
	Min	max	average
Depth, m	10.5	15.0	-
Soil temperature (T), °C	-0.3	-0.11	-0.20 (8)*
Freezing temperature, °C	-0.15	-0.06	-0.11 (8)
Particle density (ρ_s), g/cm ³	2.60	2.69	2.66 (10)
Density (ρ), g/cm ³	1.98	2.17	2.07 (10)
Dry density (ρ_d), g/cm ³	1.60	1.89	1.75 (10)
Porosity (n), %	29	40	34 (9)
Void ratio (e)	0.42	0.67	0.52 (9)
Water content (W), %	15	24	18 (10)
Liquid limit (W_L), %	20	28	24 (10)
Plastic limit (W_p), %	13	17	15 (10)
Plasticity index (I_p), %	7	11	9 (10)
Liquidity index (I_L)	0.24	0.59	0.39 (10)
Cone resistance (q_c), MPa	4.22	13.52	7.31 (10)
Long-term compression strength (σ_c) MPa	0.08	1.89	0.91 (10)

* (8) – number of tests.

Based on these findings, engineering measures were taken to minimize the heat flow from the building to the ground, including thermal insulation of the basement. A cooling system comprising two-phase thermosyphons was installed to a depth 10 m to cut down any residual heat flow. The geodetic monitoring of the structure since has shown that the differential settlement ceased and the structure has been stable since the cooling system was put into operation.

2.3 Kruzenshtern gas field

Twelve TCPTU tests were performed in the period January-February 2021 on the Sharapov Shar gulf of the Kara Sea (Figure 1, site #7). Ten of the tests reached the designed penetration depth in the range 44 m to 54 m. Early refusal of two other tests were at depths 27 m and 35 m.

The depth of water in the gulf varies between 1 and 4 m. It was unknown if the permafrost would be continuous or discontinuous at the site, and the field investigation was to characterize the ground conditions and presence of permafrost. Only one test encountered permafrost from 9 m depth with a temperature between -0.35 and -1.58°C (Figure 4).

Several peaks of high values in cone resistance and low values in sleeve friction were observed. They were not as clear as the ones at the Novy Urengoy site. However, they were interpreted as ice lenses and some of them are indicated on Figure 4.

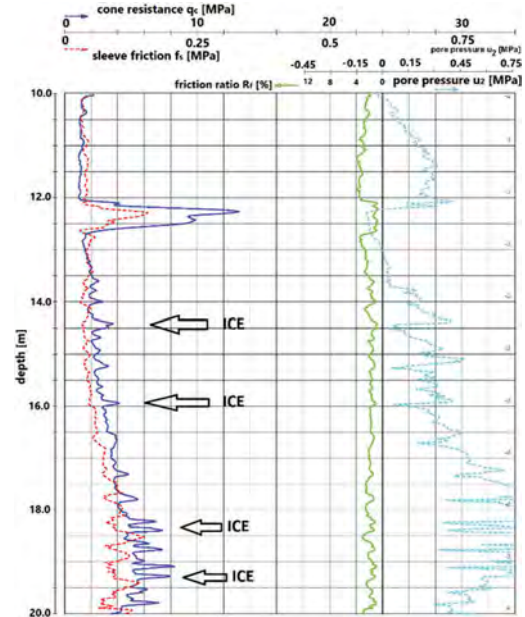


Figure 4. CPT profile in frozen soil at Sharapov Shar, Yamal peninsula.

To confirm the presence of permafrost, direct push sampling was applied close to the CPT test

location. The sampler was a regular RANGER with an inner diameter 45 mm. The collected samples confirmed the presence of frozen soil (Figure 5). The cryogenic structure is massive with rare ice layers.



Figure 5. Frozen soil samples with ice lenses collected by direct push sampler mounted on a CPT press at Sharapov Shar.

2.4 Dikson area, Kara sea

TCPTU tests were performed in the summer 2021 from a jackup platform nearshore in the area of Dikson, Kara Sea (Figure 1, site #8). Permafrost was not detected although in several locations the clay soil was found to have a temperature in the range 0 to 1°C. The clay was not frozen because of the salinity of the pore water. Conventionally, the measurement of ground temperature nearshore is problematic. To use conventional thermistors, these must be installed in a dry borehole and then monitored with time. In comparison, the TCPTU test is not complex and has a relatively low cost and required time for testing. In addition to the temperature data, a TCPTU test provides valuable data on the variability of temperature and mechanical properties with depth.

2.5 Norilsk river, Talnakh bridge

Cone penetration tests with temperature measurements (TCPTU) were performed on the right bank of the Norilsk river, located above the Arctic circle, 15 km from Talnakh city (Figure 1, site #9). The site is located in a cold region characterized by continuous permafrost, with an average annual air temperature in the Norilsk area of -9.6°C. However, the testing revealed a talik at the site formed due to the thermal impact of the Norilsk river.

The TCPTU tests detected ice rich permafrost at the site over a depth range 10 m to 30 m (Figure 6).

The ice rich permafrost was confirmed by geotechnical borehole drilling. The volumetric ice content (I_{tot}) was measured in soil laboratory. The volumetric ice content is the ratio of the volume of ice in a sample to the volume of the whole sample, expressed as a fraction (Everdingen, 2005).

The measured temperature of the ice-rich permafrost varied between -0.1 and -0.6 °C. The top layer of permafrost (10 m to 18 m) comprised clay with organic matter, a stratified cryostructure with high ice content $0.40 < I_{tot} < 0.60$. When thawed, the water content was $W_{tot}=110\%$ and density $\rho=1.36 \text{ g/cm}^3$. The layer below (18m to 30 m) comprised clay with organic matter, a stratified cryostructure and high ice content $0.60 < I_{tot} < 0.90$ (Figure 7). When thawed, the water content was $W_{tot}=263\%$ and density $\rho=1.12 \text{ g/cm}^3$.

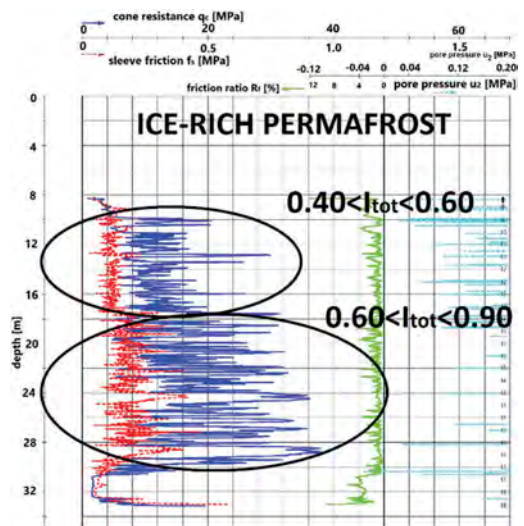


Figure 6. CPT profile in ice-rich permafrost near Norilsk.



Figure 7. Ice-rich permafrost samples collected near Norilsk.

3 STRESS RELAXATION TEST

3.1 Rheological behavior

Rheological behavior is inherent for frozen soils. The degree of rheological behavior depends on the physical properties of the frozen soil (ice content, water content, cryogenic structure, etc.). Rheological behavior is characterized by two interrelated parameters: creep and long-term strength (Vyalov, 1986). Long-term soil strength corresponds to a stress level below which no failure takes place within a practically observable period of load application. A stress in excess of the long-term strength results in failure after a certain time. In this paper we consider “practically observable period of load application” as 100 years. If the time period is different, for instance, 50 years, the term is described as the “long-term strength for 50 years”.

There are two approaches to evaluate long-term strength (Figure 8). The most common is to measure deformation under an applied constant load to describe creep, i.e. deformation change with time. The second approach measures the stress caused by a constant applied deformation to describe stress relaxation, i.e. stress change with time. The second approach is considered in this paper.

Relaxation	Creep
Stress vs time	Deformation vs time
Constant deformation	Constant stress
Relaxation period << Period of after-effect	

Figure 8. Correlation between Creep and Relaxation in the Rheological testings.

Stress relaxation is the decrease of stress with time in response to constant deformation applied to the soil. Relaxation of stress results from a redistribution of elastic and plastic deformation. All physical bodies possess both elastic and viscous properties. However, the material behavior depends on the correlation between the period of load application (i.e. the observation period) and the relaxation period. If the observation period is shorter than the

relaxation period, a body behaves as a Hookean solid. In the alternative case, it behaves like a Newtonian fluid.

The Relaxation period varies significantly for different materials. For instance, limestone 10^{11} sec (thousands of years), glass 10^{10} sec (hundreds of years), ice 10^2 sec (hundreds of seconds), water 10^{-11} sec. In the case of water, for instance, when acted on by a force lasting less than 10^{-11} sec it behaves elastically. Rocks experience load over periods of geological time and may develop viscous flow, which can be observed in folding. Ice behaves like an elastic body, failing in its brittle form if struck (or loaded) rapidly, a force applied for less than 10^2 sec (Vyalov, 1986). A long-term load causes ice to flow as a viscous material, as occurs in glaciers. Similar behavior, i.e. brittle failure under a rapid load application and viscous flow due to a long-term load, can be observed in frozen soils.

It is important that the relaxation period does not equal the period of after-effect. The process of relaxation occurs much faster than the process of creep, i.e. relaxation period significantly shorter than period of after-effect, which differs by several orders (10^n). This fact provides a key advantage for the second approach to evaluate the long-term strength which is based on stress relaxation measurements versus the first approach based on creep measurements.

3.2 Stress relaxation test procedure (SRT)

Relaxation test approach for soils was first proposed by Vyalov in 1986. It was called an “accelerated method of testing soils for long-term strength, using a dynamometric apparatus”. The method description said “if an initial stress is given which is close to the hypothetically instantaneous strength (as determined in advance), the finite value of stress will approach the ultimate long-term strength”. The stress should be measured in time.

The stress relaxation curve should then be processed by a fitting method to determine the empirical coefficients for the following equation:

$$\sigma_c = \frac{\beta}{\ln\left(\frac{t_p+1}{T}\right)} \quad (1)$$

where σ_c = long-term soil strength; t_p = measured time; and β , T are empirical coefficients.

Once the empirical coefficients are determined the long-term strength for a given period of time, for instance 100 years, may be calculated.

The proposed laboratory method was not practically useful at the time due to the low quality of measurement equipment and impossibility to determine the instantaneous strength in advance. Because of these limitations, a pure relaxation test on frozen soils is not common practice.

However, the accelerated method approach can be applied for the conditions when performing in-situ a CPT temperature dissipation test (or pore pressure dissipation test). The only requirement is that the dissipation is performed with the rods clamped (to ensure not movement). In such a case, the deformation is kept constant and the stress relaxation can be measured by the cone (q_c) and sleeve friction (f_s) sensors.

The Stress Relaxation Test (SRT) is described in detail by Sokolov (2020). A key step in the processing was to apply the fitting curve method not for the entire curve, but for the curve starting at some point. This is the point that separates two parts of the curve: the first part corresponds to the relaxation-creep stage while the second part to the relaxation stage. Once this separating point is determined it is possible to back calculate the empirical coefficients β and T for equation (1) and thereby calculate the long-term strength in compression and shear.

3.3 Results

SRT results from site #5 (Figure 1) were verified by comparing with the results of a static pile load test (Volkov, 2019, Sokolov, 2020). The common practice calculates the pile unit end bearing, q_p , from the calculated equivalent average cone resistance, q_{ca} , multiplied by an end bearing coefficient, k_c (Robertson, 2014). This approach did not work well for frozen soils because ice contributes significantly to the cone penetration resistance, but little to the long-term soil strength. Thus in case of ice rich permafrost, the end bearing coefficient, k_c , may be very low compared to common values for non-frozen soils. For instance, based on the numbers provided in Table 2, k_c (which is correlated to the relation between σ_c/q_c), varies from 0.017 to 0.086 and is quite low compared to k_c for non-frozen soils 0.2 to 0.5 (Robertson, 2014).

Table 2. CPT measured and SRT evaluated results.

Depth, m	T, °C	q_c		f_s	
		MPa	MPa	kPa	kPa
17.4	-0.41	8.96	-	153	67
20.6	-0.53	15.34	0.48	115	51
23.3	-0.49	13.65	0.48	209	23
27.6	-0.21	22.06	0.43	146	15
31.7	-0.09	1.28	0.42	75	15
32.0	+0.09	1.12	-	48	-
14.8	-0.27	15.28	0.48	114	29
17.7	-0.30	7.08	0.60	187	-
20.6	-0.21	18.27	0.49	255	16
23.5	-0.15	27.95	0.73	231	12
26.4	-0.11	31.92	0.55	294	7
30.0	-0.10	1.68	-	70	39
30.7	+0.13	2.05	-	60	-

4 CONCLUSIONS

Practical application of CPT in frozen ground has been illustrated for nine different sites with various degrees of permafrost. The CPT is able to penetrate frozen soils, including frozen sands, ice-rich soils and ice lenses. This application of CPT testing could be significantly enlarged for the current geotechnical activities in the Arctic.

Cone penetration testing provides a lot of data which can be obtained in one push performed within one working day. Perhaps most significant is that a CPT used with a temperature sensor is capable to detect frozen soils by measuring the soil temperature directly. The pore water pressure sensor provides very useful complementary data. For reference, this test has been called by the acronym TCPTU.

In addition, by using a Stress Relaxation Test (SRT) it is possible to estimate the long-term soil strength in both compression (σ_c) and shear (σ_s). The long-term strength results on one of the sites were confirmed by comparison with a static pile load test. The results on σ_c and σ_s derived for other sites also show consistency with the recommended values for pile unit end bearing and pile unit side friction.

Ice content in frozen soil plays a major role and influences strongly key parameters such as long-term strength. TCPTU testing shows great applicability for ice-rich frozen soils both to detect ice and evaluate long-term soil strength in compression and shear. Push sampling methods using the CPT equipment can recover samples for laboratory testing.

REFERENCES

- Everdingen, R.O. 2005. Multi-Language Glossary of Permafrost and Related Ground-Ice Terms: In Chinese, English, French, German, Icelandic, Italian, Norwegian, Polish, Romanian, Russian, Spanish, and Swedish, The Arctic Institute of North America, 1998 (revised 2005) – 159 pages.
- Robertson, P.K., and Cabal, K.L. 2014. Guide to Cone Penetration Testing for Geotechnical Engineering, 6th Edition, Signal Hill, California: Gregg Drilling & Testing, Inc.
- Sokolov I. 2020. Determination method for strength properties of frozen soils by cone penetration testing. PhD Thesis – Moscow State University, Moscow, 2020 – 149 pages (in Russian).
- Volkov, N., Sokolov, I. & Jewell, R. 2018. CPT Testing in Permafrost. Proceedings 4th International Symposium on Cone Penetration Testing/N. Volkov [and etc.] // – CPT'18. – Netherlands, Delft – 2018. 1258–1268.
- Volkov N.G., Sokolov I.S., 2019. Estimation of pile bearing capacity in permafrost based on stress relaxation measured by cone penetration testing. Geotechnics, Vol. XI, No. 1, pp. 68–78, <http://dx.doi.org/10.25296/2221-5514-2019-11-1-68-78>.
- Vyalov, S.S. 1986. Rheological Fundamentals of Soil Mechanics, Volume 36, 1st Edition. Elsevier. ISBN: 0444600566. 564.

A site-specific relationship between CPT data and fines content for fine grained soil in the context of liquefaction analyses

C. Vrettos

Technical University of Kaiserslautern, Germany

ABSTRACT: Fines content is a crucial factor affecting the liquefaction resistance of soils within the frame of the CPT-based cyclic stress ratio approach. In contrast to highly susceptible sands and silty sands, on one hand, and non-liquefiable clays, on the other hand, the proper identification and classification of silts is still an unresolved issue. Several empirical equations have been proposed to correlate fines content with common CPT soil behavior indices. In the frame of a site-specific study comprising pairs of CPT soundings and adjacent exploration borings, gradation characteristics of retrieved soil samples are combined with the respective values of common soil behavior indices inferred from the CPT logs to examine available predictive equations and calibrate a new hyperbolic equation. The investigation confirms the large scatter in the data and the inherent difficulty in establishing a robust correlation.

1 INTRODUCTION

Over the last years, CPT has advanced to the preferred method to assess liquefaction susceptibility in code-based design using the cyclic stress ratio approach. This holds in particular for countries outside the USA and Japan, where the Standard Penetration Test (SPT) does not constitute the primary means of site investigation via soundings. Several codes of practice include CPT-based methods as an equivalent counterpart to SPT-based methods. An example is the current draft of the new edition of the Eurocode EN 1998-5, CEN (2021), that adopted the methodology by Idriss & Boulanger (2008) and its CPT-based update by Boulanger & Idriss (2016).

In this semi-empirical method, as established in the '80s by Seed & Idriss (1983), soils other than sands were characterized with regard to liquefaction susceptibility by the fines content FC measured in the laboratory. FC is defined according to ASTM D 653-20 as the portion of soil particles finer than 0.075 mm (sieve no. 200). In EN ISO 17892-4:2016 the limit is set at the 0.063 mm sieve. An adjustment for the fines content is made by increasing the measured tip cone resistance by an increment dependent on FC .

Alternatives to consider the soil type in the cyclic stress ratio method were proposed by Robertson & Wride (1998) via a soil behavior index derived from CPT data, and by Moss et al. (2006) based on a combination of CPT tip and sleeve resistance by skipping the intermediate step. Despite its deficiencies, the fines content concept presently dominates practice and code-based design.

While in the early years the focus was placed on FC values up to 35%, evidence from seismic events and research in the last two decades revealed that fine soils may also show a degradation under high amplitude cyclic loading. It is now distinguished between two types of ultimate limit states: i) sand-like (cyclic liquefaction), and ii) clay like (cyclic softening) behavior, as elucidated among others in the recent review report by the committee of the National Academies of Sciences, Engineering, and Medicine (2016). In this context, fine-grained soils may be classified based on some measure of their consistency in terms of the water content and the Atterberg limits. A plasticity index $I_p = 15\%$ is considered as a conservative threshold beyond which the occurrence of liquefaction can be excluded. Such a classification requires collection of several samples, laboratory testing and reliable values of the in-situ water content. Even then, this information will be available only for specific points along the soil depth profile.

An evaluation based on recorded data from CPT soundings linked with a reliable general equation for FC constitutes an attractive, widely used alternative. Candidates for the independent variable in such a relationship are the well-established soil behavior type indices, as summarized in the next section. Agaiby & Mayne (2020) compiled several of these equations. The scatter in the data is considerable, in particular for silts, which constitute the crucial soil category in liquefaction hazard assessment.

The necessity to derive a site-specific predictive equation for FC in the frame of a critical project motivated the present study. The field investigations

performed, the main results of the accompanying laboratory testing program, the essential analysis steps, and the conclusions drawn are described next. Similar studies with a much larger spatial extent have been conducted for soils in Canterbury, New Zealand, among others by Lees et al. (2015).

2 EQUATIONS FOR THE FINES CONTENT

The vast majority of the suggested equations relate the fines content FC to the soil behavior index I_c proposed by Robertson & Wride (1998) to capture six of the designated zones of the SBTn-chart covering the basic soil types encountered in practice, cf. Table 1. Its current form as proposed by Robertson (2009) is:

$$I_c = \left[(3.47 - \log Q_m)^2 + (\log F_r + 1.22)^2 \right]^{0.5} \quad (1)$$

$$n = 0.381 \cdot I_c + 0.05 \cdot \left(\frac{\sigma'_{v0}}{p_a} \right) - 0.15 \leq 1.0 \quad (2)$$

where

$$F_r = \frac{f_s}{q_t - \sigma_{v0}} \cdot 100\% \quad (3)$$

$$Q_m = \left(\frac{q_t - \sigma_{v0}}{p_a} \right) \cdot \left(\frac{p_a}{\sigma'_{v0}} \right)^n \quad (4)$$

where F_r = normalized friction ratio; f_s = sleeve friction; Q_m = normalized cone resistance; q_t = tip resistance corrected for the effects of pore water pressures; n = stress normalization exponent; σ_{v0} = in-situ vertical stress; σ'_{v0} = in-situ vertical effective stress; p_a = atmospheric pressure. Except for very soft fine grained soil, it may be assumed that q_t equals the uncorrected cone resistance q_c (Robertson, 2010).

Table 1. Soil Behavior Type based on I_c .

Zone	Soil Behavior Type	I_c
2	Organic Soils – Clays	>3.6
3	Clay – silt clay to clay	2.95-3.6
4	Silt mixtures – clayey silt to silt clay	2.60-2.95
5	Sand mixtures – silty sand to sandy silt	2.05-2.60
6	Sands – clean sand to silty sand	1.31-2.05
7	Gravelly sand to dense sand	<1.31

A threshold $I_c = 2.6$ is often used to distinguish between clay-like and sand-like soils that are susceptible to liquefaction (Boulanger & Idriss, 2014).

An alternative for the soil behavior index is the modified index I_B introduced by Schneider et al. (2012) and subsequently adopted by Robertson (2016) in his charts to characterize soils:

$$I_B = 100 \cdot \frac{Q_m + 10}{70 + Q_m \cdot F_r} \quad (5)$$

Various equations relating I_c to FC have been suggested in the last decades. Some of them are considered herein in detail. One of the first has been proposed by Robertson & Wride (1998):

$$\begin{aligned} 1.64 < I_c < 2.36 \quad \text{and} \quad R_f < 0.5\% : FC = 5\% \\ 1.26 < I_c < 3.5 : FC = 1.75 \cdot (I_c)^{3.25} - 3.7 \end{aligned} \quad (6)$$

with the friction ratio

$$R_f = \frac{f_s}{q_t} \cdot 100\% \quad (7)$$

Boulanger & Idriss (2016) suggested:

$$FC = 80 \cdot (I_c + C_{FC}) - 137 \quad 0\% < FC < 100\% \quad (8)$$

where C_{FC} is a fitting parameter with a default value equal to 0 and a standard deviation ± 0.29 .

The above relationships have been examined in the frame of the extensive regional liquefaction susceptibility study on Christchurch soils by Maurer et al. (2019). Assuming a linear relationship in analogy to equation (8), regression statistics yielded for the mean estimate:

$$FC = 80.645 \cdot I_c - 128.5967 \quad (9)$$

with approximately 68% of the samples having FC within $\pm 16.56\%$ of the mean prediction. For these region-specific conditions and $FC > 10\%$, equation (6) by Robertson & Wride (1998) yields much lower values, i.e. it is too conservative. The many decimal digits in the constants of equation (9) suggest an accuracy that is not attainable.

A large database from different studies has been evaluated by Agaiby & Mayne (2020). The derived relationship reads:

$$FC = 1.3 \cdot (I_c)^{3.77} \quad (10)$$

An equation has also been obtained in terms of the modified index I_B :

$$FC = (293/I_B)^{1.65} \quad (11)$$

The observed large scatter in the data in all studies lies in the nature of I_c , which was introduced to characterize soils and not to be associated with the susceptibility to liquefaction. A linear or even power law relationship for FC vs. I_c is too simplistic if one considers the complexity of the physics of the problem, the variability of the soil composition even over short distances, the sensitivity of the CPT response as reflected in the strong fluctuation of the recorded data, as well as the uncertainty in capturing the effects of soil plasticity and grain size distribution on the CPT response.

3 SITE-SPECIFIC CORRELATIONS

The investigated site is located in Germany and is characterized by a variable stratigraphy. The top layer with a thickness of approximately 5 m consists of fillings of sand, silt and partially gravel. This is followed by alternating layers of silt, silty sand and gravel, as well as sand-silt mixtures. These soils are underlain by glacial till deposits: debris loam composed of silts and silty sands, and marly till (clays). Below this is sand with different fine-grain and gravel proportions. The encountered sediments are highly variable and hence particularly suited for checking the accuracy of the various predictive equations relating FC to I_c .

Field investigations comprised exploration borings at several locations and CPT soundings adjacent to the boreholes. Disturbed and undisturbed samples have been extracted for further testing.

The laboratory investigations included tests for particle size distribution, Atterberg limits, consistency, compressibility and shear strength.

Soil classification was conducted according to EN ISO 14688-2 in conjunction with DIN 18196. It is very similar to the USCS except for some differences in coding and in including an additional class of intermediate-plasticity for silts and clays.

The primary purpose of the investigation, and accordingly the selection of the sampling depths, was foundation design. Detailed liquefaction assessment was conducted at a later stage, since the region is characterized by low to medium seismicity.

A total of 14 CPT records were evaluated. The tests reached a depth of 20 m. Essential for the accuracy of the prediction is an appropriate geodetic survey in order to assign each sample from the boring to the correct depth along the CPT log. At each CPT location, verification checks have been performed at positions where an unambiguous identification of the soil type was possible. Spikes in the CPT records were carefully inspected, and when an abrupt change in soil type was not justified, an averaging procedure over a few centimeters centered at the location of the sample was applied. As the investigation was not planned to

validate back-analysis procedures for the CPT, the information on the sampling depth of the undisturbed samples tested in the laboratory was not precise enough to allow an exact mapping to the CPT. The accuracy was improved by incorporating the anticipated soil behavior type SBT/SBTn in the selection of the appropriate depth range for the calculation of the FC vs. I_c relationship. Hence, the identification of fines content is more accurate for the undisturbed samples.

Due to the nature of the glacial till sediments, grading for some of the samples spans over silt, sand and gravel with a large uniformity coefficient. In this case and for liquefaction hazard assessment, the adverse influence of low fines content is counterbalanced by the favorable effects of the gravel fraction that provides ample drainage. The SBTn charts presently do not include this soil type, and an interpretation solely according to I_c may be misleading. Moreover, the fill is also characterized by an inhomogeneous composition.

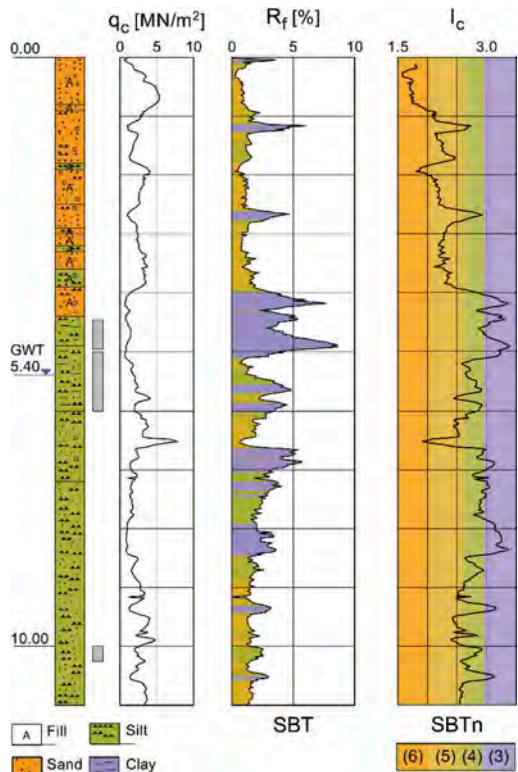


Figure 1. Results at location #13: Borehole log, position and length of extracted soil samples, CPT results, and derived I_c with colors and numbers in brackets indicating the various soil types in the SBT and SBTn charts.

Typical results and the accompanying interpretation of the field investigations at one of the locations are displayed in Figure 1. The delineation, the

Table 2. Overview of soil properties and derived soil behavior indices.

Loc.		Depth	Cl/Si/Sa/Gr	FC	I_c	I_B		w_L	I_P	
		[m]	[%]	[%]	Mean	CV	Mean	CV	[%]	
1	U	11.0 - 11.25	30.1/66.9/3.1/0.0	97.0	2.87	1.7	22.5	4.3	47.5	28.3
		18.8 - 20.0	0.0/0.7/98.7/0.6	0.7	1.79	2.9	77.0	7.9		
2	U	12.5 - 12.75	25.0/71.5/3.5/0.0	96.5	2.87	1.5	22.4	4.7	59.4	35.1
		3.5 - 4.0	6.8/17.8/66.3/9.1	24.6	2.32	7.2	39.3	30.2	17.7	5.4
4	U	12.0 - 12.25	17.3/63.0/18.5/1.1	80.3	3.00	1.4	20.6	3.2	36.2	16.9
		2.6 - 3.0	15.4/76.2/8.4/0.0	91.6	2.77	4.4	23.8	13.7	32.7	13.5
5	U	4.3 - 5.1	0.0/1.6/93.4/5.0	1.6	1.42	5.3	118.1	10.8		
		14.0 - 14.25	43.5/56.1/0.4/0.0	99.6	2.91	1.9	21.9	6.2	57.4	36.4
6	U	11.0 - 11.25	26.0/72.9/1.2/0.0	98.9	2.94	1.3	21.2	3.6	48.9	27.6
		3.0 - 3.25	21.2/44.2/30.2/4.3	65.4	2.69	2.1	24.6	13.2	39.8	23.3
7	U	9.5 - 9.75	18.7/72.7/8.6/0.0	91.4	2.66	6.6	26.4	20.4	36.5	19.6
		4.8 - 5.0	0.0/2.0/87.2/10.9	2.0	1.85	1.2	70.3	2.5		
8	U	10.0 - 10.25	5.2/40.9/53.9/0.0	46.1	2.32	7.7	39.4	23.4		
		13.0 - 13.25	16.2/62.9/20.9/0.0	79.1	2.92	1.1	21.2	3.6	47.7	26.5
9	U	18.0 - 19.0	0.0/4.9/94.8/0.3	4.9	1.82	5.0	77.0	12.8		
		10.0 - 10.25	11.0/51.2/37.8/0.0	62.2	2.83	4.0	24.0	9.8	24.8	9.2
10	U	3.0 - 3.25	11.7/62.6/23.6/2.1	74.3	2.82	5.9	24.0	20.7	29.5	14.5
		4.5 - 4.8	16.9/48.4/32.8/1.9	65.3	2.97	1.3	18.8	6.4		
11	U	5.0 - 5.25	22.6/66.5/10.6/0.3	89.1	3.12	2.0	18.8	5.9	67.5	39.0
		4.4 - 5.0	13.5/73.7/12.8/0.0	87.2	3.17	5.3	17.0	15.5	62.0	30.1
12	U	8.0 - 8.25	17.6/74.2/8.1/0.0	91.8	2.93	2.9	20.8	8.9	37.1	19.2
		4.4 - 4.9	13.3/61.9/24.1/0.8	75.2	3.05	5.0	16.6	16.0	56.0	23.0
13	U	5.0 - 6.0	9.8/73.7/16.5/0.0	83.5	2.79	6.8	23.0	19.0	25.7	8.3
		10.0 - 10.25	5.9/71.7/22.4/0.0	77.6	2.78	3.9	24.2	11.2	28.8	7.6
14	U	8.0 - 8.25	8.6/80.1/11.4/0.0	88.7	2.89	2.9	22.4	8.3	28.9	9.0

coloring, and the material symbols in the borehole logs correspond to the field description of the soil. The CPT log is given in terms of tip cone resistance q_c and friction ratio R_f . The soil type as inferred from the non-normalized SBT-chart by Robertson (2010) is indicated by different colors in the column for R_f . The last column shows the I_c profile as calculated from equations (1) to (4), and also the SBTn soil types in color. SBT- classification is the standard output of the software used, and is considered as a good approximation of the more accurate, normalized SBTn-chart for vertical effective overburden stresses up to 150 kPa (Robertson, 2010; Papamichael & Vrettos, 2018).

Data for all samples are given in Table 2 and include: sounding number (location); sampling depth; indication (U) for an undisturbed sample; material composition in terms of clay (Cl), silt (Si), sand (Sa) and gravel (Gr) content from the laboratory tests; mean value and coefficient of variation (CV) of the soil behavior index I_c and the modified index I_B (CV is the ratio of the standard deviation to the mean); liquid limit w_L and plasticity index I_P . The ground water table was encountered in depths between 5 and 7 m. For the fine-grained soil, the silt

fraction varies between 41 and 80%, the clay fraction between 5 and 43.5%.

In order to establish a relationship between I_c and FC , a single representative value I_c over the nominal depth range of the distinct disturbed/undisturbed samples extracted from the borings is required. The fluctuation of I_c over the sampling depth is considerable, and the following method is used for an automated evaluation. Samples that show for I_c over the respective depth range a coefficient of variation larger than a threshold are dismissed. Comparison of the prediction with the actual soil gradation measured in the laboratory yielded herein a threshold of 8.0. In particular, undisturbed samples extracted from the fill did not meet this criterion. If more data are available, the threshold may be set even lower.

The inherent limitations of the attainable accuracy become evident if one looks at the results for the undisturbed sample taken from the depth of 10.0 to 10.25 m at location #13, cf. Figure 1. While the identification of the soil type is correct, i.e. zone 4 in the SBTn chart matches well the laboratory gradation with 71.7% silt, the derived value I_c ranges between 2.57 and 2.92, which constitutes a significant variation if a reliable prediction of FC is sought.

The plasticity chart of EN ISO 14688-2 with all samples of fine-grained soil is presented in Figure 2. It can be seen that almost all samples classified as silts according to the grading are actually clays with respect to their soil mechanical behavior, as they plot above the A-line in the plasticity chart.

Since both FC and I_p are independent of the actual soil state in terms of consistency, it is of interest to plot the FC versus the plasticity index I_p , as shown in Figure 3. For $FC > 60\%$ there is no correlation between FC and I_p , at least for the soils encountered at the particular site.

Figure 4 Depicts the core of the investigation, i.e. data points of FC versus I_c for the samples fulfilling the coefficient of variation criterion. Figure 5 shows the corresponding data set FC versus I_B . Figure 4 includes the prediction by equations (6), (8) and (10), and Figure 5 that by equation (11).

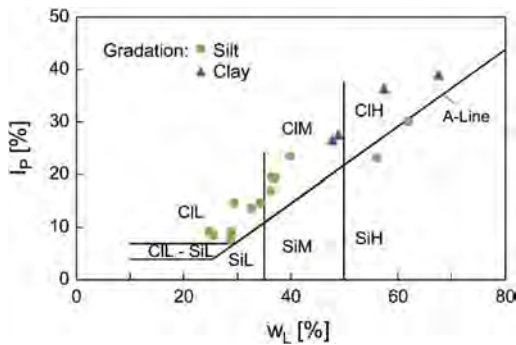


Figure 2. Sampled soil classified in the plasticity chart of EN ISO 14688-2.

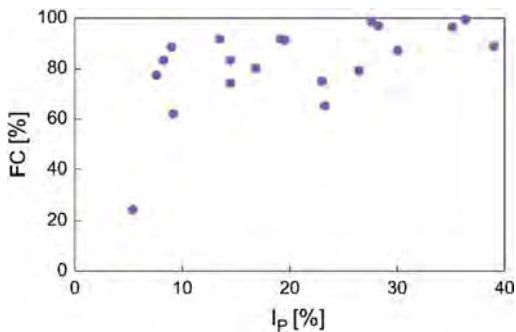


Figure 3. Fines content FC vs. plasticity index I_p .

It can be deduced from Figure 4 that for high values of I_c , i.e. for clay-like behavior, equation (6) predicts consistently lower values than actually measured, while equations (8) and (10) are closer to the laboratory results. For low I_c values (sand-like

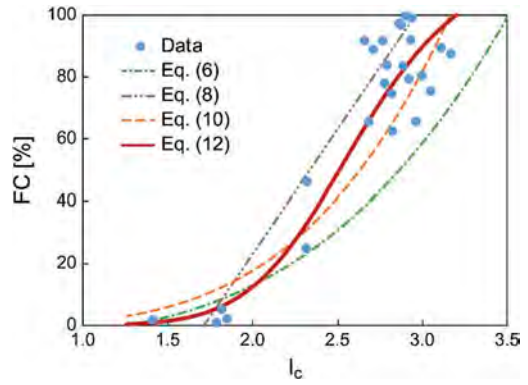


Figure 4. Fines content FC vs. soil behavior index I_c : data set, and comparison with the various predictive equations.

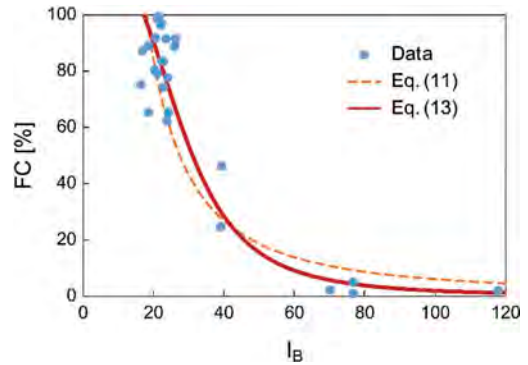


Figure 5. Fines content FC vs. modified index I_B : data set, and comparison with the predictive equations.

behavior) though, equation (6) matches the data well. As for the I_B -based relationship in Figure 5, equation (11) is a good approximation.

With regard to the I_c -based estimation of FC , it turns out that none of the three forecast equations considered is suitable for the particular site. Equation (6) is applicable for low I_c and FC values but too conservative for higher FC values. Equation (10), on the other hand, yields higher values for low FC sands (slightly non-conservative), and realistic predictions for medium and high FC values. In order to increase accuracy and avoid the unboundedness of the power-law approximations, the following hyperbolic equation that exhibits a more versatile, “S-like” form is proposed:

$$FC = a \cdot \left(1 - \frac{1}{1 + (I_c/b)^c} \right) \quad (12)$$

The engineering approximation of the data set in Figure 4 yields:

$$a = 120 ; b = 2.62 ; c = 8$$

Similarly, the following counterpart is derived for the data in Figure 5:

$$FC = \frac{d}{1 + (I_B/f)^g} \quad (13)$$

with

$$d = 120 ; f = 28 ; g = 3.3$$

Equations (12) and (13) focus on silts, which constitute the most critical soil type with the strongest variability in the composition. An accurate prediction is necessary in order to avoid i) the risk of non-conservative design due to an overestimate of fines content, and ii) non-economical design due to a false alert by too low FC estimates. The identification of liquefaction susceptible sands and silty sands of low fines content and low I_c , on the one hand, and of non-liquefiable clayey silts and clays of high I_c , on the other hand, is in general unambiguous.

4 CONCLUSIONS

CPT soundings are nowadays an integral part of modern, high-quality field investigations in earthquake-prone areas. The present study exemplarily shows the application of a state-of-the-art procedure to estimate the fines content of fine soils for subsequent use in liquefaction hazard analyses of a particular site with a strong variability in the sub-soil composition. For this type of problem, silts still constitute the type of soil with the most uncertain behavior, and gradation is surely not the most appropriate characteristic to capture it. Targeted field investigations on silts, complemented by laboratory cyclic loading tests, are urgently needed to clarify the related issues.

REFERENCES

Agaiby, S.S. & Mayne, P.W. 2020. Indirect estimation of fines content using the Modified CPT Material Index. In J.P. Hambleton, R. Makhnenko & A.S. Budge (eds) *Geo-Congress 2020: Modeling, Geomaterials, and Site Characterization (GSP 317)*: 569–582. Reston, VA: ASCE.

Boulanger, R.W. & Idriss, I.M. 2016. CPT-based liquefaction triggering procedure. *Journal of Geotechnical and Geoenvironmental Engineering* 142(2): 04015065. doi:10.1061/(ASCE)GT.1943-5606.0001388

Bray, J.D. & Sancio, R.B. 2006. Assessment of the liquefaction susceptibility of fine grained soils. *Journal of Geotechnical and Geoenvironmental Engineering* 132

(9): 1165–1177. doi:10.1061/(ASCE)1090-0241(2006)132:9(1165)

CEN - European Committee for Standardization. 2021. prEN 1998-5:2021(E). Eurocode 8 - Design of structures for earthquake resistance – Part 5: Geotechnical aspects. foundations. retaining and underground structures, Draft. September 2021.

CEN - European Committee for Standardization. 2018. EN ISO 14688–2:2018 Geotechnical investigation and testing – Identification and classification of soil – Part 2: Principles for a classification.

Idriss, I.M. & Boulanger, R.W. 2008. *Soil Liquefaction During Earthquakes*. Monograph MNO-12. Oakland: Earthquake Engineering Research Institute.

Lees, J., van Ballegooy, S. & Wentz, F.J. 2015. Liquefaction susceptibility and fines content correlations of the Christchurch soils. In *Proceedings of the 6th International Conference on Earthquake Geotechnical Engineering*, Christchurch, Paper no. 491.

Maurer, B.W., Green, R.A., van Ballegooy, S. & Wotherspoon, L. 2019. Development of region-specific soil behavior type index correlations for evaluating liquefaction hazard in Christchurch, New Zealand. *Soil Dynamics and Earthquake Engineering* 117: 96–105. doi:10.1016/j.soildyn.2018.04.059

Moss, R.E.S., Seed, R.B., Kayen, R.E., Stewart, J.P., Der Kiureghian, A. & Cetin, K.O. 2006. CPT-based probabilistic and deterministic assessment of in situ seismic soil liquefaction potential. *Journal of Geotechnical and Geoenvironmental Engineering* 132(8): 1032–1051. doi:10.1061/(ASCE)1090-0241(2006)132:8(1032).

National Academies of Sciences, Engineering, and Medicine. 2016. *State of the Art and Practice in the Assessment of Earthquake-Induced Soil Liquefaction and Its Consequences*. Washington, DC: The National Academies Press. doi: 1017226/23474.

Papamichael, S. & Vrettos, C. 2018. CPT interpretation and correlations to SPT for near-shore marine Mediterranean soils. In M.A. Hicks, F. Pisanò & J. Peuchen (eds), *Cone Penetration Testing 2018*: 499–504. London: CRC Press.

Robertson, P.K. 2016. Cone penetration test (CPT)-based soil behaviour type (SBT) classification system – an update. *Canadian Geotechnical Journal* 53: 1910–1927. doi:10.1139/cgj-2016-0044.

Robertson, P.K. 2010. Soil behaviour type from the CPT: an update. In P.K. Robertson & P.W. Mayne (eds), *Proc. 2nd International Symposium on Cone Penetration Testing, CPT'10*, Huntington Beach: 575-582.

Robertson, P.K. 2009. Interpretation of cone penetration tests – a unified approach. *Canadian Geotechnical Journal* 46(11): 1337–1355. doi:10.1139/T09-065.

Robertson, P.K. & Wride, C.E. 1998. Evaluating cyclic liquefaction potential using the cone penetration test. *Canadian Geotechnical Journal* 35(1): 151–158. doi:10.1139/t98-017.

Schneider, J.A., Hotstream, J.N., Mayne, P.W. & Randolph, M.F. 2012. Comparing the CPTu Q-F and $Q_{\Delta u_2/\sigma_{vo}}$ soil classification charts. *Géotechnique Letters* 2(4): 209–215. doi:10.1680/geolett.12.00044.

Seed, H.B. & Idriss, I.M. 1983. *Ground Motions and Soil Liquefaction during Earthquakes*. EERI Monograph Series MNO-5. Oakland: Earthquake Engineering Research Institute.

Numerical modelling of cone penetration tests in spatially variable clays

Ze Zhou Wang, Siang Huat Goh & Xiangxiang Zheng

Department of Civil and Environmental Engineering, National University of Singapore, Singapore

ABSTRACT: In soft clays, a cone factor N_{kt} is typically adopted to correlate net cone tip resistance q_t with undrained shear strength S_u . Many existing numerical studies on the estimation of N_{kt} are performed using analyses in homogeneous soil medium. However, soil properties exhibit spatial variability under real field conditions. In this study, the effects of spatial variability on the interpretation of CPT data were investigated using a finite element analysis technique, namely the Press-Replace method (PRM). This method, which can capture installation effects arising from the penetration of a piezocone, was implemented with the soil domain modelled as anisotropic random fields. Using a pre-determined N_{kt} , statistics of S_u were back-calculated using the q_t profiles obtained from different random field realizations. Comparisons of the back-calculated statistics with the true statistics used to generate the random fields revealed that the true statistics may not be fully recovered from the CPT data.

1 INTRODUCTION

In soft clays, the cone penetration test (CPT) is typically adopted to characterize the undrained shear strength through a cone factor N_{kt} as follows:

$$S_u = \frac{q_c - \sigma_{v0}}{N_{kt}} = \frac{q_t}{N_{kt}} \quad (1)$$

where σ_{v0} is the total overburden stress, q_c is the cone tip resistance corrected for cone net area ratio, and q_t is the net cone tip resistance. Although the value of N_{kt} is often obtained using laboratory data and site-specific calibration exercises, extensive analytical and numerical studies on the estimation of cone factor values have also been reported in the literature (Yu 2000; Lu et al. 2004).

Many studies are performed based on analyses that assume homogeneity in soil properties. However, it is well known that the properties of natural soils exhibit random variability in both spatial distributions and intensities under real field conditions (Phoon & Kulhawy 1999). Many studies reported that the performance of geotechnical systems can be significantly affected by the presence of spatial variability (Pan et al. 2018; Zhang et al. 2021).

Furthermore, the large deformation caused by the continuous insertion of a piezocone renders conventional small-strain numerical techniques ineffective, thus adding to the challenges in the numerical analysis of the cone penetration test. Therefore, special procedures, such as the

Arbitrary Lagrangian Eulerian (ALE) (Lu et al. 2004), the Remeshing Interpolation Technique with Small-strain (RITSS) (Zhang et al. 2020) and the Material Point Method (MPM) (Tehrani et al. 2016), have been proposed.

In the literature, numerical simulations of CPT considering both the installation effects and spatial variability have not been widely reported. This paper fused random fields and a simplified numerical procedure, the Press-Replace Method (PRM), for simulating piezocone penetration in spatially variable soils. The PRM is a simplified technique that can be implemented in standard small-strain finite-element programs without the need for additional subroutines. In addition, anisotropic random fields were adopted to realistically express the spatial variability of soil property. With the consideration of both features, the impact of spatial variability on the interpretation of CPT data can be rigorously investigated.

2 METHODOLOGY

The Press-Replace Method (PRM) is a simplified technique to simulate problems associated with continuous penetration of an object into a continuum. The PRM was first used for simulating the load-controlled penetration of a suction anchor in clay (Andersen et al. 2004) and was further used to simulate pile, cone and spudcan penetration (Engin et al. 2015; Tehrani et al. 2016; Wang & Goh 2018).

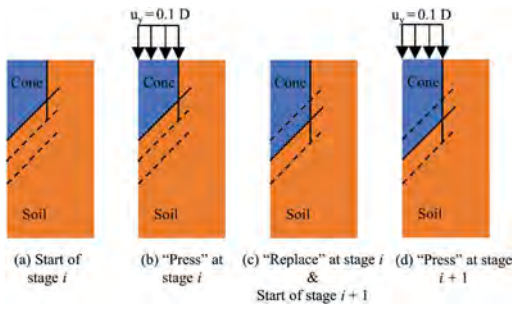


Figure 1. Illustration of the PRM technique for modelling cone penetration test.

As its name suggests, the PRM consists of two modelling phases. Figure 1 illustrates the procedures for modelling cone penetration using the method. Essentially, the entire penetration process is separated into many pairs of press-replace phases. Figure 1a illustrates the model setup at the start of an arbitrary stage i . In the next step (Figure 1b), a displacement boundary condition is prescribed to simulate the penetration. The prescribed displacement, however, corresponds to only a portion of the total penetration depth. As recommended by Engin et al. (2015), the prescribed displacement corresponds to 1/10 of the diameter or width of the penetration object. After the “press” phase, the “replace” action is performed by switching the soil body that was displaced by the piezocone in the preceding “press” phase to the cone material (Figure 1c), which marks the end of stage i . The model setup shown in Figure 1c then forms the initial condition for the next pair of press-replace phase (Figure 1d). These phases are repeated until the desired penetration depth is achieved.

3 MODEL SETUP

The finite-element software Optum G2 was used in this study. In Figure 2, the model consists of a soil domain of 0.4 m in width and 1 m in depth. An axisymmetric piezocone of 36 mm diameter (D) and 60° tip angle was modelled. The penetration started from a pre-embedment depth of 0.03 m, and a -0.0036 m step size (Engin et al. 2015) was adopted.

Interface elements were used to model the interactions between the piezocone and soil. Three types of interfaces were adopted. First, the shaft-soil interface was modelled as a fully smooth contact (Figure 2c) while fully smooth and fully rough contacts were considered for the cone-soil interface (Figure 2b). Interface extensions (Figure 2b) that are 0.0036 m, i.e. $0.1D$, in length (Engin et al. 2015), and having the same properties of the neighboring soil, were used to minimize stress oscillations around sharp corners of the cone. The model was discretized using 6490 15-node triangular elements.

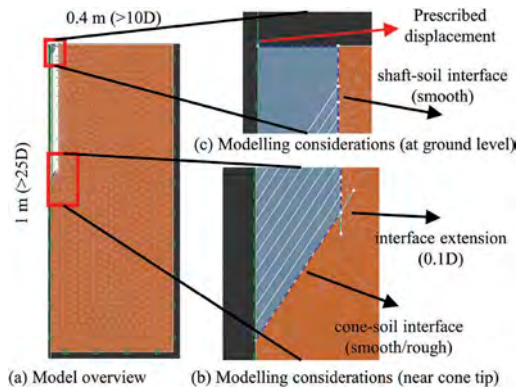


Figure 2. Model setup and relevant modelling details.

Table 1. Key parameter values used in the present study.

Parameter	Value	
	Homogeneous	Heterogeneous
Cone diameter, D	60 mm	60 mm
Cone tip-apex angle, α	60°	60°
Model width, w	0.4 m	0.4 m
Model depth, d	1.0 m	1.0 m
Unit weight, γ_{sat}	18 kN/m ³	18 kN/m ³
Earth pressure coefficient, K_0	1.0	1.0
Poisson's ratio, ν	0.5	0.5
Mean undrained shear strength, S_u	30 kPa	30 kPa
Coefficient of variance, CoV	-	0.3
Horizontal scale of fluctuation, δ_h	-	5.0 m
Vertical scale of fluctuation, δ_v	-	0.5 m
Young's modulus, E	$90S_u$; $300S_u$; $450S_u$; $600S_u$; $900S_u$ kPa	$300S_u$

The soil was modelled as a single-medium material using the Tresca model. Table 1 summarizes the key parameter values used in the present study. An S_u of 30 kPa was adopted in the analyses that assumed a homogeneous soil medium, with the Young's modulus E linearly correlated to S_u . Five separate analyses using five E/S_u correlations were carried out, and the results are compared with published results to validate the PRM method. In the RFEM analyses, a lognormal distribution was used to describe the statistical variability of both S_u and E . The correlation $E = 300S_u$, which is representative of soft clays, was adopted for the RFEM analyses. Other statistics, such as CoV, δ_h and δ_v , adopted in the present study are also representative of natural soft clays (Phoon & Kulhawy 1999).

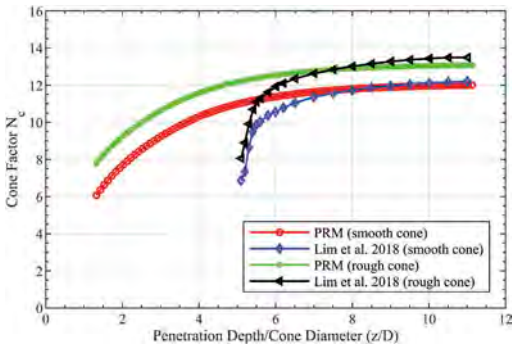


Figure 3. Comparison of cone factor values with Lim et al. (2018) ($I_r = 150$; $K_0 = 1$).

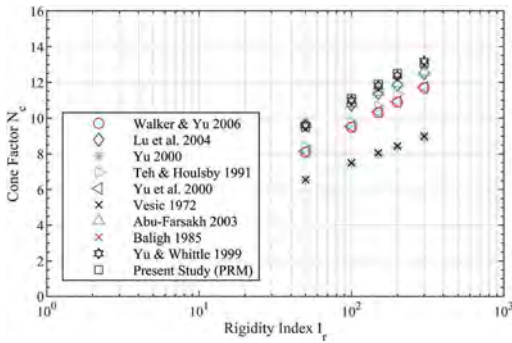


Figure 4. Comparison of cone factor values with other published results (smooth cone-soil contact).

All random fields were generated using the Karhunen-Loève (KL) expansion (Phoon et al. 2002) and a single exponential autocorrelation function. It is not easy to identify the “correct” function (Spry et al. 1988), but the single exponential autocorrelation function is more commonly used (Phoon & Kulhawy 1999). The K-L expansion was performed using 1000 terms to ensure sufficient accuracy.

4 NUMERICAL MODELLING OF CONE PENETRATION

4.1 Analysis with homogeneous soil properties

This section utilizes published results in the literature to validate the use of the PRM method. Figure 3 compares the results of the present analyses with those reported in Lim et al. (2018) who also adopted the PRM technique. All analyses indicate that the cone factor values reached a plateau at approximately $z/D > 6$, even though Lim et al. (2018) started the penetration at the depth of $z/D = 5$. According to Zhang et al. (2020), a deep penetration mechanism becomes prominent beyond this depth; therefore, a $z/D = 6$ was used in the present analyses to differentiate between a shallow and a deep penetration.

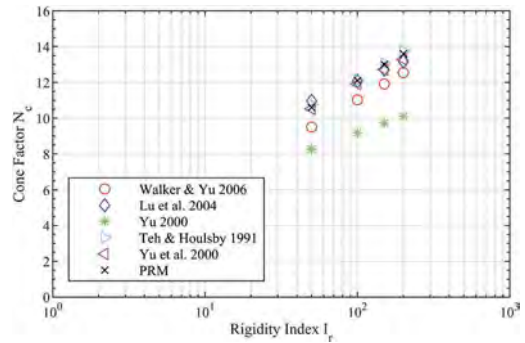


Figure 5. Comparison of cone factor values with other published results (rough cone-soil contact).

Additional analyses, using different values of the rigidity index, $I_r = G/S_u$ (Table 1), were carried out to validate the PRM against other published results. Figure 4 shows the influence of rigidity index on cone factor values for a smooth cone-soil contact. All studies indicate that the cone factors increase approximately linearly with the logarithm of I_r . The discrepancies between different published studies are likely caused by the use of different numerical simulation techniques. Nevertheless, the results obtained using the PRM agree reasonably well with other published results, indicating that the PRM is valid for simulating the large deformation cone penetration process.

Similarly, Figure 5 shows the influence of rigidity index on cone factor values for a rough cone-soil contact. The results obtained using the PRM also agree reasonably well with other published results, which further confirmed the validity of the PRM.

4.2 Random field finite-element analysis (RFEM)

Figure 6a shows an example of a random field for the undrained shear strength. Variations in S_u values were observed mainly in the vertical direction because the vertical scale of fluctuation (δ_v) is much smaller than the horizontal scale of fluctuation (δ_h). Significant fluctuations in the net cone tip resistances with respect to depth, as shown by the solid black line, were observed in Figure 6a. The profile is highly sensitive to the presence of weak and strong soils. For example, at depths of between 0.1 m and 0.2 m, the cone is penetrating through soils whose S_u values are relatively homogeneous, and hence the cone tip profile showed signs of convergence. However, as the piezocone continues to penetrate beyond 0.2m, it will encounter the presence of stronger soils at greater depths, thus causing the net cone tip resistance to pick up quickly. In contrast, the net cone tip resistance from the analysis based on the homogeneous soil medium quickly converged as the deep mechanism was mobilized at $z/D > 6$ (Figure 6b).

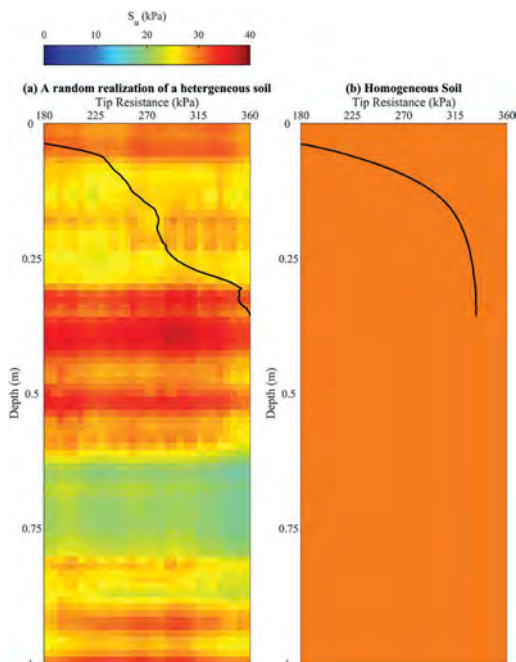


Figure 6. An example of random field and the net cone tip resistance profiles ($I_r = 150$).

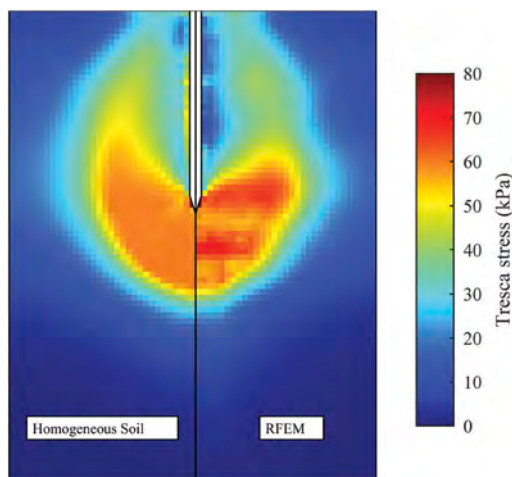


Figure 7. Comparison of Tresca stress contours ($z/D = 10$; $I_r = 150$).

Figure 7 plots contours of the Tresca stress, $(\sigma_1 - \sigma_3)/2$, where σ_1 and σ_3 are, respectively, the major and minor principal stresses at the instant when the cone tip is at $z/D = 10$, for the analysis in the homogenous soil medium and a selected RFEM realization. Both analyses mobilized a stress bulb that spans from the ground surface to approximately

4D below the cone tip. However, the variation of the stresses within the stress bulb generated by the RFEM analysis is not as smooth as that obtained in the homogeneous soil medium.

Figure 8 shows the comparison of the plastic yield zones obtained from the analysis in the homogeneous soil medium and the same selected random realization at a cone penetration of $z/D = 10$. In the homogeneous soil medium, a “butterfly” yield region was obtained that extended horizontally to 5D from the cone tip, which is in good agreement with the 4.7D and 4.65D reported by Lu et al. (2004) and Yu (2000). In contrast, the yield region obtained using the RFEM analysis for this random field realization was smaller and more irregular although the mobilized Tresca stresses were larger in some zones (Figure 7). This is attributed to the fact that the yield region propagated through weaker zones within the soil layer in order to minimize the overall energy dissipation (Zhang et al. 2020).

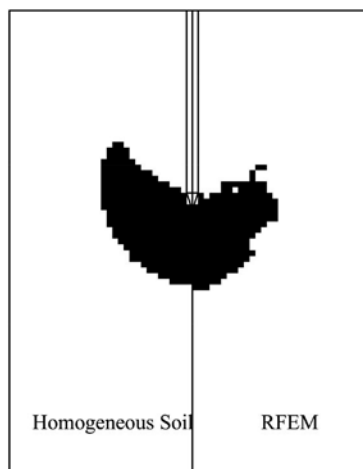


Figure 8. Comparison of yield regions ($z/D = 10$; $I_r = 150$).

The comparisons shown in Figures 7 & 8 indicate that the analysis in the homogenous soil medium that adopted highly idealized and uniform field conditions could not capture important aspects of realistic soil responses. To better understand the influence of the soil’s spatial variability on the cone response, 100 random RFEM analyses were carried out, and the results plotted in Figure 9. For each realization, fluctuations in the computed cone resistance with depth were observed, which are not unlike those recorded from field CPT measurements. Significant difference in the net cone tip resistances computed at penetration depths of $z/D = 10$ or greater were also observed across the 100 realizations. While some realizations yielded net cone tip resistances that are

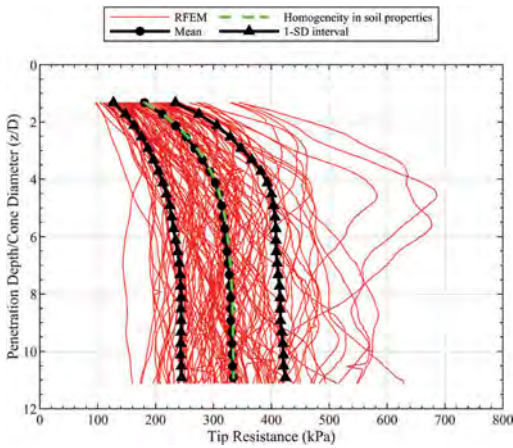


Figure 9. Net cone tip resistance profiles of 100 random field finite element analyses.

larger than 600 kPa (which is approximately 2 times the value obtained in the homogeneous soil analysis), other realizations can yield values of as low as 150 kPa. These significant differences in the computed net cone tip resistances resulting from the consideration of spatial variability cannot be captured by the analysis predicated on a homogeneous soil medium.

5 BACK-CALCULATION OF UNDRAINED SHEAR STRENGTH

As demonstrated in the preceding section, the presence of spatial variability can alter the failure mechanism and, therefore, the net cone tip resistance significantly. In this regard, the impact of spatial variability on the interpretation of CPT data was further investigated by back-calculating values of undrained shear strength S_u from the net cone tip resistances obtained from the random field finite element analyses (RFEM).

Figure 10 illustrates the procedure to back-calculate S_u , which is similar to that adopted in practice for the interpretation of CPT data in practice. A deterministic PRM analysis was first performed using a homogeneous soil medium with a constant value of S_u (Table 1) to obtain a “calibrated” cone factor, $N_{kt, homogeneous}$. This step simulates the calibration exercise that is typically used in practice to obtain the site-specific cone factor. In the second step, 100 RFEM simulations were performed, each using a heterogeneous soil medium characterized as a random field with a spatially varying undrained shear strength distribution (Table 1). The net cone tip resistances obtained from the RFEM analyses were then divided by the $N_{kt, homogeneous}$ value to arrive at the back-calculated S_u values. Only resistances computed for penetration depths of $z/D > 6$,

where the deep failure mechanism has become dominant (Figures 3 and 6), were considered for the back-calculation.

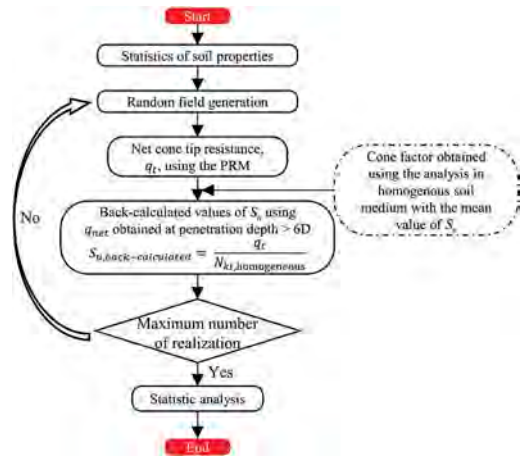


Figure 10. Procedures to back-calculate undrained shear strength values using CPT data.

Figure 11 shows the statistical distribution of the back-calculated S_u values. A lognormal distribution, represented by the solid line, was fitted to the histogram. In general, the statistical distribution of the back-calculated S_u values reasonably resembles the benchmark statistics (dashed line). However, as shown in Figure 12, while the mean back-calculated values of S_u (from the 100 RFEM analyses) are largely equal to the true (input) value, the back-calculated CoV values from the RFEM results underestimated the ‘true’ CoV (prescribed in the RFEM analyses to generate the random fields, see Table 1) by approximately 13%.

The same analyses were also repeated for the case involving a rough cone-soil contact. The results

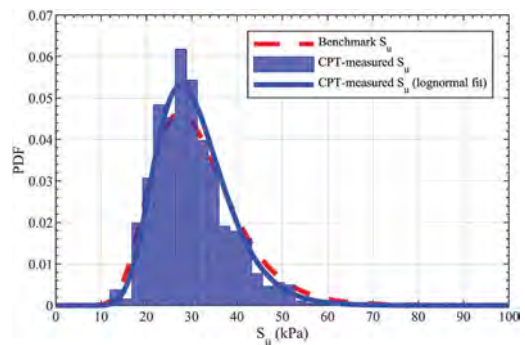


Figure 11. Statistical distribution of the back-calculated S_u (smooth cone-soil contact; $I_r = 150$).

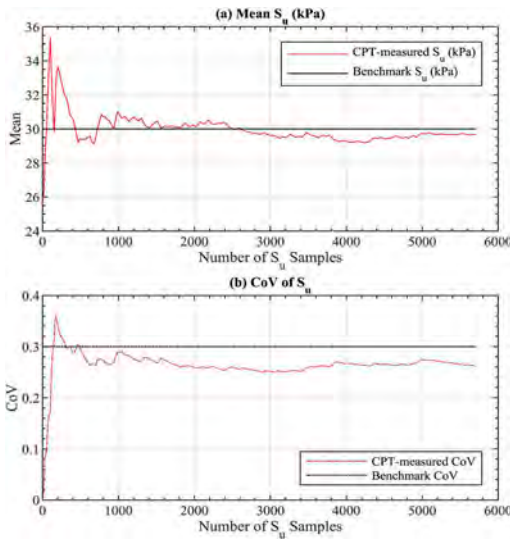


Figure 12. Convergence of the mean and CoV of the back-calculated S_u (smooth cone-soil contact; $I_r = 150$).

indicate that, while the mean back-calculated S_u agree with the true statistic, the CoV of the S_u was underestimated by approximately 16%, which is consistent with the results shown in Figure 12.

6 DISCUSSIONS

Figures 11 to 12 suggest that the conventional interpretation of CPT data that uses a “calibrated” cone factor may not fully recover the true statistics of the parameter due to the presence of spatial variability. The back-calculated data can provide a reasonable estimate of the averaged properties of in-situ soils. When only the most probable performance (Peck 1969) is required, the interpreted properties can be reliably utilized. However, when characteristic values (Orr 2007) are required for design purposes, an overestimation of the characteristic value may likely occur, resulting in an optimistic design of the geotechnical system under study. While Zhang et al. (2020) have provided a correction procedure, further research into the impact of spatial variability on the interpretation of CPT data is still warranted.

7 CONCLUSIONS

The continuous penetration of a piezocone into a statistically heterogeneous soil medium was successfully modelled using the Press-Replace Method (PRM). The performance of the PRM was rigorously validated using other published results. Using the PRM and a set of statistics that is representative of natural soft clays, the presence of spatial variability was shown to

significantly alter the failure mechanism and the net cone tip resistances. Undrained shear strength values were then back-calculated following a procedure that resembles the interpretation procedures adopted in practice. The results indicate that, while the interpreted mean S_u value from the RFEM analyses was close to the prescribed (input) value, the value of CoV was underestimated by approximately 13-16%. Further research is needed to provide an improved framework to interpret CPT data.

REFERENCES

- Abu-Farsakh, M., Tumay, M. & Voyiadjis, G., 2003. Numerical parametric study of piezocone penetration test in clays. *International Journal of Geomechanics*, 3 (2), pp.170–181.
- Andersen, K.H., Andresen, L., Jostad, H.P. & Clukey, E.C., 2004, January. Effect of skirt-tip geometry on set-up outside suction anchors in soft clay. In *International Conference on Offshore Mechanics and Arctic Engineering* (Vol. 37432, pp. 1035–1044).
- Baligh, M.M., 1985. Strain path method. *Journal of Geotechnical Engineering*, 111(9), pp.1108–1136.
- Engin, H.K., Brinkgreve, R.B.J. & Van Tol, A.F., 2015. Simplified numerical modelling of pile penetration—the press-replace technique. *International Journal for Numerical and Analytical Methods in Geomechanics*, 39 (15), pp.1713–1734.
- Lu, Q., Randolph, M.F., Hu, Y. & Bugarski, I.C., 2004. A numerical study of cone penetration in clay. *Géotechnique*, 54(4), pp.257–267.
- Lim, Y.X., Tan, S.A. & Phoon, K.K., 2018. Application of press-replace method to simulate undrained cone penetration. *International Journal of Geomechanics*, 18 (7), p.04018066.
- Orr, T.L., 2000. Selection of characteristic values and partial factors in geotechnical designs to Eurocode 7. *Computers and Geotechnics*, 26(3-4), pp.263–279.
- Peck, R.B., 1969. Advantages and limitations of the observational method in applied soil mechanics. *Geotechnique*, 19(2), pp.171–187.
- Phoon, K.K. & Kulhawy, F.H., 1999. Characterization of geotechnical variability. *Canadian geotechnical journal*, 36(4), pp.612–624.
- Phoon, K.K., Huang, S.P. & Quek, S.T., 2002. Simulation of second-order processes using Karhunen–Loeve expansion. *Computers & structures*, 80(12), pp.1049–1060.
- Pan, Y., Shi, G., Liu, Y. & Lee, F.H., 2018. Effect of spatial variability on performance of cement-treated soil slab during deep excavation. *Construction and Building Materials*, 188, pp.505–519.
- Spry, M.J., Kulhawy, F.H. and Grigoriu, M.D., 1988. *Reliability-based foundation design for transmission line structures: Volume 1, Geotechnical site characterization strategy* (No. EPRI-EL-5507-Vol. 1). Electric Power Research Inst., Palo Alto, CA (USA); Cornell Univ., Ithaca, NY (USA). Geotechnical Engineering Group.
- Teh, C.I. & Houlsby, G.T., 1991. An analytical study of the cone penetration test in clay. *Geotechnique*, 41(1), pp.17–34.
- Tehrani, F.S., Nguyen, P., Brinkgreve, R.B. & van Tol, A. F., 2016. Comparison of Press-Replace Method and

- Material Point Method for analysis of jacked piles. *Computers and Geotechnics*, 78, pp.38–53.
- Vesic, A.S., 1972. Expansion of cavities in infinite soil mass. *Journal of Soil Mechanics & Foundations Div*, 98(sm3).
- Walker, J. & Yu, H.S., 2006. Adaptive finite element analysis of cone penetration in clay. *Acta Geotechnica*, 1 (1), pp.43–57.
- Wang, Z.Z. & Goh, S.H., 2018. Spudcan installation and post installation behaviour in soft clay: The press-replace method. In *Numerical Methods in Geotechnical Engineering IX* (pp. 1503–1510). CRC Press.
- Yu, H.S. & Whittle, A.J., 1999. Combining strain path analysis and cavity expansion theory to estimate cone resistance in clay. *Unpublished notes*.
- Yu, H.S., 2000. *Cavity expansion methods in geomechanics*. Springer Science & Business Media.
- Yu, H.S., Herrmann, L.R. & Boulanger, R.W., 2000. Analysis of steady cone penetration in clay. *Journal of Geotechnical and Geoenvironmental Engineering*, 126(7), pp.594–605.
- Zhang, W., Pan, Y. & Bransby, F., 2020. Scale effects during cone penetration in spatially variable clays. *Géotechnique*, pp.1–13.
- Zhang, J.Z., Huang, H.W., Zhang, D.M., Zhou, M.L., Tang, C. & Liu, D.J., 2021. Effect of ground surface surcharge on deformational performance of tunnel in spatially variable soil. *Computers and Geotechnics*, 136, p.104229.

Some aspects of in situ testing of clay-glacial till mixture redeposited as man-made fills

J. Wierzbicki, K. Stefaniak & S. Wilczyński

Institute of Geology, Adam Mickiewicz University, Poznań, Poland

B. Brzeziński

Labortest Sp. z o.o. Sp. k., Poznań, Poland

ABSTRACT: The paper presents the results of CPTU and FVT tests carried out in soils, which filled the former brown coal excavation. In their natural state, these lands were pre-consolidated glacial till and clay. Detachment of soil from the original deposit, transport and low-energy redeposition led to the creation of multi-meter-thick non-consolidated embankments, which are now used as a construction subsoil. These embankments consolidate under their own weight, however, unlike typical geological formations, they are characterized by a decreasing influence of consolidation on the strength properties along with depth.

1 INTRODUCTION

The contemporary development of urban areas is related to, inter alia, the location of industrial facilities on the outskirts of cities. Simultaneously, the high cost of land properties within cities make it economically viable to use advanced foundation techniques in case of weak, but cheap, grounds. Therefore, more and more often commercial buildings are located in areas not previously used for construction purposes. One of the most efficient trends in such cases in Poland is the use of land reclaimed after a large scale industrial facilities as brown coal mines. Contemporary an ecological purpose makes it necessary to resign from the simple, but highly devastating from an environmental point of view, use of brown coal as an energy source. Thus, brown coal mines in Poland have been closing for a dozen of years and the rate of these changes will increase in the future. Some of the old brown coal outcrops are being changed into green areas, some of them are used for recreation with a newly built infrastructure, but some of them, especially the ones close to the cities, are going to be used as lands for clean industry facilities.

One of the good examples of such a use of reclaimed land are the areas of brown coal dumps in the vicinity of the city of Konin, in central Poland. The soil that has been dumped is a chaotic mixture of fragments of previously overconsolidated glacial till, sands and clays, very often over 20-meter thick, that consolidate naturally over time. The method of depositing man-made fill, despite the fact that the dumps are made of natural soil, leads to clear differences in

their strength and deformation characteristics, as opposed to similar soils deposited as a result of geological processes. In this case, the use of typical geotechnical procedures may cause overestimation of soil strength and stiffness. Due to a complex structure of the man-made fill the in situ tests, as CPTU, seem to be the best solution for geotechnical investigations. Nevertheless, it is worth seeing how the geotechnical properties of overconsolidated soil can be changed because of excavating and low energy redeposition. For this purpose, the results of CPTU and FVT investigations in the reclaimed land were compared with the results of investigations carried out in the areas of natural occurrence of glacial till of the same glaciation in Poland.

2 MAN-MADE FILL TEST SITE

The studies of the embankments of the brown coal mine dump were located on the southern outskirts of the central part of the former Niesłusz outcrop, which is the oldest part of the Konin mining complex (Figure 1).

The primary geological structure of this area consists of the Quaternary sediments dominated by glacial till. Two types can be distinguished: upper moraine, representing the Vistula glaciation, and lower moraine related to the Odra glaciation. In clays, there are numerous intercalations of sand-gravel and fluvio-glacial lenses, as well as varvic clays and erratic boulders (Widera 2001). These sediments lie on the Pliocene and Miocene

formations, among which brown coal accumulated in sedimentation basins is a characteristic element. Clays lay directly above the coal, intercalated with dusty sand, sandy silt or fine-grained quartz sand (Ratajczak & Hycnar 2017).



Figure 1. Location of the test sites.

Brown coal, both in Poland and around the world, is exploited almost exclusively using the opencast method. Exploitation of minerals is related to a number of activities necessary to be performed in the deposit and in its surroundings,

which, as a result, lead to the extraction of the mineral. A characteristic element of opencast mining is the removal of the overburden of various thicknesses and compositions, the mining of the mineral and its transport to the destination as well as the transport and tipping of the removed overburden (Nowak & Kozłowski 2009). Almost from the beginning of brown coal mining in the Konin region, this process has been taking place in a system in which the excavated material is transferred to belt conveyors, which are then transported to a gravity stacker that forms an embankment - a dump.

The coal deposits in the Niesłusz outcrop were exploited in the 1950s and the area was reclaimed with little investment: at the site of the dump (where the test site is located), works were undertaken to restore the land for agricultural or forest use and the largest depressions were developed as water reservoirs. The lack of success in restoring the land to agriculture and the close vicinity of a dynamically developing city meant that since the 1990s, these areas have been considered as areas for industrial and commercial development (Gilewska & Otremba 2013) (Figure 2).



Figure 2. Flat surface of the man-made fill at the Niesłusz test site.

The end of brown coal exploitation falls on circa 1961 and agricultural reclamation has been carried out since then, thus it can be assumed that the test site has been subject to consolidation for 60 years under its own weight of deposited material.

The current geological structure of the subsurface zone of the test site is between a few to over a dozen meters of embankments lying on the glacial till (Figure 3). The basic physical properties of the soil are given in Table 1 and the typical grain size distribution is showed in Figure 5.

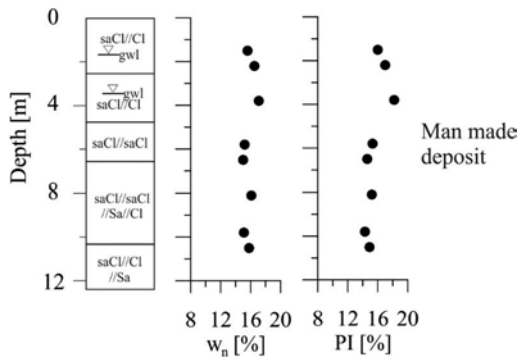


Figure 3. Typical soil profile at the Niesłusz test site (soil description according to ISO14688-2, gwI – ground water level, w_n – natural moisture, PI – plasticity index).

The ground water found in the subsoil behaves like so-called suspended waters, which can be found at different levels and do not constitute a single piezometric level.

Table 1. Typical values of physical properties of the glacial till at the Niesłusz test site.

G_s	γ	e	S_r
[-]	[kN/m ³]	[-]	[-]
2.69	19.42	0.58	0.74

where: G_s – specific gravity, γ – soil unit weight, e – void ratio, S_r – degree of saturation.

3 GLACIAL TILL TEST SITE

Research in naturally deposited glacial soil was carried out in the area of the Parsęta Lobe of the Vistula glaciation, which was formed during the local transgression of the already retreating ice sheet (Figure 1). As a result of this event, two glacial till deposits were deposited: the older, from the previous glaciation phase (the Poznań phase), pre-consolidated by the transgressing Parsęta Lobe, and the younger, from the melt out phase, normally consolidated or slightly preconsolidated (Pomeranian phase) (Figure 4).

Granulometrically, these sediments are very similar to each other, they are a mixture of sand and gravel in about 50-70%, silt in about 20% and a supplementary part of the till (Figure 5). These soils were created within approx. 4,000 years, several thousand years ago, so the aging processes did not play a decisive role in shaping their geotechnical properties. The basic physical properties of these soils are given in Table 2.

However, the different load history led to a clear differentiation of the geotechnical properties of the

sediments of both phases, which was described, among others, by Wierzbicki et al. (2008). This differentiation is visible, for example, in the natural moisture content (approx. 16% for the clays of the Pomeranian phase and approx. 11% for the clays of the Poznań phase), and especially in the values of undrained shear strength (maximum 290 kPa for clays of the Pomeranian phase and maximum 670 kPa for clays of the Poznań phase) (Wierzbicki 2010).

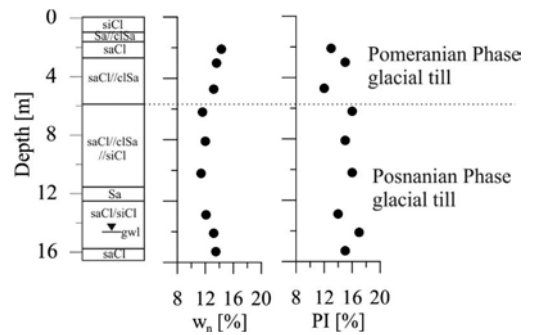


Figure 4. Typical soil profile of glacial till within the Parsęta Lobe (soil description according to ISO 14688-2, gwI – ground water level, w_n – natural moisture, PI – plasticity index).

Table 2. Typical values of physical properties of the glacial till within the Parsęta Lobe.

G_s	γ	e	S_r
[-]	[kN/m ³]	[-]	[-]
2.68	20.11	0.46	0.67

where: G_s – specific gravity, γ – soil unit weight, e – void ratio, S_r – degree of saturation.

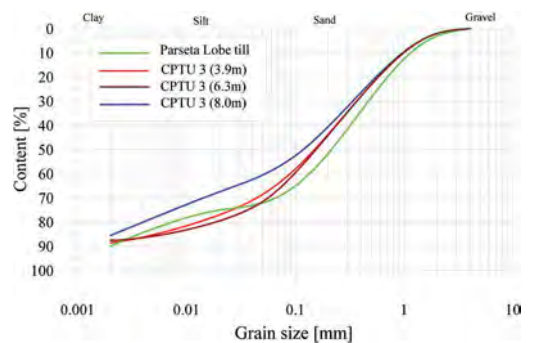


Figure 5. Typical grain size distribution of Parsęta Lobe till in comparison with grain size distribution of some samples from CPTU 3 testing point at Niesłusz test site.

4 RESULTS

The results of the research carried out on glacial deposits in their natural habitat were presented in detail by Wierzbicki (2010). On this basis, it can be concluded that the typical CPTU profile of the soils of the Vistula glaciation is shown in Figure 6.

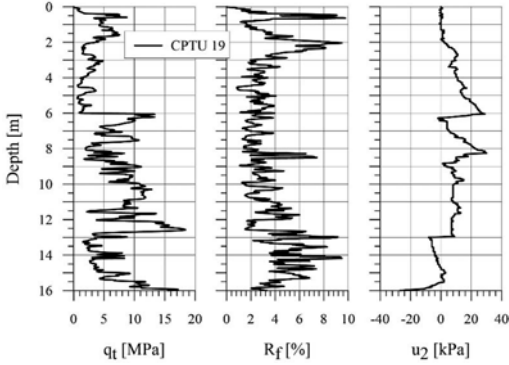


Figure 6. Typical CPTU results at glacial till test site (test no. 19) (on the basis of Wierzbicki 2010).

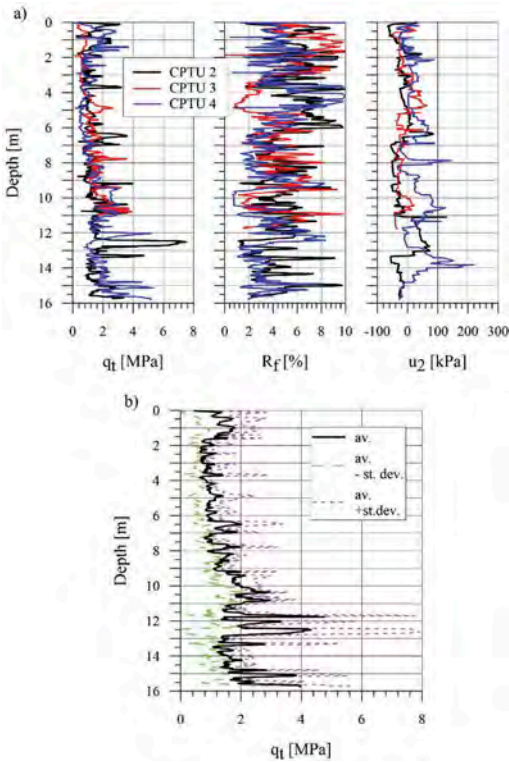


Figure 7. CPTU results at the Niesusz test site (a) tests no. 2, 3 & 4 and (b) average value of q_t (av.) with plus and minus standard deviation values (av. + st.dev. & av. - st. dev.).

The relatively low and sometimes even negative u_2 values are common in the case of the Vistula glaciation and are caused by a relatively low degree of saturation and low clay content combined with the overconsolidation effect. In case of this land, Wierzbicki (2010) also carried out a series of studies of geotechnical features, which indicate, among others, a different degree of pre-consolidation of individual parts of the profile. On the other hand, the triaxial CIU studies showed that the values of cone factor N_{kt} range from 15 to 23 (in case of sediments with high OCR and high content of gravel fraction).

As far as redeposited sediments are concerned, data from three CPTU soundings located approximately 30 m from each other were used. Boreholes were made in the same places, samples were taken for laboratory tests and FVT soundings were performed. The results of the CPTU tests indicate a general similarity of the results at individual research points (Figure 7). However, this similarity is more visible along of the entire profile rather than locally at individual depths. The results of the FVT test, as well as the CPTU test, indicate a strong local differentiation of the geotechnical features of the subsoil (Figure 8). Again, however, the general trend of strength alterations is increasing along with the depth of deposition (Figure 9). It is worth to notice that no correction for plasticity was used during the c_u (FVT) calculations, due to low plasticity of the investigated soil ($PI < 20$).

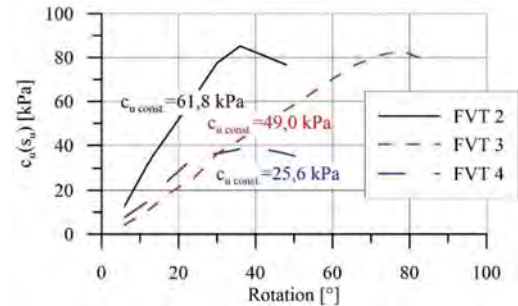


Figure 8. Results of FVT at the depth of 4,5 m at the Niesusz test site (tests no. 2, 3 & 4).

The values of N_{kt} obtained on the basis of the comparison with the results of CIU (natural sediments) and FVT (redeposited sediments), allowed to determine the undrained shear strength $c_u(s_u)$ in accordance with the Equation 1 (Figure 10).

$$c_u(s_u) = \frac{q_n}{N_{kt}} \quad (1)$$

where: $c_u(s_u)$ = undrained shear strength, q_n = nett cone resistance, N_{kt} = cone factor

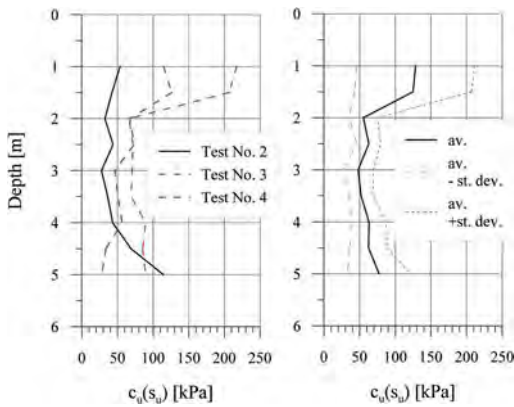


Figure 9. The undrained shear strength profiles from FVT at different testing points and the average profile of this parameter (av.) with plus and minus standard deviation values (av. + st.dev. & av. - st. dev.).

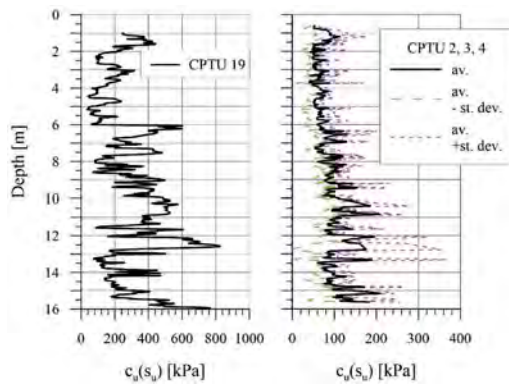


Figure 10. The undrained shear strength of glacial till (CPTU 19) and man-made fill (CPTU 2, 3, 4) on the basis of CPTU results (average values (av.) and plus and minus standard deviation values (av. + st.dev. & av. - st. dev.)). The N_{kt} value for the ranges between 13 and 17 (depending on the specific soil layer).

5 DISCUSION

In case of redeposited sediments, undrained shear strength $c_u(s_u)$, apart from low values for glacial sediments (Wierzbicki 2010), is also characterized by a clear trend increasing with depth and thus with vertical geostatic stress.

It is worth noting that a similar trend was not observed in naturally deposited land, where the the values of $c_u(s_u)$ are more related to different deposition phases and different pre-consolidation effects *than* only to the increase of depth. The different dependence of the value of $c_u(s_u)$ on the depth of occurrence in both test sites is very clearly visible after the normalization of this parameter by effective vertical stress (Figure 11).

It can be concluded that in case of redeposited sediments, the inclusion of the stress component

excessively influences the normalization, that is, the trend along with the depth is permanently negative across the entire profile. This means that the undrained shear strength of the soil increases slower and slower with increasing depth. Such an effect may be characteristic of underconsolidated deposits. It is particularly worth emphasizing that when the above dependence is presented on a semi-logarithmic scale, we observe variability around 1 in natural sediments, while in sediments redeposited with depth, we still observe a decreasing trend with depth (Figure 12). It is probable that this rule can be universal for all non-compacted man made but for now, it can be proved only in the case of fills which are 16 m thick. Thus, while the dependence of the strength properties in glacial till can be described by a logarithmic function (which is typical in most geotechnical situations), in case of the same granulometric but redeposited soil, it is not appropriate.

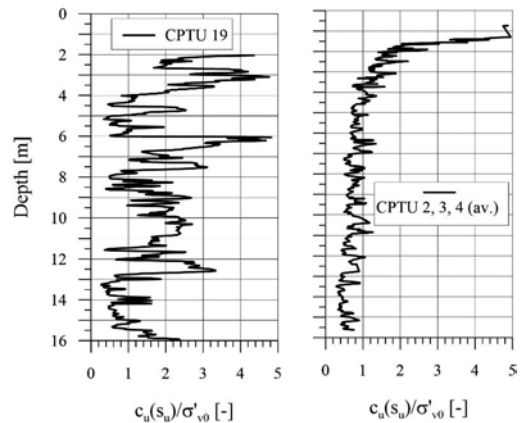


Figure 11. Undrained shear strength normalized by vertical stress for glacial till and mam-made fill profiles.

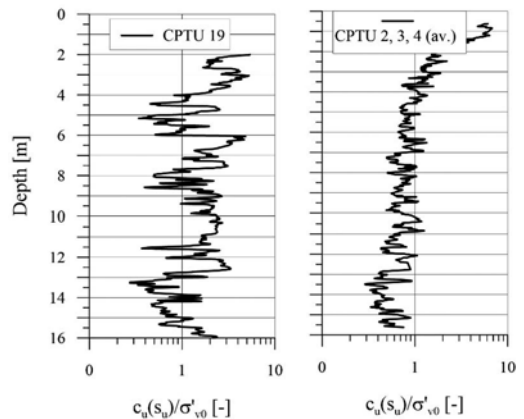


Figure 12. Undrained shear strength normalized by vertical stress in semi-log scale, for glacial till and mam-made fill profiles.

6 SUMMARY

Glacial tills, which in their natural habitat are pre-consolidated soils, lose some of their mechanical properties during excavation and transportation in the form of large fragments and redeposition. They are still soils with sufficiently good geotechnical properties to place building structures directly on them. However, the loss of strength properties is so great that the soils have the profile characteristics corresponding to under-consolidated soils and therefore susceptible to consolidation subsidence. Thus, in case of land deposited within the post outcrops of brown coal mines, the basic problem is not so much reaching the bearing limit state, but the serviceability limit state. Moreover, the research results indicate that the problem of land unconsolidation increases with depth, which makes this situation unique compared to, for example, natural soils (Radaszewski and Wierzbicki 2019).

REFERENCES

- Gilewska M. & Oremba K. 2013. Revitalisation of post-mining regions in the area of the town of Konin. *Inżynieria Środowiska* no 29, 59–67 (in Polish).
- ISO 14688-2: 2017. Geotechnical investigation and testing - Identification and classification of soil – Part 2: Principles for a classification.
- Nowak J. & Kozłowski Z. 2009. Technology of managing lignite deposits. In: Z. Kozłowski [ed.]: *Techniczno-ekonomiczny ranking zagospodarowania złóż węgla brunatnego w aspekcie założeń polityki energetycznej Polski*. Wyd. Politechniki Wrocławskiej, Wrocław (in Polish).
- Radaszewski R. & Wierzbicki J. 2019. Characterization and engineering properties of AMU Morasko soft clay. *AIMS Geosciences*, 5(2), 235–264.
- Ratajczak T & Hycnar E. 2017. Associated minerals in lignite deposits. *Wydawnictwo IGSMiE PAN* (in Polish).
- Wierzbicki, J. 2010. Evaluation of subsoil overconsolidation by means of in situ tests at the aspect of its origin. *Scientific dissertations No. 410*, University of Life Sciences in Poznań Publishing, Poland, 181–182 (in Polish).
- Widera M. 2001. Occurrence and development of accompanying minerals in lignite open-pits in Wielkopolska. *Summary of papers presented at meetings PTGeol. in Poznan X*, 61–82 (in Polish).
- Wierzbicki J., Paluszkiewicz R. & Paluszkiewicz R. 2008. Shear strength of the deposits with relation to their origin, the glacial till of Vistula glaciation case. *Landform Analysis* Vol. 9, Poznań, Poland, 390–393 (in Polish).

Cone penetration in a thin medium dense sand layer sandwiched by different clay layers – LDFE analysis

Q. Xie & Y.X. Hu

University of Western Australia, Perth, Australia

M.J. Cassidy

University of Melbourne, Melbourne, Australia

M. Zhou

South China University of Technology, Guangzhou, China

ABSTRACT: The cone penetration test (CPT) has been the most common site investigation practice for decades. This paper presents the results of large deformation finite element (LDFE) analysis that modeled a CPT into soil comprising a thin medium dense sand layer sandwiched between two clay layers of different undrained shear strengths. An extended critical state Mohr-Coulomb model is utilized to capture the stress-dependent drained behavior of sand, while Tresca failure criterion is adopted for the undrained behavior of clay. Because the sand layer and the surrounding clay layers work as a system that defines the mobilized soil stiffness and soil interface deformation, two soil layer profiles are analyzed to study cone penetration resistance responses, including soft clay on top and stiff clay at bottom, and vice versa. It is found that a peak resistance is registered in the thin sand layer, through the top and bottom clay layers show impact to the peak as well. The impact on the peak resistance from the clay layer ahead (i.e. bottom layer) weights more than the clay layer behind (i.e. top layer). The evolving soil flow mechanisms are revealed to explain the findings.

1 INTRODUCTION

1.1 Historical background

The practice of inserting a rod into soft soil to find embedded stiff layers dates back to the 19th century. However, the first recognizable form of the modern cone penetration test (CPT) was developed in Netherlands in 1934 to predict the ultimate bearing capacity of piles (Barentsen, 1936). The early forms of CPTs comprised a mechanical system of pushing rods to measure the rod tip resistance. In the late 1960s, electric penetrometers came into general usage, enabling resistance to be continuously and automatically recorded (Walker & Yu, 2010). Today the CPT is the most widely used in-situ testing method to investigate soil stratification due to its reliability and repeatability.

1.2 CPT in layered soils

The traditional design charts and formulas to identify soil properties from CPT data were formulated on uniform soils of a single layer (Silva & Bolton, 2004). To directly apply such interpretation method to layered soils can be problematic. This is because the influence zone of a cone can span a distance several

cone diameters both behind and ahead of the cone tip (Lunne et al., 2002). When the influence zone crosses layer interfaces, the measured cone resistance represents not only the properties of the local soil around the cone tip, but also the soils in adjacent layers.

The inability to accurately estimate soil properties of individual layers (particularly thin layers) in soil strata has attracted recent attention, with research focused on idealized soil profiles of two or three uniform soil layers in different sequences (e.g. weak soil over strong soil and vice versa, strong layer embedded in soft soils and vice versa). Methodologies included elastic analysis (Vreugdenhil et al., 1994, Yue & Yin, 1999), cavity expansion analysis (Mo et al., 2016), chamber testing (Tehrani et al., 2017), centrifuge testing (Mo et al., 2015) and analysis of field data (Youd & Idriss, 2001, Yost et al., 2019). Moreover, large deformation finite element (LDFE) analysis has been applied for layered clays (Ma et al., 2016, Ma et al., 2017).

For CPT in clay-sand-clay soils, an early analytical solution was obtained by elastic analysis to investigate the “error” between the resistance in a thin embedded stiff layer and the ultimate resistance in an infinitely thick layer of the same stiffness (Vreugdenhil et al., 1994). As suggested by this

study, the “error” was a function of the embedded layer thickness and the stiffness ratio between adjacent layers. The finding was later confirmed by field data (Youd & Idriss, 2001) and examined numerically (Ahmadi & Robertson, 2005). The latter suggested the “error” function only applied to thin and normally consolidated sand layers embedded in soft normally consolidated clays. Thus, caution needs to be taken to apply these formulas for different cases.

In the above studies, the stiffnesses of the top and bottom clays were assumed identical. Thus, the existing solutions may not be suitable for the situation where the top clay stiffness is different from the bottom clay, with a sand layer sandwiched in the middle. This study is set to explore the CPT in these complex soil profiles.

1.3 Objective

This study numerically investigates soil responses to cone penetration in a medium dense sand layer sandwiched by two different clay layers. The two soil layer arrangements for the top and bottom clay layers include (i) the top clay being stiffer than the bottom clay, and (ii) the top clay being softer than the bottom clay. The soil flow mechanisms will be revealed and correlated to the features observed in the cone resistance profiles. Additionally, stress history will be analyzed to further explain the cone resistance profiles.

2 METHODOLOGY

2.1 RITSS method

Cone penetration is a typical large strain problem in finite element analysis. To overcome mesh distortion in numerical analysis, the remeshing and interpolation technique with small strain (RITSS) method is deployed in this study (Hu & Randolph, 1998a). RITSS method belongs to the arbitrary Lagrangian-Eulerian (ALE) FE methods. It starts with a series of small strain incremental displacement analysis with an initial mesh, followed by updating the co-ordinates of all nodes in the mesh by the displacements calculated in the first steps and then automatically remeshing the whole domain accordingly. On the newly established mesh, the field variables will be interpolated from the old mesh. A new round of small strain analysis will be carried based on the new mesh and the process will be cycled until the desired cone penetration depth is achieved.

The FE based computer program AFENA (Carter & Balaam, 1995) is used in the study with the RITSS method implemented. *H*-adaptive mesh refinement cycles are also implemented in the program to optimize the mesh density and minimize the discretization errors (Hu & Randolph, 1998b).

2.2 Soil models

In this study, an extended Critical State Mohr-Coulomb (CSMC) model is utilized to capture the stress-dependent behavior of sand (Li et al., 2013). It introduces the critical state concept into the classical Mohr-Coulomb (MC) model by linking the friction angle and dilation angle with the soil state parameter (i.e. the difference between the current void ratio and the critical state void ratio at current stress level). Elastic parameters (i.e. Young’s modulus) are functions of the void ratio and mean effective stress. To fit the large deformation analysis computation, CSMC model balances its complexity with simplicity to avoid numerical difficulties. In contrast to the advanced model for sand, a simple Tresca model is used for clay. There is only one plastic parameter, undrained shear strength (s_u), to determine an unchanged yielding surface. Young’s modulus is assumed as proportional to the shear strength ($E = 500 \times s_u$), which is within the commonly adopted range (Hossain et al., 2005). Poisson ratio for clay is set at 0.49 for undrained analysis while that of sand is set at 0.3 for drained analysis.

The CSMC model along with the RITSS method for CPT in layered soil has been extensively verified with centrifuge tests data for two types of sand (Xie, 2020). Good agreement has been achieved providing confidence in deploying the model in this study. The sand parameters utilized in this paper are calibrated for Toyoura sand and are provided in Table 1. e_{max} and e_{min} are the maximum and minimum void ratios; ϕ_c is the critical state friction angle; A, m and n are three scaling factors.

Table 1. CSMC model parameters for Toyoura sand.

e_{max}	e_{min}	$\phi_c/^\circ$	A	m	N
0.985	0.611	32	0.5	7	0.75

3 NUMERICAL MODELLING

3.1 Problem definition

Figure 1 graphically defines the problem. A cone penetrates in clay-sand-clay soil to a depth, d , measured from the cone shoulder to the original elevation of the soil surface. The sand is medium dense ($I_D = 60\%$). The strengths of clay layers vary in two cases: Case A, top clay ($s_{ut} = 80$ kPa) is stiffer than the bottom clay ($s_{ub} = 10$ kPa) and Case B, top clay ($s_{ut} = 10$ kPa) is softer than the bottom clay ($s_{ub} = 80$ kPa). The reaction force acting on the cone, during continuous penetration, is obtained through the LDFE analysis. The cone shaft and cone face are set as fully smooth as it is normally manufactured with polished stainless steel.

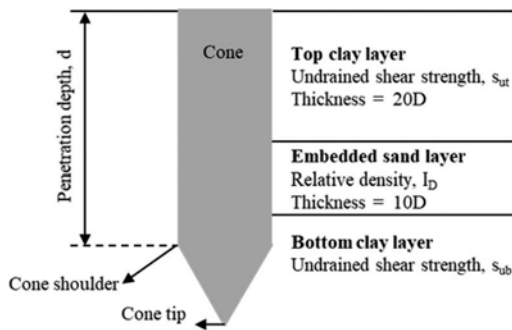


Figure 1. Cone penetration in clay-sand-clay soil.

3.2 Mesh setting

A finite element mesh setting where the cone penetrates in the bottom clay layer is depicted in Figure 2. The numerical model is simplified as 2D-axisymmetric, with the soil domain of equivalent 55D in depth and 55D in radius. The lateral side is set as a roller condition to eliminate soil horizontal movements and the bottom boundary is set as a hinge condition to eliminate both vertical and horizontal movements. The analysis uses six-node triangular elements with three Gauss points. The cone shoulder is initially buried in the soil to avoid numerical difficulties. A mesh refined zone is added adjacent to the cone, which moves with the cone, to improve numerical stability in the area of high strain concentration.

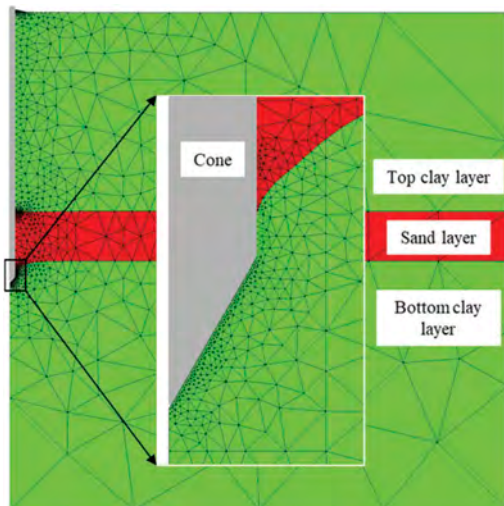


Figure 2. Mesh setting when cone penetrates in bottom clay.

4 RESULTS AND DISCUSSION

4.1 Cone resistance profiles

Figure 3 shows the cone resistance profiles of Cases A and B. There are three zones identified around the

embedded sand layer in both cases: (I) blue zone – cone resistance increases linearly and sharply with the cone tip entering the sand layer, starting from the kink point registered above the C-S interface; (II) red zone - another linear increasing stage in resistance, but with lower gradient, leading to the peak resistance in the sand layer; (III) orange zone – cone resistance decreases after the peak, and converges to the ultimate resistance in the bottom clay layer.

To illustrate the evolution of soil failure mechanisms, eight stages are denoted on the resistance profiles in Figure 3. For Case A: Stage A_1 - when the cone resistance is stabilized at its ultimate resistance in the top clay; Stage A_2 - when the resistance decreases after the stabilized resistance is reached; Stage A_3 - when the kink point is formed above the clay-sand interface; Stage A_4 - when cone resistance reaches a turning point with changed gradient; Stage A_5 - when the resistance is increasing at a reduced gradient; Stage A_6 - when the peak resistance is reached in sand; Stage A_7 to A_8 - when the resistance decreases gradually till the ultimate resistance in the bottom clay is reached. Correspondingly, eight Stages are chosen for Case B in a similar manner. The normalized penetration depths, d/D , at different stages are listed in Table 2

The differences observed between the two profiles are: (i) above the blue zone, the cone resistance shows a slight decrease before reaching the sand layer in Case A, but not in Case B; (ii) in the blue zone, the cone resistance increases more sharply in Case A than in Case B; (iii) in the red zone, the cone resistance reaches a higher peak in Case B than in Case A; (iv) in the orange zone, the cone resistance reduces more sharply in Case B than in Case A. Discussions on these observed features are provided in the following section.

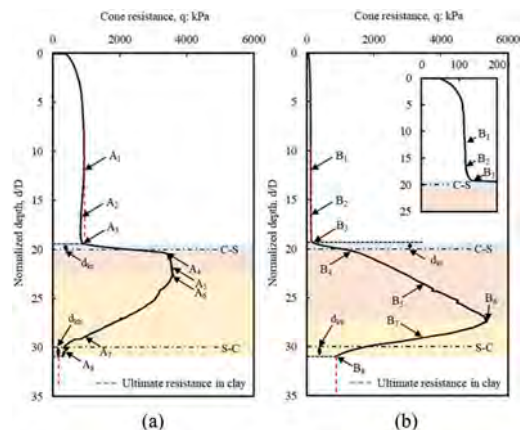


Figure 3. CPT resistance profiles in clay-sand-clay soil: (a) Case A: $s_{ut}/s_{sub} = 8$; (b) Case B: $s_{ut}/s_{sub} = 0.125$ (C-S refers to clay-sand interface while S-C refers to sand-clay interface).

Table 2. Normalized depths at different penetration stages.

Stage No.	Normalized depth (d/D)	
	Case A	Case B
1	12	12
2	16.5	16.5
3	19.3	19.25
4	20.3	20.05
5	22	23.7
6	22.7	27.3
7	29	29
8	30.2	30.85

4.2 Soil flow mechanism

4.2.1 Case A: A sand layer embedded in stiff over soft clays

Figures on the left column of Figure 4 depict the flow mechanism for Case A. In the top clay, a cavity expansion failure is formed through Stages A_1 to A_2 until the cone tip touches the sand surface at Stage A_3 . The localized failure mode should result in a constant ultimate net cone resistance as the resistance only depends on the local clay stiffness. Therefore, the reduction in resistance at Stage A_2 suggests the cone is impacted by the sand layer ahead of the cone, as soil displacements bend slightly downwards comparing with Stage A_1 . From Stage A_3 to A_4 , the cone passes through the clay-sand interface as grouped in the blue zone in Figure 3(a). Because the magnitude of mobilized stress in sand is much higher than that in clay, the resistance increases sharply over these stages, resulting in a kink registered at Stage A_3 . Soil movement is disconnected by

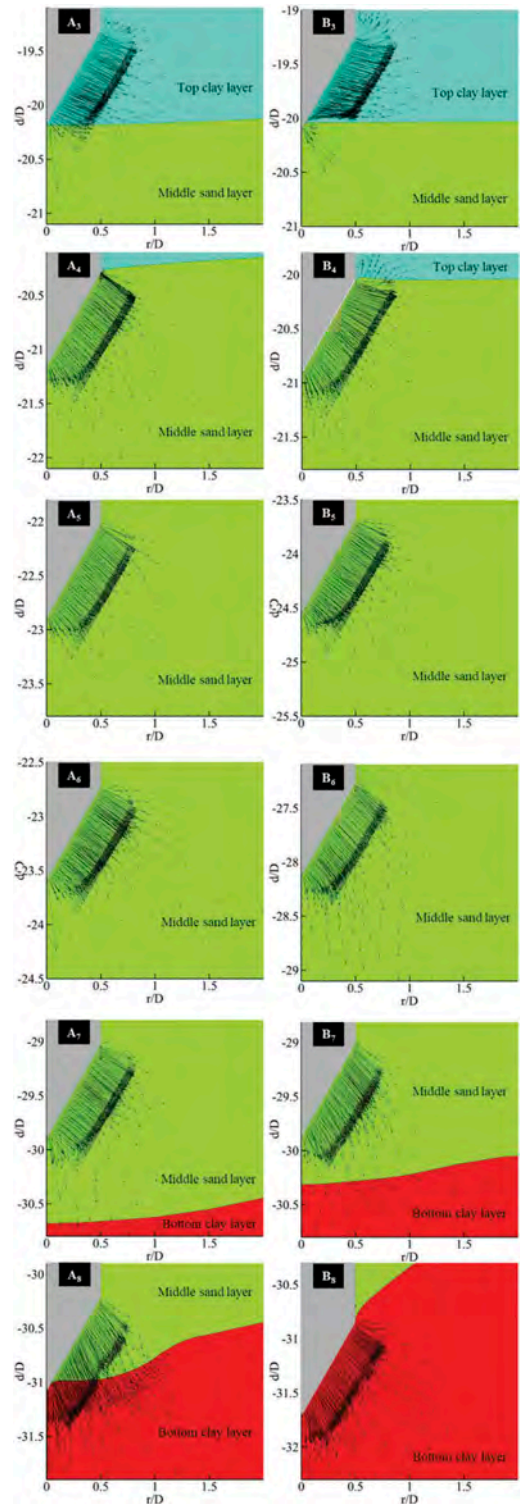
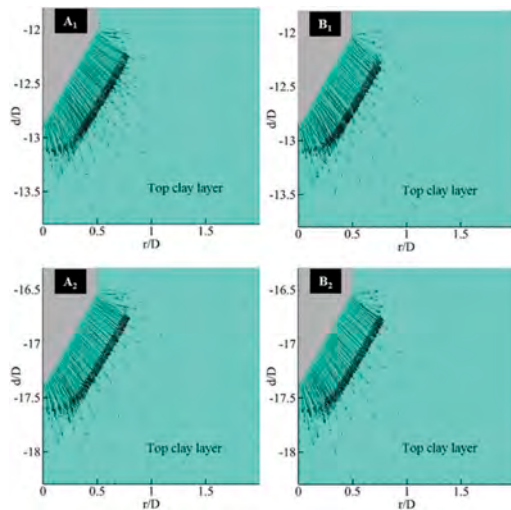


Figure 4. Soil flow mechanisms in Cases A (left) and B (right).

the layer interface: cone squeezes the top clay sideways while pushing the sand downwards. From Stage A₄, the cone shoulder detaches from the sagged interface, which marks the full cone being buried in the sand layer, and the resistance development enters a new stage as shown by the red zone in Figure 3(a). The cavity expansion merges again at Stage A₅, implying the cone senses little impact from surrounding clays except the overburden pressure. Moving to Stage A₆, the soil displacements bend downwards. This implies that the cone is sensing of the bottom soft clay, thus the cone resistance starts to reduce. From Stages A₇ to A₈, soil movements keep bending downward as the cone approaching the bottom clay. The mobilized sand keeps reducing until the resistance reaches the stable value in the bottom clay. At Stage A₈, less than 1D of sand is mobilized and the soil movement is largely attracted to the bottom clay. This reduced mobilization in sand causes the resistance to decrease in the yellow zone in Figure 3(a). The S-C interface sags extensively by $\sim 1D$, compared to $0.18D$ for the C-S interface at Stage A₃. A kink is formed far from the original elevation of the interface (e.g. $d_{kb} > 1D$).

4.2.2 Case B: A sand layer embedded in soft over stiff clays

The soil flow mechanisms for Case B are depicted in the right column of Figure 4. Many features observed in Case A can also be noted in Case B, including: (1) cavity expansion in the top clay before the cone tip touches sand (Stage B₁ to B₂); (2) cavity expansion in sand before the cone senses the bottom clay (Stage B₅); (3) the downwards bending soil displacement due to the attraction of the bottom clay (Stage B₆ to B₈). The similarities in the flow mechanisms between Cases A and Case B can explain the similar observations in the resistance profiles, while the differences between the cases are discussed below.

4.2.3 Further discussion on the profile differences

Difference (i): above the blue zone, cone resistance reduction in top clay only appears in Case A. This can be explained by the stress-dependent sand stiffness with the impacts from the surrounding clays. Figure 5 depicts the soil mean stress contours for Cases A and B. In CSMC model, sand stiffness (E_s) is a function of mean effective stress and void ratio. Extracted for Point E in Figure 5 (measured 1D from the central line and 1D below the sand surface) from the output files: $E_s = 20.8$ MPa at Stage A₂, and 10.5 MPa at Stage B₂. The stiffness of top clay (E_c) is 40 MPa in Case A and 5 MPa in Case B. Therefore, the sand layer is mobilized as a soft layer below the cone at Stage A₂, resulting the cone resistance reduction above the blue zone in Case A. This phenomenon remains until the cone penetrates into the sand layer.

Difference (ii): in the blue zone, cone resistance profile exhibits sharper increase in Case A than in

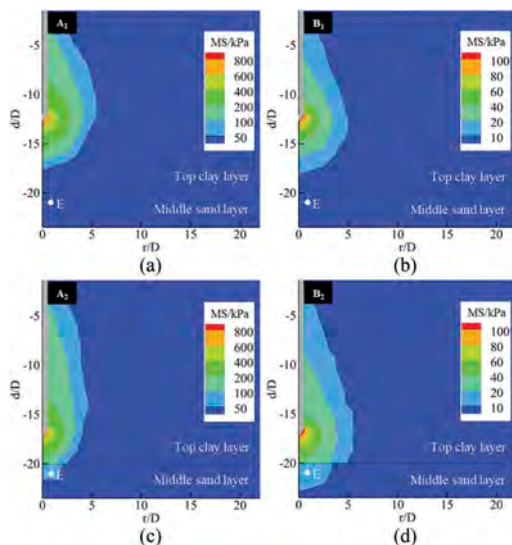


Figure 5. Mean stress contours at (a) Stage A₁, (b) Stage B₁, (c) Stage A₂, (d) Stage B₂ (MS refers the mean stress).

Case B. This may be due to the influence of the top clay layer to the mobilized sand layer. In Case A, the top clay is stiffer than that in Case B, which mobilizes higher stress in sand layer, hence a stiffer mobilized sand layer. The sand stiffness promotes a sharper increase in the cone resistance.

Difference (iii): in the red zone, the cone resistance in Case B increases with a higher gradient and lasts longer than those in Case A, and it results in a higher peak. This may be due to the influence of the bottom clay. In Case B, the bottom soil is stiffer. The stiffer bottom clay reduces the sand layer sagging and promotes higher peak resistance.

Difference (iv): in the orange zone, the cone resistance reduces more sharply in Case B than in Case A. This can also be explained by the stress-dependent behavior of sand with the impacts from surrounding clays. As discussed before, the mobilized stiffness of sand depends on its in-situ mean effective stress. Soil stiffness determines the length of sensing distance to the new layer ahead. The observation is consistent to that by Lunne et al. (2002) where a cone senses a new layer earlier in a stiff layer than in a soft layer. Thus, in Case A, the sand layer is stiffer than the bottom clay, hence the cone can sense the bottom soft clay earlier and the reduction in resistance is gradual. On the contrary, in Case B, the bottom clay is stiffer, hence the cone senses the bottom clay later and the reduction in resistance is more dramatic.

Therefore, it was observed that the top clay has more influence on the cone resistance profile in the blue zone and the zone above. The bottom clay has more influence on the cone resistance profile in the red zone and orange zone. As the peak resistance is developed in the red zone, the bottom clay has more

influence on the cone peak resistance. The peak resistance in Case A is about 2/3 of that in Case B, as the bottom clay is softer in Case A than in Case B.

5 CONCLUSION

The paper studies CPT in a thin medium dense sand layer sandwiched by two different clay layers. Two Cases of soil profiles are established, such as stiff over soft clay and vice versa. By deploying the CSMC model, the stress-dependent behaviors of sand are well captured to reveal a systematic soil responses of cone penetration into clay-sand-clay soils.

The study shows that the top clay has more influence on the cone resistance profile in the top layer and the blue zone. The bottom clay layer has more influence on the cone resistance profile in the red zone and the orange zone (refer to Figure 3 for coloring zones). A softer bottom clay in Case A induces more bending of the sand layer. A stiffer bottom clay in Case B induces higher cone peak resistance in the sand layer.

Further studies are needed to investigate more triple-layer profiles to provide guidance in CPT data interpretations.

REFERENCES

- Ahmadi, M. M. & Robertson, P. K. (2005) Thin-layer effects on the CPT q_c measurement. *Canadian Geotechnical Journal*, 42, 1302–1317.
- Barentsen, P. (1936) Short description of a field testing method with cone-shaped sounding apparatus. *Proceedings 1st International Conference on Soil Mechanics and Foundation Engineering* (pp. 6–10).
- Carter, J. P. & Balaam, N. P. (1995) AFENA users' manual. *Centre for Geotechnical Research, Department of Civil Engineering, University of Sydney, Australia*.
- Hossain, M., Hu, Y., Randolph, M. & White, D. (2005) Limiting cavity depth for spudcan foundations penetrating clay. *Géotechnique*, 55, 679–690.
- Hu, Y. & Randolph, M. F. (1998a) A practical numerical approach for large deformation problems in soil. *International Journal for Numerical and Analytical Methods in Geomechanics*, 22, 327–350.
- Hu, Y. & Randolph, M. F. (1998b) *H*-adaptive FE analysis of elasto-plastic non-homogeneous soil with large deformation. *Computers and Geotechnics*, 23, 61–83.
- Li, X., Hu, Y. & White, D. J. (2013) A large deformation finite element analysis solution for modelling dense sand. *Proc. 18th International Conference on Soil Mechanics and Geotechnical Engineering* (pp. 2359–2362).
- Lunne, T., Powell, J. J. M. & Robertson, P. K. (2002) *Cone penetration testing in geotechnical practice*, CRC Press.
- Ma, H., Zhou, M., Hu, Y. & Hossain, M. S. (2016) Interpretation of Layer Boundaries and Shear Strengths for Soft-Stiff-Soft Clays Using CPT Data: LDFE Analyses. *Journal of Geotechnical and Geoenvironmental Engineering*, 142.
- Ma, H., Zhou, M., Hu, Y. & Hossain, M. S. (2017) Interpretation of layer boundaries and shear strengths for stiff-soft-stiff clays using cone penetration test: LDFE analyses. *International Journal of Geomechanics*, 17, 06017011.
- Mo, P.-Q., Marshall, A. M. & Yu, H.-S. (2016) Interpretation of cone penetration test data in layered soils using cavity expansion analysis. *Journal of Geotechnical and Geoenvironmental Engineering*, 143, 04016084.
- Mo, P. Q., Marshall, A. M. & Yu, H. S. (2015) Centrifuge modelling of cone penetration tests in layered soils. *Géotechnique*, 65, 468–481.
- Silva, M. F. & Bolton, M. D. (2004) Centrifuge penetration tests in saturated layered sands. *Proceedings of 2nd International Conference on Site Characterization, vols. (Vol. 1, pp. 377–384)*.
- Tehrani, F. S., Arshad, M. I., Prezzi, M. & Salgado, R. (2017) Physical modeling of cone penetration in layered sand. *Journal of Geotechnical and Geoenvironmental Engineering*, 144, 04017101.
- Vreugdenhil, R., Davis, R. & Berrill, J. (1994) Interpretation of cone penetration results in multilayered soils. *International Journal for numerical and analytical methods in geomechanics*, 18, 585–599.
- Walker, J. & Yu, H. S. (2010) Analysis of the cone penetration test in layered clay. *Geotechnique*, 60, 939–948.
- Xie, Q. (2020) *Large deformation finite element analysis on cone penetration test in layered sand-clay soils*. School of Engineering, Australia, University of Western Australia.
- Yost, K. M., Cox, B. R., Wotherspoon, L., Boulanger, R. W., Van Ballegooy, S. & Cubrinovski, M. (2019) In Situ Investigation of False-Positive Liquefaction Sites in Christchurch, New Zealand: Palınurus Road Case History. *Eighth International Conference on Case Histories in Geotechnical Engineering* (pp. 436–451). *American Society of Civil Engineers*.
- Youd, T. L. & Idriss, I. M. (2001) Liquefaction resistance of soils: summary report from the 1996 NCEER and 1998 NCEER/NSF workshops on evaluation of liquefaction resistance of soils. *Journal of geotechnical and geoenvironmental engineering*, 127, 297–313.
- Yue, Z. Q. & Yin, J. H. (1999) Layered elastic model for analysis of cone penetration testing. *International journal for numerical and analytical methods in geomechanics*, 23, 829–843.

Study on SPT N -values and relative density through various soundings in full-scale chamber test ground

H. Yabe, K. Harada, T. Ito & E. Watanabe

Geotechnical Division, Fudo Tetra Corporation, Chuo-ku, Tokyo, Japan

ABSTRACT: In Japan, the evaluation of ground strength, such as the liquefaction resistance, is often carried out through the N -value of the standard penetration test (SPT), and it is used in various designs. Other soundings are also used, including the cone penetration test (CPT) and the Swedish weight sounding (SWS) that is comparatively simpler when compared with SPT, and conversion formulae to N -value have also been proposed by various researchers. In this paper, the various soundings described above (SPT, CPT, and SWS) were carried out in a sandy ground, where the density was controlled and measured by Radio Isotope (RI) method. Then, the correlation between the SPT N -value and the relative density D_r was examined. Based on the results, the N - D_r correlation was examined using the results of various soundings in a full-scale chamber test where the ground density was controlled. The results confirmed the applicability of the correlation formulae, with good correlation confirmed not only between D_r and SPT N -value, but also with the N -value estimated from each sounding.

1 INTRODUCTION

Japan has long been prone to ground disasters due to earthquakes and heavy rain, and recent events indicate that it is more prone to these hazards than ever. Countermeasure works have generally been implemented to prevent ground disasters. Ground surveys are essential when determining the necessity and the scale of countermeasure works and confirming the effectiveness after their implementation. The methods frequently used for such ground surveys include in-situ investigations (soundings) through the standard penetration test (SPT). The SPT N -values obtained have been used in the design of various facilities. For example, in the case of the sand compaction pile method used as a countermeasure against liquefaction, SPT N -value is used to determine if the implementation of the countermeasure works is necessary and to confirm the level of improvement after their execution. Also, considering that the design is carried out considering the relative density (D_r) estimated from the SPT N -values obtained, the appropriateness of SPT N -values and their evaluation (D_r -conversion) are important.

In addition to SPT, other soundings used include the cone penetration test (CPT) and the Swedish weight sounding test (SWS). Because there are cases where CPT and SWS can be implemented relatively easier than SPT, formulae to obtain the SPT N -value and D_r from the results of CPT and SWS have been developed.

The authors carried out the above-mentioned soundings in an artificially constructed sandy ground to conduct full-scale tests on ground improvement methods. The correlation between SPT N -values and D_r was examined by comparing: (1) the SPT N -values with the normalized N -values estimated from the CPT/SWS penetration resistance values; and (2) the estimated D_r obtained using available conversion formulae with the measured D_r during the construction of the full-scale test ground. This paper reports on comparative studies carried out for two cases of ground with different target relative densities.

2 OUTLINE OF FULL-SCALE TEST GROUND

The full-scale test ground is shown in Figure 1. The test ground covered an area measuring 12.2 m \times 23.4 m and a depth of 7.5 m, enabling the use of actual construction machines.

As shown in the figure, the full-scale test ground had a deck slab made of concrete and was surrounded by side walls made of steel sheet piles such that a saturated ground could be reproduced. The test ground was saturated after backfilling with sand. For this purpose, vertical pipes were installed at several locations on the sidewalls with a 50 cm thick crushed stone layer at the bottom. Water was injected and distributed through the pipes and the crushed stone layer to saturate the full-scale test ground from the bottom.

The pit sand produced in Namegata (Japan) was used to backfill the test ground. The physical properties of the pit sand are shown in Table 1 and Figure 2. Table 1 also shows the physical properties of Toyoura sand, a Japanese standard sand, for comparison.

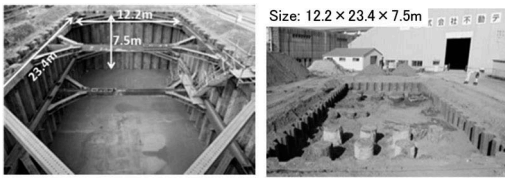


Figure 1. Photos of the full-scale chamber.

Table 1. Physical properties of the backfilling material and Toyoura sand.

Material	F _c (%)	ρ _s (g/cm ³)	e _{max}	e _{min}	e _{min} * U _c	U _c
Toyoura Sand [⊗]	0.0	2.65	0.985	0.611	0.674	1.51
Namegata Sand	4.6	2.716	1.121	0.682	0.586	2.06

e_{min}*: Minimum void ratio from compaction test

⊗Harada et al. (2003)

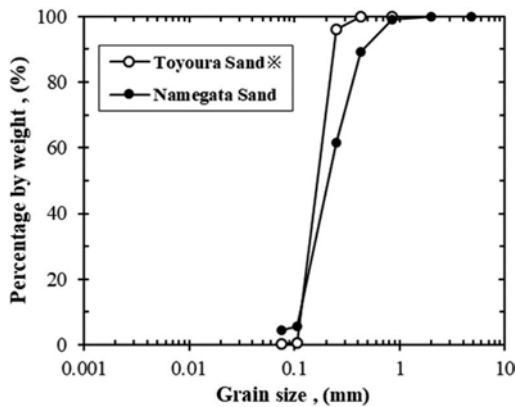


Figure 2. Grain size distribution curve of backfilling material.

3 DENSITY CONTROL DURING CONSTRUCTION OF FULL-SCALE TEST GROUND AND SOUNDING TEST RESULTS

3.1 Density control method

The full-scale test ground was constructed for each of the two cases through backfilling with sand material layer by layer, with each 0.3 m thick layer spread and compacted to the required density. More specifically, the first layer was spread to level the ground. The remaining three layers were compacted by

a roller and other equipment to ensure trafficability for the heavy machines to be used on the test ground.

The density of the full-scale test ground was controlled by measuring the relative density of each layer at 16 locations through the RI (Radio Isotope) method. Then, after completing the construction of the full-scale test ground, various soundings were conducted. Figure 3 shows the locations where the density measurement and various soundings were conducted. In the figure, the locations of the density measurement are indicated by numbers, and the sounding locations are indicated by letters (such as SPT, CPT, and SWS). Also, in Case 1, the full-scale ground was constructed with $Dr = 60\%$ while in Case 2, the ground has $Dr = 80\%$.

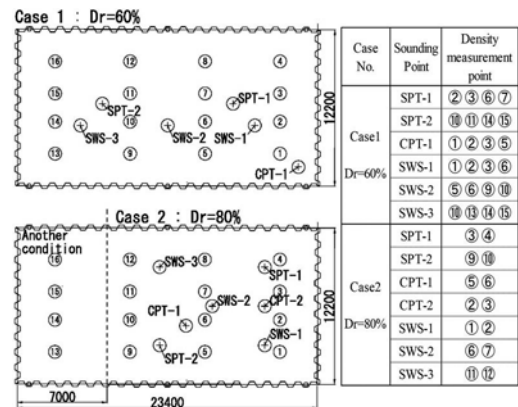


Figure 3. Relationship between the locations of density measurement and soundings within the chamber.

3.2 SPT, CPT, and SWS sounding results

Figure 4 shows the measured profiles of the penetration resistance values (SPT N -values, q_c -values, and N_{SW} values) for each sounding. Comparing the measured results for the same type of sounding conducted more than once (except for CPT in Case 1), a similar trend can be observed regardless of the measurement location. In Case 1, the values of the penetration resistance for each sounding do not change much with depth. However, in Case 2, the penetration resistance values for each sounding increases with depth, and the overall values are larger than those of Case 1 (which has lower relative density).

Figure 5 shows the RI value profiles measured in the vicinity of the sounding points. Two to four points in the vicinity of the sounding were selected based on Figure 3, and the average of the RI values is shown.

In Case 1 (target relative density $Dr = 60\%$), the overall variation of the measurement results was large, and there were places where the measurement results exceeded the control target density. However, the overall average of the measurement results, with dry density $\rho_d = 1.45$ - 1.50 g/cm³ and relative density

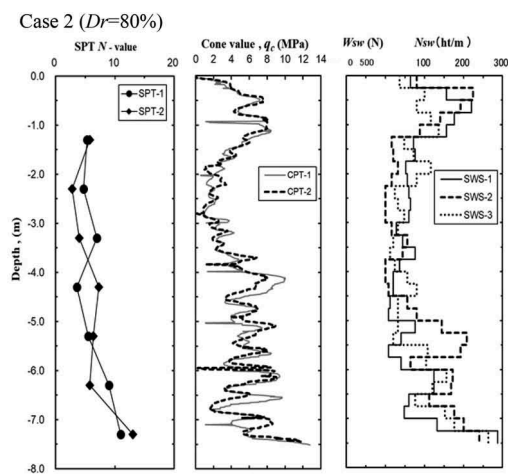
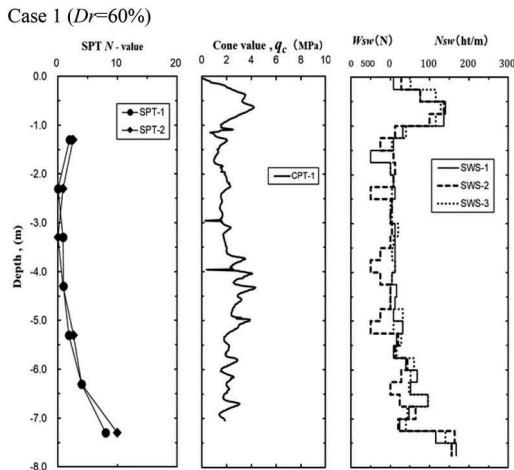


Figure 4. Results of soundings for each case.

$Dr = 55\text{--}70\%$, was within the acceptable range when compared with the target values.

In Case 2 (target relative density $Dr = 80\%$), similar variation in the measurement results was observed, with most of the values exceeding the target value. The overall average relative density was in the range of $85\text{--}100\%$, which was greater than the target value of 80% .

Comparing the profiles shown in Figures 4 and 5, there was variation in the measured RI values at various points around the sounding locations. However, the overall average RI values generally showed a similar trend to the sounding results.

4 DISCUSSION ON THE CORRELATION BETWEEN THE SOUNDING RESULTS

Table 2 shows the correlations available in the literature between Dr and penetration resistance as well as the relations between SPT N -values and CPT/SWS

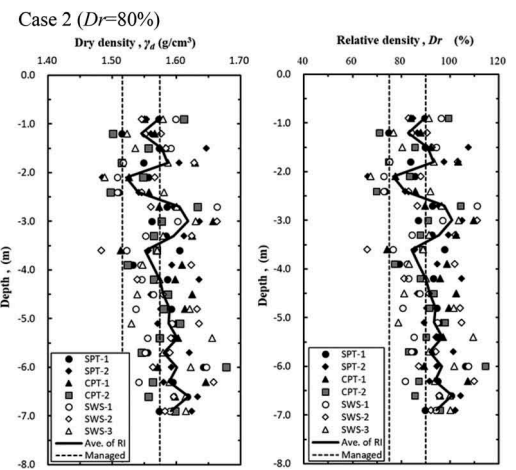
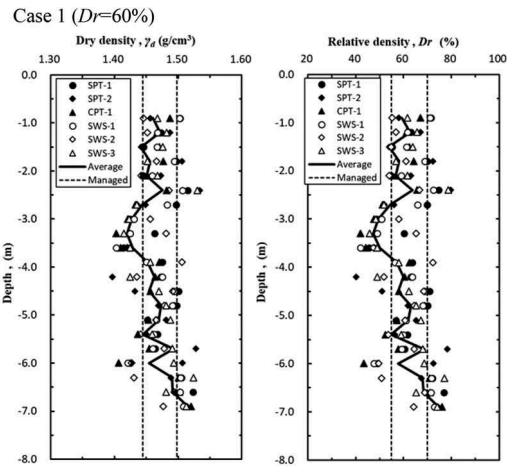


Figure 5. Results of density measurement corresponding to each sounding.

values obtained in natural or artificial grounds. The conversion formulae to obtain Dr are derived from the relation between the penetration resistance and relative density in the range of void ratios reported in the available studies shown in Figure 6.

Figure 7 shows the procedure to estimate Dr from the CPT/SWS penetration resistance and SPT N -values. What follows below is a discussion on the consistency between the sounding results in the sand layers of the full-scale test ground constructed with the controlled density and those from studies in natural ground.

4.1 Comparison between SPT N -value and normalized N -value

Figure 8 shows the comparisons between the SPT N -value and the normalized N -value calculated from the penetration resistance of CPT and SWS using the conversion formulae shown in Table 2 for the relevant cases. According to the figure, the SPT N -values

Table 2. Conversion equation each sounding test.

	Standard Penetration Test SPT	Cone Penetration Test CPT	Swedish weight Sounding Test SWS
Penetration resistance (normalized value)	N -value, N $(N_1 = \frac{170N}{\sigma_v' + 70})$ Meyerhof (1957)	Penetration resistance, q_c ($q_r > 0.2\text{MPa}$) $(q_{c1} = q_c \sqrt{\frac{98}{\sigma_v'}})$ Liao et al. (1986)	Normalized N -value, N $N = 2W_{SW} + 0.06N_{SW}$ W_{SW} : Static weights to cause static penetration of the rod N_{SW} : Number of half a turn of a handle per meter JGS (2013)
Correlating equation	N -value, N	$N_{60} = \begin{cases} 0.341I_c^{1.94} (q_t - 0.2)^{1.34 - 0.0927I_c} \\ 0 \end{cases}$ ($q_t \leq 0.2\text{MPa}$) Suzuki et al. (2003)	$N_1 = \frac{\sqrt{e_{max} - e_{min}}}{10} N'_{SW1}$ $(N'_{SW1} = (N_{SW} + 40) \sqrt{\frac{98}{\sigma_v'}})$ Tsukamoto et al. (1999)
Relative density, D_r (%)	$(N_1)_{80} = \frac{9}{(e_{max} - e_{min})^{1.7}} D_r^2$ Cubrinovski et al.(1999)	$q_{c1} = \frac{12}{(e_{max} - e_{min})^{0.8}} D_r^2$ Harada et al. (2008)	$N'_{SW1} = \frac{90}{(e_{max} - e_{min})^{2.2}} D_r^2$ Tsukamoto et al. (1999)

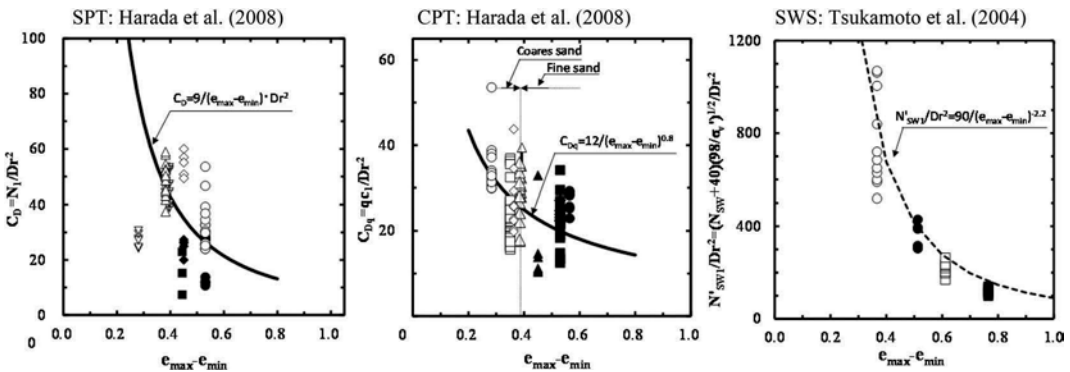


Figure 6. Relationship between the range of void ratio and gradient (SPT, CPT and SWS).

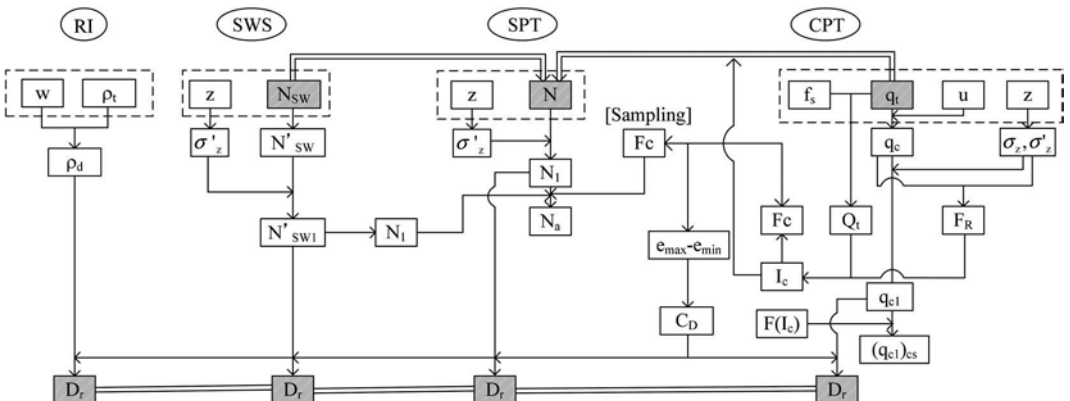


Figure 7. Correlations among each sounding test.

and the normalized N -values have distribution profiles which are similar to each other. Also, according to Figure 9, which shows the correlation between the SPT N -values and the normalized N -values (estimated from the penetration resistance of CPT and SWS using the conversion formulae), the SPT N -values correlate well with the normalized N -values.

4.2 Comparison of RI-measured D_r and sounding-estimated D_r

Figure 10 shows the comparisons between the D_r estimated from the relevant soundings (SPT, CPT, and SWS) and the D_r measured through the RI method for each respective case. The D_r obtained through the soundings was calculated from the average values of the respective cases. The RI values were the average of the measurements at the locations near the sounding locations.

From the figure, the D_r measured through the RI method is generally larger than the D_r estimated from the results of respective soundings. Also, the D_r based on CPT and SWS is close to the D_r measured through the RI method, but the D_r estimated from SPT largely differs from the D_r measured by the RI method. Similar tendencies can be found in Figure 11.

The reasons for these observed trends are considered to be threefold. The first reason is the difference between the full-scale test ground and an actual ground. The test ground was constructed by stacking sand layers each with thickness of 30 cm and saturated immediately before conducting the soundings. In contrast, the actual ground has complex strength distribution due to the stress history developed during a long accumulation period and aging effects. Thus, it is considered that the D_r measured in the full-scale test ground with younger age differs from

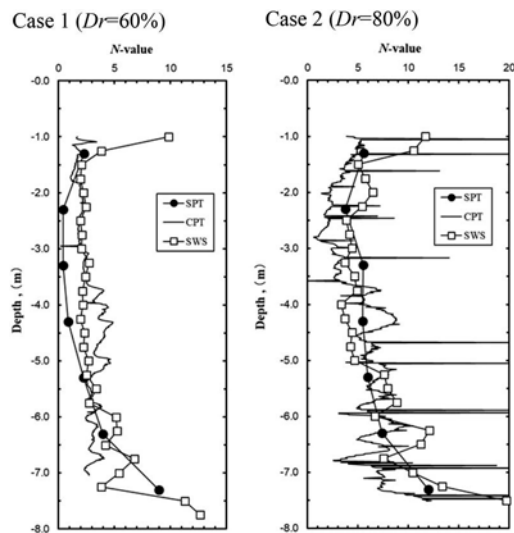


Figure 8. Measured N -values and those estimated from CPT and SWS.

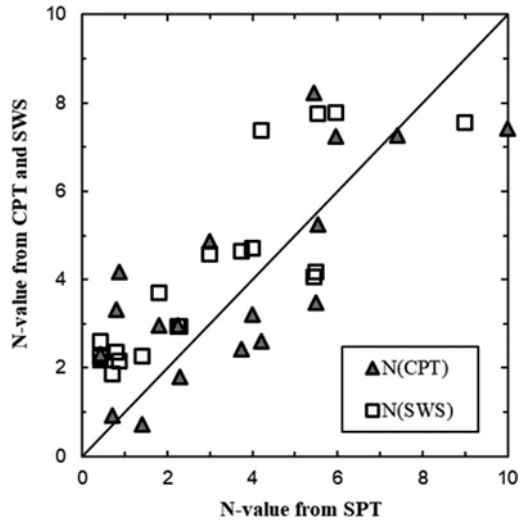


Figure 9. Comparison between measured and estimated N -value.

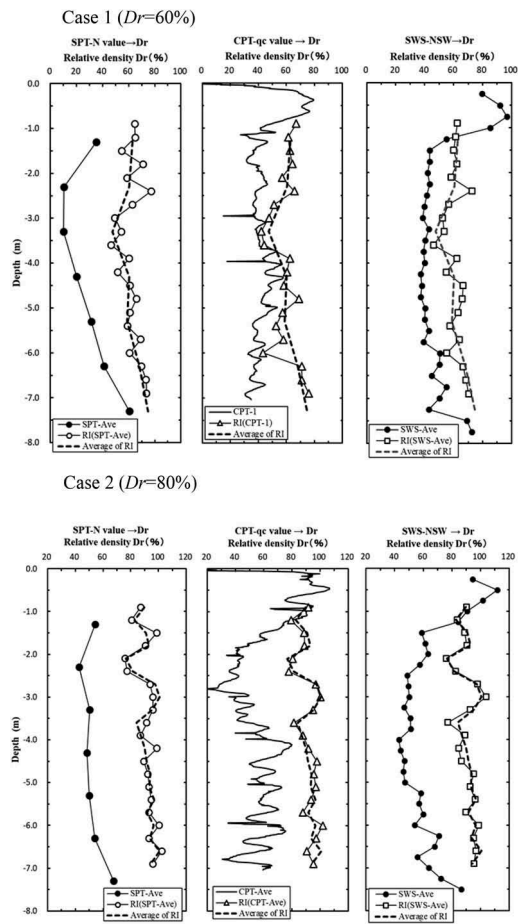


Figure 10. Measured relative density and estimated values from each sounding.

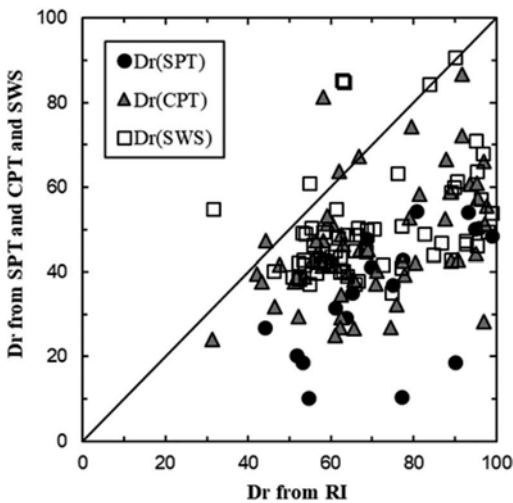


Figure 11. Comparison between measured and estimated relative density.

the Dr calculated by the conversion formulae developed for natural ground.

The second reason is the difference in penetration mechanisms. The SPT, which dynamically applies loads by dropping a hammer into the ground, tends to have a wider variation in relative density than the CPT and SWS, which statically apply loads to the ground. It is also possible that the degree of saturation of the test ground affected the Dr .

The third reason is the difference in the concepts of the minimum void ratio, e_{min} , used to calculate the relative density. There are cases where the minimum void ratios obtained through compaction tests (e_{min}^*) are smaller (denser) than the e_{min} based on its original definition (specified in standard). It is considered that there is a large difference between the measured and estimated Dr values because the conversion formulae listed in Table 2 are based on the conventional Dr , while the relative density from the RI method represents compacted state. Note that there is a significant difference between e_{min} and e_{min}^* for the backfilling sand, as shown in Table 1.

Figure 12 compares the relationship between the cyclic strength and relative density for Namegata sand and for Toyoura sand. As shown in the figure, the cyclic strength of Toyoura sand increases rapidly at relative density of 80%, while that of Namegata sand increases slowly. In other words, the actual minimum void ratio of the backfilling sand is smaller than that from the standard test, and the relative density is considered to be overestimated.

5 SUMMARY

The various soundings in the full-scale test ground confirmed that the existing correlation formulae could

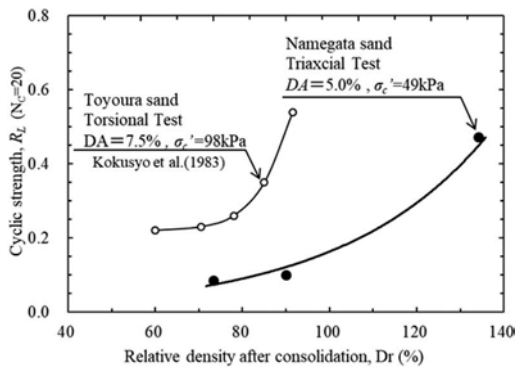


Figure 12. Relationship between cyclic strength and relative density of Namegata sand and of Toyoura sand.

be approximately applied to the correlation between control values and the Dr converted from the results of various soundings. We will continue our comparative study between the measured density in the test ground and the density obtained through the correlation formulae to further verify the accuracy of the correlation formulae.

REFERENCES

- Cubrinovski, M., Ishihara, K. 1999. Empirical correlation between SPT N-value and relative density for sandy soils. *Soils and Foundations*, 39(5): 61–71.
- Harada, K., Ishihara, K., Orense, R.P., Mukai, J. 2008. Relations between penetration resistance and cyclic strength to liquefaction as affected by Kc-conditions. *Proc. Geotechnical Earthquake Engineering and Soil Dynamics IV*, Sacramento CA, Paper 111.
- Harada, K., Yasuda, S., Niwa, T., Shinkawa, N. and Ideno, T. 2003 Evaluation of im-proved ground by compaction containing fines, *JSCCE Journal of Earthquake Engineering*, Vol. 27, No.35 (in Japanese).
- Japanese Geotechnical Society 2013. Chapter 4: Method for Swedish weight sounding test. *Geotechnical and Geoenvironmental Investigation Methods*, 331.
- Kokusho, T., Yoshida, Y., Nishi, K., Esashi, Y. 1983. A study on evaluation method of seismic stability of dense sandy ground: Part 1 - Dynamic strength properties of dense sand. *Central Research Institute of Electric Power Industry Report*, No. 383025, 1–44.
- Liao, S.C., Whitman, R.V. 1986. Overburden correction factors for SPT in sand. *J. of Geotech. Engrg.*, 112(3): 373–377.
- Meyerhof, G.G. 1957. Discussion on research on determining the density of sands by spoon penetration testing. *Proc. 4th Int. Conf. on SMFE*, 3: 110.
- Suzuki, Y., Tokimatsu, K., Sanematsu, T. 2003. Correlations between CPT data and soil characteristics obtained from SPT. *Journal of Structural and Construction Engineering*, 566: 73–80.
- Tsukamoto, Y., Ishihara, K., Sawada, S. 2004. Correlation between penetration resistance of Swedish weight sounding tests and SPT blow counts in sandy soils. *Soils and Foundations*, 44(3): 13–24.

Correcting measured CPT tip resistance for multiple thin-layer effects

K.M. Yost, J. Cooper, R.A. Green, E.R. Martin & A. Yerro
Virginia Tech, Blacksburg, VA, USA

ABSTRACT: Multiple interbedded fine-grained layers in a sand deposit have a “smoothing” effect on the measured tip resistance (q_c) from the cone penetrometer test (CPT). This can result in an underestimation of the predicted liquefaction resistance of the sand layers. Herein, the efficacies of two multiple-thin-layer correction procedures are evaluated using published calibration chamber test data. The results highlight limitations of the assessed procedures for profiles with layers less than 40 mm thick. A new approach to estimate the “true” q_c (i.e., values that would be measured in a stratum absent of multiple thin-layer effects) from measured q_c is explored. The proposed numerical optimization algorithm searches for “true” soil profiles with a finite number of layers. We compare two versions of the algorithm that numerically optimize different functions, one of which uses a logarithm to refine fine-scale details, but which requires longer calculation times to yield improved corrected q_c profiles.

1 INTRODUCTION

Cone penetrometer test (CPT) data (i.e., tip resistance, q_c , and sleeve friction, f_s) are typically reported at 1 to 2 cm depth increments. However, data measured at a given depth are not representative only of the soil at that discrete depth, but are actually averaged or “blurred” values of the “true” values that fall within a zone of influence above and below the cone tip. For example, this zone of influence can include soils that are as far away as 10 to 30 times the cone diameter (d_{cone}) ahead of the cone tip (Ahmadi and Robertson 2005). Thus, the presence of multiple interbedded fine-grained layers in a sand deposit can result in a significant underestimation of the predicted liquefaction resistance of the sand layers. This phenomenon is referred to as multiple thin-layer effects.

Several methods have been proposed to correct CPT data for multiple thin-layer effects. These procedures seek to use the measured CPT data in an interlayered soil profile and estimate the “true” CPT data that would be measured in the profile absent of multiple thin-layer effects (i.e., a true representation of the CPT data at a discrete depth in the profile). In general, approaches to correct for multiple thin-layer effects can be split into two categories: forward procedures and inverse procedures. In both cases, all procedures proposed thus far focus on correcting q_c , not f_s (though some provide methods to retroactively adjust f_s based on the corrected q_c ; complexities in correcting f_s are briefly discussed in Section 4 of this paper).

Forward procedures, like the ones proposed by Youd et al. (2001), Ahmadi and Robertson (2005), de Greef and Lengkeek (2018), and others, apply a series of corrections directly to the measured q_c (q^m) to obtain a “corrected” q_c (q^{corr}) that is a best estimate of the “true” q_c (i.e., q_c that would be measured in the profile absent of multiple thin-layer effects, q^t). Inverse procedures (e.g., Boulanger and DeJong 2018; Cooper et al. 2022) start by making a guess of q^t (q^{inv}) and then apply an artificial blurring model (representative of the blurring effect of the cone in layered soils) to q^{inv} to obtain a “simulated” q^m ($q^{m,sim}$). Then, $q^{m,sim}$ is compared to the actual q^m . If the misfit between $q^{m,sim}$ and q^m is too large, an update is automatically applied to provide a new, improved q^{inv} guess. The procedure iterates until the misfit is acceptable, at which point the last guessed q^{inv} is considered to be a best estimate of q^t .

To develop and validate multiple-thin-layer correction procedures (forward or inverse), one must know both q^m and q^t for a given layered soil profile. Typically, we only know q^m . CPT calibration chamber tests or numerical simulations can be used to obtain both q^m and q^t . In the following sections, the efficacy of existing forward and inverse procedures for correcting multiple thin-layer effects is assessed directly using calibration chamber data. Then, an alternate inverse procedure is proposed and assessed using the same calibration chamber data. Finally, a brief discussion of limitations and areas for future procedure improvement is provided.

2 ASSESSING EXISTING PROCEDURE EFFICACY

2.1 Overview of Deltares calibration chamber tests

A series of CPT calibration chamber tests performed at Deltares by de Lange (2018) were used to assess the efficacy of existing multiple-thin-layer correction procedures. Several soil profiles were considered in these tests, including layered sand-clay profiles and reference (single layer) sand profiles. The CPTs performed in the reference sand profiles were used to estimate q^t for the sand layers in the sand-clay models, where the reference sand profiles had similar relative densities (D_R) and overburden pressures (σ'_v) to the sand layers in the layered sand-clay models. No reference clay profiles were constructed, however, q^t for the clay could be estimated from one of the sand-clay models that had clay layers that were thick enough (200 mm, or $8d_{cones}$ thick) for q^t to fully develop. Details of how the tests were performed and information about the soils used to create the profiles are excluded for brevity and can be found in de Lange (2018).

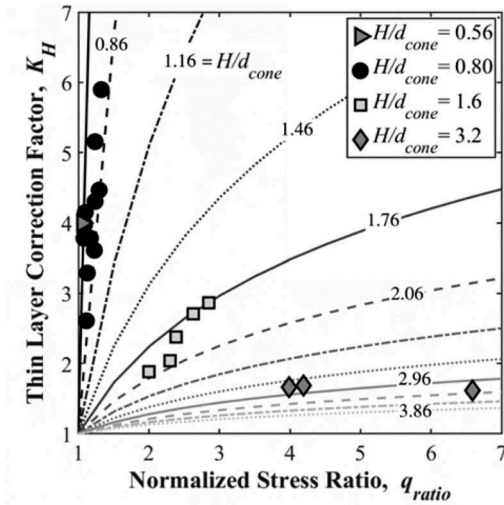


Figure 1. Thin-layer correction factor (K_H) values derived from the de Lange (2018) calibration chamber tests (shown as points) were used to define K_H curves for several normalized thin-layer thicknesses (H/d_{cone}) for the Deltares procedure (Yost et al. 2021a).

2.2 Overview of Deltares forward procedure

Trends observed by de Lange (2018) using the CPT calibration chamber dataset were used to develop a forward multiple-thin-layer correction procedure, the details of which are discussed thoroughly in Yost et al. (2021a). This procedure, termed the Deltares [DEL] procedure, consists of two parts: (1) identification of layer interfaces based on peaks and troughs in q^m , and (2) computation and application of

a correction factor K_H (a function of: layer thickness, H ; d_{cone} ; and normalized ratio between minimum and maximum q^m in a layer, q_{ratio}) that increases tip resistance in thin dense layers. In short, the DEL procedure requires an input of q^m and outputs a corrected tip resistance (q^{cor}) that is an estimate of q^t . K_H factors developed for the DEL procedure are provided in Figure 1.

2.3 Overview of BD18 inverse procedure

The Boulanger and DeJong (2018) [BD18] inverse multiple-thin-layer correction procedure proposes that q^m is equal to q^t convolved with a depth-dependent spatial filter, w_c :

$$q^m(z) = q^t(z) * w_c(z) \quad (1)$$

where $*$ represents a convolution, and q^m , q^t , and w_c are all functions of depth (z). The spatial filter w_c is a discretization of a continuous function that represents the influence of soil above and below the cone tip on q_c at a particular depth. The BD18 procedure uses an iterative splitting optimization technique to solve the misfit function defined by:

$$q^{inv} = \operatorname{argmin}_{q^t} \|q^m - q^t * w_c\|_2 \quad (2)$$

The BD18 procedure includes two steps to smooth the results to prevent them from becoming unstable: *first*, a smoothing step performed after each iteration of the inversion that computes a moving average of q^{inv} over a pre-defined smoothing window, and *second*, a low-pass spatial filtering step performed once the optimization procedure has converged to a solution. After the optimization procedure is performed, a separate interface correction procedure is applied in which sharp transitions in q^{inv} (which presumably correspond to layer interfaces) are identified. A constant value of q^{inv} (either the maximum or minimum q^{inv} identified in the transition zone) is then applied to the entire transition zone within a layer, effectively setting a single q^{inv} value for each identified soil layer.

A modified version of this procedure, termed BD18MOD, was also explored in this study. For this variant of the procedure, the recommended smoothing and filtering steps that ensure convergence of the solution were adjusted. Specifically, the smoothing window was reduced to a maximum of three q^m data points (the default smoothing window is $\max[3, \text{ceiling}(0.866d_{cone}/\Delta z)]$, where Δz is the depth interval at which the data were collected), and the low pass spatial filtering step applied after the inversion was eliminated. We found that this improved the performance of the procedure in identifying very thin layers, but also destabilized the solution, resulting in non-convergence for some scenarios.

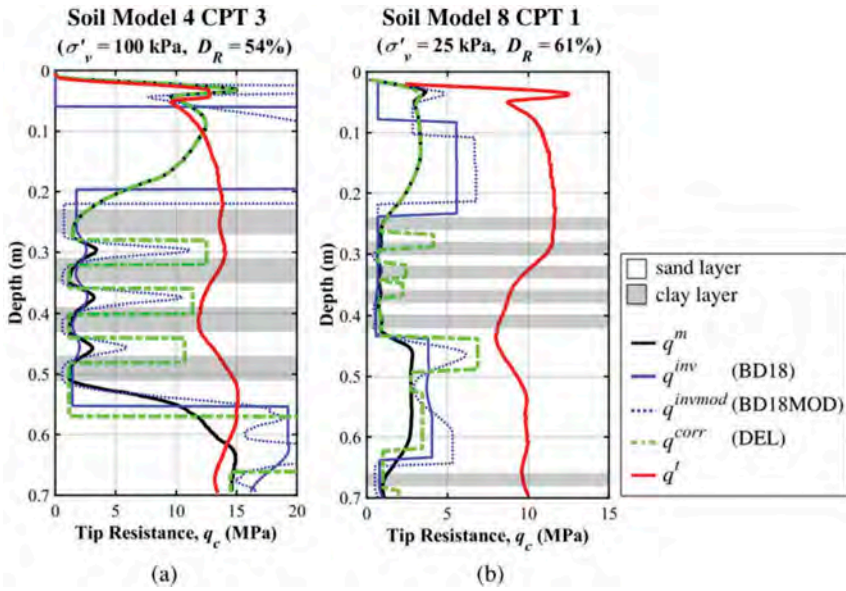


Figure 2. Results from application of multiple-thin-layer correction procedures to de Lange (2018) calibration chamber data for: (a) Soil Model 4 with 40-mm-thick clay layers; and (b) Soil Model 8 with 20-mm-thick-clay layers (Yost et al. 2021a).

2.4 Assessment of procedures using calibration chamber dataset

Direct assessments of the efficacies of the DEL forward procedure, and the BD18 and BD18MOD inverse procedures were performed using the calibration chamber data from de Lange (2018). Note that this is a biased comparison of the efficacies of the procedures, since the DEL procedure was developed and calibrated using this dataset. Regardless, the DEL and BD18/BD18MOD procedures were applied to the q^m for the layered sand-clay soil profiles reported by de Lange (2018). The resulting q^{corr} (from the DEL procedure), q^{inv} (from the BD18 procedure), and q^{invmod} (from the BD18MOD procedure) were compared with the q^t determined from the reference sand profiles. Select results from this exercise are shown in Figure 2.

As shown in Figure 2a, the DEL procedure was effective at identifying the interbedded sand layers and outputting a q^{corr} that is a good estimate of q^t for those layers. Conversely, the BD18 procedure does not identify the interbedded layers, and actually estimates a q^{inv} slightly less than the q^m (and significantly less than q^t) in the interbedded sand layers. The q^{inv} values estimated using the BD18MOD procedure in the interbedded sand layers are a better estimate of q^t , but the layer interfaces are not well defined. The performance of these procedures was similar for all soil profiles in this dataset that contained layers that were 40 mm (or $1.6d_{cone}$) thick.

For the soil profiles in the dataset with interbedded layers less than 40 mm thick, the efficacy of all procedures was poor, as exemplified in Figure 2b. None of the procedures were successful at

identifying all of the 20-mm-thick layers in this profile or providing a good estimate of q^t for those layers, although the DEL procedure did a slightly better job at identifying the layer interfaces compared to the BD18 and BD18MOD procedures.

Several other useful observations were made during this exercise. None of the procedures performed well on the reference sand (single layer) soil models (i.e., all procedures erroneously identified and attempted to correct for thin, interbedded layers that were not present). In general, the BD18MOD procedure performed better than the BD18 procedure on this dataset, however, the modifications to the smoothing steps tended to de-stabilize the solution (e.g., see phantom peak and trough between 0.4 and 0.55 m in Figure 2b). Complete results from this analysis are provided in Yost et al. (2021a).

3 PROPOSED ALTERNATIVE INVERSE PROCEDURE

Because none of the procedures discussed in the previous section were shown to be especially effective at resolving multiple thin-layer effects for profiles with thin layers less than 40 mm thick, an alternative procedure is desired. The inverse approach proposed by Boulanger and DeJong (2018) is attractive because it is fully automated and incorporates an actual description of the physics behind multiple thin-layer effects (i.e., through the blurring model described by the convolution of q^t with the spatial filter w_c). Building on this approach, we pose the inverse problem in a new way by assuming that q^t is

a piecewise constant function, and forcing guesses of q^t (i.e., q^{inv}) to be a piecewise constant function. Thus, the procedure searches for a finite number of layers in a soil profile, each having a thickness and constant q^{inv} . This approach differs from the BD18 approach, which solves for an independent q^{inv} value at every depth, and then subsequently applies a procedure to impose a constant q^{inv} within each identified layer. Reducing the number of degrees of freedom in the problem and eliminating the interface correction step results in a more computationally efficient procedure.

The inverse problem is posed to minimize the misfit function that describes the difference between the actual measured tip resistance profile (q^m) and the simulated measured tip resistance profile ($q^{m,sim}$), which is created by applying an artificial blurring filter to the q^{inv} guess. We restrict q^{inv} to be a piecewise constant function defined by N layers, each paired with a q^{inv} value. Therefore, each proposed q^{inv} profile is described by a material property vector, m , that has $2N$ components (i.e., thickness and q^{inv} for N layers), where N can be adjusted throughout the optimization. For any assumed m , we can extract the q^{inv} values represented by the piecewise function at every depth of where CPT data were measured. The q^{inv} profile resulting from this reconstruction process is denoted by $q^{inv}(m)$. The q^{inv} profile with the minimized misfit is likely to be a good estimate of the q^t profile, but numerical optimization algorithms may yield different answers depending on the choice of the misfit function. Written as an equation, this algorithm optimizes:

$$m^{inv} = \arg \min_{m \in \mathbb{R}^{2N}} \|q^m - q^{m,sim}(q^{inv}(m))\|_2 \quad (3)$$

This is not the only way to pose the optimization problem. For applications where both large-scale and fine-scale features contribute to the misfit, a logarithmic misfit function can be more appropriate and is thus proposed as an alternative to Equation 3:

$$m^{inv} = \arg \min_{m \in \mathbb{R}^{2N}} \log \left(\|q^m - q^{m,sim}(q^{inv}(m))\|_2 \right) \quad (4)$$

This procedure, including both forms of the misfit function, is detailed in Cooper et al. (2022) [Cea22] and is summarized in Figure 3.

In addition to posing the optimization problem, it is necessary to select a numerical optimization algorithm to iteratively update the q^{inv} guess. Cooper et al. (2022) utilizes a Particle Swarm Optimization (PSO) algorithm that identifies minima of the selected misfit function. PSO was selected because it is able to test many widely varying guesses of m , overcoming the challenges often associated with global versus local minima. Consequently, small adjustments to layer thicknesses or assumed q^{inv} only marginally affect $q^m - q^{m,sim}$. To optimize the PSO algorithm, two additional computational procedures are proposed. An add-one-in (AOI) algorithm is utilized to automatically add new layers between existing layers to assess whether the addition of that layer reduces the misfit function of the

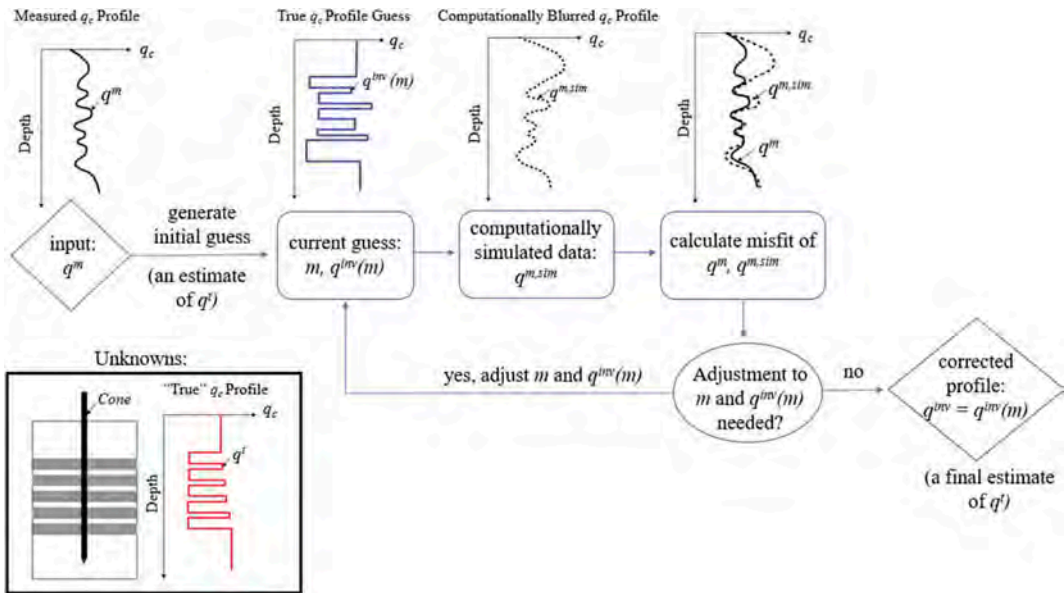


Figure 3. Cea22 inverse approach to correct for multiple-thin-layer effects in CPT tip resistance (modified from Cooper et al. 2022).

proposed profile. A leave-one-out (LOO) algorithm is utilized to remove insignificant layers from the guessed values of q^{inv} that are not physically realistic and contribute to unnecessary additional degrees of freedom.

A key component of this procedure is the application of an artificial blurring filter to the guessed value of q^{inv} . The Cea22 procedure adopts the same framework to describe this blurring as proposed by BD18 (i.e., Equation 1). However, they propose a blurring filter that is a scaled and truncated chi-squared distribution, selected for its asymmetry, smoothness, and relatively good match with the de Lange (2018) calibration chamber data:

$$q^{m,sim}(z) = (q^{m,sim}(q^t))(z) = \int_{-\infty}^{\infty} q^t(\Delta z)p(z - \Delta z)d\Delta z \quad (5)$$

where $\int_{-\infty}^{\infty} p(z)dz = 1$ and $p(z) \geq 0$ for all z . In practice, this integral is only calculated over a finite interval. This blurring function was chosen because it is simple to implement and only requires the use of a matrix convolution function (“conv” in MATLAB). This blurring function results in $q^{m,sim}$ values that represent a weighted combinations of the q^t values of the surrounding soil layers at a given depth. Although this method can quickly compute $q^{m,sim}$ for any q^{inv} guess, it is a simplification of true physics and could be improved upon in future work. This is exemplified by the difference between the actual observed q^m in the layered soil profile (shown in solid black) and the q^m derived from applying the blurring filter to the known q^t (shown in solid blue) in Figure 4, and is discussed further in Section 4.

The Cea22 procedure was applied to the de Lange (2018) calibration chamber data using the q^m derived from applying the blurring filter to q^t (i.e., the blue solid line in Figure 4), in lieu of using the actual measured q^m . It was found that the algorithm with the logarithmic misfit function (i.e., Equation 4) was more effective than the standard misfit function (i.e., Equation 3) at refining the very thin layers in the calibration chamber test soil profiles; see Figure 4. The q^{inv} resulting from the standard misfit function missed several thin layers in q^t , while the q^{inv} resulting from the logarithmic misfit detects each of the thin layers in the layered zone.

Both algorithms (standard and logarithmic misfit) had $q^{m,sim}$ closely matching q^m derived from application of the assumed blurring filter to the known q^t , indicating that the increase in computational rigor provided by the logarithmic misfit algorithm was required to achieve the detailed match between q^{inv} and q^t for this profile. Results were similar for other profiles in the de Lange (2018) dataset and are examined in more detail in Cooper et al. (2022).

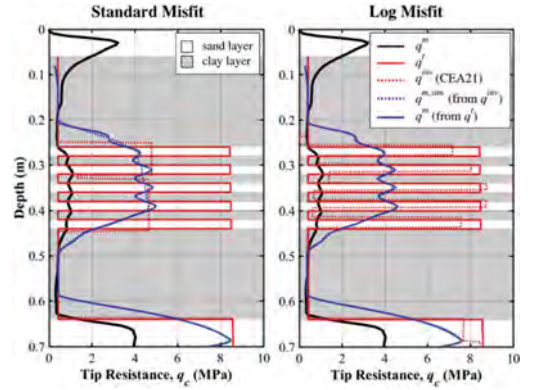


Figure 4. Comparison between Cea22 inverse procedure using the standard misfit function and the logarithmic function on data from Soil Model 9 CPT 3 from de Lange (2018) (modified from Cooper et al. 2022).

4 DISCUSSION AND CONCLUSIONS

Multiple thin-layer effects in CPT data can be addressed using forward or inverse procedures. In this paper, a new forward method (DEL procedure) and a new inverse method (Cea22 procedure) are compared to the existing inverse procedure proposed by Boulanger and DeJong (2018) [BD18] using a set of calibration chamber data collected by de Lange (2018). It is shown that neither the DEL nor the BD18 procedure are effective in correcting for multiple thin-layer effects in profiles with soil layers less than 40 mm thick, with the DEL procedure yielding slightly better results than the BD18 procedure. Because this type of profile is of particular interest for liquefaction assessment, it is desirable to improve on these procedures.

The Cea22 procedure poses the inverse problem that was first proposed by Boulanger and DeJong (2018), but in a new way - searching for a finite number of soil layers each with a thickness and constant q^t . Application of this procedure indicates that this new formulation is better able to identify thin, interbedded layers than the DEL, BD18, or BD18MOD procedures. Furthermore, the restriction on number of degrees of freedom is computationally efficient. It was shown that the logarithmic misfit function is more effective at identifying very thin layers than the standard misfit function. There are tradeoffs in using the standard versus logarithmic misfit function, namely, use of the logarithmic misfit function is significantly more computationally expensive (i.e., 5 to 10 minutes runtime for CPT soundings with several hundred data points, compared to 1 to 2 minutes for the standard misfit function). However, the use of the logarithmic misfit function is anticipated to be worth the extra computational time for highly stratified soil profiles.

Inverse procedures like the BD18 and Cea22 procedure require an artificial “blurring” that mimics

multiple thin-layer effects in CPT data. Thus far, simple blurring models have been adopted. For example, the Cea22 procedure uses a convolution of a point spread function derived from the Chi squared probability density function. As shown in Figure 4, this method does not capture well the true complexity of the physics involved with cone penetration through layered profiles and can be improved upon. If the q' is known for a profile, a q^m derived from applying the blurring filter to q' can be used as input to the multiple-thin-layer correction procedure to assess the efficacy of the procedure itself, without assessing the accuracy of the blurring filter. This is the approach taken in this paper to assess the Cea22 procedure. Developing a more accurate blurring filter is the focus of ongoing work.

A persistent challenge in developing and validating multiple-thin-layer correction procedures is the lack of available q^m and q' pairs for a given layered soil profile. These data can only come from calibration chamber tests (e.g., de Lange 2018) or from numerical simulations. Towards this end, numerical simulations of CPT in layered profiles, like those from Yost et al. (2021b), can supplement the limited available calibration chamber data and be used to develop and calibrate these methods. Numerical simulations should be calibrated and validated with laboratory calibration chamber data if possible.

Finally, all the procedures discussed in this paper focus on developing methods to correct CPT q_c for multiple thin-layer effects. However, CPT f_s is perhaps even more subject to multiple thin-layer effects owing to the large size of the sleeve friction sensor (typically ~110 to 134 mm in length). As a result, the friction sleeve will likely be in contact with multiple soil layers at once in a highly interlayered profile. Additionally, resolving the f_s for a given layer is further hampered by soil from overlying layers being dragged down into underlying layers as the cone advances, which has been observed both experimentally (i.e., de Lange 2018) and numerically (i.e., Yost et al. 2021b). Since f_s is required to compute normalized soil behavior type index (I_c) for liquefaction

triggering calculations, it is critical that future work addresses multiple thin-layer effects on f_s .

REFERENCES

- Ahmadi, M.M. & Robertson, P.K. 2005. Thin-layer effects on the CPT qc measurement. *Canadian Geotechnical Journal*, 42(5): 1302–1317.
- Boulangier, R.W. & DeJong, J.T. 2018. Inverse filtering procedure to correct cone penetration data for thin-layer and transition effects. *Proc. of Cone Penetration Testing 2018*, Hicks, Pisano, and Peuchen, eds., CRC Press, Delft, The Netherlands: 25–44.
- Cooper, J., Martin, E., Yost, K.M., Yerro-Colom, A., & Green, R.A. 2022. Robust Identification and Characterization of Thin Soil Layers in Cone Penetration Data by Piecewise Layer Optimization. *Computers and Geotechnics*, 141:104404.
- de Greef, J. & Lengkeek, H.J. 2018. Transition-and thin layer corrections for CPT based liquefaction analysis. *Proc. of Cone Penetration Testing 2018*, Hicks, Pisano, and Peuchen, eds., CRC Press, Delft, The Netherlands: 317–322.
- de Lange, D.A. 2018. CPT in Thinly Layered Soils. *In: van Elk, J., Doornhof, D., eds.*, Delft, The Netherlands.
- Yost, K.M., Green, R.A., Upadhyaya, S., Maurer, B.W., Yerro-Colom, A., Martin, E.R., & Cooper, J. 2021a. Assessment of the efficacies of correction procedures for multiple thin layer effects on Cone Penetration Tests. *Soil Dynamics and Earthquake Engineering*, 144:106677.
- Yost, K. M., Yerro, A., Green, R. A., Martin, E., & Cooper, J. 2021b. MPM Modeling of Cone Penetrometer Testing for Multiple Thin-Layer Effects in Complex Soil Stratigraphy. *Journal of Geotechnical and Geoenvironmental Engineering*. (in press)
- Youd, T. L., Idriss, I. M., Andrus, R. D., Arango, I., Castro, G., Christian, J. T., Dobry, R., Finn, W. D. L., Harder, L. F., Hynes, M. E., Ishihara, K., Koester, J. P., Liao, S. S. C., Marcuson, W. F., Martin, G. R., Mitchell, J. K., Moriwaki, Y., Power, M. S., Robertson, P. K., Seed, R. B., & Stokoe, K. H. 2001. Liquefaction Resistance of Soils: Summary Report from the 1996 NCEER and 1998 NCEER/NSF Workshops on Evaluation of Liquefaction Resistance of Soils. *Journal of Geotechnical and Geoenvironmental Engineering*, 127(10): 817–833.

Spatial interpolation of consolidation property of clays from limited CPTU dissipation data

Zening Zhao

School of Transportation, Southeast University, Nanjing, China

Wei Duan

College of Civil Engineering, Taiyuan University of Technology, Taiyuan, China

School of Transportation, Southeast University, Nanjing, China

Guojun Cai*

School of Transportation, Southeast University, Nanjing, China

School of Civil Engineering, Anhui Jianzhu University, Hefei, China

Meng Wu

School of Transportation, Southeast University, Nanjing, China

Anand J. Puppala

Zachry Department of Civil and Environmental Engineering, Texas A&M University, USA

Songyu Liu

School of Transportation, Southeast University, Nanjing, China

Surya Sarat Chandra Congress

Zachry Department of Civil and Environmental Engineering, Texas A&M University, USA

ABSTRACT: The coefficient of consolidation (c_h), an important soil property, is often estimated from the piezocone penetration test (CPTU) data. However, the number of interpreted c_h data is usually limited especially in the horizontal direction because the CPTU is usually performed vertically and the dissipation test is time-consuming. In the present study, a novel method is proposed for the interpolation of c_h data in a 2D vertical cross-section. Firstly, the original c_h is interpolated by CPTU dissipation data. Then, the c_h values are interpreted based on the dissipation data at every location including the untested locations using random field theory. Finally, real case is illustrated to prove the applicability of the proposed method. It is shown that the proposed method can reasonably interpolate the c_h at untested locations. Overall, the new method can spatially interpolate the c_h from limited CPTU dissipation data and significantly save the test time.

1 INTRODUCTION

The coefficient of consolidation (c_h), an important geotechnical parameter that reflects the consolidation property of clays, is often used to estimate the seepage characteristics and consolidation settlement of clays (Burns and Mayne, 2002; Duan et al., 2018; Zhao et al., 2021a). It can be interpreted by either laboratory-based oedometer tests or in-situ tests. Due to the drawbacks of oedometer tests being time-consuming, high cost, and disturbance of soil sample, determining c_h by in-situ tests has received extensive attention (Krage et al., 2015). Among various in-situ test methods, the piezocone penetration test (CPTU) has been widely

used to determine c_h in the field since it is fast, repeatable, and economical (Cai et al., 2011; Lunne et al., 1997; Robertson et al., 1992; Zhao et al., 2021b).

The basic principle for estimating c_h by CPTU is as follows: The excess pore pressure (Δu) can be generated around the cone during the penetration process. The penetration process will be halted when a predetermined depth is reached, then the dissipation of the penetration-induced excess pore pressure around the cone will be recorded at a certain time interval and plotted as the excess pore pressure dissipation curve. As a result, the time corresponding to 50% dissipation of the excess pore pressure (t_{50}) can be recorded and used to interpret c_h for lightly over-consolidated to

*Corresponding author
DOI: 10.1201/9781003308829-116

normally consolidated clays (Chu et al., 2002; Sully et al., 1999). For heavily over-consolidated clays, the excess pore pressure rises initially, and then gradually dissipates until it becomes zero due to the dilatatory response (Burns and Mayne, 2002; Lunne et al., 1997; Wu et al., 2021; Zhao et al., 2021a). To address this problem, Chai et al. (2014) proposed an empirical equation to correct the value of t_{50} determined from non-monotonic dissipation curves using an uncoupled plane strain radial consolidation analysis. Then, the corrected t_{50} was used in existing interpretation models.

However, the CPTU dissipation test in super soft soils and marina soils with low permeability can be time-consuming. In these cases, a single cone sounding can take over a day. Moreover, CPTU is only applicable to one-dimensional (1D) analysis, i.e., along the depth. In engineering practice, however, two- or three-dimensional (2D or 3D) geotechnical analysis is often performed in which 2D or 3D information on subsurface soil stratification and zonation is needed (Chen et al., 2016a; Duan et al., 2021; Wang et al., 2020). It is impractical to perform a large number of CPTU dissipation tests over a whole site. Fortunately, random field theory-based spatial interpolation method can provide 2D geotechnical analysis efficiently. For example, Chen et al. (2016a) used random field theory to spatially assess liquefaction-induced settlements. The visualization of the spatial map of c_h can provide useful information for guiding the design and construction of ground or subgrade treatment (Zhao et al., 2021a). Therefore, the development of a simple spatial map is appealing and expected in engineering practice.

In the present study, a novel method was proposed for the interpolation of c_h data in a 2D vertical cross-section using random field theory. Firstly, the original CPTU dissipation data was interpolated in the 2D vertical cross-section. Then, the c_h values were interpreted based on the dissipation data at every location in the 2D vertical cross-section including the untested locations. Finally, real CPTU dissipation data was illustrated to prove the applicability of the proposed method.

2 CPTU-BASED INTERPRETATION MODEL

In the past few decades, many CPTU-based theoretical and empirical interpretation models were proposed for the estimation of c_h (Baligh and Levadoux, 1986; Burns and Mayne, 2002; Cai et al., 2011; Krage et al., 2015; Robertson et al., 1992; Sully et al., 1999; Teh and Houlsby, 1991; Torstensson, 1977). One representative model proposed by Teh and Houlsby (1991) is considered in this study.

This model considers the effect of rigidity index (I_r) based on large strain path analysis and finite difference analysis:

$$c_h = \frac{T^* \sqrt{I_r}}{t_{50}} \cdot r^2 \quad (1)$$

where T^* is a modified dimensionless time factor, which is taken as 0.245 in this paper; t_{50} is the time corresponding to 50% dissipation of excess pore pressure (s); r is the radius of the CPTU cone (17.85mm).

The key to interpret c_h is to determine the time t_{50} corresponding to 50% dissipation of excess pore pressure. For non-monotonic dissipation curves, the time should be corrected. Chai et al. (2014) proposed an empirical equation to correct the value of t_{50} determined from non-monotonic dissipation curves using an uncoupled plane strain radial consolidation analysis. Then, the corrected time was used in Eq. (1). The proposed empirical equation is as follows:

$$t_{50m} = \frac{t_{50}}{1 + 18.5 \left(\frac{t_{umax}}{t_{50}} \right)^{0.67} \left(\frac{L}{200} \right)^{0.3}} \quad (2)$$

where t_{50m} is the corrected time for 50% excess pore pressure dissipation (s); t_{umax} is the time elapsed for reaching the maximum measured excess pore pressure (s).

3 RANDOM FIELD THEORY

To perform 2D analysis over the entire area of interest, random field theory is introduced in this section. The main steps are as follows (Chen et al., 2016b): 1) evaluation of c_h at individual testing locations; 2) statistical and spatial characterization of the index; 3) random field realization and Monte Carlo (MC) simulation to generate 2D c_h maps.

3.1 Spatial correlation

The semivariogram is used to describe the spatial correlation of the predicted P_L value, which can be obtained based on the half variance of two random variables separated by a distance h :

$$\gamma(\mathbf{h}) = \frac{1}{2} \text{Var}[Z(\mathbf{u}) - Z(\mathbf{u} + \mathbf{h})] \quad (3)$$

where $Z(\mathbf{u})$ is a Gaussian random variable at location \mathbf{u} . There are several semivariogram theoretical models, including the linear, spherical, exponential, and Gaussian models.

Then, the semivariogram is related to the spatial correlation $\rho(\mathbf{h})$ by:

$$\rho(\mathbf{h}) = 1 - \gamma(\mathbf{h}) \quad (4)$$

The vector distance h can account for both separation distance and orientation as:

$$h = \sqrt{\left(\frac{h_x}{a_x} \right)^2 + \left(\frac{h_y}{b_y} \right)^2} \quad (5)$$

where h_x, h_y are the scalar components of the vector h along the field's principal axes; scalar quantities a_x, a_y specify how quickly spatial dependence decreases along those axes. The ratio of $a_x/a_y = 1$ represents the correlation decreases with distance equally in all directions.

3.2 Sequential simulation process

To generate random field realizations of the variables of interest, a conditional sequential Gaussian simulation method is implemented, which has been extensively used by mining scientists and geostatisticians for natural resource evaluations and spatial prediction of geohazards. It is worth noting that a multiscale extension of this conditional sequential Gaussian simulation method has been developed in recent studies (Wang et al., 2017). The procedure can be illustrated by:

$$(Z_n|Z_p = z) \sim N\left(\Sigma_{np} \cdot \Sigma_{pp}^{-1} \cdot z, \sigma_n^2 - \Sigma_{np} \cdot \Sigma_{pp}^{-1} \cdot \Sigma_{pn}\right) \quad (6)$$

where Z_n is the next realization to be simulated; Z_p is the vector of all known and previously simulated points.

Once Z_n is simulated, it becomes a known data point in the vector of Z_p to be conditioned upon by all subsequent data locations. This process is repeated to other unknown points until all locations in the field have been simulated.

Random field models incorporate the spatial dependence of the measured parameter through the covariance matrix. The covariance of values at two separated locations could be expressed as:

$$\Sigma = \text{COV}[Z_i, Z_j] = \rho_{Z_i, Z_j} \cdot \sigma_{Z_i} \cdot \sigma_{Z_j} \quad (7)$$

where ρ_{Z_i, Z_j} is the spatial correlation (calculated by Eq. (4)) between the random variables Z_i and Z_j with standard deviations of σ_{Z_i} and σ_{Z_j} , respectively.

Once the empirical semivariogram $\gamma(h)$ is characterized, it will be plugged into the covariance matrix Eqs. (4) and (7). Thus, the unknown value Z_n at location n could be drawn using Eq. (6). The generated value is then assigned to location n and treated as known data. This process is repeated until all the unsampled locations are assigned with values. Detailed process of random field modeling may be found in Chen et al. (2016a, b).

4 ILLUSTRATIVE EXAMPLE

4.1 Interpretation of dissipation tests

The CPTU test site is located in the Yangtze River tunnel of Jiangyin, Jingjiang City, Jiangsu Province,

China. The geological formation in this area belongs to the floodplain geomorphic unit of the Yangtze River, and the depth of the groundwater level is 1.5m below the ground surface. Figure 1 shows the profiles of the CPTU site.

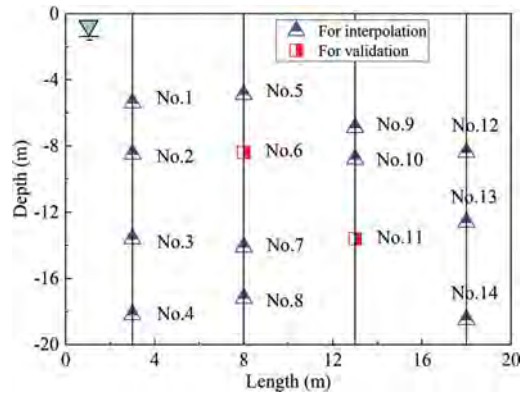


Figure 1. Layout of CPTU dissipation tests at the Yangtze River tunnel of Jiangyin, Jingjiang City, Jiangsu Province, China.

At this test site, a total of 4 CPTU boreholes were performed. The CPTU equipment is shown in Figure 2. The dissipation test was performed using a multifunctional, digital, and vehicle-mounted CPTU system produced by Vertek-Hogentogler (Randolph, OH), USA (Cai et al., 2011). The parameters of the CPTU probe are as follows: cone apex angle of 60°, a cone bottom diameter of 35.7 mm, a cross-sectional area of 10 cm², a sleeve surface area of 150 cm², the pore pressure is measured at the u_2 position, penetration rate is 20 mm/s. During the penetration process, the Δu can be measured at regular intervals. Then, the dissipation of Δu over time was recorded until the pore pressure reaches the equilibrium hydrostatic pressure. After that, the penetration was continued further to the next desired depth and the above steps were repeated. Finally, a total of 14 dissipation tests were performed in this site.

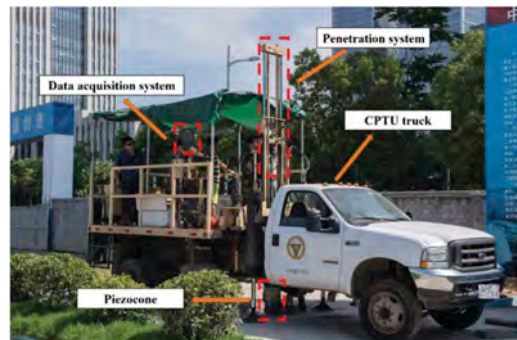


Figure 2. CPTU test equipment.

High-quality soil samples were also taken at different depths, corresponding to the depths of dissipation tests, using a stationary piston sampler. The diameter of the stationary piston sampler is 76 mm. The soil sample at the end of the tube was extruded for waxing and sealing at both ends after withdrawing the stationary piston sampler from the borehole. The collected soil samples were temporarily stored near the site before being transported back to the laboratory. In this study, unconfined compression tests and the K_o -consolidated undrained triaxial tests (CK_oU) were performed on undisturbed samples to estimate undrained shear strength (s_u) and shear modulus (G) of the soils. Then, the I_r can be calculated by $I_r = G/s_u$. Other important soil parameters such as unit weight (γ) and overconsolidation ratio (OCR) were also obtained from laboratory tests, as listed in Table 1.

It can be noted that the OCR is in the range of 1.18-1.29, indicating the clays at the test site are usually lightly over-consolidated.

The key to interpret c_h is to determine the time t_{50} corresponding to 50% dissipation of excess pore pressure. The excess pore water dissipation curves are shown in Figure 3.

Table 1. Typical soil properties in the CPTU soundings.

Sounding	γ (kN/m ³)	s_u (kPa)	E_s (MPa)	OCR
CPTU1	17.5	18.34	3.58	1.22
CPTU2	17.6	17.85	3.26	1.21
CPTU3	17.4	20.16	3.81	1.29
CPTU4	17.3	19.13	3.50	1.18

It can be noted from Figure 3 that the dissipation curves are non-monotonic dissipation curves, that is, the excess pore pressure rises initially and then gradually dissipates until it is zero. The non-monotonic dissipation curves are mainly caused by (a) shear-induced dilatancy of over-consolidated clays or dense sandy soils around the cone and (b) possible unloading effects of the soil elements moving from the vicinity of the face to the shoulder of the cone, which can cause a large gradient in pore pressure going from the cone to the shaft (Zhao et al., 2021a). Therefore, the c_h should be interpreted using Eqs. (1) and (2). The results are listed in Table 2. It can be noted that the c_h varies significantly in the spatial, it is therefore to be interpolated spatially using random field theory.

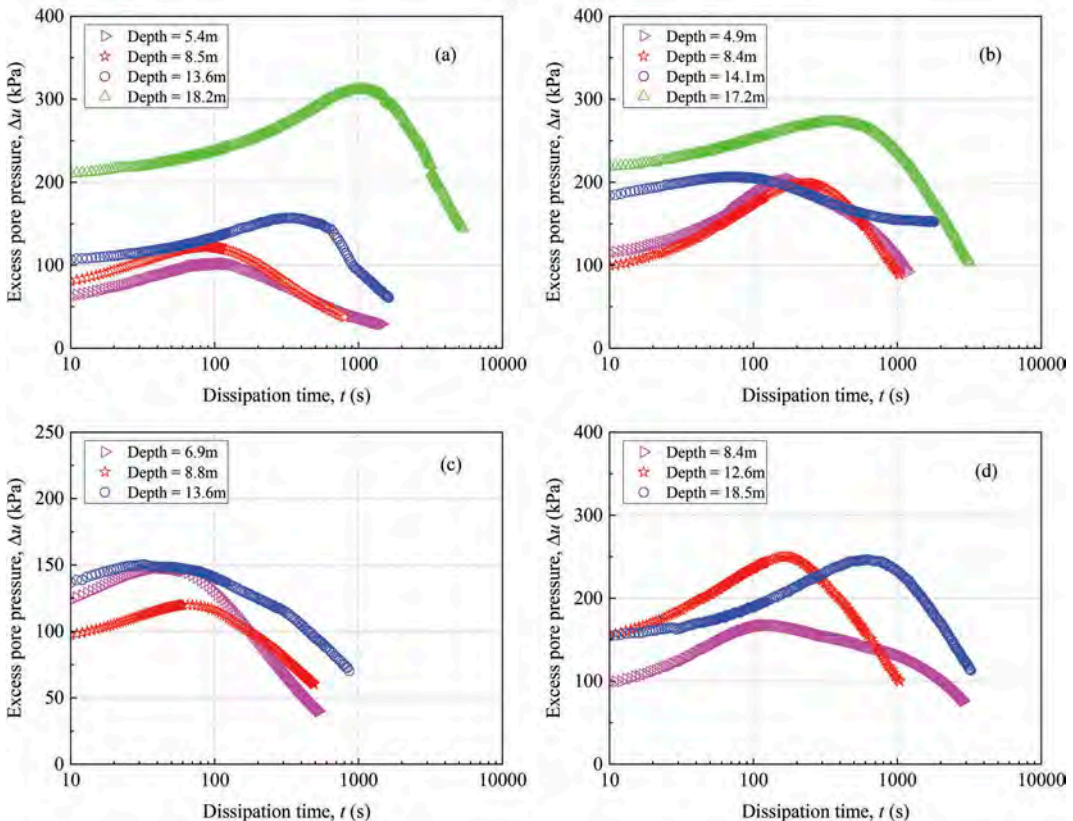


Figure 3. Dissipation curves at soundings (a) CPTU1; (b) CPTU2; (c) CPTU3; (d) CPTU4.

Table 2. Interpretation results of dissipation tests.

Sounding	No.	Depth (m)	I_r	t_{umax} (s)	t_{50} (s)	t_{50m} (s)	c_h (mm ² /s)
CPTU1	1	5.4	160	107	513	73	13.577
	2	8.5	90	98	392	58	12.754
	3	13.6	115	340	900	98	8.522
	4	18.2	95	1060	3560	470	1.618
CPTU2	5	4.9	190	195	860	111	9.685
	6	8.4	120	245	775	93	9.199
	7	14.1	160	79	1410	402	2.457
	8	17.2	90	320	2200	440	1.683
CPTU3	9	6.9	80	53	260	41	16.015
	10	8.8	110	55	420	75	9.670
	11	13.6	120	53	707	182	4.593
CPTU4	12	8.4	125	120	2520	73	13.577
	13	12.6	135	180	640	80	11.378
	14	18.5	125	580	2390	331	2.637
Mean					1156	168	8.825
SD					943	151	4.657
COV					0.816	0.894	0.528

4.2 Spatial interpolation

The length of the area is 20 m, whereas the depth of the area is 20 m. Of the 14 dissipation tests, 12 dissipation tests are used to develop the hazard map of liquefaction-induced lateral spread based on random field theory, while the other 2 dissipation tests (i.e., No. 6 and 11) are used for the validation.

As suggested by Chen et al. (2016a), the lognormal distribution is used to fit the distribution of c_h . Then, the fitted lognormal distribution is adopted to characterize the semivariogram and then generate random fields in the sequential Gaussian simulation. In the present study, the typical exponential semivariogram has been used to fit the empirical semivariogram. The grid size of the random field in this site is set as 0.1 m. A parametric analysis of MC simulation number ranging from 1,000 to 10,000 has been performed, as shown in Figure 4. It is shown that 1,000 MC simulations are enough as COV of the c_h values tends to be stable with the MCS number goes beyond 1,000.

The spatial map of c_h is shown in Figure 5. The c_h can be characterized and visualized. The c_h values at dissipation tests No. 6 and 11 are about 11.586 mm²/s and 6.325 mm²/s, respectively. It is evident that the c_h values at dissipation tests No. 6 and 11 interpolated based on random field theory are similar to the validation values, and can be viewed as the smoothed representation of the actual data. This proves the reliability of the random field theory in spatial interpolation.

The proposed method can be used to spatially interpolate any fields in the future. It can generate c_h values at untested sites and reflect the actual values in the field, which are often not available in the engineering practice. Therefore, the proposed method can significantly save the test time especially in super soft soils and marine soils.

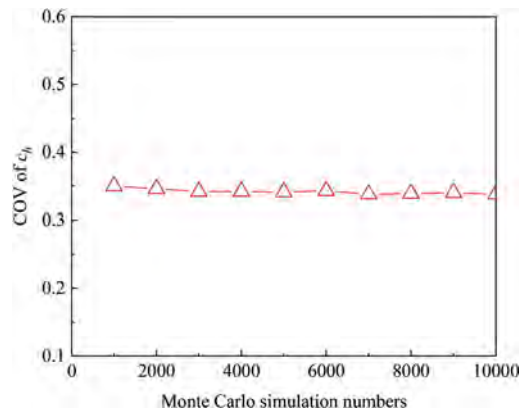


Figure 4. Variations of COV of c_h as the number of Monte Carlo simulations increases.

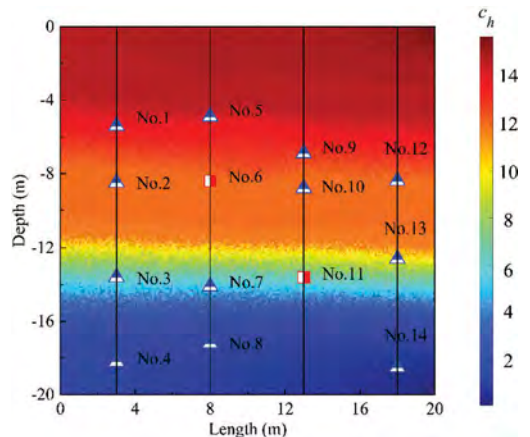


Figure 5. Spatial map of mean values of c_h in the testing site.

5 CONCLUSIONS

In this study, the random field theory was incorporated in the interpretation model of c_h , which can be used for areal interpolation and uncertainty quantification. It can provide the spatial map of c_h over a field using limited CPTU data. The spatial map can provide useful information on the need of project-specific geotechnical investigation.

The proposed method can interpolate c_h values at untested sites and reflect the actual values in the field, which are often not available in the engineering practice. Therefore, the proposed method can significantly save the test time especially in super soft soils and marine soils.

ACKNOWLEDGEMENTS

The majority of the work presented in this paper was funded by the National Key R&D Program of China (Grant No. 2020YFC1807200), the National Natural Science Foundation of China (Grant No. 41877231, No. 42072299, and No. 52108332). The financial supports are greatly acknowledged.

REFERENCES

- Baligh, M. M., & Levadoux, J. N. 1986. Consolidation after undrained piezocone penetration. II: Interpretation. *Journal of Geotechnical Engineering*, 112(7): 727–745.
- Burns, S.E. & Mayne, P.W. 2002. Analytical cavity expansion-critical state model for piezocone dissipation in fine-grained soils. *Soils and Foundations* 42(2): 131–137.
- Cai, G., Liu, S. & Puppala, A.J. 2011. Predictions of coefficient of consolidation from CPTU dissipation tests in Quaternary clays. *Bulletin of Engineering Geology and the Environment* 71(2): 337–350.
- Chai, J.C., Julfikar Hossain, M., Carter, J. & Shen, S.L. 2014. Cone penetration-induced pore pressure distribution and dissipation. *Computers and Geotechnics* 57: 105–113.
- Chen, Q., Wang, C., & Juang, C.H. 2016a. Probabilistic and spatial assessment of liquefaction-induced settlements through multiscale random field models. *Engineering Geology* 211: 135–149.
- Chen, Q., Wang, C., & Juang, C.H. 2016b. CPT-based evaluation of liquefaction potential accounting for soil spatial variability at multiple scales. *Journal of Geotechnical and Geoenvironmental Engineering* 142(2): 04015077.
- Chu, J., Bo, M.W., Chang, M.F. & Choa V. 2002. Consolidation and permeability properties of singapore marine clay. *Journal of Geotechnical and Geoenvironmental Engineering* 128(9): 724–732.
- Duan, W., Cai, G., Liu, S., Puppala, A.J. & Chen, R. 2018. In-Situ Evaluation of Undrained Shear Strength from Seismic Piezocone Penetration Tests for Soft Marine Clay in Jianguo, China. *Transportation Geotechnics* 20:100253.
- Duan, W., Congress, S.S.C., Cai, G., Liu, S., Dong, X., Chen, R. & Liu, X. 2021. A hybrid GMDH neural network and logistic regression framework for state parameter-based liquefaction evaluation. *Canadian Geotechnical Journal* 58(12): 1801–1811.
- Krage, C.P., DeJong, J.T. & Schnaid, F. 2015. Estimation of the coefficient of consolidation from incomplete cone penetration test dissipation tests. *Journal of Geotechnical and Geoenvironmental Engineering* 141(2): 06014016.
- Lunne, T., Robertson, P.K. & Powell, J.J.M. 1997. Cone Penetration Testing in Geotechnical Practice. CRC Press, London.
- Robertson, P.K., Sully, J.P., Woeller, D.J., Lunne, T., Powell, J.J.M. & Gillespie, D.G. 1992. Estimating coefficient of consolidation from piezocone tests. *Canadian Geotechnical Journal* 29(4): 539–550.
- Sully, J.P., Robertson, P.K., Campanella, R.G. & Woeller, D.J. 1999. An approach to evaluation of field CPTU dissipation data in overconsolidated fine-grained soils. *Canadian Geotechnical Journal* 36(2): 369–381.
- Teh, C.I. & Houlsby, G.T. 1991. An analytical study of the cone penetration test in clay. *Géotechnique* 41(1): 17–34.
- Torstensson, B.A. 1977. The pore pressure probe. Geoteknikdagen, Norway.
- Wang, C., Chen, Q., Shen, M., & Juang, C. H. 2017. On the spatial variability of CPT-based geotechnical parameters for regional liquefaction evaluation. *Soil Dynamics and Earthquake Engineering* 95: 153–166.
- Wang, Y., Hu, Y., & Zhao, T. 2020. CPT-based subsurface soil classification and zonation in a 2d vertical cross-section using Bayesian compressive sampling. *Canadian Geotechnical Journal* 57(7): 947–958.
- Wu, M., Cai, G., Liu, L., Jiang, Z., Wang, C. & Sun, Z. 2021. Quantitative identification of cutoff wall construction defects using Bayesian approach based on excess pore water pressure. *Acta Geotechnica* online.
- Zhao, Z., Duan, W. & Cai, G. 2021a. A novel PSO-KELM based soil liquefaction potential evaluation system using CPT and Vs measurements. *Soil Dynamics and Earthquake Engineering* 150: 106930.
- Zhao, Z., Congress, S.S.C., Cai, G. & Duan, W. 2021b. Bayesian probabilistic characterization of consolidation behavior of clays using CPTU data. *Acta Geotechnica* 1–18.



Taylor & Francis

Taylor & Francis Group

<http://taylorandfrancis.com>

Session 3: Applications



Taylor & Francis

Taylor & Francis Group

<http://taylorandfrancis.com>

Evaluation of the geotechnical behavior of mining tailings through CPTU tests in the soil improvement process for the decharacterization of upstream heightened dams

J.L. Albino

Universidade Federal de São Carlos – UFSCAR, Brazil

T.A.T. Souza J. & L.S. Machado

Universidade Federal de Viçosa – UFV, Brazil

ABSTRACT: In order to assess the pore pressure conditions, to verify the drained behavior or not of a reservoir of a tailings dam raised upstream, and to observe the evolution of the resistance of the material, CPTU surveys were carried out before and after the execution of works for the implementation of vertical geodrains in the reservoir of this dam. After the comparative tests, it was possible to indicate the safety gains of the structures resulting from the execution of the works.

Keywords: CPTU test, upstream tailing dam, pore pressure dissipation, geodrains, liquefaction

1 INTRODUCTION

The decharacterization of dams heightened by the upstream method is a legal obligation in the national territory (Brazil). This obligation is a reaction to the last dam failures in Brazil, in which the failures of the Fundão Dam in 2015 and the B1 Dam in 2019 were mainly caused by the liquefaction of the tailings. Mine tailings disposed hydraulically in dams tend to have a contractile behavior, mainly due to the initial void rate and material saturation. To carry out the decharacterization, the concern of liquefaction is also present, and it is necessary to control the possible triggers.

In this environment, companies must rethink not only their traditional approaches to mining operations, but also the development of technologies and studies of tailings disposal.

Laboratory evaluations allow testing materials in a controlled manner, under the desired conditions. However, a limitation of these analyzes is the extraction of undisturbed samples, especially those in depth and in regions of low resistance. This is because, in the sampler crimping process, the sample is disturbed, making the test results divergent from the field condition.

On the other hand, measures to assess the *in situ* tailings behavior can significantly contribute to the identification of the undrained behavior of the soil

and the susceptibility to liquefaction. Tests such as CPTU, for example, are able to assess the *in situ* conditions of the material, the development of effective stress and pore pressure along the depth.

Therefore, CPTU tests were carried out prior to the elaboration of the project to de-characterize an upstream heightened dam work located in the iron quadrangle. Since the behavior of the material was observed as susceptible to liquefaction, interventions were carried out downstream of the dam in order to turn the material initially with undrained behavior into drained behavior. These interventions were carried out with the use of vertical geodrains to accelerate the densification process, and mainly, in the dissipation of pore pressure.

The vertical geodrains contain a HDPE (High Density Polyethylene) core forming small channels. The core is wrapped in non-woven geotextile, which acts as a filter. Thus, the water captured by the drain is conducted through the small channels of the HDPE core to the surface of the land, where it is drained by the upper drainage layer, placed on the surface of the land.

After the interventions, a second battery of CPTU tests was carried out. Through these investigations, it was possible to evidence the dissipation of the pore pressure in the dam and in the tailings, causing the material to behave in a drained way. Such findings were significant for the decharacterization of the dam to be carried out safely.

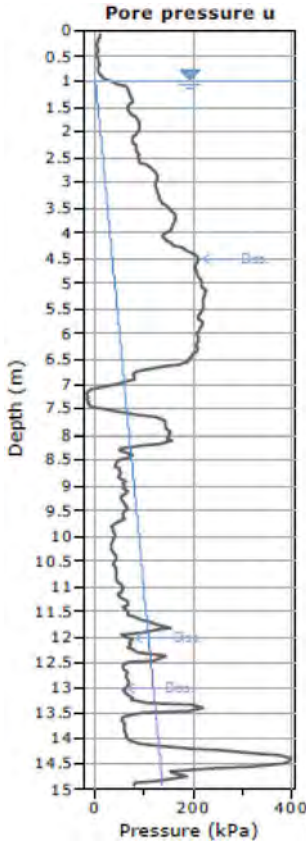


Figure 1. Pore pressure of CPTU 2017 before construction.

1.1 CPTU test

Currently, one of the main forms of sounding for simplified identification of soil properties is the CPTU. The characterization of intermediate sedimentary soils, especially silty sands, non-plastic silts, silty clays and fine-grained tailings are often complicated due to the difficulty of sampling these materials. Thus, CPTU tests can be used to determine the stratigraphic profiles, *in situ* conditions of the material and to estimate the material's geotechnical parameters. [1, 2]

With the CPTU crimping, automatic information is collected on tip resistance (q_c), resistance by lateral friction (f_s) and pore pressure at different points of the cone (u_1, u_2 e u_3). [3]

Because of the characteristic geometry of the cone, the record is disturbed by atmospheric pressure and by the difference in pore pressure value collected at different points (u_1, u_2 e u_3). Thus, it is necessary to correct the values obtained when carrying out the drilling according to the boundary conditions. Therefore, the main values that can be generated at first with the CPTU are the standardized resistance of the tip Q_m , the normalized friction ratio F_r , the friction ratio with R_f and the parameter of pore pressure as B_q . [1, 4]. The

ways of calculating these values are presented below, equations (1) to (7):

$$Q_m = [(q_t - \sigma_{vo}) / \sigma_{atm}] \times (\sigma_{atm} / \sigma'_{vo})^n \quad (1)$$

$$F_r = [f_s / q_t - \sigma_{vo}] \times 100\% \quad (2)$$

$$R_f = f_s / q_c \times 100\% \quad (3)$$

$$B_q = (u_2 - u_0) / (q_t - \sigma_{vo}) \quad (4)$$

$$q_t = q_c + (1 - a) \times u_2 \quad (5)$$

$$n = 0.381 \times I_c + 0.05 \times (\sigma'_{vo} / \sigma_{atm}) \quad (6)$$

$$I_c = \left\{ [3.47 \times \log(Q_m)]^2 + [1.22 + \log(F_r)]^2 \right\}^{0.5} \quad (7)$$

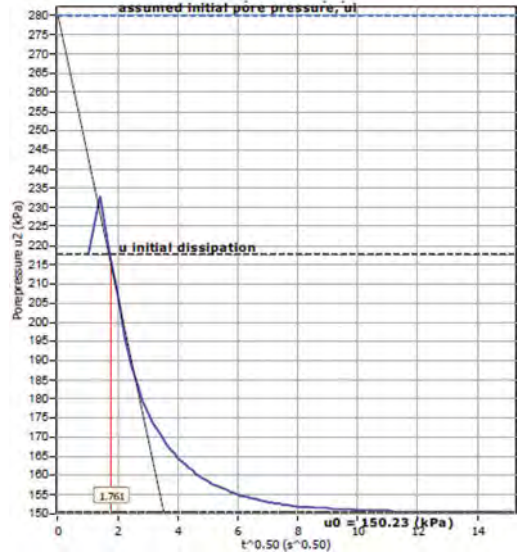


Figure 2. CPTU 2017 dissipation test (13.0 meters) before construction.

We can define the elements of the formulas written above, with q_t being the corrected true tip resistance, σ_v being the total vertical stress at depth, σ'_{vo} the vertical effective stress ($\sigma'_{vo} = \sigma_{vo} - u_0$), f_s a lateral friction resistance, q_c the penetration resistance of the tip, a being the ratio of the cone areas (A_N / A_T), u_2 is the measured pore pressure, u_0 is the equilibrium pore pressure.

1.2 Assessment of soil behavior

From the parameters obtained above, along with the CPTU drilling depth, several geotechnical characteristics of the soil can be identified.

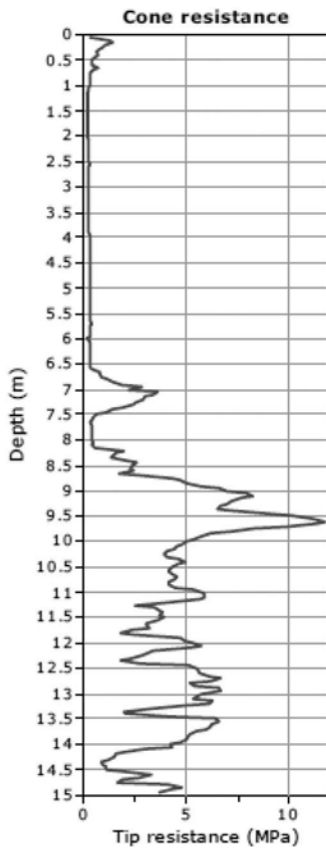


Figure 3. CPTU 2017 Cone tip resistance before construction.

With the CPTU test, it is possible to evaluate, through correlations, the following soil characteristics: stratigraphy, geotechnical profile, density coefficient (C_h e C_v), relative density (D_r), undrained resistance (S_u), sand effective friction angle (ϕ'), stress history (pre-consolidation stress, OCR), permeability coefficient (k), maximum shear modulus (G_o), deformability coefficient (m_v), modulus of deformability or Young's (E), effective friction angle (ϕ'), confined or oedometric modulus of deformation (M), sensitivity (S_t), permeability coefficients (k_h and k_v) and evaluation of susceptibility to liquefaction of a soil. [2, 8]

Another very important point is that with the records of cone tip resistance, lateral friction resistance and pore pressure, the CPTU interpretation is applied for the stratigraphic determination of the soil based on the behavior type graphs of the soil (SBTn). This proposal was presented by Robertson (1990) where plots of two abacuses are made ($Q_t \times Fr$ (%) e $Q_t \times Bq$), where the Q_t is the normalized of cone tip resistance (8) [5, 6, 7]:

$$Q_t = (q_t - \sigma_{vo}) / (\sigma_{vo} - u_0) \quad (8)$$

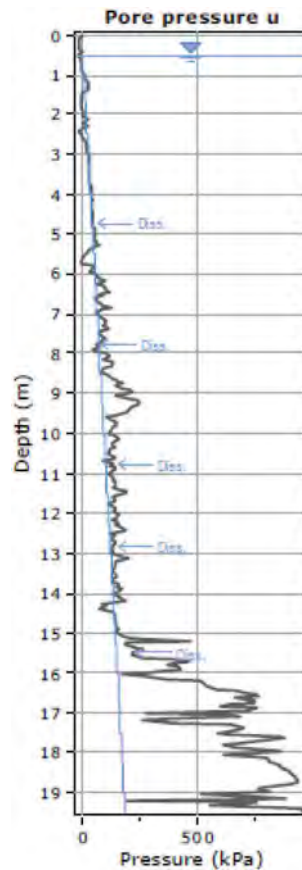


Figure 4. Pressure pore of CPTU 2020 after construction.

For this study, the pore pressure acting on the tailings will be evaluated in order to identify its reduction after the implementation of vertical geodrains in a dam's reservoir. In addition, the behavior of the material regarding the dissipation test will also be evaluated in order to assess the change from undrained to drained behavior of the tailings.

1.3 Dissipation test

The dissipation test consists of interrupting CPTU penetration and observing the pore pressure over time.

Data is logged and must occur to a minimum dissipation of 50%.

Pressures are plotted as a function of the square root of time. The graphical technique suggested by Robertson and Campanella (1989) provides a value for t_{50} , which corresponds to the time to consolidation of 50% [9].

The value of the consolidation coefficient in the radial or horizontal direction C_h was then calculated by Houlsby and Teh's (1988) theory using the following equation (9) [10]:

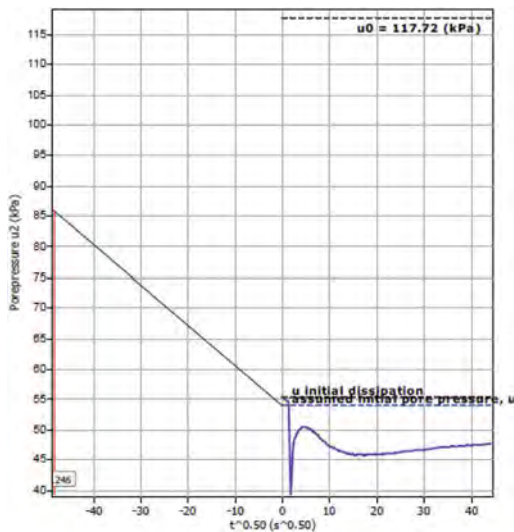


Figure 5. CPTU 2020 dissipation test (15.5 meters) after the works.

$$C_h = T \times r^2 \times I_r^{0.5} / t_{50} \quad (9)$$

Where T is the time factor given by the theory of Houlsby and Teh (1988) corresponding to the pore pressure, r piezocone radius, I_r is the stiffness index, equal to the shear modulus G divided by the undrained strength of the clay (S_u) and t_{50} the time corresponding to 50% consolidation.

Furthermore, the pore pressure dissipation during a CPTU dissipation test is controlled by the consolidation coefficient in the horizontal direction (C_h) which is influenced by a combination of soil permeability (k_h) and compressibility (M), like defined by the following equation (10):

$$k_h = C_h \times \gamma_w / M \quad (10)$$

Where M is the restricted modulus and γ_w is the unit weight of water, in compatible units.

2 RESULTS

Initially, with the performance of CPTU tests in 2017, before the geodrain implantation works, the presence of pore pressure was observed at a critical depth for the structure's safety assessments. In this condition, it was noticed that up to a depth of 6.5 m of drilling depth, there were pore pressures close to 230 kPa, thus indicating that the tailings deposited in these quotas presented an undrained behavior. Below we have Figure 1 with the representation of the result of pore pressure observed.

Furthermore, with the performance of the dissipation tests, it was observed that at the deepest point of dissipation (13.0 meters) a permeability value was found in the house of 2.56×10^{-9} m/s, classifying it in this way as waterproof material. The dissipation test will be shown below, Figure 2.

Finally, another point observed is due to the resistance of the material collected with the execution of the CPTU. For this first moment, low cone tip resistance was observed up to 6.5 m deep. The result will be shown below, Figure 3.

With the implementation of vertical geodrains in order to reduce the pore pressures acting in the critical region of the dam and provide the drained behavior and increase the local resistance of the material, new tests were carried out to verify what was foreseen in the project, the reduction of the pore pressure and the guarantee of the behavior drained by the tailings.

After performing the pore pressure tests, it was initially identified a considerable variation of the acting pore pressure up to 6.5 meters in depth. In

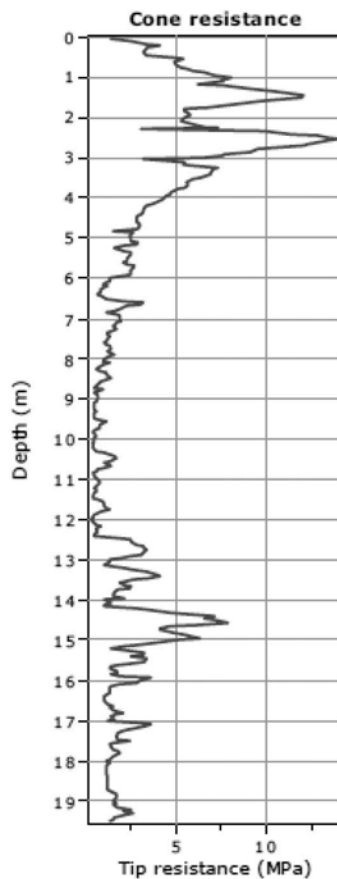


Figure 6. CPTU 2017 Cone tip resistance after the works.

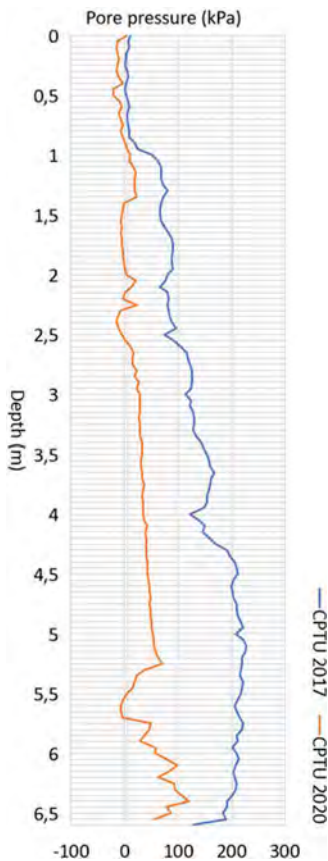


Figure 7. Comparison between the 2017 and 2020 CPTU in the critical region of pore pressure.

this condition, the behavior of the tailings presented an average pore pressure of 50 kPa and in some points a reduction of up to 200 kPa of pressure was observed. This situation can be seen in Figure 4 below.

In addition to the gains observed during the pore pressure measurement, considerable gains were also observed during the tailing's dissipation test. As can be seen in Figure 5, below, with the dissipation at the deepest point in the CPTU probe, 15.5 meters, it was identified that the permeability of the material increased to the house of 1.53×10^{-7} , thus improving the drainage capacity of the tailings around one hundred times. In this condition, the tailings started to be classified as low permeability soil.

Finally, another point is due to the resistance gain observed for the material up to 6.5 m, where the cone tip resistance initially found values close to 0.0 kPa and after the execution of the works, peaks close to 15.0 kPa were observed. This graph of the new CPTU assay is shown in Figure 6, below.

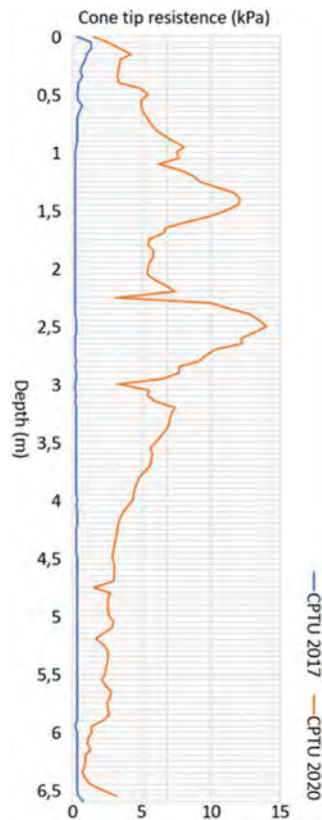


Figure 8. Comparison between the 2017 and 2020 CPTU in the critical region of cone tip strength.

3 CONCLUSION

As can be seen throughout the results presented, before the works were carried out, there were conditions of high pore pressures in the initial portion of the test. With the execution of the works, there was a considerable reduction in the critical pore pressure condition, improvement in the tailing's drainage capacity an increase in the cone tip resistance of the CPTU in this material.

A comparative graph of the pore pressure reduction in the critical region will be presented below, Figure 7.

Finally, as already mentioned, for the critical layer, up to 6.5 m, a considerable increase in material strength was also observed. A comparative graph of the increase in cone tip strength in the critical region will be presented below, Figure 8.

Therefore, carrying out the CPTU test was of great value in proving critical conditions in the field and in verifying the effectiveness of the work performed.

REFERENCES

- [1] Lunne, T.; Robertson, P.K.; Powell J.J.M. *Cone penetration testing in geotechnical practice*. Blackie Academic, EF SPON/ Routledge Publishing, 1997.
- [2] Campos, R. V. A. *Análise de investigações geotécnicas de barragens utilizando o CPTU em uma mina de ferro*. Undergraduate Thesis (Degree in Mining Engineering). Universidade Federal de Ouro Preto. Escola de Minas. Núcleo de Geotecnia, Ouro Preto, MG, 2021.
- [3] Rainer, J.; Hubert S. *Analysis of nderground stratification based on CPTu profiles using high-pass spatial filter*. *Studia Geotechnica et Mechanica*, vol. 42, no 4, 2020, p. 355–65.
- [4] Schnaid, F.; Odebrecht, E. *Ensaios de campo e suas aplicações à engenharia de fundações*. 2. ed., Oficina de Textos, São Paulo, SP, 2012.
- [5] Robertson P.K., Caval K.L. *Guide to cone penetration testing for geotechnical engineering*. 4th Edition. Gredd Drilling & Testing, Inc., California, 2010.
- [6] Jamiolkowski M.; Lo Presti D.C.F.; Manassero M. *Evaluation of relative density and shear strength of sands from CPT and DMT*. *Soil Behavior and Soft Ground Construction*, 2003, 7(119), p. 201–238.
- [7] Kim C.; Kim S.; Lee J. *Estimating clay undrained shear strength using CPTu results*. *Proceedings of the Institution of Civil Engineers Geotechnical Engineering*. 2009, 162(2), p. 119–127.
- [8] Robertson P.K. *Soil classification using the cone penetration test*. *Canadian Geotechnical Journal*, 1990, 27 (1), p. 151–159.
- [9] Campanella, R. G.; Robertson, P. K.; Davies, M. P.; Sy, A. *Use of in-situ tests in pile design*. *Proceedings 12th International Conference on Soil Mechanics and Foundation Engineering, ICSMFE*, Rio de Janeiro, Brazil, 1989, vol. 1, p. 199–203.
- [10] Houlsby G. T.; Teh C. I. *Analysis of the piezocone tests in clay*. De Ruiter J (ed.), *Penetration Testing*, Proc. 1st Isopt, Orlando, Balkema, Rotterdam, 1988, vol. 2, p. 777–783.

VCPT: An in-situ soil investigation method to validate vibratory pile-soil interaction models

D. Al-Sammarraie, S. Kreiter & T. Mörz

MARUM–Center for Marine Environmental Sciences, University of Bremen, Germany

M.O. Kluger

School of Science/Te Aka Mātuaatua, University of Waikato, Hamilton, New Zealand

M. Goodarzi

COWI – Hamburg, Germany

MARUM–Center for Marine Environmental Sciences, University of Bremen, Germany

ABSTRACT: Until now the vibratory pile driving method is not widely used because there is no reliable approach for drivability analysis. One of the main issues with the current drivability analysis methods are the inability to accurately predict the cyclic soil behavior during vibratory pile driving. In this research, the cyclic soil behavior was evaluated using a new in-situ soil investigation method, the vibratory cone penetration test (VCPT). VCPT penetrates the ground, while inducing controlled vertical cyclic strains, and measuring cone resistance, sleeve friction, and pore water pressure. Nine static CPTs and 15 VCPTs were performed at a constant frequency with three different amplitudes. The resulted cone resistance-displacement cycles were compared with the state-of-the-art soil-pile interaction models. The reduction in soil strength against vibratory loading was found to be amplitude-dependent; and it was observed that a cavity formed between the cone and soil during the upward movement of the cone for high displacement amplitudes.

1 INTRODUCTION

The notion of using vibratory pile driving to install the foundations for offshore wind turbines is increasing, because this driving technique produces less noise, causes less damage to the pile, and has a higher installation speed than impact pile driving technique (Holeyman and Whenham, 2017). The main problem of this technique is the lack of a well-established method for drivability analysis. The current drivability analysis of vibratory pile driving derives from soil-pile interaction models modified from impact pile drive analyses (Jonker, 1987, Wong et al., 1992, van Baars, 2004, Viking, 2006, Holeymann and Whenham, 2017, Lee et al., 2012). The vibratory pile driving models utilize empirical parameters, having been derived from conventional (quasi static) soil investigation methods, such as CPT and SPT, to predict the cyclic soil response during vibratory pile driving (Wong et al., 1992). The load application of the conventional soil investigation methods differs from that of vibratory pile driving. Therefore, the current soil-pile interaction models are likely unable to assess (1) degradation processes along the pile shaft and pile toe and (2) the effect of different amplitudes of vibratory pile

driving on cyclic soil behavior (Jonker, 1987, Holeymann and Whenham, 2017).

The vibratory cone penetration test (VCPT) is an in-situ soil investigation method, which penetrates the ground while inducing cyclic loads (Sasaki and Koga, 1982). The first VCPT tool utilized horizontal vibration as it was developed to investigate the liquefaction potential due to earthquake loading. More recently, VCPTs induced vertical (down-hole) vibrations (Wise et al., 1999, McGillivray et al., 2000, Mayne, 2000). The vertical cyclic motion of VCPT may be considered to resemble the motion of vibratory pile driving (Al-Sammarraie et al., 2018, Stähler et al., 2018, Viking, 2006). The measured cone resistance and displacement at the tip of the VCPT allow for evaluating the stress-displacement cycles of loading and unloading of the vibrational penetration (Al-Sammarraie et al., 2018). From these cycles, the stiffness during each individual loading and unloading cycle may be obtained (Wong et al., 1992, Lee et al., 2012). When cyclic penetration exceeds a certain amplitude threshold, the resistance at the toe decreases to zero during the upward movement and the begin of the downward movement of the penetrating object. This loss in resistance is called cavitation and is described in terms of a “cavity” even

though it is unlikely that a total empty space is formed (Massarsch and Westerberg, 1996, Rodger and Littlejohn, 1980, Viking, 2006). The degree of cavitation during vibratory pile driving is defined as the length of upward and downward movement of the penetrating object without soil contact (Massarsch and Westerberg, 1996, Massarsch et al., 2017, Vogel-sang et al., 2017, Dierssen, 1994). The cavitation and the loading and unloading stiffness during vibratory penetration have recently been investigated by utilizing the so-called Vibro-Penetration Test VPT, which is a soil investigation test that uses a vertical harmonic excitation force to drive a rod with a conical tip into the ground (Cudmani and Manthey, 2019). The VPT has a fixed relationship between frequency and potential maximum force and is furthermore influenced by the soil reaction while VCPT allows for independent variation of penetration speed, frequency and amplitude. Until now, the VCPT method was not applied to study the loading and unloading stiffness as well as the cavitation that may occur during vibratory pile driving. The influence of the displacement amplitude on the soil resistance and the loading and unloading stiffness is also still unknown.

In this study, the influence of displacement amplitudes on the degradation of cone resistance was investigated. It was explored to what extent the stiffness during loading and unloading cycles and the cavitation changed with displacement amplitudes. Finally, the obtained cyclic soil resistance were utilized to parametrize the current pile-soil interaction models developed by Dierssen (1994), Wong et al. (1992), and Jonker (1987), the results are quantified and discussed.

2 METHODOLOGY

2.1 VCPT device

The VCPT comprises a 100 kN hydraulic cylinder, a clamp, a valve unit, a displacement sensor, and a real time controller (Figure 1).

The hydraulic cylinder was used to push the rods and the cone into the ground having been controlled

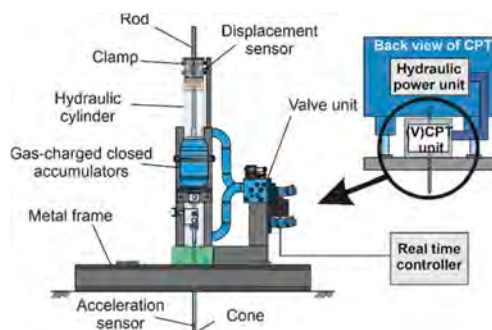


Figure 1. Vibratory cone penetration test device.

by the external displacement sensor. The displacement amplitude of VCPT, measured from the displacement sensor, is referred to as “VCPT amplitude” hereafter. The actual displacement of the cone was obtained from a three-axis acceleration sensor, which was located in the cone. This acceleration sensor had a sampling rate of 500 Hz.

2.2 Geological and geotechnical setting

The study area is located in Cuxhaven, Northern Germany. The soil deposits in the area consist mainly of very dense sand. The stratigraphy and the physical properties of the sand deposits were determined from a drill core in the vicinity of the test field (Figure 2). The stratigraphic characterization followed (Sindowski, 1965, Ehlers et al., 1984, Geo-Engineering, 2014) (Figure 3), grain size analyses were carried out according to DIN 18123 (2011), and the unit weight was provided from (Geo-Engineering, 2014).

The deposits are of Pleistocene age and consist of a 4-m-thick Middle Saalian unit composed of fine- to medium-grained sands, and an underlying 7-m-thick Older Saalian unit composed of compacted heterogeneous stratified sand deposits, with a till layer in between (Figure 3). The 60-cm-thick Drenthe till layer, composed of grains from clay to gravel size. The soil behavior types were calculated following Robertson (2009) from CPT S7 (Figure 2). Most of the sand deposits are soil behavior type 6 (sand like). Only the till layer is soil behavior type 3 and 4 (clay-like, silt-like). The sand deposits have relative densities between dense to very dense following the CPT correlation of Baldi et al. (1986).

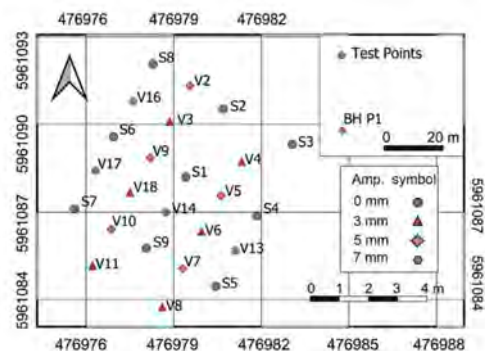


Figure 2. Maps of the layout of test points and the location of the core. The coordinate system used to create the maps was UTM zone N32.

2.3 Experimental layout

A cone with an area of 5 cm² was used to perform nine static CPTs (SCPTs hereafter) and 15 vibratory CPTs (VCPTs hereafter) in a systematic grid. In Figure 2, the letter “S” refers to SCPTs and “V”

refers to VCPT. The spacing between tests was chosen to be 1.4 m, being equivalent to 55 times cone diameter. The spacing was chosen to be larger than the minimum recommended distance between CPTs (Al-Sammarraie et al., 2020, DIN EN ISO 22476-1, 2012, BS 1377-9, 1990). The SCPTs were performed before the VCPTs.

The VCPTs were performed at a constant frequency of $f=20$ Hz and at three different VCPT amplitudes of 3, 5, and 7 mm (Figure 2). The CPT locations were determined by a DGPS system with a horizontal resolution of ± 2 cm. A theodolite with an accuracy of ± 0.3 cm was used to ensure a common height reference at the start and the end of each CPT.

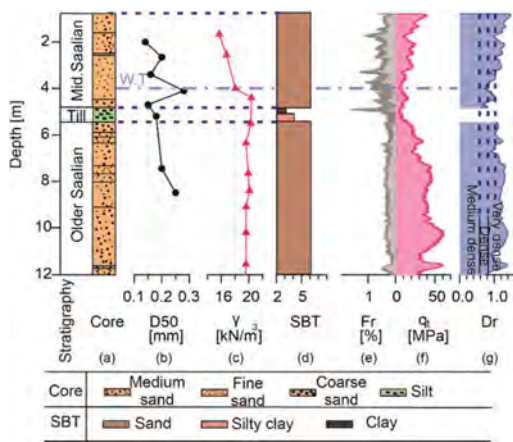


Figure 3. Stratigraphy and soil properties of test site (a) core; (b) grain size distribution (Geo-Engineering, 2014); (c) bulk unit weight (Geo-Engineering, 2014); (d) soil behavior types (SBT); (e) friction ratio; (f) corrected tip resistance; and (g) relative density derived after Baldi et al. (1986).

2.4 Evaluation of SCPTs and VCPTs datasets

The data of SCPT and VCPT were evaluated following four steps: (1) correlation, (2) cyclic behavior analyses, (3) statistics, and (4) degradation factors. Detailed explanation of the four steps is included in Al-Sammarraie (2020).

2.4.1 Correlation

The peak values of each individual cycle of the entire VCPT datasets were selected. The resulting VCPT datasets were defined as peak vibratory cone resistance, $vq_{c,p}$, peak sleeve friction, $v f_{s,p}$, and peak pore water pressure, $v u_p$. The vibratory cone resistance datasets that included the full information about each cycle is hereafter referred to as cone resistance cycles, $vq_{c,cy}$.

In order to minimize the effect of local heterogeneities and changes in the depth of specific soil

layers at small horizontal distance, all SCPT and VCPT datasets were correlated and shifted to a common depth. The cone resistance dataset of SCPT S7 was selected to be the “reference dataset” and all other SCPT and VCPT datasets were shifted to it (Figure 2) (Al-Sammarraie, 2020). After the depth shift, the depths of the SCPT and peak VCPT datasets were resampled to a common vertical depth scale with an increment of 0.5 mm.

2.4.2 Cyclic behavior analysis

In this step, the loading stiffness, K_b , and unloading stiffness, K_e , and the upward displacement with cavitation, d_{cav} , were quantified. Since the acceleration and cone resistance data were affected by noise, The cycles of cone resistance cycles, $vq_{c,cy}$, and raw acceleration, a , were stacked and averaged in order to reduce the noise level (Al-Sammarraie et al., 2018). Every second cycle of the correlated and shifted datasets of vibratory cone resistance and raw acceleration was selected and processed until the final depth of penetration of 12 m, while avoiding averaging between different of individual push-strokes. All data points of the selected cycle were added to the equivalent points of the neighboring cycles above and below and then divided by the number of cycles. This approach is similar to a moving average where the points are overlaid in phase. For cone resistance cycles and raw acceleration cycles each point is the average of 41 points. The moving average windows corresponded to a vertical length of 4 cm. The stacking and averaging process resulted in stacked cone resistance cycles, $vq_{c,cy,st}$, and stacked acceleration, a_{st} .

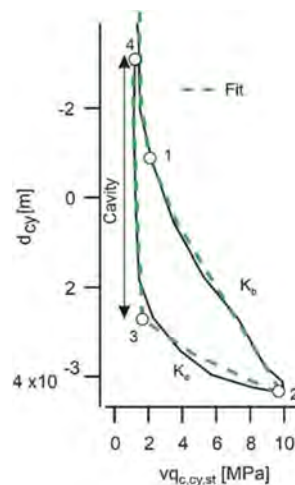


Figure 4. Fit function to determine loading stiffness, unloading stiffness and upward displacement with cavitation.

The stacked acceleration data, a_{st} was integrated twice to obtain the cyclic displacement, d_{cy} . The

constants of integration – depth and average velocity – were obtained from the displacement sensor.

The cone resistance-displacement cycles were used to determine the loading and unloading stiffnesses as well as the upward displacement with cavitation (Figure 4). This was done by using a fit function that consists of four connected linear sections to fit the cone resistance-displacement cycle (Figure 4). The loading stiffness K_b was then calculated from the slope of the second section (from point 1 to 2) and the unloading stiffness K_e from the third section (from point 2 to 3). The upward displacement with cavitation, d_{cav} , was defined as the length of the fourth section (from point 3 to 4). These steps resulted in datasets of loading stiffness, K_b , unloading stiffness, K_e , and upward displacement with cavitation, d_{cav} .

2.4.3 Statistics

The objective of the statistics step was to calculate representative datasets for different tests in the systematic grid (Figure 1). The datasets of the SCPT and VCPT that had the same VCPT amplitude, were averaged using Eq 1. The datasets of the loading/unloading stiffness and the cavitation were also averaged with respect to their corresponding VCPT using Eq 1.

$$X_r = \frac{\sum_{i=1}^n X_i}{n} \quad (1)$$

Where X_r is the representative dataset; X_i is an individual dataset; n is the total number of CPTs with the same amplitude; and i running from 1 to n .

2.4.4 Degradation factors

The degradation factors of representative cone resistance and sleeve friction was determined from Eqs. 2 and 3, in order to investigate whether or not the changes in VCPT amplitude affected the cone resistance and sleeve friction.

$$\beta_{q_c} = \frac{vq_{c,p,r}}{q_{c,r}} \quad (2)$$

Where β_{q_c} is the degradation factor of representative cone resistance (Jonker, 1987); $vq_{c,p,r}$ is the representative peak vibratory cone resistance; and $q_{c,r}$ is the representative static cone resistance.

$$\beta_{f_s} = \frac{vf_{s,p,r}}{f_{s,r}} \quad (3)$$

Where β_{f_s} is the degradation factor of representative sleeve friction; $vf_{s,p,r}$ is the representative peak vibratory sleeve friction; and $f_{s,r}$ is the representative static sleeve friction. Degradation factors with values near

zero represent high reduction, whereas values close to one represent small reduction in the representative cone resistances and sleeve frictions due to VCPT.

2.5 Pile-soil interaction models

2.5.1 Karlsruhe model

In the Karlsruhe model, four steps of the cyclic penetration are identified to describe the cyclic soil resistance-displacement behavior during vibratory penetration (Figure 5) (Dierssen, 1994, Cudmani and Manthey, 2019). The straight line between points 1 and 2 is expressed by:

$$q_T = K_b(\text{depth} - \text{depth}_1) \quad (4)$$

Where q_T is the resistance force at the toe; K_b is the loading stiffness of the soil.

When the pile moves upward the straight line between points 2 and 3 is expressed by:

$$q_T = q_{T,2} - K_e(\text{depth} - \text{depth}_2) \quad (5)$$

Where q_T is the resistance force at the toe; $q_{T,2}$ is the resistance at the toe at point 2; K_e is the unloading stiffness of the soil.

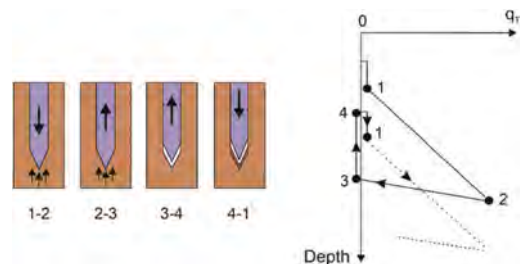


Figure 5. Description of the four phases of cyclic penetration (Dierssen, 1994).

When cyclic amplitude is large enough the resistance at the pile toe will reach zero and a cavity is formed, represented by the straight line between points 3 and 4 (Figure 5). At step between points 4 and 1', the pile moves downward while the stress at the toe remains zero because of the cavity.

The loading, K_b , and unloading stiffness, K_e , are empirical parameters, however in this study, they were obtained from the cone resistance-displacement cycle and were used as input for the fit (Figure 4). For step between points 4 and 1', the loading stiffness was restricted between values of 5-10 MPa/m, in order to account for the effect of cavity.

2.5.2 The model of Wong et al.

The cyclic penetration in this model is modeled with two equations in two parts one for the loading and one for the unloading part (Figure 6).

The first part is the loading part, which is described by (Wong et al., 1992):

$$q_l = \left[\frac{K_b w}{\left(1 + \left| \frac{K_b w}{q_0} \right|^{n_q} \right)^{\frac{1}{n_q}}} \right] F_q (1 - e^{-mw}) \quad (6)$$

And the unloading part is described in Eq.7:

$$q_u = q_c - \left[\frac{K_e (w_c - w_p)}{\left(1 + \left| \frac{K_e (w_c - w_p)}{q_0} \right|^{n_q} \right)^{\frac{1}{n_q}}} \right] F_q (1 - e^{-m(w_c - w_p)}) \quad (7)$$

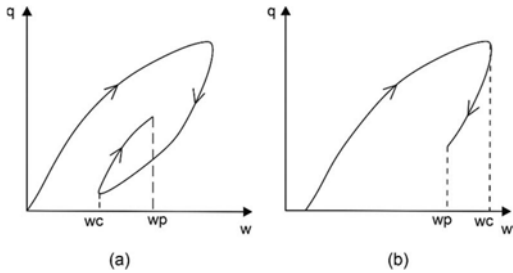


Figure 6. Loading and unloading parts and the explanation of depths of model of Wong (Wong et al., 1992): (a) Loading (b) Unloading.

Where, q_l and q_u are the loading and unloading resistance at the pile toe respectively; q_c is the unit toe resistance at the previous reversal; K_b and K_e are the loading and unloading stiffness respectively; w , w_p , and w_c , are the displacements as noted in Figure 6; q_0 is a reference value of toe resistance; F_q is the fitting factor; m is the constant which controls the magnitude of the amplitude.

The parameters K_b , K_e , q_0 , and n_q used in this model were obtained by fitting the model to the cone resistance-displacement cycles obtained from VCPT (Figure 4).

3 RESULTS

The peak vibratory cone resistances of the sand deposits were nearly always below the static cone resistance (Figure 7b). The reduction in the peak vibratory cone resistances to the static cone resistance increased with VCPT amplitude.

During VCPT, the sleeve friction was reduced with increasing amplitude until it reaches 0 MPa at

VCPT amplitude of 5 mm indicating total loss in shear stress between the sleeve and soil (Figure 7d).

The degradation factors of cone resistance decreased with increasing VCPT amplitude in the sand deposits (Figure 7c). In the silty till layer however, the degradation factors of cone resistance were close to one, indicating no effect of VCPT. The βq_c determined for different amplitudes were compared to the β -factor obtained from Jonker (1987) (Figure 7c). The degradation factor proposed by Jonker is 0.25 for sand and 0.4 for clay (the latter being considered to have similar soil properties to the silty till layer) and it is not related to changes of amplitudes.

The degradation in sleeve friction was highly affected by the VCPT amplitude in the sand deposits (Figure 7e). The silty till layer exhibited no degradation in sleeve friction during VCPT.

The representative loading and unloading stiffness values and the upward displacement with cavitation were plotted along the depth (Figure 8). In general, both loading and unloading stiffness values decreased with VCPT amplitude (Figure 8c-d). All stiffness values were very low in the silty till layer. The upward displacement with cavitation for amplitudes 5 and 7 mm exhibited approximately similar values (Figures 8e). The upward displacement with cavitation at a lower amplitude of 3 mm were lower.

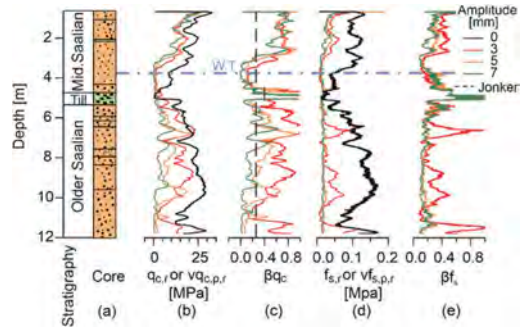


Figure 7. Degradation factors of representative cone resistance and sleeve friction for different VCPT amplitudes.

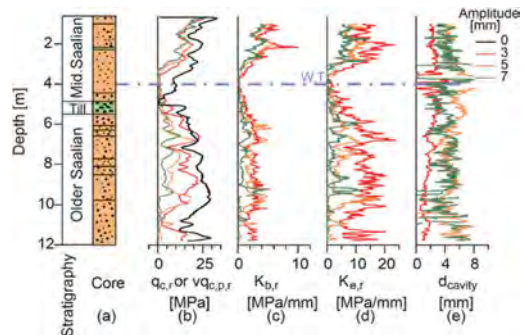


Figure 8. Loading and unloading stiffnesses and the upward displacement with cavitation plotted along the depth of penetration.

The Individual cone resistance-displacement cycles measured by VCPT at different depths were plotted and compared with the corresponding Karlsruhe and Wong fits (Figure 9). The results of Karlsruhe model agree with the cone resistance-displacement cycles for 5, and 7 mm amplitudes at depth of 8 and 10 m. For the 3 mm amplitude, the Karlsruhe model showed limitations to fully capture loading part of the resistance-displacement cycle. On the other hand the Wong model seemed to fully match the cycles at 3 mm amplitude, however larger difficulties were found when trying to capture the cyclic behaviour at 5 and 7 mm amplitudes.

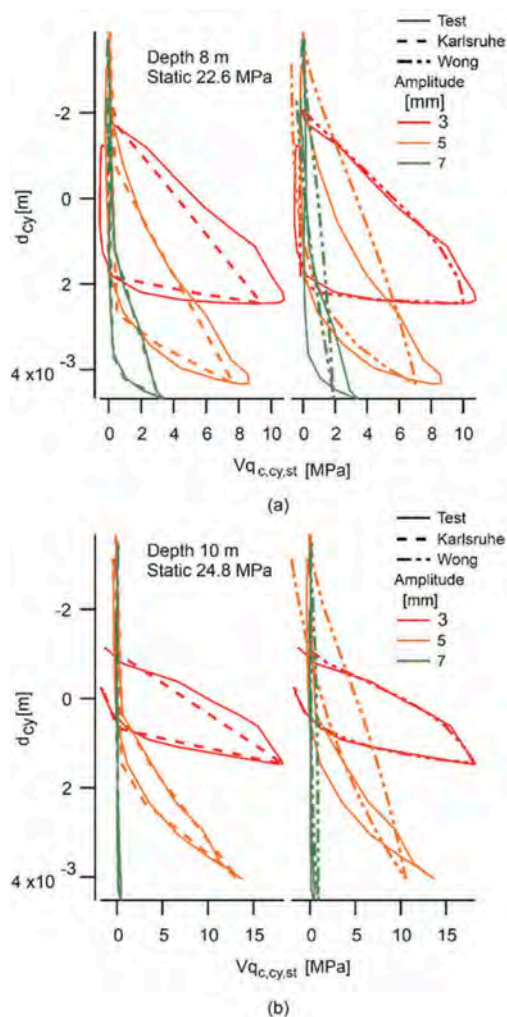


Figure 9. Stacked cyclic cone resistance – displacement behavior for the three applied amplitudes and the corresponding Karlsruhe and Wong fits at depths of a: 8 m; b: 10 m.

4 DISCUSSION

The increase in degradation of cone resistance and sleeve friction with VCPT amplitudes (Figure 7), provided practical evidence that the degradation in

soil resistance during vibratory pile driving depends on the amplitude of vibration. This conclusion agrees with previous studies about assessment of vibratory-drivability in sand, in which it was assumed that one of the important factors affecting degradation factor for piles, β , is vibration amplitude (Jonker, 1987, van Baars, 2004).

The degradation in cone resistance during VCPT may be related to the cavitation (Dierssen, 1994). During the upward movement of the cone, the unloaded soil may lose its strength, collapses and starts to flow into the cavity, which might be filled with liquified material. However, because there is only a short time interval until the reversal to the downward movement, the liquified material might have still not fully solidified (Dierssens, 1994). This process may result in remolding and/or loosening of the soil below the cone (Massarsch et al., 2017). Therefore, a reduction in cone resistance occurs when the cone gets again in contact with the soil during the downward movement.

The increase in degradation of loading and unloading stiffness with increasing amplitudes (Figure 8c-d), agrees with the degradation of the secant Young's modulus with increasing strain in triaxial tests on Ticino Sand (Yamashita et al., 2000).

The dependency of the observed cyclic behaviour on the cyclic amplitude, raises questions regarding the fruitfulness of current soil-pile interaction models to try to estimate soil cyclic resistance from the static cone resistance (Holeyman and Whenham, 2017a). Nevertheless, Wong et al. (1992) modelled the cyclic soil behaviour by including cyclic degradation of the pile-soil interface, and the loading and unloading phases during vibratory driving. However, the model utilizes empirically implemented parameters for very specific soil-pile systems, with no account for the effect of the cyclic amplitude (Eqs. 6 and 7) (Wong et al., 1992, Lee et al., 2012). Furthermore, the model does not account for the cavitation part of the cone resistance-displacement cycles which reliably occurs at higher displacement amplitudes (Figure 8e). This explains the inability of the model to capture the cone resistance-displacement cycles with amplitudes of 5 and 7 mm (Figure 9). The Karlsruhe model on the other hand accounts for cavitation part of the vibratory cycles during pile driving. Therefore, it could well match the cone resistance-displacement cycles with higher amplitudes of 5 and 7 mm (Figure 9). Although the measured cone resistance-displacement cycle differed slightly in the shape with rounder edges compared to Karlsruhe model; the ability of the Karlsruhe model to capture the cyclic soil response to the different values of the applied cyclic amplitudes (Figure 9), proved the effectiveness of utilizing the cyclic soil parameters obtained from VCPT.

5 CONCLUSION

In this study, VCPTs were performed to investigate the cyclic soil behavior in-situ. It was found that:

- 1- The degradation in vibratory cone resistance and sleeve friction increased with VCPT amplitudes. The degradation is suspected to be related to increase in cavitation.
- 2- The degradation in the loading and unloading stiffness increased with increasing VCPT amplitudes.
- 3- The parameters of the cyclic soil resistance obtained from VCPT could successfully be used in the current pile-soil interaction models.

REFERENCES

- Al-Sammarraie, D. 2020. *Vibratory cone penetration test to investigate cyclic soil behavior in-situ*. PhD, University of Bremen.
- Al-Sammarraie, D., Kreiter, S., Kluger, M. O. & Mörz, T. 2020. Reliability of CPT measurements in sand–influence of spacing. *Géotechnique*, 1–13.
- Al-Sammarraie, D., Kreiter, S., Stähler, F. T., Goodarzi, M. & Mörz, T. New Vibratory Cone Penetration Device for in-Situ Measurement of Cyclic Softening. International Symposium on Cone Penetration Testing, 2018.
- Baldi, G., Bellotti, R., Ghionna, V., Jamiolkowski, M. & Pasqualini, E. Interpretation of CPT's and CPTU's. 2nd Part: Drained Penetration" Proceeding 4th International Geotechnical Seminar, 1986 Singapore. 143–15.
- BS 1377-9 1990. Methods for test for soils for civil engineering purposes. *In-situ tests*
- Cudmani, R. & Manthey, S. 2019. A novel vibro-penetration test (VPT) for the investigation of cohesionless soils in the field. *Soil Dynamics and Earthquake Engineering*, 126, 105760.
- Dierssen, G. 1994. *Ein bodenmechanisches Modell zur Beschreibung des Vibrations-rammens in körnigen Böden*. Doctoral Thesis, University of Karlsruhe.
- DIN 18123 2011. Soil, investigation and testing–determination of grain-size distribution.
- DIN EN ISO 22476-1 2012. Geotechnical investigation and testing - Field testing *Part 1: Electrical cone and piezocone penetration test*.
- Ehlers, J., Meyer, K.-D. & Stephan, H.-J. 1984. The pre-Weichselian glaciations of north-west Europe. *Quaternary Science Reviews*, 3, 1–40.
- Geo-Engineering 2014. Geotechnical site investigation report VIBRO-project Altenwalde.
- Holeyman, A. & Whenham, V. 2017. Critical review of the Hypervib1 model to assess pile vibro-drivability. *Geotechnical and Geological Engineering*, 35, 1933–1951.
- Jonker, G. Vibratory pile driving hammers for pile installations and soil improvement projects. Offshore Technology Conference, 1987. Offshore Technology Conference.
- Lee, S.-H., Kim, B.-I. & Han, J.-T. 2012. Prediction of penetration rate of sheet pile installed in sand by vibratory pile driver. *KSCE Journal of Civil Engineering*, 16, 316–324.
- Massarsch, K. R., Fellenius, B. H. & Bodare, A. 2017. Fundamentals of the vibratory driving of piles and sheet piles. *geotechnik*, 40, 126–141.
- Massarsch, K. R. & Westerberg, E. 1996. FREQUENCY-VARIABLE VIBRATORS AND THEIR APPLICATION TO FOUNDATION ENGINEERING. *Korea Geotechnical Society*, 1996, 25–40.
- Mayne, P. W. 2000. Evaluating ground liquefaction potential by piezoviercone. Georgia Institute of Technology.
- Mcgillivray, A., Casey, T., Mayne, P. W. & Schneider, J. A. 2000. An electro-vibrocone for site-specific evaluation of soil liquefaction potential. *Innovations and Applications in Geotechnical Site Characterization*.
- Robertson, P., K., 2009. Interpretation of Cone Penetration Tests - A Unified Approach. *Can. Geotech. J.*, 46, 1337–1355.
- Rodger, A. & Littlejohn, G. 1980. A study of vibratory driving in granular soils. *Geotechnique*, 30, 269–293.
- Sasaki, Y. & Koga, Y. Vibratory cone penetrometer to assess the liquefaction potential of the ground. Proceedings, 1982. 541–555.
- Sindowski, K.-H. 1965. Die drenthestadiale Altenwalder Stauchmoräne südlich Cuxhaven. *Zeitschrift der Deutschen Gesellschaft für Geowissenschaften (ZDGG)*, 158–162.
- Stähler, F., T., Kreiter, S., Goodarzi, M., Al-Sammarraie, D. & Mörz, T. Liquefaction Resistance by Static and Vibratory Cone Penetration Tests. In: Hicks, M., A., Pisanò, F. & Peuchen, J., eds. Proceedings of the 4th International Symposium on Cone Penetration, 2018 Delft.
- Van Baars, S. 2004. Design of sheet pile installation by vibration. *Geotechnical & Geological Engineering*, 22, 391–400.
- Viking, K. The vibratory pile installation technique. Proceedings of the International Conference on Vibratory Pile Driving and Deep Soil Compaction, 2006. 65–82.
- Vogelsang, J., Huber, G. & Triantafyllidis, T. 2017. Experimental investigation of vibratory pile driving in saturated sand. *Holistic Simulation of Geotechnical Installation Processes*. Springer.
- Wise, C., Mayne, P. & Schneider, J. Prototype piezovibrocone for evaluating soil liquefaction susceptibility. *Earthquake geotechnical engineering*, 1999. 537–542.
- Wong, D., O'neill, M. W. & Vipulanandan, C. 1992. Modelling of vibratory pile driving in sand. *International Journal for numerical and analytical methods in geomechanics*, 16, 189–210.
- Yamashita, S., Jamiolkowski, M. & Presti, D. C. L. 2000. Stiffness nonlinearity of three sands. *Journal of Geotechnical and Geoenvironmental Engineering*, 126, 929–938

Monitoring ground improvement by Rammed Aggregate Piers using a combined CPTU and SDMT approach at a silty sand liquefaction-prone site in Emilia-Romagna

S. Amoroso

University of Chieti-Pescara, Pescara, Italy
Istituto Nazionale di Geofisica e Vulcanologia, L'Aquila, Italy

M.F. García Martínez, L. Tonni & G. Gottardi

University of Bologna, Bologna, Italy

P. Monaco

University of L'Aquila, L'Aquila, Italy

K.M. Rollins

Brigham Young University, Provo, Utah, USA

L. Minarelli

Istituto Nazionale di Geofisica e Vulcanologia, L'Aquila, Italy

D. Marchetti

Studio Prof. Marchetti, Rome, Italy

K.J. Wissmann

Geopier Foundation Company, Davidson, North Carolina, USA

ABSTRACT: Following the 2012 Emilia-Romagna earthquake, widespread liquefaction of silty sands was observed, providing the opportunity to gain a better understanding of the influence of fines content on liquefaction hazard and mitigation works. This paper presents the results of a thorough geotechnical investigation performed as part of a full-scale liquefaction experiment involving controlled blast tests in Bondeno, a small village that suffered liquefaction in 2012. Piezocone (CPTU) and seismic dilatometer (SDMT) tests were performed in natural and improved soils after Rammed Aggregate Pier[®] (RAP) treatment to provide accurate soil characterization and to evaluate the effectiveness of liquefaction mitigation. CPTU and SDMT results revealed a good agreement in the geotechnical characterization of the site, detecting homogenous soil properties in both the natural and treated soils and estimating CPTU-DMT coupled parameters in sandy layers (e.g. overconsolidation ratio, at-rest earth pressure coefficient), that are usually not determinable by the use of a single type of in situ test. In particular, the combined use of CPTU-DMT data provided verification of the increase in the lateral stress produced by the RAP installation. Data analyses revealed that the RAPs were an effective ground improvement technique despite the high percent of fines ($\approx 25\text{-}35\%$).

1 INTRODUCTION

Several ground improvement solutions are available to mitigate the liquefaction hazard posed by clean sands; namely, increasing the soil resistance by densification or reducing the earthquake-induced excess pore pressures through drainage or reducing the shear strains through reinforcement. Vibratory compaction methods are a common and effective form of densification for cohesionless soils (Castro 1969), as proven

by extensive research (e.g. Mitchell 1981, Vautherin et al. 2017, Amoroso et al. 2018). However, their effectiveness decreases as the fines content and plasticity increase (Mitchell 1981). Therefore, other ground improvement techniques, such as vibratory replacement, are often preferred in silty sands or sandy silts to protect the soil against liquefaction by increasing soil density, providing drainage for excess pore water pressures, and increasing the stiffness and shear resistance of the soil (Priebe 1998).

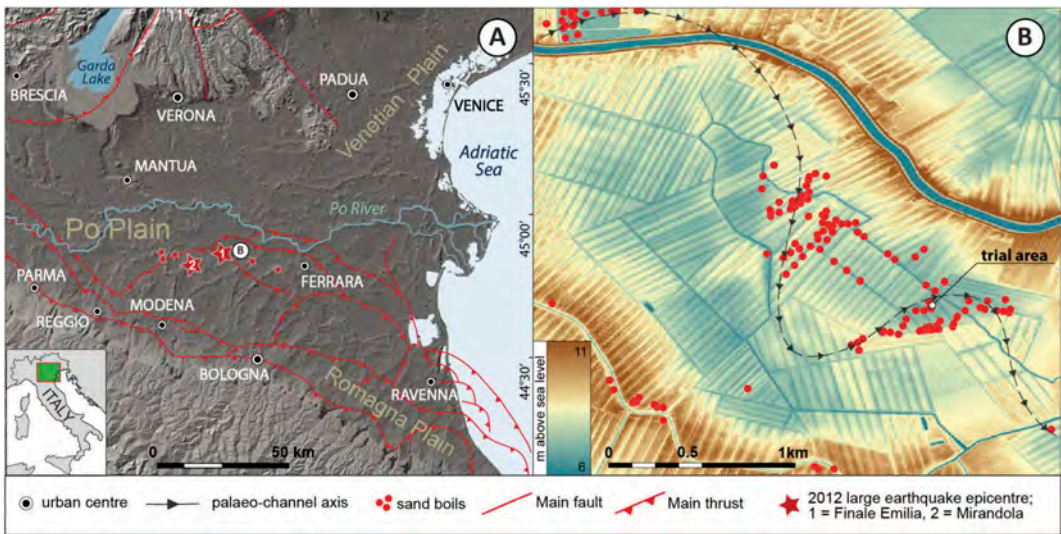


Figure 1. (a) Location of the Bondeno Test Site and of 2012 main shocks; (b) geomorphological features from LIDAR map (modified after Amoroso et al. 2020): greenish color indicates lower elevation above the sea level, while brownish color refers to higher elevation.

Examples of this type of reinforcement include Stone Columns (SC), Soil Mixed Columns (SMC), and Rammed Aggregate Piers (RAP). This last approach appears to be a promising solution in sandy silts and silty sands to increase not only the density, but also the lateral stress and shear stiffness, which is often neglected and poorly understood (Smith & Wissmann 2018, Amoroso et al. 2020).

The at-rest earth pressure coefficient (K_0) is a key parameter that should be considered with reference to liquefaction mitigation works (Schmertmann 1985, Salgado et al. 1997, Harada et al. 2010).

In this respect, in situ tests have an essential role to play in estimating the horizontal stress in granular soils before and after treatment. As argued by Masarsch et al. (2019), using cone penetration test (CPT) and flat dilatometer test (DMT) results could produce improved estimates of K_0 . Moreover, Baldi et al. (1986) and later Hossain & Andrus (2016) proposed a combined CPT-DMT K_0 -interpretation to take into account both the resistance and stress history of the soil, while the use of a CPT-only approach would have been overly affected by arching of stresses around the penetrating sleeve.

The coupling of CPT and DMT tests with down-hole geophysics (i.e. seismic piezocone SCPTU and seismic dilatometer SDMT) provides a more efficient approach to the task of geotechnical site characterization, offering clear opportunities for the economical and optimal collection of the data (Mayne et al. 2009). Therefore, direct push technologies are more relevant for understanding the changes in soil properties following ground improvement (e.g. Jendebay 1992, Amoroso et al. 2018).

This investigation presents in situ test results from a thorough geotechnical campaign performed before

and after Rammed Aggregate Pier (RAP) treatment of a silty sand site in Bondeno (Italy), a small village strongly affected by liquefaction following the 2012 Emilia-Romagna earthquake. The overall details of the research activities can be found in Amoroso et al. (2020) while details regarding the performance of the RAP group following a blast test are provided by Rollins et al. (2021) and regarding the liquefaction assessment and ground improvement are listed in Amoroso et al. (2022).

2 THE BONDENO TEST SITE (BTS)

2.1 Geological and geomorphological setting

The Bondeno Test Site (BTS) is located in the southeastern portion of the Quaternary alluvial Po Plain, one of the largest and most populous plains in Europe. The area was affected in 2012 by an intense seismic activity linked to the tectonic evolution of the fault-fold structures (Figure 1a) that form the front of the Apennine chain buried below the plain (e.g. Toscani et al. 2009).

The earthquake sequence induced widespread site effects, including liquefaction manifestations, soil fracturing and lateral spreading (Emergeo Working Group 2013). At BTS the liquefaction hazard is concentrated in a subsurface sand deposit of a Holocene Po meander (Figure 1b). Figure 1b shows the higher elevations (brownish zones) indicating fluvial ridges bounding the lower, relatively flat interfluvial depression (greenish zones). The meandering course of the paleochannel is built up within the interfluvial depression and supports the identification of the paleochannel axis together with the location of sand boils. The

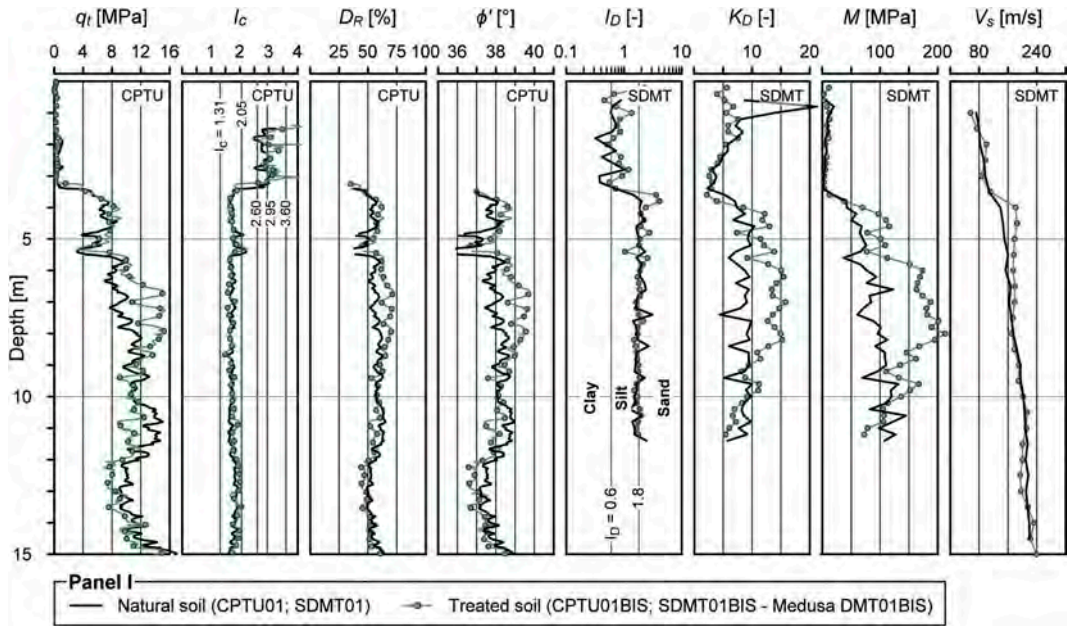


Figure 2. CPTU and SDMT interpreted results in natural (NS) and treated (TS) soils: (a) q_t , I_c , D_R , ϕ' from CPTU; (b) I_D , K_D , M , V_s from SDMT (modified after Amoroso et al. 2022).

meander base is frequently cut into upper Pleistocene coarse sand, accumulated during syn-glacial times. The meander unit geometry has been reconstructed through the analysis of remote sensing data (satellite images and LIDAR) and correlation of underground geotechnical investigations (Amoroso et al. 2020). This meander sand body is partially buried by finer grained levee sediment of historic age.

2.2 Site investigations

To assess the effectiveness of the RAP treatment at the BTS, in situ tests were performed before and after pier installations, according to the phases reported below:

- Phase I consisted of site investigations performed before the treatment (pre-RAP) and before the blast (pre-blast). Boreholes with SPTs and disturbed soil sampling, CPTUs, and SDMTs were executed up to a maximum depth of 20 m in two relatively small circular areas (10 m-diameter and 20 m-spacing) associated with the blast experiment, one for testing the natural soil (Natural Panel, NP) and one for testing the improved soil (Improved Panel, IP). This paper includes only CPTUs and SDMTs performed in the IP;
- Phase II included site investigations carried out approximately one month after the pier installation (post-RAP) and before the blast (pre-blast) within the IP. The treatment consisted of a 4×4 quadrangular grid (2 m center-to-center spacing) of RAP columns, each 9.5 m long and with a final

diameter of 0.5 m (area replacement ratio equal to 5%). Details on the construction methodology are reported in Saftner et al. (2018). Each CPTU, Medusa DMT (automated dilatometer test, Marchetti et al. 2019) and SDMT test was performed up to a maximum depth of 15 m at the exact center of four RAPs.

Further details on the site investigations performed within the full-scale liquefaction experiment through controlled blast tests are reported in Amoroso et al. (2022).

3 SITE CHARACTERIZATION

3.1 Natural soil

The stratigraphic arrangement of the subsoil beneath the test site area was deduced by the combined interpretation of borehole logs, SPTs, CPTUs, Medusa DMTs and SDMTs carried out before the RAP installation, as reported by Amoroso et al. (2020). Apart from a 0.8 m thick topsoil layer (CH, according to Unified Soil Classification System, USCS ASTM D2487-11 2011), the following well-defined stratigraphic units, also reflecting their sedimentological framework, could be identified:

- a layer of clays and silts (CL), from 0.8 to approximately 3.3-3.4 m in depth;
- a predominantly silty sand unit, approximately 9 m thick, attributable to Holocene alluvial deposits of a Po river paleochannel. Samples

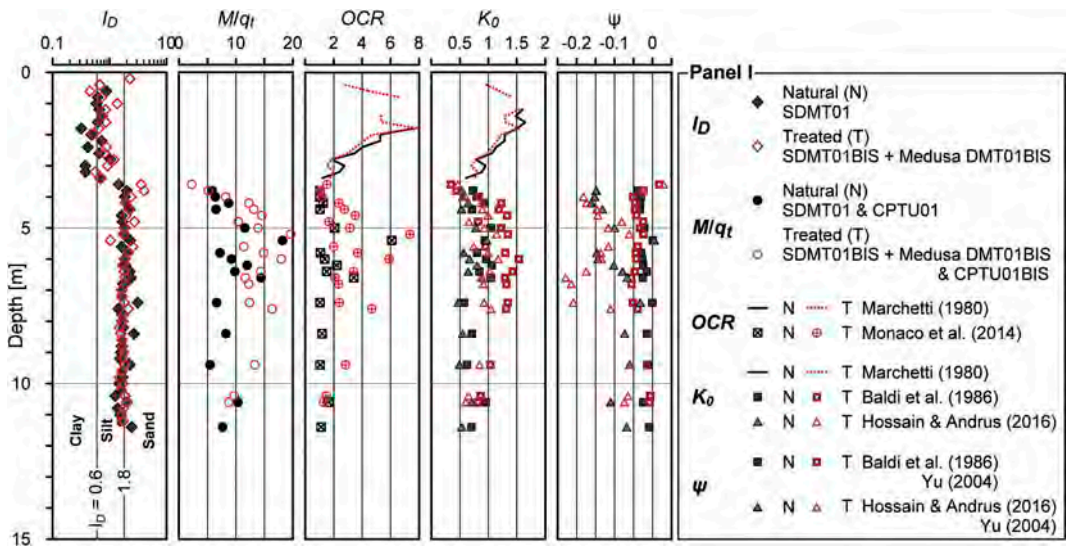


Figure 3. CPTU-DMT combined interpreted results in natural (NS) and treated (TS) soils: I_D , M/q_t , OCR , K_D , ψ (modified after Amoroso et al. 2022).

recovered from this unit can generally be classified as SM, having a FC typically in the range of 25-35%. Thin layers of coarser sediments have been occasionally found;

- a thin layer of sandy silt (ML), from 11.8-12.6 to 13.0-13.4 m in depth (interfluvial deposits);
- sands-silty sands (SP-SM) of the late Pleistocene epoch (namely, glacial braided Po River deposits), detected below 13.0-13.4 m in depth.

Figure 2 provides plots of representative piezocone and seismic dilatometer profiles carried out in the pre-RAP phase and located in the treated panel, respectively CPTU01 and SDMT01 (black lines). In particular, the CPTU profiles are shown in terms of the corrected cone resistance (q_t), soil behavior type index (I_c , Robertson 2009), relative density (D_R , Jamilokowski et al. 2001), and friction angle (φ' , Kulhawy & Mayne 1990), while the SDMT results are reported in terms of the soil material index (I_D), horizontal stress index (K_D), constrained modulus (M), and shear wave velocity V_S , according to Marchetti (1980) and Marchetti et al. (2001) correlations.

The comparative analysis of the CPTU and SDMT parameters reveals a substantial agreement between the measurements collected in the IP, thus indicating negligible horizontal spatial variability in the stratigraphic conditions of the test site.

3.2 Improved soil

Figure 2 also provides a comparison between field soil properties before and after RAP installation in the IP, in terms of both CPTU and SDMT profiles (green lines).

With regard to the piezocone profiles (Figure 2), the increase in the q_t values after column construction

appears to be particularly noticeable ($q_t = 13.10 \pm 1.76$ MPa versus 9.54 ± 1.37 MPa before installation) from 6 to 8.5 m in depth, but relatively moderate from 3.5 to 6 m. Negligible changes in the q_t profile can be observed in the silty sands below the base of the piers. Obviously, these changes in q_t affect the computed estimates of the geotechnical parameters reported in Figure 2, i.e. D_R and φ' .

The effect of RAP installation is evidently reflected by the increase in K_D (on average 48-53%), and even more in the higher M from SDMT (80-87%), at depths between 4 and 9 m (Figure 2b). The corresponding average increase in q_t is 30-35% (and in D_R is approximately 10% and is limited to a depth between 6 and 8.5 m). These results point to a significant increase in horizontal stress and stiffness resulting from pier installation, in agreement with previous observations (Saftner et al. 2018). In fact, the horizontal stress strongly influences both K_D and M estimated from DMT using the Marchetti (1980) correlation, which incorporates K_D .

The observed results are in line with previous comparisons of pre- vs. post- CPTs and DMTs executed for monitoring ground improvement (e.g. Jendebly 1992), since the RAP installation produced an average increase in M from DMT after treatment approximately 2.5 times the corresponding increase in cone penetration resistance q_c . The decrease in K_D observed in the upper crust may be due in part to the construction of an overlying working platform, but also to RAP installation under low confining stress and to seasonal variations in water content caused by fluctuation of the GWT from 1.5 m (February 2018) to 0.5 m (March 2018). No improvement was detected in the silty sands below the toe of piers, unlike RAP case histories in clean sands studied in New Zealand (e.g. Vautherin et al. 2017).

The combined interpretation of CPTU and DMT data provided information on stress history and the state parameter in sand, in both the natural and treated soils as shown in Figure 3. Filtering the data for $I_D \geq 1.8$ and $I_c \leq 2.6$, in the sand layers the ratio M/q_t (with M estimated from DMT) is shown in Figure 3. The average values of M/q_t are about 7-10 in natural soil and 13-14 in treated soil. These values are in line with the available experience from field observations before and after compaction of sand fills, reported by Marchetti et al. (2001) and Marchetti & Monaco (2018), which show an increase in the ratio M from DMT/q_c from ≈ 5 -10 before compaction to ≈ 12 -24 after compaction. The finding that compaction increases both M from DMT and q_c , but M at a faster rate, suggested the potential use of the ratio M from DMT/q_c , as a broad indicator of “equivalent” OCR in sands.

The in situ earth pressure coefficient K_0 was estimated using correlations proposed by Baldi et al. (1986), based on both DMT and CPT data, and by Hossain & Andrus (2016), which require as an additional input also OCR (in this case evaluated by Monaco et al. 2014). In the upper silty clay layer OCR and K_0 were estimated from DMT (Marchetti 1980).

The OCR s of about 1-2 estimated in the natural soil, excluding the shallow “crust”, indicate that the deposit is normally consolidated or slightly overconsolidated, with $K_0 \approx 0.5$ -0.7. As a result of the RAP installation, the “equivalent” OCR increased to about 3-3.5 and K_0 to about 0.9-1. The values of K_0 estimated according to Hossain & Andrus (2016) are lower than those estimated according to Baldi et al. (1986). The increase of M/q_t , OCR and K_0 after treatment was more pronounced at depths between 7 and 9 m.

An approximate estimate of the in situ state parameter ψ in sand from DMT was obtained according to Yu (2004), with K_0 determined by both Baldi et al. (1986) and Hossain and Andrus (2016) methods. Figure 3 shows that the input K_0 has a large influence on the calculated values of ψ , with an apparent contradiction versus the expected trend. In fact, the higher K_0 (i.e. higher OCR) estimated according to Baldi et al. (1986) should involve lower negative values of ψ compared to those obtained using K_0 from Hossain & Andrus (2016), while the opposite is observed in Figure 3. On the other hand, the reduction of ψ after treatment found using both K_0 methods is consistent with the corresponding increase of OCR and K_0 before and after treatment.

A more complete overview on the ground improvement effectiveness at BTS using in situ tests is reported in Amoroso et al. (2022).

4 CONCLUSIONS

At BTS a comprehensive comparative study based on CPTU and SDMT testing was carried out in a liquefaction-prone silty sand site improved by a group of Rammed Aggregate Piers and subjected to controlled blasting.

CPTU and SDMT tests revealed good agreement in the geotechnical characterization of the site, detecting homogenous soil properties in both the natural and improved panels. Use of both CPTU and DMT provided better estimates of soil properties in sandy layers (e.g. OCR , K_0), that are usually not determinable using a single type of in situ tests.

The comparison of the in situ tests performed pre-blast in natural and treated soils highlighted the effectiveness of the RAP treatment between 4 and 9 m depth in silty sands. The increase in the DMT parameters following treatment were more pronounced relative to those obtained from CPTU data (i.e. K_D increase ≈ 48 -53%, M increase ≈ 80 -87%, q_t increase ≈ 30 -35%), thus suggesting a higher sensitivity of DMT to the increase of horizontal stress. On the contrary, V_S measurements showed a very low sensitivity to the ground improvement. Moreover, the combined use of CPTU and DMT tests showed a significant increase of M/q_t and K_0 after treatment, supporting the use of the piers to increase the lateral soil stress and to mitigate liquefaction.

ACKNOWLEDGEMENTS

The study was primarily funded by Geopier® Foundation Company (Davidson, North Carolina, United States). A special thanks also to Releo s.r.l. (Ferrara, Italy) who provided the installation of the Rammed Aggregate Piers. The in-situ testing campaign was carried out by CIRI Edilizia e Costruzioni, University of Bologna, Italy under the research project TIRISICO (“Tecnologie Innovative per la riduzione del rischio sismico delle Costruzioni”, Project no. PG/2015/737636, POR-FESR 2014-2020). Financial contributions to this research activity were provided by INGV-FIRB Abruzzo project (“Indagini ad alta risoluzione per la stima della pericolosità e del rischio sismico nelle aree colpite dal terremoto del 6 aprile 2009”), by INGV-Abruzzo Region project (“Indagini di geologia, sismologia e geodesia per la mitigazione del rischio sismico”, L.R. n. 37/2016), and by Alma Mater Studiorum – Università di Bologna within AlmaDea research project (2017, Scient. Resp. Laura Tonni). Special thanks to Brigham Young University for contributing to the realization of the blast test experiment in terms of personnel and technical equipment; to Prof. Marco Stefani (University of Ferrara, Italy) for kindly sharing scientific information of the studied area; to Michele Perboni who kindly guested the experimental activities; to the Bondeno Municipality and to the Emilia-Romagna Region (Luca Martelli), who provided all the necessary support to realize the research in collaboration with the other local authorities.

REFERENCES

Amoroso, S., Rollins, K.M., Andersen, P., Gottardi, G., Tonni, L., García Martínez, M.F., Wissmann, K.J.,

- Minarelli, L., Comina, C., Fontana, D., De Martini, P.M., Monaco, P., Pesci, A., Sapia, V., Vassallo, M., Anzidei, M., Carpena, A., Cinti, F., Civico, R., Coco, I., Conforti, D., Doumaz, F., Giannattasio, F., Di Giulio, G., Foti, S., Loddo, F., Lugli, S., Manuel, M.R., Marchetti, D., Mariotti, M., Materni, V., Metcalfe, B., Milana, G., Pantosti, D., Pesce, A., Salocchi, A.C., Smedile, A., Stefani, M., Tarabusi, G., & Teza, G. 2020. Blast-induced liquefaction in silty sands for full-scale testing of ground improvement methods: insights from a multidisciplinary study. *Engineering Geology* 265: 105437. <https://doi.org/10.1016/j.enggeo.2019.105437>.
- Amoroso, S., Garcia Martinez, M.F., Monaco, P., Tonni, L., Gottardi, G., Rollins, K.M., Minarelli, L., Marchetti, D., & Wissmann, K.J. 2022. Comparative study of CPTU and SDMT in liquefaction prone silty sands with ground improvement. *Journal of Geotechnical and Geoenvironmental Engineering*, accepted on January 25th 2022, [https://doi.org/10.1061/\(ASCE\)GT.1943-5606.0002801](https://doi.org/10.1061/(ASCE)GT.1943-5606.0002801)
- Amoroso, S., Rollins, K.M., Monaco, P., Holtrigter, M., & Thorp, A. 2018. Monitoring ground improvement using the seismic dilatometer in Christchurch, New Zealand. *Geotechnical Testing Journal* 41 (5): 946–966. <https://doi.org/10.1520/GTJ20170376>.
- ASTM D2487-11. 2011. Standard practice for classification of soils for engineering purposes (Unified Soil Classification System). West Conshohocken, PA: ASTM International.
- Baldi, G., Bellotti, R., Ghionna, V., Jamiolkowski, M., Marchetti, S., & Pasqualini, E. 1986. Flat Dilatometer Tests in Calibration Chambers. *Proc., Specialty Conf. on Use of In Situ Tests in Geotechnical Engineering GSP 6*, 431–446. Reston, VA: ASCE.
- Castro, G. 1969. "Liquefaction of sands." Ph.D. Dissertation, Harvard University.
- Emergeo Working Group. 2013. "Liquefaction phenomena associated with the Emilia earthquake sequence of May-June 2012 (Northern Italy)." *Nat. Hazards Earth Syst. Sci.*, 13 (4), 935–947.
- Harada, K., Orense, R.P., Ishihara, K., & Mukai, J. 2010. "Lateral stress effects on liquefaction resistance correlations." *Bull. New Zeal. Soc. Earthq. Eng.*, 43(1),13–23.
- Hossain, M.A., and Andrus, R.D. 2016. "At-rest lateral stress coefficient in sands from common field methods." *J. Geotech. Geoenviron. Eng.* 142(12): 06016016. [https://doi.org/10.1061/\(ASCE\)GT.1943-5606.0001560](https://doi.org/10.1061/(ASCE)GT.1943-5606.0001560).
- Jamiolkowski, M., Lo Presti, D.C.F., & Manassero, M. 2001. "Evaluation of relative density and shear strength of sands from cone penetration test and flat dilatometer test." In *Proc. Symp. on Soil Behaviour and Soft ground Construction GSP 119*, 201–238. Reston, Virginia: ASCE.
- Jendebly, L. 1992. Deep Compaction by Vibrowing. I *Proc. Nordic Geotechnical Meeting 1*: 19–24. Lyngby (Denmark): Danish Geotechnical Society.
- Kulhawy, F.H., & Mayne, P.H. 1990. Manual on estimating soil properties for foundation design. *Report No. EL-6800*. Palo Alto, CA: Electric Power Research Institute (EPRI).
- Marchetti, D., Monaco, P., Amoroso, S., & Minarelli, L., 2019. In situ tests by Medusa DMT. *Proc. XVII Eur. Conf. on Soil Mechanics and Geotechnical Engineering*, <https://doi.org/10.32075/17ECSMGE-2019-0657>.
- Marchetti, S. 1980. In situ tests by flat dilatometer. *Journal of Geotechnical Engineering Division* 106 (3): 299–321.
- Marchetti, S., & Monaco, P. 2018. Recent improvements in the use, interpretation, and applications of DMT and SDMT in Practice. *Geotechnical Testing Journal* 41 (5): 837–850. <https://doi.org/10.1520/GTJ20170386>.
- Marchetti, S., Monaco, P., Totani, G., & Calabrese, M. 2001. The Flat Dilatometer Test (DMT) in Soil Investigations – A Report by the ISSMGE Committee TC16. *Proc. 2nd Int. Conf. on the Flat Dilatometer*, 7–48.
- Massarsch, K.R., Wersäll, C., & Fellenius, B.H. 2019. Horizontal stress increase induced by deep vibratory compaction. *Proceedings of Institution of Civil Engineers-Geotechnical Engineering* 173(3): 228–253.
- Mayne, P.W., Coop, M.R., Springman, S.M., Huang, A.B., & Zornberg, J.G. 2009. Geomaterial behavior and testing. *Proc. 17th Int. Conf. on Soil Mechanics and Geotechnical Engineering 4*: 2777–2872.
- Mitchell, J.K. 1981. Soil improvement: state-of-the-art. *Proc. 10th Int. Conf. on Soil Mechanics and Foundation Engineering 4*: 509–565.
- Monaco, P., Amoroso, S., Marchetti, S., Marchetti, D., Totani, G., Cola, S., & Simonini, P. 2014. Overconsolidation and stiffness of Venice lagoon sands and silts from SDMT and CPTU. *Journal of Geotechnical and Geoenvironmental Engineering* 140 (1): 215–227. [https://doi.org/10.1061/\(ASCE\)GT.1943-5606.0000965](https://doi.org/10.1061/(ASCE)GT.1943-5606.0000965).
- Priebe, H.J. 1998. Vibro replacement to prevent earthquake induced liquefaction. *Ground Engineering* 31(9): 30–33. UK: Emap Construct.
- Robertson, P.K. 2009. Interpretation of cone penetration tests – a unified approach. *Canadian Geotechnical Journal* 46 (11): 1337–1355.
- Rollins, K.M., Amoroso, S., Andersen, P., Tonni, L., & Wissmann, K.J. 2021. Liquefaction mitigation of silty sands using rammed aggregate piers based on blast-induced liquefaction testing. *Journal of Geotechnical and Geoenvironmental Engineering* 147 (9) [https://doi.org/10.1061/\(ASCE\)GT.1943-5606.0002563](https://doi.org/10.1061/(ASCE)GT.1943-5606.0002563)
- Saftner, D.A., Zheng, J., Green, R.A., Hryciw, R., & Wissmann, K.J. 2018. Rammed aggregate pier installation effect on soil properties. *Proceedings of Institution of Civil Engineers-Geotechnical Engineering* 171 (2): 63–73.
- Salgado, R., Boulanger, R.W., & Mitchell, J.K. 1997. Lateral stress effect on CPT liquefaction resistance correlations. *Journal of Geotechnical and Geoenvironmental Engineering* 123(8): 726–735.
- Schmertmann, J.H. 1985. Measure and use of the in situ lateral stress. *The Practice of Foundation Engineering, A Volume Honoring Jorj O. Osterberg*, 189–213.
- Smith, M.E., and Wissmann, K.J. 2018. Ground improvement reinforcement mechanisms determined for the Mw 7.8 Muisne, Ecuador, earthquake. *Proc. 5th Geotechnical Earthquake Engineering and Soil Dynamics Conference: Liquefaction Triggering, Consequences, and Mitigation*, 286–294. Washington, DC: ASCE.
- Toscani, G., Burrato, P., Di Bucci, D., Seno, S., & Valensise, G. 2009. Plio-Quaternary tectonic evolution of the northern Apennines thrust fronts (Bologna-Ferrara section, Italy): seismotectonic implications. *Italian Journal of Geosciences* 128: 605–613.
- Vautherin, E., Lambert, C., Barry-Macaulay, D., & Smith, M. 2017. Performance of rammed aggregate piers as a soil densification method in sandy and silty soils: experience from the Christchurch rebuild. *Proc. 3rd Int. Conf. on Performance-based Design in Earthquake Geotechnical Engineering*. London, UK: ISSMGE.
- Yu, H.S. 2004. James K. Mitchell Lecture – In situ soil testing: from mechanics to interpretation. *Proc. 2nd Int. Conf. on Site Characterization 1*: 3–38. London, UK: Taylor & Francis Group.

A CPT-based method for monotonic loading of large diameter monopiles in sand

S. Bascunan

Ramboll, Hamburg, Germany

K. Kaltekis

Fugro, Nootdorp, The Netherlands

B. van Dijk

Arcadis, Amersfoort, The Netherlands

K. Gavin

Delft University of Technology, Delft, The Netherlands

ABSTRACT: A joint academia-industry project, the Pile Soil Analysis (PISA) project, resulted in an empirical method for assessing the monotonic lateral loading response of large diameter monopiles. The method predicts four soil reactions, namely the distributed load and the distributed moment along the pile shaft, the pile base shear and the pile base moment. The method considers pile load test data and 3D numerical modelling. A 1D framework allows prediction of the four soil reactions. In this paper, a CPT-based approach is proposed to derive the four soil reaction components for use in a 1D model for conceptual design of monopiles in sand subject to monotonic lateral loading. The approach relies on results from 3D finite element analyses that were performed considering soil conditions for a sand site used in the PISA project (Dunkirk site). The results are compared to pile load test data from the PISA project, showing good agreement, particularly for load levels related to the serviceability limit state.

1 INTRODUCTION

Monopiles are commonly used as foundations for offshore wind turbine generators (WTGs). The current trend in the ever-growing offshore wind energy sector is for WTGs to become bigger which evidently leads to requirements for monopiles with large diameters up to 10 m to support the superstructure. It is expected that the ratio of embedded length to diameter, L/D (or slenderness ratio) of monopile foundations for the 10 MW+ next-generation wind turbines could be in the range between 2 and 6 (Panagoulas et al., 2018). Such structures are categorised as intermediate foundations according to ISO (2016).

An industry standard approach for assessing monopile lateral response was a p - y method for long slender piles, adjusted to large diameter monopiles. The p - y method is based on the Winkler assumption according to which the soil surrounding the pile is modelled as a set of uncoupled, non-linear, elastoplastic springs which define the lateral pressure (p) applied to the pile at a given depth, as a function of the lateral displacement (y). The method, however, does not capture the physics of the monopile behaviour accurately.

A joint academia-industry project, the Pile Soil Analysis (PISA) project, resulted in an empirical method for assessing the monotonic lateral loading response of large diameter monopiles. The method is based on conventional models for caisson design, predicting four soil reactions, namely the distributed load and the distributed moment along the pile shaft, the pile base shear and the pile base moment (Figure 1). The PISA schematisation excludes torsional foundation loading (Burd et al., 2020). The empirical method considers pile load test (PLT) data and 3D numerical modelling. A 1D framework allows prediction of the four soil reactions and requires, for sands, profiling of three soil parameters, namely the relative density, the vertical effective stress and the shear modulus at small strain.

In this paper, a CPT-based approach is proposed to derive the four soil reaction components for use in a 1D model for conceptual design of monopiles in sand subject to monotonic lateral loading. The approach relies on results from 3D finite element (FE) analyses that were performed considering soil conditions for a sand site used in the PISA project (Dunkirk site). The results are compared to PLT data from the

PISA project, showing good agreement, particularly for load levels related to the serviceability limit state (SLS).

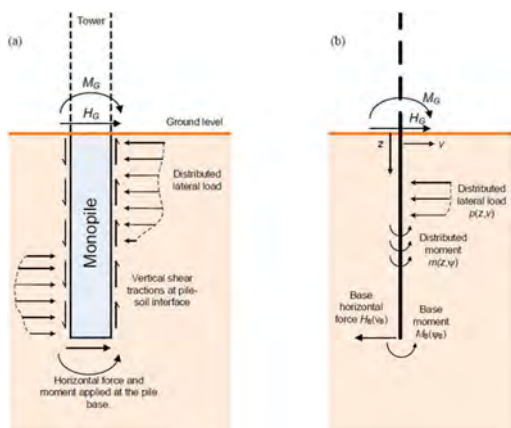


Figure 1. (a) Schematised soil reaction components acting on a laterally loaded monopile; (b) 1D design model. (after Burd et al., 2020).

2 DATABASE

Several piles driven into dense sand at the Dunkirk site were tested during the PISA project in order to investigate the effect of different design aspects such as pile geometry, load ratio, unloading/reloading behaviour and creep. In this paper, the results from three PLTs on medium diameter piles, $D = 762$ mm (i.e. DM3, DM7 and DM4; see Table 1) were compared to results from 3D FE analyses. This allowed, using the FE-derived resistance components, development of a CPT-based method.

Table 1. Geometry of PISA piles considered in this study (Taborda et al., 2020).

Pile	Diameter (m)	Length (m)	Slenderness ratio (-)	Wall Thickness (mm)
DM3	0.762	6.1	8.0	25
DM4	0.762	4.0	5.3	14
DM7	0.762	2.3	3.0	10

3 FINITE ELEMENT MODEL

3.1 General

The commercial software packages Plaxis 3D and Plaxis Monopile Design Tool, MoDeTo (Plaxis BV, 2018), were used to perform the FE analyses and extract the soil reaction curves. Through the latter, the monopile was modelled and then the FE analysis was performed in Plaxis 3D. Finally, each of the four

soil reaction curves were extracted via MoDeTo at different load steps and pile depths.

3.2 Soil model

The Dunkirk test site was characterised using a range of in situ tests and advanced laboratory testing (Zdravković et al., 2020). Several CPTs were performed next to the test pile locations and other key locations. Figure 2 presents the average cone resistance at the site. The general soil stratigraphy is shown in Table 2. The water table is found approximately at 5.4 m below ground level.

The Hardening Soil small strain model (HSsmall) was used as soil constitutive model. The model was calibrated against available soil data from the Dunkirk site, including CPTs, seismic CPTs and laboratory tests such as triaxial tests with bender element measurements. The calibration process included study of several CPT-based and empirical parameter formulations from the literature (e.g. Robertson and Cabal, 2015; Brinkgreve et al., 2010), investigation of parameter interdependency and performance of single element test predictions.

The focus of the CPT-based approach was accurate representation of the SLS, according to which the allowance for the total permanent tower axis tilt rotation is 0.5° (DNVGL, 2016). By analysing the data obtained from the PISA project, this limit is reached at approximately 30% to 50% of the maximum horizontal load applied to the monopiles during pile load testing; hence only that portion of the horizontal load-deformation curve was considered for the HSsmall calibration process.

Table 3 shows an overview of the soil parameter values for the calibrated HSsmall soil model.

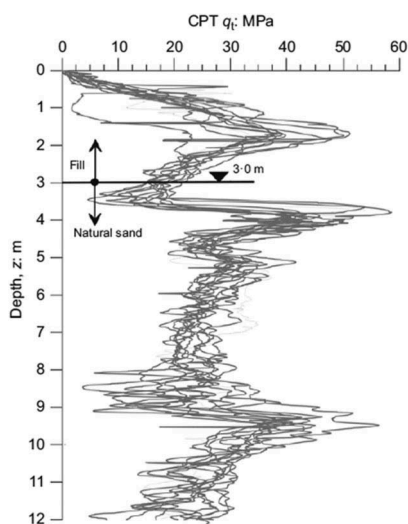


Figure 2. Cone resistance profile at the Dunkirk site (Zdravković et al., 2020).

Figure 3 illustrates the comparative results between the measured horizontal load-displacement responses from the PLTs and the predicted responses from the performed 3D FE analyses. A fairly good match is observed at the initial part of the curves, rendering the prediction of the stiffness response, which was of primary interest, satisfactory.

Additional (fictional) piles were considered in order to expand the database and check the influence of pile geometry on each of the four soil reaction components. Table 4 shows an overview of the additional piles considered for the sensitivity analyses.

4 SOIL REACTION CURVES

4.1 Distributed lateral load (p - y)

The relationship between p and y along the pile shaft has been widely studied. In recent years several formulations for p - y curves have been developed by taking into consideration the cone penetration test and considering the link between cone resistance (q_c) and in situ horizontal effective stress of the soil (Houlsby and Hitchman, 1988). An overview of some of those formulations together with their corresponding authors is shown below:

Table 2. Soil stratigraphy at the Dunkirk site (Zdravković et al., 2020).

Depth (m)	Material	Description
0 - 3	Hydraulic fill	Sand dredged from offshore Flandrian deposits
3 - 30	Flandrian sand	Marine sand deposited during three local transgressions
> 30	Ypresienne clay	Eocene marine clay located beneath the southern North Sea

Table 3. Summary of soil parameters for HSsmall model.

Depth [m]	0-3	3-5.4	5.4-9	9-12.2	12.2-15
γ' [kN/m ³]	19.1	20.8	11.0	11.8	9.8
$E_{50,ref}$ [MPa] (= $E_{oed,ref}$)	250	223	174	202	87
$E_{ur,ref}$ [MPa]	751	668	523	605	260
φ' [deg]	46	45	43	42	37
ψ [deg]	15	9	9	9	9
$\gamma_{0.7}$ [-]	1e-4	1.3e-4	1.3e-4	1.3e-4	1.3e-4
$G_{0,ref}$ [MPa]	321	285	223	259	111
R_f [-]	0.88	0.91	0.91	0.91	0.91
K_θ [-]	0.5	1.0	0.8	0.7	0.7

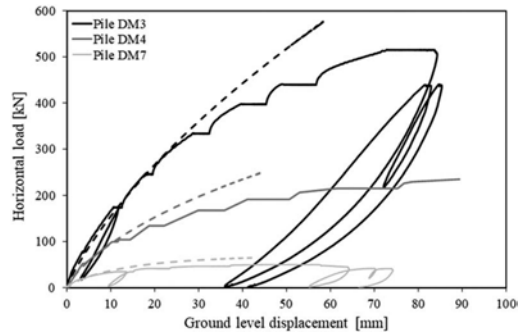


Figure 3. Comparison of ground level load-displacement for three piles tested during the PISA project (see Table 1 for details). Solid lines represent the results of the pile load tests (after Taborda et al., 2020), dashed lines represent the results of the 3D FE calculations.

Table 4. Geometry of additional (fictional) piles considered in the study.

Pile	Diameter (m)	Length (m)	Slenderness ratio (-)	Wall Thickness (mm)
DM3A	1.0	6.1	6.1	25
DM3B	1.2	6.1	5.1	25
DM3D	2.0	6.1	3.1	25
DM7B	0.762	3.0	3.9	10
DM7D	0.762	4.7	6.1	10
DM7E	0.762	3.8	5.0	10
PL1	0.762	15.0	19.7	20
PL2	0.5	15.0	30.0	25
PL3	0.6	21.0	35.0	30

$$p = \min \left(2D(\gamma'z)^{0.33} q_c^{0.67} \left(\frac{y}{D} \right)^{0.50}, Dq_c \right) \quad (1)$$

$$p = 2.84D(\gamma'D) \left(\frac{q_c}{\gamma' \cdot D} \right)^{0.72} \left(\frac{y}{D} \right)^{0.64} \quad (2)$$

$$p = 3.6D(\gamma'D) \left(\frac{q_c}{\gamma' \cdot D} \right)^{0.72} \left(\frac{y}{D} \right)^{0.66} \quad (3)$$

$$p = \begin{cases} 4.5G_{max} y, & \text{for } \frac{y}{D} \leq 0.0001 \\ p_u f(y), & \text{for } \frac{y}{D} > 0.01 \end{cases} \quad (4)$$

where Equation 1 is by Novello (1999), Equation 2 is by Dyson & Randolph (2001), Equation 3 is by Li et al. (2014), Equation 4 is by Suryasentana & Lehane (2016), D = pile diameter, γ' = effective unit weight of soil, z = depth, G_{max} = small strain shear modulus, p_u = ultimate lateral soil resistance (for more details refer to Suryasentana & Lehane, 2016) and $f(y)$ = exponential function that depends on lateral displacement (for more details refer to Suryasentana & Lehane, 2016).

Equations 1 to 4 were used to derive p - y curves which were then inserted in a 1D Timoshenko beam model for modelling of the pile-soil lateral behaviour. Long slender (fictional) piles ($L/D \geq \sim 20$) were considered so that the influence of the other three soil reaction components (distributed moment, base shear and base moment) to the overall response is negligible (see Table 4; piles PL1, PL2 and PL3). The results obtained from the 1D model were thereafter compared with results from 3D FE analyses and it was found that Equation 2 (Dyson and Randolph, 2001) was providing the better match and was thus selected to define the p - y component for this study.

4.2 Distributed moment (m - ψ)

The distributed moment (m) is caused by the vertical shear stresses along the pile shaft due to pile rotation (ψ). It is considered that m is linked to p , which is acting as a normal force along the shaft, through consideration of the pile-soil interface friction angle (δ) and the pile geometry (L and D). A fitting parameter, $F_{m\psi}$, was adopted in order to investigate the relationship between the aforementioned parameters for the range of pile geometries considered.

$$F_{m\psi} = p \cdot D \cdot \tan\delta \quad (5)$$

where δ = pile-soil interface friction angle taken as $2/3\phi'$.

By considering the maximum value of the distributed moment at every slice along the pile shaft obtained from the 3D analysis, m_{max} , the influence of L/D on the ratio $m_{max}/F_{m\psi}$ was investigated (Figure 4) and a formulation for determination of m is proposed (Equation 6). The relatively low R^2 value is attributed to the small dataset and the fact that the proposed linear trend might be less suitable as L/D increases.

$$m = 0.07 \cdot p \cdot D \cdot \tan(\delta) \cdot \left(\frac{L}{D}\right)^{0.7} \quad (6)$$

The distributed load and distributed moment are soil reactions along the pile shaft, thus the pile was divided into slices and both soil reactions were computed per slice. By considering geometric continuity

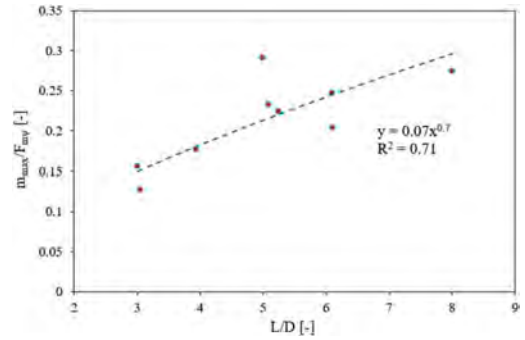


Figure 4. Distributed moment ratio as function of the slenderness ratio L/D .

of the rigid pile, the rotation can be obtained from the horizontal displacements. Figure 5 shows the distributed moment for various slices along the shaft of pile DM4, obtained both from the 3D FEA and the proposed CPT-based formulation (Equation 6).

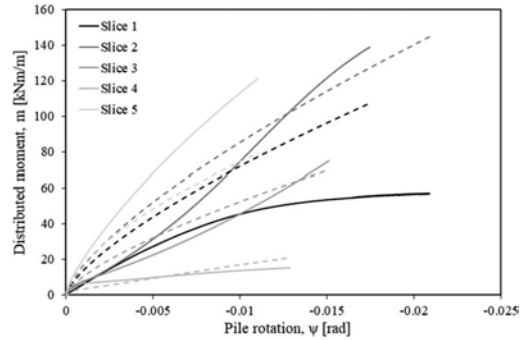


Figure 5. Pile DM4 distributed moment along each slice. Solid lines correspond to the results from 3D FE models and dashed lines correspond to the results from the proposed CPT-based formulation.

4.3 Horizontal base force (H_B)

Due to the applied force at the pile head, the base of the pile tends to move in the opposite direction, generating a horizontal base force (H_B). H_B was linked to the base displacement, v_b , via a fitting parameter, F_{HB} , which is a function of the q_c at the pile base and the pile geometry (Equation 7). Figure 6 shows the relationship between F_{HB} and the ultimate horizontal base force, $H_{B,ult}$, for all piles in the considered database.

$$F_{Hb} = \frac{q_c \cdot D^2}{(L/D)^{0.36}} \quad (7)$$

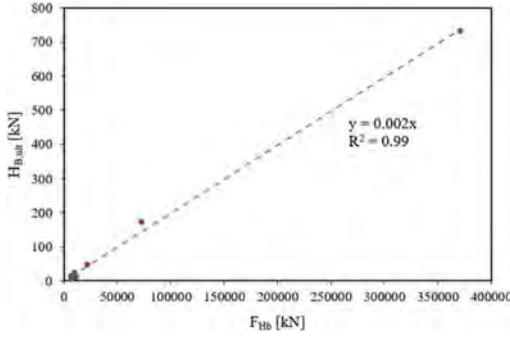


Figure 6. Fitting parameter F_{HB} versus the ultimate horizontal base force, $H_{B,ult}$.

Curve fitting with results from the Plaxis 3D models of the database resulted in the following bi-linear relationship:

$$H_B = \begin{cases} \frac{0.00235q_c}{\left(\frac{b}{D}\right)^{0.36}} \left(\frac{\pi D^2}{4}\right) \left(\frac{v_b}{0.0005D}\right), & \text{for } \frac{v_b}{D} \leq 0.0005 \\ \frac{0.00235q_c}{\left(\frac{b}{D}\right)^{0.36}} \left(\frac{\pi D^2}{4}\right), & \text{for } \frac{v_b}{D} > 0.0005 \end{cases} \quad (8)$$

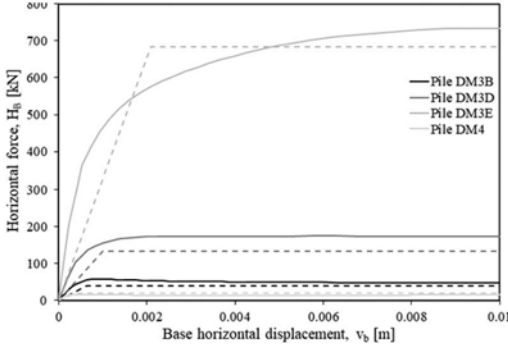


Figure 7. Pile base horizontal reactions. Solid lines correspond to the results from 3D FE models and dashed lines correspond to the results from the proposed CPT-based formulation.

Figure 7 shows the pile base horizontal reactions obtained from the 3D FEA in comparison to the reactions from the proposed CPT-based formulation (Equation 8) for a selection of piles from the database.

4.4 Base moment (M_B)

The base moment is caused by rotation of the pile toe. Similarly to the base horizontal force, the base moment relationship contains a first linear portion followed by a plateau. Curve fitting with results

from the Plaxis 3D models of the database resulted in the following bi-linear relationship:

$$M_B = \begin{cases} \frac{0.00171q_c D}{\left(\frac{b}{D}\right)^{0.52}} \left(\frac{\pi D^2}{4}\right) \left(\frac{v_b}{0.0007D}\right), & \text{for } \frac{v_b}{D} \leq 0.0007 \left[\frac{\text{rad}}{m}\right] \\ \frac{0.00171q_c D}{\left(\frac{b}{D}\right)^{0.52}} \left(\frac{\pi D^2}{4}\right), & \text{for } \frac{v_b}{D} > 0.0007 \left[\frac{\text{rad}}{m}\right] \end{cases} \quad (9)$$

Figure 8 shows the pile base moment reactions obtained from the 3D FE models and the proposed CPT-based formulation (Equation 9) for a selection of piles from the database.

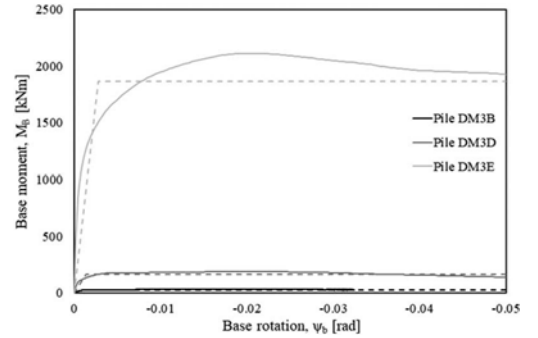


Figure 8. Pile base moment reactions. Solid lines correspond to the results from 3D FE models and dashed lines correspond to the results from the proposed CPT-based formulation.

5 PILE LATERAL RESPONSE

The four soil reaction components, as computed with the use of the proposed equations, were entered in a 1D Timoshenko beam model for modelling of the general monopile response under lateral loading. Results for the piles of Table 1 are shown in Figures 9 and 10. The predictions of the CPT-based method show in general good agreement with the PLTs and the 3D FE analyses for the initial part of the load-displacement curve, i.e. until approximately half the ultimate lateral load (Figure 9). The initial stiffness response of the monopiles is, therefore, fairly captured. Figure 10 depicts the pile deflections below ground level at different loads, all with magnitude lower than half of the ultimate lateral load. Again, a satisfactory agreement between the results of the CPT-based method, the 3D FE analyses and the PLTs is observed.

Figure 9 shows that after a certain level of ground level displacement, the response obtained from the proposed CPT-based method is stiffer than the response obtained from the 3D FE analyses and the PLTs. Therefore, a cut-off point needs to be defined beyond which the proposed

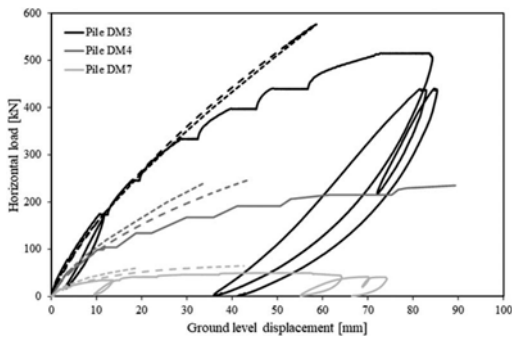


Figure 9. Comparison of ground level load-displacement for three piles tested during the PISA project. Solid lines represent the results of the pile load tests; thinly dashed lines represent the results of the 3D FE calculations; thickly dashed lines represent the results of the CPT-based method.

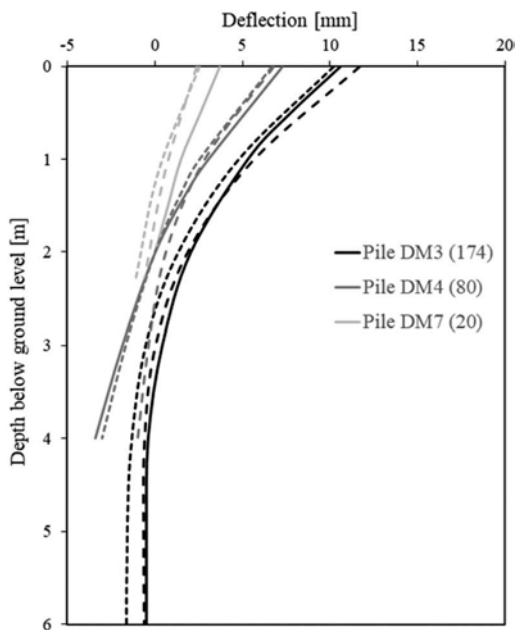


Figure 10. Comparison of deflection at and below ground level for three piles tested during the PISA project. Solid lines represent the results of the pile load tests; thinly dashed lines represent the results of the 3D FE calculations; thickly dashed lines represent the results of the CPT-based method. Values within brackets denote the applied load in kN.

method is less accurate. This point was defined by analysing, for all piles of the database, the difference in stiffness magnitude between the 3D FE analyses and the CPT-based method, at ground level and at all load levels. Consequently, it is recommended that the proposed CPT-based method is used for predictions of monopile lateral

response in which the displacements at ground level are not larger than 2% to 3% of the pile outer diameter. This level of deformation generally corresponds with the serviceability limit state of monopiles used in the offshore wind industry.

6 DISCUSSION AND CONCLUSIONS

The paper presents a CPT-based method for predicting the response of laterally loaded monopiles in a sand setting. In order to verify application of the method to full-scale monopiles and until further experience is gained with the use of this method, a FE analysis, considering typical soil conditions of the investigated site and expected pile geometry, is recommended as a minimum.

The method allows for performing monotonic conceptual design calculations for monopile foundations supporting WTGs in a time-efficient manner, requiring only CPT data. Total computing time can be reduced by up to 90 % with respect to performing 3D FE analyses.

The proposed soil reaction formulations were calibrated against soil data from the PISA sand site in Dunkirk and consider a specific limit state, i.e. the SLS. Therefore, applicability of the method to marine sites with significantly different soil conditions (e.g. in terms of strength, stiffness, sand type) than the ones at Dunkirk and/ or for different limit states should be carefully checked. In these occasions, FE analyses are required prior to implementation of the approach shown in this paper to develop a site-specific CPT-based method. Alternatively, the PISA ‘numerical-based method’ can be employed (Byrne et al., 2017).

The curve fitting process considered the individual soil reactions from the 3D FE analyses and not the actual PLTs, since modelling of each individual soil reaction component based on measured PLT data has been shown to be problematic (Foursoff, 2018).

The proposed CPT-based method provides a representation of the global monopile response under monotonic lateral loading, although the individual soil reactions at a local level can differ considerably between the FE analyses and the CPT-based formulations. The latter can be attributed to factors such as imperfect curve fitting and inherent limitations of the 1D model which cannot accurately represent all mechanisms of soil-pile interaction at a local level.

The CPT-based method should be employed in its entirety, i.e., individual soil reaction components should not be excluded from the analysis or used independently.

REFERENCES

- Brinkgeve, R. Engin, E. & Engin, H. 2010. Validation of empirical formulas to derive model parameters for sands. In *Proceedings of the 7th European Conf. on*

- Numerical Methods in Geotechnical Eng.*, Trondheim – Leiden, 137–142.
- Burd, H.J., Taborda, D.M.G., Zdravković, L., Abadie, C. N., Byrne, B.W., Houlsby, G.T., ... Potts, D.M. 2020. PISA design model for monopiles for offshore wind turbines: application to a marine sand. *Geotechnique* 70(11): 1048–1066.
- Byrne, B.W., McAdam, R., Burd, H.J., Houlsby, G.T., Martin, C.M., Beuckelaers, W.J.A.P., ... Plummer, M.A. L. 2017. PISA: new design methods for offshore wind turbine monopiles. In *Proc. of the 8th Intl. conf. on offshore site investig. and geot., smarter solutions for future offshore developments*, Vol 1: 142–161, London, UK: Soc. Underwater Tech.
- DNVGL. 2018. DNVGL-ST-0126 – Support structure for wind turbines. Oslo, Norway: DNV GL.
- Dyson, G.J. & Randolph, M.F., 2001. Monotonic lateral loading of piles in calcareous sand. *Journal of Geotechnical and Geoenvironmental Engineering*, 127(4): 346–352.
- Foursoff, W. 2018. Investigation into a new CPT-based design method for large diameter monopiles in sand. MSc thesis, Technical University of Delft, The Netherlands.
- Houlsby, G.T. & Hitchman, R. 1988. Calibration chamber tests of a cone penetrometer in sand. *Geotechnique* 38 (1): 39–44.
- International Organization for Standardization, 2016. ISO 19901–4:2016 Petroleum and Natural Gas Industries – Specific Requirements for Offshore Struc. – Part 4: Geotechnical and Foundation Design Considerations. Geneva: ISO.
- Li, W., Igoe, D. & Gavin, K. 2014. Evaluation of CPT-based p–y models for laterally loaded piles in siliceous sand. *Geotechnique Letters* 4: 110–117.
- Novello, E. 1999. From static to cyclic p–y data in calcareous sediments. 2nd Intl. Conf. on Eng. for Calc. Sedim., Perth, 17–27.
- Panagoulas, S., Brinkgeve, R.B.J., Minga, E., Burd, H.J. & McAdam, R.A. 2018. Application of the PISA framework to the design of offshore wind turbine monopile foundations. In *Proc. of the WindEurope Conf. 2018*, Hamburg, Germany.
- Plaxis BV. 2018. PLAXIS MoDeTo Manual, The Netherlands.
- Robertson, P.K., & Cabal, K.L. 2010. Estimating soil unit weight from CPT. In *Proc. of the 2nd Intl. Symposium on Cone Penetration Testing*, Huntington Beach, California.
- Suryasentana, S.K. & Lehane, B.M. 2016. Updated CPT-based p–y formulation for laterally loaded piles in cohesionless soil under static loading. *Geotechnique* 66(6): 445–453.
- Taborda, D.M.G., Zdravković, L., Potts, D.M., Burd, H.J., Byrne, B.W., Gavin, K.G., ... McAdam, R.A. 2020. Finite-element modelling of laterally loaded piles in a dense marine sand at Dunkirk. *Geotechnique* 70-11, 1014–1029
- Zdravković, L., Jardine, R.J., Taborda, D.M.G., Abadia, D., Burd, H.J., Byrne, B.W., ... Ushev, E. 2020. Ground characterisation for PISA pile testing and analysis. *Geotechnique* 70(11): 945–960.

Automatic interpretation and statistical evaluation of soil conditions for preliminary design of offshore foundations using the cone penetration test

L. Berenguer Todo Bom & M. Kanitz

Ramboll, Hamburg, Germany

ABSTRACT: The increasing need for renewable energy has led to a substantial growth of the offshore wind industry. To meet the need of the demanding timelines of the industry, while maintaining a thorough and robust design of the offshore foundations, automation is key in supporting rapid and accurate geotechnical screening of any investigated site. The preliminary design of foundations for offshore wind turbines is a crucial step to determine the feasibility of the planned structures to build an offshore wind park at the site. Therefore, an initial estimate of the ground conditions, in terms of both soil stratigraphy as well as soil strength and stiffness properties are necessary. This contribution presents a MATLAB-based tool which performs an automatic interpretation and statistical evaluation of soil conditions based on solely cone penetration testing (CPT) data. The tool derives a preliminary ground model by assembly of similar soil type and strength and stiffness parameters are determined through available CPT correlations. A depth-dependent statistical evaluation of the strength and stiffness parameters for each soil layer in the respective soil profile is computed. The output profiles can be adopted directly for the preliminary design of offshore foundations such as jacket pin-piles, suction bucket or monopiles using the PISA rule-based method.

1 GENERAL

1.1 Introduction

The increasing demand in the contribution of renewable wind power to the national energy grids of most countries in the world continues to accelerate at a rapid pace. Due to the increasing size of these structures to improve efficiency and increase energy production, the offshore environment with steadier wind speeds than on land has become very attractive for these types of investments.

The design cycles of offshore wind turbine foundation typically consist of 3 phases. An initial phase termed ‘concept’, followed by ‘Front-end engineering design’ (FEED) and ending in the ‘detailed’ stage. The geotechnical investigation campaigns are typically undertaken during the concept and FEED stages of development, where cone penetration tests (CPT) are undertaken at representative and all planned foundation locations, respectively. Whilst non-binding, important decisions concerning the foundation type and sometimes geometrical and installation methodologies are made early in the design process. Improving the methodologies and processes involved in the preliminary design of the foundations, resorting to the significant information provided by the CPT in situ testing is the main goal of this contribution.

2 BACKGROUND

2.1 Offshore foundation design practice

The most common foundation types in the offshore wind industry are the monopile and jacket structures. The monopile consists of a single tubular steel element supporting the wind turbine generator (WTG). A jacket structure consists of a welded tubular space frame with vertical or battered legs and bracing system, which is then in turn commonly fixed to the seabed by pile elements, among other foundation options.

The preliminary design of these foundations typically resorts to the methods defined in the API RP 2GEO (2014) and DNVGL-RP-C212 (2017) standards. More recent developments, namely the CPT-based methods for the calculation of axial capacity, Jardine et al. (2015) and Lehane et al. (2005), and the PISA working group publications, Byrne et al. (2020), are currently adopted already during early stages of design for jacket piles and monopiles, respectively.

The definition of a ground model and derivation of geotechnical properties is a necessary initial step for these design approaches. The following sections describe in detail an automatic procedure to undertake it supported on the CPT data.

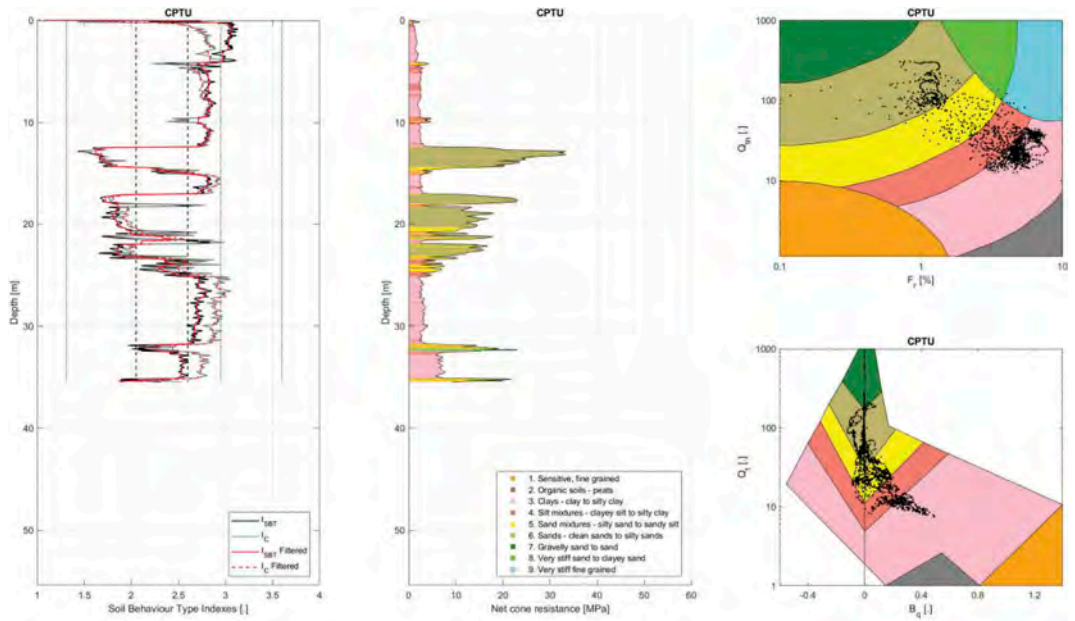


Figure 1. Soil classification based on I_c (left), based on the Robertson textural chart (middle) and Robertson chart (right).

2.2 CPT classification charts and ground model definition

CPT measurements can be used to determine the soil stratigraphy and the soil type. For this purpose, classification charts can be used that link the CPT measurements to the soil type. Robertson (1990) proposed two charts based on either the normalized cone penetration resistance with variable stress exponent Q_{tn} and the pore pressure ratio B_q or based on Q_{tn} and the normalized friction ratio F_r . These charts are subdivided into 9 regions ranging from sensitive fine grained over sand to very stiff fine-grained soil. The normalized Soil Behavior Type Index, I_c , based on Robertson and Wride (1998) is a parameter for mechanical behavior classification of the soil and defined in Equation 1.

$$I_c = \left((3.47 - \log Q_{tn})^2 + (\log F_r + 1.22)^2 \right)^{0.5} \quad (1)$$

It defines the soil as either sand (for $1.31 < I_c < 2.05$), sand/silt mixtures (for $2.05 < I_c < 2.6$), clay/silt mixtures (for $2.6 < I_c < 2.95$) or clay ($2.95 < I_c < 3.6$). Robertson (2010) additionally proposed a non-normalized Soil Behavior Type Index I_{SBT} that is based on basic CPT measurement values:

$$I_{SBT} = \left((3.47 - \log q_c/p_a)^2 + (\log R_f + 1.22)^2 \right)^{0.5} \quad (2)$$

2.3 Correlations for strength and stiffness soil parameters

For coarse-grained soils (sands), the dry density and the friction angle are evaluated based on CPT correlations. For sands, the CPT correlations according to Robertson & Campanella (1983), Equation 3, as well as Meyerhof & Hanna (1979), Equation 4, are well-established to derive the internal friction angle ϕ' :

$$\phi' = \tan^{-1} (0.1 + 0.38 \cdot \log q_t / \sigma'_{v0}) \quad (3)$$

$$\phi' = 26.8 + 4.5 \log q_c \quad (4)$$

with q_t = corrected cone resistance [MPa] and σ'_{v0} = vertical effective stress [MPa].

For fine-grained soils, the undrained shear strength C_u can be evaluated based on CPT measurements by the cone factor N_{kt} through:

$$C_u = q_{net} / N_{kt}, q_{net} = q_t - \sigma_{v0} \quad (5)$$

The shear wave velocity in sands can be derived with the CPT correlation after Baldi et al. (1989) with the cone resistance q_c [MPa] and σ'_{v0} [MPa]:

$$v_s = 277 q_c^{0.13} \sigma'_{v0}^{0.27} \quad (6)$$

For the CPT correlation of the small strain shear modulus, G_0 , in sands, the correlation after Rix and Stokoe (1991) can be used via q_c [kPa] and σ'_{v0} [kPa]:

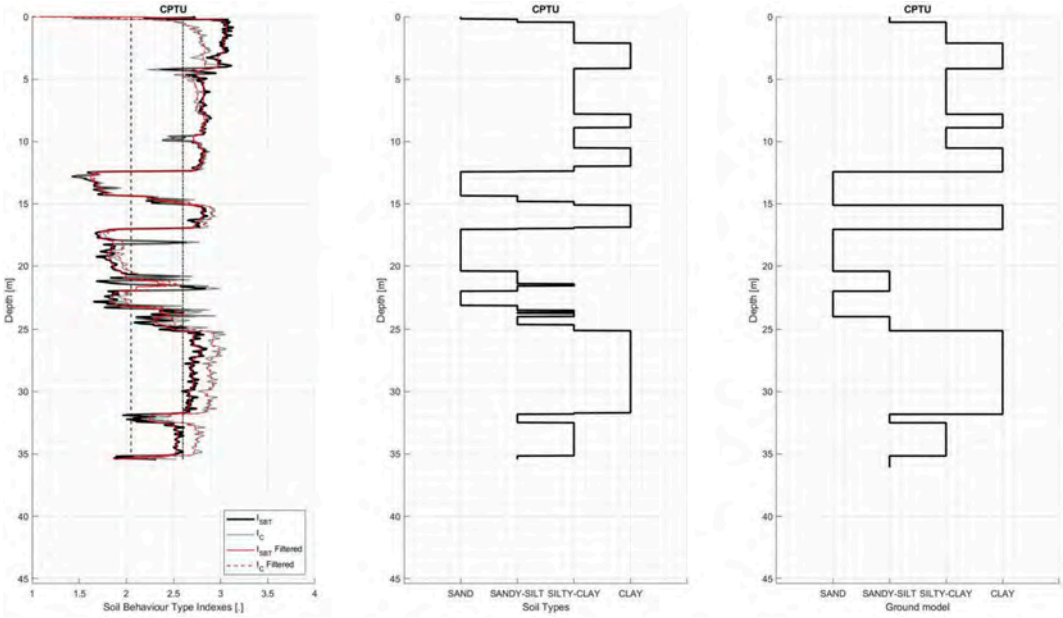


Figure 2. Identified soil types based on I_c (right), preliminary ground model (middle), simplified ground model (right).

$$G_0 = 1.634 q_c^{0.25} \sigma'_{v0}{}^{0.375} \quad (7)$$

For clays, the shear wave velocity is derived with the CPT correlation after Mayne and Rix (1995) through Equation 8 with q_c in [kPa].

$$v_s = 1.65 q_c^{0.627} \quad (8)$$

Finally, the small strain shear modulus in sands is based on the CPT correlation proposed by Mayne and Rix (1993) with q_c in [kPa]:

$$G_0 = 2.78 q_c^{1.335} \quad (9)$$

3 CPT INTERPRETATION

For a preliminary assessment of the design of the offshore wind turbine foundations, the CPT measurements at the turbine locations are analyzed. To derive the soil information, including strength and stiffness values, the cone tip resistance q_c , the sleeve friction f_s and the excess pore water pressure u_2 are required in depth. The following sections explain the necessary steps to derive a soil profile including the required soil parameters for the foundation design from the CPT measurements.

3.1 Preliminary ground model

As a first step, the soil type is determined based on either the soil textural chart, Robertson (1990) or the

soil behavior type index I_c , Robertson & Wride (1998). Figure 1 shows the derived normalized soil behavior type index I_c and I_{SBT} (left), the net cone resistance over depth including a description of the soil type based on the textural chart (middle) and the textural chart type plots for a CPT measurement (right), for a given turbine location.

Since CPT measurements can vary substantially due to repushes or small rocks at the cone tip, the soil behavior type index is filtered with a moving median function to smooth these variations. Through this investigation and presentation, the soil types present at the site are identified and an initial assessment can be made regarding the design of the foundations. In Figure 1, the location is characterized by clay layers with high thickness and embedded sand layers of medium to high thickness. Some minor stratification of the soil can also be observed in a depth of 20 m to 25 m. The textural chart additionally indicates that the location is mostly comprised of fine soils since most data points plots into section 3 (clay to silty clay) and 4 (clayey silt to silty clay). The comparison between I_c and the textural chart shows a good agreement in terms of soil classification. For preliminary ground models a low level of soil variability and stratification is preferred prior to additional soil information being available. The aim of the ground model is to identify soil units that can be characterized for the entire offshore wind farm site. Thin layers tend to do not influence the foundation design. To improve the efficiency of the analysis of the foundation design, a ground model is automatically created, neglecting thin soil layers to derive a general ground model.

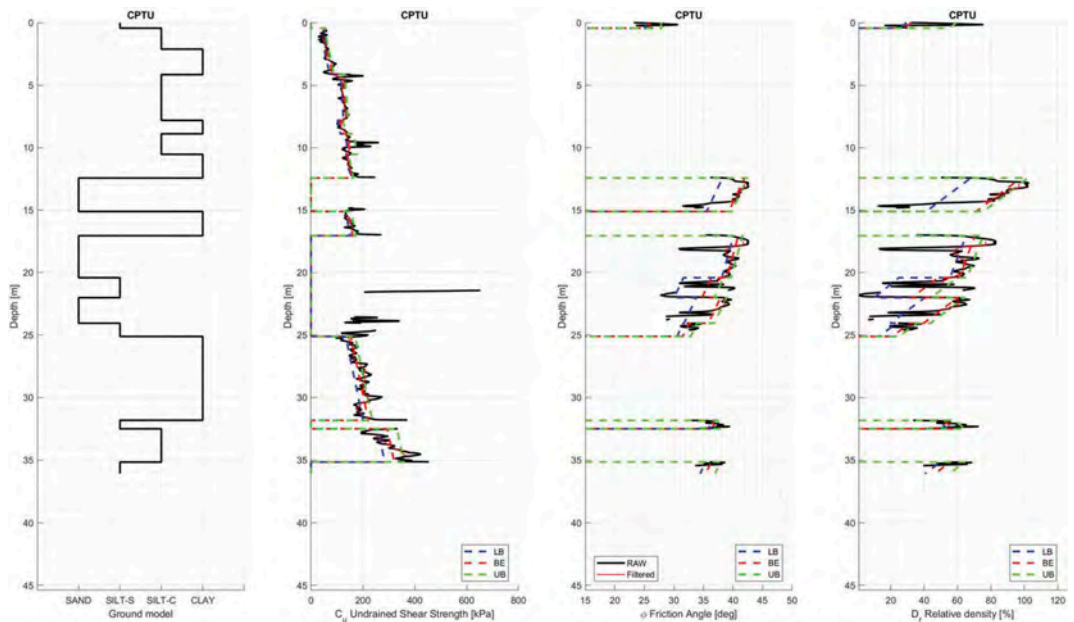


Figure 3. Derived ground model (right) with relevant soil parameters for design including lower bound, best estimate and upper bound values.

Figure 2 presents the output of this automatic procedure which details the ground model derived. On the left side of the figure, the Soil Behavior Type indexes over depth are shown as in Figure 2. In the middle, the detailed ground model is shown which is derived directly from I_c , still including thin layers.

By defining a threshold thickness of the soil layers to be acceptable in the ground model, the simplified ground model is derived (Figure 2 right). The soil layering procedure is based on a moving median approach of around 50 cm in both directions. In this analysis, the limit thickness of a soil layer is set to 0.55 m.

3.2 Determination of relevant soil parameters

Following the ground model definition, the derivation of the soil parameters relevant to the foundation design is undertaken. The CPT measurements are analyzed to derive the strength and stiffness parameter of the determined soil units. In the preliminary stage of the design process, typically, laboratory tests results of the soil are not yet available. Well-established correlations for the relevant soil parameters are hence employed to derive a first estimate of the soil properties from the in-situ CPT measurements. For all soil types, the submerged unit weight γ' and the small strain shear modulus G_0 are derived. The soil type determines which correlation (see Sec. 2.3) is used to derive G_0 . For clay and silty clay soils, the undrained shear strength c_u is determined while for sand and silty sands, the internal friction angle ϕ' and the relative density D_r are calculated. For ϕ' , the minimum

value obtained between Equation (3) and Equation (4) is adopted. The relative density is determined based on the correlation of Jamiolkowski et al. (2003). Figure 3 presents the correlated strength parameters over depth for the investigated soil profile, all of which are obtained automatically following the ground model definition.

3.3 Statistical methodology for parameter derivation

Since soil parameters can vary significantly, a statistical assessment of their distribution in depth is preferred. The local scatter present in CPT measurements should not be taken directly as input values for parameter derivation but rather statistically quantified. Figure 3 shows the soil parameters over depth for the investigated CPT profile. For the design of offshore wind turbine foundations, the statistical derivation of a lower bound (LB), upper bound (UB) and best estimate (BE) of the soil parameters, defined as the 25th, 75th and the minimum between the mean and the median, respectively, is required. Therefore, a depth-dependent statistical evaluation considering a linear variation of the soil parameter within each layer is performed for every soil unit in the preliminary ground model. These percentiles are typical assumptions in offshore foundation designs for a normal distribution of the parameters. The statistical evaluation of the mean determines if a soil parameter is constant or varying in depth as can be seen in Figure 3.

4 DESIGN APPROACHES

Different approaches can be used for the design of offshore wind turbine foundations based on design phase, client or regional specifications and the foundation type. For monopiles, the lateral bearing capacity is design-driving while for jacket-pile foundations, the axial bearing capacity is more relevant.

4.1 Monopile design approaches

For monopiles, the most used approaches are based on the API RP 2GEO (2014) or the PISA rule-based methodology proposed by Byrne et al. (2020) and Burd et al. (2020).

4.1.1 Enhanced API approach

The soil interaction curves described in the API RP 2GEO (2014) and DNVGL-RP-C212 (2017) standards do not include the local distributed moment component. This component was re-introduced by the PISA working group, Byrne et al. (2020), due to its relevance in the lateral component of resistance and therefore, in the design of large diameter pile foundations. The incorporation of the soil resistance component is usually achieved by either performing Finite Element Analyses (FEA) or adopting the PISA rule-based formulations. For the preliminary design of pile foundations, however, FEA are not usually performed and the database supporting the correlations proposed by the PISA rule-based methodology is empirically verified only for three onshore sites in northern Europe. To bridge this gap in the adequacy of the correlations to other regions of the world, and avoid conservatism in preliminary designs, a simple calculation of this component can be adopted. Considering a simple geometrical assumption, the distributed moment component can be determined from the T-z curves defined in DNVGL-RP-C212 (2017). The distributed moment component is defined in Byrne et al. (2020) as shown in Equation 10.

$$m = \frac{-1}{4} \int_0^{2\pi} t_z D^2 \cos \phi \, d\phi \quad (10)$$

The variable t_z represents the vertical shear stresses on the pile shaft, D the pile diameter and the angle ϕ is defined in the Figure 4. Assuming uniformly distributed vertical shear stresses on the pile shaft the distributed moment's component can be easily calculated. The rotation variable ψ can be simply determined by considering that the shear strain in each pile element to be negligible which results in $\theta = \psi$, since the ratio of shear stress to the pile's shear modulus, pile cross section and shear factor is assumed infinitesimal. Hence the rotation variable ψ can be simply defined from the z component of the T-z curves as shown in Equation 11.

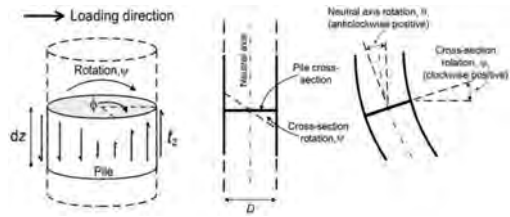


Figure 4. Pile geometrical definitions, as according to Byrne et al. (2020).

$$\psi = \tan^{-1} \left(\frac{2 \cdot z}{D} \right) \quad (11)$$

4.1.2 PISA rule-based methodology

In the PISA methodology, the lateral resistance of the monopile is determined considering the lateral soil reaction ($P-y$), the distributed moment along the pile shaft ($m-\psi$), the base shear reaction ($S-y$) and the base moment ($M_B-\psi$). The soil reaction curves are determined by a normalized analytical function that is described by the ultimate resistance, ultimate displacement, curvature of the reaction function and initial stiffness. Details of the analytical function, and correlations from soil parameters described in the previous sections to obtain the normalized parameters, can be found in Burd et al. (2020) and Byrne et al. (2020). These four parameters are either taken from the rule-based sets provided in Burd et al. (2020) and Byrne et al. (2020) or, more adequately, calibrated based on advanced 3D FE models.

4.2 Jacket piles design approach

The design of the jacket piles follows the guidelines presented in API RP 2GEO (2014). For the axial bearing capacity, the shaft friction resistance ($T-z$) and the tip resistance ($Q-w$) are determined. The T-z curves describe the relationship between mobilized soil-pile shear transfer and local pile deflection at any depth while the mobilized end bearing resistance and axial tip deflection is described by the Q-w curves. The soil parameters defined using the automated procedure described allow for an advanced preliminary design of this foundation type.

5 EXAMPLE MONOPILE MODEL

The derived ground model and geotechnical parameters can be used in the different design approaches to obtain a monopile design. In Figure 5, the results obtained from laterally loading a monopile with an outer diameter of 8.4m, wall thickness of 80mm and an embedment length of 32m in the analyzed soil profile, are shown. A lever arm of 38m of the horizontal load was considered based on the wind and wave loading conditions.

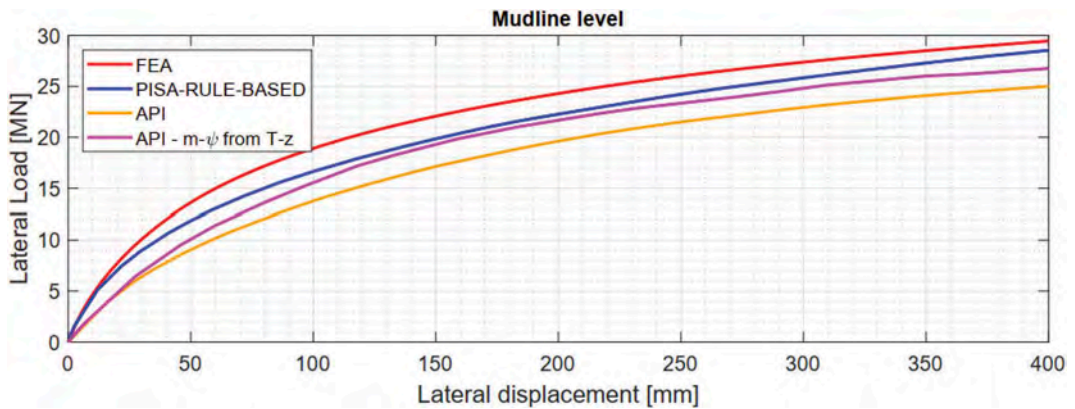


Figure 5. Global monopile lateral stiffness curves - FEA, PISA rule-based, API and enhanced API.

As additional background information, the derived load-displacement curve from advanced Finite Element Analyses (FEA), undertaken in the detailed design stage, is also plotted.

The results shown corroborate the conservatism associated with the API methodology and the significant improvement seen in both the PISA rule-based approach and the enhanced API. Moreover, the simplified calculation of the distributed moment curves option falls within the expected range of lateral monopile stiffness behavior observed in the more established approaches.

6 CONCLUSIONS

An automatic procedure to derive geotechnical ground models and parameters based on the CPT data has been described. The employed soil classification charts and parameter correlations are state of the art and the most adequate per region of the world and soil type can be adopted. Finally, a simplified approach to derive the distributed moment lateral contribution from the axial resistance curves is included. An exemplary monopile design is shown and the lateral load displacement curves plotted for different design methodologies.

REFERENCES

API RP 2GEO/ISO 19901-4, 2014. *Geotechnical and Foundation Design Considerations*, American Petroleum Institute, 2nd edition.

Baldi, G., Belotti, R., Ghionna, V. and Jamiolkowski, L.P. D., 1989. *Modulus of Sands from CPT's and DMT's*. In: Proceedings of XII ICSMFE, Rio de Janeiro.

Burd, H.J., Taborda, D.M.G., Zdravković, L., Abadie, C. N., Byrne, B.W., Houlsby, G.T., Gavin, K.G., Igoe, D.J. P., Jardine, R.J., Martin, C.M., McAdam, R.A., Pedro, A.M.G. & Potts, D.M., 2020. *PISA design model for monopiles for offshore wind turbines: application to a marine sand*. *Géotechnique*, 70(11): 1048–1066.

Byrne, B.W., Houlsby, G.T., Burd, H.J., Gavin, K.G., Igoe, D.J.P., Jardine, R.J., Martin, C.M., McAdam, R. A., Potts, D.M., Taborda, D.M.G. & Zdravković, L., 2020. *PISA Design Model for Monopiles for Offshore Wind Turbines: Application to a Stiff Glacial Clay Till*. *Géotechnique*, 70(11): 1030–1047.

DNVGL-RP-C212, *Offshore soil mechanics and geotechnical engineering*, DNVGL, August 2017.

Jamiolkowski, M., Presti, D.C., Manassero, M., 2003. *Evaluation of Relative Density and Shear Strength of Sands from CPT and DMT*. J.T. Germaine, T. C. Sheahan, R.V. Whitman (Eds.), *Soil Behavior and Soft Ground Construction*, ASCE Geotechnical Special Publication, American Society of Civil Engineers (ASCE), 119: 201–238.

Jardine, R., Chow, F., Overy, R. and Standing, J., 2005. *ICP Design Methods for Driven Piles in Sands and Clays*. Imperial College, London

Lehane, B.M., Schneider, J.A., Xu, X., 2005. *The UWA-05 method for prediction of axial capacity of driven piles in sand*. *Frontiers in Offshore Geotechnics*

Mayne, P. & Rix, G., 1993. *Gmax-qc Relationship for Clays*. *Geotechnical Testing Journal*, 16(1): 54–60.

Mayne, P. & Rix, G., 1995. *Correlations between Shear Wave Velocity and Cone Tip Resistance in Natural Clays*. *Soils and Foundation*, 35(2): 107–110.

Meyerhof, G.G. & Hanna, A.M., 1974. *Ultimate bearing capacity of foundation on sand layer overlying clay*. *Canadian Geotechnical Journal*, 11(2): 223–229.

Rix, G. & Stokoe, K., 1991. *Correlation of initial tangent modulus and cone penetration resistance*. In: 1st International Symposium on Calibration Chamber Testing (ISOCCT1), Potsdam, NY.

Robertson, P.K., 2010. *Soil behaviour type from the CPT: an update*. International Symposium on Cone Penetration Testing, CPT'10, Huntington Beach, CA, USA

Robertson, P.K. 1990. *Soil classification using the cone penetration test*. *Journal of Geotechnical and Geoenvironmental Engineering*, 27(1): 151–158, doi: 10.1139/t90-014.

Robertson, P.K. & Campanella, R.G., 1983. *Interpretation of cone penetration tests, Part I: Sand*. *Canadian Geotechnical Journal*, 20(4): 718–733.

Robertson, P.K. & Wride, C.E., 1998. *Evaluating cyclic liquefaction potential using the cone penetration test*. *Canadian Geotechnical Journal*, 35(3): 442–459.

Effect of dynamic pile driving parameters on vibratory penetration

Anchal Bhaskar, Stefan Kreiter & Dina Al-Sammarraie

MARUM—Center for Marine Environmental Sciences, University of Bremen, Germany

Tobias Mörz

MARUM—Center for Marine Environmental Sciences, University of Bremen, Germany

GeoEngineering.org

ABSTRACT: To reduce the harmful noise for marine life, generated during impact driving of offshore foundations, vibratory driving was presented as an alternative. Vibratory driving produces less noise and allows faster installation in sandy soil. This technique is cost-efficient for offshore pile installations and causes less pile fatigue than impact driving. One of the main issues with vibratory driving is the lack of a reliable driveability analysis. This is due to uncertainties in understanding of cyclic soil response during vibratory driving and the effect of different vibratory driving parameters on the soil response. In this study Vibratory Cone Penetration Test (VCPT) is used to assess the cyclic soil response during vibratory penetration. VCPT penetrates the soil while inducing cyclic loads and measures cone resistance. VCPTs were conducted in a calibration chamber to investigate the reduction of the cyclic cone resistance due to variation in frequency for the same penetration path. The VCPT results are discussed in terms of acceleration, energy, reduction ratio, which are considered as primary parameters in the different driveability analyses methods. The effect of cavitation during upward movement of the cone is investigated and discussed.

1 INTRODUCTION

With the increasing demand for renewable energy, there is an increased need to deploy offshore wind turbines around the world. Most wind turbines are constructed on pile foundations which are commonly installed by impact driving (Fischer et al. 2013). However, such construction activities adversely impact marine life due to underwater high-pressure noise generated during impact driving (Dahl et al. 2015). Alternative installation options such as vibratory pile driving, widely used in onshore engineering, have been gaining attention in offshore wind farm projects. This is because vibratory pile driving generates less noise in the water, causes less structural fatigue to the piles, enables fast installation in sandy soil, and allows easy pile handling (Tsouvalas 2020). It suffers from drawbacks such as, inefficiency in fine grained soil (Massarsch et al. 2017), and the lack reliable driveability model. It has also been proved that the bearing capacity of vibrated piles is less than that of impact driven ones (Holeyman and Whenham 2017); (O'Neill et al. 1990). The main issue with the current driveability models is the lack of understanding of the effect of dynamic pile driving parameters on the degradation of cyclic soil resistance.

Different methods have been developed to predict the degradation of the cyclic soil resistance by vibratory pile driving. The most prevalent ones are the β

value introduced by Jonker (1987) and the acceleration-based Vibdrive model using a quasi static approach (Holeyman 1993). In the former, the degradation factors were obtained from observations of full-scale vibratory pile installation in different soil types. In the latter, the effect of dynamic pile driving parameters on the degradation of cyclic soil resistance is considered implicitly by providing an empirical liquefaction factor. Until now there is no clear understanding of the effect of different dynamic pile driving parameters on the degradation of cyclic soil resistance.

Various studies have identified different key parameters influencing the degradation of soil resistance due to vibratory driving. Acceleration, frequency, displacement amplitude, energy and soil type dependent β value have been proposed as key parameters (Barkan 1962); (Rodger and Littlejohn 1980); (Jonker 1987); (O'Neill and Vipulanandan 1989); (O'Neill et al. 1990); (Wang 1994); (Viking 2002); (Cudmani and Manthey 2019). For one vibratory driver-pile combination, all these parameters are interlinked or fixed. There is no key parameter agreed upon by the past studies that dominates the degradation of soil resistance. Until now no systematic study has been made to isolate the dynamic and quasi static effects of vibratory pile driving.

There are different suggestions explaining the degradation of cyclic soil resistance during vibratory pile driving. In the work of Dierssen (1994) a total

loss of stress between the soil and the penetrating object was observed during the upward movement of the pile. This zone of total loss of stress is called cavity and the process is called cavitation. The soil is presumed to flow in this cavity and to be disturbed during this process. This disturbance is postulated to be responsible for the degradation of the cyclic soil resistance. Acceleration is also an important parameter that affect the degradation of cyclic soil resistance. This was proven in study by Barkan (1962) where steel balls placed on a unconfined dry sand bed started to penetrate when the acceleration of the whole bed exceeded a value near to the acceleration of gravity, this process is called fluidization (Barkan 1962). Furthermore, if the excess pore water pressure generated by cyclic loading reaches the value of the total stress, liquefaction and thus total loss of shear strength occurs (Kramer 1996). Therefore, liquefaction is another possible cause for the degradation of cyclic soil resistance during vibratory penetration.

The effect of various vibratory pile driving parameters can be investigated with VCPTs. The penetration of the cone is controlled by amplitude, frequency and average penetration velocity and these parameters can be varied independently. These parameters are also directly linked to the acceleration. The soil behavior itself is linked to cavitation, cyclic stress amplitude, confining stress, number of cycles and drainage. In this study the influence of dynamic parameters was isolated from quasi static influence by performing tests with different frequencies and proportionally changed average penetration velocities, leading to identical penetration paths in the depth vs average depth plane (Figure 1, 2). A change in frequency changes the dynamic parameters like acceleration and time for drainage, while leaving quasi static parameters like deformation per cycle unchanged (Figure 1).

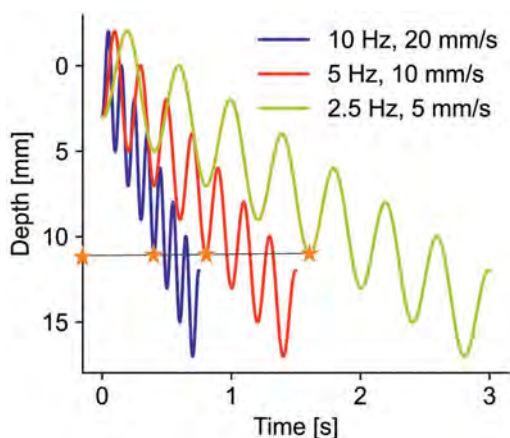


Figure 1. Illustration of VCPT penetration modes of 3 mm amplitude with varying frequency and average penetration velocity, depth vs. time. Orange stars represent the penetration after 4 cycles. Compare to Figure 2.

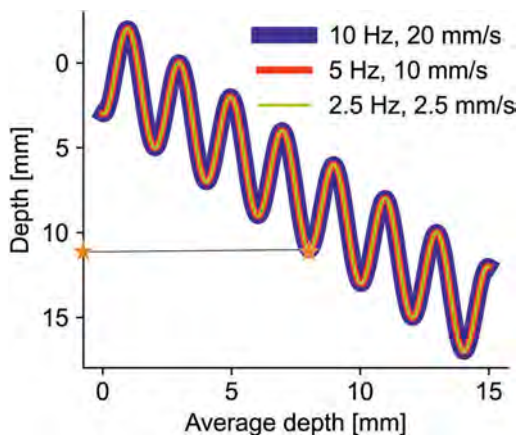


Figure 2. Illustration of VCPT penetration modes of 3 mm amplitude with varying frequency and average penetration velocity; depth vs. average depth plane. Orange stars represent the penetration after 4 cycles. Compare to Figure 1.

When the vibration amplitude of different penetration modes are the same and if the frequency and average penetration velocity for each of these penetration modes vary with the same factor, then they have the same penetration path in the depth vs. average depth plane. This is best seen in Figure 1 and 2, where the four stars marked in the time domain (Figure 1) fall in the same spot in the average depth domain (Figure 2). In fact all the points of the three penetration modes fall directly on each other in the average depth domain. If the soil reacts only quasi statically then, the resistance and other soil behavior would be the same for all three penetration modes. The differences among the three penetration modes are then the dynamic effects. This study systematically quantifies the influence of currently proposed key parameters on vibratory penetration.

Mini Vibratory Cone Penetration Tests (VCPT) were carried out in the Marum Calibration Chamber (MARCC). The VCPT, has a cone which penetrates the sample while applying vertical cyclic loading and measures the cone resistance. It was used for in-situ soil investigation to obtain dynamic soil parameters (Al-Sammarraie 2020). However, laboratory investigations eliminate the effect of inherent soil variability encountered during field investigations. Hence, this investigation is carried out in the MARCC to investigate the fundamental soil behavior.

2 METHODOLOGY

2.1 Properties of Cuxhaven Sand

The Cuxhaven Sand for the experiment comes from a sand pit in Altenwalde, Cuxhaven, Northern Germany. Cuxhaven Sand has similar properties as North Sea sand with cone resistances greater than 60

MPa in situ (Naumann et al. 2013). It is a Pleistocene glaciofluvial sand deposited in the Saalian glacial (Stähler 2020). It is uniform, well sorted, fine to medium quartz sand with less than 5% of fines (Fleischer et al. 2016). The properties of the sand is given in Table 1.

Table 1. Parameters of Cuxhaven Sand.

Property of the sand	Value
Uniformity coefficient (C_u)	3.09
Median diameter (D_{50})	0.25 mm
Minimum void ratio (e_{min})	0.48
Maximum void ratio e_{max}	0.82
Specific gravity (G_s)	2.644
Quartz content	>95%

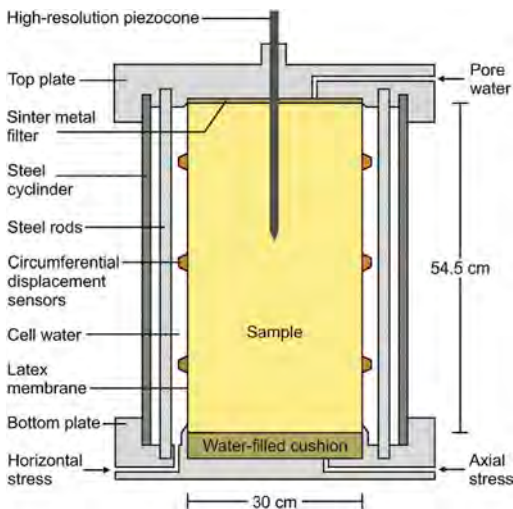


Figure 3. MARUM Calibration Chamber (MARCC).

2.2 Calibration chamber

In MARCC, the sample is fitted inside the chamber with a sinter plate on top and a water-filled cushion at the bottom (Fleischer et al. 2016). The soil sample is laterally contained in a latex membrane with a pressure-controlled cell water around it. The pore pressure is connected to the sample through small tubes located below a geotextile at the bottom of the sample and the sinter plate on top. The axial strain is computed by the volumetric changes in the water filled cushion. The axial, cell and pore pressures are controlled using three syringe pumps. The lateral strain is obtained from three lateral circumferential displacement sensors installed around the sample at height of 0.15 m, 0.25 m, 0.35 m from the top (Figure 3). The lateral stress caused by an infinite soil medium that would be around in the field is simulated in the chamber by applying Boundary Condition 5

(BC5) (Huang and Hsu 2005). Expansion is induced during CPT penetration and the stress increase with BC5 is equivalent to the reaction of an infinite half-space of the same material. The soil stiffness for this increase is based on the polynomial function obtained in lateral compression test performed prior to penetration of the cone (Kluger et al. 2021). The soil is finally penetrated with a small cone (Table 2).

Table 2. Specification of the cone in VCPT.

Cone diameter	Sampling Rate	Sample to cone ratio
12 mm	1 kHz	25

2.2.1 Sample preparation

The sample is prepared by air pluviation with a hand-held device similar to the one described in the work of Baldi et al. (1982). The sand is pluviated at a constant falling height of 0.60 m in a sample mould. The flow rate of the pluviation is adjusted by varying the aperture size of the hand-held device. The constant drop height with the chosen flow rate led to a dense sample of Cuxhaven Sand. After pluviation of the sample, a vacuum of -50 kPa is applied through the pore pressure tubes to keep the sample stable before removing the surrounding mould.

2.2.2 Saturation

The sample is saturated by increasing the vacuum at the rate of 10 kPa/steps until nearly full vacuum of ca. -100 kPa is reached. The effective stress is held constant at ca. 50 kPa by changing cell pressure and pore pressure simultaneously. Deaired deionized water is added to the sample from the pore pressure tubing at the bottom of the sample at a constant flow rate of 500 cm³/minute until the sample is saturated. Then the pore pressure and the cell pressure are increased again in 10 kPa steps holding the effective stress of ca. 50 kPa constant. Later, after the application of 300 kPa back pressure a saturation test is performed and all tests had degree of saturation of 95% i.e., Skemp-ton's B value of 0.95 was achieved (D7181 2020).

2.3 Lateral compression test

The lateral compression test determines the unique stress - strain relationship for the application of BC5 during the penetration. In this test, the cell water pressure is increased until lateral strain ϵ_h of 0.08% is reached, while keeping the axial strain fixed and maintaining a constant pore pressure. The resulted stress-strain curve is fitted by a unique fifth order polynomial function to compute the compensating pressure for the strain in BC5 (Huang and Hsu 2005). At the end of test the lateral stress is reversed back to initial stress. The influence of lateral compression test on the cone resistance was found negligible (Stähler 2020).

2.3.1 Consolidation

The consolidation stress is chosen to be equivalent to at depth of 10 m; therefore, the sample was anisotropically loaded to an effective vertical stress σ'_v of 100 kPa, horizontal effective stress σ'_h of 45 kPa. This corresponds to a lateral earth pressure of 0.45 (Fleischer et al. 2016). The sample was allowed to consolidate for a minimum of 90 minutes.

Table 3. VCPT with varying dynamic pile driving parameters investigated in MARCC.

Experiment	Name	Frequency (Hz)	Velocity (mm/s)	Amplitude (mm)
Push 1	V1	5	10	3
	V2	2.5	5	3
	V3	1	2	3
Push 2	V4	10	20	3
	V5	0.5	1	3
	V6	0.25	0.5	3
	V7	0.125	0.25	3
Push 3	S1	-	20	-

2.3.2 Vibro Penetration

The tests are performed at a constant amplitude of 3 mm with different frequencies and proportional varied average penetration velocities (Table 3). The total penetration depth is 0.42 m and a steady state penetration is expected between 0.18 m and 0.32 m from the top of the sample (Kluger et al. 2021). In two experiments, two VCPT Pushes were conducted. Each Push had 3-4 tests in the same penetration. Tests V1 to V4 were performed in Push 1 in the the first experiment, and tests V5 to V7 were performed in Push 2 in the second experiment (Table 3). At frequency greater than 10 Hz, the applied displacement amplitude of 3 mm was not completely achieved. Initially the cone penetrated for 0.18 m in the sample to reach steady state conditions with the same penetration mode. Then the frequency and average penetration velocity were changed approximately after every additional 50 mm. It was observed that after each driving parameter change, the steady state cyclic soil response was achieved in the first cycle. For comparison, a static CPT with BC5 is also conducted in a third experiment.

2.4 Data analysis

The maximum cone resistance of each cycle is the maximum cyclic cone resistance $q_{c,cyc,max}$. For every test, a dataset of cone resistance and displacement which consist of 50 to 80 steady state cycles are chosen. Two consecutive cycles were then overlaid 25 - 40 times with the following two consecutive cycles (Figure 4). This resulted in 25 - 40

independently measured points with the same phase for each point of two full sinusoidal cycles. The overlaid double cycles were then averaged yielding the mean cyclic cone resistance $q_{c,cyc,mean}$ and the mean displacement d (Figure 4).

2.5 Pile-soil interaction models

In order to compare the effect of dynamic parameters on the cyclic cone resistance $q_{c,cyc}$, following prediction models are evaluated.

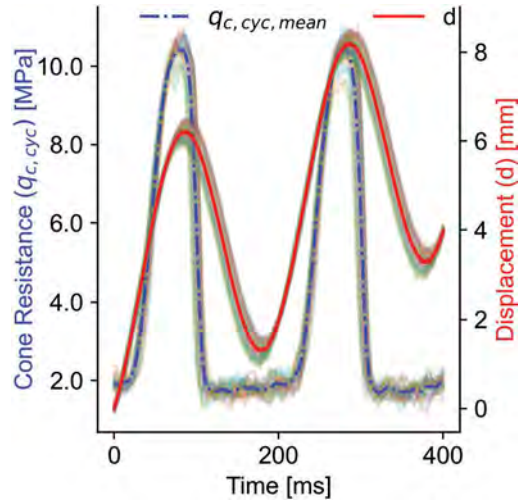


Figure 4. Stacking of 25 double cycles of cone resistance and displacement from V1 (5 Hz). The shaded colour along the mean curves represents 25 overlaid double cycles.

2.5.1 Jonker's model

Jonker estimated the cyclic cone resistance $q_{c,cyc}$ from static q_c by using the β value. This is an empirical value estimated from the past project experiences of different soil types (Jonker 1987). For comparison with the experimental results of the current study, a β value of 0.15 is used from Jonker's recommendation as a "representative value" of a clean sand.

$$q_{c,j} = \beta q_{c,static} \quad (1)$$

where, $q_{c,j}$ is the cyclic resistance based on β value [kPa], β is the empirical degradation value for cyclic cone resistance, static q_c is the static cone resistance [kPa]

2.5.2 Energy based model

The total energy dissipated for each penetration cycle was computed from the force - displacement curve (Cudmani and Manthey 2019) (Figure 5).

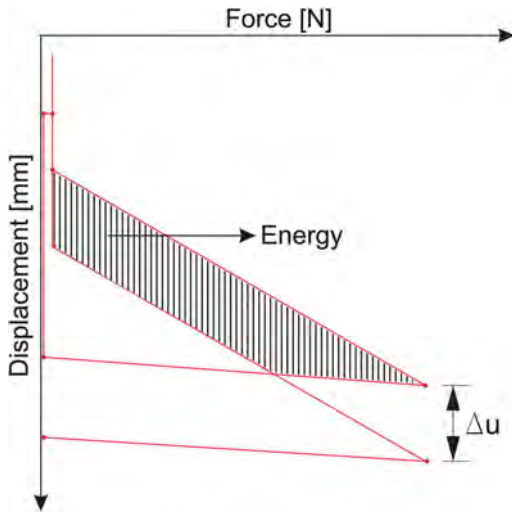


Figure 5. Energy for each cyclic cone resistance - displacement cycle of VCPT. The shaded part represents energy dissipated for each cycle in Karlsruhe model. Modified after Cudmani and Manthey (2019).

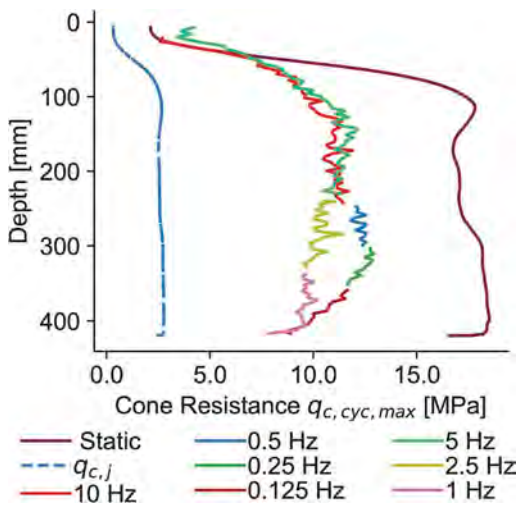


Figure 6. Static q_c vs penetration depth, $q_{c, cyc, max}$ vs penetration depth for test V1 - V7 (represented by penetrating frequency).

3 RESULTS

The maximum cyclic cone resistance $q_{c, cyc, max}$ profiles for each Push seem to be continuous even when the vibro penetration mode is changed (Figure 6). On the other hand, the vibratory penetrations as well as the static penetration are not in perfectly constant steady state conditions but undulate in a resistance range between 2 - 4 MPa. A gradual reduction in $q_{c, cyc, max}$ are observed along the bottom boundary predominantly in Push 2 (Figure 6). When

comparing the static q_c with maximum cyclic cone resistance $q_{c, cyc, max}$, there is 25 - 50% reduction in the $q_{c, cyc, max}$ for all the vibratory CPTs (Figure 6). The Jonker's model underestimates the cyclic cone resistance value $q_{c, j}$ (Figure 6).

At the steady state, the $q_{c, cyc, max}$ of the mean cyclic cone resistance value from different vibrational modes exhibited minimal changes with changing frequency (Figure 7). The energy dissipated during the penetration of each cycle was roughly proportional to the $q_{c, cyc, max}$ (Figure 7). However, the energy for tests with penetration modes of 5 and 10 Hz were low even though the $q_{c, cyc, max}$ is in comparison high.

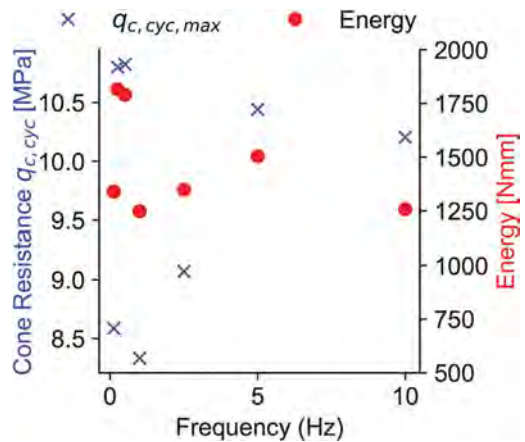


Figure 7. Maximum cyclic cone resistance at various driving frequency, Energy calculated using (Cudmani and Manthey 2019) for various driving frequency.

The reduction of cone resistance in comparison to the static penetration is also seen when looking at the full details of the penetration cycles (Figure 8). The mean cone resistance - displacement cycle is similar to Karlsruhe model, but more roundish and not exactly reaching zero (Dierssen 1994) (Figure 5, 8). During downward motion, the cone resistance rises linearly until it reaches $q_{c, cyc, max}$. In the current study, it is observed that the magnitude of cyclic cone resistance degradation remains almost unchanged even at much lower frequencies and way longer time intervals of upward motion of cone and cavitation.

From the cone resistance - displacement cycles, the upward displacement with cavitation ranged from 3.9 to 4.2 mm for all VCPTs. Both in the lowest frequency of 0.125 Hz, where 8 s are needed for the cone to reverse to downward motion and in the highest frequency of 10 Hz where only 0.1 s is spent for the start of downward motion, it was observed that the upward displacement with cavitation were nearly identical (Figure 8). When comparing the first and second cycles of cone resistance - displacement curve of each

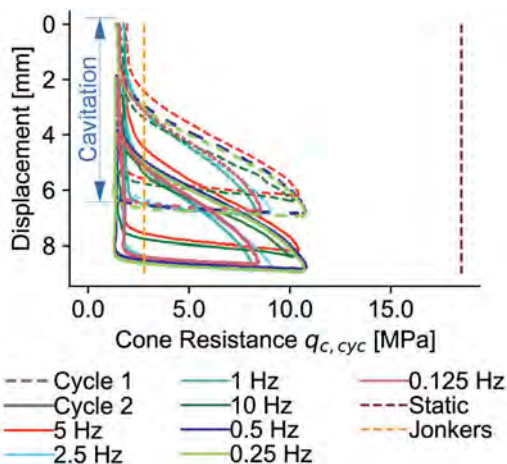


Figure 8. Mean cone resistance - displacement cycles for different vibrational modes of VCPT.

VCPT, it is clear that the cone penetrated approximately 2 mm in virgin soil in the second cycle. However, the value of $q_{c,cyc,max}$ of this cycle was still well below the static cone resistance (Figure 8).

4 DISCUSSION

The lower value of $q_{c,cyc,max}$ compared to static q_c might be attributed to cavitation as proposed by Dierssen (1994) (Figure 6). But Dierssen (1994) attributed the loss of contact from the soil mainly to the short time span for the cone to go up and to reverse for downward motion, which might indicate that the cavitation is a dynamic process. In this study however, no difference was found in the upward displacement with cavitation for 0.1 s and 8 s reversal time of the cone, therefore there seem to be no dynamic effect in the cavitation for the tested penetration modes and material. The similar values of upward displacement with cavitation might lead to approximately similar degree of remolding and loosening of the soil for all VCPTs which might be reflected in the similar reduction in the cyclic cone resistance. A relation between length of upward displacement with cavitation and reduction in the cyclic cone resistance could not be established since this length was almost constant and experiments with a lot more different penetration modes would be necessary to establish such a relation.

A classical reduction in cyclic cone resistance due to liquefaction was not expected from the beginning, because a recent field study suggested that there was no development of pore water pressure when performing vibratory CPTu (Al-Sammarraie 2020); (Wong et al. 1992); (O'Neill and Vipulanandan 1989). The non frequency i.e., time dependent reduction of $q_{c,cyc,max}$ supports the notion that liquefaction is not the main cause of cyclic cone resistance degradation

in Cuxhaven Sand, since the pore pressure would have ample time to drain at lower frequencies.

The gradual reduction in the $q_{c,cyc,max}$ for the VCPTs performed in Push 2, could be an effect of soft bottom boundary of the chamber. The influence of bottom boundary in MARCC was observed in the static CPTs (Kluger et al. 2021). However, since this gradual reduction in $q_{c,cyc,max}$ was not observed in the Push 1, the explanation of bottom boundary could be disregarded (Figure 6). The more plausible explanation for this reduction is the heterogeneity in the sand fabric and relative density that occur due to imperfect execution of the air pluviation method (Lagioia et al. 2006).

The underestimation of $q_{c,j}$ represented in Figure 6 calculated from β value is almost certainly caused by the oversimplification of the multi-variate degradation of cyclic soil resistance due to dynamic loading (Viking 2002). The proposed β values are based on data from real vibratory driver-pile combinations with amplitudes probably in the range of 6 mm, which is larger than the amplitude of 3 mm used in this study.

The proportionality between energy and $q_{c,cyc,max}$ is most likely because the general shape of the cone resistance - displacement cycle is very similar for all the VCPTs in this study. Therefore the area below the curve is proportional to the maximum value of cone resistance. If the upward displacement with cavitation would differ a lot, this proportionality would break down. The slightly lower energy dissipation at the high driving frequency, i.e., 5 Hz and 10 Hz is probably due to the inability of the system to achieve complete displacement amplitude of 3 mm (Figure 7). The dissipated energy might be an important parameter to predict the degradation of the cone resistance since both are constant and ca. proportional in this study. However, like for the cavitation, since both values are constant more data with different boundary conditions is needed to prove it. It can be concluded that the upward displacement with cavitation does not depend on frequency and average penetration velocity and that the energy is constant for same penetration path regardless of the frequency, for tested penetration modes, soil type and state.

The dynamic parameters have surprisingly little effect on the degradation of the cyclic soil resistance in this study (Figure 7), however there seem to be a complex quasi static behavior of the soil for frequencies between 0.125 and 10 Hz and corresponding maximum accelerations between 0.00185 and 11.8 m/s². With higher frequencies the dynamic effects will almost certainly appear, but its significance for the vibratory driving of monopiles with driving frequency of 20 Hz is unclear and would need further experiments, for which it is planned to upgrade the MARCC system. The observed quasi static effects are probably very important for vibratory driving of big monopiles and classic liquefaction and acceleration driven fluidization may not be the only process allowing for penetration with little resistance during vibratory driving.

5 CONCLUSION

A static CPT and several VCPTs were performed in MARCC in Cuxhaven Sand to investigate the influence of dynamic pile driving parameters on cone resistance. The degradation in the cyclic cone resistance is most likely related to the soil disturbance which might be caused during the loss of contact during the upward motion of the cone tip, a process named cavitation. The dynamic pile driving parameters, acceleration and drainage time have little to no influence on degradation of the cone resistance for tested penetration modes. Jonker's β value underestimates the cyclic cone resistance for 3 mm amplitude. The energy dissipation provides a proportional estimate of cyclic cone resistance but since both parameters were constant no conclusive relation could be determined. The penetration path in the depth vs average depth plane should be used more to discern the processes leading to the degradation in the cyclic soil resistance, to finally come to reliable driveability predictions.

ACKNOWLEDGEMENT

The authors acknowledge the support of the project "VCPTu2PDA", FKZ: 03EE3025A by the Federal Ministry for Economic Affairs and Energy (BMWi). We thank, Wolfgang Schunn, Lukas Urbainczyk for invaluable technical support with upgradation of MARCC and VCPT cone, and also Hammed Ade-niyi, Atakan Acar for assisting in lab work.

REFERENCES

- Al-Sammarraie, D. (2020). *Vibratory cone penetration test to investigate cyclic soil behavior in-situ*. Ph. D. thesis.
- Baldi, G. et al. (1982). Design parameters for sands from cpt.
- Barkan, D. D. (1962). *Dynamics of bases and foundations*. McGraw-Hill Companies.
- Cudmani, R. & S. Manthey (2019). A novel vibro-penetration test (vpt) for the investigation of cohesionless soils in the field. *Soil Dynamics and Earthquake Engineering* 126, 105760.
- D7181, A. (2020). *Standard Test Method for Consolidated Drained Triaxial Compression Test for Soils*. ASTM International, West Conshohocken, PA.
- Dahl, P. H., C. A. de Jong, & A. N. Popper (2015). The underwater sound field from impact pile driving and its potential effects on marine life. *Acoustics Today* 11(2), 18–25.
- Dierssen, G. (1994). *Ein bodenmechanisches Modell zur Beschreibung des Vibrationsrammens in körnigen Böden*. Ph. D. thesis. Karlsruhe 1994. (Veröffentlichungen des Institutes für Bodenmechanik und Felsmechanik der Universität Fridericiana in Karlsruhe. 133.) Fak. f. Bauingenieur- und Vermessungswesen, Diss. v. 9.7.1993.
- Fischer, J., H. Sychla, J. Bakker, L. de Neef, & J. Stahlmann (2013). A comparison between impact driven and vibratory driven steel piles in the german north sea. In *Proceedings Conference on Maritime Energy (COME), Hamburg*, pp. 21–22.
- Fleischer, M., S. Kreiter, T. Mörz, & M. Huhndorf (2016). A small volume calibration chamber for cone penetration testing (cpt) on submarine soils. In *Submarine Mass Movements and their Consequences*, pp. 181–189. Springer.
- Holeyman, A. (1993). An analytical model-based computer program to evaluate the penetration speed of vibratory driven sheet piles. *Geotechnique* 43(18), 65–78.
- Holeyman, A. & V. Whenham (2017). Critical review of the hypervib1 model to assess pile vibro-drivability. *Geotechnical and Geological Engineering* 35(5), 1933–1951.
- Huang, A.-B. & H.-H. Hsu (2005). Cone penetration tests under simulated field conditions. *Geotechnique* 55(5), 345–354.
- Jonker, G. (1987). Vibratory pile driving hammers for pile installations and soil improvement projects. In *Offshore Technology Conference*. OnePetro.
- Kluger, M. O., S. Kreiter, F. T. Stähler, M. Goodarzi, T. Stanski, & T. Mörz (2021). Cone penetration tests in dry and saturated ticino sand. *Bulletin of Engineering Geology and the Environment* 80(5), 4079–4088.
- Kramer, S. L. (1996). *Geotechnical earthquake engineering*. Pearson Education India.
- Lagioia, R., A. Sanzeni, & F. Colleselli (2006). Air, water and vacuum pluviation of sand specimens for the triaxial apparatus. *Soils and foundations* 46(1), 61–67.
- Massarsch, K. R., B. H. Fellenius, & A. Bodare (2017). Fundamentals of the vibratory driving of piles and sheet piles. *geotechnik* 40(2), 126–141.
- Naumann, M., C. Schnabel, J. Fritz, & D. Djuren (2013). Erstellung von baugrundabschnitten in der deutschen nordsee. *Geopotential Deutsche Nordsee Modul B* 9, 1–22.
- O'Neill, M. W., C. Vipulanadan, & D. O. Wong (1990). Evaluation of bearing capacity of vibro-driven piles from laboratory experiments. *Transportation Research Record* (1277).
- O'Neill, M. W. & C. Vipulanandan (1989). *Laboratory evaluation of piles installed with vibratory drivers*. Number 316.
- Rodger, A. & G. Littlejohn (1980). A study of vibratory driving in granular soils. *Geotechnique* 30(3), 269–293.
- Stähler, F. T. (2020). *Cone Penetration Tests in a Small Volume Calibration Chamber: Effects Related to Sand Type, Saturation State, Cyclic Pre-loading, Vibratory Penetration Mode, and Boundary Condition: Kumulative Dissertationsarbeit*. Ph. D. thesis, Universität Bremen.
- Tsouvalas, A. (2020). Underwater noise emission due to offshore pile installation: A review. *Energies* 13(12), 3037.
- Viking, K. (2002). *Vibro-driveability-a field study of vibratory driven sheet piles in non-cohesive soils*. Ph. D. thesis, Byggetenskap.
- Wang, H. (1994). *Experimental study and finite element analysis of drivability and static behavior of various piles installed by vibratory driving*. Ph. D. thesis, University of Houston.
- Wong, D., M. W. O'Neill, & C. Vipulanandan (1992). Modelling of vibratory pile driving in sand. *International Journal for numerical and analytical methods in geomechanics* 16(3), 189–210.

Application of a new q_c averaging approach for end bearing of driven piles in sand

E.J. Bittar, Y. Tian & B.M. Lehane

The University of Western Australia, Perth, Australia

ABSTRACT: CPT-based methods to estimate axial pile capacity generally relate the pile base resistance with a q_c value averaged in the vicinity of the pile tip ($q_{c,avg}$) and hence implicitly acknowledge the greater zone of influence of a full scale pile compared to a cone. To account for layered deposits (e.g. loose over dense sand), most common designs methods average the cone tip resistance over 1.5 diameters (D) above and below the cone tip or use the Dutch methodology where the averaging is conducted over a zone of $0.7D$ to $4D$ below the pile tip and $6D$ to $8D$ above the pile tip. This paper examines an alternative averaging approach based on an algorithm which allows estimation of the steady state end bearing resistance of penetrometer with the same diameter as a pile (q_p). End bearing stresses determined at a base displacement of 10% of the pile diameter ($q_{b0.1}$) in a database of instrumented static load tests on driven piles are compared with the corresponding q_p values. It is shown that the $q_{b0.1}/q_p$ ratio varies with the effective area ratio of driven piles and is independent of the pile diameter. The best-fit equation of the database of end bearing measurements provide a rational and improved means of determining end bearing of driven piles.

1 INTRODUCTION

1.1 CPT and pile end bearing resistance

Cone Penetration Test (CPT) data are widely used directly in the design of deep foundations. The similarities between a cone and a closed-ended displacement pile in terms of their geometry and installation mode provide the basis for direct correlations.

The steady-state penetration resistance for a 36 mm diameter cone (q_c) and that of a field scale displacement pile (q_b) can be expected to be theoretically equivalent in a homogeneous soil. However, natural soils comprise layers with different properties and thicknesses leading to a scale effect. This scale effect arises because of the greater sensing and development distances of the larger diameter pile. The steady-state end resistance profile of a pile (q_p) is therefore a ‘smoothened’ or filtered variant of the actual CPT q_c profile (Bittar et al., 2020a).

CPT design methods for driven piles generally assume that the base resistance at a pile base settlement of 10% of the diameter ($q_{b0.1}$) is directly proportional to the cone tip resistance q_c . The constant of proportionality (α or k_c) is less than one due to effects of partial mobilization (i.e. a settlement of 10% of the diameter, D , is not sufficient to attain steady state conditions) and due to effects of partial embedment (as the pile has not penetrated far enough to generate a steady state resistance).

The need for use of an appropriate average q_c value ($q_{c,avg}$) for estimation of pile end bearing is acknowledged in current CPT methods. Most of the CPT-based methods use the LCPC method (Bustamante & Gianeselli, 1982) where $q_{c,avg}$ is the average q_c value in the zone $1.5D$ above and below the pile tip ($q_{c,1.5D}$). However, there is a concern that the zone of influence in the LCPC method ($\pm 1.5D$ from the pile tip) is too small. Lehane (2019), for example, describes a case history where this averaging approach over-predicted the capacity of a closed-ended pile driven a distance of $2.5D$ into a sand stratum underlying a soft estuarine clay.

This paper examines an alternative q_c averaging approach based on an algorithm, devised by Boulanger & DeJong (2018), which allows estimation of the steady state end bearing resistance of a penetrometer with the same diameter as a pile (q_p). Laboratory and field experiments are described that assess the applicability of this approach. $q_{b0.1}$ values measured in a database of instrumented static load tests on driven piles are then compared with the corresponding q_p values with a view to determining a more rational means of estimating the end bearing of driven piles that allows for scale effects.

1.2 Alternative averaging technique

Boulanger & DeJong (2018) proposed a procedure to account for multiple thin-layer effects by considering

cone penetration as an inverse problem, assuming that the measured q_c is equal to the “true” q_c (q') convolved with a depth-dependent spatial filter (Yost et al., 2021). The filter is depicted in Figure 1 (where z' is the distance from the cone tip normalized by the penetrometer/pile diameter) and encapsulates experimental observations via filter parameters to represent the dependency on layers in the vicinity of the cone tip on (i) the z' value, (ii) the relative strengths (or q' values) of adjacent layers and (iii) whether the cone is above or below a given layer (i.e. negative or positive z' value).

Bittar et al., (2020a) present experimental observations showing that the procedure can provide a reasonable estimate of the steady state end resistance of a full-scale pile (q_p) value. Further comparisons with experimental observations in the laboratory and field are presented here before examining the application of the approach for estimating the end bearing resistance of driven piles in sand.

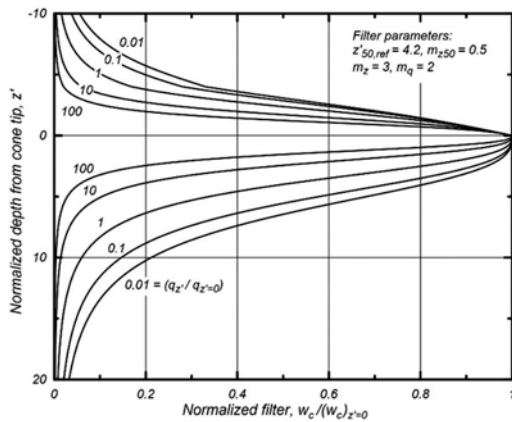


Figure 1. Normalized cone penetration filter versus normalized depth from the cone tip with lines for $q_{z'}/q_{z'=0} = 0.01, 0.1, 1, 10,$ and 100 (Boulangier & DeJong, 2018).

2 EXPERIMENTAL ASSESSMENT OF BOULANGER & DEJONG (2018)

2.1 Laboratory penetrometer testing

A number of penetration tests were conducted in a cylindrical 400 mm diameter, 400mm high steel pressure chamber. Full details of the test set-up and chamber are provided in Tian & Lehane (2022).

An illustration of the effects of development length and layering on the penetration resistance measured by a 7mm diameter cone is shown on Figure 2. The penetrometer resistances in the medium dense and dense sands (with respective relative densities, D_r , of 72% and 97%) attain a steady state after a penetration of about $6D$ in sand with $D_r = 72\%$ and about $15D$ in that with $D_r = 97\%$; the tendency for greater development distances in denser sand has been observed by Ahmadi & Robertson,

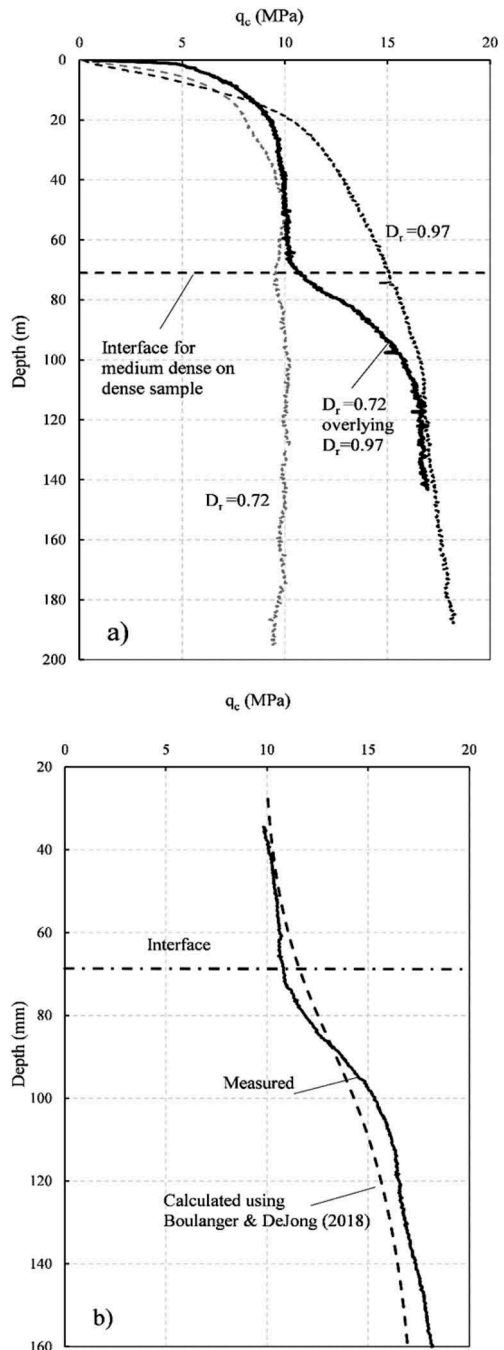


Figure 2. (a) CPT resistance in uniform and layered profiles, (b) measured and predicted CPT resistance in sample with dense sand underlying medium dense sand. Note cone diameter = 7mm and vertical effective stress = 50 kPa.

(2005), Tehrani et al., (2017) and others. Figure 2a also plots the penetration resistance in a layered profile with medium dense sand overlying dense sand. It

is seen that the penetrometer senses the dense sand at a distance of about $1D$ above the interface between the two layers and then requires a penetration of about $8D$ before reaching the steady state resistance of the dense layer.

The calculated penetration resistance, assuming steady state q_c values of 10 MPa and 18 MPa in the medium dense and dense sand respectively is compared with the measured response on Figure 2b. These calculations were performed using the default parameters proposed by Boulanger & DeJong (2018) and lead to reasonable, although certainly not perfect, predictions.

2.2 Field scale penetrometer testing

Penetrometer tests were carried out at the University of Western Australia (UWA) Shenton Park Field Station. This site, which comprises a 6m deep deposit of Aeolian sand, has been used for a range of studies with details reported in Bittar et al. (2020b), Lehane et al. (2004), and elsewhere. The penetrometer tests plotted on Figure 3 at this site were conducted using a standard 35.7mm diameter cone and a 65mm diameter closed-ended pile. Both devices were pushed at the standard rate of 20mm/s and correction for shaft friction on the pile to allow derivation of end bearing from a head load cell was determined with a high level of confidence using results from fully

instrumented jacked piles reported by Lim & Lehane (2014).

The end resistance corresponding to the 35.7mm cone was converted to a true penetration resistance (q') using the Boulanger & DeJong (2018) default parameters (noting q' is equivalent to the end resistance measured with an infinitesimally small cone). This q' profile was then used as input to calculate the penetration resistance of the 60mm diameter pile.

The calculated and measured profiles of end resistance are plotted on Figure 3. This comparison shows that the Boulanger & DeJong (2018) calculation for the 60mm diameter pile is a reasonable approximation to the measured profile, albeit overestimating resistance by up to 10% at around 0.8m depth. However, as seen on Figure 3, the calculated resistance is a substantial improvement on the standard approach of averaging q_c values within $1.5D$ of the penetrometer tip.

The comparisons made on Figures 2 and 3 provide evidence in general support of the Boulanger & DeJong (2018) algorithm for prediction of penetrometer resistance in layered sands. The value of q_p determined using this approach is equivalent to the bearing resistance of a pile with the same diameter as a penetrometer and is considered a rational means of determining an average q_c value in the vicinity of a pile tip ($q_{c,avg}$).

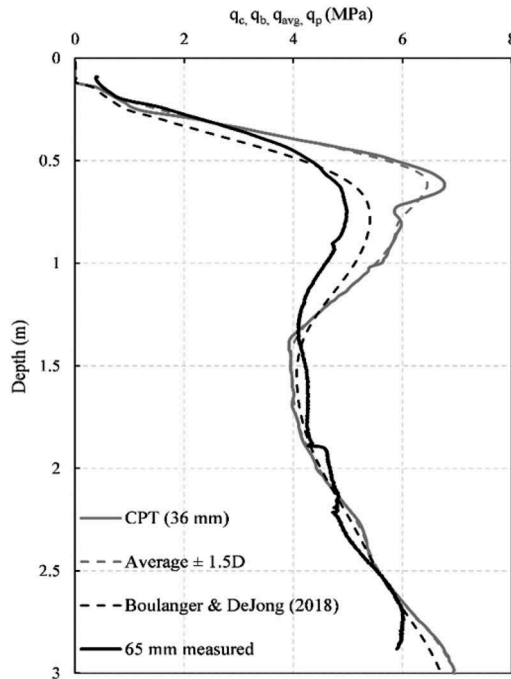


Figure 3. Measured and predicted resistance at the site: cone tip resistance, $q_{c,1.5D}$, Boulanger & DeJong method and 65mm pile tip resistance.

3 DATABASE ANALYSIS

The feasibility of employing q_p as a measure of the average q_c value near a pile tip ($q_{c,avg}$) for estimating $q_{b0.1}$ is examined here using databases of end bearing capacity measurements ($q_{b0.1}$) for closed and open ended driven piles. These databases, which are summarised in Tables 1 and 2, are an extension of those presented by Xu et al. (2008) and were used in the development of the 'Unified' CPT-based method for axial pile capacity calculation of driven piles in sand (Lehane et al., 2020).

3.1 Closed-ended driven piles

The Boulanger and DeJong (2018) algorithm was employed to determine q_p for each database pile using the published default values of the algorithm (as employed for Figure 2 and 3). These q_p values are assumed equivalent to $q_{c,avg}$ values where they are compared on Figure 3 with $q_{b0.1}$ values measured for the closed-ended pile database. A proportional relationship is observed for closed-ended piles, where:

$$q_{b0.1}/q_{c,avg} = q_{b0.1}/q_p = 0.5 \quad (1)$$

The coefficient of variation for ratios of measured $q_{b0.1}$ values to those calculated using Equation (1) is

Table 1. Database of $q_{b0.1}$ measurements for closed-ended piles.

Num.	Site name	D	L	$q_{b0.1}$	$q_{c,tip}$	q_p	$q_{b0.1}/q_p$	$q_{b0.1}/q_{c,1.5D}$
		m	m	MPa	MPa	MPa		
1	Akasaka	0.2	11	15.18	26.3	29.66	147.4	0.64
2	Drammen	0.28	8	1.14	2.86	2.72	89.5	0.42
3	Drammen	0.28	16	1.79	5	5.2	177.2	0.36
4	Hoogzand	0.36	6.8	13.96	41.16	40.91	97.5	0.38
5	Hsin Ta	0.61	34.3	3.11	7.47	5.77	310.5	0.48
6	Hunter's P	0.27	9.2	4.97	8.6	8.28	99.6	0.64
7	Kallo	0.91	9.7	8.96	27.9	27.3	108.9	0.46
8	Kallo	0.54	9.7	10.69	28.1	29.3	109.1	0.48
9	Kallo	0.62	9.8	9.73	29.2	30.1	110.2	0.43
10	Kallo	0.82	9.8	9.22	28.9	29	110	0.44
11	Kallo	0.41	9.3	10.74	25.9	25	105.3	0.5
12	Kallo	0.61	9.4	8.55	26.5	24.9	105.7	0.43
13	Pigeon R	0.36	6.9	10.96	20.25	19.94	89.6	0.57
14	Wadinxveen	0.4	9.8	6.28	8.42	8.64	73.77	0.74
15	Rio	0.7	26.5	5.46	15.07	13.63	232.05	0.46
16	Bennett	0.61	45	7.53	14.63	12.16	409.65	0.7
17	Hampton	0.69	16.8	1.85	7.17	6.99	161.16	0.35
18	Fittja Straits	0.27	12.8	2.36	6.19	5.62	134.85	0.43
19	Sermide	0.51	35.9	10.17	16.4	16.3	315	0.61
Average							0.50	0.45
ST. dev							0.11	0.13
COV							0.22	0.29

Table 2. Database of $q_{b0.1}$ measurements for open-ended piles.

Num.	Site name	D	L	IFR	A_{re}	$q_{b0.1}$	$q_{c,tip}$	$q_{\pm 1.5D}$	q_p	$q_{b0.1}/q_p$	$q_{b0.1}/q_{c,1.5D}$
		m	m			MPa	MPa	MPa	MPa		
1	Dunkirk	0.32	11.3	0.45	0.65	7	26.7	24	20.7	0.34	0.29
2	Dunkirk	0.32	11.3	0.48	0.59	6.1	26.7	24	20.7	0.3	0.25
3	Euripides	0.76	30.5	0.99	0.19	12.3	61.5	60.8	60.2	0.21	0.2
4	Euripides	0.76	38.7	0.9	0.26	9.9	50.8	50.8	50.8	0.2	0.2
5	Euripides	0.76	47	0.89	0.27	15.3	65.9	66.4	63	0.24	0.23
6	Euripides	0.76	46.7	0.82	0.33	16	63.3	63.1	63	0.25	0.25
7	Euripides	0.76	8.5	0.99	0.19	9.6	62.2	60.9	58.6	0.16	0.16
8	Euripides	0.76	16.7	0.9	0.26	9.6	51.4	51.2	51.3	0.19	0.19
9	Euripides	0.76	25	0.89	0.27	15.5	63.6	66.9	61.9	0.25	0.23
10	Hoogzand	0.36	7	0.66	0.45	10.9	37.7	42.3	32.9	0.33	0.26
11	Hoogzand	0.36	5.3	0.77	0.39	11.2	45.5	45.5	35.4	0.32	0.25
12	Pigeon	0.36	7	0.8	0.46	5.9	19.5	19.7	20.5	0.29	0.3
13	Rastanajib	0.76	25	1.13	0.09	12.3	77.1	86.8	85.9	0.14	0.14
14	Shanghai	0.91	79	0.8	0.27	5.9	23.3	23.3	23.2	0.25	0.25
15	Shanghai	0.91	79.1	0.85	0.22	5.1	23.3	23.3	23.2	0.22	0.22
16	Lafayette	0.66	31	0.7	0.5	7.4	25	26.5	25	0.29	0.28
17	Tokyo P Bay	1.5	73.5	1	0.07	8.9	80.7	84.4	72	0.12	0.11
18	Tokyo P Bay	1.5	86	1	0.07	6.4	42.1	47.9	41	0.16	0.13
19	Tokyo	2	30.6	1.08	0.01	2	30.4	23.9	21.7	0.09	0.08

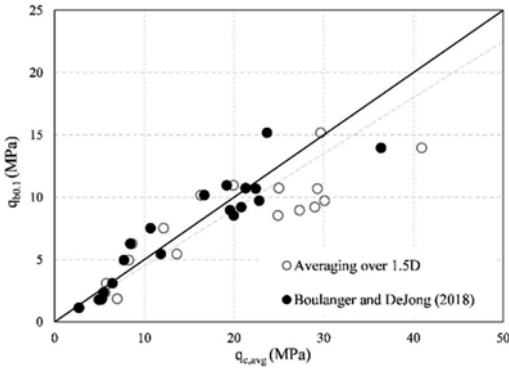


Figure 4. End bearing values $q_{b0.1}$ vs $q_{c,avg}$ for closed-ended piles with $q_{c,avg}$ equal to $q_{c,1.5D}$ and q_p .

0.22. Figure 3 also compares measured $q_{b0.1}$ values with average q_c values taken equal to $q_{c,1.5D}$. Greater scatter in the proportional relationship is seen and there is a clear tendency for the $q_{b0.1}/q_{c,1.5D}$ ratio to reduce with increasing pile diameter.

3.2 Open-ended driven piles

The mode of penetration of a pipe pile can be fully plugged, partially plugged or fully coring. The degree of sand displacement near the base can be described by the final filling ratio (FFR), which is taken to be the average incremental filling ratio (IFR) over the final 3 diameters of installation. The effective area ratio of a given open-ended pile (i.e. the ratio of the displacement induced to that of a fully plugged pile) is then given as (where D_i is the internal pile diameter):

$$A_{re} = 1 - FFR(D_i/D)^2 \quad (2)$$

When FFR data were not reported for the database piles, the value of the FFR was estimated using the following equation proposed by Lehane et al. (2020), where $d_{cpt}=35.7\text{mm}$

$$FFR = \tanh[0.3(D_i/d_{cpt})^{0.5}] \quad (3)$$

The equivalent pile diameter causing the same level of displacement is then obtained as:

$$D_{eq} = D[A_{re}]^{10.5} \quad (4)$$

Values of $q_p=q_{c,avg}$ were calculated for each open-ended pile in the database using the Boulangier and DeJong (2018) algorithm and a pile diameter of

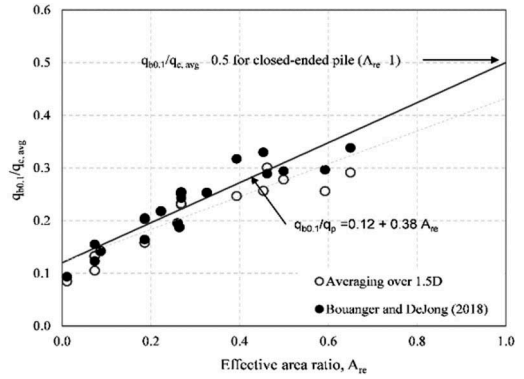


Figure 5. $Q_{b0.1}/q_p$ variation with effective area ratio for open-ended piles.

D_{eq} . A consistent linear increase in $q_{b0.1}/q_p$ with A_{re} is apparent on Figure 5 with an extrapolated $q_{b0.1}/q_p$ ratio at $A_{re} = 1$ corresponding to the best estimate for closed-ended piles on Figure 4. The best-fit linear fit to the database is:

$$q_{b0.1}/q_p = 0.12 + 0.38A_{re} \quad (5a)$$

$$A_{re} = 1 \text{ for closed - ended/plugged pile} \quad (5b)$$

This best-fit line is seen to represent all the data with good accuracy except for the case with the very low A_{re} value of 0.01 which is believed to be affected by the proximity of a low strength clay near the pile base (Randolph, 2003). Further analyses showed that Equation (5) is much better performing than an equivalent relationship using $q_{c,1.5D}$ (see data points on Figure 5) and also has no bias with respect to pile diameter and relative density of the sand.

4 CONCLUSIONS

This paper demonstrates that the Boulangier & DeJong (2018) algorithm provides a reasonable means of predicting pile/penetrometer end resistance in layered stratigraphy. This algorithm is then used to deduce steady state end bearing resistances for penetrometers with the same diameter or equivalent diameter of piles. This steady state resistance (q_p) is shown to be directly proportional to the measured end bearing of a database of driven piles at a displacements of 10% of their diameter ($q_{b0.1}$). A simple equation which includes an effective area ratio term as well as q_p is proposed (Equation 5) and is considered to provide a more rational and reliable means of assessing pile base resistance in sand.

ACKNOWLEDGMENTS

The first and second author acknowledge the support of the Australian Postgraduate Award scheme at The University of Western Australia.

REFERENCES

- Ahmadi, M. M., & Robertson, P. K. (2005). Thin-layer effects on the CPT qc measurement. *Canadian Geotechnical Journal*, 42(5), 1302–1317.
- Boulangier, R.W., & DeJong, J.T., 2018. Inverse filtering procedure to correct cone penetration data for thin-layer and transition effects. *Cone Penetration Testing 2018: Proceedings of the 4th International Symposium on Cone Penetration Testing (CPT'18)*, 21-22 June, 2018, Delft, The Netherlands, 25.
- Bittar, E., Lehane, B.M., Boulangier, R.W., & Dejong, J.T., (2020a). CPT Filter to Estimate the End Bearing of Closed-Ended Driven Piles in Layered Sands. In Proceedings of the 4th International Symposium on Frontiers in Offshore Geotechnics (pp. 520–528). Deep Foundations Institute.
- Bittar, E., Lehane, B., Watson, P., & Deeks, A. (2020b). Effect of cyclic history on the ageing of shaft friction of driven piles in sand. In 4th International Symposium on Frontiers in Offshore Geotechnics. American Society of Civil Engineers.
- Bustamante, M., & Gianeselli, L., 1982. Pile bearing capacity prediction by means of static penetrometer CPT. In Proceedings of the 2-nd European symposium on penetration testing (pp. 493–500).
- Lehane, B.M., 2019. EH Davis Memorial Lecture (2017) CPT-based design of foundations. *Australian Geomechanics Journal*, 54(4), pp.23–45.
- Lehane, B.M., Liu, Z., Bittar, E., Nadim, F., Lacasse, S., Jardine, R., Carotenuto, P., Rattley, M., Jeanjean, P., Gavin, K., Gilbert, R., Bergan-haavik, J., & Morgan, N., 2020. A new CPT-based axial pile capacity design method for driven piles in sand. *4th International Symposium on Frontiers in Offshore Geotechnics, ISFOG-4*.
- Lehane, B.M., Ismail, M.A., & Fahey, M., 2004. Seasonal dependence of in situ test parameters in sand above the water table. *Geotechnique*, 54(3), 215–218.
- Lim J.K. and Lehane B.M., 2015. Time effects on the shaft capacity of jacked piles in sand. *Canadian Geotechnical Journal*, 52(11), 1637–1648.
- Randolph, M.F., 2003. Science and empiricism in pile foundation design. *Géotechnique*, 53, 847–875.
- Tehrani, F. S., Arshad, M. I., Prezzi, M., & Salgado, R. (2017). Physical Modeling of Cone Penetration in Layered Sand. *Journal of Geotechnical and Geoenvironmental Engineering*, 144(1), 04017101.
- Tian, Y., & Lehane, B.M. 2022. Parameters affecting the CPT resistance of reconstituted sands. Proc. 5th Int. Symp. Penetration Testing, CPT22, Bologne, June 2022
- Xu, X., Schneider, J.A., & Lehane, B.M., 2008. Cone penetration test (CPT) methods for end-bearing assessment of open- and closed-ended driven piles in siliceous sand. *Canadian Geotechnical Journal*, 45(8), 1130–1141.
- Yost, K. M., Green, R.A., Upadhyaya, S., Maurer, B. W., Yerro-colom, A., Martin, E. R., & Cooper, J., 2021. Assessment of the efficacies of correction procedures for multiple thin layer effects on Cone Penetration Tests. *Soil Dynamics and Earthquake Engineering*, 144(March), 106677.

A review of a CPT based axial capacity prediction of screw piles in sand

E.J. Bittar, B.M. Lehane & S. Mahdavi
The University of Western Australia, Australia

A.P. Blake, D.J. Richards & D.J. White
The University of Southampton, UK

ABSTRACT: Screw piles are widely used in onshore engineering applications and have recently been considered as an alternative foundation solution for offshore wind turbines (OWTs) supported on jacket structures. The high loads required to support such structures demand a considerable up-scaling of the screw pile geometry typically used onshore. Driven piles followed a similar upscaling process for their use in offshore structures and the CPT tip resistance (q_c) value is now commonly used directly in design methods for both onshore and offshore driven piles. This paper evaluates the performance of a new CPT-based design method (UWA-SP-21) to predict the axial capacity of screw piles in tension and compression. To achieve this, a database of single helix load tested screw piles sand is collated and used for assessment of the method. The development of this CPT design approach reflects the process that was following for driven piles. UWA-SP21 has been developed through studies of onshore piles. The findings from this study can in the future be extrapolated appropriately to the larger pile sizes required offshore, in the same way that driven pile design has evolved.

1 INTRODUCTION

Screw (or helical) piles have been increasingly used to support a variety of structures such as pipelines, transmission towers, bridges and commercial buildings. Screw piles are steel tubes with one or more helical elements fabricated on the shaft that are screwed into the ground through the application of torque and thrust (vertical force) (Richards et al. 2019). This pile configuration increases the axial base resistance, allows a rapid, quiet and low-vibration installation, and enables reusability. These advantages have increased interest in their use as an alternative foundation solution for offshore wind turbines (OWTs) supported on jacket structures. However, given the much larger scale required to meet the axial load requirements of OWTs compared to current onshore applications, concerns have been raised regarding the large installation torque necessary for their installation (Sharif et al., 2020; Bittar et al., 2021).

The total axial resistance of a single helix pile, Q_{ult} , is usually considered as a combination of the helix bearing resistance (Q_h) and shaft resistance developed along the pile shaft (Q_s). In tension, two failure mechanisms are commonly assessed depending on the helix embedded depth (H) or embedment ratio (H/D_h), where H is the helix embedded depth and D_h the helix diameter. These failure mechanisms are known as the ‘shallow’ failure (cylindrical, conical, circular) and the ‘deep’ failure. The compression

capacity is dominated by a localized ‘deep’ failure mechanism of the helix.

The axial capacity of screw piles is often estimated using conventional bearing capacity theory or ‘semi-empirical methods’ derived from anchor test results from the laboratory or the field (Mitsch & Clemence, 1985). These so-called ‘theoretical methods’ are limited as they require estimation of appropriate soil strength parameters and the capacity estimates are very sensitive to the adopted strength parameters. In situ test data are rarely used directly in the assessment of axial capacity (Fateh et al. 2017).

In practice, an estimate of the screw pile capacity is obtained during construction via an empirical relationship with the torque measured at the end of installation. Tsuha & Aoki (2010), Spagnoli et al. (2020), and others, assume that the torsional resistance measured during installation is related directly to a pile’s axial capacity. This is because the normal forces generated on the helix that lead to its frictional and hence torque resistance are a measure of the axial resistance associated with a localized failure. The torsional resistance is also needed as a check to assess if the helix has sufficient structural strength under the application of axial load (Spagnoli & Gavin 2015).

The prediction of the installation torque for typical onshore piles is often based on one of three methods (Davidson et al. 2020), namely (i) correlation of field measured torque with anticipated or measured pile capacity (Hoyt & Clemence, 1989;

Perko, 2009); (ii) modification of empirical pile capacity design methods (Ghaly & Hanna 1991; Tsuha & Aoki, 2010; Sakr, 2015) and (iii) direct correlation with the cone penetration test (CPT) end resistance (Gavin et al. 2013; Spagnoli et al. 2016; Al-Baghdadi et al. 2017; Davidson et al. 2018a).

Although CPT-based capacity design methods for screw piles have received little attention until recently, such methods are now commonly used in the design of driven offshore piles in sand. The 22nd edition of the American Petroleum Institute (API) recommendations presents driven pile design methods, including the conventional (API) approach and four CPT-based methods. Lehane et al. (2005) performed an assessment of the reliability of the CPT methods and noted considerable improvement in their predictive performance compared with the traditional API main text approach. The commentary of the API design guidelines states that CPT methods are “fundamentally better and show statistically closer predictions of pile load test results” than the API main text approach and are preferred to the main text approach (Igoe et al. 2014).

Given the experience with offshore driven piles and the potential use of screw piles offshore, it is surprising that studies on the use of CPT q_c to design screw piles were rare until the recent studies listed above. Bittar et al. (2022) recently presented the development of one such CPT approach (UWA-SP-21) for prediction of screw pile axial capacity and the torque required for installation. This paper examines the performance of UWA-SP-21 against a database of full scale field tests involving various single-helix screw pile geometries in a range of different sands.

2 CPT METHOD FORMULATIONS FOR AXIAL CAPACITY

Informed by tests on instrumented screw piles, Bittar et al. (2022) proposed a direct application using empirical factors (β_c and α_{hi}) applied to the CPT end resistance (q_c) for the estimation of axial capacity at a displacement of 10% of the pile diameter (Q_{ult}). The proposed formulation for ultimate capacity is:

$$Q_{ult} = \sum_1^n Q_{hi} + Q_s \quad (1a)$$

$$Q_{hi} = \alpha_{hi} q_{ci} \pi D_h^2 / 4 \quad (1b)$$

$$Q_s = (\pi d_s L_s) q_{c,avg} / \beta_c \quad (1c)$$

where Q_{hi} is the axial capacity of a single helix (i) separated by more than three helix diameters (D_h) from an adjacent helix, Q_s is the axial capacity of the pile shaft, d_s is the diameter of the pile shaft, L_s is the length of the pile shaft, q_{ci} is the cone resistance at the level of the helix, $q_{c,avg}$ is average cone resistance along the pile shaft.

The method assumes that a deep localized failure mechanism applies (i.e. Figure 1b), which is expected for $H/D_h > 3$, and draws on parallel methods for the similar situation of non-displacement piles. Recommended empirical factors for α_{hi} are 0.2 for compression and 0.15 for tension. These factors are closely comparable to factors observed for footings and at the base of bored piles at a displacement of 10% of the foundation diameter (e.g. Lehane 2012) and emerge, as discussed by Lehane (2019), because of the local hemispherical expansion type mechanism of footings at this level of displacement and the proportional relationship between q_c and cavity expansion limit pressure. For evaluation of shaft capacity (Q_s), Bittar et al. (2022) proposed a β_c value of 230, which is close to the β_c value proposed for non-displacement piles by Doan & Lehane (2021). The contribution of Q_s to Q_{ult} is relatively small.

It is of interest to compare equation (1) with other formulations. For example, Gavin, et al., (2013) proposed a similar relationship but employ an α_{hi} factor of 0.065 and assume that the unit shaft friction of the shaft helix is 60% of the CPT friction sleeve value. This method was adopted by Spagnoli (2017) to evaluate torque predictions and it has to be noted that it was developed for uplift capacity only.

Perko (2009) and Tappeden (2004) amongst others use of the LCPC-1982 (LCPC) method proposed by Bustamante and Gianeselli (1982) for the calculation of screw pile capacity. It should be noted, however, that this method was established for predicting the axial capacity of conventional piles, and the applicability of the method to screw piles is questionable.

The predictive ability of the Gavin et al. (2013) and LCPC-1982 methods is examined along with that of UWA-SP-21 (i.e. Equation 1) in the following.

3 INSTALLATION TORQUE PREDICTION

The determination of Q_{ult} for helical piles in industry is typically based on an empirical relationship with torque via a dimensional torque factor, K_t (Li & Deng 2019). Hoyt & Clemence (1989) assume a direct proportional relationship between Q_{ult} and T as:

$$Q_{ult}(kN) = K_t (m^{-1}) \times T(kNm) \quad (2)$$

However, the dimensionality of the K_t factor means that the value is likely to change as piles are upscaled from onshore to offshore applications. The same authors propose a formulation for K_t that depends on the pile shaft diameter, d_s . Perko (2009) proposed the following equation which relates K_t with the shaft diameter of screw piles (d_s):

$$K_t(m^{-1}) = \frac{2.49}{[d_s(m)]^{0.92}} \quad (3)$$

Perko (2009) collected data of Q_{ult} and T for single helix screw piles data and correlated these by a linear regression (Figure 1) – which is a minor simplification of Equation 3, altering the power applied to d_s to unity. The data were from tests performed on piles with helix diameters up to 350 mm (for which $K_t \geq 6.54$, Eqn 3) and lengths up to 8 m (Spagnoli 2017). However, the torque measurements in most of this database were less than 30 kNm and the Q_{ult} vs T relationship is highly scattered in this region. As a consequence, Spagnoli (2017) suggests no unique Q_t - T correlation exist.

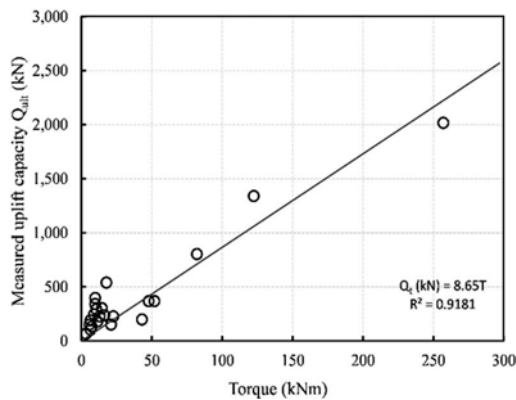


Figure 1. Torque vs. uplift capacity for previously-published case studies of single-helix piles (modified from Perko 2009).

4 DATABASE OF LOAD TESTS ON SCREW PILES IN SAND

A database of static load tests on screw piles was compiled by the authors. This database comprises 18 pile tests with 7 tests in tension and 11 in compression; the shafts of all piles were open ended. Many of the cases were derived from tests performed by Screw Pile Australia Pty Ltd while others were sourced from the literature. All the piles included in the database contain CPT results in the vicinity of the test piles.

All CPT data were digitized at depth intervals of 0.1 m. Pile capacity was defined as the load at a pile head displacement of 10% of the helix diameter ($0.1D_h$). The buoyant weight of piles tested in tension was deducted from the maximum head load to determine the tension capacity. The documented cases provided by Screw Pile Australia included piles that were typically loaded to a displacement of about 5% of D_h . The measured load displacement curves were therefore extrapolated using Chin's method (Chin 1970) to determine the ultimate capacity, defined at $0.1D_h$

(which was typically 15 to 20% higher than the measured load at a displacement of $0.05D_h$).

It is noteworthy that existing guidance on the installation of screw piles suggests that installation should be performed in a pitch-matched manner (Perko 2009) i.e. one full rotation to advance the helix by a depth equal to the helix pitch (p). No specific information regarding the advancement ratio of the database piles is available although it is expected that the ratio is somewhat less than unity as operators often allow the auger to pull itself into the ground without the assistance of additional axial thrust. Characteristics of the screw pile database are provided in Table 1.

5 METHOD PREDICTIVE PERFORMANCE

The ratio of capacities calculated using UWA-SP-21 to measured capacities (Q_m/Q_c) was evaluated and the predictive performance was expressed in terms of the mean (μ) and coefficient of variation (CoV) of the Q_m/Q_c ratios. For comparison purposes, the same approach was adopted to evaluate the CPT-method suggested by Gavin et al. (2013) and the LCPC approach mentioned previously. Measured and calculated capacities and the associated statistics are provided in Tables 2 and 3. It is observed that:

- The UWA-SP-21 method (Bittar et al. 2022) provides the lowest CoV and an average value close to unity both in compression and in tension.
- The LCPC method significantly over-predicts the capacity of screw piles in compression ($\mu=0.42$) and tension ($\mu=0.38$). This arises as the multiple on q_c in the LCPC method varies 0.3 and 0.5 while the corresponding multiple UWA-SP-21 is between 0.15 and 0.2.
- The high average value of the Gavin et al. (2013) approach ($\mu=1.37$) indicates that the method underpredicts the uplift capacity of screw piles. The CoV of Q_m/Q_c for this method is also significantly higher than that of UWA-SP-21.

UWA-SP-21 is evidently the best performing method with an excellent CoV value for Q_m/Q_c of only about 10%. The method does, however, over-predict the capacity of the database piles on average by 8% in tension and 10% in compression.

6 TORQUE PREDICTION ASSESSMENT

Table 4 lists the torques measured at the end of installation of the database piles (T_m). These were measured using a pressure gauge on a hydraulic system. The accuracy of this gauge is dependent on the rotational speed applied and the hydraulic differential pressure across the gear motor. An accuracy of $\pm 20\%$ is expected using this system. It is important for operators to know in advance what magnitude of torque is required to give confidence that the installed pile will

Table 1. Database of load tests on screw piles.

N	Pile	Site	Loading direction	L_s (m)	d_s (m)	D_h (m)	p (m)	Reference
1	S2P3	Alberta, Canada	C	4.57	0.114	0.406	0.076	Li & Deng (2019)
2	S2P1	Alberta, Canada	C	2.44	0.073	0.305	0.076	Li & Deng (2019)
3	S2P2	Alberta, Canada	C	3.05	0.089	0.356	0.076	Li & Deng (2019)
4	P1	Blessington	C	2.61	0.11	0.4	0.1	Gavin et al. (2014)
5	SC1	Port Hedland	C	6	0.219	0.6	0.1	Bittar et al. (2022)
6	SC1	Orrong Rd, Perth	C	6	0.219	0.6	0.1	Bittar et al. (2022)
7	SC2	Orrong Rd, Perth	C	8	0.219	0.6	0.1	Bittar et al. (2022)
8	SC1	Karrakatta, Perth	C	4	0.168	0.475	0.1	Bittar et al. (2022)
9	SC2	Karrakatta, Perth	C	4	0.168	0.475	0.1	Bittar et al. (2022)
10	SC1	Henry st, Perth	C	5.5	0.168	0.6	0.1	Bittar et al. (2022)
11	SC1	Ellenbrook, Perth	C	6	0.219	0.6	0.1	Bittar et al. (2022)
12	S2P3	Alberta, Canada	T	4.57	0.114	0.406	0.1	Li & Deng (2019)
13	S2P1	Alberta, Canada	T	2.44	0.073	0.305	0.1	Li & Deng (2019)
14	S2P1	Alberta, Canada	T	3.05	0.089	0.356	0.1	Li & Deng (2019)
15	T9	Alberta, Canada	T	4.9	0.273	0.762	NA	Tappeden (2007)
16	P1	Blessington	T	2.61	0.11	0.4	0.1	Gavin et al. (2014)
17	ST1	Perth airport	T	6	0.323	0.6	0.1	Bittar et al. (2022)
18	ST1	Ellenbrook, Perth	T	6	0.219	0.6	0.1	Bittar et al. (2022)

T=Tension; C=Compression

Table 2. CPT methods assessment for screw piles loaded in compression.

N	Q_c LCPC	Q_c Bittar et al. (2022)	Q_m	Q_m/Q_c LCPC	Q_m/Q_c Bittar et al. (2022)
1	365.4	162.1	135.0	0.37	0.83
2	303.0	131.3	114.0	0.38	0.87
3	360.8	160.9	143.0	0.40	0.89
4	858.3	415.0	420.0	0.49	1.01
5	3983.5	2227.8	2123.0	0.53	0.95
6	1753.3	856.2	617.0	0.35	0.72
7	2369.2	1216.0	1027.0	0.43	0.84
8	579.0	252.0	265.0	0.46	1.05
9	831.9	359.2	345.0	0.41	0.96
10	1461.4	609.1	525.0	0.36	0.86
11	3086.1	1594.8	1399.0	0.45	0.88
			Avg	0.42	0.90
			CoV	0.13	0.10

Table 3. CPT methods assessment for screw piles loaded in tension.

N	Q_t LCPC	Q_c Gavin et al. (2013)	Q_c Bittar et al. (2022)	Q_m	Q_m/Q_c LCPC	Q_m/Q_c Gavin et al. (2013)	Q_m/Q_c Bittar et al. (2022)
12	354.0	100.8	182.8	189.0	0.53	1.87	1.03
13	296.4	45.7	104.3	88.0	0.30	1.92	0.84
14	350.9	77.3	127.1	110.0	0.31	1.42	0.87
15	4154.4	2731.6	2365.4	2025.0	0.49	0.74	0.86
16	842.9	161.7	303.6	240.0	0.28	1.48	0.79
17	1484.9	770.0	601.9	554.0	0.37	0.72	0.92
18	3036.6	794.3	1219.7	1145.0	0.38	1.44	0.94
				Avg	0.38	1.37	0.89
				CoV	0.23	0.33	0.08

develop a certain axial capacity. It is therefore of interest to assess if there is a relationship between end of installation torque and axial capacity (as described in equations 2 and 3) and, furthermore, if the UWA-SP-21 method can allow a reasonable estimation of final installation torque using Equation (3).

The relevant data for this assessment are provided in Table 4 where the final installation torques are calculated using Equation (3) either (i) from the measured load test capacity, $Q_{ult,m}$ or (ii) from the ultimate capacity calculated using UWA-SP-21, $Q_{ult,c}$.

The average ratio of measured to calculated torque was 1.06 when applying Equation (3) to the measured tension capacity and was 1.03 when applying the same equation to the tension capacity calculated using UWA-SP-21. The coefficient of variation of measured to calculated torque using both approaches was about 22%, which supports the validity of a direct relationship between capacity and torque as proposed by Perko (Equation 3) - at least for the range of screw pile geometries covered by the database.

Figure 2 compares the measured uplift capacities with the final measured installation torque from the piles in the database (Table 1 and 4). The regression analysis shows great consistency when compared with the results found by Perko (2009) in Figure 1.

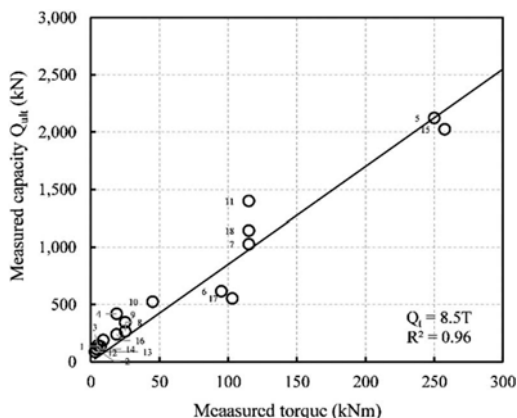


Figure 2. Measured torque vs. uplift capacity for single-helix piles in the presented database.

7 CONCLUSIONS

A database comprising 18 static load tests on single helix screw piles is presented. These piles had helix diameters ranging from 0.3m to 0.6m and lengths between 2.5m and 8m. It is demonstrated that the UWA-SP-21 CPT method (Bittar et al. 2022) provided predictions of the axial compression and tension capacity of these piles that were generally within about 12% of the measured capacities.

Table 4. Measured and calculated final installation torque for each pile in the database.

N	Pile	Loading direction	T_c from $Q_{ult,m}$	T_c from $Q_{ult,c}$	T_m	T_m/T_c from $Q_{ult,m}$	T_m/T_c from $Q_{ult,c}$
1	S2P3	C	7.4	10.0	7.0	0.95	0.70
2	S2P1	C	4.1	3.8	4.0	0.97	1.06
3	S2P2	C	6.2	5.5	5.0	0.81	0.91
4	P1	C	22.1	16.0	18.7	0.84	1.17
5	SC1	C	210.8	183.3	250.0	1.19	1.36
6	SC1	C	61.3	68.9	95.0	1.55	1.38
7	SC2	C	102.0	99.7	115.0	1.13	1.15
8	SC1	C	20.6	15.9	25.0	1.21	1.57
9	SC2	C	26.8	22.6	25.0	0.93	1.10
10	SC1	C	40.9	38.6	45.0	1.10	1.17
11	SC1	C	138.9	129.7	115.0	0.83	0.89
12	S2P3	T	10.3	10.0	9.0	0.87	0.90
13	S2P1	T	3.2	3.8	3.1	0.97	0.82
14	S2P1	T	4.8	5.5	4.2	0.88	0.76
15	T9	T	246.3	287.7	257.6	1.05	0.90
16	P1	T	12.6	16.0	18.7	1.48	1.17
17	ST1	T	78.7	92.0	103.0	1.31	1.12
18	ST1	T	113.7	129.7	115.0	1.01	0.89
					Avg	1.06	1.03
					CoV	0.21	0.22

T_m = measured torque; T_c = calculated torque using Equation 3, Perko (2009)

T_c from $Q_{t,m}$ = torque calculated from the measured $Q_{ult,m}$

T_c from $Q_{ult,c}$ = torque calculated from $Q_{ult,c}$, the capacity calculated via Bittar et. al. (2022), see Equations 1-2.

This promising predictive performance is a substantial improvement on existing approaches and arises from the simple relationship between spread footing bearing stress and CPT q_c at a displacement ratio of 10%. A combination of this method and the relationship between final installation torque and tension capacity proposed by Perko (2009) enables assessment of the torque required for installation of single helix piles to an accuracy of about 25%.

This method has the potential for scaling up to the dimensions of offshore piles, following the same research direction that has led to CPT-based methods now being favoured for predicting the capacity of driven tubular piles. This research will support the adoption of screw piles as an alternative foundation solution for offshore wind turbine jacket structures.

ACKNOWLEDGMENTS

The first author acknowledges the support of the Australian Postgraduate Award at The University of Western Australia.

REFERENCES

- Al-Baghdadi, T.A., Davidson, C., Brown, M.J., Knappett, J.A., Brennan, A., Augarde, C., Coombs, W., and Wang, L. (2017). CPT based design procedure for installation torque prediction for screw piles installed in sand. Proc. 8th Int. Conf. on Offshore Site Investigation & Geotechnics. pp. 346–353.
- Bittar E., Lehane B., Richards, D., Blake A., White D., Davidson C. and Brown, M. (2021). Field investigation to evaluate the uplift capacity and installation performance of screw piles in sand. Proc. 20th Int. Conference on Soil Mechanics and Geotechnical Engineering, Sydney 2021,
- Bittar E., Lehane B., Richards, D., Blake A., White D., Davidson C. and Brown, M. (2022). CPT-based design method for axial capacities of screw piles in sand (in press).
- Bustamante, M., and L. Ganeselli. 1982. "Pile bearing capacity prediction by means of static penetrometer CPT." Proc., 2nd European Symp. on Penetration Testing (ESOPT II), 493–500. Rotterdam, Netherlands: A.A. Balkema.
- Das, B. M. & Shukla, S. K. (2013). Earth anchors. Plantation, FL, USA: J. Ross Publishing.
- Davidson, C., Al-Baghdadi, T., Brown, M., Brennan, A., Knappett, J., Augarde, C., Coombs, W., Wang, L., Richards, D., Blake, A., and Ball, J. (2018). A modified CPT based installation torque prediction for large screw piles in sand. Proc. 4th International Symposium on Cone Penetration Testing, CPT 2018,; 255–261.
- Davidson, C., Brown, M.J., Cerfontaine, B., Al-Baghdadi, T., Knappett, J., Brennan, A., Augarde, C., Coombs, W., Wang, L., Blake, A., Richards, D., and Ball, J.D. (2020). Physical modelling to demonstrate the feasibility of screw piles for offshore jacket supported wind energy structures. *Geotechnique*. (September): 1–50
- Doan, L. V., & Lehane, B. M. (2021). CPT-Based Design Method for Axial Capacities of Drilled Shafts and Auger Cast-in-Place Piles. *Journal of Geotechnical and Geoenvironmental Engineering*, 147(8), 04021077.
- Fateh, A. M. A., Eslami, A., & Fahimifar, A. (2017). Direct CPT and CPTu methods for determining bearing capacity of helical piles. *Marine Georesources & Geotech.*, 35(2), 193–207.
- Gavin, K., Doherty, P., & Tolooiyan, A. (2014). Field investigation of the axial resistance of helical piles in dense sand. *Canadian Geotechnical Journal*, 51(11), 1343–1354.
- Hoyt, R. M., & Clemence, S. P. (1989). Uplift capacity of helical anchors in soil. In *Proceedings of the 12th International Conference on Soil Mechanics and Foundation Engineering*, Rio de Janeiro, Brazil, Vol. 2, pp. 1019–1022
- Igoe, D., Kirwan, L., & Gavin, K. G. (2014). Ageing effects and CPT based design methods for driven piles in sands. *Int. Symposium on Cone Penetration Testing*, 1073–1082.
- Lehane B.M. (2012). Foundation capacity from the CPT. Keynote Lecture, Proc. 4th Int. Conf. on Geotechnical and Geophysical Site Characterisation, 1, ISC4, Recife, Brazil, 63–82.
- Lehane, B.M., 2019. EH Davis Memorial Lecture (2017) CPT-based design of foundations. *Australian Geomechanics Journal*, 54(4), pp.23–45.
- Lehane, B.M., Schneider, J.A., and Xu, X. 2005. CPT based design of driven piles in sand for offshore structures. The University of Western Australia.
- Li, W., & Deng, L. (2019). Axial load tests and numerical modeling of single-helix piles in cohesive and cohesionless soils. *Acta Geotechnica*, 14(2), 461–475.
- Perko, H. A. (2009). *Helical piles: a practical guide to design and installation*. John Wiley & Sons.
- Richards, D., Blake, A., White, D., J. B. E., & B.M, L. (2019). Field tests assessing the installation performance of screw pile geometries optimised for offshore wind applications. Proc. 1st International Screw Pile Symposium on Screw Piles for Energy Applications (pp. 47–54).
- Sakr, M. (2015). Relationship between installation torque and axial capacities of helical piles in cohesionless soils. *Canadian Geotechnical Journal*, 52(6), 747–759.
- Sharif, Y. U., Brown, M., Ciantia, M. O., Cerfontaine, B., Davidson, C., Knappett, J., ... Ball, J. D. (2020). Using DEM to create a CPT based method to estimate the installation requirements of rotary installed piles in sand. *Canadian Geotechnical Journal*, cgj–2020–0017.
- Spagnoli, G. 2017. A CPT-based model to predict the installation torque of helical piles in sand. *Marine Georesources and Geotechnology*, 35(4): 578–585. Taylor & Francis.
- Tappenden, K. M., & Sego, D. C. (2007, October). Predicting the axial capacity of screw piles installed in Canadian soils. *OttawaGeo2007 Conference* (pp. 1608–1615).
- Tsuha, C. de H.C., and Aoki, N. 2010. Relationship between installation torque and uplift capacity of deep helical piles in sand. *Canadian Geotechnical Journal*, 47 (6): 635–647.

CPT-based liquefaction ejecta evaluation procedure

Jonathan D. Bray & Daniel Hutabarat
University of California, Berkeley

ABSTRACT: A CPT-based procedure to estimate the severity of liquefaction ejecta is presented. It employs a liquefaction ejecta demand parameter (L_D) that captures the amount of upward seepage pressure that can produce artesian flow due to elevated excess hydraulic head and a crust layer resistance parameter (C_R) that captures the strength and thickness of the nonliquefiable crust layer. L_D tends to increase systematically as ejecta severity increases at the thick, clean sand sites, and low L_D values are estimated at stratified soil sites that did not produce ejecta. C_R captures the differing performances of sites with and without a competent crust layer overlying a thick liquefiable layer with a high L_D value. The proposed $L_D - C_R$ liquefaction ejecta severity chart separates cases with severe or extreme ejecta, which have high L_D and low C_R values, from cases with minor or no ejecta, which have low L_D and high C_R values.

1 INTRODUCTION

Ejecta-induced ground failure contributed nearly 90% of the liquefaction land damage in the residential area of Christchurch, New Zealand during the 2010-2011 Canterbury earthquake sequence (van Ballegooy et al. 2014). The severity of land damage increased as more liquefied sediment was ejected. Ground-failure indices, such as Liquefaction Potential Index (LPI, Iwasaki et al. 1978) and Liquefaction Severity Number (LSN, van Ballegooy et al. 2014), often overestimated the severity of sediment ejecta produced at level-ground stratified silty soil sites in Christchurch (e.g., Maurer et al. 2014).

Hutabarat and Bray (2021a,b) performed nonlinear dynamic effective stress analysis (ESA) to find that the location of liquefaction triggering, soil layer stratification, and vertical hydraulic conductivity (k_v) profile govern the post-shaking ejecta mechanism and system response of sites that contain liquefiable layers that either produce sediment ejecta or not. The insights obtained from performing ESA are noteworthy; however, it may be infeasible to perform ESA for projects when subsurface data are limited. Cone penetration test (CPT)-based simplified procedures for evaluating liquefaction triggering have proved reliable for evaluating liquefaction triggering. A CPT-based procedure for estimating the severity of ejecta-induced ground failure for level-ground conditions is presented in this paper. The procedure quantifies two governing factors: liquefaction ejecta demand (L_D) and crust layer resistance (C_R). The L_D parameter considers the excess hydraulic head (h_{exc}) and artesian water pressure that can develop at a site, and the C_R parameter considers the thickness of the nonliquefiable crust layer and its

equivalent shear strength which suppress manifestations of liquefaction. These parameters are used to estimate the amount of ejecta likely to occur.

2 LIQUEFACTION EJECTA SEVERITY

LPI estimates the severity of liquefaction ground damage using a linear depth-weighted integration of the factor of safety against liquefaction (FS_L) to a depth of 20 m as

$$LPI = \int_0^{20\text{ m}} F(FS_L) (10 - 0.5z) dz \quad (1)$$

where $F(FS_L) = 1 - FS_L$ for $FS_L < 1.0$; $F(FS_L) = 0$ for $FS_L \geq 1.0$, and z is the depth below ground surface (m). LPI ranges from 0 to 100, where a higher value indicates more severe liquefaction-induced ground failure. LPI's performance has been evaluated extensively (e.g., Maurer et al. 2014). LSN estimates the severity of liquefaction ground damage as

$$LSN = 1000 \int \frac{\varepsilon_v}{z} dz \quad (2)$$

where $z = \text{depth} > 0$ and $\varepsilon_v =$ post-liquefaction volumetric strain estimated using Zhang et al. (2002). LSN utilizes a power-law depth-weighting function to emphasize the relative importance of shallow liquefied layers to cause severe ground failure. Additionally, Towhata et al. (2016) developed a liquefaction severity chart by comparing the LPI

values and thickness of the crust (H_1) values for cases with and without liquefaction-induced damage. Like Ishihara (1985), Towhata et al. (2016) compare liquefaction demand and crust resistance, but instead of using the thickness of the liquefiable layer (H_2), they use LPI to represent liquefaction demand.

The poor performance of these liquefaction indices in stratified silty soil sites in Christchurch is affected primarily by the limitations of simplified liquefaction triggering procedures in capturing their response (e.g., Beyzaei et al. 2018 and Cubrinovski et al. 2019). Sediment ejecta is a post-shaking hydraulic phenomenon resulting from the migration and redistribution of excess-pore-water-pressure (u_e) generated during earthquake shaking. The dissipation process of residual u_e can trigger high-gradient upward seepage that induces hydraulic fracturing in the upper crust layer. With a sufficiently high hydraulic gradient, artesian flow can be produced that exploits cracks in the crust layer to eject liquefied sediment onto the ground surface. Ejecta production is governed largely by the post-shaking upward seepage developed in the soil profile (Hutabarat and Bray 2021a,b). The amount of excess hydraulic head ($h_{exc} = u_e / \gamma_w$, where γ_w is the unit weight of water), soil's hydraulic conductivity (k_v), and the degree of soil layer stratification are key factors that largely determine the hydraulic gradient (i) and volume of upward seepage in the liquefiable layer.

ESA results indicate the h_{exc} developed at shallow depths in sites without sediment ejecta remains low during and after shaking. Low- k_v layers within a highly stratified deposit impede upward seepage so the generated h_{exc} is insufficient to produce artesian flow. Although liquefaction is triggered in isolated layers of loose sand at deeper depths, upward seepage is impeded by an overlying low- k_v layer. Liquefaction triggering in a deeper layer can also reduce the seismic demand so that liquefaction is not triggered at shallow depths. Conversely, Hutabarat and Bray (2021a,b) showed that ejecta amount largely depends on the thickness of the liquefiable high- k_v soil layer and homogeneity of the k_v -profile at sites with significant ejecta. The simulations indicated the high-hydraulic gradient upward seepage that flows within a thick, continuous, high- k_v deposit can trigger post-shaking secondary liquefaction within the sand layer directly beneath the crust. A thick, continuous, and high- k_v sand site requires more time to return to its initial hydrostatic state; thus, it can produce more ejecta. Partially stratified sites with thin and less permeable sand layers produce less upward seepage which in turn produces no or minor-to-moderate ejecta (Hutabarat and Bray 2021b).

3 CHRISTCHURCH LIQUEFACTION CASE HISTORIES

Researchers from the Univ. of Canterbury, Univ. of California at Berkeley, Univ. of Texas at Austin, and

Tonkin+Taylor investigated liquefiable sites in Christchurch with underestimations or overestimations (e.g., Cubrinovski et al. 2019). Of these sites, 44 well-investigated free-field level-ground sites were selected to represent various soil profiles, ground shaking intensities, and observed ejecta amounts. Their performance during the four Canterbury earthquakes: 2010 M_w 7.1 Darfield, 2011 M_w 6.2 February, 2011 M_w 6.0 June, and 2011 M_w 5.9 December events were considered. The 44 sites were classified as either thick, clean sand sites or partially-to-highly stratified silty soil sites to evaluate the effect of this attribute. Details of the sites are described in Hutabarat and Bray (2021b).

Figure 1 shows representative thick sand sites and stratified silty soil sites. The Robertson (2016) modified soil behavior type index (I_B) zones are used to classify the sand-like ($I_B > 32$), intermediate ($22 < I_B < 32$), and clay-like ($I_B < 22$) soil responses of the layers. Thick sand sites (Figure 1a-b) contain at least 4.5 m thick of continuous sand-like and high- k_v soils within the depth of the groundwater level (GWL) to 15 m. Stratified soil sites (Figure 1c-d) contain partially-to-highly stratified deposits of sand, intermediate, and clay soil layers where there is no continuous sand layer thicker than 4.5 m within the GWL to 15 m depth. The parameter z_{AB} highlighted in the figures is the thickness of the sand-like soil layer that may contribute to ejecta production if liquefaction is triggered measured from the top depth of z_A to the bottom depth of z_B . The parameter z_{AB} is measured from directly below the nonliquefiable crust layer to the bottom of the first continuous sand-like soil layer.

CPT-based liquefaction triggering back-analyses of all cases were performed using the Boulanger and Idriss (2016) "BI-16" procedure. The analyses considering LPI and LSN used the probability of liquefaction (P_L) of 15% to be consistent with their criteria. The liquefaction triggering calculations were performed using the median peak ground acceleration (PGA) values and a fines-content correction (C_{FC}) factor of 0.13 for Christchurch soil (Hutabarat and Bray 2022). The GWL for each site was estimated based on nearby well records and V_p measurements. Only the FS_L of soil with the Robertson (2009) SBT Index (I_c) < 2.60 is computed to calculate LPI and LSN for each case using Eqs. 1 and 2.

The distributions of LPI and LSN for each case within the two site groups categorized by ejecta severity are presented in Figure 2 with box-and-whisker plots (Tukey 1977) to evaluate their performance in estimating ejecta amounts at thick sand sites and partially-to-highly stratified soil sites. The box height represents the range of the first (Q_1) to third (Q_3) quartile of the distribution and the horizontal orange line in the box is the median value. The whiskers extend 1.5 times the interquartile range ($IQR = Q_3 - Q_1$) and data points beyond the whiskers are outliers. LPI and LSN show a flat trend of increasing ejecta amounts with increasing median values for thick sand sites (Figure 2a). There is an overlap in the

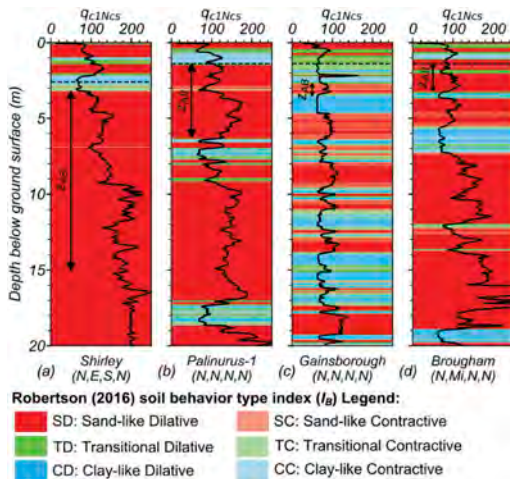


Figure 1. Examples of thick sand (a-b) and stratified soil (c-d) profiles of q_{c1Nes} , I_B , and observed ejecta severity (given below site name in the sequence of the DAR, CHC, JUN, and DEC earthquakes where N = None; Mi = Minor; Mo = Moderate; S = Severe; E = Extreme).

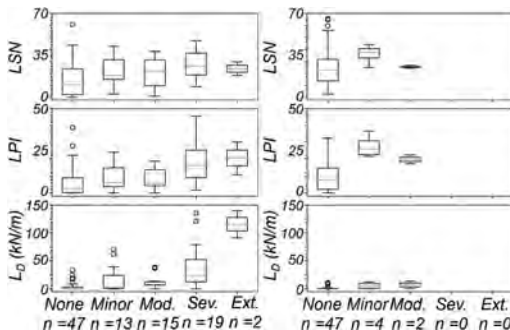


Figure 2. Box-and-whisker plots of liquefaction ejecta demand parameters grouped based on observed ejecta severity for: (a) 96 case histories with thick sand deposits and (b) 80 case histories with stratified deposits.

boxes representing the middle 50% of their distributions. There are numerous No ejecta cases above the top whisker with values higher than the Minor and Moderate top whisker. Also, LPI and LSN are not reliable for highly stratified soil sites as shown in Figure 2b. Several stratified sites have high index values but did not produce ejecta. Similar results are obtained if the input parameters are varied. The performance of the new liquefaction demand parameter (L_D) shown in Figure 2 is discussed next.

4 LIQUEFACTION DEMAND PARAMETER

Figure 3 illustrates the conceptual framework employed in the CPT-based procedure to estimate

ejecta severity. Ejecta results from high-gradient upward seepage developed in hydraulically continuous liquefied soil layers beneath the crust. For highly stratified sites, the liquefiable soil layer directly beneath the crust does not develop sufficiently high-gradient upward seepage, either because liquefaction is not triggered from reduced seismic demand due to liquefaction at depth or an underlying low- k_v soil layer impedes the upward water flow during the advection process. The intensity of the seepage is higher if a thicker liquefied layer develops h_{exc} higher than the critical head to produce artesian flow and it is composed of a high- k_v soil (Hutabarat and Bray 2021b).

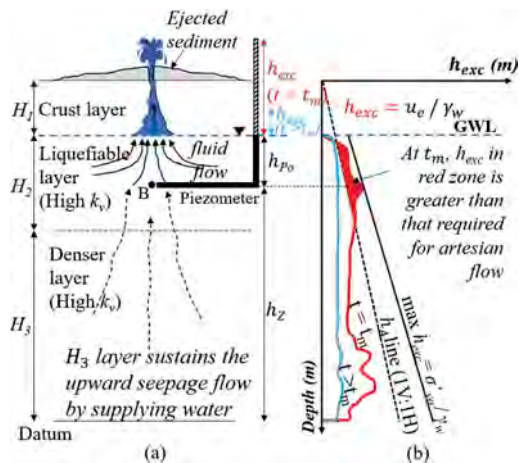


Figure 3. (a) Sediment ejecta mechanisms in a typical thick sand site and (b) Artesian Flow Potential concept.

During shaking, the elevated u_e increases the total hydraulic head. Tokimatsu and Yoshimi (1983) proposed this relationship to estimate the pore pressure ratio (r_u) as the function of FS_L :

$$r_u = 0.5 + \frac{\sin^{-1}\left(2 FS_L^{\left[\frac{1}{\alpha\beta}\right]} - 1\right)}{\pi}; \text{ for } 1.0 \leq FS_L < 3.0 \quad (3)$$

where they proposed to use $\alpha = 1.0$. The β parameter is set to -0.2, which gives $1/(\alpha\beta) = -5.0$. The inverse sine term must be calculated in radians, and $r_u = 1.0$ for $FS_L = 1.0$. The FS_L in Eq. 3 is computed using the BI-16 liquefaction triggering procedure. Once r_u is computed, the h_{exc} at each depth is estimated using

$$h_{exc} = \frac{r_u \sigma'_{v0}}{\gamma_w} \quad (4)$$

where σ'_{vo} = initial effective vertical stress and γ_w = unit weight of water (9.81 kN/m³).

Liquefaction ejecta demand from upward seepage is estimated by the head difference between a specified depth and the ground surface. A thicker H_I creates a longer travel path for water to flow, which reduces the seepage gradient and thus increases the resistance parameter. Additionally, a stronger crust provides more resistance against ejecta being produced than a weak crust.

To produce ejecta, the h_{exc} in liquefied layer must exceed a critical value h_A which is the required h_{exc} at a depth z to produce artesian flow above the ground surface to exploit cracks in the crust layer and produce a flow that transports the liquefied soil to the ground surface. The Artesian Flow Potential (AFP) concept of Hutabarat and Bray (2021a) assumes the h_A value required to cause artesian flow at a depth z is equal to z which is represented by the h_A line with slope 1H:1V down from the ground surface. AFP equals the red area in Figure 3b between the profile of h_{exc} and the h_A line when $h_{exc} > h_A$. More ejecta are produced at sites with higher AFP values that remain high after shaking.

A soil layer's k_v directly influences the upward flow of water in a soil column that can induce post-shaking secondary liquefaction at shallow depths. The water flowing upward from a deep liquefied layer can increase the h_{exc} in a shallow layer if the intermediate soil layers have high k_v values. Conversely, a low- k_v intermediate depth soil layer with sufficient thickness can restrict the upward flow of water from deep liquefiable layers. To capture this effect a normalized- k_v weighting factor is employed where a low permeability layer lowers ejecta potential and a high permeability layer increases ejecta potential. The Robertson and Cabal (2015) CPT correlation is adopted to estimate k_v using CPT data:

$$k_v(\text{m/s}) = 10^{(0.952 - 3.04I_c)}; \text{ when } 1.0 < I_c < 3.27 \quad (5)$$

A normalized k_v factor is used as the weighting function where the k_v value of clean sand calculated for $I_c = 1.8$ is selected as the baseline hydraulic conductivity. Nearly all Moderate, Severe, and Extreme ejecta cases investigated in this study contain a thick deposit of clean sand with $I_c \leq 1.8$. Soil layers where h_{exc} exceeds h_A with low I_c values and thus high k_v values are multiplied by factors greater than one, and soil layers with high I_c values and thus low k_v values are multiplied by factors less than one.

The liquefaction ejecta demand parameter (L_D) is estimated as

$$L_D(\text{kN/m}) = \gamma_w \int_{z_A}^{z_B} \frac{k_v}{k_{cs}} (h_{exc} - h_A) dz \begin{cases} \text{when } h_{exc} \geq h_A \\ 0, \text{ otherwise} \end{cases} \quad (6)$$

where z_A = depth from the ground surface to the top of the shallowest soil layer below the GWL with $I_c <$

2.6 that is at least 250-mm thick; z_B = depth from the ground surface to the top of the shallowest soil layer between the depths of z_A and 15 m with $I_c \geq 2.6$ that is at least 250-mm thick. The depth z_B will be 15 m if there is no soil layer (at least 250-mm thick) with $I_c \geq 2.6$ below z_A . L_D is calculated in these steps:

1. Estimate z_A and z_B based on the I_c profile.
2. Compute FS_L at each depth.
3. Compute r_u at each depth interval using Eq. 3.
4. Compute h_{exc} at each depth using Eq. 4.
5. Compute normalized- k_v weighting factor (k_v/k_{cs}) at each depth using Eq. 5 to calculate k_v .
6. Compute L_D using Eq. 6 where h_A is defined by the 1V:1H line shown in Figure 3b.

Figure 2 shows the distribution of the computed L_D value for each case history with its observed severity of ejecta. The results indicate:

- L_D has a lower variation than LSN and LPI as reflected by its shorter box-and-whisker box for the No ejecta cases shown in Figure 2a for the thick sand sites. Also, 87% of these cases have $L_D < 5$.
- There is some overlap of the L_D boxes of the Minor and Moderate cases shown in Figure 2a, but the median values of L_D increase systematically as the severity of ejecta increases. Some Minor-to-Moderate cases have $L_D < 5$, which overlaps with the None cases, which is likely due to the bias in the liquefaction triggering calculation.
- The Minor and Moderate L_D boxes do not overlap the Severe L_D box, and the Severe L_D box does not overlap the Extreme L_D box. More than 75% of the Severe ejecta cases have $L_D > 15$.
- L_D resolves the overestimation problem of the other liquefaction ground damage indices for the highly stratified sites (Figure 2b). The range of the None cases is smaller than the Minor and Moderate cases. The use of z_{AB} which considers the impedance of upward seepage by a low- k_v profile is primarily responsible for this improvement.

5 CRUST RESISTANCE PARAMETER

The crust layer resistance parameter (C_R) captures the strength and thickness of the nonliquefiable crust layer. It captures the differing performances of sites with and without a competent crust layer overlying a thick liquefiable layer with a high L_D value. The crust resistance parameter (C_R) is estimated as

$$C_R(\text{kN/m}) = \int_0^{H_I} s_u dz \begin{cases} s_u = K_o \sigma'_{vo} \tan(\phi_{cs}), & \text{if } I_B > 22 \\ s_u = \frac{(q_t - \sigma_{vw})}{N_{kt}}, & \text{if } I_B \leq 22 \end{cases} \quad (7)$$

where H_l (m) = thickness of the layer above z_A until the ground surface; s_u (kN/m²) = shear strength of the crust layers estimated using the CPT data; K_o = coefficient of lateral pressure, which is assumed to be 0.5; ϕ_{cs} is the critical state friction angle which is assumed to be 33 degrees; and $N_{kt} = 15$ in the tip resistance (q_t) correlation used for clay. A soil with $I_B > 22$ will have a lower s_{u-eq} than a crust layer composed of clay defined by $I_B < 22$, because the vertical effective stress is low at shallow depth. Thus, s_u represents the strength (and integrity) of the crust.

6 EJECTA SEVERITY EVALUATION PROCEDURE

The Christchurch case history data are plotted on the L_D - C_R charts shown in Figure 4 with zones for classifying ejecta severity potential. The horizontal boundary line for each zone is determined qualitatively using the Q_1 - Q_3 ranges of the box-and-whisker plot shown in Figure 2. The boundaries of the ejecta zones were adjusted for larger C_R values to bring in its effect. The classification boundaries were selected qualitatively to separate data to minimize bias and misclassifications. The bilinear boundary lines shown in Figure 4 are defined by three $[C_R, L_D]$ data points that separate adjacent zones as:

- None-to-Minor: [0, 2.5] [100, 2.5] & [250, 25]
- Minor-to-Moderate: [0, 6] [90, 6] & [250, 70]
- Moderate-to-Severe: [0, 15] [85, 15] & [250, 150]
- Severe-to-Extreme: [0, 85] [75, 85] & [200, 250]

Examination of the data plotted on the Liquefaction Severity Charts shown in Figure 4 indicates:

- The 2 Extreme ejecta cases with $L_D > 85$ and $C_R < 75$ are located at the top left part of the chart in the Extreme zone.

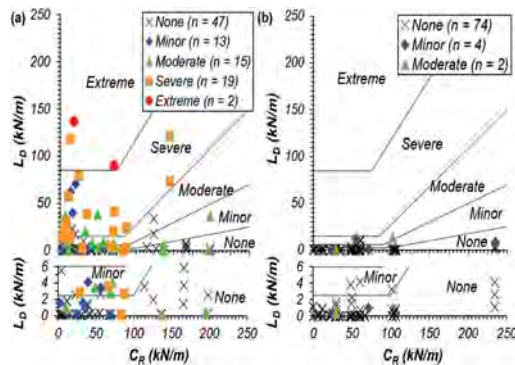


Figure 4. Ejecta severity using Liquefaction Demand (L_D) and Crust Resistance (C_R) parameters at: (a) thick sand sites and (b) stratified soil sites. The inserts show data for $L_D < 6$ kN/m.

- The Severe ejecta cases generally have lower L_D values and higher C_R values than the Extreme cases. C_R helps distinguish the severity of ejecta by shifting a data point left or right.
- C_R with L_D helps distinguish Moderate ejecta cases from Severe ejecta cases at thick sand sites; whereas it is difficult to distinguish Minor ejecta cases from Moderate and None cases.
- The No ejecta cases generally have $L_D < 2.5$ so C_R does not aid significantly in distinguishing these sites from cases with ejecta.

The $L_D - C_R$ charts (Figure 4) generally estimates ejecta severity well for the 176 case histories investigated by Hutabarat and Bray (2022). The chart resolves the overestimation problem of other indices at highly stratified soil sites (Figure 4b). The improvement is largely because L_D captures the important role of low- k_v layers in impeding upward seepage, which prevents ejecta production at stratified soil sites.

Table 1. Severity criteria used in this study.

Category	Area within 20 m covered by ejecta (%)	Best-estimate ejecta-induced settlement (mm)*
None	0	0
Minor	< 5	< 50
Moderate	5 - 20	50 - 100
Severe	20 - 50	100 - 300
Extreme	> 50	> 300

* Based on settlement measured at sites with localized ejecta.

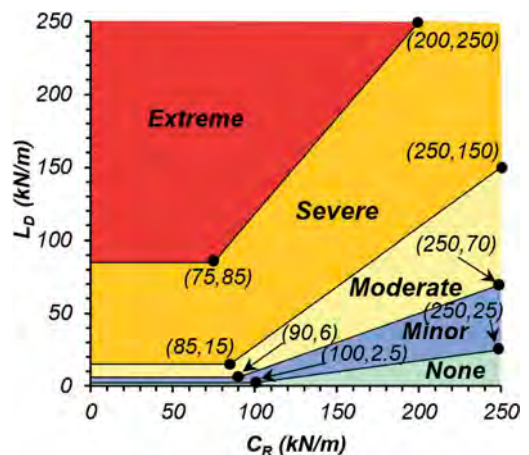


Figure 5. Liquefaction-induced ejecta severity chart.

7 CONCLUSIONS

The $L_D - C_R$ chart shown in Figure 5 provides a straightforward means to assess the severity of ejecta at a level-ground, free-field site. The proposed

chart captures two key attributes of the problem: liquefaction ejecta demand through L_D and crust resistance through C_R . Additionally, an estimate of ejecta-induced 1D free-field ground settlement is provided using the values of Table 1 based on the liquefaction severity category zone in the $L_D - C_R$ chart shown in Figure 5. Although the $L_D - C_R$ chart proved useful in evaluating ejecta potential, the chart's accuracy is hindered by the limitations of the simplified liquefaction triggering procedure used to perform the liquefaction assessment.

As discussed previously, the $L_D - C_R$ chart may produce misestimations for some cases. Often dynamic ESA can resolve these cases of overestimation or underestimation. Overall, the proposed chart with a parameter that captures liquefaction ejecta demand (L_D) and a parameter that captures crust resistance (C_R) provides reasonable estimates of ejecta severity. L_D captures the influence of depth (represented by the h_A line) and the hydraulic conductivity contrast (represented by the k_v/k_{cs} weighting factor), and C_R captures the resistance of the crust to discern when the crust might prevent ejecta formation.

Estimating k_v is challenging, and hence, estimating k_v/k_{cs} in Eq. 6 is challenging. To achieve results consistent with this study, the Robertson & Cabal (2015) CPT correlation should be used to estimate k_v . The k_v/k_{cs} weighting factor captures the post-shaking upward seepage mechanism where a high- k_v deposit tends to produce a higher rate of upward seepage that can more readily erode the crust layer. The normalized- k_v weighting factor incorporated in L_D enables it to capture important features of liquefaction induced upward seepage which are not captured by other ground failure indices.

The $L_D - C_R$ chart attempts to assess reliably the highly complex phenomenon of ejecta production in a practical manner. Investigation of additional liquefaction field case histories that produced different amounts of ejecta is warranted to refine the proposed chart. Limitations include the proposed procedure cannot capture the system site response during earthquake shaking. Additionally, the $FS_L - r_u$ relationship used in the calculation is for fine-clean sand, but it is used to estimate r_u for silty soils. Lastly, the upward seepage pressure is computed based on the unit weight of water, though the fluidized sediment will be heavier than water; however, it is difficult to estimate its value accurately, and the unit weight of water is used to keep the method straightforward. Estimating z_B is important as a thicker z_{AB} may result in an unrealistically higher L_D .

ACKNOWLEDGEMENTS

This study was funded by the Pacific Earthquake Engineering Research (PEER) Center through the Transportation Systems Research Program and the

National Science Foundation (NSF) with Grant CMMI-1561932. All opinions, findings, and conclusions expressed in this paper are those of the authors and do not necessarily reflect their views.

REFERENCES

- Beyzaei, C. Z. et al. (2018). Depositional environment effects on observed liquefaction performance in silt swamps during the Canterbury earthquake sequence. *SDEE*, Elsevier, 107, 898303–321.
- Boulanger, R. W. and Idriss, I. (2016). CPT-based liquefaction triggering procedure. *JGGE*, ASCE, 142 (2),04015065.
- Cubrinovski, M., Rhodes, A., Ntrisots, N., and Van Ballegooy, S. (2019). System response of liquefiable deposits. *SDEE*, Elsevier, 124, 212–229.
- Hutabarat, D. and Bray, J.D. (2021a). Effective stress analysis of liquefiable sites to estimate the severity of sediment ejecta. *JGGE*, ASCE, 147 (5):04021024.
- Hutabarat, D. and Bray, J.D. (2021b). Seismic response characteristics of liquefiable sites with and without sediment ejecta manifestation. *JGGE*, ASCE, 147 (6):04021040.
- Hutabarat, D. and Bray, J.D. (2022). Estimating the Severity of Liquefaction Ejecta using the Cone Penetration Test. *JGGE*, DOI: 10.1061/(ASCE)GT.1943-5606.0002744.
- Ishihara, K. (1985). Stability of natural deposits during earthquakes. Proc., 11th Int. Conf. on Soil Mechanics and Foundation Eng., ISSMGE, San Francisco, CA, 321–376.
- Iwasaki, T., Tatsuoka, F., Tokida, K., and Yasuda, S. (1978). A practical method for assessing soil liquefaction potential based on case studies at various sites in Japan. 2nd Int. Eq. Micro. Conf, San Francisco, CA, 885–896.
- Maurer, B. W., Green, R. A., Cubrinovski, M., and Bradley, B. A. (2014). "Evaluation of the liquefaction potential index for assessing liquefaction hazard in Christchurch, NZ." *JGGE*, ASCE, 140 (7).
- Robertson, P. (2009). Interpretation of cone penetration tests—a unified approach. *Can. Geotech. J.*, 46 (11),1337–1355.
- Robertson, P. (2016). CPT-based SBT classification system—an update. *Can. Geotech. J.*, 53(12),1910–1927.
- Robertson, P. K. and Cabal, K. L. (2015). 6th Ed Guide to CPT for geotechnical engineering. Gregg Drilling Testing, Inc.
- Tokimatsu, K. and Yoshimi, Y. (1983). Empirical correlation of soil liquefaction based on SPT N-value and fines content. *Soils and Foundations*, 23(4),56–73.
- Tonkin and Taylor (2013). Liquefaction vulnerability study. *Tonkin and Taylor, Ltd.* prepared for NZ EQ Comm.
- Towhata, I. et al. (2016). Qualification of residential land from the viewpoint of liquefaction vulnerability. *SDEE*, 91, 260–271.
- van Ballegooy, S. et al. (2014). Assessment of liquefaction-induced land damage for residential Christchurch. *Earthquake Spectra J.*, 30(1),31–55.
- Zhang, G., Robertson, P., and Brachman, R. W. (2002). Estimating liquefaction-induced ground settlements from CPT for level ground. *Can. Geotech. J.*, 39 (5),1168–1180.

Settlement estimations for buildings founded on saturated silty sands from CPT and DMT results

Maxwell Cáceres, Javier Fumeron & Felipe A. Villalobos

Department of Civil Engineering, Universidad Católica de la Santísima Concepción, Chile

Ricardo Moffat

LMMG Geotechnics & Faculty of Engineering and Sciences, Universidad Adolfo Ibáñez, Chile

ABSTRACT: The estimation of building settlements founded in saturated sandy and silty soils is a relevant part of foundation design. Settlement calculation methodologies are still based on SPT and plate-load tests. SPT results can have significant dispersion and soil stiffness estimations are obtained from correlations without a physical meaning and valid only for particular soils and geology conditions. Moreover, plate-load tests are normally limited to shallow depths. CPT and DMT can obtain reliable results in engineering units. These tests are operator independent and the equipment is truly standard worldwide. Results obtained using CPT and DMT equipment for an urban renovation project with buildings founded on saturated sands and silts in Concepción city in Chile, are presented. These results allow estimations of static and liquefaction-induced settlements obtained from calculation methods developed for CPT and DMT.

1 INTRODUCTION

Bearing capacity and settlements are key components in the analysis and design of foundations. Bearing capacity of shallow foundations is usually calculated adopting the Terzaghi procedure which has been extended for different conditions (geometry, loading). However, in silty sands the design becomes controlled in most of the cases by the allowable settlement and not by bearing capacity. Therefore, estimations of settlements are crucial in almost every project. Settlement estimation involves usually the determination of the soil stiffness by means of an operational deformation modulus related to the design load range, which can be obtained from laboratory tests such as triaxial tests. Alternatively, in situ tests can be carried out instead or to complement the information from laboratory. In situ testing can have benefits in terms of measuring directly in the soil without the hassles of extracting, transporting, storing and the preparation of samples. A traditional in situ test carried out in projects is the standard penetration test SPT. However, there are concerns about its reliability and result interpretation for soil stiffness due to poor reproducibility and lack of continuity (Robertson, 2012). In situ load plate test can provide a scaled footing load-displacement response. However, its applicability is limited to surface or shallow depths.

Cone penetration test CPT is versatile and reliable since results can be faster and continuously obtained

without major operator influence as with SPT (Lunne et al., 1997). A CPT based method to estimate static settlements of shallow foundations in sand requires the soil modulus of deformation E_s , which is normally obtained from the cone tip resistance.

The flat dilatometer test DMT is another in situ test which has had a particular success in the estimation of settlements of shallow foundations (Schmertmann, 1986; Schnaid, 2009; Marchetti, 2015). The settlement estimation is mainly based on the determination of the 1D dilatometer modulus M_{DMT} . Schmertmann (1986) has shown 16 case histories for different structures on sand, silt, clay, peat and mixtures of these soils where the use of M_{DMT} led to an average and standard deviation values of the estimated/measured settlement ratio s_e/s_m of 1.18 and 0.36 respectively, with s_e/s_m varying from 0.71 to 2.23 for measured settlements between 3 mm and 2.85 m. If only sand and silt and their mixtures were considered (9 cases), s_e/s_m average and standard deviation are 1.10 (0.73 – 1.34) and 0.21 for settlements between 3 and 58 mm. Moreover, other researchers have collected more cases with favourable performance of the DMT (Hayes, 1986; Monaco et al., 2006; Failmezger et al., 2015). For that reason, settlement studies based on CPT have often been benchmarked against results from the DMT (Kagawa et al., 1996; Lehane and Fahey, 2004).

This work focuses on the Aurora de Chile urban recovery project located at the Bío Bío north

riverbank in the city of Concepción, Chile, which started in 2016. The project considered the construction of 8 four-storey buildings of with 128 flats and 78 two-storey houses. As part of the geotechnical site investigation, one DMT and two CPT tests were carried out. This offers the opportunity for the comparison of settlement estimations based on results from CPT and DMT. The soils found in the project area correspond to fluvial deposits mainly of sands and silts and a mixture of them. Static settlements are determined from CPT and DMT results considering 1D deformation modulus for each soil layer and different vertical load increments. Liquefaction-induced settlement analysis based on the Ishihara (1996) chart and the liquefaction potential are performed. The latter follows the modified Seed and Idriss (1971) simplified method for CPT (Youd and Idriss, 2001) and DMT (Monaco et al. 2005; Marchetti et al. 2013).

2 STATIC SETTLEMENT ESTIMATION

Static settlement can be calculated based on a 1D compression modulus also referred to as oedometric or constrained modulus M which is commonly obtained from consolidation tests. This modulus M corresponds to the slope of a straight line between two points in the 1D effective vertical stress - vertical strain curve, which is therefore valid for that stress increment applied by a structure.

2.1 CPT-based settlement prediction

The CPT test consists in the continuous penetration through the soil of a standard steel bar with a conical tip at a constant rate of 20 mm/s. An electronically instrumented cone with load cells allows the measurement of the cone tip resistance q_c and sleeve friction resistance f_s . The use of a piezocone also allows the continuous measurement of the pore water pressure u . The CPT equipment and test procedures are standardized (ASTM D5778, 2020; EN ISO 22476-1, 2012). The CPT results can provide a detailed record for the evaluation of the ground stratigraphy and geotechnical properties (Lunne et al., 1997; Robertson, 2009a). Settlement estimations for footings in sand can be carried out by methods that use the drained elastic modulus E . 1D constrained modulus M are generally used for the estimation of long term consolidation settlements. However, for stresses below the preconsolidation stress, it can be assumed that M is approximately constant and possible to correlate with the net cone resistance ($q_t - \sigma_{v0}$) by means of DMT-CPT relationships represented in the $Q_{tn}-F_r$ chart (Robertson, 2009a, 2009b).

$$M = \alpha_M(q_t - \sigma_{v0}) \quad (1)$$

where q_t is the corrected tip resistance, σ_{v0} is the in situ vertical stress and α_M is a modulus factor:

If

$$I_c > 2.2 : \alpha_M = Q_{tn} \text{ for } Q_{tn} \leq 14 \quad (2a)$$

$$\alpha_M = 14 \text{ for } Q_{tn} > 14 \quad (2b)$$

If

$$I_c < 2.2 : \alpha_M = 0.03 \left[10^{(0.55I_c + 1.68)} \right] \quad (3)$$

where I_c is a soil behaviour type SBT index that can represent the SBT zones in the $Q_{tn}-F_r$ chart, Q_{tn} is the normalized tip resistance and F_r is the friction ratio. I_c represents the radius of a concentric circle:

$$I_c = [(3.47 - \log Q_{tn})^2 + (\log F_r + 1.22)^2]^{0.5} \quad (4)$$

$$Q_{tn} = [(q_t - \sigma_{v0})/p_a] (p_a/\sigma'_{v0})^n \quad (5)$$

$$F_r = [f_s/(q_t - \sigma_{v0})] \times 100\% \quad (6)$$

where n is an exponent which varies according to the soil type (Robertson, 2009a). α_M increases from soft soils to dense granular soils with a division around the middle for $I_c = 2.2$. Expression (9) is used to calculate static settlements, where M is obtained with (1) to (6).

2.2 DMT-based settlement prediction

The flat dilatometer test DMT provides subsurface information through two horizontal pressure readings in a circular membrane. The DMT is recognized for being a suitable test to acquire information related to the stiffness of the soil. Moreover, it is also sensitive to the soil stress history, therefore, it can provide reasonable estimations of parameters such as the coefficient of lateral earth pressure K_0 , over-consolidation ratio OCR and 1D constrained modulus M (Marchetti et al., 2001; Schnaid, 2009; Marchetti, 2015). M can be estimated according to the following expression:

$$M_{DMT} = E_D R_M (K_D, I_D) \quad (7)$$

where E_D is the dilatometer modulus, determined by the elasticity theory for the 60 mm diameter membrane displacing 1.1 mm.

$$E_D = 34.7(p_1 - p_0) \quad (8)$$

where p_0 and p_1 are the corrected lift-off and full expansion pressures, respectively. R_M is a correction factor applied to E_D , which is a function of the horizontal stress index K_D and the material index I_D ; therefore, it is calculated according to the soil type. Static settlements are calculated using the following 1D relationship:

$$S_{DMT} = \sum \frac{\Delta\sigma_v}{M_{DMT}} \Delta z \quad (9)$$

where $\Delta\sigma_v$ is the stress increment applied by buildings or embankments in the middle of a layer of thickness Δz , which can be adjusted using the theory of Boussinesq for deep layers.

3 IN SITU TESTING RESULTS

Figure 1 shows the q_t and f_s variation with depth as well as the soil behaviour type SBT interpretation for the CPT profiles. The CPT1 (Figure 1a) and CPT2 (Figure 1b) tests reached 22 and 17.5 m, respectively. The groundwater was detected at approximately 5.5 m depth from the ground level. In general, sand layers from fluvial deposits are detected with maximum thicknesses of 10 m mixed with silt and clay lenses with thicknesses that vary between 0.8 to 1.5 m.

The DMT test reached a depth of 10 m and the variation of I_D and K_D with depth are shown in Figure 2. The stratigraphy is comparable to the CPT1 profile, both coinciding in the presence of a soft layer of clay approximately 1.5 m thick at 4 m depth. It is worth noting that when $K_D = 2$ soils are normally consolidated.

In Figure 3 some of the soil parameters that are calculated based on the measurements from both test equipment are compared. Similarities can be seen between DMT and CPT1 for the profiles of unit weight γ and friction angle ϕ' , where ϕ' is around 35° in the first 4 m and 40° below 6 m. In Figure 4, the 1D compression modulus M shows low values in the first 3 m, and in the clay layer even lower values between 2 and 6 MPa according to the DMT and between 2 and 12 MPa according to CPT1.

Below 6 m, M increases with much larger values with better agreement between CPT and DMT for values in the order of 180 and 200 MPa. Figure 4 also shows the M_{DMT}/M_{CPT1} ratio, where it can be observed that CPT1 tend to overestimate M respect to DMT.

4 STATIC SETTLEMENT CALCULATIONS

Settlements are calculated with the method previously explained in 2.1 and 2.2 considering a 2 m wide square footing and founded 2 m below ground level. An increasing sequence of vertical load is considered as the stress increment $\Delta\sigma_v$.

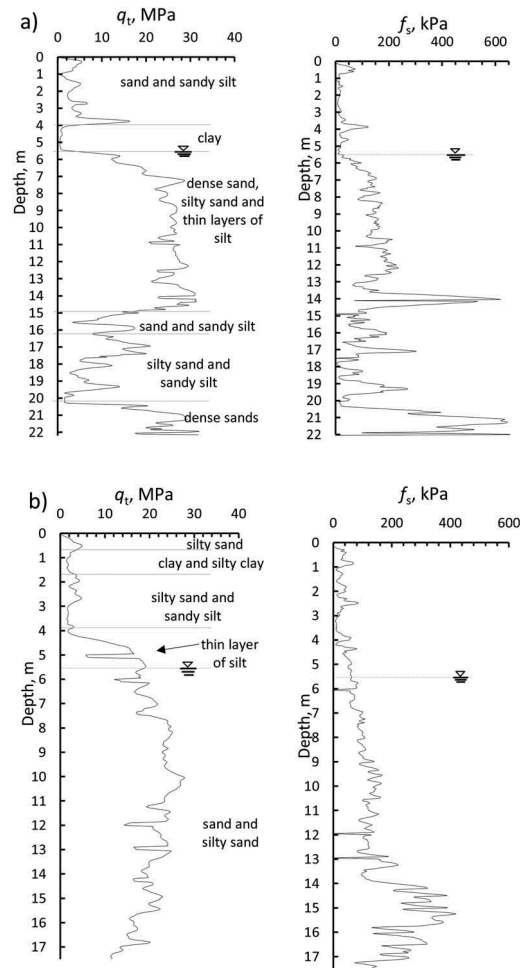


Figure 1. CPT profiles of q_t and f_s : a) CPT1 and b) CPT-2.

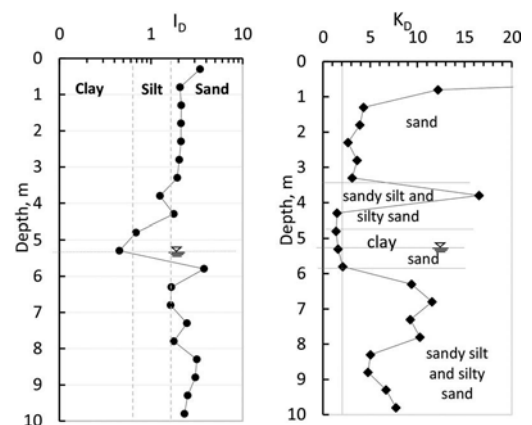


Figure 2. I_D and K_D variation with depth from DMT results.

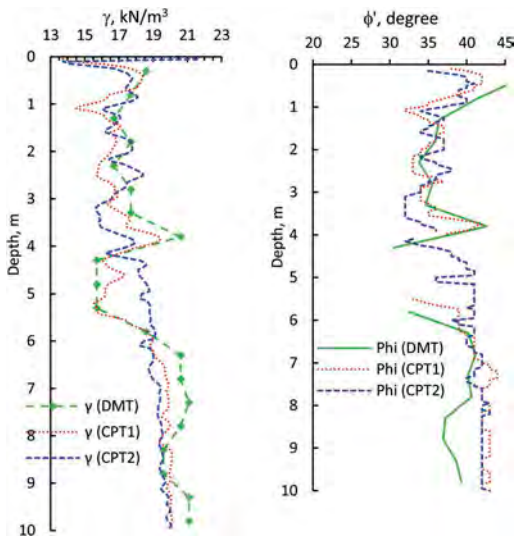


Figure 3. Comparison of the variation with depth of the unit weight γ and angle of friction ϕ' from DMT and CPT data.

Figure 5 shows the estimated settlements for each CPT and DMT test. It can be observed that DMT settlement estimations tend to be higher than those estimated with CPT. settlement estimations tend to be higher than those estimated with CPT.

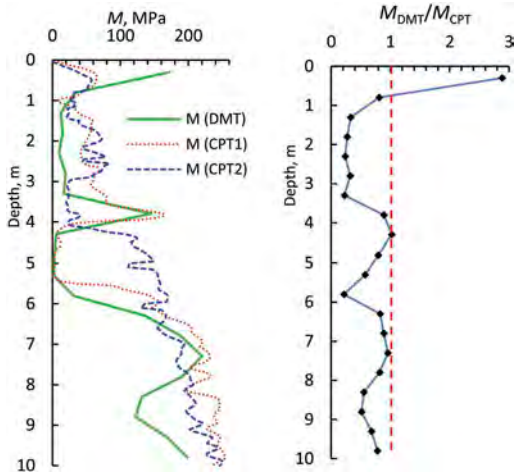


Figure 4. Variation with depth of the constrained modulus M determined from DMT and CPT and the M ratio.

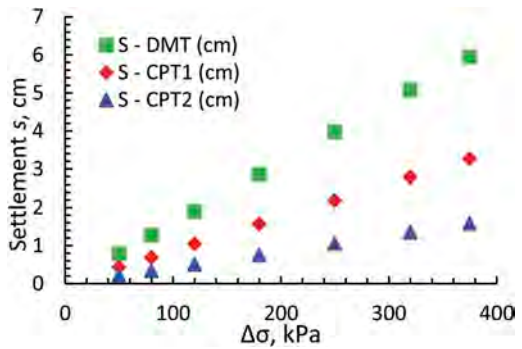


Figure 5. Shallow foundation static settlement estimated from DMT and CPT test results.

5 LIQUEFACTION ANALYSIS

5.1 Liquefaction occurrence

Chile is a highly seismic country and in particular Concepción is a region where several mega-thrust earthquakes ($M_w \geq 8.0$) have occurred (in year 1570, 1657, 1730, 1751, 1835, 1939, 1960 and 2010). Moreover, the Aurora de Chile project site is next to Bío Bío River, the largest of Chile in terms of width and water flow volume. For that reason, it is important to assess the liquefaction potential of the saturated sandy ground and the associated settlements.

The procedure to assess liquefaction potential is mainly based on the simplified method by Seed and Idriss (1971) developed initially for SPT, from which the cyclic stress ratio CSR imposed by the earthquake can be estimated.

$$CSR = 0.65(a_{\max}/g)(\sigma_{v0}/\sigma'_{v0})r_d \quad (10)$$

where r_d is a stress reduction coefficient which account for the reduction of a_{\max} with depth in absence of liquefaction. The expression used of r_d is too big to include it here (see (3) in Youd and Idriss, 2001).

For CPT data, a modified, although similar empirical procedure presented by Youd and Idriss (2001) has been adopted, where q_t is normalized and transformed to:

$$q_{t1Ncs} = K_c(q_t/p_a)/(p_a/\sigma'_{v0})^n \quad (11)$$

where K_c is a grain characteristic factor that is a function of I_c and in this form a clean sand value q_{t1Ncs} is obtained, from which the cyclic resistance ratio CRR can be determined (Robertson and Wride, 1998).

$$CRR_{7.5} = 0.833(q_{tNes}/1000) + 0.05 \text{ if } q_{tNes} < 50$$

$$CRR_{7.5} = 93(q_{tNes}/1000)^3 + 0.08 \text{ if } 50 \leq q_{tNes} < 160$$
(12)

$$K_c = 1.0 \text{ for } I_c \leq 1.64$$

$$K_c = -0.403I_c^4 + 5.581I_c^3 - 21.63I_c^2 + 33.75I_c - 17.88$$

for $I_c > 1.64$

(13)

Subsequently, a liquefaction factor of safety FS_L can be obtained as:

$$FS_L = (CRR_{7.5}/CSR)MSF K_\sigma \quad (14)$$

where MSF is a magnitude scale factor to account for earthquakes different from $M_w = 7.5$.

$$MSF = 10^{2.24/M_w - 2.56} \quad (15)$$

which results in $MSF = 0.66$ for $M_w = 8.8$. A correction factor for confining stresses higher than 100 kPa is determined as:

$$K_\sigma = (\sigma'_{v0}/p_a)^f \quad (16)$$

where f is a factor related to the site conditions such as relative density DR, ageing and overconsolidation ratio OCR. In these analyses f has been assumed either 0.65 for $DR > 60\%$ or 0.75 for $DR \leq 60\%$.

For DMT, FS_L is also calculated using (14) with the same components as for CPT, except $CRR_{7.5}$ which is determined with the following expression (Monaco et al., 2005):

$$CRR_{7.5} = 0.0107K_D^3 - 0.0741K_D^2 + 0.2169K_D - 0.1306$$
(17)

The liquefaction analyses assume $M_w = 8.8$ earthquake and a maximum acceleration $a_{max} = 0.4g$, which are actually the values recorded in the centre of Concepción during the 2010 earthquake and normally adopted in practice.

Figure 6 shows the variation with depth of the liquefaction factor of safety FS_L determined from the CPT and DMT results. The groundwater level is assumed to be at 2 m as an unfavourable condition during winter when the river water level is very high. A vertical line for $FS_L = 1$ separates where liquefaction is likely or not to occur. It can be observed that between 2 m and 3.5 or 4 m (where starts the clay layer) $FS_L < 1$ for CPT and DMT results, hence,

liquefaction is highly likely to occur there. It is worth mentioning that liquefaction has been reported along the Bio Bio river promenade during the 2010 earthquake (Verdugo et al., 2010). Liquefaction is not expected in the clay layer as shown for CPT2 and DMT. However, $FS_L < 1$ for CPT1 due to the very low values of the clay tip resistance. It is important to bear in mind that liquefaction does not occur in clay.

Below the clay layer liquefaction may still take place down to 7.5 m according to the CPT results.

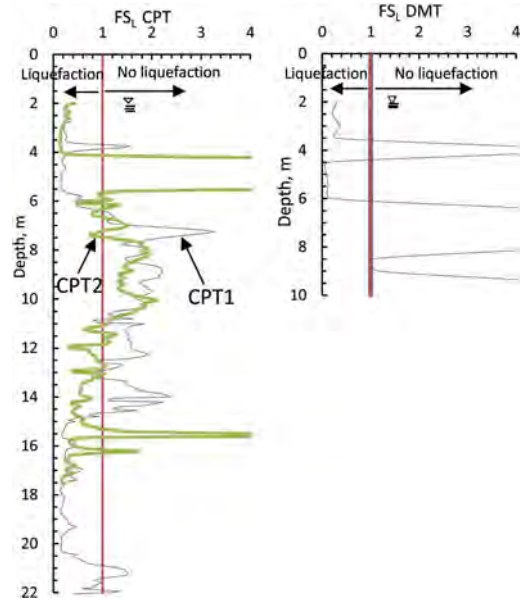


Figure 6. Liquefaction factor of safety obtained from CPT and DMT tests.

Between 7.5 and 11 m $FS_L > 1$ for CPT results, although for DMT between 8.5 and 9 m, $FS_L = 1.0 - 1.2$, which is somewhat close to CPT2 results. This zone of no liquefaction may stop propagation of liquefaction occurring below. Indeed, below 11 m $FS_L < 1.0$ and according to CPT1 a layer of 6 m thick may liquefy.

5.2 Liquefaction-induced settlements

The estimation of free-field settlements caused by earthquake-induced liquefaction is carried out usually based on the soil incremental volumetric strain ε_{vol} . Dissipation of excess pore pressure densifies the soil which may result in important volume changes leading to settlements. A chart proposed to estimate ε_{vol} as a function of FS_L and N_1 from the SPT or alternatively q_c or DR can be used (Ishihara and Yoshimine, 1992; Ishihara, 1996). From CPT and DMT data this chart was

directly used for $\epsilon_{vol} = f(FS_L, q_t)$ and $\epsilon_{vol} = f(FS_L, DR)$, respectively. The DR expressions used are a best fit to the DR- K_D plot by Reyna and Chameau (1991) for normally consolidated sands and the DR- K_D -OCR plot by Lee et al. (2011) for over-consolidated sands:

$$\begin{aligned} DR &= 50.66 \ln K_D + 7.95 \\ DR &= a \ln K_D + b \end{aligned} \quad (18)$$

Figure 7a shows the variation with depth of the increments of ϵ_{vol} for each layer analysed from CPT

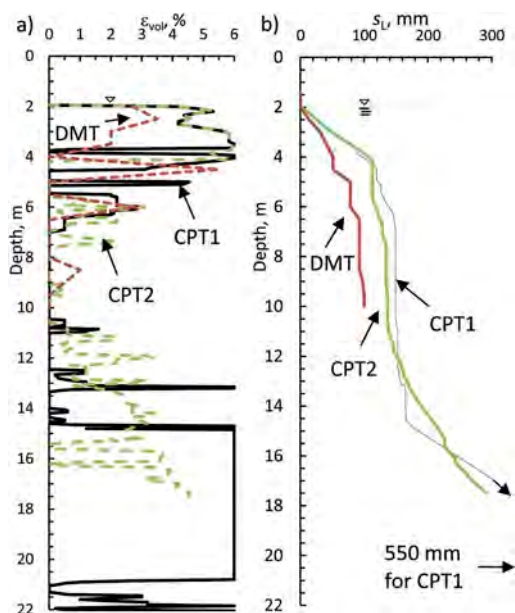


Figure 7. For CPT and DMT: a) incremental volumetric strain with depth and b) accumulated vertical displacement with depth.

and DMT data. It can be observed that in the first 2 m and below 15 m there are high values of ϵ_{vol} . The three curves are relatively close to each other denoting similar variation trends of ϵ_{vol} . Figure 7b shows the accumulated integration of ϵ_{vol} with depth which is the accumulated vertical displacement at each depth. It is clear to observe that DMT data lead to smaller settlements s_L compared with CPT data. s_L increase rate is higher in the first 4 m and then stabilises and increases again around 11 m and 15 m for CPT2 and CPT1, respectively. For the first 10 m, s_L is estimated to be around 100 mm for DMT, whereas for CPT1 $s_L \approx 150$ mm and $s_L \approx 130$ mm for CPT2. If the liquefied soil below 10 m manages to dissipate the excess pore pressure, s_L values may increase even more to values of 300 mm at 17.5 m (CPT2) and up to 550 mm at 22 m (CPT1).

It has been found that free-field liquefaction-induced settlement can become different from that occurring underneath buildings founded on shallow foundations (Bertalot, 2011). The overburden pressure imposed by a building applies large confining stresses in the soil which tend to modify settlements. Overburden increases settlements because of higher loads, but only until a certain value of bearing pressure owing to the reduction of excess pore pressure ratio with confinement (Bertalot et al., 2013). A chart has been developed to estimate building settlements s_L based on data that include the Concepción 2010 earthquake (Bertalot et al., 2013). s_L is determined based on the thickness of liquefied soil D_L , building width B and building bearing pressure q . For $B = 15$ m, $q = 50$ kPa, $s_L/D_L = 0.1$ and considering $D_L = 2, 5$ and 7 m results in $s_L = 200, 500$ and 700 mm, which are larger than those from free-field.

6 CONCLUSIONS

CPT and DMT tests were carried out in fluvial silty sands in Concepción Chile. A general good agreement was found among the results of soil profile interpretation, constrained modulus and resistance parameters. Static settlements estimated through the 1D M_{DMT} were approximately twice larger than those estimated with CPT data. Free-field liquefaction-induced settlements resulted in much larger than that from static analyses, from 100 mm (DMT) up to 150 mm (CPT) for the first 10 m. Including the confining stress imposed by a building increases even more the liquefaction-induced settlements.

REFERENCES

- ASTM D5778. 2020. Standard test method for electronic friction cone and piezocone penetration testing of soils. ASTM International, West Conshohocken, PA, USA
- Bertalot, D. 2011. An overview on field and experimental evidences concerning seismic liquefaction induced settlement of buildings with shallow foundations. *Obras y Proyectos* 10, 36–45
- Bertalot, D., Brennan, A.J. and Villalobos, F.A. 2013. Influence of bearing pressure on liquefaction-induced settlement of shallow foundations. *Géotechnique* 63(5): 391–399
- EN ISO 22476-1. 2012. Geotechnical investigation and testing. Field testing - Part 1: Electrical cone and piezocone penetration test. European Committee for Standardization CEN, Brussels, Belgium
- Failmezger, R., Till, P. Frizzel, J. & Kight, S. 2015. Redesign of shallow foundations using dilatometer tests —more case studies after DMT'06 conference. *3rd Int. Conf. on the Flat Dilatometer DMT'15*. Roma, Italy.
- Hayes, J.A. 1986. Comparison of flat dilatometer in-situ test results with observed settlement of structures and earthwork. 39th Geotechnical Conference. Ontario, Canada, 311–316.
- Ishihara, K. (1996). *Soil behaviour in earthquake geotechnics*. Oxford University Press, UK

- Ishihara, K. & Yoshimine, M. 1992. Evaluation of settlements in sand deposits following liquefaction during earthquakes. *Soils and Foundations* 32(1),173–188
- Kaggwa, W.S., Jha, R.K. & Jakska, M.B. 1996. Use of dilatometer and cone penetration tests to estimate settlements of footings on calcareous sand. *7th Australia New Zealand Conf. on Geomechanics*. Adelaide, Australia, 909–914
- Lee, M.J., Choi, S.K., Kim, M.T. and Lee, W. 2011. Effect of stress history on CPT and DMT results in sand. *Engineering Geology* 117, 259–265
- Lehane, B. & Fahey, M. 2004. Using SCPT and DMT data for settlement prediction in sand. *2nd International Conference on Geotechnical and Geophysical Site Characterization ISC2*, Millpress, Rotterdam, 1673–1679.
- Lunne, T., Robertson, P. K. & Powell, J. 1997. *Cone Penetration Testing in Geotechnical Practice*. CRC Press
- Marchetti, S. 2015. Some 2015 updates to the TC16 DMT report 2001. *3rd International Conference on the Flat Dilatometer DMT2015*, Rome, Italy, 43–65
- Marchetti, S., Monaco, P., Totani, G. & Calabrese, M. 2001. The DMT in soil investigations. ISSMGE TC 16 report. *Int. Conf. on In Situ Measurement of Soil Properties and Case Histories*. Bandung, Indonesia, 95–132
- Marchetti, S., Marchetti, D. & Villalobos, F. 2013. The seismic dilatometer SDMT for in situ soil testing. *Obras y Proyectos* 13, 20–29 (in Spanish)
- Monaco, P., Totani G. & Calabrese M. 2006. DMT predicted vs observed settlement: a review of the available experience. *DMT 2006*, Washington DC, 244–252
- Monaco, P., Marchetti, S., Totani, G. & Calabrese, M. 2005. Sand liquefiability assessment by flat dilatometer test (DMT). *16th International Conference on Soil Mechanics and Geotechnical Engineering*, IOS Press, vol. 4, 2693–2698
- Reyna, F. & Chameau, J.L. 1991. Dilatometer based liquefaction potential of sites in the Imperial Valley. *2nd International Conference on Recent Advances in Geotechnical Earthquake Engineering and Soil Dynamics*, St. Louis, Missouri, USA, 385–392
- Robertson, P.K. 2009a. Interpretation of cone penetration tests – a unified approach. *Canadian Geotechnical Journal* 46(11): 1337–1355
- Robertson, P.K. 2009b. CPT – DMT correlations. *Journal of Geotechnical and Geoenvironmental Engineering* 135 (11): 1762–1771
- Robertson, P.K. 2012. Interpretation of in-situ tests - some insights. In Coutinho & Mayne (eds.), *4th International Conference on Geotechnical and Geophysical Site Characterization, ISC4*, Porto de Galinhas, Brazil. Taylor & Francis, vol.1, 3–24
- Robertson, P.K. & Wride, C.E. 1998. Evaluating cyclic liquefaction potential using the cone penetration test. *Canadian Geotechnical Journal* 35(3),442–459
- Schmertmann, J.H. 1986. Dilatometer to compute foundation settlement. *In Situ '86, ASCE Spec. Conf. on Use of in situ Tests in Geotechn. Engineering*. Virginia Tech, Blacksburg, USA, 303–321
- Schnaid, F. 2009. *In situ testing in geomechanics: The main tests*. Taylor & Francis, Abingdon:
- Seed, H.B. & Idriss, I.M. 1971. Simplified procedure for evaluating soil liquefaction potential. *Journal of the Soil Mechanics and Foundations Division* 97(9),1249–1273
- Verdugo, R., Villalobos, F., Yasuda, S., Konagai, K., Sugano, T., Okamura, M., Tobita, T. & Torres, A. 2010. Description and analysis of geotechnical aspects associated to the large 2010 Chile earthquake. *Obras y Proyectos* 8, 25–36
- Youd, T.L. & Idriss, I.M. 2001. Liquefaction resistance of soils: summary report from the 1996 NCEER and 1998 NCEER/NSF workshops on evaluation of liquefaction resistance of soils. *Journal of Geotechnical and Geoenvironmental Engineering* 127(4),297–313

Numerical modeling of static load test in drilled shaft using CPTu results

M.A. Camacho

Independent Engineer, Cochabamba, Bolivia

C.B. Camacho

Universidad Mayor de San Simón, Cochabamba, Bolivia

V.H. Miranda

Independent Engineer, Cochabamba, Bolivia

ABSTRACT: The projects with deep foundations use information from field tests (e.g. CPTu and static load test) to predict an ultimate capacity. The static load test verifies foundation design parameters and installation method. However, this test establishes the real behavior of the drilled shaft under specific conditions and the possibility of experimenting in different conditions becomes extremely expensive and unfeasible. Therefore, the numerical modeling of the static load test becomes important because the initial soil profile and dimensions of the drilled shaft could be changed. This article presents the comparison of the load–displacement curves by numerical modeling in fine soils with that load–displacement curve through a static load test in a drilled shaft built in Cochabamba, Bolivia.

1 INTRODUCTION

The objective of a load test is to verify that the pile prototype in real conditions of the underground has enough bearing capacity. However, this test establishes the real behavior of the pile in singular conditions, and the possibility of testing in different settings make them extremely expensive and infeasible.

The necessity of developing mathematical models to predict the behavior of a pile under different conditions is evident. The implementation of a numerically model of load test allows to explore different settings demanding a little effort during its execution. These models require detailed study of the field conditions in a load test to be modeled.

The project “Nudo Viario Beijing” in the city of Cochabamba (Bolivia) is a project of great magnitude that its infrastructure required the execution of load tests (e.g., CPTu and static load tests). The present document analyzes the numerical model for the load test of a pile through the interpretation of results obtained from the field test using FB-Multiplier v.5.5 software.

2 GEOTECHNICAL MODEL

The geotechnical model based on the CPTu results analyzes the water table, the soil classification, the

soil unit weight, the friction angle, and the undrained shear strength. This data is needed for the model.

2.1 Water table

The CPTu did not find any water table (the pore pressure transducer has been damaged at the beginning of the test), however; it was evidenced that it was 2 meters below the surface, because an excavation has been carried out to that depth.

2.2 Soil classification

Figure 1 shows the evaluation of the CPTu test results using the I_{SBT} behavior index proposed by Robertson (2010). The characterization of the soil based on the fines content proposed by F. Yi (2014) allowed an identical characterization to that obtained utilizing the soil type behavior indexes (I_{SBT}), moreover, being known the percentage of fines content present in the layer, it allowed a precise definition of the type of soil.

There are 15 strata in the underground profile, 8 of them of clay and 7 of silt.

2.3 Unit weight

Within the evaluation process of the unit weight from the CPTu results, it was applied the equations proposed by Mayne (2012); Robertson & Cabal (2010). Figure 2 indicates the estimation of the unit weight values.

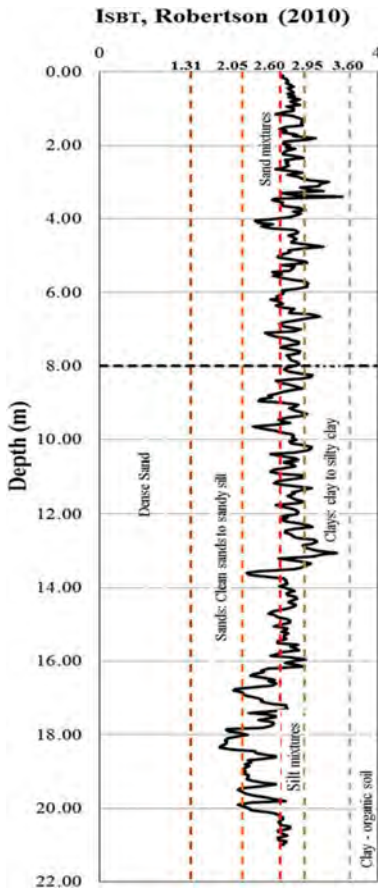


Figure 1. I_{SBT} behavior index proposed by Robertson (2010).

2.4 Undrained shear strength

Figure 3 indicates the variation of the undrained shear strength results depending on the depth. The equation proposed by Mayne & Kemper (1988) to evaluate the undrained shear strength is based on the N_{kt} factor:

$$s_u = \frac{q_t - \sigma_{vo}}{N_{kt}} \quad (1)$$

where q_t is the resistance to the corrected tip σ_{vo} is initial vertical total stress N_{kt} is a factor that varies between 10 to 20 (Ameratunga et al., 2016). The results of $N_{kt} = 12.76$ have been used.

2.5 Geotechnical model based on the results of the CPTu test

In summary, Figure 4 shows the geotechnical model based on the CPTu results for the numerical model.

The principal geotechnical parameters are indicated. The unit weight and undrained shear strength have been defined in low, medium, and high values for each clay strata. For silt strata, it was defined the friction angle with constant values between 30° and 36° .

2.6 Selection of geotechnical parameters

The unit weight and undrained shear strength data in a soil stratum vary in depth, which value is representative? The comparison between these parameters has been made (low, medium, or high values)

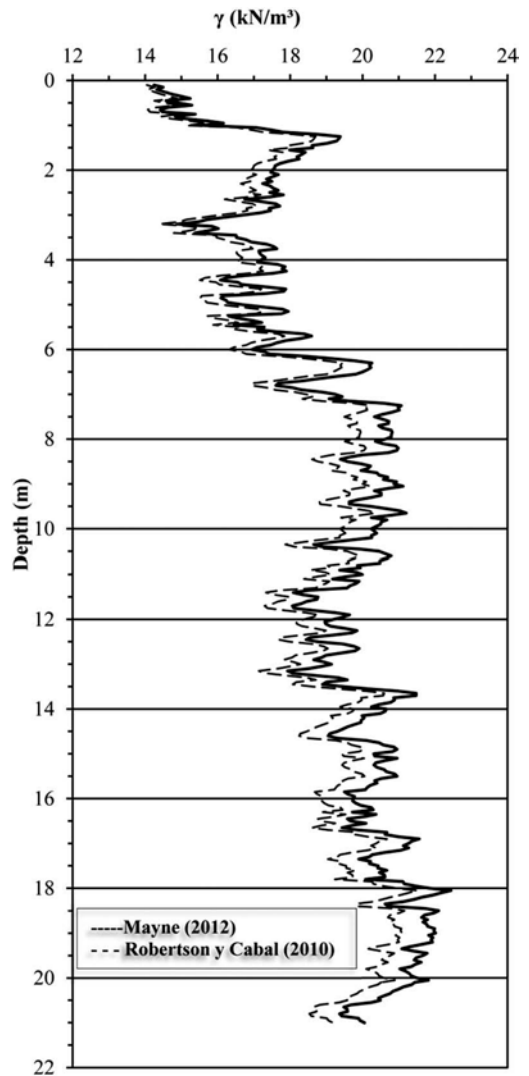


Figure 2. Unit weight estimation from CPTu results. (Mejia, 2016).

3 LOAD TEST

The static compression load test was performed on the top of the drilled shaft based on ASTM D1143–07. Figure 5 shows the results obtained reaching up to 4347 kN with a registered maximum displacement of 17,89 mm (1,50% strain based on the drilled shaft diameter).

4 SOIL–STRUCTURE INTERACTION IN FB–MULTIPLIER SOFTWARE

Due to the fact that the models for the soil and piles are not lineal, FB–Multiplier carries out an iterative solution process through a secant method for solving the non-linear equations. The software uses a Newton–Raphson iteration scheme where in each iteration the stiffnesses of the soil and piles are used to form the stiffness matrix and calculate the deformations. These deformations were used then to find the internal loads in each discretization of the piles.

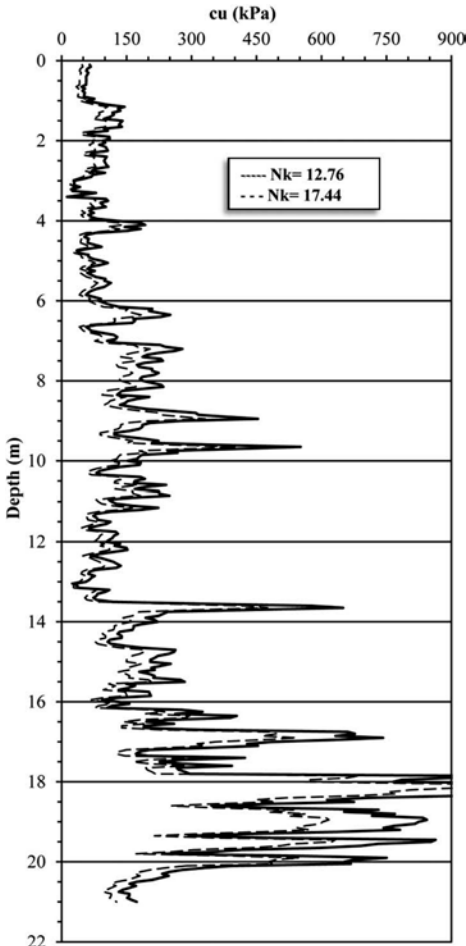


Figure 3. Undrained shear strength estimation (Mejia, 2016).

4.1 Numerical model in FB–Multiplier software

In order to get the geotechnical model of the underground, it has been carried out the numerical model of a compression load test of a drilled shaft in the FB – Multiplier software. The principal parameters used are the unit weight and the undrained shear strength since these values influence the t–z and q–z curves which are based on the research made by Reese & O’Neill (1988) and Wang & Reese (1993) for drilled shafts.

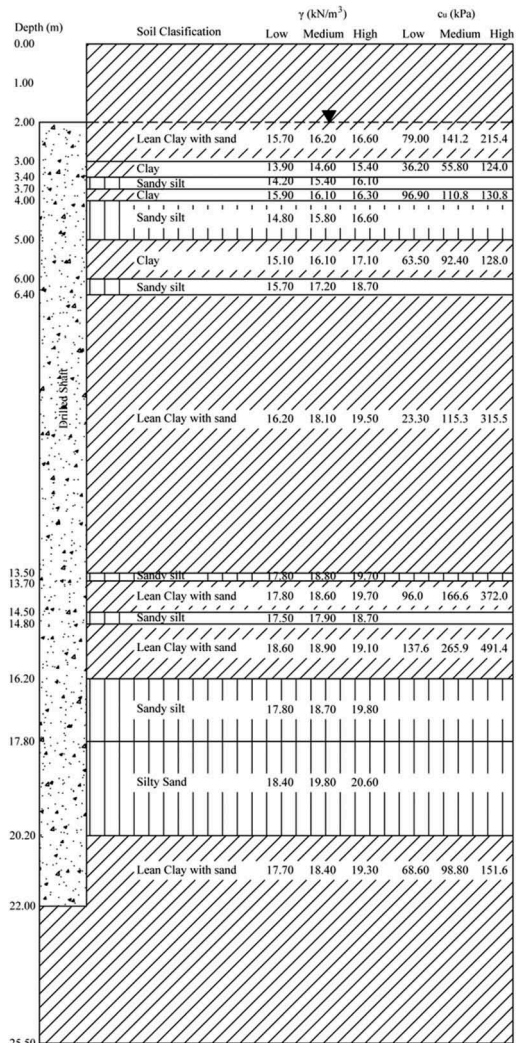


Figure 4. Geotechnical model based on the CPTu test results.

4.1.1 Global data

In the FB–Multiplier v.5.5 software, the numerical models based on the conceptual geotechnical model

have been carried out in a drilled shaft simulating the compression load test for stages.

4.1.2 Pile data

The drilled shaft considered in this study is of diameter 1,20 m, length 22 m, and made of concrete with a resistance of 41,37 MPa. The drilled shaft has been built with 24 steel bars of 25 mm. All of these parameters have been included in the FB-Multiplier software.

4.1.3 Soil parameters

The soil's parameters were defined according to the geotechnical model. It is indicated the phreatic level and each stratum was defined with the unit weight and undrained shear strength data.

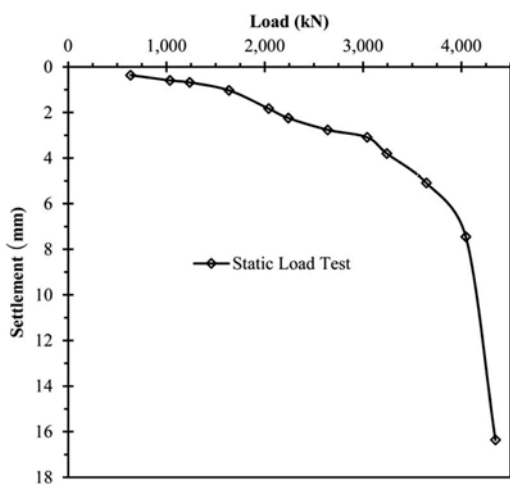


Figure 5. Load test results (Camacho & Gomez, 2016).

4.1.4 Deformations in the model

According to the results of the static load test, it has been input the displacements in the head of the drilled shaft.

Two stages of displacements were input. First, displacements between 0,20 mm to 6,95 mm with a step of 0,15 mm, and secondly, displacements between 6,95 mm to 20,15 mm with a step of 0,30 mm. Ninety load states were obtained with these displacements.

4.2 Results of the numerical model

In Table 1, the numerical model has been labeled with the names described for each case. For example, for a low undrained shear strength and a high unit weight, it has been called CPT01 curve.

The results of the sensitivity study of the geotechnical parameters that influence the t-z and q-z curves are presented in Figure 6.

The general result of the geotechnical parameters shows a proportional direct relationship between the parameters and the peak load. The higher the undrained shear strength and unit weight, the higher the peak load. Three groups of curves have stood out due to undrained shear strength, being the geotechnical parameter that defines a difference in peak loads in a range of 3000 kN. The unit weight, on the other hand, varies the peak loads in a range of 300 kN. The curves with the highest correlation to the static load test curve are the CPT02, CPT05, and CPT08. According to Table 1, all the strata have a medium undrained shear strength and each curve represents a low (CPT02), medium (CPT05), and high (CPT08) unit weight in all strata.

Table 1. Curves' names.

Undrained shear strength			
Unit weight	Low	Medium	High
Low	CPT07	CPT08	CPT09
Medium	CPT04	CPT05	CPT06
High	CPT01	CPT02	CPT03

5 RESULT ANALYSIS

The analysis has been done from a geotechnical model with low, medium, and high values of unit weight and undrained shear strength. A model has been developed in the FB-Multiplier software obtaining 9 load-displacement curves that have been compared with the executed static load test curve. From this group of 9 curves, it has been chosen 1 curve which best represents the load test in a numerical model.

5.1 Conceptual geotechnical model analysis

The CPTu test indicates a geotechnical profile as intercalation of fine-grained saturated soils, predominantly lean clays with sand (8 strata) with intercalations of sandy silt strata (7 strata).

The low, medium, and high values of the unit weight have been obtained with the correlation of the CPTu proposed by Robertson & Cabal (2010).

5.2 Load-displacement curves

From the FB-Multiplier software it has been obtained load-displacement curves. The static load test curve

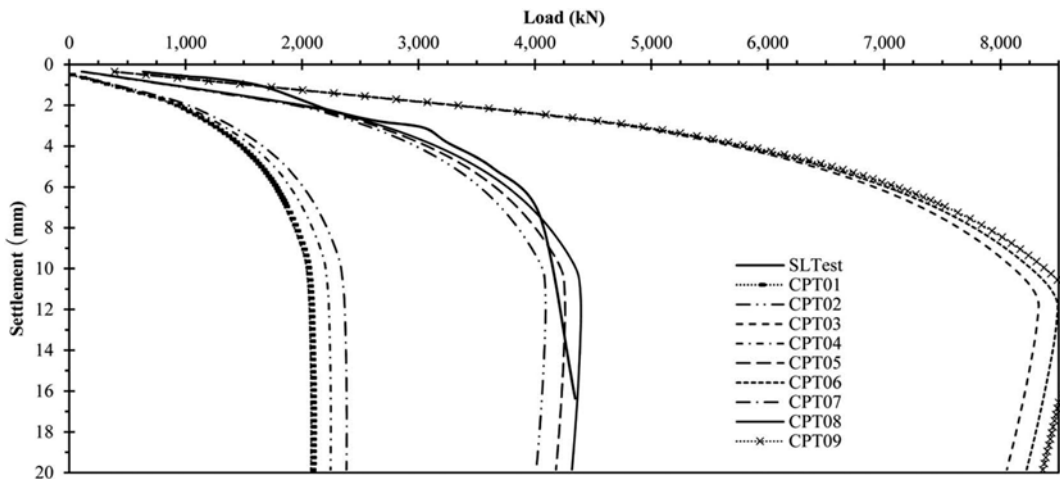


Figure 6. Load test and numerical models results based on the CPTu test.

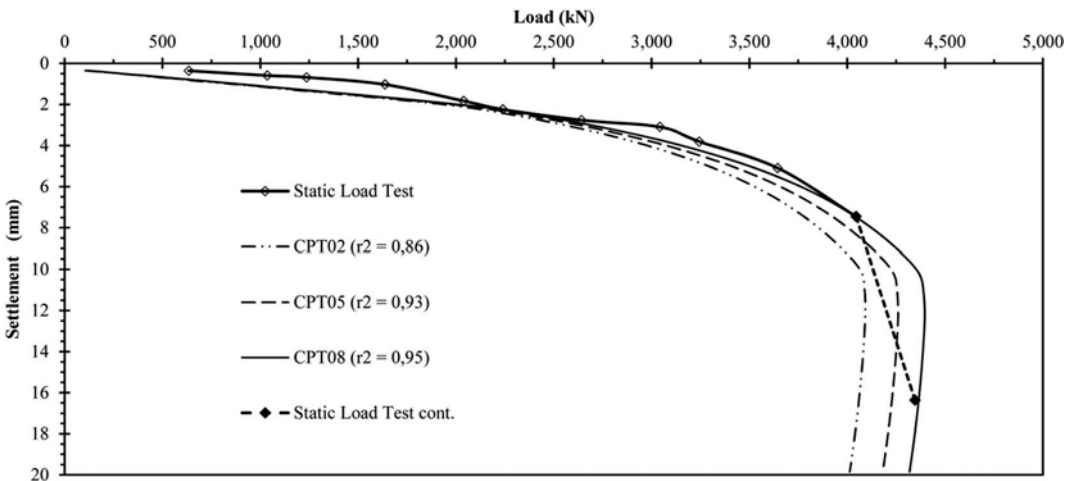


Figure 7. Load – Displacement curves from CPTu test.

plot is a group of points joined by lines. It has been observed a relationship and curvy trend between a load of 635,17 kN to 4.045,71 kN, whereas the lastest load and displacement data indicates an abrupt drop in drilled shaft capacity.

Therefore, it has been chosen to correlate the curves obtained from the numerical models with the points of the load test between 635,17 kN to 4.045,71 kN. The correlation indicator is r_2 calculated with the displacement obtained by the load.

5.3 Modeling

Figure 7 indicates 3 load–displacement curves (FB–Multiplier) that correlate with the load test. The correlation indicator r_2 varies between 0,86 to 0,95.

6 CONCLUSIONS

The geotechnical model extends from the surface to a depth of 25,50 m. where the lean clay strata with sand (75%) interspersed with sandy silt strata (25%) resulting in a slightly plastic over consolidated profile with a low expansion and variable consistency. The water table is ubicated 2 meters below the surface (Figure 4).

In the static load test, the load–displacement curve has been developed until reaching the maximum load of 4.346,64 kN and the maximum deformation of 17,89 mm was obtained in stage 12 of peak load. In the unload stage, 3,46 mm has been recovered until the end of the test.

The load test has been modeled in different scenarios from the interpretation of field test results (e.g., CPTu and static load test). It has been observed that the strength parameters that influence the t-z and q-z curves are the unit weight and the undrained cohesion. Thus, the sensitivity analysis of these two combined parameters was carried out resulting in 9 resistance states.

The load–displacement curves were obtained with the FB-Multipier software that performs the soil–pile interaction through the t-z and q-z curves. An axial displacement has been induced in the drilled shaft head (simulating the static load test) to obtain the resultant force at the same point. Ninety cases of load states have been determined and then a load–displacement curve has been plotted.

The load–displacement curves were analyzed for each geotechnical model. In addition, it has been chosen to correlate the curves obtained from the numerical models with the points of the load test between 635,17 kN to 4.045,71 kN. The correlation indicator is r_2 , calculated with the displacement obtained by the load.

The correlation indicator r_2 has varied between 0,86 and 0,95 based on the CPTu field test.

The load–displacement curve with the correlator r_2 close to 1 has been graphically observed determining that the numerical model CPT08 is appropriate to be used.

REFERENCES

- Camacho, M.A. & Gomez J. 2016. *Determinación y comparación de la capacidad portante del pilote vaciado in situ (P2-3), a partir de ensayos de campo y una prueba de carga estática en el nudo viario Beijing, Cochabamba, Bolivia*. Cochabamba: Universidad Mayor de San Simón.
- Mayne, P.W. 2012. Regional report for North America. Atlanta.
- Mejia, J. 2016. *Caracterización de suelos estratificados mediante el ensayo de penetración de piezocono CPTu*. Cochabamba: Universidad Mayor de San Simón.
- Robertson, P.K. & Cabal K.L. 2016. *Cone penetration testing for geotechnical engineering*. California: Gregg.
- Reese, L.C. & O'NEILL, M.W. 1988. *Drilled shafts: Construction and Design*. USA: FHWA Publication.
- Wang, S.T. & Reese, L.C. 1993. *COMP624P – Laterally loaded pile analysis for the microcomputer, ver. 2.0*. Springfield: FHWA Publication.

Characterization of geotechnical spatial variability in river embankments from spatially adjacent SCPT

F. Ceccato

DICEA-University of Padua, Italy

M. Uzielli

DICEA – University of Florence, Italy

Georisk Engineering S.r.l., Florence, Italy

P. Simonini

DICEA-University of Padua, Italy

ABSTRACT: characterization of the spatial variability of geotechnical properties of river embankment soils is important for the enhanced modelling and assessment of embankment stability. In practice, available data is usually limited. This study presents the results of a quantitative statistical analysis of the spatial variability of cone tip resistance from the results of 16 closely spaced SCPT carried out near a recent breach in a levee on the Panaro river in northern Italy. Two geotechnical homogeneous soil units are preliminarily identified in the levee to ensure the meaningfulness of the analysis in terms of soil type. For each unit, the horizontal and vertical spatial variability and spatial correlation structures of cone tip resistance are investigated by a two-step procedure involving the calculation of empirical semivariograms and the subsequent fitting of semivariogram models. Horizontal and vertical scales of fluctuation are estimated based on fitted semivariogram model parameters.

1 INTRODUCTION

Levee and dike collapses cause considerable financial and social losses in many countries, especially in highly developed areas. Therefore, risk assessment of river embankment stability is receiving increasing attention worldwide. The quantitative estimation of the vulnerability of embankments, which is necessary for the risk assessment process, can be pursued in the form of fragility curves from the outputs of slope stability analyses. A key parameter in slope stability analyses is soil strength, which varies spatially within soil volume due to factors such as compositional heterogeneity, level of compaction, degree of saturation, cementations, and presence of ancient breach-repairing materials.

A levee failure occurred along the Panaro River in Northern Italy on 6th December 2020. The failure was caused by a combination of concurrent causes including soil heterogeneity, relict animal burrows, presence of ancient brick elements in the embankment body, as well as of rhizomes of *Arundo Donax*.

To corroborate the interpretation of such collapse, an extensive geotechnical and geophysical campaign was conducted, including a series of 16 closely spaced

SCPT. CPT measurements have extensively proved to be well-suited for assessing inherent soil variability because a large volume of near-continuous data can be collected in a cost-effective way, the test has good repeatability, the equipment is highly standardized, and the procedure is well defined and almost independent of operator skill. The investigations revealed that the levee embankment is made of sand-silt mixtures in different proportions. While friction angle varies within a limited range (30-33 degrees), cohesion, which depends primarily on compaction level, soil suction and cementation, varies significantly even within a limited area.

This paper describes the procedures and results of a quantitative investigation into the vertical and horizontal spatial variability of cone tip resistance performed on the unsaturated silty sand of the river levee embankment. Section 2 describes the results of the geotechnical site investigation campaign along with a preliminary descriptive statistical analysis. CPT results are pre-processed to identify homogeneous soil units (Sec. 3) in which spatial soil variability is modelled through the application of geostatistical techniques (Sec. 4). Results of the geostatistical modelling process are assessed and discussed in Sec. 5

2 DESCRIPTION OF GEOTECHNICAL CAMPAIGN

The geotechnical campaign conducted in the area of the breach consisted in 12 CPTU, 2 SCPTU, 2 DMT, 2 boreholes, 7 ERT. A total of 11 undisturbed samples were collected for laboratory testing. To investigate in greater depth the spatial variability of soil strength, a short stretch of levee embankment, located approximately 150m west of the breach, was investigated through 16 seismic CPT soundings at a constant horizontal spacing of 2.5 m.

Cone tip resistance q_c and sleeve friction f_s were measured at vertical intervals of 1cm and the shear wave velocity V_s was measured at vertical intervals of 25cm with the true interval method. These tests reached a maximum depth of 5.5m. Figure 1a-b plots the complete set of results of the SCPT campaign. A smoothing procedure based on a moving average with a 40cm-wide window is applied to each SCPT vertical to remove small-scale noise.

Although the tests are very closely spaced and the boreholes show that the material is classifiable consistently as a mixture of sand and silt, simple visual inspection of Figure 1a-b reveals significant horizontal inter-sounding variations in the measured properties at the same depth, and intra-sounding, depth-wise variability in the vertical direction. While vertical variability can be expected due to in-situ stress effects and to stratigraphic layering, horizontal variability is more significant than could be foreseen given the close spacing of the soundings and the limited extension of the area. To quantify this variability,

descriptive second-moment sample statistics were calculated depth-wise for q_c , f_s , and V_s ; more specifically: mean (μ), standard deviation (σ), and coefficient of variation ($COV=\sigma/\mu$), given by the ratio of the standard deviation to the mean. Figure 1c-e plots the depth-wise mean and COV of q_c , f_s , and V_s . The grey shaded area represents the values within one sample standard deviation from the sample mean.

The depth-wise COV of tip resistance and sleeve friction varies between 0.15 and 0.6, with an average of 0.37 for q_c and 0.49 for f_s . This indicates that the horizontal variability of the deposit is relatively high, according to the “rule of thumb” provided by Harr (1987), by which coefficients of variation below 10% are considered to be “low”, between 15% and 30% “moderate”, and greater than 30%, “high”. The COV of shear wave velocity varies between 0.11 and 0.78 with an average of 0.22; indicating that the overall level of horizontal variability of this parameter is moderate.

From a geotechnical perspective, it is important to parameterize not only the degree of horizontal and vertical scatter in data measurements, but also the spatial correlation structure, i.e., whether the spatial variation of mechanical behavior as described by SCPT occurs abruptly or with continuity. The above descriptive statistical analysis is not suited to fully describe variability as it cannot provide information regarding spatial variability patterns. Moreover, the descriptive analysis does not account for the possible presence of different stratigraphic units which could display distinct geotechnical properties. In the following we focus on the variability of the tip resistance.

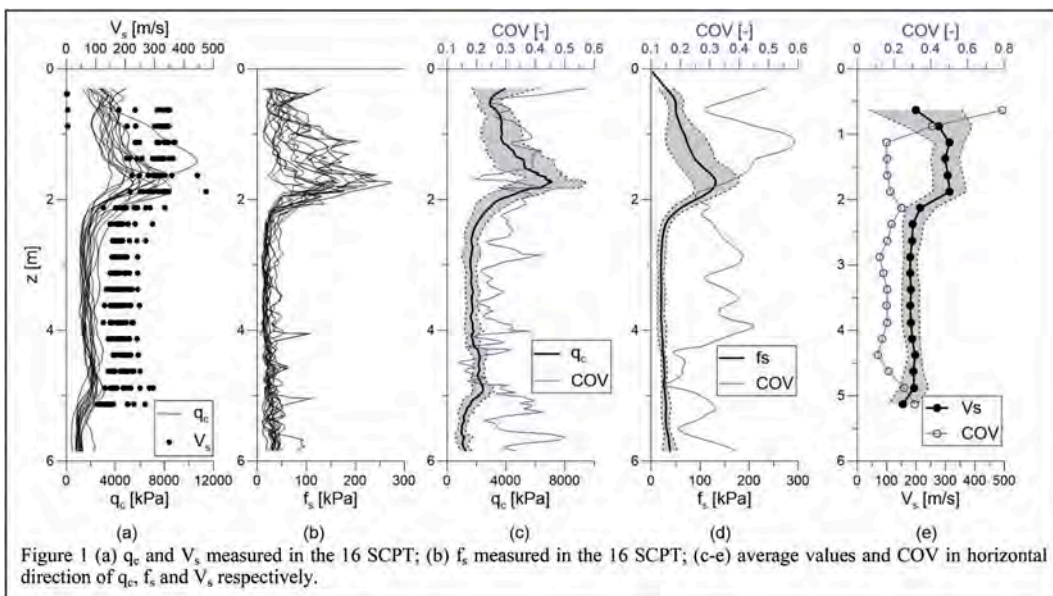


Figure 1. (a) q_c and V_s measured in the 16 SCPT; (b) f_s measured in the 16 SCPT; (c-e) average values and COV in horizontal direction of q_c , f_s and V_s respectively.

3 IDENTIFICATION OF HOMOGENEOUS SOIL UNITS

Sample statistics and spatial variability parameters aimed at characterizing specific soil types are only meaningful if conducted on soil volumes which are sufficiently homogeneous for geotechnical purposes. A moving-window procedure proposed by Uzielli et al. (2008) is employed to identify Homogeneous Soil Units (HSUs) statistically. The normalized tip resistance Q_m , normalized friction ratio F_r and soil behaviour type index I_c are computed from field measurements according to Robertson (2009).

$$Q_m = \frac{q_c - \sigma_{v0}}{p_a} * \left(\frac{p_a}{\sigma'_{v0}} \right)^n \quad (1)$$

$$F_r = \frac{f_s}{q_c - \sigma_{v0}} * 100 \quad (2)$$

$$I_{cn} = \left((3,47 - \log Q_m)^2 + (1,22 + \log F_r)^2 \right)^{0,5} \quad (3)$$

where

$$n = 0,381I_c + \frac{0,05\sigma'_{v0}}{p_a} - 0,15 \quad (4)$$

The vertical effective stress is estimated considering soil suction (s) by applying the Bishop effective stress principle

$$\sigma'_{v0} = \sigma_{v0} + sS_r \quad (5)$$

S_r is the degree of saturation computed from soil suction assuming the Van Genuchten soil water retention model (Eq. 6) with typical parameters for these soils derived from the laboratory tests, i.e., $p_0 = 5\text{kPa}$, $\lambda = 0,3$, $S_{sat} = 1$, $S_{res} = 0,16$.

$$S_r = S_{res} + (S_{sat} - S_{res}) \left(1 + \left(\frac{s}{p_0} \right)^{\frac{1}{1-\lambda}} \right)^{-\lambda} \quad (6)$$

A linear suction distribution is assumed above water level, which is 10m-deep in this site.

For each investigated depth, average values of Q_m , F_r and I_{cn} are computed over the horizontal direction and used to identify the homogeneous soil units (HSU), see Figure 2a. The procedure is based on the evaluation of the coefficient of variation (COV) of the data within a 40cm-wide moving window. Each position of the moving window defines two semi-windows of equal height above and below a centre point. The COV shows a peak at the interface between different homogeneous soil units. Q_m , F_r and I_{cn} show an increase of COV

between 1.8m and 2.3m as well as between 5.0 and 5.3m, which correspond to the transition zone between different HSU (Figure 2b). Q_m is used for the identification of HSU because it is the parameter that best captures soil compaction effects. Indeed, it is clear from the borehole that the embankment is built with silty sand but compacted at different densities. The threshold value for COV is set to 0.15.

With this procedure it is possible to identify two HSUs: Unit A (between the depths of 0.30m and 1.80m) and Unit B (between 2.35m and 5.00m).

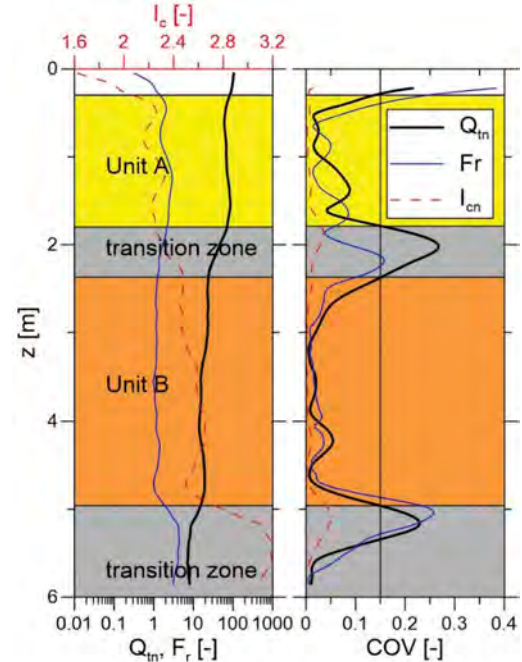


Figure 2. Identification of HSU.

4 MODELLING OF SPATIAL VARIABILITY

The spatial correlation structure of tip resistance is investigated using a geostatistical approach by means of semivariograms. Given the well-known anisotropy in geotechnical properties stemming from in-situ stress effects and other site-specific factors, horizontal and vertical variability are addressed separately. The adoption of specific geostatistical techniques and models relies heavily on the hypothesis of data stationarity, which denotes the invariance of a data set's statistics to spatial location. Stationarity can be achieved through a number of data transformation techniques. Here, data decomposition is implemented, by which the "total" spatial variability of a spatially ordered measured geotechnical property $[q(z_1...z_n)]$

in a sufficiently physically homogeneous soil unit is broken down into a trend function $[t(z_1...z_n)]$ and a set of residuals about the trend $[r(z_1...z_n)]$. In the one-dimensional case, for instance, taking depth (z) as the single spatial coordinate, decomposition is expressed by the following additive relation

$$q(z) = t(z) + r(z) \quad (7)$$

Stationarity of the residuals is verified with the Mann-Kendall test (Kendall, 1938, 1955). This non-parametric statistical test involves the calculation of the test statistic τ . Low values of τ indicate a low significance of spatial correlation (and, thus, a more probable stationarity of data), while τ values close to +1 or -1 indicate positive or negative correlation respectively.

The spatial correlation structure of residuals is investigated through a sequential process involving: (1) the calculation of empirical semivariograms; (2) the fitting of semivariogram models; and (3) the estimation of the scale of fluctuation from semivariogram model parameters. The scale of fluctuation (δ) describes the distance over which the parameters of a soil are significantly correlated. A low scale of fluctuation attests to less gradual spatial variability. The scale of fluctuation can be calculated from the values of the characteristic parameters of the semivariogram models (a : range; c_0 : nugget; c : sill) which are fitted to empirical semivariograms. Table 1 summarizes the semivariogram models used in this study and the model-specific functions used to calculate the scale of fluctuation (Elkateb et al. 2003). In the model equations given in Table 1, h is the lag distance, i.e., the distance between observations.

Table 1. Semivariogram models and analytical expressions for the scale of fluctuation (Onyejekwe et al. 2016).

Model	Equation	δ
Gaussian (GAU)	$c(1 - \exp(-\frac{h}{a})) + c_0$	$\sqrt{\pi a}$
Spherical (SPH)	$\begin{cases} c(\frac{3h}{2a} - \frac{h^3}{2a^3}) + c_0 & \text{for } h \leq a \\ c + c_0 & \text{for } h > a \end{cases}$	$0.75a$
Exponential (EXP)	$c(1 - \exp(-\frac{h^2}{a^2})) + c_0$	$2a$

4.1 Horizontal spatial variability

Horizontal spatial variability is investigated by slicing each homogeneous soil unit into 30cm-thick sub-units and conducting two-dimensional geostatistical modelling on each sub-unit. A total of 15 sub-units were obtained. The central value of the vertical

depth interval and the average tip resistance in of each sub-unit are considered as reference values for geostatistical modelling purposes. A linear trend in horizontal direction is determined for each reference depth ($q_{c,trend}(x) = a_1x + a_0$) and the residuals are calculated through data decomposition. Application of the Mann-Kendall test assessed the stationarity of the residuals of linear detrending for all sub-units.

The empirical semivariograms of the residuals for all sub-units are plotted in Figure 3. These are fitted with the Gaussian (GAU), Spherical (SPH) and Exponential (EXP) semivariogram models summarized in Table 1. Though semivariogram model fitting is performed automatically, best-fit models were subsequently scrutinized critically to assess their adequateness. The GAU and SPH model are those providing the best fits overall. An example of the best-fit model for the depth of 3.53m is shown in Figure 4.

Figure 5 plots the scale of fluctuation for each reference depth for the selected semivariogram models. GAU and SPH model provide similar values of δ , while higher values are obtained with the EXP model. The horizontal scale of fluctuation (Table 2) ranges between 3.7 and 21.1m. Average values of 6.8m, 7.4m and 11.5m are obtained for the GAU, SHP and EXP models, respectively. These average scale of fluctuations are lower than reported in other studies (e.g. (Cami et al., 2020)), but it must be considered that they highly depend not only on the database but also on the reduced horizontal spacing between soundings, which allows full exploitation of the typically existing nested correlation structure as discussed in Cami et al. (2020).

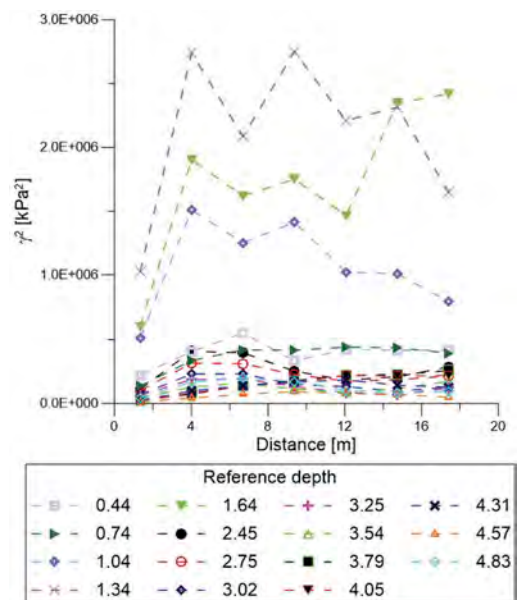


Figure 3. Empirical semivariogram in horizontal direction.

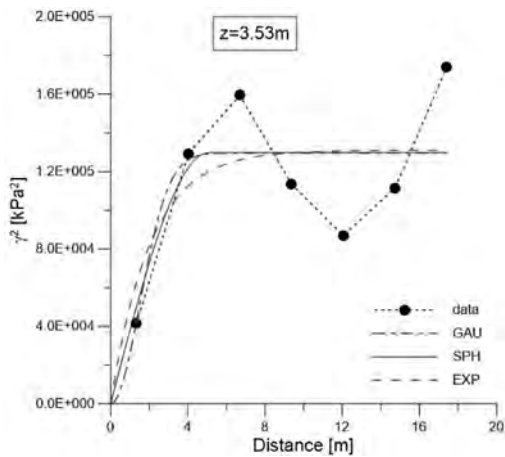


Figure 4. Best fitting semivariogram model for the reference depth of 3.53m.

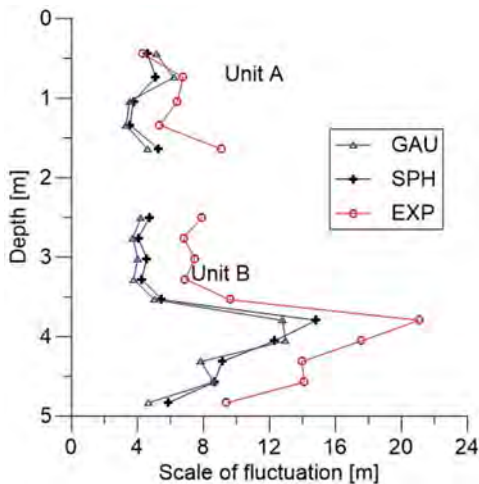


Figure 5. Horizontal scales of fluctuation by reference depth obtained from semivariogram model fitting.

4.2 Vertical spatial variability

Vertical spatial variability is investigated by soil unit and sounding. A cubic trend model ($q_{c,trend}(z) = a_3z^3 + a_2z^2 + a_1z + a_0$) is applied to each instance and the residuals are calculated. The Mann-Kendall test is performed to assess stationarity. The empirical semivariograms for all soil units and SCPT soundings are shown in Figure 6. These are fitted with the semivariogram models summarized in Table 1, yielding the vertical scales of fluctuation given in Table 3 and plotted in Figure 7.

The EXP model predicts the largest values of scale of fluctuation, followed by the SHP and GAU models. In Unit A, δ varies between 0.1m and 0.6m, thus generally lower than in Unit B, where calculated values range between 0.2m and 0.9m. These values are consistent with the results of previous studies, e.g. (Cami *et al.*, 2020).

Table 2. Horizontal scale of fluctuation calculated from semivariogram model parameters.

z[m]	GAU	SPH	EXP
0.4	5.1	4.6	4.3
0.7	6.2	5.1	6.8
1.0	3.5	3.8	6.4
1.3	3.3	3.5	5.4
1.6	4.6	5.3	9.1
2.5	4.2	4.7	7.9
2.8	3.7	4.1	6.8
3.0	4.0	4.6	7.5
3.3	3.8	4.3	6.9
3.5	5.0	5.5	9.6
3.8	12.8	14.8	21.1
4.1	13.0	12.3	17.6
4.3	7.8	9.1	14.0
4.6	8.6	8.7	14.1
4.8	4.7	5.9	9.4
Mean	6.0	6.4	9.8
Min	3.7	4.1	6.8
Max	13.0	14.8	21.1

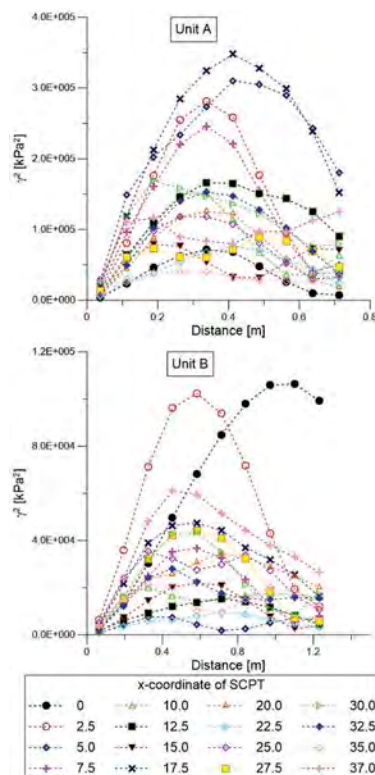


Figure 6. Empirical semivariogram in vertical direction.

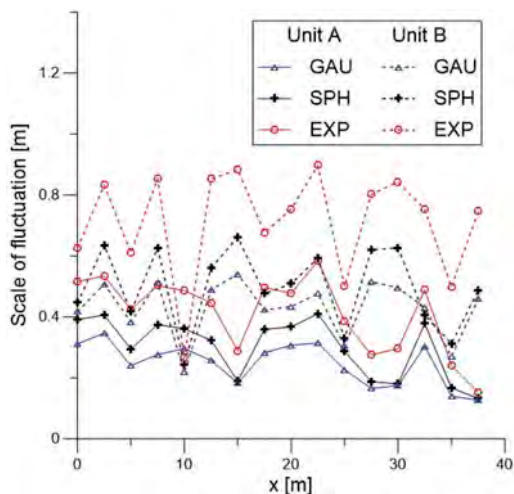


Figure 7. Vertical scales of fluctuation by semivariogram model and soil unit.

Table 3. Vertical scale of fluctuation from variogram models.

x[m]	Unit A			Unit B		
	GAU	SPH	EXP	GAU	SPH	EXP
0.0	0.3	0.4	0.5	0.4	0.4	0.6
2.5	0.3	0.4	0.5	0.5	0.6	0.8
5.0	0.2	0.3	0.4	0.4	0.4	0.6
7.5	0.3	0.4	0.5	0.5	0.6	0.9
10.0	0.3	0.4	0.5	0.2	0.2	0.3
12.5	0.3	0.3	0.4	0.5	0.6	0.9
15.0	0.2	0.2	0.3	0.5	0.7	0.9
17.5	0.3	0.4	0.5	0.4	0.5	0.7
20.0	0.3	0.4	0.5	0.4	0.5	0.8
22.5	0.3	0.4	0.6	0.5	0.6	0.9
25.0	0.2	0.3	0.4	0.3	0.3	0.5
27.5	0.2	0.2	0.3	0.5	0.6	0.8
30.0	0.2	0.2	0.3	0.5	0.6	0.8
32.5	0.3	0.4	0.5	0.4	0.4	0.8
35.0	0.1	0.2	0.2	0.3	0.3	0.5
37.5	0.1	0.1	0.2	0.5	0.5	0.7
Mean	0.2	0.3	0.4	0.4	0.5	0.7
Min	0.1	0.1	0.2	0.2	0.2	0.3
Max	0.3	0.4	0.6	0.5	0.7	0.9

5 DISCUSSION AND CONCLUSIONS

The vertical and horizontal spatial variability in cone tip resistance of the unsaturated silty sand forming a levee is investigated through statistical and

geostatistical modelling of the results of 16 closely spaced SCPT soundings. Results of the descriptive second-moment statistical analysis attest to a high degree of scatter in measured data, presumably due to the effect of partial soil saturation and other site-specific phenomena.

To supplement the outputs of the statistical analysis and to overcome its limitations with respect to the quantitative characterization of the spatial correlation structure of mechanical resistance to cone penetration, geostatistical modelling of the spatial correlation structure was conducted both in the horizontal and vertical directions for two depth intervals referring to highly homogenous soil units.

The horizontal correlation structure, parameterized by the horizontal scale of fluctuation, proved to be stronger (i.e., with cone resistance varying significantly over smaller horizontal distances) than typically assessed in existing literature. This result could be reconnected to both the high quality of the dataset (the small horizontal spacing between consecutive soundings allows the appreciation of nested correlation structures) and to the specific site effects which result in the surprisingly high degree of inter-sounding variability. Results of vertical spatial correlation modelling are fully in line with previous studies, thus attesting to the general correctness in the modelling approach.

The results obtained in the study confirm the particular site conditions which lead to the significant horizontal inter-sounding variability observed through the geotechnical testing campaign. While the complexity of the physical phenomena which lead to such variability require further and more extensive investigation, the quantitative assessment of the spatial correlation structure and its anisotropy attest to the importance of statistical and geostatistical analyses for geotechnical modelling purposes. The availability of quantitative spatial variability parameters allows the enhanced modelling of the geotechnical systems by providing realistic inputs to, for instance, limit equilibrium and numerical analyses.

ACKNOWLEDGMENTS

The authors would like to thank AIPO that financed the geotechnical site investigations.

The authors would like to acknowledge the financial support from MIUR (Redreef - PRIN 2017 Call, prot. 2017YPMBWJ)

REFERENCES

- Cami, B. *et al.* (2020) 'Scale of Fluctuation for Spatially Varying Soils: Estimation Methods and Values', *ASCE-ASME Journal of Risk and Uncertainty in Engineering Systems, Part A: Civil Engineering*, 6(4), p. 03120002. doi: 10.1061/ajrua6.0001083.
- Elkateb, T., Chalaturnyk, R. and Robertson, P. K. (2003) 'An overview of soil heterogeneity: Quantification and

- implications on geotechnical field problems', *Canadian Geotechnical Journal*, 40(1), pp. 1–15. doi: 10.1139/t02-090.
- Harr, E. M. (1987) *Reliability-based design in civil engineering*. Department of Civil Engineering, School of Engineering, North Carolina State University.
- Kendall, M. G. (1938) 'A new measure of rank correlation', *Biometrika*, 30, pp. 81–93.
- Kendall, M. G. (1955) *Rank correlation methods*. New York: Hafner Publishing Co.
- Onyejekwe, S., Kang, X. and Ge, L. (2016) 'Evaluation of the scale of fluctuation of geotechnical parameters by autocorrelation function and semivariogram function', *Engineering Geology*. Elsevier B.V., 214, pp. 43–49. doi: 10.1016/j.enggeo.2016.09.014.
- Robertson, P. K. (2009) 'Interpretation of cone penetration tests — a unified approach', *Canadian Geotechnical Journal*, 46(11), pp. 1337–1355. doi: 10.1139/T09-065.
- Uzielli, M. (2004) *Variability of stress-normalized CPT parameters and application to seismic liquefaction initiation analysis*.
- Uzielli, M., Simonini, P. and Cola, S. (2008) 'Statistical identification of homogeneous soil layers in Venice lagoon soils', in *Proceedings of the 3rd International Conference on Site Characterization ISC'3*. Taipei: Taylor & Francis. Available at: <https://flore.unifi.it/handle/2158/1181074>.

Coupling site wide CPT profiles and genetic algorithms for whole-site offshore windfarm layout optimization

J.A. Charles & S.M. Gourvenec
University of Southampton, Southampton, UK

M.E. Vardy
SAND Geophysics, Southampton, UK

ABSTRACT: Offshore windfarm layout is driven by optimizing wind potential at the selected site subject to minimum spacing between turbines. Within these constraints, this paper explores the optimization of turbine layout within a selected site based on geotechnical site conditions. Utilizing an irregular but site-wide grid of CPT profiles, a simple pile design method and a cubic interpolation of pile dimensions, heatmaps of pile length and diameter at every possible coordinate within a site can be generated, providing the opportunity for optimization of layout. This paper demonstrates the ability to optimize the location of a prescribed number of wind turbine foundations, in conjunction with other constraints such as minimum spacing, to minimize total steel usage (a simple proxy for foundation cost and embodied carbon) in the foundation system using a genetic algorithm (GA)-based approach. Existing work on windfarm layout optimization uses such techniques to maximize wind energy generation but negligible work exists on extending the methodologies to minimize foundation costs. This paper demonstrates the viability of using a set of CPT profiles with a GA-based approach for a geotechnically-informed windfarm layout and explores the effects of various meta parameters using publicly available datasets. The work demonstrated in this paper is directly relevant to ongoing advances in geophysics and machine learning that would allow for the generation of a synthetic CPT profile at any point on the site, eliminating the drawbacks of interpolation between actual CPT profiles for design parameters.

1 INTRODUCTION AND LITERATURE REVIEW

The construction of offshore windfarms is a key part of the UK government's renewable energy strategy (BEIS 2019, Supergen ORE, 2021), and internationally, the Global Wind Energy Council (GWEC) forecasts that by 2030, more than 205GW of new offshore wind capacity will be added (Global Wind Energy Council, 2020).

Securing offshore wind turbines to the seabed – whether as fixed or floating devices – requires a step change in site investigation and geotechnical design approaches. Due to the size of offshore windfarms, with Hornsea 1, currently the world's largest, covering an area of 407km² and consisting of 174 turbines (Ørsted, 2020a), ground investigation datapoints such as borehole logs and CPT profiles are relatively sparse per structure compared to e.g. a building foundation, or even an offshore hydrocarbon platform. However, using interpolation between CPTs, or synthetic CPT profiles derived from continuous seismic data, continuous ground models of a site can be derived (Vardy et al., 2017).

With continuous site investigation data, a monopile foundation can be designed at any location on a site, from which it is possible to use optimization techniques to minimize the overall foundation cost - in terms of volume of steel used - for the windfarm for a specified number and spacing of turbines. Windfarm layout optimization is typically carried out to maximize the wind energy generated based on aerodynamic considerations (Pérez et al., 2013; Samorani, 2010). This paper seeks to demonstrate that foundation efficiency can also be optimized for, and hence include geotechnical parameters as additional variables in typical wind turbine layout optimization. Combining or comparing the significance or trade-offs of these different considerations is beyond the scope of this paper, which seeks to explore and demonstrate the opportunity to include geotechnical assessment in wind farm layout optimization.

Designing a monopile at a location with a CPT profile is straightforward. Many techniques with varying complexity exist in literature and in commercial software packages (Bhattacharya, 2019, Kay et al. 2021). Designing a monopile at locations in between available CPT profiles may apply similar methods but is

associated with greater uncertainty. Since this paper aims to demonstrate a proof of concept for a geotechnically-informed windfarm layout optimization procedure, a simple cubic interpolation approach has been adopted to derive pile dimensions between locations of actual CPT profiles based on the calculated dimensions at each CPT location.

The site examined as a case study, Burbo Bank Extension (Ørsted, 2020b), located off the coast of Liverpool, UK, in the Irish Sea and has an area of the order of 40km² and around 42 CPT profiles in an irregular grid as shown in Figure 1. Coordinates are given in northings and eastings which are measured in kilometers. For Burbo Bank Extension, the maximum north-south distance is approximately 4.2km and the maximum east-west distance is approximately 11.8km. The final constructed windfarm extension consisted of 32 8MW turbines that together can power around 230,000 homes (Ørsted, 2020b). Although not utilized in this paper, the Burbo Bank Extension site investigation (and many others) feature large amounts of geophysical data. A geophysical survey involves sending seismic waves into the seafloor and determining soil properties based on reflected waves. Whereas CPT and borehole data is discrete, geophysical data is continuous, but does not directly measure physical parameters that have to date been robustly linked to engineering properties needed for geotechnical design. However, recent advances allow for synthetic CPT data to be generated from seismic data via machine learning at any point on a site with geophysical data of sufficient quality (Sauvin et al., 2019). This process, in future work, would allow for a drop-in replacement to the simple interpolation process used in this proof of concept.

This paper first details a simple CPT based pile design method and provides a brief summary of alternative/more detailed approaches. The process by which pile length and diameter are interpolated across the site is provided, along with discussions on the emerging techniques that would allow for improvements. Finally, a demonstration of how a genetic algorithm (GA) can be used to automatically select the locations for a specified number of monopiles to minimize a given condition, in this case steel volume, is presented. The general method presented here can be applied to any potential site or foundation type, and involve other constraints such as bathymetry or areas of ecological significance or anthropogenic activity.

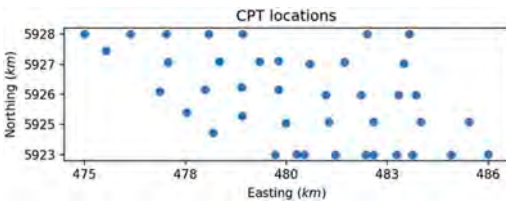


Figure 1. Locations of CPT tests at the Burbo Bank Extension.

2 GEOTECHNICAL DESIGN OF MONOPILES

There are many methods by which a monopile can be designed for a given CPT profile with varying levels of complexity. Although more complex methods such as PISA (Byrne et al., 2015) or the methodologies implemented in the web app based LAP software (Doherty, 2017, 2020) are available which consider factors such as serviceability, for this proof of concept only capacity will be considered.

The primary loading on a wind turbine foundation is horizontal loading, both hydrodynamic (wave, current) and aerodynamic (wind), taken together as 16MN for this study which is a typical value cited in literature (Lesny & Wiemann, 2005). A typical safety factor of 3 has been applied to this load for a total 48MN. Note that factoring has been applied only to the applied load and not to soil or material properties. The failure mechanism examined is rotational failure. To ensure the foundation is sufficient to resist this load, lateral resistance can be calculated at each point along the length of the pile based on the values obtained in the CPT profile. Taking moments about a representative lever arm for both wind and wave loading, 35 m in this case, the depth to the rotation point can be found. The local lateral resistance values can then be multiplied by the length they apply to and summed, with those below the point of rotation being negative.

Several equations exist to calculate discretized resistance along the pile. Equation 1 shows the piecewise resistance in clay (Truong & Lehane, 2014) and Equation 2 is the equivalent for sand (Suryasentana & Lehane, 2014). Note that there are various other possibilities for sands and clays as well as equations for other types of soil and rock (Randolph & Gourvenec, 2017).

$$p_u = Dq_{net} \left(\left(\frac{3}{4.7 + 1.6 \ln I_r} \right) + (1.5 - 0.14 \ln I_r) \tanh \left(\frac{0.65d}{D} \right) \right) \quad (1)$$

$$p_u = 2.4\sigma'_v D \left(\frac{q_c}{\sigma'_v} \right)^{0.67} \left(\frac{d}{D} \right)^{0.75} \quad (2)$$

In Equations 1 and 2, p_u refers to local lateral resistance per unit length, D is the diameter of the monopile, I_r is rigidity index (assumed to be 125 for this study), d is depth below the seafloor to the local point being calculated, σ'_v is effective vertical stress calculated at the local point, q_c is cone resistance where $q_c = Q_c/A_c$, i.e. the force required to push the cone into the ground over cone area, and q_{net} is the net cone resistance where $q_{net} = q_t - \sigma_v$, i.e. corrected cone resistance minus total vertical stress. Corrected cone resistance $q_t = q_c + u_2(1 - a)$ where u_2 is pore water pressure and a is a constant (Robertson, 1990).

As these equations are defined in terms of pile diameter (along with the pile length determining how many discretization points are to be summed together) the easiest way to size a pile is a brute force approach. Table 1 shows the range of lengths and diameters used in this study which are based on the selection used in Sauvin et al. (2019), with the addition of lower 5m and 6m diameters. It should be noted that due to the simplicity of the design criteria chosen that the possible pile dimensions in Table 1 are illustrative and not intended to represent a robust detailed design methodology for the loading conditions, and do not take into account other considerations such as installability or other failure mechanisms such as bending.

Table 1. Typical pile dimensions as used in this study.

Property					
Diameter (m)	5	6	7	7.7	8.5
Length (m)	3D	3.5D	4D	4.5D	5D

Python code was written to automatically identify soil type based on the standard Robertson charts (Robertson, 1990, 2009). For simplicity, datapoints along the CPT profiles were classified as either sand or clay allowing for automated selection of the relevant lateral resistance equation. Of the nine possible Robertson chart classifications, sensitive fine grained, organic, clay, silt-mixtures, and very stiff fine-grained were labelled as clay, and sand-mixtures, sand, gravelly sand to sand, and very stiff sand to clayey sand were labelled as sand. Figure 2 shows a plot of a Burbo Bank Extension CPT profile colored based on soil classification. The axis in the figure are normalized cone resistance $Q_t = (q_t - \sigma_v)/\sigma'_v$ and friction ratio $R_f = (f_s/q_t) \times 100\%$ where sleeve friction $f_s = F_s/A_s$ with F_s and A_s being the recorded frictional force and friction sleeve area respectively (Robertson, 1990).

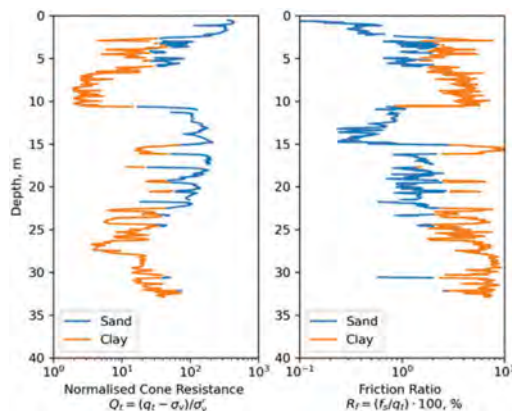


Figure 2. Example CPT profile from Burbo Bank Extension categorized into sand and clay.

3 WHOLE SITE INTERPOLATION

Although it is ideal to design a monopile that is co-located with a CPT profile, often it is necessary to design a pile that is located between actual CPT profile locations. To achieve this, a monopile was designed at each CPT location across the site, with pile length and diameter then interpolated for locations in between the discrete irregular grid.

It should be noted that this methodology has several limitations, including overlooking the actual variation in soil conditions in between CPT locations. Nonetheless, for the purpose of this proof of concept, using interpolation allows the construction of heatmaps of monopile length, diameter, and volume to be constructed over the whole site, which is a necessary step in freely selecting the location of a set of monopiles.

There are emerging techniques that would potentially eliminate the issues of this interpolation step. On a site with continuous geophysical survey data and discrete CPT data, it is possible to combine seismic inversion methods with machine learning algorithms predict a synthetic CPT profile at any location on the site (Vardy et al., 2018; Sauvin et al., 2019). This technique would potentially represent a significant improvement to site wide characterization and work is actively ongoing in this area, but has not seen widespread application, and therefore the suitability of the method for different site conditions is unclear.

It is the hope of the authors that such techniques would represent a drop-in replacement for the interpolation step presented in this paper. However, for now, cubic interpolation serves as an acceptable placeholder to allow for the demonstration of foundation-based site layout optimization.

Figure 3 shows the heatmaps generated for pile diameter, length, and volume across the site. It should be noted that due to the interpolation process it is possible that some regions on the heatmap drop below the discrete pile dimensions provided in Table 1.

Calculation of pile volume requires an additional wall thickness term. The American Petroleum Institute (API, 2005) recommend a minimum thickness t based on Equation 3. A thickness of 0.1m was found to satisfy this requirement for all pile diameters considered in this study.

$$t[mm] = 6.35 + D[mm]/100 \quad (3)$$

4 LAYOUT OPTIMISATION USING A GENETIC ALGORITHM

With heatmaps produced for required pile diameter and length across the whole site, it is possible to check the pile dimensions and hence steel volume necessary

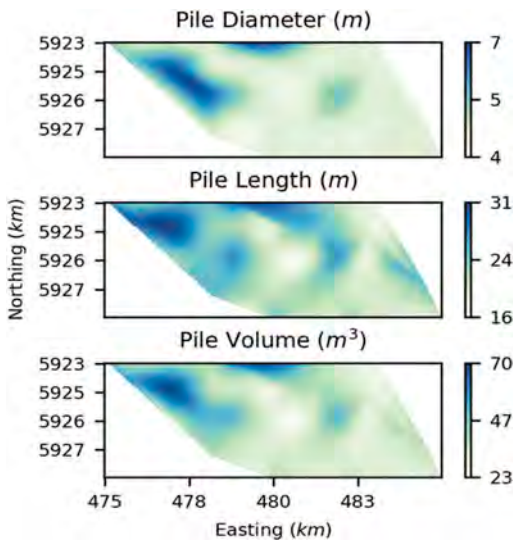


Figure 3. Heatmaps of pile diameter, length, and volume for the Burbo Bank Extension site.

at any arbitrary coordinate. It is therefore possible to sum the steel usage for a set of n arbitrarily located piles, and to compare the sums of steel usage for two different sets of piles. Using some means of optimization, in this paper, a genetic algorithm (GA), it is possible to select a set of n coordinates that minimize the required steel usage in foundations across the site.

A GA is an evolutionary algorithm (Poli et al., 2008) that mimics natural selection (Darwin, 1859). Populations of solutions (turbine layouts in this case) are ranked by fitness (steel usage in this case) with the best continuing to future generations and the less good not doing so. After many generations, the solutions tend to improve.

Although there are numerous existing libraries implementing GA functionality (e.g. Fortin et al., 2012; Gad, 2021), due to the relative simplicity of the problem, and simply being able to look up the steel usage for a given coordinate, the GA functionality for this study was implemented from scratch in Python. The steps are outlined below:

1. Generation of a specimen. Code was created to randomly select a coordinate within the site, check that specified constraints are not violated (i.e. being too close to an existing coordinate) and either add it to the list, or discard it, moving on to the next randomly selected coordinate until the desired number of coordinate positions is reached.
2. Implementation of cost function. Code was created to take a specimen as an input and calculate or look up the required steel volume for each coordinate, and then sum all values, enabling ranking of a population of specimens.
3. Creation of the next generation. Code was created to advance the population of specimens to the next generation. User specified meta-parameters

allow for a subset of specimens to advance as they are; a second subset are mutated by randomly adjusting a random selection of the associated coordinates; and a third subset is adjusted by randomly mutating the coordinates of the highest volume piles.

It is noted that advancing the best specimens without changes guarantees that the fittest solution at a given time will never become worse with additional generations. Further, for this use case the GA technique of “crossover” in which two specimens are merged has been omitted as merging half of the list of coordinates from two separate specimens without violating the distance constraint proved to not be possible without additional logic that effectively nullified any benefits of the crossover process.

There are many choices for the aforementioned meta-parameters, for example, the number of generations, the number of specimens generated, the number of specimens in each category, the rankings assigned to each category, whether or not specimens can be included in more than one category etc. Commentary and plots are provided on some meta-parameters in the following section, but an exhaustive search is beyond the scope of this paper.

5 RESULTS AND DISCUSSION

To demonstrate the methodology, the GA was run for multiple combinations of parameters. Initially, the method was used to find the optimal layout of 32 piles, the number constructed in the actual Burbo Bank Extension site development, with 100 specimens (i.e. lists of coordinates) used per generation, with 100 generations.

It should be noted that the real site layout features 32 piles packed as closely as possible along linear transects to minimize wind turbulence and maximize wind yield. An industry typical spacing would be 8 blade diameters (DNV GL Energy, 2019). Enforcing this restriction would allow no leeway to demonstrate the ability of a GA to select locations to minimize total foundation costs and as such a lower minimum spacing of 800m was enforced, representative of wind turbines of diameter 100m or spacing of the actual ~160m diameter wind turbines at 5 blade diameters.

Using smaller turbines than is currently standard or adopting smaller spacing would negatively affect energy generated, and therefore be an unattractive prospect for windfarm operators, but implementations of the presented methodology allow for fine adjustments to more traditional layouts that minimize foundation and potentially installation cost that may be beneficially offset against reduced wind power generation.

Figure 4 shows the layouts generated by the GA after 3, 20, and 60 generations. As the genetic algorithm process involves randomness it is not

deterministic and rerunning the process will likely return similar but slightly different layouts. After just 3 generations nearly every turbine is placed in a lower volume area but there are still improvements that can be seen by eye between the 3 and 20 generation layouts. The differences between 20 and 60 generations are difficult to spot in the layout maps, but small improvements can be found when examining the total site pile volume. Table 2 shows total pile volume for each of the layouts in Figure 4.

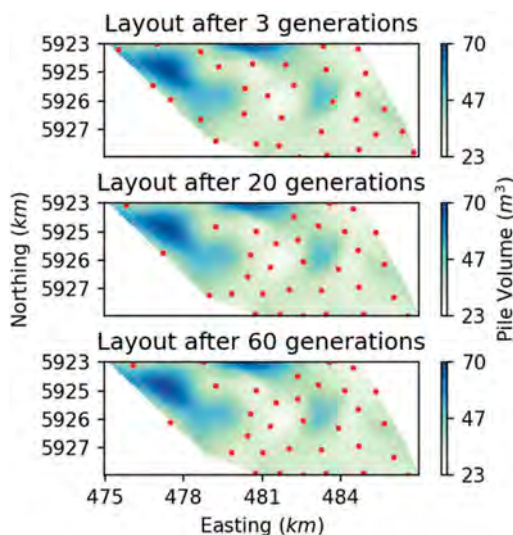


Figure 4. Layouts of 32 turbines after 3, 20, and 60 generations.

Table 2. Total pile volume per generation for the 32-pile layouts shown in Figure 4.

Generation	Total volume (m ³)	Mean volume per pile (m ³)	Difference from mean volume at CPT locations (36.96 m ³)
3	1100.8	34.4	-6.9%
20	1045.1	32.7	-11.5%
60	1039.7	32.5	-12.1%

Figure 5 shows the effects of various meta-parameters on the layout and total volume of 32 monopiles. Considering the relationship between number of generations and volume of steel used, 10 trials were carried out with the average volume plotted per generation number, and for the plot of specimens, 5 trials were carried out for each value. As stated previously, there is an infinite possibility of potential setups for parameters for a GA and the two plots presented here do not represent an exhaustive analysis but were selected due to their relative simplicity and their effects on computational time. It is evident that increasing the number of generations that the GA operates for,

provides a more optimal result, i.e. less steel used for the same number of monopiles. The implementation in fact ensures that a generation is at least as good as the one before. Most improvement happens relatively soon, within the first 10 or 20 generations, and although further improvement can be seen there are significant diminishing returns after generation 50 or so.

The relationship between number of specimens and total volume has a clear correlation but the effect is relatively modest in comparison with the number of generations. It is possible that due to the impracticality of including the GA crossover technique in the current problem formulation that the benefits of a larger population are less pronounced than they would be for a different problem. In this case, 20 specimens appear to be enough.

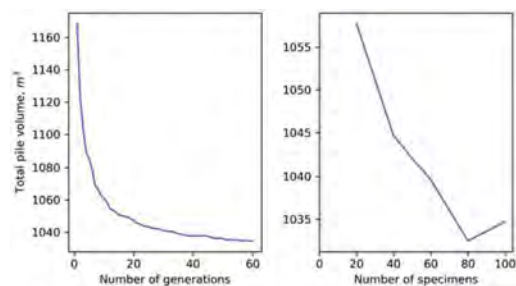


Figure 5. Effect of selected meta parameters on total pile volume.

It is important to note that there is no guarantee that a GA can find the global optimum solution, even if the improvements between generations appear to plateau. The global best solution would be the ideal solution in which there can be no improvements. GAs however can potentially tend towards a local optimum solution. A local optimum solution can be thought of as an evolutionary “dead end” in which a solution has been found that is good but is sufficiently different from the global optimum that no random mutations exist that will move from one to the other. Finding a local rather than global minima for site wide foundation cost would be more expensive but would not have safety implications.

6 CONCLUSIONS AND FUTURE WORK

Using a GA to help identify offshore windfarm site layouts that minimize foundation steel volume (and implied cost, both direct, and embodied carbon) has been illustrated. The illustrated example includes several idealizations and placeholder techniques have been used that need to be revisited to refine the approach. These include (1) Incorporating the emerging technique of generating synthetic CPT data from geophysical surveys via machine learning; (2) Additional constraints based on probabilistic analysis of the CPTs, i.e. areas in which there is high uncertainty in synthetic CPT data may be

better avoided; and (3) More complex higher order pile design approaches.

Finally, it is noted that an approach such as put forward in this paper is intended to complement, not replace other constraints and conditions for wind-farm layout optimization, such as aerodynamic effects for optimal energy generation.

ACKNOWLEDGEMENTS

This work forms part of the activities of the Centre of Excellence for Intelligent & Resilient Ocean Engineering (<https://www.southampton.ac.uk/iroe>) and the first and second authors are supported by Royal Academy of Engineering under the Chairs in Emerging Technologies scheme.

Part of the development of the GA approach presented here was carried out by University of Southampton undergraduate Etienne Martin during a summer internship organized through the Department of Civil, Maritime and Environmental Engineering and funded by the Centre of Excellence for Intelligent & Resilient Ocean Engineering.

The Burbo Bank extension dataset used was made publicly available by the Crown Estate via the Marine Data Exchange website (<https://www.marine-dataexchange.co.uk/>).

REFERENCES

- American Petroleum Institute. 2005. Recommended practice for planning, designing and constructing fixed offshore platforms—Working stress design. API RP 2A-WSD.
- Bhattacharya, S. 2019. *Design of Foundations for Offshore Wind Turbines*. John Wiley & Sons.
- BEIS, Business Energy and Industrial Strategy, Department of. 2020. Policy Paper, Offshore wind: Sector Deal. <https://www.gov.uk/government/publications/offshore-wind-sector-deal>
- Byrne, B. W., Mcadam, R., Burd, H. J., Houlsby, G. T., Martin, C. M., Zdravković, L., Taborda, D. M. G., Potts, D. M., Jardine, R. J., Sideri, M., Schroeder, F. C., Gavin, K., Doherty, P., Igoe, D., Wood, A. M., Kallehave, D., & Gretlund, J. S. 2015. New design methods for large diameter piles under lateral loading for offshore wind applications. *Frontiers in Offshore Geotechnics III*, 705–710.
- Darwin, C. 1859. *On the origin of species*. John Murray.
- DNV GL Energy. 2019. Potential to improve Load Factor of offshore wind farms in the UK to 2035. https://assets.publishing.service.gov.uk/government/uploads/system/uploads/attachment_data/file/839515/L2C156060-UKBR-R-05-D_-_potential_to_improve_Load_Factor_of_UK_offshore_wind_to_2035.pdf
- Doherty, J. P. 2017. A web based application for the lateral analysis of pile (LAP) foundations. *Proceedings of the ASME 2017 36th International Conference on Ocean, Offshore and Arctic Engineering*.
- Doherty, J. P. 2020. *Lateral Analysis of Piles User Manual*. <https://www.geocalcs.com/lap>
- Fortin, F. A., De Rainville, F. M., Gardner, M. A., Parizeau, M., & Gagné, C. 2012. DEAP: Evolutionary algorithms made easy. *Journal of Machine Learning Research*, 13, 2171–2175.
- Gad, A. F. 2021. *PyGAD: An Intuitive Genetic Algorithm Python Library*. <http://arxiv.org/abs/2106.06158>
- Global Wind Energy Council. 2020. Global Offshore Wind: Annual Market Report 2020. *Global Offshore Wind Report 2020, February*, 130.
- Kay, S., Gourvenec, S., Palix, E. & Alderlieste, E. 2021 *Intermediate Offshore Foundations*. CRC/Taylor & Francis ISBN: ISBN: 978-1-138-35353-4 (hbk) ISBN: 978-0-429-42384-0 (ebk)
- Lesny, K., & Wiemann, J. 2005. Design aspects of monopiles in German offshore wind farms. In *Proceedings of the International Symposium on Frontiers in Offshore Geotechnics* (pp. 383–389). AA Balkema Publishing.
- Ørsted. 2020a. Hornsea One: About the project. <https://hornseaprojectone.co.uk/about-the-project#project-timeline-2020>
- Ørsted. 2020b. Burbo Bank Extension Offshore Windfarm. https://orstedcdn.azureedge.net/-/media/www/docs/corp/uk/updated-project-summaries-06-19/sept-2020/200819_ps_burbo-bank-extension_v2_web-aw.ashx
- Pérez, B., Mínguez, R., & Guanque, R. 2013. Offshore wind farm layout optimization using mathematical programming techniques. *Renewable Energy*, 53, 389–399. <https://doi.org/10.1016/j.renene.2012.12.007>
- Poli, R., Langdon, W. B., & McPhee, N. F. 2008. A Field Guide to Genetic Programming. In *Wyvern* (Issue March). http://www.essex.ac.uk/wyvern/2008-04/Wyvern_April08_7126.pdf
- Randolph, M., & Gourvenec, S. 2017. *Offshore Geotechnical Engineering*. DOI: 10.1201/9781315272474
- Robertson, P. K. 1990. Soil classification using the cone penetration test. *Canadian Geotechnical Journal*, 27(1), 151–158. <https://doi.org/10.1139/t90-014>
- Robertson, P. K. 2009. Interpretation of cone penetration tests - A unified approach. *Canadian Geotechnical Journal*, 46(11), 1337–1355. <https://doi.org/10.1139/T09-065>
- Samorani, M. 2010. The Wind Farm Layout Optimization Problem. *Power*, 1–18.
- Sauvin, G., Vanneste, M., Vardy, M. E., Klinkvort, R. T., & Carl Fredrik, F. 2019. Machine Learning and Quantitative Ground Models for Improving Offshore Wind Site Characterization. *Offshore Technology Conference*, 110(9), 1689–1699. <https://doi.org/10.4043/29351-MS>
- Supergen ORE. 2021. *Delivering Net Zero: the role of Offshore Renewable Energy A COP26 Briefing note prepared by the Supergen Offshore Renewable Energy Hub*. <https://www.supergen-ore.net/uploads/Supergen-ORE-Hub-Delivering-Net-Zero-the-role-of-Offshore-Renewable-Energy-A-COP26-Brief.pdf>
- Suryasentana, S. K., & Lehane, B. M. 2014. Numerical derivation of CPT-based p-y curves for piles in sand. *Geotechnique*, 64(3), 186–194. <https://doi.org/10.1680/geot.13.P.026>
- Truong, P., & Lehane, B. 2014. Numerically derived CPT-based py curves for a soft clay modeled as an elastic perfectly plastic material. *3rd International Symposium on Cone Penetration Testing*, 975–982.
- Vardy, M. E., Vanneste, M., Henstock, T. J., Clare, M. A., Forsberg, C. F., & Provenzano, G. 2017. State-of-the-art remote characterization of shallow marine sediments: the road to a fully integrated solution. *Near Surface Geophysics*, 15(4), 387–402. <https://doi.org/10.3997/1873-0604.2017024>
- Vardy, M.E., Clare, M.A., Vanneste, M., Forsberg, C.F., & Dix, J.K. 2018. Seismic Inversion for Site Characterisation: When, Where and Why Should We Use It? OTC-28730-MS.

CPT-based model calibration for effective stress analysis of layered soil deposits

A. Chiaradonna

University of L'Aquila, L'Aquila, Italy

N. Ntritsos & M. Cubrinovski

University of Canterbury, Christchurch, New Zealand

ABSTRACT: Recent research recognized the advantages of effective stress dynamic analysis in estimating the seismic response of layered soil profiles. One of the key challenges in performing effective stress analysis is the calibration of constitutive models able to simulate complex soil behavior under seismic loading. To overcome this problem, calibration procedures have been developed to guide the definition of model parameters on the results of in-situ tests. In this study, a reference layered soil profile from Christchurch in New Zealand, which experienced liquefaction during the 2010-2011 Canterbury earthquake sequence, was used to verify the goodness of the CPT-based calibration procedure of a simplified pore water pressure model. Comparisons with the seismic response predicted using an advanced state concept-based constitutive model were also reported. Despite the simplifications adopted in the calibration process, the analysis results replicate the occurrence of liquefaction and encourage CPT-based model parameter definition for routine effective stress dynamic analyses.

1 INTRODUCTION

Recent research recognized the importance of effective stress dynamic analysis in estimating the seismic response of layered soil profiles with interbedded liquefiable and non-liquefiable soils (Cubrinovski et al. 2019). Two distinct approaches can be adopted to perform an effective stress analysis: (1) a 'loosely coupled' approach that predicts seismic-induced pore pressure build-up by adopting simplified relationships used in combination with constitutive models that address total stress (e.g., pore pressure prediction based on accumulated strains or stresses) and (2) a 'fully coupled' approach that uses a plasticity-based effective stress constitutive model to predict both the stress-strain and the pore pressure response of the soil (Tropeano et al. 2019).

One of the key challenges in performing effective stress analysis is the calibration of constitutive models able to simulate the dynamic soil behavior under seismic loading. To overcome this problem, calibration procedures have been developed to guide the definition of the parameters of advanced constitutive models based on data from in-situ tests, such as Cone Penetration Test - CPT (Ntritsos & Cubrinovski 2020). Following this philosophy, the calibration of a simplified stress-based pore water pressure model, originally based only on cyclic laboratory test data, was

generalized to include the results of field tests commonly used in engineering practice (Chiaradonna et al. 2020).

In this study, the above-mentioned simplified stress-based pore water pressure model is adopted with the two-fold goal to (1) verify the goodness of the CPT-based calibration procedure in predicting the liquefaction of a layered profile, (2) compare the model performances with those provided by an advanced state concept-based constitutive model assumed as a reference, which was calibrated on the same CPT.

To pursue these aims, a representative layered soil profile from Christchurch in New Zealand, which experienced liquefaction multiple times during the 2010-2011 Canterbury earthquake sequence, was considered in the numerical simulations. The adopted studied area was largely investigated in Cubrinovski et al. (2019), where the geotechnical model and effective-stress analyses by using the advanced state concept-based constitutive model are detailed.

One-dimensional (1D) dynamic analyses were preliminarily carried out by assuming visco-elastic linear behavior of the soils, to check that the same boundary conditions were applied in both approaches (advanced and simplified). Comparisons with equivalent linear and nonlinear codes were also provided.

Then, a 1D effective stress analysis was performed with the simplified pore water pressure model,

according to a loosely coupled approach (Chiaradonna et al. 2019). The parameters of the stress-based pore water pressure model were mainly defined on the cone tip resistance of each soil layer following the CPT-based procedure proposed by Chiaradonna et al. (2020). The same geotechnical model was also simulated through the advanced state concept-based constitutive model, whose parameters were calibrated on the same CPT data by Cubrinovski et al. (2019). Results of the 1D effective stress analyses provided insights on the capability of the loosely coupled approach to correctly predict the attainment of liquefaction in sites with complex stratigraphic conditions, also compared to the performance of a fully coupled approach assumed as reference.

2 SIMPLIFIED PORE PRESSURE MODEL AND CPT-BASED CALIBRATION

A simplified stress-based pore water pressure model, hereafter called ‘PWP model’ (Chiaradonna et al. 2018; 2019) permits the comparison of the irregular seismic loading with the soil liquefaction resistance, through an accumulation stress-based variable κ , called ‘damage parameter’. It is an incremental function of the applied load that considers the cyclic strength of the soil. This latter is expressed in terms of cyclic resistance curve, analytically described by the equation:

$$\frac{(CRR - CSR_t)}{(CSR_r - CSR_t)} = \left(\frac{N_r}{N_L} \right)^{\frac{1}{\alpha}} \quad (1)$$

where CSR is the shear stress amplitude normalized by the initial effective confining pressure; N is

the number of cycles, CSR_r is the ordinate of the curve for $N_L = 15$ (usually adopted as a reference number of cycles). For a regular shear stress history, κ is proportional to the number of cycles, N ; it is, therefore, possible to express the pore pressure ratio, r_u (ratio between the excess pore pressure and the initial effective confining pressure), as a function of the damage parameter, through the relationship proposed by the authors (Chiaradonna et al. 2018):

$$r_u = a \left(\frac{\kappa}{\kappa_L} \right)^b + (0.9 - a) \left(\frac{\kappa}{\kappa_L} \right)^d \quad (2)$$

where a , b and d are parameters that control the shape of the curve.

According to the CPT-based calibration proposed by Chiaradonna et al. (2020), The parameters of the curve $CRR-N_L$ (Eq. 1) can be computed as a function of the effective stress state and the normalized and corrected cone tip resistance, q_{c1Ncs} , of the CPT; while the parameters of the curve $r_u - N/N_L$ (Eq. 2) can be defined as a function of the fine content and relative density; this latter being usually estimated from CPT data (Robertson & Cabal 2015). In so doing, the pore water pressure model parameters can be easily calibrated directly on the results of CPTs, through the charts in Figure 1.

The PWP model was implemented in the non-linear code SCOSSA which models the soil profile as a system of consistent lumped masses, connected by viscous dampers and springs with hysteretic behavior. The non-linear shear stress-strain relationship is described by the MKZ model and the modified Masing rules. More details about the numerical implementation can be found in Tropeano et al. (2019).

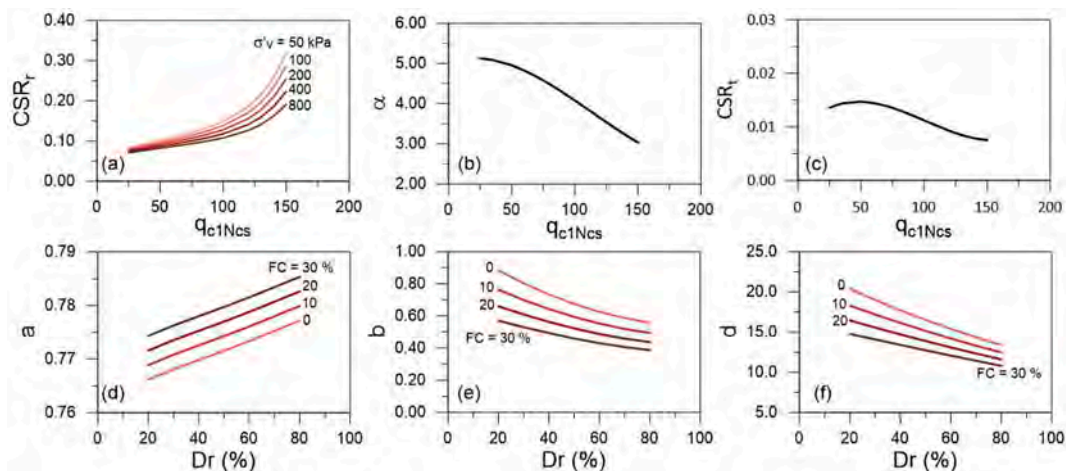


Figure 1. Parameters of the PWP model: (a) CSR_t , (b) α and (c) CSR_t of Eq. (1) as a function of q_{c1Ncs} ; (d) a , (e) b and (f) d of the Eq. (2) as a function of the fines content, FC , and the relative density, Dr .

3 ADVANCED STATE CONCEPT-BASED SOIL CONSTITUTIVE MODEL

An advanced soil constitutive model, called “Stress-Density” model (S-D Model) is formulated by Cubrinovski & Ishihara (1998a,b).

The S-D Model is a state-concept based model that accounts for the combined effects of density and confining stress on sand behavior through the state-concept framework. The benefit of this, in addition to the consistent modeling of stress-density effects on sand behavior, is that the model is a true material model with a single set of parameters representing a given soil across all relevant density-stress states.

Soil properties required for the S-D Model fall into four categories: critical state line (used to define the state of the soil relative to the reference state, the critical state); plastic stress-strain parameters (defining the shear stress-plastic shear strain relationship); stress-dilatancy parameters (providing the link between plastic shear strain and plastic volumetric strain increments); and elastic parameters (determining an incremental stress-strain relationship for elastic behavior).

The S-D Model is implemented in the finite element code DIANA-J (Corporation Taisei 1997), allowing to perform effective stress dynamic analysis according to a fully coupled approach.

4 CASE STUDY

The considered case study is the “YY-site” excited by the 22 February 2011 Canterbury earthquake. Figure 2 reports the outcrop motion of the deconvolved fault-normal component of the 22 February 2011 earthquake record at the Canterbury Aero Club (CACS) strong motion station, considered in the simulations.

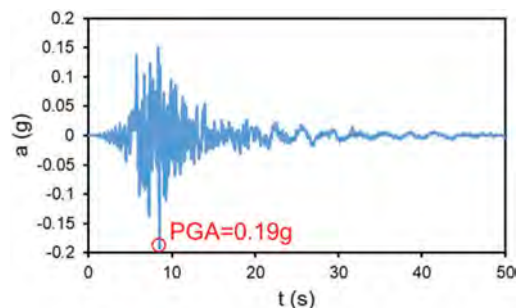


Figure 2. Reference input motion.

The soil column consists of a 20 m deposit, where eight different soil layers, named from “mat1” to “mat8”, are identified (Figure 3). The soil properties (specific gravity, G_s , porosity, n , shear wave velocity, V_s , small-strain damping, D_0 , permeability coefficient, k), of each material are the results of the soil investigations carried out by Cubrinovski et al.

(2019), and are reported in Table 1. The small-strain shear modulus of each layer was inferred from the shear wave velocity profile shown in Figure 3.

The groundwater table depth identifies the thickness of the liquefiable layer between 1.8 and 10 m depth.

This liquefiable deposit was divided into four different materials (from “mat2” to “mat5”) as a function of the normalized and corrected cone tip resistance, q_{e1Ncs} , as reported by Cubrinovski et al. (2019).

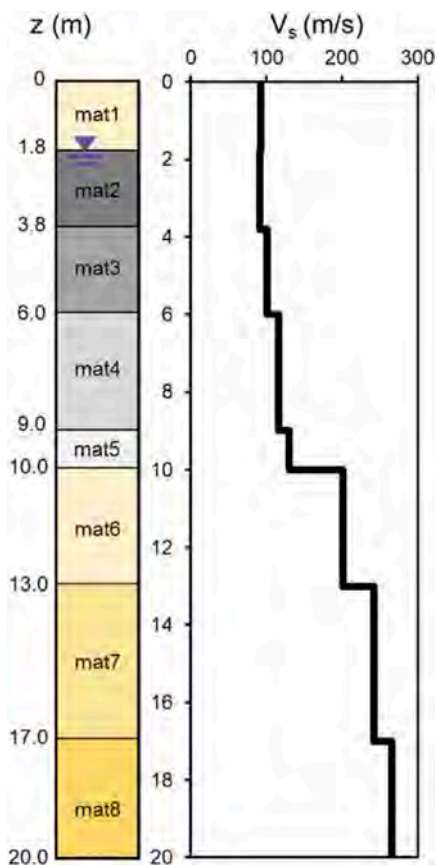


Figure 3. Layering and V_s profile.

Table 1. Soil properties.

Soil	G_s	n	V_s	D_0	k
			(m/s)	(%)	(m/s)
mat1	2.65	0.412	93	1.406	$4 \cdot 10^{-6}$
mat2	2.65	0.462	91	1.073	$4 \cdot 10^{-6}$
mat3	2.65	0.460	101	0.969	$1 \cdot 10^{-4}$
mat4	2.65	0.444	116	0.882	$2 \cdot 10^{-4}$
mat5	2.65	0.412	130	0.834	$3 \cdot 10^{-4}$
mat6	2.65	0.500	202	0.797	$1 \cdot 10^{-4}$
mat7	2.65	0.500	242	0.750	$1 \cdot 10^{-4}$
mat8	2.65	0.500	266	0.712	$1 \cdot 10^{-4}$

5 PRELIMINARY VISCO-ELASTIC LINEAR ANALYSES

Preliminarily visco-elastic linear analyses of the considered case study were performed by both loosely and fully coupled approaches, implemented in the SCOSSA and DIANA-J codes respectively. These preliminarily dynamic analyses aimed to check that the boundary conditions and small-strain soil behavior were reasonably reproduced in the same way in both approaches. To further identify possible sources of discrepancies, the same analysis was carried out with two additional computer codes widely adopted in the professional practice: the equivalent linear code in the frequency domain STRATA (Kottke et al. 2003), and the nonlinear code in the time domain Deepsoil (Hashash et al. 2016). For this latter, two conditions of the bedrock were considered, a perfectly rigid half-space, and a deformable one with a shear wave velocity of 800 m/s, a unit weight equal to 22 kN/m³ and a viscous damping ratio equal to 0.5%. The same options are available in the computer code SCOSSA. A deformable bedrock was also adopted in the analysis performed with STRATA.

In the DIANA-J code, the soil column is excited at the base by a horizontal force-time history which is proportional to the known velocity time history of the input ground motion (Ntritos & Cubrinovski 2020).

The small-strain shear modulus inferred from the V_S and damping ratio, D_0 , adopted as a target for the analyses are reported in Table 1. While the small-

strain modulus is introduced in the different codes as an elastic modulus, the small-strain damping D_0 is modeled in different ways in the adopted codes.

STRATA adopted a frequency-independent formulation, where the damping ratio is assumed to be constant with the shear strain level. The nonlinear codes SCOSSA and Deepsoil used a full Rayleigh damping formulation with two frequencies control. Finally, a full Rayleigh damping formulation with a single frequency control is used in DIANA-J. To match as close as possible the damping curves used in the different analyses, the parameters of the single-frequency control damping ratio curve in DIANA-J were defined as equivalent parameters, i.e., yielding the same damping-frequency function as the double frequency method used by SCOSSA.

The results of the visco-elastic analyses in terms of profiles of maximum acceleration, shear strain and shear stress are reported in Figure 4.

It can be observed that all the analyses showed similar responses, with amplification of the acceleration at the surface and higher shear strains attained in the liquefiable layers. Closer results can be noted in the analyses where the deformability of the seismic bedrock is considered, while higher maximum acceleration and shear strains are ascribed to the analyses where a rigid bedrock is modeled. This effect is due to the lack of radiation damping through the bedrock, which usually causes the free surface motion amplitudes of the case of deformable bedrock to be smaller than those in the case of rigid bedrock.

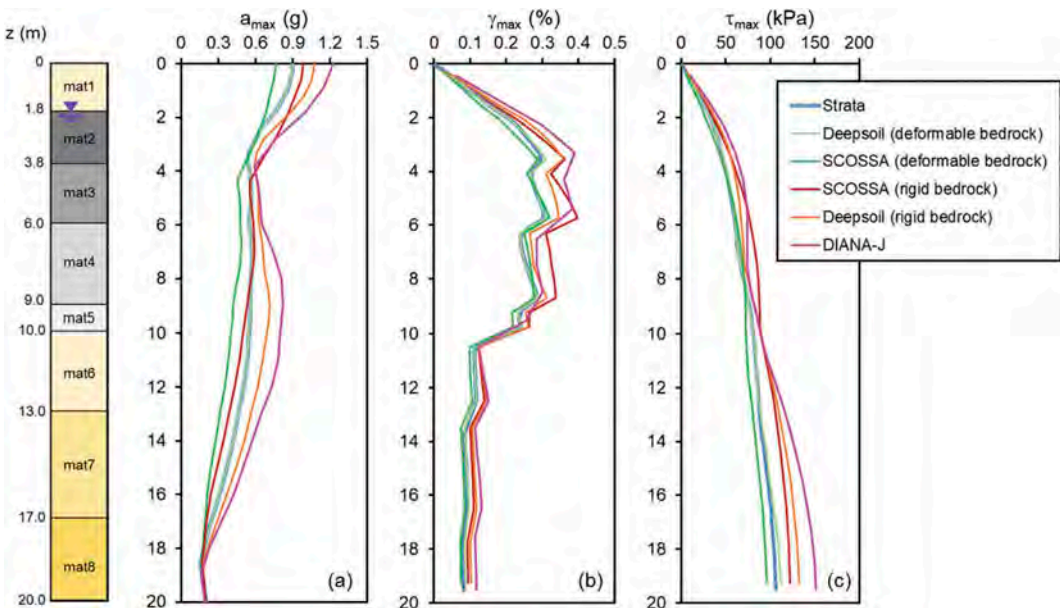


Figure 4. Vertical profiles of maximum (a) acceleration, (b) shear strain and (c) shear stress attained during the visco-elastic linear analyses.

6 NON-LINEAR EFFECTIVE STRESS ANALYSES

6.1 Loosely coupled approach

In the loosely coupled approach adopted in SCOSSA, the nonlinear and dissipative soil behavior were simulated through the definition of the normalized shear modulus, G/G_0 , and damping ratio, D , with the shear strain, γ . The curves proposed by Darendeli (2001) as a function of the effective confining pressure of each layer were adopted and analytically fitted by the MKZ model (Figure 5).

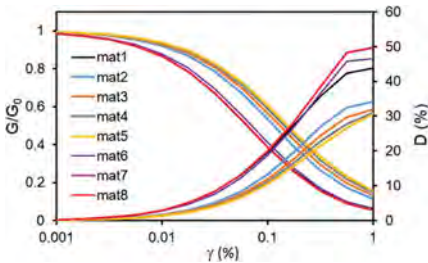


Figure 5. Normalized shear modulus and damping ratio vs shear strain.

The parameters of the PWP model to be assigned to the four liquefiable soils were defined through the charts in Figure 1, as a function of the geostatic effective vertical stress at the mean depth of each layer, the q_{c1Ncs} and fines content equal to 0. The defined curves are plotted in Figure 6 and the related model parameters are reported in Table 2.

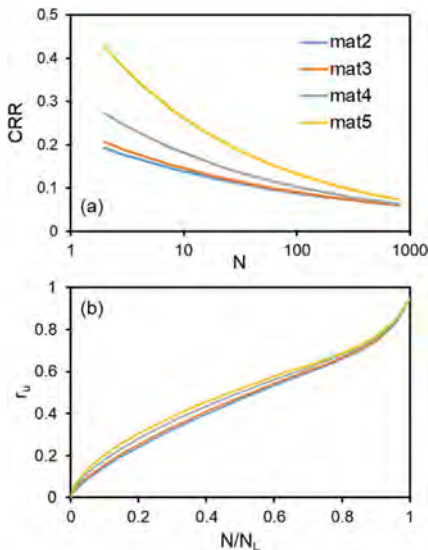


Figure 6. (a) Cyclic resistance and (b) excess pore water pressure ratio curves.

Table 2. Parameters of the PWP model.

Soil	q_{c1Ncs}	CRR - N_L			$r_u - N/N_L$		
		CSR _r	α	CSR _t	a	b	d
mat2	80	4.486	0.013	0.127	0.771	0.723	17.02
mat3	90	4.289	0.012	0.134	0.772	0.692	16.46
mat4	115	3.755	0.010	0.164	0.774	0.630	15.29
mat5	140	3.224	0.008	0.232	0.775	0.582	14.37

6.2 Fully coupled approach

For the considered soil column, the S-D Model parameters were determined by combining the use of empirical relationships and generic data for sandy soils. For non-liquefiable soils, the target cyclic stress-strain relationship is defined using strain-dependent stiffness degradation and damping ratio curves, commonly employed in site response analyses. For the liquefiable soils, the model parameters were constrained to simulate the target liquefaction resistance curves for the four soil layers determined based on the simplified liquefaction triggering procedure of Boulanger and Idriss (2014), as described in Cubrinovski et al. (2019). The model parameters and calibrated values of the considered case are reported in Cubrinovski et al. (2019), and not reported here for sake of brevity.

6.3 Results of the effective stress analyses

The results of the effective stress analyses in terms of profiles of maximum acceleration, shear strain and shear stress are reported in Figure 7. The profiles of maximum acceleration show a certain variability, with higher values of SCOSSA compared to DIANA-J in the liquefiable deposit between approximately 5 and 10 m (Figure 7a). In the remaining layers, the prediction of DIANA-J overcomes that of SCOSSA, especially at the ground level, with a predicted value of 0.38 g. The integral of the acceleration profiles in both analyses leads to a similar shear stress profile, with a slightly higher prediction provided by the analysis performed with the DIANA-J code (Figure 7b).

In the loosely coupled approach, the liquefaction condition is attained in the two shallow critical layers, mat2 and mat3, between 2 and 5 m (Figure 7c), where the lowest value of the cone tip resistance induces the lowest cyclic resistance curves (Figure 6a). It should be pointed out that at liquefaction $r_u = 0.9$ to guarantee numerical stability (Tropeano et al. 2019). In the fully coupled approach, the liquefaction is triggered in the mat2, while $r_u < 0.7$ is observed in the other liquefiable soils. The main differences

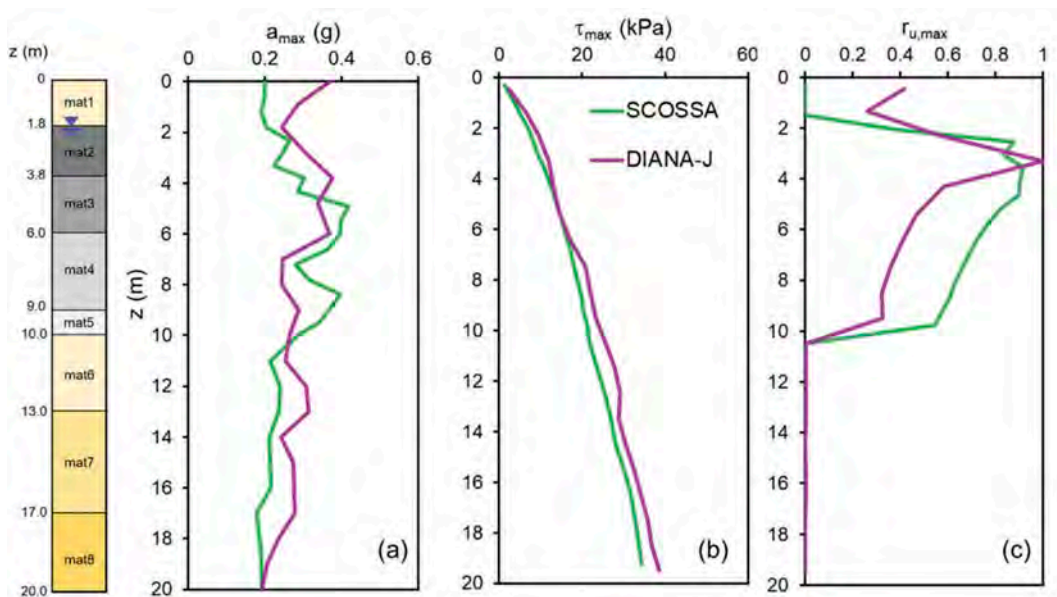


Figure 7. Vertical profiles of maximum (a) acceleration, (b) shear stress and (c) excess porewater pressure ratio attained during the nonlinear effective stress analyses.

between the two approaches are also due to the way the dissipation and redistribution of excess pore water pressure along the soil column are implemented. DIANA-J can simulate the water flow in the shallowest and unsaturated layer (mat 1), while this latter remains perfectly dry in the SCOSSA analysis.

Additionally, the simplified PWP model generated higher pore water pressure than the S-D model between 5 and 10 m, which is anyway in accordance with a quite conservative approach expected in the simplified soil modeling.

7 CONCLUSIONS

This paper investigated the performance of the CPT-based calibration procedure of a simplified PWP model in predicting the liquefaction of a layered liquefiable soil column. A case study from the liquefaction observed in Christchurch after the 2011 earthquake is considered, and also a comparison with an advanced constitutive model is provided. Some limitations of the simplified approach are mainly associated with the overestimation of the generated pore pressure induced by the seismic event. However, despite the simplifications adopted in the CPT-based calibration process, the effective stress analyses performed replicated the occurrence of liquefaction observed at the site and furtherly encourage CPT-based model parameter definition for routine effective stress dynamic analyses.

ACKNOWLEDGEMENTS

The first author was supported by the Italian Ministry of Research through the ‘Attraction and International Mobility’ project.

REFERENCES

- Boulangier, R.W. & Idriss, I.M., 2014. CPT and SPT liquefaction triggering procedures. Report No UCD/GCM-14/01, University of California at Davis, California, USA.
- Chiaradonna, A., Flora, A., d’Onofrio, A. & Bilotta, E. 2020. A pore water pressure model calibration based on in-situ test results. *Soils Found.* 60(2): 327–341
- Chiaradonna, A., Tropeano, G., d’Onofrio, A., & Silvestri, F. 2018. Development of a simplified model for pore water pressure build-up induced by cyclic loading. *Bulletin of Earthquake Engineering.* 16(9): 3627–3652
- Chiaradonna, A., Tropeano, G., d’Onofrio, A. & Silvestri, F. 2019. Prediction of non-linear soil behaviour in saturated sand: a loosely coupled approach for 1D effective stress analysis. *Proc. 7ICEGE, Rome*, June 2019.
- Corporation Taisei 1997. DIANA-J3: finite element program for effective stress analysis of two-phase soil medium. Internal report, Software science. 1997 (in Japanese).
- Cubrinovski, M. & Ishihara, K. 1998. Modelling of sand behaviour based on state concept. *Soils Found* 38 (3):115–27.
- Cubrinovski, M. & Ishihara, K. 1998. State concept and modified elastoplasticity for sand modelling. *Soils Found* 38(4):213–25.

- Cubrinovski, M., Rhodes, A., Ntritsos, N. & Van Ballegooy, S. 2019. System response of liquefiable deposits, *Soil Dynamics and Earthquake Engineering*, 124, 212–229.
- Kottke, A.R., Wang, X. & Rathje, E.M. 2003. Technical Manual for Strata. Geotechnical Engineering Center, University of Texas, Austin (USA).
- Hashash, Y. M. A., Musgrove, M. I., Harmon, J. A., Groholski, D. R., Phillips, C. A., & Park, D. 2016. DEEPSOIL 6.1, user manual. Urbana, IL, Board of Trustees of University of Illinois at Urbana-Champaign.
- Ntritsos, N. & Cubrinovski, M. 2020. A CPT-based effective stress analysis procedure for liquefaction assessment. *Soil Dynamics and Earthquake Engineering*, 131, 106063.
- Tropeano, G., Chiaradonna, A., d’Onofrio, A., and Silvestri, F., 2019. Numerical model for non-linear coupled analysis on seismic response of liquefiable soils. *Computers and Geotechnics* 105: 211–227.
- Hashash, Y.M.A., Musgrove, M.I., Harmon, J.A., Groholski, D.R., Phillips, C.A., Park, D., 2016. DEEPSOIL 6.1, User Manual. Urbana, IL, Board of Trustees of University of Illinois at Urbana-Champaign.
- Robertson P.K. & Cabal K.L. 2015. Guide to Cone Penetration Testing for Geotechnical Engineering. Gregg drilling. 6th edition.

Stress increase induced by impact precast pile driving

V. Colella

Geofondazioni Ingegneria e Lavori s.r.l., Martellago, Italy

G. Cortellazzo

University of Padua, Padua, Italy

A. Dei Svaldi

Desam ingegneria e ambiente s.r.l., Italy

S. Amoroso & L. Minarelli

University of Chieti-Pescara, Istituto Nazionale di Geofisica e Vulcanologia, Italy

K.M. Rollins

Brigham Young University, Utah, USA

ABSTRACT: The paper describes the experimental activities carried out in a test site, set up to evaluate the increase of soil stiffness and horizontal effective stress, mainly in saturated low-medium density sandy layers and in silty sand, after the driving of tapered precast piles.

The experimentation consisted in driving some prefabricated tapered piles with different energies and spacing between them in an area where some soil layers had a high liquefaction potential. To evaluate the pile driving effects on the stress state around them, preliminary CPTu and DMT tests were carried out and repeated after the driving activity.

In particular, the change of the CPTu sleeve resistances was compared with that of the DMT K_D data, to evaluate the increase in horizontal stress using different methods, a phenomenon influencing the soil susceptibility to liquefaction and the pile bearing capacity.

1 INTRODUCTION

To reduce the potential liquefaction-induced settlement in cohesionless soils, many ground improvement techniques are adopted, among them vibrocompaction, rammed aggregate piers (RAP), stone columns, drilled displacement piles, driven displacement piles, deep dynamic compaction, and blast densification (Han 2015). In particular numerous studies have been performed to evaluate the ability of deep vibratory compaction (Van Impe et al., 1994, Massarch & Fellenius 2002, Massarch et al. 2020), of drilled displacement piles (Siegel et al. 2007, Siegel et al. 2008) and RAP (Rollins et al. 2021) to mitigate the risk of liquefaction in sandy soils, while few refer to the use of driven precast tapered piles.

With deep vibratory compaction cyclic stresses are generated in the ground, resulting in a denser particle arrangement and changes in effective stresses. The installation process of drilled displacement piles

consists in displacement of soil and subsequent placement of fluid cement grout within the dislocated volume. For RAPs, the improvement mechanisms include increased lateral pressure and increased shear stiffness.

These processes can result in a measurable densification and in an increase in lateral stress. Therefore, these methods are used to mitigate cyclic liquefaction in sandy soils.

To recognize the deriving soil improvement, the most widely in situ tests used are the cone penetration test (CPT), CPT with pore water pressure measurement (CPTu), the seismic cone penetration test, the Marchetti flat dilatometer test (DMT) or the seismic dilatometer test (Mayne et al. 2009).

Indeed, the CPT and the DMT measured data enable to detect changes in strength, stiffness, and horizontal stress in the soil.

The installation process of driven precast piles determines, seemingly, similar phenomena, but there is a lack of knowledge about their quantification.

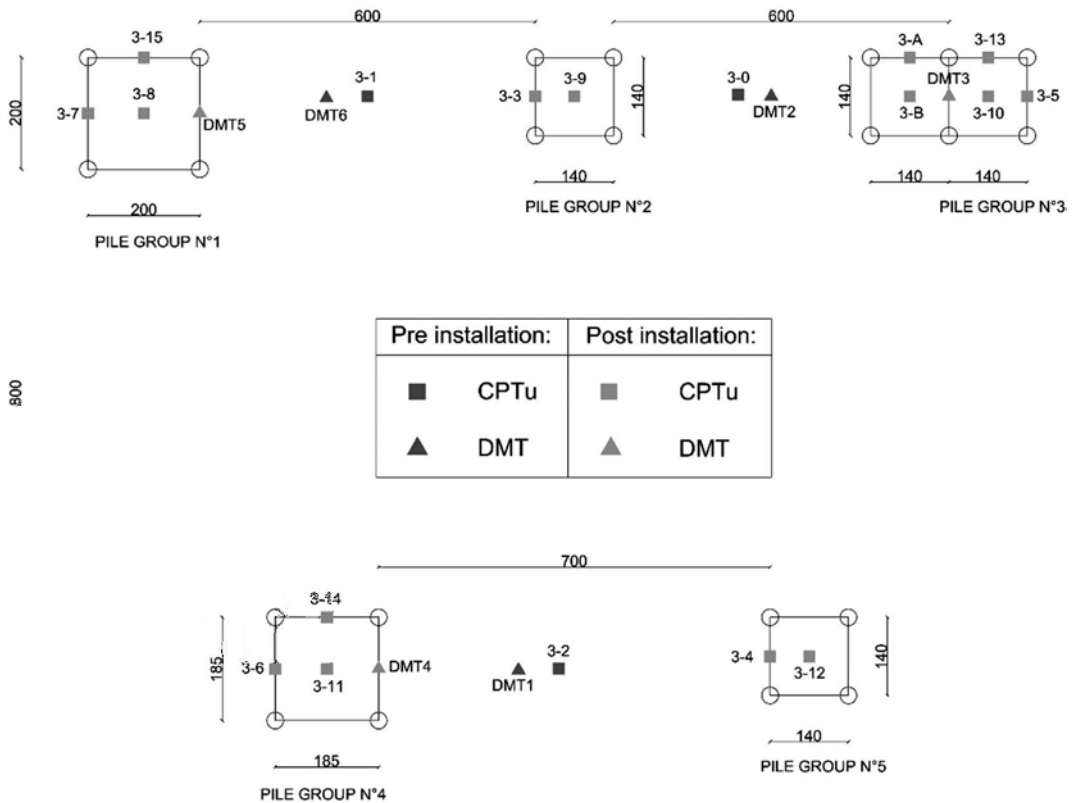


Figure 1. Configurations of pile groups and relative CPTu/DMT locations.

Therefore, the paper describes the experimental activities carried out in a test site, set up to evaluate the possible existence of these phenomena after the driving of precast piles.

The experimentation consisted in driving some prefabricated tapered piles with different energies and spacing between them in an area where some soil layers had a high liquefaction potential. To evaluate the pile driving effects on the stress state around them, preliminary CPTu and DMT tests were carried out and repeated at various distances from the pile center, after the driving activity.

One of the most interesting objectives of the research is to evaluate the change of the tip (q_t) and sleeve resistances (f_s) of the CPTu tests, comparing them with the data acquired using the DMT tests, principally the horizontal stress index K_D . Among the various phenomena influencing the soil susceptibility to liquefaction and the pile bearing capacity, the increase of horizontal stresses, resulting in a preloading effect, and its accurate determination could allow economic benefits in the design of deep foundations.

2 TEST SITE CHARACTERIZATION

2.1 Soil characteristics

The experimental site was chosen in the area where the most significant and widespread liquefaction phenomena had occurred during the 2012 Emilia seismic sequence. In particular the choice fell on an area near the Mirabello village (Ferrara, Italy), previously investigated in detail since a blast test was carried out in a neighboring area, in 2016 (Amoroso et al. 2017). During these previous studies, geological, geotechnical and geophysical characterization was carried out in proximity to the observed liquefaction evidence. The geotechnical in situ investigation included several standard penetration tests, piezocone tests, seismic dilatometer tests and deep boreholes, while geophysical tests included down-hole tests (DH1), MASWs (Multi-channel Analysis of Surface Waves), P-wave and S-wave topographies, electrical resistivity topographies (Amoroso et al. 2017). During the new research further CPTu and DMT tests were carried out in the specific test area (CPTu 3-0, 3-1 and 3-2 and DMT 1, 2 and 3 – Figure 1) to confirm the main soil characteristic recognized previously.

On the basis of the abovementioned investigations, a geotechnical model was determined and the layers with the higher probability of liquefaction were identified. In the following, the main units are listed with their Unified Soil Classification System (USCS) descriptors according to ASTM D2487-11 (2011):

- Topsoil from 0 to 1 m bgl (CH) – Layer 1;
- Silty clay from 1 to 4 m bgl (CH) – Layer 2;
- Clayey silt with sand from 4 to 6 m bgl (CL-CH) – Layer 3;
- Silty sand and sandy silt (fluvial Apeninic deposits) from 6 to 8 m bgl (ML-SM) – Layer 4;
- Silty sand (paleochannel of the Po River) from 8 to 17 m bgl (SM) – Layer 5;
- Silty sand (Syn-Glacial braided Po River deposits) from 17 to 20 m bgl (SM) – Layer 6.

2.2 Pile test characteristics

In the area four pile groups, with four piles each, and one with six piles were set up (Figure 1).

The piles were tapered precast piles 16.0 m long, with a tip/head diameter of 260/500 mm and a taper of 15 mm/m.

In pile groups N.2, N.3 and N.4 piles have the same center distance, but were driven with different energies, measured using a Pile Driving Analyser (PDA).

Chosen the installation energy of the piles ensuring the best performance as regards the improvement of the soil characteristics, two other pile groups were set up with a larger center distance than the previous ones. In Table 1 are shown the data regarding center distance and installation energy.

Table 1. Installation energy and center distance of piles in the pile groups.

Pile group	Energy (E)	Center distance (i)
	kNm	m
1	43.0	2.00
2	25.0	1.40
3	43.0	1.40
4	43.0	1.85
5	20.0	1.40

3 RESULTS

3.1 Analysis of q_t data

Figures 2, 3 and 4 show the profiles of the corrected cone tip resistance (q_t) acquired before and after the pile driving activity for the different pile groups. The CPTu tests after the pile driving were performed

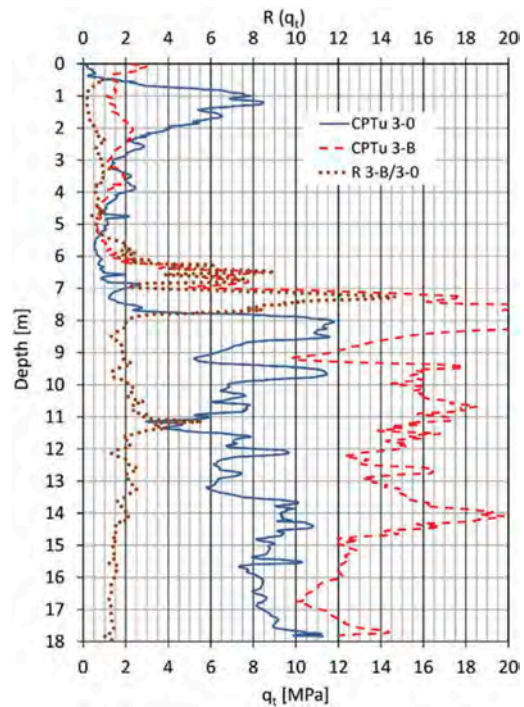


Figure 2. Corrected cone tip resistance q_t before and after pile driving and $R(q_t)$ value - Pile group N.3 [$E=43$ kNm, $i=1.4$ m].

both in the center position of the group and along one or two sides of the group of piles.

The influence of tapered precast pile installation may be represented by the ratio post-installation q_t to the pre-installation q_t , the Improvement Ratio [$R(q_t)$], defined by the following expression:

$$R(q_t) = \frac{q_{t \text{ post installation}}}{q_{t \text{ pre installation}}} \quad (1)$$

It was computed at each measurement depth and shown in the same figures.

The $q_{t \text{ post installation}}$ data differ considerably depending on both the pile driving energy used and the distance between the piles.

Considering the group of piles N.3, there is a high increase in q_t along the entire profile of the pile, after the installation, in the layers 4 and 5 (Figure 2) with an average increase of about 2 in soils with initial q_t greater than 6 MPa and even greater with values lower than 6 MPa. In the latter case, some of the very high values could depend on the comparison of different type soils (clay in the pre-installation CPTu and sand in the post-installation CPTu).

In the case of pile group N.2, the piles have the same center distance as group N.3, but they have been driven with lower energy (Table 1). $R(q_t)$ is

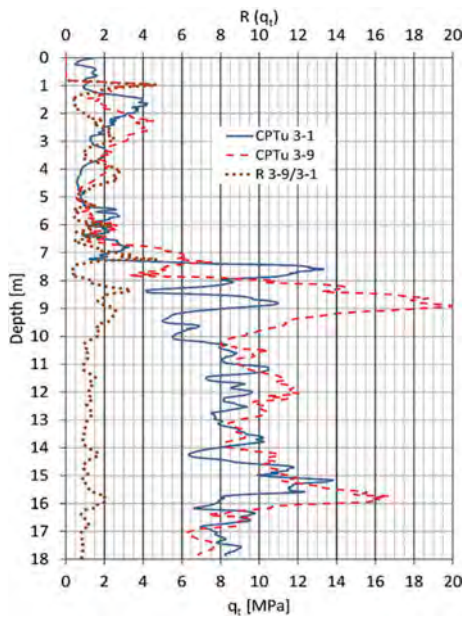


Figure 3. Corrected cone tip resistance q_t before and after pile driving and $R(q_t)$ value - Pile group N.2 [$E=25$ kNm, $i=1.4$ m].

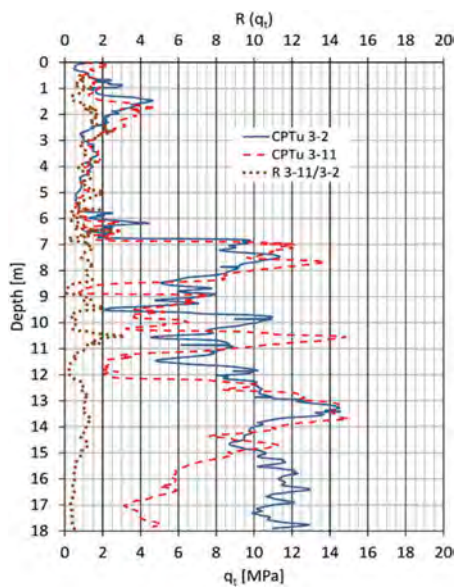


Figure 4. Corrected cone tip resistance q_t before and after pile driving and $R(q_t)$ value -Pile group N.4 [$E=43$ kNm, $i=1.85$ m].

significantly greater than 1 (Figure 3) only in the first meters of the silty sand layer 5, probably due to the effect of the lateral spreading of the soil, and is equal to 1 at deeper levels.

Finally, in the case of pile group N.4 (Figure 4), in which the piles have been driven with the same energy used for those of stand 3, but with a center

distance of approximately 1.85 m, R has a value substantially equal to one, showing a lack of improvement, albeit a probable stratigraphic variability is present at various depths. A similar situation is also observed in the case of pile group N.1.

3.2 Analysis of K_D and f_s data

A similar comparison was carried out taking into account the horizontal stress index K_D of DMT tests carried out before and after the installation of the piles. The DMTs after installation were performed along one side of the pile groups.

K_D of the dilatometric test is strictly correlated with the horizontal earth stress coefficient and therefore with the horizontal stresses.

As in the previous cases, the influence of tapered precast pile installation may be represented by the ratio post-installation K_D to the pre-installation K_D , the Improvement Ratio [$R(K_D)$], defined by the following expression:

$$R(K_D) = \frac{K_{D \text{ post installation}}}{K_{D \text{ pre installation}}} \quad (2)$$

Also in this case for pile group N.3 (Figure 5) there is a marked increase in post-installation K_D with $R(K_D)$ values between 3 and 5, while for pile group N.4 the improvement is absent, except in the loose silty sand and sandy silt layer between 6.0 and 8.0 m, having a low cone resistance (Figure 6).

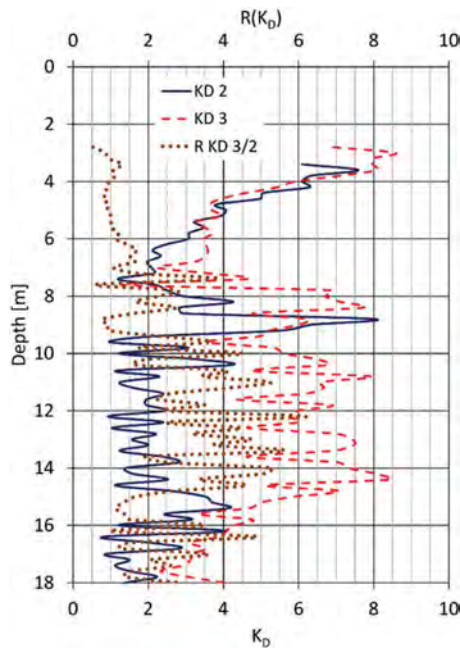


Figure 5. K_D before and after pile driving and $R(K_D)$ value - Pile group N.3 [$E=43$ kNm, $i=1.4$ m].

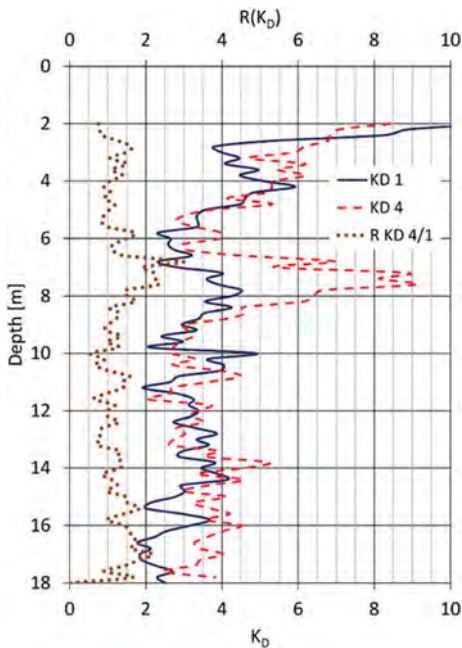


Figure 6. K_D before and after pile driving and $R(K_D)$ value - Pile group N.4 [$E=43$ kNm, $i=1.85$ m].

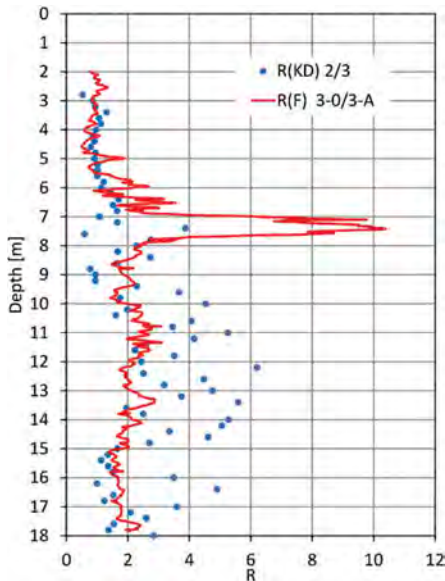


Figure 7. $R(K_D)$ and $R(F)$ - Pile group N.3 [$E=43$ kNm, $i=1.40$ m].

Robertson (2016) highlighted that the normalized CPT sleeve resistance ($F = f_s / \sigma'_{v0}$) can be used to estimate the DMT K_D ; therefore, the trend along the depth between $R(K_D)$ and $R(F)$ of various pile groups was compared, where $R(F)$ is the following expression

$$R(F) = \frac{F_{post\ installation}}{F_{pre\ installation}} \quad (3)$$

Both ratios show the same phenomena, improvement of soil characteristics in correspondence of pile group N.3 (Figure 7) and modest if not zero improvement in pile group N.4 (Figure 8). Therefore, both, again, highlight the decrease of the improvement as the distance between the piles increases. The $R(K_D)$ ratio also is more sensitive than $R(F)$ to the effects of the pile driving.

3.3 Cumulative settlement prediction

Adopting the Zhang et al. (2002) method to estimate liquefaction-induced ground settlements using CPT data, the effectiveness of the driving of piles on the decrease of the potential liquefaction effects was determined.

The Zhang approach combining the CPT estimate liquefaction resistance with laboratory test results on clean sand evaluates the liquefaction-induced volumetric strains for sandy and silty soils.

Zhang et al. (2002) assume that little or no lateral displacement occurs after the earthquake, such that the volumetric strain will be equal or close to the vertical strain. Integrating with depth the vertical strain in each soil layer, the potential liquefaction-induced ground settlement due to an earthquake is estimated by Equation 4,

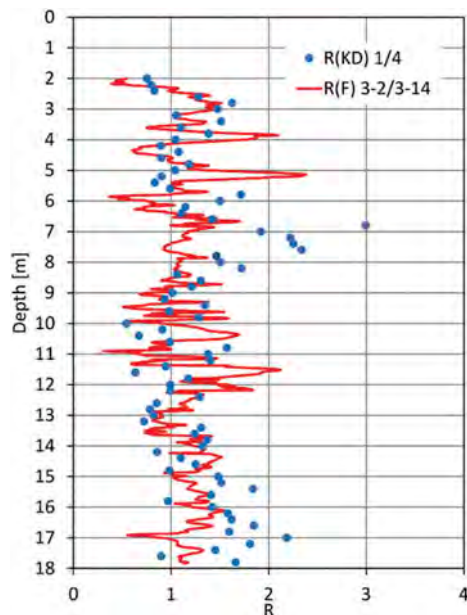


Figure 8. $R(K_D)$ and $R(F)$ - Pile group N.4 [$E=43$ kNm, $i=1.85$ m].

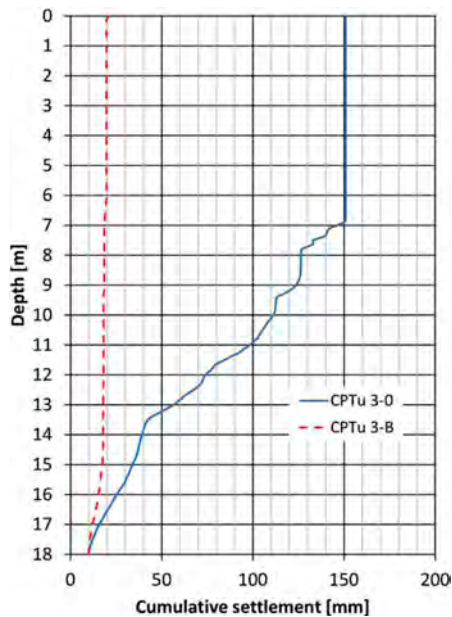


Figure 9. Post liquefaction settlement using Zhang et al. method (2002) - Pile group N.3 [$E=43 \text{ kNm}$, $i=1.4 \text{ m}$].

$$w = \sum_{i=1}^j \varepsilon_{vi} \Delta Z_i \quad (4)$$

where w is the calculated liquefaction-induced ground settlement at the CPT location; ε_{vi} is the postliquefaction volumetric strain for the soil sublayer i ; ΔZ_i is the thickness of the sublayer i ; and j is the number of soil sublayers.

The analysis of data related to the pile group N.3 (Figure 9) shows a great decrease of potential post liquefaction settlement and consequently that the improvement is large. Therefore, with groups of more piles than in this case, significant improvements can be achieved from the point of view of a potential soil liquefaction settlement lower than the virgin soil.

4 CONCLUSIONS

The CPTu and DMT in situ tests were used to evaluate the improvement of the soil characteristics due to the driving of precast tapered piles.

The data acquired using the CPT and DMT tests show that the installation of prefabricated tapered piles determines an increase of the soil resistance, pointed out by the increase in q_c , as well as a change in effective lateral stress highlighted by both the increase of F and K_D .

The phenomenon is clearly remarkable up to a distance of about 4-5 pile diameters; beyond this distance the phenomenon tends to run out.

In the present case, the driving energy played a non-negligible role in the amount of the improvement.

Referring to the potential post-liquefaction settlement due to an earthquake and determined with the

Zhang et al. (2002) calculation method, the improvement of the soil behavior achievable through the installation of driving piles was clearly highlighted.

REFERENCES

- Amoroso, S., Milana, G., Rollins, K.M., et al. 2018. The first Italian blast-induced liquefaction test (Mirabello, Emilia-Romagna, Italy): description of the experiment and preliminary results. *Annals of Geophysics* 60(5): S0556.
- ASTM D2487-11, 2011. Standard Practice for Classification of Soils for Engineering Purposes (Unified Soil Classification System).
- Fontana, D., Amoroso, S., Minarelli, L. & Stefani, M. 2019. Sand liquefaction induced by a blast test: new insights on source layer and grain size segregation mechanisms (late Quaternary, Emilia, Italy). *Journal of Sedimentary Research*, v. 89, 13–27.
- Han, J. 2015. *Principles and practices of ground improvement*. Hoboken, NJ: Wiley.
- Massarsch, K.R. & Fellenius, B.H. 2002. Vibratory compaction of coarse-grained soils. *Canadian Geotechnical Journal* 39(3): 695–709.
- Massarsch, K.R., Wersäll, C. & Fellenius, B.H. 2020. Horizontal stress increase induced by deep vibratory compaction. *Proceedings of the Institution of Civil Engineers – Geotechnical Engineering* 173(3): 228–253.
- Mayne, P.W., Coop M.R., Springman S., Huang A.B. & Zornberg, J. 2009. Geo material behavior and testing. In Hamza M, Shahien M & El-Mossallamy Y. (eds), *Proceedings of the 17th International Conference on Soil Mechanics and Geotechnical Engineering (ICSMGE)*. Millpress/IOS Press, Rotterdam, the Netherlands, vol. 4, pp. 2777–2872.
- Robertson P.K. 2016. Estimating K_0 in sandy soils using the CPT. In Lehane, Acosta-Martinez & Kelly (Eds). *Geotechnical and Geophysical Site Characterisation 5 – ISC’5, Gold Coast, Queensland, Australia, September 5 – 9, 2016*.
- Rollins, K.M., Amoroso, S.; Paul Andersen, P., Tonni, L. & Wissmann, K. 2021. Liquefaction mitigation of silty sands using rammed aggregate piers based on blast-induced liquefaction testing. *J. Geotech. Geoenviron. Eng.*, 2021, 147 (9):04021085.
- Siegel, T.C., NeSmith, W.M., NeSmith, W.M. & Cargill, P. E. 2007. Ground improvement resulting from installation of drilled displacement piles. *32nd DFI Annual Conference, Colorado Springs, CO*.
- Siegel, T.C., NeSmith, W.M. & NeSmith, W.M. 2008. Increase in Cyclic Liquefaction Resistance of Sandy Soil Due to Installation of Drilled Displacement Piles. *Earthquake Engineering and Soil Dynamics IV Conference, Sacramento CA*.
- Van Impe, V.F., De Cock, F., Massarsch, K.R. & Mengé, P. 1994. Recent experiences and developments of the resonant vibrocompaction technique. *Proceedings of International Conference on Soil Mechanics and Foundation Engineering, New Delhi, India*. Balkema, Rotterdam, the Netherlands, vol. 3, pp. 1151–1156.
- Zhang, G., Robertson, P.K. & Brachman, R.W.I. 2002. Estimating liquefaction-induced ground settlements from CPT for level ground. *Canadian Geotechnical Journal*. 39(5): 1168–1180. <http://dx.doi.org/10.1139/t02-047>

CPT based liquefaction potential of flood defences in The Netherlands

T. de Gast & K.G. Gavin

Section of Geo-Engineering, Faculty of Civil Engineering and Geosciences, Delft University of Technology, Delft, The Netherlands

P.D. Notenboom & R. Abraimi

Afdeling Kennis & Advies, Waterschap Hollandse Delta, Ridderkerk, The Netherlands

C. Reale

Department of Architecture & Civil Engineering, Centre for Infrastructure, Geotechnical and Water Engineering Research (IGWE), University of Bath, Bath, UK

ABSTRACT: The paper describes a study on the liquefaction potential of flood defences along the rivers running through the delta area of the Netherlands. The study concentrates on an area south of Rotterdam. The dykes used as primary flood defences protect an urban, rural, and industrial area of 102,400 ha. In this paper the data from more than 4200 Cone Penetration Tests, CPT traces are used to assess more than 200 km of dykes. The pore pressure, u_2 data is analysed, then used to separate the material response into contractive and dilative zones. Using the separation of liquefaction susceptible soils, and geometry of the riverbed a regional hazard map is generated. The choices for the data visualisation and their effect on the generated map are discussed and presented. The final liquefaction susceptibility map is used by the water governing authority Waterschap Hollandse Delta as a decision-making tool to improve the efficacy of liquefaction hazard assessment such as the location and return period of bathymetry measurements, and the scale of site- and laboratory investigation.

1 INTRODUCTION

In the Dutch delta, the majority of rural, industrial, and residential land are founded below mean sea level. These areas are reliant on flood defences for everyday protection. In 1953 a major flood following a heavy storm led to some of these dykes failing, which in turn led to large scale flood inundation and loss of life. Since 1953 extensive flood defences along the delta have reduced the risk of coastline flooding significantly. Dykes in the Netherlands are separated into two general types i) primary dykes which protect along the coast and rivers that have large fluctuations in water level during normal operation; and ii) regional dykes, which surround polder-systems where water levels are artificially maintained with little to no fluctuation. The responsibility to protect against inundation in the Netherlands has been given to separate water governing authorities. The water governing authority Waterschap Hollandse Delta (WSHD) are responsible for the safety of the primary and regional dykes around the Islands in the province of South Holland. There are approximately 200 km of primary dykes preventing the local area from flooding. These dykes need to be assessed frequently, considering several different failure mechanisms and their safety needs to be evaluated

and in turn reported to the national government. As part of their most recent assessment, WSHD conducted a large site-investigation campaign consisting of more than 5,000 (or exactly 5,137) Cone Penetration Tests (CPT), 800 boreholes and substantial laboratory tests on the soft deltaic soils. This study utilises this dataset to check for the potential of sand liquefaction beneath the Dykes.

Static liquefaction can occur when loose saturated cohesion less soils are loaded rapidly, for example due to slope over-steepening. Erosion of rivers in the governance area of WSHD affects the slopes of the river channel. This erosion can lead to underwater slope instability potentially leading to a static liquefaction type failure. The current assessment criteria (Rijkswaterstaat 2019) proposes a stepwise approach, where high hazard locations are identified based on their geometry, informed by both the bathymetry of the river basin and the physical geometry of the dyke. High hazard locations are then subjected to more detailed analysis. This study proposes to add to the geometrical data used to pre-screen high hazard locations by using the material behaviour chart (Robertson 2016) to identify underlying soil susceptible to liquefaction in the WSHD area.

2 GEOLOGY OF AREA

The area of investigation lies in the Rhine-Meuse delta which discharges to the North Sea. The river basin consists of silty clay and organic (clay) deposited on top of a Pleistocene sand layer typically located at depths from Dutch Ordnance Datum Level (NAP), NAP -15 m to NAP -20 m depth (≈ 15 to 20m below ground level in this low-lying coastal region). The clay and organic soil layers are intersected by several meandering streams forming channel belts, these are mapped by (Cohen, et al. 2012). Currently the rivers are ‘locked’ in place, meaning that old river channels locations have been fixed in location by engineering works. Dykes have been built to prevent flooding which can change the natural flow path of a river whilst additionally the riverbed is frequently dredged to allow for the safe operation of inland ships serving the Port of Rotterdam and maintain the discharge capacity of the river.

3 METHODOLOGY

Loose silts and fine sands will tend to contract when loaded. During regular static loading where loads are applied slowly (e.g. during construction of a building or dyke) pore pressures dissipate, and settlement occurs. However, if the rate of loading (or unloading) is high, e.g. during erosion, excess pore pressures develop and may lead to liquefaction and sudden large failure e.g. as shown in Figure 1. In dense sands this is not an issue as the particles want to dilate under loading, increasing the voids between particles and consequently the volume for water to occupy. One of the indicators of contractive/dilatative behaviour is a sand's relative density.

In an extensive site-investigation campaign WSHD has performed, 2 CPTs per 100 m length on both the top of the dyke and the inner slope (the slope facing the water being the outer slope). This dataset is used to assess the liquefaction potential



Figure 1. Example liquefaction occurrence, 1968-10-04, Oud-Kempenshofstedepolder (Tholen), by Kotvis, (1986).

along the primary dykes in the governing area of WSHD. The potential for liquefaction is determined by the layer thickness of the contractive sand or the relative density of the material when it is less than 66%. If the relative density decreases or the thickness of the contractive sand layer increases the relative risk of liquefaction in the area increases.

4 CURRENT NATIONAL GUIDELINES

The current Dutch Water Act (DWA, BWBR0025458) which came into effect on January 29th 2009, gives rules and design recommendations for the use and maintenance of Dutch water systems. The water governing authorities in the Netherlands are the primary executive organisations tasked with ensuring the water system and its defences comply with the DWA. Part of the DWA includes design rules for assessing direct and indirect failure mechanisms of dykes. With liquefaction recognised as one of the main indirect failure mechanisms, meaning that should an event happen, it will most likely not be the direct cause of a dyke failure but may contribute to one.

The recommended approach contains three assessments, each more detailed than the one before. The test are: a simple test, a detailed test, and a custom test. The methods of the simple and detailed test are prescribed in the technical guidelines whilst the custom test allows one to utilise the latest scientific insights to make the assessment.

The simple test is a geometric test with conservative assumptions. The detailed test considers soil properties, geometry, water levels and load types. The test itself determines whether there is enough dike forefront left after a liquefaction event to prevent failure (inundation). The DWA is revaluated regularly to incorporate the latest insights in water safety. The latest official code came into effect in 2017 (WBI 2017). While the next instalment is expected in 2023.

Currently there is a large difference in the complexity and as a result the level of detail required in parameter determination between the simple test and the detailed test. Incorporating information from the material behaviour chart into the simple test would allow the WSHD to identify areas more susceptible to liquefaction. This would facilitate them to focus their subsequent detailed assessments on areas with a high liquefaction hazard.

5 DETERMINING CONTRACTIVE ZONES

To identify whether a soil is contractive and subsequently susceptible to liquefaction, the following CPT based procedure developed by (Robertson 1990, Robertson 2016) has been followed. First measured q_c values are normalised into Q_t using the following relations see equations 1 to 3:

$$Q_t = \frac{q_t - \sigma_{v0}}{\sigma'_{v0}} \quad (1)$$

$$F_r = \frac{f_s}{q_t - \sigma_{v0}} * 100\% \quad (2)$$

$$q_t = q_c + u_2(1 - a) \quad (3)$$

Where Q_t is the normalized cone resistance, q_t is the cone resistance corrected for water effects, σ_{v0} is the current in-situ total vertical stress, σ'_{v0} is the current in-situ effective vertical stress, F_r is the normalized friction ratio, f_s is the measured sleeve resistance, q_c is the measured cone resistance, u_2 is the shoulder penetration pore pressure (behind cone tip) and a is the cone area ratio. When normalised CPT parameters have been obtained the soil behaviour indices I_c and I_B as well as the contractive dilative boundary (CD) can be obtained using the following relations, see Equations 4 to 8.

$$I_c = \left[(3.47 - \log Q_t)^2 + (\log F_r + 1.22)^2 \right]^{0.5} \quad (4)$$

$$Q_m = \left[\frac{q_t - \sigma_{v0}}{p_a} \right] \left(\frac{p_a}{\sigma'_{v0}} \right)^n \quad (5)$$

$$n = 0.381(I_c) + 0.05 \left(\frac{\sigma'_{v0}}{p_a} \right) - 0.15 \quad (6)$$

$$I_B = 100(Q_m + 10)(Q_m F_r + 70) \quad (7)$$

$$CD = 70 = (Q_m - 11)(1 + 0.06 F_r)^{17} \quad (8)$$

where p_a being the atmospheric reference pressure and n is the stress exponent defined by equation 6. After obtaining Q_m and F_r and using the boundaries based on I_b and CD suggested by (Robertson 2016) the soil can be classified by the soil type behaviour. The relative density, D_r of young, uncemented silica sands (Kulhawy and Mayne 1990) can be obtained using:

$$D_r = \sqrt{\frac{Q_m}{350}} \quad (9)$$

Figure 2 gives two examples of analysed CPTs using the soil behaviour chart as suggested by Robertson (2016). The following zones are named, CCS (clay-like, contractive, sensitive) CC (clay-like, contractive), CD (clay-like, dilative), TC (transitional, contractive), TD (transitional, dilative), SC (sand-like, contractive) and SD (sand-like, dilative). Figure 2a shows a CPT having a large number (606) of contractive points, and in Figure 2b fewer (296) contractive points are found.

6 IDENTIFICATION AND VISUALISATION OF LIQUEFACTION HAZARD

To identify the liquefaction potential the CPTs are automatically processed. For the calculation of

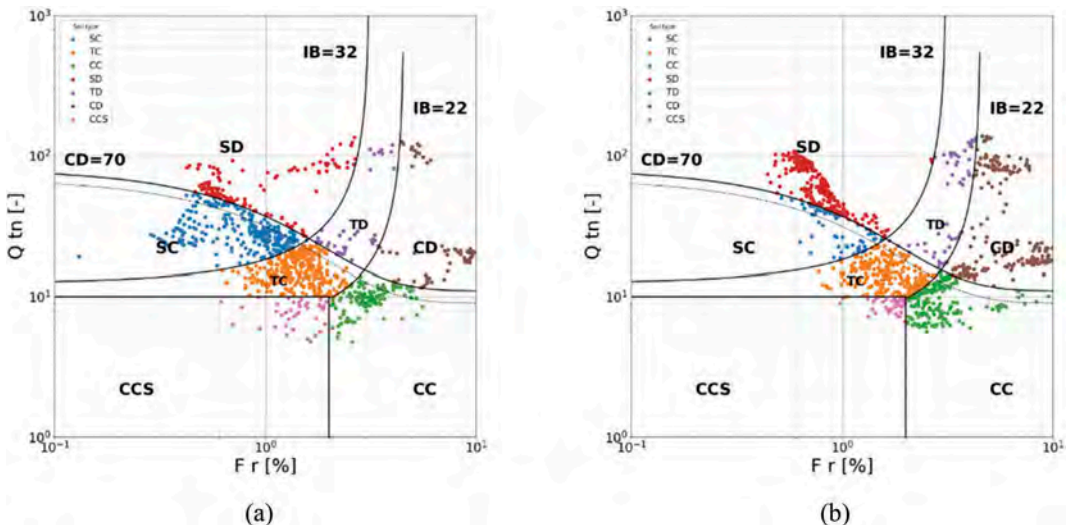


Figure 2. Example soil behaviour chart after Robertson (2016) for two CPTs a) containing a large number (606) of contractive soil points and b) containing fewer (296) contractive points.

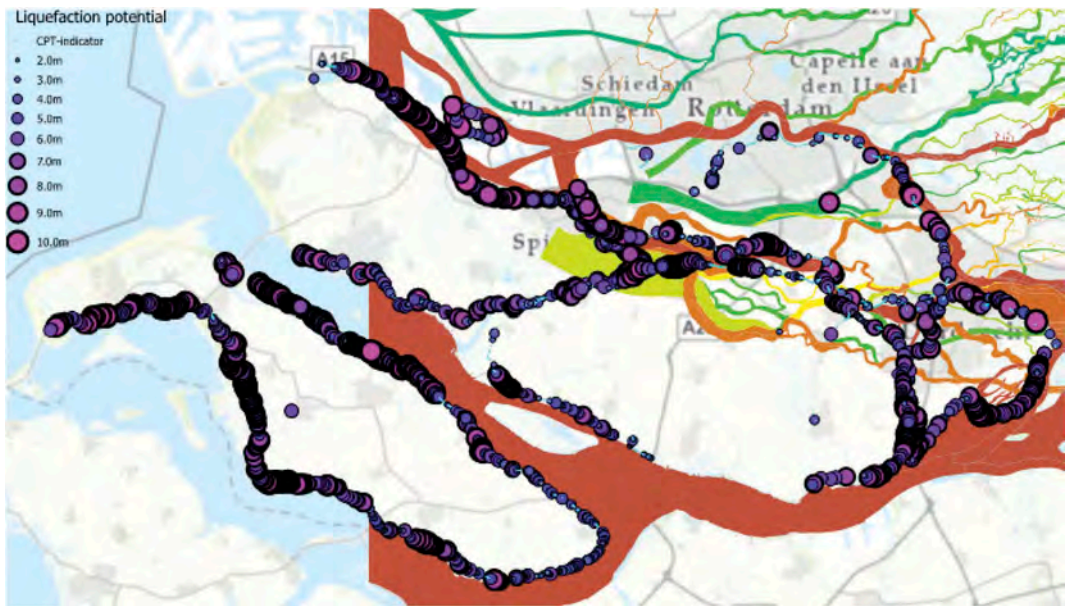


Figure 3. Governing area of WSHD overlaid with the old and current channel belts map, SC-SD-TC-TD 66% window is 200cm, CPT point size scaled to number of liquefaction susceptible points.

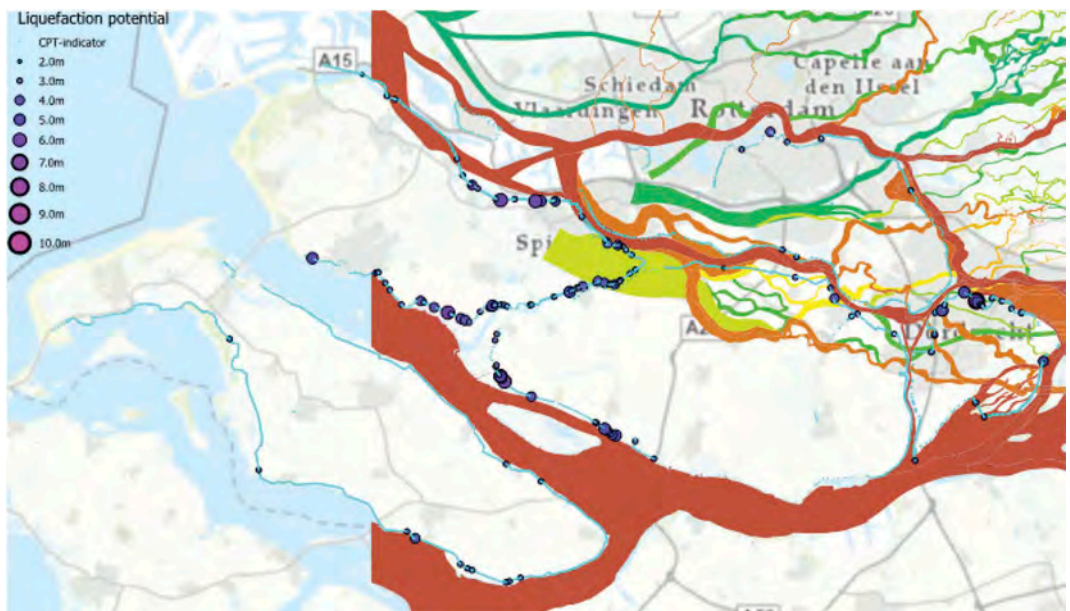


Figure 4. Governing area of WSHD overlaid with the old and current channel belts map, SC-TC 100% window is 200cm, CPT point size scaled to number of liquefaction susceptible points.

effective stress, the phreatic level is assumed to be fixed at the reference level of NAP +0.0 m with hydrostatic conditions assumed with depth. The liquefaction potential is analysed over a fixed depth of NAP +0.0 m to NAP -12.0 m. Each CPT is

analysed using a moving window approach, once points in the window are identified as being susceptible to liquefaction, they are aggregated and the total number of susceptible points at a CPT location is used as an indicator of liquefaction hazard.

For all the CPTs analysed, two different criteria of liquefaction susceptibility have been used i) contractive sands and contractive transitional soils and ii) sands and transitional soils with a relative density below 66%. A moving window is used to tally the number of liquefaction susceptible points, the liquefaction susceptible points are counted if all points meet the requirement criteria. After processing, the highest liquefaction potential is associated to the highest number of concurrent liquefiable points.

Figure 3 shows the results of a batch analysis looking within all CPTs for zones that contain a relative density below 66% for transitional soils and contractive sands, it shows that most of the locations tested in the WSHD area contain significant volumes of loosely packed sand that may be susceptible to static liquefaction. Figure 4 presents the results for 2.0 m or larger continuous contractive sands and transitional soil layers. Figure 4 still highlights a number of liquefaction prone areas in the governing area of WSHD, however much fewer are identified than when the relative density approach is used.

7 DISCUSSION AND CONCLUSIONS

This paper presents two analyses performed using a large dataset of CPTs in the governing area of Waterschap Hollandse Delta (WSHD). Each CPT profile was analysed for the liquefaction susceptibility based on relative density and contractive behaviour. Based on the relative density analysis, many dykes were shown to be built on soil profiles containing significant depths of loose sand. This loose material has the potential to liquefy but does show consistent contractive behaviour over 2.0 m depths both according to the CPT analysis. The analysis based on the soil behaviour type highlights several locations where continuous depths of soil that would exhibit contractive behaviour are observed. As this has the potential to trigger liquefaction and cause

large dyke failures to occur these areas will be more closely monitored by WSHD.

The analyses included some simplifications that can be examined in future studies. Rather than assuming hydrostatic pore pressures, an accurate assessment of in-situ pore water pressures should be conducted. The impact of dyke geometry and the resulting effective stress conditions should be included. Combining the liquefaction analysis with the geometry and bathymetry of the riverbed is an area of interest for the liquefaction susceptibility analysis. It is important to confirm the applicability of the relative density correlation and the trigger level of D_r below 66% to the Pleistocene sand layers considered. And finally, a major question remains, on what is the optimum moving window size for highlighting when contractive soil layers can cause large liquefaction induced failure.

REFERENCES

- Cohen, K., E. Stouthamer, H. Pierik and A. Geurts (2012). "Digitaal Basisbestand Paleogeografie van de Rijn-Maas Delta." *Dept. Fysische Geografie. Universiteit Utrecht. Digitale Dataset.*
- Kotvis, C (1986). Photo of liquefaction occurrence, 1968-10-04, at Oud-Kempenshofstedepolder (Tholen), *Beeldbank Zeeland*, recordnr. 6895
- Kulhawy, F. H. and P. W. Mayne (1990). Manual on estimating soil properties for foundation design. *Electric Power Research Inst., Palo Alto, CA (USA); Cornell Univ., Ithaca, NY (USA).*
- Rijkswaterstaat, (2019). Schematiseringshandleiding zettingsvloeiing. Ministerie van Infrastructuur en Waterstaat
- Robertson, P. (1990). Soil classification using the cone penetration test. *Canadian Geotechnical Journal*. 27(1), 151–158.
- Robertson, P. K. (2016). Cone penetration test (CPT)-based soil behaviour type (SBT) classification system — an update. *Canadian Geotechnical Journal* 53(12), 1910–1927.
- WBI (2017). Beoordelingsinstrumentarium (WBI2017). Ministerie van Infrastructuur en Waterstaat

Application of the CPT for liquefaction assessment of gravelly reclamations at the port of Wellington

R. Dhakal & M. Cubrinovski

University of Canterbury, Christchurch, New Zealand

J.D. Bray

University of California, Berkeley, USA

ABSTRACT: Widespread liquefaction occurred in the reclamations at CentrePort, Wellington (New Zealand) during the 2016 Kaikōura earthquake (M_w 7.8) which produced a relatively moderate seismic demand (peak horizontal ground acceleration of 0.2-0.3g at the site). Most of the damage occurred in the end-dumped fills (i.e., the Thorndon reclamation) which are comprised of 60-80% gravels and 20-40% sand-silt mixtures. This study presents results from CPT-based liquefaction assessment on a representative profile from the Thorndon reclamation using both a semi-empirical simplified method and advanced dynamic effective stress analysis. The simplified assessment results are generally consistent with observations since the CPT is able to capture the response of the finer sand-silt fraction in the matrix, which likely controlled the liquefaction behavior during the Kaikōura earthquake. The preliminary effective stress analysis provides insights on the timing and onset of liquefaction, and processes involving dynamic interactions within the deposit, thus illustrating important response characteristics which are beyond the capability of simplified methods. This paper illustrates the use of the CPT in performing conventional simplified and dynamic liquefaction analysis when applied to non-conventional or problematic soils for the assessment with reference to a well-documented case study.

1 INTRODUCTION

The cone penetration test (CPT) is commonly used for geotechnical characterization and liquefaction assessment (e.g., Boulanger and Idriss, 2014; Robertson and Wride, 1998). However, several issues exist in the use of the CPT for assessment of soil liquefaction. For example, there are challenges in the application of simplified semi-empirical CPT-based methods, developed primarily using case histories of naturally deposited sands and sands with fines, to nonstandard soils such as reclaimed gravels (Cubrinovski et al., 2019). In addition, there is a growing need for advanced numerical techniques such as seismic effective stress analysis, which can provide insights on liquefaction behavior beyond the scope of the simplified procedures. When applying an effective stress analysis, the constitutive model can be calibrated using either laboratory data on high-quality samples or empirical relationships (e.g., Ntritsos and Cubrinovski, 2020). This paper illustrates the use of the CPT for simplified and advanced liquefaction analysis for a well-documented case study of gravelly reclamation from the port of Wellington, New Zealand. In the advanced analyses, CPT-based relationships are used to calibrate the constitutive model for liquefaction evaluation of the gravelly reclamations.

2 CENTREPORT RECLAMATIONS

2.1 Reclamation history

Wellington is located at the southern tip of the North Island of New Zealand. The city was developed over the past 170 years, where the original coastline sat approximately 200 m to 500 m inland from the present coastline delineating a belt of reclaimed land. An aerial view of the port of Wellington (CentrePort) is shown in Figure 1, which was developed over several periods of major reclamation. In the most recent reclamation works (from 1965 to 1976), the area south of the buried seawall depicted in Figure 1 (i.e., the Thorndon reclamation) was constructed by end-tipping of gravelly soils sourced from nearby quarries (Cubrinovski et al., 2017). Gravelly soils were dumped into the sea to construct fills of 10 m to 22 m thickness. The fill below 2-3 m depth, aligning with the approximate depth to the water table, is uncompacted. Underlying these reclamations are Pleistocene deposits consisting of weathered alluvium, colluvium, and marine deposits. The greywacke basement rock under these deposits is at 100-150 m depth.

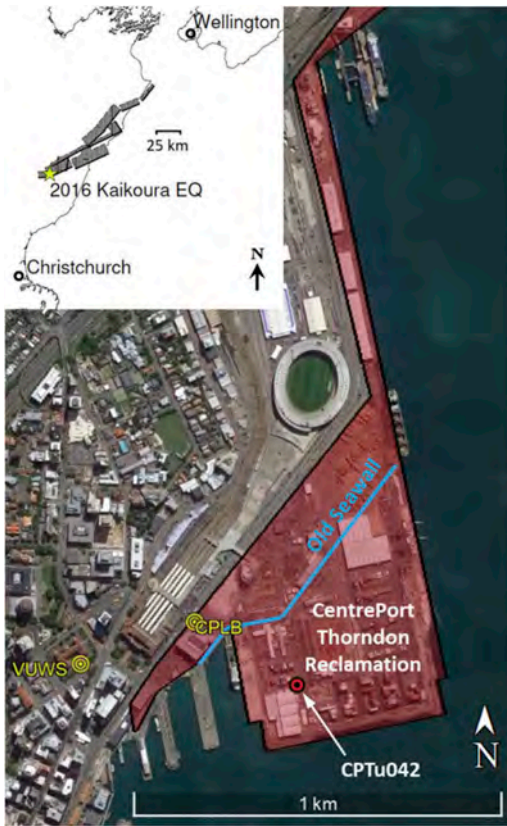


Figure 1. Aerial view of CentrePort (shaded in red), an old buried seawall, locations of two strong motion stations, and the location of one CPT (CPTu042). The inset shows the location of Wellington and the source and rupture propagation of the 2016 Kaikōura earthquake (modified from Cubrinovski et al., 2018).

2.2 Liquefaction performance during the 2016 Kaikōura earthquake

On 14 November 2016, the M_w 7.8 Kaikōura earthquake occurred in the South Island of New Zealand (location depicted in the inset of Figure 1). The closest distance from the causative faults to CentrePort was approximately 60 km, resulting in relatively long duration but moderate amplitudes of ground shaking (i.e., estimated horizontal peak ground accelerations, PGA , of 0.2–0.3g at the port).

The Kaikōura earthquake triggered widespread liquefaction that severely damaged port buildings and wharves (Cubrinovski et al., 2017). The most severe damage occurred in the Thorndon reclamation where up to 1 m horizontal movement and over half a meter of vertical settlements were observed. Large volumes of gravelly ejecta with thickness up to 150–200 mm were also observed on the ground surface (e.g., Figure 2a). Reconnaissance efforts included collection and index testing of ejected gravelly

samples, results of which are summarized in Figure 2b, which indicates the fill consists of 60% to 80% gravels (i.e., > 2 mm particle size) with the remaining 20% to 40% of the mixture consisting of silt and sand fractions. The fines content (FC) is typically between 5% and 15%.

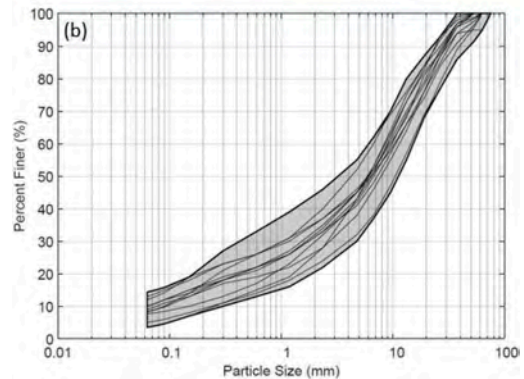


Figure 2. (a) Gravelly ejecta observed after the Kaikōura earthquake at the Thorndon reclamation (Cubrinovski et al., 2017), and (b) grain-size distribution of the Thorndon reclamation gravelly fill (Dhakal et al., 2020a).

2.3 In-situ site investigations

Comprehensive site investigation following the Kaikōura earthquake characterizes the subsurface soils at CentrePort by using over 100 CPTs, soil samples collected from over 30 boreholes, and shear-wave velocity profiles measured using direct-push and surface wave methods (Cubrinovski et al., 2018; Dhakal et al., 2020a; Dhakal et al., 2020b). The trace of measured cone tip resistance (q_c) and calculated soil behavior type index (I_c) of a representative CPT profile from the Thorndon reclamation (CPTu042) are shown in Figures 3a and 3b, respectively.

The gravel-sand-silt fill from 3 m to 14.7 m depth show characteristic values of q_c (6–8 MPa) and I_c (1.9–2.3) throughout depth despite its complex soil

composition. The relatively low penetration resistance and intermediate values of I_c for soils containing large amounts of gravel imply that these fills comprising gravel-sand-silt mixtures display soil behavior type typical for silty sand and reflects a dominant influence of the finer fractions (sand and silt) in the soil matrix. This in turn implies that the finer sand-silt fractions will have a governing role in the seismic response of the fill, despite the fact that the gravel-size particles are dominant by volume (Cubrinovski et al., 2019). The coarser gravel particles only have a minor influence, as manifested in the observed occasional spikes in q_c (associated with low I_c values).

3 SIMPLIFIED LIQUEFACTION ANALYSIS

The CPT data is used to evaluate liquefaction triggering using the Boulanger and Idriss (2014) procedure, which compares the earthquake-induced cyclic stress ratio (CSR) to the cyclic resistance ratio (CRR) of the soil to estimate a factor of safety against liquefaction triggering. The conventionally adopted criterion of $I_c < 2.6$ is used to identify soils susceptible to liquefaction. The liquefaction assessment is conducted assuming a level ground condition for a $M_w 7.8$ event with $PGA = 0.25$ g which represents the geometric mean of the shaking induced by the 2016 Kaikōura earthquake (Cubrinovski et al., 2018). The groundwater level is carefully considered in the analyses including effects of tidal fluctuations using data from nearby piezometers to estimate the water level at the location of the CPTs, at the time of the earthquake (Dhakal et al., 2020b). The probability of liquefaction triggering of $P_L = 50\%$ is used for the back-analysis of this case history instead of the deterministic value of $P_L = 16\%$, which is conventionally used in forward analysis and design. The FC is approximated as 15% in the analysis.

Figure 3 shows the computed profiles of CRR and CSR alongside the q_c and I_c data for the representative Thorndon reclamation CPT. The results in Figure 3c indicate CRR of the reclamation is well below the seismic demand imposed by the 2016 Kaikōura earthquake (i.e., the CSR). Hence, the CPT-based simplified procedure indicates that liquefaction should have been triggered throughout the depth of the Thorndon gravelly reclamation in CentrePort. As widespread liquefaction effects (e.g., soil ejecta, vertical settlements, and horizontal ground movements) were observed at the port after this event, the simplified CPT-based liquefaction triggering procedure provides results that are consistent with the field observations. This agreement reflects the fact that the sand and silt fractions in the soil matrix have a governing influence during the earthquake, which the CPT captures. On this basis, general applicability of CPT-based simplified liquefaction assessment procedures to the complex gravelly reclamations at CentrePort could be justified.

However, several challenges and limitations in the simplified liquefaction evaluation have been identified for the gravelly reclamations (Cubrinovski et al., 2019). For example, there are several areas in other gravel reclamations north of the old buried seawall (depicted in Figure 1) with poor estimates of liquefaction damage (Dhakal et al., 2020a). Furthermore, the simplified procedures provided much smaller degree of variation in the ground performance as compared to actual observations (Dhakal et al., 2020b). Therefore, additional insights are needed from more rigorous dynamic site response analyses to enhance our understanding of soil behavior and evolution of liquefaction in these reclamations.

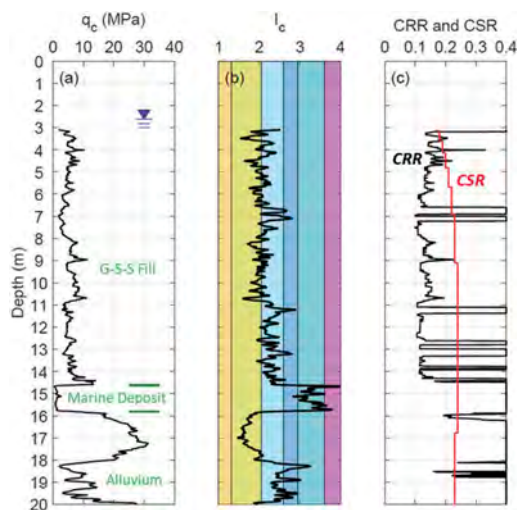


Figure 3. Profiles of CPTu042 (a) cone tip resistance (q_c), (b) soil behavior type index (I_c), and (c) cyclic stress ratio (CSR) and cyclic resistance ratio (CRR) calculated using the Boulanger and Idriss (2014) procedure under the seismic demand of the 2016 Kaikōura earthquake.

4 EFFECTIVE STRESS ANALYSIS

4.1 Numerical model

A fully coupled nonlinear effective stress analysis of saturated soil is used to perform 1D site response analysis of the Thorndon reclamation soil profile shown in Figure 3. In the analysis, an input earthquake motion is applied at the base of a 1D soil column, a finite element model comprised of 2D quadratic elements constrained to deform in simple shear mode of deformation. A key requirement in such analyses is the use of a realistic ground motion, for the site and earthquake of interest, to input at a reference subsurface layer (Ntritsos et al., 2021). Rigorous scrutiny of deconvolved motions from several nearby strong motion station (SMS) sites have shown that the deconvolved motion from a SMS site on native deposit 590 m from the location of the

analyzed soil profile (i.e., VUWS; location shown in Figure 1) is an appropriate motion for input in 1D analysis (Dhakal et al., 2022). Note that while the entire deconvolved ground motion (i.e., Figure 4b) is used as a base input motion in the dynamic analysis, the simplified analysis only uses the *PGA* of the motion (indicated in Figure 4a) recorded at the surface of the closest SMS site 330 m from the location of the analyzed soil profile (CPLB; location shown in Figure 1) in conjunction with the earthquake magnitude. By considering the entire ground motion time history, the dynamic analysis can provide insights on the timing, onset, and evolution of liquefaction throughout the depth of the fill.

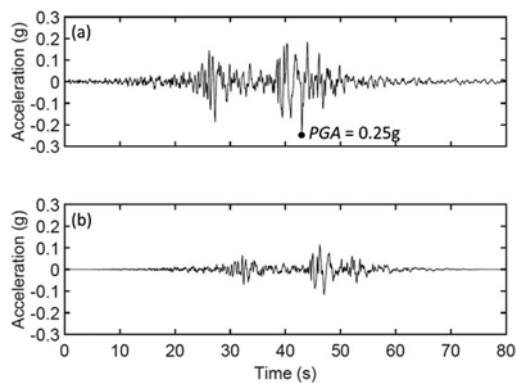


Figure 4. (a) *PGA* of the surface recorded horizontal ground acceleration at CPLB used as input for simplified liquefaction assessment, and (b) the entire horizontal ground acceleration time history of the deconvolved motion at VUWS used as input in the effective stress analysis.

4.2 Simplified CPT-based soil profiles

Unlike the simplified methods, in which a nearly continuous record of the CPT trace can be used for liquefaction calculations, discretization of the profile based on its stratification is required for the numerical model of the effective stress analysis. This study illustrates the use of the CPT in identifying the stratification for this purpose. The nearly continuous CPT profile is first discretized into several distinct layers or depth intervals over which the CPT data can be approximated by constant values of the clean-sand equivalent penetration resistance (q_{c1Ncs}) and I_c . In this study, the algorithm developed by Ntritsos and Cubrinovski (2020) is adopted for the determination of the simplified soil profile. The resulting simplified soil profile is illustrated in Figure 5 with the red solid line. The layer discretization is fine enough to allow detection of thin seams of liquefiable soils while keeping the simplified q_{c1Ncs} and I_c profiles as close as possible to the actual, more irregular, CPT traces.

Following the determination of the simplified profile, layers with $q_{c1Ncs} < 170$ and $I_c < 2.6$ are then deemed potentially liquefiable, whereas all other layers are considered as non-liquefiable. The adopted modelling approach for the liquefiable and non-liquefiable layers is summarized in Figure 5d and explained in detail in the subsequent section.

4.3 Constitutive model calibration

This study utilizes the Stress-Density model, which is an elastic-plastic constitutive model specifically tailored for analysis of soil liquefaction problems (Cubrinovski and Ishihara, 1998a; 1998b). The model is capable of accurately simulating highly nonlinear stress-strain behavior of liquefiable soils under both monotonic and irregular cyclic loading. A key feature of the model is that it utilizes the state-concept approach for modelling the effects of density and confining stress and therefore can consistently represent the behavior of sand at any density and confining stress by using the same set of material parameters.

A key requirement of the model is to accurately simulate the accumulation of shear strains and consequent development of excess pore-water pressures under cyclic loading. This ability needs to be demonstrated through a series of element-test simulations, which are also used to calibrate the key response characteristic of the constitutive model that will allow to accurately simulate target liquefaction resistance curves (LRCs). Here, LRC represents the combination of *CSR* and number of cycles (N_c) required to cause liquefaction or typically 5% double-amplitude strain, for a specific density and vertical effective stress of a given soil. Target LRCs can be obtained either from laboratory tests on soil samples or based on empirical relationships developed within the simplified triggering methods (e.g., Boulanger and Idriss, 2014). The latter approach is employed in this study, in which the Stress-Density constitutive model is calibrated to simulate LRCs derived from the Boulanger and Idriss (2014) simplified procedure, with calibration details provided in (Ntritsos and Cubrinovski, 2020). Following such calibration of the model, the only input required from the user for the analysis is a CPT profile with discretized layers of q_{c1Ncs} and I_c .

Figure 6 depicts the target LRCs based on Boulanger and Idriss (2014), shown with solid lines, for five different densities (i.e., q_{c1Ncs} values), whereas the Stress-Density model simulations of the LRCs are shown with open symbols. It illustrates that the Stress-Density model can accurately simulate LRCs, or stress-strain behavior and excess pore water pressure development, for soils with a wide range of q_{c1Ncs} (i.e., from very loose to dense soils).

Non-liquefiable layers are modelled with the Stress-Density model's pore-water pressure generation feature turned off using shear modulus and damping relationships with shear strain as target curves in the element test simulations.

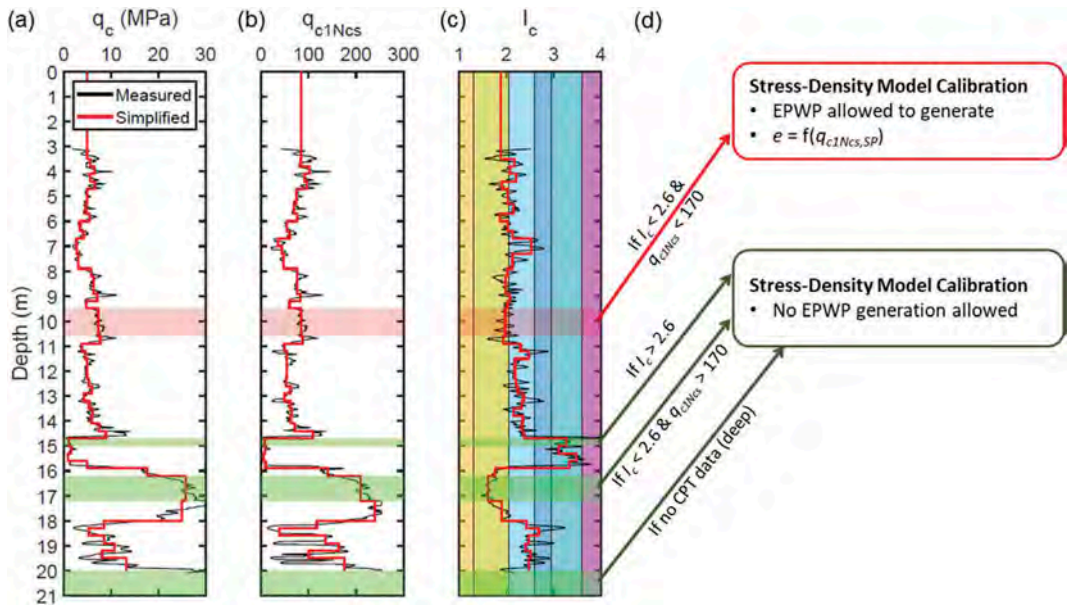


Figure 5. Profiles of CPT (a) cone tip resistance (q_c), (b) clean-sand equivalent cone tip resistance (q_{c1Ncs}), and (c) soil behavior type index (I_c) with measured data (shown in black) and simplified (layered) data (shown in red), and (d) associated modelling approaches for a liquefiable layer (shown in red) and non-liquefiable layers (shown in green).

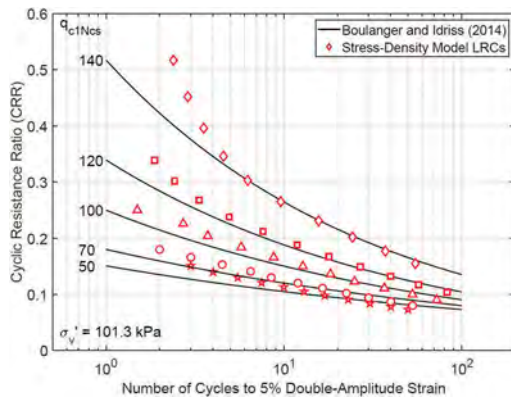


Figure 6. Semi-empirically derived target liquefaction resistance curves (solid lines; Boulanger and Idriss, 2014), and Stress-Density model simulated liquefaction resistance curves (open symbols; Ntrisots and Cubrinovski, 2020) for different clean-sand equivalent resistances (q_{c1Ncs}).

4.4 Analysis results

Figure 7 shows the results of the analysis for the selected CPT profile (CPTu042) including distribution of maximum shear strains and pore-water pressure ratios at different time sections, throughout the depth of the profile. Computed acceleration time histories at four depths are also shown. The results indicate that liquefaction occurs first in a shallower layer (6.5–8 m depth) at approximately 40 seconds after

the start of the dynamic analysis (computational time). A second, deeper layer (11.5–13 m) liquefies several seconds later. The onset of liquefaction in these two layers reduces the demand in the deposit as illustrated with the decrease in amplitude and loss of high-frequency content in the acceleration time histories. This in turn reduces pore pressure build-up and development of liquefaction in the remaining part of the profile.

These results are sensitive to key modelling decisions made by the user. For example, the shallow liquefied layer in Figure 7 includes a very thin soil layer at 7 m depth with I_c near the liquefaction susceptibility threshold of 2.6, which may have higher liquefaction resistance than that adopted in the analysis. Also, the intensity of the input ground motion will have a significant effect on how excess pore water pressures and dynamic interactions develop during the deposit. The seismic effective stress analysis provides means to investigate important mechanisms of the liquefaction response which are beyond the capacity of the simplified procedures.

5 CONCLUSIONS

This study illustrates the use of the CPT for liquefaction assessment of reclaimed gravelly soil in the port of Wellington using simplified and advanced methods. CPT data obtained in the fills composed of 60–80% gravels and 20–40% sand-silt fractions indicate the dominant influence of the finer sand-silt matrix in the fill with

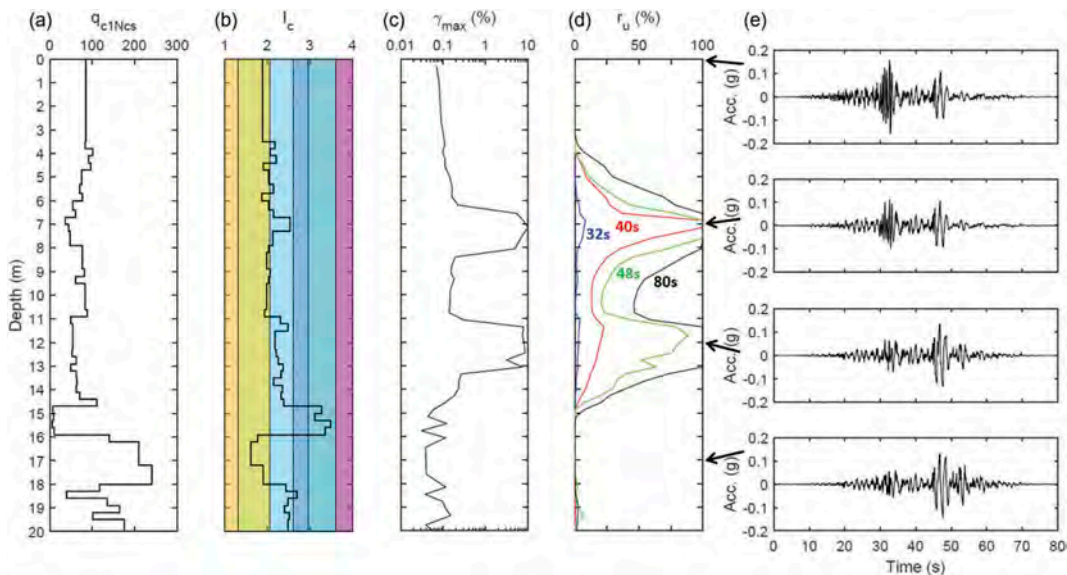


Figure 7. Results from the 1D effective stress analysis performed for CPTu042 showing (a) clean-sand equivalent cone tip resistance (q_{c1Ncs}) profile, (b) soil behavior type index (I_c) profile, (c) maximum shear strain (γ_{max}) profile, (d) excess pore-water pressure ratio (r_u) profiles at different computational times, and (e) acceleration time histories at four depths of interest.

relatively low tip resistances ($q_c = 6-8$ MPa) and soil behavior type values ($I_c = 1.9-2.3$) characteristic of sand-silt mixtures. The CPT-based simplified assessment result in relatively low cyclic resistances that are below the demand of the 2016 Kaikōura earthquake, which is generally consistent with observations. Advanced seismic effective stress analysis is also conducted through careful modeling of 1D soil layers using a sophisticated constitutive model calibrated to CPT-based semi-empirical liquefaction resistance curves. Unlike the simplified analysis which only provides a pseudo-static factor of safety, the effective stress analysis provides further details beyond the capability of simplified methods, such as the timing and onset of liquefaction, and dynamic interaction between different layers.

REFERENCES

- Boulangier, R.W. & Idriss, I.M. (2014). CPT and SPT Based Liquefaction Triggering Procedures, Report No. UCD/CGM-14/01, University of California, Davis.
- Cubrinovski, M. & Ishihara, K. (1998a). Modelling of sand behaviour based on state concept, *Soils and Foundations*, **38**(3), 115–27.
- Cubrinovski, M. & Ishihara, K. (1998b). State concept and modified elastoplasticity for sand modelling, *Soils and Foundations*, **38**(4), 213–25.
- Cubrinovski, M., Bray, J.D., de la Torre, C., Olsen, M., Bradley, B.A., Chiaro, G., Stocks, E. & Wotherspoon, L. (2017). Liquefaction Effects and Associated Damages Observed at the Wellington CentrePort from the 2016 Kaikōura Earthquake, *Bulletin of the New Zealand Society for Earthquake Engineering*, **50**(2), 152–173.
- Cubrinovski, M., Bray, J.D., de la Torre, C., Olsen, M., Bradley, B.A., Chiaro, G., Stocks, E., Wotherspoon, L. & Krall, T. (2018). Liquefaction-Induced Damage and CPT Characterization of the Reclamation at CentrePort Wellington, *Bulletin of the Seismological Society of America*, **108**(3).
- Cubrinovski, M., Ntritsos, N., Dhakal, R. & Rhodes, A. (2019). Key aspects in the engineering assessment of soil liquefaction, *Proceedings of Seventh International Conference on Earthquake Geotechnical Engineering*, Rome, Italy, June 17–20.
- Dhakal, R., Cubrinovski, M., Bray, J.D. & de la Torre, C. (2020a). Liquefaction Assessment of Re-claimed Land at CentrePort, Wellington, *Bulletin of the New Zealand Society for Earthquake Engineering*, **53**(1), 1–12.
- Dhakal, R., Cubrinovski, M. & Bray, J.D. (2020b). Geotechnical Characterization and Liquefaction Evaluation of Gravelly Reclamations and Hydraulic Fills (Port of Wellington, New Zealand), *Soils and Foundations*, **60** (6), 1507–1531.
- Dhakal, R., Cubrinovski, M. & Bray, J. (2022). Input Ground Motion Selection for Site Response Analysis at the Port of Wellington (New Zealand), *Proceedings of Fourth International Conference on Performance-Based Design in Earthquake Geotechnical Engineering*, Beijing, China, July 15–17.
- Ntritsos, N. & Cubrinovski, M. (2020). A CPT-based effective stress analysis procedure for liquefaction assessment, *Soil Dynamics and Earthquake Engineering*, **131**, 106063.
- Ntritsos, N., Cubrinovski, M. & Bradley, B.A. (2021). Challenges in the definition of input motions for forensic ground-response analysis in the near-source region, *Earthquake Spectra*, 87552930211001376.
- Robertson, P.K. & Wride, C.E. (1998). Evaluating cyclic liquefaction potential using the cone penetration test, *Canadian Geotechnical Journal*, **35**, 442–459.

Concept design of a new CPT module for direct in situ measurement of P-Y soil responses

A. Diambra, J. Creasey, J. Leonet, A. Conn, E. Ibraim & G. Mylonakis
University of Bristol, UK

D. White, B. Cerfontaine & S. Gourvenec
University of Southampton, UK

D. Igoe
Trinity College Dublin, Ireland

ABSTRACT: Due to the rapid expansion of the offshore energy market, driven by the installation of wind turbines founded on single- or multi-piled foundations, the design and optimisation of laterally loaded piles has attracted enormous interest in the last decade. Current industrial design practice, for offshore and onshore piles, typically employs lateral load-displacement springs (p - y) to model the soil response under serviceability, ultimate or fatigue limit state scenarios of this foundation type, supplemented by moment and axial springs. Correlations based on CPT data are commonly used to determine soil properties and, in turn, the stiffness and resistance of the p - y reaction curves, in advance of detailed laboratory testing that follows later in the project schedule. To extend the potential for in situ testing to support lateral pile design, this paper presents the novel idea of complementing a CPT device with a new module capable of probing the soil in such manner that the monotonic and cyclic p - y soil response (including its evolution during the foundation design life) can be directly measured in the field. The stress and strain fields induced by such a module resemble those of a miniature laterally loaded pile element and differ from circular or flat cavity expansions induced by pressuremeters or dilatometers. The new device will be developed in a collaborative research project ‘ROBOCONE’ financed by the UK and Irish research councils. The background thinking and initial conceptual design of the device, including the review and selection of appropriate motion mechanisms and instrumentation, is presented in this manuscript.

1 INTRODUCTION

Modern society demands more efficient infrastructure under stricter and more challenging operational and climatic conditions, such as offshore energy structures in harsh environments and urban developments in overly congested areas. The loading conditions are complex and time variant, and the mechanical properties of the ground can vary spatially and temporally. In this setting, a ‘whole-life’ design approach (Gourvenec, 2020; White et al. 2022), acknowledging the evolution of these actions and responses is important. Developing new technologies and methods to characterise the whole-life engineering properties of the ground is essential to meet the required safety, resilience and efficiency of geotechnical design and civil infrastructure.

The CPT has been the primary platform and manipulator for 50 years for in situ geotechnical characterisation of ground properties. CPT data have also underpinned the design of many geotechnical structures, including onshore and offshore pile foundations.

It is customary geotechnical practice to relate the parameters of lateral resistance-displacement soil springs (p - y curves), used in the design of laterally loaded piles, directly to CPT data or to soil strength and stiffness parameters inferred from CPT data (Truong and Lehane, 2014). These procedures are almost invariably based on empirically derived correlations.

The extension of the kinematic range of in situ geotechnical tests, via modern robotics, could permit the application of kinematic mechanisms and strain histories to the ground that mimic more closely the stress paths expected from the geotechnical infrastructure, such as a pile. This could allow the direct measurement of the soil ‘ p - y ’ response and its whole design life evolution, if appropriate stress and/or strain histories are imposed.

This paper presents the initial feasibility study and background thinking for the future development of a new additional ‘ p - y ’ modular section which can complement the standard CPT equipment. The work is part of a new collaborative research project

involving the University of Bristol, University of Southampton and Trinity College Dublin, financially supported by the UK-Ireland research councils.

2 CONTEXT AND NOVELTY OF THE PROPOSED DEVELOPMENT

Since its early development in the 1950s at the Dutch Laboratory for Soil Mechanics in Delft, the CPT has been considerably upgraded in the testing and control procedure as well through the inclusion of new sensors. The latter, for example, include seismic, electric resistivity and acoustic transducers (i.e. Campanella et al. 1986; Shinn et al. 1998; Houlsby and Ruck, 1998).

Alongside sensor development, the kinematic range of the CPT has also been expanded. The cone-pressuremeter combines a standard cone penetrometer with the capability of a standard pressuremeter, enabling the application of cavity expansion kinematics on surrounding soil (Houlsby & Withers, 1988).

A series of friction sleeves with torsional load and axial load sensing capabilities and with varying surface texture have also been included behind a standard cone penetrometer through recent development at the Georgia Institute of Technology (Martinez & Frost, 2018). The system is coupled with a series of pore pressure sensors, enabling the measurement of excess pore water pressure ahead and after each axial and/or torsional friction sleeve. The device can monitor both quasi-static and cyclic behaviour enabling an insight into cyclic strength degradation as well as liquefaction potential.

Other attempts have been made to impose cyclic vertical motions to simulate the cyclic response of axially loaded piles or to evaluate the cyclic liquefaction potential of soils (Diambra et al. 2014; Hosseini-Sadrabadi et al. 2019). Vibrational movements have also been imposed by Stähler et al. (2018) to assess the liquefaction resistance of soil deposits.

None of the proposed kinematic mechanisms has considered the possibility to explore the horizontal (' p - y ') soil resistance, mimicking the soil loading imposed by a laterally loaded pile. This could be achieved through an additional module behind the cone, similar to the torsional frictional sleeves. Through modern robotics, the p - y module could impose complex stress histories involving cycles of loading and unloading, similar to laboratory element testing. Relative to laboratory testing, this would eliminate the challenges of sample disturbance and re-capturing stress states as well as the time-consuming and expensive operations of drilling and sampling as well as the laboratory testing itself.

The developments within the RIGSS (Remote Intelligent Geotechnical Seabed Surveys Joint Industry Project (White et al, 2017, 2022) demonstrate the benefits of introducing robotic and smart testing in the geotechnical characterisation of shallow seabed

sediments. The present project aims at transferring some of the RIGSS capabilities to deeper soil layers.

3 OVERVIEW OF THE PROPOSED P-Y MODULE

3.1 Main principles

A diagram of the working mechanism for the proposed p - y module is shown in Figure 1. A module capable of horizontal translation is included behind the standard cone penetrometer. This device mimics the load and displacement history imposed by a laterally loaded pile element, so that the module response can be upscaled for pile design or used to determine constitutive soil parameters. The development of appropriate theoretical frameworks for the interpretation of the module response will be also a fundamental contribution of the forthcoming research project. The aim is to be able to derive full monotonic and static reaction curves and their evolution after application of particular stress histories.

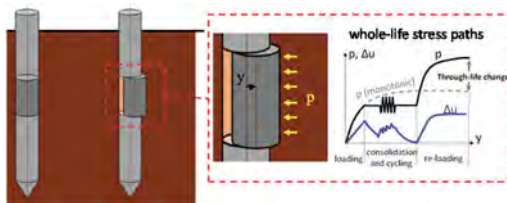


Figure 1. Diagram of the ' p - y ' CPT module and whole life stress histories that could be imposed.

The difference between the displacement field and soil reactions induced by the proposed p - y module and those produced by pressuremeters or flat dilatometers is shown in Figure 2. The proposed p - y module induces an asymmetric bulb of pressure creating a flow of soil around its cylinder, similarly to a laterally loaded pile.

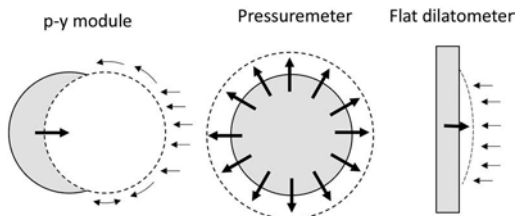


Figure 2. Cross-section of displacement field and soil reactions induced by ' p - y ' module (left), pressuremeter (middle) and flat dilatometer (right).

3.2 Application of whole-life stress histories

Robotic control and a precise actuation system is necessary in order to enable the application of complex load histories, mimicking whole-life stress histories as shown in Figure 1. Geotechnical design recognises that the strength and stiffness of ground, and therefore the performance, safety and resilience of our infrastructure, evolves through time under the exposure to in-service loadings. For example, offshore facilities on soft marine sediments can experience transient falls in strength, potentially by a factor of 2, but long-term gains by a factor of 4 due to loading episodes and consolidation (Zhou et al. 2019). Driven piles, for example in sand and chalk, can also exhibit similar levels of short-term degradation and long-term recovery depending on the loading history (Jardine and Standing, 2012; Ciavaglia et al. 2017). These advanced aspects of ground behaviour are progressively entering into engineering practice and so it is timely for in situ testing protocols to also advance in parallel, to provide the necessary site characterisation.

4 MAIN DESIGN REQUIREMENTS AND CONSTRAINTS

The initial background thinking and design of the module has revealed a number of design requirements and challenges to be addressed in order to achieve the successful development of the ‘*p-y*’ module. Among others, the following challenges have been recognized in this early stage of development. The module mechanical arrangement requires the following characteristics:

- Application of straight-line horizontal motion to the module. This may include a mechanism that transforms vertical movement or rotary motion (from a motor or other drive unit) into straight line horizontal movement.
- Ability to provide appropriate force capacity to overcome the soil resistance.
- Ability to offer adequate precision and resolution to be able to measure the stiffness of the soil over the required strain range.
- Sufficient robustness.
- Capable of hosting sensors to measure soil response, including pore water pressures.
- Resilient against soil becoming trapped between the moving parts.

Include sensors to measure soil pressure, module movements (over the very small to large displacement domain) and generated pore water pressure. Some of the above points are further elaborated in the following.

5 DEFORMATION AND CAPACITY REQUIREMENTS

5.1 Required capacity

The pushing force required to displace and bring the soil to failure can be determined by inversely applying the *p-y* theory to the translating module. The horizontal force exerted from the soil and, therefore, the required force to move a typical 44mm diameter (i.e. 15cm² cone) is shown in Figures 3 and 4 for both sands and clays for varying depth and undrained shear strength, respectively. Both sets of graphs show these forces for differing heights of the module. The required force for the sand is estimated using the *p-y* curve proposed by Reese et al. (1974), assuming a soil friction angle of 40°. The required force for the clay is estimated using both the Matlock et al. (1970) *p-y* curves for soft clay and the Reese et al. (1975) *p-y* curves for stiff clay. The relevant movements are on the order of 0.1 diameters

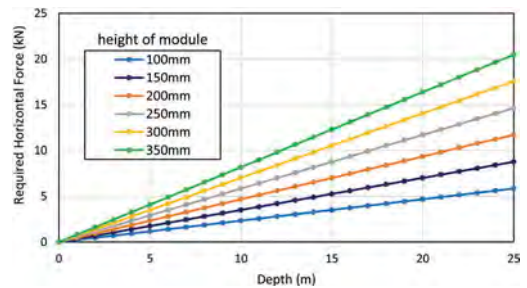


Figure 3. Required Horizontal Force vs Depth for sand to invoke lateral displacement of CPT module.

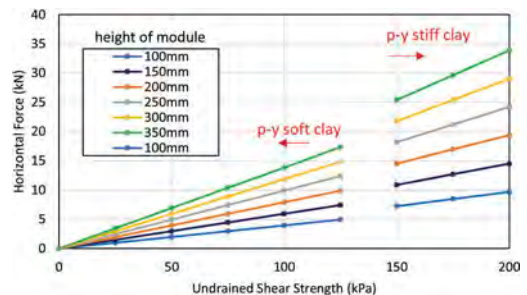
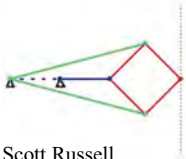
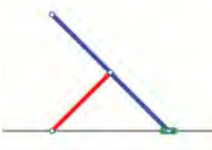
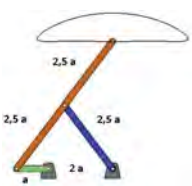
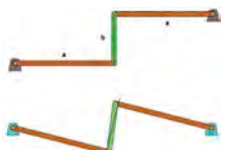

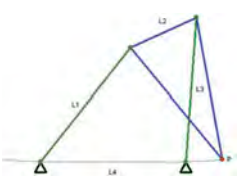
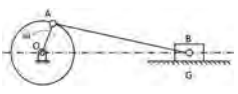


Figure 4. Required Horizontal Force vs Undrained Shear Strength for clay to invoke lateral displacement of CPT module.

5.2 Displacement resolution and control

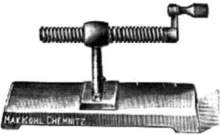
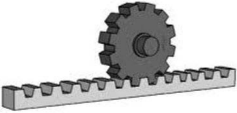
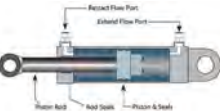
Stiffness information over the shear strain range 0.01-1% are typically important for design and can be

Table 1. Potential mechanical systems to use on the ROBOCONE 'p-y' module (based on Hricko, 2014 and ENIM, 2020).

Mechanism	Description	Strengths (+)/Weaknesses (-)
Peaucellier Lipkin 	Planar linkage transforming rotary to straight-line motion.	+ Compact + Exact straight-line - Complex revolute joints - Fragile mechanism with high stress
Scott Russell 	Linkage transforming vertical to horizontal motion. Consists of three links all equal with a rolling or sliding connection.	+ Compact + Exact straight-line - Weakness at revolute joints - Rapid wear
Hoekens 	A four bar linkage converting rotational to straight line motion.	+ Compact - Approximate straight line - Weakness due to revolute joints
Watt 	Three bars bolted together in a chain. The three bars pivot around two bolts on the central bar to move a central point in a near straight line.	+ Compact - Approximate straight line - Weakness due to revolute joints
Chebyshev 	Linkage consisting of three bars that converts rotational to straight line motion for a central point.	+ Compact - Approximate straight line - Weakness due to revolute joints
Roberts 	Linkage consisting of five bars that converts rotational to approximate straight line motion.	+ Compact - Approximate straight line - Weakness due to revolute joints
Slider crank 	A four link mechanism with three revolute joints and one sliding joint. Rotation of the crank drives linear motion.	+ Exact straight line + Resilient - High friction - Bulky due to the sliding pair

(Continued)

Table 1. (Cont.)

Mechanism	Description	Strengths (+)/Weaknesses (-)
 <p>Screw nut</p>	Very simple mechanism that converts rotational to linear motion and torque to a linear force.	+ Exact straight line + Resilient + High forces <hr/> - High wear rate - Needs accurate adjustments.
 <p>Rack-pinion</p>	A circular gear (pinion) connected to a linear gear (pinion) to convert rotational to straight line motion.	+ Exact straight line + Produces high forces + Accurate movement <hr/> - High friction - Fragile
 <p>Hydraulic pistons</p>	A hydraulic cylinder or motor that acts as a mechanical actuator used to give a unidirectional force through a unidirectional stroke.	+ Can provide high energy and force + Easily controlled using valves/levers. <hr/> - Requires maintenance to avoid leaks and fluid contamination.

obtained from tests featuring unload-reload loops. This cyclic loading can be applied with the proposed p - y module in addition to monotonic loading to investigate a wide range of soil properties. The resolution threshold of 0.01% is slightly too high to detect the small strain elastic stiffness, $G0$, and if possible a lower resolution should aim to be achieved. Precision of 1 μ m is typical of pressuremeter expansion and will be targeted in these developments.

6 REVIEW AND SELECTION OF STRAIGHT LINE MECHANISMS

Table 1 provides a review of available mechanical systems to transform a vertical or rotary motion into straight-line horizontal motion. Table 1 also considers the potential use of a hydraulic horizontal pushing system. A schematic, description and account of strengths/weaknesses are listed for each option.

The main outcome from this preliminary assessment is that many mechanical systems do not provide a perfect straight-line mechanism. As such these mechanisms have been discarded.

It appears that the Scott Russell mechanism is one of the few mechanisms that converts perfect vertical to horizontal motion. Its simplicity makes it a viable option for the proposed module, although there are concerns about its robustness. A second option could be the use of a hydraulic system with micro-pistons. These two options are analyzed in greater detail in the following section.

7 FIRST TRIALS AND ANALYSES OF STRAIGHT-LINE MECHANISM

7.1 Scott Russell mechanism

The Scott Russell linkage consists of three links, all equal length that are used to form a right-angle change of motion from vertical to horizontal linear motion as shown in Figure 5. As Point A moves vertically upwards, Point C moves horizontally assuming a rolling or sliding connection.

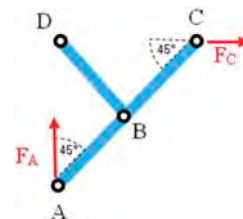


Figure 5. Scott Russell mechanism that can be used in 'p-y' module.

An initial 3-D printed prototype shown in Figure 6 has been fabricated for this mechanism type. Pulling up the vertical bar in tension triggers an outward movement of the cone while avoiding buckling of the main vertical bar. Several Scott-Russell mechanisms in series linked to a single pulling bar can be included to increase the system robustness and stability, although it appears that this mechanism may be suitable for low strength soils or

at shallow depths. It should be noted that the force conversion efficiency depends on the inclination of the bar AC in Figure 5, and it decreases as the orientation of the bar moves away from 45°.

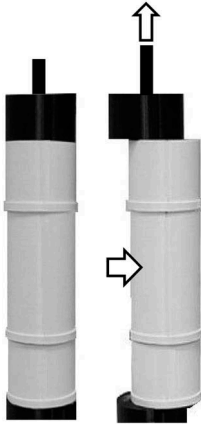


Figure 6. Initial 3-D printed prototype of the 'p-y' module with the Scott-Russell mechanism.

For the first development of a real cone, a functioning range in sands up to 10 m depth and in clays with an undrained shear strength up to 75 kPa can be assumed. According to the preliminary capacity requirements from Figures 3 and 4 with a module height of 200 mm, maximum overall horizontal forces up to 5 kN are expected for these conditions.

Considering the loss of efficiency as the inclination of the bar AB departs from the 45° (Figure 5), a vertical pull-out force equal to 10 kN could be assumed for preliminary sizing of the vertical pulling rod. This would result in a 6 mm diameter steel rod assuming a yield tensile strength for steel of 350 MPa.

A hydraulic actuation system can be used to pull the rod up and down in order to trigger the lateral movement of the *p-y* module. This may be placed within the fixed parts of the cone, either above or below the module. A cylindrical system with a diameter of 35 mm and an allowable fluid pressure of 12 MPa would be sufficient to provide the required 10 kN.

If four Scott Russell mechanisms are considered, the necessary horizontal force F_c (Figure 5) at each linkage would be 1.25 kN. The connection of the Scott Russell mechanism should be designed for a such force range.

The dimensions derived above may pose challenges considering the standard cone dimensions. Slight geometrical modification to the cone diameter and module height may prove beneficial if the Scott Russell mechanical system is adopted.

7.2 Hydraulic piston system

A miniature horizontal hydraulic drive system has also been considered where oil flow can be used to control pistons that trigger the horizontal motion of

the *p-y* module. The hydraulic system can provide high forces using simple and miniature design. The direction of oil flow, the pressure and flow rate within the circuit can be controlled using valves and hydraulic systems. This allows for more accurate control of the moving module than a mechanical system, although accuracy and precision will finally depend on the actual piston design.

A preliminary diagram of the *p-y* module with the horizontal hydraulic piston actuation is shown in Figure 7. A series of miniature pistons is placed within the fixed part of the cone, above and below the module. When oil flows inside hole 1 within the top section, pistons force the bar to move the middle section horizontally, representing the test position. Then, when oil flows in hole 2, pistons move the bar and the middle section back to its standard position.

Similar to the initial design of the Scott Russell mechanism, a required horizontal force of 5 kN is assumed for an initial sizing of the hydraulic pistons. A maximum fluid pressure of 12 MPa in the pistons is also assumed. Using fundamental pressure formula and force equilibrium, the minimum diameter of the pistons can be calculated for varying number of pistons to provide the required horizontal force. Results are provided in Table 2.

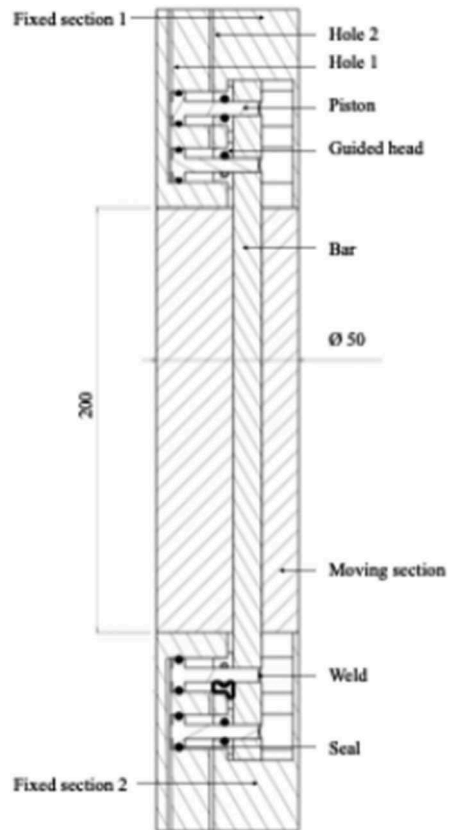


Figure 7. Diagram of 'p-y' module using hydraulic pistons system.

It appears that a configuration with four pistons of 12 mm diameter may be appropriate and sufficient. Two pistons can be placed in the top section and two in the bottom section of the cone. This configuration ensures that the soil pressure acting on the outer surface is evenly distributed over an appropriate number of pistons. It should be noted that using four pistons of 17 mm diameter will provide a twofold increase in horizontal force, suggesting that this system may be a good candidate for future upscaling to larger forces.

Table 2. Calculated minimum piston diameter, D, for varying number of pistons, n, to provide required horizontal force.

Max pressure (MPa)	No. pistons	D (mm)	F (kN)
12	2	17	5.44
12	4	12	5.43
12	6	10	5.65
12	8	8.5	5.44

8 CONCLUSIONS

This paper has presented an initial feasibility study and background thinking for the future development of a novel ‘p-y’ modular section to be attached behind a standard cone penetrometer. The module will enable in situ probing of the soil similar to a laterally loaded pile element while also imposing complex whole-life stress histories and explore how soil response changes during the design life.

A number of challenges and design requirements have been identified in this paper. Available mechanical systems to produce the desired horizontal translation of the module have been reviewed and the use of hydraulic actuation with multiple systems appear a good candidate for future developments.

The full development of the proposed module and the interpretative framework is the main objective of a collaborative research proposal ‘ROBOCONE’ involving the University of Bristol, University of Southampton and Trinity College Dublin.

ACKNOWLEDGMENTS

The authors would like to acknowledge the financial support from the Engineering and Physical Sciences Research Council (EPSRC - Ref: EP/W006235/1) and Science Foundation Ireland (SFI - Ref: 21/EPSCR/3787).

REFERENCES

Campanella, R. G., Robertson, P. K., & Gillespie, D. (1986). Seismic cone penetration test. In *Use of in situ tests in geotechnical engineering* (pp. 116–130). ASCE.

Ciavaglia, F., Carey, J., & Diambra, A. (2017). Time-dependent uplift capacity of driven piles in low to medium density chalk. *Geotechn. Letters*, 7, 90–96.

Diambra, A., Ciavaglia, F., Harman, A., Dimelow, C., Carey, J. and Nash, D.F., 2014. Performance of cyclic cone penetration tests in chalk. *Geotechnique Letters*, 4 (3), pp. 230–237.

Ecole Nationale d’Ingénieurs de Metz (ENIM). (2020). Transmission de puissance

Gourvenec, S. (2020). Whole-life geotechnical design: What is it? What’s it for? So what? And what next?: Keynote lecture. *Proc. 4th Int.l Symposium on Frontiers in Offshore Geotechnics*. DFI. pp. 206–246

Hosseini-Sadrabadi, H., Celeste, F., Chareyre, B., Dano, C., Sibille, L. and Riegel, P., 2019 Interpretation of a cyclic Cone Penetration Test (CPT) under saturated conditions: numerical and experimental approaches.

Houlsby, G. T., & Ruck, B. M. (1998). Interpretation of signals from an acoustic cone penetrometer. *Geotech. Site Characterization*, 2, 1075–1080.

Houlsby, G. T., & Withers, N. J. (1988). Analysis of the cone pressuremeter test in clay. *Geotechnique*, 38(4), 575–587.

Hricko, J. (2014). Straight-Line Mechanisms as One Building Element of Small Precise Robotic Devices. *Applied Mechanics and Materials*, 96–101.

Jardine, R. J., & Standing, J. R. (2012). Field axial cyclic loading experiments on piles driven in sand. *Soils and foundations*, 52(4), 723–736.

Marchetti, S., Totani, G., Calabrese, M and Monaco, P. (1991). P-y curves from DMT data for piles driven in clay. *DFI, Piling & Deep Foundations*, 263–272.

Martinez, A., & Frost, J. D. (2018). Undrained behavior of sand–structure interfaces subjected to cyclic torsional shearing. *J. Geotech. & Geoenvironmental Eng.*, 144(9), 04018063.

Matlock, H. (1970, April). Correlation for design of laterally loaded piles in soft clay. In *Offshore Technology Conference*. OnePetro.

Reese, L.C, Cox, W.R and Koop, F.D. (1974). Analysis of laterally loaded piles in sand. *Offshore Technology Conference*. OnePetro.

Reese, L.C, Cox, W.R, Koop, F.D. (1975). Field testing and analysis of laterally loaded piles in stiff clay. *7th Annual Offshore Technology Conference, Houston*. 672–690.

Shinn, J. D., Timian, D. A., Morey, R. M., Mitchell, G., Antle, C. L., & Hull, R. (1998). Development of a CPT deployed probe for in situ measurement of volumetric soil moisture content and electrical resistivity. *Field Analytical Chemistry & Technology*, 2(2), 103–109.

Stähler, F. T., Kreiter, S., Goodarzi, M., Al-Sammarraie, D., & Mörz, T. (2018). Liquefaction resistance by static and vibratory cone penetration tests. *Cone Penetration Testing 2018* (pp. 591–597).

Truong, P., & Lehane, B. (2014). Numerically derived CPT-based py curves for a soft clay modeled as an elastic perfectly plastic material. In *3rd Int. Symp. on Cone Penetration Testing* (pp. 975–982).

White, D. J., Doherty, J. P., Guevara, M., & Watson, P. G. (2022). A cyclic py model for the whole-life response of piles in soft clay. *Computers and Geotechnics*, 141, 104519.

White, D. J., Stanier, S. A., Schneider, M. A., O’Loughlin, C. D., Chow, S. H., Randolph, M. F., ... & Chow, F. C. (2017). Remote Intelligent Geotechnical Seabed Surveys–Technology Emerging from the RIGSS JIP. *OSIG 8th Int. Conf.Proceeding* (Vol. 1214, No. 1222, pp. 1214–1222). SUT.

Zhou, Z., O’Loughlin, C. D., White, D. J., & Stanier, S. A. (2020). Improvements in plate anchor capacity due to cyclic and maintained loads combined with consolidation. *Geotechnique*, 70(8), 732–749.

The use of dynamic probing tests and cone penetration tests to verify the effectiveness of expanding polyurethane resin injections for ground improvement

A. Dominijanni
Politecnico di Torino, Italy

M. Gabassi
Uretek Italia Spa, Italy

A. Minardi
Geotechnical Engineering Ltd, Italy

S. Pavan
Uretek Italia Spa, Italy

ABSTRACT: Injection of expanding polyurethane resins is a popular method to improve both the stiffness and the shear strength of the ground below existing foundations. The effect of the polyurethane resin expansion is to increase the soil confining stress and density around the injection holes. An estimation of the horizontal stress and volumetric strain changes that are induced within the ground is derived from the theory of cavity expansion in elasto-plastic materials. A series of case-histories is presented to document the feasibility of different *in-situ* tests to evaluate the achieved ground improvement. The tests have been performed before and after the injection of polyurethane resins and the obtained results have been compared with theoretical predictions. The considered investigation methods include the dynamic probing tests and the cone penetration tests. The preliminary results that have been achieved using an experimental miniature cone penetration test are also illustrated. The advantages and limitations of different test methods are discussed and practical indications for conducting such verifications of polyurethane resin injection effectiveness are provided.

1 INTRODUCTION

The use of polyurethane expanding resins is a widespread technique adopted to solve ground-related engineering problems. Due to their significant swelling capacity, polyurethane resins are currently deployed successfully in the following cases (Dominijanni and Manassero, 2014):

- filling and stabilization of underground cavity;
- reduction of soils hydraulic conductivity;
- heaving of pavement and foundations in settlements problems;
- ground improvement and compaction.

Ground improvement and compaction with expanding polyurethane resins aim to increase soil density and soil mechanical parameters such as stiffness and strength. This type of treatment, often performed below existing foundations, can be considered part of the treatment methods related to compaction grouting techniques. However, this type

of treatment is different from conventional compaction grouting techniques due to the physical and mechanical processes governing the expansion of the expanding polyurethane resin in the subsoil. The cavity expansion theory represents a relatively simple and reliable approach for modelling the changes in the stress state and the density of the soil induced by the expansion of the resin (Yu, 2000; ASCE, 2010; Dominijanni and Manassero, 2014).

Despite the possibility of using well-established design methodologies, the assessment of the success of the ground treatment with expanding polyurethane resins still represents a major challenge. When the ground treatment is performed before the construction of structures and buildings, it is possible to carry standard *in-situ* tests, such as cone penetration tests (CPT), to evaluate the achieved ground improvement. However, when the treatment is performed below existing structures, the use of standard *in-situ* testing equipment might not be feasible due to the space required for this type of equipment.

A solution to this issue is provided by the performance of reduced scale in situ testing, such as mini-CPT and small dynamic probing tests. This paper illustrates some examples of using these types of testing equipment, besides the adoption of CPT testing, to evaluate the effectiveness of the ground improvement with expanding polyurethane resin.

2 GROUND TREATMENT WITH POLYURETHANE RESINS

Polyurethane resins are obtained from the exothermic reaction occurring by the mixing of a polyol and an isocyanate. The swelling capacity is the key feature of this material, and it is responsible for a volume increase under unconfined conditions (null mechanical stress) of about thirty times (Dei Svaldi et al., 2005; Buzzi et al., 2008). When the resins are injected underground, the expansion process occurs in confined conditions leading to a compaction of the soil surrounding the injection point until a mechanical equilibrium between the resin and the soil is achieved. The injection can be performed at different depths using either several injection tubes with single-point injection at the bottom end of the tube or a single tube with several lateral injection points (multi-point). In both cases, the injections are performed with small tubes (external diameter of about 10-15 mm) and equipment, reducing the treatment's impact on the existing structure as much as possible.

From a design point of view, the cavity expansion theory represents an efficient tool that can be used by engineers (Yu and Houlby, 1991; Shrivastava et al., 2018). In this framework, spherical cavities expansion can be considered when single point injection tubes are adopted for the treatment. On the other hand, when multi-point injection tubes are used, it is possible to consider a cylindrical cavity expansion (Figure 1). This design approach allows engineers to estimate the amount of a specific type of resin to be injected to obtain a given increase of the soil density and mechanical parameters.

The efficiency of the treatment depends on several factors, such as the type of soil, the presence of groundwater, the soil stiffness and strength, the injection layout, the amount and type of injected resin. When compaction is the aim of the treatment, the efficiency of the treatment is higher under drained conditions (Kovacevic et al., 2000).

In fact, under drained conditions, the mean effective stress increases monotonically, and the soil compresses along a compression curve for first loading, with a consequent increase in density, stiffness and shear strength.

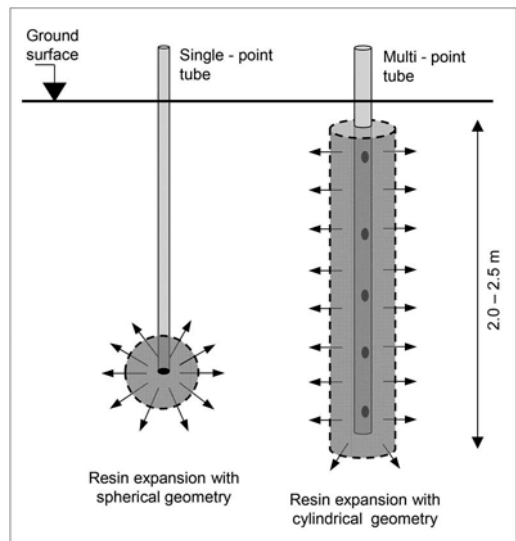


Figure 1. Schematic layout of the two types of tubes usually adopted for the injection of polyurethane resins, along with the expansion process of the injected resin.

Instead, under undrained conditions, the soil is not allowed to compress, and the mean effective stress decreases due to the formation of excess pore pressures. During the subsequent consolidation phase, the soil follows an unload/reload compression curve until the original mean effective stress is reached. However, because of the higher rigidity of the unload/reload compression curve with respect to the curve for first loading, the amount of compression is lower than that achieved under drained conditions.

Therefore, the use of polyurethane has to be firstly considered either in coarse-grained soil or in partially saturated fine-grained soil.

The evaluation of the soil geotechnical parameters is often performed with in-situ tests, such as dynamic and static penetration tests, using empirical correlations available in the scientific literature. Moreover, penetration tests may also be adopted to evaluate the efficiency of the treatment by comparing the results of the tests performed before and after the treatment in the soil surrounding the injection points. The role of in-situ testing is, therefore, fundamental not only for the design of the ground treatment but also for the assessment of the treatment efficiency.

3 IN-SITU PENETRATION TESTS

Beside the standard CPT test, the use of smaller equipment is often required to evaluate the effectiveness of the ground treatment with polyurethane resins. In the following two subsections, a brief overview of the miniature cone penetrometer (mini-CPT) and the medium-light dynamic probing penetrometer

(DPM 30-20) are introduced. These types of penetrometers have the advantage of being easy to transport, install, and use.

3.1 Mini CPT

The miniature cone penetrometer is a reduced scale cone with a diameter of 18 mm and an apex angle equal to 60°. Examples of the use of the mini cone penetrometer can be found in Squeglia and Lo Presti (2010), where this equipment has been adopted to develop an innovative methodology for the evaluation of the compaction degree of earth works, and in de Vries et al. (2018) where a comparison with standard CPT tests is illustrated. The cone is pushed downward in the soil at a constant rate equal to 2 cm/s by an electric motor. The tip resistance (q_c) is evaluated by a load cell placed above the penetrometer with maximum load of 5 kN and accuracy of 5 N.

The performance of mini-CPT tests is not common for soil geotechnical characterization. Therefore, this test method suffers of a lack of empirical correlations to estimate geotechnical parameters, as well as a direct comparison with the standard CPT test. To face this issue, mini-CPT tests are often carried out along with standard CPT or, in case this is not possible, with dynamic probing tests.

3.2 Dynamic penetrometer DMP 30-20

Dynamic probing tests (DP) consist of driving into the soil a steel cone located at the end of a set of driving rods by blowing the upper end of the rods with a specific hammer (Cestari, 2012). DP tests can be classified in different category (light, medium, heavy, super-heavy), depending on the hammer weight, falling height, cone size and geometry, rods size, etc.

In the framework of ground treatment with polyurethane resins, the use of a medium-light penetrometer, the DPM 30-20, is particularly considered in Italy. This equipment is based on the measurement of the blow number required for a penetration of the cone equal to 10 cm (N_{10}). Although this equipment is not included in any standard, its main features are similar to the standard light and medium dynamic penetrometer. The mass of hammer is 30 kg and falling height is 20 cm. The cone has a base diameter equal to 35.7 mm and an apex angle equal to 60° (Cestari, 2012).

Although the possibility to correlated the DPM 30-20 test results (N_{10}) to the standard penetration test (N_{SPT}), the main disadvantage of this type of test is represented by the absence of the measurement of the skin friction during the penetration of the cone. Therefore, the measured penetration resistance might be overestimated due to the missing contribution of the skin friction.

4 CASE STUDIES

In this section a series of case studies are presented, where the assessment of the effectiveness of the ground treatment with polyurethane resins is evaluated by performing standard CPT, mini-CPT and DPM 30-20 in situ tests. The examples refer to ground treatment works related to resin injections below shallow foundations of residential buildings.

4.1 Case a)

The first case study refers to the ground treatment performed below the plate foundation of a residential building that experienced differential settlements during construction. During the design phase, an in-situ testing investigation composed of four CPT tests was carried out. The map of the building is presented in Figure 2, along with the location of the four CPT tests. Figure 3 illustrates the tip resistance (q_c) profile obtained from the tests CPT-1 and CPT-2. From this outcome, the foundation soil can be roughly divided in a shallow layer of granular soil (mainly sand) with thickness equal to 3 m overlaying a deeper layer of fine-grained soil with a thickness equal to 7 m.

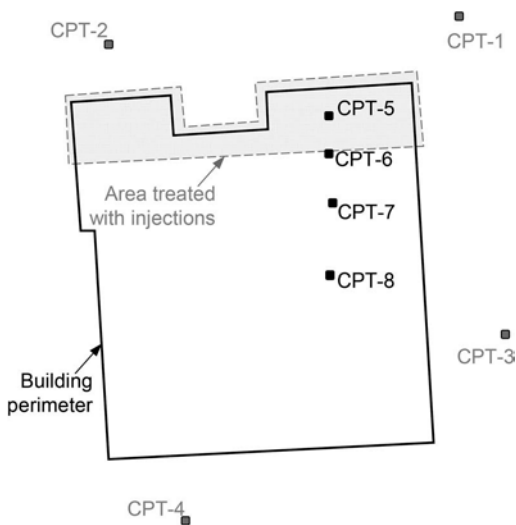


Figure 2. Map of the building along with the position of the four CPT tests (n.1 to n.4) performed before construction, the treated area with resin injections, and the four CPT tests (n.5 to n.8) performed after ground treatment.

As illustrated in Figure 2, the ground treatment was performed on the north side of the building, which was subjected to major settlements. The injection points were placed on a regular squared grid with spacing equal to 1 m, and they were performed first in correspondence of the building perimeter and then below the building. Moreover, the resin was injected first at a depth between -5 and -7 m with

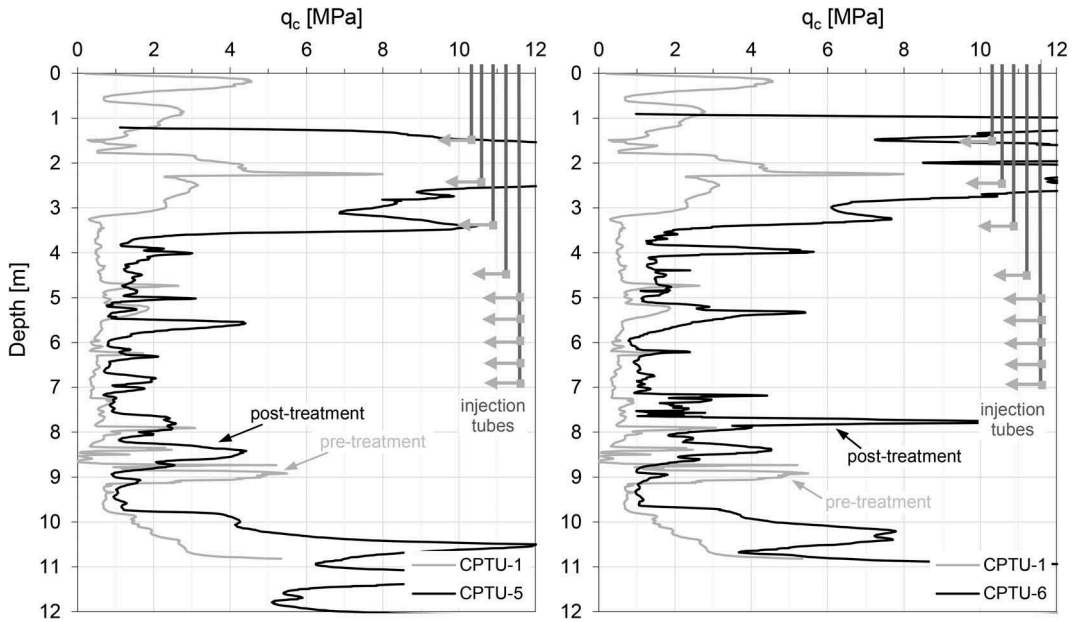


Figure 3. Comparison of tip resistance (q_c) profile between the CPT tests performed before (CPT-1) and after (CPT-5 and CPT-6) the ground treatment with polyurethane resins.

multipoint injection tubes. A second set of injection was then carried out at a shallower depth between -2 and -5 m with single-point injection tubes every 1 m.

A second series of in-situ tests, composed of four standard CPT, was performed after the ground treatment to evaluate the achieved improvement. The position of these tests is illustrated in the Figure 2 where the tests are numbered from 5 to 8. In particular, the CPT-5 and CPT-6 are carried out close the treated area, while the CPT-7 and CPT-8 are further and, therefore, less influenced by the injections.

Figure 3 shows a comparison between the tip resistance profiles obtained from the test performed before the treatment (CPT-1 is taken as a reference) and the tests performed after treatment (CPT-5 and CPT-6). In the shallow soil layer below the foundation (down to -3 m depth), a pronounced increase of the tip resistance is highlighted by both CPT tests (CPT-5 and CPT-6). The average value of q_c referred to this layer is higher than 10 MPa. On the other hand, in the depth range between -3 m and -7 m, the increase of the tip resistance exhibited by the two CPT tests is less pronounced. On average, the q_c value obtained from the two tests carried out after treatment is more than twice the average value measured before treatment.

4.2 Case b)

The second case study refers to the work carried out for the ground consolidation below an office building with dimensions equal to 15x7 m. The injections are performed along the building perimeter underneath the foundation starting from a depth equal to 1.2 m. A

combination of multi-point tubes and single point tube is adopted to treat a thickness of the ground equal to 3 m (from -1.3 m to -4.3 m). The injection points along the perimeter are spaced of 1 m.

Figure 4 shows the map of the building along with the location of the in-situ tests carried out to assess the efficiency of the treatment. Due to the presence of the existing structures, mini-CPT tests were adopted and performed in three different points. In each point, two tests were carried out one before and one after ground treatment. The two tests of each point were located close to each other to minimize the possible influence of different ground conditions.

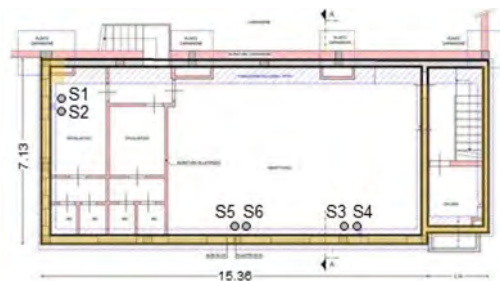


Figure 4. Map of the building illustrating the location of the mini-CPT tests performed to evaluate the efficiency of the ground treatment.

Figure 5 illustrates the tip resistance profiles of the three mini-CPT tests performed before ground treatment. From these findings, the soil can be

mainly classified as sand-silt mixture. In particular, the test S5 exhibited the lower tip resistance, highlighting the presence of silt/clayey silt below a depth equal to -3 m.

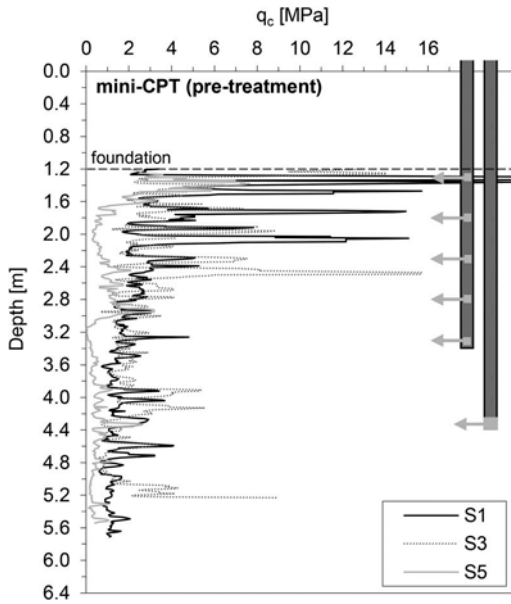


Figure 5. Tip resistance (q_c) profile of the three mini-CPT tests (S1, S3, S5) performed before the ground treatment.

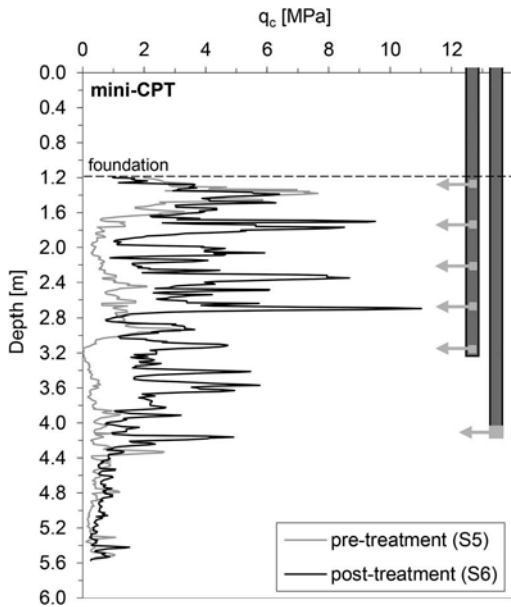


Figure 6. Comparison of the tip-resistance profiles obtained from the mini-CPT tests S5 and S6 performed before and after ground treatment.

The evaluation of the ground treatment is carried out comparing the tip resistance profiles from two

mini-CPT tests performed before and after treatment. In Figure 6 is illustrated an example obtained from the mini-CPT S5 and S6. The graph clearly highlights the increase of tip resistance measured at depths corresponding to the resin injection.

In the range between -1.3 m and -2.8 m the tip resistance increased from 1.6 MPa to 4.0 MPa, while in the range between -2.8 m and -4.3 m the tip resistance increased from 0.6 MPa to 2.4 MPa.

4.3 Case c)

The last case study illustrates the treatment with polyurethane resins of the ground foundation below an existing residential building. The treatment involved just part of the building as illustrated in the Figure 7. The injections were performed below the building foundation located at -1.2 m depth and along the perimeter of the building, with a spacing equal to 1 m, using multi-point tubes. The thickness of the soil layer treated is 2 m, from -1.2 m (depth of the foundation) to -3.2 m. The ground below the foundation is mainly composed of a mixture of loose fine soil and gravel.

In this example, the efficiency of the ground treatment was evaluated with dynamic probing tests, adopting the medium-light penetrometer DPM 30-20. As illustrated in the Figure 7, two DPM 30-20 tests were carried out: P1 before the treatment and P2 after the treatment.

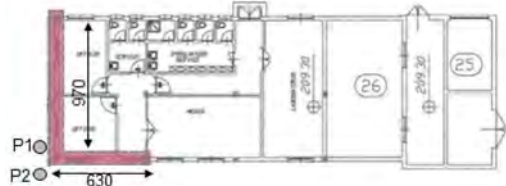


Figure 7. Map of the building along with the location of the treatment zone and the location of the DPM 30-20 tests performed before (P1) and after (P2) the ground treatment.

Figure 8 shows the results of both the two DPM 30-20 tests. From the results of the test P1, two soil layers were identified: (i) from -1.2 m to -2.3 m with an average N_{10} value equal to 7 and (ii) from -2.3 m to -3.3 m with an average N_{10} value equal to 2.4. After the treatment, the performed DPM 30-20 test highlighted an increase of the average N_{10} value for both layers. In particular, the layer 1 exhibited an average value equal to 27, while the layer 2 exhibited an average N_{10} value equal to 21.

A design tool based on the cavity expansion theory in a finite medium (Uretsek, 2021) was used to assess the achieved ground improvement in terms of increase in relative density and to verify the amount of resin injected. A perfect elasto-plastic Mohr-Coulomb model with a non-associated flow rule was adopted for the soil, considering two sets of parameters for the two different layers (Table 1). As the spacing of the injection

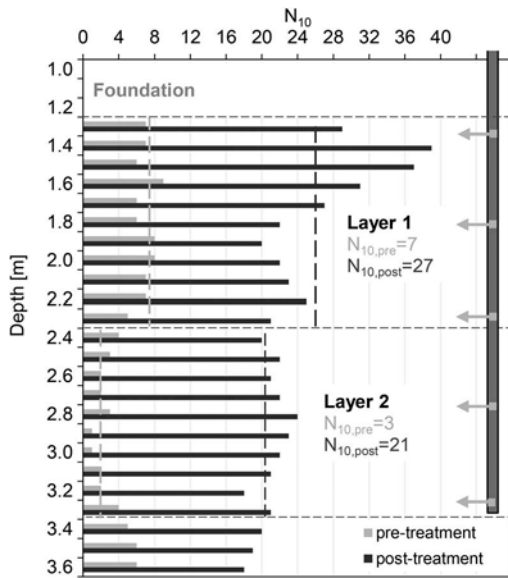


Figure 8. Comparison of the test results in terms of N_{10} obtained from the tests performed before (P1) and after (P2) the ground treatment.

holes was equal to 1 m, the radial distance of the fixed (no-displacement) boundary of the medium was set equal to 0.5 m, i.e. half of the injection hole spacing. The average increase in relative density obtained from the theoretical analyses was 12% for layer 1 (from 31% to 43%) and 21% for layer 2 (from 17% to 38%). The total amount of resin required to obtain such improvement resulted in being equal to 18.3 kg, which is in good agreement with the amount of resin injected in-situ (16.9 kg). This example highlights the potential of the cavity expansion theory to simulate ground behavior when treated with expanding polyurethane resins.

Table 1. Parameters of the soil adopted for the calculations.

Layer	1	2
Unit weight [kN/m^3]	18	18
Young modulus [MPa]	10	6
Poisson ratio [-]	0.25	0.25
Shear strength angle [$^\circ$]	34	34
Cohesion [kPa]	0	0
Dilatancy angle [$^\circ$]	-5	-8
Max void ratio [-]	0.65	0.65
Min void ratio [-]	0.30	0.30
Initial void ratio [-]	0.541	0.589

5 CONCLUSIONS

Expanding polyurethane resins represent a valid alternative to conventional grout for ground improvement and compaction. The effectiveness of the ground

treatment can be assessed by performing in-situ tests with static and dynamic penetrometers. This paper presents a series of case studies where standard CPT, mini-CPT, and DPM 30-20 tests were adopted.

The main advantage of the standard CPT test is the possibility of using the test results not only for treatment performance evaluation but also for the geotechnical characterization of the subsoil. However, it is often difficult to adopt such equipment when the treatment is carried out inside an existing structure.

The reduced size of the mini-CPT and DPM 30-20 equipment represents their main advantage. On the other hand, the lack of well-established empirical correlations to estimate soil geotechnical parameters from these tests is their main drawback.

Based on the examples presented in this work, all three in-situ tests can be regarded as suitable tools to assess the efficiency of the ground treatment with expanding polyurethane resins.

REFERENCES

- ASCE (American Society of Civil Engineers), 2010. Compaction ground consensus guide, ASCE Standard ASCE/G-1 53-10. ASCE.
- Buzzi, O., Fityus, S., Sasaki, Y., e Sloan, S., 2008. Structure and properties of expanding polyurethane foam in the context of foundation remediation in expansive soil. *Mechanics of Materials* 40,1012–1021.
- Cestari, F., 2012. *In situ geotechnical tests*. Patron editore.
- de Vries, G. T., Laban, C., & Blikendaal, E., 2018. Comparison of mini CPT cone (2 cm^2) vs. normal CPT cone (10 cm^2 or 15 cm^2) data, 2 case studies. In *Cone Penetration Testing 2018* (pp. 683–688). CRC Press.
- Dei Svaldi, A., Favaretti, M., Paschetto, A., e Vinco, G., 2005. “Modellazione analitica del miglioramento del terreno attraverso iniezioni di resina ad alta pressione d’espansione.” 6th International Conference on Ground Improvement Techniques, Coimbra, Portugal.
- Dominijanni, A., Manassero, M., 2014. Consolidamento dei terreni con resine espandenti: guida alla progettazione. McGraw-Hill.
- Kovacevic, N., Potts, D. M., & Vaughan, P. R., 2000. The effect of the development of undrained pore pressure on the efficiency of compaction grouting. *Geotechnique*, 50 (6),683–688.
- Shrivastava, N., Zen, K., Shukla, S. K., 2017. Modeling of compaction grouting technique with development of cylindrical cavity expansion problem in a finite medium. *International Journal of Geosynthetics and Ground Engineering*, 3(4),1–12.
- Squeglia, N., & Lo Presti, D. C. F., 2010. Use of mini CPT to evaluate degree of compaction in fine-grained soils. In *CPT’10. 2nd International Symposium on Cone Penetration Testing*, Huntington Beach, California.
- Uretak, 2021. SIMS 2.0 (Soil Improvement Modelling Software) – Training manual.
- Yu, H. S., Houlsby, G. T., 1991. Finite cavity expansion in dilatant soils: loading analysis. *Geotechnique*, 41(2),173–183.
- Yu, H. S., 2000. Cavity expansion methods in geomechanics. Springer Science & Business Media.

Evaluation of flow liquefaction susceptibility of a sandy-silt tailings using the CPTu

M.P. dos Santos Junior & R. César Gomes
Universidade Federal de Ouro Preto, Brazil

S.G. Silva Ribeiro
GeoFast – Geotechnical Modelling, Brazil

B.G. Delgado
CONSTRUCT-GEO, Faculdade de Engenharia da Universidade do Porto, Portugal

ABSTRACT: Flow liquefaction is a behavior observed in saturated or nearly saturated geomaterials that show a strain softening response during undrained shear, most common in very loose sands and silts as well as very sensitive clays. In the mining industry, flow liquefaction is a subject of high relevance due to the geotechnical characteristics of the tailings. Many methodologies have been developed to evaluate the susceptibility to flow liquefaction using in-situ tests, especially the CPTu test, since it provides high accuracy and good repeatability. This paper compares four methodologies based on the CPTu test to evaluate the susceptibility to flow liquefaction: i) Plewes et al. (1992), ii) Olson (2001), iii) Shuttle & Cuning (2008) and iv) Robertson (2016). The results obtained highlight the need to correct the original contour suggested by Olson (2001) for medium and high compressibility geomaterials. Furthermore, all other methods evaluated presented similar results in the overall classification.

1 INTRODUCTION

Casagrande (1975) showed that loose sands tend to contract during drained shear while dense sands tend to dilate under the same condition until it reaches the critical void ratio. If sheared under an undrained condition loose sands will generate positive excess porewater pressure, reducing the effective stress and, therefore, its shear strength, while the opposite would occur for dense sands.

Flow liquefaction is a behavior observed in saturated or nearly saturated soils that show a strain softening response in undrained shear due to its contractive behavior under drained conditions, most common in very loose sands and silts as well as sensitive clays.

As shown in Figure 1 presented by Robertson & Wride (1998), sand-like soils that are looser than the critical state will generate positive excess porewater pressure and show a strain softening behavior in undrained shear, illustrated by the Strain Softening Condition (SS). If the state prior to shear is close to the critical state, these soils can experience a limited contraction, exhibited as a Limited Strain Softening (LSS) condition in Figure 1, also referred in the literature as quasi-steady state condition. If the soil is denser than the critical state, however, it will tend to exhibit

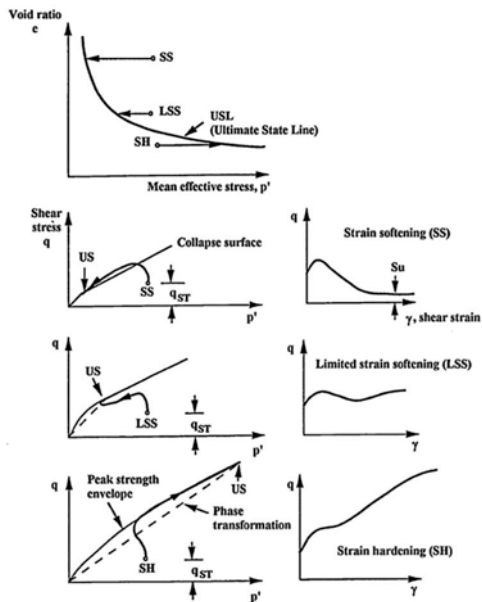


Figure 1. Typical undrained monotonic behavior of sand-like soils in triaxial compression tests - Robertson & Wride (1998).

a Strain Hardening (SH) behavior and the undrained strength will be greater than the drained strength.

2 SUSCEPTIBILITY TO FLOW LIQUEFACTION

This paper is going to evaluate the susceptibility of a sandy-silt tailings to flow liquefaction using the results of a Cone Penetration Testing (CPTu) performed in the interior of a Tailings Storage Facility (TSF). Four methodologies will be used herein to evaluate the state of the tailings: i) Plewes et al. (1992), Olson (2001), Shuttle & Cunning (2008) and Robertson (2016).

2.1 Plewes et al. (1992)

Plewes et al. (1992) suggested a relationship between the slope of the critical state line (λ_{10}) and the normalized friction ratio (F or F_r) as shown by Equation 1.

$$\lambda_{10} = \frac{F}{10} \quad (1)$$

$$F \text{ or } F_r = \frac{f_s}{(q_t - \sigma_{v0})} \times 100\% \quad (2)$$

where:

- f_s = sleeve friction resistance
- q_t = corrected cone resistance
- σ_{v0} = total vertical stress

Once the slope of the critical state line (λ_{10}) is determined the state parameter (ψ) can be calculated using the equation suggested by Shuttle & Cunning (2007).

$$Q_p (1 - B_q) + 1 = \bar{k} e^{-\bar{m}\psi} \quad (3)$$

Where Q_p is the tip resistance normalized by the mean affective stress (p'_0) and B_q is the pore pressure ratio, defined as shown below.

$$Q_p = \frac{(q_t - p_0)}{p'_0} \quad (4)$$

$$B_q = \frac{(u_2 - u_0)}{(q_t - \sigma_{v0})} \quad (5)$$

where:

- u_2 = pore pressure measured behind the cone
- u_0 = *in situ* pore pressure

As a screening-level assessment, Jefferies & Been (2016) suggested that the effective inversion coefficients, \bar{k} and \bar{m} , could be determined using Equation 6

$$\frac{\bar{k}}{M} = 3 + \frac{0.85}{\lambda_{10}} \quad (6)$$

$$\bar{m} = 11.9 - 13.3\lambda_{10} \quad (7)$$

where M is the critical friction ratio ($M=q_c/p'_c$) and λ_{10} is the slope of the critical state line (CSL) measured in $\log_{10} p' - e$ space. It was assumed $M_{tc}=1.45$ herein, using the average value of the range suggested by Jefferies & Been (2016).

2.2 Olson (2001)

Olson (2001) performed an extensive evaluation of 33 case histories of liquefaction flow failures and developed a comprehensive procedure to evaluate i) liquefaction susceptibility, ii) triggering of liquefaction and iii) post-triggering/flow failure stability.

In order to evaluate the susceptibility to flow liquefaction, Olson (2001) suggested the use of the contour proposed by Fear & Robertson (1995) based on the Standard Penetration Test (SPT). To convert the boundary from SPT to CPT, Olson (2001) used a relationship $q_c/N_{60}=0.60$, typical of clean sands, as shown in Figure 2. The contour proposed by the author to distinguish between contractive and

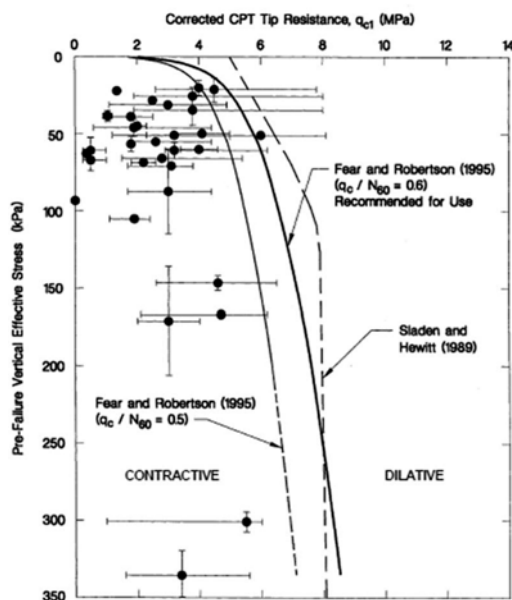


Figure 2. Boundary separating contractive from dilative behavior suggested by Olson (2001) to evaluate the susceptibility to flow liquefaction.

dilative behavior is represented by Equation 8, based on the corrected tip resistance (q_{c1}) and the vertical effective stress (σ'_{v0}).

$$\left(\sigma'_{v0}\right)_{\text{boundary}} = 1.1047 \times 10^{-2} (q_{c1})^{4.7863} \quad (8)$$

The corrected CPT tip resistance, q_{c1} , is obtained as follows:

$$q_{c1} = q_c \times C_q \quad (9)$$

where q_c is the measured cone resistance and C_q is the CPT-based overburden correction factor suggested by Kayen et al. (1992), defined by Equation 10.

$$C_q = \frac{1.8}{0.8 + \left(\frac{\sigma'_{v0}}{P_a}\right)} \quad (10)$$

where P_a is one atmosphere of pressure in the same units as σ'_{v0} .

Olson (2009) discussed the effect of compressibility on the evaluation of liquefaction susceptibility and suggested the use of the slope of the critical state line (λ_{10}) to update the original boundary suggested by Olson (2001) as shown by Figure 3. According to the author, the original boundary should only be used for low compressibility soils ($\lambda_{10} \sim 0.03$) which is

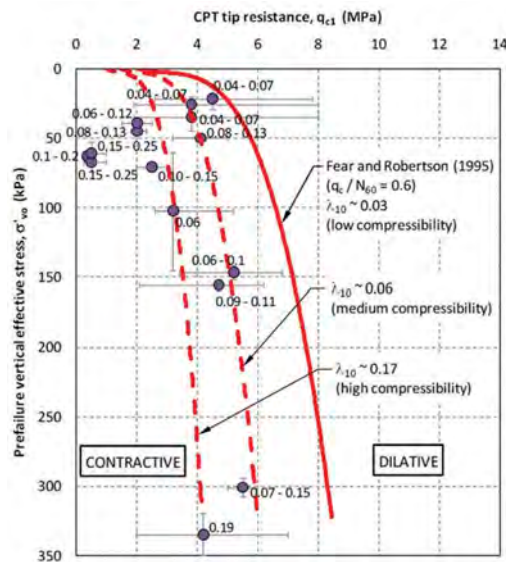


Figure 3. Contours suggested by Olson (2009) to separate contractive from dilative conditions for soils of low, medium and high compressibility.

associated with the ratio of $q_c/N_{60}=0.6$. Many investigators (Burland & Burbidge 1985; Jefferies & Davies 1993; Robertson & Campanella 1983; Schnaid & Odebrecht 2012; Stark & Olson 1995) demonstrated that the ratio q_c/N_{60} is a function of soil type (usually expressed as a function of the mean grain size - D_{50}).

This paper suggests the use of the ratio q_c/N_{60} to account for the effect of compressibility and Equation 11 is suggested for this purpose.

$$q_{c1, \text{contour}} = \frac{\left[7.69 \delta \sigma'_{v0} \left(0.209+n\right) P_a^{(1-n)}\right]}{0.8 P_a + \sigma'_{v0}} \quad (11)$$

where δ = Ratio q_c/N_{60} .

To evaluate the susceptibility to flow liquefaction it is suggested the use of Equation 12.

$$\beta = (q_{c1})_{\text{contour}} - (q_{c1})_{\text{measured}} \quad (12)$$

Therefore, $\beta > 0$ will indicate that $(q_{c1})_{\text{contour}} > (q_{c1})_{\text{measured}}$ for the same vertical effective stress, which indicates that the point in the profile is in a contractive state.

2.3 Shuttle & Cuning (2008)

Shuttle & Cuning (2007) presented a very detailed study using finite element analysis with cavity expansion theory and the NorSand Model to evaluate the liquefaction potential of a very loose silt tailings (*Rose Creek silt tailings*). Following discussions with Peter K. Robertson, Shuttle & Cuning (2008) presented a contour to distinguish between contractive and dilative behavior using the soil behavior chart suggested by Jefferies & Davies (1991), as presented in Figure 4.

Since the authors did not present the equation corresponding to the suggested contour, it is suggested herein the use of Equation 13 to be used to represent this boundary.

$$\left[Q(1 - B_q) + 1\right] = 2,35 + \frac{93,15}{\left[1 + \left(\frac{F}{25,40}\right)^{0,634}\right]^{9,93}} \quad (13)$$

where,

$$Q \text{ or } Q_t = \frac{(q_t - \sigma'_{v0})}{\sigma'_{v0}} \quad (14)$$

To characterize the behavior of the soil with depth the parameter α will be used, defined by Equation 15. Following this definition, positive values of α will indicate that $\left[Q(1-B_q)+1\right]_{\text{Contour}} > \left[Q(1-B_q)+1\right]_{\text{Measured}}$, meaning that the measured value is located below the

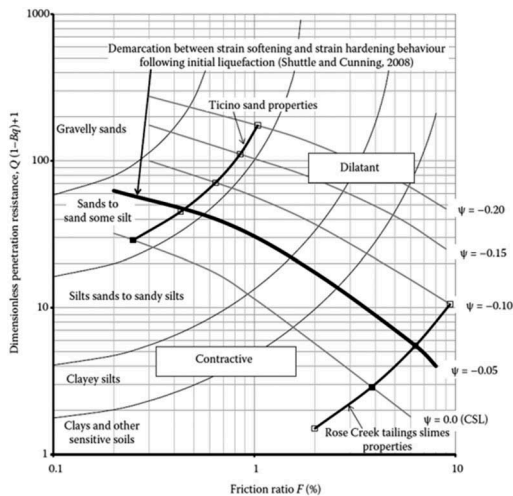


Figure 4. Boundary separating contractive from dilative behavior suggested by Shuttle & Cuning (2008) - Jefferies & Been (2016).

envelope shown in Figure 4 and, therefore, is susceptible to flow liquefaction.

$$\alpha = [Q(1 - B_q) + 1]_{Contour} - [Q(1 - B_q) + 1]_{Measured} \quad (15)$$

2.4 Robertson (2016)

Robertson (2016) updated the CPT-based normalized soil behavior type (SBTn) classification system proposed by Robertson (2009) to use behavior-based instead of textural-based descriptions, as presented in Figure 5.

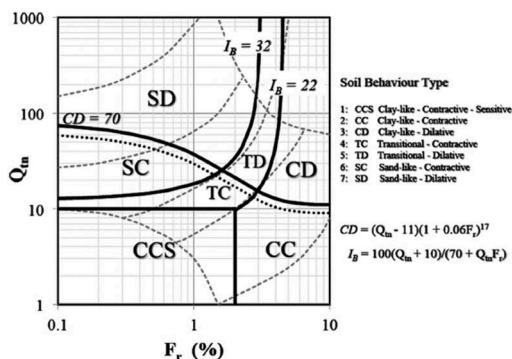


Figure 5. Updated CPT-based normalized soil behavior type chart proposed by Robertson (2016).

The author updated the soil behavior type index to use a hyperbolic shape, as indicated by Equation 16.

$$I_B = \frac{100(Q_{tn} + 10)}{(Q_{tn}F_r + 70)} \quad (16)$$

where,

$$Q_{tn} = \left[\frac{(q_t - \sigma_{v0})}{P_a} \right] \left(\frac{P_a}{\sigma'_{v0}} \right)^n \quad (17)$$

$$n = 0.381(I_c) + 0.05 \left(\frac{\sigma'_{v0}}{P_a} \right) - 0.15 \quad (18)$$

where $n \leq 1.0$.

The soil behavior type index, I_c , was first proposed by Jefferies & Davies (1993) who recognized that the boundaries between the soil behavior type zones could be approximated by concentric circles whose radius indicates the soil behavior type index. Robertson & Wride (1998) modified the definition of I_c to apply to the Robertson (1990) chart, as defined by Equation 19.

$$I_c = \left[(3.47 - \log Q_t)^2 + (\log F_r + 1.22)^2 \right]^{0.5} \quad (19)$$

Robertson (2016) suggested the use of the contour $CD=70$ (also shown in Figure 5) to differentiate soils that are contractive and dilative at large strains. The $CD=70$ boundary combines two different criteria: i) $Q_{tn,cs}=70$ for sand-like soils and $OCR=4$ for transitional and clay-like soils. Equation 20 is suggested by the author to represent the contour $CD=70$.

$$CD = 70 = (Q_{tn} - 11)(1 + 0.06F_r)^{17} \quad (20)$$

3 RESULTS

The tailings evaluated herein is a by-product of the mining of iron ore in the state of Minas Gerais/Brazil. The assessment of the tailings included the collection of disturbed samples to evaluate: i) the grain size distribution curve, ii) the water content (w), iii) the specific gravity of soil solids (G_s), iv) the unit weight (γ and γ_d), v) the liquid limit (LL) and vi) the plastic limit (PL).

The grain size distribution curves of the samples collected are shown in Figure 6. In terms of mean values, roughly 79% of the tailings corresponds to silt-sized particles, 4% to clay-sized particles and the remaining (17%) is fine sand. The fines were non-plastic and the mean values of the unit weight was $\gamma=23.4 \text{ kN/m}^3$ and $\gamma_d=19.4 \text{ kN/m}^3$.

The collected samples were also used to determine the water content (w) and these values were converted to void ratio (e) using Equation 21. The

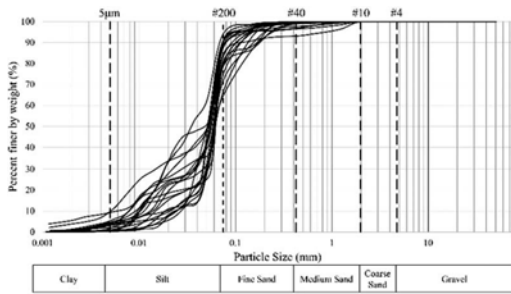


Figure 6. Grain size distribution curves of the sandy-silt tailings according to the ASTM D422-63 (2007).

mean value of water content was 21.4% and the void ratio was 0.93.

$$e = \frac{G_s \gamma_w}{\gamma_d} - 1 \quad (21)$$

The specific gravity (G_s) was determined following the procedures of the ASTM D854-14, to give a mean value of 3.8.

The normalized parameters (Q_t , F_r and B_q) from the CPTu performed on the sandy-silt tailings is shown in Figure 7. As can be seen, the initial portion of the sounding did not show excess porewater pressure up until 20m. Furthermore, below 27m the tailings exhibit a very low tip resistance and high B_q values. It is also important to notice the high heterogeneity on the tailings profile due to the interbedded layers of clay-like and sand-like behavior.

In order to evaluate the susceptibility of the tailings to flow liquefaction the contours suggested by Robertson (2016), Shuttle & Cuning (2008) and Plewes et al. (1992) are presented in Figure 8. Based on the behavior observed in the sounding, the profile

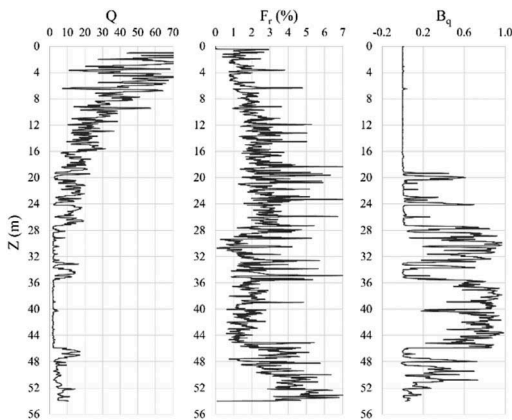


Figure 7. Normalized CPTu parameters of the sounding performed in the sandy-silt tailings.

was divided into three main regions: i) Region I: Predominantly dilative behavior (0-16m), ii) Region II: Interbedded layers of contractive and dilative behavior (16-27m) and iii) Region III: Predominantly contractive behavior (below 27m).

The results of the Fear & Robertson (1995) boundary suggested by Olson (2001) is shown in Figure 9. As can be observed, using this method most of the tailings profile is classified as contractive. In fact, only

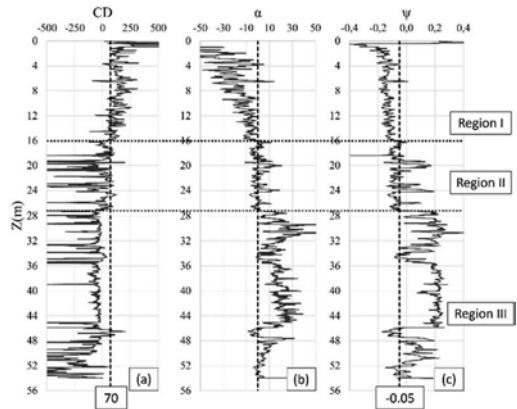


Figure 8. Evaluation of the susceptibility to flow liquefaction using a) Robertson (2016), b) Shuttle & Cuning (2008) and c) Plewes et al. (1992).

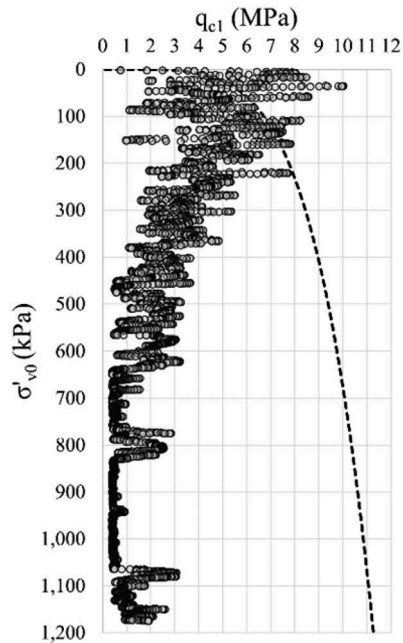


Figure 9. Results of the susceptibility to flow liquefaction using the Fear & Robertson (1995) contour suggested by Olson (2001).

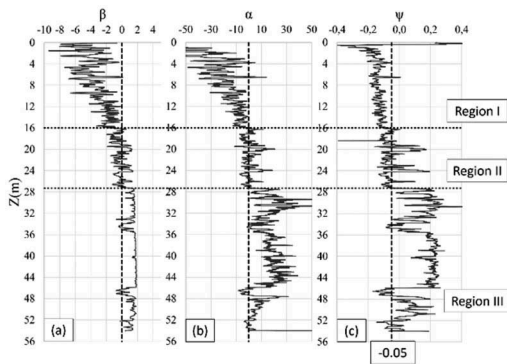


Figure 10. Evaluation of the susceptibility to flow liquefaction using a) Olson (2001) corrected for $q_c/N_{60}=0.07$, b) Shuttle & Cuning (2008) and c) Plewes et al. (1992).

the first 2m of the profile ($\sigma'_{v0}<50\text{kPa}$) was deemed to be in a dilative state.

The limitations of the original contour suggested by Olson (2001) for medium and high compressibility soils was discussed herein in the section 2.2. Equation 12 was applied in this paper to account for the effect of compressibility and it was determined the ratio q_c/N_{60} that would be necessary for the boundary suggested by Olson (2001) to yield results similar to the other methodologies evaluated. As can be seen in Figure 10, it was necessary to use a ratio of $q_c/N_{60}=0.07$ (a reduction by a factor of 8.6 in relation to the original contour) to calibrate the Fear & Robertson (1995) boundary for use with the sandy-silt tailings.

4 CONCLUSION

This paper presented an evaluation of the susceptibility to flow liquefaction of a sandy-silt tailings using four different methodologies: i) Plewes et al. (1992), ii) Olson (2001), iii) Shuttle & Cuning (2008) and iv) Robertson (2016).

The results of the study showed that for the tailings evaluated herein the contours suggested by Plewes et al. (1992), Shuttle & Cuning (2008) and Robertson (2016) yielded similar results (Figure 8).

The original boundary suggested by Olson (2001) resulted in a very conservative assessment (Figure 9). Equation 12 was used herein to account for the effect of compressibility and the ratio $q_c/N_{60}=0.07$ was used to correct the contour to yield results similar to the other methodologies evaluated.

The results of the study are useful to highlight the importance of the correction of the boundary suggested by Olson (2001) for soils of medium and high compressibility (specially tailings). Due to its inherent limitations, the authors do not recommend the use of the contour suggested by Olson (2001) to evaluate the susceptibility to flow liquefaction in soils of medium to high compressibility.

It is also important to emphasize that all these methods should be used as a screening-level assessment. Moreover, there are instances where the methodologies discussed herein can yield to different conclusions regarding the state of the soils and further investigations (including laboratory tests) would certainly be an effective tool to guide towards a better understanding of the behavior of the geomaterials.

REFERENCES

- ASTM D422-63(2007)e2. 2007. Standard Test Method for Particle-Size Analysis of Soils (Withdrawn 2016). ASTM International, West Conshohocken, PA.
- ASTM D854-14. 2014. Standard Test Methods for Specific Gravity of Soil Solids by Water Pycnometer. ASTM International, West Conshohocken, PA.
- Burland, J.B. & Burbidge, M.C. 1985. Settlement of Foundations on Sand and Gravel. *In* Proceedings of the Institute of Civil Engineers (London). pp. 1325–1381.
- Casagrande, A. 1975. Liquefaction and cyclic deformation of sands: A critical review. *In* Proceedings of the Fifth Panamerican Conference on Soil Mechanics and Foundation Engineering. pp. 79–133.
- Fear, C.E. & Robertson, P.K. 1995. Estimating the undrained strength of sand: a theoretical framework. *Canadian Geotechnical Journal*, **32**(5): 859–870. doi:10.1139/t95-082.
- Jefferies, M. G. & Been, K. 2016. Soil Liquefaction: A Critical State Approach.
- Jefferies, M.G. & Davies, M.P. 1991. Soil classification by the cone penetration test: Discussion. *Canadian Geotechnical Journal*, **28**(1): 173–176. doi:10.1139/t91-023.
- Jefferies, M.G. & Davies, M.P. 1993. Use of CPTu to Estimate Equivalent SPT N60. *Geotechnical Testing Journal*, **16**(4): 458–468. doi:10.1520/gtj10286j.
- Kayen, R.E. Mitchell, J.K. Seed, R.B. Lodge, A. Nishio, S. & Coutinho, R. 1992. Evaluation of SPT, CPT and shear wave-based methods for liquefaction potential assessment using Loma Prieta data. *In* Proceedings of the 4th Japan-U.S. Workshop on Earthquake Resistant Design of Lifeline Facilities and Countermeasures of Soil Liquefaction. pp. 177–192.
- Olson, S.M. 2001. Liquefaction Analysis of Level and Sloping Ground Using Field Case Histories and Penetration Resistance.
- Olson, S.M. 2009. Strength Ratio Approach for Liquefaction Analysis of Tailings Dams. *In* Proceedings of the University of Minnesota 57th Annual Geotechnical Engineering Conference. pp. 37–46.
- Plewes, H.D. Davies, M.P. & Jefferies, M.G. 1992. CPT based screening procedure for evaluating liquefaction susceptibility. *In* Proceedings of the 45th Canadian Geotechnical Conference.
- Robertson, P.K. 1990. Soil classification using the cone penetration test. *Canadian Geotechnical Journal*, **27**(1): 151–158. doi:10.1139/t90-014.
- Robertson, P.K. 2009. Interpretation of cone penetration tests - A unified approach. *Canadian Geotechnical Journal*, **46**(11): 1337–1355. doi:10.1139/T09-065.
- Robertson, P.K. 2016. Cone penetration test (CPT)-based soil behaviour type (SBT) classification system — An

- update. *Canadian Geotechnical Journal*, **53**(12): 1910–1927. doi:10.1139/cgj-2016-0044.
- Robertson, P.K. & Campanella, R.G. 1983. Interpretation of Cone Penetration Tests. *Canadian Geotechnical Journal*, **20**(4): 718–745.
- Robertson, P.K. & Wride, C.E. 1998. Evaluating cyclic liquefaction potential using the cone penetration test. *Canadian Geotechnical Journal*, **35**(3): 442–459. doi:10.1139/t99-102.
- Schnaid, F. & Odebrecht, E. 2012. Ensaios de Campo e suas aplicações à Engenharia de Fundações.
- Shuttle, D.A. & Cunning, J. 2007. Liquefaction potential of silts from CPTu. *Canadian Geotechnical Journal*, **44**(1): 1–19. doi:10.1139/T06-086.
- Shuttle, D.A. & Cunning, J. 2008. Reply to the discussion by Robertson on “Liquefaction potential of silts from CPTu.” *Canadian Geotechnical Journal*, **45**(1): 142–145. doi:10.1139/T07-119.
- Stark, T.D. & Olson, S.M. 1995. Liquefaction resistance using CPT and field case histories. *Journal of Geotechnical Engineering*, **121**(12): 856–869. doi:10.1061/(ASCE)0733-9410(1995)121:12(856).

Prospects on data mining approach for pile geotechnical design utilizing CPT and CPTu records: Case study: AUT database

A. Eslami & S. Heidarie Golafzani

Amirkabir University of Technology, Tehran, Iran

S. Moshfeghi

University of British Columbia (UBC), Vancouver, Canada

ABSTRACT: A comprehensive database has been compiled including CPT soundings performed adjacent to pile load test and related geotechnical information, namely AUT (Amirkabir University of Technology): Geo-CPT&Pile Database. In this paper, after a brief review of existing CPT and pile databases, the specifications of the updated AUT: Geo-CPT&Pile Database as well as different categories of data are presented. Subsequently, several procedures developed using this database from different geotechnical aspects are reviewed and introduced. These implementations are extended for appraisal of currently used CPT-based methods for pile geotechnical design by focusing on methods screening, uncertainty- reliability measures, and Performance-Based Design (PBD) approach regarding resistance factors. After all, an algorithm is presented including a formulated procedure of pile geotechnical design by means of smart database collections, reproduction of CPT profile, assortment of competitive methods, integration of geotechnical aspects i.e., capacity, load-displacement performance and resistance distribution. Correspondingly, via realizing prospects on implementation of major aspects leads towards optimum pile performance-based design upon a data mining approach.

1 BACKGROUNDS

The application of databases in geotechnical engineering returns to long decades ago since researchers tried to develop correlations among in-situ or lab measured parameters and design geotechnical parameters. Cone penetration testing (CPT) is one of reliable in-situ testing with less measurement error in comparison to others (Phoon and Kulhawy 1999). It provides continuous records with depth and due to its similarity to piles, a broad range of correlations have been made for prediction of ultimate pile bearing capacity (Eslami and Fellenius 1997). Piles are important foundation systems in geotechnical engineering facilitating construction in offshore and onshore areas or even in abnormal subsoil conditions or extreme loads imposed by superstructure in high-rise buildings and skyscrapers.

CPT-based methods differ in many areas such as the compiled CPT and pile database regarding the pile characteristics and the subsoil conditions where these piles were installed, model assumptions and simplifications, input parameters for predicting unite side and toe resistances, data processing for excess pore water pressure in back shoulder of CPT cone, failure pattern around the pile toe and so on. For instance, some methods consider loading directions or friction fatigue

in their correlations while others do not, or some methods have been develop based on total stress analysis (TSA) while some were developed based on effective stress analysis (ESA) or empirical correlations. Accordingly, various assessment criteria have been introduced to measure accuracy, precision and efficiency of these predictive methods (Eslami et al. 2019a).

The application of CPT and pile databases cannot be limited to performance assessment of predictive methods and these databases can provide us with more information.

Present study introduces a comprehensive geotechnical engineering database in the field of CPT and pile. This database named as AUT:Geo-CPT&Pile database has had different applications in the pile engineering such as reliability-based assessment of drilled displacement piles (Moshfeghi & Eslami 2019), assessing the performance of CPT-based methods in predicting axial bearing capacity of helical piles, reproduction and realization of CPT records (Jamshidi Chenari et al. 2018), predicting the load displacement behavior of driven piles regarding CPT records, and uncertainty appraisal of CPT-based methods regarding statistical, probabilistic and reliability-based criteria (Eslami et al. 2020, Heidarie Golafzani & Eslami 2021) and the

importance of relevant data-based approach in geotechnical pile design (Eslami & Heidarie Golafzani 2020). Eventually, a CPT and pile data-based approach is introduced for pile design regarding the researches have been done.

2 AUT: GEO-CPT&PILE DATABASE; AN EFFICIENT TOOL IN DATA MINING FOR GEOTECHNICAL PILE DESIGN

The AUT:Geo-CPT&Pile database has been compiled from well-published and documented geotechnical engineering sources and includes 600 records of pile loading tests along with the results of adjacent cone or piezocone penetration tests (Moshfeghi et al. 2015; Eslami et al. 2019b).

This database was primarily aimed to assess the performance of different CPT-based methods. Moshfeghi & Eslami (2018, 2019) compiled a database of forty-three and seventy-six records of driven piles installed in sandy soils and their adjacent CPT records from AUT:Geo-CPT&Pile database and studied the effect of different criteria for interpreting static pile load test records to select the most consistent approach with the CPT-based methods. Among the four selected criteria, the Brinch Hansen 80% criterion and the load at the displacement of 10% of the pile diameter were the two most consistent criteria with the CPT-based approaches. They also assessed the performance of different CPT-based methods considering wasted capacity index (WCI) and cost optimization regarding safety factor. Assessments indicate that the German (Kempfert & Becker 2010), LCPC (Bustamante & Gianeselli 1982), Meyerhof (1983), UniCone (Eslami & Fellenius 1997) and UWA-05 (Lehane et al. 2005) methods have shown the most efficient predictions at their optimum factor of safety.

Askari Fateh et al. assessed the performance of ten direct CPT-based methods for helical piles via considering thirty-seven cases of helical piles installed in different soil types. Also, the accuracy of two different assumptions of failure mechanism around helical piles was examined through comparing the predicted axial bearing capacity and measured ones in static pile load tests. Finally, they suggested a new CPT-based method to estimate the bearing capacity of helical piles (Eslami et al. 2019a).

Jamshidi et al. (2018) developed an algorithm for realization of CPT data based on non-stationary random field theory. The proposed algorithm imposes soil layering alongside inherent soil variability based on Eslami and Fellenius (1997) soil classification chart. After detection of soil layering based on the simplified proposed approach, the statistical characteristics of each soil layer are defined as multi-criteria functions, assembled into the non-stationary auto-covariance matrix and the routines continue in Monte Carlo scheme for production of CPT records.

Valikhah et al. proposed a new analytical-numerical method to estimate axial load-displacement behaviour of driven piles in granular soils using CPT records. Implementing the method of stress characteristics, they analysed the stress field below and around the pile and in effect, the failure mechanism. This failure mechanism has then been used by implementation of the kinematical approach of the limit analysis to compute the displacement field (Eslami et al. 2019a).

The application of artificial intelligence has been developed in geotechnical engineering in recent years. Implementing group method of data handling type neural networks optimized using genetic algorithms, Ardalan et al. (2009) estimated the pile unit shaft resistance.

Eslami et al. (2020b) by employing a database of instrumented pile load tests as well as CPT records correlated the pile unit shaft resistance with CPT sleeve friction. They proposed an analytical-empirical procedure for estimating pile shaft capacity considering scale effects. Factors such as mechanism and rate of penetration, size effect (i.e., length and diameter), friction fatigue are taken into account in this approach.

Heidarie Golafzani et al. (2020a, b) compiled a database of sixty driven piles installed in different soil types and studied the performance of different approaches, i.e., static analyses, SPT-based methods and CPT-based methods including twelve methods. In their studies, they considered different statistical, probabilistic and reliability-based criteria, including mean and coefficient of variation, best fitted line, 20% accuracy level, cumulative distribution function (i.e., P_{50} and $P_{90}-P_{50}$), confidence interval, root mean square error (RMSE) and efficiency ratio (i.e., the ratio of load and resistance factor (LRFD) resistance factor to the model parameter). The model parameter was defined as the ratio of measured to predicted bearing capacity. They concluded that modified first order second moment (FOSM) is less time-consuming and complicated, and leads to statistically identical resistance factors to first order reliability (FORM) method and Monte Carlo simulations (MCS). They also compared the performance of the considered approaches and methods via radar charts and deduced that CPT-based methods perform better than two other approaches.

Eslami & Heidarie Golafzani (2020) stated that selection of predictive methods for pile geotechnical design has a pivotal role in an optimum and site-specific design. Results indicated that methods prioritized by statistical, probabilistic and reliability-based criteria attain higher resistance factor in load and resistance factor design (LRFD) or lower safety factor in allowable stress design (ASD) approaches. They emphasized that the global safety factor cannot stand alone against all uncertainty sources and methods attaining similar safety factors, do not result in the same probability of failure and reliability index (i.e., β).

3 GEOTECHNICAL DATA-BASED PILE DESIGN

As reviewed, CPT and pile databases support the geotechnical designer with invaluable information about the performance of predictive methods for special pile types installed in a particular project site/with definite characterizations or even for a wide range of pile types installed in various site locations and conditions. Furthermore, databases can be mined for extra information aiding in geotechnical pile design. Figure 1 illustrates the steps for this new suggested/proposed approach.

In this approach, it is necessary to compile a database of geotechnical information about various sites including pile load test results along with adjacent CPT records to the investigated piles.

In the first step, the engineer should evaluate the site conditions in terms of its available geotechnical information and categorizes it as no testing, minimum

number of testing and comprehensive geotechnical site investigation.

If the number of tests is minimum or tests are unavailable, it is referred to the database for either gaining extra information via smart selection according to the available akin sites or data production generally such as CPT data or specifically such as P- Δ and resistance distribution if necessary. These procedures constitute the first stage of data collection.

The second stage is about processing the axial pile bearing capacity predictions. Various methods and approaches result in a wide range of predictions. Regardingly, applying miscellaneous evaluation criteria including statistical and probabilistic criteria and risk, reliability and efficiency-based criteria, leads to selection of appropriate methods according to the available site conditions, codes and local information. Indeed, this stage is dedicated to method screening leading to optimum geotechnical design. Eventually,

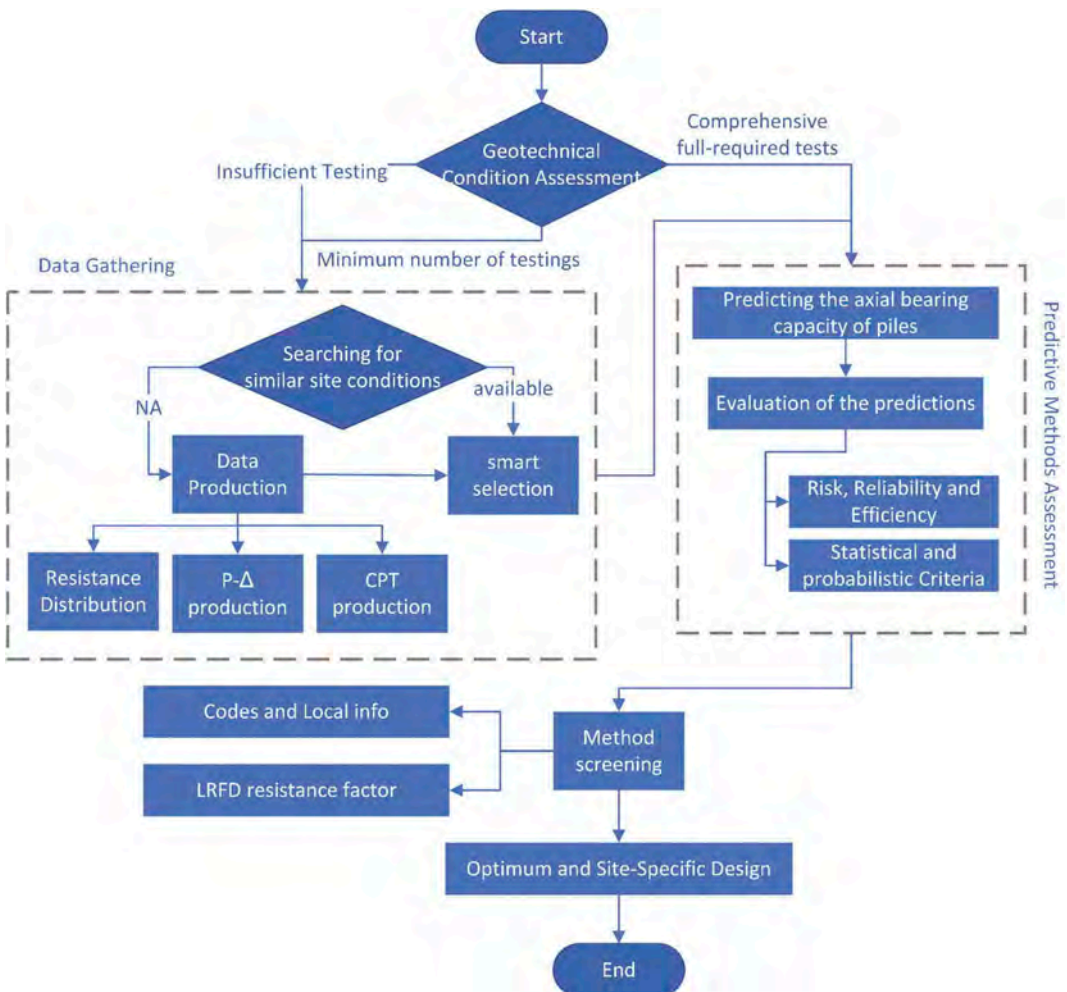


Figure 1. Geotechnical data-based pile design algorithm.

the understanding of the geotechnical engineer is improved and an optimum site-specific design approach is attained.

4 ENGINEERING IMPLEMENTATION

A database of sixty driven piles was gathered from the AUT:Geo-CPT&Pile database with their adjacent CPT records worldwide to illustrate the application of the proposed data-based geotechnical pile design approach. Most of the piles are installed in clayey soils (i.e., about 45% of the piles in the compiled database), followed by sandy soils (i.e., about 32%) and mixed soils (i.e., about 23%). According to what explained in the earlier section, for an optimum geotechnical pile design, it is appropriate to perform a comprehensive in-situ and lab tests to characterize the subsoil conditions and further consider it. In the case, the number of tests was limited or was not available for the current project, the geotechnical practitioner can gather extra information about the project site by searching through the available geotechnical site investigation reports for the nearby projects or a by smart selection from CPT and pile databases.

From the investigated database a driven pile was selected. This circular concrete pile was installed in sandy soils of Norway with embedment length of 15.5 m and diameter of 280 mm. By searching for similar site and pile conditions, a concrete square pile installed in Sweden was selected with embedment length of 12.8 m and width of 235 mm. Figure 2 provides the soil behavior classification (SBC) for these two close sites. As it is presented, the most majority of soil types are silt-sand and sand-gravel regarding the Eslami and Fellenius (1997) soil behavior classification.

Figure 3 illustrates the static pile load test (PLT) results for these two piles. Both piles behaved similarly under compression loading. As stated earlier, in case insufficient geotechnical data, Jamshidi Chenari et al. (2018) proposed a non-stationary algorithm for reproduction and realization of CPT records regarding soil stratigraphy.

Figure 4 compares the reproduced CPT records, i.e., q_c and f_s and their analogous real ones for the two investigated sites in Norway and Sweden. The geotechnical engineer can reproduce these CPT records with different inherent soil variability changing from low to high in soil characteristics reflecting the subsoil condition.

Figure 5 compares the performance of different CPT-based methods for these two piles via model parameter and it is the ratio of measured to predicted bearing capacity, i.e., Q_m/Q_p . The site conditions for these two considered piles, influence the performance of predictive methods appropriately in a similar way. For instance, if the acceptable limit for Q_m/Q_p changes from 0.8 to 1.2 as is shown in Figure 5, methods such as LCPC (Bustamante and Gianesselli

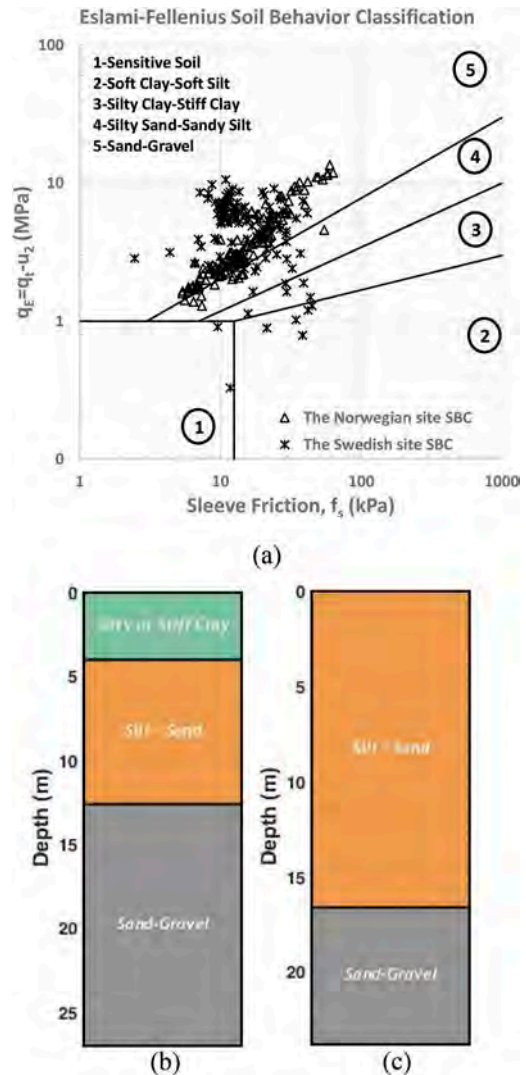


Figure 2. Soil stratigraphy; (a) soil behavior classification for the two sites (Eslami and Fellenius 1997), (b) the subsoil layering in Sweden, (c) the subsoil layering in Norway.

1983), Meyerhof (1983), UniCone (Eslami and Fellenius 1997), German (Kempfert and Becker 2010), and Modified UniCone (Niazi and Mayne 2016) have led to close predictions. However, other investigated methods, including Schmertmann (1978), Dutch (de Ruiter and Beringen 1979) and Fugro-05 (Kolk et al. 2005) resulted in less accurate predictions due to the differences mentioned earlier. Regardingly, finding matching piles with similar dimensions and embedment length installed in close or near close site conditions, enhances the geotechnical engineer to have an optimum site-specific design by selecting appropriate criteria and implementing multi-criteria decision-making models.

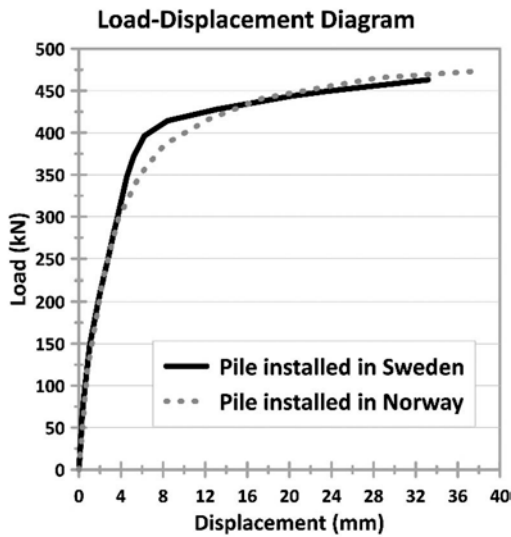


Figure 3. Pile load test results for the two considered piles.

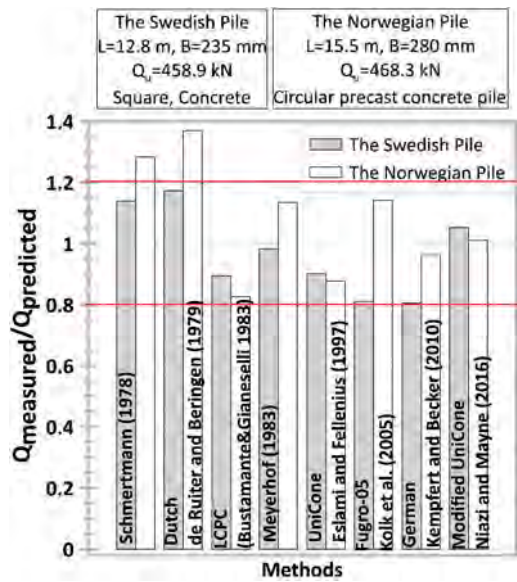


Figure 5. The performance of different CPT-based methods for these two considered piles.

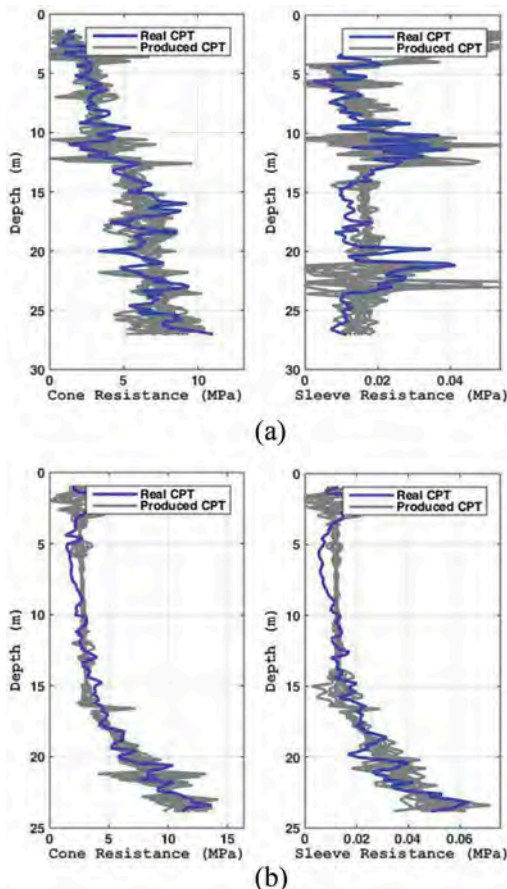


Figure 4. Reproduced CPT records for the two site conditions, (a) the Swedish site, (b) the Norwegian site.

5 CONCLUSIONS

Uncertainties are an inseparable part of geotechnical engineering, and many attempts have been made to consider their influence on geotechnical designs in the last decades. Characterizing the subsoil conditions is one of the essential steps in geotechnical designs, and CPT by producing continuous and reliable records has a crucial role in determining inherent soil variability. One of the primary applications of CPT soundings is predicting axial pile bearing capacity due to its similarity to the pile. In this regard, several methods have been developed based on CPT records. However, these methods result in a wide range of predictions according to the embedded uncertainties. To overcome the difficulties of selecting an appropriate predictive method, CPT and pile databases assist the geotechnical engineer. Accordingly, AUT:Geo-CPT&Pile database was introduced, and its implementation in various pile engineering issues was reviewed. However, the data mining of such a database is not limited to performance assessment of predictive methods, and an algorithm for data-based pile design approach is its other prospect. In this approach, with the aid of available data in the compiled database, the designer can search for the matching site and pile conditions in the absence of necessary and sufficient site geotechnical information or even reproduce and realize CPT records. After gathering adequate CPT and pile data, various predictive methods can be assessed via statistical, probabilistic, and reliability-based criteria. Eventually, the methods' screening procedure is finalized via considering codes and local info, and the superior methods are selected. Correspondingly, the final pile

geotechnical design will be an optimum pile performance-based design upon a data mining approach. The Application of this algorithm was presented through an example.

REFERENCES

- Ardalan, H., Eslami, A. and Nariman-Zadeh, N., 2009. Piles shaft capacity from CPT and CPTu data by polynomial neural networks and genetic algorithms. *Computers and Geotechnics*, 36(4), pp.616–625.
- Bustamante, M. & Gianeselli, L., 1982. Pile Bearing Capacity Prediction by Means of Static Penetrometer CPT. *Proceedings of the 2nd European Symposium on Penetration Testing*, 493–500.
- de Ruyter, J. and Beringen, F., 1979. Pile foundations for large North Sea structures. *Marine Georesources & Geotechnology*, 3(3) 267–314.
- Eslami, A. & Fellenius, B. H. 1997. Pile Capacity by Direct CPT and CPTu Methods Applied to 102 Case Histories. *Canadian Geotechnical Journal*, 34, 886–904.
- Eslami, A., Moshfeghi, S., Heidari, S., and Valikhah, F., 2019 a. AUT:Geo-CPT&Pile database updates and implementations for pile geotechnical design, *Geotechnical Engineering Journal of the SEAGS & AGSSEA*, 50(3) 74–90.
- Eslami, A., Moshfeghi, S., MolaAbasi, H. and Eslami, M. M., 2019 b. Piezocone and Cone penetration test (CPTu and CPT) applications in foundation engineering. *Butterworth-Heinemann*.
- Eslami, A., Heidarie Golafzani, S., and Moshfeghi, S., 2020a. CPT and pile database for performance-based design of pile axial bearing capacity. In *Proceedings of the 45th Annual Conference on Deep Foundations*, Deep Foundation Institute (DFI), Oxon Hill, Maryland, October 13-16, 12p.
- Eslami, A., Lotfi, S., Infante, J.A., Moshfeghi, S., and Eslami, M.M., 2020b. Pile shaft capacity from cone penetration test records considering scale effects. *International Journal of Geomechanics*, ASCE, 20(7), 13 p.
- Eslami, A. and Heidarie Golafzani, S., 2020. Relevant data-based approach upon reliable safety factor for pile axial capacity. *Marine Georesources & Geotechnology*, pp.1–14.
- Heidarie Golafzani, S., Jamshidi Chenari, R., and Eslami, A., 2020a. s, *Georisk: Assessment and management of Risk for Engineered Systems and Geohazards*, DOI:10.1080/17499518.2019.1628281.
- Heidarie Golafzani, S., Eslami, A. and Jamshidi Chenari, R., 2020b. Probabilistic Assessment of Model Uncertainty for Prediction of Pile Foundation Bearing Capacity; Static Analysis, SPT and CPT-Based Methods. *Geotechnical and Geological Engineering*, pp.1–19.
- Heidarie Golafzani, S., and Eslami, A., 2021. Uncertainty Appraisal of CPT-based Methods for Axial Pile Bearing Capacity. In *Proceedings of the 46th Annual Conference on Deep Foundations*, Deep Foundation Institute (DFI), Las Vegas, Nevada, October 12-15, 12p.
- Jamshidi Chenari, R., Kamyab Farahbakhsh, H., Heidarie Golafzani, S., and Eslami, A., 2018. Non-stationary realisation of CPT data: considering lithological and inherent heterogeneity. *Georisk: Assessment and Management of Risk for Engineered Systems and Geohazards*, 12(4) 265–278.
- Kolk, H.J., Baaijens, A.E. and Senders, M., 2005. Design criteria for pipe piles in silica sands. In *Design criteria for pipe piles in silica sands* (pp. 711–716). CRC Press/Balkema.
- Kempfert, H.G. and Becker, P., 2010. Axial pile resistance of different pile types based on empirical values. In *Deep Foundations and Geotechnical In-Situ Testing*, pp. 149–154.
- Lehane, B.M., Schneider, J.A. and Xu, X., 2005. The UWA-05 method for prediction of axial capacity of driven piles in sand. *Frontiers in offshore geotechnics: ISFOG*, pp.683–689.
- Meyerhof, G. G., 1983. Scale Effects of Ultimate Pile Capacity. *Journal of Geotechnical Engineering*, 109, 797–806.
- Niazi, F.S. and Mayne, P.W., 2016. CPTu-based enhanced UniCone method for pile capacity. *Engineering Geology*, 212, pp. 21–34.
- Phoon, K.-K. & Kulhawy, F. H., 1999. Evaluation of Geotechnical Property Variability. *Canadian Geotechnical Journal*, 36, 625–639.
- Moshfeghi, S., Eslami, A., and Hosseini, S.M.M., 2015. AUT-CPT&Pile database for piling performance using CPT and CPTu records. In *Proceedings of the 40th Annual Conference on Deep Foundations*, Deep Foundation Institute (DFI), Oakland, California, October 12-15, 10p.
- Moshfeghi, S. and Eslami, A., 2018. Study on pile ultimate capacity criteria and CPT-based direct methods. *International Journal of Geotechnical Engineering*, 12(1) 28–39.
- Moshfeghi, S. and Eslami, A., 2019. Reliability-based assessment of drilled displacement piles bearing capacity using CPT records. *Marine Georesources & Geotechnology*, 37(1) 67–80.
- Schmertmann, J.H., 1978. Guidelines for cone penetration test: performance and design (No. FHWA-TS-78-209). United States. Federal Highway Administration.

Evaluating mitigation of kinematic moments of precast driven piles in liquefiable layers using pre- and post-CPTu tests

K. Fakharian, D. Mohtashamamiri, K. Behroozian & M. Bahrami

Department of Civil & Environmental Engineering, Amirkabir University of Technology, Tehran, Iran

T. Bahrami & I.H. Attar

Pars GeoEnviro Inc., Tehran, Iran

ABSTRACT: Precast piles are driven to 23 m depth to improve the capacity of foundations located on saturated liquefiable sands on top underlain by a thick soft to medium stiff clay. Analyses show excessive kinematic moment at borderline of the two layers during liquefaction. It was decided to drive additional shorter piles (12 m) to mitigate liquefaction hoping that kinematic moments shall be reduced within allowable limits. CPTu tests were carried out before and after pile driving. The results show that q_c did not change considerably in the top saturated silty sand layer as well as the clayey soil underneath. The friction sleeve, however, increased more significantly due to radial displacement and compaction/consolidation attributed to cavity expansion during pile driving. Analyses showed that pile arrangement was not sufficient to overcome liquefaction during earthquake. However, safety factor increased sufficiently to reduce kinematic moment within the allowable limits. The details of the site operations, CPTu data before and after pile driving, analyses and interpretations are presented and discussed.

Keywords: Pizeocone Penetration Test (CPTu), Liquefaction, Precast pile, Kinematic moment

1 INTRODUCTION

Soil deposits at a site subjected to an earthquake may experience increases in pore water pressure and time-dependent vertical and lateral ground movements. As a consequence of the earthquake-induced ground movements, piles and other deep foundations will be subjected to two sources of additional lateral loading:

- a. Inertial Forces/Moments: forces and moments that are induced in the piles because of the accelerations generated within the structure by the earthquake.
- b. Kinematic Forces/Moments: forces and bending moments that are induced in the piles because of the ground movements resulting from the earthquake. Such movements will interact with the piles and because of the difference in stiffness of the piles and the moving soil, there will be lateral stresses developed between the pile and the soil, resulting in the development of shear forces and bending moments in the piles.

Tajimi (1969) and Penzien (1970) were among the first researchers to study the problem through using analytical and numerical approaches, respectively. Following these early efforts, the problem of kinematic

effects was analyzed by Blaney et al. (1976), Kagawa & Kraft (1980), Dobry & O'Rourke (1983), Nikolaou et al. (1995), Luo & Muroso (2001) and others. Determination of the kinematic forces acting on the pile depends on the liquefaction potential and soil parameters before and during liquefaction.

Conventional experiences have held that driving displacement piles into loose and medium dense sand will densify the soil volume close to the pile. Some researchers including Meyerhof (1959), Nataraja & Cook (1983), Bement & Selby (1997), Gianella et al. (2015), Stuedlein et al. (2016) and Stuedlein & Gianella (2017) and Rhyner (2018) have studied the densification effects caused by driving piles into granular soil. By changing the soil properties due to pile driving and subsequent alterations in the soil liquefaction potential, the amount of kinematic forces on the pile will change. Similarly, some have evaluated the effects of pile driving on variations of stress state and consolidation surrounding the pile shaft (e.g., Khanmohammadi & Fakharian, 2018; Fakharian & Khanmohmmnadi, 2022). Fakharian et al. (2014) evaluated the effect of surcharge pressure of the reaction system on the load-movement response of piles.

This paper presents a case study conducted to evaluate the effects of pile driving on loose, clean and silty

sand properties. The subsoil condition before pile driving was characterized using CPTu test as well as boreholes and soil sampling. Square precast concrete piles were designed and driven down to 23 m of embedment depth as the main piles or bearing piles. Analytical calculations showed excessive kinematic moments at the borderline of the two layers when liquefaction occurs. It was decided to drive additional shorter 12 m piles (compaction or improvement piles) to mitigate the liquefaction hoping that the kinematic moments shall be reduced within the allowable limits of the pile section. After driving the main piles and consolidation piles, hereinafter referred to as bearing and compaction piles, another 4 CPTu were conducted to see how the pile driving had contributed to the soil improvement between the piles. The site geological condition, CPTu data before and after pile driving, kinematic moment analyses before and after pile driving are carried out and interpretations are presented and discussed.

2 FIELD DESCRIPTION

2.1 Subsoil conditions

The trial field is located in Jask approximately 250 km south-east of Bandar-e-Abbas city in Hormozgan province, on coastal area of Gulf of Oman, Iran. Project area extends North-South, with an apparent length of 1600 m and width of 400 m. The soil stratification of the trial zone consists of three different layers (Figure 1):

Layer (I): The layer mostly consists of sand and cohesionless silt and classified as medium dense to dense silty sand. This layer has been observed from ground surface down to 8 m depth. GWT is 1.5 m deep any lies in Layer I.

Layer (II): Second layer consists of firm to stiff clay and silty clay. This layer underlying layer (I) starts from the depth of 8 m and in some areas has extended to a depth of 28 m.

Layer (III): This Layer is situated below the second layer (deeper than 28 m) and consists of medium dense to very dense sand and silty sand.

Figure 2 shows the distribution zones of clay, silt and sand with depth. In fact the red line with square points shows the border of clay-silt and the yellow line with triangle points shows the border of silt-sand. Down to 8 m, soil dominantly constitutes sand and silt, and the percentage of clay is less than 40%. From depth of 8 to about 26 m, the clay fraction is between 60 to 80%.

2.2 Main and compaction piles layout

Square 400 × 400 mm precast concrete piles were designed and driven down to 23 m of depth as the “main piles”. Ultimate bending moment of piles is 143 kNm. During liquefaction, however, analytical calculations show that kinematic moment at the borderline of the two layers (Layer I and Layer II) is greater than the

ultimate bending moment. It was decided to drive additional shorter piles (12 m) as “compaction piles” to mitigate the liquefaction hoping that the kinematic moments shall be reduced within the allowable limit of the pile section. Figure 3 shows the bearing and compaction piles layout in the trial field.

After driving the bearing and compaction piles, four CPTu tests were performed to evaluate the changes in soil condition at locations surrounded by piles and beyond. All tests were performed about 45 days after pile driving. The location of the post-pile driving tests is shown in Figure 3. CPT-10 and CPT-Ref are outside of the piling area and in a way indicates the initial state (*in situ*) of the soil. CPT-ZA3 and CPT-ZA4 are located between the bearing and compaction piles, and CPT-ZA5 is located between compaction piles.

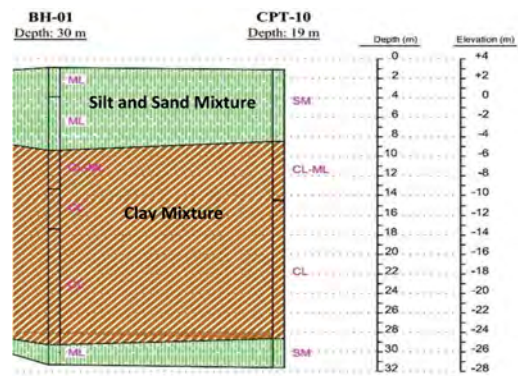


Figure 1. Geotechnical cross-section of the trial field in Jask, on Coastlines of Sea of Oman.

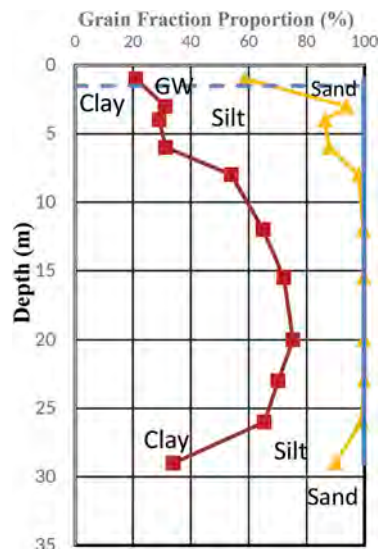


Figure 2. Grain fraction proportions with depth.

2.3 Pre- and post-driving trial tests

Results of pre- and post-driving CPTu tests are shown in Figure 4. The results after pile driving indicates that no considerable changes are observed in q_c in both layers (I) and (II) till depth 12 m, equivalent to the length of compaction piles. The friction sleeve f_s , however, has increased significantly. The pore pressure variations show that original *in situ* condition has induced higher pore pressure from starting the clayey soil of Layer II (CPT-10 and CPT-Ref). However, after pile driving, both ZA3 and ZA4 points situated in between the piles have generated negative to hydrostatic values of u down to 12 m of depth equivalent to the depth of compaction piles. This is understood to be attributed to compaction of sand as a result of increase in radial stress around the pile shaft, contributing to dilative response during shearing and hence generation of negative PWP as CPT loading is rapid hence considered as undrained. Friction ratio R_f has significantly increased within the 12 m of the compaction piles and even down to 15 m.

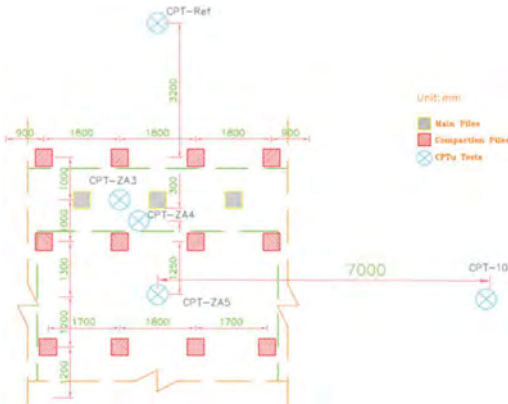


Figure 3. “Main” and “compaction” piles layout at trial field.

As shown in Figure 2, the soil has a significant percentage of fine-grained at most depths. Especially from depth of 8 m, the percentage of sand in the soil is zero indicating that the soil has very low compactibility, and as a result, q_c has not increased significantly.

Pile penetration induces soil compaction and consolidation which is manifested by an increase in horizontal effective stress, i.e., it causes the *in-situ* earth pressure coefficient, K_0 , to increase. Sleeve friction is defined as the product of horizontal effective stress and the friction coefficient at the soil–CPT sleeve interface. Assuming the coefficient of friction between the soil and CPT sleeve is constant, sleeve friction increases due to the increase in horizontal effective stress (normal to sleeve).

The analysis of CPTu results using Robertson (1990) soil classification chart (Figure 5) shows that the pile driving process has dragged the CPTu

classification results into the zone of the soils presenting the overconsolidated or cemented type.

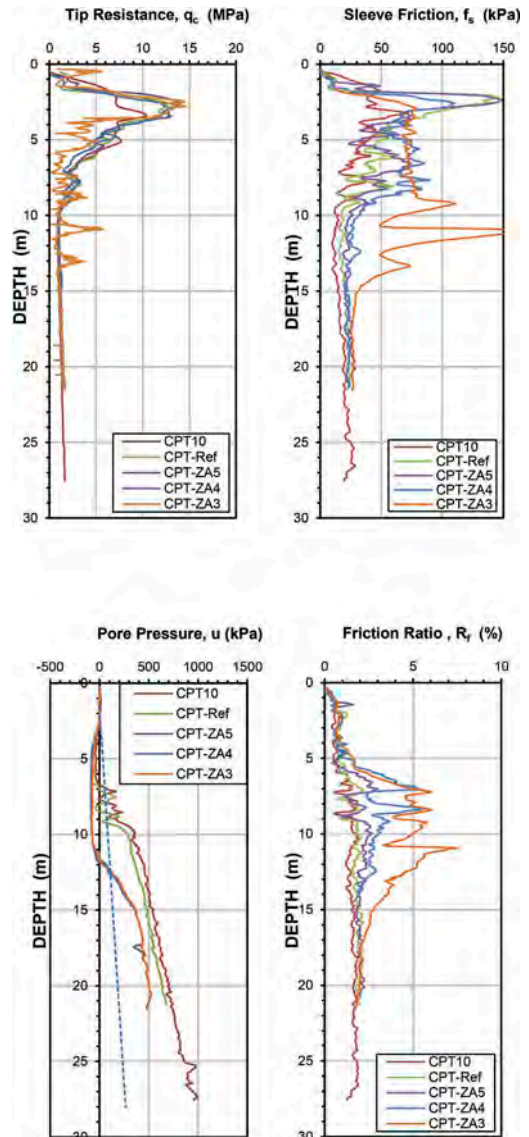


Figure 4. Pre- and post-driving CPTu results- trial field in Jask Oil Terminal project.

3 INTERPRETATIONS

3.1 Assessment of soil liquefaction potential

A procedure suggested by Robertson & Wride (1998) is used to evaluate the potential for cyclic softening and cyclic liquefaction. The procedure used the basic methodology, developed by Seed & Idriss (1971), calculating cyclic stress ratio (CSR) induced by the

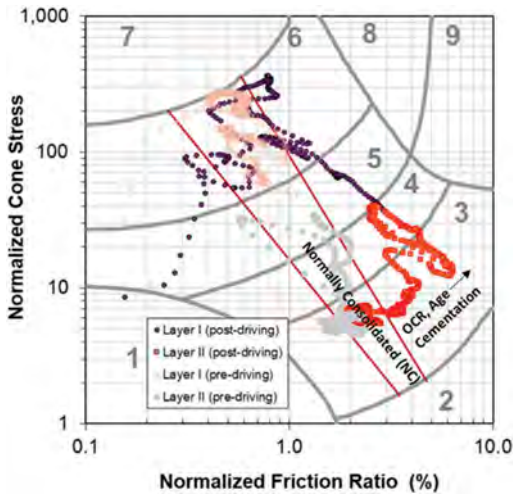


Figure 5. Robertson (1990) soil classification of pre- and post-driving CPTu results.

earthquake, and cyclic resistance ratio (CRR) of the soil. If CSR is greater than CRR, then liquefaction can occur. The proposed procedure estimates CRR based on the “sand-like” or “clay-like” classification identified by factor $I_c=2.6$. The updated procedure is well established in 2009 by Robertson (2009). Sand-like behavior is allocated to soils having $I_c < 2.5$. Such soils have the potential for cyclic liquefaction. Clay-like soils have $I_c > 2.7$ in which cyclic softening potential is recognized. The transition from sand-like to clay-like behavior generally occurs when $2.5 < I_c < 2.7$. Fine-grained soils transition depends on Atterberg Limits and Plasticity Index.

Figure 6 shows the evaluation of “cyclic liquefaction” and “cyclic softening” potential for CPT-Ref, CPT-ZA3 and CPT-ZA4. Down to 6 m depth, I_c value is lower than 2.5 where the probability of cyclic liquefaction is significant. CPT-Ref, CPT-ZA3 and CPT-ZA4 show cyclic liquefaction factor of safety (FS) lower than 1 between 4 to 6 m. Considering the effects of the main and compaction pile driving, CPT-ZA3 and CPT-ZA4 demonstrate the cyclic liquefaction safety factor is higher than the CPT-Ref in this layer (average FS of 0.74 at ZA3 point versus average FS of 0.45 at the Ref. point) Despite the higher FS, the calculations still show that cyclic liquefaction potential in this zone still exist. However, about 60% increase in FS has contributed to significant reduction of the kinematic forces induced in the piles.

The soils between 6 to 9 m are classified as transition soils. As the main and compaction piles penetrate through the soil, the CPT-ZA3 and CPT-ZA4 have shown higher sleeve friction, f_s . Thus, the soil behavior categorized in the transition zone has turned into clay-like behavior dominated by the potential for cyclic softening. As illustrated in the subjected zone

for CPT-ZA3 and CPT-ZA4, the cyclic softening FS is above 1 compared to the cyclic liquefaction FS of CPT-Ref which is lower than unity.

In depths below 9 m, calculation of potential for cyclic softening is performed, considering the domination of clay-like behavior of the soil. The uniform form of the calculated safety factor profile for the CPT-Ref (generally lower than 1) has changed due to the installation of the compaction piles down to about 12 m. This shows the effectiveness of driving compaction piles and raising FS to greater values.

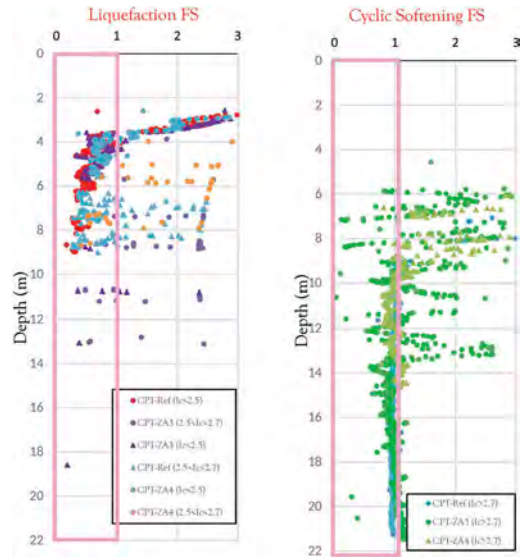


Figure 6. Changes of FS for “liquefaction” and “cyclic softening” for pre- and post-driving CPTu results.

3.2 Assessment of kinematic loading effects

The kinematic moment is evaluated using a method proposed by Nikolauou et al. (2001). In this method, pile is modeled as a beam on a dynamic Winkler foundation (BDWF), with homogenous, isotropic, and linearly elastic soil in each layer and a constant soil-damping ratio. They found that induced moments were maximum at interfaces between layers of different stiffness, and then performed a series of calculations to determine the bending moment at the interface between the two layers. The method does not consider any particular condition about the thickness of the two layers and is therefore, applicable for any depth of the layer interface.

The method proposes a reduction factor η to be applied to the maximum steady-state pile bending moment within the frequency domain to arrive at the corresponding peak value in the time domain. In the current study, the parameter η is equivalent to 0.37.

$$M_{pk} = \eta M_{res} \quad (1)$$

where M_{res} is the bending moment developed under resonant conditions and it is calculated using the following relation:

$$M_{res} = 0.042 \tau_c d^3 (L/d)^{0.3} (E_p/E_1)^{0.65} (V_{s2}/V_{s1})^{0.5} \quad (2)$$

in which d is pile diameter, L pile length, E_p Young's modulus of pile, E_1 Young's modulus of upper layer, V_{s1} average shear wave velocity in upper layer, V_{s2} average shear wave velocity in lower layer, ρ_1 the mass density of upper layer and h_1 is the thickness of upper layer.

Shear stress τ_c which is proportional to the actual shear stress is likely to develop at the interface, as a function of the free-field acceleration at the soil surface, a_s :

$$\tau_c = a_s \rho_1 h_1 \quad (3)$$

Predictions obtained using the above formula are shown in Figure 7 for the Ref point and ZA3. The magnitude of kinematic moment is significantly lower in the test results of post-driven point, CPT-ZA3. This is understood to be attributed to the effect of the main and compaction piles driven down to 23 m and 12 m, respectively.

After driving the compaction piles, the thickness of the liquefied layer has reduced from 8.5 m (left graph of Figure 7) to 5.5 m (right graph).

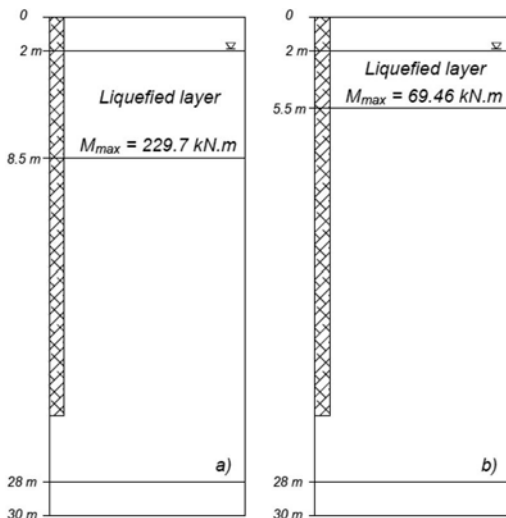


Figure 7. Schematic of kinematic loading value at interfaces between layers for a) CPT-Ref, b) CPT-ZA3.

The reduction of the maximum kinematic bending moment is resulted from: (1) increase in f_s (due to increase in lateral stress in soil) and hence reduction in liquefaction potential of the soil, (2) reduction of the liquefied layer thickness.

The presented results and the differences in CPTu parameters between the initial *in situ* condition and after the pile driving sequences are indications of effective improvement role of the driven main and compaction piles.

4 CONCLUSIONS

A case study is presented on the effect of driving “main bearing” and “compaction or improvement” piles in the silty sand to silty clay strata at a study field having high seismic and liquefaction/cyclic softening potential. CPTu tests were performed both prior and after driving the piles. Analyses were performed to evaluate the maximum kinematic moments at the interface of the two sand-like (top) and clay-like (bottom) layers. On the basis of the presented results, the main conclusions are summarized below:

- The q_c increased slightly in the top saturated layer as well as the clayey soil underneath till depth of 12 m, equivalent to the length of compaction piles.
- The friction sleeve (and hence friction ratio), however, increased more significantly due to radial displacement and compaction/consolidation attributed to cavity expansion surrounding the pile during driving.
- Liquefaction analyses show that the pile arrangement was not sufficient to overcome the liquefaction for the earthquake of the site with 0.4g acceleration and $M=7$.
- However, the factor of safety increased sufficiently to reduce kinematic moments within the allowable limits.

REFERENCES

- Bement, R. & Selby, A. 1997. Compaction of granular soils by uniform vibration equivalent to vibrodriving of piles. *Geotechnical & Geological Engineering* 15(2): 121–143.
- Blaney, G. W. 1976. Dynamic stiffness of piles. In Proc. *2nd Int. Conf. Numer. Meth. Geomech.*: 1001–1012. Blacksburg.
- Dobry, R. & O’rourke, M. (1983). Discussion of Seismic response of end-bearing piles. *Journal of Geotechnical Engineering* 109(5): 778–781.
- Fakharian, K., Meskar, M. & Mohammadlou, A.S. 2014. Effect of surcharge pressure on pile static axial load test results, *International Journal of Geomechanics, ASCE* 14(6): 40241–40249.
- Fakharian, K. & Khanmohammadi, M. 2021. Effect of OCR and pile diameter on load-movement response of piles over time embedded in clay, *International Journal of Geomechanics, ASCE*, (in press)

- Gianella, T. N., Stuedlein, A. W., & Canivan, G. J. 2015. Densification of liquefiable soils using driven timber piles. In *6th International Conference on Earthquake Geotechnical Engineering*, Christchurch, New Zealand.
- Kagawa, T., & Kraft, L. M. 1980. Lateral load-deflection relationships of piles subjected to dynamic loadings. *Soils and Foundations* 20(4): 19–36.
- Khanmohammadi M. & Fakharian K. 2018. Numerical simulation of soil stress state variations due to mini-pile penetration in clay. *International Journal of Civil Engineering, Transaction B: Geotechnical Engineering* 16(4): 409–419.
- Luo, X. & Murono, Y. 2001. Seismic analysis of pile foundations damaged in the January 17, 1995 South-Hyogo Earthquake by using the seismic deformation method. *International Conferences on Recent Advances in Geotechnical Earthquake Engineering and Soil Dynamics*. San Diego, California
- Meyerhof, G. 1959. Compaction of sands and bearing capacity of piles. *Journal of the Soil Mechanics and Foundations Division* 85(6): 1–29.
- Nataraja, M. S. & Cook, B. E. 1983. Increase in SPT N-values due to displacement piles. *Journal of geotechnical engineering* 109(1): 108–113.
- Nikolaou, A., Mylonakis, G., & Gazetas, G. 1995. *Kinematic bending moments in seismically stressed piles*. State University of New York, Buffalo, Report NCEER-95-0022, National Center for Earthquake Engineering Research
- Penzien, J. 1970. Soil-pile foundation interaction. *Earthquake engineering*: 349–381.
- Robertson, P. K. 1990. Soil classification using the cone penetration test. *Canadian Geotechnical Journal* 27(1): 151–158.
- Robertson, P. K. & Wride, C. 1998, Evaluating cyclic liquefaction potential using the cone penetration test. *Canadian Geotechnical Journal* 35(3): 442–459.
- Robertson, P. K. 2009. Interpretation of cone penetration tests—a unified approach. *Canadian geotechnical journal* 46(11), 1337–1355.
- Seed, H. B., & Idriss, I. M. 1971. Simplified procedure for evaluating soil liquefaction potential. *Journal of the Soil Mechanics and Foundations division* 97(9): 1249–1273.
- Stuedlein, A. W. & Gianella, T. N. 2017. Effects of driving sequence and spacing on displacement-pile capacity. *Journal of Geotechnical and Geoenvironmental Engineering* 143(3): 06016026.
- Rhyner, F. C. 2018. Densification of granular soils by pile driving and implications for evaluation of liquefaction. In *IFCEE 2018*: 284–300. Orlando, Florida
- Stuedlein, A. W., Gianella, T. N., & Canivan, G. 2016. Densification of granular soils using conventional and drained timber displacement piles. *Journal of Geotechnical and Geoenvironmental Engineering* 142(12): 04016075.
- Tajimi, H. 1969. Dynamic analysis of a structure embedded in an elastic stratum. *Proc. 4th World Conf. on Earthquake Eng.* Santiago.

Verification of 3D FEM analysis of ground improvement works using CPT test results

G.A. Faour & K.N. Khouri

NSCC International Ltd, Abu Dhabi, United Arab Emirates

ABSTRACT: The cone penetration test (CPT) has been widely used as one of the most well-known and reliable performance tests for ground improvement works. A comprehensive CPT testing campaign was conducted for the proposed ground improvement works of a highly technical project in Oman. The ground improvement works were evaluated based on the results of pre and post improvement CPT testing. CPT was the basis for choosing rigid inclusions (RI) and Vibro-compaction (VC) as the most suitable and economical ground improvement techniques for this project. The acceptance criteria based on the Post improvement CPT results incorporated the liquefaction potential and both allowable immediate and long-term settlements. The degree of ground improvement was evaluated by verifying that the final test results in the field met the project design criteria. It was concluded that CPT testing can be accurately correlated with multiple ground improvement acceptance criteria including liquefaction and settlement.

1 INTRODUCTION

1.1 Project description

A Development Company are constructing a 1.50 million square meters, world class multi cluster entertainment and leisure park in Barka, Oman. NSCC International was contracted for the design, construction and verification of the ground improvement works. The design was conducted to provide a cost-effective solution to mitigate liquefaction and achieve both immediate and long-term settlement criteria. The project was divided into two main areas: Retail, Dining, Entertainment (RDE) area and Theme Park area (TP). This paper elaborates on the design of the ground improvement schemes and their verification using CPT testing for these two areas.

1.2 Site investigation program

A series of one hundred additional cone penetration tests (CPT) (to compliment the borehole test results provided by the tender stage soil investigation report) were undertaken to provide a detailed evaluation of the subsurface conditions prior to construction for both RDE and TP areas. Figures 1 and 2 illustrate the approximate locations of the conducted boreholes and CPTs for both the RDE and TP areas respectively.

1.3 Subsurface conditions

The soil conditions generally consisted of sandy layers overlying silt layers which are underlain by

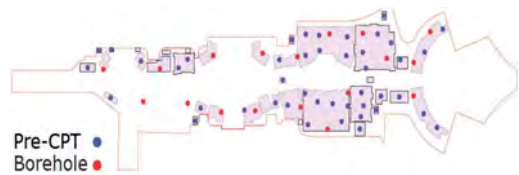


Figure 1. Pre-CPT campaign - RDE area.



Figure 2. Pre-CPT campaign - Theme Park area.

interchangeable layers of siltstone and sandstone. The sand layer was typically about 6.0m in thickness with occasional interlayering of a cohesive silt zone up to 1.0m thick encountered at 1.50m below the existing ground level. Another silt layer was found at a depth of 6.50m below the existing ground level with

a thickness of 2.0m. The underlying siltstone and sandstone layers were typically located at about 8.0m in depth. Figure 3 shows the variation of the cone penetration resistance values (q_c) with depth for the different soil strata encountered in both RDE & TP areas.

The groundwater table was encountered at about 4 to 4.50m depth below the existing ground level (-2.00m MSL); however, a conservative design groundwater table level of 0.00m MSL was considered in the design and the analysis to allow for seasonal variations.

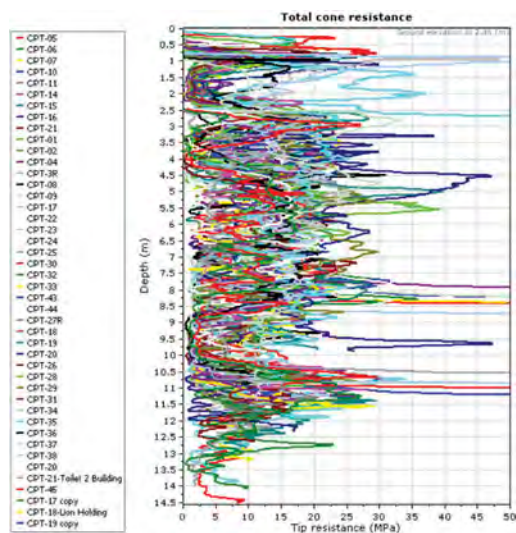


Figure 3. Variation of q_c with depth.

2 GEOTECHNICAL EVALUATION

2.1 Retail, Dining, Entertainment (RDE) area

Pre-CPT analyses were carried out to assess the liquefaction susceptibility and to estimate the resultant immediate and long-term settlement of the encountered soils under the RDE structures. The methodology to estimate the liquefaction potential requires an estimate of the cyclic stress ratio (CSR) profile caused by the design earthquake and the cyclic resistance ratio (CRR) of the ground. If the CSR is greater than the cyclic resistance ratio (CRR), liquefaction can occur. The CSR is usually estimated based on potential triggering shear stresses resulting from a 1 in 475-year design earthquake exerting a firm ground (i.e., Bedrock) peak horizontal acceleration of 0.15g. In our case this gave a potential ground surface peak horizontal acceleration of 0.23g, due to soil amplification. A simplified method to estimate CSR was developed by Seed and Idriss (1971) based on the maximum ground acceleration at the site. The results of the analyses revealed

that a soil layer of approximately 1m in thickness and susceptible to liquefaction was found at about 2.0m depth below the existing ground level; which may be underlain by thin discontinuity lenses of liquifiable soil within a zone from about 4.0m to 6.5m in depth.

In addition to the above, settlement analyses were performed for all RDE foundations by checking both immediate and long-term settlements. Based on the calculated settlement values and the Factor of Safety against liquefaction, it was deemed necessary to implement ground improvement techniques for foundations underlain by these potentially liquifiable zones to meet the project performance criteria. Several ground improvement methods were evaluated to eliminate the susceptibility of liquifiable soil and to eliminate excessive settlements. Based on the evaluation of the different ground improvement methods, the vibro-compaction method was selected to address both settlement and soil liquefaction concerns under all the RDE structures.

2.2 Theme Park (TP) area

The same analyses were repeated for the Theme Park area by analysing the pre-CPTs illustrated in Figure 2. The results of the analyses indicated that there is no risk of liquefaction for this area except for a few structures (Entry, Citadel, and Pond 11 & 12). However, our calculations show excessive long-term settlements for all structures founded in this area due to the presence of a consistent thick silt layer. Based on the above analyses, vibro-compaction was chosen to mitigate liquefaction, followed by rigid inclusions to minimise the foundations settlements. For structures which are not prone to liquefaction, only rigid inclusions were adopted. The following section depicts the full liquefaction and settlement analyses established for one of the structures in the Theme Park area, namely, the Citadel & Entry structure.

3 AN APPLICATION CASE TO CITADEL AND ENTRY STRUCTURE

3.1 Structure properties

Figure 4 portrays the overall geometry of Citadel & Entry structure along with the CPTs conducted in this area. The total area of this structure is 3,976m² with a design total service loading of 125kPa.

3.2 Liquefaction and settlement assessment

Both liquefaction and settlement analyses were implemented using the results of the conducted pre-CPTs. The results of the analyses show the presence of soil layers susceptible to liquefaction. To mitigate liquefaction risk under this structure, Vibro-compaction was performed by adopting a 3.0m triangular grid to an improvement depth of 8.50m. The grid spacing was

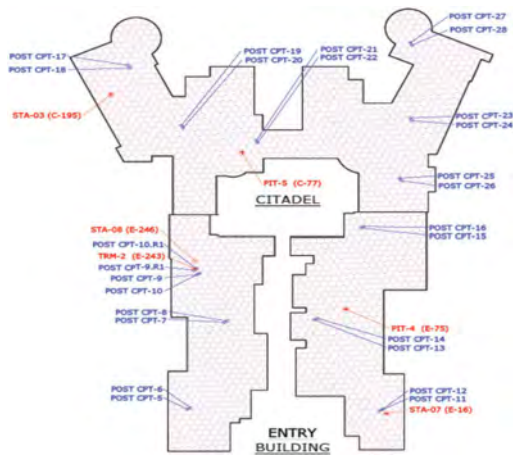


Figure 4. Citadel and entry layout.

chosen based on the results of the trial campaign conducted in that area. The effectiveness of the grid spacing was verified using the results of the zone load tests (ZLT) with four CPTs executed at the four corners of the ZLT. PLAXIS 3D analysis was carried out to compare the theoretical ZLT settlement results with the measured ones.

3.3 Liquefaction analysis using CLiq

The effectiveness of liquefaction mitigation under the Citadel & Entry structure was corroborated by carrying out a post testing campaign as shown in Figure 4. A pair of post treatment CPTUs were performed at 1/3 the distance between two Vibro-compaction points and at the centre of the triangle formed by three vibro-compaction points. Evaluation of liquefaction potential was assessed using CLiq software developed by Geologismiki using Robertson (NCEER R&W 1998, 2009). Each post-CPT pair was checked for liquefaction susceptibility by considering an earthquake magnitude of 6.0, a PGA of 0.15g at bedrock and a Factor of Safety against liquefaction of 1.25. The results of the liquefaction analysis for all post-CPTs conducted in the area are shown in Figure 5. The results confirm that liquefaction is mitigated by the vibro-compaction technique with a minimum factor of safety of 1.25 except for thin confined localized layers with thickness of approximately 0.30m. These thin layers are classified by Robertson (2011) as transition zones and are not susceptible to liquefaction. The liquefaction analyses resulted in minimum seismic vertical and horizontal settlements.

3.4 Liquefaction analysis using PLAXIS 3D

The above results were checked by carrying out liquefaction analysis using PLAXIS by adopting the UBC3D – PLM Sand Model and by defining the

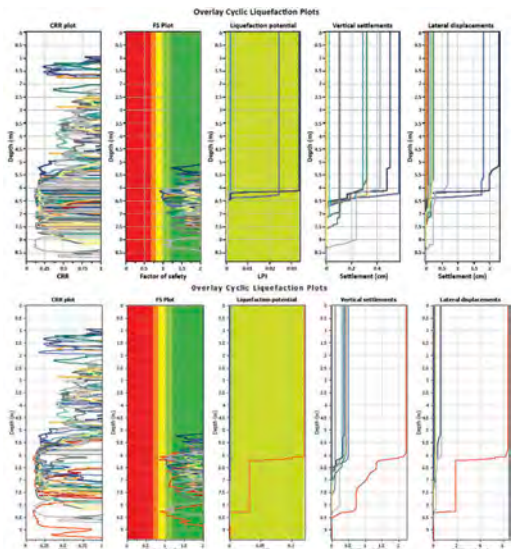


Figure 5. Liquefaction results using CLiq software.

following response spectrum curve and time history. UBC3D-PLM Sand model is an effective stress elasto-plastic model which can simulate the liquefaction behavior of sands and silty sands under seismic loading. (Tsegaye (2010), Petalas & Galavi (2012)).

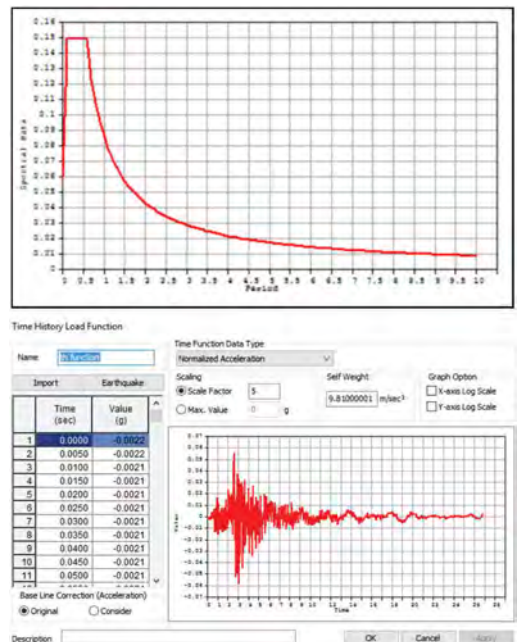


Figure 6. Earthquake parameters for PLAXIS liquefaction analysis.

The Factor of Safety against liquefaction using PLAXIS was calculated as the ratio of the excessive pore pressure changes and the initial effective pressure. Plaxis liquefaction analysis resulted in a FoS of 1.51 which is greater than the empirical factor of safety calculated using CLiq software thus confirming that the liquefaction mitigation criteria were achieved. The advantages of the dynamic analysis using UBC Sand is the ability to simulate the excess pore water pressure generation in the soil, as well as the ability of checking the amplification, liquefaction/plastic points.

3.5 Settlement analysis using Taspie

The settlement analyses of the post-CPTs indicate that the settlement criteria were not achieved by Vibro-compaction only due to the resultant settlement exceeding 25mm. Therefore, it was decided to install 450mm diameter rigid inclusions, 10.0m in length in the vibro-compacted ground, to ensure the calculated settlement be less than the allowable (25mm) under 125kPa loading. The rigid inclusions were overlain with a 40cm thick load transfer platform (LTP). The LTP plays an indispensable role in transferring the loads to the toe of the rigid inclusions and to uniformly transfer the settlement under the structure. The post-CPTs were used to derive the geotechnical parameters of the in-situ soil. As for the LTP, a compacted gravel layer was considered. Layering and material parameters of the LTP and foundation soils are listed in Table 1. The Ground level elevation is at 3.0m MSL and the ground water level is at 0.00m MSL.

Table 1. Material parameters and foundation soils.

Layer #	Thickness (m)	γ (kN/m ³)	E (Mpa)	ϕ (Deg)	ν
LTP (Gravel)	0.5	19.50	50.00	38	0.25
MD Sand 1	0.58	18.00	37.50	33	0.35
MD Sand 2	0.62	18.00	53.40	33	0.35
MD Sand 3	1.00	18.00	27.00	33	0.35
Silt	0.44	16.50	6.50	26	0.35
MD Sand 4	0.94	17.50	36.70	33	0.35
VD Sand	0.42	19.00	76.00	34	0.35

* γ : unit weight, ν : Poisson's ratio, E: elastic modulus, ϕ : drained friction angle, MD: Medium dense, VD: Very dense

The RI design is performed using Taspie by adopting a unit cell model. This software follows the general recommendations for the design and construction of rigid inclusions in ASIRI (2012).

Figure 7 displays the resultant settlement along with the stresses exerted on both soil and rigid inclusions for one of the post-CPTs pair conducted in the Citadel & Entry area.

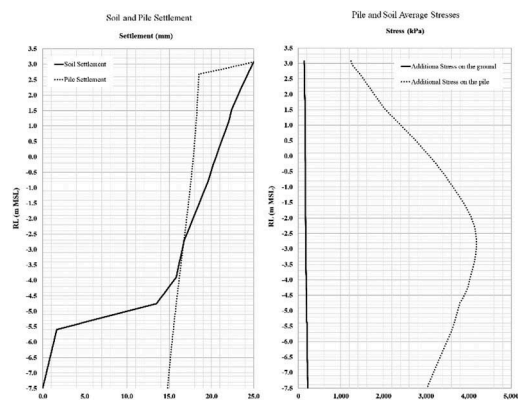


Figure 7. Load transfer mechanism (Taspie Software).

The above figure reveals that the settlement criteria was achieved with an associated settlement of approximately 25mm. The rigid inclusion settlement was approximately 14mm with a maximum stress of 4.55Mpa located at the neutral axis (-2.80m MSL).

3.6 Settlement analysis using PLAXIS 3D

To validate the estimated settlements by Taspie software, a full PLAXIS 3D finite element analysis was conducted for Citadel & Entry structure as shown in Figure 8 below. The rigid inclusions were defined as embedded beams and the slab on grade as plate elements. Soil properties illustrated in Table 1 were defined using the Mohr-Coulomb material model.

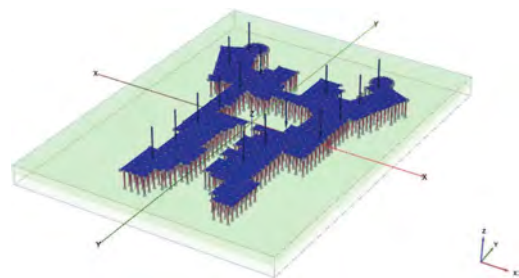


Figure 8. PLAXIS 3D View (Citadel & Entry).

The above PLAXIS 3D analysis has shown a maximum settlement of 19mm as depicted in Figure 9. Moreover, the same load transfer mechanism shown in Figure 7 using the Taspie software was also created by the PLAXIS 3D run as demonstrated in Figure 10.

3.7 Measured vs theoretical results

According to Chapter 8 of ASIRI guidelines, static load tests on an isolated inclusion in compression

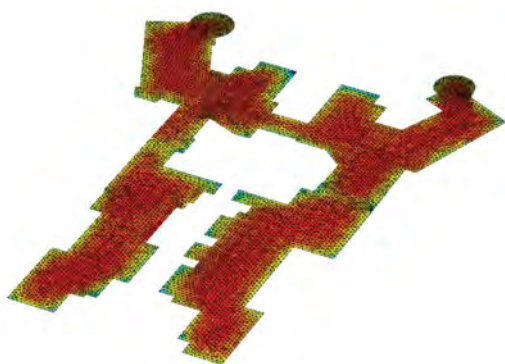


Figure 9. Settlement distribution.

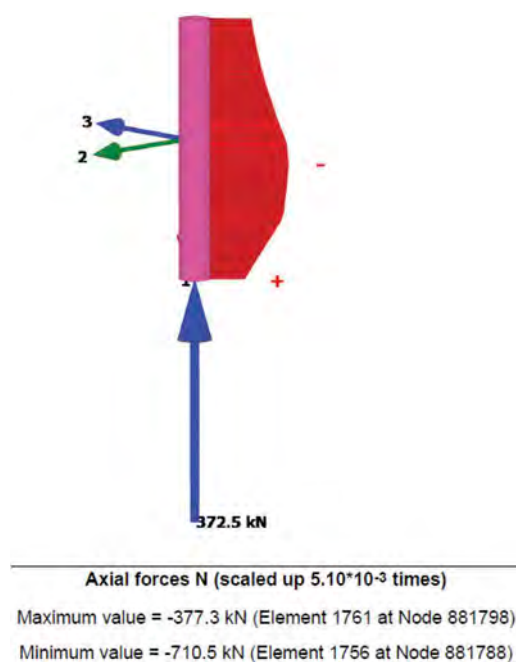


Figure 10. Load Transfer Mechanism (PLAXIS 3D).

should be conducted. Three static load tests were conducted in the Citadel & Entry area as shown in Figure 4 by applying a testing load equivalent to the sum of the head load acting on the rigid inclusion and the negative skin friction acting on the RI from its head to its neutral plane.

The effectiveness of rigid inclusions in the field response of Citadel/Entry foundation was assessed by comparing the measured settlements with the theoretical calculations using both Taspie and PLAXIS 3D software.

The following table enumerates the resultant settlement of the static tests compared with the theoretical calculations.

Table 2. Measured versus theoretical comparison.

Static Load Test	Testing Load (kN)	RI (Settlement-Taspie) (mm)	RI (Settlement-PLAXIS 3D) (mm)	RI (Settlement-Measured) (mm)
STA-07	1273	15.50	13.77	3.960
STA-08	1116	19.50	14.11	3.880
STA-03	1222	16.00	14.80	8.060

Table 2 shows that the theoretical settlements derived from both Taspie and PLAXIS 3D analyses are conservative compared to the measured settlements.

3.8 Conclusion

The CPT testing technique has proven to be an invaluable tool for calibrating and verifying the effectiveness of both Vibro-compaction and rigid inclusions techniques, particularly in its ability to identify the strength of the silt layers. The CPT testing used in both the PLAXIS 3D and Taspie software runs have resulted in conservative settlement calculations which favourably compare with the measured static load test settlements. Moreover, CPT testing has proven to be well correlated with the liquefaction acceptability criteria as calculated by carrying both static and dynamic liquefaction analyses using both CLiq and PLAXIS software respectively.

REFERENCES

- ASIRI 2012. Recommendations for design, construction, and control of foundation over soils reinforced by rigid inclusions, Presses des Ponts.
- Boulanger, R. W., and Idriss, I.M. (2005). New criteria for distinguishing between silts and clays that are susceptible to liquefaction versus cyclic failure. Proc., Technologies to Enhance Dam Safety and the Environment, 25th Annual United States Society on Dams Conf., USSD, Denver, 357–366.
- Boulanger, R. W., Meyers, M.W., Mejia, L.H., and Idriss, I. M. (1998). Behavior of a fine-grained soil during Loma Prieta earthquake. Can. Geotech. J., 35 (1), 146–158.
- Hor B. et al. 2015. A 3D FEM analysis on the performance of disconnected piled raft foundation. Japanese Geotechnical Society Special Publication 2 No.34, 1238–1243.
- Hor B. et al. 2017. Ground improvement using rigid inclusion for the foundation of LNG tanks. Proceedings of the 19th International Conference on Soil Mechanics and Geotechnical Engineering, Seoul 2017.
- Kirsch, K. (1985). Over 50 years of deep vibratory compaction: Milestones of German geotechnique. Geotechnik, Special Issue, Deutsche Gesellschaft für Erd- und Grundbau, Essen, Germany.
- Kirsch, F. and Sondermann, W. (2001). Ground improvement and its numerical analysis. In proceedings of the

- XCth ICMFE, Istanbul, Turkey. A.A. Balkema, Rotterdam, the Netherlands.
- NCEER (1997). Proceedings of the NCEER Workshop on Evaluation of Liquefaction Resistance. Technical Report NCEER-97-0022.
- Petalas, A., Galavi, V. (2012). Plaxis liquefaction model ubc3d-plm. PLAXIS knowledge base.
- Robertson et al. (1983). Interpretation of cone penetration tests. *Canadian Geotechnical Journal*, 20 (4), 718–733.
- Robertson, P.K. (1990). Soil Classification using CPT. *Canadian Geotechnical Journal*, 27(1),151–158.
- Robertson, P.K. (2011). Automatic software detection of CPT transition zones.” *Geotechnical news*, June, 2011.
- Seed, H.B., and Idriss, I.M. (1982). Ground motions and soil liquefaction during earthquakes, Earthquake Engineering Research Institute, Berkeley, Calif.
- Schmertmann, J.H. (1978). Guidelines for cone penetration test, performance, and design. Report FHWA-TS-78-209,145. US Federal Highway Administration, Washington, DC.
- Tsegaye, A. (2010). Plaxis liquefaction model. external report. PLAXIS knowledge base.
- West, J.M. (1976). The role of Ground Improvement in Foundation Engineering: Ground Treatment by Deep Compaction. The Institution of Civil Engineers, London, UK.
- Wehr, J. and Sondermann, W. (2013). Deep vibro techniques. In Kirsch, K. and Bell, A. (eds.) *Ground Improvement*. CRC Press, Taylor & Francis Group, Boca Raton, FL.
- Yoshimi, Y. (1980). Protection of structures from soil liquefaction hazards. *Geotechnical Engineering*, 11.

A comprehensive design procedure for pile groups in liquefiable soils

M. Franceschini, F. Fiorelli & E. Bandiera

Teleios Srl – Società di Ingegneria, Castel Maggiore, Bologna, Italy

ABSTRACT: Among the various strategies to mitigate the effects of soil liquefaction one of the most effective is the design of deep foundations. The designs of piles in liquefiable soils are too often concerned with the only axial bearing capacity, addressed by simply neglecting pile resistance in the liquefiable layer. This approach is inadequate to properly face the complexity of the problem. In the present paper we intend to examine this theme throughout its multiple aspects. We have synthesized a design procedure of analysis that has been already applied in some projects in different areas of Emilia-Romagna region characterized by high risk of liquefaction. The proposed design procedure is based on the most updated theories and design references concerning piles in liquefiable soil, such as those of Cubrinovsky, Olson & Stark, Rollins, Bhattacharya, Madabhushi and others, primarily referring to CPTu.

1 INTRODUCTION

When designing a structure interacting with the soil in a site subjected to a high risk of liquefaction during earthquake, there are many solutions that can be evaluated to reduce and mitigate this risk.

For foundations resting on liquefiable soil one of the most effective solutions is the use of piles. But, in this case, their design has to properly account for the effects induced on piles by liquefaction.

The phenomena involving a pile under seismic cyclic loading in presence of liquefiable soils are complicated. There are different important aspect to be accounted for: the change in shaft resistance, the reduction of base capacity also in deeper layer not directly liquefying, the equilibrium instability due to the loss of lateral support from liquefied soil and the modification of the geotechnical model under liquefaction, directly conditioning the analyses of pile groups with geotechnical numerical models.

In order to properly face the design of deep foundations on liquefiable soils we have resumed the principal bibliographic studies with the aim to build a comprehensive design procedure. In the paper we will describe in detail the various step of this procedure and we will also propose a real design example in which we have already applied this process.

2 GEOTECHNICAL MODEL

In a geotechnical design the first, and maybe most important, step is the construction of an accurate and reliable geotechnical model, i.e the parameters and

the constitutive laws that mathematically represent the mechanical response of the soil.

In the case of high risk of liquefaction, the geotechnical model valid under seismic conditions significantly differs from the static one because of liquefaction effects on soil properties. The liquefiable soil layer is described below in terms of both modified stiffness and strength parameters.

2.1 Stiffness parameters

As regards stiffness parameters we referred to the theory proposed by Cubrinovski et al. (2009). In a simplified 3-layers model, in which the central one is potentially liquefiable, the pile is modelled as a beam connected to a series of springs representing the lateral stiffness of the soil.

As expected, the stiffness offered by the liquefied soil (k_2) is significantly lower than the one of the same non-liquefied soil (k_1). The results observed in full-scale tests on piles show that the stiffness degradation factor $\beta_2 = k_1/k_2$ typically varies in a range of $1/50 \div 1/10$ for cyclic liquefaction (Figure 1). In our design procedure we chose to refer to the lower bound, i.e. to $\beta_2 = 1/50$.

The degradation factor β_2 is applied to the stiffness parameters of the liquefiable soil layer, in particular to the initial tangent value of soil elastic modulus within the numerical Boundary Element Method analyses performed adopting a non-linear hyperbolic constitutive model. The above theory (Cubrinovski et al. 2009) was originally developed for “p- δ ” curves methods: we extended the same approach to numerical BEM analyses.

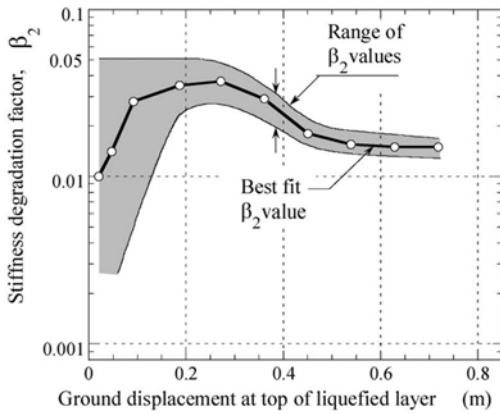


Figure 1. Degradation of stiffness in the liquefied layer observed in full-size test on piles. From Cubrinovski et al. (2009).

2.2 Strength parameters

The liquefiable soil is described in terms of strength parameters, in seismic conditions, via its residual undrained strength $s_{u(LIQ)}$, as proposed by Olson & Stark (2002).

$$\frac{s_{u(LIQ)}}{\sigma'_{v0}} = 0.03 + 0.0143 \cdot q_{c1} \pm 0.03 \quad (1)$$

for $q_{c1} \leq 6.5$ MPa

The formulation proposed in Equation 1 is valid for CPT tests. As in can be seen, it is structured to define an interval of values with an amplitude of 0.03 MPa. Many researchers have studied post-seismic conditions: residual undrained strength was evaluated on the basis of the deformed configuration of the foundation after the earthquake.

From Bowen & Cubrinovski (2008) it can be seen how, in case of cyclic liquefaction, it is safe to refer to the mean value of the interval. That is what we chose to apply in the design procedure.

3 PILE AXIAL CAPACITY

Once defined the geotechnical model, next step consists in evaluating the pile axial capacity. Many different approaches can be used: correlations with strength parameters of the soil, direct correlations with in-situ soundings (CPT & CPTu, DMT, SPT, etc.), pile load tests. As concern the design procedure, we have focused on direct methods based on CPTu: in particular, the method proposed by Eslami & Fellenius (1997) improved by Niazi (2013).

3.1 Base capacity

The axial capacity of piles in liquefiable soils is well illustrated by Madabhushi et al. (2009).

When liquefaction occurs, the degree of growth of the pore pressure can be described by the interstitial pressure ratio r_u :

$$r_u = \frac{\Delta u}{\sigma'_{v0}} \quad (2)$$

According to Equation 2, soil shows liquefaction when $r_u = 1$. Liquefaction can easily occur in superficial sandy layers. Usually, indeed, deeper coarse grained soil layers show a higher resistance to liquefaction because their higher density and also because the greater effective pressure. So, when deep foundations are designed to resist to liquefaction, it can occurs that pile toes are placed in non-liquefiable deeper sandy layer. But also in these deeper layers pore water pressure can increase, so $r_u > 0$ and so soil resistance decrease. This fact, not immediately perceivable, has to be properly taken into account in designing piles.

Starting from the model for the base resistance of a pile (Vesic 1972) and considering the effects due to the increase of pore water pressure, Knappet & Madabhushi (2008b) showed how the tip resistance of piles in liquefiable soil is related to its corresponding value in static conditions by the relation reported in Equation (3):

$$\frac{Q_{base,E}}{Q_{base,S}} = (1 - r_u)^{\frac{3 - \sin\phi}{3 \cdot (1 + \sin\phi)}} \quad (3)$$

Where r_u has been defined in Equation 2, ϕ is the angle of shearing resistance of the coarse grained soil in which the pile toe is placed while $Q_{base,E}$ and $Q_{base,S}$ are the tip bearing capacity of the pile, respectively, in seismic and static conditions.

From Equation 3 it can be seen how the resistance is related to r_u but this factor is not simple to evaluate. It would be necessary to perform advanced site effect analyses, accounting also for the liquefaction of the soil. This cannot be done in ordinary practice, so a simplified approach has been developed.

Given a liquefiable soil layer, in which liquefaction occurs ($r_u = 1$) it is assumed that excess pore pressure remain constant for depth greater than its

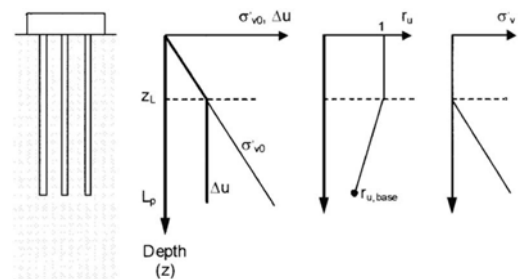


Figure 2. Effective stress conditions around piles for full liquefaction until z_L depth. From Madabhushi et al. (2009).

thickness z_L . Considering the growth of effective stresses with depth as almost linear, this lead to a bilinear shape of the factor r_u . Once the trend of r_u and the geometry of the pile are known it is easy to evaluate the interstitial pressure ratio at pile tip level L_p . It can be derived (see Figure 2).

$$r_{u, base} = \frac{z_L}{L_p} \quad (4)$$

3.2 Shaft capacity

Madabhushi et al. (2009) have extended their studies also to the shaft bearing resistance of a pile, obtaining the formulation reported in Equation 5, that follows a philosophy similar to Equation 3.

$$Q_{shaft,E} = Q_{shaft,S} \cdot (1 - r_u) = Q_{shaft,S} \cdot \frac{L_p - z_L}{L_p} \quad (5)$$

Where $Q_{shaft,E}$ and $Q_{shaft,S}$ are the shaft bearing capacity of the pile evaluated, respectively, in seismic and in static conditions.

So, in a more general way, it is possible to define the total bearing capacity of a pile in a liquefiable soil P_{bc} from Equation 6.

$$P_{bc} = Q_{base,S} \cdot (1 - r_u)^{\frac{3-\sin\phi}{3(1+\sin\phi)}} + Q_{shaft,S} \cdot \frac{L_p - z_L}{L_p} \quad (6)$$

According to Equations 5 and 6, the shaft resistance of a pile in a liquefiable soil can be significantly reduced when the factor r_u increase, but it is not strictly equal to zero. Also other researches (Rollins 2015), basing on experimental data, have demonstrated that the contribution of the liquefiable layer to shaft resistance is not null, but can decrease to about 50% of its corresponding static value. Anyway, in the present design procedure we propose to completely neglect the contribution of the liquefiable soil layers to the shaft resistance of the piles.

4 PILE INSTABILITY

Liquefaction causes the loss of lateral support of the soil to the piles and the subsequently significant variation of lateral stiffness of the foundation. In these conditions piles can face a crisis for buckling.

Pile instability due to liquefaction has been studied by Bhattacharya (2003) and Bhattacharya et al. (2004) considering a simplified model in which liquefied soil has no strength and stiffness. The pile crossing this layer will behave like an axially loaded column. Under these hypotheses the critical load P_{cr} corresponding to the loss of the elastic equilibrium is given by the well-known Euler's expression.

Anyway, experimental tests (Knappet 2006) have shown how critical loads are not so small as those predicted by theoretical formulations. This evidence has been explained with the fact that liquefied soil has a small, but not null, stiffness neglected in the theoretical model. So Euler's expression has been updated by Madabhushi et al. (2009), accounting for finite, small, stiffness of the liquefied layer by the factor $r_{u,base}$, as reported in Equation 7:

$$P_{cr} = \frac{\pi^2 \cdot E \cdot I}{(\beta \cdot r_{u,base} \cdot h)^2} \quad (7)$$

Where E and I are elastic modulus and moment of inertia of the section of the pile, h is the length of the pile crossing the liquefiable layer and β is a factor accounting for the fixity at both ends of the pile. $(\beta \cdot h)$ represent the equivalent length of the unsupported pile tract. Introducing the radius of gyration of the section r_g , the slenderness ratio λ is defined:

$$\lambda = \frac{\beta \cdot h}{r_g} \quad (8)$$

Bhattacharya & Lombardi (2012), basing on data collected from real cases, have defined an admissible domain, bounded by a slenderness ratio $\lambda = 50$ (dashed black line in Figure 3), separating deep foundations that have shown good performances from those who have not. From Figure 3 it can be seen how the choice of the limit value of slenderness $\lambda = 50$ can be excessively precautionary. For that reason we propose to refer to a limit value equal to $\lambda = 75$ (continuous red line in Figure 3).

In reality piles can suffer buckling for axial load lower than the one predicted by Equations 7 also because imperfections not accounted in theoretical models, inducing geometrical second order problem ($P-\delta$ effect). Named δ_0 the displacement induced by the horizontal action (earthquake), the total lateral

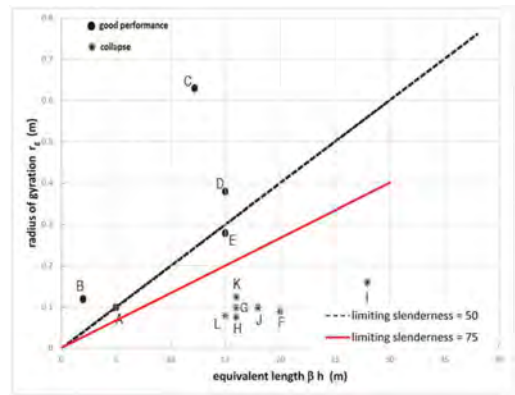


Figure 3. Admissible domain: measured performances of deep foundations after real earthquakes. From Bhattacharya & Lombardi (2012).

displacement δ in presence of a vertical action P will be greater. Equation 9 describes the normalized trend of the amplification factor δ/δ_0 .

$$\frac{\delta}{\delta_0} = \frac{1}{1 - \frac{P}{P_{cr}}} \quad (9)$$

The normalized movement δ/δ_0 is almost linear for values of vertical load $\psi = P/P_{cr} \approx 0.30$ so it can be assumed:

$$P_{ult} = \psi \cdot P_{cr} \quad (10)$$

As suggested by Bhattacharya & Lombardi (2012), and also as considered in the proposed design procedure, it is adopted $\psi = 0.35$ as limit.

According to Equations 6 and 7 both the total axial bearing capacity of the pile P_{bc} and its critical load P_{cr} depend from factor r_u . So critical values of r_u can be derived, corresponding to reaching these two limiting conditions.

Following this approach Madabhushi et al. (2009) describe a series of graphs in which, depending on pile geometry (diameter D_0 and elastic properties E , I) and required factor of safety FOS, the domain of use of the pile is defined (see Figure 4). These graphs can be derived for the specific design case considering the liquefaction conditions of the site, and can be enriched by also plotting the hyperbolic trend of $r_{u,base}$, in that way also accounting for the thickness and depth of the liquefiable layer.

The piles have to be anyway verified against their structural strength because of the stresses (bending moment and shear) due by the inertial and kinematic interaction with the superstructure.

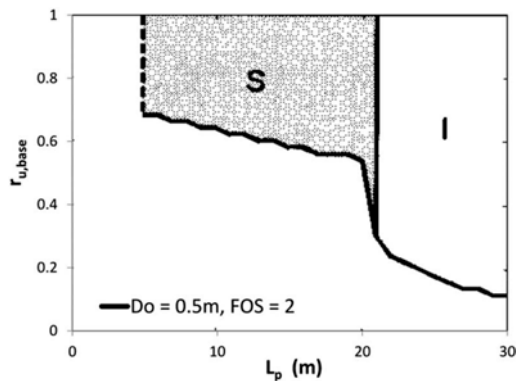


Figure 4. Design chart for a solid circular RC pile in loose sand ($D_r = 35\%$): $D_0 = 0.5\text{m}$, $\text{FOS} = 2$. From Madabhushi et al. (2009). In the blank areas the pile is verified, in those identified by “S” the pile encounter a crisis by bearing capacity while in those identified by “I” the crisis is because of instability.

5 CALCULATION METHODS

Designing a deep foundation on liquefiable soil is complex and, as seen in the previous sections, many aspects have to be properly considered to correctly face the problem. So it is clear how also the adoption of a correct method to analyze the pile group is fundamental in order to not nullify the benefits of the adopted advanced theories, as previously reported.

We used numerical BEM analyses with the software Repute, developed by Geocentric (Bond & Basile 2010, Basile 1999), adopting for the soil a non-linear hyperbolic constitutive model. In that way pile group effects and other phenomena, as pile plasticization and shadowing, can be properly accounted.

The procedures described in the previous section mainly refers to single piles. Instead we propose to extend these analyses to pile groups by adopting correct calculation methods, such as the one mentioned above, in addition to the definition of a correct geotechnical model, accounting for liquefaction (see section 2).

6 DESIGN EXAMPLE

The design procedure that we propose to design a piled foundation on liquefiable soil has been described in detail by theoretical point of view in the previous sections of the paper. Now we want to describe how this procedure has already been applied in some real case in which the authors designed deep foundations to mitigate the liquefaction risk.

The two major works in which we adopted our design procedure are the enlargement and seismic retrofit of the Cento (Ferrara, Italy) sports hall and the construction of the new Pavillion 37 as part of the revamping project of the fair quarter of Bologna (Italy). Due to the space available in the paper, we will only describe the first of these two projects.

6.1 Investigation campaign and geotechnical characterization

A first investigation campaign, consisting in four cone penetration tests with piezocone CPTu and seismic piezocone SCPTu, two flat dilatometer DMT tests, geophysical tests and laboratory ones, has been firstly carried out. From these data an high risk of liquefaction was found out so it was decided to perform an integrative campaign to better go insight the liquefaction problem. Four CPTu and dynamic laboratory tests (resonant column RC and cyclic triaxial TX CYC), on samples taken from two boreholes, have been performed.

Liquefaction risk has been assessed with different approaches: from CPTu (Robertson 2009), from DMT (Monaco et al. 2005), from dynamic lab tests.

The liquefaction potential index LPI, evaluated adopting the Sonmez (2003) approach, results ranging from the various investigations from about 8 to 18, identifying an high risk of liquefaction.

Liquefaction is induced by a layer of loose sands that extends from about 1 to 6 meters of depth from ground level. The geotechnical model in seismic condition accounting for liquefaction, reported in Table 1, has been defined according to what has been described in section 2.

Table 1. Geotechnical model in seismic conditions, accounting for liquefaction.

Layer	From -	To [m]	Undrained strength S_u [kPa]	Friction angle ϕ [°]	Tangent modulus E_0 [MPa]
Liquefiable sand	1.0	6.0	1	-	2
Clay	6.0	11.0	30	-	90
Clay	11.0	18.0	75	-	105
Sand	18.0	26.0	-	32	135
Clay	26.0	-	75	-	150

6.2 Description of the intervention

The project primarily consists in the construction of a new grandstand: this element, as enlargement of the existing sport hall, contains two reinforced concrete cores that are the principal part of the bracing system adopted to increase seismic resistance of the whole structure. These cores absorb the great amount of the seismic forces because they are designed to support and to brace the roof of the hall. Since there where no limits on this side for operating machines, we chose to adopt FDP (Full Displacement Piles) piles: due to the particular shape of the drilling tip the pile is realized without removing soil, so also a positive densifying effect is induced.

In the opposite side of the hall there is the existing tribune, supported by an RC frame. Also this zone has been involved in the seismic retrofitting, and the existing shallow foundation have been reinforced with micropiles designed according to the proposed procedure. Here they will not be discussed.

6.3 Foundation analysis

Given the loads acting on foundation from superstructures and defined the geotechnical properties of the soil, each foundation has been analyzed adopting a numerical approach: BEM analyses have been carried out with the software Repute (see section 5).

For each seismic core a deep foundation consisting in 24 FDP piles, diameter 600mm, with a length of 22.0 meters (depth of pile tip from g.l.) has been adopted. The pile cap have dimensions 12.10×9.20 meters and is 1.2m thick. The overall foundation plan is reported in Figure 5.

Following the design procedure described in the previous sections of the paper, after have being

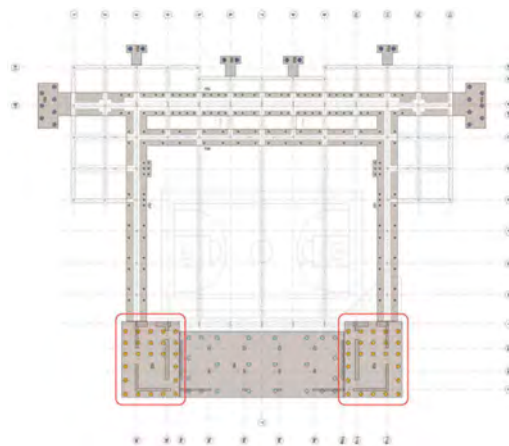


Figure 5. Foundation plan of the sport hall. In red the two seismic cores are highlighted.

defined the geotechnical model valid in seismic conditions under liquefaction, the pile ultimate axial capacity have been defined.

Pile base capacity in static conditions has been evaluated adopting the formulation proposed by Berezantsev (1965), because pile tip in placed in the lower sandy layer, finding out a value of $Q_{base,S} = 1190$ kN. Considering the development of excess pore pressures also in the lower sandy layer, it does not reach liquefaction but the tip resistance decrease. According to Equation 3 a ratio of 0.86 between the seismic and static value of base resistance has been evaluated, corresponding to a value of 0.238 for the factor $r_{u,base}$ (Eq. 4). This means that in seismic conditions the pile base resistance decrease to:

$$Q_{base,E} = 0.86 \cdot 1190 \approx 1000 \text{ kN} \quad (11)$$

Pile shaft capacity has been calculated via a direct correlation with data from CPTu adopting the method of Eslami & Fellenius (1997) improved by Niazi (2013). We referred to the 6 CPTu performed on site, finding out values of $Q_{shaft,S}$ ranging from 1390 kN to 1778 kN, with a mean value of 1600 kN.

As described in § 3.2, in our proposed design procedure the shaft capacity is completely neglected in the liquefiable layer. Adopting the same calculation procedure of the static case, in seismic conditions we found out values of $Q_{shaft,E}$ ranging from 1070 kN to 1448 kN, with a mean value of 1263 kN.

The BEM analyses of the piled foundation of the core (Figure 6) give axial forces on piles as reported in Table 2. According to the design criteria defined by the Italian code NTC pile axial capacity check is satisfied in static condition with a maximum exploitation of 81% and in seismic condition at 92%.

The last step of the design involve the check of piles against instability. It can be considered that FDP piles are rigidly connected at the top to the pile cap. The same fixity can be considered at the base, because the liquefiable sandy layer is near the ground and the piles

Table 2. Maximum axial forces on piles from BEM analyses.

Action	u.m.	Static	Seismic
Maximum compressive force	[kN]	1047	964
Maximum tensile force	[kN]	-	15
Maximum horizontal shear force	[kN]	81	79
Maximum vertical settlement	[mm]	6.9	5.9
Maximum horizontal displacement	[mm]	0.5	11.2

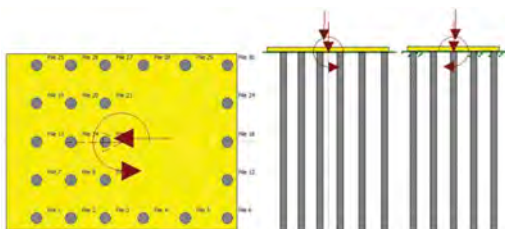


Figure 6. Repute calculation model of the piled foundation of the core.

continue below in the non-liquefiable clayey layers. Nevertheless, as a precaution, we assumed the equivalent length ($\beta \cdot h$) as twice the thickness of the liquefiable layer (equal to 5.0m, see Table 1). Considering the elastic properties of the cross-section of the piles ($E \cdot I = 159.04 \text{ MNm}^2$), the interstitial pressure ratio ($r_{u, \text{base}} = 0.238$) and limiting the critical load by the factor $\psi = 0.35$ (see Eq. 10) the ultimate axial load can be evaluated as $P_{\text{ult}} \approx 96900 \text{ kN}$, more than 100 times the maximum axial force acting on piles under seismic loading (see Table 2). The slenderness ratio $\lambda = 67$ is lower than the assumed upper admissible limit of 75.

The piled foundations, designed according to the proposed procedure, satisfy all the safety criteria.

7 CONCLUSIONS

In the paper a design procedure to correctly deal with the design of pile groups on liquefiable soil has been presented. The procedure provides guidance as concern the geotechnical model (modified strength and stiffness parameters under liquefaction), the pile axial capacity (shaft and base components) and the pile instability. Each step of the procedure is based on specific theories from various authors, in order to base the design on solid scientific bases.

Cone penetration tests are fundamental in many steps of the procedure: just think to the geotechnical characterization and the pile capacity evaluation.

The procedure is intended as a guide for designers who have to face the design of a deep foundation on liquefiable soil. This is a very sensitive problem, so we hope the guide can help geotechnical engineers in this challenging work.

REFERENCES

- Basile, F. 1999. Non-linear analysis of pile groups. *Proc. of Civil Eng., Geotech. Eng., Vol. 137, No. 2, April, pp 105-115.*
- Berezantsev, V. G. 1965. Design of deep foundations.
- Bhattacharya, S. 2003. Pile instability during earthquake liquefaction. *PhD thesis, University of Cambridge, UK.*
- Bhattacharya, S., Madabhushi, S. P. G., Bolton, M. D. 2004. An alternative mechanism of pile failure during seismic liquefaction. *Geotechnique 54 (3): 203-213.*
- Bhattacharya S., Lombardi D. 2012. Sul comportamento sismico delle fondazioni su pali in terreni liquefacibili. *Rivista Italiana Di Geotecnica 1/2012.*
- Bond, A. J., Basile, F. 2010. Repute 2.0, Software for pile design and analysis. *Reference Manual, Geocentrix Ltd, United Kingdom, 49p.*
- Bowen, H. J., Cubrinovski, M. 2008. Pseudo-static analysis of piles in liquefiable soils: parametric evaluation of liquefied layer properties. *Bulletin of the New Zealand Society for Earthquake Engineering, Vol. 41, No. 4, December 2008.*
- Cubrinovski, M., Ishihara, K. & Poulos, H. 2009. Pseudo-static analysis of piles subjected to lateral spreading. *Special Issue Bulletin of NZ Society for Earthquake Engineering.*
- De Alba, P. A. 1983. Pile settlement in liquefying sand deposit. *J. Geotech. Engng. 109 (9): 1165-1179.*
- Eslami, A., Fellenius, B.H. 1997. Pile capacity by direct CPT and CPTu methods applied to 102 case histories. *Can. Geotech. J. 34 (6): 886-904.*
- Knappet, J. A. 2006. Piled foundations in liquefiable soils: accounting for axial loads. *PhD thesis, University of Cambridge, UK.*
- Knappet, J. A., Madabhushi, S. P. G. 2008a. Liquefaction-induced settlement of pile groups in liquefiable and laterally spreading soils. *J. Geotech. Engng. 134(11).*
- Knappet, J. A., Madabhushi, S. P. G. 2008b. Designing against pile tip bearing capacity failure in liquefiable soils. *Proc. 2nd BGA Int. conf. on foundations 2: 1237-1246.*
- Madabhushi, G., Knappet, J., Haigh, S. 2009. Design of pile foundations in liquefiable soils. *London Imperial College Press.*
- Monaco, P., Marchetti, S., Totani, G. & Calabrese, M. 2005. Sand liquefiability assessment by Flat Dilatometer Test (DMT). *Proc. XVI ICSMGE, Osaka, 4, 2693-2697.*
- Niazi, F. S. 2013. An Update on Pile-CPTu Direct Correlations. *Ports 2013, ASCE.*
- Olson, S. M. & Stark, T. D. 2002. Liquefied strength ratio from liquefaction flow failure case histories. *Can. Geotech. J. 39, 629-647.*
- Robertson, P. K. 2009. Interpretation of cone penetration tests – a unified approach. *Canadian Geotechnical Journal, 46: 1337-1355.*
- Rollins, K.M., Hollenbaugh, J.E. 2015. Liquefaction Induced Negative Skin Friction from Blast-induced Liquefaction Tests with Auger-cast Piles. *6th Int. Conf. on Earth. Geotech. Enging. Christchurch, New Zealand, 1-4 Nov. 2015.*
- Sonmez, H. 2003. Modification to the liquefaction potential index and liquefaction susceptibility mapping for a liquefaction-prone area (Inegol-Turkey). *Environ. Geology 44 (7), pp. 862-871.*
- Vesic, A. S. 1972. Expansion of cavities infinite sol mass. *J. Geotech. Engng. 98 (3): 265-298.*

Deep foundations of the new Pavilion 37 – fair quarter Bologna

M. Franceschini, F. Fiorelli & E. Bandiera

Teleios Srl – Società di Ingegneria, Castel Maggiore, Bologna, Italy

Vincenzo Colella

Geofondazioni Ingegneria e Lavori Srl, Martellago, Venezia, Italy

Giampaolo Cortellazzo

Università di Padova, Padova, Italy

Andrea Dei Svaldi

Desam Ingegneria e Ambiente s.r.l., Mogliano Veneto, Treviso, Italy

ABSTRACT: The present paper concerns the design of driven precast tapered piles, that have been used within the project of the new Pavillion 37 of the fair quarter of Bologna. A particular focus will be reserved to the evaluation of the axial bearing capacity of these elements and to the prevision of their load-settlement curve. The geotechnical characterization, as well as the prediction of the axial resistance of the piles, has been mainly based on Cone Penetration Test with piezocone CPTu. The previsions will be compared with the results of a series of static load tests performed during the construction.

1 INTRODUCTION

The present paper concerns the design of deep foundation for a new exhibition hall, especially as regard the prediction of the axial bearing capacity of the piles and of their load-settlement curve.

The framework of the project and the geometry will be described first, following with the description of the geotechnical campaign and the soil characterization. Then we will assess the project prediction by comparison with the results of the static load tests performed on-site during construction.

All these evaluations are based on CPTu test, as described in the following.

2 PROJECT DESCRIPTION

Within the revamping project of the fair quarter of Bologna, the new Pavilion 37 rises as flagship of the exhibition centre with its remarkable opening roof and its planimetric dimensions of 80 x 184 meters (Figure 1). The steel structure of the roof stands on 8 reinforced concrete towers, whose foundations represent the most important and complex geotechnical elements of the whole project.

The choice was to adopt deep foundation for all the RC towers, consisting in driven precast tapered piles arranged in groups (Figure 2). The adoption of

deep foundation was basically justified by the high loads transmitted by the roof, together with the geotechnical conditions of the site.

The whole project concern also two other adjacent buildings (the so-called “Mall” and “East entrance”), not object of the present paper, whose foundations have been designed similarly.

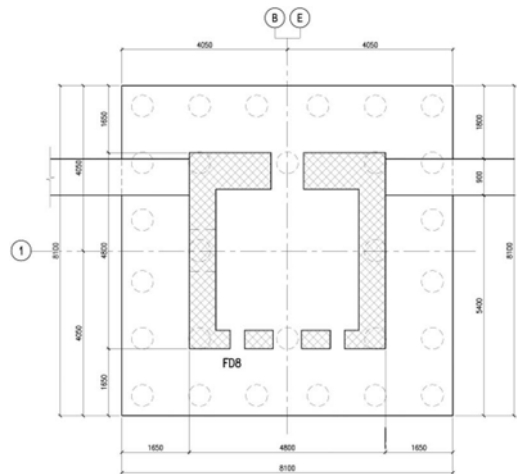


Figure 1. Typical deep foundation of the RC towers supporting the roof of the pavilion.

3 PILE DESCRIPTION

Driven precast tapered piles were used in the project. The choice was due to different aspects, both geotechnical and construction-related:

- Driven piles have good geotechnical performances. In addition, because of the installation process, an increase in density is induced in the soil.
- They are rapid to install and it is possible to control the performance of piles during driving.
- In soft soils or in presence of water neither pre-drilling nor hole support are required.
- There is no excavation material, so the organization of the construction site is clean and easier.

The adopted piles have a diameter of 53/26 cm (head/toe), a taper of 1.5 cm/m and a length of 18 meters. The piles were precasted in factory with a specific centrifugation process.

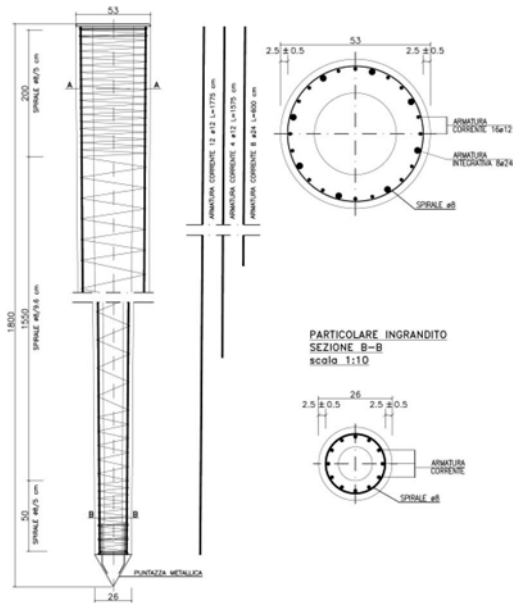


Figure 2. Typical tapered precast pile with length $L=18$ m. Vertical sections and reinforcements.

For driving were used hydraulic hammers with weight of 6 and 7 tons. The driving energy was 36 kNm and the settlement during driving was measured in the range from 5 to 7 mm/blow.

4 GEOTECHNICAL CHARACTERIZATION

The site was characterized by performing an investigation campaign consisting mainly in on-site soundings. Four cone penetration tests with piezocone CPTu, a borehole (with soil sampling and SPTs) and geophysical MASW and HVSR tests have been carried out.

The geotechnical characterization is mainly based on the interpretation of the performed CPTu. They are very effective in recognizing soil behavior and strength and stiffness parameters. In Figures 3, 4 and 5 some of the principal results from the interpretations are showed.

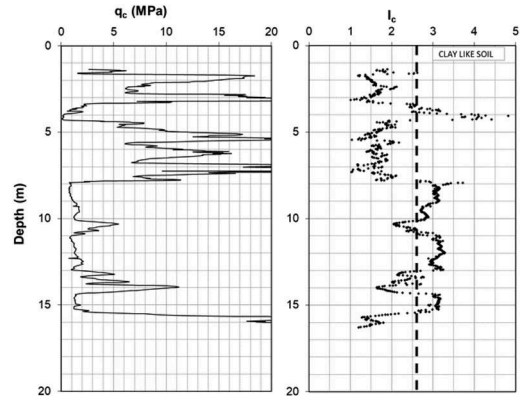


Figure 3. Point resistance and soil index vertical profiles from the interpretation of one of the performed CPTu.

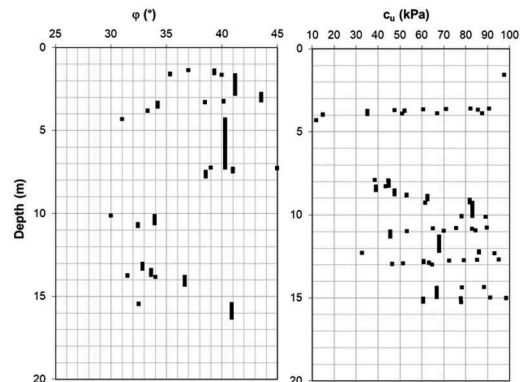


Figure 4. Friction angle and undrained strength vertical profiles from the interpretation of one of the performed CPTu.

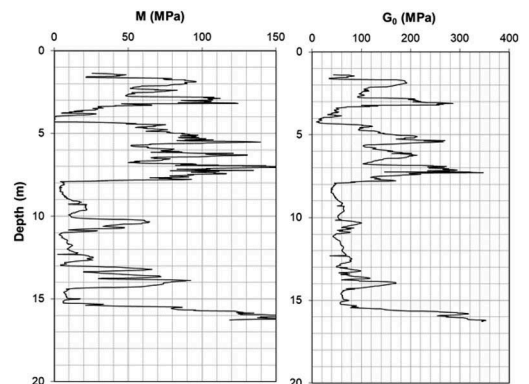


Figure 5. Confined and initial shear moduli vertical profiles from the interpretation of one of the performed CPTu.

An alternation of coarse-grained and fine-grained material was found out, described by the following geotechnical model (Table 1).

Table 1. Geotechnical model.

Layer	From [m]	To [m]	Undr. strength c_u [kPa]	Effective cohesion c' [kPa]	Friction angle ϕ [°]	Tangent modulus E_0 [MPa]
Sandy silt	0.0	8.0	-	0	32-34	200-250
Clay	8.0	15.0	60-70	5	27-30	120-170
Sandy gravel	15.0	20.0	-	0	38-40	≥ 500
Sandy to clayey silt	20.0	35.0	70-80	5	27-30	300-350

Soil stiffness was described in terms of the initial tangent modulus because the deep foundations have been analysed adopting a numerical BEM (Boundary Element Method) approach with the software Repute, developed by Geocentrix (Bond & Basile 2010, Basile 1999).

5 BEARING CAPACITY OF PILES

In the design phase, pile axial capacity has been predicted adopting calculation methods directly correlated to CPTu.

Then, during construction, pile capacity has also been evaluated by interpreting the measured load-settlement curves derived from the pile load tests, in order to validate the design predictions.

5.1 Analytical evaluation of pile capacity

We referred to different methods based, directly or indirectly, on CPTu tests. The first is the method proposed by Eslami & Fellenius (1997). In this case the beneficial effect of tapering has been taken into account by increasing the shaft capacity by a factor that, as from Nordlund (1963) and Horvath (2002), varies between about 1.5 for clayey-like soil layer to 2.0 for sandy ones. An example is reported in Figure 6.

The second method is the one proposed by Togliani (2010). This method, in particular, is specific for tapered piles and is able to directly evaluate both the shaft capacity of the pile, related to its side area, and the component related to the tapering benefit.

The axial ultimate capacity of the tapered piles, predicted applying the previous methods, is reported in Table 2, the values are referred to a limit settlement of about 10 mm.

5.2 Load tests interpretation

Four static load tests have been performed on the L=18 m tapered piles during construction, as part of the

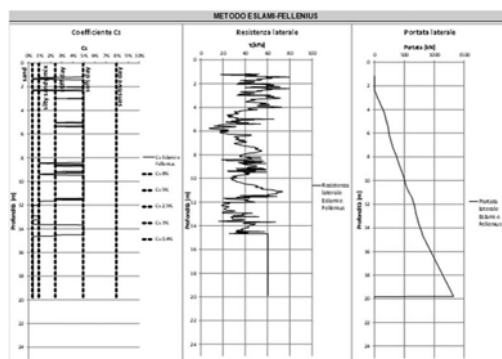


Figure 6. Tapered pile axial capacity evaluation from CPTu adopting the Eslami & Fellenius method.

Table 2. Pile axial ultimate capacity from CPTu.

CPTu sounding	Shaft capacity [kN]				Base capacity [kN]	
	Shaft	Eslami&Fellenius		Togliani		
		Taper benefit	Shaft	Taper benefit	E & F	Togliani
CPTu 1	1322	794	1306	843	340	385
CPTu 2	1593	956	1536	1180	367	416
CPTu 3	1502	1201	1527	1354	394	441
CPTu 4	1364	1228	1556	1480	344	378

acceptance testing, under a maximum vertical load approximately equal to 1.5 time the exercise load (Figure 7). The results obtained from acceptance testing are well aligned to the design prediction from direct correlations with CPTu, considering also that these load tests have not kept to failure but were intended to verify the correct installation and performance of the piles.

Moreover during the construction of a nearby building two static load tests were performed, on the same type of pile, reaching loads of 2000 kN and 2400 kN. These last two load tests have been interpreted according to the approach proposed by Chin (1970) to evaluate the ultimate capacity of the tested pile, in Figure 8 an example of the interpretation is proposed.

6 LOAD-SETTLEMENT CURVES PREVISION

The load-settlement curves, representing the response of the single pile, have been predicted adopting an analytical model (Randolph & Wroth 1978), two numerical approaches by BEM analysis with the software Repute and by FEM analysis with the software Plaxis and adopting a mixed approach based on the cavity expansion theory (Dei Svaldi et al., 2012).

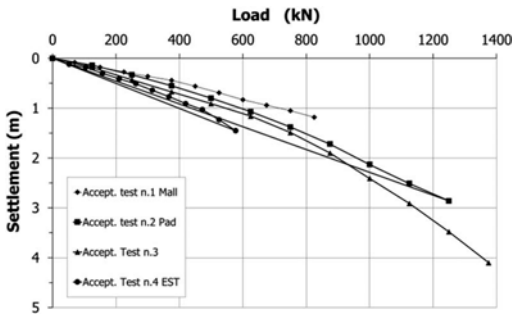


Figure 7. Acceptance testing curves.

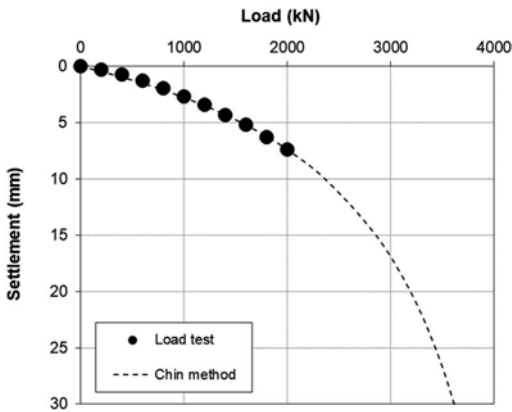


Figure 8. Interpretation of the static load test n.1 with the Chin method.

All these predictions were based on the parameters of the geotechnical model obtained from CPTu tests (Table 1).

After carrying out the load tests, the measured curves have been compared to the predicted ones, finding out what is graphically represented in Figure 9.

The design prediction does not deviate much from the experimental measures, and generally show

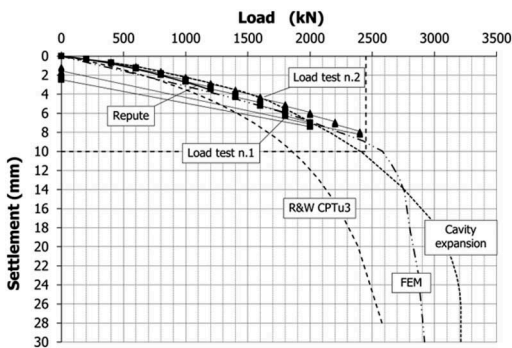


Figure 9. Load-settlement curves: comparison between design predictions and load tests.

a lower stiffness with respect to them, giving to the foundation design a certain margin of safety.

On the basis of the load-settlement curve for the single pile, a calibration analysis of the model of the deep foundation of the RC tower was carried out, by evaluating with different methods the settlements under the action of the vertical load (15785 kN). The foundation consists of a reinforced concrete raft 1.6 m thick resting on 28 tapered piles (Figure 2).

For the calibration has been adopted the following methods: the formulation proposed by Mandolini (1994), the BEM method and the traditional multi-layer one-dimensional method, where the pile-soil system was considered as a layer with stiffness modulus (Table 3) evaluated through an interaction analysis between pile, plate and soil based on the concept of efficiency (Fleming et al., 1992). Table 4 reports the results of the calibration analysis.

Table 3. Equivalent stiffness modulus of soil-pile system.

η_w	0.280	efficiency	
K_p	525	MN/m	single pile stiffness
K_{pg}	148	MN/m	pile group stiffness
E_{eq}	1108	MPa	

Table 4. Settlement of RC tower under vertical load.

	Settlement (mm)
Mandolini	
BEM	3.94
Equivalent stiffness	3.8

Once calibrated the BEM method was used to study the behaviour of the RC tower under the different load combinations in compliance with the Italian Technical Standards for Buildings (DM 17.01.2028).

An example of settlements and pile reactions under the action of ultimate state loads, obtained from BEM analysis, are shown in Figure 10.

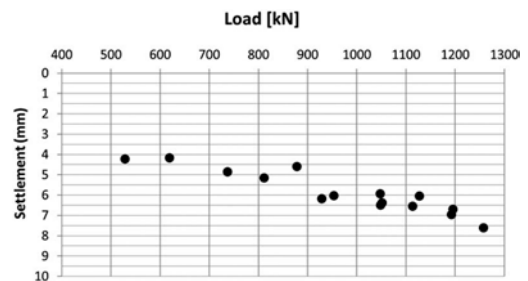


Figure 10. RC tower - settlements and reactions of the piles obtained from BEM analysis under USL loads.

7 CONCLUSIONS

The interpretative criteria of the CPTu tests allow to reliably define the stratigraphy and the mechanical characteristics of the soils at the basis of the foundation design.

For a complete design of the piled rafts it is not only important to calculate the bearing capacity of piles but also to define their behaviour through the construction of the load-settlement curve. In this context, it is possible to use complex numerical models but also simpler methods which, in any case, allow to obtain usable results for the design.

A final aspect to highlight is that in order to obtain reliable results in complex analyses with numerical methods, the calibration by comparing the results of simple analyses with other calculation methods is relevant.

REFERENCES

- Basile, F. 1999. Non-linear analysis of pile groups. *Proceedings of the Institution of Civil Engineers, Geotechnical Engineering, Vol. 137, No. 2, April*, pp 105–115.
- Bond, A. J., Basile, F. 2010. Repute 2.0, Software for pile design and analysis. *Reference Manual, Geocentrix Ltd, United Kingdom*, 49p.
- Dei Svaldi, A., Mazzucato, A. 2012 – Studio dei pali di tipo cilindrico e troncoconico infissi in terreni alluvionali - *Research Report, University IUAV of Venice*.
- Eslami, A., Fellenius, B.H. 1997. Pile capacity by direct CPT and CPTu methods applied to 102 case histories. *Can. Geotech. J. 34 (6)*886–904.
- Horvath, J. S. 2002. Static Analysis of Axial Capacity of Driven Piles in Coarse-Grain Soil. *Integrated Site Characterization and Foundation Analysis Research Project. Report No. CGT-2002-1*.
- Mandolini, A. 1994. Cedimenti di fondazioni su pali. *Ph. D. Thesis, Department of Geotech. Eng. University of Napoli Federico II*.
- Nordlund, R.L. 1963. Bearing capacity of piles in cohesionless soils. *Journal of the Soil Mechanics and foundations division, American society of civil engineers, New York, N.Y., USA, Vol. 89, No. SM3*, pp. 1–35.
- Randolph, M.F., Wroth, C.P. 1978. Analysis of deformations of vertically loaded piles. *Journal of Geotechnical Engineering, ASCE*, vol. 104, GT12, 1465–1488.
- Togliani, G. 2010. Pile Capacity Prediction using CPT - Case History. 2nd Int. Symp. on Cone Penetration Testing, Huntington Beach, CA, USA, May 2010.

Consolidation settlement of coastal areas of the Emilia-Romagna region from cone penetration tests

D. Giretti

University of Bergamo, Bergamo, Italy

V. Fioravante

University of Ferrara, Ferrara, Italy

L. Perini & L. Calabrese

Geological, seismic and soil survey of the Emilia-Romagna Region, Bologna, Italy

ABSTRACT: This paper describes an attempt to develop and calibrate a simple tool to forecast the natural subsidence of coastal Holocene deposits. An empirical correlation has been calibrated between the penetration resistance measured by a static cone penetrometric tests and i) the normal compression line NCL of fine grained, coastal deposits ii) the current void ratio and iii) the void ratio on the NCL at the site effective stress. The comparison between the site void ratio and the normally consolidated void ratio can be used to roughly estimate if the soil is overconsolidated, normally consolidated or under-consolidated/structured and, in the latter case, if the fine layer is in the condition of further developing consolidation settlement to reach the self-weight equilibrium.

1 INTRODUCTION

The vulnerability of coastal areas to climate change and, in particular, to sea level rise, is a cause for alarm at an international level. The geological survey group of the Emilia-Romagna Region (SGSS), in Italy, has carried out a study to highlight the effect of on-shore subsidence on the potential sea transgression, and the action of subsidence has resulted decisive in some areas of the coast, where the altimetric altitude is close to zero. The origins and possible evolution of subsidence need to be evaluated to limit its impact on the risk of inland sea transgression. In this context, a study has been carried out to estimate the natural component of subsidence linked to the compaction of recent coastal deposits of fine grained soils. The research has been based on three main components: i) two near shore pilot sites, well characterized from a geotechnical point of view, where subsidence rate is monitored by means of assestometric measures; ii) several site where both CPTUs and oedometric tests on fine grained samples were available, iii) a large database of CPTUs carried out in sites spread all along the Emilia-Romagna coast.

The results of CPTUs and oedometric tests on Holocene fine grained soils have been used to link the cone penetration resistance q_c to i) the compression index C_c ; ii) the altitude e_1 of the 1-D compression line in the e - $\log\sigma'_v$ plane defined at $\sigma'_v = 1$ kPa; iii) the current void ratio e_c .

A tool has been calibrated which allows to derive from a q_c profile and for fine grained layers two relevant void ratio values: the current site void ratio e_c and the void ratio the soil would have at the site effective stress if normally consolidated e_{NC} . The comparison between these values roughly indicates if the soil is overconsolidated, normally consolidated or under-consolidated/structured and, in the latter case, allows to estimate the possible consolidation settlement the layer could still develop to reach the self-weight equilibrium.

The tool has been validated for the pilot sites and used to estimate the expectable natural subsidence of fine grained deposits at selected sites of the coastal areas where CPTUs were available.

2 GEOLOGICAL SETTING AND REFERENCE SITES

The study area belongs to the outer sector of the Pliocene-Quaternary Apennine foredeep (Ricci et al. 1986), progressively affected by recent phases of compressive deformation of the Apennine chain. The Quaternary succession is over 2000 m thick and records the gradual filling of the highly subsiding basin. The land lowering due to tectonics is still active and maximum rates have been estimated about 1 mm/y (Cuffaro et al. 2010). The most recent succession (Middle Pleistocene-Holocene) is

characterized by the sedimentary cyclicity consisting of the metric alternation of sandy and highly compactable fine levels, induced by the glacial-eustatic fluctuations of the late Quaternary. The upper 30-40 metres of this succession, testify the transgressive-regressive Holocene cycle (Amorosi et al. 2003; Stefani and Vincenzi 2005.) characterized by paralic and marine deposits overlying the Pleistocenic alluvial plain in the lower portion and, in the central and upper portion, by a thick sedimentary wedge deposited by the deltaic and beach prograding systems.

From a lithological point of view, in the littoral sector, the shallowest succession is constituted by coastal and delta sands in the upper part and by thick prodelta and beach fine deposits in the lower part. The natural compaction of these recent fine deposits may be responsible for the observed subsidence (Teatini et al. 2011), that reaches maximum rates of 12 mm/year.

In the study area, sediment deposition during progradation took place through complex phases of feeding, switching and abandonment of the ancient Po delta branches; this has generated variable depositional history even for sediments that are very similar in appearance.

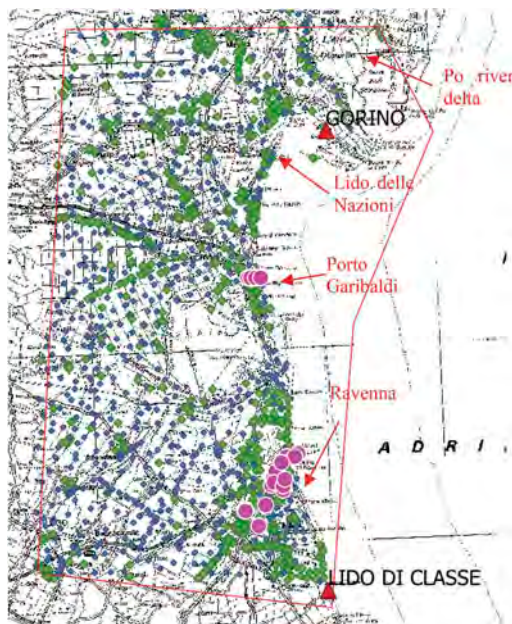


Figure 1. Location of pilot sites and available data: corings (green dots), CPTUs (blue dots) and selected tests (pink dots).

As part of the studies aimed at evaluating the natural subsidence of the superficial plio-quaternary deposits of the coastal areas, SGSS has selected two pilot sites evidenced in Figure 1 at the localities of Gorino (Ferrara Province) and Lido di Classe (Ravenna Province), where it is possible to exclude the occurrence of subsidence of anthropogenic origin. Both sites are characterized in the first 30 m of depth

by Holocene deposits of clays, silts and sands. Gorino stratigraphy is representative of the coastal deposits originated by the Po river typical of the northern sector of the regional coasts; Lido di Classe soil profile is typical of the southern sector coastal deposits, originated by the activity of Apennine rivers.

Both sites were characterized by means of continuous core drilling and undisturbed sampling, CPTU and SCPTU tests, oedometric tests on undisturbed sample of fine soil. The boreholes were equipped with settlement gauges, anchored to the Pleistocene deposits deeper than 30 m and cemented to the hole, for monitoring the subsidence of the deposit over time. The analyzes carried out so far have shown in both sites a progressive lowering of about 1 mm/year.

Gorino site (q_c profiles in Figure 2) is characterized within the first 5-6 m of depth from the ground surface by a predominantly sandy layer with frequent alternations of finer soils, followed by a clayey silty stratum up to 27-29 m of depth. This layer, made of inorganic and medium to high plasticity fines, resulted mainly normally consolidated from oedometric tests and is followed by Pleistocene sandy deposits. The ground water table is in average 0.5 m deep.

At Lido di Classe, a superficial 8 - 9 m thick layer of clean sands is followed by a dense alternation of silty sands, sandy and clayey silts up to about 24 m of depth, then by silty clays. The fine grained layers, characterized by low plasticity, are slightly over consolidated from the ground surface to 9 m of depth, overconsolidated from 9 to 15 m of depth, normally consolidated at higher depths. The ground water table is 1.7 m deep.

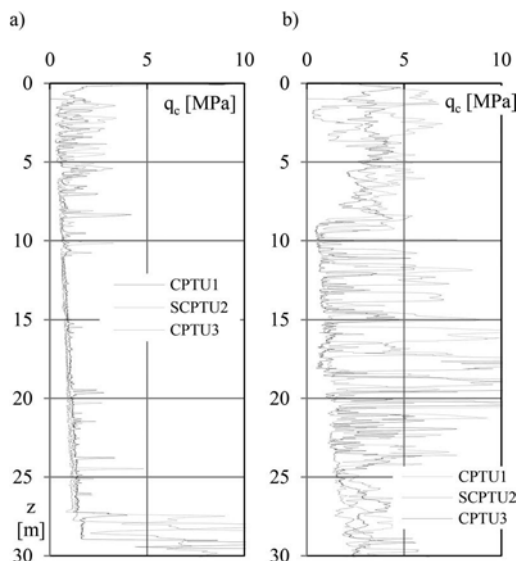


Figure 2. CPTs at pilot sites, a) Gorino, b) Lido di Classe.

In both sites, oedometric tests have been repeated also on reconstituted specimens. In some cases, the undisturbed oedometric curve lied above the intrinsic

compression line (Burland 1990), indicating presence of structure, possibly due to flocculated deposition occurred in conditions of high sedimentation rates in the delta front and proximal prodelta environment. These results are consistent with the geological and depositional history of the sites.

In both sites, the void ratio at the depths of undisturbed sampling, computed as a function of the water content and specific gravity and assuming complete saturation, resulted in some cases higher than the void ratio derived from the oedometric curve at the specific vertical stress, indicating still in progress consolidation phenomena, accordingly with the estensimetric measures, or presence of structure.

In addition to the 2 pilot sites, 5 extra sites were considered in this study, 2 located in the norther sector of the regional coast at the locality of Porto Garibaldi, 3 in the southern sector, in the area of the city of Ravenna (Figure 1), all characterized by similar geological origin and stratigraphy as the two pilot sites. For all the sites considered, CPTUs and oedometric tests on undisturbed samples were available. Figure 3 reports the grain size fractions and plastic index as a function of depth measured on the undisturbed samples overall analyzed.

3 EMPIRICAL CORRELATION

From each oedometric curve available, the compression index C_c (slope of the normal compression line in the $e - \log \sigma'_v$ plane) and the void ratio e_1 (altitude of the normal compression line at $\sigma'_v = 1$ kPa) have been derived. Figure 4 shows the C_c measures vs. depth; in Figure 5 e_1 is plotted versus C_c . A linear relation exists between C_c and e_1 , which can be expressed as:

$$e_1 = 4 \cdot C_c + 0.3 \quad (1)$$

The site void ratio at the sampling depth has been derived as a function of the measured water content w and specific gravity G_s as:

$$e_c = w \cdot G_s / S \quad (2)$$

where the degree of saturation S has been assumed equal to 1.

From the CPTU carried out nearest to the borehole from which the undisturbed samples tested in oedometer came, an average q_c value was derived at the depth of sampling. Figures 6 and 7 show the compression index C_c and the site void ratio e_c plotted versus the average q_c normalized over the atmospheric pressure p_a . C_c is in the range 0.25 – 0.5 when q_c/p_a is between 5 and 15 and decreases as the normalized cone resistance increases, indicating a decrease of compressibility as the soil resistance increases.

Despite the significant dispersion in Figures 6 and 7, and acknowledging the rather low correlation coefficients, a power function and an exponential function have been drawn to try to link C_c and e_c to the normalized cone resistance:

$$C_c = 0.48 \cdot (q_c/p_a)^{-0.167} \quad (3)$$

$$e_c = 1.127 \cdot e^{-0.015 \cdot q_c/p_a} \quad (4)$$

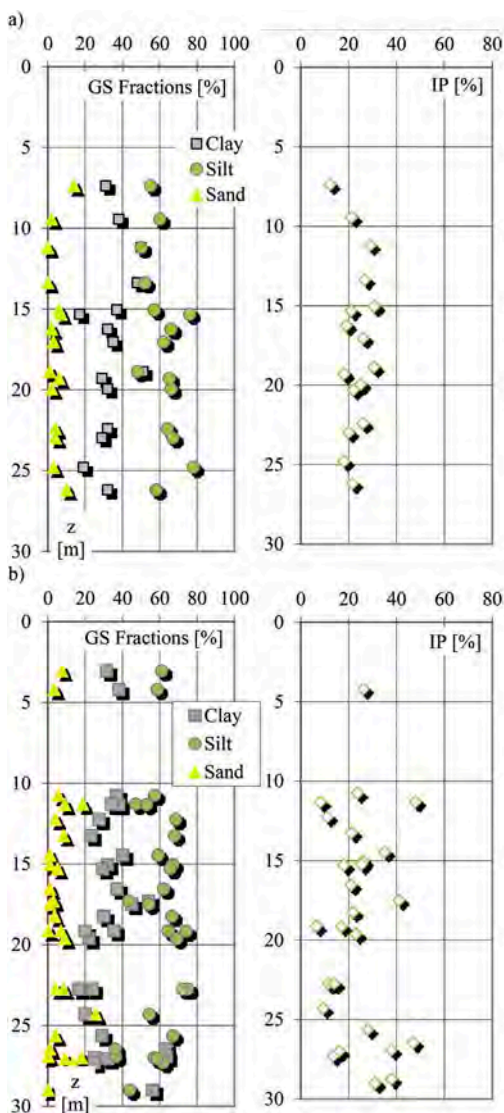


Figure 3. Grain size fraction and plastic index, a) Norther sector, b) Southern sector.

These tentative relations allow, given a generic q_c profile, to derive, for fine grain layers, C_c , e_c and e_1 according to eqs. 1, 3 and 4. The computed site void ratio e_c ,

compared with the normally consolidate void ratio e_{NC} , allows to establish if the layer is normally consolidated, overconsolidated or underconsolidated; e_{NC} can be computed at a certain depth, known e_1 and C_c , as:

$$e_{NC} = e_1 - C_c \cdot \log(\sigma'_v) \quad (5)$$

For the pilot sites, C_c and e_1 are measured quantities; e_c was computed via eq. 2 from w and G_s measured on undisturbed samples.

Figure 8 compares, for the site of Gorino:

- the profile of e_{NC_lab} computed via eq. 5 and using e_1 and C_c from laboratory measures;
- the site void ratio e_{c_lab} at sampling depth from eq. 2;
- the profile of e_{NC_CPT} computed via eq. 5 and using e_1 and C_c estimated from q_c via eqs. 3 and 1;
- the site void ratio e_{c_CPT} at sampling depth from eq.4.

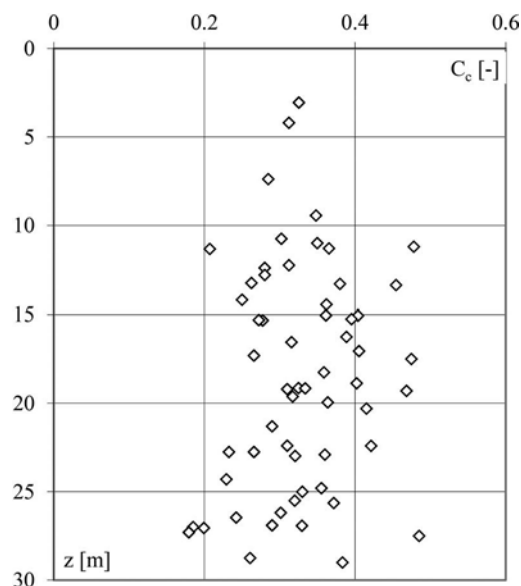


Figure 4. Compression index as a function of depth.

The discontinuities which characterise the e_{NC_lab} profile (black line) are due to change in C_c and e_1 derived from direct measures on undisturbed samples. On the other hand, the profile e_{NC_CPT} (green line) is more regular, as it mirrors the q_c profile. The comparison between e_{c_lab} value and the e_{NC_lab} profile shows that from 6 to 10 m the soil is slightly over-consolidated; between 10 and 14 m the ground is normally consolidated; at greater depths the current void ratio is greater than the normally consolidated value, indicating either that the ground on site is still subject to consolidation compression or that it is slightly structured. In the first case, subsidence settlement due to the one-dimensional compression of the layer present between 14 and 27 is of the

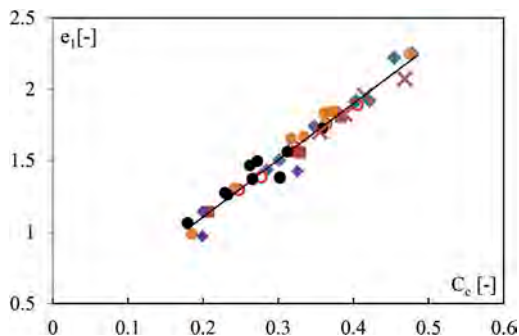


Figure 5. Altitude of the normal compression line e_1 vs. C_c .

order of 50 cm. This value is obtained as integral of the difference $\Delta e = e_{c_lab} - e_{NC_lab}$, at the depths where $e_{NC_lab} > e_{c_lab}$.

Regarding to the profile e_{NC_CPT} (obtained via Eq. 4) it can be noted that although it differs from e_{NC_lab} profile, it is in relation to e_{c_CPT} similarly to the lab profiles. In this case, the possible consolidation settlement is of the order of 74 cm.

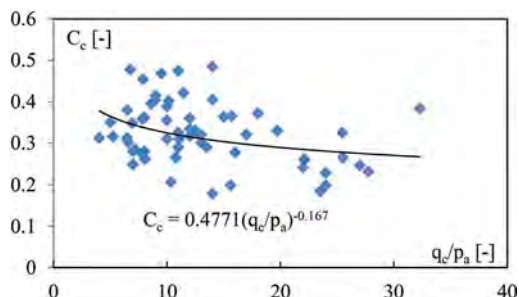


Figure 6. Compression index C_c as a function of q_c/p_a .

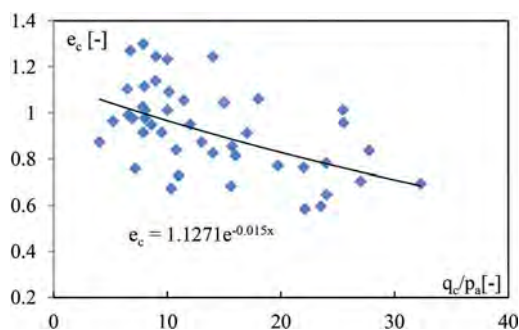


Figure 7. Site void ratio e_c as a function of q_c/p_a .

4 LARGE SCALE APPLICATION

The procedure described above was applied to CPTUs selected from the SGSS database and located in the two sectors of the regional coast evidenced in Figure 1 (blue dots). Figure 9 shows for one of the test sites (where a silty clay layer, with frequent sandy

intercalations, is present from 14 m to 30 m of depth from the ground surface, topped by a sandy deposit), the measured tip resistance q_c , lateral friction f_s , interstitial overpressure u_2 , the estimated hydrostatic profile u , the profiles of the normal consolidated void ratio e_{NC_CPT} and the current void ratio e_{c_CPT} . From the large scale application resulted that the settlements estimated for the norther sector are lower than those expected in the southern area (average value of 0.38 m in the Ferrara area and 0.58 m in the Ravenna area).

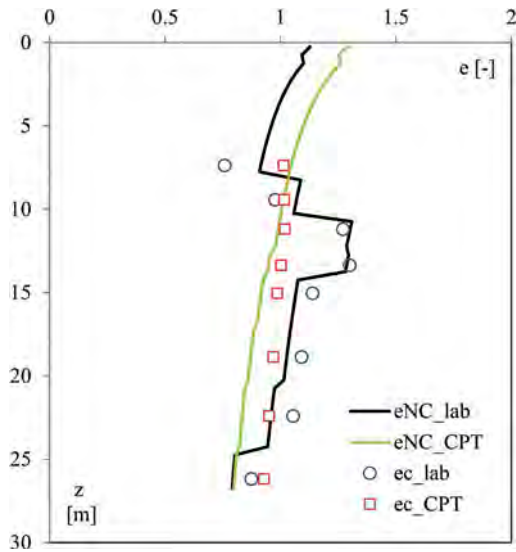


Figure 8. Gorino site: computed and measured void ratio.

Higher thickness of the layers of fine-grained soil returns higher estimated settlements. The local values of estimated consolidation settlement have been interpolated over the areas of interest to derive a map of expectable subsidence.

The function was tested to the CPTs in the northern coastal sector, between Casalborsetti and Lido di Volano. The potential settlement values for each point were interpolated with the inverse distance weighting method, obtaining the map shown in Figure 10. The spatial distribution and the range of settlements are consistent with the subsoil nature, characterized by a marked lithological heterogeneity. The lowest settlements are expected near the Reno river mouth and between Porto Garibaldi and Lido delle Nazioni where the delta and the coastal sandy deposits are thick. On the other hand, in the areas affected by the highest settlements, prodelta clays, lagoonal silts and marsh peat are prevailing.

The map provides important information to interpret the subsidence monitoring data and it also supports spatial planning, highlighting the areas most vulnerable to coastal risks, such as marine submer-sion due to land lowering.

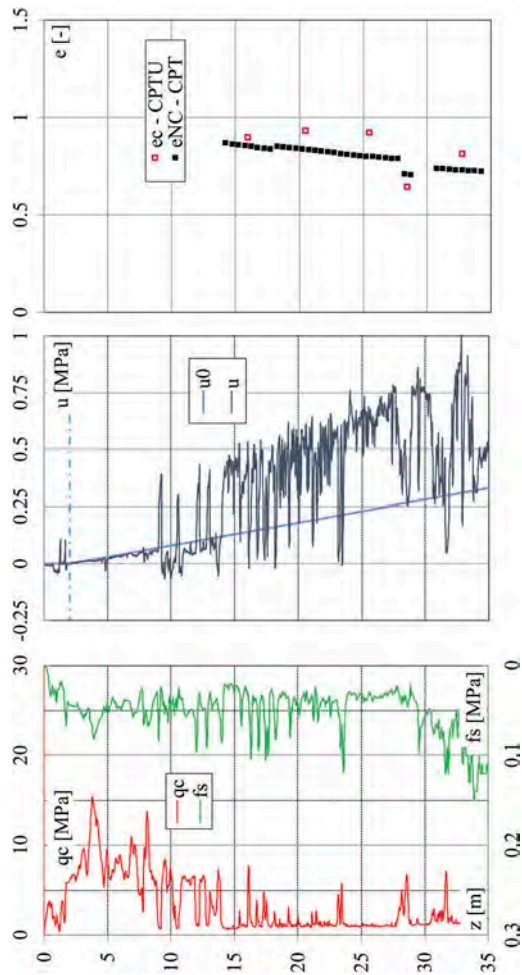


Figure 9. Application of the correlation to a CPTU.

5 CONCLUSION

The results of a significant number of CPTU and laboratory tests (particle size analyzes, Atterberg limits, oedometric tests) carried out in coastal sites characterized by the presence of recently deposited, fine-grained soil deposits, have been analyzed and interpreted to calibrate a semi-empirical correlation between the compressibility of fine grained soils and the results of static penetrometric tests.

The interpretation of all the available data allowed the elaboration of correlations between:

- the tip resistance q_c measured by a CPTU and the compression index C_c measured during the oedometric tests;
- the resistance q_c and the site void ratio e_c ;
- the compression index C_c and the altitude e_1 of the normal compression line in the $e\text{-log}\sigma'_v$ plane.

These correlations, even if characterized by significant dispersion, have been used to elaborate

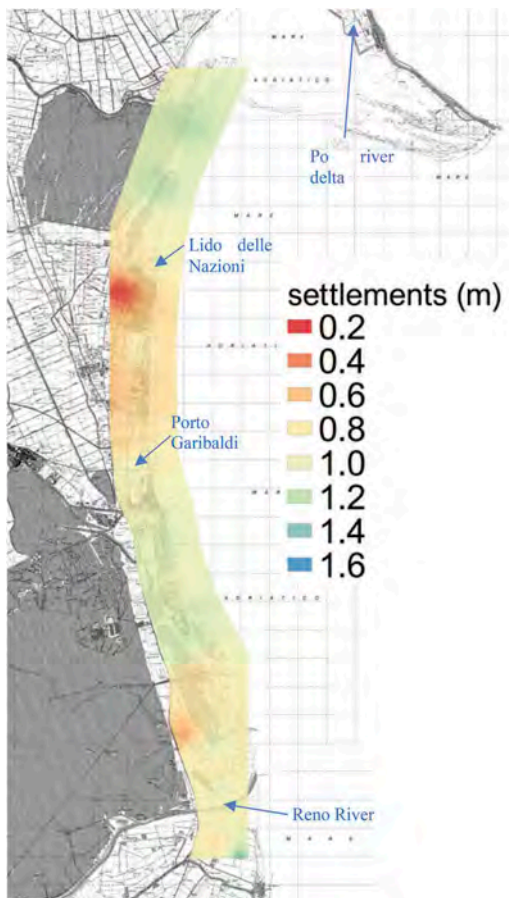


Figure 10. Map of expectable settlements in the coastal sector between Casalborsetti (RA) and Lido di Volano (FE).

a procedure that allows to evaluate, starting from the results of a CPTU, the site void ratio profile e_c of the fine-grained layers and the voids ratio profile that the fine soil would have if normally consolidated, e_{NC} . The comparison between the two profiles allows to establish if the fine soil layer is:

- overconsolidated ($e_c < e_{NC}$);
- normally consolidated ($e_c \approx e_{NC}$) or
- it has yet to reach the condition of equilibrium due to its own weight, or the soil has a structure or microcementation ($e_c > e_{NC}$); at present it is not possible to distinguish the two different conditions.

In the first two cases the layer is stable and no subsidence is expected in the absence of lithostatic load variations. In the third case, the difference between the current void index and the normal consolidated theoretical one allows to estimate any settlements that the deposit has yet to/could show due to consolidation or destructuring.

The procedure elaborated has been used to compute the possible subsidence settlement at selected sites along the Emilia-Romagna coast and to derive

expected subsidence map, which provides important information to interpret the subsidence monitoring data and supports spatial planning, highlighting the areas most vulnerable to coastal risks, such as marine submersion due to land lowering.

It should be pointed out that

- the estimated settlements is probably an upper limit, as it's not possible to distinguish underconsolidation from structuring, and its course over time is not known;
- if the difference between the current site void ratio and the normal consolidated void ratio were due to cementation or the presence of a structure, in the absence of variation in the lithostatic conditions, the soil would be stable and would not show spontaneous subsidence;
- the calibrated correlations are based on a limited sample, albeit significant, of geotechnical data that must be integrated to allow for a refinement of the proposed equations;
- nevertheless, the database employed is the first attempt of systematic collection, analysis and interpretation of compressibility data in area strongly affected by subsidence of natural and anthropic origin;
- in the definition of the empirical correlations, only coastal sites located along the regional coast were taken into consideration, therefore the calibrated equations could only have local validity and should be used only in contexts similar to those studied;
- the calibrated equations should be used only for large-scale areal considerations; for local assessments at the scale of the artefact, alternatives to the necessary geotechnical investigations on site and in the laboratory cannot be considered;
- refinement of calibrated correlations through the execution of test fields and site and laboratory geotechnical investigations is desirable.

REFERENCES

- Amorosi, A., Centineo, M.C., Colalongo, M.L., Pasini, G., Sarti, G., Vaiani S.C. 2003. Facies architecture and latest Pleistocene- Holocene depositional history of the Po Delta (Comacchio area), Italy. *J. Geol.*, 111, 39–56.
- Burland, J.B. 1990. On the compressibility and shear strength of natural clays. *Géotechnique*, 40(3), 329–378
- Cuffaro, M., Riguzzi, F., Scrocca, D., Antonioli, F., Carminati, E., Livani, L., Doglioni, C. 2010. On the geodynamics of the northern Adriatic plate. *Rend. Fis. Acc. Lincei*, 21 (Suppl.1):S253–S279.
- Ricci, Lucchi, F., 1986. The Oligocene to Recent foreland basins of the Northern Apennines. In (P.A. Allen & P. Homewood eds): *Foreland Basins*. IAS Spec. Publ., 8, 105–139.
- Stefani, M., Vincenzi, S. 2005. The interplay of eustasy, climate and human activity in the late Quaternary depositional evolution and sedimentary architecture of the Po Delta system. *Marine Geology* 222-223, 19–48.
- Teatini, P., Tosi, L., Strozzi, T. 2011. Quantitative evidence that compaction of Holocene sediments drives the present land subsidence of the Po Delta, Italy. *Journal of Geophysics Research*, 116, B08407.

A comparative study on liquefaction assessment of Rajarhat area of Kolkata by using different approaches

Abhipriya Halder

Department of Civil Engineering, Narula Institute of Technology, India

Kaustav Das, Saptarshi Nandi & Kaushik Bandyopadhyay

Department of Construction Engineering, Jadavpur University, India

ABSTRACT: Liquefaction potential assessment is of particular significance to geotechnical engineers in order to evaluate the risks for construction of high rise buildings, railway embankments, canal, road embankments, earth dams etc. in areas susceptible to liquefaction. Investigations were made at Rajarhat area of Kolkata, India by means of CPT, DMT, SPT and SDMT measurements. The main purpose of carrying out these tests is to grab a relatively rare opportunity to compare the results of all these methods for arriving at a conclusive evidence in predicting liquefaction. It was found that the results of all the in-situ techniques were relatively consistent in predicting liquefaction within a depth range of 0 to 17.0 m below the ground surface. CPT, DMT, SPT and SDMT are basically field-based in-situ tests for measurements of important geotechnical parameters and also provide reliable data for assessment of liquefaction potential of a site. In recent times Finite Element Method based (FEM), a powerful viable alternative tool is available to the geotechnical engineers for application in various fields. In the present investigation, an attempt has been made to study the assessment of liquefaction based on the numerical simulation using Finite element software in addition to all the field techniques mentioned before. The main objective of the present study is to evaluate the correlation between factor of safety against liquefaction using different in-situ test approaches as well as the FEM tool. Finally, the paper presents the correlation between the depth and factor of safety for this particular Rajarhat area of Kolkata for understanding the vulnerability of this area to liquefaction.

Keywords: Dilatometer and seismic dilatometer test, cone penetration test, standard penetration test, Finite Element Method, liquefaction potential

1 INTRODUCTION

1.1 Background

Soil plays a vital role for the proper installation of footing. Footings are placed for transferring the super-structure load to soil. Hence, proper findings out of geotechnical parameters including liquefaction susceptibility of sub-soil maintains an important role for the stability of the soil. If it is not accounted properly, the entire stability of structure can be adversely affected due to failures of the sub-soil.

Soil liquefaction is a phenomenon occurred due to vibration (generally during earthquake) to the sub-soil and results to the failure of sub-soil. During earthquake cyclic loading is triggered and passes through the sub-soil. Therefore rise of pore water pressures takes place through sub-soil in addition to

the vertical stress and it results in the loss of shear strength of saturated soil mass. This particular phenomenon is known as liquefaction. Therefore, estimation of liquefaction susceptibility of soil is important prior to any construction of structures for avoiding the future vulnerability to any calamity.

1.2 Objectives

The aim of this study is to assess the liquefaction susceptibility and evaluate the factor of safety against liquefaction by using different in-situ test approaches (i.e., SPT, CPT, DMT and SDMT) as well as the FEM (finite element method) tool (i.e., NovoLIQ and Plaxis 2D software). Finally, present the variation of factor of safety (FOS) along depth for Rajarhat area of Kolkata.

2 MATERIALS AND METHODS

2.1 Liquefaction susceptibility criteria of Rajarhat

Excessive pore water pressure generation is the cause of liquefaction. It is directly connected to the compositional characteristics of the soil i.e., fine content, gradation, plasticity index etc.

Generally, cohesion less soils (sand, silty sand or sandy silt) undergo liquefaction but this phenomenon may be also occurred on plastic & cohesive silty clay and sensitive clay (Updike et al., 1988; Kramer, 1996). Wang (1979) suggested Chinese Criteria to evaluate liquefaction susceptibility based on the earthquake observations in China.

There are four criteria which might be considered to evaluate liquefaction susceptibility for the fine grained sediments (Wang, 1979; Kramer, 1996). These criteria are given below

- 1) Fraction finer than $0.005 \text{ mm} \leq 15\%$
- 2) Liquid limit, $LL \leq 35\%$
- 3) Natural Water Content $\geq 0.9LL$
- 4) Liquidity Index ≤ 0.75

However, many researchers have followed some varying criteria on estimating the liquefaction susceptibility which unless if properly addressed, may cause the extensive damage when silty or clayey soils containing more than 15% clay size particles are found (Bray et al., 2004; Bray and Sancio, 2006).

On the other hand, based on water content (w_c), liquid limit (LL) and plasticity index (PI), Bray and Sancio (2006) had proposed a new compositional criteria obtained from the results of cyclic triaxial test to determine liquefaction susceptibility:

- 1) Highly Susceptible towards liquefaction: $PI < 12$ and $(w_c/LL) \geq 0.85$.
- 2) Moderately Susceptible towards liquefaction: $12 < PI < 18$ and $0.85 > (w_c/LL) \geq 0.8$.
- 3) Non-Susceptible towards liquefaction: $PI > 18$ and $(w_c/LL) < 0.8$.

The subsurface condition of Kolkata, Rajarhat site specify that the sedimentary deposits underlying the city involve predominantly of grain size favorable for liquefaction and this area is formed on coarse grained artificial non engineered fill. So the site may be susceptible to soil liquefaction. [Nath et al., 2018]

2.2 Methods

Different Methods used for liquefaction susceptibility analysis in this study were given below:

1. Estimation of Soil property.
2. Determination of earthquake magnitude from peer ground motion database.
3. Determination of CSR.
4. Determination of CRR from SPT, CPT and DMT tests data.

5. Computation of Factor of safety (FOS) from SPT, CPT and DMT tests data.
6. Plaxis 2D and NovoLIQ software were used as a finite element tools.

3 RESULTS AND DISCUSSIONS

3.1 Estimation of soil property

The in situ investigation was done by two numbers of boreholes of up to 30 m depth in which the standard penetration test (SPT) were performed. The cone penetration tests (CPT), Flat Dilatometer tests (DMT) and seismic Dilatometer test (SDMT) were performed up an average depth of 20m. Undisturbed soil samples were collected and unconsolidated undrained (UU) tri-axial tests were performed. In addition, the grain size distribution tests were performed on collected soil samples to obtain the fine fraction of the sub- soil.

Two numbers of CPT (CPT1 and CPT2) tests were conducted out up to a depth of 19.0m below the ground level, at Rajarhat, Kolkata. The CPT tests were carried out by using the attached CPT assembly provided with Pagani TG 63-150 penetrometer. The CPT tests were performed at 2cm/s penetration rate vertically downward. On every 200mm depth interval readings were taken.

Two numbers of DMT tests i.e., DMT1 and DMT2 (aligned to the straight line with the CPT points), were carried out by giving 500mm spacing between the respective CPT tests points. At one of the DMT points (i.e., DMT2), seismic tests (SDMT) were performed to evaluate shear wave velocity (V_s) by striking a hammer ($\approx 10\text{kg}$) to a steel plate placed at the ground level under the base of the penetrometer (Pagani TG-63/150) stand aligned perpendicular to the plane of DMT blade. This seismic test was performed on every 500mm depth interval starting from 1m below the existing ground level. This seismic test was executed during the Dilatometer Test. The shear wave velocity (V_s) measurement was done with the aid of seismic module attached to the control unit. One number of DMT test and one number of seismic dilatometer test (SDMT) were also performed up to a depth of 18.0m below ground level at this site.

CPT1 and DMT1 points were located near the Borehole1 (BH1) and the rest test points (i.e., CPT2 and DMT2) were located near the Borehole 2 (BH2), as shown in Figure 1.

3.2 Determination of earthquake magnitude from PEER GROUND MOTION DATABASE

Authentic ground motion database is needed as an important parameter of earthquakes that is likely to occur in Rajarhat area of kolkata. To get the data history of earthquake, it was collected from the website of the PEER GROUND MOTION DATABASE. From the previous earthquake database results, it

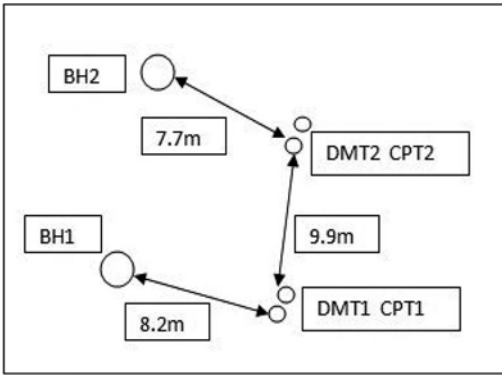


Figure 1. Location plan of the testing points.



Figure 2. Photographs of the test progress.

was observed that the earthquake magnitude in the study area is 6.5 MW (Moment Magnitude) which was used as boundary earthquake magnitude for liquefaction susceptibility analysis of the study area.

As per Indian standard (i.e., IS 1893 (Part-1): 2016), the zone wise Peak Ground Acceleration (PGA) is mentioned. On that basis Kolkata is classified into the zone III having PGA of 0.3g.

3.3 Determination of CSR

The CSR value had been determined using Equation-1, given below. The components of the equation are horizontal earthquake peak acceleration on the soil surface (a_{max}), gravity, stress reduction coefficient, and overburden stress value. All variables are formulated in the following equation:

$$CSR = \frac{\tau_{av}}{\sigma'_{vo}} = 0.65 \times \left(\frac{a_{max}}{g} \right) \times \left(\frac{\sigma_{vo}}{\sigma'_{vo}} \right) \times r_d \quad (1)$$

Where,

- a_{max} = peak horizontal acceleration on the surface of soil caused by earthquake
- g = gravitational acceleration
- σ_v = vertical overburden stress
- σ'_{vo} = effective vertical overburden stress
- r_d = coefficient of stress reduction

3.4 Determination of CRR

3.4.1 Determination of CRR from SPT

Seed & Idriss (1983 -1985) proposed $CRR_{M=7.5}$ equation as:

$$CRR_{M=7.5} = \frac{1}{34 - (N1)_{60CS}} + \frac{(N1)_{60CS}}{135} + \frac{50}{[10 \times (N1)_{60CS} + 45]^2} - \frac{1}{200} \quad (2)$$

Where:

$(N1)_{60CS}$: Corrected Value of N SPT

3.4.2 Determination of CRR from CPT

CRR from CPT had been calculated using this following graph:

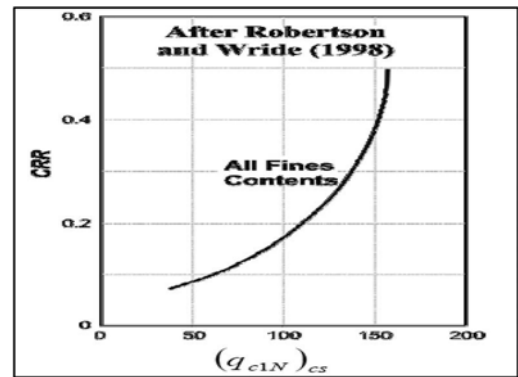


Figure 3. Graph of CRR Vs $(q_{c1N})_{cs}$ recommended by Robertson and Wride (1998).

Where:

$(q_{c1N})_{cs}$: Value of corrected cone resistance

3.4.3 Determination of CRR from DMT

Cyclic Resistance Ratio (CRR) was calculated from horizontal stress index (K_d) values using the equation proposed by Monaco et al (2005).

$$CRR = 0.0107K_d^3 - 0.0741K_d^2 + 0.2169K_d - 0.1306 \quad (3)$$

3.5 Computation of factor of safety (FOS) from SPT, CPT, DMT tests data

Furthermore, CRR value was compared to the value of CSR of each layer of soil for evaluating the value of FOS. FOS was plotted against depth, showing the value of FOS for each test depth (i.e., 200 mm). Below is a graph of the variation of factor of safety along depth for SPT tests.

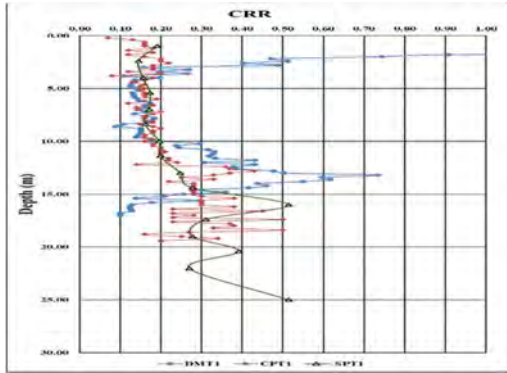


Figure 4. Variation of CRR with depth for DMT1, CPT1, SPT1 tests points.

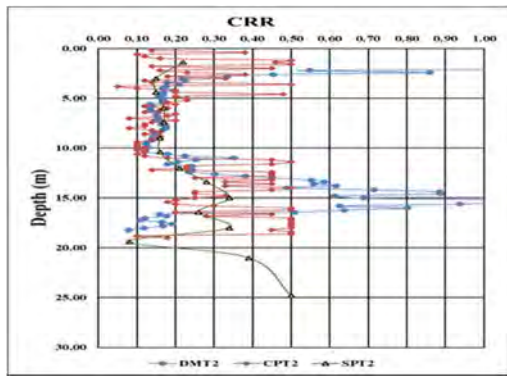


Figure 5. Variation of CRR with depth for DMT2, CPT2, SPT2 tests points.

3.6 NovoLIQ and PLAXIS 2D software were used as finite element tools

3.6.1 NovoLIQ software

NovoLIQ finite element based software had been used for liquefaction analysis based on SPT and SDMT tests data. The following graphs show the variation of FOS with depth

3.6.2 Plaxis software

Plaxis 2D finite element based software had been used for liquefaction analysis based on DMT tests data.

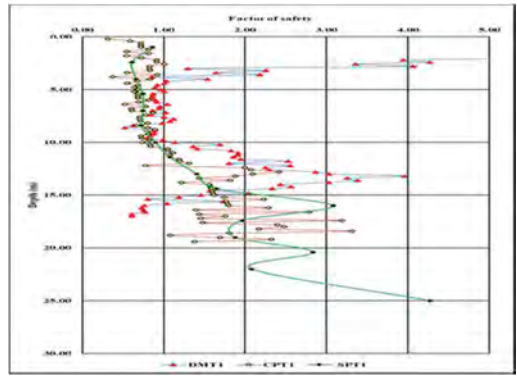


Figure 6. Variation of FOS with depth for DMT1, CPT1, SPT1 tests points.

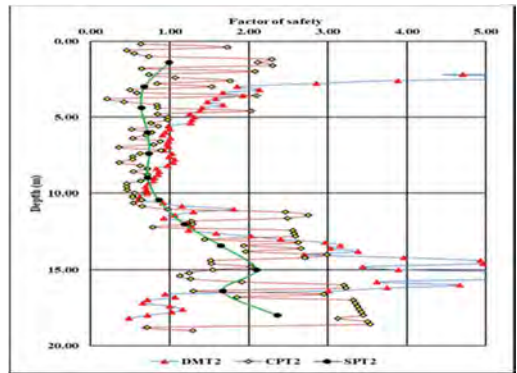


Figure 7. Variation of FOS with depth for DMT2, CPT2, SPT2 tests points.

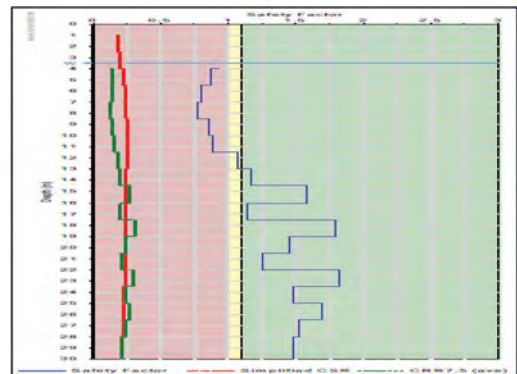


Figure 8. Variation of FOS with depth at the test location of BH-01 based on SPT.

A Plate had been assumed to be placed on the soil. The properties of the plate is given below.
 d_{eff} (effective depth) = 150mm,
 $EA = 4107919.18 \text{ kN/m}$ for isolated footing
 $EI = 7702.3 \text{ kN m}^2/\text{m}$ for isolated footing

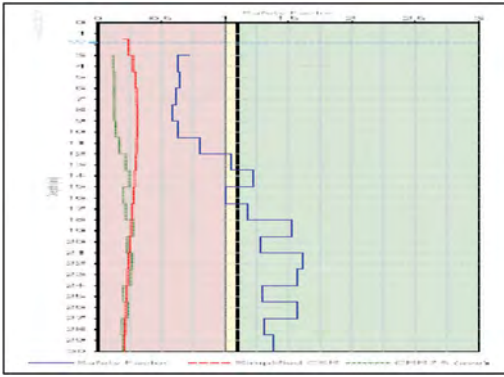


Figure 9. Variation of FOS with depth at the test location of BH-02 based on SPT.

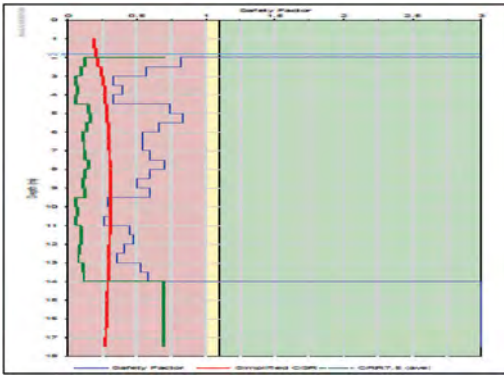


Figure 10. Variation of FOS with depth at the test location of SDMT.

On these plates a static load of 85 kPa with a earthquake of magnitude of 6.5, corresponding settlement of the foundation soil profile has been estimated. The value of the settlement had been compared with the findings of Tokimatsu, K., & Seed, H. B. (1987)., Evaluation of settlements in sands due to earthquake shaking paper.

3.7 Discussion

In this paper, the value of factor of safety against liquefaction were estimated from in-situ test's results (i.e., CPT, DMT and SPT) and had been plotted for respective tests depths. Also the computed factor of safety against liquefaction from SDMT and SPT tests had been compared and plotted by using finite element based software (i.e., Novoliq).

Apart from, the settlement of a shallow foundation had been calculated by using Plaxis2D software against earthquake magnitude of 6.5 and compared with the allowable limit proposed by Tokimatsu, K., & Seed, H. B. (1987).

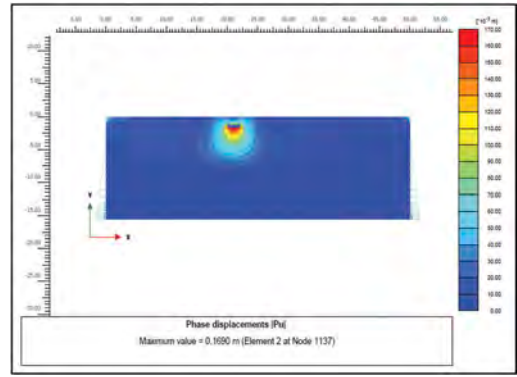


Figure 11. Settlement of 2m × 2m isolated footing when an earthquake of magnitude 6.50 is applied.

4 CONCLUSION

From the above result and discussion it can be concluded that

- For SPT, CPT and DMT, the graph of factor of safety with depth showing a similar pattern upto an average depth of 11.0m but in case DMT the graph is showing an irregularity upto an average depth of 4.0m. Soil description estimated from DMT test shows that there is a fill layer of 4.0m at the test location. Hence it can be concluded that the liquefaction analysis done by DMT is more realistic in nature with respect to CPT and SPT.
- The liquefaction Analysis done by the finite element software 'NovoLIQ' based on SPT data shows a similar pattern with conventional approach. But when liquefaction analysis is done based on SDMT data, it shows that the soil is liquefiable upto a depth of 14.0m f. Hence it can be concluded that the liquefaction analysis based on SDMT data is conservative in nature.
- The liquefaction Analysis had been done by the finite element software 'Plaxis 2D' for 2m × 2m isolated footing based on DMT data. It shows a settlement of 169mm when an earthquake of magnitude 6.50 is applied on the foundation. This value of settlement suggested that the foundation will fail due to the liquefaction effect according to the table (Tokimatsu et al., 1987) given below.

Table-1

Layer	Thickness (ft)	Settlement (in)
1	5	0.13
2	5	0.22
3	10	0.67
4	10	0.77
5	10	0.86
6	10	0.72

Hence, more research is required for liquefaction analysis of soil based on insitu tests in Kolkata.

ACKNOWLEDGMENTS

The estimation of settlements was carried out by using **PLAXIS2D V20** finite element based software received from **BENTLEY EDUCATION** for research purposes. Their kind permission to use the software is gratefully acknowledged.

The liquefaction analysis was carried out by using **NovoLIQ** finite element based software received from **A ROCSIENCE COMPANY** for research purposes. Their kind permission to use the software is gratefully acknowledged.

DMT tests were performed with the equipment received from **Studio Prof. Marchetti s.r.l., Rome, Italy**. The Cone Penetration tests were carried out by TG63/150 static/dynamic penetrometer provided by **Pagani Geotechnical Equipment**, Calendasco, Italy, (<https://www.pagani-geotechnical.com/>). Sincere thanks are extended to these companies.

Field boreholes and Laboratory tests were carried out by **Continental Consultants, Kolkata**. Contributions from Mr. B.N. Basak (Chief Consultant) from **Continental Consultants, Kolkata** is highly acknowledged.

REFERENCES

- Updike, R. G., Egan, J. A., Moriwaki, Y., Idriss, I. M., & Moses, T. L. (1988). A model for earthquake-induced translatory landslides in Quaternary sediments. *Geological Society of America Bulletin*, 100(5), 783–792.
- Kramer, S. L. (1996). *Geotechnical earthquake engineering*. Pearson Education India.
- Wang W (1979) Some findings in soil liquefaction. Water Conservancy and Hydroelectric Power Scientific Research Institute, Beijing.
- Bray, J. D., Sancio, R. B., Riemer, M. F., & Durgunoglu, T. (2004, January). Liquefaction susceptibility of fine-grained soils. In *Proc., 11th Int. Conf. on Soil Dynamics and Earthquake Engineering and 3rd Int. Conf. on Earthquake Geotechnical Engineering* (Vol.1, pp. 655–662). Stallion Press, Singapore.
- Bray, J. D., & Sancio, R. B. (2006). Assessment of the liquefaction susceptibility of fine-grained soils. *Journal of geotechnical and geoenvironmental engineering*, 132(9), 1165–1177.
- Nath, S. K., Srivastava, N., Ghatak, C., Adhikari, M. D., Ghosh, A., & Ray, S. S. (2018). Earthquake induced liquefaction hazard, probability and risk assessment in the city of Kolkata, India: its historical perspective and deterministic scenario. *Journal of Seismology*, 22(1), 35–68.
- IS:1893:2016, “Criteria for Earthquake Resistant Design of Structures,” Bureau of Indian Standards, New Delhi, 2016. [Online]. Available: <https://archive.org/details/1893Part12016>. [Accessed: 28-May-2017]
- Robertson, P. K., & Wride, C. E. (1998). Evaluating cyclic liquefaction potential using the cone penetration test. *Canadian geotechnical journal*, 35(3), 442–459.
- Monaco, P., Marchetti, S., Totani, G., & Calabrese, M. (2005). Sand liquefiability assessment by flat dilatometer test (DMT). In *Proceedings of the 16th International Conference on Soil Mechanics and Geotechnical Engineering* (pp. 2693–2698). IOS Press.
- Tokimatsu, K., & Seed, H. B. (1987). Evaluation of settlements in sands due to earthquake shaking. *Journal of geotechnical engineering*, 113(8), 861–878.

Kriging analysis on CPTU data from offshore wind farm

Rongjie He & Jinhui Li*

Department of Civil and Environmental Engineering, Harbin Institute of Technology (Shenzhen), China

Shaoli Yang

Norwegian Geotechnical Institute (NGI), Oslo, Norway

Ben He

Key Laboratory for Far-shore Wind Power Technology of Zhejiang Province; PowerChina Huadong Engineering Corporation Limited, (HDEC), Hangzhou, China

ABSTRACT: In recent years, offshore wind power has been widely developed. Because of the complexity of marine geology and the large spatial variability of soils, it is necessary to obtain CPTU data before the foundation design. However, how to reasonably interpret the CPTU data will greatly affect the reliability and safety of the offshore windfarm foundation. In addition, there is a need to predict soil conditions at the locations without CPTU data. In this study, based on the available CPTU data of offshore wind farm in east China sea, kriging method is used to interpret the CPTU data, and the soil conditions in a large area can be predicted. This method can be used to develop ground model for a large offshore wind farm, and estimate the relevant soil parameters based on CPTU data. The analysis methods can provide reference for other projects of offshore wind farm.

Keywords: offshore wind farm, CPTU, kriging method, marine geology

1 INTRODUCTION

Offshore wind power has been widely used as the clean energy in many countries. Dinh and Nguyen (2019) proposed that offshore wind power has the advantages of higher full load hours per year, longer service life and higher rotor speed comparing with onshore wind power. In practical engineering, foundation design should be carried out before the installation of offshore wind turbine.

Marine soil has the characteristics of large spatial variability (Dasaka and Zhang 2012; Ching and Phoon 2013; Li et al. 2014; Lloret-Cabot et al. 2014). Before the foundation design of the offshore wind turbine, it is necessary to obtain the CPTU data of relevant soil layers. Then the obtained CPTU data can be interpreted to get soil parameters. For example, Robertson method (Robertson and Wride, 1998) can be used to determine the classification of marine soil layer based on the CPTU data. However, due to the high cost of offshore work, the CPTU tests in a large area are usually limited. Therefore, how to predict soil conditions at

the locations without CPTU data has become an important engineering problem which needs to be solved.

Based on the above background, taking the CPTU data of offshore wind farm in east China sea as an example, this study used the Kriging method to predict the CPTU data in the unknown area, and then used the Robertson method (Robertson and Wride, 1998) to obtain the soil classification of the whole seabed profile. The predicted results can reach the 95% confidence interval in statistics. The algorithm can provide reference and guidance for the foundation design of offshore wind turbine.

2 INVESTIGATION SITE OF OFFSHORE WIND FARM

The site of the offshore wind farm is in the east China sea. The positions of the boreholes are shown in Figure 1. This site contains 27 boreholes. The drilling depth of each borehole is more than 35 m, and CPTU data is measured every 0.02 m along the

*Corresponding author
DOI: 10.1201/9781003308829-144

depth. In Figure 1, the interval of boreholes in different columns is 11000 m which is too large, so 15 boreholes in the same column are selected for analysis as shown in the frame. The measured CPTU data contain cone penetration resistance (q), sleeve friction (f) and pore pressure (u).

According to the soil samples at the site, the actual soil layers of boreholes no. 50, no. 72 and no. 77 have been already known which are shown in Figure 2. It can be seen from Figure 2 that the actual seabed geological conditions are generally divided into four layers: Ooze clay, clay, silty clay, and silty sands. The soil layers in the first 25 m are relatively homogeneous, and they are Ooze clay. The soil layers beyond 25 m vary from location to location. Figure 3 shows the typical CPTU data along depth of borehole no. 50. It can be seen that the trend of the curve at the first 25 m is increasing linearly, and the trend of the curve is much more complicated beyond 25 m.

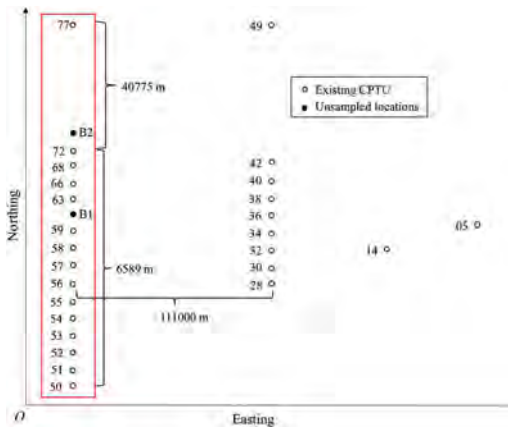


Figure 1. The position of the boreholes.

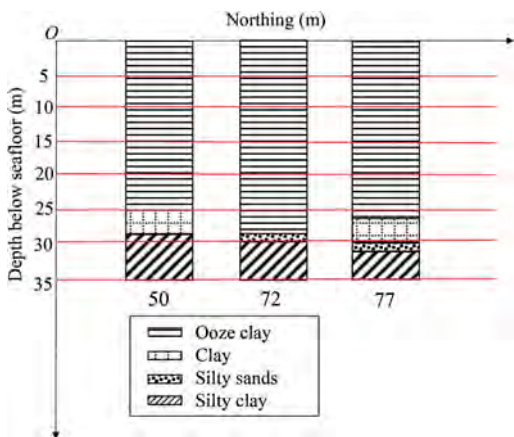


Figure 2. Soil conditions of known boreholes (Borehole no. 50, no. 72 and no. 77).

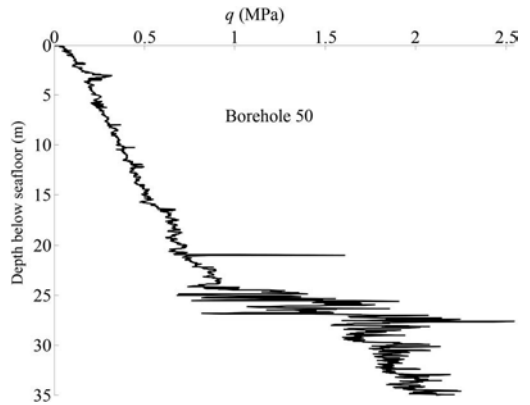


Figure 3(a). Measured cone resistance along depth below seafloor

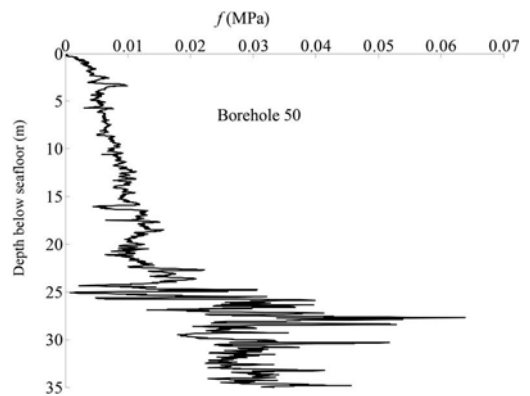


Figure 3(b). Measured sleeve friction along depth below seafloor

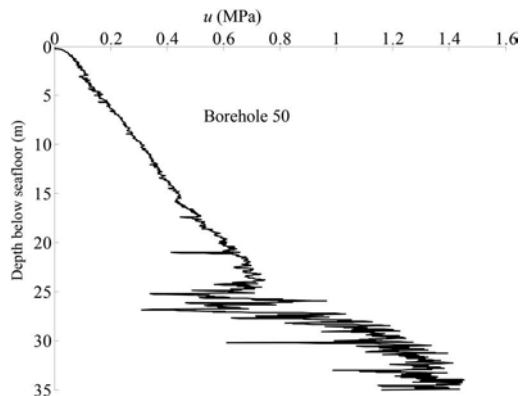


Figure 3(c). Measured pore pressure along depth below seafloor.

Figure 3. The variation of CPTU data with depth in borehole no. 50.

Based on CPTU data, the classification of soil layer can be obtained. There are many traditional

soil classification methods, such as Jefferies method (Jefferies and Davies, 1991), Olsen method (Olsen and Mitchell, 1995), Robertson method (Robertson and Wride, 1998) and so on. Liu et al. (2013) proposed that the Robertson method is suitable for the Chinese soil classification. Therefore, the Robertson method is used for soil classification in this study. The calculation formulas are shown from Equation 1 to Equation 6,

$$Q_{tn} = \frac{q_t - \sigma_{v0}}{\sigma'_{v0}} \quad (1)$$

$$F_r = \frac{f_s}{q_t - \sigma_{v0}} \times 100\% \quad (2)$$

$$B_q = \frac{u - u_0}{q_t - \sigma'_{v0}} \quad (3)$$

$$I_c = \sqrt{[3.47 - \lg(Q_{tn})]^2 + [\lg(F_r) + 1.22]^2} \quad (4)$$

$$q_t = q + (1 - a)u \quad (5)$$

$$a = d^2/D^2 \quad (6)$$

where Q_{tn} is normalized cone penetration resistance; F_r is normalized sleeve friction; B_q is normalized pore pressure; σ_{v0} is the total overburden stress; σ'_{v0} is effective overburden stress; u_0 is equilibrium pore pressure; q_t is corrected cone penetration resistance; a is the net area ratio between load cell support diameter, d , and cone diameter, D ; I_c is soil classification index. The soil types are attributed from I_c which is shown in Table 1.

Table 1. The soil classification based on Robertson method.

I_c	Soil type
$I_c > 3.6$	Ooze clay
$2.95 < I_c < 3.6$	Clay
$2.60 < I_c < 2.95$	Silty clay
$2.05 < I_c < 2.60$	Sandy silt
$1.31 < I_c < 2.05$	Silty sands
$I_c < 1.31$	Dense sand

3 KRIGING METHOD

Kriging interpolation (Liu et al., 2016) is an optimal linear unbiased interpolation method. For ordinary Kriging, there is a group of observation

points in region D , whose position coordinates are x_1, x_2, x_3 to x_n , respectively, and the corresponding observation values are $Z(x_1), Z(x_2), Z(x_3)$ to $Z(x_n)$, respectively. Then the formula of the estimated value at unknown position x_0 in region D is shown in Equation 7,

$$Z^*(x_0) = \sum_{i=1}^n \lambda_i Z(x_i) \quad (7)$$

where λ_i is the weight coefficient of Kriging interpolation. The values of λ_i should be known. The semi-variogram is used to calculate the λ_i . The semivariogram of the observation data can be calculated by Equation 8,

$$\gamma(h) = \frac{1}{2N_h} \sum_{i=1}^{N_h} [Z(x_i + h) - Z(x_i)]^2 \quad (8)$$

where N_h is the number of the observation points and h is the separation distance between different points. Based on the semivariogram values of the observation points, the Gaussian model and exponential model are usually used to fit the trend of the semivariogram which are shown in Equation 9 and Equation 10,

$$\gamma(h) = C_0 + C(1 - e^{-\frac{3h^2}{a^2}}) \quad (9)$$

$$\gamma(h) = C_0 + C(1 - e^{-\frac{3h}{a}}) \quad (10)$$

where C_0 is nugget; C is partial sill and a is range. Before fitting the semivariogram, it is essential that the data is stationary; that is, the mean and covariance of the data depend only upon separation, not on absolute location. If the data are non-stationary, treatment must be given to transform the data to a stationary set by removing the deterministic component called the trend, and the stationary residual random component is then analyzed.

After fitting the semivariogram, the weight coefficient λ_i can be calculated based on Equation 11,

$$\begin{bmatrix} \gamma_{11} & \gamma_{12} & \cdots & \gamma_{1n} & 1 \\ \gamma_{21} & \gamma_{22} & \cdots & \gamma_{2n} & 1 \\ \vdots & \vdots & & \vdots & 1 \\ \gamma_{n1} & \gamma_{n2} & \cdots & \gamma_{nn} & 1 \\ 1 & 1 & \cdots & 1 & 0 \end{bmatrix} * \begin{bmatrix} \lambda_1 \\ \lambda_2 \\ \vdots \\ \lambda_n \\ \mu \end{bmatrix} = \begin{bmatrix} \gamma_{01} \\ \gamma_{02} \\ \vdots \\ \gamma_{0n} \\ 1 \end{bmatrix} \quad (11)$$

where γ_{ij} is the modelled semivariogram values based on the distance between the two samples pertaining to

the i th and j th locations, and μ is the Lagrange parameter. The formula for calculating the variance is shown in Equation 12,

$$\sigma_{OK}^2 = \sum_{i=1}^n \lambda_i \gamma_{0i} + \mu \quad (12)$$

where σ_{OK} is the OK standard variance of the Kriging method. Assuming that the parameter is normally distributed with a mean value z_0 (estimated value) and a standard variance σ_{OK} , the 95% confidence interval of the estimation is $[z_0 - 1.96\sigma_{OK}, z_0 + 1.96\sigma_{OK}]$ (Ang and Tang, 2007).

Taking the CPTU data in depth 10 m for analysis as an example, the fitting equations of the deterministic component are shown in Equation 13, Equation 14 and Equation 15, respectively,

$$q_{trend} = 0.2871x - 34.2453 \quad (13)$$

$$f_{trend} = 0.0061x - 0.7291 \quad (14)$$

$$u_{trend} = 0.5127x - 61.5089 \quad (15)$$

where q_{trend} , f_{trend} and u_{trend} are trend values of cone penetration resistance, sleeve friction and pore pressure, and x is the longitude coordinate of the observation points.

After removing the deterministic component, the stationary residual random components are used to fit the semivariogram. In this case study, comparing with Gaussian model, exponential model has higher fitting goodness. As a result, the exponential function is used to fit the semivariogram. The number of lag distances is 105 in total. Taking about 200 m as a group, the lag distances are divided into 14 groups. The lag distances of 14 groups are averaged to obtain the best fitting results and they are shown in Figure 4.

Cheon and Gilbert (2014) indicated that it is reasonable to have a horizontal range of more than 1000 m in offshore engineering. Based on the results, the range of the three residuals are all 120 m which are reasonable. Then, the CPTU data in unknown positions can be predicted based on the modelled semivariogram.

4 PREDICTION OF SOIL TYPES

From Figure 2, there are mainly four soil layers in the seabed. According to the calculation, different soil layers have different modelled semivariograms. As a result, four modelled semivariograms were used to analyze the depths below seafloor at depth of 1m to 25 m, 26 m to 29 m, 29 m to 31 m, and 31 m to 35 m, respectively.

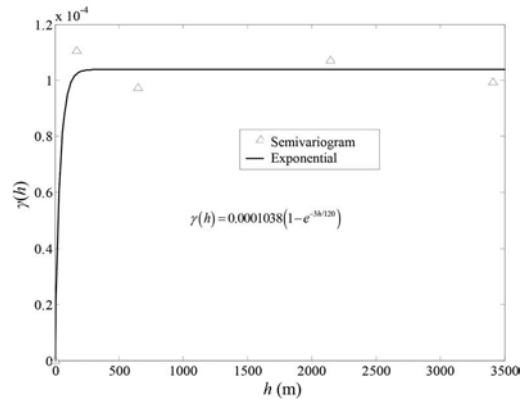


Figure 4(a). The semivariogram of cone resistance

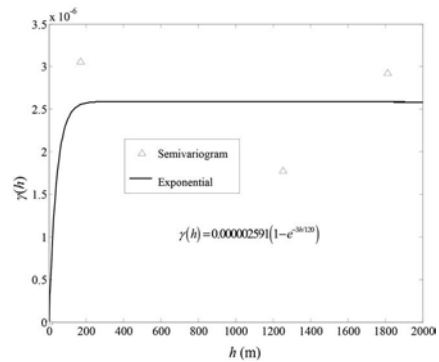


Figure 4(b). The semivariogram of sleeve friction

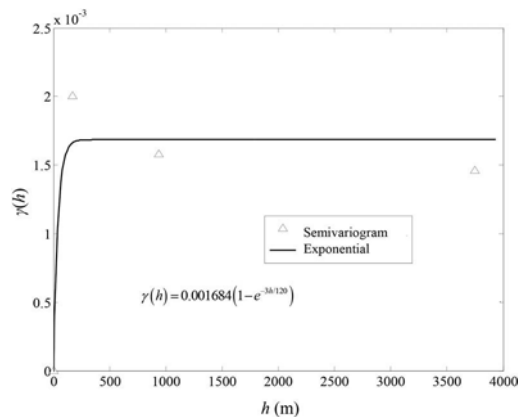


Figure 4(c). The semivariogram of pore pressure

Figure 4. The semivariogram of CPTU data in depth 10 m.

In order to verify the accuracy of the Kriging method, the soil types at boreholes no. 50 and no. 77 were predicted. The predicted results are shown in

Figure 5 and Figure 6. The results were compared with the actual soil types at the two boreholes. It can be seen that the predicted soil types are basically consistent with the actual soil types. The results prove that the Kriging method is reasonable.

B1 is the first unknown position without CPTU data which needs to be predicted. The longitude and latitude of B1 are 120.556 degree and 27.14 degree, respectively. For the depth of 15 m, 27 m, 30 m and 35 m, the estimators of cone penetration resistance of B1 are 0.521 MPa, 1.213 MPa, 2.105 MPa and 3.290 MPa; the estimators of sleeve friction of B1 are 6.7 kPa, 18 kPa, 21.3 kPa and 61.3 kPa, and the estimators of pore pressure of B1 are 0.414 MPa, 0.601 MPa, 0.808 MPa and 0.822 MPa. The 95% interval of confidence is shown in Table 2 and the predicted soil types are shown in Figure 7. For Table 2, it just means that the value will be within this interval.

Table 2. The predicted CPTU data in B1 (95% confidence interval).

Depth (m)	q (MPa)	f (kPa)	u (MPa)
15	[0.521, 0.521]	[6.690, 6.705]	[0.411, 0.418]
27	[1.106, 1.321]	[17.3, 18.7]	[0.572, 0.630]
30	[0, 8.794]	[20.80, 21.8]	[0.443, 1.173]
35	[0, 31.725]	[0.056, 0.067]	[0.176, 1.469]

B2 is the second unknown position without CPTU data which also needs to be predicted. The longitude and latitude of B2 are 120.592 degree and 27.14 degree, respectively. For the depth of 15 m, 27 m, 30 m and 35 m, the estimators of cone penetration resistance of B2 are 0.520 MPa, 1.186 MPa, 2.038 MPa and 3.066 MPa; the estimators of sleeve friction of B2 are 6.8 kPa, 17.3 kPa, 21.5 kPa and 57.3 kPa, and the estimators of pore pressure of B2 are 0.414 MPa, 0.643 MPa, 0.760 MPa and 0.827 MPa. The 95% interval of confidence is shown in Table 3. For Table 3, it just means that the value will be within this interval.

According to the soil classification criteria, the predicted soil types are the same with that at location B1, which can be seen in Figure 7.

Table 3. The prediction CPTU data in B2 (95% confidence interval).

Depth (m)	q (MPa)	f (kPa)	u (MPa)
15	[0.52, 0.52]	[6.79, 6.805]	[0.410, 0.417]
27	[1.081, 1.291]	[16.6, 18.02]	[0.622, 0.665]
30	[0, 8.636]	[0.021, 0.022]	[0.415, 1.104]
35	[0, 30.797]	[0.052, 0.062]	[0.189, 1.465]

Based on the CPTU data of boreholes, the seabed profile can be predicted and the results are shown in

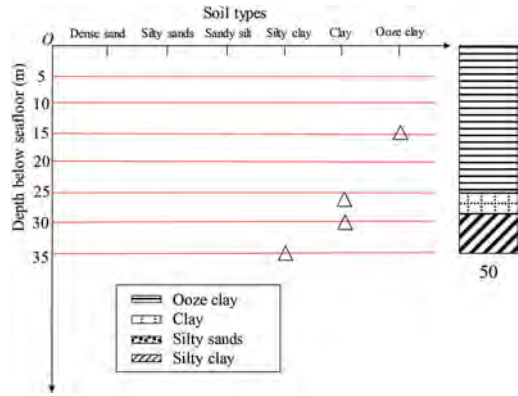


Figure 5. The comparison between prediction value and actual data in borehole no. 50.

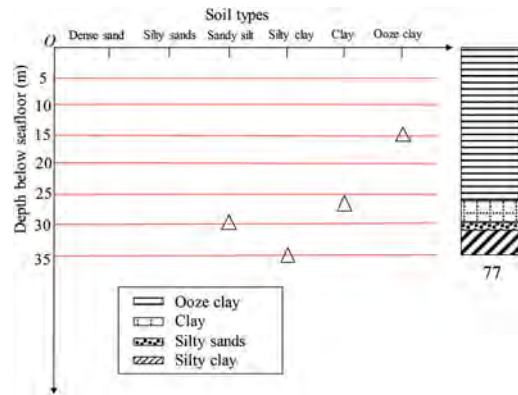


Figure 6. The comparison between prediction value and actual data in borehole no. 77.

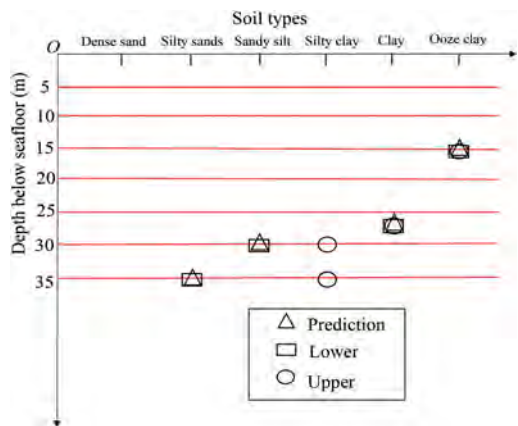


Figure 7. The prediction of soil classification in B1 and B2 (95% CI).

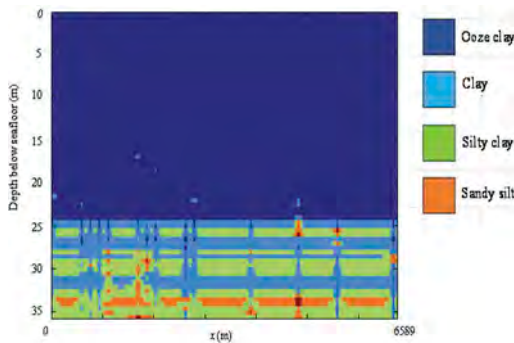


Figure 8. The prediction soil layer of seabed profile.

Figure 8. It can be seen that the seabed profile mainly has four soil layers containing ooze clay, clay, silty clay and sandy silt. In the first 25 m, the soil is homogeneous which is ooze clay. Beyond 25 m, the soil conditions become much more complex. The general conditions of soil layer are consistent with the actual soil conditions. It means that Kriging method can predict the soil conditions at unknown positions effectively, which can be used to guide the foundation design of offshore wind turbine.

5 CONCLUSIONS

In this study, the offshore wind farm in east China sea is analyzed as a case study. The results indicate that Robertson method is suitable for the soil classification in the east China sea and Kriging method can predict the soil conditions in unknown positions with 95% interval of confidence. The algorithm can be used to provide guidance and reference for the foundation design of offshore wind turbine.

ACKNOWLEDGMENTS

This study is supported by Key Laboratory for Far-shore Wind Power Technology of Zhejiang Province and Norwegian Geotechnical Institute (NGI). This

work was supported by the Natural Science Foundation of China [grant number 51979067] and Shenzhen Technology Innovation Project [grant number JCYJ20210324121402008].

REFERENCES

- Ang, A.H.S. & W.H. Tang (2007). Thin layer effects on the CPT q_c measurement. *Canadian Geotechnical Journal*, 42 (5), 1302–1307.
- Ching, J. & K.K. Phoon (2013). Probability distribution for mobilized shear strengths of spatially variable soils under uniform stress states. *Georisk*, 7 (3), 209–224.
- Cheon, J.Y. & R.B. Gilbert (2014). Modeling spatial variability in offshore geotechnical properties for reliability-based foundation design. *Structural Safety*, 49 (2014), 18–26.
- Dasaka, S.M. & L.M. Zhang (2012). Spatial variability of in situ weathered soil. *Geotechnique*, 62 (5), 375–384.
- Dinh, V.N. & H.X. Nguyen (2019). Design of an offshore wind farm layout. *Lecture Notes in Civil Engineering*, 2019, 18, 233–238.
- Jefferies, M.G. & M.P. Davies (1991). Soil classification by the cone penetration test: Discussion[J]. *Canadian Geotechnical Journal*, 28 (1), 173–176.
- Li, J.H., Huang, J., Cassidy, M.J., & R. Kelly (2014). Spatial variability of the soil at the Ballina National Field Test Facility. *Australia Geomechanics*, 49 (4), 41–47.
- Li, J.H., Cassidy, M.J., Huang, J., Zhang, L., & R. Kelly (2016). Probabilistic identification of soil stratification. *Geotechnique*, 66 (1), 16–26.
- Liu, S.Y., Cai, G.J., & H.F. Zhou (2013). Practical soil classification methods in China based on piezocone penetration tests. *Journal of Geotechnical Engineering*, 35 (10), 1765–1775 [in Chinese].
- Lloret-Cabot, M., Fenton, G.A., & M.A Hicks (2014). On the estimation of scale of fluctuation in geo-statistics. *Georisk*, 8 (2), 129–140.
- Olsen, R.S. & J.K. Mitchell (1995). CPT stress normalization and prediction of soil classification. *Proceedings of International Symposium on Cone Penetration Testing, CPT'95, Linköping, Sweden, SGI Report 3:95, 2, 257–262.*
- Robertson P.K. & C.E. Wride (1998). Evaluating cyclic liquefaction potential using the cone penetration test. *Canadian Geotechnical Journal*, 35 (3), 442–459.

Evaluation of CPT-based design method for offshore pile

B. Huang

School of Architecture and Civil Engineering, Huizhou University, China

E. Bittar

The University of Western Australia, Australia

Y. Zhang

The University of Newcastle, Australia

X. Fu

School of Civil Engineering, Wuhan University, China

ABSTRACT: In offshore engineering, it's difficult to obtain undisturbed samples. CPT-based design method of pile has become recommending method. In this paper focusing on offshore pile foundation engineering, the typical CPT-based design methods are introduced. Various design methods are evaluated in respect of friction fatigue, pile loading direction, and the plug ratio of open-ended pile in capacity contribution, and the determination of design parameters. CPT-based design methods in the clay are compared with API method. For the typical stratum in the China East Sea, the monopiles of an offshore wind farm are analysed. The calculated capacities of monopiles with different methods are compared with the measured value, and the reliability of methods are evaluated. At last according to the vertical loading condition of the offshore monopile, reasonable suggestions for the current design methods and parameters determination are given.

1 INTRODUCTION

At present, the popular methods for the vertical bearing capacity of pile foundations in offshore engineering are either based on the empirical formula of CPT tip resistance or are directly related to soil parameters, such as undrained strength, yield stress, sensitivity, internal friction angle, etc. The CPT-based design method of pile has gradually replaced design methods based on lab tests or previous experience, and it has become the preferred method for offshore pile foundation. It is generally believed that the cone tip resistance obtained by CPTu is more reliable than the sleeve friction, which is the main design method parameter. Table 1 summarizes the current design methods for offshore piles.

Fellenius (2020) pointed out that all CPT-based pile design methods are established under basically the same geological conditions for specific areas. That is to say, each method is based on limited piles and soil tests. If geological conditions are not similar, these methods are not suitable. Following the completion of a Joint Industry Project, a unified database (Lehane et al., 2017) has been developed which includes ICP, NGI, Fugro, UWA and other databases.

Among the methods applicable to sand, all but API-00 are based on CPT. It is noted that the cone tip resistance has not been corrected by pore pressure. When using these methods, the difference between the calculated results before and after the correction should be fully considered. A unified CPT-based method has been developed by the JIP group of UWA, NGI, Imperial College, Fugro, BP, Delft University of Technology, University of Texas, DNV-GL and Lloyd's Register EMEA (Lehane et al., 2020).

The methods applicable to clay include API-00, Fugro-96, NGI-05, ICP-05, UWA-13 and Fugro-10 methods, of which API-00, Fugro-96, and NGI-05 are based on the undrained strength of clay. The ICP-05 method is based on the tip resistance of CPT and is not corrected by pore pressure. UWA-13 and Fugro-10 are based on the test results of CPTu with the tip resistance of CPT corrected by pore pressure. A new Unified CPT-based method is also being developed by the JIP group.

2 DESIGN METHOD

2.1 Unified CPT-based method in sand

The unit shaft friction may be calculated from:

Table 1. Pile design methods referred.

Soil type	Design method	Reference
Sand	Unified CPT-based method	Lehane et al. (2020)
Sand	API-00	API (2000)
Sand	Fugro-05	Kolk et al. (2005)
Sand	ICP-05	Jardine et al. (2005)
Sand	NGI-05	Clausen et al. (2005)
Sand	UWA-05	Lehane et al. (2005)
Clay	API-00	API (2000)
Clay	Fugro-96	Kolk & Van Der Velde (1996)
Clay	Fugro-10	Van Dijk & Kolk (2010)
Clay	ICP-05	Jardine et al. (2005)
Clay	NGI-05	Karlsrud et al. (2005)
Clay	UWA-13	Lehane et al. (2013)

$$\tau_f = \sigma'_{rf} \tan \delta_{cv} = \frac{f}{f_c} (\sigma'_{rc} + \Delta\sigma'_{rd}) \tan 29^\circ \quad (1)$$

where σ'_{rf} is the radial effective stress at failure, σ'_{rc} is the radial effective stress after installation and equalization, $\Delta\sigma'_{rd}$ is the change in radial effective stress due to loading stress path (dilation), and f/f_c is 1 in compression and 0.75 in tension.

The radial effective stress after installation and equalization may be calculated as:

$$\sigma'_{rc} = \frac{q_c}{44} \cdot A_{re}^{0.3} \left[\max\left(\frac{h}{D}, 1\right) \right]^{-0.4} \quad (2)$$

where q_c is the cone tip resistance, A_{re} is the effective area ratio, $A_{re} = 1 - PLR \cdot (D_i/D)^2$, PLR is soil plug length ratio, h is the relative distance above the pile tip, D is the outer diameter of pile, D_i is the inner diameter of pile.

The change in radial effective stress due to loading stress path (dilation) may be estimated as:

$$\Delta\sigma'_{rd} = \left(\frac{q_c}{10}\right) \left(\frac{q_c}{\sigma'_v}\right)^{-0.33} \left(\frac{d_{CPT}}{D}\right) \quad (3)$$

where σ'_v is the vertical effective stress.

The unit end bearing may be calculated from:

$$q_{b0.1} = \bar{q}_c (0.12 + 0.38 \cdot A_{re}) \quad (4)$$

Where \bar{q}_c is the average cone tip resistance within a zone $1.5D$ above and below the pile tip in relatively homogeneous sands.

2.2 UWA-13 method in clay

The unit shaft friction is calculated from:

$$\tau_f = 0.055 \cdot q_t \cdot \left[\max\left(\frac{h}{R^*}, 1\right) \right]^{-0.2} \quad (5)$$

where q_t is the total cone tip resistance at depth z , h is the relative distance above pile tip, R^* is the equivalent radius $= (R^2 - R_i^2)^{0.5}$, R is the outer radius of pile, and R_i is the inner radius of pile.

The unit end bearing follows the recommendations of Jardine et al. (2005) for undrained loading and assumed that the open-ended piles are always plugged:

$$q_b = 0.8 \cdot \bar{q}_t; \text{ undrained, closed - ended} \quad (6)$$

$$q_b = 0.4 \cdot \bar{q}_t; \text{ undrained, open - ended(plugged)} \quad (7)$$

Where q_t is the average total cone tip resistance over $\pm 1.5D$ at pile tip.

The method ignores the effects of reversed end bearing or base suction for piles in tension.

2.3 Fugro-10 method in clay

The unit shaft friction is calculated from:

$$\tau_f = k_s \cdot q_n \quad (8)$$

$$k_s = \min \left[0.16 \cdot \left(\frac{h}{uL}\right)^{-0.3} \cdot \left(\frac{q_n}{\sigma'_{v0}}\right)^{-0.4}, 0.08 \right] \quad (9)$$

where q_n is the net cone tip resistance at depth z , σ_{v0} is the total vertical stress at depth z , σ'_{v0} is effective vertical stress at depth z , h is the relative distance above pile tip, and uL is unit length to render the expression dimensionless ($= 1.0$ m).

The unit end bearing (q_b) and reversed end bearing (q_{rb}) may be calculated from:

$$q_b = 0.7 \cdot q_{n,avg} \quad (10)$$

$$q_{rb} = \min[0.7 \cdot q_{n,avg} - u_b, 100 \text{ (kPa)}] \quad (11)$$

where $q_{n,avg}$ is the average net cone tip resistance over $\pm 1.5D$ at pile tip, and u_b is the hydrostatic pressure at pile tip (in kPa).

3 EVALUATION OF SOIL PLUG

Lehane et al. (2017) suggested in the absence of any better method, Equation (12) was therefore

employed for the calculation of plug length ratio in sand and clay. This is consistent with field test.

$$PLR = \min \left[(D_i/1.5)^{0.2}, 1 \right] \quad (12)$$

where PLR is soil plug length ratio, and D_i is the pile internal diameter expressed in metres.

Lehane et al. (2020) proposed a new empirical formula for soil length plug ratio:

$$PLR = \tan h \left[0.3(D_i/d_{CPT})^{0.5} \right] \quad (13)$$

where d_{CPT} is the diameter of standard static cone penetration, 35.7mm.

Based on the unified database (Lehane et al., 2017), the relationship between the soil plug length ratio and the pile inner diameter is plotted together, as shown in Figure 1. It can be seen that there is no obvious difference in the law of soil plugging in clay and sand, that is to say, the relationship between soil plugging and soil properties is not significant, only related to the inner diameter of pile. Equations (12) and (13) reflect that soil plugging varies with pile diameter with the same trend, especially in the range of 0.4–1.2m pile diameter. However, in terms of small diameter piles, equation (13) is closer to the actual cases.

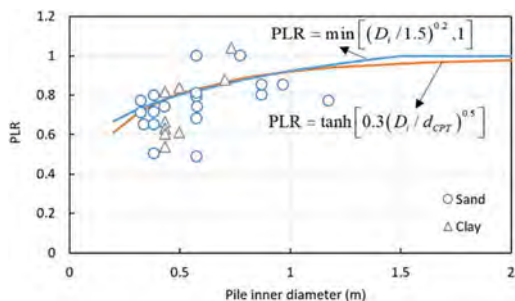


Figure 1. Relationship between plug length ratio and pile inner diameter.

The typical pile diameter to wall thickness ratio of steel pipe piles is 30–60. For offshore piles with a pile diameter greater than 1.5m, the soil plug ratios calculated by equations (12) and (13) are both greater than 0.96. So for steel pipe piles with a diameter of larger than 1.5m, there is no soil plug formed or the soil plug length ratio is equal to one which is in coring mode.

4 REVIEW OF DESIGN METHODS FOR AXIAL CAPACITY OF PILES

The Unified CPT-based method of driven pile in sand proposed by the JIP group has replaced the

API-00 method as the preferred recommended method in the new version of the API specification. According to statistical analysis of 71 piles' database, the Unified CPT-based method in sand has the lowest coefficient of variation among all the design methods of pile in sand (Lehane et al., 2020).

Unified CPT-based method, UWA-13 and Fugro-10 methods all take into account the friction fatigue effects caused by pile construction.

Through a large number of database examinations for different design methods, the reliability statistics analysis results are shown in Table 2. There are 49 piles, with diameters ranging from 0.2 to 0.8m. Compared with the pile design method in sand, the calculation results of pile capacity in clay have a larger variation coefficient. This is because there are more design parameters for piles in clay compared to sand, and they are also more complicated and diverse. Among the CPT-based design methods, the variation coefficient of the UWA-13 method is smaller than that of the Fugro-10 method. The API-00 method is a bit conservative and Fugro-10 method is sometimes unsafe compared to UWA-13 method.

Table 2. Method uncertainties for piles in clay (Lehane et al., 2017).

Method	No of sample	Q_c/Q_m		
		μ_w	σ_w	CoV _w
API-00	23	0.73	0.29	0.40
UWA-13	43	0.99	0.48	0.49
Fugro-10	43	1.17	0.69	0.59

In Table 2, Q_c is the calculated capacity, Q_m is the measured capacity, μ_w is weighted mean, σ_w is weighted standard deviation, and CoV_w is coefficient of variation.

The comparison of open-ended pile design methods in clay is shown in Table 3. It is believed that the soil inside large-diameter steel pipe pile is in soil coring mode, and there is no soil plug occurring. The API-00 method considers that the total bearing capacity is equal to the sum of the outer shaft resistance, the inner shaft resistance and the base resistance of the annulus area, and use the same unit shaft friction to calculate the inner and outer shaft resistance. Neither the UWA-13 method nor the Fugro-10 method directly mentions the inner shaft resistance in the calculation. Instead, they use the equivalent base resistance to calculate total bearing capacity of the pile, where the base area is equal to the area of the outer diameter circle. The base resistance used by the soil core is a reduction of the unit end bearing of the annulus area or closed-ended pile. The reduction factor in the Unified CPT-based method is 24% for sand, and in the UWA-13 method, it's about 40% for clay.

Table 3. Comparison of design methods for open-ended pile.

Method	Soil type	Capacity calculation
API-00	Clay sand	If $Q_{b,plug} < Q_{s,inner}$, plugged, $Q_{total} = Q_{s,outer} + Q_{b,plug} + Q_{b,ann}$; If $Q_{b,plug} \geq Q_{s,inner}$, unplugged, $Q_{total} = Q_{s,outer} + Q_{s,inner} + Q_{b,ann}$.
Unified CPT-based method	Sand	Unplugged is the same as plugged, $Q_{total} = Q_{s,outer} + Q_{b,plug} + Q_{b,ann}$.
UWA-13	Clay	Always plugged, $Q_{total} = Q_{s,outer} + Q_{b,plug} + Q_{b,ann}$.
Fugro-10	Clay	Unplugged is the same as plugged, $Q_{total} = Q_{s,outer} + Q_{b,plug} + Q_{b,ann}$.

In Table 3, Q_{total} is total bearing capacity, $Q_{s, inner}$ is inner shaft resistance, $Q_{s, outer}$ is outer shaft resistance, $Q_{b, plug}$ is base resistance of the soil plug, and $Q_{b, ann}$ is base resistance of the annulus area.

When the pile is subjected to a tension load in sand, the Unified CPT-based method uses a reduction factor of 0.75 to calculate the shaft resistance, without considering the base resistance. When the pile is subjected to a tension load in clay, none of the methods considers the reduction of the shaft resistance. Fugro-10 propose the unit end bearing when the pile is in tension, while UWA-13 method doesn't consider the base resistance of the pile in tension. API-00 does not explicitly propose a calculation of the base resistance in tension.

5 CASE ANALYSIS OF OFFSHORE PILE

5.1 Soil conditions

A field test of large diameter steel pipe piles was carried out in an offshore wind farm project. The site is about 20 km offshore, with the seabed topography of the total site area not varying much, and water depth at 8~12 m. As for regional geological information, the local Quaternary sediments within the exploration depth, the upper part is the silty clay and clay deposited in the Holocene littoral facies, and the lower part is the silty clay and silty sand deposited in the Upper Pleistocene estuary-littoral facies. According to the soil layer classification method proposed by Robertson et al. (1986), the site stratum distribution is shown in Figure 2.

CPTu cone tip resistance, shaft friction resistance, and pore pressure test results are also shown in Figure 2. It can be seen that the cone tip resistance of the clay increases linearly with depth from 4~50 m, indicating a relatively uniform soil layer. However, the shaft friction resistance changes with depth more discretely. Therefore, pile design methods only use tip

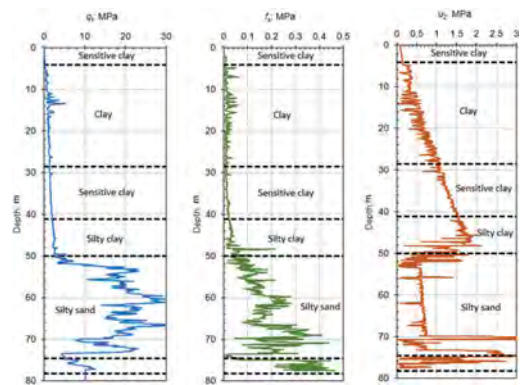


Figure 2. Profiles of tip resistance, shaft friction and pore pressure in CPTu test.

resistance as the parameter which is scientific and reasonable. The pile end is buried 69 m deep and is located in the supporting layer of silty sand.

The undrained strength of clay is determined by the empirical expression based on CPT on basis of $N_k=20$ inferred by SHANSEP method (Ladd & Foott, 1974).

5.2 Field test of offshore piles

The pile outer diameter is 1.8 m, the total pile length is 93 m, and the wall thickness is 20~40 mm. The IHC S800 hydraulic hammer is used for pile driving. There is no slipping phenomenon during the pile driving process, and the pile's embedded depth is 69 m. After pile driving, the soil plug/core is 1.45 m slightly above the mudline, and the soil plug ratio of the steel pipe pile which has an inner diameter of about 1.7 m is 1.0, which is a soil coring mode.

The vertical static compression test was carried out 44 days after the pile was driven using the slow maintained loading method, then rested for 25 days, then for the same test pile the vertical static tension test was conducted using the slow maintained loading method. Figure 3 shows the comparison between the axial compression and tension test results of the pile. The axial compression test of a single pile achieves the destruction of the soil around the pile, and the ultimate axial compression capacity is 22 MN; the axial tension test of the single pile also achieves failure, and the ultimate axial tension capacity of the single pile is 18.7 MN. When the pile head displacement is small, the compression load-displacement curve is closer to the tension test curve, and the compression curve is slightly higher than the tension curve; as the pile head displacement gradually increases, the discrepancy between compression and tension becomes larger and larger. After roughly 40 mm, both reach the limit state, and

the difference is also the largest. This is because the contribution of the base resistance of the pile in compression increases as the displacement of the pile increases, while the end resistance can be ignored in tension; in addition, at the depth of 50~74.7 m is all silty sand, and the shaft tension friction in sand is also reduced by 25% compared with compression (Lehane et al, 2020).

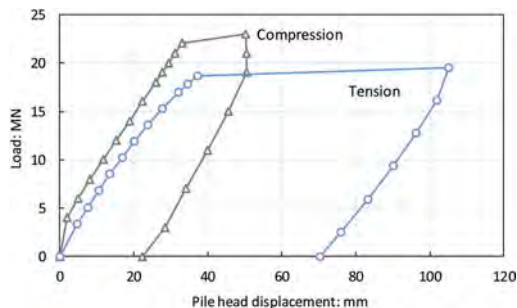


Figure 3. Comparison between axial compression and tension load-displacement curves.

5.3 Comparison between design methods

Comparisons of measured and calculated results of capacity with different design methods for compression and tension are shown in Table 4 and Table 5. It can be seen in Table 4 that all design methods are safer in calculating compression capacity, resulting in about 79%~95% of the measured value. From the calculated result of tension capacity it can be seen that in tension, the API-00 method based on undrained strength are 17% higher than the measured value, while the CPT-based design methods are 9%~13% lower than the measured value.

The UWA-13 method and Fugro-10 method, which are completely based on CPT, are safe in the calculation of compression and tension capacity.

Table 4. Comparison of measured results and calculated results of compressive capacity of different design methods.

Method	Shaft resistance (MN)	Base resistance (MN)	Total resistance (MN)	Calculated/Measured (%)
Measured	NA	NA	26.6	NA
API-00	18.1	7.0	25.1	94.5
Fugro-10	13.9	7.0	20.9	78.6
UWA-13	14.5	7.0	21.4	80.8

Note: The compression capacity measured takes into account the weight of pile and soil plug (4.6 MN). The shaft resistance and base resistance in sand use the Unified CPT-based method.

Table 5. Comparison of measured results and calculated results of tension capacity of different design methods.

Method	Shaft resistance (MN)	Base resistance (MN)	Total resistance (MN)	Calculated/Measured (%)
Measured	NA	0	14.2	NA
API-00	16.6	0	16.6	117.0
Fugro-10	12.3	0	12.3	87.1
UWA-13	12.9	0	12.9	91.2

Note: The tension capacity measured deducts the weight of pile and soil plug (4.6 MN). The shaft resistance and base resistance in sand use the Unified CPT-based method.

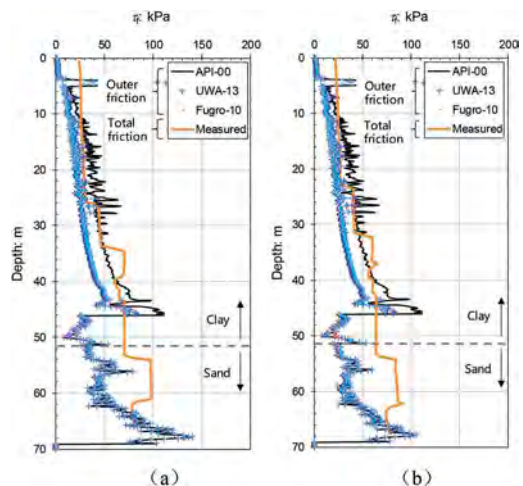


Figure 4. Shaft friction distribution with depth during ultimate bearing calculated by different methods: (a) compression; (b) tension.

The compression capacity calculated by the UWA-13 method is 81% of the measured value, and the Fugro-10 method is 79%. The UWA-13 method calculated tension capacity is 91% of the measured value and Fugro-10 method is 87%. Therefore, from this project case, UWA-13 method is slightly better than Fugro-10 method.

Figure 4 is the shaft friction distribution with depth during ultimate bearing calculated by different methods, compared with measured friction. The shaft friction of clay calculated by API-00 method is the greatest. The CPT-based methods calculate a smaller value but are very similar to each other. However, the trends of shaft friction changing with depth are almost the same.

The measured shaft friction is the sum of the inner and outer friction, and the two parts cannot be distinguished, while the shaft friction calculated by each design method is only the outer friction. Therefore, for the UWA-13 and Fugro-10 methods with

more reliable calculation results, it is obvious that the measured total friction is greater than the calculated outer friction, especially in sand below 50 m. It fully indicates that the contribution of the inner friction in the sand is more significant, and relatively the contribution of the inner friction in the clay is smaller. So the internal resistance of the soil core of the pipe pile is mainly exerted in the lower part of pile, which increases the complexity of the calculation of the internal resistance. Therefore, each design method adopts the equivalent base resistance of soil plug or core to calculate the internal resistance which is a method worth promoting.

6 CONCLUSIONS

This paper introduces and evaluates the CPT-based design methods for offshore pile under vertical load which are currently popular in the industry. The main conclusions are as follows:

- (a) The Unified CPT-based method is recommended for full-scale offshore pipe in sand. For clay, the UWA-13 method and Fugro-10 method based on CPT are recommended compared to API-00 method.
- (b) Through the case analysis of large-diameter steel pipe piles, the UWA-13 method and Fugro-10 method based entirely on CPT are conservative in the calculation of compression and tension capacity in which the calculated bearing capacity is 79%~92% of the measured value. The UWA-13 method is marginally better than Fugro-10 for the case in this paper, and Fugro-10 method is sometimes unsafe.
- (c) It is difficult in offshore engineering to determine the undrained strength of the intact clay sample. The strength parameters in different soil layers and different depths can be determined by the relatively mature SHANSEP method, but this method is only suitable for low sensitivity, unnaturally cemented and low structured cohesive soil.

ACKNOWLEDGEMENTS

The first author gratefully acknowledges the financial support by Natural Science Foundation of China (Grant No. 51978540) and China Scholarship Council (201906275010). The authors also express sincere thanks to Professor Barry Lehane, who assisted with the interpretation of CPT-based methods. We also acknowledge the assistance provided by Dylan Mo and Tommy Le.

REFERENCES

- API. 2000. API RP 2A-WSD: *Recommended Practice for Planning, Designing and Constructing Fixed Offshore Platform-Working Stress Design*, 21st Edition. API. Washington, DC.
- Clausen, C. J. F., Aas, P. M., & Karlsrud, K. 2005. Bearing capacity of driven piles in sand, the NGI approach. *In Proceedings of the 1st International Symposium Frontiers in Offshore Geotechnics*. Perth, Western Australia. pp. 677–682.
- Fellenius, B. H. 2020. *Basics of foundation design*, electronic edition.
- Jardine, R., Chow, F., Overy, R., & Standing, J. 2005. *ICP design methods for driven piles in sands and clays*. Thomas Telford, London, UK.
- Karlsrud, K., Clausen, C. J. F., & Aas, P. M. 2005. Bearing capacity of driven piles in clay, the NGI approach. *In Proceedings of the 1st Int. Symp. on frontiers in offshore geotechnics*, Perth, WA, Australia. Taylor & Francis, London, UK, vol. 1, pp. 775–782.
- Kolk, H. J., & Der Velde, E. 1996. A reliable method to determine friction capacity of piles driven into clays. *In Proceedings of Offshore Technology Conference*, Houston, Texas. Pp.337–346.
- Kolk, H. J., Baaijens, A. E. & Senders, M. 2005. Design criteria for pipe piles in silica sands. 2005. CRC Press/Balkema, 711–716.
- Ladd, C. C., & Foott, R. 1974. New design procedure for stability of soft clays. *Journal of Geotechnical and Geoenvironmental Engineering*, vol 100, GT7, 763–786.
- Lehane, B. M., Schneider, J. A., & Xu, X. 2005. The UWA-05 method for prediction of axial capacity of driven piles in sand. *In Proceedings of the 1st Int. Symp. on frontiers in offshore geotechnics*, Perth, WA, Australia. Taylor & Francis, London, UK, vol. 1, pp. 683–689.
- Lehane, B. M., Li, Y., & Williams, R. 2013. Shaft capacity of displacement piles in clay using the cone penetration test. *Journal of Geotechnical and Geoenvironmental Engineering*, 139(2), 253–266.
- Lehane, B. M., Lim, J. K., Carotenuto, P., Nadim, F., Lacasse, S., Jardine, R. J., & Van Dijk, B. F. J. 2017. Characteristics of unified databases for driven piles. *In Proceedings of the 8th International Conference of Offshore Site Investigation and Geotechnics OSIG*, London, UK. Society for Underwater Technology, vol 1, pp. 162–191.
- Lehane, B., Liu, Z., Bittar, E., Nadim, F., Lacasse, S., Jardine, R. J., ... & Morgan, N. 2020. A new CPT-based axial pile capacity design method for driven piles in sand. *In Proceedings of the 4th International Symposium on Frontiers in Offshore Geotechnics*, Austin, Texas, USA. American Society of Civil Engineers.
- Robertson, P. K., Campanella, R. G., Gillespie, D., & Greig, J. 1986. Use of piezometer cone data. *In Proceedings of in Use of in situ tests in geotechnical engineering*. ASCE, pp. 1263–1280.
- Van Dijk, B. F. J., & Kolk, H. J. 2010. CPT-based design method for axial capacity of offshore piles in clays. *In Proceedings of the International Symposium on Frontiers in offshore geotechnics II*, Perth, Australia. Taylor & Francis Group, London, pp. 555–560.

Application of CPT based 3DFE approach for estimating monopile damping in sand

D. Igoe & M.B. Mohammed
Trinity College Dublin, Ireland

ABSTRACT: Monopiles are the most popular foundation type supporting offshore wind turbines. The use of 3DFE modelling to analyse the pile response has grown significantly in recent years, supported by the introduction of the PISA framework and the development of easy to use commercial software such as PLAXIS Monopile Designer. In sands, the small-strain hardening soil (HSS) model is widely adopted for monopile design, partially due to its relatively simple set of soil input parameters. However to date there is no widely used approach for determining the required soil parameters and approaches often differ across the industry. Igoe and Jalilvand (2020) developed an approach to derive the HSS soil model parameters directly from CPT data. This procedure has been validated by the authors for monotonic loading against a database of large-scale field tests including PISA field tests in the Dunkirk marine SAND. This paper examines the use of the 3DFE approach under cyclic loading to determine soil damping for monopiles. The results from the 3DFE analysis are compared to field test data and show a good match with the damping estimated under two-way cyclic loading.

1 BACKGROUND

1.1 Introduction

The global offshore wind market has grown rapidly over the past decade with an average 30% increase per year since 2010 (International Energy Agency, 2019). Monopile foundations, which are large diameter steel tubes driven into the ground, represent around 80% of all offshore wind turbine foundations installed to date and will likely remain the most common foundation solution for offshore wind for at least the next 10 years. The geotechnical design of monopiles is governed by the response to lateral loads and overturning moments. Initially, monopiles were designed using the industry standard API p-y method (API RP2GEO 2014), which was adopted from the oil and gas industry. However, in recent years it became evident that the API p-y method was not suitable for the design of large diameter monopiles (Kallehave et al. 2015). The recently completed PISA project (Burd et al. 2020a,b, Byrne et al. 2020a,b), was formed to develop new design methods for large diameter monopiles. The PISA project proposed a new approach for the geotechnical design of monopiles which was calibrated from a suite of 3DFE analysis, which were validated against large-scale field tests. The new approach, termed the ‘PISA design model’, is an enhanced form of the p-y method, which is extended to include additional components of soil resistance which are significant for low slenderness piles ($2 < L/D < 6$). Site specific soil reaction curves can be calibrated from

3DFE analyses undertaken for a range of pile geometries and load eccentricities. The commercial software, Plaxis Monopile Designer, has been developed to allow industry practitioners to simply apply the new PISA design model (Brinkgreve et al. 2020). The developments from the PISA project have accelerated the use of 3DFE for monopile design in industry. Despite the widespread use of 3DFE analysis for monopile design, there is no industry standard approach to deriving the required soil input parameters. Igoe and Jalilvand (2020) developed an approach to derive the HSS soil model parameters directly from CPT data, which is used in this paper.

Offshore wind turbines are flexible structures which are dynamically sensitive and offshore loading is primarily cyclic and dynamic in nature. While significant improvement in monopile design was achieved through the PISA project, the project focused on monotonic loading, to define ‘backbone curves’, which could be extended in the future to account for cyclic and dynamic effects. Accurately calculating the damping of the structure is critical to prevent excessive fatigue damage over the lifetime of the structure. Consequently, the PISA ‘Soil Damping Project’ was a supplementary piece of field testing within the PISA project, focused on obtaining the pile-soil response under two-way cyclic lateral loading at very low load amplitudes. A review of monopile damping is provided in Malekjafarian et al. (2021). This paper presents the development of a 3DFE modelling approach, using CPT data to derive the soil parameters, in order

to estimate monopile damping. The results from the 3DFE are compared to the damping values measured from the PISA field tests.

2 PISA DAMPING FIELD TESTS

The PISA project field tests in sand were undertaken at a test site at Loon Plage, near Dunkirk in northern France. The Dunkirk site consists of a normally consolidated dense to very dense sand, with a top 3 m comprising very dense fill material, below which is a dense natural sand. The ground water level was at about 5.4 m depth. The site was chosen for its extensive pre-existing site investigation history, including in-situ field characterisation alongside substantial suites of laboratory testing (Byrne et al 2020b). The pile test program was designed to provide a high-quality dataset which could be used for validation of 3DFE modelling. The damping tests involved undertaking 2-way cyclic loading on a single pile, designated DM1. The geometry for pile DM1 is provided in Table 1 below. The load test setup for 2-way loading is described in Byrne et al 2020c (see Figure 1). The main loading is applied by a hydraulic actuator located at a height, h , 10 m above the ground. The hydraulic actuator reacts against a much larger (2.0 m) diameter reaction pile. To apply two-way loading and to ensure that the hydraulic loading system is always in tension, a back-stay system with a dead load was used. Although the back-stay imposes a very small additional vertical load to the test pile due to the angle of loading, this has a negligible effect on the lateral response. Results from the PISA Damping Project were presented in Beuckalaers (2017) and are used for comparison with the 3DFE modelling approach developed in this paper.

Table 1. Pile DM1 geometry.

Test	D (m)	L (m)	L/D	t (mm)	h (m)
DM1	0.762	3.97	5.21	14	10.02

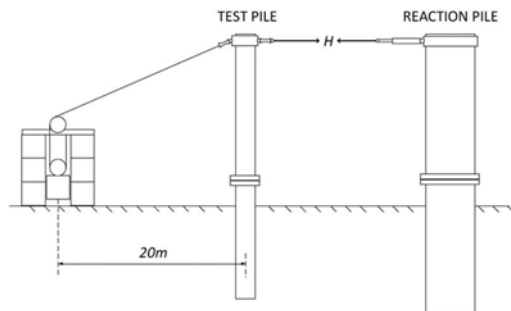


Figure 1. Load test setup for DM1 pile (from Byrne et al. 2020b).

3 3D FE MODELING

3.1 Soil model

Pile DM1 was modelled in 3DFE using the commercially available finite element software Plaxis 3D v21. The soil elements are modelled as ten-node tetrahedral elements. For sand deposits, Igoo and Jalilvand (2020) developed a procedure to calculate the soil model input parameters for the HSS soil model directly from Cone Penetration Test (CPT) data. The new approach adopted some widely used CPT correlations and was validated against a database of lateral load field tests. This procedure offers a consistent approach to develop all the required soil input parameters and offers improved predictions of the piles monotonic response compared with the current state of the art Plaxis Monopile designer recommendations (Panagoulas, et al 2018).

The CPT data was first used to derive the sand relative density using the expression proposed by Kulhawy and Mayne (1990) as follows:

$$D_R = \sqrt{\frac{Q_m}{305 \times OCR^{0.15}}} \quad (1)$$

$$Q_m = \left(\frac{q_t - \sigma_{v0}}{p_{ref}} \right) \left(\frac{p_{ref}}{\sigma'_{v0}} \right)^n \quad (2)$$

$$n = 0.381 \cdot I_c + 0.05 \frac{\sigma'_{v0}}{p_{ref}} - 0.15. \quad (3)$$

$$I_c = \sqrt{\frac{(3.47 - \log_{10} Q_m)^2 + (1.22 + \log_{10} F_r)^2}{}} \quad (4)$$

$$F_r = \frac{f_s}{q_t - \sigma_{v0}} \quad (5)$$

where q_t is the CPT cone resistance corrected for pore water effects, p_{ref} is a reference stress (atmospheric pressure) taken as ≈ 100 kPa and n is a stress exponent which varies between 0 and 1 depending on soil type and stress level. The Over Consolidation Ratio (OCR) was determined using the following formula from Mayne (2001):

$$OCR = \left[\frac{1.33 * q_t^{0.22}}{K_{0NC} * \sigma'_{vo}^{0.31}} \right]^{\frac{1}{\sin \alpha' - 0.27}} \quad (6)$$

The OCR is used in the determination of relative density, see Eq. (1), but is not input into the plaxis models directly. Instead the coefficient of lateral earth pressure, K_0 , is input into Plaxis, which is calculated using the approach proposed by Mayne and Kulhawy (1982)

$$K_0 = K_{0NC} * OCR^{\sin\varphi'} \quad (7)$$

$$K_{0NC} = 1 - \sin\varphi' \quad (8)$$

Igoe and Jalilvand recommend a maximum OCR of 20 was assumed, to avoid unrealistically high K_0 values at shallow depths. The soil peak friction angle was determined using the CPT correlation by Bolton (1986):

$$\varphi' = \varphi'_{cv} + 3(D_R(10 - \ln p') - 1) \quad (9)$$

where φ'_{cv} is the critical state friction angle, was determined from lab test data at each site ($\varphi'_{cv} = 32$ degrees can be assumed in the absence of such data) and p' is the mean effective stress. The stiffness parameters were derived from CPT cone resistance, starting with the small strain shear modulus:

$$G_0 = \alpha(q_t \cdot \sigma'_{v0} \cdot p_{ref})^{\frac{1}{3}} \quad (10)$$

where $\alpha = 185$ was used for Dunkirk Sand (verified against shear wave velocity measurements). The remaining stiffness inputs required for the analysis were derived from the G_0 adjusted for reference stress levels (and therefore indirectly from the CPT cone resistance) as follows (in MPa):

$$G_0^{ref} = G_0 / \left(\frac{K_{0NC} \cdot \sigma'_{v0}}{p_{ref}} \right)^m \quad (11)$$

where m is the stress exponent taken as 0.5 in cohesionless soils.

$$E_0^{ref} = 2(1 + \nu)G_0^{ref} \quad (12)$$

$$E_{ur}^{ref} = 10^{\log(0.00464 \cdot (E_0^{ref})^{1.724})} \quad (13)$$

$$E_{50}^{ref} = \frac{E_{ur}^{ref}}{3} \quad (14)$$

$$E_{oed}^{ref} = E_{50}^{ref} \quad (15)$$

Full details of the correlations used are provided in Igoe and Jalilvand (2020). An unsaturated soil unit weight of 17.7 kN/m³ and the reference shear strain, $\gamma_{0.7} = 1.5 \times 10^{-4}$ was used in the analysis. The other soil parameters calculated are provided in Table 2.

3.2 Pile model

The pile is modelled at full scale in half-space assuming “wished-in-place” condition. The pile is modelled by shell elements using a linear elastic

material model (Young’s modulus, E , and Poisson’s ratio, ν). Interface elements are added to the pile shaft plate (both internal and external surfaces of the pile). The interfaces have zero thickness and are composed of 12-node elements which consist of pairs of nodes which link the 6-noded plate elements to the soil. The reduction in interface shear strength when slip occurs is accounted for using the strength reduction factor R_{inter} which is selected depending on the soil type and available geotechnical data. An R_{inter} value of 0.7 was used for the sand-steel interface. The vertical model boundaries were set at ± 6 m in the direction of loading and 4m in the perpendicular direction, while the bottom boundary extended to 13.2m as shown in Figure 2.

Table 2. Soil Parameters used to model Pile DM1.

Depth [m]	E_{50}^{ref} [kPa]	E_{oed}^{ref} [MPa]	E_{ur}^{ref} [MPa]	ϕ [°]	ψ [°]	G_0^{ref} [MPa]	K_0 [-]
0	90.0	91.5	269.9	43.7	15.9	234.2	2.43
1.2	166.9	166.9	500.7	47.9	21.6	331.9	2.27
2.1	77.4	77.4	232.1	42.1	13.7	212.5	1.39
3.3	87.8	87.8	263.4	42.6	14.4	228.7	1.35
3.6	122.1	122.1	366.4	45.2	17.9	276.9	1.55
4.2	80.3	80.3	241.0	41.9	13.4	217.2	1.16
6.3	67.2	67.2	201.7	40.5	11.6	195.9	0.98
7.8	53.4	53.4	160.2	38.9	9.6	171.4	0.82
8.2	64.3	64.3	192.8	39.9	10.8	190.8	0.88

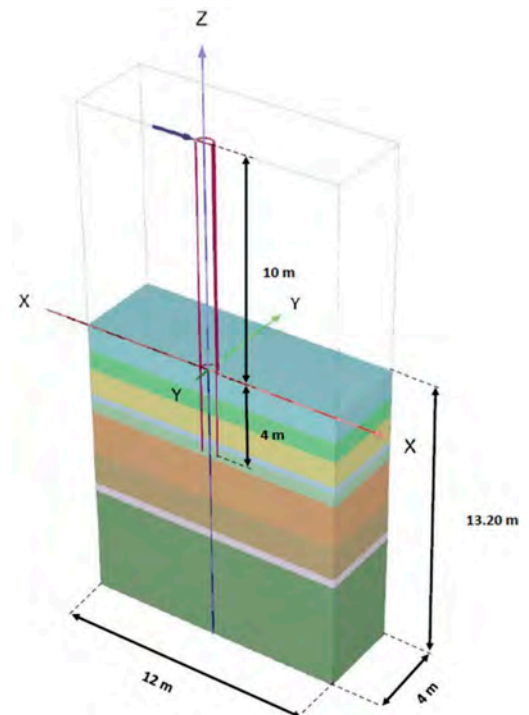


Figure 2. Plaxis model for pile DM1.

3.3 Loading

In order to simplify the calculations and reduce the model run time, the loading was applied as a static analysis using the ‘plastic’ calculation type. The pile was loaded applying a prescribed load to the top of the pile stick-up (as seen in Figure 2). Four separate cyclic load levels of 4, 10, 15 and 20 kN were considered in the analysis. For each load level, 5 cycles were applied, and the 5th cycle loop was used to obtain the damping ratio from displacement and rotation response extracted from the results of Plaxis 3D output. Each cycle was applied in three phases. The first phase applied positive loading, the second phase the pile is loaded in the opposite direction and the third phase the load is brought back to zero. The damping ratio was calculated using a Python code that determines the area of the loop and also elastic potential energy and then uses the equation below to determine the damping ratio:

$$\zeta = \frac{1}{4\pi} \frac{E_{diss}}{E_{el}} \quad (16)$$

where E_{diss} = dissipated energy during a load cycle; E_{el} = elastic stored energy. The global monopile damping is divided into load-displacement damping ratio ζ_v which is calculated from the horizontal load-displacement response and, moment-rotation damping ratio ζ_ψ which is calculated from the moment-rotation response. The area of the loop is calculated using Gauss’s area formula. The elastic energy is calculated by finding the area of the shaded triangle shown in Figure 3 in which σ indicates the horizontal force or the moment and ϵ indicates the displacement or the rotation. It is important to note that in most cases the hysteresis loops do not close in the unload-reload loops. For that case, the initial point at which the loop starts is changed to the final point so as to close the loops for the damping ratio calculation. In order to determine the total damping from both the horizontal displacement and rotational component, the dissipated energy and elastic energy from both components are added together.

$$E_{diss(total)} = E_{diss(v)} + E_{diss(\psi)} \quad (17)$$

$$E_{el(total)} = E_{el(v)} + E_{el(\psi)} \quad (18)$$

4 RESULTS AND DISCUSSION

The results from the 3DFE modelling of pile DM1 are presented below. The load-displacement response and moment-rotation response from the 5th cycle for each load level is shown in Figures 4 and 5 respectively. As expected, the higher load levels result in larger areas enclosed in each cycle. The damping for each load level was calculated from these loops and compared to

the measure response from the DM1 field test, as report in Beuckelaers (2017). The calculated damping ratios from the load-displacement and moment-rotation responses are compared to the measure response from the DM1 field test (as reported in Beuckelaers 2017) and presented in Figures 6 and 7 respectively. It is evident that the 3DFE underpredicts the damping measured from the load-displacement response at low load levels but matches the field tests well at the higher load levels. For the moment-rotation response, the 3DFE predicts the damping well at low load levels but overpredicts at the higher load levels.

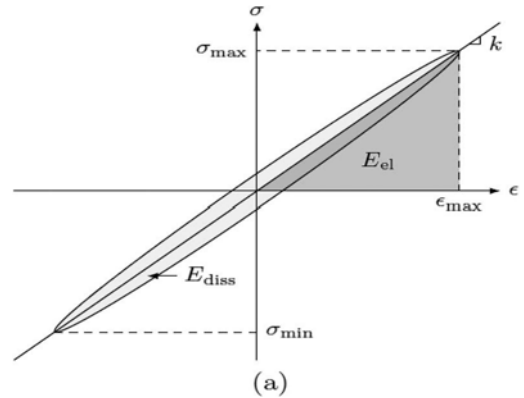


Figure 3. Hysteretic soil stress-strain response (from Beuckelaers, 2017).

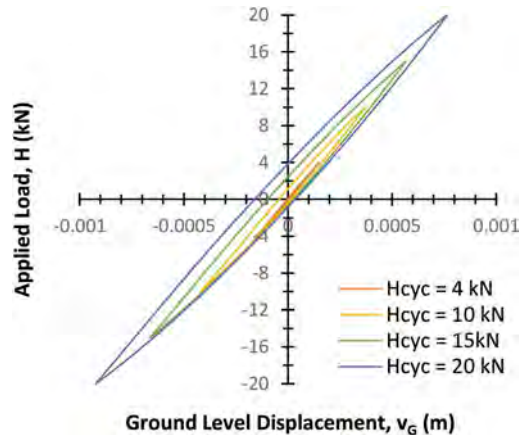


Figure 4. Load-Displacement response from 5th cycle of each load level from 3DFE model of pile DM1.

A comparison of the total damping ratios is provided in Figure 8. It is evident that overall the 3DFE is able to provide a reasonably good match for the damping ratio measured in the field tests at low load levels. At higher load levels the 3DFE overestimates the total damping measured.

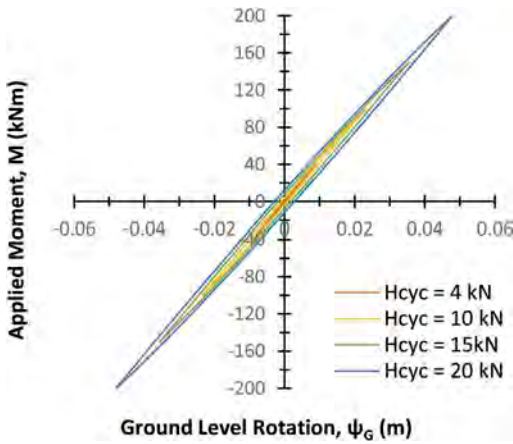


Figure 5. Moment-Rotation response from 5th cycle of each load level from 3DFE model of pile DM1.

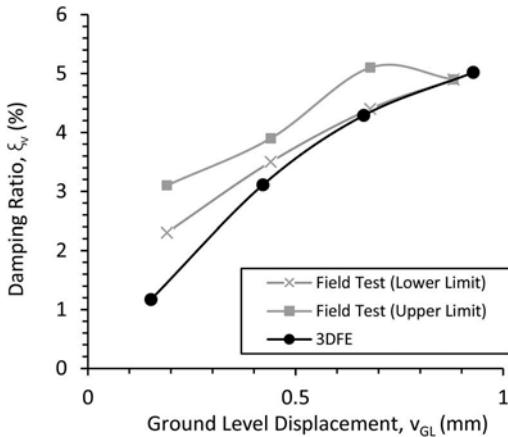


Figure 6. Comparison between 3DFE and field test damping ratios from load-displacement response (field test data from Beuckelaers 2017).

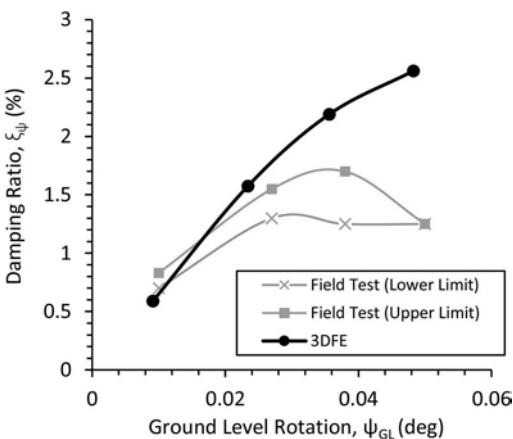


Figure 7. Comparison between 3DFE and field test damping ratios from moment-rotation response (field test data from Beuckelaers 2017).

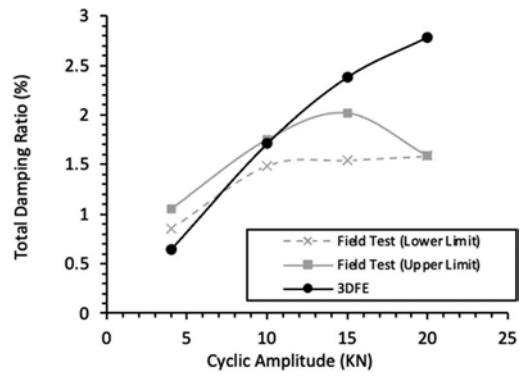


Figure 8. Comparison between 3DFE and field test total damping ratios (field test data from Beuckelaers 2017).

5 CONCLUSIONS

This paper presents the results from 3DFE modelling of monopile field experiments to determine foundation damping. The small-strain hardening soil (HSS) model was adopted along with a CPT based approach to calibrate the soil parameters developed by Igoe and Jalilvand (2020). The CPT based approach for deriving the soil input parameters had previously been validated against monopile field tests under monotonic loading. This paper examines the use of the 3DFE approach under cyclic loading to determine the monopile soil damping. The results from the analysis are compared to field test data and show a good match with the damping estimated under two-way cyclic loading, particularly at low load levels. At higher load levels the 3DFE tended to over-predict the damping compared with the measured values. The authors are currently undertaking further cyclic monopile field tests which can be used for validation of the 3DFE damping approach.

ACKNOWLEDGEMENTS

This publication has emanated from research conducted with the financial support of the Sustainable Energy Authority of Ireland (SEAI) grant number 19/RDD/511.

REFERENCES

- API (2014). "API RP2GEO: Geotechnical and Foundation Design Considerations."
- Benz, T., Schwab, R., and Vermeer, P. (2009). "Small-strain stiffness in geotechnical analyses." *Bautechnik*, 86(SUPPL. 1), 16–27.
- Beuckelaers, W.J.A.P. (2017) Numerical Modelling of Laterally Loaded Piles for Offshore Wind Turbines. University of Oxford Ph.D. Dissertation. (January 2017), 485–491.
- Bolton, M. D. (1986). "The strength and dilatancy of sands." *Géotechnique*, 36(1), 65–78.

- Brinkgreve, R. B. J., Engin, E., and Swolfs, W. M. (2018). "Plaxis 3D Materials Manual."
- Brinkgreve, R., Engin, E., and Engin, H. (2010). "Validation of empirical formulas to derive model parameters for sands." *Numerical Methods in Geotechnical Engineering*, (June), 137–142.
- Brinkgreve R, Lisi D, Lahoz M, Panagoulas S. (2020) "Validation and Application of a New Software Tool Implementing the PISA Design Methodology", *Journal of Marine Science and Engineering*, 8(6):457. <https://doi.org/10.3390/jmse8060457>
- Burd, H.J., Taborda, D.M.G., Zdravković, L., Byrne, B.W., Houlsby, G.T., Gavin, K., Igoe, D., Jardine, R.J., Martin, C.M., McAdam, R.A., Potts, D.M., (2020), "PISA Design Model for Monopiles for Offshore Wind Turbines: Application to a Dense Marine Sand", *Geotechnique*, 70 (11), pp. 1048–1066, [10.1680/jgeot.18.p.277](https://doi.org/10.1680/jgeot.18.p.277).
- Burd, H.J., Beuckelaers, W.J.A.P., Byrne, B.W., Gavin, K., Houlsby, G.T., Igoe, D., Jardine, R.J., Martin, C.M., McAdam, R.A., Muir Wood, A., Potts, D.M., Skov Gretlund, J., Taborda, D.M.G. and Zdravković, L. (2020). New data analysis methods for instrumented monopile field tests, *Geotechnique*, 70(11), pp. 961–969, doi.org/10.1680/jgeot.18.PISA.002.
- Byrne, B., MacAdam, R., Burd, H. and Houlsby, G. (2015). "New design methods for large diameter piles under lateral loading for offshore wind applications." *Proceedings to the Third International Symposium on Frontiers in Offshore Geotechnics in Oslo, Norway*.
- Byrne, B.W., Houlsby, G.T., Burd, H.J., Gavin, K., Igoe, D., Jardine, R.J., Martin, C.M., McAdam, R.A., Potts, D.M., Taborda, D.M.G. and Zdravković, L., (2020), "PISA Design Model for Monopiles for Offshore Wind Turbines: Application to a Stiff Glacial Clay Till", 70 (11), pp. 1030–1047, [10.1680/jgeot.18.p.255](https://doi.org/10.1680/jgeot.18.p.255)
- Byrne, B.W., McAdam, R.A., Burd, H.J., Beuckelaers, W.J.A.P., Gavin, K., Houlsby, G.T., Igoe, D., Jardine, R.J., Martin, C.M., Muir Wood, A., Potts, D.M., Skov Gretlund, J., Taborda, D. and Zdravković, L. (2020). "Monotonic lateral loaded pile testing in a stiff glacial clay till at Cowden", 70 (11), pp. 970–985, doi.org/10.1680/jgeot.18.PISA.003.
- Byrne, B.W., McAdam, R.A., Beuckelaers, W.J.A.P., Burd, H.J., Gavin, K., Houlsby, G.T., Igoe, D., Jardine, R.J., Martin, C.M., Potts, D.M., Taborda, D.M.G. and Zdravković, L. (2020). "Cyclic laterally loaded medium scale field pile testing for the PISA project", *Proceedings to the Fourth International Symposium on Frontiers in Offshore Geotechnics in Houston, USA*.
- Igoe, D. and Jalilvand, S. (2020). "3D finite element modelling of monopiles in sand validated against large scale field tests." *Proceedings to the Fourth International Symposium on Frontiers in Offshore Geotechnics in Houston, USA*.
- Kirsch, F., Richter, T., and Coronel, M. (2014). "Geotechnische Aspekte bei der Gründungsdimensionierung von Offshore-Windenergieanlagen auf Monopfählen mit sehr großen Durchmesser." *Stahlbau Spezial 2014 – Erneuerbare Energien*, 83 (SUPPL. 2), 61–67.
- Kulhawy, F. H., and Mayne, P. W. (1990)., *Manual on Estimating Soil Properties for Foundation Design.* EPRI-EL-6800.
- Mayne, P. W., and Kulhawy, F. (1982). "K₀ - OCR relationships in soils." *Journal of Geotechnical Engineering Division*, 108(6), 851–872.
- Malekjafarian, A., Jalilvand, S., Igoe, D., Doherty, P., (2020), *Foundation damping for offshore wind turbines on monopile supports: a review*, *Marine Structures*, Volume 77, May 2021, doi.org/10.1016/j.marstruc.2021.102937
- Minga, E. and Burd, H. (2019). "Validation of the PLAXIS MoDeTo 1D model for dense sand".
- Page, A.M., Skau, K.S., Jostad, H.P. & Eiksund, G.R. (2017) *A New Foundation Model for Integrated Analyses of Monopile-based Offshore Wind Turbines*. *Energy Procedia*. [Online] 137, 100–107. Available from: [doi:10.1016/j.egypro.2017.10.337](https://doi.org/10.1016/j.egypro.2017.10.337).
- Panagoulas, S., Brinkgreve, R. and Zampich, L. (2021) "Plaxis Monopile Designer CE V21 Manual".
- Robertson, P. K., and Cabal, K. (2014). "Guide to Cone Penetration Testing for Geotechnical Engineering - 6th Edition".
- Schnaid, F., and Yu, H. S. (2007). "Interpretation of the seismic cone test in granular soils." *Geotechnique*, 57 (3), 265–272.

The use of CPTU for driven piles designed in a backfilled opencast ‘marl hole’ in an important post-industrial revolution area within the UK

D. Illingworth & C. Burton

Piledesigns Limited, UK

L. Dhimitri & D. Ward

In Situ Site Investigation, UK

P. Shelton

Phil Shelton Geotechnical Consultancy Limited, UK

ABSTRACT: The Etruria Formation has historically been an important resource for the pottery and brick-making industry in the Stoke-on-Trent area and was mainly exploited using opencast methods – or ‘marl holes’ as they were commonly known. These ‘marl holes’ some of which have been reported to be more than 100m deep, have been subsequently backfilled generally with non-organic pottery, brickmaking and domestic waste. This paper explores the redevelopment of land over a backfilled ‘marl hole’ at a site in Hanley, Stoke-on-Trent, Staffordshire, UK, for residential properties. The development posed a number of challenges for the design of the foundations due to the historical legacy of the site. Driven steel tubular piles were chosen as a suitable system as there is precedent with this foundation solution, which has been frequently adopted for buildings within the area. However, some of the key challenges for this site included the presence of ‘high walls’ along the edges of the opencast works where driven piles could be deviated off the sides along with the uncertainty regarding socket lengths of piles driven into the underlying solid strata. To establish a 3D ground model for the ‘marl pit’, underlying strata, piezocone tests (CPTU) were seen as the most cost-effective and practicable method of site characterisation. Using this data, piles were installed, test/production piles were installed, driven to a set/penetration into the bedrock criteria and then compared to this ground model.

1 INTRODUCTION

This paper discusses the use of piezocone tests, CPTU for characterizing a backfilled opencast site for pile design.

1.1 Site description

The site is situated to the south of Hanley, which forms one of the six towns that make up the City of Stoke-on-Trent, in North Staffordshire, United Kingdom.

The proposed development is made up of a series of low-rise (2–3 storey) self-contained residential units. While the current topography shows a generally flat ground surface, this conceals the historical legacy of this part of Stoke.

1.2 Comments on the geology regarding the proposed development

The geological structure of the North Staffordshire Coalfield, presented in Figure 1, is a syncline, plunging towards the south-south-west, with the

productive Coal Measures at the centre of the coal-field and the Etruria Formation forming the outline, particularly along the eastern limb of the syncline (Rees et al., 1998).

It is no coincidence that the six towns forming the city of Stoke (Tunstall, Burslem, Hanley, Stoke, Fenton and Longton) are aligned along the eastern syncline limb above the Etruria Formation.

Unlike the North Staffordshire coal mining, the Etruria was generally exploited by opencast methods – or ‘marl holes’ as they were called. The outcrop of the Etruria, along the eastern limb of the syncline forms a line of many marl excavations of varying sizes. At Fenton, less than 10 km south-south-east of Hanley, the marl pit is reported to have been more than 100m deep.

The British Geological Survey (BGS) no longer recognises the term ‘marl’ and so now the Etruria Marl is officially known as the Etruria Formation.

Published information from the BGS suggests this proposed development site is underlain by Glacial Devensian deposits and in turn Carboniferous bedrock. These are mainly formed of a sequence of the

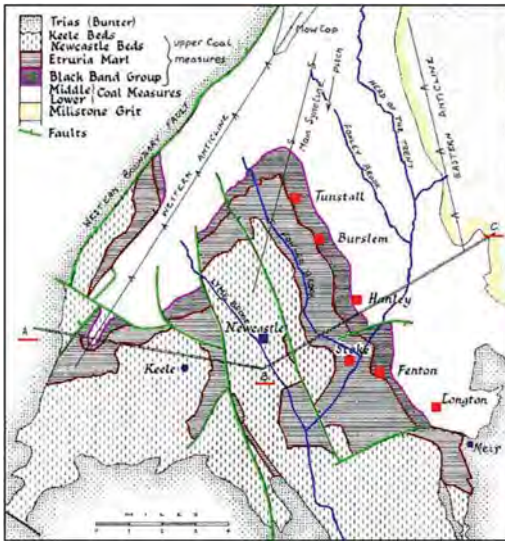


Figure 1. Geological map of North Staffordshire, modified from Millott (1937).

Etruria Formation, which is of Middle Carboniferous age, from 308 to 319 million years ago. It comprises of mudstones, siltstones and sandstones that overlay part of the North Staffordshire productive Coal Measures (Pennine Upper Coal Measures).

Reference to historical data indicates the site sits partly over an old marl pit. Data for an adjacent site indicates that the main extent of this old pit, known as the Mousehole Marl Pit, was to the north-east of the current development. The remainder of the site considered in this paper also appears to straddle the side of this old pit.

The Etruria Formation has a few unique properties that have made it a very important resource for the pottery and brickmaking industry. Firstly, it has a relatively high natural carbonate content common with non-marine semi-lacustrine ‘marl’ deposits. However, the source material for the Etruria was eroded material from an older Midlands volcanic sequence. Therefore, it has a relatively high iron content that gives rise to the natural colour variations. While the formation is mainly of clay and silt grain size, the Etruria also includes regular sandstone layers termed ‘esplays’. These are laterally discontinuous with few recognised as named horizons.

No published records are available for the Mousehole Marl Pit, which is known to extend beneath the proposed development. Following the exploitation of the Etruria Formation, the marl holes were backfilled with non-organic pottery and brickmaking waste. Much of the backfilling was undertaken during the 1960s, 1970s and 1980s (or before), when domestic waste was largely ash, glass and metal goods and it is expected that these products are also present.

Furthermore, there have been many anecdotal reports of industrial waste being dumped within the marl holes during times when the controls on waste disposal were less rigorous than now.

The following photograph presented in Figure 2 shows the nature of the excavations from a nearby well documented marl hole at Daisy Bank. While these pits were active, the high walls were steep probably between 45° and 50° overall, but locally up to 60°.



Figure 2. Air photos depicting the full extent of the Daisy Bank Brickworks, English Heritage (1927).

In respect of future development over the marl holes, probably the worst case is construction over the marl hole sides, often termed the ‘high walls’.

2 INTERFACE DELINIATION BETWEEN THE MADE GROUND AND MUDSTONE

2.1 Ground conditions

Field work was undertaken in two phases. The first phase took place in September 2019 where 9 boreholes were performed, six to shallow depths to nearly 6m and three deeper boreholes to a maximum of nearly 24m. On the deepest borehole, groundwater was encountered at 16.5m. Ground conditions at the borehole locations comprised a layer of made ground overlying natural strata considered to be Upper Coal Measures Formation.

Most of this initial investigation terminated in the made ground and no Glacial deposits were found. The made ground was mainly granular loose to medium sandy gravel with occasional cohesive material present in thin layers, typically soft to firm clay. Mudstone was only encountered in a couple of boreholes found below the made ground and was described as very weak rock.

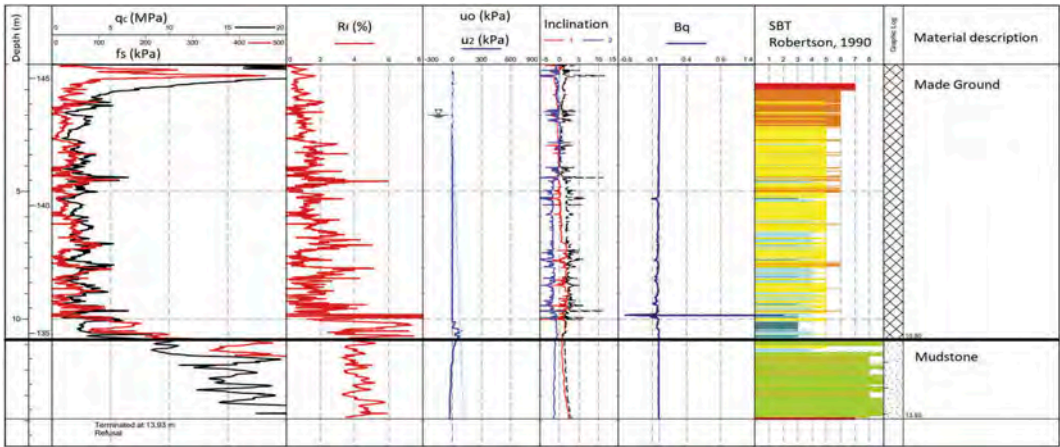


Figure 3. Typical CPTU profile for this site.

During the second phase of site investigation, 52 CPTUs were carried out to a maximum depth of 31.5m.

2.2 CPTU interpretation

The delineation of the interface between the made ground and the mudstone was assessed by the cone resistance, q_c , friction sleeve, f_s , porewater pressure, u_2 and inclination. Figure 3 represents a typical CPTU profile from this site.

The typical site level was 145.5m AOD. CPTU results indicate bedrock from between 3-30m depth. Although CPTUs provided a site coverage, it was found that there is no evidence for bedrock between 128 and 124m AOD.

The increase in q_c and f_s with greater depths were immediately noticed when cone was penetrating the mudstone. Results from 42 CPTUs with a penetration of more than 1m into this strata suggest that within mudstone $q_c > 5.5$ MPa, $f_s > 250$ kPa and u_2 has a significant drop to negative measured values. The negative porewater pressure indicates suction. Smoother inclination measurements are another indication that Mudstone is a uniform deposit.

To allow further review of the CPTU results within the mudstone, the data points recorded were plotted in the Robertson 1990 soil behaviour type, SBT chart, as presented in Figure 4.

The majority of results for Etruria Formation fall in zones 8-9, sand to clayey sand and very stiff fine grained, respectively. It is also noticed that some results plot in zones 3-4, which represent clay and silt mixtures.

Figure 5 presents a typical CPTU cross section for this site. The data shows that the rockhead was encountered at shallower depths in the south west of the site. In the eastern boundary of the site, mudstone occurs at greater depths. These results are used to

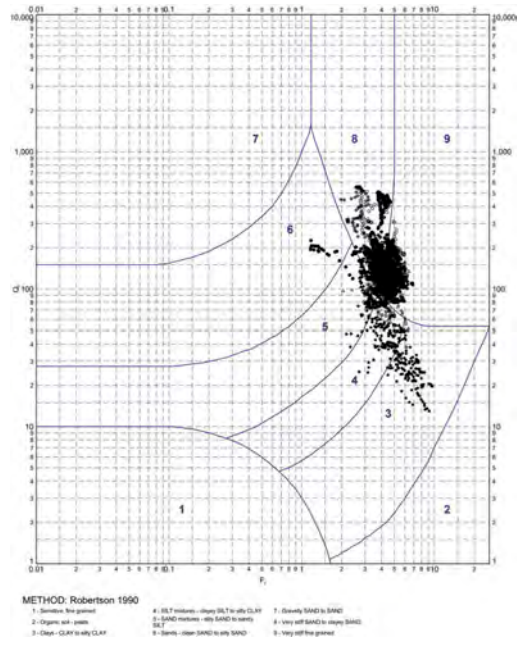


Figure 4. Mudstone results plotted on Robertson 1990 SBT chart.

develop the ground model for this site, which is also included in the paper.

A simplified graph of friction ratio, R_f (%) for mudstone to show the variation of results is presented in Figure 6. Black graphs present the minimum and maximum R_f within the deposit, meanwhile the red graph presents the averaged results. It is seen that this parameter may vary greatly in mudstone and cannot be trusted as the main parameter to interpret it.

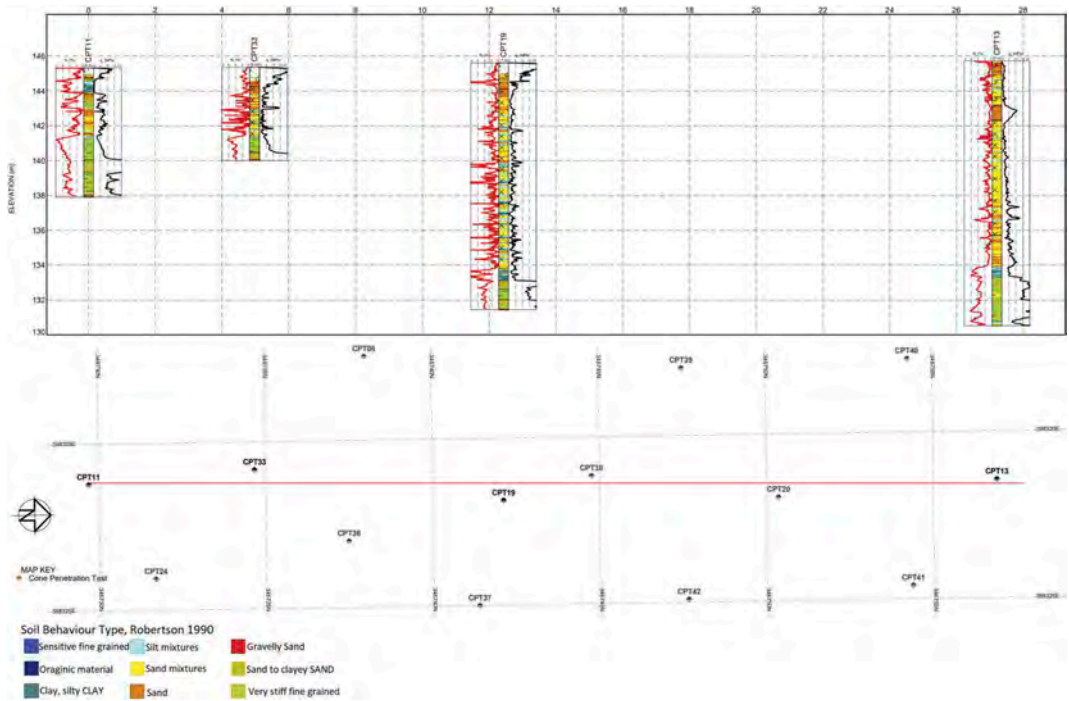


Figure 5. Cross section showing the mudstone coming in at a shallower depth to the south and much deeper to the north of the site.

Although CPTU provided a good site coverage, it was found that there were no probes relating to datum levels of between 128 and 124mAOD. Consequently, CPTU data were provided within two zones and between approximate levels of 141 to 128mAOD and 124 to 115mAOD. These are referred to as the upper and lower zones. The stratigraphic plots indicate distinct differences between the upper and lower zones. Although the results show some consistency several distinct layers can also be seen. In particular a more cohesive layer, with typical $R_f = 6-8\%$ between 140-138mAOD, and then some more sandy horizons averaging $R_f = 1\%$ between 133-130mAOD. The lower zone indicates significantly more variation with values of R_f varying from as low as 1% to as high as 9%.

After reviewing the scatter in these results it is suggested that the big variation in R_f results within the deposit can be mainly explained by lithological variations within the marl.

2.3 Discussion of CPTU results

Findings from CPTU tests regarding the delineation of the interface between the made ground and the mudstone for this site are in line with historical facts and previous experiences from investigations of backfilled opencast 'marl holes'.

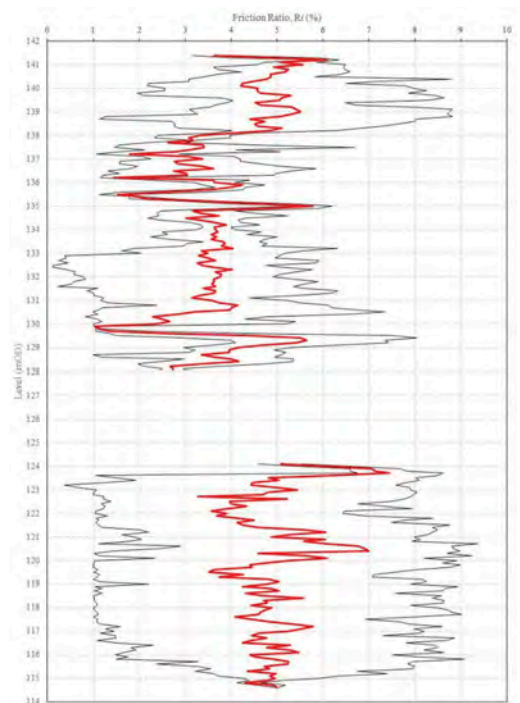


Figure 6. Friction Ratio (R_f) variation.

Among 52 tests carried out in total, only a few tests were refused at shallow depths, due to obstacles encountered in the first meters of backfilled material. 42 CPTU tests penetrated through the mudstone, 18 of which with a penetration of more than 2m into this material, which allowed us to review the results and the findings of this paper were crucial for the ground model and foundation design. Etruria Formation, interpreted as mudstone behaves as very stiff fine grained material, plotting in zone 9 in Robertson 1990 SBT when $q_c > 5.5$ MPa and $f_s > 250$ kPa and as sand to clayey sand when $q_c > 15$ MPa and $f_s > 500$ kPa, plotting in zone 8.

Porewater pressure can be another important measured parameter to interpret Mudstone, due to the sudden drop in the interface with made ground and large suction developed as the penetration continues. Another important indication of the penetration in mudstone is the inclination in both directions, which becomes uniform soon after the start of penetration through this deposit.

3 GROUND MODEL

The ground model for this site was developed based on CPTU results that had penetrated into the natural strata beneath the made ground.

For some tests where sensible assessment of this rockhead boundary was unclear, or the CPTU test appeared to have deviated or refused on an obstruction within the made ground, a repeat test was carried out.

Based on the CPTU results a model of the pit was constructed using the contouring package Surfer. Surfer interpolates irregularly spaced XYZ data into a regularly spaced grid. The grid data can then be interpreted using gridding and mapping modelling tools to produce 2D or 3D maps such as contour, shaded relief and surface maps. In addition, calculations such as bilinear interpolation can be carried out where the Z value at the XY location can be calculated from the nearest four grid nodes. In Figures 7 and 8 the marl hole contour profiles is shown, including the pile positions, shown in red.

The initial Surfer plots in Figures 7 and 8 provide a profile of the western high wall of the marl hole. This model was used to check that installed piles have a suitable penetration into the natural strata.

In reviewing the updated ground model, the data shows that rockhead occurs at 144-143m AOD along the western boundary of the site. There is a fairly shallow gradient towards the east until typical rockhead falls to 141-140m AOD. Thereafter the plot shows a steeper incline representing the western edge of the marl hole. Rockhead falls to about 123-122m AOD and then thereafter the gradient is more gradual towards the eastern site boundary.

Nearer the eastern site boundary rockhead levels are typically 120m AOD although with some further reduced levels. Reviewing the steeper part of the

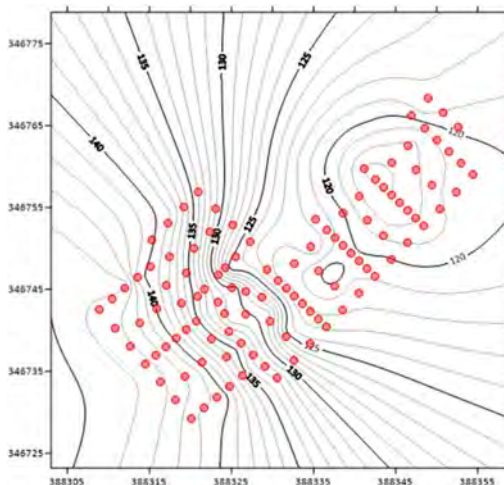


Figure 7. Marl Hole Contour Profile 2D.

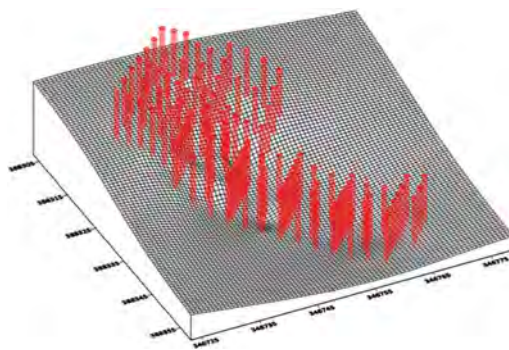


Figure 8. Marl Hole Contour Profile 3D.

western edge of the marl pit the average gradient appears to be about 50 degrees although locally this is indicated as increasing to almost 65 degrees. These back analysed gradients are comparable with those previously indicated for marl pits in the area.

From the results of the CPTU tests a suitable ground model showing the profile of the made ground/bedrock interface across the site has been established in relation to the proposed pile locations. The CPTU testing has provided data which indicates a good profile for the interface, and which looks reasonable when comparing all the available information. Where CPTU results looked anomalous, they have been discounted.

In reviewing and analysing the CPTU data, at least 1-2m bedrock penetration was typically considered sufficient to provide confidence that the probe attained a suitable penetration into the natural material.

This surfer ground model has been used to review the toe depths of the installed piles against the interpolated mudstone levels. It may be noted that the

surfer ground model has been considered as more reliable than particular pile driving records.

4 FOUNDATIONS

The foundation proposal was to adopt top driven tubular steel piles with a 178mm diameter tubular steel section considered. The driving system employed was using a 5.5 tonne hammer. It may also be noted, based on experience, that it was expected that the proposed newly installed piles would achieve a penetration at least comparable to the CPTU tests.

From the piling works a typical penetration of approximately 3 to 4m into natural strata was achieved. This was considered appropriate as it is anticipated that for the proposed piles, using an efficient energy input, a greater penetration compared to the CPTU tests, should be achieved.

As noted in monitoring the installation data all piles used within the foundation system showed reasonable penetration into the mudstone. Only one pile indicated an anomaly, taken as possible deviation, and which was subsequently replaced.

5 CONCLUSIONS

CPTU tests were used to provide a cost effective method to profile and establish a ground model for the backfilled opencast marl hole in Stoke on Trent. There was an initial concern on using CPTU to get to depths due to equipment limitations to penetrate through hard strata and rocks.

At the end of the site investigation program, CPTUs provided effective information for the

ground model, which allowed a suitable piling solution to be installed for the site.

From reviewing 42 CPTUs, it may be suggested that Robertson 1990 normalized SBT chart is a good classification method to interpret the mudstone in an accurate way. It provides more consistent results, indicating the behaviour of the deposit as overconsolidated cemented weak rock, plotting data points for this deposit in soil zones 8-9.

Possible inconsistencies in CPTU based classification should be attributed to physical complexity, which may affect the overall behaviour of the deposit especially in the upper zone, where some soils show a more clay-like behaviour and some others a more sand-like behaviour.

REFERENCES

- Lunne, T. *et al.* 1997. *Cone Penetration Testing in Geotechnical Practice*. Spon Press, London, UK.
- Millott, J. O'N. 1937. *The Coal Seams of North Staffordshire*. Physical and Chemical Survey of the National Coal Resources No. 39, Department of Scientific and Industrial Research.
- Robertson, P.K. *et al.* 1986. *Use of Piezometer Cone Data*. Proceedings of the ASCE Speciality Conference In Situ '86: Use of In Situ Tests in Geotechnical Engineering. ASCE (American Society of Civil Engineers), New York, NY, USA.
- Rees, J.G. *et al.* 1998. *Geology of the country around Stoke-on-Trent: Memoir for 1:50000 geological sheet 123 (England & Wales)*. Memoirs of the Geological Survey of Great Britain, England and Wales.
- Robertson, P.K. 1990. *Soil Classification Using the Cone Penetration Test*. Canadian Geotechnical Journal 27(1): 151–158.
- Robertson, P.K. and Cabal, K.L. 2015. *Guide to Cone Penetration Testing 6th Edition*. Gregg Drilling & Testing Inc, Signal Hill, CA, USA.

Consolidation settlement prediction using cone penetration testing

M. Kermani

Golder Associates Ltd., Montreal, Canada

F. Esford

Golder Associates Ltd., Vancouver, Canada

ABSTRACT: A reduction in the local groundwater table surrounding a mine, in the Abitibi-Témiscamingue region of Quebec, Canada, has led to dissipation of porewater pressure and displacement of the ground surface. The mechanical behavior of the site's fine-grained soil has been studied in the laboratory (consolidation tests) and in-situ tests, particularly cone penetration tests (CPT). Additionally, displacements of the ground surface have been monitored for over 10 years. The consolidation settlements due to the groundwater table drawdown were calculated based on tip resistance values measured during the CPT. By comparing the calculated magnitudes and trends of vertical displacement with measured values, the consolidation calculation method using CPT data was validated. At some locations, there was a good match between the calculated and measured trends. At other survey monuments, the measured displacements were greater than calculated values. It was concluded that additional mechanisms were contributing to the displacements. The possible influence of these mechanisms varies spatially within the studied site.

1 INTRODUCTION

1.1 Problem statement

The studied area is a mine site in the Abitibi-Témiscamingue region of Quebec, Canada. During mine production, conditions both underground and on surface of the mine began to change. The groundwater level declined and inflows to the underground workings increased.

Subsequently, investigations were carried out to understand the conditions and mechanisms associated with the ground surface movements.

As mining progresses, the owner continues to monitor the area, including measuring: surface displacements, bedrock deformations, elevation of the phreatic surface (through monitoring wells, vibrating wire piezometers, and CPT dissipation tests.), water infiltration into the underground workings, blast monitoring, and micro-seismic activity. Data is regularly reviewed and potential interactions between mining activities and site conditions are assessed by a multidisciplinary team.

For the sake of this study, samples, in-situ test data, and displacement monitoring data recorded at fixed survey monuments have been provided by Agnico Eagle Mines Limited (AEM).

1.2 Objectives

This paper makes use of the gathered data during the past 10 years, particularly the in-situ testing and

displacement monitoring to assess and estimate the consolidation settlements. Using cone penetration testing data, the validity of the Fellenius (2011) method for estimation of the tangent modulus based on CPT tip resistance values, and the Janbu (1967) method for estimation of consolidation settlements for the studied site are evaluated. To estimate the initial and final vertical effective stresses, the porewater pressure before drawdown and actual porewater pressure were considered. The vertical and lateral coefficients of consolidation were estimated from laboratory oedometer tests and in-situ CPT dissipation tests. Then by using Terzaghi's one-dimensional consolidation theory, settlement versus time plots were generated. For locations where it was estimated that primary consolidation was achieved by 95%, secondary compression settlements were also added to the settlement prediction time plots. Note that in this article all stresses are effective stress, unless otherwise noted.

1.3 Studied site's stratigraphy

The studied site is in the Abitibi-Témiscamingue region of Quebec province in Canada. The stratigraphic profile generally consists of (from top to bottom):

- A desiccated layer of firm to stiff, brown, clay or silty clay, typically 2 m in thickness. The desiccated layer is associated with the annual

fluctuation in the phreatic level and freeze-thaw cycles.

- A soft to firm, sensitive, grey, lacustrine (Lake Barlow-Ojibway clay), varved silty-clay to clay, of low to high plasticity, with a water content close to or above the liquid limit. Varves of silty clay to clay are reported to vary between 2 and 20 mm thick and silt between 1 and 15 mm thick. The undrained shear strength typically varies from 14 to 45 kPa, and sensitivity varies from 5 to 40. The clay is primarily saturated. It can reach thicknesses up to 30 m.
- A cohesionless, grey, silt and/or sand layer or mixture of silty sand or sandy silt, with occasional cobbles. The thickness varies from 2 to 25 m. The silt/sand was initially reported as loose to compact and saturated however, due to the reduction of the groundwater level, the majority of the silt/sand layer in the vicinity of the mine is now unsaturated. As a result, the compactness of this material has increased. It is now reported to be compact to dense at depth.
- A compact to very dense till unit that is variable in composition is discontinuously present. In general, the till is well graded and composed of sand and gravel, some silt and some clay, and occasional cobbles and boulders.
- Bedrock.

2 METHODOLOGY

2.1 Field observations

The field observation data on the displacements include survey monuments and inclinometers. As most of the survey monuments were installed after the onset of displacements, they have not captured the complete deformation history. Therefore, data from the satellite imagery analysis (InSAR) at the location of each survey monument was also used to supplement the measurements. Figure 1 shows an example of how the displacement from satellite (PALSAR and TSX satellite data) measurements has been added to survey monument data to estimate the total displacement since the onset of movements. Conversely, when both sets of data were available, the surface measurements were used to verify the precision of the satellite data. Note the satellite displacement data is measured along the line of sight. The PALSAR data had a grid size pixel spacing of 15 m and TSX had a 6 m spacing.

2.2 Janbu (1967) tangent modulus method

The tangent modulus method was developed by Janbu in the 1960's upon the assumption that the soil modulus of material can be estimated by dividing stress by strain. The modulus decreases as the stress

increases. Janbu proposed an empirical equation for the change in modulus with the stress level.

$$M_t = m\sigma_r(\sigma/\sigma_r)^{1-\alpha} \quad (1)$$

where: M_t = tangent modulus; σ_r = reference stress; σ = effective stress in the direction of strain; m = modulus number; α = dimensionless stress exponent. Both m and α depend on the material type and can be obtained from laboratory tests on high quality samples or in-situ tests (CPT in this study).

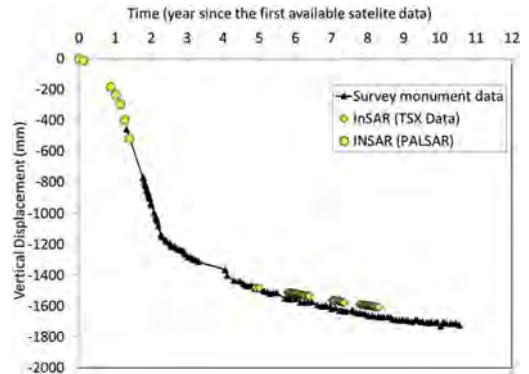


Figure 1. Vertical displacement data from surveying combined with satellite data at a specific location.

This approach has been used to calculate the magnitude of future, primary consolidation settlements (after the date each CPT was pushed). These CPTs were generally pushed after partial or full drawdown of the water table had occurred, which in turn altered the initial in-situ conditions. Therefore, this approach was found to be of interest because it considers the soil conditions, as well as porewater pressure at the time the CPT was pushed and allows estimating the settlements going forward with a higher precision.

Two different equations are derived from Janbu (1967) method, one for the fine-grained material, and one for granular materials. The settlement of the clay layer is calculated according to the following equation:

$$\varepsilon = \frac{1}{m_r} \ln \frac{\sigma_p}{\sigma_0} + \frac{1}{m} \ln \frac{\sigma_1}{\sigma_p} \quad (2)$$

and the settlement of the silt and sand layer are calculated according to the following equation:

$$\varepsilon = \frac{1}{5m_r} (\sqrt{\sigma_p} - \sqrt{\sigma_0}) + \frac{1}{5m} (\sqrt{\sigma_1} - \sqrt{\sigma_p}) \quad (3)$$

Where: ε = strain induced by an increase in effective stress; m_r = recompression modulus number; m = modulus number; σ_0 = initial effective stress (kPa);

σ_1 = final effective stress (kPa), and σ_p = preconsolidation stress (kPa).

In order to obtain an upper bound for the settlements, a simplifying assumption was made that the soil was in a normally consolidated state (OCR=1). By this assumption, the modulus number m remains the only compressibility material property to estimate the consolidation settlement. As explained in the next section, Fellenius (2011) has proposed an empirical equation that correlates the modulus number to the CPT tip resistance.

2.3 Fellenius (2011) method

Fellenius (2011) suggests the following equation for the estimation of the modulus number based on basic CPT data:

$$m = a \left[\left(\frac{q_t}{(\sigma_r \sigma_v)^{0.5}} \right) \left(\frac{3}{1 + 2K_0} \right)^{0.5} \right]^{0.5} \quad (4)$$

where: a = empirical modulus modifier which depends on soil type; q_t = unadjusted cone resistance (but corrected for pore pressure); σ_v = the vertical effective stress; σ_r = the reference stress, here 100 kPa; and K_0 = the coefficient of lateral earth pressure at rest. The term $3/(1 + 2K_0)$ varies between 1.2 and 1 for a soil with K_0 between 0.5 and 1. This term was assumed to be unity, which provides conservative values for the modulus number.

The modulus modifier, “ a ” was estimated based on the Soil Behaviour Type (SBT) determined from the CPT data (Table 1).

Table 1. Modulus modifier values based on SBT (from Massarsch et al., 1997).

SBT (Jeffries and Davies, 1993)	Modulus modifier, a
0, 1 and 2	3
3	5
4	12
5	15
6	22
7	28
8	35

Figure 2 schematically shows the state of stresses in the clay unit at the location of a given CPT. The total and effective stresses at the moment the CPT was pushed are shown in the figure. The soil unit weight was estimated using Shelby tube samples, as well as interpretation of CPT data. The pore pressure at the moment the CPT was pushed needs to be considered for the calculation of the actual effective stress. CPT dissipation tests provided reliable values for the calculations. If the difference between

saturated and wet unit weights are neglected, the final effective stress after dissipation of pore pressure would equal the current total stress (the red dashed line). For each CPT, the red curve showing the preconsolidation pressure was found using CPT data. The preconsolidation pressure was calculated for each 10 cm increment of the soil using the following correlation:

$$\sigma'_p = (q_t - \sigma_{v0}) / N_{\sigma t} \quad (5)$$

where σ_{v0} is the vertical total stress and the parameter $N_{\sigma t}$ is assumed to be 3.4 for Eastern Canada clays (Demers and Leroueil, 2002). Then the values were validated by laboratory oedometer tests and field vane tests (FVT). Equation 6 was used to estimate the preconsolidation pressure from the FVTs (Mesri, 1988).

$$S_{u(mob)} = 0.22\sigma'_p \quad (6)$$

where $S_{u(mob)}$ is the undrained shear strength mobilized on the failure surface in the field. According to Bjerrum (1973), the shear strength from FVT is close to $S_{u(mob)}$ for clays with plasticity indexes close to 20%, which is the case for the studied site.

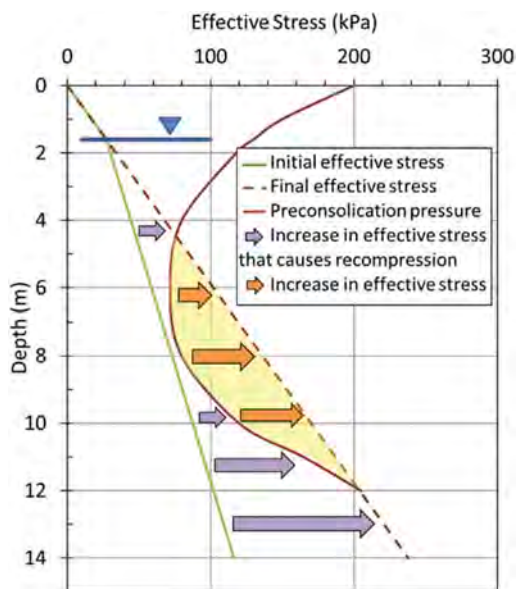


Figure 2. Schematic of the state of stresses considered for consolidation calculations.

The consolidation settlement is a function of the difference between the actual and final effective stress (the difference between the green line and red dashed line). For the zone between the actual effective stress and the preconsolidation pressure, the calculations were done using the recompression modulus m_r (indicated by the grey arrows), and for the zone

between preconsolidation pressure line and final effective stress, the modulus number was used, as presented in equation 1 (indicated by the orange arrows).

2.4 Distribution of settlement through time

As explained in the previous sections, the magnitudes of settlements were calculated using the Janbu (1967) and Fellenius (2011) methods. To estimate the distribution of the calculated settlement through time, the rate of consolidation needed to be considered. The rate of consolidation was calculated according to Terzaghi's well-known one-dimensional consolidation theory. The time factor T_v was calculated from the below equation:

$$T_v = \frac{c_v t}{H_{dr}^2} \quad (7)$$

where t is the time to obtain a certain degree of consolidation, H_{dr} is the length of the longest drainage path, and c_v is the vertical coefficient of consolidation. The consolidation ratio U (%) was calculated using empirical equations (Holtz et al., 2011) as a function of T_v .

Considering the varved nature of the clay, the coefficient of consolidation in the horizontal direction is clearly higher than the vertical direction. In order to adopt a representative coefficient of consolidation for clay, both laboratory oedometer tests and CPT dissipation tests were considered. A slower rate, $c_v = 13.6 \text{ m}^2/\text{yr}$, was determined from average vertical coefficients of consolidation from several laboratory oedometer tests. A faster rate, $c_v = 63.1 \text{ m}^2/\text{yr}$, was adopted from average radial coefficients of consolidation based on the interpretation of CPT dissipation tests. Plotting the estimated settlements versus measured displacement during 10 years of monitoring showed that the slower rate provided a better match with the measurements. This is coherent with the mechanism of consolidation in the site, which is ground water table drawdown and the downward drainage of water. If the consolidation calculation method presented in this article is to be used for other sites, the consolidation mechanism and the direction of drainage needs to be considered. For instance, if wicked drains are installed, radial coefficient of consolidation could be more representative of site conditions.

2.5 Secondary compression

Where the consolidation was estimated to have been complete by 95%, the secondary compression settlements were also added to the consolidation settlements, using the conventional method:

$$S = \frac{C_\alpha}{1 + e_{0p}} L_0 \log \frac{t}{t_p} \quad (8)$$

where S is the magnitude of secondary compression, C_α is the secondary compression index, L_0 is the initial thickness of the consolidating layer, t_p is the duration of the primary consolidation stage, e_{0p} is the void ratio at the beginning of secondary compression, and t is the time interval of interest that begins from the start of consolidation. C_α was estimated using one-dimensional laboratory consolidation test results on high-quality large diameter samples carefully collected from the same geologic formation at another site in the region.

The determination of the beginning of secondary compression has always been controversial among geotechnical engineers. When calculating secondary compression settlement during a specific period of time (between times t_1 and t_2), when the secondary compression has started before t_1 , the following equation can be derived from equation 8:

$$S_2 - S_1 = \frac{C_\alpha}{1 + e_{0p}} L_0 \log \frac{t_2}{t_1} \quad (9)$$

Therefore, the time of the beginning of secondary compression does not influence the results.

3 RESULTS

Figure 3a shows the initial and final effective vertical stresses along with the preconsolidation pressures for each 10 cm soil increment. The preconsolidation pressures from CPT were validated with laboratory oedometer test, as well as field vane tests (FVT). There is generally a good agreement between CPT, FVT and oedometer test results. At depths between 6 m and 9 m, FVT tends to overestimate the σ'_p , possibly because of higher plasticity of clay in these depths. To carry out the consolidation calculations, the preconsolidation pressure from CPT data was used.

As shown in equations 2 and 3 and Figure 2, the compression of clay is a function of the effective stress change from the preconsolidation pressure to the final effective stress, and the modulus number. Figure 3b shows the modulus numbers calculated using equation 4 based on the CPT data for each 10 cm of soil increment. An advantage of the consolidation settlement calculation method presented in this article is that at each elevation a specific soil modulus is considered and the variability throughout the soil column is taken into account. A step change is observed in the calculated modulus numbers at depth 11 m. This is because the SBT changes from 3 to 1 at this depth, meaning that the soil becomes more plastic, and the modulus modifier, a , changes from 5 to 3 (see Table 1).

Considering the equation 2 and relating the modulus number to the conventional consolidation test parameters, the modulus number can be estimated directly from oedometer test results using the following equation:

$$m = \ln 10 \frac{(1 + e_0)}{C_c} \quad (10)$$

where C_c is the compression index and e_0 is the initial void ratio. The modulus numbers estimated based on consolidation test results are shown along with the values from CPT tests (Fellenius 2011 equation) in Figure 3b. The laboratory modulus numbers are slightly greater than CPT values. But there is generally a good match between field and laboratory values. Note that for the consolidation calculations, Fellenius (2011) was used to estimate the compression modulus m in clay. The recompression modulus number m_r in clay, as well as both moduli for silt/sand units were estimated based on laboratory consolidation tests.

Figure 3c shows the cumulative ultimate settlement calculated for each depth. As expected, the majority of settlements occur at the depths where the clay pre-consolidation pressure is close to the current effective stress (6 m to 20 m). Additionally, it can be observed that greater settlements are calculated between depths 11 m and 20 m, where the modulus numbers are smaller compared to depths 6 m to 11 m.

Figure 4 shows the consolidation calculation vs. time for two of the studied CPTs from the date each CPT was pushed, along with the measured vertical displacement at a nearby survey monument. The survey monument readings show some variations due to freeze-thaw cycles but minimum values (fall readings) show the vertical displacement trend and magnitude.

The consolidation calculations estimate the settlements, from the moment the CPT was pushed and considers the geotechnical properties of the encountered soil at the time of the test. For each CPT the settlement vs. time predictions are presented with two different consolidation rates (faster and slower) considering two different coefficients of consolidation, as explained in section 2.4.

The 2011 CPT with the slower rate has captured the general trend of the settlements from the test date. However, the measured total ground displacement has exceeded the calculated total settlement. The higher c_v (from CPT) appears to overestimate the rate of consolidation. The consolidation calculations are carried out for the 2017 CPT with the updated pore water pressure regime, and soil geotechnical characteristics at the time the cone was pushed. It appears that the 2017 CPT data has captured well the ground displacements for the years following the test. The 2017 CPT was located closer to the survey monument (15 m vs. 25 m for the 2011 CPT). The fact that the 2011 CPT provided results which deviated from the measured values could be attributed to the spatial variability of the stratigraphy. Note that for this location, based on the dissipation tests, the 95% primary consolidation has not been attained. Therefore, the secondary compression settlements are not considered.

The mismatch between measured and predicted settlements was observed for some monuments. The

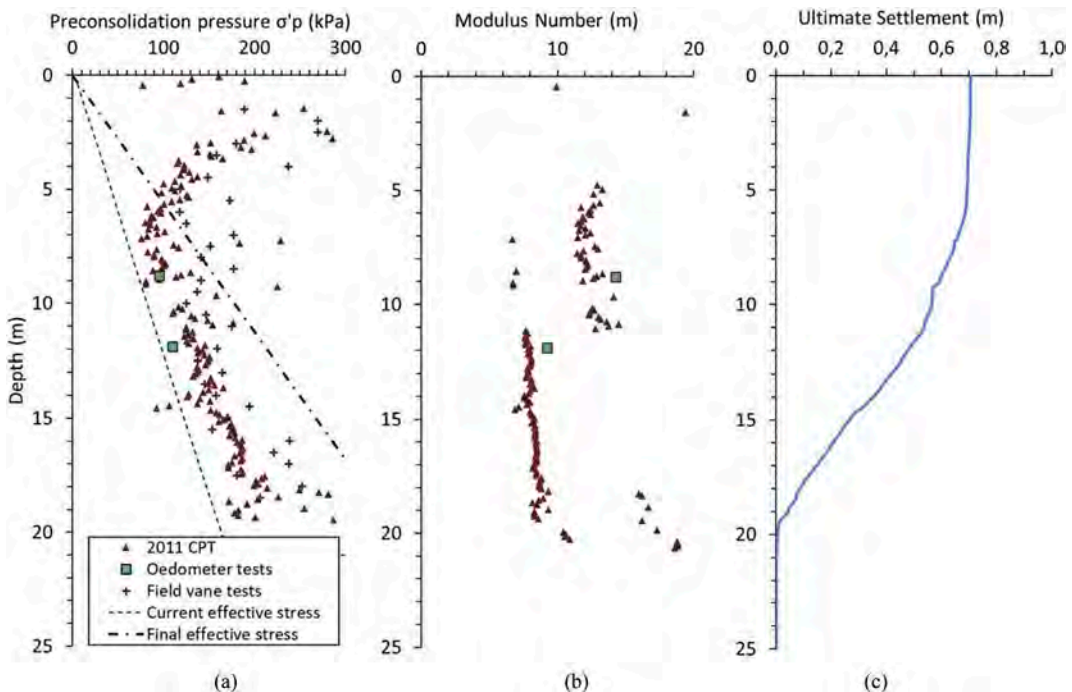


Figure 3. Example of calculation of a) initial and final state of stresses, b) modulus number, and c) ultimate settlement.

discrepancy was concluded to be associated with, but not limited to factors such as the following:

Stratigraphic variation: The CPTs were sometimes up to 50 m away from the reference survey monument. Several drilling and site investigation programs on the site have shown that the stratigraphy is highly variable. So, the stratigraphy encountered in the CPT may not necessarily be the same as the subsurface layers below the survey monument.

Further phreatic surface drawdown: The overall ground water table at the site was assumed to remain constant from the moment the study was carried out. Any additional drawdown of the water table (in the partially drained areas) could increase the estimated settlements.

Lateral movements: Lateral movements could contribute to the vertical displacements by reducing the soil confinement.

Development of suction in soil: It was assumed in this study that the final porewater pressure in elevations above the phreatic surface will become zero. Soil-Water Characteristic Curve testing indicated that most of the clay layer will remain in a saturated state in long-term. However, considering that the phreatic surface is below the bottom of the clay layer, it is possible that negative pore pressures (suction) develop in clay, which would increase the final effective stresses beyond the estimated values (higher than the actual total stress). Higher final effective stress would lead to greater deformations in clay, than what is calculated considering a zero final porewater pressure. The installation of vibrating wire piezometers in clay would allow estimating the vertical effective stress with more precision.

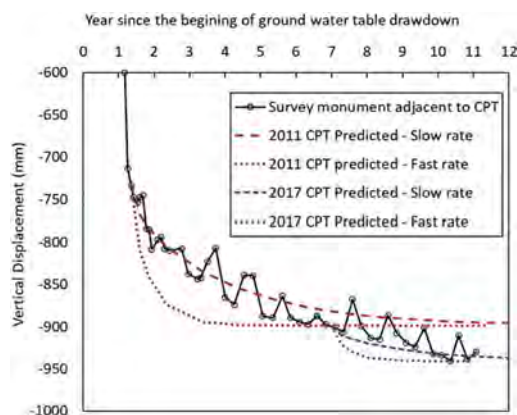


Figure 4. Example of measured and predicted settlement vs. time plots.

4 CONCLUSIONS

In this article, a consolidation settlement calculation method using CPT data was presented. A case study

of a site where a decline in the phreatic surface has led to consolidation settlements was presented. The results showed that the method can capture the consolidation settlement-time curves. A discussion is presented on the reasons why for some survey monuments, the match between measured and predicted settlements was less accurate.

This method can be used to create a contour map of the predicted consolidation settlements for a site with low stratigraphic variability. It is recommended to space out the CPTs to cover the zone of interest, and to carry out more CPTs close to the sensitive structures to obtain more reliable data. A combination of CPTs and traditional boreholes is recommended to collect high quality samples for laboratory testing to validate the calculations parameters. As CPTs can be carried out faster and at a lower cost, they should be used to capture the variability in site stratigraphy.

It should be noted that the studied case is different from conventional consolidation problems where adding a load forces the porewater out of the soil matrix and leads to an increase in the effective stress. In the studied case, the increase in effective stress is caused by a decline in groundwater table. Therefore, as the groundwater table is below the bottom of the clay layer, negative porewater pressure (suction) could be generated in the clay which may lead to greater effective stress and larger deformations. This aspect is presently being evaluated by measuring potential suction in fine-grained soil layers on the site.

ACKNOWLEDGEMENTS

The authors acknowledge the contribution of Agnico Eagle Mines Limited (AEM) in providing the information, support and guidance in the studies associated with this article. Further the authors would like to acknowledge the contributions of a former colleague, Gerd Janssen, in developing this approach for estimating the settlements.

REFERENCES

- Fellenius, B. H., 2011. Basics of foundation design. *Electronic edition*. www.Fellenius.net, 362 p.
- Holtz, R. D., Kovacs, W. D. Sheahan, T. C. 2011. An introduction to geotechnical engineering. Second Edition.
- Jeffries, M.G. and Davies, M.P. 1993. Use of CPTu to Estimate Equivalent SPT N60, *Geotechnical Testing Journal, ASTM, 16*: 458–168
- Massarsch, K.R., Westerberg, E., and Broms, B.B., 1997. Footings supported on settlement-reducing vibrated soil nails. *14th, Hamburg 97*, Vol. 3, pp. 1533–1539.
- Mesri, G. 1988. A reevaluation of $S_{u(mob)} = 0.22\sigma'_p$ using laboratory shear tests. *Canadian Geotechnical Journal*. Vol. 26, 162–164
- Demers, D., & Leroueil, S. 2002. Evaluation of preconsolidation pressure and the overconsolidation ratio from piezocone tests of clay deposits in Quebec. *Canadian Geotechnical Journal*, 39(1), 174–192.

3D FE derivation of CPT based soil reaction curves for monopile lateral static design in sand

Louis-Marin Lapastoure

*Department of Civil, Structural & Environmental Engineering, Trinity College Dublin, Dublin, Ireland
Gavin and Doherty Geosolutions Ltd, Dublin, Ireland*

David Igoe

Department of Civil, Structural & Environmental Engineering, Trinity College Dublin, Dublin, Ireland

ABSTRACT: This paper aims to offer novel correlation between all 4 components of PISA soil reaction curves for monopile modelling and Cone Penetration Testing (CPT) data. This approach requires minimum user inputs and offers a consistent approach to develop site-specific soil reaction curves when CPT data are made available. The procedure developed by Igoe and Jalilvand was used to derive small-strain hardening (HS-small) soil model parameters from a range of CPT profile. HS-small parameters are then used to model the monopile response to static lateral loading in sand using Plaxis 3D. This procedure has been validated by the authors against a database of large-scale field tests including PISA tests in the Dunkirk marine sand. Soil reaction curves were directly extracted from the Plaxis models then applied into Timoshenko beam elements to match the 3D FE response and validated the extraction process. It is demonstrated that current CPT based correlations do not match the shape nor the ultimate reaction of 3D FE extracted soil reaction curves. It is also shown that all four components of soil reactions are required to accurately model monopiles which are short and rigid.

1 INTRODUCTION

1.1 Context

Monopiles are the main foundation type supporting about 80% of the installed offshore wind turbines to date in Europe (Wind Europe, 2020). The traditional industry design approach for monopile was adopted from the oil and gas industry. The ‘p-y’ approach recommended in the main design standards (API 2011, DNV 2013) was validated against a rather small database of long slender piles with diameter smaller than 1 m. On the contrary, monopiles are now designed with a low slenderness ratio ($L/D \approx 3$) and a large diameter up to 10 m. Since 2014, it is warned that the API approach has “not been calibrated for monopiles with larger diameters and are in general not valid for such monopiles” (DNV 2014).

The recently completed PISA project was developed with the aim of improving on the traditional API design approach for monopile. In the PISA design model, pile-soil interactions are not limited to the distributed lateral reaction (p-y curves) but also include distributed moment, base shear and base moment (Burd et al. 2020). The PISA framework has now been implemented into the commercial software PLAXIS Monopile Designer (formerly MoDeTo) and is being commonly used in the industry (Minga and Burd

2019). It offers the option to extract site-specific soil reaction curves from 3D finite element models. However, this can be seen as computationally costly and requires careful calibration of the 3DFE soil input parameters.

Soil strength and stiffness parameters are often determined using correlations with Cone Resistance Testing (CPT) results, and therefore researchers have been looking at correlating soil reaction curves with CPT directly. Broms (1964) originally proposed relationship between ultimate lateral reaction, p_u , as a function of the cone resistance, q_c , in silica sands as per equation (1) where D is the pile diameter, p' is the mean effective stress and p_a is a reference stress taken as 100 kPa.

$$\frac{p_u}{D} = 0.1959 \cdot \left(\frac{q_c}{p_a}\right)^{0.4719} \cdot \left(\frac{p'}{p_a}\right)^{-0.6281} \quad (1)$$

Suryasentana and Lehane (2014) developed new p-y formulations for piles in sand based entirely on 3D finite element modelling, as opposed to back analysis of small scale instrumented laterally loaded pile tests as was the traditional approach. Equation (2) below has been calibrated against FE models using the hardening soil model (HS) in Plaxis 3D

foundation and validated against lateral pile field tests with diameters of about 0.6 m and pile penetrations of 17 m ($L/D > 28$). γ denotes the soil unit weight and Z the depth at which the soil reaction is calculated.

$$\frac{p_u}{D} = 2.4 \cdot \gamma \cdot Z \cdot \left(\frac{q_c}{\gamma \cdot Z} \right)^{0.67} \left(\frac{Z}{D} \right)^{0.75} \quad (2)$$

However, these CPT based correlations are not compatible with the PISA framework and, as only the p-y response is considered, they might not be suitable for modelling monopiles (similarly to API).

1.2 Proposed approach

It is proposed here (see Figure 1) to use 3D finite element modelling to derive CPT based correlations of soil reaction curves including distributed lateral reaction, distributed moment, base shear and base moment (as per PISA framework).

Soil parameters required as inputs for the 3D FE are directly derived from CPT profiles as per the approach proposed by Igoe and Jalilvand (2020). This approach requires minimum user inputs and has been validated against a database of lateral pile field tests including PISA tests in the Dunkirk marine sand.

All components of soil reaction are extracted from the 3D FE models for a range of pile geometries and CPT profiles. CPT based correlations are calibrated from this database of soil reaction curves and by matching the 3D FE and 1D FE mudline responses.

The approach is then validated against large scale pile field tests (the same database used by Igoe and Jalilvand 2020).

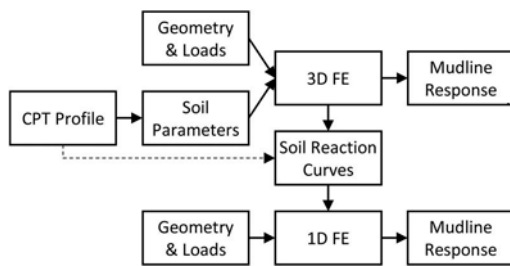


Figure 1. Flowchart of the proposed approach.

2 PLAXIS 3D FINITE ELEMENT MODELLING

This section presents how the 3D finite element models are set up in PLAXIS 3D and how results are being post-processed.

2.1 Model set up

Monopiles are modelled at full scale and half space using the commercially available finite element package PLAXIS 3D (see Figure 2). They are modelled with linear elastic plate elements with Young's modulus of 210 GPa and Poisson's ratio of 0.3. Since the lateral response is the main concern, the self-weight of the monopile is omitted. The piles are assumed wished in-place with no effect of the installation taken into account.

This study is limited to monopile modelling in sand. The hardening soil model with small-strain stiffness (HS-small) is an improvement of the HS model used by Suryasentana and Lehane (2014). It has been successfully used to accurately model monopile lateral response in sand (Igoe and Jalilvand 2020), and thus is considered here. Vertical interfaces are added between the pile shaft and the soil to allow for differential displacements, to introduce an interface strength reduction factor (set to 0.7 here) and to allow extraction of soil distributed reactions (distributed lateral load and distributed moment). At pile toe, an additional horizontal interface is added to allow for extraction of base reactions (base shear and base moment) but with no strength reduction considered.

The lateral loading as a result of wind and wave action is applied as a prescribed displacement at a height, e , above mudline. Burd et al. (2020) showed that there is negligible effect of the loading eccentricity on soil reaction curves. Hence the value of e is taken as 60 m (a mean value to represent both wave and wind dominated scenarios). The lateral loading is applied in the y direction. The size of the domain is taken as 12D in the direction of loading and 4D in the perpendicular direction as recommended in the PLAXIS Monopile Designer manual (Panagoulas et al. 2021), where D is the monopile diameter. The depth of the model is here set to 80 m with 16 soil layers of 5 m thickness each. This is to ensure the soil domain is large enough to avoid boundary effects.

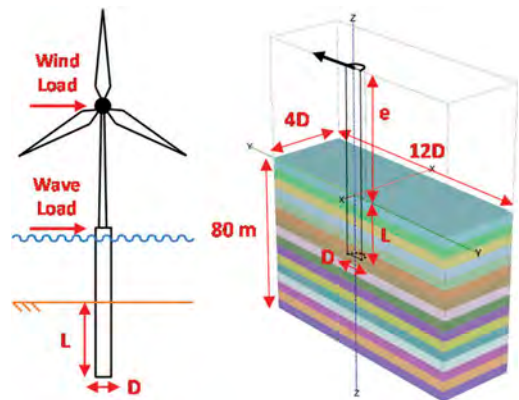


Figure 2. Description of the monopile model in Plaxis 3D.

2.2 Soil parameters

Igoe and Jalilvand (2020) developed an approach to derive all of the required HS-small input parameters using widely used CPT correlations. All correlations used are summarised in Table 1. The approach has been validated against a database of large scale field tests including PISA tests in the Dunkirk marine sand and offers better predictive accuracy metrics than correlations suggested for the Plaxis Monopile Designer (Panagoulas et al. 2021).

By re-arranging the correlations presented in Table 1, synthetic CPT profiles for constant sand relative density are generated. Relative densities of 30% (loose), 50% (medium dense), 70% (dense) and 90% (very dense) are considered. At this stage, only normally consolidated state is considered with OCR set to 1. A constant ratio sleeve friction to cone resistance, f_s/q_c , of 1% is assumed. The constant volume friction angle is taken as 32 degrees for all profiles. The soil unit weight is taken ranging from 17 kN/m³ to 20 kN/m³ depending (linearly) on relative density. Finally, the small strain shear modulus profiles are estimated from the cone resistance with α set to 185 as recommended by Igoe & Jalilvand (2021).

Table 1. Correlations used by Igoe & Jalilvand (2021).

Correlations	References
$E_{50}^{ref} = E_{ur}^{ref} / 3$	Brinkgreve et al. (2010)
$E_{oed}^{ref} = E_{50}^{ref}$	Brinkgreve et al. (2010)
$E_{ur}^{ref} = 0.00464 \cdot E_0^{ref \cdot 1.724}$ Where $E_0^{ref} = 2(1 + \nu)C_0^{ref}$	Modified after Kirsh et al. (2014)
$m = 0.5$	Benz et al. (2009)
$\varphi' = \varphi'_{cv} + 3(D_R(10 - \ln p'_0) - 1)$	Bolton (1986)
$D_R = \sqrt{\frac{Q_m}{305 \times OCR^{0.15}}}$	Kulhawy & Mayne (1990)
$Q_m = \left(\frac{q_t - \sigma_{v0}}{p_{ref}}\right) \left(\frac{p_{ref}}{\sigma'_{v0}}\right)^n$ $n = 0.381 \cdot I_c + 0.05 \frac{\sigma'_{v0}}{p_{ref}} - 0.15$	Roberston & Cabal (2014)
$I_c = \sqrt{\frac{(3.47 - \log_{10} Q_m)^2 + (1.22 + \log_{10} F_r)^2}{}}$ $F_r = \frac{f_s}{q_t - \sigma_{v0}}$	
$\sin \psi' = \frac{\sin \varphi' - \sin \varphi'_{cv}}{1 - \sin \varphi' \sin \varphi'_{cv}}$	Brinkgreve et al. (2018)
$G_0 = \alpha(q_t \cdot \sigma'_{v0} \cdot p_{ref})^{1/3}$	Schnaid and Yu (2007)
$\gamma_{0.7} = 1.5 \cdot 10^{-4}$	Benz et al. (2009)
$G_0^{ref} = G_0 \left(\frac{p_{ref}}{p'_0}\right)^m$	Brinkgreve et al. (2018)
$K_0 = (1 - \sin \varphi') \times OCR^{\sin \varphi'}$	Mayne & Kulhawy (1982)

2.3 Monopile geometry

To allow for the calibration of the CPT based correlations, a range of monopile geometries is considered. Literature showed that there is negligible effect of the pile wall thickness and load eccentricity on the soil reaction curves so these are kept constant as $t = D/110$ and $e = 60$ m, respectively (representative values based on experience). Outside diameters (D) of 6 m, 8 m, 10 m and 12 m are considered. Slenderness ratios (L/D) of 2, 3, 4, 5 and 6 are considered. This results in pile embedded length (L) ranging from 12 m to 72 m. Hence a total of 20 geometries are considered for each soil profile covering recent, current and future design.

2.4 Soil reaction curves extraction

Unlike Suryasentana and Lehane (2014), soil reaction curves are not calculated from the derivative of shear and bending moment diagrams. The approach briefly presented in the PLAXIS Monopile Designer manual (Panagoulas et al. 2021) has been preferred as it allow for extraction of all components of the soil reaction.

Distributed lateral load and distributed moment are calculated from integration of the normal and tangential stresses acting on monopile shaft (vertical interface). Soil reactions are integrated along 1 m (ΔZ) intervals as shown on Figure 3 and as per equations (3) and (4). Resulting lateral forces, F_y , and vertical forces, F_z , are calculated at each of the 6 Gaussian stress points of each interface elements as per equations (5) and (6), respectively. Where σ_n , τ_1 and τ_2 are the stresses directly extracted from Plaxis, X and Y are the coordinates of the stress point, D is the pile diameter, A is the area of the interface element and w is the weight of the stress point (0.11 for stress points 1 to 3 and 0.22 for stress points 4 to 6).

$$p(Z) = \frac{\int_{Z-\Delta Z/2}^{Z+\Delta Z/2} F_y(z) dz}{\Delta Z} \quad (3)$$

$$dM(Z) = \frac{\int_{Z-\Delta Z/2}^{Z+\Delta Z/2} y \times F_z(z) dz}{\Delta Z} \quad (4)$$

$$F_y = wA \left(\frac{2Y}{D} \sigma_n - \frac{2X}{D} \tau_2 \right) \quad (5)$$

$$F_z = wA \tau_1 \quad (6)$$

The base shear and base moments are calculated from the horizontal interface. This is not detailed here as the approach is very similar. All calculations are repeated for each load increment

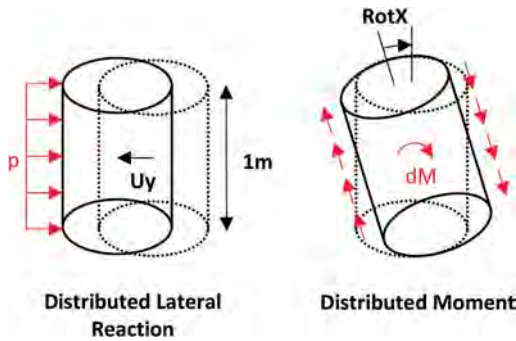


Figure 3. Integration of distributed lateral reaction and distributed moment.

in order to build the full reaction curves. These are then saved in a formatted .csv file for later use.

3 PRELIMINARY RESULTS

With 4 relative densities considered and 20 monopile geometries for each soil profile, the database consists in 80 3D FE models. On average, it took 1 hour to set up, run and process each model on a relatively high capacity computer (Intel(R) Xeon(R) W-1270P CPU @ 3.80GHz, 32 GB DDR4). The computation times were greatly reduced thanks to the automation of most aspects of the PLAXIS modelling through the PYTHON scripting interface. The database has been recently completed and this section presents and discuss preliminary results obtained.

3.1 Comparison 1D FE – 3D FE responses

In order to make sure soil reaction curves are being correctly extracted from PLAXIS, 3D FE and 1D FE monopile response are compared.

For the sake of conciseness, only one model with pile diameter of 10 m, embedment length of 30 m in 70% relative density sand (case RD70%_D10L30) is presented in Figure 4 but all other models show similar results. Both load-displacement (top of the figure) and moment-rotation (bottom of the figure) curves compare relatively well when all reaction components are considered in the 1D FE model. However, when only p-y curves are being considered, the 1D FE response is found to be considerably softer than the 3D FE response. This is in agreement with findings from the PISA project (Byrne et al. 2015) and confirms the need of CPT based correlations including all components of pile-structure interactions and not limited to p-y curves only.

To add to this qualitative assessment, Table 2 compare initial stiffnesses, SLS rotations and ultimate capacities from 1D FE and 3D FE for the same

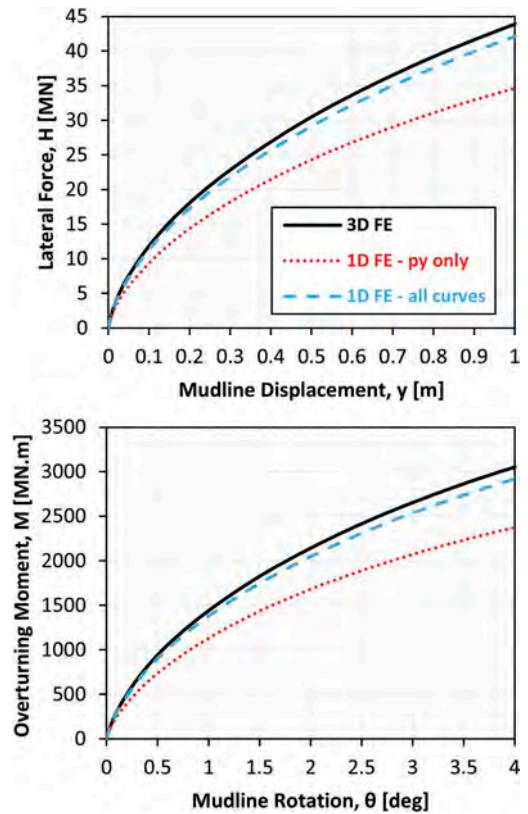


Figure 4. Comparison of 1D FE and 3D FE monopile lateral responses for case RD70%_D10L30.

model. The initial stiffness and ultimate capacity are defined at a mudline displacement of $D/10000$ and $D/10$, respectively. From experience, monopiles are subjected to strict serviceability requirements leading to low utilization in ULS GEO checks ($\approx 1/2$). When the load partial factor of ≈ 1.35 and material partial factor of 1.15 is considered, the SLS load is approximately defined as 1/3 of the ultimate capacity. One may consider that the 1D FE with p-y only may be considered overly conservative with underestimation of the initial stiffness and the ultimate capacity by 16.4% and 21.1%, respectively. The “SLS” rotation is overestimated by 47.7%. When adding other component of soil reactions to the 1D FE model, the match is much better with only a 4% underestimation of initial stiffness and ultimate capacity. The “SLS” rotation is only overestimated by 6.9%.

This quantitative assessment has been repeated for all 80 models. Only results pertaining to the estimation of ultimate capacity are presented in Figure 5 but the other two metrics show the same trend. For a typical slenderness ratio (L/D) of 3, the pile ultimate capacity is underestimated by more than 20% if only ‘p-y’ curves are used in 1D FE while the error is reduced to about 5% when all components are

Table 2. Comparison of 1D FE and 3D FE initial stiffnesses, SLS rotations, and ultimate capacities for case RD70%_D10L30.

Model	Initial Stiffness [MN/m]	SLS Rotation [deg]	Ultimate Capacity [MN]
3D FE	244.4	0.450	43.9
1D FE	204.2	0.664	34.6
py only	(- 16.4 %)	(+ 47.7 %)	(- 21.1 %)
1D FE	234.5	0.481	42.1
all curves	(- 4.0 %)	(+ 6.9 %)	(- 4.0 %)

considered. For any L/D, the error is always larger when considering p-y curves only which suggests the need for the other component of soil reaction (distributed moment, base shear and base moment). For the p-y only scenario there is a clear trend for the errors to reduce when L/D increases. This is in agreement with the results of Byrne et al. (2015) and it explains why approaches validated for slender piles (API 2011, Broms 1964, Suryasantana and Lehane 2014) had satisfactory results for slender piles. However, for current monopile design with L/D of as low as 3, these approaches are no longer applicable.

It is not yet clear why the errors with all curves included tend to slightly increase with L/D. However, the errors are deemed small enough (typically less than 5%) and the extracted soil reaction curves are deemed satisfactory.

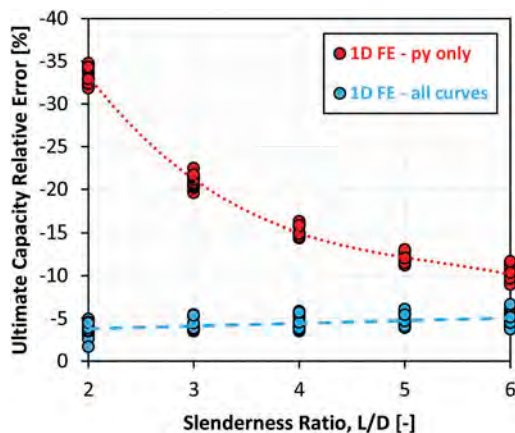


Figure 5. Comparison of ultimate capacity relative errors.

3.2 Comparison soil reaction curves

For the same case (RD70%_D10L30), Figure 6 shows the distributed lateral reaction curves (p-y curve) at a depth of 4.5 m as extracted from the 3D FE model and calculated as per API (2011), PISA rule (Burd

et al. 2020) and Broms (1964). Input parameters required for API (friction angle) and PISA rule (relative density) are calculated as per approach set out in Table 1. Broms (1964) approach is directly based on the synthetic CPT profiles presented in section 2.2.

Figure 6 Highlights the need to not only correctly match the ultimate reaction but also accurately describe the shape of the reaction curves. Broms (1964) overly simplify the problem by considering that the full reaction is mobilised at any displacement. In the API (2011), a hyperbolic tangent function is considered with the initial stiffness being a function of sand peak effective friction angle and depth. Although both approaches underestimate the ultimate capacity they will result in stiffer response in most practical cases (until a displacement of about 3% of pile diameter). On the contrary, the initial part of the PISA rule curve match relatively well with 3D FE. Although the ultimate capacity is underestimate again, they will result in similar response in most practical case.

In the PISA framework each of the reaction curves (distributed lateral reaction, distributed moment, base shear and base moment) are fitted with 4 parameters: the initial stiffness, the curvature, the ultimate reaction and the displacement at which the ultimate reaction is reached. This results in a total of 16 functions to correlate with CPT.

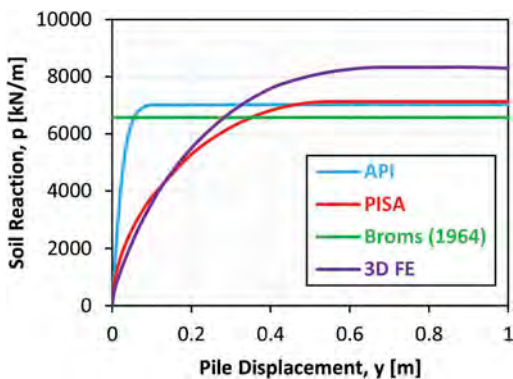


Figure 6. Comparison of distributed lateral reactions (p-y curves) at 4.5 m depth for case RD70%_D10L30.

4 ALTERNATIVE APPROACH

To date, no satisfactory CPT based correlations could be achieved due to a number of limitations with the current approaches. The main one (see sketch on Figure 7) is the lack of reaction close to pile point of rotation due to insufficient displacement. Although the pile is pushed until failure (mudline displacement larger than 10% of the pile diameter), the ultimate reactions are only reached for the top first 30%-40% of the pile length. No reaction at all is recorded close to point of rotation (at about 70% of pile length).

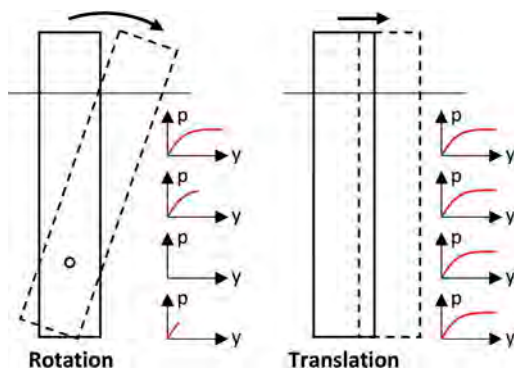


Figure 7. Limitation of the current rotation approach and proposed alternative approach.

An alternative approach is being considered where the pile would be laterally translated rather than rotated. This would allow for full mobilisation of reaction at any depth. Some components of the soil reaction may not be captured (distributed moment, base moment) and will still need to be extracted from the original models or correlated with the other component (distributed lateral reaction, base shear).

On-going works are focusing on comparing p - y curves extracted from both approaches to make sure they are comparable.

5 CONCLUSION

This paper presents a novel approach to derive CPT based correlation of soil reaction curves including distributed lateral reaction (p - y curves) but also distributed moment, base shear and base moment. This approach relies on finite element modelling in Plaxis 3D and the CPT based correlation of hardening soil model with small strain stiffness (HS-small) parameters developed by Igoe and Jalilvand (2020).

A total of 80 FE models are considered based on a range of pile geometry and synthetic CPT profiles for relative densities ranging from 30% (loose sand) to 90% (very dense sand).

All soil reaction curves are directly extracted from Plaxis 3D. Soil reactions are calculated from integration of stress at the pile-soil interface rather than derivation of pile shear force and bending moment profiles with depth. These are incorporated in a 1D FE solver and the obtained responses are compared with 3D FE to ensure the reaction curves are correctly extracted. Both initial stiffness, ultimate capacity and rotation under representative SLS loads are found to match well. By comparing the 1D FE responses when only p - y curves are considered, it is shown that existing approaches relying on p - y curves solely are not satisfactory for monopile modelling with slenderness ratio (L/D) of about 3.

Comparison of 3D FE extracted curves with existing approach shows that the ultimate distributed lateral soil reaction seems to be currently underestimated, but this may not necessarily translate into an under-estimation of the pile response depending on the curve stiffness (and the account of other soil reaction components).

Current work is focusing on the derivation of CPT based correlations for all soil reaction curves including distributed lateral load, distributed moment, base shear and base moment. However, no satisfactory results could be obtained so far.

It is being investigated if the current 3D modelling approach should be revised. The current approach involves rotation of the monopile around a point of rotation. There is no pile displacement close to the point of rotation and hence no soil reactions making most of the data extracted from the 3D FE models unusable. An alternative approach is being considered where the pile is being laterally translated in order to record soil reaction along the whole length of the monopile rather than only the top 30%-40%.

ACKNOWLEDGEMENT

The research conducted in this publication was funded by the Irish Research Council Postgraduate Employment-based Programme under grant number EBPPG/2019/4.

REFERENCES

- API (2011). "API RP2GEO: Geotechnical and Foundation Design Considerations."
- Benz, T., Schwab, R., and Vermeer, P. (2009). "Small-strain stiffness in geotechnical analyses." *Bautechnik*, 86(SUPPL. 1), 16–27.
- Bolton, M. D. (1986). "The strength and dilatancy of sands." *Géotechnique*, 36(1), 65–78.
- Brinkgreve, R. B. J., Engin, E., and Swolfs, W. M. (2018). "Plaxis 3D Materials Manual."
- Brinkgreve, R., Engin, E., and Engin, H. (2010). "Validation of empirical formulas to derive model parameters for sands." *Numerical Methods in Geotechnical Engineering*, (June), 137–142.
- Burd, H., Taborda, D., Zdravković, L., Abadie, C., Byrne, B., Houlsby, G., Gavin, K., Igoe, D., Jardine, R., Martin, C., McAdam, R., Pedro, A. and Potts, D. (2020). "PISA design model for monopiles for offshore wind turbines: application to a marine sand." *Géotechnique*, 70:11, 1048–1066.
- Byrne, B., MacAdam, R., Burd, H. and Houlsby, G. (2015). "New design methods for large diameter piles under lateral loading for offshore wind applications." *Proceedings to the Third International Symposium on Frontiers in Offshore Geotechnics in Oslo, Norway*.
- DNV (2013). DNV OS-J101: Design of offshore Wind Turbine Structures.
- DNV (2014). DNV OS-J101: Design of offshore Wind Turbine Structures.

- Igoe, D. and Jalilvand, S. (2020). "3D finite element modeling of monopiles in sand validated against large scale field tests." Proceedings to the Fourth International Symposium on Frontiers in Offshore Geotechnics in Houston, USA.
- Kirsch, F., Richter, T., and Coronel, M. (2014). "Geotechnische Aspekte bei der Gründungsdimensionierung von Offshore-Windenergieanlagen auf Monopfählen mit sehr großen Durchmessern." *Stahlbau Spezial 2014 – Erneuerbare Energien*, 83 (SUPPL. 2), 61–67.
- Kulhawy, F. H., and Mayne, P. W. (1990). „Manual on Estimating Soil Properties for Foundation Design.” EPRI-EL-6800.
- Mayne, P. W., and Kulhawy, F. (1982). "K₀ - OCR relationships in soils." *Journal of Geotechnical Engineering Division*, 108(6),851–872.
- Minga, E. and Burd, H. (2019). "Validation of the PLAXIS MoDeTo 1D model for dense sand".
- Panagoulas, S., Brinkgreve, R. and Zampich, L. (2021) "Plaxis Monopile Designer CE V21 Manual".
- Petrasovits, G., and Award, A. 1972. "Ultimate lateral resistance of a rigid pile in cohesionless soil." *Proc., 5th European Conf. on SMFE 3, The Spanish Society for Soil Mechanics and Foundation*, 407–412.
- Prasad, Y. V. S. N., and Chari, T. R. 1999. "Lateral capacity of model rigid piles in cohesionless soils." *Soils Found.*, 39(2), 21–29.
- Robertson, P. K., and Cabal, K. (2014). "Guide to Cone Penetration Testing for Geotechnical Engineering - 6th Edition".
- Schnaid, F., and Yu, H. S. (2007). "Interpretation of the seismic cone test in granular soils." *Géotechnique*, 57 (3),265–272.
- Suryasentana, S., and Lehane, B. M. (2014). "Numerical derivation of CPT-based p-y curves for piles in sand", 64(3)
- Wind Europe (2020). "Offshore wind in Europe: key trends and statistics."

CPT-based assessment of densification induced by stone column installation

F. Marchi, E. Zambianchi, A. Boschi, A. Mastrangelo & G. Marchi

ENSER Srl, Faenza, Italy

G. Gottardi & L. Tonni

UNIBO, Bologna, Italy

ABSTRACT: The use of CPTs for liquefaction susceptibility assessment has become increasingly common in design practice. In the past, the design of densification soil improvement methods against liquefaction has been commonly based on experience, large scale field tests and, possibly, validation after the intervention. Nevertheless, a design method to assess quantitatively the densification effect induced by stone column installation can be developed following a workflow based on CPTs, in order to estimate the efficiency of the soil improvement and to check the compliance with safety requirements before accessing the site. As by common practice, the assessment of liquefaction susceptibility is performed by means of CPT data and related empirical methods. The design method proposed in this paper is based on the estimation of modifications induced by the soil densification technique, easily detectable by the CPT profile, in order to carry out a liquefaction susceptibility analysis. The approach is applied in particular to a well-documented case study in Northern Italy (Bondeno, Ferrara province), providing a consistent dataset of piezocone tests carried out before and after soil treatment through stone columns, as part of a blast-induced liquefaction experiment. In this way, a clear comparison between pre- and post- intervention conditions along the CPT profiles with depth can be performed, thus allowing a validation of the design methodology.

1 INTRODUCTION

Among the ground improvement solutions available to mitigate the liquefaction hazard, densification is probably the most common and widespread. In particular, vibratory compaction methods are a common and effective form of densification for cohesionless soils (Castro 1969), as proven by extensive research (e.g. D'Apollonia 1954, Mitchell 1981, Baez 1995, Adalier and Elgamal 2004, Wissmann et al. 2015, Vautherin et al. 2017, Amoroso et al. 2018). In spite of its large application in the last decades, design methods to quantify and predict the efficiency of the improvement are not commonly reported in technical manuals.

Soil improvement has been mainly calibrated through real scale field tests; such type of tests presents, however, some issues to face. Real scale tests can be difficult to perform in a design phase, since often the executor of the treatment has not been chosen yet or the permission to operate in the area is not ready. Finally, real scale tests are expensive and need to be designed too.

In the following, a workflow will be described in order to obtain a prediction of the improvement efficiency. The proposed workflow is based on the CPT data. In fact, CPTs are cost effective site investigations and several simplified procedures for liquefaction

susceptibility assessment have been developed and validated in the last decades (e.g. Seed and Idriss 1971, Robertson and Wride 1998, Idriss and Boulanger 2008, Boulanger and Idriss 2014).

The results of the design workflow will be applied to the data coming from the field tests performed in connection with a full-scale controlled blast test in Bondeno (FE), Italy. A detailed geotechnical investigation of the site is presented by Amoroso et al. (in press).

2 THEORETICAL WORKFLOW

In case of real scale field test, common practice suggests following a number of steps:

1. performing investigations on the natural soil (CPT in the present study, PRE index will be used to address these data),
2. assessing liquefaction susceptibility on the data collected,
3. performing the soil improvement treatment,
4. performing new investigations (POST-M index will be used to address these data) in order to compare them with the pre-treatment ones,
5. assessing liquefaction susceptibility on the base of post-treatment data collected.

A soil improvement is recognized to be successful when the liquefaction susceptibility detected in the post-treatment phase is neglectable or tolerable.

The proposed workflow will follow the same steps. Point 4 will be done trying to predict a theoretical post-treatment CPT data (POST-P index will be used to address this data), modifying artificially the cone resistance q_c and sleeve friction f_s measurements, and finally assessing liquefaction susceptibility on the base of this predicted post-treatment test. In the following, the proposed procedure for the determination of the POST-P CPT parameters will be presented in detail.

With reference to the different CPT measurements ($q_{c,PRE}$, $f_{s,PRE}$), the cone resistance is assumed as the main parameter for the procedure. In particular the procedure will be applied to the normalized cone penetration resistance for clean sands, $Q_{tn,cs,PRE}$, defined as per Robertson & Wride (1998). The densification treatment in fact has its proper application on clean sands. Accordingly, it is then possible to back-calculate $q_{t,cs,PRE}$ and $q_{c,cs,PRE}$ from $Q_{tn,cs,PRE}$, according to the following relationships:

$$q_{t,cs,PRE} = \sigma_{v0} + p_a \frac{Q_{tn,cs,PRE}}{(p_a / \sigma'_{v0})^n} \quad (1)$$

$$q_{c,cs,PRE} = q_{t,cs,PRE} - u \cdot (1 - a) \quad (2)$$

where p_a = atmospheric pressure; σ_{v0} = vertical total stress; σ'_{v0} = vertical effective stress; u = pore pressure; a = cone area ratio.

Using the Jamiolkowsky et al. (2001) correlation, it is then possible to obtain the relative density ($D_{R,cs,PRE}$) and then the void ratio of the untreated soil ($e_{0,cs,PRE}$):

$$D_{R,cs,PRE} = \frac{1}{C_2} \cdot \ln \left[\frac{q_{c,cs,PRE} / p_a}{C_0 \cdot (\sigma'_{v0} / p_a)^{C_1}} \right] \quad (3)$$

$$e_{0,cs,PRE} = e_{max,cs} - D_{R,cs,PRE} \cdot (e_{max,cs} - e_{min,cs}) \quad (4)$$

where $C_0 = 17.68$; $C_1 = 0.50$; $C_2 = 3.10$ according to Jamiolkowsky et al. (2001) whereas $e_{max,cs}$ and $e_{min,cs}$ are assumed in this study equal to 1 and 0.4 respectively, in agreement with relevant ranges of the maximum and minimum void ratio shown by Cubrinovski & Ishihara (2002).

On the basis of the value assumed by the void ratio, it is possible to quantify the improvement induced by the densification treatment. In particular, the void ratio of the soil after treatment, $e_{0,cs,POST-P}$ can be inferred from a correlation originally proposed by Mitchell (1981) to predict sand compaction due to pile installation. Accordingly, $e_{0,cs,POST-P}$ is given by:

$$e_{0,cs,POST-P} = e_{0,cs,PRE} - A_r \cdot (1 + e_{0,cs,PRE}) \quad (5)$$

where A_r is the substitution ratio defined as the area of the treating element divided by the area of the treated mesh, as also explained in Figure 1. For the A_r values generally considered in practical applications, equation (5) results in values of $e_{0,cs,POST-P}$ within the range of values typically assumed by the void ratio.

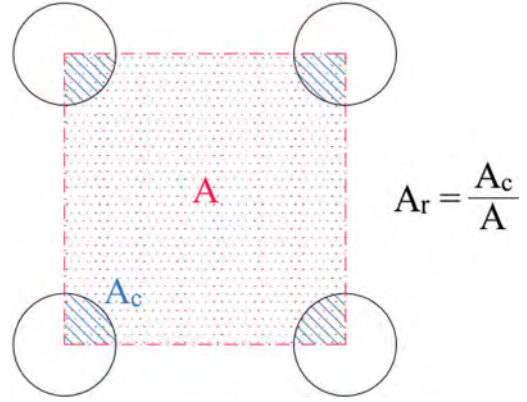


Figure 1. Definition of the A_r parameter.

Based on the improved void ratio, the procedure can be applied backward, giving:

$$D_{R,cs,POST-P} = \frac{e_{max,cs} - e_{0,cs,POST-P}}{e_{max,cs} - e_{min,cs}} \quad (6)$$

$$q_{c,cs,POST-P} = p_a \cdot C_o \cdot \left(\frac{\sigma'}{p_a} \right)^{C_1} \cdot e^{-C_2 \cdot D_{R,cs,POST-P}} \quad (7)$$

$$q_{t,cs,POST-P} = q_{c,cs,POST-P} + u \cdot (1 - a) \quad (8)$$

By applying again equations (1) and (2), it is then possible to back-calculate $q_{t,POST-P}$ and $q_{c,POST-P}$. The procedure presented above only involves the parameters defined from cone penetration resistance, whereas the sleeve friction resistance has not been touched yet. A disconnected modification in one of these two parameters would lead to a change in the soil behavior type index (I_c), that is mainly related to the soil class. Assuming that the improvement will not change the soil type, $f_{s,POST-P}$ can be back calculated from the improved cone penetration resistance.

A new profile of the CPT can be then predicted ($q_{c,POST-P}$, $f_{s,POST-P}$). Ordinary procedures to assess liquefaction susceptibility can be performed on the new profile in order to evaluate the efficiency of the soil improvement treatment on a theoretical base.

An additional evaluation has to be performed to assess the suitability of soils for vibratory compaction,

since it is documented in literature that only soils with low fines content react properly to vibratory compaction (Massarsch, 1991).

3 VERIFICATION ON BLAST TEST DATA

Bondeno blast test site offered the occasion to verify if the theoretical framework gives a good prediction of the soil improvement efficiency. The site has been widely investigated in natural conditions, before treatment (Phase I), after the soil improvement (Phase II) and after the blast-induced shaking (Phase III). The soil improvement consisted of a number of 4 x 4 columns in quadrangular grid (2m center-to-center spacing) of Rammed Aggregate Piers (RAP) columns (Saftner et al., 2018), each 9.5m long and with a final diameter of 0.5m ($A_r \approx 5\%$) (Amoroso et al., in press).

Among the available cone penetration tests carried out in the test site, CPT01 performed in Phase I (also referred in the following to as CPT01_PRE) and CPT01bis performed in Phase II (also referred to as CPT01bis_POST-M) have been chosen to test the procedure described above.

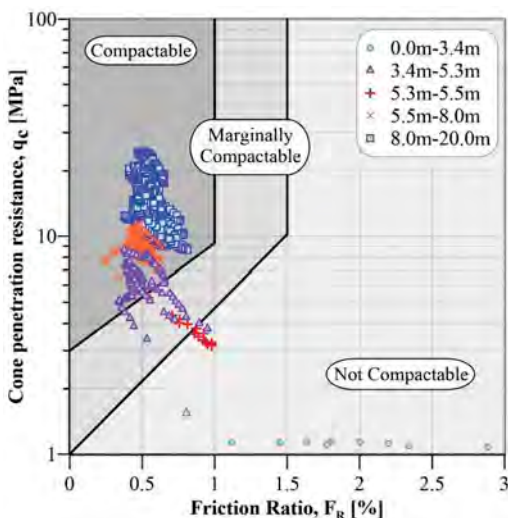


Figure 2. Soil classification for assessment of deep compaction based on CPT (Massarsch, 1991).

In particular:

- CPT01 is the test performed before the soil improvement treatment ($q_{c,PRE}$);
- CPT01 will be modified following the workflow exposed in section 2 in order to predict the post-treatment cone resistance profile ($q_{c,POST-P}$);
- CPT01bis is the test carried out after the installation of the RAPs, providing the profile of the measured cone resistance ($q_{c,POST-M}$).

As reported in Amoroso et al. (in press), the Bondeno test site subsoil consists of a silty-clayey hard topsoil in the upper 3.5m, with an average plasticity index (PI) of 20%, followed by a non-plastic silty sand with fine content typically in the range 25-35% and therefore classified as SM.

Suitability for vibratory compaction of CPT01_PRE has been evaluated following Massarsch (1991); Figure 2 shows that the cone penetration data points, in terms of tip resistance q_c and friction ratio F_R (calculated as $100 \cdot q_c/f_s$), fall in the domain of compactable materials.

Figure 3 provides a comparison between CPT01 and CPT01bis, carried out at a distance of 1.5m. Profiles of q_t , soil behaviour type index I_c , relative density D_R , fine content F_C , Factor of Safety against liquefaction SF and Liquefaction Potential Index LPI are provided. The plot clearly shows where and how the soil improvement affected the degree of compaction of the natural soil, taking into account that RAP length was 9.5m.

Liquefaction analyses have been performed following the procedure suggested by Boulanger & Idriss (2014).

4 FINAL RESULTS

Following the theoretical workflow presented in section 2, data from CPT01_PRE test have been elaborated to produce a design prediction of the treated soil. The prediction will be referred to as CPT01_POST-P. A comparison between measured and predicted profiles is presented in Figure 4.

The comparison in terms of q_t shows a very good agreement from 5.5m to 8.0m in depth. In the lower part of the treatment (from 8.0m to 9.5m) the efficiency of the soil improvement seems to decrease; this can be related to the influence of the end depth of the treatment. Getting closer to the tip of the columns, the basic hypothesis of two-dimensional behavior in the horizontal plane, on which eq. (5) relies, can no longer be considered as strictly valid. Three-dimensional effects probably have some influence in the soil volume, causing a decrease in the densification effect.

In the range between 3.4m and 5.3m, the agreement is still quite good, although the predicted q_t profile shows values higher than those measured. The same comments apply to the values of D_R .

The evaluations related to liquefaction susceptibility, expressed in terms of SF and LPI, show similar trend, though the suggested workflow seems to slightly overestimate the efficiency of the soil improvement. Considering the result on LPI, the distribution along depth suggests the same differences discussed above. In particular, from 5.5m down to the end of the test the agreement between prediction and measured data is extremely good. More significant differences are observed in the range 3.4m - 5.3m depth. Results from comparison between CPT01_POST-P and

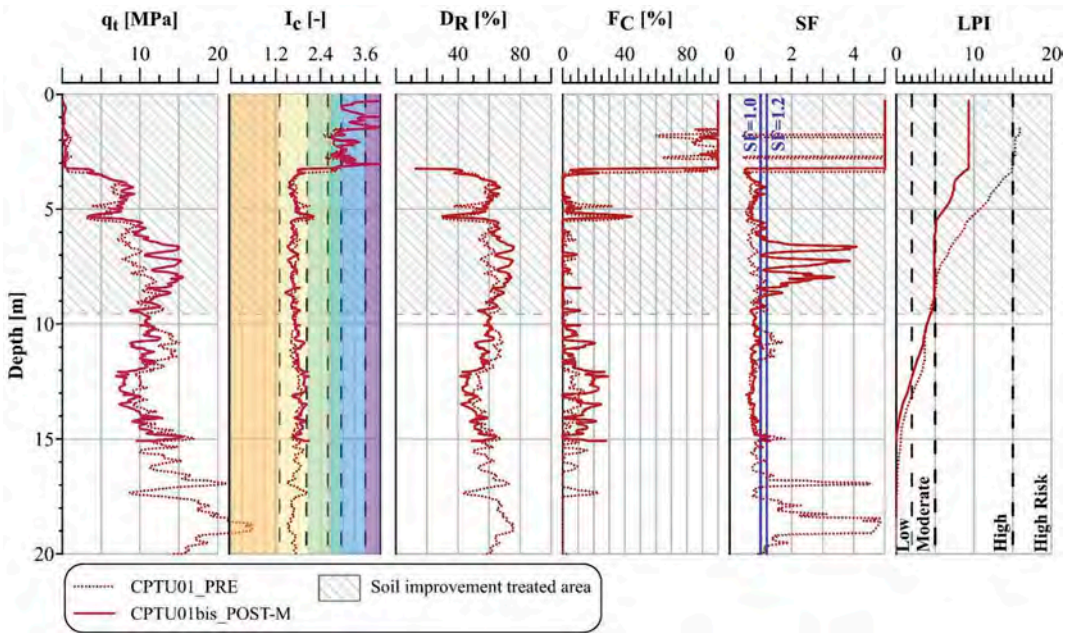


Figure 3. Comparison between pre-treatment (CPTU01_PRE) and post-treatment (CPTU01bis_POST-M) investigations.

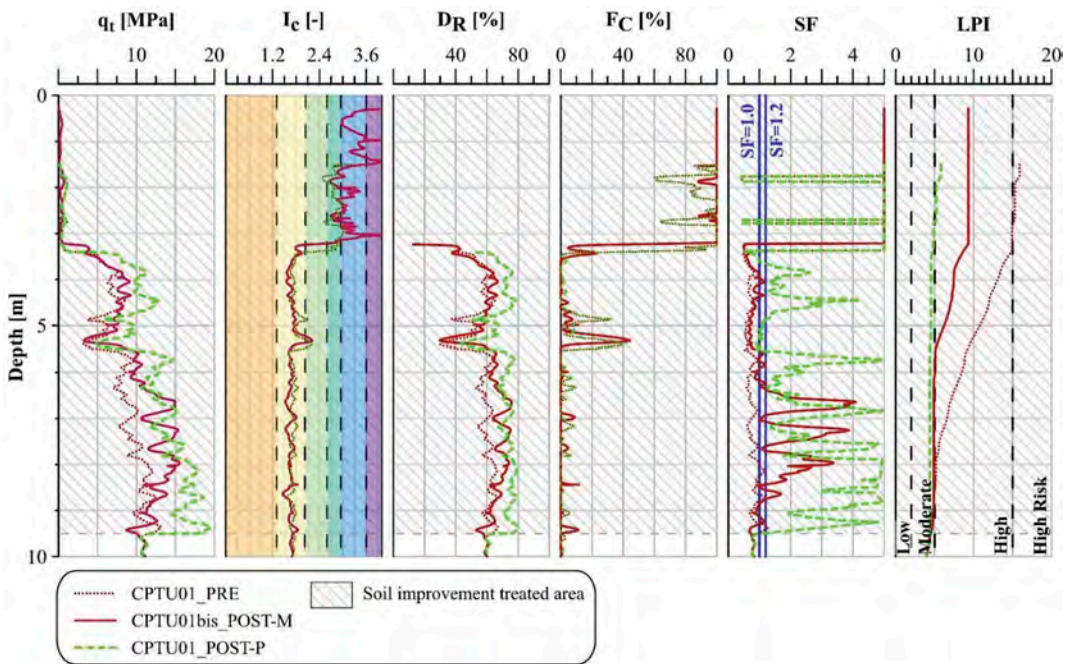


Figure 4. Comparison between pre-treatment (CPTU01_PRE) and post-treatment investigations, as measured in CPTU01bis_POST-M and predicted in CPTU01_POST-P.

Table 1. Numerical evaluation of predictions.

z m	Soil	q _t MPa	D _R %	SF
3.4-5.3	CPT01_PRE	6.39	56	0.66
	CPT01bis_POST-M	7.09 (+11%)	57 (+3%)	0.80 (+20%)
	CPT01bis_POST-P	9.65 (+51%)	69 (+24%)	1.59 (+139%)
5.8-8.0	CPT01_PRE	8.94	60	0.76
	CPT01bis_POST-M	12.33 (+38%)	69 (+15%)	1.85 (145%)
	CPT01bis_POST-P	13.45 (+50%)	73 (+22%)	2.76 (+264%)
3.4-9.5	CPT01_PRE	7.66	57	0.71
	CPT01bis_POST-M	9.86 (+29%)	63 (+11%)	1.36 (+91%)
	CPT01bis_POST-P	11.55 (+51%)	70 (+23%)	2.20 (+209%)

CPT01bis_POST-M, taking CPT01_PRE as reference, are summarized in Table 1. The percentage increment of q_t, D_R and SF after treatment is given in brackets.

5 CONCLUSIONS

The theoretical workflow proposed in this paper is a guideline for the quantification of soil improvement effectiveness in densification treatment against liquefaction. Following the procedure, it is possible to obtain a design prediction of the soil improvement based only on CPT data. This simple approach is very useful in a design phase where in situ tests are commonly available for liquefaction assessment, but it is hardly possible to carry out full-scale field tests.

The application of the workflow on a case-study in Bondeno (FE) allowed to evaluate the performance of the method by comparing predictions with verification tests. The overall result gives a good agreement in the lower liquefiable layer, though further analyses need to be performed in order to verify local differences with depth. In addition, only one CPT was available for the verification of the workflow, verifying the approach on other test couples performed in different sites with different soil conditions is needed.

The workflow seems to slightly overestimate the soil improvement beneficial effects. This can be related to a variety of factors. A general efficiency factor is a possible solution in order to take into account different aspects related to the installation method. The procedure would also need to be extended through the implementation of efficiency factors accounting for marginally compactable soils (with higher fine and/or plastic contents) and for the reduction of soil treatment efficiency approaching the treatment tip. It is in fact reasonable to consider

that, close to the column tip, the efficiency of the treatment will gradually decrease to zero, while in the method described in this paper the densification effect is solely quantified on the horizontal displacement of the soil.

ACKNOWLEDGEMENTS

The study presented in the paper was based on the data collected within a Blast Test experiment, carried out with the financial support of Istituto Nazionale di Geofisica e Vulcanologia (INGV), CIRI Edilizia e Costruzioni - University of Bologna, Geopier® Foundation Company, and Releo srl.

REFERENCES

- Adalier, K. & Elgamil, A. 2004. Mitigation of liquefaction and associated ground deformations by stone columns. *Eng. Geol.*, 72(3-4): 275–291.
- Amoroso, S., Rollins, K.M., Monaco, P., Holtrigter, M., & Thorp, A. 2018. Monitoring ground improvement using the seismic dilatometer in Christchurch, New Zealand. *Geotech. Test. J.*, 41 (5): 946–966. <https://doi.org/10.1520/GTJ20170376>.
- Amoroso, S., Martínez, M.F.G., Monaco, P., Tonni, L., Gottardi, G., Rollins, K.M., Minarelli, L., Marchetti, D., Wissmann, K.J. Comparative study of CPTU and SDMT in a silty sand liquefaction-prone site improved by Rammed Aggregate Piers and subject to controlled blasting. *Journal of Geotechnical and Geoenvironmental Engineering* (in press).
- Baez, J.I. 1995. A design model for the reduction of soil liquefaction by vibrostone columns. *Ph.D dissertation*, Univ. of Southern California.
- Boulanger, R.W. & Idriss, I.M. 2014. CPT and SPT based liquefaction triggering procedures. *Rep. No. UCD/CGM-14/01*. Davis, CA: Center for Geotechnical Modeling, Dept. of Civil and Environmental.
- Castro, G. 1969. Liquefaction of sands. *Ph.D. Dissertation*, Harvard University.
- Cubrinovski, M. & Ishihara, K. 2002. Maximum and minimum void ratio characteristics of sands. *Soil and Foundations*, Vol.42, No.6, 65–78.
- D'Appolonia, E. 1954. Loose sands - their compaction by vibroflotation. In *Proc., Symp. on Dynamic Testing of Soils*: 138–162. West Conshohocken, PA: ASTM International.
- Idriss, I.M. & Boulanger, R.W. 2008. Soil liquefaction during earthquakes. *Report No. MNO-12*. Oakland, CA: Earthquake Engineering Research Institute.
- Jamiolkowski, M., Lo Presti, D.C.F., Manassero, M., 2001. Evaluation of Relative Density and Shear Strength of Sands from CPT and DMT. *ASCE Geotechnical Special Publication* No. 119: 201–238.
- Massarsch, K.R., 1991. Deep Soil Compaction Using Vibratory Probes. In *Robert C. Bachus, Ed., American Society for testing and Material, ASTM, Symposium on Design, Construction, and Testing of Deep Foundation Improvement: Stone Columns and Related Techniques*, *ASTM Special Technical Publication, STP 1089*: 297–319.
- Mitchell, J.K. 1981. Soil improvement: state-of-the-art. In *Proc. 10th Int. Conf. on Soil Mechanics and Foundation Engineering*, Vol. 4: 509–565.

- Robertson, P.K. & Wride, C.E. 1998. Evaluating cyclic liquefaction potential using the cone penetration test. *Can. Geotech. J.*, 35(3): 442–459.
- Robertson, P.K. & Cabal, K.L., 2015. Guide to Cone Penetration Testing for Geotechnical Engineering, 6th edition.
- Saftner, D.A., Zheng, J., Green, R.A., Hryciw, R. and Wissmann, K.J. 2018. Rammed aggregate pier installation effect on soil properties. *P. I. Civil Eng. Ground Impr.* 171 (2), 63–73.
- Seed, H.B. & Idriss, I.M. 1971. Simplified procedure for evaluating soil liquefaction potential. *J. Geotech. Engrg. Div.*, ASCE, 97(9): 1249–1273.
- Vautherin, E., Lambert, C., Barry-Macaulay, D., & Smith, M. 2017. Performance of rammed aggregate piers as a soil densification method in sandy and silty soils: experience from the Christchurch rebuild. In *Proc., 3rd Int. Conf. on Performance-based Design in Earthquake Geotechnical Engineering*.
- Wissmann, K.J., van Ballegooy, S., Metcalfe, B.C., Dismuke, J.N., & Anderson, C.K. 2015. Rammed aggregate pier ground improvement as a liquefaction mitigation method in sandy and silty soils. In *Proc., 6th Int. Conf. on Earthquake Geotechnical Engineering*.

Geopier Impact technology for liquefaction risk mitigation based on CPTu investigations

G. Martinez & K. Wissmann

Geopier Foundation Company, Davidson, USA

M. Franceschini, E. Bandiera & F. Fiorelli

Teleios Srl-Società di Ingegneria, Castel Maggiore, Bologna, Italy

ABSTRACT: The present paper is focused on the Impact Rammed Aggregate Pier system, a ground improvement technology developed by Geopier Foundation Company. From extensive in-situ tests also including blast tests, Impact elements have proven to be very effective at densifying in-situ granular soils and increasing the factor of safety against liquefaction. The intent of the paper is to verify the methods that are used to evaluate liquefaction mitigation with Impact piers. One method to evaluate the mitigation of liquefaction risk for design of Impact piers is to estimate the increase in CPT tip resistance q_c expected after installation of the Impact elements. In the paper we will consider CPTu tests performed before and after Impact installations in various sites worldwide to attempt to verify the accuracy of formulas from literature and to try to understand which aspects can be refined in future studies. The future aim is to possibly modify the formulas to account for local soil conditions in the Emilia-Romagna region in Italy.

1 INTRODUCTION

Among the various technologies for soil improvement, stone columns are a method extensively used all around the world with different technological variants.

In addition to their demonstrated capacity to increase soil resistance and to reduce foundation settlements against static loads, the increasing interest in soil improvement methods for geotechnical seismic engineering has led to an advance in the study of gravel columns for liquefaction mitigation purposes.

The proposed paper focuses on a specific type of gravel column, the Rammed Aggregate Pier (RAP) Impact technology developed by Geopier Foundation Company. The Impact technology is a displacement system that produces highly compacted gravel columns together with vibro-densification of the in-situ granular soils. Successfully used in several hundred sites worldwide, the Impact system has also proven to be very effective at densification and controlling liquefaction compared to other methods such as timber piles and reinforced gravel rafts (EQC, 2015).

Since predicting densification is a very useful tool for the design engineer when liquefaction mitigation is required, the authors recognize the importance of having reliable predictive correlations and having knowledge of which regions in the world these correlations may need to be modified for. The aim of the article is to present the state of the art of predictive methods for

estimating densification based on Piezocone Penetration Tests (CPTu). One method available in literature will be presented and its reliability will be assessed by means of comparison with pre and post-installation CPTu tests performed in various sites around the world.

The future aim of the authors is to develop correlations specific to the local soil conditions in the Emilia-Romagna region in Italy, where the authors have already designed several projects for liquefaction mitigation.

2 RAMMED AGGREGATE PIER ELEMENTS

Rammed Aggregate Pier elements are a ground improvement technology developed over the last 25 years by Geopier Foundation Company. The RAP installation method creates a densified column of aggregate surrounded by a stiffened matrix soil, with the aim of providing settlement control and allowing for higher bearing capacities.

RAP installation methods can be classified as either “drill and fill”, such as the GP3 system for non-caving soils, or “displacement” such as the Impact system.

2.1 Impact system

The advantage of the Impact system is that it allows for the construction of a Rammed Aggregate Pier element by displacement of the in-situ soil, aided by the use of a vibratory hammer.

The use of this technology is particularly suitable in the case of loose sand deposits below the groundwater table and for soils where it is not possible to carry out drilling without supporting the walls of the drilled cavities.

The mandrel consists of a steel tube with a specially designed compaction chamber at the tip for achieving high vertical compaction of the aggregate and, consequently, lateral expansion of the cavity. A sacrificial plate is typically used for the initial drive of the mandrel, after which the mandrel is filled with gravel to begin construction of the pier. The mandrel is subsequently raised by about 90 cm, allowing the aggregate to flow into the displaced cavity, and then lowered to compact the gravel, forming layers 30/35 cm thick. The achievable depths are typically up to 15 m, with constructed diameters ranging from 50 to 60 cm. The construction methodology has been described in detail by Majchrzak et al. (2010).

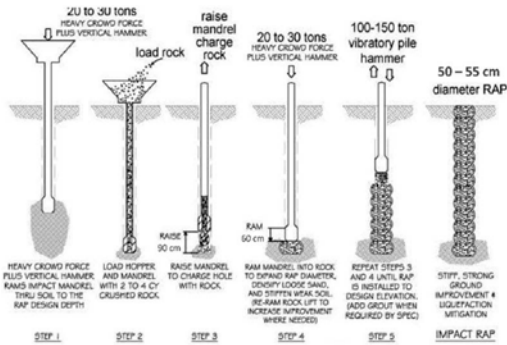


Figure 1. RAP Impact installation sequence.

The installation process is quick and clean (dry installation), and the displacement process produces minimal spoils. The end result of this construction method is a very stiff aggregate column, with the added benefit of densification of the surrounding sandy matrix soil.

3 LIQUEFACTION MITIGATION WITH RAP GROUND IMPROVEMENT ELEMENTS

The Impact technology finds its core applications on structures transmitting medium to medium-high loads, such as industrial sheds or buildings of medium height, tanks, silos, embankments or floorings.

Another specialty use of the RAP Impact technology is its application in reducing liquefaction risk in loose to medium dense sandy soils below the groundwater table. The high vertical compaction and vibratory energy applied during Impact pier installations expands the cavity created by the driven

mandrel and densifies the surrounding granular soil, thereby reducing this risk.

Used in a large number of projects worldwide including Italy, the effectiveness of the system in mitigation of liquefaction risk has been demonstrated by both on-site tests and real case histories. In addition, their effectiveness in mitigating liquefaction in clean sandy soils has been well documented by Farrell et al. (2010); Majchrzak et al. (2010); Wissmann et al. (2015) and Saftner et al. (2016).

The effectiveness of RAP Impact elements for liquefaction mitigation in siltier soil has been demonstrated from the full-scale data set collected at Bricceno Bridge embankment; a site reinforced with RAP elements that performed well after the Muisne Mw 7.8 earthquake (Smith & Wissmann, 2018; Amoroso et al., 2020; Salocchi et al., 2020). Finally, full-scale blast-induced liquefaction tests were recently carried out in Bondeno, Italy (Amoroso et al., 2020; Rollins et al., 2021) to directly evaluate the effectiveness of RAP Impact elements in mitigating liquefaction hazards in silty sands. Also in this case, improvement with Impact elements was effective in reducing liquefaction-induced settlements to acceptable levels in comparison with the untreated soil.

4 PREDICTION OF LIQUEFACTION MITIGATION WITH CPTU

From a design point of view, there are formulations and methods available in literature to quantify the improvement of the soil matrix after installation of Impact piers for liquefaction risk mitigation. These are based on in-situ CPTu investigations, which are usually the only data provided to the engineer at the design stage.

A popular method to quantify the improvement of the soil matrix after installation of Impact piers is to estimate the densification expected after the installation of the piers. Estimating the increase in CPT tip resistance q_c is a common way of considering densification and this will be the method of focus in this paper. By using the increased q_c , which is dependent on the soil type, depth and other parameters, and by referring to the pre-improvement sleeve friction f_s and soil behavior type index I_c , it is possible to evaluate the updated Factor of Safety against liquefaction.

Additional methods such as evaluation of Shear Stress Attraction (Green et al., 2008; Rayamajhi et al., 2012), the increase in lateral confinement stress and Cyclic Resistance Ratio CRR (Salgado et al., 1997), and use of the stiffness of the Impact piers to reduce post-liquefaction deformations (Rollins et al., 2021) are beyond the scope of this paper.

4.1 New Zealand-based correlation

The study undertaken by Vautherin et al. (2017), provides correlations for predicting the degree of densification after Impact pier installations. The study is based on a large database of CPT data spread among 80 sites across Christchurch, New Zealand. The sites were treated with Impact piers after the full-scale trials in 2013 indicated their effectiveness in reduction of liquefaction risk (EQC, 2015).

The authors introduced the ratio Q_c to indicate improvement, and is defined as the ratio between the post treatment q_c and the pre – treatment q_c .

The relationships for Q_c in clean sand are given by equation 1 and 2 as a function of the effective confinement stress σ'_{v0} .

For $\sigma'_{v0} < 30$ kPa:

$$Q_c \text{ ratio} = 4.0 - 0.076 \cdot \sigma'_{v0} \quad (1)$$

For $\sigma'_{v0} > 30$ kPa:

$$Q_c \text{ ratio} = 1.69 \quad (2)$$

In silty soils, with soil behavior type index I_c comprised between 1.8 and 2.4, the correlations proposed for Q_c are presented below. The authors of the Vautherin (2017) paper highlight that these three equations should not be used for design given the large scatter observed in the data.

For $1.8 < I_c < 2.0$:

$$Q_c \text{ ratio} = 2.7 - 0.015 \cdot \sigma'_{v0} \quad (3)$$

With $R^2 = 0.16$. For $2.0 < I_c < 2.2$:

$$Q_c \text{ ratio} = 2.0 - 0.01 \cdot \sigma'_{v0} \quad (4)$$

With $R^2 = 0.06$. For $2.2 < I_c < 2.4$:

$$Q_c \text{ ratio} = 1.7 - 0.007 \cdot \sigma'_{v0} \quad (5)$$

With $R^2 = 0.03$.

Impact piers in most of the sites were installed at an area replacement ratio (ARR) of 8%. ARR values of 5 to 8% are typically used in liquefaction mitigation projects.

5 PREDICTION ASSESSMENT

The scope of this paper is to both verify the accuracy of the densification formulas from literature, and to attempt to identify areas for improvement for future studies.

In order to assess the reliability of the correlations available, we have considered CPTu tests performed in Christchurch, New Zealand and Bondeno, Italy

both before and after installation of Impact elements; and comparisons are made between the predicted q_c increments and the measured q_c increments.

5.1 Christchurch, New Zealand sites

The pre and post-installation CPTs presented below were performed during the full-scale trials carried out in Christchurch, New Zealand in 2013 (EQC, 2015). The tests were performed in three different trial sites (Site 3, Site 4 and Site 6), in which Rammed Aggregate Pier (RAP) columns were installed to 4m depth with a triangular spacing of about 1.50 m, 2.00 m and 1.80 m on-center resulting in Area Replacement Ratios of approximately 14.5%, 8% and 5%, respectively (Amoroso et al., 2015). In all the sites, pre and post-installation CPTu tests were performed in both natural and treated soil to investigate the effects of RAP Impact installations on soil properties, with post-installation CPTs performed at the center of a pier group.

Figures 2-4 plot the measured pre and post installation CPT tip resistance q_c and the predicted q_c using Equations 1-5 as well as the soil behavior type index I_c obtained from the CPTu carried out in untreated and treated soil. The predicted q_c values were plotted separately for $I_c < 1.8$ and $I_c > 1.8$.

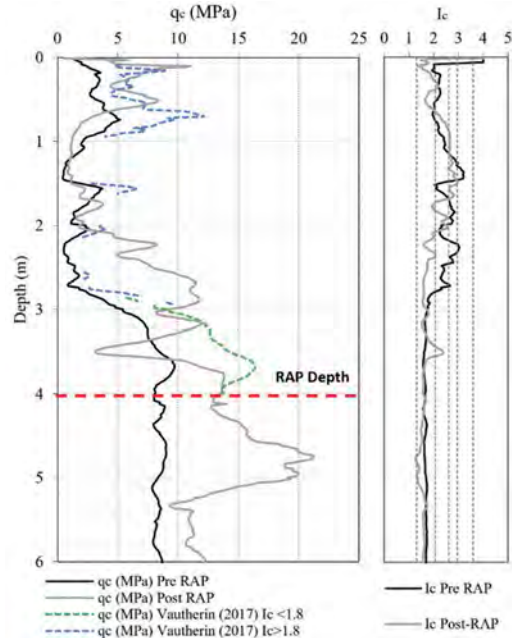


Figure 2. Comparison of measured pre and post-installation q_c profile with depth and predicted ones according to exposed correlations and I_c for site 3.

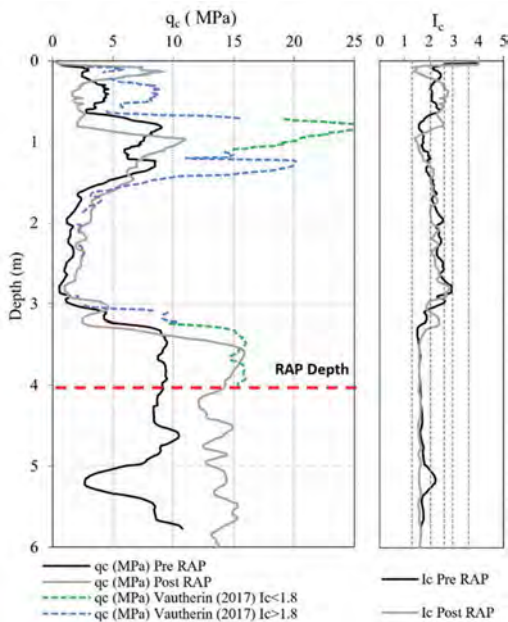


Figure 3. Comparison of measured pre and post- q_c profile with depth and predicted ones according to exposed correlations and I_c for site 4.

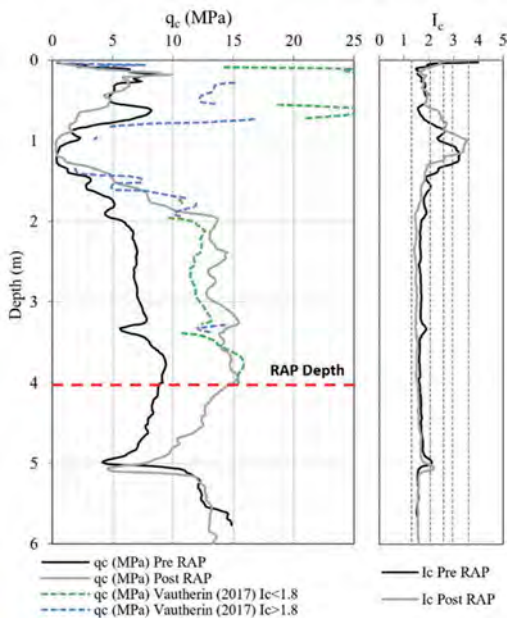


Figure 4. Comparison of measured pre and post- q_c profile with depth and predicted ones according to exposed correlations and I_c for site 6.

5.2 Bondeno test site, Italy

A full-scale trial for blast induced liquefaction was carried out in Bondeno, Italy in 2018. The test was carried

out to assess the effectiveness of RAP elements for liquefaction mitigation (Rollins et al., 2021). In the study, 16 RAP elements were installed to a depth of 9.5 m in a square grid pattern at a spacing of 2m on-center, resulting in an ARR of 5%. The post-installation CPT was performed at the center of a group of four piers. The pre and post-installation CPT results are provided in Figure 5 below obtained from Rollins et al. (2021).

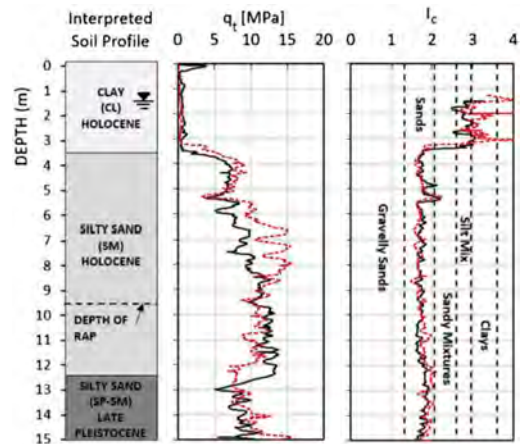


Figure 5. CPTu profile pre and post RAP treatment at the Bondeno test site (Rollins et al., 2021). Pre-RAP q_c data is plotted in black and post-RAP q_c data is plotted in red.

The authors were not able to obtain the CPT data file to plot all the measured and predicted increases in q_c with depth as was done for the New Zealand sites.

5.3 Composite results

We proceeded to analyze several representative layer data points in each of the CPTs from all four sites to compare the predicted and measured increases in CPT tip resistance q_c directly. The points were selected at depths where the pattern of the peaks and valleys of the pre and post-improvement q_c suggest that a similar layer was detected in both CPTs. Points where the post-improvement q_c was lower than the pre-improvement q_c were not selected. It is noted that pre and post-improvement soil behavior type index I_c values may not be closely matched for the selected points since the post-improvement q_c and sleeve friction f_s are different than the pre-improvement values after densification has occurred.

The data points chosen are tabulated in Table 1. Data points for the New Zealand Site 3 were only selected between 0m and 1m depth as the stratigraphy below 1m was more dissimilar between the pre and post-improvement CPTs. The pre and post-improvement q_c values for the Bondeno site were visually approximated using Figure 5 as the CPT data files were not available. The data between 3.5 and 6m depth at this site was discarded due to observed issues

with aggregate flow during pier installations and the corresponding lack of cavity expansion (densification). It is noted that Figure 5 plots the total cone resistance q_c ; though, the difference between q_i and q_c may be small for the points selected as most points of the Bondeno data points have I_c values of less than 1.8.

Table 1. Selected data points for comparison. Pre-improvement and post-improvement data tabulated in the same row were considered to pertain to the same soil layer.

Site	Pre-improvement data points		Post-improvement data points (Measured)	
	Depth (m)	q_c (MPa)	Depth (m)	q_c (MPa)
NZ Site 3	0.44	2.70	0.34	4.41
	0.74	5.17	0.51	8.38
NZ Site 4	0.79	8.75	0.99	10.72
	1.71	2.37	1.79	3.48
	2.0	1.3	2.14	2.59
	2.5	1.13	2.5	2.33
	3.34	8.94	3.56	15.72
NZ Site 6	4.0	9.09	4.0	14.28
	1.5	3.15	1.5	5.12
	2.0	5.84	2.0	13.7
	2.5	6.96	2.5	14.03
	3.0	7.21	3.0	13.42
Bondeno	3.5	8.06	3.5	14.22
	4.0	9.12	4.0	15.05
	6.8	9.9	6.8	15.0
	7.0	8.3	7.0	10.9
	7.15	9.3	7.25	15.4
	7.75	10.5	7.95	15.4
	8.2	9.9	8.2	14.4
	8.6	12.0	8.6	14.0

The predicted post-improvement q_c values were subsequently estimated with the Vautherin et al (2017) equations using the pre-improvement q_c values in Table 1 and the respective effective confinement stress σ'_{v0} and soil behavior type index I_c for each data point tabulated. The predicted and measured increases in CPT tip resistance q_c (Δq_c) were subsequently estimated and plotted in Figure 6. The results suggest good agreement between the Vautherin et al (2017) correlation and the measured q_c values for the New Zealand sites and suggest that the correlation overpredicts the increase in q_c for the Bondeno site soils. It is possible that aggregate flow negatively impacted densification even below 6m depth at the Bondeno site.

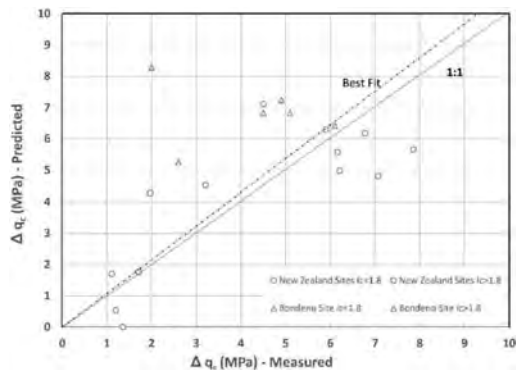


Figure 6. Comparison of predicted increase in q_c with measured increase in q_c profile for all sites.

6 DISCUSSION AND FUTURE DEVELOPMENTS

This study indicated that the correlations used for estimating improvement in q_c show generally good agreement with post-installation q_c measurements, despite the uncertainties and variables that can affect these correlations.

The degree that a soil layer can be densified, which can be expressed in terms of increase in the tip resistance q_c in CPTu tests, is a function of the lithology and confinement stress. Little difference in densification was evident between the Impact pier spacings of 1.5 to 2m used in the Christchurch trials. Additional research could be undertaken to consider the normalized CPT tip resistance q_{c1n} proposed by Boulanger (2003), which automatically eliminates the influence of the soil's effective overburden pressure.

Moreover, New Zealand case histories show that in, certain soils, densification occurred below the bottom depth of the columns. Clearly this is not considered in the bibliographical formulas and is an area that needs an in-depth study.

It is also evident that the greatest accuracy is found in the tests carried out in Christchurch. This is because some areas of the city, following the Canterbury Earthquake Sequence in New Zealand in 2010-2011, were home to a unique large-scale study on the efficacy of the Impact technology along with other type of ground improvement. Thus, a large amount of data and site measurements on the effect of RAP Impact installation has been derived from the Christchurch area.

The final goal is to develop more accurate tools to improve the accuracy of RAP Impact pier designs for liquefaction risk mitigation. The authors, together with the licensed Geopier installer in Italy, have designed and constructed several liquefaction risk mitigation projects with RAP Impact elements in the Emilia-Romagna region, including the cities of Ravenna, Cervia and Forli. In these sites, "pre and post" CPTu investigations are being carried out to form part of

a future local database. Eventually, a new general correlation could be proposed, or the correlations could be specialized to be specific to the Emilia-Romagna region. This is an ambitious goal and is expected to be developed over a medium-long term time frame. The authors hope to include the pre and post-installation CPTu tests performed at Bondeno test site (Figure 5) into the future Emilia-Romagna local database.

7 CONCLUSION

The Impact pier technology developed by Geopier Foundation Company is a ground improvement method employed worldwide for reduction in site requiring liquefaction risk mitigation. The displacement and vibro-compaction construction technique improve the surrounding sandy soils by means of densification which subsequently reduces the risk of liquefaction.

Numerous tests and bibliographic case histories have demonstrated the effectiveness of this technology for liquefaction risk mitigation. In addition, predictive methods are available for the designer to estimate the densification of the soil based on lithology.

The main purpose of the article was to test the reliability of these methods by means of post-installation CPTu data from sites around the world. The predictive correlations appear to be a useful assessment tool to help in predicting liquefaction mitigation using Impact during the geotechnical design. Nevertheless, further efforts need to be made to extend the existing databases and eventually to specialize them geographically by studying and evaluating site-specific correlations. In this direction the authors are already carrying out more in-depth studies, focused on design phase, that may be the subject of future publications.

ACKNOWLEDGMENTS

The authors would like to thank Sara Amoroso for providing the data of on-site tests presented here.

REFERENCES

- Amoroso, S., K. M. Rollins, P. Andersen, G. Gottardi, L. Tonni, M. F. Garcia Martinez, K. Wissmann, L. Minarelli, C. Comina, D. Fontana, P. M. De Martini, P. Monaco, A. Pesci, V. Sapia, M. Vassallo, M. Anzidei, A. Carpena, F. Cinti, R. Civico, I. Coco, D. Conforto, F. Doumaz, F. Fannattasio, G. Di Giulio, S. Foti, F. Loddo, S. Lugli, M. R. Manuel, D. Marchetti, M. Mariotti, V. Materni, B. Metcalfe, G. Milana, D. Pantosti, A. Pesce, A. C. Salocchi, A. Smedile, M. Stefani, G. Tarabusi, & G. Teza (2020). Blast-induced liquefaction in silty sands for full scale testing of ground improvement methods: Insights from a multidisciplinary study. *Eng. Geol.* 265 (Feb): 105437.
- Amoroso, S., K. M. Rollins, K. Wissmann, & L. Minarelli (2020). Estimation of lateral spreading by SPT, CPTU and DMT following the 2016 Mw7.8 Ecuador earthquake. *Proc. ISC'6 Conference*, Budapest, Hungary.
- Amoroso, S., K. M. Rollins, P. Monaco, & A. Thorp (2015). Use of SDMT testing for measuring soil densification by ground improvement. *3rd International Conference on the Flat Dilatometer*, Christchurch, New Zealand.
- Boulanger, R.W. (2003). State normalization of penetration resistance and the effect of overburden stress on liquefaction resistance. *Proc. 11th international conference on soil dynamics and earthquake engineering and 3rd international conference on earthquake geotechnical engineering*. University of California, Berkeley.
- EQC (2015). Residential Ground Improvement Main Report. Findings from trials to manage liquefaction vulnerability. <https://www.eqc.govt.nz/assets/Publications-Resources/Residential-Ground-Improvement-Findings-from-trials-to-manage-liquefaction-vulnerability-report.pdf>
- Farrell, T.M., K. Wallace, & J. Ho (2010). Liquefaction mitigation of three projects in California. *Fifth International Conference on Recent Advances in Geotechnical Engineering and Soil Dynamics and Symposium in Honor of Professor I.M. Idriss*, San Diego, California.
- Green, R.A., C. G. Olgun, & K. J. Wissmann (2008). Shear stress redistribution as a mechanism to mitigate the risk of liquefaction. *ASCE GSP-181, Geotechnical Earthquake Engineering and Soil Dynamics IV*.
- Majchrzak, M., T. Farrell, & B. Metcalfe (2010). Innovative soil reinforcement method to control static and seismic settlements. *Contemporary Topics in Ground Modification, Problem Soils, and Geo-support. Geotechnical Special Publication No. 187. ASCE Press, Reston, Va.*, 313–320.
- Rayamajhi, D., T. V. Nguyen, A. Ashford, & R. W. Boulanger (2012). Effect of discrete columns on shear stress distribution in liquefiable soil. *ASCE Geo-Congress, 1908–1917*.
- Rollins, K.M., S. Amoroso, P. Andersen, L. Tonni, & K. Wissmann (2021). Liquefaction mitigation of silty sands using Rammed Aggregate Piers based on blast-induced liquefaction testing. *Journal of Geotechnical and Geoenvironmental Engineering Volume 147 Issue 9*.
- Salgado, R., R. W. Boulanger, & J. K. Mitchell (1997). Lateral stress effects on CPT liquefaction resistance correlations. *Journal of Geotechnical and Geoenvironmental Engineering, Vol. 123, No. 8*.
- Salocchi, A. C.; L. Minarelli, S. Lugli, S. Amoroso, K. M. Rollins, D. Fontana (2020). Liquefaction source layer for sand blows induced by the 2016 megathrust earthquake (Mw 7.8) in Ecuador (Boca de Briceño). *Journal of South American Earth Sciences. - ISSN 0895-9811. - 103*, pp. 1–10.
- Smith, M. E. & K. Wissmann (2018). Ground improvement reinforcement mechanisms determined for the Mw 7.8 Muisne, Ecuador, earthquake. *5th Geotechnical Earthquake Engineering and Soil Dynamics Conference: Liquefaction Triggering, Consequences, and Mitigation - GEESDV*, Austin, Texas, GSP 290, pp. 286–294
- Vautherin, E., C. Lambert, D. Barry-Macaulay, & M. Smith (2017). Performance of Rammed Aggregate Piers as a soil densification method in sandy and silty soils: experience from the Christchurch rebuild. *3rd International Conference on Performance-based Design in Earthquake Geotechnical Engineering*. Vancouver, BC, Canada, No. 215.
- Wissmann, K. J., S. van Ballegooy, B. Metcalfe, J. N. Dismuke, & C. K. Anderson (2015). Rammed Aggregate Pier ground improvement as a liquefaction mitigation method in sandy and silty Soils. *6th International Conference on Earthquake Geotechnical Engineering*. Christchurch, New Zealand.

Estimating bearing capacity of polar snow using the Cone Penetration Test (CPT)

A.B. McCallum & G. White

School of Science, Technology and Engineering, University of the Sunshine Coast, Sippy Downs, Australia

ABSTRACT: Increased access to the polar regions requires increased infrastructure. Design and construction of this infrastructure can only be achieved by accurately estimating surface bearing capacity. We reviewed contemporary methods for determining bearing capacity in soils and applied these to data obtained from almost 100 cone penetration tests conducted in Antarctica. Numerous direct and indirect methods exist to enable estimation of surface bearing capacity in polar snow, but the preferred method is the rate-controllable, friction-sleeve equipped, cone penetration test (CPT). Application of this and similar techniques is essential to ensure the correct design and construction of infrastructure in ever-more trafficked polar regions.

1 INTRODUCTION

As our climate changes, contestation for polar resources is increasing (Dodds and Hemmings, 2015). This results in increased polar operations and the need for increased supporting infrastructure. White and McCallum (2018) reviewed the design and construction of pavements of snow and ice, including measures of snow bearing capacity.

Abele (1990) says that although the strength of snow can be determined by various methods, there are three primary measurement techniques: surface loading, sample strength testing, or probing, in which a penetrative device is forced into the snow obtaining a proxy for snow strength. Of these, probing is the preferred means of assessing in situ strength because it allows the profile of the snow bearing strength to be measured on undisturbed in situ material (McCallum, 2013).

Numerous instruments have been used historically to probe snow, such as the Swiss Rammsonde (Haefeli, 1936) or the Standard Penetration Test (SPT) or Drop Cone Penetrometer (DCP); more recently lightweight penetrometers have been developed for alpine snow (predominantly avalanche) work (Schneebeili and Johnson, 1998). However, because polar snow is a rate-sensitive material (McCallum, 2017a) a robust, hydraulically-driven, constant-rate penetrometer, such as that used for the Cone Penetration Test (CPT), is preferable for assessing physical characteristics of hard polar snow, to depth (~5 m), from which snow bearing capacity might be estimated. The existence of a friction-sleeve further increases the usefulness of this tool (McCallum, 2017b).

In this paper we validate direct derivation of bearing capacity in polar snow from rate-controllable, friction-sleeve equipped, cone penetration test data.

2 BACKGROUND

Many authors have examined the derivation of bearing capacity and/or settlement of geomaterials, either directly or indirectly. Direct measurement of bearing capacity is derived directly from CPT data after consideration is given to differences in the cone shape, size and penetration rate, by applying modification factors. In contrast, indirect measurement includes measuring material parameters derived from CPT data, and then converting to bearing strength via standard equations. The indirect approach is the common and conventional method for polar snow. These indirect methods use the application of standard bearing capacity theory (Terzaghi, 1943), cavity expansion theory (Yu, 2000) and various numerical models.

The measurement of snow bearing capacity is informed by the practices applied to other geomaterials, such as soil. Many approaches for direct bearing capacity derivation in soils are described in Lunne (1997), including those by Schmertmann (1978), Meyerhof (1976) and Tand (1995). Additionally, Eslami and Gholami (2006) presented an analytical model to directly derive ultimate bearing capacity from cone resistance and Lee and Salgado (2005) proposed a method to directly estimate the bearing capacity of circular footings on sands based on the cone penetration test.

Mayne, who has written extensively on the application of both methods (e.g., Mayne (2020)) noted in

a recent report (Dagger et al., 2018), that many techniques (particularly indirect techniques) are now obsolete and calculation of bearing capacity from cone penetration test data is now the preferable method.

Having briefly examined these techniques in soil, we now briefly inspect similar methods that have been considered for polar snow.

3 HISTORICAL ESTIMATION OF BEARING CAPACITY IN POLAR SNOW

Abele (1963) examined the correlation between snow compressive strength and penetration resistance, as measured by the Rammsonde. Furthermore, Mellor and Smith (1966) examined the impact of temperature on Rammsonde measurements in homogeneous snow. They showed that Rammsonde hardness varied with snow temperature similarly to unconfined compressive strength. Salm (1971) examined the rheological behaviour of snow under high stresses and Mellor (1975) extensively examined snow mechanics, including the rheology, elastic and viscoelastic behaviour, creep behaviour, failure and shear strength. Mellor (1975) noted that the derivation of strength measurements for snow from Rammsonde penetration resistance data is somewhat 'arbitrary' but upon further examination (because of the utility of the Rammsonde) he concluded that correlation between ram resistance and uniaxial compressive strength in snow is important, but variations in snow density and microstructure complicate the relationship, meaning a universal correlation is unlikely to be found.

Barthelemy (1975) summarised snow-road construction techniques and examined the conversion of Rammsonde penetration resistance to hardness values, and additionally related evident relationships between Ramm hardness, confined shear strength and expected bearing potential.

More recently, Petrovic (2003) briefly examined a wide array of snow and ice mechanical properties and Shapiro et al. (1997) in re-reviewing the state of snow mechanics presented an indirect calculation for settlement based on snow density but highlighted that estimating the natural snow's bearing capacity is not easily determined, again because of variations in both density and microstructure/bonding. Models are being developed to assist in such estimation, but necessary empirical data for complex snow load response does not exist (Shapiro et al, 1997).

Land and Harrison (1995) examined the stress-deformation behaviour of snow of various densities and Scapozza and Bartelt (2003) used a specially constructed triaxial testing device to examine the behaviour of snow of different density at different strain rates and confining pressures, also examining the work hardening that occurs after initial failure. So, historically, the estimation of bearing capacity in snow has proven difficult, either directly or indirectly, because of the variability in snow density and microstructure, which also changes with temperature.

The US Army Cold Regions Research and Engineering Laboratory (CRREL) has used an indirect method to estimate bearing capacity for polar infrastructure such as roads, runways and buildings. White and McCallum (2018) recently reviewed this approach; an example nomogram from which necessary snow hardness/strength criteria must be met for various aircraft is shown (Figure 1).

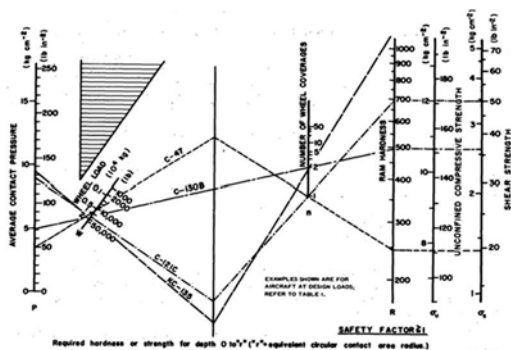


Figure 1. Required hardness (or strength) of a snow pavement for various wheel load conditions (from Abele, 1990).

For surface polar infrastructure, Blaisdell and Weale (2006) examined bulk and differential settlement into the snowpack of a foundation on a deep snowpack at the South Pole (stratigraphy was not described) and Geduhn and Enss (2006) assessed the service life of Neumayer Station, Antarctica, defining failure in terms of settlement and establishing a stress amount to be avoided in order to deny the onset of tertiary creep (McCallum, 2012). Aside from White and McCallum's review of ice and snow runway pavements (White and McCallum, 2018), limited additional consideration of bearing capacity derivation (direct or indirect) for polar snow is apparent.

4 CONTEMPORARY ESTIMATION OF BEARING CAPACITY IN POLAR SNOW

Because snow bearing strength is rate-sensitive, temperature dependant and variable with depth/location, McCallum (2012) postulated that a hydraulically-driven, constant-rate, friction-sleeve equipped penetrometer, could be useful to assess bearing capacity of polar infrastructure, such as snow roads and runways. McCallum conducted almost 100 CPTs in Antarctica and presented initial postulations on the direct and indirect derivation of surface bearing capacity for polar snow, in layered and nonlayered situations (McCallum, 2012). He focussed on direct methods for layered and unlayered snow, in terms of both ultimate (elastic deformation only) and allowable (plastic deformation/settlement occurs) bearing capacity. Typical CPT data considered (Figure 2) and McCallum's postulations

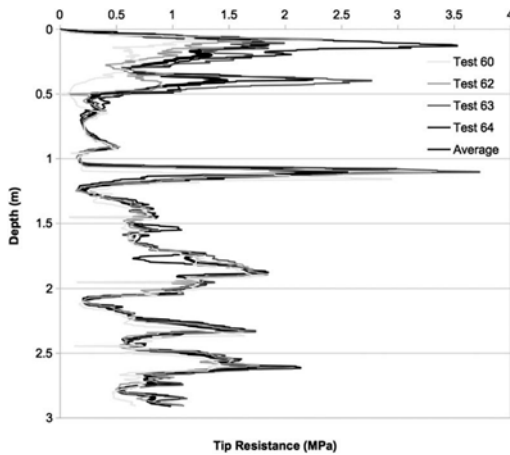


Figure 2. Example CPT data from which McCallum (2012) derived his relationships, for snow of particular initial density.

Table 1. Methods to derive BC from CPT data.

Method	Relationship	BC (kPa) for q_{cavg} of 2 MPa
Ultimate homogeneous (Method 1)	$q_{cavg}/\sim 3$	~ 667
Ultimate homogeneous (Method 2)	$q_{cavg}/\sim 2.2$	~ 909
Allowable homogeneous	$q_{cavg}/\sim 1.5$	~ 1330
Ultimate layered	Depends on strata	N/A
Allowable layered	Depends on strata	N/A
Allowable homogeneous (direct)	$q_{cavg}/\sim 2.4$	~ 840

(Table 1) are presented; q_{cavg} is average tip resistance (MPa).

We now briefly further examine the direct and indirect estimation of bearing capacity in both homogeneous and layered snow.

Homogeneous snow

Homogeneous snow can be considered elastic (Poulos and Davis, 1974) prior to initial failure (McCallum, 2012) and ultimate or allowable bearing capacities can be estimated either indirectly or directly.

Indirect Methods

Kartashov (1965) examined the relationship between settlement and pressure, for snow of varying density and determined a power-law relationship (Equation 1):

$$P = A \left\{ \frac{\Delta h}{h} \right\}^\alpha = A \left\{ \frac{\gamma - \gamma_0}{\gamma} \right\}^\alpha \quad (1)$$

where A and α are parameters; h is the initial sample height; Δh is settlement; γ_0 is initial specific weight and γ is final specific weight, with parameters of state A and α depending on microstructure, initial density, temperature and loading rate.

Abele and Gow (1976) examined settlement of compacted snow due to compressive stress and established stress-deformation (pressure-sinkage) relationships that depended on initial density and temperature.

Shoop (1993) examined field terrain characterization for vehicle trafficability on snow using the Rammsonde and other devices, from which bearing capacity could be indirectly calculated; specifics were not given.

Fellin and Lackinger (2007) used cohesion values obtained from rapid unconfined uniaxial compression tests to design strip footings for cable car towers founded upon glacial ice, and Masterson comprehensively examined ice bearing capacity and construction (Masterson, 2009).

Lee (2010) modelled plate indentation in snow using FEA (ABAQUS), calculating an initial yield strength in compression using the Drucker-Prager cohesion (Pa) and snow friction angle. Lee back-calculated these data from indentation tests via an optimization procedure.

McCallum (2012) deliberated extensively on the derivation of strength and bearing capacity (Table 1) from CPT in polar snow, presenting an equation to derive ultimate (elastic) bearing capacity (MPa) for homogeneous snow of initial density $\sim 450 \text{ kg m}^{-3}$ (Equation 2):

$$BC = 2.8(q_{cavg}/1.7)/(0.5/0.587M) \quad (2)$$

Where M equals 5.3 for snow of initial density $\sim 450 \text{ kg m}^{-3}$ (McCallum, 2012). McCallum (2012) also built on Johnson's work (Johnson, 2003) to show how his Statistical Micromechanical Theory of Cone Penetration in Granular Materials might be applied to estimate shear strength from CPT for the cohesive granular material, polar snow.

McCallum (2013) presented preliminary relationships to derive snow density from both CPT tip resistance and CPT sleeve friction. Strong qualitative relationships were evident, but quantitative relationships were not significantly examined. Additionally, he presented initial deliberations on deriving snow shear strength from CPT tip resistance data; but this derivation relied on knowing initial snow density values.

Further to this work, McCallum (2014) applied relationships developed by Robertson (2010) for soil, to show that a statistically significant relationship exists between CPT sleeve friction and snow density.

Direct Methods

Irwin (1991), though controlled laboratory experiments in manufactured snow, derived an expression for footing load (bearing capacity) based on pressure-bulb depth, shear stress and compressive stress, derived directly from Rammsonde hardness data, for snow of variable density, temperature, ageing and grain size. This built on previous work in natural snow (Irwin, 1989) and incorporated volumetric compaction of the snow under the footing and shear resistance around the cylindrical perimeter.

McCallum (2012) built on this theory and devised a direct derivation of allowable bearing capacity for polar snow (Table 1) from CPT data by incorporating empirically observed differences in cone shape, size and penetration rate, also incorporating compaction ahead of the penetrating cone.

McCallum (2018b) also applied Einav's work (Einav, 2007a; 2007b) on breakage mechanics theory to postulate on the estimation of pile end bearing capacity from polar snow CPT data.

Non-homogeneous snow

In the more-complicated case of non-homogeneous snow, less indirect and direct methods have been examined.

Indirect Methods

Sturm et al. (2004) used a micromechanical theory to convert high-resolution micro-penetrometer data to snow bond strength and Geduhn and Enns (2006) examined the stress dependent creep behaviour of snow and ice to assess the bearing capacity and settlement of columns used to support Germany's Antarctic Station Neumayer III. They used an idealised depth-density curve to represent actual site stratigraphy.

To estimate the extent of vertical stress transfer within layered snow, estimation of elastic modulus is necessary. Marshall (2005) used ABAQUS to model surface loading within a layered snowpack. He refined a statistical-micromechanical model (Johnson and Schneebeli, 1999) to define a macroscopic elastic modulus based on mini-penetrometer data, concluding that this method could prove valid for (larger diameter) CPT data.

McCallum (2012) subsequently derived macroscopic elastic modulus measurements directly from CPT tip-resistance (for snow of assumed density), obtaining results consistent with values reported by Mellor (1975), concluding that the results were strain rate dependant. McCallum went on to examine ultimate and allowable bearing capacity of layered polar snow, using CPT-derived modulus data, subsequently generating plots of vertical stress diminution with depth using the FEM package Pdisp (Oasys Ltd, 2009).

Subsequent to McCallum's work the Avatech SP1 and SP2 Smartprobes (Avatech, 2014) were developed to measure snowpack stratigraphy and

resistance to penetration, but retrieved data are relative, not absolute, and a measure of neither snow strength nor bearing capacity is attained.

Most recently, Haehnel et al. (2019) examined the Phoenix compacted snow airfield near McMurdo Station, Antarctica, to determine strength necessary to support a C-17 aircraft. They defined strength depth profiles in terms of uniaxial compressive strength, determined via numerous variable-rate penetrative methods, including the Rammsonde (RAM), Dynamic Cone Penetrometer (DCP) and the Russian Snow Penetrometer (RSP). They used elastic modulus estimated from snow density (kg m^{-3}) (Shapiro et al., 1997) as input into a back-calculation tool "FAA Backcalculation" (BAKFAA V. 2.0*) from which Major principal stresses versus depth were predicted, for different aircraft at varying snow densities. Subsequently, they generated recommended structural design strengths for the runway, to a depth of 1 m, in terms of unconfined uniaxial compressive strengths, derived from penetrometer strength indices for both the RSP and RAM (e.g., Equation 3 for deriving unconfined uniaxial compressive strength from RAM data (Abele, 1990).

$$\sigma = 0.37R^{0.55} \quad (3)$$

No additional contemporary indirect methods to derive bearing capacity in non-homogeneous polar snow are known to exist.

Direct Methods

McCallum (2012) examined existing direct methods for soil such as Meyerhof (1976) and Schmertmann (1978) to estimate what the ultimate bearing capacity of snow might be as a percentage of CPT tip resistance. Although he considered the direct manipulation of CPT data due shape, size and penetration rate to derive bearing capacity in homogeneous snow (previously discussed), he did not examine the direct derivation of surface bearing capacity from CPT data in layered non-homogeneous polar snow.

No other research is known to exist that considers the derivation of bearing capacity in layered polar snow directly from CPT data.

5 APPLICATION OF CONTEMPORARY SOIL METHODS TO POLAR SNOW

The limited research on direct snow bearing strength measurements, coupled with the low reliability of indirect measurement, indicates there is significant advantage in applying contemporary soil bearing strength methods, such as those proposed by Dagger (2018) and Lehane (2019).

Lehane (2019) examined how CPT end-resistance (q_t) can be used to directly predict bearing capacity for driven and bored piles in sand, silts and clays, and shallow foundations on sand; he also examined

shaft friction correlations (similar to McCallum's work in snow (McCallum, 2018)). Contemporaneously, the behaviour of shallow foundations on snow is of most interest. Lehane (2019) deduced a direct relationship between CPT tip resistance and shallow foundation settlement (Equation 4).

$$q_{0.1} = 0.16q_{c,average} \quad (4)$$

where $q_{0.1}$ equals the applied bearing pressure where foundation settlement divided by foundation width equals 0.1, and $q_{c, average}$ equals average cone tip resistance. This relationship is very similar to that derived by Mayne (2012) where ultimate surface footing bearing capacity equals 18% of mean CPT tip resistance. It is interesting how both these formulations are of a similar order to McCallum's initial formulation (Table 1; McCallum (2012)).

However, snow is not sand, and although Lehane's derivation (from Terzaghi's initial formulation (Terzaghi, 1956)) considers the effects of horizontal stress, soil compressibility/stiffness, friction angle and consolidation, it does not incorporate cohesion, which snow immediately gains upon formation (Szabo, 2007). Boufrina (2018) also examined design of shallow foundations directly from CPT data but they also did not consider cohesion.

Robertson (2010) briefly considered direct and indirect estimation of shallow foundation bearing capacity from CPT data in cohesive soils (Equations 5 & 6 respectively). Indirect:

$$q_f = N_c s_u + \gamma D \quad (5)$$

Where q_f is ultimate bearing capacity, N_c is a function of footing width and shape, s_u is undrained shear strength (corrected for Bjerrum's correction (Bjerrum (1973))), γ is soil unit weight and D equals depth of footing. Direct:

$$q_f = K_{su} q_{c(av)} + \gamma D \quad (6)$$

Where q_f is ultimate bearing capacity, K_{su} varies from 0.3 to 0.6 depending on footing B/D and shape, and soil OCR and sensitivity, γ is soil unit weight and D equals depth of footing.

For a surface footing, application of the indirect equation suggests a bearing capacity of $\sim 5.s_u$. This is very close to McCallum's derived relationship between CPT tip resistance and shear strength for polar snow of density 400 kg m^{-3} of $\sim 4.5.s_u$ (McCallum, 2012). Robertson's indirect relationship is directly applicable to snow, for snow of density 407 kg m^{-3} . Contemporary indirect methods to estimate surface footing bearing capacity for cohesive soils, can probably be used for polar snow.

Examining Robertson's direct equation, for a surface footing, suggests that (depending on footing B/D etc.) bearing capacity equals $\sim 0.5. q_{c(av)}$. This is very similar to McCallum's direct derivation of $\sim 0.42. q_{c(av)}$. Again, application of a direct soil method for cohesive soils to polar snow appears useful.

Dagger (2018) emphasise that traditional (indirect) techniques are no longer required because direct methods from CPT exist for square, rectangular and circular shallow footings. They propose robust direct methods for all soils and propose a general direct CPT method, but derivation is particular to footing width and accepted settlement, and is not easily comparable here.

6 CONCLUSION

Many techniques, both indirect and direct, exist to estimate surface bearing capacity in soils; far less research has been conducted into snow, a cohesive, rate-sensitive material, whose evolving microstructure depends on initial density and ongoing temperature gradients.

Indirect techniques for snow have been derived (McCallum, 2012 etc.), but in soils, such techniques are no longer preferable, because robust direct-derivation methods now exist (Dagger, 2018).

Direct methods derived for snow, such as those postulated by McCallum (McCallum, 2012), agree well with accepted methods for cohesive soils (Robertson, 2010). Therefore, the preferred method for deducing surface bearing capacity of polar snow, is through application of rate-controllable, friction-sleeve equipped, cone penetration test (CPT) data.

ACKNOWLEDGEMENTS

McCallum's CPT research in Antarctica was supported by the Menzies Foundation, Lankelma Limited (UK) and the British Antarctic Survey.

REFERENCES

- Abele, G., 1963. A correlation of unconfined compressive strength and ram hardness of processed snow, USA CRREL Technical Report 85.
- Abele, G., 1990. Snow Roads and Runways, USA CRREL Monograph 90-3.
- Abele, G. and Gow, A. J., 1976. Compressibility Characteristics of Compacted Snow, USA CRREL Report 76-21.
- Bjerrum, L. 1973. Problems of Soil Mechanics and Construction on Soft Clays and Structurally Unstable Soils. In Proc., Eighth International Conference on Soil Mechanics and Foundation Engineering, Moscow, Vol.3, pp. 111-159.
- Dagger, Saftner, Mayne, 2018. Cone Penetration Test Design Guide for State Geotechnical Engineers, Minnesota DoT.

- Dodds, K. and Hemmings, A.D., 2015. Polar Oceans: Sovereignty and the Contestation of Territorial and Resource Rights
- Eslami, A. and Gholami, M., 2006. Bearing capacity analysis of shallow foundations from CPT data, Proceedings of the 16th International Conference on Soil Mechanics and Geotechnical Engineering.
- Haefeli, R., 1936. "Beitrag zur geologie der schweiz geotechn.". Serie-Hydr, 3.
- Irwin, G. J., Mohamed, A. M. O., Alammawi, S. and Yong, R. N., 1991. Prediction of load carrying capacity of deep snow by ramsonde hardness, Journal of Terramechanics, Vol. 28.
- Johnson, J. and Schneebeli, M., 1999. Characterizing the microstructural and micromechanical properties of snow, Cold Regions Science and Technology.
- Kartashov, S. N., 1965. Mechanical properties of snow and firn", in: "Symposium international sur les aspects scientifiques des avalanches de neige", 69, Union de Geodesie et Geophysique internationale.
- Lee J., and Salgado R., 2005. Estimation of bearing capacity of circular footings on sand based on Cone Penetration Test, Journal of Geotechnical and Geoenvironmental Engrg 131 (4).
- Lehane, B. M., 2019, CPT-based design of foundations, E. H. Davis Memorial Lecture (2017).
- Shapiro, L. H., Johnson, J., Sturm, M. and Blaisdell, G.L., 1997. Snow Mechanics. Review of the State of Knowledge and Applications, USA CRREL Technical Report 97-3.
- Lunne, T., Robertson, P. and Powell, J., 1997. Cone Penetration Testing in Geotechnical Practice, Soil Mechanics and Foundation Engineering, Vol. 46.
- Marshall, H. P., 2005. Snowpack spatial variability: towards understanding its effect on remote sensing measurements and snow slope stability, PhD Thesis, University of Colorado.
- Mayne, P. W., 2020. The 26th Széchy Lecture: Use of in-situ geotechnical tests for foundation systems. Proceedings of the Széchy Károly Emlékkonferencia, published by the Hungarian Geotechnical Society, Budapest: 12–73.
- McCallum, A. B., 2012. Cone Penetration Testing in Polar Snow, PhD thesis, University of Cambridge.
- McCallum, A. B., 2013. CPT: A valuable tool for investigating polar snow, NZ Journal of Hydrology, 52(2).
- McCallum, A. B., 2014. Direct estimation of snow density from CPT, Proceedings 3rd International Symp. on CPT.
- McCallum, A. B., 2017. CPT in Antarctic firn: an introduction to interpretation, Journal of Glaciology, 60 (219).
- McCallum, A. B., 2017. Assessing mass balance with the cone penetration test, Journal of Glaciology, 63 (239).
- McCallum A. B., 2018. Applying breakage mechanics theory to estimate bearing capacity from CPT in polar snow, Proceedings 4th International Symp. on CPT.
- McCallum, A. B. and Wiegand, A., 2018. Simple Method for Estimating Snow Strength Using CPT Sleeve Friction Data. Journal of Cold Regions Engineering, Vol. 32 (4).
- Mellor and Smith, 1966. Strength studies of snow, USA CRREL Research Report 168.
- Meyerhof, G.G., 1976. Bearing capacity and settlement of pile foundations (11th Terzaghi Lecture).
- Petrovic, J.J., 2003. Mechanical properties of ice and snow Journal of Materials Science, 38 (1-6).
- Poulos, H. G. and Davis, E. H., 1974. Pile Foundation Analysis and Design, University of Sydney.
- Schmertmann, J. H., 1978. Guidelines for cone penetration test: performance and design, Technical Report, US Federal Highway Administration.
- Schneebeli, M., and Johnson, J. B., 1998. "A constant-speed penetrometer for high resolution snow stratigraphy". Annals of Glaciology, 26, pp. 107–111.
- Shoop, S., 1993. Terrain Characterization for Trafficability, USA CRREL Report 93-6.
- Szabo, D. and Schneebeli, M. 2007. Subsecond sintering of ice, Applied Physics Letters, Vol. 90 (15).
- Tand, K.E., Warden, P.E. and Funegård, E.G. (1995). Predicted-measured bearing capacity of shallow footings on sand. Proceedings, Intl. Symp. on Cone Penetration Testing, Vol. 2.
- Terzaghi, K., 1943. Theoretical Soil Mechanics, John Wiley & Sons.
- White, G. and McCallum, A. B., 2018. Review of ice and snow runway pavements, International Journal of Pavement Research and Technology, Vol. 18 (3).
- Yu, H. S., 2000. Cavity Expansion Methods in Geomechanics, Springer Science + Business Media.

The use of CPT based metamodels to predict the performance of offshore anchor piles

A Mentani & L. Govoni

University of Bologna, Bologna, Italy

F. Bourrier

French National Research Institute for Agriculture, Food and Environment, Grenoble, France

ABSTRACT: The paper presents the development of metamodels for the prediction of the load-displacement response of steel piles driven in sand subjected to pull-out. Two metamodels are created for the evaluation of the tensile capacity and initial stiffness of the pile. They were developed based on the outcomes of a finite element testing campaign, employing models of parameters derived from the tip resistance of cone penetration tests. Two hundreds finite element simulations, which included various soil-pile configurations, were required to calibrate accurate metamodels. Assessment of the procedure was carried out with reference to available data on a model pile and related cone penetration test results. The approach relies on particularly simplified finite element models, but it can be extended to accommodate modelling features of higher complexity. The results find application to the design of offshore piles used as anchors for floating structures.

1 INTRODUCTION

The paper focuses on the drained, static load-displacement response of steel open-ended piles subjected to pull-out. In the offshore environment, tensile loading conditions may become critical for piles employed as anchor foundations, particularly when used with vertical or taut line moorings. In the context of offshore wind exploitation, these solutions offer an attractive alternative to catenaries, as they may allow to contain the area over which a floating wind farm would extend, aiding with a reduction of the investment costs (Castro-Santos & Diaz-Casas 2016).

The tensile response of offshore piles is traditionally estimated using the shaft load-transfer curve approach, combined with ultimate shaft friction prediction methods. The development of load-transfer curves dates back to the Fifties and several formulations are now available as comprehensively reviewed in Bohn et al. (2017). In sand, the tensile capacity is now estimated according to cone penetration test-based procedures (CPT-methods), which predictive performance was assessed in Schneider et al. (2008). The approach is very accurate and its implementation straightforward, however, uncertainties may arise when selecting the most suitable formulation among those available (Foglia et al. 2017, Schmoor et al. 2018).

Finite element or finite difference models can be also employed to describe the pile tensile load-

displacement curve (De Nicola & Randolph 1993; van Tol & Broere 2006; De Gennaro et al. 2008).

The implementation and calibration of these models can be, however, a complex and computationally onerous task. To overcome this limitation, metamodelling techniques can be employed, as they allow to store the results of finite element analyses in simple mathematical functions, which have the advantage of an easy implementation and low computational cost (Sudret 2008).

In this paper, metamodels are developed to predict some behavioural features of piles driven in a homogeneous sand bed. Building up on the experience matured in the context of the CPT-methods over the last decade, a simple CPT-based Finite Element (FE) modelling strategy is adopted to investigate the pile response when subjected to a tensile load through a parametric study. A Polynomial Chaos Expansion (PCE) metamodel (Xiu & Karniadakis 2002) is built from the results obtained by the FE study. The prediction capacity of the developed metamodel is then assessed with respect to selected data included in the ZJU-ICL experimental database of piles driven in sand (Yang et al. 2015).

2 FE SIMULATION PROGRAMME

A FE parametric study was carried out, in which an upward vertical displacement was applied to

a wished in place model pile. They were total stress, small-strain and static analyses and the software suite Abaqus FEA (ABAQUS 2014) was used to the scope.

2.1 Details of the FE models

The FE models used in the parametric study involved a pile foundation of diameter D , length L and wall thickness t . The pile is subjected to a drained axial pull-out test from a uniform sand deposit, that is characterised by a constant value of the relative density D_r and a constant effective unit weight ($\gamma' = 10 \text{ kN/m}^3$). The models were axial-symmetric, with zero displacement boundaries set at a distance of $15D$ from the pile shaft and $10D$ down the pile tip. A sensitivity study was carried out which showed that, to avoid any convergence issues, a very fine uniform mesh was required in the vicinity of the pile (Figure 1).

Assuming a fully plugged failure, the pile was modelled as a solid, deformable element, obeying to a linear elastic constitutive law. It features a uniform cross section. The equivalent density and elastic properties were calculated to account for the section geometry on the pile weight and axial deformation.

The soil response was modelled as linear-elastic and perfectly plastic, failing according to the Mohr-Coulomb criterion. Model parameters are derived from an artificial cone tip resistance ($q_{c,FE}$). The particular form of the trend is generated according to the relation given by Jamiolkowski et al. (2003) as this was also used in the interpretations made in the ZJU-ICL database (Yang et al. 2015).

$$q_{c,FE} = 20 \cdot \exp\left(\frac{D_r}{0.35}\right) \cdot p_a \cdot \left(\frac{\sigma'_{v0}}{p_a}\right)^{0.5} \quad (1)$$

where p_a = atmospheric pressure and σ'_{v0} = in situ vertical effective stress.

The soil's Young modulus was prescribed to vary with the artificial cone tip resistance according to Robertson (2009)

$$E' = \alpha_E \cdot q_{net,FE} \quad (2)$$

where

$$\alpha_E = 0.015 \cdot (10^{0.55I_c + 1.68}) \quad (3)$$

applies to the net tip resistance and I_c = soil behaviour type index. Soil peak strength and dilation angles were implemented in the FE models according to well-established Bolton (1986) correlation. The critical state interface friction angle was taken constant ($\delta_{cv} = 29^\circ$), as it is generally done for steel driven piles in case interface tests are not available

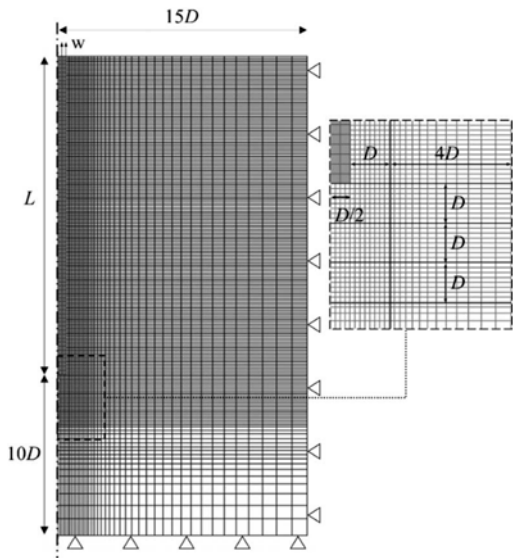


Figure 1. Distribution of the mesh size along the FE models geometry and applied boundary conditions.

(Schneider et al. 2008). Piles were wished in place, therefore the effects of installation on the soil stress state prior to loading was implemented to ensure that the radial stress on the pile was, at any soil depth, that predicted by Jardine et al. (1998)

$$\sigma'_h = 0.029 \cdot q_{c,FE} \cdot \left(\frac{\sigma'_{v0}}{p_a}\right)^{0.13} \cdot \left(\frac{L-z}{R^*}\right)^{-0.38} \quad (4)$$

where $R^* = 0.25 \cdot [D^2 - (D - 2t)^2]^{0.5}$.

2.2 Sampling and results

Five independent input variables were considered in the design of the FE test programme. The pile was described by three variables, whose range was established to encompass the geometries encountered in the ZJU-ICL experimental database. Two variables were used for the definition of the soil model: the relative density and the modulus factor, α_E , which were

Table 1. Input variables for the FE test programme.

Input variable	Range
Pile diameter D [m]	0.20 – 1.00
Pile slenderness L/D [-]	10 – 70
Pile wall thickness ratio D/t [-]	10 – 100
Soil density D_r [%]	40 – 100
Soil modulus factor α_E [-]	3 – 10

allowed to vary within a realistic range for clean sands (i.e., $I_c = 1.31 - 2.05$). All the input variables are collected in Table 1, along with their domain of variation.

The FE analyses were conducted with certain combination of the input variables by using the Latin Hypercube Sampling technique (LHS, McKay et al. 1979). According to the LHS, each input variable range is divided into intervals of equal probability. The number of intervals is equivalent to the sample dimension and the location of the design point (i.e. the combination of inputs) is taken randomly within the interval. This method allows for an optimum coverage of the input variable domain and the sample size can be easily increased.

In this study, the five input variables were first combined to create a LH sample of size 50 (S_{50}), which was increased to 100 (S_{100}) and then to 200 (S_{200}). In Figure 2, the results of the 200 simulations are shown in terms of normalised vertical force ($V/(\gamma'DL^2)$) and displacement (w/D). Two outputs variables were identified along the curves, the normalised tensile capacity ($V_{ult}/(\gamma'DL^2)$) and the normalised initial stiffness ($K_i/(\gamma'L^2)$), which was evaluated as the initial tangent to the curve.

The input combinations and the resulting outputs were then used for the development and calibration of the PCE metamodels. To validate the metamodels further FE analyses were performed on a new sample of size 50 (S_{val}).

3 DEVELOPING METAMODELS

A metamodel (MM) or surrogate model is the model of a model, and metamodeling is the process of generating such MMs. A metamodel is an explicit mathematical algorithm representing the relation between input

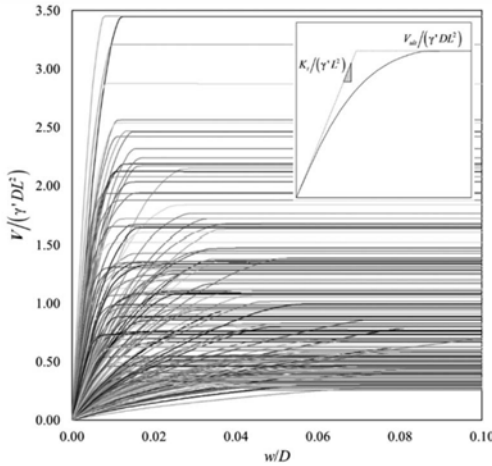


Figure 2. Results of the FE test programme in terms of dimensionless force and displacement.

and output variables and it approximates the complex and implicit function defined by the emulated model (this model is either deterministic or random). They are generally grouped into classification and regression types. When the aim is to predict a continuous target variable, as in the case examined in this paper, the regression type, such as the PCE, is to be used. In this work, the open-source Python package OpenTURNS (Baudin et al. 2016) was used to build the MMs.

3.1 Details of the PCE

A given model is described by a vector \mathbf{X} in which a finite number of input random variables are gathered. The response vector \mathbf{Y} , which collects the output quantities, can be represented as the application of a mathematical model to the input vector. The PCE is an algorithm which approximate this function, and the chaos representation of the response vector is defined as the linear combination of selected multivariate orthonormal basis, $\Psi_k(\mathbf{Z})$, and their corresponding coefficient α_k as represented by

$$\mathbf{Y} = f(\mathbf{X}) \approx \hat{f}(\mathbf{X}) = \sum_{k \in K} \alpha_k \Psi_k(\mathbf{Z}) \quad (5)$$

with \mathbf{Z} obtained by applying an isoprobabilistic transform to the input vector ($\mathbf{Z} = \mathbf{T}(\mathbf{X})$).

The choice of the family of orthonormal basis (e.g., Legendre, Hermite, Krawtchouk) depends on the distribution type of the input variables, which are rescaled by the isoprobabilistic transform into common distribution types (e.g., uniform, normal, binomial). The following step consists on the determination of the coefficients, α_k , associated to each polynomial basis. These coefficients are estimated according to a suitable regression strategy (Sudret 2008). The most common are the least squares strategy that minimise the quadratic error between the model response and the polynomial approximation, and the integration strategy, which uses the inner product rules, thanks to the orthogonality and normality property of the polynomial basis.

3.2 Calibration and validation of the PCE

Two MMs were calibrated using the results of the FE test programme as follows. The combinations of the five input variables listed in Table 1 were collected in the input vector \mathbf{X} , and the selected outputs (i.e., the normalised pile tensile capacity load and tangent initial stiffness) represented two response surfaces (i.e., \mathbf{Y}). A uniform distribution of the input variable was selected as the most suitable to be applied to sample created with the LHS technique. Consequently, the Legendre orthonormal polynomial basis were chosen as associated to this distribution type. As for the evaluation strategy to compute the

polynomials coefficients, the least squares method was selected as it was shown to provide more accurate results, if compared to the integration strategy.

The calibration (i.e. the identification of coefficient α_k) of the two MMs was carried out using the results of the FE test programme originated by the created samples (S_{50} , S_{100} , S_{200}). Accordingly, three MMs (MM_{50} , MM_{100} , MM_{200}) were created for each of the two outputs ($V_{ult}/(\gamma' DL^2)$, $K_r/(\gamma' L^2)$) to explore the influence of the sample size on their accuracy. To the aim, the validation set of input-output combinations (S_{val}) was used, with the predictive coefficient, Q^2 , defined by

$$Q^2 = 1 - \frac{\sum_{i=1}^N (Y_i - \hat{f}(X_i))^2}{Var(Y)} \quad (6)$$

where N is the size of the validation sample ($N=50$) and $Var(Y)$ is the variance of the FE model outputs.

The MMs predictions are compared with the results of the FE testing campaign with reference to the two considered outputs: the tensile capacity (Figure 3a) and the initial stiffness (Figure 3b). Different markers are used to identify the MM's predictions built on different sample sizes. Some scatter is observed in the prediction of MM calibrated with the smaller sample size (MM_{50}), particularly at low and high output values and this is particularly evident for the prediction of the tensile capacity. The increase in the sample size, reduces the error at either end of the output distribution, with MM_{200} ensuring an excellent accuracy, consistent for both the outputs and estimated to be larger than 0.98.

4 ASSESSMENT OF THE PROCEDURE

4.1 Experimental data

The data used to explore the approach potential as a predictive tool were selected among those available in ZJU-ICL experimental database. The database was developed with the scope of validating the CPT-methods for axial pile capacity. Therefore, the results of the pile loading tests are always accompanied by the relevant CPT tip resistance profiles.

Among all, the data of a pile subjected to pull-out was chosen. The selection was made to ensure that the foundation and the soil had characteristics consistent with the FE models used in the calibration procedure and that are describable through the proposed set of input. The adopted pile was steel, open-ended driven, the soil was uniform, dense, fine to medium flandrian marine sand. The q_c profile at the test location is shown in Figure 4a.

The q_c data were processed to estimate the relative density at the pile location according to equation

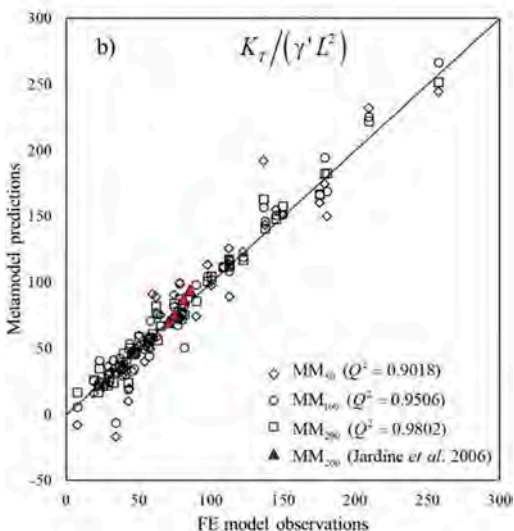
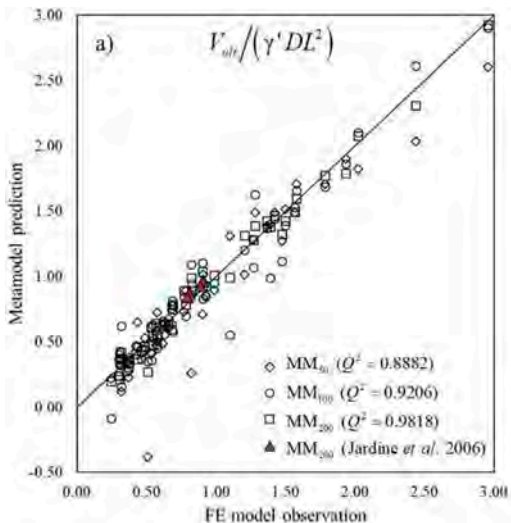


Figure 3. Accuracy of the MMs in predicting: (a) the tensile capacity; (b) the initial stiffness.

1. For a further and likely estimate of the results, the expression suggested by ISO standards (ISO, 2016) for the implementation of the CPT-methods was also employed

$$D_r = \frac{1}{2.96} \cdot \ln \left(\frac{q_c/p_a}{24.94 \cdot (p'_m/p_a)} \right)^{0.46} \quad (7)$$

where p'_m = effective mean in situ stress.

The profiles of relative density estimated with equations 1 and 7 are shown in Figure 4b, along with their average values. Application of equation 1

to the two average relative density values returns the artificial tip resistance profiles inserted in Figure 4a, which are implemented in the FE models according to the procedure described in section 1.1.

Table 2 collects the input data used for the FE and MMs. These includes the experimental pile geometry, the average relative densities, and two values of α_E , corresponding to possible upper and lower bound for I_c , estimated using the information on the test site available in Jardine et al. (2006).

Table 2. Input data for FE and MM.

D [m]	L/D [-]	D/t [-]	D_r [%]	α_E [-]
0.457	42.23	33.8	72.04; 76.25	5
			72.04; 76.25	7

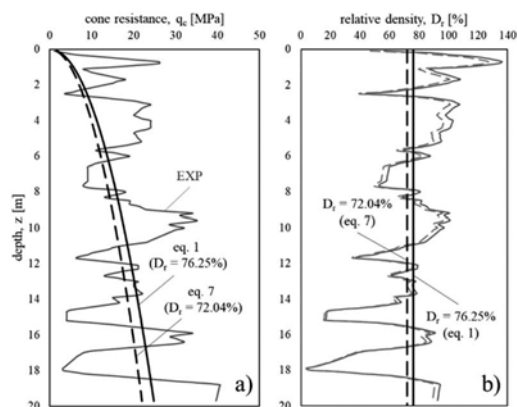


Figure 4. a) CPT data at the pile test location (redrawn from Yang et al. 2015 and artificial profile): (a) evolution of the cone resistance q_c and (b) relative density D_r depending on depth.

4.2 FE models and MM prediction

The data in Table 2 were employed first to assess the FE strategy presented in section 1.1. This validation plays a crucial role in the development of MMs, as their performance relies upon the robustness of the mechanical models they stem from.

Four FE analyses were performed (as detailed in Table 2) and the results are shown to compare well with the experimental data in terms of load-displacement curves (Figure 5). A close approximation of the initial stiffness and non-linearity prior to failure are observed, with the experimental capacity falling in the rather narrow band defined by the results obtained with the two sets of FE simulations performed with the two different estimates of relative density. The average FE capacity is 1443 kN, very close to the experimental data (1450 kN). The initial

experimental stiffness (about 380 MN/m) is slightly underestimated by the FE models, which predicted an average value of 310 MN/m and 270 MN/m with α_E equal to 5 and 7, respectively. A better fit could be obtained with a larger value of the modulus factor.

To assess the ability of the MM to reproduce the experimentally observed behaviour, the most accurate MMs were used (MM₂₀₀). The predictions for the different input combinations of Table 2 are inserted in Table 3.

These results are compared with those predicted with the FE models in Figure 3 (triangular markers), showing consistency of the MM₂₀₀ accuracy. Combining the outputs of the two MMs a bi-linear response can be drawn and a direct comparison with the experimental load-displacement curve can be pursued, as depicted in Figure 6. As the MMs were built to predict selected behavioural features, they were not expected to capture the entire curve, but to provide a good estimation of the initial experimental stiffness and tensile capacity. Capacity values well compared with the results of API and NGI methods: 1450 kN and 1559 kN, respectively. A slightly higher estimate was observed when compared to the prediction of the UWA, ICP and Fugro approaches, respectively 1304 kN, 1310 kN and 1100 kN.

The results were obtained using a very simplified FE strategy and produced encouraging results. A better implementation of the q_c profile as input

Table 3. Predictions of MM₂₀₀.

Outputs	$D_r = 72\%$;	$D_r = 72\%$;	$D_r = 76\%$;	$D_r = 76\%$;
	$\alpha_E = 5$	$\alpha_E = 7$	$\alpha_E = 5$	$\alpha_E = 7$
V_{ult} [kN]	1597	1478	1641	1433
K_t [MN/m]	350	326	280	261

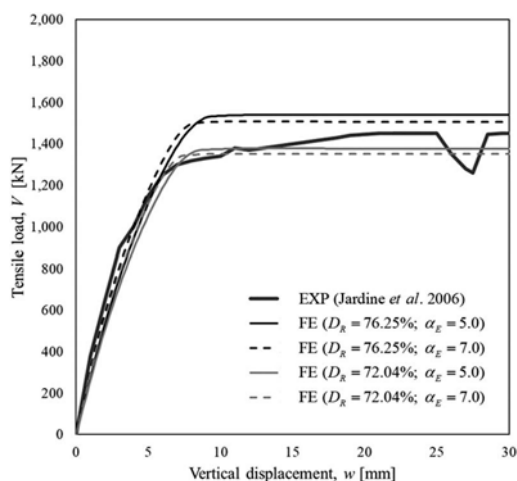


Figure 5. Experimental and FE load-displacement curves.

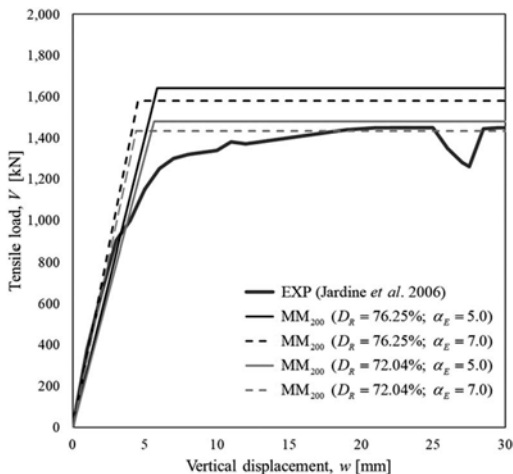


Figure 6. Experimental and MM₂₀₀ load-displacement curves.

variable should be pursued for a more reliable procedure. A possible way could be to follow the approach recently proposed by Cai et al. 2021.

5 CONCLUDING REMARKS

The paper has presented the development of a novel procedure for the prediction of the tensile response of steel displacement piles in sand. The approach has made use of a metamodelling technique, employed to store the results of a FE test programme with the aim of make them available for preliminary design purposes.

The FE models were simple, with soil parameters easily identifiable from CPT results. The modelling choices largely relied on the recent advance in the prediction of the axial capacity of offshore piles in sand with the CPT-based methods, thanks to which, available empirical correlations, had been validated on a large database of model tests.

The results obtained, although preliminary, have shown that:

- a simple CPT-based FE modelling strategy can produce results which compare well with experimental data, encouraging further validation;
- MMs can be built using a relatively small number of FE simulations and provide very accurate results over wide domains of input variables;
- inputs of MMs can be easily identified based on the interpretation of CPT data and produces good estimate of the experimental response.

Overall, the implementation of MMs is rather straightforward, avoiding the laborious FE modelling activities. MMs also run at a negligible

computational cost and are therefore suitable to parametric studies, which can be, in turn, interpreted in a probabilistic framework. The procedure, here presented in its essential steps, can be further extended to accommodate modelling features of higher complexity, increasing the number of input variables and can be employed to predict other behavioural aspects, increasing the numbers of outputs.

ACKNOWLEDGEMENT

This work forms part of the activities of the project SEAFLOWER, which has received funding from the European Union's Horizon 2020 research and innovation programme, under the Marie Skłodowska-Curie grant agreement No 891826.

REFERENCES

- ABAQUS 2014. Analysis User's Manual. Version 6.14, Dassault Systemes Simulia, Inc.
- Baudin, M., Lebrun, R., Iooss, B., Popelin, A-L. 2016. OpenTURNS: an industrial software for uncertainty quantification in simulation. In R. Ghanem, D. Higdon & H. Owhadi (eds.) *Handbook of uncertainty quantification*. Springer International Publishing.
- Bohn, C., Lopes dos Santos, A., Frank, R. 2017. Development of axial pile load transfer curves based on instrumented load tests. *Journal of Geotechnical and Geoenvironmental Engineering* 143 (1):04016081.
- Bolton, M.D. 1986. The strength and dilatancy of sands. *Geotechnique* 36(1): 65–78.
- Castro-Santos, L. & Diaz-Casas, V. 2016. *Floating Offshore Wind Farms*. Switzerland: Springer International Publishing.
- Cai, Y., Bransby, F., Gaudin, C., Uzielli, M. 2021. A framework for the design of vertically loaded piles in spatially variable soil. *Computers and Geotechnics* 134: 104140.
- Foglia, A., Wefer M., Forni, F. 2017. *Large-Scale Experiments and Load Transfer Analysis of Piled Foundations Supporting an Offshore Wind Turbine*. Offshore Site Investigation Geotechnics, 8th International Conference Proceeding, pp. 1078-1083(6).
- De Nicola, A. & Randolph, M.F. 1993. Tensile and compressive shaft capacity of piles in sand. *Journal of Geotechnical Engineering* 119(12): 1952–1973.
- De Gennaro, V., Frank, R., Said, I. 2008. Finite element analysis of model piles axially loaded in sands. *Rivista Italiana di Geotecnica* 2: 44–62.
- ISO (International Organization for Standardization) 2016. 19901-4: Petroleum and natural gas industries – specific requirements for offshore structures. Part 4: Geotechnical and foundation design considerations. Geneva, Switzerland.
- Jamiolkowski, M.B., Lo Presti, D.F.C., Manassero, M. 2003. Evaluation of relative density and shear strength of sands from CPT and DMT. *Soil Behaviour and Soft Ground Construction. ASCE, Geotechnical Special Publication* 119: 201–238.
- Jardine, R.J., Overy, R.F., Chow, F.C. 1998. Axial capacity of offshore piles in dense North Sea sands. *Journal of Geotechnical and Geoenvironmental Engineering* 124 (2): 171–178.

- Jardine, R.J., Standing, J.R. & Chow, F.C. 2006. Some observations of the effects of time on the capacity of piles driven in sand. *Géotechnique* 56(4): 227–244.
- McKay, M.D., Beckman, R.J., Conover, W.J. 1979. A comparison of three methods for selecting values of input variables in the analysis of output from a computer code. *Technometrics* 21(2): 239–245.
- Robertson, P.K. 2009. Interpretation of cone penetration tests – a unified approach. *Canadian Geotechnical Journal* 46: 1337–1355.
- Schmoor, K.A., Achmus, M., Foglia, A., Wefer, M. 2018. Reliability of design approaches for axially loaded offshore piles and its consequences with respect to the North Sea. *Journal of Rock Mechanics and Geotechnical Engineering* 10(6): 1112–1121.
- Schneider, J.A., Xiangtao, X., Lehane, B. 2008. Database assessment of CPT-based design methods for axial capacity of driven piles in siliceous sands. *Journal of Geotechnical and Geoenvironmental Engineering* 134(9): 1227–1244.
- Sudret, B. 2008. Global sensitivity analysis using polynomial chaos expansions. *Reliability Engineering and System Safety* 93: 964–979.
- van Tol, A.F. & Broere, W. 2006. Modelling the bearing capacity of displacement piles in sand. *ICE Proceedings Geotechnical Engineering* 159(3): 195–206.
- Xiu, D. & Karniadakis, G.E. 2002. The Wiener-Askey Polynomial Chaos for stochastic differential equations. *SIAM Journal on Scientific Computing* 24(2): 619–644.
- Yang, Z.X., Jardine, R.J., Guo, W.B., Cow, F. 2015. A new and openly accessible database of tests on piles driven in sands. *Géotechnique Letters* 5: 12–20.

Spatial interpolation of sparse PCPT data to optimise infrastructure design

M.P. O'Neill, M.F. Bransby, J. Doherty & P. Watson

ARC Research Hub for Transforming energy Infrastructure through Digital Engineering (TIDE), Oceans Graduate School, The University of Western Australia, Australia

ABSTRACT: In an offshore setting the geotechnical data available to infrastructure designers is usually sparse, and judgement is required in using information from sampled locations to estimate design parameters at unsampled locations. Recent interest in data-centric methods has seen advances in the interpolation of sparse data via statistical and analytical approaches. This paper demonstrates the implementation of one such approach, applying Bayesian Compressive Sensing and Markov Chain Monte Carlo techniques to sparse two-dimensional PCPT data. Through a simplified case study, the paper highlights how the method incorporates estimation uncertainty and its associated impact on the geotechnical design of a representative foundation.

1 INTRODUCTION

1.1 Background

In an offshore project, the number of piezocone penetrometer tests (PCPTs) performed either for a development layout or along a given alignment (e.g. a subsea pipeline or power cable) may be limited by technical constraints and high costs – and hence data is almost always sparse. In addition, infrastructure layouts may change and investigated locations may no longer align. Therefore, geotechnical designers are often required to employ a significant degree of engineering judgement in using the available data (at ‘sampled’ locations) to estimate PCPT profiles, and by extension soil design parameters, at untested (or ‘unsampled’) locations. The consequential risks to fabrication and installation costs and satisfactory in-service performance can be significant.

From a geotechnical perspective, the intrinsic balance in such judgement is the trade-off between (i) the risk of *underestimating uncertainty at any point* and therefore giving an ‘unconservative’ design profile which exposes the designed infrastructure to risk of failure to install or to fail during its service life, versus (ii) the cost of *overestimating uncertainty at any point* and generating a ‘conservative’ design profile which will lead to increased fabrication and installation costs. Such trade-offs have generally been achieved using engineering judgement, with no formal methodologies (apart from anecdotal records of installation risk or in-service failure) available to assess which side of the balance general practice lies for different types of site investigation (SI) data, seabed conditions and infrastructure.

Recent improvements in off-the-shelf computational capability have seen growing interest in the application of data-centric methods to analyse and use measured data, with recent publications highlighting advances in the interpolation, and in some cases extrapolation, of data via statistical and analytical approaches (e.g. Zhao et al. 2020, Cai et al. 2018, Rahman et al. 2021, Shi & Wang 2021, Wang et al. 2021). Such approaches provide a tool which can be used to question how design profiles are selected from various types of SI data and quantify whether these profiles result in appropriate installation and operational reliability when incorporated into code-based design.

1.2 Purpose of study

This paper describes a study to investigate the potential benefits and consequent challenges of using advanced statistical methods (that considers proximity of SI data to the designed infrastructure) to select inputs for geotechnical design. One particular method (Zhao et al. 2020) uses a two-dimensional (2D) Bayesian compressive sensing-Markov Chain Monte Carlo (hence termed ‘BCS’) approach, which is compared to a simpler ‘standard’ approach using an offshore field PCPT dataset.

The study incorporates the BCS and standard analysis results into a simple geotechnical design assessment of a representative foundation. By comparing the findings of the foundation assessment, the study highlights the benefit an advanced statistical approach provides in addressing uncertainty (risk) in the estimation of soil strength for foundation design.

2 FIELD PCPT DATA

2.1 Overview

The field PCPT data were obtained at a deep-water site offshore north-western Australia. The sediments across the site comprised high plasticity carbonate muddy silts and silty muds. For this study the five PCPTs located along the example survey line (PCPT1 to PCPT5) highlighted on Figure 1 were considered. The tests were conducted at approximately regular intervals along the line, with a horizontal distance (x) of 142 m separating PCPT5 from PCPT1. Data were recorded at regular depth increments (Δz) of 0.02 m

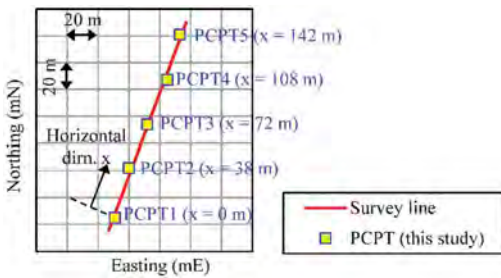


Figure 1. PCPT locations.

Profiles of the measured (field) net cone resistance (q_{net-f}) and excess pore pressure ratio (B_{q-f}) versus depth below mudline (z) obtained at the five PCPT locations are presented on Figure 2 down to $z = 20$ m. A cursory review of the data indicates four soil types (units; U1 to U4) exhibiting similar overall trends with depth across the survey line down to 20 m depth, as illustrated on Figure 2. It is noted that across the survey line (relative to x) q_{net-f} is reasonably uniform with no significant ‘outliers’. For sites with higher variability the estimation of soil strength would require a greater amount of input (measured) data.

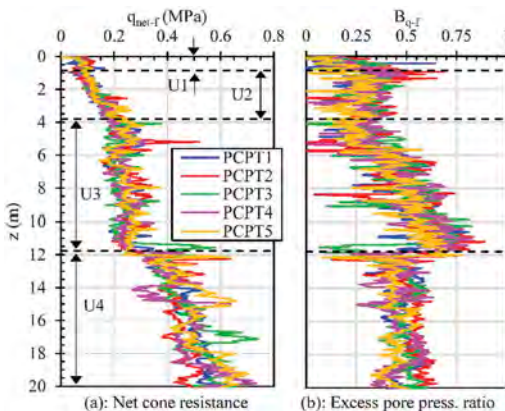


Figure 2. PCPT measured net cone resistance & excess pore pressure ratio.

2.2 Sampled data case scenarios

For this study three ‘sampled data’ case scenarios were assessed:

- Case 1 considered q_{net-f} from all five PCPTs as input;
- Case 2 considered q_{net-f} from PCPT1/3/4/5 as input and excluded PCPT2 ($x = 38$ m);
- Case 3 considered q_{net-f} from PCPT1/3/5 as input and excluded PCPT2 ($x = 38$ m) and PCPT4 ($x = 108$ m).

For Case 2 and Case 3 the excluded PCPTs were considered to be unsampled (unseen) data.

3 BCS ANALYSIS OF FIELD PCPT DATA

The BCS method proposed by Zhao et al. (2020) for assessing sparse geotechnical data allows for the formal treatment of uncertainty in the estimation of geotechnical parameters at unsampled locations. The method is relatively fast, computationally efficient and well suited to non-stationary data (i.e. multi-layered soil stratigraphies with spatially varying soil properties and soil layer boundaries).

3.1 BCS analysis parameters

A 2D BCS analysis was undertaken for each case, extending across the 142 m long survey line and down to 20 m depth, using horizontal and vertical spatial increments of $\Delta x = 1.0$ m and $\Delta z = 0.02$ m respectively. The analysis adopted natural log values of the input q_{net-f} data to avoid negative estimated net cone resistance (q_{net-e}) values and to reflect the generally log-normally distributed nature of the sampled q_{net-f} data (see Lacasse 1994, Griffiths et al. 2009).

Each BCS analysis comprised 10,500 iterations. Results from the first 500 iterations were discarded, as these were assumed to represent the numerical stabilisation phase of the analysis. In order to ensure the final results were statistically independent, the results from every 20th iteration (from the remaining 10,000 iterations) were saved while those from the other iterations were also discarded. Hence, each BCS analysis comprised 500 independent q_{net-e} sets across the full 20 m by 142 m z - x cross-section.

The study did not account for measurement uncertainty in the PCPT data (this will be addressed as part of future/ongoing development of the approach).

3.2 BCS analysis results

Results from the Case 1 BCS analysis are presented on Figure 3 as z - x heat maps showing the mean and coefficient of variation (COV) of the estimated net cone resistance (q_{net-m} and $q_{net-cov}$ respectively) determined from the 500 independent q_{net-e} cross-sections, with the PCPT locations (input q_{net-f} data) high-lighted. The q_{net-m} map shows a similar soil unit structure across

the survey line as that inferred from the measured data (see Figure 2). The $q_{\text{net-cov}}$ map provides an informative illustration of the predictive functionality of the BCS method. The COV at the PCPT locations is near-zero; this is to be expected, since at these locations q_{net} is measured (known; i.e. $q_{\text{net-f}}$) and the corresponding estimated values are considered to be reliable. Conversely, in between the PCPTs the COV is relatively high, since at these locations no information on $q_{\text{net-f}}$ is available. Note the COV increases as the horizontal distance from the nearest sampled location also increases.

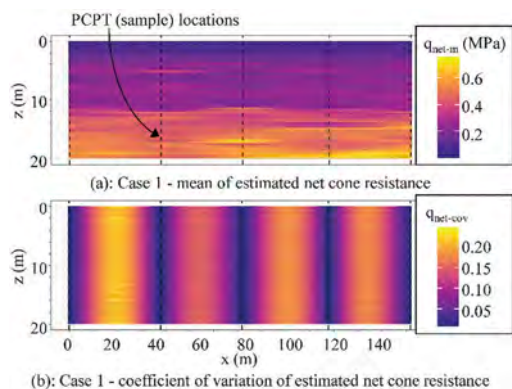


Figure 3. Case 1 BCS analysis – mean & COV of estimated net cone resistance.

Figure 4 provides a useful demonstration of the overall structure of the BCS analysis results. The figure shows plots of $q_{\text{net-m}}$ and the 10th and 90th percentile ($[P10, q_{\text{net-p10}}]$ and $[P90, q_{\text{net-p90}}]$ respectively) estimated net cone resistance versus horizontal distance along the survey line (x) at a depth (z) of 8 m for the three cases. On each plot the locations of the PCPT measured $q_{\text{net-f}}$ included in the respective analysis input are highlighted. The $q_{\text{net-m}}$, $q_{\text{net-p10}}$ and $q_{\text{net-p90}}$ profiles essentially represent near-smooth continuous functions of x . At the PCPT locations the $q_{\text{net-f}}$ values constrain the range of $q_{\text{net-e}}$, while as the horizontal distance from the nearest PCPT increases the $q_{\text{net-e}}$ range also increases (as reflected by the widening range between $q_{\text{net-p10}}$ and $q_{\text{net-p90}}$).

Further insight into the BCS analysis functionality may be obtained by interrogating estimated net cone resistance versus depth profiles at specific locations along the survey line. Figure 5a shows the measured ($q_{\text{net-f}}$) profile for PCPT2 ($x = 38$ m), together with the mean, P10 and P90 estimated profiles from the Case 2 BCS analysis at $x = 38$ m. In this scenario where the PCPT2 measured $q_{\text{net-f}}$ was excluded from the BCS analysis input, we can assess the performance of the BCS method in predicting $q_{\text{net-f}}$. The mean estimated $q_{\text{net-m}}$ profile shows generally reasonable agreement with the measured profile, although locally there is some mismatch. Comparing the mean estimated and measured profiles, the Case 2 average normalised

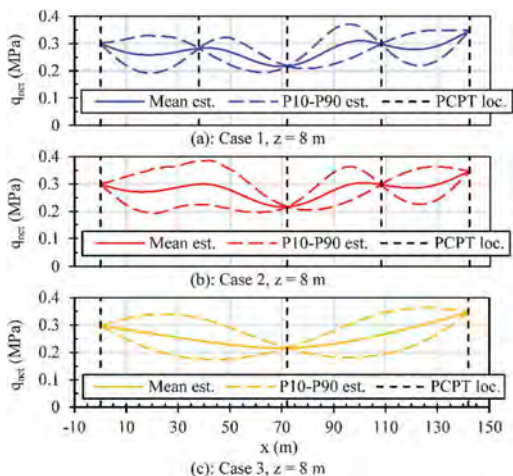


Figure 4. Case 1, Case 2 & Case 3 BCS analyses – mean estimated & P10-P90 estimated net cone resistance at 8 m depth.

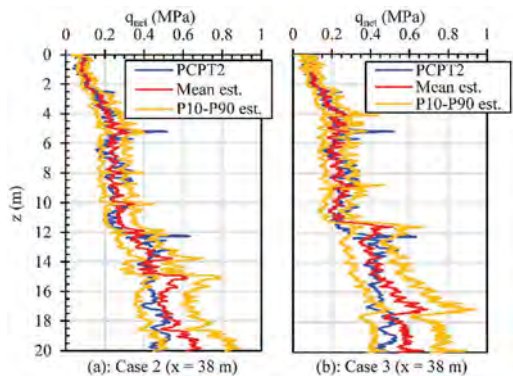


Figure 5. Case 2 & Case 3 BCS analyses – measured, mean estimated & P10-P90 estimated net cone resistance at PCPT2.

prediction error for PCPT2 (expressed as the average absolute value of $[q_{\text{net-m}} - q_{\text{net-f}}]/q_{\text{net-f}}$) was 16.9 %. Furthermore, with the exception of a handful of specific abrupt changes in the measured $q_{\text{net-f}}$, the $q_{\text{net-p10}}$ and $q_{\text{net-p90}}$ profiles bound the $q_{\text{net-f}}$ profile well.

A similar set of profiles at $x = 38$ m are presented on Figure 5b for the Case 3 analysis. The overall agreement between $q_{\text{net-m}}$ and $q_{\text{net-f}}$ is similar to that observed for Case 2. For Case 3 the average normalised prediction error for PCPT2 was 17.1 %.

4 FOUNDATION DESIGN ASSESSMENT

A simplistic design assessment of a representative foundation was undertaken which utilised the results of the BCS analyses (in the form of estimated soil strength along the survey line z - x cross-section), in addition to an alternative estimate of soil strength based on a more standard approach.

4.1 Standard assessment of field PCPT data

A ‘standard’ assessment of field PCPT data across a specified survey area or line for the purpose of foundation design often involves assuming that the seabed forms a single soil zone in the area of interest (covering the planned infrastructure and investigated locations). The available data is compiled and simple percentile (or quantile) profiles of the data versus depth are generated. These profiles are normally independent of horizontal location and apply right across the survey area or line.

For this study the standard assessment was based on the quantile regression (QR) ‘zonation’ approach (Uzielli et al. 2019). An example of this approach is illustrated on Figure 6, which shows the Case 1 (five PCPTs) measured q_{net-f} versus depth data. Included on the same figure are the corresponding 10th and 90th quantile (Q10 and Q90 respectively) representative design profiles of the Case 1 q_{net-f} data. The QR profiles were generated considering the same soil units inferred from the field PCPT data (see Figure 2).

4.2 Foundation design scenario

The simple deterministic foundation design scenario considered a circular caisson foundation with nominal outer diameter (D) values of 2 m and 10 m, an embedment length (L) ranging between 5 m and 20 m, and a skirt wall thickness (t) defined by $D/t = 50$.

The design considered the foundation in-place vertical capacity and installation resistance. The capacity (V_{cap}) was simplistically assumed to comprise the sum of end bearing across the full caisson base ($q_b = N_c s_{u-b} A_b$, N_c = bearing capacity factor, s_{u-b} = average undrained shear strength across the caisson base, A_b = caisson base area) and skin friction across the outer caisson wall ($f_o = \alpha s_{u-o} A_o$, α = adhesion factor, s_{u-o} = average undrained shear strength across the outer caisson wall, A_o = outer caisson wall area).

The installation resistance (V_{inst}) was simplistically assumed to comprise the sum of end bearing across the caisson wall tip area ($q_t = N_c s_{u-b} A_t$,

where A_t = caisson wall tip area), friction across the outer caisson wall (f_o) and friction across the inner caisson wall ($f_i = \alpha s_{u-i} A_i$, where s_{u-i} = average undrained shear strength across the inner caisson wall, A_i = inner caisson wall area). In all cases it was assumed $N_c = 9$ and $\alpha = 0.6$, while s_{u-b} , s_{u-o} and s_{u-i} were determined assuming $s_u = q_{net}/N_{kt}$ where N_{kt} = cone factor = 15.

4.3 Foundation design example

A set of foundation design assessment results is presented on Figure 7 in terms of V_{cap} and V_{inst} versus L for $D = 2$ m and a caisson centre horizontal location (x_c) of 38 m (coincident with PCPT2). The V_{cap} and V_{inst} values were calculated considering soil strengths based on the Case 1 and Case 3 BCS estimated q_{net} values (P10 for V_{cap} , P90 for V_{inst}) and Case 3 QR estimated q_{net} values (Q10 for V_{cap} , Q90 for V_{inst}). Since the PCPT2 q_{net-f} data was included in the Case 1 analysis input, the Case 1 BCS-estimated V_{cap} and V_{inst} values for $D = 2$ m at $x = 38$ m closely reflect the soil strength profile derived directly from the PCPT2 measured q_{net-f} .

Figure 7a shows for all values of L the Case 3 BCS-P10 V_{cap} is lower than the Case 3 QR-Q10 V_{cap} , which in turn is generally lower than the Case 1 BCS-P10 V_{cap} . For Case 3 at $x = 38$ m (midway between the closest PCPTs, PCPT1 and PCPT3) no information on q_{net-f} is available, and therefore the BCS estimated strength range is sufficiently wide (about the mean, reflecting higher uncertainty) such that the Case 3 BCS-P10 strength is less than the Case 3 QR-Q10 strength (and the Case 1 BCS-P10 strength, which is assumed to be similar to the PCPT2 q_{net-f}).

The opposite trend is shown on Figure 7b for V_{inst} , implying the Case 3 BCS-P90 strength is greater than the Case 3 QR-Q90 strength (and the Case 1 BCS-P90 strength, which again is assumed to be similar to the PCPT2 q_{net-f}).

Considering a scenario represented by Case 3 and a design requirement to select an appropriate L for a $D = 2$ m caisson at $x = 38$ m, the results presented

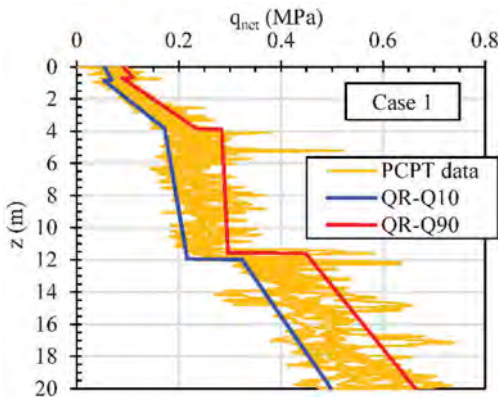


Figure 6. Case 1 – Q10-Q90 design net cone resistance.

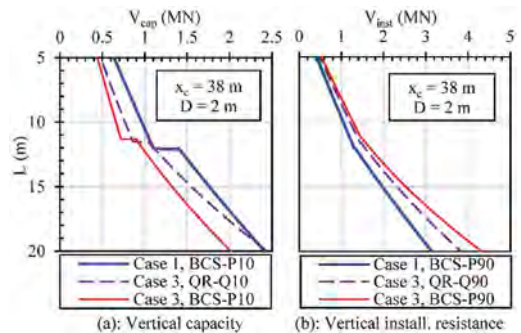


Figure 7. Case 1 & Case 3 – example foundation vertical capacity & installation resistance versus embedment length.

on Figure 7 highlight the implications of the decision on if the caisson sizing should adopt an estimated soil strength based on the available (in-hand) data, or whether additional data (in the form of a PCPT) should be acquired at $x = 38$ m. If it were decided not to acquire additional data, the design may adopt the relatively conservative Case 3 BCS estimates for V_{cap} and V_{inst} as these account for the relationship between location (x) and uncertainty in the estimated soil strength. Conversely, if the additional PCPT was performed, the designers could adopt the less conservative Case 1 BCS V_{cap} and V_{inst} estimates. If no extra PCPT was performed and the designers adopted the simpler traditional approach, the resulting QR-based estimate of soil strength would underestimate uncertainty and lead to a design that may be unconservative (by an amount represented by the difference between the Case 3 QR and BCS estimates for V_{cap} and V_{inst}).

4.4 Overview of foundation design assessment

A summary of the foundation design assessment findings is provided in Table 1 in terms of the capacity ratio (R_{cap}) equal to the BCS estimated V_{cap} divided by the QR estimated V_{cap} , and the installation resistance ratio (R_{inst}) equal to the BCS estimated V_{inst} divided by the QR estimated V_{inst} . By normalising the BCS-based capacity and installation resistance values against their QR counterparts, the R_{cap} and R_{inst} results highlight the ability of the BCS method to account for location-specific confidence in soil strength. Note the R_{cap} and R_{inst} values contained in Table 1 are average values for $5 \text{ m} \leq L \leq 20 \text{ m}$. Results are presented for $x_c = 72 \text{ m}$, 55 m and 38 m , $D = 2 \text{ m}$ and 10 m , and for the three different cases.

The same results are plotted on Figure 8 in terms of average R_{cap} and R_{inst} values versus the corresponding representative horizontal separation distance of the caisson centre from the nearest PCPT locations ($s_{rep} = [s_1 s_2] / [s_1^2 + s_2^2]^{0.5}$, where s_1 and s_2 = horizontal distance from the caisson centre to the immediately adjacent PCPTs situated each side of the caisson centre location; values of s_{rep} are listed in Table 1). Included on the plots are approximate trendline fits to the results.

The results indicate a general trend of R_{cap} decreasing and R_{inst} increasing with increasing s_{rep} (i.e. greater separation between the caisson and known soils data). For caissons centred about a PCPT location ($s_{rep} = \text{zero}$), the BCS estimated capacity is shown to be higher than the corresponding QR estimated value ($R_{cap} > 1.0$), while the BCS estimated installation resistance is lower than the corresponding QR estimated value ($R_{inst} < 1.0$). Hence, these results suggest for $s_{rep} = \text{zero}$ the QR approach tends to overestimate the level of soil strength uncertainty.

Conversely, for caissons situated some distance away from the closest PCPT locations (high s_{rep}), the BCS estimated capacity is shown to be slightly lower than the corresponding QR estimated value ($R_{cap} < 1.0$), while the BCS estimated installation

Table 1. Foundation design assessment results.

Found Centre	Case	Reprsnt. Sep. Dist.	Average Capacity		Average Install. Resist.	
			Ratio R_{cap}		Ratio R_{inst}	
x_c	s_{rep}		D=2m	D=10m	D=2m	D=10m
72	1	0.0	1.18	1.15	0.82	0.84
	2	0.0	1.18	1.15	0.82	0.85
	3	0.0	1.16	1.13	0.81	0.83
55	1	12.0	0.99	0.98	0.98	0.98
	2	16.2	0.96	0.96	1.06	1.06
	3	16.2	0.95	0.95	0.98	0.98
38	1	0.0	1.20	1.14	0.86	0.88
	2	25.3	0.95	0.95	1.10	1.10
	3	25.3	0.87	0.86	1.09	1.09

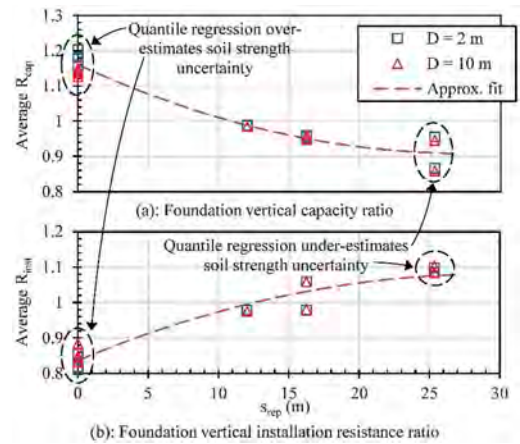


Figure 8. Foundation average capacity & installation resistance ratios versus representative horizontal separation distance from nearest PCPTs.

resistance is generally slightly higher than the corresponding QR estimated value ($R_{inst} > 1.0$). Hence, this suggests for high s_{rep} the QR approach tends to slightly underestimate soil strength uncertainty.

The results listed in Table 1 also show that for caissons centred about a PCPT location ($s_{rep} = \text{zero}$), as the caisson outer diameter (D) increases R_{cap} decreases slightly while R_{inst} increases slightly. This reflects the increasing level of uncertainty in the BCS estimated strength across the caisson footprint as it expands beyond the PCPT location. For caissons situated away from the closest adjacent PCPT locations (relatively high s_{rep}) the opposite trend is expected, although the results indicate minimal change in R_{cap} and R_{inst} with increasing D . This suggests the foundation must be situated within some limiting distance from the nearest adjacent PCPT for D to influence R_{cap} and R_{inst} .

5 CONCLUSIONS

5.1 *Interpolation of PCPT data and impact on foundation design*

The study outlined in this paper provides a demonstration of the application of an advanced statistical approach to interpolating sparse field PCPT data (specifically net cone resistance) to improve geotechnical design inputs for a representative foundation. The findings of the foundation design assessment (summarised in Table 1 and Figure 8) provide a concise quantitative example of the benefit offered by such approaches in addressing the spatial variation in soil strength uncertainty caused by the layout of an SI. This benefit encapsulates both the opportunity to rationally reduce foundation size requirements when soil strength uncertainty is low (near SI locations), and the need to fully account for risk by increasing foundation size requirements when soil strength uncertainty is high (further from SI locations).

5.2 *Next steps – interpolation of data*

As part of future/ongoing development of the application of advanced statistical approaches to interpolate sparse data, a near-term goal will be to investigate options for incorporating additional sources of geodata into approaches such as the Zhao et al. (2020) BCS method featured in this paper. One potential source is geophysical data which may inform the spatial alignment of soil unit boundaries and the identification and selection of soil unit types and possibly soil classification properties.

The BCS approach may also be expanded to a three-dimensional (3D) spatial framework. Such analyses would require significantly more computational time and resources. However, in situations where data is available over a specific spatial footprint or survey area, and for the scenario where the position of future infrastructure within the footprint changes, such a capability would be beneficial.

5.3 *Next steps – applications of interpolated data*

As demonstrated by the foundation design assessment, the potential geotechnical engineering applications of statistical analysis methods which consider spatial distribution of seabed uncertainties are significant. A possible future application involves using predicted soil properties at unsampled locations as input to a suite of forecasting-costing-optimisation tools, which may be used to facilitate planning of future geotechnical SIs and inform real-time decision-making for current SIs. Similarly, in the context of an offshore setting the tools may be employed in the optimisation of infrastructure design (e.g. pipelines, cables, platforms, offshore wind turbines and subsea structures). The goal will be to use these tools in a project setting to undertake quantitative cost-benefit assessments in order to provide answers to questions

such as “do we need to acquire additional geo-data?”, “where should we locate our infrastructure?” and “what size does our infrastructure need to be?”.

ACKNOWLEDGEMENTS

This research is supported by the ARC ITRH for Transforming energy Infrastructure through Digital Engineering (TIDE, <http://TIDE.edu.au>) which is led by The University of Western Australia (UWA), delivered with The University of Wollongong and a number of Australian and international research partners, and funded by the Australian Research Council, INPEX Operations Australia, Shell Australia, Woodside Energy, Fugro Australia Marine, Wood Group Kenny Australia, RPS Group, Bureau Veritas and Lloyd’s Register Global Technology (grant No. IH200100009). The second author holds the Fugro Chair in Geotechnics at UWA, whose support is gratefully acknowledged. The fourth author leads the Shell Chair in Offshore Engineering research team at UWA, which is supported by Shell Australia.

REFERENCES

- Cai, Y., Li, J., Li, X., Li, D. & Zhang, L. 2018. Estimating soil resistance at unsampled locations based on limited CPT data. *Bulletin of Engineering Geology & the Environment* 2019, 78:3637–3648, <https://doi.org/10.1007/s10064-018-1318-2>.
- Griffiths, D.V., Huang, J. & Fenton, G.A. 2009. Influence of spatial variability on slope reliability using 2-D random fields. *Journal of Geotechnical & Geoenvironmental Eng.*, Vol. 135, No. 10, pp. 1367–1378.
- Lacasse, S. 1994. Reliability & probabilistic methods. *Proc. 13th Int. Conf. Soil Mechanics & Foundation Engineering*, New Delhi, India, pp. 225–227.
- Rahman, Md.H., Abu-Farsakh, M.Y. & Jafari, N. 2021. Generation & evaluation of synthetic cone penetration test (CPT) data using various spatial interpolation techniques. *Canadian Geotechnical Journal*, 58: 224–237 (2021), <http://dx.doi.org/10.1139/cgj-2019-0745>.
- Shi, C. & Wang, Y. 2021. Non-parametric machine learning methods for interpolation of spatially varying non-stationary & non-Gaussian geotechnical properties. *Geoscience Frontiers*, 12 (2021) 339–350, <https://doi.org/10.1016/j.gsf.2020.01.011>.
- Uzielli, M., Zei, M. & Cassidy, M.J. 2019. Probabilistic assignment of design undrained shear strength using quantile regression. *Proc. 7th Int Symp. Geotechnical Safety & Risk*, pp. 188–193.
- Wang, Y., Shi, C. & Li, X. 2021. Machine learning of geological details from borehole logs for development of high-resolution subsurface geological cross-section & geotechnical analysis. *Georisk: Assessment and Management of Risk for Engineering Systems & Geohazards*, <https://www.tandfonline.com/action/showCitFormats?doi:10.1080/17499518.2021.1971254>.
- Zhao, T., Xu, L. & Wang, Y. 2020. Fast non-parametric simulation of 2D multilayer cone penetrometer test (CPT) data without pre-stratification using Markov Chain Monte Carlo simulation. *Engineering Geology*, 273 (2020) 105670, <https://doi.org/10.1016/j.enggeo.2020.105670>.

Use of CPT as a soil mixing verification tool: Some practical observations

A. O'Brien & I. Murray

GE Solutions Consulting Ltd., Whitburn, UK

ABSTRACT: Mass soil mixing is a versatile ground improvement technology for marginal and brownfield sites. Dry soil mixing is relatively common in the UK for the improvement of ground with very wet and/or organic materials. Wet mixing is less commonplace and involves introduction of a fluid grout with simultaneous rotavating of the soil with a mixing tool. This paper presents the results of CPT investigations into wet mixed soils with a view to use the results as a means to verify the strength and consistency of the mixed materials. A high volume of data has been extracted from two active sites. CPT soundings are found to be purposeful in terms of demonstrating the overall improvement effect and integrity of the mixed soil volume spatially and with depth. Existing CPT testing of mass mixed soil is very limited and this testing has allowed the mixed soil to be compared to existing CPT soil behaviour indexes to give an insight into their usefulness for characterising mixed material and its behaviour.

1 INTRODUCTION

Mass wet soil mixing involves disaggregation over large areas / volumes of soil using a rotavating tool. Mixing usually takes place within discrete “cells” and the mixing depth is typically limited up to 5-7m depending on the application and native soil conditions. The rotavating tool spins at high revolutions per minute (in the order of 80-90rpm) and grout is injected under medium pressure (typically up to 50bar). The result is a completely fluidised cell, homogenising the native soils and engendering the required strength with curing time.

Post-construction behaviour is usually assessed via limited in situ testing, such as plate bearing tests supplemented with laboratory strength testing of samples recovered during construction, typically to establish a specified unconfined compressive strength. However, because of the nature of the mixing process, there is scope for small inclusions of unmixed material to remain where mixing effort is not adequate. Cone penetration testing is a practical means to establish the strength and consistency of the mixed soil body, particularly where pre-construction and post-construction soundings are undertaken to allow quantification of the improvement effect.

The use of the cone penetration test for these purposes needs careful consideration if the data is to be used for anything more than a comparison of pre-construction and post-construction conditions. The

nature of the soil mixing process is such that the entire matrix of the soil is de-structured with hydration & cementation subsequently forming an entirely new macro- and microscopic condition. The mixed materials would fall outside of the normal soil behaviour type / index categorization, which is obviously limited to natural materials. However, if found to be reliable, the use of CPT to re-parameterise the mixed material would have significant technical and commercial benefits including spatial quality control, estimating spatial variability of the mixed area and development of geotechnical parameters for the mixed soil, thereby mitigating the need for high-frequency laboratory testing.

It is noted that the use of CPT in soil mixing applications is currently typically limited to deep columns (e.g., Puppala et al., 2005; Ilander et al., 1999), which are necessarily more focused and higher intensity mixing efforts and this is a distinction which must be made for mass mixing, which attempts to productively improve larger soil volumes, typically to a lower strength than deep soil mixed columns.

2 THE SITES

Two sites have been examined in this study, denoted as BWB and JSR – both are active sites in western Scotland. Site BWB was predominantly firm non-organic lightly overconsolidated horizons of sandy, silty clay or sandy silt with occasional

lenses of silty sand. The groundwater regime is ill-defined on this site and is potentially subject to a hydraulic gradient, but is known to be within the mixed horizon. The minimum mixed depth for the BWB site is 6m.

Site JSR was characterised by very soft silty clay with inclusions of organic materials and occasional bands of organic materials up to 1m in thickness. The organic materials are nominally described as amorphous peat. The site is low-lying between glacial drumlins. The groundwater table is, again, ill-defined but typical equilibrium water level is within the mixed horizon. The minimum mixed depth for the JSR site is 4.0m.

2.1 Mass mix procedure

For both sites, a target mixing depth was established and achieved. Cement was added via a neat cementitious grout (CEM I only) with added cement proportions measured between 12-15% of the bulk unit weight of the native soil. This is a typical proportion for this type of mixing in order to control both material bulking and overall injected volume. Curing time post-mixing varied in a narrow range of 25-35 days when the CPTs were undertaken at both sites.

3 COMPARISON OF PRE- AND POST-CONSTRUCTION CPT DATA

All CPT data in this study was collected using 15cm² subtraction piezocones manufactured by Geomil Equipment B.V. The data procedures were consistently in accordance with EN ISO 22476-1:2012 and all CPTs achieved Application Class 2, noting that the soil type prohibited achievement of Application Class 1 as a practical matter.

Porewater pressure measurements were measured at the cone shoulder (u_2) position.

3.1 Tip resistance

Corrected cone tip resistances for both sites are presented in Figures 1 & 2 for the BWB and JSR sites respectively. Based on mean corrected tip resistance, post-construction improvement in tip resistance was estimated as a multiplier of 6.11, with a standard deviation of 2.71 for the BWB site (mean pre-construction tip resistance of 1.16MPa, standard deviation of 0.518MPa). The equivalent multiplier for the JSR site is 4.86 with a standard deviation of 2.27 (mean pre-construction tip resistance of 0.30MPa, standard deviation of 0.11MPa).

3.2 Sleeve friction

Sleeve friction for both sites are presented in Figures 3 & 4 for the BWB and JSR sites respectively. Based on mean sleeve friction, post-construction improvement in sleeve friction was estimated as

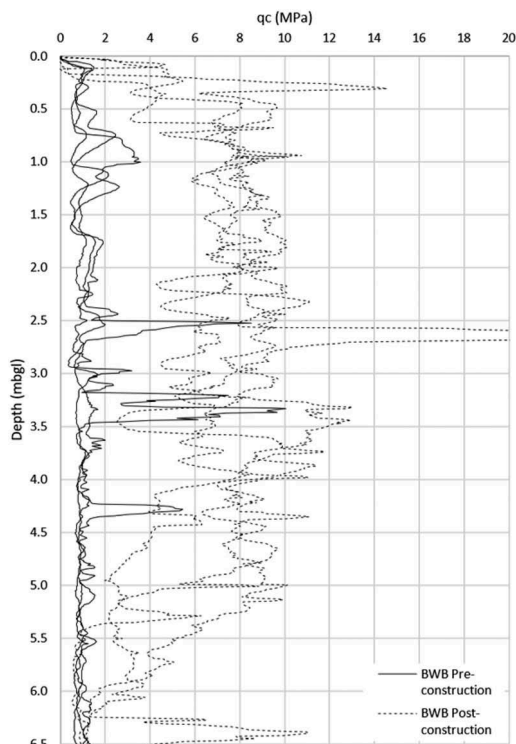


Figure 1. BWB site tip resistances.

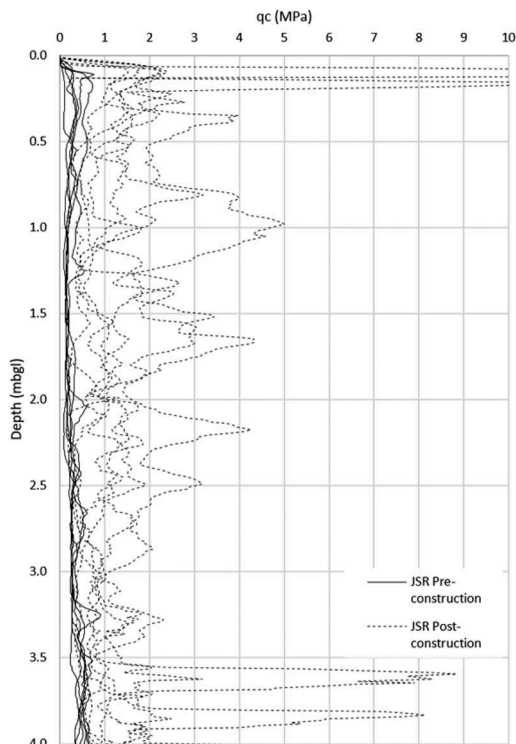


Figure 2. JSR site tip resistances.

a multiplier of 5.33 with a standard deviation of 1.94 for the BWB site (mean pre-construction sleeve friction of 50.5kPa, standard deviation of 17.93kPa). The equivalent multiplier is 4.55 with a standard deviation of 2.17 for the JSR site (mean pre-construction sleeve friction of 12.77kPa, standard deviation of 5.08kPa). A statistical summary of the primary measured parameters are presented in Table 1.

3.3 Dynamic porewater pressure

Dynamic porewater pressure profiles are presented in Figures 5 & 6 for the BWB & JSR sites respectively. A rational statistical examination of these profiles is not possible; however, a number of observations can be made. Pre-construction dynamic porewater pressure, noting that cone saturation was tightly controlled and dissipation tests were run in order to assure saturation of the cone where appropriate, is invariably negative/approaching cavitation pressure or inconsistently and modestly positive (u2 where positive is typically less than 50kPa).

Post-construction, large dynamic porewater pressures are generated, particularly for the BWB site. The large porewater pressures are generated generally towards the middle of the mixed horizon and are observed to revert towards pre-construction behaviour at the base of the mixed horizon. Cavitation pressures were established over some of the mixed horizon at the BWB site and more consistently towards the base of the mixed horizon at the JSR site. There are no noted operational reasons for this occurrence.

3.4 Friction ratio

Comparison of pre- and post-post construction friction ratio observes a degree of inverse proportionality. Figure 7 presents a comparison of friction ratio pre- and post-construction based on average values. It is observed that where the pre-construction friction ratio is initially low (<4%), there is a tendency for post-construction friction ratio to be elevated. Where the

Table 1. Statistical summary of measured parameters for BWB & JSR sites.

Measured parameter	Stat.	Site BWB		Site JSR	
		Pre	Post	Pre	Post
Corrected cone resistance (MPa)	Mean	1.160	6.469	0.301	1.298
	Median	0.990	7.066	0.294	1.221
	St. Dev.	0.518	2.331	0.105	0.441
	COV	0.447	0.360	0.350	0.340
Sleeve friction (kPa)	Mean	50.502	258.010	12.766	49.394
	Median	47.346	273.448	12.264	47.356
	St. Dev.	17.934	87.605	5.077	10.389
	COV	0.355	0.340	0.398	0.210

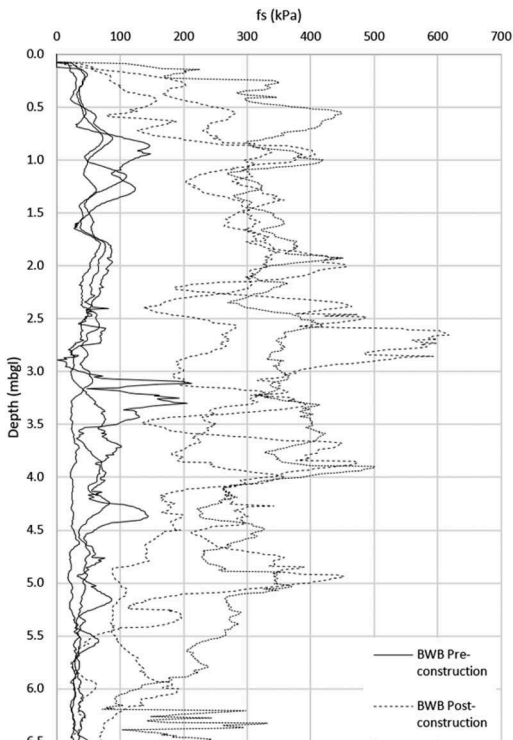


Figure 3. BWB site sleeve friction.

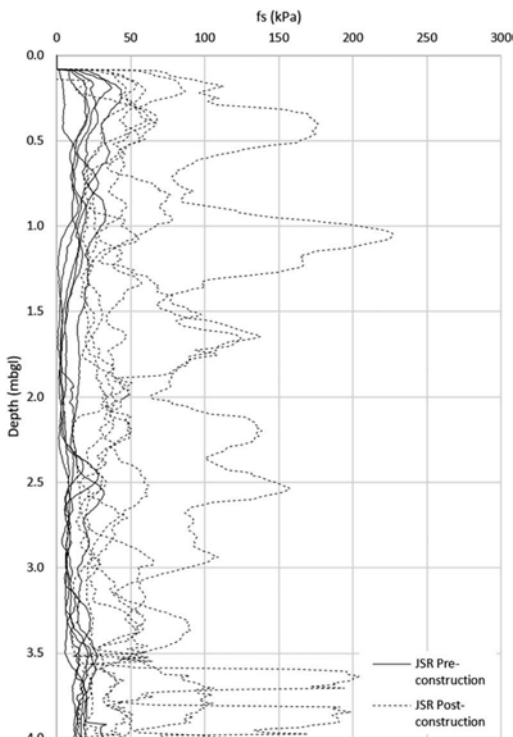


Figure 4. JSR site sleeve friction.

pre-construction friction ratio is $>5\%$, there is a tendency for the post-construction friction ratio to be reduced. Between 4% and 5%, there is a transition zone where friction ratio could be either reduced or elevated when compared to pre-construction levels.

3.5 Soil behaviour index / type

Normalised soil behaviour indexes (I_c), calculated based on the work of Robertson (2009), for both sites are presented in Figures 8 & 9 below for the BWB & JSR sites respectively using routine procedures for normalising the input parameters. The soil behaviour indexes are observed to undergo a marked shift post-construction.

Examining soil behaviour type more broadly, the shifts are in the main from normally to lightly over-consolidated fine-grained soils towards very stiff fine-grained soils, capturing the cemented structure. More recent soil behaviour index methods (e.g., Robertson, 2016) would have categorised the mixed soil as *Clay-like / Dilative* or *Transitional / Dilative* with estimates of the lower B_q parameter indicative of increasing microstructure (cementation, bonding). The SBT charts for the BWB & JSR charts are presented respectively in Figures 10 & 11, while the mean shift in soil behaviour type is shown in Figure 12.

4 OBSERVATIONS

The direct measurements of cone tip resistance and sleeve friction are observed to increase post-mixing. Mean tip resistance increased by between 558% (site BWB) and 430% (site JSR) for respective mean pre-construction tip resistances of 1.16MPa and 0.3MPa. Similarly, mean sleeve friction increased by between 511% and 387% for respective mean pre-construction sleeve friction of 50.5kPa and 12.8kPa. The CPT is observed to be purposeful in demonstrating that achieved improvement is less at the base of the mixed horizon at the time of the measurements.

The naïve coefficient of variation (noting that mean values were used in these calculations on the basis of consistent sample sizes) reduces for the measurement of tip and sleeve resistance over both sites, though not markedly, mainly owing to the lack of stratification over both sites i.e., there are no dominant horizons in the pre-mixed zone. The magnitude of the reduction in variation is most pronounced in the measurement of sleeve friction for the JSR site where the pre-construction variation was greatest of the parameters measured (0.398 pre-construction, 0.210 post construction).

There is marked facility to set up high excess porewater pressures post-construction. Pre-construction soils expressed dilative behaviour and cavitation resulting in negative u_2 measurements. However, post-construction, and most pointedly at the BWB site, very high excess porewater pressures were measured.

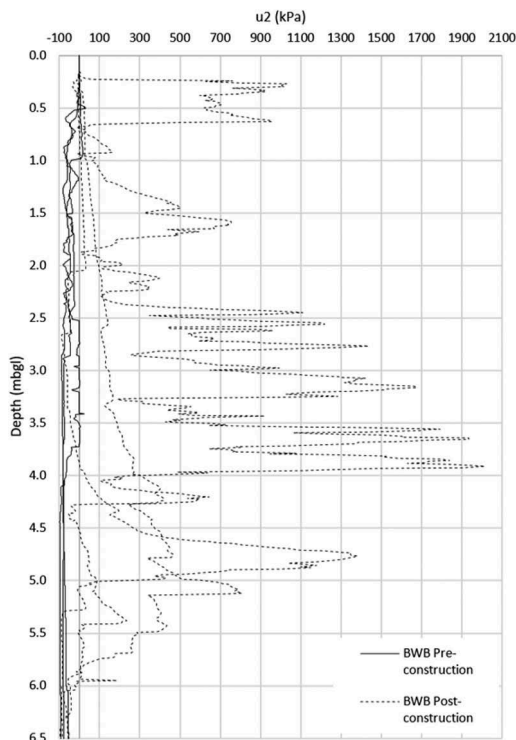


Figure 5. BWB site dynamic porewater pressure (u_2).

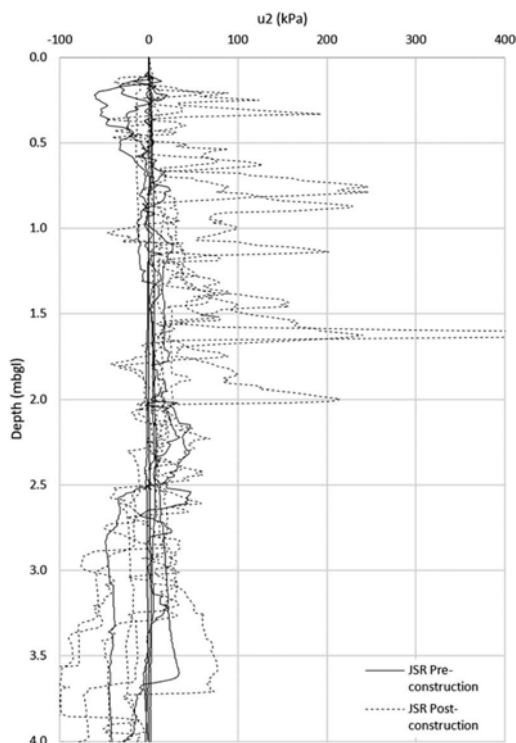


Figure 6. JSR site dynamic porewater pressure (u_2).

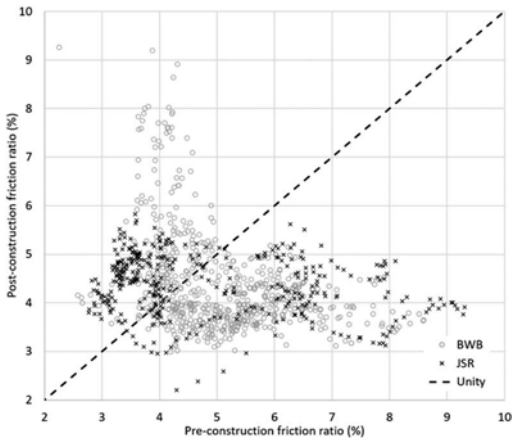


Figure 7. Pre- / post-construction friction ratio comparison.

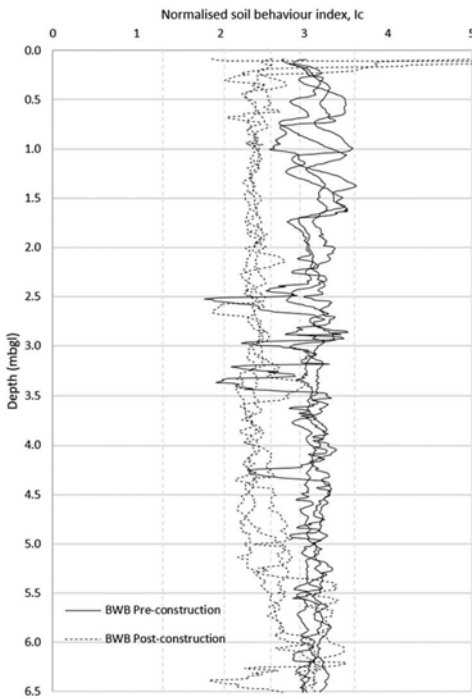


Figure 8. I_c for BWB site.

As noted, the friction ratio measurements appear to show a trend of inverse proportionality with the presence of a transitional zone of between 4%-5% where post-construction estimate has been observed to be both higher and lower than pre-construction estimates.

Soil behaviour index/type were found to markedly shift post-construction using traditional methods (see Figure 12). The SBT chart shows indicatively the average shift pre- to post-construction. The main point to

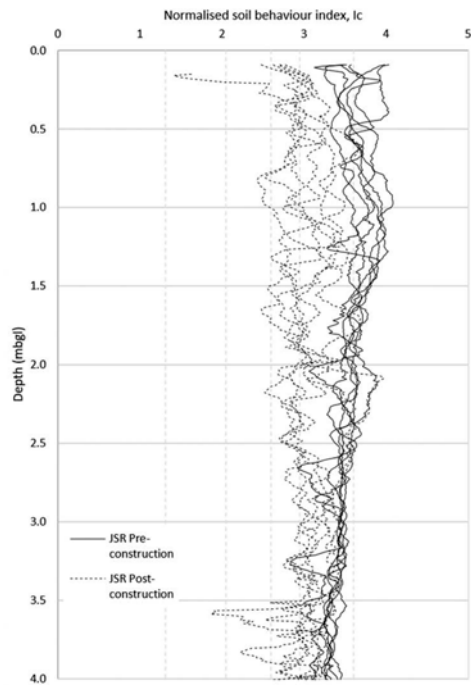


Figure 9. I_c for JSR site.

extract from this chart is the trajectory of the soil behaviour type which is towards a very stiff and fine-grained categorisation which is indicative of the cemented nature of the material. As noted, more modern SBT methods would identify the materials as cohesive or transitional and dilative. However, the magnitude of dynamic porewater pressures established

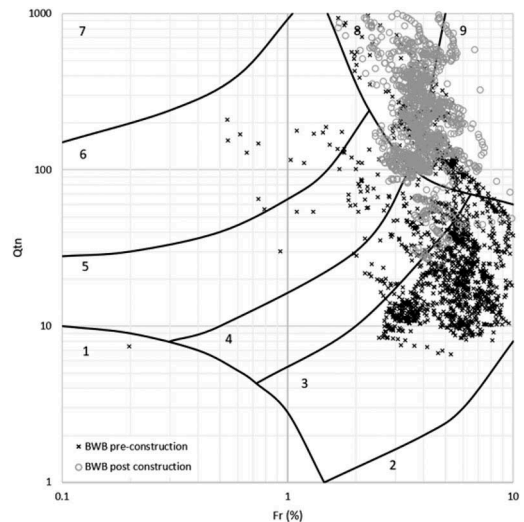


Figure 10. Soil behaviour type chart for BWB site.

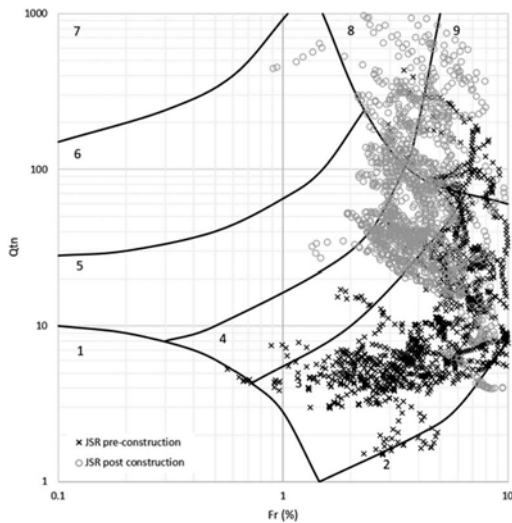


Figure 11. Soil behaviour type chart for JSR site.

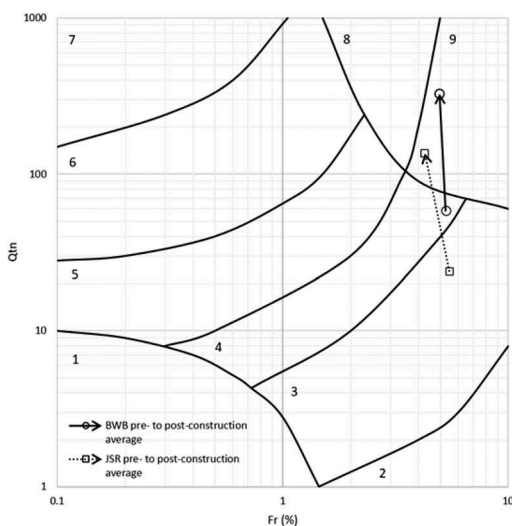


Figure 12. Soil behaviour type chart for both sites showing trajectory of mean shift in behaviour.

post-mixing is not consistent with dilative material categorisation.

While sub-optimal as a categorisation tool, soil behaviour index may have some utility as a measure of the integrity of the mixed soil, particularly where the expected behaviour of the soil pre-construction is well defined. This is because the soil behaviour index takes into account both tip and sleeve resistance and can be stress-normalised. With regard to stress normalisation, variation in the bulk density of the mixed material when compared to the native soil bulk density, should be accounted for.

5 RECOMMENDATIONS FOR FUTURE WORK

It is clear that current SBT methods are effective in capturing the effect of the mixing effort, however, even with more modern methods which consider soil fabric / microstructure more actively, current SBT methods are not optimal for a final categorisation. Key to this is the observation regarding the contractive / dilative behaviour and the marked facility to set up substantial excess porewater pressures. It appears justified that the assumption of undrained behaviour is reasonable for design incorporating wet soil mixing of this nature and to that end, extraction of undisturbed samples for more detailed laboratory (triaxial) testing would be purposeful to establish an appropriate N_k factor for mixed soil.

As noted, the efficacy of the mixing toward the base of the mixed horizon is less than through the main body of the mixed horizon. However, there are a number of other effects that should be investigated as contributory here. For example, the oscillation of the mixing tool, which is typically excavator-mounted in mass mix applications, could yield small unmixed inclusions which would distort CPT results at the base. Also, the exothermic effects of curing merit further consideration in strength achievement in particular, how the ambient ground temperature can be contributory to suppression or acceleration of curing rate which would be most pronounced at the native soil interface. CPT (with thermal measurement capability) would be purposeful in investigating this in situ as extracted samples can be subject to storage and temperature variations that are not representative of the in-situ condition.

REFERENCES

- Puppala, A.J, Bhadriraju, V. & Porbaha, A. 2005. SPT and CPT based methods to address shear strength of deep mixed soil cement columns. Proceedings of the 16th International Conference on Soil Mechanics and Geotechnical Engineering, Millpress Science Publishers/IOS Press 1257–1260
- Ilander, A., Halkola, H., Lahtinen, P. & Kettunen, A. 1999. EuroSoilStab – Kivikko test embankment – Construction and research Proceeding of Dry Mix Methods for Deep Soil Stabilisation. Bredenberg, Holm & Broms (eds), Balkema, Rotterdam 347–354
- EN ISO 22476-1:2012. Geotechnical investigation and testing – Field testing – Part:1: Electrical cone and piezocone penetration test
- Robertson, P.K. 2009. Interpretation of cone penetration tests – a unified approach. Canadian Geotechnical Journal, 46: 1337–1355.
- Robertson P.K. 2016. Cone penetration test (CPT)-based soil behaviour type (SBT) classification system — an update. Canadian Geotechnical Journal, 53: 1910–1927

Liquefaction damage assessment using Bayesian belief networks

L. Paoella, A. Baris & G. Modoni

University of Cassino and Southern Latium, Italy

R.L. Spacagna & S. Fabozzi

CNR IGAG, Area della Ricerca Roma 1, Italy

ABSTRACT: The seismic and liquefaction risk assessment implies introducing methods based on different hypotheses and dealing with different levels of uncertainty affecting the whole process from triggering to surficial manifestation. In this context, soft computing methods, like Bayesian Belief Networks (BBN) and artificial intelligence algorithms, provide the logic framework for cause-effect relationships and the statistical statement to manage uncertainties. Taking advantage of the significant amount of geotechnical data and post-earthquake surveys, an application of BBN versus the forecasting of liquefaction-induced ground damage is proposed considering three main shocks of the 2010 – 2011 Christchurch (New Zealand) Earthquakes Sequence. The BBN algorithms are firstly employed to identify significant variables and learn the relationships among them, then a direct and graphical link between input and target data is created. The quantitative validation of the built architecture enables to advantageously queried the net to predict the result of new datasets.

1 INTRODUCTION

The chain phenomena describing the liquefaction process involve numerous and complex relationships that rule the origin, propagation, surficial manifestation, and induced structural and infrastructural damage. In the field of Earthquake Engineering, the cause-effect relationships starting from the probability of occurrence of a predefined intensity measure have been translated into the PEER convolutive integral (Cornell and Krawinkler, 2000), which develops the performance-based earthquake engineering approach.

In recent years, the development of soft computing methods and the progress in artificial intelligence A.I. provide robust and reliable instruments capable of dealing with large amounts of data in a reasonable time, controlling the quality of results and quantifying uncertainties. Artificial Neural Networks (ANNs) and Bayesian Belief Networks (BBNs) have been advantageously used in various engineering applications to identify the most significant variables, learn the relationships and dependencies among them, and link the input data to the target. After scrutinizing the new data collection campaigns following the 2012 Emilia (Italy) Earthquake sequence, Paoella et al. (2019) developed artificial neural networks and Monte Carlo simulations to relate the Ishihara-based geotechnical model to the observed ground liquefaction in the municipality of San Carlo. Ching and Phoon (2017) developed a method based on the sparse Bayesian learning (SBL) approach to analyze

site-specific measurements like cone penetration test (CPT) data for probabilistic site characterization. A detailed study has been carried out by Tesfamariam (2013) about liquefaction risk that calibrates four different BBN structures and defines a procedure to assess the liquefaction risk at the regional and single building levels. Tang et al. (2018) compare ANN technology and BNNs in describing the liquefaction ground severity demonstrating that the Bayesian model achieves better accuracy for each damage state. Taking advances from previous experiences and the considerable amount of geotechnical data, a BN model for liquefaction prediction is proposed in this work. The best structure is obtained after the processing of ≈ 9000 CPTs available from the New Zealand Geotechnical Database and testing each performance against three main events of the 2010-2011 Canterbury Earthquake Sequence. In a preliminary analysis, the back analysis enables the reconnaissance of the critical layer, *i.e.*, the sandy stratum most likely to undergo liquefaction during the 2010-2011 Christchurch earthquake sequence. The obtained results have shown that, if opportunely guided, the model can relate pre-defined representative variables to liquefaction ground evidence, the latter available from specific post-earthquake surveys. In a subsequent step, more detailed evaluations have been performed on such a critical layer, and a set of site-specific soil fragility functions is proposed. Uncertainties at different levels are accounted for through statistical and probabilistic terms, displaying

and controlling each variable. In conclusion, an alternative approach to large areas studies (Spacagna et al., 2021) and traditional liquefaction severity indicators often evaluated deterministically is presented by developing a set of fragility functions.

2 BAYESIAN BELIEF NETWORKS

A Bayesian Network falls in the category of probabilistic graphical modeling (PGM) technique that is to compute uncertainties by using the probability concept (Pearl, 1988). It is represented as a directed acyclic graph (DAG) which contains a set of nodes and links, relating parent nodes to the children ones. A directed acyclic graph evaluates the uncertainty of an event occurring based on the conditional probability distribution of each random variable. A conditional probability table is used to represent this distribution of each variable in the network.

To understand the meaning, it is necessary to introduce the inference algorithm that is based on the Bayes theorem and conditional independence as follows:

$$P(B|A) = \frac{P(A|B)P(B)}{P(A)} \quad (1)$$

It introduces joint probability, a measure of two events happening simultaneously *i.e.*, $P(A|B)$, and the conditional probability of an event B, which is the probability that event B occurs given that an event A has already occurred. The Bayesian Networks satisfy the Local Markov Property, stating that a node is conditionally independent of its non-descendants, given its parents. In the example of Figure 1, $P(D|A, B)$ is equal to $P(D|A)$ because D is independent of its non-descendent, B. This property aids us in simplifying the Joint Distribution. The Local Markov Property leads us to the concept of a Markov Random Field, which is a random field around a variable that is said to follow Markov properties.

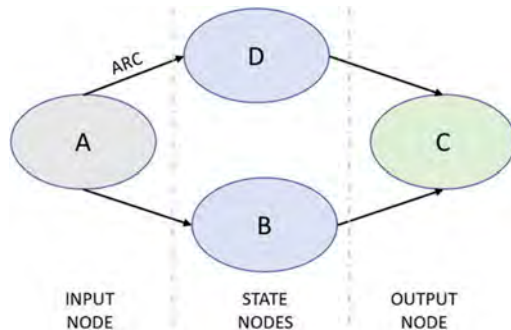


Figure 1. Scheme of a sample Bayesian Network.

Proven that the probability of a random variable depends on his parents, a Bayesian Network can be generalized as shown in Eqn. 2:

$$P(X_1, \dots, X_n) = \prod_{i=1}^n p(X_i | \text{Parents}(X_i)) \quad (2)$$

2.1 Bayesian Networks for liquefaction hazard

In general, the assessment of liquefaction hazard moves from subsequent steps, which translate the soil propensity to liquefy, the triggering analysis, and the liquefaction-induced ground deformation (Bird et al., 2005). Therefore, a BN model for liquefaction hazard requires introducing three types of nodes: 1) input nodes that include soil parameters (e.g., relative density, plasticity, fine contents), site conditions (groundwater depth, thickness and position homogeneous layers, distance from geological features like rivers/paleochannels) and seismic intensity measures (peak ground acceleration, Magnitude, duration, epicentral distance); 2) state nodes which combine input into intermediate variables (*i.e.*, the classification of soil susceptibility, the probability of triggering the phenomenon), and 3) output nodes describing the severity of liquefaction-induced ground observations.

Hu et al. (2016) provided an example of a net that constructed a model for liquefaction potential evaluation considering 12 factors. In this study, a revised approach is proposed, to link geotechnical and geological susceptibility to free field liquefaction ground evidence via the Arias Intensity, without evaluating traditional liquefaction severity indicators, *i.e.*, simplifying an intermediate step that unavoidably introduces noises.

After selecting representative variables for liquefaction, several net models are automatically generated and tested. With this regard, updating the net calculates the probability of having a particular combination of input variables given the evidence, allowing to determine the size, position, and strength characterization of the most likely layer experiencing liquefaction during the considered Earthquake sequence. On this layer, more detailed studies are carried out. The development of a probability model for liquefaction occurrence considers different crust thickness, H_c , thick, H_l , and average resistance, mean crr , of the potentially liquefiable layer. The maximum likelihood criterion is applied to fit the histograms data to lognormal functions (Baker, 2013).

2.2 Management of uncertainty and Validation

Among the advantages of the proposed method there, is an immediate and reliable graphic tool that displays input variables and their relationships. Uncertainties in data estimates and the validity of basic assumptions (like the three-layer hypothesis) can be managed at different levels. In addition, the probabilistic model

allows practitioners to make predictions for future situations with a certain level of confidence. Validation criteria are required to assess the reliability of the obtained results. The metrics used in this study are borrowed from the binary validation methods Lusted (1971), which introduces the concept of Receiver Operative Characteristic Curves obtained by combining specificity and sensitivity; the Area Under the Curve (AUC) is a global proxy of the estimate quality. In addition, the Kappa statistics method is used to assess the agreement between the actual and expected results (Witten and Frank, 2005). Kappa statistics is defined in Equation 3: Pa is the fraction of agreement and Pe is the fraction of random agreement used to correct for values. Pa is a summation of the diagonal values of the confusion matrix.

$$K = \frac{Pa - Pe}{1 - Pe} \quad (3)$$

3 THE CASE STUDY OF CHRISTCHURCH (NEW ZEALAND)

3.1 The 2010-2011 Canterbury Earthquake Sequence

The city of Christchurch ($\approx 370'000$ inhabitants in 2011), in the Canterbury Region of the South Island of New Zealand, was repeatedly struck by earthquakes during the 2010-2011 seismic sequence known as Christchurch Earthquake Sequence (C.E.S) The most noticeable were: the Mw 7.1 Darfield event of September 4th 2010, the (Mw 6.2) Christchurch Earthquake of February 22nd 2011, resulting in 185 fatalities and diffuse devastation to dwellings and infrastructures and the Mw 6.0 June 13th 2011. Liquefaction played a significant role in causing the removal of 900'000 tons of liquefied soil, the demolition of 8'000 buildings (Cubrinovski, 2013; Tonkin & Taylor, 2013), and an economic loss of NZ\$30 billion only on the residential sector (NZ Parliament).

3.2 Creation of databases and variables management

Taking advantage of the significant amount of geotechnical data, a general framework to develop BBN is developed. The strategy to reach such goals include: i) database construction and preliminary processing of CPT data; ii) sensitivity and correlation analyses; iii) automated training of different nets and validation test. In addition, a probabilistic model is derived from the output of the structure showing the best performance.

The database creation includes the collection and homogenization into a standardized format of many CPTs from the New Zealand Geotechnical Database. Out of 30'000 stratigraphies available on the whole

Christchurch area, around 9'000 CPT profiles with a depth greater than 10m have been considered. In a preliminary phase, the Equivalent Soil Profile (ESP) method defined by Millen et al. (2020) is applied to determine the liquefaction susceptibility. This criterion converts a CPT profile into a three-layered equivalent one, defined by H_c , H_l and crr of the potentially liquefiable layer, with an error term used to confirm the consistency with the hypothesis of three-layered profile. The following analysis include three variables (*i.e.*, crust thickness, liquefiable thickness, and resistance), which define 22 homogeneous soil classes for liquefaction susceptibility taken from Millen et al. (2020) criterion. The groundwater table is not explicitly accounted since it is already considered in evaluating the crust thickness. In addition, the ESP normed error representing a check factor for the consistency with the 3-layered profile hypothesis is considered. On the other hand, the distance from riverbeds is assumed as a proxy for geological susceptibility. Seismic hazard is characterized for three earthquakes among the main events of the 2010-2011 C.E.S., *i.e.*, the Sept 2010 Mw7.1 Darfield earthquake, the Mw6.2 Feb 2011, and the Mw6.0 Jun 2011 Christchurch Earthquakes. For each of them, the Arias Intensity is evaluated elaborating the records of Central Christchurch strong motion stations. These scenarios are modeled through the fault distance and the Arias Intensity selected in place of the pair PGA-magnitude since it embeds the intensity and duration of the shaking. On the other hand, the liquefaction ground observation is classified as "YES" and "NO". The subsequent diagnostic inference showing the correlation between each variable and the observed liquefaction is reported in Figure 2. Just as an example of traditional severity indices, the van Ballegooy et al. (2014) Liquefaction Severity Number (LSN) which combines triggering with a hyperbolic weight function, is presented in Figure 2.

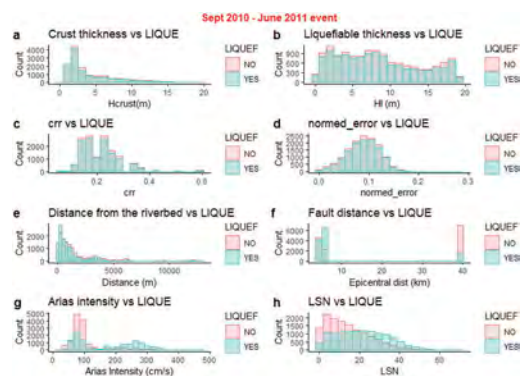


Figure 2. Sensitivity analysis of selected variables versus liquefaction ground observations: a) non-liquefiable crust thickness (m); b) thick of potentially liquefiable layer (m); c) mean crr; d) normed error (Millen et al., 2020); e) distance of investigated profile from riverbeds (m); e) epicentral distance (km); g) Arias (1970) Intensity (cm/s); h) LSN (van Ballegooy et al., 2014).

Although each variable of Millen et al. (2020) method seems to correlate to liquefaction poorly, if considered alone, from Figure 2, it is intuitive to observe that liquefaction occurrence increases with proportionally with the seismic shaking (see Arias Intensity) and close to riverbeds. The herein analyzed seismic scenarios remark that the relationship between seismic moment magnitude M_w and observed liquefaction is here strongly affected by the epicentral distance that made the Mw6.0 (located at approximately 5km from the City Center) and Mw6.2 February event, whose epicenter was around 6-7km South of Christchurch, more severe than the Mw7.1 Darfield event (epicenter 45km West of Christchurch).

In the following analysis, the existing dependencies among input variables are evaluated by calculating the Pearson coefficient; the resulting correlation matrix is plotted in Figure 3, whose coefficient font size is proportional to the correlation found. The massive amount of raw data, the lack of a predefined standard in the format, in conjunction with a certain level of subjectivity connected to post-earthquake rapid surveys, results in a non-negligible noise affecting the whole dataset. Therefore, Figure 3 shows a partial moderate/strong correlation between parameters introduced to quantify liquefaction susceptibility, which can be merged into one variable (*i.e.*, the ESP soil class) and between Arias Intensity and liquefaction severity indicators like LSN. However, to reduce the intermediate steps resulting in error, in the following process Arias Intensity is directly assumed as Engineering Demand Parameter for a given soil configuration, providing an alternative approach to traditional liquefaction severity indicators. In addition, the preliminary classification of variables applied by Millen et al. (2020) has been increased to investigate other geometric configurations better.

3.3 Training and validation of Bayesian Belief Networks for liquefaction

To generate a BBN for liquefaction assessment, the local score metrics are considered for structure learning. Following the typical steps in assessing the liquefaction-induced permanent ground deformation, seven structures of Bayesian Belief Networks are trained and tested comparing the performance versus the liquefaction prediction capability for the Sept 2010 Mw7.1 Darfield earthquake, the Mw6.2 Feb 2011, and the Mw6.0 Jun 2011 Christchurch Earthquakes. Bearing in mind the results displayed in Figure 3, these networks architecture is built in the “Genie Academy” environment (Genie, 2020 <https://www.bayesfusion.com/>) by introducing different search algorithms. PC (Spirtes et al., 1993) uses independences observed in data (established employing classical independence tests) to infer the structure that has generated them and is the most adequate for continuous datasets; Naive Bayes and its improved version, *i.e.*, Tree Augmented Naive Bayes (TAN) and Augmented Naive Bayes (ANB), Bayesian search (BS), and Greedy thick thinning (GTT), respectively defined by Cooper and Herkovits (1992), and Cheng et al. (1997). Additionally, a background knowledge is provided to the PC algorithm to build an expert-guided network based on engineering judgment. The expert-guided model is displayed in Figure 4. The net is based on the PC algorithm customized on the phenomenon knowledge. In particular, the combination of H_c , H_l , and crr provides the equivalent soil profile class by introducing the normed error as the first control factor. The geological susceptibility is separately considered; therefore, the distance from the riverbed is considered and modeled as an independent variable. On the right side of the net, the epicentral distance and Arias Intensity can be observed; the net learned both a dependency among each other and liquefaction ground evidence. Conditional and prior probabilities are specified and, in turn, employed to perform belief updating and extract posterior beliefs. The quality measure can be judged with several criteria like the Bayesian approach or minimum description length (Bouckaert et al., 2011). The score of the whole network can be decomposed as the sum (or product) of individual node scores in a way that enables local scoring and searching methods. The performance of each algorithm is summarized in Table 1 that shows the result of the 5-fold cross-validation test, which splits the whole dataset into 5 panels and estimates how the model is expected to perform when used to make predictions on data not used during the training of the model. The AUC, in conjunction with the K statistics, is used to rank the best learning structure. Although a perfect match exists when K statistics is equal to 1.0, realistically, for a site investigation on a regional scale, a $K=0.5$ match is more appropriate (Demshar, 2020).

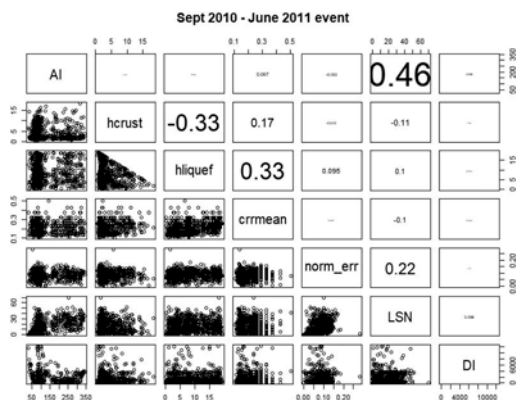


Figure 3. Correlation matrix of the considered variables for liquefaction.

Table 1. Summary of validation results for the above defined Bayesian networks.

BBN	SCORE			
	AUC	K-stat.	OSR	PRECISION
PC	0.81	0.442	0.72	0.70
Naïve Bayes	0.79	0.431	0.72	0.72
ANB	0.77	0.458	0.73	0.71
TAN	0.82	0.447	0.72	0.71
BS	0.81	0.421	0.72	0.56
GTT	0.81	0.460	0.73	0.69
Expert-guided*	0.81	0.461	0.73	0.70

* Ranked as the best structure because of the highest K-statistics and the physical accounting of cause-effect relationships governing the liquefaction phenomenon.

Once the general performance is evaluated through the AUC, the features of the Christchurch critical layer have been searched by setting the evidence of liquefaction and discarding those profiles not ascribable to the three-layered model (Paolella et al., 2020). It is found that, for the considered seismic scenarios, the critical layer for liquefaction is shallow ($H_c < 3m$ in 60% of cases), mid-size to large ($H_l > 3m$ in 81% of cases) and can be modeled with a $crr < 0.30$ (93%of cases) (Figure 4).

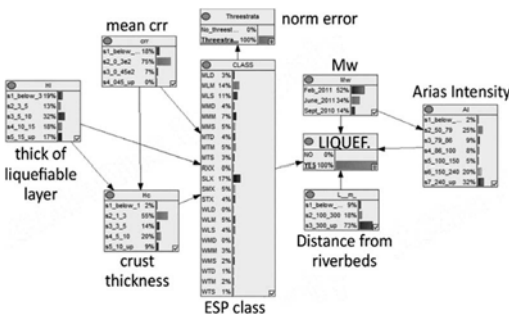


Figure 4. Back analysis of Christchurch earthquake scenarios with the selected expert-guided net.

3.4 A probabilistic model for liquefaction triggering analysis

The automated processing of such a number of CPT data and the availability of post-event damage surveys provides a unique chance to test the performance of current criteria and develop new models. About the latter task, the probability of observing liquefaction given the critical layer has been better investigated by splitting the liquefiable thickness range into three classes, i.e. $3 < H_l \leq 5m$, $5 < H_l \leq 10m$, $10 < H_l \leq 15m$

curves have been derived on these configurations. A fragility curve like the one shown in Equation 4 evaluates the probability of observing liquefaction given an intensity measure (IM) idealized by a typical lognormal distribution:

$$p(L|IM) = \phi\left(\frac{LN\left(\frac{IM}{IM_m}\right)}{\beta}\right) \quad (4)$$

where ϕ denotes the Gaussian cumulative distribution function, IM_m is the median distribution and β is the logarithmic standard deviation. Even though that minor literature exists about the modeling of soil liquefaction vulnerability with this approach (Geyin and Maurer, 2020), fragility curves are generally adopted in procedures to assess seismic and liquefaction risk on buildings (Fotopoulou et al., 2018), road and embankments (Syner-G, 2013) and pipelines (Liu et al., 2015; Baris et al., 2020). Fragility functions are developed as an extension of deterministic models, allowing practitioners to make provisions linked to probabilistic seismic hazard analyses. After the experience of Baker (2013) in structural modelling, the maximum likelihood method is here applied to reach the appropriate data fitting. Assuming that the number of liquefaction/no liquefaction observations from each experiment is independent of observations from other experiments, the probability of observing z_j liquefaction occurrence in n_j motions having $IM = x_j$ is provided by the binomial distribution (Equation 5).

$$P(z_j \text{ evidence in } n_j \text{ experiments}) = \binom{n_j}{z_j} p_j^{z_j} (1 - p_j)^{n_j - z_j} \quad (5)$$

where p_j is the probability that a ground motion with $IM = x_j$ will trigger liquefaction. The maximum likelihood is thus implemented to find the fragility function capable of predicting p_j with the highest probability of fitting experimental data. When analysis data are obtained at multiple IM levels, we take the product of the binomial probabilities (from Equation 5) at each IM level to obtain the likelihood for the entire data set.

$$Likelihood = \prod_{j=1}^m \binom{n_j}{z_j} p_j^{z_j} (1 - p_j)^{n_j - z_j} \quad (6)$$

where m is the number of IM levels and Π is a product over all levels.

The pairs of IM_m and β obtained for each soil configuration by maximizing Equation 6 are reported in Table 2; in addition, the maximum observed value of

arias intensity is indicated, meaning that discretion should be used in using the obtained fragility functions out from the suggested range. Figure 5 displays both the suit of functions showed in Table 2 and the interpolated experimental points; a graphical comparison among each other is presented in Figure 5d. It reflects the positive correlation between thick of liquefiable layer Hl and liquefaction occurrence for a given shaking.

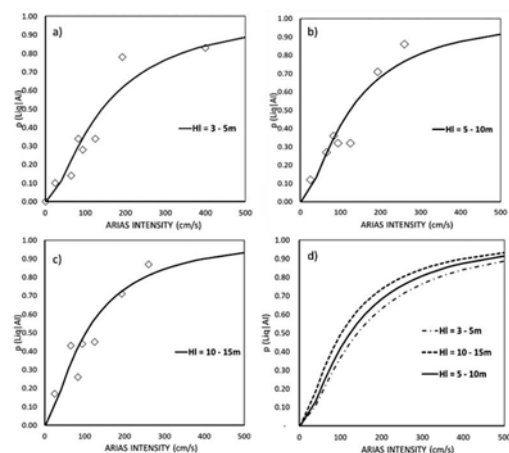


Figure 5. Probability of observing liquefaction manifestations given the AI, for each profile configuration: a) $3 < Hl \leq 5m$; b) $5 < Hl \leq 10m$; c) $10 < Hl \leq 15m$; d) general comparison.

Table 2. Summary of fragility function parameters.

Hl(m)	IMm	β	Arias Intensity (cm/s) range
3-5	142.3	1.03	<350
5-10	123.8	1.02	<350
10-15	102.6	1.06	<350

4 CONCLUSIONS

After processing $\approx 30'000$ CPTs, seven structures of Bayesian Networks are tested against the liquefaction ground evidence induced by three main shocks of the 2010 – 2011 Christchurch Earthquake Sequence. The validation criteria ranked the “expert-guided” Net as the best architecture. It accounts for the cause-effect relationships ruling the phenomenon introducing new variables that better describe the geological/geotechnical susceptibility (e.g., epicentral and riverbeds distances) not considered by traditional liquefaction severity indicators. The robustness of the proposed method herein is quantified by an AUC equal to 0.81, *i.e.*, $\approx 15\%$ higher than traditional indices, which cannot manage all the uncertainties connected with

the randomness of seismic source, spatial variability, and error propagation (Paolella et al., 2020). The Bayesian Network-based back analysis located the Christchurch critical sandy layer at a relatively small depth ($Hc < 3m$), and a very low relative density is found on it ($crr < 0.3$). The following analysis defined a set of soil fragility curves that couple the liquefaction susceptibility of such a critical layer to the seismicity of the area via the Arias Intensity measure. Their applicability should respect the Arias Intensity range reported in Table 2, requiring additional analyses and judgment if this value is exceeded.

REFERENCES

- Arias A., 1970: “A measure of earthquake intensity”. Seismic design for nuclear power plants, R. J. Hansen, ed., MIT Press, Cambridge, Mass.
- Baker J. W., 2013: “Efficient analytical fragility function fitting using dynamic structural analysis”, Earthquake Spectra.
- Baris A., Spacagna R. L., Paolella L., Koseki J. & Modoni G., 2020: “Liquefaction fragility of sewer pipes derived from the case study of Urayasu (Japan)”. Bulletin of Earthquake Engineering, Springer B.V. 2020.
- Bird, J., Crowley, H., Pinho, R., Bommer, J.; 2005: “Assessment of building response to liquefaction induced differential ground deformation”. Bulletin of the New Zealand Society for Earthquake Engineering, 38-4, Dec. 2005, 215–234.
- Bouckaert R.R., 2011: “WEKA Manual for version 3-7-5”.
- Cheng, J., David A. B. & Weiru L., 1997: “An Algorithm for Bayesian Belief Network Construction from Data”. Proceedings of AI & Statistics, pages 83-90.
- Cornell, C.A., and Krawinkler, H. 2000. “Progress and Challenges in Seismic Performance Assessment”. PEER Center News, 3, 1–3.
- Ching J., Phoon K.K., 2017: “Characterizing uncertain site-specific trend function by sparse Bayesian learning”. ASCE Journal of Engineering Mechanics, 143(7), 04017028.
- Cooper G. F., and Herskovits E. A., 1992: “A Bayesian method for the induction of probabilistic networks from data”. Machine Learning, 9:309–347.
- Cubrinovski M., 2013: “Liquefaction-Induced Damage in the 2010-2011 Christchurch (New Zealand) Earthquakes”. In: Proceedings of the 7th International Conference on Case Histories in Geotechnical Engineering, 29 Apr–4 May, Chicago, Illinois.
- Demshar J., 2020: “Development of Liquefaction Hazard Map Using a Geostatistical Method”. University of Minnesota, ProQuest LLC.
- Fotopoulou S., Karafagka S., Pitilakis K., 2018, Vulnerability assessment of low-code reinforced concrete frame buildings subjected to liquefaction-induced differential displacements, Soil Dynamics and Earthquake Engineering 110 (2018) 173–184.
- GeNIe, (2020). BayesFusion, LLC. Retrieved from <http://www.bayesfusion.com/>.
- Geyn M., and Maurer B. W., 2020: “Fragility functions for liquefaction-induced ground failure”. Journal of Geotechnical and Geoenvironmental Engineering, © ASCE, ISSN 1090-0241.
- Hu, J., Tang, X., and Qiu, J.: Assessment of Seismic liquefaction potential based on Bayesian network constructed

- from domain knowledge and history data, *Soil Dyn. Earthq. Eng.*, 89, 49–60, 2016.
- Liu M., Giovinazzi S. and Lee P., 2015: “Seismic fragility functions for sewerage pipelines”. (ASCE), Pipelines Conference 2015, 23-26 August, Baltimore (MD), USA.
- Lusted L.B., 1971, Signal detectability and medical decision making. *Science* 171: 1217–1219.
- Millen M., Viana da Fonseca A., Quintero J., Ferreira C., Oztoprak S., Bozbey I., Oser C., Aysal N., Kosic M., Logar J., 2020: “Equivalent soil profiles to integrate in situ tests results and soil-structure interaction in liquefiable soils. The Adapazari case-study”. *Bull Earthq Eng (Special issue)*.
- Paolella L., Salvatore E., Spacagna R. L., Modoni G., Ochmanski M., 2019: “Prediction of Liquefaction Damage with Artificial Neural Networks”, *Atti 7ICEGE* 2019.
- Paolella L., Spacagna R. L., Chiaro G., Modoni G., 2020: “A simplified vulnerability model for the extensive liquefaction risk assessment of buildings”. *Bulletin of Earthquake Engineering*, 2020.
- Pearl J., 1988: “Probabilistic Reasoning in Intelligent Systems: Networks of Plausible Inference”. San Francisco, California: Morgan Kaufmann Publishers, Inc.
- Spacagna R.L., Porchia A., Fabozzi S., Cesarano M., Peronace E., Romagnoli G., 2021: Seismic liquefaction assessment in Calabria region in Southern Italy: a geostatistical approach at regional and sub-regional scale. *International Journal of Geosciences* (accepted).
- Spirtes P., Glymour c., and R. Scheines. 1993: “Causation, Prediction and Search”. Springer Verlag, Berlin.
- SYNER-G, 2013: “Systemic Seismic Vulnerability and Risk Analysis for Buildings, Lifeline Networks and Infrastructures Safety Gain”. ISBN: 978-92-79-33135-0. DOI: 10.2788/23242. Web-site: <http://www.vce.at/SYNER-G/files/project/proj-overview.html>
- Tang X., Bai X., Hu J. H., Qiu J., 2018: “Assessment of liquefaction-induced hazards using Bayesian networks based on standard penetration test data”. *Natural Hazards and Earth System Sciences* 18(5):1451–1468.
- Tesfamariam S., 2013: “Seismic risk analysis using Bayesian belief networks”. In *Handbook of seismic risk analysis and management of civil infrastructure systems*, S. Tesfamariam and K. Goda editors, Woodhead Publishing Limited, pp.175–208.
- Tonkin & Taylor, Ltd. (2013): “Liquefaction Vulnerability Study”. Report to Earthquake Commission. Tand T ref. 52020.0200/v1.0, prepared by S. van Ballegooy and P. Malan, available at <https://canterburygeotechnicaldatabase.projectorbit.com>.
- van Ballegooy S., Malan P., Lacrosse V., Jacka M.E., Cubrinovski M., Bray J.D., O'Rourke T.D., Crawford S. A., Cowan H., 2014: “Assessment of Liquefaction-Induced Land Damage for Residential Christchurch”. *Earthquake Spectra* (30) No. 1: pages 31–55, February 2014.
- Witten I.H., Frank E., 2005: “Data mining: Practical Machine Learning Tools and Techniques. Burlington, MA: Elsevier pp. 143–185.

Geotechnical zoning of deltaic and alluvial soils of Guayaquil (Ecuador) using CPT and N_{kt} calibration based on FVT

J. Paredes & F. Illingworth

Subterra, Ecuador

R. Luque

Geosismica, Ecuador

ABSTRACT: This document summarizes the results obtained from geotechnical zoning analysis in the city of Guayaquil and its surroundings, which stratigraphy consists mostly of alluvial and estuarine deltaic soils, by compiling over 600 CPTs and 800 boreholes. Products generated include a map of rigid stratum depth with high impedance contrast as well as spatial distribution of liquefaction susceptibility using a simplified methodology. Furthermore, shear strength s_u peak and remolded have been evaluated by comparing CPT-borehole pairs and 26 sites with CPT and electric FVT. It has been found that s_u peak from laboratory tests adjusts well to the FVT s_u remolded and f_s , suggesting sample disturbance. It has been verified that N_{kt} values measured with FVT are lower than average reported values in previews studies, possibly due to diatoms identified in scanning electron microscope (SEM). F_r based estimates appear to yield an upper limit of N_{kt} factor in Guayaquil soft clays, while s_u maps for 5 m soil segments are provided from CPT-based N_{kt} values.

1 INTRODUCTION

Guayaquil is located on the Ecuadorian coast, and has a flat relief in most of its extension. Geologically, the soils correspond to the Holocene with a large alluvial plain and estuarine deltaic deposit, located at the foot of the Chongón-Colonche Mountain Range. Due to the geological characteristics of Guayaquil, a large percentage of sites include soils susceptible to liquefaction or profiles with a thick upper layer of soft clay and organic material. Moreover, the tectonic environment rich in dissolved silica, favors the existence of diatoms, elements that provide a characteristic geotechnical behavior.

Geotechnical investigation in Guayaquil has been predominantly conventional drilling and sampling, from the 1950s to the present, but in the last decade, emphasis has been placed on in situ testing, especially through CPTu soundings. In this document, the experience from 615 CPTs in Guayaquil and the surrounding area is synthesized along with 143 electric field vane tests (FVT), carried out in an effective area of 450 km². In situ results have been integrated with existing boreholes.

The common state of practice in Guayaquil is to perform unconfined compression tests or use handheld devices (torvane, penetrometer) to determine undrained shear strength s_u in clays, and measure N_{60} (standard penetration number, corrected) in order to

estimate liquefaction potential of granular soils. While considering testing procedures, CPT estimates provide a more accurate and efficient alternative. However, it is imperative to calibrate CPT geotechnical parameters in unconventional soils, with measurements obtained from other in situ and laboratory tests (Mayne, 2007b; Robertson, 2009; Robertson, 2012). Therefore, this report analyzes: 1) back-calculated N_{kt} values from FVT measurements and 2) a simplified geotechnical zoning of Guayaquil considering highly compressible top stratum, shear strength s_u , and susceptibility to liquefaction (LSN, LPI and settlements).

2 IN-SITU INVESTIGATION

The database considered for developing a compressible-top-layer zoning map consists of 1432 soundings: 615 CPTs (95% down to refusal conditions), and 817 boreholes from several companies. In addition, 26 FVT profiles were evaluated, delivering 143 s_u values (Figure 1). SEM images were taken at 14 sites to corroborate the existence of amorphous microstructures.

For CPTu tests, a standard 10 cm² cone, compression type, with 150 cm² sleeve was used. The pore pressure filter (u_2 position) is made out of bronze, and saturated with silicone oil. The piezocone is pushed at 2 cm/s with a 15-ton Pagani TG-63

equipment recording measurements every cm. FVTs have been carried out by pushing the vane housing with the same penetrometer and further advancing 50x100 mm vanes, 25 cm from penetrated depth. Torque is applied from the surface at one-meter intervals with Geomil GVT-100 tester. The data acquisition system records the resistance as a function of angular rotation of the vane from initial position until peak and remolded resistance is measured.

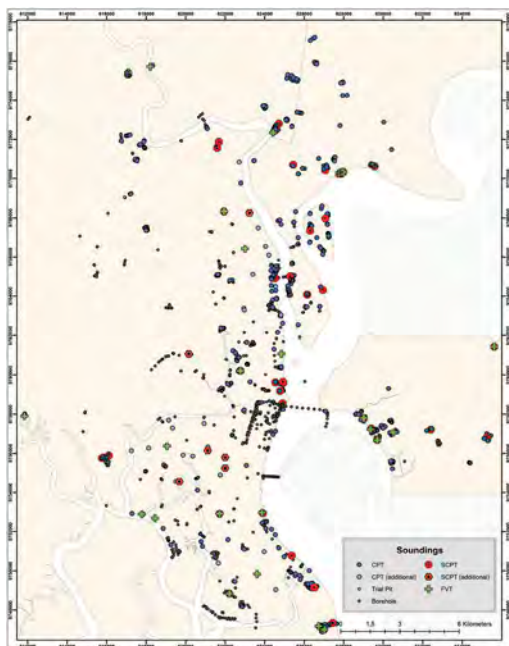


Figure 1. Location of soundings.

A preliminary classification of each sounding was necessary to determine profile types and potential geotechnical problems. It was found that 38% of profiles have a top soft clay stratum with variable thickness from 3 to 30 m, 24% presented susceptibility of liquefaction in the first 20 m and 11% of profiles include both conditions. Also, 10% of profiles presented organic material content or more than 30 m of soft clay while 10% of soils consisted of high impedance contrast within the top 25 m. This totals 93% of the profiles in which an exhaustive geotechnical analysis is required on most medium risk projects. In 83% of soundings where a thick soft clay layer or loose sand is present, is convenient to use CPTu for a better identification of sandy intercalations and suitable characterization of soft layers, both in terms of strength and compressibility.

3 N_{kt} MEASUREMENT

Piezocoone, along with vane testing, was performed at 26 different sites, less than 1.5 m apart and in 7

cases, also near boreholes. Vane measurements were taken between 1 and 17 m (avg. 5.6 m) while recorded peak values vary between 10 and 240 kPa (avg. 64 kPa). Different CPT parameters at FVT depth location were compared for trend evaluation: corrected cone resistance (q_t), normalized cone resistance (Q_m), normalized friction ratio (F_r), normalized pore pressure ratio (B_q), normalized SBT_n Index (I_c). Tip values of q_t range between 0.1 and 4.4 MPa, those of I_c between 2.1 and 3.8, B_q between -0.3 and 1.0, and F_r between 1% and 11%.

The bearing factor N_{kt} for cone tip resistance was back-calculated first, using a single q_t value at vane test depth and secondly, with an average q_t value ± 25 cm from FVT depth, to consider lenses variability across the distance between both tests. The lower the standard deviation of q_t (σ_{qt}), the closer both N_{kt} values are. Hence, by filtering measurements with $\sigma_{qt} > 0.2$ MPa, 95% of N_{kt} values range between 3 and 12 ($N_{kt-avg} = 7.4$).

There are limitations regarding the procedure and interpretation of the vane failure mechanism, as explained by Bjerrum (1972), Ladd & Foott (1977), among others. Even when considering a correction factor $\mu = 0.80$, according to Bjerrum, for an plasticity index (PI) of 50% (conservative in most data points analyzed), estimated N_{kt} values are in the range of 4 to 15, with an average of 9.3. Thus, relatively low values of N_{kt} should be expected in the upper compressible stratum of Guayaquil.

While no correlation was detected with F_r , inversely proportional trends have been identified with I_c and B_q and directly proportional with Q_m and OCR. However, none of the correlations provides an acceptable adjustment coefficient. Figure 2 illustrates the correlation between N_{kt} and Q_m , which could be considered the best trend found among normalized parameters.

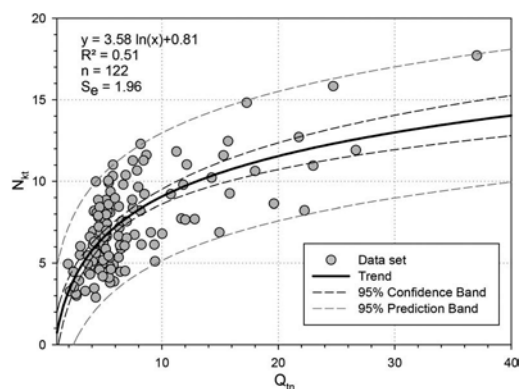


Figure 2. Back-calculated N_{kt} values as a function of Q_m .

Furthermore, the N_{kt} range has been analyzed graphically among FVTs_u and net cone resistance ($q_{net} = q_t - \sigma_v$) considering 136 measurements with $\sigma_{qt} < 1$ MPa. Three sub-datasets corresponding to

different geotechnical zones (106 values) have been compared: alluvial, deltaic-estuarine of Guayaquil and Durán. The q_{net} - s_u relation is shown in Figure 3 with slopes between 8 and 10, which corresponds to plausible Guayaquil N_{kt} values.

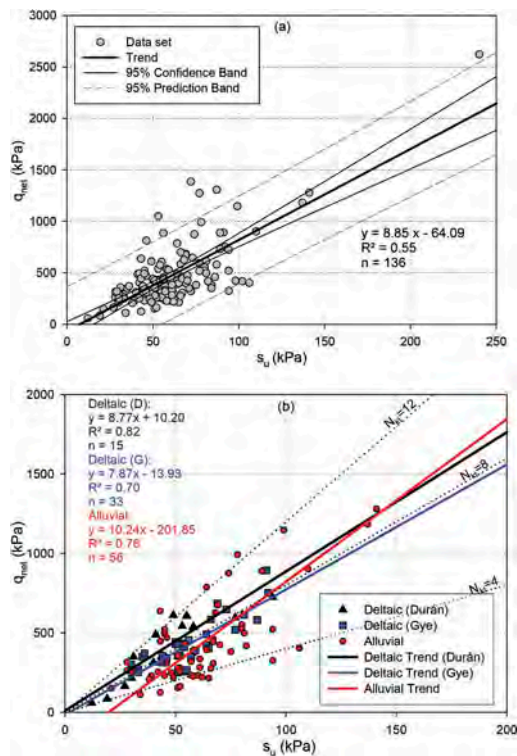


Figure 3. Correlation between q_{net} and s_u from field vane tests: (a) 136 measurements with $\sigma_{qt} < 1$ MPa; (b) three sub-datasets for geotechnical zones.

Based on evaluated trends the following can be concluded: 1) N_{kt} values are low compared to average values of conventional soils and 2) a correlation for N_{kt} with normalized parameters such as B_q or F_r (Mayne & Peuchen, 2018; Robertson, 2012), seem unfit for the available data from Guayaquil.

Although laboratory tests are commonly used to determine s_u in Guayaquil, sample quality is poor in many cases. According to Lunne et al. (1997) criterion, based on void ratio initial (e_o) and void ratio variation (Δe_c), 50 consolidation tests were analyzed resulting in 90% of samples having $\Delta e_c/e_o > 0.04$ and 60% > 0.07 , so the quality of sampling is generally low or medium. In addition, when comparing CPTs and boreholes from 40 sites, laboratory s_u peak tends to adjust to CPT f_s , and similarly to in-situ remolded s_u at sites where FVT was also available. As an example, Figure 4 illustrates this matter in two profiles, suggesting resistance loss due to samples disturbance.

Hence, Robertson N_{kt} - F_r correlation has proven to be more appropriate than readily available laboratory

tests for preliminary and somewhat conservative estimates in Guayaquil alluvial and deltaic soils. In addition, an upper N_{kt} limit of 12 is proposed for the NC clay deposit, while site specific CPT-FVT pairing along with laboratory tests would be necessary for evaluating site specific behavior. Therefore, an

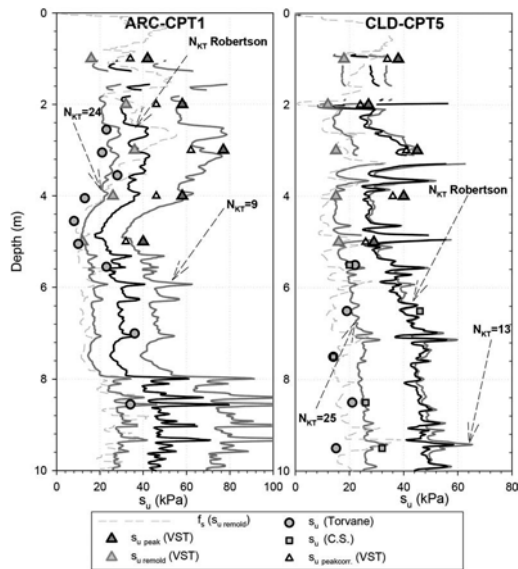


Figure 4. Comparison between s_u values from CPT, FVT, unconfined compression and torvane tests.

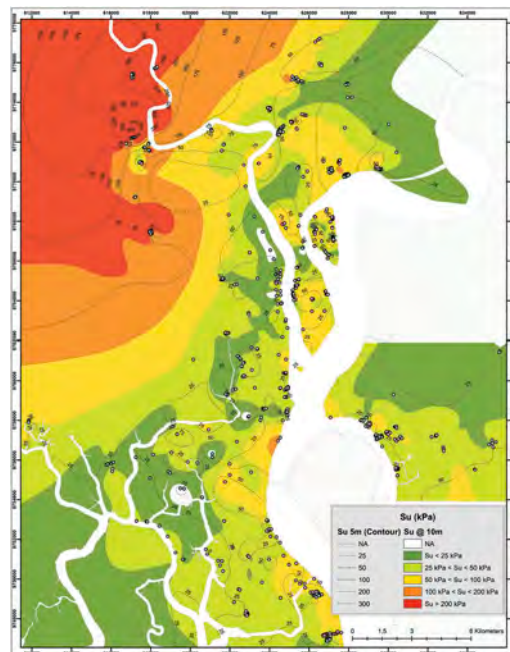


Figure 5. Spatial distribution of estimated s_u in Guayaquil from 0 to 5 m and 5 to 10 m soil segments.

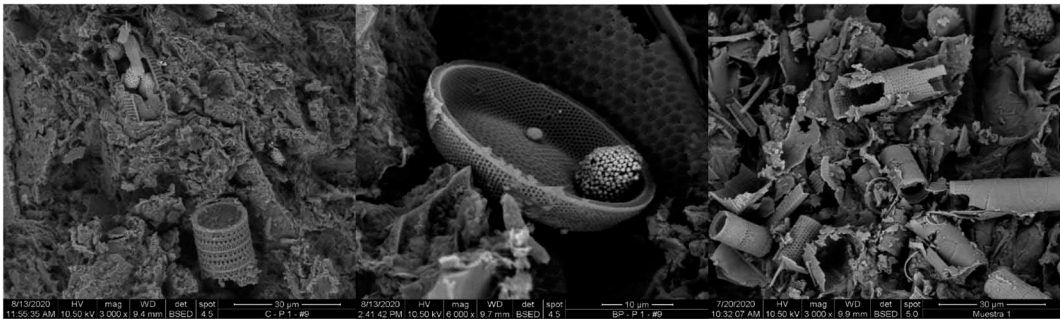


Figure 6. SEM images from samples obtained in alluvial and estuarine deltaic deposits of Guayaquil (South East-D1, Durán and Kennedy-D3).

interpolation has been performed in ArcGIS for average values of estimated s_u in 5 m soil segments, except for segments which are predominantly granular soils (>55% SBTn 5-8). Figure 5 shows maps generated for 0-5 m and 5-10 m segments.

4 PRESENCE OF MICROFOSSILS

Diatom microfossils have been found in several marine and lacustrine deposits, such as those in Japan, Mexico and Colombia. The presence of diatoms in two estuarine locations in Guayaquil has been widely discussed (Vera, 2014).

Diatoms are eukaryotic unicellular algae, with a frustule composed of SiO_2 that fossilizes after the death of the microorganism. They are found in marine environments with dissolved silica, very common in places with high tectonic activity (Díaz-Rodríguez, 2011). Diatoms modify the static and dynamic response of soils. A higher diatom content increases porosity, compressibility and dilatation (Díaz-Rodríguez et al., 1998; Shiwakoti & Tanaka, 2002). Besides, s_u increases proportionally with diatom content (Wiemer & Kopf, 2017). Diatoms may cause a deviation from existing N_{kt} trends per normalized CPT parameters and also provide an explanation for encountered relatively low N_{kt} values.

Abundant presence of diatoms and framboidal pyrites has been found in sites with low N_{kt} . In 13 out of 14 sites, SEM images identified a wide range of diatoms from different species. Figure 6 shows the microstructure identified in three different sectors. As diatoms exist in soil microstructure, and consequently higher $s_{u\text{-peak}}$ values are measured, it is reasonable to obtain higher sensitivity values ($S_t = s_{u\text{-peak}}/s_{u\text{-rem}}$) as well, compared to a diatom-free soil matrix. Although measured S_t values from FVT range between 1.1 and 12.8, with an average of 2.5, several tests show 5 to 10 kPa oscillation around remolded values. So, reported S_t average could be higher, perhaps close to 4 considering lowest measured values. At such low values it is difficult to accurately determine soil sensitivity. Besides, it is

worth noting that f_s values lower than 5 kPa have been reported in several CPTs, demonstrating the presence of very soft and possibly sensitive soils. Further research with additional testing is required to establish a more specific range of S_t by geotechnical zones.

Previous studies indicate that S_t is inversely proportional to N_{kt} (Robertson, 2012; Mayne & Peuchen, 2018), which would support the low range values of N_{kt} obtained in Guayaquil. Nevertheless, no relationship between measured sensitivity and N_{kt} has been observed, possibly due to the difficulty of determining the exact remolded value in highly sensitive soft soils or due to the need of precisely determining diatom content, which has not been the case.

5 GEOTECHNICAL ZONING OF COMPRESSIBLE STRATUM AND SOIL LIQUEFACTION

Other parameters evaluated from the database were: 1) thickness of top compressible layer or depth of rigid stratum, 2) liquefaction potential, 3) SBTn Index I_c , 4) relative density D_r of granular materials, 5) OCR and 6) coefficient of consolidation c_v (Paredes, 2020). This report illustrates zoning maps with regards to the compressible layer and soil liquefaction potential.

A preliminary qualitative and quantitative evaluation of the rigid stratum depth was performed to determine the first and foremost impedance contrast with the upper clay deposit. Supported by dozens of pile driving analyses, this stratum would correspond to a pile bearing capacity of 2500 kPa for a 50 cm square section. For defining such stratum, Q_m must be greater than 100 (N_{60} greater than 45 blows in sands) and thickness greater than 2 m. If the identified layer was less than 2 m thick and located above a second soft clay layer, then the following layer with Q_m and thickness greater than 100 and 2 m, respectively, was considered. The thickness variation of the upper compressible stratum has been calculated by means of a global interpolation process with local adjustment and iterative finite differences (topo to raster), which

allows generating smooth curves and considering boundaries. Figure 7 illustrates the interpolation map, with depth contours between 0 and 50 m.

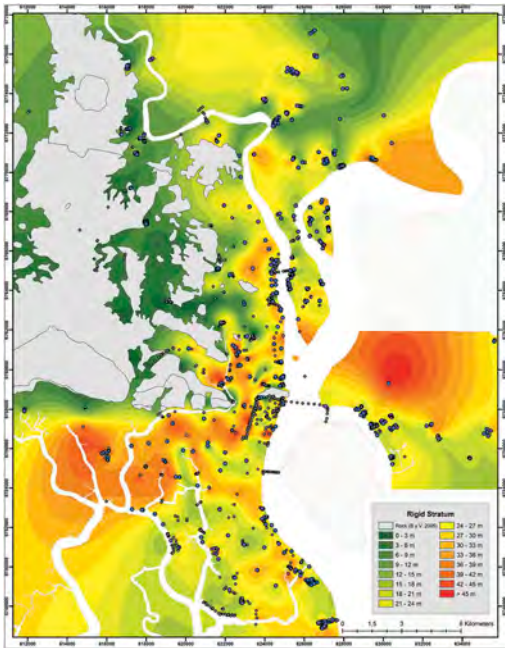


Figure 7. Rigid stratum depth map from 1432 soundings (615 CPTs). Rock outcrop (Benitez & Vera, 2006).

This map provides a rapid identification of depths in which pile installation may complicate if appropriate measures are not considered. Also, it constitutes a preliminary drainage or compressibility boundary with regards to settlements analyses. Although, the presence of soft to firm clays greater than 20-meter thick has been confirmed in most of the estuarine area, certain sectors south-west of the city are noteworthy, where dense soils have been identified at shallower depths as well as sandbars.

Due to the abundance of soft soils in Guayaquil, this map results beneficial for the construction industry and real state. Based on the map, an exploration campaign could be targeted towards potential geotechnical issues and project risks.

In an effort to develop liquefaction potential maps, the factor of safety FS was calculated for each sounding in Guayaquil database, considering a seismic demand of $M_w=7.5$ and $PGA=0.4$ g (according to the PSHA disaggregation carried out by Beauval et al., 2018). Subsequently, LPI (Iwasaki & Tokida, 1981) and LSN (Tonkin & Taylor Ltd, 2013) indices were calculated as well as post-liquefaction vertical free field deformations for the first 20 m (Sett @ 20m), and for the entire profile (Zhang, Robertson, & Brachman, 2002). Figures 8 and 9 illustrates the interpolated maps.

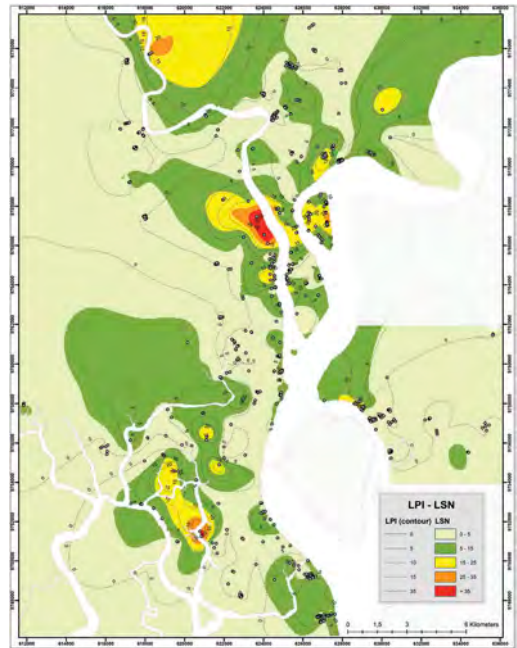


Figure 8. Spatial distribution of LPI and LSN.

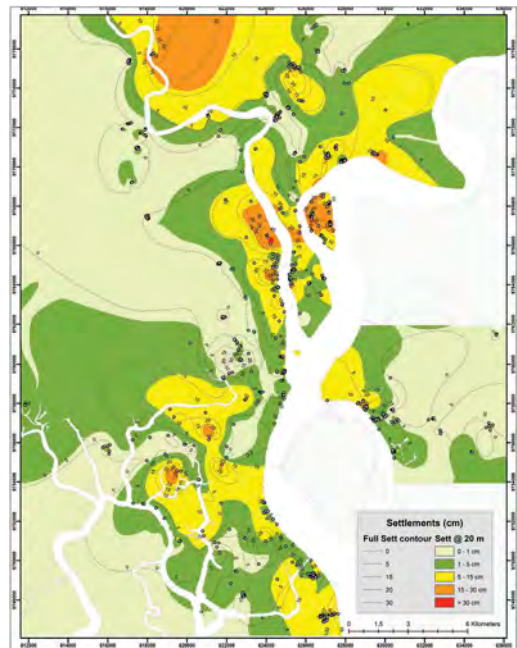


Figure 9. Spatial distribution of free field post-liquefaction settlements down to 20 m and complete profile.

Results indicate that 20% of CPTs have $LPI > 10$, 8% $LSN > 20$, 20% $Sett@20m > 15$ cm and 35% Sett in the entire profile > 15 cm. The low percentage of moderate LSN is due to the strong influence

of upper layers with high fines content that, in most cases mitigate damage at ground surface. Zones where estimated post-liquefaction deformations in the entire profile is greater than 15 cm, even though $Sett@20m$ is lower, are especially relevant for pile design projects to ensure the neutral plane is below liquefiable layers.

According to LSN and LPI, sectors with highest risk and damage associated with liquefaction are those located north, in the alluvial zone. However, low LSN values south-east of Isla Mocolí and at the first five kilometers of Ave. Puntilla-Samborondón are notable, since before mapping a high liquefaction potential would have been expected due to its geotechnical location in alluvial zones. On the contrary, for estuarine deltaic areas where predominantly thick clayey layers are expected, some soil profiles are prone to liquefaction due to the presence of sandy layers in the top 20 m.

6 CONCLUSIONS

A database of 615 CPTs, 26 FVT profiles and 817 boreholes have been used to perform a geotechnical zoning of 1) top compressible stratum, 2) liquefaction potential, and 3) undrained shear strength s_u for the city of Guayaquil and surroundings.

Diatoms have been identified in the soils of Guayaquil, and the presence of these microstructures possibly relates to the low N_{kt} values measured in FVT. Although a valid trend is not observed between N_{kt} and $F_r-B_{q_0}$, there is a direct proportionality with Q_{in} . Average values of N_{kt} varying between 8 and 10 have been found for different geotechnical zones.

There is high variability and heterogeneity in the alluvial and estuarine soil deposits from Guayaquil, based on different geotechnical zoning maps. Moreover, the database highlights the suitability of CPTu investigation in soft compressible soils given that drainage conditions are better determined when detecting a sandy intercalation that may have not been characterized while sampling. Likewise, CPT liquefaction analysis is more reliable since it would consider sandy or clayey lenses that might aggravate or alleviate foundation damage. Finally, pile driving analysis with CPT has been highly beneficial in several construction projects for Guayaquil soil deposits, by modeling with great precision intercalations of dense soils that hinders pile penetration while estimating shaft resistance accurately. Further research hopes to provide detailed field results from case studies.

REFERENCES

Benítez, S., & Vera, X. (2006). *Estudio Geológico de la ciudad de la ciudad de Guayaquil. Informe final de Investigación y Estudio del comportamiento dinámico del subsuelo*. IIFIUC, Universidad Católica Santiago de Guayaquil.

Beauval, C., Marinier, J., Yépez, H., Audin, L., Nocquet, J.-M., Alvarado, A., Baize, S., Aguilar, J., Singaicho, J., & Jomard, H. (2018). A New Seismic Hazard Model for Ecuador. *Bulletin of the Seismological Society of America* 108 (3). doi:10.1785/0120170259

Bjerrum, L. (1972). Embankments on Soft Ground. *Proc. ASCE Esp. Conf. on Performance of Earth and Earth-Supported Structures*.

Díaz-Rodríguez, J., Lozano-Santa Cruz, R., Dávila-Alcocer, V., Vallejo, E. & Girón, P. (1998). Physical, chemical, and mineralogical properties of Mexico City sediments: a geotechnical perspective. *Canadian Geotechnical Journal* 35 (4): 600–610.

Díaz-Rodríguez, A. (2011). Diatomaceous soils: monotonic behavior. *International Symposium on Deformation Characteristics of Geomaterials*. Seúl: Civil Engineering Department, National University of Mexico. DOI: 10.13140/2.1.3322.5606

Iwasaki, T., Tokida, K., & Tatsuoka, F. (1981). Soil Liquefaction Potential Evaluation with Use of the Simplified Procedure. *International Conferences on Recent Advances in Geotechnical Earthquake Engineering and Soil Dynamics*. 12.

Ladd, C., & Foott, R. (1974). New design procedure for stability of soft clays. *J. of the Geotech. Eng. Div.*, 100 (GT7), 763–786.

Lunne, T., Berre, T., & Strandvik, S. (1997). Sample disturbance effects in soft low plastic Norwegian clay. *Symposium on Recent Developments in Soil and Pavement Mechanics*: 81–102.

Mayne, P. (2007b). Invited Overview Paper: In-situ test calibrations for evaluating soil parameters, Characterization & Engineering Properties of Natural Soils, Vol. 3 (Proc. IS-Singapore), Tay-lor & Francis Group, London: 1602–1652.

Mayne, P., & Peuchen, J. (2018). Evaluation of CPTu N_{kt} cone factor for undrained strength of clays. *Proceedings of the 4th International Symposium on Cone Penetration Testing (CPT'18)* (pp. 423–429). Delft, (ND): CRC Press.

Paredes, J. (2020, noviembre). Evaluación de parámetros geotécnicos de los depósitos de suelos ubicados en la llanura aluvial y en el complejo deltaico estuarino de Guayaquil. *Master's Thesis. Escuela Superior Politécnica del Litoral (ESPOL)*, Guayaquil, Ecuador.

Robertson, P. (2009a). Interpretation of cone penetration tests – a unified approach. *Canadian Geotechnical Journal* 46, 1337–1355.

Robertson, P. (2012). Interpretation of in situ tests - some insights. *J.K. Mitchell lecture, Proceedings of ISC'4*, (pp. 3–24). Recife, Brazil.

Shiwakoti, D., Tanaka, H., Tanaka, M., & Locat, J. (2002). Influences of diatom microfossils on engineering properties in soils. *Soils and Foundations Vol. 42 No. 3*, 1–17.

Tonkin & Taylor Ltd. (2013). Liquefaction Vulnerability Study. Report to Earthquake Commission, ref. 52020.0200/v1.0, prepared by S. van Ballegooy and P. Malan.

Vera, X. (2014). Seismic Response of a Soft, High Plasticity, Diatomaceous Naturally Cemented Clay Deposit. Doctoral Thesis. University of California, Berkeley.

Wiemer, G., & Kopf, A. (2017). Influence of diatom microfossils on sediment shear strength and slope stability. *Geochemistry, Geophysics, Geosystems* 18, 333–345.

Zhang, G., Robertson, P., & Brachman, R. (2002). Estimating liquefaction-induced ground settlements from CPT for level ground. *Canadian Geotechnical Journal*, 39, 1168–1180.

Use of piezocone with dissipation tests CPTu_Δu, in tailings dams in Mexico: Case history

J.L. Rangel-Núñez

Universidad Autónoma Metropolitana, Plantel Azcapotzalco, Mexico

E. Ibarra-Razo & R. Flores-Eslava

inGeum Ingeniería, Mexico

ABSTRACT: This paper describes and analyzes several aspects observed during the exploration of mine tailings deposits in Mexico using the CPTu_Δu test: high ground temperatures, interstratification, chemical reaction, dissipation curves with negative pore pressure, and S-wave profile. It was observed that the use of sensors with temperature compensation for the q_T and f_s measurements produces satisfactory results if temperature changes are not abrupt. For the case of the dynamic pore pressure sensor u_2 , where no temperature compensation was made, the measurements are within the range mentioned in the standard except in the case when the temperature increases to values of 50°C or higher. The presence of high interstratification between thin layers of hard and soft soils, with different degrees of saturation, leads to errors in the measurement of the tip resistance and can produce deviations from the verticality of the cone, making it necessary to carry out corrections. The different types of dissipation curves observed in the tailings dams studied, where the soils are partially saturated, are generally the same as those described by Sully *et al.* (1999), with the particularity that in some cases, the equilibrium pressure reaches negative values. Finally, the S-wave profile obtained with correlations reproduces the general trend of the measured S-wave profile. Nevertheless, it was not possible to capture the variations in this type of deposit. In the case history described in this paper, the maximum values were not reproduced. Therefore, in this type of deposit, it is advisable the direct measurement of the shear wave and to use the smaller intervals of measurement according to the technique used.

1 INTRODUCTION

The design, execution and interpretation of an exploration campaign require experience and knowledge of both geology and exploration techniques to achieve satisfactory results. The case of tailings dams is a particular challenge because this type of deposit presents peculiarities, namely: they are very young, *i.e.*, compaction or consolidation is sometimes in the process; chemical processes may still be developing that can affect measurements, mainly in gold mines; the different sequences and forms of deposition using different types of debris induce a highly variable heterogeneity and anisotropy in the mechanical properties of the deposit.

All the mentioned aspects have an impact on the geotechnical exploration campaign. For example, the number of stages of the exploration campaign could increase, as well as, the field and laboratory tests. Undisturbed soil sampling is difficult, it is not possible to use the correlations commonly employed to estimate mechanical properties and it is often necessary to carry out modifications of the processes of execution of the field tests, such as increasing the rotation speed in shear vane tests.

One of the techniques used to characterize soils in tailings dams is the seismic piezocone with dissipation testings (sCPTu_Δu test); however, it has been observed that for this type of deposit there are factors that make it difficult to perform the test and their interpretation.

This paper describes and analyzes several aspects observed during the exploration of mine tailings deposits in Mexico using the sCPTu_Δu test, that is: high ground temperature, interstratification, chemical reaction with the soil and evaluation of the dissipation test and s-wave velocity profile.

In deposits where it is difficult to use any field exploration techniques, as in the case of tailings dams, the execution of a piezocone test requires following procedures that ensure the quality of the tests in order to eliminate factors that hinder its interpretation and finally to reliably obtain both the stratigraphic profile and the geotechnical model of the deposit.

In order to validate exploration with CPTu_Δu in tailings deposits, it is advisable to observe the following aspects: verification of zeros at the beginning and end of the test, performing repeatability tests more frequently, changing filters and verifying their saturation, evaluating tip and shaft continuously,

measure verticality, measure temperature, control driving speed and in general carry out continuous maintenance of the equipment.

2 FACTORS AFFECTING THE INTERPRETATION OF THE PIEZOCONE TESTS

A variety of CPTu $_{\Delta u}$ and sCPTu $_{\Delta u}$ tests have been carried out in several Mexican tailings dams where aspects that have hindered the performance and interpretation of these tests have been observed. Some of them, which are particular aspects of exploration in tailings dams, are described below.

2.1 High ground temperature

During the exploration of a tailings dam of a gold mine in northern Mexico, where high ambient temperatures arise, the piezocone temperature before driving was 25°C, and during the test, it gradually increased to a maximum value of 50°C, in other words, twice the ambient temperature. High temperatures can affect the measurements of the parameters q_T and f_s when the equipment does not have compensating temperature sensors. If the cone has compensating temperature sensors, according to the manufacturer, the sensors can stabilize the measurements if:

- The temperature gradient should be uniform as the piezocone is driven, *i.e.* not present abrupt temperature changes.
- The compensation is performed for temperature variations or changes in the piezocone of up to 50°C (temperature variation in the piezocone with respect to that adopted at ambient temperature). For a temperature variation of up to 50°C, a change in the voltage output of the load sensor of up to 10 microvolts is compensated.
- The output voltage of the load sensor for the full-scale output (FSO=75 MPa) is 8.7 mV, so that 10 microvolts correspond to 0.115% of the output voltage for the full scale; in terms of stress, it represents a compensation of approximately 86.20 kPa for a maximum temperature change or variation of 50°C (1.72 kPa/°C), so that for the case studied where there was an increase of 25°C, there would be a compensation of 43.1 kPa.

However, for the pore pressure sensor, the equipment does not perform any temperature compensation, so that the measurements of u_2 and Δu may be erroneous. In this sense, two experiments were proposed to evaluate these effects using corrections for q_T and f_s .

The first experiment consisted of gradually increasing the temperature of the water in which the piezocone was submerged under controlled conditions, from 4°C to 45°C, while recording the variations in the zero readings of the tip, shaft and pore pressure sensors: the first parameters (q_T and f_s) were

registered to validate the temperature compensation already described and in the case of the pore pressure, the objective was to observe the influence of the temperature in their measurements.

Figure 1 shows the results obtained in the first experiment for each of the variables studied. it can be seen that for the q_c and f_s sensors, the measurement variations are very small, falling within the interval error indicated in ASTM D5778-12. Regarding the pore pressure, u_2 , where the measurements were performed without compensating temperature, the results indicate variations of about 8kPa for low temperatures and 13kPa for high temperatures. Although, although they are small values, for a class 1 cone the value determined for high temperatures is in the limit according to the ASTM standard. On the other hand, this temperature effect can induce errors for the interpretation of dissipation tests, so it is advisable to provide the cone with compensating temperature in the tailing deposit are expected.

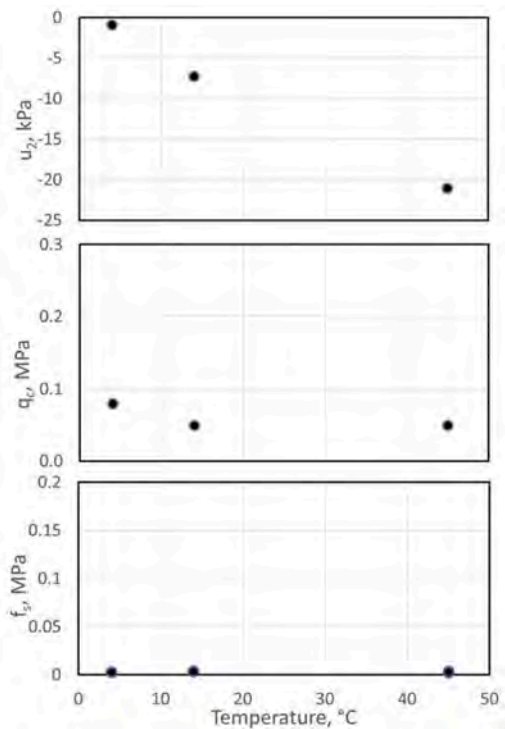


Figure 1. Effect of temperature on pore pressure (u_2), tip (q_c) and shaft (f_s) sensors.

The second experiment consisted of evaluating the repeatability of the piezocone testing under field conditions. To do this, two CPTs were executed, two meters apart for each other, in an area where variable temperatures between 41.5 and 44°C were recorded during the extraction stage. The temperature in the piezocone was measured with a digital thermometer. Figure 2 shows the results obtained in both boreholes

and it can be seen that this temperature gradient generated during the driving of the equipment does not affect the measurements, considering an ambient temperature of 25°C at the beginning of the driving.

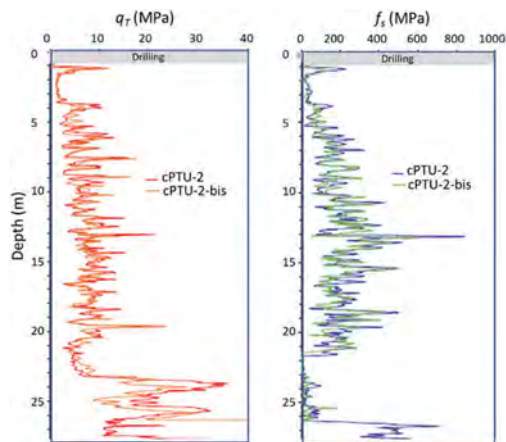


Figure 2. Repeatability survey.

2.2 Interstratification

The presence of high interstratification between thin layers of hard and soft soils, with different degrees of saturation, causes sudden changes in the tip resistance. Moving from a hard to a soft stratum leads to errors, low values in the measurement of the tip resistance (Figure 3), making it necessary to carry out corrections (Boulanger and DeJong, 2018) and the instrumentation must guarantee low hysteresis in order to obtain trustworthy data.

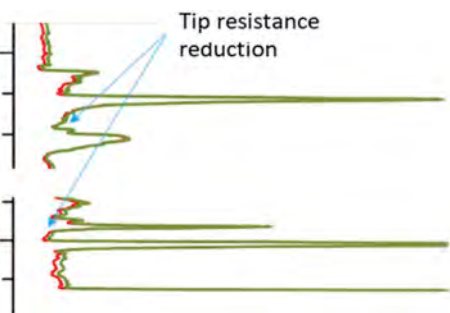


Figure 3. Alternation between hard and soft lenses or layers produces reductions on q_T values.

Likewise, since the measurement of the parameters q_T and f_s is carried out at a given time but not at the same depth, and the alternation in the stiffness of the soil can produce deviations in the verticality of the cone, it is necessary to make depth corrections. Therefore, the interpretation of the records is not immediate since post-processing is required. In addition to

this, interstratification makes it difficult to interpret dissipation tests because drainage and soil saturation conditions are often different, so it is common to observe that dissipation curves have different and unusual shapes.

2.3 Dissipation curves

Dissipation tests were carried out using piezocones with u sensor located at position 2 (u_2). The dissipation tests were executed at various sites of tailings dams, where there are clays and silty clays and no groundwater level. Figure 4 shows the main types of dissipation curves observed in the tailings dams studied:

- With monotonic decay up to the equilibrium pressure, u_0 , either positive or negative.
- A maximum is present and the equilibrium pressure may be positive or negative.
- With monotonic growth up to the equilibrium pressure.

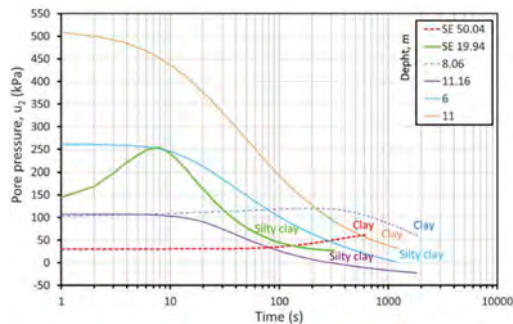


Figure 4. Main types of dissipation curves observed in the studied tailings dams.

According to the criteria presented by Sully *et al.* (1999), monotonic decreasing curves with a positive value are of type I and II and occur in normally consolidated fine soils; those with a maximum value are of type III if the initial pressure is higher than the equilibrium pressure, but if the initial pressure is lower, they are of types IV and V. According to this classification, all types of curves are present in the tailings dams studied, with the particularity that there are negative equilibrium pore pressures, although with small magnitude, between 0kPa and -50kPa.

In the literature, methods have been proposed to determine the value of the pressure increase $\Delta u = u_T - u_0$ generated during piezocone driving and determined in dissipation tests following the nomenclature shown in Figure 5 (Burns and Mayne, 1998; Sully *et al.*, 1999; Paniagua *et al.*, 2016; Imre *et al.*, 2018), however, these methods are only applicable for type I to III curves. For the other cases, it is difficult to determine the value of Δu due to the number of factors involved: fastening of the driving rods, position of the sensor, drainage and saturation conditions of the soil, soil type, to mention the most important ones.

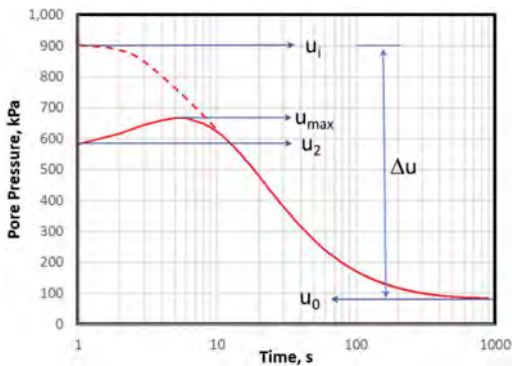


Figure 5. Nomenclature used for conventional dissipation curves.

Considering the hypothesis that the dynamic pore pressure u_2 is given by eqs 1 and 2 (Burns and Mayne, 1998), and given that the octahedric component produces only positive increases in pore pressure, the shear component, which depends on the dilative/contractive behavior of the soil, would be one of the factors responsible for the suction generated in the driving process for the dissipation curve types III to V. The decrease of the initial pore pressure in the dissipation test can also be caused by the abrupt stop of the driving (Kurup and Tumay, 1995), by the actual drainage conditions, by the saturation conditions of the soil, by the movement of the bars after stopping the driving, among other factors.

$$u_2 = u_0 + \Delta u \quad (1)$$

$$\Delta u = \Delta u_{oct} + \Delta u_{shear} \quad (2)$$

As previously mentioned, all the tests were performed in tailings deposits where there is no groundwater level, so the soils are partially saturated. For comparison purposes, Figure 6 shows dissipation tests carried out in the clays and silty clays of

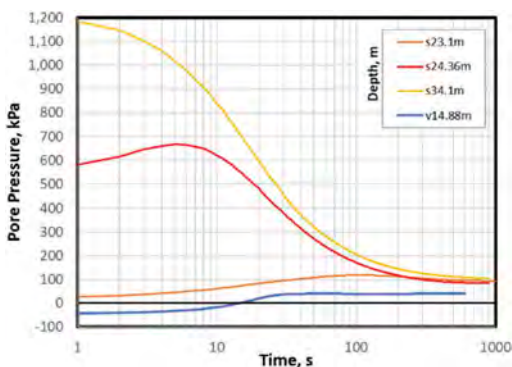


Figure 6. Main types of dissipation curves observed in clayey soils in Mexico City.

Mexico City, where the groundwater level is superficial, and although the deposit is saturated, there are significant drops in pore pressures. Curves with behavior similar to that observed in the tailings dams are observed, but there is a case where u_2 starts at negative values.

2.4 Chemical reaction

It is common that after driving the cone, the probe gets dirty, mainly in fine soils, and has to be cleaned to start a new drilling, but a relevant aspect that was observed in drillings on mining deposits, was the generation of an impregnated oxide layer in the piezocone after the execution of a probe (Figure 7), which is difficult to remove with the process that is commonly done even using a brush with steel bristles. One of the important characteristics of the deposits where this aspect was observed was that there was a constant emanation of gaseous ammonia (NH_3) generated as a consequence of the leaching process. The most feasible and efficient solution to remove this oxide layer was to immerse the removable parts of the piezocone, such as the shaft jacket and the apex in acetic acid (CH_3COOH), as well as to clean the fixed parts with the same compound and with the help of a toothbrush.



Figure 7. Piezocone with oxide induced by the minerals that make up the tailings deposit.

2.5 S-wave velocity profile

The tailings dams are formed by deposits of very young soils, some of them still in the process of compaction or consolidation, where the definition of the stratigraphic profile and the evaluation of the mechanical properties of each stratum is difficult, mainly because there is heterogeneity, both vertical and horizontal, and it is also difficult to obtain unaltered samples. Therefore, in this type of deposits, field techniques are used, especially sCPTu Δu and VST tests, because it is possible to define the stratigraphic profile and determine, either directly or indirectly, the mechanical properties of each unit, particularly

parameters such as modulus of stiffness at small deformations (G_0), permeability coefficient (k) and undrained shear strength (s_u), in order to carry out stability analyses.

The velocity profiles obtained at one site from the sCPTu are presented in Figure 8. In this case, the determination of the S-wave velocity profile is performed with two procedures: direct measurement by means of the seismic modulus and by means of empirical correlations. It is observed that, although the correlation generates satisfactory results, it was not able to reproduce the alternation of values, especially the maximum values.

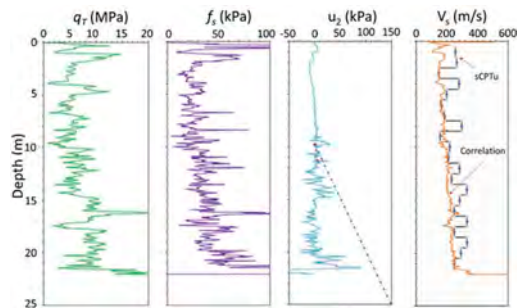


Figure 8. Determination of the S-wave profile by correlations and with the seismic modulus.

3 CONCLUSIONS

This paper describes and analyzes several aspects observed during the exploration of mine tailings deposits in Mexico using the CPTu Δu test: high ground temperatures, interstratification, chemical reaction, dissipation curves, and S-wave profile.

High temperatures can affect measurements of the parameters q_T , f_s , u_2 , and Δu when the equipment does not have compensators, but if they do exist, it is required that temperature changes are not abrupt so that the sensor can stabilize during the measurement. For this reason, experiments were carried out in this type of deposits using equipment with compensators, finding that the variations of q_T and f_s measurements were found to be within the error range indicated in the standards (ASTM D5778-12). Regarding the dynamic pore pressure, u_2 , where the measurement was performed without a temperature compensator, the results indicate variations of about 13kPa, which, although small, can induce errors for the interpretation of dissipation tests.

The second factor analyzed was the presence of high interstratification between thin layers of hard and soft soils, with different degrees of saturation. Moving from a hard to a soft stratum leads to errors in the measurement of the tip resistance, making it necessary to carry out corrections (Boulanger and DeJong, 2018). Also, since the measurement of q_T and f_s parameters is performed at a given time, but not at the

same depth, and the alternation in soil hardness can produce deviations from the verticality of the cone, it is necessary to carry out depth corrections. Therefore, the interpretation of the logs in this type of terrain is not immediate, since post-processing is required.

The different types of dissipation curves observed in the tailings dams studied, where the soils are partially saturated, are generally the same as those described in Sully *et al* (1999), with the particularity that in some cases the equilibrium pressure has negative values.

A case is described in which a chemical reaction occurs in the piezocone during its driving, which may affect the readings. Ammonia generated as a consequence of the leaching process induces oxidation, so it is necessary to perform continuous maintenance of such equipment, and for the type of deposits studied vinegar proved to be the best substance for cleaning the cones.

Finally, velocity profiles are determined for two sites of tailings dams through correlations with the value of q_T and the one determined with the seismic modulus. It is observed that the profile obtained with correlations reproduces the general trend but it is not possible to capture the variations of the shear wave velocity in this type of deposits, in the particular case, the maximum values are not reproduced, therefore, in this type of deposits it is advisable the direct measurement of the shear wave and to use the smaller intervals of measurement according to the technique used.

REFERENCES

- ASTM D5778–12 “Standard Test Method for Electronic Friction Cone and Piezocone Penetration Testing Of Soils”.
- Boulanger R.W. and DeJong J.T., (2018), “Inverse filtering procedure to correct cone penetration data for thin-layer and transition effects”, *Penetration Testing 2018*, Hicks, Pisano and Peuchen (Eds), Delft University of Technology, The Netherlands, 25–44
- Burns S.E. and Mayne P.W. (1998), “Monotonic and dilatatory pore pressure decay during piezocone test in clay”, *Canadian Geotechnical Journal* 35, 1063–1073.
- Kurup P.U. and Tumay M.T. (1995), “Piezocone dissipation curves with initial excess pore pressure variation”, *Proc. Int. Symposium on Cone Penetration Testing, CPT’95*, Linköping, Sweden, 195–200.
- Imre E., Schanz T., Bates L. and Fityus S. (2018), “Evaluation of complex and/or short CPTu dissipation test”, *Cone Penetration Testing 2018*, Hicks, Pisano and Peuchen (Eds), Delft University of Technology, The Netherlands, 351–357
- Paniagua P., Carrol R., L’Heureux J.S., and Nordal S. (2016), “Monotonic and dilatatory excess pore water dissipation in silt following CPTu at variable penetration rate”, *Proc. IS Osaka-Engineering Practice and Performance of Soft Deposits*, Osaka, Japan, 147–152
- Sully P.J., Robertson P.K., Campanella R.G., and Woeller D.J. (1999), “An approach to evaluation of field CPTu dissipation data in over consolidated fine-grained soils”, *Canadian Geotechnical Journal* 36, 369–381.

Assessment of the spatial variability of a Croatian flood embankment using the cone penetration test

C. Reale

University of Bath, UK

M.S. Kovačević & M. Bacic

University of Zagreb, Croatia

K.G. Gavin

Delft University of Technology, The Netherlands

ABSTRACT: Understanding how soil varies spatially is necessary in order to accurately quantify the reliability of geotechnical infrastructure. For long linear infrastructure such as flood embankments, incorporating vertical and horizontal scales of fluctuation can have a significant impact on stability assessments. This paper presents preliminary results and discussion from a field test designed to determine the vertical and horizontal scales of fluctuation of a Croatian flood embankment. A series of 15 CPTUs were carried out over a 200m length of the embankment with a Multi-channel Analysis of Surface Waves (MASW) survey done on the same section. CPT spacing was designed specifically to determine horizontal variation with multiple CPTs carried out in close proximity to each other. There was significant variation in soil stratigraphy over the embankment section with pockets of increased strength and stiffness showing up in the MASW and CPT results. This paper discusses dealing with horizontal correlation in challenging deposits and presents initial findings from the underlying sand layer.

1 INTRODUCTION

Soil properties vary as a function of space and time. Quantifying exactly how they vary is of upmost importance in determining the capacity of geotechnical structures (De Gast, Vardon and Hicks, 2020). This is particularly important for aged linear infrastructure, which underwent less rigorous design than its modern counterparts and has a lower safety margin as a result (Reale *et al.*, 2016; Reale, Xue and Gavin, 2017). It is infeasible and inadvisable to replace such infrastructure en-masse, moreover it is likely unnecessary given that the structures have remained stable so far. Instead, a better approach is to quantify the uncertainties present in the material in order to accurately assess the risk of failure. Such an approach could be applied consistently with a risk-based decision methodology to decide which assets to improve or replace (Reale, Xue and Gavin, 2016).

Random field theory considers soil properties at a given location as random variables. Within a zero mean stationary random field, the spatial variation between one point and another in the same structure can be described by their correlation structure. Statistically modelling spatial variability presumes a stationary random field. Such an assumption may be hard to achieve in reality given that soil is not really

stochastic but it is convenient to model it as such, as information is limited (Phoon, 2008). If a dataset is not stationary, then estimation of soil statistics may be subject to bias. To prevent this, the dataset should undergo transformation to achieve stationarity, data decomposition is frequently adopted to this end. Phoon *et al.* (2003) describe a modified Bartlett hypothesis test that can be used to check stationarity.

If one is concerned about the average properties within some volume of soil (e.g. the average shear strength or average resistance of a material) then areas of high value balance areas of low value so that the variance of the average goes down as the volume of soil mobilised becomes larger. Point variations such as those listed by (Phoon & Kulhawy, 1999) are typically much higher than spatially averaged variations. Spatial averaging therefore reduces uncertainty. The net result of which is lower failure rates which are more consistent with those observed in reality (Phoon, 2008). Depending on the scale of fluctuations involved spatial averaging can have a significant impact on the stability of linear infrastructure.

Random field theory has been successfully used to generate one dimensional, two dimensional and three dimensional geological models (Zhu and Zhang, 2013; Lloret-Cabot, Fenton and Hicks, 2014) and applied to various geotechnical

problems such as bearing capacity of foundations (Fenton and Griffiths, 2003; Srivastava and Babu, 2009), water flow (Renato et al., 2006), two dimensional slope stability (Srivastava, Babu and Haldar, 2010; Santoso, Phoon and Quek, 2011; Tabarrokhi, Ahmad and Banaki, 2013; Li et al., 2014), three dimension slope stability (Hicks and Spencer, 2010), scour (Prendergast, Reale and Gavin, 2018) and suction caisson design (Remmers et al., 2019).

This study describes the initial findings from a series of CPTs investigating the horizontal and vertical variability of a flood embankment in Croatia, the findings will be utilised in a wider study to investigate the stability of the flood defenses and to assess their potential for liquefaction.

2 METHODOLOGY

Decomposition can be used to investigate a CPTs underlying spatial correlation structure where a trend function is fitted to and extracted from a dataset using least squares or some similar approach. This removes any underlying trend from the data leaving behind some fluctuating component. The correlation structure of this fluctuating component can then be determined.

After removing any discernible trend, the soil property (in this case q_c) for a normal distribution can be described by Equation 1.

$$q_c = \mu + \sigma \mathbf{G} \quad (1)$$

where μ is the mean value described at some depth z using Equation 2, σ is the standard deviation at the same depth and \mathbf{G} is a matrix containing n spatially correlated normal random processes of zero mean and unit variance which account for the spatial correlation structure of the soil.

$$\mu(z) = a_i + b_i z \quad (2)$$

where a_i is the mean trends value at the beginning of the i th layer, b_i is the slope of the trendline in question and z is the depth.

After removing the linear depth trend of each q_c profile in the dataset, the standard deviation of the detrended tip resistances can be calculated. Dividing an individual detrended tip resistance by its respective standard deviation transforms the tip resistance variation into the standard normal space. i.e. it produces normal random fields with a mean of zero and a standard deviation of 1. Variations within these normal random fields can be used to estimate the spatial correlation structure $\hat{\rho}(\tau_j)$ of the tip resistance with depth or horizontal distance, see Equation 3.

$$\hat{\rho}(\tau_j) = \frac{1}{\sigma^2(n-j)} \sum_{i=1}^{n-j} (X_i - \mu)(X_{i+j} - \mu) \quad (3)$$

where $j = 0, 1, \dots, n-1$ with n being the number of data points, $\tau_j = j\Delta\tau$ is the lag distance between the two points in question where $\Delta\tau$ is the distance between two adjacent points, μ is the estimated mean, σ is the standard deviation and X is the random soil property in this case tip resistance. A Markov correlation function (Lloret-Cabot, Fenton and Hicks, 2014; Kasama and Whittle, 2015) was used to approximate the spatial correlation structure, see Equation 4. It is important to note, that many correlation functions exist and the choice of correlation function will depend on the goodness of fit achieved with the underlying correlation structure. The scale of fluctuation θ , is varied until the correlation structure obtained from Equation 3 is described by the correlation function i.e. until the difference between $\hat{\rho}(\tau)$ and $\rho(\tau)$ is negligible.

$$\rho(\tau_j) = \exp\left(\frac{-2|\tau_j|}{\theta}\right) \quad (4)$$

For horizontal spatial variation the Equation 4 holds except there is a greater distance between measurement points and the spacing between points is unlikely to be uniform. In practice this complicates the process as it becomes difficult to determine when like is being compared with like. The authors compared the top of the sand layer in each CPT as if they occurred at the same depth and determined horizontal correlations across CPT using a 1m moving window therein.

3 TEST SITE

The CPT test location is located next to a embankment in central Croatia, in Orle Municipality, around 25 km from Zagreb. The embankment is part of a flood defence network which protects the wider area from the influence of the Odra and Sava rivers. CPTs were performed over a 200m length at the following spacings [0 m, 2 m, 5 m, 10 m, 25 m, 50 m, 75 m, 100 m, 125 m, 150 m, 175 m, 190 m, 195 m, 198 m, 200 m], see Figure 1, to a depth of 15 m. The first soil layer at the site was a clay of variable thickness, with deeper deposits of between 7m and 8m found on either end of the 200m test length. Layer thickness reduced to approximately 2m in the middle of the test length. Underneath the clay was a dense sand deposit to great depth. The full set of CPT traces demonstrated a lot of variability, particularly within the sand layer and at transition depths, see Figure 2.

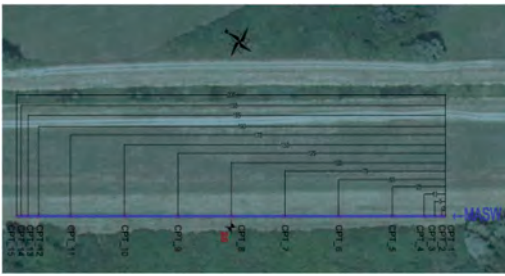


Figure 1. CPT traces and MASW were performed along the blue line adjacent to the embankment.

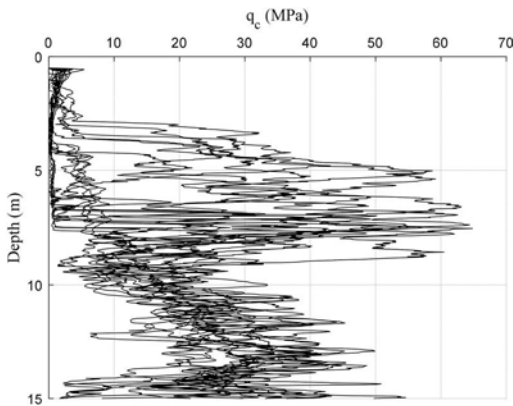


Figure 2. 15 CPT traces across the site.

Multi-Channel Analysis of Surface Waves (MASW) was also performed at the site, see Figure 3, which corroborated the assumed stratigraphy showing deeper deposits of low shear wave velocity at either end of the test length. The presence of localized deposits of increased stiffness can also be seen within the sand layer, demonstrating the variability of the material.

Due to the complex layering present in the upper clay layer the initial spatial variability interrogation is focused in the lower sand layer from a depth of 10 to 15m where the soil behaves more consistently across the site, see Figure 4.

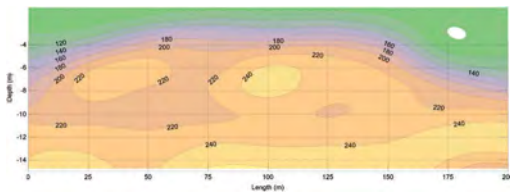


Figure 3. Shear wave velocities from MASW performed at the site, demonstrating the variability in the depth of the sand layer across the site.

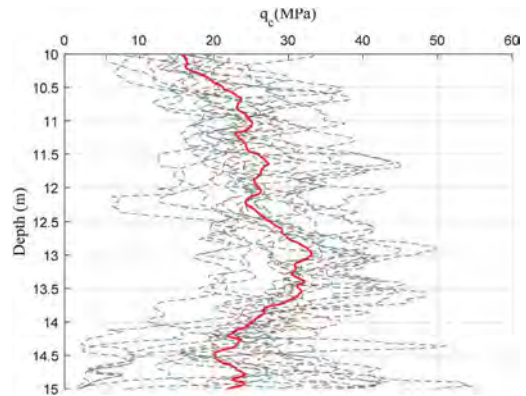


Figure 4. CPT traces from 10 to 15m with the mean qc profile shown in red.

4 RESULTS

The CPT traces in the lower sand layer were detrended, normalised and the underlying correlation structure was determined using the procedure described in section 2. Equation 4 was then fitted to the underlying structure by optimizing the scale of fluctuation. The vertical scale of fluctuation θ_V was found to be 0.82 m with the 95% confidence intervals ranging from 0.78 m to 0.85 m. A strong goodness of fit with achieved using the Markov correlation function with an R-square of 0.9358 and an RMSE of 0.0528.

The same procedure was followed for horizontal correlation with intermediate points interpolated to facilitate curve fitting. Initial results indicated that the horizontal scale of fluctuation was approximately 8.39 m with a 95% confidence interval range of 7.45 m to 9.33 m.

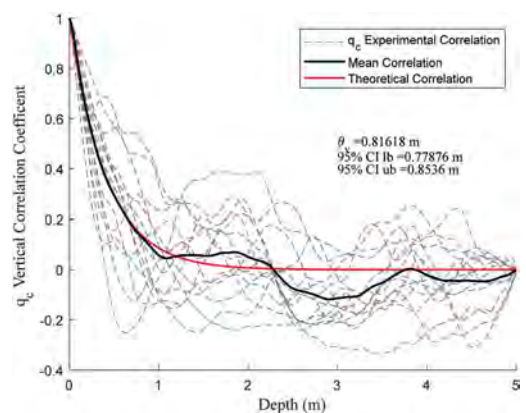


Figure 5. Vertical correlation structure found in the lower sand layer.

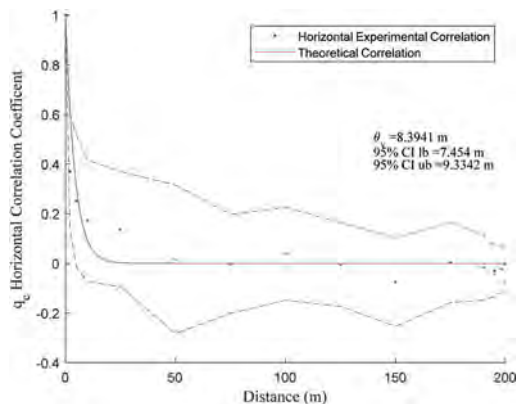


Figure 6. Initial horizontal correlation structure found in the lower sand layer.

5 DISCUSSION AND CONCLUSIONS

This paper presents initial results from a site investigation to investigate spatial variability in Croatia. Initial work was focused on the underlying sand layer which behaved more consistently than the finer surface deposits. Initial results suggest that horizontal variability is an order of magnitude greater than the vertical variability. However significant uncertainty exists in determining the horizontal correlation structure. One issue stems, from the variability in layer depth across the site, as the boundary of the sand layer is inclined. This makes it difficult to correlate “like with like” across the site as merely correlating CPTs at the same depth could result in correlating across layer boundaries. To overcome this the authors considered the top of the sand layer in each CPT as the start point of the analysis and used a moving window of 1m to determine horizontal correlations below those point. As there is no continuous measurement in the horizontal direction, there needs to be a methodology to ensure that the correct data is being used to determine the mean autocorrelation behavior horizontally. Different averaging procedures will be investigated, while different window sizes to determine the effect of sample size on scales of fluctuation. The analysis will also be rerun to consider the start point at intermediate CPT locations to check consistency across the site. Some consideration also needs to be paid to stationarity. This is difficult to ensure in the vertical direction, but much more so in the horizontal direction where there are much more limited discrete measurement points which makes the implementation of stationarity checks such as Bartlett statistics challenging. This will be investigated moving forward.

REFERENCES

- Fenton, G. A. and Griffiths, D. V (2003) ‘Bearing-capacity prediction of spatially random $c - \phi$ soils’, *Canadian Geotechnical Journal*, 40(1), pp. 54–65. doi: 10.1139/t02-086.
- De Gast, T., Vardon, P. J. and Hicks, M. A. (2020) ‘Assessment of soil spatial variability for linear infrastructure using cone penetration tests’, *Géotechnique*, pp. 1–15. doi: 10.1680/jgeot.19.sip.002.
- Hicks, M. and Spencer, W. (2010) ‘Influence of heterogeneity on the reliability and failure of a long 3D slope’, *Computers and Geotechnics*, 37(7–8), pp. 948–955. doi: 10.1016/j.compgeo.2010.08.001.
- Kasama, K. and Whittle, A. J. (2015) ‘Effect of spatial variability on the slope stability using Random Field Numerical Limit Analyses’, *Georisk: Assessment and Management of Risk for Engineered Systems and Geohazards*, 10(1), pp. 42–54. doi: 10.1080/17499518.2015.1077973.
- Li, D.-Q. et al. (2014) ‘Effect of spatially variable shear strength parameters with linearly increasing mean trend on reliability of infinite slopes’, *Structural Safety*, 49, pp. 45–55. doi: 10.1016/j.strusafe.2013.08.005.
- Lloret-Cabot, M., Fenton, G. and Hicks, M. (2014) ‘On the estimation of scale of fluctuation in geostatistics’, *Georisk: Assessment and Management of Risk for Engineered Systems and Geohazards*, 8(2), pp. 129–140. doi: 10.1080/17499518.2013.871189.
- Phoon, K.-K., Quek, S.-T. and An, P. (2003) ‘Identification of Statistically Homogeneous Soil Layers Using Modified Bartlett Statistics’, *Journal of Geotechnical and Geoenvironmental Engineering*, 129(7), pp. 649–659. doi: 10.1061/(asce)1090-0241(2003)129:7(649).
- Phoon, K. (2008) *Reliability-based design in geotechnical engineering: computations and applications*. Edited by K. Phoon. Taylor and Francis.
- Phoon, K. and Kulhawy, F. (1999) ‘Characterization of geotechnical variability’, *Canadian Geotechnical Journal*, 36(4), pp. 612–624.
- Prendergast, L. J., Reale, C. and Gavin, K. (2018) ‘Probabilistic examination of the change in eigenfrequencies of an offshore wind turbine under progressive scour incorporating soil spatial variability’, *Marine Structures*, 57, pp. 87–104. doi: 10.1016/j.marstruc.2017.09.009.
- Reale, C. et al. (2016) ‘Multi-modal Reliability Analysis of Slope Stability’, *Transportation Research Procedia*, 14, pp. 2468–2476. doi: 10.1016/j.trpro.2016.05.304.
- Reale, C., Xue, J. and Gavin, K. (2016) ‘System reliability of slopes using multimodal optimisation’, *Géotechnique*, 66(5), pp. 413–423. doi: 10.1680/jgeot.15.P.142.
- Reale, C., Xue, J. and Gavin, K. (2017) ‘Using Reliability Theory to Assess the Stability and Prolong the Design Life of Existing Engineered Slopes’, in *Risk Assessment and Management in Geotechnical Engineering: from Theory to Practice*, ASCE Geotechnical Special Publication in Memory of the Late Professor Wilson H. Tang, pp. 61–81. doi: 10.1061/9780784480731.006.
- Remmers, J. et al. (2019) ‘Geotechnical installation design of suction buckets in non-cohesive soils: A reliability-based approach’, *Ocean Engineering*, 188, p. 106242. doi: 10.1016/j.oceaneng.2019.106242.
- Santoso, A., Phoon, K. and Quek, S. (2011) ‘Effects of soil spatial variability on rainfall-induced landslides’, *Computers & Structures*, 89(11–12), pp. 893–900.

- Srivastava, A. and Babu, G. (2009) 'Effect of soil variability on the bearing capacity of clay and in slope stability problems', *Engineering Geology*, 108(1–2), pp. 142–152.
- Srivastava, A., Babu, G. and Haldar, S. (2010) 'Influence of spatial variability of permeability property on steady state seepage flow and slope stability analysis', *Engineering Geology*, 110(3–4), pp. 93–101.
- Tabarrokhi, M., Ahmad, F. and Banaki, R. (2013) 'Determining the factors of safety of spatially variable slopes modeled by random fields', *Journal of Geotechnical and Geoenvironmental Engineering*, 139(12), pp. 2082–2095.
- Zhu, H. and Zhang, L. (2013) 'Characterizing geotechnical anisotropic spatial variations using random field theory', *Canadian Geotechnical Journal*, 50(7), pp. 723–734. doi: 10.1139/cgj-2012-0345.

Prediction of bearing capacity and settlement using penetrometer design method for shallow foundation and load transfer curves

P. Reiffsteck & F. Szymkiewicz

GERS-SRO, Université Gustave Eiffel, IFSTTAR, Marne la Vallée, France

M.A. Benz Navarrete & T.A. Luong

Research and Development, Sol-Solution, Riom Cedex, France

ABSTRACT: This paper presents a simple, economic, and sound design method that could be easily implemented worldwide, based on a new generation version of Dynamic Cone Penetrometer Test (DCPT) devices giving access to the whole cone resistance versus penetration depth of the cone curve, to predict the bearing capacity, as well as to estimate the load – settlement curve of a shallow foundation which is partly inspired from the French Penetrometer design method. A methodology is then proposed in this study for the conception of shallow foundation based on load transfer curves obtained from DCPT.

1 INTRODUCTION

Spread foundations are the most extensively used geotechnical structures in civil engineering world, as they are simple to construct and the most cost-effective choice for support of a building furthermore. These foundations are implemented for all kinds of structure from small individual buildings to bridges.

For the conception of shallow foundations including the evaluation of bearing capacity and its settlement, the conventional methods such as c and φ method (Skempton, 1951) (Terzaghi, 1943) and the one-dimensional approach often overestimate limit load and underestimate settlement, which leads to a non-conservative design or differential settlement, both being detrimental to the structures (Poulos & Carter, 2001).

Static and dynamic cone penetration tests (respectively, CPT and DCPT) are the techniques in the ground investigation and foundation design, which are widely used in many countries around the world. However, in conventional procedures, these tests only allow a fairly assessment of soil deformation since no direct relationship between load and settlement (stress strain relation) is obtained during the test. Thus, the development of a new test protocol and equipment of Cone Penetrometer Test in its dynamic version are improved not only to ensure the advantages of economy and simple operation, but also improve the measurement capacity to derive various soil parameters and increase their reliability.

The dynamic cone loading test (DCLT), developed very recently in France (Benz, et al., 2013) (Escobar Valencia, et al., 2013), consists of analyzing the

measurements made during the dynamic penetrometer driving to obtain a dynamic cone load-penetration curve at cone-soil interface, which is qualitatively comparable to the expansion curve obtained by the pressuremeter as well as settlement curve obtained during shallow foundation loading test.

This paper then introduces a methodology for the calibration of the transfer curves from the DCPT tests, therefore, to predict the load – settlement curve for the conception of the shallow foundations.

2 DYNAMIC CONE LOADING TEST (DCLT)

2.1 Description of DCLT apparatus

The instrumented dynamic cone penetrometer (DPT) has been designed and based on the same functional principle as the P.A.N.D.A. (*from French Pénéromètre Autonome Numérique Assisté par ordinateur*).

It is an instrumented lightweight DPT which is driven with variable energy (Gourvès & Barjot, 1995) provided by the operator by means of a hand-hammer mass. For each blow, the energy supplied as well as total penetration is directly measured (Benz Navarrete, 2009). The new version of P.A.N.D.A. used in this work, includes new sensors and the general principle is based on wave equation solution. A general description of the device as well as the theoretical implemented approach is presented by (Benz Navarrete, et al., 2021).

After each hammer blow, instrumented anvil records strain, acceleration, and displacement. An example of raw measurements performed during the test is shown in Figure 1.b.

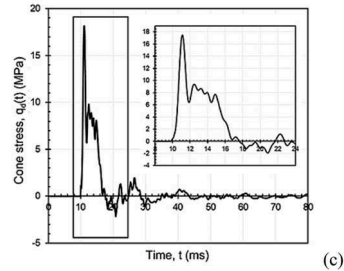
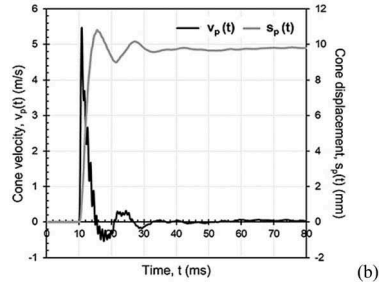
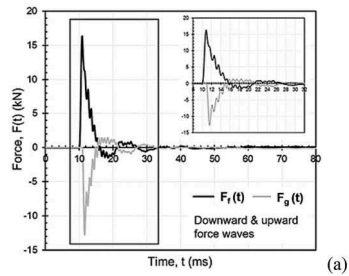
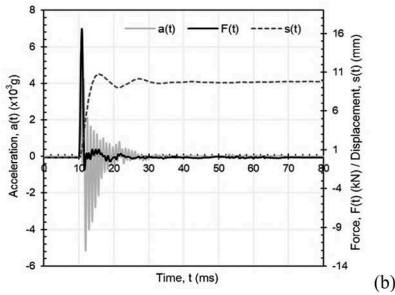
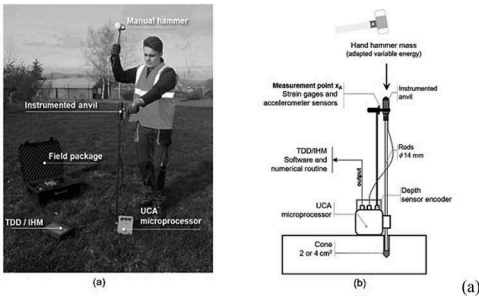


Figure 1. (a) Dynamic penetrometer P.A.N.D.A.3 (Benz et al. 2013) and (b) raw measurements (acceleration, force, and displacement).

Penetrometer is composed of rods with a diameter of 14 mm and 500 mm in length and of overflowing conical tips with a cross-section of 2 or 4 cm² (respectively, 15.9 or 22.5 mm in diameter). In accordance with the ISO-22476-2 Standard (2005), the apex angle of cones is 90°. To avoid the effects of skin friction on the rods, the use of overflowing conical tips (having a larger diameter than that of the rods) has proved to be sufficient. However, jacking or mud injection can be implemented in necessary (ISO 22476-2).

2.2 Getting DCLT curves

The derivation of mechanical parameters is based on pile dynamic, rapid shocks, Split Hopkinson Pressure Bars (SPHB) as well as rock percussion borehole tests (Rausche, 1970; Karlsson, et al., 1989; Bussac, et al., 2002; Omidvar, et al., 2014; Omidvar, et al., 2015).

Figure 2 shows for each blow, by supposing no skin friction along the rods and from measurements carried out in the upper end of rod string (close to the anvil), elementary downward and upward waves are decoupled. From that, force $F_p(t)$, velocity $v_p(t)$ and settlement $s_p(t)$ are then computed at cone/soil interface (Benz, et al., 2013) (Escobar Valencia, et al., 2013) and (Tran, et al., 2019). Dynamic Cone Load-penetration (DCLT) curves are obtained by plotting cone resistance $q_d(t)$ as a function of its settlement $s_p(t)$ (Figure 3).

Cone resistance $q_d(t)$, shown in Figure 3, represents the total soil resistance under dynamic loading. DCLT

Figure 2. Example of (a) force decoupled waves in measurement point x_A , and reconstructed cone signals (b) velocity and displacement; and (c) cone stress.

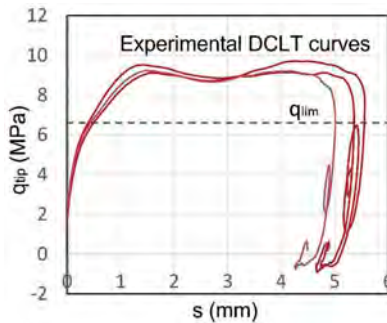


Figure 3. Field Dynamic Cone Loading (DCLT) curves (Jossigny, France).

curve can be modelled by a perfectly elasto-plastic and dashpot model, where total soil resistance $q_d(t)$ is the sum of pseudo-static q_{ps} , damping $q_{dyn}(t)$ and inertial q_{in} resistances (Eq. (1)) which can be neglected due to the low mass of penetrometer. Pseudo-static resistance q_{ps} is displacement dependent and modelled by a non-linear elastic perfectly plastic law

while $q_{dyn}(t)$, is penetration rate dependent and modelled with a radiation dashpot (Eq. (2)).

$$qd(t) = q_{ps} + q_{dyn}(t) + q_{in} \quad (1)$$

$$qd(t)A_p = Qd = k_b u + c_b \dot{u} + m_p \ddot{u} \quad (2)$$

In Eq. (2), \ddot{u} , \dot{u} , and u are, respectively, acceleration, velocity, and displacement at penetrometer's cone/soil interface. Qd is the total strength and A_p the cone section. c_b and k_b are the dashpot and spring constant (El Naggar & Novak, 1996), defined by:

$$k_b = \frac{4G_s R_{(H)}}{(1 - \nu_s)} \quad (3)$$

$$c_b = \frac{3.4R_{(H)}^2 \sqrt{G_s \rho_s}}{(1 - \nu_s)} \quad (4)$$

Where, $R_{(H)}$ is equivalent radius introduced by (Holeyman, 1988) and computed according to (Novak & Beredugo, 1972; El Naggar & Novak, 1994). G_s , ρ_s and ν_s are respectively shear modulus, density, and Poisson's ratio of soil.

Plastic resistance or soil limit resistance q_{lim} is obtained from velocity, displacement, and strength signal according to the Unloading Point Method proposed by (Middendorp et al. 1992; Hölscher et al. 2012) and explained by (Brown 1994, 2016).

Moreover, spring constant or dynamic stiffness k_{dyn} is determined from DCLT experimental measurements by mean of FRF transfer functions (Davis 1975; Paquet and Briard 1976; Tran et al. 2019). For the case of a rigid embedded foundation subject to transient dynamic loading, it is assumed that at low frequencies, k_{dyn} is close to k_b . Knowing k_b and assuming Poisson's ratio ν_s , shear modulus G_s can be obtained from Eq. (3). Moreover, Elastic modulus (E_s) can be then obtained by applying the theory of elasticity. Other elastic parameters can be deduced.

In practice, DCLT curves are analyzed as follows:

- Assessment of dynamic stiffness k_b from FRF curves,
- Determination of shear modulus G_s (Eq. (3)).
- Elastic modulus (E_s) assessment from G_s and ν_s .
- Determination of soil limit resistance q_{lim} from DCLTs curves and Eq. (2) according to UPM method:
 - From cone velocity signal $v_p(t)$, find the moment (t_0) where $v_p(t)$ is zero after the blow.
 - Confirm that the t_0 moment coincides with maximum tip displacement $s_p(t)$ is at its maximum.
 - From strength signal $F_p(t)$, computed average value $F_p(t)^*$ at ($t_0 \pm dt$) moment (with $dt \approx 0,1ms$).

- Limit resistance assessment is obtained after inertial correction, $q_{lim} = F_p(t)^* - m_p \cdot a(t_0)$; where m_p is the mass of penetrometer and $a(t_0)$ is average acceleration at t_0 .

In this way, knowing E_s and q_{lim} , DCLT curves can be modeled by a nonlinear elastic plastic model as the Simplified Hyperbolic one presented below.

2.3 Simplified hyperbolic model adjustment to DCLT

The possibility to establish the cone resistance–penetration curve of DCLT is to fit a predetermined curve type suitable for reproducing the test from the experimental curves, with the choice set on the characteristic features of the curve which are the modulus E_s and the limit resistance q_{lim} . A similar development has been proposed by (Elhakim, 2005).

To reproduce the curves in a systematic way based on the parameters that are the cone resistance and the dynamic modulus, we will use a hyperbola formulation. The final version homogenizes the terms of the formula and systemizes the determination of the A_i parameters, closer to the method proposed by (Baud & Gambin, 2008), the deformation ε :

$$\begin{aligned} \varepsilon = \frac{s}{h_e} &= A_1 + A_2 q + \frac{A_4}{A_6 - q} \\ A_1 &= -\frac{A_4}{A_6} & A_2 &= \frac{\beta}{E_{dyn}} \\ A_4 &= \frac{(\alpha - \beta)(1 - x)}{E_{dyn}} q_d^2 & A_6 &= q_d = q_{lim} \end{aligned} \quad (5)$$

Where, $x = \frac{q_2}{q_d}$ a non dimensional term, where q_2 is the inflection point at the end of the linear part, corresponding to the conventional definition of $p_{LM} = 1.7p_{fM}$. We can therefore estimate x with a value around 0,6 to 0,7.

$\alpha = \frac{s_2 E}{q_2 h_e} = (1 - \nu^2) \frac{b}{h_e} C_f$, a non dimensional term, with $C_f = 0.79$ corresponding to the form coefficient of the rigid circular cone of P.A.N.D.A, an influence depth $h_e = \frac{\pi R}{4} (1 - \nu^2)$ (Butterfield & Banerjee, 1971), b and R being respectively diameters and radius of the cone.

β is equal to 0.95α , this ratio allowing to decrease the initial slope, in order to guide the hyperbola with an upward concavity.

Figure 4 shows the adjustment curves modelled by this version, based on data of DCLT tests that are the tip resistance, q_d and the dynamic modulus, E_{dyn} at the depth from 1 m to 1.25 m, in Jossigny site and at the depth from 1.75 m to 2 m, in Cran site.

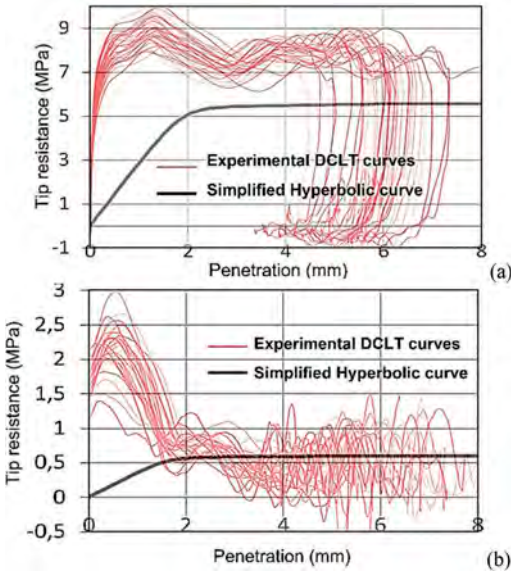


Figure 4. Curve adjusted in (a) Jossigny from 1 to 1.25 m and (b) Cran from 1.75 to 2 m.

3 PROPOSED DESIGN METHOD

3.1 Bearing capacity

Bearing capacity of the foundation is computed using the French penetrometer design direct method with slight modification (AFNOR, 2013).

$$q_{net} = q_0 + k_d \cdot q_{de} \quad (6)$$

$$k_d = k_{d0} + \left(a + b \cdot \frac{D_e}{B} \right) \cdot \left(1 - e^{-c \frac{D_e}{B}} \right) \quad (7)$$

With the q_{net} the net pressure under the foundation, q_0 the total vertical stress at the base of the foundation after construction, k_d the penetrometer bearing capacity coefficient, q_{de} the equivalent cone resistance, D_e and B respectively, the equivalent embedment depth and the width of foundation and k_{d0} , a , b , c and d the coefficients tabulated according to the type of soil and the shape of the foundation.

3.2 The load-settlement curve approach

As shown in Figure 5, a similar approach to the Load Settlement Curve Method proposed by Briaud has been developed to access the full load settlement curve (Briaud, 2007). The principle is based on the similarity of the cone resistance – penetration curve acquired by the DCLT at each hammer blow with the loading – settlement curve of the shallow foundation.

This transformation based on full-scale tests and numerical simulations is achieved using the equation

5 and real load pressure anticipated up to q_{net} obtained with equation 6. Results obtained with the proposed method are compared with settlement predicted by Schmertmann method as proposed by Eurocode 7 part 2.

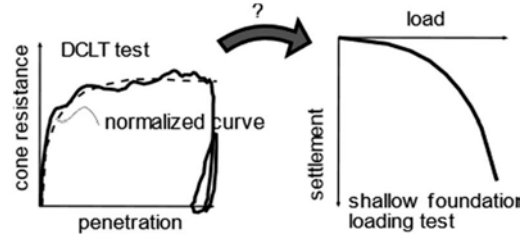


Figure 5. Principle of the similitude between shallow foundation loading test and DCLT.

4 FOUNDATION LOADING TESTS

4.1 Loading procedure

Several loading tests of $B = 1; 0.71$ m square and 0.6 m circular footings have been performed on several sites. Ground investigation using P.A.N.D.A (DCLT), PMT, CPT, SPT and other techniques helped to define the ground model.

Foundations were loaded, using load steps of a 30-minutes duration, until failure occurred, with an average number of 10 steps. The Figure 6 and 7 show schematically the equipment used for shallow foundation loading tests.

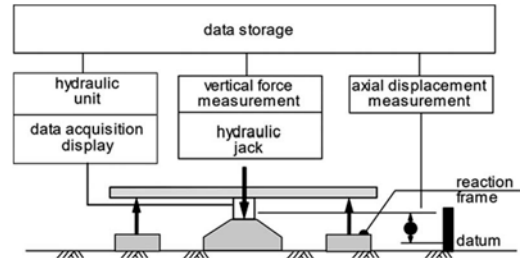


Figure 6. Schematic shallow foundation loading test.

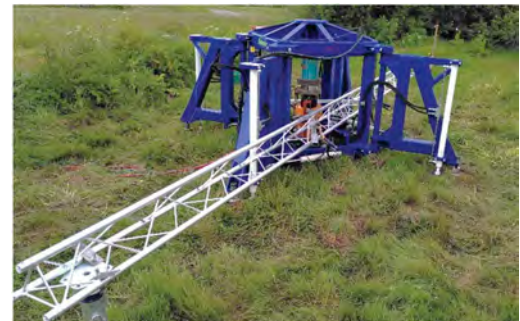


Figure 7. Foundation loading test in Cran.

4.2 Sites presentation and tests performed

Table 1 summarizes information on two sites of different soil types where foundation and DCLT tests have been performed. Based on the results of several shallow foundation load test for each site, a mean curve can be fitted (by least-squares method).

Table 1. Sites and number of DCLT test.

Site	Soil type	DCLT test	
		Quantity	DCLT curves /ml
Jossigny	Silty	6	130 c/ml
Cran	Marine clay	9	128 c/ml

Figure 8 presents the mean loading – settlement curve for Jossigny site for the case of 1m square foundations and two experimental curves for Cran site for the case of a 0.6 m circular footing.

4.3 Tests results and comparison to prediction

The bearing capacity prediction using the pressuremeter and penetrometer methods, proposed in the French national application standard of Eurocode 7 NF P94-261 for shallow foundation design, is presented in Figures 9 and 10.

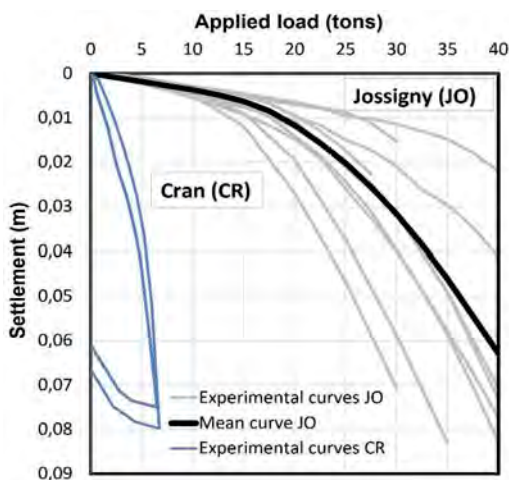


Figure 8. Mean curve of foundation load tests performed on Jossigny (Square 1x1m) and Cran (Circular D = 0,6m) sites.

The cumulative distribution curves of ratios between calculated and measured bearing capacity coefficients are compared with Normal law distribution function.

The DCLT method results superimposed well on the ones obtained using pressuremeter method as proposed by NF P94-261. The safety level of the bearing capacity is represented by the deviation from an average value of 1. Figure 9 shows that the prediction of these methods tends to a conservative

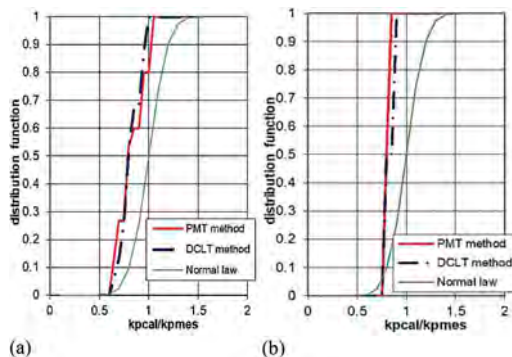


Figure 9. Distribution curves of the experimental and computed bearing capacity ratio for (a) square 1x1m footing in Jossigny and (b) circular D = 0.6 m footing in Cran.

prediction of bearing capacity, for Jossigny as well as Cran sites, especially the results from DCLT method.

Figure 10 shows settlement prediction, by four design methods: the French Application Standard of EC7 (NF P94-261), the Load

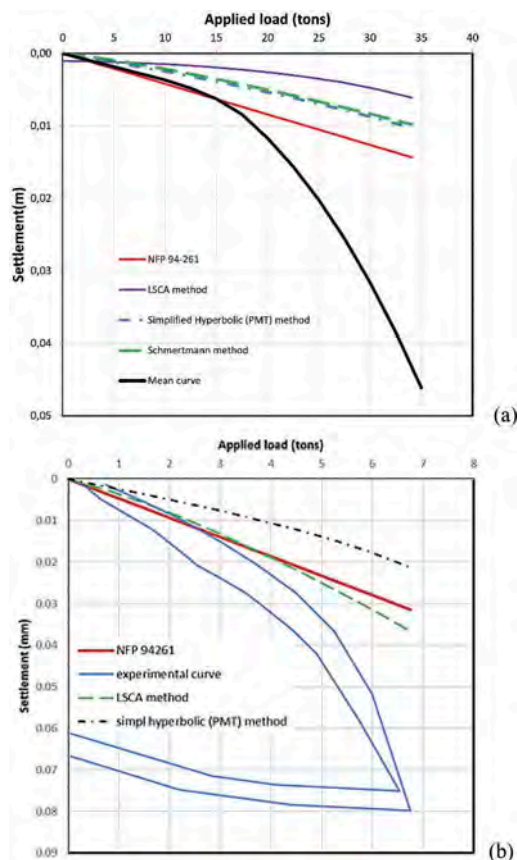


Figure 10. Comparison of experimental and predicted settlement curves. For (a) 1x1 m square foundation on silt in Jossigny and (b) D = 0,6 m circular foundation on marine clay in Cran.

Settlement Curve Approach (LSCA) proposed by (Briaud, 2007), the Simplified Hyperbolic (SH) model for PMT and the Schmertmann method, for a square footing in Jossigny and circular footing in Cran. We also note that the values of the respective conventional bearing capacity of soil in Jossigny and in Cran are respectively about 36 and 6 tons.

Figure 10a, compares the mean experimental curve (Figure 8) to computed settlement. The predicted settlement obtained with NF P94-261 and Schmertmann methods and the SH model for PMT well match the experimental mean curve, in the first half the loading phase. However, the LSCA method underestimates the settlement. One drawback of this method is the non-zero settlement for a loading close to zero.

Figure 10b shows the case of marine clay in Cran. The NF P94-261 method gives an acceptable settlement prediction while the two others present a non-conservative result.

When the loading is over 50% of bearing capacity, the four methods all underestimate the settlement of the real foundation. The calculated curve of the LSCA method is always farthest from the experimental mean curves while NF P94-261 method is the closest prediction.

5 CONCLUSIONS

This paper presents a method to predict bearing capacity of shallow foundations from the cone resistance and dynamic modulus of the newly developed Dynamic Cone Loading Test. A database of tests has been collected to validate the proposed design method whose results show a good agreement with the real foundation loading test results. However, the enrichment of more data from dynamic penetrometer and foundation loading tests in different sites is needed to better define the model factor of this method.

ACKNOWLEDGEMENTS

This project was carried out within the framework of collaborative research program Emerg3R grant.

REFERENCES

- AFNOR, 2013. Justification of geotechnical work - National application standards for the implementation of Eurocode 7 - Shallow foundations - NF P94-261. p. 160.
- Baud, J.-P. & Gambin, M. P., 2008. Homogenising MPM Tests Curves by Using a Hyperbolic Model. *Geotechnical and Geophysical Site Characterization, Proc. ISC'3*, 1–4 April.
- Benz Navarrete, M., 2009. *Mesures dynamiques lors du battage du pénétromètre Panda 2*, s.l.: University of Clermont-Auvergne.
- Benz Navarrete, M., Pierre, B. & Roland, G., 2021. Application of wave equation theory to improve dynamic cone penetration test for. *Journal of Rock Mechanics and Geotechnical Engineering*, p. 31.
- Benz, M., Escobar, E., Gourvès, R. & et al, 2013. Dynamic measurements of the penetration test - Determination of the tip's dynamic load-penetration curve. *In: 18th International Conference on Soil Mechanics and Geotechnical Engineering: Challenges and Innovations in Geotechnics, ICSMGE 2013*.
- Briaud, J.-L., 2007. Spread Footings in Sand: Load Settlement Curve Approach. *Journal of Geotechnical and Geoenvironmental Engineering*, pp. 905–920.
- Brown, M., 2016. Design methods based upon rapid pile load tests. *ISSMGE - ETC 3 Int Symp Des Piles Eur*.
- Brown, D., 1994. Evaluation of Static Capacity of Deep-Foundations from Statnamic Testing. *Geotech Test J 17*, p. 403–414.
- Bussac, M., Collet, P., Gary G & Othman, R., 2002. An optimisation method for separating and rebuilding one-dimensional dispersive waves from multi-point measurements. Application to elastic or viscoelastic bars. *J Mech Phys Solids 50*, pp. 321–349.
- Butterfield, R. & Banerjee, P., 1971. A rigid disc embedded in an elastic half space. *Geotechnical Engineering*, pp. 2: 35–52.
- El Naggar, M. & Novak, M., 1994. Non-Linear Model for Dynamic Axial Pile Response. *J Geotech Eng 120*, p. 308–329.
- El Naggar, M. & Novak, M., 1996. Nonlinear analysis for dynamic lateral pile response. *Soil Dyn Earthq Eng 15*, p. 233–244.
- Elhakim, A., 2005. *Evaluation of shallow foundation displacements using soil small-strain*, Atlanta: s.n.
- Escobar Valencia, E., Benz Navarrete, M., Gourvès, R. & Breul, P., 2013. Dynamic Cone Penetration Tests in Granular Media: Determination of the tip's Dynamic Load-Penetration Curve. *AIP Conf Proc 1542*, pp. 389–392.
- Gourvès, R., 1979. Méthode et dispositif pour la mesure in situ de caractéristique de déformation des sols. p. 14.
- Gourvès, R. & Barjot, R., 1995. Le pénétromètre dynamique léger PANDA. *In: 11ème Congrès Européens de Mécanique des sols et des travaux de fondations*, pp 83–88.
- Holeyman, A., 1988. Modelling of dynamic behaviour at the pile base. *Proc Third Int Conf Appl Stress Theory to Piles*, p. 174–185.
- Hölscher, P., Brassinga, H., Brown, M. & et al, 2012. *Rapid Load Testing on Piles Interpretation Guidelines*, Boca Raton, Florida: CRC Press Taylor & Francis Group.
- Karlsson, L., Lundberg, B. & Sundin, K., 1989. Experimental study of a percussive process for rock fragmentation. *Int J Rock Mech Min Sci 26*, pp. 45–50.
- Middendorp, P., Bermingham, P. & Kuiper, B., 1992. Statnamic load testing of foundation piles. *In: Proceedings of the Fourth International Conference on Application of Stress Wave Theory to Piles*, pp 581–582.
- Novak, M. & Beredugo, Y., 1972. Vertical vibration of embedded footings. *J Soil Mech Foudation Div ASCE 98*, p. 1291–1310.
- Omidvar, M., Iskander, M. & Bless, S., 2014. Response of granular media to rapid penetration. *Int J Impact Eng 66*, pp. 60–82.
- Omidvar, M., Malioche, J., Bless, S. & Iskander, M., 2015. Phenomenology of rapid projectile penetration into granular soils. *Int J Impact Eng 85*, p. 146–160.
- Pan, C., Zhang, R., Luo, H. & Shen, H., 2016. Baseline correction of vibration acceleration signals with inconsistent initial velocity and displacement. *Adv Mech Eng 8*, pp. 1–11.

- Paquet, J. & Briard, M., 1976. Contrôle Non Destructif Des Pieux En Béton. *Ann Inst Tech Batim Trav Publics*, p. 49–80.
- Poulos, H. & Carter, J., 2001. Foundations and retaining structures - research and practice. *Proc Int Conf Soil Mech Found Eng*, p. 80.
- Rausche, F., 1970. *Soil response from dynamic analysis and measurement on piles*, s.l.: Case Western Reserve University.
- Skempton, . A. W., 1951. *The bearing capacity of clays*. London, Building Research Congress, Div. I.
- Terzaghi, K., 1943. Die Berechnung der Durchlässigkeitsziffer des Toneseaus dem Verlauf der hydrodynamischen Spannungser schinungeen. *Sitzungsberichte de Akadennie der wissehsahaften*, 132, (Abt., II a).
- Tran, Q., Benz Navarrete, M. & Breul, P., 2019. Soil dynamic stiffness and wave velocity measurement through dynamic cone penetrometer and wave analysis. *Geotech Eng XXI Century Lessons Learn Futur challenges NP López-Acosta al 1–8*.

Probabilistic analysis of gyttja undrained strength from CPTU data for slope stability analysis

S. Rios, L. Sousa & A. Viana da Fonseca

CONSTRUCT-GEO, Faculty of Engineering, University of Porto, Porto, Portugal

P. Milheiro-Oliveira

CMUP, Faculty of Engineering, University of Porto, Porto, Portugal

O. Hededal

COWI A/S, Kongens Lyngby, Denmark

ABSTRACT: The design of an artificial peninsula near Copenhagen led to an extensive experimental campaign where a significant number of CPTU tests were performed. The CPTU data presented a significant dispersion due to material heterogeneity, which motivated a probabilistic analysis of the soft soil undrained strength. For that purpose, a probabilistic density function of the undrained strength ratio was estimated and introduced as input in a limit equilibrium slope stability analysis. This enables the evaluation of the probabilistic density function of the factor of safety, the probability of failure and the reliability index instead of a single deterministic factor of safety. This information can be used by the designer or project owner to choose between different solutions based on the required level of risk.

1 INTRODUCTION

1.1 Probabilistic analysis in geotechnical engineering

The main concern of an engineer when designing a certain structure is its safety. In geotechnical engineering, designers have to deal with the uncertainties related to the geological materials, the variability existing in nature, and simplified models. The conventional way of coping with these uncertainties, is to use a deterministic factor of safety. A factor of safety of 1.5, for example, is often used to account for the combination of uncertainties in the ground, in the analysis parameters and the calculation method. There is the general perception that a design with a safety factor higher than 1.5 has to be safe. However, a factor of safety of 1.5 represents a spectrum of failure probabilities, which depend on the uncertainties in the analysis. As shown by Lacasse and Nadim (1996) a design with a high factor of safety can have higher failure probability than another with a lower factor of safety, if the involved uncertainties are large. This means that a higher factor of safety does not imply a smaller risk, because it is affected by the uncertainties in the analysis (Lacasse et al., 2019).

At present, Eurocodes (Eurocode 0, CEN, 2002) are based in the statement that "a structure shall be designed and executed in such a way that it will,

during its intended life with appropriate degrees of reliability and in an economic way sustain all actions and influences likely to occur during execution and use, and remain fit for the use for which it is required".

As the deterministic scenario may underestimate the risk, it is recommended to adopt a reliability-based-design instead of the usual factor of safety. Basic reliability measures include probability of failure and reliability index. These can be used to verify the margin of safety defined as the difference between resistance and load. Reliability index refers to the number of standard deviations between the mean safety margin (M) and failure, being defined as:

$$\beta = \frac{M_{mean}}{SD} \quad (1)$$

where SD is the standard deviation of the safety margin.

The reliability index, β , can be related to the failure probability (p_f) by the expression:

$$p_f = \Phi(-\beta) \simeq 10^{-\beta} \quad (2)$$

where Φ represents the cumulative distribution function of the standardised normal distribution.

This work presents an attempt of applying a probabilistic approach to describe the undrained strength ratio in a slope stability situation.

1.2 Lynetteholmen project

The case study presented in this work concerns the construction of an artificial peninsula, built outside the Copenhagen harbor, in an area called Lynetteholm. This artificial peninsula will span over 282 hectares over the North of Refshaleøen and will be delimited to the north by Nordhavn and to the west by the Trekroner. The main purpose for its construction is to prevent the city of Copenhagen from the occurrence of floods and storm surges. In fact, it is predicted that by the end of 2100, the sea level will rise between 54 cm (under the “Paris agreement”) and 74 cm (“business as usual” scenario), according to the Geological Survey of Denmark and Greenland. Lynetteholm is expected to be completed in 2070. The hope is that the first homes can begin building in 2035.

The artificial peninsula will be mainly built with hydraulic fill contained by earth supporting structures such as sheet pile walls and embankments. Then perimeter design layout will be arranged with sand and rock in the front to form beaches.

2 SITE CONDITIONS

2.1 Site geology

Formerly below the Scandinavian Ice Shield, the area has now an upper layer of filling material resulting mainly from dredging, although ashes, slags, rubble, concrete rubble and other man made components can be included. Mixed with the fill or immediately below, post-glacial marine deposits are found consisting mainly in gyttja. On top of the gyttja layers, slag that was thrown overboard from steamships is frequently found. Gyttja is a very soft and odorous soil that originates from remains of plants and animals rich in fats and proteins. The material consists of both organic matter and inorganic (clay, silt, fine sand, shells or limescale). During its formation, varying quantities of inorganic material are mixed with the organic and when examined, a lower loss of filament and water content is found which is common for peat (Larsson, 1990).

2.2 Geotechnical data

COWI carried out extensive geotechnical studies in order to obtain factual geological, geotechnical and hydrogeological data for the area. The geotechnical studies included 301 CPTU tests and 191 boreholes. Based on boreholes and CPTU, a thickness map was developed (Figure 1) indicating the thickness of soft postglacial deposits, including gyttja, peat and clay. The thickness of the organic post-glacial deposits is greatest in the former meltwater valleys, where up to 6-9 m thick layers of gyttja and peat were taken.

CPTU data (Figure 2) revealed low values of the corrected cone resistance (q_t) defined as follows:

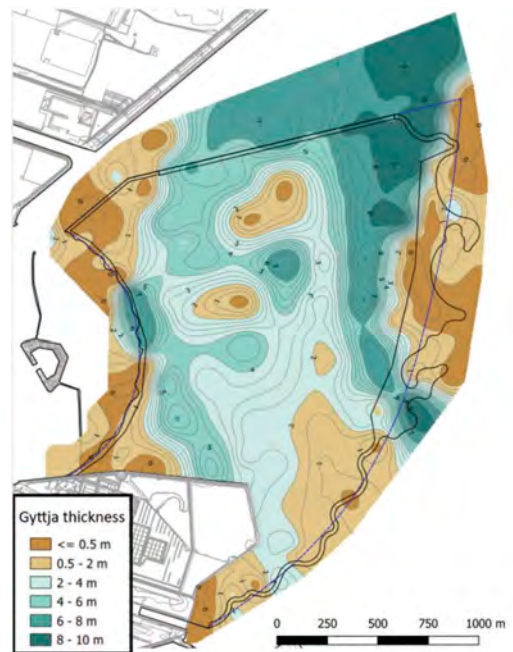


Figure 1. Gyttya thickness map.

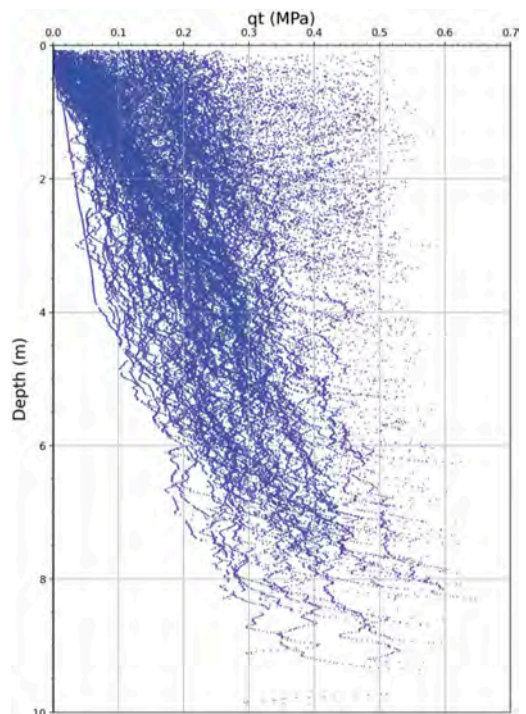
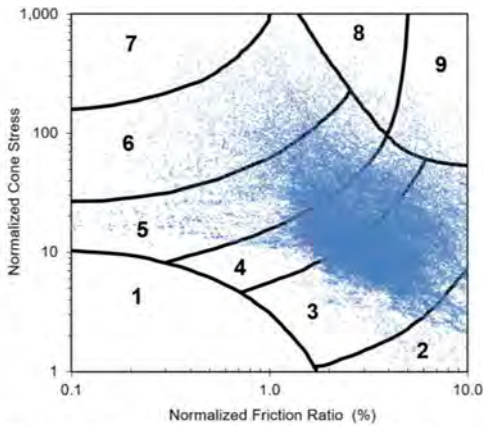


Figure 2. Corrected cone resistance (q_t) evolution with depth for all CPTU data.

$$q_t = q_c + u_2(1 - a) \quad (3)$$

where q_c is the tip cone resistance, u_2 is the pore pressure measured behind the cone, and a is the area factor calculated as the ratio of the cross sectional area of the load cell, A_n , by the projected area of the cone, A_c , ($a=A_n/A_c$). In this case, two different cones were used for the CPTU campaign. A number of 193 tests were conducted by a piezocone with $a=0.6$ and 106 tests with $a=0.8$.

Figure 2 plots q_t values with depth, ranging in the interval of 0 to 0.6 MPa, where a significant dispersion is observed. To better understand the type of material present, the results were analysed by the unified approach proposed by Robertson (2009) which have indicated a clayey/silty behavior with no relevant sensitivity (Figure 3)



1 Sensitive, fine grained	6 Sands – clean sand to silty sand
2 Organic soils - clay	7 Gravely sand to dense sand
3 Clay – silty clay to clay	8 Very stiff sand to clayey sand
4 Silt mixtures – clayey silt to silty clay	9 Very stiff fine grained
5 Sand mixtures – silty sand to sandy silt	

Figure 3. CPTU data plotted in the Robertson (2009) soil behavior chart.

3 UNDRAINED STRENGTH

3.1 Laboratory data

Based on 5 boreholes, 15 valid anisotropically consolidated undrained triaxial compression tests (CAUC) were conducted to determine the gytja undrained shear strength (Table 1).

From that data summarized in Table 1, the evaluation of the undrained shear strength ($C_{U,TC}$) was plotted against the vertical effective stress after the consolidation, σ'_{v0} , obtaining the following linear regression:

$$C_{U,TC} = 0.26 \cdot \sigma'_{v0} + 5.4 \text{ (kPa)} \quad (4)$$

Table 1. Undrained strength obtained in the triaxial tests.

Triaxial NO.	$C_{U,TC}$ (kPa)	σ'_{v0}	C_u/σ'_{v0}
BH_P_34_1	4.2	12.1	0.35
BH_P_34_2	14.3	41.0	0.35
BH_P_34_3	58.5	186.3	0.31
BH_P_33_1	16.3	28.3	0.58
BH_P_33_2	21.8	58.3	0.37
BH_P_33_3	60.5	205.4	0.29
BH_P_25_3.1	6.5	12.0	0.54
BH_P_25_3.2	16.5	44.0	0.38
BH_P_25_3.3	60.5	185.0	0.33
BH_P_25_8.1	16.0	33.0	0.48
BH_P_25_8.2	84.0	217.0	0.39
BH_P_25_8.3	63.5	214.0	0.30
BH_P_84_1	13.5	29.3	0.46
BH_P_84_2	22.0	44.0	0.50
BH_P_84_3	47.5	195.0	0.24

3.2 Undrained strength from empirical correlations

Mayne and Peuchen (2018) have proposed an empirical correlation to obtain the parameter N_{kt} from the B_q parameter of the CPTU interpretation (equation 5)

$$N_{kt} = 10.5 - 4.6 \cdot \ln(B_q + 0.1) \quad (5)$$

B_q being given by equation (6) where q_{net} is the net cone resistance ($q_{net} = q_t - \sigma_{v0}$),

$$B_q = \frac{(u_2 - u_0)}{q_{net}} \quad (6)$$

N_{kt} can then be used to calculate the undrained strength using the following well-known relation:

$$C_u = \frac{q_{net}}{N_{kt}} \quad (7)$$

Considering only the CPTU tests performed near the boreholes where the samples for the triaxial tests were retrieved and the CPTU data at the depths at which those samples were taken, the following results were obtained (Table 2).

It is clear from this data that much higher undrained strength ratios (C_u/σ'_{v0}) were obtained from the CPTU data interpreted with Mayne and Peuchen (2018) correlation (Table 2) in comparison with the laboratory data presented in Table 1. These values are also very high taking into account that the soil under study concerns a normally consolidated material where an undrained strength ratio between 0.2 and 0.4 was expected. This might be explained by two main reasons: i) this empirical correlation has not been developed for gytja; ii) the site is very

Table 2. Undrained strength obtained in the CPTU tests by the Mayne and Peuchen (2018) correlation.

N_{kt}	C_u (kPa)	C_u/σ'_{v0}
14.3	9.5	0.91
15.6	8.3	0.77
15.7	8.3	0.86
13.3	17.8	0.80
13.9	19.5	0.90
13.5	17.8	0.82
17.5	7.6	0.86
15.6	9.4	0.88
14.8	10.9	0.93
13.3	18.2	0.66
13.1	15.4	0.59
13.8	15.9	0.60
11.7	23.7	1.04
12.0	21.4	1.02
12.2	23.3	1.05

heterogeneous where it is possible that gytija is mixed with other man-made materials.

3.3 Proposed approach

In these conditions, an average N_{kt} value was adopted considering only the five CAUC tests performed with lower effective stresses (<60 kPa) considered more representative of the effective stresses acting at gytija according to Figure 1. To avoid differences between effective stresses of CPTU tests and the effective stresses of CAUC test, the undrained strength coming from CAUC tests was calculated with equation (4) for the depth at which the CPTU data was taken. The results are presented in Table 3 from where an average N_{kt} value of 19.2 was taken (Sousa, 2020).

Table 3. N_{kt} values obtained in 5 CAUC tests.

Borehole	$C_{u,TC\ avg}$ (kPa)	CPTU	$q_{net, avg}$ (MPa)	N_{kt}
BH_P_25	7.7	CPT_A_235	0.133	17.2
BH_P_33	12.5	CPT_A_193	0.208	16.6
BH_P_34	11.2	CPT_A_179	0.237	21.2
BH_P_84	8.1	CPT_P_84	0.135	16.7
BH_P_84	11.3	CPT_P_84	0.277	24.5

Then, the undrained strength obtained in all the 80 000 CPTU measurements was calculated with this N_{kt} value using equation (7). The results are plotted in Figure 4, which represents the histogram of all the undrained strength ratio values.

It is clear that, even using a quite high N_{kt} value, there are still a significant number of undrained strength ratios above 0.4. This may be associated to the

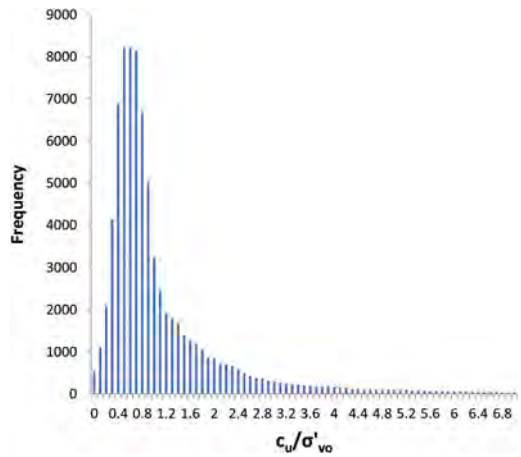


Figure 4. Histogram of all the undrained strength ratio values.

heterogeneity of the material and the presence of man-made materials, namely slag, mixed with the soft soil.

4 PROBABILISTIC ANALYSIS

For the data presented in Figure 4, a probabilistic density function was fitted using a Lognormal distribution (equation (8)),

$$f(x) = \frac{e^{-\frac{(\ln((x-\theta)/m))^2}{2\sigma^2}}}{(x-\theta)\sigma\sqrt{2\pi}} \quad (8)$$

where σ is the Lognormal standard deviation (or shape parameter), m is the Lognormal mean (or scale parameter) and θ is the offset of the Lognormal mean (or the location parameter). This case, the following estimates of the parameters were obtained to adjust the histogram of Figure 4: $\sigma=0.852$, $m=0.720$ and $\theta=0.04$, as presented in Figure 5.

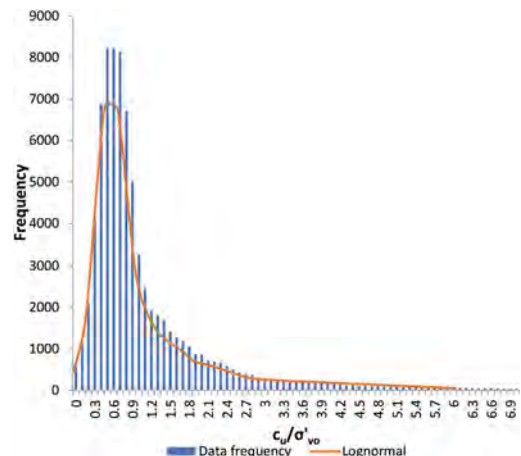


Figure 5. Lognormal fit to the undrained strength ratio.

5 SLOPE STABILITY ANALYSIS

The probabilistic distribution of the undrained strength as described above was included in a slope stability analysis using the limit equilibrium software SLOPE/W from GEOSTUDIO®. The aim of this work was to analyze the gytija stability during its excavation. The retaining support structures built in the perimeter of the area to contain the hydraulic fill, will be founded in the layers below gytija. For this reason, the gytija will be excavated in those areas. Slope stability analysis are needed because submarine landslides caused by failures in the gytija layer can cause tsunamis and/or disturbances in the submarine environment with impact on its biodiversity.

In these conditions, limit equilibrium analysis using the Morgenstern-Price method were performed considering the gytija undrained strength as a random variable whose distribution is the one indicated in equation (8). The probabilistic procedure used herein was the Monte Carlo method, integrated in SLOPE/W, considering a total amount of 500 MC samples. This was applied to a slope of 9 m high and 45° of inclination, as illustrated in Figure 6.

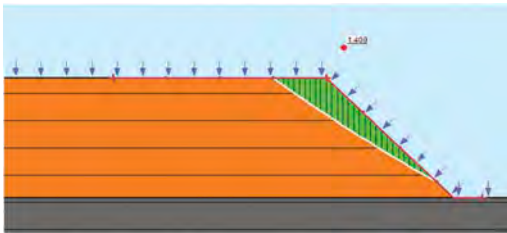


Figure 6. Slope used in the gytija stability analysis.

The results of the probabilistic distribution of the factor of safety (FS) are indicated in Figure 7, where a minimum FS of 1.43 and a maximum FS of 9.40 were obtained with an average of 2.64. In addition, a reliability index of 1.45 was obtained for this case.

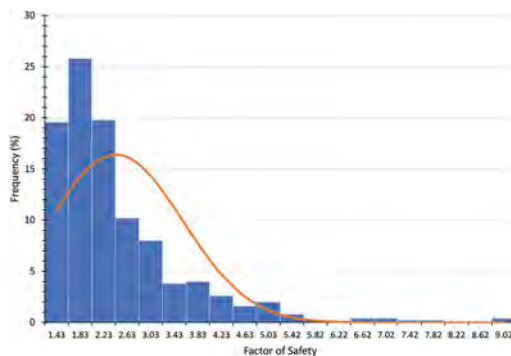


Figure 7. Probabilistic density function of the factor of safety.

6 CONCLUSIONS

Geotechnical engineering design is progressively moving from a deterministic approach to a probabilistic approach. This enables the consideration of natural variability and the uncertainties associated to geotechnical parameters. It also enables to quantify the probability of failure and the reliability index associated to a certain design, which can be used by designers or project owners to decide upon different options depending on the required level of risk. In this work, the large amount of CPTU data performed for the construction of an artificial peninsula close to Copenhagen was used to perform a probabilistic analysis of the soft soil undrained strength ratio. The probabilistic density function of this variable was then introduced in a slope stability analysis by the limit equilibrium method. The results indicated that for a slope of 9 m high and 45° of inclination, the reliability index associated to the probability of failure was 1.45, which is quite low. This means that although a deterministic factor of safety of 1.4 was obtained, the reliability associated with the studied design is low.

ACKNOWLEDGMENTS

This work was financially supported by: Base Funding - UIDB/04708/2020 of the CONSTRUCT - Instituto de I&D em Estruturas e Construções - funded by national funds through the FCT/MCTES (PIDDAC) and by UTD/MAT/00144/2019. It also received European Commission funds from the ERASMUS program. The authors express gratitude to By og Havn A/S for permission to use geotechnical data from the Lynetteholmen project.

REFERENCES

- Casagrande, A. (1965). The role of the 'calculated risk' in earthwork and foundation engineering. 91.
- CEN (2002). Eurocode 0 - basis of structural design. European Committee for Standardization, Brussels
- Khan, F., & Malik, A. (2013). Probability and sensitivity analysis of the slope stability of Naulong dam. Pakistan Journal of Engineering and Applied Sciences, vol 13, 54-64.
- Lacasse, S., Nadim, F. 1996. Uncertainties in characterizing soil properties. Uncertainty in the Geologic Environment: From Theory to Practice (Uncertainty '96), ASCE GSP 158 (49-75).
- Lacasse, S., Nadim, F., Liu, Z.Q., Eidsvig, T.M.H., Le, T. M.H., Lin, C.G. (2019). Risk assessment and dams - Recent developments and applications. Proceedings of the XVII ECSMGE- Geotechnical Engineering foundation of the future, Reykjavik, Iceland
- Larsson, R. (1990). Behavior of organic clay and gytija. Rapport-Statens geotekniska institut, 38.
- Mayne, P., & Peuchen, J. (2018). Evaluation of CPTU N_{kt} cone factor for undrained strength of clays. Proceedings

- of the Cone Penetration Testing Conference, Delft, Netherlands, 423–429.
- Peck, R. B. (1969). Advantages and Limitations of the Observational Method in Applied Soil Mechanics. *Géotechnique*, 19(2), 171–187. doi:10.1680/geot.1969.19.2.171
- Robertson, P.K. (2009). Interpretation of cone penetration tests —a unified approach. *Can. Geotech. J.*, 46(11), 1337–1355
- Sousa, L. (2020). Probabilistic undrained strength evaluation of soft soil for slope stability design. MSc Thesis presented to the Faculty of Engineering of University of Porto, Portugal

Monitoring ground improvement using in situ tests in Guayaquil, Ecuador

F. Ripalda, D. Falquez & D. Besenon

ESPOL Polytechnic University, Escuela Superior Politécnica del Litoral, ESPOL, Department of Earth Sciences, Guayaquil, Ecuador

R. Luque

Geosísmica, Guayaquil, Ecuador

F. Illingworth

Subterra, Guayaquil, Ecuador

S. Amoroso

*University of Chieti Pescara, Pescara, Italy
Istituto Nazionale di Geofisica e Vulcanologia, Italy*

ABSTRACT: The present work describes the use of the seismic dilatometer test (SDMT) and the piezocone test (CPTu), to assess the effects of ground improvement at a wastewater treatment plant in Guayaquil, Ecuador. The ground improvement consisted of 15 m-long, 0.55 m-diameter and 2 m-spacing stone columns built with vibro-replacement technique. The tests were carried out both in natural and in treated soils to compare the variation of the geotechnical parameters in the analyzed deposits. The results show specific sensitivity of the DMT over the CPTu tests to the ground improvement into the layer composed of sands and sandy silts, while VS values show a limited increase in the treated area.

1 INTRODUCTION

Ground improvement involves different techniques to modify soil response under different conditions. Ground modification performance is based on assessing problematic soils, liquefaction potential, soil instability, insufficient bearing capacity and excessive settlement, seepage. U.S. Army Corps of Engineers (1999).

Mitchell (2008) discussed the applications and limitations of these densification methods, and the author noted that the degree of improvement given by the deep dynamic compaction, vibro-compaction and blasting is greater in clean sands since it decreases as the fines content (FC) increases. Nevertheless, several studies have documented mitigation works using various FC values (including rather high percentages), highlighting an improvement given by the vibro-replacement stone columns, Mackiewicz & Camp (2007) used an improvement index (I_i), given by the ratio between the cone resistance (q_c) after and before the treatment minus one, to provide an improvement of $0.3 < I_i < 2.8$ for $FC < 5\%$, and of $0 < I_i < 1.6$ for $15\% < FC < 40\%$. (Luehring et al. 2001) showed an increase of 95% for the corrected SPT blow count (N_{160}), and 180% for the normalized corrected cone

resistance q_{c1N} , using vibro-replacement stone columns in combination with vertical drains in deposits with $FC < 65\%$. Mitchell & Wentz (1991) showed a 100% increase for the corrected cone resistance for overburden stress, (q_{c1}), and a 45% increase for the SPT corrected penetration resistance, (N_1)₆₀, when comparing pre and post-treatment results in soil layers with $FC < 55\%$. Vibro-replacement stone columns installation may have the double beneficial effect to cause densification of the surrounding soil during installation and facilitate the dissipation of the excess of pore water pressure developed during an earthquake, by providing a shorter path of drainage, Adalier & Elgamal (2004).

Therefore, the effectiveness verification of the improvement using in situ tests becomes relevant since these investigations allow a quick assessment, which compares selected geotechnical parameters obtained before and after the treatment. Numerous authors (Schmertmann 1986, Mackiewicz & Camp 2007, Mitchell 2008, Monaco et al. 2014, Bałachowski & Kurek 2015, Wotherspoon et al. 2015, Massarsch & Fellenius 2019, Massarsch et al. 2020) evaluate the change of the soil characteristics using different in situ tests and their parameters: SPT blow count N_{SPT} in the standard penetration test (SPT),

horizontal stress index K_D and constrained modulus M in the flat dilatometer test (DMT), corrected cone resistance q_t in the piezocone penetrometer test (CPTu). Other studies (e.g., Wotherspoon et al. 2015, Hwang et al. 2017, Comina et al. 2021) have applied shear wave velocity V_S in the geophysical measurements provided by invasive or non-invasive tests (e.g., seismic piezocone SCPTu, seismic dilatometer SDMT, down-hole DH, cross-hole CH, multichannel analysis of surface waves MASW). Moreover, several research discusses the change in the at-rest lateral earth pressure coefficient K_0 , the overconsolidation ratio OCR and the ratio M/q_t when monitoring the densification effectiveness and the lateral stress increase. A combination of CPT and DMT tests is performed to estimate the parameters mentioned above, as suggested in previous studies (e.g., Baldi et al. 1986, Marchetti et al. 2001, Amoroso et al. 2018, 2020, Massarsch et al. 2020)

The present study describes the effects of ground improvement using SDMT and CPTu tests. In this regard, CPTu and SDMT tests and V_S measurements were executed in natural and treated soils, to compare the geotechnical parameters, to assess liquefaction before and after treatment.

2 COMBINATION OF SDMT AND CPTU FOR MONITORING GROUND IMPROVEMENT

Single-parameters derived from SDMT and CPTu tests can detect the modification in soil characteristics due to improvement works. As stated by various authors (e.g. Schmertmann 1986, Balachowski & Kurek 2015, Amoroso et al. 2018, 2020, Massarsch & Fellenius 2019, Massarsch et al. 2020), these parameters can be identified in the horizontal stress index K_D and the constrained modulus M from DMT, the corrected cone resistance q_t (or the cone resistance q_c) and the relative density D_R from CPT. K_D is directly derived from the corrected DMT membrane lift-off pressure reading and contains information about the stress history of the soil. Concurrently M is a function of the three DMT intermediate parameters (horizontal stress index K_D , dilatometer modulus E_D and material index I_D). q_t (or q_c) is a direct measurement from CPT, while D_R is usually based on correlations as a function of the cone resistance and effective stress, Juang et al. (1996). According to previous ground improvement studies related to densification techniques (e.g. Massarsch & Fellenius 2002, 2019, Massarsch et al. 2019), the horizontal stress also increases after compaction, making K_D (and therefore M) more sensitive than q_t (and consequently D_R) to detect the modifications induced by the treatment.

Moreover, the coupled CPT-DMT parameters, such as K_0 , OCR, can help identify the treatment effectiveness in sandy soils. The present research estimated K_0 using the more recent relationship proposed by Hossain & Andrus (2016):

$$K_0 = 0.72 + 0.456 \log OCR + 0.035K_D - 0.194 \log^{qc/\sigma'_{v0}} \quad (1)$$

where σ'_{v0} is the vertical effective stress.

To estimate OCR in sands the approximation by Monaco et al. (2014) was used:

$$OCR = 0.0344(M/q_t)^2 - 0.4174(M/q_t) + 2.2914 \quad (2)$$

3 IN SITU TESTS

The results presented in this study belong to a trial site located within a wastewater treatment plant (WTP) in Guayaquil, Ecuador. Figure 1, shows the location where CPTu and SDMT tests were performed before the stone columns (SC) installation, natural soil (NS), and after SC installation, treated soil (TS), up to 16-20 m depth. NS soil testing is identified as CPTu1_NS and SDMT1_NS, while surveys after SC installation are detected as CPTu2_TS and SDMT2_TS. The SC were in a staggered arrangement with 2 m spacing. Additional information regarding the NS condition was obtained from the borehole, SPTs (SPTP3_NS) and CPTu tests (CPTu14_NS) performed during the WTP construction.

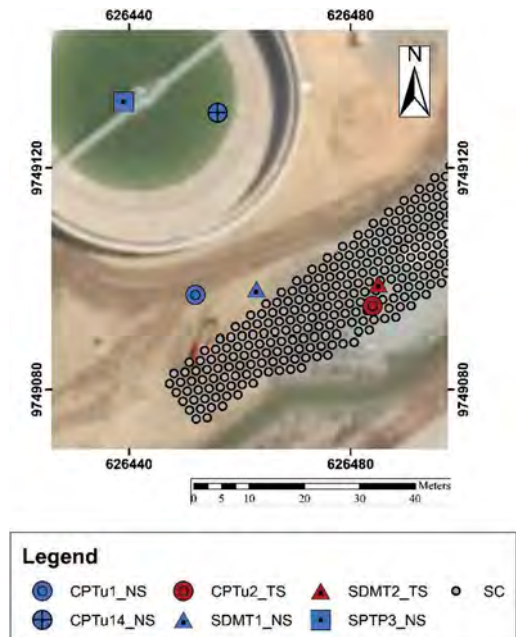


Figure 1. Location of the water treatment plant at “Las Esclusas”, in-situ tests and stone columns.

For the execution of CPTus and SDMTs, the shallow compacted fill layer ($\approx 0.6-0.8$ m thick) was removed, to prevent damage to the geotechnical

equipment. Table 1 summarizes the basic information of the in-situ tests used for verifying the ground improvement effectiveness. The ground-water table (GWT) fluctuations, at the trial site, were strongly influenced by the Guayas river tide, following the Navy Oceanographic and Antarctic Institute measurements, INOCAR (2021).

Table 1. Summary information of the in situ tests at the trial site.

Field test	Depth (m)	GWT depth* (m)
SPTP3_NS	19.0	2.0
CPTu14_NS	20.8	2.7
SDMT1_NS	20.4	3.4
SDMT2_TS	20.6	3.4
CPTu1_NS	17.6	3.8
CPTu2_TS	19.0	3.8

* Note: Measured from the ground surface post filling.

3.1 Geotechnical description

Figure 2 summarize the soil profile in both soil conditions using CPTu and SDMT tests at the Guayaquil trial site. Beneath the shallow fill, the soil is variable, but four clearly defined layers can be observed. The first layer is approximately 2 m thick and varies from silt to clay, as described by: the soil behavior index (I_c) profile that intercalates between 2.6 and 3.4, the material index (I_D) values which are between 0.2 and 1.1. Underlying this layer, loose to medium dense sand mixtures ($2\text{MPa} < q_t < 8\text{MPa}$; $2 < K_D < 9$) are present with a maximum depth of ≈ 10 m. These non-plastic sands and silty sands are mainly characterized by $I_c < 2.6$ and $I_D > 1.2$. A lens of variable thickness, comprised of silt mixtures ($2.6 < I_c < 3.0$, $0.6 < I_D < 1.1$) is present within the sandy layer between ≈ 7 and 10 m depth. Finally, below 10-11 m depth, normally to moderately overconsolidated clays are encountered, according to OCR approximation by Marchetti et al. (2001). This finding associates the following DMT and CPTu parameters: $2.2 < K_D < 3.3$, with $3.1 < I_c < 3.9$, $0.2 < q_t < 2.0$ and $0.2 < I_D < 0.6$.

4 GROUND IMPROVEMENT

Figures 2 and 3 show the variation of the CPTu, DMT and combined (CPTu and SDMT) parameters in natural soil (NS) and treated soil (TS), estimated according to Robertson & Cabal (2015). The relative density (D_R) estimation is based on the correlations proposed by Kulhawy & Mayne (1990). I_c profiles present a very slight variability of the soil before and after treatment, which makes quite comparable the data within the depth of the SC improvement where

the silty sand to sandy silt layer ($I_c < 2.6$) is located. However, for some depth intervals between 4 and 10 m, q_t ($\approx 4.2\text{-}6$ m, 8-9 m, 9.6-10.4 m depth), and D_R ($\approx 4.5\text{-}6$ m, 8-9 m depth) values in the NS are somewhat higher than in TS. This rise is observed when the I_c increases in the TS, and it behaves more like fine-grained soil. Figure 3 also compares the CPTu- D_R values with the ones evaluated from SPT, Skempton (1986). The D_R SPT-based values in the NS are in good agreement with the related CPTu ones from ≈ 6 to 8 m depth, while between 8 and 11 m depth, the SPT-based method overpredicts the relative density. The SPT-based overestimations of D_R can be attributed to the lens of silt mixtures detected only by CPTu and SDMT.

The DMT parameters, were calculated using the Marchetti et al. (2001) formulae. The equilibrium pore pressure, u_0 , obtained from the third DMT pressure reading (p_z) into the sandy layers, well determined the GWT location. The effectiveness of the treatment is noticeable from ≈ 2 to 6 m depth, by looking at K_D and M and profiles (Figures 2, 3); in this depth range, $I_D > 0.6$ predominate in both soil conditions. The increase in K_D profile is clearly defined in this depth interval and a 52% increment is observed after the treatment. The shear wave velocity V_s (Figure 3) also provides some increase after improvement, but limited between 4 and 6 m. A specific lateral soil heterogeneity is distinguishable in the NS and TS, I_D profiles between ≈ 6 to 8 m depth: the TS exhibits a fine-grained soil behavior, considering the lower I_D values ($0.3 < I_D < 1.2$ corresponding to silty clay to silt), while the NS of the same layer results mostly silty-sandy ($1.2 < I_D < 2.3$). This response helps to understand why for the same depth interval, the horizontal stress index K_D and the constrained modulus M are much lower despite the SC installation. The analysis of CPTu and DMT combined parameters is displayed in Figure 3 to monitor ground improvement effectiveness. The OCR and K_0 estimations were performed both in fine-grained and incoherent soils. Specifically, for $I_D < 1.2$, OCR and K_0 were estimated by DMT using Marchetti et al. (2001) formulae, while for sandy layers ($I_c < 2.6$ and $I_D > 1.2$) the combined CPT-DMT approach was used according to Equation 2 from Monaco et al. (2014) for OCR and to Equation 1 from Hossain & Andrus (2016) for K_0 . The OCR and K_0 profiles detect the effectiveness of the SC treatment between ≈ 2.6 and 6.6 m depth. Below 6.6 m, the NS and TS trend remains unchanged despite the SC installation.

Table 2 summarizes the average test results of the single and combined parameters in the layer where the increase was better noticed for $I_c < 2.6$ and $I_D > 1.2$, approximately between 3.2 and 6.6 m depth. The improvement was calculated by relating the difference between TS and NS to NS results, expressed as a percentage. The CPTu conventional indicators of improvement show an increment of 6% for q_t and 7% for D_R , while for

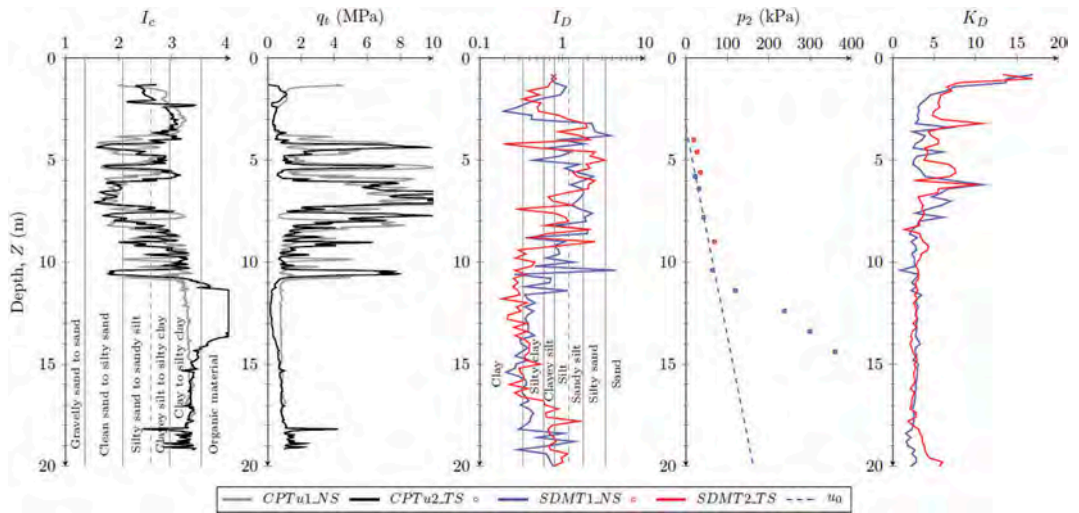


Figure 2. CPTu and SDMT basic parameters in both soil conditions (natural and treated soil) at the Guayaquil trial site.

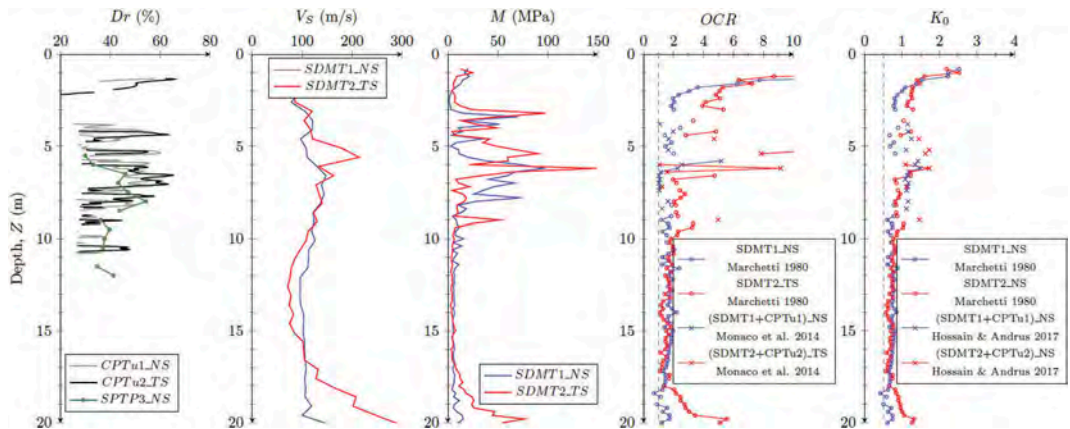


Figure 3. CPTu and SDMT estimated parameters in terms of D_R , V_S , M , OCR and K_0 at the Guayaquil trial site.

Table 2. Summary of average parameters (pre and post treatment) between 3.2 and 6.6 m depth: q_t , D_R , K_D , M , V_S , OCR , K_0 .

	q_t (MPa)	D_R (%)	K_D	M (Mpa)	V_S (m/s)	OCR	K_0
NS	5.0	42.5	5.0	43.6	121.2	3.1	1.3
TS	5.3	45.7	6.2	61.9	152.8	6.1	1.5
Inc. (%)	6.0	7.6	22.4	42.0	26.1	98.4	15.8

the SDMT parameters, K_D increased 22%, M 42% and V_S 26%. For the combined CPTu and SDMT parameters, K_0 increased just 16%, while OCR increased 98%

5 CONCLUSIONS

Despite the length of the SCs, the effectiveness of the treatment resulted noticeable only between 3.2 to 6.6 m depth, where the sand mixtures were detected by in situ tests. Below this layer a lens of silt mixtures, with higher FC (up to 46%) approximately between 7 to 10 m depth, and of a cohesive soil layer, from 10-11 m depth, were identified.

The evaluation of the soil improvement between 3.2 to 6.6 m depth was mainly detected by using the combined CPTu and SDMT parameters, with a 98 % increment in OCR and 15% increment in K_0 . The relatively low increment in K_0 can be attributed to the high initial K_0 condition in NS ($K_0 \approx 1.27$), as already noticed by Schmertmann (1985). In the CPTu based effectiveness assessment, q_t and D_R

have a similar increase (6% and 7.5% respectively), although the NS and TS were related to quite homogeneous subsoil, as detectable looking at I_c . Furthermore, SDMT single parameters, K_D , M , V_S , provided a more evident SC improvement, even still limited, 22%, 42% and 26% respectively. Therefore, at the Guayaquil trial site the densification provided by the SCs resulted merely perceived by the CPTu tests probably also due to the lateral soil variability.

ACKNOWLEDGEMENT

Special thanks to Studio Prof. Marchetti (Italy) for kindly providing the SDMT apparatus.

Special thanks also to Hidalgo e Hidalgo S.A. for sharing information for the present research.

REFERENCES

- Adalier, K. & Elgamal, A. (2004) 'Mitigation of liquefaction and associated ground deformations by stone columns', *Engineering Geology*, 72(3–4), pp. 275–291.
- Amoroso, S., Rollins, K., Monaco, P., Holtrigter, M. & Thorp, A. (2018) 'Monitoring ground improvement using the seismic dilatometer in Christchurch, New Zealand', *Geotechnical Testing Journal*, 41(5), pp. 946–966.
- Amoroso, S., Rollings, K., Andersen, P., Gottardi, G., Tonni, L., García Martínez, M., Wissman, K., et al. (2020) 'Blast-induced liquefaction in silty sands for full-scale testing of ground improvement methods: Insights from a multidisciplinary study', *Engineering Geology*, 265, p. 105437.
- Balachowski, L. & Kurek, N. (2015) 'Vibroflotation Control of Sandy Soils Using DMT and CPTU', in *The 3rd International Conference on the Flat Dilatometer*, pp. 185–190.
- Baldi, G., Bellotti, R., Ghioma, V., Jamiolkowski, M., Marchetti, S. & Pasqualini, E. (1986) 'Flat Dilatometer Tests in Calibration Chambers', in *Proc. In Situ '86 ASCE Spec. Conf. on Use of In Situ Tests in Geotechnical Engineering*. Virginia Tech, Blacksburg, pp. 431–446.
- Comina, C., Mandrone, G., Arato, A., Chicco, J., Duò, E. & Vacha, D. (2021) 'Preliminary Analyses of an Innovative Soil Improving System by Sand/Gravel Injections—Geotechnical and Geophysical Characterization of a First Test Site', *Engineering Geology*, 293, p. 106278.
- Hossain, A. M. & Andrus, R. D. (2016) 'At-Rest Lateral Stress Coefficient in Sands from Common Field Methods', *Journal of Geotechnical and Geoenvironmental Engineering*, 14(12), pp. 06016016–1–06016016–5.
- Hwang, S., Roberts, J., Stokoe, K., Cox, B., van Ballegooy, S. & Soutar, C. (2017) 'Utilizing Direct-Push Crosshole Seismic Testing to Verify the Effectiveness of Shallow Ground Improvements: A Case Study Involving Low-Mobility Grout Columns in Christchurch, New Zealand', in *Proceedings of Grouting 2017*. Honolulu, Hawaii, pp. 415–424.
- INOCAR (2021) Instituto Oceanográfico y Antártico de la Armada - Tabla de mareas puertos del Ecuador (Oceanographic and Antarctic Institute of the Navy - Table of tides of ports of Ecuador) . See <https://www.inocar.mil.ec/web/index.php/productos/tabla-mareas#busqueda-de-datos-de-mareas> (accessed 2021 Mar 22).
- Juang, C., Huang, X., Holtz, R. & Chen, J. (1996) 'Determining relative density of sands from CPT using fuzzy sets', *Journal of Geotechnical Engineering*, 122(1), pp. 1–6.
- Kulhawy, F. H. & Mayne, P. W. (1990) Manual on estimating soil properties for foundation design. (No. EPRI-EL-6800). Electric Power Research Inst., Palo Alto, CA (USA); Cornell Univ., Ithaca, NY (USA). Geotechnical Engineering Group.
- Luehring, R., Snorteland, N., Stevens, M. & Mejia, L. (2001) Liquefaction Mitigation of a Silty Dam Foundation Using Vibro-Stone Columns and Drainage Wicks: A Case History at Salmon Lake Dam. *Water Oper. Manage. Bull.* (198): 1–15
- Mackiewicz, S. M. & Camp, W. M. (2007) 'Ground Modification: How Much Improvement?' *Geo-Denver 2007*, Denver, Colorado, United States, p.9.
- Marchetti, S., Monaco, P., Totani, G. & Calabrese, M. (2001) The Flat Dilatometer Test (DMT) in Soil Investigations— A Report by the ISSMGE Committee TC16. *Proceedings of In Situ 2001, International Conference on In Situ Measurement of Soil Properties*, Bali, Indonesia. ISSMGE, London, UK, p.42.
- Massarsch, K. & Fellenius, B. H. (2019) 'Evaluation of vibratory compaction by in situ tests', *ASCE Journal of Geotechnical and Geoenvironmental Engineering*, 145(12), pp. 1–15.
- Massarsch, K., Wersäll, C. & Fellenius, B.H. (2019) 'Horizontal stress increase induced by deep vibratory compaction', in *Proceedings of the Institution of Civil Engineers: Geotechnical Engineering*, pp. 1–26.
- Massarsch, K., Wersäll, C., Fellenius, B.H., Bałachowski, L., Kurek, N. & Konkol, J. (2020) 'Discussion: Horizontal stress increase induced by deep vibratory compaction', *Proceedings of the Institution of Civil Engineers: Geotechnical Engineering*, 173(4), pp. 370–375.
- Massarsch, K. & Fellenius, B. H. (2002) 'Vibratory compaction of coarse-grained soils', *Canadian Geotechnical Journal*, 39(3), pp. 695–709.
- Mitchell, J. K. (2008) 'Mitigation of liquefaction potential of silty sands', in Symposium Honoring Dr. John H. Schmertmann for His Contributions to Civil Engineering at Research to Practice in Geotechnical Engineering. New Orleans, Louisiana, United States, pp. 433–451.
- Mitchell, J. K. & Wentz, F. J. (1991) Performance of Improved ground. During the Loma Prieta Earthquake, *UCB/EERC-91/12*, Earthquake Engineering Research Center, University of California, Berkeley, p. 100.
- Monaco, P., Amoroso, S., Marchetti, S., Marchetti, D., Totani, G., Cola, S. & Simonini, P. (2014) 'Overconsolidation and Stiffness of Venice Lagoon Sands and Silts from SDMT and CPTU', *ASCE Journal of Geotechnical and Geoenvironmental Engineering*, 140, pp. 215–227.
- Robertson, P. & Cabal, K. (2015) *Guide to Cone Penetration Testing for Geotechnical Engineering*. 6th edn. Signal Hill, CA: Gregg Drilling & Testing.
- Schmertmann, J., Baker, W., Gupta, R. & Kessler, K. (1986) 'CPT/DMT quality control of ground modification at a power plant', in *Specialty Conference-In Situ '86*. Blacksburg, VA, pp. 985–1001.

- Schmertmann, J. H. (1985) *Measure and Use of the In Situ Lateral Stress, Practice of Foundation Engineering. A Volume Honoring Jorj O. Osterberg*. The Department of Civil Engineering, Northwestern University, pp. 189–213.
- Skempton, A. W. (1986) ‘Standard penetration test procedures and the effects in sands of overburden pressure, relative density, particle size, ageing and overconsolidation’, *Géotechnique*, 36(3), pp. 425–447.
- U.S. Army Corps of Engineers (1999) Guidelines on Ground Improvement for Structures and Facilities, ETL 1110-1-185. Available at: <http://usacetechnicalletters.tpub.com/ETL-1110-1-185/ETL-1110-1-1850002.htm> (Accessed: 6 October 2020).
- Wotherspoon, L., Cox, B., Stokoe II, K., Ashfield, D. & Phillips, R. (2015) ‘Utilizing Direct-Push Crosshole Testing to Assess the Effectiveness of Soil Stiffening Caused by Installation of Stone Columns and Rammed Aggregate Piers’, in *Proceedings of the 6th International Conference on Earthquake Geotechnical Engineering - 6ICEGE*. Christchurch, New Zealand.

Plate anchor capacity estimation through CPT tip resistance in sand

A. Roy & S.H. Chow

Department of Infrastructure Engineering, the University of Melbourne, Australia

ABSTRACT: Reliable estimation of plate anchor uplift capacity in sand through analytical and empirical equations is often complicated due to uncertainties in estimation of soil properties required in the equations. In order to address this uncertainty, this study proposes a correlation to estimate plate anchor vertical uplift capacity in sand based on cone tip resistance measured from cone penetrometer tests (CPT). The correlation was established using a database of reported centrifuge experiments on circular, rectangular and strip anchors in loose and dense silica sand at various embedment depths and g -levels, along with the corresponding centrifuge CPTs performed in the same testing boxes. The centrifuge cone tip resistances were also depth-corrected to remove the effect of shallow embedment. Through regression analyses, the correlation between plate anchor capacity and cone tip resistance in dimensionless form was developed, with different coefficients fitted for circular, rectangular and strip anchors respectively.

1 INTRODUCTION

Plate anchors are routinely used onshore as foundations for structures subjected to high uplift or lateral loads. With a recent global thrust in harnessing energy from cleaner renewable energy sources, plate anchors are also likely to find increased application in mooring offshore renewable energy devices owing to their cost- and capacity-effectiveness relative to other anchors and piles. Such renewable energy devices are likely to be located in much shallower water where the seabeds of interest include coarser-grained deposits. Hence, reliable estimation of plate anchor uplift capacity in coarser-grained soils will be of interest for geotechnical practitioners.

One of the most widely used soil exploration methods in coarser-grained offshore deposits is cone penetration tests (CPT). As undisturbed core sample collection for coarser-grained soils requires specialised equipment and becomes expensive for offshore sites, CPT data is often the only source of geotechnical information available during the early planning stages for offshore projects. Considering that behaviour in sands is highly dependent on initial fabric, stress levels and relative density (R_D) (Been et al. 1991, Gajo & Wood 1999), a continuous CPT profile can macroscopically capture such effects with respect to the change in soil stratigraphy. As compared to a traditional ‘operational’ friction angle (ϕ) based approach, there is great value in direct application of cone tip resistance (q_c) profiles in design approaches, because it will significantly improve reliability in prediction by eliminating uncertainties in estimation of a back-analysed ϕ . Such q_c based design approaches have been reported for bearing capacity problems on footings and spudcans (Lee & Salgado, 2005, Liu & Lehane 2020,

Pucker et al. 2013) and pile foundations (Schneider et al. 2010) over the last two decades, but is yet to be explored in uplift capacity problems.

This paper explores the test results from an elaborate set of reported centrifuge experiments (vertical uplift tests) on circular, rectangular and strip anchors with companion cone penetrometer tests in different densities at various embedment depths, g -levels and OCR levels. The cone tip resistance (q_c) measured in the centrifuge were depth-corrected to remove the effect of shallow embedment. A correlation between plate anchor capacity and cone tip resistance is then developed using a regression analysis on the database of centrifuge anchor tests.

2 EXPERIMENTAL DATABASE DETAILS

The anchor database comprised of 91 uplift tests across 20 sand samples reported from two different centrifuge studies:

- Tests reported by Roy et al. (2021a,b) on strip, rectangular and circular plate anchors in silica sand of relative density, $R_D \sim 70\%$ and $R_D \sim 45\%$ (details in Table 1 and Table 2). These tests were conducted at gravitation accelerations ranging between 20g and 100g, and embedment ratios (H/B or H/D , where H is depth of the plate anchor, B is the anchor width and D is the anchor diameter) of 2 to 6 to investigate the behaviour of plate anchors under different stress levels (hence at different g) and load inclination. For the current study, only vertical uplift tests from the respective samples are included in the database.

- Tests reported by Hao et al. (2018) on circular plates and single helices in sand of $R_D = 85-95\%$ at $20g$ (details in Table 3) at anchor embedment ratios (H/D) in the range 2 to 10;

Table 1. Anchor database in loose sand (after Roy et al. 2021a).

Sample No., R_D (%) (and $\gamma(kN/m^3)$)	Anchor code	g	OCR	H/B or H/D	Anchor factor, N_γ
D1, 76.72 (16.61)	ST_3	30	1	1.95	2.28
	ST_2	30	1	1.95	2.14
	ST_1	50	1	1.95	2.18
	R_2	30	1	2.00	3.49
	R_3	50	1	2.00	3.37
	R_1	100	1	2.05	3.38
D2, 73.5 (16.52)	ST_2	30	1	2.70	2.51
	ST_3	50	1	2.70	2.30
	R_2	30	1	2.70	3.73
	R_3	50	1	2.95	3.82
	R_1	100	1	2.68	3.25
	C_1	33.3	1	1.80	4.18
	C_2	66.6	1	1.80	3.43
D3, 75.28 (16.58)	ST_1	30	1	3.95	4.17
	ST_2	50	1	3.95	3.99
	R_3	30	1	4.00	7.11
	R_1	50	1	4.00	6.34
	R_2	100	1	4.00	6.15
	C_1	33.3	1	2.70	7.32
	C_2	66.6	1	2.70	6.68
D4, 75.14 (16.57)	ST_1	30	1	3.85	4.01
	ST_2	50	1	3.96	3.60
	R_1	30	1	3.81	5.98
	R_3	50	1	3.95	5.89
	R_2	100	1	3.85	5.59
	C_1	33.3	1	2.53	6.31
	C_2	66.6	1	2.57	6.12
D5, 69.53 (16.41)	R_4	20	1	1.80	2.96
	C_3	20	1	1.93	4.33
D6, 71.1 (16.45)	R_5	20	1	3.03	4.29
	C_3	20	1	2.90	8.28
D7, 74.35 (16.54)	R_4	20	1	3.77	6.55
	C_5	30	1	5.94	14.46
D9, 78 (16.65)	C_4	30	3	5.9	17.22
	C_7	30	5	5.87	18.21
	R_6	30	1	6.05	8.95
	R_5	30	1	5.8	8.58
	R_8	30	3	5.9	9.1
	R_7	30	5	5.93	9.2

These uplift tests involved anchors with different geometry (strip (ST) with aspect ratio 8:1, rectangular

(R) with aspect ratio 2:1, circle (C), helix (H)) as listed in Tables 1-3 and Figure 1. All these tests were conducted in a fine sub-angular silica sand, commonly identified as the UWA Silica sand with properties as summarised in Table 4. The samples for the centrifuge tests were prepared using air pluviation technique and anchor testing setup can be found in the respective papers.

Table 2. Anchor database in loose sand (after Roy et al. 2021 a,b).

Sample No., R_D (%) (and $\gamma(kN/m^3)$)	Anchor code	g	OCR	H/B or H/D	Anchor factor, N_γ
L1, 42.8 (15.68)	ST_2	30	1	1.75	1.31
	ST_3	50	1	1.75	1.33
	ST_1	100	1	1.75	1.26
	R_3	30	1	1.80	2.01
	R_2	50	1	1.80	1.90
	R_1	100	1	1.85	1.90
L2, 48.9 (15.84)	ST_2	30	1	2.75	1.56
	ST_1	50	1	2.75	1.60
	ST_3	100	1	2.75	1.56
	R_1	30	1	2.8	1.98
	R_2	20	1	2.75	2.82
	R_5	20	1	1.90	2.29
	R_4	33.3	1	1.83	1.72
L3, 45.7 (15.76)	C_1	33.3	1	1.90	2.61
	ST_2	30	1	3.60	2.38
	ST_3	50	1	3.85	2.35
	ST_1	75	1	3.70	2.25
	R_3	30	1	3.80	3.93
	R_2	50	1	3.80	3.86
	R_1	100	1	3.73	3.75
L4, 47.35 (15.8)	C_1	33.3	1	2.53	4.70
	C_2	66.6	1	2.53	4.70
L5, 47.37 (15.79)	R_4	20	1	1.83	2.13
	C_3	20	1	1.90	2.39
L6, 48.67 (15.83)	R_4	20	1	2.87	3.33
	C_3	20	1	2.77	4.19
L7, 50.21 (15.87)	R_4	20	1	4.07	4.51
	C_3	20	1	3.90	6.04
	C_6	30	1	5.78	9.73
	C_7	30	3	5.92	9.92
	C_5	30	5	5.95	12.27
	C_4	30	5	5.85	11.40
	R_8	30	1	5.78	6.46
	R_7	30	3	5.92	6.95
R_6	30	5	5.93	8.97	
R_5	30	5	5.9	8.69	

Companion cone penetrometer tests were also conducted in these reported studies at $20g$ using a 10 mm diameter cone penetrometer (d_{cone}).

Figure 2 presents q_c profiles measured across: (a) the 13 sand samples reported in Roy et al. (2021) at 20g performed at the start of testing, and (b) q_c profiles from the 13 sand samples in Hao et al. (2019). These q_c profiles are used to estimate the relative density (R_D) of the samples using a $q_c - R_D$ relation proposed by Roy et al. (2019) for the UWA silica sands, that accounts for effective vertical stress (σ'_v), relative density and normalised penetration depth (z_m/d_{cone}):

$$q_c = C_0 P_a (\sigma'_v / P_a)^{C_1 + C_3 (1 - f_D) + f_D \Delta C_{1oc}} (e)^{C_2 + f_D \Delta C_{2oc}} R_D \quad (1a)$$

$$f_D = \exp(-C_4 (z_m / d_{cone})^{-C_5}) \quad (1b)$$

where the constants for UWA Silica sand were obtained as $C_0 = 8.5$, $C_1 = 0.89$, $C_2 = 3.3$, $C_3 = 0.36$, $C_4 = 1049.2 R_D^{7.25}$, $C_5 = 3.7$ respectively. ΔC_{1-oc} and ΔC_{2-oc} are constants that account for the decreased compressibility of the sands under OC condition, the details of which are explained in Roy et al. (2019). It is worth noting that the effect of shallow embedment on q_c for centrifuge CPTs are incorporated through a varying depth factor (f_D) in Equation 1. Using Equation 1, relative density at the anchor locations was back-analysed as $R_D = 41 - 51\%$ for the loose sand and $R_D = 69 - 76\%$ in the dense sand reported by Roy et al. (2021a). For the tests reported by Hao et al (2019) on circular plates, the R_D was $\sim 85 - 96\%$.

Table 3. Anchor database in very dense sand at 20g and OCR = 1 (after Hao et al., 2019).

Relative density (%) (unit weight) (kN/m ³)	Anchor code	H/D	q_a (kPa)	N_y
96.2 (17.07)	H	3	182.29	8.9
86.7 (16.87)	H	4	340.12	12.6
86.4 (16.86)	H	6	861.68	21.3
96.2(17.07)	H	6	966.73	23.6
90 (16.94)	H	7.5	1285.68	25.3
86.4 (16.86)	H	8	1407.82	26.1
96.4 (17.07)	H	8	1731.80	31.7
88.8 (16.91)	H	9	1991.16	32.7
96.1 (17.07)	H	9	2156.46	35.1
96.2 (17.07)	H	9	2070.69	33.7
96.4 (17.07)	H	10	2465.23	36.1
90 (16.94)	H	10.5	2169.90	30.5
86.7 (16.87)	H	2	78.28	5.8
85.8 (16.84)	C	3	181.87	9.0
85.8 (16.84)	C	6	860.86	21.3
85.8 (16.84)	C	9	1879.34	31.0

For anchor tests conducted at different g -levels or OCRs within the same sample (see samples D1-D7, D9 in Table 1 and L1-L7 in Table 2), a q_c profile at the respective g -level or OCR was required to generate the correlate to anchor capacity. However, CPT tests at all g -levels as those of the anchor tests were

not possible due to the space constraints in the strong-boxes; as such Equation (1) was subsequently used in such cases to establish the respective q_c profile. The validity of such an approach is confirmed by the good agreement between the measured and simulated $q_c - z_m/d_{cone}$ profiles using Equation (1) at two different R_D and g -levels in a separate CPT study as shown in Figure 3.

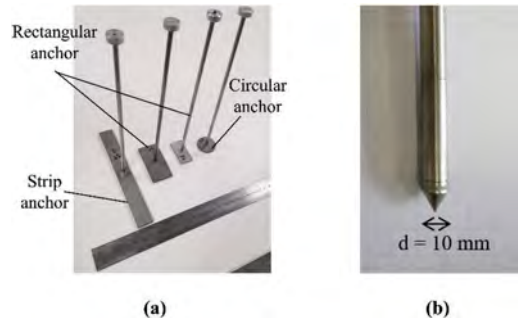


Figure 1. Model plate anchors and piezocone (after Roy et al. 2021a, b).

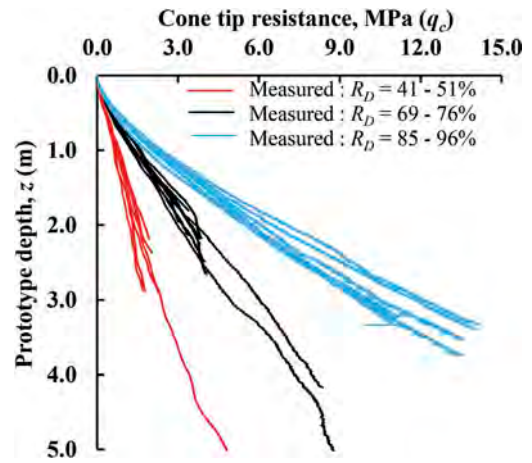


Figure 2. Measured q_c profiles in loose, dense (Roy et al., 2021a) and very dense sand (Hao et al., 2019).

Table 4. Physical properties of UWA silica sand.

Soil properties	UWA Silica sand
Angularity	Sub-rounded to sub-angular
Maximum void ratio ^a	0.789
Minimum void ratio ^a	0.512
Specific gravity ^b	2.67
Uniformity coefficient (U)	1.73
Mean particle size (d_{50})	0.2 mm

^a Maximum and minimum void ratios calculated as per AS 1289.5.5.1

^b Specific gravity calculated as per AS 1289.3.5.1

3 ESTABLISHING N_γ - q_c CORRELATIONS

3.1 Anchor capacity factor

The mobilised peak anchor capacity (q_a) in this paper is reported in dimensionless form as peak anchor factor ($N_\gamma = q_a/\sigma'_{vo}$, where σ'_{vo} is the effective overburden stress). The q_a and N_γ for each anchor test is tabulated in Tables 1-3. The N_γ is typically attained within normalized displacement (δ/B or δ/D) of 15% in medium dense ($R_D = 48\%$) and 7-12% in dense sand ($R_D = 70\%$), as reported in Roy et al. (2021a,b). At a given H/B , the highest N_γ is observed from circular plates whereas the least is observed from strip anchors.

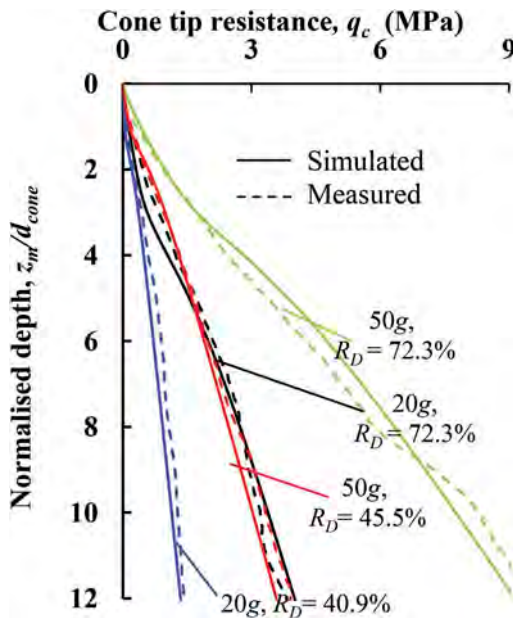


Figure 3. Comparison of measured and simulated $q_c - z_m/d_{cone}$ profiles at different R_D and g -levels.

3.2 Correcting q_c for shallow embedment effects

The q_c profiles from centrifuge samples undergo shallow penetration and need to be corrected for effects of shallow embedment (Bolton *et al.* 1999). For example, if the results for a prototype anchor having $D = 0.6$ m at H/D of 2 was to be simulated, a model anchor plate with diameter of 30 mm (as reported in the database) would have to be embedded at a sample depth of 60 mm at 20g. With centrifuge penetrometers having $d_{cone} = 10$ mm, the anchor placement depth would be located within a penetrating distance of $6d_{cone}$, resulting in a shallow failure mechanism for the penetrometer. For corresponding prototype anchors having $D = 0.6$ m, it would have to be embedded at a depth of 1.2 m in field (for $H/D = 2$); a penetrometer in such conditions would have penetrated by $\sim 33d_{cone}$ (considering a standard cone diameter of 35.8 mm) to reach embedded depth for the anchor, resulting in a deep

failure mechanism. As per reported studies by Bolton *et al.* (1999) and Liu & Lehane (2020), the critical normalised depth governing the transition from shallow to a deep mechanism for a cone penetration test usually ranges between 5 and 15. So, cone profiles from centrifuge samples would produce a smaller q_c value at shallow depths than the corresponding prototype samples at similar stress and density levels. Hence, correction is necessary to obtain an equivalent q_c value under the effect of similar stress and density levels but independent of penetrating distance. This can be readily worked out using the correlations by use of depth factor $f_d = 1$.

The depth-corrected q_c profiles simulated using $f_d = 1$ in Equation (1) is shown in Figure 4 for two different densities at two different stress levels. These profiles show that the effect of depth correction on q_c is more pronounced as the g -level and the R_D increases. For the measured (uncorrected) centrifuge q_c profiles in Figure 4, a shallow failure mechanism results in an increased concave upwards curvature at the shallower penetration depths. In contrast, the simulated (depth-corrected) profiles are convex-shaped at the shallow penetration depths. The simulated and measured profiles tend to merge with each other at z/d_{cone} value greater than 8.

3.3 Obtaining average q_c values

The anchor tests reported in Table 1-3 were conducted at stress levels ranging from 20g to 100g. In order to obtain a correlation between N_γ and q_c , a representative q_c value in the influencing domain was necessary at the corresponding g level of the anchor test. Numerical studies have confirmed that (Al Hakeem and Aubeny, 2019, Hao *et al.* 2014), for plate anchor uplift under drained conditions, the failure mechanism significantly mobilises a soil on top of the anchor plate up to a distance of $2D$ or $2B$. Based on this evidence, a representative q_c value (termed as $q_{c,avg}$) was taken as the average over a distance of $2D$ or $2B$ over the top of the anchor using the depth-corrected simulated q_c profiles obtained by correlations in Equation 1. This zone encompasses the distance required to mobilise peak N_γ for all anchor types and embedment ratios.

3.4 Correlation for anchors

Figure 5 presents the average cone tip resistance ($q_{c,avg}$) vs. mobilised peak anchor capacity (q_a) data at all g levels for circular anchor. The data shows q_a linearly with an increase in $q_{c,avg}$ for all anchor types. However, at a particular value of $q_{c,avg}$, q_a values from loose sand are observed to be higher than those in dense sand. Now, in order to inter-compare q_a at similar $q_{c,avg}$ values in loose and dense sand, an anchor would have to be located at a much deeper depth (or higher σ'_v) for the loose sand than for the dense sand. This suggests that there appears to be a significant contribution of σ'_v in governing peak N_γ . This hints that a stress normalised $q_{c,avg}$ value would be necessary to reliable correlation.

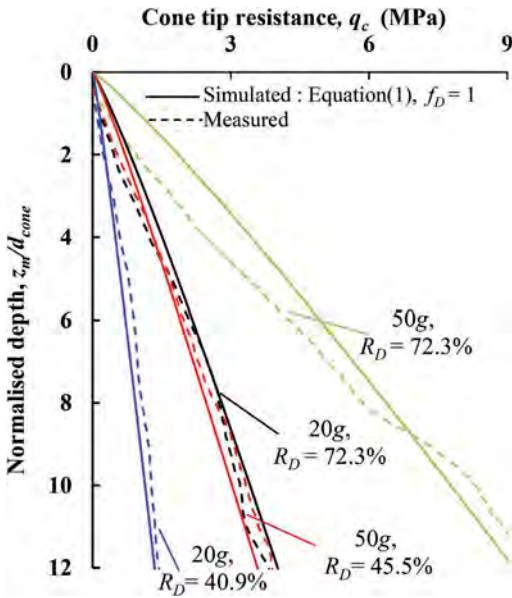


Figure 4. Comparison of measured cone profiles and simulated cone profiles using $f_D = 1$ at different g -levels in loose and dense sand.

In order to capture the effects of stress on the penetration resistance, Sharp et al. (2010) suggested the use of a normalised tip resistance term q_{c1N} :

$$q_{c1N} = (q_c/P_a)(P_a/\sigma'_v)^m, \quad (2)$$

where P_a is the atmospheric pressure, σ'_v is the effective overburden stress and m is a stress exponent term ranging from 0.3 to 0.8 that better accounts for the effects of σ'_v for a given problem. Trial iterations with using $m = 1$ across all densities (i.e. without using any R_D dependent normalisation), showed that insufficient overlap across all datasets, thus hindering the development of a unique correlation. This suggested that a density dependent m value needs to be used to ensure sufficient overlap between the datasets.

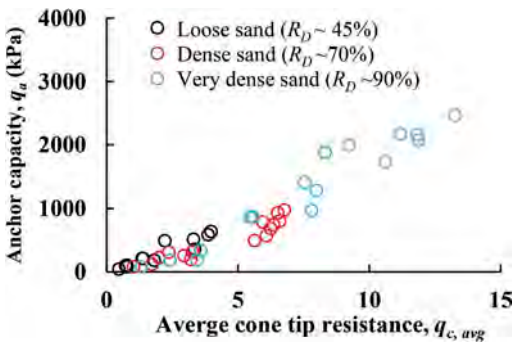


Figure 5. Variation of peak anchor capacity with average cone tip resistance in loose and dense sands for circular anchors.

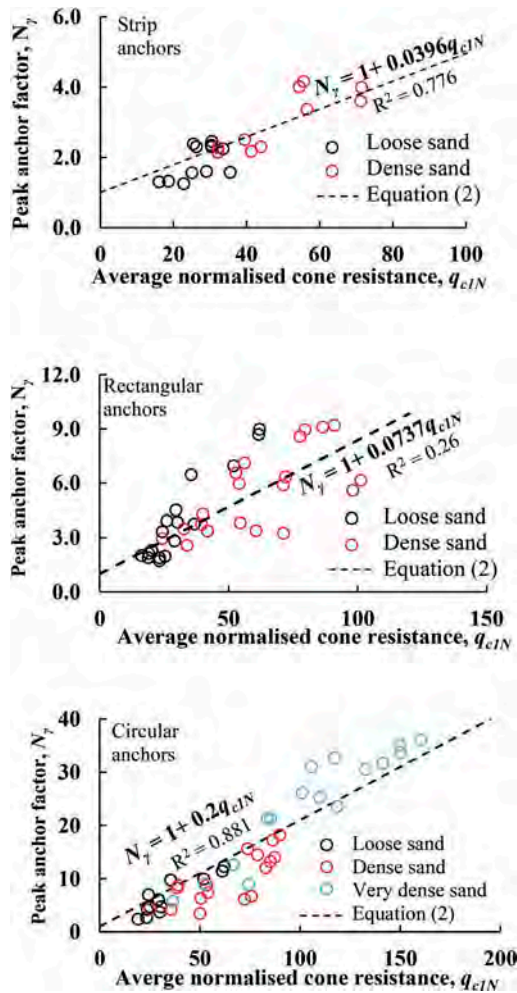


Figure 6. Correlation of N_γ with q_{c1N} in loose and dense sand for (a) strip anchors, (b) rectangular anchors and (c) circular anchors.

The value of m was therefore evaluated using an optimisation routine to produce the greatest overlap in loose and dense sand data by a relative shift in the abscissa of the $N_\gamma - q_{c1N}$ plot. This was achieved iteratively resulting in a value of $m = 0.6$ in loose sands ($R_D \sim 45\%$), 0.4 in dense sands ($R_D \sim 70\%$) and 0.39 in very dense sands ($R_D \sim 90\%$). More anchor experimental data at $R_D < 40\%$ would be required to draw an unambiguous conclusion on the precise values of m in very loose sand. In absence of such data, it is assumed that m would take an upper bound of 0.8 at very low R_D values, therefore the exponent m used to obtain q_{c1N} can be expressed as:

$$m = 0.41(R_D(\%)/100)^{-0.24} \quad (3)$$

Applying the optimized m in Equation (2), the correlation between q_{c1N} and N_{γ} is established as shown in Figure 6 and presented in Equation (4):

$$N_{\gamma} = 1 + f_u q_{c1N} \quad (4)$$

where f_u is a coefficient dependent on anchor shape and is equal to 0.0396, 0.0784 and 0.2 for strip, rectangular and circular plates respectively. The R^2 values for the respective correlations for strip, rectangular and circular plate anchors are 0.776, 0.26 and 0.881 respectively. The significantly lower R^2 of 0.26 for the rectangular anchors is due to greater scatter in the experimental dataset at lower q_{c1N} levels and suggests that more experimental data would be required to obtain a reliable correlation. The f_u values also indicate that the anchor capacity increases in the order of strip, rectangular and circular anchors, which agree with existing studies (e.g. Murray and Geddes 1987).

4 CONCLUSIONS

A correlation between anchor capacity factor (N_{γ}) and normalized cone tip resistance (q_{c1N}) has been established based on a collected database of centrifuge tests on strip, rectangular and circular anchors at varying g -levels in loose and dense sands. The centrifuge cone profiles were depth-corrected to remove the effect of shallow embedment and make them inter-comparable with prototype tests. The results indicated that a varying stress exponent factor is necessary to account for the effect of overburden stress in loose and dense sands and to establish a unique correlation. It is desired to validate the proposed N_{γ} - q_{c1N} correlation using field anchor and companion CPT data. The results can also be used to readily compute anchor capacity through CPT profiles when the soil fabric has been disturbed due to installation effects, which is a distinct advantage when compared to other methods relying on in-situ inputs of density and friction angles.

ACKNOWLEDGEMENTS

The authors acknowledge the financial support from the Australian Research Council Discovery Grant Scheme DP190100914.

REFERENCES

- Been, K., Jefferies, M. G. & Hachey, J. 1999. The critical state of sands. *Géotechnique* 41(3): 365–381. doi: 10.1680/geot.1991.41.3.365.
- Bolton, M. D., Gui, M.W., Garnier, J., Corte, J.F., Bagge, G., Laue, J. & Renzi, R. 1999. Centrifuge cone penetration tests in sand. *Géotechnique* 49(4): 543–552. doi: 10.1680/geot.1999.49.4.543.
- Gajo, A. & Wood, D. M. 1999. A kinematic hardening constitutive model for sands: the multiaxial formulation. *International Journal for Numerical and Analytical Methods in Geomechanics* 23: 925–965.
- Al Hakeem, N. & Aubeny, C. 2019. Numerical Investigation of Uplift Behavior of Circular Plate Anchors in Uniform Sand. *Journal of Geotechnical and Geoenvironmental Engineering* 145(9): doi: 10.1061/(asce)gt.1943-5606.0002083.
- Hao, D., Wang, D., O’ Loughlin, C.D. & Gaudin, C. 2019. Tensile monotonic capacity of helical anchors in sand: interaction between helices. *Canadian Geotechnical Journal* 56(10):1534–1543. doi: 10.1139/cgj-2018-0202.
- Hao, D., Fu, S. & Rong, C. 2014. Numerical Analysis of Uplift Capacity of Circular Plate Anchor in Sand. *Journal of geotechnical engineering* 19: 18947–18961.
- Lee, J. & Salgado, R. 2005. Estimation of Bearing Capacity of Circular Footings on Sands Based on Cone Penetration Test. *Journal of Geotechnical and Geoenvironmental Engineering* 131(4): 442–452.
- Liu, Q. & Lehane, B. M. 2020. A centrifuge investigation of the relationship between the vertical response of footings on sand and CPT end resistance. *Géotechnique* 71 (5):1–11. doi: 10.1680/jgeot.19.p.253.
- Murray E.J. & Geddes, J.D. 1987. Uplift of anchor plates in sand. *Journal of Geotechnical and Geoenvironmental Engineering* 113(3): 202–215.
- Pucker, T., Bienen, B. & Henke, S. 2013. CPT based prediction of foundation penetration in siliceous sand. *Applied Ocean Research* 41: 9–18. doi: 10.1016/j.apor.2013.01.005.
- Roy, A., Chow, S., O’ Loughlin, C.D. & Randolph, M.F. 2021a. Towards a simple and reliable method for calculating uplift capacity of plate anchors in sand. *Canadian Geotechnical Journal* 58(9): 1314–1333. doi: 10.1139/cgj-2020-0280.
- Roy, A., O’ Loughlin, C.D., Chow, S. & Randolph, M.F. 2021b. Inclined loading of horizontal plate anchors in sand. *Géotechnique*: doi: 10.1680/jgeot.20.P.119
- Schneider, J. A., Xu, X. & Lehane, B. M. 2010. End bearing formulation for CPT based driven pile design methods in siliceous sands. *2nd International Symposium on Cone Penetration Testing* 3(May): 8.
- Sharp, M. K., Dobry, R. & Phillips, R. 2010. CPT-Based Evaluation of Liquefaction and Lateral Spreading in Centrifuge. *Journal of Geotechnical and Geoenvironmental Engineering* 136(10):1334–1346. doi: 10.1061/(ASCE)GT.1943-5606.0000338.

CPT results and installation parameters for CFA piles in pyroclastic soils

G. Russo & M. Ramondini

Department of Civil and Environmental Engineering, University of Napoli Federico II, Italy

A. Vecchietti

Department of Engineering, University of Perugia, Italy

G. Russo

Department of Earth Science, Environment and Resources, University of Napoli Federico II, Italy

ABSTRACT: A large number of bored CFA piles was installed during the construction of a big treatment plant in Poggiomarino (Naples), where the subsoil is formed by sub-horizontal strata of alluvial soils of pyroclastic origin interbedded with organic silt layers, overlying the pyroclastic base formation. The installation parameters of CFA piles (rate of revolution, rate of penetration, torque, etc.) have been recorded during construction. In the paper the statistical correlation between CPT results and monitoring data of CFA piles installation was analysed. The statistical correlation allowed evaluating the bearing capacity of each CFA pile based on the monitoring of installation data. The correlation was developed by considering different pile groups located around the CPT verticals, in order to analyse the sensitivity to the spatial variability of geotechnical subsoil properties. The statistical based prediction of bearing capacity was validated by considering two load tests on pilot CFA piles at the study site.

1 INTRODUCTION

The CFA or Continuous Flight Auger pile is a rather widespread pile type in USA also called auger cast piles. They are installed by first inserting an auger under the combined action of a torque and an axial force. The auger retrieval is carried out while concrete is pumped through the central stem.

With this technology is possible and is more and more frequent the monitoring of installation parameters during the pile construction. These parameters are connected to the step of auger insertion and to the final stage of auger retrieval and concrete downwards pumping.

In the drilling phase, the tube advancement takes place with an intermediate mechanism between that of a screw and that of a *coclea*. Named v the speed of advancement, n the speed of rotation and l the pitch of the auger, in a time Δt there is a volume of displaced soil:

$$V_d = \frac{\pi}{4} d_0^2 v \Delta t \quad (1)$$

and a volume of soil removed from the auger and taken to the surface:

$$V_a = \frac{\pi}{4} (d^2 - d_0^2) (nl - v) \Delta t \quad (2)$$

If $v=nl$, the volume removed is null, the auger advances into the ground without any removal of the surrounding soil.

If $v=0$, the auger turns without advancing and works as a an archimedean coclea screw by continuously removing soil. To obtain an overall compression effect, it should be $V_d \geq V_a$, and therefore:

$$v \geq nl \left(1 - \frac{d_0^2}{d^2} \right) = v_{crit} \quad (3)$$

The second member of the equation (3) represents the critical penetration speed v_{crit} , of the auger into the ground.

The paper is dedicated to determine a statistical correlation between CPT results on one side and installation parameters of the CFA piles recorded during the pile construction at the site of the large treatment plant in Poggiomarino (Napoli, Italy) on the other side.

A further correlation aimed at the prediction of the bearing capacity of piles on the basis of the installation recorded parameters has been developed and tested using the results of static design load tests on several piles instrumented with strain gauges along the pile shaft

2 GEOTECHNICAL INVESTIGATIONS AND SUBSOIL CONDITIONS

The whole area has been investigated between 1998 and 1999, the available in-situ tests include n. 5 boreholes (20-50m) with undisturbed/disturbed samples for laboratory tests, 19 CPT (14-30m), 7 CPTU (16-51m), 4 SCPTU (16-39m).

Two main lithotypes, whose main physical and mechanical characteristics are reported in Table 1, characterize the site (Figure 1): a lacustrine/alluvial soil constituted by pyroclastic sand and silt with organic or peat levels, with a thickness of 15÷18 m is found above the *Ignimbrite Campana* formation, made of pozzolana (silty sands) and grey tuff levels, that extends down to 50 m (max. borehole depth). Cone penetration resistance q_c is between 2 ÷ 3 MPa in the mostly silt, organic levels while $q_c = 50 \div 70$ MPa in the sandy levels; in the pozzolana layer, q_c ranges between 5 ÷ 200 MPa.

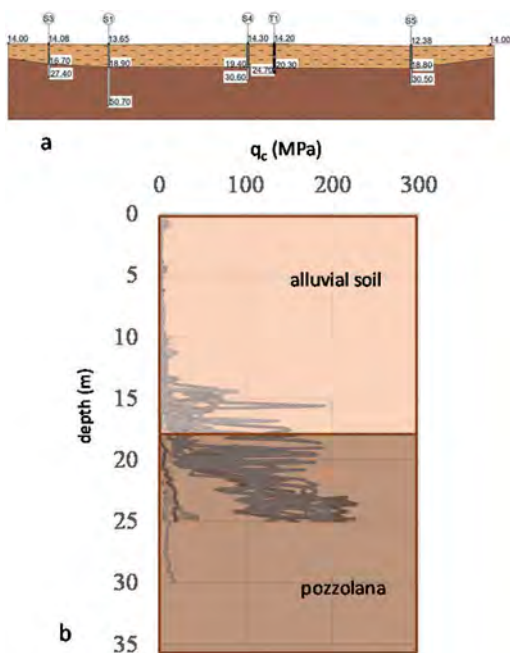


Figure 1. Subsoil profile (a) and CPT results (b) of the investigated area.

Data referring to the alluvial soil are scattered, with grain size distribution ranging from sandy silt to silty sand; the unit weight γ ranges between 14 and 20 kN/m³, the water content $w=20-60\%$, with corresponding value of the porosity $n=40-60\%$. Some thin levels with high organic content have been detected at various depths, with lower values of γ (11-12 kN/m³) and higher values of w and n (respectively 80-200% and 65-80%). The base formation of pozzolana (silty sand) is more uniform: the unit weight γ ranges between 14 and 16 kN/m³, the water content w is

generally higher than 40%, the porosity n ranges between 55% and 65%. The few available lab data on the shear strength and estimation deriving from the interpretation of CPT tests lead to an overall value of the friction angle $\phi' = 28^\circ$ for the alluvial soils, $\phi' = 35^\circ$ for the base formation of pozzolana.

Table 1. Main physical and mechanical parameters of subsoil layers.

Layer	depth [m]	γ [kN/m ³]	ϕ' [°]	c' [kPa]	E_{ed} [MPa]
Alluvial soil	0.0÷18.0	15.8	28	0	0.5÷5.0
Pozzolana	18.0÷50.0	15.6	35	0	20.0

3 INSTALLATION PARAMETERS OF CFA PILES AND IN SITU LOAD TESTS

In this study a group of 65 piles with 27 m length and 0.8 m diameter belonging to the biological treatment tank have been considered, as reported in Figure 2.

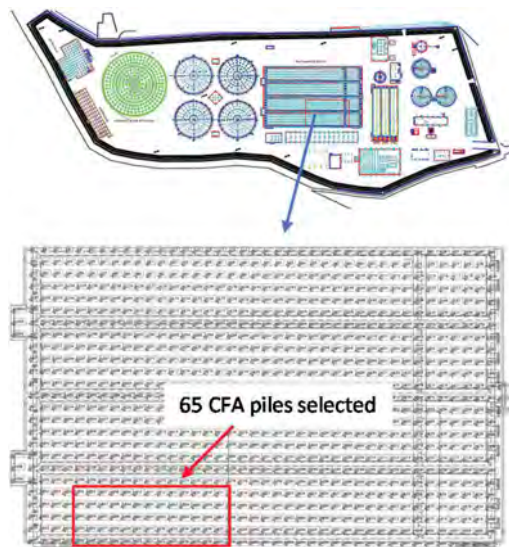


Figure 2. Investigated area with details of biological treatment tank foundation; the red square evidences the set of 65 CFA piles selected for this study.

The drilling machines were equipped with Jean-Lutz recording system that allowed for continuous monitoring of installation parameters. Rate of revolution, rate of penetration and torque with depth were recorded every 8 cm. Conversion of operating pressure in torque (kNm) was performed with reference to a specific relationship for the drilling machine provided by the manufacturer. Torque has been considered as the most relevant installation parameter in this study, for its close relation with the subsoil characteristics. An increase of

soil resistance along the depth results in increase of torque applied for continuing the pile installation and *vice versa*. Profiles of average values of torque and box-plots of statistical parameters with depth for the n. 65 piles considered in the study are reported in Figure 3.

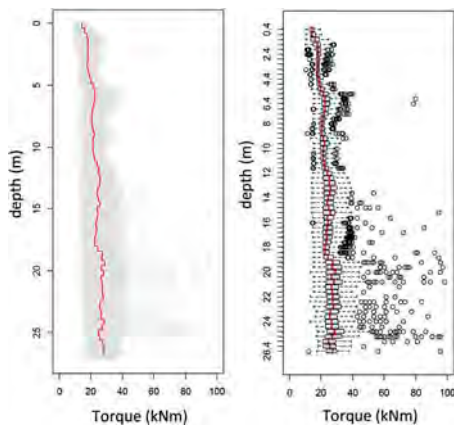


Figure 3. Measured values of torque along depth: average values and boxplot representation.

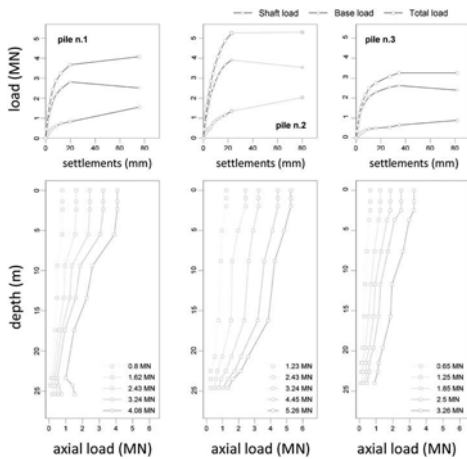


Figure 4. Results of piles load tests: axial loads vs. settlements and axial loads vs. depth curves.

Load tests to failure on three instrumented CFA piles belonging to the foundations were conducted (Mandolini et al., 2002). Vertical displacements were measured by means of four dial gages and precision levelling. All the test piles were equipped with the removable tape extensometers (Bustamante and Jezequel, 1991) whose results were also compared with vibrating wire gages installed in a central pipe (Russo, 2005). The main results of the load tests are listed in Table 2, while the axial load-settlement curves (total load Q , shaft load, S and base load P) and the axial load distributions along the pile shaft as an example are reported for all the tested piles in Figure 4. In Figure 5 is shown the torque registered during the tested piles.

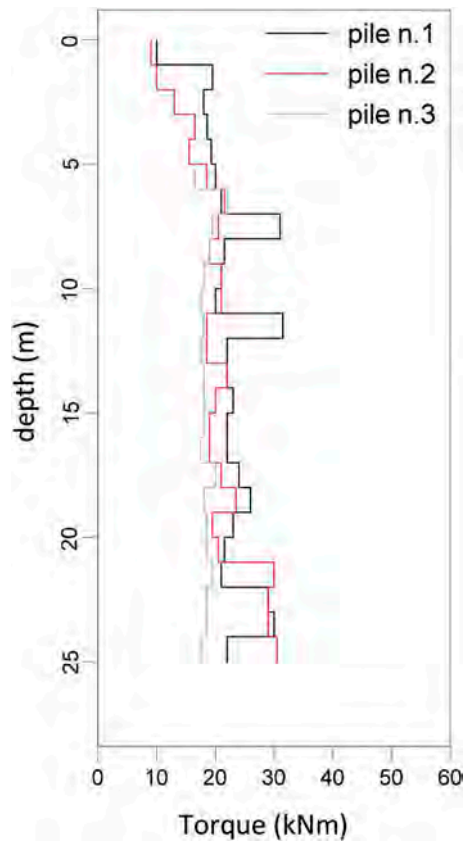


Figure 5. Measured values of torque along depth for test piles.

Table 2. Load tests results.

	d	L	Q_{max}	w_{max}	P_{max}	S_{max}
Load test	[m]	[m]	[MN]	[mm]	[MPa]	[MPa]
	a*	b*	c*			
pile n.1	0.8	24.0	4.08	75.6	1.55	2.81
pile n.2	0.6	22.5	3.26	81.9	0.89	2.59
pile n.3	0.8	24.1	5.30	22.8	1.36	3.94

d = diameter; L = length; Q_{max} = maximum axial load; w_{max} = maximum settlement; P_{max} = maximum tip resistance; S_{max} = maximum shaft resistance.

4 STATISTICAL ANALYSIS

Statistical correlations between the relevant parameters were investigated with R numerical code (R Core Team, 2013). CPT tip resistance q_c and torque M_t recorded during the drilling of 65 piles of the biological treatment tank and CPT results in the proximity of the area were first considered. A sensitivity analysis was performed, aimed at investigating correlations at difference distances scales, considering three ranges,

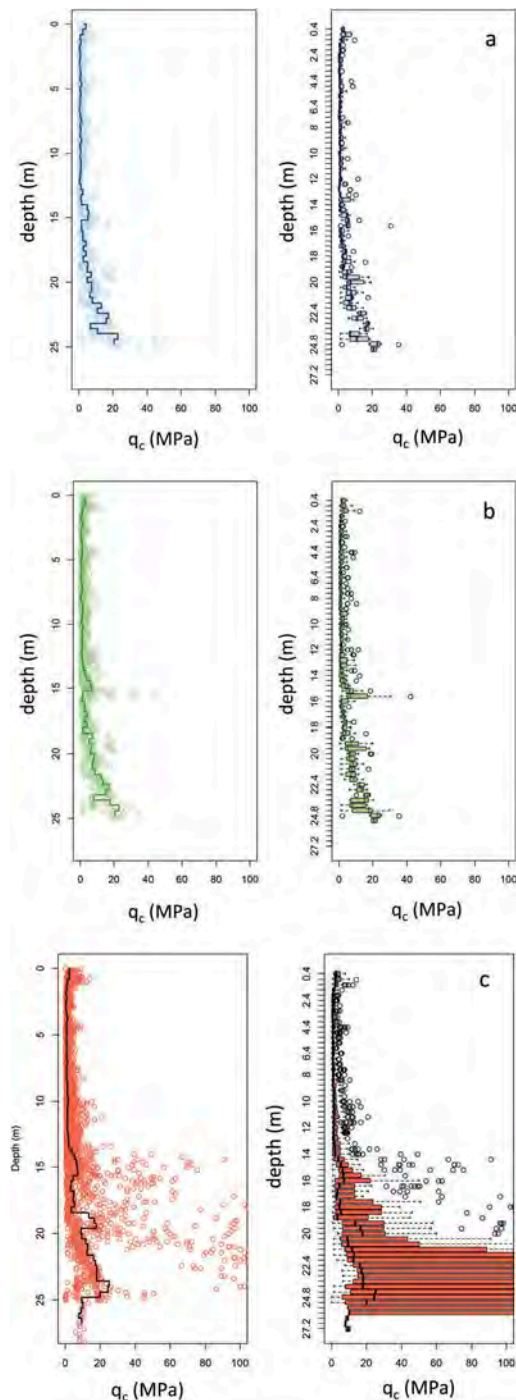


Figure 6. CPTs tip resistance q_c vs. depth: average trends and boxplots for a) n.4 CPTs, b) n.7 CPTs, c) n.29 CPTs.

from the nearest CPTs around the selected piles up to all available CPTs in the investigated area (namely n.4 CPTs located close to the selected piles, n.7 CPTs

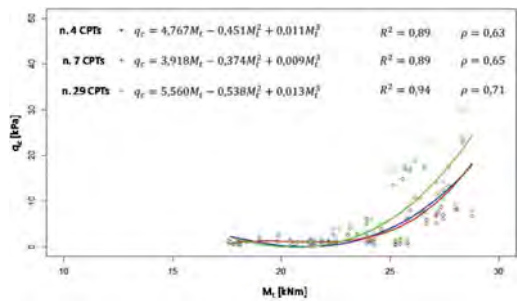


Figure 7. CFA piles: regression functions of $q_c=f(M_t)$ for the three selected set of CPTs.

located within the biological tank foundation, n. 29 CPTs performed within the plant perimeter). For each group of selected CPTs, the tip resistance q_c varies with depth as shown in boxplots of Figure 6, highlighting similar trends of q_c with depth regardless the number of data selected, thus confirming the homogeneity of subsoil profile in the considered area.

Regression analyses of average values of M_t and q_c with depth confirmed that correlation coefficients ρ for each set of selected CPTs were similar (namely $\rho = 0.63$ for n.4 CPTs set, $\rho = 0.66$ for n.7 CPTs set, $\rho = 0.71$ for n. 29 CPTs set), denoting a positive, moderate correlation between the two variables. The function $q_c = f(M_t)$ was determined by means of non-linear regression analysis. Polynomial regression models were used with the constrain that $q_c = 0$ for $M_t = 0$. The three functions are reported in Figure 7. The assessment of the “goodness of fit” was provided through the absence of trends of residuals (not shown), and a close relation between measured q_c and fitted q_c trends with depth for the three levels of analysis.

The statistical correlation between M_t and the unshaft resistance s of test piles was also analyzed. The distribution of s with depth was evaluated from the measured variation of axial load along the test pile shaft. The function $s = f(M_t)$ derived by the non-linear regression analysis between $s(z)$ and measured $M_t(z)$ is reported in Figure 8.

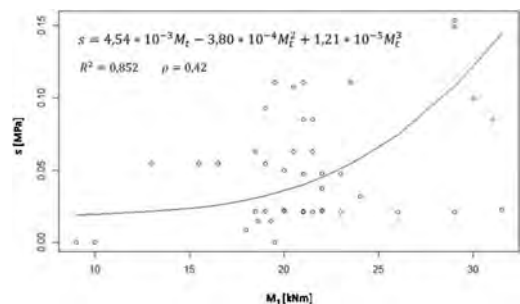


Figure 8. Test piles: regression function of $s=f(M_t)$ from the results of load tests.

5 PREDICTION OF UNIT SHAFT RESISTANCE

To assess the suitability of inferring CFA pile shaft resistance from installation parameters, the derived relations from statistical analysis were used for calculating the shaft resistance of selected CFA piles and compared with the results of load tests.

The average shaft resistance of the selected CFA piles was evaluated following the relation (Viggiani et al., 2012):

$$s(z) = \alpha q_c(z)$$

where α is a coefficient varying from 0.02 ($q_c < 2$ MPa, very loose soil) to 0.07 ($q_c > 25$ MPa, dense soil) and the tip resistance q_c was evaluated as function of the average torque $M_t(z)$.

The shaft bearing capacity of test piles has been calculated by integrating along the pile length the function $s = f(M_t)$ obtained through the statistical analysis.

The shaft resistance inferred from load test results was considered as benchmark for the predictions of shaft resistances based on the regression functions with installation parameters. Only test piles n.1 and n.3 were considered, having those piles the same diameter of CFA piles set considered in the study (i.e. $d = 0.8$ m). In Table 3 the calculated shaft resistances of CFA piles (both ordinary and test piles) and the shaft resistance inferred from load tests are reported.

Table 3. Comparison between calculated and measured pile shaft resistances.

Load test	S_{max}	$S [s = f(q_c(M_t))]$			$S [s = f(M_t)]$
	[MPa]	[MPa]			[MPa]
		a*	b*	c*	
pile n.1	2.52	3.17	3.19	3.90	3.51
pile n.3	3.54	3.73	3.50	3.95	2.95

* a = n.4 CPTs; b = n.7 CPTs; c = n.29 CPTs

With reference to the integral shaft resistance S calculated referring to the function $s = f(q_c(M_t))$, the results highlight an overestimation of the shaft resistance for pile test n.1, whereas for pile n.3 the estimate can be considered as satisfactory, whenever the level of the analysis performed. As shown by Mandolini et al. (2012), test pile n.1 is characterized by a rate of penetration v_p along the pile shaft lower than the critical value v_{crit} , whereas for test pile n. 3 the rate of penetration is higher than v_{crit} . The effects of the installation procedure of test piles n.1 on the soil mass,

closer to the effects of bored piles, may explain the overestimation of shaft resistance based on the correlation function $s = f(q_c(M_t))$.

The correlation function $s = f(M_t)$ seems to be less effective in the estimation of both test piles shaft resistance, probably due to the limited number of M_t data on test piles available for the statistical regression.

6 CONCLUSIONS

CFA piles are generally considered as replacement piles because there is a rather large volume of soil removed during the construction. It has long been recognized however that the careful control of the installation parameters via monitoring tools on board of the equipment used to install the pile may positively influence the performance of the pile under live loading. Particularly the comparison between the advancement velocity, v , of the auger and the critical velocity v_{crit} allow to evaluate at least qualitatively the net effect of the installation of the auger on the surrounding soil.

In this paper following the path already outlined by the authors in previous published works (Mandolini & Russo, 2008, Mandolini et al. 2012,) a correlation between CFA installation parameters and soil response during the widely used CPT investigation tool has been outlined. The best correlation has been found between the tip resistance q_c of the CPT and the torque M_t . A direct statistical correlation between this last value and the shaft unit friction of piles load tested to failure has been also established. Finally it is also well known that CPT is a valid tool to directly obtain bearing capacity of piles at the design stage. In this paper the load tests available carried out on instrumented CFA piles have allowed to compare shaft capacity derived by statistical correlations with installation parameters and that one directly measured during loading tests on three CFA piles. Two comparisons have been carried out: one based on direct correlation with the measured torque on tested pile and the other based on indirect correlation between the torque and the shaft capacity passing via the correlation with the CPT tip resistance. The comparison is indeed rather satisfactory, particularly for the second type of correlation, showing that another step has been done in the direction of reliable pile performance prediction on the basis of a careful controlled installation process.

ACKNOWLEDGEMENTS

The Authors are grateful to Maria Vicario, Sara Ersilia Sansone and Sara Polidoro for their effort in performing the statistical analyses during their Master thesis works.

REFERENCES

- Mandolini A., Ramondini, M., Russo, G., Viggiani, C., 2002. Full scale loading tests on instrumented CFA piles. In *Deep Foundations 2002: An International Perspective on Theory, Design, Construction, and Performance* (pp. 1088–1097).
- Viggiani, C., Mandolini, A., Russo, G., 2012. *Piles and Pile Foundations*. Spon Press.
- Bustamante, M., and Jezequel, J.F. (1991). La mesure des deformations a l'aide des estensiometeres amovible. LCPC Methode d'essai n°34 LEPC, Paris
- Russo G. 2004 Full load test on instrumented micropiles. Proc. of Inst. of Civil Eng. Geotech. Eng. 157 (GE3), 127–135
- Mandolini A, Russo G. 2008. Statistical Analysis of CFA piles construction. *Proc. of 5th International Geotechnical Seminar Deep Foundations on Bored and Auger Piles*, BAP V, Ghent, 8–10 September 2008, ISBN 978-88-6342-027-2

Validation of CPT-based methods for estimation of footing settlement in sand

V.A. Sakleshpur, M. Prezzi & R. Salgado

Lyles School of Civil Engineering, Purdue University, West Lafayette, IN, USA

ABSTRACT: A variety of design methods have been proposed to estimate the settlement of footings in sand using cone penetration test (CPT) results. Yet, due to the limited number of well-documented, high-quality footing load tests, efforts still need to be made to assess the performance of these methods. This paper presents two case histories of full-scale, instrumented load tests performed on axially loaded, square footings in silica sand reported in the literature. The performance of the traditional Schmertmann method and more modern CPT-based methods are evaluated through a detailed comparison between the predicted footing load-settlement curves and those obtained from footing load test measurements. For the case histories considered, these modern methods are shown to generally produce more accurate, reliable, and consistent predictions of footing response in sand than the traditional Schmertmann method.

1 INTRODUCTION

Schmertmann's method (Schmertmann 1970, Schmertmann et al. 1978) is widely used in foundation engineering practice to predict the settlement of footings in sand using cone penetration test (CPT) data. The method is based on the following observations: (1) footing settlement results from vertical strains that start at some value at the base of the footing, peak at some depth below the footing base, and then approach zero below a certain depth, and (2) the representative elastic modulus of each sublayer within the influence zone of the footing is determined from the representative cone resistance for that sublayer. The genesis and shortcomings of Schmertmann's method have been critically reviewed by Pantelidis (2020). The main shortcoming of the method is that it is based on linear elasticity and does not account for modulus degradation with increasing footing settlement level.

Over the past two decades, several methods have been proposed for estimation of footing settlement in sand using CPT results. These methods may be broadly classified into three categories: (1) methods based on Schmertmann's approach but with some modifications and improvements (Lee et al. 2008, Lee & Salgado 2002, Mohamed et al. 2013, O'Loughlin & Lehane 2010), (2) methods that fit an equation to load test data after normalizing the unit load and settlement of the footing with respect to cone resistance and footing size, respectively (Mayne et al. 2012, Mayne & Dasenbrock 2018, Mayne & Illingworth 2010), and (3) methods that approximate the shape

of the footing load-settlement curve by an initial linear component followed by a nonlinear (parabolic) component (Gavin et al. 2009).

The reliability and accuracy of design methods in predicting the settlement of footings in sand can be assessed by comparing the predictions with measured results from instrumented footing load tests. In this paper, two case histories (Briaud & Gibbens 1997, Lehane et al. 2008) comprising a total of nine instrumented, full-scale load tests performed on square footings in sand at Perth, Australia (four footings), and Texas, USA (five footings), are documented. The footing load-settlement curves predicted by four CPT-based design methods (Schmertmann et al. 1978, Lee & Salgado 2002, Gavin et al. 2009, and Mayne et al. 2012) were compared with the data obtained from the footing load tests.

Of these, the method by Mayne et al. (2012) is a purely direct CPT-based method, i.e. the method relies only on CPT data (e.g. cone resistance q_c) to the exclusion of other variables. The other three methods are indirect or soil property-based methods; for example, the method by Schmertmann et al. (1978) requires the estimation of a representative Young's modulus E from q_c and the calculation of a strain influence factor I_z ; the method by Lee & Salgado (2002) accounts for the dependency of the ratio E/q_c on footing settlement level w , footing size B , and relative density D_R ; while the method by Gavin et al. (2009) requires the small-strain Young's modulus E_0 as input in addition to q_c . A summary of the equations involved in these design methods can be found in Sakleshpur et al. (2021a).

2 CASE HISTORIES

2.1 UWA footing load tests (Lehane et al. 2008)

2.1.1 Site description and cone resistance profiles

Lehane et al. (2008) reported the results of four, instrumented, footing load tests performed at the University of Western Australia (UWA) test site at Shenton Park, Perth, Australia. The soil profile at the site consists of 5–7 m of poorly graded, medium-dense, siliceous dune sand overlying weakly cemented Tamala limestone. The sand layer is of Holocene age and was formed from the chemical weathering (dissolution) of limestone with subsequent erosion, transportation, and re-deposition by wind (Lehane et al. 2008, Schneider 2007). The presence of small quantities (< 5%) of remnant carbonates from the parent limestone provides the potential for very light cementation and bonding between the sand particles (Lim & Lehane 2014). The groundwater table is typically located at a depth of about 5.5 m, just above the limestone layer. The degree of saturation S of the sand layer is typically less than 15% and varies seasonally by up to about 5% (Lehane et al. 2004, 2008, Lim & Lehane 2014). Table 1 summarizes the properties of Shenton Park sand; the sand particles are sub-angular to sub-rounded in shape.

Table 1. Properties of Shenton Park sand (Lehane et al. 2004, Schneider et al. 2008).

Property	Unit	Value
Particle sizes D_{10} , D_{50} , D_{60}	mm	0.21, 0.42, 0.47
Coefficient of uniformity C_U	—	2.24
Fines content	%	< 5
Unit weight γ_m^*	kN/m ³	16.14–16.63
Minimum void ratio e_{min}	—	0.45
Maximum void ratio e_{max}	—	0.81
Relative density D_R	%	35–55
Critical-state friction angle ϕ_c^{**} (°)	(°)	32

* Based on *in situ* sand replacement density tests.

** Based on isotropically-consolidated ($p' = 100$ kPa) triaxial compression tests performed on specimens reconstituted to $e_0 = 0.60$ ($D_R = 58.3\%$).

Figure 1 Shows the cone resistance profiles obtained from four CPT soundings performed at the site. Based on self-boring pressuremeter test (SBPMT) results, Lehane et al. (2008) stated that the coefficient of lateral earth pressure at-rest K_0 decreases from 0.70 at a depth of 1.3 m to a relatively constant value of 0.43 below a depth of 2.3 m. Using this information, we considered a constant K_0 value of 0.70 between 0–1.3 m depth, a linear decrease in K_0 from 0.70 to 0.43 between 1.3–2.3 m depth, and a constant K_0 value of 0.43 for depths greater than 2.3 m (Sakleshpur et al. 2021b).

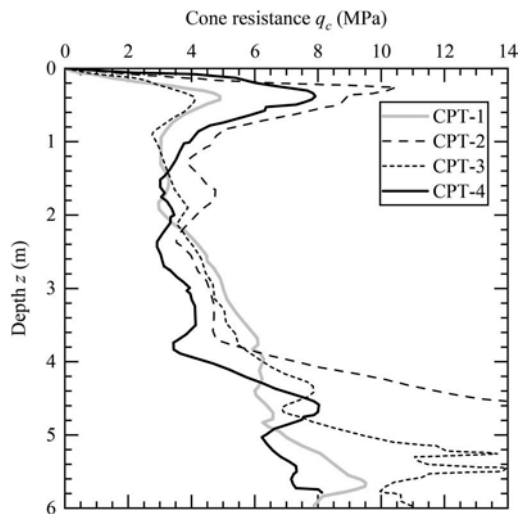


Figure 1. Cone resistance profiles obtained from four CPT soundings performed at Shenton Park [digitized from Schneider (2007)].

2.1.2 Footing dimensions and loading details

Table 2 summarizes the width, thickness, and embedment depth of four square footings constructed inline at the site. The center-to-center distance between the footings is about 5.5 m for footings 1 and 2, 5.2 m for footings 2 and 3, and 4.1 m for footings 3 and 4 (Schneider 2007). The four CPT soundings, CPT-1 to CPT-4, were performed at a horizontal distance of about 3 m from the centerline of footings 1–4, respectively (Schneider et al. 2008). The soundings were performed about nine days after the footings were constructed and six days before they were tested (Schneider 2007). The footings were loaded up to a maximum value of about 200 kN in increments of 15–20 kN using the reaction provided by a 25-tonne CPT truck; each load increment was maintained for about 10 minutes (Lehane et al. 2008).

Table 2. Dimensions of Shenton Park footings (Lehane et al. 2008).

Footing	Width B (m)	Embedment depth D (m)	Thickness t (m)
1	1.5	1.0	1.0
2	1.0	1.0	1.0
3	1.0	0.5	0.5
4	0.67	1.0	1.0

2.1.3 Comparison between predicted and measured load-settlement curves

Figure 2 compares the load-settlement curves of footings 1–4 obtained from the footing load tests at Shenton Park with those predicted using the methods of Schmertmann et al. (1978), Lee & Salgado (2002), Gavin et al. (2009), and Mayne et al. (2012). For aged, normally consolidated silica sand, the parameter λ in

the Lee & Salgado (2002) method was set to a value of 0.53 (Sakleshpur et al. 2021b), while the E/q_c ratio in the Schmertmann et al. (1978) method was set to a value of 3.5 (Robertson & Campanella 1989). The following points should be noted for the Gavin et al. (2009) method: (1) The normalized yield settlement level w_y/B and small-strain Poisson's ratio ν_0 were set to values of 0.03% and 0.15, respectively, (2) The depth profiles of small-strain shear modulus G_0 obtained from the results of two seismic cone penetration tests performed at the site were averaged to obtain a representative G_0 profile, and the small-strain Young's modulus E_0 was then determined using the relationship $E_0 = 2G_0(1 + \nu_0)$, and (3) The effect of time-dependent settlement (creep) was considered by setting the values of parameters t and t_R as 600 seconds and 100 seconds, respectively; t = time elapsed since the application of the load increment, and t_R = reference time corresponding to the onset of creep settlement.

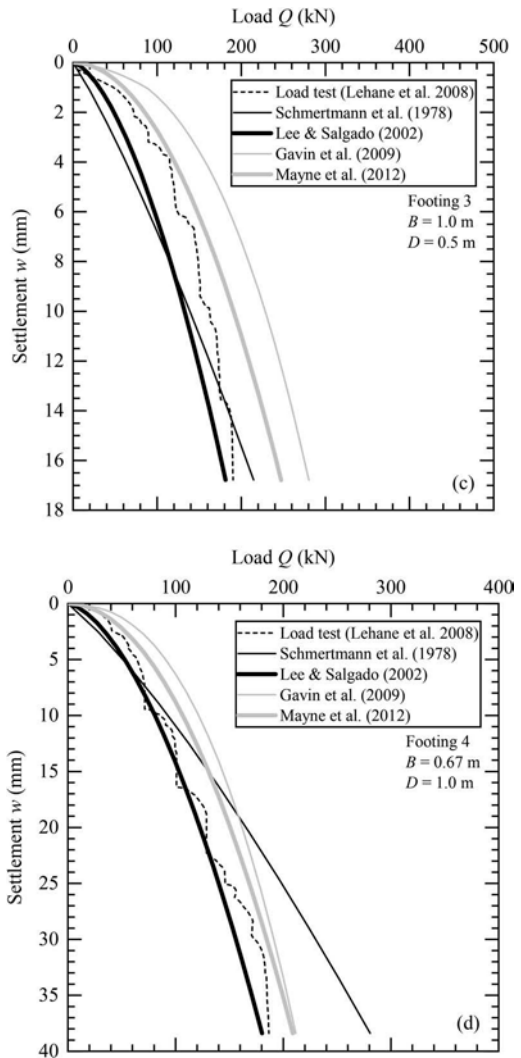
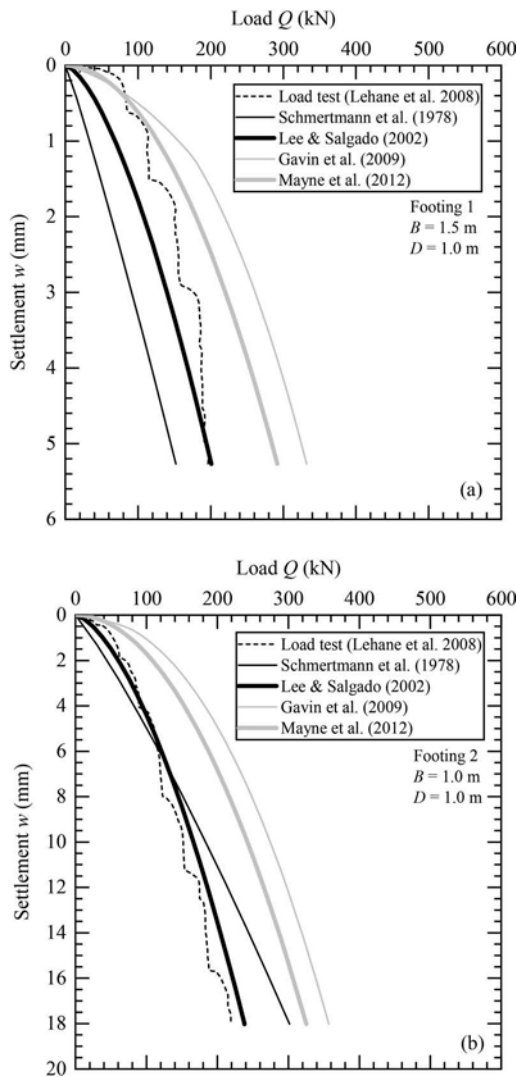


Figure 2. Comparison between predicted and measured load-settlement curves at Shenton Park for (a) Footing 1, (b) Footing 2, (c) Footing 3, and (d) Footing 4.

Although unload-reload tests were performed on the footings, the unload-reload loops of the measured load-settlement curves were not included in Figure 2 for simplicity. According to Lehane et al. (2008), some of these loops were unplanned and arose due to on-site difficulties with the pump for the hydraulic jack. It can be seen from Figure 2 that the load-settlement curves obtained using the Lee & Salgado (2002) method are either in good agreement (e.g. footings 2 and 4) or slightly conservative (e.g. footings 1 and 3) with respect to the UWA footing load test data than those obtained using the other methods considered in this study.

2.2 Texas A&M footing load tests (Briaud & Gibbens 1997)

2.2.1 Site description and cone resistance profiles

Briaud & Gibbens (1997) reported the results of five, instrumented, footing load tests performed at the National Geotechnical Experimentation Site on the Texas A&M University Riverside Campus near College Station, Texas, USA. The soil profile at the site consists predominantly of medium-dense, silty fine silica sand of Pleistocene age up to a depth of 11 m. The fines content at the site generally varies from about 8% near the ground surface to 35% at a depth of 9 m; the fines are nonplastic. The silty sand layer is overconsolidated due to the desiccation of the fines and the removal of 0.5–1.5 m of overburden prior to the construction of the footings. Below the silty sand layer, there is a very stiff, marine clay deposit of Eocene age extending down to a depth of about 33 m. The liquid limit LL and plasticity index PI of the clay layer are 40% and 21%, respectively. The groundwater table was observed at a depth of 4.9 m from the ground surface. Table 3 summarizes the properties of the silty sand layer at the site.

Table 3. Properties of silty sand layer at Texas A&M (Briaud & Gibbens 1997).

Property	Unit	Value
Specific gravity G_s	—	2.64–2.66
Mean particle size D_{50}	mm	0.15–0.20
Coefficient of uniformity C_U	—	1.8–2.4
Unit weight γ_m	kN/m ³	15.28–15.65
Minimum void ratio e_{min}	—	0.62–0.65
Maximum void ratio e_{max}	—	0.91–0.94
Relative density D_R	%	55
Critical-state friction angle ϕ_c^*	(°)	34.2

* Based on consolidated, drained triaxial compression test results.

Figure 3 shows the cone resistance profiles obtained from five CPT soundings performed at the site. It can be seen that the cone resistance q_c obtained from sounding CPT-7 is very low (≈ 300 kPa) at a depth of 3 m. The corresponding values of sleeve resistance f_s and friction ratio f_s/q_c were also reported to be very low at this depth (Briaud & Gibbens 1997). However, results obtained from adjacent CPT soundings (CPT-2 and CPT-6) reveal that the cone resistance at a depth of 3 m is about 6 MPa, which is 20 times greater than that obtained from sounding CPT-7. In addition, results obtained from an SPT boring (SPT-1) adjacent to CPT-7 show that the SPT blow count at a depth of 3 m is equal to 22 (Briaud & Gibbens 1997). Therefore, we believe that the very low q_c values observed for sounding CPT-7 near a depth of 3 m may not reflect the true soil state below footing 3. Accordingly, for a depth of about 2.0–3.5 m, instead of using the q_c profile obtained directly from sounding CPT-7, we considered the cone resistance to increase linearly from 4.2–6.5 MPa within this depth range.

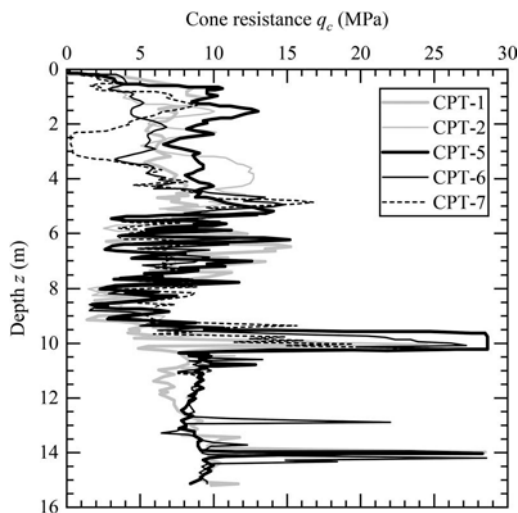


Figure 3. Cone resistance profiles obtained from five CPT soundings performed at Texas A&M [digitized from Briaud & Gibbens (1997)].

2.2.2 Footing dimensions and loading details

Table 4 summarizes the as-built dimensions and embedment depths of the footings. The footings were loaded using the reaction provided by four 0.91-m-diameter, 21.3-m-long, belled drilled shafts (with 60° under-reamed bells of 2.7 m base diameter) and one 0.91-m-diameter, 5-m-long, cylindrical drilled shaft. The footings were loaded in increments equal to 1/10th of the footing capacity estimated by Briaud & Gibbens (1999) using traditional bearing capacity calculation methods. Each load increment was typically maintained for 30 minutes. The layout of the footings and CPT soundings at the site can be found in Briaud & Gibbens (1997) – CPTs 1 and 2 correspond to footings 5 and 4, respectively, while CPTs 5–7 correspond to footings 1–3, respectively.

Table 4. As-built dimensions of Texas A&M footings (Briaud & Gibbens 1999).

Footing	Length $L \times$ width B [as-built (m)]	Embedment depth D (m)	Thickness t (m)
1	3.004 \times 3.004	0.762	1.219
2	1.505 \times 1.492	0.762	1.219
3	3.023 \times 3.016	0.889	1.346
4	2.496 \times 2.489	0.762	1.219
5	0.991 \times 0.991	0.711	1.168

2.2.3 Comparison between predicted and measured load-settlement curves

Figure 4 compares the load-settlement curves of footings 1–5 obtained from the footing load tests at Texas A&M with those predicted using the methods of Schmertmann et al. (1978), Lee & Salgado (2002), Gavin et al. (2009), and Mayne et al. (2012).

For overconsolidated silica sand, the parameter λ in the Lee & Salgado (2002) method was set to a value of 0.91 (Sakleshpur et al. 2021b), while the E/q_c ratio in the Schmertmann et al. (1978) method was set to a value of 6.0 (Robertson & Campanella 1989). The following points should be noted for the Gavin et al. (2009) method: (1) The values of w_v/B and v_0 were set to 0.03% and 0.15, respectively, (2) The depth profiles of small-strain shear modulus G_0 obtained from the results of *in situ* cross-hole tests performed at the site were averaged to obtain a representative G_0 profile from which the values of the small-strain Young's modulus E_0 were obtained, and (3) The effect of time-dependent settlement (creep) was not included in the analysis of this case history because the equation to model the creep response was developed by Lehane et al. (2008) primarily for the Shenton Park site.

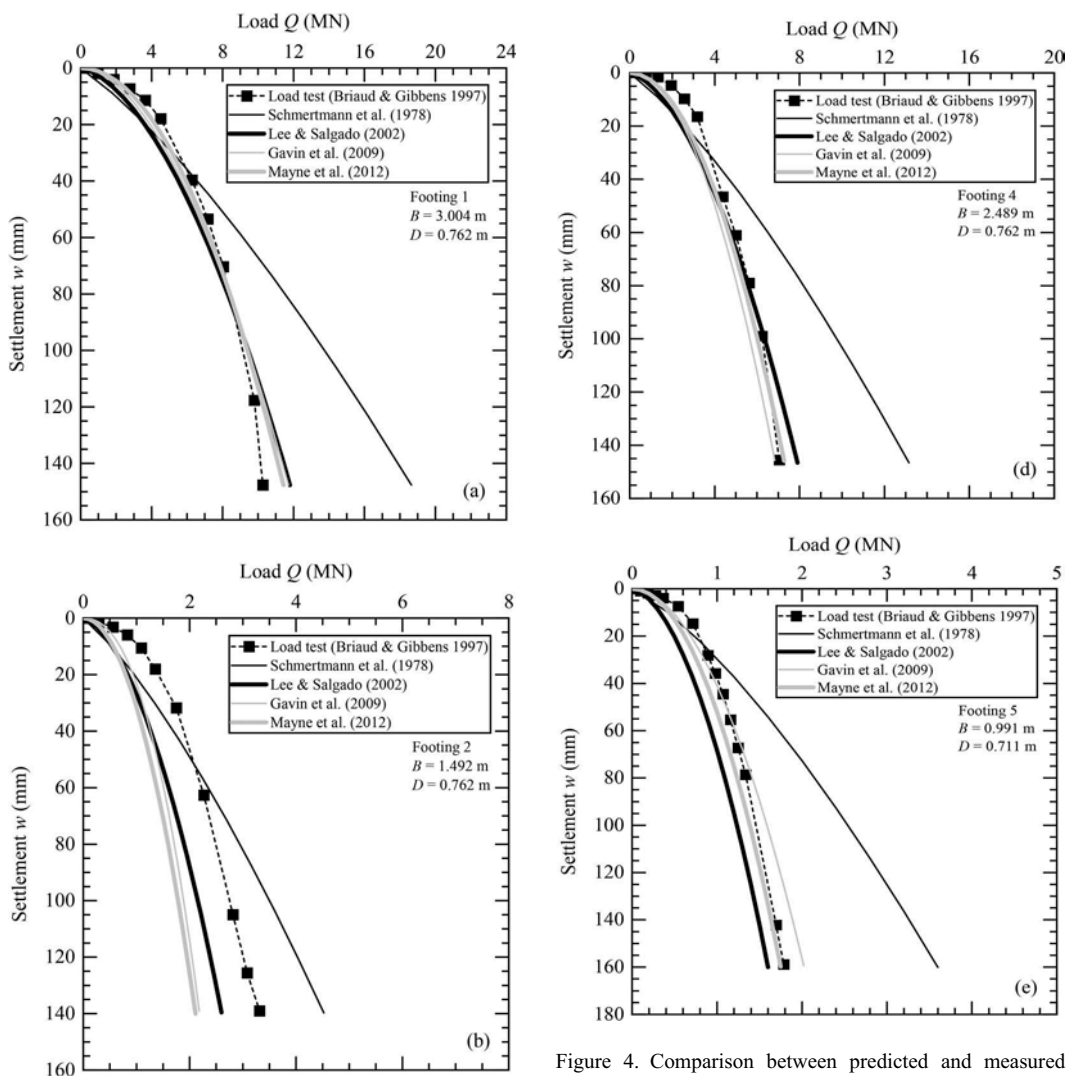


Figure 4. Comparison between predicted and measured load-settlement curves at Texas A&M for (a) Footing 1, (b) Footing 2, (c) Footing 3, (d) Footing 4, and (e) Footing 5.

The data points on the measured load-settlement curves shown in Figure 4 correspond to the footing settlements obtained at the end of each load increment during the load tests; for simplicity, all unload-reload cycles have been removed from these curves. It can be seen from Figure 4 that the load-settlement curves obtained using all the methods, except that of Schmertmann et al. (1978), are in fairly good agreement with the Texas A&M footing load test data over a wide range of settlement levels. The load-settlement response obtained using the Schmertmann et al. (1978) method tends to be unconservative when the load or settlement level increases beyond the range to which the representative Young's modulus applies.

The method by Gavin et al. (2009) is sensitive to the value of relative settlement w_s/B up to which the small-strain Young's modulus E_0 is assumed to operate. For example, in the UWA case history, if the value of w_s/B is decreased from 0.03% [the value suggested by Gavin et al. (2009)] to 0.005% (Lehane et al. 2008), the footing load-settlement curves obtained using the Gavin et al. (2009) method would be in better agreement with the load test data. In contrast, the method by Mayne et al. (2012) was developed based on statistical (regression) analysis of a footing load test database; both the UWA and Texas A&M footings were a part of this database.

3 CONCLUSIONS

The paper presents two case histories of axial load tests performed on full-scale, instrumented, square footings in silica sand. The load-settlement curves obtained from the test results for each of the nine footings were reported. Four CPT-based footing design methods were used to predict the load-settlement curves of the test footings in both case histories. The estimated load-settlement curves were compared with those obtained from the footing load tests to assess the performance of the design methods. Among the four footing design methods, the Lee & Salgado (2002) method generally provides the most accurate load-settlement estimates for the case histories considered in this paper. Finally, from a practical standpoint, the paper demonstrates the applicability of CPT data and CPT-based methods for estimation of footing settlement in sand.

REFERENCES

Briaud, J.-L. & Gibbens, R. 1997. *Large-scale load tests and data base of spread footings on sand*. Report No. FHWA-RD-97-068. McLean, VA: Federal Highway Administration.

Briaud, J.-L. & Gibbens, R. 1999. Behavior of five large spread footings in sand. *Journal of Geotechnical and Geoenvironmental Engineering* 125(9): 787–796.

Gavin, K., Adekunte, A. & O'Kelly, B. 2009. A field investigation of vertical footing response on sand. *Proceedings of the ICE-Geotechnical Engineering* 162(5): 257–267.

Lee, J. & Salgado, R. 2002. Estimation of footing settlement in sand. *International Journal of Geomechanics* 2(1): 1–28.

Lee, J., Eun, J., Prezzi, M. & Salgado, R. 2008. Strain influence diagrams for settlement estimation of both isolated and multiple footings in sand. *Journal of Geotechnical and Geoenvironmental Engineering* 134(4): 417–427.

Lehane, B.M., Ismail, M.A. & Fahey, M. 2004. Seasonal dependence of in situ test parameters in sand above the water table. *Geotechnique* 54(3): 215–218.

Lehane, B.M., Doherty, J.P. & Schneider, J.A. 2008. Settlement prediction for footings on sand. *Deformation characteristics of geomaterials; Proc. 4th intern. symp., Atlanta, GA*, Vol. 1, 133–150. Amsterdam: IOS Press.

Lim, J.K. & Lehane, B.M. 2014. Characterisation of the effects of time on the shaft friction of displacement piles in sand. *Géotechnique* 64(6): 476–485.

Mayne, P.W. & Illingworth, F. 2010. Direct CPT method for footing response in sands using a database approach. *Cone penetration testing; Proc. 2nd intern. symp., Huntington Beach, CA, 9-11 May*, Vol. 3, 315–322.

Mayne, P.W., Uzielli, M. & Illingworth, F. 2012. Shallow footing response on sands using a direct method based on cone penetration tests. *Full-scale testing and foundation design: Honoring Bengt H. Fellenius (GSP 227); Proc. GeoCongress 2012, Oakland, CA, 25–29 March*, 664–679. Reston, VA: ASCE.

Mayne, P.W. & Dasenbrock, D. 2018. Direct CPT method for 130 footings on sands. *Innovations in geotechnical engineering: Honoring Jean-Louis Briaud (GSP 299); Proc. IFCEE 2018, Orlando, FL, 5–10 March*, 135–146. Reston, VA: ASCE.

Mohamed, F.M.O., Vanapalli, S.K. & Saatcioglu, M. 2013. Generalized Schmertmann equation for settlement estimation of shallow footings in saturated and unsaturated sands. *Geomechanics and Engineering* 5(4): 343–362.

O'Loughlin, C.D. & Lehane, B.M. 2010. Nonlinear cone penetration test-based method for predicting footing settlements on sand. *Journal of Geotechnical and Geoenvironmental Engineering* 136(3): 409–416.

Pantelidis, L. 2020. A critical review of Schmertmann's strain influence factor method for immediate settlement analysis. *Geotechnical and Geological Engineering* 38(1): 1–18.

Robertson, P.K. & Campanella, R.G. 1989. *Guidelines for geotechnical design using the cone penetrometer test and CPT with pore pressure measurement*. 4th Edition, Columbia, MD: Hogentogler & Co.

Sakleshpur, V.A., Prezzi, M., Salgado, R. & Zaheer, M. 2021a. *CPT-based geotechnical design manual, Volume 2: CPT-based design of foundations (methods)*. West Lafayette, IN: Purdue University (in press).

Sakleshpur, V.A., Prezzi, M., Salgado, R. & Zaheer, M. 2021b. *CPT-based geotechnical design manual, Volume 3: CPT-based design of foundations (example problems)*. West Lafayette, IN: Purdue University (in press).

Schmertmann, J.H. 1970. Static cone to compute static settlement over sand. *Journal of the Soil Mechanics and Foundations Division* 96(3): 1011–1043.

Schmertmann, J.H., Hartmann, J.P. & Brown, P.R. 1978. Improved strain influence factor diagrams. *Journal of the Geotechnical Engineering Division* 104(8): 1131–1135.

Schneider, J.A. 2007. *Analysis of piezocone data for displacement pile design*. Ph.D. Dissertation. Perth, Australia: The University of Western Australia.

Schneider, J.A., Fahey, M. & Lehane, B.M. 2008. Characterisation of an unsaturated sand deposit by in situ testing. *Geotechnical and Geophysical Site Characterization 3; Proc. 3rd intern. conf., Taipei, 1–4 April*, 633–638. CRC Press.

Derivation of SRD for driven piles from CPT data

J.A. Schneider

U.S. Army Corps of Engineers, St. Paul, MN, USA

M.F. Randolph & J.P. Doherty

The University of Western Australia, Australia

ABSTRACT: Measurements from the cone penetration test are analogous to parameters used in assessing the static component of the soils pile driving resistance. This paper presents comparisons of pile driving data from 610 mm open ended pipe piles driven through lake clays into underlying glacial till, with estimates of driving resistance using the web-based software, IMPACT. IMPACT uses a continuum-based soil model that explicitly separates internal and external shaft friction in the soil-pile model. CPT based expressions for evaluating the static resistance to driving include factors that account for end condition, friction fatigue and differences in the diameter of the CPT and the pile. Evaluation of static tension load test results requires additional estimates of setup and relative contribution of driving resistance from the soil plug.

1 INTRODUCTION

Data from cone penetration tests (CPT) are ideal for assessing the ‘static resistance to driving’ (SRD) of a pile as well as for evaluating long-term axial capacity after installation and equalization. Pile-soil interaction parameters can be derived from the cone data, including values of end-bearing resistance and maximum values of shaft friction relevant in the current vicinity of the pile tip.

The sleeve friction measurement, while conceptually similar to pile shaft friction, has complications in application to assessing both long-term static resistance and short-term pile driving resistance. This is illustrated in Figure 1 by comparing average long term shaft friction from pile load tests ($\tau_{f,avg}$) in clay to average CPT sleeve friction ($f_{s,avg}$). The ratio of $\tau_{f,avg}/f_{s,avg}$ ranges from over three to approximately 0.5. For low values of $f_{s,avg}$, setup, or the increase in capacity with time due to equalization of pore water pressures tends to control the ratio. For high values of $f_{s,avg}$, the ratio is less than unity, implying that friction fatigue, or the reduction in local friction with continued pile penetration, tends to dominate long term pile friction when compared to CPT sleeve friction.

For the case of pile driving, evaluation of pile shaft friction from CPT sleeve friction would seem to be simpler than attempting to assess setup for evaluating the long-term capacity. However, viscous rate effects and separating the contribution of internal as compared to external shaft friction for open ended piles still require additional analysis and interpretation. This paper presents interpretation of pile drivability, stress

wave analysis, and pile load testing for a case history of an open-ended pile in clay. The stress waves are analyzed systematically to provide insight into the derivation of the SRD from CPT parameters.

Dynamic analysis of piles, including drivability studies and stress-wave analysis following a dynamic test, is presented in this paper, using the web-based software, IMPACT. The software allows input of CPT data as the basis for assessing relevant pile-soil interaction parameters, with several published recommendations for estimating pile SRD from CPT data being included as options. However, the web-app allows the user to input their own algebraic expressions relating, for example, maximum shaft friction to cone tip resistance for any given soil behaviour type, and similarly for the friction degradation functions and the end-bearing resistance. Application of the web-app is illustrated with an example field study where dynamic stress-wave data were measured during driving of an open-ended pile in lake clay overlying glacial till.

2 SITE CHARACTERIZATION, FARGO, ND

Data discussed in this paper were collected as part of a load test program at the Diversion Inlet Structure, in Fargo, ND, USA. Site characterization included piezocone penetration tests (CPTU), prebored pressuremeter tests (PMT), standard borings and index testing, as well as laboratory triaxial and oedometer tests.

Figure 2 shows results of a CPTU performed adjacent to the pile driving locations, along with PMT and index test results collected in the area. The site

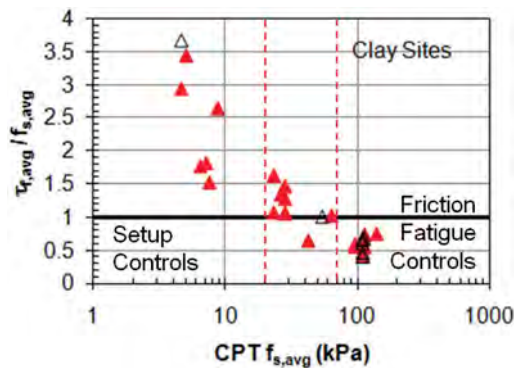


Figure 1. Comparison of ratio of average pile shaft friction to average CPT sleeve friction (database used discussed in Schneider 2010).

consisted of approximately 13 m of lake clays underlain by glacial till. Most CPTs were terminated at the top of the till. The CPTU shown had the deepest penetration in the till, of about 2.5 m. CPT refusal in the clay till was typically associated with sharp changes in cone inclination which exceeded 1 degree over a 1 m push length.

3 PILES AND DRIVING DATA

Two 18.3 m long, 610 mm diameter x 19 mm wall thickness ($D/t = 32$) open ended pipe piles were driven with a Delmag D46-32 hammer to a depth of approximately 16.2 m. Each pile was monitored with a pile driving analyzer (PDA) during installation. One pile (TP-7) was statically load tested after a setup time of 120 days. The second pile, TP-8, was restruck at 125 days after installation.

Figure 3 shows the collected pile driving data (blowcount, stroke, and transferred energy) adjacent to the CPTU cone tip resistance. In addition to the measured CPTU data, the geometric mean of tip resistance taken either from 4 equivalent diameters (D_{eq}) above the cone tip to 2 D_{eq} below the cone tip, or from 4 diameters (D) above the cone tip to 2 diameters below, are shown. The equivalent pile diameter of 210 mm represents a solid circle with the same area of steel as the pile annulus. Average cone tip resistance and sleeve friction were used in analyses.

The Delmag D46-32 hammer has a rated energy of 165 kN-m. Hammer efficiencies ranged from 35% in the lake clays to 45% in the glacial till for TP-7 and from 40% to 55% for TP-8.

4 DRIVABILITY ANALYSIS

The background and workflow for an IMPACT pile drivability analysis is discussed by Randolph (2008)

and Doherty et al. (2020). Equations based on the Alm & Hamre (2001) drivability method were used in this paper to account for friction fatigue. The method includes friction fatigue that leads to a reduction in local shaft friction (τ_s) with height (h) above the pile tip (in m) according to

$$\tau_s = \tau_{min} + (\tau_{max} - \tau_{min}) \exp(-hk) \quad (1)$$

The rate of friction fatigue (k) increases with normalized cone tip resistance according to

$$k = (q_t / \sigma'_v)^{0.5} / 80 \quad (2)$$

The soils at the site are predominantly clayey. The maximum shaft friction is evaluated from CPTU sleeve friction, and the minimum shaft friction is related to normalized cone tip resistance by

$$\tau_{max} = f_s (\sigma'_v / 100 kPa)^{0.13} \quad (3)$$

$$\tau_{min} = \frac{q_t}{250} \left(1 - \frac{q_t / p'_0}{400} \right) \quad (4)$$

The end bearing in clays is taken as 60% of the cone tip resistance.

Soil stiffness was based on secant unload-reload modulus from pressuremeter tests. This resulted in ratios of G/q_b of approximately 30 and G/τ_s of 200. Poisson's ratio was taken as 0.5. Viscous rate effects were used to evaluate dynamic shaft friction (τ_d) using a power law function of

$$\tau_d = \tau_s \left[1 + \alpha \left(\frac{\Delta v}{v_{ref}} \right)^\beta \right] \quad (5)$$

where v_{ref} is 1 m/s and Δv is the relative velocity between the pile and the soil. The parameter β was taken as unity for all soils. Softer clays used an α of 0.2, while heavily overconsolidated clays (Till) used an α of 0.06.

Comparisons between measured and calculated blowcounts using impact and a continuum soil model are shown in Figure 4. Two cases were analyzed: (1) with the plug friction taken as 1 percent of the external friction, and (2) with the plug friction equal to the external friction. The small amount of friction for the first case was primarily to maintain numerical stability. Minimal to zero plug friction is often used for drivability studies of open-ended piles.

Both cases overpredict blow counts in the upper lake clays, but show good agreement in the glacial till at the end of driving.

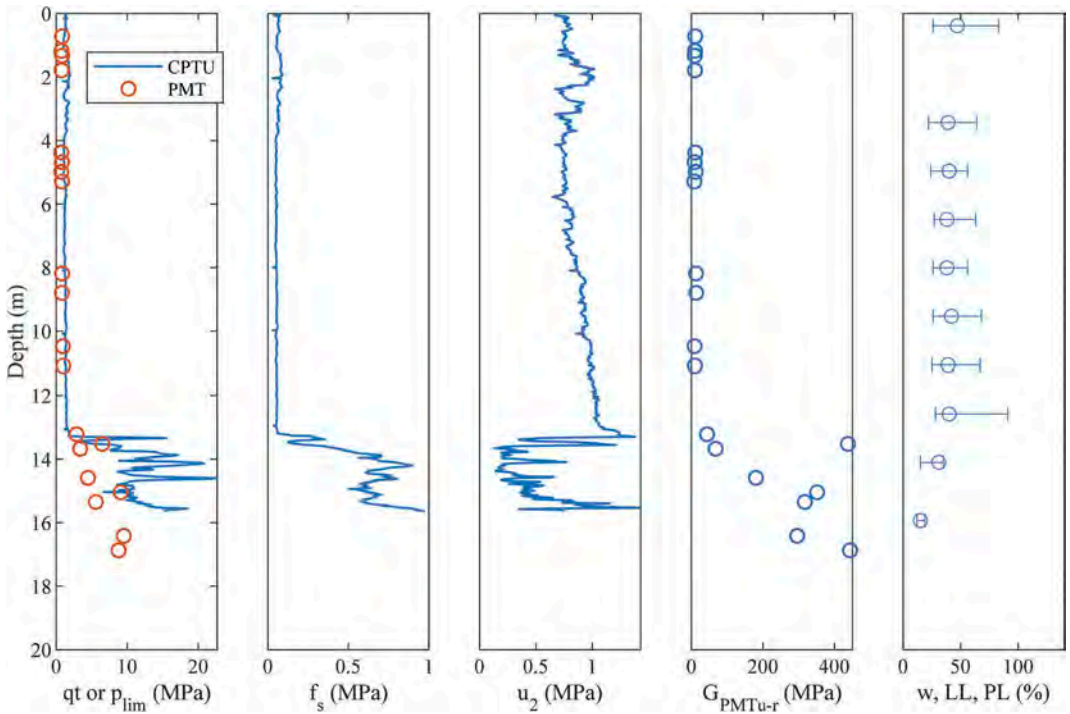


Figure 2. Site characterization data from the Fargo Diversion Inlet Structure site.

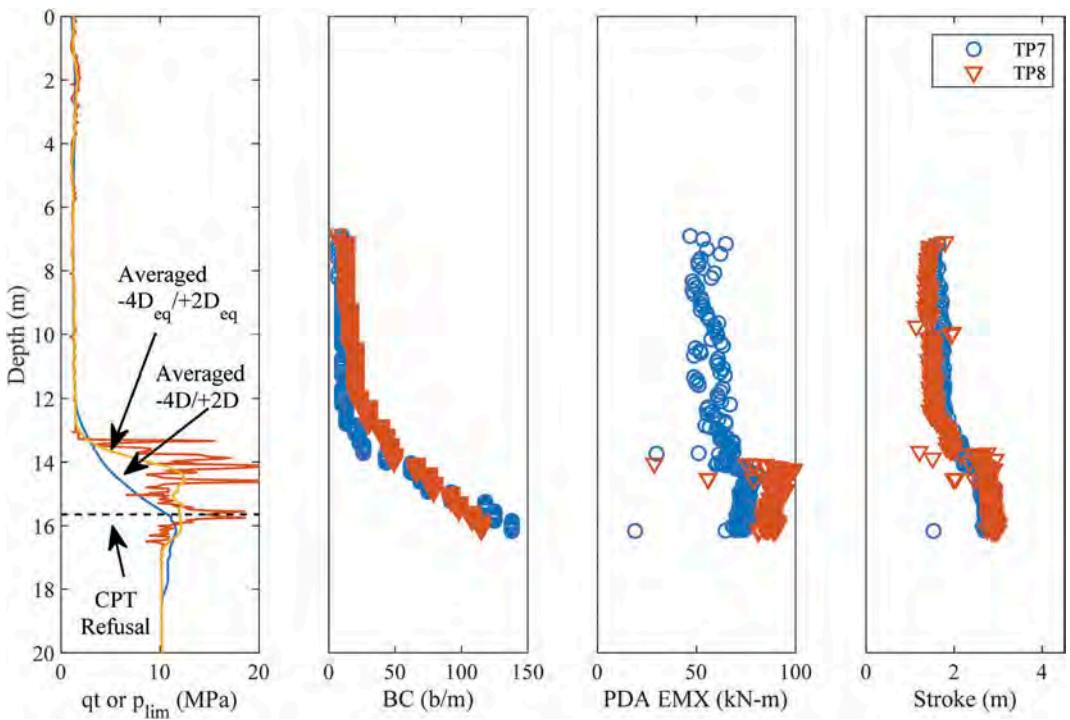


Figure 3. Pile driving data from the Fargo Diversion Inlet Structure site.

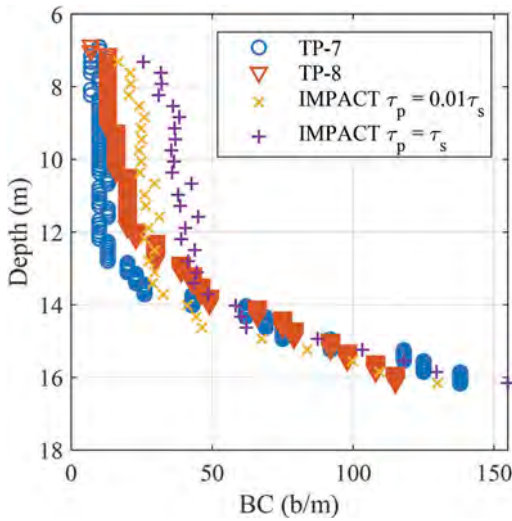


Figure 4. Comparison of Impact predictions of blowcount based on CPT data to measured results using Alm & Hamre (2001) method, and $\tau_{f,in} = 0.01\tau_{f,out}$ and $\tau_{f,in} = \tau_{f,out}$.

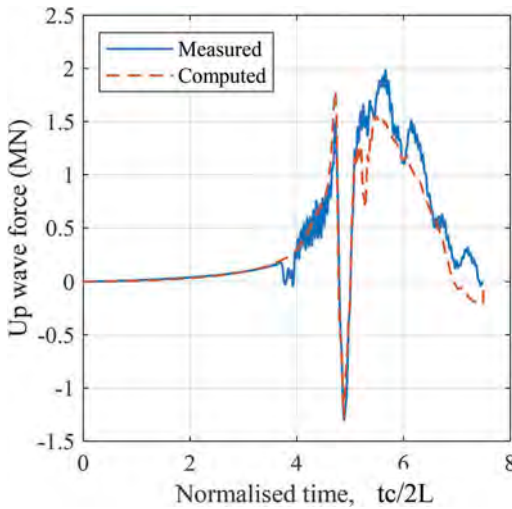


Figure 5. Comparison of measured and calculated wave up for TP-7 assuming resistance distribution from Alm & Hamre (2001) and $\tau_{f,in} = 10$ kPa.

5 SIGNAL MATCHING

Signal matching was undertaken using the downward travelling stress-wave as input and comparing the calculated and measured upward travelling stress waves (see, for example, Randolph 2003). The upward travelling wave is

$$F_u = 0.5(F - Zv) \quad (6)$$

where F is the force, v is the velocity, and Z is the pile impedance, EA/c . EA is the cross-sectional rigidity and c is the wave speed in the pile.

Stress wave measurements are presented for three cases: (i) the end of driving for TP-7 (300th blow); (ii) the end of driving for TP-8 (350th blow); and (iii) the beginning of restrike collected 125 days after driving on TP-8 (6th blow).

The first comparison in Figure 5 for TP-7 uses the recommended end bearing and shaft friction based on the Alm & Hamre (2001) method. The match between the measured and calculated upward traveling wave is good. However, the method assumes no internal shaft resistance for a coring case. This has historically been a reasonable assumption, since commercial wave equation analysis software does not explicitly model the soil plug. To logically step through the relationship between CPT and pile SRD parameters, modeling the soil plug explicitly becomes more useful.

A series of four analyses of upward traveling stress waves are shown in Figures 6 through 9 for pile TP-8 at the end of driving (EOD). Details of the analyses are:

1. Assume CPT parameters apply directly to the pile driving analysis with full internal friction, $\tau_s = f_s$, $q_b = q_t$, $\tau_p = \tau_s$ (Figure 6).
2. Essentially remove internal pile plug friction $\tau_p = 0.01\tau_s$ (Figure 7).
3. Reduce external friction using friction fatigue, increasing internal friction over lower two diameters of the pile (Figure 8).
4. Improve fit, increasing end bearing (Figure 9). Two more (5th and 6th) analyses are presented for the TP-8 beginning of restrike (BOR) blow to explore setup mechanisms, the results of which

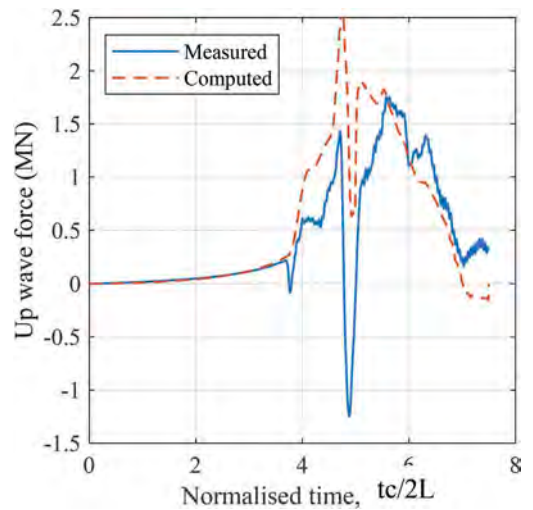


Figure 6. Comparison of measured and calculated wave up for TP-8 assuming $q_b = q_c$, $\tau_f = f_s$, and $\tau_{f,in} = \tau_{f,out}$ (Step 1).

are compared to static load test response in the next section.

5. Increase external friction to account for setup (Figure 10).
6. Increase internal friction to account for different pile response during restrrike (Figure 11).

Figures 6 and 7 show a calculated up wave force greater than the measured up wave force, for a normalized time between approximately 4 and 5. This indicates overprediction of soil resistance to

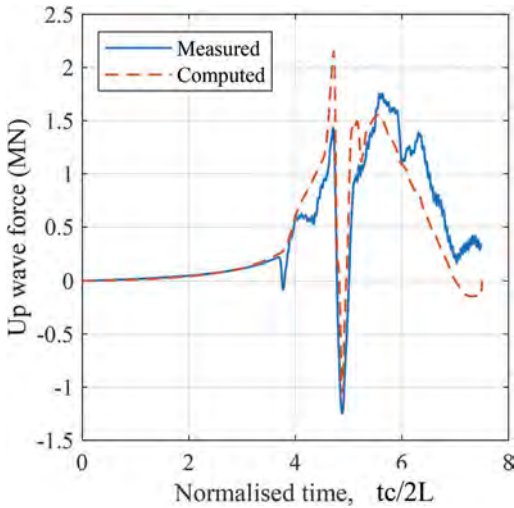


Figure 7. Comparison of measured and calculated wave up for TP-8 assuming $q_b = q_c$, $\tau_f = f_s$, and $\tau_{f,in} = 10$ kPa (Step 2).

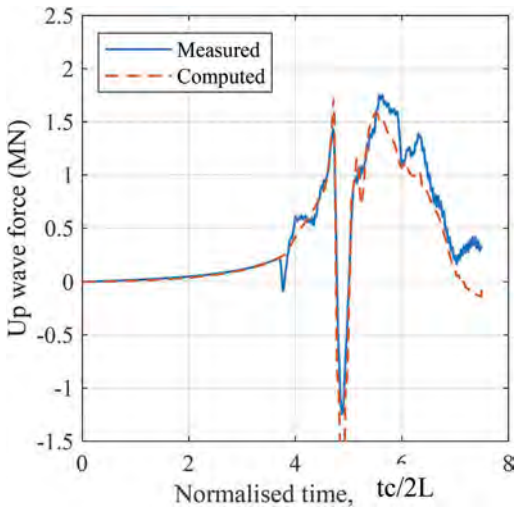


Figure 8. Comparison of measured and calculated wave up for TP-8 assuming $q_b = q_c$, but reducing τ_f for friction fatigue and adding some internal friction at bottom of pile (Step 3).

driving using CPT parameters, even when no internal friction from the plug is assumed.

Friction fatigue was used to reduce external friction. A greater rate of degradation (k) was needed for the till soils as compared to the softer lake clays. Some internal friction was needed for an acceptable match. A constant internal shaft friction of 700 kPa, approximately equal to the CPT sleeve friction, was used over the lower two diameters near the pile tip. A reasonable match for this case is shown in Figure 8.

The match was slightly improved in Figure 9, by increasing the annular base resistance from q_t to $1.4q_t$. The higher q_b is considered reasonable since

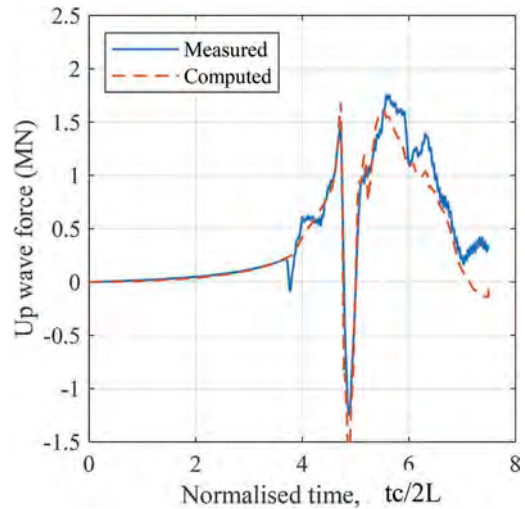


Figure 9. Improving fit from Step 3 by increasing $q_b = 1.4q_c$ (Step 4).

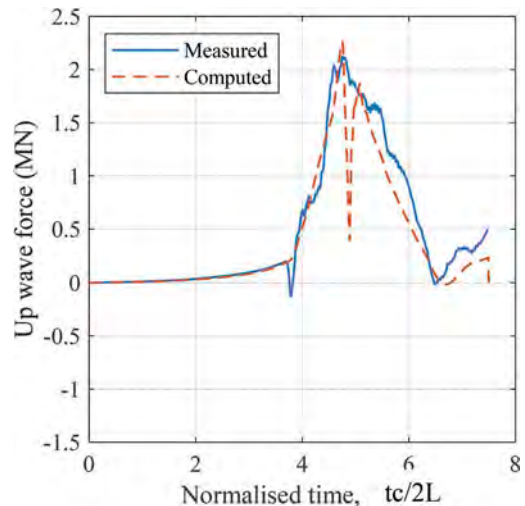


Figure 10. Matching TP-8 restrrike blow through increasing external friction.

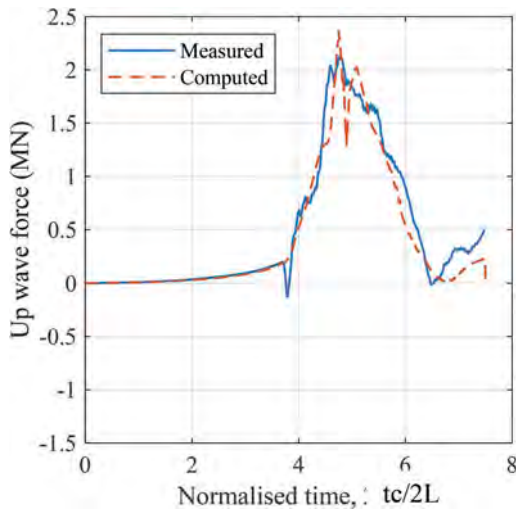


Figure 11. Improving restrike match for TP-8 by increasing internal friction.

CPT refusal was met (following increased inclination) prior to the termination tip elevation of the pile. It is likely that higher resistance layers exist in the till.

A restrike blow performed on TP-8 was recorded 125 days after pile installation, as shown in Figure 10. Compared to Figure 9, a significant increase in measured up wave resistance is shown. A two-step procedure was used to match the restrike blow:

1. The external friction was increased to match the peak up force.
2. The internal friction was increased to improve the overall fit.

The first estimate of external friction was based on using CPT sleeve friction directly, with no friction fatigue degradation. The match in Figure 10 was surprisingly good. This is not to imply that CPT sleeve friction is always a good match for long term pile capacity (see Figure 1). However, the comparison was reasonable for this pile. Increasing the plug length to 20D, and keeping the internal friction equal to the external friction leads to the best match using this technique, as shown in Figure 11.

6 LOAD TEST COMPARISON

A static load test was performed on TP-7 120 days after pile installation. The load-displacement curve is shown in Figure 12. The contributions of internal and external shaft friction, as well as annular base resistance and total plugged and unplugged capacity are shown in Table 1. The restrike blow for TP-8 showed an increase in capacity by a factor of approximately 1.3 compared to TP-8 at the end of driving. The

interpretation of the external shaft capacity from the restrike blow was approximately 10% less than the load test capacity.

Table 1. Summary of soil resistance inferred from dynamic measurements and static load tests.

	TP-7 EOD ¹	TP-8 EOD ²	TP-8 RS ²	TP-7 SLT
External Shaft (kN)	3899	2883	3794	4200
Internal Shaft (kN)	36	811	2988	
Base (kN)	257	581	581	
Unplugged (kN)	4192	4276	7364	
Plugged (kN)	6025	7704	8614	

¹ Assumed minimal internal friction

² Analysed using progressive CPT procedure

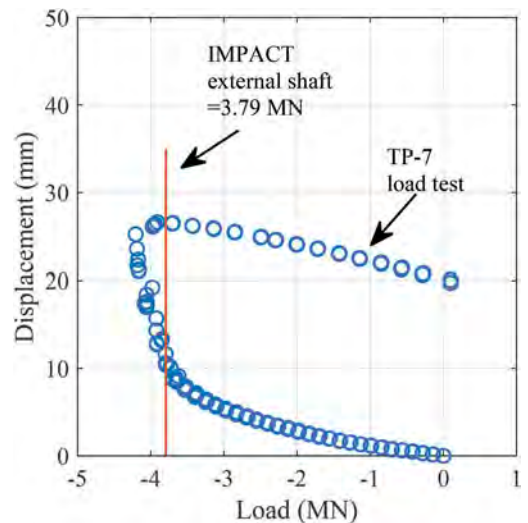


Figure 12. Comparison of external shaft friction from PDA signal matching to tension load test results on TP-7.

A point of interest from Table 1 comes from looking at the internal shaft friction. For TP-7, the analysis assumed that essentially all shaft friction is external. This is a common assumption for analysis of open-ended pipe piles, leading to three follow-on effects: (i) the effects of friction fatigue are underestimated; (ii) the effects of soil setup are underestimated; (iii) if plug resistance is ignored when interpreting restrikes, tension capacity could be significantly overpredicted.

7 CONCLUSIONS

This paper focused on analyses that highlight the mechanisms controlling the relationship between

soil-pile resistance and CPT parameters. Insights related to both soil resistance to driving and static capacity highlighted effects of friction fatigue and setup at this clayey site. The CPT is an excellent tool to constrain parameters used in pile analyses. However, additional mechanisms need to be included such that rational decisions can be made during installation as well as in relation to long term capacity.

DISCLAIMER

The views expressed are those of the authors and do not necessarily represent those of the U.S. Army Corps of Engineers.

REFERENCES

- Alm, T. and Hamre, L. (2001). Soil model for driveability predictions based on CPT interpretations. Proc. 15th International Conference on Soil Mechanics and Geotechnical Engineering, Istanbul, Turkey, 2, 1297–1302, 2001.
- Doherty, J.P., Randolph, M.F. and Schneider, J.A. (2020). Analyzing the driving performance of pile foundations using data driven models. Proceedings, ISFOG 2020: 664–673.
- Randolph, M.F. (2003). Science and empiricism in pile foundation design. *Géotechnique*, 53(10): 847–875.
- Randolph, M.F. (2008). IMPACT: Dynamic analysis of pile driving. Users' manual, version 4.2.
- Schneider, J.A. (2009). Uncertainty and bias in evaluation of LRFD ultimate limit state for axially loaded driven piles, *The Journal of the Deep Foundation Institute*, 3 (2): 25–36.

New method for assessing soil liquefaction resistance using a cyclic cone penetrometer

A. Sharma, P. Rapanakis, E. Incardona, C. Dano, L. Sibille & B. Chareyre

University of Grenoble Alpes, CNRS, Grenoble INP, 3SR, Grenoble, France

H.H. Sadrabadi

Equatech R&D, Equaterre, Annecy, France

ABSTRACT: This paper introduces a new methodology and machinery to extract soil properties and assess its liquefaction susceptibility. A mechanical Gouda tip cone penetrometer is used to apply a cyclic load on the soils. This test aims a load closer to real world liquefaction events, more robustness and a cheaper cost than a conventional CPTu. Since the cone tip used for the test does not have a pore pressure sensor, nor a friction sleeve and electrical or optical cables, it is of low maintenance, easy to operate and can be used to drill through gravel or any dense layer to reach layers of interest without digging a borehole, saving time and money. The liquefaction resistance is found using the response of soils to cyclic loading on the cone tip. The methodology also involves measuring the change of tip resistance before and after applying a cyclic load and correlates it to the volume changes that took place during it. For this, an experimental campaign was carried out in a new calibration chamber using a mini cone with stress and pore pressure changes measured independently in the soil during the cyclic load. The different response to cyclic load of clean Fontainebleau GA39 sand under different vertical stresses, saturation conditions and created by different sample preparation methods is studied. In turn, the pore pressure increase and the corresponding number of cycles during the cyclic cone penetration tests are compared with similar results from cyclic compressive triaxial tests. This allows us to find a relation between the loading applied in the two methods to cause a similar increase of pore pressure. Hence, a method is suggested to compare the loading applied by the cone penetrometer to the Cyclic Stress Ratio(CSR) expected in a liquefaction event. Eventually, using the CSR and CRR defined, the liquefaction susceptibility of the soils can be calculated.

1 INTRODUCTION

A new cone penetration testing methodology is introduced to predict liquefaction and extract soil properties. The cone we use for our tests is a mechanical Gouda tip (Figure 1) which lacks any sensors inside the tip. Instead, the tip resistance is measured using the force transmitted by the internal rods and recorded by a force sensor on the surface. The test uses a cone of standard 10 cm² surface area for the field experiments, while for the laboratory experiments, we use a miniature cone of 4 cm² to minimize boundary effects.

The loading devices, both at the site and in the laboratory, involves two different driving mechanisms. One for the constant penetration, to measure the tip resistance against penetration at a constant speed and to reach the desired depth for the cyclic test. The other is a cyclic jack capable of applying the cyclic load to the internal rod of the Gouda tip without moving the external rods. This jack is constrained in its total drive length (6 cm for laboratory and 10 cm for field experiments). For the laboratory experiments, a calibration chamber has been newly

developed in the 3SR laboratory to facilitate better placement of independent pore pressure and total stress sensors and for better control of saturation con-

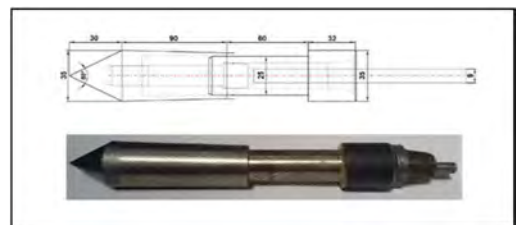


Figure 1. The schematic(top, sizing in mm) and image of the Gouda tip used for the field test.

ditions. The boundary conditions applied are fixed lateral and bottom boundaries, while the vertical stress is applied from top using a pressurized membrane with a hole in the center to allow the cone to enter the calibration chamber. The tip opening is measured using the internal measurement of the cyclic

jack and using a LVDT attached to a frame at the head of the cyclic jack. Under normal driving, the length of internal rods are chosen to ensure that the tip is slightly open (<0.5 cm) and all the tip force is transferred to the force sensor attached at the piston of the cyclic jack. The cyclic jack acts as a rigid frame for the internal rods and the force sensor during static driving. During the cyclic loading, the cyclic jack applies the load directly on the internal rods, which moves the front end of the tip without moving the external rods.

2 METHODOLOGY

The traditional CPTu relies on empirical relationships that use the pore pressure, the friction sleeve readings and the cone penetration resistance for predicting liquefaction resistance (Idriss & Boulanger 2006, Robertson 1990). These empirical relations are developed from comprehensive databases of tests done in-situ and in calibration chambers.

However, the dependency on empirical relationships, the complexity of use and susceptibility of the sensors to damage and malfunction leads to uncertainties in CPTu tests. Also, these tests are relatively expensive to perform, involves equipment with high maintenance cost and may also require boreholes to traverse through hard strata. As such, the CPTu test becomes an unpractical solution for a large number of geotechnical problems. Besides, the empirical relations used to predict liquefaction susceptibility and other soil properties may need to be adapted for local soil conditions.

Our novel approach tries to overcome a few of these shortcomings and provide a cost effective and reliable method to find liquefiable layers under all field conditions.

We use a mechanical Gouda tip to apply stress-controlled cycles on depths of interest. For each test, the outer rod of the cone penetrometer will be fixed, and the tip of the cone will be used to apply a cyclic load in accordance with the patented loading mechanism on the tip using the internal rods. The maximum displacement of the tip during each cyclic CPT test is 6 cm in the lab and 10 cm on the field. It is limited by the dimensions of the Gouda cone or/ and the maximum displacement of the jack applying the cyclic load. As such, in each cyclic test, we measure the properties of a layer of depth around 10 cm while the zone of influence of each test may be as high as 72 cm as is the case in conventional CPTu (Rogers 2006). The loading applied to the soil can be divided into eight steps which involve two pushes at a constant speed for 1 cm penetration, waiting times after each push while applying a constant force, and uniform stress cycles after the waiting time. The frequency used for the cyclic loading was 1 Hz, and the amplitude of cycles was decided based on the tip resistance measured during the initial push.

The number of cycles required for a given displacement, the displacement of tip during the waiting time, the rate of displacement during cycles, and the change of tip resistance before and after cycles are a few significant results being looked into to distinguish between different soil types and extract soil properties, especially the liquefaction susceptibility. The density of the soil, the stress state the soil exists in, are a few of the parameters that can affect the response of the soil and vary these results.

3 CHARACTERIZATION OF SAND

All the tests were performed on clean Fontainebleau GA39 sand whose main properties are summarized in Table 1.

Table 1. GA39 sand properties, from the supplier SIL-BECO, France.

SiO ₂ (%)	G _S (-)	d ₁₀ (mm)	d ₅₀ (mm)	d ₆₀ (mm)	C _u	e _{max}	e _{min}
>99.1	2.56	0.087	0.113	0.122	1.1	1.01	0.56

The sand grain shape is sub-angular, sub-rounded (Rimoy 2013). The grain size distribution of this sand falls directly under soils that are traditionally prone to liquefaction.

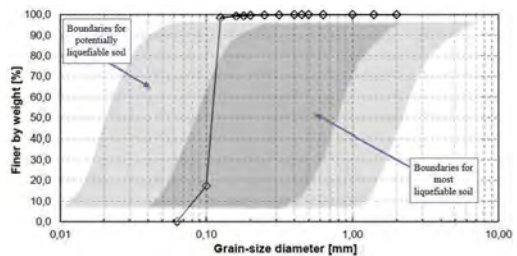


Figure 2. Grain size distribution for sand prone to liquefaction and Fontainebleau GA39 sand.

A number of laboratory experiments were performed to characterize the sand properties, its interaction with the cone, and the effect of sample preparation. Direct shear interface tests between smooth steel used to make the cone and the sand at constant normal stress resulted in a friction angle of 13.1°. We also performed constant head permeameter tests to study the effect of the sample preparation method on permeability. Moist tamping specimen created more permeable samples than those created by dry pluviation, which were more permeable than those created by dry tamping. In all cases, the order of magnitude of permeability was similar (10^{-5} m/s) and corresponded to those expected from fine sand.

However, the values varied between 3.4 to 7.1×10^{-5} m/s. These permeability values correspond to conditions of completely drained conditions during normal cone penetration. (McNeilan and Bugno, 1985).

Also, as a part of this study 20 tri-axial tests (6 drained, 14 un-drained) were performed to study the effect of sample preparation, back pressure, initial confining stress on very loose (Relative density <15%) or loose sand specimens (Relative density <35%). For the drained tests in Figure 3, we see a clear distinction

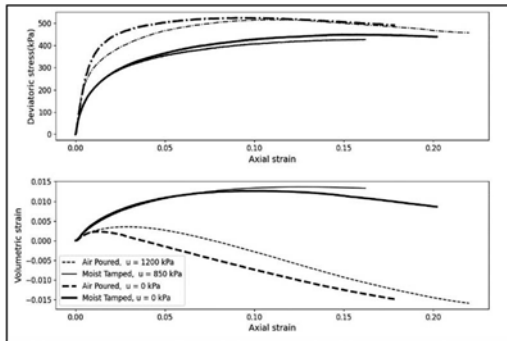


Figure 3. Varying drained behaviour for different sample preparation methods at 200 kPa confining stress.

in volumetric strain for tests done at similar confining stresses (200 kPa) based on sample preparation method even when all the samples fell in loose or very loose category. The relative density for the two air poured sample was 25% ($\pm 2.5\%$) and was the minimum the authors could achieve with this method of

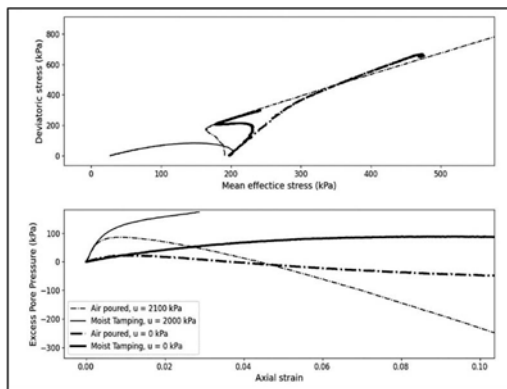


Figure 4. Varying behaviour of samples during un drained triaxial tests.

sample preparation. The moist tamped sample resulted in much looser samples. The samples discussed in Figure 3 had a relative density of -13.3% ($\pm 0.3\%$) We observed that moist tamped loose sample contracted while shearing but the air poured sample dilated.

These effects can be caused due to the density difference as well as the difference of method of sample preparation. However the shear stress were quite close at high axial strain as expected at critical state.

Also, the effect of back pressure is quite small for samples prepared by same method and having simi-

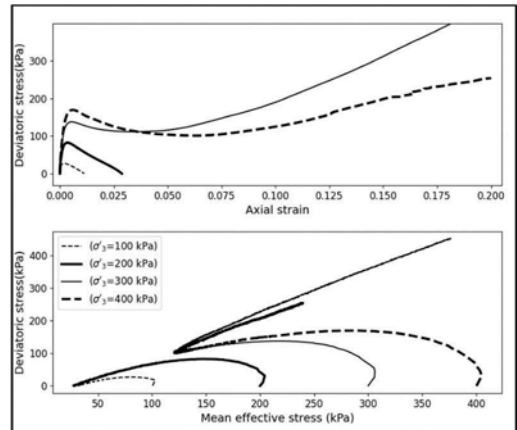


Figure 5. Difference of behaviour of moist tamped sample based on initial confining stress.

lar initial density. As such the specimen in the calibration chamber which is saturated without a back pressure should behave similarly as the one saturated using a high back pressure.

For un drained tests too, the initial density of the air poured sample shown in Figure 4 was higher (27% & 35%) for air poured samples as compared to moist tamped samples (-7% & -1%). The behaviour of the specimen even under the same initial confining pressure (200 kPa) varied depending on the method of sample preparation and the resulting relative density. It was observed that even loose air poured samples dilated (negative pore pressure) hence showing no tendency to liquefy. While very loose moist tamped sample had a development of pore pressure as the axial strain increased, as such may be prone to liquefaction.

Therefore, we will be able to control the initial state of the soil sample in the calibration chamber by either preparing the sample by moist tamping or air pouring. In particular the control of initial relative density can be used to create samples that are susceptible to liquefaction or not for this sand.

Lastly, in Figure 5 we can observe the un drained response of four moist tamped samples with relative density of $-4.5 \pm 3\%$ when initial confining stress is changed. We can observe a change of behaviour when initial confining stress changes from 200 to 300 kPa giving us an indication as to what depths on the field and what vertical stresses in the calibration chamber can be used to differentiate between liquefiable and non-liquefiable cases for these kinds of samples.

4 CYCLIC CPT TESTS IN LABORATORY

For preliminary tests, we performed cyclic penetration tests on the same Fontainebleu GA39 placed in a cylindrical container (35 cm Ø and 40 cm depth) at a depth

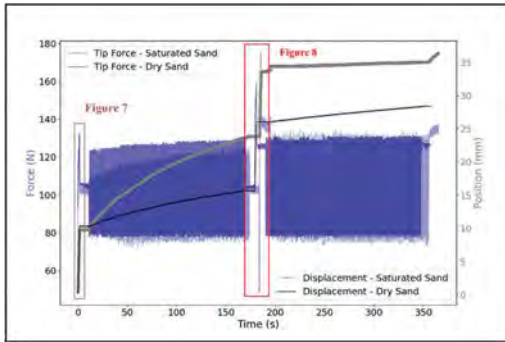


Figure 6. The difference of behaviour of saturated and dry sand to cyclic penetration test.

of 15 cm without applying a confining pressure. We created the sample by air pouring and observed a relative density of $28 \pm 2\%$ and performed tests in dry and saturated state. We observed that the total tip penetration caused by the cyclic CPT test is less in the dry state than in the saturated state (Figure 6). However, the tip resistance measured during static penetration at

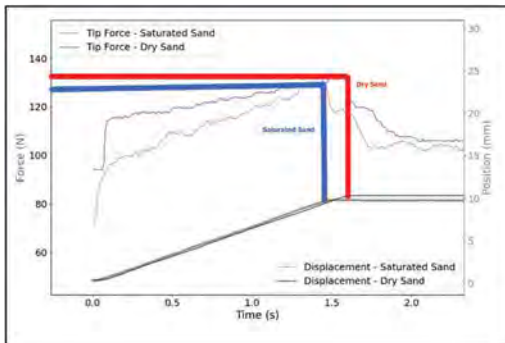


Figure 7. Similar behaviour of the two saturation conditions to static penetration.

constant speed (normal CPT) were very close for the dry and the saturated sample (Figure 7). (drained penetration – as expected from permeability values). Also, the response of the soil to a second penetration, after applying the cyclic load, is different in the two saturated conditions. We saw a distinct increase of penetration resistance after applying the cyclic load in saturated sand (Figure 8). This increase may be due to the compaction of the saturated soil due to the cyclic

loading. Thus the test can play a major role in distinguishing the saturation condition of the soil without a pore pressure measurement and this is an useful information for calculating the liquefaction probability.

It can also be observed that the penetration of the tip in dry sample continues for the second round of cycles almost with the same rate as during the first round of cycles. However, in the saturated sample, the rate of displacement continuously decreases during the first round (between ~ 20 to ~ 150 seconds in Figure 6) and reduces drastically for the second round of cyclic loading. This occurs even when the maximum and the minimum amplitude of the two sets of cycles remain similar. This decrease of the penetration rate is an indication of densification of the saturated sample due to the first cyclic loading and the second 1 cm push. This effect is more pronounced in the saturated sample.

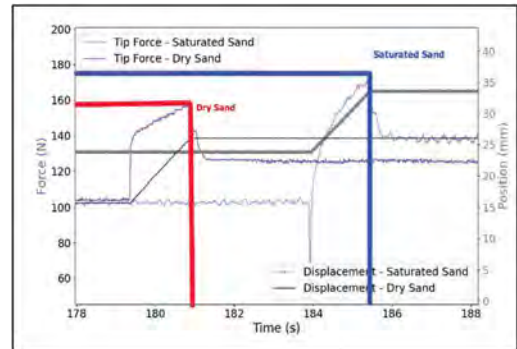


Figure 8. Different behaviour of the two saturation conditions to static penetration after the cyclic load.

5 FIELD EXPERIMENTS

During the initial investigation, we have performed cyclic tests next to a CPTu test. The CPTu tests were performed at a building site at *Le Bourget du Lac*, France. This CPTu test was used to find the Soil Behaviour Index (I_c) (Robertson 1990). The test indicated a compacted layer for 1.8 m depth and a predominantly saturated clay like soil till a depth of 8.5 m. However, a sand like layer was observed between a depth of 3.8 and 4.2 m. We performed the cyclic CPT tests just outside and inside of this layer. In two of these tests, performed at 3.2 m (clay like soil - I_c value of 3.1) and at 4 m depth (sand like soil - I_c value of 2.3) we observed two different behaviours. Figure 9 shows the results of two of cyclic CPT tests.

It was observed that the tip resistance during the initial static push of 1 cm is higher for the sand like layer and as such the cyclic load applied was also higher (compared to clay like layer). In the clay like soil we observed rapid tip opening during the stress controlled cycling loading while the same in sandy soil is much

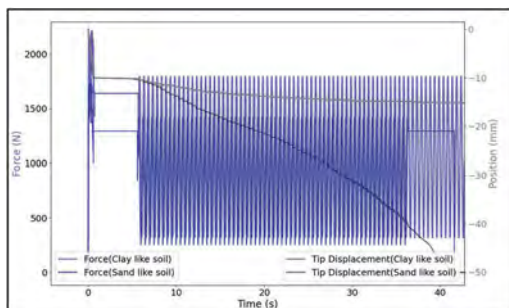


Figure 9. Field tests done on soil of two different type at similar depths.

slower. Also, the total tip displacement in the sandy soil remained less than 5 mm even after 180 cycles, while 35 cycles of lesser amplitude resulted in almost 40 mm of the tip opening in clay like layer. These results are encouraging as with this cyclic test, different responses for soils with different I_c values can be observed. As such, the cyclic CPT may be used to identify different soil types.

6 CONCLUSION

A new cyclic cone penetration test is presented and the benefits are listed. Primary results indicates its effectiveness in differentiating between different saturation state of the soil and also to differentiate soils at almost identical depth but different soil behaviour index. This can add to the information from existing geotechnical tests and help engineers better predict soil properties and also liquefaction susceptibility of soil. The laboratory experiments provide us with the framework to differentiate liquefiable and non-liquefiable conditions of the Fontainebleau GA39 sand and provide us with variable to be tested during the calibration chamber testing.

7 PERSPECTIVE

The laboratory equipment became functional only a week before the final submission of this paper. The preliminary results are encouraging and motivating to study the effect of vertical stress, the density of the sand on the response of soil to cyclic CPT. The results obtained from the laboratory testing regarding the effect of the sample preparation method, max effective stress to permit liquefaction etc., can be used to decide parameters for experiments in the calibration chamber. The evaluation of pore pressure around the tip in different cases and the corresponding tip displacement will be studied to differentiate between liquefiable and non-liquefiable cases. Field experiments are limited by a max cyclic force of 3500 N on a 3.57 cm dia cone. Thus only shallow depths could be investigated till now and leaves scope for improvement. Comparison of CPTu test results and our cyclic CPT test on similar specimens performed in identical conditions will further help us validate our method to predict soil properties, including liquefaction susceptibility.

REFERENCES

- Idriss IM & Boulanger RW, 2004. Semi-empirical procedures for evaluating liquefaction potential during earthquakes. *Soil Dynamics and Earthquake Engineering*
- McNeilan TW & Bugno WT 1985. Jackup Rig Performance in Predominantly Silty Soils, The offshore Technology Conference.
- Rimoy SP, 2013 Ageing and axial cyclic loading studies of displacement piles in sands. PhD thesis, Imperial College London London, UK,.
- Robertson PK, 1990. Soil Classification Using the Cone Penetration Test. *Canadian Geotechnical Journal*, 27: pp. 151–158.
- Rogers JD, 2006. Subsurface exploration using the standard penetration test and the cone penetrometer test. *Environmental and Engineering Geosciences*. Vol. XII, No. 2. pp. 161–179.

Evaluation of deformation modulus during Cone Loading Tests (CLT) and settlement of shallow foundations

A. Teyssier, M. Rispal & C. Jacquard

Fondasol, Avignon, France

P. Reiffsteck

GERS-SRO, University Gustave Eiffel, IFSTTAR, Marne-la-Vallée, France

ABSTRACT: The static loading of a piezocone is one of the only in-situ tests leading to a measure of compression of soil under the cone, shear stress on the shaft and pore pressure between these two points. These three load-deformations curves give valuable information usually impossible to reach with another ground investigation technique. The incremental loading of the cone up to failure, called Cone Loading Test (CLT), provides the vertical loading/unloading soils curve. From this curve, an estimation of deformation modulus, which is a key parameter in structure design such as foundations, is possible. CLT's deformation modulus will be compared to modulus obtained from traditional investigation methods (Menard pressuremeter tests). An experimental survey, including pressuremeter tests (PMT), Cone penetration test (CPT) and shallow foundation loadings tests, was undertaken to compare the results with CLT moduli measurements. A calculation procedure, based on CLT's deformation modulus, is proposed to design shallow foundations settlement. The article presents prediction of long-term foundation settlements (i.e. effect of time) both with the conventionnel methods and the new CLT method.

1 INTRODUCTION

The common ground investigation methods provide many parameters to characterize soils.

Each method measures different parameters relative to resistance and/or deformation. However, the variability of soils and the costs of the tests, represent limits, all parameters cannot be directly measured in-situ, and some are obtained from empirical correlations, with limited validity.

The Cone Penetration Test with pore water pressures measurements, or piezocone (CPTu) is worldwide used (EN ISO 22476-1). It is highly documented and known as a reliable method to measure soils mechanical parameters of fine-grained soils and coarse soils up to a maximal diameter of 20 mm. It provides the static cone resistance (q_c or q_t , the total cone resistance with piezocone), the sleeve friction (f_s), and the pore pressure (u_2). From these parameters, the soil resistance, the permeability and the liquefaction potential can be obtained. Though the CPT does not allow a direct soil nature identification, the Robertson and Cabal correlations (2014) permit an estimation of the lithology encountered during the test.

As all penetration methods, the CPT does not provide a measurement of the deformation modulus, needed to calculate ground settlements and to consider

their impact on structures. The Cone Loading Test (CLT) was developed (Arbaoui, 2006; Ali, 2010), in this aim. The CLT is an hybrid test combining the classical probing and an incremental loading of the cone, to obtain resistance and deformability parameters.

The test consists in interrupting the penetration at a chosen depth, and then applying an incremental load on the cone up to failure. Once the yield point is reached, an incremental unloading is performed. This allows the drawing of a loading/unloading curve giving settlements beneath the cone from the applied pressure (Figure 1 and Figure 2).

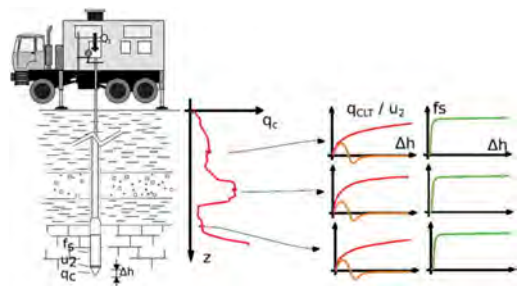


Figure 1. Cone Loading Test principles (Reiffsteck, 2017).

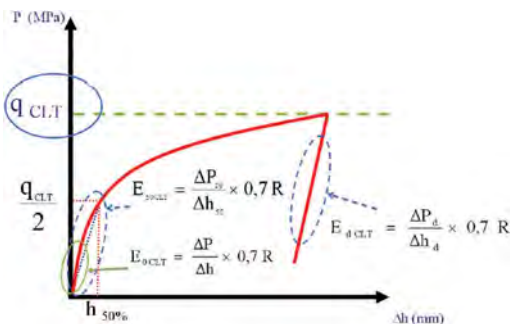


Figure 2. Determination of deformation modulus $E_{0,CLT}$, $E_{50,CLT}$ and $E_{d,CLT}$ according to the pressure versus deformation curve (Ali., 2010).

The limit cone resistance from the CLT is named q_{CLT} . This is the maximum loading reached at the yield point during the CLT test just before the soil collapses. This load is generally smaller than the classical cone resistance (q_c) because it is measured with an almost zero penetration rate.

Three different values of deformation modulus are calculated from the curve:

- $E_{0,CLT}$: the initial tangent modulus, estimated with the slope of the first linear part of the loading curve.
- $E_{50,CLT}$: the modulus at 50% loading, calculated with P_{50} which is half of the limit cone resistance (q_{CLT}) and with h_{50} the associated deformation.
- $E_{d,CLT}$: the unloading modulus, estimated from the slope of the unloading curve.

According to Ali (2010), every modulus is affected by a coefficient of $0,7R$, where R is the conical radius and 0.7 is a coefficient taking into account the conic driving, its geometry, and the disturbed soil.

2 THE CONE LOADING TEST

2.1 The CPT penetrometer

The test is performed with a heavy static penetrometer vehicle, at a constant speed of 2 cm/s . The thrust can reach 200 kN .

The cone penetrometer, in compliance with the EN ISO 22476-1 standards, allows independent measurements of the cone resistance (q_c), the sleeve friction (f_s), the pore pressure (u_2) and the vertical inclination. These measurements are collected in real time inside the CPT truck by a connecting cable that is threaded inside the push rods.

The data acquisition system is located at the surface and synchronized in real time to store the cone resistance and depth measurements at the same time.

2.2 The loading system

The additional thrust device consists in an hydraulic cylinder placed between rods and the thrust head of the penetrometer. This jack, controlled by a pressure limiter, is powered by a hydraulic power pack. It allows to apply a controlled thrust on rods independently from the evolution of the soil reaction force.

2.3 Instrumentations and measures

At the beginning of a CLT test, a dissipation test is done and recorded by the data acquisition system of the penetrometer. At the same moment, the thrust device at the surface allows the measurement of the pressure in the hydraulic jack, and so the total thrust force on rods corresponding to the q_c value expected. The displacement is measured at the top of rods as it is represented in Figure 3.

In this study, CLT tests has been performed at shallow depth ($1, 2$ and 3m), allowing to neglect the effect of rods compression.

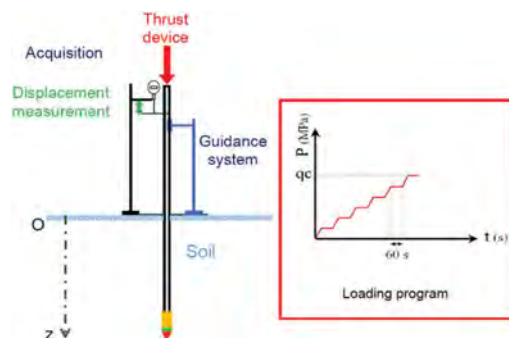


Figure 3. Schematic representation of CLT Test equipment.

3 EXPERIMENTAL SURVEY

To meet the objectives (and allow comparisons), conventional investigations (PMT, CPT, shallow foundation loading tests) were needed.

The data is issued from the "Jossigny-France" site, located on Figure 4:



Figure 4. Location of Jossigny site (Google Earth).

3.1 Site description and in situ tests performed

The Jossigny site is located along the A4 highway, East of Paris (“Aire de Ferrières”). The area is relatively flat and horizontal, and composed of homogeneous clayey silts on the top 6 meters.

The in-situ tests undertaken were:

- 5 pressuremeter boreholes (PMT) down to 3 and 6 m
- 6 mechanical cone penetration tests with “Gouda cone” down to 3 and 6 m
- 17 shallow foundation loading test, using a 1 m × 1 m footing and a axially centered force.

The results of measured cone resistance (q_c) are given in Figure 5.

The results of measured Ménard Modulus (E_M) are presented in Figure 6, together with the representation of the harmonical mean calculated for each meter using the results of the different boreholes.

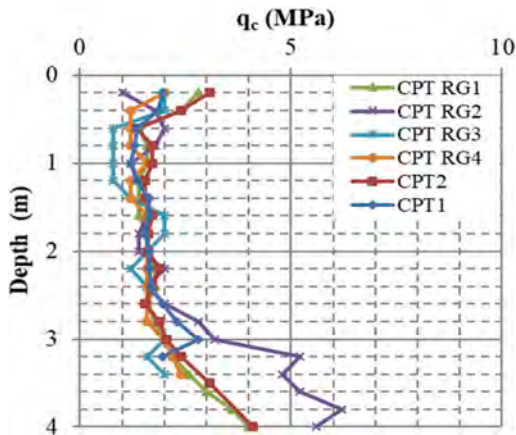


Figure 5. Cone resistance (q_c) measures for Jossigny site.

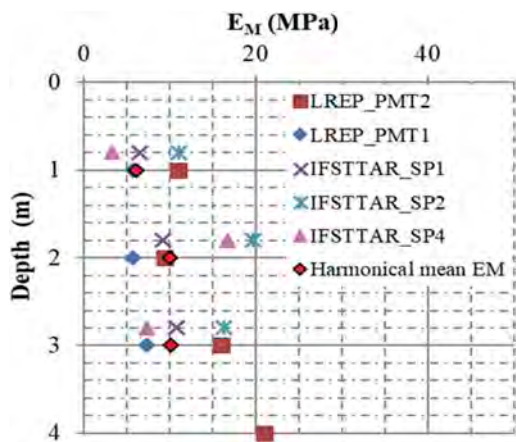


Figure 6. Ménard pressuremeter modulus (E_M) results for Jossigny site.

The Figure 7 shows the results of the different shallow foundation loading tests. The experimental foundations are one-meter squares and are directly laid on the ground (no embedding).

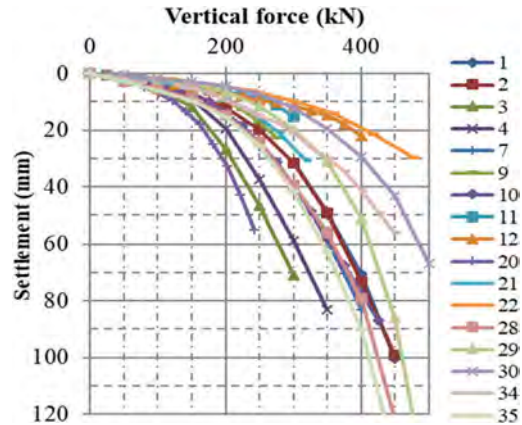


Figure 7. Vertical shallow foundations loading tests for Jossigny site.

3.2 Cone loading tests and results

This study considers three CLT tests (CLT1, CLT3, CLT4), from the Jossigny site.

The CLT tests were performed and interpreted in compliance with the operating procedure defined by Ali (2010). The test starts after a 10 min waiting time, for pore pressure dissipation. The cone is loaded following different stages; every loading stage is maintained during 1 min. Displacements are measured at 30 and 60 sec.

Figure 8 shows a result of a CLT test. Figure 9 shows the results of the different CLT tests realized at the Jossigny site. The different values of CLT moduli obtained are represented in Figure 10.

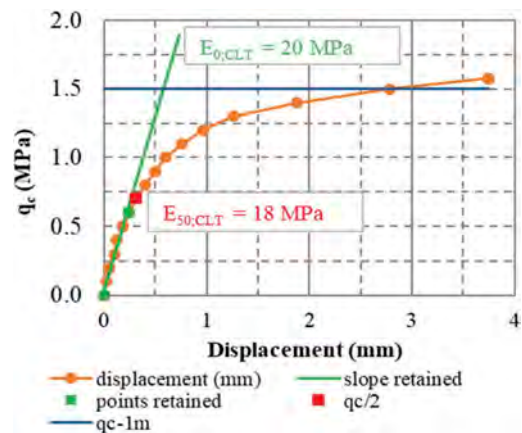


Figure 8. Example of a CLT test interpretation – Jossigny-CLT1-1m.

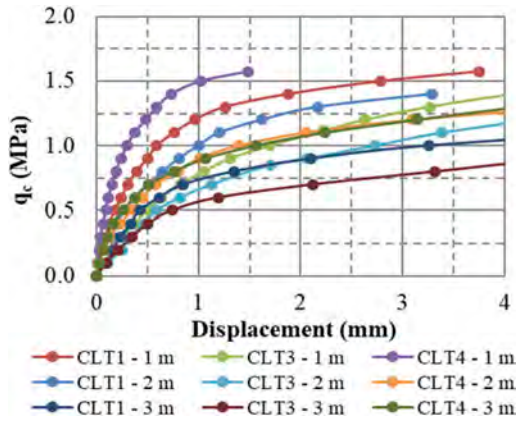


Figure 9. CLT tests for Jossigny site.

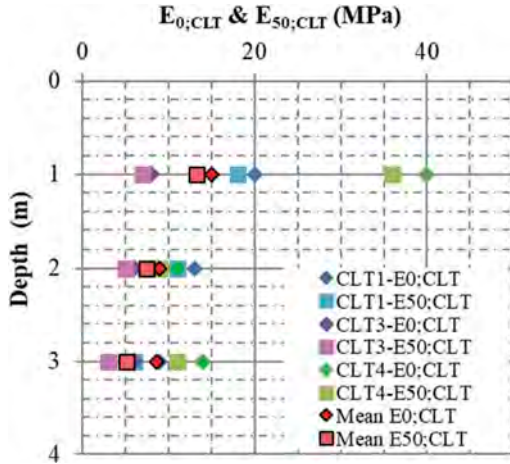


Figure 10. CLT moduli for Jossigny site.

The CLT moduli measured on the the Jossigny site are in the same order of magnitude as the pressuremeter moduli at the same depths. The $E_{0,CLT}$ average value at 1 m is slightly higher; this average value is probably affected by a stiffer soil encountered beneath the surface on the CLT4 test.

3.3 Synthesis of Jossigny site

In this study, several metric layers are distinguished in clayey silts (0-1, 1-2, 2-3 and 3-6m). Table 1 summarizes the geotechnical characteristics:

Young moduli are derived from the relation (1), (2) and (3) from NF P94-261-J.2.2:

$$E_y = \alpha_E (q_c - \sigma_{v0}) \quad (1)$$

If $I_c < 2.2$:

$$\alpha_E = 0.015 \cdot 10^{0.55I_r + 1.68} \quad (2)$$

If $I_c > 2.2$:

$$\alpha_E = \frac{Q_T}{1.2} \text{ for } Q_T < 14 \quad (3)$$

$$\alpha_E = 11.7 \text{ for } Q_T > 14$$

A mean Young modulus of 18.7 MPa and a mean initial tangent CLT modulus of 10.2 MPa are considered for the top three meters of clayey silts.

Table 1. Geotechnical characteristics of Jossigny site.

Depth (m)	q_c (MPa)	E_M (MPa)	I_c^* (-)	α_E^{**} (-)	E_y (MPa)	$E_{0,CLT}$ (MPa)
0-1	1.3	6.2	2.35	11.7	15.1	15
1-2	1.7	10	2.75	11.7	19.7	8.9
2-3	2.0	10.2	3.02	11.7	23.1	8.6
3-6	4.1	21	2.80	11.7	47.3	-

* I_c : Soil behavior type index

** α_E : Correlation coefficient on penetrometer method

4 DISCUSSION

4.1 CLT loadings and shallow foundations loading tests

CLT loadings (red envelope curves) and shallow foundations loading tests curves are compared, in normalized axis (values divided by maximum values), in Figure 11.

At 1 m depth, and for small values of load, there is a good match between shallow foundation loading tests and CLT loading tests. Then, the initial tangent CLT moduli can be considered as similar as the initial tangent moduli for shallow foundation loading tests.

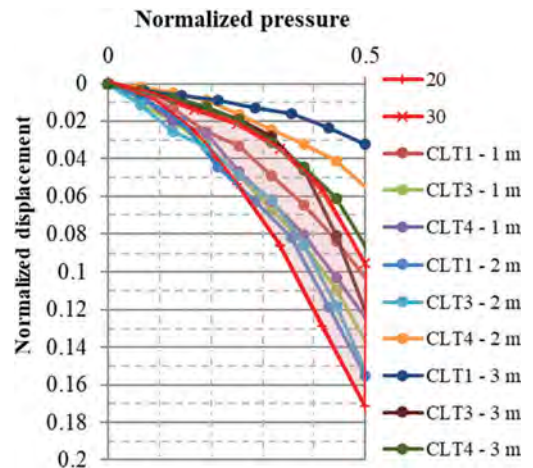


Figure 11. CLT loadings and shallow foundation loading tests (red) for Jossigny site.

4.2 CLT moduli and settlement calculations

Settlement results with different methods based on penetrometer and pressuremeter data are compared to the settlement measured during shallow foundation loading test n°1, which is almost an average of all the foundation loading tests realized:

- Method 1: Boussinesq method, NF P94-261-J.4.1
- Method 2: Homogeneous soil (mean moduli on 3 meters), NF P94-261-J.3.1
- Method 3: Schmertmann method, NF P94-261-I
- Method 4: Multi-elastic method, according to Steimbrenner (1934) and Bowles (1996)
- Method 5: Pressuremeter method, NF P94-261-H

Then the initial tangent CLT moduli are used in these calculation methods instead of Young moduli.

Calculations are realized with small loading stages (V_d), between 0 and 204 kN, to remain in the elastic domain of deformations.

The results are presented in Figure 12 and in Table 2.

Table 2. Settlement predictions with the five methods using E_Y moduli and $E_{0,CLT}$ moduli.

V_d (kN)	1 (mm)	1 _{CLT} (mm)	2 (mm)	2 _{CLT} (mm)
1	0.04	0.07	0.02	0.04
45.4	4.5	6.9	1.9	3.5
90.9	8.9	13.8	3.8	7.0
136.4	13.4	20.7	5.7	10.5
159.1	15.7	24.1	6.7	12.3
181.8	17.9	27.6	7.6	14.0
204.5	20.1	31.0	8.6	15.8

V_d (kN)	3 (mm)	3 _{CLT} (mm)	4 (mm)	4 _{CLT} (mm)
1	0.05	0.05	0.06	0.09
45.4	2.9	3.9	2.9	4.0
90.9	6.6	8.7	5.8	8.0
136.4	10.7	14.1	8.8	12.0
159.1	12.9	17.1	10.2	14.0
181.8	15.2	20.1	11.7	16.0
204.5	17.6	23.2	13.1	17.9

V_d (kN)	5 (mm)
1	0.02
45.4	1.8
90.9	3.5
136.4	5.3
159.1	6.2
181.8	7.0
204.5	7.9

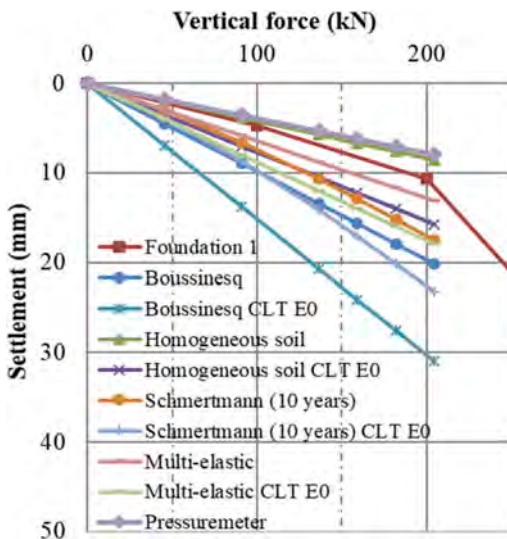


Figure 12. Settlement predictions with different calculation methods and with $E_{0,CLT}$ moduli.

First, we can note a good match of values between the loading observed for foundation n°1 and the settlement obtained with the homogeneous soil method (2), the multi-elastic method (4) and the pressuremeter method (5)

For the four different methods, settlement predictions using the CLT moduli are always higher than predictions using the Young Moduli.

To consider the initial tangent CLT moduli in calculation methods, a coefficient named ψ must be determined. This coefficient is applied to the initial tangent modulus to obtain the same deformation than with elastic moduli, according to equation (4). Only penetrometer methods are considered for the determination of these coefficients.

$$E_{calc} = E_{0,CLT} \times \psi \quad (4)$$

This coefficient is calculated for each method with the ratio of settlement predictions between elastic moduli and CLT moduli, for every loading case. For all methods, the ratio remains constant for all loads. The mean is calculated for each method.

Results of ψ coefficients are given in Table 3:

Table 3. ψ coefficient applied to $E_{0,CLT}$ modulus, for each penetrometer settlement prediction method.

Method	1	2	3	4
ψ	1.54	1.84	1.27	1.37

Using this coefficient, for clayey silts, it is possible to consider CLT moduli for different calculation procedures.

However, it is necessary to consider the context.

The penetrometer calculation method presented here was used only in the elastic domain in clayey silts.

The incidence of the Soil Behavior Type index on the determination of the Young modulus is preponderant, linked to the lithological nature.

5 CONCLUSIONS

The Cone Loading Test is a loading/unloading test than can easily be coupled with a static cone penetration test campaign to measure a soil deformability parameter at different depths.

This study, based on Jossigny's clayey silts proposes a method to consider CLT moduli in traditional method of settlement predictions from penetrometer data. This method requires the use of a coefficient ψ which applies to CLT moduli. This coefficient varies depending on the calculation method but also on the stiffness and the lithological nature of soils.

In the future it would be necessary to carry out new surveys, firstly in clayey silts to confirm the ψ coefficient table, then in other type of soils (sands, ...) to complete the table of ψ coefficient for every method of settlement design of shallow foundations. Indeed, a complete table will allow the use of CLT moduli measurements for every calculation procedure.

REFERENCES

- Ali H., Reiffsteck P., Baguelin F., Van de Graaf H., Bacconnet C., Gourvès R. 2010. Settlement of pile using Cone Loading Test: Load Settlement Curve Approach, CPT 10, Huntington Beach Los Angeles.
- Ali H., Reiffsteck P., Thorel L., Gaudin C. 2010. Influence factors study of cone loading test in the centrifuge, CPT'10, Huntington Beach, P. Robertson Ed.
- Ali H. 2010. "Caractérisation améliorée des sols par l'essai de chargement de pointe au piezocone – Application au calcul des fondations profondes", (Improved characterization of soils by the Cone Loading Test – Application to calculation of deep foundations) Doctoral degree, University Blaise Pascal – Clermont-Ferrand II, (in French) [online] Available at: <https://tel.archives-ouvertes.fr/tel-00629642>.
- Arbaoui H., Gourvès R., Bressolette Ph., Bodé L. 2006. "Mesure de la déformabilité des sols in situ à l'aide d'un essai de chargement statique d'une pointe pénétrométrique", (Measurement of soils deformability in situ using a static loading test with a penetrometer cone) *Can. Geotech. J.*, (in French), 43(4) 355–369.
- Bowles J.E. 1996. *Foundation analysis and Design*, 5th edition McGraw-Hill
- Khoury N., Zaman M., Ghabchi R., Kazmee H. 2010. Stability and permeability of proposed aggregate bases in Oklahoma, School of Civil Engineering and Environmental Science – The University of Oklahoma, [online] Available at: www.okladot.state.ok.us/reports/rad_spr2-i2196-fy2009-rpt-final-zaman [Accessed: 13/11/2015]
- NF P94–261. 2013. *Justification des ouvrages géotechniques - Normes d'application nationale de l'Eurocode 7 - Fondations superficielles*.
- Reiffsteck P., Van de Graaf H., Jacquard C., 2018. Assessment of pile bearing capacity and load-settlement behavior, based on cone loading test (CLT) results, CPT18, 4th Int Symp. on Cone Penetration Testing, Delft.
- Reiffsteck P., Bacconnet C., Gourvès R., van de Graaf H. C., Thorel L. 2009. Measurements of soil compressibility by means of cone penetrometer, *Soils and Foundations*, 49(3) 397–408.
- Reiffsteck P., Bacconnet C., Gourvès R., Godde E., Van De Graaf H. 2008. Determination of elastic modulus from stress controlled cone penetration test, 3rd International conference on Site Characterization, Taipei, pp. 1135–1138.
- Robertson P.K., Cabal. K.L. 2014. *Guide to cone penetration testing*, Gregg Drilling & Testing, Inc., 6th edition.
- Steinbrenner W. 1934. "Tafeln zur Setzungsberechnung, Die Straße, vol. 1, pp. 121–124
- Teyssier A., Reiffsteck P., Jacquard C., Rispal M. 2021. Evaluation of modulus deformation and drainage condition during Cone Loading Tests. ISC6.
- Teyssier A., Reiffsteck P., Jacquard C., Rispal M. 2020. "Détermination de modules de déformation au cours d'essais CLT – Application au calcul de tassement des fondations", (Determination of deformation modulus during CLT tests – Application to settlement calculation of foundations), JNGG2020 (in french)

Assessment of the potential for liquefaction using CPTu in the tailings dam I – Feijão

M. Tincopa

Universidad de Ingeniería y Tecnología - UTEC, Peru

G. Carnero-Guzman

Golder Associates Pty. Ltd., Australia

ABSTRACT: In Brazil in 2019, the failure of the tailings dam I - Feijão costed a total of 7 billion dollars in civil and environmental reparation. The report of the expert panel that evaluated the failure of dam I concluded that the failure was due to static liquefaction, which is one of the most common dam failures in the world. However, the identification of the liquefaction potential has challenges such as identifying the behavior of the tailings (contractive and dilative behavior) and extracting undisturbed samples for sophisticated laboratory tests. CPTu is a fast and reliable field test, and, through empirical relationships, the liquefaction potential of soil can be estimated using the state parameter (ψ). The objective of this article is to present the results of piezocone (CPTu) in the different in situ geotechnical campaigns in Feijão Dam with focus on the state parameter (ψ) data used to determine the liquefaction potential. The methodology used herein is that $\psi > -0.05$ means contractive behavior or high change of potential for liquefaction. The results show that the CPTu tests in dam I - Feijão showed that there was high liquefaction potential during the geotechnical campaigns (2005, 2016, and 2018) by using this procedure.

1 INTRODUCTION

Tailings dams are structures made up of mining waste coming from mineral processing (Vick, 1990). Unfortunately, some significant failures in tailing dams occurred in recent years. In this regard, static liquefaction has been one of the most damaging failure modes for tailings facilities as shown in Table 1.

Particularly, a recent failure in tailings dam No. 1 of Vale's external link Córrego do Feijão iron ore mine near Brumadinho (Minas Gerais – Brazil) triggered the urgency for a global tailings management standard. This conclusion was drawn from the official expert panel report (Robertson et al. 2019), where the causes of the disaster were assessed.

The Expert Panel looked in detail at available monitoring, laboratory, field data and undertook a back analysis of historical InSAR data. The upstream construction method deployed by Vale at Brumadinho and the lack of adequate drainage were found responsible for the dam failure.

The mechanisms involved in the dam failure were creep and static liquefaction (sudden loss of soil strength). Specifically, static liquefaction can be assessed by the state parameter. As shown in Been (2016), this parameter is defined as the difference between the in-situ void ratio and critical state locus

(CSL) void ratio (defined in Figure 1). The value indicates if the soil is whether contractive (loose) or dilatant (dense). Commonly, this evaluation is conducted during the characterization of tailing dams which is a difficult and overestimated problem in geotechnical engineering. However, extremely relevant to prevent failure of the structure, which can lead to significant negative impacts on the economy, surrounding properties, and lives of the population (Draves & Fox 1998; Hudson-Edwards et al. 2003).

Characterization of tailings dams is needed to minimize the risk of failure. For instance, liquefaction potential is a crucial analysis that requires a tailings characterization. The pressure to minimize geotechnical characterization costs without a consistent approach for assessing the tailings material means that empirical methods derived from sand and clay research work are often inappropriately applied (Been 2016; Macedo & Vergaray 2021). Nevertheless, the empirical methods still used on the industry.

This article focuses on the evaluation of static liquefaction using the state parameter. A similar study on fundão tailings dam failure was conducted by Reid (2019). Nevertheless, the current paper focuses on the state parameter (ψ) from the CPTu data presented in the panel expert report (Robertson et al. 2019).

The paper concludes that using the CPTu test (ASTM 5778-20) to measure the state parameter is

an excellent practical approach applicable to other case scenarios.

Table 1. Summary of recent tailings dam failures.

Description	Location/ Year	Consequences
Aberfan	UK/1968	144 dead from static liquefaction caused by increased groundwater pressure
Aznalcollar	Spain/ 1998	Brittle foundation failure causing dam failure and widespread downstream contamination
Kingstong Fly ash	USA/ 2008	Static undrained failure of fine-grained volcanic ash, causing significant environmental pollution
Mt Polley	Canada/ 2014	Rapid foundation failure resulted in the dam rupture and one of the most significant environmental disasters in modern Canadian history
Fundão	Brazil/ 2015	Static liquefaction with at least 17 deaths and estimated damage of billions of dollars
Brumadinho	Brazil/ 2019	It triggered the urgency for a global tailings management standard which ICMM published in 2020

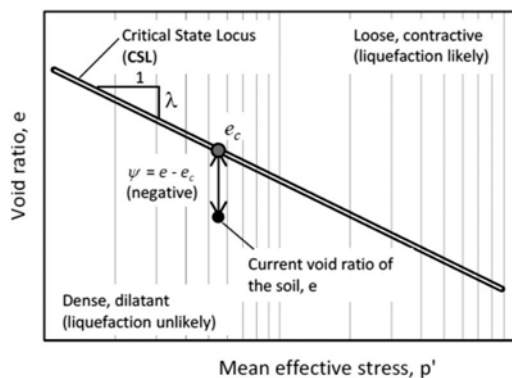


Figure 1. Definition of state parameter (retrieved from Been 2016).

2 DETERMINATION OF THE STATE PARAMETER

2.1 Field data

The raw CPTu data available previous of the failure dam included 28 CPTu tests completed as part of geotechnical investigations in 2005, 2016 and 2018 (see Annex B, Robertson et al. 2019). Figure 2 shows the locations of the CPTu tests in dam I, Feijão.

The field test data presented in this paper were obtained from the results of tests performed during the following geotechnical field explorations:

- CPTu tests performed by In Situ Geotecnia Ltda. in 2005;
- CPTu tests conducted by Fugro In Situ Geotecnia Ltda. in 2016; and
- CPTu tests performed by Fugro In Situ Geotecnia Ltda. in 2018.

For this paper, three CPTu, namely CPTu2005-07, CPTu2016-04, and CPTu2018-19 were selected by considering the executed year and close location as shown inside the red circle on Figure 2.

To obtain the usable set of data from these probes, the tip resistance (q_t), pore pressure (u) and friction ratio (R_f) records provided in graphical form in the panel Appendix B were transferred into AutoCAD version 2022 software and scaled, and then data from the probes were extracted at 0.25 m intervals. By doing so, the range of relevant CPTu calculations to estimate various engineering properties could be made in particular to analyze ψ . It is worth mentioning that the three CPTu could not reach more than 50 m although there are commercial push rigs capable of reaching around 100 m depth. Deeper investigations are relevant because the potential failure mechanism of a tailings dam may be found on the foundation or nearby.

2.2 Subsurface conditions and state parameter estimation using CPTu data

The subsurface soil conditions at the site were characterized by using normalized soil type behavior (SBT) charts to interpret the soil type encountered during testing. SBT charts group soils that exhibit similar engineering behavior properties allowing interpretation of soil type based on the normalized tip resistance and friction ratio results. Fine ($I_c > 2.6$) and Coarse ($I_c < 2.6$) tailings were assumed by using the SBT charts.

Various methods are available to calculate the in-situ state parameter from CPTu data. The methods of Robertson (2009), Plewes et al. (1992) and Jefferies and Been (2016) were used in this assessment.

The Robertson (2009) and Plewes et al. (1992) methods are empirical and do not require laboratory testing or numerical analysis but rely on relationships developed from a database of mainly silica-based sandy soils. The method developed by Jefferies and Been (2016) is a more site-specific approach that relies on numerical simulations and incorporates index and laboratory testing data.

The next section discusses the three methods examined to characterize the in-situ state parameter of Fine and Coarse Tailings.

2.2.1 Robertson (2009) method (PKR)

The Robertson (2009) method uses corrected tip resistance (q_t) and sleeve friction (f_s) from CPTu

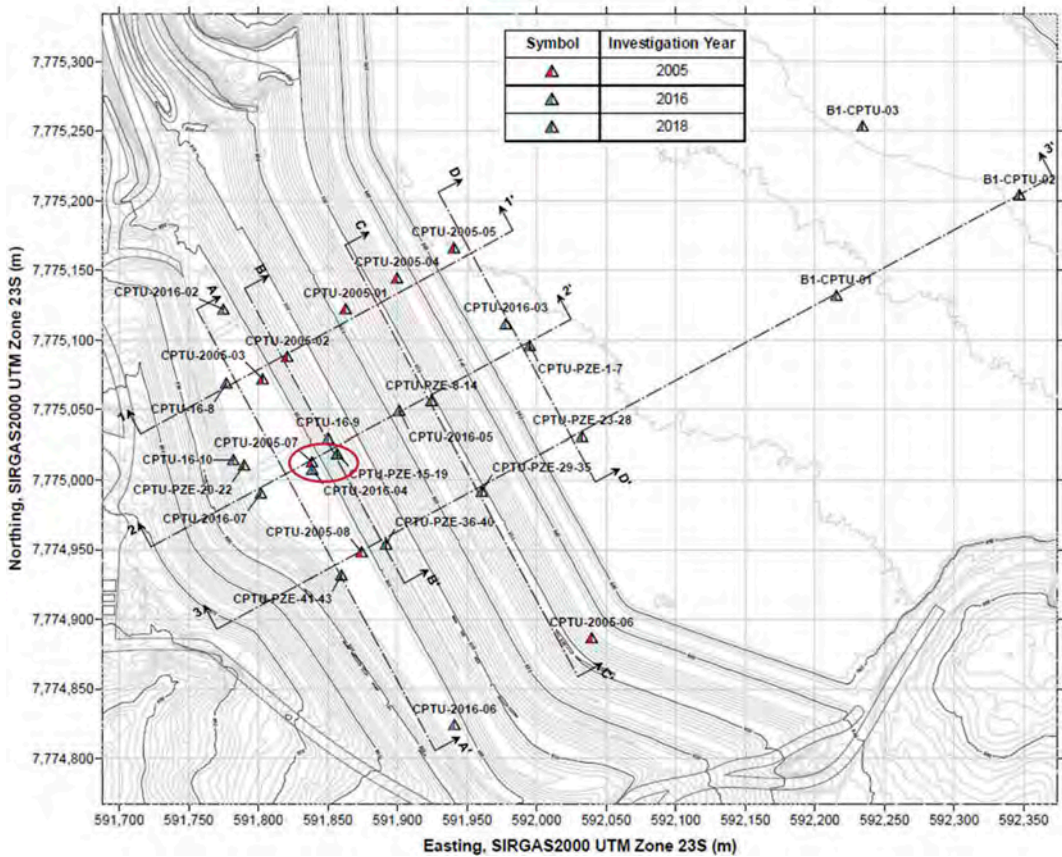


Figure 2. Location plan of CPTu tests (modified and retrieved from Robertson et al. 2019).

data to calculate a stress-normalized tip resistance (Q_{tn}) using Equation 1.

$$Q_{tn} = \left(\left(\frac{q_t - \sigma_v}{p_a} \right) \right) \left(\frac{p_a}{\sigma'_v} \right)^n \quad (1)$$

Where,

- σ_v = in-situ total vertical stress
- σ'_v = in-situ effective vertical stress
- p_a = atmospheric pressure
- n = stress exponent ($n \leq 1$)

The stress-normalized tip resistance (Q_{tn}) is adjusted to account for fines content, mineralogy and plasticity using the correction factor K_c , to calculate an equivalent clean sand value ($Q_{tn,cs}$), as shown in Equation 2.

$$Q_{tn,cs} = K_c Q_{tn} \quad (2)$$

Where,

- $K_c = 1.0$, if $I_c \leq 1.64$
- $K_c = 5.581I_c^3 - 0.403I_c^4 - 21.63I_c^2 + 33.75I_c - 17.88$, if $I_c > 1.64$

The in-situ state parameter (ψ) is then calculated using Equation 3.

$$\psi = 0.56 - 0.33 \log(Q_{tn,cs}) \quad (3)$$

2.2.2 Plewes Et Al. (1992) method (Plewes)

The Plewes et al. (1992) method normalizes q_t using mean effective stress and dynamic pore water pressure and relates it to (ψ) using Equation 4, 5, 6 and 7.

$$Q_p(1 - B_q) + 1 = \bar{k} \exp(-\bar{m} \psi) \quad (4)$$

$$B_q = \Delta u / (q_t - \sigma_{v0}) \quad (5)$$

$$\bar{k} / M_{tc} = 3 + 0.85 \lambda_{10} \quad (6)$$

$$\bar{m} = 11.9 - 13.3 \lambda_{10} \quad (7)$$

$$Q_p = (q_t - p_0) / p'_0 \quad (8)$$

Where,

Q_p = tip resistance normalized by mean effective stress

B_q = normalized exceed pore pressure
 M_{lc} = critical state friction ratio
 λ_{10} = slope of the critical state line
 \bar{k} & m = semi-empirical parameters for estimating ψ
 p_0 = mean total stress
 p'_0 = mean effective stress
 Δu = exceed pore pressure

While the method provides empirical relationships for estimating λ_{10} and M_{lc} , it also indicates that development of the soil's CSL through triaxial testing on intact or reconstituted soil samples can be used to refine estimates of λ_{10} and M_{lc} and provide an estimate of (ψ) that is more soil specific. The calculation of (ψ) was completed using a λ_{10} value of 0.09 and a M_{lc} value of 1.38. These values were calculated by laboratory testing. Additionally, the later stress coefficient (K_0) of 0.5 was selected as reported by Robertson et al. (2019).

2.2.3 Cavity expansion method - Jefferies and Been (2016)

Jefferies and Been (2016) method uses the critical state parameters discussed in Plewes et al. (1992). However, this method uses numerical simulations of the spherical cavity expansion treated as an analogue to the CPTu technique. These simulations are used to develop site-specific values of \bar{k} and m (see method of Plewes, et al. (1992)), to calculate \bar{k} from CPTu data. These analyses used the NorSand constitutive model with the inputs of laboratory tests (Robertson et al. 2019). Jefferies and Been (2016) method was not used in the current paper since it is an extension of Plewes et al. (1992).

3 RESULTS AND DISCUSSION

A histogram represents a frequency distribution. Figure 3 shows histograms of the state parameter during field exploration stages. Two range of (ψ) can be identified, namely dilatant range (from -0.3 to -0.05) and contractive range (from -0.05 to 0.2). The tendency of the state parameter in each year showed an increased on the range values highest than -0.05. Consequently, this range meant a contractive tailings that was liquefaction susceptibility. Robertson's and Plewes' methods presented a similar contractive trend on the CPTu2018-19, but not in the CPTu2005-07 and the CPTu2016-04. It can be noted that CPTu2018-19 presented Fine tailings along with the depth profile. Consequently, Robertson's method results for such layers might not be as accurate as for the Coarse tailings encountered in the profile.

Both methods showed that the distribution of state parameter moved to the contractive range over time (i.e. 2005, 2016 and 2018). The observed behavior in Figure 3 is consistent with the range of states parameters often seen on tailings dam (Reid and Jefferies 2017).

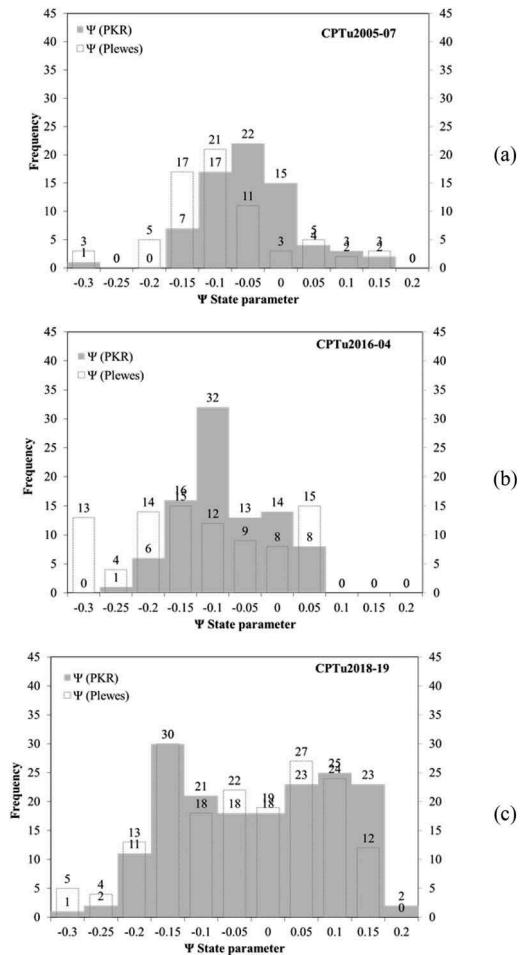


Figure 3. Histogram of the state parameter estimation based on Robertson (2009) and Plewes et al (1992) (a) CPTu2005-07, (b) CPTu2016-04, (c) CPTu2018-19.

Using the Robertson's and Plewes' methods described above, estimates of (ψ) were calculated for both fine and coarse tailings at each CPTu location, as shown in Figure 4.

The analysis of ψ shows that CPTu2005-07 presented contractive range ($\psi > -0.05$). Over time, the analysis of ψ for CPTu2016-04 and CPTu2018-19 showed an increment in areas with a high value of ψ which translate into high liquefaction potential. Therefore, the results herein point out that liquefaction potential increases as time goes. Consequently, the results should have been a warning during the operation of the dam.

Interestingly, the CPTu2018-19 presented the highest depth (~45 m) between the three CPTu. Conversely, CPTu2005-07 and CPTu2016-04 presented a shallow depths (around 25 m). The relevance of deep CPT data relies on identify the layers for liquefaction potential. This was clearly found on CPTu2018-19.

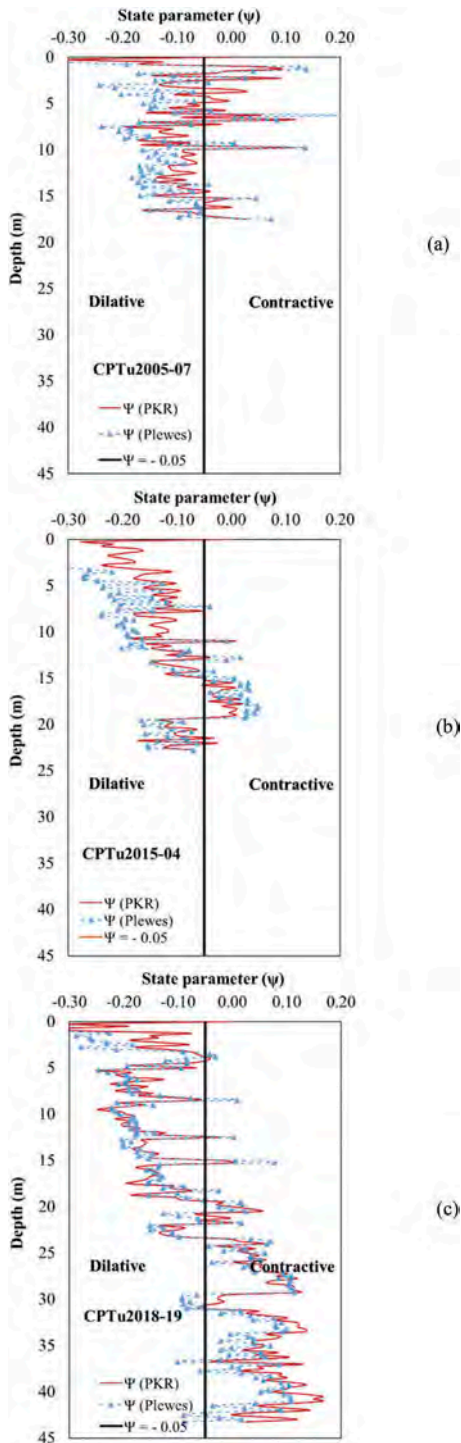


Figure 4. State parameter based on PKR and Plewes methods (a) CPTu2005-07, (b) CPTu2016-04, (c) CPTu2018-19.

For the three CPTu selected, a state parameter greater than -0.05 is identified at different depths, which was established as zones susceptible to liquefaction (Plewes 1992), as presented in Figure 4. Most of the tailings dam failure showed a high value of state parameter before the failure (contractive behavior).

Additionally, histograms of the 28 CPTu data from Feijão were reproduced in the expert panel report. The histograms were overlain for the Coarse and Fine Tailings in Figures 5a and 5b, showing the distributions of these data used in the analyses. In this analysis, Robertson (2009) method was ultimately not used for the Fine Tailings because the method is not appropriate given the similarity in the slope of the CSL for the Coarse and Fine Tailings. Fine tailings showed a high frequency on the higher range of state parameter (Figure 5b) which should have been a warning for operation purposes.

Overall, the main trend of the Feijão dam is that the fine tailings were mainly contractive and the state parameter were captured by using the two methods as discussed in Figure 3, 4 and 5. Moreover, the contractive tailings was identified at high depth and increased the frequency over time.

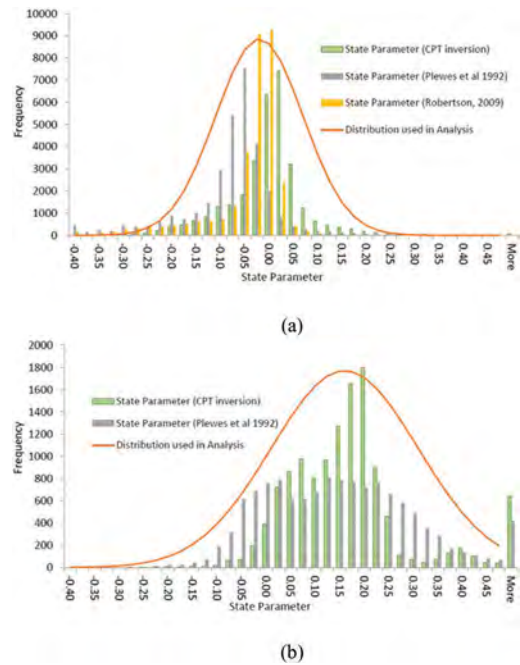


Figure 5. State Parameter (Ψ) Distribution for (a) Coarse Tailings and (b) Fine Tailings (Retrieved from Robertson et al. 2019).

4 CONCLUSIONS

In general, the results indicated that the three methods agree well with the state parameter for coarse tailings.

For fine tailings, Plewes' method and Jefferies and Been's method resulted in a similar state parameter ψ .

However, Plewes' method was more even. Both methods show that the state parameter (ψ) of fine tailings was significantly higher than coarse tailings. Therefore, both fine and coarse tailings are likely to exhibit potential flow liquefaction.

The three CPTu selected showed that the liquefaction potential is high as time goes by. As a recommendation, designed makers should be considering this key indicator in their decision for the physical stability of the tailing dams.

The histograms of state parameter illustrated a tendency for high-frequency values of ψ (right side of the gauss curve) which can be an indicator for contractive behavior of tailings body.

5 DATA AVAILABILITY STATEMENT

The CPTu data that were digitized and interpreted as part of this work are available at https://drive.google.com/drive/folders/1jGH0MePCuVKWnEskUsr_esu7ITPVQxBZ?usp=sharing

REFERENCES

- American Society for Testing and Materials. (2020). *Standard test method for electronic friction cone and piezocone penetration testing of soils*. ASTM International.
- Been, K. (2016). *Characterizing mine tailings for geotechnical design*. Australian Geomechanics, 51(4), 59–78.
- Draves J. F., Fox M. G (1998) *Effects of a mine tailings spill on feeding and metal concentrations in yellow perch (Perca flavescens)*. Environmental Toxicology and Chemistry, 17 (8), 1626–1632.
- Hudson-Edwards K. A., Macklin M. G., Jamieson H. E. et al. (2003) The impact of tailings dam spills and clean-up operations on sediment and water quality in river systems: the Ríos Agrio-Guadamar, Aznalcóllar, Spain. Applied Geochemistry, 18 (2), 221–239.
- ICMM 2020, retrieved from <https://www.icmm.com/en-gb/annual-reports/2020>
- Macedo J. & Vergaray L. (2020) *Properties of Mine Tailings for Static Liquefaction Assessment*. Canadian Geotechnical Journal. <https://doi.org/10.1139/cgj-2020-0600>.
- Jefferies, M., & Been, K. (2016). Soil variability and characteristic states. Soil Liquefaction: A Critical State Approach. CRC Press, 203–224.
- Plewes, H.D., Davies, M.P., & Jefferies, M.G. (1992). *CPT based screening procedure for evaluating liquefaction susceptibility*. Proceedings from The 45th Canadian Geotechnical Conference, 41–49. Richmond, BC: BiTech Publishers Ltd.
- Reid, D., & Jefferies, M. (2017). State parameter as a geological principle in tailings. In *Proceedings of Tailings and Mine Waste* (pp. 305–314).
- Reid, D. (2019). Additional analyses of the Fundao tailings storage facility: in situ state and triggering conditions. *Journal of Geotechnical and Geoenvironmental Engineering*, 145(11), 04019088.
- Robertson PK, Melo L, Williams DJ, Wilson GW (2019). *Report of the Expert Panel on the Technical Causes of the Failure of Feijão Dam I*. December 12 2019. <http://www.b1technicalinvestigation.com/pt/>. Accessed 29 Dec 2019
- Robertson, P.K. (2009). *Interpretation of cone penetration tests – a unified approach*. Canadian Geotechnical Journal, 46(11), 1337–1355.
- Vick, S. G. (1990). Planning, Design, and Analysis of Tailings Dams [B]. doi:<http://dx.doi.org/10.14288/1.0394902>

Is CPT a suitable in situ test for characterizing gravelly sands?

G. Togliani

Geologist, Massagno, Switzerland

ABSTRACT: A recent study (Han et al, 2019) showed that CPTs performed in sandy soils with a variable but sometimes significant gravel content, despite special operational measures (alternating drilling and CPT), frequently provide unrealistic q_c values which adversely affect the piles capacity predictions even using the most representative CPT-based design methods. However a series of SPT verticals are also available and the conversion of N_{30} into q_c values has allowed, via a number of steps, the development of four virtual CPTu, two of which were then used for the pile capacity predictions This procedure has proven to be effective, so that, even employing far less authoritative methods, were obtained sufficiently approximate shaft and toe resistances.

1 INTRODUCTION

This paper is based on the study of Han et al. (2019) concerning the load response of two pipe piles driven in a gravelly sand alluvium (Lafayette, Indiana, USA), one open-ended and the other closed-ended ($D=0.61$ m and $L=17.3$ m) but only the last one is debated because it is affected by fewer unknowns.

The variable but frequently significant gravel content has made CPTs execution problematic, so much so that, for CPT3, it was necessary to refer to a drill-and-push procedure in order to go deeper than 30m.

It is precisely for this reason that to obtain a complete test it was necessary to combine CPT2 and CPT3, via digitizing both with the result shown in Figure 1 (CPT2-3).

Anyway, the most serious problem was created by the gravel dragging effect that made the q_c values poorly reliable, increasing them, randomly, in an unlikely manner.

Nevertheless, the q_c values, albeit with a few local corrections, were likewise used to calculate the piles capacities applying five of the most representative methods known to date, logically with poor results.

In contrast, some SPT verticals, one of which is represented in Figure 1 (SPT2), were not considered for the same goal maybe fearing similar results due to a ratio $[(q_c/Pa)/N]$ close to 10 as suggested by literature for gravelly sands or, again, to the generally accepted SPT limitations, surprisingly emphasized, however, only in recent years although innate.

Some grain size analysis, which results are summarized in Table 1, complete the soils description.

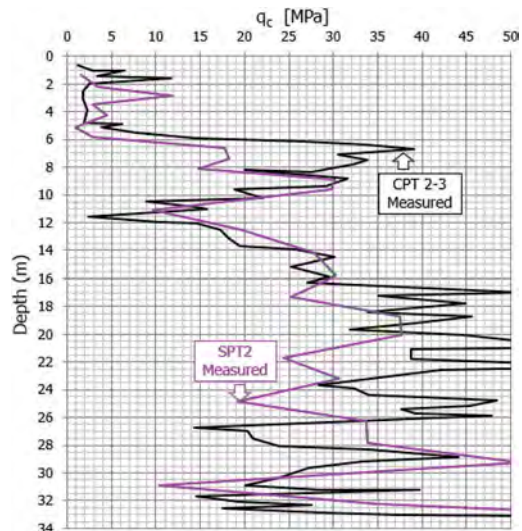


Figure 1. q_c and N_{SPT} plots.

Table 1. Geostatigraphy at test site.

Depth m	Soil Type	Gravel Content (%)	D50 mm	USCS
0.0-5.5	Clayey silt	-	-	-
5.5-8.2	Sand with gravel	4	0.4	SP
8.2-10.4	Sandy Gravel	49	4.5	SP
10.4-19.1	Sand with gravel	10	0.9	SP
19.1-22.6	Gravelly sand	43	4.1	SP
22.6-32.6	Gravelly sand	28	1.1	SP

2 CPT AND SPT MATCHING

Comparing the two curves in Figure 1, it is rather singular to note that with q_c values, over 6 m depth, almost always above 30 MPa and with frequent peaks of 40/50 MPa, the SPT has only two N_{30} values above 50, both, moreover, at depths greater than 29 m when the energy is decidedly declining.

Considering that, anyway, also the SPT values despite the more favorable scale effect (cone section of 20 cm² against 15 cm² for CPT), are influenced by the gravel presence, it is reasonable to assume that the poorly graded sandy matrix has a density index that, barely, achieves the medium dense state.

The author, noting the above, then thought to verify what results were provided by some of the most known methods for the piles design via SPT (Shariatmadari et al., 2008), summarizing them in Table 2 together with the measured one, corrected for residual load, and those obtained by Han et al. (2019) using CPT based methods described by themselves.

Table 2. CEP capacities.

Static Loading Test & Design Methods	Toe (kN)	Shaft (kN)	Capacity (kN)
Measured (corrected)	2403	2157	4560
Purdue (CPT)	4350	2825	7175
ICP05 (CPT)	3616	2055	5671
UWA05 (CPT)	5026	2624	7650
NGI05 (CPT)	3817	3665	7482
Fugro05 (CPT)	4204	3167	7371
Meyerhof (SPT)	3000	1082	4082
Decourt (SPT)	3465	2135	5600
Bazaara (SPT)	1843	2164	3998
Shariatmadari (SPT)	3101	1389	4490

By examining the table contents, it is evident that the approximation of the predictions obtained using SPT methods is better than those produced via CPT, so justifying the attempt to generate more likely q_c values by creating virtual CPTu starting from the N_{30} values of SPT2, even knowing their limits.

On the matter, remembering that Jefferies et al. (1993) claim that the best SPT is the one obtained by suitably processing a CPTu, then the author assumed that, in specific, the opposite could also be true

However in developing this procedure within sandy-gravel alluviums, the q_c values derived via D_{50} (Robertson et al., 1983), or using I_c [Lunne et al. (1997), Robertson (2012)], or $f(I_c)$ according to Ahmed et al. (2013), were ignored because with a mean value around 1 for D_{50} , I_c anyway ≤ 1.50 and consequently $f(I_c) > 550$, we always get too high q_c values.

Instead, new q_c profiles were obtained using for the conversion four different approaches [Jefferies et al., Bustamante, Dutch modified, Togliani (2016)].

The next Table 3 and Table 4 are helpful in understanding the way followed to carry out the mentioned conversions over the pile whole length.

Table 3. Conversion coefficients guides.

α (Guide)	Zone (I_c Guide)
1.2 (GW, GP, GM, GP)	7 $I_c < 1.25$
1.1 (GM-ML, GC-CL)	7 $I_c < 1.25$
1.0 [SW, (GW)]	6 $1.25 < I_c < 1.80$
0.9 [SW (SM), SP]	6 $1.25 < I_c < 1.80$
0.8 (SC, SM-ML)	5 $1.80 < I_c < 2.40$
0.7 (SC-CL)	5 $1.80 < I_c < 2.40$
0.6 (ML, CL-ML)	4 $2.40 < I_c < 2.67$
0.5 (CL)	3 $2.67 < I_c < 3.22$
0.4 (OL, OH, MH)	2 $I_c > 3.22$
0.3 (Pt)	2 $I_c > 3.22$

Table 4. Conversion coefficients application.

Depth (m)	N_{30}	USCS	α	Zone	I_c
1.3	2	SC, SM-ML	0.8	5	2.20
2.2	3	SC, SM-ML	0.8	5	2.20
2.9	12	SP[SW (GW)]	1.0	6	1.50
3.4	3	SC, SM-ML	0.8	5	2.20
4.3	4	SC, SM-ML	0.8	5	2.20
5.1	1	SC, SM-ML	0.8	5	2.20
5.8	3	SC, SM-ML	0.8	5	2.20
6.6	18	SP[SW (GW)]	1.0	6	1.50
7.4	19	SP[SW (GW)]	1.0	6	1.50
8.1	15	SP[SW (GW)]	1.0	6	1.50
8.9	30	SP[SW (GW)]	1.0	6	1.50
9.6	30	SP[SW (GW)]	1.0	6	1.50
11.1	10	SP[SW (GW)]	1.0	6	1.50
12.5	20	SP[SW (GW)]	1.0	6	1.50
14.2	28	SP[SW (GW)]	1.0	6	1.50
15.8	30	SP[SW (GW)]	1.0	6	1.50
17.3	25	SP[SW (GW)]	1.0	6	1.50

Based on previous suggestions, the q_c values, for the Jefferies et al. approach, were obtained solving the original equation (1993), just according to q_c instead of N_{30} , choosing for I_c a value compatible with the results of the grain size analyses (Table 1):

$$q_c(\text{bar}) = 8.5N_{30} (1 - I_c/4.6) \quad (1)$$

Instead, using Bustamante et al. (1993), q_c values were derived according with nomogram in Figure 2.

The Dutch modified method already described by Togliani et al. (2004) and Togliani et al. (2015), is based on the following equation:

$$q_c(\text{bar}) = \alpha(M^2H)/[Ae(m + M1)] \quad (2)$$

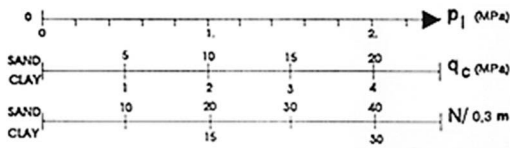


Figure 2. Bustamante et al. (1993) Nomogram.

where: α = conversion coefficient (Table 3)
 $M=63.5$ kg, $H=76$ cm, $A=20$ cm²
 e =set per blow, $m= 6$ kg/m, $M1=70$ kg

Finally, the Togliani method, created for personal use in 2016, refers to equation below:

$$q_c(\text{MPa}) = \alpha[N_{30}/\log(\sigma'_v)] \quad (3)$$

where: σ'_v is in kPa

Subsequently, pertinent f_s values were estimated via q_c elevating it to 0.4 (if $q_c < 1.5$ MPa), to 0.55 (if $q_c > 30$ MPa), to 0.47 for intermediate q_c values as illustrated in the graph below, which serves also as a check involving the well-known Euripides Project.

For the study by Han et al., 2019 (Lafayette) a change was introduced to mitigate the gravel impact [if $q_c > 1.5$ MPa, $f_s = q_c^{0.45}$ (with f_s and q_c in kPa)].

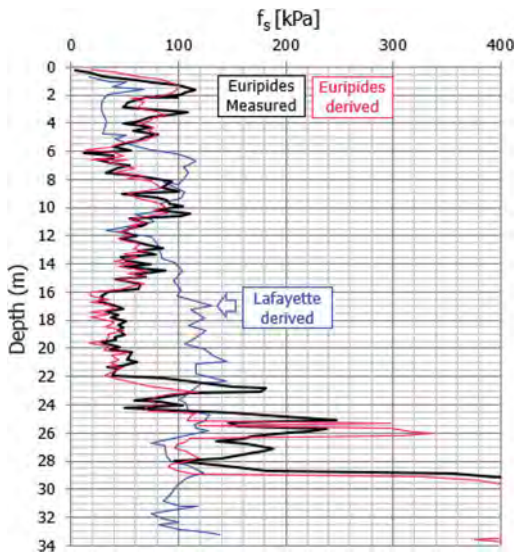


Figure 3. Virtual f_s .

At last, the virtual CPTu were completed equalizing the u_2 to u_0 values (soils classified as SP assume that their permeability is high), processing which via CPeT-IT interpretation software (supervised by P.K. Robertson), new N_{30} values were derived to compare with those measured, thus closing the loop.

3 VIRTUAL AND REAL N_{30} , q_c VALUES

Applying the procedure suggested in the previous paragraphs, the four curves relating to both q_c and N_{30} values were determined and compared with the measured ones in Figure 4 and in Figure 5.

In this regard, we highlight the amazing match of the curves referred to N_{30} values both measured and predicted according to Togliani, 2016.

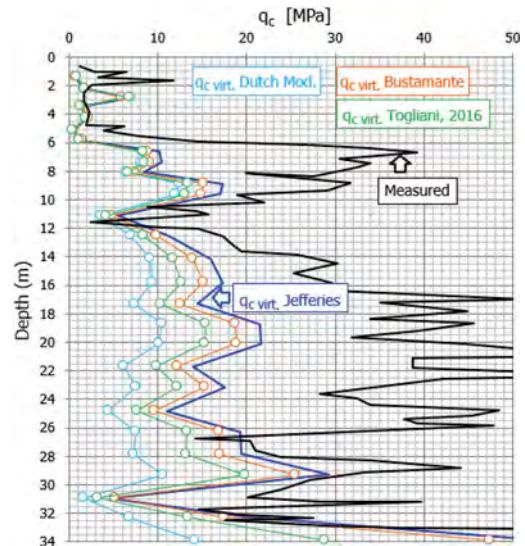


Figure 4. q_c Synoptic plots.

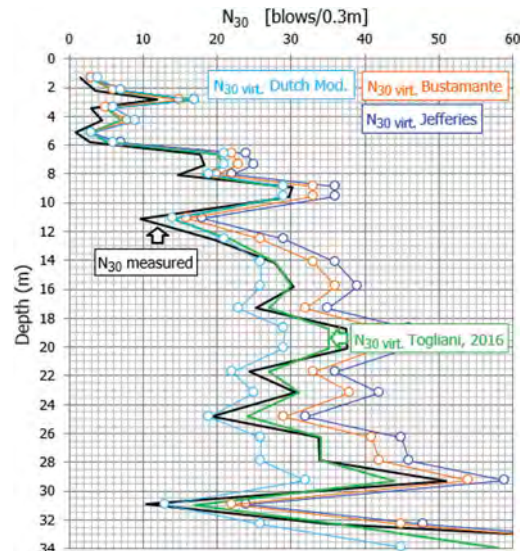


Figure 5. N_{30} Synoptic plots.

The above synoptic graphs show that the approach of Jefferies et al. (1993) for q_c and the one of Togliani (2016) for N_{30} , are those closest to the measured values and, for this reason, were chosen for the piles capacity prediction, applying the methods below:

1. ICP05 selected, as reference and comparison, among those used by Han et al.(2019);
2. Décourt (1995) by employing the N_{30} values obtained from the two virtual CPTu;
3. LCPC (1982) method, being the precursor among those using only the q_c values;
4. Togliani 2008 ($q_c \& R_f$) and 2018 ($q_c \& K^*_G$).

4 CPT/SPT-BASED DESIGN METHODS

ICP05, LCPC and Décourt methods are well-known and widely used and therefore do not need any explanation.

For ICP05, however, it should be noted that, in the specific case, the q_c values used have not been subjected to any filtering, that those of the natural unit weights γ_n were obtained from virtual CPTu processing (CPeT-IT), as well as the interface friction angles ($\delta_c = \phi_{peak}^{0.95}$, arbitrarily decided in this case where q_c is only virtual and specific measured values are missing).

With this option, δ_c , at least in gravelly sand, is ranging anyway between 29° and 32° and so in agreement, with the suggestion of Salgado et al. (2011), by which $\delta_c = 0.9\phi_c$.

Both Togliani methods, are usually updated according to new experiences especially related to international piles capacity prediction events, which is why we report below their latest version.

- 1 $q_c \& R_f$ Method (2008): Unit Friction (q_s)

$$q_s = \beta q_c^{0.4} \quad \text{if } f_s \leq 20 \text{ kPa} \quad (4)$$

$$q_s = \beta \{ q_c^{0.52} [0.9(0.4 \ln R_f)] \} \quad \text{if } R_f \geq 1.5 \quad (5)$$

$$q_s = \beta \{ q_c^{0.51} [0.8 + (1 - R_f/8)] \} \quad \text{if } 1 \leq R_f < 1.5 \quad (6)$$

$$q_s = \beta \{ q_c^{0.53} [0.8 + (1.1 - R_f/8)] \} \quad \text{if } R_f < 1 \quad (7)$$

- 2 $q_c \& K^*_G$ Method (2018): Unit Friction (q_s)

$$q_s = \beta (q_c^{0.3+x}) \quad \text{if } 3 < SBT < 7 \quad (8)$$

$$q_s = \beta (q_c^{0.2+x}) \quad \text{if } SBT \geq 7 (q_c < 30 \text{ MPa}) \quad (9)$$

$$q_s = \beta (q_c^{0.2+x}) \quad \text{if } SBT \leq 3 \quad (10)$$

where SBT= Soil Behavior Type

$$x = \log(K^*G^a)$$

$\alpha = 0.11$ (driven precast and pipe piles)

$\alpha = 0.10$ (cast in situ piles)

- 3 Both Methods (2018): Unit Base (q_b)

$$q_b = q_{c\text{toe}} [\lambda + 0.05 L_{\text{pile}} / D_{\text{pile}}] \quad (11)$$

where: $q_{c\text{toe}}$ goes from +8 d_{toe} to -4 d_{toe} , range considered for homogeneity reasons also for ICP05 predictions

Table 5 summarizes the correspondent pile type co-efficients.

Table 5. Pile type coefficients.

Pile Type	β	λ
Driven/Jacked (precast, pipe closed-ended)	1.00	0.30
Drill Displacement	0.90	0.25
Pipe (open-ended)	0.70	0.20
CFA, Bored (cased-cohesionless)	0.60	0.15
Bored (polymer, bentonite-upper bond)	0.60	0.10
Bored (cased-cohesive)	0.50	0.10
Bored (bentonite-lower bond)	0.40	0.05

About λ we note that at least doubles if $SBT < 3$, when the whole length “+8 d_{toe} to -4 d_{toe} ” develops in a dense/consistent soil without gravel or an Expander Body is present, while it reduces to 1.5λ in gravelly soils.

5 CEP: CPT/SPT-BASED METHODS RESULTS

The first group of results is that of the already known representative methods (Han et al. 2019), none of which fall within $\pm 20\%$ of the generally admitted tolerances (red lines), where especially the toe resistance is overestimated in a remarkable amount while, among all the methods, only ICP05 correctly evaluates the shaft resistance (Figure 6).

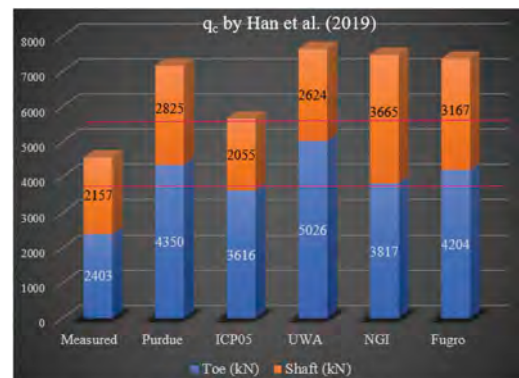


Figure 6. Pile capacity by representative methods.

When using q_c values derived by Jefferies et al. (1993) conversion approach, three methods are within the accepted tolerances not only for pile capacity (ICP05, LCPC, Togliani 2018) but also for its toe and shaft components while Togliani 2008 suffers from a notable overestimation of the latter that extends, for Decourt, also to toe resistance (Figure 7).

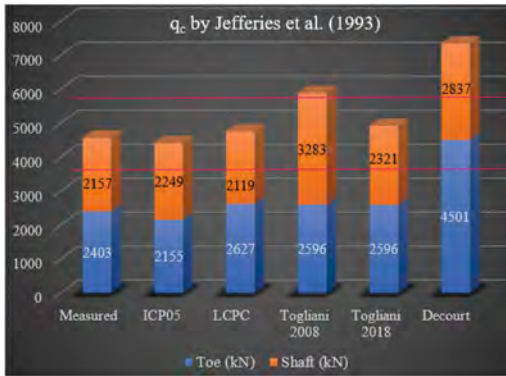


Figure 7. Pile capacity using q_c by Jefferies et al (1993).

The circumstance that, for ICP05, in the face of much lower q_c values (Jefferies et al., 1993) we obtain a higher shaft resistance than Han et al. (2249 kN vs. 2055 kN, respectively), is probably due to the different evaluation of the interface friction angles.

Lastly, applying the method of conversion from N_{SPT} to q_c developed by Togliani in 2016, only Togliani 2008 and 2018 meet the requirements for pile capacity but it is exclusively Togliani 2018 that satisfies both components.

Among other methods, the approximation is sufficient for shaft resistance for both ICP05 and Decourt while LCPC is underestimating both components (Figure 8).

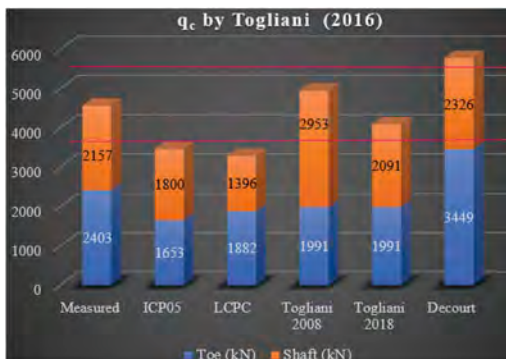


Figure 8. Pile capacity using q_c by Togliani (2016).

6 PILE UNIT FRICTION DERIVED FROM VS

The author has only at the last moment known the outcome of three dynamic loading tests performed on bored piles with a diameter of 1.5 m and a length of 16 m placed in sandy gravel with cobbles, for the first 6-12 m consisting of medium-dense, dense fill followed by dense, very dense alluvial deposit.

This is the reason why the matter is treated in a concise way making visible first, in Figure 9, the grain size of the soils of interest (at 9 m and 10 m bricks are still present while GWT is at depth of 15 m)

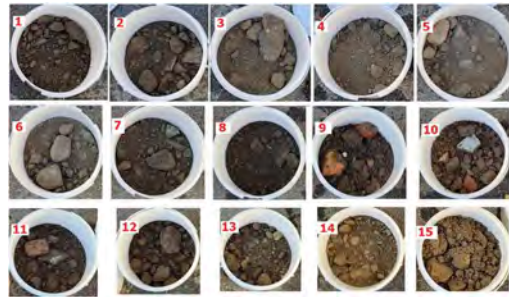


Figure 9. Samples collected during a pile execution.

The deep foundations were necessary for the covering of the Swiss Federal Railways Maintenance Center in Biasca.

The piles are distributed on two rows for a length of about 500 m for whose geotechnical characterization were available a continuous coring borehole with punctual SPT each 2-3m and a tomographic seismic profile that covered the entire length.

In this way it was possible to have a vertical log of the shear waves per meter depth at each pile that allowed to try a correlation between V_s and unit friction (q_s), finally applied and proving promising so as to be tested for our pile after the appropriate modifications (in comparison, in fact, there are a cast in situ bored pile and a driven closed ended steel pipe whose capacity prediction comes, for more, from parameters found in a virtual CPTu).

The proposed equation is:

$$q_s = V_s^{0.95 - I_c/10} \quad (12)$$

where: q_s is in kPa, V_s is in m/sec and I_c is the Soil Behavior Type Index

Despite being totally improvised, the above equation predicts a shaft resistance close to that measured, then showing a good potential (Figure 10).

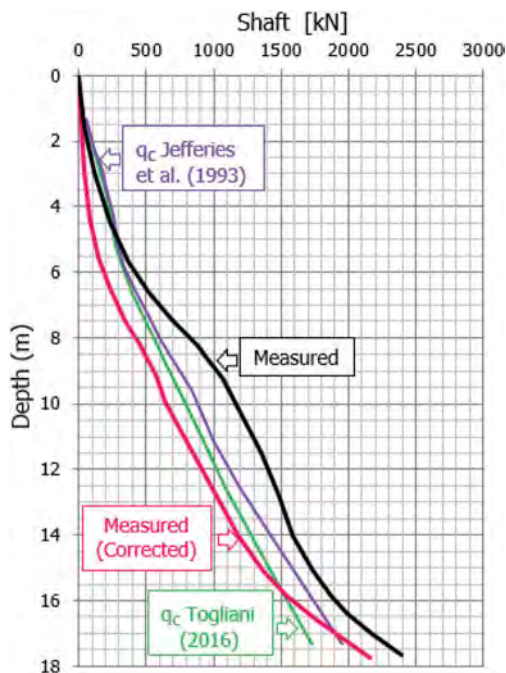


Figure 10. Shaft resistance prediction vs measure.

7 CONCLUSION

The above leads to the following final remarks:

1. if an alluvial sand is frequently gravelly, a CPT is not a suitable in situ test to propose, being the static penetration often problematic and the q_c values too frequently unrealistic especially due to dragging gravel effect. Always applying the rule that “garbage in, garbage out”, any pile capacity prediction where such values are directly used, is then condemned to failure whatever the representativity of the methods used;
2. fortunately, in this case, SPTs were also available, processing which made it possible to create alternative q_c values that proved valid even when applying pile design methods derived from personal experiences and therefore mainly intended for practical use, such as those of the author, that, in the 2018 updated version ($q_c \& K \cdot G$), proved to be the most performing;
3. in sandy soils with a variable but sometimes significant gravel content, punctual SPTs, carried out in continuous core drilling, would be more effective by replacing the standard sampler, useless in this case, with a conical point thus allowing to extend the test well beyond the zone remolded by the decompression/structural change that frequently affects the values recorded in the standard length of 0.45 m. Alternating the recovery of samples to SPTs, in incoherent soils even several meters long, we are able to obtain a sort

of continuous and reliable DPSH and also, in cohesive soils, to bypass the casing requirement that should characterize the dynamic continuous penetration tests of better quality. This way of performing SPTs, already described (Togliani et al., 2004), has never been disappointed the author which, on the contrary, has often benefited from it and in any case obtained information that has allowed him to make better-informed decisions. Of course, in cohesionless sands without gravel, it should be remembered that when interpreting the results, the replacement of the standard sampler with a conical point will generate different and greater values as we go from small displacement to full displacement conditions;

4. the lesson learned, especially for the practitioners, is that SPT, which is still the most popular and used in situ test although its validity is being questioned more and more, in certain contexts is providential and therefore, where present, should always be considered at least as a comparison.
5. last but not least, the use of Vs for the pile unit friction prediction seems to be able to help in predominantly gravelly soils with cobbles in which the usual in situ tests are difficult to perform and their outcome uncertain as well as questionable and, for this reason, other tests, in different scenarios, would be beneficial.

ACKNOWLEDGMENT

A grateful thought is addressed to the late friend and colleague Giorgio Beatrizotti for his consistent encouragement to develop the practice on in situ tests, of which he was a great supporter.

REFERENCES

- Ahmed, S.M., Agaiby, S.W., Abdel-Rahman, A.H. *A unified CPT-SPT correlation for non-crushable and crushable co-hesionless soils*. Ain Shams Engineering Journal (2014)
- Bustamante, M., and Gianeselli, L. (1982). *Pile Bearing Capacity by Means of Static Penetrometer CPT*. ESOPT II
- Bustamante, M. & L. Gianeselli (1993). *Design of auger displacement piles from in situ tests*. 2nd Intern. Geotechnical Seminar: Deep Foundations on Bored and Auger Piles CPeT-IT v.3.0. CPT interpretation software. Geologismiki
- Decourt, L. 1995. *Prediction of load-settlement relationships for foundations on the basis of the SPT-T*. Ciclo de Conferencias Internacionales, Leonardo Zeevaert, UNAM, Mexico.
- Han, F., Ganju, E., Salgado, R., Prezzi, M., & Zaheer, M. (2019). *Experimental study of the load response of large diameter closed-ended and open-ended pipe piles installed in alluvial soil* (Joint Transportation Research Program Publication No. FHWA/IN/JTRP-2019/03). West Lafayette, IN: Purdue University

- Jardine, R., Chow, F., Overy, R., Standing, J. 2005. *ICP design methods for driven piles in sands and clays*. Thomas Tel- ford Publishing
- Jefferies, M.G., and Davies, M.P., 1993. *Use of CPTU to estimate equivalent SPT N60*. Geotechnical Testing Journal, ASTM,
- Robertson, P.K. 2016. *Cone penetration test (CPT)- based soil behaviour type (SBT) classification system — an update*. Canadian Geotechnical Journal, 53(12)1910–1927
- Salgado, R., Woo, S. I., & Kim, D. (2011). *Development of load and resistance factor design for ultimate and serviceability limit states of transportation structure foundations* (Joint Transportation Research Program Publication
- Shariatmadari, N., Eslami, A., Karimpour-Fard, M. (2008). *Bearing Capacity of Driven Piles in Sand from SPT – Applied to 60 Case Histories*. Iranian Journal of Science & Technology
- Togliani, G. Beatrizotti, G. 2004. *Experimental In Situ Test Sites*. ISC-2 Proceedings. Porto, September, 19-22, 2004
- Togliani, G. 2008. *Pile capacity prediction for in situ tests*. Proceedings ISC-3 April 1-4, 2008. 1187-1192. Taylor & Francis Group, London, UK
- Togliani, G., Calzolari, L., Menghini, A. 2015. *Governolo (Italy) Experimental Site: In Situ Test Comparisons and Mutual Conversions*. DMT'15 Proceedings
- Togliani, G. 2018. *Soil Behaviour and Pile Design: Lesson Learned from Some Prediction Events - Part 1: Aged and Residual Soils-Part 2: Unusual NC Soils*. CPT'18 Proceedings

A CPT-based diameter-dependent m - θ spring model for lateral pile analysis

J. Tott-Buswell & L.J. Prendergast

Department of Civil Engineering, University of Nottingham, Nottingham, UK

ABSTRACT: Offshore Wind Turbines (OWT) are a successful renewable energy solution; however, emerging turbine sizes require pile geometries beyond the calibration range of existing design standards. This necessitates soil sampling and rigorous finite element modelling, which is problematic for quick design estimates. Cone Penetration Test (CPT)-based p - y methods can provide preliminary deflection estimates, although their applicability becomes increasingly uncertain as pile slenderness ratios, length normalized by diameter (L/D), reduce. This is due to the increase in diameter incurring additional resistances that p - y models alone cannot account for. To incorporate the additional resistance, this paper defines a CPT-based moment-rotation (m - θ) model by rescaling empirically derived axial capacity functions (known as τ - w curves). Various monopile dimensions are simulated and pile-head displacements are compared for CPT-based p - y models with and without m - θ springs. The net effect of incorporating m - θ springs increases as monopile diameters (and rigidity) increase and diminishes as piles increase in slenderness.

1 INTRODUCTION

1.1 Current monopile design process

There are two fundamental solutions to the increasing demand in renewable energy within the offshore wind sector. These are; increasing the radius of the blade-swept area to generate more energy per OWT, and optimizing the windfarm construction process. However, the foundation geometries required to facilitate the large moments induced by emerging wind turbine dimensions extend beyond the applicability of current design practices, requiring advanced 3D finite element modelling (Doherty and Gavin, 2011; API, 2014; Burd et al., 2017). Such design methodologies call for soil sample investigations which are often difficult to undertake in offshore environments and are impractical for preliminary design estimates. It would therefore be beneficial to develop a model which takes advantage of early measurements for soil strength properties, such as the Cone Penetration Test (CPT) (Reale et al., 2021), to gain a preliminary performance evaluation of OWT monopiles, optimizing the design process.

1.2 The p - y model using CPT data

The p - y method for piles simplifies the physical system to one-dimension using a series of discretized nonlinear springs that represent the lateral soil pressures p as a function of lateral pile displacement y . Each spring is linked through linear-elastic Euler-Bernoulli beam elements. For sands, the API

design methodology recommends curves empirically derived from piles with slenderness ratios (L/D) much greater than the geometries expected for emerging monopiles (Reese et al., 1974; Murchinson and O’Niell, 1986), therefore their applicability in the design of OWT foundations is increasingly questionable.

CPT-based p - y curves have been developed based on taking the cone tip end resistance (q_c) and empirically deriving exponential functions for the p - y relationship (Dyson and Randolph, 2001; Li et al., 2014; Suryasentana and Lehane, 2014). However, it has been demonstrated that their effectiveness at encapsulating lateral soil resistance decreases as L/D reduces, and their suitability for the problem relies on the range at which they were empirically calibrated (Li et al., 2014). This notion limits the traditional model configuration to lateral springs that employ p - y curves calibrated for specific pile size configurations; however, they are unable to fully account for all resistances. Therefore, further modifications must be made to traditional p - y methods to account for the presence of these additional resistance mechanisms induced by the increased rigidity of monopiles.

1.3 Distributed moment resistance

It is becoming apparent that the lateral resistance of piles with stockier geometries are not solely dependent on lateral soil pressures (Lam, 2013; Murphy et al., 2018; Burd et al., 2020; Fu et al., 2020). The

increase in diameter size introduces a distributed moment along the shaft as well as additional lateral and overturning resistances at the pile tip. These additional resistances are termed “diameter effects”. The distributed moment stems from the interface shear friction acting at a distance from the cross-section’s center of rotation, generating a -moment m along the pile shaft proportional to its rotation θ . This is outside of the modelling capabilities of a lateral spring element and can be effectively modelled through rotational spring elements in tandem with the distributed p - y springs. Larger diameters additionally lead to base resistances, which are not considered in this paper.

The aim of this paper is to define an appropriate m - θ spring function to describe the distributed moment impeding global rotation using q_c only, improving current CPT-based p - y models and enhancing geometric versatility. Such a model can provide the first step towards a strong preliminary evaluation of OWT monopile performance due to the convenience of CPT extraction in offshore environments.

2 METHODOLOGY

2.1 P - y function

The monopile’s embedded length L and the CPT q_c profile are both discretized into lengths L_{inc} such that the q_c values can be averaged over length L_{inc} (giving $q_{c,avg}$). This informs evenly discretized points along the monopile, thereby characterizing the p - y and m - θ springs (Figure 1). The p - y springs used in this paper are informed through Equation 1 which were empirically derived by Suryasentana and Lehane (2014) for low L/D monopiles in sand.

$$\frac{p}{\gamma z D} = 2.4 \left(\frac{q_c}{\gamma z} \right)^{0.67} \left(\frac{z}{D} \right)^{0.75} \times \left\{ 1 - \exp \left[-6.2 \left(\frac{z}{D} \right)^{-1.2} \left(\frac{\gamma}{D} \right)^{0.89} \right] \right\} \quad (1)$$

where γ is the unit weight of the soil (assumed 20 kN/m³ for dense sand applications), z is the spring depth and D in the diameter of the monopile. The initial stiffness of the p - y spring is determined based on a correlation to small-strain shear modulus, see Suryasentana and Lehane (2016).

2.2 M - θ function

The m - θ spring model is derived from principles based on the axial capacity design for monopiles. τ - w vertical springs represent the uniform soil-pile interface friction when loaded vertically as shown in Figure 2a. The τ - w

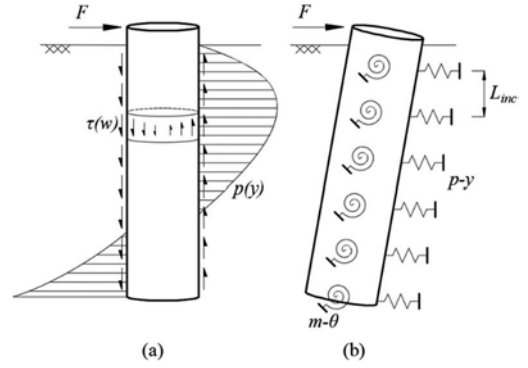


Figure 1. (a) Soil resistances on a monopile under lateral load and (b) the one-dimensional discretised model (neglecting base diameter effects).

relationship is described through a quadratic equation defined by Randolph (2003) in Equations 2 and 3.

$$\tau(w) = G_0 \left(\frac{w}{2D} \right) \left[1 - \frac{w}{2w_f} \right] \quad (2)$$

$$w_f = \frac{4D\tau_f}{G_0} \quad (3)$$

Where w is the vertical displacement, w_f is the maximum vertical displacement at which the shear resistance is fully mobilized, and G_0 is the initial stiffness which can be approximated from q_c using the relationship $G_0 \approx nq_{c,avg}$ (Schnaid et al., 2004). n is taken as 6 for dense soils (Prendergast et al., 2013). The maximum shear stress τ_f is shown in Equation 4 as defined in UWA-05 (Lehane et al., 2005).

$$\tau_f = \frac{f_t}{f_c} \tan \delta_f \times \left[0.03b q_c A_{re}^{0.3} \left[\max \left(\frac{H}{D}, 2 \right) \right]^{0.5} + \Delta\sigma'_{rd} \right] \quad (4)$$

where $f_t/f_c = 1$ and $b = 1$ for piles in compression, H is the distance from pile tip to a given soil horizon, and $A_{re} = 1 - \text{IFR}(D_t/D)^2$ is the effective area ratio. IFR (Incremental Filling Ratio) is taken as 1. For the present study, the angle of friction δ_f is assumed 35° and the change in radial stress due to dilation $\Delta\sigma'_{rd}$ is assumed negligible.

A pile section under rotation experiences varied shear resistance magnitudes proportional to the distance from the axis of rotation. The origin of this varied shear resistance due to an overturning moment is recognized to be related to the uniform friction due to vertical loading as shown in Figure 2b.

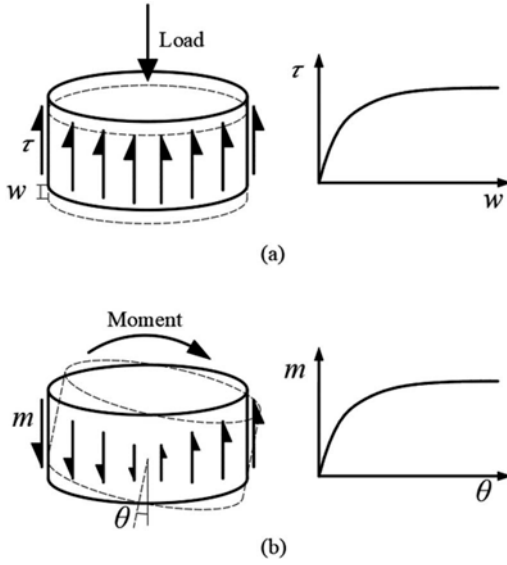


Figure 2. Pile section under (a) vertical uniform friction and (b) vertical varied friction.

It is therefore possible to scale the original τ - w function and transform to m - θ form. Figure 3 illustrates the scaling theory. This model assumes that the axis of rotation is at the center of the pile cross section for all depths and the p - y and m - θ springs remain uncoupled.

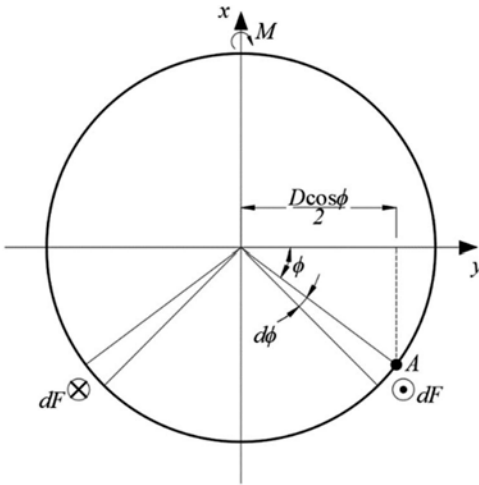


Figure 3. Derivation of total moment about a pile's cross-section (adapted from Fu et al. (2020)).

The vertical displacement w for any point around the rotating pile section in Figure 3 is given by Equation 5.

$$w = \frac{\theta D}{2} \cos \phi \quad (5)$$

where ϕ is the radial coordinate within the pile cross section. The total moment per meter m caused by incremental force dF on the lever arm $0.5D \cos \phi$ is given by the integral defined in Equation 6.

$$m = 2 \int_{-\frac{\pi}{2}}^{\frac{\pi}{2}} \frac{D}{2} \cos \phi dF \quad (6)$$

Substituting $dF = \tau dA$ (where $dA = 0.5D d\phi$) into Equation 6 gives m as a function of $\tau(w)$.

$$m = \frac{D^2}{2} \int_{-\frac{\pi}{2}}^{\frac{\pi}{2}} \tau(w) \cos \phi d\phi \quad (7)$$

Further substituting Equation 4 and 5 into 7, then solving the integral gives the total moment m as a quadratic function in terms of θ (Eq. 8).

$$m(\theta) = \begin{cases} a\theta - b\theta^2, & \theta < \theta_f \\ m_f, & \theta \geq \theta_f \end{cases} \quad (8a)$$

$$a = \frac{G_0 D^2 \pi}{16}, \quad b = \frac{G_0^2 D^2}{96 \tau_f} \quad (8c)$$

Where m_f and θ_f are the maximum moment per meter and maximum rotation, respectively. m_f is computed based on taking advantage of the parabolic properties of Equation 8a. The function is illustrated in Figure 4 and the key parameters are highlighted in Table 1.

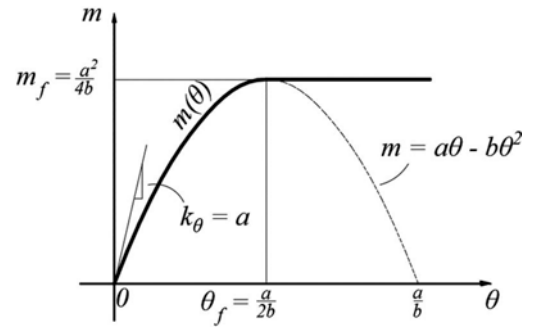


Figure 4. Parabolic relationship of m - θ .

Table 1. m - θ function key parameters.

Parameter	Definition
Maximum moment, m_f	$\frac{a^2}{4b} = \frac{3}{32} \pi^2 D^2 \tau_f$
Failure rotation, θ_f	$\frac{a}{2b} = 3\pi \tau_f / G_0$
Initial stiffness, k_θ	$a = \frac{1}{16} \pi D^2 G_0$

Note that the failure moment m_f , failure rotation θ_f and initial stiffness k_θ are in some scaled form that is reflective of the soil's conventional properties, enabling a quick specification of the moment-rotation interaction. The described methodology for deriving the $m-\theta$ function is not limited to the CPT $\tau-w$ curves derived by Randolph (2003) and can be replaced with any $\tau-w$ definition. The initial stiffness k_θ can also be used for small-strain dynamic analysis to determine natural frequencies (Prendergast and Gavin, 2016).

The numerical model implementing the above procedure is developed in MATLAB using its proprietary programming language to compute the monotonic lateral response of a series of piles with varying L/D . The secant stiffness of the springs defined in Equations 1 and 8 characterize the global stiffness matrix and the displacements are iterated until convergence to compute pile deflections using the Direct Stiffness method. Diameter effects induced at the pile tip are neglected.

2.3 CPT profile

An idealized CPT profile is generated based on the formulations derived by Lunne and Christoffersen (1983) as follows:

$$q_c = 60 \left(\sigma'_v \right)^{0.7} \exp(2.91 D_r) \quad (9)$$

where D_r is the relative density and is taken as 0.8 for dense sand and σ'_v is the vertical effective stress. The vertical effective stress was calculated by assuming a bulk unit weight of 20 kN/m³ and dry soil conditions. Equation 9 is used to inform spring characteristics in Equations 1 and 8.

It is noted that the current iteration of the model does not account for monopile tip effects, which can have a significant influence on the lateral displacements when the diameter size is substantially large (Murphy et al., 2018). The currently proposed framework is therefore an iteration towards an all-encompassing versatile resistance model informed through preliminary offshore soil data.

3 RESULTS AND DISCUSSION

Two models are developed to observe the influence of the $m-\theta$ springs for various monopile geometries. The $py-m\theta$ model includes $n = 100$ lateral and rotational spring elements defined by Equations 1 and 8, respectively, to capture the monotonic soil-structure interaction, whereas the py -only model is simply the traditional $p-y$ methodology with $n = 100$ lateral spring elements. An independent study showed that an increase in n had negligible effects on the model's performance. Both models implement the same CPT profile derived from Equation 9.

The embedded length of the pile is 24m and the outer diameter is set to 8m, 4m, 2m and 1m to investigate model performance with various L/D ratios ($L/D = 3, 6,$

12 and 24, respectively). A horizontal force is applied at the mudline and the pile head displacements are calculated. The results are shown in Figure 5.

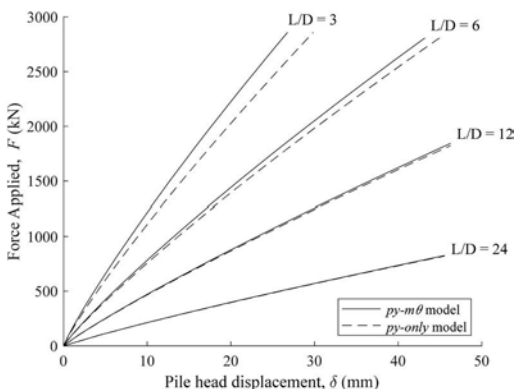


Figure 5. Comparison of pile head displacement between $py-m\theta$ and py -only models.

It is clear from Figure 5 that the increase in slenderness ratio results in the $py-m\theta$ model converging towards the traditional $p-y$ model, as the rotational spring elements exhibit negligible influence for lateral monotonic loading. This is due to the distributed moment m being proportional to D^2 as described in Equation 8. Conversely, a decrease in L/D amplifies the effect of the $m-\theta$ springs, which is indicative of the physical behavior of a monopile experiencing a distributed moment along its embedded depth. Therefore, the proposed model has demonstrated adaptability towards monopile modeling when the dimensions are varied. Further, the model's inherent modular framework allows for alternative spring functions and is not limited to the expressions used in this paper. Thus, defining $m-\theta$ functions does not require quantifying $m-\theta$ relationships experimentally, but instead selecting an appropriate axial resistance model.

An alternative approach to the problem is to calibrate $p-y$ functions that are specifically tailored for a given range of pile dimensions, which would include contributions of the distributed moment in the lateral springs. However, this restricts the model to a specific range of slenderness ratios and would incorporate physical resistances that the mechanical analogy is not intended for. It is therefore important to note that it would be preferable to use a $p-y$ function appropriate for slender piles in this proposed framework to ensure that only lateral resistances are considered in the lateral spring (as best as possible).

4 CONCLUSION

With demand outpacing research in the offshore wind sector, the need for an efficient preliminary design tool for laterally loaded monopiles is apparent. CPTs can provide initial strength profiles for offshore sites where soil sampling can be impractical for initial

performance estimates of OWTs. This paper presents an elegant method to include the distributed moments that arise from the increased cross-sectional dimensions for monopile foundations. The rotational springs are included with the traditional p - y methodology that should be already familiar to practicing engineers. The m - θ function is derived from CPT-based τ - w relationships due to the similarity in the origin of their resistances. The vertical soil-pile stresses τ mobilized from vertical displacements w are rescaled to define the relationship between the distributed moment m mobilized by pile rotation θ .

A series of monotonic pushover simulations were undertaken for various slenderness ratios of p - y models with and without m - θ springs. It was demonstrated that the increase in diameter resulted in a larger contribution from the rotational spring elements, accurately representing the likely resistance behavior of monopiles with low L/D values. Increasing the slenderness resulted in the model converging towards the p - y only model, highlighting the versatility of such a modular framework.

Defining the m - θ relationship has been simplified to selecting an appropriate τ - w function informed through q_c data. The next stage for this framework is to include a model for pile tip diameter effects that can be characterized by CPT data. Additionally, the initial rotational stiffness of the rotational spring facilitates a potential improvement to the evaluation of natural frequencies via small-strain analysis.

ACKNOWLEDGEMENTS

The first author wishes to acknowledge funding for his PhD under EP/R513283/1 EPSRC Standard Research Scholarship (DTP) at the Faculty of Engineering, University of Nottingham.

REFERENCES

- API (2014) *API RP 2GEO: Geotechnical and foundation design considerations*. Washington, DC, USA: API.
- Burd, H. J., Abadie, C. N., Byrne, B. W., Houlby, G. T., Martin, C. M., McAdam, R. A., Jardine, R. J., Pedro, A. M. G., Potts, D. M., Taborda, D. M. G., Zdravković, L. and Andrade, M. P. (2020) 'Application of the PISA design model to monopiles embedded in layered soils', *Géotechnique*, 70(11), pp. 1067–1082. doi: 10.1680/jgeot.20.PISA.009.
- Burd, H. J., Byrne, B. W., McAdam, R. A., Houlby, G. T., Martin, C. M., JAP Beuckelaers, W., Zdravković, L., Taborda, D. M. G., Potts, D. M., Jardine, R. J., Gavin, K., Doherty, P., Igoe, D. J. P., Skov Gretlund, J., Pacheco Andrade, M. and Muir Wood, A. (2017) 'Design aspects for monopile foundations', in *TC 209 workshop on foundation design for offshore wind structures, 19th ICSMGE*, pp. 35–44.
- Doherty, P. and Gavin, K. (2011) 'Laterally loaded monopile design for offshore wind farms', *Proceedings of the Institution of Civil Engineers - Energy*, 165(1), pp. 7–17. doi: 10.1680/ener.11.00003.
- Dyson, G. J. and Randolph, M. F. (2001) 'Monotonic Lateral Loading of Piles in Calcareous Sand', *Journal of Geotechnical and Geoenvironmental Engineering*, 127(4), pp. 346–352. doi: 10.1061/(ASCE)1090-0241(2001)127:4(346).
- Fu, D., Zhang, Y., Aamodt, K. K. and Yan, Y. (2020) 'A multi-spring model for monopile analysis in soft clays', *Marine Structures*, 72(July 2019). doi: 10.1016/j.marstruc.2020.102768.
- Lam, I. P. O. (2013) 'Diameter effects on p-y curves', in R. B., B. and A., E. (eds) *Deep Marine Foundations: A Perspective on the Design and Construction of Deep Marine Foundations*. Hawthorne, NJ, USA: Deep Foundations Institute.
- Lehane, B. M., Schneider, J. A. and Xu, X. (2005) 'The UWA-05 method for prediction of axial capacity of driven piles in sand', *Frontiers in offshore geotechnics: ISFOG*, pp. 683–689.
- Li, W., Igoe, D. and Gavin, K. (2014) 'Evaluation of CPT-based P – y models for laterally loaded piles in siliceous sand', *Géotechnique Letters*, 4(2), pp. 110–117. doi: 10.1680/geolett.14.00021.
- Lunne, T. and Christoffersen, H. P. (1983) 'Interpretation of Cone Penetrometer Data for Offshore Sands', in *Offshore Technology Conference*. Offshore Technology Conference. doi: 10.4043/4464-MS.
- Murchinson, J. R. and O'Niell, M. W. (1986) 'Evaluation of p-y relationships in cohesionless soils', *International Journal of Rock Mechanics and Mining Sciences & Geomechanics Abstracts*, 23(3), p. 109. doi:10.1016/0148-9062(86)91228-3.
- Murphy, G., Igoe, D. J. P., Doherty, P. and Gavin, K. (2018) '3D FEM approach for laterally loaded monopile design', *Computers and Geotechnics*, 100, pp. 76–83. doi: 10.1016/j.compgeo.2018.03.013.
- Prendergast, L. J. and Gavin, K. (2016) 'A comparison of initial stiffness formulations for small-strain soil-pile dynamic Winkler modelling', *Soil Dynamics and Earthquake Engineering*, 81, pp. 27–41. doi: 10.1016/j.soildyn.2015.11.006.
- Prendergast, L. J., Hester, D., Gavin, K. and O'Sullivan, J. J. (2013) 'An investigation of the changes in the natural frequency of a pile affected by scour', *Journal of Sound and Vibration*, 332(25), pp. 6685–6702. doi: 10.1016/j.jsv.2013.08.020.
- Randolph, M. F. (2003) 'Load transfer analysis of axially loaded piles', *RATZ manual version 4.2*. University of Western Australia.
- Reale, C., Tott-Buswell, J. and Prendergast, L. J. (2021) 'Impact of Geotechnical Uncertainty on the Preliminary Design of Monopiles Supporting Offshore Wind Turbines', *ASCE-ASME J Risk and Uncert in Engrg Sys Part B Mech Engrg*, 7(4), pp. 1–10. doi: 10.1115/1.4051418.
- Reese, L. C., Cox, W. R. and Koop, F. D. (1974) 'Analysis of Laterally Loaded Piles in Sand', in *All Days*. Reston, Virginia: OTC, pp. 95–105. doi: 10.4043/2080-MS.
- Schnaid, F., Lehane, B. M. and Fahey, M. (2004) 'Insitu test characterisation of unusual soils', in *Proceedings of the 2nd International Conference on Geotechnical and Geophysical Site Characterisation*. Porto, pp. 49–74.
- Suryasentana, S. K. and Lehane, B. M. (2014) 'Numerical derivation of CPT-based p-y curves for piles in sand', *Géotechnique*, 64(3), pp. 186–194. doi: 10.1680/geot.13.P.026.
- Suryasentana, S. K. and Lehane, B. M. (2016) 'Updated CPT-based p – y formulation for laterally loaded piles in cohesionless soil under static loading', *Géotechnique*, 66(6), pp. 445–453. doi: 10.1680/jgeot.14.P.156.

An investigation into the use of the Vibdrive and β -methods for calculating the SRV of offshore piled foundations

M.P. Trubshaw & T. Joseph

Ramboll, London, UK

G. Giuliani

COWI, London, UK

ABSTRACT: Offshore piled foundations are typically installed using an impact hammer. Increasingly, more attention is being given to use of vibratory hammers due to added benefits of prolonged pile life, reduced installation noise, and reduced risk of observing pile-run. This paper considers a case study in the North Sea, consisting of six positions where piles are installed in layered sands and clays. The Cone Penetration Test (CPT) data for the positions have been used in calculating the Soil Resistance to Vibratory Driving (SRV) as part of the Vibdrive method, from Holeyman (2002). This method has been compared with the SRV calculated using the non-CPT based β -method, from Jonker (1986). By varying the SRV used in driveability predictions, the results can be compared with the available driving records. It was found that the CPT based Vibdrive method consistently produced more representative results while still maintaining a conservative prediction.

1 INTRODUCTION

The foundations of offshore wind farms represent approximately 25% of the construction cost. Currently, the predominant type of offshore windfarm foundations are monopiles, which accounted for 88% of foundations installed in 2016, Moscoso (2018). The traditionally used installation technique is impact driving. Adopted worldwide, it is the preferred method and considered the lowest risk approach. However, there is increasing interest in vibratory driving as this technique surpasses many of the inherent problems of impact driving. This includes the generation of lower stresses into the pile thereby increasing its design life, it is 3-4 times faster at pile installation than impact driving and can be combined with faster handling procedures allowing for serial installation.

There is currently a lack of driving data for vibro installed piles in the public domain. This lack of available data prevents the development of more reliable methods of predicting the installation resistance of vibro-installed piles. As vibro-driving predictions are better understood, there is greater potential for this method to be more widely used. This paper will provide a case study of the application of two SRV calculation techniques, and how the subsequent analysis compares to the driving records. This work adopts the current industry approach to determine the driveability of impact driven piles and makes amendments to the soil input, accounting for liquefaction

induced by vibro-driving. Using this process a link is made between the two installation methods.

The SRV is calculated using the industry standard β -Method and the CPT-based Vibdrive method. There are other methods used to predict the vibro-driveability of offshore piles, some of these consist of advanced numerical models that aim to account for the forces involved, Viking (2002).

The case study is located in the southern North Sea and consists of monopiles with transition pieces. Vibro-driving was initially used until refusal, after which the impact hammer was used to achieve target penetration. The vibro-driving records, pile geometry, and hammer information were made available for six positions, along with corresponding CPT data.

2 SITE CHARACTERISATION

The soils at the investigated site are known to be dominated by medium dense to extremely dense sand with two large formations of medium plasticity clays.

The Friction Ratio (R_f) and Cone Tip Resistance (q_c) for the six positions considered in this investigation are presented in Figure 1. It can be observed that Location 4 is a significant outlier with R_f values of generally greater than 4 % from 4 m to 26 m depth. Likewise, Location 5 exhibits an R_f of greater than 4 % between 2 m and 12 m depth. At these locations, the q_c values are generally less than

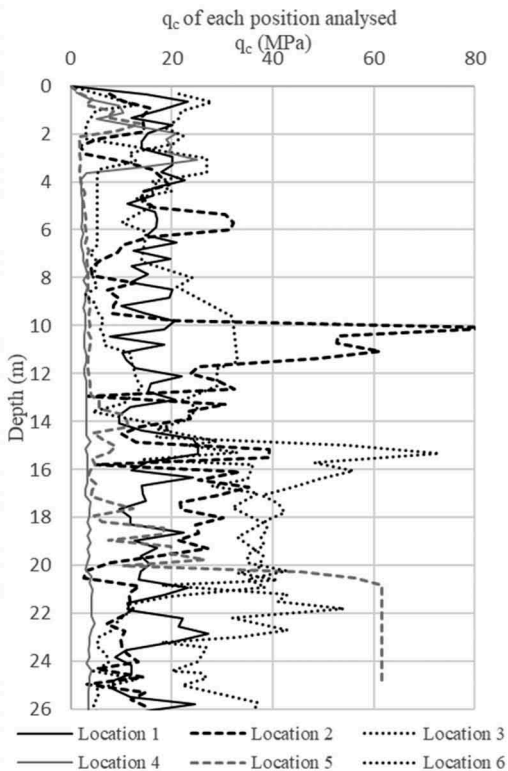
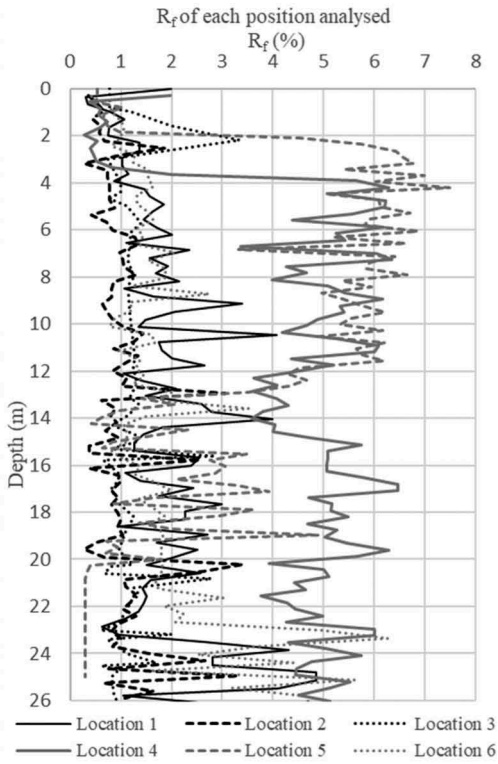


Figure 1. Measured R_f and q_c values for each location.

5 MPa within these depth ranges, and overall, less than 20 MPa. Indicating predominantly cohesive soils.

In contrast for Locations 1, 2, 3, and 6, the R_f values predominantly vary between 0.5 % and 4 %, and the q_c values are generally higher. These indicate a more silty to increasingly sandy material. The significant variability of the R_f values also indicates there is a large amount of interbedding present in the soil column.

3 METHODOLOGY

The SRV calculation for the β -method and Vibdrive method are described below:

3.1 β -method

Unit Shaft Resistance (τ)

$$\left(k_0 \cdot \sigma_v' \cdot \tan \delta\right) \cdot \beta \quad (1)$$

Unit End Bearing (q)

$$\left(N_q \cdot \sigma_v'\right) \cdot \beta \quad (2)$$

where k_0 = the lateral earth pressure at rest; σ_v' = the vertical effective stress; $\delta = \varphi - 5$ degrees; φ = angle of internal soil friction, β = factor applied to account for residual yield stress of the soil and N_q is an end bearing factor (DNV-GL, 2019).

β values are expected to range from 0.1 to 0.45 based on the soil type, as shown in Jonker (1987), however for this assessment it was observed that a β value of 0.6 for both the shaft and end bearing resistances was considered more appropriate.

3.2 Vibdrive method

Unit Shaft Resistance (τ)

$$\tau_d = (1 - e^{-\alpha})\tau_l + \tau_s \cdot e^{-\alpha} \quad (3)$$

$$\tau_l = \tau_s \left[(1 - \psi) e^{\frac{1}{FR}} + \psi \right] \quad (4)$$

$$\tau_s = \frac{1}{2}(2III) \quad (5)$$

$$\alpha = \frac{me \cdot \omega^2 \sin(\omega t)}{M_{dyn}} \quad (6)$$

where τ_d = vibratory shaft resistance; τ_l = liquified shaft resistance, τ_s = static shaft resistance; α = acceleration ratio, me = eccentric moment, ω = angular frequency, M_{dyn} = dynamic mass ψ = empirical liquefaction factor, FR = friction ratio; III = the average sleeve friction resistance between the level of the

sleeve and an equal distance ($III = b/2$) below and above the sleeve, and b = the diameter of the pile.

Unit End Bearing (q)

$$q_d = (1 - e^{-a})q_1 + q_s \cdot e^{-a} \quad (7)$$

$$q_l = q_s \left[(1 - \psi)e^{\frac{-I}{Rk}} + \psi \right] \quad (8)$$

$$q_s = \frac{1}{2}(I + II) \quad (9)$$

where q_d = vibratory toe resistance; q_l = liquefied toe resistance; q_s = static toe resistance; I = the average cone penetration resistance between the level of the base and a distance ($I = b/4$) above the base, b = pile diameter; II = the average cone penetration resistance between the level of the base and a distance ($II = 3b/4$) below the base.

The toe SRV can be seen for four locations in Figure 2. It can be observed that a significantly greater SRV is calculated using the Vibdrive method than the β -method.

3.3 Dynamic factors

The values of maximum elastic deformation corresponding to the maximum elastic force (quake) and the dynamic loading effect of the soil (damping) for the purpose of driveability predictions are summarised in Table 1. Both quake and damping values are based on information from Sinke (2020) and WEAP (2010).

Table 1. Dynamic factors used for analysis.

Quake (mm)		Damping (s/m)	
Toe	Shaft	Toe	Shaft
2.5	2.5	0.5	0.15

3.4 Software

The driveability analysis was carried out using the software GRLWEAP 2010, Offshore Version. This analysis is based on the stress wave theory and uses a lumped mass approach developed by Smith (1960). The pile is divided into discrete masses, interconnected by springs, and each interacting with the soil through a series of springs and dampers. The motions and forces within a foundation pile when driven by a specific hammer are simulated by the software. It carries out a dynamic analysis that represents the stress wave propagation (inclusive of reflection) throughout all sections of the pile.

The program computes the following for a vibro-driving case:

- The penetration rate (sec/m) for the pile to reach design penetration;
- Frequency (Hz) over the length of the pile;

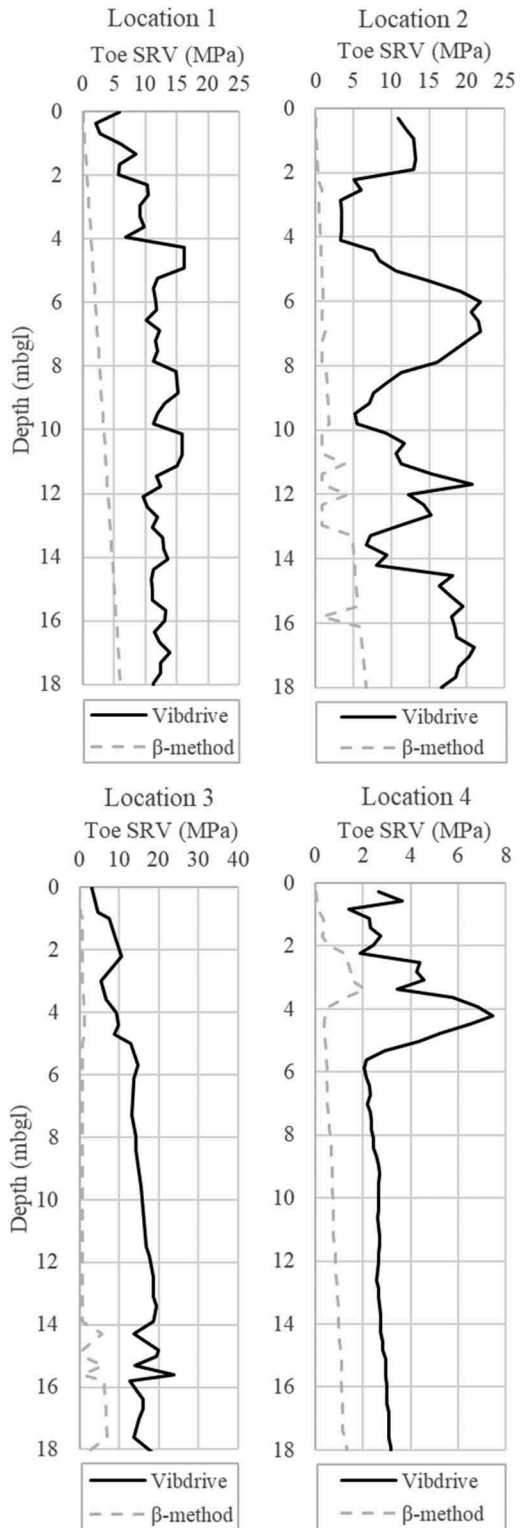


Figure 2. Calculated Toe SRV using the β -Method and the Vibdrive Method.

- The axial stresses in the pile over its cross sectional area;
- Max power (kW).

3.5 Hammer properties

The vibro-hammer analysed here is made up of four separate vibrators. The combined properties of the hammer are summarised in Table 2.

Table 2. Hammer Properties.

Hammer Property	Value
Eccentric moment (kgm)	920
Dynamic Mass (kg)	76188
Max Frequency (Hz)	23.3
Clamp Weight (kN)	1494.5
Maximum Power (kW)	3552

3.6 Driving records

Driving records were available for each foundation location and typically included:

- The start and end time of each period of operation;
- The cumulative penetration [cm];
- The centrifugal force for each period of operation (MN);
- The revolutions per minute (RPM) of the eccentric moments;
- The hydraulic driving pressure (bar);
- Hydraulic clamp pressure (bar).

The refusal criteria for the vibro hammer are considered as below:

- Penetration speed < 2.0 mm/s is calculated for 1.5 consecutive meters;
- Penetration speed < 1.0 mm/s is calculated for 0.5 consecutive meters;
- Maximum movement of 250 mm in 300 seconds of operation at full frequency.

3.7 Pile geometry

The pile design comprised non-uniform, open-ended, large diameter steel piles. The general pile geometry and key properties assumed are summarised below:

- Gain/loss factors - taken as 1 for this study;
- Pile lengths between 54 m and 71 m;
- Varying diameters between 4700 mm and 6500 mm from the pile head to pile tip;
- Wall thickness between 57 mm to 110 mm;
- Steel yield stress of 355 MN/m²;
- Steel elastic modulus of 210 GN/m².

The pile geometry varies slightly for each position.

3.8 Available data

To be able to undertake this assessment, four key pieces of information are required:

- Driving data;
- Soil information (CPT data);
- Pile geometry;
- Hammer make and model.

For this case study the full driving data was available for four locations. Two locations (Location 5 and Location 6) had partial driving data consisting of the self-weight penetration (SWP), average penetration speed, and refusal depth. The q_c and sleeve friction (f_s) data was available for all locations, however, the measured porewater pressure was not available which limited the soil characterisation undertaken.

4 RESULTS

Plots for four locations showing the predicted driving time with depth using the β -Method and the Vibdrive method compared with the driving record are shown in Figure 3. Locations 1, 2 and 3 are from the more granular material whereas Location 4 represents the more clay dominated material. The two locations which formed part of the study but only have partial driving records are included in Table 3.

Table 3. Summary of results for Location 5 and Location 6.

Driving Data	Location 5	Location 6
SWP (m)	4	1
Average Penetration Speed (s/m)	166.7	88.5
Refusal Depth (m)	37.7	31.7
Vibdrive		
SWP (m)	2	3
Average Penetration Speed (s/m)	138.8	27.2
Refusal Depth (m)	7	9
β - Method		
SWP (m)	16	6
Average Penetration Speed (s/m)	9.2	53.8
Refusal Depth (m)	37.7	11

4.1 Self-weight penetration

The SWP is the penetration into the seabed prior to driving. Dynamic soil resistance is therefore not active during this stage of pile installation. Under- or over-predictions of SWP affects the accuracy of the remaining driveability estimate.

Generally, the SWP was underpredicted using the Vibdrive method, with Location 1 and 2 predicting no SWP and Location 3 predicting 1m of SWP. This compares to the driving records which showed 4 m, 2 m, and 5 m respectively of SWP. For Location 4, the Vibdrive method predicted 2 m SWP which

compares to 3 m from the driving record. The β -method significantly overpredicted the SWP for all locations with 9 m predicted for Locations 1 and 2, 8 m for Location 3 and 14 m for Location 4.

4.2 Penetration rate

It can be observed that for all locations, the β -method underpredicts the driving record suggesting a faster penetration speed will be achieved. In contrast, the Vibdrive method generally overpredicts the driving record suggesting a slower penetration speed. Prior to refusal, the Vibdrive method matches reasonably well with the driving records.

For Location 1 there is a good match until 12 m, where the pile is predicted to refuse. This coincides with a slight spike in the q_c and a drop in the R_f . The transition to a relatively more sandy layer may be the cause of the refusal.

Location 2 is a generally more sandy and granular profile. The Vibdrive method shows two points of refusal at 5 m and 8 m. From 12 m it underpredicts the driving record. The Vibdrive method has not been found to best capture the installation resistance very well at this location.

Location 3 consists of predominantly silty material. The Vibdrive method showed an early refusal when it encountered a particularly sandy layer at 3 m. It then showed another theoretical refusal at 11 m following a gradual rise in penetration rate.

At Location 4, which has a notably higher R_f value indicating clay material, the Vibdrive method predicts a good match to about 6 m, and then an early refusal at 7 m.

5 DISCUSSION

The Vibdrive method has been shown to consistently predict a more conservative result in terms of the SWP, penetration speed, and refusal depth while the β -method is shown to underpredict the result.

The refusal of the Vibdrive method occurs predominantly in the more cohesive soil profiles. This could suggest that the method overpredicts the soil resistance in cohesive material. For the β -method, the dynamic effect is incorporated by the β -factor and considered during the SWP, before the actual vibro-driving starts. This assumption may lead to an overprediction of the SWP. Therefore, based on the results observed, it is suggested that a combination of both methods may provide a representative range of SWP when undertaking vibro-installation assessments.

The results show that for both the granular and cohesive profiles presented in this study, the CPT based Vibdrive method generally produced a better match to the measured results and a more conservative prediction. However, the Vibdrive method also predicted refusal depths that may not always be realistic. This may be due to limitations of the

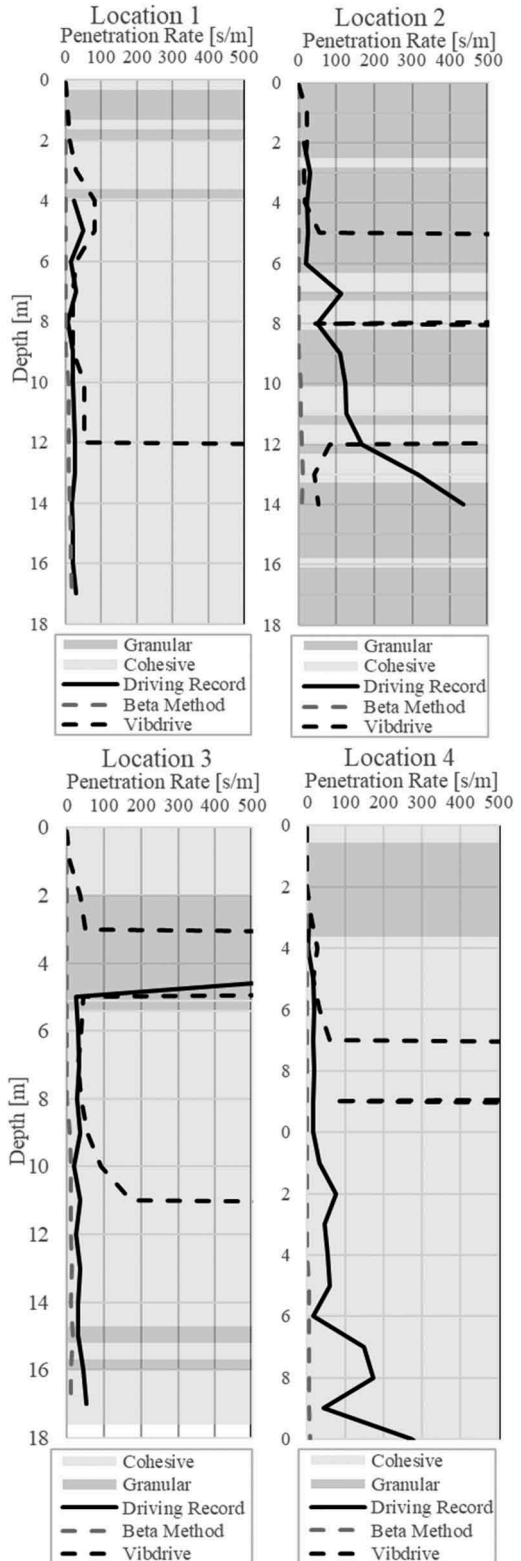


Figure 3. Results of the driveability predictions compared to the driving records of four locations.

method in capturing the actual variability of the process or other phenomena that need to be accounted for.

The β -method, on the contrary, predicts a much lower penetration rate than shown by the driving records. This can be due to a combination of factors such as the derivation of the geotechnical parameters and the selection of β -factors in determining the shaft and end bearing resistances. These would benefit from site-specific calibration through further back-analysis.

Further refinement of the Vibdrive method is required to produce a less conservative result. The associated research will require greater information on the soil conditions, which should include such details as the porewater pressure, unavailable for this study, but would give better insight into the liquefaction potential of the soil under vibratory loading. Using this information, in addition to the CPT data, a more complete ground model can be derived, and it will be possible to identify under which conditions the method best performs and what are its limitations. It should also be emphasised that the results from this study represent a small sample size and further work is required using different sites to gain more reliable conclusions and recommendations.

While appreciating the existing limitations, the current work does demonstrate that the existing methods can give acceptable estimates of the vibro-installation effort required. Based on the predictions of SWP, SRV and penetration rates, the CPT-based Vibdrive method consistently produced better results while still maintaining a conservative prediction. This method is therefore recommended to be taken forward for further improvement.

6 CONCLUSION

The results of this case study show there are still discrepancies between the current methods used to predict the vibro-driving behavior of offshore monopile installations and the actual driving records observed. The results have proven that many unknowns are not adequately captured by the methods analysed and further work needs to be done.

The misalignment shown by the two methodologies in respect of the driving record suggests that this is an area in which more research should be undertaken to remove more of the variations in predictions.

The Vibdrive method applied to this site was found to overpredict the driving record while the β -Method was found to underpredict the driving record. The use of both the β -Method and Vibdrive method provides an envelope of probable driving behavior.

The Vibdrive method, based on CPT data, was found to predict early refusal. This was often triggered when the pile progressed into a different soil type.

Further work is needed to understand the impact that both methods have in calculating SRV in different soil types. However, based on the case studies assessed, the Vibdrive method predicts a more representative driving behavior while maintaining conservatism. Once further driving records and back analysis data has been gathered from other sites, more robust conclusions can be made and inform advances in the application of the methods. This will enable greater certainty in the design of vibro-driven monopiles, and greater savings to be made in their design.

7 RECOMMENDATIONS FOR ADDITIONAL WORK

Further work into this field is required to improve the database of case studies with more driving records and soil data made available to allow research to be undertaken and improve the prediction of vibro driveability in a variety of soil conditions.

CPT data is still considered a valid starting point to investigate even further the performance of pile driving through a vibro hammer.

ACKNOWLEDGEMENTS

The authors would like to thank Jan Dührkop for the assistance in identifying and attaining the relevant data. The authors would also like to thank Ramboll for their support in proving the relevant data and information required to undertake this assessment.

REFERENCES

- Del Prado Mazza, N.M. 2018 Vibrodriveability analysis on sandy soils. Ecole polytechnique de Louvain, Université catholique de Louvain.
- DNV, Offshore soil mechanics and geotechnical engineering. Offshore Standard DNVGL-RP-C212.
- Holeyman, A.E. 2002. Soil behavior under vibratory driving. In Proceedings of the International Conference on Vibratory Pile Driving and Deep Soil Compaction, Transvibe 2002 (pp. 3–19).
- Jonker, G. 1987, April. Vibratory pile driving hammers for pile installations and soil improvement projects. In Offshore Technology Conference. OnePetro.
- Smith, E. A. L. 1960. Pile driving analysis by the wave equation. Journal of the soil mechanics and foundations division, 86(4),35–61.
- Sinke, J.M. 2020. A probabilistic approach to sheet pile driveability predictions by vibro hammers. MSc Thesis, Delft University of Technology.
- Viking, K. 2002. Vibro-Driveability. A field study of vibratory driven sheet piles in non-cohesive soils. Doctoral Thesis. Department of Civil and Architectural Engineering. Royal Institute of Technology (KTH). Stockholm, Sweden.

Potential of the Cone Pressuremeter Test for obtaining stiffness degradation for offshore wind turbine monopile foundations

G.W. Tucker, C.T. Leth, L. Krogh & P. Ladefoged

Ørsted

T. Lunne

Norwegian Geotechnical Institute

M. Taylor

In Situ Site Investigation

ABSTRACT: The piezocone (CPTU) offers a quick and repeatable investigation tool with instantly available high-resolution data. For these reasons it is both technically and commercially attractive to further instrument the CPTU to acquire additional measurements with more sensors either within the cone itself or as add-on modules behind the cone. Many ideas for further instrumentation of the CPTU have been conceptualised or tested but one that could offer direct benefit for offshore wind turbine foundation design is the Cone Pressuremeter (CPM). This in situ tool includes a pressuremeter module behind the standard cone that can measure ground displacement or expansion as a function of pressure applied during the loading, unloading and reloading of the surrounding soil when penetration is paused. From these measurements a number of soil parameters may be interpreted including the stiffness degradation (G/G_0) of the soil when combined with reliable in situ or laboratory measured G_0 values. With increasingly larger wind turbines being used and deeper water sites selected for construction, soil stiffness is an increasingly critical input for the design of many offshore wind turbine foundations. CPM testing has been trialed in the field onshore at a glacial till site and a medium to very dense sand site. The results of the CPM are compared in this paper to site specific results for the self-boring pressuremeter and advanced laboratory-based alternatives. The practical considerations of using the CPM offshore in seafloor mode are also reviewed.

1 INTRODUCTION

The piezocone (CPTU) is the main in situ tool for offshore geotechnical site investigations related to the design of offshore wind turbine foundations. It is a relatively fast test to perform and process, particularly in seafloor (non-drilling) mode, that provides continuous data for the entire investigation depth. These advantages inspire continuous development of the CPTU where many add on modules are considered and developed to investigate specific soil properties.

Following the general trends in offshore wind of increasing turbine sizes and larger water depths the soil stiffness becomes increasingly important for laterally loaded foundation design, for example the initial stiffness (G_0) and the stiffness degradation (G/G_0) required for the PISA design method (e.g. Byrne et al, 2017).

Current practice allows determination of initial stiffness in situ by seismic cone piezometer (SCPTU) and P-S logging and in the laboratory by use of advanced tests like the resonant column test and the bender

element add on to triaxial tests. The knowledge on stiffness degradation can be derived from in situ pressuremeter tests and testing in the laboratory by use of resonant column tests and direct simple shear tests.

An onshore research campaign has been carried out to investigate the use of a cone pressuremeter (CPM), a CPTU with a pressuremeter module, with the objectives of investigating its practical application and benchmarking its results to the self-boring pressuremeter (SBP) and advanced laboratory tests. With the assumption that G_0 is known from other in situ tests (e.g. SCPTU) the applicability of the CPM for offshore use is explored. This assessment also assumes the requirement to deploy the CPM in seafloor mode to maximise the associated operational benefits.

2 BACKGROUND

The concept of mounting a pressuremeter module behind a cone penetrometer was first applied in the early 1980s. Jezequel et al. (1982) developed

a pressio penetrometer for shallow offshore surveys. The device had a diameter of 89 mm and was installed using a vibrating hammer device. Robertson et al. (1984) placed a 60° solid cone on to the base of a 75 mm diameter SBP. Due to the large diameter of these devices, special equipment was required for their installation. The pressuremeter data proved to be successful for the design of laterally loaded piles.

These early devices were superseded by smaller diameter devices known as CPMs, which comprised of a pressuremeter module mounted behind a standard electrical cone penetrometer. These devices could be installed by CPTU jacking equipment, either cone truck or seafloor frame, and enable pressuremeter tests to be performed as part of the CPTU operations. The first CPM, for which the most results have been published, was designed and built by Cambridge In Situ, originally to a specification of Fugro Netherlands. This device was described by Withers et al. (1986) and has been slightly modified afterwards to improve the operation.

Considerable research and development was carried out on the use of the CPM and the interpretation of the results in the late 1980s and the 1990s. Work was carried out by Powell & Shields (1995) and others. Over the last 20 years the CPM has not been used so much but its use may prove useful in the near future with an application in offshore wind foundation design.

3 TESTING

3.1 *Equipment and method*

The CPM considered here (Figure 1) comprises of a cylindrical 47 mm diameter pressuremeter module placed behind either a 46.7 mm diameter (15 cm²) or a 36 mm diameter (10 cm²) instrumented CPTU cone. This configuration can record live data during penetration through the soil, as well as being able to undertake a pressuremeter test and dissipation test when pushing is temporarily paused.



Figure 1. CPM equipment.

The combined CPM module is approximately 1.30 m in length. It has a central expanding section which is covered by a tough rubber membrane 250 mm in length and its centre point being 630 mm behind the instrumented cone tip. The expanding section can be pressurised internally by oil using a manual hydraulic pump or compressed air using cylinder stored gas and a manual control unit. Oil is typically only used for marine surveys, whereby the

complex internal electronics are more protected from the ingress of saltwater in the event of a membrane burst.

Testing is generally carried out in accordance with ISO 22476-6. Pressure applied to the inside of the instrument forces the membrane to expand against the test pocket wall. The radial displacement of the inside boundary of the membrane is measured at three points equally distributed at 120° around the centre of the expanding section by free moving arms. This displacement and the pressure necessary to cause the movement is continuously monitored by electronic transducers contained within the instrument.

Testing trials were performed in the field with the CPM either by pushing the instrument in from ground level, or by undertaking a pre-push using a 63 mm diameter dummy cone to approximately 1.00 m above each pressuremeter test depth. The CPM was inserted using a 20 tonne track mounted CPTU rig with 36 mm diameter push rods. The rods were then released from the top drive hydraulic pushing clamps at which point a pressuremeter test was simultaneously initiated. The pressuremeter tests were carried out in a nominal stress-controlled manner using a manually operated gas control box to pressurise the instrument at an appropriate rate for the ground conditions.

During the tests a number of pressuremeter unload-reload loops were performed in order to provide data for determining shear modulus. Loading was continued until uneven expansion around the probe occurred such that the operator deemed the risk of damage to the probe via a membrane burst too high if loading was continued, or the strain capacity of the CPM was approached, typically around 60 %. Upon full unloading and deflation of the membrane, the dissipation test was terminated, and the CPM was either pushed to the next pressuremeter test depth further down or withdrawn from the ground.

The CPM is classed as a full displacement pressuremeter as it increases the state of stress in the test material as it is inserted. The early stages of the pressuremeter test should therefore always be treated with a degree of caution as the material has already been partially disturbed from its original state.

The SBP used (Figure 2) for comparison purposes to the CPM comprises of a cylindrical instrument with an integral cutter, of the same diameter as the main body of the instrument, that is drilled into the ground using a top drive rotary drilling rig. The rotary rig provides rotation to the SBP cutter through RW size 27.8 mm diameter inner rods and thrust to advance the pressuremeter via non-rotating 50.8 mm diameter outer rods. Water or drilling mud is flushed by the rig pump down the inner rods and returns up through the annulus between the inner and outer rods to remove the cuttings and provide lubrication and cooling to the cutter. The outside of the pressuremeter remains in contact with the ground relatively undisturbed during insertion.



Figure 2. SBP equipment.

The SBP probe is approximately 1.20 m in length. It has a central section 493 mm in length covered by a rubber membrane. Pressure applied to the inside of the instrument, via compressed air, forces the membrane to expand against the test pocket wall.

The larger diameter of the SBP (63.1 mm) compared to the CPM (47 mm) means that the radial displacement of the inside boundary of the membrane can be measured by six free moving arms, equally distributed at 60° around the centre of the expanding section. Analysis using a greater number of measured points generally increases the reliability of pressuremeter test results. The radial displacement and pressure necessary for the expansion of the membrane are continuously monitored by transducers contained within the instrument body.

The SBP is also equipped with pore water pressure transducers, which are opposite facing, positioned at the midpoint of the membrane.

3.2 Site details and scope

Trials were performed with the CPM at two test sites with ground conditions similar to some commonly encountered at offshore wind farm developments.

The first site was located in Cowden, England and was selected to test overconsolidated clays within glacial tills. Groundwater level was estimated to be at 3.0 m below ground level (bgl) based on piezometer readings and CPTU dissipation tests. In total seven pressuremeter tests were performed using the CPM at three locations between 6.7 m bgl and 18.2 m bgl. For comparison purposes, a further seven pressuremeter tests were performed using the SBP at two locations between 7.0 m bgl and 18.7 m bgl. In addition, borehole samples were taken to perform a suite of laboratory testing for classification of the site and further comparison to the CPM.

The second site was located in Cuxhaven, Germany and comprised mainly of medium dense to very dense fine to medium sands. Groundwater level was estimated to be at 2.75 m bgl based on falling head tests in standpipes with time (slug tests). At this site six pressuremeter tests were performed using the CPM between 3.0 m bgl and 7.0 m bgl at three locations. A further six SBP tests were performed at three locations between 3.0 m bgl and 7.5 m bgl.

4 RESULTS AND ANALYSIS

4.1 Reliability of test data

The maximum distances between CPM and SBP test locations at both sites are summarised in Table 1.

Table 1. Maximum distance between CPM locations, between SBP locations and between all (CPM and SBP) locations.

Site	CPM only	SBP only	All
Cowden (CO)	2.8 m	1.5 m	5.0 m
Cuxhaven (CU)	1.5 m	3.0 m	5.0 m

For each site, the cone resistance (q_c), sleeve friction (f_s) and penetration pore water pressure (u_2) profiles with depth at each CPM location were compared to evaluate the similarity of soil conditions, as shown in Figure 3 and Figure 4. Pre-pushing was performed using a dummy cone, at Cowden to 15.1 m bgl and 15.5 m bgl for Tests CO-CPM-1A and CO-CPM-2A respectively and at Cuxhaven to 3.9 m bgl for Test CU-CPM-1, so it was not possible to compare these CPTU profiles to the others. Overall the ground conditions were comparable for the two sets of tests and hence not considered a major uncertainty for evaluating the repeatability of the CPM test results.

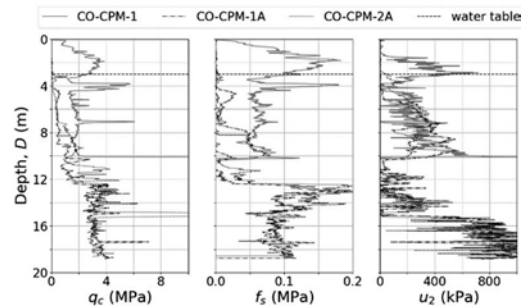


Figure 3. CPTU profiles with depth at CPM positions for the Cowden site.

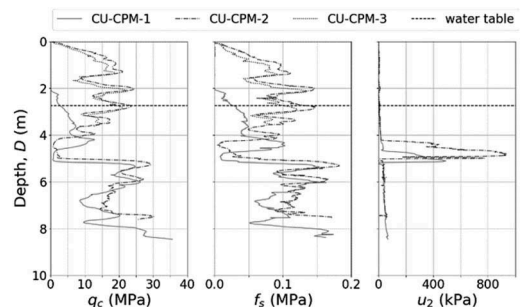


Figure 4. CPTU profiles with depth at CPM positions for the Cuxhaven site.

For the interpretation of stiffness degradation, average arm displacements from the CPM and SBP data were used as per standard practice. A review of the datasets confirmed that average arm displacements were generally representative of the response for each individual pressuremeter arm with applied pressure. Examples of this are shown in Figure 5 for the CPM and Figure 6 for the SBP for Cowden.

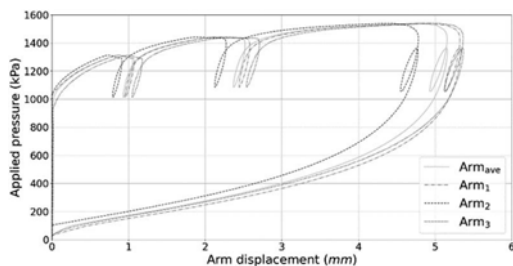


Figure 5. Comparison of individual and average arm displacements for a representative CPM (CO-CPM-1A, 15.5 m bgl).

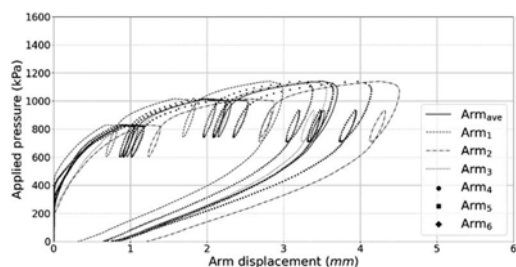


Figure 6. Comparison of individual and average arm displacements for a representative SBP (CO-SBP-1, 15.5 m bgl).

The repeatability of the applied pressure versus average arm displacement plots was reviewed to further evaluate the reliability of the data. Examples from Cowden are shown for pairs of CPM tests and pairs of SBP tests at similar depths in Figure 7 and Figure 8 respectively.

The ‘lift off’ pressures at the start of the CPM tests in Figure 7 were within approximately 10 % of each other. This was also found to be the case for the other pair of CPM tests available at Cowden. The difference in maximum pressure at the end of the two pairs of CPM tests were 3 % and 8 % respectively. For Cuxhaven, three pairs of CPM tests were available for comparison and the difference in ‘lift off’ pressures typically differed by approximately 200 kPa to 300 kPa and maximum pressures differed by between approximately 10 % and 35 %.

The only pair of SBP tests available from Cowden were within 7 % of the maximum pressure of each other while there was a nominal difference in ‘lift off’ pressures. Unfortunately, the SBP tests performed at Cuxhaven were significantly influenced by disturbance of the test pocket.

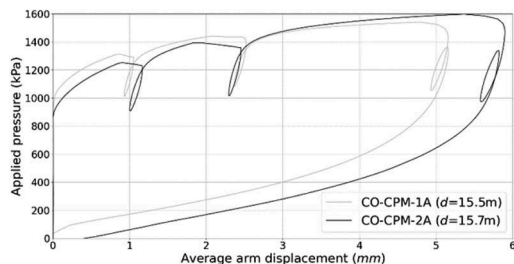


Figure 7. Comparison of applied pressure versus average arm displacement for CPM tests.

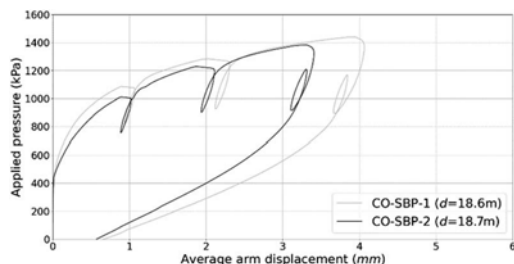


Figure 8. Comparison of applied pressure versus average arm displacement for SBP tests.

An additional comparison was made for CPM tests from Cowden with historical CPM tests at similar depths performed by Building Research Establishment (1996) where ground conditions were broadly similar enough for comparison purposes. It was found that plots of applied pressure versus average arm displacement were consistent between the two sites.

Finally, applied pressure versus average arm displacement plots for CPM tests were compared to SBP tests at the same depth to benchmark the CPM data against the SBP data. An example from Cowden is shown in Figure 9.

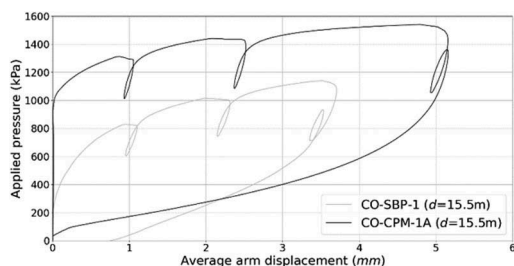


Figure 9. Comparison of applied pressure versus average arm displacement for CPM and SBP tests.

It was consistently observed across both sites that the CPM recorded a higher ‘lift off’ pressure and maximum applied pressure than the SBP, as was reported by Powell & Shields (1995). As the CPTU displaces

the surrounding soil during penetration before the pressuremeter test is performed, the applied pressure at a given displacement is higher than would be expected for the in situ conditions. In theory the SBP insertion method does not displace any soil and hence in situ conditions should not be disturbed, however in practice this requires a high degree of operator control, and so may be considered a disadvantage compared to the CPM. It was observed from the results of Cuxhaven that inserting the SBP in coarser grained soils is very challenging. These differences in measurements between the CPM and SBP may influence the reliability of other interpreted parameters but not the G/G_0 curves.

4.2 Stiffness degradation

Shear modulus was interpreted from the average gradient of the unload-reload loops performed during each CPM and SBP test using Bolton and Whittle (1999).

At Cowden interpreted shear modulus with shear strain was very similar for unload-reload loops from the same CPM test, and for pairs of CPM tests at the same depth. Figure 10 shows three stiffness degradation curves per pressuremeter test derived from the three corresponding unload-reload loops performed (loop 1-3). Very good repeatability was seen for loops from three pairs of CPM and SBP tests at similar depths. A fourth pair at 15.5 m bgl (CO-CPM-1A and CO-SBP-1), had very similar stiffness degradation profiles to CO-CPM-1A at 17.0 m and CO-SBP-1 at 17.7 m bgl. The only instance with poor repeatability was at 7.0 m bgl comparing CO-CPM-1 to CO-SBP-1, where the latter experienced leakage of the pressuremeter membrane.

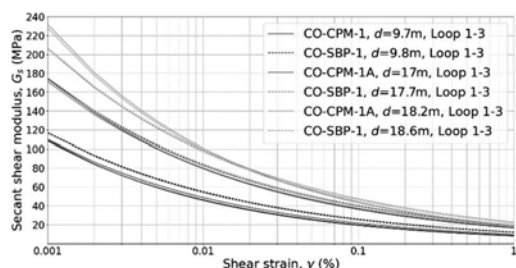


Figure 10. Comparison of shear modulus versus shear strain for CPM and SBP tests at the Cowden Site.

Figure 11 shows that at Cuxhaven the repeatability of unload-reload loops from the same CPM test was still good, except for CU-CPM-2 at 5.5 m bgl. However, repeatability between loops from different CPM locations at the same depth and between loops from CPM and SBP locations at the same depth were comparatively poorer than at Cowden, with stiffness at a given strain differing by up to a factor of two approximately. The difference in performance at the two sites was deemed to be influenced by the quality

of the CPM test pocket that could be achieved in this instance, where considerable disturbance was observed for the coarser soils.

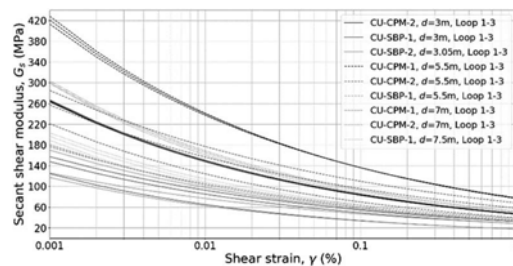


Figure 11. Comparison of shear modulus versus shear strain for CPM and SBP tests at the Cuxhaven Site.

For use in the design of laterally loaded foundations, shear modulus versus shear strain is normalised by G_0 . As an example, data from Cowden was normalised using G_0 values from laboratory Bender element and resonant column tests. The outcome was compared to historical pressuremeter and laboratory data presented by Powell & Butcher (2003) as shown in the example in Figure 12. Good agreement was found between the Cowden CPM data and the historical pressuremeter data. Relationships proposed by Vucetic & Dobry (1991) and Hardin & Drnevitch (1972) were not found to be good fits.

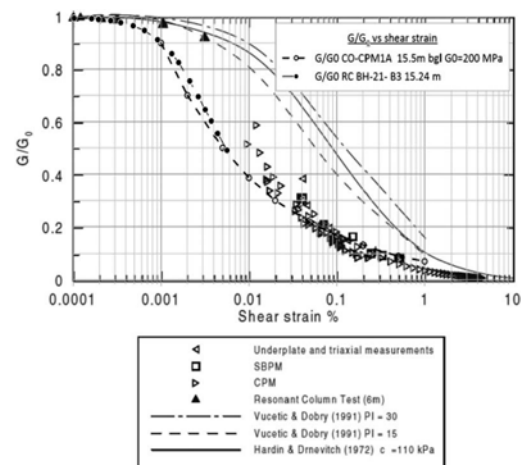


Figure 12. G/G_0 from CPM and resonant column tests at 15.5 m bgl compared with data from Powell & Butcher (2003).

In practice the sensitivity of the measurement by the pressuremeter arms are considered accurate only to 0.01 % shear strain. However, the interpreted curve has been presented to 0.001 % shear strain for information and does not appear unreasonable compared to resonant column data. Verification work is needed to confirm if the method for establishing the

G/G_0 curve is representative of the lateral deformation experienced by the monopile.

5 APPLICABILITY FOR OFFSHORE USE

The CPM pressuremeter module is primarily designed for testing in superficial deposits, such as loose to medium dense sands and soft to very stiff clays. The CPM was found to be easily susceptible to damage if pushing through dense granular material or till deposits containing coarse gravel or cobble size fragments. In general, it is not recommended to advance the instrument in its current design through granular material that is dense to very dense ($q_c > 18$ MPa), or very high strength cohesive material (typically $q_c > 4$ MPa), as there is increased risk of damaging the membrane, or in the worst case bending the instrument body. Pre-pushing using a dummy cone was often required to advance the instrument to the required test depths, however this will not be practical for offshore testing.

For deployment offshore in seafloor mode, the body of the instrument would require strengthening and the electronics module made more robust with improved watertight sealing. The deployment and operation of the instrument would also need careful consideration if it is to be combined with currently available seafloor pushing systems, especially the control umbilical and instrument inflation system.

6 CONCLUSIONS

CPM tests have been carried out at two very different sites to investigate the use of the add on tool.

Analysis of the obtained stiffness results for over-consolidated clays showed very good repeatability in the CPM tests, and a direct comparison of the results from CPM and SBP tests showed good compliance for the unload-reload loops.

CPM testing in medium to very dense sands showed a fair repeatability for stiffness based on unload-reload loops from the same CPM test but much less so when loops were compared from different locations. The granular nature of the soils presented operational challenges with forming the test pocket which affected test quality and generally being able to insert the CPM in these soils.

The two sites that were tested represent the typical range of fine to coarse soils encountered offshore. The equipment presently available for CPM testing appears to be susceptible to damage in these soils and measures to ease the penetration (i.e. use of dummy cone) would not be compatible in seafloor mode. Thus, there is potential for further exploring the instrument and its development, including increasing its robustness.

A G/G_0 curve has been established from CPM and laboratory tests at Cowden and comparison with historical data shows a very good compliance, though deviating from the general relationships

proposed in literature. Overall, the results show the potential of the CPM for offshore wind turbine foundation design. Further investigation and validation of reliable G/G_0 curves from the CPM when combined with other in situ tests used to estimate G_0 may help mature the CPM for this application in the future.

ACKNOWLEDGEMENTS

The authors thank Ørsted for giving permission to publish this work, and Rob Cooke and John Holt of In Situ Site Investigation for reviewing this paper. The authors would like to recognise In Situ Site Investigation and Russell Geotechnical Innovations for performing the field and laboratory testing respectively that formed the basis of this paper.

REFERENCES

- Bolton, M.D. & Whittle R.W. 1999. A non-linear elastic/perfectly plastic analysis for plane strain undrained expansion tests. *Geotechnique* 49(1): 133–141
- Building Research Establishment 1996. The development of semi-empirical design procedures for foundations. *Factual report – Cowden Report no. T3-01, Rev. R1.*
- Byrne, B.W., McAdam, R.A., Burd, H.J., Houlby, G.T., Martin, C.M., Beuckelaer, W.J.A.P., Zdravković, L., Tabor, D.M.G., Potts, D.M. & Jardine, R.J. 2017. PISA: New design methods for offshore wind turbine monopiles. *Proceedings of the 8th International Conference on Offshore Site Investigation and Geotechnics, London: Society for Underwater Technology.*
- Hardin, B.O. & Drnevich, V.P. 1972. Shear modulus and damping in soils – measurement and parameter effects. *American Society of Civil Engineers, Journal of the Soil Mechanics and Foundations Division* 98(6): 603–624.
- Jezequel, J.F., Lamy, J. L. & Perrier, M. 1982. The LPC-TLM pressuremeter. *Proceedings of the Symposium on the Pressuremeter and its Marine Applications, Paris: 275–287.*
- Powell, J.J.M. & Butcher, A.P. 2003. Characterisation of a glacial till at Cowden, Humberside. *Workshop, Characterisation and Engineering Properties of Natural Soils: 983-1020.* Singapore, 2002.
- Powell, J.J.M. & Shields, C.H. 1995. Field studies of the full displacement pressuremeter in clays. *Proceedings of 4th International Symposium, The Pressuremeter and its New Avenues, Sherbrooke, Canada: 239–246.* Rotterdam: Balkema.
- Robertson, P.K., Hughes, J.M.O., Campanella, R.G. & Sy, A. 1984. Design of laterally loaded displacement piles using a driven pressuremeter. *Laterally Loaded Deep Foundations: Analysis and Performance, ASTM Special technical publication, STP 835 : 229–38.*
- Vucetic, M. & Dobry, R. 1991. Effect of soil plasticity on cyclic response. *American Society of Civil Engineers, Journal of Geotechnical Engineering* 117(1): 89–107.
- Withers, N.J Schaap, L.H.J. & Dalton, C.P. 1986. The development of a full displacement pressuremeter. *Proceedings of the 2nd International Symposium on the Pressuremeter and its Marine Applications, College Station, Teaxs, ASTM Special technical publication, STP 950 : 38–56.*

Centrifuge study on the CPT based p - y models for the monopiles

Huan Wang & Daan Veldhuijzen van Zanten
Delft University of Technology, The Netherlands

Dirk de Lange
Deltares, The Netherlands

Federico Pisanò, Ken Gavin & Amin Askarinejad
Delft University of Technology, The Netherlands

ABSTRACT: The p - y load transfer method is the most widely used for the design of monopile foundations. Recently, many CPT based p - y models were proposed experimentally or numerically to overcome the uncertainty in deriving stiffness and strength parameters of soil from in-situ testing. This paper aims to evaluate the performance of existing CPT based p - y models for predicting the monopile behavior, by conducting a series of centrifuge tests in dense Geba sand. Four different diameter ($D = 0.9$ m, 1.8 m, 1.25 m and 2.5 m) monopiles with two aspect ratios (L/D) of 3.6 and 5 were studied. The lateral load was applied at two different loading eccentricities of $0.67L$ and L above the ground surface. It was found that the model of Novello (1999) model gave the best overall prediction (at both small and large deflection) for the tests in this study, while the model of Dyson and Randolph (2001) model always underestimate the pile response. Compared with the Novello (1999), the model of Suryasentana and Lehane (2014) and Li et al. (2014) will overestimate the pile response at large deflection, but, can well predict the pile response at small deflection. In all cases, the API p - y model significantly overestimates the response with a factor more than 2. The experimental observations in this study proves the feasibility and reliability of developing CPT based p - y model for monopile.

1 BACKGROUND

For a typical wind farm, the foundations can take up more than 30% of the total cost and play an important role in the economic feasibility of the whole project (Byrne et al. 2015). Due to large horizontal forces and overturning moments from the wind, wave and currents, the lateral response of foundations is the key factor in the design. Among all the foundation types, monopiles are the most preferred for supporting offshore wind turbines (OWTs) and have been used in around 80% of total installations in Europe (Ramírez et al. 2020). The loads on OWT's in typical water depths of 10 to 40 m and in the dense sands found in offshore areas of Europe can be effectively resisted by large diameter (D) monopiles with low aspect ratios (L/D , where L is embedded length of monopile). The diameters of monopiles installed in Europe are usually larger than 6 m and the aspect ratios are less than 8. Meanwhile, monopiles with diameter of 10 m and aspect ratio of 3 are under consideration for the turbine with larger capacity in deeper waters (Kirkwood 2016, Negro et al. 2017).

Among all the existing methods for the design of a laterally loaded pile, the p - y load transfer method is

the most widely used. In this method, the monopile is modelled by a series of beam elements while the soil is represented by a series of non-interacting, non-linear springs distributed along the pile. The p - y curves are used to represent non-linear relationships between the net soil resistance (p) at a given depth per unit length and the lateral deflection of a pile at that depth (y) (Suryasentana & Lehane 2014).

The p - y model in current design guidelines API (2011) and DNV GL (2014) was originally proposed by Reese et al. (1974) based on a series of field tests and has been used successfully in the oil and gas industry for many decades. However, extensive studies have reported that the API p - y model is not suitable for the design of large diameter monopiles (Doherty & Gavin 2012). Furthermore, the API (2011) uses the friction angle (ϕ') of a soil as the only input to define the p - y curves. In real projects, empirical correlations with in-situ test results (e.g. CPT, SPT) are used to determine the sand friction angle. The uncertainties in those empirical correlations will further exacerbate the method's already high sensitivity to the chosen ϕ' , leading to the unsafe design of the foundation.

To avoid difficulties in selecting appropriate strength parameters and to properly model in-situ

soil complexity, several researchers have suggested ways of using the tip resistance (q_c) from the cone penetration test (CPT) to determine the relationship between the soil resistance and the lateral deflection of a pile. Such approaches have the advantage that they are direct methods that are not susceptible to the subjectivity associated with the inference of friction angle values (Suryasentana & Lehane 2014).

Although many CPT based p - y models were proposed for the laterally loaded piles in sand, no systematic studies were performed to quantify the accuracy of the models for predicting the response of monopiles. In this study, a series of centrifuge tests in dense Geba sand were performed on monopiles with a wide range of configurations. The newly developed mini-CPT at TU Delft centrifuge lab was used to obtain the q_c profiles of the test samples. Beam simulations were performed using the existing CPT based p - y models and the API model. The performance of existing CPT-based p - y models is systematically evaluated.

2 CPT BASED P-Y MODELS

Salgado & Randolph (2001) performed a series of numerical analysis and concluded that the cone tip resistance depends both on horizontal stress, the sand friction angle and the sand's stiffness characteristics. Similarly, the behaviour of laterally loaded pile is also governed by the horizontal soil stress, the sand friction angle and the sand's stiffness characteristics. Therefore, it is possible to correlate the p - y curve of laterally loaded monopile with the measured in-situ cone tip resistance (q_c) of cone penetration test (CPT) (Suryasentana & Lehane 2014).

Novella (1999) and Dyson & Randolph (2001) performed a series of centrifuge tests on piles driven in calcareous sand and proposed the first power-law CPT based expression for p - y curves. Although the proposed formulation provided reasonable fits to the experimental data from which they were derived, the applicability of these expressions to the large diameter monopile is not clear. Li et al. (2014) performed six static lateral loading field tests and proposed an updated power-law model for piles driven in siliceous sand. Recently, Suryasentana & Lehane (2014) performed systematic analysis on monopile in homogeneous soil by three-dimensional finite element model. A non-linear elasto-plastic soil model was adopted to simulate the behavior of sand. The corresponding cone tip resistance of CPT profile was derived numerically using a cavity expansion simulation. Parametric studies were conducted to investigate the influence of cross section shape, pile diameter, pile bending stiffness and soil non-homogeneity. An exponent CPT-based p - y formulation was then proposed and validated by full-scale field tests.

Compared with the power-law model, the exponent function can capture the ultimate limit resistance of pile at large deflection. Details of each CPT based p - y model are summarized in Table 1. As shown in the table, except Suryasentana & Lehane (2014), all the other p - y models adopted the power-law function, which means that the soil resistance (p) will keep increasing with pile deflection (y). Furthermore, it can be seen that in all the models, the soil resistance (p) is related to the q_c by a power of around 0.7 (0.67-0.72).

Table 1. Existing CPT-based p - y models.

Reference	CPT-based p - y model
Novello (1999)	$p = 2D(\sigma'_v)^{0.33}(q_c)^{0.67}\left(\frac{y}{D}\right)^{0.5}$
Dyson and Randolph (2001)	$p = 1.35\gamma D^2\left(\frac{q_c}{\sigma'_v}\right)^{0.72}\left(\frac{y}{D}\right)^{0.58}$
Suryasentana and Lehane (2014)	$p = 2.4\sigma'_v D\left(\frac{q_c}{\sigma'_v}\right)^{0.67}\left(\frac{z}{D}\right)^{0.75}$ $\left(1 - \exp\left(-6.2\left(\frac{z}{D}\right)^{-1.2}\left(\frac{y}{D}\right)^{0.89}\right)\right)$
Li et al. (2014)	$p = 3.6D(\gamma'D)\left(\frac{q_c}{\gamma'D}\right)^{0.72}\left(\frac{y}{D}\right)^{0.66}$

3 CENTRIFUGE MODELLING

All of the centrifuge model tests in this study were carried out at the Geo-engineering Section of TU Delft using the beam centrifuge with a nominal diameter of the rotating arm of 2.5 m. The centrifuge is capable of performing tests at a maximum acceleration of 300g with the maximum carrying capacity of 30 kg (Zhang & Askarinejad 2019).

A total of seven monotonic lateral loading tests were performed in this study at two different centrifugal accelerations of 50g and 100g. Two model piles with diameter of 18 mm and 25 mm were used to model the prototype monopile foundations with diameters of 0.9 m and 1.25 m at 50g and 1.8 m and 2.5 m at 100g, respectively. The two model piles were made of aluminum pipe with the elastic modulus and a poisson's ratio of 71.7 GPa and 0.33, respectively. The wall thickness of 18 mm and 25 mm diameter piles are 1 mm and 1.5 mm, respectively, so as to meet the equivalent section bending stiffness of typical monopile in offshore wind projects (Negro et al., 2017). Most existing monopile foundations in offshore wind farms have an aspect ratio of less than 5. Therefore, two aspect ratios of 3.6 and 5 were investigated in this study. Considering the large overturning moment on offshore wind turbines, the lateral load was applied at two eccentricities of $0.67L$ and L above the ground surface. Details of the test program are summarized in Table 2.

Table 2. Centrifuge test program.

NO.	Acceleration	D^* (m)	L/D	e/L
1	50	0.9	5	0.67
2	50	0.9	5	1.0
3	100	1.8	5	0.67
4	100	1.8	5	1.0
5	50	1.25	3.6	0.67
6	100	2.5	3.6	0.67
7	100	2.5	3.6	1.0

Note: * denotes the pile diameter at prototype scale.

All the tests were performed in dry Geba sand with a relative density of 80%. The sand is sub-angular to sub-rounded, with a median grain size (d_{50}) of 0.11 mm. The maximum and minimum void ratios are 1.07 and 0.64, respectively. The sample seabed was prepared by first “raining” the sand from a sand bucket with holes at a pre-calibrated height and then vibrate to densify it to the target density. To obtain the q_c profile of the test sample, a mini-CPT was developed at TU Delft. Figure 1 shows a sketch of the developed mini-CPT at TU Delft centrifuge lab. As shown in the figure, the penetrator has a diameter of 7.5 mm with a standard 60 degrees cone tip. The cone tip is made of steel and connected with a steel inner rod. The inner rod has a diameter slightly smaller than the outer tube. A Teflon ring is installed between the inner rod and the outer tube, allowing to constrain the verticality of the rod without applying additional friction force.

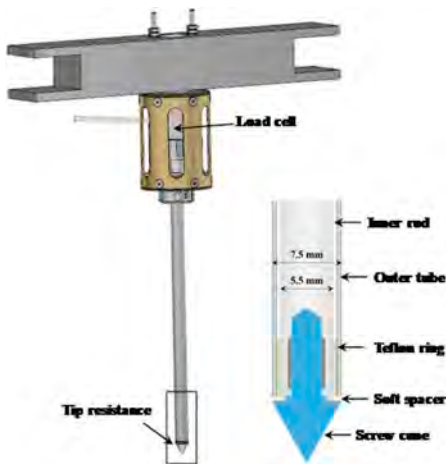


Figure 1. Sketch of the mini-CPT.

During the test, the soil pressure acting on the cone tip will be transferred to the inner tube and measured as a total force by the load cell connected with the inner tube. The load cell has a measurement range of 2.65 kN, which is equal to a tip resistance (q_c) of 60 MPa. The whole penetrator is designed in

a modular mode, which allows for changing the component independently based on the requirement of the tests. The penetrator has a maximum depth of 150 mm, which is equivalent to a depth of 7.5 m and 15 m in prototype at a centrifuge acceleration of 50g and 100g, respectively. The mini-CPT can be easily installed on the 2D loading actuator. Photos of the mini-CPT installed on the actuator and the sample surface after the penetration are presented in Figure 2.

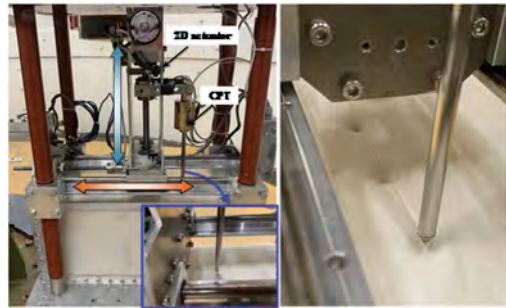


Figure 2. Photo of the mini-CPT.

In lateral loading tests, the two-dimensional (2D) servo actuator is used to apply lateral loads on the pile head. A specially designed loading head was designed to allow loading the model pile without inducing any rotational fixity. The loading head is connected with a beam-type loading cell, which monitors the applied force. Displacement potentiometers were also installed to calculate the pile deflection at loading point.

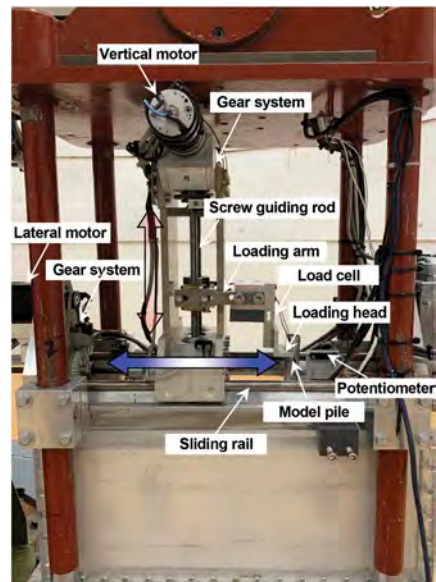


Figure 3. A typical model setup for the lateral loading test.

4 INTERPRETATION OF RESULTS

In the following sections, all results are interpreted in prototype scale, unless stated otherwise.

4.1 Q_c profiles from mini-CPT

Figure 4 shows the typical q_c profiles of the test sample at the centrifugal acceleration of 50g and 100g. In each sample, CPT tests with different distances between two penetrations and different penetration velocities were performed. It was found that a distance of around $13D_{CPT}$ (D_{CPT} is the diameter of the mini-CPT) is required to eliminate the boundary effect or any interaction between penetrations. In addition, since the tests are in dry sand, no rate effect is observed. The q_c profiles in Figure 4 are from tests in the same sample but at different locations. Based on the excellent consistency of the results, it can be concluded that the sample preparation method used in this study is reliable and repeatable. The prepared sample is very uniform.

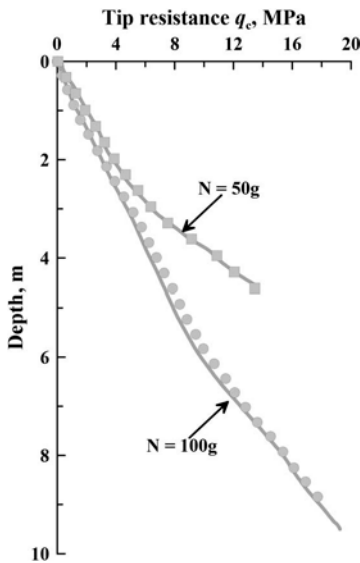
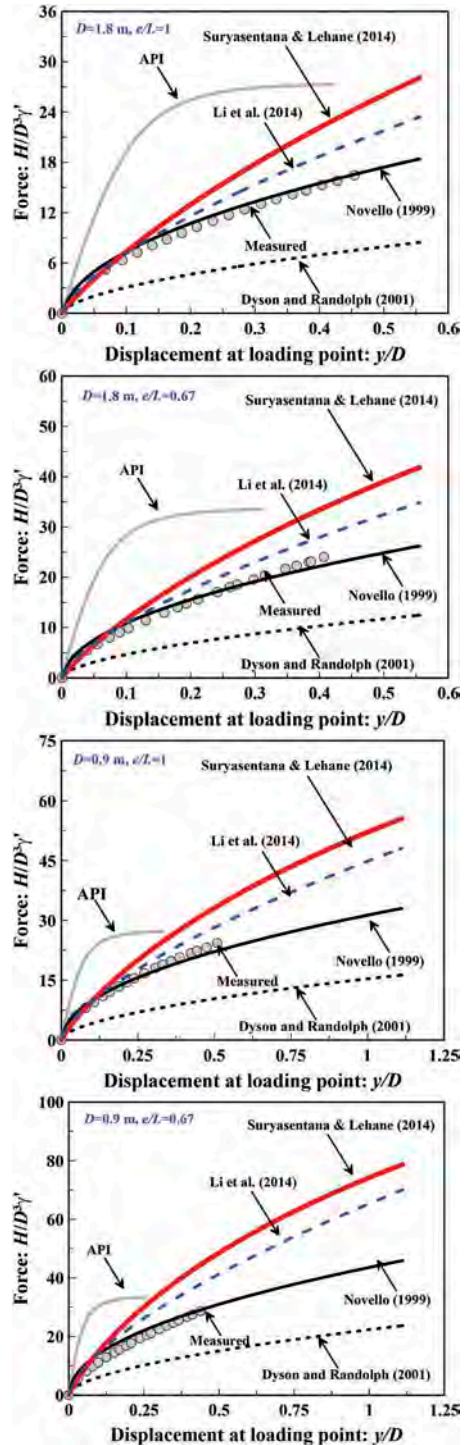


Figure 4. q_c profiles from mini-CPT: (a) tests at 50 g; (b) tests at 100g.

4.2 Measured and computed pile response

Figure 5 presents measured load-deflection curves at the loading point for all the tests in this study. As shown, the reaction force of model pile increases with the pile deflection with no sign of reaching the ultimate capacity. This hardening response of monopile in sand has been widely reported in other studies. In the same figure, the computed response with the API p - y model and the existing CPT based p - y models were also included. It can be seen that in all the cases, the API model will significantly

overestimate the pile response, especially at small deflection. According to the DNV GL (2014), the maximum allowable rotation of the offshore wind turbine is 0.5 degrees, which equivalent of a pile head deflection of around 0.14 m for the



1.8 m diameter pile tests in this study. As shown in Figure 5a and 5b, in this deflection range, the pile response can be overestimated by a factor of more than 2 for the API model. However, it should be noted that due to the hardening behaviour of monopile, as shown in Figure 5a-5g, the API p - y model tends to underestimate the ultimate lateral capacity of the monopile.

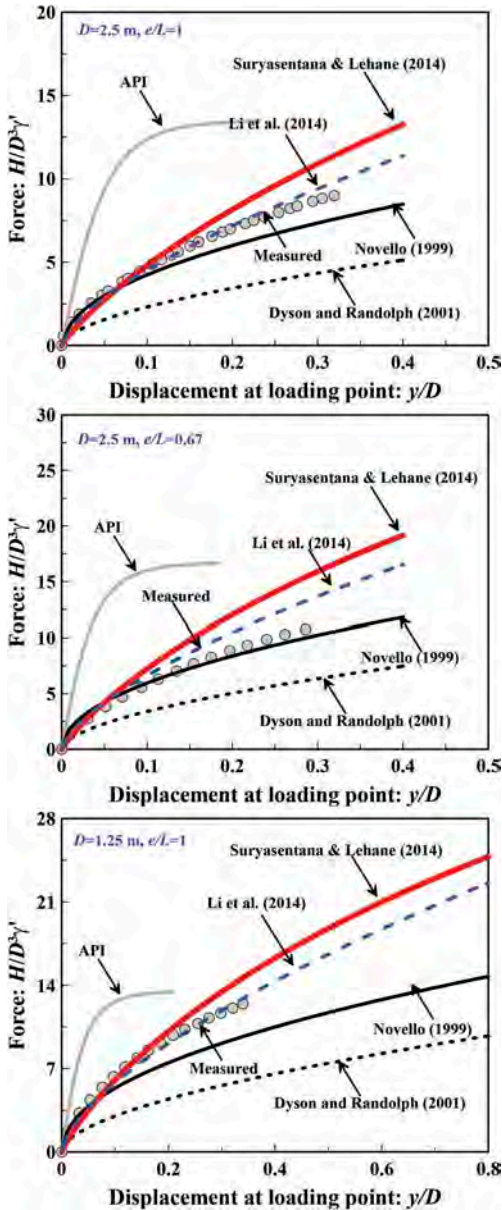


Figure 5. Measured and computed pile response.

Compared with the API model, the CPT based p - y models generally give better prediction of pile response, except for the model of Dyson &

Randolph (2001), which will always underestimate the pile response. This may be caused by the way of incorporating the vertical stress in the model. As shown in Table 2, in the model of Dyson & Randolph (2001), the q_c is normalized by the vertical effective stress (σ'_v). Compared with the power coefficient of around 0.33 in Novello (1999)'s and Suryasentana & Lehane (2014)'s model, p - y curves in Dyson and Randolph (2001) is related to the vertical effective stress (σ'_v) by a power coefficient of -0.72, which will cause the reduction of soil resistance compared to Novello (1999) and Suryasentana & Lehane (2014).

Among all the CPT based p - y models, the Novello (1999)'s model gave the best overall prediction for the series of tests in this study at both small and large pile deflection. On the contrary, the model of Suryasentana & Lehane (2014) and Li et al. (2014) can capture the pile behaviour at small deflection, but will overestimate the pile response at larger deflection. It is believed that the inaccuracy of Li et al. (2014)'s model should be related to the insufficient consideration of the influence of vertical stress and depth. As shown in Table 2, Li et al. (2014)'s model is defined mainly by pile diameter without considering the vertical effective stress (σ'_v). As for the Suryasentana & Lehane (2014)'s model, the overestimation may be attributed to the inaccurate input of the ultimate soil resistance used in the model, since the pile deflection in simulations of Suryasentana & Lehane (2014) are less than 10% D . The ultimate soil resistance was not reached in most cases.

Although the model of Novello (1999) gave best prediction in this study, it should be noted that the power-law function used in the model will eventually overestimate the pile ultimate capacity since the soil resistance (p) will keep increase with pile deflection (y) in the power-law function. On the other hand, the exponent function used in Suryasentana & Lehane (2014) has the feature to reach an ultimate value at large deflection. Based on the experimental observation from this study, it is recommended to combine the Novello (1999)'s model into the Suryasentana & Lehane (2014)'s model in the future study or even using a different function as the back-bone curve, for example, the hyperbolic function and hyperbolic tangent function.

5 SUMMARY

A series of centrifuge CPT tests and monotonic laterally loaded pile tests in dense Geba sand were performed in this study. Performance of the API p - y model and the existing CPT based p - y models were systematical evaluated. Based on the experimental observation, following conclusions were drawn:

1. The newly developed mini-CPT at TU Delft centrifuge lab can provide reliable q_c profile of the test sample. For the Geba sand used in this study, a distance of $13D_{CPT}$ (D_{CPT} is the diameter of the mini-CPT) is required to eliminate any boundary effect or interaction between penetrations.
2. The API p - y model significantly overestimate the pile response in all the tests, especially at the small pile deflection with a factor more than 2. But at large deflection, due to the hardening response of monopile in sand, the API p - y model tends to underestimate the ultimate lateral capacity of monopile.
3. All the CPT based p - y models, except Dyson & Randolph (2001)'s model, can give better prediction than the API model. The model of Dyson & Randolph (2001) underestimate the pile response due to the inaccurate consideration of the vertical stress (σ'_v).
4. The Novello (1999)'s model gave the best overall prediction for the series of tests in this study at both small and large pile deflection. On the contrary, the Suryasentana and Lehane (2014)'s and Li et al. (2014)'s model can only capture the pile response at small deflection. The inaccuracy of Li et al. (2014) may be caused by the insufficient consideration of the vertical effective stress in the model, while the overestimation of Suryasentana & Lehane (2014) is attributed to the inaccurate input of the ultimate soil resistance.
5. The experimental results in this study proved the feasibility of using the CPT based p - y model in monopile design.

However, it should be noted that the experimental observation is only limited to the specific pile configurations and the uniform dry sand in this study. More studies should be performed in the future on additional model piles and in different sands or layered soils to develop the CPT based p - y models with general applicability.

REFERENCES

- API (American Petroleum Institute). (2011). Geotechnical and foundation design considerations. API RP 2GEO. Washington, DC: API.
- Byrne, B. W., Mcadam, R., Burd, H. J., Houlsby, G. T., Martin, C. M., Zdravkovic, L., Taborda, D. M. G., Potts, D. M., Jardine, R. J., Sideri, M., Schroeder, F. C., Gavin, K., Doherty, P., Igoe, D., Muir Wood, A., Kallehave, D. & Skov Grethund, J. (2015). New design methods for large diameter piles under lateral loading for offshore wind applications. In 3rd International Symposium on Frontiers in Offshore Geotechnics - ISFOG. Oslo, Norway, 705–710.
- DNV, GL. (2014). DNV-OS-J101–Design of offshore wind turbine structures. DNV GL: Oslo, Norway.
- Doherty, P., and Gavin, K. (2012). Laterally loaded monopile design for offshore wind farms. Proceedings of the Institution of Civil Engineers-Energy, 165(1),7–17.
- Dyson, G. J., & Randolph, M. F. (1998). Installation effects on lateral load-transfer curves in calcareous sands. In Centrifuge 98, 545–550.
- Kirkwood, P. B. (2016). Cyclic lateral loading of monopile foundations in sand, PhD Thesis, University of Cambridge.
- Li, W., Igoe, D., & Gavin, K. (2014). Evaluation of CPT-based p - y models for laterally loaded piles in siliceous sand. Géotechnique Letters, 4(2),110–117.
- Negro, V., López-Gutiérrez, J. S., Esteban, M. D., Alberdi, P., Imaz, M., and Serraclara, J. M. (2017). Monopiles in offshore wind: Preliminary estimate of main dimensions. Ocean Engineering, 133, 253–261.
- Novello, E. A. (1999). From static to cyclic p - y data in calcareous sediments. In Proc. 2nd Int. Conf. on Engineering for Calcareous Sediments (pp. 17–27).
- Ramírez, L., Fraile, D., Brindley, G. (2020). Offshore wind in Europe: Key trends and statistics 2019.
- Salgado, R., & Randolph, M. F. (2001). Analysis of cavity expansion in sand. International Journal of Geomechanics, 1(2),175–192.
- Suryasentana, S. K., & Lehane, B. M. (2014). Numerical derivation of CPT-based p - y curves for piles in sand. Géotechnique, 64(3),186–194.
- Zhang, W., & Askarinejad, A. (2019). Centrifuge modelling of submarine landslides due to static liquefaction. Landslides, 16(10),1921–1938.

Using near-surface CPT data to predict foundation skirt embedment in partially drained carbonate sands

H.M. Wroth, M.F. Bransby & C.D. O’Loughlin

Centre for Offshore Foundation Systems, Oceans Graduate School, The University of Western Australia, Australia

M.F. Silva, M. Cocjin, N. Levy & H.E. Low

Fugro Australia Marine, Australia

ABSTRACT: A series of CPT and skirt penetration tests have been conducted in carbonate silty sand in a range of drainage conditions ranging from fully drained to fully undrained. The drainage transition response for each has been quantified in order to provide guidance in how to use the results from field CPTs to predict soil resistance during the installation of skirted foundations.

1 INTRODUCTION

1.1 Background

Skirted foundations are a type of shallow foundation featuring vertical plates (‘skirts’) that extend up to beneath the underside of the foundation. They are frequently used offshore to secure subsea infrastructure to the sea floor. They are popular because they are installed by being simply craned onto the seabed where the self-weight of the structure pushes the skirts into the seabed. The skirts provide higher foundation capacity by contributing to sliding resistance (through the additional passive resistance that develops at the skirt face) and by moving the failure mechanism deeper in the soil, often mobilising higher soil strength. Reviews of their role in increasing foundation capacity are provided in Murff & Millar (1977) and Bransby et al. (2017). The skirts can also add some additional scour protection to the structure by delaying undermining. In carbonate silty sand conditions the skirts are kept short (e.g. often 200-300 mm long) because of the high seabed strength gradient.

Ease of installation leads to short installation durations and consequently a cheaper foundation solution because it requires less vessel time, but relies on the self-weight of the structure being sufficient to install the skirts. However, the approach requires confident prediction of maximum likely seabed resistance to skirt penetration whereby an overestimation of the resistance may result in unnecessary ballast increasing project outlay, whereas an underestimation may pose a risk of early refusal during installation requiring expensive mitigation (Bransby et al., 2015).

The most common design method utilises inputs direct from cone penetrometer tests (CPTs) in the depth range of the skirt length (which may be as small as 0.2 m in coarser-grained seabeds). In particular, skirt tip resistance, q_b (= total base resistance, Q_b divided by skirt base area, A_b) is linked empirically with net cone resistance, q_{net} , so that $q_b = \beta q_{net}$ although there is some dispute on the particular value of scaling factor, β , to use, particularly in carbonate soils. This uncertainty is further exacerbated when the soil drainage conditions during cone penetration may be different to those during installation of the skirted foundation. In addition, skirt skin friction, q_s (= total skirt resistance through interface shear, Q_s divided by skirt area, A_s) can be either related directly to CPT sleeve friction, q_s or empirically to net cone tip resistance, q_{net} .

The aim of the work reported here is to improve understanding of the relationship between skirt tip resistance and net cone resistance for a carbonate silty sand. This was achieved through a series of laboratory tests in which model scale CPTs and skirt penetration tests were undertaken using a carbonate silty sand taken from the North West Shelf of Australia. Samples were prepared at a density typically found on the seabed and probed with cones and skirts at a range of velocities from virtually drained to undrained (spanning an approximately four order of magnitude velocity range). Because of the shallow depth of interest (say 0.2 m) and the small thickness of typical skirts (say 8 – 12 mm), the skirt tests were conducted at full-scale. Furthermore, the size of the skirts allowed skirt tip resistance to be measured separately from skin friction and thus permitted a comparison of each component to the CPT equivalents.

This paper first describes the soil, apparatus and testing performed before presenting the results from the experiments and describing their implications for design.

2 EXPERIMENTAL METHODS

2.1 Overview

Two samples of carbonate silty sand were prepared in sample containers ('strongboxes') of plan dimensions 650 by 390 mm and depth 325 mm. In these samples 10 mm diameter cone penetrometer and 2, 4, and 8 mm thickness skirt penetration tests were conducted at different rates.

2.2 Sample preparation

The soil used was a carbonate silty sand with a fines content of 44%, median grain size, $d_{50} = 0.085$ mm and a carbonate content of 92% (O'Beirne et al., 2020) and was sampled from the North West Shelf of Australia in approximately 100 m water depth. Sufficient material was available to make a sample of depth 220 mm in the selected strongbox.

A 20 mm layer of dense coarse sand was first placed at the base of the strongbox to create a drainage layer that was covered by multiple layers of geofabric to prevent loss of fines. The carbonate silty sand was mixed by hand to the targeted moisture content of about 45%, and placed in layers by hand into the strongbox. The strongbox was then moved to a large consolidometer and a vertical stress of 100 kPa was applied in one increment through a lid to the top surface of the sample and allowed to consolidate with the lid settlement monitored during consolidation. On reaching equilibrium the sample was unloaded to approximately 0 kPa and allowed to swell. This process was repeated twice, such that the sample experienced three cycles of loading to 100 kPa and back to 0 kPa before it was removed from the large consolidometer and equilibrated under self-weight ready for cone or skirt testing.

The above procedure generated a repeatable dense sample (of moisture content of approximately 36%) which is believed to be in a density state representative of wave-trafficked sediment on the North-West Shelf at about 100 m water depth. Consequently, skirt testing was performed at full scale, investigating the performance of the very short skirts which are typically used in carbonate silty sands and sandy silts on the North West Shelf.

2.3 Measurement of coefficient of consolidation

Measurement of the coefficient of consolidation of each sample is critical for generalising the results of the skirt penetration tests. Consequently, two different approaches were used to quantify the coefficient of consolidation. The first was interpretation of the

oedometer-style results generated when loading and unloading the sample in the large consolidometer during sample preparation to obtain c_v , whereas the second was interpretation of u_2 pore pressure dissipation data during pauses in cone penetration to obtain c_h .

From the oedometer-type loading events the average value across the two samples was $c_v = 84.5$ m²/yr. The CPT dissipation tests were conducted by penetrating the 10 mm piezocone described below at a rate of 64 mm/s to a depth of 120 mm and holding position whilst recording the u_2 pore pressure. Interpretation using the method of Teh & Houlsby (1991) gave an average value $c_h = 100$ m²/yr.

2.4 Cone penetrometer tests

The cone penetrometer tests were conducted using a model scale (laboratory) cone penetrometer, with dimensions that are scaled down (by a factor of ~3.6) from the standard 10 cm² field geometry (ISO 2014). This resulted in cone diameter of 10 mm and sleeve length of 37.5 mm. The model cone measures tip and sleeve resistance through independent load cells, and pore pressure at the cone shoulder (i.e. at the u_2 position).

Tests were conducted using one of two electro-mechanical actuators. The first 'standard' actuator is capable of vertical penetration rates in the range 0.001 mm/s to 3 mm/s to reach a cone penetration depth of 185 mm, whereas the other 'high speed' actuator is capable of penetration rates up to 72 mm/s, but restricted, by travel limits, to a penetration depth of 120 mm.

The test programme included a range of different penetration rate CPTs from 0.003 mm/s with the standard actuator (which were conducted overnight) to

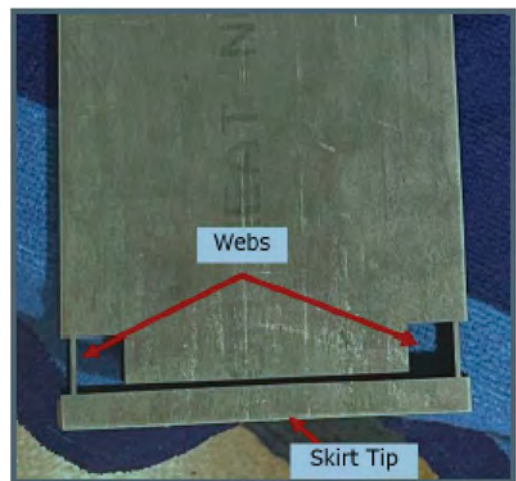


Figure 1. Instrumentation of the skirt tip. Strain gauges were placed on the webs.

64 mm/s with the high speed actuator (which took two seconds). The cone was extracted at 3 mm/s in all tests.

2.5 Skirt penetration tests

Skirts of four different thicknesses (2, 4, 8 and 12 mm) were fabricated from Grade 316 stainless steel, with dimensions listed in Table 1. These values were chosen to investigate the effect of thickness on installation resistance and cover practical skirt thickness ranges of 6 to 12 mm.

Table 1. Dimensions of the fabricated test skirts.

Skirt thickness t (mm)	2	4	6	8
Skirt breadth b (mm)	20	40	80	120
Skirt length L (mm)	400	400	400	400
Instrumented?	N	N	Y	N



Figure 2. Skirt testing apparatus.

The same roughness characteristics for all skirts was achieved by sand blasting each skirt. After treatment, an absolute roughness, R_a , of approximately 3 microns was measured for all skirts. Based on a series of ‘sled’ interface tests performed on the same soil by O’Brien et al. (2020), this interface roughness was expected to have a drained residual interface coefficient, μ between 0.55 and 0.6.

The 8 mm skirt features a strain gauged web zone immediately behind the skirt tip (see Figure 1), allowing direct measurement of skirt tip resistance. During

testing, an S-shaped load cell was placed in-line between the actuator and skirt plate in order to measure the total soil resistance to skirt penetration (and so deduce the skirt friction alone by comparing this to the resistance measured by the skirt tip load cell).

Tests were conducted by starting the skirt tip immediately above the soil surface and penetrating the skirt into the seabed at a prescribed rate whilst logging the vertical load, vertical displacement and the skirt tip load cell (when relevant). The experimental apparatus during skirt testing is shown in Figure 2.

3 RESULTS: CONE PENETRATION RESISTANCE

Depth profiles of cone tip resistance for all the cone penetration tests are shown on Figure 3. Multiple tests were conducted at the faster velocities (> 1 mm/s) to investigate repeatability (which appears to be reasonable, see Figure 4), but only single tests were conducted at the slower rates of 0.003, 0.01, 0.03, 0.1 and 0.3 mm/s.

There is an approximately linearly-increasing tip resistance for the slowest (drained) tests so that q_{net}/σ'_v remains almost constant with a cone q_{net} gradient of about 2.2 MPa/m. This is a typical near-surface value in a medium dense carbonate sand deposit offshore.

In contrast, a maximum q_{net} is mobilised in about 3 or 4 cone diameters of penetration for the fastest tests and this resistance does not increase significantly with depth thereafter. This resistance was also associated with mobilisation of a maximum negative pore pressure, $u_2 = 30$ kPa after which the pore pressure did not decrease further. This limit may be due to an early mobilisation of a ‘deep’ mechanism in undrained conditions or because of generation of cavitation conditions.

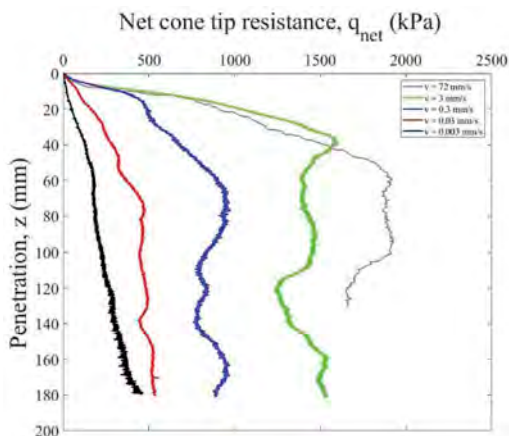


Figure 3. Cone tip penetration resistance curves for CPTs conducted at a range of velocities.

The variation in cone tip resistance with penetration rate is examined in more detail in Figure 4, which plots the net cone resistance, q_{net} , divided by a reference net cone resistance, $q_{net,ref}$ (taken here as that during the slowest (0.003 mm/s) cone test) against the dimensionless velocity, vD/c_v (where $c_v = 84.5 \text{ m}^2/\text{yr}$ as noted earlier). Results are shown for a penetration depth, $z = 40 \text{ mm}$ (4D) and 100 mm (10D).

At both depths, results suggest that undrained conditions are achieved for all tests with $vD/c_v \geq 20$ (approximately consistent with Finnie and Randolph, 1994), Randolph & Hope (2003) and Silva & Bolton (2004), and there is no further change in net cone resistance with increasing velocity. A 10 cm^2 field cone conducted at 2 cm/s (as in the ISO standard condition) would generate $vD/c_v = 274$ in this soil sample and therefore measure undrained soil resistance.

The difference in q_{net} is small between the two slowest cone tests and suggests that close to drained conditions were achieved with $vD/c_v \leq 0.05$. This suggests a range of partially drained behaviour when $0.05 < V < 10$ giving a velocity range of 200 times.

The ratio of undrained to drained net cone resistance is approximately 12 and 6.5 at penetration depths of 4D and 10D respectively – both noticeably higher than for clays. A higher ratio at shallower depths is consistent with the previous observation that drained cone resistance is proportional to effective stress level (and hence depth), whereas undrained cone resistance reaches a maximum at shallow depth and then becomes approximately constant with depth.

The evolution of cone resistance with V can be described using a ‘back-bone’ curve of the form:

$$\frac{q}{q_d} = a - \frac{(a-1)}{\left(1 + (V/V_{50})^d\right)} \quad (1)$$

where $a = q_{ud}/q_d$, with the subscripts ‘d’ and ‘ud’ denoting drained and undrained resistances respectively. Eq. 1 adopts q rather than q_{net} to permit application to both the cone and skirt data. As applied to

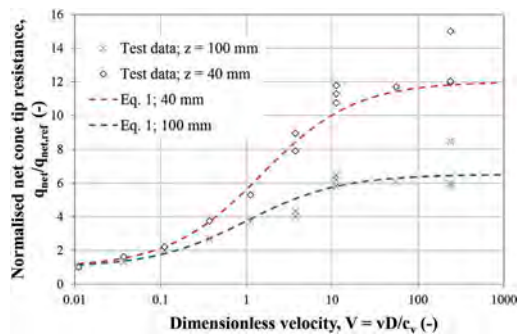


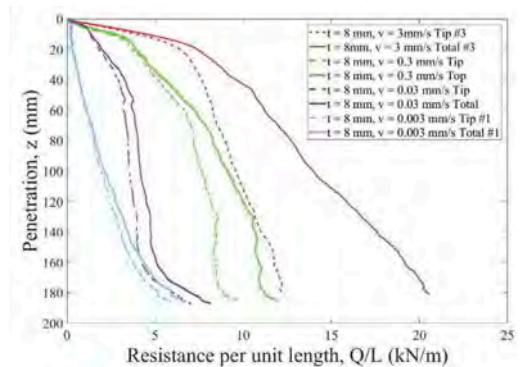
Figure 4. Evolution of normalised net cone tip penetration resistance with dimensionless penetration velocity at depths of 40 mm (4D) and 100 mm (10D).

the cone data, q denotes the net cone resistance, with the best agreement with the measurements obtained using $a = 12$, $d = 0.8$ and $V_{50} = 1.5$ at $z = 40 \text{ mm}$, and $a = 6.5$, $d = 0.8$ and $V_{50} = 1.0$ at $z = 100 \text{ mm}$.

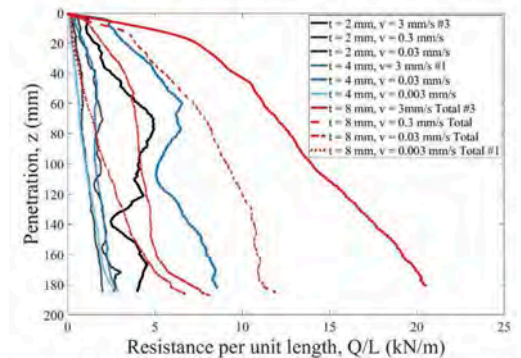
4 RESULTS: SKIRT PENETRATION

Figure 5 shows depth profiles of total and tip resistance for the three skirt thicknesses from tests involving penetration velocities in the range 0.003 to 18.75 mm/s. For clarity, total and tip resistance for the 8 mm instrumented skirt is shown separately on Figure 5a, whereas only total resistance is available for the 2 and 4 mm skirts and so is plotted compared to the total resistance for the 8 mm skirts on Figure 5b.

For the slowest tests, the resistance is almost proportional to depth up to about $z = 160 \text{ mm}$, beyond which the influence of boundary effects at the bottom of the box on the obtained results becomes apparent for the 8 mm skirt. Furthermore, for the slowest tests, the total resistance measured by the load cell located at the top of the skirt is very similar to the load measured by the tip load cell, implying a very small skin friction. In contrast, for the fastest test (18.75 mm/s) the total resistance is larger, varies non-linearly with depth and



(a) Selected results for 8 mm skirts



(b) Selected results for 2, 4 and 8 mm thickness skirts

Figure 5. Skirt penetration resistance curves for skirt tests conducted at range of velocities (selected tests).

the skirt friction is approximately 25% of the tip resistance (i.e. $Q_s/Q_t \approx 0.25$). Intermediate Q_s/Q_t values are observed for the tests at intermediate velocities.

Skirt tip resistance (from the 8 mm skirt penetration tests), normalised by the value for the slowest test, is plotted against dimensionless velocity, $V (=vt/c_v)$, where t is the skirt thickness) on Figure 6 for depths, $z = 40$ and 100 mm (i.e. at the same depths as the cone data on Figure 4). The variation in normalised skirt tip resistance with V is approximately similar to the equivalent for the cone (Figure 4): the resistance maximises at $V > 10$ and appears to be close to drained at $V = 0.01$; and the ratio of undrained to drained resistance is approximately 11 and 5 at depths of 40 mm and 100 mm respectively.

Figure 6 also includes skirt tip backbone curves using Eq. 1, where the best fit to the data was obtained using $a = 5$, $d = 1$ and $V_{50} = 0.3$ for $z = 100$ mm and $a = 12$, $d = 0.6$ and $V_{50} = 0.4$ for $z = 40$ mm. These parameters are summarised together with those for the cone on Table 2, and suggest that higher velocities are required to ensure no drainage occurs for shallower depths.

Figure 7 compares tests with different skirt thicknesses using total rather than tip resistance as the 2 and 4 mm skirts were too thin to instrument to measure tip resistance independently. To investigate scaling, the data from the different skirt thicknesses are plotted against velocity (v ; in mm/s) on Figure 7a, normalised velocity (vt/c_v ; dimensionless) on Figure 7b, and in normalised movement time ($T = c_v(z/v)/t^2$; dimensionless) on Figure 7c. As expected, faster velocities are required to achieve undrained conditions for the 2 mm skirt, although the vD/c_v normalisation shown in Figure 7b does not appear quite sufficient to explain the trend. The normalisation using dimensionless travel time gives an interesting relationship which warrants further investigation, but is not believed to provide sufficient evidence to overturn the expected vD/c_v drainage scaling.

Table 2. Equation 1 parameters for cone and skirt data at depth, $z = 40$ and 100 mm: tip resistance.

Skirt thickness, t or cone diameter, D (mm)	z (mm)	a	V_{50}	d
Cone, 10	40	12	1.5	0.8
	100	6.5	1.0	0.8
Skirt, 8	40	12	0.4	0.6
	100	5	0.3	1.0

5 IMPLICATIONS FOR DESIGN

The results from both the CPTs and skirt tests are presented in dimensionless velocity space showing the transition in resistance from undrained and drained soil response. By considering the field drainage conditions for the two devices (which

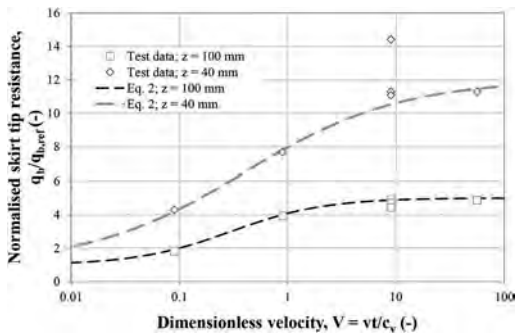
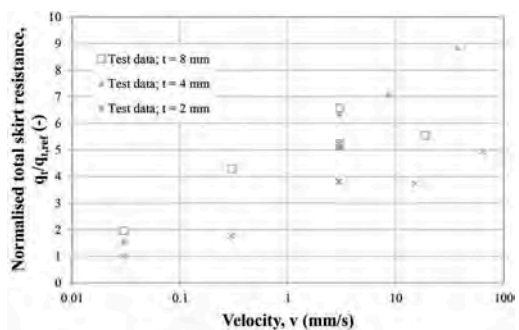
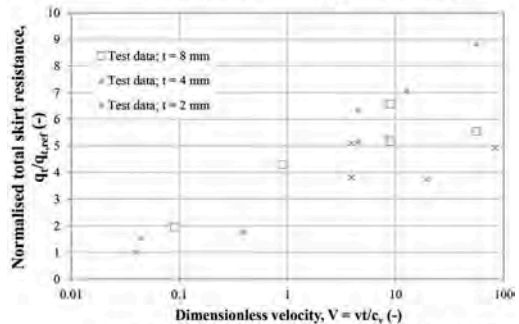


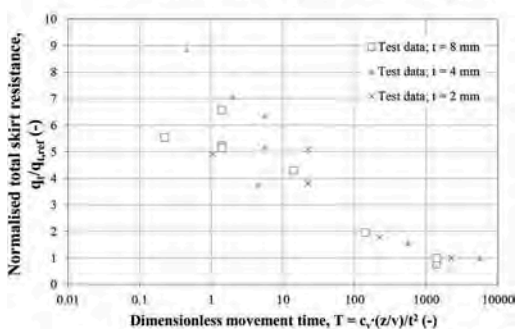
Figure 6. Normalised skirt tip penetration resistance versus dimensionless velocity for 8 mm instrumented skirt.



(a) Resistance plotted against velocity



(b) Resistance plotted against normalised velocity



(c) Resistance plotted against normalised travel time

Figure 7. Normalised skirt tip penetration resistance versus velocity or time for 2, 4 and 8 mm skirts ($z = 100$ mm).

depends on the coefficient of consolidation of the soil and the foundation set-down velocity), improved advice is given about how to predict skirt installation resistance from CPT results in the field.

Calculations were performed to quantify the scaling between the skirt tip resistance, q_b and cone tip resistance q_c (i.e. $\beta = q_b/q_c$) for skirts of thickness, $t = 12$ mm penetrated in soils with different coefficients of consolidation values at different velocities (Figure 8). It was assumed that a 10 cm^2 cone was penetrated at 2 cm/s as in ISO (2014). For fully drained conditions, the cone gradient was approximated to 2.2 MPa/m as measured for the slowest conducted cone, and the skirt tip penetration resistance gradient approximated as 1.8 MPa/m . Equation (1) and the parameters for $z = 100 \text{ mm}$ listed in Table 2 were used to describe the drainage backbone curves. Consequently, for every skirt velocity and c_v combination, the vt/c_v value for the skirt and the vD/c_v for the cone and the above information could be used to calculate β .

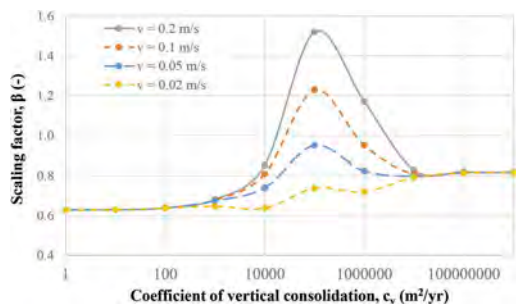


Figure 8. Required scaling factor β for soils with different c_v values for a skirt of 12 mm thickness penetrating at different velocities ($z = 100 \text{ mm}$).

For high c_v values (for a coarse-grained soil), both the skirt penetration and cone penetration is drained and the drained ratio is 0.8 (i.e. the ratio of the cone tip and skirt tip resistance gradients = $1.8/2.2$). In contrast, if c_v is very low (for a clay or silt), the soil around both the penetrating skirt and the penetrating cone is undrained and the ratio becomes equal to a constant undrained ratio, $\beta \approx 0.62$. These ratios are broadly consistent with shape factors describing the difference in bearing resistance for plane strain versus axisymmetric shallow and deep foundations in drained and undrained conditions.

However, if the soil has intermediate c_v (such as with a silty sand or sandy silt – or for a fast-penetrating skirt in sand) the cone may be drained (generating less tip resistance), but the skirt would be partially drained (with more resistance).

Consequently, the cone resistance has to be scaled up for these conditions because of the drainage difference.

Figure 8 shows calculated values of scaling factor, β , for a likely range of set-down velocities (0.05 m/s to 0.2 m/s) for a typical skirt thickness (12 mm). The curve suggests that if the soil c_v is not well known (and it is normal to have some orders of magnitude of uncertainty in c_v for these types of soil), that there may be a need to use a β value larger than 1 in order to capture the largest likely skirt tip resistance from the CPT data. Interestingly, however, a curve for a slower velocity (0.02 m/s) reveals that the system may self-correct – increasing resistance from higher velocity may reduce installation velocity and therefore reduce installation resistance. This is true for the dilatant response observed for the soil investigated here, whereas for a contractant response the soil resistances will increase as the skirt penetration velocity reduces, which may lead to premature refusal.

6 CONCLUSIONS

A series of full-scale skirt penetration experiments were conducted in a carbonate silty sand sample, in a density state typically found offshore, to investigate how seabed resistance varies with penetration velocity due to changing soil drainage conditions. By comparing the drainage transition curve for the skirted foundations with a separately measured curve for a CPT, recommendations were generated for scale factors to obtain skirt tip resistance from cone tip resistance. The calculations revealed that a larger than currently recommended value (of larger than 1) may be required for some intermediate soils where standard cone penetration rates lead to almost drained soil response, whereas likely skirt penetration velocities provoke partially drained or undrained response. Further work is required to generalise this behaviour.

ACKNOWLEDGEMENTS

The second author holds the Fugro Chair in Geotechnics whose support is gratefully acknowledged

REFERENCES

- Bransby, M., Xie, Y., & White, D. J. (2015). Strategies for Quantifying the Installation Reliability of Skirted Subsea Foundations *ASME 2015 34th International Conference on Ocean, Offshore and Arctic Engineering*, St. John's, Canada.
- Bransby, F., Randolph, M. F., O'Driscoll, D., Zhu, H., & Drummen, T. (2017). Optimising Foundation Skirt Geometries for Reliable Foundation Capacity and Installation. *ASME 2017 36th International Conference on Ocean, Offshore and Arctic Engineering*, Trondheim, Norway

- Finnie, I. M. S., & Randolph, M. F. (1994). Punch-Through and Liquefaction Induced Failure of Shallow Foundations on Calcareous Sediments *7th International conference on the behaviour of offshore structures*, Cambridge; MA.
- ISO 2014. ISO 19901-8: Petroleum and natural gas industries — Specific requirements for offshore structures — Part 8: Marine soil investigations.
- O'Beirne, C., O'Loughlin, C., Watson, P., & White, D. (2020). *Centrifuge modelling of Pipe Clamping Mattresses (PCMs) as axial restraint for the Perseus over Goodwyn flowline*. UWA research report.
- Murff, J.D. and Miller, T.W. 1977. Stability of offshore gravity structure foundations by the upper bound method. In *Offshore Technology in Civil Engineering: Hall of Fame Papers from the Early Years: Volume Two* (pp. 106–113). ASCE.
- Randolph, M.F. and Hope, S. (2004). Effect of cone velocity on cone resistance and excess pore pressure. *Int. Symp. Eng. Practice and Performance of soft deposits*, Osaka, 1470152.
- Silva, M.F. and Bolton, M.D. (2005). Interpretation of centrifuge piezocone tests in dilatant, low plasticity silts. *In International Conference on Problematic Soils* (pp. 27–34).
- Teh, C. I., & Houlsby, G. T. (1991). An analytical study of the cone penetration test in clay. *Geotechnique* 41.

The role of cone penetration testing in the Dogger Bank offshore wind farm

Tor Inge Yetginer-Tjelta, Jérôme De Sordi & Leonardo Caferri
Equinor, Stavanger, Norway

Mike Rose
SSE Renewables, Perth, Scotland

Callum Duffy
Logos Geoservices Ltd, Oxford, UK

Tom Lunne, Øyvind Blaker, Stein Strandvik & Vaughan Meyer
NGI, Oslo, Norway

ABSTRACT: The cone penetration test is the preferred tool for measuring the in-situ soil conditions for offshore wind farm developments. This preference stems from the consistent and reliable data quality, low relative cost, and speed of data acquisition which enables developers to characterise large areas with numerous structure locations to support foundation concept feasibility studies, installation risk assessments and geotechnical engineering analyses to optimise the foundation design by reducing the uncertainty in soil input parameters. However, the interpretation of CPT data is largely dependent on site-specific or published correlations, which can present challenges when relying on the CPT as the primary tool for stratigraphic profiling, interpretation of soil behaviour and for defining geotechnical parameters for engineering design. This paper presents recent developments and processes that enabled the delivery of an optimised CPT based geotechnical design basis for the Dogger Bank Wind Farm. The processes and tools that enabled this approach comprised a novel SI strategy, focussed CPT interpretation and CPT tool development. The strategic approach for the novel SI strategy is presented and the individual elements described. Challenges and limitations associated with the interpretation of CPT data are discussed, including size and scale effects, resolution, calibration with laboratory and large-scale field test data and rate effects. Finally, the challenges with using statistical methods to derive design values from CPT records are briefly discussed.

1 INTRODUCTION

The Dogger Bank offshore wind farm comprises three project areas (Dogger Bank A, B and C) within the Dogger Bank Offshore Development Zone, located 125 to 290 km off the east coast of Yorkshire, UK. The development zone covers ca. 8660 km² and water depths range from 18 to 63 m (Dogger Bank Wind Farm, 2022).

Dogger Bank has a complex geology, resulting from the different depositional environments and post-depositional processes that have formed it over the last 120 000 years (Cotterill, et al., 2017a & b). Dogger Bank is generally accepted to be a complex of highly deformed glacial till, created as the ice sheets from Britain and Scandinavia oscillated across the area, bringing eroded soils with them that were often left in ridges (terminal moraines) at the front of the ice. As the ice moved backwards and forwards these soils were “rucked up” forming features known

as push-moraines, which were then overridden and eroded by later glacial advances. Between these ridges shallow lakes developed. The soils are therefore typically non-sedimented and have been deposited and reshaped by a number of different environments ranging from tundra, permafrost, sub-glacial, pro-glacial - through to temperate - including lacustrine, fluvial and estuarine or lagoonal and to changes as the sea level rose and flooded the Dogger Bank about 7000 years ago. Thus, desiccation due to drying, evapotranspiration and freezing are considered to be important post-depositional processes in the geologic history of the Dogger Bank soils. The resulting variability in the soil conditions are significant for the ground investigations and the ensuing characteristic values of soil properties derived for geotechnical design of the monopile foundations. At Dogger Bank, seafloor CPTs were the primary intrusive ground investigation tool performed at each wind turbine generator (WTG) location. The CPT

data were a key input to the ground model developed for the site, which combined high quality 3D seismic profiling and targeted borehole locations from which site-specific CPT correlations were developed.

2 CHALLENGES AND LIMITATIONS ASSOCIATED WITH INTERPRETATION OF CPT DATA

The soils present at Dogger Bank are, in general, not classic sedimented clays and sands, or conventional glacial lodgement tills or glaciomarine tills. The Dogger Bank soils must therefore not be forced into a classical framework for sedimented soils nor the correlations that have been developed for such soils. It follows that a key challenge with the Dogger Bank site is the natural variability encountered in the geotechnical parameters, especially for the clays of the Dogger Bank Formation. This variability is primarily attributed to the different depositional environments and varying post-depositional processes to which the soils have been subjected, as discussed above. Consequently, the soils vary in composition (particle size distribution and plasticity), stress and strain histories, and in their current state (in situ stresses, density) and fabric. Coupled with this natural variability are possible sample disturbance effects (including effects of dissolved gas coming out of solution when sample is recovered to deck (Lunne et al. 2001), uncertainty with in situ stress conditions, limitations with laboratory testing, and scale effects. A further complication when using CPT data to develop site-specific correlations, is that these data are invariably noncoincident with the other test data used to develop the correlation. Examples of the variability in geotechnical parameters are given below.

For low to medium overconsolidation (OCR) ratio clays, it has been shown that the preconsolidation stress (p_c') assessed from oedometer tests usually correlates well with the undrained shear strength from anisotropically consolidated triaxial compression (CAUC) tests (s_{uc}), as shown in Figure 1. The post-depositional processes to which the Dogger Bank clays have been subjected have imposed stress histories that are very different to simple vertical loading, unloading and reloading. Consequently, very large scatter is evident in the $s_{uc} - p_c'$ dataset shown in Figure 1 for the Dogger Bank clays.

It should be emphasized that the p_c' and OCR values derived from oedometer tests performed on these soils are “apparent” values. Correlations developed from loading-unloading-reloading data, such as those linking p_c' and s_{uc} and those linking OCR and in situ horizontal stress (or the later earth pressure at rest, K_0), therefore do not apply to the Dogger Bank clays. As noted by Yetginer & Tjelta (2021), the inability to reliably estimate p_c' , OCR and K_0 increases the uncertainty in laboratory test results for these soils.

Figure 2 presents plots of corrected cone resistance (q_t) versus depth for Upper Dogger Bank

clay. The cone resistance data have been filtered to remove sand-like layers based on expected Soil Behaviour Type (SBT), however some spikes in the q_t data are still present. It is seen that q_t increases with depth, but that there is variability in the cone resistance. This variability leads to challenges and uncertainties when developing cone resistance based geotechnical parameter correlations.

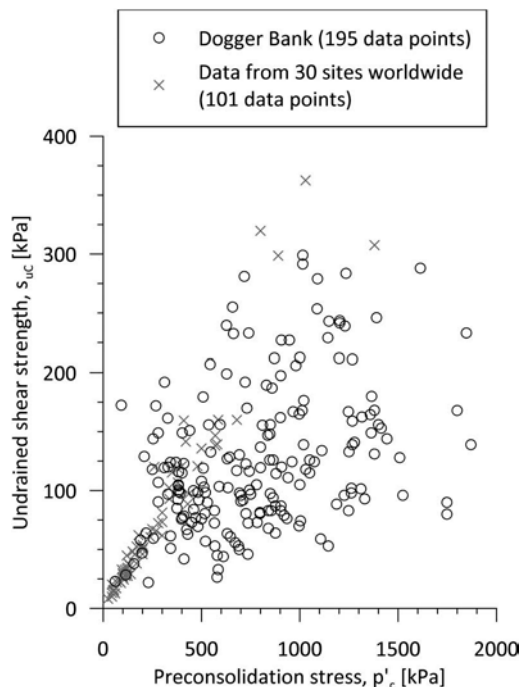


Figure 1. Preconsolidation stresses from oedometer tests compared with undrained shear strengths from anisotropically consolidated triaxial compression tests (updated from DeGroot et al., 2019).

Figure 3 shows considerable variation of N_{kt} -factor versus depth (where $N_{kt} = q_{net}/s_{uc}$), despite efforts to filter the data based on sample quality and sampling techniques. Possible explanations for this scatter include:

- 1) The presence of fissures and planes of weakness in the clay fabric which influence the measured undrained shear strength.
- 2) Sample disturbance effects which are difficult to quantify in overconsolidated/non-sedimented clays and possibly includes dissolved gas coming out of solution.
- 3) Uncertainties in the selected q_t value due to non-coincident borehole and CPT data (i.e. the physical inability to measure q_t on the soil sample tested in the laboratory).
- 4) Limitations in laboratory testing procedures, including the inability to reliably estimate p_c' , OCR and K_0 , as noted previously.

3 EVOLVEMENT OF A NOVEL SOIL INVESTIGATION STRATEGY

Soil investigation (SI) for the Dogger Bank offshore wind farm has been conducted in three principal phases. These phases were not conceived entirely at the outset but developed organically to address arising challenges and constraints.

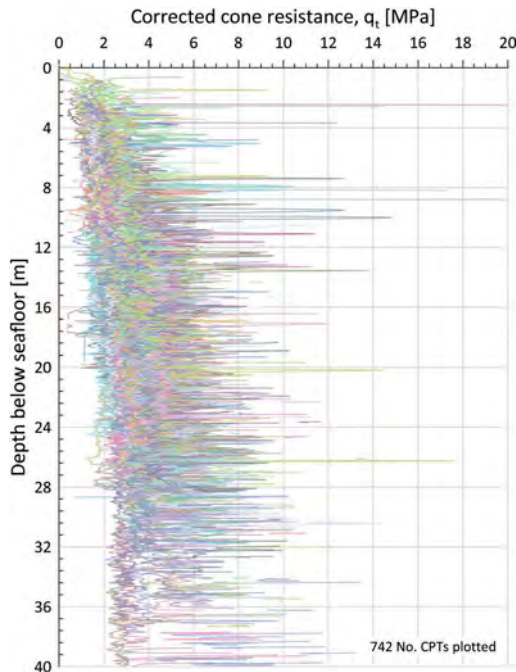


Figure 2. Corrected cone resistance versus depth for Upper Dogger Bank clay.

Phase I:

An initial phase with regional geophysical and geotechnical investigations (incorporating boreholes and CPTUs) and including study of geological information. All information was integrated into a regional ground model that was used for wind farm layout and foundation feasibility studies. Routines to provide “synthetic CPT data” from the ground model at untested locations were also developed (Forsberg et al. 2017).

Development of site-specific correlations between CPT data and geotechnical parameters started during this phase. Two of the most important challenges were:

- 1) Available seafloor CPT equipment did not give sufficiently deep penetrations for the expected monopile embedment’s.
- 2) The “normal” approach of correlating corrected cone resistance (q_t) to undrained shear strength (s_u) resulted in exceptionally large scatter in the derived N_{kt} factors.

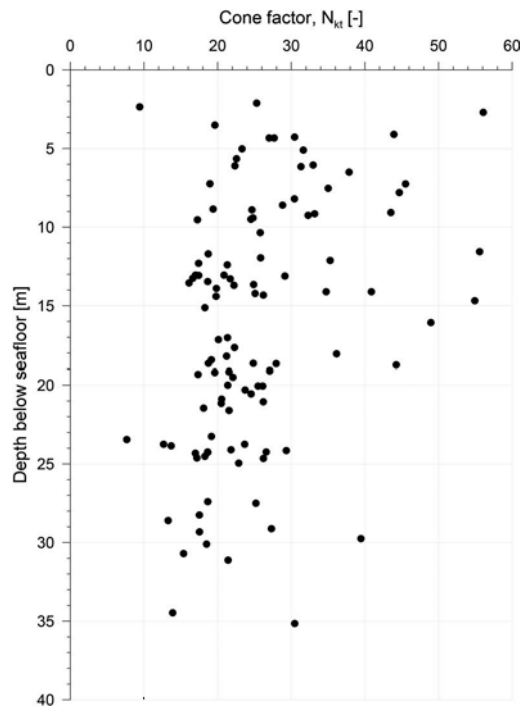


Figure 3. Example variation in N_{kt} -factor versus depth for clay from the Dogger Bank Formation.

Phase II

A hypothesis that the scatter in apparent p_c' , $s_{u,c}$ and N_{kt} data is a function of sampling, testing, and/or scale (fabric) effects was tested by deployment of spudcan penetration tests (see Section 5.1) and detailed soil characterization, including seismic CPTs at a small number of carefully selected “focus” locations. These focus locations provided detailed information on the soils, including the depositional and post-depositional regimes, for the various geological units identified at each location. CPT correlations were then developed using the data gathered at the focus locations. Phase II also included the trialling of enhanced seafloor CPT equipment with the aim to achieve penetrations beyond the expected monopile embedment’s, and finalization of the CPT interpretation scheme.

Phase III

In order to optimise project execution, the Phase III SI and final Geotechnical Design Basis (GBD) production were squeezed into a 10-month period.

The final phase of SI comprised at least one enhanced (deep) seafloor CPTU at each WTG location. Seismic CPTs and soil borings were performed at selected locations identified from the updated ground model.

Due to the lack of soil sampling at turbine locations, a complementary 3D Ultra High Resolution Seismic (UHRS) survey was also conducted. This survey and associated detailed geological

interpretation provided a high reliability of regional geological unitisation, which was critical given the lack of sampling at WTG locations.

The key elements to the success of the soil investigation strategy are:

- 1) Enhanced CPTs extending below monopile embedment depths, enabling reliance on CPTs as the primary WTG location specific dataset, and thereby minimising the final survey campaign period and laboratory testing period;
- 2) Integration of CPT, borehole and interpreted 3D UHRS geophysical survey data;
- 3) A geological model developed by the BGS (Cotterill, et al., 2017a & b);
- 4) Site- and unit-specific CPT-correlations for geotechnical parameters;
- 5) Spudcan penetration tests to validate the ‘operational shear strength’ and application of regional unit specific N_{kt} -factors.

4 RECENT DEVELOPMENTS WITH CPT EQUIPMENT

For monopile foundations it is generally necessary to obtain soil parameter data to a depth of 40 – 50 m bsf. Using seafloor CPTs to obtain the required data is approximately 10 times more efficient than using combined down-hole sampling and CPT boreholes. Thus, there is a significant productivity gain in being able to penetrate to 45-50 m bsf with seafloor CPTs. However, from a CPT and monopile design perspective, the very dense sands of the Eem Formation, present at a depth of 30 – 40 m bsf at the Dogger Bank site are important. Seafloor CPT refusal was invariably encountered in the upper few metres of this unit, with q_c values of up to 150 MPa being recorded. This presented a challenge for the project and led to enhancements of the standard CPT equipment, such as using lubrication behind the cone to reduce rod friction. However, even with lubrication, it can be difficult, or even impossible, to penetrate a deep very dense sand layer. A new approach where water is flushed through holes near the cone tip has been developed and successfully used at the Dogger Bank Offshore Wind Farm. The development of these enhanced CPTs for Dogger Bank project has been successful due to close cooperation between the soil investigation contractor and the wind farm developer, as presented in Tjelta et al. (2022).

These enhancements increased the seafloor CPT penetration depth, as indicated in Table 1 and thus permitted efficient use of the CPT data to derive full depth geotechnical design parameter profiles at each WTG location.

Table 1. Summary of seafloor CPT penetration depths for the Dogger Bank project area.

Year	No. CPTs*	Final penetration depth (m bsf)		
		Minimum	Maximum	Average
2010	97	3.8	40.2	22.5
2012	87	8.9	40.1	27.2
CPT equipment enhancements from 2018 onwards				
2018	35	12.4	40.0	27.5
2019	100	14.3	45.6	38.8
2020	120	7.5	50.3	40.1
2021	98	23.5	58.8	44.5

* excluding tests with premature refusal and seismic CPTs

5 IMPROVEMENTS IN CPT INTERPRETATION

5.1 Giant “CPTs”

A novel feature of the Dogger Bank SI strategy was the use of large scale plate loading tests in the form of spudcans from a jack-up unit to assess the mass *operational* undrained shear strengths for the clay units at selected focus locations (Yetginer & Tjelta, 2021). Back-analysis of spudcan penetrations recorded from these jacking trials resulted N_{kt}^* factors for most clay units in the range 18-22 with a best estimate of 20. The corresponding reduced range in undrained shear strengths avoided designing foundations for a potentially unrealistic low strength for capacity, yielding large foundations, and then an equally unrealistic high strength for installation, resulting in high refusal risk.

Corrected CPT cone resistance measurements were interpreted both individually and collectively (over the wider jacking footprint area) to derive design undrained shear strength profiles for input into the back-analysis calculations. Location specific average operational N_{kt}^* factors were fine-tuned to best match the predicted spudcan penetration behaviour with the observed offshore penetration record. Spudcan penetration predictions were made by means of both traditional bearing capacity calculations using NGI’s in-house SPLAT software (Zhang et al., 2015) and Large Deformation Finite Element (LDFE) analyses using Abaqus. Example details from a back-analysis are shown in Figure 4.

Results from the spudcan penetration tests help to highlight that scale and fabric effects are an important consideration for the Dogger Bank clays. Comparison of the laboratory CAUC

1 Herein N_{kt}^* denotes the factor used to infer the mass operational shear strength, whereas N_{kt} denotes the factor used to estimate the undrained shear strength in triaxial compression, s_{UC} .

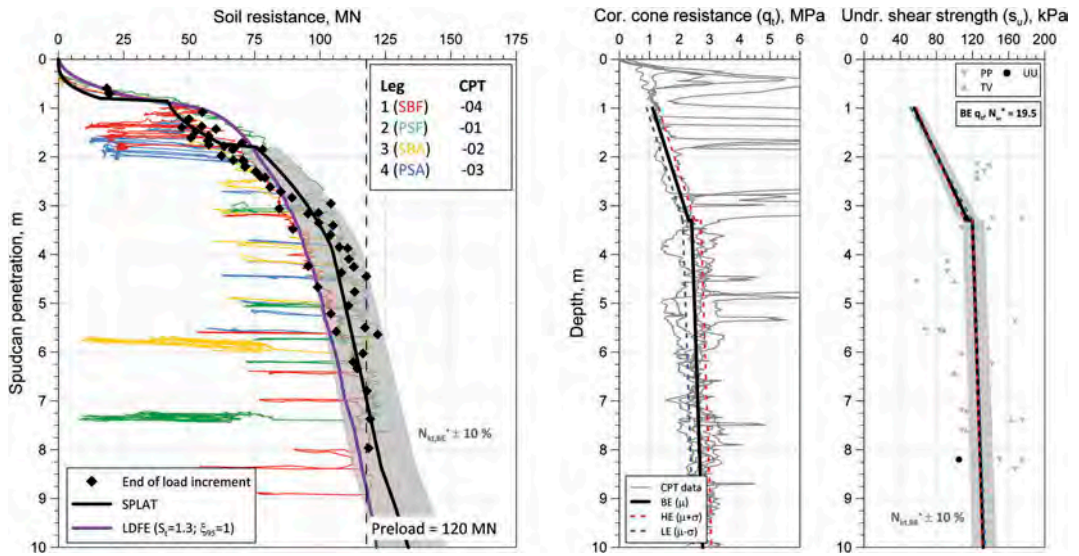


Figure 4. Example details from back analysis of recorded spudcan penetrations using SPLAT and large deformation finite element (LDFE) analyses.

strengths and the mass operational undrained shear strengths determined from back-analysis of spudcan penetration records at Dogger Bank, suggests the data shows a positive scale effect, with undrained strength increasing with increasing sample size. The size of the spudcans are comparable to the diameter of a monopile and the scale of the penetration tests is such that the varying responses due to natural variability and to different behaviour patterns in undrained shear (e.g. Hight et al., 2003) are integrated to some extent. The resulting range in N_{kt} values applicable to back-calculated strengths are lower than for the laboratory tests.

Differences in the kinematic restraints between the field and laboratory tests as well as rate-effects are noted to contribute to this observation.

The cost of performing the spudcan penetration tests were comparable to those for an SI vessel, particularly when these tests could be timed with existing operations. Such tests also have the advantage of providing valuable information for future WTG installation operations.

5.2 V_s and G_{max} correlations

Soil unit specific correlations for shear wave velocity (v_s) were developed in terms of net cone resistance (q_{net}) and in situ effective vertical stress (σ'_{v0}):

$$v_s = \beta_0 \cdot q_{net}^{\beta_1} \cdot \sigma'_{v0}{}^{\beta_2} \quad (4.1)$$

where β_0 , β_1 and β_2 are best-fit empirical factors. The unit for q_{net} and σ'_{v0} is kPa and that for v_s is m/s. The small strain shear modulus (G_{max}) is evaluated from:

$$G_{max} = \rho \cdot v_s^2 \quad (4.2)$$

where ρ is the soil density.

The correlations are primarily developed from sea-floor and downhole seismic CPTs (SCPTs). Data from borehole suspension logging as well as bender element measurements performed during triaxial, direct simple shear and resonant column laboratory tests were also considered. Figure 5 presents a comparison of measured versus calculated shear wave velocity for Upper and Lower Dogger Bank clay. As with the N_{kt} dataset, there is also variability in the v_s data. This suggests that factors such as the depositional environment and varying post-depositional processes to which the soils have been subjected also influence the shear stiffness of the soil.

Shear wave velocities determined at the end of consolidation in triaxial tests using bender elements typically give v_s values which are lower than those determined in situ (Figure 6). Such observations are not uncommon and highlight the importance of in situ shear wave velocity measurements for structures, such as monopiles, which are sensitive to the small strain stiffness response of the soil.

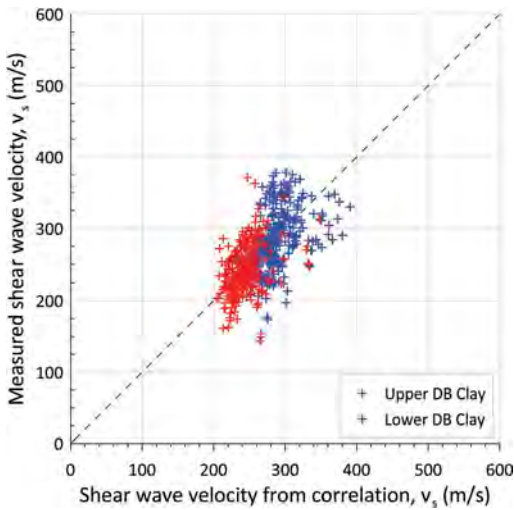


Figure 5. Measured versus calculated shear wave velocity for Upper and Lower Dogger Bank clay.

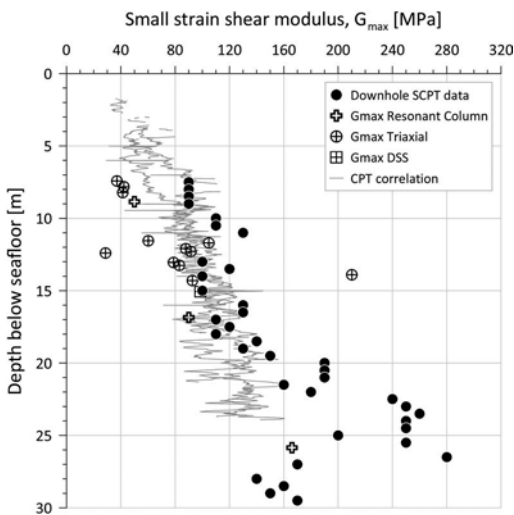


Figure 6. Example G_{max} data from investigations at a focus location.

6 FINAL CPT DATA INTERPRETATION SCHEME

A key advantage with CPT testing is the speed with which the data can be acquired, processed and interpreted to provide geotechnical engineering parameters. This is advantageous for the development of offshore wind farm projects which may have 100 or more WTGs. For the Dogger Bank WTG locations, continuous seafloor CPT data permitted semi-automatic processing and analysis of data and thus:

- 1) Rapid development of geotechnical design profiles (preliminary profiles available in a matter of minutes);
- 2) Early phase monopile driveability predictions for identifying the potential risk of refusal during installation.

The geotechnical design profiles can also be used in automated routines for monopile design, such as those presented by Klinkvort et al. (2020).

Design parameter profiles for each WTG monopile foundation were developed from the site-specific CPT data acquired at each location coupled with the ground model developed for the Dogger Bank site. Figure 7 presents an example design parameter profile, showing q_t together with interpreted parameter profiles for undrained shear strength (s_u), relative density (D_r), peak drained effective stress friction angle (ϕ'), small strain shear modulus (G_{max}) and soil behaviour type (SBT).

Figure 8 presents example soil resistance to driving (SRD) and blow count predictions derived automatically from the site-specific CPT data. These predictions proved very valuable and indicated that monopile installation should be nonproblematic (earlier estimations made using composite CPT profiles gave strong indications for driving refusal).

7 INTEGRATION OF 3D UHRS SURVEY DATA

At each WTG location, refined interpretation of the 3D UHRS seismic data was performed to validate the variations in the CPT data accounted for in the characteristic design profiles. These detailed interpretations focused primarily on the continuity of soil layers within a 40×40 m box surrounding each CPT position, as shown in Figure 9. Such interpretations provide confidence that the CPT-derived stratigraphic profiles are representative for the much larger scale application of monopile foundation design.

8 STATISTICAL INTERPRETATION OF CPT DATA

The continuous nature of seafloor CPT data lends itself towards the development of design parameter profiles using statistical methods. However, this approach has some challenges, as discussed below.

Linear regression can be used to derive a best estimate (i.e. central estimation) trend for q_t data over a specified depth interval. For such data, which can be considered to have a single independent variable, the confidence on the mean value, \bar{q}_t , together with the predictive interval (e.g. 5 and 95% percentiles) can be estimated from DNV (2012).

It is important to emphasise that the formulations in DNV (2012) only apply where there is a single independent variable. Where multiple variables are present, such as when geotechnical parameters are derived from CPT-based correlations (e.g. s_u or G_{max}), an

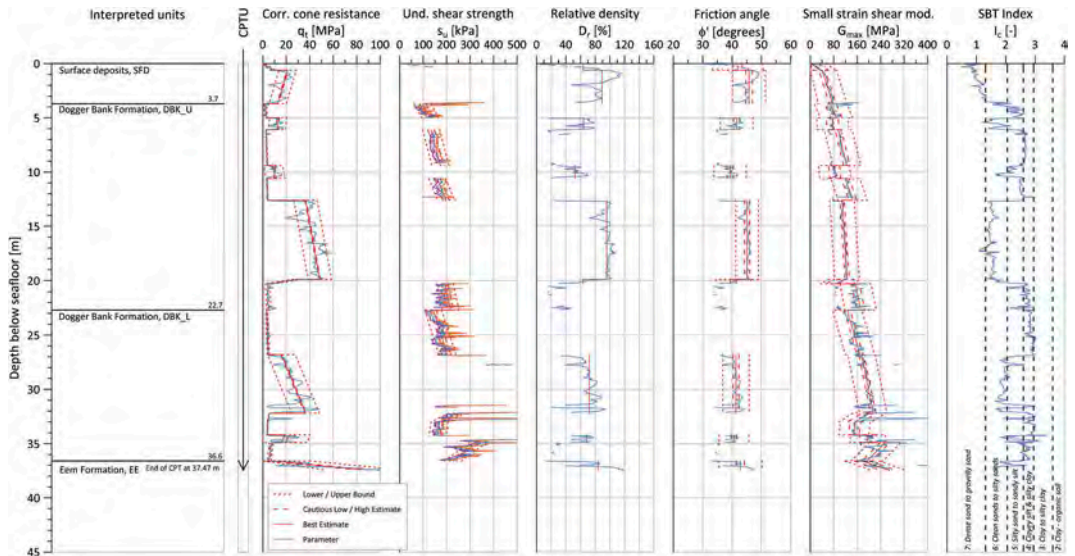


Figure 7. Example design parameter profile for a WTG location.

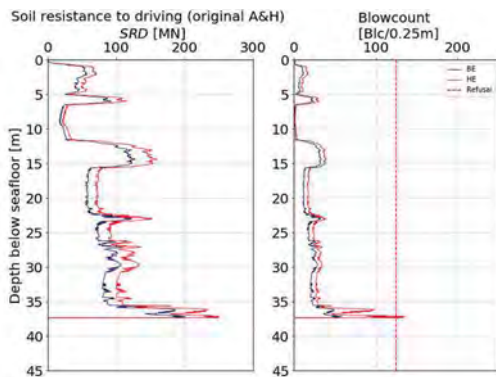


Figure 8. Example SRD and blow count predictions.

alternative methodology needs to be adopted which also considers the uncertainty in the correlation itself. One such method is the first-order second-moment (FOSM) method, which determines the stochastic moments of a function with random input variables using a first-order Taylor series (Haldar & Mahadevan, 2000). However, this approach is also not without its challenges and limitations, which include:

- 1) Assessment of the statistical uncertainty associated with each coefficient and exponent in the correlation formula. Such information may not be readily available.
- 2) Assessment of the equivalent number of independent data points for CPT data.

Coupled with this are how the design parameter profiles should be defined. Treatment of these topics is beyond the scope of this paper, but it is emphasized

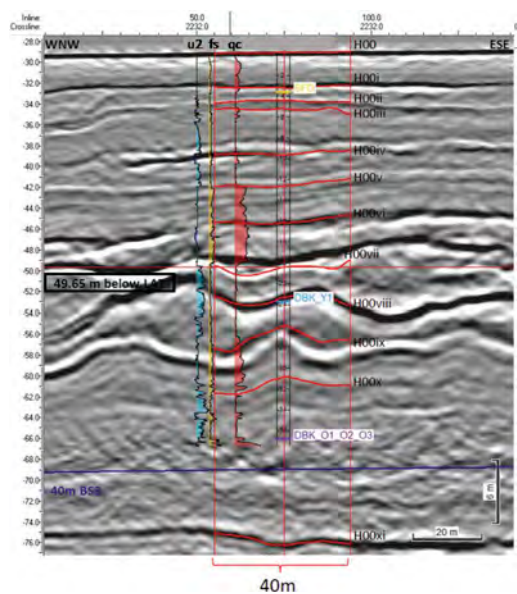


Figure 9. Example showing correlation between interpreted geophysical profile and CPT data (image courtesy of Geosurveys/MMT).

that these are important topics which the industry should address.

9 CONCLUDING REMARKS

The Dogger Bank project has demonstrated that the CPT can be used as the primary intrusive site investigation tool for offshore wind farm projects despite

complex geology and challenging ground conditions comprising stiff clays and very dense sands. A novel soil investigation strategy evolved for the project which addressed these challenges as they arose and had the following key elements:

- 1) Enhanced CPTs extending below monopile embedment depths. This enabled CPTs to be the primary intrusive SI dataset for each monopile location which had significant project timeline benefits. In order to attain target CPT penetration depths, innovative technical developments comprising rod lubrication and/or water injection at the cone tip were developed. The developments were the result of close collaboration between the SI contractor and the project developer.
- 2) Development of a reliable ground model which integrated CPT and borehole information with interpreted 3D UHRS geophysical survey data and the regional geological model for the site.
- 3) Development of site- and unit-specific CPT correlations for geotechnical parameters. Laboratory testing necessary for the development of these correlations was programmed early in the project timeline, where possible.
- 4) Innovative use of spudcan penetration tests to validate the operational undrained shear strength of the clays and enable application of regional unit specific N_{kt} -factors. Such tests highlight the value of large scale in situ testing of soils.

The CPT tool developments outlined in this paper, together with the novel site investigation strategy developed for the Dogger Bank wind farm, indicate the CPT will continue to have a central role in future offshore wind projects. However, it is contended that CPT tool development now probably lies in front of CPT interpretation, especially when it comes to the determination of design parameter profiles inferred from CPT data and associated coupling with statistical analysis.

ACKNOWLEDGEMENTS

The work presented herein was undertaken for the Dogger Bank project and the authors gratefully acknowledge the project's permission to publish this work. The authors are also grateful for the assistance given by various colleagues from Equinor, SSE and NGI in the preparation of this paper. The understanding of Dogger Bank geology and processes and integration with geotechnics that led to this CPT strategy would not have been possible without the early works by David Long and Carol Cotterill from the BGS, the late Leo James from RPS, Carl Fredrik Forsberg from NGI and Prof. Don DeGroot (University of Massachusetts Amherst). The authors also gratefully acknowledge the work performed for the project by BGS, Fugro, Geo, Geosurveys, MMT, RPS and Prof. David Hight (GCG).

REFERENCES

- Cotterill, C., Phillips, E., James, L., Forsberg, C.F. & Tjelta, T.I. (2017a). How understanding past landscapes might inform present-day site investigations: a case study from Dogger Bank, southern central North Sea. *Near Surface Geophysics*, 2017, 15, 403–413.
- Cotterill, C., Phillips, E., James, L., Forsberg, C.F., Tjelta, T.I., Carter, G. & Dove, D. (2017b). The evolution of the Dogger Bank, North Sea: A complex history of terrestrial, glacial and marine environmental change. *Quaternary Science Reviews* 171 (2017), 136–153.
- DeGroot, D.J., Lunne, T., Ghanekar, R., Knudsen, S., Jones, C.D. & Tjelta, T.I. (2019). Engineering properties of low to medium overconsolidation ratio offshore clays. *AIMS Geosciences. Special Issues: Characterization and Engineering Properties of Natural Soils used for Geotesting*. Vol. 5(3): 535–567. <http://dx.doi.org/10.3934/geosci.2019.3.535>
- DNV (2012). *Statistical Representation of Soil Data*, DNV-RP-C207, January 2012.
- Dogger Bank Wind Farm (2022). <https://doggerbank.com/about/>
- Forsberg, C.F., Lunne, T., Vanneste, M., James, L., Tjelta, T. I., Barwise, A. and Duffy, C. (2017). Synthetic CPTs from Intelligent Ground Models based on the integration of geology, geotechnics and geophysics as a tool for conceptual foundation design and soil investigation planning. *Proc. SUT Conference*, London, September, 2017.
- Haldar, A & Mahadevan S. (2000). *Probability, Reliability, and Statistical Methods in Engineering Design*. John Wiley & Sons New York/ Chichester,UK, 2000.
- Hight, D.W., McMillan, F., Powel, J.J.M, Jardine, R.J. & Allenou, C.P. (2003). Some characteristics of London Clay, *Characterisation and Engineering Properties of Natural Soils – Tan et al. (eds.), Swets & Zeitlinger, Lisse*, pp. 851–907.
- Hight, D.W., Ellison, R.A. & Page, D.P. (2004). *Engineering in the Lambeth Group*, CIRIA C583, London 2004.
- Klinkvort, R. T., Sturm, H., Page, A. M., Zhang, Y., & Jostad, H. P. (2020). A Consistent, Rigorous and Super-Fast Monopile Design Approach, In Z. Westgate (Ed.), *4th International Symposium on Frontiers in Offshore Geotechnics*, Austin, Texas. November 8-11, 2021. Hawthorne: Deep Foundations Institute.
- Lunne, T., Berre, T., Strandvik, S., Andersen, K.H. and Tjelta, T.I. (2001) Deepwater Sample Disturbance Due to Stress Relief. *Proc. OTRC Conf.*, April 2001, pp. 64–85.
- Marsland, A. (1974). Comparison of results from static penetration tests and large in situ plate tests in London Clay. *Proc. of the European Sym. on Penetration Testing*, Stockholm, 2.2: 245–252.
- Yetginer-Tjelta T.I., Bødtker S., Rose, M., Lunne, T., Meyer, V. & Duffy, C. (2022). Development of an enhanced CPT tool for offshore wind projects. *Proc. 5th Int. Symp. on Cone Penetration Testing, CPT'22*, Bologna, Italy, 8-10 June 2022.
- Yetginer, G. & Tjelta, T.I. (2020). Bridging knowledge between old and new energy projects. *Proceedings International Symposium on Frontiers in Offshore Geotechnics (ISFOG)*, Austin, Texas, USA, August 2020 (Proceedings issued 2020, conference delayed until 2022).
- Zhang, Y., Khoa, H.D.V., Meyer, V. & Cassidy, M.J. (2015). Jack-up spudcan penetration analysis: review of semi-analytical and numerical methods. *Proceedings International Symposium on Frontiers in Offshore Geotechnics (ISFOG)*, Oslo, Norway, 10-12 June 2015.

Procedures to evaluate seismic settlement in dry sand based on CPT data – an update

Fred Yi

Mid Pacific Engineering Inc., California, USA

ABSTRACT: The seismic settlement of dry sands becomes one of the major geological hazards in areas where loose sandy deposits exist, and groundwater is relatively deep as human activities and urban development moving towards these areas. Research related to the evaluation of seismic settlement of dry sand seems paused for a period since pioneer work of Silver and Seed (1971) in the early 1970's. Later research related to the topic was found by Tokimatsu and Seed (1987) and Pradel (1998). Both papers were based on the use of Standard Penetration Test (SPT). Yi (2010) was the first attempting to evaluate the seismic settlement of dry sand using Cone Penetration Test (CPT) data. In this paper, the procedures to evaluate seismic settlement in dry sand based on CPT data was summarized and the relationship between volumetric strain and cyclic shear strain was updated for CPT data by considering various effects such as fine contents and overburden pressure based on the most recent research findings.

1 INTRODUCTION

Cone Penetration Tests (CPT) have become one of the most used and accepted in situ testing methods for soil investigation in recent year due to its advantages such as the continuation of sampling, the repeatability, and economical efficiency. Various papers were published by researchers for the interpretation and application of CPT data since Robertson and Campanella, as the pioneer, published two major papers in 1983 on the interpretation of CPT data. Most of the later publications were contributed to the interpretations or the application in liquefaction potential evaluations (Robertson, 2009; Robertson & Wride, 1998; Mayne, 2007). In the inland areas where groundwater is relatively deep and soil deposits consist of aeolian accumulations, one of the important applications of CPT is the evaluation of seismic dry sand settlement. Yi (2010a) was the first attempting this application by correlating laboratory test results of volumetric strain of dry sand (Silver & Seed, 1971) and CPT tip resistance. About the same time, Robertson and Shao (2010) also addresses this topic by converting CPT data into equivalent Standard Penetration Test (SPT) blowcounts and applying calculation method developed for SPT data (Pradel, 1998). Since then, the evaluations of seismic dry sand settlement were widely performed in California. In recent years, it is discovered that the cyclic volumetric strain of dry sand is significantly affected by the amount of fines (Yee et al., 2014; Stewart 2014). In this paper, the procedures to evaluate

seismic settlement in dry sand based on CPT data was summarized and the relationship between volumetric strain and cyclic shear strain was updated for CPT data by considering various effects such as fine contents and overburden pressure based on the most recent research findings. The approaches were compared with the results predicted by currently used methods.

2 SEISMIC SETTLEMENT OF DRY SAND

In the simplified method, the evaluation of the seismic settlement of dry sand generally follows the following procedures:

1. Calculate shear stress, τ_{av} .
2. Calculate cyclic shear strain, γ .
3. Calculate volumetric strain, ε_v .
4. Correct for various factors.
5. Calculate accumulated settlement, S_v .

The details of each step were discussed in the following sections.

2.1 Evaluation of cyclic shear stress

Seed & Idriss (1971) proposed an equation to calculate of the average equivalent uniform cyclic shear stress caused by an earthquake as

$$\tau_{av} = 0.65 \cdot (a_{max}/g) \cdot \sigma_{v0} \cdot r_d \quad (1)$$

where a_{max} is the peak horizontal acceleration at ground surface generated by the earthquake, g is the acceleration of gravity, σ_{v0} is the total vertical overburden stresses, and r_d is a stress reduction coefficient. Seed & Idriss (1971) assumed τ_{av} being 65% of the peak cyclic stress. The choice of 0.65 is somewhat arbitrary but has been in use ever since (Idriss & Boulanger, 2008).

Various equations have been proposed to calculate r_d (Seed & Idriss 1971; Lao & Whitman 1986, Seed et al. 2003). The author recommends the equation proposed by Idriss (1999).

$$r_d = \exp[\alpha(z) + \beta(z) \cdot M] \quad (2)$$

$$\alpha(z) = -1.012 - 1.126 \sin(z/11.73 + 5.133) \quad (2a)$$

$$\beta(z) = 0.106 + 0.118 \sin(z/11.28 + 5.142) \quad (2b)$$

where z is the depth below ground surface in meters.

2.2 Evaluation of cyclic shear strain

Utilizing the nonlinear relationship between the shear modulus ratio (G/G_0) and shear strain, the cyclic shear strain induced in the soil can be determined by the following equation.

$$\gamma = \frac{\tau_{av}}{G_0 \cdot (G/G_0)} \quad (3)$$

where G_0 is the maximum shear modulus of the soil. Robertson (2009) proposed a relationship between G_0 and corrected cone resistance, q_t .

$$G_0 = \alpha_G(q_t - \sigma_{v0}) \quad (4)$$

where α_G is the shear modulus factor. For an average unit weight of 18 kN/m³, Robertson obtained

$$\alpha_G = 0.0188 \left[10^{(0.55I_c + 1.68)} \right] \quad (5)$$

where I_c is Soil Behavior Type index.

Due to the nonlinear relationship, the calculation of γ in Eq. 3 usually requires iterations. Using the relationships between the shear modulus and the shear strain obtained experimentally by Iwasaki et al. (1978), Pradel (1998) formulated an equation which avoids the iterative process.

$$\gamma = \left[\frac{1 + a \cdot \exp(b \cdot \tau_{av}/G_0)}{1 + a} \right] \cdot \frac{\tau_{av}}{G_0} \times 100 (\%) \quad (6a)$$

where

$$a = 0.0389(p/p_a) + 0.124 \text{ and } b = 6400(p/p_a)^{-0.6} \quad (6b)$$

where p is the average stress, p_a is the atmospheric pressure. For at-rest condition,

$$p = \left(\frac{1 + 2K_0}{3} \right) \sigma_{v0} \quad (6c)$$

K_0 is the coefficient of lateral earth pressure at rest. Mayne and Kulhawy (1982) found that K_0 depends on the internal frictional angle (φ) of soil and the overconsolidation ratio (OCR) as shown in following equation.

$$K_0 = (1 - \sin \varphi) OCR^{\sin \varphi} \quad (7)$$

2.3 Evaluation of volumetric strain

Under cyclic loading, loose dry sands tend to compress, resulting a settlement at ground surface, termed as seismic dry sand settlement or seismic compression. For clean sand, laboratory tests of past research indicate that the compositional factors principally affecting the seismic compression potential of clean sands is relative density (D_R) and the magnitude of the cyclic shear strain (γ). Volumetric strain generally decreases with increasing relative density and increases with increasing cyclic shear strain.

2.3.1 Relative density

Relative density (D_R) is one of the important parameters affecting the settlement of dry sand under seismic loading. Several correlations between relative density and CPT resistance were proposed in past years (Tatsuoka et al., 1990; Jamiolkowski et al, 2001; Idriss & Boulanger, 2004). Those correlations are generally fallen in a band as shown in Figure 1. Yi (2010) recommended an average correlation as expressed in Eq. 8.

$$D_R = 77.29 \log(q_{c1N}) - 94.36 (\%), \quad (25 \leq q_{c1N} \leq 250) \quad (8)$$

2.3.2 Volumetric strain of clean sand

The relationship between volumetric strain and shear strain of dry sand, termed as volumetric strain material model (VSMM) by UCLA research group, was built based on laboratory tests. The pioneer work

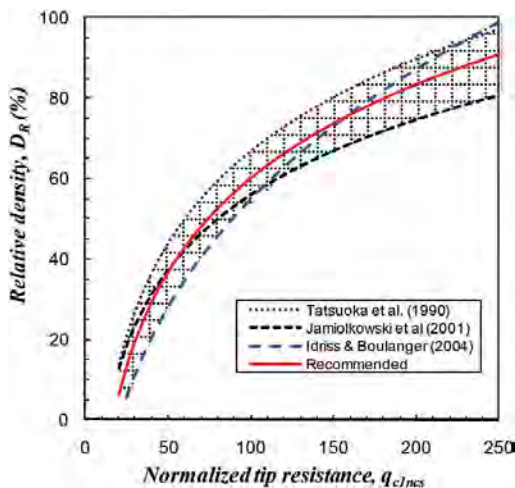


Figure 1. Relations between relative density and equivalent normalized clean sand resistance (after Yi, 2010).

was performed by Silver & Seed (1971). They conducted a series of one-directional cyclic shear tests on dry sand with relative densities of 45, 60, and 80%, and obtained relationships between volumetric and shear strains as shown in Figure 2. These relationships were widely used in the seismic dry sand settlement analysis for SPT data (Tokimatsu & Seed, 1987; Pradel, 1998). Yi (2010) applied the relationships in Figure 2 to CPT tip resistance as shown in Eq. 9.

$$\epsilon_{vc,M=7.5} = 10^n \gamma, \quad n = 18.4 / (q_{c1Ncs})^{0.61} - 1 \quad (9)$$

where q_{c1Ncs} is normalized tip resistance of clean sand.

The test results shown in Figure 2 are based solely on a single clean quartz material (Crystal Silica No. 20). Additional data have been compiled since then on other materials. Unfortunately, the database is inadequate to systematically investigate the effects of compositional and environmental factors on seismic compression susceptibility. The research group in UCLA (Steward & Whang, 2003; Steward et al. 2004; Duku et al., 2008) expanded the database by performing cyclic simple shear tests on various different clean sands. The representative results for $D_R=60\%$ are shown in Figure 4.

Based on the new test results, a new empirical relationship between volumetric strain associated with 15 cycles of loading, $(\epsilon_v)_{N=15}$, and the uniform cyclic shear strain amplitude, γ_c , was developed by UCLA group (Duku et al., 2008).

$$(\epsilon_v)_{N=15} = a(\gamma_c - \gamma_r)^b (\%) \quad (10)$$

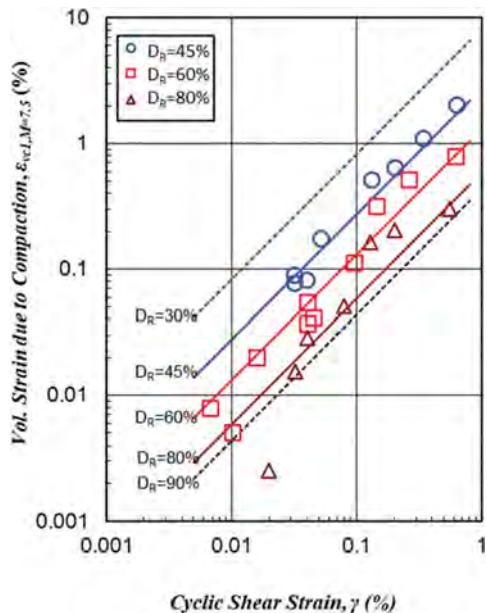


Figure 2. Relationship between volumetric strain and shear strain for dry clean sands (after Silver & Seed 1971).

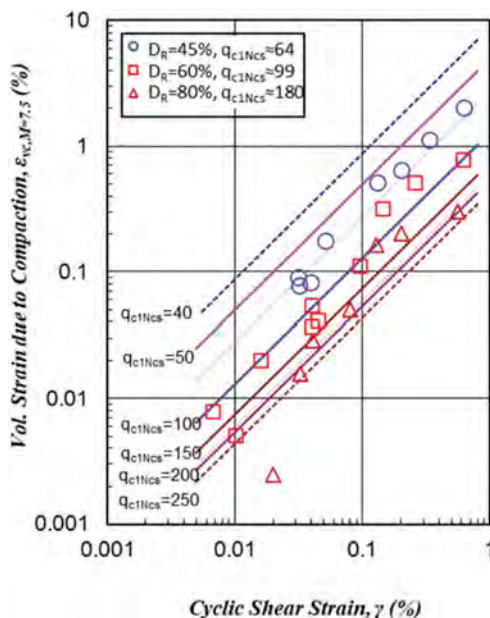


Figure 3. Relationship between volumetric strain, shear strain and normalized CPT tip resistance for dry clean sands (after Yi, 2010).

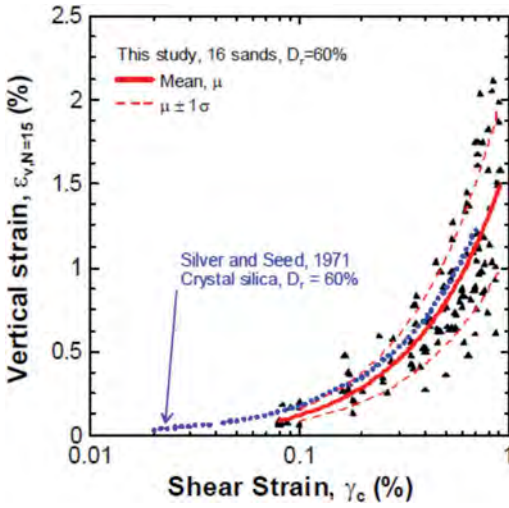


Figure 4. Volumetric strain versus shear strain of 16 clean sands (after Steward & Whang, 2003).

where γ_{tv} is volumetric threshold strain, and a and b are material specific constants. A typical range of γ_{tv} for sands is 0.01–0.03%. For average conditions,

$$a = 5.38 \cdot \exp(-0.023 \cdot D_R) \quad (10a)$$

$$b = 1.2 \quad (10b)$$

By introducing Eq. 8 into Eq. 10, we obtained

$$(\varepsilon_v)_{N=15} = 47.133(q_{c1N})^{-0.772}(\gamma_c - 0.02)^{1.2} \quad (11)$$

that applies to average conditions of clean sand.

2.4 Effects of low plasticity fines

The VSMM developed based on laboratory test results of clean sands limits its application in real engineering practice due to the existence of fines in the subsurface soil materials in most of the project sites. The surface settlement may be over-estimated resulting in over design.

Yee et al. (2014) performed a series of cyclic simple shear tests using natural soils with low plasticity fines contents (FC) between 14 and 35% and natural soils based artificial mixtures with FC values of between 10 and 100%. The effects of fines on seismic compression are expressed by the ratio of the parameter a of Eq. 10 for an arbitrary fines contents to clean sand value ($FC=0$).

$$K_{FC} = (a)_{FC}/(a)_{FC=0} \quad (12)$$

Yee et al. (2014) discovered that this correction factor is generally independent of D_R . The regression of test data shows

$$\begin{aligned} K_{FC} &= 1 & (FC = 0 - 10\%) \\ K_{FC} &= e^{[-0.042(FC-10)]} & (FC = 10\% - FC_L) \\ K_{FC} &= 0.35 & (FC \geq FC_L) \end{aligned} \quad (13)$$

where FC_L is limiting fines content (~35%).

2.5 Other effecting factors

According to Yee et al. (2014), other major factors affect the seismic compression are number of strain cycles (N), overburden pressure (σ_v) and degree of saturation (S). The effects of these factors can be expressed as below:

Effect of Number of Strain Cycles:

$$C_N = \varepsilon_{v,N}/\varepsilon_{v,N=15} = 1 + R \cdot \ln(N/15) \quad (14)$$

where $R = -0.026 \ln(\gamma_c - \gamma_{tv}) + 0.26$ based on regression.

Effect of Overburden Pressure:

$$K_{\sigma,\varepsilon} = (a)_{\sigma}/(a)_{\sigma=1atm} = (\sigma_v/p_a)^{-0.29} \quad (15)$$

where p_a = atmospheric pressure.

Effect of Saturation:

$$K_S = (a)_S/(a)_{S=0} \quad (16)$$

$$\begin{aligned} K_S &= 1 - 0.017S & (S < 30\%) \\ K_S &= 0.5 & (30\% \leq S < 50\%) \\ K_S &= 0.05S - 2 & (50\% \leq S < 60\%) \\ K_S &= 1 & (S \geq 60\%) \end{aligned} \quad (17)$$

2.6 Volumetric strain for any soil conditions

By introducing above discussed factors, the volumetric strain after 15 cycles of loading for any low plasticity sandy and silty soils and at any stress and saturation conditions can be expressed as

$$\varepsilon_{v,N=15} = K_{FC} \cdot K_{\sigma,\varepsilon} \cdot K_S \cdot (\varepsilon_{v,N=15})_{cs} \quad (18)$$

where $(\varepsilon_{v,N=15})_{cs}$ is the volumetric strain of clean sand after 15 cycles of loading calculated using Eq. 10 or 11.

2.7 Volumetric strain at any loading cycle (N)

Eq. 18 is only applicable when there are 15 equivalent uniform strain cycles ($N=15$), typically corresponding to an earthquake magnitude of 7.5. For any loading cycles or earthquake magnitude, the effect of number of strain cycles (Eq. 14) should be incorporated.

$$\varepsilon_{v,N} = C_N \cdot \varepsilon_{v,N=15} = \left[1 + R \ln\left(\frac{N}{15}\right) \right] \cdot \varepsilon_{v,N=15} \quad (19)$$

2.8 Equivalent number of uniform strain cycles

Liu et al. (2001) developed empirical regression equations to evaluate the equivalent number (N) of uniform stress cycles of earthquake shaking as a function of magnitude (M), site-source distance (r), site condition ($S=0$ for rock, $S=1$ for soil), and near-fault rupture directivity effects, using a strong motion data set for tectonically active regions.

$$\ln(N) = \ln \left[\frac{\left(\frac{\exp(b_1 + b_2(M - 5.8))}{10^{1.5M + 16.05}} \right)^{-1/3}}{4.9 \cdot 10^6 \beta} + Sc_1 + rc_2 \right] \quad (20)$$

where r is in km. Stewart et al. (2002) found that the weighting factor set, $b_1 = 1.53$, $b_2 = 1.51$, $c_1 = 0.75$, $c_2 = 0.095$, $\beta = 3.2$, is appropriate for evaluation of equivalent number of uniform strain cycles (N). Figure 5 shows the variation of N with

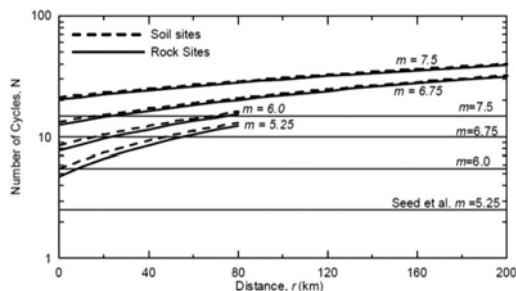


Figure 5. Variation of median values of N with distance and magnitude from Liu et al. (2001) along with recommendations of Seed et al. (1975) (after Stewart & Whang, 2003).

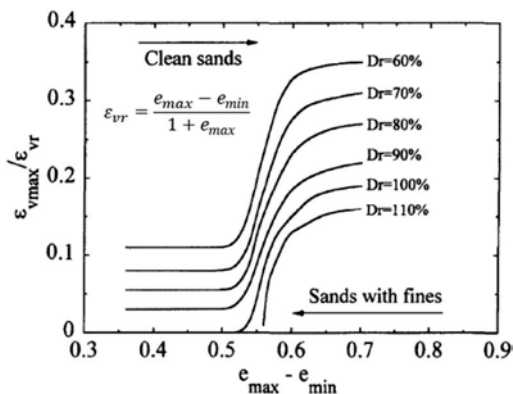


Figure 6. Chart correlating $\varepsilon_{vmax}/\varepsilon_{vr}$ and void ratio range (after Tsukamoto et al. 2004).

source distance for earthquake magnitude from 5.25 to 7.5.

2.9 The potential maximum volumetric strain

In computer programming, one should carefully define the conditions of for each equation to avoid calculating unrealistic mathematic number, e.g., Eq. 6 may calculate very high shear strain if G/G_0 is smaller than 0.1 and consequently Eq. 11 may calculate relatively high mathematic volumetric strain value. In order to evaluate realistic value, an upper bound of the potential maximum volumetric strain, ε_{vmax} , is necessary. This issue was discussed by Tsukamoto et al. (2004) and Yi (2010b). Theoretically, the maximum volumetric strain of sandy material is controlled by void ratio “breath” $e - e_{min}$. Based on laboratory test results of various soils from clean sand to silty sand, Tsukamoto et al. (2004) created a generalized chart correlating the value of $\varepsilon_{vmax}/\varepsilon_{vr}$ and the void ratio range, $e_{max} - e_{min}$, with a series of D_R constant curves as shown in Figure 6. From this diagram, it is possible to estimate the value of $\varepsilon_{vmax}/\varepsilon_{vr}$ for a soil with a given relative density D_R and grain composition represented by the void ratio range $e_{max} - e_{min}$. However, for most of the cases, the grain composition, i.e., e_{max} and e_{min} is unknown resulting a difficulty in direct application of Figure 6. The author analyzed the e_{max} and e_{min} of 25 different soils. Using the mediums of e_{max} and e_{min} , the potential maximum volumetric strain could be expressed as following equation.

$$\varepsilon_{vmax} = 0.274(100 - D_R)(in\%) \quad (21)$$

Without further measured data of soil grain composition, the author suggests using Eq. 21 as the upper bond of the calculated volumetric strain.

2.10 Calculation of total settlement

Eq. 10 was developed based on cyclic simple shear tests. According to Pyke et al. (1975), “the settlement caused by combined horizontal motions are about equal to the sum of the settlement caused by the components acting alone.” As such, the volumetric strain for any magnitude should be calculated using the following equation to account for the effects of multidirectional shaking and earthquake magnitude.

$$\varepsilon_v = 2 \cdot \varepsilon_{v,N} (< \varepsilon_{vmax}) \quad (22)$$

The seismic settlement of dry sand can be evaluated by equating the vertical strain to the volumetric strain and then integrating the vertical strains over the depth interval of concern using following equation:

$$S_{v,1D} = \int_0^{Z_{max}} \varepsilon_v \cdot dz \quad (23)$$

2.11 Summary of procedures

The updated procedures for evaluating seismic settlement of dry sand are summarized in Figure 7 in the form of a flow chart. The flow chart clearly shows the step-by-step process involved in using the proposed integrated method based on the CPT data for evaluating seismic dry sand settlement and indicates the recommended equations for each step of the process.

3 APPLICATION OF THE UPDATED PROCESURES

An example of the seismic dry sand settlement using the updated procedures based on CPT data is shown in Figure 8 for a site located in southern California. Based on soil behavior type, soil profile generally consists of clean sand to sandy silt layers with few thin clay to silty clay and clayey sand to very stiff sand layers. The majority of calculated fines contents ranges from less than 5% to near 50%.

Seismic settlement was calculated using methods proposed by Tokimatsu & Seed (1987), Pradel’s (1998), Yi (2010) and the updated method of this paper. The comparison of calculated shear strain, volumetric strain and accumulated settlement is shown in Figure 8. The shear strain based on proposed and Yi (2010) methods are about identical. The volumetric strain of

proposed method was corrected for fines contents and overburden pressure. The correction for saturation was omitted due to the lack of data. Overall, the calculated accumulated settlement based on UCLA correction is approximate 28 to 54% of the previous methods. This agrees with the case histories reported by Lew & Tran (2012). Lew & Tran (2012) reported a case history of a site consisted mainly sandy silt profile. The observed settlement was reported approximately 20% of that predicted by currently used methods.

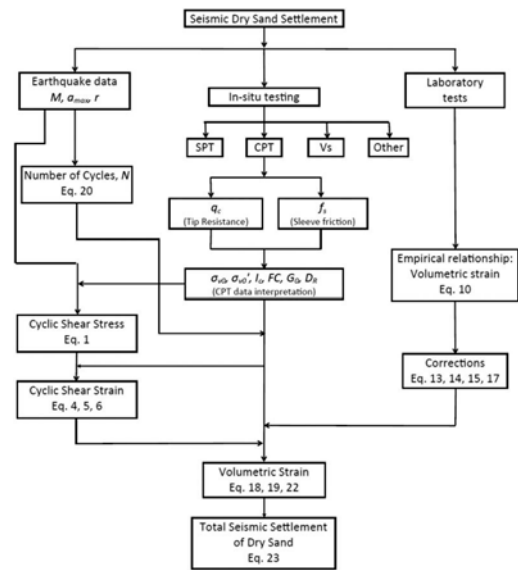


Figure 7. Flow chart illustrating the application of procedure.

4 CONCLUSIONS

This paper updated the procedures for evaluating seismic settlement in dry sand based on CPT data. Efforts were made for the update of the correlation between volumetric strain and shear strain and various corrections such as fines content and overburden pressure utilizing the laboratory test results obtained by UCLA research group. The procedure has been presents in the order of the calculation sequence through a set of equations. The performance of the proposed method was verified by comparing the results obtained using existing methods for field investigation data. The outcome indicates that the proposed method could provide better prediction of seismic dry sand settlement especially for silty soils.

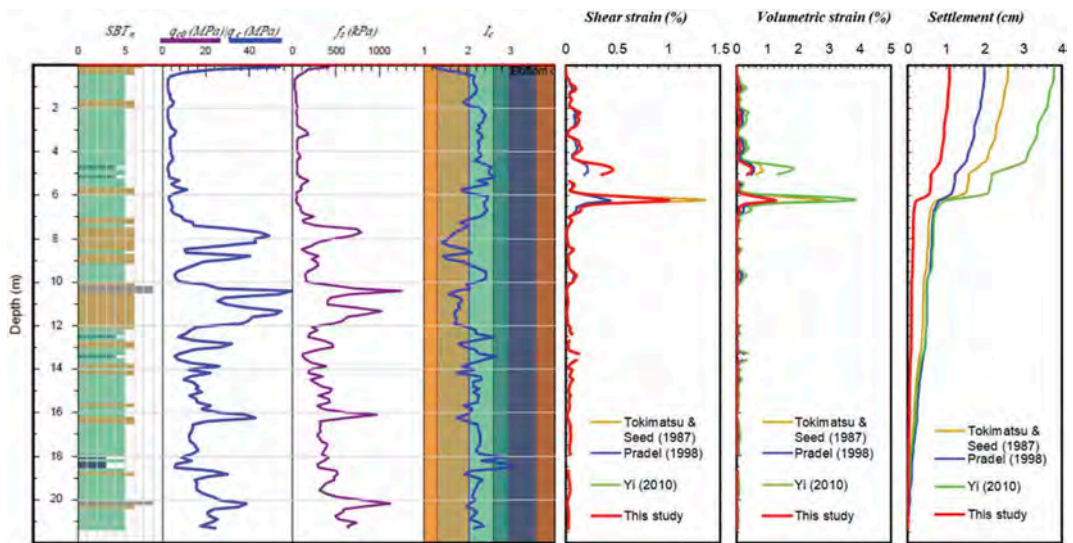


Figure 8. Comparison of shear strain, volumetric strain, and settlement with previous methods.

REFERENCES

- Duku, P. M., Stewart, J. P., Whang, D. H., & Yee, E. (2008). Volumetric strains of clean sands subject to cyclic loads, *J. Geotech. & Geoenv. Engrg.*, ASCE, 134 (8), 1073–1085
- Idriss, I.M., & Boulanger, R.W. (2004). Semi-empirical procedures for evaluating liquefaction potential during earthquakes. *11th ICSDEE/3rd ICEGEP Proceedings*, D. Doolin et al., eds., Stallion Press, Vol. 1, 32–56.
- Idriss, I. M., & Boulanger, R. W. (2008). *Soil Liquefaction During Earthquake*, Earthquake Engineering Research Institute (EERI) Publication MNO-12.
- Iwasaki, T., Tatsuoka, F. & Takagi, Y. (1978) Shear moduli of sand under cyclic torsional shear loadings, *Soils and Foundations*, 18(1), 39–56
- Jamiolkowski, M., LoPresti, D.C.F., & Manassero, M. (2001). Evaluation of Relative Density and Shear Strength of Sands from Cone Penetration Test and Flat Dilatometer Test, *Soil Behavior and Soft Ground Construction (GSP119)*, ASCE, Reston, Va., 2001, pp. 201–238.
- Lew, M., & Tran, L. (2012). Case History of Observed Liquefaction-Induced Settlement versus Predicted Settlement, *Proc., 15th World Conference on Earthquake Engineering*, Lisbon, Portugal, 2012.
- Liu, A. H., Stewart, J. P., Abrahamson, N. A. & Moriwaki, Y. (2001). Equivalent number of uniform stress cycles for soil liquefaction analysis, *J. Geotech. and Geoenv. Engrg.*, ASCE, 127 (12), 1017–1026.
- Pradel, D. (1998). Procedure to evaluate earthquake-induced settlements in dry sandy soils, *J. Geotech. & Geoenv. Engrg.*, ASCE, 124 (4), 364–368.
- Pyke, R., Seed, H.B., Chan, C.K. (1975). Settlement of sands under multidirectional shaking, *J. Geotech. Engrg.*, ASCE, 101 (4), 379–398.
- Robertson, P.K. (2009). Interpretation of Cone Penetration Tests - a unified approach. *Canadian Geotechnical Journal*, 46 pp 1337–1355
- Seed R.B. & et al. (2003). *Recent Advances in Soil Liquefaction Engineering: A Unified and Consistent Framework*, UC Berkeley, Report No. EERC 2003-06.
- Seed, H.B., & Idriss, I.M. (1971). Simplified procedure for evaluating soil liquefaction potential, *J. Soil Mech. and Found. Div.*, 97 (9), 1249–273.
- Silver, M. L., & Seed, H. B. (1971). Volume changes in sand during cyclic loading, *J. Soil Mech. and Found. Div.*, 97 (9), 1171–182.
- Stewart, J. P. & Whang, D. H. (2003) Simplified procedure to estimate ground settlement from seismic compression in compacted soils, *Proc. 2003 Pacific Conference on Earthquake Engineering*, Christchurch, New Zealand, Paper 46.
- Stewart, J. P., Whang, D. H., Moyneur, M., & Duku, P. (2004). *Seismic compression of As-compacted Fill Soils with Variable Levels of Fine Content and Fine Plasticity*, CUREE Publication No. EDA-05.
- Tatsuoka, F., Zhou, S., Sato, T., & Shibuya, S. (1990). *Method of evaluating liquefaction potential and its application. Rep. on Seismic hazards in the soil deposits in urban areas*, Ministry of Education of Japan, 75–109 (in Japanese).
- Tokimatsu, K. & Seed, H.B. (1987). Evaluation of settlements in sands due to earthquake shaking, *J. Geot. Engrg.*, 113 (8), 861–878.
- Tuskamoto, Y., Ishihara, K. & Sawada, S. (2004). Settlement of Silty Deposits Following Liquefaction During Earthquakes, *Soils and Foundations*, Vol. 44, No. 5, 135–148
- Yi, F. (2010a). Case Study of CPT Application to Evaluate Seismic Settlement in Dry Sand, *The 2nd International Symposium on Cone Penetration Testing*, Huntington Beach, California, USA, May 9-11, 2010.
- Yi, F. (2010b). Procedure to Evaluate Seismic Settlement in Dry Sand Based on Shear Wave Velocity, *The 9th U.S. National and 10th Canadian Conference on Earthquake Engineering (9USN/10CCEE)*, Toronto, Canada, July 25-29, 2010.
- Yoshimine, M., Nishizaki, H., Amano, K. & Hosono, Y. (2006). Flow deformation of liquefied sand under constant shear load and its application to analysis of flow slide of infinite slope, *Soil Dyn. and Earthquake Engrg.*, 26 (2-4), 253–264.

Author Index

- Abraimi, R. 889
Adams, N. 275
Agaiby, S.S. 552
Albino, J.L. 793
Al-Sammarraie, D. 799, 825
Amorosi, A. 294
Amoroso, S. 190, 806, 883, 1071
Angeles, M. 728
Arroyo, M. 332, 339, 591
Askarinejad, A. 1143
Attar, I.H. 926
Augustesen, A.H. 176, 275, 420
- Bacic, M. 1053
Bahrami, M. 387, 926
Bahrami, T. 387, 926
Bandiera, E. 938, 944, 1004
Bandyopadhyay, K. 955
Barati Nia, A. 282
Baris, A. 708, 1035
Bartczak, K. 288
Barth, R. 275
Barwise, A. 275, 420
Bascunan, S. 812
Bassi, A. 300
Bates, L. 473
Baziw, E. 109, 115
Behroozian, K. 926
Bellio, M. 247
Benz Navarrete, M.A. 1058
Berbert, L.A. 427
Berenguer Todo Bom, L. 819
Bersan, S. 646
Bertolini, I. 294, 300
Besenzon, D. 1071
Bhaskar, A. 825
Bicalho, K.V. 677
Bilici, C. 275
Bisht, V. 16
Bittar, E. 3, 967
Bittar, E.J. 832, 838
Blake, A.P. 838
Blaker, Ø. 138, 1156
- Borgström, K. 452
Boschi, A. 998
Bøtker-Rasmussen, S. 176, 266
Bottaro, F. 247
Bourrier, F. 1016
Brand, F. 617
Bransby, M.F. 214, 1023, 1149
Bray, J.D. 844, 894
Brinkgreve, R.B.J. 503, 509, 540
Bruno, L. 294
Brzeziński, B. 760
Buò, B. Di 356
Burbury, D. 275, 420
Burton, C. 979
- Cáceres, M. 850
Cafferri, L. 1156
Cai, G. 363, 784
Calabrese, L. 949
Camacho, C.B. 857
Camacho, M.A. 857
Capotosto, A. 247
Carey, T.J. 325
Cargill, E. 559
Carnero-Guzman, G. 1113
Carotenuto, P. 275, 420
Carpentier, S. 641
Carrington, T. 220
Cassidy, M.J. 766
Cavallaro, A. 311
Ceccato, F. 863
Cerfontaine, B. 900
César Gomes, R. 913
Chareyre, B. 1102
Charles, J.A. 870
Chen, R. 363
Chia, R.W.L. 317
Chiaradonna, A. 325, 876
Chow, S.H. 1077
Ciantia, M.O. 623
Cocjin, M. 1149
Colella, V. 883, 944
Collico, S. 332, 339
- Congress, S.S.C. 363
Conn, A. 900
Cooper, J. 778
Cordeiro, D. 584
Corrales, S. 345
Cortellazzo, G. 883, 944
Coughlan, M. 345
Creasey, J. 900
Cubrinovski, M. 876, 894
- da Fonseca, A.V. 683
Dano, C. 1102
Danziger, F.A.B. 306
Das, K. 955
De Backer, G. 121
de Gast, T. 889
De La Rosa R., J.M. 351
de Lange, D.A. 126
de Lange, D. 1143
De Sordi, J. 1156
De Vries, G. 288
de Wit, S. 275, 420
Dei Svaldi, A. 883, 944
DeJong, J.T. 282, 325, 368
Delgado, B.G. 913
Deu, A. 332, 339
DeVincenzi, M. 332, 339
Dhakal, R. 894
Dhimitri, L. 651, 979
Di Buò, B. 132, 356, 497, 552
Diambra, A. 900
Dias, H. 275, 420
Dijkstra, J. 480
Dodaro, E. 414
Doherty, J. 1023
Doherty, J.P. 1095
Dominijanni, A. 907
Dong-Woo, M. 164
Donohue, S. 345
dos Santos Junior, M.P. 913
Duan, W. 363, 784
Duffy, C. 266, 1156
D'Ignazio, M. 132, 356

- Entezari, I. 374
Erbrich, C. 275
Esford, F. 985
Eslami, A. 598, 920
Exley, B. 381
- Fabozzi, S. 1035
Fabris, C. 445
Fakharian, K. 387, 926
Falquez, D. 1071
Faour, G.A. 932
Farhadi, M.S. 394, 400
Ferreira, C. 584, 683
Fetrati, M. 407
Fiera, F. 715
Fioravante, V. 275, 414, 420, 949
Fiorelli, F. 938, 944, 1004
Fityus, S. 473
Flores López, F.A. 351
Flores-Eslava, R. 1048
Franceschini, M. 938, 944, 1004
Franken, T. 203
Freire, M.M. 427
Freudenthaler, T. 697
Fu, X. 967
Fumeron, J. 850
- Gabassi, M. 907
Galavi, V. 407
Gallipoli, D. 247
Gao, L. 577
García Martínez, M.F. 806
Gavin, K. 812, 1143
Gavin, K.G. 889, 1053
Gens, A. 591
Ghanekar, R.K. 183
Gharehaghajlou, A. 445
Giacheti, H.L. 670
Giretti, D. 275, 414, 420, 949
Giuliani, G. 1131
Goh, S.H. 317, 753
Gomez Bautista, D. 722
Gómez Meyer, E. 220
Goodarzi, M. 407, 799
Gottardi, G. 209, 294, 300, 414, 432, 806, 998
Gourvenec, S. 900
Gourvenec, S.M. 870
Govoni, L. 1016
Gragnano, C.G. 414
- Green, R.A. 778
Gu, X.Q. 703
Gundersen, A.S. 138
- Haasnoot, J. 646
Haelterman, K. 121
Haikola, M. 132, 497
Halder, A. 955
Hammer, H.B. 438, 690
Harada, K. 772
Hauser, L. 445, 617
He, B. 961
He, R. 961
Hededal, O. 1065
Hegedüs, M. 473
Heidarie Golafzani, S. 598, 920
Hov, S. 452
Hu, J. 703
Hu, Y.X. 766
Hu, Y. 459
Huang, B. 967
Huffman, A.P. 282
Hutabarat, D. 844
- Ibarra-Razo, E. 1048
Ibraim, E. 900
Igoe, D. 900, 973, 991
Illés, Z. 466
Illingworth, D. 979
Illingworth, F. 636, 979, 1071
Imre, E. 473
Incardona, E. 1102
Ingarfield, S. 214, 275
Isaev, O.N. 144, 151
Isaksson, J. 480
Ito, T. 772
- Jaber, R. 158
Jacobsz, S.W. 604
Jacoby, J. 381
Jacquard, C. 1107
Jang, I. 164
Jannuzzi, G.M.F. 306
Jewell, R.A. 741
Joseph, T. 1131
- Kádár, I. 466
Kaltekis, K. 486, 812
Kang, H. 164
Kanitz, M. 819
Karlsson, M. 480
- Karthikeyan, M. 170
Kashkooli, M. 387
Kermani, M. 985
Kheffache, A. 722
Khin, P.S. 610
Khouri, K.N. 932
Kim, H. 528
Kluger, M.O. 799
Knuuti, M. 497
Koreta, O. 176
Kortbawi, M.E. 368
Kovačević, M.S. 1053
Kreiter, S. 407, 799, 825
Krogh, L. 138, 176, 183, 275, 420, 1137
Kwon, O. 164
- Lacasse, S. 3
Ladefoged, P. 1137
Lagosha, D. 491
Länsivaara, T. 132, 356, 394, 400, 497
Lapastoure, L.-M. 991
Lehane, B.M. 3, 734, 832, 838
Lengkeek, H.J. 503, 509, 540
Leonet, J. 900
Leth, C.T. 1137
Levy, N. 1149
Li, J. 961
Lindeboom, R. 420
Lindeboom, R.C.J. 275
Liu, S. 363, 784
Liu, Z. 3
Long, M. 28, 345, 515
Lontzetidis, K. 521
Low, H.E. 214, 1149
Lundvig, K. 176
Lunne, T. 138, 183, 220, 266, 275, 400, 420, 1137, 1156
Luong, T.A. 1058
Luque, R. 1042, 1071
L'Heureux, J.S. 356, 400
L'Heureux, J.-S. 438, 515, 630, 690
- Ma, Q.Z. 577
Machado, L.S. 793
Mahdavi, S. 838
Mahler, A. 466
Makra, A. 528

- Mántaras, F.M. 534
 Marchetti, D. 190, 617, 715, 806
 Marchi, F. 998
 Marchi, G. 998
 Marchi, M. 294, 300
 Marcolongo, M. 209
 Marques, M.E.S. 427
 Marte, R. 445, 617, 697
 Martin, E.R. 778
 Martinez, G. 1004
 Marzouk, I. 540
 Mastrangelo, A. 998
 Mayne, P.W. 374, 546, 552, 559
 McCallum, A.B. 1010
 McConnell, A.J. 197
 Menegaz, T. 566
 Mentani, A. 1016
 Meyer, V. 266, 1156
 Milheiro-Oliveira, P. 1065
 Minardi, A. 907
 Minarelli, L. 806, 883
 Miranda, V.H. 857
 Młynarek, Z. 570
 Mo, P.Q. 577
 Modoni, G. 708, 1035
 Moffat, R. 850
 Mohammed, M.B. 973
 Mohr, H. 258
 Mohtashamamiri, D. 926
 Molina-Gómez, F. 584
 Monaco, P. 94, 190, 570, 806
 Monforte, L. 591
 Morton, D.J. 521
 Mörz, T. 407, 799, 825
 Moshfeghi, S. 920
 Moug, D.M. 282, 368
 Murray, I. 1029
 Mylonakis, G. 900
- Nadim, F. 3
 Naghibi, M.H. 598
 Nagy, G. 466
 Nagy, L. 466
 Nandi, S. 955
 Narainsamy, Y. 604
 Nenci, N. 715
 Nguyen, T.D. 610
 Nierwinski, H.P. 566
 Nordal, S. 438, 690
 Notenboom, P.D. 889
 Ntritsos, N. 876
- Oberhollenzer, S. 445, 617, 697
 Odebrecht, E. 534, 566
 Oliynyk, K. 623
 Ooms, B. 235
 O'Brien, A. 1029
 O'Loughlin, C.D. 1149
 O'Neill, M.P. 1023
- Paduli, F. 540
 Pagani, E. 715
 Paniagua, P. 356, 452, 552, 630
 Pant, S. 214
 Paolella, L. 708, 1035
 Parasie, N. 203
 Paredes, J. 636, 1042
 Pavan, S. 907
 Pereira, F.S. 534
 Perini, L. 949
 Perini, M. 715
 Peters, D.J. 126
 Peuchen, J. 203, 220, 486, 546, 641
 Pfeifer, S. 617
 Pham, Q.N. 610
 Pinheiro, A.V.S. 306
 Pippi, M. 646
 Pisanò, F. 1143
 Powell, J.J.M. 651
 Prendergast, L.J. 1126
 Presti, D.L. 715
 Prezzi, M. 16, 1089
 Puppala, A.J. 363, 784
 Pynch, A. 381
- Ramondini, M. 1083
 Ramsey, N. 657, 664
 Ranalli, M. 432
 Randolph, M.F. 214, 1095
 Rangel-Núñez, J.L. 241, 1048
 Rapanakis, P. 1102
 Reale, C. 889, 1053
 Reiffsteck, P. 1058, 1107
 Richards, D.J. 838
 Rios, S. 1065
 Ripalda, F. 1071
 Rispal, M. 1107
 Robertson, P.K. 521
 Rocchi, I. 209
 Rocha, B.P. 670
 Rodrigues, R.A. 670
 Rodriguez, A. 332, 339
- Rollins, K.M. 806, 883
 Rose, M. 266, 1156
 Rosso, A. 300
 Roy, A. 1077
 Russo, G. 1083
- Sacchetto, M. 253
 Sadrabadi, H.H. 1102
 Safaqaq, O. 214
 Sakleshpur, V.A. 1089
 Salgado, R. 16, 1089
 Santos, M.D. 677
 Santos, R. 183
 Sastre Jurado, C. 722
 Schnaid, F. 534, 566
 Schneider, J.A. 1095
 Schweiger, H.F. 445, 617
 Selänpää, J. 356, 497
 Seo, J. 164
 Shahgholian, R. 683
 Sharafutdinov, R.F. 151
 Sharma, A. 1102
 Sharp, J. 374
 Shelton, P. 979
 Shin, C. 164
 Sibille, L. 1102
 Silva, M.F. 1149
 Silva Ribeiro, S.G. 913
 Simonini, P. 863
 Siviero, M. 715
 Skrede, H. 438, 690
 Slowiok, M. 697
 Soage Santos, R. 55, 220
 Sokolov, I.S. 741
 Sokolov, I. 1, 491
 Song, Y. 703
 Sougla, M.-C. 420
 Sougla, M.-C. 275
 Sousa, L. 1065
 Souza J., T.A.T. 793
 Spacagna, R.L. 708, 1035
 Stacul, S. 715
 Stanier, S.A. 258
 Stark, N. 158
 Stefaniak, K. 760
 Stelzer, R. 138
 Storteboom, O. 229, 235, 241
 Strandvik, S. 1156
 Stuyts, B. 722
 Surya Sarat Chandra Congress 784
 Szymkiewicz, F. 1058

Tamagnini, C. 623
 Tanaka, C. 728
 Tao, X.L. 577
 Tarantino, A. 247
 Tassi, M.C. 427
 Taylor, M. 1137
 Teyssier, A. 1107
 Tho, K.K. 657
 Thunder, B. 381
 Tian, Y. 734, 832
 Tincopa, M. 1113
 Togliani, G. 1119
 Tonni, L. 209, 294, 300,
 394, 432, 806, 998
 Totani, F. 190
 Totani, G. 190
 Tott-Buswell, J. 1126
 Trafford, A. 345
 Trubshaw, M.P. 1131
 Tschuchnigg, F. 540
 Tucker, G.W. 138, 183,
 1137

 Uzielli, M. 81, 432, 863

 Vaezian, H. 387
 van den Bosch, J. 275
 van Dijk, B. 812
 van Duinen, T.A. 126
 van Erp, F. 641
 van Kesteren, W. 641

 van Zanten, D.V. 1143
 Vandeweyer, V. 641
 Vardy, M.E. 870
 Vecchiotti, A. 1083
 Verastegui-Flores, R.D. 121
 Verbeek, G. 109, 115
 Verhagen, J. 229
 Vervaele, W. 121
 Viana da Fonseca, A. 584,
 1065
 Villalobos, F.A. 850
 Vincke, L. 121
 Vinco, G. 253
 Vink, R. 646
 Volkov, N.G. 741
 Volkov, N. 225, 491
 Vrettos, C. 747
 Vu, A.T. 610

 Wang, A. 363
 Wang, H. 1143
 Wang, Y. 459
 Wang, Z.Z. 317, 753
 Ward, D. 979
 Wassenaar, E.J.C. 197
 Watanabe, E. 772
 Watson, P. 1023
 Westgate, Z.J. 214
 White, D. 900
 White, D.J. 66, 258, 838
 White, G. 1010

 Wierzbicki, J. 570, 760
 Wilczyński, S. 760
 Wissmann, K. 1004
 Wissmann, K.J. 806
 Wong, J.Y. 728
 Woollard, M. 229, 235,
 241
 Wroth, H.M. 1149
 Wu, M. 784

 Xie, Q. 766

 Yabe, H. 772
 Yang, S. 961
 Yannie, J. 480
 Yerro, A. 778
 Yetginer, G. 220
 Yetginer-Tjelta, T.I. 266,
 1156
 Yi, F. 1164
 Yost, K.M. 778
 Yu, H.S. 577

 Zakatov, D.S. 151
 Zambianchi, E. 998
 Zhang, Y. 967
 Zhao, Z. 363, 784
 Zheng, X. 753
 Zhou, M. 766
 Ziotopoulou, K. 325,
 368